



# Modern Aspects of Rare Earths and their Complexes

V.S. Sastri

J.-C. Bünzli

V. Ramachandra Rao

G.V.S. Rayudu

J.R. Perumareddi

ELSEVIER B.V.  
Sara Burgerhartstraat 25  
P.O. Box 211, 1000 AE Amsterdam, The Netherlands

© 2003 Elsevier B.V. All rights reserved.

This work is protected under copyright by Elsevier, and the following terms and conditions apply to its use:

#### Photocopying

Single photocopies of single chapters may be made for personal use as allowed by national copyright laws. Permission of the Publisher and payment of a fee is required for all other photocopying, including multiple or systematic copying, copying for advertising or promotional purposes, resale, and all forms of document delivery. Special rates are available for educational institutions that wish to make photocopies for non-profit educational classroom use.

Permissions may be sought directly from Elsevier's Science & Technology Rights Department in Oxford, UK: phone: (+44) 1865 843830, fax: (+44) 1865 853333, e-mail: [permissions@elsevier.com](mailto:permissions@elsevier.com). You may also complete your request on-line via the Elsevier homepage (<http://www.elsevier.com>), by selecting 'Customer Support' and then 'Obtaining Permissions'.

In the USA, users may clear permissions and make payments through the Copyright Clearance Center, Inc., 222 Rosewood Drive, Danvers, MA 01923, USA; phone: (+1) (978) 7508400, fax: (+1) (978) 7504744, and in the UK through the Copyright Licensing Agency Rapid Clearance Service (CLARCS), 90 Tottenham Court Road, London W1P 0LP, UK; phone: (+44) 207 631 5555; fax: (+44) 207 631 5500. Other countries may have a local reprographic rights agency for payments.

#### Derivative Works

Tables of contents may be reproduced for internal circulation, but permission of Elsevier is required for external resale or distribution of such material.

Permission of the Publisher is required for all other derivative works, including compilations and translations.

#### Electronic Storage or Usage

Permission of the Publisher is required to store or use electronically any material contained in this work, including any chapter or part of a chapter.

Except as outlined above, no part of this work may be reproduced, stored in a retrieval system or transmitted in any form or by any means, electronic, mechanical, photocopying, recording or otherwise, without prior written permission of the Publisher.

Address permissions requests to: Elsevier's Science & Technology Rights Department, at the phone, fax and e-mail addresses noted above.

#### Notice

No responsibility is assumed by the Publisher for any injury and/or damage to persons or property as a matter of products liability, negligence or otherwise, or from any use or operation of any methods, products, instructions or ideas contained in the material herein. Because of rapid advances in the medical sciences, in particular, independent verification of diagnoses and drug dosages should be made.

#### First edition 2003

#### Library of Congress Cataloging in Publication Data

A catalog record from the Library of Congress has been applied for.

#### British Library Cataloguing in Publication Data

A catalogue record from the British Library has been applied for.

ISBN: 0 444 51010 9

Ⓢ The paper used in this publication meets the requirements of ANSI/NISO Z39.48-1992 (Permanence of Paper).

Printed in The Netherlands.

# MODERN ASPECTS OF RARE EARTHS AND THEIR COMPLEXES

**DR. V.S. SASTRI**

Sai Ram Consultants  
Ottawa, Canada

**DR. JEAN-CLAUDE BÜNZLI**

Swiss Federal Institute of Technology  
Lausanne, Switzerland

**DR. V. RAMACHANDRA RAO**

Professor Emeritus  
Nagpur University  
Nagpur, India

**DR. G.V.S. RAYUDU**

Professor of Nuclear Medicine  
Rush University  
Chicago, USA

**DR. J.R. PERUMAREDDI**

Professor of Chemistry  
Florida Atlantic University  
Boca Raton, Florida, USA



ELSEVIER

2003

Amsterdam - Boston - Heidelberg - London - New York - Oxford - Paris  
San Diego - San Francisco - Singapore - Sydney - Tokyo

---

## PREFACE

---

The rare earth elements form a fascinating group, resembling each other very closely in both physical and chemical properties. The close similarity of the behaviour of the elements led to difficulties in isolation of the elements in a state of high purity. Now that the separation and purification of these elements have been achieved, the chemistry and the industrial applications of the rare earth elements are drawing the attention of many scientists in the world, especially countries which possess vast reserves of rare earth minerals. Some of the applications of mixed rare earths are as metallurgical additives for ferrous and non-ferrous metals, fluid cracking catalysts, lighter flints, polishing compounds in glasses, carbon arc cores for lighting and hydrogen absorbing alloys for rechargeable batteries. Some of the salient applications of high-purity rare earth elements are cathode ray tubes, automotive catalytic converters, permanent magnets in computer technology and sound systems, lasers, phosphors, electric motors, optical fibres, and possible future applications such as in coloured pigments for plastics and paints, new catalysts, refrigeration systems and solid oxide fuel cells.

In order to use rare earths successfully in various applications, a good understanding of the chemistry of these elements is of paramount importance. Nearly three to four decades have passed since titles such as *The Rare Earths* edited by F.H. Spedding and A.H. Daane, *The chemistry of the Rare Earth Elements* by N.E. Topp and *Complexes of the Rare Earths* by S.P. Sinha were published. There have been many international conferences and symposia on rare earths, as well as the series of volumes entitled *Handbook of Physics and Chemistry of Rare Earths* edited by K.A. Gschneidner and L. Eyring. Thus, there is a need for a new title covering modern aspects of rare earth complexes along with the applications.

The present title consists of twelve chapters. The first chapter is an introduction covering definition, classification, properties, world reserves, methods of processing from ores, methods of separation both classical and modern, and analytical chemistry of rare earths, including classical and modern methods.

The second chapter deals with quantum chemical considerations, s, p, d and f orbitals, electronic configurations, Pauli's principle, spin-orbit coupling and levels, energy level diagrams, Hund's rules, Racah parameters, oxidation states, HSAB principle, coordination number, lanthanide contraction, interconfiguration fluctuations. This is followed by a chapter dealing with methods of determination of stability constants, stability constants of complexes, thermodynamic consideration, double-double effect, inclined w plot, applications of stability constant data.

The fourth chapter deals with complexes of rare earth elements with a variety of complexing agents, such as monocarboxylic acids, dicarboxylic acids, polycarboxylic acids like citric, nitrilotriacetic, ethylenediamine tetraacetic; beta diketones, ligands with

nitrogen donors, macrocyclic ligands, ligands with sulphur donors, phosphines, cyanate, thiocyanate, selenocyanate, perchlorate, decaborates, acyclic and macrocyclic Schiff's bases, carboranes, selenides and tellurides.

Structural chemistry of lanthanide complexes dealing with low coordination numbers, 6-, 7- and 8-coordination, dodecahedra, square antiprisms, hexagonal bipyramids, cubes and other structures, 9-coordination, high coordination numbers and organometallic structures is discussed in the fifth chapter.

Organometallic complexes such as tris, bis and monocyclopentadienyl complexes, cyclooctatetraenyl complexes, cyclopentadienyl–cyclooctatetraenyl complexes, indenyl complexes, fluorenyl complexes, complexes with other aromatic ligands, callixerene complexes, NMR spectroscopy of organometallic complexes, vibrational spectra, and catalytic applications form the theme of the sixth chapter.

Kinetics and mechanisms complex formation involving rate expressions, rate laws, dissociative and associative pathways, techniques used in probing reaction mechanisms, crystal field effects are discussed in the following chapter.

Crystal field theory, intensities of  $4f-4f$  transitions, Judd–Ofelt theory of electric–dipole transitions, covalency model of hypersensitivity, dynamic coupling mechanism, solution spectra, spectral data for complexes, solvent effects, fluorescence and photochemistry of lanthanide complexes are dealt with in spectroscopy of lanthanide complexes.

Photoelectron spectroscopy of rare earths involving typical spectra, core levels, splitting due to exchange, spin–orbit coupling, binding energies, states arising due to ionization of  $f^n$  configuration, interconfiguration fluctuation and surface oxidation phenomena are discussed in the next chapter. The following chapter deals with the important topic of lanthanide NMR shift reagents and their applications in elucidating structures. The penultimate topic deals with ecological, physiological and environmental aspects along with some interesting biological applications.

In the final chapter, applications such as in metallurgy of steels, corrosion inhibition, catalysis, paints, cinema arc carbon and search light electrodes, polishing powders in optics, permanent magnets, ceramic superconductors, lasers, garnet films for magnetic bubble memory applications, nuclear applications, X-ray phosphors for medical radiology, fiber optics, photonics, electronics, magnetic resonance imaging (MRI) high-tech applications and fuel cells are elucidated.

The authors studied in schools headed by pioneers in rare earth chemistry, have a combined experience of one hundred and fifty years in inorganic chemistry, rare earth complex chemistry, nuclear and radiochemistry of rare earths and supramolecular chemistry. The present monograph is a product of this rich experience.

V.S. Sastri  
J.-C.G. Bünzli  
V.R. Rao  
G.V.S. Rayudu  
J.R. Perumareddi

chapter 1

---

INTRODUCTION

---

---

# CONTENTS

---

1. Rare earth reserves . . . . .	5
2. Rare earth markets . . . . .	5
3. Formation of lanthanide ores . . . . .	8
4. Rare earth sources . . . . .	10
5. Recovery of rare earths from ores . . . . .	16
6. Separation of rare earths . . . . .	19
7. Ion exchange chromatography . . . . .	22
8. Displacement chromatography . . . . .	22
9. Liquid–liquid ion-exchange chromatography . . . . .	26
10. Solvent extraction . . . . .	28
11. Recovery of rare earths from monazite . . . . .	33
12. Preparation of rare earth metals . . . . .	46
13. Analytical chemistry of rare earths . . . . .	47
14. Spectrophotometric method of analysis of rare earth elements . . . . .	61
15. Emission spectroscopy . . . . .	63
16. Neutron activation analysis . . . . .	63
17. X-ray spectroscopy . . . . .	65
18. Atomic absorption, flame emission, electrothermal atomization, inductively coupled mass spectrometry . . . . .	66
19. Inductively coupled plasma mass spectrometry (ICPMS) . . . . .	68
20. High pressure liquid chromatography (HPLC) . . . . .	68
20.1. Separation of rare earths by “dynamic coating” ion-interaction chromatography . . . . .	68
References . . . . .	69

The name rare earths is a misnomer since these elements are neither rare nor earths. The name rare earths referring to elements with atomic numbers 58 to 71 may have arisen because they were initially isolated as oxides which, in some ways, resemble calcium, magnesium and aluminum oxides known as common earths. A chronological summary of the discovery of the elements is given in Table 1.1.

The descriptive classification of rare earths is as follows:

Light earths (La to Eu)	Middle earths (Sm to Ho)	Heavy earths (Gd to Lu)
Lanthanium—57	Samarium—62	Gadolinium—64
Cerium—58	Europium—63	Terbium—65
Praseodymium—59	Gadolinium—64	Dysprosium—66
Neodymium—60	Terbium—65	Holmium—67
Promethium—61	Dysprosium—66	Erbium—68
Samarium—62	Holmium—67	Thulium—69
Europium—63		Ytterbium—70
		Lutetium—71

The natural abundance of the rare earths is given in Table 1.2.

Clearly, La, Ce and Nd are quite abundant followed by Pr, Sm, Gd, Dy, Er and Yb of moderate abundance and followed by Eu, Tb, Ho, Tm and Lu present in the range of 0.3 to

TABLE 1.1  
Chronological order of discovery of rare earths.

Rare earths	Discoverer	Year
Discovery of yttria	Gadolin	1794
Discovery of ceria	Berzelius, Hisinger	1804
Discovery of lanthana	Mosander	1839
Discovery of didymia	Mosander	1841
Discovery of yttria, terbia and erbia	Mosander	1843
Discovery of ytterbia	DeMarignac	1878
Discovery of scandia	Nilson	1879
Discovery of thulia and holmia	Cleve	1879
Discovery of dysprosia	De Boisbaudrau	1886
Discovery of lutetia and ytterbia	Urbain and Von Welsbach	1907
Discovery of samaria	De Boisbaudrau	1879
Discovery of gadolinia	De Boisbaudrau	1886
Isolation of neodymium and praseodymium	Von Welsbach	-
Discovery of europium	Demarcay	1901
Discovery of promethium	Marinsky and Coryell	1948



TABLE 1.2  
Natural abundance of rare earth elements [1].

Element	Z	Abundance (g/ton)
La	57	19
Ce	58	44
Pr	59	5.6
Nd	60	24
Pm	61	Radioactive
Sm	62	6.5
Eu	63	1.0
Gd	64	6.3
Tb	65	1.0
Dy	66	4.3
Ho	67	1.2
Er	68	2.4
Tm	69	0.3
Yb	70	2.6
Lu	71	0.7

TABLE 1.3  
Some physical properties of rare earth metals [2].

Element	Symbol	At. no.	At. wt.	Terrestrial abundance (ppm)	M.P. (°C)	B.P. (°C)	Density (g/cm <sup>3</sup> )	Crystal structure
Yttrium	Y	39	88.90	28	1522	3338	4.469	hcp
Lanthanum	La	57	139.91	18	918	3464	6.145	dhcp
Cerium	Ce	58	140.12	46	798	3433	6.770	fcc
Praseodymium	Pr	59	140.90	5.5	931	3520	6.773	dhcp
Neodymium	Nd	60	144.24	24	1021	3074	7.007	dhcp
Promethium	Pm	61	147.00	—	1042	3000*	7.260	dhcp
Samarium	Sm	62	150.35	6.5	1074	1794	7.520	rhomb
Europium	Eu	63	151.96	1.0	822	1529	5.243	bcc
Gadolinium	Gd	64	157.25	6.4	1313	3273	7.900	hcp
Terbium	Tb	65	158.92	0.9	1356	3230	8.229	hcp
Dysprosium	Dy	66	162.50	4.5	1412	2567	8.550	hcp
Holmium	Ho	67	164.93	1.2	1474	2700	8.755	hcp
Erbium	Er	68	167.26	2.5	1529	2868	9.066	hcp
Thulium	Tm	69	168.93	0.2	1545	1950	9.321	hcp
Ytterbium	Yb	70	173.04	2.7	819	1196	6.965	fcc
Lutetium	Lu	71	174.97	0.8	1663	3402	9.840	hcp

hcp, hexagonal close packed; dhcp, double C hexagonal close packed; rhomb, rhombohedral; fcc, face centered cubic; bcc, body centered cubic.

\*Estimated.

1.2 g/ton. From these data it is clear that rare earths are not rare in the sense of their natural abundance.

Some physical properties of the rare earth elements are given in Table 1.3.

## 1. Rare earth reserves

The world reserves of rare earths are summarized in Table 1.4. The reserve base encompasses current economic reserves, marginally economic reserves and sub-economic reserves. The locations of the major rare earth deposits in the world are depicted in Fig. 1.1.

Some possible future resources of rare earths in India are given in Table 1.5.

## 2. Rare earth markets

The broad applications of rare earths and the detailed metallurgical applications are given in Tables 1.6 and 1.7, respectively.

Rare earth consumption in various industries in the world is given in Table 1.8.

TABLE 1.4  
World resources of rare earths ( $\times 10^3$  metric tons of rare earths oxide REO) [3].

Country	Major ore type	Reserves	Reserve base
<i>North America</i>			
USA	Bastnasite-bearing carbonatite	4900	5200
Canada	Uranium ores	<u>182</u>	<u>197</u>
		5100	5400
<i>South America</i>			
Brazil	Beach placers, carbonatite and alkaline rocks	20	73
<i>Europe</i>			
USSR	By-product of apatite processing carbonatite	450	500
Finland/Norway/Sweden	Alkaline rocks	<u>50</u>	<u>55</u>
		500	500
<i>Africa</i>			
Malagasy Repub.	Beach placers (monazite)	50	55
Repub. of S.A.	Monazite vein	357	321
Egypt	Fluviatile placers (monazite)	100	110
Malawi	Carbonatite	297	330
Burundi	Carbonatite	<u>1.1</u>	<u>1.3</u>
		820	830
<i>Asia</i>			
Malaysia	Alluvial tin placers (monazite and xenotime)	30	35
India	Beach placers (monazite)	2220	2500
Korea	Placers (monazite)	45	50
Sri Lanka	Beach placers (monazite)	13	14
China	Fe-carbonate formations	36 000	38 000
Thailand	Beach placers	<u>1</u>	<u>1</u>
		38 000	41 000
Australia	Heavy mineral placers (monazite)	<u>184</u>	<u>200</u>
World total		45 000	48 000

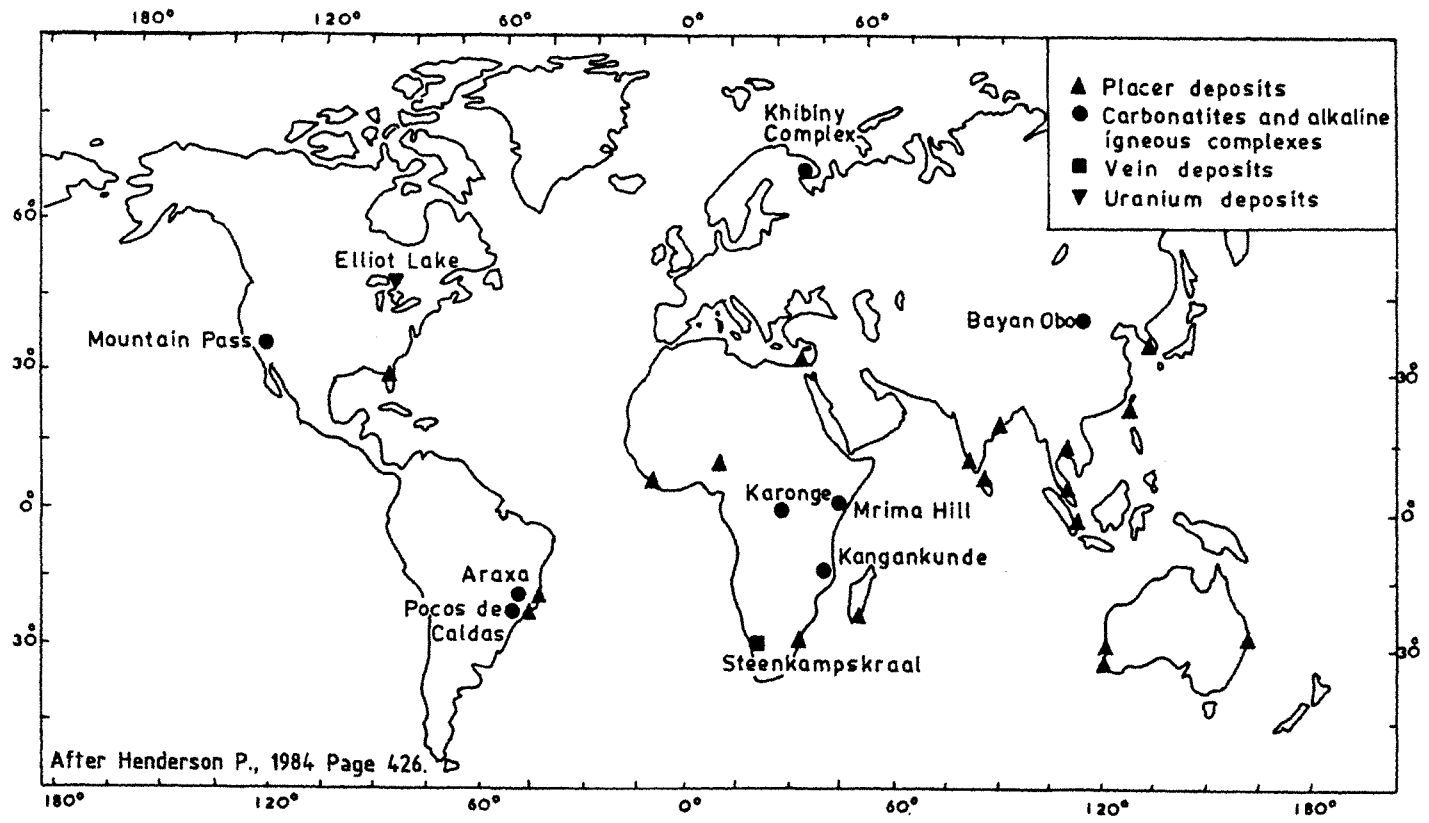


Fig. 1.1. Location of the major rare earth deposits of the world [3].

TABLE 1.5  
Promising geological environments and target areas for rare earth deposits in India [3].

Type	Geology	Mineralogy	Examples of target areas in India
Placer	Coastal and inland placers	Monazite	Coastal stretches of Indian seaboard and inland placers of Tamilnadu, MP, Bihar and West Bengal Siri River, M.P.
	Coastal and inland placers	Xenotime	
Sedimentary	Quartz-pebble conglomerates and associated formations	Monazite, uraninite, brannerite	Karnataka
	Carbonate (dolomite) hosted RE-Fe deposits	Bastnasite, monazite and RE apatite	Specified areas yet to be identified
	Re in phosphorites	RE mainly in colophonite	Mussoorie (U.P.) and Udaipur (Rajasthan)
Metamorphic	Marble/skarn, biotite schist hosted Re mineralization	Monazite, columbite and apatite	Parts of Tirunelveli-Tiruchinapalli, Tamilnadu, Dungarpur, Rajasthan, Sauser Series, M.P., Khetri-Khandala areas in Sikar Dt, Rajasthan
	Migmatized sillimanite biotite schist and gneiss, paragneiss and schists U-mineralized shear zones	Monazite, xenotime (occur as minerals)	Khondalites and associated calc-silicate rocks of Eastern Ghats
	Iron and manganese ores (of Proterozoic age)	Brannerite, xenotime, monazite Cerite, orthite, bastnasite and other RE minerals	Singhbhum Thrust Belt, Bihar Mn-horizons of the Sauser Series, M.P.
Igneous	Syngenetic concentrations in igneous rocks, eluvial deluvial/alluvial concentrations from disseminations in	Monazite, xenotime, thorite, thoregummite, samarskite, fergusonite	Granites of Kunkuri (M.P.) and Kanigiri (A.P.)
	(a) granites and (b) carbonatites and alkaline rocks	Pyrochlore	Amba Dungar (Gujarat) Sung Valley (Meghalaya), Newania, Kishangarh, Mundwara, Sarnu, Dandali, Sarodia (Rajasthan), Koraput (Orissa), Kundalur, Medupally, Kunnavaram, Giddalur, Chelima (A.P.), Kullampatti, Sivamalai, Kadavur, Elagiri and Sevathur, Tamilnadu
	Pegmatites irregularly distributed masses in zoned and hydrothermally altered pegmatites	Fergusonite, samarskite, ytrotantalite, yttrifluorite, etc.	In Pegmatites of Bihar, Nellore (A.P.), Rajasthan, Karnataka, Tamilnadu and M.P.

TABLE 1.6  
RE products used in each market application [4].

Market	Application	RE element
Catalyst	Fluid cracking catalyst	All RE mixture
	Automobile catalyst	Ceric RE mixture
	Others	Ce, La, Nd
Glass	Decolourizing	Ce-rich compounds
	Colourizing	Ce, Er, Nd, Pr
	Polishing	All RE mixture, ceric RE mixture
Ceramics	Glazed ceramic tiles	Ce, Pr
Metallurgy	Cast iron	All RE mixture
	Flints	Ce, La
	Steel	
	Al, Mg alloys	Ce, Nd, Pr and mixture
	Refractory alloys	Y
Other markets	Magnets	Sm, Pr, Ce, Nd, Dy, Er, Gd
	Phosphors for TV lamps and X-ray screens	Y, Gd, Eu, La, Tb, Tm
	Electronics (YAG, YIG, GGG)	Y, Gd, Nd, Tb
	Nuclear	Gd, Eu
	Special glasses (fibers, lenses, etc.)	Y, Gd, La
	Fine ceramics: YZ, PSZ, Si <sub>3</sub> N <sub>4</sub>	Y, La, Ce
	Capacitors	Nd, La, Sm

The rare earths consumption pattern as a function of time (years) in tons is depicted in Fig. 1.2.

It is obvious that the curve does not show a smooth rise and it has peaks and troughs. The non-uniformity of the curve can be explained by a comparison of old technology with new technology and also use of new products in place of rare earth products already in use. Technology changes citing the element affected and the newly developed products as replacements of rare earth products already in use are given in Tables 1.9 and 1.10.

Based on factors such as population growth, gross national product and indexes of industrial activity, numerical estimates for demand of rare earths obtained by Jolly (Mineral Facts and Problems, Bur. Mines Bulletin, 667, 1975) are given in Table 1.10a.

The present and future scenarios for rare earths in India as given by Drs. Kalam and Rajan in *Materials Processing Technology by 2020*, Technology Information Forecasting Council are summarized in Scheme 1.1.

### 3. Formation of lanthanide ores

Nature concentrates rare earth ores into useful ores by three processes. Minerals like monazite occur in small concentrations in common rocks that resist weathering and have high densities. They remain intact when their host rocks weather away. These are moved by water and enriched into placer deposits when less dense minerals are removed from them.

TABLE 1.7  
Metallurgical applications of rare earths.

Areas of application	Brief details
Flints For lighters, sparking toys, industrial torches and miner's safety lamps	Misch metal alloyed with 23% Fe called ferrocerium with additives like Mg/Cu is either cast or extruded to make flints
Cast irons	Cerium or misch metal as inoculant to modify the graphite morphology from flakes to nodular
Steels High strength low alloy steels (line pipe, structural) and steels for fatigue intensive applications (axles, bearings, rail steels)	Misch metal or rare earth silicon alloy for controlling shapes of sulfide inclusions and thereby improving transverse impact strength
Copper alloys (OFHC copper and leaded brasses)	Yttrium or misch metal for improving the oxidation resistance of OFHC copper and elimination of hot tearing in leaded brasses
Magnesium alloys (cast or wrought alloys)	Alloying with 1–3% misch metal reduces the microporosity
Aluminum alloys (for electrical conductors)	Misch metal addition improves tensile strength, heat resistance, vibration resistance and corrosion resistance
Superalloys Cobalt based	Lanthanum addition (~ 0.08%) improves the oxidation resistance by changing the character of oxides at elevated temperatures
Permanent magnet alloys for producing magnets of high coercivity and high energy products	AB <sub>5</sub> type where A is rare earth metal (misch metal, samarium, praseodymium) and B is cobalt. These are either cast or fabricated by powder metallurgy routes
Corrosion inhibitors Rare earth salts	Mostly cerium salts are used as corrosion inhibitors

TABLE 1.8  
Consumption of rare earths (percent weight).

	1973	1974	1975	1976	1977	1984	1985
Catalysts	29	34	36	38	39	43	33
Metallurgy	46	44	45	32	34	22	25
Glass/ceramics	24	20	17	28	26	31	37
Phosphors/electronics/others	3	2	2	2	1	4	5

Pegmatites is another way of concentration of rare earths. Pegmatites are formed due to the crystallization of magma bodies. During crystallization of the magma, the lanthanides are concentrated into lanthanide bearing minerals. Large amounts of lanthanides are present in magmas which give rise to highly alkali basalts. If titanium is predominant, the magma crystallizes as perovskite along with the rare earths. When carbonatites are present in the magma we get a lanthanide mineral like apatite. Thus placer deposits have

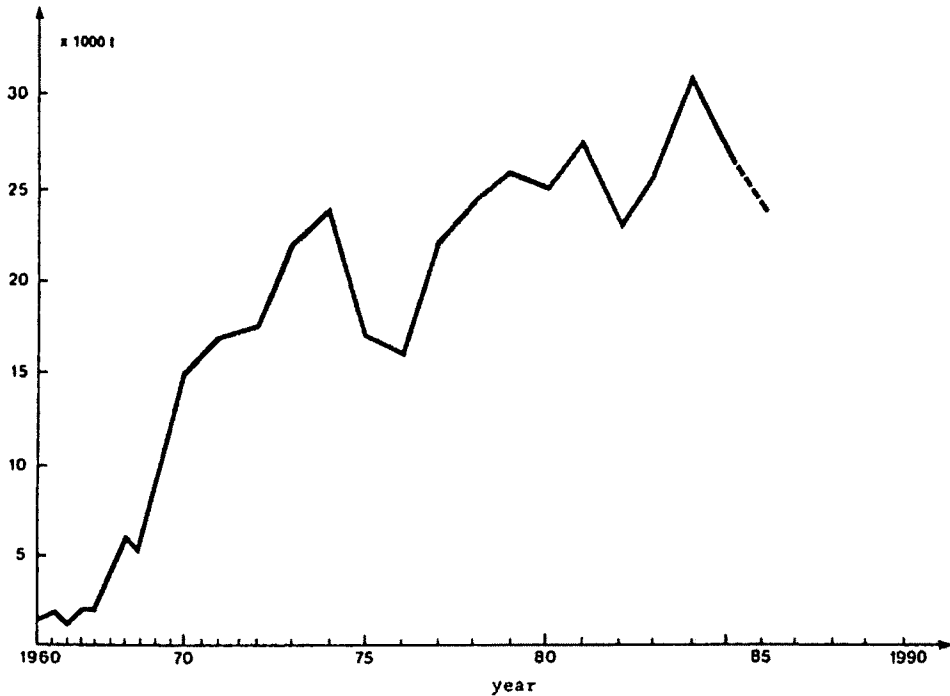


Fig. 1.2. Rare earths consumption (REO equivalent) [4].

apatites, allanite, monazite, xenotime and zircon. Pegmatites have all the forms associated with placer deposits and fluorite. Alkali rock complexes give rise to apatite, perovskite and bastnasite.

#### 4. Rare earth sources

The important minerals, their grades and specifications are given below.

Minerals	Grades and specifications
Monazite (Ce,La,Y,Th)PO <sub>4</sub>	A rare-earth phosphate. Most concentrates contain 55–65% REO including 2% Y <sub>2</sub> O <sub>3</sub> . Marketable REO content 55% (minimum)
Bastnasite (Y,Ce)(CO <sub>3</sub> )F	A fluoro carbonate of cerium/yttrium—concentrates contain 60% REO raised to 70% REO by acid leaching and 85% by leaching and calcining Y <sub>2</sub> O <sub>3</sub> low (0.1–0.3%)
Xenotime (YPO <sub>4</sub> )	A phosphate of yttrium—concentrates contain 25% Y <sub>2</sub> O <sub>3</sub> which may be upgraded to 60% Y <sub>2</sub> O <sub>3</sub> and 40% REO
Loparite (Nb-perovskite)	A titanate of Ca, Na, Ce with 30% REO
Iron ore RE	Adsorbed on Fe-Mn ores

TABLE 1.9  
Technology changes [4].

Old technology	New technology	Element affected
Auer gas mantles	Incandescent lamps	Th, Ce
Sulfide inclusion shape control	Extreme steel desulfurisation with calcium	La, Ce
Arc carbon rod filled with RE fluoride	High pressure halogen lamps	Ce fluoride RE fluoride
Lighter flints	Piezoelectric ceramics	Misch metal
Gadolinium gallium garnet for magnetic bubble memories	Ram silicon memories magnetic tapes and discs	Gd
Cathode ray tube* for TV display	Liquid crystal displays	Y, Eu

\*In progress for small size screens.

TABLE 1.10  
Product change within the same technology [4].

Application	Existing product	Substitution product
Graphite nodularization in casting	Misch metal	Magnesium
Neutron absorption in nuclear submarines	Europium	Hafnium
White opacifier for ceramic glazing	Cerium	Tin, zirconium
Hydrogen storage	Lanthanum–nickel alloy	Iron–titanium alloy
High strength permanent magnets	Samarium cobalt	Neodymium iron boron

TABLE 1.10a  
Summary of forecasts of US and rest-of-world rare earth elements (including yttrium) demand 1974 and 2000 (short tons REO and  $Y_2O_3$ ).

	1974	2000 forecast range		Probable		Probable average annual growth rate 1974–2000 (percent)
		Low	High	1985	2000	
United States						
Annual demand	15 500	24 000	50 000	22 000	34 000	3.1
Cumulative	–	510 000	782 000	207 000	625 000	–
Rest-of-world						
Annual demand	11 500	25 000	50 000	19 000	40 000	4.9
Cumulative	–	457 000	699 000	168 000	608 000	–
World						
Annual demand	27 000	49 000	100 000	41 000	74 000	3.9
Cumulative	–	967 000	1 481 000	375 000	1 233 000	–

Of these, bastnasite is the only mineral worked primarily for rare earths and both monazite and xenotime are mostly by-products of mining ilmenite, rutile, cassiterite, zircon or gold. Apatite and some multi oxide minerals like pyrochlore, euxenite, brannerite and loparite (a niobium titanate) are also commercial sources of rare earths, but production of RE from these is limited.



Present Scenario (1997)		Rare earths, potential for India	Future Scenario (2010)	
<b>Resources</b>		<b>Core technologies</b>	<b>Production of rare earths</b>	
Global 62 MT (China 80%, US 11%, rest India & EU)		* Recovery of metals (Nd, Sm) (mineral → oxide → metal) * Value addition of RE materials * Application engineering for use of rare earths in high tech areas like, catalysts, phosphors, magnets, special ceramics and metallurgy * Applications to sensors, guidance, automation, etc.	India 15 000 tonnes per year (India could have an export niche). High growth expected: 12–15%. Thorium applications in a major way—India's leadership	
<b>Production India</b>			<b>Global market</b>	
5000 Tpy India 2.7 MT (largest thorium deposits)			\$900 million; India to have good share of production	
<b>Global market</b>			<b>Demand (India)</b>	
\$400 million of Nd-Fe-B (high energy magnets); Indian production limited			15 tonnes/year	
<b>Demand (India)</b>			<b>Nd-Fe-B</b>	
7 tonnes/year			Magnets of 85 MGOe	
<b>Nd-Fe-B</b>				
Up to 35 MGOe developed				

Scheme 1.1.

TABLE 1.11  
Average rare earth content of the major ore minerals (%) [2].

Element	Monazite		Bastnasite		Xenotime	
La	23	} 93	32	} 98.7		} 10.6
Ce	46		50			
Pr	5		4			
Nd	19		13			
Sm	3	} 4.7	0.5	} 0.75	1.2	} 4.8
Eu	0.01		0.1		0.01	
Gd	1.7		0.15		3.6	
Tb	0.16	} 0.9	*	} 4.6	1.0	} 4.6
Dy	0.5				7.5	
Ho	0.09				2.0	
Er	0.13				6.2	
Tm	0.01				1.27	
Yb	0.06				6.0	
Lu	0.006				0.63	
Y	2	2		60.0		

\* Almost absent.

The average rare earth content of the three major minerals; namely, monazite, bastnasite and xenotime is given in Table 1.11.

TABLE 1.12  
Rare earth and yttrium contents of major source minerals [5] (percent of total rare earth oxide).

	Bastnasite		Monazite				Xenotime		
	California	China	Eastern Australia	Western Australia	Florida	India	China	Malaysia	
La <sub>2</sub> O <sub>3</sub>	32.00	27.00	20.20	23.90	17.47	23.00	23.35	0.50	
CeO <sub>2</sub>	49.00	50.00	45.30	46.03	43.73	46.00	45.69	5.00	
Pr <sub>6</sub> O <sub>11</sub>	4.40	5.00	5.40	5.05	4.98	5.50	4.16	0.70	
Nd <sub>2</sub> O <sub>3</sub>	13.50	15.00	18.30	17.38	17.47	20.00	15.74	2.20	
Sm <sub>2</sub> O <sub>3</sub>	0.50	1.10	4.60	2.53	4.87	4.00	3.05	1.90	
Eu <sub>2</sub> O <sub>3</sub>	0.10	0.20	0.10	0.05	0.16	–	0.10	0.20	
Light REO	99.50	98.30	93.90	94.94	88.68	98.50	92.09	10.50	
Gd <sub>2</sub> O <sub>3</sub>	0.30	0.40	2.00	1.49	6.56	–	2.03	4.00	
Tb <sub>4</sub> O <sub>7</sub>	0.01	–	0.20	0.04	0.26	–	0.10	1.00	
Dy <sub>2</sub> O <sub>3</sub>	0.03	–	1.15	0.69	0.90	–	1.02	8.70	
Ho <sub>2</sub> O <sub>3</sub>	0.01	–	0.05	0.05	0.11	–	0.10	2.10	
Er <sub>2</sub> O <sub>3</sub>	0.01	1.00	0.40	0.21	0.04	1.50	0.51	5.40	
Tm <sub>2</sub> O <sub>3</sub>	0.02	–	trace	0.01	0.03	–	0.51	0.90	
Yb <sub>2</sub> O <sub>3</sub>	0.01	–	0.20	0.12	0.21	–	0.51	6.20	
Lu <sub>2</sub> O <sub>3</sub>	0.01	–	trace	0.04	0.03	–	0.10	0.40	
Y <sub>2</sub> O <sub>3</sub>	0.10	0.30	2.10	2.41	3.18	–	3.05	60.80	
Heavy REO total	0.50	1.70	6.10	5.06	11.32	–	7.93	89.50	
Total	100.00	100.00	100.00	100.00	100.00	100.00	100.00	100.00	
Total REO in marketable concentrates	60–70%		←————— 55–60% —————→						42.51

Analysis adjusted to 100% REO.

TABLE 1.13  
RE content in Chinese Fe-Fe-RE ore deposits [6].

	Re <sub>2</sub> O <sub>3</sub> (%)	Light RE (LRE) Heavy RE (HRE)	Eu
I Bayan Obo ores			
Massive Nb-RE-Fe ore	2.0	44.6	0.57
Banded Nb-RE-Fe ore	9.0	62.2	0.56
Aegerine Nb-RE-Fe ore	3.5	49.4	0.67
Dolomite Nb-RE-Fe ore	0.36	16.5	0.86
Riebekite Nb-RE-Fe ore	1.5	54.4	0.74
Aegerine Nb-RE ore	8.0	49.2	0.97
Dolomite Nb-RE ore	4.0	40.8	0.40
II Dianyi rocks			
Banded magnetite saderite ore	0.14	4.8	1.49
Banded magnetite saderite ore	0.18	3.1	2.49
Massive magnetite saderite ore	0.23	6.8	2.56
Banded magnetite saderite ores	0.46	3.7	2.85
III Minsong			
RE-bearing magnetite dolomite	0.36	10.0	0.85
RE-bearing magnetite dolomite	0.78	14.0	0.82
Biotite-quartz-schist	0.03	7.0	0.70

HRE (Gd-Lu, Y).

TABLE 1.14  
Ores used for 1985 production [4].

Ore	1985 tons/REO
Bastnasite	11 000
Monazite	10 500
Others (RECl <sub>3</sub> , xenotime, concentrates...)	5 500
Total	27 000

TABLE 1.15  
Rare earths (REO) production (tons) in some countries [2].

	1973	1974	1975	1976	1977
USA	15245	16652	10430	11834	13521
Australia	3835	3270	4158	4906	9571
Brazil	1439	1196	1176	1452	NA
India	3500	3273	2500	3100	4000
Malaysia	1943	1787	3285	1879	NA
Others	NA	703	697	696	NA

TABLE 1.16  
List of main RE manufacturers [4].

"Have been"	Existing
Thorium Ltd. (UK)	Rhone Poulenc (F-USA)
Steetley (UK)	Rare Earth product (Johnson Matthey) (UK)
Th. Goldschmidt (FRG)	Treibacher CW (Austria)
Tukako (J)	Megon (Norway)
Haeino Kako (J)	Molycorp (USA)
Kindai Chem (J)	Research Chemicals (USA)
Sanko RE (J)	Grace (USA)
Toda ND (J)	Mitsubishi Chemical Industries (J)
Nihon Kigenso (J)	Santoku (J)
Honjo Metal (J)	Mitsui metal (J)
Sankin (J)	Shin Etsu chem (J)
	Shin Nihon metal (J)
	Seimi Chemical (J)
	Nippon Yttrium Company (J)
	Nissan Kigenso (J)
	Tohoku/Metal and Chemicals (J)
	China
	USSR
	Nuclemon (Brazil)
	Fluminense
	Indian Rare Earths (India)

TABLE 1.17  
Pricing pattern of rare earths [2].

Material	Base quantity	\$ per lb contained REO
Concentrate		
Bastnasite (70% REO)	TL*	0.76
Lanthanum (75% REO)	TL*	0.85
Rare earth chloride	TL*	0.64
Oxides (99.9% min)		
	lbs	
Cerium	200	6.75
Europium	25	710.00
Lanthanum	300	6.00
Samarium	50	30.00
Yttrium	50	34.50

TL\* = truck load.

The rare earth and yttrium contents of major mineral sources occurring in various parts of the world are given in Table 1.12.

The rare earth content of Chinese iron rare earth ore deposits occurring in three regions is given in Table 1.13.

The amounts of the ores used for production of rare earth oxides are given in Table 1.14. The amounts of rare earth oxide produced in some parts of the world are given in Table 1.15.

The main manufacturers of rare earths are listed in Table 1.16.

Some costs associated with the production of rare earths as of 1980 are given in Table 1.17.

## 5. Recovery of rare earths from ores

Generally speaking, there are two processes for the extraction of rare earths from monazite. One of the processes involves sulfuric acid digestion and this is illustrated in Fig. 1.3.

The second method of recovery of rare earths from monazite involves caustic soda digestion and is illustrated in Fig. 1.4.

Recovery of rare earths as chlorides by hydrochloric acid digestion of bastnasite is illustrated in Fig. 1.5.

Xenotime, which is an orthophosphate like monazite, can be processed by either the sulfuric acid process or by caustic fusion. The caustic fusion method is illustrated in Fig. 1.6.

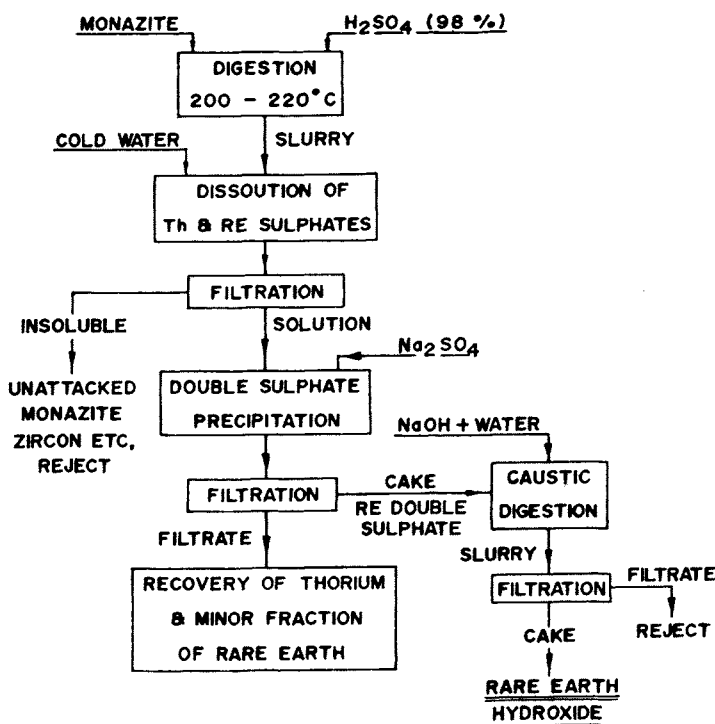


Fig. 1.3. Sulphuric acid process for the recovery of rare earths from monazite [2].

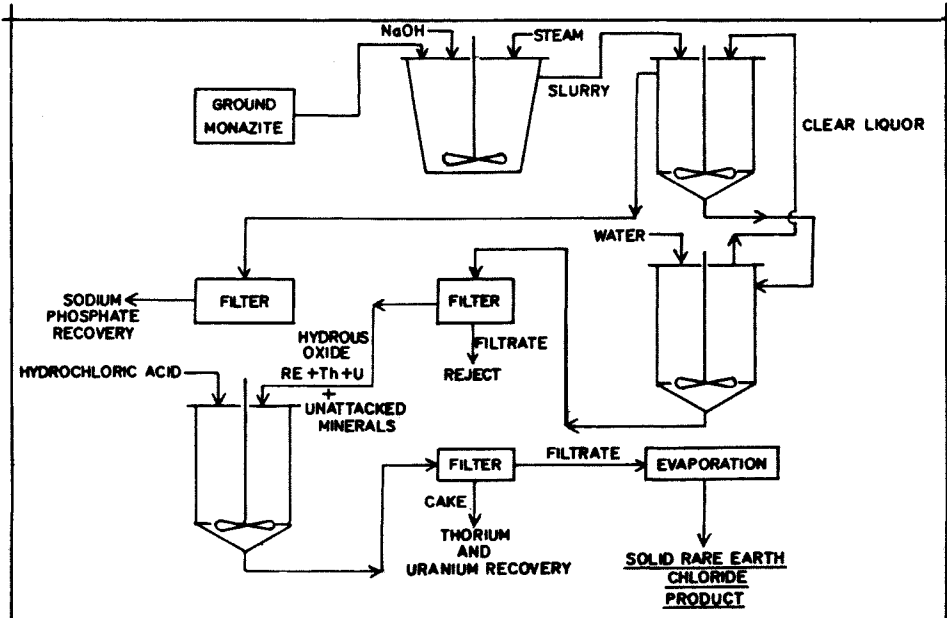


Fig. 1.4. Caustic soda digestion process for recovery of rare earths from monazite [2].

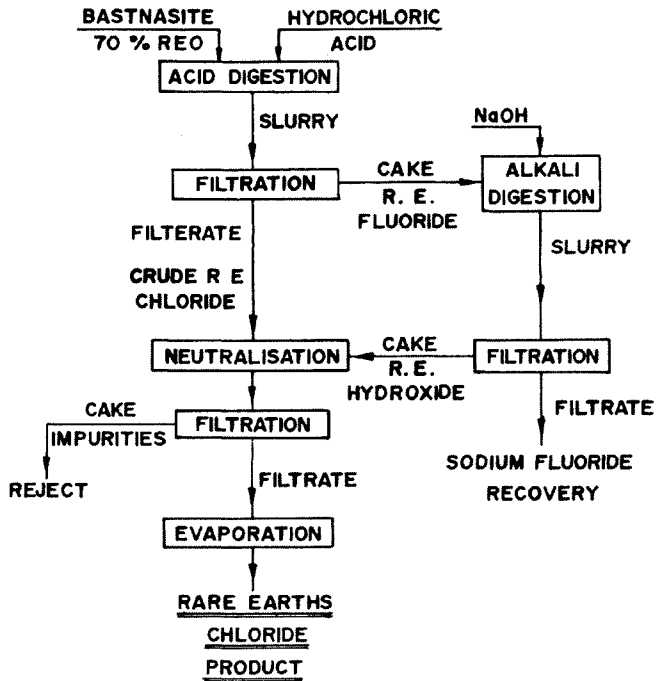
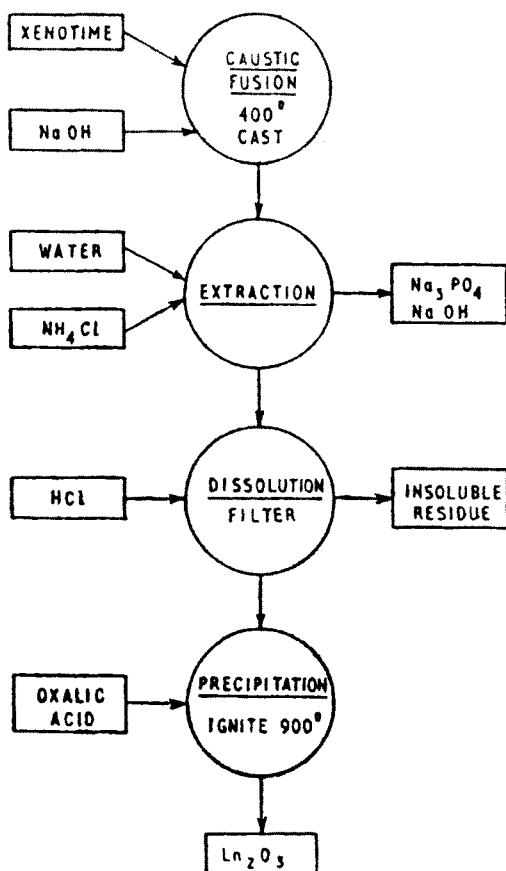


Fig. 1.5. Production of rare earths chloride from bastnasite [2].



XENOTIME: ALKALINE BREAKDOWN

Fig. 1.6. Recovery of rare earths from xenotime.

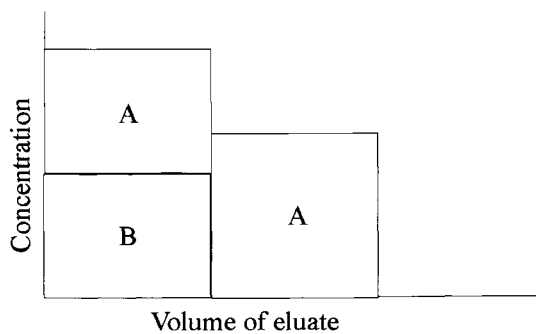


Fig. 1.7. Separation of A and B.

TABLE 1.18  
Commercial ion exchangers [8].

Type and name	Capacity (m-eq./g)
Cation exchangers:	
<i>Strong acid: phenolic methylene sulfonic</i>	
Amberlite IR-100	1.75
Dowex 30	4.00
Duolite C-3	3.25
Wolfatit K	2.50
Zeo-Rex	2.70
<i>Strong acid: nuclear sulfonic</i>	
Amberlite IR-120	4.20
Dowex 50	4.25
Wolfatit KS	2.45
Permutit Q	4.10
<i>Medium acid: sulfonated coal</i>	
Zeo-Karb	3 (pH 7)
<i>Weak acid: carboxylic</i>	
Amberlite IRC-50	10.0
Permutit 216	5.3
Wolfatit C	7.0
<i>Aluminosilicate gel</i>	
Decalso	3
Anion exchangers:	
<i>Strong base: quaternary amine</i>	
Amberlite IRA-400	2.3
Dowex 1	2.4
Permutit S	2.4
<i>Weak base: primary, secondary and tertiary amine</i>	
Amberlite IR-4B	10.0
Duolite A-2	7.0
De-Acidite 515	9.3

## 6. Separation of rare earths

Classical methods of separation [7] are (1) fractional crystallization, (2) precipitation and (3) thermal reactions. Fractional crystallization is an effective method for lanthanides at the lower end of the series, which differ in cation radius to a large extent. The separation of lanthanum as a double nitrate,  $\text{La}(\text{NO}_3)_3 \cdot 2\text{NH}_4\text{NO}_3 \cdot 4\text{H}_2\text{O}$ , from praseodymium and other trivalent lanthanide with prior removal of cerium as  $\text{Ce}^{4+}$  is quite a rapid process and is of commercial significance. Other examples are separation of yttrium earths as bromates,  $\text{RE}(\text{BrO}_3)_3 \cdot 9\text{H}_2\text{O}$  and use of simple nitrates, sulfates and double sulfate and alkali metal rare earth ethylenediamine tetraacetate complex salts in fractional crystallization separation.



TABLE 1.19  
Association constants of rare earth cations with aminocarboxylic acids [9].

Rare earth element	Complexing agent							
	EDTA	TRILO		HEEDTA	DCTA	DTPA	EGTA	EEDTA
	log $K$	log $K_1$	log $K_2$	log $K$	log $K$	log $K$	log $K$	log $K$
La	15.50	10.64	7.37	13.22	16.26	19.96	15.84	16.29
Ce	15.98	10.91	7.98	14.08	16.76	—	16.06	17.13
Pr	16.40	11.04	8.18	14.39	17.31	21.85	16.17	17.61
Nd	16.61	11.22	8.43	14.71	17.68	22.24	16.59	17.81
Sm	17.14	11.29	9.20	15.15	18.38	22.84	17.75	18.25
Eu	17.35	11.36	—	15.21	18.62	22.91	—	—
Gd	17.37	11.38	9.35	15.10	18.77	23.01	17.50	18.21
Tb	17.93	11.54	—	15.10	19.50	23.21	17.80	18.31
Dy	18.30	11.65	9.40	15.08	19.69	23.46	17.84	18.29
Ho	18.74	11.79	—	15.06	—	—	17.90	18.17
Er	18.85	11.94	—	15.17	20.68	23.18	18.00	18.18
Tm	19.32	12.13	—	15.38	20.96	22.97	17.96	18.01
Yb	19.51	12.29	9.22	15.64	21.12	23.01	18.22	18.06
Lu	19.83	12.44	—	15.79	21.51	—	18.48	17.92
Y	18.09	11.33	9.02	14.49	19.15	22.40	17.16	17.79

EDTA	Ethylenediaminetetraacetic acid
TRILO	Nitritotriacetic acid
HEEDTA	$\beta$ -hydroxyethylenediaminetriacetic acid
DCTA	1,2-diaminocyclohexanetetraacetic acid
DTPA	Diethylenetriaminepentaacetic acid
EGTA	1,2-bis(2-di(carboxymethyl)aminoethoxy)ethane
EEDTA	2,2-bis(2-di(carboxymethyl)amino)ethyl ether

Fractional precipitation is similar to fractional crystallization technique but takes advantage of basicity differences and solubility differences. Separation of yttrium from yttrium earths by fractional precipitation is an example of differences in basicity. Separation of yttrium earths from cerium earths by double alkali sulfate precipitation in the form of double sulfates is an example of fractional precipitation.

Change in oxidation state can be used effectively because of the large solubility changes accompanying the changes in oxidation state. Examples of this method of separation are (i) separation of cerium by oxidation to  $\text{Ce}^{4+}$  and (ii) reduction of Eu, Sm and Yb to divalent state. Differences in solubility products of  $\text{RE}(\text{OH})_3$  can be profitably used in their separation by fractional precipitation. For example,  $K_{\text{sp}}$  values of  $\text{La}(\text{OH})_3$  and  $\text{Lu}(\text{OH})_3$  are  $10^{-19}$  and  $10^{-24}$ , respectively, and these values show that it is possible to preferentially precipitate the bulk of rare earths in the presence of ammonium ion leaving  $\text{La}^{3+}$  in solution.

Homogeneous precipitation may be more useful in precipitation separation of rare earths. This involves addition of reagents which release the precipitating agent slowly in solution. Addition of trichloroacetic acid and dimethyl oxalate in place of  $\text{Na}_2\text{CO}_3$  and

TABLE 1.20  
Separation factors for Dowex 1 with 90% MeOH–10% (1 M HNO<sub>3</sub>) [10].

Pair	$\alpha_z^{z+1}$	Pair	$\alpha_z^{z+1}$	Pair	$\alpha_z^{z+1}$
Lu–Yb	1.0	Dy–Tb	1.1	Pm–Nd	2.6
Yb–Tm	1.0	Tb–Gd	1.3	Nd–Pr	2.2
Tm–Er	1.0	Gd–Eu	1.6	Pr–Ce	1.7
Er–Ho	1.0	Eu–Sm	1.9	Ce–La	1.7
Ho–Dy	1.0	Sm–Pm	2.3		

TABLE 1.21  
Averaged values of individual separation factors for adjacent pairs of lanthanons being eluted with EDTA and its homologues (calculated from 9 sets of stability constant data) [10].

Pair	$\alpha_z^{z+1}$	Pair	$\alpha_z^{z+1}$	Pair	$\alpha_z^{z+1}$
Lu–Yb	1.6	Gd–Eu	1.1	Dy–Y	1.6
Yb–Tm	1.8	Eu–Sm	1.5	Y–Tb	1.5
Tm–Er	2.0	Sm–Pm	(1.8)		
Er–Ho	2.0	Pm–Nd	1.9		
Ho–Dy	2.0	Nd–Pr	2.0		
Dy–Tb	2.7	Pr–Ce	2.4		
Tb–Gd	3.5	Ce–La	3.3		

TABLE 1.22  
Separation factors observed in liquid-ion exchange chromatography with HDEHP and HEHP under various conditions.

Pair	HDEHP [11] (25°C)		HDEHP [12] (40°C)	HDEHP [13] (60°C)		HEHP [14] (20°C)	
	HCl	HNO <sub>3</sub>	HCl	HCl	HClO <sub>4</sub>	HCl	HNO <sub>3</sub>
La–Ce	2.8	2.7	3.1	2.4	4.7	3.3	–
Ce–Pr	1.5	(1.3)	1.7	1.5	1.3	1.5	–
Pr–Nd	1.3	(1.2)	1.4	1.4	1.4	1.3	–
Nd–Pm	2.7	2.1	2.3	1.9	2.1	2.8	–
Pm–Sm	3.2	2.7	2.2	2.3	2.6	3.6	–
Sm–Eu	2.2	2.1	2.2	2.0	1.8	2.3	–
Eu–Gd	1.5	1.7	1.6	1.4	1.5	1.6	1.8
Gd–Tb	5.0	5.5	4.4	3.3	5.2	5.4	5.9
Tb–Dy	2.6	3.0	2.2	1.9	1.9	2.1	2.3
Dy–Ho	2.1	2.2	2.0	1.9	1.8	1.9	2.0
Ho–Er	2.8	2.7	2.5	2.7	2.7	2.9	3.0
Er–Tm	3.4	3.5	2.5	1.8	3.3	3.8	4.0
Tm–Yb	2.8	3.1	2.7	3.1	2.2	3.2	3.4
Yb–Lu	1.9	1.9	1.8	2.1	1.8	3.0	2.1

TABLE 1.23  
Separation of rare earths by ion exchange.

Rare earths	Eluant	Condition	Reference
Y group rare earths	5% citrate	pH 3.28, 100°C	[15]
Eu–Sm, Y–Th	0.5 M citrate	pH 3.04, 87°C	[16]
Sm–Eu–Tb	0.5 M malate	pH 2.99, 87°C	[16]
Sm–Eu–Tb	0.3 M glycolate	pH 4, 87°C	[16]
Tb–Y–Er–Tm–Lu	0.25 glycolate	pH 3.5	[17]
	0.05% Aerosol OT		
Y–Tb, Eu–Sm	0.24 M lactate	pH 5.0, 87°C	[16]
Ce–Pr–Nd–Sm	1 M lactate	87°C	[18]
Y–Eu–Sm–Pm–Nd, Pr	1 M lactate	pH 3.25, 87°C	[19]
Rare earths	0.2–0.4 M $\alpha$ -hydroxybutyric acid	pH 4–4.6, 87°C	[20]
Sm–Pr–Nd–La	0.5 M NTA	pH increased stepwise from 3.5 to 4.2	[21]
Tb–Eu–Sm	0.026 M EDTA	pH 3.62	[16]
Rare earths	0.017 M EDTA	–	[22]
Tm, Er, Ho, Dy, Tb	0.2 M HIBA	–	[22a]

$\text{Na}_2\text{C}_2\text{O}_4$  to effect precipitation are examples of homogeneous precipitation. Fractional precipitation with these reagents in the presence of complexing agents could be applied in the separation of rare earths. It is useful to recognize that these classical methods have been replaced by (i) ion exchange chromatography, (ii) liquid-liquid ion exchange and (iii) solvent extraction methods for the separation of rare earths both on micro and macro levels.

## 7. Ion exchange chromatography

The first successful separations of rare earths by this technique was achieved fifty years ago. Two techniques used in the separation of rare earths are (i) displacement chromatography and (ii) elution chromatography. Commercial ion exchangers involving both cation exchangers and anion exchangers are listed in Table 1.18.

## 8. Displacement chromatography

This technique depends on the differences in affinity of ions to the resin. In the case of cation exchange resins, the sorption affinity increases with increase in charge,  $\text{M}^{3+} > \text{M}^{2+} > \text{M}^+$ . For ions of the same charge, the sorption affinity increases with decrease in the size of the aquo ion. In the case of rare earth ions, the affinity is in the order:  $\text{La}^{3+} > \text{Ce}^{3+} > \text{Pr}^{3+} > \text{Nd}^{3+} > \text{Sm}^{3+} > \text{Eu}^{3+} > \text{Gd}^{3+} > \text{Tb}^{3+} > \text{Dy}^{3+} > \text{Y}^{3+} > \text{Ho}^{3+} > \text{Er}^{3+} > \text{Tm}^{3+} > \text{Yb}^{3+} > \text{Lu}^{3+} > \text{Sc}^{3+}$ .

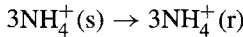
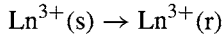
In the case of separation of two ions A and B, it is necessary that the selectivity coefficient  $[K_c]_B^A$  is defined by the equation

$$[K_c]_B^A = \frac{(A)_r(B)_s}{(B)_r(A)_s}$$

where r and s refer to resin and solution phases, be favorable. In separation of A and B, it is necessary that A and B differ considerably in their affinities for the resin and that a third species C having greater affinity than A and B for the resin be available to displace A and B, which are initially sorbed on the resin column. When the affinity of A is less than B for the cation exchange resin, then it is possible to separate A from B as shown in Fig. 1.7.

In the case of rare earth ions, the charge is the same and the differences in size are small and hence it is difficult to separate them by this technique.

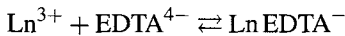
In elution chromatography or displacement development chromatography, the ion exchange column is loaded with the ions to be separated and then eluted with a complexing agent which forms complexes with the sorbed ions on the column. There is a competition set-up between the ions for the resin and the eluting complexing agent to form complexes of high stability constants. If the ions sorbed on the column form complexes with a marked difference in stability constant value, a fair separation of the sorbed ions can be achieved. Let us consider ethylenediaminetetracetic acid (EDTA) the well-known complexing agent and the  $\text{NH}_4^+$  form of the resin and a lanthanide ion ( $\text{Ln}^{3+}$ ). Initially  $\text{Ln}^{3+}$  and  $\text{NH}_4^+$  ions compete for the resin sites and we may write:



For each  $\text{Ln}^{3+}$  ion, three  $\text{NH}_4^+$  ions are displaced. The relative affinity of the competing ions may be written as:

$$K_{\text{NH}_4^+}^{\text{Ln}^{3+}} = \frac{(\text{NH}_4^+)_s^3 (\text{Ln}^{3+})_r}{(\text{NH}_4^+)_r^3 (\text{Ln}^{3+})_s}$$

Complexation of  $\text{Ln}^{3+}$  by EDTA may be written as



and the complexation constant  $K_c$  is

$$K_c = \frac{(\text{Ln EDTA}^-)}{(\text{Ln}^{3+})(\text{EDTA}^-)}$$

Denoting  $M_r$  and  $M_s$  as metal concentrations in the resin and solution phases, respectively, the distribution factor  $K_d$  is the ratio  $M_r/M_s$ .

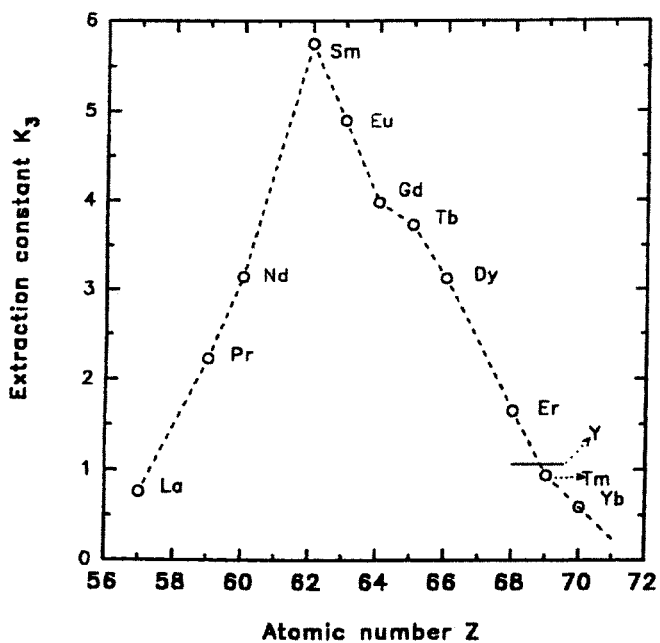


Fig. 1.8. Effective extraction constant of the trisolvate  $(TBP)_3 \cdot Ln(NO_3)_3$  versus lanthanide atomic number  $Z$ . Extraction system  $Ln(NO_3)_3-H_2O-TBP$  100 vol%.

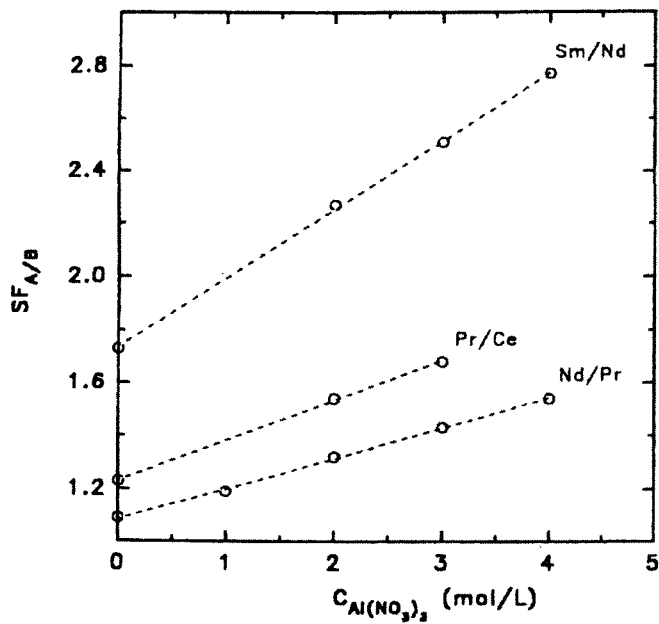


Fig. 1.9. Separation factors of selected lanthanide pairs versus aluminum nitrate concentration. Data from Ref. [24].

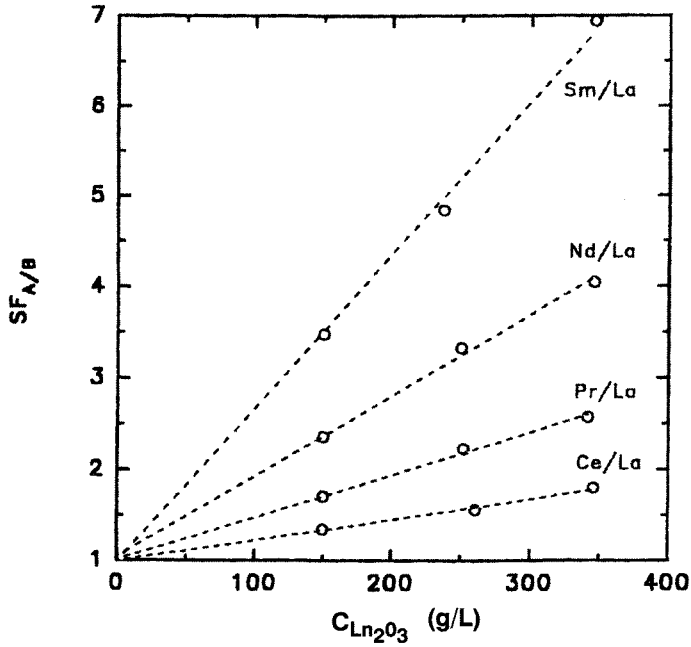


Fig. 1.10. Separation factors of selected lanthanide pairs versus lanthanide nitrate concentration. Data from Ref. [24].

When anionic complexes are formed,  $M_r = (Ln^{3+})_r$ ,  $M_s = (Ln^{3+})_s + LnEDTA^- \approx (LnEDTA^-)$ . Then we may write

$$K_d = \frac{K_{NH_4^+}^{Ln^{3+}} (NH_4^+)^3 (H^+)^4}{K_c K_a (EDTA) (NH_4^+)^3}$$

where  $K_a = K_1 \cdot K_2 \cdot K_3 \cdot K_4$  of EDTA.

In the case of a pair of rare earth ions, the affinities for the resin are nearly the same and the separation factor for the pair  $K_s$  or  $\alpha_z^{z+1}$  becomes

$$K_s = \frac{K_{d1}}{K_{d2}} = \frac{K_{c1}}{K_{c2}} = \alpha_z^{z+1}$$

Thus the separation of the two lanthanide ions from each other depends upon their respective complex formation constants. The lanthanide whose stability constant is higher will desorb and elute from the column in preference to the lanthanide whose stability constant is lower.

It is necessary, therefore, to examine data pertaining to complex formation constants of rare earth ions with ligands. The readily available data with some aminocarboxylic acid are given in Table 1.19. There is a significant difference in the stability constant values of

TABLE 1.24  
Separation factors for HDEHP-HCl and HDEHP-HClO<sub>4</sub>, toluene–water systems at 25°C [10].

Pair	HCl	HClO <sub>4</sub>	Pair	HCl	HClO <sub>4</sub>
La–Ce	2.4	3.0	Gd–Tb	3.2	5.0
Ce–Pr	2.8	2.1	Tb–Dy	2.0	2.1
Pr–Nd	1.7	1.4	Dy–Ho	2.1	1.9
Nd–Pm	2.1	2.2	Ho–Er	2.1	2.3
Pm–Sm	2.4	3.1	Er–Tm	2.5	2.5
Sm–Eu	2.2	1.9	Tm–Yb	1.8	3.1
Eu–Gd	1.6	1.4	Yb–Lu	2.2	1.9

rare earth metals with EDTA and DCTA as ligands and hence these reagents are promising eluting agents in the separation of rare earth ions and this is borne out by their use in practical separation of rare earths.

Separation factors for adjacent rare earth pairs on Dowex 1 resin with 90% methanol–10% 1 M nitric acid are given in Table 1.20. The data show that the separation factors are in the range of 1.0 to 2.6.

Averaged values for the separation factors for adjacent pairs of lanthanides eluted with EDTA and its homologues are given in Table 1.21. The separation factors are in the range of 1.5 to 3.5 showing considerable improvement in separation factors. In the majority of cases, the separation factors with EDTA as an eluant are greater than the values obtained in methanol–nitric acid medium, which is expected based on the stability constant data for rare earth EDTA complexes.

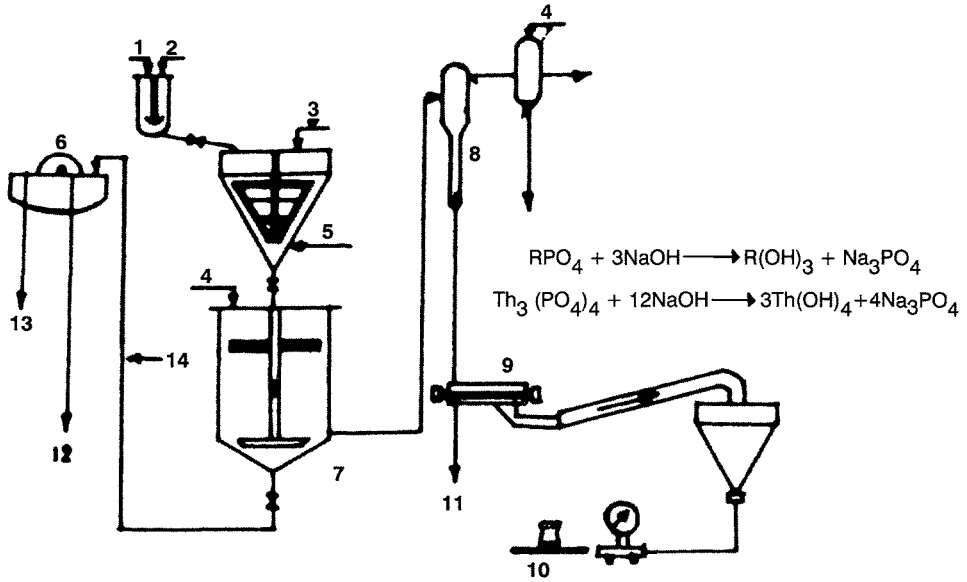
## 9. Liquid–liquid ion-exchange chromatography

Some solvent extraction reagents can be considered as ion-exchange media. For example, protonated tertiary amines and quaternary ammonium ions symbolized as  $R_3NH_4^+$  and  $R_4N^+$  are anion exchangers and dialkyl orthophosphate and alkyl phosphonate are cation exchangers. These reagents can be deposited as thin films on inert materials and used as ion exchangers. Since the films are thin, the problem of slow diffusion encountered in solid-ion exchangers is overcome with a reduction in value of height equivalent to theoretical plate.

Typical cation exchange extractants are di-2-ethylhexyl orthophosphoric acid (HDEHP), di-n-octyl orthophosphoric acid (HDOP) and hexylphenyl phosphonic acid (HEHP). Some data on the separation factors for adjacent pairs of lanthanides are given in Table 1.22.

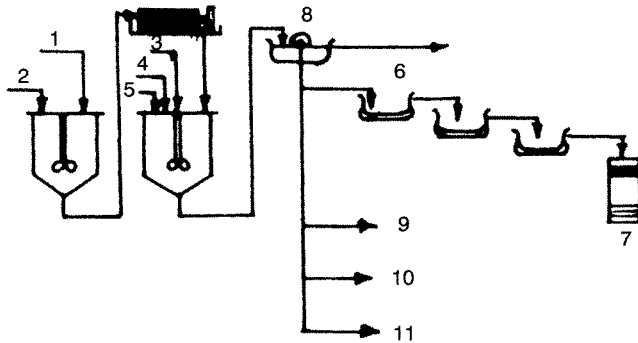
Quantitative separations of rare earths have been achieved on a micro scale with different complexing agents as elements and some of the data are summarized in Table 1.23.

Large scale separation of rare earths involve use of EDTA and NTA with the resin in cupric state. Zinc form resin has also been used with NTA. In some cases HEDTA is useful and in some cases superior to EDTA and NTA since resins in hydrogen form can be used. EDTA is probably the best reagent for the separation of the entire series of rare earths.



- |                 |                      |                                       |
|-----------------|----------------------|---------------------------------------|
| 1. MONAZITE     | 6. FILTER            | 11. MOTHER LIQUOR                     |
| 2. CAUSTIC LYE  | 7. LEACHING          | 12. SETTLING                          |
| 3. CAUSTIC SODA | 8. CRYSTALLISER      | 13. TO R.E. EXTRACTION                |
| 4. WATER        | 9. CENTRIFUGE        | 14. RARE EARTHS AND THORIUM HYDROXIDE |
| 5. STEAM        | 10. PRODUCT - T.S.P. |                                       |

Fig. 1.11. Processing of monazite [25].



- |                                    |                       |                                |
|------------------------------------|-----------------------|--------------------------------|
| 1. R.E. & TH. Hydroxide Slurry     | 5. BaCl <sub>2</sub>  | 9. To Solvent Extraction Plant |
| 2. Hydrochloric acid               | 6. R.E. Chloride      | 10. R.E. Fluoride Plant        |
| 3. Na <sub>2</sub> S               | 7. Cast R.E. Chloride | 11. R.E. Oxide Plant           |
| 4. Na <sub>2</sub> SO <sub>4</sub> | 8. Filter             |                                |

Fig. 1.12. Rare earth extraction [25].



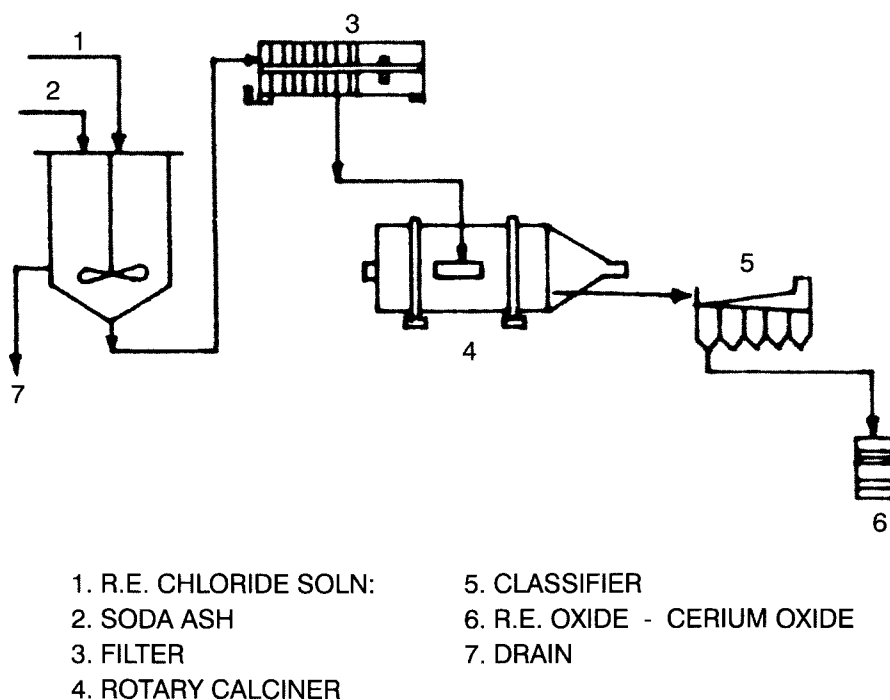


Fig. 1.13. Production of rare earth/cerium oxide [25].

## 10. Solvent extraction

In principle, this method can be used for the separation of all the rare earth elements, although it has been used on a large scale only for the separation of light and middle rare earth elements. In any separation technique, it is necessary to (i) eliminate the limitations exercised by the need to exceed the solubility product of the desired element, (ii) eliminate the limitations imposed on the ultimate purity of the desired element by contaminating impurities, (iii) increase the single step difference between a pair of lanthanides and (iv) achieve more easily multiplication of stages. Solvent extraction separation of rare earths meets all the aforementioned conditions except the last requirement, since achieving multiple stages means the use of many mixer-settlers. This technique does not possess the integrating effect of an ion exchange chromatographic column.

Although many early studies on the solvent extraction of rare earth chloride into alcohols, ether, ketone, rare earth thiocyanates into butanol, rare earth nitrates into n-hexanol were done, extraction of rare earth nitrates by tri-n-butyl phosphate (TBP) proved to be the most promising system. The general step of extraction is:



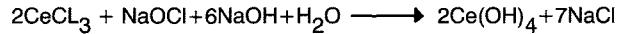
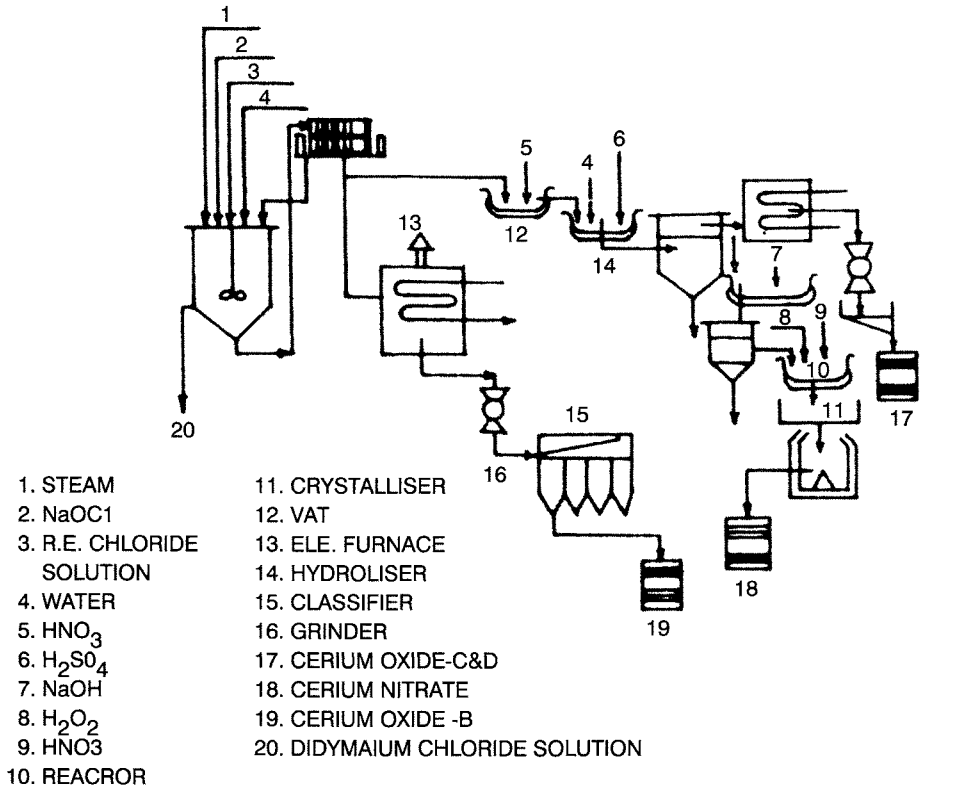


Fig. 1.14. Cerium recovery [25].

where aq and org refer to aqueous and organic phases, respectively. Now we may write:

$$K = \frac{[\text{La}(\text{NO}_3)_3(\text{TBP})_3 \text{ org}]}{[\text{La}_{\text{aq}}^{3+}][\text{NO}_3 \text{ aq}]^3[\text{TBP}_{\text{org}}]^3}$$

The distribution coefficient  $D = \frac{[\text{La}(\text{NO}_3)_3(\text{TBP})_3 \text{ org}]}{[\text{La}_{\text{aq}}^{3+}]}$

$$D = K[\text{NO}_3^-]_{\text{aq}}^3[\text{TBP}]_{\text{org}}^3$$

In order to separate a pair of rare earths, the separation factor  $\beta$  or  $\alpha^{z+1}$  which is the ratio  $\frac{D_{\text{La1}}}{D_{\text{La2}}}$  has to be reasonably high. Separation factors between adjacent rare earths vary from 1.5 to 2.5 depending upon the system. Separation factors are in the range of 1.5 to 2.0 for TBP systems.

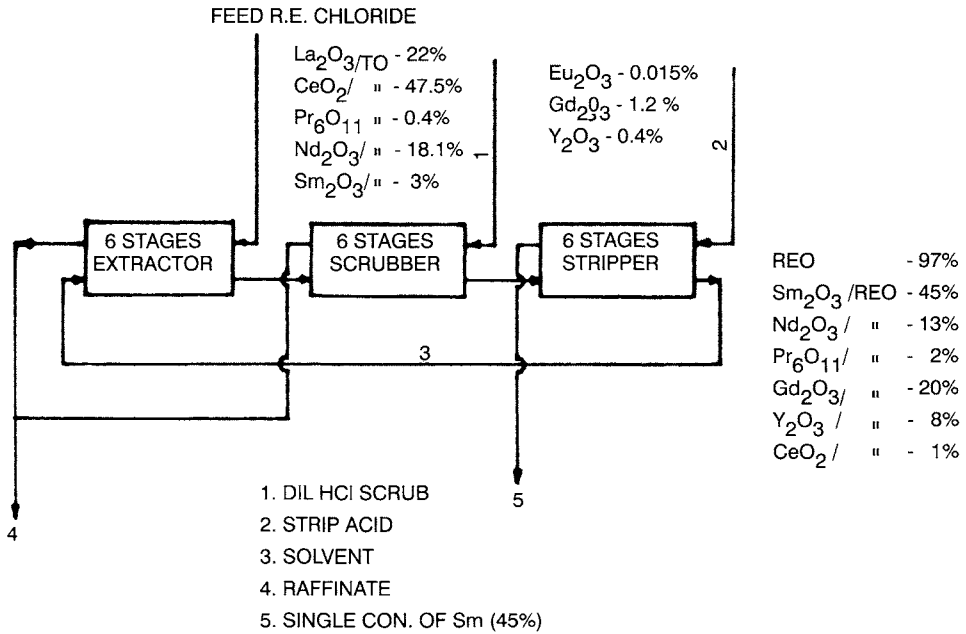


Fig. 1.15. Production of samarium concentrate [25].

Based on the Mikulin–Sergievskii–Dannus model, the separation factor for a pair of lanthanides may be written as [23]:

$$SF_{A/B} = \frac{K_{3(A)}}{K_{3(B)}} \exp[(s_{(3)B}^* - s_{(3)A}^*)(1 - a_{H_2O})] \left( \frac{F_A(a_{H_2O})}{F_B(a_{H_2O})} \right)^4$$

where  $K_{3(A)}$ ,  $s_{3(A)}^*$  and  $K_{3(B)}$ ,  $s_{3(B)}^*$  refer to  $(TBP)_3 \cdot A(NO_3)_3$  and  $(TBP)_3 \cdot B(NO_3)_3$  respectively. It is important to point out that  $K_{3(Ln)}$  and  $s_{3(Ln)}^*$  depend on the initial organic phase composition even if the concentration of TBP does not appear explicitly in the expression for  $SF_{A/B}$ .

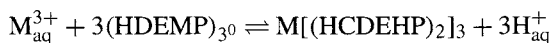
The extraction constants of lanthanides with TBP vary as shown in Fig. 1.8.

Separation factors can be increased by adding a salting-out agent such as  $Al(NO_3)_3$  and the effect of variation of concentration of  $Al(NO_3)_3$  on the separation factor of Sm–Nd, Pr–Ce and Nd–Pr is shown in Fig. 1.9.

Separation factors of lanthanide pairs is also a function of lanthanide nitrate concentration as shown in Fig. 1.10.

High purity La, Pr and Nd salts have been obtained by TBP extraction from 13–14 M  $HNO_3$  in 10–14 stages.

Extraction with di-2-ethylhexyl orthophosphoric acid (HDEHP) at low acidities involves a cation exchange mechanism.



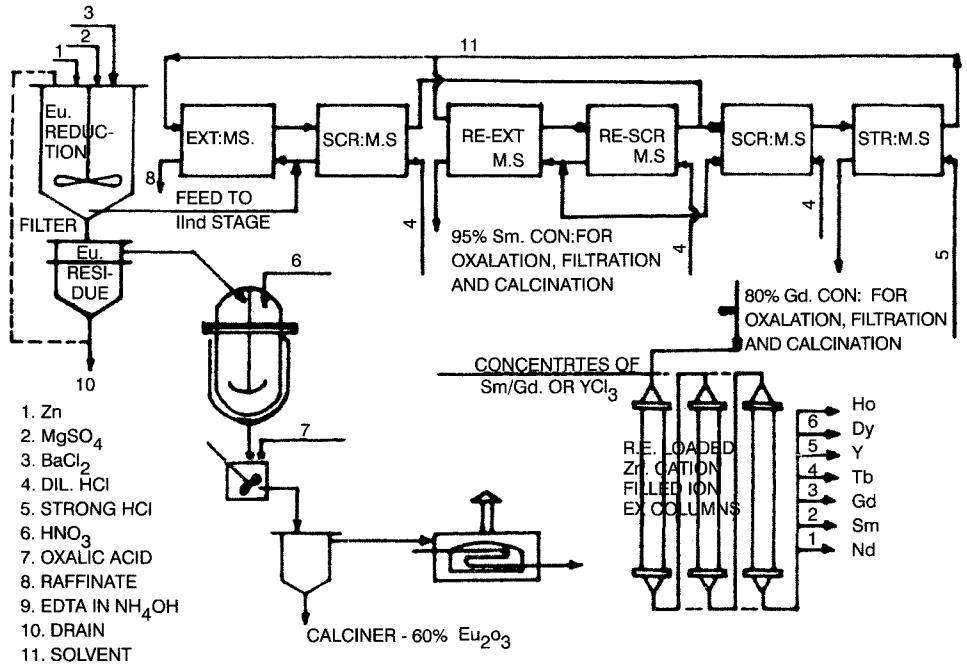
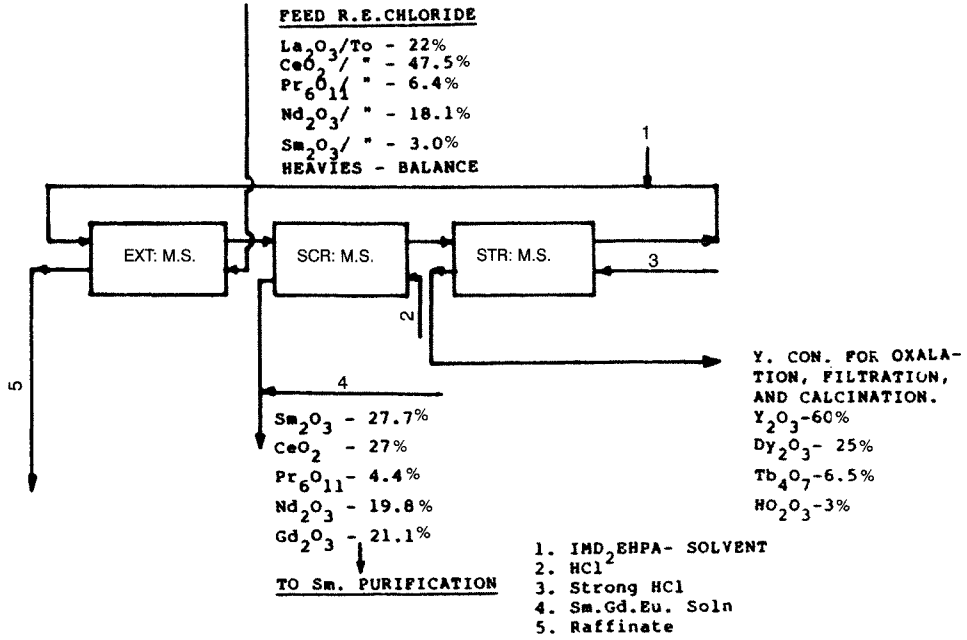


Fig. 1.16. Separation and purification of rare earths by solvent extractions [25].

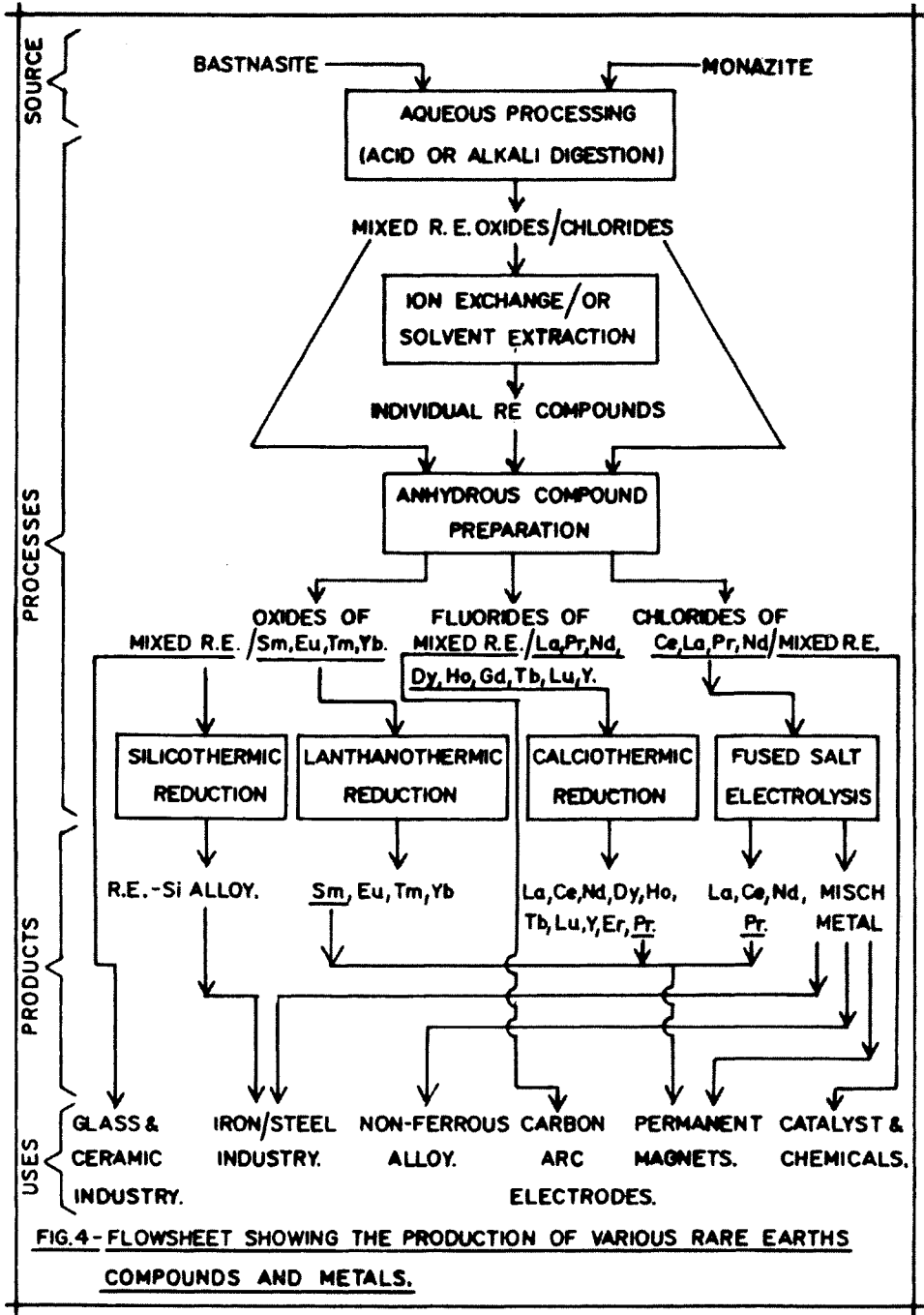


Fig. 1.17. Flowsheet showing the production of various rare earth compounds and metals [2].

TABLE 1.25  
Processes for the production of rare earth metals [2].

Process	Electrolysis	Ca-reduction	La-reduction
Starting material	Chlorides	Chlorides/fluorides	Oxides
Reduction process	Molten salt electrolysis in inert atmosphere	Calciothermic reduction in protective atmosphere	Lanthanothermic reduction in vacuum
Post reduction treatment	Vacuum melting	(i) Vacuum distillation of excess reductant and reductant halides (ii) Purification with respect to contamination from container (a) Holding above the melting point to get rid of Ta picked up during reduction (for Ce, La, Pr and Nd) (b) Vacuum distillation of metals and their collection on the condensers (Y, Gd, Tb, Lu, Dy, Ho, Er)	
Metals	Ce, La, Pr, Nd	Ce, La, Pr, Nd, Y, Gd, Tb, Lu, Dy, Ho, Er	Sm, Eu, Tm, Yb

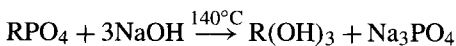
The separation factors obtained with HDEHP in HCl and HClO<sub>4</sub> media range between 1.4 and 5 (Table 1.24).

HDEP has been found useful for the commercial production of Eu from bastnasite and for the purification of yttrium.

Long-chain amines have been used for the extraction of lanthanides and the separation factors are not high. Quaternary ammonium compounds behave like anion exchangers and the separation factors are not attractive. Among this class of extractants, the intensely studied are the two commercial extractants, Alamine 336 and Aliquat 336.

## 11. Recovery of rare earths from monazite

The use of various techniques discussed so far is well illustrated by the processing steps adopted in the economic recovery of rare earths from monazite in India [25]. The first step in the processing of monazite is digestion with caustic soda and this is schematically shown in Fig. 1.11. The main reaction that takes place during digestion may be written as:



The thorium is converted to thorium hydroxide

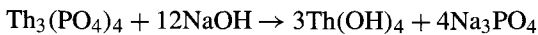
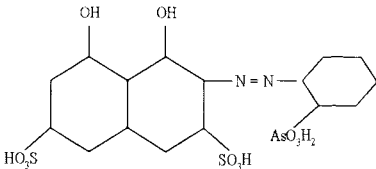


TABLE 1.26  
General qualitative reagents for rare earths elements.

Reagent	Conditions	Sensitivity ( $\mu\text{g/ml}$ )	Reference
Oxalic acid	Weak acidic medium	6.3–6.9	[26,27]
Hydrofluoric acid	Neutral or weak acid medium	–	[28]
Ammonia	–	–	[28]
8-Hydroxy quinoline	pH 4.5–9.5	0.6–3.7	[29,30]
2-Methyl-8-hydroxy quinoline	pH 9.5	3–36	[29,30]
Cupferron (nitroso phenyl hydroxylamine)	Neutral pH	1.6–18.0	[26]
Sodium d-camphorate	At 30–35°C or in ethanol	< 1000	[31]
Pyrocatechol	Precipitate in presence of ethylenediamine, pyridine or quinoline	5–100	[32]
Dihydroxy tartaric acid	Neutral or weakly acid medium	10–100	[33]
Diphen-2,2'-dicarboxylic acid	pH 4–5 in 50% ethanol $\text{Ce}^{3+}$ precipitates	< 300	[34]
Quinalizarin-1,2,5,8-tetrahydroxy anthraquinone	pH 5.5	1	[35]
Na alizarin sulphonate	Red precipitate	–	[36]
Pyrogallol 4-carboxylic acid	Purple, brown precipitate	–	[37]
Murexide	Pink to orange-yellow compounds	20	[37,38]
$  \begin{array}{c}  \text{HN} - \text{CO} \quad \quad \text{C} \quad \text{NH} \\    \quad   \quad \quad   \quad   \\  \text{OC} \quad \text{C} - \text{N} = \text{C} \quad \text{CO} \\    \quad    \quad \quad   \quad   \\  \text{HN} - \text{C} \quad \quad \text{OC} - \text{NH} \\    \\  \text{ONH}_4  \end{array}  $			
Neothoron, arsenazo I		0.1	[39]
			
2-( <i>o</i> -arsenophenylazo)-1,8-dihydroxy-3,6-naphthalene disulfonic acid			

The rare earths and thorium hydroxides are then treated with HCl (30%) to attain a pH of 3.2 at 70°C. This step in the recovery of rare earths is schematically shown in Fig. 1.12. Rare earths are obtained as soluble chlorides leaving behind insoluble  $\text{Th}(\text{OH})_4$ . Rare earth chlorides are treated with  $\text{Na}_2\text{SO}_4$  and  $\text{BaCl}_2$  to free the rare earths from Pb, Ra and Th. It is also treated with  $\text{Na}_2\text{S}$  to remove Pb, Fe, Th and U.

Rare earths are then precipitated as the carbonates by the addition of  $\text{Na}_2\text{CO}_3$ . The process is schematically shown in Fig. 1.13.

TABLE 1.27  
Specific qualitative reagents for rare earth elements.

Element	Reagent	Conditions	Sensitivity (g/ml)	Ref.
La	Ammonium acetate in the presence of I <sub>2</sub>	1 N NH <sub>4</sub> OH	700	[40]
	Aniline yellow S	Neutral or weakly acid	1	[41]
	Monochrome Bordeaux C	pH 9-9.4	1.5	[42]
Ce	KIO <sub>3</sub>	Precipitated from acid media	-	[43]
	KIO <sub>4</sub>	pH 2-7	10	[44]
	Dibenzoylmethane	Ce(C <sub>15</sub> H <sub>11</sub> O <sub>2</sub> ) <sub>4</sub> ppt	-	[45]
	H <sub>2</sub> O <sub>2</sub>	NH <sub>4</sub> OH + H <sub>2</sub> O <sub>2</sub>	7	[46]
	Sodium acetate	Excess reagent at 50-60°C	10	[47]
	Phosphomolybdic and silicomolybdic acids	Weakly basic medium	15	[48]
	<i>o</i> -toluidine	Neutral medium, acetate buffer	10	[49]
	(4,4-diamino-3,3-dimethyl diphenyl)			
	Phenetine (4-ethoxyl aminobenzene)	Neutral medium	30	[50]
	<i>p</i> -sulfanilic acid	Weakly acid medium	20	[51]
	Arsanilic acid	Weak or strong acid medium	10	[52]
	Pyrogallol	Alkaline medium	14	[53]
	Gallein	pH 11.4, Ce <sup>3+</sup> give blue or violet colour	1.2	[54]
	Brucine	Acid medium, Ce <sup>4+</sup> give intense red colour	8	[55]
	Morphine	Alkaline medium, brown precipitate	10	[56]
	Malachite green	Alkaline medium, Ce <sup>4+</sup> gives blue green colour	3	[57]
		Fe <sup>3+</sup> + dimethyl glyoxime	Alkaline medium, Ce <sup>3+</sup> detected	~ 1
	Diphenylamine	Ce <sup>4+</sup> give blue colour	3	[59]
	Sulphinic acids	Acetate buffer, Ce <sup>4+</sup> forms orange yellow precipitate	-	[60]
Pr	MnSO <sub>4</sub> solution	Pr <sub>6</sub> O <sub>11</sub> in acetate solution gives pink violet colour	1	[61]
	Malachite green	Pr <sub>6</sub> O <sub>11</sub> in acetate solution gives blue green colour	0.3	[62]
Sm	Calcium amalgam	SmCl <sub>3</sub> in ethanol gives red SmCl <sub>2</sub>	~ 0.1	[63]
	Mg + HCl	SmCl <sub>3</sub> in ethanol gives red SmCl <sub>2</sub>		
Eu	Cacotheline	Eu <sup>3+</sup> reduced by Zn + HCl gives purple colour with cacotheline	3	[64]
Yb	KIO <sub>3</sub>	Acid medium, YbCl <sub>3</sub> reduced by Na amalgam gives yellow colour	-	[65]
	Oxalic acid and naphthoresorcinol	Yb <sup>3+</sup> reduced by Na amalgam gives red colour	~ 3	[66]
Rare earths	Specific reagents	-	-	[67,68]



TABLE 1.28  
Gravimetric determination of rare earth elements.

Reagent	Conditions	Heat treatment	Weighing form	Ref.
Oxalic acid	0.1–0.3 M excess reagent in hot acid solution	Drying in vacuum desiccator	$\text{Ln}_2(\text{C}_2\text{O}_4)_3 \cdot n\text{H}_2\text{O}$ La ( $n = 8$ ) Ce ( $n = 10$ ) Pr ( $n = 9$ ) Y ( $n = 7$ )	[69]
		Ignition		
		360–400°C	$\text{CeO}_2$	[70]
		790–800°C	$\text{Pr}_6\text{O}_{11}$	[71]
		730–750°C	$\text{Tb}_4\text{O}_7$	[71]
		550–730°C	$\text{La}_2\text{O}_2\text{CO}_3$	[70]
		Not below 800°C	$\text{Ln}_2\text{O}_3$ For all elements except Ce, Pr, Tb	[70,71] [72,73]
$\text{NH}_3$ or NaOH	Small excess of precipitant	850–900°C	$\text{Ln}_2\text{O}_3$	[74]
$\text{K}_4\text{Fe}(\text{CN})_6$	Small excess of precipitant in 40–60% ethanol	Dry in air or desiccator	$\text{KLn}[\text{Fe}(\text{CN})_6 \cdot n\text{H}_2\text{O}]$ La ( $n = 7$ ) $\text{Ce}^{3+}$ ( $n = 2$ ) Nd ( $n = 5$ )	[75]
$\text{Na}_3\text{PO}_4$ or $\text{Na}_2\text{HPO}_4$ or $\text{NaH}_2\text{PO}_4$	0.001 M excess reagent at pH 4.5	900°C	$\text{LnPO}_4$ (except Ce)	[76]
$\text{KIO}_3$	0.25 M excess from 4–5 N $\text{HNO}_3$	40–50°C for 10 minutes	$2\text{Ce}(\text{IO}_3)_4 \cdot \text{KIO}_3 \cdot 8\text{H}_2\text{O}$	[77]
$\text{NH}_4\text{IO}_3$	0.05–0.2 M excess of iodate in 0.5–1.0 M $\text{HNO}_3$ and 3 g persulphate	800–900°C	$\text{CeO}_2$	[78]
$\text{KIO}_4$	Excess reagent, pH 2.7	Dry in vacuum desiccator	$\text{CeHfO}_6\text{H}_2\text{O}$	[79]
		700–800°C	$\text{CeO}_2$	[80]
8-hydroxy quinoline	pH 4.8–5.8 for La pH 4.4–5.5 for Ce	Dry at 110–120°C	$\text{Ln}(\text{C}_9\text{H}_6\text{ON})_3$	[81]
		La 800°C		
		Nd, Sm, Gd, Y at 700–750°C	Oxides	[81]
		Ce 420°C, Pr 575°C		
		La, Nd, Gd 650°C Sm 610°C, Pr, Y 570°C Ce 380°C	Oxides	[82]

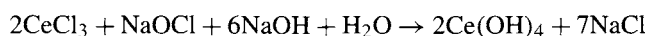
TABLE 1.28  
(Continued.)

Reagent	Conditions	Heat treatment	Weighing form	Ref.
5,7-di-halo-8-hydroxy quinoline	In presence of NH <sub>4</sub> -acetate at room temperature	580–810°C for Cl 520–760°C for Br 350–590°C for I derivatives	Oxides	[83]
Cupferron	pH 3–4; 0.01–0.02 M rare earth salts, 0.15 M excess reagent	Dry at 110–120°C	Ln(C <sub>6</sub> H <sub>5</sub> N <sub>2</sub> ) <sub>3</sub> Ln = La, Ce, Pr, Nd, Sm, Y	[84]
		La, Sm, Y 459–600°C Ho 610°C Eu 570°C, Yb 520°C Tb, Dy, Er 550°C	Oxides	[85]
Neocupferron	pH 3–4; 0.01–0.02 M rare earth salts; 0.15 M excess reagent, <i>T</i> < 50°C	Nd 750°C Pr, Sm 660°C La 610°C Eu, Tb 570°C Dy, Er, Y 540°C Ce, Gd, Yb 490°C Ho 450°C	Oxides	[85,86]
Salicylic acid	pH 3–7 adjusted with ammonia	Dry at 100–105°C	La(C <sub>7</sub> H <sub>5</sub> O <sub>3</sub> ) <sub>3</sub> ·5H <sub>2</sub> O	[87]

TABLE 1.29  
Volumetric methods of analysis of rare earth elements.

Element	Titrant	Conditions	Ref.
Ce(IV)	Oxalic acid	Hot solution, presence of ICl or MnSO <sub>4</sub>	[88]
	Ti <sub>2</sub> (SO <sub>4</sub> ) <sub>3</sub>	Diphenylamine indicator	[89]
	V(II)SO <sub>4</sub>		[90]
	KI, thiosulphate	pH 4–5	[91]
	Arsenious acid	Hot solution, MnSO <sub>4</sub> catalyst	[88]
	Ferrous sulfate	Hot solution, 70°C	[92]
Ce(III)	Sodium hypobromite		[93]
	KMnO <sub>4</sub>	Neutral solution	[92]
	K <sub>3</sub> Fe(CN) <sub>6</sub>	Alkaline solution	[94]
Pr	KMnO <sub>4</sub>	Reduce Pr with FeSO <sub>4</sub>	[95]
Eu	K <sub>2</sub> Cr <sub>2</sub> O <sub>7</sub>	Reduction with Jones reductor, FeCl <sub>3</sub> added, diphenylamine indicator	[96]
	Thiosulphate	Reduction by Jones reductor, add I <sub>2</sub>	[97]
Tb	Iodometric method	Ce and Pr should be absent	[98]
Yb	K <sub>2</sub> Cr <sub>2</sub> O <sub>7</sub>	Reduction by alkali metal amalgam, FeCl <sub>3</sub> added	[96]
Sm <sup>2+</sup>	Mohr's salt	Add excess K <sub>2</sub> Cr <sub>2</sub> O <sub>7</sub> to Sm <sup>2+</sup>	[99]

The mixed rare earth oxides containing cerium can be separated by oxidation of cerium to cerium(IV) by hypochlorite.



The cerium recovery is illustrated schematically in Fig. 1.14.

The cerium oxide obtained on calcination is treated with nitric acid and then hydrolysed in the presence of sulfate to give basic sulfate of 99.9% purity. The cerium-free rare earth chlorides are subjected to a solvent extraction step to produce a samarium concentrate as shown in Fig. 1.15.

The rare earth chlorides are adjusted to a density of 1.3, acidity of 0.05 N and fed into a 12 stage mixer settler and contacted with D<sub>2</sub>EHPA with kerosene as a diluent. The aqueous to organic ration is kept at 1:3 to enable extraction of all the samarium. The lighter rare earths are scrubbed off in a 12 stage scrubbing unit with HCl. The scrubbed solvent is led to a 6-stage stripping unit where it is stripped with 6 N HCl. The stripped solution is a concentrate of all the heavy rare earths, Y and Gd and has 45% of Sm. The mixer settler units are used to produce individual concentrates of Eu, Sm, Gd, and Y and this is schematically shown in Fig. 1.16. The rare earth chlorides are fed into 12-stage mixer settlers where 1 M D<sub>2</sub>EHPA is used as the extractant. The raffinate is recirculated to the main plant and evaporated to yield mixed chloride. The organic phase is scrubbed in a 12-stage mixer settler with dilute HCl to remove lighter rare earths. The organic phase is

TABLE 1.30  
Complexometric titration methods of analysis of rare earth elements.

Element	Titrant	Indicator	Conditions	Ref.
Rare earths	EDTA	Alizarin red	Th at pH 1.5–2.2 REE at pH 4.5 with sulphosalicylic acid and ascorbic acid	[100]
Rare earths	EDTA (0.01 M)	Alizarin red + methylene blue	pH 4 acetate buffer. Hot solution	[101]
Rare earths	EDTA	Arsenazo I	REE pH 5.5	[102]
	0.05 M EDTA	Arsenazo I	REE pH 5.5	[103]
	0.0005 M EDTA	Arsenazo I	Microdetermination of REE by paper chromatography	[104]
	Citric acid	Arsenazo I	Microdetermination of REE in urotropin buffer	[104]
Rare earths Th, Ce <sup>3+</sup> Sc, La, Nd, Er, Y	EDTA	PAR 4-(2-pyridylazo)	pH 6.0	[105]
		Resorcinol		[106]
Sc, rare earths	EDTA, DTPA	1-(2-pyridylazo) 2-naphthol PAN	Acetate buffer Sc pH 2.5 RE pH 4–10	[107]
Th, Sc, RE	EDTA	Methylthymol blue	Acid medium	[108]
Rare earths, Sc, La, Ce, Gd, Y	EDTA	Xylenol orange	Sc, La pH 5–5.2	[109]
			Ce, Gd, Y pH 5.6–6.0 Acetate and hexamethylene tetraamine buffer	[110]
Rare earths	EDTA	Xylenol orange	Back titration	[111]
Rare earths	0.1–0.01 M EDTA	Bromopyrogallol red	Acetate buffer	[112]
La, Ce, Th	EDTA	Chrome Azurol S	Pyridine buffer Th pH 1–2	[113]
Rare earths	EDTA	Erichrome black T	Hexamethylene tetraamine buffer	[114]
	EDTA	Erichrome black T	pH 10 back titration by Zn	[115]
	EDTA	Erichrome black T	Microdetermination at pH 8–9 in presence of tartaric or citric acid	[116]
Rare earths	EDTA	Omegachrome black-blue G	Determination of REE	
Rare earths	Sulfosalicylic acid	Aluminon (aurintricarboxylic acid)	Sensitivity 6 µg/ml	[117]
Rare earths	NTA (nitriolo-triacetic acid)	Murexide		[118]

TABLE 1.31  
Methods based on precipitation reactions for the analysis of rare earths.

Element	Reagent	Method	Ref.
Rare earths	Oxalate	Potentiometry	[119]
		High-frequency conductimetry	[120]
Rare earths	Alkali NaOH	Glass electrode	[121]
Rare earths	$K_4Fe(CN)_6$	Potentiometry	[122]
		High-frequency conductimetry	[120]
Rare earths	$K_2Cr_2O_7$	High-frequency conductimetry	[120]
Rare earths	Oxalate to precipitate metal ions	$KMnO_4$ titration	[123]
	Precipitate titrated with $KMnO_4$		
Rare earths	Ferrocyanide to precipitate REE	Excess ferrocyanide determined by cerimetry with Fe-phenanthroline complex as indicator	[124]
Rare earths	$KIO_3$ to precipitate RE.	Potentiometry $IO_3^-$ titrated with persulphate	[125]
	Excess $IO_3^-$ —determined		
La, Y	8-hydroxyquinoline as precipitant.	Bromatometric titration	[126]
	Precipitate dissolved in 2 N HCl		

TABLE 1.32  
Polarographic methods of analysis of rare earths elements.

Element	$E_{1,2}$ (V)	Conditions	Ref.
Eu	-0.67 to -0.73	In monazite	[127]
Eu, Yb		Differential polarography	[128]
Yb	-1.40 to -1.46	0.1 N $NH_4Cl$	[129,130]
Ce	-0.16	Sensitivity 0.1% in Th and U 0.5% in Y, 1% in Fe, Zn, 3% in Al 5% in V, Ni, La, Sc	[131]
Sm	-1.71 to -1.81		[132]
Rare earths	Azo dyes for complexing	Characteristic waves	[133]
Rare earths		Polarographic analysis	[134-138]
U, rare earths	Complexing agents	Polarography	[138a]

scrubbed with 2.75 M HCl in a third mixer settler and then the organic phase is stripped in a 6-stage stripper with 6 M HCl. The strip solution contains 60% yttrium.

Sodium carbonate is added to the 2.75 M solution for neutralization followed by acetic acid, metallic Zn powder is added when Eu(III) is reduced to Eu(II). Then barium chloride and magnesium sulfate are added to precipitate  $EuSO_4$ . In further processing an 8-stage extractor containing 1 M  $D_2EHPA$  is used. The organic phase is scrubbed in 5-stage scrubbers with 2 M HCl. The scrub solution and raffinate are recirculated. The organic is contacted with 1.5 M HCl in a 7-stage unit when all the Sm and a trace of Gd pass into aqueous phase. The organic is then stripped with 5 M HCl to yield 80-85%  $Gd_2O_3$ .

TABLE 1.33  
Molar absorptivity of rare-earth ions at analytical wavelengths\*.

$\lambda$ (nm)	Molar absorptivity, $\epsilon$ (liter/mole-cm)									
	Pr	Nd	Sm	Eu	Gd	Dy	Ho	Er	Tm	Yb
272.8	1.13	0.210	0.166	0.335	4.20	0.215	0.227	0.698	0.685	0.365
287.0	0.511	1.185	—	0.132	—	0.140	<b>3.59</b>	0.316	0.521	0.266
350.4	—	2.60	0.052	—	—	<b>2.54</b>	0.057	0.096	0.145	—
354.0	—	<b>5.20</b>	0.087	—	—	0.737	0.047	0.382	0.454	—
361.1	—	0.042	0.453	0.053	—	0.271	<b>2.34</b>	0.296	0.801	—
365.0	—	0.025	0.244	0.062	—	<b>2.10</b>	0.331	<b>1.94</b>	0.154	—
379.6	—	0.067	0.052	0.299	—	0.252	0.047	<b>7.18</b>	—	—
394.2	—	0.025	0.148	<b>3.06</b>	—	0.233	0.123	0.096	—	—
401.5	—	—	<b>3.31</b>	0.097	—	0.187	0.038	0.086	—	—
444.2	10.49	—	0.044	—	—	0.047	0.454	0.306	—	—
450.8	1.29	0.025	—	—	—	0.261	4.16	0.497	—	—
521.6	—	<b>4.41</b>	—	—	—	—	0.047	2.10	—	—
523.5	—	1.68	—	—	—	—	0.076	<b>3.20</b>	—	—
537.0	—	—	—	—	—	—	<b>5.16</b>	0.076	—	—
575.5	0.102	<b>6.93</b>	—	—	—	—	—	—	—	—
640.4	—	—	—	—	—	—	3.53	0.153	—	—
683.0	—	0.336	—	—	—	—	—	—	<b>2.56</b>	—
739.5	—	<b>7.20</b>	—	—	—	—	—	—	0.058	—
794.0	—	<b>11.78</b>	—	—	—	0.084	—	0.143	0.579	—
908.0	—	—	—	—	—	<b>2.46</b>	0.113	—	—	0.089
974.0	—	—	0.052	—	—	0.047	—	1.29	—	<b>2.12</b>

\*The spectra were recorded by a Cary-14 recording spectrophotometer with a wavelength scale calibrated with reference to mercury lines. Cells with  $l = 10$  mm were used (20 mm cell for Yb, and 50 mm cell for Tb). All solutions contained 20 mg of oxide in 1 ml of 1 M HClO<sub>4</sub> (except in the case of Er, 10 mg/ml, the figures in bold type refer to the coefficients at the wavelengths used (or recommended) for determining the respective element).

TABLE 1.34  
Spectrophotometric methods for the rare earth elements.

Element	$\lambda$ (nm)	Conditions	Working range (mg/ml)	Sensitivity	Accuracy (%)	Ref.
Ce	253.6	1 N H <sub>2</sub> SO <sub>4</sub> $\epsilon = 650-750$ Ce 40-100% in mixtures with other REE	0.04-0.2	-	$\pm 1$	[140]
		NaF-ZrF <sub>4</sub> UF <sub>4</sub> matrix $\epsilon = 770$	0-0.4		$\pm 10$	[141]
	295.5	In HCl medium $\epsilon = 58$	0.14-2.8		$\pm 8$	[142]
	295.5	Different media $\epsilon = 10.5-25.6$	0.2-7			[143]
Gd	272.8	As chloride $\epsilon = 2.3$	6.7-25		$\pm 10$	[144]
	272.8	As chloride or perchlorate $\epsilon = 3.2$	20-60			[145]
Tb	219.8	HClO <sub>4</sub> medium $\epsilon = 320$	0.001-0.8			[146]
Pr	444	Mixture of REE chloride solutions		0.07	15-20	[147]
	444	Mixture of nitrate solutions		0.008%	5	[147]
	444	Monazite chloride, nitrate solution	0-20			[148]
	444	Chlorides	1.5-12.5		1	
Nd	588	In absence of Nd				[147]
	522	In presence of Pr, Y earths				[147]
	522	Chlorides	3.5-25		1	[144]
	576	Nitrates salt	0.3-30%		2-3	[147]
	576			0.13	15-20	[147]
	576			0.008%	6	[147]
	741	Chlorides or nitrates	0-20			[148]
	796	Mixture of REE				
Sm	402	Chloride solution		1%	1.5-2.5	[149]
	402			0.03%	6	[147]
	402	Chlorides or nitrates Mixture of REE	0-20		5%	[148]
	402	Chlorides	5-25		1%	[144]
	402	Various media	1-27 mg			[150]
	1090	Various media	1-60			[151]
Eu	394	Chlorides	5-25		1	[144]
Ho	640			0.2	15-20	[147]
Er	523			0.33	15-20	[147]
	653					
Tm	379	Chlorides	4.2-18.5		1	[144]
	683			0.33	15-20	[147]
Yb	683	Chlorides	6.6-54		1	[144]
	975	Chlorides	9-72		1	[144]

TABLE 1.35  
Spectrophotometric analysis of rare earths with organic reagents.

Reagent	Element	$\lambda$ (nm)	$\epsilon$	Conditions	Sensitivity	Range ( $\mu\text{g/ml}$ )	Accuracy (%)	Ref.
8-hydroxyquinoline	La	365	5230	0.1 N HCl	–	4–20	0.3	[152]
	Ce	495	~ 6700	CHCl <sub>3</sub>	1	2–30	–	[153]
5,7-dibromo hydroxy quinoline	Ce(III)	513	–	CHCl <sub>3</sub>	–	1–20	–	[154]
Alizarin S	REE	550		pH 4.67	0.7	3–40		[155]
	Y	550			0.3	2.5–25		
	La	520		60% acetone	0.06			[156]
	Y	510		60% acetone	0.06			
	La, Ce, Y	530	$(8-10) \times 10^3$	pH 7, acetate buffer, boric acid		1.4–5	$\pm 1$	[157]
Pyrocatechol violet	Y (Nd, Sm)	665	25900	pH 8.4–9.0	–	1.8 (upper limit)	$\pm 3$	[158]
Bromo pyrogallol red	REE, Y	665	$(41-49) \times 10^3$	pH 6–7.5	–	0.5–3.5	–	[159]
	Ce	675	$56 \times 10^3$					
Naphthazirin	REE, Y	601–606	$(9.6-11.2) \times 10^3$	Pure elements	–	1–6 for REE 0.6–3 for Y	–	[160]
Gallic acid	Ce(III)	–	–	NH <sub>4</sub> OH + Na <sub>2</sub> CO <sub>3</sub> medium	–	14–28 21–42	–	[161]
2',6'-dichloro hydroxy dimethyl fuchson di-carbolic acid	Ce(III)	–	–	pH 7.5 acetate buffer	–	0.8–4	–	[162]
Methylene blue	Ce(IV)	510	9510	pH > 9.6	–	0–8	–	[163]
Tiron, pyrocatechol disulphonate	Ce(IV)	500		pH > 7	–	4–100	–	[164]
		500	4414		–	4–60	–	[165]
Aluminon	REE	530–550	–	pH 8, acetate buffer	–	6 (lower limit)	$\pm 5$	[166]
Hematoxylin	La	600	–	pH 6.2	–	130–260	$\pm 2$	[167]
	Y	650	–	–	–	27–200	$\pm 2$	



TABLE 1.35  
(Continued.)

Reagent	Element	$\lambda$ (nm)	$\epsilon$	Conditions	Sensitivity	Range ( $\mu\text{g/ml}$ )	Accuracy (%)	Ref.
$(\text{NH}_4)_2\text{MoO}_4$	REE	820–830	–	Indirect method	–	–	–	[168]
Stilbazo	Y	540	$6 \times 10^4$	pH 7, acetate buffer	–	0.2–1.4	$\pm 2$	[169]
Neothoron	REE	550–565	$(13.5\text{--}15) \times 10^3$	pH 6–10	–	2 (upper limit)	–	[170]
Arsenazo I	Y	550	$13.5 \times 10^3$	Pure solutions	–	–	–	
	REE	570	$29 \times 10^3$	Pure solution, pH 8	$\sim 0.04$	–	–	[171]
	REE	$\sim 570$	–	pH 6–7.5	–	1–30	$\pm 5\text{--}\pm 20$	[172]
Arsenazo III	REE	655	–	Sc pH 1.8	–	0.01–2	$\pm 2\text{--}\pm 15$	[173]
	Y	605	–	REE, Y pH 2–3	–	–	–	
	Sc	675	–	–	–	–	–	
Ferroin	Ce	505	–	pH 2.5–2.8	–	0.2–10	–	[174]
$\text{Na}_2\text{MoO}_4$	Ce	360	–	0.2 N $\text{H}_2\text{SO}_4$	–	1–16	–	[175]
$\text{H}_2\text{O}_2$	Ce	430–465	645	–	–	41–200	–	[176]
			$\sim 800$	–	–	5–50	–	[177]
Anthranitic acid	Ce	–	–	1:1 $\text{HNO}_3$	–	0.1–0.65 mg	–	[178]
<i>o</i> -toluidine I	Ce	410	9500	pH 0–4	–	0.1–3	–	[179]
<i>o</i> -toluidine II								
<i>o</i> -dianisidine	Ce	469	–	20% $\text{H}_2\text{SO}_4$	–	0–10	–	[180]
Leuco base of Malachite green	Ce	610	–	1 N $\text{H}_2\text{SO}_4$	–	0.3–4	–	[181]
Veratrole (1,2-dimethoxy benzene)	Ce	350–475	–	1 N $\text{H}_2\text{SO}_4$	–	14–140	–	[182]
Strychnine			–	–	–	3.2–18.2	–	[183]

TABLE 1.36  
Emission spectroscopic methods of analysis.

Sample	Impurities	Concentration range (%)	Sensitivity (%)
La	Ce, Pr, Nd	0.05–1.0	0.02–0.03
	Sm, Eu, Gd	–	0.03
Ce	La, Pr, Nd	0.01–1.0, 0.05–2.0	0.005–0.03
Sm	Eu	0.005–1.0	–
	Nd, Eu, Gd, Dy, Y	0.003–1.0	0.001–0.05
Eu	Sm	–	0.005
Gd	Nd, Sm	0.05–1.0	0.02
	Eu, Tb	0.1–2.0	0.05
	Dy, Ho, Y	0.05–2.0	0.02
Tb	Sm, Gd, Dy, Y	0.02–1.0	0.005–0.03
Dy	Y, Tb, Ho, Er	0.02–1.0	0.007–0.1
Ho	Dy, Er, Y	0.01–1.0	0.005–0.04
Er	Ho, Tm	0.005–1.0	0.0001–0.005
	Dy, Ho, Tm, Yb	0.01–1.0	–
	Y	0.01–1.0	0.0007
Tm	Er, Yb	0.005–1.0	–
	Ho, Er, Yb, Lu, Y	0.02–1.0	0.0002–0.02
Yb	Sm, Er, Tm, La, Y, Sc	0.01–1.0	0.002–0.005
Lu	Tm, Yb, Y, Sc	0.02–1.0	0.0005–0.005
Y	La, Pr, Nd	0.01–0.44	–
	Sm, Gd, Tb, Dy, Ho, Er	0.01–2.0	0.005–0.05

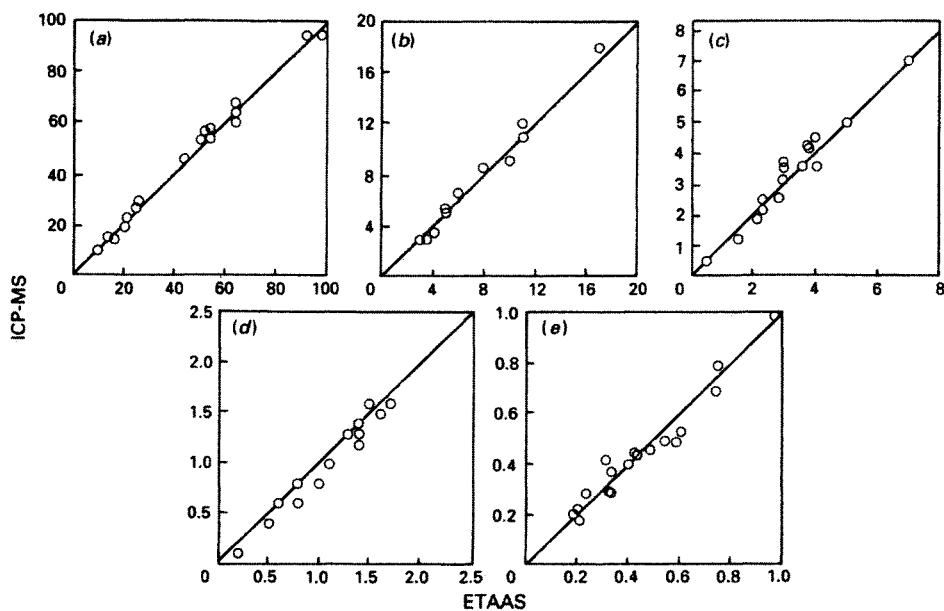


Fig. 1.18. Inter-method correlation plots for ETAAS versus ICP-MS: (a) Nd; (b) Sm; (c) Er; (d) Ho; and (e) Tm. Analyte concentration in  $\mu\text{g g}^{-1}$ .

TABLE 1.37

Sensitivity of determination of individual rare-earth elements by activation analysis, compared with sensitivity of other analytical methods\* [185].

Element	Isotope used for determination	Sensitivity ( $\mu\text{g/ml}$ )			
		Activation analysis		Emission spectroscopy (Cupspark)	Flame photometry
		X-10 reactor, neutron flux $5 \times 10^{11} \text{ cm}^{-2} \text{ s}^{-1}$	LITR reactor, neutron flux $10^{13} \text{ cm}^{-2} \text{ s}^{-1}$		
La	La <sup>140</sup>	0.002	0.00001	0.05	5.0
Ce	Ce <sup>141</sup>	0.1	0.005	0.5	20.0
	Ce <sup>143</sup>	0.2			
Pr	Pr <sup>142</sup>	0.002	0.0001	0.2	100
Nd	Nd <sup>147</sup>	0.1	0.005	0.2	50
	Nd <sup>149</sup>	0.1			
Sm	Sm <sup>153</sup>	0.0006	0.00003	0.2	100
Eu	Eu <sup>152</sup>	0.00003	0.0000015	0.02	
Gd	Gd <sup>161</sup>	0.02	0.001	0.1	10.0
Tb	Tb <sup>160</sup>	0.004	0.0002		
Dy	Dy <sup>165</sup>	0.00003	0.0000015	0.5	10.0
Ho	Ho <sup>166</sup>	0.0004	0.00002	0.2	
Er	Er <sup>171</sup>	0.02	0.001	0.5	
Tm	Tm <sup>170</sup>	0.002	0.0001	0.05	
Yb	Yb <sup>175</sup>	0.002	0.0001	0.1	
Lu	Lu <sup>177</sup>	0.0003	0.000015	2.0	
Y	Y <sup>90</sup>	0.01	0.0005	0.01	50

\*The time of irradiation necessary for the accumulation of long-lived isotopes is 30 days, but in the case of short-lived isotopes the time of irradiation was selected in accordance with the saturation conditions. One ml of the solution was taken for the activation analysis. For the other analytical methods, the sensitivity data was recalculated to correspond to a sample volume of 1 ml, and the relative error to  $\pm 10\%$ . The threshold of the determination corresponds to 40 decays per second.

The Sm solution is then adjusted to a pH of 0.23 followed by solvent extraction in a 6-stage extractor. The raffinate is about 95% Sm<sub>2</sub>O<sub>3</sub> which is precipitated as oxalate and ignited to obtain Sm<sub>2</sub>O<sub>3</sub>.

The final stage involves ion exchange chromatography with the resin in zinc form and the columns of 60 cm dia  $\times$  300 cm height are used. EDTA is used as the eluting agent and individual rare earths of 99.9% purity are obtained.

## 12. Preparation of rare earth metals

The three main processes by which rare earth metals are produced may be listed as (i) electrolysis, (ii) calcium reduction and (iii) lanthanum reduction. The three processes are summarized in Table 1.25.

Bastnasite and monazite are the main sources for the production of rare earth metals and their compounds. A flow sheet illustrating the sources, processes, the products that can be obtained and their uses or applications is given in Fig. 1.17.

TABLE 1.38  
Main analytical lines in the X-ray spectra of rare earth elements.

Element	Transition	Wavelength, X (in first order of reflection)	Remarks
La	$L_{\beta 1}$	2453.87	Any other line of the L series can also be used
Ce	$L_{\beta 1}$	2351.0	
Pr	$L_{\beta 2}$	2204.1	Slight interference by La
	$L_{\alpha 1}$	2457.7	
Nd	$L_{\beta 1}$	2253.9	
	$L_{\alpha 1}$	2365.3	
	$L_{\beta 1}$	2162.2	
Sm	$L_{\beta 2}$	2031.4	Strong interference by Pr Strong interference by Dy Used to analyze rich concentrates
	$L_{\alpha 1}$	2195.0	
	$L_{\beta 1}$	1993.6	
Eu	$L_{\beta 2}$	1878.1	
	$L_{\alpha 1}$	2116.3	
	$L_{\beta 1}$	1916.3	
Gd	$L_{\beta 2}$	1808.2	Ce interferes
	$L_{\alpha 1}$	2041.9	
Tb	$L_{\beta 1}$	1842.5	Ho interferes
	$L_{\alpha 1}$	1971.5	
Dy	$L_{\beta 1}$	1772.7	Th and Tm interfere
	$L_{\alpha 1}$	1904.90	
Ho	$L_{\beta 1}$	1706.6	Gd and U interfere
	$L_{\alpha 1}$	1841.0	
Er	$L_{\beta 1}$	1643.5	Y interferes
	$L_{\alpha 1}$	1780.68	
	$L_{\alpha 2}$	1792.02	
	$L_{\beta 1}$	1584.09	
Tm	$L_{\beta 2}$	1510.94	Strong interference by Sm
	$L_{\alpha 1}$	1722.8	
Yb	$L_{\alpha 1}$	1668.50	Used to analyze rich concentrates
Lu	$L_{\alpha 1}$	1616.17	
	$L_{\alpha 2}$	1626.90	
	$L_{\gamma 1}$	1219.76	

### 13. Analytical chemistry of rare earths

The classic method for the isolation of the rare earth group which is used for both qualitative and quantitative determination involves three methods. In the first method, rare earths are precipitated as fluorides in acidic medium. The elements precipitated include Mg, Cu, Fe, rare earths Th, Ca and Sr. The second method consists of precipitation as hydroxides resulting in the removal of alkaline-earth elements like calcium from the mineral. In the third method rare earths are precipitated as oxalates from moderately acidic solutions and the elements Ca, Zn, Pb, Cu, Cd, and Ag may be coprecipitated. In early times the above methods were repeated several times to isolate, the rare earth group in a relatively pure form.

TABLE 1.39

Characteristics of the main lines and bands of rare earth elements in oxygen–hydrogen flame spectra [184].

Element	$\lambda$ (nm)	Band half-width (nm)	Sensitivity, div ( $\mu\text{g/ml}$ )	Interfering elements, div ( $\mu\text{g/ml}$ )
La	442	5	9	None
	560	—	0	Heavy REE starting from Gd
	741	10	8	None
	791	10	8	None
Pr	604	5	3	Y 40, Gd 20, Tb 8, Sm 6, Dy 3, Nd 1
Nd	663	8	4	Eu 4, Sm 4
	700	15	3	None
	712	8	3	None
Sm	614	18	8	Y 80, Gd 27, Eu 5, Tb 3, Dy 2
	624	10	9	Y 40, Gd 32, Eu 11, Tb 2
	640	10	8	Eu 8, Gd 2, Nd 1
	652	10	8	Eu, 8, Nd 1
Eu	459	Line	22	Tb 2, Sm 1
	463	Line	18	Gd 8, Tb 2, Sm 1
	466	Line	15	Gd 8, Tb 2
Gd	464	5	8	Eu 18, Sm 1
	622	20	32	Y 40, Eu 11, Sm 9, Dy 2, Tb 2, Nb 1
Tb	535	5	10	Yb 10, Tm 5, Ho 3, La 3, Y 1
	573	5	11	Dy 18, Yb 9, Gd 7, Er 2, Tm 2, Y 2
	598	5	13	Y 80, Gd 27, Eu 13, Sm 4, Pr 1
Dy	528	5	15	Yb 10, Ho 6, Tm 2
	540	5	11	Tm 9, Tb 8, Gd 2, Yb 2
	549	5	10	Er 8, Tm 8, La 3, Gd 2, Tb 2
	573	10	18	Ho 10, Yb 9, Tb 8, Gd 5
	583	5	15	Gd 15, Tb 8, Ho 4, Y 4
Ho	516	8	10	Lu 20, Er 5, Dy 5, Tm 2, Y 2, Yb 2
	532	5	6	Yb 12, Tm 7, Dy 5, Tb 4, Gd 1
	566	10	25	La 8, Gd 7, Tb 7, Er 6, Tm 5, Yb 4
	504	12	12	Y 3, Yb 2
	552	18	13	Dy 8, Tb 5, Yb 5, Gd 3, La 3
Tm	482	5	7	Y 12, Yb 6, Gd 1
	494	10	10	Gd 4, Yb 2
	540	12	9	Dy 11, Gd 3, La 3, Ho 2, Tb 2, Yb 2
Yb	399	Line	60	None
Lu	468	5	25	Eu 10, Gd 4, Y 4, Tb 1
	517	5	25	Ho 10, Er 6, Dy 5, Y 2
Y	482	5	12	Tm 7, Yb 6, Gd 2
	598	8	80	Gd 27, Eu 13, Tb 13, Sm 6, Dy 2, Lu 2, Pr 1
	614	8	80	Gd 27, Sm 8, Eu 5, Tb 3, Pr 1

\*Data obtained with the ORNL grating spectrophotometer, using the RCA-6217 (380–700 nm) and 16-PMI Farnsworth (700–900 nm) photomultipliers. Dynode voltage, 100 v; slit width, 0.25 mm, gas flow rates: O<sub>2</sub>, 5100 ml/min; H<sub>2</sub>, 3600 ml/min: metal concentration in the form of complexes with TTA (0.1 M solution in hexane) 50  $\mu\text{g/ml}$ ; except Nd, 100  $\mu\text{g/ml}$ ; and Pr, 500  $\mu\text{g/ml}$ .

TABLE 1.40

Operating parameters and sensitivities for yttrium and certain rare earths in the nitrous oxide-acetylene flame [186].

Element	Wavelength (nm)	Spectral band-width (nm)	Lamp current (mA)	Sensitivity (ppm/1% absorption)		
				This work	Jaworowski et al.	Van Loon et al.
Y	410.24	0.33	10	3.2	4 <sup>†</sup>	1.8
Nd	492.45	0.17	5	9.4	20 <sup>*</sup>	‡
Sm	429.67	0.17	10	7.6	20 <sup>†</sup>	‡
Eu	459.40	0.33	10	0.35	1.5 <sup>*</sup>	0.7
Dy	421.17	0.08	15	0.40	4 <sup>†</sup>	1.0
Ho	410.38	0.08	15	0.67	‡	2.0
Er	400.80	0.17	10	0.46	2 <sup>*</sup>	0.8
Tm	371.79	0.33	15	0.21	‡	1.0
Yb	398.80	0.33	5	0.07	‡	0.3

\* Chloride in 80% ethyl alcohol.

† Chloride in 80% methyl alcohol.

‡ Not determined.

TABLE 1.41

Determination \* of certain lanthanides and yttrium in some rare earth minerals and comparison with previously published X-ray fluorescence values, where available (all results average of 2–6 determinations are given as %) [186].

Oxides	Britholite		Cenosite		Allanite	Chevkinite <sup>¶</sup>
	This work	Hughson & Sen Gupta	This work	Pouliot et al.	This work	This work
Y <sub>2</sub> O <sub>3</sub>	0.44	0.4	26.2	25.27	0.20	0.30
La <sub>2</sub> O <sub>3</sub>	5.9	5.6	—	—	4.75	4.00
Nd <sub>2</sub> O <sub>3</sub>	7.5	8.0	0.20	0.19	1.80	1.30
Sm <sub>2</sub> O <sub>3</sub>	1.3	1.5	0.22	0.27	‡	1.00
Eu <sub>2</sub> O <sub>3</sub>	0.29	**	0.13	**	0.07	0.05
Dy <sub>2</sub> O <sub>3</sub>	0.22	**	3.06	3.10	‡	‡
Ho <sub>2</sub> O <sub>3</sub>	0.04	**	1.07	**	0.10	0.01
Er <sub>2</sub> O <sub>3</sub>	0.03	**	2.65	3.53	‡	‡
Tm <sub>2</sub> O <sub>3</sub>	0.006	**	0.45	**	‡	‡
Yb <sub>2</sub> O <sub>3</sub>	0.012	**	2.33	2.71	< 0.05	< 0.05

\* Yttrium and rare earths were determined by atomic absorption; lanthanum was determined by flame emission.

\*\* Not determined.

† From Picnoe river, north of Otter Lake, Quebec, Canada.

‡ Not detected.

¶ From Pitt Prospect, Pontiac County, Quebec, Canada.

Some qualitative analytical reagents for the detection of rare earths elements are given in Tables 1.26 and 1.27. Gravimetric, volumetric, complexometric, precipitation and polarographic methods of analysis of rare earths are summarized in Tables 1.28 to 1.32.

TABLE 1.42

Determination\* of certain lanthanides and yttrium in rocks and some minerals containing small amounts of these elements and comparison with other values, where available (all results, average of two determinations, are given as ppm in the sample) [186].

Element	Syenite Rock-1**		Syenite Rock-2**		Syenite Rock-3**		Limonite Gossan <sup>¶</sup>	Apatite <sup>¶¶</sup>	Sphene <sup>¶¶</sup>
	This work	Reported median or values	This work	Median of other values	This work	Median of other values	This work	This work	This work
Y	425	450	120	140	600	710	79	1260	1890
La	200	220	88	88	1250	1400	1023	1961	597
Nd	260	302	75	<100 <sup>†</sup>	700	840	-***	2744	2058
Sm	70	<100, 245	17	17, <20 <sup>‡</sup>	108	80, 130 <sup>‡</sup>	-***	517	604
Eu	9	8, 15	2.3	2	14	15	43	78	104
Dy	76	100, 135	21	<80 <sup>†</sup>	118	110 <sup>†</sup>	26	261	436
Ho	18	2, 21	7	?	22	?	-***	61	105
Er	48	42, 57	13	?	52	?	?	131	219
Tm	9.6	5	2.5	?	10.5	?	-***	20	38
Yb	55	70	16	16	55	62	< 9	88	176

\* Yttrium and rare earths were determined by atomic-absorption; lanthanum was determined by flame-emission.

\*\* Spectroscopy Society of Canada standard reference material.

\*\*\* Not detected.

<sup>†</sup> Single result only from one source.

<sup>‡</sup> Two results only from two sources.

<sup>¶</sup> From Springiron Lake, British Columbia, Canada.

<sup>¶¶</sup> From Turners Island, Ontario, Canada.

TABLE 1.43

Operating parameters in the determination of rare-earth elements with the IL555 flameless atomizer [186].

Purge gas: Argon	Flow-rate: 15 ft <sup>3</sup> /h					
Operation mode: Auto	Temperature feedback: On					
Auto clean cycle: On	Sample size: 5–25 $\mu$ l					
Indicated temperature: $^{\circ}$ C	75	100	500	750	2500	2500
Time setting: ( $\times 5$ s):	5	5	3	3	0	1

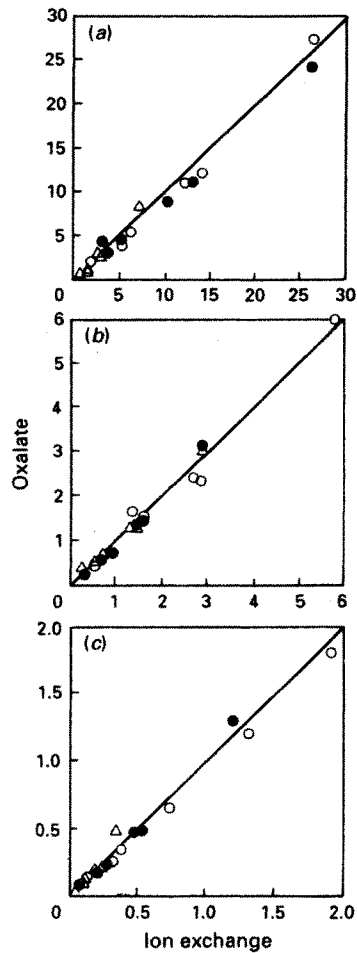


Fig. 1.19. Inter-method correlation plots for oxalate versus ion-exchange pre-concentration of Y and REE from CCRMP reference materials TDB-1, WGB-1, UMT-1, WMG-1 and WMS-1. (a)  $\circ$ , Y;  $\bullet$ , Nd; and  $\Delta$ , Sm. (b)  $\circ$ , Dy;  $\bullet$ , Er; and  $\Delta$ , Yb. (c)  $\circ$ , Eu;  $\bullet$ , Ho; and  $\Delta$ , Tm. Analyte concentrations in  $\mu\text{g g}^{-1}$ .



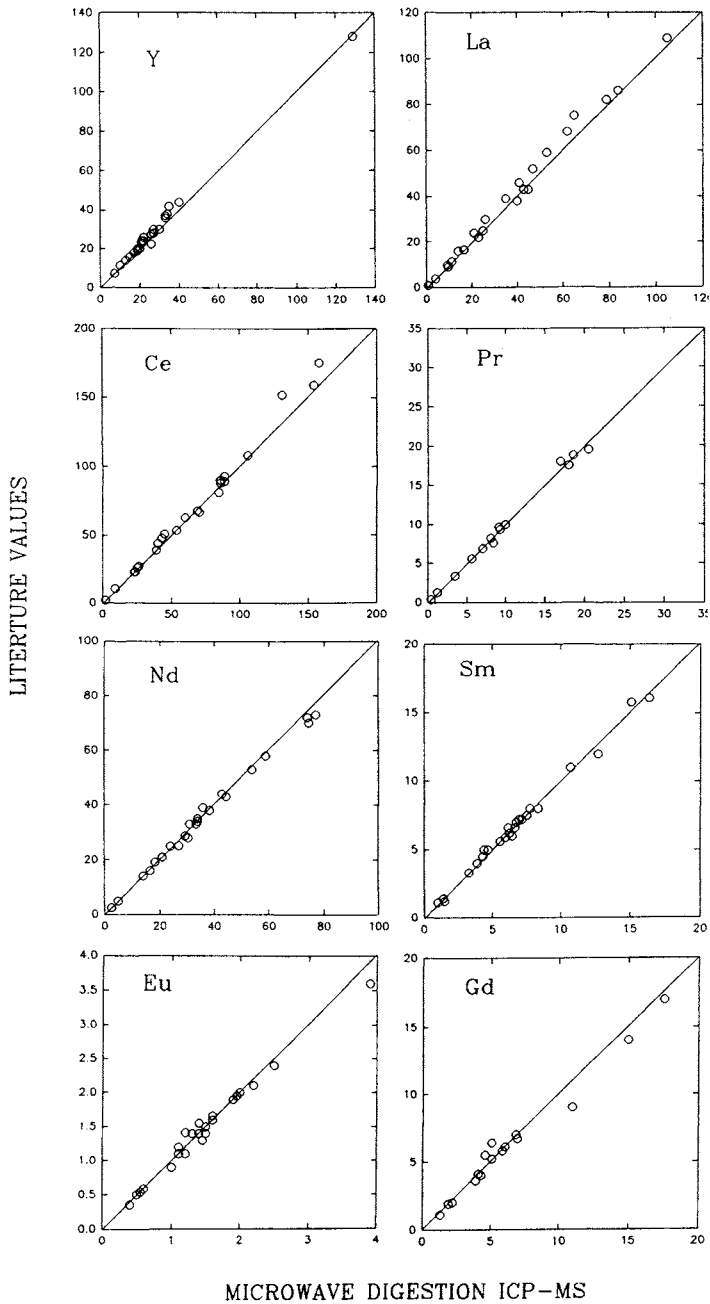


Fig. 1.20. Correlation plots for the microwave digestion ICP-MS results versus the literature values for Y, La, Ce, Pr, Nd, Sm, Eu and Gd in some international reference samples of rocks and sediments (concentration is given in micrograms per gram) [198].

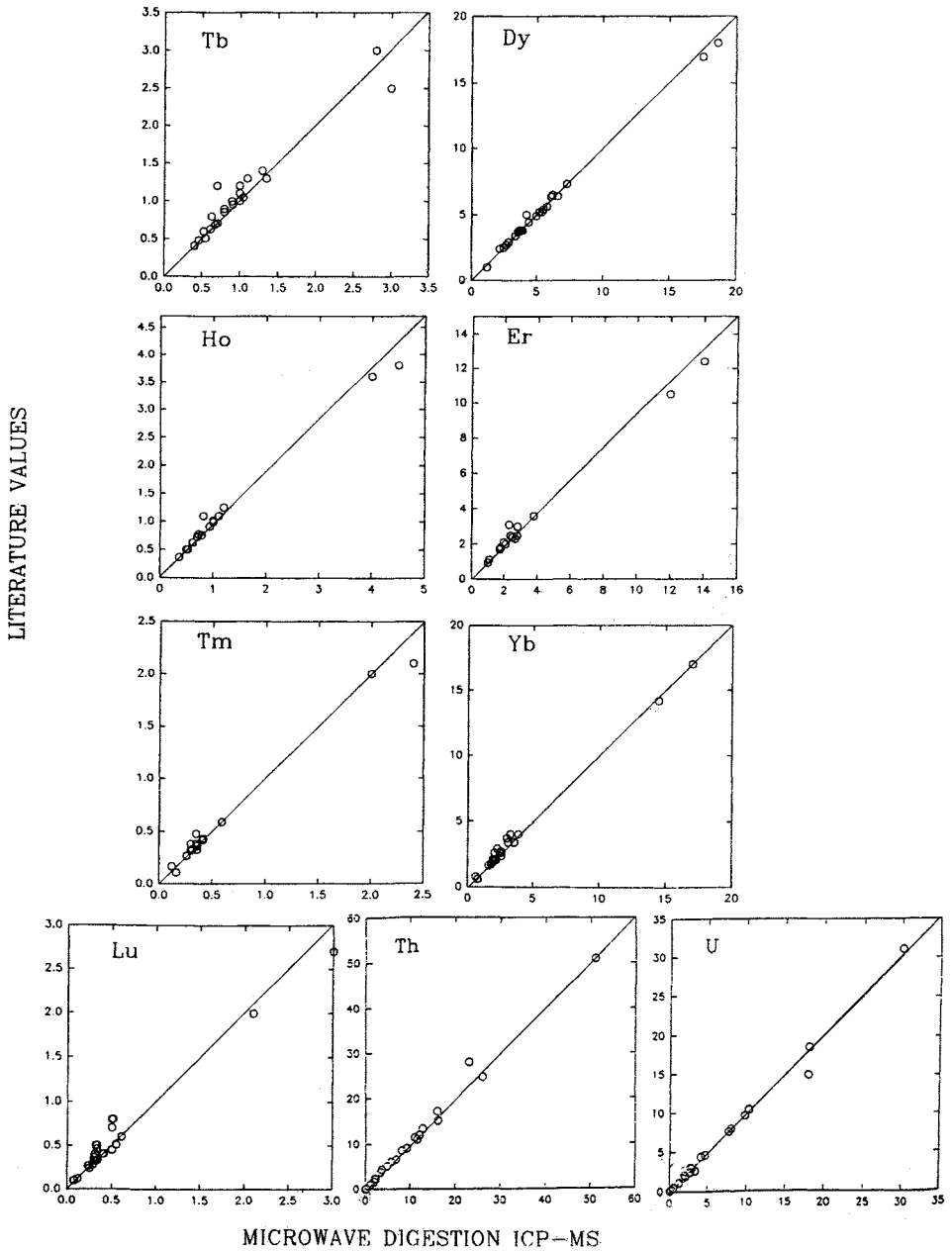


Fig. 1.21. Correlation plots for the microwave digestion ICP-MS results versus the literature values for Tb, Dy, Ho, Er, Tm, Yb, Lu, Th and U in some international reference samples of rocks and sediments (concentration is given in micrograms per gram) [198].

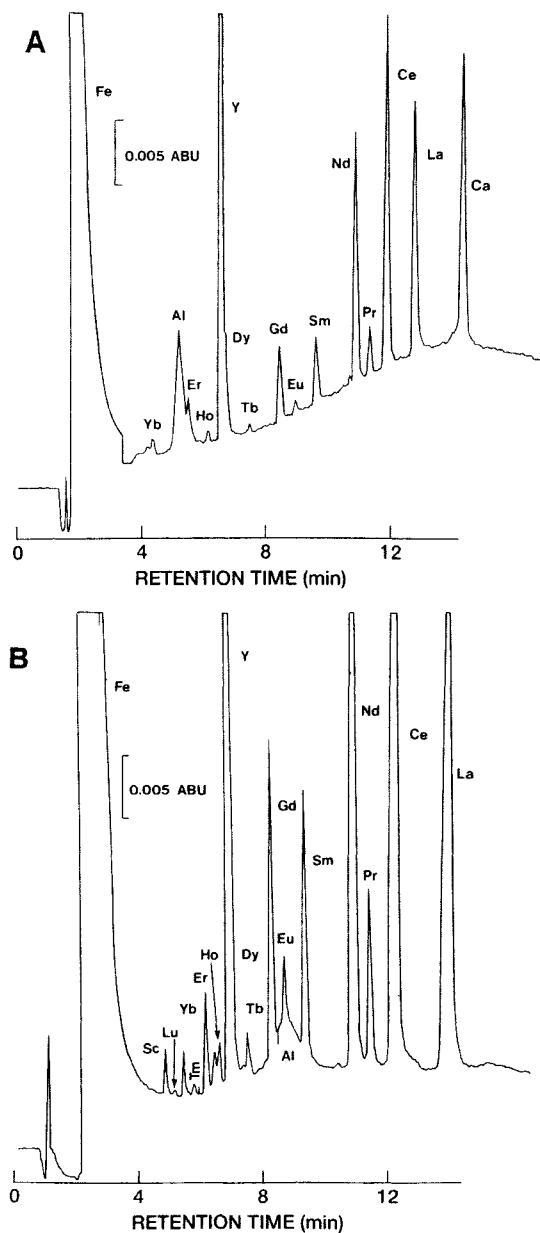


Fig. 1.22. Direct injection of aluminium processing solution. Conditions: Supelcosil LC-18-DB column; gradient programme at a flow-rate of 1.0 ml/min from 1.05 M HIBA to 0.4 M HIBA over 10 min. and held at 0.4 M for 5 min.; modifier, 1-octanesulphonate at 0.01 M; (A), eluents at pH 4.5; (B), eluents at pH 3.8; detection at 658 nm after post-column reaction with Arsenazo III; sample injected, 50  $\mu$ l; sample dilution, (A) 10 ml to 100 ml, (B) 20 ml to 50 ml.

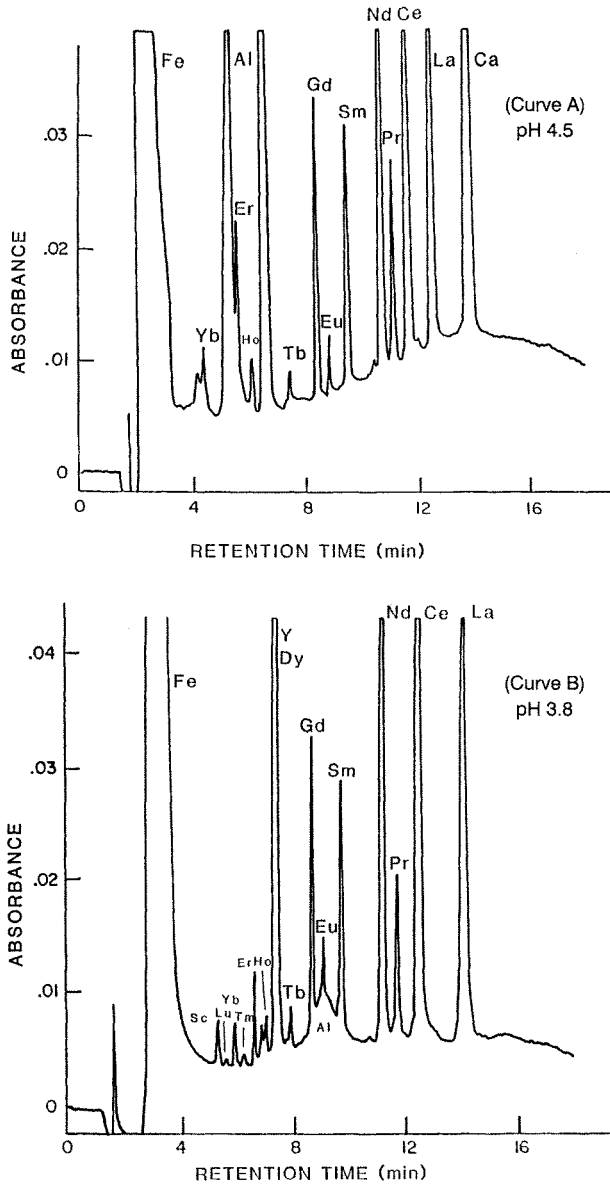


Fig. 1.23. Direct injection of aluminum processing solution. Conditions: Supelco LC-18 DB column; gradient program at a flow rate of 1.0 ml/min from 0.05 mol/l HIBA to 0.4 mol/l HIBA over 10 min and held at 0.4 mol/l for 5 min; modifier, 1-octanesulfonate at  $1 \times 10^{-2}$  mol/l; Curve (A), eluents at pH 4.5; Curve (B), eluents at pH 3.8; detection at 658 nm after post-column reaction with Arsenazo III; sample, 50  $\mu$ l; sample dilution, 20 ml per 50 ml.

TABLE 1.44

Instrumental parameters in the determination of rare earth elements by graphite-furnace atomic-absorption spectrometry [186].

Element	Wavelength (nm)	Light-source (hollow-cathode lamp)	Current (mA)	Special bandpass (nm)	Furnace temperature (°C)
Dy	421.2	Westinghouse	3	0.15	2500
Er	400.8	Westinghouse	6	0.3	2500
Eu	459.4	Westinghouse	4.5	0.15	2500
Gd	368.4	Westinghouse	14	0.15	2700
Ho	410.4	Westinghouse	10	0.15	2500
Lu	336.0	Varian Techtron	17	0.3	2700
Nd	492.5	Westinghouse	10	0.15	2500
Pr	495.1	Cathodeon	12	0.5	2300
Sm	429.7	Westinghouse	6	0.3	2700
Tb	432.7	Cathodeon	11	0.3	2700
Tm	371.8	Westinghouse	19	0.5	2500
Y	410.2	Westinghouse	6	0.3	2500
Yb	398.8	Westinghouse	5	0.3	2500

TABLE 1.45

Sensitivity\* of rare earth elements in the determination by graphite-furnace atomic-absorption spectrometry and comparison with other published values [186].

Element	Furnace temperature (°C)	Sensitivity*	
		This work (pyrolytically-coated furnace) (g)	L'vov and Pelieva (tantalum-foil lined furnace) (g)
Dy	2500	$1.1 \times 10^{-11}$	$4.0 \times 10^{-11}$
	2700	$8.8 \times 10^{-12}$	
Er	2500	$2.3 \times 10^{-11}$	$6.0 \times 10^{-11}$
Eu	2500	$4.7 \times 10^{-12}$	$3.0 \times 10^{-11}$ (at 2400°C)
Gd	2500	$2.7 \times 10^{-9}$	$2.5 \times 10^{-9}$ (at 2550°C)
	2700	$4.0 \times 10^{-10}$	
Ho	2500	$1.2 \times 10^{-11}$	$6.0 \times 10^{-11}$
Lu	2725	$2.0 \times 10^{-10}$	$3.0 \times 10^{-10}$ (at 2500°C)
Nd	2500	$1.1 \times 10^{-9}$	$3.5 \times 10^{-9}$
	2550	$2.6 \times 10^{-10}$	
Pr	2300	$3.0 \times 10^{-9}$	$3.6 \times 10^{-9}$ (at 2600°C)
Sm	2500	$2.1 \times 10^{-10}$	$1.0 \times 10^{-9}$ (at 2400°C)
	2700	$7.0 \times 10^{-11}$	
Tb	2500	$7.0 \times 10^{-10}$	$4.0 \times 10^{-10}$ (at 2600°C)
Tm	2500	$3.0 \times 10^{-12}$	$2.0 \times 10^{-11}$ (at 2400°C)
Y	2500	$1.8 \times 10^{-10}$	$6.0 \times 10^{-11}$
Yb	2500	$1.0 \times 10^{-12}$	$4.0 \times 10^{-12}$

\*Defined as the weight of the element that gives an absorbance of 0.0044 measured as a peak-height.

TABLE 1.46  
Determination of yttrium and the rare earth elements in South African reference sample NIM-18/69 by graphite-furnace and flame atomic-absorption spectrometry [186].

Constituent	This work	Other values <sup>d</sup>	Average of other value
CeO <sub>2</sub> (%)	0.40 <sup>e</sup>	0.48, 0.41, 0.48 0.11 <sup>*</sup> , 0.40, 0.51 0.40, 0.43, 0.50	0.45
Dy <sub>2</sub> O <sub>3</sub> (ppm)	68 <sup>a</sup> 68 <sup>b</sup>	42, 40, 66, 60 101, 100, 7 <sup>*</sup>	68
Er <sub>2</sub> O <sub>3</sub> (ppm)	24 <sup>a</sup> 26 <sup>b</sup>	10, 19, 1 <sup>*</sup>	15
Eu <sub>2</sub> O <sub>3</sub> (ppm)	50 <sup>a</sup> 56 <sup>b</sup>	50, 50, 46, 56 44, 98, 22	52
Gd <sub>2</sub> O <sub>3</sub> (ppm)	150 <sup>a</sup> 154 <sup>b</sup>	117, 141, 140 101, 140, 245 23 <sup>*</sup>	147
Ho <sub>2</sub> O <sub>3</sub> (ppm)	11.2 <sup>a</sup> 11.5 <sup>b</sup>	6, 9, 3 <sup>*</sup>	8
La <sub>2</sub> O <sub>3</sub> (%)	0.21 <sup>a</sup>	0.29, 0.20, 0.25, 0.36 0.30, 0.22, 0.18	0.26
Lu <sub>2</sub> O <sub>3</sub> (ppm)	4.8 <sup>b</sup>	1.1	1
Nd <sub>2</sub> O <sub>3</sub> (%)	0.16 <sup>a</sup> 0.16 <sup>b</sup> 0.15 <sup>c</sup>	0.18, 0.12, 0.17, 0.096, 0.10, 0.15, 0.30, 0.084	0.15
Pr <sub>6</sub> O <sub>11</sub> (ppm)	520 <sup>a</sup> 580 <sup>b</sup>	749, 372, 468, 271, 946, 500, 760, 161	528
Sm <sub>2</sub> O <sub>3</sub> (ppm)	215 <sup>a</sup> 213 <sup>b</sup>	280, 161, 238, 301, 50 <sup>*</sup> , 60 <sup>*</sup> , 325, 141	241
Tb <sub>4</sub> O <sub>7</sub> (ppm)	31 <sup>b</sup>	14, 14	14
Tm <sub>2</sub> O <sub>3</sub> (ppm)	2.9 <sup>a</sup> 3.0 <sup>b</sup>	5, 2, 2	3
Y <sub>2</sub> O <sub>3</sub> (ppm)	334 <sup>a</sup> 330 <sup>b</sup> 328 <sup>c</sup>	270, 191, 161 221, 200, 281, 315	234
Yb <sub>2</sub> O <sub>3</sub> (ppm)	15.7 <sup>a</sup> 15.7 <sup>b</sup> 15.7 <sup>c</sup>	10, 10, 13, 9, 18, 3 <sup>*</sup>	12

<sup>a</sup>Flame atomic-absorption value; <sup>b</sup>graphite-furnace atomic-absorption value; <sup>c</sup>arc-emission spectrographic value;

<sup>d</sup>Stock, Steele and Copelowitz; <sup>e</sup>semi-quantitative arc-emission spectrographic value.

\*Rejected in calculating the average of other values in the last column.

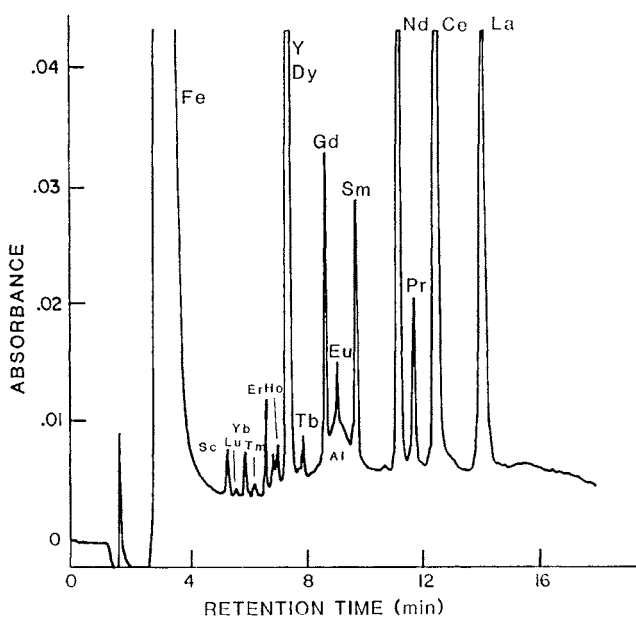


Fig. 1.24. Effect of pH on the retention time of the rare earths. Conditions: Supelco LC-18 DB column; gradient program at a flow rate of 1.0 ml/min from 0.05 mol/l HIBA to 0.4 mol/l HIBA over 10 min and held at 0.4 mol/l for 5 min; modifier, concentration of 1-octanesulfonate at  $1 \times 10^{-2}$ .

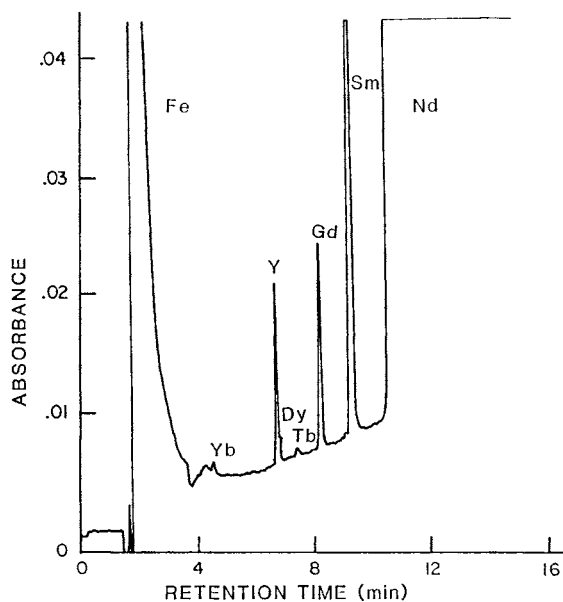


Fig. 1.25. Effect of pH on the retention time of metals ions. Conditions: Supelco LC-18 DB column; gradient program at a flow rate of 1.0 ml/min from 0.05 mol/l HIBA to 0.4 mol/l HIBA over 10 min and held at 0.4 mol/l for 5 min; modifier, concentration of 1-octanesulfonate at  $1 \times 10^{-2}$ .

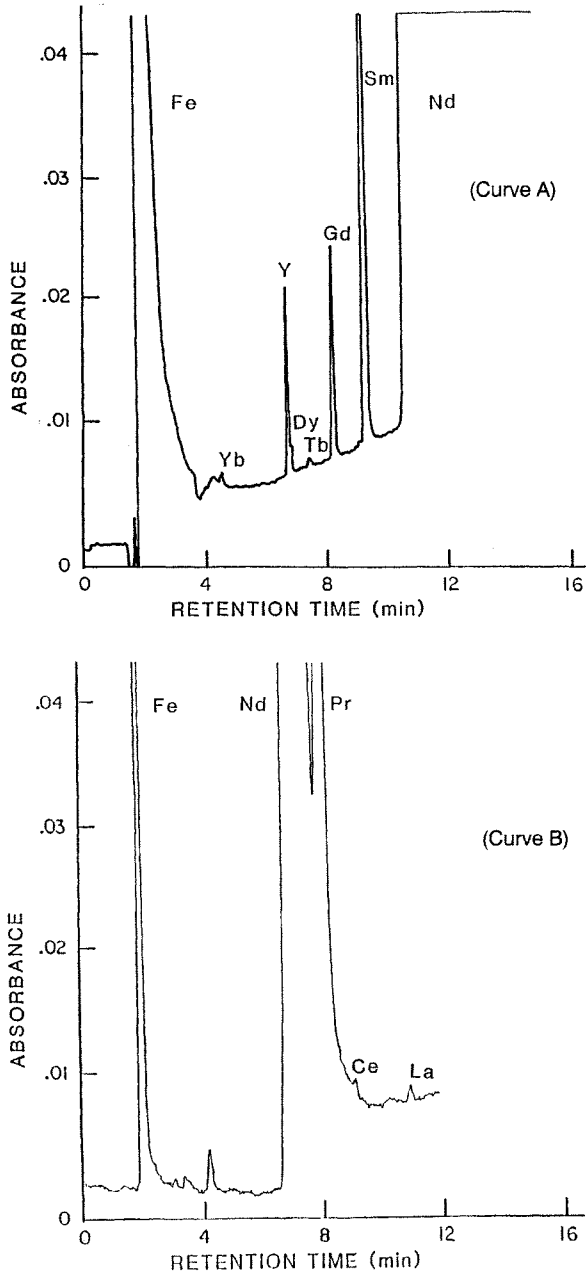


Fig. 1.26. Direct injection of a solution of neodymium (80%)-iron (20%) alloy. Conditions: Supelco LC-18 DB column; curve (A), gradient program at pH 4.5 from 0.05 mol/l HIBA to 0.4 mol/l HIBA in 10 min at flow rate of 1.0 ml/min; modifier, 0.01 mol/l 1-octanesulfonate; sample size, 50  $\mu$ l; sample dilution, 0.965 g per 100 ml. Curve (B), gradient program at pH 4.5 from 0.25 mol/l HIBA to 0.5 mol/l HIBA in 8 min at 1.0 ml/min; modifier, 0.02 mol/l 1-octanesulfonate; sample size, 50  $\mu$ l; sample dilution, 0.965 g per 100 ml and 5 ml/100 ml.



TABLE 1.47  
Sensitivities of determinations [188].

Element	Atomic absorption sensitivity (ppm/1% absorption)	Spectrophotometric sensitivity of Th-Arsenazo III colour reaction ( $\mu\text{g}/\text{cm}^2$ )	Minimum determinable concentration (ppm in original sample)		
			Flame emission	OES* (photoelectric)	OES* (photographic)
Y	3.2			40	20
La			50	100	50
Ce				200	500
Nd	9.4				150
Sm	7.6				
Eu	0.35				
Dy	0.40				
Ho	0.67				
Er	0.46				
Tm	0.21				
Yb	0.07			4	2
Th		0.02			

\*OES, optical emission spectrometry.

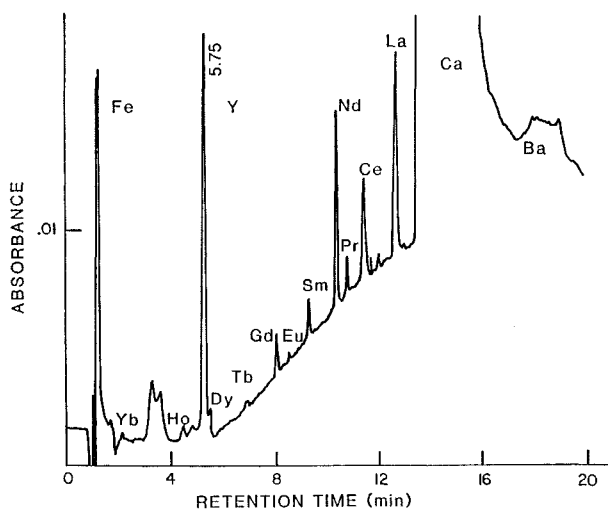


Fig. 1.27. Direct injection of solution of limestone sample. Conditions: Supelco LC-18 DB column; concentration and pH gradient program at a flow rate of 1.5 ml/min from 0.06 mol/l HIBA at pH 3.8 to 0.5 mol/l HIBA at pH 4.5 11 min; modifier, 0.02 mol/l 1-octanesulfonate; detection as for Fig. 1.23; sample injection, 50  $\mu\text{l}$  sample dilution, 0.6 g in 25 ml.

TABLE 1.48  
Sensitivities for Sc, Y and the lanthanides in pyrolytically-coated and tantalum foiled-lined graphite furnaces [193].

Element	Atomization temperature (°C)	Sensitivity*		Sensitivity enhancement factor (PCF/TaF) at 2600°C
		Pyrolytically-coated furnace (PCF)	Ta-foil lined furnace (TaF)	
Sc	2600	$1.3 \times 10^{-10}$	$1.2 \times 10^{-11}$	10.8
	2700	$1.0 \times 10^{-10}$		
Y	2600	$2.6 \times 10^{-9}$	$2.8 \times 10^{-10}$	9.3
	2700	$1.3 \times 10^{-9}$		
La	2600	$4 \times 10^{-8}$	$2 \times 10^{-9}$	20
	2700	$2 \times 10^{-8}$		
Ce	2600	$2 \times 10^{-7}$	$5 \times 10^{-9}\dagger$	40
	2700	$0.8 \times 10^{-7}$		
Pr	2600	$1.6 \times 10^{-8}$	$1.5 \times 10^{-9}$	10.7
	2700	$1 \times 10^{-8}$		
Nd	2600	$3 \times 10^{-9}$	$2 \times 10^{-10}$	15
	2700	$1.5 \times 10^{-9}$		
Sm	2600	$1 \times 10^{-9}$	$7 \times 10^{-11}$	14.3
	2700	$0.8 \times 10^{-9}$		
Eu	2600	$5.5 \times 10^{-11}$	$4 \times 10^{-12}$	13.8
	2700	$3.4 \times 10^{-11}$		
Gd	2600	$2.1 \times 10^{-8}$	$7.3 \times 10^{-10}$	28.8
	2700	$1.4 \times 10^{-8}$		
Tb	2600	$6.4 \times 10^{-9}$	$3.2 \times 10^{-10}$	20
	2700	$4.1 \times 10^{-9}$		
Dy	2600	$2 \times 10^{-10}$	$2 \times 10^{-11}$	10
	2700	$1.4 \times 10^{-10}$		
Ho	2600	$5.5 \times 10^{-10}$	$3.1 \times 10^{-11}$	17.7
	2700	$2.8 \times 10^{-10}$		
Er	2600	$4.4 \times 10^{-10}$	$1.3 \times 10^{-11}$	33.8
	2700	$2.8 \times 10^{-10}$		
Tm	2600	$3.7 \times 10^{-11}$	$4 \times 10^{-12}$	9.3
	2700	$1.8 \times 10^{-11}$		
Yb	2600	$3.3 \times 10^{-12}$	$5.4 \times 10^{-13}$	6.1
	2700	$2.5 \times 10^{-12}$		
Lu	2600	$4.9 \times 10^{-9}$	$1.4 \times 10^{-10}$	35
	2700	$3.5 \times 10^{-9}$		

\* Defined as the weight of the element in g which produces a change, compared with a pure solvent or blank, of 0.0044 absorbance unit.

† Value obtained previously.

#### 14. Spectrophotometric method of analysis of rare earth elements

Characteristic absorption bands of rare earth ions in the UV-VIS region due to the electronic transitions in the 4f shell have been used for the quantitative determination of

TABLE 1.49  
Operating parameters for electrothermal AAS determination of the rare-earth elements [194].

Element	Step number	Temperature (°C)	Time (s)	Argon gas flow (l/min)
Ce, Pr, Nd, Tb,	1	75	15	3
Ho, Er, Tm and Lu	2	90	60	3
	3	120	10 <sup>†</sup>	3
	4	850	10	3
	5	1800	10	3
	6	1800	2	0
	7	2700 <sup>‡</sup>	1.3	0*
	8	2700 <sup>‡</sup>	2	0*
	9	2800 <sup>‡</sup>	5 <sup>§</sup>	3

\* Read command initiated.

<sup>†</sup> 60 s for Lu in a tantalum foil-lined furnace.

<sup>‡</sup> 2600°C for Lu as above.

<sup>§</sup> 1 s Lu as above.

TABLE 1.50  
Wavelengths used for ICPAES determinations [194].

Element	Wavelength (nm)	Element	Wavelength (nm)
Na	588.99	Co	228.62
Mg <sub>1</sub>	279.08	Ni	231.60
Mg <sub>2</sub>	383.83	Cu	324.75
Al	308.22	Zn	213.86
Si <sub>1</sub>	251.61	Sr	407.77
Si <sub>2</sub>	288.16	Y	371.03
P	178.29	Zr	343.80
K	766.49	Ba	233.5
Ca <sub>1</sub>	317.93	La	333.75
Ca <sub>2</sub>	315.89	Ce	413.77
Ti	337.20	Sm	359.26
V	292.40	Eu	381.97
Cr	267.72	Gd	335.05
Mn <sub>1</sub>	257.61	Dy	353.17
Fe <sub>1</sub>	259.94	Yb	328.94
Fe <sub>2</sub>	261.19	Th	283.73

\* Subscript 1 or 2 after the symbol indicates that the corresponding wavelength is the most or least sensitive, respectively.

rare earth elements with sensitivities as low as 0.1 mg/ml. The values of molar absorptivity of rare earth ions at analytical wavelengths are given in Table 1.33.

Spectrophotometric methods of analysis of rare earths are given in Tables 1.34 and 1.35.

TABLE 1.51  
Determination of thorium, yttrium and the rare-earth elements (%) in Oka-2 [194].

Constituent	Found* (this work)	Standard deviation ( <i>s</i> )	Range of CCRMP values	Number of contributing laboratories	Methods used <sup>¶</sup>	Mean of CCRMP values $\pm 2s$
ThO <sub>2</sub>	3.38 <sup>†</sup>	0.045	3.11–3.57	25	A, B, C, D, E, F, G,	3.34 $\pm$ 0.25
Y <sub>2</sub> O <sub>3</sub>	0.50 <sup>‡</sup> 0.40 <sup>†</sup>	0.010 0.007	0.27–0.37	4	A, E, F, H	0.31 $\pm$ 0.08
La <sub>2</sub> O <sub>3</sub>	5.84 <sup>‡</sup>	0.055	5.51–6.21	11	A, D, E, F, H	5.8 $\pm$ 0.5
CeO <sub>2</sub>	15.5 <sup>‡</sup> 15.4 <sup>§</sup>	0.100 0.145	12.87–16.02	12	A, D, E, F, H	14.4 $\pm$ 1.8
Pr <sub>6</sub> O <sub>11</sub>	1.70 <sup>§</sup>	0	1.37–2.18	9	A, D, F, H	1.8 $\pm$ 0.5
Nd <sub>2</sub> O <sub>3</sub>	7.70 <sup>§</sup>	0.12	6.11–7.68	10	A, D, F, H	6.7 $\pm$ 1.0
Sm <sub>2</sub> O <sub>3</sub>	1.30 <sup>‡</sup>	0	0.86–1.21	11	A, D, F, H	1.0 $\pm$ 0.2
Eu <sub>2</sub> O <sub>3</sub>	0.30 <sup>‡</sup>	0	0.20–0.37	12	A, D, F, H	0.26 $\pm$ 0.09
Gd <sub>2</sub> O <sub>3</sub>	0.73 <sup>‡</sup>	0.005	0.28–0.80	10	A, D, F, H	0.6 $\pm$ 0.3
Tb <sub>4</sub> O <sub>7</sub>	0.053 <sup>§</sup>	0.001	0.033–0.076	10	A, D, F, H	0.06 $\pm$ 0.03
Dy <sub>2</sub> O <sub>3</sub>	0.26 <sup>‡</sup>	0.007	0.131–0.318	9	A, D, E, F, H	0.19 $\pm$ 0.11
Ho <sub>2</sub> O <sub>3</sub>	0.0094 <sup>§</sup>	0.0001	0.0186–0.0282	4	D, F, H	0.023 $\pm$ 0.008
Er <sub>2</sub> O <sub>3</sub>	0.0122 <sup>§</sup>	0.0003	0.0053–0.1000	3	A, D, F, H	0.06 $\pm$ 0.04 <sup>a</sup>
Tm <sub>2</sub> O <sub>3</sub>	0.0011 <sup>§</sup>	0	0.0017–0.0034	3	D, F, H	0.003 $\pm$ 0.002
Yb <sub>2</sub> O <sub>3</sub>	0.0108 <sup>‡</sup>	0.0003	0.0076–0.0171	5	D, E, F, H	0.013 $\pm$ 0.008
Lu <sub>2</sub> O <sub>3</sub>	0.0010 <sup>¶</sup>	0	0.0006–0.0017	6	D, F	0.0012 $\pm$ 0.0007

\* Mean of 5 values.

<sup>†</sup> Determined by ICPAES after fusion of the sample with lithium meta- and tetraborates.

<sup>‡</sup> Determined by ICPAES after preconcentration by fluoride and oxalate precipitations.

<sup>§</sup> Determined by ETAAS after preconcentration.

<sup>¶</sup> Determined by ETAAS in a tantalum foil-lined furnace after preconcentration.

<sup>¶</sup> A, X-ray fluorescence spectrometry; B, spectrophotometry; C, gamma-ray spectrometry; D, neutron activation analysis; E, ICPAES; F, direct coupled plasma emission spectrometry; G, titrimetry; H, inductively-coupled plasma mass spectrometry.

<sup>a</sup> Mean  $\pm s$ .

## 15. Emission spectroscopy

Alternating or direct current arcs and spark discharge are common methods of excitation for emission spectroscopic analysis of rare earth elements. Emission spectra of rare earth elements contain a large number of lines. The three arbitrary groups are (i) spectra of La, Eu, Yb, Lu and Y, (ii) more complicated spectra of Sm, Gd and Tm, (iii) even more complicated spectra of Ce, Nd, Pr, Tb, Dy and Er. Rare earths have been analyzed with spectrographs of high resolution and dispersion up to 2 Å/mm. Some salient information is presented in Table 1.36.

## 16. Neutron activation analysis

This technique is highly sensitive in the determination of rare earth elements. The sensitivities obtained by this technique exceed many orders of magnitude obtained by

TABLE 1.52

Sensitivities of Sc, Y and REE elements as obtained with a pyrolytic graphite coated graphite tube furnace using the Hitachi Z-9000 simultaneous multi-element atomic absorption spectrometer and comparison with some previous values [197].

Element	Atomization temperature (°C)	Sensitivity* (pg)	
		This work with Hitachi Z-9000	Previous values with Varian GTA-95 <sup>†</sup>
Sc	2600	423 <sup>‡</sup>	130 <sup>§</sup>
Y	2700	—	1300
	3000	480	—
	2700	—	1500
Nd	2800	4160	—
	2900	1900	—
	3000	1300	—
	2700	—	800
Sm	3000	330	—
	2700	—	34
Eu	2800	51	—
	3000	18	—
	2600	195	—
Dy	2700	—	140
	2800	255	—
	2700	—	280
Ho	2800	130	—
	2900	70	—
	3000	32	—
	2700	—	280
Er	2800	136	—
	2900	67	—
	3000	32	—
	2600	20	—
Tm	2700	—	18
	2800	15	—
	2900	10	—
	3000	6	—
Yb	2200	3.8	—
	2600	11 <sup>  </sup>	3.3 <sup>¶</sup>

\* Defined as the mass of the element in picograms that produces a change in absorbance, compared with a pure solvent or blank, of 0.0044.

<sup>‡</sup> At 326.9 nm.

<sup>§</sup> At 391.2 nm.

<sup>¶</sup> At 398.8 nm.

<sup>||</sup> At 246.5 nm.

other techniques such as emission spectroscopy and flame photometry. The main drawback is it is slow and time consuming. Some data on the sensitivity of the method are given in Table 1.37. Individual photopeaks of rare earths in ocean sediments, auto glasses and precious metal ores were identified in neutron activated samples using Ge(Li) spectrometry [185a].

TABLE 1.53

Determination of Sc, Y and eight REE in three new CCRMP candidate reference rocks by multi-element ETAAS using a Hitachi Z-9000 spectrometer and comparison of results with those obtained by ICP-AES and ICP-MS (results in  $\mu\text{g g}^{-1}$ ) [197].

Sample	Element	ETAAS ( <i>n</i> )	ICP-AES ( <i>n</i> )	ICP-MS ( <i>n</i> )
TDB-1 (Diabase Rock)	Sc	33, 36	–	33, 30
	Y	23 ± 5 (4)	31 ± 4.5 (11)	26 ± 5 (6)
	Nd	27 ± 1.6 (6)	26 ± 2.2 (9)	23 ± 5.7 (6)
	Sm	9.3 ± 1.7 (6)	6.8 ± 0.4 (11)	6.4 ± 0.7 (6)
	Eu	1.9 ± 0.1 (8)	1.9 ± 0.1 (11)	1.9 ± 0.3 (6)
	Dy	5.5, 5.7	6.4 ± 0.4 (11)	5.8 ± 0.5 (7)
	Ho	0.93, 0.97	–	1.10 ± 0.22 (6)
	Er	2.8 ± 0.2 (6)	–	3.2 ± 0.7 (6)
	Tm	0.34 ± 0.02 (10)	–	0.39 ± 0.13 (6)
	Yb	2.5, 2.5	2.9 ± 0.5 (11)	2.9 ± 0.6
WGB-1 (Gabbro Rock)	Sc	30, 34	–	30, 33
	Y	18 ± 1.6 (4)	14 ± 3.3	14 ± 3.5
	Nd	15 ± 2 (6)	13 ± 1	11 ± 3.4
	Sm	3.4 ± 0.9 (6)	2.7 ± 0.2 (6)	2.6 ± 0.7 (6)
	Eu	1.3 ± 0.16 (4)	1.3 ± 0.10 (11)	1.3 ± 0.50 (6)
	Dy	2.8 ± 0.2 (4)	2.8 ± 0.2 (11)	2.6 ± 0.5 (6)
	Ho	0.46, 0.47	–	0.51 ± 0.09 (6)
	Er	1.4 ± 0.5 (3)	–	1.5 ± 0.3 (6)
	Tm	0.22 ± 0.10 (5)	–	0.20 ± 0.02 (6)
	Yb	1.4 ± 0.1 (4)	1.4 ± 0.1 (11)	1.5 ± 0.3 (6)
UMT-1 (Ultramafic Rock)	Sc	14, 16	–	14, 18
	Y	9.5 ± 1.6 (4)	6.5 ± 0.6 (11)	6.5 ± 2.5 (6)
	Nd	5 ± 0.8 (6)	5 ± 0.9 (11)	3.3 ± 1.1 (6)
	Sm	1.3 ± 0.2 (6)	1.3 ± 0.2 (11)	1.3 ± 0.4 (6)
	Eu	0.32 ± 0.04 (6)	0.35 ± 0.03 (11)	0.35 ± 0.12 (4)
	Dy	1.8 ± 0.3 (4)	1.5 ± 0.2 (11)	1.3 ± 0.5 (6)
	Ho	0.23, 0.20	–	0.26 ± 0.06 (6)
	Er	0.8 ± 0.2 (8)	–	0.8 ± 0.2 (6)
	Tm	0.10 ± 0.02 (8)	–	0.10 ± 0.03 (6)
	Yb	0.9 ± 0.2 (4)	0.7 ± 0.1 (11)	0.8 ± 0.2 (6)

## 17. X-ray spectroscopy

This is a classic method for the analysis of rare earths. L-spectra of the elements in the region 1500–2500 Å show that for each element it is possible to select 2–5 lines for analysis. These analytical lines are given in Table 1.38. By this method rare earths in a complex mixture can be analyzed. The emission method has a sensitivity of 0.1 to 0.01%. The time of analysis is 1.5–2.0 h. The method has been used in the analysis of minerals, alloys, etc.

X-ray fluorescence analysis has been applied to rare earth minerals and has the same sensitivity as X-ray emission and analysis time is 0.5–4 h with a single element in 10 minutes.

TABLE 1.54

Determination of Sc, Y, and eight REE in three new CCRMP candidate reference rocks by multi-element ETAAS using a Hitachi Z-9000 spectrometer and comparison of results obtained by ICP-AES and ICP-MS (results in  $\mu\text{g/g}^{-1}$ ) [197].

Sample	Element	ETAAS ( <i>n</i> )	ICP-AES ( <i>n</i> )	ICP-MS ( <i>n</i> )
WPR-1 (Peridotite)	Sc	10, 6	–	8.4, 4.2
	Y	9, 8	$4.7 \pm 0.3$ (9)	$4.7 \pm 2.1$ (4)
	Nd	$5.5 \pm 3.7$ (4)	$5.9 \pm 1.4$ (7)	$2.7 \pm 1$ (4)
	Sm	$1.5 \pm 0.9$ (4)	$1.0 \pm 0.2$ (9)	$1.0 \pm 0.3$ (4)
	Eu	0.3, 0.3	$0.3 \pm 0.05$ (9)	$0.28 \pm 0.14$ (4)
	Dy	1.8, 1.5	$1.3 \pm 0.4$ (9)	$1.2 \pm 0.9$ (4)
	Ho	0.13, 0.11	–	$0.18 \pm 0.04$ (4)
	Er	$0.55 \pm 0.20$ (4)	–	$0.54 \pm 0.17$ (4)
	Tm	0.13, 0.16	–	$0.07 \pm 0.02$ (4)
	Yb	$0.57 \pm 0.02$ (6)	$0.5 \pm 0.10$ (9)	$0.50 \pm 0.20$ (4)
WMG-1 (Mineralized Gabbro)	Sc	20, 21	–	21, 21
	Y	13, 12	$12 \pm 1$ (9)	$12 \pm 1.8$ (8)
	Nd	$12 \pm 4.5$ (6)	$11 \pm 1$ (7)	$9 \pm 0.4$ (7)
	Sm	2.9, 2.9	$2.8 \pm 0.2$ (10)	$2.4 \pm 0.2$ (8)
	Eu	0.8, 0.9	$0.74 \pm 0.03$ (9)	$0.71 \pm 0.03$ (8)
	Dy	3.2, 3.2	$2.3 \pm 0.1$ (9)	$2.3 \pm 0.13$ (8)
	Ho	0.40, 0.43	–	$0.48 \pm 0.03$ (8)
	Er	$1.3 \pm 0.45$ (5)	–	$1.1 \pm 0.3$ (8)
	Tm	$0.2 \pm 0.04$ (5)	–	$0.2 \pm 0.02$ (8)
	Yb	$1.6 \pm 0.2$ (4)	$1.1 \pm 0.2$ (9)	$1.2 \pm 0.2$ (8)
WMS-1 (Massive Sulfide Mineral)	Sc	1.8, 1.3	–	1.4, 1.0
	Y	5.9, 5.0	$2 \pm 0.2$ (9)	$2.1 \pm 0.6$ (9)
	Nd	$4.3 \pm 1.1$ (7)	$3.8 \pm 1.1$ (6)	$1.9 \pm 0.3$ (9)
	Sm	$0.6 \pm 0.1$ (4)	$0.6 \pm 0.1$ (6)	$0.5 \pm 0.1$ (9)
	Eu	0.1, 0.1	$0.14 \pm 0.04$ (9)	$0.11 \pm 0.02$ (9)
	Dy	0.7, 0.8	$0.44 \pm 0.1$ (9)	$0.4 \pm 0.1$ (9)
	Ho	$0.08 \pm 0.01$ (5)	–	$0.08 \pm 0.01$ (9)
	Er	$0.31 \pm 0.03$ (7)	–	$0.24 \pm 0.04$ (9)
	Tm	$0.06 \pm 0.01$ (4)	–	$0.03 \pm 0.01$ (9)
	Yb	$0.30 \pm 0.04$ (6)	$0.23 \pm 0.04$ (9)	$0.25 \pm 0.07$ (9)

## 18. Atomic absorption, flame emission, electrothermal atomization, inductively coupled mass spectrometry

The atomic absorption method of analysis has undergone many changes since it was discovered. The sensitivity of this method of analysis has been improved by (i) sampling in organic solvents, (ii) switching from oxy-acetylene flame to nitrous oxide-acetylene flame, (iii) replacing flame atomization by graphite furnace atomization or electrothermal atomization, (iv) inductively coupled plasma atomic emission and (v) inductively coupled plasma mass spectrometry. All these techniques have been used in the analysis of rare earth elements. Some salient features of the techniques used in rare earth element analysis are given in Tables 1.39–1.54 and Figs 1.18 and 1.19.

TABLE 1.55  
Instrumental operating conditions and data acquisition parameters [198].

Condition/parameter	Result
ICP mass spectrometer	
R.f. power (kW)	1.0
Plasma argon gas flow rate (1 min <sup>-1</sup> )	15
Auxiliary argon gas flow rate (1 min <sup>-1</sup> )	0.9
Nebulizer argon gas flow rate (1 min <sup>-1</sup> )	0.9
Sampler skimmer	Nickel
Data acquisition	
Dwell time (ms)	100
Scan mode	peak hopping
Points across peak	1
Sweeps reading <sup>-1</sup>	10
Number of replicates	2

TABLE 1.56  
List of isotopes of yttrium, rare earth elements and thorium together with ruthenium and rhenium employed in this work [198].

Group 1	Group 2
<sup>89</sup> Y	<sup>151</sup> Eu
<sup>139</sup> La	<sup>159</sup> Tb
<sup>140</sup> Ce	<sup>160</sup> Gd
<sup>141</sup> Pr	<sup>160</sup> Dy
<sup>143</sup> Nd	<sup>165</sup> Ho
<sup>147</sup> Sm	<sup>166</sup> Er
<sup>101</sup> Ru <sup>a</sup>	<sup>169</sup> Tm
	<sup>174</sup> Yb
	<sup>175</sup> Lu
	<sup>232</sup> Th
	<sup>238</sup> U
	<sup>185</sup> Re <sup>b</sup>

<sup>a</sup>Used as an internal standard to correct for instrumental drift and matrix effects on Group 1 elements.

<sup>b</sup>Used as an internal standard to correct for instrumental drift and matrix effects on Group 2 elements.

TABLE 1.57  
Results obtained for neodymium metal [199].

Rare earth	Yb	Y	Dy	Tb	Gd	Sm	Pr	Ce	La
Conc. (ppm)	2.7	12.8	2.2	0.6	20.9	141	420 × 10 <sup>2</sup>	85	60



TABLE 1.58  
Comparison of HPLC and ICP emission spectrometry results for limestone sample.

Rare earth	HPLC (ppm)	IPC (ppm)
La	6.3	6.8
Ce	4.5	4.7
Pr	1.0	–
Nd	5.3	6.8
Sm	1.2	0.5
Eu	< 0.5	0.2
Gd	0.9	1.2
Tb	< 0.5	–
Dy	1.2	1.4
Y	12.8	14
Ho	0.8	–
Er	–	–
Tm	< 1	–
Yb	1.4	1.1
Lu	< 1	–

## 19. Inductively coupled plasma mass spectrometry (ICPMS)

The operating parameters and the isotopes used in this technique are given in Tables 1.55 and 1.56. Correlation plots obtained by this technique in the determination of rare earths are given in Figs 1.20 and 1.21.

## 20. High pressure liquid chromatography (HPLC)

### 20.1. Separation of rare earths by “dynamic coating” ion-interaction chromatography

Dynamic ion-exchange chromatography is used in the laboratory to determine rare earths in a variety of samples. This includes mine tailings, metallurgical processing solutions, sediments, steels, and alloys. In this technique a hydrophobic ion (such as octanesulphonate), which is present in the eluent, is dynamically sorbed onto the hydrophobic surface of a reversed-phase to provide a charged surface that can be used for ion-exchange separations. The eluent also contains a complexing agent such as HIBA to elute the rare earths. The advantages of this approach include rapid mass transfer characteristics, good reproducibility, and the ability to vary ion-exchange capacity. Changes in capacity along with eluent pH and addition of an organic modifier can be used to adjust the selectivity of the separation. With an on-line post-column reaction, using Arsenazo III and monitored at 658 nm, detection limits are in the low nanogram range.

An example of the application of dynamic ion-exchange chromatography for the direct separation of rare earths is shown in Fig. 1.22. The sample was a sodium hydroxide leach solution from an aluminium processing operation and contained high concentrations of sodium, iron and aluminium. Due to matrix interference, these solutions could not be accurately analysed by inductively coupled plasma emission spectroscopy. Fig. 1.22 shows the chromatogram when the sample was separated by dynamic ion-exchange

chromatography with eluent pH 4.5 while B refers to chromatogram obtained with eluent pH 3.8.

Dynamic ion exchange chromatography has been used in a variety of metallurgical samples for the determination of rare earths and yttrium. Optimization of the effective capacity of the dynamic ion exchanger with respect to factors such as eluent pH, concentration of  $\alpha$ -hydroxy isobutyric acid (HIBA) permitted the direct analysis of rare earths in the presence of large amounts of salt, matrix metal ions and acids. Eluted rare earths are determined by spectrophotometry at 658 nm, after an on-line post column reaction with Arsenazo III. Results obtained on aluminum processing solution, neodymium-iron alloy and limestone rock are given in Tables 1.57 and 1.58 and Figs 1.23 to 1.27.

A comparison of the results obtained by high pressure liquid chromatography (HPLC) with results obtained by other techniques such as inductively coupled plasma emission spectroscopy (ICPES) showed good agreement and HPLC procedures are found to be economical in terms of analysis time.

## References

- [1] V.M. Goldschmidt, *J. Chem. Soc.*, 655, 1937.
- [2] T.K.S. Murty, C.K. Gupta, in: *Science and Technology of Rare Earth Materials*, ed. E.C. Subbarao, W.E. Wallace, pp. 3–23, Academic Press, 1980.
- [3] P. Mahadevan, *Material Science Forum* **30**, 13–32, 1988.
- [4] P.G. Falconnet, *Material Science Forum* **30**, 1–12, 1988.
- [5] U.S. Department of Interior, *Mineral Facts and Problems, Bureau of Mines, Bull.*, 675, 1985.
- [6] T. Guanghzi, Z. Zhenhua, Q. Yuzhuo, *Precambrian Research* **27**, 131, 1985.
- [7] *The Rare Earths*, eds. F.H. Spedding, A.H. Daane, John Wiley Sons, Ltd., New York, 1961.
- [8] R. Kunin, R.J. Myers, *Ion Exchange Resins*, Wiley, New York, 1950.
- [9] N.E. Topp, *The Chemistry of Rare Earth Elements*, Elsevier, New York, 1965.
- [10] K.A. Gschneinder, L. Eyring, *Handbook of Physics and Chemistry of Rare Earths*, Chapter 22, North Holland Publishing Company, 1978.
- [11] R.J. Sochaska, S. Siekierski, *J. Chromatography* **16**, 376, 1964.
- [12] J. Bosholm, H. Grosse-RuyKen, *J. Prakt. Chem.* **26**, 83, 1964.
- [13] T.B. Pierce, P.F. Peck, R.S. Hobbs, *J. Chromatography* **12**, 81, 1963.
- [14] T. Fidelis, T. Siekierski, *J. Chromatography* **17**, 542, 1965.
- [15] B.H. Ketelle, G.E. Boyd, *J. Am. Chem. Soc.* **73**, 1862, 1951.
- [16] S.W. Mayer, E.C. Freiling, *J. Am. Chem. Soc.* **75**, 5647, 1953.
- [17] D.C. Stewart, M.H. Studier, J.F. Mech, J.E. Gindler, P.R. Fields, A.M. Friedman, H. Diamond, M.M. Petharam, R.K. Sjoblom, R.F. Barnes, *Proc. Int. Conf. Peaceful Uses Atomic Energy, Geneva 1955* **7**, 321, 1956.
- [18] E.C. Freiling, L.R. Bunney, *J. Am. Chem. Soc.* **76**, 1021, 1954.
- [19] J.G. Cunningham, M.L. Sizeland, H.H. Willis, J. Eakins, E.R. Mercer, *J. Inorg. & Nuclear Chem.* **1**, 163, 1955.
- [20] G.R. Chopin, R.J. Desilva, *J. Inorg & Nuclear Chem.* **3**, 153, 1956.
- [21] L. Holleck, L. Hartinger, *Angew. Chem.* **68**, 412, 1956.
- [22] F.W. Cornish, G. Phillips, A. Thomas, *Can. J. Chem.* **34**, 1461, 1956; (a) G.V.S. Rayudu, L. Yaffe, *Can. J. Chem.* **41**, 2544, 1963.
- [23] B. Mokili, C. Poitrenaud, *Solvent Extraction and Ion Exchange* **15**, 455, 1997.
- [24] G.V.V. Korpusov, *Proc. Int. Solvent Extr. Conf. (ISEC '88)*, Moscow, 1988.
- [25] N.S. Narayanan, S. Thulasidoss, T.V. Ramachandran, T.V. Swaminathan, K.R. Prasad, *Materials Science Forum* **30**, 45, 1988.
- [26] W. Wendlandt, D.W. Hayes, *Science* **126**, 451, 1957.
- [27] P. Wegner, G. Gutzeit, *Manuel de Chimie analytique qualitative mineral*, Geneva, 1933.

- [28] F.P. Treadwell, W.T. Hau, *Analytical Chemistry, I. Qualitative Analysis*, Wiley, New York, 1949.
- [29] W.W. Wendlandt, *Science* **125**, 1042, 1957.
- [30] W.W. Wendlandt, R.G. Sewell, *Anal. Chim. Acta* **21**, 94, 1959.
- [31] Ya.Ya. Dodonov, S.B. Pirkes, *Zh. O. Kh.* **26**, 379, 1956.
- [32] G. Beck, *Mikrochim. Acta* **337**, 1956.
- [33] G. Beck, *Mikrochim. Acta* **1495**, 1956.
- [34] M. Bobtelsky, A.H. Ben-Bassat, *Bull. Soc. Chim. France* **1138**, 1958.
- [35] A.S. Komarovskii, I.M. Korenman, *Z. Anal. Chem.* **94**, 247, 1933.
- [36] I.M. Kolthoff, R. Elmquist, *J. Am. Chem. Soc.* **53**, 1217, 1931.
- [37] F.H. Pollard, J.F.W. Mcomie, H.M. Stevens, *J. Chem. Soc.* **3435**, 1954.
- [38] G. Beck, *Anal. Chim. Acta* **1**, 69, 1947.
- [39] K. Emi, K. Toei, K. Furukawa, *Nippon Kagaku Zasshi* **79**, 681, 1958.
- [40] D. Krüger, E. Tschirsch, *Ber.* **62**, 2776, 1929.
- [41] I.M. Kolthoff, *Emich Festschrift*, 189, 1930.
- [42] F.S. Frum, *Trudy Po Khimii i Khimicheskoi Tekhnologii* **1**, 132, 1958.
- [43] E. Negrusz, *Chem. Anal.* **3**, 813, 1958.
- [44] M. Venugopalan, K.J. George, *Naturwiss.* **43**, 348, 1956.
- [45] L. Wolf, D. Stather, *J. Prakt. Chem.* **6**, 259, 1958.
- [46] R. Marc, *Ber.* **35**, 2370, 1902.
- [47] L.M. Dennis, W.H. Magee, *J. Am. Chem. Soc.* **16**, 649, 1894.
- [48] R.E. Kitson, M.G. Mellon, *Ind. Eng. Chem., Anal. Ed.* **16**, 466, 1944.
- [49] L.M. Kul'berg, *Zavodskaya Laboratoriya* **7**, 905, 1938.
- [50] P.E. Wenger, Y. Rusconi, R. Duckert, *Helv. Chim. Acta* **27**, 1479, 1944.
- [51] E. Montignie, *Bull. Soc. Chim.* **6**, 889, 1939.
- [52] Y.F. Miller, *Ind. Eng. Chem., Anal. Ed.* **9**, 181, 1937.
- [53] F.M. Shemyakin, *Doklady AN SSSR* **15**, 347, 1937.
- [54] F.S. Frum, *Trudy Po Khimii i Khimicheskoi Tekhnologii* **1**, 132, 1958.
- [55] F.M. Shemyakin, V.A. Volkova, *Zh. O. Kh.* **9**, 698, 1939.
- [56] F.M. Shemyakin, *Doklady AN SSSR* **14**, 113, 1937.
- [57] L.M. Kul'berg, *Microchemie* **21**, 35, 1936.
- [58] G. Beck, *Pharm. Acta Helv.* **13**, 304, 1938.
- [59] R. Lang, *Mikrochim. Acta* **3**, 116, 1938.
- [60] T.P. Forrest, D.E. Ryan, *Can. J. Chem.* **36**, 1674, 1958.
- [61] M.N. Ambrozhi, A.M. Gol'tsev, *Nauchnye Doklady Vysshei Shkoly Khimiya i Khimicheskaya Tekhnologiya* No. 3, 491, 1958.
- [62] M.N. Ambrozhi, L.M. Kul'berg, A.G. Fedorova, *Uchenye Zapiski Saratovskogo Gosudarstvennogo Universiteta* **43**, 149, 1956.
- [63] A. Brukl, *Z. Angew. Chem.* **52**, 151, 1939.
- [64] G. Beck, *Mikrochim. Acta* **3**, 141, 1938.
- [65] M.N. Ambrozhi, E.F. Luchnikova, *Nauchnyi Ezhegodnik Saratovskogo Gosudarstvennogo Universiteta za 1954 g.* **486**, 1955.
- [66] T. Moeller, H.E. Kremers, *Ind. Eng. Chem., Anal. Ed.* **17**, 793, 1965.
- [67] E. Jungreis, E. Levy, *Talanta* **10**, 708, 1963.
- [68] V.P. Rao, D. Satyanarayana, *Z. Anal. Chem.* **197**, 409, 1963.
- [69] N.E. Ballou, *Radiochemical Studies of Fission Products*, Vol. 3, p. 1673, McGraw-Hill, N.Y., 1951.
- [70] W.W. Wendlandt, *Anal. Chem.* **30**, 58, 1958.
- [71] W.W. Wendlandt, *Anal. Chem.* **31**, 408, 1959.
- [72] E. Duval, *Anal. Chim. Acta* **10**, 321, 1954.
- [73] V.M. Padmanabhan, S.C. Saraiya, A.K. Sundaram, *J. Inorg. Nucl. Chem.* **12**, 356, 1960.
- [74] S.S. Moosath, *J. Inorg. Nucl. Chem.* **11**, 286, 1959.
- [75] I.V. Tannanaev, G.B. Seifer, *Zh. N. Kh.* **1**, 53, 1956.
- [76] A.G. Buyers, E. Geisbrecht, L.F. Audrieth, *J. Inorg. Nucl. Chem.* **5**, 133, 1957.
- [77] Yu.A. Chernikov, T.A. Uspenskaya, *Zavodskaya Laboratoriya* **9**, 276, 1940.
- [78] H.H. Willard, Yu.S. Tsai, *Anal. Chem.* **25**, 1754, 1953.
- [79] J.S. Fritz, J.E. Abbink, *Anal. Chem.* **34**, 1080, 1962.
- [80] G.P. Aleksandrov, V.S. Tikhonova, *Ukr. Khimicheskii Zhurnal* **22**, 379, 1956.
- [81] W.W. Wendlandt, *Anal. Chim. Acta* **15**, 109, 1956.
- [82] W.W. Wendlandt, *Anal. Chim. Acta* **17**, 274, 1957.
- [83] W.W. Wendlandt, *Anal. Chim. Acta* **17**, 428, 1957.
- [84] W.W. Wendlandt, *Anal. Chim.* **27**, 1277, 1955.
- [85] W.W. Wendlandt, *Anal. Chim. Acta* **21**, 116, 1959.
- [86] W.W. Wendlandt, J.M. Bryant, *Anal. Chim. Acta* **13**, 550, 1959.
- [87] Ya.I. Fialkov, V.I. Ermolenko, *Zh. N. Kh.* **4**, 359, 1959.
- [88] J.P. Watson, *Analyst* **76**, 177, 1951.
- [89] K. Emi, *J. Soc. Chem. Ind., Japan* **44**, 854, 1941.

- [90] P.C. Banerjee, *J. Indian Chem. Soc.* **15**, 475, 1938.
- [91] R. Pribil, V. Simon, J. Dolezal, *Coll. Czechoslov. Chem. Commun.* **16**, 88, 1951.
- [92] L. Weiss, H. Sieger, *Z. Anal. Chem.* **113**, 305, 1938.
- [93] O. Tomicek, M. Jasek, *J. Am. Chem. Soc.* **57**, 2409, 1935.
- [94] G.W. Leonard, H.J. Keily, D.N. Hume, *Anal. Chim. Acta* **16**, 185, 1957.
- [95] A. Malaguti, *Ann. Chim. (Rome)* **44**, 195, 1954.
- [96] D.C. Foster, H.E. Kremers, *Anal. Chem.* **25**, 1921, 1953.
- [97] H.N. McCoy, *J. Am. Chem. Soc.* **58**, 1577, 1936.
- [98] G.Ya. Gornyi, in: *Redkozamel'nye Elementy*, ed. D.I. Ryabchikov, Nauka, Moscow, 1963.
- [99] A.I. Popov, W.W. Wendlandt, *Proc. Iowa Acad. Sci.* **60**, 300, 1953.
- [100] K.Y. Bril, S. Halzer, B. Rethy, *Anal. Chem.* **31**, 1353, 1959.
- [101] G. Brunisholz, R. Cahen, *Helv. Chim. Acta* **39**, 324, 1956.
- [102] J.S. Fritz, R.T. Oliver, D.J. Pietrzyk, *Anal. Chem.* **30**, 1111, 1958.
- [103] R.S. Lauer, N.S. Poluektov, *Zavodskaya Laboratoriya* **25**, 391, 1959.
- [104] V.I. Kuznetsov, L.A. Okhanova, *Zavodskaya Laboratoriya* **25**, 1162, 1959.
- [105] P. Wehber, *Z. Anal. Chem.* **166**, 186, 1959.
- [106] L. Sommer, M. Hnilickova, *Naturwiss.* **45**, 544, 1958.
- [107] C.K. Lu, *Chemist Analyst* **47**, 93, 1958; **44**, 96, 1955.
- [108] J. Körbl, R. Pribil, *Chem. Listy* **51**, 1061, 1957.
- [109] J. Körbl, R. Pribil, *Chemist Analyst* **45**, 102, 1956.
- [110] V.P. ShvedoV, A.P. Stepanov, *Radiokhimiya* **1**, 112, 1959.
- [111] J. Kinnunen, B. Wennerstrand, *Chemist Analyst* **46**, 92, 1957.
- [112] A. Jenickova, V. Suk, M. Malat, *Chem. Listy* **50**, 760, 1956.
- [113] M. Malat, M. Tenerova, *Chem. Listy* **51**, 2135, 1957.
- [114] G. Brunisholz, R. Cahen, *Helv. Chim. Acta* **39**, 2136, 1956.
- [115] J.A.R. Genge, J.E. Salmon, *Lab. Practice* **6**, 695, 1957.
- [116] H. Flaschka, *Mikrochim. Acta* **1**, 55, 1955.
- [117] L. Holleck, L. Hartinger, E. Eckhardt, *Angew. Chem.* **65**, 347, 1953.
- [118] G. Beck, *Anal. Chim. Acta* **1**, 69, 1947.
- [119] I.A. Atanasiu, *Z. Anal. Chem.* **112**, 15, 19, 1938, **113**, 276, 1938.
- [120] A.K. Majumdar, B.K. Mitra, *Anal. Chim. Acta* **21**, 29, 1959.
- [121] P. Kuan, H.T. Ming, *Bull. Chem. Soc., Japan* **28**, 309, 1955.
- [122] P. Spacu, *Z. Anal. Chem.* **104**, 119, 1936.
- [123] P.H.M.P. Brinton, H.A. Pagel, *J. Am. Chem. Soc.* **45**, 1460, 1923.
- [124] G.S. Deshmukh, M. Venugopalan, *J. Ind. Chem. Soc.* **33**, 299, 1956.
- [125] G. Spacu, P. Spacu, *Z. Anal. Chem.* **128**, 229, 1947.
- [126] A.S. Murthy, T.P. Sarma, Bh.S.V.R. Rao, *Z. Anal. Chem.* **145**, 418, 1955.
- [127] V.T. Athavale, R.G. Dhaneswar, M.M. Mehta, *Anal. Chim. Acta* **23**, 71, 1960.
- [128] P.R. Pomeroy, R.A. White, G.H.R. Gwatkins, *Metallurgia* **46**, 157, 1952.
- [129] A. Iwase, *Nippon Kagaku Zasshi* **81**, 95, 1960.
- [130] H.A. Laitinen, W.A. Taebel, *Ind. Eng. Chem. Anal. Edn.* **13**, 825, 1941.
- [131] J. Dolezal, J. Novak, *Chem. Listy* **52**, 2060, 1958.
- [132] A. Purushotam, Bh.S.V.R. Rao, *Anal. Chim. Acta* **12**, 589, 195.
- [133] T.M. Florence, L.E. Smythe, *Nature* **187**, 771, 1960.
- [134] O.P. Agrawal, R.C. Kapoor, *Talanta* **10**, 316, 1963.
- [135] P.G. Desideri, *J. Electroanal. Chem.* **2**, 39, 1961.
- [136] L.C. Hall, D.A. Flanigan, *Anal. Chem.* **35**, 2108, 1963.
- [137] F.J. Miller, H.E. Zittel, *J. Electroanal. Chem.* **7**, 116, 1964.
- [138] S. Misumi, Y. Masuda, *Anal. Chim. Acta* **28**, 188, 1963; (a) G.V.S. Rayudu, Bh.S.V.R. Rao, *J. Sci. & Ind. Res.* **17B**, 363, 1958.
- [139] C.V. Banks, D.W. Klingman, *Anal. Chim. Acta* **15**, 356, 1956.
- [140] L. Greenhaus, A.M. Feibush, L. Gordon, *Anal. Chem.* **29**, 1531, 1957.
- [141] J.C. White, R.F. Apple, *Talanta* **2**, 176, 1959.
- [142] L. Holleck, G. Liebold, G. Wiedmann, *Angew. Chem.* **68**, 522, 1956.
- [143] N. Iordanov, K. Daiev, *Izv. Inst. Po. Obschcha. Neorg. Khim. Org. Khim. Bulgar. Akad. Nauk* **9**, 19, 1962.
- [144] T. Moeller, J.C. Brantley, *Anal. Chem.* **22**, 433, 1950.
- [145] T. Moeller, F.A.J. Moss, *J. Am. Chem. Soc.* **73**, 3149, 1951.
- [146] E.I. Onstott, C.J. Brown, *Anal. Chem.* **30**, 172, 1958.

- [147] Methods of Determination and Analysis of Rare Elements, Collection of Papers, Moscow, IL, 1961.
- [148] A.W. Wylie, *J. Soc. Chem. Ind. (London)* **69**, 143, 1950.
- [149] R. Raisin-Streden, W. Dauschan, O. Zemek, *Mikrochim. Acta* **512**, 1956.
- [150] Z. Hagiwra, *Kogyo Kagaku Zasshi* **59**, 1383, 1956.
- [151] G. Muto, M. Mamiya, *Nippon Kagaku Zasshi* **79**, 809, 1958.
- [152] K.S. Bergstrasser, *Anal. Chem.* **30**, 1630, 1958.
- [153] I.P. Alimarin, E.S. Przhevaliskii, I.V. Puzdrenkova, A.P. Gdovina, *Trudy Komissii po Analiticheskoi Khimii* **8**, 152, 1954.
- [154] A. Misumi, T. Taketatsu, Y. Ide, *C.A.* **53**, 12940, 1959.
- [155] R.W. Rinehart, *Anal. Chem.* **26**, 1820, 1959.
- [156] V.R. Rao, A.S. Murty, Bh.S.V.R. Rao, *J. Sci. Ind. Res. India* **14B**, 190, 1955.
- [157] I.M. Kolthoff, R. Elmquist, *J. Am. Chem. Soc.* **53**, 1271, 1951.
- [158] J.P. Young, J.C. White, B.G. Ball, *Anal. Chem.* **32**, 928, 1960.
- [159] J. Herrington, K.C. Stead, *Anal. Chim. Acta* **22**, 180, 1960.
- [160] T.P. Moeller, M. Tecotzky, *J. Am. Chem. Soc.* **77**, 2649, 1955.
- [161] F.M. Shemyakin, *Zavodskaya Laboratoriya* **3**, 1090, 1934.
- [162] S. Misumi, *C.A.* **49**, 773, 1955.
- [163] H. Goto, Y. Kakita, *Nippon Kagaku Zasshi* **79**, 1524, 1958.
- [164] B. Sarma, *J. Sc. Ind. Research* **14B**, 538, 1955.
- [165] B. Sarma, *J. Sc. Ind. Research* **15B**, 692, 1956.
- [166] L.D. Holleck, D. Eckhardt, L. Hartinger, *Z. Anal. Chem.* **146**, 103, 1955.
- [167] T.P. Sarma, Bh.S.V.R. Rao, *J. Sci. Ind. Res.* **14B**, 450, 1955.
- [168] E.B. Sandell, *Colorimetric Determination of Traces of Metals*, Inter Sci., 2nd edn, p. 252, NY, 1950.
- [169] L.S. Serdyluk, G.P. Fedorova, *Zh. A. Kh.* **15**, 287, 1960.
- [170] S. Shibata, F. Takeuchi, T. Matsumi, *Anal. Chim. Acta* **21**, 177, 1959.
- [171] J.S. Fritz, M.J. Richard, W.J. Lane, *Anal. Chem.* **30**, 1776, 1958.
- [172] F.V. Zaikovskii, V.S. Bashmukova, *Zh. A. Kh.* **14**, 50, 1959.
- [173] V.I. Kuznetsov, N. Cheming, G.E. Myasoedova, L.A. Okhanova, *Acta Chimica Sinica* **27**, 24, 1961.
- [174] R.K. Korbel'nik, *Zh. A. Kh.* **11**, 419, 1956.
- [175] Z.F. Shakhova, S.A. Gavrilova, *Zh. A. Kh.* **13**, 211, 1958.
- [176] A.A. Tikhonova, *Zavodskaya Laboratoriya* **19**, 779, 1953.
- [177] M. Malinek, M. Klir, *Chem. Listy* **50**, 1317, 1956.
- [178] F.M. Shemyakin, L.M. Budanova, K.D. Gavrilova, *Trudy Komissi po Analiticheskoi Khimii* **3**, 246, 1951.
- [179] N. Iordanov, K. Daiev, *Zh. A. Kh.* **15**, 443, 1960.
- [180] G. Popa, I. Paralescy, D. Mircea, *Z. Anal. Chem.* **167**, 329, 1959.
- [181] P. Szarvas, M. Popovicz, *Acta Univ. Debrecen* **1**, 187, 1954.
- [182] H.N. Antoniadis, *Chemist Analyst* **44**, 34, 1955.
- [183] V. Voicu, I. Dema, *Acad. Rep. Populaire Romaine, Studi Cercetari Chim.* **7**, 423, 1959.
- [184] T.C. Rains, H.P. House, O. Menis, *Anal. Chim. Acta* **22**, 315, 1960.
- [185] W.W. Meinke, *Science* **121**, 177, 1955; (a) G.V.S. Rayudu, *Proc. 50<sup>th</sup> CIC Union*, Toronto **50**, 65, 1967.
- [186] J.G. Sen Gupta, *Talanta* **23**, 343, 1976, **28**, 31-36, 1981.
- [187] J.C. Van Loon, J.H. Galbraith, H.M. Aarden, *Analyst* **96**, 47, 1971.
- [188] J.G. Sen Gupta, *Geostandards Newsletter* **1**, No. 2, 149, 1977.
- [189] J.G. Sen Gupta, *Anal. Chim. Acta* **138**, 295, 1982.
- [190] J.G. Sen Gupta, *Talanta* **31**, 1053, 1984.
- [191] J.G. Sen Gupta, *Talanta* **31**, 1045, 1984.
- [192] J.G. Sen Gupta, *Talanta* **28**, 31, 1981.
- [193] J.G. Sen Gupta, *Talanta* **32**, 1-6, 1985.
- [194] J.G. Sen Gupta, *Talanta* **34**, 1043, 1987.
- [195] J.G. Sen Gupta, *Can. J. Appl. Spectr.* **38**, 145, 1993.
- [196] J.G. Sen Gupta, *Geostandards Newsletter* **18**, 111, 1996.
- [197] J.G. Sen Gupta, *J. Analyt. Atomic Spectroscopy* **8**, 93, 1993.
- [198] J.G. Sen Gupta, N.B. Bertrand, *Talanta* **42**, 1595, 1995.
- [199] D.J. Barkley, L.A. Bennett, J.R. Charbonneau, L.A. Pokrajac, *J. Chromatography* **606**, 195, 1992.
- [200] D.J. Barkley, P.A. Eichorn, L.A. Pokrajac, *MSL, Canmet* 91-18 (J).

chapter 2

---

GENERAL ASPECTS

---

---

# CONTENTS

---

1. Quantum chemical considerations . . . . .	75
2. Quantum numbers . . . . .	78
3. Electron configurations and its consequences . . . . .	84
4. Spin-orbit coupling . . . . .	91
5. Oxidation states . . . . .	96
5.1. Oxidation states of the lanthanides . . . . .	101
6. Size variation in lanthanides . . . . .	102
7. Interconfigurational fluctuations and their consequences . . . . .	104
8. Hirst's model . . . . .	105
9. Ionic radii and coordination number . . . . .	110
10. Chemical polarizability and soft character . . . . .	112
11. Some recent developments . . . . .	117
12. Electronic configuration and multiplet structure . . . . .	119
13. Spin-pairing energy . . . . .	122
References . . . . .	125

## 1. Quantum chemical considerations

It is useful to discuss some preliminaries of quantum mechanics before the discussion of  $f$ -orbitals in lanthanides. Consider the simplest system; namely, the hydrogen atom consisting of a single electron interacting with a proton. The Schrödinger equation for a particle of mass  $m$ , the electron in a central field produced by the nucleus is

$$\nabla^2 \Psi + \frac{2m}{\hbar^2} (W - V) \Psi = 0,$$

where  $W$  is the total energy,  $V$  is the potential energy as a function of the position

$$(x, y, z) \text{ of } m, \quad \hbar = \frac{h}{2\pi}, \quad \nabla^2 = \frac{\partial^2}{\partial x^2} + \frac{\partial^2}{\partial y^2} + \frac{\partial^2}{\partial z^2}.$$

The Schrödinger equation is a second order differential equation and the solutions  $\Psi(x, y, z)$  must satisfy the equation.

The conditions of wave function  $\Psi$  are (i) they must be single-valued, continuous and differentiable at every point in space, (ii) they must be finite for all values of  $x$ ,  $y$  and  $z$ , (iii) the wave functions must be normalized (i.e.)  $\int |\Psi|^2 d\tau = 1$ , (iv) any two solutions to the wave equation must be orthogonal  $\int \Psi_i^* \Psi_j d\tau = 0$ . The orthonormality condition requires  $\int \Psi_i^* \Psi_j d\tau = \delta_{ij}$  where  $\delta_{ij}$  is Kronecker or Dirac delta function and  $\delta_{ij} = 1$  if  $i = j$  and  $\delta_{ij} = 0$  if  $i \neq j$ .

Consider a spherically symmetric field around the atomic nucleus and using polar coordinate system in Fig. 2.1. We can write the relations between rectangular and polar coordinates as

$$x = r \sin \theta \cos \varphi \quad y = r \sin \theta \sin \varphi \quad z = r \cos \theta$$

$$d\tau = dx dy dz = r^2 dr \sin \theta d\theta d\varphi.$$

The coordinates, description and boundaries are as follows.

Coordinate	Description	Boundaries	Volume element
$r$	distance from nucleus	$0 \rightarrow \infty$	$r^2 dr$
$\theta$	angle from $z$ axis	$0 \rightarrow \pi$	$\sin \theta d\theta$
$\varphi$	angle from $x$ axis	$0 \rightarrow 2\pi$	$d\varphi$



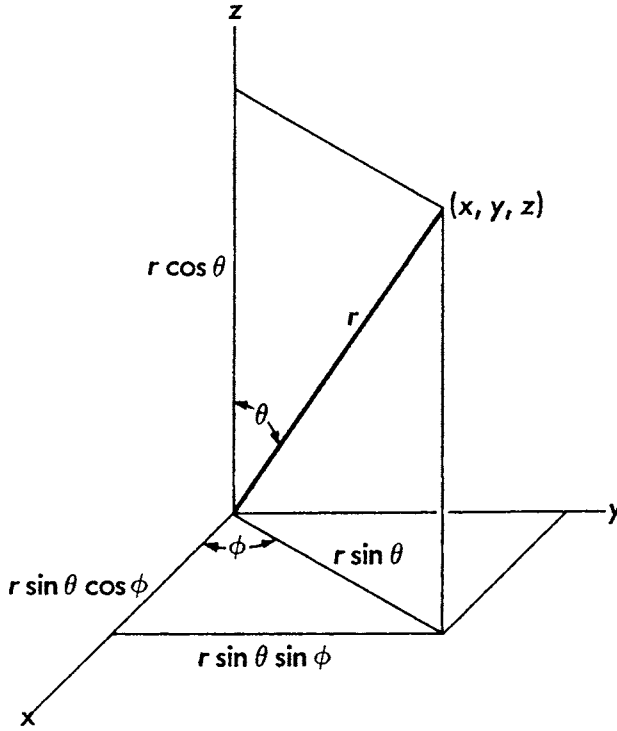


Fig. 2.1. Polar and rectangular coordinates.

The nucleus at the centre has a positive charge  $Ze$ , where  $e$  is the numerical value of the charge of electron and hence the Hamiltonian operator for an electron in the central field can be written as

$$\mathcal{H} = \frac{-\hbar^2}{2m} \nabla^2 - \frac{Ze^2}{r}.$$

Expressing  $\nabla^2$  in polar coordinates, the Schrödinger equation for the system can be written as

$$\left[ \frac{1}{r^2} \frac{\partial}{\partial r} \left( r^2 \frac{\partial}{\partial r} \right) + \frac{1}{r^2 \sin \theta} \frac{\partial}{\partial \theta} \left( \sin \theta \frac{\partial}{\partial \theta} \right) + \frac{1}{r^2 \sin^2 \theta} \frac{\partial^2}{\partial \varphi^2} \right] \Psi + \frac{2m}{\hbar^2} \left[ W + \frac{Ze^2}{r} \right] \Psi = 0.$$

The equation is a second order differential equation in three variables and a possible guessed solution is

$$\Psi(r, \theta, \varphi) = R(r)Y(\theta\varphi).$$

On substituting the solution we get

$$\begin{aligned} \frac{1}{R(r)} \frac{\partial}{\partial r} \left( r^2 \frac{\partial R(r)}{\partial r} \right) + \frac{2m}{\hbar^2} \left( W + \frac{Ze^2}{r} \right) r^2 \\ = - \frac{1}{Y(\theta\varphi) \sin \theta} \frac{\partial}{\partial \theta} \left( \sin \theta \frac{\partial Y(\theta\varphi)}{\partial \theta} \right) - \frac{1}{Y(\theta\varphi) \sin \theta} \frac{\partial^2 Y(\theta\varphi)}{\partial \varphi^2}. \end{aligned}$$

Since  $r$ ,  $\theta$  and  $\varphi$  are freely varying independent coordinates we can write

$$\begin{aligned} \frac{1}{\sin \theta} \frac{\partial}{\partial \theta} \left( \sin \theta \frac{\partial Y}{\partial \theta} \right) + \frac{1}{\sin^2 \theta} \frac{\partial^2 Y}{\partial \varphi^2} + \lambda Y = 0, \\ \frac{1}{r^2} \frac{d}{dr} \left( r^2 \frac{dR}{dr} \right) + \left[ \frac{2m}{\hbar^2} \left( W + \frac{Ze^2}{r} \right) - \frac{\lambda}{r^2} \right] R = 0, \end{aligned}$$

where  $\lambda$  is a constant and  $Y$  for  $Y(\theta\varphi)$  and  $R$  for  $R(r)$ .

The Schrödinger equation consists of two second order differential equations with one dependent on  $\theta$  and  $\varphi$  and the other on  $r$ . There are many solutions which satisfy the conditions, namely that the wave function must be single-valued, continuous, differentiable at every point in space and must be finite for all values of  $x$ ,  $y$ , and  $z$  but it is also necessary that the constant  $\lambda = l(l+1)$  where  $L = 0, 1, 2, 3$ , etc. When  $L = 0$ ,  $Y = a$  constant and is a solution for the angular part of the equation. Normalizing this solution  $1/\sin \theta d\theta d\varphi$ , we get  $Y = \sqrt{1/4\pi}$ .

The radial function can be calculated by using the relationship

$$R_{n,l}(r) = Nr \rho^l l_{n+l}^{2l+1}(\rho) e^{-\rho/2},$$

where  $Nr$  is normalization constant,  $\rho = 2Zr/na_0$ ,  $z$  is nuclear charge,  $a_0$  is Bohr radius,  $0.529 \text{ \AA}$  (52.9 pm),  $l$  is polynomial  $(\rho^{(n-l-1)} - \rho^{(n-l-2)} + \text{constant})$ .

Consider 1s orbital ( $n = 1, l = 0$ )

$$R_{1,0}(r) = N \rho^0 (\rho^{(1-0-1)}) e^{-\rho/2} = N e^{-\rho/2} = N e^{-r/a_0} \quad \text{since } \rho = \frac{2(1)r}{1a_0}.$$

For 2s orbital  $n = 2, l = 0$

$$R_{2,0}(r) = N \rho^0 (\rho^{(2-0-1)}) e^{-\rho/2} = N \rho e^{-r/2a_0} \quad \text{since } \rho = \frac{2(1)r}{2a_0}.$$

For 2p orbital  $n = 2, l = 1$

$$R_{2,1}(r) = N \rho^1 (\rho^{(2-1-1)}) e^{-\rho/2} = N \rho e^{-r/2a_0} \quad \text{since } \rho = \frac{2(1)r}{2a_0}.$$

The plots for hydrogen-like wave functions of radial function  $R(r)$  versus  $r$ , the distance from the nucleus and the probability distribution function  $4\pi r^2 [R(r)]^2$  versus  $r$  are shown

in the literature. It is to be noted that there is a node in the case of 2s orbital where there is no electron density. The following are some rules for drawing radial wave functions: (i) number of nodes =  $n - l - 1$ ; (ii) where  $l = 0$  (i.e.) for s orbital the wave function is non-zero at  $r = 0$  or origin; and, (iii) when  $l \neq 0$  the wave function starts at origin, (0,0).

## 2. Quantum numbers

In simple terms, the Schrödinger equation describes the energy levels and other properties of electrons in atoms and molecules. The Schrödinger equation is

$$\hat{H}\Psi = E\Psi,$$

where  $\hat{H}$  is the Hamiltonian operator which contains derivatives that operate on the wave function,  $E$  is the energy of the electron,  $\Psi$  is the wave function that describes the behaviour of the electron. In the case of the hydrogen atom we may write

$$H = \frac{\hbar^2}{2\mu} \nabla^2 - \frac{Ze^2}{r},$$

where the first term and the second term on the right-hand side are kinetic energy and potential energy operators,  $\hbar = h/2\pi$ .  $\mu$  the reduced mass is equal to  $M_e M_{\text{nuc}} / (M_e + M_{\text{nuc}})$ ,  $\nabla^2$  is Laplacian which is the differential with respect to polar coordinates and  $Z$  is the charge of the nucleus. In atoms, wave functions are known as orbitals.

Principal quantum number  $n$  gives the energy of an orbital.

$$E = -\frac{RZ^2}{n^2}, \quad \text{where} \quad R = \frac{2\pi^2\mu Z^2 e^4}{(4\pi E_0)^2 h^2} = \frac{-R}{n^2}, \quad R \text{ is Rydberg constant.}$$

The values of  $n$  are  $1, 2, 3, 4, \dots$ . The second or azimuthal quantum number  $l$  gives orbital angular momentum (i.e., the rotation about the nucleus) which determines the shape of the orbital.

$$L(M) = \sqrt{l(l+1)}\hbar.$$

The value of  $l$  can be 0, 1, 2, 3, ... ( $n - 1$ ) for a given  $n$  value. The orbitals corresponding to  $l$  are s, p, d, f. The third quantum number  $M_L$  is the magnetic quantum number which gives the  $Z$ -component of orbital angular momentum to determine the orientation of an orbital

$$L_Z(M_Z) = M_L \hbar.$$

$M_L$  can have values 0,  $\pm 1$ ,  $\pm 2$ ,  $\pm 3$ , ...  $\pm l$  for a given  $l$  value.

The three quantum numbers  $n$ ,  $l$ ,  $m_L$  together define an atomic orbital. The fourth quantum number  $M_S$  is intrinsic or spin and can have two values:

$$m_s \quad \begin{array}{cc} \frac{1}{2} & -\frac{1}{2} \\ + & - \\ \alpha & \beta \end{array}$$

The orbitals are defined by  $n$ ,  $l$  and  $m_l$  and are denoted in the case of  $n = 2$ ,  $l = 1$ ,  $m_l = 0, -1, +1$  as  $\begin{smallmatrix} 2p_0 \\ (2,1,0) \end{smallmatrix}$ ,  $\begin{smallmatrix} 2p_{-1} \\ (2,1,-1) \end{smallmatrix}$ ,  $\begin{smallmatrix} 2p_1 \\ (2,1,1) \end{smallmatrix}$ . These orbitals which differ by  $m_l$  only have the same radial function but different angular functions.

We will now examine the angular dependence of the hydrogen-like orbitals. In terms of spherical harmonics the solution to the Schrödinger equation may be written as

$$Y_l^{m_l}(\theta, \varphi) = \Theta_{lm_l}(\vartheta) \Phi_{m_l}(\varphi)$$

$$\Phi_{m_l}(\varphi) = \sqrt{\frac{1}{2\pi}} e^{im_l\varphi}$$

$$\Theta_{lm_l}(\theta) = N_\theta \rho_l^{|m_l|} \cos \theta, \quad \text{where } N_\theta \text{ is normalization constant}$$

$$\text{and } \rho_l^{|m_l|} \cos \theta = (1 - \cos^2 \theta)^{m_l \frac{1}{2}} \frac{d^{|m_l|}}{d \cos \theta} \rho_l^0(\cos \theta), \quad \text{where } m_l = 0$$

$$\rho_l^0(\cos \theta) = \frac{1}{2^l \cdot l!} \frac{d^l}{d \cos^l \theta} (\cos^2 \theta - 1)^l.$$

During calculations substitute  $\cos \theta$  by  $Z$ .

In the case of s orbital  $l = 0$ ,  $m_l = 0$ .

$$\begin{aligned} Y_0^0 &= N_\theta \rho_0^0(\cos \theta) \cdot \Phi_0(\varphi) \\ &= N_\theta \cdot 1 \cdot \sqrt{\frac{1}{2\pi}} e^0 \quad \text{since } \rho_0^0(\cos \theta) = 1 \\ &= N_\theta \sqrt{\frac{1}{2\pi}}. \end{aligned}$$

For p orbitals  $l = 1$ ,  $m_l = 0, +1, -1$  we have

$$\begin{aligned} Y_0^0 &= N_\theta \rho_1^0(\cos \theta) \cdot \Phi_0(\varphi) \\ \rho_1^0(\cos \theta) &= \frac{1}{2^1 \cdot 1} \frac{d}{d \cos \theta} (\cos^2 \theta - 1) = \cos \theta \\ Y_1^0 &= N_\theta \cos \theta \sqrt{\frac{1}{2\pi}} \sim \frac{Z}{r} (P_Z). \end{aligned}$$

When  $l = 1, m_l = 1$

$$Y_1^{+1} = N_\theta \rho_1^{+1}(\cos \theta) \cdot \Phi_1(\varphi)$$

$$\rho_1^{+1}(\cos \theta) = (1 - \cos^2 \theta)^{\frac{1}{2}} \frac{d^1}{d \cos \theta} \rho_1^0(\cos \theta) = \sin \theta$$

$$\Phi(\varphi) = \sqrt{\frac{1}{2\pi}} e^{i\varphi}$$

$$Y_1^{+1} = N_\theta \sin \theta \sqrt{\frac{1}{2\pi}} e^{i\varphi}$$

$$Y_1^{-1} = N_\theta \sin \theta \sqrt{\frac{1}{2\pi}} e^{-i\varphi}.$$

It is to be noted that any linear combination of solutions is also a solution and imaginary functions can be combined to give a real solution which is the case when  $m_l \neq 0$ .

Now  $(Y^+ + Y^-)$  and  $(Y^+ - Y^-)$  are also solutions as shown below.

$$\begin{aligned} \frac{1}{\sqrt{2}}(Y_1^+ + Y_1^{-1}) &= \frac{1}{\sqrt{2}} \sin \theta (e^{i\theta} + e^{-i\theta}) \\ &= \frac{1}{\sqrt{2}} \sin \theta \cos \varphi \sim \frac{x}{r} (p_x). \end{aligned}$$

Since  $e^{\pm i\alpha} = \cos \alpha \pm i \sin \alpha$ .

The second combination or solution is

$$\begin{aligned} \frac{1}{i\sqrt{2}}(Y_1^+ - Y_1^{-1}) &= \frac{1}{i\sqrt{2}} \sin \theta (e^{i\theta} - e^{-i\theta}) \\ &= \frac{1}{i\sqrt{2}} \sin \theta 2i \sin \varphi = \frac{y}{r} (p_y). \end{aligned}$$

In the case of d orbitals  $l = 2, m_l = 0, +1, -1, +2, -2$

$$Y_2^0 = N_\theta \rho_2^0(\cos \theta) \sqrt{\frac{1}{2\pi}} e^0$$

$$\rho_2^0(\cos \theta) = \frac{1}{2^2 \cdot 2} \frac{d^2}{d \cos \theta^2} (\cos^2 \theta - 1) = \frac{1}{2} (3 \cos^2 \theta - 1)$$

$$Y_2^0 = \frac{1}{2} (3 \cos^2 \theta - 1) \sqrt{\frac{1}{2\pi}} \sim \frac{Z^2 - r^2}{r^2} (d_{Z^2})$$

$$Y_2^{\pm 1} = N_\theta \rho_2^{\pm 1}(\cos \theta) \sqrt{\frac{1}{2\pi}} e^{\pm i\varphi}$$

$$\rho_2^{\pm 1}(\cos \theta) = (1 - \cos^2 \theta)^{\frac{1}{2}} \frac{d}{d \cos \theta} \rho_2^0(\cos \theta) = \sin \theta 3 \cos \theta$$

$$Y_2^{\pm 1} = 3 \cos \theta \sin \theta \sqrt{\frac{1}{2\pi}} e^{\pm i\varphi}.$$

The first real solution is

$$\frac{1}{\sqrt{2}}(Y_2^1 + Y_2^{-1}) = \frac{1}{\sqrt{2}}(3 \cos \theta \sin \theta \cdot 2 \cos \varphi) \sim \frac{zx}{r^2} (d_{xz}).$$

The second real solution is

$$\begin{aligned} \frac{1}{\sqrt{2}}(Y_2^1 - Y_2^{-1}) &= \frac{1}{i\sqrt{2}}(3 \cos \theta \sin \theta \cdot 2i \sin \varphi) \\ &= \frac{1}{\sqrt{2}}(3 \cos \theta \sin \theta \cdot 2 \sin \varphi) \sim \frac{yz}{r^2} (d_{yz}). \end{aligned}$$

When  $l = 2$ ,  $m_l = +2, -2$

$$\begin{aligned} Y_2^{\pm 2} &= N_\theta \rho_2^{\pm 2}(\cos \theta) \sqrt{\frac{1}{2\pi}} e^{\pm 2i\varphi} \\ \rho_2^{\pm 2}(\cos \theta) &= (1 - \cos^2 \theta)^2 \frac{d^2}{d \cos^2 \theta} \rho_2^0(\cos \theta) = (1 - \cos^2 \theta) \cdot 3 = 3 \sin^2 \theta \\ Y_2^{\pm 2} &= 3 \sin^2 \theta \sqrt{\frac{1}{2\pi}} e^{\pm 2i\varphi}. \end{aligned}$$

The first real solution is

$$\frac{1}{\sqrt{2}}(Y_2^2 + Y_2^{-2}) = \frac{1}{\sqrt{2}} 3 \sin^2 \theta \cdot 2 \cos 2\varphi \sim \frac{x^2 - y^2}{r^2} (d_{x^2-y^2}).$$

The second real solution is

$$\frac{1}{\sqrt{2}}(Y_2^2 - Y_2^{-2}) = \frac{1}{\sqrt{2}}(3 \sin^2 \theta \cdot 2 \sin 2\varphi) \sim \frac{xy}{r^2} (d_{xy}).$$

The shapes of s,  $p_x$ ,  $p_y$ ,  $p_z$ , d orbitals and f orbitals are given in Figs 2.2a and 2.2b.

We now consider spherical harmonic expressions for f orbitals. The derivation of the expression for  $P_3^0$  is as follows.

$$\begin{aligned} P_3^0(Z) &= \frac{1}{8 \cdot 6} \frac{d^3}{dZ^3} (Z^2 - 1)^3 = \frac{1}{48} \frac{d^3}{dZ^3} (Z^6 - 3Z^4 + 3Z^2 - 1) \\ &= \frac{1}{48} \frac{d^2}{dZ^2} (6Z^5 - 12Z^3 + 6Z) = \frac{1}{48} \frac{d}{dZ} (30Z^4 - 36Z^2 + 6) \\ &= \frac{1}{48} (120Z^3 - 72Z) = \frac{5}{2} Z^3 - \frac{3}{2} Z = \frac{1}{2} (5Z^3 - 3Z) = \frac{1}{2} (5 \cos^3 \theta - 3 \cos \theta) \end{aligned}$$

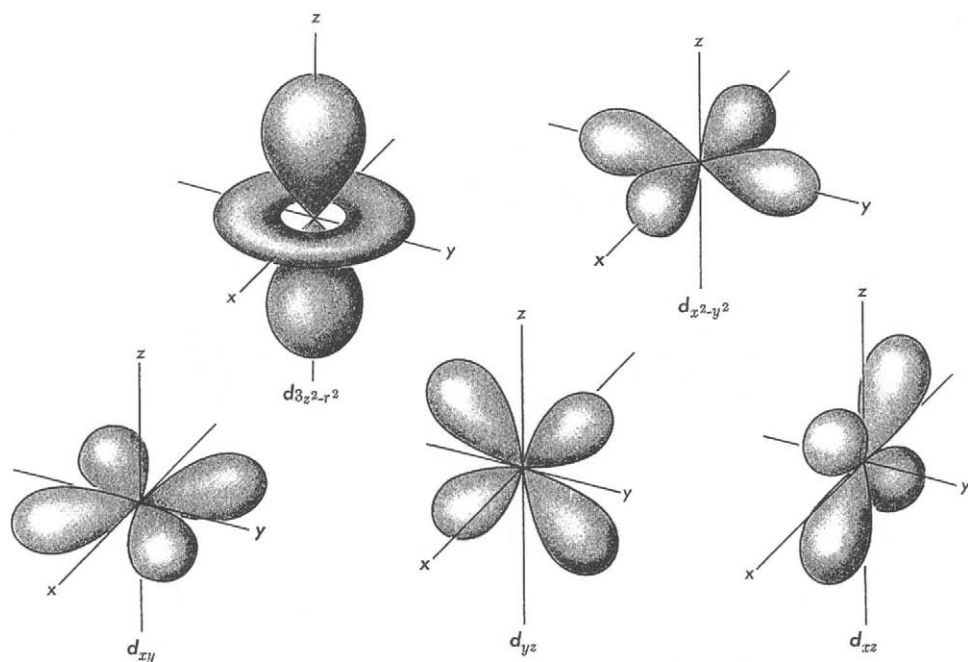


Fig. 2.2a. Atomic orbitals for the hydrogen atom, drawn as enclosure surfaces as described in the text. The lobes are derived from  $\Psi^2$  and must be everywhere positive. The lobes have been given the signs, however, of the original wave function  $\Psi$ , as this is information that becomes important when considering bonding via overlap of such orbitals.

$$\begin{aligned}
 P_3^{\pm 1}(Z) &= (1 - Z^2)^{\frac{1}{2}} \frac{d}{dZ} \left( \frac{5}{2} Z^3 - \frac{3}{2} Z \right) = (1 - Z^2)^{\frac{1}{2}} \left( \frac{15}{2} Z^2 - \frac{3}{2} \right) \\
 &= \sin \theta \left( \frac{15}{2} \cos^2 \theta - \frac{3}{2} \right) \\
 P_3^{\pm 2}(Z) &= (1 - Z^2)^{\frac{3}{2}} \frac{d^2}{dZ^2} \left( \frac{5}{2} Z^3 - \frac{3}{2} Z \right) = (1 - Z^2) \frac{d}{dZ} \left( \frac{15}{2} Z^2 - \frac{3}{2} \right) \\
 &= (1 - Z^2) \cdot 15Z = \sin^2 \theta \cdot 15 \cos \theta.
 \end{aligned}$$

For  $f$  orbitals  $l = 3$ ,  $m_l = 0, \pm 1, \pm 2, \pm 3$ .

$$\begin{aligned}
 P_3^0(\cos \theta) &= \frac{1}{2} (5 \cos^3 \theta - 3 \cos \theta) \\
 P_3^{\pm 1}(\cos \theta) &= (A \cos^2 \theta - B) \sin \theta \\
 P_l^{|m_l|}(\cos \theta) &= (A \cos^{l-|m_l|} \theta - B \cos^{l-|m_l|-2} \theta + C \cos^{l-|m_l|-1} \theta \dots) \sin^{|m_l|} \theta \\
 P_3^{\pm 3}(Z) &= (1 - Z^2)^{\frac{3}{2}} \cdot 15 = 15 \sin^3 \theta.
 \end{aligned}$$

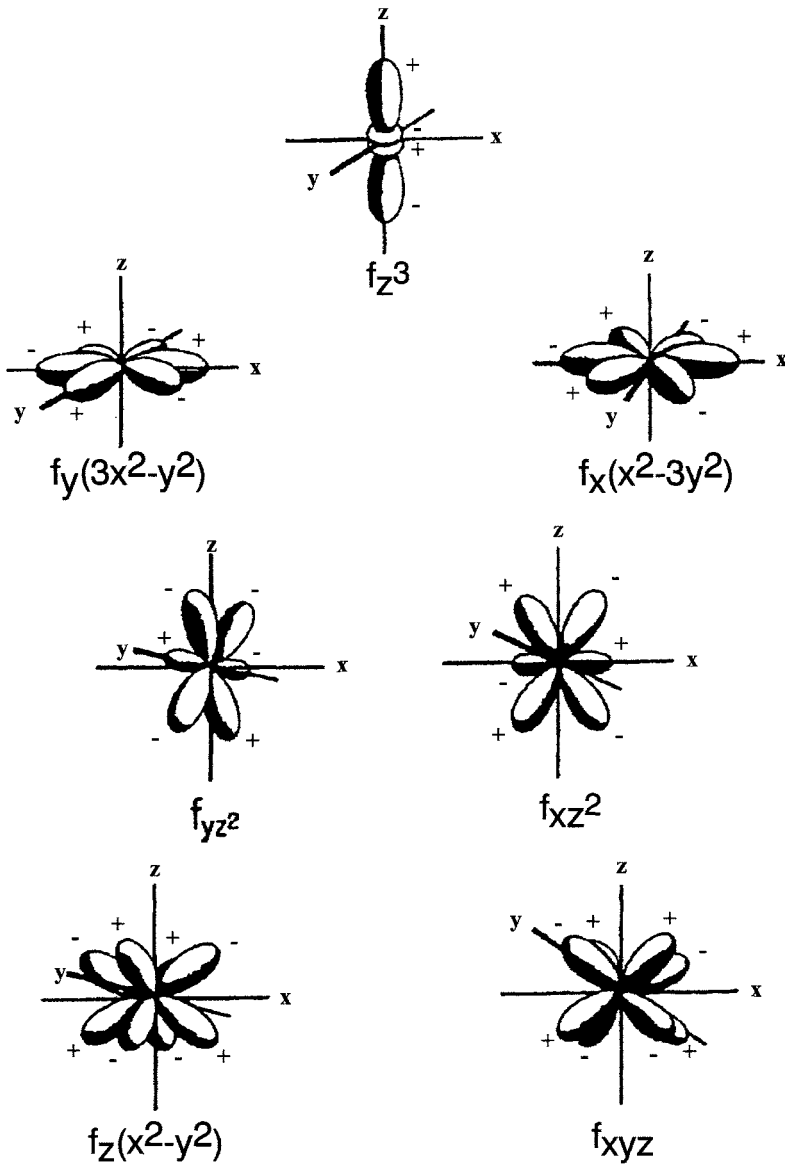


Fig. 2.2b. Representation of the seven real  $f$  orbitals. Pairs of functions in a given row are related by rotation about the  $z$ -axis.

We may now write for the first orbital

$$Y_3^0 = N_\theta P_3^0(\cos\theta) \sqrt{\frac{1}{2\pi}} e^0 = N_\theta \left( \frac{5}{2} \cos^3\theta - \frac{3}{2} \cos\theta \right) \sqrt{\frac{1}{2\pi}} \sim \frac{Z^3}{r^3} - \frac{Z}{r} \sim Z^3.$$



For the second and third orbitals

$$Y_3^{\pm 1} = N_\theta P_3^{\pm 1}(\cos \theta) \sqrt{\frac{1}{2\pi}} e^{\pm i\varphi} = N_\theta (\cos^2 \theta \sin \theta - \sin \theta) \sqrt{\frac{1}{2\pi}} e^{\pm i\varphi}$$

$$\frac{1}{\sqrt{2}}(Y_3^1 + Y_3^{-1}) = \frac{1}{\sqrt{2}} [(\cos^2 \theta \sin \theta - \sin \theta) \cdot 2 \cos \varphi] \sim \frac{XZ^2}{r^3 \cos \varphi} - \frac{X}{r} \sim XZ^2$$

$$\frac{1}{\sqrt{2}}(Y_3^1 - Y_3^{-1}) = \frac{1}{i\sqrt{2}} (\cos^2 \theta \sin \theta - \sin \theta \cdot 2i \sin \theta) \sim \frac{Z^2 Y}{r^3 \sin \varphi} - \frac{Y}{r} \sim YZ^2.$$

For  $m_l = 2$  we can write

$$Y_3^{\pm 2} = N_\theta P_3^{\pm 2}(\cos \theta) \sqrt{\frac{1}{2\pi}} e^{\pm 2i\varphi}$$

since  $P_3^{\pm 2} = \cos \theta \sin^2 \theta$

$$Y_3^{\pm 2} = N_\theta (\cos \theta \sin^2 \theta) \sqrt{\frac{1}{2\pi}} e^{\pm 2i\varphi}$$

$$\frac{1}{\sqrt{2}}(Y_3^2 + Y_3^{-2}) = \frac{1}{\sqrt{2}} (\cos \theta \sin^2 \theta \cdot 2 \cos 2\varphi) \sim Z(x^2 - y^2)$$

$$\frac{1}{i\sqrt{2}}(Y_3^2 - Y_3^{-2}) = \frac{1}{i\sqrt{2}} (\cos \theta \sin^2 \theta \cdot 4i \sin 2\varphi) \sim Z(xy).$$

For  $m_l = 3$  we can write

$$Y_3^{\pm 3} = N_\theta P_3^{\pm 3}(\cos \theta) \sqrt{\frac{1}{2\pi}} e^{\pm 3i\varphi}$$

since  $P_3^{\pm 3} = \sin^3 \theta$

$$Y_3^{\pm 3} = N_\theta (\sin^3 \theta) \sqrt{\frac{1}{2\pi}} e^{\pm 3i\varphi}$$

$$\frac{1}{\sqrt{2}}(Y_3^3 + Y_3^{-3}) = \frac{1}{\sqrt{2}} (\sin^3 \theta \cdot 2 \cos 3\varphi) \sim x(x^2 - 3y^2)$$

$$\frac{1}{i\sqrt{2}}(Y_3^3 - Y_3^{-3}) = \frac{1}{i\sqrt{2}} (\sin^3 \theta \cdot 4i \sin 3\varphi) \sim y(3x^2 - y^2).$$

The  $f$  orbitals are shown in Fig. 2.2b.

### 3. Electron configurations and its consequences

Pauli's exclusion principle states that in a single atom, no two electrons can have the same values for the four quantum numbers  $n$ ,  $l$ ,  $m_l$  and  $m_s$ . The ground state electron configuration in various periods is

Period	Electron configuration
1	$1s^2$
2	$2s^2 2p^6$
3	$3s^2 3p^6$
4	$4s^2 3d^{10} 4p^6$
5	$5s^2 4d^{10} 5p^6$
6	$6s^2 4f^{14} 5d^{10} 6p^6$
7	$7s^2 5f^{14} 6d$

During ionization, in general s electrons are removed before p electrons and some exceptions to this rule are

$^{24}\text{Cr}$	$1s^2 2s^2 2p^6 3s^2 3p^6 4s^1 3d^5$
$^{42}\text{Mo}$	$1s^2 2s^2 2p^6 3s^2 3p^6 4s^2 3d^{10} 4p^6 5s^1 4d^5$
$^{29}\text{Cu}$	$1s^2 2s^2 2p^6 3s^2 3p^6 4s^1 3d^{10}$
$^{47}\text{Ag}$	$1s^2 2s^2 2p^6 3s^2 3p^6 4s^2 3d^{10} 4p^6 5s^1 4d^{10}$
$^{79}\text{Au}$	$1s^2 2s^2 2p^6 3s^2 3p^6 4s^2 3d^{10} 4p^6 5s^2 4d^{10} 5p^6 6s^1 5d^{10}$

Russell–Saunders terms ( $L$ ,  $S$ ) refer to energy states arising out of an electronic configuration when electron repulsions are included. The terms are denoted as  $L$ , the orbital angular momentum and  $S$ , the spin angular momentum. We will now summarize the various attributes in one-electron and many electron systems.

Property	One-electron system	Many electron system
Orbital angular momentum	$l = 0, 1, 2, 3$ s p d f	$L = 0, 1, 2, 3, \dots$ S P D F
Z-component of orbital angular momentum	$m_L = l, l - 1, 0 \dots -l$	$M_L = L, L - 1, \dots -L$
Orbital degeneracy	$\#m_l = 2l + 1$	$\#M_L = 2L + 1$
Spin angular momentum	$s = 1/2$	$S = 0, 1/2, 1, 3/2 \dots$
Component of spin angular momentum	$m_s = +1/2$ or $-1/2$	$M_S = S, S - 1, \dots -S$
Spin degeneracy	$\#m_s = 2s + 1$	$\#M_S = 2S + 1$
Total degeneracy (orbital and spin)	$2(2l + 1)$	$\#M_S = (2S + 1)(2L + 1)$
Term notation	$2L$	$2S+1L$

Now consider an electron in a p orbital with  $l = 1$  and  $s = 1/2$ . The total degeneracy in this case is  $(2L + 1)(2S + 1) = 3 \cdot 2 = 6$ . The possible combinations for one p electron may be written as

spin	+	+	+	-	-	-
$m_l$	+1	0	-1	+1	0	-1

Thus one obtains six possible combinations.

Degeneracy can also be obtained from the formula

$$\left. \begin{aligned} np^x &= \binom{6}{x} = \frac{6!}{x!(6-x)!} \\ nd^x &= \binom{10}{x} = \frac{10!}{x!(10-x)!} \\ nf^x &= \binom{14}{x} = \frac{14!}{x!(14-x)!} \end{aligned} \right\} \begin{array}{l} x \text{ is the number of electrons} \\ \text{in orbitals of a given } l \text{ value} \end{array}$$

Microstates are the atomic states that result from interactions between electrons in a many electron system ( $m_l$  and  $m_s$  values). The microstate table lists all the possible microstates for a given electron configuration arranged according to the  $M_L$  and  $M_S$  values. In the case of a  $np^2$  configuration the microstate table will be of the form

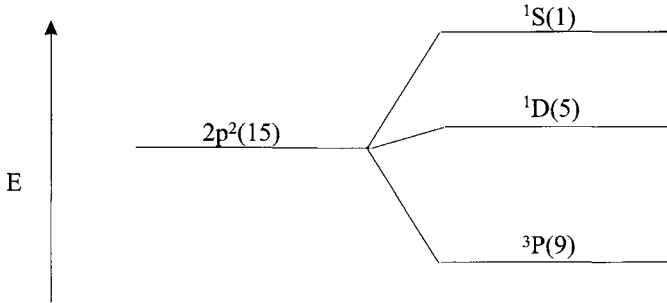
$M_L$	$M_S$	+1	0	-1
+2			$\begin{matrix} + & - \\ (+1 & +1) \end{matrix}$	$\begin{matrix} 1D \\ 1 \end{matrix}$
+1	$\begin{matrix} + & + \\ (+1 & 0) \end{matrix}$	$\begin{matrix} 1D \\ 3P \end{matrix}$	$\begin{matrix} + & - \\ (+1 & 0) \end{matrix}$	$\begin{matrix} 3P \\ - & - \\ (+1 & 0) \end{matrix}$
0	$\begin{matrix} + & + \\ (+1 & -1) \end{matrix}$	$\begin{matrix} 1D \\ 3P \end{matrix}$	$\begin{matrix} + & - \\ (+1 & -1) \end{matrix}$	$\begin{matrix} 3P \\ 1S \\ + & - \\ (0 & 0) \\ - & - \\ (+1 & -1) \end{matrix}$
-1	$\begin{matrix} + & + \\ (-1 & 0) \end{matrix}$	$\begin{matrix} 1D \\ 3P \end{matrix}$	$\begin{matrix} + & - \\ (-1 & 0) \end{matrix}$	$\begin{matrix} 3P \\ - & - \\ (-1 & 0) \end{matrix}$
-2			$\begin{matrix} 1D \\ + & - \\ (-1 & -1) \end{matrix}$	

The unique microstate is  $\begin{matrix} + & - \\ (+1 & +1) \end{matrix}$ , with  $M_L = 2$ ,  $L = 2$  (note that there are no higher  $M_L$  values),  $M_S = 0$ ,  $S = 0$  (note that there are no higher  $M_S$  values for given  $M_L$ ).

The term is denoted as  $^{2S+1}L = {}^1D$  which means singlet D state. The total degeneracy in this case is  $(2L + 1)(2S + 1) = 5$ . Note that there are five microstates belonging to  ${}^1D$ . Hence the term is written as  ${}^1D(5)$ . From gleaning the table of microstates, we see that there are  ${}^1S(1)$  and  ${}^3P(9)$ . The ground state from the three terms  ${}^1S(1)$ ,  ${}^1D(5)$  and  ${}^3P(9)$  is chosen or assigned according to Hund's rules.

Hund's rules are: (i) the greater the spin multiplicity, the lower is the energy of the state; (ii) among two states of the same spin multiplicity, the state with the higher  $L$  value will be the lower energy state.

The energy level diagram for the  $2p^2$  system will look like



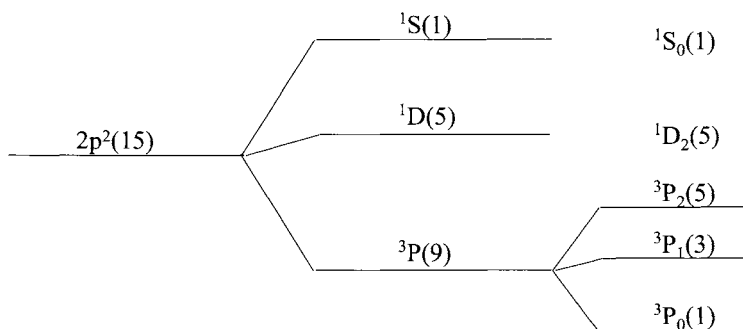
The splitting of energy levels is due to electron repulsions which is denoted by  $\sum \frac{e^2}{r_{ij}}$ .

In the case of the  $3d^2$  system, the microstate table is as given below, consisting of a total of 45 states.

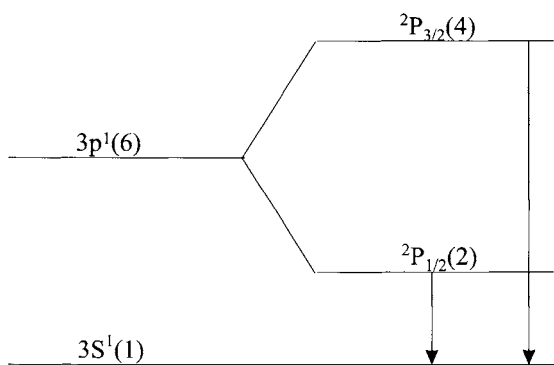
Values of $M_L, M_S$ for $(3d)^2$ configuration			
$M_L$	$M_S$		
	1	0	-1
4		+ - (2, 2)	
3	++ (2, 1)	+ - - + (2, 1)(2, 1)	- - (2, 1)
2	++ (2, 0)	+ - - + + - (2, 0)(2, 0)(1, 1)	- - (2, 0)
1	+++ + (1, 0)(2, -1)	+ - - + (1, 0)(1, 0)	- - - - (1, 0)(2, -1)
		+ - - + (2, -1)(2, -1)	
0	+ + + + (2, -2)(1, -1)	+ - - + (2, -2)(2, -2)	
		+ - (1, -1)	- - - - (2, -2)(1, -1)
		- + + - (1, -1)(0, 0)	
-1	+ + + + (-1, 0)(1, -2)	+ - - + (-1, 0)(-1, 0)	- - - - (-1, 0)(1, -2)
		+ - - + (-2, 1)(-2, 1)	
-2	+ + (-2, 0)	+ - - + + - (-2, 0)(-2, 0)(-1, -1)	- - (-2, 0)
-3	+ + (-2, -1)	+ - - + (-2, -1)(-2, -1)	- - (-2, -1)
-4		+ - (-2, -2)	

We may now consider the  $2p^2$  configuration and draw the energy level diagram including the spin-orbit levels as follows.

Consider



the two emission lines of sodium on excitation. The excited state configuration of sodium is  $3S^1 3p^1$  for which  $L + S = 1 + 1/2 = 3/2$ ,  $L - S = 1/2$  and this may be represented as



The energy expression for spin-orbit levels can be obtained thus

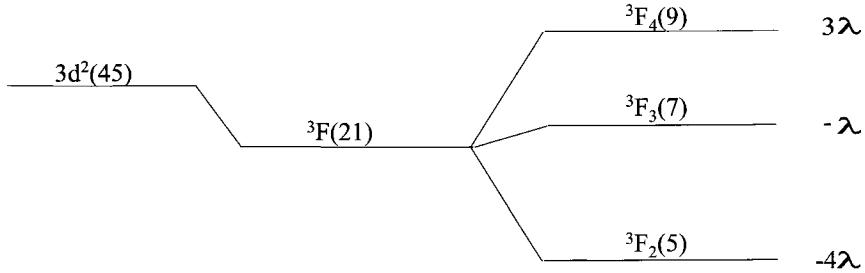
$$J^2 = (L + S)^2 = L^2 + 2LS + S^2$$

$$LS = 1/2(J^2 - L^2 - S^2)$$

$$E(LS) = 1/2[J(J + 1) - L(L + 1) - S(S + 1)]$$

$$E(LS) = \lambda/2[J(J + 1) - L(L + 1) - S(S + 1)].$$

In the case of the  $3d^2$  system, the energy level diagram can be represented as



It is necessary that the centre of gravity principle is obeyed.

$$\sum (\text{degeneracy})(\text{energy}) = 0.$$

The degeneracy of the  $nd^2$  system is

$$\binom{10}{2} = \frac{10!}{2!8!} = 45.$$

According to the table, there are 45 microstates. The unique microstates are

- (a)  $\left( +2 \quad \bar{2} \right) \quad {}^1G(9)$   
 $M_L = 4 \quad L = 4(G)$   
 $M_S = 0 \quad S = 0 \quad 2S + 1 = 1$   
 Total degeneracy =  $(2S + 1)(2L + 1) = 9$
- (b)  $\left( +2 \quad +1 \right) \quad {}^3F(21)$   
 $M_L = 3 \quad L = 3(F)$   
 $M_S = 1 \quad S = 1 \quad 2S + 1 = 3$   
 $(2S + 1)(2L + 1) = 21$   
 $\left( +2 \quad +0 \right) \quad M_L = 2L = 3(F)$   
 $M_S = 1 \quad S = 1 \quad 2S + 1 = 3$
- (c)  $\left( +2 \quad \bar{0} \right) \quad {}^1D(5)$   
 $M_L = 2 \quad L = 2(D)$   
 $M_S = 0 \quad S = 0 \quad 2S + 1 = 1$   
 $(2S + 1)(2L + 1) = 5$

$$(d) \left( \begin{array}{cc} + & + \\ +1 & 0 \end{array} \right) \quad {}^3P(9)$$

$$M_L = 1 \quad L = 1(P)$$

$$M_S = 1 \quad S = 1 \quad 2S + 1 = 3$$

$$(2S + 1)(2L + 1) = 9$$

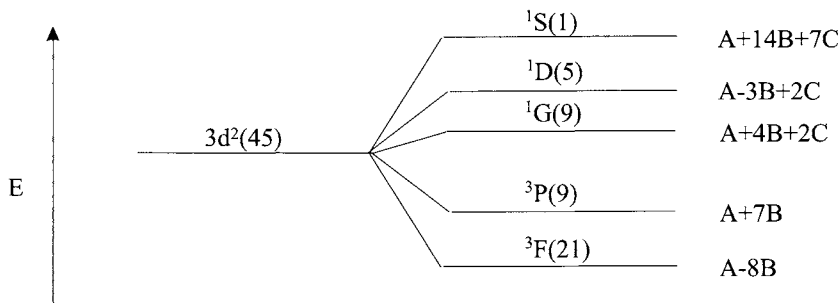
$$(e) \left( \begin{array}{cc} + & - \\ +2 & -2 \end{array} \right) \quad {}^1S(1)$$

$$M_L = 0 \quad L = 0(S)$$

$$M_S = 0 \quad S = 0 \quad 2S + 1 = 1$$

$$(2S + 1)(2L + 1) = 1.$$

Applying Hund's rules we conclude that  ${}^3F$  to be the ground state. The orbital energy diagram of the  $d^2$  system along with the corresponding Racah parameters is given below. Racah parameters (A, B and C) are energy expressions describing electron repulsions by integrals designated by A, B and C.



The case of excited electronic configuration is also treated similarly. For instance, a configuration such as  $2p^1 3p^1$  has  $l_1 = 1, l_2 = 1, L = 2, 1, 0$  and  $S = 1, 0$  and gives rise to 36 states with the possible terms  ${}^3D(15), {}^3P(9), {}^3S(3), {}^1D(5), {}^1P(3)$  and  ${}^1S(1)$ .

The procedure for the determination of ground state term without the tedious task of obtaining all the terms consists of: (i) listing all possible  $M_L$  and  $M_S$  values and (ii) applying Hund's rules. As an example, consider  $nd^2$  configuration. We have

$$\begin{array}{cccc} + & + & + & + \\ +2 & +1 & 0 & -1 & -2 \end{array} \quad \begin{array}{cccc} - & - & - & - \\ +2 & +1 & 0 & -1 & -2 \end{array}$$

$$M_L = 3 \quad L = 3(F)$$

$$M_S = 1 \quad 2S + 1 = 3$$

Hence  ${}^3F$  is the ground state.

Principle of hole formalism: according to this principle the equivalence

$$p^x = p^{x-6}; \quad d^x = d^{10-x}; \quad f^x = f^{14-x}$$

holds good. Consider application of this principle to  $\text{Co}^{2+}(3d^7)$  using this hole formalism  $3d^7 \equiv 3d^3$ .

For  $d^3$  configuration we have

$$\begin{array}{cccccc}
 + & + & + & + & - & - & - & - & - \\
 +2 & +1 & 0 & -1 & -2 & +2 & +1 & 0 & -1 & -2 \\
 M_L = 3 & & & & L = 3(\text{F}) & & & & & \\
 M_S = 3/2 & & & & S = 3/2 & & & & & 2S + 1 = 4.
 \end{array}$$

Hence  $^4\text{F}$  is the ground state.

It is to be noted that  $2S + 1$  of the ground state term corresponds to the sum of the number of unpaired electrons and one. The terms discussed thus far arise due to electron repulsions.

#### 4. Spin-orbit coupling

Spin-orbit interactions give rise to spin-orbit levels characterized by  $J$ , the total angular momentum.  $M_J$  is known as the component of total angular momentum and it is written as

$$\begin{aligned}
 m_J &= J, J - 1 \dots - J \\
 \text{Degeneracy} &= 2J + 1.
 \end{aligned}$$

$J$  values are obtained by coupling  $L$  and  $S$

$$J = (L + S), (L + S - 1) \dots |L - S|$$

Consider the three terms  $^1\text{S}(1)$ ,  $^1\text{D}(5)$  and  $^3\text{P}(9)$  of  $\rho^2$  configuration

					Term notation
$^1\text{S}(1)$	$L = 0$	$S = 0$	$J = 0$	$(2J + 1) = 1$	$^1\text{S}_0(1)$
$^1\text{D}(5)$	$L = 2$	$S = 0$	$J = 2$	$(2J + 1) = 5$	$^1\text{D}_2(5)$
$^3\text{P}(9)$	$L = 1$	$S = 1$	$J = 2$	$(2J + 1) = 5$	$^3\text{P}_2(5)$
			$J = 1$	$(2J + 1) = 3$	$^3\text{P}_1(3)$
			$J = 0$	$(2J + 1) = 1$	$^3\text{P}_0(1)$

It is to be noted in general that the lower the  $J$  value, the lower is the energy for half-filled electron configurations and the trend is reversed for electron configurations that are more than half-filled. Thus in the case of the two configurations  $2p^2$  and  $2p^4$  the energy level diagram will be similar except in the placement of its spin-orbit levels ( $J$  levels).

The various terms and the number of  $J$  levels for rare earths of different electronic configurations are given in Table 2.1.



TABLE 2.1  
Terms of  $f^q$  configurations of  $\text{Ln}^{3+}$  free ions.

Configuration	$\text{Ln}^{3+}$	Terms	Number of terms	Number of levels with different $J$
$f^1, f^{13}$	$\text{Ce}^{3+}, \text{Yb}^{3+}$	$^2\text{F}$	1	2
$f^2, f^{12}$	$\text{Pr}^{3+}, \text{Tm}^{3+}$	$^1\text{SDGI } ^3\text{PFH}$	7	13
$f^3, f^{11}$	$\text{Nd}^{3+}, \text{Er}^{3+}$	$^2\text{PDFGHIKL } ^4\text{SDFGI}$ $2\ 2\ 2\ 2$	17	41
$f^4, f^{10}$	$\text{Pm}^{3+}, \text{Ho}^{3+}$	$^1\text{SDFGHIKLN } ^3\text{PDFGHIKLM } ^5\text{SDFGI}$ $24\ 4\ 2\ 3\ 2\ 3\ 2\ 4\ 3\ 4\ 2\ 2$	47	107
$f^5, f^9$	$\text{Sm}^{3+}, \text{Dy}^{3+}$	$^2\text{PDFGHIKLMNO } ^4\text{SPDFGHIKLM } ^6\text{PFH}$ $45\ 76\ 7\ 55\ 32\ 23\ 44\ 3\ 32$ $^1\text{SPDFGHIKLMNQ } ^3\text{PDFGHIKLMNO}$ $4\ 6\ 48\ 4\ 73\ 42\ 2\ 65\ 97\ 9\ 66\ 33$	73	198
$f^6, f^8$	$\text{Eu}^{3+}, \text{Tb}^{3+}$	$^5\text{SPDFGHIKL } ^7\text{F}$ $3\ 23\ 2\ 2$	119	295
$f^7$	$\text{Gd}^{3+}$	$^2\text{SPDFGHIKLMNOQ } ^4\text{SPDFGHIKLMN}$ $257\ 101\ 09\ 97\ 54\ 2\ 226\ 57\ 5\ 53\ 3$ $^6\text{PDFGHI } ^8\text{S}$	119	327

Some properties of lanthanides along with scandium and yttrium are given in Table 2.2.

The most conventional ground-state electronic configuration based on emission spectral data along with the terms are given in Table 2.3.

As seen from the table there is no gradual filling of  $f$  and the two configurations,  $4f^{n-1}5d^16s^2$  and  $4f^n6s^2$  appear as ground states. Relative energy relationships between these two configurations for lanthanides are shown in Fig. 2.3.

It is clear from Fig. 2.3 that half-filled ( $f^7$ ) and filled ( $f^{14}$ ) orbitals show greater stability than elements with other  $f^n$ -configuration [1]. This is also true for monovalent ( $\text{Ln}^+$ ) and divalent ( $\text{Ln}^{2+}$ ) ions but does not hold good in the case of  $\text{Ln}^{3+}$  ions which have regularly increasing  $f^n$  configuration.

The ground state configuration of lanthanides,  $4f^{n-1}5d^16s^2$  or  $4f^n6s^2$  does not determine the chemical behaviour of these elements. In forming  $\text{Ln}^{3+}$  ions, an  $f$  electron is removed. Lanthanides differ from transition elements in that  $4f$  orbitals are shielded and are not available for reactions. Thus lanthanides resemble more closely alkaline earths and the scandium group than transition elements in their chemistry.

The anomalous position of lanthanum and lutetium in the conventional periodic table has been recognized and the debate as to the placement of lanthanum and actinium or lutetium and lawrencium in group III B along with scandium and yttrium has received considerable attention [2]. Early spectroscopic work indicated ground state electronic configurations of  $[\text{Xe}]4f^{13}5d^16s^2$  for ytterbium and  $[\text{Xe}]4f^{14}5d^16s^2$  for lutetium with lutetium as the last member of the lanthanide series. The ground state configurations of La, Sc and Y were assigned as  $[\text{Xe}]5d^16s^2$ ,  $[\text{Ar}]3d^14s^2$  and  $[\text{Kr}]4d^15s^2$  respectively in group III B. Based on further spectroscopic work, all the rare earths have been assigned  $(\text{Xe})4f^n6s^2$  with the

TABLE 2.2  
Some properties of scandium, yttrium, and the lanthanides.

Z	Name	Symbol	Electron configuration	Valences	M <sup>3+</sup> radius (Å)	M <sup>3+</sup> colour
21	Scandium	Sc	[Ar]3d <sup>1</sup> 4s <sup>2</sup>	3	0.68	Colourless
39	Yttrium	Y	[Kr]4d <sup>1</sup> 5s <sup>2</sup>	3	0.88	Colourless
57	Lanthanum	La	[Xe]5d <sup>1</sup> 6s <sup>2</sup>	3	1.06	Colourless
58	Cerium	Ce	[Xe]4f <sup>1</sup> 5d <sup>1</sup> 6s <sup>2</sup>	3, 4	1.03	Colourless
59	Praseodymium	Pr	[Xe]4f <sup>3</sup> 6s <sup>2</sup>	3, 4	1.01	Green
60	Neodymium	Nd	[Xe]4f <sup>4</sup> 6s <sup>2</sup>	3	0.99	Lilac
61	Promethium	Pm	[Xe]4f <sup>5</sup> 6s <sup>2</sup>	3	0.98	Pink
62	Samarium	Sm	[Xe]4f <sup>6</sup> 6s <sup>2</sup>	2, 3	0.96	Yellow
63	Europium	Eu	[Xe]4f <sup>7</sup> 6s <sup>2</sup>	2, 3	0.95	Pale pink
64	Gadolinium	Gd	[Xe]4f <sup>7</sup> 5d <sup>1</sup> 6s <sup>2</sup>	3	0.94	Colourless
65	Terbium	Tb	[Xe]4f <sup>9</sup> 6s <sup>2</sup>	3, 4	0.92	Pale pink
66	Dysprosium	Dy	[Xe]4f <sup>10</sup> 6s <sup>2</sup>	3	0.91	Yellow
67	Holmium	Ho	[Xe]4f <sup>11</sup> 6s <sup>2</sup>	3	0.89	Yellow
68	Erbium	Er	[Xe]4f <sup>12</sup> 6s <sup>2</sup>	3	0.88	Lilac
69	Thulium	Tm	[Xe]4f <sup>13</sup> 6s <sup>2</sup>	3	0.87	Green
70	Ytterbium	Yb	[Xe]4f <sup>14</sup> 6s <sup>2</sup>	2, 3	0.86	Colourless
71	Lutetium	Lu	[Xe]4f <sup>14</sup> 5d <sup>1</sup> 6s <sup>2</sup>	3	0.85	Colourless

TABLE 2.3  
Ground-state "outer" electronic configurations.

Atomic number	Symbol	Configuration (spectroscopic term)			
		Ln <sup>0</sup>	Ln <sup>+</sup>	Ln <sup>2+</sup>	Ln <sup>3+</sup>
57	La	5d <sup>1</sup> 6s <sup>2</sup> ( <sup>2</sup> D <sub>3/2</sub> )	5d <sup>2</sup> ( <sup>3</sup> F <sub>2</sub> )	5d <sup>1</sup> ( <sup>2</sup> D <sub>3/2</sub> )	4f <sup>0</sup> ( <sup>1</sup> S <sub>0</sub> )
58	Ce	4f <sup>1</sup> 5d <sup>1</sup> 6s <sup>2</sup> ( <sup>1</sup> G <sub>4</sub> )	4f <sup>1</sup> 5d <sup>1</sup> 6s <sup>2</sup> ( <sup>2</sup> G <sub>7/2</sub> )	4f <sup>2</sup> ( <sup>3</sup> H <sub>4</sub> )	4f <sup>1</sup> ( <sup>2</sup> F <sub>5/2</sub> )
59	Pr	4f <sup>3</sup> 6s <sup>2</sup> ( <sup>4</sup> I <sub>9/2</sub> )	4f <sup>3</sup> 6s <sup>1</sup> ( <sup>5</sup> I <sub>4</sub> )	4f <sup>3</sup> ( <sup>4</sup> I <sub>9/2</sub> )	4f <sup>2</sup> ( <sup>3</sup> H <sub>4</sub> )
60	Nd	4f <sup>4</sup> 6s <sup>2</sup> ( <sup>5</sup> I <sub>4</sub> )	4f <sup>4</sup> 6s <sup>1</sup> ( <sup>6</sup> I <sub>7/2</sub> )	4f <sup>4</sup> ( <sup>5</sup> I <sub>4</sub> )	4f <sup>3</sup> ( <sup>4</sup> I <sub>9/2</sub> )
61	Pm	4f <sup>5</sup> 6s <sup>2</sup> ( <sup>6</sup> H <sub>5/2</sub> )	4f <sup>5</sup> 6s <sup>1</sup> ( <sup>7</sup> H <sub>2</sub> )	4f <sup>5</sup> ( <sup>6</sup> H <sub>5/2</sub> )	4f <sup>4</sup> ( <sup>5</sup> I <sub>4</sub> )
62	Sm	4f <sup>6</sup> 6s <sup>2</sup> ( <sup>7</sup> F <sub>0</sub> )	4f <sup>6</sup> 6s <sup>1</sup> ( <sup>8</sup> F <sub>1/2</sub> )	4f <sup>6</sup> ( <sup>7</sup> F <sub>0</sub> )	4f <sup>5</sup> ( <sup>6</sup> H <sub>5/2</sub> )
63	Eu	4f <sup>7</sup> 6s <sup>2</sup> ( <sup>8</sup> S <sub>7/2</sub> )	4f <sup>7</sup> 6s <sup>1</sup> ( <sup>9</sup> S <sub>4</sub> )	4f <sup>7</sup> ( <sup>8</sup> S <sub>7/2</sub> )	4f <sup>6</sup> ( <sup>7</sup> F <sub>0</sub> )
64	Gd	4f <sup>7</sup> 5d <sup>1</sup> 6s <sup>2</sup> ( <sup>9</sup> D <sub>2</sub> )	4f <sup>7</sup> 5d <sup>1</sup> 6s <sup>1</sup> ( <sup>10</sup> D <sub>5/2</sub> )	4f <sup>7</sup> 5d <sup>1</sup> ( <sup>9</sup> D <sub>2</sub> )	4f <sup>7</sup> ( <sup>8</sup> S <sub>7/2</sub> )
65*	Tb	4f <sup>9</sup> 6s <sup>2</sup> ( <sup>6</sup> H <sub>15/2</sub> )	4f <sup>9</sup> 6s <sup>1</sup> ( <sup>7</sup> H <sub>8</sub> )	4f <sup>9</sup> ( <sup>6</sup> H <sub>15/2</sub> )	4f <sup>8</sup> ( <sup>7</sup> F <sub>6</sub> )
66	Dy	4f <sup>10</sup> 6s <sup>2</sup> ( <sup>5</sup> I <sub>8</sub> )	4f <sup>10</sup> 6s <sup>1</sup> ( <sup>6</sup> I <sub>17/2</sub> )	4f <sup>10</sup> ( <sup>5</sup> I <sub>8</sub> )	4f <sup>9</sup> ( <sup>6</sup> H <sub>15/2</sub> )
67	Ho	4f <sup>11</sup> 6s <sup>2</sup> ( <sup>4</sup> I <sub>15/2</sub> )	4f <sup>11</sup> 6s <sup>1</sup> ( <sup>5</sup> I <sub>8</sub> )	4f <sup>11</sup> ( <sup>4</sup> I <sub>15/2</sub> )	4f <sup>10</sup> ( <sup>5</sup> I <sub>8</sub> )
68	Er	4f <sup>12</sup> 6s <sup>2</sup> ( <sup>3</sup> H <sub>6</sub> )	4f <sup>12</sup> 6s <sup>1</sup> ( <sup>4</sup> H <sub>13/2</sub> )	4f <sup>12</sup> ( <sup>3</sup> H <sub>6</sub> )	4f <sup>11</sup> ( <sup>4</sup> I <sub>15/2</sub> )
69	Tm	4f <sup>13</sup> 6s <sup>2</sup> ( <sup>2</sup> F <sub>7/2</sub> )	4f <sup>13</sup> 6s <sup>1</sup> ( <sup>3</sup> F <sub>4</sub> )	4f <sup>13</sup> ( <sup>2</sup> F <sub>7/2</sub> )	4f <sup>12</sup> ( <sup>3</sup> H <sub>6</sub> )
70	Yb	4f <sup>14</sup> 6s <sup>2</sup> ( <sup>1</sup> S <sub>0</sub> )	4f <sup>14</sup> 6s <sup>1</sup> ( <sup>2</sup> S <sub>1/2</sub> )	4f <sup>14</sup> ( <sup>1</sup> S <sub>0</sub> )	4f <sup>13</sup> ( <sup>2</sup> F <sub>7/2</sub> )
71	Lu	4f <sup>14</sup> 5d <sup>1</sup> 6s <sup>2</sup> ( <sup>2</sup> D <sub>3/2</sub> )	4f <sup>14</sup> 6s <sup>2</sup> ( <sup>1</sup> S <sub>0</sub> )	4f <sup>14</sup> 6s <sup>1</sup> ( <sup>2</sup> S <sub>1/2</sub> )	4f <sup>14</sup> ( <sup>1</sup> S <sub>0</sub> )

\*Ground states of Tb<sup>0</sup> and Tb<sup>+</sup> may be 4f<sup>8</sup>5d<sup>1</sup>6s<sup>2</sup> and 4f<sup>8</sup>5d<sup>1</sup>6s<sup>1</sup>, respectively.

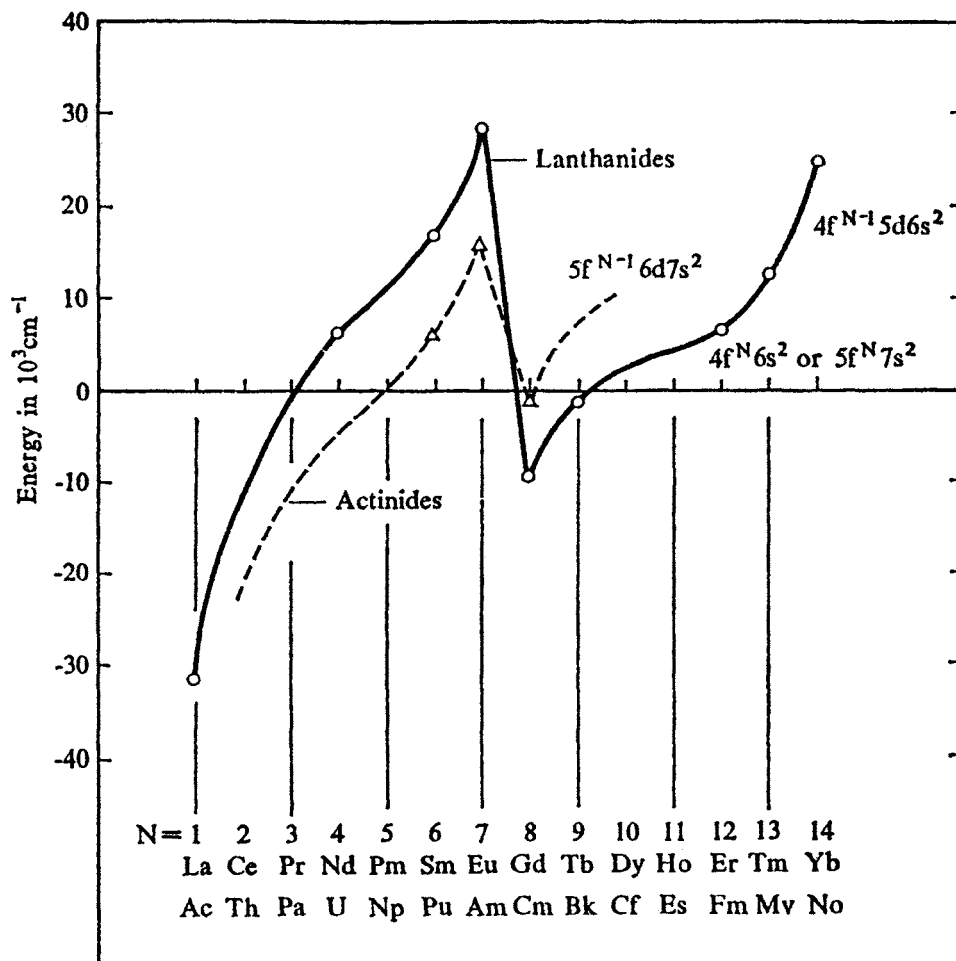


Fig. 2.3. Relative energy relationships between  $f^n s^2$  and  $f^{n-1} d^1 s^2$  ground-state electronic configurations.

exception of La, Gd, and Lu which have ground state configuration of  $[\text{Xe}]4f^{n-1}5d^1 6s^2$ . Thus  $[\text{Xe}]4f 6s^2$  and not  $[\text{Xe}]4f^{n-1}5d^1 6s^2$  is the ideal ground state configuration of lanthanides. Thus ytterbium and lutetium have  $[\text{Xe}]4f^{14} 6s^2$  and  $[\text{Xe}]4f^{14} 5d^1 6s^2$  ground state configurations respectively. Thus Yb and Lu differ by a d electron and Lu becomes the first member of 6d block elements.

Although thorium has the configuration  $[\text{Rn}]6d^2 7s^2$  it is considered as an  $f$  block element with an irregular configuration. This lends support to the supposition that La and Ac should be considered as  $f$  block elements with irregular configurations derived from the ideal configurations  $[\text{Xe}]4f^1 6s^2$  and  $[\text{Rn}]5f^1 7s^2$  respectively. Thus La and Ac should be considered as the first member of the  $f$ -block rather than Ce and Th. By the same token Yb and No can be considered as the last members of the  $f$  block and not Lu and Lr and not

TABLE 2.4  
Periodic trends in various properties for the first part of the d-block [2].

Atomic Radii* (A)	Sum of the First Two Ionization Potentials* (eV)	Melting Point <sup>b</sup> (°K)	Electronegativity <sup>b</sup> (Allred-Rochow) Scale
Sc 1.570 Y 1.693 La 1.915 versus Sc 1.570 Y 1.693 Lu 1.553	Sc 19.45 Y 18.61 La 17.04 versus Sc 19.45 Y 18.61 Lu 20.85	Sc 1812 Y 1803 La 1193 versus Sc 1812 Y 1803 Lu 1925	Sc 1.20 Y 1.11 La 1.08 versus Sc 1.20 Y 1.11 Lu 1.14
Ti 1.477 Zr 1.593 Hf 1.476	Ti 20.40 Zr 19.76 Hf 20.40	Ti 1940 Zr 2130 Hf 2495	Ti 1.32 Zr 1.22 Hf 1.23
V 1.401 Nb 1.589 Ta 1.413	V 20.94 Nb 20.78 Ta 23.90	V 2188 Nb 2741 Ta 3253	V 1.45 Nb 1.23 Ta 1.33
Cr 1.453 Mo 1.520 W 1.360	Cr 23.25 Mo 22.85 W 25.68	Cr 2173 Mo 2893 W 3653	Cr 1.56 Mo 1.30 W 1.40
Mn 1.278 Tc 1.391 Re 1.310	Mn 23.07 Tc 22.10 Re 24.47	Mn 1517 Tc 2473 Re 3453	Mn 1.70 Tc 1.36 Re 1.46
Fe 1.227 Ru 1.410 Os 1.266	Fe 24.08 Ru 23.96 Os 25.70	Fe 1809 Ru 2700 Os 3290	Fe 1.64 Ru 1.42 Os 1.52
		Ni 1728 Pd 1825 Pt 2042	Ni 1.75 Pd 1.35 Pt 1.44
		Co 1768 Rh 2233 Ir 2727	Co 1.70 Rh 1.45 Ir 1.55

La and Ac as the first members of d blocks in periods 6 and 7. Thus Lu and Lr are placed in group III B along with Sc and Y.

The electronic configurations of La and Ac considering core plus valence electron are similar to those of Sc and Y and not that of Lu and Lr, is an argument that fails in the light of intraperiod and intragroup similarities discussed below.

The nine d-block elements of period 6 viz. Hf to Hg have [Xe]4f<sup>14</sup> core like lutetium and not just the [Xe] core of the lanthanum. Similarly, in passing down the columns of the d-block from Ti to Zn, the addition of 4f subshell is encountered in moving from period 5 to 6. The periodic trends in atomic radii, sum of the first two ionization potentials, melting

TABLE 2.5  
A comparison of various properties of Sc and Y versus those of Lu and La [2].

Property	Sc	Y	Lu	La
Highest common oxidation state	3+	3+	3+	3+
Precipitation of sulfate in fractional crystallization	Y group	Y group	Y group	Ce group
Structure of metal at room temperature	hcp	hcp	hcp	special double hcp
Structure of oxide (M <sub>2</sub> O <sub>3</sub> )	$\frac{3}{\infty}[AB_{6/4}]c$	$\frac{3}{\infty}[AB_{6/4}]c$	$\frac{3}{\infty}[AB_{6/4}]c$	special hex. CN-7 A-M <sub>2</sub> O <sub>3</sub> struct.
Structure of chloride (MX <sub>3</sub> )	$\frac{2}{\infty}[AB_{6/2}]m$	$\frac{2}{\infty}[AB_{6/2}]m$	$\frac{2}{\infty}[AB_{6/2}]m$	$\frac{3}{\infty}[AB_{9/3'}]h$
Presence of low-lying nonhydrogenic <i>f</i> -orbitals	No	No	No	Yes
d-Block-like structure for conduction band	Yes	Yes	Yes	No
Superconductivity	No	No	No	Yes (4.9 K)

point and electronegativity for the first part of the d-block are summarized in Table 2.4. All the properties show that Lu resembles Sc and Y more closely than La.

A comparison of some properties of Sc and Y with those of Lu and La is given in Table 2.5. All these properties favour the placement of lutetium and lawrencium, rather than lanthanum and actinium in group III B.

The revised form of the medium-length form of the periodic table is given in Table 2.6.

## 5. Oxidation states

In general, the most common and stable oxidation state of lanthanides is +3. Examples of lanthanides in +2 oxidation state are LnCl<sub>2</sub> (Ln = Nd, Sm, Eu, Dy, Tm and Yb), LnBr<sub>2</sub> (Ln = Sm, Yb, Eu), LnI<sub>2</sub> (Ln = Nd, Sm, Eu, Dy, Tm, Yb, La, Ce, Pr, Gd), LnF<sub>2</sub> (Ln = Sm, Eu, Yb), LnS, LnSe and LnTe (Ln = Sm, Eu, Tm and Yb), LnSO<sub>4</sub> (Ln = Sm, Eu), LnCO<sub>3</sub> (Ln = Sm, Eu and Yb), EuC<sub>2</sub>O<sub>4</sub>, LnD<sub>2</sub>, LnH<sub>2</sub> (Ln = Eu, Yb). Tetrapositive state containing compounds involving Ce, Pr, Nd, Tb and Dy have been characterized. Some examples are LnF<sub>4</sub> (Ln = Ce, Pr, Tb), LnO<sub>2</sub> (Ln = Ce, Pr, Tb).

The electron configurations of the various oxidation states of lanthanides are given in Table 2.7.

Among the divalent lanthanides Eu(II) is the most stable in aqueous solutions. The +4 oxidation state is relatively stable in the case of Ce, Pr and Tb and the Ce<sup>4+</sup> chemistry is extensive in this group. The ionization of lanthanum can be written as

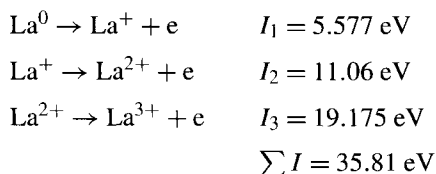


TABLE 2.6

Revised version of the currently popular medium-length block form of the periodic table.

												I H 1.008											2 He 4.003						
		IA IIA												IIIA IVA VA VIA VIIA															
PERIOD	3 Li 6.939	4 Be 9.012											5 B 10.811	6 C 12.011	7 N 14.007	8 O 15.999	9 F 18.998	10 Ne 20.183											
PERIOD	11 Na 22.990	12 Mg 24.312											VIII	IB IIB															
PERIOD	19 K 39.102	20 Ca 40.08	21 Sc 44.956	22 Ti 47.90	23 V 50.942	24 Cr 51.996	25 Mn 54.938	26 Fe 55.847	27 Co 58.933	28 Ni 58.71	29 Cu 63.54	30 Zn 65.37	31 Ga 69.72	32 Ge 72.59	33 As 74.922	34 Se 78.95	35 Br 79.909	36 Kr 83.80											
PERIOD	37 Rb 85.47	38 Sr 87.62	39 Y 88.905	40 Zr 91.22	41 Nb 92.906	42 Mo 95.94	43 Tc <sup>*</sup> [99]	44 Ru 101.07	45 Rh 102.91	46 Pd 106.4	47 Ag 107.870	48 Cd 112.40	49 In 114.82	50 Sn 118.69	51 Sb 121.75	52 Te 127.60	53 I 126.90	54 Xe 131.30											
PERIOD	55 Cs 132.91	56 Ba 137.3	57 La 174.97	58 Ce 176.49	59 Pr 190.95	60 Nd 193.85	61 Pm <sup>*</sup> [160.2]	62 Sm 192.2	63 Eu 195.09	64 Gd 196.97	65 Tb 200.59	66 Dy 204.37	67 Ho 207.19	68 Er 208.98	69 Tm 210	70 Yb <sup>*</sup> [210]	71 Lu <sup>*</sup> 222												
PERIOD	87 Fr <sup>*</sup> [223]	88 Ra <sup>*</sup> 226	103 Lr <sup>*</sup> [261]	104 Ku <sup>*</sup> [260]																									

LANTHANIDE SERIES										57 La 138.91	58 Ce 140.12	59 Pr 140.91	60 Nd 144.24	61 Pm <sup>*</sup> [147]	62 Sm 150.35	63 Eu 151.96	64 Gd 157.25	65 Tb 158.92	66 Dy 162.50	67 Ho 164.93	68 Er 167.27	69 Tm 168.93	70 Yb <sup>*</sup> 173.05
ACTINIDE SERIES										89 Ac <sup>*</sup> 227	90 Th <sup>*</sup> 232.03	91 Pa <sup>*</sup> 231	92 U <sup>*</sup> 238.03	93 Np <sup>*</sup> [237]	94 Pu <sup>*</sup> [242]	95 Am <sup>*</sup> [243]	96 Cm <sup>*</sup> [247]	97 Bk <sup>*</sup> [247]	98 Cf <sup>*</sup> [251]	99 Es <sup>*</sup> [254]	100 Fm <sup>*</sup> [257]	101 Md <sup>*</sup> [258]	102 No <sup>*</sup> [259]

TABLE 2.7

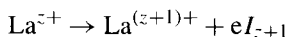
Distinguishing electronic configurations describing best characterized oxidation states.

Symbol	Configuration			
	0	+2	+3	+4
La		5d <sup>1</sup>	6s <sup>2</sup>	4f <sup>0</sup> (La <sup>3+</sup> )
Ce	4f <sup>1</sup>	5d <sup>1</sup>	6s <sup>2</sup>	4f <sup>1</sup> (Ce <sup>3+</sup> ) 4f <sup>0</sup>
Pr	4f <sup>3</sup>		6s <sup>2</sup>	4f <sup>2</sup> (Pr <sup>3+</sup> ) 4f <sup>1</sup>
Nd	4f <sup>4</sup>		6s <sup>2</sup>	4f <sup>3</sup> (Nd <sup>3+</sup> ) 4f <sup>2</sup>
Pm	4f <sup>5</sup>		6s <sup>2</sup>	4f <sup>4</sup> (Pm <sup>3+</sup> )
Sm	4f <sup>6</sup>		6s <sup>2</sup>	4f <sup>5</sup> (Sm <sup>3+</sup> )
Eu	4f <sup>7</sup>		6s <sup>2</sup>	4f <sup>6</sup> (Eu <sup>3+</sup> )
Gd	4f <sup>7</sup>	5d <sup>1</sup>	6s <sup>2</sup>	4f <sup>7</sup> (Gd <sup>3+</sup> )
Tb	4f <sup>9</sup>		6s <sup>2</sup>	4f <sup>8</sup> (Tb <sup>3+</sup> ) 4f <sup>7</sup>
Dy	4f <sup>10</sup>		6s <sup>2</sup>	4f <sup>9</sup> (Dy <sup>3+</sup> ) 4f <sup>8</sup>
Ho	4f <sup>11</sup>		6s <sup>2</sup>	4f <sup>10</sup> (Ho <sup>3+</sup> )
Er	4f <sup>12</sup>		6s <sup>2</sup>	4f <sup>11</sup> (Er <sup>3+</sup> )
Tm	4f <sup>13</sup>		6s <sup>2</sup>	4f <sup>12</sup> (Tm <sup>3+</sup> )
Yb	4f <sup>14</sup>		6s <sup>2</sup>	4f <sup>13</sup> (Tm <sup>3+</sup> )
Lu	4f <sup>14</sup>	5d <sup>1</sup>	6s <sup>2</sup>	4f <sup>14</sup> (Lu <sup>3+</sup> )

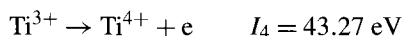
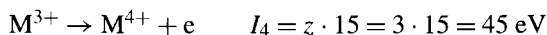
The total ionization energy  $\sum I = 35.81$  eV to be compensated by  $\Delta H_{\text{hydr}}$  which is  $-784$  Kcal/mole and that La(III) aquo ions are stabilized. Further ionization producing La(IV)



involves  $I_4$  of 45.95 eV and cannot be compensated by the additional hydration energy and hence La(IV) is not favoured. As a general rule one can write



and that such a process is not favoured when  $I_{z+1} > z \cdot 12$  eV in the case of lanthanides. Using the empirical rule,  $I_4$  of cerium is 36 eV to 39 eV depending on whether  $z \cdot 12$  or  $z \cdot 13$  is used. This value is close to the experimental value of  $I_4 = 36.76$  eV. In the case of transition metals, the empirical rule may be written as



Instead of considering the total hydration energy of the  $\text{M}^{z+}$  ion, it is possible to consider the difference in hydration energy of  $\text{M}^{(z-1)+}$  and  $\text{M}^{z+}$  ions to compare them with  $I_z$ . Then we may write [3]

$$I_{\text{ch}} = E^0 + 4.5 \text{ eV} = I_z - (2z - 1)k,$$

where  $k = 5.3$  eV for 3d elements and 4.3 eV for lanthanides.

Using the empirical equations in the case of Ti(III) and Ce(III) we have

$$\text{Ti(III): } E^0 = 43.27 - 7 \times 5.3 - 4.5 = +1.7 \text{ V}$$

$$\text{Ce(III): } E^0 = 36.76 - 7 \times 4.3 - 4.5 = +2.2 \text{ V}$$

In the case of europium we have

$$\text{Eu(II): } E = 24.7 - 5 \times 4.3 - 4.5 = -1.3 \text{ V (expt. } -0.4 \text{ V)}$$

The ionization energies of lanthanides to yield Ln(III) and Ln(IV) are given in Table 2.8. It is seen from the data that all the ions have a ground state configuration of  $[\text{Xe}]4f^n$  with the exception of  $\text{La}^{2+}$  and  $\text{Gd}^{2+}$ .

There is a regular increase in  $I_3$  and  $I_4$  values with  $f^n$  for  $n = 1$  to 7 and then for  $n = 8$  to 14. The highest values of  $I_3$  correspond to the existence of Eu(II) and Yb(II) and lowest value of  $I_4$  corresponding to the stability of Ce(IV).

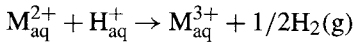
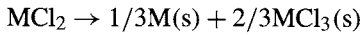
Using  $E^0$  values of  $-0.4$  V for Eu(II) and  $-1.1$  V for Yb(II),  $k$  values may be calculated from the equation

$$k = (I_3 - E^0 - 4.5)/5.$$

TABLE 2.8  
 Ionization energies (in eV) of monoatomic  $4f^4$  systems  $M^{+2}$ ,  $M^{+3}$  and  $M^{+4}$  (the ground states of  $\text{La}^{+2}$  and  $\text{Gd}^{+2}$  would show  $I_3$ , 0.89 and 0.295 eV higher, respectively).

$q$	$R^{+2}$	$I_3$	$R^{+3}$	$I_4$	$R^{+4}$	$I_5$
1	La	18.28	Ce	36.76	Pr	57.53
2	Ce	20.20	Pr	38.98	Nd	60.0
3	Pr	21.62	Nd	40.41	Pm	61.7
4	Nd	22.14	Pm	41.1	Sm	62.7
5	Pm	22.3	Sm	41.37	Eu	63.2
6	Sm	23.43	Eu	42.65	Gd	64.8
7	Eu	24.70	Gd	44.01	Tb	66.5
8	Gd	20.34	Tb	39.79	Dy	62.1
9	Tb	21.91	Dy	41.47	Ho	63.9
10	Dy	22.79	Ho	42.48	Er	65.1
11	Ho	22.84	Er	42.65	Tm	65.4
12	Er	22.74	Tm	42.69	Yb	65.6
13	Tm	23.68	Yb	43.74	Lu	66.8
14	Yb	25.03	Lu	45.19	Hf	68.36

The calculated values of 4.01 and 4.33 eV for Eu(II) and Yb(II) differ by 0.32 eV which can be attributed to decreasing ionic radius. The variation of  $I_3$  along the series is depicted in Fig. 2.4. The variation of  $I_3$  shows irregularities at half-filled shell ( $f^7$ ), three-quarter filled shell and quarter-filled shell. These irregularities are due to discontinuities in the changes in the  $4f$  electron repulsion energy [4]. The  $\Delta G^0$  values refer to



The type of variation of  $I_3$  or  $\Delta G^0$  observed is not seen in the case of reactions such as complex formation between rare earths and EDTA and the enthalpy of formation of trichlorides because in the latter reactions,  $4f$  electrons are conserved.

Deviations from regular smooth variation of properties of lanthanides occur at quarter-, half- and three-quarter filled  $4f$  configurations which have been attributed to tetrad effect. This effect has been attributed to small changes in Racah parameters when the ligands around the metal change during the reactions. The half-filled shell effect and the quarter- and three-quarter shell effects are caused by changes in  $E^1$  and  $E^3$  in the theoretical ionization potential expressions for  $f^n$  ions [4].

$n$	$E$	$n$	$E$	$n$	$E$
1	$U$	6	$U - 5E^0 - 9E^1$	11	$U - 10E^0 - 9E^1$
2	$U - E^0 + 9E^3$	7	$U - 6E^0$	12	$U - 11E^0 - 9E^1 - 12E^3$
3	$U - 2E^0 + 12E^3$	8	$U - 7E^0 - 9E^1$	13	$U - 12E^0 - 9E^1 - 9E^3$
4	$U - 3E^0$	9	$U - 8E^0 - 9E^1 + 9E^2$	14	$U - 13E^0 - 9E^1$
5	$U - 4E^0 - 12E^3$	10	$U - 9E^0 - 9E^1 + 12E^2$		



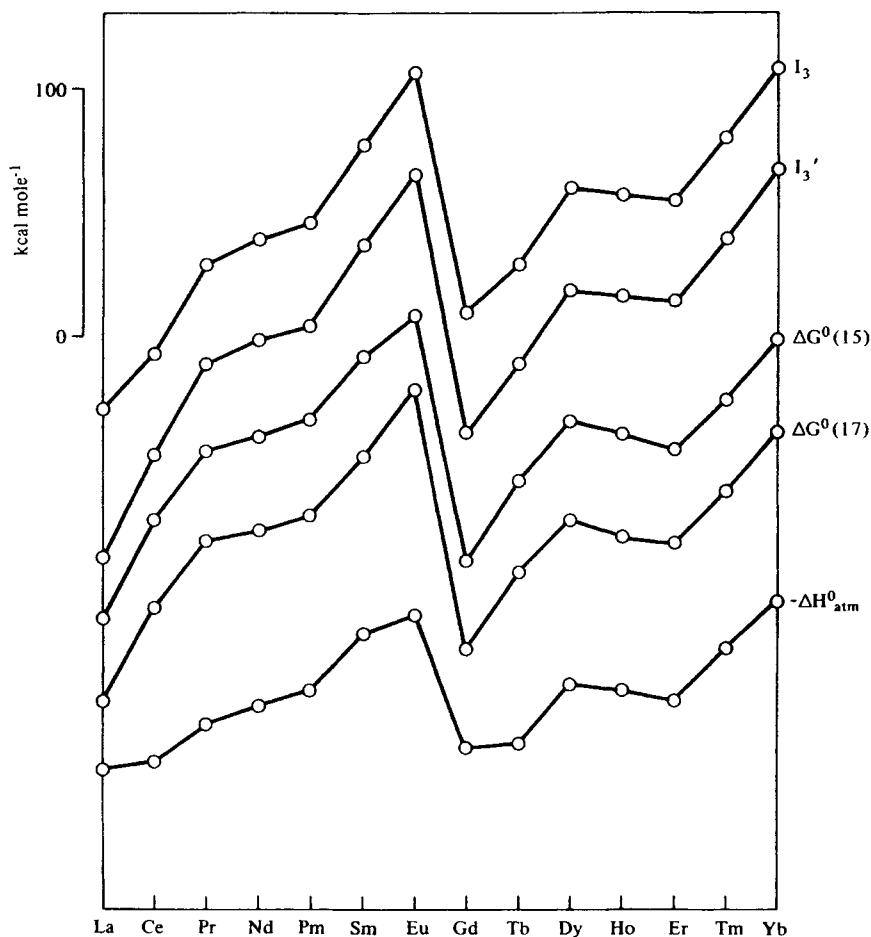


Fig. 2.4. Variations in the energies of various lanthanide processes [4].

The ionization energy  $E$  is the sum of  $U$  the coulombic energy of an  $f$  electron and  $E^0$ ,  $E^1$ ,  $E^2$  and  $E^3$  are the Racah parameters which represent repulsion energy. When  $n = 8$ , we have a term  $-9E^1$  and  $E^3$  at three-quarter shell and these terms are responsible for the observed effects. For configurations  $f^1$  to  $f^7$  exchange energy loss, which is proportional to the number of parallel spin interactions that are destroyed, increases from 0 to 6. In  $f^8$  configuration the spin of the eighth electron is opposed to the other seven electrons and when  $f^8$  ionizes no parallel spin interactions are destroyed. The 0–6 pattern repeats for  $f^8$  to  $f^{14}$  and this accounts for the half-filled shell effect. Thus the variation of  $I_3$  can be understood in terms of increasing nuclear charge and exchange energy losses.

In lanthanide compounds such as  $\text{LnBr}_3$  the absorption spectra contain bands in the charge transfer region involving electron transfer from ligand to metal. From energies of electron transfer bands it is possible to relate the redox potential with the electron transfer bands. This type of relationship leads to  $E^0[\text{Tm}^{3+}/\text{Tm}^{2+}] = -2.5 \text{ V}$ ,  $E[\text{Pr}^{4+}/\text{Pr}^{3+}] =$

TABLE 2.9  
Values of  $E^0[M^{3+}/M^{2+}]$  estimated by spectroscopic correlation.

M	$E^0[M^{3+}/M^{2+}]$ (V) <sup>a</sup>	M	$E^0[M^{3+}/M^{2+}]$ (V) <sup>a</sup>
La	(-3.1)	Gd	(-3.9)
Ce	(-3.2)	Tb	(-3.7)
Pr	(-2.7)	Dy	(-2.6)
Nd	(-2.6)	Ho	(-2.9)
Pm	(-2.6)	Er	(-3.1)
Sm	-1.55	Tm	(-2.3)
Eu	-0.35	Yb	-1.15

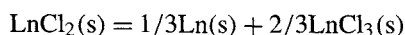
<sup>a</sup>Estimated values are in parentheses.

TABLE 2.10  
Thermodynamic properties lanthanide redox processes [4].

M	$\Delta G^0$ (kcal mole <sup>-1</sup> )	$E^0[M^{3+}/M^{2+}]'$ (V)	$E^0[M^{3+}/M^{2+}]$ (V)
La	(-73)	(-5.8)	(-3.8)
Ce	(-33)	(-4.2)	(-3.5)
Pr	(-6)	(-3.0)	(-3.0)
Nd	(0 ± 4)	(-2.8)	(-2.8)
Pm	(7)	(-2.5)	(-2.5)
Sm	32 ± 5	-1.50 ± 0.2	-1.50 ± 0.2
Eu	(48 ± 3)	-0.35 ± 0.03	-1.50 ± 0.03
Gd	(-50)	(-4.9)	(-3.6)
Tb	(-17)	(-3.5)	(-3.5)
Dy	(6)	(-2.6)	(-2.6)
Ho	(1)	(-2.9)	(-2.9)
Er	(-6)	(-3.0)	(-3.0)
Tm	(15)	(-2.1)	(-2.1)
Yb	38 ± 5	-1.10 ± 0.1	-1.10 ± 0.1

3.2 V and  $E[Tb^{4+}/Tb^{3+}] = 3.1$  V. The important point involved in this method is the linear relationship between charge transfer band energies and redox potentials. Some data obtained in this way are given in Table 2.9.

An alternate approach involving thermodynamic calculation for the reaction



leads to  $\Delta G^0$  and  $E[M^{3+}/M^{2+}]$  values given in Table 2.10.

### 5.1. Oxidation states of the lanthanides

It is clear that both the thermodynamic and spectroscopic approaches agree well with respect to the estimation of redox potentials and stabilities of lanthanides in different oxidation states.

## 6. Size variation in lanthanides

The variation of atomic and crystal radii of Lanthanides along with those of Sc and Y is obvious from the data in Table 2.11 and Fig. 2.5.

There is a regular increase in both atomic radius and crystal radius with an increase in atomic number as exemplified by Sc(21), Y(39) and La(57). As one progresses further, both atomic and crystal radii decrease with increasing atomic number with the exception of atomic radii of Eu and Yb. The observed decrease in size is known as the lanthanide contraction. The lanthanide contraction is attributed to imperfect shielding of one  $f$  electron by another  $f$  electron. As the nuclear charge and  $4f$  electron population increase, imperfect shielding due to the directional nature of the orbitals results in each  $4f$  electron being pulled towards the nucleus. This results in contraction of the  $4f^n$  disposition and hence a decrease in the size of atoms and ions. The contraction is evident in  $\text{Ln}^{3+}$  ions with the exception of  $\text{Gd}^{3+}$  ion which has a half-filled shell  $f^7$ . A similar trend is observed with  $\text{Ln}^{2+}$  and  $\text{Ln}^{4+}$  ions although the data are limited. Anomalous positions of Eu and Yb in the atomic radii are worth noting.

TABLE 2.11  
Atomic and crystal radii.

Atomic number	Symbol	Atomic radius <sup>a</sup> (Å)	Crystal radius (Å)		
			+2 <sup>b</sup>	+3 <sup>c</sup>	+4 <sup>b</sup>
21	Sc	1.641 (a)		0.68 <sup>b</sup>	
39	Y	1.801 (a)		0.88 <sup>b</sup>	
57	La	1.877 (a)		1.061	
58	Ce	1.824 $\gamma$		1.034	0.92
59	Pr	1.828 (a)		1.013	0.90
60	Nd	1.821		0.995	
61	Pm	(1.810) <sup>d</sup>		(0.979) <sup>d</sup>	
62	Sm	1.802 (a)	1.11	0.964	
63	Eu	2.042	1.09	0.950	
64	Gd	1.802 (a)		0.938	
65	Tb	1.782 (a)		0.923	0.84
66	Dy	1.773		0.908	
67	Ho	1.766		0.894	
68	Er	1.757		0.881	
69	Tm	1.746	0.94	0.869	
70	Yb	1.940 (a)	0.93	0.858	
71	Lu	1.734		0.848	
89	Ac	1.878		1.11 <sup>b</sup>	

<sup>a</sup>For coordination number = 12 and modification listed. Non-hexagonal crystal structures =  $\gamma$ -Ce, fcc; a-Sm, rhomb; Eu, bcc; a-Yb, fcc; Ac, fcc. Data from A.H. Daane, in: The Rare Earths, John Wiley, New York (1961), Ch. 13; K.A. Gschneider, *ibid.*, Ch. 14 (see Table 22).

<sup>b</sup>W.H. Zachariasen, in: The Actinide Elements, McGraw-Hill, New York (1954), p. 775.

<sup>c</sup>D.H. Templeton and C.H. Dauben, *J. Am. Chem. Soc.* 76 (1954) 5237.

<sup>d</sup>Estimated.

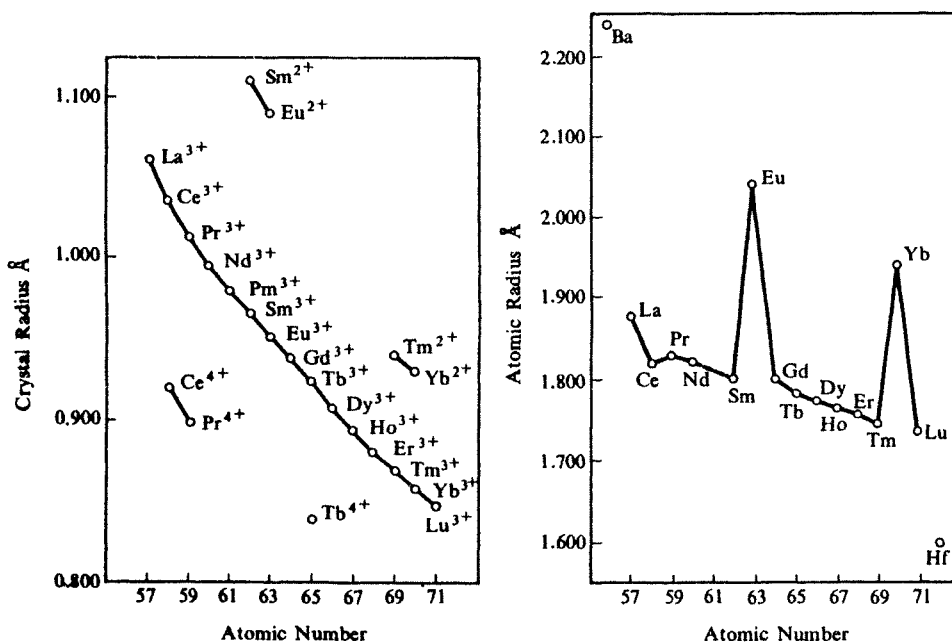


Fig. 2.5. Variations in atomic and crystal radii. *The Chemistry of the Lanthanides*, Reinhold Book Corporation, New York (1963), pp. 21, 22.

The implications [6] of the explanation of the lanthanide contraction given above are (i) the size of the lanthanide atoms or ions is determined by the  $4f^n$  subshell and (ii) the contraction of the size is due to the angular part of the  $4f$  wave functions. These implications have recently been questioned and it is useful to examine the problem in some detail.

The decrease in radius in moving from  $\text{La}^{3+}$  to  $\text{Lu}^{3+}$  is 117.2 to 100.1 pm which is less than 114–88 pm for elements  $\text{Ca}^{2+}$  to  $\text{Zn}^{2+}$ . In the case of  $\text{Sc}^{3+}$  to  $\text{Ga}^{3+}$ , the radius decreases from 88.5 to 76 pm. This comparison shows that the percent contraction is greater in the case of  $\text{Sc}^{3+}$  to  $\text{Ga}^{3+}$  and  $\text{Ca}^{2+}$  to  $\text{Zn}^{2+}$  series than lanthanides series. The fact is that the magnitude of the lanthanide contraction is small and the usual interpretation of magnetic and spectroscopic properties of the lanthanides are inconsistent with the idea of considerable shielding of  $4f$  electrons from the chemical environment of the ion by the  $5s^25p^6$  configuration. Thus the implication that the size of lanthanide atoms or ions is determined by the  $4f^n$  subshell must be incorrect.

In the third transition series the  $4f$  shell is complete and has spherical symmetry and angular effect. Any effect must be due to the radial part of the appropriate wave functions. Thus so far as the effects on the third series of transition elements are concerned the second implication that the contraction is due to the angular part of the  $4f$  wave functions does not appear to be convincing.

Using Slater's rules the radius  $R_m$  of the maximum is a spherical charge density function which can be calculated using the formula

$$R_m = n^{*2} Z^{*-1} \times 52.9 \text{ pm},$$

where  $Z^*$  and  $n^*$  are the effective nuclear charge and effective quantum number, respectively. In the case of  $\text{Gd}^{3+}$ ,  $R_m = (5p^6)$  69 pm and  $(4f^7)$  24 pm which means  $4f^7$  is located deep inside the ions.  $R_m$  for  $4f^n$  is slightly more than one-third of that of  $5p^6$ . The radius of  $f$  shell falls by the 32 percent in going from  $\text{Ce}^{3+}$  to  $\text{Ln}^{3+}$  (35.6 to 24.4 pm) which is greater than 21% in the case of  $5p^6$  (80.0 to 63.2 pm). From this it is clear that the  $f$  shell contracts rapidly well inside the outermost core electrons.

For Gd the ratio of the electron densities of  $4f^7/(5p^6 + 5s^2) + 0.21$  at  $R_m$  ( $5p^6$ ) decreases to 0.07 at the ionic radius of Gd. Thus  $4f^7$  contributes 10% to the electron density in the outer regions which is not a negligible contribution to the size. Although this is the case  $5s^2 5p^6$  configurations is a radius-determining configuration with minor contribution from  $4f$  which increases along the series. As the  $f$  shell occupancy increases more rapidly than  $f$  orbital density and the ionic radius decreases from the contraction, the small effects of  $f$  electrons act in opposition to the contraction.

Having shown the angular part of the  $4f$  wave functions to be insignificant, the explanation for the contractions may be sought in the radial part of the wave function. There is only one radial maximum for  $4f$ , and within  $R_m(4f)$  there will be small shielding of other electrons by  $4f$  electrons. The third radial maximum of  $5p^6$  and the fourth radial maximum of  $5s$  orbitals lie inside the maximum of  $4f$ . Thus there is penetration of  $5s$  and  $5p$  orbitals into  $4f$  and consequent dependence of size on nuclear charge. Thus the lanthanide contraction may be viewed as penetration effects on size and orbital energies of polyelectronic atoms. In terms of shielding, the significant shielding is for  $5s^2 5p^6$  configuration and not for  $4f$  electrons.

## 7. Interconfigurational fluctuations and their consequences [7]

In the case of normal rare earth intermetallic compounds, it is quite plausible to assume that the rare earth has well-defined  $4f^n$  configuration with an oxidation state of +3. Thus the behaviour of the rare earth ion in a metallic system is similar to insulators. The  $4f$  electrons are strongly correlated in atomic type configurations characterized by total angular momentum quantum levels,  $J$  in accordance with Hund's rules.

Rare earth ions interact with conduction electrons giving rise to spin density oscillations in the conduction electron cloud which is responsible for the magnetic ordering of rare earth metals. The interaction, however, does not result in appreciable width of the energy levels of the ion. As a first approximation, the rare earth metallic system can be considered as an assembly of rare earth ions with a well-defined magnetic moment interacting among themselves through the conduction electrons.

The above description of intermetallics has proved to be inadequate in the case of some intermetallic compounds of Ce, Sm, Eu, Tm and Yb. The experimental data in these systems suggest that the rare earth ions fluctuate between two electronic configurations of  $4f^n$  and  $4f^{n-1}$  but appear identical in time average. An important consequence of

the fluctuation of configuration is the demagnetization of the  $4f$  shell with TmSe as an exception. This phenomenon exhibited by rare earth ions is referred to in the literature in many ways, namely valence fluctuations, interconfiguration fluctuation, mixed valence and intermediate valence. On an average, the rare earth ion in such a context has a non-integral  $4f$  electron occupancy which reflects itself in many physical properties such as lattice parameters, magnetic susceptibility, Mössbauer isomeric shift and Hall coefficient. Ce metal and SmS are the two best studied systems exemplifying interconfiguration fluctuations.

Many models have been postulated to account for the interconfiguration fluctuations (ICF) in rare earth intermetallic compounds. We will consider Hirst's model which assumes that the  $4f$  electrons are highly correlated and preserve their atomic-like features during the valence fluctuation. Both the X-ray photoelectron spectra and the magnetic susceptibility of rare earth intermetallic compounds can be successfully explained on the basis of Hirst's model [8,11].

### 8. Hirst's model

The Hamiltonian of the  $4f$  rare earth ions may be written as

$$\mathcal{H} = \mathcal{H}_{\text{ion}} + \mathcal{H}_{\text{intra}} + \mathcal{H}_{\text{inter}}$$

and

$$\mathcal{H}_{\text{ion}} = -V_n + U_n(n-1)/2,$$

where  $\mathcal{H}_{\text{intra}}$  represents the energy involving interactions giving rise to metal-like  $L$ ,  $S$  terms and crystal field splittings of  $J$  levels,  $\mathcal{H}_{\text{inter}}$  is the energy of interaction between conduction electrons and the localized  $4f$  electrons,  $-V_n$  is the attractive potential energy of  $n$   $4f$  electrons on the rare earth ion and  $U_n(n-1)/2$  is the coulomb repulsion among the  $4f$  electrons taken as pairs.

Let us consider an assembly of rare earth ions placed in a sea of nearly free conduction electrons. Let  $E_{\text{exc}}^-$  be the energy required for the process

$$4f^n \rightarrow 4f^{n-1} + e$$

and the released electron be placed at the Fermi level  $E_F$  of the conduction band. This process is shown in Fig. 2.6.

The figure shows both  $4f^n \rightarrow 4f^{n-1}$  and  $4f^n \rightarrow 4f^{n+1}$  transitions and the energies involved in the transitions may be written as

$$E_{\text{exc}}^- = (E_{n-1} - E_n) + E_F$$

$$E_{\text{exc}}^+ = (E_{n+1} - E_n) - E_F$$

where  $E_{n-1}$ ,  $E_{n+1}$  and  $E_n$  are the energies of ground states of  $4f^{n-1}$ ,  $4f^{n+1}$  and  $4f^n$  configurations, respectively. The particular  $4f^n$  configuration is stable when the energies

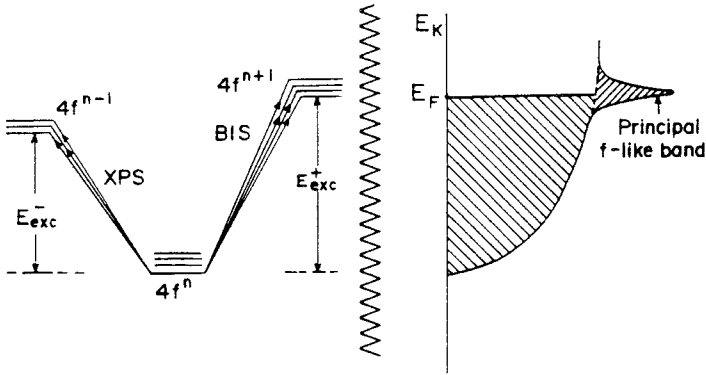


Fig. 2.6. Configuration-based energy levels of a rare earth ion with stable configuration  $4f^n$ . The  $4f^n \rightarrow 4f^{n-1}$  transitions are the XPS transitions whereas the  $4f^n \rightarrow 4f^{n+1}$  transitions are BIS transitions.

are favourable (i.e.) when  $E_{exc}^-$  and  $E_{exc}^+$  are positive. When  $E_{exc}^-$  or  $E_{exc}^+$  approaches zero the rare earth ion is considered to be at 'configuration crossover' and the transitions



are favoured with the electron emission or absorption in the sea of conduction electrons and  $E_{exc}^-$  and  $E_{exc}^+$  varies between a positive value and negative value.

We now turn to the interaction between the conduction electrons and the  $4f$  electrons of the rare earth ions. The strength of the interaction,  $\Delta$  is of the order of 0.1 eV. This interaction results in introduction of a small width to the energy levels of localized and highly correlated  $4f$  electrons. However when the rare earth ion is at the point of configuration crossover, this interaction produces a strong mixing between  $4f^n$  and  $4f^{n-1}$  or  $4f^n$  and  $4f^{n+1}$  as the case may be. The main criterion for the stability of  $4f^n$  configuration against fluctuations may be stated as

$$E_{exc}^\pm > \Delta \quad \text{and not} \quad U > \Delta.$$

Although  $U$  is of the order of 10 eV, the rare earth ion experiences rapid inter-configurational fluctuations if  $E_{exc}^\pm \sim \Delta$ . The large value of  $U$  (10 eV) in comparison to 0.1 eV for  $\Delta$  is responsible for preserving the atomic-like features of the rare earth ion during the interconfigurational fluctuations.  $\mathcal{H}_{\text{Inter}}$  causes strong mixing between the two configurations which gives rise to a narrow  $f$ -like band at the Fermi level, named by Hirst as the principal band. This band is due to the fact that the rare earth ion is at the point of configuration crossover and is typical of systems undergoing interconfiguration fluctuations. The density of states  $\rho(E)$  of such a system would appear like Fig. 2.6, namely a smooth function superimposed with a pronounced peak maximum at energy,  $E = E_F$ , where  $E_F$  refers to Fermi level.

According to the model the period  $\tau$  of the interconfigurational fluctuation is given by the width,  $dE(\approx h\tau)$  of the principal band. The average valence  $V$  is given by

$$\tau \bar{v} = n\tau_n + (n-1)\tau_{n-1},$$

where  $\tau_n$  and  $\tau_{n-1}$  are the residence times of the rare earth ion in  $4f^n$  and  $4f^{n-1}$  configurations.

Rare earth compounds exhibiting intermediate valence are common in the case Ce, Sm, Eu, Tm and Yb. Ce and Yb form compounds which exhibit intermediate valence more often than other rare earths. Typical examples of Ce compounds are CePd<sub>3</sub>, CeSn<sub>3</sub>, CeAl<sub>3</sub>, CeN and CeB<sub>4</sub>. Some of the compounds exhibiting intermediate valence are [9] YbAl<sub>2</sub>, YbCu<sub>2</sub>Si<sub>2</sub>, Yb<sub>4</sub>Sb<sub>3</sub>; EuCu<sub>2</sub>Si<sub>2</sub>, EuRh<sub>2</sub>, SmS, TmSe. There are two methods by which a rare earths ion attains the interconfiguration fluctuation state namely: (i) by varying temperature and pressure and (ii) alloying with other material. Ce metal and SmS are examples where ICF occurs by alloying with another material as well as by varying conditions such as variation of temperature and pressure.

In the case of Sm metal, the Sm atoms on the surface are in +2 state and the Sm atoms in the interior in +3 state. This observation shows that the energy  $E_{exc}^+$  which stabilizes the +3 state in the bulk and prevents it in going to +2 state, experience a reduction at the surface thereby placing the Sm atoms at the configuration crossover. A similar phenomenon has also been observed in the case of Yb ions in YbAu<sub>2</sub>.

Fine particles of metallic Eu and Yb have been shown to exhibit valence transition with critical particle sizes of 50 Å for Eu and 35 Å for Yb. At these critical particle sizes, there is a reduction in the lattice constant with no change in the critical fcc structure. There appears to be a change in valence from +2 to +3. This effect may be due to a shift in the position of Fermi level,  $E_F$  such that  $E_{exc}^-$  approaches zero resulting in the ions at the configuration crossover. ICF state can in general result in lattice constant anomaly due to the fractional occupation of the  $4f$  shells. Thus once ICF is identified in a system, valence fluctuation can be studied by many techniques.

The methods by which the phenomenon of interconfiguration fluctuations may be studied are: (i) determination of lattice constant, (ii) magnetic susceptibility measurements, (iii) Mössbauer spectroscopy, (iv) measurement of electrical resistivity, (v) Hall effect, (vi) X-ray absorption spectroscopy and (vii) X-ray photoelectron emission spectroscopy. It is useful to note that a suite of techniques must be used to detect ICF phenomenon in a system. Nuclear magnetic resonance is sparingly used because not all the systems exhibiting ICF contain magnetically active nuclei.

The utility of some of the methods in the study of materials exhibiting ICF can be illustrated by considering the well-known compounds EuCu<sub>2</sub>Si<sub>2</sub> and YbCu<sub>2</sub>Si<sub>2</sub>. The average valence of Eu in EuCu<sub>2</sub>Si<sub>2</sub> depends upon temperature and pressure while that of Yb in YbCu<sub>2</sub>Si<sub>2</sub> is nearly independent of temperature and pressure. These compounds are tetragonal with a space group  $D_{4h}$  and resemble ThCr<sub>2</sub>Si<sub>2</sub> structure and have two chemical formulae per unit cell. The four copper atoms in the unit cell are equivalent and results in one resonance signal for each copper nucleus in the nuclear magnetic spectrum (NMR). Quadruple interaction in SmCu<sub>2</sub>Si<sub>2</sub>, EuCu<sub>2</sub>Si<sub>2</sub> and YbCu<sub>2</sub>Si<sub>2</sub> compounds [10] has been



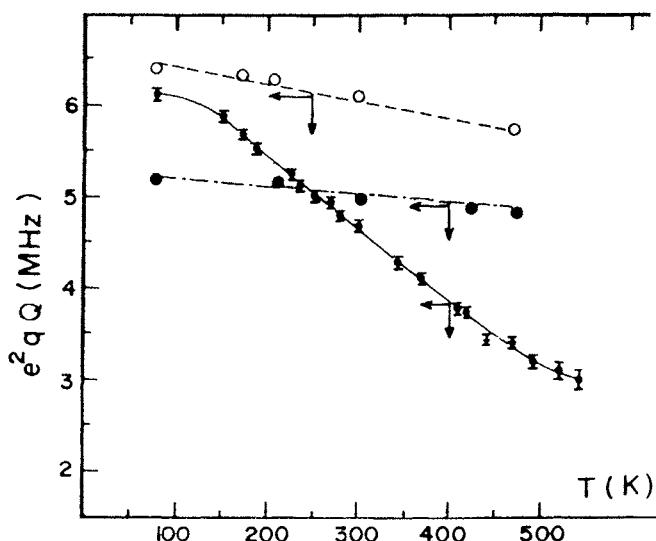


Fig. 2.7. Temperature dependence of quadrupole coupling constant  $e^2qQ$  of  $^{63}\text{Cu}$ ;  $\circ$ ,  $\text{SmCu}_2\text{Si}_2$ ;  $\Phi$ ,  $\text{EuCu}_2\text{Si}_2$ ;  $\bullet$ ,  $\text{YbCu}_2\text{Si}_2$ .

studied. The NMR signal splits into 21 components and the interaction frequency is given by

$$\omega_Q = 3e^2qQ/21(21 - 1)\hbar$$

and the Larmor precession frequency by

$$\omega_L = \gamma H_0.$$

When the interaction frequency  $\omega_Q$  is not small in comparison to the Larmor precession frequency,  $\omega_L$ , the resonance transitions other than the principal one,  $1/2 \leftrightarrow -1/2$  are generally difficult to observe. In such a situation the value of  $e^2qQ$  is obtained from the splitting of the principal transition. The values of  $e^2qQ$  obtained as a function of temperature are plotted in Fig. 2.7.

From NMR Spectra obtained as a function of temperature and applied field, the values of electric field gradient (EFG) represented as  $e^2qQ$  in MHz are obtained. EFG values plotted as a function of temperature in Fig. 2.7 for  $\text{EuCu}_2\text{Si}_2$  show strong temperature dependence while  $\text{YbCu}_2\text{Si}_2$  and  $\text{SmCu}_2\text{Si}_2$  show a slight temperature dependence. The electric field gradient fluctuations are due to rare earth charge fluctuations which have a frequency of about  $\sim 10^{12}/\text{s}$ . The NMR signal is due to the average EFG at the Cu nuclide. The average valence in  $\text{YbCu}_2\text{Si}_2$  is independent of temperature while  $\text{EuCu}_2\text{Si}_2$  exhibits strong dependence on temperature. The anomalous temperature dependence of  $\text{EuCu}_2\text{Si}_2$  is due to the dependence of average valence on temperature although both Eu and Yb compounds are ICF Systems.

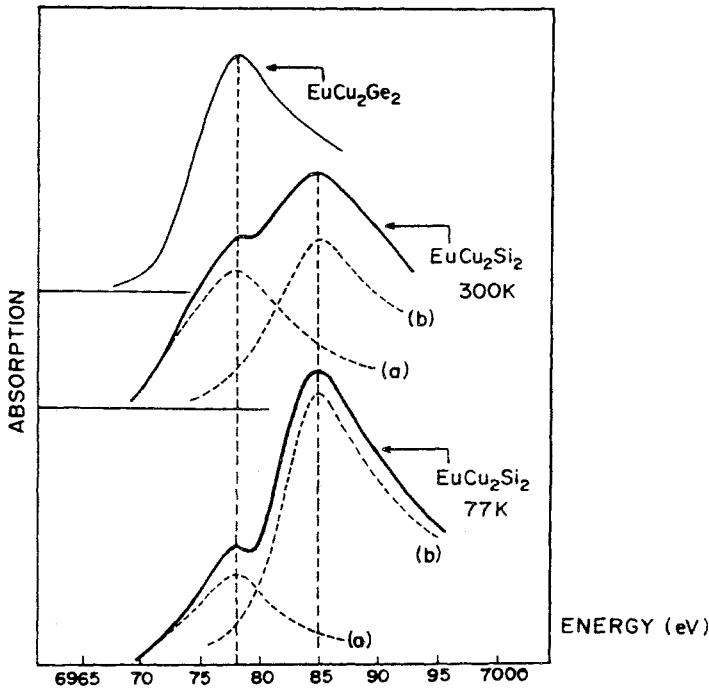


Fig. 2.8. The X-ray absorption spectrum of the mixed valence system  $\text{EuCu}_2\text{Si}_2$  at 300 and 77 K. The peaks (a) and (b) of the deconvoluted profiles refer to  $\text{Eu}^{2+}$  and  $\text{Eu}^{3+}$ , respectively.  $\text{EuCu}_2\text{Ge}_2$  has been chosen as the reference for divalent europium [9].

In the case of the single phase alloy  $\text{Sm}_{0.5}\text{Yb}_{0.5}\text{Cu}_2\text{Ge}_2$  the NMR signal due to copper was not detected and the resonance line broadening beyond the point of detection due to spatial fluctuation of EFG at the copper nuclei explains the reason why rare earths in  $\text{EuCu}_2\text{Si}_2$  and  $\text{YbCu}_2\text{Si}_2$  'appear' identical to the copper nuclei.

Knight shifts (K.S.) also provide useful information on the magnetic state of the rare earths ion in compounds of the type  $\text{CePt}_{2-x}\text{Rh}_x$ . Cerium is trivalent in  $\text{CePt}_2$  and nearly tetravalent in  $\text{CeRh}_2$ . In mixed alloys  $\text{CePt}_{2-x}\text{Rh}_x$  cerium is expected to be in an intermediate valence state (i.e.) between 3 and 4. With alloys  $0 \leq x \leq 0.75$ , the knight shift of  $^{195}\text{Pt}$  has been found to be the same as in  $\text{CePt}_2$ , with a positive value and temperature dependent. This signifies with alloys,  $0 \leq x \leq 0.75$  cerium is in the trivalent state. When the alloys with  $1.25 \leq x \leq 1.75$  the Knight shift was small and independent of temperature signifying the presence of tetravalent cerium.

X-ray absorption edge studies [9] on  $\text{EuCu}_2\text{Si}_2$ ,  $\text{YbCu}_2\text{Si}_2$  and  $\text{Sm}_4\text{Bi}_3$  show in general absorption profiles consisting of two peaks which can be further resolved into two absorption edges belonging to two valence states of the rare earth under consideration. The X-ray absorption spectrum of the mixed valence systems  $\text{EuCu}_2\text{Si}_2$  at 300 and 77 K is shown in Fig. 2.8. For comparison, the reference spectrum of  $\text{EuCu}_2\text{Ge}_2$  is also shown. The peaks (a) and (b) of the deconvoluted profiles correspond to  $\text{Eu}^{2+}$  and  $\text{Eu}^{3+}$  states, respectively. As is obvious the +3 state peak intensity increases and the +2 state peak

intensity decreases when the temperature decreases from 300 to 77 K. In the case of  $\text{Sm}_4\text{Bi}_3$  the ratio of peak intensities of +2 to +3, states of 3:1 was observed showing the formula of  $\text{Sm}_4\text{Bi}_3$  to be  $\text{Sm}_{\frac{2}{3}}^{2+}\text{Sm}_{\frac{1}{3}}^{3+}\text{Bi}_3$  rather than  $\text{Sm}_{\frac{2}{3}}^{2+}\text{Sm}_{\frac{1}{3}}^{3+}\text{Bi}_3$ .

## 9. Ionic radii and coordination number $N$

In the chemistry of rare earths one frequently encounters statistically disordered, non-stoichiometric compounds, even of cubic symmetry [3]. It is obvious that many inorganic compounds do not contain distinct molecules. Considering  $\text{NaCl}$  as an example, each  $\text{Na}^+$  ion is surrounded by six  $\text{Cl}^-$  ions in an octahedral disposition and each  $\text{Cl}^-$  ion is surrounded by an octahedron of six  $\text{Na}^+$  ions. Thus the coordination number is 6 for both the cation and anion. In  $\text{CsCl}$  both cation and anion have  $N = 8$ . In a way  $\text{CaF}_2$  can be considered as a super-structure of  $\text{CsCl}$  lacking half the cations but retaining cubic symmetry. In  $\text{CaF}_2$ ,  $\text{Ca}^{2+}$  has  $N = 8$  with  $8\text{F}^-$  ions forming a cube and  $\text{F}^-$  ions have  $N = 4$  with 4  $\text{Ca}^{2+}$  ions forming a tetrahedron. Many  $\text{CaF}_2$ -type minerals are non-stoichiometric and yttrifluorite is an example ( $\text{Ca}_{1-x}\text{Y}_x\text{F}_{2+x}$ ). In this mineral  $x = 0.3$  and the excess fluoride is situated on the empty cation positions. Normally anion deficiency is observed as in the case of thorinite,  $\text{Th}_{1-x}\text{R}_x\text{O}_{2-0.5x}$  where  $\text{R} =$  lanthanides. Disordered fluorite structure occurs in  $\text{Er}_{0.5}\text{Zr}_{0.5}\text{O}_{1.75}$  which lacks an eighth of an oxide. The compound  $\text{Dy}_2\text{Zr}_2\text{O}_7$  has a cubic superstructure of fluorite, pyrochlore where  $\text{Dy(III)}$  has  $N = 8$  in a distorted cube and  $\text{Zr(IV)}$  has  $N = 6$  in a distorted octahedron. The pyrochlore structure of  $\text{Er}_2\text{Ti}_2\text{O}_7$  has  $\text{Ti(IV)}$  pulling oxide anions away from  $\text{Er(III)}$ . Some disordered mixed oxide structures have epitaxial layer structures.

Considerations of crystal structures of compounds of rare earths show small and systematic deviations from high symmetries. Perovskites of the formula  $\text{RMO}_3$  when  $\text{R(III)}$  is large and  $\text{M(III)}$  is small have non-cubic symmetry.  $\text{LaRO}_3$ , where  $\text{R} = \text{Er, Tm, Yb}$  belong to perovskite group but decompose above  $650^\circ\text{C}$  giving rise to mixed oxides. Perovskites of the type  $\text{La}_{1-x}\text{Eu}_x\text{AlO}_3$  have low local symmetry and  $N = 12$  does not mean roughly equal  $\text{La-O}$  distances.

The three types of oxides are: (i) hexagonal A-type  $\text{R}_2\text{O}_3$ , where  $\text{R}$  has  $N = 7$  with two triangles in planes perpendicular on the axis containing the seventh neighbour atom; the oxides readily dissolve in acids; (ii) complicated low-symmetry B-type and (iii) cubic C-type with  $N = 6$  also exemplified by  $\text{Sc}_2\text{O}_3$  do not dissolve in acids readily. A quarter of  $\text{M}$  (metal) in C-type is surrounded similar to  $\text{Ti}$  in pyrochlore  $\text{Er}_2\text{Ti}_2\text{O}_7$  while the remaining metal has six oxide neighbours very far from forming a regular octahedron. These irregular structures are much more regular when seen from the point of view of the oxygen atom. Actually these oxides have to a good approximation four atoms of  $\text{M}$  in a circumscribing regular tetrahedron as is the case in basic beryllium acetate  $\text{Be}_4\text{O}(\text{CH}_3\text{COO})_6$  which has a hexagonal structure. In the case of  $\text{Cr}_2\text{O}_3$ ,  $\text{Fe}_2\text{O}_3$  and  $\text{Ga}_2\text{O}_3$ , we have  $N = 4$  for oxide,  $N = 6$  for  $\text{M(III)}$  which is closer to octahedron than in the case of C-type rare earth oxides. In general, in a compound  $\text{M}_a\text{X}_b$ , where all  $\text{M}$  atoms and  $\text{X}$  atoms are equivalent.

$$N \text{ (number of M-X contacts) for M} = b/aN_x.$$

It should be noted the coordination number,  $N$  for trivalent lanthanides does not bear the same relevance and context as the transition elements, Fe(3d), Pd(4d) and Pt(5d). The  $4f^n$  electron population does not influence  $N$  in moving along the lanthanides series while the d electron population has considerable influence on  $N$  in the transition metals. Taking nickel as an example we have compounds of Ni(IV), Ni(III), Ni(II) and Ni(0). The majority of the compounds are of Ni(II) such as  $\text{Ni}(\text{H}_2\text{O})_6^{2+}$ ,  $\text{Ni}(\text{NH}_3)_6^{2+}$  which have  $N = 6$  and an octahedral disposition. The compound  $\text{KNiF}_3$  is a cubic perovskite with  $N = 6$  and also paramagnetic. When Ni(II) forms diamagnetic complexes  $N = 4$  with a square planar disposition. Tetrahedral  $\text{NiCl}_4^{2-}$  with  $N = 4$  tetragonal-pyramidal  $\text{Ni}(\text{CN})_5^{3-}$  with  $N = 5$  are also known.

Unlike d transition elements,  $4f$  orbitals in rare earths hardly have any influence on bonding in trivalent lanthanide compounds. This does not mean that covalent bonding does not play a role, but it is difficult to obtain evidence for such a situation. Consider the dissolution of strongly calcined  $\text{CeO}_2$  and  $\text{ThO}_2$  in boiling sulphuric acid. The dissolution process is slow and it may be due to the large Madelung potential in the fluorite-type crystals which leads to a high Arrhenius activation energy for dissolution but in part also due to covalent bonding in  $\text{CeO}_2$  and  $\text{ThO}_2$ . The X-ray emission spectra of  $\text{CeO}_2$  and  $\text{ThO}_2$  show evidence of covalent bonding in these oxides involving oxygen 2p orbitals with Ce  $4f$  and Th  $5f$  orbitals. It should be pointed out that it is very difficult to obtain evidence for covalent bonding because in the linear combination of the atomic orbitals (LCAO) model it is due to the five empty 5d orbitals and the empty 6s orbital. Similar difficulty is encountered in explaining covalent bonding in Cu(I), Zn(II) and Ga(III) compounds which may in part be due to empty 4s orbitals and to a lesser extent to the three empty 4p orbitals.

Many models are available to explain the covalent nature of compounds. Molecular orbital (MO) calculations in molecules based on LCAO are not quite satisfactory because they relate to weak effects compared with the binding energy of a nucleus with  $+Z$  charge surrounded by  $Z$  electrons. The binding energies are not much greater than bond disassociation energies and MO approach based on LCAO is not quite satisfactory in explaining the extent of the covalent nature. Valence shell electron-pair repulsion (VSEPR) theory not based on LCAO is quite satisfactory in explaining the behaviour of non-transitional group elements. This theory requires the spherical region of valence shells to be divided between bulky lone-pairs and bonding electron pairs having smaller angular requirements when the other atom has a higher electronegativity. The weakness of this theory is that it is an empirical fact that elements boron to fluorine have four electron pairs while the subsequent elements have six pairs of electrons. This can be rationalized by Kimball's concept of non-overlapping spheres each containing a pair of electrons giving rise to tetrahedral and octahedral distribution of spheres. Kimball's model results in unusually high values of kinetic energy of electrons in the spheres. Changes in kinetic energy have been thought to be the driving force behind covalent bonding. Kinetic operator and the Virial theorem which states that the electronic kinetic energy in any stationary state cancels exactly half the potential energy determine the average radius of 1s electron in a hydrogen atom. The main difficulty in describing in terms of electron pairs is that we are not certain that all chemical bonds can be assigned two electrons in a significant way. According to the 18-electron rule,  $N$  of  $d^n$  systems is  $\frac{1}{2}(18 - n)$  when  $n$  is even. This rule has enjoyed some success in organometallic complexes but there are many exceptions

like square planar  $d^8 \text{Ni}(\text{CN})_4^{2-}$  and linear  $d^{10} \text{Cu}(\text{CN})_2^-$ . And there are difficulties in assigning  $2N$  electrons to covalent bonding resulting in NaCl-type oxides, nitrides and carbides (NiO, LaN, HfC) which have  $N = 6$  in excess of 4 valence orbitals and in  $\text{CaF}_2$ -type  $\text{Be}_2\text{C}$  with  $N = 8$  for carbon.

The coordination number,  $N$  of lanthanides varies significantly and no intrinsic property of  $4f$  group atoms predetermines a high propensity for a given  $N$  value and symmetry as is common with transition elements like  $3d^3 \text{Cr(III)}$ ,  $3d^6 \text{Co(III)}$ ,  $3d^8 \text{Ni(II)}$ ,  $4d^6 \text{Rh(III)}$ , and  $5d^6 \text{Ir(III)}$  and  $\text{Pt(IV)}$ . In the case of lanthanides,  $N$  takes on values from 3 to 16 as shown by examples given below.

$N = 3$	$\text{RBr}_3, \text{RI}_3, \text{RN}_3$
$N = 4$	$\text{LuC}_4\text{Er(III)S}_4$
$N = 6$	$\text{RCl}_6^{3-}, \text{RBr}_6^{3-}, \text{RI}_6^{3-}, \text{Cs}_2\text{NaEuCl}_6$
$N = 7, 8, 9$	
$N = 12$	$[\text{Mg}(\text{H}_2\text{O})_6^{2+}]_2[\text{R}(\text{O}_2\text{NO})_6^{3-}]_2 \cdot 6\text{H}_2\text{O}$ $\text{Nd(III)O}_{12}$ icosahedron
$N = 16$	$\text{Ce}(\text{C}_8\text{H}_8)_2^-$ $(\text{C}_2\text{H}_5)_3\text{YbCNC}_6\text{H}_{11}$

The electronic densities as determined by X-ray diffraction appear to be superposition of atomic quantities with the exception of the hydrogen atom. Spectroscopic techniques give the instantaneous picture although atoms are in motion. Rotational spectra give a time-average picture. Electron diffraction gives time-average interatomic distances like X-ray diffraction but is lacking in anisotropic information derived from spatial orientation in the crystal. No matter which technique is used, it will be difficult to define  $N$  when one obtains a distribution of non-equivalent distances between atoms. As an example,  $\text{LaF}_3$  may be considered. La has eleven fluorine neighbouring atoms with two fluorines at long distances with the effective  $N = 9$ .

## 10. Chemical polarizability and soft character [12]

According to the geochemical classification of elements, the two major categories are:

- lithophilic elements: alkali, alkaline-earth metals, Al, Ti, Si, Y, Zr, Nb, lanthanides, Hf, Ta, Th, U occur as silicates, mixed oxides,
- chalcophilic elements: Cu, Zn, As, Se, Ag, Cd, Sb, Te, Hg, Tl, Pb, Bi occur as sulphur bearing minerals,
- intermediate elements: Ni, Ge, In, Sn occur both as silicates and sulphides.

From the study of complexes, Ahrlund, Chatt and Davies arrived at a classification scheme comprising A-type and B-type central atoms corresponding to lithophilic and chalcophilic elements.

- A-type (lithophilic): high affinity for fluoride and oxygen-bearing ligands,
- B-type (chalcophilic): affinity for  $\text{I}^-$ ,  $\text{Br}^-$ , S bearing ligands,  $\text{PH}_3$ ,  $\text{NH}_3$ ,  $-\text{NH}_2$ .

According to Abegg and Bodländer, noble materials with positive  $E^0$  (relative to hydrogen) preferentially form complexes with  $I^-$ ,  $S^{2-}$  and  $CN^-$  corresponding to B-type classification. Seen from the point of view of classical methods of qualitative analysis, metal ions precipitated by  $H_2S$  are chalcophilic or B-type and metals precipitated as hydroxides are in general lithophilic or A-type elements. Trends of this nature have also been observed in complex formation constants with multidentate ligands. All these observations led to Pearson's hard and soft acid base principle (HSAB). According to HSAB classification, we have:

- A-type atoms and other antibases—hard acids.
- Fluoride, oxygen containing ligands—hard bases.
- B-type metals (antibases)—soft acids.
- Iodide, cyanide, phosphine, sulphur-bearing ligands—soft bases.

According to the HSAB principle, hard acids react preferentially with hard bases and soft acids react preferentially with soft bases. It is clear from the above description of the various factors leading to the enunciation of the HSAB principle that the general concepts underlying the HSAB principle are not new. To a good approximation, hardness is synonymous with electrovalent bonding while softness is not the same as covalent bonding.

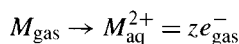
Consider the halides and the properties associated with them, such as electronegativity. The electronegativities for  $F^-$ ,  $Cl^-$ ,  $Br^-$  and  $I^-$  are 3.9, 3.0, 2.8 and 2.5, respectively, and the order is  $F^- > Cl^- > Br^- > I^-$  which is also the hardness order. The electronegativities obtained from electron transfer spectra and from ionization energies in photoelectron spectra are not necessarily associated with the hard or soft behaviour. Viewed from the optical electronegativities of central atoms, there is some correlation between softness and oxidizing character with some exceptions like Tl(III) and Hg(II). Tl(III) has higher ionization energy, I than Mn(I), although the chemical shift of I of inner shells contains a substantial contribution from the interatomic relaxation effect corresponding to chemical polarization. This observation shows less correlation with the softness of the central atom. When considering the increase in polarizability from  $F^-$  to  $I^-$  it is necessary to bear in mind: (i) that the electric dipolar polarizability  $\alpha$  for weak field strengths are much smaller for species like hydride ( $-I$ ) and fluoride ( $-I$ ) than gaseous  $H^-$  and  $F^-$  and (ii) that  $\alpha$  values of cations have very little to do with softness. Some  $\alpha$  values in  $\text{Å}^3$  and given below.

F(-I)	0.8	Cl(-I)	3.0	Br(-I)	4.2	I(-I)	6.3
Ne	0.39	Ar	1.63	Kr	2.46	Xe	4.0
Na(I)	0.3	K(I)	1.2	Rb(I)	1.9	Cs(I)	2.9
Mg(II)	0.1	Ca(II)	0.9	Sr(II)	1.4	Ba(II)	2.4
Al(III)	0.0	Sc(III)	1.1	Y(III)	1.5	La(III)	2.2
Zn(II)	0.9	Mn(II)	1.3	Ag(I)	2.3	Ce(IV)	4.0
Cu(II)	1.0	Cd(II)	1.7	Cd(II)	1.7	Hf(IV)	1.7
				In(III)	1.6	Th(IV)	2.7

The value of  $\alpha$  is larger for isoelectronic halide than noble gas and smaller for isoelectronic cations. The  $\alpha$  values do not show dramatic decrease as a function of

oxidation state as expected for gaseous ions. On the other hand the  $\alpha$  values reach a minimum between M(II) and M(III). In normal circumstances,  $\alpha$  is proportional to the summation over all excited states of the oscillator strength divided by the square of the wave number of the transition. This approach leads to high values of  $\alpha$  for Pt(IV), 4 to 5 Å<sup>3</sup> for Ti(IV), 2.2 Å<sup>3</sup> for Fe(III). The  $\alpha$  values increase from 2.2 Å<sup>3</sup> for La(III) to 2.4 Å<sup>3</sup> for Ce(III) and then decrease to 1.6 Å<sup>3</sup> for Yb(III). Further from a comparison of  $\alpha$  values of Ca(II) with Cu(II), Ag(I) with Cs(I) and Cd(II) with Ba(II) it becomes increasingly clear  $\alpha$  appears to have little to do with polarization.

Many attempts have been made to define physical quantities that relate to softness and the parameter  $\sigma_A$  of Ahrlund as the energy of the process



divided by  $Z$  appears to be somewhat relevant as seen from the values given below [3].

H(I)	2.3	K(I)	1.0	Fe(III)	3.1	Sr(II)	0.8	La(III)	0.6
Li(I)	0.0	Ca(II)	0.7	Ni(II)	2.0	Y(III)	0.6	Ce(IV)	2.0
Be(II)	1.2	Sc(III)	1.2	Cu(II)	3.1	Cd(II)	3.6	Hg(II)	5.1
Na(I)	0.9	Cr(II)	2.1	Zn(II)	3.1	In(III)	3.3	Tl(I)	2.7
Mg(II)	1.4	Mn(II)	2.0	Ga(III)	2.9	Cs(I)	1.2	Tl(II)	4.3
Al(III)	1.6	Fe(II)	2.0	Rb(I)	1.0	Ba(II)	0.9	Pb(II)	3.6

These values reflect more closely softness defined by the HSAB principle. There are some discrepancies and the main drawback is that this approach tends to overestimate the softness to an extent proportional to  $Z$ . Neglecting the distinction between enthalpy and free energy  $\sigma_A$  can be written as

$$\sigma_A = (E^0 + 4.5) - (\Delta H_{\text{atom}}/Z),$$

where  $E^0$  is the standard oxidation potential of the metal,  $\Delta H_{\text{atom}}$  is the heat of atomization and  $Z$  the charge. It is useful to note that the hydrogen electrode constant 4.5 produces a constant shift in  $\sigma_A$  and the monoatomic  $I_n$  values are not necessary. Thus one gets 1.29 for Mg(II), 0.64 for Y(III) and 0.71 for La(III) in fair agreement with the values quoted earlier. The following values for  $\sigma_A$  are obtained by this approach.

Cr(III)	2.6	Pd(II)	3.5				
Co(III)	3.4	Ag(I)	2.35				
Cu(I)	1.55	Bi(III)	4.1				
Ce(III)	0.72	Pr(III)	0.93	Nd(III)	1.05	Sm(III)	1.51
Gd(III)	0.85	Dy(III)	1.18	Er(III)	1.07	Tm(III)	1.45

The values of  $\sigma$  for Sm and Tm are high and these elements have low heats of ionization.

Klopman developed a theory [13] applied to chemical reactivity based on the quantum mechanical perturbation method. This method emphasizes the importance of charge and frontier orbital-controlled effects. The frontier orbitals are the highest occupied molecular orbitals (HOMO) of the donor base atom and the lowest unoccupied molecular orbital (LUMO) of the acceptor atom in the acid molecule. When the difference in energy between HOMO and LUMO ( $E_{\text{HOMO}} - E_{\text{LUMO}}$ ) is large, no electron transfer occurs and charge controlled interaction or ionic forces dominate in the resulting compound. When  $E_{\text{HOMO}} - E_{\text{LUMO}}$  is small there results electron transfer from donor to acceptor and the resulting compound is covalent in nature. Hard-hard interactions are charge-controlled and soft-soft interactions are frontier-controlled. By considering ionization potentials, electron affinities, ionic sizes and solvation energies, Klopman calculated a set of characteristic numbers  $E^\ddagger$  for many cations which are presented in Table 2.12.

The data show good correlation with hard and soft behaviour of the ions as a Lewis acid or base. The  $E^\ddagger$  values consist of the energies of the frontier orbitals and the changes in solvation energy after the electron transfer or covalent bond formation. In the case of  $\text{Al}^{3+}$ , it is the de-solvation energy that makes it a hard acid. It is to be noted that all cations would become softer in less polar solvents. In the gas phase they would become softest. Similarly soft anions in solution would become hard in the gas phase.

Consider the application of the quantum mechanical perturbation method to the analysis of interaction of systems R and S. The total perturbation energy from such an interaction is comprised of contributions from neighbouring effects resulting in ion-pair formation without electron transfer and partial charge transfer due to covalent bonding. This approach also takes into account solvation effects.

When the perturbation is small, the total perturbation energy,  $\Delta E_{\text{total}}$  is given by

$$\Delta E_{\text{total}} = -q_R q_S \frac{\Gamma}{\epsilon} + \Delta_{\text{solv}} + \sum_{\substack{m \\ \text{occ}}} \sum_{\substack{n \\ \text{unocc}}} \left[ \frac{2(C_R^m)^2 (C_S^n)^2 \beta^2}{E_m^* - E_n^*} \right],$$

where  $q_R$  and  $q_S$  are total initial charges on atoms R and S, respectively.  $\Gamma$  is the coulomb repulsion term between R and S,  $\epsilon$  is the local dielectric constant of the solvent  $E_m^*$  and  $E_n^*$  are energies of the highest occupied molecular orbital of the donor and lowest unoccupied molecular orbital of the acceptor respectively.

When  $|E_m^* - E_n^*| \gg 4\beta^2$  very little charge transfer takes place, and  $\Delta E_{\text{total}}$  total reduces to

$$\Delta E_{\text{total}} = -q_R q_S \frac{\Gamma}{\epsilon} + \Delta_{\text{solv}} + 2 \sum_{\substack{m \\ \text{occ}}} (C_R^m)^2 \sum_{\substack{n \\ \text{unocc}}} (C_S^n)^2 \gamma,$$

where  $\gamma = \beta^2 / (E_m^* - E_n^*)$  average.

In this case the charges on the atoms R and S are dominant factors and the resulting interaction is charge-controlled. This type of reaction occurs when the donor atom is difficult to ionize or polarize (i.e.)  $E_m^*$  is of low value and the acceptor atom exhibits a slight tendency to accept electrons (i.e.)  $E_n^*$  is large and when both atoms are small and



TABLE 2.12  
Calculated softness character (empty frontier orbital energy) of cations and donors [13].

Ion	Orbital energy (eV)	De-solvation energy (eV)	$E_m^\ddagger$ (eV)	
Al <sup>3+</sup>	26.04	32.05	6.01	Hard
La <sup>3+</sup>	17.24	21.75	4.51	Hard
Ti <sup>4+</sup>	39.46	43.81	4.35	Hard
Be <sup>2+</sup>	15.98	19.73	3.75	Hard
Mg <sup>2+</sup>	13.18	15.60	2.42	Hard
Ca <sup>2+</sup>	10.43	12.76	2.33	Hard
Fe <sup>3+</sup>	26.97	29.19	2.22	Hard
Sr <sup>2+</sup>	9.69	11.90	2.21	Hard
Cr <sup>3+</sup>	27.33	29.39	2.06	Hard
Ba <sup>2+</sup>	8.80	10.69	1.89	Hard
Ga <sup>3+</sup>	28.15	29.60	1.45	Hard
Cr <sup>2+</sup>	13.08	13.99	0.91	Hard
Fe <sup>2+</sup>	14.11	14.80	0.69	Borderline
Li <sup>+</sup>	4.25	4.74	0.49	Borderline
H <sup>+</sup>	10.38	10.8	0.42	Borderline
Ni <sup>2+</sup>	15.00	15.29	0.29	Borderline
Na <sup>+</sup>	3.97	3.97	0	Borderline
Cu <sup>2+</sup>	15.44	14.99	-0.55	Soft
Tl <sup>+</sup>	5.08	3.20	-1.88	Soft
Cd <sup>2+</sup>	14.93	12.89	-2.04	Soft
Cu <sup>+</sup>	6.29	3.99	-2.30	Soft
Ag <sup>+</sup>	6.23	3.41	-2.82	Soft
Tl <sup>3+</sup>	27.45	24.08	-3.37	Soft
Au <sup>+</sup>	7.59	3.24	-4.35	Soft
Hg <sup>2+</sup>	16.67	12.03	-4.64	Soft
			$E_n^\ddagger$	
F <sup>-</sup>	6.96	5.22	-12.18	Hard
H <sub>2</sub> O	15.8	(-5.07)	-(10.73)	Hard
OH <sup>-</sup>	5.38	5.07	-10.45	Hard
Cl <sup>-</sup>	6.02	3.92	-9.94	Hard
Br <sup>-</sup>	5.58	3.64	-9.22	Hard
CN <sup>-</sup>	6.05	2.73	-8.78	
SH <sup>-</sup>	4.73	3.86	-8.59	Soft
I <sup>-</sup>	5.02	3.29	-8.31	Soft
H <sup>-</sup>	3.96	3.41	-7.37	Soft

strongly solvated. Charge-controlled reaction is hard-hard interaction in terms of HSAB theory.

When  $|E_m^* - E_n^*| \approx 0$  interaction between frontier orbitals (HOMO and LUMO) is important and a frontier-controlled reaction involving electron transfer occurs.  $\Delta E_{\text{total}}$  may then be written as

$$\Delta E = 2C_R^m C_S^n \beta,$$

TABLE 2.13  
Type and rate of reaction between hard and soft reagents.

Donor $E_m^*$	Acceptor $E_n^*$	$E_m^* - E_n^*$	$\Gamma$	$\beta$	Reactivity	
High (soft) Large orbital	High (hard) Small orbital	Medium	Small	Very small	Undefined	Low
	Low (soft) Large orbital	Small	Very small	Large	Frontier controlled	High
Low (hard) Small orbital	High (hard) Small orbital	Large	Large	Small	Charge controlled	High
	Low (soft) Large orbital	Medium	Small	Very small	Undefined	Low

which depends on the frontier orbital electron density,  $C_R^m$ ,  $C_S^n$ . Such an interaction involves polarizability of the reactants and low solvation energies. This type of interaction is called soft-soft interaction in terms of HSAB theory. Table 2.13 given below summarizes the different types of reactions.

### 11. Some recent developments

Using density functional theory, the electronic chemical potential,  $\mu$  and absolute hardness,  $\eta$  have been introduced by Pearson [14]. A chemical system is characterized by its electronic chemical potential,  $\mu$ , and by its absolute hardness,  $\eta$ . These are exactly defined as

$$\mu = \left( \frac{\partial E}{\partial N} \right)_v,$$

$$\eta = \frac{1}{2} \left( \frac{\partial \mu}{\partial N} \right)_v,$$

where  $N$  is the number of electrons and  $v$  is the potential due to the nuclei and any external potential. The operational and approximate definitions given by Pearson are

$$-\mu = (I + A)/2 = \chi,$$

$$\eta = (I - A)/2,$$

where  $I$  and  $A$  are the ionization potential and electron affinity, respectively. The softness  $\sigma$ , is the inverse of hardness,

$$\sigma = 1/\eta.$$

Some values of  $\sigma_p$  due to Pearson are given for selected ions in Table 2.14.

The  $\sigma_p$  values do not show a well-defined and discernible trend and not even to the extent of  $\sigma_A$  of Ahrland as discussed earlier.

TABLE 2.14  
 $\sigma_p$  values of some selected ions.

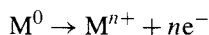
Li <sup>+</sup>	0.029	K <sup>+</sup>	0.073	Fe <sup>3+</sup>	0.083	Sr <sup>2+</sup>	0.061	La <sup>3+</sup>	0.065
Be <sup>2+</sup>	0.015	Ca <sup>2+</sup>	0.051	Ni <sup>2+</sup>	0.118	Y <sup>3+</sup>	0.049	Hg <sup>2+</sup>	0.130
Na <sup>+</sup>	0.047	Sc <sup>3+</sup>	0.041	Cu <sup>2+</sup>	0.121	Cd <sup>3+</sup>	0.097	Tl <sup>+</sup>	0.140
Mg <sup>2+</sup>	0.031	Cr <sup>2+</sup>	0.138	Zn <sup>2+</sup>	0.092	In <sup>3+</sup>	0.077	Tl <sup>3+</sup>	0.096
Al <sup>3+</sup>	0.022	Mn <sup>2+</sup>	0.111	Ga <sup>3+</sup>	0.059	Cs <sup>+</sup>	0.094	Pb <sup>2+</sup>	0.118
		Fe <sup>2+</sup>	0.138	Rb <sup>+</sup>	0.087				

It is worthwhile to point out some obvious anomalies in HSAB theory. Some ligands do not show definite hard or soft behaviour. Consider OH<sup>-</sup> which reacts with most central atoms in M(II) and M(III) with the exceptions of Ca, Sr, Ba, Eu and Ra irrespective of the softness of the central atom. This behaviour is probably due to the consecutive deprotonation of ligated water molecules to hydroxy and then to oxo complexes which is pH dependent and due to increase in ionic potential  $Z/r_{ion}$ .

Many consider H<sup>+</sup> as a hard acid when compared with the small Li<sup>+</sup> ion. This in fact is not the observed trend because H<sub>aq</sub><sup>+</sup> has great affinity for H<sup>-</sup>, CH<sub>3</sub><sup>-</sup> and CN<sup>-</sup> and hence can be regarded as a soft acid. This argument can be countered by the observation of pH 3 of aqueous HF solution which is 10 times higher than the expected value. This may be explained by the strong hydrogen bonding present in aqueous solutions of HF and also the fact that hard complexes are formed endothermally in aqueous solution with positive  $\Delta H$  and negative  $\Delta G$ . On the other hand the reactions between soft central atoms of soft ligands have negative  $\Delta H$  and  $\Delta G$  values with a more moderate change in entropy. Thus the entropy of fluoride and some oxygen-containing ligands coupled with high stability of aquo ions leads to difficulties in explanations based on simple models.

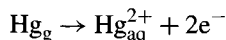
It is useful to note  $\Delta H_{hyd}/Z^2$  value 3.37 eV for Ba<sup>2+</sup> is lower than 3.75 of Sr<sup>2+</sup> and 4.12 for Ca<sup>2+</sup>; 4.75 eV for Hg<sup>2+</sup>, 4.82 eV for Tl<sup>3+</sup> and 3.82 eV for Pb<sup>2+</sup> in spite of higher ionic radii than Cd<sup>2+</sup>, In<sup>3+</sup> and Sr<sup>2+</sup>, respectively. Thus we lack a detailed understanding of hydration energy although rough proportionality to  $Z^2$  supports electrostatic arguments. However one can argue that since  $I_z$  of M<sup>+z-1</sup> tends to be proportional to  $Z$  with a total energy of  $k(Z^2 + Z)$  relative to ground state of neutral atom, the hydration energy must compensate more or less for the quadratic dependence on  $Z$ .

It is useful to note that the process



is generally endothermic although in the case of Ca<sup>2+</sup> the heat of formation is positive and this paradox can be explained by the fact that electrons with zero energy relative to vacuo are not available in aqueous solutions. The condition for thermodynamics equilibrium at 25°C with 1 atm of H<sub>2</sub> is  $E^0 = 0.059$  pH or  $I_{chem} = 4.5-0.059$  pH and in the case of oxidizing solution with 0.2 atm O<sub>2</sub> as found in air  $I_{chem} = 5.7-0.059$  pH. Thus reactions producing electrons with an energy of -4 eV proceed by evolution of hydrogen. In the case of complexes like Hg(CN)<sub>4</sub><sup>2-</sup> with  $\log \beta_4 = 41.5$ ,  $\Delta H = -63$  kcal/mole, the

covalent bond compensates or pays back 2.8 eV of the  $2\sigma_A = 10.2$  eV lacking when the reaction



takes place.

In conclusion it can be stated that Klopman's  $E^\ddagger$  parameters describe the softness of ions better than Pearson's  $\sigma = 1/\eta$  parameter. It can also be said that one of the shortcomings of Pearson's HSAB principle is that it cannot predict  $\Delta H$  or  $\Delta G$  as an explicit function such as the sum of two products of two parameters, one characterizing the acid and the other the base. In spite of the limitations, the HSAB principle is useful in rationalizing and understanding the behaviour of metal ions.

## 12. Electronic configuration and multiplet structure [3]

As pointed out before the 5d group can conveniently start with lutetium followed by Hf, Ta, W. There is no particular reason to place 4f rare earths elements as an inclusion in the 5d group. Lanthanides are not trivalent simply because their neutral atoms contain  $(Z - 57)$  4f electrons but because eleven of the fourteen rare earths resemble barium with  $q = (Z - 56)$  and  $6s^2$  configuration. There is no profound difference between the chemistry of four lanthanum-like ground states, La, Ce, Gd, and Lu and the remaining eleven rare earths. The reasons for trivalence are: (i)  $I_3$  for  $M^{2+} \rightarrow M^{3+} + e^-$  is small compared with  $5k$  ( $k = 4.3$  eV for rare earths), that  $M_{\text{aq}}^{2+}$  ions have negative  $E^0$  values and evolve  $\text{H}_2$ , (ii)  $I_4$  for  $M^{3+} \rightarrow M^{4+} + e^-$  is large compared with  $7k$  and that  $E^0$  for  $M_{\text{aq}}^{3+}$  is positive to evolve oxygen. The value of  $I_4 - I_3$  for rare earth is high and this is not due to crossing a closed shell configuration as in the case of  $\text{Al}^{3+}$  whose  $I_3 = 24.45$  eV in losing 3s electron and  $I_4 = 120$  eV for depleting Ne core. In the case of lanthanides  $I_4$  is higher than  $I_3$  by 20 eV even though the 4f electron is removed. In short, the electron affinity of a partly filled 4f shell is smaller than the corresponding ionization energy,  $I$ .

Hartree-Fock calculations in solving the Schrodinger equation for many electron atoms yield negative eigen values  $E$  which are not in keeping with the actual chemistry. An approximate relation for the binding energy of  $Z$  electrons to the nucleus of charge  $Z$  is  $-Z^{2.4}$  rydberg where a rydberg is equal to 13.6 eV. This relationship deviates considerably for  $Z = 90$  due to relativistic reasons. Considering the atomic core consisting of strongly bound, closed shells as the zero-point of energy, and an electron bound to the core can alleviate the deviation problem. When the ionic charge is  $+Z$ , Rydberg's relation for binding energy may be written as

$$-\varepsilon_{\text{nl}} = -(Z + 1)^2 \text{rydberg}(n - d)^2,$$

where  $d$  the Rydberg defect decreases in the order  $s > p > d > f$  electrons and varies very little with the principal quantum number,  $n$ .

Consider the baricentre of the relativistic effect of spin-orbit coupling. The two  $j$  values are  $(l + 1/2)$ ,  $(l - 1/2)$  for positive  $l$  values corresponding to  $(2l + 2)$  and  $2l$  states and

separated by  $(l + \frac{1}{2}) \zeta_{nl}$  where  $\zeta$  is the Lande parameter. The baricentre is located  $\frac{1}{2}l\zeta$  below the higher of the two  $j$  levels. It may be noted that

$$\zeta_{nl} \propto (Z + 1)^2 Z^2$$

and under identical conditions  $\zeta_{nL}$  varies in the order

External p electrons > d electrons > f electrons.

In typical cases  $\zeta_{nL}$  is about a few percent of  $\epsilon_{nL}$ .

In the case of two electrons in two different shells outside the atomic core, many energy levels characterized by a quantum number,  $J$  are observed, each corresponding to  $(2J + 1)$  states. In terms of Russell–Saunders coupling one has quantum numbers  $S$  and  $L$  and each containing  $(2S + 1)(2L + 1)$  states when one of the electrons has  $l = 0$ , the terms with  $S = 0$  (singlet) and  $S = 1$  (triplet) are obtained if  $l = l$  of the other electron. The triplet at lower energy has three times the states of a singlet and the baricentre of this configuration is located a quarter of the  $S \rightarrow T$  distance above the triplet energy.

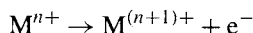
In the case of two electrons ( $nl$ ) and ( $n'l'$ ) many terms arise from  $L = (l+l')$ ,  $(l+l' - 1)$ ,  $(l+l' - 2) \dots (|l - l'| + 1)|l - l'|$  with  $S = 0$  and  $S = 1$ . When the two electrons are in ( $nl$ ), we have  $(2l + 1)(4l + 1)$  states occurring with terms  $^1S, ^3P, ^1D, ^3F, ^1G, ^3H, ^1I \dots ^3(2L - 1), ^1(2L)$ . In the case of  $f^3, f^{11}$  configurations we get

$^4S, ^4D, ^4F, ^4G, ^4I, ^2P, ^2D, ^2D, ^2F, ^2F, ^2G, ^2G, ^2H, ^2H, ^2I, ^2K, ^2L$ .

The number of states,  $J$ -levels and terms are

	$q$							
	0.14	1.13	2.12	3.11	4.10	5.9	6.8	7
States	1	14	91	364	1001	2002	3003	3432
$J$ -levels	1	2	13	41	107	195	295	327
$S, L$ terms	1	1	7	17	47	73	119	119
Hund	$^1S$	$^2F$	$^3H$	$^4I$	$^5I$	$^6H$	$^7F$	$^8S$
Highest $L$	$^1S$	$^2F$	$^1I$	$^2L$	$^1N$	$^2O$	$^1Q$	$^2Q$

In order to understand the properties of lanthanide compounds of  $4f^n$  configuration with the high number of energy levels and the ionization energies for



it is useful to evaluate the baricentre of each configuration by weighting the energies of each  $J$ -level with the number  $(2J + 1)$  states and when needed supplementing the observed  $J$ -levels with the calculated positions of missing  $J$ -levels. The baricentre obtained this way refers to the actual  $J$ -levels belonging to a given configuration including conceivable differences of correlation energy in the monoatomic entities. Interelectronic repulsion

TABLE 2.15  
One and two electron parameters [3].

	$\epsilon_{4d}$	$\epsilon_{5s}$	$\epsilon_{5p}$		$A^*(4d4d)$	$A^*(4d5s)$	$A^*(4d5p)$	$A^*(5s5s)$	$A^*(5s5p)$
Rb	1.74	4.22	2.60						
Sr <sup>+</sup>	9.18	11.03	8.06	Sr	7.19	5.83	4.84	5.58	4.34
Y <sup>2+</sup>	20.46	19.59	15.25	Y <sup>+</sup>	9.68	7.44	6.45	6.32	5.70
Zr <sup>3+</sup>	34.22	29.51	24.05	Zr <sup>2+</sup>	11.78	9.30	8.06	6.45	6.45
	$\epsilon_{4f}$	$\epsilon_{5d}$	$\epsilon_{6s}$		$A^*(4f4f)$	$A^*(4f5d)$	$A^*(4f5s)$	$A^*(5d5d)$	$A^*(5d6s)$
Cs	0.87	2.11	3.84	Ba	—	—	3.10	6.32	5.33
Ba <sup>+</sup>	3.97	9.30	10.04	La <sup>+</sup>	12.89	9.30	6.94	8.06	6.45
La <sup>2+</sup>	18.10	18.97	17.48	Ce <sup>2+</sup>	17.23	11.16	8.31	9.55	7.81
Ce <sup>3+</sup>	36.57	30.38	26.04	Pr <sup>3+</sup>	19.34	12.15	8.80	7.93	—
Pr <sup>4+</sup>	57.16	42.90	35.21						

parameter  $A^*(nl, n'l')$  is defined for the energy of the baricentre of  $(n, l)'(n'l)'$  [or  $(nl)^2$  giving  $A^*(nl, nl)$ ] of  $M^{(n-2)+}$  outside the closed shells of ground state of  $M^{n+}$  using the latter ground state as the zero-point energy

$$-\epsilon_{nl} - \epsilon_{n'l'} + A^*(nl, n'l').$$

The two one-electron energies are obtained from the Rydberg relation

$$-\epsilon_{nl} = (Z - 1)^2 \text{rydberg} / (n - d)^2.$$

The baricentres of  $(4l + 2)n(4l' + 2)$  or  $(2l + 1)(4l + 1)$  states are known with good precision. One and two electron parameters for some selected monoatomic entities containing one electron (Cs, Ba<sup>+</sup>, La<sup>2+</sup>, Ce<sup>3+</sup>, Pr<sup>4+</sup>) and two electrons (Ba, La<sup>+</sup>, Ce<sup>2+</sup>, Pr<sup>3+</sup>) outside the xenon closed shells are given in Table 2.15. The values of  $\epsilon_{nl}$  for Rb, Sr<sup>+</sup>, Y<sup>2+</sup> and Zr<sup>3+</sup> and interelectronic repulsion parameter  $A^*(nl, n'l')$  for Sr, Y<sup>+</sup> and Zr<sup>2+</sup> are also given for 4d, 5s, 5p electrons outside the krypton closed shells.

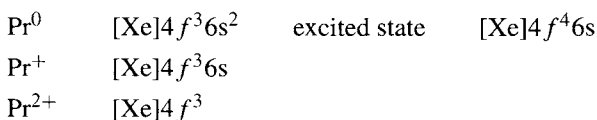
The important conclusion that can be drawn from the data is that 4f electrons are distinctly external before barium and are located inside closed shells after cerium. The Rydberg defect  $d$  increases from 0.31 in Ba<sup>+</sup> to 1.40 in La<sup>2+</sup> and the interelectronic repulsion parameter  $A^*(4f, 4f)$  is 13 eV in La<sup>+</sup> and 19.3 eV in Pr<sup>3+</sup> in comparison to  $A^*(5s, 5s)$  value of 6.3 eV for Y<sup>+</sup>. The interelectronic repulsion parameters  $A^*$  bear a close relationship with the reciprocal average radius of the orbital involved. We can define a generalized baricentre polynomial involving  $A^*$  for any element containing  $x$  electrons in the  $nl$  shell and  $y$  electrons in the  $n'l'$  shell as

$$-x\epsilon_{nl} - y\epsilon_{n'l'} + \frac{1}{2}x(x-1)A^*(nl, nl) + xyA^*(nl, n'l') + \frac{1}{2}y(y-1)A^*(n'l', n'l').$$

The above equation can be applied to three or more partly filled shells as well with coefficients of  $A^*$  being  $\frac{1}{2}q(q-1)$  for  $q$  electrons in the same shell and  $q_1q_2$  for  $q_1$  electrons in one shell repelling  $q_2$  electrons in another shell.

In general a linear dependence of the baricentre energies on the occupation numbers of the two shells is expected but in reality the dependence is non-linear. The non-linear dependence becomes clear when it is noted that  $A^*(nl, n'1')$  is considerably smaller than the arithmetic average value of  $A^*(nl, nl)$  and  $A^*(n'1', n'1')$  when the average radii of  $n1$  and  $n'1'$  are different. This is illustrated by a comparison of  $d$  or  $f$  orbital with  $s$  orbital.  $\text{Sc}^+$  has the configuration  $[\text{Ar}]3d4s$  at equal distance below  $[\text{Ar}]3d^2$  and  $[\text{Ar}]4s^2$ . Similarly  $\text{La}^+$  with the configuration  $[\text{Xe}]5d6s$  is below  $[\text{Xe}]5d^2$  and  $[\text{Xe}]6s^2$ . The two configurations  $[\text{Xe}]4f^2$  and  $[\text{Xe}]4f5d$  almost coincide in  $\text{Ce}^{2+}$  but the baricentre of  $[\text{Xe}]5d^2$  occurs 5 eV higher. The hypothetical configuration  $[\text{Xe}]4f^4$  of neutral cerium is expected to give  $\text{Ce}^+$  with configuration  $[\text{Xe}]4f5d^2$ .

In the case of praseodymium we have



In the case of  $\text{Pr}^{2+}$  with the configuration  $[\text{Xe}]4f^25d$  it is 1.6 eV higher in energy. The baricentre of  $[\text{Xe}]4f^3$  is about 2.4 eV above the ground state  $\text{Pr}^{2+}$ , 3.2 eV above that of  $[\text{Xe}]4f^25d$  and 4.7 eV above that of  $[\text{Xe}]4f^26s$ . This observed inconsistency in the baricentre of energy states may be compared with the observed ground state energy of  $\text{Pr}^{2+}$  relative to  $\text{Pr}^{5+}$  is  $-952$  and of the baricentre of  $[\text{Xe}]4f^3$  at  $933$  which may be considered to be in reasonable agreement. From this discussion it can be concluded that the value of  $A^*(4f, 4f)$  is not constant.

### 13. Spin-pairing energy

The overall separation between  $[\text{Xe}]4f^q$  of  $M^{n+}$  and  $[\text{Xe}]4f^{q-1}$  of  $M^{(n-1)+}$  is primarily determined by the interelectronic repulsion parameter  $A^*(4f, 4f)$  since the coefficient changes by  $(q-1)$ . The value of  $A^*(4f, 4f)$  varies with  $q$  in a non-uniform manner which may be explained by the fact that the baricentre of all the states having the maximum  $S$  value is located below, the baricentre of the configuration of  $4f^q$  for  $q$  between 2 and 12. In practice the fraction of all having  $S_{\max}$  decreases sharply near the half-filled shell.

$q$	$S_{\max}$
2.12	7/13
3.11	5/13
4.10	25/143
5.9	9/143
6.8	7/429
7	1/429

The baricentre of all the states of  $L^q$  of a given value of  $S$  and the baricentre at higher energy of all states of  $(S-1)$  are separated by  $2DS$  where  $D$  is a definite linear

combination of Slater–Condon–Shortley parameters or of Racah parameters. It is well-known that the singlet and triplet baricentres of a two-electron system are separated by  $2D$ . The same linear combination of interelectronic repulsion parameters can be used for all  $q$  with same  $l$  and can be used for  $f^4, f^5, f^6$  and  $f^7$  with three or four alternate values of  $S$ . The separation  $2DS$  is the difference quotient of  $-DS(S+1)$  and the deviation of the baricentre of all the states with a given  $S$  value from baricentre of all the states of  $1^q$  may be written as

$$D[\langle S(S+1) \rangle - S(S+1)],$$

where the average value of  $\langle S(S+1) \rangle$  for the whole configuration

$$\begin{aligned} \langle S(S+1) \rangle &= \frac{1}{4}q(q+2) - \frac{2l+2}{4l+1} \frac{1}{2}q(q-1) && \text{(Racah's theory)} \\ &= \frac{3}{4}q - \frac{3}{8l+2} \frac{1}{2}q(1+1) && \text{(Pauli's exclusion principle)} \\ &= \frac{3q(4l+2-q)}{16l+4} && \text{(Pauli's hole-equivalence).} \end{aligned}$$

In Racah's formalism,  $S_{\max}$  for  $q \leq (2l+1)$  is  $1/2q$  and the coefficient for  $1/2q(q-1)$  indicates what multiple of  $D$  might be added to  $A^*$  if desired. According to Pauli's exclusion principle  $\langle S(S+1) \rangle$  decreases from the value of  $3/4q$  as for non-equivalent electrons in which case it is multiplied by a factor  $1 - (q-1)/(4l+1)$ . In the hole formalism  $((4l+2-q)$  and  $q$  electrons are symmetric. The values of the coefficients in the equation

$$D[\langle S(S+1) \rangle - S(S+1)]$$

are reported and tabulated in the literature.

When a partly filled  $f$  shell is considered,  $S_{\max}$  corresponds to a spin-pairing stabilization reaching a minimum of  $-168D/13$  at  $q = 7$  and the general value of  $-8D/13[1/2q(q-1)]$  for  $q$  below 7.

Although  $D$  can be written as

$$D = \frac{2l+3}{2l+2} \cdot K_{\text{av}} - \frac{9}{8}E'$$

for  $f$  electrons, where  $K_{\text{av}}$  is the average value of the exchange integral of the two-electron operator, it is not strictly appropriate to relate  $2DS$  with the multiple of  $K_{\text{av}}$ . When there are several terms with  $S_{\max}$  of differing energy, the lowest has a lower energy than the baricentre of all states with  $S_{\max}$ . In the case of  $4f^q$   $L$  value of the ground term is the determining factor. We have further stabilization in terms of  $E^3$  values as given below.

$q = 2, 12$	${}^3\text{H}$	$-9E^3$
$q = 5, 9$	${}^6\text{H}$	$-9E^3$
$q = 3, 11$	${}^4\text{I}$	$-24E^3$
$q = 4, 10$	${}^5\text{I}$	$-24E^3$



It is useful to note that  $E^3 \approx +1/10E'$ .

Refined spin-pairing energy theory introduced by Jorgensen involves adding coefficients to  $E^3$  and spin-orbit coupling stabilization values to the lowest  $J$ -levels by  $-1/2(L+1)\zeta_{4f}$  for  $q \leq 7$  and  $-1/2L\zeta_{4f}$  for  $q > 7$ , with  $V$  as the zero-point energy and  $(E - A)$  as a parameter due to the stabilization of  $4f$  electrons from one element to another. For  $q = 1$  to 14 we have the expressions for the spin-pairing

$$\begin{aligned}
 q = 1 & \quad V + 2\zeta_{4f} \\
 q = 2 & \quad V + (E - A) + 8/13D + 9E^3 + \zeta_{4f} \\
 q = 3 & \quad V + 2(E - A) + 16/13D + 12E^3 + 1/2\zeta_{4f} \\
 q = 4 & \quad V + 3(E - A) + 24/13D \\
 q = 5 & \quad V + 4(E - A) + 32/13D - 12E^3 - 1/2\zeta_{4f} \\
 q = 6 & \quad V + 5(E - A) + 40/13D - 9E^3 - \zeta_{4f} \\
 q = 7 & \quad V + 6(E - A) + 48/13D - 2\zeta_{4f} \\
 q = 8 & \quad V + 7(E - A) - 48/13D + 3/2\zeta_{4f} \\
 q = 9 & \quad V + 8(E - A) - 40/13D + 9E^3 + \zeta_{4f} \\
 q = 10 & \quad V + 9(E - A) - 32/13D + 12E^3 + 1/2\zeta_{4f} \\
 q = 11 & \quad V + 10(E - A) - 24/13D \\
 q = 12 & \quad V + 11(E - A) - 16/13D - 12E^3 - 1/2\zeta_{4f} \\
 q = 13 & \quad V + 12(E - A) - 8/13D - 9E^3 - \zeta_{4f} \\
 q = 14 & \quad V + 13(E - A) - 3/2\zeta_{4f}
 \end{aligned}$$

energy for the removal of an electron from  $4f^q$  to from  $4f^{q-1}$ . It is experimentally known that the ionization energy for  $q = 7$  is marginally larger than  $q = 14$  in condensed matter which means  $7(E - A) = 48D/13$ . Thus the ionization energies are comparable for  $q$  and for  $(7 + q)$  electrons. In the absence of definite answers to problems such as assuming invariant parameters for a given oxidation state or making allowance for smooth variation from one element to the other,  $(E - A)$  is evaluated as a parameter from the experimental data, a typical value being  $3000 \text{ cm}^{-1}$ .  $D$  is fixed as  $6500 \text{ cm}^{-1}$  because of its divisibility by 13. A fixed value of  $500 \text{ cm}^{-1}$  for  $E^3$  is assumed or allowed to vary from known value of  $460 \text{ cm}^{-1}$  in Pr(III)  $q = 2$  to  $630 \text{ cm}^{-1}$  for  $q = 2$  in Tm(III). Spin-orbit coupling is known to increase smoothly from  $\zeta_{4f} = 650 \text{ cm}^{-1}$  for  $q = 1$  in Ce(III) to  $2950 \text{ cm}^{-1}$  for  $q = 13$  in Yb(III). When  $(E - A) = 3200 \text{ cm}^{-1}$ ,  $D = 6500 \text{ cm}^{-1}$ ,  $E^3 = 500 \text{ cm}^{-1}$ , empirical values of  $\zeta_{4f}$  are

$q = 1$	1300	$q = 2$	12 500	$q = 3$	20 900
$q = 4$	21 600	$q = 5$	22 200	$q = 6$	30 200
$q = 7$	40 300	$q = 8$	800	$q = 9$	11 900

$q = 10$	19 800	$q = 11$	20 000	$q = 12$	20 000
$q = 13$	27 200	$q = 14$	37 200		

From  $q = 1$  to 3 the values increase, followed by a plateau between  $q = 3$  to 5 followed by an increase from  $q = 5$  to 7. This behaviour is repeated between  $q = 8$  to 14. This observation is known as the double zig-zag curve. The data from ionization energies of gaseous ions suggest  $(E - A)$  values higher than the values that are cited above. When  $D = 6500 \text{ cm}^{-1}$ ,  $E^3 = 500 \text{ cm}^{-1}$ ,  $I_3$  of  $M^{2+}$  gives a value of  $(E - A) = 4200 \text{ cm}^{-1}$  and a still larger value for  $I_4$ . It should be noted that the mean value of  $I$  for  $q = 7$  and 8 should be close to the mean value of  $I$  for  $q = 1$  and 14 at equal distance.

Mean value of  $I_4$  for  $Gd^{3+}$  and  $Tb^{3+}$  is higher than  $I_4$  or  $Ce^{3+}$  but only 3.29 eV below  $I_4$  of  $Lu^{3+}$ .  $I_5$  of  $Pr^{4+}$  is 6.74 eV below the mean value of  $I_5$  for  $Tb^{4+}$  and  $Dy^{4+}$  which is 4.1 eV below  $I_5$  of  $Hf^{4+}$ . Thus it is clear that definite values cannot be given to the two distances, although it should be  $13(E - A)/2$ . This can probably be explained by assuming  $(E - A)$  decreases with  $Z$  since  $(E - A)$  is the difference between two large parameters and  $A$  includes interelectronic repulsion parameter,  $A^*$ . The value of  $A^*(4f, 4f)$  is 19.34 eV (or  $156\,000 \text{ cm}^{-1}$ ) for  $Pr^{3+}$  may be assumed to increase just as  $E^3$  to the same extent. In this case the increase would be  $5000 \text{ cm}^{-1}$  per unit  $Z$ . This argument does not explain the observation in the gaseous ions. Thus the baricentre polynomial model is useful in explaining the vast changes in  $A^*$  in going from one configuration to another. The refined spin-pairing energy theory can also explain the spectra of M(II) in  $CaF_2$  matrix, M(III) in  $CaF_2$  matrix, variation of energy difference between the lowest  $J$ -level of  $[Xe]4f^q-15d$  and the lowest  $J$  level of  $[Xe]4f^q$  with  $q$ , difference between lowest  $J$ -level of  $[Xe]4f^q-15d6s$  and  $[Xe]4f^q6s$  in gaseous  $M^+$  and the difference between the lowest  $J$ -level of  $[Xe]4f^q-15d6s^2$  and  $[Xe]4f^q6s^2$  in neutral  $M^0$  atoms.

## References

- [1] M. Fred, Lanthanide/Actinide Chemistry, Vol. 71, p. 200, Advances in Chemistry Series, American Chemical Society, Washington, D.C., 1967.
- [2] W.B. Jensen, J. Chem. Education **59**, 684, 1982.
- [3] C.K. Jorgensen, in: Handbook of Physics and Chemistry of Rare Earths, eds. K.A. Gschneidner, Jr., L. Eyring, p. 111, North Holland Publishing Company, 1979.
- [4] D.A. Johnson, in: Advances in Inorg. Chemistry and Radiochemistry, eds. H.J. Emeleus, A.G. Sharpe, Vol. 20, pp. 1-131, Academic Press, 1977.
- [5] T. Moeller, The Chemistry of the Lanthanides, Reinhold Book Corporation, New York, 1963.
- [6] D.R. Lloyd, J. Chem. Education **63**, 502, 1986.
- [7] L.C. Gupta, in: Science and Technology of Rare Earth Materials, eds. E.C. Subbarao, W.E. Wallace, p. 155, Academic Press, New York, 1980.
- [8] L.L. Hirst, AIP Conf Proc. **24**, 11, 1975.
- [9] T.K. Hatwar, R.M. Nayak, M.N. Ghatikar, B.D. Padalia, E.V. Sampatkumaran, L.C. Gupta, R. Vijayaraghavan, Solid State Commun., 1980.
- [10] B.C. Sales, R. Viswanathan, J. Low Temp. Phys. **23**, 449, 1976.
- [11] A. Jayaraman, in: Handbook on Physics and Chemistry of Rare Earths, eds. K.A. Gschneidner Jr., L. Eyring, Vol. 2, p. 575, North Holland Publishing Company, 1979.
- [12] R.G. Pearson, Hard and Soft Acids and Bases, Dowden, Hutchinson & Ross, Inc, Stroudsburg, Pennsylvania, 1973.
- [13] G. Klopman, J. Am. Chem. Soc. **90**, 223, 1968.
- [14] R.G. Pearson, Inorg. Chem. **27**, 734, 1983.
- [15] J.A. Wilson, A generalized configuration-dependent band model for lanthanide compounds and conditions for interconfiguration fluctuations, pp. 58-90, Bell Laboratories, Murray Hill, New Jersey 07974.

chapter 3

---

## STABILITY OF COMPLEXES

---

---

# CONTENTS

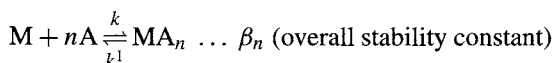
---

1. Methods . . . . .	134
2. Stability of rare earth complexes in solution . . . . .	150
3. Thermodynamic considerations . . . . .	160
4. Stability of macrocyclic complexes . . . . .	168
5. Double–double effect . . . . .	170
6. Applications . . . . .	176
References . . . . .	177
Appendix . . . . .	180

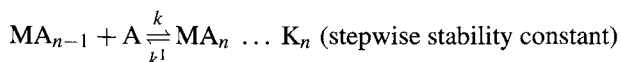
Stability constants of complexes may be determined by: (i) kinetic and (ii) equilibrium methods. In the present discussion, attention will be focused on mononuclear complexes and the fact that the activity coefficients of all the species can be held effectively constant by using suitable ionic media. The kinetic approach is applicable when: (i) the rates of formation and dissociation of a complex are sufficiently slow and (ii) accessible to experimental measurement by suitable techniques. Using the law of mass equation

$$\text{equilibrium constant } K = \frac{\text{rate constant of forward reaction}}{\text{rate constant of reverse reaction}} = k/k^1$$

the above gives the stability constant provided: (i) there is only one species in solution and (ii) there is only one rate-determining step involved. The ratio of forward and reverse reaction rate constants of a general nature may be written as [1]



and similarly we may write



The kinetic approach is of restricted utility because it is applicable to: (i) slow reactions, (ii) some transition metal ions, (iii) the role played by the electronic structure of the central metal ion. The equilibrium approach is more convenient than the kinetic approach and hence discussed here in a detailed manner. In general when a metal M complexes with a ligand A and forms complexes of the type MA, MA<sub>1</sub> ... MA<sub>N</sub> we may write for the total concentrations of M and A as

$$M = [M] + [MA] + [MA_2] + \dots + [MA_N] = m \sum_0^N \beta_n a^n \quad (3.1)$$

$$A = [A] + [MA] + 2[MA_2] + \dots + N[MA_N] = a + m \sum_1^N n \beta_n a^n \quad (3.2)$$

provided mononuclear complexes are formed and the terms 'm' and 'a' represent the free concentrations of metal ion and ligand, respectively.

When the system is inert or made inert, the equilibrium concentrations of some or all the species in solution can be determined analytically and hence the stability constants

evaluated. In labile systems, free concentrations of metal ions may be determined by potentiometry or polarography and hydrogen ions and many anions by potentiometry. When there is a distinct difference in colors of the solutions, such as complexes with chromophores, UV-vis spectroscopy may be used in the determination of the equilibrium concentration of one of the species. Competitive reaction technique may also be used to determine free concentrations of metal ( $m$ ) and ligand ( $a$ ). Knowledge of the values of ' $m$ ' and ' $a$ ' coupled with values of either  $[M]$  or  $[A]$  can be used to determine the stability constants.

Usually the common situation is such that values of either ' $m$ ' or ' $a$ ' as a function of  $[A]$  and  $[M]$  are obtained. Sometimes it is necessary to use secondary concentration variables to calculate the stability constants. Suppose we have values of  $[M]$  and  $[MA_c] = m$  and  $c = 0$ , we can define the fraction  $a_c$  of total  $M$  in the form of  $MA_c$ .

We may then write

$$a_c = \frac{[MA_c]}{[M]} = \frac{[MA_c]}{[M] + [MA] + [MA_2] + \dots} = \frac{\beta_c a^c}{\sum_0^N \beta_n a^n} \quad (3.3)$$

The number of ligands bound to the metal is given by [1]

$$\bar{n} = \frac{A - a}{M} \quad (3.4)$$

$$\bar{n} = \frac{[MA] + 2[MA_2] + \dots}{[M] + [MA] + [MA_2] + \dots} = \frac{\sum_1^N n \beta_n a^n}{\sum_0^N \beta_n a^n} \quad (3.5)$$

where  $a_c$  represents the degree of formation of the complex  $MA_c$  and  $\bar{n}$  the ligand number. Plot of  $\bar{n}$  vs.  $\log a$  results in the formation curve [1].

It is useful to note that  $a_c$  and  $\bar{n}$  are functions of ' $a$ ' only provided the system consists of a mononuclear complex. In the case of polynuclear complexes  $a_c$  and  $\bar{n}$  are dependent on both ' $a$ ' and the concentration of  $M$ . When mixed complexes  $MA_n L_m$  are formed,  $a_c$  and  $\bar{n}$  are functions of concentrations of both ligands  $A$  and  $L$ . Thus it is necessary in any system to confirm that the experimental values of  $a_c$  and  $\bar{n}$  are functions of ' $a$ ' only before calculating the stability constants. Once this condition is satisfied,  $N$  sets of values  $\bar{n}$ ,  $a$  or  $a_c$  should be sufficient for the determination of  $N$  values of  $\beta_n$ .

From equations (3.3) and (3.5) we obtain

$$\frac{d \log a_c}{d \log a} = c - \bar{n} \quad (3.6)$$

and the value of  $\bar{n}$  can be obtained from the slope of the plot of  $\log a_c$  vs.  $\log a$ . Integration of equation (3.6) gives

$$\log \alpha_c = \int (c - \bar{n}) d \log a + \text{constant} \quad (3.7)$$

from which the value of  $a_c$  is calculated knowing  $a$ ,  $\bar{n}$  and the integration constant. When  $c = 0$  we get

$$\log \frac{M}{m} = \int_0^a \bar{n} d \log a \quad (3.8)$$

Since  $M$  is known, the value of  $m$  can be obtained by integrating the curve involving  $\bar{n}$  vs.  $\log a$ . The free ligand concentration 'a' can be calculated from the values of  $\bar{n}$  and  $a_c$  using the relationship

$$\log a = \int \frac{1}{c - \bar{n}} d \log a_c + \text{constant} \quad (3.9)$$

The distribution of  $M$  among various mononuclear complexes as a function of free ligand concentration may appear as curves [2] shown in Fig. 3.1.

The ligand number,  $\bar{n}$  can be determined by four methods. The values of  $\bar{n}$  can be calculated from equation (3.4) provided  $M$  and  $A$  are known and that 'a' can be measured. When very strong complexes are involved,  $A \gg a$  in the concentration range where  $A < NM$  and the value of  $\bar{n}$  can be obtained from the relationship

$$\bar{n} \simeq \frac{A}{M}$$

without the knowledge of 'a'.

Note that this method is not applicable in the case of weak complexes or when tracer concentrations of  $M$  are present because the term  $A - a$  in equation (3.4) does not differ from zero.

Using equation (3.4) we may write

$$A = \bar{n}M + a \quad (3.10)$$

Thus for a series of "corresponding" solutions having the same unknown values of  $\bar{n}$  and 'a' but containing different total concentrations of  $A$  and  $M$ , a plot of  $A$  vs.  $M$  yields a straight line whose slope is  $\bar{n}$  and intercept 'a'. Alternatively the equations (3.4) and (3.5) may be solved algebraically to obtain values of  $\bar{n}$  and 'a'. Then the "correspondence" between two or more solutions may be established using a property which is a function of 'a' only, provided large concentrations of  $M$  can be used. The equation (3.6) can be written as

$$\frac{d \log x_c}{d \log a} = c - \bar{n} \quad (3.11)$$

where  $x_c$  is a property proportional to  $a_c$ . The most commonly used property is  $x_0 = 10^E$  where  $E$  is the potential of a cell reversible to metal ions and  $x_{c(>0)} = D_M$ , where  $D_M$  is the distribution ratio of  $M$  between two immiscible solvents. Equation (3.11) is in particular applicable when  $A - a \sim 0$  and tracer concentrations of  $M$  are involved.

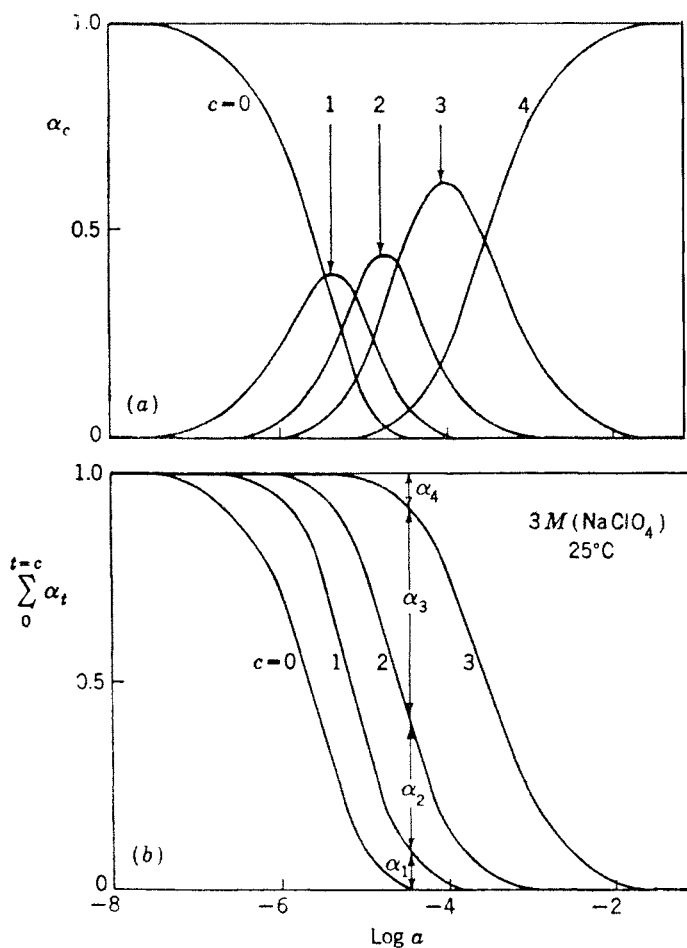


Fig. 3.1.

Colligative properties of solutions measure the sums of all the species in solution.

$$S = \sum_0^N [MA_n] + a = M + a \quad (3.12)$$

and hence

$$\bar{n} = \frac{A + M - S}{M} \quad (3.13)$$

The procedures used when free ligand concentration 'a' is not measured are outlined below. The simplest approach is to assume  $a \sim A$  and obtain the value of 'a' by successive



approximation. In case  $x_c$  or  $\alpha_c$  is determined as a function of  $A$ , approximate values of  $\bar{n}$  may be obtained graphically using the relationship

$$\frac{d \log x_c}{d \log a} \sim c - \bar{n} \quad (3.14)$$

The resulting values of  $\bar{n}$  are used in equation (3.4) to obtain preliminary values of 'a' and subsequent plot of  $\log x_c$  vs.  $\log a$  gives better values of  $\bar{n}$ .

When the value of 'm' is obtained experimentally by a technique such as potentiometry, the calculation of free ligand concentration can be done by using the concept of average number of ligands per complex [3] ( $\bar{v}$ )

$$\bar{v} = \frac{A - a}{M - m} \quad (3.15)$$

$$\bar{v} = \frac{\sum_1^N n \beta_n a^n}{\sum_1^N \beta_n a^n} \quad (3.16)$$

Initial values of  $\bar{n}$  are obtained from equation (3.14) and the values of  $\bar{v}$  are estimated using the relationships

$$\bar{v} \sim 1 \quad \text{in the range} \quad 0 < \bar{n} < 1.5$$

$$\bar{v} \sim \bar{n} \quad \text{in the range} \quad 1.5 < \bar{n} < N$$

Approximate values of free ligand concentration 'a' may be obtained from equation (3.15), using the values of  $\bar{v}$  and the experimentally obtained values of  $M$ ,  $m$  and  $A$ . Another procedure for determining free ligand concentration involves the relationship between a property  $X$  and the total ligand concentration  $A$  for a number of values of  $M$ . Plots of  $X$  vs.  $A_B$  are made followed by lines parallel to  $x$ -axis to obtain the relationship between  $A$  and  $M$  at different values of  $X$ . At the point  $M = 0$ , the free ligand concentration equals the total ligand concentration (i.e)  $a = A$  and extrapolation of the functions  $A(M)_x$  to cut the  $A$  axis gives the corresponding pairs of values  $X_{M=0}$  and 'a'. Although this method necessitates a vast amount of experimental data, its advantage is that the method is devoid of successive approximation. This procedure is of little utility when complexes of high stability are considered. In such cases, alternate procedures may be used. In one such procedure, the equation (3.6) is modified to give

$$\log \frac{a_2}{a_1} = \int_{F_0(a_1)}^{F_0(a_2)} \frac{1}{\bar{n}} d \log F_0, \quad (3.17)$$

where  $F_0 = 1/a_0$ . When pairs of values  $a_0$  and  $\bar{n}$  are known experimentally, the plot of  $1/\bar{n}$  vs.  $\log F_0$  can be integrated between the limits of  $F_0$  of known  $a_2$  value and unknown  $a_1$  value of ligand concentration. The value of  $\bar{n}$  may be obtained as a slope from the plot of  $M$  vs.  $A_x$  for corresponding solutions and the free ligand concentration  $a_2$  as the intercept of a line from a plot of  $M$  vs.  $A_x$  for which  $\bar{n} = N$  and  $A > NM$ .  $F_0$  is measured

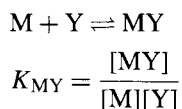
potentiometrically and the free ligand concentration  $a_1$  corresponding to each value of  $\bar{n}$  can be calculated from equation (3.17).

It is well known that a cyanide ligand is involved in the formation of extremely strong metal cyanide complexes, in which case equation (3.9) can be used to obtain  $\bar{n}$  valid in the range  $0 < A < NM$ . In this system,  $a_2$  can be calculated by preparing solutions with excess ligand such that all M is in the form of the highest complex  $MA_N$ . In such a case  $\bar{n} = N$ ,  $[MA_N] = M$  and  $a = A - NM$ . Since 'm' is experimentally measured, the overall stability constant  $\beta_n = M/ma^N$  could be calculated for a number of solutions. Taking the average value of  $\beta_n$ , measured value of 'm' the value of 'a' is calculated for the solution in which  $MA_N$  is completely formed and a negligible amount of ligand is left. In such a solution,  $\bar{n} = A/M = N$ . The free ligand concentration in all other solutions may then be calculated from the experimental values of  $\bar{n}$  and  $F_0$  using equation (3.17).

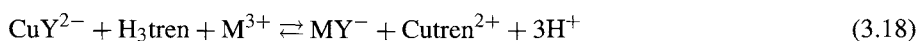
## 1. Methods

In this section it will be useful to discuss some common experimental methods used in the determination of stability constants of rare earth complexes. Ethylenediamine tetraacetate anion (EDTA) is a hexadentate and forms complexes with trivalent rare earth ion readily. The pioneering studies of Schwarzenbach [4] on the determination of stability constants of rare earth EDTA complexes by potentiometry and polarography can be considered to illustrate the principles involved in the determination of stability constants.

Denoting the rare earth metal as M and EDTA by Y we may write



The approach used makes use of the reaction



where 'tren' stands for trihydrochloride of  $\beta, \beta', \beta''$ -triaminotriethylene. The above reaction produces three protons which can be neutralized by three moles of NaOH in the buffer region of pH 4 to 5.5. The equilibrium constant for the above reaction may be written as

$$K = \frac{[MY][Cutren][H^+]^3}{[CuY][H_3tren][M]} = \frac{K_{cutren} \cdot K_{MY}}{\bar{K}_{H_3tren} \cdot K_{CuY}} \quad (3.19)$$

where  $K_{Cutren} = 10^{19.1}$ ,  $K_{CuY} = 10^{18.38}$ ,  $K_{H_3tren} = 10^{28.44}$ .

The mixture is mixed with a known volume and concentration of NaOH, equilibrated and the resulting pH measured. Representing NaOH by "a" the following equations are used in the calculation of K.

$$[Cu]_t = 10^{-3} = [CuY] + \alpha[Cutren]$$

TABLE 3.1  
Values of  $K_{MY}$  for rare earth ions [4].

Metal ion	log $K_{MY}$
La <sup>3+</sup>	14.72
Ce <sup>3+</sup>	15.39
Pr <sup>3+</sup>	15.75
Nd <sup>3+</sup>	16.06
Sm <sup>3+</sup>	16.55
Eu <sup>3+</sup>	16.69
Gd <sup>3+</sup>	16.70
Tb <sup>3+</sup>	17.25
Dy <sup>3+</sup>	17.57
Ho <sup>3+</sup>	17.67
Er <sup>3+</sup>	17.98
Tm <sup>3+</sup>	18.59
Yb <sup>3+</sup>	18.68
Lu <sup>3+</sup>	19.06
Y <sup>3+</sup>	17.38

$$[M]_t = 10^{-3} = [MY] + [M]$$

$$[Y]_t = 10^{-3} = [CuY] + [MY]$$

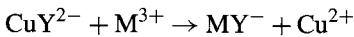
$$[tren]_t = 10^{-3} = [Cutren] + [H_3tren]$$

$$[H]_t = (3 - a) \times 10^{-3} = [H] + 3[H_3tren]$$

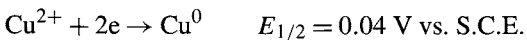
$$\alpha = 1 + \frac{[H]^3 \times \bar{K}_{Htren}}{[H_3tren]K_{cutren}}$$

From the knowledge of the values of  $\bar{K}_{H_3tren}$ ,  $K_{CuY}$ ,  $K_{Cutren}$  and combining with the calculated values of  $K$ , the values of  $K_{MY}$  are obtained. The resulting values of  $K_{MY}$  for the rare earth ions are given in Table 3.1.

An alternative method consisting of polarography was applied to the reaction.



and the stability constants for the formation of  $MY^-$  were evaluated. The method is based on the fact that free  $Cu^{2+}$  and complexed  $Cu^{2+}$  ion can be measured polarographically because the polarogram consists of two distinct waves due to the reaction



and reduction of  $CuY^{2-}$  with  $E_{1/2}$  of  $-0.32$  V. Between the two waves the diffusion current,  $i_d$  remains constant which is proportional to the concentration of free uncomplexed  $Cu^{2+}$  ion present in solution. The stability constants obtained by this method are given in the Table 3.2.

TABLE 3.2  
Stability constants of rare earths by polarography.

Rare earth ( $M^{3+}$ )	$\log K_{MY}$ [4]
Ce	15.6
Pr	15.8
Nd	16.0
Sm	16.3
Eu	16.5
Gd	16.6
Tb	17.38
Dy	17.75
Ho	18.31
Er	18.55
Tm	19.07
Yb	19.39
Lu	19.65
Y	17.56

The values of stability constants obtained for rare earth metal ions by the two methods are shown in Fig. 3.2. The agreement between the values obtained by the two methods is quite good for Ce, Pr and Nd extending up to Gd. The differences in the values is more prominent in the case of heavy rare earths (i.e.) from Dy to Lu. The large increase in the stability constant  $K_{MY}$  from  $La^{3+}$  to  $Ce^{3+}$  is paralleled by a rapid decrease in ionic radius from La to Ce.

Another example of the potentiometric technique as applied to the reaction of hydroxy naphthoic acids with  $M(III)$  ions, where  $M = Y, La, Ce, Pr, Nd$  and  $Sm$  may be considered to illustrate the Bjerrum method of analysis in the determination of stability constants [5]. The approach consists of potentiometric titration of (i) complexing agent with  $NaOH$  and (ii) mixture of metal and complexing agent with  $NaOH$  at constant ionic strength by using  $1\ M$  ( $NaClO_4$ ). Formation curves for the ligand are shown in Fig. 3.3 and the formation number,  $\bar{n}_A$  is calculated by the equation (3.20)

$$\bar{n}_A = \gamma - \frac{(v_2 - v_1)(N + E^0)}{(V^0 + v_1)T_L^0}, \quad (3.20)$$

where  $\gamma$  is the number of replaceable hydrogen ions ( $\gamma = 2$  in this case),  $E^0$  and  $T_L^0$  are the initial concentrations of  $HClO_4$  and naphthoic acid, respectively,  $v_1$  and  $v_2$  are the volumes of base of normality  $N$  required for titrations at a given  $pH$ , and  $V^0$  is the initial volume of the solution. Accurate values of  $pK_1$  are obtained from the equation (3.21) in the range  $1 < \bar{n}_A < 2.0$ .

$$\log \frac{\bar{n}_A - 1}{Z - \bar{n}_A} = pK_1 - pH \quad (3.21)$$

The formation of metal complexes is indicated by the considerable shift along the volume axis of the metal–ligand titration curve as compared to the ligand titration curve. The study assumes a negligible extent of hydrolysis of  $M(III)$ , and the formation of polynuclear

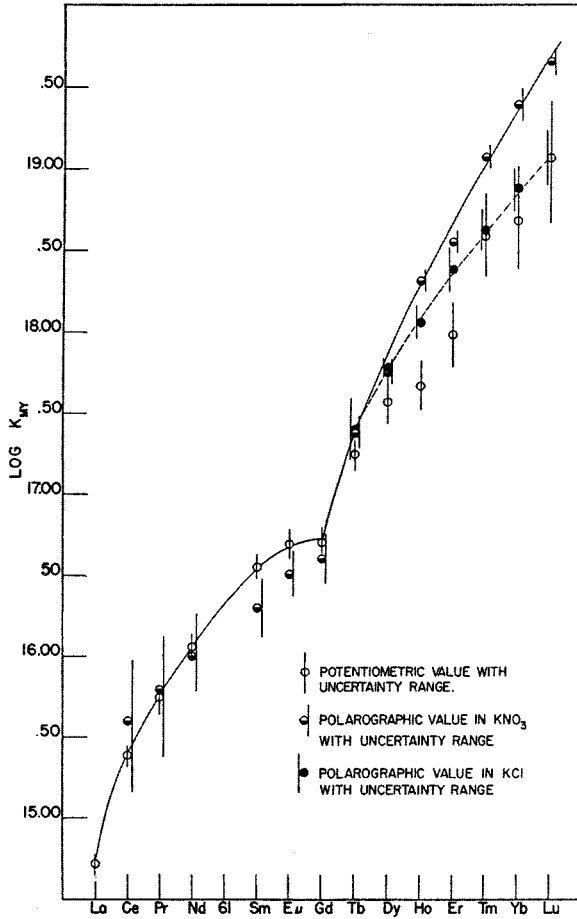


Fig. 3.2.

complexes. Under these conditions  $\bar{n}$ , the metal–ligand formation  $\bar{n}$  is obtained from equation (3.22)

$$\bar{n} = \frac{(v_3 - v_2)N + E + T_L^0(\gamma - \bar{n}_A)}{(v^0 + v_2)T_M^0\bar{n}_A}, \tag{3.22}$$

where  $v_3$  and  $v_4$  are the volumes of the base consumed in the titration of the metal complex and ligand, respectively, and  $T_M^0$  is the initial concentration of M(III) ions. The other quantities are the same as in equation (3.20). The method of Irving and Rossotti was used in calculating  $\bar{n}$  values and the  $\bar{n}$  values in B values (i.e. pH meter readings) range of 3 to 5.5 were continuous and the maximum value of 5.5 indicated the formation of 1:1 complex. The  $\bar{n}$  values at different B values showed an irregular trend above B value of 5.5 and up to 7.0. These abrupt changes may be attributed to the dissociation of the complex MLH and also the hydrolysis of the metal ion.

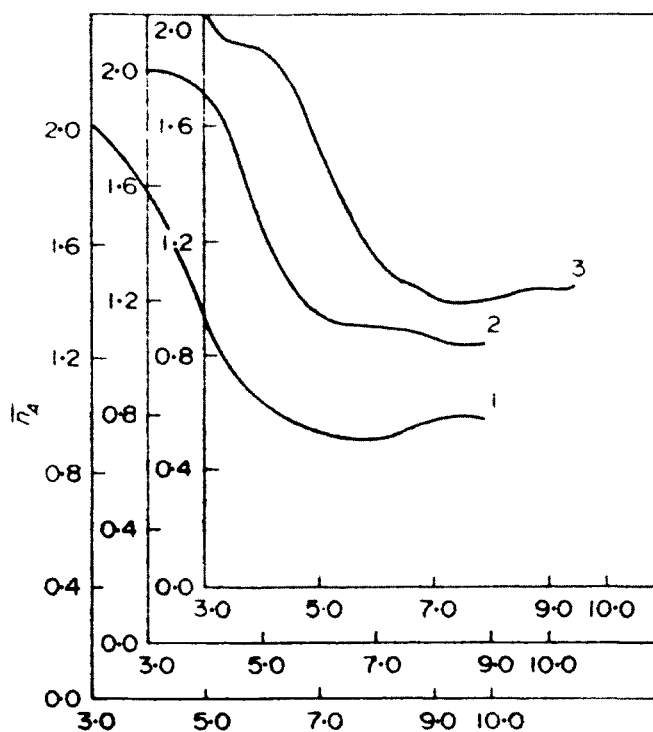


Fig. 3.3.

The values of  $pL = -\log[L]$ , where  $[L]$  is free ligand concentration have been calculated using equation (3.23)

$$pL = \frac{1 + ([H^+]/K_1) + ([H^+]/K_1K_2)}{T_L^0 - \bar{n}T_M^0} \times \frac{V^0 + v_3}{V^0} \quad (3.23)$$

The  $pL$  values at various  $\bar{n}$  values were evaluated and  $\log K_1$  determined by pointwise calculations. Typical formation curves of  $\bar{n}$  vs.  $pL$  are shown in Fig. 3.4.  $\log K_1$  obtained from the curves by noting the  $pL$  values at  $\bar{n} = 0.5$ . Pointwise calculations were used to obtain accurate values of  $\log K_1$ . The formation function used in these calculations is given by equation (3.24)

$$\log \frac{\bar{n}}{1 - \bar{n}} = \log K_1 - pL \quad (3.24)$$

By using the least squares method, equation (3.24) was solved and the resulting  $\log K_1$  are presented in Table 3.3.

The ionic nature of these complexes is illustrated by the correlation of the stability of  $M(III)$ , where  $M = Ce, Pr, Nd$  and  $Sm$  with hydroxy naphthoic acids versus  $e^2/r$  as shown in Fig. 3.5.

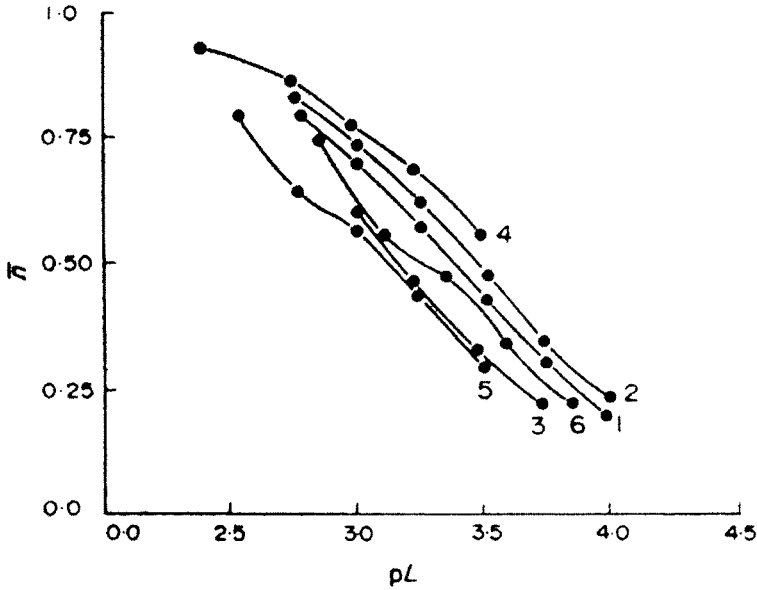


Fig. 3.4.

TABLE 3.3  
log  $K_1$  of lanthanide(III) complexes [5].

Ligand	Y(III)	La(III)	Ce(III)	Pr(III)	Nd(III)	Sm(III)
2-hydroxy-1-naphthoic acid	5.28	5.37	5.08	5.49	5.06	5.31
2-hydroxy-1-naphthoic acid	4.72	6.00	4.97	5.48	5.56	5.90
1-hydroxy-2-naphthoic acid	4.97	5.55	4.73	4.96	4.07	5.22

The spectrophotometric method applied to the determination of the composition and stability constant of the complex formed between Sc(III), Y(III) and La(III) with the chromogenic agent Alizarin Red S (ARS) shows the utility of the method when distinct differences in absorption spectra are present. Some of the conditions that must be satisfied for this method to be valid are: (i) the complexing agent (ARS) and the metal complex to have distinct absorption spectra so that the concentrations of the ligand, free metal ion and the metal complex in solution can be determined experimentally, (ii) the metal complex should be stable in a given pH range, (iii) composition of the complex can be established by different methods such as the method of continuous variations, slope ratio method and mole ratio method. In the case of the La(III)–ARS system, the complex has absorption maximum at 520 nm compared to the ligand which has its maximum at 420 nm [6,7]. The continuous variation method for the La(III)–ARS system is illustrated in Fig. 3.6. The curves show a maximum at the ratio of La/La + ARS of 0.3 to give the complex composition of La(ARS)<sub>2</sub>. The second approach used in determining the composition of the complex, namely, mole ratio method, consisted of determining the absorbance at 530 nm

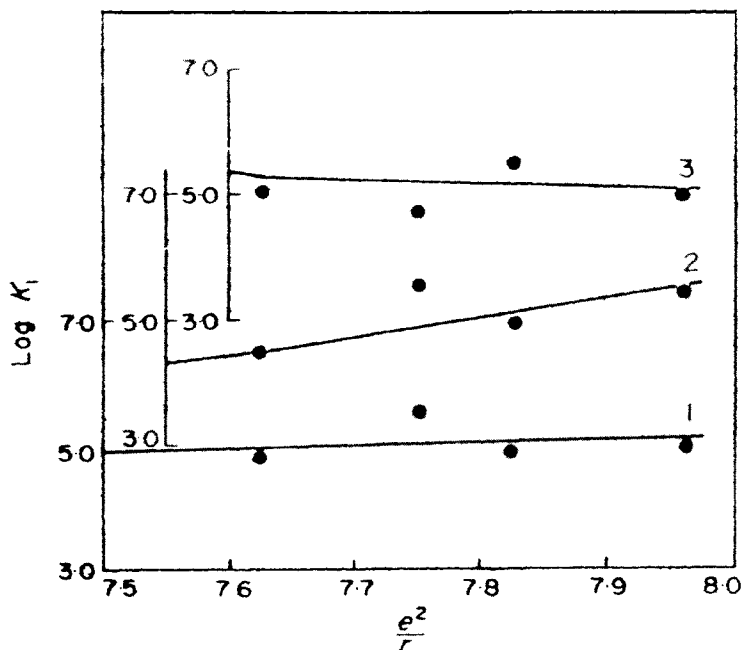
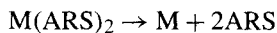


Fig. 3.5.

of a series of solutions containing different mole ratios of La/ARS. The resulting data are plotted as measured absorbance vs. mole ratio of La/ARS. Fig. 3.7 illustrates this method and it is obvious from the figure that La:ARS is in the ratio 1:2 indicating the formation of  $\text{La}(\text{ARS})_2$  complex in solution.

The third approach in establishing the composition of the complex consists of measuring the absorbance of two sets of solutions at two suitable wavelengths. The solutions consist of a fixed metal ion but variable ARS concentration in one and fixed ARS but variable metal ion in another. The measured absorbance at a chosen wavelength is plotted against the amount of variable component. The ratio of the slopes of the resulting lines at the two wavelengths gives the number of ligand molecules in the complex. This approach is illustrated in Fig. 3.8 for the system La-ARS.

Having established the composition of the complex, the stability constant of the complex was determined by (i) mole ratio method and (ii) continuous variations method. In the former method, the equilibrium considered is



whose initial concentrations are  $\text{M}(\text{ARS})_2 = c$ ,  $\text{M}$  and  $2\text{B} = 0$  with  $\alpha$ , the degree of dissociation, equilibrium concentrations of  $\text{M}(\text{ARS})_2 = c(1 - \alpha)$ ,  $\text{A} = \alpha c$ ,  $\text{B} = 2\alpha c$ . In such a case, the dissociation constant may be written as

$$K = \frac{(\alpha c)(2\alpha c)^2}{c(1 - \alpha)}$$



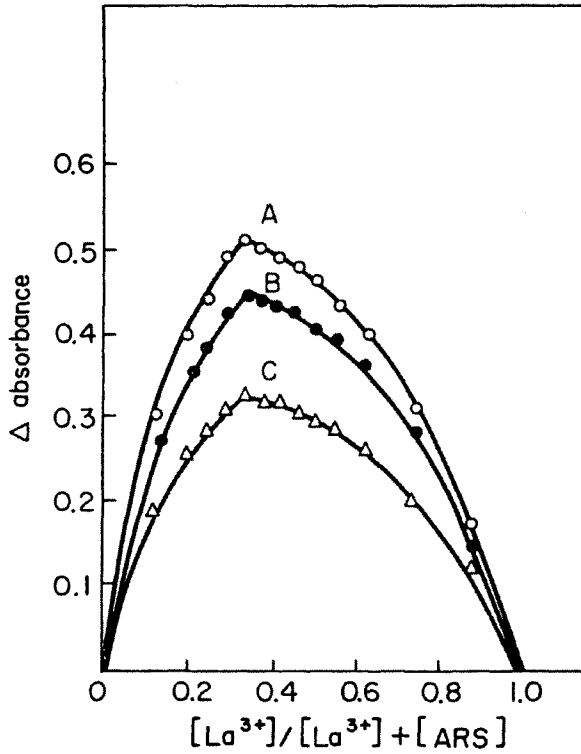


Fig. 3.6.

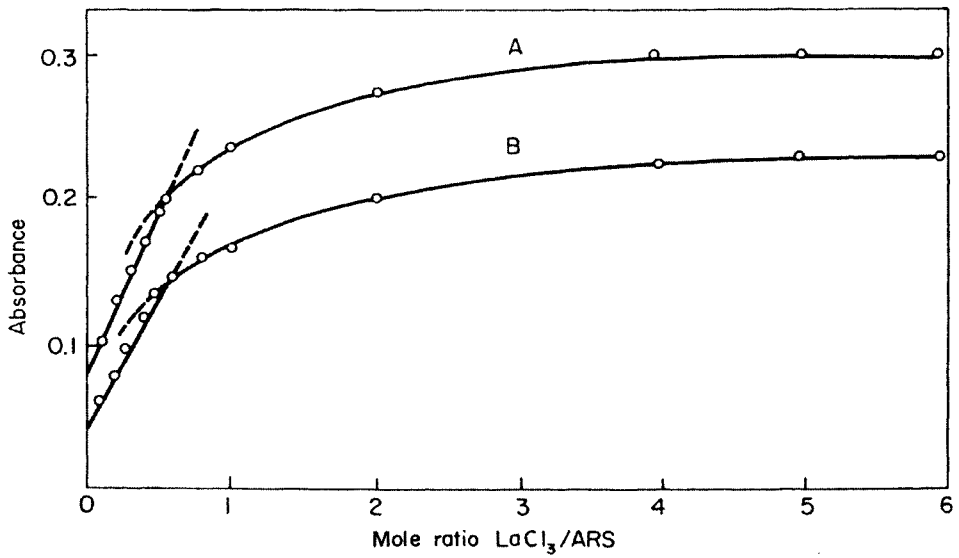


Fig. 3.7.

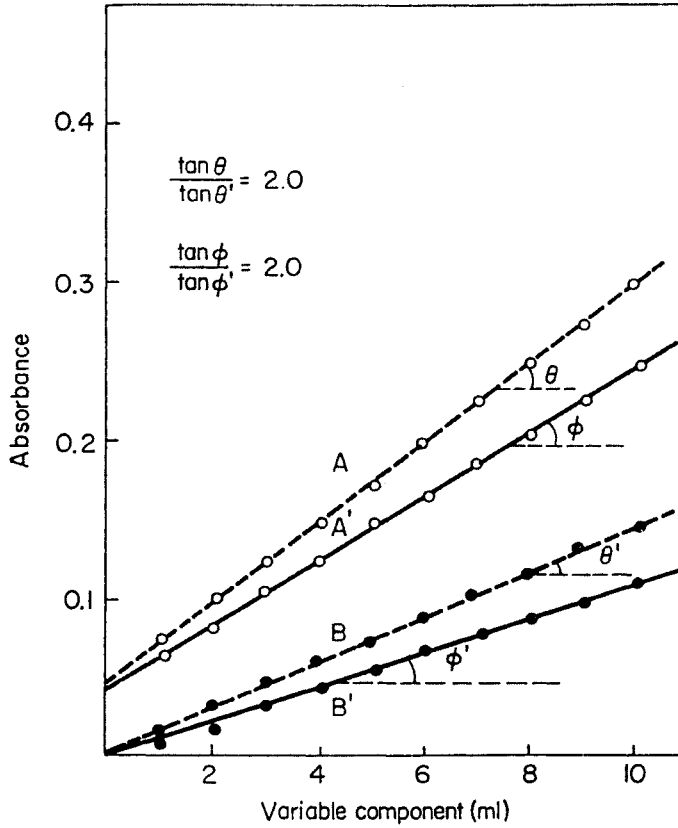


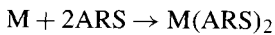
Fig. 3.8.

and  $\alpha$  is obtained from the relation

$$\alpha = \frac{E_m - E_s}{E_m}$$

where  $E_m$  is the maximum extinction when all the reagent is in the form of complex and  $E_s$  is the extinction at the stoichiometry.

In the continuous variations method for the reaction



the formation constant  $K$  is given by

$$K = \frac{M(ARS)_2}{M(ARS)^2} = \frac{x}{(a-x)(b-2x)^2}, \quad (3.25)$$

TABLE 3.4  
Stability constant of La(ARS)<sub>2</sub> at 25°C [6].

Method	pH	log <i>K</i>	Δ <i>G</i> <sup>0</sup> (kcal)
Mole ratio	4.0	8.6 ± 0.2	-11.9 ± 0.2
Continuous variations	4.0	8.3 ± 0.1	-11.5 ± 0.1

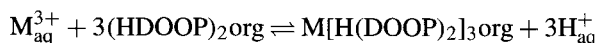
where *x* is the complex concentration at equilibrium, *a* and *b* are initial concentrations of metal ion and ARS. Taking two different initial concentrations but with same value of *x*

$$K = \frac{x}{(a-x)(b-2x)^2} = \frac{x}{(a^1-x)(b^1-2x)^2} \quad (3.26)$$

The value of *x* the extent of complex formation can be calculated and hence the value *K*. The resulting data are given in Table 3.4.

The data in the table summarized above show good agreement thus showing the relevance of different approaches as a necessary condition in obtaining information on the stability constant. The structure has been suggested for the complex based on experiments involving ion exchange retention on IR-45.

The solvent extraction method involves the distribution of metal into two different phases such as aqueous and organic phases. Knowledge of the distribution constants can be used in the determination of stability constants of chloro and nitrate complexes of rare earth metal ions. This method has been successfully applied to the determination of stability constants of MCl<sup>2+</sup> and MNO<sub>3</sub><sup>2+</sup>, where M = La, Ce, Pr, Eu, Tm, Yb and Lu. The method consists of equilibrating an aqueous solution of metal ion [8] 1 M in H<sup>+</sup> and 1 M in perchlorate and chloride in the case of chloride and 1 M in perchlorate and nitrate in the case of nitrate complexes with dioctyl phenyl phosphoric acid (HDOOP) in toluene as the organic phase. The distribution coefficient or constant is obtained by determining the metal ion concentration in both aqueous and organic phase after equilibration. The extraction of the lanthanide ion into the organic phase from the aqueous phase may be represented by the reaction



The distribution ratio *K* for M<sup>3+</sup> may be written as

$$K = k_1 [\text{H}(\text{DOOP})_2]_{\text{org}}^3 / [\text{H}^+]_{\text{aq}}^3 \quad (3.27)$$

In order to establish the absence of anions ClO<sub>4</sub><sup>-</sup>, Cl<sup>-</sup>, or NO<sub>3</sub><sup>-</sup> in the metal M<sup>3+</sup> extracted the inverse third power dependence on H<sup>+</sup> ion is proved by a plot of log *K* vs. log[H<sup>+</sup>] whose slope is -3.0 (Fig. 3.9).

Similar dependence on [H<sup>+</sup>] is also established in the medium of HNO<sub>3</sub> and NaNO<sub>3</sub> to show the absence of extraction of MNO<sub>3</sub><sup>2+</sup> into the organic phase. The succeeding step is to show the variation of *K* with the concentration of X<sup>-</sup> = Cl<sup>-</sup>, NO<sub>3</sub><sup>-</sup> by extraction

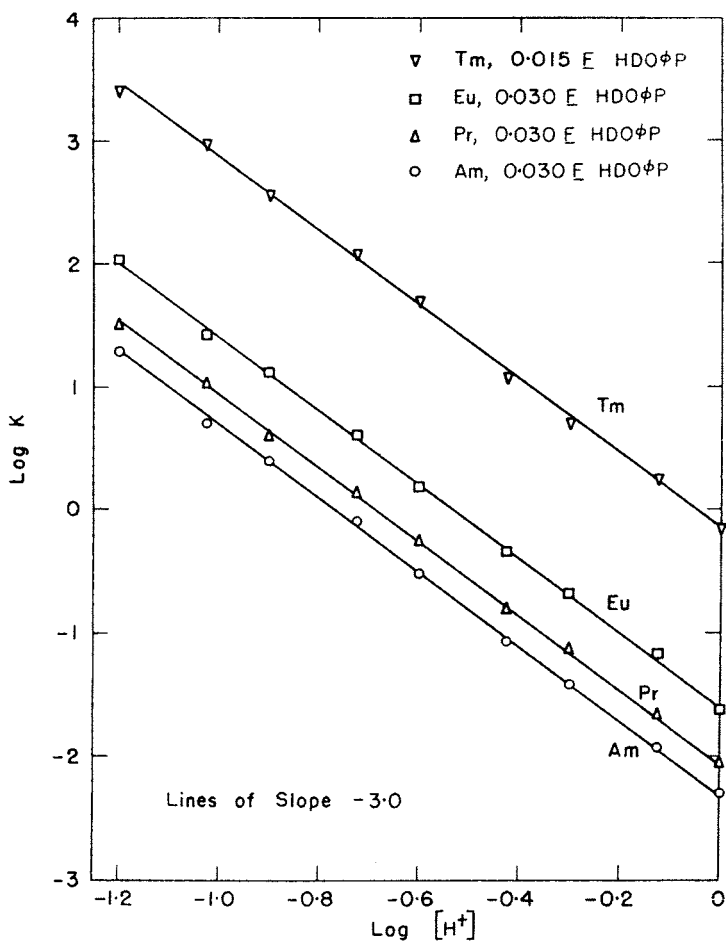


Fig. 3.9.

TABLE 3.5  
Stability constants for  $\text{MX}^{2+}$ ,  $\mu = 1.00$ ,  $22 \pm 1^\circ\text{C}$ .

M(III)	$K_c$ for $\text{MX}^{2+}$	
	$\text{X}^- = \text{Cl}^-$	$\text{X}^- = \text{NO}_3^-$
La	$0.9 \pm 0.3$	$1.3 \pm 0.3$
Ce	$0.9 \pm 0.3$	$1.3 \pm 0.3$
Pr	$0.9 \pm 0.3$	$1.7 \pm 0.3$
Eu	$0.9 \pm 0.3$	$2.0 \pm 0.3$
Tm	$0.8 \pm 0.3$	$0.7 \pm 0.2$
Yb	$0.6 \pm 0.2$	$0.6 \pm 0.2$
Lu	$0.4 \pm 0.2$	$0.6 \pm 0.2$
Am	$0.9 \pm 0.2$	$1.8 \pm 0.3$

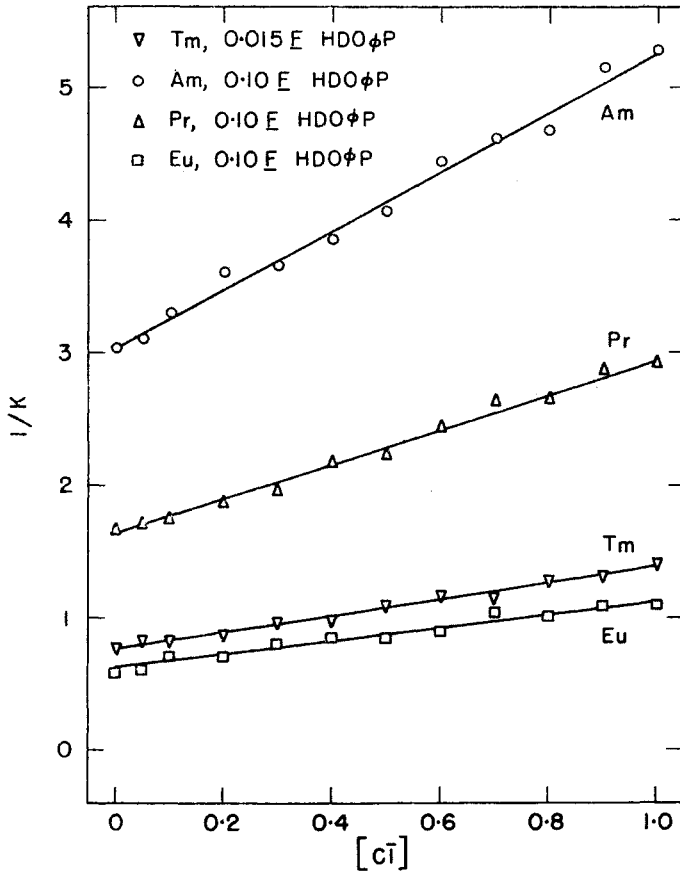


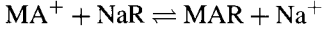
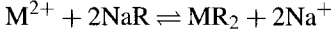
Fig. 3.10.

into HDOOP at a fixed amount of toluene. The experimentally determined  $K$  values as a function of varying concentration of  $X^- = \text{Cl}^-, \text{NO}_3^-$  at constant ionic strength,  $\mu = 1.0$  are plotted with  $1/K$  as ordinate and the anion concentration on the abscissa. A typical plot in the case of rare earth ions  $M^{3+}$  ( $M = \text{Eu}, \text{Tm}, \text{Pr}$ ) is shown in Fig. 3.10 for the chloride medium containing  $\text{HCl}$  and  $\text{HClO}_4$ . From the slope and zero intercept values of the straight lines in Fig. 3.10, the stability constant of the complex  $\text{MCl}^{2+}$  was calculated. A similar procedure in the case of nitrate was adopted to determine the stability constants of  $\text{MNO}_3^{2+}$  complexes, where  $M = \text{Pr}, \text{Eu}, \text{Tm}$ . The resulting values obtained by this technique are summarized in Table 3.5.

Comparative values obtained for  $\text{CeCl}^{2+}$  obtained by other techniques are 1.25 and 1.73 at  $\mu = 0.6$  and 1.0, respectively. In the case of  $\text{CeNO}_3^{2+}$  complex, the value of 1.4 at  $\mu = 0.9$  obtained by other techniques shows good agreement with the value of 1.3 at  $\mu = 1.0$ .

The ion exchange method of determination of stability constants can be illustrated by the complex formation of  $\text{Ho}$  and  $\text{Yb}$  with acetyl acetone as the ligand. It is necessary to elucidate some principles involved in the ion exchange method in the determination

of stability constants of complexes [9]. Consider a metal ion  $M^{2+}$  and  $MA^+$  complex, the sodium form of the ion exchange resin in equilibrium. Then we have the exchange reactions



We may then write

$$\frac{MR_2}{[M^{2+}]} = k_0 \frac{(NaR)^2}{[Na^+]^2} \quad (3.28)$$

$$\frac{(MAR)}{[MA^+]} = k_1 \frac{(NaR)}{[Na^+]} \quad (3.29)$$

$k_0$  and  $k_1$  are constant at a fixed value of  $C_{MR} = (MR_2) + (MAR)$ , where  $MR_2$ ,  $MAR$  are moles of  $M^{2+}$  and  $MA^+$ , respectively, contained in one unit weight of ion exchanger at equilibrium.

$$\text{Let } l_0 = k_0 \frac{(NaR)^2}{[Na^+]^2}; \quad l_1 = k_1 \frac{(NaR)}{[Na^+]} \quad (3.30)$$

When  $C_M$ , the total concentration of  $M^{2+}$  in the ion exchange resin is low in comparison with ionic strength, then  $[Na^+]$  is constant in all the solutions. We may then write for  $(NaR)$ :

$$(NaR) = a - 2(MR_2) - (MAR) \quad (3.31)$$

$$(NaR) = a - 2(2 - \bar{n}_R)C_{MR} \quad (3.32)$$

where 'a' is the exchange capacity and  $\bar{n}_R = (MAR)/C_{MR}$ . Using the definition of  $C_{MR}$  and equations (3.28)–(3.30)

$$C_{MR} = l_0[M^{2+}] + l_1[MA^+] \quad (3.33)$$

Combining the expressions  $[MA^+] = \beta_1[M^{2+}][A^-]$ ,  $C_M = [M^{2+}][A^-]$ ,  $C_M = [M^{2+}]x$  with equation (3.33) and defining  $l_1\beta_1/l_0 = l$  we get

$$\phi = l_0 \frac{1 + l[A^-]}{x} \quad (3.34)$$

From equations (3.30) and (3.31) and (3.32) at constant 'a' value (or pH),  $C_{MR}$  is very small, that the term  $(2 - \bar{n}_R)C_{MR}$  in equation (3.32) becomes negligible and  $l_0$ ,  $l_1$  and  $l$  are constants. Thus we have

$$\bar{n}_R = \frac{l[A^-]}{1 + l[A^-]} \quad (3.35)$$

It is necessary  $C_{MR}$  should be low and kept constant so that equation (3.34) with constant  $l$  and  $l_0$  can be used within a concentration range of  $[A^-]$  that is large enough for the calculation of stability constants of complexes. In order to calculate  $C_{MR}$  and  $\phi$  the following equation is used

$$C_{MR} = \frac{v}{m}(C'_M - C_M\delta), \quad (3.36)$$

where  $v$  is initial volume of the solution,  $m$  = the weight of the resin,  $v\delta$  the volume at equilibrium and  $C'_M$  is the initial concentration of  $M^{2+}$  in solution and  $C'_M$ ,  $C_M$  and  $\delta$  are experimentally obtained. Because of swelling of the resin and  $\delta < 1$  and is the quotient between the initial and final concentrations of the ligand in solutions at  $C_M = 0$ , the value of  $\delta$  is independent of  $C_A$  at constant ionic strength.

As an approximation of  $\bar{n}$ , the following relationship can be used

$$\bar{n} \simeq -\frac{C_A}{\phi} \left( \frac{\partial \phi}{\partial C_A} \right)_{C_{MR}} \quad (3.37)$$

and this relationship is obtained from equation (3.34) by letting  $l \simeq 0$  and  $C_A \simeq [A^-]$ . Then the  $[A^-]$  values are calculated from the relationship  $[A^-] = C_A - \bar{n}$ .  $C_M$  and this approximation is satisfactory since  $C_M$  is small. Having determined  $\phi$  as a function of  $[A^-]$  when  $l$  and  $l_0$  are constants, we now turn to calculate  $\beta_j$  stability constants. The product  $\phi x$  is differentiated twice with respect to  $[A^-]$  and from equation (3.34) we get

$$\phi'' x + 2\phi' x' + \phi' X'' = 0$$

where

$$\phi' = \frac{d\phi}{d[A^-]}, \quad \phi'' = \frac{d^2\phi}{d[A^-]^2}$$

$$x = 1 + \sum_{j=1}^N \beta_j [A^-]^j, \quad x_j = (x_{j-1} - \beta_{j-1})/[A^-]$$

Substituting for  $x$ ,  $x'$ ,  $x''$  we can write

$$\phi'' + \sum_{j=1}^N \alpha_j \beta_j = 0 \quad (3.38)$$

By graphically plotting  $\phi$  as a function of  $[A^-]$  one can determine  $\phi'$  and similarly  $\phi''$  from a plot of  $\phi'$  vs.  $[A^-]\phi''$  and  $\alpha_j$  are obtained at  $N$  values of  $[A^-]$  in the concentration range used. Thus there are  $N$  equations from which the stability constants  $\beta_j$  can be evaluated. The quotient  $\phi$  between the total concentration of the central group adsorbed on the resin ( $C_{MR}$ ) and in solution,  $C_M$  at equilibrium is written as

$$\phi = \frac{l_0 + l_1 \beta_1 [A^-]}{x} \quad (3.39)$$

The function  $\phi$  on graphical extrapolation to  $[A^-] = 0$  leads to the relation

$$l_0 = \lim_{[A^-] \rightarrow 0} \phi \quad (3.40)$$

Thus knowing  $l_0$  the function  $\phi$  can be written as

$$\phi_1 = (l_1\phi^{-1} - 1)[A^-]^{-1} \quad (3.41)$$

By letting  $l = l_1\beta_1l_0^{-1} = 1$  and using it, and extrapolation of  $\phi_1$  to  $[A^-] = 0$  leads to the expression

$$\beta - 1 = \lim_{[A^-] \rightarrow 0} \phi_1 \quad (3.42)$$

A new function  $f$  containing  $l_0$  and  $\beta_1 - l$  is defined as

$$f = \frac{l_0\phi^{-1}\{(\beta_1 - l)[A^-] - 1\} + 1}{[A^-]^2} \quad (3.43)$$

It is also possible to rewrite equation (3.39) as

$$f = \beta_1\phi_1 - \sum_{j=2}^N \beta_j[A^-]^{j-2} \quad (3.44)$$

Using the approach and methodology of Fronaeas, the ion exchange method has been successfully applied for the complex formation Ho and Yb with acetyl acetone. Dowex 50 in the sodium form and  $^{166}\text{Ho}$   $^{175}\text{Yb}$  radio tracers were used. The fundamental relations used are [10]

$$\phi_1 = (l_0\phi^{-1} - 1)[A^-] \quad \lim_{[A^-] \rightarrow 0} \phi = l_0 \quad (3.45)$$

$$f = \frac{l_0\phi^{-1}\{(K_1 - l)[A^-] - 1\} + 1}{[A^-]^2} \quad \lim_{[A^-] \rightarrow 0} \phi_1 = K_1 - l \quad (3.46)$$

$$l = \frac{k_a K_1 (\text{NaR})^3}{l_0 [\text{Na}]^3} \quad \lim_{[A^-] \rightarrow 0} f = f_0 \quad (3.47)$$

The significance of all the quantities are the same as in the previous equation, except for  $K_1$  and  $K_a$  which represent the stability constant of  $M(\text{AcAc})$  and equilibrium ion exchange constant, respectively.

The least squares method was used in the calculation of  $(K_1 - l)$ ,  $f_0$  and  $K_1$ . Experimentally, values of  $\phi$ ,  $f$ ,  $\Delta\phi_1/[A^-]$  and  $\Delta f/[A^-]$  at different values of  $[A^-]$  in the range  $3.12 \times 10^{-4}$  to  $1.32 \times 10^{-3}$  M for Ho and  $1.6 \times 10^{-4}$  to  $1.06 \times 10^{-3}$  M for Yb were obtained. The resulting data are given in Table 3.6. The table also gives data on the stability constants obtained by the potentiometric method. The values of  $\log K_1$  and  $\log K_2$  obtained by the two methods show fair agreement considering the limitations inherent in the two methods.



TABLE 3.6

Step-wise complexity constants  $K_n$  determined by ion exchange method and by potentiometric method [1].

Method	$\log K_1$		$\log K_2$		$\log K_3$	
	Ho	Yb	Ho	Yb	Ho	Yb
Ion exchange	5.65	5.7	4.76	4.45	—	—
Potentiometric	6.05	6.18	4.68	4.86	3.40	3.60

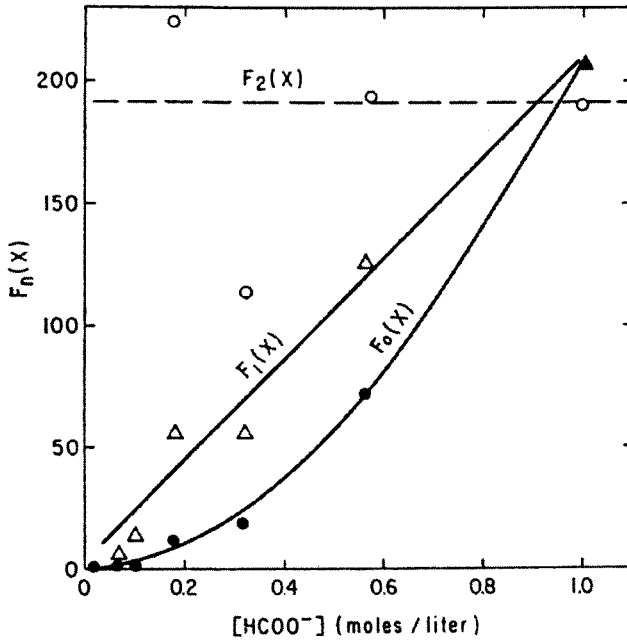


Fig. 3.11.

Chronopotentiometry and polarography were used in studying Eu(III) formate complexes [11]. At constant ionic strength of 1 M by means of  $\text{NaClO}_4$  and a pH 4.3 formate concentration is varied from 0.01 to 1.0 M keeping Eu at  $1.60 \times 10^{-4}$  M. In formate medium, the polarographic reduction of Eu(III) at the dropping mercury electrode is irreversible as evidenced by a plot of  $E$  the potential vs.  $\ln i/i_d - i$  a value of 0.5 for  $n$ . The chronopotentiometric reduction of Eu(III) was reversible and the plot of  $E$  vs.  $\ln(\tau^{1/2} - t^{1/2})/t^{1/2}$  gave a value of 0.9 for  $n$ . This difference in reversibility is attributed in part to the adsorption of formic acid on the electrode surface and the longer contact time between the electrode and solution in the chronopotentiometric process. The polarographic approach consisted of defining a function

$$F_0(x) = \text{anti log} \left\{ \frac{0.43nF}{RT} [(E_{1/2})_s - (E_{1/2})_s - (E_{1/2})_c] \right\} \quad (3.48)$$

and then plotting  $F_n(x)$  vs. formate concentration as shown in Fig. 3.11.

A least squares plot of  $F_1(x)$  vs. formate concentration gave a value of 16.3 for the intercept  $K_1$  and a slope of 197 which is in good agreement with the value of 192 for  $K_2$  derived from  $F_2(x)$ . The slope of  $F_2(x)$  is zero and thus the major species present in solution are  $\text{Eu}(\text{HCOO})_2^+$ ,  $\text{Eu}(\text{HCOO})_2^{2+}$  and  $\text{Eu}^{3+}$ .

In the chronopotentiometric method, the quarter wave potentials are used and the corresponding function may be written as

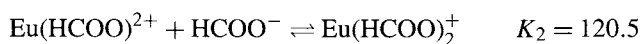
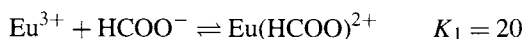
$$F_0(x) = \text{anti log} \left\{ \frac{0.43nF}{RT} [(E_{1/4})_s - (E_{1/4})_c] \right\},$$

where subscripts for  $E_{1/4}$ , s and c refer to aquo ion and complex ion, respectively. The uncertainty in  $E_{1/4}$  is about  $\pm 0.5$  mV with a consequent scatter in calculated points.  $F_1(x)$  is assumed to be linear and the  $F_0(x)$ ,  $F_1(x)$  and  $F_2(x)$  values are given in the table below.

Chronopotentiometric data for Eu(III) formate system.

$[\text{HCOO}^-]$ (M)	$E_{1/4}$	$F_0(x)$	$F_1(x)$	$F_2(x)$
0.00	-0.535	1.00		
0.10	-0.557	2.36	13.6	
0.316	-0.605	15.4	45.5	
0.562	-0.613	21.0	35.6	22.9
1.00	-0.642	6.2	64.2	41.4 $K_2 = 45.4$
Reverse				
0.00	-0.535	1.00		
0.01	-0.532	1.00		
0.10	-0.567	3.49	24.9	
0.178	-0.594	10.00	50.6	106
0.316	-0.624	32.3	98.9	238
0.562	-0.627	36.3	62.8	71.3
1.00	-0.655	117	116	93.2 $K_2 = 127$

From the data, it is evident the scatter in chronopotentiometric data is large and that the polarographic method gives fairly reliable data for  $K_1$  and  $K_2$ .



The distribution diagram for Eu(III) among the various complexes in the presence of formate is shown in Fig. 3.12.

## 2. Stability of rare earth complexes in solution

Some of the important techniques used in the determination of stability constants have already been discussed together with some examples. The values for the formation constants of rare earth complexes with inorganic and organic ligands are given in

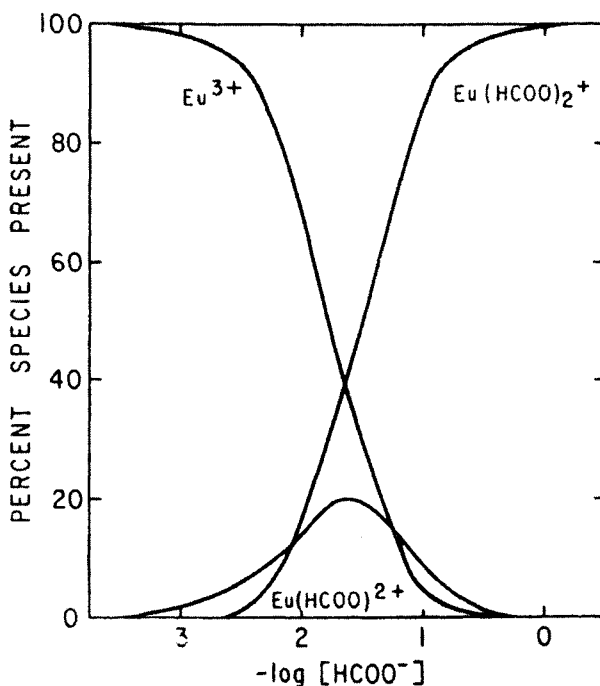


Fig. 3.12.

Tables 3.10 and 3.11, respectively (see Appendix). These tables of data are by no means encyclopedic in nature. In general, it is difficult to ascertain the absolute accuracy of a given set of data and hence several sets of data are given for some ligands. In general, the values obtained by the ion exchange method tend to be less precise and accurate than those obtained by potentiometric titration.

Stability constant data have been obtained both from the practical point of view of developing new and improved techniques of separation of individual rare earths and the more fundamental view of obtaining a deeper insight into the structure and bonding in the complexes. Thus comparisons of the data are useful and require care because significant variations in the reported data can result from small changes in conditions such as ionic strength and temperature. In general, the reported data are based on concentration rather than activity.

Although a large number of ligands have been studied, data are not available for all the elements in some cases and also many ligands are substituted molecules of the same parent molecule. Thus the complexing behaviour of a parent ligand (PL) and substituted parent ligand (SPL) will not differ drastically as far as the trend in the stability constant values is concerned. The available data for ligands that have been studied with all the rare earths completely indicate that it is not easy to interpolate or extrapolate in other systems where data are available for only a few rare earth metal ions. Thus although there is a large body of data on the stability constants (Table 3.11, see Appendix) it is difficult to rationalize the data in general terms. Hence some salient features will be mentioned.

The crystal radii of the rare earth metal ions decrease in a regular manner along the series. There is vast data suggestive of the formation of predominantly ionic complexes in the case of rare earth ions. Based on electrostatic theory, a direct relationship between the stability constant values and the atomic number of the rare earth metal ion is predicted [12]. In most of the complexes, this correlation of  $\log K_1$  with  $Z$  holds good for La to Eu although in some cases the europium complexes are less stable than the samarium complexes. Further, this simple relationship is not valid when the heavy rare earth ions Tb to Lu are considered.

Thus there is a need for alternate considerations when the data for elements following gadolinium are considered. According to Moeller [13] the trends in the formation constant data for rare earths past gadolinium may qualitatively be divided into three groups. The first group consists of ligands which show a regular increase in formation constants along the series. This does not imply that the ligands follow the simple electrostatic model since the slope of the plot of  $\log K_1$  vs.  $1/r$ , where  $r$  is the ionic radius is not the same as in the case of elements preceding gadolinium. Some typical ligands belonging to this group are glycolic acid, lactic acid, iminodiacetic acid  $\alpha$ -hydroxyisobutyric acid, nitrotriacetic acid (NTA), ethylenediamine  $N,N'$ -diacetic acid, and ethylenediamine  $N,N,N',N'$ -tetraacetic acid (EDTA).

The second group of ligands have complex formation constants for the elements past gadolinium which are very nearly the same.

The ligands showing this behaviour are acetic acid, mercaptoacetic acid, methoxyacetic acid, acetylacetone, dipicolinic acid and  $N'$ -(2-hydroxyethyl)ethylenediamine  $N,N,N'$ -triacetic acid.

The third group behaviour is typified by 2,2'-bis[di(carboxymethyl)amino]diethyl ether and diethylenetriamine  $N,N,N',N',N'$ -pentaacetic acid. The formation constants for elements after gadolinium show a slight increase initially followed by a decrease. The manner in which the formation constants vary across the series as a function of  $1/r$  is shown in the Fig. 3.13.

In the case of a majority of ligands, the gadolinium complex is less stable than one would expect based on the simple electrostatic model. This has been known as the "gadolinium break" which cannot be explained in terms of steric hindrance since this anomaly is present even with ligands which offer no steric hindrance.

The position of yttrium in rare earth chemistry has always been interesting and this is also the case with respect to complex formation. The electrostatic model suggests placement of yttrium between holmium and thulium. It has been shown that it is not the case [14]. When one considers the stability constant data of group 1 ligands, yttrium is similar to the heavy rare earths. When the second group of ligands is considered, yttrium exhibits a behaviour similar to the lighter rare earth elements.

The trends in the stability constants of 2:1 and higher complexes are difficult to analyze because of the onset of steric effects and the magnitude of errors involved in the measurements. The group classification of the ligand remains unaltered in the case of data that are reliable and accurate.

The position of yttrium in 2:1 complexes shifts totally from the 1:1 complexes. With ligands of the second group such as mercapto acetic acid, yttrium resembles the heavy rare earths. In the case of iminodiacetic acid, yttrium forms a complex whose formation constant is more in keeping with the light rare earths.

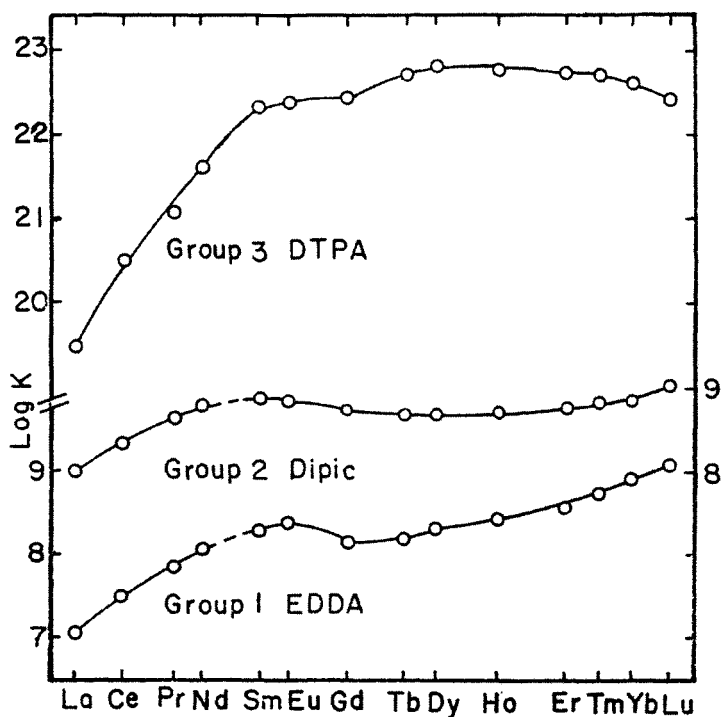


Fig. 3.13.

There are three main considerations involved in explaining the trends in the formation constants. The three considerations are: (i) crystal field effects, (ii) increase in coordination number and (iii) steric factors. The possible involvement of crystal field effects is useful in explaining the trends in the stability constant for ligands in the first group, since the change in  $\log K_1$  values with increasing atomic number is similar to the trend in d transition elements. The break in gadolinium is easily explained since  $f^7$ , a half-filled configuration, should have no crystal field stabilization. Yttrium also does not have any crystal field stabilization and this explains the reason why yttrium complexes do not occupy the expected place when the plot is based on the radius of the yttrium ion. Crystal field stabilization in holmium and dysprosium complexes with  $\alpha$ -hydroxyisobutyric acid has been postulated on this basis [15]. Ligand field effects have been applied by Yatsimirskii successfully in explaining the trends in stability of aminocarboxylic acid and carboxylic acid complexes of rare earths [16]. Schwarzenbach [17] showed that many properties of rare earths such as ionic radii, heats of dissolution of halides, molar volumes of basic sulphates, some basic properties of hydroxides and stability constants of some complexes exhibit a discontinuity at gadolinium known as "gadolinium break". The change in some properties of rare earth compounds is illustrated in Fig. 3.14. The stability constants of the complexes are related to the heat of formation and the deviation from the linear relationship shown by the change in the properties can be attributed to the extrastabilization energy. The ionic radii, molar volumes, and basic properties are determined by the effective charge of

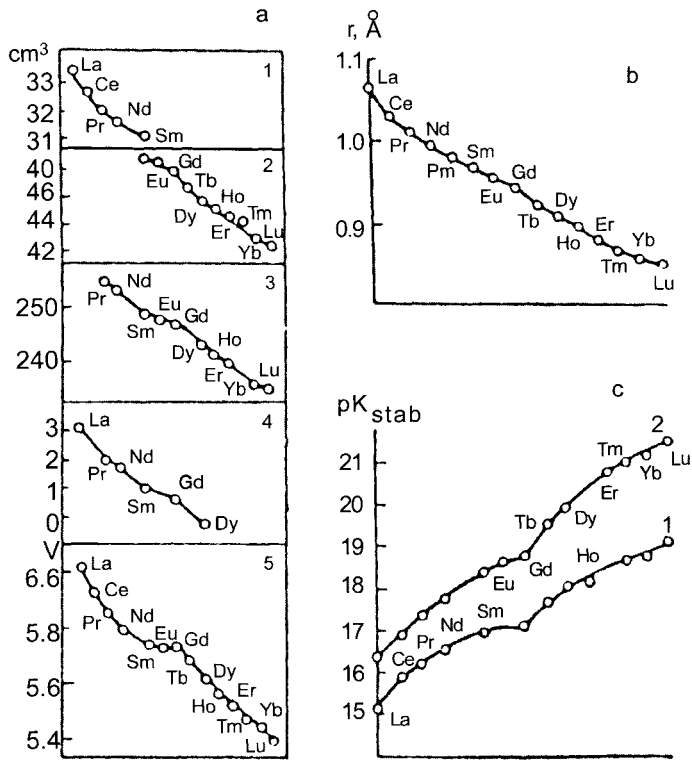


Fig. 3.14.

the atomic core (i.e.) basic properties decrease with increase in the effective charge. The effective charge of the core in rare earth series increases due to the incomplete screening of the nucleus by the f electrons. If the screening effect of the f electrons in different orbitals were the same, the effective charge, and hence related properties, would change with an increase in the number of electrons. In a ligand field the f electrons become non-equivalent. The electrons in orbitals whose axes are directed away from the ligands, namely,  $f_{xyz}$ ,  $f_{x(y^2-z^2)}$ ,  $f_{y(z^2-x^2)}$ ,  $f_{z(x^2-y^2)}$  in the case of an octahedral environment screen the positive charge of the nucleus to a lesser extent than the electrons in orbitals whose axes are directed towards the ligands. Hence the effective charge of the core should increase more sharply as orbitals of low energy are filled (i.e.)  $f_{xyz}$ ,  $f_{x(y^2-z^2)}$ ,  $f_{y(z^2-x^2)}$ ,  $f_{z(x^2-y^2)}$ . Since La is not an f system and in gadolinium and lutetium the f electrons are distributed regularly throughout all the orbitals there should be no ligand field effect for these elements.

Thus the energy of formation of complexes in the rare earth series should vary in the same manner as the molar volumes and basic properties of hydroxides should vary in the opposite manner. It is clear from Fig. 3.14 that the ionic radii, molar volumes and the basic properties of hydroxides show negative deviations. The central members of the cerium subgroup show maximum deviations. The deviations shown by the yttrium subgroup are smaller than the cerium subgroup. This situation is analogous to the behaviour of transition

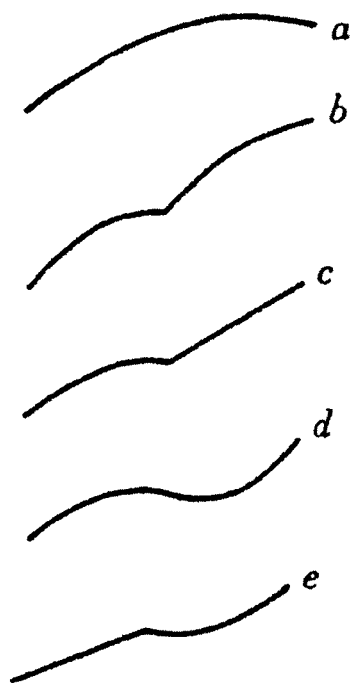


Fig. 3.15.

elements. The deviation from the linear relationship with respect to ionic radii, hydration energies, heats of formation are greater for  $d^1$ – $d^4$  elements than  $d^6$ – $d^9$  elements.

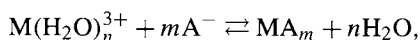
The data on the stability constants with some organic ligands have been classified into five groups depending on the manner in which they vary with atomic number. The five types of variation are illustrated in Fig. 3.15. In the first group (a) the variation of  $\log K$  vs. atomic number shows a convex curve with a maximum in the region of Tb and Er. This group consists of diethylenetriamine pentaacetate and bispicolinate complexes of rare earths. In the second group the deviations are positive in both subgroups of rare earths. The ligands showing the behaviour are ethylenediamine tetraacetic acid and cyclohexanediamine tetraacetate.

The third group (curve c) shows positive deviations in the cerium subgroup with no deviations in the yttrium subgroup. Some typical ligands showing this behaviour are nitrilo triacetic acid and 8-hydroxyquinoline-5-sulphonic acid. In the fourth group, positive deviations in the cerium subgroup and negative deviations in the yttrium subgroup are exhibited (curve d). Ligands exhibiting this trend are acetates, glycolates, gluconates and *N*-hydroxyethyl ethylenediamine tetraacetate. Acetylacetonates belonging to the fifth group show no deviations in the cerium subgroup and negative deviations for elements in the yttrium subgroup (curve e).

Assuming that the interaction between the metal and ligands to be predominantly electrostatic, the energy of formation of the complex ( $E$ ) consists of: (i)  $U$ , the energy of interaction of the spherically symmetrical core of the central metal ion with ligands and

(ii) the extrastabilization energy,  $\Delta E$ . The change in the stability constants for complexes of La, Gd and Lu gives an idea of the manner in which  $U$  varies for the rare earth elements since  $\Delta E = 0$  for La, Gd and Lu. If  $\log K$  vs.  $Z$  is a straight line then this gives the dependence of the magnitude of  $U$  on atomic number. However, in practice, the plot of  $\log K$  vs.  $Z$  for complexes of La, Gd and Lu gives a convex curve with a maximum lying in the yttrium group in the case of bulky ligands. This has been explained [16] by analysing the dependence of the energies of formation of the complexes on the radius of the ligands.

For complex formation, the following equilibrium may be written



where  $M^{3+}$  is a rare earth ion. We see that six water molecules are replaced by six ligands ( $m = n = 6$ ) and then the energy of formation of an octahedral complex is given by the equation

$$U = -6(Z - S_p)e^2/(r_i + r_A) + 6Ze\mu/(r_i + r_w)^2 - C,$$

where  $U$  is the energy of formation of complex,  $e$  the charge on electron,  $r_i$ ,  $r_A$ , and  $r_w$  radii of rare earth, ligand and water, respectively,  $S_p$  the coefficient of mutual repulsion of the ligands,  $\mu$  the dipole moment of water and  $Z$  the charge on the rare earth ion. The constant  $C$  consists of heats of hydration of ions and ligands and heat of vaporization of six water molecules. The foregoing equation gives the dependence of the energy of formation of the complex on the radius of anion or ligand A. The calculations of  $A^- = F^-$  ( $r_{A^-} = 1.33 \text{ \AA}$ ) showed an increase in  $U$  with a decrease in the radius of the rare earth ion. For larger anions the dependence is different and a flat portion is obtained near the end of the rare earth series. For anions of  $r \simeq 2.0 \text{ \AA}$  the curve for energy of formation of complexes shows a maximum which is displaced from elements of yttrium group to cerium group elements with increasing radius of the anion. For anions of  $r > 2.0 \text{ \AA}$  the curve for the energy of formation of complexes decreases with decreasing radius.

An analogous explanation may be given for the variation of energies of formation of rare earth complexes with multidentate ligands. The observed change in the stability constants of complexes of La, Gd and Lu (either straight line or convex curve) has been attributed to change in the electrostatic interaction with change in the ratio of the radii of the central metal ion and the ligands. The extent of deviation of the observed  $\log K$  from the straight line or curve is attributed to the extrastabilization energy of the complexes.

In the complex formation reaction where water molecules are replaced by ligand A



the reaction involves the replacement of field due to water molecules by the field due to ligand A. Thus the extrastabilization energy  $\Delta E'$  is the difference in the extrastabilization energies for water and ligand. We may write

$$\Delta E = \rho 14D_q$$



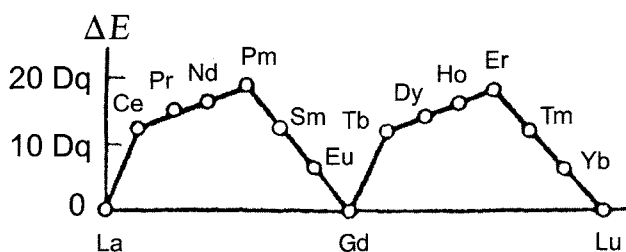


Fig. 3.16.

where

$$\rho = 6/7n_1 + 3/7n_2 - 3/7n_3 \quad \text{for an octahedron and}$$

$$\rho = 3/7n_1 - 1/7n_2 - 6/7n_3 \quad \text{for a tetrahedron and cube}$$

$$\Delta E^1 = \rho_A 14D_{qA} - \rho_{H_2O} 14D_{qH_2O},$$

where  $\rho_A$  and  $\rho_{H_2O}$  are factors which depend on the electronic structure of the central metal ion and the geometric configuration of the complex,  $D_{qA}$  and  $D_{qH_2O}$  are field strengths for ligand and water, respectively.

If the configuration of the complex is preserved in the reaction where water is replaced by ligand A,  $\rho_A$  and  $\rho_{H_2O}$  are equal and the gain or loss of energy is determined by  $D_q$  since the value of  $D_q$  depends on the radius of the central metal ion, the ratio of  $D_q$  values for water and ligand must be based on the fact that this quantity changes in the rare earth series. It should also be recognized that the decrease in extrastabilization in crystals with a decrease in the radius of the rare earth metal ion has been established [18].

If the changes in  $D_q$  for water and the ligand are the same, then the difference  $D_{qA} - D_{qH_2O} = \Delta D_q$  remains constant and  $\Delta E'$  should vary as shown in Fig. 3.16. A similar change has been observed for the variation of the stability constants of rare earth ethylenediamine tetraacetate and cyclohexanediamine tetraacetate complexes (Fig. 3.15).

In the case of most of the complexes, the extrastabilization energy in aqueous solutions,  $\Delta E'$  decreases for the elements in the yttrium group elements and in some cases becomes negative or zero (Fig. 3.15, curves c, d and e). This change in  $\Delta E'$  can be attributed to the fact that  $D_{qA}$  and  $D_{qH_2O}$  change in a different manner with a change in the radius of the rare earth ion. The dependence of  $D_q$  on the average nucleus–electron distance for the metal ion ( $\bar{r}$ ), the metal–ligand distance ( $R$ ) and the charge and deformability of the ligand for transition metals with  $O_h$  symmetry are given by the equations

$$10D_q = 5/3Ze(r^{-4}/R^5)$$

for ionic ligands and

$$10D_q = 5(\mu_0 + \mu_i)e(\bar{r}^{-4}/R^5)$$

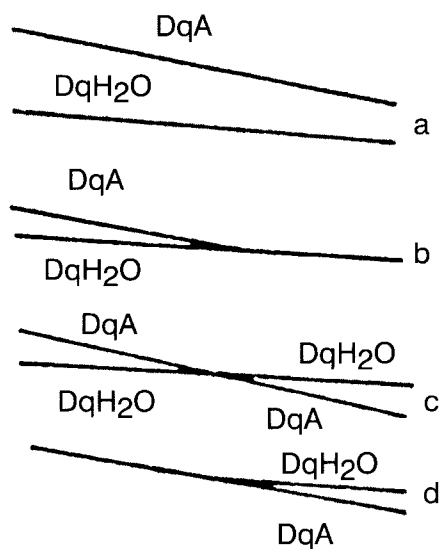


Fig. 3.17.

for the dipole ligands, where  $Ze$  is the charge of the ligand and  $\mu_0$  and  $\mu_i$  are the moments of the permanent and induced dipoles.

In the case of rare earths  $\bar{r}$  changes more sharply than  $R$ , and  $D_q$  value decreases in the series. This change should be less marked for water because the metal–ligand distance is smaller and appears to a higher power than in the case of an ionic ligand.

The following cases of changes in  $D_{qH_2O}$  and  $D_{qA}$  are possible, depending upon the strength of the ligand field: (i) the ligand field strength of  $A^-$  is greater than the ligand field strength of water. This case refers to curve 'a' in Fig. 3.17. The difference in changes in  $D_{qA}$  and  $D_{qH_2O}$  leads to a decrease in  $\Delta D_q$  and a decrease in the extrastabilization energy for the yttrium group, (ii) the second is when the ligand field strengths of  $A^-$  and  $H_2O$  are similar. In this case, the strength of the field due to water when encountering the yttrium group may be either equal (curve b in Fig. 3.17) or greater (curve c Fig. 3.17) than the strength of the ligand field. In the former case  $\Delta E' = 0$  for the yttrium group and  $\Delta E'$  will be negative in the latter case. If for the cerium group of elements  $D_{qA} = D_{qH_2O}$ ,  $D_{qA}$  will become smaller than  $D_{qH_2O}$  in going to the yttrium group of elements as shown by curve 'd' in Fig. 3.17.

Thus crystal field theory can in principle explain all the trends of variation of stability constants shown in Fig. 3.15.

The extrastabilization energy for complex formation in solution may be written as

$$\Delta E' = 2.30RT(\log K_{\text{stab}} - \log K'_{\text{stab}}),$$

where  $K_{\text{stab}}$  is the experimentally determined value of the stability constant of the complex and  $K'_{\text{stab}}$  is the value obtained by interpolation from a straight line joining points of values for La, Gd and Lu.

TABLE 3.7  
Calculated  $\Delta D_q$  values for EDTA complexes.

Metal	$\log K_{\text{stab}} - \log K'_{\text{stab}}$	$\Delta E$	$\rho$	$14\Delta D_q$
La	0	0	0	0
Ce	0.4	530	12/14	620
Pr	0.44	585	14/14	585
Nd	0.50	663	16/14	580
Pm	0.50	663	18/14	520
Sm	0.37	490	12/14	575
Eu	0.20	266	6/14	620
Gd	0	0	0	0
Tb	0.30	410	12/14	480
Dy	0.40	544	14/14	544
Ho	0.40	544	16/14	475
Er	0.33	450	18/14	350
Tm	0.25	340	12/14	400
Yb	0.12	163	6/14	380
Lu	0	0	0	0

Assuming  $\rho$  remains constant on formation of the complex, we have

$$\Delta E^1 = \rho 14D_q$$

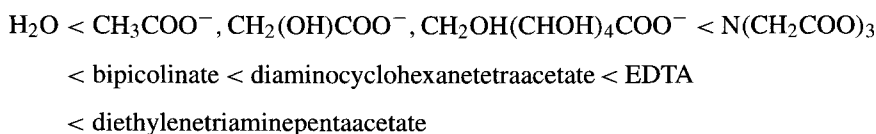
Knowing the value of  $\rho$  one can determine  $\Delta D_q$ .

Ethylenediaminetetraacetate, a sexadentate ligand is assumed to form an octahedral complex with rare earth ions. Thus  $\rho$  was calculated for different electronic configurations using the equation

$$\rho = 6/7n_1 + 3/7n_2 - 3/7n_3$$

The values of  $\rho$  for a regular octahedron,  $\Delta E$  and  $14\Delta D_q$  for the case of complex formation between rare earth ions and ethylenediaminetetraacetate obtained by calculations [16] are given in Table 3.7. The data show that the calculated values of  $14\Delta D_q$  are fairly constant for the cerium group of elements, followed by a decrease for the yttrium group of elements.

For elements of the cerium group, the values of maximum extrastabilization energy for a given ligand has been used to compare the field strengths for different ligands. Based on the deviations for complexes of the same type (MA) the ligands have been arranged in the following order of increasing field strength:



The above order pertains to the cerium group of elements. The order changes for the yttrium group of elements and appears to be as shown below:

carboxylic acids < water ~ nitrolotriacetate

This approach is interesting but appears to be of limited utility because it has not been pursued further and cannot explain all the observations.

The increase in coordination number is another way of explaining the gadolinium discontinuity. This can occur when the ligand has more than six donor atoms in the molecule. The stability constants of rare earth complexes of rare earths with diethylenetriamine pentaacetic acids are greater than the ethylenediamine tetraacetic acid which is suggestive of a coordination number greater than six in the former complexes. The increase in a coordination number is also likely in rare earth complexes (2:1) with nitrolotriacetic acid (2:1 complexes) and ethylenediamine *N,N'*-diacetic acid [19] (2:1 complexes). Coordination number 7 has been suggested for rare earth complexes of EDTA with a water molecule occupying the seventh position [20].

The third interpretation invokes steric effects. This consideration has been used with the assumption that the larger coordination number and octahedral configuration are involved. Steric factors are certainly important in explaining the trends in the stability constants of nitrolotriacetic acid complexes, as well as complexes with diethylenetriaminepentaacetic acid and dipicolinic acid [13].

### 3. Thermodynamic considerations

From earlier discussions, it is obvious that the stability constant data cannot be rationalized in terms of known specific factors. Naturally this leads to a close examination of thermodynamic data for the formation of complexes in solution. The stability constant is directly related to free energy change ( $\Delta G$ ) and is a reflection of the enthalpy  $\Delta H$  and entropy  $\Delta S$  associated with the formation of the complex. Since most of the systems studied are in aqueous medium, the change in enthalpy upon complexation reflects the bond energy toward the lanthanide ion ( $\text{Ln}^{3+}$ ) between the ligand and the coordinated water molecules. The coordinated water molecules may include water molecules outside the primary coordination sphere and it is best called as "hydration sphere". Hence the measured enthalpy change includes the energy necessary for rearranging the hydrogen bonds in the vicinity of the complex compound. The entropy change is related to both the changes in the number of particles in the system and to changes in the modes of motion of the particles. Chelation is favoured by entropy change in terms of initially coordinated water molecules. The majority of the rare earth chelate complexes are entropy stabilized.

The enthalpy and entropy data for the formation of some rare earth complexes are given in Table 3.12 (see Appendix). The data given are not extensive and also very few systems have been studied calorimetrically. The variation in the enthalpy values for most of the ligands are not regular in the rare earth series. Maximum and minimum values occur at various points in the series. This behaviour cannot be properly explained by invoking ligand-field effects. The sinusoidal type of variation of  $\Delta H$  for some ligands may require destabilization if the ligand field is significant. Ligand field effects may also

be less significant because of the screening of 4f electrons. It is also reasonable to expect that complexes containing Ln–O bonds to behave similar to the Ln–H<sub>2</sub>O bond as far as the ligand field is concerned. It is not totally correct to discard ligand field effects in explaining the thermodynamic data. This is suggested by an earlier discussion of stability constants and by the thermochemical studies of lanthanide complexes [21]. For 1:3 complexes, a plot of  $\Delta H_3$  vs. atomic number shows a regular variation and a ligand field stabilization of a few hundred calories between La<sup>3+</sup> and Gd<sup>3+</sup> and Gd<sup>3+</sup> and Lu<sup>3+</sup>. Six coordination, lack of hydration and octahedral configuration are suggested for the 1:3 complexes with dipicolinate and diglycolate ligands.

In the case of nitriloacetate complexes, the changes in enthalpy have been explained in terms of the consequences of lanthanide contraction: (i) increasingly exothermic complexation with decreasing crystal radius and (ii) decreasing exothermic complexation with decreasing hydration of the cation [22]. In the case of dipicolinates and diglycolates these effects become small as the coordination sphere loses water molecules. Thus  $\Delta H_3$  and  $\Delta S_3$  vary more regularly than  $\Delta H_1$  and  $\Delta S_1$ .

Conductance measurements of lanthanides at infinite dilution give three size ranges, namely La<sup>3+</sup>–Nd<sup>3+</sup>, Pm<sup>3+</sup>–Tb<sup>3+</sup> and Dy<sup>3+</sup>–Lu<sup>3+</sup> which is the order of increasing size. The smaller the hydration sphere, the less exothermic is the complexation reaction. Thus there is a corresponding decrease in the  $\Delta S$  value since fewer water molecules are released in this reaction.

Roughly there are three groups: (i) La<sup>3+</sup>–Eu<sup>3+</sup>, (ii) Ho<sup>3+</sup>–Eu<sup>3+</sup> and (iii) Gd<sup>3+</sup>–Dy<sup>3+</sup>. The third group Gd<sup>3+</sup>–Dy<sup>3+</sup> belongs to a borderline group, having constant but different  $\Delta S$ . Other complications which come into play are steric hindrance due to bulky ligands, hydration numbers of Ln<sup>3+</sup> ions. These complications cause difficulties in the interpretation of the data. Change in coordination number is certainly a significant factor and in general, the more negative  $\Delta H$  value, the more positive the value of  $\Delta S$ .

Choppin [24] examined some aspects of lanthanide-organic ligand interaction in aqueous solutions. An interpretation of thermodynamic parameters ( $\Delta G$ ,  $\Delta H$  and  $\Delta S$ ) of complexation have been given in terms of hydration, inner versus outer sphere character, stability vs. chelate ring size and ligand charge polarization.

It is important to recognize that in solution as well as in crystals, the coordination number of lanthanides is often 8 or 9. Radial distribution functions [24] and neutron scattering [25] have been interpreted to show a coordination number of 9 for lighter lanthanides and 8 for the heavier lanthanides with the transition occurring between Nd<sup>3+</sup> and Tb<sup>3+</sup>. Luminescence decay rates [26] of Tb<sup>3+</sup> and Eu<sup>3+</sup> in D<sub>2</sub>O–H<sub>2</sub>O mixtures yielded a value of 9 for Tb and 9.6 for Eu. Raman studies [27] of Eu(III) and Gd(III) in chloride solutions showed the primary hydration sphere to increase with decrease in water fraction content. It appears that coordination numbers of 8 and 9 appear to be present in other solvents as well. Some examples worth noting are Ln(TTA)<sub>3</sub> · (TBP)<sub>2</sub> (TTA: theonyl trifluoroacetone, TBP: tributyl phosphate), where the coordination number is 8; Eu(ClO<sub>4</sub>)<sub>3</sub> in acetonitrile has a coordination number of 9 which becomes 8 in dimethylformamide [28]. This large variable coordination numbers of lanthanides are probably due to the combined effects of the ionic nature of bonds and steric effects. The non-linear nature of the variation of the energy of formation of complex formation,  $\Delta G_{10n}$  or  $\log B_{10n}$  (where  $n$  = number of ligands) with  $Z$  atomic number has already been noted. Free energy variation is more

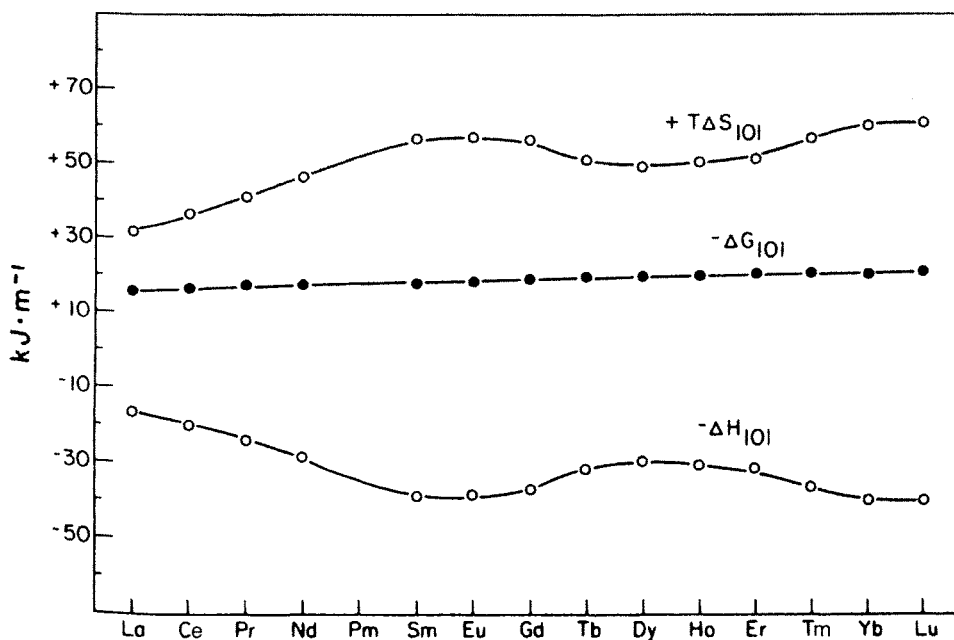


Fig. 3.18.

regular while the enthalpy and entropy variation is irregular as seen in Fig. 3.18. In general a linear relationship exists between enthalpy and entropy values for complex formation for the same ligand for different lanthanides. Thus the relationship suggests a compensational effect in which the enthalpy and entropy changes reflect hydrational changes on complexation. The free energy expression is

$$\Delta G_{101} = \Delta G_R + \Delta G_H = \Delta G_R + \Delta H_H - T(\Delta S_R + \Delta S_H)$$

also

$$|\Delta H_H| > |\Delta H_R| \quad \text{and} \quad |\Delta S_H| > |\Delta S_R|$$

The subscript R stands for cation-anion interaction and H for hydration energy changes on complexation. If upon complexation the net hydration decreases, both  $\Delta H_H$  and  $\Delta S_H$  will be positive. Because  $\Delta H_{101}$  and  $\Delta S_{101}$  are found to be positive for organic ligands in solutions, the hydration terms are larger than the reaction terms. When the hydration terms cancel then

$$\Delta H_H \simeq T \Delta S_H; \quad \Delta G_H \simeq 0$$

In such a case  $\Delta G_{101} \simeq \Delta G_R$ . This means that the free energy of complex formation is reflective of lanthanide-ligand interaction. Thus the value of  $\Delta H_{101}$  and  $\Delta S_{101}$  can be interpreted to a first approximation in terms of hydrational changes [29].

TABLE 3.8  
Calculated percentages of inner sphere  $\text{LnNO}_3^{2+}$  complexation.

Ln(III)	Ionic strength (%)	Method	Innersphere	Ref.
La	ca.0.5	NMR	27	[31]
Pr	4	spec	32	[32]
Sm	4	spec	35	[32]
Eu	0.1	spec	18	[33]
Eu	0.5	spec	58	[34]
Dy	ca.0.5	NMR	44	[35]
Er	4	spec	70	[32]
Er	$f_{\text{H}_2\text{O}} = 0.16$ (in DMSO)	ultrasonic	50	[36]

Lanthanide complexes with inorganic ligands such as  $\text{Cl}^-$ ,  $\text{Br}^-$ ,  $\text{I}^-$ ,  $\text{SCN}^-$ ,  $\text{NO}_3^-$  and sulphate can be either inner sphere  $\text{LnX}^{2+}$  or outer sphere or solvent separated complexes,  $\text{Ln}(\text{H}_2\text{O})_n^{3+}\text{X}^-$ . In the case of halides the complexes are thought to be outer sphere  $\text{Ln}(\text{H}_2\text{O})_n\text{X}^{2+}$ , although there is evidence for the existence of anionic complexes like  $\text{LnCl}_4^-$ . Similarly  $\text{EuSCN}^{2+}$  is supposed to have both inner sphere and outer sphere character [23].

Based on the stability constants for overall complexation,  $\beta_{101}^T$  which can be separated into two parts, namely inner sphere,  $\beta_{101}^i$  and outer sphere,  $\beta_{101}^o$  at different ionic strengths, the values of inner and outer sphere percentages have been calculated (Table 3.8).

The inner sphere and outer sphere character was also ascertained in the case of halates and chloroacetates of lanthanides by calorimetry and solvent extraction techniques. Another aspect of the study is to ascertain the relationship between  $\text{p}K_a$  and inner and outer sphere character [30].

$\text{EuClO}_3^{2+}$	$\text{p}K_a - 2.7$	outer sphere
$\text{EuBrO}_3^{2+}$	$\text{p}K_a - 2.3$	both inner and outer sphere
$\text{EuIO}_3^{2+}$	$\text{p}K_a = 0.7$	inner sphere

For organic ligands the data are as follows:

Ligand	$\text{p}K_a$	Percent innersphere in $\text{LnAc}^{2+}$
Acetate	4.8	100
Trichloroacetate	-0.5	0
Dichloroacetate	1.1	22
Chloroacetate	2.7	50

The relationship between  $\log \beta_{101}$  and  $\text{p}K_a$  of the ligand for the haloacetate complexes is as shown in Fig. 3.19.

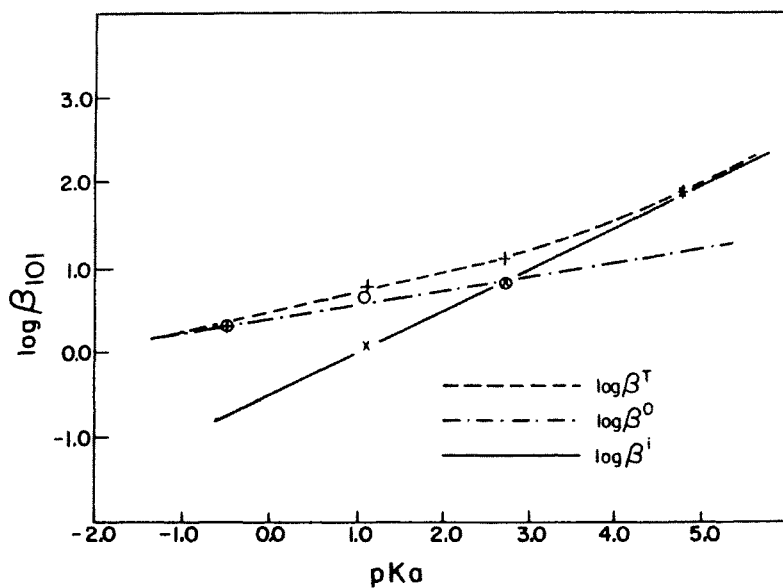


Fig. 3.19.

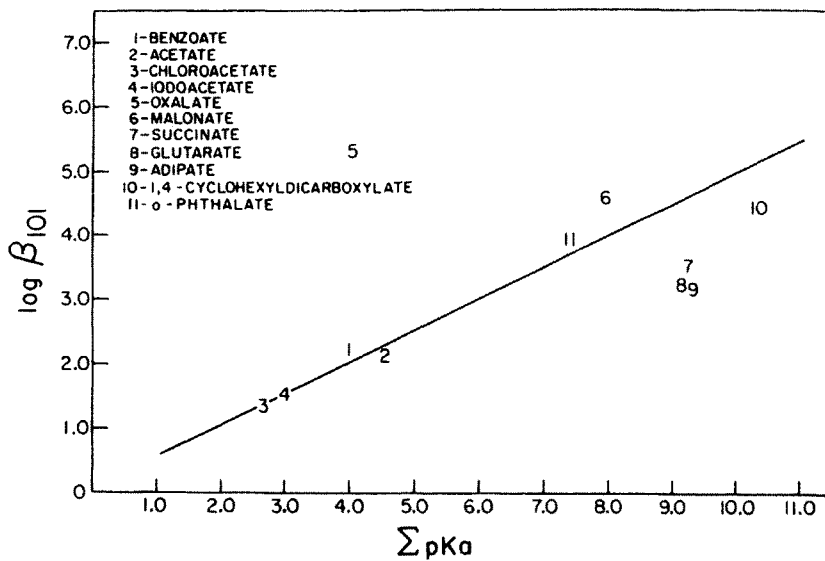


Fig. 3.20.

Another aspect to be considered is the stability of chelate rings as a function of the ring size. Carboxylic acids of the formula  $(CH_2)_nCOOH$ , where  $n = 0$  to 4 form complexes with lanthanides with different sizes of the chelate ring [23]. A plot of  $\log \beta_{101}$  for  $Sm^{3+}$  versus  $\sum pK_a$  of the ligands is shown in Fig. 3.20.



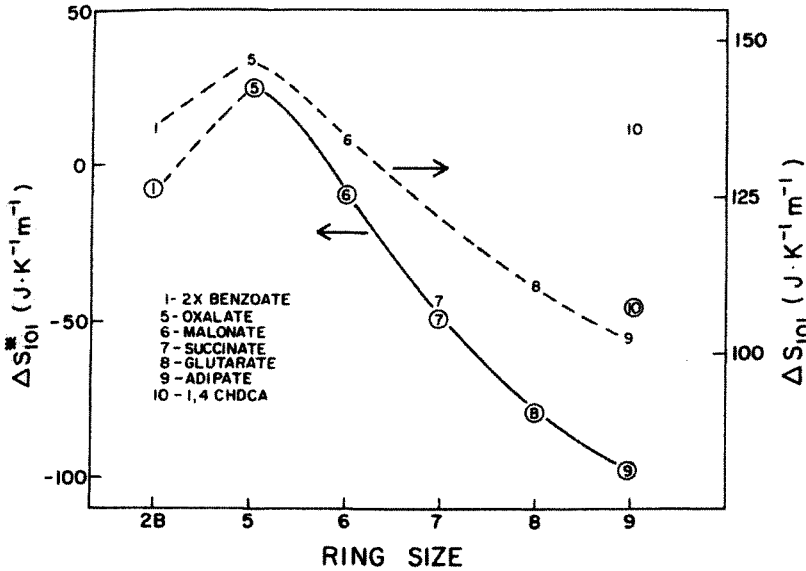
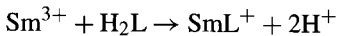


Fig. 3.21.

The figure shows that the oxalate which forms a five-membered ring has the highest stability followed by malonate (6-membered ring). Succinate, glutarate and adipate form 7, 8 and 9 membered rings and are less stable. The Sm(III) CHCDA probably has a "boat" structure and hence more stable than the 9-membered adipate complex. The boat structure involves less entropy loss upon complexation. In all these complexes, the  $\log \beta_{101}$  values are greater than 3.0 for succinate, glutarate and adipate suggesting bidentate character of the ligands.

As the size of the chelate ring increases, the increase in strain should reflect in the entropy  $\Delta S_{101}$  with ring size. Hence the entropy  $\Delta S_{101}$  value of the reaction



may be appropriate to use for the correlation of entropy with the chelate ring size in the lanthanide complexes. Thus a correlation of  $\Delta S_{101}$  and  $\Delta S_{101}^*$  with ring size for complexes with ligands of the formula  $(\text{CH}_2)_n\text{COO}^-$ , where  $n = 0$  to 4 (for oxalate through adipate) has been made. Such a correlation is shown in Fig. 3.21. The correlation of  $\Delta S_{101}$  is not as good as that of  $\Delta S_{101}^*$ . The values for 1,4-CHCDA indicate a loss of  $\approx 40 \text{ J K}^{-1} \text{ mol}^{-1}$  upon chelation with probably a boat structure than with an alkyl chain structure.

As far as  $\Delta H_{101}$  values are concerned they are expected to be more exothermic and increase with increase in  $\sum pK_a$ . The values on complexation become more positive contrary to the expectation.

Oxalate	+4.8 kJ mol <sup>-1</sup>	Glutarate	+9.2 kJ mol <sup>-1</sup>
Malonate	+11.2 kJ mol <sup>-1</sup>	Adipate	+3.6 kJ mol <sup>-1</sup>
Succinate	+18.2 kJ mol <sup>-1</sup>		

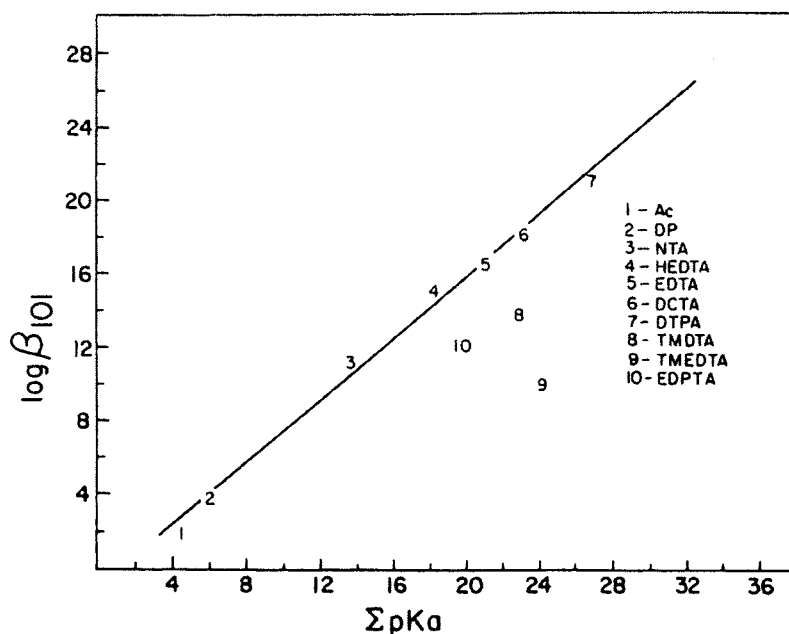


Fig. 3.22.

Succinate, glutarate and adipate have  $\sum pK_a \sim 9.2$  and the observed trend could be due to shorter Ln-O bond distances.

Rare earth aminopolycarboxylate complexes have been studied extensively because of their utility in the preparation of highly pure rare earths. Studies are still continuing on these complexes and efforts are being made on understanding the factors that contribute to their stability. The  $\Delta S_{101}$  values for an individual lanthanide and a series of these ligands appear to be a function of the number of carboxyl groups in the ligand [37]. For Eu(III) complexes  $\Delta S_{101}$  values are about  $70 \text{ J K}^{-2} \text{ m}^{-1}$  per carboxyl group which are similar to the acetate system. This observation means that the dominant entropy effect is the dehydration of the carboxyl group. The endothermic enthalpy values were less than the values expected for the interaction with four carboxylate groups indicating a strong exothermic Ln-N interaction. This interpretation is strongly supported by NMR data on the Ln-EDTA system. Thus compensation of hydration effects appear to be applicable as with simpler ligands. This leads to a linear relationship between  $\log \beta_{101}$  and  $\sum pK_a$  of the ligand as shown in Fig. 3.22. The ligands that fit the linear relationship are five-membered rings containing the rings  $\text{O-Ln-N}$  or  $\text{N-Ln-N}$ . TMDTA and TMEDTA form 6 and 7-membered  $\text{N-La-N}$  rings, respectively. EDPDA forms two six and two five-membered rings. The complexes which have larger rings are less stable. The difference between the experimental value of  $\log \beta$  and the value expected from the line denoted as  $\Delta \log \beta$  appears to indicate the extent of Ln-N bonding.

TMDTA	6-membered ring	$\Delta \log \beta \simeq 2.4 \text{ N-Ln-N}$
TMEDTA	7-membered ring	$\Delta \log \beta \simeq 4.6 \text{ N-Ln-N}$
EDPDA	6-membered ring	$\Delta \log \beta \simeq 2.0 \text{ O-Ln-N}$

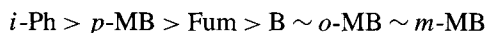
Nuclear magnetic resonance (NMR) has provided useful information on the structure and nature of bonding in the lanthanide aminocarboxylate complexes [39]. The splitting of  $^1\text{H}$  spectra reflect the lifetimes of Ln–O and Ln–N bonds and the differences in the shifts of similar protons (the four acetate groups in EDTA) yield information on the structure of the complex. The symmetric ligand structure of LnEDTA is indicated by the same extent of shift of the protons of the four acetate groups. The Ln–O bonds were shortlived while the Ln–N bonds were long lived relative to the NMR time scale of  $\simeq 10^{-4}$ – $10^{-7}$  s. The Ln–N bond lifetime increased in moving along the La–Lu series. The EDPDA complexes showed similar asymmetry and bond lifetimes like HEDTA and MEDTA. The spectra of TMDTA and TMEDTA complexes showed increase in the size of  $\overbrace{\text{N-Ln-N}}$  ring [40].

Intraligand charge polarization is one of the factors involved in explaining the variation of  $\log \beta_{101}$  values with  $\text{p}K_a$  of substituted carboxylic acids. Inductive and resonance effects in the ligands may oppose or reinforce each other and will be enhanced by highly charged cations. Conjugated  $\pi$  ligand systems should exhibit intraligand polarization more readily than saturated ligands because resonance effects are stronger than inductive effects.

Studies on the fumarate and isophthalate complexes yielded  $\log \beta_{101}$  values greater than the values expected from the  $\sum \text{p}K_a$  of the ligands [41,42]. This discrepancy was explained in terms of stabilization due to polarization of the ligand charge by the lanthanide cation. Further studies with the following ligands involving substituted benzoates (Fig. 3.23) showed stability constants for 1:1 complex to be in the order



From the  $\text{p}K_a$  values the expected order of stability is



The disagreement can be explained by the resonance and inductive charge polarization present in  $p\text{-MB}$  and fumarate complexes.

The relationship between  $\text{p}K_a$  and  $\log \beta_{101}$  from the correlation of  $\text{p}K_a$  with  $\log \beta_{101}$  of the complexes is shown in Fig. 3.23. From the correlation of  $\text{p}K_a$  with  $\log \beta_{101}$  the intraligand polarization effects are small in acetate and maleate and the  $\text{p}k_a^1$  value of 5.5 for fumarate and isophthalate represents charge saturation of the carboxylates. In the case of  $o\text{-MB}$  and  $m\text{-MB}$  only inductive polarization is possible and has a  $\text{p}k_a^1$  of 4.7. From this correlation one can define the maximum value of  $\log \beta$  which in the case of Eu is  $\simeq 2.8$  ( $-\Delta G_{101} \simeq 16 \text{ kJ mol}^{-1}$ ).

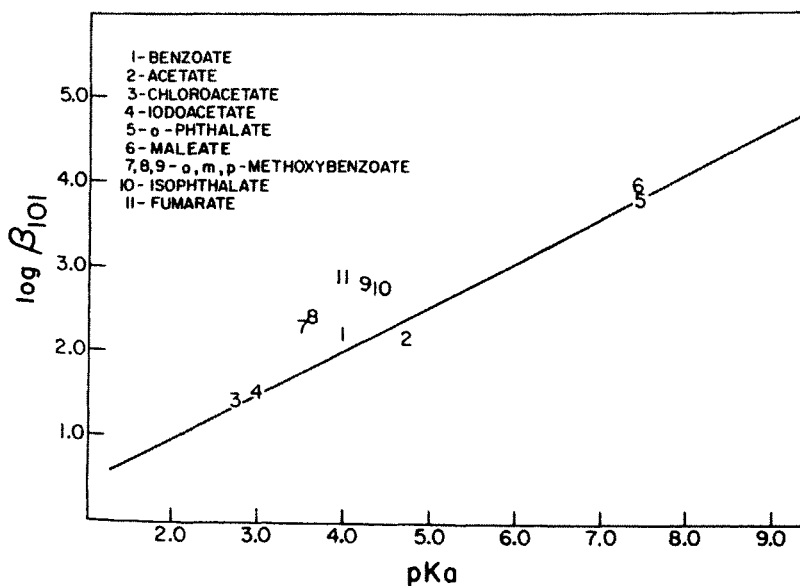


Fig. 3.23.

#### 4. Stability of macrocyclic complexes

Stability constants of rare earths with a variety of macrocyclic ligands are presented in Tables 3.13 to 3.19 (see Appendix) and the associated references are given at the bottom of the tables. As is the case with noncyclic ligands, stability constants are determined by several different techniques. One should be careful when comparing the values, since different conditions and techniques might have been applied. Stability constants for the complexes of cations with macrocyclic compounds are often influenced by the relative sizes of the cations and the cavities of the macrocycles, and hence the macrocycles have specific selectivities to various cations. It is naturally expected that macrocyclic compounds also exhibit unique selectivities to lanthanides.

The stabilities of lanthanide complexes with 18C6 were systematically [44–46] investigated in methanol and in propylene carbonate. This stability decreases with increase in the atomic number of the lanthanide (Tables 3.13 and 3.14, see Appendix). This stability trend is opposite to those for most of the complexes with noncyclic ligands. A similar trend is observed for complexes with butylbenzo substitutes [48]. The stability of the complex of the cyclohexano-substituted crown ether has also a similar trend, though the number of elements investigated is small. On the other hand, the 1:1 complexes of 12C4 and of 15C5 have nearly the same stabilities over the lanthanide series, although the 15C5 complex seems to be slightly more stable for the lighter lanthanides. These results are in agreement with the structures of the complexes. The stabilities of the lanthanide complexes with 12C4 and with 15C5 are only slightly influenced by the relative sizes of the ligand cavity and the cation, because the metal ions are located slightly apart from the crown ether rings due

to the larger sizes of the cations relative to the cavities. On the other hand, lanthanide ions are located in the center of the polyether ring in the 18C6 complexes though the ring size is larger than the size of La, which is the largest element of the lanthanide series. With an increase in the atomic number of the lanthanide, or a decrease in the ionic size, the difference in size between the lanthanide and the hole of the macrocycle increases. The distortion in the polyether increases in order to maintain the distance between the coordinating oxygens and the metal at the lengths suitable for coordination. Consequently, the stability of the complex decreases with increasing atomic number of the lanthanide. The stability trends of the 1:2 complexes with 12C4 and 15C5 are similar to those of the 1:1 18C6 complexes, though the data are limited [49]. The behavior is at least partly due to a structural effect. The two crown ethers of the 1:2 complexes (considered to be sandwich type) are brought closer together with a decrease in ionic diameter of the lanthanide, and the steric interactions become more significant in decreasing the stability of the complexes.

The stability constants of lanthanide complexes with *t*-butylbenzo-15C5 and -18C6 are 3 and 3 to 5 orders of magnitude lower than those of complexes with unsubstituted 15C5 and 18C6, respectively. The decrease is attributed to the decrease in the charge density on the oxygen atoms due to the withdrawing effect of the phenyl ring. The increase in the rigidity of the ligand caused by the substitution also yields destabilization. The effect of the rigidity is more significant and the decrease in stability caused by the substitution is larger in the case of complexes of 18C6 and the substituted 18C6. The larger rigidity improves the selectivity between lanthanides. The La(III)/Yb(III) selectivity,  $\log \beta_1$ , is 2.57 with *t*-butylbenzo-18C6 (for trifluormethane sulfonate complex in propylene carbonate [48]), while  $\Delta \log \beta_1$  is 1.25 with 18C6.

DB30C10 forms 1:1 complexes though the original cavity size is quite large, as previously stated. The stabilities of the complexes exhibit an unusual [49] trend in that a maximum is observed at Gd(III). Massaux and Desreux attributed this behavior to the structural change at Gd. The polyether experiences deformation in order to wrap around the lanthanides. The deformation causes intramolecular repulsions and strains leading to destabilization of the complexes. The contraction of cavity size accompanying the decrease in ionic radius progressively decreases the stability from La to Gd. It seems likely that a structural change occurs after Gd because the macrocycle is no longer able to reduce the cavity size.

The macrocycles containing amine groups in the ring, diaza-15C5 and diaza-18C6 [(2.1) and (2.2)] give more stable complexes than those of the corresponding crown ethers (Table 3.15). The values of  $\log \beta$  for the two diazacrown ethers are 8 to 9.9 log units and 7.5 to 9.2 log units larger, respectively. The increase in stability is due to the higher polarization of NH groups, at least to some extent. The stability constants of complexes with diazacrown ether (2.1) are smaller than those of complexes with cryptand (2.2.1), and the difference,  $\Delta \log \beta_1$ , is about 4, being likely to indicate a so-called macrobicyclic effect. However, such a difference is not observed between (2.2) and (2.2.2) or between (2.1) and (2.1.1). It seems that the difference observed between (2.1) and (2.2.1) may not be simply attributable to the macrobicyclic effect. The complexes of the cryptands (2.1.1), (2.2.1), and (2.2.2) are much more stable than those of crown ethers, and the stability constants are measured even in the strongly coordinating solvents such as water and DMSO (Tables 3.16, 3.17). The difference in stability of complexes with N-containing

macrocycles between individual lanthanides is small in any solvent. The stability constants of the lanthanide complexes are in the order (2.2.1) > (2.2.2) > (2.1.1) in propylene carbonate, but are nearly the same with the three cryptands in water and DMSO. The interaction of these solvents with the lanthanide through the holes between the aliphatic chains of the ligands is considered to decrease the specificities of the metal ions. The acetic acid substitutes of the diazacrown ethers, 1,7-diaza-4, 10, 13-trioxacyclopentadecane-*N,N*<sup>1</sup>-diacetic acid [DACDA, (2.2)DA], form very stable complexes in aqueous solution ( $\log \beta > 10$ ) (Table 3.16). The stability of the complex with DACDA exhibits a similar trend with that of the complexes with the corresponding crown ether, 18C6, decreasing with the increase in atomic number from La ( $\log \beta_1 = 12.2$ ) to Lu ( $\log \beta_1 = 10.8$ ). On the other hand, the complexes of DAPDA have a different stability trend, with a maximum around Eu, and the selectivity is poor [51]. The complexes of the polyazamacrocyclic polyacetic acids with no ether bonds, 1,4,7,10-tetraazacyclododecane-*N,N,N',N''*-tetraacetic acid (DOTA), 1,4,8,11-tetraazacyclotetradecane-*N,N',N'',N'''*-tetraacetic acid (TETA), and 1,4,7-triazacyclononane-*N,N',N''*-triacetic acid (NOTA), form very stable complexes ( $\log \beta_1 > 13$ ) in water, especially DOTA, which gave exceedingly stable complexes ( $\log \beta_1 = 23\text{--}25$  in water). The complexes are more stable than the DTPA complexes that have been accepted to be the most stable ones. Other authors reported even higher stability constant values for the DOTA complexes ( $\log \beta_1 = 28\text{--}29$ ) [50]. Thermodynamic data on  $\Delta H$  and  $\Delta S$  show that  $\Delta S$  is the major contributor to the stability of macrocyclic complexes of rare earths.

## 5. Double–double effect

This effect originates in the various f electron configurations of lanthanides and actinides. This effect is based on the correlation observed between the full pattern of the effect and the sequence of values of the L quantum number [52]. The correlation consists of the occurrence of the same double symmetry in (a) the series of L quantum number values of the ground terms of f element ions and (b) the sequence of relatively stabilized or destabilized f electron configurations (i.e.) the double–double effect. Accordingly

- $f^0, f^3, f^4, f^7, f^{10}, f^{11}$  and  $f^{14}$  are relatively stable configurations while the four pairs  $f^1\text{--}f^2$ ,  $f^5\text{--}f^6$ ,  $f^8\text{--}f^9$  and  $f^{12}\text{--}f^{13}$  are relatively destabilized configurations,
- $f^0, f^3, f^4, f^7, f^{10}, f^{11}, f^{14}$  stable, even L values, S = 0, I = 6 terms,
- $f^1\text{--}f^2, f^5\text{--}f^6, f^8\text{--}f^9, f^{12}\text{--}f^{13}$  unstable, odd L values, F = 3, H = 5 terms.

The double–double effect is illustrated in Fig. 3.24. It is to be noted that elements of relative stable configuration form complexes of less negative  $\Delta G$  values (i.e.) the ease of complex formation is less.

The double–double effect finds confirmation by the singularities of the  $f^3\text{--}f^4$ ,  $f^7$  and  $f^{10\text{--}11}$  configurations in terms of spin-pairing energies [53]. The theory of spin-pairing is based on the fact that for a given configuration  $l^q$ , the energy difference between the centre of gravity of all (S - 1) terms and the centre of gravity of all S terms is equal to 2DS, where D is a linear combination of interelectronic integrals in the Condon–Shortley

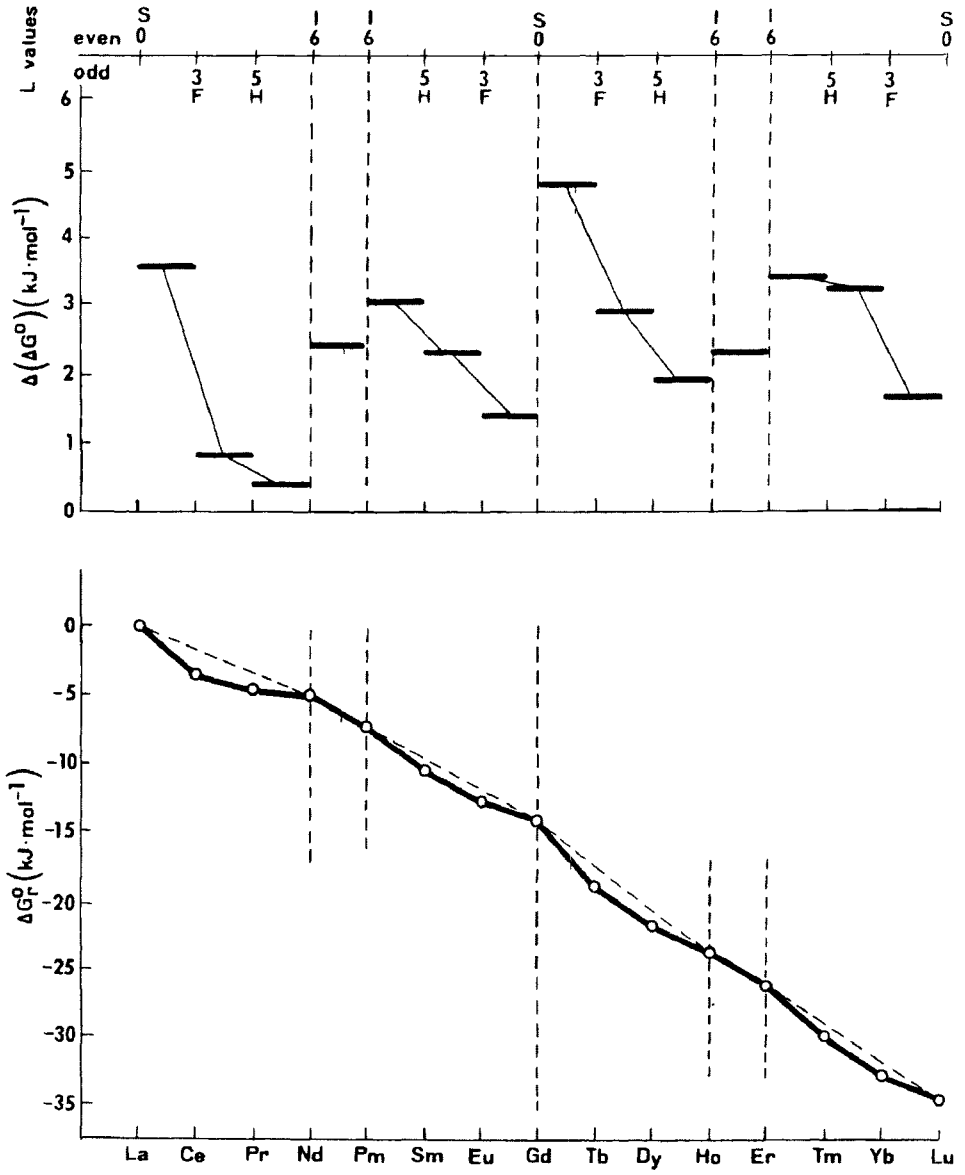


Fig. 3.24.

theory. The lowest term with maximum S value is situated below the baricentre of the whole configuration to an extent of

$$-4(q^2 - q)D/13$$

for  $q \leq 7$  while  $q$  is replaced by  $14 - q$  for other configurations. In the above equation  $D$  is a spin-pairing energy parameter equal to  $6500 \text{ cm}^{-1}$  for the  $4f$  elements and  $3900 \text{ cm}^{-1}$  for  $5f$  elements. For configurations  $f^q$  where more than one term represents the maximum of  $S$ , the lowest term is further stabilized

$$-21E^3 \text{ for } q = 3, 4, 10 \text{ and } 11$$

$$-9E^3 \text{ for } q = 2, 5, 9 \text{ and } 12$$

where  $E^3$ , the Racah parameter, is about one-tenth of  $D$ . Thus the stabilization of ground electronic states of  $f^q$  configuration relative to the baricentre of the whole configuration is as follows.

Configuration	Term	Stabilization energy
$f^2, f^{12}$	$^3H$	$-8D/13 - 9E^3$
$f^3, f^{11}$	$^4I$	$-24D/13 - 21E^3$
$f^4, f^{10}$	$^5I$	$-48D/13 - 21E^3$
$f^5, f^9$	$^6H$	$-80D/13 - 9E^3$
$f^6, f^8$	$^7F$	$-120D/13$
$f^7$	$^8S$	$-168D/13$

There is no such stabilization in  $f^0, f^{14}$  ( $^1S$  terms) and  $f^1, f^{13}$  ( $^2F$  terms) systems. The double-double effect is supposed to result from the decrease of phenomenological parameters of interelectronic repulsion with increasing covalency of metal-ligand bonding. The degree of covalent bonding is related to the nephelauxetic effect which becomes more pronounced with higher reducing power of ligands and higher oxidizing power of the central metal ion.

The coefficients of  $D$ -dependent terms display symmetry with respect to  $f^7$  configuration along with two subgroups  $f^0-f^7$  and  $f^7-f^{14}$ , changes in coefficients of  $E^3$  show the symmetry in the two subgroups. Assuming that both parameters of interelectronic repulsion  $D$  and  $E^3$  decrease by one percent Fig. 3.25a is drawn. The combined stabilization is shown in Fig. 3.25b. Superposition of stabilization originating from the expression  $-21E^3$  and  $-9E^3$  in plotting the value of  $4(q^2 - q)D/13$  as a function of  $q$  gives the singularities of  $f^3-f^4$  and  $f^{10}-f^{11}$  configurations (i.e.) two sub-pairs within the groups  $f^0-f^7$  and  $f^7-f^{14}$ .

Fig. 3.25c is drawn assuming a decrease of one percent in  $E^3$  and 0.25 percent in  $D$ . The above assumption is based on the premise that  $E^3$  has a greater nephelauxetic effect on the ground state energy than  $D$ . From Fig. 3.25 the singularities of the central pairs  $f^3-f^4$  and  $f^{10}-f^{11}$  are seen to be pronounced. From this it is seen that the stabilization of the ground terms relative to the baricentre of the whole configuration, plotted as a function of  $q$  shows the same double symmetry as the double-double effect. The double symmetry can also be seen in the sequence of ground terms when the total orbital angular momentum  $L$  is plotted against  $q$  (i.e. two maxima in the plot). The two maxima are due to two central pairs within the two subgroups  $f^0-f^7$  and  $f^7-f^{14}$ . The plots of  $L$  vs.  $q$  and  $S$  vs.  $q$  are given in Fig. 3.26



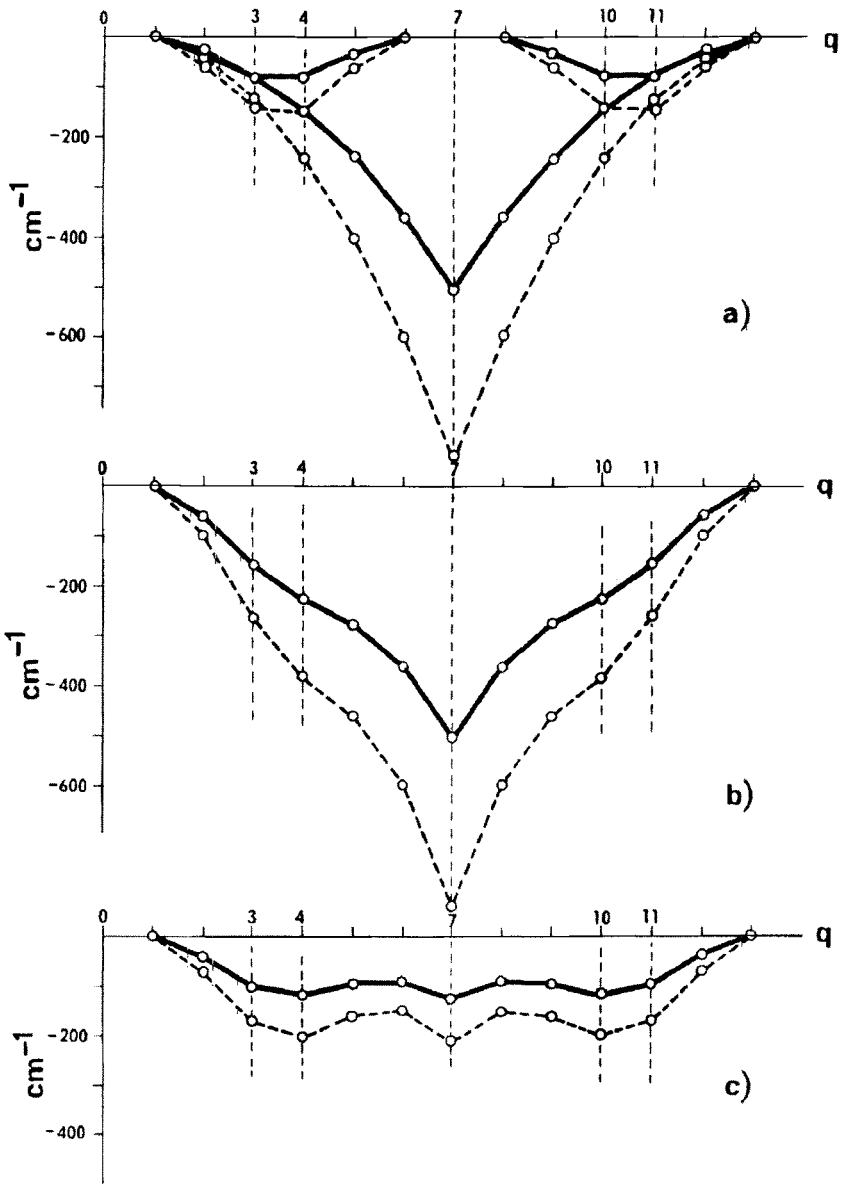


Fig. 3.25.

and these plots show the maxima due to two central pairs within the two subgroups  $f^0-f^7$  and  $f^7-f^{14}$ .

It is probably useful to view the stability constants and the associated thermodynamic parameters in terms of spin-pairing energy or the double-double effect. In the case of

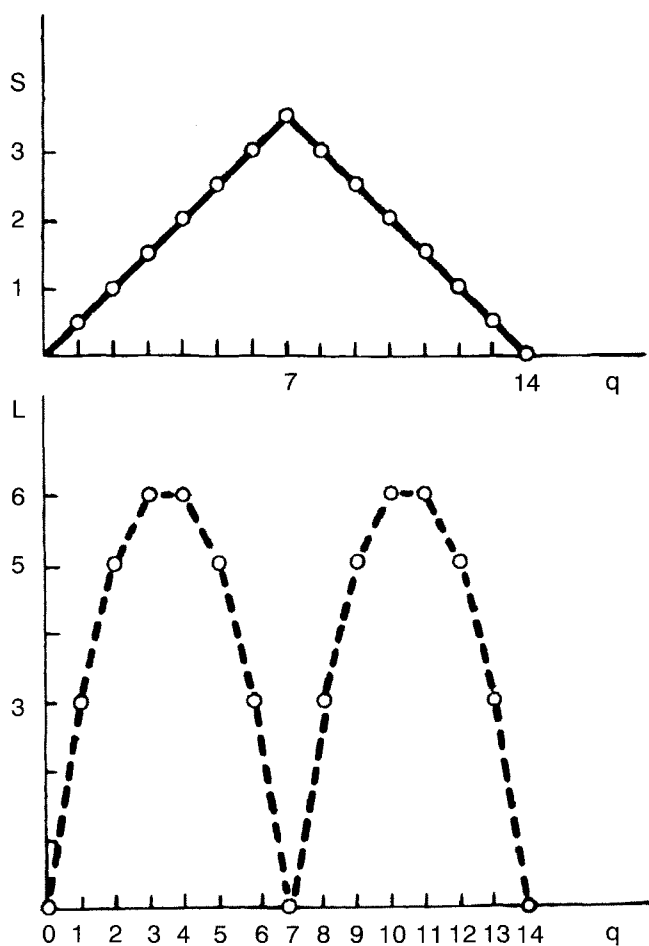


Fig. 3.26.

free energy of complex formation, it reflects the stabilization of ground state terms for the complex and aquo ion. The experimentally observed double-double effect is greater when there is a pronounced change in  $E^1$ ,  $E^3$  parameters under the nephelauxetic action of the ligands. Thus the effect of nephelauxetic action of the ligands in expanding the partly filled shell of the central ion, and a decrease in interelectronic repulsion parameters  $E^1$  and  $E^3$  are of primary importance in interpreting the experimental data such as stability constants or thermodynamic parameters in the series of lanthanides. Siekierski [54] defined the separation  $\bar{\alpha}$  as

$$\bar{\alpha} = \frac{\sum_1^n \frac{(\beta_3)_{z+1}}{(\beta_3)_z}}{n},$$

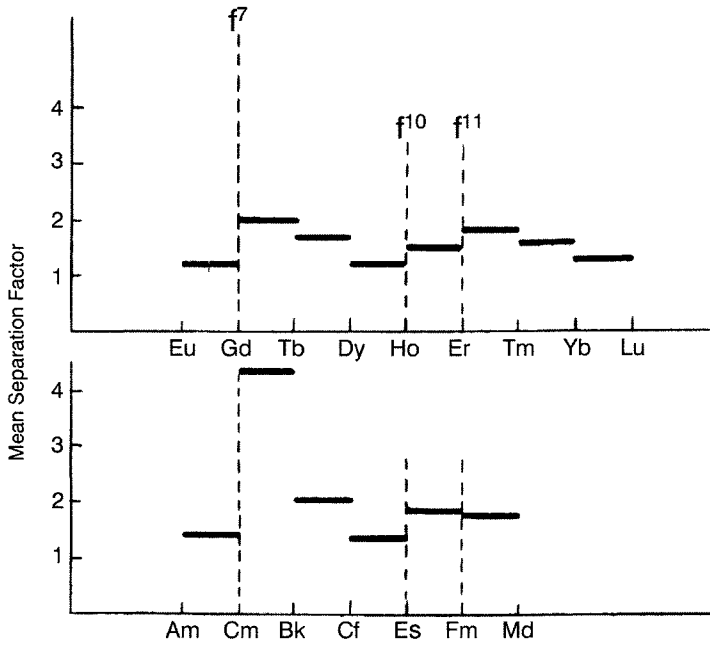


Fig. 3.27.

where  $Z$  is the atomic number and  $n$  the number of ligands. A plot of  $\bar{\alpha}$ , mean separation for lanthanides and their complexes with over 30 ligands, is given in Fig. 3.27. The double-double effect is clearly seen in the figure.

In general, most of the properties of lanthanides and their variation allow one to classify them into subgroups, namely,  $f^0-f^3$ ,  $f^4-f^7$ ,  $f^7-f^{10}$  and  $f^{10}-f^{14}$ . The properties of lanthanide ions and their complexes vary linearly with the total orbital angular momentum ( $L$ ) values and give rise to a four segmented "inclined W" shape. Also the lanthanides have been classified into four groups when  $\text{Ln}^{3+}$  is involved.

		0	I	II	III
1.	$f^2$	La	Ce	Pr	Nd
2.	$f^{4+q}$	Pm	Sm	Eu	Gd
3.	$f^{7+q}$	Gd	Tb	Dy	Ho
4.	$f^{11+q}$	Er	Tm	Yb	Lu

The largest difference in properties is between elements of group 0 and I and the smallest difference is between elements of groups II and III. The double-double effect that is reflected in four subgroups is similar to the observations of Moeller [13] who grouped  $\text{La}^{3+}-\text{Nd}^{3+}$ ,  $\text{Pm}^{3+}-\text{Tb}^{3+}$ ,  $\text{Dy}^{3+}-\text{Lu}^{3+}$  into three groups.

## 6. Applications

Fractional crystallization and precipitation are classical methods of separation of rare earth metal ions. Complex forming agents may be used to give better separations than simple or double salts. Some of the complexing agents used in fractionation separation are given below.

	Reference
Reagent	
Mandelic acid	[55]
Dimethyl phosphates	[56]
NH <sub>4</sub> [LnEDTA]	[57]
Complexing agent	
EDTA in oxalate precipitation	[58]
NTA in oxalate precipitation	[13]

Rare earths separation has been achieved by formation of species of the formula Ln(NO<sub>3</sub>)<sub>3</sub>·3TBP, where TBP is tributyl phosphate. This process is solvent extraction which is widely used at present in the production of rare earths in pure form.

Reagents	Reference
Tributylphosphate	[59]
2-ethylhexyl phenyl phosphonate	[60]

The complex formation constants of rare earth ions with a variety aminopolycarboxylic acids are sufficiently different for the purpose of separation of the ions by ion-exchange methods.

Reagent	Reference
EDTA (cation exchange)	[61]
NTA (cation exchange)	[62]
Triphosphate (cation exchange)	[63]
DTPA (cation exchange)	[64]
EDTA (anion exchange)	[65]
Citrate (anion exchange)	[66]

The important analytical application is complexometric titration with EDTA for the individual determination or as a group [67].

Spectrophotometric methods for the analytical determination of rare earths using complexing agents have been developed. Although some reagents give high sensitivity these methods suffer from interferences due to other cations, anions and chelating agents [13].

TABLE 3.9  
Solvent extraction of lanthanides with crown ethers.

Organic phase	Aqueous phase [Ln(III)]	Ln:L:A <sup>a</sup>	Remarks	Ref.
12C4-PhNO <sub>2</sub>	Ln(NO <sub>3</sub> ) <sub>3</sub> -picrate (La-Lu)	1:2	Tb and Yb are best extracted	[71]
15C5, DB18C6-PhNO <sub>2</sub>		1:1		
15C5, 18C6, DB18C6-CHCl <sub>3</sub>	Ln(NO <sub>3</sub> ) <sub>3</sub> -picrate (La-Lu)	1:2:3	K <sub>e</sub> decreases from Ce to Lu	[72]
ButB15C5, BrB15C5-PhNO <sub>2</sub>	Picrate (Ce, Nd, Sm, Eu, Tm, Yb, Lu)	1:2:3	Ce > Nd > Sm > Eu > Tm > Yb > Lu	[73]
DB18C6, DC18C6-CH <sub>2</sub> Cl <sub>2</sub>	Picrate (La-Lu)			[74]
MeB15C5-CHCl <sub>3</sub>	Picrate (Ce, Nd, Eu, Tm, Yb)	1:2:3	Nd > Eu > Ce > Tm > Yb	[75]
15C5, 18C6, DC18C6, DC24C8 + (BuO) <sub>2</sub> -(CH <sub>2</sub> CH <sub>2</sub> O) <sub>n</sub> C <sub>6</sub> H <sub>6</sub>	Nitrate (La-Lu)		Synergistic extraction	[76]
DC18C6, DC15C5-CH <sub>2</sub> Cl <sub>2</sub>	Picrate (La-Gd)	1:2:3		[77]
15C5 + HTTA-CHCl <sub>3</sub>	Acetate	1:2:3 <sup>b</sup>	Synergistic effect (Eu > Tm > Yb)	[78]
But15C5 + DNSA-CH <sub>3</sub> C <sub>6</sub> H <sub>5</sub> <sup>c</sup>	Perchlorate (Ce, Pm, Eu, Tm)		Synergistic extraction	[79]
DB16C5AA-CHCl <sub>3</sub> + C <sub>6</sub> H <sub>13</sub> OH <sup>d</sup>	Chloride, nitrate, sulfate (La-Lu)		La > Pr > Sm > Eu > Tb, Er > Yb, Lu	[80]

<sup>a</sup>Lanthanide:ligand:anion ratio in the extracted species.

<sup>b</sup>TTA is the anion.

<sup>c</sup>DNSA is dinonylnaphthalene sulfonic acid.

<sup>d</sup>DB16C5AA is dibenzo-16-crown-5-oxyacetic acid.

The specific selectivity of macrocyclic compounds for cations has been successfully used in the separation of lanthanides.

Separation of Pr and Er	Chromatography	[68]
Separation of Sm and Gd	Chromatography	[69]
Separation of La-Sm and Tb-Lu groups using DOTA	Ion exchange	[70]

Solvent extraction studies for the separation of rare earths using crown ethers are summarized in Table 3.9.

## References

- [1] J. Bjerrum, *Metal Amine Formation in Aqueous solution*, P. Haase & Son, Copenhagen, 1957.
- [2] J.Z. Hearon, J.B. Gilbert, *J. Am. Chem. Soc.* **77**, 2594, 1955.
- [3] D.L. Martin, F.J.C. Rossotti, *Proc. Chem. Soc.* **60**, 1959.
- [4] E.J. Wheelwright, F.H. Spedding, G. Schwarzenbach, *J. Am. Chem. Soc.* **75**, 4196, 1953.
- [5] Y.H. Deshpande, D.V. Jahagirdhar, V. Ramachandra Rao, *J. Inorg. Nucl. Chem.* **37**, 1761, 1975.
- [6] S.P. Sangal, *Microchemical Journal* **9**, 26, 1965.

- [7] K.N. Munshi, S.N. Sinha, S.P. Sangal, A.K. Dey, *Microchemical Journal* **7**, 474, 1963.
- [8] D.F. Peppard, G.W. Mason, I. Hucher, *J. Inorg. Nucl. Chem.* **24**, 881, 1962.
- [9] S. Fronaeus, *Acta Chem. Scand.* **5**, 859, 1951; **6**, 1200, 1952.
- [10] J. Prasilova, *J. Inorg. Nucl. Chem.* **24**, 661, 1962.
- [11] D.J. Macero, L.B. Anderson, P. Malachuk, *J. Electroanal. Chem.* **10**, 76, 1965.
- [12] I. Grenthe, W.C. Fernelius, *J. Am. Chem. Soc.* **82**, 6258, 1960.
- [13] T. Moeller, D.F. Martin, L.C. Thompson, R. Ferrus, G.R. Feistel, W.J. Randall, *Chem. Rev.* **65**, 1, 1965.
- [14] I. Grenthe, W.C. Fernelius, *Rare Earth Research*, ed. E.V. Kleber, The Macmillan Co., NY, 1961.
- [15] G.R. Choppin, J.A. Chopoorian, *J. Inorg. Nucl. Chem.* **22**, 97, 1961.
- [16] K.B. Yatsimirskii, N.A. Kostromina, *Russ. J. Inorg. Chem.* **9**, 971, 1964.
- [17] G. Schwarzenbach, R. Gut, *Helv. Chim. Acta* **39**, 1589, 1956.
- [18] R.L. White, J.P. Andelin, *Phys. Rev.* **115**, 1435, 1959.
- [19] L.C. Thompson, *J. Inorg. Nucl. Chem.* **24**, 1083, 1962.
- [20] J.L. Hoard, G.S. Smith, M. Lind, *Advances in the Chemistry of Coordination Compounds*, ed. S. Kirschner, pp. 296–302, The Macmillan Co., NY, 1961.
- [21] L.A.K. Staveley, D.R. Markham, M.R. Jones, *Nature* **211**, 1172, 1966.
- [22] I. Grenthe, *Acta Chem. Scand.* **18**, 293, 1964.
- [23] G.R. Choppin, *J. Less Common Metals* **112**, 193, 1985.
- [24] A. Habenschuss, F.H. Spedding, *J. Chem. Phys.* **70**, 2797, 3758, 1979.
- [25] A.H. Narten, R.L. Hahn, *Science* **217**, 1249, 1982.
- [26] W.D. Horrocks, Jr., D.R. Sidnick, *J. Am. Chem. Soc.* **101**, 334, 1979.
- [27] H. Kanno, J. Hiraishi, *J. Phys. Chem.* **86**, 1488, 1982.
- [28] J.C. Bunzli, J.R. Yersin, C. Mabillard, *Inorg. Chem.* **21**, 1471, 1982.
- [29] G.R. Choppin, *Proc. 12<sup>th</sup> Rare Earth Conf.*, Vol. 1, Vail, Co, p. 130, 1976.
- [30] P.L. Rinaldi, S.A. Khan, G.R. Choppin, G.C. Levy, *J. Am. Chem. Soc.* **101**, 1350, 1979.
- [31] J. Reuben, *J. Phys. Chem.* **79**, 2154, 1975.
- [32] A. Anagnostopoulos, P.O. Sakehlaridis, *J. Inorg. Nucl. Chem.* **32**, 1740, 1970.
- [33] J.C. Bunzli, J.R. Yersin, *Inorg. Chem.* **18**, 605, 1979.
- [34] P.J. Breen, W.D. Horrocks, Jr., *Inorg. Chem.* **22**, 536, 1982.
- [35] J. Reuben, D. Fiat, *J. Chem. Phys.* **51**, 4909, 1969.
- [36] H.B. Silber, L.V. Kromer, *J. Inorg. Nucl. Chem.* **42**, 103, 1980.
- [37] G.R. Choppin, M.P. Goedken, T.F. Gritmon, *J. Inorg. Nucl. Chem.* **39**, 2025, 1977.
- [38] I. Grenthe, *J. Am. Chem. Soc.* **83**, 360, 1960.
- [39] R.J. Day, C.N. Reilly, *Anal. Chem.* **36**, 1073, 1964; **37**, 1326, 1965.
- [40] P.A. Baisden, G.R. Choppin, B.B. Garrett, *Inorg. Chem.* **16**, 1367, 1977.
- [41] G.R. Choppin, P.A. Bertrand, Y. Hasegawa, E.N. Rizkalla, *Inorg. Chem.* **21**, 3722, 1982.
- [42] G.R. Choppin, A. Dadgar, R. Stampfli, *J. Inorg. Nucl. Chem.* **35**, 875, 1973.
- [43] G.R. Choppin, T. Liu, *J. Less Common Met.* **94**, 406, 1983.
- [44] R.M. Izatt, J.D. Lamb, J.J. Christensen, B.L. Haymore, *J. Am. Chem. Soc.* **99**, 8344, 1977.
- [45] J. Zhou, D. Wang, He Huaxue Yu Fangshe Huaxue **4**, 174, 1982.
- [46] J. Zhou, X. Wu, He Huaxue Ye Fangshe Huaxue **6**, 78, 1984.
- [47] M.C. Almasio, F. Arnaud-Neu, M.J. Schwing-Weill, *Helv. Chim. Acta* **66**, 1296, 1983.
- [48] J. Massaux, J.F. Desreux, C. Delhambre, G. Duyckaerts, *Inorg. Chem.* **19**, 1893, 1980.
- [49] J. Massaux, J.F. Desreux, *J. Am. Chem. Soc.* **104**, 2967, 1982.
- [50] M.F. Loncin, J.F. Desreux, E. Merciny, *Inorg. Chem.* **25**, 2646, 1986.
- [51] C.A. Chang, V.O. Ochaya, *Inorg. Chem.* **25**, 355, 1986; **22**, 3866, 1983.
- [52] I. Fidelis, *Acad. Polon. Sci. Ser. Sci. Chim.* **18**, 681, 1970.
- [53] C.K. Jorgensen, *Struct. Bonding* **13**, 199, 1973.
- [54] S. Siekierski, *J. Inorg. Nucl. Chem.* **32**, 519, 1970.
- [55] B. Weaver, *Anal. Chem.* **26**, 476, 1954.
- [56] J.K. Marsh, *J. Chem. Soc.* 554, 1939.
- [57] G. Brunisholz, *Chimia* **11**, 97, 1957.
- [58] I. Grenthe, *J. Am. Chem. Soc.* **83**, 360, 1961.
- [59] D. Scargill, K. Alcock, J.M. Fletcher, E. Hesford, H.A.C. McKay, *J. Inorg. Nucl. Chem.* **4**, 304, 1957.
- [60] D.F. Peppard, G.W. Mason, I. Hucher, *J. Inorg. Nucl. Chem.* **18**, 245, 1961.
- [61] J.E. Powell, F.H. Spedding, *Chem. Eng. Progr. Symp. Ser.* **55**, 24, 101, 1959.
- [62] L. Wolf, J. Massone, *J. Chem. Tech.* **10**, 290, 1958.

- [63] P.R. Subbaraman, K.S. Rajan, J. Gupta, Z. Anorg. Allgem. Chem. **304**, 191, 1960.
- [64] J. Loriers, J. Tuesnu, Compt. Rend. **239**, 1643, 1955.
- [65] J. Minczewski, R. Dybczynski, J. Chromat. **7**, 568, 1962.
- [66] G.M. Kolosova, M.M. Senyavich, Chem. Abstr. **54**, 20, 611h, 1960.
- [67] H. Flascha, A.J. Barnard Jr., W.C. Broad, Chemist-Analyst **47**, 78, 1958.
- [68] R.B. King, P.R. Heckley, J. Am. Chem. Soc. **96**, 3118, 1974.
- [69] Y. Zhai, X. Chen, Z. Su, M. Tan, Lanzhou Daxue Xuebao, Ziran Kexueban **4**, 174, 1984.
- [70] E. Merciny, J.F. Desreux, J. Fuger, Anal. Chim. Acta **189**, 301, 1986.
- [71] L.M. Tsai, J.S. Shih, S.C. Wu, Analyst **108**, 1108, 1983.
- [72] Y. Hasegawa, M. Masuda, K. Hirose, Y. Fukuhara, Solvent Extr. Ion Exch. **5**, 255, 1987.
- [73] Y. Yang, Y. Ding, Q. Wang, Z. Yao, G. Pan, He Huaxue Yu Fangshe Huaxue **4**, 21, 1982.
- [74] Y. Kao, J. Ni, *ibid.* **5**, 146, 1983.
- [75] W. Wang, B. Chen, Z.K. Jin, A. Wang, J. Radioanal. Chem. **76**, 49, 1983.
- [76] V.V. Yaskin, A.T. Fedorova, A.V. Volkov, B.N. Laskorin, Dokl. Akad. Nauk SSSR **277**, 1417, 1984.
- [77] Z. Duang, J. Zou, D. Wang, He Huaxue Yu Fangshe Huaxue **8**, 193, 1986.
- [78] H.F. Aly, S.M. Khalia, J.D. Navratill, M.T. Saba, Solv. Extr. Ion Exch. **3**, 623, 1985.
- [79] D.D. Ensor, G.R. McDonald, C.G. Pippin, Anal. Chem. **58**, 1814, 1986.
- [80] T. Jian, C.M. Wai, Anal. Chem. **58**, 3233, 1986.

## Appendix

TABLE 3.10  
Stability constants of rare earth complexes with inorganic ligands.

Metal-L	Method	Temp. (°C)	Medium	log of equilibrium constant			Ref.
La <sup>3+</sup> -OH <sup>-</sup>	Diss		0.1 LiClO <sub>4</sub>	-7.4 ( $K_1^*$ )			1
Pr <sup>3+</sup>	Diss		0.1 LiClO <sub>4</sub>	-7.1			1
Nd <sup>3+</sup>	Diss		0.1 LiClO <sub>4</sub>	-7.0			1
Pm <sup>3+</sup>	Diss		0.1 LiClO <sub>4</sub>	-6.5			1
Sm <sup>3+</sup>	Diss		0.1 LiClO <sub>4</sub>	-4.4			1
Eu <sup>3+</sup>	Diss		0.1 LiClO <sub>4</sub>	-4.8			1
Gd <sup>3+</sup>	Diss		0.1 LiClO <sub>4</sub>	-7.1			1
Tb <sup>3+</sup>	Diss		0.1 LiClO <sub>4</sub>	-5.2			1
Dy <sup>3+</sup>	Diss		0.1 LiClO <sub>4</sub>	-5.6			1
Ho <sup>3+</sup>	Diss		0.1 LiClO <sub>4</sub>	-5.7			1
Er <sup>3+</sup>	Diss		0.1 LiClO <sub>4</sub>	-5.5			1
Tm <sup>3+</sup>	Diss		0.1 LiClO <sub>4</sub>	-4.4			1
Yb <sup>3+</sup>	Diss		0.1 LiClO <sub>4</sub>	-4.3			1
Lu <sup>3+</sup>	Diss		0.1 LiClO <sub>4</sub>	-3.5			1
M <sup>3+</sup> -ReO <sub>4</sub> <sup>-</sup>	Sp		1 (HReO <sub>4</sub> )	Pr, $K_1 = -0.92$			2
				Ho, $K_1 = -0.76$			2
				Er, $K_1 = -0.82$			2
				Tm, $K_1 = -0.89$			2
Nd <sup>3+</sup> -ReO <sub>4</sub> <sup>-</sup>			Var HReO <sub>4</sub>	$K_1 = 1.22, \beta_2 = 1.37$			3
M <sup>3+</sup> -Fe(CN) <sub>6</sub> <sup>4-</sup>							
La <sup>3+</sup>	Con	40-70		$K_s [K^+La^{3+}L^{4-}] = -8.7$			4
Ce <sup>3+</sup>	Con	20-30		$K_s [K^+Ce^{3+}L^-] = -9.20$			4
M <sup>3+</sup> -Fe(CN) <sub>6</sub> <sup>3-</sup>				$K_1$	$\Delta H_1$	$\Delta S_1$	
La	Cal	25	0 corr	3.70	0.85	19.8	5
Pr	Cal	25	0 corr	3.64	0.87	19.5	5
Nd	Cal	25	0 corr	3.77	0.80	19.9	5
Sm	Cal	25	0 corr	3.72	0.91	20.1	5
Eu	Cal	25	0 corr	3.65	0.98	20.0	5
Gd	Cal	25	0 corr	3.59	1.04	19.9	5
Tb	Cal	25	0 corr	3.76	0.94	20.4	5
Dy	Cal	25	0 corr	3.68	1.02	20.3	5
Ho	Cal	25	0 corr	3.66	1.06	20.3	5
Er	Cal	25	0 corr	3.68	1.04	20.3	5
Tm	Cal	25	0 corr	3.67	1.05	20.3	5
Yb	Cal	25	0 corr	3.66	1.04	20.2	5
Lu	Cal	25	0 corr	3.69	1.01	20.3	5
M <sup>3+</sup> -SCN <sup>-</sup>	Dis	30	1 NH <sub>4</sub> ClO <sub>4</sub>	La $K_1 = 0.12 \beta_2 = 0.22$			6
				Eu $K_1 = 0.13 \beta_2 = 0.29$			6
				Tb $K_1 = 0.23 \beta_2 = 0.34$			6
				Lu $K_1 = 0.21 \beta_2 = 0.35$			6
Ce <sup>3+</sup>	Dis	25	2 NH <sub>4</sub> NO <sub>3</sub>	$K_1 = 0.30 \beta_2 = 0.20$			7
Pr <sup>3+</sup>	Sp		3 LiClO <sub>4</sub>	$K_1 = 0.10$ to 0.50			8
Ho <sup>3+</sup>	Sp		3 LiClO <sub>4</sub>	$K_1 = 0.10$ to 0.40			8



(Continued.)					
Metal-L	Method	Temp. (°C)	Medium	log of equilibrium constant	Ref.
Azide					
La <sup>3+</sup> -N <sub>3</sub> <sup>-</sup>	E	25	3(NaClO <sub>4</sub> )	K <sub>1</sub> = 0.64	9
Nitrate, NO <sub>3</sub> <sup>-</sup>	Sp		HNO <sub>3</sub> var	β[M <sup>3+</sup> + 3L <sup>-</sup> + HL ⇌ ML <sub>3</sub> HL]	10
				Pr = -0.52	10
				Nd = -1.67	10
				Eu = -0.44	10
				Dy = -0.50	10
				Ho = -0.74	10
				Er = -0.76	10
				Yb = -1.29	10
				β[ML <sub>3</sub> HL + 2HL ⇌ ML <sub>3</sub> (HL) <sub>3</sub> ]	10
				Pr = -1.41	10
				Nd = -1.46	10
				Eu = -1.40	10
				Dy = -1.59	10
				Ho = -1.12	10
				Er = -0.87	10
				Yb = -1.41	10
La <sup>3+</sup>	Var		1 (KNO <sub>3</sub> )	K <sub>1</sub> = 1.5 ev LaL <sub>3</sub>	11
Ce <sup>3+</sup>	Δν		1 (NaClO <sub>4</sub> )	K <sub>1</sub> = 0.46	12
Hypophosphite, PO <sub>2</sub> H <sub>2</sub> <sup>-</sup>					
Pr <sup>3+</sup>	Sp		Var	K <sub>1</sub> = 1.33	13
Nd <sup>3+</sup>	Sp		Var	K <sub>1</sub> = 1.10	13
Er <sup>3+</sup>	Sp		Var	K <sub>1</sub> = 1.47	13
M <sup>3+</sup> -PO <sub>4</sub> <sup>3-</sup>					
La <sup>3+</sup>	Dis	25	1 (NH <sub>4</sub> ClO <sub>4</sub> )	β[La <sup>3+</sup> + H <sub>2</sub> L <sup>-</sup> ] = 1.61	14
Nd <sup>3+</sup>	Sp		POCl <sub>3</sub>	ev NdL <sub>3</sub> <sup>6-</sup>	15
Pyrophosphate, P <sub>2</sub> O <sub>7</sub> <sup>4-</sup>					
Y <sup>3+</sup>	I.ex	25	0.1 (NaClO <sub>4</sub> )	β <sub>2</sub> = 9.7	
Triphosphate, P <sub>2</sub> O <sub>10</sub> <sup>5-</sup>					
La <sup>3+</sup>	Gl	-	0.1 (NaClO <sub>4</sub> )	β <sub>2</sub> = 15.81, HL <sup>4-</sup> ; K <sub>1</sub> = 4.63, HL <sup>4-</sup> ; K <sub>1</sub> K <sub>2</sub> = 8.32	196
Pr <sup>3+</sup>	Gl	-	0.1 (NaClO <sub>4</sub> )	β <sub>2</sub> = 16.95, HL <sup>4-</sup> ; K <sub>1</sub> = 4.86, HL <sup>4-</sup> ; K <sub>1</sub> K <sub>2</sub> = 8.64	196
Sm <sup>3+</sup>	Gl	-	0.1 (NaClO <sub>4</sub> )	β <sub>2</sub> = 16.98, HL <sup>4-</sup> ; K <sub>1</sub> = 4.89, HL <sup>4-</sup> ; K <sub>1</sub> K <sub>2</sub> = 8.66	196
Eu <sup>3+</sup>	Gl	-	0.1 (NaClO <sub>4</sub> )	β <sub>2</sub> = 16.91, HL <sup>4-</sup> ; K <sub>1</sub> = 4.90, HL <sup>4-</sup> ; K <sub>1</sub> K <sub>2</sub> = 8.68	196
Gd <sup>3+</sup>	Gl	-	0.1 (NaClO <sub>4</sub> )	β <sub>2</sub> = 16.92, HL <sup>4-</sup> ; K <sub>1</sub> = 4.91, HL <sup>4-</sup> ; K <sub>1</sub> K <sub>2</sub> = 8.72	196
Dy <sup>3+</sup>	Gl	-	0.1 (NaClO <sub>4</sub> )	β <sub>2</sub> = 17.12, HL <sup>4-</sup> ; K <sub>1</sub> = 4.94, HL <sup>4-</sup> ; K <sub>1</sub> K <sub>2</sub> = 8.84	196
Er <sup>3+</sup>	Gl	-	0.1 (NaClO <sub>4</sub> )	β <sub>2</sub> 17.41, HL <sup>4-</sup> ; K <sub>1</sub> = 5.00, HL <sup>4-</sup> ; K <sub>1</sub> K <sub>2</sub> = 9.05	196
Yb <sup>3+</sup>	Gl	-	0.1 (NaClO <sub>4</sub> )	β <sub>2</sub> = 17.95, HL <sup>4-</sup> ; K <sub>1</sub> = 5.20, HL <sup>4-</sup> ; K <sub>1</sub> K <sub>2</sub> = 9.29	196
Y <sup>3+</sup>	Gl	-	0.1 (NaClO <sub>4</sub> )	β <sub>2</sub> = 17.21, HL <sup>4-</sup> ; K <sub>1</sub> = 4.97, HL <sup>4-</sup> ; K <sub>1</sub> K <sub>2</sub> = 8.87	196

(Continued.)

Metal-L	Method	Temp. (°C)	Medium	log of equilibrium constant	Ref.
	Gl	25-45	0.1 (KNO <sub>3</sub> )	$\beta_2 = 8.0$ (25°), $\Delta H_{\beta_2} = -2.5$ (La)	17
	Gl	25-45	0.1	$\beta_2 = 8.2$ (25°), $\Delta H_{\beta_2} = -2.4$ (Ce)	17
	Gl	25-45	0.1	$\beta_2 = 8.3$ (25°), $\Delta H_{\beta_2} = -2.4$ (Pr)	17
	Gl	25-45	0.1	$\beta_2 = 8.5$ (25°), $\Delta H_{\beta_2} = -4.5$ (Nd)	17
	Gl	25-45	0.1	$\beta_2 = 8.7$ (25°), $\Delta H_{\beta_2} = -6.8$ (Sm)	17
	Gl	25-45	0.1	$\beta_2 = 8.8$ (25°), $\Delta H_{\beta_2} = -6.9$ (Eu)	17
	Gl	25-45	0.1	$\beta_2 = 8.9$ (25°), $\Delta H_{\beta_2} = -6.9$ (Gd)	17
	Gl	25-45	0.1	$\beta_2 = 9.1$ (25°), $\Delta H_{\beta_2} = -6.8$ (Tb)	17
	Gl	25-45	0.1	$\beta_2 = 9.2$ (25°), $\Delta H_{\beta_2} = -4.7$ (Dy)	17
	Gl	25-45	0.1	$\beta_2 = 9.3$ (25°), $\Delta H_{\beta_2} = -6.8$ (Ho)	17
	Gl	25-45	0.1	$\beta_2 = 9.5$ (25°), $\Delta H_{\beta_2} = -6.7$ (Er)	17
	Gl	25-45	0.1	$\beta_2 = 9.7$ (25°), $\Delta H_{\beta_2} = -6.7$ (Tm)	17
M <sup>n+</sup> +H <sub>2</sub> O					
Y <sup>3+</sup>	Mag, kin	104	Var	$\beta[\text{Y}(\text{EDTA})\text{L}_{n-1}^-, \text{L}] = -2.0$	18
	EMF	20	0.1 KNO <sub>3</sub>	$\beta[\text{Y}(\text{EDTA})\text{L}_{n-1}^-, \text{L}] = -2.0$	18
				Sm = 0.7, Eu = 0.15, Gd = -0.15, Tb = -1.0	19
				Dy = -1.05, Ho = -1.38, Er = -2.00	18
Pr <sup>3+</sup>	Sp		EtOH-H <sub>2</sub> O	$K_6 = 0.53$	20
M <sup>3+</sup> +SO <sub>4</sub> <sup>2-</sup>	Cal	25	0 corr	$\Delta H_1 = 3.50$ (La), 3.78 (Ce), 3.92 (Pr), 4.15 (Nd), 4.34 (Sm), 4.13 (Eu), 4.10 (Gd), 4.02 (Tb), 3.58 (Dy), 3.54 (Ho), 3.39 (Er), 3.15 (Tm), 2.90 (Yb), 3.54 (Lu)	21
	Con	25	0 corr	$K_1 = 3.65$ (La), 3.67 (Ce), 3.67 (Pr), 3.68 (Nd), 3.68 (Sm), 3.67 (Gd), 3.60 (Ho), 3.58 (Er), 3.51 (Yb), 3.52 (Lu)	22
	Oth	25	0 corr	$K_1 = 3.62$ (Pr), 3.64 (Nd), 3.66 (Sm), 3.66 (Eu), 3.66 (Gd), 3.64 (Tb), 3.61 (Dy), 3.59 (Ho)	23
	Kin	25	0 corr	$K_1 = 3.62$ (La), 3.64 (Nd), 3.65 (Gd), 3.61 (Dy)	24
	Cal	25	0 corr	$\Delta H_1 = 3.13$ , $\Delta S_1 = 27$ (La); $\Delta H_1 = 3.42$ , $\Delta S_1 = 28.3$ (Sm); $\Delta H_1 = 3.70$ , $\Delta S_1 = 29.0$ (Tb); $\Delta H_1 = 3.37$ , $\Delta S_1 = 27.6$ (Er)	22, 25
	Cal	25	0 corr	$K_1 = 1.67$ (La), 1.30 (Pr), 1.50 (Nd), 1.74 (Eu), 1.55 (Gd), 1.51 (Tb), 1.2 (Dy), 1.3 (Ho), 1.45 (Er), 1.55 (Tm), 1.6 (Yb)	22, 25
La <sup>3+</sup>	Dis	25	1 (NaClO <sub>4</sub> )	$K_1 = 1.77$ , $\beta_2 = 2.66$ ( $l = 0.5$ )	27
Ce <sup>3+</sup>	Kin	25	5 (NaClO <sub>4</sub> )	$\beta[\text{CeL}_2 + \text{HL}^- = \text{CeHL}_3] = 0.53$	28
Ce <sup>3+</sup>	$\Delta\nu$	30	1 (NaClO <sub>4</sub> )	$K_1 = 1.76$ , $\Delta\nu_1 = 15.1$ cm <sup>3</sup>	29
Eu <sup>3+</sup>	Sp	25	0 corr	$K_1 = 3.67$	31
				$\Delta H_1 = 6.2$ (also $\Delta S$ )	
	Sp	25	var, p atm	$K_1 = 3.68$ ( $p = 1$ ), 3.44 ( $p = 545$ ), 3.29 ( $p = 983$ ), 3.11 ( $p = 1497$ )	32
	Dis	25	0 corr	$k_1 = 3.87$ , $\beta_2 = 5.75$ , $\beta_3 = 5.09$	33

(Continued.)					
Metal-L	Method	Temp. (°C)	Medium	log of equilibrium constant	Ref.
Tb <sup>3+</sup>	Oth	25	2 (NaClO <sub>4</sub> )	$K_1 = 1.59$ (luminescence quenching)	34
M <sup>3+</sup> -F <sup>-</sup>	Lit	25		$K_1 = 2.67$ (La), 2.81 (Ce), 3.01 (Pr), 3.09 (Nd), 3.12 (Sm), 3.19 (Eu), 3.31 (Gd), 3.43 (Tb), 3.46 (Dy), 3.52 (Ho), 3.54 (Er), 3.56 (Tm), 3.58 (Yb), 3.60 (Lu) $K_1 = 3.6$ (La), 4.0 (Ce), 4.26 (Gd) $\beta_4 = 18.49$	
Sc <sup>3+</sup>	Dis	25	0.5 (NaClO <sub>4</sub> )	$K_1 = 6.17, \beta_2 = 11.44, \beta_3 = 15.46,$ $\beta_4 = 18.49$	36
Y <sup>3+</sup>	Dis	25	0.5 (NaClO <sub>4</sub> )	$K_1 = 3.89, \beta_2 = 7.11, \beta_3 = 10.30$	36
Eu <sup>3+</sup>	IseF	25	0.5 (NaClO <sub>4</sub> )	$K_1 = 3.40$	37
Chloride, Cl <sup>-</sup>					
M <sup>3+</sup> -Cl <sup>-</sup>					196
La <sup>3+</sup>	Dist	22	1 (HClO <sub>4</sub> )	$K_1 = 0.05$	196
La <sup>3+</sup>	Sol	25	0.5	$K_1 = 0.46$	196
Ce <sup>3+</sup>	Dist	22	1 (HClO <sub>4</sub> )	$K_1 = 0.05$	196
Pr <sup>3+</sup>	Dist	22	1 (HClO <sub>4</sub> )	$K_1 = 0.05$	196
Sm <sup>3+</sup>	Sol	25	0.5	$K_1 = 0.46$	196
Eu <sup>3+</sup>	Dist	22	1 (HClO <sub>4</sub> )	$K_1 = 0.05$	196
Tm <sup>3+</sup>	Dist	22	1 (HClO <sub>4</sub> )	$K_1 = 0.10$	196
Yb <sup>3+</sup>	Dist	22	1 (HClO <sub>4</sub> )	$K_1 = 0.22$	196
Yb <sup>3+</sup>	Sol	25	0.5	$K_1 = 0.56$	196
Lu <sup>3+</sup>	Dist	22	1 (HClO <sub>4</sub> )	$K_1 = 0.40$	196
Lu <sup>3+</sup>	Sol	25	0.5	$K_1 = 0.48$	196
Y <sup>3+</sup>	Dist	-	3	$K_1 = 0.89-0.13$	196
Y <sup>3+</sup>	Red	15-35	0 cor	$K_1 = 0.38$ (15°), 0.36 (25°), 0.32 (35°) ( $\Delta H_1 = -0.3, \Delta S_1 = -1$ )	196
La <sup>3+</sup>	Sol	25	0 corr	$K_3[\text{La}^{3+}(\text{OH}^-)_2\text{Cl}^-] = -15.51$ (fresh), $-16.76$ (aged)	196
Pr <sup>3+</sup>	Sp	25	3 (LiClO <sub>4</sub> )	$K_1 = 0.85,$	39
	Sp	25	ProH	$K_1 = 1$ (1 (LiClO <sub>4</sub> ))	41
Nd <sup>3+</sup>	Sol, Sp	25	HCl var	$K_1 = -0.1$ (outer sphere)	42
	Sp		MeOH	$K_1 = 1.8\beta_2 = 2.0$ (0.5 (LiClO <sub>4</sub> ))	43
Pm <sup>3+</sup>	Oth	15	HCl var	$K_1 = 0.7, K_2(?) = -0.8$ (paper electrophoresis)	44
Sm <sup>3+</sup>				$K_1 = 0.96$	39
Eu <sup>3+</sup>	Sp	25	W%MeOH	$K_1 = 0.04$ (W = 0), $K_1 = 0.55$	39
Tb <sup>3+</sup>	Oth	20		1 ev TbL <sub>4</sub> <sup>-</sup> , TbL <sub>5</sub> <sup>3-</sup> , TbL <sub>6</sub> <sup>3-</sup> , Tb <sub>2</sub> L <sub>7</sub> <sup>-</sup> (refractometry)	46
Ho <sup>3+</sup>	Sp	25	3 (LiClO <sub>4</sub> )	$K_1 = 0.82$	39
Er <sup>3+</sup>	Sp	25	3 (LiClO <sub>4</sub> )	$K_1 = 0.71$	39
Yb <sup>3+</sup>	Sp	25	W%MeOH	$K_1 = -0.11$ (W = 0), 0.34 (W = 50) (3 (LiClO <sub>4</sub> ))	39
M <sup>3+</sup> -ClO <sub>3</sub> <sup>-</sup>					
Eu <sup>3+</sup>	Dis	2-40	1 NaClO <sub>4</sub>	$K_1 = 0.08$ (20°)	49
Tb <sup>3+</sup>	Dis	2-30	1 NaClO <sub>4</sub>	$K_1 = 0.00$ (20°)	49
M <sup>3+</sup> -ClO <sub>4</sub> <sup>-</sup>					
Nd <sup>3+</sup>	Sol, Sp	25	HL var	$K_1 = -1.77$	42
Er <sup>3+</sup>	Sp	25	%MeOH	$K_1 = 0.6$	50

*(Continued.)*

Metal-L	Method	Temp. (°C)	Medium	log of equilibrium constant	Ref.
$M^{3+}-Br^-$					
$Pr^{3+}$				$K_1 = -0.23 (W = 0)$	
	Sp	25	PrOH	$K_1 = 0.4 \text{ to } 0.9 (1 (LiClO_4))$	41
$Nd^{3+}$	Sp	25	PrOH	$K_1 = 0 \text{ to } 0.5 (1 (LiClO_4))$	41
$Sm^{3+}$	Sp	25	W%MeOH	$K_1 = -0.16 (W = 0)$	48
$Ho^{3+}$	Sp	25	W%MeOH	$K_1 = -0.62 (W = 0)$	48
$Er^{3+}$	Sp	25	PrOH	$K_1 = 0.5 \text{ to } 0.9 (1 (LiClO_4))$	41
$M^{3+}-BrO_3^-$					
$Eu^{3+}$	Dis	2-40	1 NaClO <sub>4</sub>	$K_1 = 0.62 (20^\circ)$	49
$Tb^{3+}$	Dis	2-40	1 NaClO <sub>4</sub>	$K_1 = 0.54 (20^\circ)$	49
$M^{3+}-IO_3^-$					
$Eu^{3+}$	Dis	2-40	1 NaClO <sub>4</sub>	$K_1 = 0.90 (20^\circ)$	49
$Tb^{3+}$	Dis	2-40	1 NaClO <sub>4</sub>	$K_1 = 0.82 (20^\circ)$	49
$Eu^{3+}$	Dis	0-40	1 NaClO <sub>4</sub>	$K_1 = 1.15 (25^\circ), \Delta H_1 = 2.65$	51

## References for Table 3.10

1. R. Guillaumont, B. Desire, M. Galin, *Radiochem. Radioanalyt. Letters* 8, 189.
2. K.I. Petrov, N.A. Orlin, V.E. Plyushchev, *Zhur. Neorg. Khim.* 15, 439, 442.
3. K.I. Petrov, N.A. Orlin, V.E. Plyushchev, *Zhur. Neorg. Khim.* 14, 2739.
4. A. Bellomo, D. Demarco, A. Casale, *Talanta* 20, 355.
5. R. Stampfli, G.R. Choppin, *J. Inorg. Nuclear Chem.* 34, 205.
6. P.K. Khopkar, J.N. Mathur, *J. Inorg. Nuclear Chem.* 36, 3819.
7. R. Chiarizia, P.R. Danesi, G. Scibona, L. Magon, *J. Inorg. Nuclear Chem.* 35, 3595.
8. V.S. Netsvetaeva, I.M. Batyaev, *Zhur. Neorg. Khim.* 19, 1256.
9. F. Maggio, L. Bellerito, V. Romano, T. Bizzino, *Attic Acad. Sci. LeH Arti Palermo* 4, 33, 195, 1973-74.
10. A.E. Klygin, I.D. Smirnova, N.S. Kolyada, E.N. Malkina, A.M. Gertseva, V.A. Lekae, D.M. Zavrashnova, *Zhur. Neorg. Khim.* 15, 622.
11. J. Knoeck, *Analyst Chem.* 41, 2069.
12. T.G. Spiro, A. Revesz, J. Lee, *J. Amer. Chem. Soc.* 90, 4000.
13. N.S. Poluektov, R.S. Lauer, S.F. Ognichenko, *Zhur. Neorg. Khim.* 15, 2133.
14. V.K. Rao, C.J. Sharani, C.L. Rao, *Radiochim. Acta* 14, 31.
15. P. Brun, P. Caro, *Compt. Rend.* 273c, 894.
16. A.A. Elesin, A.A. Zaitsev, V.A. Karaseva, I.I. Nazarova, I.V. Petukhova, *Radiokhimiya* 14, 374.
17. M.M.T. Khan, P.R. Reddy, *J. Inorg. Nucl. Chem.* 35, 179.
18. R.H. Betts, R.H. Voss, *Can. J. Chem.* 51, 538.
19. G. Geier, U. Karlen, *Helv. Chim. Acta* 54, 135.
20. R.K. Chernova, L.K. Sukhova, T.N. Efimova, *Zhur. Neorg. Khim.* 19, 1245.
21. D.P. Fay, N. Purdie, *J. Phys. Chem.* 73, 3462.
22. M.M. Farrow, N. Purdie, *J. Solution Chem.* 2, 503.
23. M.M. Farrow, N. Purdie, *J. Solution Chem.* 2, 513.
24. J. Reidler, H.B. Silber, *J. Phys. Chem.* 77, 1275.
25. M.M. Farrow, N. Purdie, W.D. White, *J. Solution Chem.* 3, 395.
26. H.K.J. Powell, *JCS Dalton* 1108, 1974.
27. A. Aziz, S.J. Lyle, *J. Inorg. Nuclear Chem.* 32, 1925.
28. S.K. Mishra, Y.K. Gupta, *J. Chem. Soc. (A)* 2918, 1970.
29. T.G. Spiro, A. Revesz, J. Lee, *J. Amer. Chem. Soc.* 90, 4000.
30. A. Qadeer, *Z. Phys. Chem. (Frankfurt)* 91, 301.
31. C.F. Hale, F.H. Spedding, *J. Phys. Chem.* 76, 1887.
32. C.F. Hale, F.H. Spedding, *J. Phys. Chem.* 76, 2925.
33. W.J. McDowell, C.F. Colemam, *J. Inorg. Nucl. Chem.* 34, 2837.

34. B.M. Antipenko, I.M. Batyaev, T.A. Privalova, *Zhur. Neorg. Khim.* 18, 607.
35. L.R. Batisanova, *Uspekhi Khim.* 40, 945.
36. A. Aziz, S.J. Lyle, *J. Inorg. Nuclear Chem.* 31, 3471.
37. A. Aziz, S.J. Lyle, *Anal. Chim. Acta* 47, 49.
38. N.N. Kozachenko, I.M. Batyaev, V.E. Mironov, *Zhur. Neorg. Khim.* 15, 888.
39. N.N. Kozachenko, I.M. Batyaev, *Zhur. Neorg. Khim.* 16, 125.
40. E.P. Mignonsin, G. Duyckaerts, *Analyt. Letters* 2, 153.
41. A.I. Krutous, I.M. Batyaev, *Zhur. Neorg. Khim.* 19, 1234.
42. G.A. Shutova, K.B. Yatsimirskii, T.V. Malkova, *Zhur. Neorg. Khim.* 13, 2708.
43. A.A. Zholdakov, L.N. Lugina, N.K. Davydenko, *Zhur. Neorg. Khim.* 16, 2373.
44. B. Marin, T. Kikindai, *Compt. Rend.* 268c, 129.
45. N.N. Kozachenko, I.M. Batyaev, *Zhur. Neorg. Khim.* 16, 1841.
46. P. Spacu, E. Ivan, *Rev. Roumaine Chim.* 13, 1177.
47. P. Spacu, I. Albescu, E. Ivan, *Rev. Roumaine Chim.* 13, 425.
48. N.N. Kozachenko, N.A. Panteleeva, V.S. Netsvetaeva, I.M. Batyaev, *Zhur. Neorg. Khim.* 18, 1776.
49. R. Roulet, R. Chenaux, *Helv. Chim. Acta* 55, 1959.
50. H.B. Silber, *J. Phys. Chem.* 78, 1940.
51. G.R. Choppin, S.L. Bertha, *J. Inorg. Nucl. Chem.* 35, 1309.

TABLE 3.11  
Stability constants of rare earth complexes with organic ligands.

Metal	Method	Temp. (°C)	Medium	log of equilibrium constant	Ref.		
Formic acid							
Eu <sup>3+</sup>	Pol	25	1 NaClO <sub>4</sub>	$K_1 = 1.30, K_2 = 2.08$	1		
Methyl phosphonic acid, CH <sub>5</sub> O <sub>3</sub> P							
Pm <sup>3+</sup>	Iex	25	→ 0	$K(\text{Pm}^{3+} + \text{HL} = \text{PmHL}^{2+}) = 2.67$	2		
Hydroxymethyl phosphonic acid, CH <sub>5</sub> O <sub>4</sub> P							
Pm <sup>3+</sup>	Iex	25	0.2 NH <sub>4</sub> ClO <sub>4</sub>	$K(\text{Pm}^{3+} + \text{HL} = \text{PmHL}^{2+}) = 1.65$ $K[\text{PmHL}^{2+} + \text{HL} = \text{Pm}(\text{HL})_2^+] = 13.3$	3		
C <sub>2</sub> H <sub>2</sub> O <sub>4</sub> , oxalic acid							
Ce <sup>3+</sup>	Sol	20	1 NaClO <sub>4</sub>	$K_1 = 4.49, \beta_2 = 7.91, \beta_3 = 10.30, \beta_4 = 11.75$	4		
Er <sup>3+</sup>	Sol	18–30	0.1	$K_1(18^\circ) = 2.92, \beta_2(18^\circ) = 5.70, \beta_3(18^\circ) = 8.64$	5		
Eu <sup>3+</sup>	Sol	20	1 NaClO <sub>4</sub>	$K_1 = 5.04, \beta_2 = 8.70, \beta_3 = 11.57, \beta_4 = 13.09$	4		
La <sup>3+</sup>	Dis	25	0.5 NaClO <sub>4</sub>	$K_1 = 4.47, \beta_2 = 8.00$	6		
Lu <sup>3+</sup>	Sol	20	1 NaClO <sub>4</sub>	$K_1 = 5.28, \beta_2 = 9.53, \beta_3 = 12.74, \beta_4 = 14.68$	4		
Pm <sup>3+</sup>	Dis	20	0.1 NH <sub>4</sub> Cl	$\beta_2 = 8.3, \beta_3 = 11.8$	7		
Sm <sup>3+</sup>	Sol	25	0.5	$K_1 = 6.62$	8		
Tb <sup>3+</sup>	Sol	20	1 NaClO <sub>4</sub>	$K_1 = 5.08, \beta_2 = 8.86, \beta_3 = 11.85, \beta_4 = 13.42$	4		
Tm <sup>3+</sup>	Iex	18	0.1	$K_1 = 3.40, \beta_2 = 3.45, \beta_3 = 1.0$	9		
C <sub>2</sub> H <sub>4</sub> O <sub>2</sub> , acetic acid							
Ce <sup>3+</sup>	Dis	2–47	2.0 NaClO <sub>4</sub>	$K_1 = 1.70 (25^\circ)$	10		
Eu <sup>3+</sup>	Dis	0–55	2.0 NaClO <sub>4</sub>	$K_1 = 1.90 (25^\circ)$	10		
La <sup>3+</sup>	Oth	20	0.2	$\beta_3 = 2.97$	11		
Nd <sup>3+</sup>	Pot	?	2 NaClO <sub>4</sub>	$K_1 = 1.90$	12		
	Qh	?	0.5 NaClO <sub>4</sub> 0–70% dioxane	$\beta_2 = 3.64, \beta_3(60\%) = 7.63$	13		
Pr <sup>3+</sup>	Pot	?	2 NaClO <sub>4</sub> 0–80% EtOH	$K_1 = 1.96, \beta_2 = 2.83, \beta_3 = 3.83, \beta_4 = 3.58$ $\beta_5(60\%) = 7.70, \beta_6(80\%) = 12.44$	12 12		
Tb <sup>3+</sup>	Oth	25	2.0 NaClO <sub>4</sub>	$K_1 = 1.00, K_2 = 0.78, K_3 = 0.60$	13		
Y <sup>3+</sup>	Oth	–	–	$\beta_2 = 3.74$	14		
La <sup>3+</sup>	–	–	$\mu = 0.1$	$K_1 = 2.02, K_2 = 1.24$	16		
Ce <sup>3+</sup>	–	–	$\mu = 0.1$	$K_1 = 2.09, K_2 = 1.44$	16		
Pr <sup>3+</sup>	–	–	$\mu = 0.1$	$K_1 = 2.18, K_2 = 1.45$	16		
Nd <sup>3+</sup>	–	–	$\mu = 0.1$	$K_1 = 2.22, K_2 = 1.54$	16		
Sm <sup>3+</sup>	–	–	$\mu = 0.1$	$K_1 = 2.30, K_2 = 1.58$	16		
C <sub>2</sub> H <sub>4</sub> O <sub>2</sub> S, HSCH <sub>2</sub> CO <sub>2</sub> H, mercapto acetic acid (thioglycolic acid), HL							
Metal	Method	<i>I</i>	<i>T</i> (°C)	log <i>K</i> <sub>1</sub>	log <i>K</i> <sub>2</sub>	log $\beta_2$	Ref.
La <sup>3+</sup>	Gl	0.1 M NaClO <sub>4</sub>	20	1.98	1.00	2.98	195
La <sup>3+</sup>	Gl	2 M NaClO <sub>4</sub>	25	1.42	0.70	2.12	195
La <sup>3+</sup>	Gl	0.1 M KCl	30	2.27	2.35	4.62	195
Ce <sup>3+</sup>	Gl	0.1 M NaClO <sub>4</sub>	20	1.99	1.04	3.03	195
Ce <sup>3+</sup>	Gl	2 M NaClO <sub>4</sub>	25	1.43	0.70	2.13	195
Ce <sup>3+</sup>	Gl	0.1 M KCl	30	2.28	2.36	4.64	195
Pr <sup>3+</sup>	Gl	0.1 M NaClO <sub>4</sub>	20	2.03	1.04	3.07	195
Pr <sup>3+</sup>	Gl	0.1 M KCl	30	2.40	2.44	4.84	195
Nd <sup>3+</sup>	Gl	2 M NaClO <sub>4</sub>	20	2.07	1.20	3.27	195
Nd <sup>3+</sup>	Gl	0.1 M NaClO <sub>4</sub>	25	1.49	0.78	2.27	195
Nd <sup>3+</sup>	Gl	0.1 M KCl	30	2.48	2.52	5.00	195
Sm <sup>3+</sup>	Gl	0.1 M NaClO <sub>4</sub>	20	2.11	1.36	3.47	195

(Continued.)									
Metal	Method	<i>I</i>	<i>T</i> (°C)	log <i>K</i> <sub>1</sub>	log <i>K</i> <sub>2</sub>	log β <sub>2</sub>	Ref.		
Sm <sup>3+</sup>	Gl	2 M NaClO <sub>4</sub>	25	1.81	0.90	2.71	195		
Eu <sup>3+</sup>	Gl	0.5 M (NaClO <sub>4</sub> )	20	1.55	0.72	2.27	195		
Eu <sup>3+</sup>	Gl	0.1 M NaClO <sub>4</sub>	20	2.07	1.34	3.41	195		
Eu <sup>3+</sup>	Gl	2.0 M NaClO <sub>4</sub>	25	1.75	0.78	2.53	195		
Gd <sup>3+</sup>	Gl	0.1 M NaClO <sub>4</sub>	20	2.01	1.30	3.31	195		
Gd <sup>3+</sup>	Gl	2 M NaClO <sub>4</sub>	25	1.64	0.78	2.42	195		
Tb <sup>3+</sup>	Gl	0.1 M NaClO <sub>4</sub>	20	1.96	1.26	3.22	195		
Tb <sup>3+</sup>	Gl	2 M NaClO <sub>4</sub>	25	1.63	0.78	2.41	195		
Dy <sup>3+</sup>	Gl	0.1 M NaClO <sub>4</sub>	20	1.93	1.32	3.25	195		
Ho <sup>3+</sup>	Gl	0.1 M NaClO <sub>4</sub>	20	1.92	1.32	3.24	195		
Ho <sup>3+</sup>	Gl	2 M NaClO <sub>4</sub>	25	1.32	0.84	2.16	195		
Er <sup>3+</sup>	Gl	0.1 M NaClO <sub>4</sub>	20	1.94	1.43	3.26	195		
Er <sup>3+</sup>	Gl	2 M NaClO <sub>4</sub>	25	1.28	0.90	2.18	195		
Tm <sup>3+</sup>	Gl	0.1 M NaClO <sub>4</sub>	20	1.98	1.11	3.09	195		
Yb <sup>3+</sup>	Gl	0.1 M NaClO <sub>4</sub>	20	1.98	1.32	3.30	195		
Yb <sup>3+</sup>	Gl	2 M NaClO <sub>4</sub>	25	1.32	0.90	2.22	195		
Lu <sup>3+</sup>	Gl	0.1 NaClO <sub>4</sub>	20	2.01	1.30	3.31	195		
Y <sup>3+</sup>	Gl	0.1 M NaClO <sub>4</sub>	20	1.91	1.28	3.19	195		
Y <sup>3+</sup>	Gl	2 M NaClO <sub>4</sub>	25	1.49	0.70	2.19	195		
C <sub>2</sub> H <sub>4</sub> NO <sub>2</sub> , CH <sub>3</sub> CONOH, acethydroxamic acid, HL									
Metal	Method	<i>I</i>	<i>T</i> (°C)	<i>K</i> <sub>1</sub>	<i>K</i> <sub>2</sub>	β <sub>2</sub>	<i>K</i> <sub>3</sub>	β <sub>3</sub>	Ref.
La <sup>3+</sup>	Gl	0.1 NaNO <sub>3</sub>	20	5.16	4.17	9.33	2.55	11.88	201
Ce <sup>3+</sup>	Gl	0.1 NaNO <sub>3</sub>	20	5.45	4.34	9.79	3.0	12.8	201
Sm <sup>3+</sup>	Gl	0.1 NaNO <sub>3</sub>	20	5.96	4.77	10.73	3.68	14.41	201
Gd <sup>3+</sup>	Gl	0.1 NaNO <sub>3</sub>	20	6.10	4.76	10.86	3.07	13.93	201
Dy <sup>3+</sup>	Gl	0.1 NaNO <sub>3</sub>	20	6.52	5.36	11.91	4.04	15.95	201
Yb <sup>3+</sup>	Gl	0.1 NaNO <sub>3</sub>	20	6.61	5.59	12.20	4.29	16.49	201
Eu <sup>3+</sup>		μ = 0.1		2.31	1.60				16
Gd <sup>3+</sup>				2.16	1.60				16
Tb <sup>3+</sup>				2.07	1.59				16
Dy <sup>3+</sup>				2.03	1.61				16
Ho <sup>3+</sup>				2.00	1.59				16
Er <sup>3+</sup>				2.01	1.59				16
Tm <sup>3+</sup>				2.02	1.59				16
Yb <sup>3+</sup>				2.03	1.64				16
Lu <sup>3+</sup>				2.05	1.64				16
Metal	Method	Temp. (°C)	Medium	log of equilibrium constant				Ref.	
C <sub>2</sub> H <sub>4</sub> O <sub>3</sub> , hydroxy acetic acid									
Eu <sup>3+</sup>	Dis	0.5–52	2.0 NaClO <sub>4</sub>	<i>K</i> <sub>1</sub> = 2.52 (25°)				17	
C <sub>2</sub> H <sub>4</sub> O <sub>3</sub> , glycollic acid									
La <sup>3+</sup>	Gl	20	0.1 NaClO <sub>4</sub>	<i>K</i> <sub>1</sub> = 2.55, <i>K</i> <sub>2</sub> = 1.69, <i>K</i> <sub>3</sub> = 0.78, β <sub>2</sub> = 4.24, β <sub>3</sub> = 5.02				194	
Ce <sup>3+</sup>	Gl	20	0.1 NaClO <sub>4</sub>	<i>K</i> <sub>1</sub> = 2.69, <i>K</i> <sub>2</sub> = 1.85, <i>K</i> <sub>3</sub> = 0.84, β <sub>2</sub> = 4.54, β <sub>3</sub> = 5.38				194	
Pr <sup>3+</sup>	Gl	20	0.1 NaClO <sub>4</sub>	<i>K</i> <sub>1</sub> = 2.78, <i>K</i> <sub>2</sub> = 1.90, <i>K</i> <sub>3</sub> = 1.18, β <sub>2</sub> = 4.68, β <sub>3</sub> = 5.86				194	
Nd <sup>3+</sup>	Gl	20	0.1 NaClO <sub>4</sub>	<i>K</i> <sub>1</sub> = 2.89, <i>K</i> <sub>2</sub> = 1.96, <i>K</i> <sub>3</sub> = 1.26, β <sub>2</sub> = 4.85, β <sub>3</sub> = 6.11				194	

<i>(Continued.)</i>					
Metal	Method	Temp. (°C)	Medium	log of equilibrium constant	Ref.
Sm <sup>3+</sup>	Gl	20	0.1 NaClO <sub>4</sub>	$K_1 = 2.91, K_2 = 2.10, K_3 = 1.56,$ $\beta_2 = 5.01, \beta_3 = 6.57$	194
Eu <sup>3+</sup>	Gl	20	0.1 NaClO <sub>4</sub>	$K_1 = 2.93, K_2 = 2.14, K_3 = 1.45,$ $\beta_2 = 5.07, \beta_3 = 6.52$	194
Gd <sup>3+</sup>	Gl	20	0.1 NaClO <sub>4</sub>	$K_1 = 2.79, K_2 = 2.06, K_3 = 1.15,$ $\beta_2 = 4.85, \beta_3 = 6.00$	194
Tb <sup>3+</sup>	Gl	20	0.1 NaClO <sub>4</sub>	$K_1 = 2.82, K_2 = 2.09, K_3 = 1.11,$ $\beta_2 = 4.91, \beta_3 = 6.02$	194
Dy <sup>3+</sup>	Gl	20	0.1 NaClO <sub>4</sub>	$K_1 = 2.92, K_2 = 2.05, K_3 = 1.58,$ $\beta_2 = 4.97, \beta_3 = 6.55$	194
Ho <sup>3+</sup>	Gl	20	0.1 NaClO <sub>4</sub>	$K_1 = 2.99, K_2 = 2.05, K_3 = 1.53,$ $\beta_2 = 5.04, \beta_3 = 6.57$	194
Er <sup>3+</sup>	Gl	20	0.1 NaClO <sub>4</sub>	$K_1 = 3.00, K_2 = 2.18, K_3 = 1.66,$ $\beta_2 = 5.18, \beta_3 = 6.84$	194
Tm <sup>3+</sup>	Gl	20	0.1 NaClO <sub>4</sub>	$K_1 = 3.06, K_2 = 2.26, K_3 = 1.67,$ $\beta_2 = 5.32, \beta_3 = 6.99$	194
Yb <sup>3+</sup>	Gl	20	0.1 NaClO <sub>4</sub>	$K_1 = 3.13, K_2 = 2.24, K_3 = 1.74,$ $\beta_2 = 5.37, \beta_3 = 7.11$	194
Lu <sup>3+</sup>	Gl	20	0.1 NaClO <sub>4</sub>	$K_1 = 3.15, K_2 = 2.33, K_3 = 1.80,$ $\beta_2 = 5.48, \beta_3 = 7.28$	194
Y <sup>3+</sup>	Gl	20	0.1 NaClO <sub>4</sub>	$K_1 = 2.79, K_2 = 2.09, K_3 = 0.90,$ $\beta_2 = 4.88, \beta_3 = 5.78$	194
C <sub>2</sub> H <sub>8</sub> N <sub>2</sub> , ethylenediamine					
La <sup>3+</sup> -L	Cal	23	CH <sub>3</sub> CN	$K_1 = 9.5, K_2 = 7.5, K_3 = 6.2, K_4 = 3.3$	19
Tb <sup>3+</sup>	Cal	23	CH <sub>3</sub> CN	$K_1 = 10.4, K_2 = 8.4, K_3 = 6.2, K_4 = 3.2$	19
Yb <sup>3+</sup>	Cal	23	CH <sub>3</sub> CN	$K_1 = 11.5, K_2 = 8.4, K_3 = 6.2, K_4 = 3.8$	19
C <sub>2</sub> H <sub>5</sub> O <sub>2</sub> N, aminoacetic acid					
Nd <sup>3+</sup> -L	Sp	?	0.1NdCl <sub>3</sub>	$K_1 = 4.74$ $K_3 = 0.83$	20 21
C <sub>2</sub> H <sub>5</sub> O <sub>5</sub> P, phosphonoacetic acid					
Pm <sup>3+</sup>	Iex	25	→ 0	$K[\text{Pm}^{3+} + \text{HL}^{2-} = \text{PmHL}^+] = 5.15$ $K[\text{Pm}^{3+} + 2\text{HL}^{2-} = \text{Pm}(\text{HL})_2^-] = 8.50$ $K[\text{Pm}^{3+} + \text{H}_2\text{L}^- = \text{PmH}_2\text{L}^{2+}] = 2.75$	22
C <sub>2</sub> H <sub>7</sub> O <sub>4</sub> P, dimethyl phosphoric acid					
La <sup>3+</sup>	Kin	25	0	$K_1 = 0.73$	23
Nd <sup>3+</sup>	Kin	25	0	$K_1 = 0.85$	23
Yb <sup>3+</sup>	Kin	25	0	$K_1 = 1.45$	23
C <sub>2</sub> H <sub>8</sub> O <sub>7</sub> P <sub>2</sub> , hydroxyethylidenediphosphoric acid					
Pr <sup>3+</sup>	Sp	?	pH 10.0	$K[\text{PrOH}^{2+} + 2\text{L}^{5-} = \text{Pr}(\text{OH})\text{L}_2^{8-}] = 4.26$	24
C <sub>3</sub> H <sub>4</sub> O <sub>4</sub> , malonic acid					
M <sup>3+</sup> -L <sup>-</sup>					
Ce <sup>3+</sup>	Gl	25	1.0 NaClO <sub>4</sub>	$K_1 = 3.23, \beta_2 = 5.23$	25
Dy <sup>3+</sup>	Gl	25	1.0 NaClO <sub>4</sub>	$K_1 = 3.85, \beta_2 = 6.35, \beta_3 = 7.59$	25
Er <sup>3+</sup>	Gl	25	1.0 NaClO <sub>4</sub>	$K_1 = 3.85, \beta_2 = 6.39, \beta_3 = 7.61$	25
Eu <sup>3+</sup>	Gl	25	1.0 NaClO <sub>4</sub>	$K_1 = 3.72, \beta_2 = 6.24$	25
Gd <sup>3+</sup>	Gl	25	1.0 NaClO <sub>4</sub>	$K_1 = 3.73, \beta_2 = 6.24$	25
Ho <sup>3+</sup>	Gl	25	1.0 NaClO <sub>4</sub>	$K_1 = 3.83, \beta_2 = 6.37, \beta_3 = 7.67$	25
La <sup>3+</sup>	Gl	25	1.0 NaClO <sub>4</sub>	$K_1 = 3.07, \beta_2 = 5.14$	25
Lu <sup>3+</sup>	Gl	25	1.0 NaClO <sub>4</sub>	$K_1 = 3.88, \beta_2 = 6.42, \beta_3 = 7.88$	25



(Continued.)

Metal	Method	Temp. (°C)	Medium	log of equilibrium constant	Ref.
Nd <sup>3+</sup>	Gl	25	1.0 NaClO <sub>4</sub>	$K_1 = 3.38, \beta_2 = 5.92$	25
Pr <sup>3+</sup>	Gl	25	1.0 NaClO <sub>4</sub>	$K_1 = 3.27, \beta_2 = 5.61$	25
Sm <sup>3+</sup>	Gl	25	1.0 NaClO <sub>4</sub>	$K_1 = 3.67, \beta_2 = 6.07$	25
Tb <sup>3+</sup>	Gl	25	1.0 NaClO <sub>4</sub>	$K_1 = 3.82, \beta_2 = 6.38$	25
Tm <sup>3+</sup>	Gl	25	1.0 NaClO <sub>4</sub>	$K_1 = 3.85, \beta_2 = 6.42, \beta_3 = 7.62$	25
Yb <sup>3+</sup>	Gl	25	1.0 NaClO <sub>4</sub>	$K_1 = 3.87, \beta_2 = 6.43, \beta_3 = 7.79$	25
C <sub>3</sub> H <sub>6</sub> O <sub>2</sub> , propanoic acid					
Ce <sup>3+</sup>	Pot	25	0.5 NaClO <sub>4</sub>	$K_1 = 1.85, \beta_3 = 3.01$	26
Eu <sup>3+</sup>	Gl	25	0.5 NaClO <sub>4</sub>	$K_1 = 1.93, \beta_2 = 3.24, \beta_3 = 3.86$	27
La <sup>3+</sup>	Pot	25	0.5 NaClO <sub>4</sub>	$K_1 = 1.24, \beta_2 = 2.10$	26
Nd <sup>3+</sup>	Pot	25	0.5 NaClO <sub>4</sub>	$K_1 = 1.94, \beta_2 = 3.23$	26
Pr <sup>3+</sup>	Pot	25	0.5 NaClO <sub>4</sub>	$K_1 = 1.85, \beta_2 = 3.06$	26
C <sub>3</sub> H <sub>4</sub> O <sub>6</sub> , dihydroxypropanedioic acid					
H <sup>+</sup>	Gl	23–25	0.2 (KCl)	$K_1 = 3.50, K_2 = 1.75$	28
Ce <sup>3+</sup>	Gl	23–25	0.2 (KCl)	$K_1 = 3.68 + 0.03$	28
Dy <sup>3+</sup>	Gl	23–25	0.2 (KCl)	$K_1 = 3.82 + 0.05$	28
Er <sup>3+</sup>	Gl	23–25	0.2 (KCl)	$K_1 = 3.67 + 0.08$	28
Eu <sup>3+</sup>	Gl	23–25	0.2 (KCl)	$K_1 = 4.05 + 0.15$	28
Gd <sup>3+</sup>	Gl	23–25	0.2 (KCl)	$K_1 = 3.83 + 0.15$	28
Ho <sup>3+</sup>	Gl	23–25	0.2 (KCl)	$K_1 = 3.71 + 0.06$	28
La <sup>3+</sup>	Gl	23–25	0.2 (KCl)	$K_1 = 3.25 + 0.03$	28
Lu <sup>3+</sup>	Gl	23–25	0.2 (KCl)	$K_1 = 3.65 + 0.06$	28
Nd <sup>3+</sup>	Gl	23–25	0.2 (KCl)	$K_1 = 3.94 + 0.08$	28
Pr <sup>3+</sup>	Gl	23–25	0.2 (KCl)	$K_1 = 3.76 + 0.04$	28
Sm <sup>3+</sup>	Gl	23–25	0.2 (KCl)	$K_1 = 4.06 + 0.07$	28
Tb <sup>3+</sup>	Gl	23–25	0.2 (KCl)	$K_1 = 3.56 + 0.11$	28
Tm <sup>3+</sup>	Gl	23–25	0.2 (KCl)	$K_1 = 3.67 + 0.06$	28
Yb <sup>3+</sup>	Gl	23–25	0.2 (KCl)	$K_1 = 3.96 + 0.06$	28
C <sub>3</sub> H <sub>6</sub> O <sub>3</sub> , 3-hydroxy propanoic acid					
Ce <sup>3+</sup>	Gl, Cal	25	2.0 NaClO <sub>4</sub>	$K_1 = 1.57$	29
Dy <sup>3+</sup>	Gl, Cal	25	2.0 NaClO <sub>4</sub>	$K_1 = 1.45$	29
Er <sup>3+</sup>	Gl, Cal	25	2.0 NaClO <sub>4</sub>	$K_1 = 1.32$	29
Eu <sup>3+</sup>	Gl, Cal	25	2.0 NaClO <sub>4</sub>	$K_1 = 1.64$	29
Gd <sup>3+</sup>	Gl, Cal	25	2.0 NaClO <sub>4</sub>	$K_1 = 1.61$	29
Ho <sup>3+</sup>	Gl, Cal	25	2.0 NaClO <sub>4</sub>	$K_1 = 1.48$	29
La <sup>3+</sup>	Gl, Cal	25	2.0 NaClO <sub>4</sub>	$K_1 = 1.56$	29
Lu <sup>3+</sup>	Gl, Cal	25	2.0 NaClO <sub>4</sub>	$K_1 = 1.40$	29
Nd <sup>3+</sup>	Gl, Cal	25	2.0 NaClO <sub>4</sub>	$K_1 = 1.66$	29
Pr <sup>3+</sup>	Gl, Cal	25	2.0 NaClO <sub>4</sub>	$K_1 = 1.62$	29
Sm <sup>3+</sup>	Gl, Cal	25	2.0 NaClO <sub>4</sub>	$K_1 = 1.75$	29
Tb <sup>3+</sup>	Gl, Cal	25	2.0 NaClO <sub>4</sub>	$K_1 = 1.54$	29
Tm <sup>3+</sup>	Gl, Cal	25	2.0 NaClO <sub>4</sub>	$K_1 = 1.45$	29
Y <sup>3+</sup>	Gl, Cal	25	2.0 NaClO <sub>4</sub>	$K_1 = 1.43$	29
Yb <sup>3+</sup>	Gl, Cal	25	2.0 NaClO <sub>4</sub>	$K_1 = 1.51$	29
C <sub>3</sub> H <sub>6</sub> O <sub>3</sub> , 2-hydroxy propanoic acid (lactic acid)					
Eu <sup>3+</sup>	Dis	25	2.0	$K_1 = 2.48, \beta_2 = 4.56, \beta_3 = 5.83$	30
La <sup>3+</sup>	Pot	25	NaClO <sub>4</sub>	$K_1 = 3.34$	31
Lu <sup>3+</sup>	Pot	25	NaClO <sub>4</sub>	$K_1 = 3.85$	31

*(Continued.)*

Metal	Method	Temp. (°C)	Medium	log of equilibrium constant	Ref.
Pm <sup>3+</sup>	Iex	?	?	$\beta_2 = 5.38$	32
Pr <sup>3+</sup>	Iex	20	0.2 NaClO <sub>4</sub>	$K_1 = 2.46, \beta_2 = 4.27, \beta_3 = 5.62$	33
C <sub>3</sub> H <sub>5</sub> O <sub>2</sub> N, isonitrosoacetone, HL					
H <sup>+</sup>	Gl	20	0.1 NaClO <sub>4</sub> , 50% v/v dioxan	$K_1 = 9.70 + 0.04$	34
Ce <sup>3+</sup>	Gl	20	0.1 NaClO <sub>4</sub> , 50% v/v dioxan	$K_1 = 4.90$	34
Dy <sup>3+</sup>	Gl	20	0.1 NaClO <sub>4</sub> , 50% v/v dioxan	$K_1 = 5.88$	34
Er <sup>3+</sup>	Gl	20	0.1 NaClO <sub>4</sub> , 50% v/v dioxan	$K_1 = 5.99$	34
Eu <sup>3+</sup>	Gl	20	0.1 NaClO <sub>4</sub> , 50% v/v dioxan	$K_1 = 5.81$	34
Gd <sup>3+</sup>	Gl	20	0.1 NaClO <sub>4</sub> , 50% v/v dioxan	$K_1 = 5.68$	34
Ho <sup>3+</sup>	Gl	20	0.1 NaClO <sub>4</sub> , 50% v/v dioxan	$K_1 = 5.95$	34
La <sup>3+</sup>	Gl	20	0.1 NaClO <sub>4</sub> , 50% v/v dioxan	$K_1 = 4.73$	34
Lu <sup>3+</sup>	Gl	20	0.1 NaClO <sub>4</sub> , 50% v/v dioxan	$K_1 = 6.11$	34
Nd <sup>3+</sup>	Gl	20	0.1 NaClO <sub>4</sub> , 50% v/v dioxan	$K_1 = 5.24$	34
Pr <sup>3+</sup>	Gl	20	0.1 NaClO <sub>4</sub> , 50% v/v dioxan	$K_1 = 5.08$	34
Sm <sup>3+</sup>	Gl	20	0.1 NaClO <sub>4</sub> , 50% v/v dioxan	$K_1 = 5.60$	34
Tb <sup>3+</sup>	Gl	20	0.1 NaClO <sub>4</sub> , 50% v/v dioxan	$K_1 = 5.79$	34
Tm <sup>3+</sup>	Gl	20	0.1 NaClO <sub>4</sub> , 50% v/v dioxan	$K_1 = 6.07$	34
Y <sup>3+</sup>	Gl	20	0.1 NaClO <sub>4</sub> , 50% v/v dioxan	$K_1 = 5.98$	34
Yb <sup>3+</sup>	Gl	20	0.1 NaClO <sub>4</sub> , 50% v/v dioxan	$K_1 = 6.19$	34
C <sub>3</sub> H <sub>6</sub> O <sub>2</sub> N <sub>2</sub> , methylglyoxime, H <sub>2</sub> L					
H <sup>+</sup>	Gl	20	0.1 NaClO <sub>4</sub> , 50% v/v dioxan	$K_1 = 12.45 + 0.10, K_2 = 11.50 + 0.04$	34
Ce <sup>3+</sup>	Gl	20	0.1 NaClO <sub>4</sub> , 50% v/v dioxan	$K_1 = 6.22, K_2 = 5.29$	34
Dy <sup>3+</sup>	Gl	20	0.1 NaClO <sub>4</sub> , 50% v/v dioxan	$K_1 = 6.94, K_2 = 5.99$	34
Er <sup>3+</sup>	Gl	20	0.1 NaClO <sub>4</sub> , 50% v/v dioxan	$K_1 = 7.19, K_2 = 6.08$	34
Eu <sup>3+</sup>	Gl	20	0.1 NaClO <sub>4</sub> , 50% v/v dioxan	$K_1 = 6.96, K_2 = 5.99$	34
Gd <sup>3+</sup>	Gl	20	0.1 NaClO <sub>4</sub> , 50% v/v dioxan	$K_1 = 6.70, K_2 = 5.78$	34

(Continued.)

Metal	Method	Temp. (°C)	Medium	log of equilibrium constant	Ref.
Ho <sup>3+</sup>	Gl	20	0.1 NaClO <sub>4</sub> , 50% v/v dioxan	$K_1 = 7.07, K_2 = 6.12$	34
La <sup>3+</sup>	Gl	20	0.1 NaClO <sub>4</sub> , 50% v/v dioxan	$K_1 = 6.07, K_2 = 5.18$	34
Lu <sup>3+</sup>	Gl	20	0.1 NaClO <sub>4</sub> , 50% v/v dioxan	$K_1 = 7.27, K_2 = 6.00$	34
Nd <sup>3+</sup>	Gl	20	0.1 NaClO <sub>4</sub> , 50% v/v dioxan	$K_1 = 6.48, K_2 = 5.50$	34
Pr <sup>3+</sup>	Gl	20	0.1 NaClO <sub>4</sub> , 50% v/v dioxan	$K_1 = 6.37, K_2 = 5.43$	34
Sm <sup>3+</sup>	Gl	20	0.1 NaClO <sub>4</sub> , 50% v/v dioxan	$K_1 = 6.72, K_2 = 5.73$	34
Tb <sup>3+</sup>	Gl	20	0.1 NaClO <sub>4</sub> , 50% v/v dioxan	$K_1 = 6.79, K_2 = 5.85$	34
Tm <sup>3+</sup>	Gl	20	0.1 NaClO <sub>4</sub> , 50% v/v dioxan	$K_1 = 7.27, K_2 = 6.15$	34
Y <sup>3+</sup>	Gl	20	0.1 NaClO <sub>4</sub> , 50% v/v dioxan	$K_1 = 6.43, K_2 = 5.74$	34
Yb <sup>3+</sup>	Gl	20	0.1 NaClO <sub>4</sub> , 50% v/v dioxan	$K_1 = 7.42, K_2 = 6.04$	34
C <sub>3</sub> H <sub>6</sub> O <sub>2</sub> S, 2-mercaptopropanoic acid, H <sub>2</sub> L					
Ce <sup>3+</sup>	Gl	25	2.0 (NaClO <sub>4</sub> )	$K(\text{Ce}^{3+} + \text{HL}^- = \text{CeHL}^{2+}) = 1.36$	35
Dy <sup>3+</sup>	Gl	25	2.0 (NaClO <sub>4</sub> )	$K(\text{Dy}^{3+} + \text{HL}^- = \text{DyHL}^{2+}) = 1.58$	35
Er <sup>3+</sup>	Gl	25	2.0 (NaClO <sub>4</sub> )	$K(\text{Er}^{3+} + \text{HL}^- = \text{ErHL}^{2+}) = 1.53$	35
Eu <sup>3+</sup>	Gl	25	2.0 (NaClO <sub>4</sub> )	$K(\text{Eu}^{3+} + \text{HL}^- = \text{EuHL}^{2+}) = 2.00$	35
Gd <sup>3+</sup>	Gl	25	2.0 (NaClO <sub>4</sub> )	$K(\text{Gd}^{3+} + \text{HL}^- = \text{GdHL}^{2+}) = 1.75$	35
Ho <sup>3+</sup>	Gl	25	2.0 (NaClO <sub>4</sub> )	$K(\text{Ho}^{3+} + \text{HL}^- = \text{HoHL}^{2+}) = 1.53$	35
La <sup>3+</sup>	Gl	25	2.0 (NaClO <sub>4</sub> )	$K(\text{La}^{3+} + \text{HL}^- = \text{LaHL}^{2+}) = 1.23$	35
Lu <sup>3+</sup>	Gl	25	2.0 (NaClO <sub>4</sub> )	$K(\text{Lu}^{3+} + \text{HL}^- = \text{LuHL}^{2+}) = 1.51$	35
Nd <sup>3+</sup>	Gl	25	2.0 (NaClO <sub>4</sub> )	$K(\text{Nd}^{3+} + \text{HL}^- = \text{NdHL}^{2+}) = 1.93$	35
Pr <sup>3+</sup>	Gl	25	2.0 (NaClO <sub>4</sub> )	$K(\text{Pr}^{3+} + \text{HL}^- = \text{PrHL}^{2+}) = 1.89$	35
Sm <sup>3+</sup>	Gl	25	2.0 (NaClO <sub>4</sub> )	$K(\text{Sm}^{3+} + \text{HL}^- = \text{SmHL}^{2+}) = 2.06$	35
Tb <sup>3+</sup>	Gl	25	2.0 (NaClO <sub>4</sub> )	$K(\text{Tb}^{3+} + \text{HL}^- = \text{TbHL}^{2+}) = 1.65$	35
Tm <sup>3+</sup>	Gl	25	2.0 (NaClO <sub>4</sub> )	$K(\text{Tm}^{3+} + \text{HL}^- = \text{TmHL}^{2+}) = 1.48$	35
Y <sup>3+</sup>	Gl	25	2.0 (NaClO <sub>4</sub> )	$K(\text{Y}^{3+} + \text{HL}^- = \text{YHL}^{2+}) = 1.70$	35
Yb <sup>3+</sup>	Gl	25	2.0 (NaClO <sub>4</sub> )	$K(\text{Yb}^{3+} + \text{HL}^- = \text{YbHL}^{2+}) = 1.43$	35
C <sub>4</sub> H <sub>4</sub> O <sub>4</sub> , cis-butenedioic acid (maleic acid), H <sub>2</sub> L					
Dy <sup>3+</sup>	Gl	25	0.1 (NaClO <sub>4</sub> )	$K_1 = 3.75 \pm 0.01, K_2 = 2.09 \pm 0.03$	36
	Gl	25	0.1 (NaClO <sub>4</sub> )	$K_1 = 3.74 \pm 0.01$	37
Er <sup>3+</sup>	Gl	25	0.1 (NaClO <sub>4</sub> )	$K_1 = 3.65 \pm 0.01, K_2 = 2.06 \pm 0.01$	36
	Gl	25	0.1 (NaClO <sub>4</sub> )	$K_1 = 3.64 \pm 0.01$	37
Eu <sup>3+</sup>	Gl	25	0.1 (NaClO <sub>4</sub> )	$K_1 = 3.83 \pm 0.01, K_2 = 2.15 \pm 0.02$	36
	Gl	25	0.1 (NaClO <sub>4</sub> )	$K_1 = 3.83 \pm 0.01$	37
Gd <sup>3+</sup>	Gl	25	0.1 (NaClO <sub>4</sub> )	$K_1 = 3.80 \pm 0.01, K_2 = 2.11 \pm 0.02$	36
	Gl	25	0.1 (NaClO <sub>4</sub> )	$K_1 = 3.79 \pm 0.01$	37
Ho <sup>3+</sup>	Gl	25	0.1 (NaClO <sub>4</sub> )	$K_1 = 3.67 \pm 0.01, K_2 = 2.02 \pm 0.02$	36
	Gl	25	0.1 (NaClO <sub>4</sub> )	$K_1 = 3.67 \pm 0.01$	37
La <sup>3+</sup>	Gl	25	0.1 (NaClO <sub>4</sub> )	$K_1 = 3.45 \pm 0.01, K_2 = 1.98 \pm 0.01$	36
	Gl	25	0.1 (NaClO <sub>4</sub> )	$K_1 = 3.44 \pm 0.01$	37

(Continued.)

Metal	Method	Temp. (°C)	Medium	log of equilibrium constant	Ref.
Lu <sup>3+</sup>	Gl	25	0.1 (NaClO <sub>4</sub> )	$K_1 = 3.60 \pm 0.01, K_2 = 2.08 \pm 0.02$	36
Nd <sup>3+</sup>	Gl	25	0.1 (NaClO <sub>4</sub> )	$K_1 = 3.66 \pm 0.01, K_2 = 2.14 \pm 0.02$	36
	Gl	25	0.1 (NaClO <sub>4</sub> )	$K_1 = 3.66 \pm 0.01$	37
Pr <sup>3+</sup>	Gl	25	0.1 (NaClO <sub>4</sub> )	$K_1 = 3.64 \pm 0.01, K_2 = 2.16 \pm 0.02$	36
	Gl	25	0.1 (NaClO <sub>4</sub> )	$K_1 = 3.63 \pm 0.01$	37
Sm <sup>3+</sup>	Gl	25	0.1 (NaClO <sub>4</sub> )	$K_1 = 3.83 \pm 0.01, K_2 = 2.19 \pm 0.02$	36
Tb <sup>3+</sup>	Gl	25	0.1 (NaClO <sub>4</sub> )	$K_1 = 3.75 \pm 0.01, K_2 = 2.08 \pm 0.01$	36
Tm <sup>3+</sup>	Gl	25	0.1 (NaClO <sub>4</sub> )	$K_1 = 3.62 \pm 0.01, K_2 = 2.02 \pm 0.02$	36
Y <sup>3+</sup>	Gl	25	0.1 (NaClO <sub>4</sub> )	$K_1 = 3.62 \pm 0.01, K_2 = 1.94 \pm 0.03$	36
Yb <sup>3+</sup>	Gl	25	0.1 (NaClO <sub>4</sub> )	$K_1 = 3.64 \pm 0.01, K_2 = 2.09 \pm 2.09$	37
				$K_1 = 3.64$	
C <sub>4</sub> H <sub>4</sub> O <sub>4</sub> , fumaric acid					
Ce <sup>3+</sup>	Gl	25	0.1 NaClO <sub>4</sub>	$K_1 = 2.80$	37
Dy <sup>3+</sup>	Gl	25	0.1 NaClO <sub>4</sub>	$K_1 = 2.80$	37
Er <sup>3+</sup>	Gl	25	0.1 NaClO <sub>4</sub>	$K_1 = 2.80$	37
Eu <sup>3+</sup>	Gl	25	0.1 NaClO <sub>4</sub>	$K_1 = 2.86$	37
Gd <sup>3+</sup>	Gl	25	0.1 NaClO <sub>4</sub>	$K_1 = 2.88$	37
Ho <sup>3+</sup>	Gl	25	0.1 NaClO <sub>4</sub>	$K_1 = 2.80$	37
La <sup>3+</sup>	Gl	25	0.1 NaClO <sub>4</sub>	$K_1 = 2.74 \pm 0.01$	37
Lu <sup>3+</sup>	Gl	25	0.1 NaClO <sub>4</sub>	$K_1 = 2.81 \pm 0.02$	37
Nd <sup>3+</sup>	Gl	25	0.1 NaClO <sub>4</sub>	$K_1 = 2.74 \pm 0.01$	37
Pr <sup>3+</sup>	Gl	25	0.1 NaClO <sub>4</sub>	$K_1 = 2.84 \pm 0.01$	37
Sm <sup>3+</sup>	Gl	25	0.1 NaClO <sub>4</sub>	$K_1 = 2.83 \pm 0.01$	37
Tb <sup>3+</sup>	Gl	25	0.1 NaClO <sub>4</sub>	$K_1 = 2.77 \pm 0.01$	37
Tm <sup>3+</sup>	Gl	25	0.1 NaClO <sub>4</sub>	$K_1 = 2.81 \pm 0.02$	37
Yb <sup>3+</sup>	Gl	25	0.1 NaClO <sub>4</sub>	$K_1 = 2.80 \pm 0.02$	37
C <sub>4</sub> H <sub>6</sub> O <sub>4</sub> , butanedioic acid (succinic acid), H <sub>2</sub> L					
Er <sup>3+</sup>	Sol	25	0.5	$K_1 = 4.54$	38
La <sup>3+</sup>	Sol	25	0.5	$K_1 = 3.77$	38
Sm <sup>3+</sup>	Sol	25	0.5	$K_1 = 4.96$	38
C <sub>4</sub> H <sub>6</sub> O <sub>5</sub> , diglycollic acid					
Dy <sup>3+</sup>	Qh	5-50	1.0 NaClO <sub>4</sub>	$K_1 = 5.42, \beta_2 = 10.09$	39
Er <sup>3+</sup>	Pot	20	1.0 NaClO <sub>4</sub>	$K_1 = 5.47, \beta_2 = 10.16, \beta_3 = 13.41$	40
Gd <sup>3+</sup>	Pot	20	1.0 NaClO <sub>4</sub>	$K_1 = 5.49, \beta_2 = 10.03, \beta_3 = 13.22$	40
Ho <sup>3+</sup>	Pot	20	1.0 NaClO <sub>4</sub>	$K_1 = 5.40, \beta_2 = 10.07, \beta_3 = 13.46$	40
Lu <sup>3+</sup>	Pot	20	1.0 NaClO <sub>4</sub>	$K_1 = 5.79, \beta_2 = 10.75, \beta_3 = 13.42$	40
Pr <sup>3+</sup>	Qh	5-50	1.0 NaClO <sub>4</sub>	$K_1 = 5.35, \beta_2 = 9.27, \beta_3 = 11.82$	39
Sm <sup>3+</sup>	Qh	5-50	1.0 NaClO <sub>4</sub>	$K_1 = 5.62, \beta_2 = 10.01$	39
Tb <sup>3+</sup>	Pot	20	1.0 NaClO <sub>4</sub>	$K_1 = 5.42, \beta_2 = 10.08, \beta_3 = 13.41$	40
Yb	Qh	5-50	1.0 NaClO <sub>4</sub>	$K_1 = 5.70, \beta_2 = 10.54$	39
C <sub>4</sub> H <sub>6</sub> O <sub>5</sub> , malic acid					
Dy <sup>3+</sup>	Gl	25	0.1 NaClO <sub>4</sub>	$K_1 = 4.78, K_2 = 3.33$	41
Er <sup>3+</sup>	Gl	25	0.1 NaClO <sub>4</sub>	$K_1 = 4.96, K_2 = 3.29$	41
Eu <sup>3+</sup>	Gl	25	0.1 NaClO <sub>4</sub>	$K_1 = 4.85, K_2 = 3.26$	41
Gd <sup>3+</sup>	Gl	25	0.1 NaClO <sub>4</sub>	$K_1 = 4.76, K_2 = 3.23$	41
Ho <sup>3+</sup>	Gl	25	0.1 NaClO <sub>4</sub>	$K_1 = 4.90, K_2 = 3.35$	41
La <sup>3+</sup>	Gl	25	0.1 NaClO <sub>4</sub>	$K_1 = 4.37, K_2 = 2.79$	41
Lu <sup>3+</sup>	Gl	25	0.1 NaClO <sub>4</sub>	$K_1 = 5.08, K_2 = 3.59$	41

<i>(Continued.)</i>					
Metal	Method	Temp. (°C)	Medium	log of equilibrium constant	Ref.
Nd <sup>3+</sup>	Gl	25	0.1 NaClO <sub>4</sub>	$K_1 = 4.77, K_2 = 3.17$	41
Pr <sup>3+</sup>	Gl	25	0.1 NaClO <sub>4</sub>	$K_1 = 4.65, K_2 = 3.09$	41
Sm <sup>3+</sup>	Gl	25	0.1 NaClO <sub>4</sub>	$K_1 = 4.89, K_2 = 3.27$	41
Tb <sup>3+</sup>	Gl	25	0.1 NaClO <sub>4</sub>	$K_1 = 4.77, K_2 = 3.26$	41
Tm <sup>3+</sup>	Gl	25	0.1 NaClO <sub>4</sub>	$K_1 = 5.01, K_2 = 3.49$	41
Y <sup>3+</sup>	Gl	25	0.1 NaClO <sub>4</sub>	$K_1 = 4.91, K_2 = 3.28$	41
Yb <sup>3+</sup>	Gl	25	0.1 NaClO <sub>4</sub>	$K_1 = 5.05, K_2 = 3.53$	41
C <sub>4</sub> H <sub>6</sub> O <sub>6</sub> , tartaric acid					
Dy <sup>3+</sup>	Gl	25	0.05	$K_1(0) = 4.13$	42
Er <sup>3+</sup>	Gl	25	0–40% ethanol	$K_1(0) = 4.14$	42
Eu <sup>3+</sup>	Gl	25	0–40% ethanol	$K_1(0) = 4.33$	42
Gd <sup>3+</sup>	Gl	25	0–40% ethanol	$K_1(0) = 4.15$	42
Ho <sup>3+</sup>	Gl	25	0–40% ethanol	$K_1(0) = 4.14$	42
La <sup>3+</sup>	Gl	25	0–40% ethanol	$K_1(0) = 3.74$	42
Lu <sup>3+</sup>	Gl	25	0–40% ethanol	$K_1(0) = 4.32$	42
Nd <sup>3+</sup>	Gl	25	0–40% ethanol	$K_1(0) = 4.20$	42
Pm <sup>3+</sup>	Dis	20	0.1 NH <sub>4</sub> Cl	$K_1 = 3.9, \beta_2 = 6.8$	43
Pr <sup>3+</sup>	Gl	25	0.05	$K_1(0) = 4.08$	42
Sm <sup>3+</sup>	Gl	25	0.05	$K_1(0) = 4.27$	42
Tb <sup>3+</sup>	Gl	25	0.05	$K_1(0) = 4.06$	42
Y <sup>3+</sup>	Gl	25	0.05	$K_1(0) = 4.03$	42
Yb <sup>3+</sup>	Gl	25	0.05	$K_1(0) = 4.26$	42
C <sub>4</sub> H <sub>8</sub> O <sub>2</sub> , butanoic acid					
Ce <sup>3+</sup>	Ql	25	0.5 NaClO <sub>4</sub>	$K_1 = 1.73$	44
La <sup>3+</sup>	Ql	25	0.5 NaClO <sub>4</sub>	$K_1 = 1.64, \beta_2 = 2.43$	44
Nd <sup>3+</sup>	Ql	25	0.5 NaClO <sub>4</sub>	$K_1 = 1.76, \beta_2 = 2.88, \beta_3 = 6.92$	44
Pr <sup>3+</sup>	Ql	25	0.5 NaClO <sub>4</sub>	$K_1 = 1.89, \beta_2 = 2.83, \beta_3 = 6.83$	44
C <sub>4</sub> H <sub>8</sub> O <sub>2</sub> , isobutyric acid					
Yb <sup>3+</sup>	Gl	25	0.1	$K_1 = 2.01, K_2 = 1.60$	45
La <sup>3+</sup>	Gl	25	0.1	$K_1 = 1.64, K_2 = 2.16$	46
Ce <sup>3+</sup>	Gl	25	0.1	$K_1 = 1.79, K_2 = 2.32$	46
Pr <sup>3+</sup>	Gl	25	0.1	$K_1 = 1.92, K_2 = 3.18$	46
Nd <sup>3+</sup>	Gl	25	0.1	$K_1 = 1.98, K_2 = 3.10$	46
Sm <sup>3+</sup>	Gl	25	0.1	$K_1 = 2.05, K_2 = 3.30$	46
Eu <sup>3+</sup>	Gl	25	0.1	$K_1 = 1.98, K_2 = 3.10$	46
Gd <sup>3+</sup>	Gl	25	0.1	$K_1 = 1.87, K_2 = 3.28$	46
Tb <sup>3+</sup>	Gl	25	0.1	$K_1 = 1.82, K_2 = 2.84$	46
Dy <sup>3+</sup>	Gl	25	0.1	$K_1 = 1.74, K_2 = 2.57$	46
Ho <sup>3+</sup>	Gl	25	0.1	$K_1 = 1.70, K_2 = 2.92$	46
Er <sup>3+</sup>	Gl	25	0.1	$K_1 = 1.69, K_2 = 2.59$	46
Tm <sup>3+</sup>	Gl	25	0.1	$K_1 = 1.69, K_2 = 2.28$	46
Yb <sup>3+</sup>	Gl	25	0.1	$K_1 = 1.78, K_2 = 3.10$	46
Lu <sup>3+</sup>	Gl	25	0.1	$K_1 = 1.81, K_2 = 2.32$	46
Y <sup>3+</sup>	Gl	25	0.1	$K_1 = 1.60, K_2 = 2.71$	46
Hydroxyisobutyric acid (HIB), trihydroxyisobutyric acid (THIB)					
M <sup>3+</sup>	M <sup>3+</sup> -HIB		M <sup>3+</sup> -THIB		Ref.
	log $K_1$	log $K_2$	log $K_1$	log $K_2$	
La	2.22	3.67	2.40	3.88	47
Ce	2.37	4.01	2.61	4.45	47

(Continued.)						
$M^{3+}$		$M^{3+}$ -HIB		$M^{3+}$ -THIB		Ref.
		log $K_1$	log $K_2$	log $K_1$	log $K_2$	
Pr		2.48	4.12	2.75	4.69	47
Nd		2.54	4.32	2.81	4.62	47
Sm		2.63	4.60	2.86	5.07	47
Eu		2.71	4.92	2.80	5.00	47
Gd		2.71	4.97	2.69	4.99	47
Tb		2.87	5.21	2.71	4.88	47
Dy		2.95	5.32	2.66	4.87	47
Ho		2.98	5.42	2.71	4.89	47
Er		3.03	5.54	2.79	4.83	47
Tm		3.13	5.62	2.85	4.97	47
Yb		3.18	5.76	2.90	5.07	47
Lu		3.21	5.85	2.94	5.19	47
Y		2.88	5.32	2.65	4.67	47
Metal	Method	Temp. (°C)	Medium	log of equilibrium constant		Ref.
$C_4H_6O_4S$ , thiodiglycolic acid						
$Ce^{3+}$	GI	25	1.0 NaClO <sub>4</sub>	$K_1 = 2.66, \beta_2 = 4.49$		48
$Er^{3+}$	GI	25	1.0 Na (ClO <sub>4</sub> )	$K_1 = 2.36, \beta_2 = 3.85$ $K(Er^{3+} + H^+ + L^{2-} = ErHL^{2+}) = 5.14$ $K(Er^{3+} + H^+ + 2L^{2-} = ErHL_2) = 7.21$		48
$Pr^{3+}$	GI	25	1.0 NaClO <sub>4</sub>	$K_1 = 2.74, \beta_2 = 4.39$		48
$Sm^{3+}$	GI	25	1.0 Na (ClO <sub>4</sub> )	$K_1 = 2.90, \beta_2 = 4.68$ $K(Sm^{3+} + H^+ + L^{2-} = SmHL^{2+}) = 5.59$ $K(Sm^{3+} + H^+ + 2L^{2-} = SmHL_2) = 7.82$		48
$Tb^{3+}$	GI	25	1.0 Na (ClO <sub>4</sub> )	$K_1 = 2.52, \beta_2 = 4.12$ $K(Tb^{3+} + H^+ + 2L^{2-} = TbHL^{2+}) = 5.21$ $K(Tb^{3+} + H^+ + 2L^{2-} = TbHL_2) = 7.30$		48
$Yb^{3+}$	GI	25	1.0 Na (ClO <sub>4</sub> )	$K_1 = 2.36, \beta_2 = 2.76$ $K(Yb^{3+} + H^+ + 2L^{2-} = YbHL^{2+}) = 5.10$ $K(Yb^{3+} + H^+ + 2L^{2-} = YbHL_2) = 7.27$		48
<i>N</i> -acetylglycine						
$Er^{3+}$	pH	25	0.1 NaClO <sub>4</sub>	$K_1 = 1.51$		49
$Eu^{3+}$	Dis	5-35	1 NaClO <sub>4</sub>	$K_1 = 1.96, \Delta H = 4.5, \Delta S = 24$		49
$La^{3+}$	pH	25	0.1 (NaClO <sub>4</sub> )	$K_1 = 1.61 \pm 0.03$		49
$Nd^{3+}$	pH	25	0.1 (NaClO <sub>4</sub> )	$K_1 = 1.86 \pm 0.03$		49
$Sm^{3+}$	pH	25	0.1 (NaClO <sub>4</sub> )	$K_1 = 1.88 \pm 0.04$		49
$Tb^{3+}$	Dis	5-35	1 (NaClO <sub>4</sub> )	$K_1(5^\circ) = 1.42 \pm 0.05$ $K_1(15^\circ) = 1.53 \pm 0.05$ $K_1(25^\circ) = 1.65 \pm 0.07$ $K_1(35^\circ) = 1.74 \pm 0.06$ $\Delta H = 4.3 \pm 0.6, \Delta S = 22 \pm 4$		49
$C_4H_7O_4N$ , aspartic acid						
$Dy^{3+}$	GI	25 ± 0.05	0.1 KCl	$K_1 = 5.85 \pm 0.04, \beta_2 = 10.78 \pm 0.15$		50
$Er^{3+}$	GI	25 ± 0.05	0.1 KCl	$K_1 = 6.08 \pm 0.04, \beta_2 = 10.93 \pm 0.15$		50
$Eu^{3+}$	GI	25 ± 0.05	0.1 KCl	$K_1 = 5.62 \pm 0.04, \beta_2 = 9.77 \pm 0.15$		50
$Gd^{3+}$	GI	25 ± 0.05	0.1 KCl	$K_1 = 5.74 \pm 0.04, \beta_2 = 10.50 \pm 0.15$		50
$Ho^{3+}$	GI	25 ± 0.05	0.1 KCl	$K_1 = 5.91 \pm 0.04, \beta_2 = 10.81 \pm 0.15$		50
	GI	30	0.1 (NaClO <sub>4</sub> )	$K_1 = 6.36$		
$Lu^{3+}$	GI	25 ± 0.05	0.1 KCl	$K_1 = 6.25 \pm 0.05, \beta_2 = 11.58 \pm 0.15$		50

(Continued.)

Metal	Method	Temp. (°C)	Medium	log of equilibrium constant	Ref.										
Nd <sup>3+</sup>	Gl	25 ± 0.05	0.1 KCl	$K_1 = 5.36 \pm 0.04, \beta_2 = 9.26 \pm 0.15$	50										
Pr <sup>3+</sup>	Gl	25 ± 0.05	0.1 KCl	$K_1 = 5.20 \pm 0.04, \beta_2 = 8.80 \pm 0.15$	50										
Sm <sup>3+</sup>	Gl	25 ± 0.05	0.1 KCl	$K_1 = 5.55 \pm 0.04, \beta_2 = 9.72 \pm 0.15$	50										
Tb <sup>3+</sup>	Gl	25 ± 0.05	0.1 KCl	$K_1 = 5.80 \pm 0.04, \beta_2 = 10.28 \pm 0.15$	50										
Tm <sup>3+</sup>	Gl	25 ± 0.05	0.1 KCl	$K_1 = 6.10 \pm 0.04, \beta_2 = 11.10 \pm 0.15$	50										
Yb <sup>3+</sup>	Gl	25 ± 0.05	0.1 KCl	$K_1 = 6.18 \pm 0.04, \beta_2 = 11.45 \pm 0.15$	50										
IMDA, HIMDA, NTA (refs 51, 52, 53)															
Ligand	M <sup>3+</sup>														
	La	Ce	Pr	Nd	Sm	Eu	Gd	Tb	Dy	Ho	Er	Tm	Yb	Lu	Y
IMDA															
log $K_1$	5.88	6.18	6.44	6.50	6.64	6.73	6.68	6.78	6.88	6.97	7.09	7.22	7.42	7.61	6.78
log $K_2$	4.09	4.53	4.78	4.89	5.24	5.38	5.39	5.46	5.43	5.50	5.59	5.68	5.85	6.12	5.25
HIMDA															
log $K_1$	8.00	8.46	8.64	8.80	9.10	9.10	9.01	9.08	9.08	9.18	9.24	9.35	9.38	9.50	9.22
log $K_2$	5.98	6.56	6.86	7.13	7.77	7.91	8.04	8.19	8.30	8.13	7.98	7.88	7.74	8.02	7.61
NTA															
log $K_1$	10.47	10.70	10.88	11.11	11.33	11.3	11.43	11.5	11.62	11.7	11.9	12.1	12.08	12.4	11.41
log $K_2$	7.24	7.84	8.18	8.47	9.18	9.18	9.26	9.38	9.41	9.35	9.26	9.23	9.29	9.42	8.95
Metal	Method	Temp. (°C)	Medium	log of equilibrium constant	Ref.										
C <sub>4</sub> H <sub>8</sub> O <sub>2</sub> N <sub>2</sub> , dimethyl glyoxime															
Dy <sup>3+</sup>	Gl	20	0.1 NaClO <sub>4</sub> , 50% v/v dioxan	$K_1 = 8.24, K_2 = 7.28$	54										
Er <sup>3+</sup>	Gl	20	0.1 NaClO <sub>4</sub> , 50% v/v dioxan	$K_1 = 8.51, K_2 = 7.52$	54										
Eu <sup>3+</sup>	Gl	20	0.1 NaClO <sub>4</sub> , 50% v/v dioxan	$K_1 = 8.19, K_2 = 7.09$	54										
Gd <sup>3+</sup>	Gl	20	0.1 NaClO <sub>4</sub> , 50% v/v dioxan	$K_1 = 7.99, K_2 = 6.98$	54										
Ho <sup>3+</sup>	Gl	20	0.1 NaClO <sub>4</sub> , 50% v/v dioxan	$K_1 = 8.41, K_2 = 7.49$	54										
La <sup>3+</sup>	Gl	20	0.1 NaClO <sub>4</sub> , 50% v/v dioxan	$K_1 = 7.42, K_2 = 6.31$	54										
Lu <sup>3+</sup>	Gl	20	0.1 NaClO <sub>4</sub> , 50% v/v dioxan	$K_1 = 8.53, K_2 = 7.33$	54										
Nd <sup>3+</sup>	Gl	20	0.1 NaClO <sub>4</sub> , 50% v/v dioxan	$K_1 = 7.81, K_2 = 6.84$	54										
Pr <sup>3+</sup>	Gl	20	0.1 NaClO <sub>4</sub> , 50% v/v dioxan	$K_1 = 7.68, K_2 = 6.63$	54										
Sm <sup>3+</sup>	Gl	20	0.1 NaClO <sub>4</sub> , 50% v/v dioxan	$K_1 = 8.01, K_2 = 6.97$	54										
Tb <sup>3+</sup>	Gl	20	0.1 NaClO <sub>4</sub> , 50% v/v dioxan	$K_1 = 8.11, K_2 = 7.18$	54										
Tm <sup>3+</sup>	Gl	20	0.1 NaClO <sub>4</sub> , 50% v/v dioxan	$K_1 = 8.63, K_2 = 7.57$	54										
Y <sup>3+</sup>	Gl	20	0.1 NaClO <sub>4</sub> , 50% v/v dioxan	$K_1 = 7.95, K_2 = 7.02$	54										
Yb <sup>3+</sup>	Gl	20	0.1 NaClO <sub>4</sub> , 50% v/v dioxan	$K_1 = 8.75, K_2 = 7.50$	54										

(Continued.)

Metal	Method	Temp. (°C)	Medium	log of equilibrium constant	Ref.	
C <sub>4</sub> H <sub>11</sub> O <sub>4</sub> P, diethylphosphoric acid, HL						
Ce <sup>3+</sup>	Est	25	Dil	$K_1 = 1.36$	55	
Dy <sup>3+</sup>	Kin	25	Dil	$K_1 = 1.96 \pm 0.05$	55	
Er <sup>3+</sup>	Kin	25	Dil	$K_1 = 2.08 \pm 0.02$	55	
Eu <sup>3+</sup>	Est	25	Dil	$K_1 = 1.71$	55	
Gd <sup>3+</sup>	Kin	25	Dil	$K_1 = 1.75 \pm 0.06$	55	
Ho <sup>3+</sup>	Est	25	Dil	$K_1 = 2.00$	55	
La <sup>3+</sup>	Kin	25	Dil	$K_1 = 1.82$	56	
	Kin	25	Dil	$K_1 = 1.24 \pm 0.03$	55	
Lu <sup>3+</sup>	Kin	25	Dil	$K_1 = 2.35 \pm 0.06$	55	
Nd <sup>3+</sup>	Kin	25	Dil	$K_1 = 2.02$	56	
	Est	25	Dil	$K_1 = 1.47$	55	
Pm <sup>3+</sup>	Est	25	Dil	$K_1 = 1.54$	55	
Pr <sup>3+</sup>	Kin	25	Dil	$K_1 = 1.41 \pm 0.03$	55	
Sm <sup>3+</sup>	Kin	25	Dil	$K_1 = 1.67 \pm 0.04$	55	
Tm <sup>3+</sup>	Est	25	Dil	$K_1 = 2.18$	55	
Yb <sup>3+</sup>	Kin	25	Dil	$K_1 = 2.81$	56	
	Kin	25	Dil	$K_1 = 2.22 \pm 0.05$	55	
C <sub>5</sub> H <sub>6</sub> O <sub>4</sub> , itaconic acid						
Dy <sup>3+</sup>	?	25	1.0 NaClO <sub>4</sub>	$K_1 = 2.22,$ $K[\text{Dy}^{3+} + \text{H}^+ + \text{L}^- = \text{Dy}(\text{HL})^{2+}] = 6.4$ $K[\text{Dy}^{3+} + 2\text{H}^+ + 2\text{L}^- = \text{Dy}(\text{HL})_2^+] = 12.62$	57	
Er <sup>3+</sup>	?	25	1.0 NaClO <sub>4</sub>	$K_1 = 2.27,$ $K[\text{Er}^{3+} + \text{H}^+ + \text{L}^{2-} = \text{Er}(\text{HL})^{2+}] = 6.24$ $K[\text{Er}^{3+} + 2\text{H}^+ + 2\text{L}^{2-} = \text{Er}(\text{HL})_2^+] = 12.23$ $K(\text{Er}^{3+} + \text{H}^+ + 2\text{L}^{2-} = \text{ErHL}_2) = 8.40$	57	
Gd <sup>3+</sup>	?	25	1.0 NaClO <sub>4</sub>	$K_1 = 2.18,$ $K[\text{Gd}^{3+} + \text{H}^+ + \text{L}^{2-} = \text{Gd}(\text{HL})^{2+}] = 6.49$ $K[\text{Gd}^{3+} + 2\text{H}^+ + 2\text{L}^{2-} = \text{Gd}(\text{HL})_2^+] = 12.76$	57	
Nd <sup>3+</sup>	?	25	1.0 NaClO <sub>4</sub>	$K_1 = 2.00,$ $K[\text{Nd}^{3+} + \text{H}^+ + \text{L}^{2-} = \text{Nd}(\text{HL})^{2+}] = 16.37$ $K[\text{Nd}^{3+} + 2\text{H}^+ + 2\text{L}^{2-} = \text{Nd}(\text{HL})_2^+] = 12.53$	57	
Sm <sup>3+</sup>	?	25	1.0 NaClO <sub>4</sub>	$K_1 = 2.07,$ $K[\text{Sm}^{3+} + \text{H}^+ + \text{L}^{2-} = \text{Sm}(\text{HL})^{2+}] = 16.48$ $K[\text{Sm}^{3+} + 2\text{H}^+ + 2\text{L}^{2-} = \text{Sm}(\text{HL})_2^+] = 12.72$	57	
C <sub>5</sub> H <sub>8</sub> O <sub>2</sub> , acetyl acetone						
M <sup>3+</sup>	$\mu$		log $K_1$	log $K_2$	log $K_3$	
La	0.1		4.96	3.45	2.5	58
Ce	0.1		5.09	3.3	2.9	58
Pr	0.1		5.27	3.93	3.2	58
Nd	0.1		5.30	4.10	3.20	58
Sm	0.1		5.59	4.46	2.90	58
Eu	0.1		5.87	4.48	3.29	58
Gd	0.1		5.90	4.48	3.41	58
Tb	0.1		6.02	4.61	3.41	58
Dy	0.1		6.03	4.67	3.34	58
Ho	0.1		6.05	4.68	3.40	58
Er	0.1		5.99	4.68	3.38	58



(Continued.)

$M^{3+}$	$\mu$		$\log K_1$	$\log K_2$	$\log K_3$	
Tm	0.1		6.09	4.76	3.48	58
Yb	0.1		6.18	4.86	3.60	58
Lu	0.1		6.23	4.77	3.63	58
Y	0.1		5.87	4.98	3.25	58
Metal	Method	Temp. (°C)	Medium	log of equilibrium constant		Ref.
$C_5H_8O_4$ , methylsuccinic acid, $H_2L$						
$H^+$	Gl	25	0.1 (NaClO <sub>4</sub> )	$K_1 = 5.35, K_2 = 3.88$		59
$Dy^{3+}$	Gl	25	0.1 (NaClO <sub>4</sub> )	$K_1 = 3.17 \pm 0.01, K_2 = 1.96 \pm 0.03$		59
$Er^{3+}$	Gl	25	0.1 (NaClO <sub>4</sub> )	$K_1 = 3.08 \pm 0.01, K_2 = 2.07 \pm 0.06$		59
$Eu^{3+}$	Gl	25	0.1 (NaClO <sub>4</sub> )	$K_1 = 3.37 \pm 0.01, K_2 = 1.65 \pm 0.07$		59
$Gd^{3+}$	Gl	25	0.1 (NaClO <sub>4</sub> )	$K_1 = 3.33 \pm 0.01, K_2 = 1.79 \pm 0.08$		59
$Ho^{3+}$	Gl	25	0.1 (NaClO <sub>4</sub> )	$K_1 = 3.08 \pm 0.01, K_2 = 2.01 \pm 0.05$		59
$La^{3+}$	Gl	25	0.1 (NaClO <sub>4</sub> )	$K_1 = 2.95 \pm 0.01, K_2 = 1.64 \pm 0.07$		59
$Lu^{3+}$	Gl	25	0.1 (NaClO <sub>4</sub> )	$K_1 = 3.07 \pm 0.02, K_2 = 2.06 \pm 0.09$		59
$Nd^{3+}$	Gl	25	0.1 (NaClO <sub>4</sub> )	$K_1 = 3.26 \pm 0.01, K_2 = 1.75 \pm 0.05$		59
$Pr^{3+}$	Gl	25	0.1 (NaClO <sub>4</sub> )	$K_1 = 3.21 \pm 0.01, K_2 = 1.68 \pm 0.07$		59
$Sm^{3+}$	Gl	25	0.1 (NaClO <sub>4</sub> )	$K_1 = 3.41 \pm 0.01, K_2 = 1.64 \pm 0.06$		59
$Tb^{3+}$	Gl	25	0.1 (NaClO <sub>4</sub> )	$K_1 = 3.22 \pm 0.01, K_2 = 1.83 \pm 0.04$		59
$Tm^{3+}$	Gl	25	0.1 (NaClO <sub>4</sub> )	$K_1 = 3.08 \pm 0.02, K_2 = 2.06 \pm 0.10$		59
$Y^{3+}$	Gl	25	0.1 (NaClO <sub>4</sub> )	$K_1 = 3.12 \pm 0.01, K_2 = 1.79 \pm 0.05$		59
$Yb^{3+}$	Gl	25	0.1 (NaClO <sub>4</sub> )	$K_1 = 3.07 \pm 0.01, K_2 = 2.08 \pm 0.04$		59
$C_5H_8O_4$ , glutaric acid						
$La^{3+}$	Sol	25	0.5	$K_1 = 3.10$		60
	Gl	25	0.05	$K_1(0\%) = 3.02 \pm 0.06,$ $K_1(25\%) = 3.24 \pm 0.04,$ $K_1(40\%) = 3.52 \pm 0.02$		61
			0–40% (v/v) ethanol	$K_1(40\%) = 3.52 \pm 0.02$		
$Sm^{3+}$	Sol	25	0.5	$K_1 = 3.68$		60
$Y^{3+}$	Gl	25	0.05	$K_1(0\%) = 3.25 \pm 0.05,$ $K_1(25\%) = 3.50 \pm 0.01,$ $K_1(40\%) = 3.7 \pm 0.02$		60
			0–40% (v/v) ethanol	$K_1(40\%) = 3.7 \pm 0.02$		61
$C_5H_{10}O_4$ , 2,2-bis(hydroxymethyl)propionic acid, HL						
$Er^{3+}$	Gl	25	0.1 (NaClO <sub>4</sub> )	$K_1 = 2.28 \pm 0.01, K_2 = 1.60 \pm 0.02$		62
$Eu^{3+}$	Gl	25	0.1 (NaClO <sub>4</sub> )	$K_1 = 2.46 \pm 0.01, K_2 = 1.69 \pm 0.02,$ $K_3 = 1.12 \pm 0.08$		62
$Gd^{3+}$	Gl	25	0.1 (NaClO <sub>4</sub> )	$K_1 = 2.37 \pm 0.01, K_2 = 1.63 \pm 0.02,$ $K_3 = 1.23 \pm 0.08$		62
$Ho^{3+}$	Gl	25	0.1 (NaClO <sub>4</sub> )	$K_1 = 2.28 \pm 0.01, K_2 = 1.64 \pm 0.02$		62
$La^{3+}$	Gl	25	0.1 (NaClO <sub>4</sub> )	$K_1 = 2.06 \pm 0.01, K_2 = 1.48 \pm 0.03,$ $K_3 = 1.21 \pm 0.09$		62
$Lu^{3+}$	Gl	25	0.1 (NaClO <sub>4</sub> )	$K_1 = 2.34 \pm 0.01, K_2 = 1.63 \pm 0.02$		62
$Nd^{3+}$	Gl	25	0.1 (NaClO <sub>4</sub> )	$K_1 = 2.37 \pm 0.01, K_2 = 1.59 \pm 0.03,$ $K_3 = 1.32 \pm 0.09$		62
$Pr^{3+}$	Gl	25	0.1 (NaClO <sub>4</sub> )	$K_1 = 2.30 \pm 0.01, K_2 = 1.59 \pm 0.03,$ $K_3 = 1.36 \pm 0.08$		62
$Sm^{3+}$	Gl	25	0.1 (NaClO <sub>4</sub> )	$K_1 = 2.48 \pm 0.01, K_2 = 1.67 \pm 0.03,$ $K_3 = 1.30 \pm 0.03$		62
$Tb^{3+}$	Gl	25	0.1 (NaClO <sub>4</sub> )	$K_1 = 2.30 \pm 0.01, K_2 = 1.60 \pm 0.04,$ $K_3 < 1$		62
$Tm^{3+}$	Gl	25	0.1 (NaClO <sub>4</sub> )	$K_1 = 2.31 \pm 0.01, K_2 = 1.62 \pm 0.02$		62

*(Continued.)*

Metal	Method	Temp. (°C)	Medium	log of equilibrium constant	Ref.
Y <sup>3+</sup>	Gl	25	0.1 (NaClO <sub>4</sub> )	$K_1 = 2.17 \pm 0.01, K_2 = 1.56 \pm 0.04$	62
Yb <sup>3+</sup>	Gl	25	0.1 (NaClO <sub>4</sub> )	$K_1 = 2.30 \pm 0.01, K_2 = 1.61 \pm 0.02$	62
C <sub>5</sub> H <sub>12</sub> O <sub>3</sub> , 2-hydroxy-2methylbutanoic acid (methylethylglycolic acid), HL					
H <sup>+</sup>	Gl	25	0.1 (KNO <sub>3</sub> )	$K_1 = 3.73$	63
Ce <sup>3+</sup>	Gl	25	0.1 (KNO <sub>3</sub> )	$K_1 = 2.51, K_2 = 1.72, K_3 = 1.20$	63
Dy <sup>3+</sup>	Gl	25	0.1 (KNO <sub>3</sub> )	$K_1 = 3.16, K_2 = 2.54, K_3 = 1.72$	63
Er <sup>3+</sup>	Gl	25	0.1 (KNO <sub>3</sub> )	$K_1 = 3.32, K_2 = 2.73, K_3 = 1.98$	63
Eu <sup>3+</sup>	Gl	25	0.1 (KNO <sub>3</sub> )	$K_1 = 2.90, K_2 = 2.30, K_3 = 1.60$	63
Gd <sup>3+</sup>	Gl	25	0.1 (KNO <sub>3</sub> )	$K_1 = 2.94, K_2 = 2.34, K_3 = 1.58$	63
Ho <sup>3+</sup>	Gl	25	0.1 (KNO <sub>3</sub> )	$K_1 = 3.24, K_2 = 2.63, K_3 = 1.85$	63
La <sup>3+</sup>	Gl	25	0.1 (KNO <sub>3</sub> )	$K_1 = 2.35, K_2 = 1.58, K_3 = 1.30$	63
Lu <sup>3+</sup>	Gl	25	0.1 (KNO <sub>3</sub> )	$K_1 = 3.45, K_2 = 2.85, K_3 = 2.05$	63
Nd <sup>3+</sup>	Gl	25	0.1 (KNO <sub>3</sub> )	$K_1 = 2.65, K_2 = 1.84, K_3 = 1.32$	63
Pr <sup>3+</sup>	Gl	25	0.1 (KNO <sub>3</sub> )	$K_1 = 2.54, K_2 = 1.77, K_3 = 1.11$	63
Sm <sup>3+</sup>	Gl	25	0.1 (KNO <sub>3</sub> )	$K_1 = 2.80, K_2 = 2.15, K_3 = 1.51$	63
Tb <sup>3+</sup>	Gl	25	0.1 (KNO <sub>3</sub> )	$K_1 = 3.10, K_2 = 2.48, K_3 = 1.73$	63
Tm <sup>3+</sup>	Gl	25	0.1 (KNO <sub>3</sub> )	$K_1 = 3.37, K_2 = 2.76, K_3 = 1.92$	63
2,3-Dihydroxypyridine					
Ce <sup>3+</sup>	Gl	25	0.1 NaClO <sub>4</sub> , 50% dioxan	$K_1 = 7.33$	64
Er <sup>3+</sup>	Gl	25	0.1 NaClO <sub>4</sub> , 50% dioxan	$K_1 = 8.62$	64
Gd <sup>3+</sup>	Gl	25	0.1 NaClO <sub>4</sub> , 50% dioxan	$K_1 = 8.34$	64
La <sup>3+</sup>	Gl	25	0.1 NaClO <sub>4</sub> , 50% dioxan	$K_1 = 7.13$	64
Nd <sup>3+</sup>	Gl	25	0.1 NaClO <sub>4</sub> , 50% dioxan	$K_1 = 7.57$	64
Pr <sup>3+</sup>	Gl	25	0.1 NaClO <sub>4</sub> , 50% dioxan	$K_1 = 7.41$	64
Sm <sup>3+</sup>	Gl	25	0.1 NaClO <sub>4</sub> , 50% dioxan	$K_1 = 8.18$	64
UO <sub>2</sub> <sup>2+</sup>	Gl	25	0.1 NaClO <sub>4</sub> , 50% dioxan	$K_1 = 9.35, K_2 = 8.27$	64
	Gl	25	0.1 NaClO <sub>4</sub> , 50% dioxan	$K_1 = 8.14, K_2 = 6.82$	64
Yb <sup>3+</sup>	Gl	25	0.1 NaClO <sub>4</sub> , 50% dioxan	$K_1 = 8.83$	64
C <sub>2</sub> H <sub>7</sub> O <sub>3</sub> N, isonitrosoacetylacetone, HL					
H <sup>+</sup>	Gl	20	0.1 NaClO <sub>4</sub> , 50% dioxan	$K_1 = 8.48 \pm 0.04$	54
Ce <sup>3+</sup>	Gl	20	0.1 NaClO <sub>4</sub> , 50% dioxan	$K_1 = 3.96, K_2 = 3.00$	54
Dy <sup>3+</sup>	Gl	20	0.1 NaClO <sub>4</sub> , 50% dioxan	$K_1 = 4.94, K_2 = 3.58$	54
Er <sup>3+</sup>	Gl	20	0.1 NaClO <sub>4</sub> , 50% dioxan	$K_1 = 5.26, K_2 = 3.72$	54
Eu <sup>3+</sup>	Gl	20	0.1 NaClO <sub>4</sub> , 50% dioxan	$K_1 = 4.69, K_2 = 3.53$	54

(Continued.)

Metal	Method	Temp. (°C)	Medium	log of equilibrium constant	Ref.
Gd <sup>3+</sup>	Gl	20	0.1 NaClO <sub>4</sub> , 50% dioxan	$K_1 = 4.52, K_2 = 3.58$	54
Ho <sup>3+</sup>	Gl	20	0.1 NaClO <sub>4</sub> , 50% dioxan	$K_1 = 5.14, K_2 = 3.73$	54
La <sup>3+</sup>	Gl	20	0.1 NaClO <sub>4</sub> , 50% dioxan	$K_1 = 3.86, K_2 = 2.87$	54
Lu <sup>3+</sup>	Gl	20	0.1 NaClO <sub>4</sub> , 50% dioxan	$K_1 = 5.33, K_2 = 3.50$	54
Nd <sup>3+</sup>	Gl	20	0.1 NaClO <sub>4</sub> , 50% dioxan	$K_1 = 4.17, K_2 = 3.22$	54
Pr <sup>3+</sup>	Gl	20	0.1 NaClO <sub>4</sub> , 50% dioxan	$K_1 = 4.07, K_2 = 3.10$	54
Sm <sup>3+</sup>	Gl	20	0.1 NaClO <sub>4</sub> , 50% dioxan	$K_1 = 4.48, K_2 = 3.47$	54
Tb <sup>3+</sup>	Gl	20	0.1 NaClO <sub>4</sub> , 50% dioxan	$K_1 = 4.78, K_2 = 3.40$	54
Tm <sup>3+</sup>	Gl	20	0.1 NaClO <sub>4</sub> , 50% dioxan	$K_1 = 5.38, K_2 = 3.77$	54
Y <sup>3+</sup>	Gl	20	0.1 NaClO <sub>4</sub> , 50% dioxan	$K_1 = 5.19, K_2 = 3.68$	54
C <sub>5</sub> H <sub>8</sub> O <sub>3</sub> N <sub>2</sub> , methylacetylgyoxime, H <sub>2</sub> L					
H <sup>+</sup>	Gl	20	0.1 NaClO <sub>4</sub> , 50% v/v dioxan	$K_1 = 11.24 \pm 0.10, K_2 = 10.17 \pm 0.04$	54
Ce <sup>3+</sup>	Gl	20	0.1 NaClO <sub>4</sub> , 50% v/v dioxan	$K_1 = 5.05, K_2 = 4.11$	54
Dy <sup>3+</sup>	Gl	20	0.1 NaClO <sub>4</sub> , 50% v/v dioxan	$K_1 = 5.90, K_2 = 5.05$	54
Er <sup>3+</sup>	Gl	20	0.1 NaClO <sub>4</sub> , 50% v/v dioxan	$K_1 = 6.19, K_2 = 5.23$	54
Eu <sup>3+</sup>	Gl	20	0.1 NaClO <sub>4</sub> , 50% v/v dioxan	$K_1 = 5.74, K_2 = 4.80$	54
Gd <sup>3+</sup>	Gl	20	0.1 NaClO <sub>4</sub> , 50% v/v dioxan	$K_1 = 5.60, K_2 = 4.73$	54
Ho <sup>3+</sup>	Gl	20	0.1 NaClO <sub>4</sub> , 50% v/v dioxan	$K_1 = 6.04, K_2 = 5.19$	54
La <sup>3+</sup>	Gl	20	0.1 NaClO <sub>4</sub> , 50% v/v dioxan	$K_1 = 4.98, K_2 = 4.02$	54
Lu <sup>3+</sup>	Gl	20	0.1 NaClO <sub>4</sub> , 50% v/v dioxan	$K_1 = 6.30, K_2 = 5.01$	54
Nd <sup>3+</sup>	Gl	20	0.1 NaClO <sub>4</sub> , 50% v/v dioxan	$K_1 = 5.30, K_2 = 4.30$	54
Pr <sup>3+</sup>	Gl	20	0.1 NaClO <sub>4</sub> , 50% v/v dioxan	$K_1 = 5.17, K_2 = 4.19$	54
Sm <sup>3+</sup>	Gl	20	0.1 NaClO <sub>4</sub> , 50% v/v dioxan	$K_1 = 5.59, K_2 = 4.60$	54
Tb <sup>3+</sup>	Gl	20	0.1 NaClO <sub>4</sub> , 50% v/v dioxan	$K_1 = 5.76, K_2 = 4.89$	54
Tm <sup>3+</sup>	Gl	20	0.1 NaClO <sub>4</sub> , 50% v/v dioxan	$K_1 = 6.28, K_2 = 5.21$	54

*(Continued.)*

Metal	Method	Temp. (°C)	Medium	log of equilibrium constant	Ref.
Y <sup>3+</sup>	Gl	20	0.1 NaClO <sub>4</sub> , 50% v/v dioxan	$K_1 = 5.63, K_2 = 4.88$	54
Yb <sup>3+</sup>	Gl	20	0.1 NaClO <sub>4</sub> , 50% v/v dioxan	$K_1 = 6.42, K_2 = 5.14$	54
C <sub>5</sub> H <sub>10</sub> O <sub>3</sub> N <sub>2</sub> , L-alanyl-glycine, HL					
Eu <sup>3+</sup>	Gl	25	0.1 (KCl)	$K_1 = 2.55$	65
Gd <sup>3+</sup>	Gl	25	0.1 (KCl)	$K_1 = 2.40$	65
Ho <sup>3+</sup>	Gl	25	0.1 (KCl)	$K_1 = 2.45$	65
Nd <sup>3+</sup>	Gl	25	0.1 (KCl)	$K_1 = 2.30$	65
Yb <sup>3+</sup>	Gl	25	0.1 (KCl)	$K_1 = 2.80$	65
C <sub>5</sub> H <sub>10</sub> O <sub>3</sub> N <sub>2</sub> , glycyl-DL-alanine, HL					
Eu <sup>3+</sup>	Gl	25	0.1 (KCl)	$K_1 = 2.60$	65
Gd <sup>3+</sup>	Gl	25	0.1 (KCl)	$K_1 = 2.40$	65
Ho <sup>3+</sup>	Gl	25	0.1 (KCl)	$K_1 = 2.55$	65
Nd <sup>3+</sup>	Gl	25	0.1 (KCl)	$K_1 = 2.30$	65
Yb <sup>3+</sup>	Gl	25	0.1 (KCl)	$K_1 = 2.80$	65
C <sub>5</sub> H <sub>10</sub> O <sub>3</sub> N <sub>2</sub> , glutamine					
Ce <sup>3+</sup>	Gl	25	0.1 (NaClO <sub>4</sub> )	$\beta_2 = 7.09$	66
La <sup>3+</sup>	Gl	25	0.1 (NaClO <sub>4</sub> )	$\beta_2 = 6.43$	66
Nd <sup>3+</sup>	Gl	25	0.1 (NaClO <sub>4</sub> )	$\beta_2 = 7.06$	66
Pr <sup>3+</sup>	Gl	25	0.1 (NaClO <sub>4</sub> )	$\beta_2 = 7.51$	66
Y <sup>3+</sup>	Gl	25	0.1 (NaClO <sub>4</sub> )	$\beta_2 = 8.05$	66
C <sub>5</sub> H <sub>10</sub> O <sub>4</sub> N <sub>2</sub> , glycyl-DL-serine, HL					
H <sup>+</sup>	Gl	25	0.1 (KCl)	$K_1 = 8.24, K_2 = 3.04$	65
Eu <sup>3+</sup>	Gl	25	0.1 (KCl)	$K_1 = 2.50$	65
Gd <sup>3+</sup>	Gl	25	0.1 (KCl)	$K_1 = 2.50$	65
Ho <sup>3+</sup>	Gl	25	0.1 (KCl)	$K_1 = 2.60$	65
Nd <sup>3+</sup>	Gl	25	0.1 (KCl)	$K_1 = 2.25$	65
Yb <sup>3+</sup>	Gl	25	0.1 (KCl)	$K_1 = 2.80$	65
C <sub>6</sub> H <sub>6</sub> O <sub>2</sub> , 1,2-dihydroxybenzene (catechol, pyrocatechol), H <sub>2</sub> L					
Dy <sup>3+</sup>	Pot	25	0.1 (NaCl)	$K_1 = 11.34 \pm 0.07$	67
Er <sup>3+</sup>	Pot	25	0.1 (NaCl)	$K_1 = 11.43 \pm 0.07$	67
Eu <sup>3+</sup>	Pot	25	0.1 (NaCl)	$K_1 = 11.17 \pm 0.07$	67
Nd <sup>3+</sup>	Pot	25	0.1 (NaCl)	$K_1 = 10.50 \pm 0.07$	67
Pr <sup>3+</sup>	Pot	25	0.1 (NaCl)	$K_1 = 10.31 \pm 0.07$	67
Gd <sup>3+</sup>	Pot	25	0.1 (NaCl)	$K_1 = 11.20 \pm 0.07$	67
Ho <sup>3+</sup>	Pot	25	0.1 (NaCl)	$K_1 = 11.42 \pm 0.07$	67
La <sup>3+</sup>	Pot	25	0.1 (NaCl)	$K_1 = 9.46 \pm 0.07$	67
Lu <sup>3+</sup>	Pot	25	0.1 (NaCl)	$K_1 = 11.31 \pm 0.07$	67
Tm <sup>3+</sup>	Pot	25	0.1 (NaCl)	$K_1 = 11.56$	67
Yb <sup>3+</sup>	Pot	25	0.1 (NaCl)	$K_1 = 11.67$	67
C <sub>6</sub> H <sub>6</sub> O <sub>3</sub> , 3-hydroxy-2-methyl-4-pyrone (maltol), HL					
Dy <sup>3+</sup>	Gl	30	0.1 (NaClO <sub>4</sub> )	$K_1 = 6.88, K_2 = 5.61, K_3 = 4.12$	68
Er <sup>3+</sup>	Gl	30	0.1 (NaClO <sub>4</sub> )	$K_1 = 6.98, K_2 = 5.68, K_3 = 4.21$	68
Eu <sup>3+</sup>	Gl	30	0.1 (NaClO <sub>4</sub> )	$K_1 = 6.72, K_2 = 5.31, K_3 = 3.80$	68
Gd <sup>3+</sup>	Gl	30	0.1 (NaClO <sub>4</sub> )	$K_1 = 6.58, K_2 = 5.33, K_3 = 3.95$	68
La <sup>3+</sup>	Gl	30	0.1 (NaClO <sub>4</sub> )	$K_1 = 5.76, K_2 = 4.41, K_3 = 3.17$	68
Nd <sup>3+</sup>	Gl	30	0.1 (NaClO <sub>4</sub> )	$K_1 = 6.22, K_2 = 4.92, K_3 = 3.54$	68

(Continued.)

Metal	Method	Temp. (°C)	Medium	log of equilibrium constant	Ref.
Pr <sup>3+</sup>	Gl	30	0.1 (NaClO <sub>4</sub> )	$K_1 = 6.13, K_2 = 4.83, K_3 = 3.55$	68
Sm <sup>3+</sup>	Gl	30	0.1 (NaClO <sub>4</sub> )	$K_1 = 6.51, K_2 = 5.19, K_3 = 3.73$	68
Y <sup>3+</sup>	Gl	30	0.1 (NaClO <sub>4</sub> )	$K_1 = 6.70, K_2 = 5.39, K_3 = 3.88$	68
Yb <sup>3+</sup>	Gl	30	0.1 (NaClO <sub>4</sub> )	$K_1 = 7.06, K_2 = 5.83, K_3 = 4.39$	68
C <sub>6</sub> H <sub>6</sub> O <sub>4</sub> , 3-hydroxy-5-(hydroxymethyl)-4-pyrone (kojic acid), HL					
Dy <sup>3+</sup>	Gl	30	0.1	$K_1 = 6.39, K_2 = 5.47, K_3 = 4.35$	69
Er <sup>3+</sup>	Gl	30	0.1	$K_1 = 6.31, K_2 = 5.46, K_3 = 4.40$	69
Eu <sup>3+</sup>	Gl	30	0.1	$K_1 = 6.15, K_2 = 5.10, K_3 = 4.03$	69
Gd <sup>3+</sup>	Gl	30	0.1	$K_1 = 6.09, K_2 = 5.12, K_3 = 4.05$	69
La <sup>3+</sup>	Gl	30	0.1	$K_1 = 5.35, K_2 = 4.21, K_3 = 3.31$	69
Nd <sup>3+</sup>	Gl	30	0.1	$K_1 = 5.80, K_2 = 4.83, K_3 = 4.03$	69
Pr <sup>3+</sup>	Gl	30	0.1	$K_1 = 5.77, K_2 = 4.77, K_3 = 3.89$	69
Sm <sup>3+</sup>	Gl	30	0.1	$K_1 = 6.03, K_2 = 5.02, K_3 = 3.94$	69
Y <sup>3+</sup>	Gl	30	0.1	$K_1 = 6.18, K_2 = 5.19, K_3 = 4.15$	69
Yb <sup>3+</sup>	Gl	30	0.1	$K_1 = 6.53, K_2 = 5.70, K_3 = 4.82$	69
C <sub>6</sub> H <sub>8</sub> O <sub>6</sub> , ascorbic acid, H <sub>2</sub> L					
Er <sup>3+</sup>	Sp	?	?	$K(\text{Er}^{3+} + \text{HL}^- = \text{ErHL}^{2+}) = 0.5$	70
	Sp	?	?	$K_1 = 9.03$	
Eu <sup>3+</sup>	Sp	?	?	$K(\text{Eu}^{3+} + \text{HL}^- = \text{EuHL}^{2+}) = 0.8$	71
Ho <sup>3+</sup>	Sp	?	?	$K(\text{Ho}^{3+} + \text{HL}^- = \text{HoHL}^{2+}) = 1.0$	70
Nd <sup>3+</sup>	Sp	?	?	$K_1 = 8.65$	72
M <sup>3+</sup> -citric acid (L)					
La <sup>3+</sup> -L <sub>2</sub>				9.45	73, 74
Ce <sup>3+</sup> -L <sub>2</sub>				9.65	73, 74
Nd <sup>3+</sup> -L <sub>2</sub>				9.69	73, 74
Pm <sup>3+</sup> -L <sub>2</sub>				9.75	73, 74
Eu <sup>3+</sup> -L <sub>2</sub>				9.80	73, 74
C <sub>6</sub> H <sub>10</sub> O <sub>3</sub> , ethylacetoacetate, HL					
Dy <sup>3+</sup>	Gl	30	0.1 (NaClO <sub>4</sub> ), 75% acetone	$K_1 = 6.78, K_2 = 5.80$	75
Er <sup>3+</sup>	Gl	30	0.1 (NaClO <sub>4</sub> ), 75% acetone	$K_1 = 6.88, K_2 = 6.08$	75
Eu <sup>3+</sup>	Gl	30	0.1 (NaClO <sub>4</sub> ), 75% acetone	$K_1 = 6.62, K_2 = 5.70$	75
Gd <sup>3+</sup>	Gl	30	0.1 (NaClO <sub>4</sub> ), 75% acetone	$K_1 = 6.30, K_2 = 5.35$	75
La <sup>3+</sup>	Gl	30	0.1 (NaClO <sub>4</sub> ), 75% acetone	$K_1 = 5.48, K_2 = 4.80$	75
Nd <sup>3+</sup>	Gl	30	0.1 (NaClO <sub>4</sub> ), 75% acetone	$K_1 = 6.08, K_2 = 5.30$	75
Pr <sup>3+</sup>	Gl	30	0.1 (NaClO <sub>4</sub> ), 75% acetone	$K_1 = 5.88, K_2 = 5.22$	75
Sm <sup>3+</sup>	Gl	30	0.1 (NaClO <sub>4</sub> ), 75% acetone	$K_1 = 6.40, K_2 = 5.70$	75
Y <sup>3+</sup>	Gl	30	0.1 (NaClO <sub>4</sub> ), 75% acetone	$K_1 = 6.40, K_2 = 5.53$	75
Yb <sup>3+</sup>	Gl	30	0.1 (NaClO <sub>4</sub> ), 75% acetone	$K_1 = 6.96, K_2 = 6.16$	75

(Continued.)

Metal	Method	Temp. (°C)	Medium	log of equilibrium constant		Ref.
<b>C<sub>6</sub>H<sub>10</sub>O<sub>4</sub>, hexanedioic acid (adipic acid), H<sub>2</sub>L</b>						
H <sup>+</sup>	Gl	30	0.1 (NaClO <sub>4</sub> )	$K_1 = 5.03, K_2 = 4.12$		76
Er <sup>3+</sup>	Sol	25	0.5	$K_1 = 2.43$		77
La <sup>3+</sup>	Sol	25	0.5	$K_1 = 3.96$		77
Sm <sup>3+</sup>	Sol	25	0.5	$K_1 = 3.77$		77
<b>C<sub>6</sub>H<sub>5</sub>O<sub>2</sub>N, pyridine-2-carboxylic acid (picolinic acid), HL</b>						
Dy <sup>3+</sup>	Gl	25	0.1 (KNO <sub>3</sub> )	$K_1 = 4.16, K_2 = 3.54, K_3 = 2.74, K_4 = 2.11$		78
Er <sup>3+</sup>	Gl	25	0.1 (KNO <sub>3</sub> )	$K_1 = 4.26, K_2 = 3.68, K_3 = 2.84, K_4 = 2.08$		78
Eu <sup>3+</sup>	Gl	25	0.1 (KNO <sub>3</sub> )	$K_1 = 3.99, K_2 = 3.46, K_3 = 2.86, K_4 = 2.18$		78
Gd <sup>3+</sup>	Gl	25	0.1 (KNO <sub>3</sub> )	$K_1 = 3.98, K_2 = 3.43, K_3 = 2.83, K_4 = 2.26$		78
Ho <sup>3+</sup>	Gl	25	0.1 (KNO <sub>3</sub> )	$K_1 = 4.19, K_2 = 3.58, K_3 = 2.76, K_4 = 1.95$		78
La <sup>3+</sup>	Gl	25	0.1 (KNO <sub>3</sub> )	$K_1 = 3.51, K_2 = 2.95, K_3 = 2.28, K_4 = 1.30$		78
Lu <sup>3+</sup>	Gl	25	0.1 (KNO <sub>3</sub> )	$K_1 = 4.41, K_2 = 3.86, K_3 = 2.98, K_4 = 2.23$		78
Nd <sup>3+</sup>	Gl	25	0.1 (KNO <sub>3</sub> )	$K_1 = 3.88, K_2 = 3.36, K_3 = 2.74, K_4 = 2.04$		78
Pr <sup>3+</sup>	Gl	25	0.1 (KNO <sub>3</sub> )	$K_1 = 3.83, K_2 = 3.30, K_3 = 2.65, K_4 = 2.00$		78
Sm <sup>3+</sup>	Gl	25	0.1 (KNO <sub>3</sub> )	$K_1 = 3.97, K_2 = 3.46, K_3 = 2.83, K_4 = 2.20$		78
Tb <sup>3+</sup>	Gl	25	0.1 (KNO <sub>3</sub> )	$K_1 = 4.08, K_2 = 3.48, K_3 = 2.76, K_4 = 2.18$		78
Tm <sup>3+</sup>	Gl	25	0.1 (KNO <sub>3</sub> )	$K_1 = 4.33, K_2 = 3.75, K_3 = 2.87, K_4 = 2.04$		78
Yb <sup>3+</sup>	Gl	25	0.1 (KNO <sub>3</sub> )	$K_1 = 4.40, K_2 = 3.83, K_3 = 2.95, K_4 = 2.11$		78
<b>C<sub>6</sub>H<sub>5</sub>O<sub>2</sub>N, pyridine-3-carboxylic acid (nicotinic acid), HL</b>						
H <sup>+</sup>	Gl	25	0.2 (KNO <sub>3</sub> )	$K_1 = 4.60 \pm 0.03$		79
	Sp	20	0.5 NaNO <sub>3</sub>	$K_1 = 4.70, K_2 = 2.09$		79
Ce <sup>3+</sup>	Gl	25	0.2 (NaClO <sub>4</sub> )	$K_1 = 1.98$		79
Dy <sup>3+</sup>	Gl	25	0.2 (NaClO <sub>4</sub> )	$K_1 = 2.19$		79
Er <sup>3+</sup>	Gl	25	0.2 (NaClO <sub>4</sub> )	$K_1 = 2.21$		79
Eu <sup>3+</sup>	Gl	25	0.2 (NaClO <sub>4</sub> )	$K_1 = 2.10$		79
Gd <sup>3+</sup>	Gl	25	0.2 (NaClO <sub>4</sub> )	$K_1 = 2.08$		79
Ho <sup>3+</sup>	Gl	25	0.2 (NaClO <sub>4</sub> )	$K_1 = 1.63$		79
La <sup>3+</sup>	Gl	25	0.2 (NaClO <sub>4</sub> )	$K_1 = 1.90 \pm 0.07$		79
Lu <sup>3+</sup>	Gl	25	0.2 (NaClO <sub>4</sub> )	$K_1 = 2.19$		79
Nd <sup>3+</sup>	Gl	25	0.2 (NaClO <sub>4</sub> )	$K_1 = 2.03$		79
Pr <sup>3+</sup>	Gl	25	0.2 (NaClO <sub>4</sub> )	$K_1 = 2.01$		79
Sm <sup>3+</sup>	Gl	25	0.2 (NaClO <sub>4</sub> )	$K_1 = 2.07$		79
Tb <sup>3+</sup>	Gl	25	0.2 (NaClO <sub>4</sub> )	$K_1 = 2.09$		79
Y <sup>3+</sup>	Gl	25	0.2 (NaClO <sub>4</sub> )	$K_1 = 2.39$		79
Yb <sup>3+</sup>	Gl	25	0.2 (NaClO <sub>4</sub> )	$K_1 = 2.18$		79
<b>C<sub>6</sub>H<sub>5</sub>NO<sub>2</sub>, 2-picolinic acid, HL</b>						
				log $\beta_2$	log $\beta_3$	
La <sup>3+</sup>	Gl	25	0.1 KNO <sub>3</sub>	6.28	8.9	205
Ce <sup>3+</sup>	Gl	25	0.1 KNO <sub>3</sub>	6.56	9.5	205
Pr <sup>3+</sup>	Gl	25	0.1 KNO <sub>3</sub>	6.96	9.9	205
Nd <sup>3+</sup>	Gl	25	0.1 KNO <sub>3</sub>	6.92	10.0	205
Sm <sup>3+</sup>	Gl	25	0.1 KNO <sub>3</sub>	7.40	10.6	205
Eu <sup>3+</sup>	Gl	25	0.1 KNO <sub>3</sub>	7.48	10.6	205
Gd <sup>3+</sup>	Gl	25	0.1 KNO <sub>3</sub>	7.34	10.5	205
Tb <sup>3+</sup>	Gl	25	0.1 KNO <sub>3</sub>	7.62	10.8	205
Dy <sup>3+</sup>	Gl	25	0.1 KNO <sub>3</sub>	7.76	10.7	205
Ho <sup>3+</sup>	Gl	25	0.1 KNO <sub>3</sub>	7.72	10.9	205

(Continued.)

Metal	Method	Temp. (°C)	Medium	log of equilibrium constant		Ref.
Er <sup>3+</sup>	Gl	25	0.1 KNO <sub>3</sub>	7.86	10.9	205
Tm <sup>3+</sup>	Gl	25	0.1 KNO <sub>3</sub>	7.98	11.2	205
Yb <sup>3+</sup>	Gl	25	0.1 KNO <sub>3</sub>	8.12	11.4	205
Lu <sup>3+</sup>	Gl	25	0.1 KNO <sub>3</sub>	8.20	11.4	205
Y <sup>3+</sup>	Gl	25	0.1 KNO <sub>3</sub>	7.36	10.0	205
C <sub>6</sub> H <sub>5</sub> O <sub>3</sub> N, 3-hydroxypyridine-2-carboxylic acid, H <sub>2</sub> L						
H <sup>+</sup>	Gl	30	0.1 (NaClO <sub>4</sub> )	$K_2 = 5.17$		80
Er <sup>3+</sup>	Gl	30	0.1 (NaClO <sub>4</sub> )	$K(\text{Er}^{3+} + \text{HL}^- = \text{ErHL}^{2+}) = 3.88$ $K[\text{ErHL}^{2+} + \text{HL}^- = \text{Er}(\text{HL})_2^+] = 13.50$		80
Gd <sup>3+</sup>	Gl	30	0.1 (NaClO <sub>4</sub> )	$K(\text{Gd}^{3+} + \text{HL}^- = \text{GdHL}^{2+}) = 3.46$ $K[\text{GdHL}^{2+} + \text{HL}^- = \text{Gd}(\text{HL})_2^+] = 13.24$		80
La <sup>3+</sup>	Gl	30	0.1 (NaClO <sub>4</sub> )	$K(\text{La}^{3+} + \text{HL}^- = \text{LaHL}^{2+}) = 3.18$ $K[\text{LaHL}^{2+} + \text{HL}^- = \text{La}(\text{HL})_2^+] = 13.04$		80
Pr <sup>3+</sup>	Gl	30	0.1 (NaClO <sub>4</sub> )	$K(\text{Pr}^{3+} + \text{HL}^- = \text{PrHL}^{2+}) = 3.28$ $K[\text{PrHL}^{2+} + \text{HL}^- = \text{Pr}(\text{HL})_2^+] = 13.22$		80
Sm <sup>3+</sup>	Gl	30	0.1 (NaClO <sub>4</sub> )	$K(\text{Sm}^{3+} + \text{HL}^- = \text{SmHL}^{2+}) = 3.54$ $K[\text{SmHL}^{2+} + \text{HL}^- = \text{Sm}(\text{HL})_2^+] = 13.29$		80
C <sub>6</sub> H <sub>5</sub> O <sub>4</sub> Cl, 3-chloro-5-hydroxy-2-hydromethyl-4-pyrone (chlorokojic acid), HL						
H <sup>+</sup>	Gl	30	0.1	$K_1 = 7.54$		81
Dy <sup>3+</sup>	Gl	30	0.1	$K_1 = 6.13, K_2 = 5.38$		81
Er <sup>3+</sup>	Gl	30	0.1	$K_1 = 6.19, K_2 = 5.44$		81
Eu <sup>3+</sup>	Gl	30	0.1	$K_1 = 5.98, K_2 = 5.21$		81
Gd <sup>3+</sup>	Gl	30	0.1	$K_1 = 5.98, K_2 = 5.14$		81
La <sup>3+</sup>	Gl	30	0.1	$K_1 = 5.28, K_2 = 4.48$		81
Nd <sup>3+</sup>	Gl	30	0.1	$K_1 = 5.73, K_2 = 4.92$		81
Pr <sup>3+</sup>	Gl	30	0.1	$K_1 = 5.70, K_2 = 4.82$		81
Sm <sup>3+</sup>	Gl	30	0.1	$K_1 = 5.83, K_2 = 5.08$		81
Y <sup>3+</sup>	Gl	30	0.1	$K_1 = 6.00, K_2 = 5.32$		81
Yb <sup>3+</sup>	Gl	30	0.1	$K_1 = 6.28, K_2 = 5.69$		81
C <sub>6</sub> H <sub>6</sub> O <sub>8</sub> S <sub>2</sub> , 4,5-dihydroxybenzene-1,3-disulphonic acid (catechol-3,4-disulphonic acid, tiron), H <sub>4</sub> L						
Dy <sup>3+</sup>	Gl	25	0.1 (NaClO <sub>4</sub> )	$K_1 = 14.36$ $K(\text{Dy}^{3+} + \text{HL}^{3-} = \text{DyHL}) = 5.59$		82
Er <sup>3+</sup>	Gl	25	0.1 (NaClO <sub>4</sub> )	$K_1 = 14.48$ $K(\text{Er}^{3+} + \text{HL}^{3-} = \text{ErHL}) = 5.45$		82
Gd <sup>3+</sup>	Gl	25	0.1 (NaClO <sub>4</sub> )	$K_1 = 14.10$ $K(\text{Gd}^{3+} + \text{HL}^{3-} = \text{GdHL}) = 5.92$		82
Ho <sup>3+</sup>	Gl	25	0.1 (NaClO <sub>4</sub> )	$K_1 = 14.39$ $K(\text{Ho}^{3+} + \text{HL}^{3-} = \text{HoHL}) = 5.42$		82
Sm <sup>3+</sup>	Gl	25	0.1 (NaClO <sub>4</sub> )	$K_1 = 13.92$ $K(\text{Sm}^{3+} + \text{HL}^{3-} = \text{SmHL}) = 5.72$		82
Tb <sup>3+</sup>	Gl	25	0.1 (NaClO <sub>4</sub> )	$K_1 = 14.14$ $K(\text{Tb}^{3+} + \text{HL}^{3-} = \text{TbHL}) = 5.71$		82
Tm <sup>3+</sup>	Gl	25	0.1 (NaClO <sub>4</sub> )	$K_1 = 14.36$ $K(\text{Tm}^{3+} + \text{HL}^{3-} = \text{TmHL}) = 5.67$		82
Y <sup>3+</sup>	Gl	25	0.1 (NaClO <sub>4</sub> )	$K_1 = 13.72$ $K(\text{Y}^{3+} + \text{HL}^{3-} = \text{YHL}) = 5.13$		82
Yb <sup>3+</sup>	Gl	25	0.1 (NaClO <sub>4</sub> )	$K_1 = 14.43$ $K(\text{Yb}^{3+} + \text{HL}^{3-} = \text{YbHL}) = 5.65$		82

*(Continued.)*

Metal	Method	Temp. (°C)	Medium	log of equilibrium constant	Ref.
La <sup>3+</sup>	Gl	25	0.1 (NaClO <sub>4</sub> )	$K_1 = 12.87$	82
Nd <sup>3+</sup>	Gl	25	0.1 (NaClO <sub>4</sub> )	$K_1 = 13.69$	82
				$K(\text{Nd}^{3+} + \text{HL}^{3-} = \text{NdHL}) = 5.61$	
Pr <sup>3+</sup>	Gl	25	0.1 (NaClO <sub>4</sub> )	$K_1 = 13.47$	82
C <sub>6</sub> H <sub>7</sub> ON, 2-aminophenol, L					
Dy <sup>3+</sup>	Gl	25	0.12 (NaClO <sub>4</sub> ), 50% (CH <sub>3</sub> ) <sub>2</sub> SO	$K_1 = 3.98, K_2 = 3.16$	83
			0.12 (NaClO <sub>4</sub> ), 50% dioxan	$K_1 = 5.25, K_2 = 4.32$	
			0.12 (NaClO <sub>4</sub> ), 50% ethanol	$K_1 = 4.75, K_2 = 3.66$	
Er <sup>3+</sup>	Gl	25	0.12 (NaClO <sub>4</sub> ), 50% (CH <sub>3</sub> ) <sub>2</sub> SO	$K_1 = 4.41, K_2 = 3.97$	83
			0.12 (NaClO <sub>4</sub> ), 50% dioxan	$K_1 = 5.52, K_2 = 4.14$	
			0.12 (NaClO <sub>4</sub> ), 50% ethanol	$K_1 = 4.89, K_2 = 4.11$	
Gd <sup>3+</sup>	Gl	25	0.12 (NaClO <sub>4</sub> ), 50% (CH <sub>3</sub> ) <sub>2</sub> SO	$K_1 = 3.80, K_2 = 2.86$	83
			0.12 (NaClO <sub>4</sub> ), 50% dioxan	$K_1 = 5.04, K_2 = 4.33$	
			0.12 (NaClO <sub>4</sub> ), 50% ethanol	$K_1 = 4.48, K_2 = 3.37$	
Ho <sup>3+</sup>	Gl	25	0.12 (NaClO <sub>4</sub> ), 50% (CH <sub>3</sub> ) <sub>2</sub> SO	$K_1 = 4.23, K_2 = 3.67$	83
			0.12 (NaClO <sub>4</sub> ), 50% dioxan	$K_1 = 5.32, K_2 = 4.32$	
			0.12 (NaClO <sub>4</sub> ), 50% ethanol	$K_1 = 4.79, K_2 = 3.92$	
La <sup>3+</sup>	Gl	25	0.12 (NaClO <sub>4</sub> ), 50% (CH <sub>3</sub> ) <sub>2</sub> SO	$K_1 = 3.54, K_2 = 2.98$	83
			0.12 (NaClO <sub>4</sub> ), 50% dioxan	$K_1 = 4.50, K_2 = 3.14$	
			0.12 (NaClO <sub>4</sub> ), 50% ethanol	$K_1 = 3.59, K_2 = 2.48$	
Nd <sup>3+</sup>	Gl	25	0.12 (NaClO <sub>4</sub> ), 50% (CH <sub>3</sub> ) <sub>2</sub> SO	$K_1 = 3.72, K_2 = 3.15$	83
			0.12 (NaClO <sub>4</sub> ), 50% dioxan	$K_1 = 4.62, K_2 = 3.67$	
			0.12 (NaClO <sub>4</sub> ), 50% ethanol	$K_1 = 4.31, K_2 = 3.18$	
Tb <sup>3+</sup>	Gl	25	0.12 (NaClO <sub>4</sub> ), 50% (CH <sub>3</sub> ) <sub>2</sub> SO	$K_1 = 3.82, K_2 = 2.84$	83
			0.12 (NaClO <sub>4</sub> ), 50% dioxan	$K_1 = 5.14, K_2 = 4.24$	
			0.12 (NaClO <sub>4</sub> ), 50% ethanol	$K_1 = 4.65, K_2 = 3.61$	
Tm <sup>3+</sup>	Gl	25	0.12 (NaClO <sub>4</sub> ), 50% (CH <sub>3</sub> ) <sub>2</sub> SO	$K_1 = 4.48, K_2 = 4.02$	83



(Continued.)

Metal	Method	Temp. (°C)	Medium	log of equilibrium constant	Ref.
Yb <sup>3+</sup>	Gl	25	0.12 (NaClO <sub>4</sub> ), 50% dioxan	$K_1 = 5.65, K_2 = 4.34$	83
			0.12 (NaClO <sub>4</sub> ), 50% ethanol	$K_1 = 5.01, K_2 = 4.20$	
			0.12 (NaClO <sub>4</sub> ), 50% (CH <sub>3</sub> ) <sub>2</sub> SO	$K_1 = 4.54, K_2 = 4.08$	
			0.12 (NaClO <sub>4</sub> ), 50% dioxan	$K_1 = 5.82, K_2 = 4.52$	
			0.12 (NaClO <sub>4</sub> ), 50% ethanol	$K_1 = 5.12, K_2 = 4.30$	
C <sub>6</sub> H <sub>7</sub> O <sub>2</sub> N, isonitrosoacetophenone, HL					
H <sup>+</sup>	Gl	20	0.1 NaClO <sub>4</sub> , 50% v/v dioxan	$K_1 = 9.92 \pm 0.04$	34
Ce <sup>3+</sup>	Gl	20	0.1 NaClO <sub>4</sub> , 50% v/v dioxan	$K_1 = 5.80, K_2 = 5.08$	34
Dy <sup>3+</sup>	Gl	20	0.1 NaClO <sub>4</sub> , 50% v/v dioxan	$K_1 = 6.18, K_2 = 5.66$	34
Er <sup>3+</sup>	Gl	20	0.1 NaClO <sub>4</sub> , 50% v/v dioxan	$K_1 = 6.37, K_2 = 5.67$	34
Eu <sup>3+</sup>	Gl	20	0.1 NaClO <sub>4</sub> , 50% v/v dioxan	$K_1 = 6.19, K_2 = 5.57$	34
Gd <sup>3+</sup>	Gl	20	0.1 NaClO <sub>4</sub> , 50% v/v dioxan	$K_1 = 6.05, K_2 = 5.40$	34
Ho <sup>3+</sup>	Gl	20	0.1 NaClO <sub>4</sub> , 50% v/v dioxan	$K_1 = 6.28, K_2 = 5.64$	34
La <sup>3+</sup>	Gl	20	0.1 NaClO <sub>4</sub> , 50% v/v dioxan	$K_1 = 5.72, K_2 = 4.92$	34
Lu <sup>3+</sup>	Gl	20	0.1 NaClO <sub>4</sub> , 50% v/v dioxan	$K_1 = 6.53, K_2 = 5.49$	34
Nd <sup>3+</sup>	Gl	20	0.1 NaClO <sub>4</sub> , 50% v/v dioxan	$K_1 = 5.94, K_2 = 5.24$	34
Pr <sup>3+</sup>	Gl	20	0.1 NaClO <sub>4</sub> , 50% v/v dioxan	$K_1 = 5.86, K_2 = 5.14$	34
Sm <sup>3+</sup>	Gl	20	0.1 NaClO <sub>4</sub> , 50% v/v dioxan	$K_1 = 6.02, K_2 = 5.48$	34
Tb <sup>3+</sup>	Gl	20	0.1 NaClO <sub>4</sub> , 50% v/v dioxan	$K_1 = 6.14, K_2 = 5.51$	34
Tm <sup>3+</sup>	Gl	20	0.1 NaClO <sub>4</sub> , 50% v/v dioxan	$K_1 = 6.49, K_2 = 5.61$	34
Y <sup>3+</sup>	Gl	20	0.1 NaClO <sub>4</sub> , 50% v/v dioxan	$K_1 = 6.32, K_2 = 5.62$	34
Yb <sup>3+</sup>	Gl	20	0.1 NaClO <sub>4</sub> , 50% v/v dioxan	$K_1 = 6.64, K_2 = 5.57$	34
C <sub>6</sub> H <sub>9</sub> O <sub>2</sub> N <sub>3</sub> , 2-amino-3-(4-imidazolyl)propanoic acid (histidine), HL					
Dy <sup>3+</sup>	Gl	25	3.0 NaClO <sub>4</sub>	$K_1 = 4.40 \pm 0.06, \beta_2 = 9.14 \pm 0.07$ $K(\text{Dy}^{3+} + \text{H}^+ + \text{L}^- = \text{DyHL}^{3+}) = 11.16 \pm 0.16$	
Er <sup>3+</sup>	Gl	25	3.0 NaClO <sub>4</sub>	$K_1 = 4.49 \pm 0.08, \beta_2 = 8.99 \pm 0.09$ $K(\text{Er}^{3+} + \text{H}^+ + \text{L}^- = \text{ErHL}^{3+}) = 11.18 \pm 0.09$	

(Continued.)

Metal	Method	Temp. (°C)	Medium	log of equilibrium constant	Ref.
Gd <sup>3+</sup>	Gl	25	3.0 NaClO <sub>4</sub>	$K_1 = 4.39 \pm 0.10, \beta_2 = 8.61 \pm 0.10$ $K(\text{Gd}^{3+} + \text{H}^+ + \text{L}^- = \text{GdHL}^{3+}) = 11.47 \pm 0.08$	
La <sup>3+</sup>	Gl	25	3.0 NaClO <sub>4</sub>	$K_1 = 4.10 \pm 0.12, \beta_2 = 5.40 \pm 0.15$ $K(\text{La}^{3+} + \text{H}^+ + \text{L}^- = \text{LaHL}^{3+}) = 11.75 \pm 0.18$	
Nd <sup>3+</sup>	Gl	25	3.0 NaClO <sub>4</sub>	$K_1 = 4.40 \pm 0.09, \beta_2 = 6.59 \pm 0.14$ $K(\text{Nd}^{3+} + \text{H}^+ + \text{L}^- = \text{NdHL}^{3+}) = 11.77 \pm 0.07$	
Pr <sup>3+</sup>	Gl	25	3.0 NaClO <sub>4</sub>	$K_1 = 4.36 \pm 0.03, \beta_2 = 6.20 \pm 0.13$ $K(\text{Pr}^{3+} + \text{H}^+ + \text{L}^- = \text{PrHL}^{3+}) = 11.77 \pm 0.07$	
Sm <sup>3+</sup>	Gl	25	3.0 NaClO <sub>4</sub>	$K_1 = 4.46 \pm 0.07, \beta_2 = 8.71 \pm 0.08$ $K(\text{Sm}^{3+} + \text{H}^+ + \text{L}^- = \text{SmHL}^{3+}) = 11.78 \pm 0.05$	
Yb <sup>3+</sup>	Gl	25	3.0 NaClO <sub>4</sub>	$K_1 = 4.23 \pm 0.10, \beta_2 = 9.83 \pm 0.05$ $K(\text{Yb}^{3+} + \text{H}^+ + \text{L}^- = \text{YbHL}^{3+}) = 11.40 \pm 0.14$	
C <sub>6</sub> H <sub>11</sub> O <sub>5</sub> N, <i>N</i> -hydroxyethyliminodiacetic acid, H <sub>2</sub> L					
La <sup>3+</sup>	Gl	25	0.1 KNO <sub>3</sub>	log $\beta_2 = 13.90$	204
Ce <sup>3+</sup>	Gl	25		log $\beta_2 = 14.12$	204
Pr <sup>3+</sup>	Gl	25		log $\beta_2 = 14.45$	204
Nd <sup>3+</sup>	Gl	25		–	204
Sm <sup>3+</sup>	Gl	25		log $\beta_2 = 15.74$	204
Eu <sup>3+</sup>	Gl	25		log $\beta_2 = 16.26$	204
Gd <sup>3+</sup>	Gl	25		log $\beta_2 = 16.08$	204
Tb <sup>3+</sup>	Gl	25		log $\beta_2 = 16.42$	204
Dy <sup>3+</sup>	Gl	25		log $\beta_2 = 16.40$	204
Ho <sup>3+</sup>	Gl	25		log $\beta_2 = 16.36$	204
Er <sup>3+</sup>	Gl	25		log $\beta_2 = 16.34$	204
Tm <sup>3+</sup>	Gl	25			204
Yb <sup>3+</sup>	Gl	25		log $\beta_2 = 16.37$	204
Lu <sup>3+</sup>	Gl	25			204
Y <sup>3+</sup>	Gl	25			204
C <sub>6</sub> H <sub>10</sub> O <sub>2</sub> S, ethyl thioacetacetate, HL					
Er <sup>3+</sup>	Gl	30	0.1, 75% acetone	$K_1 = 7.56, K_2 = 6.22, K_3 = 6.00$	85
Eu <sup>3+</sup>	Gl	30	0.1, 75% acetone	$K_1 = 7.30, K_2 = 6.00, K_3 = 5.60$	85
Gd <sup>3+</sup>	Gl	30	0.1, 75% acetone	$K_1 = 7.08, K_2 = 5.75, K_3 = 5.46$	85
La <sup>3+</sup>	Gl	30	0.1, 75% acetone	$K_1 = 6.76, K_2 = 5.50, K_3 = 4.60$	85
Nd <sup>3+</sup>	Gl	30	0.1, 75% acetone	$K_1 = 7.11, K_2 = 5.92, K_3 = 5.26$	85
Pr <sup>3+</sup>	Gl	30	0.1, 75% acetone	$K_1 = 7.00, K_2 = 5.60, K_3 = 5.00$	85
Sm <sup>3+</sup>	Gl	30	0.1, 75% acetone	$K_1 = 7.20, K_2 = 5.96, K_3 = 5.52$	85
Y <sup>3+</sup>	Gl	30	0.1, 75% acetone	$K_1 = 7.02, K_2 = 6.02, K_3 = 5.57$	85
Yb <sup>3+</sup>	Gl	30	0.1, 75% acetone	$K_1 = 7.64, K_2 = 6.42, K_3 = 6.25$	85
M <sup>3+</sup> -L, triglycine, C <sub>6</sub> H <sub>11</sub> O <sub>4</sub> N <sub>3</sub>					
Eu <sup>3+</sup>	Gl	25	0.1 (KCl)	$K_1 = 2.55$	65
Gd <sup>3+</sup>	Gl	25	0.1 (KCl)	$K_1 = 2.20$	65
Ho <sup>3+</sup>	Gl	25	0.1 (KCl)	$K_1 = 2.35$	65
Nd <sup>3+</sup>	Gl	25	0.1 (KCl)	$K_1 = 2.15$	65
Yb <sup>3+</sup>	Gl	25	0.1 (KCl)	$K_1 = 2.50$	65
C <sub>6</sub> H <sub>12</sub> O <sub>7</sub> , gluconic acid					
La <sup>3+</sup>	Gl	25	0.02 KCl	$\beta_1 = 2.38 \quad \beta_2 = 4.28$	203
Pr <sup>3+</sup>	Gl	25	0.02 KCl	$\beta_1 = 2.66 \quad \beta_2 = 4.70$	203
Nd <sup>3+</sup>	Gl	25	0.02 KCl	$\beta_1 = 2.70 \quad \beta_2 = 5.06$	203

(Continued.)

Metal	Method	Temp. (°C)	Medium	log of equilibrium constant	Ref.
Sm <sup>3+</sup>	Gl	25	0.02 KCl	$\beta_1 = 2.76$ $\beta_2 = 4.88$	203
Eu <sup>3+</sup>	Gl	25	0.02 KCl	$\beta_1 = 2.74$ $\beta_2 = 4.97$	203
Gd <sup>3+</sup>	Gl	25	0.02 KCl	$\beta_1 = 2.66$ $\beta_2 = 4.76$	203
Tb <sup>3+</sup>	Gl	25	0.02 KCl	$\beta_1 = 2.47$ $\beta_2 = 4.67$	203
Dy <sup>3+</sup>	Gl	25	0.02 KCl	$\beta_1 = 2.40$ $\beta_2 = 4.57$	203
Ho <sup>3+</sup>	Gl	25	0.02 KCl	$\beta_1 = 2.42$ $\beta_2 = 4.51$	203
Er <sup>3+</sup>	Gl	25	0.02 KCl	$\beta_1 = 2.50$ $\beta_2 = 4.53$	203
Yb <sup>3+</sup>	Gl	25	0.02 KCl	$\beta_1 = 2.80$ $\beta_2 = 4.68$	203
Lu <sup>3+</sup>	Gl	25	0.02 KCl	$\beta_1 = 2.85$ $\beta_2 = 4.78$	203
Y <sup>3+</sup>	Gl	25	0.02 KCl	$\beta_1 = 2.40$ $\beta_2 = 4.52$	203
C <sub>6</sub> H <sub>13</sub> O <sub>4</sub> N, <i>N,N</i> -bis(2'-hydroxyethyl)glycine, HL					
Ce <sup>3+</sup>	Gl	30	0.1 (KCl)	$K_1 = 5.09 \pm 0.04$ , $K_2 = 3.75 \pm 0.08$	86
Dy <sup>3+</sup>	Gl	30	0.1 (KCl)	$K_1 = 5.55 \pm 0.04$ , $K_2 = 4.44 \pm 0.08$ , $\beta_2 = 9.99 \pm 0.03$	86
Er <sup>3+</sup>	Gl	30	0.1 (KCl)	$K_1 = 5.38 \pm 0.04$ , $K_2 = 4.11 \pm 0.08$ , $\beta_2 = 9.49 \pm 0.03$	86
Eu <sup>3+</sup>	Gl	30	0.1 (KCl)	$K_1 = 5.60 \pm 0.04$ , $K_2 = 4.65 \pm 0.08$ , $\beta_2 = 10.25 \pm 0.03$	86
Gd <sup>3+</sup>	Gl	30	0.1 (KCl)	$K_1 = 5.84$ , $K_2 = 4.76$ , $\beta_2 = 10.60$	86
Ho <sup>3+</sup>	Gl	30	0.1 (KCl)	$K_1 = 5.51 \pm 0.04$ , $K_2 = 4.19 \pm 0.08$ , $\beta_2 = 9.70 \pm 0.03$	86
La <sup>3+</sup>	Gl	30	0.1 (KCl)	$K_1 = 4.95 \pm 0.04$ , $K_2 = 3.65 \pm 0.08$ , $\beta_2 = 8.60 \pm 0.03$	86
Lu <sup>3+</sup>				-	
Nd <sup>3+</sup>	Gl	20	0.03, 0-80% ethanol	$K_1(0\%) = 5.77 \pm 0.08$	86
Pr <sup>3+</sup>	Gl	20	0.03 (KCl), 0-80% ethanol	$K_1(0\%) = 5.44 \pm 0.03$	88
Sm <sup>3+</sup>	Gl	30	0.1 (KCl)	$K_1 = 5.54 \pm 0.04$ , $K_2 = 4.38 \pm 0.08$ , $\beta_2 = 9.92 \pm 0.03$	86
Tb <sup>3+</sup>	Gl	30	0.1 (KCl)	$K_1 = 5.48 \pm 0.04$ , $K_2 = 3.72 \pm 0.08$ , $\beta_2 = 9.20 \pm 0.03$	86
Tm <sup>3+</sup>	Gl	30	0.1 (KCl)	$K_1 = 5.52 \pm 0.04$ , $K_2 = 4.13 \pm 0.08$ , $\beta_2 = 9.65 \pm 0.03$	86
Yb <sup>3+</sup>	Gl	20	0.03 (KCl), 0-80% ethanol	$K_1(0\%) = 5.45 \pm 0.03$ ,	88
C <sub>6</sub> H <sub>15</sub> O <sub>4</sub> P, dipropylphosphoric acid, HL					
La <sup>3+</sup>	Kin	25	→ 0	$K_1 = 1.92$	89
Yb <sup>3+</sup>	Kin	25	→ 0	$K_1 = 3.12$	89
C <sub>6</sub> H <sub>12</sub> O <sub>3</sub> N <sub>2</sub> S, glycyl-DL-methionine, HL					
Eu <sup>3+</sup>	Gl	25	0.1 (KCl)	$K_1 = 2.60$	90
Gd <sup>3+</sup>	Gl	25	0.1 (KCl)	$K_1 = 2.50$	90
Ho <sup>3+</sup>	Gl	25	0.1 (KCl)	$K_1 = 2.60$	90
Nd <sup>3+</sup>	Gl	25	0.1 (KCl)	$K_1 = 2.40$	90
Yb <sup>3+</sup>	Gl	25	0.1 (KCl)	$K_1 = 2.85$	90
M <sup>3+</sup> -glycyl-DL-methionine					
Eu <sup>3+</sup>	Gl	25	0.1 KCl	$K_1 = 2.60$	90
Gd <sup>3+</sup>	Gl	25	0.1 KCl	$K_1 = 2.50$	90
Ho <sup>3+</sup>	Gl	25	0.1 KCl	$K_1 = 2.60$	90

(Continued.)

Metal	Method	Temp. (°C)	Medium	log of equilibrium constant					Ref.
Nd <sup>3+</sup>	Gl	25	0.1 KCl	$K_1 = 2.40$					90
Yb <sup>3+</sup>	Gl	25	0.1 KCl	$K_1 = 2.85$					90
2,6-pyridinedicarboxylic acid (dipicolinic acid), H <sub>2</sub> L									
Metal	Method	<i>I</i>	<i>T</i> <sub>1</sub> (°C)	log <i>K</i> <sub>1</sub>	log <i>K</i> <sub>2</sub>	log β <sub>2</sub>	log <i>K</i> <sub>3</sub>	log β <sub>3</sub>	Ref.
La <sup>3+</sup>	Cu-Hg	0.5 M NaClO <sub>4</sub>	20	7.98	5.81	13.79	4.27	18.06	197
Ce <sup>3+</sup>	Cu-Hg	0.5 M NaClO <sub>4</sub>	20	8.34	6.08	14.42	4.38	18.80	197
Pr <sup>3+</sup>	Cu-Hg	0.5 M NaClO <sub>4</sub>	20	8.63	6.47	15.10	4.84	19.94	197
Nd <sup>3+</sup>	Cu-Hg	0.5 M NaClO <sub>4</sub>	20	8.78	6.72	15.50	5.06	20.56	197
Sm <sup>3+</sup>	Cu-Hg	0.5 M NaClO <sub>4</sub>	20	8.86	7.02	15.88	5.35	21.23	197
Eu <sup>3+</sup>	Cu-Hg	0.5 M NaClO <sub>4</sub>	20	8.84	7.14	15.98	5.51	21.49	197
Gd <sup>3+</sup>	Cu-Hg	0.5 M NaClO <sub>4</sub>	20	8.74	7.32	16.06	5.77	21.83	197
Tb <sup>3+</sup>	Cu-Hg	0.5 M NaClO <sub>4</sub>	20	8.68	7.43	16.11	5.92	22.03	197
Dy <sup>3+</sup>	Cu-Hg	0.5 M NaClO <sub>4</sub>	20	8.69	7.49	16.18	5.95	22.13	197
Ho <sup>3+</sup>	Cu-Hg	0.5 M NaClO <sub>4</sub>	20	8.72	7.51	16.23	5.85	22.08	197
Er <sup>3+</sup>	Cu-Hg	0.5 M NaClO <sub>4</sub>	20	8.77	7.62	16.39	5.74	22.13	197
Tm <sup>3+</sup>	Cu-Hg	0.5 M NaClO <sub>4</sub>	20	8.83	7.71	16.54	5.50	22.04	197
Yb <sup>3+</sup>	Cu-Hg	0.5 M NaClO <sub>4</sub>	20	8.85	7.76	16.61	5.12	21.73	197
Lu <sup>3+</sup>	Cu-Hg	0.5 M NaClO <sub>4</sub>	20	9.03	7.77	16.80	4.68	21.48	197
Y <sup>3+</sup>	Cu-Hg	0.5 M NaClO <sub>4</sub>	20	8.46	7.27	15.73	5.61	21.34	197
Metal	Method	Temp. (°C)	Medium	log of equilibrium constant					Ref.
C <sub>7</sub> H <sub>6</sub> O <sub>2</sub> , 2-hydroxycyclohepta-2,4,6-trien-1-on-3 (tropolone), HL									
Ce <sup>3+</sup>	Gl	25	0.1 KNO <sub>3</sub>	$K_1 = 6.56, K_2 = 5.20, K_3 = 4.36$					91
Er <sup>3+</sup>	Gl	25	0.1 KNO <sub>3</sub>	$K_1 = 7.54, K_2 = 6.37, K_3 = 5.24, K_4 = 3.96$					91
Eu <sup>3+</sup>	Gl	25	0.1 KNO <sub>3</sub>	$K_1 = 7.10, K_2 = 5.71, K_3 = 4.81$					91
Gd <sup>3+</sup>	Gl	25	0.1 KNO <sub>3</sub>	$K_1 = 7.04, K_2 = 5.86, K_3 = 4.82, K_4 = 3.30$					91
Ho <sup>3+</sup>	Gl	25	0.1 KNO <sub>3</sub>	$K_1 = 7.4, K_2 = 6.20, K_3 = 5.20, K_4 = 3.77$					91
La <sup>3+</sup>	Gl	25	0.1 KNO <sub>3</sub>	$K_1 = 6.19, K_2 = 4.93, K_3 = 4.19,$					91
Lu <sup>3+</sup>	Gl	25	0.1 KNO <sub>3</sub>	$K_1 = 7.69, K_2 = 6.64, K_3 = 5.44, K_4 = 3.96$					91
Nd <sup>3+</sup>	Gl	25	0.1 KNO <sub>3</sub>	$K_1 = 6.77, K_2 = 5.44, K_3 = 4.40$					91
Pr <sup>3+</sup>	Gl	25	0.1 KNO <sub>3</sub>	$K_1 = 6.61, K_2 = 5.33, K_3 = 4.45$					91
Sm <sup>3+</sup>	Gl	25	0.1 KNO <sub>3</sub>	$K_1 = 6.91, K_2 = 5.68, K_3 = 4.60$					91
Tb <sup>3+</sup>	Gl	25	0.1 KNO <sub>3</sub>	$K_1 = 7.15, K_2 = 6.03, K_3 = 4.82, K_4 = 3.38$					91
Tm <sup>3+</sup>	Gl	25	0.1 KNO <sub>3</sub>	$K_1 = 7.60, K_2 = 6.39, K_3 = 5.40, K_4 = 3.80$					91
Y <sup>3+</sup>	Gl	25	0.1 KNO <sub>3</sub>	$K_1 = 7.18, K_2 = 6.08, K_3 = 5.01, K_4 = 3.42$					91
Yb <sup>3+</sup>	Gl	25	0.1 KNO <sub>3</sub>	$K_1 = 7.85, K_2 = 6.50, K_3 = 5.48, K_4 = 3.90$					91
C <sub>7</sub> H <sub>6</sub> O <sub>3</sub> , 2-hydroxybenzoic acid (salicylic acid), H <sub>2</sub> L									
Eu <sup>3+</sup>	Gl	25	0.1 (NaCl)	$K_1 = 5.81, K_2 = 5.11, K_3 = 3.23$					92
Gd <sup>3+</sup>	Gl	25	0.1 (NaCl), 99.9% methanol	$K_1 = 6.16, K_2 = 4.88, K_3 = 3.42$					92
Ho <sup>3+</sup>	Gl	25	0.1 (NaCl), 99.9% methanol	$K_1 = 6.27, K_2 = 4.48, K_3 = 3.51$					92
La <sup>3+</sup>	Gl	25	0.1 (NaCl), 99.9% methanol	$K_1 = 5.32, K_2 = 4.28, K_3 = 3.11$					92
Lu <sup>3+</sup>	Gl	25	0.1 (NaCl), 99.9% methanol	$K_1 = 5.82, K_2 = 4.87, K_3 = 3.79$					92
Nd <sup>3+</sup>	Gl	25	0.1 (NaCl), 99.9% methanol	$K_1 = 5.25, K_2 = 4.96, K_3 = 3.16$					92

(Continued.)

Metal	Method	Temp. (°C)	Medium	log of equilibrium constant	Ref.
Pr <sup>3+</sup>	Gl	25	0.1 (NaCl), 99.9% methanol	$K_1 = 5.36, K_2 = 4.75, K_3 = 3.57$	92
Sm <sup>3+</sup>	Gl	25	0.1 (NaCl), 99.9% methanol	$K_1 = 5.75, K_2 = 4.67, K_3 = 3.24$	92
Tb <sup>3+</sup>	Gl	25	0.1 (NaCl), 99.9% methanol	$K_1 = 6.15, K_2 = 4.77, K_3 = 3.42$	92
C <sub>7</sub> H <sub>8</sub> O <sub>2</sub> , 1,2-dihydroxy-4-methylbenzene (4-methylcatechol), H <sub>2</sub> L					
H <sup>+</sup>	Gl	25	0.12 (NaClO <sub>4</sub> ), 50% dioxan	$K_1 = 5.77, K_2 = 4.62$	
Dy <sup>3+</sup>	Gl	25	0.12 (NaClO <sub>4</sub> ), 50% (CH <sub>3</sub> ) <sub>2</sub> SO	$K_1 = 4.40, K_2 = 4.08$	93
			0.12 (NaClO <sub>4</sub> ), 50% dioxan	$K_1 = 5.67, K_2 = 4.48$	93
			0.12 (NaClO <sub>4</sub> ), 50% ethanol	$K_1 = 5.09, K_2 = 3.86$	93
Er <sup>3+</sup>	Gl	25	0.12 (NaClO <sub>4</sub> ), 50% (CH <sub>3</sub> ) <sub>2</sub> SO	$K_1 = 4.60, K_2 = 4.12$	93
			0.12 (NaClO <sub>4</sub> ), 50% dioxan	$K_1 = 5.77, K_2 = 4.62$	93
			0.12 (NaClO <sub>4</sub> ), 50% ethanol	$K_1 = 5.27, K_2 = 4.33$	93
			0.12 (NaClO <sub>4</sub> ), 50% (CH <sub>3</sub> ) <sub>2</sub> SO	$K_1 = 4.13, K_2 = 3.82$	93
Gd <sup>3+</sup>	Gl	25	0.12 (NaClO <sub>4</sub> ), 50% (CH <sub>3</sub> ) <sub>2</sub> SO	$K_1 = 5.28, K_2 = 4.13$	93
			0.12 (NaClO <sub>4</sub> ), 50% dioxan	$K_1 = 4.83, K_2 = 3.73$	93
			0.12 (NaClO <sub>4</sub> ), 50% ethanol	$K_1 = 4.49, K_2 = 4.23$	93
			0.12 (NaClO <sub>4</sub> ), 50% (CH <sub>3</sub> ) <sub>2</sub> SO	$K_1 = 5.76, K_2 = 4.49$	93
Ho <sup>3+</sup>	Gl	25	0.12 (NaClO <sub>4</sub> ), 50% dioxan	$K_1 = 5.15, K_2 = 4.09$	93
			0.12 (NaClO <sub>4</sub> ), 50% ethanol	$K_1 = 3.82, K_2 = 3.50$	93
			0.12 (NaClO <sub>4</sub> ), 50% (CH <sub>3</sub> ) <sub>2</sub> SO	$K_1 = 4.60, K_2 = 3.47$	93
			0.12 (NaClO <sub>4</sub> ), 50% dioxan	$K_1 = 3.95, K_2 = 2.75$	93
La <sup>3+</sup>	Gl	25	0.12 (NaClO <sub>4</sub> ), 50% ethanol	$K_1 = 4.00, K_2 = 3.70$	93
			0.12 (NaClO <sub>4</sub> ), 50% (CH <sub>3</sub> ) <sub>2</sub> SO	$K_1 = 5.09, K_2 = 4.08$	93
			0.12 (NaClO <sub>4</sub> ), 50% dioxan	$K_1 = 4.66, K_2 = 3.45$	93
			0.12 (NaClO <sub>4</sub> ), 50% ethanol	$K_1 = 4.25, K_2 = 3.97$	93
Nd <sup>3+</sup>	Gl	25	0.12 (NaClO <sub>4</sub> ), 50% (CH <sub>3</sub> ) <sub>2</sub> SO	$K_1 = 5.51, K_2 = 4.49$	93
			0.12 (NaClO <sub>4</sub> ), 50% dioxan		
			0.12 (NaClO <sub>4</sub> ), 50% ethanol		
Tb <sup>3+</sup>	Gl	25	0.12 (NaClO <sub>4</sub> ), 50% (CH <sub>3</sub> ) <sub>2</sub> SO		
			0.12 (NaClO <sub>4</sub> ), 50% dioxan		

(Continued.)

Metal	Method	Temp. (°C)	Medium	log of equilibrium constant	Ref.
			0.12 (NaClO <sub>4</sub> ), 50% ethanol	$K_1 = 5.00, K_2 = 3.78$	93
Tm <sup>3+</sup>	Gl	25	0.12 (NaClO <sub>4</sub> ), 50% (CH <sub>3</sub> ) <sub>2</sub> SO	$K_1 = 4.74, K_2 = 4.55$	93
			0.12 (NaClO <sub>4</sub> ), 50% dioxan	$K_1 = 5.80, K_2 = 4.81$	93
			0.12 (NaClO <sub>4</sub> ), 50% ethanol	$K_1 = 5.36, K_2 = 4.50$	93
Yb <sup>3+</sup>	Gl	25	0.12 (NaClO <sub>4</sub> ), 50% (CH <sub>3</sub> ) <sub>2</sub> SO	$K_1 = 4.82, K_2 = 4.59$	93
			0.12 (NaClO <sub>4</sub> ), 50% dioxan	$K_1 = 5.86, K_2 = 4.64$	93
			0.12 (NaClO <sub>4</sub> ), 50% ethanol	$K_1 = 5.49, K_2 = 4.62$	93
C <sub>7</sub> H <sub>10</sub> O <sub>4</sub> , 1,1-cyclopentanedicarboxylic acid, H <sub>2</sub> L					
Dy <sup>3+</sup>	Gl	25	0.1 (KNO <sub>3</sub> )	$K_1 = 4.29, \beta_2 = 6.81$	94
Er <sup>3+</sup>	Gl	25	0.1 (KNO <sub>3</sub> )	$K_1 = 4.24, \beta_2 = 6.76$	94
Eu <sup>3+</sup>	Gl	25	0.1 (KNO <sub>3</sub> )	$K_1 = 4.17, \beta_2 = 6.70$	94
Gd <sup>3+</sup>	Gl	25	0.1 (KNO <sub>3</sub> )	$K_1 = 4.18, \beta_2 = 6.67$	94
Ho <sup>3+</sup>	Gl	25	0.1 (KNO <sub>3</sub> )	$K_1 = 4.25, \beta_2 = 6.74$	94
Lu <sup>3+</sup>	Gl	25	0.1 (KNO <sub>3</sub> )	$K_1 = 4.22, \beta_2 = 6.65$	94
Tb <sup>3+</sup>	Gl	25	0.1 (KNO <sub>3</sub> )	$K_1 = 4.26, \beta_2 = 6.78$	94
Tm <sup>3+</sup>	Gl	25	0.1 (KNO <sub>3</sub> )	$K_1 = 4.25, \beta_2 = 6.82$	94
Yb <sup>3+</sup>	Gl	25	0.1 (KNO <sub>3</sub> )	$K_1 = 4.26, \beta_2 = 6.88$	94
C <sub>7</sub> H <sub>12</sub> O <sub>3</sub> , 3-methyl ethylacetoacetate. HL					
H <sup>+</sup>	Gl	30	0.1, 75% acetone	$K_1 = 12.80$	95
Dy <sup>3+</sup>	Gl	30	0.1, 75% acetone	$K_1 = 8.36$	95
Er <sup>3+</sup>	Gl	30	0.1, 75% acetone	$K_1 = 8.62$	95
Eu <sup>3+</sup>	Gl	30	0.1, 75% acetone	$K_1 = 8.22$	95
Gd <sup>3+</sup>	Gl	30	0.1, 75% acetone	$K_1 = 8.08$	95
La <sup>3+</sup>	Gl	30	0.1, 75% acetone	$K_1 = 7.07$	95
Nd <sup>3+</sup>	Gl	30	0.1, 75% acetone	$K_1 = 7.84$	95
Pr <sup>3+</sup>	Gl	30	0.1, 75% acetone	$K_1 = 7.75$	95
Sm <sup>3+</sup>	Gl	30	0.1, 75% acetone	$K_1 = 8.05$	95
Y <sup>3+</sup>	Gl	30	0.1, 75% acetone	$K_1 = 8.20$	95
Yb <sup>3+</sup>	Gl	30	0.1, 75% acetone	$K_1 = 8.66$	95
C <sub>7</sub> H <sub>4</sub> O <sub>7</sub> N <sub>2</sub> , 2-hydroxy-3,5-dinitrobenzoic acid (3,5-dinitrosalicylic acid), H <sub>2</sub> L					
Ce <sup>3+</sup>	Gl	23–25	0.2 (LiCl)	$K_1 = 4.83 \pm 0.07$	96
Dy <sup>3+</sup>	Gl	23–25	0.2 (LiCl)	$K_1 = 5.48 \pm 0.03$	96
Er <sup>3+</sup>	Gl	23–25	0.2 (LiCl)	$K_1 = 5.43 \pm 0.05$	96
Eu <sup>3+</sup>	Gl	23–25	0.2 (LiCl)	$K_1 = 5.40 \pm 0.04$	96
Gd <sup>3+</sup>	Gl	23–25	0.2 (LiCl)	$K_1 = 5.27 \pm 0.08$	96
Ho <sup>3+</sup>	Gl	23–25	0.2 (LiCl)	$K_1 = 5.38 \pm 0.02$	96
La <sup>3+</sup>	Gl	23–25	0.2 (LiCl)	$K_1 = 4.51 \pm 0.04$	96
Lu <sup>3+</sup>	Gl	23–25	0.2 (LiCl)	$K_1 = 5.51 \pm 0.04$	96
Nd <sup>3+</sup>	Gl	23–25	0.2 (LiCl)	$K_1 = 4.90 \pm 0.06$	96
Pr <sup>3+</sup>	Gl	23–25	0.2 (LiCl)	$K_1 = 4.95 \pm 0.04$	96
Sm <sup>3+</sup>	Gl	23–25	0.2 (LiCl)	$K_1 = 5.14 \pm 0.08$	96
Tb <sup>3+</sup>	Gl	23–25	0.2 (LiCl)	$K_1 = 5.46 \pm 0.03$	96

(Continued.)

Metal	Method	Temp. (°C)	Medium	log of equilibrium constant	Ref.
Tm <sup>3+</sup>	Gl	23–25	0.2 (LiCl)	$K_1 = 5.61 \pm 0.03$	96
Y <sup>3+</sup>	Gl	23–25	0.2 (LiCl)	$K_1 = 5.41$	96
Yb	Gl	23–25	0.2 (LiCl)	$K_1 = 5.60$	96
C <sub>7</sub> H <sub>6</sub> O <sub>5</sub> S, 2-carboxybenzenesulphonic acid (2-sulphobenzoic acid), H <sub>2</sub> L					
H <sup>+</sup>	Gl	25	0.2 (KCl)	$K_1 = 3.78 \pm 0.04, K_2 = 1.55 \pm 0.04$	97
Ce <sup>3+</sup>	Gl	25	0.2 (KCl)	$K_1 = 2.1$	97
La <sup>3+</sup>	Gl	25	0.2 (KCl)	$K_1 = 2.4$	97
Nd <sup>3+</sup>	Gl	25	0.2 (KCl)	$K_1 = 2.4$	97
Pr <sup>3+</sup>	Gl	25	0.2 (KCl)	$K_1 = 2.0$	97
Sm <sup>3+</sup>	Gl	25	0.2 (KCl)	$K_1 = 2.5$	97
C <sub>7</sub> H <sub>6</sub> O <sub>6</sub> S, 5-sulphosalicylic acid					
Ce <sup>3+</sup>	Gl	20	1.0 (Na,H)ClO <sub>4</sub>	$K_1 = 6.03, K_2 = 4.88$	98
Dy <sup>3+</sup>	Gl	20	1.0 (Na,H)ClO <sub>4</sub>	$K_1 = 7.15, K_2 = 5.86$	98
Er <sup>3+</sup>	Gl	20	1.0 (Na,H)ClO <sub>4</sub>	$K_1 = 7.20, K_2 = 5.82$	98
Eu <sup>3+</sup>	Gl	20	1.0 (Na,H)ClO <sub>4</sub>	$K_1 = 6.79, K_2 = 5.67$	98
Gd <sup>3+</sup>	Gl	20	1.0 (Na,H)ClO <sub>4</sub>	$K_1 = 6.93, K_2 = 5.90$	98
Ho <sup>3+</sup>	Gl	20	1.0 (Na,H)ClO <sub>4</sub>	$K_1 = 7.18, K_2 = 5.80$	98
La <sup>3+</sup>	Gl	20	1.0 (Na,H)ClO <sub>4</sub>	$K_1 = 5.92, K_2 = 4.81$	98
Lu <sup>3+</sup>	Gl	20	1.0 (Na,H)ClO <sub>4</sub>	$K_1 = 7.33, K_2 = 5.97$	98
Nd <sup>3+</sup>	Gl	20	1.0 (Na,H)ClO <sub>4</sub>	$K_1 = 6.35, K_2 = 5.50$	98
Pr <sup>3+</sup>	Gl	20	1.0 (Na,H)ClO <sub>4</sub>	$K_1 = 6.23, K_2 = 5.01$	98
Sm <sup>3+</sup>	Gl	20	1.0 (Na,H)ClO <sub>4</sub>	$K_1 = 6.77, K_2 = 5.79$	98
Tb <sup>3+</sup>	Gl	20	1.0 (Na,H)ClO <sub>4</sub>	$K_1 = 6.95, K_2 = 5.91$	98
Tm <sup>3+</sup>	Gl	20	1.0 (Na,H)ClO <sub>4</sub>	$K_1 = 7.28, K_2 = 5.87$	98
Yb <sup>3+</sup>	Gl	20	1.0 (Na,H)ClO <sub>4</sub>	$K_1 = 7.32, K_2 = 8.6$	98
C <sub>7</sub> H <sub>7</sub> O <sub>2</sub> N, 2-aminobenzoic acid (anthranilic acid), HL					
H <sup>+</sup>	Gl	25	0.1 (NaClO <sub>4</sub> )	$K_1 = 4.79, K_2 = 1.97$	99
Er <sup>3+</sup>	Gl	25	0.1 (NaCl), methanol	$K_1 = 7.35, K_2 = 5.97, K_3 = 3.69, K_4 = 2.38$	100
Eu <sup>3+</sup>	Gl	25	0.1 (NaCl), methanol	$K_1 = 7.01, K_2 = 5.80, K_3 = 3.26, K_4 = 2.52$	100
Gd <sup>3+</sup>	Gl	25	0.1 (NaCl), methanol	$K_1 = 7.15, K_2 = 5.84, K_3 = 3.35, K_4 = 2.65$	100
Ho <sup>3+</sup>	Gl	25	0.1 (NaCl), methanol	$K_1 = 7.35, K_2 = 5.75, K_3 = 3.56, K_4 = 2.40$	100
La <sup>3+</sup>	Gl	25	0.1 (NaCl), methanol	$K_1 = 6.05, K_2 = 4.82, K_3 = 3.04, K_4 = 2.64$	100
Lu <sup>3+</sup>	Gl	25	0.1 (NaCl), methanol	$K_1 = 7.29, K_2 = 6.28, K_3 = 3.83, K_4 = 2.49$	100
Nd <sup>3+</sup>	Gl	25	0.1 (NaCl), methanol	$K_1 = 6.58, K_2 = 5.55, K_3 = 3.26, K_4 = 2.50$	100
Pr <sup>3+</sup>	Gl	25	0.1 (NaCl), methanol	$K_1 = 6.48, K_2 = 5.60, K_3 = 3.40, K_4 = 2.46$	100
Sm <sup>3+</sup>	Gl	25	0.1 (NaCl), methanol	$K_1 = 6.94, K_2 = 5.42, K_3 = 3.26, K_4 = 2.55$	100
Tb <sup>3+</sup>	Gl	25	0.1 (NaCl), methanol	$K_1 = 7.25, K_2 = 5.85, K_3 = 3.06, K_4 = 2.82$	100
Yb <sup>3+</sup>	Gl	25	0.1 (NaCl), methanol	$K_1 = 7.22, K_2 = 6.17, K_3 = 3.64, K_4 = 2.94$	100

(Continued.)					
Metal	Method	Temp. (°C)	Medium	log of equilibrium constant	Ref.
C <sub>7</sub> H <sub>7</sub> O <sub>3</sub> N, 2-hydroxybenzohydroxamic acid (salicylohydroxamic acid), H <sub>2</sub> L					
Dy <sup>3+</sup>	Gl	25	0.1 (NaClO <sub>4</sub> ), 75% acetone	$K(\text{Dy}^{3+} + \text{HL}^- = \text{DyHL}^{2+}) = 7.72$ $K[\text{DyHL}^{2+} + \text{HL}^- = \text{Dy}(\text{HL})_2^+] = 7.00$ $K[\text{Dy}(\text{HL})_2^+ + \text{HL}^- = \text{Dy}(\text{HL})_3] = 5.06$	102
Er <sup>3+</sup>	Gl	25	0.1 (NaClO <sub>4</sub> ), 75% acetone	$K(\text{Er}^{3+} + \text{HL}^- = \text{ErHL}^{2+}) = 7.82$ $K[\text{ErHL}^{2+} + \text{HL}^- = \text{Er}(\text{HL})_2^+] = 7.03$ $K[\text{Er}(\text{HL})_2^+ + \text{HL}^- = \text{Er}(\text{HL})_3] = 5.10$	102
Eu <sup>3+</sup>	Gl	25	0.1 (NaClO <sub>4</sub> ), 75% acetone	$K(\text{Eu}^{3+} + \text{HL}^- = \text{EuHL}^{2+}) = 7.40$ $K[\text{EuHL}^{2+} + \text{HL}^- = \text{Eu}(\text{HL})_2^+] = 6.84$ $K[\text{Eu}(\text{HL})_2^+ + \text{HL}^- = \text{Eu}(\text{HL})_3] = 5.04$	102
Gd <sup>3+</sup>	Gl	25	0.1 (NaClO <sub>4</sub> ), 75% acetone	$K(\text{Gd}^{3+} + \text{HL}^- = \text{GdHL}^{2+}) = 7.35$ $K[\text{GdHL}^{2+} + \text{HL}^- = \text{Gd}(\text{HL})_2^+] = 6.80$ $K[\text{Gd}(\text{HL})_2^+ + \text{HL}^- = \text{Gd}(\text{HL})_3] = 4.60$	102
La <sup>3+</sup>	Gl	25	0.1 (NaClO <sub>4</sub> ), 75% acetone	$K(\text{La}^{3+} + \text{HL}^- = \text{LaHL}^{2+}) = 6.30$ $K[\text{LaHL}^{2+} + \text{HL}^- = \text{La}(\text{HL})_2^+] = 5.96$ $K[\text{La}(\text{HL})_2^+ + \text{HL}^- = \text{La}(\text{HL})_3] = 4.90$	102
Nd <sup>3+</sup>	Gl	25	0.1 (NaClO <sub>4</sub> ), 75% acetone	$K(\text{Nd}^{3+} + \text{HL}^- = \text{NdHL}^{2+}) = 7.03$ $K[\text{NdHL}^{2+} + \text{HL}^- = \text{Nd}(\text{HL})_2^+] = 6.64$ $K[\text{Nd}(\text{HL})_2^+ + \text{HL}^- = \text{Nd}(\text{HL})_3] = 5.10$	102
Pr <sup>3+</sup>	Gl	25	0.1 (NaClO <sub>4</sub> ), 75% acetone	$K(\text{Pr}^{3+} + \text{HL}^- = \text{PrHL}^{2+}) = 6.94$ $K[\text{PrHL}^{2+} + \text{HL}^- = \text{Pr}(\text{HL})_2^+] = 6.50$ $K[\text{Pr}(\text{HL})_2^+ + \text{HL}^- = \text{Pr}(\text{HL})_3] = 4.98$	102
Sm <sup>3+</sup>	Gl	25	0.1 (NaClO <sub>4</sub> ), 75% acetone	$K(\text{Sm}^{3+} + \text{HL}^- = \text{SmHL}^{2+}) = 7.20$ $K[\text{SmHL}^{2+} + \text{HL}^- = \text{Sm}(\text{HL})_2^+] = 6.77$ $K[\text{Sm}(\text{HL})_2^+ + \text{HL}^- = \text{Sm}(\text{HL})_3] = 5.01$	102
Y <sup>3+</sup>	Gl	25	0.1 (NaClO <sub>4</sub> ), 75% acetone	$K(\text{Y}^{3+} + \text{HL}^- = \text{YHL}^{2+}) = 7.24$ $K[\text{YHL}^{2+} + \text{HL}^- = \text{Y}(\text{HL})_2^+] = 6.50$	102
Yb <sup>3+</sup>	Gl	25	0.1 (NaClO <sub>4</sub> ), 75% acetone	$K(\text{Yb}^{3+} + \text{HL}^- = \text{YbHL}^{2+}) = 8.13$ $K[\text{YbHL}^{2+} + \text{HL}^- = \text{Yb}(\text{HL})_2^+] = 7.25$	102
C <sub>7</sub> H <sub>12</sub> O <sub>3</sub> N <sub>2</sub> , L-prolylglycine, HL					
H <sup>+</sup>	Gl	25	0.1 (KCl)	$K_1 = 8.97, K_2 = 3.28$	90
Eu <sup>3+</sup>	Gl	25	0.1 (KCl)	$K_1 = 3.10$	90
Gd <sup>3+</sup>	Gl	25	0.1 (KCl)	$K_1 = 3.00$	90
Ho <sup>3+</sup>	Gl	25	0.1 (KCl)	$K_1 = 3.25$	90
Nd <sup>3+</sup>	Gl	25	0.1 (KCl)	$K_1 = 2.75$	90
Yb <sup>3+</sup>	Gl	25	0.1 (KCl)	$K_1 = 3.50$	90
C <sub>8</sub> H <sub>14</sub> O <sub>3</sub> , 3-ethylethylacetoacetate, HL					
H <sup>+</sup>	Gl	30	0.1, 75% acetone	$K_1 = 13.15$	95
Dy <sup>3+</sup>	Gl	30	0.1, 75% acetone	$K_1 = 9.10$	95
Er <sup>3+</sup>	Gl	30	0.1, 75% acetone	$K_1 = 9.17$	95
Eu <sup>3+</sup>	Gl	30	0.1, 75% acetone	$K_1 = 9.04$	95
Gd <sup>3+</sup>	Gl	30	0.1, 75% acetone	$K_1 = 8.86$	95
La <sup>3+</sup>	Gl	30	0.1, 75% acetone	$K_1 = 7.58$	95
Nd <sup>3+</sup>	Gl	30	0.1, 75% acetone	$K_1 = 8.43$	95
Pr <sup>3+</sup>	Gl	30	0.1, 75% acetone	$K_1 = 8.22$	95
Sm <sup>3+</sup>	Gl	30	0.1, 75% acetone	$K_1 = 8.79$	95
Y <sup>3+</sup>	Gl	30	0.1, 75% acetone	$K_1 = 9.03$	95
Yb <sup>3+</sup>	Gl	30	0.1, 75% acetone	$K_1 = 9.23$	95



<i>(Continued.)</i>					
Metal	Method	Temp. (°C)	Medium	log of equilibrium constant	Ref.
$C_8H_5O_6N_5$ , <i>N</i> -(4'-Hydroxy-2',6'-dioxo-1',3'-diazin-5'-yl)-5-imino(perhydro-1,3-diazine-2,4,6-trione) (purpuric acid) (murexide = $L \cdot NH_3$ ), $H_3L$					
$Dy^{3+}$	Sp	12	0.1 (NaClO <sub>4</sub> ), 50% ethanol	$K(Dy^{3+} + H_2L^- = DyH_2L^{2+}) = 4.52$	103
$Gd^{3+}$	Sp	12	0.1 (NaClO <sub>4</sub> ), 50% ethanol	$K(Gd^{3+} + H_2L^- = GdH_2L^{2+}) = 4.91$	103
$Ho^{3+}$	Sp	12	0.1 (NaClO <sub>4</sub> ), 50% ethanol	$K(Ho^{3+} + H_2L^- = HoH_2L^{2+}) = 4.43$	103
$Tb^{3+}$	Sp	12	0.1 (NaClO <sub>4</sub> ), 50% ethanol	$K(Tb^{3+} + H_2L^- = TbH_2L^{2+}) = 4.68$	103
$C_8H_8O_2N_2$ , phenylglyoxime, $H_2L$					
$H^+$	Gl	20	0.1 NaClO <sub>4</sub> , 50% v/v dioxan	$K_1 = 12.70, K_2 = 11.72$	
$Ce^{3+}$	Gl	20	0.1 NaClO <sub>4</sub> , 50% v/v dioxan	$K_1 = 6.46, K_2 = 5.64$	54
$Dy^{3+}$	Gl	20	0.1 NaClO <sub>4</sub> , 50% v/v dioxan	$K_1 = 7.23, K_2 = 6.39$	54
$Er^{3+}$	Gl	20	0.1 NaClO <sub>4</sub> , 50% v/v dioxan	$K_1 = 7.48, K_2 = 6.54$	54
$Eu^{3+}$	Gl	20	0.1 NaClO <sub>4</sub> , 50% v/v dioxan	$K_1 = 7.11, K_2 = 6.19$	54
$Gd^{3+}$	Gl	20	0.1 NaClO <sub>4</sub> , 50% v/v dioxan	$K_1 = 7.01, K_2 = 6.10$	54
$Ho^{3+}$	Gl	20	0.1 NaClO <sub>4</sub> , 50% v/v dioxan	$K_1 = 7.36, K_2 = 6.51$	54
$La^{3+}$	Gl	20	0.1 NaClO <sub>4</sub> , 50% v/v dioxan	$K_1 = 6.38, K_2 = 5.52$	54
$Lu^{3+}$	Gl	20	0.1 NaClO <sub>4</sub> , 50% v/v dioxan	$K_1 = 7.43, K_2 = 6.27$	54
$Nd^{3+}$	Gl	20	0.1 NaClO <sub>4</sub> , 50% v/v dioxan	$K_1 = 6.60, K_2 = 5.88$	54
$Pr^{3+}$	Gl	20	0.1 NaClO <sub>4</sub> , 50% v/v dioxan	$K_1 = 6.55, K_2 = 5.73$	54
$Sm^{3+}$	Gl	20	0.1 NaClO <sub>4</sub> , 50% v/v dioxan	$K_1 = 6.88, K_2 = 6.06$	54
$Tb^{3+}$	Gl	20	0.1 NaClO <sub>4</sub> , 50% v/v dioxan	$K_1 = 7.12, K_2 = 6.23$	54
$Tm^{3+}$	Gl	20	0.1 NaClO <sub>4</sub> , 50% v/v dioxan	$K_1 = 7.55, K_2 = 6.52$	54
$Y^{3+}$	Gl	20	0.1 NaClO <sub>4</sub> , 50% v/v dioxan	$K_1 = 6.82, K_2 = 5.97$	54
$Yb^{3+}$	Gl	20	0.1 NaClO <sub>4</sub> , 50% v/v dioxan	$K_1 = 7.67, K_2 = 6.42$	54
$C_8H_8O_2Se$ , 1-(2'-selenoyl)butane-1,3-dione (selenoylacetone), HL					
$Eu^{3+}$	Dis	25	0.1 (KNO <sub>3</sub> )	$K_1 = 6.24, \beta_2 = 12.29, \beta_3 = 17.88$	105
$Nd^{3+}$	Dis	25	0.1	$K_1 = 5.62, K_2 = 5.42, K_3 = 4.48$	104
$C_8H_9O_4N$ , dehydroacetic acid oxime, $H_2L$					
$Ce^{3+}$	Gl	35	0.01 NaClO <sub>4</sub> , 50% dioxan	$[Ce^{3+} + nHL^- = Ce(HL)_n^{(3-n)+}]$ , $K(n=1) = 3.95, K(n=2) = 7.08$	106

(Continued.)					
Metal	Method	Temp. (°C)	Medium	log of equilibrium constant	Ref.
Dy <sup>3+</sup>	Gl	35	0.01 NaClO <sub>4</sub> , 50% dioxan	[Dy <sup>3+</sup> + nHL <sup>-</sup> = Dy(HL) <sub>n</sub> <sup>(3-n)+</sup> ], K(n = 1) = 4.57, K(n = 2) = 8.35	106
Er <sup>3+</sup>	Gl	35	0.01 NaClO <sub>4</sub> , 50% dioxan	[Er <sup>3+</sup> + nHL <sup>-</sup> = Er(HL) <sub>n</sub> <sup>(3-n)+</sup> ], K(n = 1) = 4.83, K(n = 2) = 8.55	106
Eu <sup>3+</sup>	Gl	35	0.01 NaClO <sub>4</sub> , 50% dioxan	[Eu <sup>3+</sup> + nHL <sup>-</sup> = Eu(HL) <sub>n</sub> <sup>(3-n)+</sup> ] K(n = 1) = 4.52, K(n = 2) = 8.19	106
Gd <sup>3+</sup>	Gl	35	0.01 NaClO <sub>4</sub> , 50% dioxan	[Gd <sup>3+</sup> + nHL <sup>-</sup> = Gd(HL) <sub>n</sub> <sup>(3-n)+</sup> ] K(n = 1) = 4.37, K(n = 2) = 7.86	106
Ho <sup>3+</sup>	Gl	35	0.01 NaClO <sub>4</sub> , 50% dioxan	[Ho <sup>3+</sup> + nHL <sup>-</sup> = Ho(HL) <sub>n</sub> <sup>(3-n)+</sup> ] K(n = 1) = 4.69, K(n = 2) = 8.52	106
La <sup>3+</sup>	Gl	35	0.01 NaClO <sub>4</sub> , 50% dioxan	[La <sup>3+</sup> + nHL <sup>-</sup> = La(HL) <sub>n</sub> <sup>(3-n)+</sup> ] K(n = 1) = 3.85, K(n = 2) = 6.88	106
Lu <sup>3+</sup>	Gl	35	0.01 NaClO <sub>4</sub> , 50% dioxan	[Lu <sup>3+</sup> + nHL <sup>-</sup> = Lu(HL) <sub>n</sub> <sup>(3-n)+</sup> ] K(n = 1) = 4.90, K(n = 2) = 8.31	106
Nd <sup>3+</sup>	Gl	35	0.01 NaClO <sub>4</sub> , 50% dioxan	[Nd <sup>3+</sup> + nHL <sup>-</sup> = Nd(HL) <sub>n</sub> <sup>(3-n)+</sup> ] K(n = 1) = 4.18, K(n = 2) = 7.57	106
Pr <sup>3+</sup>	Gl	35	0.01 NaClO <sub>4</sub> , 50% dioxan	[Pr <sup>3+</sup> + nHL <sup>-</sup> = Pr(HL) <sub>n</sub> <sup>(3-n)+</sup> ] K(n = 1) = 4.08, K(n = 2) = 7.36	106
Sm <sup>3+</sup>	Gl	35	0.01 NaClO <sub>4</sub> , 50% dioxan	[Sm <sup>3+</sup> + nHL <sup>-</sup> = Sm(HL) <sub>n</sub> <sup>(3-n)+</sup> ] K(n = 1) = 4.40, K(n = 2) = 7.97	106
Tb <sup>3+</sup>	Gl	35	0.01 NaClO <sub>4</sub> , 50% dioxan	[Tb <sup>3+</sup> + nHL <sup>-</sup> = Tb(HL) <sub>n</sub> <sup>(3-n)+</sup> ] K(n = 1) = 4.45, K(n = 2) = 8.08	106
Tm <sup>3+</sup>	Gl	35	0.01 NaClO <sub>4</sub> , 50% dioxan	[Tm <sup>3+</sup> + nHL <sup>-</sup> = Tm(HL) <sub>n</sub> <sup>(3-n)+</sup> ] K(n = 1) = 4.92, K(n = 2) = 8.52	106
Y <sup>3+</sup>	Gl	35	0.01 NaClO <sub>4</sub> , 50% dioxan	[Y <sup>3+</sup> + nHL <sup>-</sup> = Y(HL) <sub>n</sub> <sup>(3-n)+</sup> ] K(n = 1) = 4.16, K(n = 2) = 7.38	106
Yb <sup>3+</sup>	Gl	35	0.01 NaClO <sub>4</sub> , 50% dioxan	[Yb <sup>3+</sup> + nHL <sup>-</sup> = Yb(HL) <sub>n</sub> <sup>(3-n)+</sup> ] K(n = 1) = 5.03, K(n = 2) = 8.53	106
C <sub>8</sub> H <sub>12</sub> O <sub>8</sub> N <sub>2</sub> , ethylenediamine- <i>N,N'</i> -dimalonic acid					
Ce <sup>3+</sup>	Gl	25	0.1 KNO <sub>3</sub>	K <sub>1</sub> = 11.90	107
Dy <sup>3+</sup>	Gl	25	0.1 KNO <sub>3</sub>	K <sub>1</sub> = 11.28	107
Er <sup>3+</sup>	Gl	25	0.1 KNO <sub>3</sub>	K <sub>1</sub> = 11.29	107
Eu <sup>3+</sup>	Pol	25	0.1 KNO <sub>3</sub>	K <sub>1</sub> = 11.04	107
Gd <sup>3+</sup>	Pol	25	0.1 KNO <sub>3</sub>	K <sub>1</sub> = 10.78	107
Ho <sup>3+</sup>	Gl	25	0.1 KNO <sub>3</sub>	K <sub>1</sub> = 11.29	107
La <sup>3+</sup>	Gl	25	0.1 KNO <sub>3</sub>	K <sub>1</sub> = 10.33	107
Lu <sup>3+</sup>	Gl	25	0.1 KNO <sub>3</sub>	K <sub>1</sub> = 11.39	107
Nd <sup>3+</sup>	Pol	25	0.1 KNO <sub>3</sub>	K <sub>1</sub> = 10.46	107
Pr <sup>3+</sup>	Pol	25	0.1 KNO <sub>3</sub>	K <sub>1</sub> = 10.50	107
Sm <sup>3+</sup>	Pol	25	0.1 KNO <sub>3</sub>	K <sub>1</sub> = 10.97	107
Tb <sup>3+</sup>	Gl	25	0.1 KNO <sub>3</sub>	K <sub>1</sub> = 11.44	107
Tm <sup>3+</sup>	Pol	25	0.1 KNO <sub>3</sub>	K <sub>1</sub> = 11.32	107
Y <sup>3+</sup>	Pol	25	0.1 KNO <sub>3</sub>	K <sub>1</sub> = 10.47	107
Yb <sup>3+</sup>	Gl	25	0.1 KNO <sub>3</sub>	K <sub>1</sub> = 11.42	107
C <sub>8</sub> H <sub>16</sub> O <sub>3</sub> N <sub>2</sub> , glycyl-DL-leucine, HL					
Eu <sup>3+</sup>	Gl	25	0.1 (KCl)	K <sub>1</sub> = 2.45	65
Gd <sup>3+</sup>	Gl	25	0.1 (KCl)	K <sub>1</sub> = 2.30	65

(Continued.)					
Metal	Method	Temp. (°C)	Medium	log of equilibrium constant	Ref.
Ho <sup>3+</sup>	Gl	25	0.1 (KCl)	$K_1 = 2.60$	65
Nd <sup>3+</sup>	Gl	25	0.1 (KCl)	$K_1 = 2.40$	65
Yb <sup>3+</sup>	Gl	25	0.1 (KCl)	$K_1 = 2.85$	65
C <sub>8</sub> H <sub>16</sub> O <sub>3</sub> N <sub>2</sub> , DL-leucylglycine					
H <sup>+</sup>	Gl	25	0.1 KCl	$K_1 = 8.07, K_2 = 3.28$	65
Eu <sup>3+</sup>	Gl	25	0.1 KCl	$K_1 = 2.45$	65
Gd <sup>3+</sup>	Gl	25	0.1 KCl	$K_1 = 2.25$	65
Ho <sup>3+</sup>	Gl	25	0.1 KCl	$K_1 = 2.40$	65
Nd <sup>3+</sup>	Gl	25	0.1 KCl	$K_1 = 1.85$	65
Yb <sup>3+</sup>	Gl	25	0.1 KCl	$K_1 = 2.60$	65
C <sub>8</sub> H <sub>19</sub> O <sub>4</sub> P, phosphoric acid <i>O, O</i> -dibutylester (dibutylphosphoric acid), HL					
Ce <sup>3+</sup>	Kin	25	?	$K_1 = 2.12 \pm 0.01$	108
Dy <sup>3+</sup>	Kin	25	?	$K_1 = 2.97 \pm 0.01$	108
La <sup>3+</sup>	Kin	25	→ 0	$K_1 = 2.02$	109
Lu <sup>3+</sup>	Kin	25	?	$K_1 = 3.55 \pm 0.03$	108
Nd <sup>3+</sup>	Kin	25	→ 0	$K_1 = 2.20$	109
Pm <sup>3+</sup>	Kin	25	?	$K_1 = 2.40 \pm 0.03$	108
Tm <sup>3+</sup>	Kin	25	?	$K_1 = 3.29 \pm 0.01$	108
Yb <sup>3+</sup>	Kin	25	→ 0	$K_1 = 3.49$	109
C <sub>8</sub> H <sub>18</sub> O <sub>10</sub> N <sub>2</sub> P <sub>2</sub> , ethylenedinitrilo- <i>N, N</i> -bis(methylphosphonic acid)- <i>N', N'</i> -diacetic acid, H <sub>6</sub> L					
Ce <sup>3+</sup>	Ix	20	0.1 (NH <sub>4</sub> <sup>+</sup> )	$K_1 = 16.70 \pm 0.04$ $K(\text{Ce}^{3+} + \text{H}_n\text{L}^{(6-n)-} = \text{CeH}_n\text{L}^{(3-n)-})$ $K(n=1) = 11.51 \pm 0.05,$ $K(n=2) = 8.66 \pm 0.06$	110
Y <sup>3+</sup>	Ix	20	0.1 (NH <sub>4</sub> <sup>+</sup> )	$K_1 = 18.82 \pm 0.05$ $K(\text{Y}^{3+} + \text{H}_n\text{L}^{(6-n)-} = \text{YH}_n\text{L}^{(3-n)-})$ $K(n=1) = 13.80 \pm 0.05,$ $K(n=2) = 11.92 \pm 0.07$	110
C <sub>8</sub> H <sub>22</sub> O <sub>6</sub> N <sub>2</sub> P <sub>2</sub> , 2,2'-(ethylenediimino)bis(isopropylphosphoric acid)					
Ce <sup>3+</sup>	Tp	25	0.1	$K_1 = 17.20$	111
Pm <sup>3+</sup>	Tp	25	0.1	$K_1 = 17.23$	111
C <sub>8</sub> H <sub>24</sub> O <sub>12</sub> N <sub>2</sub> P <sub>4</sub> S, thiobis(ethylene nitrilo)tetra(methyl phosphonic acid)					
Ce <sup>3+</sup>	Iex	20	0.1 KCl	$K_1 = 12.07$	112
Y <sup>3+</sup>	Iex	20	0.1 KCl	$K_1 = 13.01$	112
C <sub>9</sub> H <sub>10</sub> O <sub>3</sub> , 2-hydroxy-2-phenylpropanoic acid					
Pm <sup>3+</sup>	Iex, pH	20	0.2 NaClO <sub>4</sub>	$K_1 = 2.34, \beta_2 = 4.06, \beta_3 = 5.08$	113
Pr <sup>3+</sup>	Iex, pH	20	0.2 NaClO <sub>4</sub>	$K_1 = 2.45, \beta_2 = 4.20, \beta_3 = 5.11$	113
C <sub>9</sub> H <sub>6</sub> O <sub>3</sub> N <sub>2</sub> , 5-nitro-8-hydroxyquinoline					
Ce <sup>3+</sup>	Gl	25	0.1 NaClO <sub>4</sub> , 60% dioxan	$\beta_3 = 16.95$	114
C <sub>9</sub> H <sub>7</sub> ON, 8-hydroxyquinoline					
Dy <sup>3+</sup>	Gl	30	0.3 NaClO <sub>4</sub> , 50% dioxan	$K_1 = 9.20, K_2 = 8.31$	115
Er <sup>3+</sup>	Gl	30	0.3 NaClO <sub>4</sub> , 50% dioxan	$K_1 = 9.39, K_2 = 8.59$	115
Gd <sup>3+</sup>	Gl	30	0.3 NaClO <sub>4</sub> , 50% dioxan	$K_1 = 9.03, K_2 = 8.18$	115
Ho <sup>3+</sup>	Gl	30	0.3 NaClO <sub>4</sub> , 50% dioxan	$K_1 = 9.24, K_2 = 8.51$	115

(Continued.)

Metal	Method	Temp. (°C)	Medium	log of equilibrium constant	Ref.
La <sup>3+</sup>	Gl	30	0.3 NaClO <sub>4</sub> , 50% dioxan	$K_1 = 8.48, K_2 = 7.73$	115
Lu <sup>3+</sup>	Gl	30	0.3 NaClO <sub>4</sub> , 50% dioxan	$K_1 = 9.79, K_2 = 8.61$	115
Nd <sup>3+</sup>	Gl	30	0.3 NaClO <sub>4</sub> , 50% dioxan	$K_1 = 8.88, K_2 = 8.25$	115
Pm <sup>3+</sup>	Dis	?	→ 0, 50% dioxan	$K_1 = 6.91, \beta_2 = 13.25, \beta_3 = 19.08$	115
Pr <sup>3+</sup>	Gl	30	0.3 NaClO <sub>4</sub> , 50% dioxan	$K_1 = 8.75, K_2 = 8.05$	115
Sm <sup>3+</sup>	Gl	30	0.3 NaClO <sub>4</sub> , 50% dioxan	$K_1 = 9.05, K_2 = 8.26$	115
Y <sup>3+</sup>	Gl	30	0.3 NaClO <sub>4</sub> , 50% dioxan	$K_1 = 9.09, K_2 = 8.15$	115
Yb <sup>3+</sup>	Gl	30	0.3 NaClO <sub>4</sub> , 50% dioxan	$K_1 = 9.67, K_2 = 8.65$	115
C <sub>9</sub> H <sub>7</sub> O <sub>2</sub> N, 8-hydroxyquinoline <i>N</i> -oxide, HL					
H <sup>+</sup>	Gl	30	0.3 NaClO <sub>4</sub> , 50% dioxan	$K_1 = 10.30 \pm 0.02$	115
Ce <sup>3+</sup>	Gl	30	0.3 NaClO <sub>4</sub> , 50% dioxan	$K_1 = 6.76 \pm 0.03$	115
Dy <sup>3+</sup>	Gl	30	0.3 NaClO <sub>4</sub> , 50% dioxan	$K_1 = 7.08 \pm 0.05$	115
Er <sup>3+</sup>	Gl	30	0.3 NaClO <sub>4</sub> , 50% dioxan	$K_1 = 7.25 \pm 0.02$	115
Gd <sup>3+</sup>	Gl	30	0.3 NaClO <sub>4</sub> , 50% dioxan	$K_1 = 7.10 \pm 0.03$	115
Ho <sup>3+</sup>	Gl	30	0.3 NaClO <sub>4</sub> , 50% dioxan	$K_1 = 7.12 \pm 0.04$	115
La <sup>3+</sup>	Gl	30	0.3 NaClO <sub>4</sub> , 50% dioxan	$K_1 = 6.68 \pm 0.04$	115
Lu <sup>3+</sup>	Gl	30	0.3 NaClO <sub>4</sub> , 50% dioxan	$K_1 = 7.70 \pm 0.03$	115
Nd <sup>3+</sup>	Gl	30	0.3 NaClO <sub>4</sub> , 50% dioxan	$K_1 = 6.96 \pm 0.03$	115
Pr <sup>3+</sup>	Gl	30	0.3 NaClO <sub>4</sub> , 50% dioxan	$K_1 = 6.80 \pm 0.05$	115
Sm <sup>3+</sup>	Gl	30	0.3 NaClO <sub>4</sub> , 50% dioxan	$K_1 = 7.12 \pm 0.04$	115
Tm <sup>3+</sup>	Gl	30	0.3 NaClO <sub>4</sub> , 50% dioxan	$K_1 = 7.40 \pm 0.02$	115
Y <sup>3+</sup>	Gl	30	0.3 NaClO <sub>4</sub> , 50% dioxan	$K_1 = 7.21$	115
Yb <sup>3+</sup>	Gl	30	0.3 NaClO <sub>4</sub> , 50% dioxan	$K_1 = 7.65$	115
C <sub>9</sub> H <sub>11</sub> O <sub>2</sub> N, 3-phenylalanine, HL					
Er <sup>3+</sup>	Gl	25	0.1 (KCl)	$K_1 = 4.35, K_2 = 3.9$	117
Gd <sup>3+</sup>	Gl	25	0.1 (KCl)	$K_1 = 4.25$	117
La <sup>3+</sup>	Gl	25	0.1 (KCl)	$K_1 = 3.8$	117

(Continued.)					
Metal	Method	Temp. (°C)	Medium	log of equilibrium constant	Ref.
Lu <sup>3+</sup>	Gl	25	0.1 (KCl)	$K_1 = 4.45, K_2 = 3.5$	117
Nd <sup>3+</sup>	Gl	25	0.1 (KCl)	$K_1 = 4.2$	117
Tb <sup>3+</sup>	Gl	25	0.1 (KCl)	$K_1 = 4.3, K_2 = 3.5$	117
Ce <sup>3+</sup>	Gl	25	0.1 (KCl)	$K_1 = 3.52$	117
C <sub>9</sub> H <sub>11</sub> O <sub>3</sub> N, 2-amino-3-(4'-hydroxyphenyl)propanoic acid (tyrosine), H <sub>2</sub> L					
Gd <sup>3+</sup>	Gl	25	0.1 (KCl)	$K(\text{Gd}^{3+} + \text{HL}^- = \text{GdHL}^{2+}) = 4.35$ $K[\text{GdHL}^{2+} + \text{HL}^- = \text{Gd}(\text{HL})_2^+] = 4.2$	117
La <sup>3+</sup>	Gl	25	0.1 (KCl)	$K(\text{La}^{3+} + \text{HL}^- = \text{LaHL}^{2+}) = 4.2$	117
Lu <sup>3+</sup>	Gl	25	0.1 (KCl)	$K(\text{Lu}^{3+} + \text{HL}^- = \text{LuHL}^{2+}) = 4.55$ $K[\text{LuHL}^{2+} + \text{HL}^- = \text{Lu}(\text{HL})_2^+] = 4.5$	117
Nd <sup>3+</sup>	Gl	25	0.1 (KCl)	$K(\text{Nd}^{3+} + \text{HL}^- = \text{NdHL}^{2+}) = 4.1$	117
Tb <sup>3+</sup>	Gl	25	0.1 (KCl)	$K(\text{Tb}^{3+} + \text{HL}^- = \text{TbHL}^{2+}) = 4.35$ $K[\text{TbHL}^{2+} + \text{HL}^- = \text{Tb}(\text{HL})_2^+] = 4.3$	117
Er <sup>3+</sup>	Gl	25	0.1 (KCl)	$K(\text{Er}^{3+} + \text{HL}^- = \text{ErHL}^{2+}) = 4.4$ $K[\text{ErHL}^{2+} + \text{HL}^- = \text{Er}(\text{HL})_2^+] = 4.1$	117
C <sub>9</sub> H <sub>5</sub> ONl <sub>2</sub> , 8-hydroxy-5,7-diiodoquinoline, HL					
H <sup>+</sup>	Gl	35	0.1 NaClO <sub>4</sub> , 75% dioxan	$K_1 = 8.80, K_2 = 0.92$	118
Ce <sup>3+</sup>	Gl	35	0.1 NaClO <sub>4</sub> , 75% dioxan	$K_1 = 6.35, K_2 = 5.40, K_3 = 4.70$	118
Dy <sup>3+</sup>	Gl	35	0.1 NaClO <sub>4</sub> , 75% dioxan	$K_1 = 7.20, K_2 = 6.05, K_3 = 5.40$	118
Er <sup>3+</sup>	Gl	35	0.1 NaClO <sub>4</sub> , 75% dioxan	$K_1 = 7.45, K_2 = 6.15, K_3 = 5.40$	118
Eu <sup>3+</sup>	Gl	35	0.1 NaClO <sub>4</sub> , 75% dioxan	$K_1 = 7.15, K_2 = 6.05, K_3 = 5.35$	118
Gd <sup>3+</sup>	Gl	35	0.1 NaClO <sub>4</sub> , 75% dioxan	$K_1 = 7.00, K_2 = 5.80, K_3 = 5.20$	118
Ho <sup>3+</sup>	Gl	35	0.1 NaClO <sub>4</sub> , 75% dioxan	$K_1 = 7.30, K_2 = 6.15, K_3 = 5.50$	118
La <sup>3+</sup>	Gl	35	0.1 NaClO <sub>4</sub> , 75% dioxan	$K_1 = 6.10, K_2 = 5.30, K_3 = 4.50$	118
Lu <sup>3+</sup>	Gl	35	0.1 NaClO <sub>4</sub> , 75% dioxan	$K_1 = 7.70, K_2 = 6.15, K_3 = 4.90$	118
Nd <sup>3+</sup>	Gl	35	0.1 NaClO <sub>4</sub> , 75% dioxan	$K_1 = 6.75, K_2 = 5.80, K_3 = 5.10$	118
Pr <sup>3+</sup>	Gl	35	0.1 NaClO <sub>4</sub> , 75% dioxan	$K_1 = 6.50, K_2 = 5.70, K_3 = 4.90$	118
Sm <sup>3+</sup>	Gl	35	0.1 NaClO <sub>4</sub> , 75% dioxan	$K_1 = 6.95, K_2 = 5.90, K_3 = 5.15$	118
Tb <sup>3+</sup>	Gl	35	0.1 NaClO <sub>4</sub> , 75% dioxan	$K_1 = 7.10, K_2 = 5.95, K_3 = 5.35$	118
Tm <sup>3+</sup>	Gl	35	0.1 NaClO <sub>4</sub> , 75% dioxan	$K_1 = 7.60, K_2 = 6.10, K_3 = 5.20$	118
Yb <sup>3+</sup>	Gl	35	0.1 NaClO <sub>4</sub> , 75% dioxan	$K_1 = 7.75, K_2 = 6.10, K_3 = 5.05$	118
C <sub>9</sub> H <sub>7</sub> ON <sub>3</sub> S, <i>o</i> -(2-thiazolylazo) cresol, HL					
Ce <sup>3+</sup>	Sp	25	0.1 (KNO <sub>3</sub> ), 10% dioxan	$K_1 = 8.57$	119

(Continued.)

Metal	Method	Temp. (°C)	Medium	log of equilibrium constant	Ref.
Dy <sup>3+</sup>	Sp	25	0.1 (KNO <sub>3</sub> ), 10% dioxan	$K_1 = 9.71, K_2 = 8.69$	119
Er <sup>3+</sup>	Sp	25	0.1 (KNO <sub>3</sub> ), 10% dioxan	$K_1 = 8.57, K_2 = 9.43$	119
Eu <sup>3+</sup>	Sp	25	0.1 (KNO <sub>3</sub> ), 10% dioxan	$K_1 = 9.57$	119
Gd <sup>3+</sup>	Sp	25	0.1 (KNO <sub>3</sub> ), 10% dioxan	$K_1 = 9.61, K_2 = 8.65$	119
Ho <sup>3+</sup>	Sp	25	0.1 (KNO <sub>3</sub> ), 10% dioxan	$K_1 = 9.61, K_2 = 9.12$	119
La <sup>3+</sup>	Sp	25	0.1 (KNO <sub>3</sub> ), 10% dioxan	$K_1 = 8.17$	119
Nd <sup>3+</sup>	Sp	25	0.1 (KNO <sub>3</sub> ), 10% dioxan	$K_1 = 9.01$	119
Pr <sup>3+</sup>	Sp	25	0.1 (KNO <sub>3</sub> ), 10% dioxan	$K_1 = 8.91$	119
Sm <sup>3+</sup>	Sp	25	0.1 (KNO <sub>3</sub> ), 10% dioxan	$K_1 = 9.41, K_2 = 8.54$	119
Tb <sup>3+</sup>	Sp	25	0.1 (KNO <sub>3</sub> ), 10% dioxan	$K_1 = 9.65$	119
Yb <sup>3+</sup>	Sp	25	0.1 (KNO <sub>3</sub> ), 10% dioxan	$K_1 = 9.69, K_2 = 9.90$	119
C <sub>9</sub> H <sub>6</sub> O <sub>4</sub> NBrS, 7-bromo-8-hydroxy-5-quinoline-sulphonic acid, H <sub>2</sub> L					
H <sup>+</sup>	Gl	25	0.1 (NaClO <sub>4</sub> )	$K_1 = 7.32 \pm 0.03, K_2 = 4.38 \pm 0.03,$ $K_3 < 2$	120
Ce <sup>3+</sup>	Gl	30	0.1 (NaClO <sub>4</sub> )	$K_1 = 4.81 \pm 0.04, K_2 = 4.19 \pm 0.08,$ $K_3 = 3.6 \pm 0.8$	120
Dy <sup>3+</sup>	Gl	30	0.1 (NaClO <sub>4</sub> )	$K_1 = 5.45 \pm 0.04, K_2 = 4.85 \pm 0.08,$ $K_3 = 4.1 \pm 0.8$	120
Er <sup>3+</sup>	Gl	30	0.1 (NaClO <sub>4</sub> )	$K_1 = 5.69 \pm 0.04, K_2 = 4.81 \pm 0.08,$ $K_3 = 4.0 \pm 0.8$	120
Eu <sup>3+</sup>	Gl	30	0.1 (NaClO <sub>4</sub> )	$K_1 = 5.43 \pm 0.04, K_2 = 4.70 \pm 0.08,$ $K_3 = 4.3 \pm 0.8$	120
Gd <sup>3+</sup>	Gl	30	0.1 (NaClO <sub>4</sub> )	$K_1 = 5.21 \pm 0.04, K_2 = 4.64 \pm 0.08,$ $K_3 = 4.0 \pm 0.8$	120
Ho <sup>3+</sup>	Gl	30	0.1 (NaClO <sub>4</sub> )	$K_1 = 5.59 \pm 0.04, K_2 = 4.89 \pm 0.08,$ $K_3 = 4.1 \pm 0.8$	120
La <sup>3+</sup>	Gl	30	0.1 (NaClO <sub>4</sub> )	$K_1 = 4.68 \pm 0.04, K_2 = 4.03 \pm 0.08,$ $K_3 = 3.4 \pm 0.8$	120
Lu <sup>3+</sup>	Gl	30	0.1 (NaClO <sub>4</sub> )	$K_1 = 5.82 \pm 0.04, K_2 = 4.50 \pm 0.15$	120
Nd <sup>3+</sup>	Gl	30	0.1 (NaClO <sub>4</sub> )	$K_1 = 5.09 \pm 0.04, K_2 = 4.43 \pm 0.08,$ $K_3 = 4.0 \pm 0.8$	120
Pr <sup>3+</sup>	Gl	30	0.1 (NaClO <sub>4</sub> )	$K_1 = 4.97 \pm 0.04, K_2 = 4.30 \pm 0.08,$ $K_3 = 3.9 \pm 0.8$	120
Sm <sup>3+</sup>	Gl	30	0.1 (NaClO <sub>4</sub> )	$K_1 = 5.30 \pm 0.04, K_2 = 4.57 \pm 0.08,$ $K_3 = 4.2 \pm 0.8$	120
Tb <sup>3+</sup>	Gl	30	0.1 (NaClO <sub>4</sub> )	$K_1 = 5.32 \pm 0.04, K_2 = 4.77 \pm 0.08,$ $K_3 = 4.1 \pm 0.8$	120

(Continued.)					
Metal	Method	Temp. (°C)	Medium	log of equilibrium constant	Ref.
Tm <sup>3+</sup>	Gl	30	0.1 (NaClO <sub>4</sub> )	$K_1 = 5.82 \pm 0.04, K_2 = 4.73 \pm 0.08,$ $K_3 = 3.9 \pm 0.08$	120
Y <sup>3+</sup>	Gl	30	0.1 (NaClO <sub>4</sub> )	$K_1 = 5.50 \pm 0.04, K_2 = 4.86 \pm 0.08,$ $K_3 = 4.2 \pm 0.08$	120
Yb <sup>3+</sup>	Gl	30	0.1 (NaClO <sub>4</sub> )	$K_1 = 5.93 \pm 0.04, K_2 = 4.64 \pm 0.08,$ $K_3 = 3.8 \pm 0.8$	120
C <sub>10</sub> H <sub>8</sub> N <sub>2</sub> , 2,2'-bipyridyl, L Gd <sup>3+</sup>	Cal	25	CHCl <sub>3</sub>	(GdA <sub>3</sub> + nL = GdA <sub>3</sub> L <sub>n</sub> ) $K(n=1) = 3.71 \pm 0.10,$ $K(n=2) = 7.50 \pm 0.08,$ where A = 4,4,4-trifluoro- 1-(2-thienyl)-1,3-butanedione	121
La <sup>3+</sup>	Cal	25	CHCl <sub>3</sub>	(LaA <sub>3</sub> + nL = LaA <sub>3</sub> L <sub>n</sub> ), $K(n=1) = 3.25 \pm 0.10,$ $K(n=2) = 7.50 \pm 0.20,$ where A = 4,4,4-trifluoro- 1-(2-thienyl)-1,3-butanedione	121
Lu <sup>3+</sup>	Cal	25	CHCl <sub>3</sub>	(GdA <sub>3</sub> + nL = GdA <sub>3</sub> L <sub>n</sub> ), $K(n=1) = 4.75 \pm 0.10,$ $K(n=2) = 7.75 \pm 0.22,$ where A = 4,4,4-trifluoro- 1-(2-thienyl)-1,3-butanedione	121
C <sub>10</sub> H <sub>10</sub> O <sub>2</sub> , 1-phenylbutane-1,3-dione (benzoylacetone), HL Eu <sup>3+</sup>	Dis	25	0.1 KNO <sub>3</sub>	$K_1 = 6.89, \beta_2 = 13.37, \beta_3 = 19.62$	122
C <sub>10</sub> H <sub>12</sub> O <sub>2</sub> , 3-isopropyltropolone Gd <sup>3+</sup>	Gl	24	0.1 (NaCl), 80% methanol	$K_1 = 8.8, K_2 = 7.33, K_3 = 6.1, K_4 = 4.6$	123
Ho <sup>3+</sup>	Gl	24	0.1 (NaCl), 80% methanol	$K_1 = 9.2, K_2 = 7.7, K_3 = 6.5, K_4 = 5.2$	123
La <sup>3+</sup>	Gl	24	0.1 (NaCl), 80% methanol	$K_1 = 7.88, K_2 = 6.35, K_3 = 5.0, K_4 = 3.4$	123
Nd <sup>3+</sup>	Gl	24	0.1 (NaCl), 80% methanol	$K_1 = 8.4, K_2 = 6.99, K_3 = 5.7, K_4 = 4.2$	123
Pr <sup>3+</sup>	Gl	24	0.1 (NaCl), 80% methanol	$K_1 = 8.3, K_2 = 6.85, K_3 = 5.5, K_4 = 4.1$	123
Sm <sup>3+</sup>	Gl	24	0.1 (NaCl), 80% methanol	$K_1 = 8.7, K_2 = 7.29, K_3 = 6.0, K_4 = 4.6$	123
Tb <sup>3+</sup>	Gl	24	0.1 (NaCl), 80% methanol	$K_1 = 9.1, K_2 = 7.6, K_3 = 6.3, K_4 = 4.9$	123
Y <sup>3+</sup>	Gl	24	0.1 (NaCl), 80% methanol	$K_1 = 9.0, K_2 = 7.5, K_3 = 6.2, K_4 = 4.8$	123
C <sub>10</sub> H <sub>16</sub> O <sub>2</sub> , 2-butanoylcyclohexanone (2-butyrylcyclohexanone), HL H <sup>+</sup>	Gl	30	0.1	$K_1 = 12.56$	124
Dy <sup>3+</sup>	Gl	30	0.1	$K_1 = 9.88, K_2 = 9.02, K_3 = 8.63$	124
Er <sup>3+</sup>	Gl	30	0.1	$K_1 = 10.72, K_2 = 8.95, K_3 = 9.03$	124
Eu <sup>3+</sup>	Gl	30	0.1	$K_1 = 9.92, K_2 = 8.92, K_3 = 8.09$	124
Gd <sup>3+</sup>	Gl	30	0.1	$K_1 = 9.42, K_2 = 8.78, K_3 = 8.45$	124
La <sup>3+</sup>	Gl	30	0.1	$K_1 = 8.52, K_2 = 7.33$	124
Nd <sup>3+</sup>	Gl	30	0.1	$K_1 = 9.43, K_2 = 8.53, K_3 = 8.59$	124

(Continued.)

Metal	Method	Temp. (°C)	Medium	log of equilibrium constant	Ref.
Pr <sup>3+</sup>	Gl	30	0.1	$K_1 = 9.20, K_2 = 8.53, K_3 = 8.02$	124
Sm <sup>3+</sup>	Gl	30	0.1	$K_1 = 9.69, K_2 = 8.79, K_3 = 8.44$	124
Y <sup>3+</sup>	Gl	30	0.1	$K_1 = 9.13, K_2 = 8.02$	124
Yb <sup>3+</sup>	Gl	30	0.1	$K_1 = 10.81, K_2 = 9.76, K_3 = 9.61$	124
C <sub>10</sub> H <sub>7</sub> O <sub>2</sub> N, quinoline-2-carboxylic acid, HL					
H <sup>+</sup>	Gl	30	0.1 (NaClO <sub>4</sub> )	$K_1 = 4.92$	125
Ce <sup>3+</sup>	Gl	30	0.1 (NaClO <sub>4</sub> )	$K_1 = 2.48, K_2 = 2.23$	125
Dy <sup>3+</sup>	Gl	30	0.1 (NaClO <sub>4</sub> )	$K_1 = 2.62, K_2 = 2.53$	125
Er <sup>3+</sup>	Gl	30	0.1 (NaClO <sub>4</sub> )	$K_1 = 2.67, K_2 = 2.63$	125
Eu <sup>3+</sup>	Gl	30	0.1 (NaClO <sub>4</sub> )	$K_1 = 2.59, K_2 = 2.47$	125
Gd <sup>3+</sup>	Gl	30	0.1 (NaClO <sub>4</sub> )	$K_1 = 2.58, K_2 = 2.48$	125
La <sup>3+</sup>	Gl	30	0.1 (NaClO <sub>4</sub> )	$K_1 = 2.43, K_2 = 2.21$	125
Nd <sup>3+</sup>	Gl	30	0.1 (NaClO <sub>4</sub> )	$K_1 = 2.57, K_2 = 2.35$	125
Pr <sup>3+</sup>	Gl	30	0.1 (NaClO <sub>4</sub> )	$K_1 = 2.53, K_2 = 2.26$	125
Sm <sup>3+</sup>	Gl	30	0.1 (NaClO <sub>4</sub> )	$K_1 = 2.64, K_2 = 2.45$	125
Y <sup>3+</sup>	Gl	30	0.1 (NaClO <sub>4</sub> )	$K_1 = 2.58, K_2 = 2.46$	125
Yb <sup>3+</sup>	Gl	30	0.1 (NaClO <sub>4</sub> )	$K_1 = 2.70, K_2 = 2.58$	125
C <sub>10</sub> H <sub>7</sub> O <sub>2</sub> N, quinoline-8-carboxylic acid, HL					
H <sup>+</sup>	Gl	30	0.1 (NaClO <sub>4</sub> )	$K_1 = 6.84$	125
Ce <sup>3+</sup>	Gl	30	0.1 (NaClO <sub>4</sub> )	$K_1 = 2.48$	125
Er <sup>3+</sup>	Gl	30	0.1 (NaClO <sub>4</sub> )	$K_1 = 2.78$	125
Eu <sup>3+</sup>	Gl	30	0.1 (NaClO <sub>4</sub> )	$K_1 = 2.64$	125
Gd <sup>3+</sup>	Gl	30	0.1 (NaClO <sub>4</sub> )	$K_1 = 2.61$	125
La <sup>3+</sup>	Gl	30	0.1 (NaClO <sub>4</sub> )	$K_1 = 2.43$	125
Nd <sup>3+</sup>	Gl	30	0.1 (NaClO <sub>4</sub> )	$K_1 = 2.55$	125
Pr <sup>3+</sup>	Gl	30	0.1 (NaClO <sub>4</sub> )	$K_1 = 2.47$	125
Sm <sup>3+</sup>	Gl	30	0.1 (NaClO <sub>4</sub> )	$K_1 = 2.64$	125
Y <sup>3+</sup>	Gl	30	0.1 (NaClO <sub>4</sub> )	$K_1 = 2.60$	125
Yb <sup>3+</sup>	Gl	30	0.1 (NaClO <sub>4</sub> )	$K_1 = 2.86$	125
C <sub>10</sub> H <sub>10</sub> OS, 3-mercapto-1-phenylbut-2-en-1-one, HL					
H <sup>+</sup>	Gl	30	0.1 (NaClO <sub>4</sub> ), 75% acetone	$K_1 = 8.12$	126
Dy <sup>3+</sup>	Gl	30	0.1 (NaClO <sub>4</sub> ), 75% acetone	$K_1 = 4.00, K_2 = 3.57, K_3 = 3.28$	126
Er <sup>3+</sup>	Gl	30	0.1 (NaClO <sub>4</sub> ), 75% acetone	$K_1 = 4.18, K_2 = 3.70, K_3 = 3.45$	126
Gd <sup>3+</sup>	Gl	30	0.1 (NaClO <sub>4</sub> ), 75% acetone	$K_1 = 3.92, K_2 = 3.38, K_3 = 3.02$	126
La <sup>3+</sup>	Gl	30	0.1 (NaClO <sub>4</sub> ), 75% acetone	$K_1 = 3.42, K_2 = 2.98, K_3 = 2.70$	126
Nd <sup>3+</sup>	Gl	30	0.1 (NaClO <sub>4</sub> ), 75% acetone	$K_1 = 3.80, K_2 = 3.41, K_3 = 3.16$	126
Pr <sup>3+</sup>	Gl	30	0.1 (NaClO <sub>4</sub> ), 75% acetone	$K_1 = 3.71, K_2 = 3.34, K_3 = 2.97$	126
Sm <sup>3+</sup>	Gl	30	0.1 (NaClO <sub>4</sub> ), 75% acetone	$K_1 = 4.03, K_2 = 3.55, K_3 = 3.11$	126
Y <sup>3+</sup>	Gl	30	0.1 (NaClO <sub>4</sub> ), 75% acetone	$K_1 = 3.85, K_2 = 3.42, K_3 = 3.18$	126



(Continued.)					
Metal	Method	Temp. (°C)	Medium	log of equilibrium constant	Ref.
Yb <sup>3+</sup>	Gl	30	0.1 (NaClO <sub>4</sub> ), 75% acetone	$K_1 = 4.33, K_2 = 3.82, K_3 = 3.55$	126
C <sub>10</sub> H <sub>12</sub> O <sub>4</sub> N <sub>2</sub> , <i>N</i> -(2-pyridylmethyl) iminodiacetic acid					
Ce <sup>3+</sup>	Iex	25	0.1 NH <sub>4</sub> ClO <sub>4</sub>	$K_1 = 8.34, \beta_2 = 15.68$	127
C <sub>10</sub> H <sub>12</sub> O <sub>4</sub> N <sub>2</sub> , <i>N</i> -(2-methyl pyridyl) iminodiacetic acid					
Ce <sup>3+</sup>	Iex	25	0.1	$K_1 = 8.34, \beta_2 = 15.68$	127
Ethylenediamine tetraacetic acid, EDTA					
La <sup>3+</sup>				14.72	128
Ce <sup>3+</sup>				15.39	128
Pr <sup>3+</sup>				15.75	128
Nd <sup>3+</sup>				16.06	128
Sm <sup>3+</sup>				16.55	128
Eu <sup>3+</sup>				16.69	128
Gd <sup>3+</sup>				16.70	128
Tb <sup>3+</sup>				17.25	128
Dy <sup>3+</sup>				17.57	128
Ho <sup>3+</sup>				17.67	128
Er <sup>3+</sup>				17.98	128
Tm <sup>3+</sup>				18.59	128
Yb <sup>3+</sup>				18.68	128
Lu <sup>3+</sup>				19.06	128
Y <sup>3+</sup>				17.38	128
C <sub>10</sub> H <sub>12</sub> NO <sub>4</sub>					
La <sup>3+</sup>	Gl	25	0.1 KNO <sub>3</sub>	$\log K_1 = 7.80, \log K_2 = 5.90$	206
Ce <sup>3+</sup>	Gl	25	0.1 KNO <sub>3</sub>	$\log K_1 = 8.30, \log K_2 = 6.44$	206
Pr <sup>3+</sup>	Gl	25	0.1 KNO <sub>3</sub>	$\log K_1 = 8.53, \log K_2 = 6.95$	206
Nd <sup>3+</sup>	Gl	25	0.1 KNO <sub>3</sub>	$\log K_1 = 8.64, \log K_2 = 7.18$	206
Sm <sup>3+</sup>	Gl	25	0.1 KNO <sub>3</sub>	$\log K_1 = 8.92, \log K_2 = 7.96$	206
Eu <sup>3+</sup>	Gl	25	0.1 KNO <sub>3</sub>	$\log K_1 = 8.92, \log K_2 = 8.02$	206
Gd <sup>3+</sup>	Gl	25	0.1 KNO <sub>3</sub>	$\log K_1 = 8.76, \log K_2 = 8.01$	206
Tb <sup>3+</sup>	Gl	25	0.1 KNO <sub>3</sub>	$\log K_1 = 8.87, \log K_2 = 8.17$	206
Dy <sup>3+</sup>	Gl	25	0.1 KNO <sub>3</sub>	$\log K_1 = 9.00, \log K_2 = 8.03$	206
Ho <sup>3+</sup>	Gl	25	0.1 KNO <sub>3</sub>	$\log K_1 = 9.07, \log K_2 = 7.80$	206
Er <sup>3+</sup>	Gl	25	0.1 KNO <sub>3</sub>	$\log K_1 = 9.25, \log K_2 = 7.65$	206
Tm <sup>3+</sup>	Gl	25	0.1 KNO <sub>3</sub>	$\log K_1 = 9.40, \log K_2 = 7.61$	206
Yb <sup>3+</sup>	Gl	25	0.1 KNO <sub>3</sub>	$\log K_1 = 9.60, \log K_2 = 7.73$	206
Lu <sup>3+</sup>	Gl	25	0.1 KNO <sub>3</sub>	$\log K_1 = 9.72, \log K_2 = 7.75$	206
Y <sup>3+</sup>	Gl	25	0.1 KNO <sub>3</sub>	$\log K_1 = 8.63, \log K_2 = 7.38$	206
C <sub>6</sub> H <sub>16</sub> O <sub>8</sub> N <sub>2</sub> , ethylenediamine- <i>N,N'</i> -succinic acid, H <sub>4</sub> L					
Dy <sup>3+</sup>	Pol	25	0.1 (KNO <sub>3</sub> )	$K_1 = 13.59$	129
Er <sup>3+</sup>	Pol	25	0.1 (KNO <sub>3</sub> )	$K_1 = 13.63$	129
Eu <sup>3+</sup>	Pol	25	0.1 (KNO <sub>3</sub> )	$K_1 = 13.54$	129
Gd <sup>3+</sup>	Pol	25	0.1 (KNO <sub>3</sub> )	$K_1 = 13.45$	129
Ho <sup>3+</sup>	Pol	25	0.1 (KNO <sub>3</sub> )	$K_1 = 13.60$	129
La <sup>3+</sup>	Pol	25	0.1 (KNO <sub>3</sub> )	$K_1 = 11.98$	129
Lu <sup>3+</sup>	Pol	25	0.1 (KNO <sub>3</sub> )	$K_1 = 14.32$	129
Pr <sup>3+</sup>	Pol	25	0.1 (KNO <sub>3</sub> )	$K_1 = 12.969$	129
Sm <sup>3+</sup>	Pol	25	0.1 (KNO <sub>3</sub> )	$K_1 = 13.46$	129

(Continued.)

Metal	Method	Temp. (°C)	Medium	log of equilibrium constant	Ref.
Tb <sup>3+</sup>	Pol	25	0.1 M KNO <sub>3</sub>	$K_1 = 13.51$	129
Tm <sup>3+</sup>	Pol	25	0.1 M KNO <sub>3</sub>	$K_1 = 14.00$	129
<i>N'</i> -(2-hydroxyethyl)ethylenediamine- <i>N,N,N'</i> -triacetic acid, H <sub>3</sub> L					
La <sup>3+</sup>	Hg	20	0.1 M KNO <sub>3</sub>	$\log K_1 = 13.82$	130
La <sup>3+</sup>	Gl	25	0.1 M KNO <sub>3</sub>	$\log K_1 = 13.46$	130
La <sup>3+</sup>	Gl	25	0.1 M KNO <sub>3</sub>	–	130
La <sup>3+</sup>	Gl	25	0.1 M KCl	$\log K_1 = 13.22$	130
Ce <sup>3+</sup>	Hg	20	0.1 M KNO <sub>3</sub>	$\log K_1 = 14.45$	130
Ce <sup>3+</sup>	Gl	25	0.1 M KNO <sub>3</sub>	$\log K_1 = 14.11$	130
Ce <sup>3+</sup>	Gl	25	0.1 M KCl	$\log K_1 = 14.08$	130
Pr <sup>3+</sup>	Hg	20	0.1 M KNO <sub>3</sub>	$\log K_1 = 14.96$	130
Pr <sup>3+</sup>	Gl	25	0.1 M KNO <sub>3</sub>	$\log K_1 = 14.61$	130
Pr <sup>3+</sup>	Gl	25	0.1 M KNO <sub>3</sub>	–	130
Pr <sup>3+</sup>	Gl	25	0.1 M KCl	$\log K_1 = 14.39$	130
Nd <sup>3+</sup>	Hg	20	0.1 M KNO <sub>3</sub>	$\log K_1 = 15.16$	130
Nd <sup>3+</sup>	Gl	25	0.1 M KNO <sub>3</sub>	$\log K_1 = 14.86$	130
Nd <sup>3+</sup>	Gl	25	0.1 M KNO <sub>3</sub>	–	130
Nd <sup>3+</sup>	Gl	25	0.1 M KCl	$\log K_1 = 14.71$	130
Sm <sup>3+</sup>	Hg	20	0.1 M KNO <sub>3</sub>	$\log K_1 = 15.64$	130
Sm <sup>3+</sup>	Gl	25	0.1 M KNO <sub>3</sub>	$\log K_1 = 15.28$	130
Sm <sup>3+</sup>	Gl	25	0.1 M KNO <sub>3</sub>	–	130
Sm <sup>3+</sup>	Gl	25	0.1 M KCl	$\log K_1 = 15.15$	130
Sm <sup>3+</sup>	Pol	25	0.1 M KNO <sub>3</sub>	$\log K_1 = 15.3$	130
Eu <sup>3+</sup>	Hg	20	0.1 M KNO <sub>3</sub>	$\log K_1 = 15.62$	130
Eu <sup>3+</sup>	Gl	25	0.1 M KNO <sub>3</sub>	$\log K_1 = 15.35$	130
Eu <sup>3+</sup>	Gl	25	0.1 M KNO <sub>3</sub>	–	130
Eu <sup>3+</sup>	Gl	25	0.1 M KCl	$\log K_1 = 15.21$	130
Gd <sup>3+</sup>	Hg	20	0.1 M KNO <sub>3</sub>	$\log K_1 = 15.44$	130
Gd <sup>3+</sup>	Gl	25	0.1 M KNO <sub>3</sub>	$\log K_1 = 15.22$	130
Gd <sup>3+</sup>	Gl	25	0.1 M KNO <sub>3</sub>	–	130
Gd <sup>3+</sup>	Gl	25	0.1 M KCl	$\log K_1 = 15.10$	130
Gd <sup>3+</sup>	Pol	25	0.1 M KNO <sub>3</sub>	$\log K_1 = 15.4$	130
Tb <sup>3+</sup>	Hg	20	0.1 M KNO <sub>3</sub>	$\log K_1 = 15.55$	130
Tb <sup>3+</sup>	Gl	25	0.1 M KNO <sub>3</sub>	$\log K_1 = 15.32$	130
Tb <sup>3+</sup>	Gl	25	0.1 M KNO <sub>3</sub>	–	130
Tb <sup>3+</sup>	Gl	25	0.1 M KCl	$\log K_1 = 15.10$	130
Dy <sup>3+</sup>	Hg	20	0.1 M KNO <sub>3</sub>	$\log K_1 = 15.51$	130
Dy <sup>3+</sup>	Gl	25	0.1 M KNO <sub>3</sub>	$\log K_1 = 15.30$	130
Dy <sup>3+</sup>	Gl	25	0.1 M KNO <sub>3</sub>	–	130
Dy <sup>3+</sup>	Gl	25	0.1 M KCl	$\log K_1 = 15.08$	130
Dy <sup>3+</sup>	Pol	25	0.1 M KNO <sub>3</sub>	$\log K_1 = 15.3$	130
Ho <sup>3+</sup>	Hg	20	0.1 M KNO <sub>3</sub>	$\log K_1 = 15.55$	130
Ho <sup>3+</sup>	Gl	25	0.1 M KNO <sub>3</sub>	$\log K_1 = 15.32$	130
Ho <sup>3+</sup>	Gl	25	0.1 M KNO <sub>3</sub>	–	130
Ho <sup>3+</sup>	Gl	25	0.1 M KCl	$\log K_1 = 15.06$	130
Ho <sup>3+</sup>	Pol	25	0.1 M KNO <sub>3</sub>	$\log K_1 = 15.4$	130
Er <sup>3+</sup>	Hg	20	0.1 M KNO <sub>3</sub>	$\log K_1 = 15.61$	130

(Continued.)					
Metal	Method	Temp. (°C)	Medium	log of equilibrium constant	Ref.
Er <sup>3+</sup>	Gl	25	0.1 M KNO <sub>3</sub>	log $K_1 = 15.42$	130
Er <sup>3+</sup>	Gl	25	0.1 M KNO <sub>3</sub>	–	130
Er <sup>3+</sup>	Gl	25	0.1 M KCl	log $K_1 = 15.17$	130
Er <sup>3+</sup>	Pol	25	0.1 M KNO <sub>3</sub>	log $K_1 = 15.4$	130
Tm <sup>3+</sup>	Hg	20	0.1 M KNO <sub>3</sub>	log $K_1 = 16.00$	130
Tm <sup>3+</sup>	Gl	25	0.1 M KNO <sub>3</sub>	log $K_1 = 15.59$	130
Tm <sup>3+</sup>	Gl	25	0.1 M KNO <sub>3</sub>	–	130
Tm <sup>3+</sup>	Gl	25	0.1 M KCl	log $K_1 = 15.38$	130
Tm <sup>3+</sup>	Pol	25	0.1 M KNO <sub>3</sub>	log $K_1 = 15.5$	130
Yb <sup>3+</sup>	Hg	20	0.1 M KNO <sub>3</sub>	log $K_1 = 16.17$	130
Yb <sup>3+</sup>	Gl	25	0.1 M KNO <sub>3</sub>	log $K_1 = 15.88$	130
Yb <sup>3+</sup>	Gl	25	0.1 M KNO <sub>3</sub>	–	130
Yb <sup>3+</sup>	Gl	25	0.1 M KCl	log $K_1 = 15.64$	130
Yb <sup>3+</sup>	Pol	25	0.1 M KNO <sub>3</sub>	log $K_1 = 15.8$	130
Lu <sup>3+</sup>	Hg	20	0.1 M KNO <sub>3</sub>	log $K_1 = 16.25$	130
Lu <sup>3+</sup>	Gl	25	0.1 M KNO <sub>3</sub>	log $K_1 = 15.88$	130
Lu <sup>3+</sup>	Gl	25	0.1 M KNO <sub>3</sub>	–	130
Lu <sup>3+</sup>	Gl	25	0.1 M KCl	log $K_1 = 15.79$	130
Lu <sup>3+</sup>	Pol	25	0.1 M KNO <sub>3</sub>	log $K_1 = 16.0$	130
Y <sup>3+</sup>	Hg	20	0.1 M KNO <sub>3</sub>	log $K_1 = 15.03$	130
Y <sup>3+</sup>	Gl	25	0.1 M KNO <sub>3</sub>	log $K_1 = 14.65$	130
Y <sup>3+</sup>	Gl	25	0.1 M KNO <sub>3</sub>	–	130
Y <sup>3+</sup>	Gl	25	0.1 M KCl	log $K_1 = 14.49$	130
Y <sup>3+</sup>	Pol	25	0.1 M KNO <sub>3</sub>	log $K_1 = 14.8$	130
C <sub>10</sub> H <sub>19</sub> O <sub>4</sub> N <sub>3</sub> , DL-leucylglycylglycine, HL					
H <sup>+</sup>	Gl	25	0.1 (KCl)	$K_1 = 7.85, K_2 = 3.31$	90
Eu <sup>3+</sup>	Gl	25	0.1 (KCl)	$K_1 = 2.40$	90
Gd <sup>3+</sup>	Gl	25	0.1 (KCl)	$K_1 = 1.95$	90
Ho <sup>3+</sup>	Gl	25	0.1 (KCl)	$K_1 = 2.00$	90
Nd <sup>3+</sup>	Gl	25	0.1 (KCl)	$K_1 = 1.75$	90
Yb <sup>3+</sup>	Gl	25	0.1 (KCl)	$K_1 = 2.30$	90
C <sub>10</sub> H <sub>20</sub> O <sub>4</sub> N <sub>2</sub> , N,N'-diethylethylenedinitrilo-N,N'-diacetic acid, H <sub>2</sub> L					
H <sup>+</sup>	Gl	25	0.1 (KNO <sub>3</sub> )	$K_1 = 10.42, K_2 = 6.31$	131
Dy <sup>3+</sup>	Gl	25	0.1 (KNO <sub>3</sub> )	$K_1 = 7.0$	131
Er <sup>3+</sup>	Gl	25	0.1 (KNO <sub>3</sub> )	$K_1 = 7.0$	131
Eu <sup>3+</sup>	Gl	25	0.1 (KNO <sub>3</sub> )	$K_1 = 7.1$	131
Gd <sup>3+</sup>	Gl	25	0.1 (KNO <sub>3</sub> )	$K_1 = 6.9$	131
Ho <sup>3+</sup>	Gl	25	0.1 (KNO <sub>3</sub> )	$K_1 = 6.9$	131
Lu <sup>3+</sup>	Gl	25	0.1 (KNO <sub>3</sub> )	$K_1 = 7.1$	131
Tb <sup>3+</sup>	Gl	25	0.1 (KNO <sub>3</sub> )	$K_1 = 7.0$	131
Tm <sup>3+</sup>	Gl	25	0.1 (KNO <sub>3</sub> )	$K_1 = 7.1$	131
Y <sup>3+</sup>	Gl	25	0.1 (KNO <sub>3</sub> )	$K_1 = 6.8$	131
Yb <sup>3+</sup>	Gl	25	0.1 (KNO <sub>3</sub> )	$K_1 = 7.1$	131
C <sub>10</sub> H <sub>7</sub> O <sub>5</sub> NS, 1-hydroxy-2-nitrosophthalene-5-sulphonic acid, H <sub>2</sub> L					
H <sup>+</sup>	Gl	25	0.01 (KCl)	$K_1 (\rightarrow 0) = 7.32, K_1(0.1) = 6.91$	132
Nd <sup>3+</sup>	Gl	25	0.1 (KCl)	$K_1 = 3.83, \beta_2 = 6.9$	132
Pr <sup>3+</sup>	Gl	25	0.1 (KCl)	$K_1 = 3.50, \beta_2 = 6.3$	132

(Continued.)					
Metal	Method	Temp. (°C)	Medium	log of equilibrium constant	Ref.
$C_{10}H_7O_5NS$ , 2-hydroxy-1-nitrosophthalene-6-sulphonic acid, $H_2L$					
$H^+$	Gl	25	0, 0.1 (KCl)	$K_1(\rightarrow 0) = 7.60, K_1(0.1) = 7.22$	132
$Eu^{3+}$	Pot	25	$\rightarrow 0$	$K_1 = 5.60, \beta_2 = 9.47$	132
$Gd^{3+}$	Sp	?	?	$K_1 = 2.25$	132
$Nd^{3+}$	Gl	25	0.1 (KCl)	$K_1 = 4.52, \beta_2 = 8.2$	132
$Pr^{3+}$	Gl	25	0.1 (KCl)	$K_1 = 4.25, \beta_2 = 7.7$	132
$C_{10}H_{16}O_{13}N_5P_3$ , adenosine-5'-triphosphoric acid (ATP), $H_4L$					
$Ce^{3+}$	Gl	35	0.1 (KNO <sub>3</sub> )	$K(CeA^- + L^{4-} = CeAL^{5-}) = 4.4 \pm 0.1$ , where $H_4A = EDTA$	133
$Dy^{3+}$	Gl	35	0.1 (KNO <sub>3</sub> )	$K(DyA^- + L^{4-} = DyAL^{5-}) = 5.5 \pm 0.1$ , where $H_4A = EDTA$	133
$Er^{3+}$	Gl	35	0.1 (KNO <sub>3</sub> )	$K(ErA^- + L^{4-} = ErAL^{5-}) = 6.2 \pm 0.1$ , where $H_4A = EDTA$	133
$Eu^{3+}$	Gl	35	0.1 (KNO <sub>3</sub> )	$K(EuA^- + L^{4-} = EuAL^{5-}) = 4.8 \pm 0.2$ , where $H_4A = EDTA$	133
$Gd^{3+}$	Gl	35	0.1 (KNO <sub>3</sub> )	$K(GdA^- + L^{4-} = GdAL^{5-}) = 4.6 \pm 0.2$ , where $H_4A = EDTA$	133
$Ho^{3+}$	Gl	35	0.1 (KNO <sub>3</sub> )	$K(HoA^- + L^{4-} = HoAL^{5-}) = 5.8 \pm 0.1$ , where $H_4A = EDTA$	133
$La^{3+}$	Gl	35	0.1 (KNO <sub>3</sub> )	$K(LaA^- + L^{4-} = LaAL^{5-}) = 4.3 \pm 0.1$ , where $H_4A = EDTA$	133
$Nd^{3+}$	Gl	35	0.1 (KNO <sub>3</sub> )	$K(NdA^- + L^{4-} = NdAL^{5-}) = 4.6 \pm 0.1$ , where $H_4A = EDTA$	133
$Pr^{3+}$	Gl	35	0.1 (KNO <sub>3</sub> )	$K(PrA^- + L^{4-} = PrAL^{5-}) = 4.5 \pm 0.1$ , where $H_4A = EDTA$	133
$Sm^{3+}$	Gl	35	0.1 (KNO <sub>3</sub> )	$K(SmA^- + L^{4-} = SmAL^{5-}) = 4.7 \pm 0.1$ , where $H_4A = EDTA$	133
$Tb^{3+}$	Gl	35	0.1 (KNO <sub>3</sub> )	$K(TbA^- + L^{4-} = TbAL^{5-}) = 5.3 \pm 0.1$ , where $H_4A = EDTA$	133
$Tm^{3+}$	Gl	35	0.1 (KNO <sub>3</sub> )	$K(TmA^- + L^{4-} = TmAL^{5-}) = 6.8 \pm 0.2$ , where $H_4A = EDTA$	133
$Y^{3+}$	Gl	35	0.1 (KNO <sub>3</sub> )	$K(YA^- + L^{4-} = YAL^{5-}) = 5.2 \pm 0.1$ , where $H_4A = EDTA$	133
$C_{10}H_{27}O_6N_3P_2$ , iminobis[ethyleneimino(dimethyl)methylenephosphonic acid] (diethylenetriamine- $N,N'$ -doisopropylphosphonic acid), $H_4L$					
$H^+$	Gl	25	0.1 (KCl)	$K_1 = 11.20, K_2 = 10.40, K_3 = 6.55, K_4 = 5.39$	134
$Eu^{3+}$	Gl	25	0.1 (KCl)	$K_1 = 12.92 \pm 0.10$ $K(Eu^{3+} + H_2L^{2-} = EuHL^+) = 6.19 \pm 0.07$	134
$C_{11}H_8O_4$ , 3-acetyl-4-hydroxycoumarin, HL					
$H^+$	Gl	35	0.1 NaClO <sub>4</sub>	$K_1 = 5.05$	135
$Ce^{3+}$	Gl	35	0.1 NaClO <sub>4</sub> , 50% dioxan	$K_1 = 3.32, K_2 = 2.52$	135
$Dy^{3+}$	Gl	35	0.1 NaClO <sub>4</sub> , 50% dioxan	$K_1 = 3.98, K_2 = 3.04$	135
$Er^{3+}$	Gl	35	0.1 NaClO <sub>4</sub> , 50% dioxan	$K_1 = 4.21, K_2 = 3.12$	135
$Eu^{3+}$	Gl	35	0.1 NaClO <sub>4</sub> , 50% dioxan	$K_1 = 3.92, K_2 = 2.97$	135

(Continued.)

Metal	Method	Temp. (°C)	Medium	log of equilibrium constant	Ref.
Gd <sup>3+</sup>	Gl	35	0.1 NaClO <sub>4</sub> , 50% dioxan	$K_1 = 3.73, K_2 = 2.82$	135
Ho <sup>3+</sup>	Gl	35	0.1 NaClO <sub>4</sub> , 50% dioxan	$K_1 = 4.09, K_2 = 3.08$	135
La <sup>3+</sup>	Gl	35	0.1 NaClO <sub>4</sub> , 50% dioxan	$K_1 = 3.23, K_2 = 2.45$	135
Nd <sup>3+</sup>	Gl	35	0.1 NaClO <sub>4</sub> , 50% dioxan	$K_1 = 3.64, K_2 = 2.70$	135
Pr <sup>3+</sup>	Gl	35	0.1 NaClO <sub>4</sub> , 50% dioxan	$K_1 = 3.47, K_2 = 2.59$	135
Sm <sup>3+</sup>	Gl	35	0.1 NaClO <sub>4</sub> , 50% dioxan	$K_1 = 3.78, K_2 = 2.84$	135
Tb <sup>3+</sup>	Gl	35	0.1 NaClO <sub>4</sub> , 50% dioxan	$K_1 = 3.88, K_2 = 2.93$	135
Tm <sup>3+</sup>	Gl	35	0.1 NaClO <sub>4</sub> , 50% dioxan	$K_1 = 4.34, K_2 = 3.08$	135
Y <sup>3+</sup>	Gl	35	0.1 NaClO <sub>4</sub> , 50% dioxan	$K_1 = 4.02, K_2 = 3.08$	135
Yb <sup>3+</sup>	Gl	35	0.1 NaClO <sub>4</sub> , 50% dioxan	$K_1 = 4.46, K_2 = 2.92$	135
C <sub>11</sub> H <sub>12</sub> O <sub>3</sub> , ethyl benzoylacetate, HL					
H <sup>+</sup>	Gl	25	0.1 NaClO <sub>4</sub> , 75% acetone	$K_1 = 11.27 \pm 0.02$	136
Dy <sup>3+</sup>	Gl	25	0.1 NaClO <sub>4</sub> , 75% acetone	$K_1 = 8.62, K_2 = 7.20$	136
Er <sup>3+</sup>	Gl	25	0.1 NaClO <sub>4</sub> , 75% acetone	$K_1 = 8.77, K_2 = 7.50$	136
Eu <sup>3+</sup>	Gl	25	0.1 NaClO <sub>4</sub> , 75% acetone	$K_1 = 8.50, K_2 = 7.18$	136
Gd <sup>3+</sup>	Gl	25	0.1 NaClO <sub>4</sub> , 75% acetone	$K_1 = 8.27, K_2 = 6.84$	136
La <sup>3+</sup>	Gl	25	0.1 NaClO <sub>4</sub> , 75% acetone	$K_1 = 7.49, K_2 = 6.42$	136
Nd <sup>3+</sup>	Gl	25	0.1 NaClO <sub>4</sub> , 75% acetone	$K_1 = 8.07, K_2 = 7.01$	136
Pr <sup>3+</sup>	Gl	25	0.1 NaClO <sub>4</sub> , 75% acetone	$K_1 = 7.90, K_2 = 6.78$	136
Sm <sup>3+</sup>	Gl	25	0.1 NaClO <sub>4</sub> , 75% acetone	$K_1 = 8.40, K_2 = 6.98$	136
Y <sup>3+</sup>	Gl	25	0.1 NaClO <sub>4</sub> , 75% acetone	$K_1 = 8.56, K_2 = 7.18$	136
Yb <sup>3+</sup>	Gl	25	0.1 NaClO <sub>4</sub> , 75% acetone	$K_1 = 8.84, K_2 = 7.30$	136
C <sub>11</sub> H <sub>18</sub> O <sub>2</sub> , 2-(3'-methylbutanoyl)cyclohexane (2-isovaleryl cyclohexanone), HL					
H <sup>+</sup>	Gl	30	75% acetone	$K_1 = 12.30$	69
Dy <sup>3+</sup>	Gl	30	75% acetone	$K_1 = 9.43, K_2 = 9.01, K_3 = 8.30$	69
Er <sup>3+</sup>	Gl	30	75% acetone	$K_1 = 10.04, K_2 = 9.79, K_3 = 8.41$	69
Eu <sup>3+</sup>	Gl	30	75% acetone	$K_1 = 9.74, K_2 = 9.11, K_3 = 8.76$	69
Gd <sup>3+</sup>	Gl	30	75% acetone	$K_1 = 9.49, K_2 = 8.93, K_3 = 8.09$	69

(Continued.)					
Metal	Method	Temp. (°C)	Medium	log of equilibrium constant	Ref.
La <sup>3+</sup>	Gl	30	75% acetone	$K_1 = 8.95, K_2 = 7.49$	69
Nd <sup>3+</sup>	Gl	30	75% acetone	$K_1 = 9.54, K_2 = 8.55, K_3 = 7.93$	69
Pr <sup>3+</sup>	Gl	30	75% acetone	$K_1 = 9.43, K_2 = 8.51, K_3 = 7.62$	69
Sm <sup>3+</sup>	Gl	30	75% acetone	$K_1 = 9.63, K_2 = 9.08, K_3 = 8.17$	69
Y <sup>3+</sup>	Gl	30	75% acetone	$K_1 = 9.56, K_2 = 9.60$	69
Yb <sup>3+</sup>	Gl	30	75% acetone	$K_1 = 10.18, K_2 = 9.34, K_3 = 8.90$	69
C <sub>11</sub> H <sub>18</sub> O <sub>2</sub> , 2-butanoyl-6-methylcyclohexanone (2-butyryl-6-methylcyclohexanone), HL					
H <sup>+</sup>	Gl	30	75% acetone	$K_1 = 12.97$	69
Dy <sup>3+</sup>	Gl	30	75% acetone	$K_1 = 10.62, K_2 = 10.07$	69
Er <sup>3+</sup>	Gl	30	75% acetone	$K_1 = 10.70, K_2 = 10.11$	69
Eu <sup>3+</sup>	Gl	30	75% acetone	$K_1 = 10.58, K_2 = 10.24$	69
Gd <sup>3+</sup>	Gl	30	75% acetone	$K_1 = 10.32, K_2 = 9.94$	69
La <sup>3+</sup>	Gl	30	75% acetone	$K_1 = 10.31, K_2 = 9.58$	69
Nd <sup>3+</sup>	Gl	30	75% acetone	$K_1 = 10.69, K_2 = 10.08$	69
Pr <sup>3+</sup>	Gl	30	75% acetone	$K_1 = 10.40, K_2 = 9.30$	69
Sm <sup>3+</sup>	Gl	30	75% acetone	$K_1 = 10.75, K_2 = 10.26$	69
Y <sup>3+</sup>	Gl	30	75% acetone	$K_1 = 10.58, K_2 = 9.90$	69
Yb <sup>3+</sup>	Gl	30	75% acetone	$K_1 = 10.74, K_2 = 9.84$	69
C <sub>11</sub> H <sub>20</sub> O <sub>2</sub> , 2,2,6,6-tetramethylhepta-3,5-dione (dipivaloyl methane), HL					
H <sup>+</sup>	pH	21	CH <sub>3</sub> OH	$K_1 = 14.3 \pm 0.2$	137
Er <sup>3+</sup>	Pot	21	CH <sub>3</sub> OH	$K_1 = 13.6, K_2 = 10.4, K_3 = 5.5$	137
Nd <sup>3+</sup>	Pot	21	CH <sub>3</sub> OH	$K_1 = 12.7, K_2 = 9.80, K_3 = 4.4$	137
C <sub>11</sub> H <sub>9</sub> O <sub>2</sub> N <sub>3</sub> , 1,3-dihydroxy-4-(2'-pyridylaza)benzene (pyridylazoresorcinol) (PAR), H <sub>2</sub> L					
Dy <sup>3+</sup>	Sp	20	0.1 (KCl)	$K(\text{Dy}^{3+} + \text{HL}^- = \text{DyHL}^+) = 3.48$	138
Er <sup>3+</sup>	Sp	20	0.1 (KCl)	$K(\text{Er}^{3+} + \text{HL}^- = \text{ErHL}^+) = 3.66$	138
Eu <sup>3+</sup>	Sp	20	0.1 (KCl)	$K(\text{Eu}^{3+} + \text{HL}^- = \text{EuHL}^+) = 3.50$	138
Gd <sup>3+</sup>	Sp	20	0.1 (KCl)	$K(\text{Gd}^{3+} + \text{HL}^- = \text{GdHL}^+) = 3.52$	138
Ho <sup>3+</sup>	Sp	20	0.1 (KCl)	$K(\text{Ho}^{3+} + \text{HL}^- = \text{HoHL}^+) = 3.60$	138
La <sup>3+</sup>	Sp	20	0.1 (KCl)	$K(\text{La}^{3+} + \text{HL}^- = \text{LaHL}^+) = 2.69$	138
Lu <sup>3+</sup>	Sp	20	0.1 (KCl)	$K(\text{Lu}^{3+} + \text{HL}^- = \text{LuHL}^+) = 3.81$	138
Nd <sup>3+</sup>	Sp	20	0.1 (KCl)	$K(\text{Nd}^{3+} + \text{HL}^- = \text{NdHL}^+) = 3.45$	138
Pr <sup>3+</sup>	Sp	20	0.1 (KCl)	$K(\text{Pr}^{3+} + \text{HL}^- = \text{PrHL}^+) = 3.35$	138
Sm <sup>3+</sup>	Sp	20	0.1 (KCl)	$K(\text{Sm}^{3+} + \text{HL}^- = \text{SmHL}^+) = 3.49$	138
Tb <sup>3+</sup>	Sp	20	0.1 (KCl)	$K(\text{Tb}^{3+} + \text{HL}^- = \text{TbHL}^+) = 3.43$	138
C <sub>11</sub> H <sub>9</sub> O <sub>4</sub> N, 3-acetyl-4 hydroxycoumarin oxime, H <sub>2</sub> L					
M <sup>3+</sup> -HL	Gl	35	0.01 NaClO <sub>4</sub> , 50% dioxan	$\text{M}^{3+} + n\text{HL}^- = \text{M}(\text{HL})_n^{(3-n)+}$	
Ce <sup>3+</sup>				$K(n=1) = 3.16, K(n=2) = 5.52$	135
Dy <sup>3+</sup>				$K(n=1) = 3.73, K(n=2) = 6.61$	135
Er <sup>3+</sup>				$K(n=1) = 3.90, K(n=2) = 6.83$	135
Eu <sup>3+</sup>				$K(n=1) = 3.73, K(n=2) = 6.63$	135
Gd <sup>3+</sup>				$K(n=1) = 3.52, K(n=2) = 6.19$	135
Ho <sup>3+</sup>				$K(n=1) = 3.82, K(n=2) = 6.69$	135
La <sup>3+</sup>				$K(n=1) = 3.02, K(n=2) = 5.24$	135
Lu <sup>3+</sup>				$K(n=1) = 4.03, K(n=2) = 6.66$	135
Nd <sup>3+</sup>				$K(n=1) = 3.43, K(n=2) = 6.06$	135
Pr <sup>3+</sup>				$K(n=1) = 3.31, K(n=2) = 5.79$	135
Sm <sup>3+</sup>				$K(n=1) = 3.62, K(n=2) = 6.39$	135

(Continued.)					
Metal	Method	Temp. (°C)	Medium	log of equilibrium constant	Ref.
Tb <sup>3+</sup>				$K(n=1) = 3.63, K(n=2) = 6.40$	135
Y <sup>3+</sup>				$K(n=1) = 3.35, K(n=2) = 5.91$	135
Yb <sup>3+</sup>				$K(n=1) = 4.15, K(n=2) = 6.92$	135
C <sub>11</sub> H <sub>12</sub> O <sub>2</sub> N <sub>2</sub> , 2-amino-3-(indol-3'-yl)propanoic acid (tryptophan), HL					
H <sup>+</sup>	Gl	25	0.1 (KCl)	$K_1 = 9.39 \pm 0.02$	139
	Gl	25	1 (NaNO <sub>3</sub> )	$K_1 = 9.43, K_2 = 2.44$	139
Ce <sup>3+</sup>	Pot	20	0.1 (KCl)	$K_1 = 4.6 \pm 0.2$	140
Er <sup>3+</sup>	Gl	25	0.1 (KCl)	$K_1 = 5.1, K_2 = 4.5$	139
	Gl	25	0.1 (KCl)	$K_1 = 5.3 \pm 0.3, K_2 = 4.5 \pm 0.2$	139
Eu <sup>3+</sup>	Pol	25	?	$K_1 = 6.80$	141
Gd <sup>3+</sup>	Gl	25	0.1 (KCl)	$K_1 = 5.0, K_2 = 4.6$	139
	Gl	25	0.1 (KCl)	$K_1 = 5.2 \pm 0.1, K_2 = 4.6 \pm 0.1$	139
La <sup>3+</sup>	Gl	25	0.1 (KCl)	$K_1 = 4.45, K_2 = 4.1$	
	Gl	25	0.1 (KCl)	$K_1 = 4.5 \pm 0.1, K_2 = 4.1 \pm 0.1$	139
Lu <sup>3+</sup>	Gl	25	0.1 (KCl)	$K_1 = 5.2, K_2 = 4.7$	139
	Gl	25	0.1 (KCl)	$K_1 = 5.3 \pm 0.3, K_2 = 4.7 \pm 0.1$	139
Nd <sup>3+</sup>	Gl	25	0.1 (KCl)	$K_1 = 4.4 \pm 0.1, K_2 = 4.4 \pm 0.1$	139
Tb <sup>3+</sup>	Gl	25	0.1 (KCl)	$K_1 = 5.0, K_2 = 4.7$	139
C <sub>11</sub> H <sub>13</sub> O <sub>6</sub> N, 1,2-dihydroxybenzenemethyleneiminodiacetic acid, H <sub>4</sub> L					
H <sup>+</sup>	Gl	25	0.1 (KCl)	$K_1 = 12, K_2 = 10.96, K_3 = 8.50, K_4 = 2.60$	134
Eu <sup>2+</sup>	Gl	25	0.1 (KCl)	$K(\text{Eu}^{2+} + \text{HL}^{3-} = \text{EuHL}^-) = 4.52 \pm 0.04$	134
Eu <sup>3+</sup>	Gl	25	0.1 (KCl)	$K(\text{Eu}^{3+} + \text{HL}^{3-} = \text{EuHL}) = 13.63 \pm 0.03$	134
C <sub>11</sub> H <sub>13</sub> O <sub>6</sub> N, 1,4-dihydroxybenzene-2-methyleneiminodiacetic acid, H <sub>4</sub> L					
H <sup>+</sup>	Gl	25	0.1 (KCl)	$K_1 = 12, K_2 = 11.17, K_3 = 8.33, K_4 = 2.65$	134
Eu <sup>2+</sup>	Gl	25	0.1 (KCl)	$K(\text{Eu}^{2+} + \text{HL}^{3-} = \text{EuHL}^-) = 5.17 \pm 0.03$	134
Eu <sup>3+</sup>	Gl	25	0.1 (KCl)	$K(\text{Eu}^{3+} + \text{HL}^{3-} = \text{EuHL}) = 12.15 \pm 0.02$	134
				$K(\text{Eu}^{3+} + \text{H}_2\text{L}^{2-} = \text{EuH}_2\text{L}^+) = 6.66 \pm 0.02$	
				$K(\text{Eu}^{3+} + \text{H}_3\text{L}^- = \text{EuH}_3\text{L}^{2+}) = 3.21 \pm 0.02$	
C <sub>11</sub> H <sub>13</sub> O <sub>6</sub> N, 2,3-dihydroxybenzyliminodiacetic acid, H <sub>4</sub> L					
Gd <sup>3+</sup>	Pot	?	?	$K(\text{Gd}^{3+} + \text{HL}^{3-} = \text{GdHL}) = 14.4$	142
La <sup>3+</sup>	Pot	?	?	$K(\text{La}^{3+} + \text{HL}^{3-} = \text{LaHL}) = 12.7$	142
C <sub>11</sub> H <sub>13</sub> O <sub>6</sub> N, 2,5-dihydroxybenzyliminodiacetic acid, H <sub>4</sub> L					
Gd <sup>3+</sup>	Gl	25	~0	$K(\text{Gd}^{3+} + \text{HL}^{3-} = \text{GdHL}) = 14.4$	142
C <sub>11</sub> H <sub>13</sub> O <sub>6</sub> N, 2,6-dihydroxybenzyliminodiacetic acid, H <sub>4</sub> L					
Gd <sup>3+</sup>	Pot	?	?	$K(\text{Gd}^{3+} + \text{HL}^{3-} = \text{GdHL}) = 12.4$	142
La <sup>3+</sup>	Pot	?	?	$K = 10.6$	142
C <sub>11</sub> H <sub>14</sub> O <sub>4</sub> N, glycyl-DL-tyrosine, H <sub>2</sub> L					
H <sup>+</sup>	Gl	25	0.1 (KCl)	$K_2 = 8.30, K_3 = 3.01$	65
Eu <sup>3+</sup>	Gl	25	0.1 (KCl)	$K(\text{Eu}^{3+} + \text{HL}^- = \text{EuHL}^{2+}) = 2.85$	65
Gd <sup>3+</sup>	Gl	25	0.1 (KCl)	$K(\text{Gd}^{3+} + \text{HL}^- = \text{GdHL}^{2+}) = 2.65$	65
Nd <sup>3+</sup>	Gl	25	0.1 (KCl)	$K(\text{Nd}^{3+} + \text{HL}^- = \text{NdHL}^{2+}) = 2.70$	65
Yb <sup>3+</sup>	Gl	25	0.1 (KCl)	$K(\text{Yb}^{3+} + \text{HL}^- = \text{YbHL}^{2+}) = 2.85$	65
C <sub>11</sub> H <sub>14</sub> O <sub>3</sub> N <sub>2</sub> , glycyl-DL-phenylalanine, HL					
H <sup>+</sup>	Gl	25	0.1 (KCl)	$K_1 = 8.22, K_2 = 3.35$	65
Eu <sup>3+</sup>	Gl	25	0.1 (KCl)	$K_1 = 2.65$	65
Gd <sup>3+</sup>	Gl	25	0.1 (KCl)	$K_1 = 2.40$	65
Ho <sup>3+</sup>	Gl	25	0.1 (KCl)	$K_1 = 2.45$	65
Nd <sup>3+</sup>	Gl	25	0.1 (KCl)	$K_1 = 2.25$	65
Yb <sup>3+</sup>	Gl	25	0.1 (KCl)	$K_1 = 2.75$	65

(Continued.)

Metal	Method	Temp. (°C)	Medium	log of equilibrium constant	Ref.
$C_{11}H_{14}NO_4C_6H_5CH_2NH(CH_2COOH)_2$ , <i>N</i> -benzyliminodiacetic acid, $H_2L$					
$La^{3+}$	Iex	25	0.1 KCl	$\log K_1 = 6.47, \log K_2 = 5.42$	202
$Ce^{3+}$	Iex	25	0.1 KCl	$\log K_1 = 6.78, \log K_2 = 5.59$	202
$Pr^{3+}$	Iex	25	0.1 KCl	$\log K_1 = 6.92, \log K_2 = 5.65$	202
$Nd^{3+}$	Iex	25	0.1 KCl	$\log K_1 = 6.61, \log K_2 = 5.67$	202
$Sm^{3+}$	Iex	25	0.1 KCl	$\log K_1 = 7.10, \log K_2 = 5.82$	202
$Gd^{3+}$	Iex	25	0.1 KCl	$\log K_1 = 7.04, \log K_2 = 5.75$	202
$Tb^{3+}$	Iex	25	0.1 KCl	$\log K_1 = 7.22, \log K_2 = 5.91$	202
$Ho^{3+}$	Iex	25	0.1 KCl	$\log K_1 = 7.38, \log K_2 = 5.97$	202
$Er^{3+}$	Iex	25	0.1 KCl	$\log K_1 = 7.49, \log K_2 = 6.10$	202
$Y^{3+}$	Iex	25	0.1 KCl	$\log K_1 = 7.10, \log K_2 = 5.71$	202
$C_{11}H_{19}N_2O_8 (HOOCCH_2)_2NCH_2CH_2-N(CH_2COOH)_2$ , propylenediaminetetraacetic acid (PDTA), $H_4L$					
$La^{3+}$	M-Hg	20	0.1 $KNO_3$	$\log K_1 = 16.42$	207
$Ce^{3+}$	M-Hg	20	0.1 $KNO_3$	$\log K_1 = 16.79$	207
$Pr^{3+}$	M-Hg	20	0.1 $KNO_3$	$\log K_1 = 17.17$	207
$Nd^{3+}$	M-Hg	20	0.1 $KNO_3$	$\log K_1 = 17.54$	207
$Sm^{3+}$	M-Hg	20	0.1 $KNO_3$	$\log K_1 = 17.97$	207
$Eu^{3+}$	M-Hg	20	0.1 $KNO_3$	$\log K_1 = 18.26$	207
$Gd^{3+}$	M-Hg	20	0.1 $KNO_3$	$\log K_1 = 18.21$	207
$Tb^{3+}$	M-Hg	20	0.1 $KNO_3$	$\log K_1 = 18.64$	207
$Dy^{3+}$	M-Hg	20	0.1 $KNO_3$	$\log K_1 = 19.05$	207
$Ho^{3+}$	M-Hg	20	0.1 $KNO_3$	$\log K_1 = 19.30$	207
$Er^{3+}$	M-Hg	20	0.1 $KNO_3$	$\log K_1 = 19.61$	207
$Tm^{3+}$	M-Hg	20	0.1 $KNO_3$	$\log K_1 = 20.08$	207
$Yb^{3+}$	M-Hg	20	0.1 $KNO_3$	$\log K_1 = 20.25$	207
$Lu^{3+}$	M-Hg	20	0.1 $KNO_3$	$\log K_1 = 20.56$	207
$Y^{3+}$	M-Hg	20	0.1 $KNO_3$	$\log K_1 = 18.78$	207
$C_{11}H_{18}O_8N_2$ , 1,3-diaminopropane- <i>N,N,N',N'</i> -tetraacetic acid (trimethylenedinitrilo- <i>N,N,N',N'</i> -tetraacetic acid), $H_4L$					
$H^+$		20	0.1 ( $KNO_3$ )	$K_1 = 10.46, K_2 = 8.02, K_3 = 2.47, K_4 = 1.88$	143
$Ce^{3+}$	pH, ix	20	0.1 ( $KNO_3$ )	$K_1 = 11.70, \Delta G = -15.69, \Delta H = 3.60,$ $\Delta S = 65.8, K(CeHL = CeL^- + H^+) = -4.55$	143
$Dy^{3+}$	pH, ix, Pol	20	0.1 ( $KNO_3$ )	$K_1 = 14.65, \Delta G = -19.65, \Delta H = 4.56,$ $\Delta S = 82.6$	143
$Eu^{3+}$	pH, ix	20	0.1 ( $KNO_3$ )	$K_1 = 13.54, \Delta G = -18.15, \Delta H = 5.95,$ $\Delta S = 82.2$	143
$Er^{3+}$	ix, Pol	20	0.1 ( $KClO_4$ )	$\Delta G = -18.15, \Delta H = 5.81, \Delta S = 81.7$	143
$Er^{3+}$	ix, Pol	20	0.1 ( $KNO_3$ )	$K_1 = 14.80, \Delta G = -19.86, \Delta H = 4.21,$ $\Delta S = 80.7$	143
$Gd^{3+}$	pH, ix, Pol	20	0.1 ( $KNO_3$ )	$K_1 = 13.70, \Delta G = -18.37, \Delta H = 4.95,$ $\Delta S = 79.2$	143
$La^{3+}$	pH	20	0.1 ( $KNO_3$ )	$K_1 = 11.23, \Delta G = -15.05, \Delta H = 3.78,$ $\Delta S = 63.7, K(LaHL = LaL^- + H^+) = -4.67$	143
$Lu^{3+}$	ix	20	0.1 ( $KNO_3$ )	$K_1 = 15.54, \Delta G = -20.88, \Delta H = 3.53,$ $\Delta S = 83.4$	143
$Nd^{3+}$	pH, ix, Pol	20	0.1 ( $KNO_3$ )	$K_1 = 12.34, \Delta G = -16.17, \Delta H = 4.2,$ $\Delta S = 69.5, K(NdHL = NdL^- + H^+) = -4.03$	143
$Pr^{3+}$	pH	20	0.1 ( $KNO_3$ )	$K_1 = 11.99, \Delta G = -16.06, \Delta H = 3.92,$ $\Delta S = 68.1$	143



(Continued.)					
Metal	Method	Temp. (°C)	Medium	log of equilibrium constant	Ref.
Sm <sup>3+</sup>	pH, ix, Pol	20	0.1 (KNO <sub>3</sub> )	$K_1 = 13.14, \Delta G = -17.72, \Delta H = 5.65,$ $\Delta S = 79.4$	143
		20	0.1 (KClO <sub>4</sub> )	$\Delta G = -17.72, \Delta H = 5.52, \Delta S = 78.9$	143
Yb <sup>3+</sup>	ix, Pol	20	0.1 (KNO <sub>3</sub> )	$K_1 = 15.42, \Delta G = -20.70, \Delta H = 3.65,$ $\Delta S = 80.3$	143
C <sub>12</sub> H <sub>11</sub> O <sub>2</sub> F <sub>7</sub> , 1,1,1,2,2,3,3-heptafluoro-7,7-dimethyl-4,6-octanedione, HL					
H <sup>+</sup>	Sp	24-26	0.1 Et <sub>4</sub> NClO <sub>4</sub>	$K_1 = 6.7$	144
Eu <sup>3+</sup>	Dis	24-26	0.1 Et <sub>4</sub> NClO <sub>4</sub>	$\beta_2 = 11.9 \pm 0.2, \beta_3 = 18.4 \pm 0.2$	144
Gd <sup>3+</sup>	Dis	24-26	0.1 Et <sub>4</sub> NClO <sub>4</sub>	$\beta_2 = 12.7 \pm 0.2, \beta_3 = 18.7$	144
Pr <sup>3+</sup>	Dis	24-26	0.1 Et <sub>4</sub> NClO <sub>4</sub>	$\beta_2 = 18.0 \pm 0.2$	144
Sm <sup>3+</sup>	Dis	24-26	0.1 Et <sub>4</sub> NClO <sub>4</sub>	$\beta_3 = 18.4$	144
Tm <sup>3+</sup>	Dis	24-26	0.1 Et <sub>4</sub> NClO <sub>4</sub>	$\beta_2 = 13.4, \beta_3 = 19.4$	144
C <sub>12</sub> H <sub>20</sub> O <sub>8</sub> N <sub>2</sub> , (1,2-butylenedinitrilo)tetraacetic acid, H <sub>4</sub> L					
H <sup>+</sup>	Gl	20	0.1 (KNO <sub>3</sub> )	$K_1 = 10.98, K_2 = 6.05, K_3 = 3.04, K_4 = 2.1$	145
Ce <sup>3+</sup>	Gl	20	0.1 (KNO <sub>3</sub> )	$K_1 = 17.15$	145
Dy <sup>3+</sup>	Pol	20	0.1 (KNO <sub>3</sub> )	$K_1 = 19.48 \pm 0.10$	145
Er <sup>3+</sup>	Pol	20	0.1 (KNO <sub>3</sub> )	$K_1 = 20.11 \pm 10.14$	145
Eu <sup>3+</sup>	Pol	20	0.1 (KNO <sub>3</sub> )	$K_1 = 18.38 \pm 0.10$	145
Gd <sup>3+</sup>	Pol	20	0.1 (KNO <sub>3</sub> )	$K_1 = 18.56 \pm 0.10$	145
Ho <sup>3+</sup>	Pol	20	0.1 (KNO <sub>3</sub> )	$K_1 = 19.80 \pm 0.12$	145
La <sup>3+</sup>	Pol	20	0.1 (KNO <sub>3</sub> )	$K_1 = 16.58 \pm 0.15$	145
Lu <sup>3+</sup>	Pol	20	0.1 (KNO <sub>3</sub> )	$K_1 = 20.97 \pm 0.17$	145
Nd <sup>3+</sup>	Pol	20	0.1 (KNO <sub>3</sub> )	$K_1 = 17.77 \pm 0.12$	145
Pr <sup>3+</sup>	Pol	20	0.1 (KNO <sub>3</sub> )	$K_1 = 17.49 \pm 0.13$	145
Sm <sup>3+</sup>	Pol	20	0.1 (KNO <sub>3</sub> )	$K_1 = 18.25 \pm 0.10$	145
Tb <sup>3+</sup>	Pol	20	0.1 (KNO <sub>3</sub> )	$K_1 = 19.03 \pm 0.10$	145
Tm <sup>3+</sup>	Pol	20	0.1 (KNO <sub>3</sub> )	$K_1 = 20.52 \pm 0.17$	145
Yb <sup>3+</sup>	Pol	20	0.1 (KNO <sub>3</sub> )	$K_1 = 20.87 \pm 0.16$	145
C <sub>12</sub> H <sub>20</sub> O <sub>8</sub> N <sub>2</sub> , (DL-2,3-butylenedinitrilo)tetraacetic acid, H <sub>4</sub> L					
Dy <sup>3+</sup>	Pol	20	0.1	$K_1 = 19.93$	146
	Sp	20	0.1 (NaClO <sub>4</sub> )	$K_1 = 19.83$	147
Er <sup>3+</sup>	Pol	20	0.1	$K_1 = 20.68$	146
	Sp	20	0.1 (NaClO <sub>4</sub> )	$K_1 = 20.30$	147
Eu <sup>3+</sup>	Pol	20	0.1	$K_1 = 18.61$	146
	Sp	20	0.1 (NaClO <sub>4</sub> )	$K_1 = 18.54$	147
Gd <sup>3+</sup>	Pol	20	0.1	$K_1 = 18.84$	146
	Sp	20	0.1 (NaClO <sub>4</sub> )	$K_1 = 18.64$	147
Ho <sup>3+</sup>	Pol	20	0.1	$K_1 = 20.27$	146
	Sp	20	0.1 (NaClO <sub>4</sub> )	$K_1 = 19.97$	147
Lu <sup>3+</sup>	Pol	20	0.1	$K_1 = 21.33$	146
Nd <sup>3+</sup>	Pol	20	0.1	$K_1 = 17.70$	146
	Sp	20	0.1 (NaClO <sub>4</sub> )	$K_1 = 17.60$	147
Pr <sup>3+</sup>	Pol	20	0.1	$K_1 = 17.49$	146
	Sp	20	0.1 (NaClO <sub>4</sub> )	$K_1 = 17.39$	147
Sm <sup>3+</sup>	Pol	20	0.1	$K_1 = 18.32$	146
	Sp	20	0.1 (NaClO <sub>4</sub> )	$K_1 = 18.22$	147
Tb <sup>3+</sup>	Pol	20	0.1	$K_1 = 19.45$	146
	Sp	20	0.1 (NaClO <sub>4</sub> )	$K_1 = 19.15$	147

(Continued.)

Metal	Method	Temp. (°C)	Medium	log of equilibrium constant	Ref.
Tm <sup>3+</sup>	Pol	20	0.1	$K_1 = 20.96$	146
	Sp	20	0.1 (NaClO <sub>4</sub> )	$K_1 = 20.44$	147
Yb <sup>3+</sup>	Pol	20	0.1	$K_1 = 21.29$	146
C <sub>12</sub> H <sub>20</sub> O <sub>8</sub> N <sub>2</sub> , (meso-2,3-butylenedinitrilo)tetraacetic acid, H <sub>4</sub> L					
H <sup>+</sup>	Gl	20	0.1 (KNO <sub>3</sub> )	$K_1 = 11.22, K_2 = 6.29, K_3 = 2.69, K_4 = 1.76$	147
Dy <sup>3+</sup>	Pol	20	0.1	$K_1 = 17.01$	146
	Sp	20	0.1 (NaClO <sub>4</sub> )	$K_1 = 17.16$	147
Er <sup>3+</sup>	Pol	20	0.1	$K_1 = 17.55$	146
	Sp	20	0.1 (NaClO <sub>4</sub> )	$K_1 = 17.59$	147
Eu <sup>3+</sup>	Pol	20	0.1	$K_1 = 16.57$	146
	Sp	20	0.1 (NaClO <sub>4</sub> )	$K_1 = 17.05$	147
Gd <sup>3+</sup>	Pol	20	0.1	$K_1 = 16.51$	146
	Sp	20	0.1 (NaClO <sub>4</sub> )	$K_1 = 17.03$	147
Ho <sup>3+</sup>	Pol	20	0.1	$K_1 = 17.25$	146
	Sp	20	0.1 (NaClO <sub>4</sub> )	$K_1 = 17.36$	147
Lu <sup>3+</sup>	Pol	20	0.1	$K_1 = 18.11$	146
	Sp	20	0.1 (NaClO <sub>4</sub> )	$K_1 = 18.10$	147
Nd <sup>3+</sup>	Pol	20	0.1	$K_1 = 16.06$	146
	Sp	20	0.1 (NaClO <sub>4</sub> )	$K_1 = 16.47$	147
Pr <sup>3+</sup>	Pol	20	0.1	$K_1 = 15.81$	146
	Sp	20	0.1 (NaClO <sub>4</sub> )	$K_1 = 16.10$	147
Sm <sup>3+</sup>	Pol	20	0.1	$K_1 = 16.47$	146
	Sp	20	0.1 (NaClO <sub>4</sub> )	$K_1 = 16.74$	147
Tb <sup>3+</sup>	Pol	20	0.1	$K_1 = 16.72$	146
	Sp	20	0.1 (NaClO <sub>4</sub> )	$K_1 = 17.02$	147
Tm <sup>3+</sup>	Pol	20	0.1	$K_1 = 17.87$	146
	Sp	20	0.1 (NaClO <sub>4</sub> )	$K_1 = 17.87$	147
Yb <sup>3+</sup>	Pol	20	0.1	$K_1 = 18.11$	146
	Sp	20	0.1 (NaClO <sub>4</sub> )	$K_1 = 18.08$	147
C <sub>12</sub> H <sub>20</sub> O <sub>8</sub> N <sub>2</sub> , ethylenediiminodi-2-pentanedioic acid, H <sub>4</sub> L					
H <sup>+</sup>	Gl	30	0.1 (KNO <sub>3</sub> )	$K_1 = 9.75, K_2 = 8.93, K_3 = 4.85, K_4 = 3.75$	148
Ce <sup>3+</sup>	Gl	25	0.1 (KNO <sub>3</sub> )	$K_1 = 7.23 \pm 0.08$	149
Dy <sup>3+</sup>	Gl	25	0.1 (KNO <sub>3</sub> )	$K_1 = 8.80 \pm 0.07$	149
Er <sup>3+</sup>	Gl	25	0.1 (KNO <sub>3</sub> )	$K_1 = 8.99 \pm 0.07$	149
Eu <sup>3+</sup>	Gl	25	0.1 (KNO <sub>3</sub> )	$K_1 = 7.92 \pm 0.04$	149
Gd <sup>3+</sup>	Gl	25	0.1 (KNO <sub>3</sub> )	$K_1 = 8.02 \pm 0.09$	149
Ho <sup>3+</sup>	Gl	25	0.1 (KNO <sub>3</sub> )	$K_1 = 8.90 \pm 0.07$	149
	Gl	30	0.1 (NaClO <sub>4</sub> )	$K_1 = 8.46$	150
La <sup>3+</sup>	Gl	25	0.1 (KNO <sub>3</sub> )	$K_1 = 6.56 \pm 0.06$	149
Lu <sup>3+</sup>	Gl	25	0.1 (KNO <sub>3</sub> )	$K_1 = 9.50 \pm 0.06$	149
Nd <sup>3+</sup>	Gl	30	0.1 (KNO <sub>3</sub> )	$K_1 = 7.79 \pm 0.05$	151
	Gl	25	0.1 (KNO <sub>3</sub> )	$K_1 = 7.70 \pm 0.09$	149
Pr <sup>3+</sup>	Gl	30	0.1 (KNO <sub>3</sub> )	$K_1 = 7.22 \pm 0.06$	151
	Gl	25	0.1 (KNO <sub>3</sub> )	$K_1 = 7.21 \pm 0.08$	149
Sm <sup>3+</sup>	Gl	30	0.1 (KNO <sub>3</sub> )	$K_1 = 8.22 \pm 0.03$	151
	Gl	25	0.1 (KNO <sub>3</sub> )	$K_1 = 7.82 \pm 0.05$	149
Tb <sup>3+</sup>	Gl	25	0.1 (KNO <sub>3</sub> )	$K_1 = 8.62 \pm 0.05$	149
Y <sup>3+</sup>	Gl	25	0.1 (KNO <sub>3</sub> )	–	149
Yb <sup>3+</sup>	Gl	25	0.1 (KNO <sub>3</sub> )	–	149

(Continued.)					
Metal	Method	Temp. (°C)	Medium	log of equilibrium constant	Ref.
C <sub>12</sub> H <sub>20</sub> O <sub>9</sub> N <sub>2</sub> , (HO <sub>2</sub> CCH <sub>2</sub> ) <sub>2</sub> NCH <sub>2</sub> CH <sub>2</sub> OCH <sub>2</sub> CH <sub>2</sub> N(CH <sub>2</sub> CO <sub>2</sub> H) <sub>2</sub> , 2,2'-bis[di(carboxymethyl)amino]diethyl ether, H <sub>4</sub> L					
La <sup>3+</sup>	Hg	20	0.1 M KNO <sub>3</sub>	log K <sub>1</sub> = 16.00	199
La <sup>3+</sup>	Pol	20	0.1 M KNO <sub>3</sub>	log K <sub>1</sub> = 16.29	199
Ce <sup>3+</sup>	Iex	20	0.1 M NH <sub>4</sub> Cl	log K <sub>1</sub> = 17.87	199
Ce <sup>3+</sup>	Hg	20	0.1 M KNO <sub>3</sub>	log K <sub>1</sub> = 16.69	199
Ce <sup>3+</sup>	Pol	20	0.1 M KNO <sub>3</sub>	log K <sub>1</sub> = 17.13	199
Pr <sup>3+</sup>	Hg	20	0.1 M KNO <sub>3</sub>	log K <sub>1</sub> = 17.36	199
Pr <sup>3+</sup>	Pol	20	0.1 M KNO <sub>3</sub>	log K <sub>1</sub> = 17.61	199
Nd <sup>3+</sup>	Hg	20	0.1 M KNO <sub>3</sub>	log K <sub>1</sub> = 17.67	199
Nd <sup>3+</sup>	Pol	20	0.1 M KNO <sub>3</sub>	log K <sub>1</sub> = 17.81	199
Sm <sup>3+</sup>	Hg	20	0.1 M KNO <sub>3</sub>	log K <sub>1</sub> = 18.19	199
Sm <sup>3+</sup>	Pol	20	0.1 M KNO <sub>3</sub>	log K <sub>1</sub> = 18.25	199
Eu <sup>3+</sup>	Hg	20	0.1 M KNO <sub>3</sub>	log K <sub>1</sub> = 18.3	199
Eu <sup>3+</sup>	Pol	20	0.1 M KNO <sub>3</sub>	log K <sub>1</sub> = 18.38	199
Gd <sup>3+</sup>	Hg	20	0.1 M KNO <sub>3</sub>	log K <sub>1</sub> = 18.13	199
Gd <sup>3+</sup>	Pol	20	0.1 M KNO <sub>3</sub>	log K <sub>1</sub> = 18.21	199
Tb <sup>3+</sup>	Hg	20	0.1 M KNO <sub>3</sub>	log K <sub>1</sub> = 18.31	199
Tb <sup>3+</sup>	Pol	20	0.1 M KNO <sub>3</sub>	log K <sub>1</sub> = 18.31	199
Dy <sup>3+</sup>	Hg	20	0.1 M KNO <sub>3</sub>	log K <sub>1</sub> = 18.21	199
Dy <sup>3+</sup>	Pol	20	0.1 M KNO <sub>3</sub>	log K <sub>1</sub> = 18.29	199
Ho <sup>3+</sup>	Hg	20	0.1 M KNO <sub>3</sub>	log K <sub>1</sub> = 18.13	199
Ho <sup>3+</sup>	Pol	20	0.1 M KNO <sub>3</sub>	log K <sub>1</sub> = 18.17	199
Er <sup>3+</sup>	Hg	20	0.1 M KNO <sub>3</sub>	log K <sub>1</sub> = 17.99	199
Er <sup>3+</sup>	Pol	20	0.1 M KNO <sub>3</sub>	log K <sub>1</sub> = 18.18	199
Tm <sup>3+</sup>	Hg	20	0.1 M KNO <sub>3</sub>	log K <sub>1</sub> = 17.83	199
Tm <sup>3+</sup>	Pol	20	0.1 M KNO <sub>3</sub>	log K <sub>1</sub> = 18.01	199
Yb <sup>3+</sup>	Hg	20	0.1 M KNO <sub>3</sub>	log K <sub>1</sub> = 17.85	199
Yb <sup>3+</sup>	Pol	20	0.1 M KNO <sub>3</sub>	log K <sub>1</sub> = 18.06	199
Lu <sup>3+</sup>	Hg	20	0.1 M KNO <sub>3</sub>	log K <sub>1</sub> = 17.75	199
Lu <sup>3+</sup>	Pol	20	0.1 M KNO <sub>3</sub>	log K <sub>1</sub> = 17.92	199
Y <sup>3+</sup>	Hg	20	0.1 M KNO <sub>3</sub>	log K <sub>1</sub> = 17.54	199
Y <sup>3+</sup>	Pol	20	0.1 M KNO <sub>3</sub>	log K <sub>1</sub> = 17.79	199
(2,2'-oxydiethylene)dinitrilo tetraacetic acid (EEDTA), H <sub>4</sub> L					
Nd <sup>3+</sup>	Sp	20	0.5	K <sub>1</sub> = 17.34	152
C <sub>12</sub> H <sub>20</sub> O <sub>10</sub> N <sub>2</sub> , (2,3-dihydroxytetramethylenedinitrilo)tetraacetic acid, H <sub>4</sub> L					
Dy <sup>3+</sup>	oth	?	?	K(2Dy <sup>3+</sup> + L <sup>6-</sup> = Dy <sub>2</sub> L) = 27.23, high-frequency titration	153
Er <sup>3+</sup>	Pot	25	0.1 (KCl)	K(Er <sup>3+</sup> + H <sub>2</sub> L <sup>4-</sup> = ErH <sub>2</sub> L <sup>-</sup> ) = 13.6 K(Er <sup>3+</sup> + HL <sup>5-</sup> = ErHL <sup>2-</sup> ) = 18.34	154
Gd <sup>3+</sup>	Pot	25	0.1 (KCl)	K(Gd <sup>3+</sup> + H <sub>2</sub> L <sup>4-</sup> = GdH <sub>2</sub> L <sup>-</sup> ) = 13.06 K(Gd <sup>3+</sup> + HL <sup>5-</sup> = GdHL <sup>2-</sup> ) = 17.15	154
La <sup>3+</sup>	Oth	?	?	K(2La <sup>3+</sup> + L <sup>6-</sup> = La <sub>2</sub> L) = 19.27, high-frequency titration	153
Nd <sup>3+</sup>	Oth	?	?	K(2Nd <sup>3+</sup> + L <sup>6-</sup> = Nd <sub>2</sub> L) = 21.57, high-frequency titration	153
Yb <sup>3+</sup>	Oth	?	?	K(2Yb <sup>3+</sup> + L <sup>6-</sup> = Yb <sub>2</sub> L) = 25.91, high-frequency titration	153

(Continued.)

Metal	Method	Temp. (°C)	Medium	log of equilibrium constant	Ref.
		25	0.1 (KCl)	$K(\text{Yb}^{3+} + \text{H}_2\text{L}^{4-} = \text{YbH}_2\text{L}^-) = 12.62$ $K(\text{Yb}^{3+} + \text{HL}^{5-} = \text{YbHL}^{2-}) = 18.27$ $K(2\text{Yb}^{3+} + \text{HL}^{5-} = \text{Yb}_2\text{HL}^+) = 2.96$ $K(2\text{Yb}^{3+} + \text{L}^{6-} = \text{Yb}_2\text{L}) = 8.04$	154
$\text{C}_{12}\text{H}_9\text{O}_2\text{NSe}$ , picolinoyl-2-acetoselenophene, HL					
$\text{Ce}^{3+}$	Dis, Sp	20	0.1 $\text{NaClO}_4$	$K_1 = 9.24, K_2 = 8.14, K_3 = 7.03$	155
$\text{C}_{13}\text{H}_{10}\text{O}_2\text{Se}$ , benzoyl-2-selenoylmethane, HL					
$\text{Eu}^{3+}$	Dis	25	0.1 $\text{KNO}_3$	$K_1 = 5.5, \beta_2 = 11.04, \beta_3 = 16.08$	156
$\text{C}_{13}\text{H}_{11}\text{O}_2\text{N}$ , <i>N</i> -phenylbenzohydroxamic acid ( <i>N</i> -benzoyl- <i>N</i> -phenylhydroxylamine)					
$\text{Dy}^{3+}$	Gl	25	0.1 $\text{NaClO}_4$	$K_1 = 8.60, K_2 = 6.50, K_3 = 5.50$	157
$\text{Er}^{3+}$	Gl	25	0.1 $\text{NaClO}_4$ , 75% acetone	$K_1 = 8.75, K_2 = 6.70, K_3 = 5.90$	157
$\text{Eu}^{3+}$	Gl	25	0.1 $\text{NaClO}_4$ , 75% acetone	$K_1 = 8.45, K_2 = 6.42$	157
$\text{Gd}^{3+}$	Gl	25	0.1 $\text{NaClO}_4$ , 75% acetone	$K_1 = 8.36, K_2 = 6.32$	157
$\text{La}^{3+}$	Gl	25	0.1 $\text{NaClO}_4$ , 75% acetone	$K_1 = 7.28, K_2 = 5.76, K_3 = 4.74$	157
$\text{Nd}^{3+}$	Gl	25	0.1 $\text{NaClO}_4$ , 75% acetone	$K_1 = 7.88, K_2 = 6.30, K_3 = 5.03$	157
$\text{Pr}^{3+}$	Gl	25	0.1 $\text{NaClO}_4$ , 75% acetone	$K_1 = 7.70, K_2 = 6.20, K_3 = 5.00$	157
$\text{Sm}^{3+}$	Gl	25	0.1 $\text{NaClO}_4$ , 75% acetone	$K_1 = 8.28, K_2 = 6.35, K_3 = 5.15$	157
$\text{Y}^{3+}$	Gl	25	0.1 $\text{NaClO}_4$ , 75% acetone	$K_1 = 8.00, K_2 = 6.32$	157
	Gl	25	0.1 $\text{NaClO}_4$ , 75% acetone	$K_1 = 7.73, \beta_2 = 14.73, \beta_3 = 20.81$	158
$\text{Yb}^{3+}$	Gl	25	0.1 $\text{NaClO}_4$ , 75% acetone	$K_1 = 9.17, K_2 = 6.95, K_3 = 6.15$	157
$\text{C}_{13}\text{H}_{12}\text{ON}_4$ , 1,5-diphenyl-1,2,4,5-tetraazapent-1-en-3-one (1,5-diphenylcarbazone)					
$\text{H}^+$	pH	20	0.1 $\text{NaClO}_4$ , 50% ethanol	$K_1 = 9.30$	159
$\text{Ce}^{3+}$	pH	20	0.1 $\text{NaClO}_4$ , 50% ethanol	$K_1 = 3.20$	159
$\text{Dy}^{3+}$	pH	20	0.1 $\text{NaClO}_4$ , 50% ethanol	$K_1 = 3.65$	159
$\text{Er}^{3+}$	pH	20	0.1 $\text{NaClO}_4$ , 50% ethanol	$K_1 = 3.80$	159
$\text{Eu}^{3+}$	pH	20	0.1 $\text{NaClO}_4$ , 50% ethanol	$K_1 = 3.65$	159
$\text{Gd}^{3+}$	pH	20	0.1 $\text{NaClO}_4$ , 50% ethanol	$K_1 = 3.45$	159
$\text{Ho}^{3+}$	pH	20	0.1 $\text{NaClO}_4$ , 50% ethanol	$K_1 = 3.70$	159
$\text{La}^{3+}$	pH	20	0.1 $\text{NaClO}_4$ , 50% ethanol	$K_1 = 3.05$	159
$\text{Lu}^{3+}$	pH	20	0.1 $\text{NaClO}_4$ , 50% ethanol	$K_1 = 3.90$	159

<i>(Continued.)</i>					
Metal	Method	Temp. (°C)	Medium	log of equilibrium constant	Ref.
Nd <sup>3+</sup>	pH	20	0.1 NaClO <sub>4</sub> , 50% ethanol	$K_1 = 3.40$	159
Pr <sup>3+</sup>	pH	20	0.1 NaClO <sub>4</sub> , 50% ethanol	$K_1 = 3.30$	159
Sm <sup>3+</sup>	pH	20	0.1 NaClO <sub>4</sub> , 50% ethanol	$K_1 = 3.50$	159
Tb <sup>3+</sup>	pH	20	0.1 NaClO <sub>4</sub> , 50% ethanol	$K_1 = 3.55$	159
Tm <sup>3+</sup>	pH	20	0.1 NaClO <sub>4</sub> , 50% ethanol	$K_1 = 3.75$	159
Yb <sup>3+</sup>	pH	20	0.1 NaClO <sub>4</sub> , 50% ethanol	$K_1 = 3.80$	159
C <sub>13</sub> H <sub>12</sub> N <sub>4</sub> S, diphenylthiocarbazon					
Ce <sup>3+</sup>	pH	20	0.1 NaClO <sub>4</sub>	$K_1 = 1.50$	
Dy <sup>3+</sup>	pH	20	0.1 NaClO <sub>4</sub> , ethanol	$K_1 = 2.05$	159
Er <sup>3+</sup>	pH	20	0.1 NaClO <sub>4</sub> , ethanol	$K_1 = 2.20$	159
Eu <sup>3+</sup>	pH	20	0.1 NaClO <sub>4</sub> , ethanol	$K_1 = 2.00$	159
Gd <sup>3+</sup>	pH	20	0.1 NaClO <sub>4</sub> , ethanol	$K_1 = 1.80$	159
Ho <sup>3+</sup>	pH	20	0.1 NaClO <sub>4</sub> , ethanol	$K_1 = 2.15$	159
La <sup>3+</sup>	pH	20	0.1 NaClO <sub>4</sub> , ethanol	$K_1 = 1.40$	159
Lu <sup>3+</sup>	pH	20	0.1 NaClO <sub>4</sub> , ethanol	$K_1 = 2.30$	159
Nd <sup>3+</sup>	pH	20	0.1 NaClO <sub>4</sub> , ethanol	$K_1 = 1.75$	159
Pr <sup>3+</sup>	pH	20	0.1 NaClO <sub>4</sub> , ethanol	$K_1 = 1.65$	159
Sm <sup>3+</sup>	pH	20	0.1 NaClO <sub>4</sub> , ethanol	$K_1 = 1.90$	159
Tb <sup>3+</sup>	pH	20	0.1 NaClO <sub>4</sub> , ethanol	$K_1 = 1.95$	159
Tm <sup>3+</sup>	pH	20	0.1 NaClO <sub>4</sub> , ethanol	$K_1 = 2.25$	159
Yb <sup>3+</sup>	pH	20	0.1 NaClO <sub>4</sub> , ethanol	$K_1 = 2.30$	159
C <sub>13</sub> H <sub>15</sub> O <sub>6</sub> N, 2-benzylnitritotriacetic acid, H <sub>3</sub> L					
H <sup>+</sup>	?	25	0.1	$K_1 = 9.59, K_2 = 2.51, K_3 = 2.0$	160
Ce <sup>3+</sup>	?	25	0.1	$K_1 = 11.2, K_2 = 7, 67$	160
Er <sup>3+</sup>	?	25	0.1	$K_1 = 11.8, K_2 = 9.16$	160
Gd <sup>3+</sup>	?	25	0.1	$K_2 = 8.97$	160
Ho <sup>3+</sup>	?	25	0.1	$K_2 = 9.03$	160
La <sup>3+</sup>	?	25	0.1	$K_1 = 10.86, K_2 = 6.90$	160
Nd <sup>3+</sup>	?	25	0.1	$K_1 = 11.5, K_2 = 8.28$	160
Pr <sup>3+</sup>	?	25	0.1	$K_1 = 11.3, K_2 = 7, 97$	160

(Continued.)					
Metal	Method	Temp. (°C)	Medium	log of equilibrium constant	Ref.
Sm <sup>3+</sup>	?	25	0.1	$K_1 = 11.6, K_2 = 8.86$	160
Tb <sup>3+</sup>	?	25	0.1	$K_2 = 9.01$	160
Y <sup>3+</sup>	?	25	0.1	$K_2 = 8.94$	160
C <sub>13</sub> H <sub>18</sub> N <sub>2</sub> O <sub>8</sub> , trimethylenediamine- <i>N,N,N',N'</i> -tetraacetic acid (TMTA), H <sub>4</sub> L					
La <sup>3+</sup>	Gl	20	0.1 KNO <sub>3</sub>	log $K = 11.23$	208
Ce <sup>3+</sup>	Gl	20	0.1 KNO <sub>3</sub>	log $K = 11.75$	208
Nd <sup>3+</sup>	Gl	20	0.1 KNO <sub>3</sub>	log $K = 12.36$	208
Sm <sup>3+</sup>	Gl	20	0.1 KNO <sub>3</sub>	log $K = 13.21$	208
Eu <sup>3+</sup>	Gl	20	0.1 KNO <sub>3</sub>	log $K = 13.58$	208
Gd <sup>3+</sup>	Gl	20	0.1 KNO <sub>3</sub>	log $K = 13.74$	208
Dy <sup>3+</sup>	Gl	20	0.1 KNO <sub>3</sub>	log $K = 14.40$	208
Er <sup>3+</sup>	Gl	20	0.1 KNO <sub>3</sub>	log $K = 14.72$	208
Yb <sup>3+</sup>	Gl	20	0.1 KNO <sub>3</sub>	log $K = 15.10$	208
Y <sup>3+</sup>	Gl	20	0.1 KNO <sub>3</sub>	log $K = 15.88$	208
C <sub>13</sub> H <sub>22</sub> O <sub>8</sub> N <sub>2</sub> , 3-methyl-1,2-diaminobutane- <i>N,N,N',N'</i> -tetraacetic acid, H <sub>4</sub> L					
H <sup>+</sup>	Gl	20	0.1 (KNO <sub>3</sub> )	$K_1 = 11.25, K_2 = 5.64, K_3 = 3.33, K_4 = 2.4$	161
Ce <sup>3+</sup>	Pol	20	0.1 (KNO <sub>3</sub> )	$K_1 = 16.98 \pm 0.12$	161
Dy <sup>3+</sup>	Pol	20	0.1 (KNO <sub>3</sub> )	$K_1 = 19.39 \pm 0.12$	161
Er <sup>3+</sup>	Pol	20	0.1 (KNO <sub>3</sub> )	$K_1 = 19.97 \pm 0.14$	161
Eu <sup>3+</sup>	Pol	20	0.1 (KNO <sub>3</sub> )	$K_1 = 18.30 \pm 0.11$	161
Gd <sup>3+</sup>	Pol	20	0.1 (KNO <sub>3</sub> )	$K_1 = 18.44 \pm 0.11$	161
Ho <sup>3+</sup>	Pol	20	0.1 (KNO <sub>3</sub> )	$K_1 = 19.70 \pm 0.13$	161
La <sup>3+</sup>	Pol	20	0.1 (KNO <sub>3</sub> )	$K_1 = 16.41 \pm 0.17$	161
Lu <sup>3+</sup>	Pol	20	0.1 (KNO <sub>3</sub> )	$K_1 = 20.79 \pm 0.19$	161
Nd <sup>3+</sup>	Pol	20	0.1 (KNO <sub>3</sub> )	$K_1 = 17.57 \pm 0.14$	161
Pr <sup>3+</sup>	Pol	20	0.1 (KNO <sub>3</sub> )	$K_1 = 17.28 \pm 0.11$	161
Sm <sup>3+</sup>	Pol	20	0.1 (KNO <sub>3</sub> )	$K_1 = 18.12 \pm 0.14$	161
Tb <sup>3+</sup>	Pol	20	0.1 (KNO <sub>3</sub> )	$K_1 = 18.97 \pm 0.11$	161
Tm <sup>3+</sup>	Pol	20	0.1 (KNO <sub>3</sub> )	$K_1 = 20.38 \pm 0.14$	161
Yb <sup>3+</sup>	Pol	20	0.1 (KNO <sub>3</sub> )	$K_1 = 20.65 \pm 0.20$	161
C <sub>14</sub> H <sub>12</sub> O <sub>2</sub> , benzoic acid, HL					
Pm <sup>3+</sup>	ix, pH	20	0.2 NaClO <sub>4</sub>	$K_1 < 2.15, \beta_2 < 4.0, \beta_3 < 5.0$	162
Pr <sup>3+</sup>	ix, pH	20	0.2 NaClO <sub>4</sub>	$K_1 < 2.15, \beta_2 < 4.0, \beta_3 < 5.3$	162
C <sub>14</sub> H <sub>8</sub> O <sub>7</sub> S, 1,2-dihydroxyanthraquinone-3-sulphonic acid (Alizarin Red S), H <sub>3</sub> L					
Dy <sup>3+</sup>	Sp	?	50% v/v acetone	$K_1 = 7.05, \beta_3 = 17.50,$ borax buffers	163
Er <sup>3+</sup>	Sp	?	50% v/v acetone	$K_1 = 7.87, \beta_3 = 17.90,$ borax buffers	163
C <sub>14</sub> H <sub>9</sub> O <sub>3</sub> N, 1-amino-4-hydroxyanthraquinone, HL					
Ce <sup>3+</sup>	Sp	30	?	$K_1 = 9.29$	164
La <sup>3+</sup>	Sp	30	?	$K_1 = 5.21$	164
Nd <sup>3+</sup>	Sp	30	?	$K_1 = 5.43$	164
Pr <sup>3+</sup>	Sp	30	?	$K_1 = 5.39$	164
Sm <sup>3+</sup>	Sp	30	?	$K_1 = 5.35$	164
C <sub>14</sub> H <sub>9</sub> O <sub>6</sub> N <sub>7</sub> , 1,5-bis(2-hydroxy-4-nitrophenyl)-3-cyanoformazan, H <sub>3</sub> L					
La <sup>3+</sup>	Sp	25	0.1 NaClO <sub>4</sub>	$K[\text{La}^{3+} + 2\text{H}^+ + 2\text{L}^{3-} = \text{La}(\text{HL})_2^-] = 46.4$	165
C <sub>14</sub> H <sub>22</sub> O <sub>8</sub> N <sub>2</sub> , ( <i>trans</i> -1,2-cyclohexylenedinitrilo)tetraacetic acid (CDTA), H <sub>4</sub> L					
Ce <sup>3+</sup>	Tp	25	0.1	$K_1 = 16.68$	166

(Continued.)

Metal	Method	Temp. (°C)	Medium	log of equilibrium constant	Ref.
Eu <sup>2+</sup>	Pol	?	1.0	$K_1 = 10.69 \pm 0.09$	167
Eu <sup>3+</sup>	Dis	20	0.1 (NH <sub>4</sub> Cl)	$K_1 = 18.51$	168
C <sub>14</sub> H <sub>22</sub> O <sub>8</sub> N <sub>4</sub> , 1,2-diaminocyclohexane- <i>N,N,N',N'</i> -tetraacetic acid					
La <sup>3+</sup>	Pol	20	0.1 M KNO <sub>3</sub>	log $K_1 = 16.18$	194
La <sup>3+</sup>	Hg	20	0.1 M KNO <sub>3</sub>	log $K_1 = 16.35$	194
Ce <sup>3+</sup>	Pol	20	0.1 M KNO <sub>3</sub>	log $K_1 = 16.96$	194
Pr <sup>3+</sup>	Pol	20	0.1 M KNO <sub>3</sub>	log $K_1 = 17.37$	194
Pr <sup>3+</sup>	Hg	20	0.1 M KNO <sub>3</sub>	log $K_1 = 17.23$	194
Nd <sup>3+</sup>	Pol	20	0.1 M KNO <sub>3</sub>	log $K_1 = 17.66$	194
Nd <sup>3+</sup>	Hg	20	0.1 M KNO <sub>3</sub>	log $K_1 = 17.69$	194
Sm <sup>3+</sup>	Pol	20	0.1 M KNO <sub>3</sub>	log $K_1 = 18.55$	194
Sm <sup>3+</sup>	Hg	20	0.1 M KNO <sub>3</sub>	log $K_1 = 18.63$	194
Eu <sup>3+</sup>	Pol	20	0.1 M KNO <sub>3</sub>	log $K_1 = 18.99$	194
Eu <sup>3+</sup>	Hg	20	0.1 M KNO <sub>3</sub>	log $K_1 = 18.77$	194
Gd <sup>3+</sup>	Pol	20	0.1 M KNO <sub>3</sub>	log $K_1 = 19.02$	194
Gd <sup>3+</sup>	Hg	20	0.1 M KNO <sub>3</sub>	log $K_1 = 18.80$	194
Tb <sup>3+</sup>	Pol	20	0.1 M KNO <sub>3</sub>	log $K_1 = 19.58$	194
Tb <sup>3+</sup>	Hg	20	0.1 M KNO <sub>3</sub>	log $K_1 = 19.30$	194
Dy <sup>3+</sup>	Pol	20	0.1 M KNO <sub>3</sub>	log $K_1 = 20.02$	194
Dy <sup>3+</sup>	Hg	20	0.1 M KNO <sub>3</sub>	log $K_1 = 19.69$	194
Ho <sup>3+</sup>	Pol	20	0.1 M KNO <sub>3</sub>	log $K_1 = 20.27$	194
Ho <sup>3+</sup>	Hg	20	0.1 M KNO <sub>3</sub>	log $K_1 = 19.89$	194
Er <sup>3+</sup>	Pol	20	0.1 M KNO <sub>3</sub>	log $K_1 = 20.66$	194
Er <sup>3+</sup>	Hg	20	0.1 M KNO <sub>3</sub>	log $K_1 = 20.20$	194
Tm <sup>3+</sup>	Pol	20	0.1 M KNO <sub>3</sub>	log $K_1 = 20.87$	194
Tm <sup>3+</sup>	Hg	20	0.1 M KNO <sub>3</sub>	log $K_1 = 20.46$	194
Yb <sup>3+</sup>	Pol	20	0.1 M KNO <sub>3</sub>	log $K_1 = 21.33$	194
Yb <sup>3+</sup>	Hg	20	0.1 M KNO <sub>3</sub>	log $K_1 = 20.80$	194
Lu <sup>3+</sup>	Pol	20	0.1 M KNO <sub>3</sub>	log $K_1 = 21.39$	194
Lu <sup>3+</sup>	Hg	20	0.1 M KNO <sub>3</sub>	log $K_1 = 20.91$	194
Y <sup>3+</sup>	Pol	20	0.1 M KNO <sub>3</sub>	log $K_1 = 19.81$	194
Y <sup>3+</sup>	Hg	20	0.1 M KNO <sub>3</sub>	log $K_1 = 19.41$	194
C <sub>14</sub> H <sub>22</sub> O <sub>10</sub> N <sub>3</sub> , (HO <sub>2</sub> CCH <sub>2</sub> ) <sub>2</sub> NCH <sub>2</sub> CH <sub>2</sub> NCH <sub>2</sub> (CH <sub>2</sub> CO <sub>2</sub> H)CH <sub>2</sub> N(CH <sub>2</sub> CO <sub>2</sub> H) <sub>2</sub> , diethylenetriamine- <i>N,N,N',N',N''</i> -pentaacetic acid, H <sub>5</sub> L					
La <sup>3+</sup>	Pol	20	0.1 M KNO <sub>3</sub>	log $K_1 = 19.35$	200
La <sup>3+</sup>	Gl	25	0.1 M KCl	log $K_1 = 19.96$	200
La <sup>3+</sup>	Hg	25	0.1 M KNO <sub>3</sub>	log $K_1 = 19.1$	200
La <sup>3+</sup>	Hg	25	0.1 M KNO <sub>3</sub>	log $K_1 = 19.48$	200
Ce <sup>3+</sup>	Gl	20	0.1 M KCl	log $K_1 = 20.40$	200
Ce <sup>3+</sup>	Pol	20	0.1 M KNO <sub>3</sub>	log $K_1 = 20.10$	200
Ce <sup>3+</sup>	Hg	25	0.1 M KNO <sub>3</sub>	log $K_1 = 20.5$	200
Pr <sup>3+</sup>	Gl	25	0.1 M KCl	log $K_1 = 21.85$	200
Pr <sup>3+</sup>	Hg	25	0.1 M KNO <sub>3</sub>	log $K_1 = 21.07$	200
Nd <sup>3+</sup>	Gl	25	0.1 M KCl	log $K_1 = 22.24$	200
Nd <sup>3+</sup>	Hg	25	0.1 M KNO <sub>3</sub>	log $K_1 = 21.60$	200
Sm <sup>3+</sup>	Gl	25	0.1 M KCl	log $K_1 = 22.84$	200
Sm <sup>3+</sup>	Hg	25	0.1 M KNO <sub>3</sub>	log $K_1 = 22.34$	200
Eu <sup>3+</sup>	Gl	25	0.1 M KCl	log $K_1 = 22.91$	200

(Continued.)

Metal	Method	Temp. (°C)	Medium	log of equilibrium constant	Ref.
Eu <sup>3+</sup>	Hg	25	0.1 M KNO <sub>3</sub>	log $K_1 = 22.39$	200
Gd <sup>3+</sup>	Gl	25	0.1 M KCl	log $K_1 = 23.01$	200
Gd <sup>3+</sup>	Hg	25	0.1 M KNO <sub>3</sub>	log $K_1 = 22.46$	200
Tb <sup>3+</sup>	Gl	25	0.1 M KCl	log $K_1 = 23.21$	200
Tb <sup>3+</sup>	Hg	25	0.1 M KNO <sub>3</sub>	log $K_1 = 22.71$	200
Dy <sup>3+</sup>	Gl	25	0.1 M KCl	log $K_1 = 23.46$	200
Dy <sup>3+</sup>	Hg	25	0.1 M KNO <sub>3</sub>	log $K_1 = 22.82$	200
Ho <sup>3+</sup>	Hg	25	0.1 M KNO <sub>3</sub>	log $K_1 = 22.78$	200
Er <sup>3+</sup>	Gl	25	0.1 M KCl	log $K_1 = 23.18$	200
Er <sup>3+</sup>	Hg	25	0.1 M KNO <sub>3</sub>	log $K_1 = 22.74$	200
Tm <sup>3+</sup>	Gl	25	0.1 M KCl	log $K_1 = 22.97$	200
Tm <sup>3+</sup>	Hg	25	0.1 M KNO <sub>3</sub>	log $K_1 = 22.72$	200
Yb <sup>3+</sup>	Gl	25	0.1 M KCl	log $K_1 = 22.97$	200
Yb <sup>3+</sup>	Hg	25	0.1 M KNO <sub>3</sub>	log $K_1 = 22.62$	200
Lu <sup>3+</sup>	Hg	25	0.1 M KNO <sub>3</sub>	log $K_1 = 22.44$	200
Y <sup>3+</sup>	Gl	25	0.1 M KCl	log $K_1 = 22.40$	200
Y <sup>3+</sup>	Hg	25	0.1 M KNO <sub>3</sub>	log $K_1 = 22.05$	200
C <sub>14</sub> H <sub>23</sub> O <sub>10</sub> N <sub>3</sub> , [( <i>N</i> -carboxymethyl-2,2'-iminodiethylene)dinitrilo]tetraacetic acid (diethylenetriaminopentaacetic acid) (DTPA), H <sub>5</sub> L					
Ce <sup>3+</sup>	Sp	?	?	$K_1 = 19.8 \pm 0.4$	169
	Tp	25	0.1	$K_1 = 21.20$	166
Gd <sup>3+</sup>	Sp	18–22	?	$K_1 = 22.46 \pm 0.08$	170
	Sp	18–22	dil	$K_1 = 22.46 \pm 0.08$	170
La <sup>3+</sup>	Sp	18–22	dil	$K_1 = 19.23 \pm 0.03$	170
	Sp	18–22	?	$K_1 = 19.23 \pm 0.03$	170
Lu <sup>3+</sup>	Sp	18–22	?	$K_1 = 22.32 \pm 0.09$	170
	Sp	18–22	dil	$K_1 = 22.32 \pm 0.03$	170
Nd <sup>3+</sup>	Sp	?	0.5 (KCl)	$K_1 = 22.95 \pm 0.2$	170
	Sp	20	0.6	$K_1 = 21.05 \pm 0.08$	170
Pr <sup>3+</sup>	Sp	18–20	0.003	$K_1 = 21.79$	170
Eu <sup>2+</sup>	Pol	?	0.1	$K_1 = 10.2 \pm 0.1$	170
Y <sup>3+</sup>	Sp	18–22	dil	$K_1 = 21.95 \pm 0.03$	170
	Sp	18–22	?	$K_1 = 21.95 \pm 0.3$	170
C <sub>14</sub> H <sub>24</sub> O <sub>8</sub> N <sub>2</sub> , ethylenediamine- <i>N,N'</i> -diacetic- <i>N,N'</i> -di-2-butyric acid, H <sub>4</sub> L					
Ce <sup>3+</sup>	Pol	20	0.1 KNO <sub>3</sub>	$K_1 = 14.77$	171
Dy <sup>3+</sup>	Pol	20	0.1 (KNO <sub>3</sub> )	$K_1 = 17.58$	171
Er <sup>3+</sup>	Pol	20	0.1 (KNO <sub>3</sub> )	$K_1 = 18.19$	171
Eu <sup>3+</sup>	Pol	20	0.1 (KNO <sub>3</sub> )	$K_1 = 16.31$	171
Gd <sup>3+</sup>	Pol	20	0.1 (KNO <sub>3</sub> )	$K_1 = 16.48$	171
Ho <sup>3+</sup>	Pol	20	0.1 (KNO <sub>3</sub> )	$K_1 = 17.85$	171
La <sup>3+</sup>	Pol	20	0.1 (KNO <sub>3</sub> )	$K_1 = 14.13$	171
Lu <sup>3+</sup>	Pol	20	0.1 (KNO <sub>3</sub> )	$K_1 = 18.90$	171
Nd <sup>3+</sup>	Pol	20	0.1 (KNO <sub>3</sub> )	$K_1 = 15.35$	171
Pr <sup>3+</sup>	Pol	20	0.1 (KNO <sub>3</sub> )	$K_1 = 15.09$	171
Sm <sup>3+</sup>	Pol	20	0.1 (KNO <sub>3</sub> )	$K_1 = 16.00$	171
Tb <sup>3+</sup>	Pol	20	0.1 (KNO <sub>3</sub> )	$K_1 = 17.13$	171
Tm <sup>3+</sup>	Pol	20	0.1 (KNO <sub>3</sub> )	$K_1 = 18.45$	171
Yb <sup>3+</sup>	Pol	20	0.1 (KNO <sub>3</sub> )	$K_1 = 18.70$	171



(Continued.)

Metal	Method	Temp. (°C)	Medium	log of equilibrium constant	Ref.
$C_{14}H_{24}O_{10}N_2$ , (HO <sub>2</sub> CCH <sub>2</sub> )NCH <sub>2</sub> CH <sub>2</sub> OCH <sub>2</sub> CH <sub>2</sub> OCH <sub>2</sub> CH <sub>2</sub> N(CH <sub>2</sub> CO <sub>2</sub> H) <sub>2</sub> , 1,2-bis[2-di(carboxymethyl)aminoethoxy]ethane, H <sub>4</sub> L					
La <sup>3+</sup>	Hg	20	0.1 M KNO <sub>3</sub>	log $K_1 = 15.55$	199
La <sup>3+</sup>	Hg	20	0.1 M KNO <sub>3</sub>	log $K_1 = 15.84$	199
Ce <sup>3+</sup>	Hg	20	0.1 M KNO <sub>3</sub>	log $K_1 = 15.70$	199
Ce <sup>3+</sup>	Hg	20	0.1 M KNO <sub>3</sub>	log $K_1 = 16.06$	199
Pr <sup>3+</sup>	Hg	20	0.1 M KNO <sub>3</sub>	log $K_1 = 16.05$	199
Pr <sup>3+</sup>	Hg	20	0.1 M KNO <sub>3</sub>	log $K_1 = 16.17$	199
Nd <sup>3+</sup>	Hg	20	0.1 M KNO <sub>3</sub>	log $K_1 = 16.28$	199
Nd <sup>3+</sup>	Hg	20	0.1 M KNO <sub>3</sub>	log $K_1 = 16.59$	199
Sm <sup>3+</sup>	Hg	20	0.1 M KNO <sub>3</sub>	log $K_1 = 16.88$	199
Sm <sup>3+</sup>	Hg	20	0.1 M KNO <sub>3</sub>	log $K_1 = 17.25$	199
Eu <sup>3+</sup>	Hg	20	0.1 M KNO <sub>3</sub>	log $K_1 = 17.10$	199
Eu <sup>3+</sup>	Hg	20	0.1 M KNO <sub>3</sub>	log $K_1 = 17.77$	199
Gd <sup>3+</sup>	Hg	20	0.1 M KNO <sub>3</sub>	log $K_1 = 16.94$	199
Gd <sup>3+</sup>	Hg	20	0.1 M KNO <sub>3</sub>	log $K_1 = 17.50$	199
Tb <sup>3+</sup>	Hg	20	0.1 M KNO <sub>3</sub>	log $K_1 = 17.27$	199
Tb <sup>3+</sup>	Hg	20	0.1 M KNO <sub>3</sub>	log $K_1 = 17.80$	199
Dy <sup>3+</sup>	Hg	20	0.1 M KNO <sub>3</sub>	log $K_1 = 17.42$	199
Dy <sup>3+</sup>	Hg	20	0.1 M KNO <sub>3</sub>	log $K_1 = 17.84$	199
Ho <sup>3+</sup>	Hg	20	0.1 M KNO <sub>3</sub>	log $K_1 = 17.38$	199
Ho <sup>3+</sup>	Hg	20	0.1 M KNO <sub>3</sub>	log $K_1 = 17.90$	199
Er <sup>3+</sup>	Hg	20	0.1 M KNO <sub>3</sub>	log $K_1 = 17.40$	199
Er <sup>3+</sup>	Hg	20	0.1 M KNO <sub>3</sub>	log $K_1 = 18.00$	199
Tm <sup>3+</sup>	Hg	20	0.1 M KNO <sub>3</sub>	log $K_1 = 17.48$	199
Tm <sup>3+</sup>	Hg	20	0.1 M KNO <sub>3</sub>	log $K_1 = 17.96$	199
Yb <sup>3+</sup>	Hg	20	0.1 M KNO <sub>3</sub>	log $K_1 = 17.78$	199
Yb <sup>3+</sup>	Hg	20	0.1 M KNO <sub>3</sub>	log $K_1 = 18.22$	199
Lu <sup>3+</sup>	Hg	20	0.1 M KNO <sub>3</sub>	log $K_1 = 17.81$	199
Lu <sup>3+</sup>	Hg	20	0.1 M KNO <sub>3</sub>	log $K_1 = 18.48$	199
Y <sup>3+</sup>	Hg	20	0.1 M KNO <sub>3</sub>	log $K_1 = 16.82$	199
Y <sup>3+</sup>	Hg	20	0.1 M KNO <sub>3</sub>	log $K_1 = 17.16$	199
$C_{14}H_{24}O_8N_2$ , ethylenedinitrilo- <i>N,N'</i> -diacetic- <i>N,N'</i> -di(2-butanoic) acid, H <sub>4</sub> L					
H <sup>+</sup>	Gl	20	0.1	$K_1 = 10.42, K_2 = 6.09, K_3 = 2.69, K_4 = 1.8$	171
Ce <sup>3+</sup>	Gl	20	0.1	$K_1 = 14.8$	171
Dy <sup>3+</sup>	Gl	20	0.1	$K_1 = 17.6$	171
Er <sup>3+</sup>	Gl	20	0.1	$K_1 = 18.2$	171
Eu <sup>3+</sup>	Gl	20	0.1	$K_1 = 16.3$	171
Gd <sup>3+</sup>	Gl	20	0.1	$K_1 = 16.5$	171
Ho <sup>3+</sup>	Gl	20	0.1	$K_1 = 17.9$	171
La <sup>3+</sup>	Gl	20	0.1	$K_1 = 14.1$	171
Lu <sup>3+</sup>	Gl	20	0.1	$K_1 = 18.9$	171
Nd <sup>3+</sup>	Gl	20	0.1	$K_1 = 15.4$	171
Pr <sup>3+</sup>	Gl	20	0.1	$K_1 = 15.1$	171
Sm <sup>3+</sup>	Gl	20	0.1	$K_1 = 16.0$	171
Tb <sup>3+</sup>	Gl	20	0.1	$K_1 = 17.1$	171
Tm <sup>3+</sup>	Gl	20	0.1	$K_1 = 18.5$	171
Yb <sup>3+</sup>	Gl	20	0.1	$K_1 = 18.7$	171

(Continued.)

Metal	Method	Temp. (°C)	Medium	log of equilibrium constant	Ref.
C <sub>14</sub> H <sub>24</sub> O <sub>8</sub> N <sub>2</sub> , 4-methyl-1,2-diaminopentan- <i>N,N,N',N'</i> -tetraacetic acid, H <sub>4</sub> L					
H <sup>+</sup>	Gl	20	0.1 (KNO <sub>3</sub> )	$K_1 = 11.00, K_2 = 5.91, K_3 = 3.05, K_4 = 2.1$	161
Ce <sup>3+</sup>	Pol	20	0.1 (KNO <sub>3</sub> )	$K_1 = 17.02 \pm 0.13$	161
Dy <sup>3+</sup>	Pol	20	0.1 (KNO <sub>3</sub> )	$K_1 = 19.47 \pm 0.13$	161
Er <sup>3+</sup>	Pol	20	0.1 (KNO <sub>3</sub> )	$K_1 = 19.99 \pm 0.14$	161
Eu <sup>3+</sup>	Pol	20	0.1 (KNO <sub>3</sub> )	$K_1 = 18.45 \pm 0.12$	161
Gd <sup>3+</sup>	Pol	20	0.1 (KNO <sub>3</sub> )	$K_1 = 18.48 \pm 0.11$	161
Ho <sup>3+</sup>	Pol	20	0.1 (KNO <sub>3</sub> )	$K_1 = 19.71 \pm 0.14$	161
La <sup>3+</sup>	Pol	20	0.1 (KNO <sub>3</sub> )	$K_1 = 16.45 \pm 0.17$	161
Lu <sup>3+</sup>	Pol	20	0.1 (KNO <sub>3</sub> )	$K_1 = 20.92 \pm 0.19$	161
Nd <sup>3+</sup>	Pol	20	0.1 (KNO <sub>3</sub> )	$K_1 = 17.65 \pm 0.15$	161
Pr <sup>3+</sup>	Pol	20	0.1 (KNO <sub>3</sub> )	$K_1 = 17.32 \pm 0.12$	161
Sm <sup>3+</sup>	Pol	20	0.1 (KNO <sub>3</sub> )	$K_1 = 18.20 \pm 0.14$	161
Tb <sup>3+</sup>	Pol	20	0.1 (KNO <sub>3</sub> )	$K_1 = 18.99 \pm 0.12$	161
Tm <sup>3+</sup>	Pol	20	0.1 (KNO <sub>3</sub> )	$K_1 = 20.40 \pm 0.18$	161
Yb <sup>3+</sup>	Pol	20	0.1 (KNO <sub>3</sub> )	$K_1 = 20.74 \pm 0.18$	161
C <sub>14</sub> H <sub>24</sub> O <sub>10</sub> N <sub>2</sub> , [(ethylenedioxy)diethylenedinitrilo]tetraacetic acid (EGTA), H <sub>4</sub> L					
Nd <sup>3+</sup>	Sp	20	0.5	$K_1 = 16.16$	172
C <sub>14</sub> H <sub>25</sub> O <sub>9</sub> N <sub>3</sub> [( <i>N</i> -(2-hydroxyethyl)-2,2'-iminodiethylene)dinitrilo]tetraacetic acid, H <sub>4</sub> L					
H <sup>+</sup>	Gl	?	0.1 (KCl)	$K_1 = 9.30, K_2 = 8.00, K_3 = 3.54, K_4 = 2.58$	173
Dy <sup>3+</sup>	Pol	?	0.1 (KCl)	$K_1 = 13.97$	173
Er <sup>3+</sup>	Pol	?	0.1 (KCl)	$K_1 = 13.87$	173
Gd <sup>3+</sup>	Pol	?	0.1 (KCl)	$K_1 = 13.45$	173
La <sup>3+</sup>	Pol	?	0.1 (KCl)	$K_1 = 11.35$	173
Lu <sup>3+</sup>	Pol	?	0.1 (KCl)	$K_1 = 13.35$	173
Nd <sup>3+</sup>	Pol	?	0.1 (KCl)	$K_1 = 13.07$	173
Sm <sup>3+</sup>	Pol	?	0.1 (KCl)	$K_1 = 13.45$	173
Y <sup>3+</sup>	Pol	?	0.1 (KCl)	$K_1 = 13.21$	173
C <sub>15</sub> H <sub>25</sub> O <sub>10</sub> N <sub>3</sub> , [( <i>N</i> -carboxyethyl-2,2'-iminodiethylene)dinitrilo]tetraacetic acid, H <sub>5</sub> L					
H <sup>+</sup>	Pot	?	?	$K_1 = 9.31, K_2 = 8.14, K_3 = 4.70, K_4 = 2.97, K_5 = 2.58$	174
Dy <sup>3+</sup>	Pot	?	0.1 (KCl)	$K_1 = 16.71$	174
Er <sup>3+</sup>	Pot	?	0.1 (KCl)	$K_1 = 16.46$	174
	Pot	?	?	$K_1 = 16.49$	174
Eu <sup>3+</sup>	Pot	?	0.1 (KCl)	$K_1 = 16.46$	174
Gd <sup>3+</sup>	Pot	?	0.1 (KCl)	$K_1 = 16.71$	174
	Pot	?	?	$K_1 = 18.4$	174
Ho <sup>3+</sup>	Pot	?	0.1 (KCl)	$K_1 = 16.71$	174
La <sup>3+</sup>	Pot	?	0.1 (KCl)	$K_1 = 15.0$	174
	Pot	?	0.1 (KCl)	$K_1 = 16.69$	174
Lu <sup>3+</sup>	Pot	?	0.1 (KCl)	$K_1 = 16.28$	174
	Pot	?	?	$K_1 = 18.59$	174
Nd <sup>3+</sup>	Pot	?	0.1 (KCl)	$K_1 = 16.14$	174
	Pot	?	?	$K_1 = 18.18$	174
Pr <sup>3+</sup>	Pot	?	0.1 (KCl)	$K_1 = 15.70$	174
Sm <sup>3+</sup>	Pot	?	0.1 (KCl)	$K_1 = 16.16$	174
	Pot	?	?	$K_1 = 18.4$	174
Tb <sup>3+</sup>	Pot	?	0.1 (KCl)	$K_1 = 16.71$	174

(Continued.)

Metal	Method	Temp. (°C)	Medium	log of equilibrium constant	Ref.
Tm <sup>3+</sup>	Pot	?	0.1 (KCl)	$K_1 = 16.71$	174
Y <sup>3+</sup>	Pot	?	0.1 (KCl)	$K_1 = 16.52$	174
Yb <sup>3+</sup>	Pot	?	0.1 (KCl)	$K_1 = 16.46$	174
C <sub>16</sub> H <sub>20</sub> O <sub>8</sub> N <sub>2</sub> , (1-phenylethylenedinitrilo)tetraacetic acid, H <sub>4</sub> L					
H <sup>+</sup>	Gl	20	0.1 (KNO <sub>3</sub> )	$K_1 = 9.95, K_2 = 5.42, K_3 = 3.23, K_4 = 2.10$	175
Dy <sup>3+</sup>	Pol	20	0.1 (KNO <sub>3</sub> )	$K_1 = 18.42 \pm 0.14$	175
Er <sup>3+</sup>	Pol	20	0.1 (KNO <sub>3</sub> )	$K_1 = 19.01 \pm 0.15$	175
Eu <sup>3+</sup>	Pol	20	0.1 (KNO <sub>3</sub> )	$K_1 = 17.25 \pm 0.12$	175
Gd <sup>3+</sup>	Pol	20	0.1 (KNO <sub>3</sub> )	$K_1 = 17.40 \pm 0.11$	175
Ho <sup>3+</sup>	Pol	20	0.1 (KNO <sub>3</sub> )	$K_1 = 18.69 \pm 0.13$	175
La <sup>3+</sup>	Pol	20	0.1 (KNO <sub>3</sub> )	$K_1 = 15.49 \pm 0.15$	175
Lu <sup>3+</sup>	Pol	20	0.1 (KNO <sub>3</sub> )	$K_1 = 19.83 \pm 0.20$	175
Nd <sup>3+</sup>	Pol	20	0.1 (KNO <sub>3</sub> )	$K_1 = 16.56 \pm 0.12$	175
Pr <sup>3+</sup>	Pol	20	0.1 (KNO <sub>3</sub> )	$K_1 = 16.29 \pm 0.11$	175
Sm <sup>3+</sup>	Pol	20	0.1 (KNO <sub>3</sub> )	$K_1 = 17.09 \pm 0.12$	175
Tb <sup>3+</sup>	Pol	20	0.1 (KNO <sub>3</sub> )	$K_1 = 17.96 \pm 0.14$	175
Tm <sup>3+</sup>	Pol	20	0.1 (KNO <sub>3</sub> )	$K_1 = 19.34 \pm 0.16$	175
Yb <sup>3+</sup>	Pol	20	0.1 (KNO <sub>3</sub> )	$K_1 = 19.68 \pm 0.19$	175
C <sub>16</sub> H <sub>28</sub> O <sub>8</sub> N <sub>2</sub> , ethylenediamine- <i>N,N'</i> -diacetic- <i>N,N'</i> -di-2-isovaleric acid, H <sub>4</sub> L					
H <sup>+</sup>	Gl	20	0.1 (KNO <sub>3</sub> )	$K_1 = 10.38, K_2 = 5.60, K_3 = 3.02, K_4 = 1.9$	171
Ce <sup>3+</sup>	Gl	20	0.1 (KNO <sub>3</sub> )	$K_1 = 11.54$	171
Dy <sup>3+</sup>	Gl	20	0.1 (KNO <sub>3</sub> )	$K_1 = 14.41$	171
	Pol	20	0.1 (KNO <sub>3</sub> )	$K_1 = 14.45$	171
Er <sup>3+</sup>	Gl	20	0.1 (KNO <sub>3</sub> )	$K_1 = 14.91$	171
	Pol	20	0.1 (KNO <sub>3</sub> )	$K_1 = 14.99$	171
Eu <sup>3+</sup>	Gl	20	0.1 (KNO <sub>3</sub> )	$K_1 = 13.23$	171
Gd <sup>3+</sup>	Gl	20	0.1 (KNO <sub>3</sub> )	$K_1 = 13.39$	171
	Pol	20	0.1 (KNO <sub>3</sub> )	$K_1 = 13.47$	171
Ho <sup>3+</sup>	Gl	20	0.1 (KNO <sub>3</sub> )	$K_1 = 14.70$	171
	Pol	20	0.1 (KNO <sub>3</sub> )	$K_1 = 14.71$	171
La <sup>3+</sup>	Gl	20	0.1 (KNO <sub>3</sub> )	$K_1 = 10.78$	171
Lu <sup>3+</sup>	Pol	20	0.1 (KNO <sub>3</sub> )	$K_1 = 15.77$	171
Nd <sup>3+</sup>	Gl	20	0.1 (KNO <sub>3</sub> )	$K_1 = 12.09$	171
Pr <sup>3+</sup>	Gl	20	0.1 (KNO <sub>3</sub> )	$K_1 = 11.93$	171
Sm <sup>3+</sup>	Pol	20	0.1 (KNO <sub>3</sub> )	$K_1 = 12.87$	171
Tb <sup>3+</sup>	Gl	20	0.1 (KNO <sub>3</sub> )	$K_1 = 14.07$	171
	Pol	20	0.1 (KNO <sub>3</sub> )	$K_1 = 14.00$	171
Tm <sup>3+</sup>	Gl	20	0.1 (KNO <sub>3</sub> )	$K_1 = 15.20$	171
	Pol	20	0.1 (KNO <sub>3</sub> )	$K_1 = 15.31$	171
Yb <sup>3+</sup>	Gl	20	0.1 (KNO <sub>3</sub> )	$K_1 = 15.38$	171
	Pol	20	0.1 (KNO <sub>3</sub> )	$K_1 = 15.55$	171
C <sub>16</sub> H <sub>28</sub> O <sub>8</sub> N <sub>2</sub> , ethylenediamine- <i>N,N'</i> -diacetic- <i>N,N'</i> -di-2-valeric acid					
H <sup>+</sup>	Gl	20	0.1 (KNO <sub>3</sub> )	$K_1 = 10.47, K_2 = 6.15, K_3 = 2.79, K_4 = 1.9$	171
Ce <sup>3+</sup>	Pol	20	0.1 (KNO <sub>3</sub> )	$K_1 = 14.77$	171
Dy <sup>3+</sup>	Pol	20	0.1 (KNO <sub>3</sub> )	$K_1 = 17.63$	171
Er <sup>3+</sup>	Pol	20	0.1 (KNO <sub>3</sub> )	$K_1 = 18.16$	171
Eu <sup>3+</sup>	Pol	20	0.1 (KNO <sub>3</sub> )	$K_1 = 16.39$	171
Gd <sup>3+</sup>	Pol	20	0.1 (KNO <sub>3</sub> )	$K_1 = 16.60$	171

(Continued.)					
Metal	Method	Temp. (°C)	Medium	log of equilibrium constant	Ref.
Ho <sup>3+</sup>	Pol	20	0.1 (KNO <sub>3</sub> )	$K_1 = 17.85$	171
La <sup>3+</sup>	Pol	20	0.1 (KNO <sub>3</sub> )	$K_1 = 14.12$	171
Lu <sup>3+</sup>	Pol	20	0.1 (KNO <sub>3</sub> )	$K_1 = 18.92$	171
Nd <sup>3+</sup>	Pol	20	0.1 (KNO <sub>3</sub> )	$K_1 = 15.38$	171
Pr <sup>3+</sup>	Pol	20	0.1 (KNO <sub>3</sub> )	$K_1 = 15.11$	171
Sm <sup>3+</sup>	Pol	20	0.1 (KNO <sub>3</sub> )	$K_1 = 16.07$	171
Tb <sup>3+</sup>	Pol	20	0.1 (KNO <sub>3</sub> )	$K_1 = 17.16$	171
Tm <sup>3+</sup>	Pol	20	0.1 (KNO <sub>3</sub> )	$K_1 = 18.45$	171
Yb <sup>3+</sup>	Pol	20	0.1 (KNO <sub>3</sub> )	$K_1 = 18.75$	171
C <sub>16</sub> H <sub>9</sub> ON <sub>2</sub> Br <sub>3</sub> , 1-(2,4,6-tribromophenylazo)-2-naphthol, HL					
Ce <sup>3+</sup>	Kin	25	0.02	$K_1 = 4.54$	176
Dy <sup>3+</sup>	Kin	25	0.02	$K_1 = 5.18 \pm 0.03$	176
Er <sup>3+</sup>	Kin	25	0.02	$K_1 = 5.40 \pm 0.05$	176
Eu <sup>3+</sup>	Kin	25	0.02	$K_1 = 4.92 \pm 0.07$	176
Gd <sup>3+</sup>	Kin	25	0.02	$K_1 = 5.03 \pm 0.03$	176
Ho <sup>3+</sup>	Kin	25	0.02	$K_1 = 5.28 \pm 0.06$	176
La <sup>3+</sup>	Kin	25	0.02	$K_1 = 4.42 \pm 0.06$	176
Lu <sup>3+</sup>	Kin	25	0.02	$K_1 = 5.71 \pm 0.02$	176
Nd <sup>3+</sup>	Kin	25	0.02	$K_1 = 4.65 \pm 0.07$	176
Pm <sup>3+</sup>	Kin	25	0.02	$K_1 = 4.75 \pm 0.10$	176
Pr <sup>3+</sup>	Kin	25	0.02	$K_1 = 4.60 \pm 0.07$	176
Sm <sup>3+</sup>	Kin	25	0.02	$K_1 = 4.87 \pm 0.06$	176
Tb <sup>3+</sup>	Kin	25	0.02	$K_1 = 5.12 \pm 0.04$	176
Tm <sup>3+</sup>	Kin	25	0.02	$K_1 = 5.45 \pm 0.04$	176
Yb <sup>3+</sup>	Kin	25	0.02	$K_1 = 5.56 \pm 0.07$	176
C <sub>16</sub> H <sub>12</sub> O <sub>4</sub> N <sub>2</sub> S, 1-(2'-hydroxy-1'-naphthylazo)-4-benzenesulphonic acid, H <sub>2</sub> L					
Eu <sup>3+</sup>	Spj	rt	dil	$\beta_2 = 7.32$	177
La <sup>3+</sup>	Spj	rt	dil	$\beta_2 = 7.52$	177
Sm <sup>3+</sup>	Spj	rt	dil	$\beta_2 = 7.34$	177
C <sub>16</sub> H <sub>13</sub> O <sub>11</sub> N <sub>2</sub> S <sub>2</sub> As, 2-(2'-arsonophenylazo)chromotropic acid (arsenazo I), H <sub>6</sub> L					
Ce <sup>3+</sup>	Sp	19-21	0.1	$K(\text{Ce}^{3+} + \text{H}_2\text{L}^{4-} = \text{CeH}_2\text{L}^-) = 8.47 \pm 0.02$	178
Dy <sup>3+</sup>	Sp	19-21	0.1	$K(\text{Dy}^{3+} + \text{H}_2\text{L}^{4-} = \text{DyH}_2\text{L}^-) = 8.27 \pm 0.01$	178
Er <sup>3+</sup>	Sp	19-21	0.1	$K(\text{Er}^{3+} + \text{H}_2\text{L}^{4-} = \text{ErH}_2\text{L}^-) = 8.28 \pm 0.01$	178
Eu <sup>3+</sup>	Sp	19-21	0.1	$K(\text{Eu}^{3+} + \text{H}_2\text{L}^{4-} = \text{EuH}_2\text{L}^-) = 8.36 \pm 0.02$	178
Gd <sup>3+</sup>	Sp	19-21	0.1	$K(\text{Gd}^{3+} + \text{H}_2\text{L}^{4-} = \text{GdH}_2\text{L}^-) = 8.34 \pm 0.04$	178
Ho <sup>3+</sup>	Sp	19-21	0.1	$K(\text{Ho}^{3+} + \text{H}_2\text{L}^{4-} = \text{HoH}_2\text{L}^-) = 8.27 \pm 0.03$	178
La <sup>3+</sup>	Sp	19-21	0.1	$K(\text{La}^{3+} + \text{H}_2\text{L}^{4-} = \text{LaH}_2\text{L}^-) = 8.64 \pm 0.02$	178
Lu <sup>3+</sup>	Sp	19-21	0.1	$K(\text{Lu}^{3+} + \text{H}_2\text{L}^{4-} = \text{LuH}_2\text{L}^-) = 8.42 \pm 0.01$	178
Nd <sup>3+</sup>	Sp	19-21	0.1	$K(\text{Nd}^{3+} + \text{H}_2\text{L}^{4-} = \text{NdH}_2\text{L}^-) = 8.66 \pm 0.04$	178
Pr <sup>3+</sup>	Sp	19-21	0.1	$K(\text{Pr}^{3+} + \text{H}_2\text{L}^{4-} = \text{PrH}_2\text{L}^-) = 8.50 \pm 0.02$	178
Sm <sup>3+</sup>	Sp	19-21	0.1	$K(\text{Sm}^{3+} + \text{H}_2\text{L}^{4-} = \text{SmH}_2\text{L}^-) = 8.39 \pm 0.03$	178
Tb <sup>3+</sup>	Sp	19-21	0.1	$K(\text{Tb}^{3+} + \text{H}_2\text{L}^{4-} = \text{TbH}_2\text{L}^-) = 8.28 \pm 0.01$	178
Tm <sup>3+</sup>	Sp	19-21	0.1	$K(\text{Tm}^{3+} + \text{H}_2\text{L}^{4-} = \text{TmH}_2\text{L}^-) = 8.33 \pm 0.02$	178
Y <sup>3+</sup>	Sp	19-21	0.1	$K(\text{Y}^{3+} + \text{H}_2\text{L}^{4-} = \text{YH}_2\text{L}^-) = 9.60 \pm 0.03$	178
Yb <sup>3+</sup>	Sp	19-21	0.1	$K(\text{Yb}^{3+} + \text{H}_2\text{L}^{4-} = \text{YbH}_2\text{L}^-) = 8.35 \pm 0.03$	178
C <sub>17</sub> H <sub>14</sub> O <sub>2</sub> N <sub>2</sub> , 1-phenyl-3-methyl-4-benzoylpyrazol-5-one, HL					
Ce <sup>3+</sup>	Dis, Sp	20	0.1 (NaClO <sub>4</sub> )	$K_1 = 6.54, K_2 = 5.55, K_3 = 4.46$	179

(Continued.)					
Metal	Method	Temp. (°C)	Medium	log of equilibrium constant	Ref.
Er <sup>3+</sup>	Dis	25	CHCl <sub>3</sub>	$K(\text{ErA}^{3+} + 3\text{L}^- = \text{ErAL}_3)$ = 2.29, where A = tributyl phosphate = 7.56, where A = piperidine = 8.26, where A = 1,10-phenanthroline	179
Gd <sup>3+</sup>	Dis	25	CHCl <sub>3</sub>	$K(\text{GdA}^{3+} + 3\text{L}^- = \text{GdAL}_3) = 1.56,$ where A = tributyl phosphate $K(\text{GdA}^{3+} + 3\text{L}^- = \text{GdA}_2\text{L}_3)$ = 6.23, where A = piperidine = 7.43, where A = 1,10-phenanthroline	179
Nd <sup>3+</sup>	Dis	25	CHCl <sub>3</sub>	$K(\text{NdA}_2^{3+} + 3\text{L}^- = \text{NdA}_2\text{L}_3)$ = 2.63, where A = tributyl phosphate = 8.10, where A = piperidine	179
C <sub>18</sub> H <sub>20</sub> O <sub>6</sub> N <sub>2</sub> , ethylenedinitrilo- <i>N,N'</i> -bis(2'-hydroxyphenyl)- <i>N,N'</i> -diacetic acid, H <sub>4</sub> L					
H <sup>+</sup>	Pot	?	?	$K_1 = 11.68, K_2 = 9.15, K_3 = 4.72, K_4 = 3.20$	180
Pr <sup>3+</sup>	Pot	?	?	$K(\text{Pr}^{3+} + \text{HL}^{3-} = \text{PrHL}) = 8.97$	180
Tb <sup>3+</sup>	Pot	?	?	$K(\text{Tb}^{3+} + \text{HL}^{3-} = \text{TbHL}) = 9.05$	180
Yb <sup>3+</sup>	Pot	?	?	$K(\text{Yb}^{3+} + \text{HL}^{3-} = \text{YbHL}) = 9.07$	180
C <sub>20</sub> H <sub>14</sub> O <sub>5</sub> N <sub>2</sub> S, 1-(1-hydroxy-2-naphthylazo)-2-naphthol-4-sulphonic acid (solochrome 6BN), 2-hydroxy-4-[(1-hydroxy-2-naphthyl)azo]-1-naphthalene sulphonic acid					
H <sup>+</sup>	Gl	25	0.1 (NaClO <sub>4</sub> )	$K_1 = 12.25, K_2 = 6.51$	181
Ce <sup>3+</sup>	Sp	?	?	$K_1 = 5.72$	182
Nd <sup>3+</sup>	Sp	?	?	$K_1 = 5.16$	182
C <sub>20</sub> H <sub>14</sub> O <sub>5</sub> N <sub>2</sub> S, [3-hydroxy-4-(2-hydroxy-1-naphthoylazo)naphthalene-1-sulphonic acid]					
H <sup>+</sup>	Sp	?	?	$K_1 = 13.5, K_2 = 7.3$	183
Ce <sup>3+</sup>	Sp	?	98% ethanol	$K(?) = 5.20 \pm 0.8$	183
La <sup>3+</sup>	Sp	?	98% ethanol	$K(?) = 5.20 \pm 0.8$	183
Nd <sup>3+</sup>	Sp	?	98% ethanol	$K(?) = 5.20 \pm 0.8$	183
Pr <sup>3+</sup>	Sp	?	98% ethanol	$K(?) = 5.20 \pm 0.8$	183
Sm <sup>3+</sup>	Sp	?	98% ethanol	$K(?) = 5.20 \pm 0.8$	183
C <sub>21</sub> H <sub>14</sub> O <sub>3</sub> , 6,7-dihydroxy-2,4-diphenylbenzopyranol, HL					
H <sup>+</sup>	Sp	?	?	$K_1 = 8.58, K_2 = 2.72$	184
Nd <sup>3+</sup>	Sp	?	?	$K(\text{NdOH}^{2+} + \text{L}^- = \text{NdOHL}^+) = 9.31$	184
Y <sup>3+</sup>	Sp	?	?	$K(\text{YOH}^{2+} + \text{L}^- = \text{YOHL}^+) = 9.36$	184
C <sub>22</sub> H <sub>20</sub> O <sub>13</sub> , 5-carboxy-1,3,4,6-tetrahydroxy-8-methyl-2-(1'-oxo-2',3',4',5'-tetrahydroxyhexyl)-anthraquinone (carminic acid), H <sub>5</sub> L					
H <sup>+</sup>	Sp	?	0.1	$K_4 = 8.81 \pm 0.01, K_5 = 5.87 \pm 0.01$	185
Gd <sup>3+</sup>	Sp	?	0.1	$K[\text{GdOH}^{2+} + 2\text{H}_3\text{L}^{2-} = \text{GdOH}(\text{H}_3\text{L})_2^{2-}]$ = 16.90	185
La <sup>3+</sup>	Sp	?	0.1	$K[\text{LaOH}^{2+} + 2\text{H}_3\text{L}^{2-} = \text{LaOH}(\text{H}_3\text{L})_2^{2-}]$ = 15.19	185
Lu <sup>3+</sup>	Sp	?	0.1	$K[\text{LuOH}^{2+} + 2\text{H}_3\text{L}^{2-} = \text{LuOH}(\text{H}_3\text{L})_2^{2-}]$ = 19.29	185
Y <sup>3+</sup>	Sp	?	0.1	$K[\text{YOH}^{2+} + 2\text{H}_3\text{L}^{2-} = \text{YOH}(\text{H}_3\text{L})_2^{2-}]$ = 17.76	185
C <sub>22</sub> H <sub>18</sub> O <sub>14</sub> N <sub>4</sub> S <sub>2</sub> As <sub>2</sub> , 2,7-bis(2'-arsonophenylazo)chromotropic acid (Arsenazo III), H <sub>8</sub> L					
H <sup>+</sup>	Sp	?	?	$K_1 = 12.43, K_2 = 10.18, K_3 = 8.43, K_4 = 6.96$ $K_5 = 4.96, K_6 = 3.53, K_7 = 2.91, K_8 = 0.79$	186
Ce <sup>3+</sup>	Sp	19-21	?	$K(\text{Ce}^{3+} + \text{H}_4\text{L}^{4-} = \text{LaH}_4\text{L}^-) = 14.88 \pm 0.12$	186
Dy <sup>3+</sup>	Sp	19-21	?	$K(\text{Dy}^{3+} + \text{H}_4\text{L}^{4-} = \text{DyH}_4\text{L}^-) = 16.66 \pm 0.03$	186

(Continued.)

Metal	Method	Temp. (°C)	Medium	log of equilibrium constant	Ref.
Er <sup>3+</sup>	Sp	19-21	?	$K(\text{Er}^{3+} + \text{H}_4\text{L}^{4-} = \text{ErH}_4\text{L}^-) = 16.39 \pm 0.12$	186
Eu <sup>3+</sup>	Sp	19-21	?	$K(\text{Eu}^{3+} + \text{H}_4\text{L}^{4-} = \text{EuH}_4\text{L}^-) = 15.85 \pm 0.29$	186
Gd <sup>3+</sup>	Sp	19-21	?	$K(\text{Gd}^{3+} + \text{H}_4\text{L}^{4-} = \text{GdH}_4\text{L}^-) = 15.75 \pm 0.12$	186
Ho <sup>3+</sup>	Sp	19-21	?	$K(\text{Ho}^{3+} + \text{H}_4\text{L}^{4-} = \text{HoH}_4\text{L}^-) = 16.57 \pm 0.09$	186
La <sup>3+</sup>	Sp	19-21	?	$K(\text{La}^{3+} + \text{H}_4\text{L}^{4-} = \text{LaH}_4\text{L}^-) = 14.87 \pm 0.07$	186
Lu <sup>3+</sup>	Sp	19-21	?	$K(\text{Lu}^{3+} + \text{H}_4\text{L}^{4-} = \text{LuH}_4\text{L}^-) = 15.05 \pm 0.14$	186
Nd <sup>3+</sup>	Sp	19-21	?	$K(\text{Nd}^{3+} + \text{H}_4\text{L}^{4-} = \text{NdH}_4\text{L}^-) = 15.43 \pm 0.31$	186
Pr <sup>3+</sup>	Sp	19-21	?	$K(\text{Pr}^{3+} + \text{H}_4\text{L}^{4-} = \text{PrH}_4\text{L}^-) = 15.38 \pm 0.12$	186
Sm <sup>3+</sup>	Sp	19-21	?	$K(\text{Sm}^{3+} + \text{H}_4\text{L}^{4-} = \text{SmH}_4\text{L}^-)$ $= 15.73 \pm 0.34$	186
Tb <sup>3+</sup>	Sp	19-21	?	$K(\text{Tb}^{3+} + \text{H}_4\text{L}^{4-} = \text{TbH}_4\text{L}^-) = 16.29 \pm 0.25$	186
Y <sup>3+</sup>	Sp	19-21	?	$K(\text{Y}^{3+} + \text{H}_4\text{L}^{4-} = \text{YH}_4\text{L}^-) = 16.07 \pm 0.13$	186
Yb <sup>3+</sup>	Sp	19-21	?	$K(\text{Yb}^{3+} + \text{H}_4\text{L}^{4-} = \text{YbH}_4\text{L}^-) = 14.98 \pm 0.19$	186
C <sub>23</sub> H <sub>18</sub> O <sub>9</sub> S, 4'-hydroxy-3,3'-dimethyl-2''-sulphofuchsonone-5,5'-dicarboxylic acid (eriochrome cyanine R), H <sub>4</sub> L					
H <sup>+</sup>	Sp	25	0.1 (Na,NH <sub>4</sub> )Cl	$K_1 = 12.1, K_2 = 5.45, K_3 = 2.32, K_4 < 1$	187
Gd <sup>3+</sup>	Sp	25	?	$\beta_2 = 9.8$	187
Ho <sup>3+</sup>	Sp	25	?	$\beta_2 = 9.8$	187
Lu <sup>3+</sup>	Sp	25	?	$\beta_2 = 9.2$	187
Nd <sup>3+</sup>	Sp	25	?	$\beta_2 = 9.6$	187
Pr <sup>3+</sup>	Sp	25	?	$\beta_2 = 10.6$	187
Sm <sup>3+</sup>	Sp	25	?	$\beta_2 = 9.6$	187
Tm <sup>3+</sup>	Sp	25	?	$\beta_2 = 9.6$	187
Yb <sup>3+</sup>	Sp	25	?	$\beta_2 = 9.1$	187
Gd <sup>3+</sup>	Sp	25	?	$\beta_2 = 9.8$	187
C <sub>23</sub> H <sub>16</sub> O <sub>9</sub> Cl <sub>2</sub> S, 2'',6''-dichloro-4'-hydroxy-3,3'-dimethyl-3''-sulphofuchsonone-5,5'-dicarboxylic acid (chrome Azurol S), H <sub>4</sub> L					
La <sup>3+</sup>	Sp	?	?	$K[\text{LaOH}^{2+} + 3\text{A} + \text{H}_3\text{L}^- = \text{LaOHA}_3(\text{H}_3\text{L})^+]$ $= 17.87$ , where A = 1,10-phenanthroline	188
Y <sup>3+</sup>	Sp	?	?	$K[\text{YOH}^{2+} + \text{A} + \text{H}_3\text{L}^- = \text{YOHA}(\text{H}_3\text{L})^+]$ $= 12.50$ , where A = 1,10-phenanthroline	188
C <sub>31</sub> H <sub>32</sub> O <sub>13</sub> N <sub>2</sub> S, 5,5'-bis-N,N-bis(carboxymethyl)aminomethyl-4'-hydroxy-3,3'-dimethyl-fuchsonone-2''-sulphonic acid (xylenol orange), H <sub>6</sub> L					
Ce <sup>3+</sup>	Sp	?	?	$K(\text{Ce}^{3+} + \text{H}_2\text{L}^{4-} = \text{CeH}_2\text{L}^-) = 6.45$	189
La <sup>3+</sup>	Sp	?	?	$K(\text{La}^{3+} + \text{H}_2\text{L}^{4-} = \text{LaH}_2\text{L}^-) = 6.43$	189
Nd <sup>3+</sup>	Sp	?	?	$K(\text{Nd}^{3+} + \text{H}_2\text{L}^{4-} = \text{NdH}_2\text{L}^-) = 6.5$	189
Pr <sup>3+</sup>	Sp	?	?	$K(\text{Pr}^{3+} + \text{H}_2\text{L}^{4-} = \text{PrH}_2\text{L}^-) = 6.48$	189
Sc <sup>3+</sup>	Sp	?	?	$K(\text{Sc}^{3+} + \text{H}_2\text{L}^{4-} = \text{ScH}_2\text{L}^-) = 6.5$	189
Sm <sup>3+</sup>	Sp	?	?	$K(\text{Sm}^{3+} + \text{H}_2\text{L}^{4-} = \text{SmH}_2\text{L}^-) = 6.52$	189
Y <sup>3+</sup>	Sp	?	?	$K(\text{Y}^{3+} + \text{H}_2\text{L}^{4-} = \text{YH}_2\text{L}^-) = 7.4$	189
C <sub>18</sub> H <sub>30</sub> O <sub>12</sub> N <sub>4</sub> , triethylenetetraminehexaacetic acid (TTHA), H <sub>6</sub> L					
H <sup>+</sup>	Gl	20	0.1 KNO <sub>3</sub>	$K_1 = 10.65, K_2 = 9.54, K_3 = 6.10,$ $K_4 = 4.03, K_5 = 2.68, K_6 = 2.28$	190
Ce <sup>3+</sup>	Sp	?	?	$K_1 = 19.20$	191
Er <sup>3+</sup>	Red	25	0.1 KNO <sub>3</sub>	$K_1 = 23.40$	192
La <sup>3+</sup>	Gl	25	0.1 KNO <sub>3</sub>	$K_1 = 16.7$	193
Ho <sup>3+</sup>	Gl	25	0.1 KNO <sub>3</sub>	$K_1 = 15.4$	193
Nd <sup>3+</sup>	Gl	25	0.1 KNO <sub>3</sub>	$K_1 = 16.6$	193
Sm <sup>3+</sup>	Gl	25	0.1 KNO <sub>3</sub>	$K_1 = 15.7$	193

## References for Table 3.11

1. D.J. Macero, L.B. Anderson, P. Malachosky, J. Electroanal. Chem. **10**, 76, 1965.
2. M.S. Borisov, A.A. Elesin, I.A. Lebedev, Radiokhimiya **8**, 166, 1967.
3. A.A. Elesin, A.A. Zaitsev, N.A. Ivanovitch, V.A. Karaseva, G.N. Yakolylev, Radiokhimiya **14**, 546, 1972.
4. I. Grenthe, G. Gardhammar, E. Rundcrntz, Acta Chem. Scand. **23**, 93, 1969.
5. I.V. Kolosov, Z.F. Andreeva, Zhur. Neorg. Khim. **14**, 664, 1969.
6. A. Aziz, S.J. Lyle, J. Inorg. Nucl. Chem. **32**, 1925, 1970.
7. I. Stary, Radiokhimiya **8**, 504, 1966.
8. S.A. Merkusheva, V.N. Kumok, N.A. Skurik, V.V. Serebrinnikov, Radiokhimiya **12**, 175, 1970.
9. Z.F. Andreeva, V.N. Bezuevskaya, I.V. Kolosov, Z.N. Shevtsova, I. Timiryazev, Selskokhoz. Akad. 200, 1967.
10. G.R. Choppin, J.K. Schneider, J. Inorg. Nucl. Chem. **32**, 3283, 1970.
11. M. Tomus, M. Totan, Stud. Univ. Babes-Bolyai, Chem. **49**, 1968.
12. P.K. Migal, N.G. Chebotar, Zhur. Neorg. Khim. **15**, 1218, 1970.
13. P.K. Migal, N.G. Chebotar, A.N. Sorochinskaya, Zhur. Neorg. Khim. **18**, 607, 1973.
14. B.M. Antipenko, I.M. Batyaev, T.A. Privalova, Zhur. Neorg. Khim. **12**, 2.11, 1967.
15. G. Marcu, A. Botar, Stud. Univ. Babes-Bolyai, Ser. Chem. **12**, 211, 1967.
16. F.H. Spedding, Jaffe, J. Amer. Chem. Soc. **76**, 882, 1954.
17. G.R. Choppin, G. Degischer, J. Inorg. Nucl. Chem. **34**, 3473, 1973.
18. G.S. Manku, R.C. Chadha, J. Inorg. Nucl. Chem. **34**, 357, 1972.
19. J.H. Forsberg, T. Moeller, Inorg. Chem. **8**, 889, 1969.
20. L.S. Sukhanova, L.I. Martynenko, Zhur. Neorg. Khim. **14**, 397, 1969.
21. L.S. Sukhanova, A.E. Elikhilyali, T.N. Saprykina, L.I. Martynenko, Vest. Moskovsk. Univ. **14**, 1, 59, 1973.
22. A.A. Elesin, A.A. Zaitsev, S.S. Kazakova, G.N. Yakolev, Radiokhimiya **14**, 541, 1972.
23. E.I. Sinyavskaya, Z.Z. Sheka, Radiokhimiya **8**, 410, 1966.
24. A.I. Kirillov, L.A. Turkina, N.A. Vlasov, Izvest. Vuz. Khim. **16**, 846, 1973.
25. I. Dellien, I. Grenthe, Acta Chem. Scand. **25**, 1387, 1971.
26. P.K. Migal, N.G. Chebotar, A.M. Sorochinskaya, Zhur. Neorg. Khim. **16**, 1823, 1971.
27. A. Aziz, S.J. Lyle, J.E. Newbery, J. Inorg. Nucl. Chem. **33**, 1757, 1971.
28. A.V. Lapitskaya, S.B. Pirkes, Zhur. Neorg. Khim. **18**, 1204, 1973.
29. A.D. Jones, G.R. Choppin, J. Inorg. Nucl. Chem. **31**, 3523, 1969.
30. A. Aziz, S.J. Lyle, J. Inorg. Nucl. Chem. **33**, 3407, 1971.
31. L.P. Lisovaya, N.A. Skorik, Zhur. Neorg. Khim. **18**, 1134, 1973.
32. H. Deelstra, F. Verbeek, Bull. Soc. Chim. Belges **76**, 557, 1967.
33. K. Winkler, K.B. Zaborenko, Z. Physik. Chem. **238**, 348, 1968.
34. G.C.S. Manku, Z. Anorg. Allgem. Chem. **382**, 202, 1971.
35. G.R. Choppin, L.A. Martinez-Perez, Inorg. Chem. **7**, 2657, 1968.
36. R. Roulet, J. Feuz, T. VuDuc, Helv. Chim. Acta **53**, 1876, 1970.
37. G.R. Choppin, A. Dadgar, R. Stamfli, J. Inorg. Nucl. Chem. **35**, 875, 1973.
38. S.A. Merkusheva, V.N. Kumok, N.A. Skorik, V.V. Serebrennikov, Radiokhimiya **12**, 175, 1970.
39. I. Grenthe, H. Ots, Acta Chem. Scand. **26**, 1217, 1972.
40. I. Grenthe, H. Ots, Acta Chem. Scand. **26**, 1229, 1972.
41. R. Roulet, J. Feux, T. VuDuc, Helv. Chim. Acta **53**, 1876, 1970.
42. G.N. Shabanova, N.A. Skorik, Zhur. Obshechi Khim. **42**, 204, 1972.
43. I. Stary, Radiokhimiya **8**, 509, 1966.
44. P.K. Migal, A.M. Sorochinskaya, Zhur. Neorg. Khim. **16**, 3243, 1971.
45. M.E. Clark, J.L. Bear, J. Inorg. Nucl. Chem. **32**, 3569, 1970.
46. Stagg, Powell, Inorg. Chem. **3**, 242, 1964.
47. G.R. Choppin, Chopoorian, J. Inorg. Nucl. Chem. **22**, 97, 1961.
48. I. Dellien, I. Grenthe, G. Hessler, Acta Chem. Scand. **27**, 2431, 1973.
49. R. Roulet, R. Chenaux, T. VuDuc, Helv. Chim. Acta **54**, 916, 1971.
50. R. Dreyer, J. Redlich, R. Shre, Z. Physik. Chem. (Leipzig) **238**, 417, 1968.
51. Thompson, Inorg. Chem. **1**, 490, 1962.
52. Thompson, Lorrans, Inorg. Chem. **2**, 594, 1963.

53. G. Schwarzenbach, H. Gut, *Helv. Chim. Acta* **39**, 1589, 1956.
54. G.C.S. Manku, Z. *Anorg. Allgen. Chem.* **382**, 202, 1971.
55. A.I. Mikhailichenko, N.N. Guseva, E.V. Sklenskaya, M.Kh. Karapetyants, *Zhur. Neorg. Khim.* **16**, 3101, 1971.
56. E.J. Sinyavskaya, Z.A. Sheka, *Radiokhimiya* **8**, 410, 1966.
57. H. Schurmans, H. Thun, F. Verbeck, W. Vanderleen, *J. Electroanal. Chem. Interfacial Electrochem.* **38**, 209, 1972.
58. Dutt, Bandhopadhyay, *J. Inorg. Nucl. Chem.* **26**, 729, 1964.
59. R. Roulet, J. Feuz, T. VuDuc, *Helv. Chim. Acta* **53**, 1876, 1970.
60. S.A. Merkusheva, V.N. Kumok, N.A. Skorik, V.A. Serebrennikov, *Radiokhimiya* **12**, 175, 1970.
61. E.I. Chutakova, N.A. Skorik, *Zhur. Neorg. Khim.* **18**, 2723, 1973.
62. R. Roulet, T. VuDuc, *Helv. Chim. Acta* **53**, 1873, 1970.
63. J.E. Powell, A.R. Chugtai, J.W. Ingemanson, *Inorg. Chem.* **8**, 2216, 1969.
64. D.P. Goel, Y. Dutt, R.P. Singh, *J. Inorg. Nucl. Chem.* **32**, 2119, 1970.
65. P. Fiege, D. Mocker, R. Dreyer, R. Munze, *J. Inorg. Nucl. Chem.* **35**, 3269, 3629, 1973.
66. R.C. Tewari, M.N. Srivastava, *J. Inorg. Nucl. Chem.* **35**, 3044, 1973.
67. D.V. Pakhomova, V.N. Kumok, V.V. Serebrennikov, *Zhur. Neorg. Khim.* **14**, 1434, 1969.
68. N.K. Dutt, U.V.M. Sharma, *J. Inorg. Nucl. Chem.* **32**, 1035, 1970.
69. N.K. Dutt, U.V.M. Sharma, *J. Inorg. Nucl. Chem.* **32**, 2261, 1972.
70. K.P. Stolyarov, I.A. Amantova, *Vest. Leningr. Univ.* **4**, 155, 1966.
71. K.P. Stolyarov, I.A. Amantova, *Vest. Leningr. Univ.* **4**, 155, 1966.
72. N.S. Poluetkov, N.P. Efrushina, *Ukrain. Khim. Zhur.* **36**, 164, 1970.
73. Stepanov, Merkulova, *Radiokhimiya* **1**, 668, 1959.
74. T.V. Beloedova, L.V. Kazakova, N.A. Skorik, *Zhur. Neorg. Khim.* **17**, 1580, 1972.
75. N.K. Dutt, S. Rahut, *J. Inorg. Nucl. Chem.* **31**, 3177, 1969.
76. V.D. Khanoikar, D.V. Jahagirdar, D.D. Khanolkar, *J. Inorg. Nucl. Chem.* **35**, 971, 1973.
77. S.A. Merkusheva, V.N. Kumok, N.A. Skorik, V.V. Serebrennikov, *Radiokhimiya* **12**, 175, 1970.
78. J.E. Powell, J.W. Ingemanson, *Inorg. Chem.* **7**, 2459, 1968.
79. C. Petitfaux, J.P. Barbier, J. Faucherre, *Bull. Soc. Chim. France* 3441, 1970.
80. N.K. Dutt, K. Nag, *J. Inorg. Nucl. Chem.* **31**, 1867, 1969.
81. N.K. Dutt, S. Sanyal, U.U.M. Sharma, *J. Inorg. Nucl. Chem.* **34**, 2261, 1972.
82. L.D. Shtenke, N.A. Skorik, V.N. Kumok, *Zhur. Neorg. Khim.* **15**, 1214, 1970.
83. J.L. Bear, M.E. Clark, *J. Inorg. Nucl. Chem.* **31**, 1517, 1969.
84. A.D. Jones, D.R. Williams, *J. Chem. Soc. (A)* 3138, 1970.
85. N.K. Dutt, S. Rahut, *J. Inorg. Nucl. Chem.* **32**, 1033, 1970.
86. Y. Masuda, H. Sakai, S. Misumi, *Japan Analyst* **22**, 1577, 1973.
87. N.A. Kostromina, E.D. Romanenko, *Zhur. Neorg. Khim.* **13**, 1848, 1968.
88. N.A. Kostromina, E.D. Romanenko, *Zhur. Neorg. Khim.* **15**, 1782, 1970.
89. E.I. Sinyavskaya, Z.A. Sheka, *Radiokhimiya* **8**, 410, 1966.
90. P. Fiege, D. Mocker, R. Dreyer, R. Munze, *J. Inorg. Nucl. Chem.* **34**, 3269, 1973.
91. D. L. Campbell, T. Moeller, *J. Inorg. Nucl. Chem.* **31**, 1077, 1969.
92. I.M. Batyaev, N.L. Puzankova, *Zhur. Neorg. Khim.* **18**, 981, 1973.
93. J.L. Bear, M.E. Clark, *J. Inorg. Nucl. Chem.* **31**, 2811, 1969.
94. J.E. Powell, D.K. Johnson, *J. Inorg. Nucl. Chem.* **33**, 3586, 1971.
95. N.K. Dutt, S. Rahut, *J. Inorg. Nucl. Chem.* **33**, 1725, 1971.
96. S.B. Pirkes, M.T. Shestakova, A.V. Lapitskaya, *Zhur. Neorg. Khim.* **17**, 395, 1972.
97. E.A. Didenko, S.B. Pirkes, *Zhur. Neorg. Khim.* **18**, 73, 1973.
98. A. Cassol, P. Di Bernardo, R. Portanova, L. Magon, *Gaz. Chim., Ital.* **102**, 1118, 1972.
99. S. Takata, E. Kyuno, R. Tsuchiya, *Bull. Chem. Soc., Japan* **41**, 3416, 1968.
100. N.L. Belkova, I.M. Batyaev, V.R. Mironov, *Zhur. Neorg. Khim.* **15**, 2138, 1970.
101. N.K. Dutt, T. Seshadri, *J. Inorg. Nucl. Chem.* **31**, 2153, 1969.
102. T. Seshadri, *Talanta* **17**, 168, 1969.
103. J.L. Bear, C.T. Lin, *J. Inorg. Nucl. Chem.* **34**, 2368, 1972.
104. V.M. Peshkova, I.P. Efimov, N. Magdesieva, *Zhur. Analyt. Khim.* **21**, 499, 1966.



105. A.S. Beryland, A.I. Byrke, L.I. Martynenko, *Zhur. Neorg. Khim.* **13**, 2106, 1968.
106. G.C.S. Manku, *Austral. J. Chem.* **24**, 25, 1971.
107. I.P. Gorelov, V.A. Babich, *Zhur. Neorg. Khim.* **17**, 641, 1972.
108. A.I. Mikhailichenko, N.N. Guseva, E.V. Sklenskaya, M.Kh. Karapetyants, *Zhur. Neorg. Khim.* **16**, 3101, 1971.
109. E.J. Sinyavskaya, Z.A. Sheka, *Radiokhimiya* **8**, 410, 1966.
110. L.I. Tikhonova, *Zhur. Fiz. Khim.* **44**, 3118, 1970.
111. A.B. Shalinets, *Radiokhimiya* **113**, 566, 1971.
112. L.I. Tikhonova, L.I. Ivanova, *Zhur. Neorg. Khim.* **16**, 1238, 1971.
113. K. Winkler, K.B. Zaborenko, *Z. Physik Chem.* **238**, 348, 1968.
114. H. Steger, A. Corsini, *J. Inorg. Nucl. Chem.* **35**, 1621, 1973.
115. R.D. Gupta, G.S. Manku, A.N. Bhat, B.D. Jain, *Austr. J. Chem.* **23**, 1387, 1970.
116. N.E. Brezhneva, V.I. Levin, M.G. Ratnikova, V.S. Novoselov, *Radiokhimiya* **12**, 259, 1970.
117. I.M. Batyaev, R.S. Fogileva, *Zhur. Neorg. Khim.* **17**, 391, 1972.
118. G.C.S. Manku, *J. Inorg. Nucl. Chem.* **33**, 285, 1971.
119. F. Kai, Y. Sadakane, H. Yokoi, H. Aburada, *J. Inorg. Nucl. Chem.* **35**, 2128, 1973.
120. G.C.S. Manku, *Bull. Chem. Soc., Japan* **46**, 1704, 1973.
121. A.S. Kertes, E.F. Kassierer, *Inorg. Chem.* **11**, 2108, 1972.
122. A.S. Berlyand, A.I. Byrke, L.I. Martynenko, *Zhur. Neorg. Khim.* **13**, 2106, 1968.
123. N.K. Davidenko, A.A. Zholdokov, *Zhur. Neorg. Khim.* **13**, 2955, 1968.
124. N.K. Dutt, S. Sanyal, *J. Inorg. Nucl. Chem.* **34**, 651, 1972.
125. N.K. Dutt, K. Nag, *J. Inorg. Nucl. Chem.* **31**, 1867, 1969.
126. N.K. Dutt, K. Nag, T. Seshadri, *J. Inorg. Nucl. Chem.* **31**, 1435, 1969.
127. S.H. Eberle, I. Bayat, *Inorg. Nucl. Chem. Letters* **5**, 229, 1969.
128. E.J. Wheelwright, F.H. Spedding, G. Schwarzenbach, *J. Am. Chem. Soc.* **75**, 4196, 1953.
129. V.A. Babich, I.P. Gorelov, *Zhur. Analit. Khim.* **26**, 1832, 1971.
130. T. Moeller, D.F. Martin, L.C. Thompson, R. Ferrus, G.R. Feistel, W.J. Randall, *Chem. Rev.* **65**, 1, 1965.
131. J.E. Powell, T.V. Swaminathan, *J. Chromatog.* **76**, 459, 1973.
132. O. Maikitie, H. Saarinen, L. Lindroos, K. Seppovaara, *Acta Chem. Scand.* **24**, 740, 1970.
133. M.M. Taqui Khan, P. R. Reddy, *J. Inorg. Nucl. Chem.* **34**, 967, 1972.
134. M.I. Gromova, M.N. Litivina, V.M. Peshkova, *Zhur. Analit. Khim.* **27**, 270, 1972.
135. G.C.S. Manku, *Austral. J. Chem.* **24**, 925, 1971.
136. N.K. Dutt, S. Rahut, S. Sur, *J. Inorg. Nucl. Chem.* **33**, 121, 1971.
137. A.S. Berlyand, L.I. Martynenko, *Vest. Moskovsk. Univ.* **6**, 729, 1971.
138. V.I. Egorova, V.N. Kumok, *Zhur. Obshch. Khim.* **4**, 1786, 1971.
139. I.M. Batyaev, R.S. Fogileva, *Zhur. Neorg. Khim.* **17**, 391, 1972.
140. E.M. Ragozina, D.K. Popov, T.M. Ponikarova, *Zhur. Obshch. Khim.* **38**, 1959, 1968.
141. S. Lal, *Austral. J. Chem.* **25**, 1571, 1972.
142. N.M. Dyatlova, V.Ya. Temkina, *Koordinat. Khim.* **1**, 66, 1975.
143. G. Anderegg, F. Wenk, *Helv. Chim. Acta* **52**, 173, 1970.
144. T.R. Sweet, D. Brengartner, *Anal. Chim. Acta* **52**, 173, 1970.
145. V. Novak, E. Dvorakova, J. Majer, *Chem. Zvesti* **23**, 161, 1969.
146. E. Dvorakova, J. Majer, *Chem. Zvesti* **20**, 233, 1966.
147. H.M.N.H. Irving, K. Sharpe, *J. Inorg. Nucl. Chem.* **33**, 203, 217, 1971.
148. O.P. Sunar, C.P. Trivedi, *J. Inorg. Nucl. Chem.* **33**, 3993, 1971.
149. I.P. Gorelov, V.A. Babich, *Zhur. Obshch. Khim.* **42**, 434, 1972.
150. O.P. Sunar, S. Tak, C.P. Trivedi, *Inorg. Nucl. Chem.* **35**, 314, 1973.
151. O.P. Sunar, S. Tak, C.P. Trivedi, *Indian J. Chem.* **10**, 1108, 1972.
152. N.A. Kostromina, G.A. Komashiko, *Zhur. Neorg. Khim.* **13**, 1041, 1968.
153. R.P. Latovsky, N.M. Dyatlova, I.A. Seliverstova, *Zhur. Neorg. Khim.* **12**, 3351, 1967.
154. I.A. Seliverstova, O.I. Samoilo, N.M. Dyatlova, Y.G. Yashunskii, *Zhur. Obshch. Khim.* **37**, 2463, 1967.
155. I.P. Efimov, L.S. Voronets, L.G. Makarova, V.M. Peshkova, *Vestnik Moskov. Univ., series II Khim.* **24**, No. 4, 121, 1969.

156. A.S. Beryland, A.I. Byrke, L.I. Martynenko, *Zhur. Neorg. Khim.* **13**, 2106, 1968.
157. K.R. Gupta, S.G. Tandon, *J. Indian Chem. Soc.* **47**, 972, 1970.
158. J.P. Shukla, S.G. Tandon, *Talanta* **19**, 711, 1972.
159. G.C.S. Manku, *J. Inorg. Nucl. Chem.* **33**, 3173, 1971.
160. R. Hering, W. Kruger, G. Kuhn, *Z. Chem.* **2**, 374, 1962.
161. V. Novak, L. Lucansky, J. Majer, *Chem. Zvesti* **22**, 733, 1968; **23**, 161, 1969.
162. K. Winkler, K.B. Zaborenko, *Z. Physik. Chem.* **238**, 348, 1968.
163. A.I. Kochubei, A.I. Tolubara, Yu.T. Usatenko, *Zhur. Analit. Khim.* **28**, 500, 1973.
164. A.K. Jain, V.P. Aggarwala, P. Chand, S. Garg, *Talanta* **19**, 1481, 1972.
165. B.W. Budesinsky, J. Svec, *Inorg. Chem.* **10**, 313, 1971.
166. A.B. Shalinets, *Radiokhimiya* **13**, 566, 1971.
167. N.N. Tananaeva, N.A. Kostromina, *Zhur. Neorg. Khim.* **18**, 674, 1973.
168. I. Stary, *Radiokhimiya* **8**, 509, 1966.
169. J. Prasilova, J. Havlicek, *J. Inorg. Nucl. Chem.* **32**, 953, 1970.
170. V.T. Krumina, K.V. Astakhov, S.A. Barkov, *Zhur. Fiz. Khim.* **43**, 1196, 1969.
171. V. Novak, E. Dvorkova, M. Svicekova, J. Majer, *Chem. Zvesti* **23**, 861, 1969.
172. N.A. Kostromina, G.A. Komashko, *Zhur. Neorg. Khim.* **13**, 1041, 1968.
173. V.F. Vasilyeva, O.Yu. Lavrova, N.M. Dyatlova, V.G. Yashchunskii, *Zhur. Obshch. Khim.* **38**, 473, 1968.
174. V.F. Vasilyeva, O.Yu. Lavrova, N.M. Dyatlova, V.G. Yashanskii, *Zhur. Obshch. Khim.* **36**, 674, 1966.
175. V. Novak, E. Dvorakova, M. Svicekova, J. Majer, *Chem. Zvesti* **23**, 330, 1969.
176. N.N. Guseva, E.V. Sklenskaya, M.Kh. Karapetiyants, A.I. Mikhailichenko, *Radiokhimiya* **14**, 132, 1972.
177. P. Spacu, S. Plostinaru, *Rev. Roumaine Chim.* **14**, 591, 1969.
178. P.K. Spitsyn, V.S. Shvarev, G.K. Zvonareva, *Izvest. VUZ. Khim.* **14**, 28, 1971.
179. L.G. Tomlova, I.P. Efimov, V.M. Beshkova, *Zhur. Analit. Khim.* **28**, 666, 1973.
180. V.Ya. Temkina, M.N. Risina, L.V. Krinitskaya, R. Lastovskii, *Zhur. Obshch. Khim.* **38**, 2207, 1968.
181. S.P. Mushran, O. Prakash, R. Murti, *J. Inorg. Nucl. Chem.* **35**, 2119, 173.
182. R.K. Chernova, G.M. Borisova, *Izvest. VUZ. Khim.* **15**, 21, 1972.
183. S.M.F. Rahman, M. Ahmad, J. Ahmad, *J. Indian Chem. Soc.* **45**, 531, 1968.
184. N.S. Pouektov, M.A. Sandu, *Zhur. Analit. Khim.* **24**, 1472, 1969.
185. N.S. Poluektov, R.S. Lauer, M.A. Sandu, *Zhur. Analit. Khim.* **25**, 2118, 1970.
186. P.K. Spitsyn, V.S. Shvarev, T.P. Popyvanov, *Zhur. Neorg. Khim.* **17**, 966, 1972.
187. S.P. Mushran, O. Prakash, P. Sanyal, *J. Prakt. Chem.* **38**, 125, 1968.
188. L.I. Ganago, L.A. Alinovskaya, *Zhur. Analit. Khim.* **29**, 494, 1973.
189. O.A. Tataev, E.T. Beschetnova, *Sbornik Soobshch. Dagest. Univ. Khim.* **38**, 2015, 1968.
190. G. Anderegg, W.E. Van Der Linden, *Chimia (Aarau)* **23**, 191, 1969.
191. M.B. Hafez, R. Guillamont, *Bull. Soc. Chim. France* 1047, 1969.
192. L. Harju, *Anal. Chim. Acta* **50**, 475, 1970.
193. A. Yingst, A.E. Martell, *J. Am. Chem. Soc.* **91**, 6927, 1969.
194. R.H. Karraker, PhD Thesis, Iowa State University, 1962.
195. R.S. Kolat, PhD Thesis, Iowa State University, 1962.
196. T. Moeller, D.F. Martin, L.C. Thompson, R. Ferrus, G.R. Feistel, W.J. Randall, *Chem. Revs.* **65**, 1, 1965.
197. I. Grenthe, *J. Am. Chem. Soc.* **83**, 360, 1961.
198. J. Olivard, *Arch. Biochem. Biophys.* **88**, 382, 1960.
199. J.L. Mackey, M.A. Hiller, J.E. Powell, *J. Phys. Chem.* **66**, 311, 1962.
200. L.C. Thompson, PhD Thesis, University of Illinois, 1960.
201. G. Anderegg, F.L.L. Epplattener, G. Schwarzenbach, *Helv. Chim. Acta* **46**, 1400, 1963.
202. R. Hering, W. Krueger, G. Kuehn, *Z. Chem.* **2**, 374, 1962.
203. N.A. Kostromina, *Zhur. Neorg. Khim.* **8**, 1900, 1963.
204. M.M. Dyatlov, *Russ. J. Inorg. Chem.* **10**, 612, 1964.
205. L.C. Thompson, *Inorg. Chem.* **3**, 1319, 1964.
206. L.C. Thompson, *Inorg. Chem.* **3**, 1015, 1964.
207. H.M.N.H. Irving, J.P. Conesa, *J. Inorg. Nucl. Chem.* **26**, 1945, 1964.
208. F.L. Epplattener, G. Anderegg, *Helv. Chim. Acta* **47**, 1792, 1964.

TABLE 3.12  
Heats and entropies of formation of rare earth complexes.

Metal	$\Delta H_1^0$ (kcal/mole)	$\Delta S_1^0$ (e.u./mole)	$\Delta S_1^0 + \bar{S}^0 \text{Ln}$ (e.u./mole)	Ref.
Glycolic acid				
Ce <sup>3+</sup>	-0.44	8.9	-27	1
Gd <sup>3+</sup>	-0.40	9.9	-32	
Malonic acid				
La <sup>3+</sup>	4.8	39	4	
Gd <sup>3+</sup>	5.1	42	0	2
Lu <sup>3+</sup>	5.2	44	-4	
Lactic acid				
Ce <sup>3+</sup>	-0.83	7.9	-28	1
Gd <sup>3+</sup>	-0.54	9.8	-32	1
$\alpha$ -hydroxyisobutyric acid				
Ce <sup>3+</sup>	-0.83	8.4	-28	1
Gd <sup>3+-</sup>	-0.89	9.9	-32	1
Ethylenediamine- <i>N,N,N',N'</i> -tetraacetic acid				
La <sup>3+</sup>	-4.1	53	18	3, 4
Ce <sup>3+</sup>	-2.94	60.8	25	3, 4
Ce <sup>3+</sup>	-2.43	64.8	29	3, 4
Pr <sup>3+</sup>	-3.20	61.4	24	3, 4
Nd <sup>3+</sup>	-3.62	61.3	23	3, 4
Nd <sup>3+</sup>	-2.98	65.8	27	3, 4
Sm <sup>3+</sup>	-3.35	64.4	24	3, 4
Eu <sup>3+</sup>	-2.56	67.6	27	3, 4
Gd <sup>3+</sup>	-1.73	71.2	29	3, 4
Gd <sup>3+</sup>	-1.11	75.7	34	3, 4
Tb <sup>3+</sup>	-1.11	75.5	33	3, 4
Dy <sup>3+</sup>	-1.21	77.3	34	3, 4
Ho <sup>3+</sup>	-1.36	78.0	34	3, 4
Er <sup>3+</sup>	-1.71	78.3	33	3, 4
Tm <sup>3+</sup>	-1.87	79.1	33	3, 4
Yb <sup>3+</sup>	-2.31	79.2	32	3, 4
Lu <sup>3+</sup>	-2.51	79.1	32	3, 4
Y <sup>3+</sup>	-0.59	77.5	30	3, 4
Y <sup>3+</sup>	+0.32	83.8	37	3, 4
<i>N'</i> -(2-hydroxyethyl)ethylenediamine- <i>N,N,N'</i> -triacetic acid				
La <sup>3+</sup>	-2.20	54.2	20	5
Ce <sup>3+</sup>	-3.06	54.4	18	5
Pr <sup>3+</sup>	-4.45	52.0	15	5
Nd <sup>3+</sup>	-4.25	53.8	15	5
Sm <sup>3+</sup>	-4.65	54.4	16	5
Eu <sup>3+</sup>	-4.81	54.1	13	5
Gd <sup>3+</sup>	-4.66	54.1	12	5
Tb <sup>3+</sup>	-3.39	58.8	16	5
Dy <sup>3+</sup>	-2.12	62.8	19	5
Ho <sup>3+</sup>	-1.14	66.3	22	5
Er <sup>3+</sup>	-0.32	69.4	24	5
Tm <sup>3+</sup>	0.92	74.5	29	5

(Continued.)

Metal	$\Delta H_1^0$ (kcal/mole)	$\Delta S_1^0$ (e.u./mole)	$\Delta S_1^0 + \bar{S}^0 \text{Ln}$ (e.u./mole)	Ref.			
Yb <sup>3+</sup>	0.36	74.0	27	5			
Lu <sup>3+</sup>	0.22	73.4	26	5			
Y <sup>3+</sup>	-0.29	66.1	19	5			
1,2-diaminocyclohexane- <i>N,N,N',N'</i> -tetraacetic acid							
La <sup>3+</sup>	3.55	86.7	52	6			
Pr <sup>3+</sup>	5.00	95.6	58	6			
Nd <sup>3+</sup>	5.00	97.6	59	6			
Sm <sup>3+</sup>	5.00	102.00	62	6			
Eu <sup>3+</sup>	5.54	104.5	63	6			
Gd <sup>3+</sup>	5.75	105.3	64	6			
Tb <sup>3+</sup>	5.00	105.1	62	6			
Dy <sup>3+</sup>	3.09	100.5	57	6			
Ho <sup>3+</sup>	1.18	95.0	51	6			
Er <sup>3+</sup>	0.12	92.8	48	6			
Tm <sup>3+</sup>	-1.59	88.3	42	6			
Yb <sup>3+</sup>	-4.49	80.2	33	6			
Lu <sup>3+</sup>	-4.92	79.2	32	6			
Y <sup>3+</sup>	4.23	103.0	56	6			
Diethylenetriamine- <i>N,N,N',N',N''</i> -pentaacetic acid							
La <sup>3+</sup>	-5.7	70.0	35	7			
Pr <sup>3+</sup>	-7.1	72.0	35	7			
Nd <sup>3+</sup>	-5.8	79.4	41	7			
Sm <sup>3+</sup>	-8.2	74.7	34	7			
Eu <sup>3+</sup>	-8.1	75.3	34	7			
Gd <sup>3+</sup>	-7.5	77.6	36	7			
Tb <sup>3+</sup>	-7.7	78.1	36	7			
Dy <sup>3+</sup>	-8.0	77.6	34	7			
Ho <sup>3+</sup>	-7.6	78.7	34	7			
Er <sup>3+</sup>	-7.3	79.6	34	7			
Tm <sup>3+</sup>	-5.5	85.5	39	7			
Yb <sup>3+</sup>	-5.5	85.1	38	7			
Lu <sup>3+</sup>	-4.6	87.2	41	7			
Y <sup>3+</sup>	-5.2	83.4	36	7			
Nitrilotriacetic acid							
Metal	$\Delta H_1^0$ (kcal/mole)	$\Delta H_2^0$ (kcal/mole)	$\Delta S_1^0$ (e.u./mole)	$\Delta S_1^0 + \bar{S}^0 \text{Ln}$ (e.u./mole)	$\Delta S_2^0$ (e.u./mole)	$\Delta S_1^0 + \Delta S_2^0 + \bar{S}^0 \text{Ln}$ (e.u./mole)	Ref.
La <sup>3+</sup>	2.05	-2.43	54.3	20	25.0	45	8
Ce <sup>3+</sup>	1.25	-3.06	53.8	18	25.6	43	8
Pr <sup>3+</sup>	0.45	-3.72	52.2	15	24.9	40	8
Nd <sup>3+</sup>	0.68	-3.78	53.8	15	26.1	41	8
Sm <sup>3+</sup>	0.40	-4.37	54.1	14	26.5	40	8
Eu <sup>3+</sup>	0.93	-5.08	55.8	15	25.0	40	8
Gd <sup>3+</sup>	1.02	-5.80	56.2	14	22.9	37	8
Tb <sup>3+</sup>	1.71	-5.21	58.8	16	25.4	42	8
Dy <sup>3+</sup>	2.25	-5.61	61.3	18	24.2	42	8
Ho <sup>3+</sup>	2.63	-5.15	63.3	19	25.5	44	8
Er <sup>3+</sup>	2.51	-3.87	63.5	18	29.4	48	8
Tm <sup>3+</sup>	1.90	-2.36	62.3	16	34.3	51	8

(Continued.)

Metal	$\Delta H_1^0$ (kcal/mole)	$\Delta H_2^0$ (kcal/mole)	$\Delta S_1^0$ (e.u./mole)	$\Delta S_1^0 + \bar{S}^0 \text{Ln}$ (e.u./mole)	$\Delta S_2^0$ (e.u./mole)	$\Delta S_1^0 + \Delta S_2^0 + \bar{S}^0 \text{Ln}$ (e.u./mole)	Ref.
Yb <sup>3+</sup>	2.09	-1.86	63.7	17	36.3	53	8
Lu <sup>3+</sup>	1.98	-1.11	63.8	16	39.4	56	8
Y <sup>3+</sup>	2.69	-4.19	61.6	15	26.9	42	8

References of Table 3.12

1. Chopoorian, Ph.D. Thesis, Florida State University, 1961.
2. E. Gelles, G.H. Nancollas, Trans. Farad. Soc. **52**, 680, 1956.
3. J.L. Mackey, J.E. Powell, F.H. Spedding, J. Am. Chem. Soc. **84**, 2047, 1962.
4. L.A.K. Staveley, T. Randall, Discussions Faraday Society **26**, 157, 1958.
5. T. Moeller, R. Ferrus, J. Inorg. Nucl. Chem. **20**, 261, 1961.
6. T. Moeller, T.M. Hseu, J. Inorg. Nucl. Chem. **24**, 1635, 1962.
7. T. Moeller, L.C. Thompson, J. Inorg. Nucl. Chem. **24**, 499, 1962.
8. T. Moeller, R. Ferrus, Inorg. Chem. **1**, 19, 1962.

TABLE 3.12a  
Enthalpy and entropy of formation of rare earth complexes.

Cation	$\Delta H_1$ (kcal/mole)	$\Delta H_2$ (kcal/mole)	$\Delta H_3$ (kcal/mole)	$\Delta S_1$ (e.u./mole deg.)	$\Delta S_2$ (e.u./mole deg.)	$\Delta S_3$ (e.u./mole deg.)	Ref.
C <sub>2</sub> H <sub>4</sub> O <sub>2</sub> , CH <sub>3</sub> COOH, acetic acid, all data taken at 25°C and <i>I</i> = 2.00 M (NaClO <sub>4</sub> )							
La <sup>3+</sup>	2.181 ± 0.010	3.786 ± 0.059	4.62 ± 0.14	14.6	24.2	29.4	1
Ce <sup>3+</sup>	2.092 ± 0.011	3.664 ± 0.059	5.11 ± 0.17	14.8	24.8	31.8	1
Pr <sup>3+</sup>	1.719 ± 0.012	4.154 ± 0.071	3.61 ± 0.20	14.2	27.8	27.3	1
Nd <sup>3+</sup>	1.708 ± 0.008	3.486 ± 0.038	4.36 ± 0.11	14.6	25.7	30.7	1
Sm <sup>3+</sup>	1.453 ± 0.014	2.876 ± 0.028	3.773 ± 0.050	14.2	24.7	30.5	1
Gd <sup>3+</sup>	1.868 ± 0.009	3.245 ± 0.032	3.543 ± 0.070	14.8	25.3	29.1	1
Dy <sup>3+</sup>	2.925 ± 0.011	4.439 ± 0.036	4.309 ± 0.052	17.6	28.7	32.0	1
Ho <sup>3+</sup>	3.167 ± 0.022	5.009 ± 0.037	4.533 ± 0.039	18.3	30.2	32.6	1
Er <sup>3+</sup>	3.276 ± 0.027	5.509 ± 0.034	5.166 ± 0.041	18.5	31.8	34.3	1
Yb <sup>3+</sup>	3.507 ± 0.018	6.065 ± 0.071	6.58 ± 0.12	19.5	33.7	38.7	1
Y <sup>3+</sup>	3.262 ± 0.016	5.390 ± 0.025	5.243 ± 0.027	18.1	30.6	33.3	1
C <sub>14</sub> H <sub>24</sub> N <sub>2</sub> O <sub>10</sub> , (HO <sub>2</sub> CCH <sub>2</sub> ) <sub>2</sub> N(CH <sub>2</sub> ) <sub>2</sub> O(CH <sub>2</sub> ) <sub>2</sub> O(CH <sub>2</sub> ) <sub>2</sub> N(CH <sub>2</sub> COOH) <sub>2</sub> , <i>O, O'</i> -bis(β-aminoethyl)ethylene-glycol- <i>N, N'</i> -tetraacetic acid							
La <sup>3+</sup>	-5.46			53.6			
C <sub>4</sub> H <sub>8</sub> O <sub>2</sub> , (CH <sub>3</sub> ) <sub>2</sub> CHCOOH <i>i</i> -butyric acid							
La <sup>3+</sup>	3.47	2.50		18.8			2
Ce <sup>3+</sup>	3.33	2.55		18.6			2
Pr <sup>3+</sup>	3.02	2.51		18.4			2
Nd <sup>3+</sup>	2.84	2.36		18.3			2
Sm <sup>3+</sup>	2.66	2.08		18.1			2
Eu <sup>3+</sup>	2.91	1.85		18.8			2
Gd <sup>3+</sup>	3.45	1.66		20.1			2
Tb <sup>3+</sup>	4.38	1.46		22.6			2
Dy <sup>3+</sup>	5.04	1.79		24.5			2
Ho <sup>3+</sup>	5.31	2.55		25.3			2
Er <sup>3+</sup>	5.49	3.43		25.8			2

(Continued.)

Cation	$\Delta H_1$ (kcal/mole)	$\Delta H_2$ (kcal/mole)	$\Delta H_3$ (kcal/mole)	$\Delta S_1$ (e.u./mole deg.)	$\Delta S_2$ (e.u./mole deg.)	$\Delta S_3$ (e.u./mole deg.)	Ref.
Tm <sup>3+</sup>	5.39	4.10		25.5			2
Yb <sup>3+</sup>	5.35	3.97		25.4			2
Lu <sup>3+</sup>	5.35	3.65		25.5			2
Y <sup>3+</sup>	5.36	3.22		25.5			2

C<sub>4</sub>H<sub>8</sub>O<sub>6</sub>, (HO<sub>2</sub>CH<sub>2</sub>)<sub>2</sub>OH<sub>2</sub>O, diglycolic acid, *I* = 1.00 M (NaClO<sub>4</sub>) and *T* = 25.00°C

La <sup>3+</sup>	-0.070 ± 0.016	-0.828 ± 0.021	-0.474 ± 0.040	22.3	35.6	45.2	3
Ce <sup>3+</sup>	-0.401 ± 0.017	-1.270 ± 0.023	-1.764 ± 0.032	22.2	36.5	45.4	3
Pr <sup>3+</sup>	-0.680 ± 0.016	-1.712 ± 0.021	-2.500 ± 0.030	22.1	36.4	44.7	3
Nd <sup>3+</sup>	-0.848 ± 0.014	-2.103 ± 0.019	-3.000 ± 0.024	22.1	36.4	45.4	3
Sm <sup>3+</sup>	-1.048 ± 0.017	-2.878 ± 0.023	-4.291 ± 0.028	21.8	35.5	43.9	3
Eu <sup>3+</sup>	-0.781 ± 0.019	-2.943 ± 0.021	-4.507 ± 0.024	22.6	35.9	45.0	3
Gd <sup>3+</sup>	-0.360 ± 0.019	-2.672 ± 0.022	-4.590 ± 0.027	23.5	36.3	44.0	3
Tb <sup>3+</sup>	0.765 ± 0.021	-1.877 ± 0.023	-4.464 ± 0.026	27.0	39.2	45.4	3
Dy <sup>3+</sup>	1.323 ± 0.022	-1.081 ± 0.019	-4.413 ± 0.022	28.8	42.0	46.1	3
Ho <sup>3+</sup>	1.591 ± 0.023	-0.261 ± 0.025	-4.384 ± 0.029	29.6	44.6	46.0	3
Er <sup>3+</sup>	1.660 ± 0.072	0.699 ± 0.078	-4.202 ± 0.093	30.1	48.2	46.2	3
Tm <sup>3+</sup>	1.574 ± 0.056	1.165 ± 0.061	-3.189 ± 0.076	30.5	50.8	47.8	3
Yb <sup>3+</sup>	1.423 ± 0.056	1.046 ± 0.028	-3.857 ± 0.036	30.2	51.0	47.1	3
Lu <sup>3+</sup>	1.230 ± 0.021	0.781 ± 0.022	-3.819 ± 0.030	30.0	50.9	47.2	3
Y <sup>3+</sup>	1.732 ± 0.031	0.489 ± 0.035	-3.709 ± 0.040	30.0	46.4	47.2	3

C<sub>7</sub>H<sub>5</sub>NO<sub>4</sub>, dipicolinic acid (pyridine-2,6-dicarboxylic acid), *I* = 1.00 M (NaClO<sub>4</sub>) and *T* = 25.00°C

La <sup>3+</sup>	-3.125 ± 0.020	-6.401 ± 0.028	-8.631 ± 0.033	25.8	41.3	53.2	3
Ce <sup>3+</sup>	-3.547 ± 0.027	-7.140 ± 0.037	-10.296 ± 0.043	26.1	41.6	50.9	3
Pr <sup>3+</sup>	-3.913 ± 0.026	-7.869 ± 0.037	-11.370 ± 0.043	26.1	42.3	52.4	3
Nd <sup>3+</sup>	-4.012 ± 0.043	-8.109 ± 0.059	-11.883 ± 0.068	26.5	43.2	53.5	3
Sm <sup>3+</sup>	-4.283 ± 0.053	-8.971 ± 0.070	-13.265 ± 0.081	25.9	42.1	52.0	3
Eu <sup>3+</sup>	-4.073 ± 0.055	-9.123 ± 0.046	-13.732 ± 0.053	26.6	42.0	51.5	3
Gd <sup>3+</sup>	-3.582 ± 0.036	-8.731 ± 0.046	-13.619 ± 0.0053	27.8	43.7	53.5	3
Tb <sup>3+</sup>	-2.689 ± 0.017	-8.007 ± 0.017	-13.811 ± 0.019	30.5	46.4	53.7	3
Dy <sup>3+</sup>	-2.169 ± 0.031	-7.158 ± 0.037	-13.820 ± 0.043	32.4	49.7	54.2	3
Ho <sup>3+</sup>	-1.946 ± 0.033	-6.166 ± 0.033	-13.557 ± 0.038	33.2	52.4	54.8	3
Er <sup>3+</sup>	-1.850 ± 0.035	-5.752 ± 0.032	-13.406 ± 0.037	33.8	55.4	55.5	3
Tm <sup>3+</sup>	-1.834 ± 0.043	-5.471 ± 0.050	-12.870 ± 0.061	34.2	57.0	57.0	3
Yb <sup>3+</sup>	-1.925 ± 0.025	-5.785 ± 0.029	-12.907 ± 0.035	34.0	56.3	55.4	3
Lu <sup>3+</sup>	-2.191 ± 0.033	-5.995 ± 0.059	-12.658 ± 0.049	33.9	56.4	55.2	3
Y <sup>3+</sup>	-1.438 ± 0.028	-5.311 ± 0.034	-12.236 ± 0.040	33.8	53.9	55.9	3

Glycolic acid, *I* = 2.00 M (NaClO<sub>4</sub>) and *T* = 25.00°C, ref. 1

Cation	$\Delta H_1$ (kcal/mole)	$\Delta H_2$ (kcal/mole)	$\Delta H_3$ (kcal/mole)	$\Delta H_4$ (kcal/mole)	$\Delta S_1$ (e.u./mole deg)	$\Delta S_2$ (e.u./mole deg)	$\Delta S_3$ (e.u./mole deg)	$\Delta S_4$ (e.u./mole deg)
La <sup>3+</sup>	0.633 ± 0.021	1.055 ± 0.035	1.680 ± 0.085	2.19 ± 0.39	7.9	13.6	16.3	15.8
Ce <sup>3+</sup>	0.810 ± 0.017	1.599 ± 0.030	2.268 ± 0.037	2.99 ± 0.11	8.0	12.9	15.8	15.1
Nd <sup>3+</sup>	1.193 ± 0.016	2.188 ± 0.021	3.479 ± 0.037	4.00 ± 0.08	7.4	12.4	13.6	14.0
Sm <sup>3+</sup>	1.039 ± 0.031	2.404 ± 0.045	3.686 ± 0.055	4.94 ± 0.12	8.1	12.5	14.2	12.6
Gd <sup>3+</sup>	0.614 ± 0.020	1.734 ± 0.034	3.515 ± 0.045	4.27 ± 0.07	9.3	14.4	14.5	14.8
Dy <sup>3+</sup>	0.164 ± 0.034	0.608 ± 0.069	1.737 ± 0.086	2.58 ± 0.17	11.0	18.4	21.1	20.9

(Continued.)

Cation	$\Delta H_1$ (kcal/mole)	$\Delta H_2$ (kcal/mole)	$\Delta H_3$ (kcal/mole)	$\Delta H_4$ (kcal/mole)	$\Delta S_1$ (e.u/mole deg)	$\Delta S_2$ (e.u/mole deg)	$\Delta S_3$ (e.u/mole deg)	$\Delta S_4$ (e.u/mole deg)
Er <sup>3+</sup>	0.19 ± 0.04	0.60 ± 0.02	1.28 ± 0.05	1.43 ± 0.15	11.3	18.9	23.1	25.2
Yb <sup>3+</sup>	0.288 ± 0.045	0.768 ± 0.080	1.66 ± 0.12	0.59 ± 0.29	11.4	19.4	23.3	29.0
Y <sup>3+</sup>	0.073 ± 0.022	0.173 ± 0.034	0.895 ± 0.042	0.92 ± 0.08	11.1	19.6	23.0	25.5
Cation	$\Delta H_1$ (kcal/mole)	$\Delta H_2$ (kcal/mole)	$\Delta H_3$ (kcal/mole)	$\Delta S_1$ (e.u/mole deg)	$\Delta S_2$ (e.u/mole deg)	$\Delta S_3$ (e.u/mole deg)	Ref.	
C <sub>4</sub> H <sub>7</sub> NO <sub>4</sub> , HN(CH <sub>2</sub> CO <sub>2</sub> H) <sub>2</sub> , iminodiacetic acid, <i>I</i> = 0.1 M (KNO <sub>3</sub> ) and <i>T</i> = 20°C								
La <sup>3+</sup>	0.17	-0.16		25.6	43.6		4	
C <sub>3</sub> H <sub>6</sub> O <sub>2</sub> , CH <sub>3</sub> CH <sub>2</sub> COOH, propionic acid								
La <sup>3+</sup>	2.47	1.66	$\mu = 2$	15.3	9.6		4	
Ce <sup>3+</sup>	2.16	1.77	$\mu = 2$	14.9	10.5		4	
Pr <sup>3+</sup>	1.89	1.68	$\mu = 2$	14.5	10.6		4	
Nd <sup>3+</sup>	1.78	1.47	$\mu = 2$	14.8	10.2		4	
Sm <sup>3+</sup>	1.56	1.33	$\mu = 2$	14.5	10.0		4	
Eu <sup>3+</sup>	1.76	0.99	$\mu = 2$	15.0	9.3		4	
Gd <sup>3+</sup>	2.22	0.86	$\mu = 2$	15.9	8.9		4	
Tb <sup>3+</sup>	3.03	0.65	$\mu = 2$	18.1	8.5		4	
Dy <sup>3+</sup>	3.67	0.83	$\mu = 2$	19.8	8.9		4	
Ho <sup>3+</sup>	3.90	1.63	$\mu = 2$	20.5	11.1		4	
Er <sup>3+</sup>	3.96	2.32	$\mu = 2$	20.6	12.9		4	
Tm <sup>3+</sup>	3.98	2.83	$\mu = 2$	20.7	14.2		4	
Yb <sup>3+</sup>	3.77	2.73	$\mu = 2$	20.1	14.0		4	
Lu <sup>3+</sup>	3.82	2.50	$\mu = 2$	20.4	13.5		4	
Y <sup>3+</sup>	3.88	2.02	$\mu = 2$	20.4	12.2		4	
C <sub>12</sub> H <sub>20</sub> N <sub>2</sub> O <sub>8</sub> , (HO <sub>2</sub> CCH <sub>2</sub> ) <sub>2</sub> N(CH <sub>2</sub> ) <sub>4</sub> N(CH <sub>2</sub> CO <sub>2</sub> H) <sub>2</sub> , tetramethylene-diamine- <i>N,N,N',N'</i> -tetraacetic acid								
La <sup>3+</sup>	1.88			48.2			4	
SCN, thiocyanate, <i>I</i> = 1.00 M (NaClO <sub>4</sub> , <i>T</i> = 25°C								
Nd <sup>3+</sup>	-5.47 ± 0.20			-14.7 ± 0.7			5	
Eu <sup>3+</sup>	-0.05 ± 0.03			-0.4 ± 0.2			5	
C <sub>11</sub> H <sub>18</sub> N <sub>2</sub> O <sub>8</sub> , (HO <sub>2</sub> CCH <sub>2</sub> ) <sub>2</sub> N(CH <sub>2</sub> ) <sub>3</sub> N(CH <sub>2</sub> CO <sub>2</sub> H) <sub>2</sub> , trimethylene-diamine- <i>N,N,N',N'</i> -tetraacetic acid								
La <sup>3+</sup>	3.76				64.2		4	
HSCH <sub>2</sub> COOH, thioglycolic acid, <i>I</i> = 2.00 M (NaClO <sub>4</sub> , <i>T</i> = 25°C								
La <sup>3+</sup>	1.486 ± 0.023	3.89 ± 0.09		11.5	22.7		6	
Sm <sup>3+</sup>	1.335 ± 0.032	3.31 ± 0.10		12.7	23.5		6	
Er <sup>3+</sup>	2.380 ± 0.085	5.44 ± 0.22		13.8	28.2		6	

## References for Table 3.12a

1. I. Grenthe, Acta Chem. Scand. **18**, 293, 1964.
2. G.R. Choppin, A.J. Graffeo, Inorg. Chem. **4**, 1254, 1965.
3. I. Grenthe, Acta Chem. Scand. **17**, 2487, 1963.
4. G. Anderegg, Helv. Chim. Acta **47**, 1801, 1964.
5. G.R. Choppin, J. Ketels, J. Inorg. Nucl. Chem. **27**, 1335, 1965.
6. I. Grenthe, Acta Chem. Scand. **18**, 283, 1964.

TABLE 3.13  
Stability constants for complexes between Ln (CF<sub>3</sub>SO<sub>3</sub>)<sub>3</sub> and crown ethers in anhydrous propylene carbonate.

Ln	12C4		15C5		But15C5	18C6	But <sub>2</sub> DB18C6	DB30C10
	1:1	1:2	1:1	1:2	1:1	1:1	1:1	1:1
La	5.00 ± 0.12	6.98 ± 0.15	6.49 ± 0.15	10.18 ± 0.11	3.26 ± 0.04	8.75	5.14 ± 0.05	4.29 ± 0.04
Ce					3.62 ± 0.04		4.95 ± 0.03	4.10 ± 0.03
Pr	5.27 ± 0.08	7.09 ± 0.10	6.22		3.60 ± 0.08	8.60	4.79 ± 0.05	4.12 ± 0.04
Nd	5.19 ± 0.09	6.74 ± 0.12	6.55 ± 0.13	8.65 ± 0.04	3.75 ± 0.04		4.58 ± 0.06	4.10 ± 0.05
Sm	5.17 ± 0.10	6.76 ± 0.14	6.11		3.45 ± 0.04	8.10	4.00 ± 0.04	3.75 ± 0.03
Gd					3.02 ± 0.05		3.62 ± 0.13	3.53 ± 0.04
Tb	5.15 ± 0.13	6.09 ± 0.20	5.96 ± 0.14	7.66 ± 0.19	2.85 ± 0.05		3.50 ± 0.08	4.07 ± 0.06
Dy					2.90 ± 0.12	7.90	3.40 ± 0.07	
Ho			5.66		2.80 ± 0.08		3.29 ± 0.15	
Er			5.33		2.82 ± 0.07	7.67	3.16 ± 0.05	4.48 ± 0.05
Tm					2.81 ± 0.05		2.94 ± 0.09	
Yb	4.94 ± 0.09		5.53		2.80 ± 0.10	7.50	2.57 ± 0.09	4.76 ± 0.04
Lu	5.00 ± 0.11		5.83 ± 0.16	7.89 ± 0.22	2.80 ± 0.06		2.51 ± 0.06	4.80 ± 0.05
Ref.	1	1	1, 2	1	1	2	3	1

References for Table 3.13

1. J. Massaux, J.F. Desreux, J. Am. Chem. Soc. **104**, 2967, 1982.
2. M.C. Almasio, F. Arnaud-Neu, M.J. Sching-Weill, Helv. Chim. Act. **66**, 1296, 1983.
3. J. Massaux, J.F. Desreux, C. Delchambre, G. Duyckerts, Inorg. Chem. **19**, 1893, 1980.



TABLE 3.14  
Stability constants for rare earth complexes with crown ethers and cryptands in methanol.

Ln	B15C5	NitrB	15C5	(2.1)	18C6	DC18C6	(2.2.1)	(2.2.2)
Y	2.38	3.36		8.66				10.34
La	2.13	2.34		7.08	3.29 ± 0.03	2.49	8.28	9.4
Ce	2.30				3.57 ± 0.20	2.05		8.4
Pr	2.18	2.45		7.94	2.63 ± 0.28	1.62	9.31	
Nd	2.27	2.70		7.86	2.44 ± 0.16	<1..3	9.86	
Sm	2.37	2.81		7.00	2.03 ± 0.07		9.70	
Eu				8.59	1.84 ± 0.14		10.57	
Gd	2.35	2.98		7.67	1.32 ± 0.12		10.14	
Tb				8.29			10.26	
Dy	2.60	3.36	8.96				10.45	
Ho			8.81				10.86	
Er	2.40	3.40	8.70				10.78	
Tm			9.46				11.61	
Yb							12.00	
Lu	2.41	3.60						
Ref.	1	1	2	3	4		2	5

NitrB = nitribenzo-15C5.

References for Table 3.14

1. W. Xiao, Z. Ji, R. Lou, N. Dong, Y. Ren, X. Liu, S. Yu, X. Ni, Z. Qin, *New Frontiers in Rare Earth Science*, Science Press, Beijing, Vol. 1, p. 208, ed. G. Xu and J. Xia, 1985.
2. M.C. Almasio, F. Arnad-Neu, M.J. Schwing-weill, *Helv. Chim. Acta* **66**, 1296, 1983.
3. R.M. Izatt, J.D. Lamb, J.J. Christensen, B.L. Haymore, *J. Am. Chem. Soc.* **99**, 8344, 1977.
4. J. Zhou, D. Wang, *He Huaxue Yu Fangshe Huaxue* **4**, 174, 1982; J. Zhou, X. Wu, *He Huaxue yu Fangshe Huaxue* **6**, 78, 1984.
5. G. Anderegg, *Helv. Chim. Acta* **64**, 1790, 1981.

TABLE 3.15

Stability constants for complexes between  $\text{Ln}(\text{CF}_3\text{SO}_3)_3$  and various diazacrown ethers and cryptates in propylene carbonate.

Ln	(2.1)	(2.2)	(2.1.1)	(2.2.1)	(2.2.2)	
	1:1	1:1	1:1	1:1	1:1	1:1
La	14.4	16.5	15.1	18.6	16.1	
Pr	14.5	16.1		18.7		15.9
Sm	14.9	16.5	15.3	19.0	17.3	16.0
Eu	14.65	16.5	15.2	19.0	17.2	
Gd		16.5	15.4		16.8	
Tb						16.6
Dy	14.15	16.9	15.4	19.0	17.1	
Er	14.8	16.9	15.5	19.2		
Yb	15.4	16.9	15.6	19.1	18.0	17.6
Ref.	1	2	2	1	2	3

## References for Table 3.15

1. M.C. Almasio, F. Arnaud-Neu, M.J. Schwing-Weill, *Helv. Chim. Acta* **66**, 1296, 1983.
2. F. Arnaud-Neu, E.L. Lufouilou, M.J. Schwing-Weill, *J. Chem. Soc. Dalton Trans.* 262, 1986.
3. G. Gillain, P. Berthelemy, J. Massaux, J.F. Desreux, *J. Chem. Soc. Dalton Trans.* 2847, 1984.

TABLE 3.16

Stability constants ( $\log \beta_1$ ) of rare earth complexes with cryptands and macrocyclic polyacetic acids in water.

Ln	TETA	DOTA	(2.1)DA	(2.2)DA	(2.1.1)	(2.2.1)	(2.2.2)
Y			10.85 ± 0.02				
La	14.51 ± 0.06	23.0	10.11 ± 0.06	12.21 ± 0.13		6.59 ± 0.09	6.45 ± 10.3
Ce		23.4	10.89 ± 0.08	12.23 ± 0.04		6.58 ± 0.04	6.37 ± 0.08
Pr		23.0	11.31 ± 0.05	12.22 ± 0.06			
Nd	14.51 ± 0.06	23.0	11.60 ± 0.07	12.12 ± 0.04			
Sm	14.97 ± 0.03	23.0	11.72 ± 0.09	12.02 ± 0.10	6.8 ± 0.2	6.76 ± 0.02	5.94 ± 0.06
Eu	15.46 ± 0.02	23.5	11.85 ± 0.11	11.93 ± 0.09		6.8 ± 0.2	5.90 ± 0.09
Gd	15.75 ± 0.04	24.7	11.66 ± 0.10	11.70 ± 0.06		6.7 ± 0.1	
Tb		24.7	11.52 ± 0.10	11.57 ± 0.04		6.6 ± 0.1	
Dy	16.04 ± 0.02	24.8	11.55 ± 0.07	11.18 ± 0.10			
Ho		24.8	11.34 ± 0.08	11.30 ± 0.08	6.21		6.2 ± 0.2
Er	16.49 ± 0.02	24.8	11.15 ± 0.06	11.10 ± 0.02	–	6.60 ± 0.8	
Tm		24.7	10.79 ± 0.09	11.10 ± 0.02	6.8 ± 0.4	6.88 ± 0.05	
Yb	16.55	25.02	10.76 ± 0.03	10.90 ± 0.04	6.51 ± 0.09		
Lu		25.4	10.33 ± 0.09	10.84 ± 0.02	6.55 ± 0.09		
Ref.	1	1	2	3	4	2	5

## References for Table 3.16

1. M.F. Loncin, J.F. Desreux, E. Merciny, *Inorg. Chem.* **25**, 2646, 1986.
2. W.P. Cacheris, S.K. Nickle, A.D. Sherry, *Inorg. Chem.* **26**, 958, 1987.
3. C.A. Chang, V.O. Ochaya, *Inorg. Chem.* **25**, 355, 1986.
4. C.A. Chang, M.E. Rowland, *Inorg. Chem.* **22**, 3866, 1983.
5. J.H. Burns, J.F. Baes, *Inorg. Chem.* **13**, 85, 1981.

TABLE 3.17  
Stability constants for lanthanide complexes with crown ethers and cryptands.

Ligand	Ln:L	Anion	Ln	$\log \beta_n$	Solvent	Ref.
12C4	1:1	TFA	La	>7	CD <sub>3</sub> CN	1
15C5	1:2	PF <sub>6</sub> <sup>-</sup>	La	7.4 ± 0.2	CD <sub>3</sub> CN	2
			Pr	4.4 ± 0.2	CD <sub>3</sub> CN	2
			Nd	3.8 ± 0.2	CD <sub>3</sub> CN	2
			Sm	3.2 ± 0.2	CD <sub>3</sub> CN	2
18C6	1:1	NO <sub>3</sub> <sup>-</sup>	La	<1.23	DMF	3
			La	4.4 ± 0.2	CD <sub>3</sub> CN	4
			Ce	4.5 ± 0.2	CD <sub>3</sub> CN	4
			Pr	3.7 ± 0.2	CD <sub>3</sub> CN	4
			Nd	3.5 ± 0.2	CD <sub>3</sub> CN	4
		TFA	Eu	2.6 ± 0.2	CD <sub>3</sub> CN	4
			Yb	2.3 ± 0.2	CD <sub>3</sub> CN	4
			La	>6	CD <sub>3</sub> CN	1
			Sm	4.4 ± 0.2	CD <sub>3</sub> CN	1
			Pr	3.86 ± 0.05	DMSO	5
(2.1.1)	1:1	Cl <sup>-</sup>	Nd	3.97 ± 0.14	DMSO	5
			Gd	3.87 ± 0.14	DMSO	5
			Ho	3.80 ± 0.05	DMSO	5
			Yb	4.43 ± 0.11	DMSO	5
			Pr	3.47 ± 0.07	DMSO	5
(2.2.1)	1:1	Cl <sup>-</sup>	Nd	3.01 ± 0.31	DMSO	5
			Gd	3.26 ± 0.09	DMSO	5
			Ho	3.11 ± 0.23	DMSO	5
			Yb	4.00 ± 0.23	DMSO	5
			Pr	3.22 ± 0.07	DMSO	5
(2.2.2)	1:1	Cl <sup>-</sup>	Nd	3.26 ± 0.14	DMSO	5
			Gd	3.45 ± 0.11	DMSO	5
			Ho	3.47 ± 0.15	DMSO	5
			Yb	4.11 ± 0.11	DMSO	5

## References for Table 3.17

1. J.C.G. Bunzli, A. Giorgetti, *J. Less. Comm. Metals* **112**, 355, 1985.
2. J.C.G. Bunzli, A. Giorgetti, *Inorg. Chim. Acta* **110**, 225, 1985.
3. R.D. Boss, A.I. Popov, *Inorg. Chem.* **24**, 3660, 1985.
4. J.C. Bunzli, D. Wessner, *Helv. Chim. Acta* **64**, 582, 1981.
5. R. Pizer, R. Selzer, *Inorg. Chem.* **22**, 1359, 1983.

TABLE 3.18  
Stability constants ( $\log K_{ML}$ ) of macrocyclic complexes of lanthanides at 25°C and  $\mu = 0.2 \text{ M NaNO}_3^a$ .

Metal ion	Macrocyclic					1	5
	2	3	4	DTPA <sup>b</sup>			
La <sup>3+</sup>	12.74	13.57	19.11	19.5			
Ce <sup>3+</sup>	13.12	14.16	19.59	20.3		23.0 <sup>c</sup>	19.7 <sup>d</sup>
Nd <sup>3+</sup>	13.76	14.85	20.36	21.6			
	14.51 <sup>e</sup>						
Sm <sup>3+</sup>	14.47	15.35	21.24	22.3			
	14.97 <sup>e</sup>						
Eu <sup>3+</sup>	14.66	15.59	22.68	22.4		28.2 <sup>f</sup>	
	15.46 <sup>e</sup>						
Gd <sup>3+</sup>	14.73	15.88	22.95	22.5		24.6 <sup>c</sup>	21.1
	15.75 <sup>e</sup>						
Tb <sup>3+</sup>	14.81	15.91	23.15	22.7		28.6 <sup>f</sup>	
Ho <sup>3+</sup>	14.95	16.48	23.88	22.8			
Tm <sup>3+</sup>	15.15	16.61	24.09	22.7			
Lu <sup>3+</sup>	15.31	16.71	24.26	22.4		29.2 <sup>f</sup>	23.0 <sup>d</sup>
						25.5 <sup>c</sup>	
Y <sup>3+</sup>	14.77	16.07	24.04	22.1		24.9	21.1
Dy <sup>3+</sup>	16.04 <sup>e</sup>						
Er <sup>3+</sup>	16.49 <sup>e</sup>						
Yb <sup>3+</sup>	16.55 <sup>e</sup>						

<sup>a</sup>  $K_{ML} = [ML][M]^{-1}[L]^{-1} (\text{M}^{-1})$ . Three titrations were conducted for each system. The standard deviations at the 95% confidence level for the complexation constants are 0.05 unless otherwise noted (ref. 1).

<sup>b</sup>Ref. 2, <sup>c</sup>ref. 3, <sup>d</sup>ref. 4, <sup>e,f</sup>ref. 5. At 80°C and  $\mu = 1.0 \text{ M NaCl}$  (ref. 5) determined by gravimetric method (refs 7 and 8).

#### References for Table 3.18

1. M. Kondama, T. Koike, A.B. Mahatma, E. Kimura, *Inorg. Chem.* **30**, 1270, 1991.
2. A.E. Martell, R.M. Smith, *Critical Stability constants*, Vol. 6, Plenum, New York, 1989.
3. W.P. Cacheris, S.K. Nickle, A.D. Sherry, *Inorg. Chem.* **26**, 958, 1987.
4. K. Kumar, C.A. Chang, M.F. Tweedle, *Inorg. Chem.* **32**, 587, 1993.
5. M.F. Loncin, J.F. Desreux, E. Merciny, *Inorg. Chem.* **25**, 2646, 1986.
6. S.I. Kang, R.S. Ranganathan, J.E. Emswiler, K. Kumar, J.Z. Gougoutas, M.F. Malley, M.F. Tweedle, *Inorg. Chem.* **32**, 2912, 1993.
7. R. Delgado, J.J.R. Frausto de Silva, *Talanta* **29**, 850, 1982.
8. H. Stetter, W. Frank, R. Mertens, *Tetrahedron* **37**, 767, 1981.

TABLE 3.19  
Stability constants of some macrocyclic complexes.

Complex	log <i>K</i>	Ref.
Gd (1)	24.6	1
Ce (1)	23.0	1
Gd (2)	13.7	2
Ce (2)	—	
Gd (3)	15.1	3
Gd (4)	14.7	3
Gd (5)	10.4	3
Ce (6)	19.7	4
Gd (6)	21.0	4
Lu (6)	23.0	4
Gd (8)	25.3	5

## References for Table 3.19

1. W.P. Cacheris, S.K. Nickle, A.D. Sherry, *Inorg. Chem.* **26**, 958, 1987.
2. E. Brucher, A.D. Sherry, *Inorg. Chem.* **29**, 1555, 1990.
3. E. Brucher, S. Cortes, F. Chavez, A.D. Sherry, *Inorg. Chem.* **30**, 2092, 1991.
4. K. Kumar, C.A. Chang, M.F. Tweedle, *Inorg. Chem.* **32**, 587, 1993.
5. S.I. Kang, R.S. Ranganathan, J.E. Emswiler, K. Kumar, J.Z. Gougoutas, M.F. Malley, M.F. Tweedle, *Inorg. Chem.* **32**, 2912, 1993.

## chapter 4

---

**PART A: LANTHANIDE COMPLEXES**  
**PART B: MACROCYCLIC COMPLEXES**

---

---

# CONTENTS

---

Part A . . . . .	262
1. Introduction . . . . .	262
2. Lanthanide compounds as starting materials . . . . .	262
3. Anhydrous solutions for preparation of complexes . . . . .	263
4. Preparation of anhydrous salts as starting materials . . . . .	263
5. Synthesis of lanthanide complexes . . . . .	265
6. Lanthanide complexes with carboxylic acids, amino acids and phosphorus acids [22–24] . . . . .	265
7. Lanthanide complexes with polyamino polyacetic acids . . . . .	266
8. Lanthanide complexes with diketones and Schiff bases . . . . .	266
9. Lanthanide complexes of non-ionizable ligands . . . . .	267
10. Metal-template synthesis . . . . .	268
11. Lanthanide complexes with macromolecules . . . . .	269
12. Lanthanide complexes with specific guests . . . . .	270
13. Characterization of complexes . . . . .	271
14. Lanthanide complexes in solutions . . . . .	275
15. Complexes in non-aqueous solutions . . . . .	278
16. Formation of perchlorate complexes . . . . .	278
17. Complex formation with trifluoromethane sulfonate . . . . .	279
18. Formation of halide complexes . . . . .	280
19. Complex formation with thiocyanate . . . . .	282
20. Complex formation with nitrate . . . . .	283
21. Solid rare earth complexes . . . . .	285
22. Inorganic ligands . . . . .	285
22.1. Halides and pseudohalides . . . . .	285
23. Complexes with pseudohalides . . . . .	287
24. Complexes with oxyanions . . . . .	288
25. Oxygen donors . . . . .	289
25.1. Carbonyl oxygen donors . . . . .	291
25.2. 1,3-Diketones as oxygen donors . . . . .	292
25.3. Alcohols as oxygen donors . . . . .	293
25.4. Polycyclic ethers as oxygen donors . . . . .	294
25.5. Oxygen donors such as (C <sub>6</sub> H <sub>5</sub> ) <sub>3</sub> PO, DMSO, HMPA, pyridine <i>N</i> -oxide . . . . .	294
26. Nitrogen donors . . . . .	295
27. Unidentate ammonia and amines . . . . .	296

28. Bidentate donor ligands . . . . .	297
29. Multidentate ligands . . . . .	298
30. Nitrogen–oxygen donors . . . . .	299
31. Other donor atoms . . . . .	301
<b>Part B . . . . .</b>	<b>303</b>
32. Macrocyclic complexes: historical outlook . . . . .	303
33. The problematic of metal and lanthanide ion complexation by macrocyclic ligands . . . . .	309
33.1. The lock and key principle . . . . .	309
33.2. The induced fit principle . . . . .	311
33.3. Thermodynamic considerations . . . . .	314
33.4. Kinetics . . . . .	314
33.5. Concluding remark . . . . .	315
33.6. Definitions and scope of the following sections . . . . .	315
34. Complexes with coronands and cryptands . . . . .	316
34.1. Simple coronands . . . . .	316
34.2. Simple cryptands . . . . .	322
34.3. Stabilization of lanthanide low oxidation states . . . . .	325
34.4. Applications of lanthanide coronates and cryptates . . . . .	327
34.5. Template effect . . . . .	332
35. Complexes with porphyrins and phthalocyanines . . . . .	334
35.1. Analytical applications . . . . .	338
35.2. Texaphyrins and their medical applications . . . . .	339
36. Coronands fitted with pendant arms . . . . .	341
36.1. Lariat crown ethers . . . . .	341
36.2. Cyclen derivatives . . . . .	343
37. Calixarenes . . . . .	350
37.1. Simple calix[ <i>n</i> ]arenes ( <i>n</i> = 4, 5, 6, 8, see Fig. 4.8) . . . . .	352
37.2. Substituted calix[ <i>n</i> ]arenes ( <i>n</i> = 4, 6, 8) . . . . .	356
37.3. Calix-crowns, calix-cryptands and extended networks . . . . .	361
38. Metallacrowns . . . . .	364
39. Conclusion and further reading . . . . .	368
<b>References . . . . .</b>	<b>368</b>



## Part A

### 1. Introduction

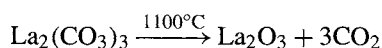
The first step in the study of metal complexes is the synthesis or preparation of the complex of interest followed by physicochemical characterization of the complex. Lanthanides rarely behave like transition metal cations and hence the need for different precautions in handling them. The fundamental characteristics and behavior of lanthanides in solution is useful for embarking on the synthesis of lanthanide complexes. Some properties of lanthanides, which are useful, and of direct interest for practical purposes will be recalled here.

- (i) The 4f valence electrons of the lanthanides are situated in the inner orbitals and are not directly available for bonding. The lanthanides form essentially electrostatic bonds and hence their complexes are labile. Hence it is difficult to predict the conformation of a lanthanide complex, and it is difficult to isolate optical isomers of a lanthanide complex.
- (ii) The lanthanides have a wide range of coordination numbers, e.g. 3 to 12. The stoichiometry and the conformation of a lanthanide complex often depends on the method of preparation. The lanthanide contraction can affect the stoichiometry and structure of the complexes of light and heavy lanthanides. In some cases isolation of complexes of lanthanides is possible either with members in the beginning or at the end of the lanthanide series.
- (iii) Lanthanides interact strongly with negatively charged groups because of the electrostatic nature of the coordination bonds. For example polydentate inorganic anions like nitrate ( $\text{NO}_3^-$ ) and sulphate ( $\text{SO}_4^{2-}$ ) form stable lanthanide compounds which can prevent the formation of lanthanide complexes with poorly coordinating ligands.
- (iv) Lanthanide cations hydrolyze readily to form hydroxy lanthanides and ultimately form insoluble hydroxides. Thus careful control of the pH of lanthanide salt solutions is necessary. Lanthanide complexes formed and isolated from aqueous solutions yield solid complexes with water of hydration. Complete dehydration of the complexes may result in partial decomposition of the complexes and the ultimate formation of hydroxy lanthanide species.

### 2. Lanthanide compounds as starting materials

Highly pure lanthanide oxides (99.99% purity) that are commercially available can be used as starting materials for the preparation of lanthanide complexes after treatment at  $1100^\circ\text{C}$

to convert residual carbonates into the oxides.



Hydrated chlorides, nitrates or perchlorates can be easily prepared by the dissolution of lanthanide oxides with concentrated HCl, HNO<sub>3</sub> or HClO<sub>4</sub>, respectively.

Aqueous solutions of known concentration can be obtained by adding enough deionized water to cover a weighed amount of oxide, followed by the addition of a small excess of mineral acid and heated at 80°C to achieve complete dissolution. The mixture is evaporated to dryness under a stream of air and the resulting solid dissolved in a small amount of water. The water and excess acid are again eliminated by heating the solution under a current of air and the dissolution–evaporation is repeated until the pH of the solution is in the range of 5–6. After the final evaporation, the hydrated salt is dissolved in a known volume of water to give a solution of known concentration.

Hydrated lanthanide salts may also be obtained by the addition of an excess of lanthanide oxide to a concentrated acid solution, heating at 80°C until the pH is between 5 and 6. The residual oxide is removed by filtration, and the filtrate is subjected to rotary evaporation. This procedure may lead to the presence of oxo and hydroxy species in solution. At present hydrated lanthanide salts of 99.9% purity are available commercially. Salts of the highest purity are generally used in spectroscopic and magnetic studies. The purity of lanthanide salts can be determined by complexometric titration with ethylenediamine tetraacetic acid [1].

### 3. Anhydrous solutions for preparation of complexes

Synthesis of several lanthanide complexes requires anhydrous conditions. Hydrated lanthanide salts undergo decomposition in the process of dehydration under vacuum at elevated temperatures. Thus special procedures are required for the preparation of anhydrous salts.

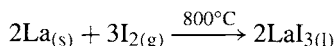
One of the methods involves the addition of an excess of triethylorthoformate to a lanthanide salt in acetonitrile and refluxing for 5 hours [2]. In another procedure the hydrated salt in acetonitrile or *n*-butanol is refluxed through a Soxhlet extractor packed with 3 Å molecular sieves [3]. After 12 hours the molecular sieves are replaced and the water content analysed by Karl Fischer titration. The process is repeated until the solution is practically free from water.

Anhydrous lanthanide adducts with dimethyl formamide (DMF) [4], dimethyl sulphoxide [5] (DMSO) and hexamethyl phosphoramide [6] may be used for the synthesis of anhydrous complexes as long as their solvation does not interfere with the preparative reaction [7].

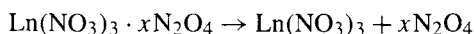
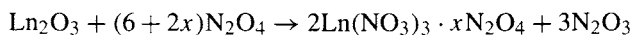
### 4. Preparation of anhydrous salts as starting materials

Anhydrous lanthanide halides have been prepared and documented [8]. The method involves either

- (i) The reaction of the metal with HX (X = Cl, Br, I) or halogen vapour (Cl<sub>2</sub>, Br<sub>2</sub>, or I<sub>2</sub>).  
 (ii) The chlorination of lanthanide oxides with thionyl chloride or ammonium chloride [9].  
 The iodination of lanthanides [10] takes place as below



Lanthanide halides are hygroscopic and should be handled in a glovebox. Dehydration of lanthanide nitrates leads to the formation of oxynitrates [11] in the case of heavy lanthanides. Synthesis of lanthanide nitrates has been reported by the reactions [12]

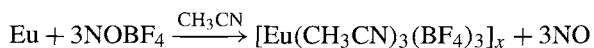


The initial starting materials for the preparation of lanthanide complexes must be such that the counterions do not compete with the ligand in the formation of complexes. Among the lanthanide salts the complex formation tendency is in the order  $\text{SO}_4^{2-} > \text{NO}_3^- > \text{ClO}_4^-$  and hence lanthanide perchlorates are the preferred starting materials for the synthesis of complexes.

The dehydration of lanthanide perchlorates to obtain the anhydrous salt has been studied [13–15]. Lighter lanthanide perchlorate lose the water of hydration readily at 200°C under vacuum while the heavier lanthanide salts produced insoluble basic salts. Anhydrous heavier lanthanide perchlorates have been obtained by extraction with anhydrous acetonitrile. Utmost precaution should be exercised in the purification of lanthanide perchlorate, since the mixture of lanthanide perchlorate and acetonitrile can lead to an explosion. An alternate approach involves the addition of triethylorthoformate to the mixture or refluxing the solvent through a Soxhlet extractor packed with molecular sieves [3]. In view of the hazardous nature of perchlorates, alternate materials such as lanthanide trifluoromethane sulfonates have received some attention. Lanthanide triflates are thermally stable, soluble in organic solvents, unreactive to moisture and are weak coordinating agents. Triflic acid is stronger than perchloric acid [17]. Lanthanide perchlorates and triflate have the same reduction potentials in aprotic solvents and the dissociation of the triflates is less than the perchlorates in acetonitrile [17].

Synthesis of lanthanide triflates is achieved by adding an excess of lanthanide oxide to a concentrated solution of triflic acid in water at 80°C. The reaction is complete when the solution has a pH of 6.0. The solution is filtered, and evaporated in a rotary evaporator. The resulting solid is dried in a vacuum at 100°C for 12 hours.

The lanthanide triflates may also be obtained by the addition of triflic acid to lanthanide carbonates in ethanol or acetonitrile [18]. Filtration and concentration of the filtrate yield a solid salt which is washed with solvent. Lanthanide salts of poorly coordinating anions such as  $\text{PF}_6^-$ ,  $\text{BF}_4^-$  or  $\text{B}(\text{C}_6\text{H}_5)_4^-$  have been also used in the synthesis of lanthanide complexes as starting materials. Adducts of acetonitrile with europium tetrafluoroborate ( $\text{BF}_4^-$ ) and hexafluorophosphate ( $\text{PF}_6^-$ ) have been prepared [19]



The hexafluorophosphate adducts tend to decompose but the complexes with the corresponding amides are stable even after dehydration [20].

Lanthanide alcoholates such as those of 2-propanol have been synthesized [21], for the purpose of using them as starting materials for complexes. The alcoholates are in particular useful for the synthesis of lanthanide complexes with ligands containing acidic coordinating groups. The synthesis is carried out in an anhydrous organic solvent and the lanthanide alcoholate is used for the deprotonation of the acidic group of the ligand.

## 5. Synthesis of lanthanide complexes

The leading references for the synthesis and properties of various lanthanide complexes are given below.

Ligand	Reference
Polyamines, amino acids, polyaminopoly carboxylic acids	[22]
Schiff bases, oximes, amides, cryptands	[23]
Alcohols, ketones, ethers	[24]
Carboxylic acids	[25]
Ligands containing S, Se, Si, P, As	[26]

## 6. Lanthanide complexes with carboxylic acids, amino acids and phosphorus acids [22–24]

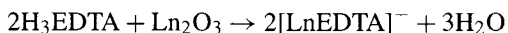
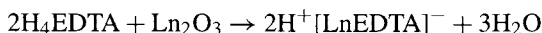
The classical procedure consists of adding an aqueous or methanolic solution of the ligand or its sodium salt to an equimolar solution of a lanthanide chloride and the resulting precipitate isolated by filtration. The pH of the mixture is usually adjusted to 5 or higher with  $\text{NH}_4\text{OH}$  or  $\text{NaOH}$  solution in order to form a complex. The mixture is evaporated until crystals are obtained. If the pH of the solution is above 6.0, hydroxo species form unless the chelate has a high stability constant. The optimum pH range for complex formation may be calculated from the stability constant of the complex and the protonation constant of the ligand [27].

The complexes may also be prepared by the addition of a solution of carboxylic ligand to an equivalent amount of: (i) a lanthanide carbonate [28], (ii) hydroxide [29] or (iii) oxide [30] with a slight excess of the latter. The insoluble part is filtered and the filtrate evaporated to obtain crystalline complex. Anhydrous lanthanide complexes of small chain carboxylic acids may be prepared by: (i) the dissolution of lanthanide carbonate in excess of the carboxylic acid, followed by heating to obtain complete dissolution of the suspension and partial evaporation of the solution to obtain the crystals [31], (ii) anhydrous lanthanide is converted into the corresponding monochloroacetate by the addition of an excess of monochloroacetic acid, followed by heating under reflux at reduced pressure for 2 h. Then ether is added to precipitate the salt [32], (iii) the addition of dimethyl formamide and benzene to lanthanide acetates and distillation of the water azeotropes to obtain anhydrous complexes. The last procedure yielded lighter lanthanide complexes solvated with dimethyl formamide [33]. The DMF may be removed by heating in a vacuum at  $120^\circ\text{C}$ .

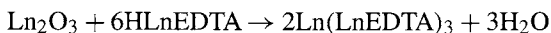
## 7. Lanthanide complexes with polyamino polyacetic acids

Ethylenediamine tetraacetic acid (EDTA) and 1,4,7,10-tetraazacyclododecane-*N,N',N'',N'''*-tetraacetic acid (DOTA) are typical of this family of ligands. The general method of preparation of the complexes consists of mixing solutions of the lanthanide salt and the ligand in the acidic form followed by raising the pH to 6.0 or higher. It should be noted that the kinetics of complexation with EDTA is fast while it is very slow in the case of tetraazacyclododecane tetraacetic acid. The reaction with the latter ligand is so slow that synthesis is carried out at 80°C and the base such as NaOH is added over a period of several hours [34]. In the case of kinetically inert complexes it is preferable to follow the direct reaction of the stoichiometric amount of ligand with lanthanide oxide or hydroxide and concentration of the mixture to obtain the complex. In some cases crystallization may be difficult [35], and one obtains a glassy deposit. Addition of ethanol to the reaction mixture is an alternative to obtain a crystalline complex. Addition of a layer of ethanol above the aqueous mixture induces slow diffusion of ethanol into the water layer and resulted in crystallization of the complex [36].

Another method of synthesis involves the direct reaction of stoichiometric amounts of ligand in acid form and lanthanide oxide, hydroxide or carbonate in suspension in hot water. The mixture is heated under reflux until total dissolution is obtained.



The sodium salt may be obtained by adding a dilute NaOH solution to attain pH 5.0. One of the main precautions is that the synthesis be done with dilute solutions. For example nitrilotriacetic acid (NTA) complexes have been synthesized using 0.02 M solutions and at higher dilutions in the case of heavy lanthanides [37]. Use of an excess of lanthanide oxide should be avoided since reactions of the following type may take place [38]



When the oxide is in excess and the ligand concentration is small, a hydroxylated form of the complex is formed. Species of the type  $\text{Ln}_2(\text{OH})_2\text{EDTA}$  or  $\text{Ln}_5(\text{OH})_7(\text{EDTA})_2$  have been obtained by the addition of NaOH to LnEDTA solutions [39]. Reversed-phase chromatography may be used in identification of various species in solution [40].

## 8. Lanthanide complexes with diketones and Schiff bases

The  $\beta$ -diketones and Schiff bases containing acidic substituents are ionizable and may be slightly soluble in water. The  $\beta$ -diketone complexes are used as NMR shift reagents. Their luminescence properties are also useful.

The aqueous methanolic solution of lanthanide nitrate or chloride is mixed with a stoichiometric amount of diketone in methanol and the pH of the mixture is adjusted to 6.0

by the addition of methanolic ammonia or NaOH. If there is no precipitation, the solution is concentrated by evaporation [41–45].

Solvent extraction technique has been used in the synthesis of tris chelates of 1,1,1,5,5,6,6,7,7,7-decafluoro-2,4-heptanedione. An aqueous solution of lanthanide chloride is equilibrated with an ether solution of ammonium diketonate, with the condition of an excess of lanthanide in the aqueous phase to prevent the formation of the tetrakis complex [46].

Hydrated lanthanide diketonates may be dehydrated under vacuum over  $P_4O_{10}$ .

To avoid the complication of hydrolysed product or partial decomposition during dehydration, anhydrous diketonate complexes can be prepared by the reaction of diketonate with lanthanide 2-propanolate [47] in benzene, with a lanthanide hydride or with metallic europium [48].

Anhydrous  $\beta$ -diketonate complexes may be obtained by sublimation of the solid hydrated complexes [49]. Hydrated complexes may be dissolved in a solvent that forms an azeotrope with water and the solvent is cycled over molecular sieves to achieve complete dehydration [50].

Lewis bases like aliphatic or aromatic amines, sulphoxides, phosphorous derivatives form adducts with  $\beta$ -diketonates, by recrystallization of the hydrated lanthanide  $\beta$ -diketonates in a solution of the substrate [51,52]. The adducts have also been prepared by extraction of lanthanide salt with a stoichiometric mixture of the  $\beta$ -diketone and a Lewis base. Alternatively it can be prepared by increasing the pH of an ethanolic–water solution of lanthanide salt,  $\beta$ -diketone and the organic substrate.

Lanthanide tetrakis  $\beta$ -diketonates can be prepared by any of the procedures described above for the adducts [55]. Preparation of Ce(IV) tetrakis- $\beta$ -diketonate is described in the literature [56].

Lanthanides form complexes with Schiff bases or imines quite readily. The important ligands are obtained by the condensation of an amine with salicylaldehyde derivative or a  $\beta$ -diketone. Schiff base complexes have been prepared by the reaction of ligand with a lanthanide 2-propanolate. The solvent medium is benzene and the liberated propanol during the complexation reaction is removed by distillation as alcohol–benzene azeotrope [57,58].

Since Schiff bases are relatively acidic, the complexes can be prepared with a hydrated lanthanide salt in pure ethanol. A mild base such as sodium acetate or triethylamine can be added slowly to achieve deprotonation [59].

Schiff base complexes of lanthanides derived from  $\beta$ -diketones and imines can be prepared [60] in acetone–water medium by dropwise addition of ammonia to adjust the pH to 5–6. In the absence of addition of ammonia simple adducts between lanthanide salt and imine are formed [61].

## 9. Lanthanide complexes of non-ionizable ligands

Lanthanide complexes of poorly coordinating ligands such as aldehydes and ketones [24], esters [25], and ligands containing sulphur and phosphorus [26] have been prepared. The procedure consists of mixing a solution of hydrated lanthanide salt with a solution of the

ligand in an organic solvent such as ethanol, acetone or acetonitrile followed by heating for a few hours. Usually crystallization occurs. If there is no crystallization, the solvent is removed under vacuum or a second solvent is added until the appearance of turbidity.

Lanthanide complexes of amines are prepared in an anhydrous medium to avoid precipitation of lanthanide hydroxides. In one of the procedures, a solution of ethylenediamine in acetonitrile is mixed with a solution of anhydrous lanthanide nitrate or perchlorate [13, 62, 63].

Lanthanide complexes with macrocyclic polyethers [64] have been obtained by mixing solutions of the ligand and solution of a hydrated lanthanide salt [65].

The ratio of the size of the metal ion and the radius of the internal cavity of the macrocyclic polyether determines the stoichiometry of these complexes. The stoichiometry of these complexes also depends on the coordinating ability of the anion associated with the lanthanide. For example, 12-crown-4 ether forms a bis complex with lanthanide perchlorate in acetonitrile while a 1:1 complex is formed when lanthanide nitrate is used in the synthesis [66]. Unusual stoichiometries of M:L are observed when L = 12 crown-4 ether and M is lanthanide trifluoroacetate [67]. In the case of 18-crown-6 ligand and neodymium nitrate a 4:3 stoichiometry has been observed for M:L. The composition of the complex [68] has been found to be two units of  $[\text{Nd}(18\text{-crown-6})(\text{NO}_3)_2]^{4+}$  and  $[\text{Nd}(\text{NO}_3)_6]^{3-}$ . A similar situation is encountered [69] when L = 2.2.2 cryptand and one has  $[\text{Eu}(\text{NO}_3)_5 \cdot \text{H}_2\text{O}]^{2-}$  anions and  $[\text{Eu}(2.2.2)\text{NO}_3]^+$  cations. It is important to note that traces of moisture can lead to polynuclear macrocyclic complexes containing hydroxy lanthanide ions. Thus it is imperative that the synthesis of macrocyclic complexes be performed under anhydrous conditions.

Synthesis of anhydrous macrocyclic complexes of lanthanides involve the use of dimethyl formamide adducts like  $\text{Eu}(\text{ClO}_4)_3(\text{DMF})_8$  as the starting material in the preparation of dinuclear complex with octaphenol tertiary butyl calix[8]arene [70]. Lanthanide complexes with crown ethers [3] and cryptands [71] have been synthesized in acetonitrile by drying solutions of  $\text{Ln}(\text{ClO}_4)_3$  or  $\text{Ln}(\text{NO}_3)_3$  through refluxing the acetonitrile–water azeotrope and with a Soxhlet extractor filled with molecular sieves. Since the perchlorate salts are explosive, they have been replaced by trifluoromethane sulfonates (triflates) [72] and tetrafluoroborates [19] in the synthesis of macrocyclic complexes. The cryptate complexes have been prepared by drying nitrate salts of lanthanides in acetonitrile by adding triethyl orthoformate [2]. The europium and terbium cryptates have been prepared by using the exchange reaction of sodium bromide complexes of macrobicyclic polypyridine cryptands and anhydrous  $\text{Ln}(\text{NO}_3)_3$  or  $\text{LnCl}_3$  where Ln = Eu, Tb in chloroform–acetonitrile mixtures [73].

## 10. Metal-template synthesis

Schiff base macrocyclic complexes of lanthanides have been prepared by a metal-template condensation of a diamine and 2,6-diacetyl or 2,6-diformyl derivative of pyridine or *p*-cresol [74]. The yield of these complexes depends on the radius of the metal ion and the donor ability of the counterion [75]. The acetate anion gave high yields while chloride and perchlorate anions gave poor yields [76]. In general the template synthesis

is done by refluxing the reactants in anhydrous methanol for several hours. Traces of moisture produces complexes containing lanthanide hydroxy species. An ingenious method of synthesis of polyaza macrocyclic complexes of lanthanides avoiding the possible presence of hydroxo lanthanide has been devised. The method consists of the condensation of 2,2',2''-triaminotriethylamine with triflate in anhydrous acetonitrile yielding a cyclic aliphatic polyamine that encapsulates the lanthanide ion. Bis(dimethylaminomethane) may be used as a coupling agent and this permits a condensation without the production of water and hence prevents the formation of lanthanide hydroxide [72].

### 11. Lanthanide complexes with macromolecules

It has been pointed out elsewhere (Chapter 11) that the similar ionic radii of  $\text{Ca}^{2+}$  ion and  $\text{Ln}^{3+}$  and their likelihood of occupying similar coordination sites permits the substitution of  $\text{Ca}^{2+}$  by  $\text{Ln}^{3+}$  ions in biologically significant macromolecules [77].

Aqueous aliquots of the macromolecule and lanthanide salt, both in the same buffer of known pH and ionic strength are mixed. Slow evaporation of the mixture containing an excess of lanthanide salt results in crystallization of the complex. Centrifugation and decantation of the supernatant liquid gives the solid complex. Repeated extraction with alcohol will remove the excess lanthanide salt [78].

Substitution of  $\text{Ca}^{2+}$  by  $\text{Ln}^{3+}$  is achieved by soaking calcium containing crystals of the macromolecule in a solution of a lanthanide ion. Soaking times are two days in the case of thermolysin [79] and four weeks in the case lysozyme [80].

In the process of lanthanide complex formation with the porphyrins, the ligand loses two protons and yields lanthanide hydroxy porphyrin or lanthanide porphyrin X, where  $\text{X} = \text{Cl}^-$ ,  $\text{Br}^-$ ,  $\text{NO}_3^-$ , etc. Many lanthanide complexes with substituted porphyrins have been prepared by heating a mixture of porphyrin and the lanthanide salt in imidazole melt in the range 210–240°C. When the complex formation is complete the solvent (i.e.) imidazole is eliminated by either sublimation [81] or by dissolution of the mixture in benzene, followed by washing with water [82]. Further purification requires column chromatography. The starting material can be anhydrous lanthanide chloride or hydrated lanthanide acetylacetonate. After purification the final product tends to be a monohydroxy lanthanide porphyrin complex.

Mixed complexes such as lanthanide porphyrin diketonates have been prepared and these are soluble in organic solvents [83,84]. These mixed complexes are prepared in organic solvents like 4-phenylpyridine, or 1,2,4-trichlorobenzene with refluxing. After the reaction is complete, the solvent is removed by distillation under reduced pressure and the product purified by column chromatography.

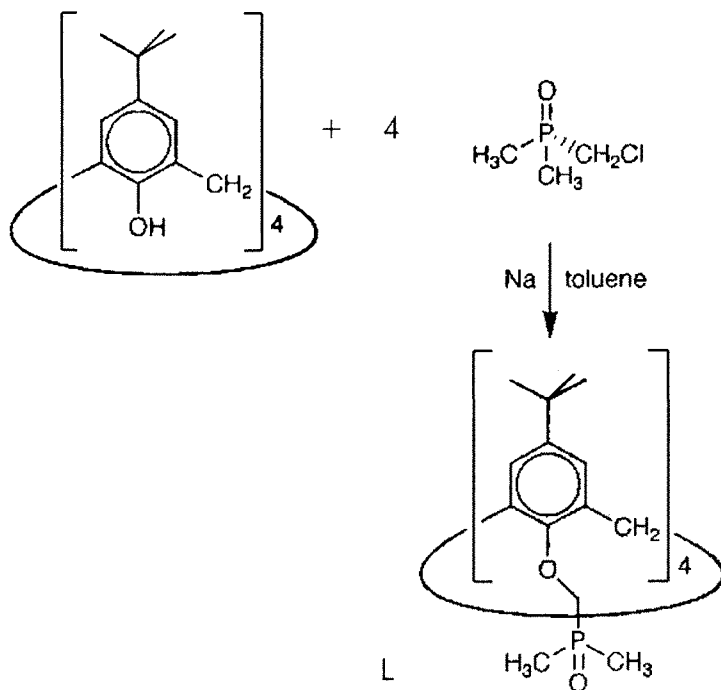
Phthalocyanines are tetraaza tetrabenzo analogues of porphyrins. Lanthanide complexes with phthalocyanines are prepared by the condensation of phthalonitrile (4 moles) with a lanthanide salt. The monocomplexes were prepared by heating a 1:4 mixture of lanthanide salt:phthalonitrile at 275°C. The molten solution solidified after an hour and purification of the complex is done by removal of excess phthalonitrile and impurities with organic solvents. Final purification is done by chromatography [85]. The bis complexes are prepared in a similar fashion but with a large excess of phthalonitrile [86]. Mixed ligand



complexes of lanthanides of the type  $\text{Ln}_2(\text{phthalocyanine})(\text{diketone})_4$  have been prepared by refluxing  $\text{Ln}(\text{diketone})_3$  with di-lithium salt of phthalocyanine in dry benzene [87]. Mixed ligand complexes of other stoichiometries have been obtained by removing benzene under vacuum and dissolving the solid in solvents like dichloromethane.

## 12. Lanthanide complexes with specific guests

There is vast amount of literature involving studies of rare earth complexes with specific guests under the umbrella of supramolecular chemistry. The ligands involved in this area of rare earth complexes are not usually available commercially. In fact the ligands are designed and synthesized and later the rare earth complexes of the synthesized ligands are prepared. An example is cited here to illustrate the scheme involved in the preparation of lanthanide supramolecular complexes.



The ligand *p-t*-butylcalix[4]arene fitted with phosphinoyl arms is synthesized by refluxing the tetrasodium derivative of *p-t*-butylcalix[4]arene and chloro(dimethylphosphinoyl)methane in toluene or xylene [88]. The resulting ligand L is reacted with lanthanum perchlorate in acetonitrile to obtain 1:1 and 1:2 complexes,  $\text{LaL}$  and  $\text{LaL}_2$ . The majority of the supramolecular complexes of rare earths involves the use of organic solvents like toluene, hexane or acetonitrile for the synthesis of both the ligands and lanthanide complexes.

### 13. Characterization of complexes

The synthesis of the complex is followed by the most important step of characterization of the complex. The composition and the structural features of both the ligand and complex have to be established before embarking on further studies. There exist many methods by which the composition and structural features of the complexes are studied. Some of the methods are: (i) elemental analysis, (ii) X-ray crystallography, (iii) UV-Vis absorption spectra, (iv) infrared spectroscopy, (v) Raman spectroscopy, (vi) thermal methods of analysis such as thermogravimetry, differential thermal analysis, (vii) nuclear magnetic resonance spectroscopy (proton, multinuclear), (viii) electrospray mass spectrometry. Depending upon the complexity of the system, some or all the methods are used in the studies of complexes.

Up to about the 1960's, elemental analysis coupled with absorption spectra and infrared spectra and X-ray crystallography were the primary methods used in the studies of complexes. Later on with the developments in nuclear magnetic resonance (NMR) spectroscopy, especially multinuclear NMR, this technique has been invariably used in the studies of structural features of lanthanide complexes. To illustrate these points some references to literature are herein pointed out. The studies on the rare earth 1,3-diketones, where 1,3-diketones are acetyl acetone, benzoyl acetone, dibenzoyl methane and 2-thienoyl trifluoroacetone totally relied on elemental analysis, UV-Vis and IR spectra to establish the nature of the complexes [89]. The important role played by X-ray crystallography in the elucidation of the structures of lanthanide complexes has been extensively discussed in Chapter 5 and the use of this technique goes as far back as the 1960's. Nevertheless it continues to play a major role in the studies of lanthanide complexes.

The system consisting of lanthanide complexation [88] with *p-t*-butyl calix[4]arene fitted with phosphinoyl pendant arms is considered to illustrate the use of many modern techniques in the elucidation of the composition and structural features of the complexes. The ligand studied is a substituted calix[4]arene, L = 5,11,17,23-tetra-*t*-butyl-25,26,27,28-tetrakis(dimethyl-phosphinoyl methoxy) calix[4]arene. The ligand is synthesized by refluxing the tetrasodium derivative of *p-t*-butyl calix[4]arene and chloro(dimethyl phosphinoyl)methane in toluene or xylene. The elemental analysis shows the isolated product has the composition L·2H<sub>2</sub>O. The IR spectrum of the ligand showed an intense  $\nu(\text{P}=\text{O})$  band at 1158 cm<sup>-1</sup> which shifts to 1171 cm<sup>-1</sup> when the ligand L·2H<sub>2</sub>O is converted to L by heating at 120°C.

White monoclinic crystals were obtained from acetonitrile-diisopropyl ether with the composition L·2CH<sub>3</sub>CN. X-ray crystal structure points to discrete molecules in a cone conformation with one acetonitrile in the upper rim and the second solvent molecule in an interstitial position (Fig. 4.1).

The mean bond length of 1.487 Å was observed for P=O bond. The molecules adopt the same enantiomeric form,  $\Delta$ , with four phosphinoyl arms in  $\delta\delta\delta\delta$  arrangement. The observed dihedral angles between aromatic rings A and C, and B and D are 39° and 54° indicating the presence of a regular cone.

The <sup>1</sup>H, <sup>13</sup>C NMR spectra and the distortionless enhancement by polarization transfer data lead to a ligand displaying a time-averaged C<sub>4</sub> symmetry in acetonitrile solution. In support of this symmetry only four singlets have been observed for the aromatic carbon

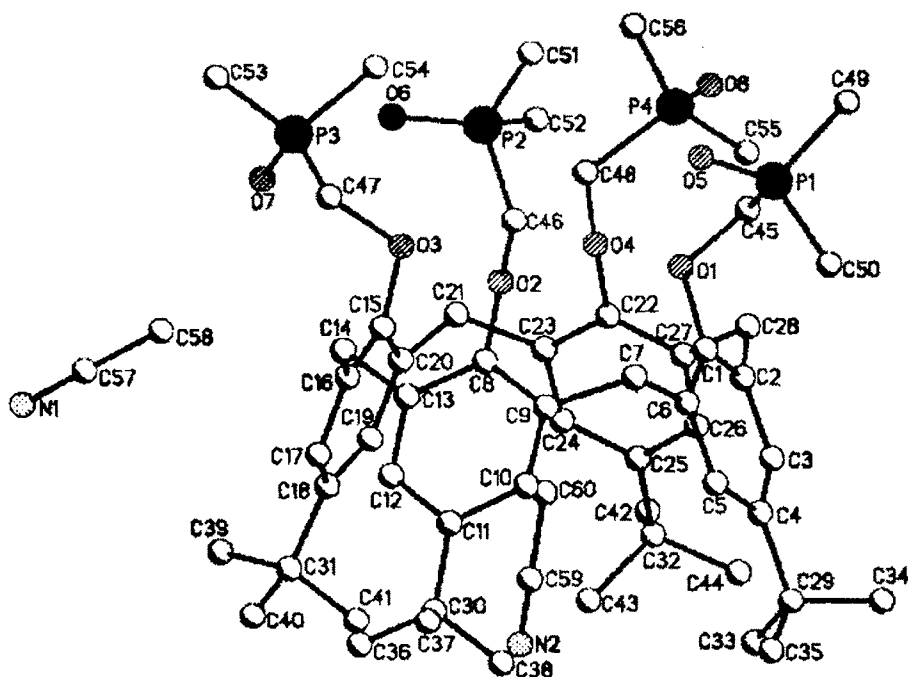


Fig. 4.1. View of L-2MeCn showing the atom-numbering scheme. (Reproduced with permission).

atoms in the  $^{13}\text{C}\{-^1\text{H}\}$  spectrum- $\delta$ 125.68 (CH) and 133.57, 146.04 and 153.25 (quaternary carbon atoms). The cone conformation in solution is confirmed by the AB spin system observed in the  $^1\text{H}$  NMR spectrum for the bridging methylene protons. The interaction of the ligand with  $\text{La}(\text{ClO}_4)_3$  has been studied by  $^{31}\text{P}\{^1\text{H}\}$  NMR spectroscopy and the data were fitted to a model involving  $\log \beta_1 = 13.4 \pm 1.3$  and  $\log \beta_2 = 19 \pm 1.8$ . The chemical shifts and the coupling constants for the complexes identified are given in Table 4.1.

The speciation was also confirmed by electrospray-mass spectroscopy. The data showed  $[\text{LaL}_2]$  at  $m/z$  of 719.1 along with acetonitrile adducts of  $[\text{LaL}]^{3+}$ , such as  $[\text{LaL}\cdot\text{CH}_3\text{CN}]^{3+}$  at  $m/z$  of 395.6 and  $[\text{LaL}\cdot 2\text{CH}_3\text{CN}]^{3+}$  at  $m/z$  of 409.6. For larger  $[\text{La}^{3+}]_t/[\text{L}]_t$  values the observed species are  $\text{CH}_3\text{CN}$  adducts of  $\text{LaL}$  and  $[\text{LaL}\cdot\text{ClO}_4]$  at  $m/z$  of 623.8.

Spectrophotometric studies showed the presence of two complexes with  $\log \beta_1 = 11.4 \pm 1.5$  and  $\log \beta_2 = 19.6 \pm 1.8$  for  $[\text{LaL}]^{3+}$  and  $[\text{LaL}_2]^{3+}$  complexes. The spectrophotometric titration curve involving the plot of absorbance versus  $R = [\text{La}^{3+}]_t/[\text{L}]_t$  is shown in Fig. 4.2.

The spectral data for the various species are:

L, 278.4 nm	$[\text{LaL}]^{3+}$ , 276 nm	$[\text{LaL}_2]^{3+}$ , 279.5 nm
$\varepsilon = 3780 \text{ M}^{-1} \text{ cm}^{-1}$	$\varepsilon = 1660 \text{ M}^{-1} \text{ cm}^{-1}$	$\varepsilon = 9970 \text{ M}^{-1} \text{ cm}^{-1}$

TABLE 4.1

The  $^1\text{H}$  and  $^{31}\text{P}\{-^1\text{H}\}$  chemical shifts ( $\delta$ ) and coupling constants ( $J/\text{Hz}$ , in parentheses) for the complexed species identified during the titration of L by  $\text{La}(\text{ClO}_4)_3 \cdot x\text{H}_2\text{O}$  in  $\text{CD}_3\text{CN}$  at 298 K.<sup>a</sup>

Observed nucleus	Species 1 [LaL <sub>2</sub> ] <sup>3+</sup>	$\Delta\delta^b$	Species 3 <sup>c</sup> [LaL <sub>2</sub> ] <sup>3+</sup>	$\Delta\delta^b$	Species 4 <sup>d</sup> [LaL <sub>2</sub> ] <sup>3+</sup>	$\Delta\delta^b$
H(ax)	4.63(d) (12.2)	-0.19	4.46(d) (12.8)	-0.36	4.05(d) (12.8)	-0.77
H(eq)	3.58(d) (12.8)	+0.28	3.65(d) (12.8)	+0.35	3.90(d) (12.8)	+0.60
Aryl H	7.30(s)	+0.22	7.41(s)	+0.33	7.59(s) (1.8)	+0.51
CH <sub>2</sub> P(O)	4.78(s, br)	+0.14	4.51(d) (3.6)	-0.13	5.11(d) (14.0) 4.26(dd), (14.0, 4.3)	
P(O)(CH <sub>3</sub> ) <sub>2</sub>	1.69(d) (13.4)	+0.26	1.79(d) (13.4)	+0.36	2.02(d) (14.0)	+0.59
C(CH <sub>3</sub> ) <sub>3</sub>	1.21(s)	+0.06	1.23(s)	+0.08	1.21(s)	+0.06
$^{31}\text{P}\{-^1\text{H}\}$	48.1	+10.7	50.9	+13.5	60.9	+23.5

<sup>a</sup>s = singlet, d = doublet, dd = doublet of doublets, br = broad.

<sup>b</sup> $\Delta\delta = \delta(\text{bound}) - \delta(\text{free})$ .

<sup>c</sup>In presence of traces of water.

<sup>d</sup>Under anhydrous conditions.

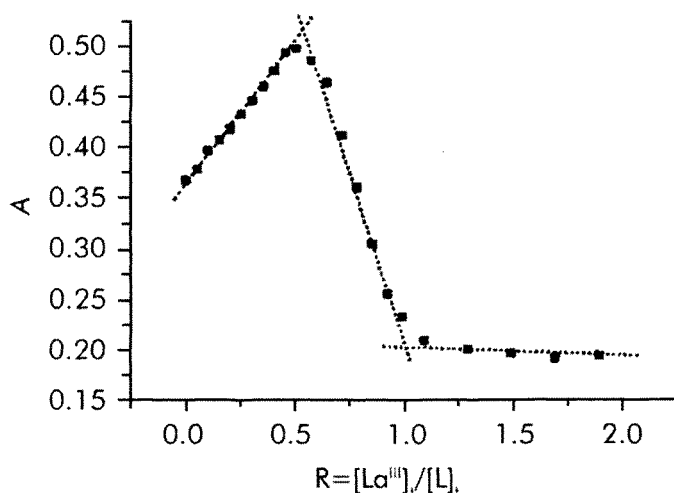


Fig. 4.2. Spectrophotometric titration of L by  $\text{La}(\text{ClO}_4)_3 \cdot x\text{H}_2\text{O}$  in MeCN at 295 K: variation of A (280 nm) vs.  $[\text{La}^{\text{III}}]_t : [\text{L}]_t$ .

The structure of the complexes can be gleaned from the  $^1\text{H}$  NMR spectra of L, 1:1 and 1:2 La:L complexes as shown in Fig. 4.3. It is to be noted that  $\text{LaL}_2$  and hydrated  $\text{LaL}$  species give the same signal multiplicity indicating  $\text{C}_4$  symmetry of L. This is not the same for the anhydrous  $[\text{LaL}]^{3+}$  complex in so far as the  $\text{CH}_2\text{P}(\text{O})_t$  protons,  $\text{H}_p$  are concerned.

The shift of aromatic protons with respect to free ligand L is interpreted to reflect the participation of ether oxygen atoms in coordination to the metal ion which increases with an increase in metal-oxygen interaction. In support of this the following  $\Delta\delta$  value has been observed:  $[\text{LaL}_2]^{3+}$ , +0.22 ppm;  $[\text{LaL}]^{3+} \cdot \text{H}_2\text{O}$ , +0.33 ppm;  $[\text{LaL}]^{3+}$ , 0.51 ppm. The M-O interaction is confirmed by the proton signals of ring methylene bridge  $\text{H}_a$ .

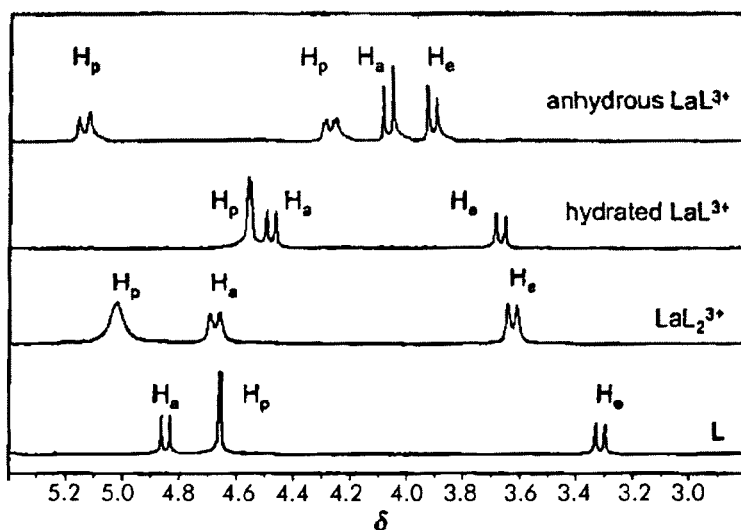


Fig. 4.3. Part of the  $^1\text{H}$  NMR spectra of L and its 1:1 and 1:2 complexes with  $\text{La}^{\text{III}}$  in  $\text{CD}_3\text{CN}$  at 298 K displaying the signals of the methylene protons (ring,  $\text{H}_a$  and  $\text{H}_e$ ; arm,  $\text{H}_p$ ). (Reproduced with permission).

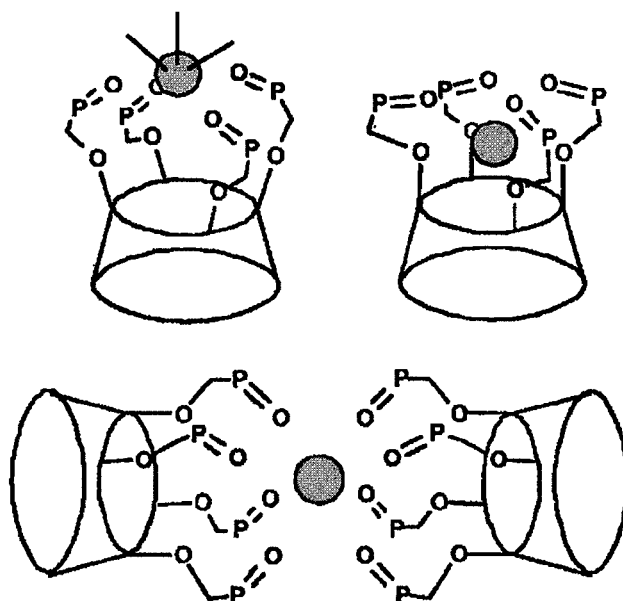


Fig. 4.4. Scheme representation of the solution structure of both hydrated (top left) and anhydrous (top right)  $[\text{LaL}]^{3+}$  and of  $[\text{LaL}_2]^{3+}$  (bottom), as inferred from NMR data. (Reproduced with permission).

$\text{H}_e$ . The values  $d(\text{H}_a)$  decrease and the values of  $d(\text{H}_e)$  increase in the order:  $[\text{LaL}]^{3+}$  anhydrous  $>$   $[\text{LaL}]^{3+}$  hydrated  $>$   $[\text{LaL}_2]^{3+}$ . This order shows the proximity of the proton and the metal ion. Different multiplicity is observed for  $\text{CH}_2\text{PO}$  protons for anhydrous

TABLE 4.2  
Crystal data and structure refinement for L·2CH<sub>3</sub>CN.

Formula	C <sub>60</sub> H <sub>90</sub> N <sub>2</sub> O <sub>8</sub> P <sub>4</sub>
M	1091.22
T (K)	143(2)
Crystal system	Monoclinic
Space group	P2 <sub>1</sub> /c
a (Å)	12.717(3)
b (Å)	18.034(4)
c (Å)	26.811(5)
β (deg)	102.60(3)
U (Å <sup>3</sup> )	6001(2)
Z	4
Reflections collected	13 510
Independent reflections	7161 ( $R_{\text{int}} = 0.0552$ )
$R_1, wR_2 [I > 2\sigma(I)]$	0.0550, 0.1207
All data	0.1051, 0.1349

[LaL]<sup>3+</sup> than for [LaL]<sup>3+</sup> hydrate and [LaL<sub>2</sub>]<sup>3+</sup> species. The differing multiplicity of the species-doublet for L ( $J_{\text{HP}} = 2.2$  Hz); [LaL]<sup>3+</sup>·H<sub>2</sub>O ( $J_{\text{HP}} = 3.6$  Hz); [LaL<sub>2</sub>]<sup>3+</sup>-singlet [LaL]<sup>3+</sup>-AB spin system ( $J_{\text{HH}} = 14$ ,  $J_{\text{HP}} = 3.6$  Hz). These data have been interpreted in terms of a significant geometrical change. In the presence of water four P=O groups and water molecules coordinate to the metal ion and under anhydrous conditions acetonitrile is unable to compete with ether oxygen atoms and as a consequence the metal ion moves into a deeper position in the calixarene cavity as depicted in Fig. 4.4. The proposed structures for the complexes are supported by the infrared spectral data. The  $\nu(\text{P}=\text{O})$  vibration is split into two components in the 1:1 complexes and red-shifted with respect to the frequency for anhydrous L by a margin which depends on the solvation of the complexes. For example for 1:1 complexes the observed shifts are La 25.5 cm<sup>-1</sup>, Eu 17.7 cm<sup>-1</sup> for hydrated samples increase to La 27.18 cm<sup>-1</sup>, Eu 36.18 cm<sup>-1</sup>. The shift for  $\nu(\text{P}=\text{O})$  in 1:2 complexes for Tb is ~ 50 cm<sup>-1</sup>.

The crystal structure data of the ligand L are given in Table 4.2.

#### 14. Lanthanide complexes in solutions

Lanthanides form many types of complexes in both aqueous and non-aqueous solutions and have been studied extensively. In the early stages the main interest was in the development of efficient ligands for the separation of lanthanides by the ion-exchange technique. The second thrust was the study of complexes in non-aqueous solutions which can be used in the solvent extraction separation of lanthanides.

In aqueous solutions the most common complex is aquo ion,  $[\text{M}(\text{H}_2\text{O})_n]^{3+}$  when the counter anion is an innocent or non-complexing anion. The value of 'n' is known and is not constant in the lanthanide series. However a value of 9 for n for elements La to Nd and a value of 8 for elements Tb–Lu is proposed [90]. For ions from Nd<sup>3+</sup> to Tb<sup>3+</sup> steric factors play a critical role with an equilibrium mixture of 8-coordinated and 9-coordinated aquo

TABLE 4.3  
Representative types of rare earth complexes in solution [93].

Inorganic ligands	Organic ligands
$RX^{2+}$ (X = F, Cl, Br, I)	$R(C_2H_3O_2)_n^{(3-n)+}$ ( $n = 1-3$ )
$RX_2^+$ (X = Cl, Br)	$R(HOCH_2COOC_2H_3O_2)_n^{(3-n)+}$ ( $n = 1-4$ )
$RCIO_4^{2+}$	$R(EDTA)^-$
$RNO_3^{2+}$	$R(NTA)_n^{(3-3n)+}$ ( $n = 1, 2$ )
$R(P_2O_7)_n^{(3-4n)+}$ ( $n = 1, 2$ )	$R(HEDTA)(IMDA)^{2-}$
	$R(HEDTA)(OH)^-$
	$R(\beta\text{-diketone})_n^{(3-n)+}$ ( $n = 1-3$ )
	$R(PDC)_n^{(3-2n)+}$ ( $n = 1-3$ )
	$R(NO_3)_3 \cdot 3TBP$ (kerosene as solvent)

ions with the equilibrium shifting gradually toward 8-coordination. The solution chemistry of lanthanides in both aqueous and non-aqueous solutions is complicated by concentration effects which can lead to both inner and outer sphere anion coordination. Inner sphere complexes of halides, nitrate, sulphate [91] and perchlorate [92] have been identified. As a result, the interpretation of data obtained from conductance, density, partial molal volumes, reaction dynamics, formation constants and spectral measurements can be very complicated.

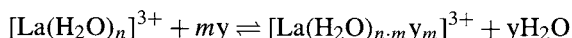
In aqueous solutions it is needless to state that any complexing ion or ligand has to compete with water molecules for coordination to the metal ion and also should not be so basic in nature that lanthanide hydroxide/hydroxo species are precipitated. With respect to non-aqueous solutions, the limitation is the solubility of ligands in organic solvents in the formation of lanthanide complexes in non-aqueous solutions. Some typical rare earth complexes in solution are given in Table 4.3.

Stability constants have been measured in aqueous solutions for a large number of both inorganic and organic ligands (Chapter 3). Rare earth ions are hard acids or class (a) metals and their complexes tend to be with oxygen donor ligands. Extensive studies have been made with ligands such as carboxylic, hydroxycarboxylic and substituted amino carboxylic acids. Comparatively inorganic ligands form weak complexes in aqueous solutions. The relative tendency of the various donor groups to coordinate to lanthanides has been estimated from the stability constants for the appropriate N-substituted iminodiacetic acid [93]. The extra stabilization ( $\Delta \log K$ ) imparted by some donor groups was found to be the same for each lanthanide as follows [94].

	Group				
	HO-	CH <sub>3</sub> O-	CH <sub>3</sub> S-	Pyridine	Methyl pyridine
$\Delta \log K$	2.9	1.6	0.00	3.3	1.0

Except for the anomalous pyridyl group, the above values confirm the hard nature of lanthanides.

The stability constants data and their interpretation have been discussed at length for reactions in aqueous solution (Chapter 3). Depending upon



the nature of complexes the formation constants have been determined by various techniques such as potentiometry, conductimetry or spectrophotometry. The stability constant data are given in tables (Chapter 3).

Some representative data range for La to Lu for 1:1 complexes are given below.

	Ligand				
	Acetate	Glycolate	Diglycolate	EDTA	IMDA
log <i>K</i>	1.58–2.04	2.19–2.72	4.93–5.64	15.5–19.83	2.8–4.30

Some of the important features are: (i) the values of the stability constant are large but not as large as those of transition elements, (ii) the stability constants along the lanthanide series do not follow the same trend for the ligands, acetate, glycolate, diglycolate, EDTA and IMDA, (iii) the stability constants do not increase monotonically with decrease in ionic radius. Factors other than simple ionic interaction have to be invoked to explain the stability constant data. Factors such as the nature of the aquated ion, the extent of aquation of the complex, changes in coordination number, and steric effects in the ligands must have important roles [93].

The thermodynamic data,  $\Delta H$  and  $\Delta S$  for some complexes have been presented and discussed (Chapter 3). The enthalpy changes ( $\Delta H$ ) for complex formation reactions are related to the difference in energy between the cation–ligand bond and cation–coordinated solvent molecule bond. Both of these will also encompass the effects due to a change in solvation and changes in the bulk solvent [95]. As is the case with the stability constants, the enthalpy change in the case where L = acetate, glycolate, diglycolate, EDTA and IMDA does not vary monotonically from La to Lu. In fact  $\Delta H$  values become more positive with a slight decrease at the end of the lanthanide series.

The entropy factor is most important for many complexes. The entropy factor is related to the change in the number of particles and the changes in vibrational modes of these particles. For complexation reactions in aqueous solutions, release of coordinated water molecules contributes to the entropy change and more favorably upon chelation. The changes in  $\Delta H$  and  $\Delta S$  can also be rationalized in terms of changes in the hydration number of lanthanide ions [91], or of the complex itself. For some complexation reactions it was found that the more negative  $\Delta H$  value meant the less positive value for  $\Delta S$  [96]. In the case of 1:1 complexes with unidentate ligands,  $\Delta H$  should disfavour the outer sphere complex formation. This has been found to be the case when the ligand is nitrate or thiocyanate ion. This means that the hydration sphere is undisturbed. When  $\Delta H$  is unfavourable and  $\Delta S$  is favourable, inner sphere complexation occurs as is the case with the fluoride or carboxylate ion. In this case, the primary hydration sphere of the lanthanide is disturbed [91].

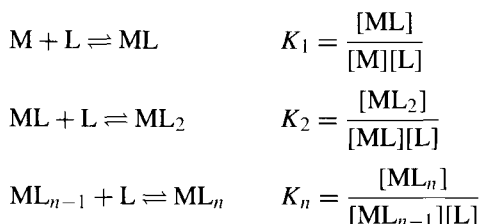
Studies on the thermodynamics of lanthanide complex formation with ligands like ethylenediamine (en) and diethylenetriamine (dien) in acetonitrile to form  $[\text{M}(\text{en})_n]^{3+}$



where  $n = 1$  to 4 and  $[\text{M}(\text{dien})_n]^{3+}$  with  $n = 1$  to 3, showed that the complex formation is enthalpy stabilized and that entropy changes deter complex formation. These results have to a certain extent overcome the uncertainty encountered in the interpretation of the results obtained on the thermodynamic parameters in aqueous solutions.

### 15. Complexes in non-aqueous solutions

Similar to aqueous solutions studies on lanthanide complex formation in non-aqueous solutions involve complex equilibria characterized by equilibrium constants and stability constants which have been discussed in detail in Chapter 3. To recall, we define the equilibrium constants and stability constants as follows:



The products of individual stability constants give cumulative formation constants

$$\begin{aligned} \beta_1 &= K_1 \\ \beta_2 &= K_1 \cdot K_2 = \frac{[\text{ML}_2]}{[\text{M}][\text{L}]^2} \\ \beta_n &= \prod_{i=1}^n K_i = \frac{[\text{ML}_n]}{[\text{M}][\text{L}]^n} \end{aligned}$$

Many methods have been used in the studies of lanthanide complex formation in non-aqueous solutions. Some commonly used methods are given below:

Diffraction techniques	La, Nd in methanol	[97,98]
Luminescence	Lanthanides	[99]
Infrared spectroscopy	Lanthanides	[100,101]
Ultrasonic absorption	Lanthanides	[102]
Nuclear magnetic resonance	Lanthanides	[103,104]
Electron paramagnetic resonance	Gd(III), Eu(II)	[105,106]
Spectrophotometry	Lanthanides	[107]
Conductimetry	La	[108]
Calorimetry	La, Gd, Yb	[109]

### 16. Formation of perchlorate complexes

Perchlorate ion is usually considered to be an innocent anion and perchlorate salts are generally used in maintaining constant ionic strength in the studies of aqueous solutions

TABLE 4.4  
Perchlorate vibrations [99,110,111].

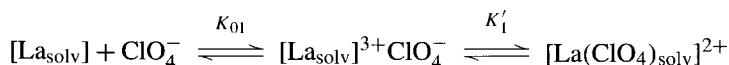
$\equiv\text{Cl}-\text{O}\cdots\text{Ln} (\text{C}_{3v})$	$\text{ClO}_4^- (\text{T}_d)$	$\text{>Cl}\cdots\text{O}\cdots\text{Ln} (\text{C}_{2v})$
$\nu_4(\text{E}) \nu_{\text{as}}(\text{ClO}) 1160 \text{ cm}^{-1}$	$\nu_3(\text{T}_2) \nu_{\text{as}}(\text{ClO}) 1090\text{--}1100 \text{ cm}^{-1}$	$\nu_8(\text{B}_2) \nu_{\text{as}}(\text{ClO}_2) 1200 \text{ cm}^{-1}$ $\nu_6(\text{B}_1) \nu_{\text{as}}(\text{ClO}_2) 1140 \text{ cm}^{-1}$ $\nu_1(\text{A}_1) \nu_{\text{s}}(\text{ClO}_2) 990 \text{ cm}^{-1}$
$\nu_1(\text{A}_1) \nu_{\text{s}}(\text{ClO}_3) 1030 \text{ cm}^{-1}$		
$\nu_2(\text{A}_1) \nu(\text{ClO}) 930 \text{ cm}^{-1}$	$\nu_1(\text{A}_1) \nu_{\text{s}}(\text{ClO})$ Raman only, $930 \text{ cm}^{-1}$	$\nu_2(\text{A}_1) \nu_{\text{s}}(\text{ClO}_2) 930 \text{ cm}^{-1}$
$\nu_3(\text{A}_1) \nu_{\text{as}}(\text{ClO}_3) 650 \text{ cm}^{-1}$	$\nu_4(\text{T}_2) \nu_{\text{as}}(\text{ClO}_2) 625 \text{ cm}^{-1}$	$\nu_3(\text{A}_1) \nu_{\text{s}}(\text{ClO}_2) 650 \text{ cm}^{-1}$ $\nu_7(\text{B}_1) \nu_{\text{as}}(\text{ClO}_2) 640 \text{ cm}^{-1}$ $\nu_9(\text{B}_2) \nu(\text{ClO}_2) 610 \text{ cm}^{-1}$
$\nu_5(\text{E}) \nu_{\text{as}}(\text{ClO}_3) 620 \text{ cm}^{-1}$		
$\nu_6(\text{E}) \nu(\text{ClO}_2) 470 \text{ cm}^{-1}$	$\nu_2(\text{E}) \nu_{\text{s}}(\text{ClO}_2)$ Raman only, $460 \text{ cm}^{-1}$	$\nu_4(\text{A}_1) \nu_{\text{s}}(\text{ClO}_2) 450 \text{ cm}^{-1}$ $\nu_5(\text{A}_2)$ torsion, Raman only
6 modes	4 modes	9 modes

of complexes. In fact, perchlorate can form either inner sphere or outer sphere complexes depending on the nature of the solvent.

Solvent	Complex type
DMSO	No inner sphere complex
DMF	No inner sphere complex
Anhydrous methanol	Inner sphere complex
Anhydrous acetonitrile	Inner sphere complex
Methanol + water	Both inner and outer sphere complexes

Perchlorate vibrations for free perchlorate, monodentate and bidentate obtained with lanthanides in acetonitrile are given in Table 4.4.

The equilibrium given below is considered for rationalization of the observations



The equilibrium constants  $K_1 = K_{01} K'_1$  have been evaluated and the resulting values have been given in Table 4.5. The interaction of lanthanides with perchlorate is strong enough to warrant care in interpreting data on the stability constants in the presence of a large excess of perchlorate used to maintain constant ionic strength.

## 17. Complex formation with trifluoromethane sulfonate

Trifluoromethane sulfonate salts of lanthanides are used as starting materials for the preparation of other lanthanide complexes instead of perchlorates for safety reasons.

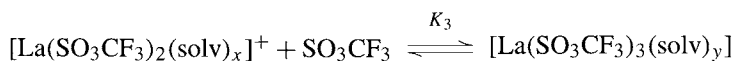
TABLE 4.5  
Stability constants of perchlorate complexes.

R	$\log K_1 \text{ClO}_4^-$	Ref.
Gd	n.a.	—
Tb	$1.9 \pm 0.4$	[99,110]
Dy	$1.8 \pm 0.4$	[111]
Ho	$1.8 \pm 0.3$	[111]
Er	$2.1 \pm 0.4$	[99,110]
Tm	$2.7 \pm 0.5$	[111]
Yb	n.a.	—
Lu	n.a.	—
Yb	$2.4 \pm 0.4$	[111]

TABLE 4.6  
Stability constants for  $\text{La}(\text{trifl})_3$ .

$\log K_3 (\text{SO}_3\text{CF}_3^-)$	Ref.
2.5	[112]
2.6	[112]
2.5	[112]
2.5	[112]
2.5	[112]
2.4	[112]
2.3	[112]
2.3	[112]

Studies on the interactions of trifluoromethane sulfonate with Ln(III) ion by FT-IR technique showed that only  $K_3$  could be determined and the values are given in Table 4.6.



## 18. Formation of halide complexes

Studies on the formation of chlorocomplexes when Ln = Pr, Sm, Nd, by UV-Vis and IR spectroscopy in propylene carbonate [113] showed the formation of  $[\text{MCl}]^{2+}$  and  $[\text{MCl}_2]^+$  with the following values for the overall stability constants.

M	$\beta_1$	$\beta_2$
Pr	54	$1.6 \times 10^3$
Nd	92	$5.2 \times 10^3$
Sm	80	$1.0 \times 10^3$

TABLE 4.7

Overall stability constants for the formation of lanthanide chloro- and bromo-complexes in anhydrous methanol, ethanol, and propanol, as determined by spectrophotometry.

X/R	$\beta$ ( $RX^{2+}$ )	$\beta$ ( $RX_2^+$ )	Conditions		Ref.
			T (°C)	Solution	
Methanol					
Cl-La	1500 ± 200	—	23		[104]
Cl-Pr	5.4	4.4		LiClO <sub>4</sub> 4 M	[114]
	7.10 ± 0.30	—	25	LiClO <sub>4</sub> 3 M	[115]
Cl-Nd	16.8	26.8		LiClO <sub>4</sub> 4 M	[114]
	8.35 ± 0.25		25	LiClO <sub>4</sub> 3 M	[115]
	63 ± 1	100 ± 2		Isomolar mixture of LiCl and LiClO <sub>4</sub> (0.5 M)	[116]
Cl-Sm	13.0	35		LiClO <sub>4</sub> 4 M	[114]
	9.16 ± 0.24	—	25	LiClO <sub>4</sub> 3 M	[115]
Cl-Ho	6.60 ± 0.20	—	25	LiClO <sub>4</sub> 3 M	[115]
Cl-Er	5.15 ± 0.20	—	25	LiClO <sub>4</sub> 3 M	[115]
Ethanol					
Cl-Ho	8.65 ± 0.55	—	25	LiClO <sub>4</sub> 3 M	[117]
Cl-Er	6.16 ± 0.55	—	25	LiClO <sub>4</sub> 3 M	[117]
<i>n</i> -propanol					
Cl-Pr	298 ± 15	—	25	LiClO <sub>4</sub> 1 M	[118]
	298 ± 14	—	25	LiClO <sub>4</sub> 1 M	[119]
Cl-Nd	10.8 ± 14.9	—	25	LiClO <sub>4</sub> 1 M	[118]
Cl-Ho	12.37 ± 0.62	—	25	LiClO <sub>4</sub> 1 M	[118]
Cl-Er	4.32 ± 0.22	—	25	LiClO <sub>4</sub> 1 M	[118]
Methanol					
Br-Pr	1.33 ± 0.30	—	25	LiClO <sub>4</sub> 3 M	[120]
Br-Nd	1.55 ± 0.22	—	25	LiClO <sub>4</sub> 3 M	[120]
Br-Sm	1.87 ± 0.25	—	25	LiClO <sub>4</sub> 3 M	[120]
Br-Ho	0.97 ± 0.14	—	25	LiClO <sub>4</sub> 3 M	[120]
Br-Er	0.70 ± 0.15	—	25	LiClO <sub>4</sub> 3 M	[120]
Methanol					
Br-Pr	4.84 ± 0.90	—	25	LiClO <sub>4</sub> 3 M	[120]
Br-Er	3.30 ± 0.30	—	25	LiClO <sub>4</sub> 3 M	[120]
<i>n</i> -propanol					
Br-Pr	9.50 ± 0.48	—	25	LiClO <sub>4</sub> 1 M	[118]
Br-Nd	4.30 ± 0.22	—	25	LiClO <sub>4</sub> 1 M	[118]
Br-Ho	17.50 ± 0.88	—	25	LiClO <sub>4</sub> 1 M	[118]
Br-Er	9.06 ± 0.45	—	25	LiClO <sub>4</sub> 1 M	[118]

These values reflect moderate interaction between Ln(III) and the chloride ion. The overall stability constants for the formation of chloro and bromo complexes of lanthanides ( $\beta(MX)^{2+}$  and  $\beta(MX_2^+)$ ) are given in Table 4.7.

The stability constants in absolute methanol show a slight increase in the series Pr–Nd–Sm followed by a decrease for the heavy Ho and Er. The values in methanol are three times greater than in 50% methanol and 8–9 times larger than in aqueous solutions. The estimated values for  $\beta_1$  are: Pr, 0.71; Nd, 0.82; Sm, 1.24; Ho, 0.50; Er, 0.47.

Studies using X-ray diffraction and  $^{139}\text{La}$  and  $^{35}\text{Cl}$  NMR showed the presence of  $[\text{LaCl}_3(\text{EtOH})_5]$  and  $[\text{La}_2\text{Cl}_4(\text{MeOH})_{10}]^{2+}$  in ethanol and methanol solutions, respectively [121].

Considering the possibility of perchlorate complexation, and correcting for this effect  $K_1 = 63$  and  $K_2 = 100^{-1}$  are obtained for  $\text{NdCl}_2^{2+}$ ,  $\text{NdCl}_2^+$  formation. The general picture that emerges is a weak La-Cl interaction in methanol and a coordination number between 8 and 9 for methanolato and chloro complexes.

The data for bromo complexes were obtained in aqueous methanolic solutions and outer-sphere bromo complexes with  $K_1 = 1.3\text{--}1.9$  were obtained for Pr, Nd, Sm, which are larger than the values of Ho (0.97) and Er (0.70). Chloro and bromo complex formation in dimethyl formamide studied by titration calorimetry [122] showed the evidence for  $\text{MCl}_2^{2+}$ ,  $\text{MCl}_2^+$ ,  $\text{MCl}_3$ , and  $\text{MCl}_4^-$  species in solutions. In the case of bromide, monobromo and dibromo inner sphere complexes have been detected. The stepwise formation constants could not be determined for iodo complexes due to the small value of enthalpies of reaction. The stability constants data obtained in DMF are given in Table 4.8.

The thermodynamic parameters (i.e.) the enthalpy and entropy values showed the formation of inner-sphere chloro complexes in the case of all the lanthanides. The enthalpies for the formation of monobromo complexes of lanthanides are also positive but smaller in magnitude than the corresponding chloro complexes. The complex formation enthalpies follow the sequence  $\Delta H^0(\text{Cl}) > \Delta H^0(\text{Br}) > \Delta H^0(\text{I})$  which is unusual for hard metal(III) ions.

Complex formation in dimethyl acetamide studied by calorimetry resulted in data given in Table 4.9.

The enthalpy variation is endothermic and is suggestive of the formation of weakly bonded complexes. The values of  $\log K$  and  $\Delta H$  show a break at gadolinium which may be due to electronic effects and change in coordination. The formation constants and the enthalpy value for bromo complexes of La and Nd showed that bromo complexes are less stable than chloro complexes ( $\text{Cl}^- > \text{Br}^-$ ) for La and the order is  $\text{Br}^- > \text{Cl}^-$  for  $\text{Nd}^{3+}$  ion. The data have been interpreted in terms of inner-sphere complexes in the case of both chloride and bromide [125]. Studies in DMSO medium showed that no Pr-Cl could be detected while  $\text{Er}^{3+}$  formed inner-sphere  $[\text{ErCl}]^{2+}$  complex [98].

## 19. Complex formation with thiocyanate

Thiocyanate can bond through nitrogen or sulfur atoms in monodentate configuration or through both nitrogen and sulfur in a bidentate configuration. This is known as an ambidentate ligand. Studies on the complex formation of  $\text{Ln} = \text{La, Nd, Tb, Ho, Tm}$  and  $\text{Yb}$  with thiocyanate in dimethyl formamide by calorimetry, and Raman spectroscopy have been made [126] and  $\log K_1$  values of  $\sim 1.5\text{--}1.8$   $\text{mol}^{-1}$ ,  $\Delta H_1^0$  of  $\sim 7.4\text{--}9.0$   $\text{kJ mol}^{-1}$ ,  $\Delta S_1^0$  of  $\sim 57\text{--}66$   $\text{J}^{-1} \text{mol}^{-1} \text{K}^{-1}$  were obtained. The  $\Delta H_1^0$  value is positive and much smaller than the value of  $\text{MCl}_2^{2+}$  complex and slightly larger than that of  $\text{MBr}^+$  complexes. In general we have the sequence  $\Delta H_1^0(\text{Cl}) \gg \Delta H_1^0(\text{NCS}) > \Delta H_1^0(\text{Br})$ .

The thermodynamic parameters of the thiocyanato complexes are similar to those of lanthanide bromo complexes and the latter are outer-sphere complexes in DMF. Contrary to this  $^{89}\text{Y}$  NMR spectra suggest an inner-sphere  $\text{Y(III)-NCS}$  complex.

TABLE 4.8

Stability constants for the formation of  $[RX_n]^{(3-n)+}$  complexes ( $X = Cl^-, Br^-$ ) in DMF containing 0.2 M  $Et_4NClO_4$ , at 25°C, as determined by titration calorimetry; [R], between 0.003 and 0.03 M. Uncertainties refer to three standard deviations.

R	$\log K_1$	$\log K_2$	$\log K_3$	$\log K_4$	Ref.
R/Cl <sup>-</sup> (inner sphere)					
Y	2.3 ± 0.2	2.1 ± 0.2	1.4 ± 0.3	1.1 ± 0.2	[122]
La	3.04 ± 0.06	2.15 ± 0.08	0.43 ± 0.16	–	[123]
Ce	3.25 ± 0.09	2.16 ± 0.08	1.36 ± 0.13	0.24 ± 0.29	[123]
Pr	3.25 ± 0.09	2.13 ± 0.09	1.42 ± 0.14	0.49 ± 0.14	[123]
Nd	3.26 ± 0.10	2.01 ± 0.09	1.35 ± 0.13	0.63 ± 0.12	[123]
Sm	3.00 ± 0.11	1.89 ± 0.10	1.50 ± 0.13	0.95 ± 0.09	[123]
Eu	3.15 ± 0.23	2.05 ± 0.15	1.66 ± 0.17	1.03 ± 0.10	[123]
Gd	2.80 ± 0.13	1.97 ± 0.12	1.44 ± 0.18	1.11 ± 0.13	[123]
Tb	2.63 ± 0.16	2.17 ± 0.14	1.38 ± 0.20	1.34 ± 0.15	[123]
Dy	2.57 ± 0.11	2.19 ± 0.11	1.46 ± 0.13	1.43 ± 0.08	[123]
Ho	2.61 ± 0.21	2.39 ± 0.19	1.63 ± 0.21	1.46 ± 0.16	[123]
Er	2.47 ± 0.2	2.42 ± 0.20	1.81 ± 0.10	1.41 ± 0.09	[123]
Tm	2.57 ± 0.2	2.76 ± 0.15	2.04 ± 0.10	1.55 ± 0.06	[123]
Yb	2.70 ± 0.2	2.61 ± 0.18	2.35 ± 0.13	1.73 ± 0.05	[123]
Lu	2.82 ± 0.2	2.48 ± 0.15	2.41 ± 0.11	1.71 ± 0.06	[123]
R/Br <sup>-</sup> (outer sphere)					
Y	1.8 ± 0.4	–	–	–	[122]
La	1.4 ± 0.2	0.4 ± 0.3	–	–	[122]
Nd	1.6 ± 0.3	0.5 ± 0.3	–	–	[122]
Tb	1.6 ± 0.5	1.0 ± 0.4	–	–	[122]
Tm	2.1 ± 0.4	–	–	–	[122]

Infrared evidence shows N-bonding to lanthanides. The near constancy of the thermodynamic parameters for thiocyanato complexes is due to small N-end and lack of geometry change along the lanthanide series. In alcoholic solutions, inner-sphere thiocyanato complex formation has been observed [127] with cerium (III).

## 20. Complex formation with nitrate

Interaction of the nitrate ion with lanthanide(III) in acetonitrile solution was studied by conductivity, vibrational spectroscopy and luminescence spectroscopy. Bidentate nitrate with approximate  $C_{2v}$  local symmetry was detected. FT-IR spectral evidence for the formation of  $[La(NO_3)_5]^{2-}$ , where La = Nd, Eu, Tb and Er with coordination number 9.9 has been obtained [128]. Two inequivalent nitrate ions bound to lanthanides were detected by vibrational spectroscopy. The inequivalent nature varied with different lanthanides. For example three equivalent nitrate groups for La and Yb, one nitrate different from the other two for Eu ion were detected. Vibrational spectral data point towards strong La-NO<sub>3</sub> interaction in acetonitrile [129]. Stability constants for lanthanide nitrate complexes are given in Table 4.10.

In aqueous methanol  $[Eu(NO_3)]^{2+}$ ,  $[Eu(NO_3)_2]^+$  and  $[Eu(NO_3)_3]$  species have been detected. Under the same experimental conditions the stoichiometries of the nitrate

TABLE 4.9

Stability constants and  $\Delta H_1$  and  $\Delta H_2$  values for the formation of chloro- and bromo-complexes in DMA at 298 K.

R	$K_1$ (mol <sup>-1</sup> )	$K_2$ (mol <sup>-1</sup> )	$\Delta H_1$ (kJ mol <sup>-1</sup> )	$\Delta H_2$ (kJ mol <sup>-1</sup> )	Ref.
R/Cl <sup>-</sup>					
Y	156 ± 1	220 ± 31	20.4 ± 0.1	30.7 ± 0.3	[124]
La	212 ± 1	62 ± 9	26.1 ± 0.1	36.0 ± 0.4	[124]
Ce	242 ± 1	37 ± 5	28.2 ± 0.1	27.7 ± 0.3	[124]
Pr	167 ± 1	30 ± 4	35.5 ± 0.2	37.8 ± 0.4	[124]
Nd <sup>a</sup>	58 ± 1	–	24.1 ± 0.1	–	[124]
Sm	109 ± 1	21 ± 3	25.9 ± 0.1	18.9 ± 0.2	[124]
Eu	81 ± 1	50 ± 7	23.4 ± 0.1	21.5 ± 0.2	[124]
Gd	17 ± 1	51 ± 9	13.2 ± 0.1	-0.111 ± 0.001	[124]
Tb	128 ± 1	38 ± 5	17.7 ± 0.1	22.2 ± 0.2	[124]
Dy	66 ± 1	144 ± 20	17.4 ± 0.1	18.1 ± 0.2	[124]
Ho	190 ± 1	166 ± 23	17.8 ± 0.1	26.1 ± 0.3	[124]
Er	205 ± 1	57 ± 8	9.9 ± 0.1	9.5 ± 0.1	[124]
Tm	284 ± 1	232 ± 33	22.1 ± 0.1	35.9 ± 0.4	[124]
Yb	221 ± 1	1462 ± 205	17.4 ± 0.1	22.8 ± 0.2	[124]
Lu	293 ± 1	233 ± 33	30.7 ± 0.2	49.0 ± 0.5	[124]
R/Br <sup>-</sup>					
La	165 ± 1	48 ± 7	32.6 ± 0.2	45.6 ± 0.4	[125]
Nd	115 ± 1	–	33.6 ± 0.2	–	[125]

TABLE 4.10

Stability constants of lanthanide–nitrate complexes in various solvents.

R	Solvent	Conditions			$K_1$	$K_2$	$K_3$	Ref.
		$T$ (°C)	$I$	Electrolyte				
Methanol <sup>a</sup>								
Nd	$X_w = 0.04$	25	3.0	NaNO <sub>3</sub> , KNO <sub>3</sub>	83.12 ± 1.4	5.56 ± 1.0	–	[130]
Eu	$X_w = 0.01$	25	3.0	NaClO <sub>4</sub>	168.4 ± 14.8	114.6 ± 5.2	41.1 ± 3.6	[107]
Er	$X_w = 0.13$	25	3.0	NaNO <sub>3</sub> , KNO <sub>3</sub>	110.15 ± 15.05	40.83 ± 5.59	12.27 ± 1.4	[130]
<i>n</i> -propanol								
Pr		25	1.0	LiClO <sub>4</sub>	1.24–3.57	–	–	[131]
Nd		25	1.0	LiClO <sub>4</sub>	3.13–8.54	–	–	[131]
Ho		25	1.0	LiClO <sub>4</sub>	2.29	–	–	[131]
Er		25	1.0	LiClO <sub>4</sub>	3.76	–	–	[131]
<i>N,N</i> -dimethylacetamide								
La		25			17 ± 1	16 ± 2	–	[125]
Nd		25			25 ± 1	92 ± 13	–	[125]

<sup>a</sup>  $X_w$  is the water mole fraction; the data for other water mole fractions and other temperatures are available in the given reference.

complexes were different for Nd(III) and Er(III) from Eu(III). These differences have been attributed to changes in coordination number. The enthalpy and entropy changes showed differences between Nd(III) and the other lanthanides which are attributed to the degree of outer-sphere complexation of Nd(III).

Using  $^{15}\text{N}$  NMR spectroscopy, lanthanide complexation with nitrate in aqueous methanol, and aqueous acetone, the formation of mononitrato, bisnitrato complexes of Er(III),  $[\text{Ce}(\text{NO}_3)]^{2+}$ ,  $[\text{Ce}(\text{NO}_3)_2]^+$ , tetranitrato, either penta- or hexanitrato complexes were detected. It is significant that  $[\text{Ce}(\text{NO}_3)_3]$  could not be detected and that the nitrate complexes are not formed sequentially [132].

Complexation of lanthanides with nitrate in dimethyl formamide [110] studied by IR, Raman and electronic absorption spectroscopy showed evidence for the formation of  $[\text{Nd}(\text{NO}_3)_n]$ , where  $n = 1$  to 3. In the case of Eu(III), evidence pointed to the presence of  $[\text{Eu}(\text{NO}_3)_2 \cdot (\text{DMF})_x]$  and  $[\text{Eu}(\text{NO}_3)_3 \cdot (\text{DMF})_y]$ .

The following data were obtained in dimethyl acetamide for La and Nd by calorimetric titration technique.

Metal	$K_1$	$K_2$	$\Delta H$ ( $\text{kJ mol}^{-1}$ )	$\Delta H_2$ ( $\text{kJ mol}^{-1}$ )
La	17	16	48.2	23.1
Nd	25	92	1.0	8.3

Complexation of lanthanides in dimethyl sulfoxide with nitrate ion studied with Er(III) and Y(III) showed [98] coordination of 1.5 nitrate groups to the metal ion and 6 DMSO molecules. The nitrate is probably in a bidentate disposition with M–O(1) bond length of 2.38 Å and M–O(2) length of 2.57 Å. The overall coordination number for Er(III) is close to 9, similar to the solid complex of the composition  $\text{Er}(\text{NO}_3)_3 \cdot 6\text{DMSO}$ .

Interaction of lanthanide(III) salts with neutral donors like acetonitrile, DMSO, nitromethane, dimethyl formamide has been studied and documented in the literature [133].

In Table 4.11 the coordination numbers of lanthanides in the solid state and in solution are compared.

## 21. Solid rare earth complexes

The field of rare earth complexes is quite large and hence it is important to define the scope of discussion to be presented here. We will confine the discussion to representative types of ligands which form solid rare earth complexes and have been identified and characterized. The coverage will of necessity be brief and not encyclopedic in nature. However, as far as possible, examples of all the major types of complexes will be given, especially complexes of unusual significance. Some reviews on solid rare earth complexes of common ligands have appeared in the literature [134–136].

## 22. Inorganic ligands

### 22.1. Halides and pseudohalides

Representative examples of rare earth complexes with halides and pseudohalides are given in Table 4.12. Some oxyanions such as nitrates are included in a separate listing. The formulas given for halide complexes as hexahalides are misleading since these compounds are extended lattice compounds and are not always octahedral.



TABLE 4.11  
Comparison of coordination numbers determined in the solid state and in solution [133].

Complex	Site symmetry	CN (solid state)	CN (solution)
R(NO <sub>3</sub> ) <sub>3</sub> · <i>n</i> DMSO <sup>a</sup>			
La(NO <sub>3</sub> ) <sub>3</sub> ·4DMSO	C <sub>2v</sub>	10	9.4 <sup>b</sup> , 10.2 <sup>c</sup>
Pr(NO <sub>3</sub> ) <sub>3</sub> ·4DMSO	C <sub>2v</sub>	10	9.2 <sup>b</sup> 9.9 <sup>c</sup>
Nd(NO <sub>3</sub> ) <sub>3</sub> ·4DMSO	C <sub>2v</sub>	10	9.5 <sup>b</sup> 9.6 <sup>c</sup>
Sm(NO <sub>3</sub> ) <sub>3</sub> ·4DMSO	C <sub>2v</sub>	10	9.2 <sup>b</sup> 9.6 <sup>c</sup>
Eu(NO <sub>3</sub> ) <sub>3</sub> ·4DMSO	C <sub>2v</sub>	10	8.9 <sup>b</sup> 9.0 <sup>c</sup>
Tb(NO <sub>3</sub> ) <sub>3</sub> ·3DMSO	D <sub>3h</sub>	9	8.9 <sup>b</sup> 9.0 <sup>c</sup>
Er(NO <sub>3</sub> ) <sub>3</sub> ·3DMSO	D <sub>3h</sub>	9	8.9 <sup>b</sup> 9.0 <sup>c</sup> 9.0 <sup>d</sup>
Tm(NO <sub>3</sub> ) <sub>3</sub> ·3DMSO	D <sub>3h</sub>	9	8.3 <sup>b</sup> 8.8 <sup>c</sup>
Yb(NO <sub>3</sub> ) <sub>3</sub> ·3DMSO	D <sub>3h</sub>	9	8.3 <sup>b</sup> 8.3 <sup>c</sup>
Lu(NO <sub>3</sub> ) <sub>3</sub> ·3DMSO	D <sub>3h</sub>	9	8.3 <sup>b</sup> 8.4 <sup>c</sup>
R(ClO <sub>4</sub> ) <sub>3</sub> · <i>n</i> DMSO			
R(ClO <sub>4</sub> ) <sub>3</sub> ·8DMSO (R = La–Gd)		8	7.8–7.2 <sup>f</sup> 8.7–7.7 <sup>g</sup>
R(ClO <sub>4</sub> ) <sub>3</sub> ·7DMSO (R = Tb–Lu)		7	7.2–6.6 <sup>f</sup> 7.6–7.4 <sup>g</sup>
Sm[(CH <sub>3</sub> CN) <sub>9</sub> ](AlClCH <sub>3</sub> CN)			9

<sup>a</sup>Data from single-crystal X-ray diffraction.

<sup>b</sup>Data for R<sub>DMSO</sub> = [DMSO]<sub>t</sub>/[R(III)]<sub>t</sub> = 4.

<sup>c</sup>Data for R<sub>DMSO</sub> = [DMSO]<sub>t</sub>/[R(III)]<sub>t</sub> = 6.

<sup>d</sup>Data from X-ray diffraction measurements; 1 M solutions of Er(NO<sub>3</sub>)<sub>3</sub> in DMSO.

<sup>e</sup>Data from IR and powder X-ray diffraction measurements.

<sup>f</sup>R<sub>DMSO</sub> = 8.

<sup>g</sup>R<sub>DMSO</sub> = 12.

This is the case with fluoro complexes and the crystal structure of (NH<sub>4</sub>)<sub>2</sub>CeF<sub>6</sub> shows the coordination is nearly square antiprismatic with cerium having eight fold coordination [140]. However the compounds Cs<sub>2</sub>NaMF<sub>6</sub> and analogous chloride have octahedral coordination [139]. Raman spectra of the chloro compounds of La, Pr, Nd and Er have been obtained [146–148]. Raman spectra along with the far infrared spectra of Nd and Er show the octahedral coordination of the lanthanide ion. For these complexes the location of A<sub>1g</sub> band is as follows: La = 274 cm<sup>-1</sup>; Pr = 281 cm<sup>-1</sup>; Nd = 278 cm<sup>-1</sup>; Er = 289 cm<sup>-1</sup>.

The number and spacings of the lines due to electronic transitions of the Pr complex suggest a weakly distorted structure which is supported by electron spin resonance results [149].

TABLE 4.12  
Representative complexes with halides and pseudohalides<sup>a</sup>.

Halide ions		Ref.
MRF <sub>4</sub>	(R = La–Lu, Y, Sc)	[137]
M <sub>3</sub> RF <sub>6</sub>	(R = La–Lu, Y, Sc)	[137]
M <sub>2</sub> CeF <sub>6</sub>		[137]
Cs <sub>3</sub> RF <sub>7</sub>	(R = Ce, Pr, Nd, Tb, Dy)	[137]
M <sub>3</sub> RCl <sub>6</sub>		[138]
M <sub>3</sub> R <sub>2</sub> Cl <sub>9</sub>		[137]
M <sub>2</sub> CeCl <sub>6</sub>		[137]
Cs <sub>2</sub> NaRCl <sub>6</sub>	(R = La–Lu, Y, Sc)	[139]
M <sub>3</sub> RBr <sub>6</sub>		[138]
M <sub>3</sub> RI <sub>6</sub>		[140]
Pseudohalide ions		
M <sub>3</sub> R(NCS) <sub>6</sub>	(R = Pr–Lu, Y, Sc)	[141]
M <sub>3</sub> R(NCSe) <sub>6</sub>	(R = Pr–Er, Y)	[142]
M <sub>3</sub> R(NCO) <sub>6</sub>	(R = Eu–Yb, Y, Sc)	[143]
M <sub>3</sub> R(NCO) <sub>3</sub> (NO <sub>3</sub> ) <sub>3</sub>	(R = La–Yb)	[145]
M <sub>3</sub> R(NCO) <sub>3</sub> X <sub>3</sub>	(X = Cl, NCS; R = Dy, Er, Yb, Y)	[144]

<sup>a</sup>In this and subsequent tables M signifies an alkali metal or organic ammonium, phosphonium, etc., cation. If the scandium complex has been prepared, this will be specifically noted.

The octahedral coordination for the solid complexes [(C<sub>6</sub>H<sub>5</sub>)<sub>3</sub>PH]<sub>3</sub>MX<sub>6</sub> and [(C<sub>5</sub>H<sub>5</sub>)<sub>3</sub>NH]<sub>3</sub>MX<sub>6</sub>, where X = Cl was assigned from visible spectral results [138]. This coordination is also supported by far infrared and Raman spectral data [150]. The totally symmetric stretching frequency varies from 252 cm<sup>-1</sup> for Nd to 263 cm<sup>-1</sup> for Yb similar to Cs<sub>2</sub>NaMCl<sub>6</sub> complexes. These anionic halide complexes of low-coordination seem to be stabilized by the presence of large counter cations. Analogous compounds with tetrabutyl ammonium cation are also known [151].

### 23. Complexes with pseudohalides

The preparation and the crystal structure of [(C<sub>4</sub>H<sub>9</sub>)<sub>4</sub>N]Er(NCS)<sub>6</sub> have been reported and the complex has six-coordination [152]. These complexes are quite stable, soluble in organic solvents and melt with decomposition. There are some difficulties encountered in assigning coordination numbers as illustrated [153] by the complexes K<sub>4</sub>Nd(NCS)<sub>7</sub>·4H<sub>2</sub>O and K<sub>4</sub>Eu(NCS)<sub>7</sub>·6H<sub>2</sub>O. These complexes contain eight-coordinate lanthanide in [Ln(NCS)<sub>4</sub>(H<sub>2</sub>O)<sub>4</sub>]<sup>-</sup> unit and the coordination polyhedron is a dodecahedron in which each trapezoid contains two water molecules on the A vertices and two nitrogen atoms from the (NCS) groups on the B vertices. The remaining three thiocyanate ions are not coordinated to the lanthanide ion.

We have noted that N-bonded thiocyanate complexes dissociate readily in solution. Mixed ligand complexes of lanthanides with thiocyanates and L = ethanol, pyridine, triphenyl phosphorous oxide, phenanthroline, etc. have been synthesized.

Complexes with cyanate were prepared [143] by reaction of anhydrous lanthanide chlorides with an excess of tetraethylammonium cyanate in absolute ethanol. The complex has the formula  $[(C_2H_5)_4N]_3Ln(NCO)_6$ , where  $Ln = Eu, Gd, Dy, Ho, Er,$  and  $Yb$  and they are indicated to be six-coordinate and cyanate is N-bonded as evidenced by IR spectra [147]. Mixed complexes  $[(C_2H_5)_4N]_3[Ln(NCO)_3X_3]$ , where  $Ln = Dy, Er$  and  $Yb$  and  $X = Cl, NCS$  have been synthesized and they appear to be of six-coordinate [144]. Mixed complexes of the type  $[(C_2H_5)_4N]_3[Ln(NCO)_3(NO_3)_3]$ , where  $Ln = La, Pr, Nd, Sm, Eu, Gd, Er$  and  $Yb$  have been synthesized and the IR spectra shows N-bonded cyanate, bidentate nitrate and the overall coordination number amounting to nine [145].

Complexes of lanthanides with selenocyanate of the type  $[n\text{-}But_4N]_3[Ln(NCSe)_6]$ , where  $Ln = Pr, Nd, Sm, Dy, Ho$  and  $Er$  have been reported and the IR spectra indicate that they are N-bonded. Selenocyanate complexes dissociate more readily than the thiocyanate complexes in solution. From the molar absorptivities in the visible region, it is inferred that they deviate significantly from the octahedral symmetry. This may arise from the non-linearity of  $M\text{-}NCSe$  moiety. Mixed ligand selenocyanate complexes of  $La, Ce, Pr$  and  $Nd$  have been reported with various nitrogen and oxygen donor ligands but in all the cases the selenocyanate group is coordinated only as a monodentate ligand through the nitrogen [154].

## 24. Complexes with oxyanions

Some examples of complexes formed with oxyanions are given in Table 4.13.

Oxanions form both inner- and outer-sphere complexes in aqueous solutions with lanthanide ions but the number of genuine solid complexes is small. The structures of some nitrate complexes has been elucidated in Chapter 5 dealing with structural chemistry of lanthanide complexes.

The crystal structure of  $(NH_4)Ce(NO_3)_6$  shows monoclinic symmetry with each  $Ce(IV)$  atom coordinated by six bidentate nitrate groups and the symmetry around the cerium atom approximating closely to  $T_h$ . The bond lengths and bond angles for  $Ce(IV)$  and  $Ce(III)$  nitrate complexes are given in Table 4.14 for comparison.

Because of the higher charge and polarizing power of  $Ce^{4+}$  ion the metal–oxygen bond distances in its complex are shorter than the  $M\text{-}O$  bond distances in the  $Ce(III)$  nitrate complex.

The structure of  $(PhEtP)_2Ce(NO_3)_5$  shows it to have 10-coordinate cerium and the stereochemistry of the bidentate nitrate groups being based on trigonal bipyramid [158]. Complexes of the type  $[(C_4H_9)_4N]_3La(NO_3)_6$ , where  $La = La, Ce, Pr, Nd, Sm$  and  $[(C_4H_9)_4N]_2[La(NO_3)_5]$ , where  $La = Nd, Ho, Tm,$  and  $Yb$  have been synthesized emphasizing the role of size of the cation in determining the coordination number [159]. The complex nitrates  $K_3Pr_2(NO_3)_9$  has distorted icosahedral disposition [160].

There exist many mixed complexes of lanthanides of organic ligands and nitrate ions. From their formulae it can be concluded that nitrate ions are coordinated to the lanthanide ions either as a monodentate or as a bidentate ligand. The actual disposition of the nitrate group may be ascertained from the infrared and Raman spectra [155]. The ionic nitrate and bound nitrate differ in symmetry.

TABLE 4.13  
Classes of nitrate complexes formed by lanthanide elements [155].

Valence state	Class of complex		Formed for
III	$M_2^I M^{III}(NO_3)_5 \cdot xH_2O$	$M^{III}$	La, Ce, Pr, Nd
		$M^I$	Variously, Na, K, Rb, Cs, Tl, $NH_4$ and $Ph_4P$
		$x$	1 (Na, K), 2 (K, Cs) or 4 (Rb, Cs, $NH_4$ )
	$M_3^II M_2^{III}(NO_3)_{12} \cdot 24H_2O$	$M^{III}$	La, Ce, Pr, Nd, Sm, Eu, Gd, Er
		$M^I$	Variously, Mn, Fe, Co, Ni, Cu, Zn, Mg, Cd

TABLE 4.14  
Interatomic distances and angles for nitrate groups in nitrate-complexes.

Compound		Bond lengths (Å)					Interbond angles (deg)			Ref.
		<i>a</i>	<i>b</i>	<i>r</i> <sub>1</sub>	<i>r</i> <sub>2</sub>	<i>r</i> <sub>3</sub>	<i>a</i> <sub>1</sub>	<i>a</i> <sub>2</sub>	<i>a</i> <sub>3</sub>	
$Mg_3Ce_2(NO_3)_{12} \cdot 24H_2O$	$NO_3(1)$	2.616	2.636	1.262	1.257	1.225				[157]
	$NO_3(2)$	2.612	2.675	1.259	1.268	1.220				
$(NH_4)_2Ce(NO_3)_6$	$NO_3(1)$	2.497	2.530	1.280	1.287	1.243	124.1	120.7	115.2	[156]
	$NO_3(2)$	2.510	2.488	1.272	1.289	1.235	124.5	120.9	114.6	
	$NO_3(3)$	2.514	2.512	1.280	1.286	1.225	115.6	120.5	113.9	

Ionic nitrate  $D_{3h}$  has 4 vibrations (3 IR active 1 Raman active), coordinated nitrate  $C_{2v}$  has 6 IR active, and 6 Raman active vibrations. The doubly degenerate  $\nu_4$  band of ionic nitrate ( $700\text{ cm}^{-1}$ ) is split into  $\nu_3$  and  $\nu_4$  upon coordination. Further Raman polarization studies can distinguish between monodentate from bidentate nitrate and bridging nitrate groups. As an example  $La(HMPA)_3(NO_3)_3$  has both ionic and coordinated nitrate [161].

Complexes with coordinated nitrite with the formula  $Cs_2Na Ln(NO_2)_6$ , where  $Ln = La-Er$  and  $Rb_2NaLn(NO_2)_6$ , with  $Ln = La-Nd$  have been identified with  $T_h$  symmetry and weak  $La-N$  bond [162].

Hexakis (nitrito) europate(III) has been synthesized [163] whose IR spectrum shows it to have  $T_h$  symmetry.

In general perchlorate is an innocent anion. However, complexes of the type  $La(HMPA)_4(ClO_4)_3$  have been isolated and their IR and Raman spectra gave evidence for the presence of both ionic and coordinated perchlorate [164]. The Raman band at  $436\text{ cm}^{-1}$  indicated perchlorate with  $C_{2v}$  symmetry and as a bidentate ligand.

Rare earth ions are hard acids and in general prefer hard bases in complex formation. Thus it is not surprising that rare earth ions form a variety of complexes with oxygen donor ligands such as: (i) carboxylic and hydroxy carboxylic acids, (ii) carbonyl ligands, (iii) 1,3-diketones, (iv) alcohols and alkoxides, (v) polyethers and (vi) compounds such as pyridine *N*-oxide,  $(C_6H_5)_3PO$ ,  $(C_6H_5)_3AsO$ , DMSO, HMPA, etc.

## 25. Oxygen donors

Carboxylic and hydroxy carboxylic acids form complexes readily with lanthanides with high stability constants (Chapter 3) and they have been widely used in the ion exchange

TABLE 4.15

Representative complexes with carboxylic and hydroxycarboxylic acids [165,166].

$R(C_2H_3O_2)_3 \cdot 4H_2O$	(R = Sm–Lu)
$R_2(C_2O_4)_3 \cdot 10H_2O$	
$R_2(C_2O_4)_3 \cdot 6H_2O$	(R = Ho–Lu, Sc)
$R_2(\text{malonate})_3 \cdot 8H_2O$	(R = Ce–Gd)
$R_2(\text{malonate})_3 \cdot 6H_2O$	(R = Ce–Eu)
$Sc(OH)(\text{malonate}) \cdot 2H_2O$	
$R(C_2H_3O_2)_3 \cdot o\text{-phen}$	
$M[R(C_2H_3O_2)_4] \cdot xH_2O$	
$M_2[R(C_2H_3O_2)_5] \cdot xH_2O$	
$M_3[R(C_2H_3O_2)_6] \cdot xH_2O$	
$M[R(C_2O_4)_2] \cdot xH_2O$	
$R(\text{tartrate})Cl \cdot xH_2O$	
$R(\text{citrate}) \cdot xH_2O$	
$K_3R(\text{citrate})_2 \cdot 3H_2O$	

method for the separation and purification of rare earths. Many complexes of carboxylic and hydroxy carboxylic acids have been synthesized and characterized, and for the sake of brevity they are not included here [165]. Most of these complexes are in hydrated form and their structures are complex with carboxyl groups in bridging disposition between metal ions. Some typical complexes are listed in Table 4.15. Detailed X-ray structural studies of oxalate complexes show the oxalate groups serving as bridging ligands and the larger lanthanides and smaller lanthanides have a coordination number of nine and eight, respectively.

Two types of malonate groups have been identified with one in a six-membered chelate ring and the other in a non-chelated form [166].

Glycolic acid complexes of rare earths have been studied in detail and tris glycolate complexes of lanthanides with coordination number greater than six through the sharing of carboxylate groups by polyhedra as well as chelation of glycolate has been reported [167]. Similar findings of bridging carboxylate and chelated carboxylate in the case of nicotinic and isonicotinic acid complexes have been documented [168].

Diglycolic acid, a terdentate ligand forms nine-coordinate complexes with rare earths [169]  $Na_3[Ln(OCOCH_2OCH_2OCO)_3] \cdot 2NaClO_4 \cdot 6H_2O$  in which two carboxyl groups are unidentate with metal–ether oxygen interaction. The metal–ether oxygen interaction is weaker than metal–carboxyl oxygen interaction and this is reflected in the greater bond distance of the former interaction.

Nitriiotriacetate forms lanthanide complexes extensively (Chapter 3) and the structures of many compounds have been determined [165]. The monohydrate praseodymium compound is 9-coordinate in a distorted tricapped trigonal prism or a distorted singly-capped trigonal prism. In the analogous dehydrated complex the metal ion is 8-coordinate with a distorted triangular-faced dodecahedral arrangement of five acetate and two water oxygen atoms and one nitrogen atom bound to the metal. In the trihydrated compound the 9-coordinate arrangement may be described as a distorted singly capped square antiprism [171].

In the monoclinic complex  $[\text{HLa}(\text{H}_2\text{O})_4\text{EDTA}] \cdot 3\text{H}_2\text{O}$  La is 10-coordinate. The complex has been studied and the structure reported [170]. In the complexes of the type  $\text{M}^+[\text{Ln}(\text{EDTA})] \cdot 8\text{H}_2\text{O}$  the lanthanide is 9-coordinate and the ligand is in one hemisphere and the three water molecules in another hemisphere [170].

### 25.1. Carbonyl oxygen donors

This class of complexes is vast and only a few chosen types of complexes deem discussion. Some examples of the complexes are given in Table 4.16.

The counter anion has a decisive effect on the type of complex formed with *N,N,N',N'*-tetramethyl urea (TMU).

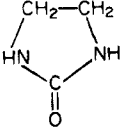
Anion	Complex type	Lanthanides	Reference
$\text{ClO}_4^-$	$\text{Ln}(\text{TMU})_6(\text{ClO}_4)_3$	For all lanthanides	[174]
$\text{Cl}^-$	$\text{Ln}(\text{TMU})_{3,5}\text{Cl}_3$ (dimer?)		[175]
	$\text{Ln}(\text{TMU})_3\text{Cl}_3$		[173]
$\text{NO}_3^-$	$\text{Ln}(\text{TMU})_3(\text{NO}_3)_3$ coord. nitrate		[176]
$\text{NCS}^-$	$\text{Ln}(\text{TMU})_5(\text{NCS})_3$	Ln = La–Nd	
	$\text{Ln}(\text{TMU})_4(\text{NCS})_3$	Ln = Sm–Er	[177]
	$\text{Ln}(\text{TMU})_3(\text{NCS})_3$	Ln = Tm–Lu	

In these complexes anion coordination must be present with the exception of perchlorate. Lanthanide contraction may also be an influencing factor. The molecular structure [189] of  $\text{Eu}(\text{TMU})_3(\text{NO}_3)_3$  shows the presence of bidentate nitrates with a coordination number of nine. The coordination polyhedron is neither the tricapped trigonal prism nor the monocapped square antiprism which may be due to the small bite of nitrate ligand. The dimethyl acetamide (DMA) complexes behave similarly as those of tetramethyl urea (TMU) with less steric requirements as evidenced by the synthesis of [180–182]  $\text{La}(\text{DMA})_8(\text{ClO}_4)_3$ , La = La–Nd;  $\text{La}(\text{DMA})_7(\text{ClO}_4)_3$ , La = Sm–Er;  $\text{La}(\text{DMA})_6(\text{ClO}_4)_3$ , La = Tm–Lu.

The complexes formed with diamides, diacetamide [190], di-*n*-butyramide [191], *N,N*-dimethylacetacetamide [184], tetramethyl malonamide [185] and tetramethyladipamide [192] have been synthesized. The complexes have the general formula  $\text{Ln}(\text{diamide})_4(\text{ClO}_4)_3$ . In the case of adipamide the complexes had the formulation  $\text{Ln}(\text{diamide})_3(\text{ClO}_4)_3$ . All the complexes had uncoordinated perchlorate ion as evidenced by its  $T_d$  symmetry. With other anions as counter ions the number of coordinated diamide ligands decreased.

The complexes formed with cyclopropylene urea (CPU) have the formula [193]  $\text{Ln}(\text{CPU})_8\text{X}_3$ , where  $\text{X} = \text{ClO}_4^-, \text{NO}_3^-$ . Complexes of this composition have been synthesized with all the lanthanides when the anion is perchlorate. When X = nitrate it was possible to synthesize complexes for the early lanthanides (i.e.) La to Gd. In both cases the anions are not coordinated as evidenced by IR spectra. Europium complexes, with  $\text{X} = \text{ClO}_4^-, \text{NO}_3^-, \text{I}^-, \text{PF}_6^-$  have been found to be of the same symmetry around Eu(III) as evidenced by their emission spectra [178].

TABLE 4.16  
Representative complexes with ligands having carbonyl groups.

Compound		Reference
$RCl_3 \cdot 6H_2NCONH_2$	(R = La–Sm, Ho)	[172]
$RCl_3 \cdot 5(1,3\text{-dimethylurea})$	(R = La, Ce, Pr, Nd, Sm, Gd, Ho)	[173]
$R(ClO_4)_3 \cdot 6(\text{tetramethylurea})$	(R = La–Lu, Y)	[174]
$RCl_3 \cdot 3(\text{tetramethylurea})$	(R = La–Lu, Y)	[173]
$R(NO_3)_3 \cdot 3(\text{tetramethylurea})$	(R = La–Lu, Y)	[176]
$R(NCS)_3 \cdot x(\text{tetramethylurea})$	(x = 5, R = La–Nd) (x = 4, R = Sm–Er, Y) (x = 3, R = Tm–Lu)	[177]
$R(ClO_4)_3 \cdot 8(N,N'\text{-ethyleneurea})$		[178]
$RCl_3 \cdot 8(N,N'\text{-ethyleneurea})$	(R = La–Tm)	[173]
$R(NO_3)_3 \cdot x(N,N'\text{-ethyleneurea})$	(x = 8, La, Ce) (x = 6, Ho, Tm)	[173]
$RCl_3 \cdot 3(\text{biuret}) \cdot 3H_2O$	(R = La–Ho)	[173]
$RI_3 \cdot 8DMF$	(R = La–Gd)	[179]
$R(ClO_4)_3 \cdot xDMA$	(x = 8, R = La–Nd) (x = 7, R = Sm–Er, Y) (x = 6, R = Tm–Lu)	[180]
$R(NO_3)_3 \cdot xDMA$	(x = 4, R = La–Pr) (x = 3, R = Sm–Lu, Y)	[181]
$R(NCS)_3 \cdot xDMA$	(x = 5, R = La–Nd) (x = 4, R = Sm–Lu, Y)	[182]
$R(ClO_4)_3 \cdot 8(\gamma\text{-butyrolactam})$		[183]
$R(NO_3)_3 \cdot x(\gamma\text{-butyrolactam})$	(x = 8, R = La–Gd) (x = 3, R = Dy, Er, Yb)	[183]
$R(ClO_4)_3 \cdot x(N\text{-methyl-}\gamma\text{-butyrolactam})$	(x = 8, R = La–Gd) (x = 7, R = Dy, Er, Yb, Y)	[183]
$R(ClO_4)_3 \cdot 4(N,N\text{-dimethylacetoacetamide})$		[184]
$R(ClO_4)_3 \cdot 4TMMA$		[185]
$R(NO_3)_3 \cdot 2TMMA$		[185]
$RCl_3 \cdot 2TMMA$		[186]
$R(NCS)_3 \cdot 4TMMA$	(R = La–Yb, Y)	[186]
$Lu(NCS)_3 \cdot 3TMMA$		[186]
$RX_3 \cdot 6(\text{antipyrene})$	(X = $ClO_4$ , I, NCS, $B(C_6H_5)_4$ )	[187]
$R(NO_3)_3 \cdot 3(\text{antipyrene})$		[188]

### 25.2. 1,3-Diketones as oxygen donors

This class of ligands are very good chelating ligands forming highly stable five-membered rings. Some representative examples are given in Table 4.17.

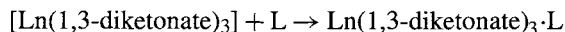
The potential lasing action of rare earth diketonates has been studied [203]. The complexes  $Ln(1,3\text{-diketone})_3$  tend to add on one or more ligands such as water. Dehydration of the hydrated complexes leads to decomposition or formation of polymeric

TABLE 4.17  
Representative complexes with  $\beta$ -diketonates ligands.

Compound		Reference
R(acac) <sub>3</sub> ·xH <sub>2</sub> O	(x = 1 or 3)	[194]
(R(DPM) <sub>3</sub> )	(R = La–Lu, Y, Sc)	[195]
R(fod) <sub>3</sub> ·xH <sub>2</sub> O	(x = 0 or 1)	[196]
	(x = 0 for Sc)	
R(acac) <sub>2</sub> OH		[194]
M[R(hexafluoroacetylacetonato) <sub>4</sub> ]	(R = La–Lu, Y, Sc)	[197]
R( $\beta$ -diketonate) <sub>3</sub> ·xL	(x may be 1 or 2 depending on L and $\beta$ -diketonate;	[197]
	L = triphenylphosphine oxide, <i>o</i> -phen. dipy, terpy, DMSO, etc.)	[197]
	(R = La–Lu, Y)	[199]
R(acac) <sub>3</sub>		[200]
R(DBM) <sub>3</sub>		
R(DBA) <sub>3</sub>		
R(TTA) <sub>3</sub>		
R(pongamal) <sub>3</sub>	pongamal = C <sub>18</sub> H <sub>13</sub> O <sub>4</sub>	[201]
R(curcumin)Cl <sub>2</sub> ·2H <sub>2</sub> O	curcumin = C <sub>21</sub> H <sub>19</sub> O <sub>6</sub>	[202]

hydroxo compounds [194]. With large substituents such as *t*-butyl groups in the diketone it is possible to obtain the anhydrous complex [195].

When the ligand has small substituents, a fourth diketonate may be added [198] to yield M[La(1,3-diketone)<sub>4</sub>], where M is a univalent cation either inorganic or organic. It is also useful to note that the fourth ligand need not necessarily be a diketonate, it may be



and L can be Ph<sub>3</sub>PO, dipyrindyl, terpyridyl, *o*-phenanthroline, pyridine-*N*-oxide. These complexes have been synthesized. Such an addition reaction has the useful application in that Ln(DPM)<sub>3</sub> and Ln(fod)<sub>3</sub> are valuable NMR shift reagents. These  $\beta$ -diketone complexes are useful in many studies since the metal ion is shielded from the environment around the complexes in addition to their solubility in many organic solvents.

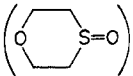
### 25.3. Alcohols as oxygen donors

We have noted the affinity of lanthanides for water and this affinity is extended to alcohols to form alcoholates [180]. Alcoholates are generally unstable. Lanthanide triisopropoxide has been synthesized and characterized [204]. The lanthanide triisopropoxide may be used as a starting material in the preparation of other alkoxides by alcoholysis. Triisopropoxides of lanthanides are reported to be in dimeric and tetrameric forms as evidenced by mass spectrometry.

Compounds of the type Ln[Al(OC<sub>3</sub>H<sub>7</sub>)<sub>4</sub>]<sub>3</sub> have been reported [205]. The compounds are monomeric in benzene and a structure consists of a six-coordinate lanthanide ion in which one half of the isopropoxide ions form bridges of the type Ln–O–Al.



TABLE 4.18  
Representative complexes with ligands of the type N–O.

Complex	Reference
$R(\text{ClO}_4)_3 \cdot 8(\text{pyridine-}N\text{-oxide})$	[206]
$\text{RI}_3 \cdot 8(\text{pyridine-}N\text{-oxide})$	[207]
$R(\text{ClO}_4)_3 \cdot 4(2,2'\text{-dipyridyl-1,1-dioxide})$	[208]
$R(\text{ClO}_4)_3 \cdot 6\text{HMPA}$	(R = La–Lu, Y, Sc) [209]
$\text{RCl}_3 \cdot 3\text{HMPA}$	(R = La–Lu, Y, Sc) [211]
$R(\text{NO}_3)_3 \cdot 3\text{HMPA}$	(R = La, Nd) [212]
$R(\text{NO}_3)_3 \cdot 3.5\text{HMPA}$	(R = Sm, Gd) [212]
$R(\text{NO}_3)_3 \cdot 4\text{HMPA}$	(R = Dy–Yb) [212]
$R(\text{ClO}_4)_3 \cdot 6(\text{trimorpholinophosphine oxide})$	(R = La–Lu, Y, Sc) [213]
$\text{RCl}_3 \cdot 3(\text{trimorpholinophosphine oxide})$	(R = La–Lu, Y, Sc) [214]
$R(\text{NCS})_3 \cdot 4(\text{C}_6\text{H}_5)_3\text{PO}$	(R = La–Sm) [215]
$R(\text{NCS})_3 \cdot 3(\text{C}_6\text{H}_5)_3\text{PO}$	(R = Sm–Lu, Y) [215]
$\text{Sc}(\text{NCS})_3 \cdot 3(\text{C}_6\text{H}_5)_3\text{PO}$	[216]
$R(\text{NCS})_3 \cdot 3(\text{C}_6\text{H}_5)_3\text{AsO}$	(R = Ce, Pr) [215]
$R(\text{ClO}_4)_3 \cdot x\text{DMSO}$	(x = 8, R = La–Nd) [217]
	(x = 7, R = Sm–Ho, Y)
	(x = 6, R = Er–Lu)
$R(\text{ClO}_4)_3 \cdot x(\text{thioxane oxide})$	(x = 9, R = La–Nd) [186]
	(x = 8.5, R = Sm)
	(x = 8, R = Eu–Er)
	(x = 7, R = Tm–Lu, Y)
$R(\text{PF}_6)_3 \cdot 8(\text{thioxane oxide})$	[218]
$R(\text{NCS})_3 \cdot x(\text{thioxane oxide})$	(x = 5, R = La–Tb) [219]
	(x = 4, R = Dy–Lu, Y)

#### 25.4. Polycyclic ethers as oxygen donors

This fascinating family of complexes is discussed at length under the title ‘Macrocyclic complexes’.

#### 25.5. Oxygen donors such as $(\text{C}_6\text{H}_5)_3\text{PO}$ , DMSO, HMPA, pyridine *N*-oxide

This family of adduct compounds is extensive and some examples are given in Table 4.18.

The complexes are similar to complexes cited with carbonyl ligands. The similarities are particularly the anion coordination possibility and the different coordination numbers for complexes with a given ligand depending upon the anion. All the complexes have the group L–O, where L = P, As, N, S and the coordination to the metal is through oxygen, L<sub>n</sub>–O–L where L = N, S, P, As. The evidence for this is based on infrared spectra for most of the complexes and the X-ray diffraction method of determination of some structures.

It appears that careful control of reaction conditions is absolutely necessary in the synthesis of L<sub>n</sub> HMPA complexes [218]. The complex L<sub>n</sub>(HMPA)<sub>6</sub>(ClO<sub>4</sub>)<sub>3</sub> was found to contain ionic perchlorate based on infrared spectra [210]. However the complex L<sub>n</sub>(HMPA)<sub>4</sub>(ClO<sub>4</sub>)<sub>3</sub> had both ionic and coordinated perchlorate [220].

Examination of pyridine-*N*-oxide complexes shows regular behaviour with the largest number of ligands when the counter anion  $X^- = ClO_4^-, I^-, PF_6^-$  [206,207]. Eight ligands are coordinated throughout the lanthanides. In the case of a bidentate ligand, 2,2'-dipyridyl-1,1'-dioxide complexes of the composition  $Ln(dipyO_2)_4(ClO_4)_3$  have been characterized [208].

As discussed earlier, the sulfoxide group is a good donor for hard rare earth ions (section on non-aqueous solvents). Dimethyl sulfoxide forms complexes with different numbers of organic ligands coordinated depending on the anion and the size of the lanthanide ion [221]. We thus have [217]:  $Ln(DMSO)_8(ClO_4)_3$ ,  $Ln = La-Nd$ ;  $Ln(DMSO)_7(ClO_4)_3$ ,  $Ln = Sm-Ho$ ;  $Ln(DMSO)_6(ClO_4)_3$ ,  $Ln = Er-Lu$ .

With iodide the complexes [222] are  $Ln(DMSO)_8I_3$  for  $Ln = La-Er$ . When  $PF_6^-$  is the anion one has  $Ln(DMSO)_7(PF_6^-)_3$  for both heavy and lighter lanthanides. It appears that experimental conditions have to be controlled very carefully in the synthesis of these complexes.

With diphenyl sulfoxide,  $Ln(DPSO)_6(ClO_4)_3$  complexes containing ionic perchlorate and  $Ln(DPSO)_8I_3$  for  $Ln = La-Y$  have been reported [221,222]. The above on repetition yielded  $Ln(DPSO)_7(ClO_4)_3$  for  $Ln = Sm, Eu, Yb$ . This family of complexes lack structural data.

When the ligand L is triphenyl phosphine oxide, complexes of the following types and composition are formed:  $Ln(NO_3)_3L_2 \cdot EtOH$ ,  $Ln(NO_3)_3L_3$ ,  $Ln(NO_3)_3L_3(Me_2CO)_2$ ,  $Ln(NO_3)_3L_4 \cdot Me_2CO$ ,  $Ln(NO_3)_3L_4 \cdot EtOH$ ,  $[Ln(NO_3)_2L_4]NO_3$ ,  $LnCl_3L_3$ ,  $LnCl_3L_4$ ,  $Ln(NCS)_3L_3$ ,  $Ln(NCS)_3L_4$ .

The  $[NdL_4(ClO_4)_2]ClO_4$  complex has both ionic and bound perchlorate [218]. With L=triphenyl arsine oxide the complex types formed are [215]  $Ln(NCS)_3L_3$ ,  $Ln(NO_3)_3L_2 \cdot EtOH$ ,  $Ln(NO_3)_3L_3$ ,  $Ln(NO_3)_3L_4$ . Triphenyl arsine oxide complexes appear to be stronger than the phosphine oxide based on the higher dipole moment of arsine.

Complexes of phosphinamides and substituted phosphinamides with lanthanides have been synthesized, characterized and the complexes with the latter ligand have reduced number of coordinated ligands in keeping with the steric effects generated due to N-substitution [223].

## 26. Nitrogen donors

The impetus for the development of synthesis and characterization of complexes of lanthanides with organic nitrogen donor ligands is due to the search for more efficient luminescent rare earth compounds. One of the difficulties is the risk of precipitating lanthanide hydroxides in the process of synthesis of lanthanide complexes with organic amines. In the early stages, lanthanide complexes of heterocyclic bases of low basicities were prepared in aqueous alcoholic media [224]. In the synthesis section it was appropriately pointed out the need for the anhydrous conditions and involved procedures for the preparation of lanthanide complexes of ligands of non-ionizable nature. Some representative complexes of both aliphatic and aromatic amines are listed in Table 4.19.

TABLE 4.19  
Representative complexes with ligands having nitrogen donor atoms.

Heterocyclic	
$R(o\text{-phen})_2X_3 \cdot (H_2O \text{ or } C_2H_5OH)_n$	(X = Cl, NO <sub>3</sub> , SCN, SeCN; n = 0–5)
$R(o\text{-phen})_3X_3$	(X = SCN, SeCN)
$R(o\text{-phen})_4(CIO_4)_3$	
$R(\text{dipy})_2X_3 \cdot (H_2O \text{ or } C_2H_5OH)_n$	(X = Cl, NO <sub>3</sub> , SCN, SeCN; n = 0–5)
$R(\text{dipy})_3X_3$	(X = SCN, SeCN)
$R(\text{terpy})X_3 \cdot nH_2O$	(X = Cl, Br, NO <sub>3</sub> ; n = 0–3)
$R(\text{terpy})_2X_3$	(X = Cl, Br, CIO <sub>4</sub> )
$R(\text{terpy})_3(CIO_4)_3$	
Aliphatic	
$[R(\text{en})_4(NO_3)](NO_3)_3$	(R = La–Sm)
$[R(\text{en})_4](NO_3)_3$	(R = Eu–Yb)
$[R(\text{en})_3(NO_3)_2][NO_3]$	(R = Gd–Ho)
$[R(\text{en})_4Cl]Cl_2$	(R = La, Nd)
$[R(\text{en})_4]Cl_3$	(R = Sm–Lu)
$[R(\text{en})_3Cl_2]Cl$	(R = Gd, Er)
$[Sc(\text{en})_3]Cl_3$	
$[Sc(\text{en})_2Cl_2]Cl$	
$[R(\text{en})_4Br]Br_2$	(R = La)
$[R(\text{en})_4]Br_3$	(R = Nd, Gd)
$[R(\text{en})_3Br_2]Br$	(R = Gd)
$[Sc(\text{en})_3]Br_3$	
$[Sc(\text{en})_2Br_2]Br$	
$[R(\text{en})_4](CIO_4)_3$	(R = La–Nd)
$[R(\text{dien})_3](NO_3)_3$	(R = La–Gd)
$[R(\text{dien})_2(NO_3)_2](NO_3)$	(R = La–Yb)
$[R(\text{trien})_2](NO_3)_3$	(R = Pr–Eu)
$[R(\text{trien})_2](CIO_4)_3$	(R = La–Ho)

## 27. Unidentate ammonia and amines

Compounds of the formula  $LnCl_3 \cdot xNH_3$ , where  $x = 1-8$  have been prepared by the reaction of the components. These compounds are labile. Variable stoichiometry depends upon the reaction conditions and the lanthanide involved.

Another ammonia bearing compound  $Ln[OC(CF_3)_3](NH_3)_3$  has been prepared by the reaction of  $LnCl_3$  in ether with  $HOC(CF_3)_3$  at  $-80^\circ C$ , followed by bubbling anhydrous gaseous ammonia through the solution at room temperature [226].

Reaction of methylamine with anhydrous lanthanide chlorides yielded compounds of the formula [227]  $LnCl_3 \cdot xCH_3NH_2$ , where  $x = 1$  to 5.

Benzidine forms a complex of the formula  $LnCl_3H_2NC_6H_4C_6H_4NH_2 \cdot 2THF$  when benzidine in tetrahydrofuran (THF) is reacted with  $LaCl_3$  in absolute ethanol. The coordination number of six has been assigned, on the basis of conductance data. Coordination through  $-NH_2$  group is indicated by the shifts in frequencies of  $-NH_2$  bending mode and C–N stretching mode [228]: Eu(III) dibenzoyl methide forms 1:1 and 2:1 adducts with *N*-butylamine, aniline, piperidine, pyridine and quinoline. Aniline forms 1:1 adduct  $Eu(DBM)_3 \cdot \text{aniline}$  while other amines form  $Eu(DBM)_3 \cdot 2L$ . The absence of IR

band at  $1700\text{ cm}^{-1}$  indicated [229] Ln–O bonding with DBM and a coordination number greater than six for Eu(III).

Lanthanide nitrates and perchlorates form complexes with substituted pyridines in acetonitrile with net enthalpies of less than  $-3\text{ kcal/mol}$  for 1:1 adducts of Pr(III) and Nd(III) perchlorates and nitrates. When L:M ratio is greater than six 3:1 adducts were formed [230]. Adducts like  $\text{LnCl}_3 \cdot x\text{CH}_3\text{CN}$  with  $x = 1-3$  have been synthesized and characterized by X-ray diffraction and infrared spectroscopy [231].

## 28. Bidentate donor ligands

Bidentate nitrogen donor ligands confer more stability due to the formation of chelate rings with the metal ion. The ligands belonging to this category and forming complexes are: (i) phenylhydrazine,  $\text{C}_6\text{H}_5\text{NHNH}_2$ , (ii) 2,7-dimethyl-1,8-naphthyridine (2,7-dmnapy), (iii) ethylenediamine (en), (iv) propylenediamine (pn), (v) 2,2'-bipyridyl (Bipy), (vi) 1,10-phenanthroline (phen). Phenyl hydrazine forms complexes of the type [232]  $\text{Ln}(\text{C}_6\text{H}_5\text{NHNH}_2)_2(\text{H}_2\text{O})\text{Cl}_3$ . The NH stretching,  $\text{NH}_2$  bending and N–N stretching modes shifted to lower frequencies upon complexation. The observed frequencies are NH stretching  $3110-3190\text{ cm}^{-1}$ ;  $\text{NH}_2$  bending  $1570-1588\text{ cm}^{-1}$ ; N–N stretching  $887-895\text{ cm}^{-1}$ . A coordination number of 8 is appropriate.

Complexes with 2,7-dimethyl-1,8-naphthyridine of the formula [233]  $\text{Ln}(2,7\text{-dmnapy})_2(\text{NO}_3)_3$  have been identified containing coordinated nitrate groups  $\text{C}_{2v}$  symmetry. A coordination number ten for these complexes seems plausible. The IR data for ionic and coordinated nitrate groups are given below.

Infrared absorptions characteristic of  $\text{D}_{3h}$  and  $\text{C}_{2v}$  nitrate groups.

Type	$\text{NO}_3^-$	$\text{cm}^{-1}$	Assignment
$\text{D}_{3h}$ -ionic			
$\text{A}_2^{\text{II}} \dots$	$\nu_2$	831	NO, deformation
$\text{E}^{\text{I}} \dots$	$\nu_3$	1390	NO, asymmetric stretching
$\text{E}^{\text{I}} \dots$	$\nu_4$	720	Planar rocking
$\text{C}_{2v}$ -coordinated			
$\text{A}_1 \dots$	$\nu_2$	1034–970	N–O stretching
$\text{B}_2 \dots$	$\nu_6$	800–781	Non-planar rocking
$\text{B}_1 \dots$	$\nu_4$	1531–1481	Asymmetric stretching
$\text{A}_1 \dots$	$\nu_1$	1290–1253	$\text{NO}_2$ symmetric stretching
$\text{A} \dots$	$\nu_3$	740	$\text{NO}_2$ bending
$\text{B}_1 \dots$	$\nu_5$	713	Planar rocking

With ethylenediamine complexes of the formula  $\text{Ln}(\text{en})_3\text{X}_3$  and  $\text{Ln}(\text{en})_4\text{X}_3$ , where  $\text{X} = \text{Cl}^-$ ,  $\text{Br}^-$ ,  $\text{NO}_3^-$ ,  $\text{ClO}_4^-$  have been characterized. IR data indicate that the tris and tetrakis complexes of the lighter lanthanides La–Sm, contain both ionic and coordinated nitrate groups. By contrast tetrakis complexes of heavier lanthanides, Eu–Yb contain ionic nitrate. This is possibly due to steric factors resulting from decreasing cationic radius that force the nitrate out of the coordination sphere of the lanthanides. A coordination number of 8 for tris complexes and a number of 9 for lighter lanthanide tetrakis complexes appears reasonable [234]. The thermodynamic parameters obtained show enthalpy stabilization for

these complexes in sharp contrast to more common entropy stabilization. Large stepwise enthalpy changes are indicative of an absence of strong  $\text{Ln}^{3+}$ -acetonitrile interaction making acetonitrile a useful medium for the studies of complexes.

The complexation with 1,2-propanediamine gives rise to both tris and tetrakis complexes with both coordinated and ionic nitrate groups. In the case of heavier lanthanides only ionic nitrate is indicated. A coordination number of 8 or 9 for the nitrate-containing species has been suggested [235].

Bipyridyl complexes [236] of the formula  $\text{Ln}(\text{bipy})_2\text{Cl}_3 \cdot n\text{H}_2\text{O}$  for  $\text{Ln} = \text{La-Ho}$  and  $\text{Ln}(\text{bipy})\text{Cl}_3 \cdot n\text{H}_2\text{O}$  for  $\text{Ln} = \text{Er-Lu}$  have been characterized. Other complexes include  $\text{Ln}(\text{bipy})_2\text{Cl}_3 \cdot \text{C}_2\text{H}_5\text{OH}$  ( $\text{Ln} = \text{Sm, Tb}$ ),  $\text{Ln}(\text{bipy})_2\text{Cl}_3$  ( $\text{Ln} = \text{Eu-Lu}$ ). The IR spectra of all these complexes show the displacement of the molecular ligand band at  $990 \text{ cm}^{-1}$  to higher frequencies indicating the Ln-N bonding.

The nitrate complexes  $\text{Tb}(\text{NO}_3)_3(\text{bipy})_2$ ,  $\text{Ln}(\text{bipy})_2(\text{NO}_3)_3 \cdot \text{H}_2\text{O}$  ( $\text{Ln} = \text{Dy, Ho}$ ) have been synthesized and characterized. The anhydrous complexes have coordinated nitrate groups suggesting a coordination number of ten for  $\text{Ln}(\text{bipy})_2(\text{NO}_3)_3$ . The molecular geometry is that of a bicapped triangularly faced dodecahedron [237] of  $D_2$  symmetry with Ln-O bond length of  $2.605 \text{ \AA}$  and two Ln-N bond lengths of  $2.665$  and  $2.648 \text{ \AA}$ .

Mixed complexes of the type  $\text{Ln}(\text{bipy})_2(\text{NCS})_3$  have been isolated containing both coordinated and uncoordinated groups. Because of the overlap of the bipyridine and thiocyanate band, unequivocal assignment is not possible [238]. Analogous selenocyanate complexes  $\text{Ln}(\text{bipy})_3(\text{NCSe})_3$  with N-bonded selenocyanate and a coordination number of 9 have been reported.

Lanthanide complexes of 1,10-phenanthroline (phen) have been obtained as chlorides, nitrates, sulfates, perchlorates acetates, thiocyanates and selenocyanates from various solvents.

Complexes of the type  $\text{Ln}(\text{phen})_3\text{Cl}_3$  and  $\text{Ln}(\text{phen})_3\text{Cl}_3 \cdot \text{H}_2\text{O}$  with bidentate phenanthroline and lighter lanthanides forming the hydrated complex have been reported [240]. With nitrate complexes of the type  $\text{Ln}(\text{phen})_2(\text{NO}_3)_3$  containing  $\text{C}_{2v}$ , coordinated nitrate groups amounting to a coordination number 10 have been reported [238].

Both tris and tetrakis phenanthroline perchlorates,  $\text{Ln}(\text{phen})_3(\text{ClO}_4)_3$  and  $\text{Ln}(\text{phen})_4(\text{ClO}_4)_3$  are known. Coordinated perchlorate of  $\text{C}_{3v}$  symmetry has been detected. This is true of only lighter lanthanides and only ionic perchlorate being detected in the heavier lanthanide complexes [241]. The complexes of the type [239]  $\text{Ln}(\text{phen})_3(\text{NCS})_3$  show no evidence for Ln-NCS bonding while the corresponding  $\text{Ln}(\text{phen})_3(\text{NCSe})_3$  shows the Ln-NCSe bonding with a coordination number of 9.

## 29. Multidentate ligands

Terpyridyl is a terdentate ligand and behaves like bipyridyl, and *o*-phenanthroline. The three terpyridyl ligands coordinate to the lanthanide when the anion is perchlorate. The emission spectrum of the Eu(III) complex points to  $D_3$  symmetry which has been confirmed by the determination of the structure [242].

The ligand bis(2'-quinolyl)-2,6-pyridine is similar to terpyridyl and complexes formed with this ligand are different from those of terpyridyl in that only one ligand molecule is

coordinated even with perchlorate as the anion. The complex is solvated by three molecules of water [243]. The molar conductivities suggest that the thiocyanate and nitrate complexes are non-electrolytes and the perchlorate complexes 3:1 electrolytes which is in agreement with the IR spectra.

The synthesis of lanthanide complexes [244] with multidentate diethylenetriamine (dien) gave rise to two types of complexes,  $\text{Ln}(\text{dien})_3(\text{NO}_3)_3$  for  $\text{Ln} = \text{La} - \text{Gd}$ , and  $\text{Ln}(\text{dien})_2(\text{NO}_3)_3$  for  $\text{Ln} = \text{La} - \text{Yb}$ . The tris complexes contain ionic nitrate while the bis complexes contain both ionic and coordinated nitrate ions. The coordination number is nine in the tris complexes while it is not known with certainty in the bis complexes. With triethylene triamine (tren) two types of complexes [ $\text{Ln}(\text{tren})(\text{NO}_3)_3$ ] and  $\text{Ln}(\text{tren})_2(\text{NO}_3)_3$  have been isolated. In the bis complexes both ionic and coordinated nitrate groups are present for larger lanthanides (La–Nd) but only ionic nitrate for smaller lanthanides (Sm–Yb). When perchlorate is the anion [245]  $\text{Ln}(\text{tren})(\text{ClO}_4)_3$  ( $\text{Ln} = \text{Pr}, \text{Gd}, \text{Er}$ ) and  $\text{Ln}(\text{tren})_2(\text{ClO}_4)_3$  for  $\text{Ln} = \text{La}, \text{Pr}, \text{Nd}, \text{Gd}, \text{Er}$  complexes were obtained. The monocomplexes contain coordinated perchlorate ions while the bis complexes contain ionic perchlorate ions.

The ligand 1,2-bis(pyridine- $\alpha$ -aldimino)ethane has four nitrogen atoms for coordination and forms 1:1 solid complexes with lanthanide [246] chlorides, nitrates, thiocyanates or salicylates. Infrared spectra show evidence for nitrate coordination and pyridyl coordination. Attempts to isolate bis complexes were futile although there is spectral evidence for their existence in solution.

The synthesis and isolation of porphyrin, phthalocyanine complexes have been discussed briefly in the synthesis section [82–87].

### 30. Nitrogen–oxygen donors

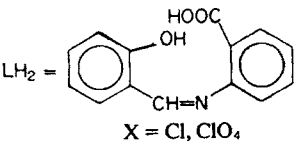
Aminopolycarboxylic acids are typical of oxygen–nitrogen donor ligands and while the solution chemistry of lanthanide interactions with this ligand is extensive, solid state characterization is sparse. Some representative complexes with this class of ligands are given in Table 4.20. Heterocyclic nitrogen-bearing ligands are typified by 8-hydroxyquinoline and dipicolinic acid (dpc).

Schiff bases related compounds form the third group containing both nitrogen and oxygen donors. Complexes of Schiff base derived ligand will be discussed at length under the section ‘Macrocyclic complexes’.

Preparation and characterization of lanthanide complexes of aminopolycarboxylic acids in the solid state has been difficult along with some conflicting results. These complexes are hydrated and it has been difficult to distinguish between coordinated water and lattice water. The structures of  $\text{H}[\text{La}(\text{EDTA})(\text{H}_2\text{O})_4] \cdot 3\text{H}_2\text{O}$  have been determined and lanthanum is ten coordinate in the complex [252]. The thermogravimetric and differential thermal analysis of lanthanide complexes of EDTA shows different patterns of decomposition of monohydrate and multihydrate complexes. The different thermal behaviour is probably due to the structural differences in the mode of bonding of EDTA to the metal. These complexes are polymeric in nature with carboxyl bridging groups [253].

The difficulties in the synthesis of iminodiacetic acid complex serve as typical of this family of complexes. Mixing  $\text{NdCl}_3$  solution with  $\text{Nd}_2(\text{IMDA})_3$  solution yielded

TABLE 4.20  
Representative complexes with ligands having nitrogen and oxygen donor atoms.

Aminopolycarboxylic acids		[165]
R(IMDA)Cl·xH <sub>2</sub> O	(R = La–Lu, Y, Sc)	
R <sub>2</sub> (IMDA) <sub>3</sub> ·H <sub>2</sub> O	(R = La–Lu, Y, Sc)	
K[R(IMDA) <sub>2</sub> ·xH <sub>2</sub> O]	(R = La–Lu, Y, Sc)	
M <sub>3</sub> [R(IMDA) <sub>3</sub> ]·xH <sub>2</sub> O	(R = La–Lu, Y, Sc)	
R(NTA)·xH <sub>2</sub> O	(R = La–Lu, Y, Sc)	
K <sub>3</sub> R(NTA) <sub>2</sub> ·xH <sub>2</sub> O	(R = La–Lu, Y, Sc)	
HR(EDTA)·xH <sub>2</sub> O	(R = La–Lu, Y, Sc)	
MR(EDTA)·xH <sub>2</sub> O	(R = La–Lu, Y, Sc)	
Heterocyclic nitrogen–oxygen		
Na <sub>3</sub> [R(PDC) <sub>3</sub> ]·xH <sub>2</sub> O		[247]
R(8-hydroxyquinolate) <sub>3</sub>		[248]
Schiff bases		
R <sub>2</sub> (salen) <sub>3</sub> ·(C <sub>2</sub> H <sub>5</sub> OH or H <sub>2</sub> O) <sub>n</sub>		[249]
[R(LH) <sub>2</sub> (H <sub>2</sub> O)]X		[250]
		
R(N-alkylsalicylidineiminato) <sub>3</sub> ·xH <sub>2</sub> O		[251]

Nd<sub>2</sub>(IMDA)<sub>3</sub>·2HCl·7H<sub>2</sub>O containing >NH<sub>2</sub><sup>+</sup> group. The same components at pH > 4.5 gave Nd(IMDA)Cl·3H<sub>2</sub>O which had the geometry of a distorted tricapped trigonal prism, with IMDA as tridentate chelate.

Pyridine-2,6-dicarboxylic acid (PDC) forms a complex Na<sub>3</sub>[Ce(C<sub>7</sub>H<sub>3</sub>NO<sub>4</sub>)<sub>3</sub>]·15H<sub>2</sub>O in the form of triclinic crystals. Other complexes of the type Ln(DPC)(DPCH)·6H<sub>2</sub>O for Ln = La–Tb and Ln(DPCH)<sub>3</sub>·3H<sub>2</sub>O for Ln = Sm–Yb have been characterized. The complexes in each series are isostructural as evidenced by IR and X-ray data. The formula Ln(DCPH)<sub>3</sub>H<sub>2</sub>O is supported by the lack of change in C=O vibrational frequency upon dehydration of the complex. The complex is nine-coordinate. Presence of bridging carboxylate groups in Ln(DPC)(DPCH)·6H<sub>2</sub>O is speculated [254].

The complexation with Schiff bases is ambiguous. Lanthanides form complexes with *t*-butylsalicylideneimine (Sal) of the formula La(Sal)<sub>2</sub>·3H<sub>2</sub>O with the loss of phenolic proton and the ligand in the anionic form is bonded to the lanthanide [251]. In contrast, complexes of the type [Y(SalH)<sub>3</sub>Cl<sub>2</sub>]Cl containing neutral ligand have been reported based on elemental analysis and conductivity data [255].

Complexes of lanthanide nitrates with Schiff derivatives of acetylacetone, 2,4-pentanedioneanil, and 2,4-pentanedionebenzylamine of the formula [Ln(L–LH)<sub>3</sub>(NO<sub>3</sub>)](NO<sub>3</sub>)<sub>2</sub>, where Ln = lighter lanthanides and [Ln(L–LH)<sub>2</sub>(NO<sub>3</sub>)](NO<sub>3</sub>)<sub>2</sub>, where Ln = Yb have been isolated from acetone and characterized [256]. In these complexes the ligand does not lose a proton and is in neutral form. In the case of the ligand bisalicylaldehydeethylenediamine, lanthanide complexes are formed with the loss of a phenolic proton [249].

The complexes formed between lanthanide isopropoxides and 2-hydroxy-1-naphthylidene-*n*-butylamine and 2-hydroxy-1-naphthylideneaniline in benzene show the formation of different products with different molar ratios of the reactants. In these complexes the ligand is coordinated in the anionic form to the lanthanide [275]. It has been pointed out earlier in the synthesis section that it is necessary to synthesize these complexes in anhydrous media because of the weaker donor capacity of the ligands.

### 31. Other donor atoms

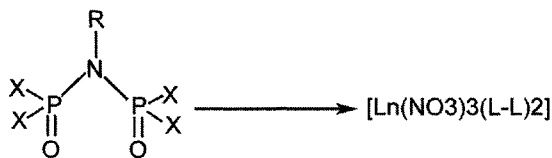
Apart from oxygen and nitrogen as donor ligands there exist a very small number of complexes with other donors. Although the interaction is weak between lanthanides and sulfur, some complexes have been isolated and characterized. Thiourea reacts with lanthanide [257] acetates to give  $\text{Ln}(\text{Ac})_3(\text{tu}) \cdot n\text{H}_2\text{O}$  with  $n = 2$  for  $\text{Ln} = \text{La}, \text{Ce}$ ;  $n = 1$  for  $\text{Ln} = \text{Pr}, \text{Nd}$ ;  $n = 0.5$  for  $\text{Ln} = \text{Sm}$ ;  $n = 2$  for  $\text{La}, \text{Ce}, \text{Pr}$ ;  $n = 1$  for  $\text{Ln} = \text{Nd}-\text{Dy}$ . The splitting of  $\text{NH}_2$  band at  $1617 \text{ cm}^{-1}$  has been observed as evidence for  $\text{Ln}-\text{S}$  bond formation. Propionate complexes of the composition  $\text{Ln}(\text{tu})_3(\text{C}_3\text{H}_5\text{O}_2)_3 \cdot 3\text{H}_2\text{O}$ ;  $\text{Ln} = \text{Nd}, \text{Sm}, \text{Gd}$  have been reported [258]. Complexes of lanthanides with substituted thioureas like naphthyl-, diphenyl-, di-isopropyl-, allyl- and *o*-tolyl-thiourea have been characterized with  $\text{Ln}-\text{S}$  interaction [259].

The reaction of lanthanide monochloroacetates with *R*-substituted tetrazoline-5 thione ( $\text{R} = \text{C}_6\text{H}_5, \text{OCH}_3, \text{Cl}, \text{o}-\text{C}_6\text{H}_4 \cdot \text{CH}_3$ ) resulted in complexes of the formula  $\text{Ln}(\text{tzt})_3$  for  $\text{Ln} = \text{La}-\text{Sm}$  with infrared data suggestive of the bidentate nature of the ligand and the compounds are polymeric in nature [260].

Treatment of anhydrous lanthanide(III) bromides with the sodium salt of *N,N*-diethyldithiocarbamate (dtc) in absolute ethanol yielded  $\text{Ln}(\text{dtc})_3$  for  $\text{Ln} = \text{La}-\text{Lu}-\text{Pm}$ . Reaction of  $\text{Ln}(\text{dtc})_3$  with *N,N*-diethyldithiocarbamate and tetraethyl ammonium bromide in ethanol yielded  $[(\text{C}_2\text{H}_5)_4\text{N}][\text{Ln}(\text{dtc})_4]$ . All the tetrakis complexes are isostructural while two series of isostructural tris complexes exist, one for  $\text{Ln} = \text{La}-\text{Nd}$  and the other for  $\text{Ln} = \text{Sm}-\text{Lu}$ . The tris complexes are probably 6-coordinate, and the tetrakis complexes 8-coordinate [261,262].

There is an isolated example in which phosphine selenides and tellurides transfer selenium or tellurium to unsaturated lanthanide complexes to form bridging dimers [263].

Diphosphazane dioxide complexes of lanthanides have potential application in the solvent extraction separation of lanthanides. Reaction of lanthanide nitrate with  $\text{X}_2\text{P}(\text{O})\text{NPr}^i-\text{P}(\text{O})\text{X}_2(\text{L}-\text{L})$  yields the bis chelate complexes  $\text{Ln}(\text{NO}_3)(\text{L}-\text{L})_2$ . The structure of the praseodymium complex has been determined by X-ray diffraction and the space group is  $\text{P}_{32}$ . There are two independent molecules in the unit cell which differ in orientation of the phenyl group. The metal ion is ten-coordinated [264].

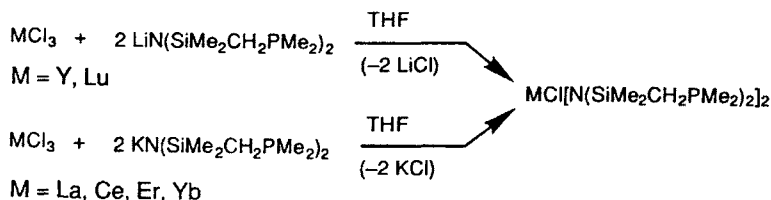


$\text{R} = \text{CH}_3, \text{X} = \text{OPh}$

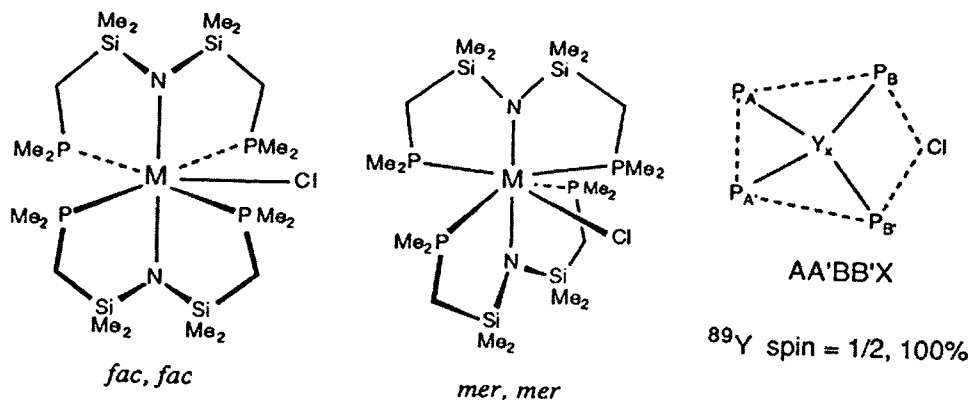
$\text{R} = \text{CHME}_2, \text{X} = \text{Ph}$



Authentic phosphine complexes of lanthanides have been synthesized by the scheme



These complexes are seven-coordinate and geometries based on pentagonal bipyramid satisfy the low temperature NMR data and the scheme is shown below [265].



Decaborate complexes of Yb(II), Eu(II) and Sm(II) of the formula  $[\text{CH}_3\text{CN}]_6\text{Yb}(\text{B}_{10}\text{H}_{14})$  have been synthesized [266] by the reduction of  $\text{B}_{10}\text{H}_{14}$  by lanthanides in liquid ammonia. The product is extracted with  $\text{CH}_3\text{CN}$ . The boron cage is bound to lanthanide through  $\text{Ln-H-B}$  bonds. The synthetic scheme is shown below. The Yb complex has been shown to be 8-coordinate in the solid state and its molecular structure has been determined.

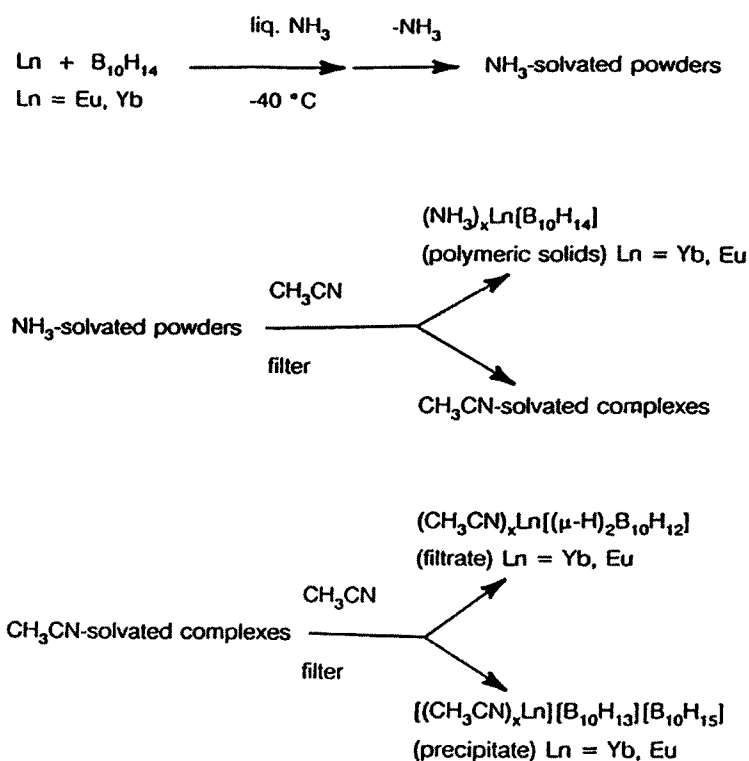
Carborane complexes of lanthanides have been discussed at length in the literature [267, 268].

Metal fullerene complexes containing lanthanides such as Gd have been synthesized and their use as a contrast agent in MRI has been explored [269,270]. The polyhydroxylated Gd- $\text{C}_{82}$  complex showed twenty times better signal enhancement for water protons compared with Magnevist. But these reagents distribute into the bones of rats instead of being excreted which is a disadvantage in clinical applications. To overcome this disadvantage, the complex  $\text{Gd-C}_{60}[\text{C}(\text{COONa})_2]_{10}$  has been synthesized and tested. This complex is excreted in rats and shows promise as a contrast agent.

## Part B

### 32. Macrocyclic complexes: historical outlook

Cyclic molecules and macrocycles have always fascinated chemists and since the recognition of the benzene ring structure by August Kekulé von Stradonitz, organic chemists have devoted a great deal of effort analysing natural macrocycles and synthesizing new ones. However, and curiously, the use of macrocycles for the complexation of metal ions is a relatively new field despite the fact that the basic principles of metal-ion coordination chemistry have been laid out at the beginning of the 20<sup>th</sup> century by Alfred Werner (Nobel laureate in 1913). A starting point of host–guest (macrocycle–metal ion) chemistry is the isolation of nonactin in 1955, a natural antibiotic produced by various



Scheme 4.1. Synthesis and separation of products from Ln/B<sub>10</sub>H<sub>14</sub> reaction in liquid ammonia.

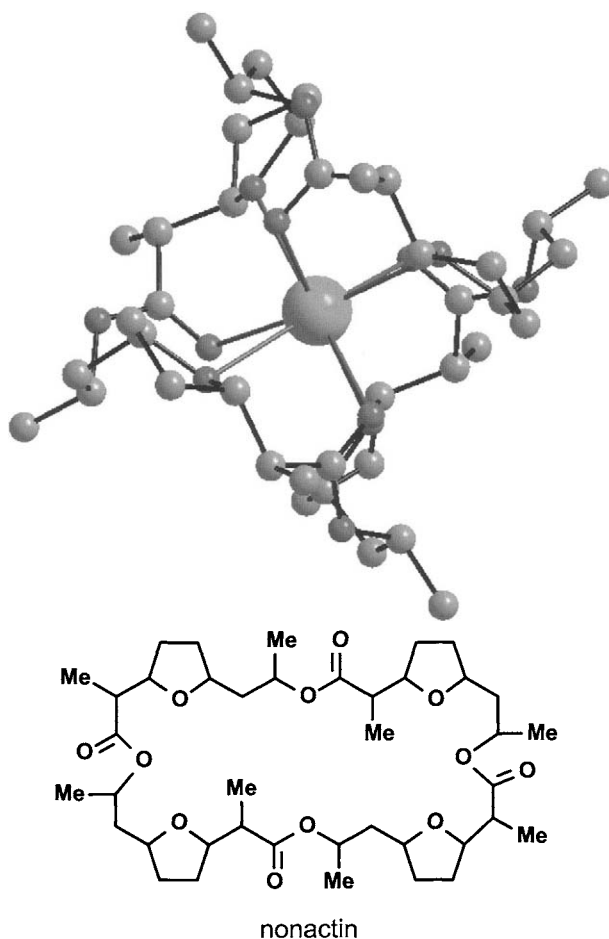


Fig. 4.5. Structure of the potassium complex with nonactin (redrawn from B.T. Kilbourn et al., *J. Molec. Biol.* **30**, 559, 1967).

strains of *actinomyces*. Nonactin is a cyclic molecule with a 32-membered ring containing 24 carbon and 8 oxygen atoms; however, no one speculated at the time that this cyclic molecule could be a suitable receptor for cations. Naturally occurring ionophores (i.e. substances having the ability to transfer ions from an aqueous medium into a hydrophobic phase) were discovered at the beginning of the 1960's and were found to be essential components of the transport of alkali ions through biological membranes. In 1967, the crystal structure of the nonactin potassium complex was published (Fig. 4.5) and revealed an eight coordinated cation by four ether atoms from tetrahydrofuran rings and four oxygen atoms from ester groups, these eight donor atoms forming a nearly perfect cube. The complex is globular, with a polar cavity inside and hydrophobic groups outside, which makes it lipid soluble and provides an elegant method to achieve lipid solubility for cations.

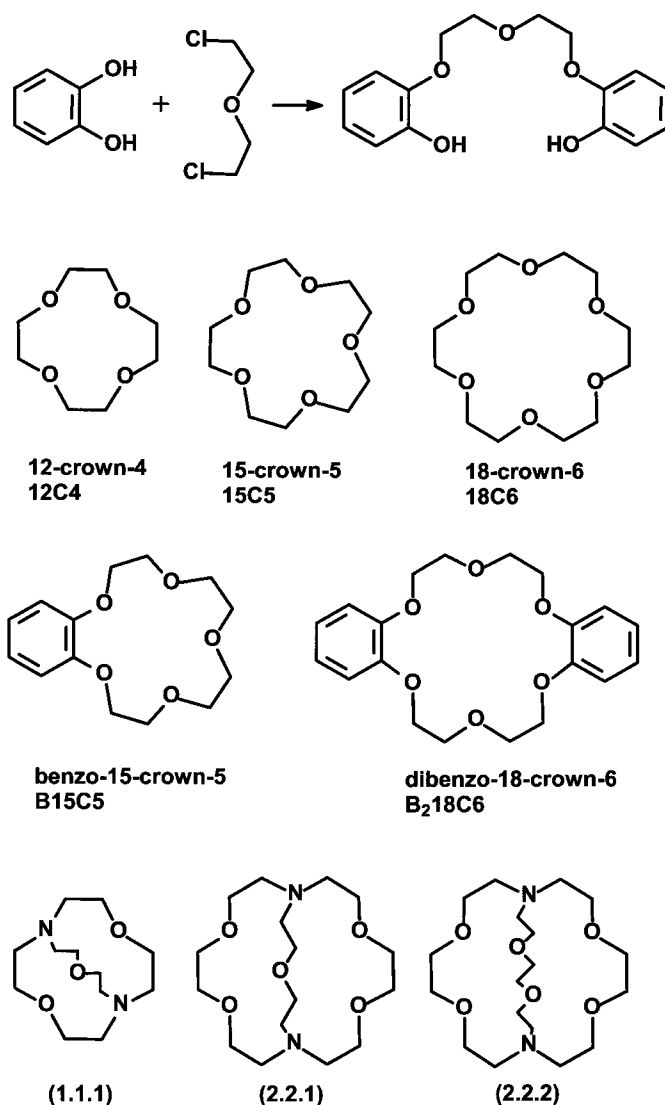


Fig. 4.6. (Top) Reaction that eventually led to the serendipitous synthesis of dibenzo-18-crown-6 ether. (Middle) common crown ethers with their usual denomination. (Bottom) some cryptands with their denomination.

The positive charge of the potassium ions is so effectively screened from the outside that the anions do not interact with it and simply lie in empty spaces left between complex cations.

The same year, Charles J. Pedersen (who shared in 1987 the Nobel prize in chemistry with J.-M. Lehn and D.J. Cram) published his first communication on crown ethers, which are cyclic molecules obtained by repeating a  $-\text{CH}_2-\text{CH}_2-\text{O}-$  motif (Fig. 4.6) and their complexes with metal salts. He described the formation of stable complexes between

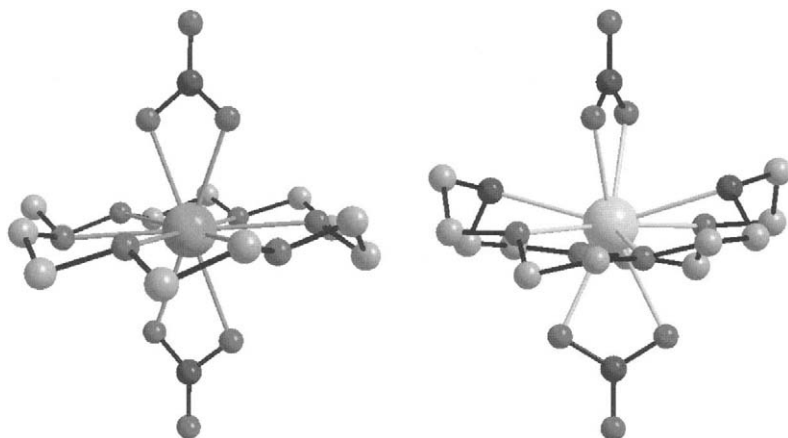


Fig. 4.7. (Left) Structure of the complex cation  $[\text{Nd}(\text{NO}_3)_2(18\text{C}6)]^+$  with  $C_{2h}$  symmetry found in  $[\text{Nd}(\text{NO}_3)_2(18\text{C}6)_3][\text{Nd}(\text{NO}_3)_6]$ ; redrawn from J.-C.G. Bünzli et al., *Inorg. Chim. Acta* **54**, L43, 1981. (Right) Structure of the complex cation  $[\text{Eu}(\text{NO}_3)_2\text{Me}_2(2.2)]^+$ ; redrawn from J.-C.G. Bünzli et al., *Helv. Chim. Acta* **69**, 288, 1986.

dibenzo-18-crown-6 ( $B_218C6$ ) and dicyclohexyl-18-crown-6 ( $Cy_218C6$ ) and salts of La(III) and Ce(III), henceforth giving the start of a new subject in lanthanide coordination chemistry. Pedersen was a chemist working in the Elastomer Chemicals Department of the Dupont Chemical Company's research facility in Wilmington, Delaware and, as a matter of fact, he was interested in preparing non-cyclic phenolic derivatives for the complexation of divalent cations. As he proceeded to synthesize a bis(phenol) derivative, he obtained a mixture from which a tiny quantity of white silky crystals separated. Analysis of these crystals showed them to be dibenzo-18-crown-6. A preliminary structure of the 1:1 complex between  $\text{La}(\text{NO}_3)_3$  and  $B_218C6$  was published in 1976 and revealed a 12-coordinate La(III) ion bound to the six oxygen atoms from the macrocycle and to three bidentate nitrate ions. These initial studies on crown ether complexes with lanthanide ions were followed by numerous ones and it soon appeared that subtle differences in the ligand flexibility and in crystallisation conditions could yield different species. In particular, a commonly observed entity turned out to be the  $\text{LnX}_2^+$  cation inserted into various crown ether cavities (with  $X = \text{NO}_3^-$ ,  $\text{Cl}^-$  or  $\text{ClO}_4^-$ ); the left part of Fig. 4.7 shows the structure of the  $[\text{Nd}(\text{NO}_3)_2(18\text{C}6)]^+$  cation in which the metal ion lies on an inversion centre.

Simultaneous with this activity at Dupont, Jean-Marie Lehn, who had just returned from postdoctoral studies with Professor Woodward at Harvard University, started to develop considerations on the host topology needed to recognize a given molecular (or cationic) species. He realized that adding a third donor group strand would allow a complete encapsulation of the guest species and that modulating the size of the donor strands would lead to specific recognition of a given cation. The corresponding receptors were obtained by replacing two ether functions of the crown ethers by two nitrogen bridges connected by a third  $-\text{CH}_2(-\text{CH}_2-\text{O}-\text{CH}_2)_n-\text{CH}_2-$  chain (Fig. 4.6). The first results were published in 1969 and the new hosts were named cryptands. They better shield the metal ion from

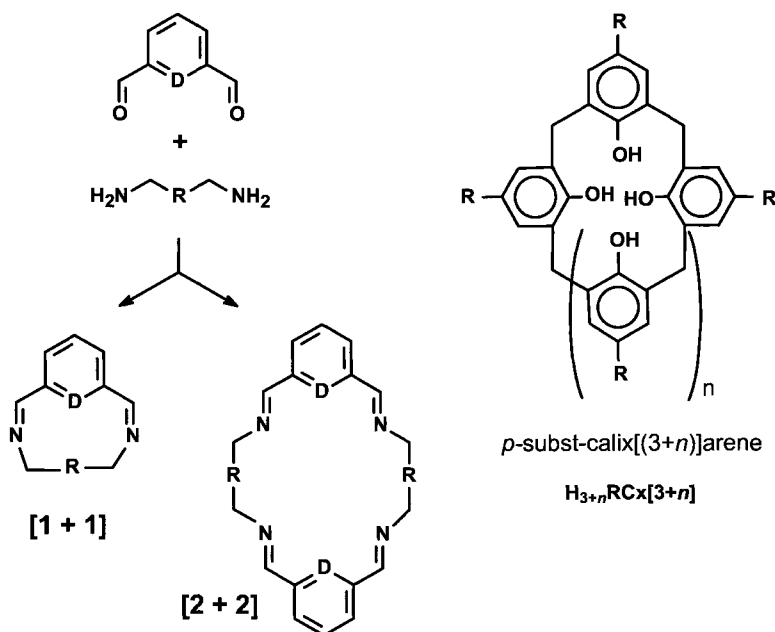


Fig. 4.8. Common cyclic [1 + 1] and [2 + 2] Schiff bases and calixarenes.

outside interactions in comparison with crown ether complexes which remain amenable to equatorial interactions above and under the mean plane of the macrocycle. Three years later, the first complex of lanthanum nitrate with a tetraaza-hexaoxa-macrotricyclic cryptand was isolated, while a more systematic study with the classic (2.2.1) and (2.2.2) cryptands appeared in 1977.

Other classes of macrocyclic compounds with biological relevance are the porphyrins and the phthalocyanines which were systematically studied at the beginning of the 1970's, after the initial work by I.S. Kirin on phthalocyanine complexes  $\text{LnPc}_2$  published in 1965. At that time, nuclear magnetic resonance spectroscopy was emerging as a powerful analytical tool. However, the large number of protons in heme complexes was prohibiting a complete assignment in view of the relatively low-field instruments available, so that researchers were looking for tools able to spread the resonances. Lanthanide-based shift reagents proved to be ideal for this task and it is the main reason why 1:1 lanthanide complexes with phthalocyanines and porphyrins were isolated and characterized in 1973 and 1974, respectively.

Again at the beginning of the 1970's, other classes of synthetic macrocycles were being investigated, not necessarily in connection with biological problems. For instance, the rich chemistry of Schiff base derivatives (Fig. 4.8) was being developed and yielded the first macrocyclic complexes in 1979 (Fig. 4.9). Another type of interesting macrocyclic molecules are the calixarenes (Fig. 4.8) the history of which can be traced back to the first experiments, in Berlin in 1872, of Adolf von Baeyer (Nobel prize in chemistry in 1905) who treated *p*-substituted phenols with formaldehyde in the presence of acid or base.

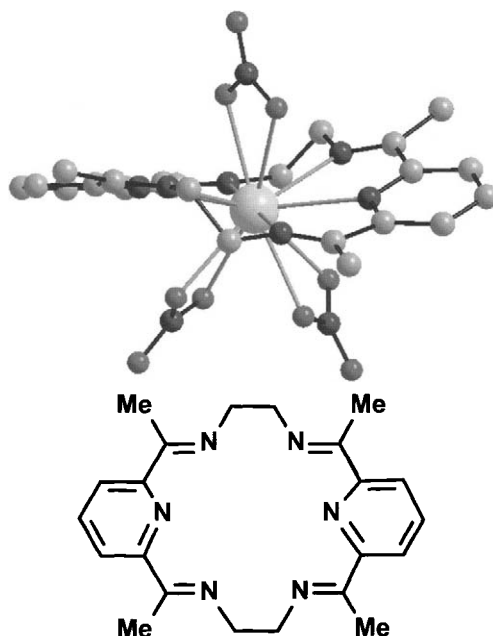


Fig. 4.9. Structure of the neutral complex  $[La(NO_3)_3L]$  redrawn from J.D.J. Backer-Dirks et al., *J. Chem. Soc. Chem. Commun.* 774, 1979.

He only obtained ill-defined tar-like compounds, which were eventually exploited by Leo Henrik Baekeland, a bright Belgian scientist who earned a PhD degree from the University of Ghent at 21 and who immigrated to the United States; in 1907, Baekeland filed for a patent describing the first modern synthetic plastic material, Bakelite. Since phenol reacts at both the *ortho* and *para* positions to yield highly cross-linked polymers, Alois Zincke and Erich Ziegler from the University of Graz in Austria decided to simplify the problem by substituting the phenol in its *para* position with a *t*-butyl group. They postulated a cyclic tetrameric structure for the compound isolated in 1944, but a definitive proof was given in 1950 only. It turned out that an entire new class of cyclic compounds could be obtained by a one-pot synthesis and they were named “calixarenes” by C.D. Gutsche in 1970 because the cyclic tetramer adopts a cone conformation reminiscent of the shape of a Greek crater (calix). The first lanthanide complexes (with *p-t*-butylcalix[8]arene) were characterized in 1987.

In conclusion, macrocyclic complexes of lanthanide ions represent a fairly new field of investigation, since it really started in the mid 1970's, which has sustained considerable development during the last three decades. The receptors synthesised so far have added a new dimension to the coordination chemistry of these ions with potential applications in extraction and separation processes, in controlling energy transfer processes and in the engineering of spectroscopic probes for analytical and biomedical sensors. In the following, we first discuss the problematic of lanthanide ion complexation by macrocyclic receptors before describing the main classes of lanthanide macrocyclic complexes, including bimetallic entities.

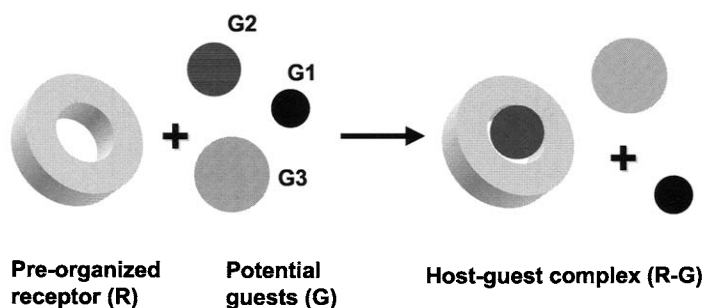
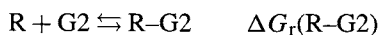


Fig. 4.10. Illustration of the *lock-and-key* principle for the complexation of spherical entities.

### 33. The problematic of metal and lanthanide ion complexation by macrocyclic ligands

#### 33.1. The lock and key principle

It is Emil Fisher who stated this principle in 1896 to explain the specificity of biological processes which are based on molecular recognition. Indeed, in biological systems, molecules are usually active only if they are attached onto a specific receptor. The fixation must be selective, which implies a strict match between the receptor and the host, hence the lock-and-key image to illustrate the specific interaction. The principle is illustrated in Fig. 4.10: a receptor programmed to selectively interact with spherical metal ions of a given size (one speaks of a pre-organized receptor R, the host, and of guests, G) is brought into contact with several spherical cations of varying sizes. According to the molecular programming, the interaction is maximized with G2, giving rise to the stable host-guest complex R-G2; therefore, the free enthalpy of reaction  $\Delta G_r(\text{R-G2})$  is more negative than  $\Delta G_r(\text{R-G1})$  or  $\Delta G_r(\text{R-G3})$ :



The maximization of the host-guest interaction does not necessarily need very strong R-G bonds; on the contrary, the latter are often weak, so-called non-covalent, interactions such as in the case of metal ions, the stability of the host-guest complex relies primarily on stronger ion-dipole bonds or hydrogen bonds for organic guests (or even more subtle van der Waals interactions); on the other hand, the number of interactions is important. In the case of a metal ion, this number must be close to the coordination number of the ion to fully benefit from the chelate effect which contributes to  $\Delta G_r$  by a large positive  $\Delta S_r$  value. For instance in water:



Furthermore, host-guest interaction is also favoured if the interacting atoms of each entity have the same degree of softness or, respectively, hardness. If the receptor features soft bases as donor atoms (i.e. S, P) they will preferentially interact with soft Lewis acids (e.g.



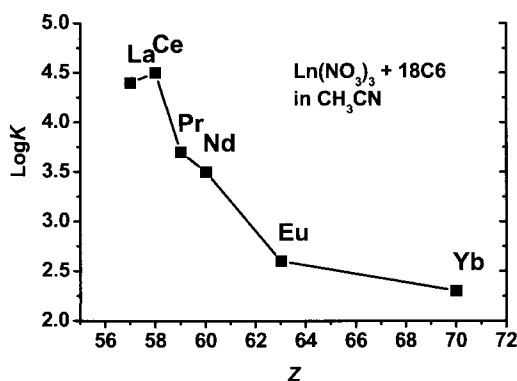


Fig. 4.11. Stability constants of the 1:1 complexes between lanthanide trinitrates and 18-crown-6 in acetonitrile, as determined by NMR spectroscopy (redrawn from J.-C.G. Bünzli et al., in: *The Rare Earths in Modern Science and Technology*, eds G.J. McCarthy, J.J. Rhyne, H.B. Silber, Vol. 2, 1980, p. 99ff, Plenum Press, New York).

Hg<sup>2+</sup>, Cd<sup>2+</sup>, Cu<sup>+</sup>). Since lanthanide ions are hard cations, their complexation therefore requires hard donor atoms such as oxygen or nitrogen.

The principle also requires that the receptor is pre-organized, which means that its conformation in the free state is similar to the conformation in the host-guest complex. Crown ethers and cryptands are typical examples. Their cavity is pretty well defined and can be modulated depending upon the ion one wishes to coordinate. For instance, 18C6 complexes potassium one hundred times better than sodium and cryptand (2.2.2) complexes potassium about 20–25 times better than cryptand (2.2.1). The ionic diameter difference between potassium and sodium is about 0.76 Å (76 pm) which roughly matches the difference in cavity diameter between 18C6 and 15C5 ethers or between (2.2.2) and (2.2.1) cryptands, making ion recognition design relatively easy.

With lanthanide ions, however, the task is more difficult: the ionic radius difference between lanthanum and lutetium amounts to only about 0.15 Å while the ionic radius of two consecutive trivalent lanthanide ions differs by a mere 0.01–0.015 Å. This means that a fine tuning of the receptor to accommodate a specific lanthanide ion is not possible: for instance, the addition of a –CH<sub>2</sub>–CH<sub>2</sub>–O– unit to a crown ether increases the cavity diameter by 0.5–0.7 Å, a difference three to four times as large as the contraction of the ionic radius along the entire Ln(III) series! The stability constants of the 1:1 complexes between lanthanide trinitrates and 18-crown-6 have been determined in acetonitrile by <sup>1</sup>H-NMR (Fig. 4.11). They clearly show that 18C6 cannot distinguish between La(III) and Ce(III). However, the data display some discrimination towards the heavier lanthanide ions, which seems to contradict our previous statement. In fact, 18-crown-6 has a somewhat too large cavity diameter (2.6–3.2 Å as estimated from several crystal structure determinations of complexes with mono- and divalent ions) for most of the Ln(III) ions, except maybe the lighter ones: for a coordination number of nine, the ionic diameter of Ln(III) ions amount to 2.43 (La), 2.39 (Ce), 2.36 (Pr), 2.32 (Nd), and 2.24 Å (Eu). Therefore, the *lock-and-key* principle seems to work between (La, Ce) and (Pr, Nd) on one hand and between the latter pair and Eu on the other hand, the stability difference being approximately one order of magnitude each time. In fact, the stability difference is not larger because the crown ethers

are not completely rigid molecules and can somewhat adapt to the size of the metal ion they complex. This, by the way, is also true for the cryptands. The image of the *lock-and-key* principle is therefore not completely adequate here.

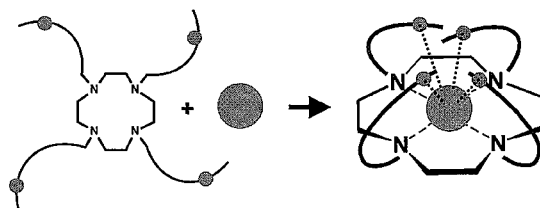
### 33.2. The induced fit principle

The increasing demand for improved selectivity in the complexation of lanthanide and other transition metal ions (for instance in the cases of nuclear waste management and heavy metal recycling) has led to the consideration of the *induced fit* principle which uses flexible receptors in order to optimise the interactions between the donor atoms and the metal ion. In fact, the receptor cavity is built upon complexation thanks to the flexibility introduced into the complexation agents which are now termed *predisposed ligands*. There are several advantages to this approach. Firstly, the heavy synthetic chore in designing and synthesizing pre-organized receptors coded for the recognition of a single metal ion is made easier when the *induced fit* principle is applied. Secondly, the maximisation of the metal–donor interactions creates an enthalpic contribution which more than overcomes the entropic cost for the formation of the induced complexation cavity so that the resultant complexes are usually more stable compared to those with crown ethers and cryptands which do not exactly fit the ion diameter.

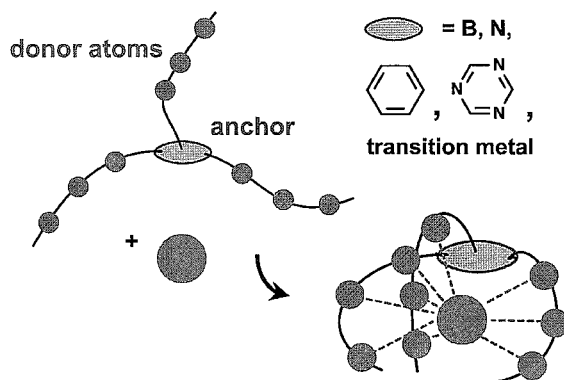
Several types of ligands are amenable to produce a host cavity upon reaction with metal ions. They are schematically described on Fig. 4.12.

- (i) Large, flexible macrocycles have the ability to wrap around metal ions. One early example is the potassium complex of dibenzo-30-crown-10 ether in which the two halves of the macrocycle fold and face each other so that the ten oxygen atoms can coordinate to the metal ion. With respect to lanthanide ions, large calixarenes or Schiff base macrocyclic ligands play the same role. For instance, Fig. 4.13 shows how a di-anionic Schiff base macrocyclic ligand wraps around two Gd(III) ions to yield a double-propeller conformation with the two metal ions held a relatively short distance (3.97 Å), given their tripositive charge, and allowing magnetic interaction between the two metallic centres. The two phenolic oxygen bridges both metal ions and the coordination sphere is completed to ten coordination by four nitrate ions.
- (ii) Another class of ligands consists of macrocycles grafted with functionalised pendant arms, such as cyclen (1,4,7,10-tetraazacyclododecane) derivatives (see top of Fig. 4.12) or calixarenes (Fig. 4.8). The donor atoms of the ring participate in the binding, but to prevent interaction with either anions or solvent molecules, as seen for instance with simple crown ethers (see Fig. 4.7), the remaining coordination positions of the metal ion are blocked by interactions with the functionalised arm. With cyclen derivatives, the coordination cavity is achieved by the four nitrogen atoms of the ring and by four additional donor atoms located on each dangling arm. With respect to the commonly observed nine coordination of the trivalent lanthanide ions, one position remains free for interaction with solvent molecules, an essential feature in the design of contrast agents for magnetic resonance imaging in medicine, especially that large stabilities are obtained. For instance, the tetracarboxylate derivative of cyclen, DOTA, is among the strongest complexation agents for Ln(III) ions, with log  $K$ 's ranging between 24 and 26 in water. This is 17–20 orders of magnitude larger than the observed

## Ligands with pendant arms



## Podands



## Self-assembly processes

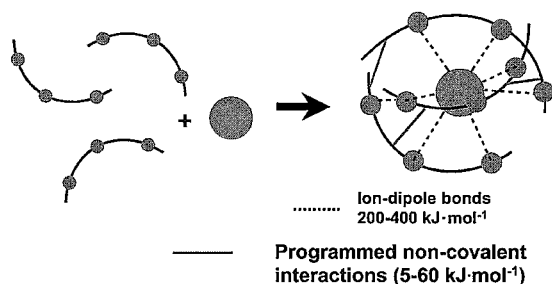


Fig. 4.12. Illustration of the *induced fit* principle in the case of a cyclen derivative, DOTA (top), of podands (middle) and of self-assembly processes (bottom).

stability constants with the cryptand (2.2.1), which demonstrates the superiority of the *induced fit* approach versus the *lock-and-key* principle for the design of lanthanide ion receptors. With calixarenes, the situation may be more complicated and the phenoxy donor groups do not necessarily contribute to the coordination sphere of the Ln(III) ions.

- (iii) A similar approach can be realised by using podands. Here, the functionalised pendant arms are no more attached onto a coordinating macrocycle but simply onto a single atom (boron, nitrogen are usual examples as well as transition metal ions) or a small

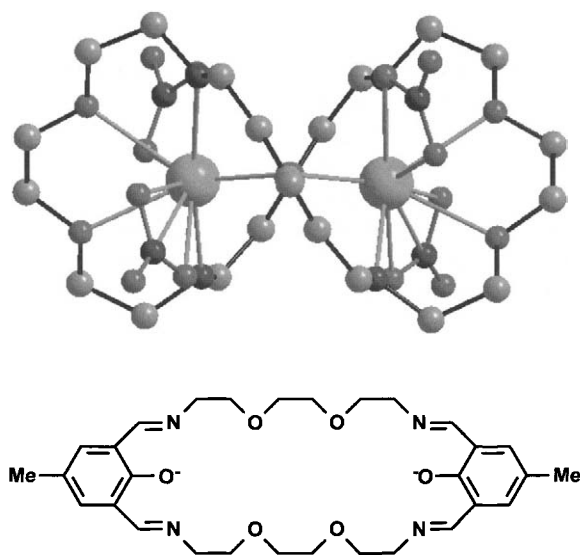


Fig. 4.13. Structure of the dimetallic gadolinium complex with a ditopic macrocyclic Schiff base,  $[\text{Gd}_2(\text{L}^{2-})(\text{NO}_3)_4]$ . Redrawn from I.A. Kahwa et al., *J. Chem. Soc., Chem. Commun.* 1531, 1989.

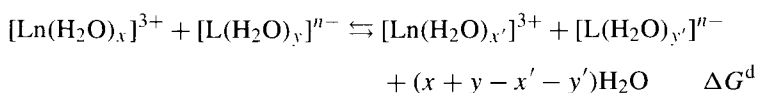
aromatic ring such as benzene. This strategy is particularly used when the design of a lanthanide-containing molecular edifice with programmed functionalities requires the presence of bidentate or tridentate pendant arms. Their grafting onto a macrocycle is not always straightforward from a synthetic viewpoint, hence the use of smaller anchors. Ligands with four arms are usually built from small aromatic rings, while tri-armed receptors are often engineered from a single atom. The advantage of this technology is that the number of donor atoms can be easily varied by changing both the number of arms and the denticity. However, since these ligands are less pre-disposed than the macrocycles fitted with pendant arms, the orientation of the arms to build the correct hosting cavity requires more conformational work, which is detrimental to the stability of the final molecular edifice. One remedy is to make use of non-covalent interactions, such as H-bonding, to position the arms in the right conformation prior to complexation.

- (iv) Finally, a more subtle way of building an induced cavity is to resort to a self-assembly process. Here, small polydentate and functionalised molecules are designed in such a way that upon reaction with a metal ion, they will wrap around the cation generating strong ion-dipole bonds. In addition, and this is the difference with respect to the previously described methods, weak non-covalent interactions are programmed so that the ligand strands are held together. Again, H-bonds may be used but also, and more commonly,  $\pi$ - $\pi$  interactions between aromatic moieties of the ligands. Examples of lanthanide complexes exhibiting secondary intramolecular interactions between ligand strands are the complexes derived from bis(benzimidazole)pyridine.

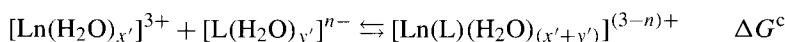
### 33.3. Thermodynamic considerations

From the thermodynamic viewpoint, in aqueous solution, the enthalpy and entropy changes on formation of complexes is usually more influenced by changes in the hydration of cations and ligands (especially if the latter are anionic) than by the cation–ligand interaction itself. Complexation always results in a decrease in the hydration of the ions and of the ligands, which provides a positive entropy change, reflecting the increase in randomness of the system. In the particular case of multidentate ligands, this results in a large chelate effect. The more the ligand is pre-organized, respectively pre-disposed, the larger the chelate effect (in the case of macrocyclic ligands, one speaks of “macrocyclic effect”). The entire complexation process between a  $\text{Ln}^{3+}$  ion and a charged ligand  $\text{L}^{n-}$  may be viewed as follows, based on the electrostatic model:

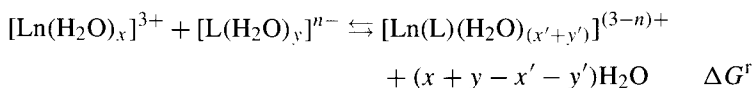
(i) Dehydration step



(ii) Complexation step



Therefore, the total variation of free Gibbs energy for the reaction:



can be expressed at constant pressure and temperature as:

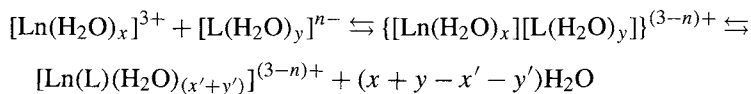
$$\Delta G^r = \Delta G^d + \Delta G^c = \Delta H^d + \Delta H^c - T(\Delta S^d + \Delta S^c)$$

Usually, there is a compensation effect, that is  $\Delta H^d \approx -T\Delta S^d$  so that  $\Delta G^d \approx 0$ . Experimentally,  $\Delta S^r$  is positive (especially for macrocyclic ligands), and so is very often  $\Delta H^r$  (which means that usually, the Ln–L bonds are weaker than the Ln–OH<sub>2</sub> ones) so that complexation reactions in water are entropy driven and, moreover, a linear relationship between  $\Delta H^r$  and  $\Delta S^r$  holds for the Ln(III) series of cations. One has, however, to be cautious when this approach is applied to polydentate ligands. The thermodynamic parameters may also reflect other factors such as the formation of stable 5-membered chelate rings. When another solvent is considered, the solvation enthalpy is much smaller than in water and the above considerations may no more hold.

### 33.4. Kinetics

Trivalent lanthanide ions are known as being kinetically very labile, with water exchange rates in the range  $10^7$ – $10^9$  s<sup>-1</sup>. Complexation reactions with non-cyclic, simple, ligands

or self-assembly processes are also quite fast. In general, the reaction sequence fits within the Eigen–Tamm mechanism:



The first step is diffusion-controlled and is the fastest step in the complexation process. It leads to the formation of an outer-sphere complex which, in a subsequent stage yields the inner-sphere complex. The overall rate of complex formation with simple ligands (such as  $\text{SO}_4^{2-}$ ) may be as fast as the water exchange processes. For multidentate ligands, the rate determining step is usually the ring-closure step, and the overall formation constant becomes small: for instance, the *pseudo* first-order rate constant for the formation of the lutetium complex with dtpa (a branched polyaminocarboxylate, diethylenetriaminepentaacetic acid) amounts to  $4.6 \text{ min}^{-1}$  at pH 7.8 and 298 K. For macrocyclic ligands, and in non-aqueous solvents, the situation may be dramatically different. For instance, the *pseudo* first-order rate constant at pH 7.8 and 298 K for the formation of the Lu(III) complex with the above-mentioned tetra-anionic macrocyclic DOTA ligand amounts to only  $6.3 \times 10^{-3} \text{ min}^{-1}$ , which is almost three orders of magnitude smaller than with dtpa and corresponds to a half-life of 110 min. It therefore takes several days to reach thermodynamic equilibrium under these experimental conditions. Since the metal ion competes with proton, the reaction rate is lowered when the pH is decreased. Longer spans of time are needed to reach equilibrium with cryptands (up to several weeks).

### 33.5. Concluding remark

In the absence of steric constraints, lanthanide ions display large coordination numbers; these are somewhat adjustable. The design of a convenient receptor for Ln(III) ions must include a large number of donor atoms, as to meet their coordination requirements by saturating the inner coordination sphere. The receptor, either the initial ligand or the final self-assembled entity, should also comply with other criteria, for instance pre-organization of the coordination sites or as much predisposition of the arms as possible, in order to minimize the entropy cost of conformation change upon complexation. However, retaining some fluxionality will help keep a relatively fast rate of complexation. With this in mind, it seems that applying the *induced fit* principle to the construction of suitable receptors for the trivalent lanthanide ions offers wider possibilities than the more limited *lock-and-key* principle.

### 33.6. Definitions and scope of the following sections

At this stage, it is helpful to summarise some definitions and to identify the classes of compounds which will be described in the subsequent sections. Definitions are collected in Table 4.21. As can be seen, some definitions overlap. For instance, the distinction between podands and chelating agents is rather thin so that some authors use these terms indifferently. Other differences are also subtle, e.g. between cryptands and sepolchrand.

TABLE 4.21  
Definitions pertaining to coordination and macrocyclic chemistry.

Term	Definition
Ionophore	Substance having the ability to promote the transfer of ions from an aqueous solution into a hydrophobic phase
Ligand	Anion or neutral molecule which binds a metal cation
Chelating agent	Ligand featuring several donor atoms able to bind a metal cation
Chelate	Metal ion complex with a chelating agent
Denticity	Number of donor atoms in a chelating agent
Macrocyclic	Cyclic molecule with a large number of atoms in its ring
Coronand	Macrocyclic ligand featuring several donor atoms in its main ring
Coronate	Metal ion complex with a coronand
Crown ether	Macrocyclic polyether (coronand featuring O-donor atoms)
Aza crown	Macrocyclic polyamine (coronand featuring N-donor atoms)
Calixarene	Macrocyclic obtained by the condensation of phenol rings with formaldehyde and amenable to substitution both on the phenolic functions and on the para positions of the phenol rings
Cryptand	Macropolycyclic ligand forming a cage
Cryptate	Metal ion complex with a cryptand
Sepulchrand	Macropolycyclic polyamine ligand (a form of cryptand leading to extremely inert metal ion complexes)
Sepulchrates	Metal ion complex with a sepulchrand
Podand	Ligand featuring several functionalised groups attached onto a single atom or onto a small aromatic ring
Podate	Metal ion complex with a podand
Chelate effect	Favourable entropic effect generated by a multidentate chelating agent with respect to the complexation by monodentate ligands
Macrocyclic effect	Increase of stability generated by the use of a macrocyclic ligand with respect to its non-cyclic analogue
Template effect	Process in which the presence of a metal ion facilitates the formation of a macrocycle by bringing together the reacting strands and leading to one-pot syntheses

In the following, we shall discuss the complexation of lanthanide ions with a limited number of classes of macrocyclic ligands, in view of the overwhelming literature in the field: coronands, cryptands, phthalocyanines and porphyrins, coronands bearing pendant arms, and calixarenes. Whenever possible, we shall put the emphasis on functional coordination compounds, namely on luminescent complexes, on compounds displaying contrast agent ability for magnetic resonance imaging, analytical potential, as well as selectivity in extraction and separation processes. Both monometallic and dimetallic edifices will be described.

### 34. Complexes with coronands and cryptands

#### 34.1. Simple coronands

The interaction between the simple crown ethers with lanthanide ions is weak in water. However, in non-aqueous media, the interaction is stronger, which allows one to form and isolate complexes. The stoichiometry of the crown ether coronates depends upon several factors: the relative size of the ligand cavity and the ionic diameter, the nature

TABLE 4.22

Selected values of the ratio  $D_i/C_d$  (ionic diameters of Ln(III) ions/ cavity diameter of complexed crown ether) versus coordination number. The cavity diameters of the complexed crown ethers are taken from crystallographic data (12C4: 1.35 Å, 15C5: 1.9 Å, 18C6: 2.5 Å). The best fit is given in bold characters.

Ln	Crown	CN=8	CN=9	CN=10	CN=12
La	12C4	1.72	1.80	1.88	2.01
	15C5	1.22	1.28	1.34	1.43
	18C6	0.93	0.97	<b>1.02</b>	1.09
Nd	12C4	1.64	1.73	1.81	1.92
	15C5	1.17	1.23	1.29	1.36
	18C6	0.89	0.93	<b>0.98</b>	1.04
Gd	12C4	1.56	1.64	1.73	1.84
	15C5	1.11	1.17	1.23	1.31
	18C6	0.84	0.89	0.94	<b>0.99</b>
Er	12C4	1.49	1.57	1.65	1.76
	15C5	1.06	1.12	1.17	1.25
	18C6	0.80	0.85	0.89	<b>0.95</b>
Lu	12C4	1.44	1.52	1.61	1.72
	15C5	<b>1.03</b>	1.08	1.15	1.22
	18C6	0.78	0.82	0.87	0.93

of the counterion, the solvent and the presence or absence of water molecules. When the anion is a small, strongly coordinating entity such as the nitrate, its binding to the metal ion diminishes the charge density of the cation and weakens the ligand–Ln(III) interaction. A similar effect arises when strongly coordinating solvents are used. The reported metal:ligand ratios range from 2:1 (for instance with 12C4 and  $\text{CF}_3\text{CO}_2^-$ ) to 3:2 ( $\text{Cy}_2\text{18C6}$ ,  $\text{NO}_3^-$ ), 4:3 (18C6,  $\text{NO}_3^-$ ), 1:1 (most of the cases), 1:2 (12C4, 15C5 and  $\text{ClO}_4^-$ ). However, crystal structure determinations show that the complex entity is either a 1:1 complex (see Fig. 4.7) or, in rare cases, a sandwich-type complex (12C4, 15C5, 18C6 and either  $\text{ClO}_4^-$  or  $\text{PF}_6^-$ ).

The thermodynamic parameters for the complexation of crown ethers to lanthanide ions have been determined for several systems and we shall first focus our attention on the cation–cavity fit which is modelled by the ratio  $R$  between the ionic diameter of the cation,  $D_i$ , and the cavity diameter  $D_c$ , as estimated from crystallographic determinations of metal complexes. Table 4.22 lists selected values of  $R = D_i/D_c$  and it immediately occurs that if it is difficult to adjust the cavity for a given Ln(III) ion, this difficulty is somewhat eased if one is able to modify the coordination number of the metal ion. And precisely, lanthanide ions are known to be able to adapt to varying environments by changing their coordination numbers. If the ionic radius varies only by about 16% from La(III) to Lu(III), it increases by more than 30% upon increasing the coordination number of a given Ln(III) ion from 6 to 12, or by about 17–20% in going from CN = 8 to CN = 12, which is a more reasonable span of coordination numbers for macrocyclic complexes. It is therefore not surprising that for each Ln(III) ion listed in Table 4.22, a ratio  $R$  between 0.95 and 1.03 can be found, that is close to the ideal ratio of 1. In reality, adjusting the coordination number to the required number to achieve a perfect fit is not always feasible, since the only possibility is to bind anions (or solvent molecules) axially, that is above and below the mean plane of the



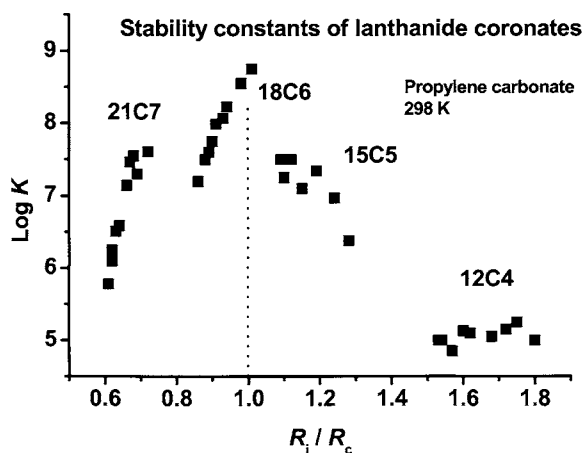


Fig. 4.14. Stability constants of Ln(III) coronates versus the ratio  $D_i/D_c$  ratio (assuming an "average" coordination number of 9) as determined in propylene carbonate at 298 K by potentiometric measurement (counterion:  $\text{ClO}_4^-$ ). Redrawn from J.-C.G. Bünzli et al., *Inorg. Chem.* **28**, 2638, 1989.

macrocyclic ligand. In Fig. 4.7, a 10-coordination is achieved for the Nd(III) ion by complexation of two bidentate nitrate ions. Since these ions are strongly coordinating however, the Nd(III)–18C6 interaction is modest ( $\log K = 3.5$  in acetonitrile). The importance of the ion–cavity fit is illustrated in Fig. 4.14 in which the stability constants for the 1:1 complexes of lanthanide trifluoromethanesulfonates (triflates) with 12C4, 15C5, 18C6 and 21C7 in propylene carbonate at 298 K and  $\mu = 0.1 \text{ M}$  ( $\text{Et}_4\text{NClO}_4$ ) are plotted versus the ratio  $R$ : the largest values are close to  $R = 1$  and the curve is reasonably symmetrical around  $R = 1$ . When the ratio  $R$  is larger than 1, sandwich complexes form, especially with 12C4 and 15C5, but, also, with 18C6 in the presence of a very weakly coordinating anion such  $\text{PF}_6^-$ .

However, as pointed in Section 33, another important factor is the flexibility of the macrocyclic ligand, which somewhat offsets the *lock-and-key* behaviour of the crown ethers towards Ln(III) ions as shown in Fig. 4.11. To illustrate this, the stability constants for the formation of neutral  $[\text{Ln}(\text{NO}_3)_3(\text{L})]$  complexes with 15C5 and B15C5 in anhydrous acetonitrile at 298 K are plotted for the lighter lanthanide ions in Fig. 4.15. With 15C5, there is a linear decrease in  $\log K$  as a function of the atomic number; the macrocycle is slightly flexible, so that it can somewhat adapt its conformation to fit the ion diameter; in which case, it is an induced fit. On the other hand, B15C5 is much more rigid due to the presence of the benzene substituent and cannot adapt so easily to the ion size. A first consequence is a decrease in stability with respect to 15C5 by more than one order of magnitude for La(III) and Ce(III) and two orders of magnitude for Pr(III); the decrease in stability in going from La(III) to Pr(III) is much more pronounced than with the unsubstituted crown ether. From Pr(III) on, the stability remains almost constant, with a slight increase with  $Z$  due to the increased charge density on the Ln(III) ions; therefore, the rigidity of B15C5 causes a behaviour close to the *lock-and-key* principle. Complete thermodynamic data have been gathered for the complexation of the lighter lanthanide nitrates (La–Gd) with simple crown ethers 15C5, 16C5 and 18C6. Interestingly,  $\Delta H$  ranges

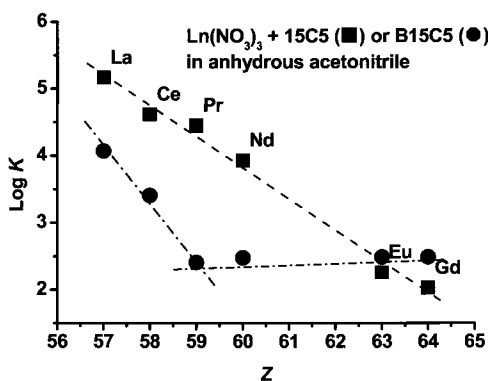


Fig. 4.15. Stability constants of Ln(III) nitrate complexes with 15C5 and B15C5 in anhydrous acetonitrile. Redrawn from Y. Liu et al., *J. Phys. Chem.* **97**, 4548, 1993, and D.-Q. Huang, *Acta. Chim. Sin.* **48**, 452, 1990.

from  $-28$  to  $-46$   $\text{kJ mol}^{-1}$  in the case of 15C5 and from  $+12$  to  $+21$   $\text{kJ mol}^{-1}$  for B15C5, which points to the better ligand–Ln(III) interaction with 15C5. The entropic contribution to  $\Delta G$ ,  $-T\Delta S$ , is unfavourable for 15C5 ( $+3$  to  $+30$   $\text{kJ mol}^{-1}$ ) while it is favourable for B15C5 ( $-26$  to  $-36$   $\text{kJ mol}^{-1}$ ), consistent with the larger pre-organization of the latter ligand.

The macrocyclic effect has been measured for the unsubstituted 12C4, 15C5, 18C6 and 21C7 ethers. Stability constants have been determined in propylene carbonate for the complexes between lanthanide trifluoromethanesulfonates and both the cyclic crown ethers containing from four to seven oxygen atoms, and their open chain analogues, the linear polyethers termed 12P4 (2,5,8,11-tetraoxadodecane), 15P5 (2,5,8,11,14-pentaoxapentadecane), 18P6 (2,5,8,11,14,17-hexaoxaoctadecane) and 21P7 (2,5,8,11,14,17,20-heptaaxaheneicosane). Data are reported in Fig. 4.16. As shown by the structure of the  $[\text{Ln}(\text{NO}_3)_2(18\text{P6})]^+$  cation (Fig. 4.17), the conformation adopted by the ligand is very similar to the one displayed by the corresponding macrocyclic ligand (compare Fig. 4.7), except for some helicity induced by the steric repulsion of the two methyl groups. Therefore, the difference in the stability constants of the 1:1 coronates (Table 4.23) can be attributed to the macrocyclic effect: the formation of the podates is less favoured compared to that of the coronates in view of the conformational work to be achieved by the linear ligand in order to reach a ring-like structure. Kinetic and solvation differences may also contribute to the macrocyclic effect. Analysing the data of Fig. 4.16 in more detail shows that for a given coronate, the macrocyclic effect is more or less constant for the lanthanide series:  $\Delta \log K_1 = 1.0 \pm 0.3$  (12C4),  $3.1 \pm 0.2$  (18C6), and  $0.9 \pm 0.2$  (21C7). The behaviour for 15C5 is somewhat different: the macrocyclic effect increases 200 fold from La to Tb and then stays approximately constant, with a magnitude five times larger than the macrocyclic effect for 18C6. There is a gradual shift of the maximum of stability from the 18C6 coronates with lighter lanthanide ions to the 15C5 coronates with the heavier lanthanide ions. Two factors may be invoked to explain these data. The first one is the fit between the ion diameter and the cavity diameter (see Table 4.22). The relative constancy of the macrocyclic effect for the 18C6 coronates may be traced back to the flexibility of

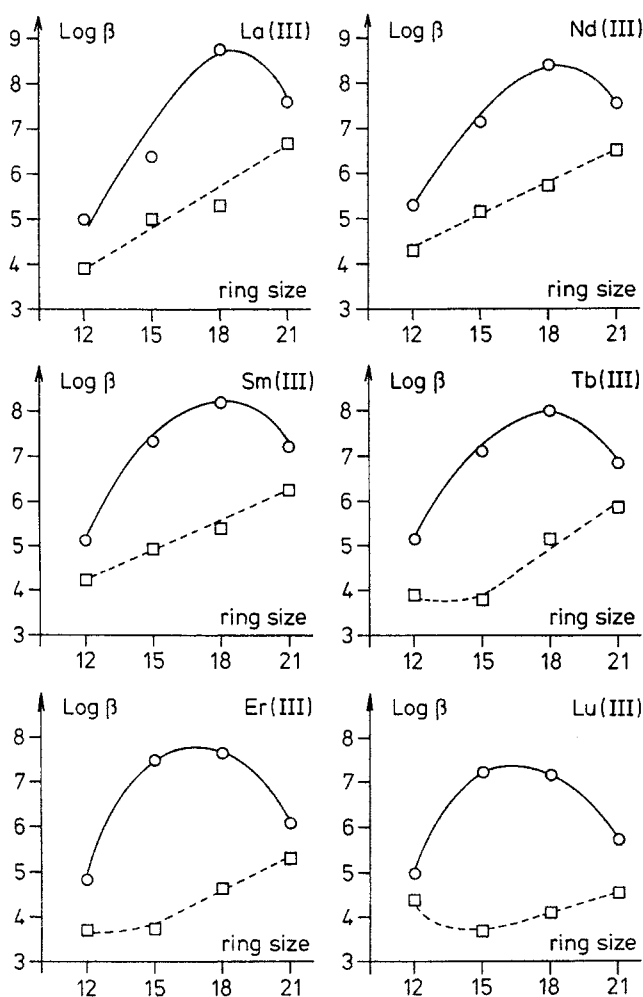


Fig. 4.16. Stability constants of Ln(III) coronates and podates versus the ring or chain size, in propylene carbonate at 298 K,  $\mu = 0.1$  M ( $\text{Et}_4\text{NClO}_4$ ). Redrawn from J.-C.G. Bünzli et al., *Inorg. Chem.* **28**, 2638, 1989.

the macrocycle, which adapts to the ion size; a similar argument holds for the 21C7 coronates, but here the macrocyclic effect is much smaller due to the large conformational work needed to fit the large cycle to the lanthanide ions. Note that the macrocyclic effect is small for the 12C4 coronates too because the ions are not encapsulated into the too small macrocycle which has a marked tendency to form sandwich complexes. The second parameter is related to solvation changes along the lanthanide series and/or to structure and composition changes in the complexes. These effects are subtle and not easy to decipher. For instance, as mentioned above, the nature of the anion has a marked effect: the 18C6 coronates are 4–6 orders of magnitude more stable with lanthanide trifluoromethanesulfonate (respectively perchlorate) than with nitrate as counterion.

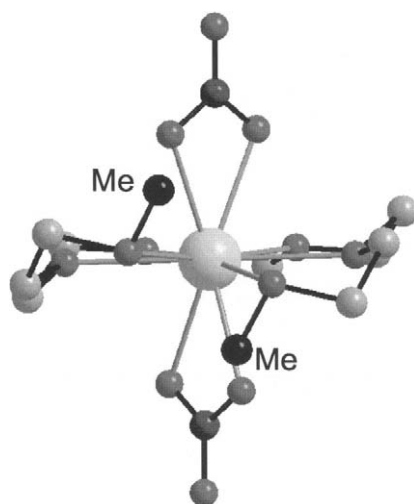


Fig. 4.17. Structure of the complex cation  $[\text{La}(\text{NO}_3)_2(18\text{P}6)]^+$  (redrawn from J.-C.G. Bünzli et al., *Helv. Chim. Acta* **67**, 1121, 1984).

TABLE 4.23

Macrocyclic effect expressed as  $\Delta \log K_1$  (coronate-podate) for various ring sizes in anhydrous propylene carbonate at 298 K,  $\mu = 0.1$  M. Standard deviations are given within parentheses ( $2\sigma$ ).

Ln	4	5	6	7
La	1.08(17)	1.33(6)	3.45(24)	0.93(18)
Pr	1.63(16)	1.57(8)	3.41(20)	1.03(10)
Nd	0.90(21)			1.06(12)
Sm	0.92(25)	2.31(11)	3.05(26)	0.62(24)
Eu			2.7(5)	0.64(11)
Tb	1.25(22)	3.30(18)	2.85(10)	0.72(10)
Er	1.15(13)	3.77(12)	3.04(13)	0.79(6)
Yb	0.38(26)	3.55(16)		
Lu	0.59(28)	3.78(10)	3.06(9)	1.21(6)

The stability of the coronates depends markedly upon the nature of the donor atoms, as shown on Fig. 4.18. When two ether functions of 15C5 are replaced by amine groups to yield a ligand termed (2.1), the stability of the lanthanide coronates jumps by eight to nine orders of magnitude. At first sight, this is surprising because nitrogen is a softer donor atom than oxygen. One explanation is that the extra flexibility added to the macrocycle by the amine group may provide a considerably better match between the ion and the cavity. One also notes that the nitrogen lone pair is easily polarisable by the large cationic charge on the metal ion. Replacing two ether functions of 18C6 by two amine groups has approximately the same effect. The extra flexibility of the ligand is shown on Fig. 4.7 in which the structures of  $[\text{Nd}(\text{NO}_3)_2(18\text{C}6)]^+$  and  $[\text{Eu}(\text{NO}_3)_2\text{Me}_2(2.2)]^+$  are compared (Me<sub>2</sub>(2.2) is the *N,N*-dimethyl substituted coronand (2.2)). In fact, when the six ether

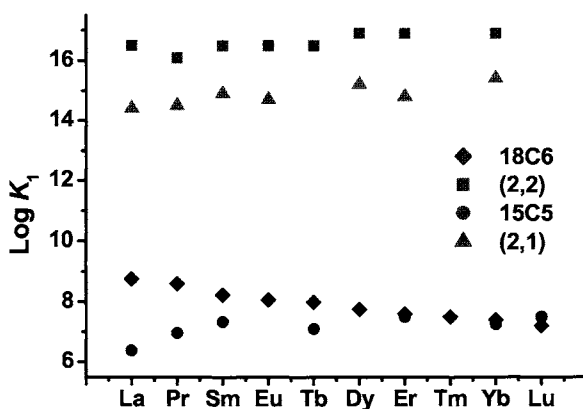


Fig. 4.18. Stability constants of Ln(III) coronates in propylene carbonate at 298 K and  $\mu = 0.1$  M ( $\text{Et}_4\text{NClO}_4$ ). From data reported by J.-C.G. Bünzli, in: Handbook on the Physics and Chemistry of Rare Earths, eds K.A. Gschneidner, Jr., L. Eyring, Vol. 9, Ch. 60, North Holland, Amsterdam, 1987.

functions of 18C6 are replaced by six amine functions, to yield  $\text{N}_6$ 18C6, interaction in water becomes sizeable, with  $\log K_1(\text{La}) = 5.7$ , while negligible interaction is seen with the parent crown ether.

Finally, the stability of the coronates can also be tuned by grafting substituents on the ring carbon atoms. In particular, the presence of a *t*-butyl-phenyl substituent on 15C5 decreases  $\log K_1$  by three orders of magnitude, compared to 15C5.

### 34.2. Simple cryptands

Most of the reasoning made with coronands can be applied to the cryptands. Indeed, these ligands provide a cavity which may be adapted depending on the size of the three chains anchored on the nitrogen atoms. Similarly to the crown ethers, the addition of an extra  $-\text{CH}_2-\text{CH}_2-\text{O}-$  fragment to one chain modifies substantially the cavity size, excluding a fine recognition for a given lanthanide ion. Finally, the chains have some flexibility so that they may fold back to leave the metal ion interact with other donor groups as in the Pr(III) dimer of (2.2.1) cryptand, which is bridged by two  $\mu$ -OH groups,  $[\text{Pr}(2.2.1)(\mu\text{-OH})_2\text{Pr}(2.2.1)]^{4+}$ , as illustrated on top of Fig. 4.19. Each praseodymium ion is nine coordinate, being bound to the five oxygen and two nitrogen atoms from the ligand and to the two bridging hydroxide groups. The dimer is perfectly symmetric, its two parts being related by an inversion centre. In this case, the cation is not completely enclosed in the host and the complex is described as being “exclusive” rather than “inclusive”. The flexibility of the chains also allows interaction either with an anion or with a solvent molecule, even in the case of an “inclusive” cryptate, as shown in the bottom of Fig. 4.19 in the case of the  $[\text{Eu}(\text{ClO}_4)(2.2.2)]^{2+}$  cryptate. Here the Eu(III) ion is ten coordinate by the eight donor atoms of the cryptand and by a bidentate perchlorate anion. There are several other examples of similar structures, for instance  $[\text{LaCl}(2.2.2)(\text{H}_2\text{O})]^{2+}$ ,  $[\text{La}(\text{CF}_3\text{SO}_3)(2.2.2)]^{2+}$ , or  $[\text{Nd}(\text{NO}_3)(2.2.2)]^{2+}$ .

Interestingly, the stability constants of the lanthanide cryptates with the simple cryptands (2.1.1), (2.2.1) and (2.2.2) in propylene carbonate, reported on Fig. 4.20, are not much

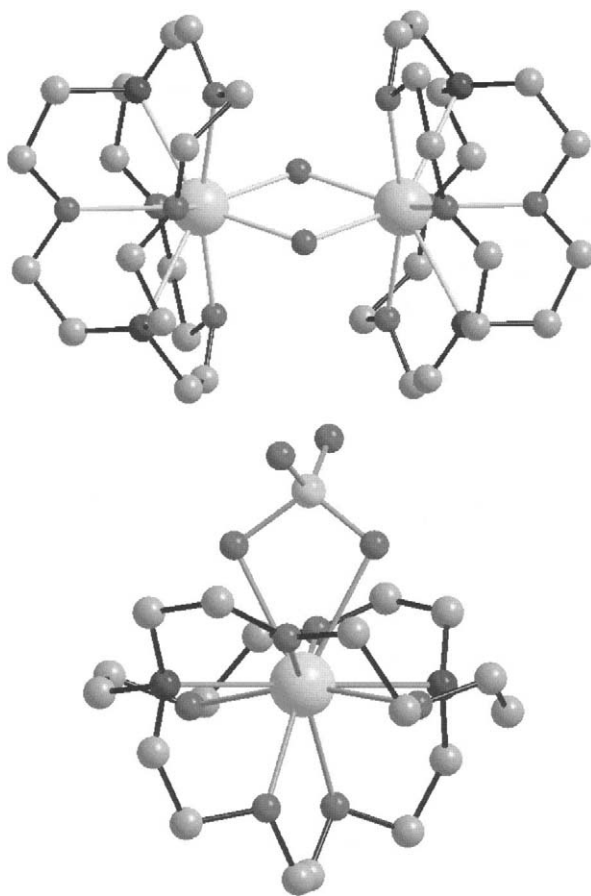


Fig. 4.19. (Top) Dimeric structure of a Pr(III) cryptate with (2.2.1) in which the two monomers are connected through two  $\mu$ -OH links (redrawn from J. Rebizant et al., *J. Incl. Phenom. Mol. Recogn. Chem.* 5, 505, 1987. (Bottom) Structure of the  $[\text{Eu}(\text{ClO}_4)(2.2.2)]^{2+}$  cation showing the coordination of a perchlorate anion between two arms of the cryptand receptor. Redrawn after M. Ciampolini et al., *J. Chem. Soc., Dalton Trans.* 974, 1979.

larger than the corresponding data with the nitrogen-containing coronands (2.1) and (2.2). In fact, when the cryptand has no guest, it compensates for the vacant cavity by rotating one methylene group inward and extending somewhat. The three triethylenedioxy chains connecting each nitrogen atom lie approximately parallel to each other and the N...N distance is quite long, reaching 7 Å for (2.2.2). Therefore, upon complexation, a considerable conformational change has to be performed by the host molecule. The stability constants increase slightly with the atomic number, reflecting the increased charge density of the cation, showing no size-discrimination within the series. However, there is a size-discriminating effect between the cryptands: as expected from the size of its cavity, the macrotricyclic (2.2.1) yields the largest stability constants. The (2.1.1) cryptand is too small and, on average, the stability of the corresponding cryptates is 3–4 orders of magnitude smaller. The (2.2.2) cryptand is too large, its mean cavity diameter being

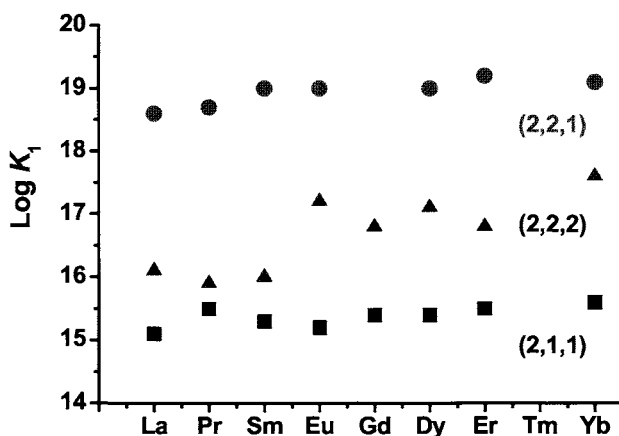


Fig. 4.20. Stability constants of lanthanide cryptates in propylene carbonate at 298 K and  $\mu = 0.1$  M ( $\text{Net}_4\text{ClO}_4$ ). From data reported by J.-C.G. Bünzli, in: Handbook on the Physics and Chemistry of Rare Earths, eds K.A. Gschneidner, Jr., L. Eyring, Vol. 9, Ch. 60, North Holland, Amsterdam, 1987.

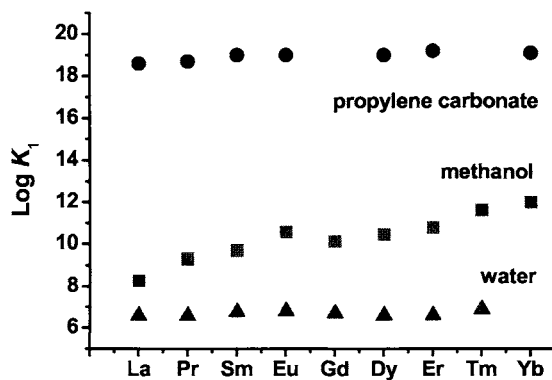
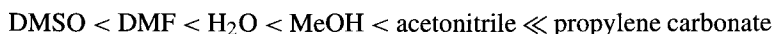


Fig. 4.21. Stability constants of the (2.2.1) cryptates in propylene carbonate, methanol and water at 298 K. From data reported by J.-C.G. Bünzli, in: Handbook on the Physics and Chemistry of Rare Earths, eds K.A. Gschneidner Jr., L. Eyring, Vol. 9, Ch. 60, North Holland, Amsterdam, 1987.

estimated to 2.8 Å; however, its larger flexibility results in larger stability constants than with (2.1.1), which are on average only 2–3 orders of magnitude smaller than the corresponding ones for the (2.2.1) cryptates. The influence of the solvent is dramatic (Fig. 4.21). While (2.2.1) cryptates have  $\log K_1$  in the range 18–19 in propylene carbonate, a non-protic solvent, they range between 8 (La) and 12 (Lu) in methanol and are as low as 6–7 in water. That is, cryptand (2.2.1) the size of which is relatively well adapted to the ionic diameter of the Ln(III) ions is a much less effective complexing agent than EDTA (ethylenediaminetetraacetate) for these ions ( $\log K_1$  ranges between 15 (La) and 20 (Lu) for EDTA chelates), in spite of the encapsulating nature of the resulting host–

guest complex. Generally speaking, the stability of lanthanide cryptates increases in the following solvent sequence:



which is nearly in agreement with the solvating properties of the solvents as expressed by their Gutmann donor numbers (14.1 for acetonitrile, 15 for propylene carbonate, 18 for water, 19 for methanol, 26.6 for DMF, and 29.8 for DMSO), with the exception of propylene carbonate. It is noteworthy that the stability constants are much lower in acetonitrile than in propylene carbonate; in the former solvent,  $\log K_1$  is relatively constant for Sm, Eu and Yb, between 11.3 and 11.6, that is almost 8 orders of magnitude smaller than in propylene carbonate. Some insight into an explanation for this may be gained from the thermodynamic parameters for the formation of lanthanide (2.2.1) cryptates. In propylene carbonate, they are clearly enthalpy stabilized ( $-75$  to  $-146 \text{ kJ mol}^{-1}$ ), with a favourable entropic contribution ( $-T\Delta S_f$ ) for the lighter lanthanide ions ( $-29 \text{ kJ mol}^{-1}$  at 298 K for La) which fades out in the middle of the series and eventually becomes unfavourable towards the end ( $+37 \text{ kJ mol}^{-1}$  at 298 K for Er). In acetonitrile, the enthalpic contribution is comparable (between  $-75$  and  $-126 \text{ kJ mol}^{-1}$ ), but the entropy is now unfavourable, with contribution of  $+12 \text{ kJ mol}^{-1}$  for La and  $+42 \text{ kJ mol}^{-1}$  for Nd at 298 K. The decrease of the entropy with increasing atomic number may be interpreted as arising from the smaller solvation number for the heavier lanthanide ions and, possibly, an incomplete de-solvation. The single ion enthalpies of transfer from propylene carbonate to acetonitrile determined for the (2.2.1) and (2.2.2) cryptates are independent of the ligands but vary with the lanthanide ions, indicating that the cation recognition is performed by the solvent and not by the cryptand! Therefore, the complete shielding of the cation by the cryptand (sometimes called the "extrathermodynamic assumption") is not a good model for lanthanide cryptates, as suggested by the crystal structures shown on Fig. 4.19.

### 34.3. Stabilization of lanthanide low oxidation states

In solution, lanthanide ions usually exist in the +3 oxidation state, with a few exceptions. Tetravalent cerium and divalent europium are relatively stable in water, as well as divalent samarium and ytterbium in tetrahydrofuran. Ln(III)/Ln(II) reduction potentials (in water, versus normal hydrogen electrode) are indeed equal to  $-0.35 \text{ V}$  (Eu),  $-1.15 \text{ V}$  (Yb) and  $-1.55 \text{ V}$  (Sm) while they are well above 2 V for the other lanthanides. Recently, the work of William Evans at the University of California, Irvine, has shown that the reductive chemistry of the lanthanides can be extended to almost all the elements, provided elaborate organometallic ligands (based on cyclopentadienyl derivatives) and peculiar experimental conditions are used. Since the coronands and cryptands are somewhat flexible ligands, it has been realised at the beginning of their use as host for spherical metal ions that they may stabilise low oxidation states of the lanthanides since the ionic radii of the Ln(II) ions are usually  $0.16\text{--}0.20 \text{ \AA}$  larger than the radii of Ln(III) ions. In several solvents, including water, dimethylformamide and methanol, the reduction of trivalent lanthanide coronates and cryptates always occurs at a higher potential than the reduction of the uncomplexed cations. In some instances, e.g. in water, the cyclic voltammograms of the uncomplexed ions are irreversible, which is not the case for the encapsulated cations. The difference in



TABLE 4.24

Stabilisation of Ln(II) ions by macrocycles (1:1 coronates or cryptates, 298 K, lanthanide trifluoromethanesulfonates,  $\mu = 0.1 \text{ M Net}_4\text{ClO}_4$ ).

Ln	Ligand	Solvent <sup>a</sup>	log $K_{\text{II}}$	log( $K_{\text{II}}/K_{\text{III}}$ )
Sm	18C6	PC	8.9	0.8
		(2.2)	11.2	-5.3
	(2.2.1)	PC	15.6	-3.4
		W	9.2	4.2
	(2.2.2)	PC	17.6	0.3
		W	12.2	6.3
Eu	18C6	W	2.7	b
		AN	b	2.0
	(2.2)	AN	5.0	-4.1
		(2.2.1)	AN	9.3
	(2.2.2)	W	10.2	3.4
		DMSO	5.3	b
		AN	12.9	1.5
		W	13.0	7.1
		DMSO	5.8	b
		W	2.4	b
Yb	18C6	W	2.4	b
	(2.2.1)	W	b	5.5

<sup>a</sup>AN = acetonitrile, PC = propylene carbonate, DMSO = dimethylsulfoxide, W = water.

<sup>b</sup>Not determined.

the formal redox potential  $\Delta E_f$  between the complex and uncomplexed one-electron redox couples is related to the difference in Gibbs free energy for these processes by the so-called Nernst–Peter equation:

$$\Delta E_{1/2} = \frac{2.303RT}{F} \log \frac{K_{\text{II}}}{K_{\text{III}}} = \frac{\Delta G_{\text{II}}^0 - \Delta G_{\text{III}}^0}{F}$$

Some data are collected in Table 4.24. Several effects affect the stabilisation of Ln(II) over Ln(III). We have previously seen that the stability of the Ln(III) cryptates is inversely proportional to Gutmann's donor number of the solvent. This is not the case for the Ln(II) coronates and cryptates, the stability of which is more or less independent of the solvent. This leads to large variations in the stabilisation of Ln(II) over Ln(III) depending upon the solvent. Stabilisation in propylene carbonate or acetonitrile is small (at most two orders of magnitude) or even negative, while good results are obtained in water for (2.2.1) or (2.2.2) cryptates, up to seven orders of magnitude. In DMSO, the Eu(II) cryptates with (2.2.1) and (2.2.2) have sizeable stability whereas Eu(III)—and generally speaking Ln(III)—cryptates do not form to an appreciable extent. Use of the Nernst–Peter equation leads to negative values for log  $K_{\text{III}}$ . A thermodynamic study shows that the Eu(II) cryptates with (2.2.1) and (2.2.2) are stabilised by a large enthalpic effect in DMSO ( $-50.2$  and  $-36.0 \text{ kJ mol}^{-1}$ , respectively) and destabilised by an unfavourable entropic contribution ( $+17.1$  and  $+5.6 \text{ kJ mol}^{-1}$ , respectively). The nature of the counter ion has also a marked influence on the Ln(II) stabilisation.

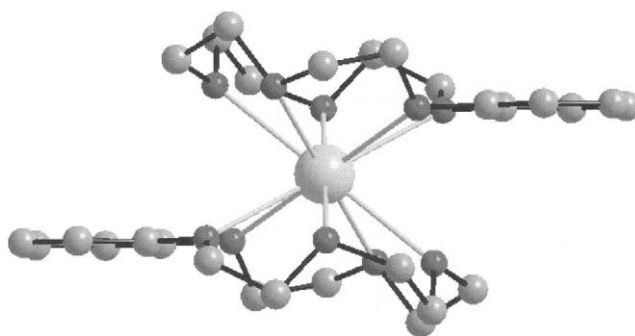


Fig. 4.22. Structure of the sandwich complex between Eu(II) and benzo-15-crown-5 ether. Redrawn from P. Starynowicz, K. Bukietynska, *Eur. J. Inorg. Chem.* 1835, 2002.

Several Ln(II) coronates and cryptates have been isolated, but few crystal structures are known. One example is given in Fig. 4.22 in which Eu(II) is sandwiched between two B15C5 coronands. The metal ion lies on an inversion centre and is ten coordinate with an environment close to a pentagonal antiprism, with approximate  $D_{5d}$  geometry. From the Eu–O distances, an ionic radius of about 1.39 Å can be calculated, as compared to the standard value of 1.33 Å, which means that the Eu–O bond lengths are somewhat longer than usual.

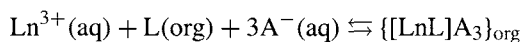
A great deal of work has been carried out by the group of Professor Gin-Ya Adachi at the University of Osaka to design luminescent polymers doped with Eu(II) macrocyclic compounds. Indeed, Eu(II) is a component of blue phosphors (materials emitting light and used in fluorescent lamps or cathode-ray tube displays) because it presents a broad and intense emission band with a maximum between 420 and 480 nm. This transition originates from the  $4f^65d$  electronic configuration and terminates on the  $^8S_{1/2}$  level of the  $4f^7$  electronic configuration. Interesting results have been obtained, but practical applications could not be developed in view of the relatively poor resistance of these materials to degradation caused by photophysical processes.

#### 34.4. Applications of lanthanide coronates and cryptates

##### 34.4.1. Extraction and separation processes

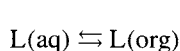
In view of their size discriminating effect and of the presence of a hydrophilic cavity and a hydrophobic exterior, coronands and cryptands have been tested in separation and extraction processes. Applications range from metal separation and recycling, to nuclear waste management, analytical methods (ion-selective electrodes, chromatography) and determination of the stoichiometry and stability of complexes extracted into an organic phase. This field has generated a vast number of studies and it is out of the scope of the present chapter to provide a detailed review. The first studies were concerned with the separation of alkali metal ions, since there are not many good complexation agents for these metals, but they were soon extended to alkaline-earth and transition metals, including 4f and 5f cations. The overall equations for the extraction of a metal ion  $Ln^{3+}$  from an aqueous phase into an organic phase in the presence of a macrocyclic ligand L dissolved

into an organic phase and of an anion  $A^-$  can be formulated as follows

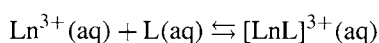


$$K_{\text{ex}} = \frac{\{[\text{LnL}]\text{A}_3\}_{\text{org}}}{[\text{Ln}^{3+}(\text{aq})][\text{L}(\text{aq})][\text{A}^-(\text{aq})]^3}$$

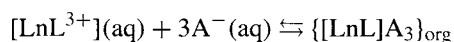
where  $\{[\text{LnL}]\text{A}_3\}_{\text{org}}$  is the extracted ion pair. Commonly used anions in lanthanide extraction processes are picrate and trichloroacetate. This overall equilibrium can be broken down into several equilibria:



$$D_{\text{L}} = \frac{\text{L}(\text{org})}{\text{L}(\text{aq})}$$



$$K_{\text{LnL}} = \frac{[\text{LnL}]^{3+}(\text{aq})}{[\text{Ln}^{3+}(\text{aq})][\text{L}(\text{aq})]}$$



$$K'_{\text{ex}} = \frac{\{[\text{LnL}]\text{A}_3\}_{\text{org}}}{[\text{Ln}^{3+}(\text{aq})][\text{A}^-(\text{aq})]^3}$$

$$K_{\text{ex}} = \frac{K_{\text{LnL}} \cdot K'_{\text{ex}}}{D_{\text{L}}}$$

If a non-polar solvent is used as an organic phase, dissociation of the ion pair in this solvent is negligible, whereas it is supposed to be complete in water. Note that in practice, relatively high concentrations are used so that they should be replaced by activities. The distribution ratio of the metal ion is equal to:

$$D_{\text{Ln}} = \frac{[\text{Ln}(\text{org})]_{\text{tot}}}{[\text{Ln}(\text{aq})]_{\text{tot}}} = \frac{\{[\text{LnL}]\text{A}_3\}_{\text{org}}}{[\text{Ln}^{3+}(\text{aq})] + [\text{LnL}(\text{aq})]}$$

The distribution coefficient of the ligand is one of the most important factors governing the magnitude of  $K_{\text{ex}}$ : the smaller  $D_{\text{L}}$  is, the larger the  $K_{\text{ex}}$  value will be. However, if the ligand itself is very soluble in water, the LnL complex will probably also be quite soluble, which in turn is unfavourable for a high extractability in the organic phase. A balance has therefore to be found.

When lanthanide ions  $10^{-5}$  M are extracted by 18-crown-6 ether  $10^{-2}$  M in 1,2-dichloroethane at 298 K in presence of 1 M trichloroacetate and at pH 3.0, distribution coefficients vary by three orders of magnitude between La (7.6) and Eu (0.004) and the difference between two consecutive lanthanide ions is large enough to obtain a good separation (for instance:  $D_{\text{Pr}} = 0.56$ ,  $D_{\text{Nd}} = 0.10$ ). This is comparable to the distribution coefficients obtained with one of the commonly used commercial extractants, di-2-ethylhexyl-phosphoric acid, and this performance may be increased by a factor 3–7 by addition of EDTA (ethylenediaminetetraacetate) in the aqueous solution. However, the improvement over the performance of commercial extraction agents is not large enough to trigger the development of extraction and separation processes entirely based on coronands, except in very specific cases. For instance  $^{90}\text{Y}$  has radioactive properties suitable for its use

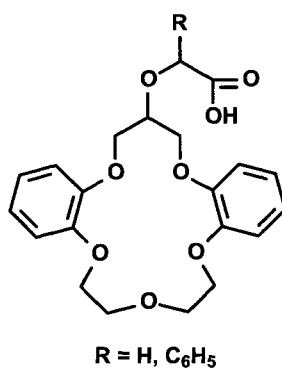


Fig. 4.23. A substituted 16-crown-5 ether used in extraction and separation studies.

in the production of labelled monoclonal antibodies for tumour therapy. It is produced from its parent isotope  $^{90}\text{Sr}$  and must therefore be separated from it to a high degree of purity. Ionisable crown ethers (i.e. crown ethers bearing a pendant arm fitted with a carboxylic acid function) such as *sym*-dibenzo-16-crown-5-oxyacetic acid and its derivatives (Fig. 4.23) can achieve purities larger than 99.9% in a single solvent extraction step from an aqueous solution into chloroform: the  $D_M$  values are 0.01 and 19 for Sr(II) and Y(III), respectively (at 298 K, metal concentration  $10^{-4}$  M, ligand concentration  $5 \times 10^{-3}$  M, pH 6.0). The same crown ether derivatives are highly efficient in separating the lanthanide ions from tetravalent thorium with a purity of 99.9% reached for Th(IV) in the organic phase, chloroform.

#### 34.4.2. Bioanalytical applications

Cryptands could also be used for this type of separation processes; however their cost, which is much higher than the cost of coronands, prevented development of practical extraction processes based on the macrotricyclic ligands. They have, however, found applications in biomedical analysis. For instance, the cryptand (bpy.bpy.bpy), obtained by linking three bipyridine units to two nitrogen bridgeheads, yields a stable and luminescent cryptate with Eu(III),  $[\text{Eu}(\text{bpy.bpy.bpy})]^{3+}$ , which is used in homogeneous fluoroimmunoassays. In these analyses (Fig. 4.24), an antigen (the analyte) is specifically reacted with two different antibodies, via biochemical reactions. Antibody A bears the Eu cryptate grafted onto it via a functional side chain. Antibody B bears an energy acceptor, which is an organic molecule (a chemically engineered allophycocyanin) absorbing in the red and having a large molar absorption coefficient. A UV light pulse is shined onto the solution and light is absorbed by the (bpy.bpy.bpy) cryptand. The energy is first transferred onto the triplet state of the cryptand via an intersystem crossing and secondly onto the Eu(III) ion. In principle, once excited the metal ion should give off a brilliant red luminescence with main lines at 590, 620, and 720 nm. However, the presence of the monoclonal antibody B at a not too large distance (10–20 Å) induces a third energy transfer process via a dipole–dipole mechanism onto the allophycocyanin. The latter finally emits red light at 660 nm. The experiment is performed in time-resolved mode, which allows for the elimination of the luminescence background emitted by the biological material

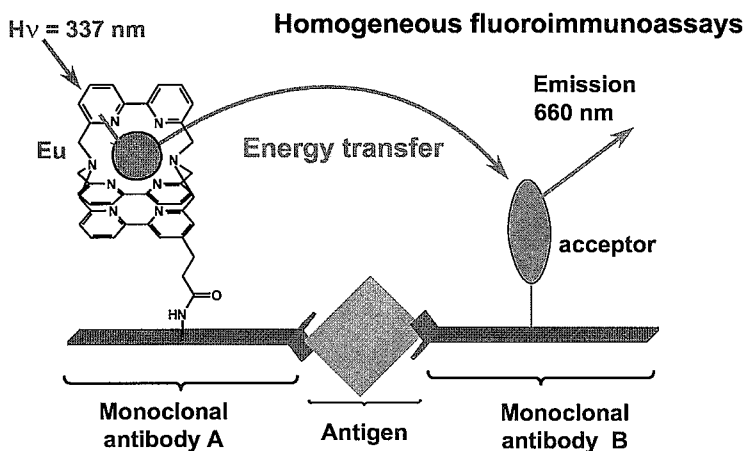


Fig. 4.24. Use of the europium cryptand  $[\text{Eu}(\text{bpy}.\text{bpy}.\text{bpy})]^{3+}$  in homogeneous fluoroimmuno-assays. Redrawn from Bünzli et al., *J. Alloys & Compounds* **303–304**, 66, 2000.

itself. Indeed, the latter is a fast decaying process (nano- to microsecond range), while the luminescence of Eu(III) is a slow, phosphorescence process (millisecond range). Moreover, since the experiments can be repeated every 1–2 milliseconds, signal averaging improves considerably the signal-to-noise ratio, henceforth the sensitivity of the analysis, which is in the range  $10^{-13}$ – $10^{-15}$  M. The light emitted by the Eu(III) ion coupled to the monoclonal antibody A and that emitted by this ion in the triplex are separated spectrally, which avoids chemical separation of the un-reacted monoclonal antibody A. This technique is now widely used in hospitals for common blood and urine analyses. It can also be applied for probing interactions in life sciences, such as protein–protein interactions or DNA hybridisation and these applications are presently triggering a wide interest among analytical chemists, biochemists and medical doctors.

A derivative of the (bpy.bpy.bpy) cryptand, obtained by modifying one of the chains,  $L_{\text{bpy}}$ , forms a di-protonated cryptate with  $\text{EuCl}_3$  in water at acidic pH,  $[\text{EuCl}_3(\text{H}_2L_{\text{bpy}})]^{2+}$  in which the metal ion is coordinated to the four bipyridyl and two bridgehead nitrogen atoms, and to the three chlorine ions (Fig. 4.25). The polyamine chain is not involved in the metal ion coordination, due to the binding of the two acidic protons within this triamine subunit. In solution, when chlorides are replaced by perchlorate ions, two water molecules coordinate onto the Eu(III) ion at low pH and one at neutral pH, a pH at which de-protonation of the amine chain occurs, allowing it to coordinate to the metal ion. As a result, the intensity of the luminescence emitted by Eu(III) is pH dependent since water molecules deactivate the metal ion in a non-radiative way. Henceforth, this system can be used as a pH sensor. Several other europium cryptates have been developed as luminescent labels for microscopy.

Recently, it has been proposed that the Eu(II) cryptate with (2.2.2) is a good contrast agent for magnetic resonance imaging (see section on cyclen derivatives below). Firstly, the electronic configuration of the ion is identical to the one of Gd(III); secondly, two water molecules can interact with the Eu(II) ion, which is ten coordinate in water, instead of

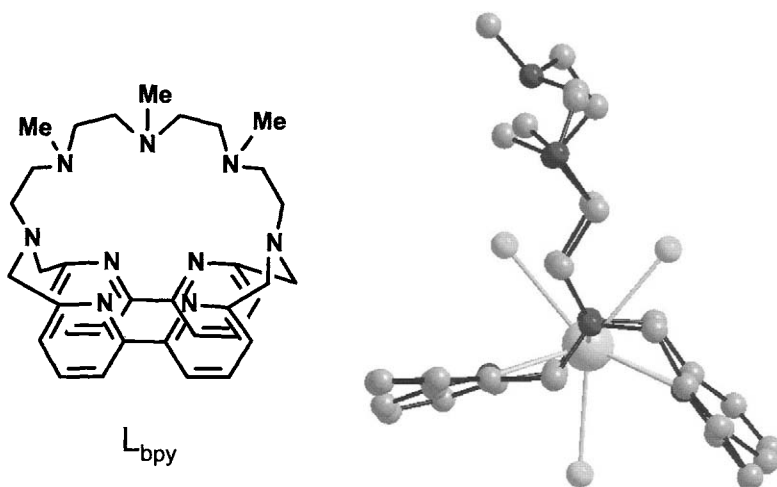


Fig. 4.25. Structure of the protonated cryptate  $[\text{EuCl}_3(\text{H}_2\text{L})]^{2+}$ . Redrawn from C. Bazzicalupi et al., Chem. Commun. 561, 2000.

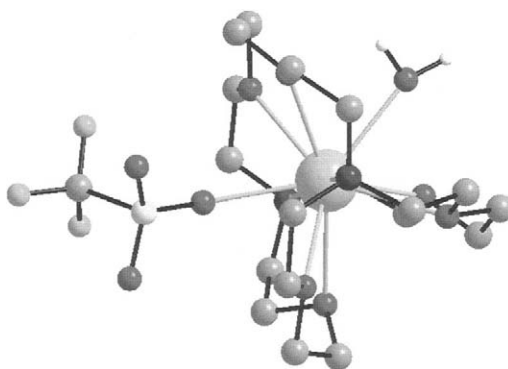


Fig. 4.26. Structure of  $[\text{Sr}(\text{CF}_3\text{SO}_3)(2.2.2)(\text{H}_2\text{O})]^+$  as a model for the structure of the corresponding cryptate with Eu(II). Redrawn from L. Burai et al., Chem. Commun. 2366, 2002.

only one in most of the Gd(III)-containing contrast agents, increasing the proton relaxivity. This is demonstrated by the crystal structure of the homologous Sr(II) cryptate (Sr(II) has the same ionic radius as divalent Eu) shown on Fig. 4.26. One clearly sees one water molecule interacting between two chains of the ligand, as well as one trifluoromethanesulfonate ion; in aqueous solution, the latter dissociates and is replaced by a second water molecule (as proved by <sup>17</sup>O-NMR measurements). Thirdly, the water exchange rate is larger than for Gd(III) contrast agents and the electron spin relaxation slower, two favourable factors. Finally the stability of the cryptate in water is large enough to be compatible with biomedical applications. Overall, this cryptate can be considered as being a synthon for the design of new contrast agents that could be redox-switched. Indeed, the Eu(III) ion has no effect on the proton relaxivity and therefore is not a potential contrast agent.

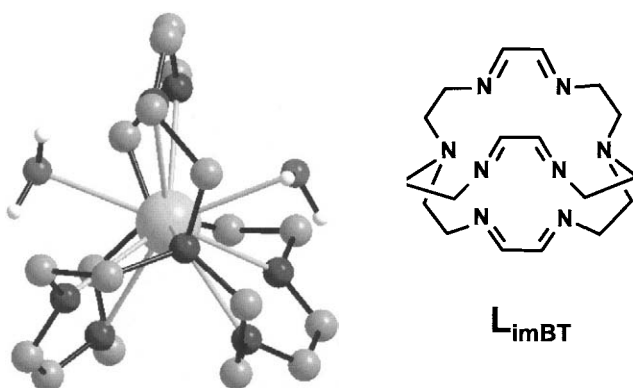


Fig. 4.27. Structure of the di-aqua gadolinium cryptate with  $L_{imBT}$ . Redrawn from S.W.A. Bligh et al., *J. Chem. Soc., Dalton Trans.* 3711, 1998.

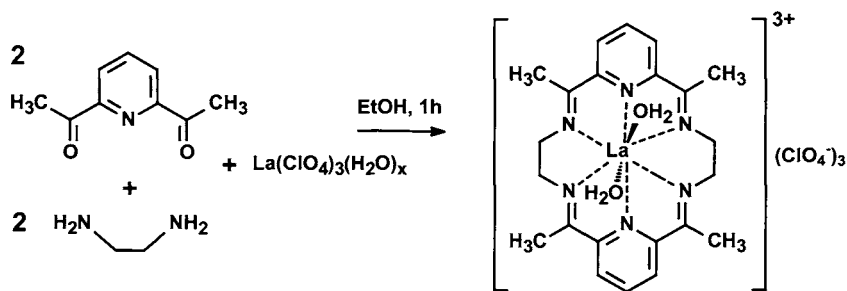


Fig. 4.28. Template effect used to synthesize a La(III) coronate. From W. Radecka-Paryzek, *Inorg. Chim. Acta* 45, L147, 1980.

As for the luminescent pH sensor described above, sensors relying on a change in relaxivity may also be designed that are pH sensitive. An example is the iminocryptand  $L_{imBT}$  which encapsulates the Gd(III) ion but has sufficient space between its imine chains to let two water molecules interact with the metal ion (Fig. 4.27). Above  $pH = 8$ , one of the water molecules is de-protonated and an hydroxo form of the cryptate is present. Therefore, the relaxivity (which is a measure of the efficiency of a contrast agent) is pH dependent and this cryptate works as a pH sensitive stain.

#### 34.5. Template effect

The synthesis of some coronands and cryptands involve several synthetic steps and, sometimes, high dilution techniques to avoid unwanted polymerisation, which considerably adds to the cost of the synthesis. In some instances, it is possible to simplify the synthetic procedure by using a templating agent, that is, a metal ion which pre-organizes the reactants in such a way that they do not polymerise and have the right orientation to yield the desired compound. One of the first examples of such template reaction in lanthanide macrocyclic chemistry was demonstrated by Wanda Radecka-Paryzek who isolated via a one-pot pro-

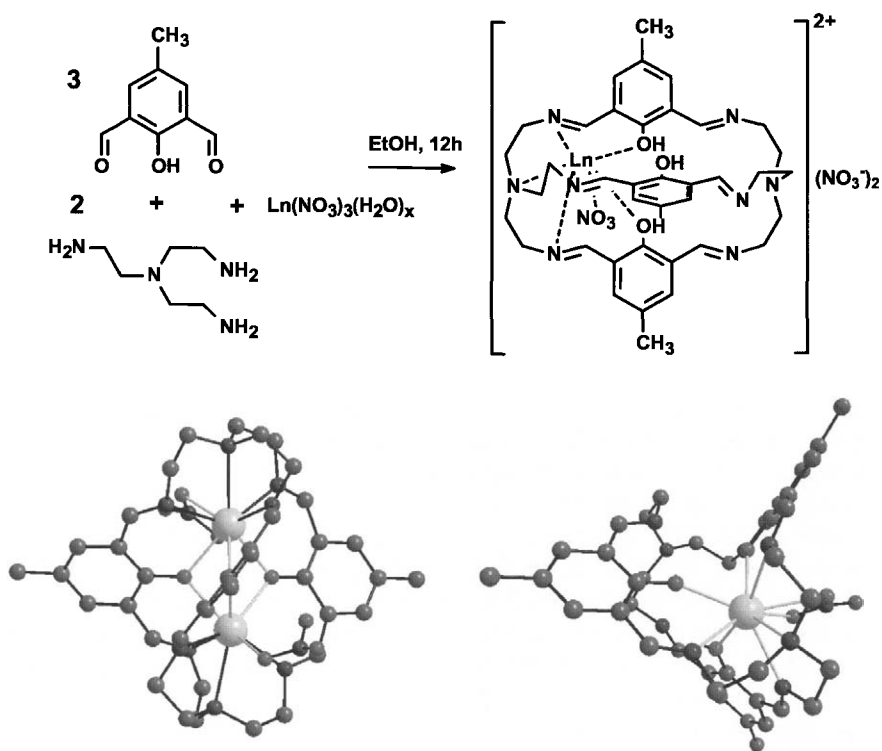


Fig. 4.29. Template effect used to synthesize a Nd(III) cryptate and its structure (bottom, right); redrawn from C. Platas-Iglesias et al., *Inorg. Chem.* **38**, 3190, 1999. Bottom left: structures of the 2:1 Dy(III) cryptate with the same ligand; redrawn from C. Platas-Iglesias, *J. Chem. Soc. Dalton Trans.* 611, 2000.

cedure a lanthanum coronate (Fig. 4.28). The author simply mixed hydrated lanthanum perchlorate and 2,6-diacetylpyridine in ethanol and after heating the solution to reflux, she added a solution of ethylenediamine in ethanol. A yellow-orange precipitate formed after one hour, which turned out to be the coronate depicted in Fig. 4.9.

An even more impressive process is the assembly of lanthanide cryptates from three molecules of 2,6-diformyl-4-methylphenol, three molecules of tris(2-aminoethyl)amine and one molecule of hydrated lanthanide trinitrate in ethanol to yield the monometallic cryptand  $[\text{Ln}(\text{NO}_3)(\text{L})](\text{NO}_3)_2$  shown for  $\text{Ln}=\text{Nd}$  on Fig. 4.29. If two molecules of lanthanide salt are used, a bimetallic cryptate forms, the ligand becoming trianionic:  $[\text{Ln}(\text{NO}_3)_2(\text{L}-3\text{H})](\text{NO}_3)$ ; the structure for  $\text{Ln}=\text{Dy}$  is also shown on the bottom left of Fig. 4.29; interestingly, the  $\text{Dy} \cdots \text{Dy}$  distance is quite short, 3.48 Å, and the cryptand adopts an *sss* *endo-endo* conformation. An antiferromagnetic interaction has been found in the GdGd cryptate, with  $J = -0.194 \text{ cm}^{-1}$ . The 1:1 cryptates can be used as starting materials for the isolation of 3d-4f dimetallic complexes with Zn(II), Cu(II) and Ni(II), for instance  $[\text{Ln}(\text{NO}_3)(\text{L}-3\text{H})\text{Zn}](\text{NO}_3)$ . In these entities, the ligand is helically wrapped around the two metal ions, leading to pseudo  $C_3$  symmetry and the three five-membered chelate rings of the ligand backbone coordinating the Ln(III) ion adopt a  $(\lambda\lambda\lambda)_5$  or  $(\delta\delta\lambda)_5$  conformation



while the three pseudo chelate rings formed by the coordination of the ligand to Zn(II) adopt a  $(\lambda'\lambda'\lambda')_5$  or a  $(\delta'\delta'\delta')_5$  conformation. The trianionic form of the cryptand acts as a fairly good sensitiser for the luminescence of Eu(III) and Tb(III) at low temperature. A ferromagnetic interaction takes place between Gd and Cu in the GdCu cryptate with  $J = 2.2 \text{ cm}^{-1}$ .

### 35. Complexes with porphyrins and phthalocyanines

Tetrapyrrole derivatives such as porphyrins or phthalocyanines (Fig. 4.30) are highly stable and have exceedingly delocalised  $\pi$  systems. Consequently, they exhibit a wide range of intriguing optical, electrical, magnetic and spectroscopic properties which render them useful in the fields of materials science, catalysis, biology and medicine. Since lanthanide ions have similarly fascinating properties, their combination with porphyrins and phthalocyanines has been investigated quite early, starting in the mid 1960's by the work of Kirin et al. who isolated  $\text{Ln}(\text{Pc})_2$  complexes ( $\text{Ln} = \text{Pr}, \text{Nd}, \text{Er}, \text{Lu}$ ) which are now well known electrochromic materials. Bis(porphyrinato) complexes  $\text{Ln}(\text{Por})_2$  have been first reported by Buchler et al. in 1983. Since the lanthanide ions are larger than the core size of the rings in Pp and Pc complexes, the metal centres are usually situated out of the ring. Generally speaking, two main types of complexes have been isolated: (i) half-sandwiches (1:1), in which the coordination sphere of the lanthanide ion is completed by the binding of small uni- or bidentate ligands and (ii) 1:2, sandwich compounds (double-decker complexes) in which the metal ions are inserted between two parallel rings. The former compounds are good and specific NMR shift reagents which have been used to probe the structure of proteins; they are also interesting precursors for the synthesis of sandwich compounds. Other stoichiometries include 2:2 and 2:3 complexes, the latter being referred to as "triple decker" compounds (Fig. 4.30). When the ligands are fully deprotonated, either 1:1 or 2:3 stoichiometries are found while 1:2 complexes mainly form with tetravalent cerium.

The structure of two cerium complexes with octaethylporphyrin are reported in Fig. 4.31. On the left hand side, tetravalent cerium is sandwiched between two macrocyclic ligands. It is eight coordinate in an almost perfect square antiprism geometry: the porphyrin rings are rotated by about  $42^\circ$  with respect to their eclipsed conformation. The macrocycles are convex and somewhat distorted from planarity. The right hand side of the figure features a Ce(III) triple decker, with an inversion centre located between the two cerium ions. Therefore, the two external macrocycles have exactly the same orientation with respect to the internal one. The metal ions are again eight coordinate, but the coordination polyhedra are more distorted with respect to the ideal square antiprism than the one of the Ce(IV) ion; the mean value of the rotational angle of two macrocycles is  $24.5^\circ$ . Since the internal ring is coordinated to two Ce(III) ions, the distance between the latter and the metal ion is substantially longer than with respect to the external ligands (ca. 1.9 versus 1.4 Å).

In solution, the porphyrin rings undergo free rotation, unless this process is hindered by sterically demanding substituents. For instance, if four dimethoxyphenyl groups are grafted in the R positions of the porphyrin depicted in Fig. 4.30, the ring rotation is sufficiently slowed down for the enantiomeric rotamers to be separated by chiral high performance

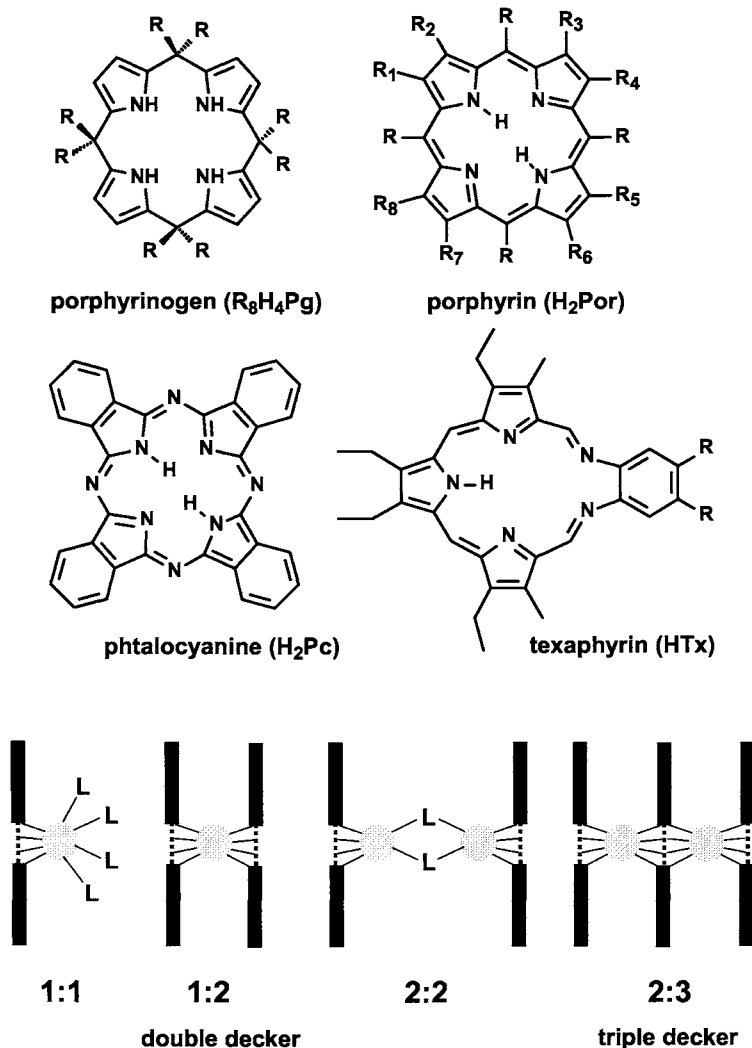


Fig. 4.30. Formulae of tetrapyrrole-based ligands, together with a schematic representation of the potential structures of the complexes.

liquid chromatography. On the NMR time scale, no rotation is seen up to  $110^\circ\text{C}$  and no ligand exchange is observed, although there is a slow racemisation. The reduction of Ce(IV) into Ce(III) accelerates the rate of racemisation approximately 300-fold. In an important study, Seiji Shinkai has exploited the chirality of the rotamers for molecular recognition of chiral dicarboxylic acids (Fig. 4.32). He designed a tetrasubstituted porphyrin with pyridine groups (R position, see Fig. 4.30). Each nitrogen atom of the pyridine moieties may bind a carboxylic acid function through a hydrogen bond. If a chiral dicarboxylic acid is chosen in which the acid functions are separated by a  $C_2$  spacer, two

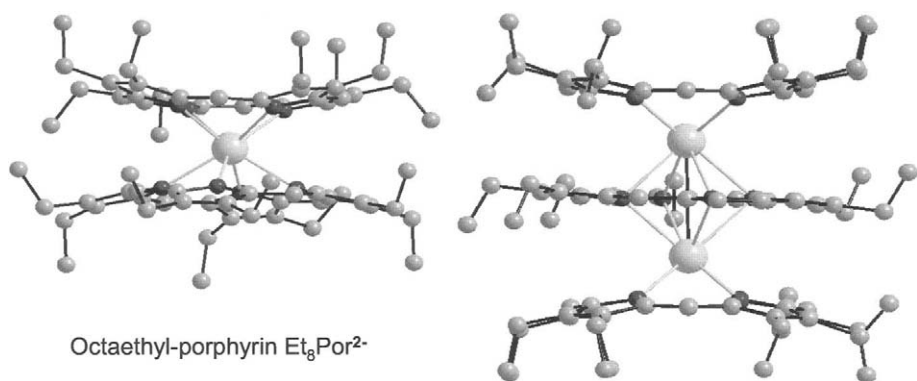


Fig. 4.31. Structures of two complexes of cerium with octaethylporphyrin: double-decker (or sandwich)  $\text{Ce}^{\text{IV}}(\text{Et}_8\text{Por})_2$  (left) and triple-decker  $\text{Ce}_2^{\text{III}}(\text{Et}_8\text{Por})_3$  (right). Redrawn from J.W. Buchler et al., *J. Am. Chem. Soc.* **108**, 3652, 1986.

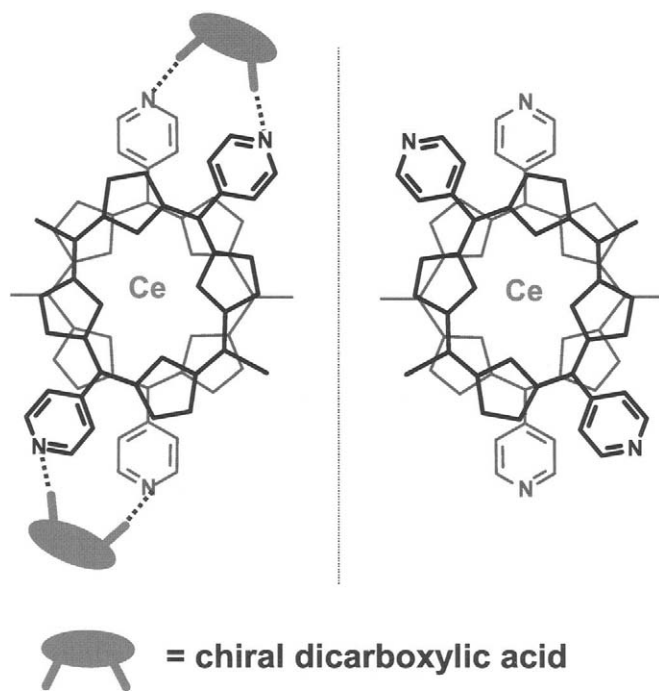


Fig. 4.32. Chiral recognition and induction of molecular memory in  $\text{Ce}(\text{IV})$  complexes with a substituted porphyrin. Redrawn from S. Shinkai et al., *J. Chem. Soc., Perkin Trans. I* 3259, 1999.

interactions are generated with a particular rotamer, which locks the top and bottom rings of the sandwich  $\text{Ce}(\text{IV})$  complex, preventing ring rotation. The supramolecular binding of a second guest is now facilitated by what is called a positive allosteric effect. Addition of

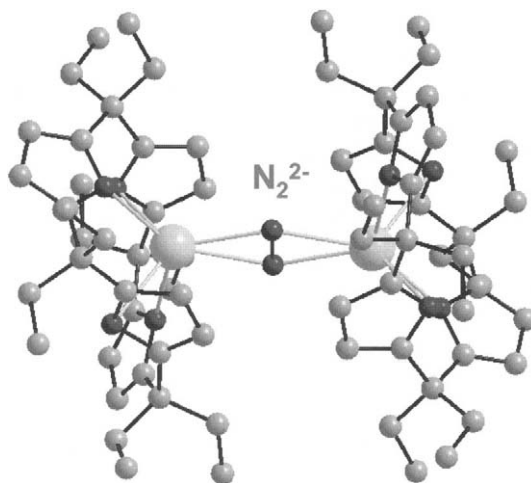


Fig. 4.33. Activation of a dinitrogen molecule by complexation two Nd(III) ions bonded to *meso*-octaethylporphyrinogen, forming a  $N_2^{2-}$  anion. Only the central part of the structure is shown. Redrawn after E. Campazzi et al., Chem. Commun. 2603, 1998.

a base to the solution will destroy the hydrogen bonds and the racemisation process will start. However, the latter is very slow, with a half life of three hours at room temperature (one year at  $-37^\circ\text{C}$ ), so that, the authors speak of molecular memory.

Another fascinating application is the use of lanthanide sandwich complexes with *meso*-octaethylporphyrinogen (Fig. 4.30) to induce the activation of small molecules. In the case of dinitrogen activation, complexes with 1:1 stoichiometry  $\text{Na}[\text{Ln}(\text{Et}_8\text{Pg})](\text{solv})_x$  are first formed by reacting  $\text{Et}_8\text{H}_4\text{Pg}$  in tetrahydrofuran (THF) with metallic sodium and, subsequently, with lanthanide trichloride ( $\text{Ln}=\text{Pr}, \text{Nd}$ ). The 1:1 intermediates are then reduced by metallic sodium under dinitrogen atmosphere and in the presence of traces of naphthalene to yield  $\text{Na}_4\{[\text{Ln}(\text{Et}_8\text{Pg})]_2(\text{N}_2)\}(\text{THF})_4$  which can be recrystallized in dimethoxyethane (Pr) or dioxane (Nd). Fig. 4.33 illustrates the activation of dinitrogen by two Nd(III) ions; each lanthanide ion is connected to one macrocyclic ligand and to the two nitrogen atoms of a dinitrogen di-anion acting as a bridging ligand. One sodium ion is also bonded to each nitrogen atom from the di-anion and complete their coordination sphere by interacting with one nitrogen atom from a pyridine unit and a solvent molecule. That dinitrogen is effectively reduced to its  $-2$  state is proven by the N–N distance ( $1.23 \text{ \AA}$ ), while magnetic susceptibility measurements confirm that the Nd(III) ions retain their  $+3$  oxidation state and the absence of magnetic interaction between them. The compounds are stable and no loss of  $\text{N}_2$  is observed, even under vacuum. Similarly, acetylene and ethylene can be activated to yield complexes with a structure close to the one depicted on Fig. 4.33, except that  $N_2^{2-}$  is replaced by  $C_2^{2-}$  or  $C_2H_4^{2-}$ .

Phthalocyanine triple decker complexes have been used by N. Ishikawa et al. in 2002 to detect f–f interactions in a series of homodimetallic  $\text{PcLnPcLnPc}^*$  compounds, where  $\text{Pc}^*$  denotes a phthalocyanine octa-substituted by butoxy groups. The temperature dependence of the magnetic susceptibility of these triple deckers has been compared to the same data

for compounds in which one paramagnetic Ln(III) ion is replaced by a diamagnetic Y(III) ion. The observed variations point to ferromagnetic interactions occurring between (Tb, Tb), (Dy, Dy) and (Ho, Ho) pairs, while the interaction between the (Er, Er) and (Tm, Tm) pairs is antiferromagnetic. These data, as well as the fact that the (Yb, Yb) interaction is almost negligible can be rationalized on the basis of a ligand-field analysis.

Porphyryns have low lying triplet states, between 12 500 and 14 500  $\text{cm}^{-1}$ , so that they are ideally suited to sensitise the luminescence of lanthanide ions emitting in the near infrared, such as Nd(III) and Yb(III). Indeed, f-f transitions are forbidden and therefore one has to resort to energy transfer processes from the matrix in which the ion is inserted in the case of ionic compounds, or from the ligand in coordination compounds. In the latter, the transfer usually goes through the triplet state of the ligand because it is long-lived as are the excited states of the lanthanide ions. For an efficient transfer, the energy of the triplet state must lie about 2–5000  $\text{cm}^{-1}$  above the excited state. A great deal of ytterbium and neodymium complexes with substituted porphyrins have therefore been studied. Indeed, the Yb(III) luminescence originates from the  $^2F_{5/2}$  level, located slightly above 10 000  $\text{cm}^{-1}$ , and terminates on the  $^2F_{7/2}$  level. Its wavelength is approximately 1  $\mu\text{m}$ . The Nd(III) luminescence includes three transitions from  $^4F_{3/2}$  to  $^4I_{13/2,11/2,9/2}$  corresponding to bands around 0.9, 1.06 and 1.35  $\mu\text{m}$ . The corresponding complexes with phthalocyanines are non-luminescent because the triplet states lie at too low energy. The overall quantum yields remain modest, between 0.2 and  $5 \times 10^{-3}$  for Nd(III) and Yb(III) porphyrinates, because de-excitation processes induced by high-energy vibrations are very effective in view of the small energy gap between the excited and ground states (10 000–11 000  $\text{cm}^{-1}$ ). Nevertheless, the photophysics of lanthanide porphyrinates is attractive because it could be of great help in medicine. For instance, hematoporphyrin derivatives are known to accumulate in malignant tumours and are used in medical diagnosis and photodynamic therapy of cancer. It is noteworthy that the Yb(III) complex with *meso*-tetra(3-pyridyl)porphyrin displays a substantial quantum yield (1.4%) when inserted into micelles formed by the non-ionic surfactant Triton X-100, a medium that can be considered as a model for biological tissues.

### 35.1. Analytical applications

Bis(phthalocyanine) lanthanide compounds  $\text{LnPc}_2$ , similar to other metallophthalocyanines, have physical properties that can be exploited to develop analytical sensors and actuators, especially for gases. For instance,  $\text{LnPc}_2$  complexes have high intrinsic conductivities, in the range  $10^{-6}$  to  $10^{-3}$   $\text{S cm}^{-1}$  at 300 K, and they react with electron donor or electron acceptor gases. Selectivity may be tuned by changing the metal ion and/or by incorporating functional groups on the aromatic rings. The sensors are based on the Langmuir–Blodgett film technology, which provides means for a precise control of the surface, the organisation and the thickness of the films. With the idea of developing an electronic nose, researchers from the University of Valladolid in Spain have explored the possibility of using  $\text{LnPc}_2$  Langmuir–Blodgett films to analyse olive oil aroma. The exposure of the films to olive oil aroma causes a fast and reversible increase of the resistivity which is very selective depending on the nature of the oil (Fig. 4.34). An array formed by five sensors has been designed which, coupled with pattern recognition techniques, is able to discriminate between olive oils of different qualities.

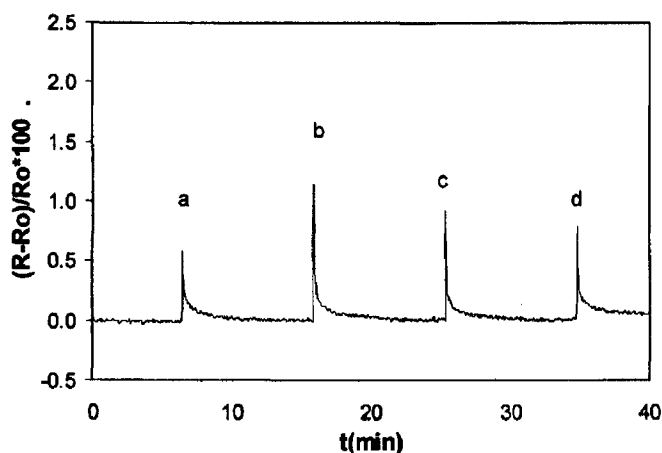


Fig. 4.34. Typical response of a  $\text{LuPc}_2$  Langmuir-Blodgett film expressed as the fractional change in resistance  $(\Delta R/R) \times 100$  towards (a) refined olive oil; (b) lampante olive oil; (c) extra virgin olive oil and (d) ordinary olive oil. Reproduced with permission from N. Gutierrez et al., *Sensors and Actuators B* **77**, 437, 2001.

### 35.2. *Texaphyrins and their medical applications*

At the end of the 1980's, John Sessler from the University of Texas at Austin developed a new class of pyrrole-based expanded porphyrins that he named "texaphyrins" (see Figs 4.30, 4.35). Like the porphyrins, texaphyrins are fully aromatic and highly coloured. They are, however dark green rather than purple, their lowest energy transition falling at 700 nm instead of 620 nm for porphyrins. Texaphyrins are mono-ionic ligands with a central core 20% larger than that of porphyrins and they are capable of binding a variety of metal cations, including lanthanide ions, and stabilizing a number of unusual coordination geometries. Lanthanide complexes with several texaphyrin derivatives have been studied ( $R = \text{CH}_3$ ,  $\text{OCH}_3$ ,  $\text{O}(\text{CH}_2)_3\text{OH}$  for instance). The structure of the gadolinium complex with the texaphyrin HTex1 contains cationic species  $[\text{Gd}(\text{NO}_3)(\text{MeOH})_2(\text{Tex1})]^+$  with a nine coordinate metal ion (Fig. 4.35); the Gd(III) ion is ligated by the five nitrogen atoms of the ligand, one bidentate nitrate ion and two molecules of methanol; it sits at approximately 0.6 Å from the plane of the five nitrogen atoms.

Both porphyrins and texaphyrins are difficult to oxidise, but it turns out that lanthanide complexes with texaphyrins are far easier to reduce than typical metalloporphyrins. For example, the following potentials have been measured versus normal hydrogen electrode in DMF:  $E_{1/2} = -0.041$  and  $-0.044$  V for Gd and La complexes with HTex2 (Fig. 4.36) as compared to  $-1.41$  V for a Zn(II) octaethylporphyrinate. This fact, coupled with the observation that texaphyrins show the tumour selectivity characteristics of many porphyrins, led to testing GdTex2 as an enhancing agent in X-ray radiation therapy. In addition, the GdTex2 complex presents a sizable relaxivity so that it is detectable by magnetic resonance imaging techniques, allowing non-invasive evaluation of its localization in tissues (and, of course of its elimination from tissues). It has been demonstrated that this agent works particularly well in vivo, and clinical tests are under way.

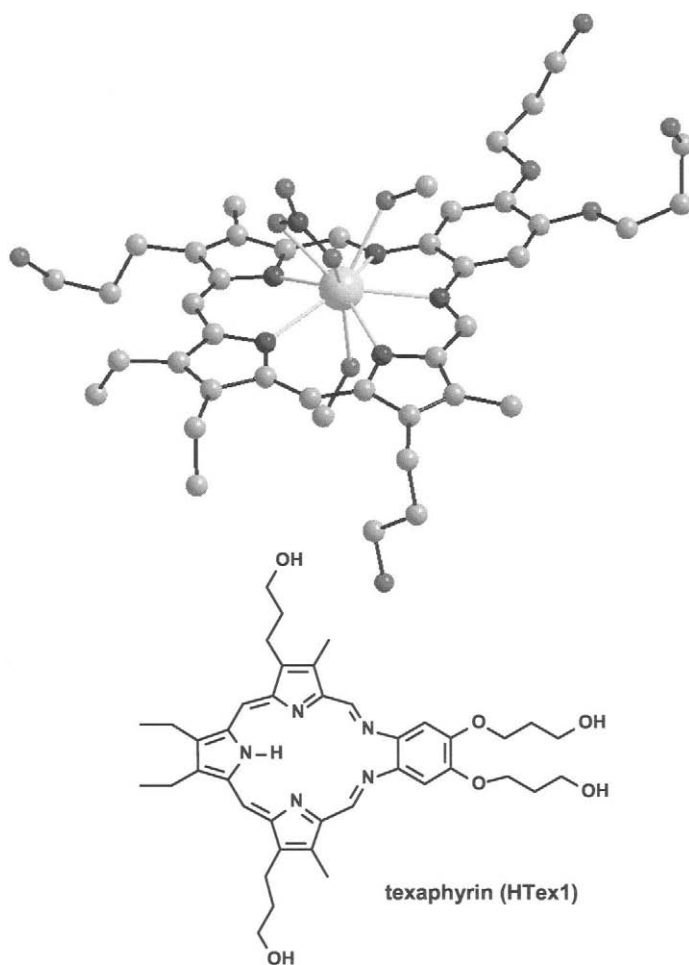


Fig. 4.35. Structure of  $[\text{Gd}(\text{NO}_3)_2(\text{MeOH})_2\text{Tex1}]^+$ , redrawn from J.L. Sessler et al., *Inorg. Chem.* **32**, 3175, 1993.

Another method for curing cancer is photodynamic treatment. In this type of treatment, a photosensitiser is administered via intravenous injection and localizes in the cancerous region. Visible light is used to activate the sensitiser and to produce singlet oxygen, the cytotoxic agent. Adequate photosensitisers are not easy to find and very few have been approved by the American Federal Drug Administration, among them, a sodium porphyrinate. It turned out that LuTex2 can do the job, being a good sensitiser for the singlet oxygen production. Additionally, it has several advantages over the previous sensitisers: it is water-soluble, which renders its administration easy, it is a well defined compound and its absorption maximum is at 732 nm, a wavelength at which most of the body tissues are transparent. It produces singlet oxygen with a yield between 20 and 70% depending on the experimental conditions. The compound has been tested *in vivo* and is presently in phase II of clinical tests.

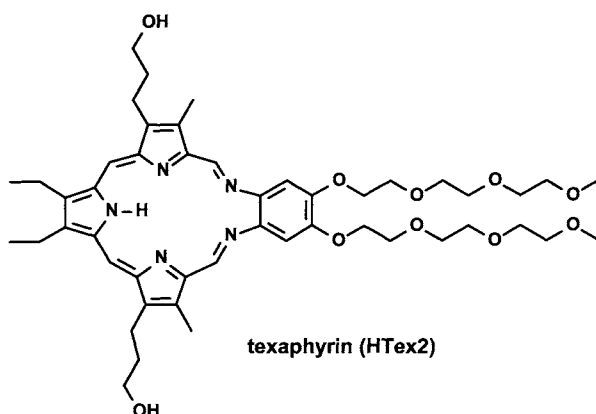


Fig. 4.36. Developed formula of HTex2.

### 36. Coronands fitted with pendant arms

#### 36.1. Lariat crown ethers

The application of the *induced fit* principle requires the grafting of pendant arms on coronands; these usually bear additional donor atoms in order to better match the coordination requirements of the lanthanide ions and, also, in order to protect them from solvent interaction. Sometimes, such structural modifications are solely done to improve the solubility of the resulting complexes. These coronands represent a large number of novel structures and have been prepared by numerous research groups. One example of a coronand fitted with one additional arm has already been presented when discussing the  $^{90}\text{Y}/^{90}\text{Sr}$  separation (Fig. 4.23). Introducing sidearms is usually easier when oxygen atoms of the ring are replaced by nitrogen atoms, which are designated as being the “pivots”. When the sidearm(s) can co-operate in the cation binding, the resulting coronands are termed “lariat crown ethers”, but this name is now loosely applied to nearly any structure having a sidearm, whether or not binding is involved. The term “lariat” comes from the image that the derivatised coronand binds the cation in much the same way as a lasso is used to rope and tie a farm animal. When two or more arms are attached to the macrocycle, this image breaks down, so that the Latin word *bracchium* (arm) is used: two-armed coronands are called *bibracchial lariat ethers* (sometimes referred to as *BiBLEs*); likewise, three-armed systems are now *tribracchial lariat ethers*.

The introduction of a side-chain can alter considerably the properties of the coronates. As an example, the quantum yield of the blue-green  $\text{Eu}(\text{II})$  emission ( $460\text{--}490\text{ nm}$ ,  $4f^65d \rightarrow 4f^7$ ) of the 1:2 coronate with 12C4 in methanol increases from 3.6% to 14% if the parent 12-crown-4 ether is replaced by the lariat ether  $\text{MeO}12\text{C}4\text{N}$  (10-(2-methoxyethyl)-1,4,7-trioxa-10-azacyclododecane) sketched in Fig. 4.37. On the other hand an opposite effect is obtained with the 15-membered coronands, mainly because the stoichiometry of the complex with 15-crown-5 ether in solution is 1:3 (quantum yield 28% in methanol) whereas it is only 1:1 with the lariat ether ( $Q = 0.3\%$ !).



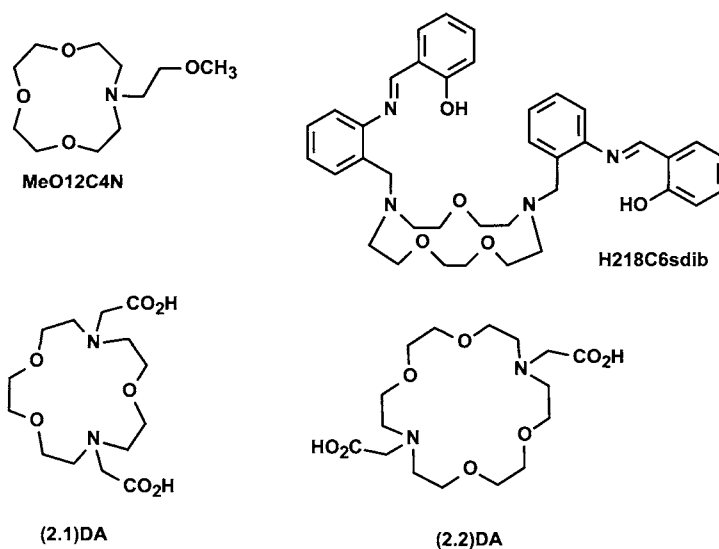


Fig. 4.37. Chemical structures of some lariat crown ethers.

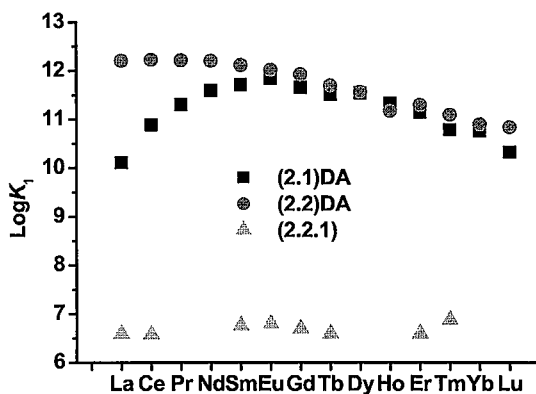


Fig. 4.38. Stability constants in water at 298 K and  $\mu = 0.1$  M, for lanthanide complexes with the (2.2.1) cryptand and the bibracchial lariat ethers (2.1)DA and (2.2)DA. From data reported by J.-C.G. Bünzli, in: Handbook on the Physics and Chemistry of Rare Earths, eds K.A. Gschneidner Jr., L. Eyring, Vol. 9, Ch. 60, North Holland, Amsterdam, 1987.

Increasing the stability of the coronates is also one of the goals achieved by introducing pendant arms. As an example, the stability constants, in water and at 298 K, of the 1:1 complexes with two coronates fitted each with two carboxylic acid arms, (2.1)DA and (2.2)DA (see Fig. 4.37), are plotted in Fig. 4.38, along with similar data for the cryptates with (2.2.1). With respect to the latter, the bibracchial lariat coronates are 5–6 orders of magnitude more stable, mainly in view of the anionic carboxylate coordinating groups. The stability difference between the two series of coronates is only sizeable for lanthanum

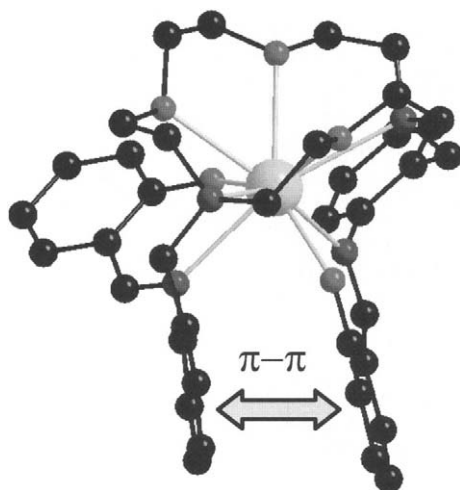


Fig. 4.39. Structure of  $[\text{Ce}(\text{15C5sdb})]^+$  showing the  $\pi-\pi$  interaction inducing a cryptand-like cavity. Redrawn from M. Gonzales-Lorenzo et al., *Inorg. Chem.*, 2003, in press.

(2 orders of magnitude) and diminishes quickly with increasing atomic number to fade off at Eu.

If the substituents on the arms are chosen in such a way that they may interact via non-covalent interactions, an induced cryptand-like cavity may be generated. This is the case with the di-deprotonated form of the bibracchial lariat ether *N,N'*-bis(2-salicylaldiminobenzyl)-1,10-diaza-15-crown-5 ( $\text{H}_2\text{18C6sdb}$ ). The receptor is prepared in situ by the condensation of *N,N'*-bis(2-aminobenzyl)-1,10-diaza-15-crown-5 and salicylaldehyde and the complexes are isolated by reacting the lariat ether with lanthanide perchlorates in 2-propanol. The X-ray crystal structure of  $[\text{Ce}(\text{15C5sdb})](\text{ClO}_4)\cdot\text{C}_3\text{H}_8\text{O}$  shows two different complexes. In both of them, the metal ion is nine-coordinated by the five donor atoms of the macrocycle and by the four donor atoms of the two arms, arranged in a distorted monocapped square antiprismatic geometry. The metal ion is deeply buried in the cavity of the di-anionic receptor which presents a cryptand-like structure in the solid state due to the formation of a second macroring through  $\pi-\pi$  interaction between one of the phenol rings and one of the benzyl rings. Indeed, the coordination of both side arms to the Ce(III) ion brings the aromatic rings close together and nearly parallel, and so that weak intra-molecular  $\pi-\pi$  interactions are possible, the distance between the two aromatic planes being 3.82 and 3.97 Å for the two complex molecules and the dihedral angles 16° and 12°, respectively (Fig. 4.39).

### 36.2. Cyclen derivatives

One of the most studied class of macrocyclic ligands in lanthanide coordination chemistry is without any doubt the molecules derived from cyclen, a 12-membered ring bearing four amino functions. In particular, its tetracarboxylic derivative  $\text{H}_4\text{DOTA}$  (see Fig. 4.40) was synthesized in 1976 by a German chemist, H. Stetter from the University of Aachen,

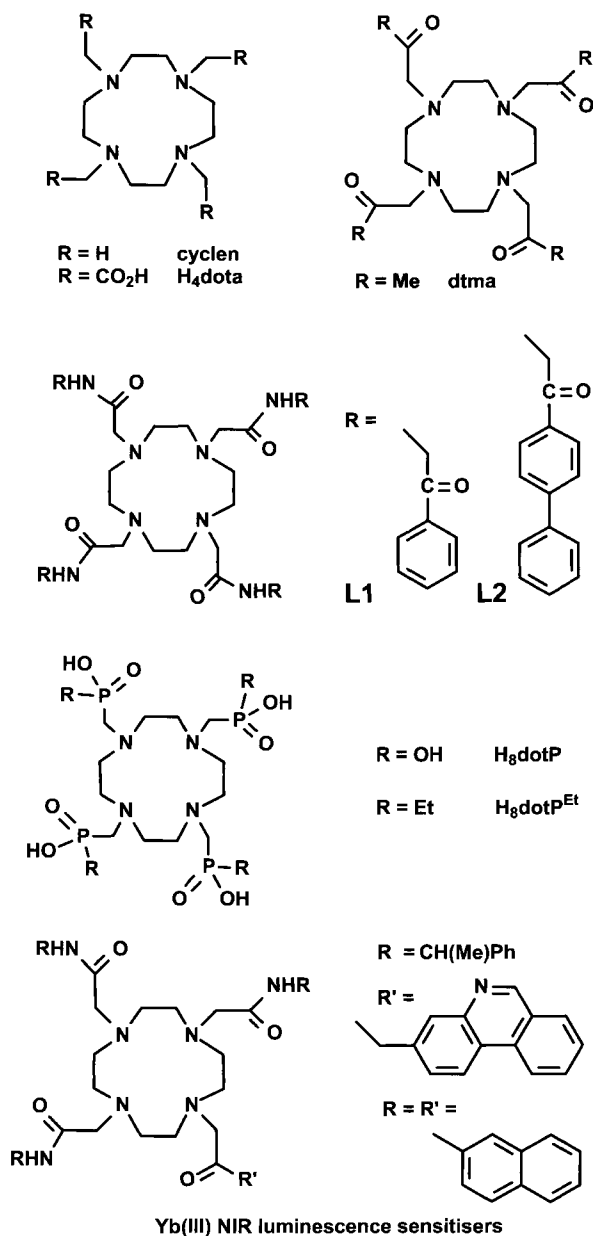


Fig. 4.40. Chemical structure of some cyclen derivatives.

who isolated complexes with divalent transition metal and alkaline-earth cations. The tetracarboxylic acid has  $pK_a$  values of 11.1, 9.69, 4.84 and 3.95 ( $\mu = 0.1$  M KCl). Three years later, a young Belgian chemist, Jean François Desreux from the University of Liège, discovered that DOTA forms highly stable complexes with lanthanide ions, with  $\log K_1$  in

the range 25–28, and that these complexes are also highly kinetically inert. At that time, the medical industry was looking for good contrast agents able to enhance the sharpness of magnetic resonance images and trivalent gadolinium was an obvious candidate in view of its  $7/2$  spin.

Indeed, magnetic resonance imaging (MRI) relies on the fact that in the presence of a magnetic field, hydrogen nuclei have two nuclear spin states with different energy; when a radiofrequency field of adequate energy is applied, that is matching the energy difference between the proton spin states, the higher energy level is populated. When the field is turned off, the proton nuclei return to their ground state in order to reach again thermal equilibrium, inducing a radiofrequency signal in a suitably positioned coil and so the concentration of protons can be monitored. In medical imaging, magnetic gradients are used, which define the spatial coordinates of the resonating protons and therefore, a two- or three-dimensional image can be obtained. The chemical environment of a proton affects the rate of return to thermal equilibrium; direct loss of energy to the environment is characterised by a longitudinal relaxation time  $T_1$  (the de-excitation decay is exponential) while interactions with other protons represent another de-activation path, characterised by a transverse relaxation time  $T_2$ . If the experiment is carried out in a pulse mode, not only can the concentration of protons be determined but, also, the relaxation times. From a physiological viewpoint, the measured signal mainly comes from the protons of water in the tissues and the relaxation times depend on the nature of a given tissue. For instance,  $T_1$  ranges from 150 and 500 ms, while  $T_2$  is shorter (40–150 ms). Moreover, these times are different for normal tissues and pathology. Small quantities of paramagnetic species can considerably reduce the  $T_1$  and  $T_2$  relaxation times. This occurs because the magnetic field associated with the spin of unpaired electrons oscillates at the frequency at which the hydrogen nuclei precess in a magnetic field (the Larmor frequency), allowing energy transfer between the protons and the spins, which adds a third de-excitation path. Henceforth the reduction in both  $T_1$  and  $T_2$ . If the magnetic species can be brought close to the carcinogenic cells, one will be able to better differentiate the radiofrequency signal emitted by its protons upon relaxation compared to that from normal tissue. The effect is proportional to the number of unpaired electrons and the ability to reduce the relaxation time is called “relaxivity” and is measured in  $\text{s}^{-1} \text{mM}^{-1}$ .

However, Gd(III) is very toxic ( $\text{LD}_{50}$  for gadolinium chloride is  $0.4 \text{ mmol kg}^{-1}$  for mice) because its ionic radius is almost equal to that of Ca(II), resulting in competition with calcium in a number of calcium-dependent systems. Many proteins exhibit a higher binding affinity up to 1000 fold for Gd(III) compared with Ca(II) in view of the higher charge density of the former cation. Therefore, Gd(III) has to be inserted into a very stable and highly inert complex before being injected into patients. Ligand DOTA does the job very well and in 1988, a French company, Guerbet SA, filed a patent for meglumine gadoterate,  $[\text{Gd}(\text{DOTA})(\text{H}_2\text{O})]^{-}(\text{mg})^{+}$ , under the registered trade mark Dotarem<sup>™</sup>. The structure of  $[\text{Gd}(\text{DOTA})]^{-}$  is shown on Fig. 4.41, where one clearly sees the folding of the four carboxylate groups, the monocapped square antiprismatic coordination geometry and the exchanging water molecule. The latter is essential; indeed the effect of the paramagnetic ion on the relaxation of the protons only occurs when the distance is relatively short and therefore a crucial factor in determining the relaxivity of a potential contrast agent is the water exchange rate, which is very fast for the trivalent gadolinium ion ( $10^9 \text{ s}^{-1}$ ); the water

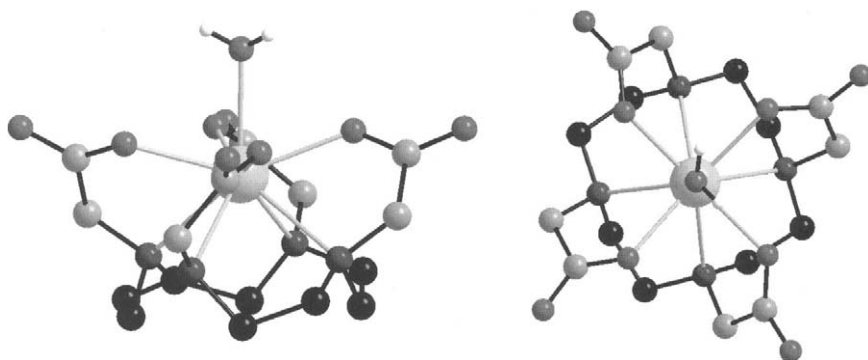
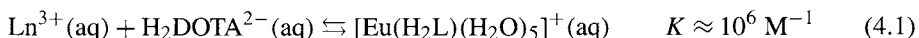


Fig. 4.41. Two views of the structure of  $[\text{Gd}(\text{DOTA})]^-$  showing the encapsulation of the metal ion by the four pendant arms (left) and the  $C_4$  symmetry (right, top view). Redrawn from C.A. Chang et al., *Inorg. Chem.* **32**, 3501, 1993.

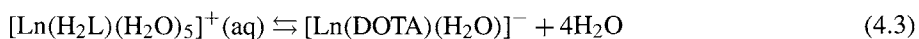
exchange mechanism is dissociative and steric crowding at the water site will enhance the exchange rate. On the other hand, the formation of the  $[\text{Ln}(\text{DOTA})(\text{H}_2\text{O})]^-$  species is rather slow since it corresponds to considerable rigidification of the ligand. Detailed kinetic studies show the following reaction mechanism to be operative:



In a first step, an intermediate species forms rapidly upon mixing the lanthanide ion with  $\text{H}_4\text{DOTA}$ . Both excited state luminescence lifetime determinations (for  $\text{Eu}^{3+}$ ) and molecular mechanics calculations are consistent with a structure in which the lanthanide ion is coordinated to four carboxylate groups, well away from the nitrogen atoms of the macrocycle, two of which are protonated. This intermediate may react with a hydroxide group to form a monoprotonated neutral species in a rapid equilibrium.



Finally, the monoprotonated species rearranges into the final product:



The rate of conversion of  $[\text{Ln}(\text{H}_2\text{L})(\text{H}_2\text{O})_5]^+(\text{aq})$  into  $[\text{Ln}(\text{DOTA})(\text{H}_2\text{O})]^-$  is pH-dependent and ranges from  $7.2 \times 10^{-4}$  to  $7.9 \times 10^{-2}$  for  $\text{Ln} = \text{Eu}$  as the pH is raised from 3.8 to 5.8; similar values are obtained for  $\text{Ln} = \text{Gd}$ . Dissociation of the  $\text{Gd}$ -DOTA complex is also very slow and its half-life in a 0.1 M solution of hydrochloric acid is larger than one month. The usual dose for an experiment is  $0.1 \text{ mmol kg}^{-1}$ , there are few side effects and excretion is reasonably fast (75% in three hours).

Since the introduction of Dotarem<sup>TM</sup>, a wealth of studies have been devoted to this complex and to complexes with coronands derived from the cyclen framework, both for contrast agent capability and, more recently, for analytical sensors based on relaxivity

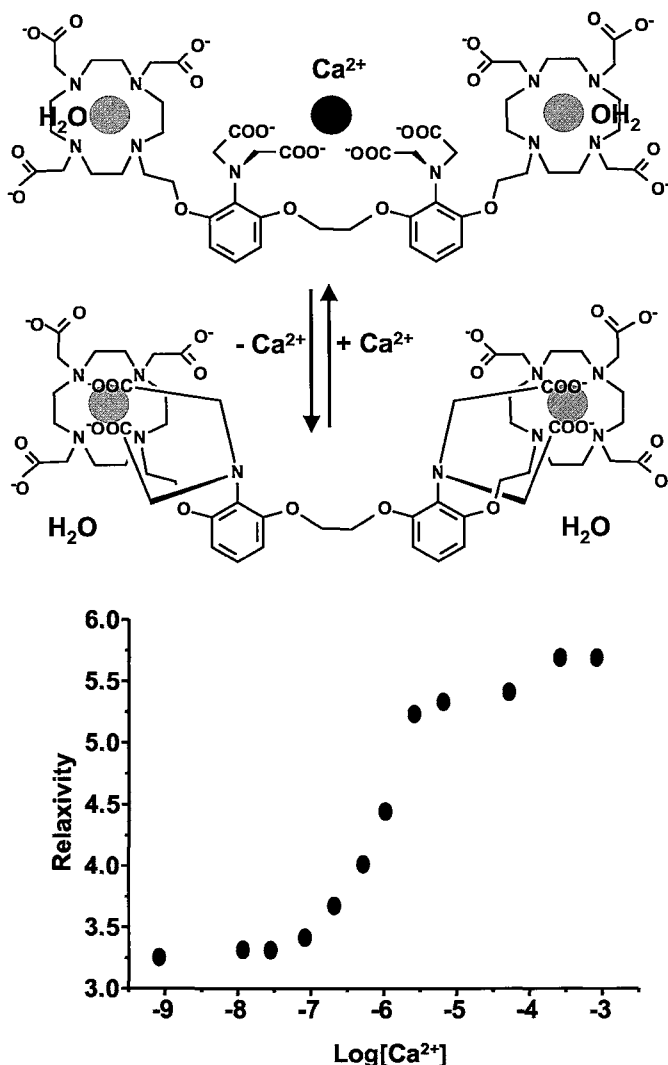


Fig. 4.42. Supramolecular calcium sensor based on relaxivity measurement. From W.H. Li et al., *J. Am. Chem. Soc.* **121**, 1413, 1999.

switching. One typical example is a calcium-sensor proposed by Thomas Meade from CalTech (Fig. 4.42). The sensor is built from a known and selective calcium complexation agent to which are attached two  $[\text{Gd}(\text{DOTA})]^-$  macrocycles. When the calcium ion is bound, the Gd(III) coordination sphere is completed by a water molecule and the relaxivity of the supramolecular edifice is high. Upon calcium release, the carboxylic arms of the central units bend over the DOTA units to bind the Gd(III) ions, expelling the water molecules, so that the relaxivity is now almost zero. The device is therefore a direct measure of the calcium concentration in solution.

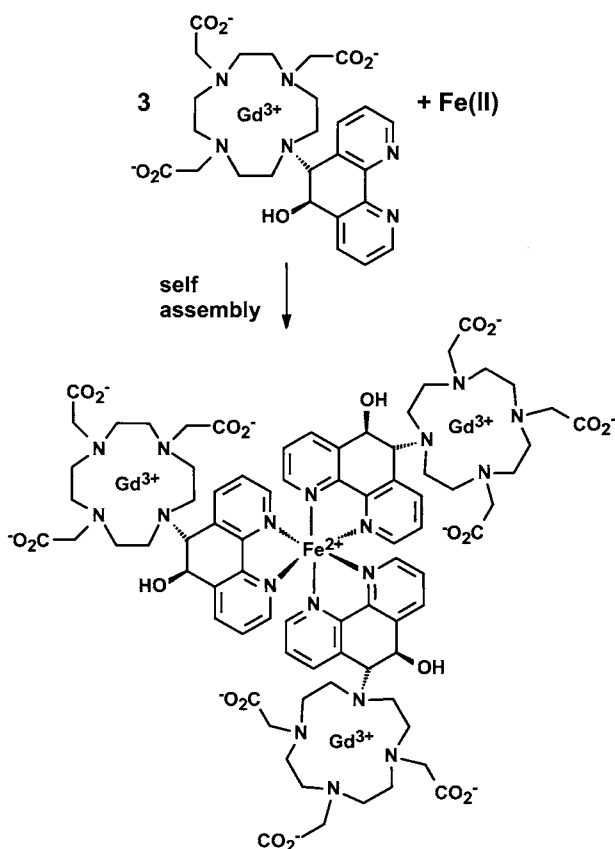


Fig. 4.43. Self-assembly of a polymetallic contrast agent. Redrawn from V. Jacques, J.-F. Desreux, *Top. Cur. Chem.* **221**, 123–164, 2002.

Further developments involve testing the capability of tetraazacycles bearing phosphonic and methylphosphonic acid pendant arms (see Fig. 4.40) as well as the synthesis of elaborate polymetallic entities containing several paramagnetic ions. One example of the latter is sketched in Fig. 4.43. A Gd–DOTA complex is modified to accommodate a derivatised phenanthroline group which is known as being a good complexation agent for divalent iron. If three of these complexes are self-assembled with Fe(II), a new tetrametallic entity forms with a relaxivity 145% larger than that of  $[\text{Gd}(\text{DOTA})(\text{H}_2\text{O})]^-$ . These assemblies can be made iron-dependent and lead to iron sensors.

The good encryption of lanthanide ions in DOTA-type molecules has also prompted the development of luminescent probes based on this structure, particularly by substituting DTMA, 1,4,7,10-tetrakis(methylcarbamoylmethyl)-1,4,7,10-tetraazacyclododecane. For instance, phenacyl and phenylphenacyl substituents have been grafted onto DTMA and the corresponding ligands, L1 and L2 (Fig. 4.40) form stable 1:1 complexes in water with lanthanide ions ( $\log K_1 \approx 12\text{--}13$  at 295 K). The structure of  $[\text{Tb}(\text{L1})(\text{H}_2\text{O})]^{3+}$  (Fig. 4.44) shows the ion well encapsulated into the cavity formed by the macrocyclic platform and

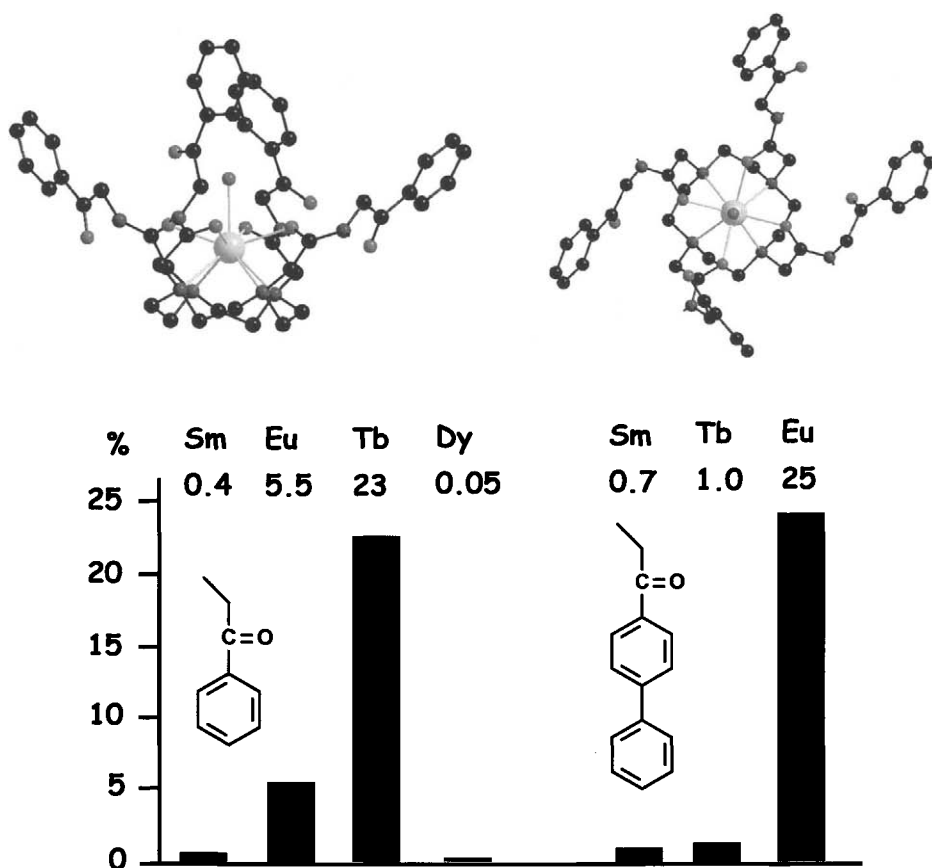


Fig. 4.44. (Top) Two views of the  $[\text{Tb}(\text{L1})\text{H}_2\text{O}]^{3+}$  complex. (Bottom) Sensitisation of the luminescence of several Ln(III) ions by ligands L1 (left) and L2 (right). Redrawn after G. Zucchi et al., *Inorg. Chem.* **41**, 2459, 2002.

the four pendant arms. The metal ion is nine coordinate, a water molecule being bound in the axial position. Again, the edifice has a symmetry close to  $C_4$ , the coordination polyhedron is a monocapped square antiprism and the absolute configuration is  $\Delta(\lambda\lambda\lambda\lambda)$ . In complexes with the phenacyl substituent, the triplet states lie at  $24\,550\text{ cm}^{-1}$  and is ideally suited for sensitising the luminescence from the Tb(III) ion. The quantum yield for an aerated solution in water is 23%, upon ligand excitation. In addition, Sm(III), Eu(III) and Dy(III) are also sensitised. With the phenylphenacyl substituent, the energy of the triplet state is lower, at  $20\,080\text{ cm}^{-1}$ , which prevents an efficient energy transfer onto Tb(III) since the  $\text{Tb}(^5\text{D}_4)$  level has approximately the same energy, resulting in a back-transfer process. On the other hand, the ligand is ideal for the sensitisation of the Eu(III) luminescence, the quantum yield being 26%.

An elaborate supramolecular sensor has been engineered by attaching a permethylated cyclodextrin to a terbium–DOTA complex. The cyclodextrin acts as a scavenger for



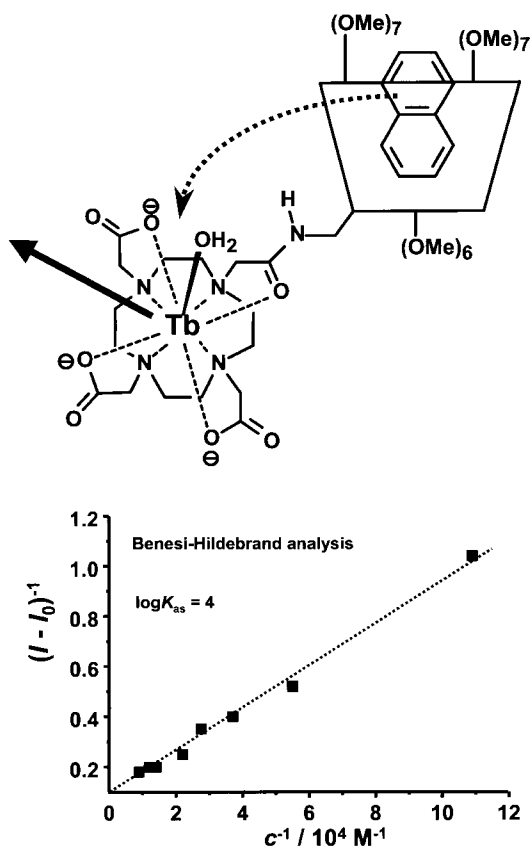


Fig. 4.45. Luminescent sensor for polyaromatic hydrocarbons (e.g. anthracene) based on a derivatised Tb(III)-DOTA complex. Redrawn from D. Parker et al., J. Chem. Soc., Perkin Trans. 2, 1329, 2000.

polyaromatic hydrocarbons which insert themselves into its cavity. When the cyclodextrin has no host in its cavity, the Tb(III) luminescence is rather weak. When a host is complexed, for instance anthracene (see Fig. 4.45), it transfers energy to the Tb(III) ion which in turns emits a bright green luminescence. A Hildebrandt–Benesi analysis shows the association constant between anthracene and the permethylated cyclodextrin to be  $\log K_{as} = 4$ . Luminescent sensors for the determination of pH,  $pO_2$ , or cations and anions in physiological solutions and based on Eu(III) and Tb(III) complexes with derivatised cyclens have been proposed. Since the cyclen complexes are inherently chiral, they are also used to design chirality sensors, particularly when they emit in the IR (e.g. Yb(III), see Fig. 4.40 for some of the ligands used).

### 37. Calixarenes

Calix[*n*]arenes are a family of macrocycles prepared by condensation reactions between *para*-substituted phenols and formaldehyde (see Fig. 4.8). In a way, they can be thought

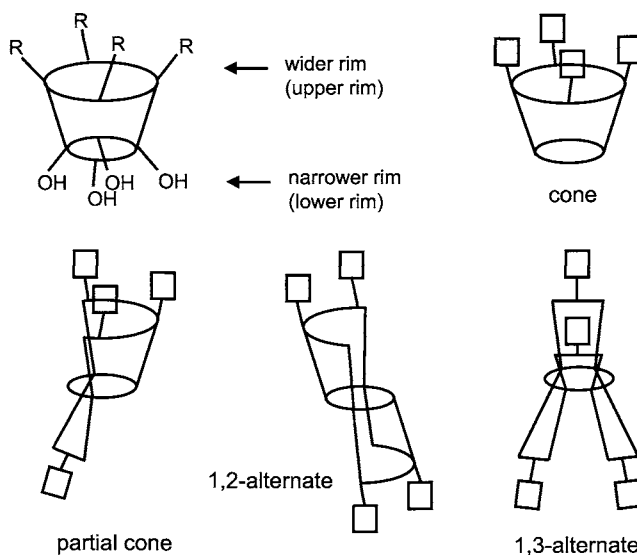


Fig. 4.46. Conformers of calix[4]arene.

of as being a special class of coronands fitted with pendant arms. Calixarenes with an even number of phenol groups are easier to synthesize than those with an odd number of phenol groups. Calix[4]arenes can take several conformations. The most usual one is when the four alkyl substituents are on the same side, resulting in a cone conformation (Fig. 4.46). Initially, the rim bearing the alkyl substituents was termed “upper rim”; however, to avoid potential confusion, the current practice is to name it “wider rim”. The other conformers are the partial cone one in which one alkyl substituent lies opposite to the three other ones, the 1,2-alternate and the 1,3-alternate. Most of the lanthanide complexes with calix[4]arene derivatives contain the ligand in the cone conformation. Calixarenes are particularly attractive macrocyclic ligands and some of the reasons are listed below.

- (i) Their framework can be regarded as a platform with two rims onto which functional groups can be separately grafted to modify either the coordination behaviour or the lipophilicity (which is important for solubility).
- (ii) The calixarene framework is sufficiently flexible to adapt its conformation to a potential metal guest.
- (iii) The size of the induced cavity can be modulated both by adjusting the  $n$  number and, also, the size of the pendent-arm substituents.
- (iv) The number and the geometrical arrangement of the ligating pendant arms can be varied to match the coordination requirements of the metal ions.
- (v) Calixarenes can be modified as to accommodate two different metal ions, henceforth allowing the study of intermetallic interactions (e.g. magnetic interactions).
- (vi) The wider rim, which is usually more lipophilic, can accommodate organic molecules and therefore, the ligand may act as an inorganic–organic receptor.

During the last fifteen years, a great deal of effort have been devoted to the synthesis of suitable calix[ $n$ ]arene receptors for lanthanide ions, mainly with the purpose of developing

extraction and separation processes, particularly within the problematic of nuclear waste management, as well as luminescent stains.

### 37.1. Simple calix[*n*]arenes ( $n = 4, 5, 6, 8$ , see Fig. 4.8)

Simple calix[*n*]arenes bearing no substituent on the narrower rim and *p-t*-butyl groups on the wider rim form complexes with lanthanide ions. The stoichiometry is 2:2 for  $n = 4$  and 5, 1:2 for  $n = 6$ , but one ligand molecule is not coordinated, and 2:1 for  $n = 8$ . Some 1:1 complexes with the latter are also known, and this stoichiometry is often seen with derivatised calix[4]arenes. The synthesis of the complexes is usually performed in organic solvents, often DMF, DMSO or THF, and in the presence of a base to help deprotonate the ligand. As a result, the isolated complexes contain several solvent molecules, both interacting in the inner coordination sphere and interstitial, and are efflorescent. In the case of calix[8]arene, varying the strength of the base results in different stoichiometry for the complexes: when the base is weak, 1:1 complexes are isolated, whereas dimetallic entities form with a strong base. In dimetallic complexes (2:2 or 2:1 stoichiometry) phenoxide groups act as bridges between the two metal ions, sometimes complemented by solvent molecules.

The structures of the europium complexes with *p-t*-butylcalix[*n*]arenes ( $n = 4, 5, 6$ , and 8) are reported in Fig. 4.47. The 2:2 complex with calix[4]arene is a centrosymmetric dimer with the two ligand molecules adopting the cone conformation. One phenoxide function of each calixarene acts as a bridge. The Eu(III) ion is coordinated to four phenoxide and one hydroxyl oxygen atoms and its coordination sphere is completed by the binding of two DMF molecules, which leads to a rather uncommon seven coordinate ion. Another DMF molecule is included in each ligand cavity. The Eu–Eu distance is short: 3.91 Å, that is within the range allowing electronic and magnetic interaction between the two metal centres.

The structure of the dimeric 2:2 complex with *p-t*-butylcalix[5]arene is fairly similar. The dimer is also centrosymmetric, but the calixarenes adopt a partial 1,2-alternate conformation. The Eu(III) ions are connected through one phenoxide group of each trianionic ligand; they are eight coordinate, being bound to four phenoxide and two hydroxyl oxygen atoms from the ligands and to two DMSO molecules. The Eu–Eu distance is only marginally shorter than the distance observed in the calix[4]arene dimer, 3.89 Å. Similar dimers have been found with d-transition metal ions.

The isolation of lanthanide complexes with *p-t*-butylcalix[6]arene has proved more difficult, owing to the fact that the ligand is large and flexible, although its cavity is not large enough to accommodate two metal ions. In the isolated 1:2 complex, one calixarene molecule is neutral and uncoordinated. The coordinated macrocycle is deprotonated twice, has a hinged “3-up-3-down” conformation and acts as a monodentate ligand. The Eu(III) ion is bound to the less hindered of the two inequivalent tripod sites of the calixarene. The unidentate nature of the calix[6]arene is somewhat surprising; it may be explained both by the presence of a hydroxyl group linked to the metal ion and by the formation of two strongly interacting hydrogen-bonding networks within each compartment of the ligand. The Eu(III) ion is again eight coordinate, being additionally ligated by six DMF molecules.

The dimetallic complexes with *p-t*-butylcalix[8]arene containing DMF molecules,  $[\text{Ln}_2(\text{H}_2\text{butCx}[8])(\text{DMF})_5] \cdot (\text{DMF})_4$  are efflorescent and exhibit polymorphism associated

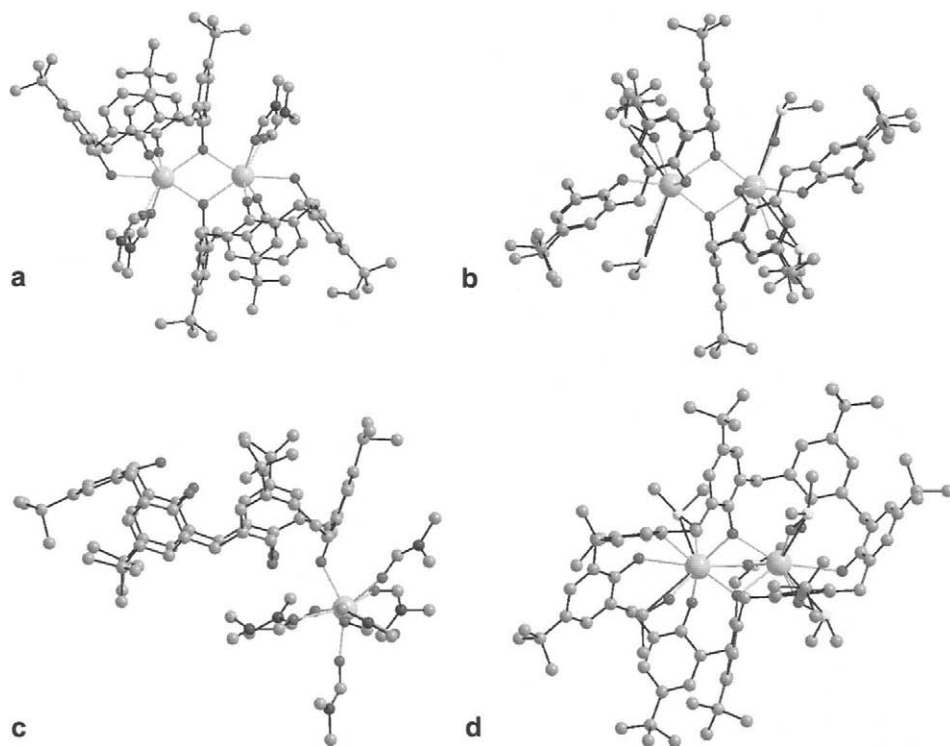


Fig. 4.47. Structures of europium complexes with simple *p-t*-butyl calixarenes. (a)  $[\text{Eu}_2(\text{HbutCx}[4])_2(\text{DMF})_4](\text{DMF})_7$ , redrawn from B.M. Furphy et al., *J. Chem. Soc., Dalton Trans.* 2217, 1989; (b)  $[\text{Eu}_2(\text{H}_2\text{butCx}[5])_2(\text{DMSO})_4](\text{THF})_{10}$ , redrawn from L.J. Charbonnière et al., *J. Chem. Soc., Dalton Trans.* 505, 1998; (c)  $[\text{Eu}(\text{OH})(\text{H}_4\text{butCx}[6])(\text{DMF})_4]\cdot\text{H}_6\text{butCx}[6](\text{DMF})_4$ , redrawn from L.M. Engelhardt, *Austr. J. Chem.* **41**, 1465, 1988; (d)  $[\text{Eu}_2(\text{H}_2\text{butCx}[8])(\text{DMF})_5](\text{DMF})_4$ , redrawn from B.M. Furphy et al., *Inorg. Chem.* **26**, 4231, 1987.

with different degrees of solvation, whereas the dimethylsulfoxide adducts  $[\text{Ln}_2(\text{H}_2\text{butCx}[8])(\text{DMSO})_5]$  form a single isomorphous series. The ligand adopts a kind of a two-bladed propeller conformation. It can be viewed as if the calix[8]arene would consist of two calix[4]arenes in the cone conformation and placed side by side in a *transoid* configuration. This conformation creates an oxophylic platform and brings the oxygen atoms closer to each other than in the free ligand which has an undulated conformation, as in the 1:1 complexes. In this way, the coordination of two metal ions becomes possible. The two Eu(III) ions are bridged by two phenoxide groups and by one DMSO molecule; they are surrounded by eight oxygen atoms from four phenoxide and one phenol groups and three DMSO molecules. The distance between the two metal ions is 3.63 Å. Owing to this short interionic distance, an antiferromagnetic interaction has been evidenced in the Gd(III) dimetallic complex  $[\text{Gd}_2(\text{H}_2\text{butCx}[8])(\text{DMF})_5]$  and a fit of the magnetic susceptibility versus temperature using a simple coupling model for the two ions with  $S = 7/2$  yielded  $g = 1.97$  and  $J = -0.063 \text{ cm}^{-1}$ , pointing to a very weak interaction.

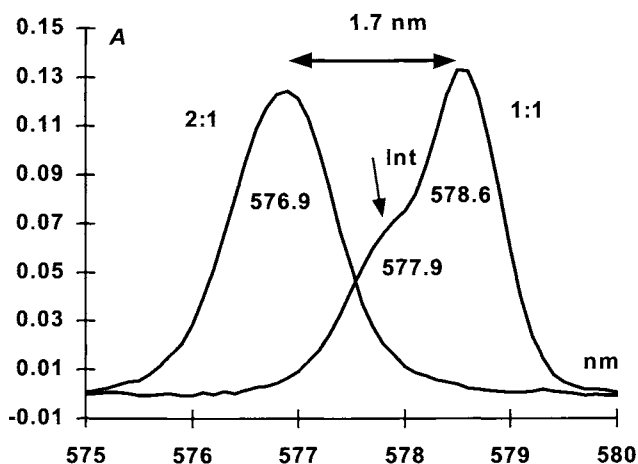
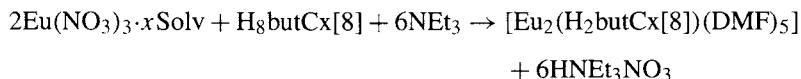


Fig. 4.48. Absorption spectra of the  $\text{Eu}(^5\text{D}_0 \leftarrow ^7\text{F}_0)$  transition for the dimetallic ( $9.9 \times 10^{-3}$  M) and monometallic ( $2.7 \times 10^{-3}$  M) complexes with *p-t*-butylcalix[8]arene, at 298 K, in DMF; the shoulder at 577.9 nm corresponds to a reaction intermediate. Reproduced with permission from J.-C.G. Bünzli et al., in: Calixarenes for Separations, ACS Symposium Series, eds G.J. Lumetta, R.D. Rogers, A. Gopalan, Vol. 757, Ch. 14, American Chemical Society, Washington D.C., 2000.

### 37.1.1. Kinetics of formation

The formation of the 2:1 complexes with *p-t*-butylcalix[8]arene in DMF goes through several reaction intermediates, as demonstrated by a spectrophotometric study based on the weak  $^5\text{D}_0 \leftarrow ^7\text{F}_0$  transition of the Eu(III) ion. The overall reaction is the following:



This transition (Fig. 4.48), which is unique for a given Eu(III) chemical environment, has been monitored versus time after mixing the lanthanide salt and the ligand in the presence of an excess of triethylamine. The results point to a very fast initial formation of the 1:1 complex  $[\text{Eu}(\text{NO}_3)(\text{H}_6\text{butCx}[8])(\text{DMF})_4]$  (half-life in the ms range) which then slowly transforms into the bimetallic 2:1 assembly with a half-life of 5500 s in the presence of an 18-fold excess of triethylamine. It is noteworthy that this second reaction is 6 times slower in the presence of a 4-fold excess of  $\text{Et}_3\text{N}$  and becomes incomplete when only one equivalent of base per Eu(III) ion is added.

This kinetic aspect is understandable since the conformation of the calixarene in the 1:1 complex is like the one adopted in the free ligand, while a substantial conformational change occurs upon formation of the bimetallic edifice, leading to the two-bladed propeller conformation of the macrocycle. The detailed investigation of the  $^5\text{D}_0 \leftarrow ^7\text{F}_0$  transition under numerous conditions of temperature, pressure, concentration, and also upon addition of acid and base led to a model in which the 1:1 to 2:1 transformation goes through two reaction intermediates (Fig. 4.49), one charged species corresponding to the dissociation of the nitrate anion and a neutral species which forms upon the third deprotonation

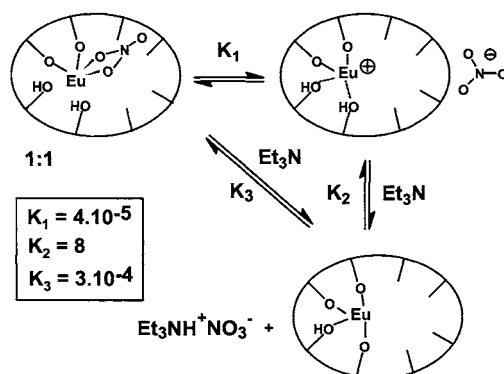
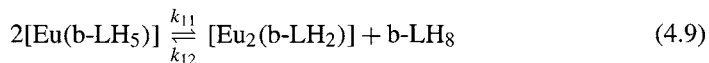
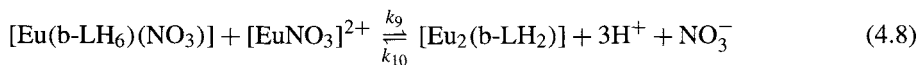
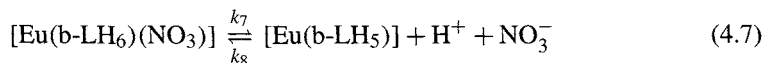
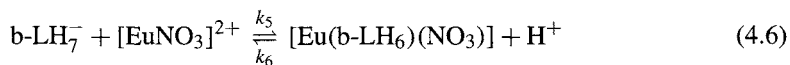


Fig. 4.49. Proposed reaction intermediates in the formation of the bimetallic Eu(III) complex with *p-t*-butylcalix[8]arene from the 1:1 complex in DMF. Reproduced with permission from J.-C.G. Bünzli et al., in: Calixarenes for Separations, ACS Symposium Series, eds. G.J. Lumetta, R.D. Rogers, A. Gopalan, Vol. 757, American Chemical Society, Washington D.C., 2000.

of the calixarene. A complete mechanism for the formation of the complexes in DMF has been proposed on the basis of a study of the fast reaction step by a stopped-flow method, monitoring the ligand-to-metal charge transfer band, by conventional UV-visible spectrophotometry ( ${}^5D_0 \leftarrow {}^7F_0$  transition) and by a multi-level stochastic simulation (H<sub>8</sub>butCx[8] is abbreviated b-LH<sub>8</sub>):



The main path to the formation of the bimetallic complex is reaction (4.8). A variable-temperature thermodynamic study of the equilibria involved in the complex formation demonstrates that the energetic drive for the formation of both 1:1 and 2:1 complexes is in fact provided by triethylamine which captures the protons released in the process. Taking the presence of NEt<sub>3</sub> into account leads to  $\log K_3 = 4$  ( $\Delta G_r^0(3) = -23 \text{ kJ mol}^{-1}$ ) and to  $\log K_5 = 5$  ( $\Delta G_r^0(5) = -29 \text{ kJ mol}^{-1}$ ). The larger value of  $K_5$  with respect to  $K_3$  points to a cooperative effect induced by the change in the conformation of the macrocycle.

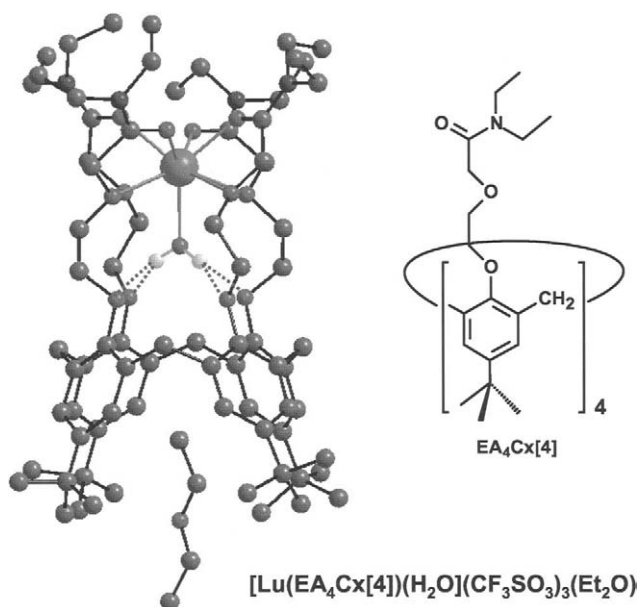


Fig. 4.50. Structure of [Lu(EACx[4])(H<sub>2</sub>O)(Et<sub>2</sub>O)](CF<sub>3</sub>SO<sub>3</sub>)<sub>3</sub>·Et<sub>2</sub>O. Redrawn from F. de M. Ramirez et al., J. Chem. Soc., Dalton Trans. 3205, 2001.

### 37.2. Substituted calix[n]arenes ( $n = 4, 6, 8$ )

Both lower rim and upper rim substitutions have been used to modify the coordination strength of the calixarenes and the properties of the resulting edifices. We shall only give a few examples here, with an emphasis on the efforts aimed at designing efficient luminescent probes and extraction agents.

To start with, let us see how the principles of supramolecular chemistry may be used to organise a pre-disposed ligand to form an adequate cavity. The aim is to design a predisposed host bearing relatively long arms and able to build an induced protective cavity upon complexation with lanthanide ions (Fig. 4.50). Ether-amide pendant arms were chosen because the amide function is a good sensitizer of the Tb(III) luminescence. In solution, the ligand adopts the classical cone conformation with an averaged C<sub>4</sub> symmetry. In acetonitrile, it reacts with hydrated lanthanide trifluoromethanesulfonates to yield stable cationic 1:1 complexes (log *K* in the range 8.6–9.6), despite the fact that the coordinated atoms belong to relatively weak donor (hydroxyl groups from the phenol moieties and from ether functions). One of the positive contributions to the construction of the edifice is the fact that the lanthanide ions act as nine coordinate ions: in addition to the eight oxygen atoms from the ligand, an oxygen atom from a water molecule is coordinated onto the metal ion. This molecule is included into the induced cavity and stabilizes it by hydrogen bonding to the phenolic oxygen atoms. Additionally the calixarene hosts a diethylether molecule in the wider, lipophilic cavity, so that it acts as an inorganic-organic receptor. The terbium luminescence is reasonably well sensitised, the quantum yield in acetonitrile and at 295 K being 5.8%.

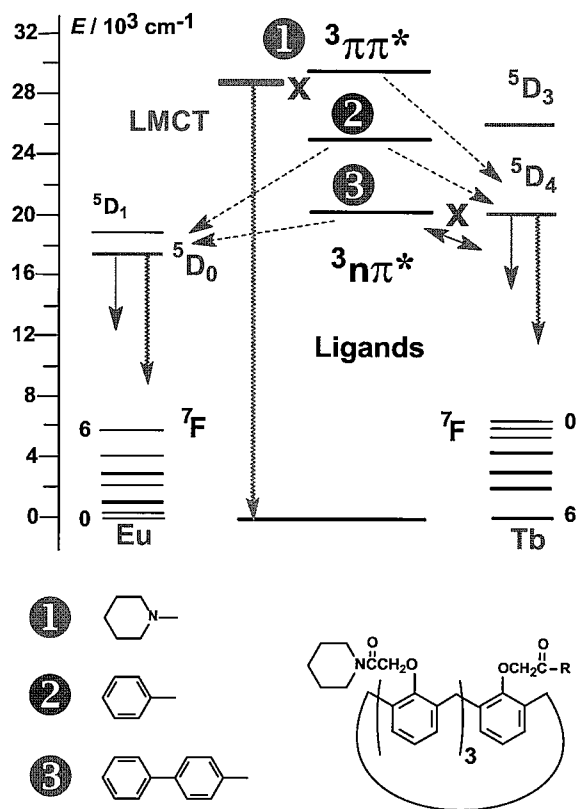


Fig. 4.51. Schematic energy diagram showing the influence of the pendant arm substituent on the sensitisation of the Eu(III) and Tb(III) ions by substituted calix[4]arenes. Redrawn from N. Sato, S. Shinkai, *J. Chem. Soc., Perkin Trans. 2*, 621, 1993.

### 37.2.1. Designing luminescent probes

In an effort to design luminescent probes, Nariaki Sato and Seiji Shinkai from the University of Fukuoka in Japan have derivatised calix[4]arenes in order to enhance the ligand-to-metal energy transfer processes. Among others, they have synthesised the three calixarenes depicted on Fig. 4.51. With the calixarene bearing four piperidine groups, the triplet state arises from the phenol units; it lies at about  $30\,000\text{ cm}^{-1}$  and energy transfer onto Tb(III) occurs (quantum yield in acetonitrile for the metal-centred luminescence at 298 K:  $Q = 16\%$ ); in the case of the Eu(III) complex, there is a ligand-to-metal charge-transfer state (LMCT, one could label it as C=O-to-Eu) which efficiently deactivates the excited state of the metal ion ( $Q = 0.17\%$ ). With the phenacyl substituent, the  $^3n\pi^*$  state lies at about  $26\,000\text{ cm}^{-1}$ , that is below the LCMT and both Tb(III) and Eu(III) are sensitised ( $Q = 27$  and  $6\%$ , respectively). The smaller quantum yield displayed by the europium complex is mainly due to a smaller energy gap between the lowest excited state and the highest sub-level of the  $^7F$  ground state, compared to terbium. When the phenylphenacyl substituent is introduced, its  $^3n\pi^*$  state lies below the  $^5D_4$ (Tb) excited



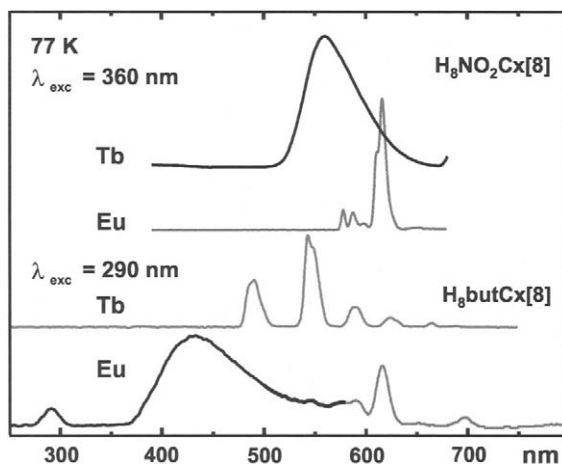


Fig. 4.52. Influence of the para substituent on the photophysical properties of Eu(III) and Tb(III) dimetallic complexes with calix[8]arenes. Redrawn from F. Ihringer et al., *Inorg. Chim. Acta* **246**, 195, 1996.

state and energy cannot be transferred onto this ion ( $Q = 0.008\%$ ), while energy transfer onto Eu(III) is as efficient as previously ( $Q = 6.1\%$ ). This is a nice demonstration that a relatively small change in one pendant arm can dramatically alter the photophysics of the corresponding complexes with Ln(III) ions. Another similar, even more dramatic example since it involves much simpler chemistry, is depicted on Fig. 4.52. The dimetallic complex between Tb(III) and *p-t*-butylcalix[8]arene is reasonably luminescent in DMF, with a quantum yield close to 5%. Looking at the emission spectrum of the corresponding Eu(III) coordination compound, one sees that energy is only partly transferred onto the metal ion and the emission from the ligand triplet state dominates the emission spectrum. This is partly due to a too large energy difference between this triplet state and the excited  $^5D_0(\text{Eu})$  state and, mainly, to the presence of a LMCT state which de-excites the metal ion non-radiatively. When the *p-t*-butyl groups are replaced by electron attracting  $\text{NO}_2$  groups, both the stoichiometry and the structure of the dimetallic complexes remain the same, but the photophysical properties change dramatically. The LMCT state is pushed towards higher energies and the triplet state appears at much lower energy. As a result, energy transfer onto the Tb(III) ion can no more occur, and only the triplet state emission is seen in the emission spectrum. On the other hand, transfer onto the Eu(III) ions is operative and since non-radiative de-activation through the LMCT state is minimized, the red emission of the metal ion is the only luminescence given off by the sample.

Derivatization of calix[ $n$ ]arenes (mainly  $n = 4$ ) has been systematically investigated. Some of the best results are summarized in Table 4.25, the corresponding ligands being sketched in Fig. 4.53. The first compounds to be studied have been the complexes of the tetraacetamide ligand Cx1; they are water soluble and about one water molecule is found to coordinate the metal ion in the inner coordination sphere. A substantial quantum yield is found for TbCx1 in water, 20%. In fact, the energy transfer from the ligand singlet state to the triplet state and to the  $^5D_4$  excited level of Tb(III) is 35%, the difference between these two yields being accounted for by non-radiative processes. On the other hand, the EuCx1

TABLE 4.25

Largest quantum yields reported for Eu(III) and Tb(III) complexes with derivatised calix[4]arenes. From data reported by N. Sabbatini et al., in *Calixarenes 2001*, Z. Asfari, V. Böhmer, J.M. Harrowfield, J. Vicens, eds, Dordrecht: Kluwer Academic Publishers, 2001, Ch. 31.

Ligand <sup>a</sup>	Solvent	Q(Eu) (%)	Ligand <sup>a</sup>	Solvent	Q(Tb) (%)
Cx2	CH <sub>3</sub> CN	15	Cx1	H <sub>2</sub> O	20
Cx3	CH <sub>3</sub> CN	16	Cx5	CH <sub>3</sub> CN	16
Cx4	CH <sub>3</sub> CN	19	Cx6	H <sub>2</sub> O	13
			Cx7	CH <sub>3</sub> CN	
			Cx8	CH <sub>3</sub> CN	27

<sup>a</sup>See Fig. 4.53 for formulae.

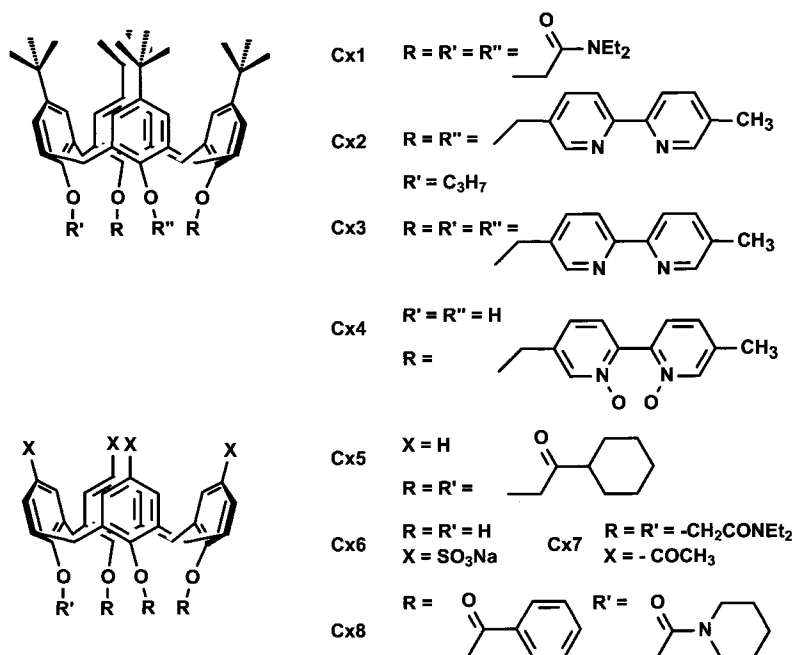


Fig. 4.53. Substituted calixarenes for lanthanide-containing luminescent probes.

complex is only faintly luminescent due to quenching through the LMCT state. In order to better sensitise the luminescence of Eu(III), one has to resort to dipyriddy substituents (Cx2, Cx3, Cx4) which increase the quantum yields in the range 15 to 19% in acetonitrile. The triplet state of these ligands lies at too low energy to present an efficient energy transfer onto the Tb(III) ion. The latter is better sensitised when carbonyl or acetamide groups are present on the substituents (Cx5–Cx8). It is noteworthy that larger calixarenes are not better in transferring energy onto the lanthanide ions. The only substantial quantum yield is the

one obtained with *p*-sulfonyl-calix[8]arene, 20% in water for Tb(III), whereas this figure is ten times lower with the corresponding parent calix[6]arene.

The gadolinium complex with Cx1 displays a reasonable relaxivity and it has been assessed as a potential contrast agent for magnetic resonance imaging. Its stability constant is however too low to make this complex a good candidate for *in vivo* applications. Until now, no calixarene derivative has proved efficient in this field, contrary to the pendant-arm substituted coronands.

### 37.2.2. Extraction and separation processes

An important application of lanthanide complexes with calixarenes is the development of separation and extraction processes. Calixarenes substituted with carboxylic acid arms were among the first ones studied in view of the extraction of Ln(III) ions by cation-exchange technology. The advantage of such extractants is that they can be almost quantitatively back-extracted at low pH (1–2). However the highest mutual separation factors reported rarely exceed 2. The stoichiometry of the extracted species is a function of several parameters including the ligand lipophilicity, the number of donor atoms, the solvent composition and the concentration and pH ranges. Calix[6]arenes are more efficient at lower pH compared to the calix[4]arenes, except in the case of co-extraction with sodium which pre-organizes the carboxylic arms allowing an easier complexation of the Ln(III) ion. A more rational design of calixarene extractants was achieved by introducing monodentate P(O) donor groups. Narrower-rim substitution achieves a satisfactory separation between light and heavy Ln(III) ions, which is less than the case of wider-rim substitution. The best results so far have been obtained with bidentate donor groups featuring one carbonyl and one phosphoryl function: the carbamoylphosphine oxides (CMPO), which were grafted onto calix[*n*]arene frameworks, mainly for *n* = 4. The calixarenes substituted at the wider rim show a good mutual separation of lanthanide ions and preference for trivalent actinide ions. In 1999, Volker Böhmer from the Johannes-Gutenberg University in Mainz reported interesting results obtained with the CMPO-substituted calixarene depicted in Fig. 4.54.

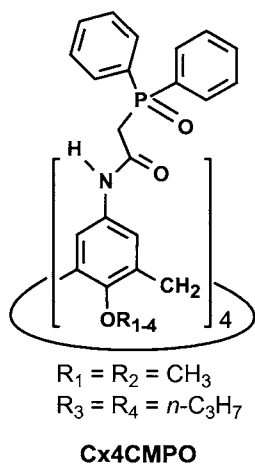


Fig. 4.54. Substituted calix[4]arene used in extraction and separation studies.

Maximum extraction occurs from 1 to 3 M  $\text{HNO}_3$  into *o*-nitrophenyl-hexyl-ester and the following separation factors were measured with respect to trivalent americium for 1 mM ligand concentration and  $10^{-4}$  M metal ions:  $S_f(\text{Am/Ln or Cm}) = 2.00$  (La), 52 (Ce), 1.72 (Nd), 2.78 (Sm), 5.15 (Eu), 7.15 (Cm). Following this study numerous CMPO-substituted calix[4]arenes have been synthesized and tested.

### 37.3. Calix-crowns, calix-cryptands and extended networks

With new synthetic methods no longer limiting the imagination of chemists, the calixarene framework has been combined with crown ether and cryptand moieties to ensure a better shielding cavity. Examples of ligands used to sensitize the luminescence of the Eu(III) and Tb(III) ions are shown in Fig. 4.55 and the corresponding data are listed in Table 4.26. In particular, the ligands Cx10 and Cx12–Cx14 which bear a bipyridyl moiety can efficiently transfer energy on both ions and the quantum yields measured in acetonitrile are rather

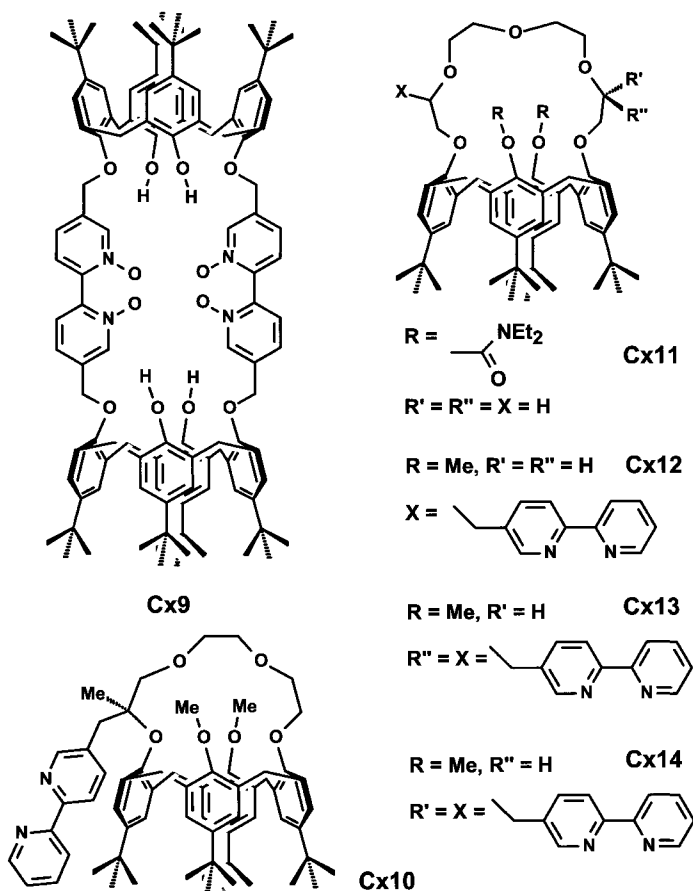


Fig. 4.55. Examples of calix-cryptands and calix-crowns.

TABLE 4.26

Largest quantum yields reported for Eu(III) and Tb(III) complexes with calixcrowns and calixcryptands. From data reported by N. Sabbatini et al., in *Calixarenes 2001*, Z. Asfari, V. Böhmer, J.M. Harrowfield, J. Vicens, eds, Dordrecht: Kluwer Academic Publishers, 2001, Ch. 31.

Ligand <sup>a</sup>	Solvent	$Q(\text{Eu})$ (%)	$Q(\text{Tb})$ (%)
Cx9	CH <sub>3</sub> OH	11	0
Cx10	CH <sub>3</sub> CN	18	32
Cx11	CH <sub>3</sub> CN	0	15
Cx12	CH <sub>3</sub> CN	32	35
Cx13	CH <sub>3</sub> CN	23	39
Cx14	CH <sub>3</sub> CN	28	37

<sup>a</sup>See Fig. 4.55 for formulae.

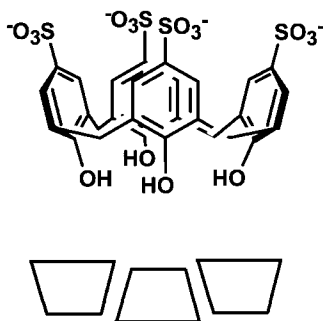


Fig. 4.56. *p*-sulfonatocalix[4]arene and schematic representation of its crystal packing.

large for lanthanide complexes, lying in the range 18–32% and 32–39% for Eu and Tb, respectively. The Eu(III) complex with ligand Cx11 is non-luminescent at room temperature because of the quenching by the LMCT state as discussed above, while ligand Cx9 possesses a triplet state with a too low energy to avoid back transfer from the Tb(III) ion onto the ligand, which explains that the complex with the latter ion is non-luminescent.

An innovative chemistry aiming at self-assembling bi-layers, capsules and tubular arrays using complexes with *para*-sulfonated-calixarenes as synthons, among others, has been developed by Jerry L. Atwood from the University of Missouri-Columbia and Colin L. Raston from the University of Leeds. The starting point is the observation that highly charged species are important (i) in crystal engineering of complex species in the solid state, (ii) in the formation of micelle-like species and nano-structures in solution, and (iii) in developing enzyme models. The small calix[4,5]arenes substituted at the wider rim by sulfonato groups were chosen because of their bowl-shape (cone) conformation, which minimizes any pre-organization energy during the binding of hydrophilic moieties into the cavity. Larger oligomers have non-cone conformations which are lower in energy. The *p*-sulfonatocalix[4,5]arenes are therefore shaped like a truncated cone, with hydrophilic wider and narrower rims separated by a hydrophobic mid-region. The solid state packing of crystal structures containing *p*-sulfonatocalix[4,5]arenes are dominated by these structure-

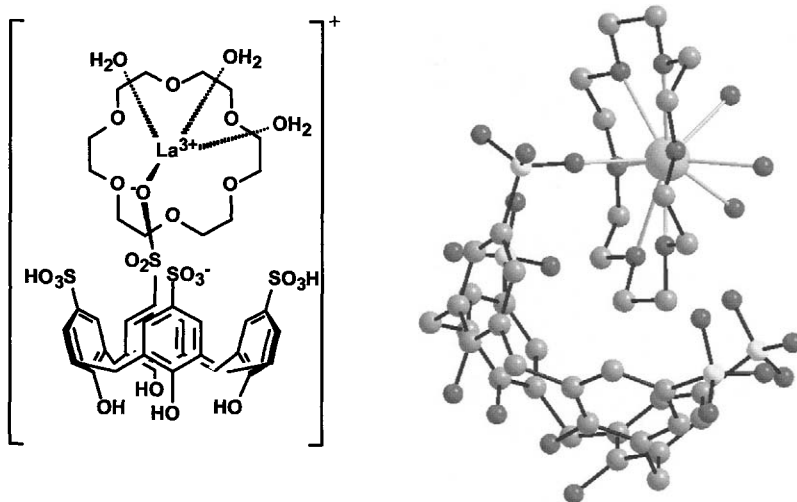


Fig. 4.57. "Ferris-wheel" structure formed with lanthanum chloride interacting with *p*-sulfonatocalix[4]arene and 18-crown-6. Redrawn from A. Drljaca et al., Chem. Commun. 1135, 1999.

directing topological characteristics, resulting in an up-down arrangement (Fig. 4.56). Since the calixarene cavity is a potential host for organic molecules (see Fig. 4.50), this may be exploited to create a second or even a third coordination sphere for a metal ion or for encapsulating organic molecules. For instance, the reaction of lanthanum chloride with *p*-sulfonatocalix[4]arene and 18-crown-6 in water in the pH range 2.5–3 yields a "ferris-wheel" type structure (Fig. 4.57). The lanthanide ion is bound symmetrically by the six oxygen atoms from the crown ether and, additionally, by three water molecules and one oxygen atom from a sulfonate group grafted onto the calixarene. The La–crown complex is further held into the cavity of the calixarene by Van der Waals interactions and there is an interaction between the coordinated water molecules and the sulfonate groups of another complex cation. The complementarity between the curvatures of the crown and calixarene molecules is achieved by splaying two opposite phenol groups. The entire structure forms an infinite helical array of the supercations, chloride counterions and water through hydrogen bonding associations. With smaller cations, another type of supramolecular structure is obtained, featuring capsules into which an uncoordinated crown ether molecule is enclosed (Fig. 4.58). In this structure, the lanthanide cations are bound to the 1,3-sulfonate groups of the calixarene with two calixarene subunits encapsulating the 18-crown-6 molecule. There are two metal ion sites, both with seven water molecules and one coordinated sulfonate group. They are involved in hydrogen bonding leading to the dimerization of calix units in two distinct modes. One mode involves a head-to-head dimerization to form a capsule; the other one builds an S-shape motif and involves the partially occupied  $[\text{Ln}(\text{H}_2\text{O})_7]^{3+}$  aquo-ions disordered over two adjacent sites (occupancy: 1/3). Finally, the crown ether molecule is held into the capsule by hydrogen bonds. A similar capsule is obtained with Sc(III) and is shown in Fig. 4.59. Other fascinating structures have been obtained upon changing the composition of the

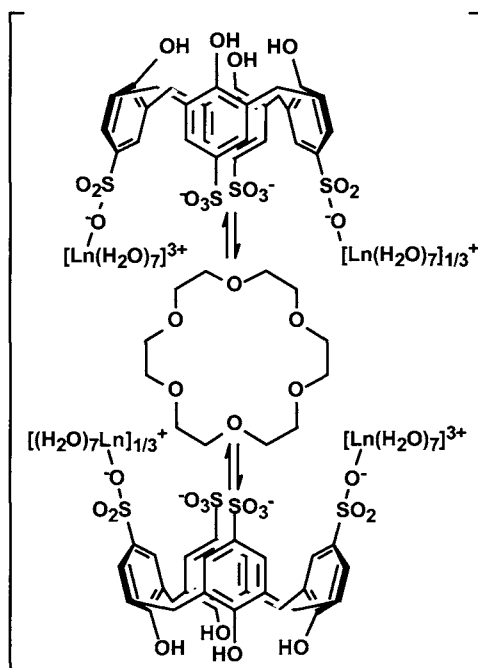


Fig. 4.58. Capsule structure formed with lanthanide ions in the presence of *p*-sulfonatocalix[4]arene and 18-crown-6 ether. Redrawn after J.L. Atwood et al., *Coord. Chem. Rev.* **222**, 3, 2001.

mixtures and adding small molecules (e.g. pyridine *N*-oxide) to link sub-units between them.

### 38. Metallacrowns

Until now, the hosts we have been describing have all been synthesised by elaborate organic syntheses. There is an alternate approach to the problem of engineering recognition agents: the exclusive use of heteroatoms, particularly metal ions. Indeed, in organic-based hosts, the conformations are governed by the tetrahedral and trigonal geometries of carbon, nitrogen and oxygen, which is not the case if metals are used as ring constituents. Moreover, the metal ions possess functional properties (spectroscopic, magnetic, chemical) that may be of high interest, henceforth the development of what are known as metallacrowns. These receptors are obtained by substituting the methylene bridges in crown ethers by a transition metal and a nitrogen atom. The schematic diagram in Fig. 4.60 shows the similarity between 12C4 ether and a metallacrown having 12 atoms in its ring, including four Fe(III) ions. The nomenclature adopted for metallacrowns is related to crown ethers, but requires further elaboration. First, both the nature of the metal ion and of the other atom (usually N) must be given; secondly, some indication on the nature of the ligand bearing the nitrogen donor atom should also be given (as well as the oxidation state of the metal ion, not shown on the figure). The first metallacrowns

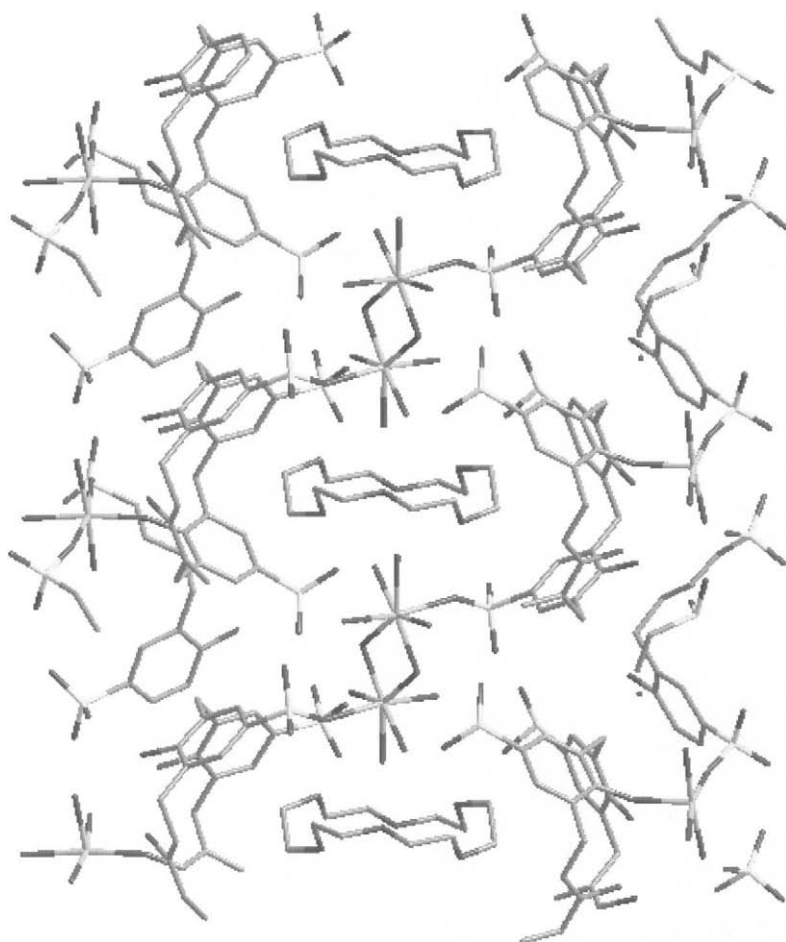


Fig. 4.59. Capsule-type packing in the complex  $\{(p\text{-sulfonatocalix[4]arene})(18\text{C}6)_{1/2}\text{-[Sc(OH)}_2(\text{H}_2\text{O})_8]_{1/2}\text{-[Sc(H}_2\text{O)}_4]\}$ . Redrawn from H.R. Webb et al., Chem. Eur. J. 7, 3616, 2001.

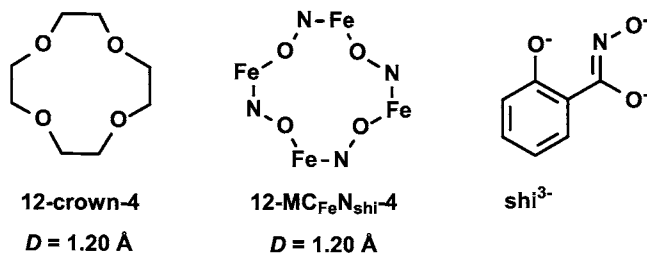


Fig. 4.60. Schematic diagram of a metalla 12-crown-4.



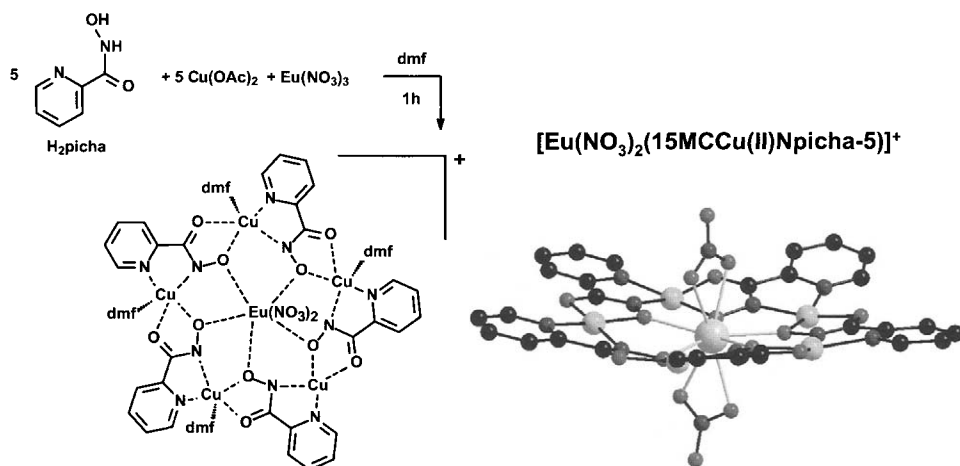


Fig. 4.61. Synthesis and structure of  $[Eu(NO_3)_2(15MCCu(II)Npicha-5)]^+$ . Redrawn from A.J. Stemmler et al., *Inorg. Chem.* **38**, 2807, 1999.

were prepared using hydroxamic acids, for instance salicylhydroxamic acid,  $H_3SHI$ , or its trianion,  $SHI^{3-}$ . At first, the more common metallacrowns had 9, 12 and 15 atoms in their ring, but presently large macro-rings can be obtained, featuring up to 50 or 60 atoms. With respect to lanthanide ion complexation the new approach was pioneered at the beginning of the 1990's by Richard Winpenny from the University of Edinburgh, who was looking for copper-lanthanide precursors of superconducting materials. Lanthanide encapsulation complexes with copper or nickel metallacrowns are easily obtained in high yield from one-pot syntheses involving planar ligands such as picoline hydroxamic acid ( $H_2picha$ ) or non-planar amino hydroxamic acids, the metal acetate and the appropriate trivalent lanthanide nitrate. In the 15-metallacrown-5 [ $15-Cu(II)(picha)-5$ ] shown on Fig. 4.61, four of the five  $Cu(II)$  cations are five coordinate, being loosely bound to one DMF molecule, while the fifth one is strictly square planar. In all the complexes, the  $Ln(III)$  ion is generally pentagonal bipyramidal being coordinated to five oxygen atoms from the metallacycle and solvent molecules or nitrate ions in the axial positions. In the case of  $Eu(III)$ , two bidentate nitrate ions are bound on either side of the metallacycle. The cavity of the latter presents an estimated radius of 1.2 Å, which matches fairly exactly the  $Eu(III)$  ionic radius for a coordination number of nine. The circular arrangement of the d-transition metal ions implies interesting magnetic properties. For instance, the  $Gd(NO_3)_3$  complex of [ $15-Cu(II)(picha)-5$ ] displays ferromagnetic coupling of the  $Gd(III)$  ion to the five  $Cu(II)$  ions and its relaxivity is quite large ( $9.8 \text{ mM}^{-1}\text{s}^{-1}$  at  $20^\circ\text{C}$  and 30 MHz). Much larger metallacycles may be obtained; for instance, the reaction of  $N,N'$ -ethylene-bis(pyridine-2-one) with hydrated lanthanide nitrates in methanol or acetonitrile yields a range of metallacyclic complexes, the structure of one of which is shown in Fig. 4.62. Here, six  $Tb(III)$  ions are connected in a 54-membered cycle. The compound forms a continuous array of metallacyclic rings, with cavities hosting acetonitrile molecules.

Similarly to the metallacrowns, metallacalixarenes can be synthesized, as exemplified by a palladium metallacalix[4]arene obtained by a self-assembly process from  $Pd(II)en$  (en

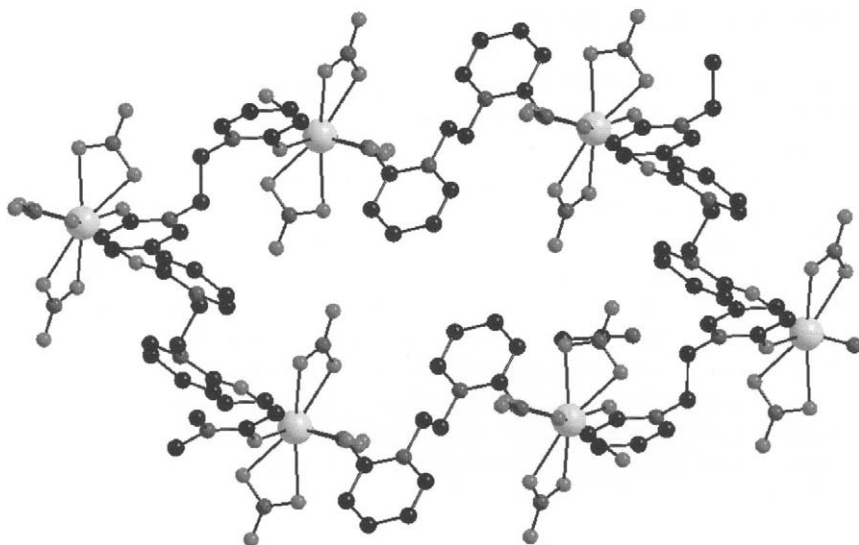


Fig. 4.62. 54-membered ring generated by reacting *N,N'*-ethylenebis(pyridine-2-one) with terbium nitrate. Redrawn from D.L.M. Goodgame et al., *Inorg. Chim. Acta* **272**, 131, 1998.

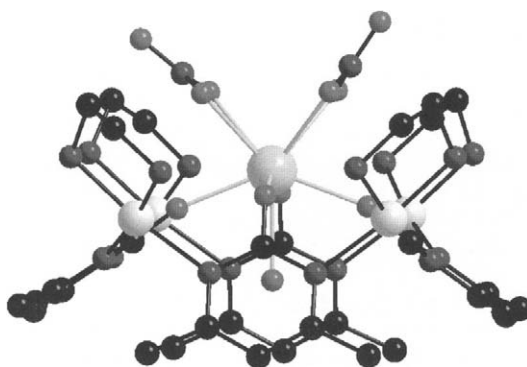


Fig. 4.63. Structure of a palladium metallacalix[4]arene encapsulating a Gd(III) ion. Redrawn from J.A.R. Navarro, J.M. Salas, *Chem. Commun.* 235, 2000.

is 1,2-diaminoethane) and 4,6-dimethyl-2-hydroxypyrimidine (dmpymo). This inorganic host with O...O separations of about 4 Å is ideally suited for the complexation of a Gd(III) ion which strongly binds the four dmpymo oxygen atoms (Fig. 4.63). The four Pd(II) centres lie in a plane forming an almost perfect square with approximately 5.7 Å sides. The Gd(III) ion binding to the dmpymo forces the four pyrimidine moieties to orient in the same direction. Additionally, two bidentate nitrate ions complete the coordination sphere of the lanthanide ion, along with a water molecule which is entirely incorporated into the host.

### 39. Conclusion and further reading

In the above sections, we have tried to give a general overview of the macrocyclic chemistry of lanthanide ions; this view remains incomplete since we have deliberately not covered several fields of interest such as chiral macrocyclic complexes, cyclodextrins, podands, particularly pyrazolylborate ligands which form an easily adaptable induced cavity around the metal ions, organometallic chemistry, or the intercalation compounds with fullerenes which display fascinating properties. Moreover, we have tried to put the emphasis on functional compounds, but most of the examples given belong to biomedical, luminescence and extraction applications, and the chemical applications have been somewhat shadowed. Nevertheless, we hope that this part of the chapter devoted to lanthanide complexes has made the reader aware of the very imaginative ways that chemists have found to fine-tune the inner coordination sphere of the rare-earth ions with the aim of maintaining or, better, enhancing, their unique physico-chemical and chemical properties. The interested reader can refer to the following articles and books to better his understanding of the matter reviewed.

- Coronates, cryptates and their applications [271–275].
- Complexes with porphyrins and phthalocyanines [276–279].
- Coronands fitted with pendant arms [280–282].
- Calixarenes [283,284].
- Metallacrowns [285].
- Polymetallic assemblies [286].

### References

- [1] I.M. Kolthoff, P.J. Elving (eds), *Treatise on Analytical Chemistry*, Vol. 8. Part. II, p. 54, Interscience-Wiley, NY, 1963.
- [2] O.A. Gansow, A.R. Kausar, *Inorg. Chim. Acta* **95**, 1–6, 1985.
- [3] J.F. Desreux, A. Renard, G. Duyckaerts, *J. Inorg. Nucl. Chem.* **39**, 1587, 1977.
- [4] C.E. Higgins, W.H. Baldwin, *Chem. Div. Ann. Progr. Rep. ORNL-4791*, p. 46, 1972.
- [5] V.N. Krishnamurthy, S. Soundararajan, *J. Inorg. Nucl. Chem.* **29**, 517, 1967.
- [6] J.T. Donoghue, E. Fernandez, J.A. McMillan, D.A. Peters, *J. Inorg. Nucl. Chem.* **31**, 1431, 1969.
- [7] R.R. Thomas, V. Chebolu, A. Sen, *J. Am. Chem. Soc.* **108**, 4096, 1986.
- [8] *Handbook on the Physics and Chemistry of Rare Earths*, eds K.A. Gschneidner, Jr., L. Eyring, Vol. 4, p. 89, North Holland, Amsterdam, 1979.
- [9] G. Meyer, P. Ax, *Mat. Res. Bull.* **17**, 1447, 1982.
- [10] J.D. Corbett, *Inorg. Synth.* **22**, 31, 39, 1983.
- [11] J.-C.G. Bunzli, E. Moret, J.-R. Yersin, *Helv. Chim. Acta* **61**, 762, 1978.
- [12] T. Moeller, V.D. Aftandilian, G.W. Cullen, *Inorg. Synth.* **5**, 37, 1957.
- [13] J.H. Forsberg, T. Moeller, *Inorg. Chem.* **8**, 889, 1969.
- [14] J.-C.G. Bunzli, J.-R. Yersin, C. Mabillard, *Inorg. Chem.* **21**, 1471, 1982.
- [15] J.-C.G. Bunzli, C. Mabillard, *Inorg. Chem.* **25**, 2750, 1986.
- [16] N.E. Dixon, G.A. Lawrence, P.A. Lay, A.M. Sargeson, H. Taube, *Inorg. Synth.* **24**, 243, 1986.
- [17] T. Fujinaga, I. Sakamoto, *Pure Appl. Chem.* **52**, 1389, 1980.
- [18] A. Seminara, E. Rizzarelli, *Inorg. Chim. Acta* **40**, 249, 1980.
- [19] M. Albin, A.C. Goldstone, A. Sommerville Withers, W. Dew Horrocks, Jr., *Inorg. Chem.* **22**, 3182, 1983.
- [20] G. Vincentini, L.B. Zinner, *Inorg. Synth.* **23**, 180, 1985.

- [21] R.C. Mehrotra, J.M. Batwara, *Inorg. Chem.* **9**, 2505, 1970.
- [22] J.H. Forsberg, T. Moeller, *Rare Earth Elements*, in: *Gmelin Handbook of Inorganic Chemistry*, Vol. D1, Springer-Verlag, Berlin, 1980.
- [23] E.R. Birnbaum, J.H. Forsberg, *ibid.*, Vol. D2, 1982.
- [24] E.R. Birnbaum, J.H. Forsberg, Y. Marcus, *ibid.*, Vol. D3, 1981.
- [25] E.R. Birnbaum, *ibid.*, Vol. D5, 1984.
- [26] E.R. Birnbaum, J.H. Forsberg, *ibid.*, Vol. D4, 1986.
- [27] D.D. Perrin, I.G. Sayce, *Talanta* **14**, 833, 1967.
- [28] B.S. Mathur, T.S. Srivastava, *J. Inorg. Nucl. Chem.* **32**, 3277, 1970.
- [29] W. Brzyska, W. Ferenc, *Pol. J. Chem.* **56**, 15, 1982.
- [30] K.W. Rillings, J.E. Roberts, *Thermochim. Acta* **21**, 409, 1977.
- [31] Yu.G. Sakharov, I.Ya. Evtushenko, N.N. Sakharova, *Russ. J. Inorg. Chem.* **15**, 1349, 1970.
- [32] R.C. Paul, G. Singh, G.S. Gothra, *Indian J. Chem.* **11**, 294, 1973.
- [33] T. Moeller, V. Galasyn, J. Xavier, *J. Inorg. Nucl. Chem.* **15**, 259, 1960.
- [34] J.F. Desreux, *Inorg. Chem.* **19**, 1319, 1980.
- [35] R.I. Badalova, L.I. Martynenko, V.I. Spitsyn, *Russ. J. Inorg. Chem.* **16**, 1556, 1971.
- [36] P.G. Jones, *Chem. Brit.* **17**, 222, 1981.
- [37] N.D. Mitrofanova, L.I. Martynenko, A.I. Grigor'ev, *Russ. J. Inorg. Chem.* **9**, 174, 1964.
- [38] T. Moeller, F.A.J. Moss, R.H. Marshall, *J. Am. Chem. Soc.* **77**, 3182, 1955.
- [39] L.I. Martynenko, *Russ. J. Inorg. Chem.* **6**, 1366, 1961.
- [40] J.J. Hagan, S.C. Taylor, M.F. Tweedle, *Anal. Chem.* **60**, 514, 1988.
- [41] C.S. Springer, D.W. Meek, R.E. Sievers, *Inorg. Chem.* **6**, 1105, 1967.
- [42] D.G. Karraker, *J. Inorg. Nucl. Chem.* **33**, 3713, 1971.
- [43] E.W. Berg, J.J.C. Acosta, *Anal. Chim. Acta* **40**, 101, 1968.
- [44] T. Shigematsu, M. Matsui, K. Utsunomijya, *Bull. Chem. Soc. Japan* **42**, 1278, 1969.
- [45] S.J. Lyle, A.D. Witts, *Inorg. Chim. Acta* **5**, 481, 1971.
- [46] M.F. Richardson, R.E. Sievers, *Inorg. Chem.* **10**, 498, 1971.
- [47] J.K. Przystal, W.G. Boss, I.B. Liss, *J. Inorg. Nucl. Chem.* **33**, 679, 1971.
- [48] I.B. Liss, W.G. Boss, I.B. Liss, *J. Inorg. Nucl. Chem.* **39**, 443, 1977.
- [49] K.J. Eisenstraut, R.E. Sievers, *Inorg. Synth.* **11**, 94, 1968.
- [50] J.F. Desreux, J. Massaux, G. Duyckaerts, *J. Inorg. Nucl. Chem.* **40**, 1159, 1978.
- [51] J.J. Uebel, R.M. Wing, *J. Am. Chem. Soc.* **94**, 8910, 1972.
- [52] J. Selbin, N. Ahmad, N. Bhacca, *Inorg. Chem.* **10**, 1383, 1971.
- [53] F. Halverson, J.S. Brinen, J.R. Leto, *J. Chem. Phys.* **41**, 157, 1964.
- [54] L.R. Melby, N.J. Rose, E. Abramson, J.C. Caris, *J. Am. Chem. Soc.* **86**, 5117, 1964.
- [55] R. Belcher, J. Majer, R. Perry, W.I. Stephen, *J. Inorg. Nucl. Chem.* **31**, 471, 1969; *ibid.* p. 1715.
- [56] T.J. Pinnavaia, R.C. Fay, *Inorg. Synth.* **12**, 77, 1970.
- [57] S.K. Agarwal, J.P. Tandon, *Syn. Reactive Inorg. Metal. Org. Chem.* **4**, 387, 1974.
- [58] S.P. Mital, R.V. Singh, J.P. Tandon, *ibid.* **10**, 327, 1980.
- [59] R.F. Venteicher, Ph.D. Thesis, Univ. Microfilms, Ann Arbor, 1975.
- [60] A.K. Srivastava, V.B. Rana, M. Mohan, M.P. Jain, *J. Inorg. Nucl. Chem.* **37**, 723, 1975.
- [61] M. Mohan, *Gazz. Chim. Ital.* **107**, 309, 1977.
- [62] J.H. Forsberg, C.A. Wathen, *Inorg. Chem.* **10**, 1379, 1971.
- [63] J.H. Forsberg, T.M. Kubik, T. Moeller, K. Guewa, *Inorg. Chem.* **10**, 2656, 1971.
- [64] J.-C.G. Bunzli, *Handbook of Physics of Chemistry of Rare Earths*, Vol. 9, Chap. 60, North-Holland, Amsterdam, 1987.
- [65] D. Wessner, J.-C.G. Bunzli, *Inorg. Synth.* **23**, 149, 1985.
- [66] J.F. Desreux, G. Duyckaerts, *Inorg. Chim. Acta* **35**, L313-L315, 1979.
- [67] J.-C.G. Bunzli, D. Wessner, *Isr. J. Chem.* **24**, 313, 1984.
- [68] J.-C.G. Bunzli, B. Klein, D. Wessner, K.-J. Shenk, G. Chapuis, G. Bombieri, G. de Paoli, *Inorg. Chim. Acta* **54**, L43-L46, 1981.
- [69] G. Yang, S. Liu, Z. Jin, *Inorg. Chim. Acta* **131**, 125, 1987.
- [70] B.M. Murphy, J.M. Harrowfield, D.L. Kepert, B.W. Skelton, A.H. White, F.R. Wilner, *Inorg. Chem.* **26**, 4231, 1987.
- [71] J. Rebizant, M.R. Spirlet, P.P. Barthelemy, J.F. Desreux, *J. Incl. Phenom.* **5**, 505, 1987.
- [72] P.H. Smith, K.N. Raymond, *Inorg. Chem.* **24**, 3469, 1985.
- [73] B. Alpha, J.-M. Lehn, G. Mathis, *Angew. Chem.* **26**, 266, 1987.

- [74] D.E. Fenton, P.A. Vigato, *Chem. Soc. Rev.* **17**, 69, 1988.
- [75] P.A. Vigato, D.E. Fenton, *Inorg. Chim. Acta* **139**, 39, 1987.
- [76] L. De Cola, D.L. Smailes, L.M. Vallarino, *Inorg. Chem.* **25**, 1729, 1986.
- [77] W. Dew Horrocks, Jr., D.R. Sudnick, *Acc. Chem. Res.* **14**, 384, 1981.
- [78] G. Yonuschot, C.W. Mushrush, *Biochemistry* **14**, 1677, 1975.
- [79] B.W. Mathesws, L.H. Weaver, *Biochemistry* **13**, 1719, 1974.
- [80] K. Kurachi, L.C. Sieker, L.H. Jenson, *J. Biol. Chem.* **250**, 7663, 1975.
- [81] W. Dew Horrocks, Jr., E.G. Hove, *J. Am. Chem. Soc.* **100**, 4386, 1978.
- [82] M. Gouterman, C.D. Schumaker, T.S. Srivastava, T. Yonetani, *Chem. Phys. Lett.* **40**, 456, 1976.
- [83] C.P. Wong, W. Dew Horrocks, Jr., *Tetrahedron Letters* 2637, 1975.
- [84] W. Dew Horrocks, Jr., C.P. Wong, *J. Am. Chem. Soc.* **98**, 7157, 1976.
- [85] I.S. Kirin, P.N. Moskalev, Yu.A. Makashev, *Russ. J. Inorg. Chem.* **10**, 1065, 1965.
- [86] A.G. Mckay, J.F. Boas, G.J. Troup, *Aust. J. Chem.* **27**, 955, 1974.
- [87] H. Sugimoto, T. Higashi, A. Maeda, Y. Hirai, J. Teraoka, M. Mori, *J. Less Common Met.* **112**, 387, 1985.
- [88] L.L. Saulnier, S. Varbanov, R. Scopelliti, M. Elhabiri, J.-C.G. Bunzli, *J. Chem. Soc., Dalton Trans.* 3919, 1999.
- [89] D. Purushotham, V. Ramachandra Rao, B.H.S.V. Raghava Rao, *Anal. Chim. Acta* **33**, 182, 1965.
- [90] A. Habenschuss, F.H. Spedding, *Proc. of 11<sup>th</sup> Rare Earth Conf., Traverse City, Vol. 2*, pp. 909–918, U.S. Atomic Energy Commission, Oak Ridge, 1974.
- [91] G.R. Choppin, *Pure Appl. Chem.* **27**, 23–41, 1971.
- [92] H.B. Silber, *J. Phys. Chem.* **78**, 1940, 1974.
- [93] T. Moeller, D.R. Martin, L.C. Thompson, R. Ferrus, G.R. Fiestel, W.J. Randall, *Chem. Rev.* **65**, 1, 1965.
- [94] L.C. Thompson, B.L. Shafer, J.A. Edgar, K.D. Mannila, *Adv. Chem. Ser.* **71**, 169, 1967.
- [95] T. Moeller, MTP (Med. Sci. Tech.) Publ. Co., *Int. Rev. Sci., Inorg. Chem. Series One* **7**, 275, 1972.
- [96] G.R. Choppin, W.F. Strazik, *Inorg. Chem.* **4**, 1250, 1965.
- [97] D.L. Wertz, S.T. Finch, *Inorg. Chem.* **18**, 1590, 1979.
- [98] G.H. Johnsson, H. Yokoyama, H. Ohtaki, *J. Solution Chem.* **20**, 1991.
- [99] J.C.G. Bunzli, C. Mabillard, J.R. Yersin, *Inorg. Chem.* **21**, 4214, 1982.
- [100] I.M. Batyaev, S.M. Shilov, V.B. Zaharova, *Russ. J. Inorg. Chem.* **30**, 43, 1985.
- [101] A. Milicic-Tang, J.C.G. Bunzli, *Inorg. Chim. Acta.* **192**, 201, 1992.
- [102] H.B. Silber, R.L. Campbell, *J. Less Common Metals* **149**, 265, 1989.
- [103] C. Cossy, A.E. Merbach, *Pure Appl. Chem.* **60**, 1785, 1988.
- [104] J.C.G. Bunzli, A.E. Merbach, R.M. Nielson, *Inorg. Chim. Acta* **139**, 151, 1987.
- [105] W.B. Mims, J.L. Davis, *J. Chem. Phys.* **65**, 3266, 1976.
- [106] R. Janakiraman, L. Kevan, *J. Chem. Phys.* **75**, 1658, 1981.
- [107] H.B. Silber, M.S. Strozier, *Inorg. Chim. Acta* **128**, 267, 1987.
- [108] A.N. Campbell, E.M. Kartzmark, *J. Chem. Eng. Data* **29**, 168, 1984.
- [109] M.J. Blandamer, J. Burgess, J. Kijowski, *Inorg. Chim. Acta* **58**, 155, 1982.
- [110] J.C.G. Bunzli, J.R. Yersin, C. Mabillard, *Inorg. Chem.* **21**, 1471, 1982.
- [111] J.C.G. Bunzli, V. Kasperek, *Inorg. Chim. Acta* **182**, 101, 1991.
- [112] P. Di Bernardo, G.R. Choppin, R. Portanova, P.L. Zanonato, *Inorg. Chim. Acta* **207**, 85, 1993.
- [113] M. Hamze, J. Meullemestre, F. Vierling, *J. Less Common Met.* **146**, 75, 1989.
- [114] M. Hamze, J. Meullemestre, M.J. Schwing-Weill, F. Vierling, *J. Less Common Met.* **118**, 153, 1986.
- [115] N.N. Kozachenko, I.M. Batyaev, *Russ. J. Inorg. Chem.* **16**, 66, 1971.
- [116] A.A. Zholdakov, L.N. Lugina, N.K. Davidenko, *Russ. J. Inorg. Chem.* **16**, 1265, 1971.
- [117] N.N. Kozachenko, I.M. Batyaev, *Russ. J. Inorg. Chem.* **16**, 978, 1971.
- [118] A.I. Krutous, I.M. Batyaev, *Russ. J. Inorg. Chem.* **18**, 1451, 1973.
- [119] A.I. Krutous, I.M. Batyaev, *Russ. J. Inorg. Chem.* **19**, 671, 1974.
- [120] N.N. Kozachenko, N.A. Panteleeva, V.S. Netsvetaeva, I.M. Batyaev, *ibid.* **18**, 938, 1973.
- [121] L.S. Smith, Jr., D.C. McCain, D.L. Wertz, *J. Am. Chem. Soc.* **98**, 5125, 1976.
- [122] R. Takahashi, S. Ishiguro, *J. Chem. Soc. Faraday Trans.* **87**, 3379, 1991.

- [123] S. Ishiguro, R. Takahashi, *Inorg. Chem.* **30**, 1854, 1991.
- [124] P.L.O. Volpe, A.P. Chagas, C. Airoidi, *J. Inorg. Nucl. Chem.* **42**, 1321, 1980.
- [125] C. Airoidi, P.L.O. Volpe, A.P. Chagas, *Polyhedron* **1**, 49, 1982.
- [126] R. Takahashi, S. Ishiguro, *J. Chem. Soc. Faraday Trans.* **88**, 3165, 1992.
- [127] A.G. Svetashev, M.P. Tsvirko, *Teor. Eksp. Khim.* 108–113, 1991.
- [128] C. Mabillard, Ph.D. Thesis No. 505, Ecole Polytechnique Federale, Lausanne, Switzerland, 1983.
- [129] J.C.G. Bunzli, *J. Alloys Compounds* **192**, 266–270, 1993.
- [130] H.B. Silber, R. Bakshandefar, L.A. Contreras, F. Gaizer, M. Gonslaves, S. Ismail, *Inorg. Chem.* **29**, 4473, 1990.
- [131] A.I. Krutous, I.M. Batyaev, *Russ. J. Inorg. Chem.* **19**, 671, 1974.
- [132] A. Fratiello, V. Kubo-Andersen, E. Marinez, D. Matejka, R. Perrigan, B. Yao, *J. Solution Chem.* **21**, 651, 1992.
- [133] J.C.G. Bunzli, A. Milicic-Tang, *Handbook on the Physics and Chemistry of Rare Earths*, Vol. 21, Chapter 145, Elsevier Science, B.V., 1995.
- [134] J.H. Forsberg, *Coord. Chem. Rev.* **10**, 195–226, 1973.
- [135] T. Moeller, MTP (Med. Sci. Tech. Publ.) Co., *Int. Rev. Sci., Inorg. Chem. Series One* **7**, 65–110, 1975.
- [136] P.T. Moseley, MTP, *Int. Rev. Sci., Inorg. Chem., Series One* **7**, 65–110, 1972.
- [137] D. Brown, D.G. Holah, *Chem. Commun.* 1545–1546, 1968.
- [138] J.L. Ryan, C.K. Jorgensen, *J. Phys. Chem.* **70**, 2845, 1966.
- [139] L.R. Morss, M. Siega, L. Stenger, N. Edelstein, *Inorg. Chem.* **9**, 1771, 1970.
- [140] J.L. Ryan, *Inorg. Chem.* **8**, 2053, 1969.
- [141] J.L. Burmeister, S.D. Patterson, E.A. Deardoff, *Inorg. Chim. Acta* **3**, 105, 1969.
- [142] J.L. Burmeister, E.A. Deardoff, *Inorg. Chim. Acta* **4**, 97–100, 1970.
- [143] R.L. Dieck, T. Moeller, *J. Inorg. Nucl. Chem.* **35**, 3781, 1973.
- [144] R.L. Dieck, T. Moeller, *J. Less Common Metals* **33**, 355, 1973.
- [145] R.L. Dieck, T. Moeller, *J. Inorg. Nucl. Chem.* **36**, 2283, 1974.
- [146] G.N. Papatheodorou, *Inorg. Nucl. Chem. Lett.* **11**, 483, 1975.
- [147] H.D. Amberger, R.D. Fischer, G.G. Rosenbauer, B. Bunsenges, *Phys. Chem.* **79**, 1226, 1975.
- [148] Y.A. Barbanel, R.B. Dooshin, V.V. Kolin, N.K. Michaelov, G.P. Choodnovska, *Koord. Khim* **1**, 411, 1975.
- [149] R.W. Schwartz, S.F. Watkins, C.J. O'Connor, R.L. Carlin, *J. Chem. Soc., Faraday Trans.* **72**, 565, 1976.
- [150] M. Choca, J.R. Ferraro, K. Nakomoto, *Coord. Chem. Rev.* **12**, 295, 1974; *J. Inorg. Chem.* **37**, 1425, 1975.
- [151] I.M. Walker, L. Rosenthal, M.S. Quereshi, *Inorg. Chem.* **10**, 2463, 1971.
- [152] J.L. Martin, L.C. Thompson, L.J. Radinovich, M.D. Glick, *J. Am. Chem. Soc.* **90**, 4493, 1968.
- [153] P.I. Lazarev, V.M. Ionov, L.A. Aslanov, M.A. Porai-Koshits, *Russ. J. Struct. Chem.* **14**, 151, 1973.
- [154] A.H. Norbury, in: *Advances in Inorganic Chemistry and Radio Chemistry*, eds H.J. Emelius, A.G. Sharpe, Vol. 17, Acad. Press, NY, 1975.
- [155] D. Brown, in: *Int. Rev. Science, Inorg. Chem., Series Two*, Vol. 7, Butterworths, London, 1975.
- [156] T.A. Beineke, J. Delgaudio, *Inorg. Chem.* **7**, 715, 1962.
- [157] A. Zalkin, J.D. Forrester, D.H. Templeton, *J. Chem. Phys.* **39**, 2881, 1963.
- [158] A.R. Al-Karaghoul, J.S. Wood, *Chem. Commun.* **135**, 1970.
- [159] I.M. Walker, D.H. Weeden, *Inorg. Chem.* **12**, 772, 1973.
- [160] W.T. Carrall, S. Siegel, J.R. Ferraro, B. Tani, E. Gebert, *Inorg. Chem.* **12**, 560, 1973.
- [161] J.A. Sylvanovich, Jr., S.K. Madan, *J. Inorg. Nucl. Chem.* **34**, 1675, 1972.
- [162] J.C. Barnes, R.D. Peacock, *J. Chem., Soc. A* 558–562, 1971.
- [163] M.R. Roser, L.R. Corruccini, *Phys. Rev. B.* **41**, 2539, 1990.
- [164] R.P. Scholer, A.E. Merbach, *Inorg. Chim. Acta* **15**, 15–20, 1975.
- [165] K.W. Bagnall, MTP (Med. Sci. Tech.) Publ. Co., *Int. Rev. Sci., Inorg. Chem. Series Two* **7**, 41, 1975.
- [166] E. Hansson, Thesis, On the Structures of Solid Rare Earth Oxalates, and Malonates, Lund, 1973.
- [167] I. Grenthe, H. Ots, *Acta Chem. Scand.* **26**, 1229, 1972.
- [168] J. Kay, J.W. Moore, M.D. Glick, *Inorg. Chem.* **11**, 2818, 1972.
- [169] J. Albertsson, Thesis, On the Stereochemistry of 9-coordinate Lanthanide Compounds, Lund, 1972.

- [170] M.D. Lind, B. Lee, J.L. Hoard, *J. Am. Chem. Soc.* **87**, 1611, 1965.
- [171] L.L. Martin, R.A. Jacobson, *Inorg. Chem.* **11**, 2789, 1972.
- [172] G. Condorelli, A. Seminara, *Boll. Sedute. Acad. Gionia Sci. Natur. Catania* **9**, 87–92, 1967.
- [173] A. Seminara, G. Condorelli, *Ann. Chim. (Rome)* **59**, 990, 1969.
- [174] E. Giesbrecht, M. Kawashita, *J. Inorg. Nucl. Chem.* **32**, 2461, 1970.
- [175] M. Perrier, R. Najjar, G. Vicentini, *An. Acad. Brasi, Cieno.* **42**, 439, 1970.
- [176] G. Vicentini, R. Najjar, *Inorg. Nucl. Chem.* **6**, 571, 1970.
- [177] M. Perrier, G. Vicentini, *J. Inorg. Nucl. Chem.* **36**, 555, 1973.
- [178] M.C. Vanderveer, MSc. Thesis, University of Minnesota, 1972.
- [179] T. Moeller, V. Galasyn, *J. Inorg. Nucl. Chem.* **12**, 259, 1960.
- [180] T. Moeller, G. Vincentini, *J. Inorg. Nucl. Chem.* **27**, 1477, 1965.
- [181] G. Vicentini, E. de Carvalho Filho, *J. Inorg. Nucl. Chem.* **28**, 2987, 1966.
- [182] G. Vicentini, R. Najjar, C. Airoidi, *An. Acad. Brasil. Cienc.* **41**, 375, 1969.
- [183] W.V. Miller, S.K. Madan, *J. Inorg. Nucl. Chem.* **30**, 3287, 1968; 2785, 1968.
- [184] M. Perrier, G. Vicentini, *J. Inorg. Nucl. Chem.* **36**, 1187, 1974.
- [185] G. Vicentini, R. Isuyama, *An. Acad. Brasil. Cienc.* **44**, 423, 1972.
- [186] G. Vicentini, M. Perrier, *J. Inorg. Nucl. Chem.* **36**, 77–79, 1974.
- [187] R.W. Bashoum, R.L. Dieck, T. Moeller, *Inorg. Nucl. Chem. Lett.* **9**, 773–776, 1973.
- [188] S.S. Krishnamurthy, S. Soundararajan, *J. Less Common Metals* **13**, 619–625, 1967.
- [189] C. Chich, G.E. Togood, T.D. Boyle, C.M. Burgess, *Acta Crystallogr.* **B32**, 1008, 1976.
- [190] C. Airoidi, Y. Gushikem, *J. Inorg. Nucl. Chem.* **34**, 3921, 1972.
- [191] Y. Gushikem, C. Airoidi, O.L. Alves, *ibid.* **35**, 1159, 1973.
- [192] G. Vicentini, R. Isuyama, *ibid.* **37**, 2018, 1975.
- [193] C.M. Burgess, G.E. Toogood, *Inorg. Nucl. Chem. Lett.* **7**, 761–766, 1971.
- [194] G.W. Pope, J.F. Steinbach, W.F. Wagner, *J. Inorg. Nucl. Chem.* **20**, 304, 1961.
- [195] K.J. Eisenstraut, R.E. Sievers, *J. Am. Chem. Soc.* **87**, 5254–5266, 1965.
- [196] C.S. Springer, Jr., D.W. Meek, R.E. Sievers, *Inorg. Chem.* **6**, 1105, 1967.
- [197] L.R. Melby, N.J. Rose, E. Abramson, J.C. Caris, *J. Am. Chem. Soc.* **86**, 5117, 1964.
- [198] H. Bauer, J. Blanc, D.L. Ross, *J. Am. Chem. Soc.* **86**, 5125, 1964.
- [199] J. Selbin, N. Ahmad, N. Bhacca, *Inorg. Chem.* **10**, 1383, 1971.
- [200] D. Purushotham, V. Ramachandra Rao, B.H.S.V. Raghava Rao, *Anal. Chim. Acta* **33**, 182–197, 1965.
- [201] V. Ramachandra Rao, et al., *Ind. J. Chem.* **3**, 321, 1965; *Curr. Sci.* **35**, 12, 1965; *ibid.* **38**, 110, 1969.
- [202] P.V. Talakar, V. Ramachandra Rao, *Ind. J. Chem.* **7**, 943, 1969.
- [203] V. Ramachandra Rao, J.A. Marinsky, unpublished results, SUNY, Buffalo, NY, 1964.
- [204] D.C. Bradley, *Adv. Inorg. Chem. Radiochem.* **15**, 290, 1972.
- [205] R.C. Mehrotra, M.M. Agarwal, A. Mehrotra, *Syn. Inorg. Metal-Org. Chem.* **3**, 181, 1973.
- [206] V.N. Krishnamurthy, S. Soundararajan, *Can. J. Chem.* **45**, 189, 1967.
- [207] L. Ramakrishnan, S. Soundararajan, *Monotsch. Chem.* **106**, 625, 1975.
- [208] D.M. Mehs, S.K. Madan, *J. Inorg. Nucl. Chem.* **30**, 3017, 1968.
- [209] E. Giesbrecht, L.B. Zinner, *Inorg. Nucl. Chem. Lett.* **5**, 575, 1969.
- [210] J.T. Donoghue, E. Fernandez, J.M. Mc Millan, D.A. Peters, *J. Inorg. Nucl. Chem.* **31**, 1431, 1969.
- [211] J.T. Donoghue, D.A. Peters, *ibid.* **31**, 467–470, 1969.
- [212] J.A. Sylvanovich, Jr., S.K. Madan, *ibid.* **34**, 1675–1683, 1972.
- [213] J.T. Donoghue, *Bull. Chem. Soc., Japan* **43**, 932–934, 1970.
- [214] J.T. Donoghue, E. Fernandez, *ibid.* **43**, 271–273, 1970.
- [215] D.R. Cousins, F.A. Hart, *J. Inorg. Nucl. Chem.* **30**, 3009–3015, 1968.
- [216] N.P. Crawford, G.A. Melson, *J. Chem. Soc. A* 1049–1052, 1969.
- [217] F. Kutek, *Coll. Czech. Chem. Commun.* **33**, 1341–1345, 1968.
- [218] O.A. Serra, L.C. Thompson, *Inorg. Chem.* **15**, 504–507, 1976.
- [219] G. Vicentini, A.M.S. Vieira, *An. Acad. Brasil. Cienc.* **45**, 371–376, 1973.
- [220] M.T. Dumey, R.S. Marianelli, *Inorg. Nucl. Chem. Lett.* **6**, 895–902, 1970.
- [221] S.K. Ramalingam, S. Soundararajan, *J. Inorg. Nucl. Chem.* **29**, 1763, 1967.

- [222] D.K. Koppikar, S. Soundararajan, *ibid.* **38**, 174–176, 1975.
- [223] G. Vicentini, L.B. Zinner, L. Rothschild, *Inorg. Chim. Acta.* **9**, 213–216, 1974.
- [224] F.A. Hart, F.P. Laming, *Proc. Chem. Soc.*, London **107**, 1963.
- [225] T. Moeller, R.L. Dieck, J.E. McDonald, *Revue de chimie Minerale* **10**, 177–188, 1973.
- [226] D.K. Huggins, W.B. Fox, U.S. Patent No. 631081, Dec. 28, 1971.
- [227] W.W. Wendlandt, *Science* **122**, 197, 1955; *J. Am. Chem. Soc.* **77**, 857, 1955.
- [228] S.M.K. Rahman, J. Ahmad, M.M. Haq, *J. Inorg. Nucl. Chem.* **34**, 1460, 1972.
- [229] R.G. Charles, R.C. Ohlmann, *ibid.* **27**, 119, 1965; *J. Chem. Phys.* **40**, 3131, 1964.
- [230] E.R. Birnbaum, T. Moeller, *J. Am. Chem. Soc.* **91**, 7274, 1969.
- [231] J. Mac Cordick, C. Burn, *Chem.-Ztg. Chem. App.* **94**, 848, 1970.
- [232] S.M.F. Rahman, J. Ahmad, M.M. Haq, *J. Inorg. Nucl. Chem.* **33**, 4351, 1971.
- [233] D.G. Hendricker, R.J. Foster, *ibid.* **34**, 1949, 1972.
- [234] J.H. Forsberg, T. Moeller, *Inorg. Chem.* **8**, 883, 1969; *ibid.* 889, 1969.
- [235] L.J. Charpentier, T. Moeller, *J. Inorg. Nucl. Chem.* **32**, 3575, 1970.
- [236] L.I. Labanov, V.A. Smirnova, *Russ. J. Inorg. Chem.* **12**, 243, 1967.
- [237] A.R. Al-Kharaghoul, J.S. Wood, *J. Am. Chem. Soc.* **90**, 6548, 1968.
- [238] F.A. Hart, F.P. Laming, *J. Inorg. Nucl. Chem.* **27**, 1825, 1965.
- [239] A.M. Golub, M.V. Kopa, V.M. Skopenko, G.W. Zinzadse, *Z. Anorg. Allgem. Chem.* **375**, 302, 1970.
- [240] B.M. Bansal, D. Damien, G. Kohly, *Inorg. Nucl. Chem. Lett.* **5**, 509, 1969.
- [241] R.C. Grandey, T. Moeller, *J. Inorg. Nucl. Chem.* **32**, 333, 1970.
- [242] G.H. Frost, F.A. Hart, C. Heath, M.B. Hursthouse, *Chem. Commun.* **1421**, 1969.
- [243] S. Gurrieri, S. Musumeci, E. Rizzarelli, A. Seminars, *J. Inorg. Nucl. Chem.* **38**, 259, 1976.
- [244] J.H. Forsberg, C.A. Wathen, *Inorg. Chem.* **10**, 1971.
- [245] M.F. Johnson, J.H. Forsberg, *Inorg. Chem.* **15**, 734, 1976.
- [246] D.A. Durham, F.A. Hart, *J. Inorg. Nucl. Chem.* **31**, 145, 1969.
- [247] J. Albertsson, *On the Stereochemistry of 9-coordinate Lanthinoid Compounds*, Thesis, Lund, 1972.
- [248] D.E. Jackson, Ph.D. Dissertation, Univ. of Illinois, 1950.
- [249] N.K. Dutt, K. Nag, *J. Inorg. Nucl. Chem.* **30**, 2493, 1968.
- [250] G.F. Desa, E. Giesbrecht, L.C. Thompson, *ibid.* **37**, 109, 1975.
- [251] S. Yameda, K. Yamanonchi, H. Kuma, S. Ynth, *Inorg. Metal-Org. Chem.* **1**, 9–12, 1971.
- [252] M.D. Lind, B. Lee, J.L. Hoard, *J. Am. Chem. Soc.* **87**, 1611–1612, 1965.
- [253] J.L. Mackey, N.N. Greenwood, *J. Inorg. Nucl. Chem.* **34**, 1529, 1972; **33**, 3699, 1971.
- [254] D.L. Hoof, D.G. Tisley, R.A. Walton, *J. Chem. Soc. Dalton Trans.* 200–204, 1973.
- [255] H. Kuma, S. Yamada, *Inorg. Chim. Acta* **15**, 213–215, 1975.
- [256] S.K. Agarwal, J.P. Tandon, *Syn. React. Inorg. Metal-Org. Chem.* **4**, 387, 1975.
- [257] D.G. Karraker, *J. Inorg. Nucl. Chem.* **31**, 2833, 1969.
- [258] N.N. Sakharova, Yu.G. Sakharova, *Russ. J. Inorg. Chem.* **15**, 922, 1970.
- [259] A.U. Malik, *J. Inorg. Nucl. Chem.* **32**, 1743, 1970.
- [260] L. Agarwal, U. Agarwal, *ibid.* **34**, 2255, 1972.
- [261] D. Brown, D.G. Holah, *Chem. Commun.* **1545**, 1968.
- [262] D. Brown, D.G. Holah, C.E.F. Rickard, *J. Chem. Soc. (A)* **786**, 1970.
- [263] J.G. Brennan, R.A. Andersen, A. Zalkin, *Inorg. Chem.* **25**, 1761, 1986.
- [264] K. Aparna, S.S. Krishnamurthy, M. Nethaji, *Z. Anorg. Allg. Chem.* **621**, 1913, 1995.
- [265] M.D. Fryzuk, T.S. Haddad, *J. Am. Chem. Soc.* **110**, 8263, 1988; *Chem. Commun.* 1990.
- [266] J.P. White, III, S.G. Shore, *Inorg. Chem.* **31**, 2756, 1992.
- [267] A.K. Saxena, N.S. Hosmane, *Chem. Revs.* **93**, 1081–1124, 1993.
- [268] N.S. Hosmane, J.A. Maguire, *Phosphorus, Sulfur, Silicon* **124–125**, 263–273, 1997.
- [269] H.C. Dorn, *Chem. Eng. News*, p. 54, Sep. 20, 1999.
- [270] R. Dani, *Chem. Eng. News*, p. 32, June 17, 2002.
- [271] J.-C.G. Bünzli, *Complexes with synthetic ionophores*, in: *Handbook on the Physics and Chemistry of Rare Earths*, eds K.A. Gschneidner, Jr., L. Eyring, Vol. 9, Ch. 60, pp. 321–394, Elsevier Science Publ., Amsterdam, 1987.
- [272] P. Guerriero, S. Tamburini, P.A. Vigato, *From mononuclear to polynuclear macrocyclic or macrocyclic complexes*, *Coord. Chem. Rev.* **139**, 17–243, 1995.



- [273] V. Alexander, Design and synthesis of macrocyclic ligands and their complexes of lanthanides and actinides, *Chem. Rev.* **95**, 273–342, 1995.
- [274] J. Jiang, N. Higashiyama, K.I. Machida, G.Y. Adachi, The luminescent properties of divalent europium complexes of crown ethers and cryptands, *Coord. Chem. Rev.* **170**, 1–29, 1998.
- [275] G. Mathis, Biological applications of rare earth cryptates, in: *Rare Earths*, eds R. Saez Puche, P. Caro, pp. 285–315, Editorial Complutense, Madrid, 1998.
- [276] D.K.P. Ng, Half-sandwich tetrapyrrole complexes of rare earths and actinides, in: *Handbook on the Physics and Chemistry of Rare Earths*, eds Gschneidner, Jr., L. Eyring, G.H. Lander, Vol. 32, Ch. 210, pp. 611–653, Elsevier Science B.V., Amsterdam, 2001.
- [277] Y. Korovin, N. Rusakova, Infrared 4f-luminescence of lanthanides in the complexes with macrocyclic ligands, *Rev. Inorg. Chem.* **21**, 299–329, 2001.
- [278] N. Ishikawa, T. Ino, Y. Kaizu, *J. Phys. Chem. A* **106**, 9543–9550, 2002.
- [279] T.D. Mody, L. Fu, J.L. Sessler, *Prog. Inorg. Chem.* **49**, 551–598, 2001.
- [280] H.C. Aspinall, Chiral lanthanide complexes: coordination chemistry and applications, *Chem. Rev.* **1807–1850**, 2002.
- [281] V. Jacques, J.F. Desreux, New classes of MRI contrast agents, *Top. Curr. Chem.* **221**, 123–164, 2002.
- [282] I. Lukes, J. Kotek, P. Vojtisek, P. Herrmann, Complexes of tetraazacycles bearing methylphosphinic/phosphonic acid pendant arms with copper(II), zinc(II) and lanthanides(III). A comparison with their acetic acid analogues, *Coord. Chem. Rev.* **216**, 287–312, 2001.
- [283] *Calixarenes for Separations*, eds G.J. Lumetta, R.D. Rogers, A. Gopalan, ACS Symposium Series, Vol. 757, American Chemical Society, Washington DC, 2000.
- [284] *Calixarenes 2001*, eds Z. Asfari, V. Böhmer, J.M. Harrowfield, J. Vices, Kluwer Academic Press, Dordrecht, 2001.
- [285] V.L. Pecoraro, A.J. Stemmler, B.R. Gibney, J.J. Bodwin, W. Hsin, J.W. Kampf, A. Barwinski, Metallacrowns: a new class of molecular recognition agents, *Prog. Inorg. Chem.* **45**, 83–177, 1997.
- [286] J.-C. G. Bünzli, C. Piguet, Lanthanide-containing molecular and supramolecular polymetallic functional assemblies, *Chem. Rev.* **102**, 1897–1928, 2002.

chapter 5

---

STRUCTURAL CHEMISTRY OF  
LANTHANIDE COMPLEXES

---

---

# CONTENTS

---

1. Complex formation . . . . .	377
2. Coordination numbers . . . . .	378
3. Low coordination number . . . . .	380
4. Complexes with coordination number 4 . . . . .	382
5. Coordination number 5 . . . . .	383
6. Coordination number 6 . . . . .	383
7. Coordination number 7 . . . . .	387
8. Coordination number 8 . . . . .	394
8.1. Dodecahedron . . . . .	397
8.2. Square antiprism . . . . .	401
8.3. Cubes . . . . .	404
9. Coordination number 9 . . . . .	405
10. Coordination number 10 . . . . .	410
11. Complexes of high coordination numbers . . . . .	414
References . . . . .	417

## 1. Complex formation

The tendency of a metal ion to form complexes depends strongly on a number of factors. These factors for rare earth ions are different from those of transition metals. The trivalent rare earth ions have the electronic configuration  $4f^n 5s^2 5p^6$ , where  $n = 0$  to 14. The figure representing the square of the radial wave functions for the 4f, 5s, 5p and 6s electrons of  $Gd^{3+}$  versus the electron–nucleus distance shows clearly that the 4f orbitals are inner orbitals with respect to 5s and 5p orbitals. The outer  $5s^2$  and  $5p^6$  sub shells shield inner 4f electrons from outer interactions, which determine most of the properties of the lanthanide(III) ions. The  $Ln^{3+}$  ions are essentially spherical and present an environment very similar to alkali and alkaline earth ions towards complex formation. Since the 4f orbitals are not available for chemical bonding and are sufficiently shielded, the crystal field stabilization energy is of the order of  $100\text{ cm}^{-1}$  which is small as compared to  $\sim 30000\text{ cm}^{-1}$  in the case of d-transition elements. Hence the bonding in lanthanide complexes will be mostly ionic in nature and the geometrical arrangement of the ligands will not be dictated so much by bonding requirements but by steric requirements.

The ionic radii of trivalent lanthanides are given in Table 5.1.

It is clear from the table that with the exception of the scandium, the ionic radii are quite large, and in fact, are among the largest values for any trivalent ions. These large radii mean that the ionic potential (charge to radius ratio) is relatively low which results in a very low polarizing ability. This is reflected in the predominantly ionic character in the metal–ligand bonds. Another major effect of large ionic radii is the influence on the coordination number of the rare earth complexes. These two factors result in rare earth complexes having a coordination number greater than six.

TABLE 5.1  
Ionic radii of the trivalent rare earth in six-coordination\* [1,2].

Symbol	Radius (Å)	Symbol	Radius (Å)
Sc	0.68	Gd	0.938
Y	0.88	Tb	0.923
La	1.061	Dy	0.908
Ce	1.034	Ho	0.894
Pr	1.013	Er	0.881
Nd	0.995	Tm	0.869
Pm	(0.979)	Yb	0.858
Sm	0.964	Lu	0.848
Eu	0.950		

\*Lanthanide values from Templeton and Dauben [1], scandium and yttrium values from Zachariasen [2].

TABLE 5.2

Basic properties of trivalent rare-earth ions and of  $\text{Ca}^{II}$ : electronic structure, ionic radii for coordination numbers 6, 9, and 12.

Ion	El. struct.	$r_i(6)$ (Å)	$r_i(9)$ (Å)	$r_i(12)$ (Å)
Ca	[Ar]	0.99	1.18	n.a.
Sc	[Ar]	0.75	0.93	1.06
Y	[Kr]	0.90	1.08	1.22
La	[Xe]	1.03	1.22	1.36
Ce	[Xe]4f <sup>1</sup>	1.01	1.20	1.34
Pr	[Xe]4f <sup>2</sup>	0.99	1.18	1.32
Nd	[Xe]4f <sup>3</sup>	0.98	1.16	1.30
Pm	[Xe]4f <sup>4</sup>	0.97	1.14	1.28
Sm	[Xe]4f <sup>5</sup>	0.96	1.13	1.27
Eu	[Xe]4f <sup>6</sup>	0.95	1.12	1.25
Gd	[Xe]4f <sup>7</sup>	0.94	1.11	1.24
Tb	[Xe]4f <sup>8</sup>	0.92	1.10	1.23
Dy	[Xe]4f <sup>9</sup>	0.91	1.08	1.22
Ho	[Xe]4f <sup>10</sup>	0.90	1.07	1.21
Er	[Xe]4f <sup>11</sup>	0.89	1.06	1.19
Tm	[Xe]4f <sup>12</sup>	0.88	1.05	1.18
Yb	[Xe]4f <sup>13</sup>	0.87	1.04	1.17
Lu	[Xe]4f <sup>14</sup>	0.86	1.03	1.16

The electron configuration along with the ionic radii of lanthanides of coordination numbers 6, 9 and 12 are given in Table 5.2.

It is obvious from the table that the ionic radii of lanthanides are very similar to the ionic radius of the  $\text{Ca}^{2+}$  ion. Further, the ionic radii of lanthanides differ by about 0.3 Å in changing the coordination environment from 6 to 12. The differences of 0.3 Å in ionic radius between coordination number 6 and 12 makes the lanthanides(III) ions highly adaptable to many coordination environments. This has led to the development of a wide array of macrocyclic molecular complexes with exciting properties. From this point of view, lanthanides have been known as the chameleons of coordination chemistry [5].

From Fig. 5.1, it is seen clearly that the ionic radii strongly depend on the coordination numbers. The ionic radii span the values of  $\text{Ca}^{2+}$  ions which is suggestive of the fact that  $\text{Ln}^{3+}$  ions can replace  $\text{Ca}^{2+}$  ions in coordination compounds.

## 2. Coordination numbers

Many factors affect coordination numbers and coordination polyhedra. It was recognized during 1962–1975 that the chemistry of yttrium and lanthanides is dominated by large coordination numbers. Although the structure of  $\text{Nd}(\text{BrO}_3)_3 \cdot 9\text{H}_2\text{O}$  had been determined as early as 1939 by Helmholtz [6] and shown that the central neodymium ion was bound to nine water molecules in a face-centred trigonal prismatic structure, the commonly held opinion was that the rare earth ions formed six-coordinate, octahedral complexes [7]. This notion was based on the known octahedral, six-coordination known at that time for the most

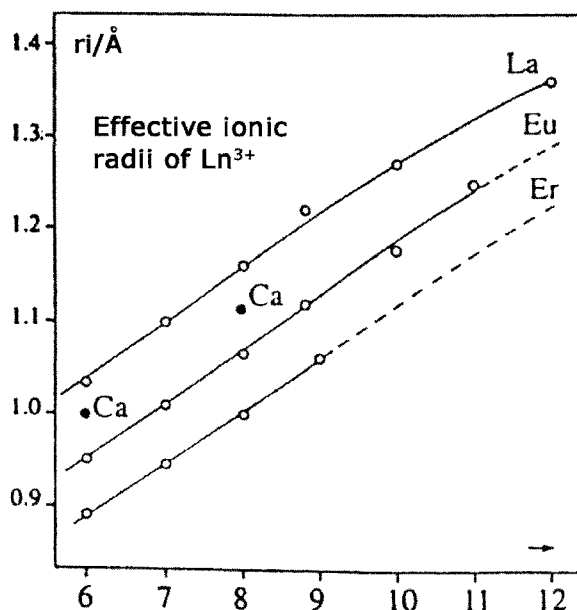


Fig. 5.1. Effective ionic radii of trivalent lanthanide ions vs coordination number (4).

trivalent metal ions of both d-transition and representative metals. Further, many of the rare earth complexes had formulations, which could be construed as six-coordinate complexes.

Studies on the stability constants of 2:1 complexes of nitriloacetic acid with yttrium and lanthanides [8] and 1:1 complex of diethylene-triaminepentaacetic acid with Ce(III) ion [9] were suggestive of the tendency of lanthanides to adopt large coordination numbers. Other studies involving stability constants of complexes with multi donor ligands, solvent extractions of rare earths, stability constants of mixed ligand complexes, and the synthesis of rare earth tetrakis- $\beta$ -diketonate complexes were also suggestive of coordination numbers greater than six for lanthanides [7]. Finally Hoard and coworkers [10] provided conclusive evidence against six coordination by their studies involving crystal and molecular structures of complexes with the formulas  $\text{NH}_4\text{La}(\text{EDTA}) \cdot 8\text{H}_2\text{O}$  and  $\text{HLa}(\text{EDTA}) \cdot 7\text{H}_2\text{O}$  with coordination numbers 9 and 10 for La, respectively. Many structural investigations [11] have been done and the compounds invariably have coordination numbers greater than six. In fact, compounds with coordination numbers less than seven are very rare for yttrium and lanthanides.

The chemical composition of rare earth complexes cannot by itself reveal the coordination number of the central metal ion. There are many complexes containing hydrated water molecules and coordinated water molecules. The nitrilotriacetic acid (NTA) complexes of Pr and Dy have the formulae  $\text{PrNTA} \cdot 3\text{H}_2\text{O}$  and  $\text{DyNTA} \cdot 4\text{H}_2\text{O}$ , respectively. The praseodymium complex is a nine-coordinate system with one molecule of water in the hydrated form [12] and the dysprosium complex is eight-coordinate with two molecules of water of hydration [13]. These structures cannot be predicted from the composition of the complexes. The complex  $\text{Nd}(\text{NO}_3)_3 \cdot 4\text{DMSO}$  is ten-coordinate [14] since the nitrate

groups act as bidentate ligands. The complex  $\text{Lu}(\text{NO}_3)_3 \cdot 3\text{DMSO}$  is nine-coordinate [15] with nitrate groups as bidentates. This also cannot be predicted from the stoichiometry of the complexes.

The coordination number can sometimes be established by coordinated physical measurements such as conductance, molecular weight measurement, infrared, UV-VIS-near IR, and emission spectroscopy [16]. The coordination numbers of solid complexes can be obtained by X-ray diffraction methods. Infrared spectroscopy and the conductance methods were used in the determination of the coordination numbers of  $\text{Nd}(\text{NO}_3)_3 \cdot 4\text{DMSO}$  and  $\text{Dy}(\text{NO}_3)_3 \cdot 3\text{DMSO}$  complexes [17].

Coordination numbers of complexes in solution are more difficult to determine and are usually inferred from spectroscopic and conductance data.

The existence of rare earth complexes with larger coordination numbers is due to the large size of rare earth ions and the predominant ionic nature of the bond. Since there is no strong, directional bonding, the disposition of the ligands is influenced by the size of the rare earth ion, and the properties of the ligands. Steric factors also influence the arrangement of ligands in rare earth complexes. In the absence of steric factors, the rare earth ions appear to have a coordination number of eight or higher. In the case of dipivoyl methane complexes the bulky *t*-butyl groups permit only tris-chelates formation and not tetrakis-chelates [18]. The trisdipivoyl methane complexes tend to add on ligands like pyridine, picoline or *o*-phenanthroline to form seven- or eight-coordinate species. On the other hand tetrakis-dibenzoyl methane complexes of rare earths are easily formed [20].

The coordination numbers of seven and eight are well-known for each rare earth ion. Higher coordination numbers depend critically on the size of the rare earth ion as well as the nature of the ligands. As pointed out earlier, dysprosium in  $\text{DyNTA} \cdot 4\text{H}_2\text{O}$  is eight coordinate and praseodymium in  $\text{PrNTA} \cdot 3\text{H}_2\text{O}$  is nine coordinate. Thus the change in coordination number is dependent on the steric interactions and the size of the central metal ion. Rare earth complexes with coordination numbers greater than nine are limited to terbium and lighter lanthanides, namely lanthanum to gadolinium.

The coordination number of six which is common for d-transition metals and scandium, is rather rare in the case of lanthanides. Authentic six-coordinate rare earth complexes are few. Some known six-coordinate complexes are  $\text{LnCl}_6^{3-}$  and  $\text{Ln}(\text{NCS})_6^{3-}$ . From the composition, it is clear that these are anionic complexes and that the high total negative charge and packing considerations preclude from the coordination of more uninegative ions than six.

We will now examine some examples of rare earth complexes spanning coordination numbers three to twelve. The examples given are illustrative and no claim is made as to coverage of an exhaustive list of compounds. It is also necessary to bear in mind that the coordination polyhedron for complexes with large coordination numbers is rarely uniquely determined and that it is generally possible to describe the polyhedron as related to more than one of the ideal structures. The description of the polyhedron is usually influenced by the compounds with which comparisons are made [21].

### 3. Low coordination number

The compounds of the general formula  $\text{M}[\text{N}(\text{SiMe}_3)_2]_3$ , where M represents Sc, Y, La, Ce, Pr, Nd, Sm, Eu, Gd, Ho, Yb and Lu have been synthesized and characterized [22].

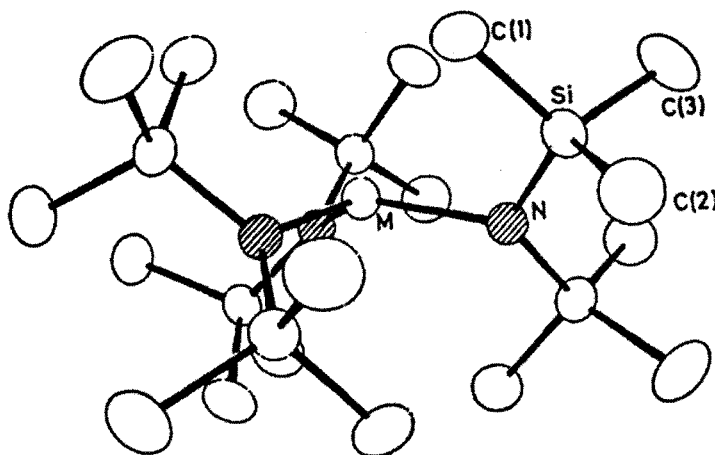


Fig. 5.2. The molecular structure of  $R\{N(\text{SiMe}_3)_2\}_3$  ( $R = \text{Sc, Eu}$ ) (reprinted with permission from Ghotra, J.S. Hursthouse, M.B. and Welch, A.J., 1973, *J. Chem. Soc., Chem. Comm.*, 669–670).

TABLE 5.3  
Theoretical explanation of the pyramidal structure of  $\text{NdL}_3$ .

Bond angle of N–Nd–N (degree)	Overlap interval of Nd–N	Mulliken bond order				Net charge on N
		Nd(6s)–N	Nd(6p)–N	Nd(5d)–N	Nd–N	
120	–0.172	0.079	0.116	0.435	0.630	0.637
115	0.386	0.084	0.111	0.452	0.641	0.503
100	0.438	0.094	0.103	0.457	0.654	0.421
90	0.293	0.095	0.100	0.456	0.651	0.415
80	0.055	0.093	0.097	0.452	0.642	0.433

The compounds of scandium, europium and ytterbium are isomorphous and it appears that all the compounds have the same structure. The structures of scandium and europium compounds determined [23] are different from those of the analogous compounds of iron and aluminum. The iron compound has a three-coordinate planar structure which permits the delocalization of the  $\pi$  electrons. In the case of scandium and europium compounds, there is three-coordination but the ligands are in pyramidal arrangement with N–M–N bond angle of  $116^\circ$ . Pyramidal coordination can be explained in terms of ionic bonding. The structures involving large lanthanide ions imply the presence of a considerable amount of ligand steric effect. The zero dipole moment in solution indicates planar structure and packing modes in solid state may be important. The molecular structure of the compound is shown in Fig. 5.2.

The electronic structure and chemical bonding of the neodymium compound  $\text{Nd}[N(\text{SiMe}_3)_2]_3$  has been studied by the INDO method [24]. The net charge on the Nd atom was found to be 0.254 and from this it is concluded that the Nd–N bonds have a co-



valent character. The covalence is attributed to the participation of 5d, 6s, and 6p orbitals of the atom and the three f electrons are 99% or more localized on the Nd atom. In Table 5.3 the Mulliken bond order, net charge on nitrogen, bond angle and the overlap integral are given. The Mulliken bond order of the Nd–N bond is maximum at N–Nd–N bond angle of  $100^\circ$  which explains the pyramidal structure.

Since the orbitals 5d, 6s and 6p participate, the lanthanide should have a high coordination tendency resulting in polymerization or reaction with other neutral ligands or solvent molecules. The presence of bulky trimethyl silicon offers steric hindrance and prevents polymerization.

#### 4. Complexes with coordination number 4

Complexes of the coordination number 4 are scarce. The only complex [25] of this coordination number is  $[\text{Li}(\text{C}_4\text{H}_8\text{O})][\text{Lu}(\text{C}_8\text{H}_9)_4]$ . The anion is tetrakis (2,6-dimethyl phenyl) luteate(III) and its structure is shown in Fig. 5.3.

The complex has a tetrahedral configuration with Lu–C bonds of 2.42–2.50 Å bond length. The bulky 2,6-dimethylphenyl group provides steric limitations in the complex. Ytterbium complex isomorphous with lutetium is also known. The electronic structure and the nature of chemical bonding of the lutetium complex was studied by the INDO method [26]. The MO's of  $\text{Lu}(\text{C}_8\text{H}_9)_4^-$  ion and the charge distribution are shown in Figs 5.4 and 5.5, respectively.

The net charge on lutetium is 0.948 and the Lu–C bond is predominantly covalent with 31% ionic characters and the Mulliken bond order of Lu–C bond is 0.497.

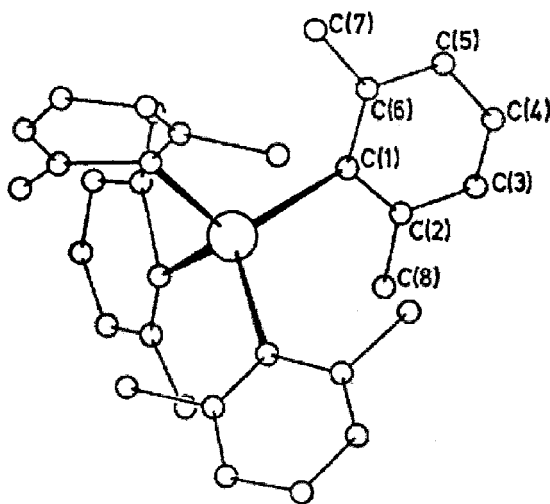


Fig. 5.3. The structure of the anion  $\text{Lu}(\text{C}_8\text{H}_9)_4^-$  (reprinted with permission from Coton, S.A., F.A. Hsrt, M.B. Hursthouse, and A.J. Welch, 1972, *J. Chem. Soc., Chem. Comm.*, 1225–1226).

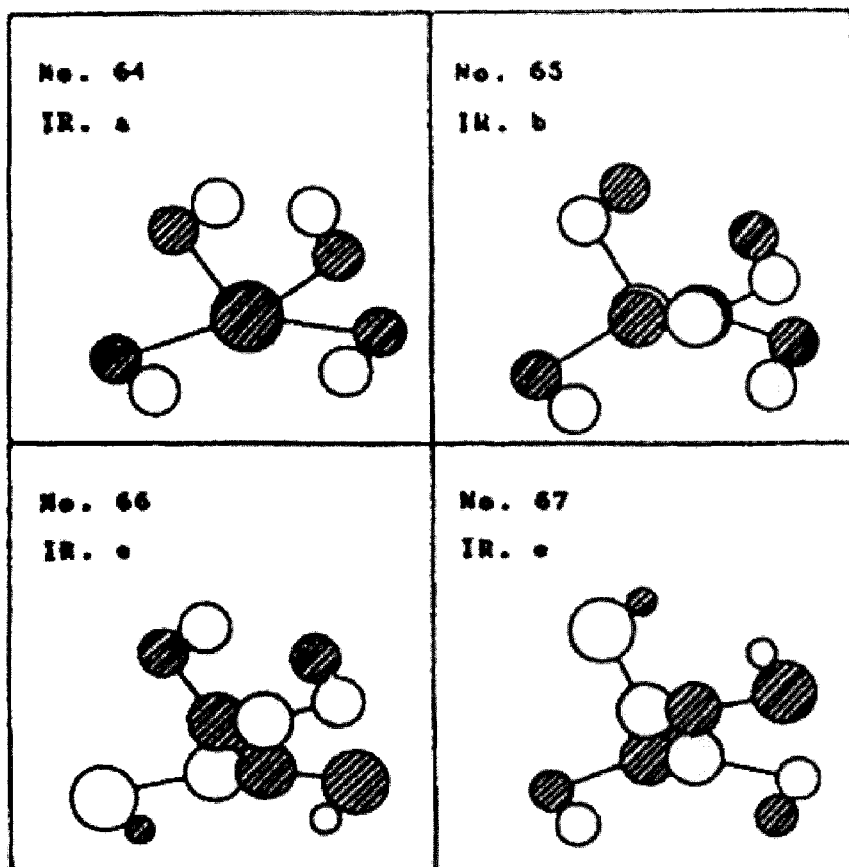


Fig. 5.4. Schematic diagram of some MO's of  $\text{Lu}(\text{2,6-dimethylphenyl})_4^-$ .

### 5. Coordination number 5

Formation of  $\text{La}_2\text{O}_2\{\text{N}(\text{SiMe}_3)_2\}_3(\text{Opph}_3)_2$  by the reaction of  $\text{La}\{\text{N}(\text{ScMe}_3)_2\}_3$  with an excess of triphenylphosphine oxide has been reported [27]. Considering the peroxy group as a bidentate, the complex is five-coordinate. Similar compounds containing praseodymium, samarium and europium have been synthesized. Another example of a five-coordinate complex is  $\text{LnCl}_3(\text{phenanthroline})$  whose structure has not been reported so far. The molecular structure of  $\text{La}_2\text{O}_2\{\text{N}(\text{SiMe}_3)_2\}_3(\text{Opph}_3)_2$  is shown in Fig. 5.6.

### 6. Coordination number 6

The structure of a genuine six-coordinate lanthanide complex namely,  $\text{Er}(\text{NCS})_6^{3-}$  in  $\text{C}_4\text{H}_9\text{O}_3\text{NEr}(\text{NCS})_6$  was determined by Martin and coworkers [28]. Earlier spectroscopic studies predicted the octahedral disposition of this complex [29]. The geometrical

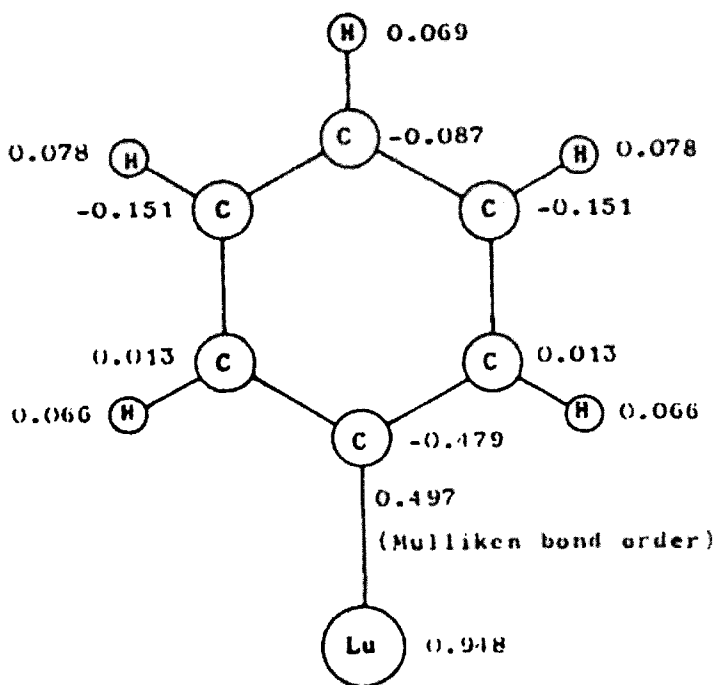


Fig. 5.5. Net charge distribution of  $\text{LuPh}_4^-$ .

arrangement predicted for six unidentate ligands is octahedral with distortions of a tetragonal or rhombic nature if the ligands are not identical. Complexes of the type  $\text{Ln}(\text{bidentate})_3^{n+}$  are expected to be octahedral with trigonal prismatic distortions with progressive decrease in the 'bite' of the bidentate ligand.

All the hexaisothiocyanato complexes of praseodymium to lutetium and yttrium are isostructural. The formula of the lanthanum complex is  $(\text{C}_4\text{H}_9)_4\text{La}(\text{NCS})_7$  but its structure is not known. Since lanthanum is large it may adopt six-coordination less readily. Another example of six-coordination is hexakis antipyrene yttrium(III) iodide whose structure is shown in Fig. 5.7. The antipyrene ligand is large and the six oxygen atoms coordinated to yttrium form an octahedron with  $S_6$  molecular symmetry.

Among the chelate complexes, the tris-dipivaloylmethane complexes of lanthanides from holmium to lutetium have been synthesized. The structures of these six-coordinate complexes have been determined. The coordination polyhedron of the erbium complex [30],  $\text{Er}(\text{DPM})_3$  consists of three, planar bidentate DPM ligands and deviates very slightly from the ideal trigonal prismatic structure. The larger lanthanide ions do not correspond to the six-coordinate complexes with DPM, but instead dimerize and give rise to seven-coordinate complexes [31]. This process of dimerization and formation of seven coordinate complexes with DPM can be attributed to the large ionic radii of the lighter lanthanides. The structure of  $\text{Er}(\text{DPM})_3$  complex is shown in Fig. 5.8. The coordination polyhedra of 7-coordinate hydrates of lanthanide chelates generally exhibit the geometry

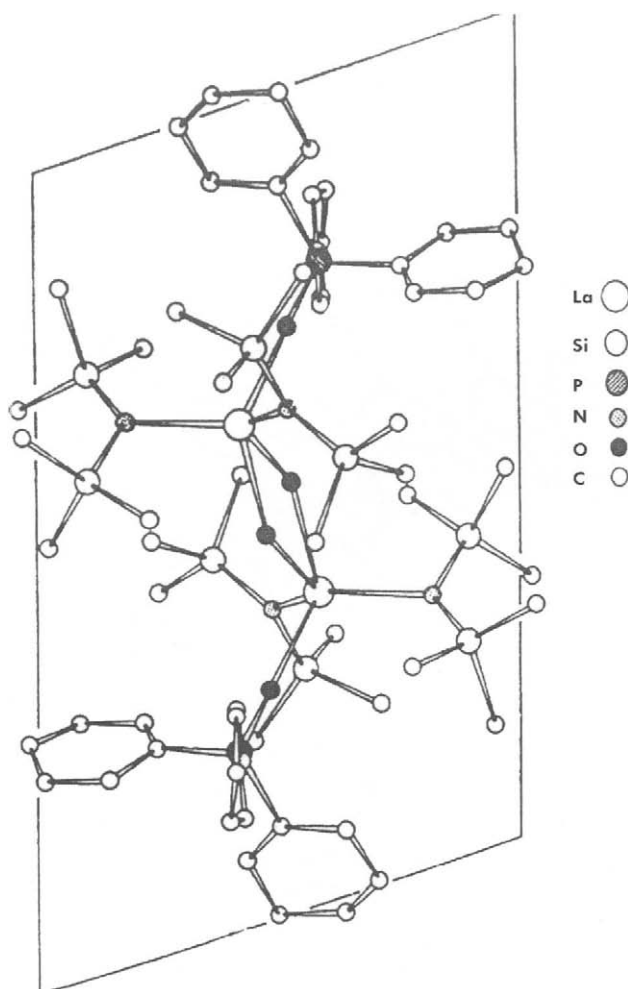


Fig. 5.6. The molecular structure of  $\text{La}_2\text{O}_2\{\text{N}(\text{SiMe}_3)_2\}(\text{OPPh}_3)_2$  (reprinted with permission from Bradley, D.C., J.S. Ghotra, F.A. Hart, M.B. Hursthouse, and P.R. Ruithby, 1974, *J. Chem. Soc., Chem. Comm.*, 40–41).

of a monocapped trigonal prism. The relationship between this polyhedron and the trigonal prism of the anhydrous  $\text{Ln}(\text{DPM})_3$ , is evidence for a hydration mechanism involving the replacement of one of the ligand oxygen atoms by water. The displaced oxygen atom of the ligand is then drawn back into the coordination sphere as the cap.

Crystal structures which have been shown to include hexa-coordinate metal atoms are given in Tables 5.4 and 5.5.

For hexa-coordination, the metal atoms are usually found in their highest oxidation state corresponding to a minimum radius for the element. The experimental results support theoretical analysis [44], in that the optimum arrangement of six monodentate ligands around a metal atom is octahedral. In the case of non-identical ligands, the metal–ligand

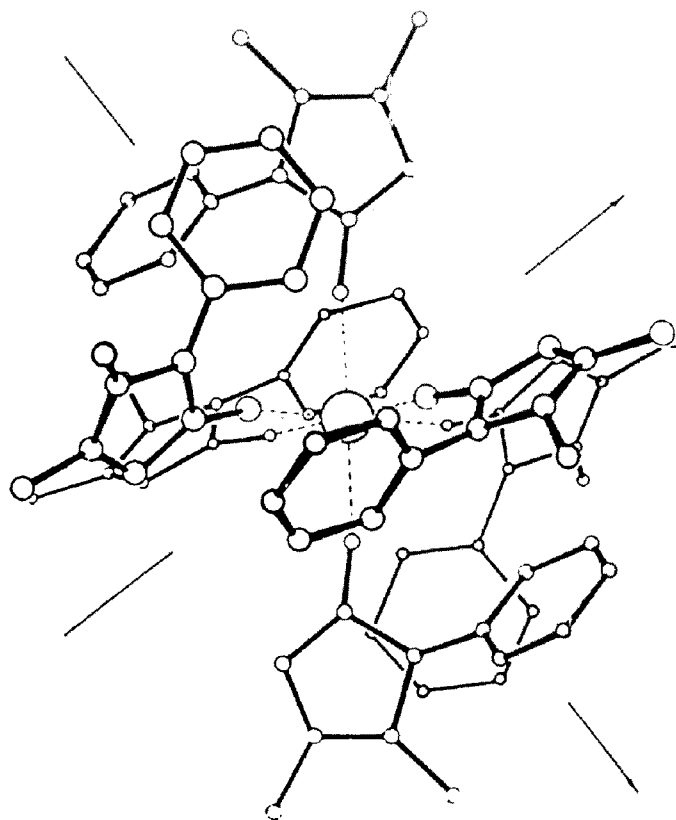


Fig. 5.7. The molecular structure of the hexakisantipyrenytrium(III) cation (reprinted with permission from Baker, R.W. and J.W. Jeffery, 1974, *J. Chem. Soc., Dalton Trans.*, 229–232).

TABLE 5.4  
Structures containing hexa-coordinate metal atoms.

Compound	Distortion	Metal in highest oxidation state	Reference
Octahedral	—	—	—
Gd(DMP) <sub>3</sub> Cl <sub>3</sub>	—	yes	[32]
Y(C <sub>11</sub> H <sub>12</sub> N <sub>2</sub> O) <sub>6</sub> I <sub>3</sub>	—	yes	[33]
Na[Yb(NH <sub>2</sub> ) <sub>4</sub> ]	—	yes	[34]
Eu <sub>4</sub> Al <sub>2</sub> O <sub>9</sub>	—	—	[35]
NaSmGeO <sub>4</sub>	—	—	[36]
Y <sub>2</sub> SiO <sub>5</sub>	—	—	[37]
Y <sub>2</sub> Si <sub>2</sub> O <sub>7</sub>	Irregular	yes	[38]
Y <sub>2</sub> BeO <sub>4</sub>		yes	[39]
Er <sub>2</sub> Si <sub>2</sub> O <sub>7</sub>		—	[40]
LiEu <sub>3</sub> O <sub>4</sub>		—	[41]
Ho <sub>2</sub> S <sub>3</sub>		yes	[42]

dmp = 2,6-dimethyl-4-pyrone.

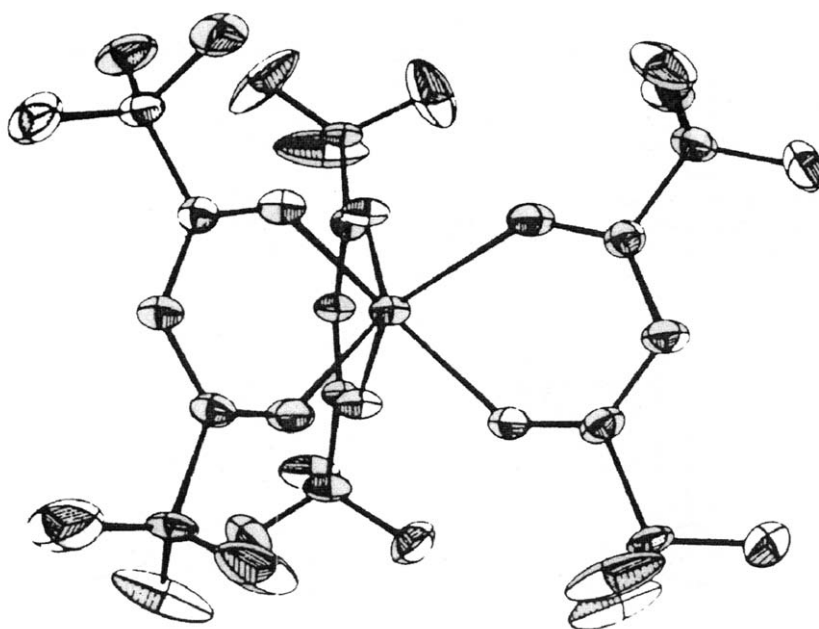


Fig. 5.8. Trigonal prismatic coordination in  $\text{Er}(\text{DPM})_3$  (reprinted with permission from de Villiers, J.P.R. and J.C.A. Boeyens, 1971, *Acta Crystallogr.* B27, 2335–2340).

TABLE 5.5  
Structures containing hexa-coordinate metal atoms.

Compound	Configuration	Metal in highest oxidation state	Reference
Other polyhedra			
$\text{Er}(\text{DPM})_3$	Trigonal prism	yes	[30]
$\beta\text{-Pr}_2\text{Si}_2\text{O}_7$	Irregular		[43]

DPM = 2,2,6,6-tetramethylheptane:3,5-dionato.

bond lengths vary or the angles between them differ from  $90^\circ$  resulting in either tetragonal or rhombic distortions.

## 7. Coordination number 7

There are many complexes of lanthanides of coordination number seven [11]. There are many polyhedra for this coordination number, namely pentagonal bipyramid ( $D_{5h}$ ) capped octahedron ( $C_{3v}$ ), tetragonal base trigonal base ( $C_s$ ), capped trigonal prism ( $C_{2v}$ ) and capped trigonal prism ( $C_{3v}$ ). Inter ligand repulsivities have been studied as the function of the form of power law used for energy comparisons between different polyhedra for several coordination numbers [45,46]. The order of preference for the different idealized

TABLE 5.6

Equal distance–equal charges repulsivities for various 7-coordinate polyhedra (after King [44]).

Polyhedron	Symmetry	Repulsivity
Pentagonal bipyramid	$D_{5h}$	10.250
Capped octahedron	$C_{3p}$	10.276
Tetragonal base trigonal base	$C_s$	10.446 & 10.446 (2 isomers)
Capped trigonal prism	$C_{2p}$	10.785
Capped trigonal prism	$C_{3p}$	10.793 & 10.969 (2 isomers)

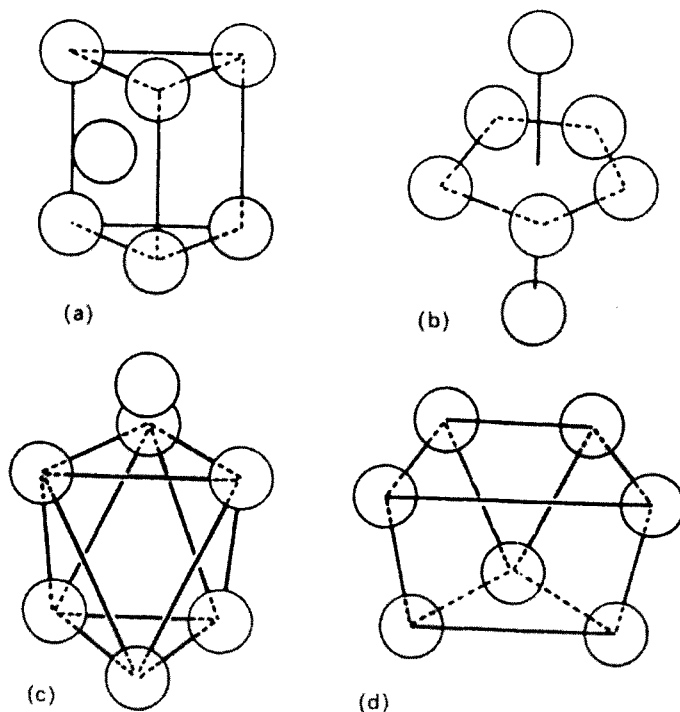


Fig. 5.9. Idealised polyhedra for 7-coordination.

form changes when the power law is varied only in the case of 7-coordination. The relative repulsivities for 7-coordinate polyhedra calculated [44] on the basis of the inverse square law are given in Table 5.6.

The order of preference of the polyhedra given in Table 5.6 is confirmed by the observation that the first four polyhedra have been reported in the structures reported for Lanthanide complexes. The idealized shapes of the four favoured polyhedra are shown in Fig. 5.9. It is necessary to exercise utmost care in the consideration of specific 7-coordination in view of the very small differences of spatial arrangement between the various ideal geometries.

TABLE 5.7  
Structures incorporating lanthanide atoms in 7-coordination.

Compound	Basic structural unit	Reference
Capped trigonal prism		
Pr(DPM) <sub>3</sub>	Binuclear	[31]
Dy(DPM) <sub>3</sub> H <sub>2</sub> O	Monomer	[48]
Er <sub>8</sub> O(DPM) <sub>10</sub> (OH) <sub>12</sub>	Octanuclear	[49]
Lu(FOD) <sub>3</sub> H <sub>2</sub> O	Monomer	[50]
Y <sub>2</sub> TiO <sub>5</sub>	Lattice	[51]
Gd <sub>2</sub> S <sub>3</sub>	Lattice	[52]
NaNd <sub>3</sub> (GeO <sub>4</sub> ) <sub>2</sub> (OH) <sub>2</sub>	Lattice	[53]
Other polyhedra	Configuration	
Ho(PhCOCHCOPh) <sub>3</sub> H <sub>2</sub> O	Distorted capped octahedron	[54]
La <sub>2</sub> TiO <sub>5</sub>	Distorted capped octahedron	[55]
EuI <sub>2</sub>	Tetragonal base-trigonal base	[56]
YbCl <sub>2</sub>	Tetragonal base-trigonal base	[57]
Er <sub>2</sub> Ge <sub>2</sub> O <sub>7</sub>	Distorted pentagonal bipyramid	[58]
Eu <sub>4</sub> Al <sub>2</sub> O <sub>9</sub>	Irregular	[35]
α-Pr <sub>2</sub> Si <sub>2</sub> O <sub>7</sub>	Detailed shape of polyhedra not available	[59]
β-Pr <sub>2</sub> Si <sub>2</sub> O <sub>7</sub>	Detailed shape of polyhedra not available	[43]
Gd <sub>2</sub> Si <sub>2</sub> O <sub>7</sub>	Detailed shape of polyhedra not available	[60]
Gd <sub>2</sub> (MoO <sub>4</sub> ) <sub>3</sub>	Detailed shape of polyhedra not available	[62]
β-Gd <sub>2</sub> (MoO <sub>4</sub> ) <sub>3</sub>	Detailed shape of polyhedra not available	[62]
YbOOH	Detailed shape of polyhedra not available	[63]
Pr <sub>10</sub> S <sub>14</sub> O	Detailed shape of polyhedra not available	[64]
7Gd <sub>2</sub> O <sub>3</sub> · 9SiO <sub>2</sub>	Detailed shape of polyhedra not available	[65]
Complexes	Basic polyhedron	
Ho(C <sub>6</sub> H <sub>5</sub> COCHCOC <sub>6</sub> H <sub>5</sub> ) <sub>3</sub> · H <sub>2</sub> O	Mono-capped octahedron	[54]
Y(C <sub>6</sub> H <sub>5</sub> COCHCOCH <sub>3</sub> ) <sub>3</sub> · H <sub>2</sub> O	Mono-capped octahedron	[66]
Dy(DPM) <sub>3</sub> · H <sub>2</sub> O	Mono-capped trigonal prism	[48]
Lu(DPM) <sub>3</sub> · C <sub>6</sub> H <sub>7</sub> N	Mono-capped trigonal prism	[67]
Yb(acac) <sub>3</sub> · H <sub>2</sub> O	Mono-capped trigonal prism	[68]
Eu(DPM) <sub>3</sub> · DMSO	Pentagonal bipyramid	[69]

DPM = 2,2,6,6-tetramethylheptane-3,5-dionato(dipivaloyl methane).

FOD = 1,1,1,2,2,3,3-heptafluoro-7,7-dimethyl-4,6-octane dionato.

This problem has been well illustrated in the literature [47]. It has also been pointed out that the energy differences between the different idealized geometrical shapes are probably small compared with the intermolecular forces generated by ordering. Some compounds with structures incorporating lanthanide atoms in seven coordination are given in Table 5.7. Depending on the nature of the solvent such as water or dimethyl sulphoxide, the polyhedron can be either a monocapped trigonal prism or a pentagonal bipyramid and this is illustrated by the complexes listed in Table 5.7.



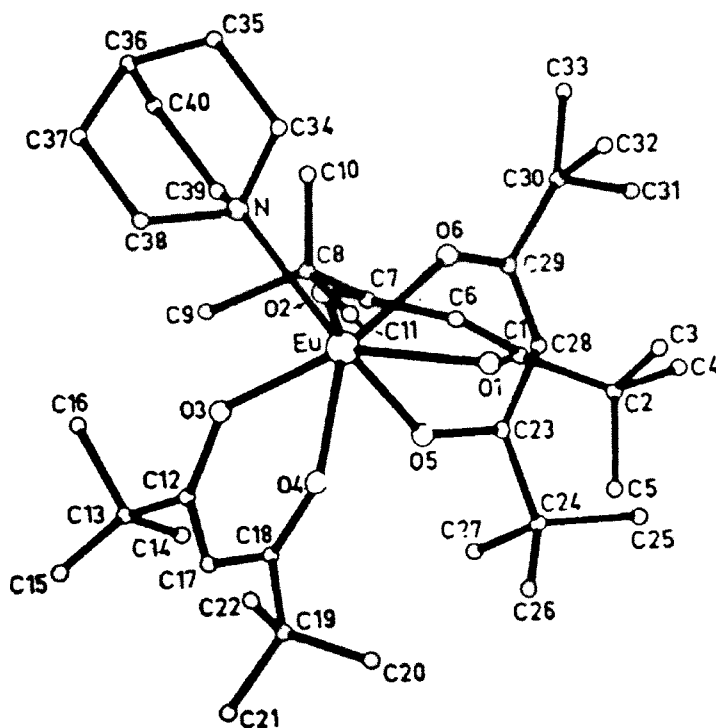


Fig. 5.10. The molecular structure of the quinuclidine adduct of  $\text{Eu}(\text{DPM})_3$  (reprinted with permission from Bye, E., *Acta Chem. Scand.* A28, 731–739).

The complexes studied are of the general formula  $[\text{Ln}(\text{bidentate})_3(\text{unidentate})]^{n+}$  where the bidentate is a  $\beta$ -diketone. From a consideration of ligand–ligand repulsion energies using a “normalized bite” of one 1.22 the preferred coordination polyhedra for these complexes have been determined [70]. The “normalized bite” is defined as the distance between the two donor atoms divided by the metal to donor atom distance. This led to three favored coordination polyhedra, namely: (1) Mono-capped octahedron, (2) a figure with no elements of symmetry which is a capped trigonal prism in loose terms, (3) a polyhedron figure lying in between a pentagonal bipyramid and a capped trigonal prism. It is important to note that the differences necessary to stabilize one structure over another are very subtle. All the geometries cited earlier have been confirmed by the synthesis of rare earth complexes containing  $\text{Ln}(\text{DPM})_3$  unit which adds on a unidentate ligand to form a seven coordinate complex.

The quinuclidine complex of  $\text{Eu}(\text{DPM})_3$  gives rise to a polyhedron consisting of a distorted octahedron formed by six oxygen atoms with quinuclidine nitrogen located above the center of one of the faces, resulting in overall threefold symmetry. The molecular structure [71] of  $[\text{Eu}(\text{DPM})_3 \cdot \text{quinuclidine}]$  is shown in Fig. 5.10.

The complex compounds such as  $\text{Eu}(\text{DPM})_3$  with 3,3-dimethylthietane-1-oxide and  $\text{Lu}(\text{DPM})_3$  with 3-methyl pyridine have been synthesized and the geometries adapted by

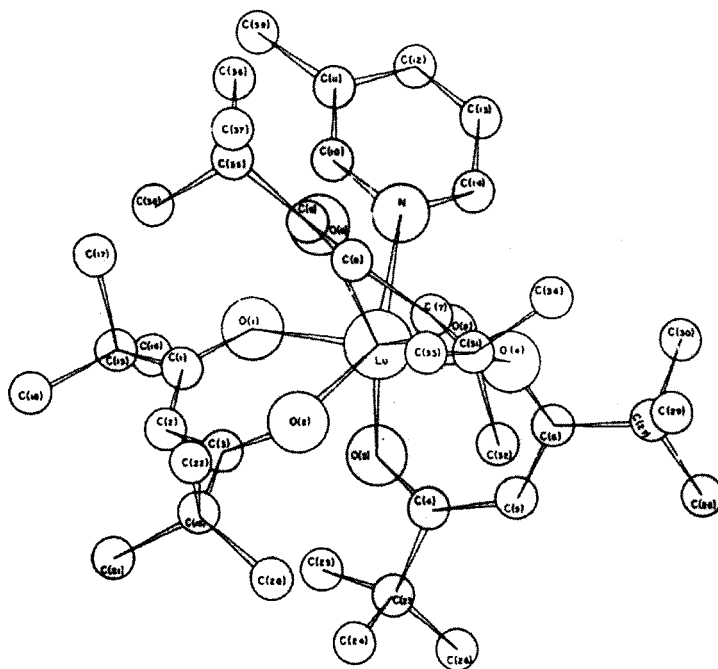


Fig. 5.11. The molecular structure of 3-methylpyridine-Lu(DPM)<sub>3</sub> (reprinted with permission from S.J.S. Wasson, D.E. Sands, W.F. Wagner, *Inorg. Chem.*, 12, 187–190).

these complexes may best be described as a capped trigonal prism. Earlier, the effect of size (i.e.) the radii of metal ions and its influence in favouring different geometries was briefly mentioned, but here we have complexes of metal ions of different radii adopting the same geometry. It was suggested from the structure of Pr<sub>2</sub>(DPM)<sub>6</sub> that 7 coordination is impossible when M–O distances are less than 2.27 Å. Contrary to this suggestion, M–O distances of 2.33 Å in Eu(DPM)<sub>3</sub> and 2.24 Å in Lu(DPM)<sub>3</sub> have been observed. The molecular structure [67] of Lu(DPM)<sub>3</sub> · 3-methylpyridine is given in Fig. 5.11.

The complex Eu(DPM)<sub>3</sub> · DMSO is a 7 coordinate structure with 2 slightly distorted pentagonal bipyramid geometries [69]. Since dimethyl sulphoxide forms a strong bond with rare earth ions, the existence of the complex in the forms of distorted pentagonal bipyramids is borne out by theory and practice [70]. This complex provides unequivocal evidence for the existence of 7 coordinate complexes in a deformed manner.

The theory of repulsive forces for estimating preferred polyhedra is based on minimizing the repulsive forces between atoms. An alternative approach has been suggested. This approach involves optimizing the arrangement of seven atoms at equal distances from a central reference point in such a way that all pairs of atoms subtend an angle of ~77° at the center. Polyhedra which comply with this condition have been reported for praseodymium atoms in the dimeric complex Pr<sub>2</sub>(DPM)<sub>6</sub>. Two out of the seven oxygen atoms in each coordination sphere have only three near neighbors, while the other five

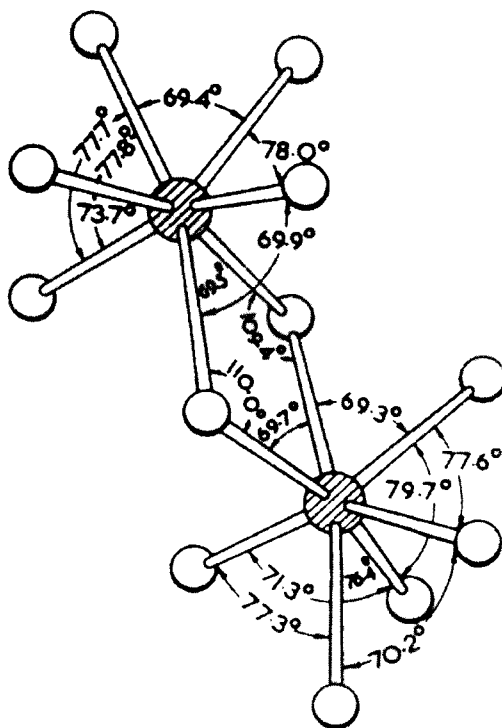


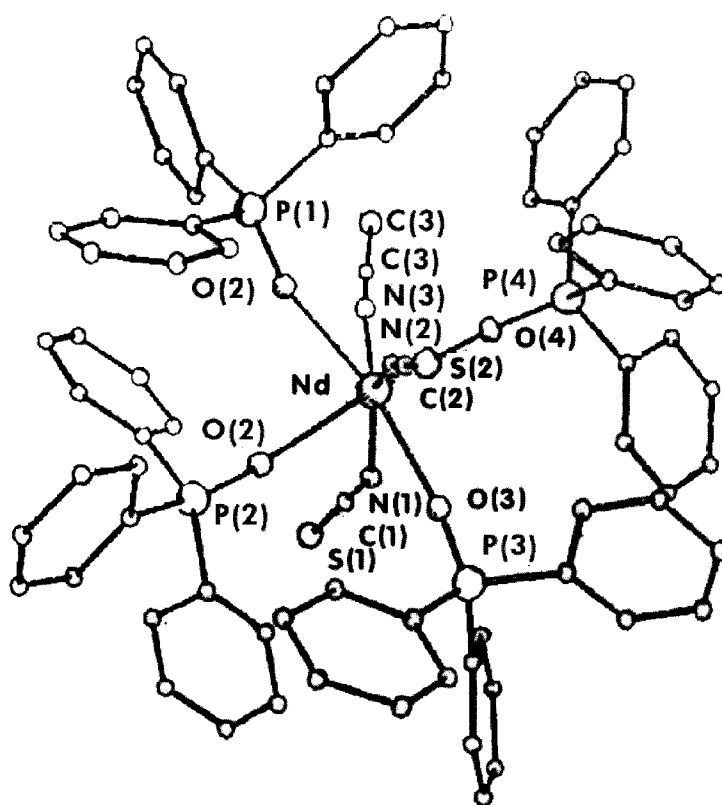
Fig. 5.12. The coordination geometry of the  $\text{Pr}_2\text{O}_{12}$  system (from Erasmus and Boeyens [31]).

have four near neighbors. The shape of polyhedra resemble that of the  $C_{2v}$  trigonal prism. The coordination geometry of the  $\text{Pr}_2\text{O}_{12}$  system is shown in Fig. 5.12.

A similar arrangement has been described [48] with seven oxygen atoms for the complex  $\text{Dy}(\text{DPM})_3 \cdot \text{H}_2\text{O}$ . The water molecule which completes the 7-coordination is hydrogen bonded to two oxygen atoms of a center of symmetry related formula unit so that two formula units are held together by hydrogen bonds in a dimer. The crystal structure of  $\text{Lu}(\text{FOD})_3 \cdot \text{H}_2\text{O}$  resembles that of  $\text{Dy}(\text{DPM})_3\text{H}_2\text{O}$ .

The complex  $\text{Ho}(\text{PhCOCHOPh})_3$  involves distortion of the holmium coordination polyhedron from a capped octahedral arrangement. This complex is similar to  $\text{Eu}(\text{DPM})_3 \cdot \text{quinuclidine}$ .

An interesting structure is provided by  $\text{Er}_8\text{O}(\text{DPM})_{10}(\text{OH})_{12}$ , the hydrolysis product of  $\text{Er}(\text{DPM})_3$ . In the hydrolysis product, the erbium atoms are each chelated to one DPM ligand and cluster around a central oxygen atom in inner and outer spheres of four atoms each. The inner sphere atoms surround the central oxygen tetrahedrally and are also bonded to five hydroxyl groups, each of which is shared with two other erbium atoms. The coordination number of the inner erbium atoms is eight and that of the outer erbium atoms, where each has a DPM bonded at one position, is seven. The tertiary butyl groups are all directed outwards.

Fig. 5.13. Structure of  $\text{Nd}(\text{NCS})_3(\text{Ph}_3\text{PO})_4$ .

It is difficult to describe oxides and other simple compounds with respect to the geometries they adopt.

The crystal structure of the complex  $\text{Nd}(\text{NCS})_3(\text{Ph}_3\text{PO})_4$  shows it to be seven coordinate with monoclinic structure [72] and space group  $P21/e$ . The unit cell parameters are

$$\begin{array}{lll}
 a = 13.211(7) \text{ \AA} & B = 102.19^\circ(5) & Z = 4 \\
 b = 23.544(14) \text{ \AA} & F(000) = 2924 e & d_{\text{calc}} = 1.370 \text{ g/cm}^3 \\
 c = 22.821(18) \text{ \AA} & V = 6943 \text{ \AA}^3 & d_{\text{exp}} = 1.375 \text{ g/cm}^3
 \end{array}$$

The molecular structure and the coordination sphere are shown in Figs 5.13 and 5.14, respectively. The molecule has an approximate  $C_s$  symmetry with three Nd–N bonds of 2.50 Å length and four dative bonds of bond length of 2.39 Å for Nd–O bonds.

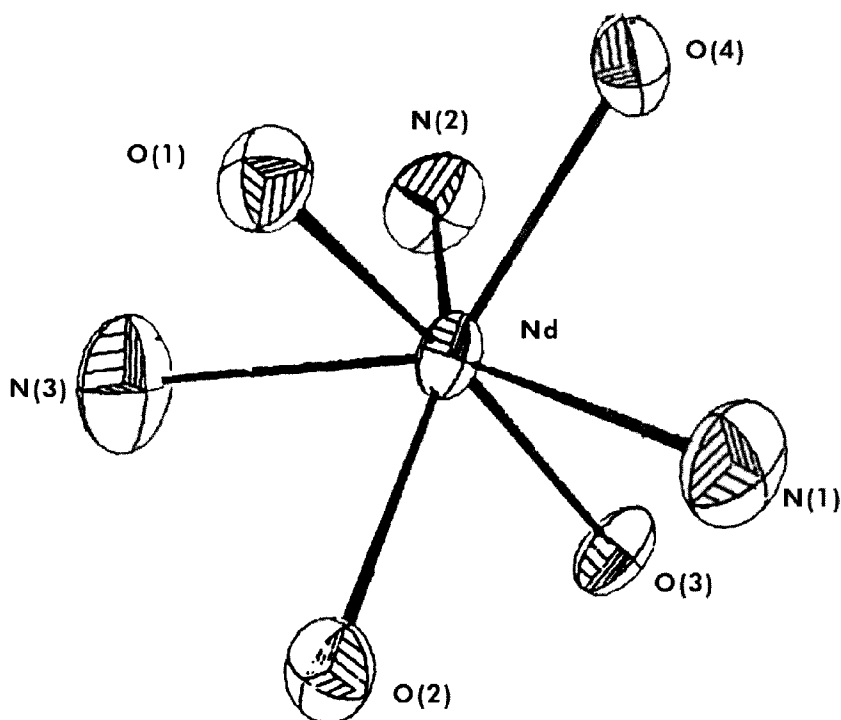


Fig. 5.14. The coordination sphere of neodymium.

TABLE 5.8  
Equal distance–equal charge repulsivities for 8-coordinate polyhedra (after King [44]).

Polyhedron	Point group symmetry	Repulsivity
Square antiprism	$D_{4d}$	14.337
Dodecahedron(triangular faces)	$D_{2d}$	14.390, 14.354*
Bicapped octahedron	$D_{3d}$	14.501
Truncated octahedron	$D_{2h}$	14.783
4.4 Bicapped trigonal Prism	$C_{2v}$	14.878
Distorted cube	$C_{2v}$	15.658
Cube	$O_h$	15.667

\*Two isomers.

## 8. Coordination number 8

Lanthanide complexes with octa-coordination are well-known. The relative stabilities of various coordination polyhedra based on interligand repulsivities are given in Table 5.8.

The geometry of octa-coordination has been extensively discussed in the literature [47, 73,74]. The two most common configurations are the square antiprism ( $D_{4d}$ ) and the

dodecahedron with triangular faces ( $D_{2d}$ ). The coulombic energy difference between these two basic types of polyhedra are very small and the preference for one or the other is governed by chelate ligand requirements or molecular packing forces.

The antiprism is characterized by two shape parameters, namely:

- (1) The ratio of the length of the side of a triangular face to that of the edge of the square face ( $1/S$ ) and
- (2) the angle between the  $\bar{8}$  axis and the vector from the central atom to one of the ligands ( $\theta$ ) (Fig. 5.15a). The 'most favorable' values for the two parameters [75] are  $1/S = 1.057$ ,  $\theta = 57.3$  degrees. The hard sphere model for the antiprism leads to the values  $1 = S$  and  $\theta = 59.25$  degrees.

The dodecahedron may be characterized by three parameters (Fig. 5.15b), namely:

- (i)  $\theta_A$  the angle between M–A bond vector and  $\bar{4}$  axis of the polyhedron
- (ii)  $\theta_B$  the angle between the M–B bond and the  $\bar{4}$  axis and
- (iii) the ratio of bond lengths, M–A/M–B. The most favourable values are  $\theta_A = 35.2$  deg,  $\theta_B = 73.5$  deg and M–A/M–B = 1.03. The values for a hard sphere model are  $\theta_A = 36.9$  deg,  $\theta_B = 69.5$  deg and M–A/M–B = 1.

The conversion of antiprismatic conformation into a dodecahedron arrangement involves a small spatial rearrangement and hence it is not easy to decide which idealized geometry to choose in crystal structures for which the shape of the polyhedron is not certainly fixed by elements of symmetry.

Due to the unsatisfactory nature of the two shape parameters  $1/S$  and  $\theta$  in distinguishing between antiprism and dodecahedron, Lippard and Russ [76] proposed alternative criteria such as

- (i) the angle between the best planes through the atoms AABB and B'B'A'A' (i.e.) interpenetrating trapezoids (Fig. 5.15b) and
- (ii) 'd' the average deviation of the ligand atoms from these planes.

Although these parameters serve as a test, comprehensive analysis is deemed necessary for a satisfactory way of distinguishing between distorted polyhedra.

When bidentate ligands are involved in 8-coordinate complexes, many isomeric forms are possible for each polyhedron. The six isomers for a dodecahedron and the three isomers for a square antiprism are listed in Table 5.9.

The two important factors that determine the geometry of neutral bidentate complexes [75] are ligand–ligand repulsion energies and matching of the ring span of the bidentate ligand with the appropriate polyhedron edges. Thus for neutral tetrakis complexes with M–L distances of 2.30 Å or greater, the dodecahedron ( $D_{2d}$ ) or the square antiprism ( $D_2$ ) are stable configurations. The tetrakis acetylacetonate complex of Ce(IV) has square antiprism geometry corresponding to the  $D_2$  symmetry isomer.

The influence of bidentate ligands on the stereochemistry of 8-coordinate complexes has been analyzed by calculation of ligand–ligand repulsion energies [77]. Based on this analysis for complexes  $M(\text{monodentate})_4(\text{bidentate})_2$  or  $M(\text{bidentate})_4$  with ligands of small bites, dodecahedron ( $D_{2d}$ ) is the preferred geometry. When the bite of the ligand increases, square antiprism geometry is preferred. When the bite of the ligand becomes

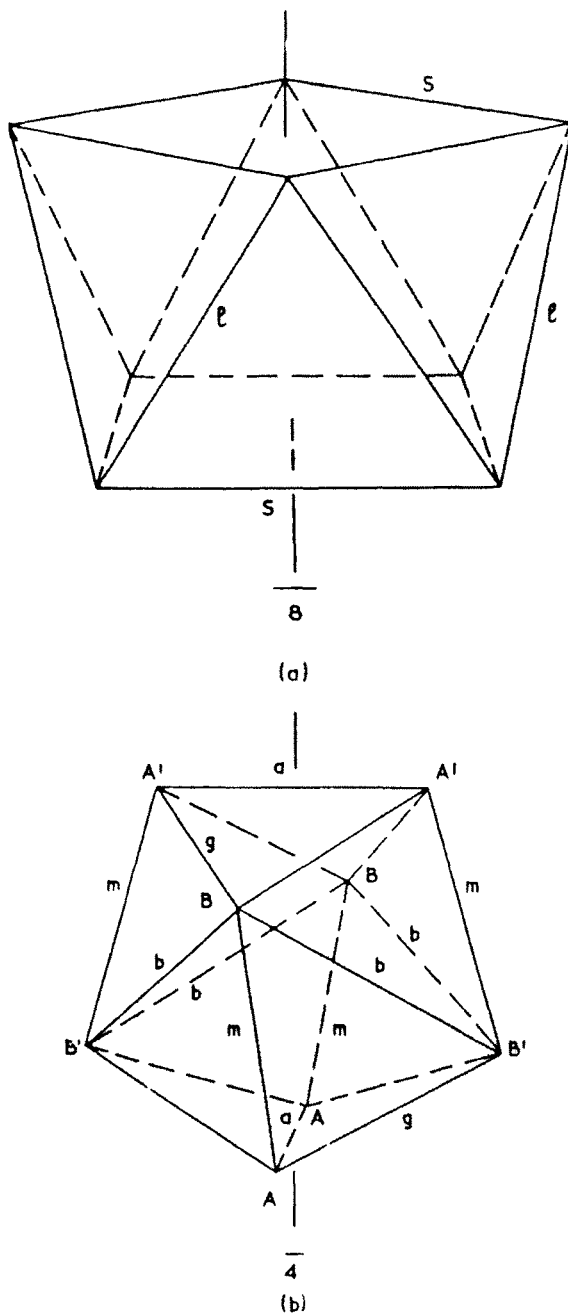


Fig. 5.15. Idealised 8-coordinate polyhedra. (a) Square antiprism. (b) Dodecahedron with triangular faces (symmetry related vertices are labelled with capital letters and edges with small letters).

TABLE 5.9  
Stereoisomers for tetrakis (bidentate) octa-coordinate polyhedra.

Dodecahedron	Symmetry	Occupied edges of dodecahedron*
	D <sub>2d</sub>	(m,m,m,m)
	S <sub>4</sub>	(g,g,g,g)
	D <sub>2</sub>	(g,g,g,g)
	D <sub>2</sub>	(a,a,b,b)
	C <sub>2</sub>	(m,m,g,g)
	C <sub>1</sub>	(a,b,m,g)
Square antiprism	Symmetry	Occupied edges of square antiprism*
	D <sub>4</sub>	(1,1,1,1)
	D <sub>2</sub>	(s,s,s,s)
	C <sub>2</sub>	(1,1,s,s)

\*The notation of polyhedron edges corresponds to that used in Fig. 5.15.

equal to the distance between donor atoms observed for complexes containing monodentate ligands three geometries, namely, D<sub>2</sub> square antiprism, D<sub>4</sub> square antiprism and D<sub>2d</sub> dodecahedron are likely. These predictions are borne out by known crystal structures.

The two other polyhedra possible for 8-coordination are hexagonal bipyramid and cube. Hexagonal bipyramid is energetically unfavourable. The eight ligands at the corners of a cube result in non-bonding repulsions. Cubic coordination requires f orbital participation and is a possible configuration for some lanthanide compounds. Some structures of lanthanide compounds with octa-coordination are given in Table 5.10.

### 8.1. Dodecahedron

There are many compounds of lanthanides exhibiting coordination polyhedra close to a dodecahedron with triangular faces. There remains a great interest in the various environments and ligand combinations for which the dodecahedral arrangement is favourable.

The structure of Dy(NTA)(H<sub>2</sub>O)<sub>2</sub> consists of dysprosium atoms having five acetate oxygen atoms, two water molecules and one nitrogen atom situated at the corners of the distorted dodecahedron. Each nitrilotriacetate ligand is a hexadentate with one acetate oxygen atom uncoordinated to any metal atom and two carboxylate oxygen atoms coordinated to metal atoms in neighboring molecules. Thus the structure is polymeric [84].

Polymeric structures containing dodecahedrally coordinated metal atoms are encountered among the carboxylates of heavier lanthanides. Erbium in [Er(HOCH<sub>2</sub>COO)-(OCH<sub>2</sub>COO)(H<sub>2</sub>O)]H<sub>2</sub>O is coordinated to eight oxygen atoms contributed by hydroxyacetate, oxyacetate and water molecule [89]. The acetate groups act as bridging ligands and the resulting structure is shown in Fig. 5.16.

The dodecahedra occur in pairs sharing a pair of oxygen atoms at a common edge and their shape is distorted from the ideal shape. Thus there are two intersecting trapezoids with angles  $\theta_A = 34.5^\circ$  and  $37.4^\circ$ ;  $\theta_B = 73.2^\circ$  and  $69.5^\circ$ . There are two types of metal atoms in the crystal structure [88] of Er(HOCH<sub>2</sub>COO)<sub>3</sub> · 2H<sub>2</sub>O. Each metal is bonded to eight oxygen atoms forming a distorted dodecahedron. One Er is in the form of the



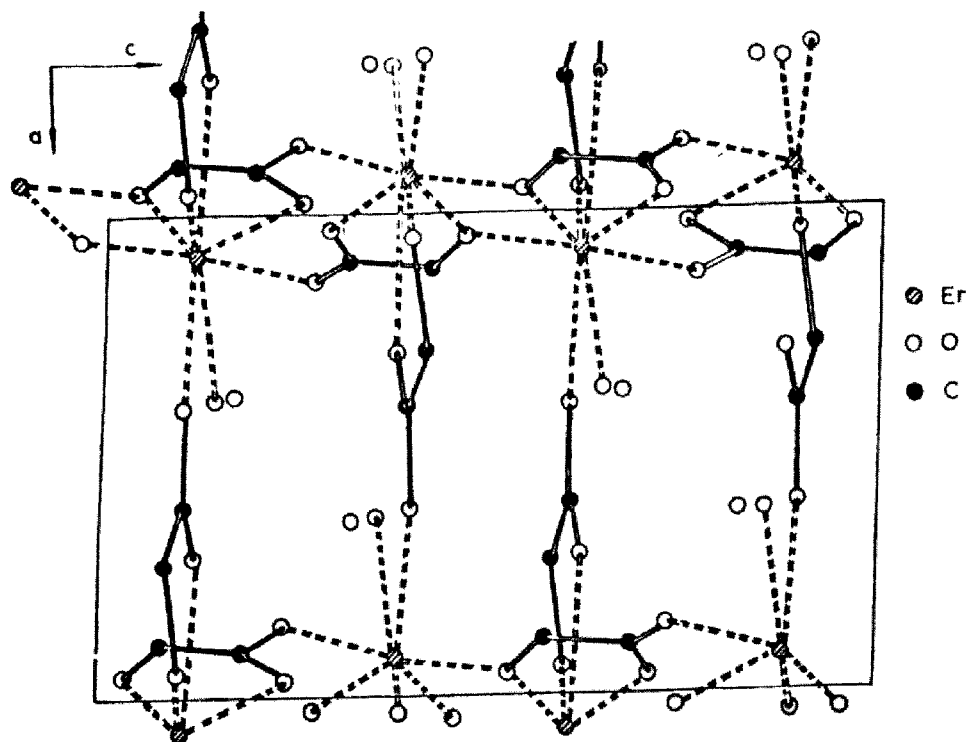
TABLE 5.10  
Structures incorporating octa-coordinate metal atoms.

Compound	Elements (M) for which structure is available	Symmetry of stereoisomer	Reference
<b>Dodecahedral</b>			
Th(DTC) <sub>4</sub>		D <sub>24</sub>	[78]
CsM(HFA) <sub>4</sub>	Am, Eu, Y	D <sub>2</sub>	[79]
Rb <sub>2</sub> UF <sub>6</sub>			[80]
ThSiO <sub>4</sub>			[81]
(NH <sub>4</sub> ) <sub>3</sub> CEF <sub>7</sub> · H <sub>2</sub> O			[82]
Pr <sub>2</sub> (FOD) <sub>6</sub> · 2H <sub>2</sub> O (also C <sub>2v</sub> BCTP)			[83]
KGd(CO <sub>3</sub> ) <sub>2</sub> · 3H <sub>2</sub> O			[13]
(NTA)M · 2H <sub>2</sub> O	Dy–Lu		[84]
MCl <sub>3</sub> · 6H <sub>2</sub> O	Eu, Gd, Dy, Ho		[85]
NH <sub>4</sub> (trop) <sub>4</sub> Ho		D <sub>24</sub>	[86]
Ho(acac) <sub>3</sub> · 4H <sub>2</sub> O			[87]
M(HOCH <sub>2</sub> COO) <sub>3</sub> · 2H <sub>2</sub> O	Tb–Lu		[88]
[M(HOCH <sub>2</sub> COO)(OCH <sub>2</sub> COO)H <sub>2</sub> O] · H <sub>2</sub> O	Gd–Lu		[89]
α-Nd <sub>2</sub> (MoO <sub>4</sub> ) <sub>3</sub>			[90]
ErPO <sub>4</sub>			[91]
<b>Square antiprismatic</b>			
(PCN) <sub>2</sub> U			[92]
β-M(acac) <sub>4</sub>	Ce, U	D <sub>2</sub>	[93]
La(C <sub>5</sub> H <sub>5</sub> NO) <sub>8</sub> (ClO <sub>4</sub> ) <sub>3</sub>	La–Lu		[94]
M(DMP) <sub>8</sub> (ClO <sub>4</sub> ) <sub>3</sub>	La–Sm		[32]
M(nicotinate) <sub>3</sub> (H <sub>2</sub> O) <sub>2</sub>	La–Lu		[95]
M(isonicotinate) <sub>3</sub> (H <sub>2</sub> O) <sub>2</sub>	La–Pr		[96]
M(isonicotinate) <sub>3</sub> (H <sub>2</sub> O) <sub>2</sub>	Er–Lu		[97]
Nd <sub>2</sub> (C <sub>4</sub> H <sub>5</sub> O <sub>4</sub> N) <sub>3</sub> 2HCl · 7H <sub>2</sub> O			[98]
HpipM(BA) <sub>4</sub>	La–Lu		[99]
Eu(acac) <sub>3</sub> (phen)		(D <sub>2</sub> )	[100]
Eu(DPM) <sub>3</sub> (py) <sub>2</sub>			[101]
HM(BA) <sub>4</sub> · xNHEt <sub>2</sub>	La–Gd		[102]
HGd(BA) <sub>4</sub> · n pip (n ≈ 1)			[103]
[M(C <sub>5</sub> H <sub>4</sub> NCOOH) <sub>3</sub> (H <sub>2</sub> O) <sub>2</sub> ]Cr(NCS) <sub>6</sub>	La–Lu		[97]
(4-picoline) <sub>2</sub> Ho(dpm) <sub>3</sub>			[104]
(K,Nd)Nd[WO <sub>4</sub> ] <sub>2</sub>			[105]
DyMn <sub>2</sub> O <sub>5</sub>			[106]
Y <sub>2</sub> SiBe <sub>2</sub> O <sub>7</sub>			[107]
NaNd <sub>3</sub> (GeO <sub>4</sub> ) <sub>2</sub> (OH) <sub>2</sub>			[54]
Nd(TTA) <sub>3</sub> · pip · H <sub>2</sub> O	Nd		[124]
Compound	Nearest regular shape(s)		Reference
<b>Intermediate and distorted polyhedra</b>			
Nd(acac) <sub>3</sub> · 2H <sub>2</sub> O	A and C <sub>2v</sub> BCTP		[108]
NdCl <sub>3</sub> · 2C <sub>6</sub> H <sub>12</sub> N <sub>4</sub> · 14H <sub>2</sub> O	D and A		[109]
Nd <sub>2</sub> (SO <sub>4</sub> ) <sub>3</sub> · 8H <sub>2</sub> O	D and A		[110]
Nd <sub>2</sub> O <sub>2</sub> CO <sub>3</sub>	BCO		[111]
Eu(acac) <sub>3</sub> · 3H <sub>2</sub> O	C <sub>2v</sub> BCTP		[112]
Er <sub>8</sub> O(DPM) <sub>10</sub> (OH) <sub>12</sub>	BCTP		[49]
BaTM <sub>2</sub> F <sub>8</sub>	Cube		[113]

TABLE 5.10  
(Continued.)

Compound	Nearest regular shape(s)	Reference
LaVO <sub>4</sub>		[114]
$\alpha$ -Pr <sub>2</sub> Si <sub>2</sub> O <sub>7</sub>		[115]
$\beta$ -Pr <sub>2</sub> Si <sub>2</sub> O <sub>7</sub>		[43]
Pr <sub>2</sub> Sr <sub>3</sub> (BO <sub>3</sub> ) <sub>4</sub>		[116]
CsPr(MoO <sub>4</sub> ) <sub>2</sub>		[117]
Nd <sub>4</sub> Re <sub>2</sub> O <sub>11</sub>		[118]
NdWO <sub>4</sub> OH	Cube	[119]
Eu <sub>2</sub> SiO <sub>4</sub>	Cube	[120]
La(OH) <sub>2</sub> Cl	C <sub>2v</sub> BCTP	[121]
Gd <sub>2</sub> S <sub>3</sub>	C <sub>2v</sub> BCTP	[52]
Nd <sub>2</sub> WO <sub>6</sub>	Cube	[122]
LaTaO <sub>4</sub>	Cube	[123]

D, dodecahedron; A, square antiprism; BCTP, bicapped trigonal prism; BCO, bicapped octahedron; DTC, *N,N*-diethyldithiocarbamate; HFA, hexafluoroacetylacetonato; FOD, 1,1,1,2,2,3,3-heptafluoro-7,7-dimethyl-4,6-octane dionato; NTA, nitrilotriacetato; acac, acetylacetonato; PCN, phthalocyaninato; DMP, 2,6-dimethyl-4-pyrone; BA, benzoyacetonato; pip, piperidine; DPM, 2,2,6,6-tetramethylheptane-3,5-dionato; py, pyridine; phen, 1,10-phenanthroline; trop, troponato.

Fig. 5.16. A projection of the structure of  $\text{Er}(\text{HOCH}_2\text{COO})(\text{OCH}_2\text{COO})(\text{H}_2\text{O}) \cdot \text{H}_2\text{O}$  (from Grenthe [89]).

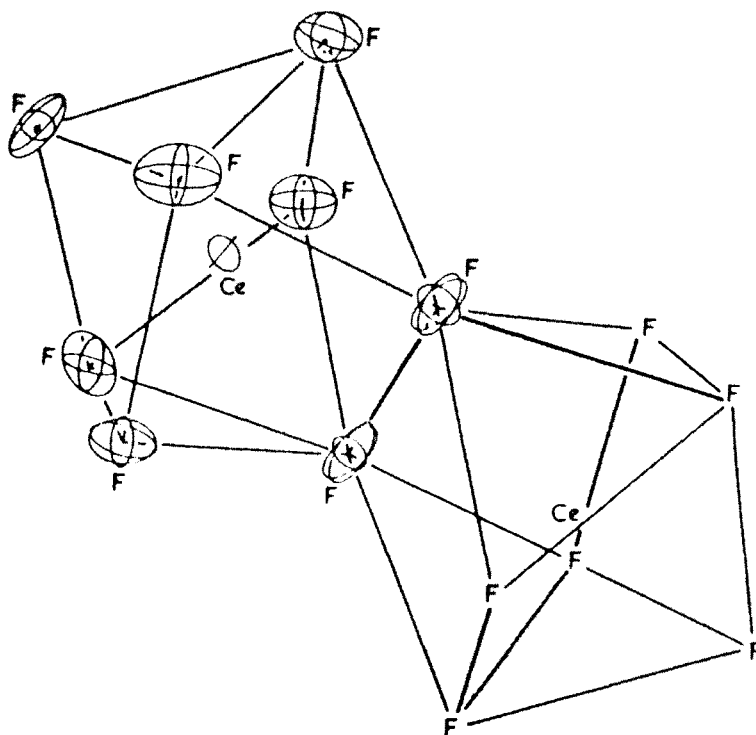


Fig. 5.17. Structure of the dimeric anion in  $(\text{NH}_4)_3\text{CeF}_7 \cdot \text{H}_2\text{O}$  (from Ryan and Pennemap [82]).

complex anion,  $[\text{Er}(\text{HOCH}_2\text{COO})_4]^-$  and the other Er is in the form of a complex cation,  $[\text{Er}(\text{HOCH}_2\text{COO})_2(\text{H}_2\text{O})_4]^+$ . Both the complex cation and anion are linked together in two dimensions by hydrogen bonds forming layers to the 'ab' plane. The glycolate ligands form chelates along the m edges of both dodecahedra.

The complex  $(\text{NH}_4)_3\text{CeF}_7 \cdot \text{H}_2\text{O}$  exists as a dimer in which the dodecahedra share an edge [82]. Each cerium atom is surrounded by eight fluorine atoms to form a distorted dodecahedron. The two dodecahedra are joined along an edge to form the centrosymmetric  $[\text{Ce}_2\text{F}_{14}]^{6-}$  ion as shown in Fig. 5.17.

The tetrakis hexafluoro acetylacetonates of Eu and Y are isomorphous and adopt the  $D_2$  dodecahedral arrangement with the chelate rings spanning the g edges of the polyhedron. In this structure as well as in the case of  $\text{NH}_4[\text{Pr}(\text{TTA})_4] \cdot \text{H}_2\text{O}$ , the rings interconnect the trapezoids of the dodecahedron. The structure of the yttrium complex is in accord with a strong ion-pair with the cesium ion surrounded by eight fluorine atoms from two neighboring  $\text{Y}(\text{HFA})_4^-$  moieties. The coordination dodecahedron in the complex  $[\text{Y}(\text{HFACAc})_4]^-$  viewed down the two-fold axis through the yttrium ion is shown in Fig. 5.18.

In the complex  $\text{NH}_4[\text{Ho}(\text{tropolanto})_4]$  m edges are spanned since the complex has a small bite [125]. A similar situation of sharing m edges is encountered in isoquinolinium tetrakis[4,4,4-trifluoro-1-(2-thienyl)-1,3-butanedione]cerium(III) and the dodecahedron is

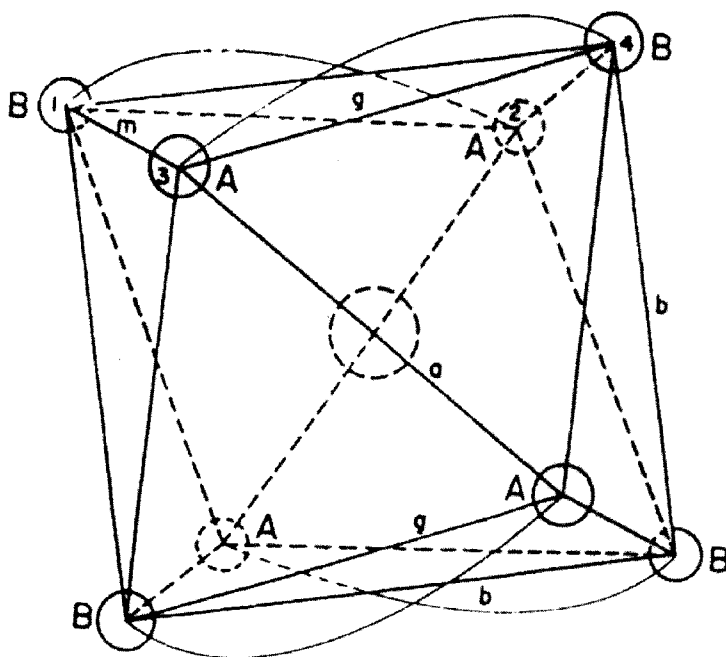


Fig. 5.18. Coordination dodecahedron in the tetrakis (hexafluoroacetylacetonato)yttrate(III) ion viewed down the two-fold axis through the yttrium ion (reprinted with permission from Bennett, M.J., F.A. Cotton, P. Legzdins and S.J. Lippard, 1968, *Inorg. Chem.* 7, 1770–1776).

distorted by the formation of a hydrogen bond from the isoquinolinium ion to one of the chelated oxygen atoms [126].

In general, the majority of the complexes of the  $[M(\text{bidentate})_3(\text{unidentate})_2]^{n+}$  type have square antiprismatic stereochemistry. There are some exceptions to this generalization. The complex  $\text{Nd}(\text{TTA})_3(\text{opph}_3)_2$  has a dodecahedral configuration [127] with two chelate rings spanning the 9 edges and the third spanning the  $m$  edge as shown in Fig. 5.19.

The compound  $\text{Pr}_2(\text{fod})_6 \cdot 2\text{H}_2\text{O}$  is an interesting compound and it contains dimeric eight coordinate groups [83]. The complex has one praseodymium atom with dodecahedral configuration with the second metal atom having bicapped trigonal prismatic structure. The chelate rings are very similar to those in the seven-coordinate  $\text{Pr}_2(\text{DPM})_6$  complex.

## 8.2. Square antiprism

The lanthanide complexes adopting the square antiprismatic geometry are given in Table 5.8. The complexes  $[\text{Ce}(\text{acac})_4]$  and  $\text{Hpip}[\text{Eu}(\text{COCHCOCH}_3)_4]$  adopt this geometry [93,102] with the chelate rings spanning the  $S$  edges. The complex  $[\text{Y}(\text{acac})_3(\text{H}_2\text{O})_2]\text{H}_2\text{O}$  is best described as a slightly distorted square antiprism involving a subtle interplay of interligand steric effects, crystal packing effects and bonding considerations [68]. On the other hand, the complex  $[\text{Ho}(\text{acac})_3(\text{H}_2\text{O})_2]$  adopts dodecahedral geometry [108]. In the complex  $\text{tris-}[4,4,4\text{-trifluoro-1-(2-thienyl)-1,3-butanediono}]\text{Eu} \cdot 2\text{H}_2\text{O}$  the two water

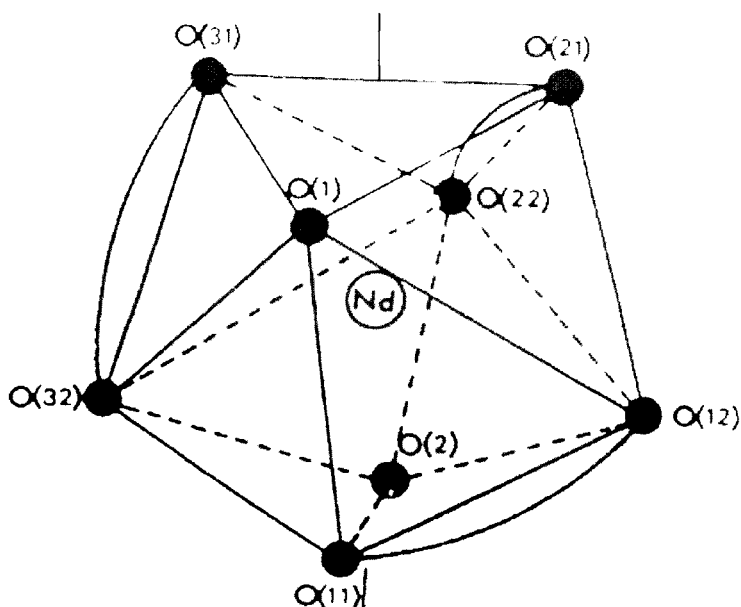


Fig. 5.19. The coordination polyhedron in  $\text{Nd}(\text{TTA})_3(\text{Oph}_3)_2$  (reprinted with permission from Leipoldt, J.G., L.D.C. Bok, A.E. Laubscher and S.S. Bosson, 1975, *J. Inorg. Nucl. Chem.* 37, 2477–2480).

molecules are diagonally opposite one another on one square face. Thus one chelate ring spans S edges and the other two span the L edges [128].

The complexes  $[\text{Eu}(\text{DPM})_3(\text{py})_2]$ ,  $[\text{Ho}(\text{DPM})_3(4\text{-picoline})_2]$  which are important from the point of view of lanthanide shift reagents, are basically square antiprismatic in geometry. The two nitrogen atoms in the complexes are on opposite square faces located as far as possible from one another. The molecular structure of  $[\text{Eu}(\text{DPM})_3(\text{py})_2]$  is shown in Fig. 5.20.

In sharp contrast the DPM complexes of Eu with attached pyridine, the corresponding  $[\text{Eu}(\text{DPM})_3 \cdot (\text{DMF})_2]$  complex is square antiprismatic with the two DMF molecules in *cis* positions on the same square face [69], the three chelate rings span the S edges. It is obvious from this that any extrapolation of structures from solid to solution must be done with extreme caution.

The complex octakis (pyridine-*N*-oxide) $\text{La}(\text{III})$  perchlorate is an example involving eight unidentate ligands giving rise to a square antiprismatic structure with almost perfect  $D_4$  symmetry. Detailed coordinations suggest that the complex is distorted toward the cube. The molecular structure of  $[\text{La}(\text{PyNO})_8]$  is shown in Fig. 5.21.

The small influence of hydrogen bonding on molecular geometry is well illustrated by the structures of lanthanide complexes with pyridine-3-carboxylate [95] (nicotinate ion), pyridine-4-carboxylate (isonicotinate ion) and nicotinic acid [96]. The structure of  $\text{La}_2(\text{C}_5\text{H}_4\text{NCOO})_6(\text{H}_2\text{O})_4$  consists of two  $\text{La}(\text{III})$  ions related by a center of symmetry, with four bridging carboxylate groups, and an additional carboxyl group chelating to each metal ion. The coordination sphere has two water molecules per metal ion and the coordination of each metal ion in the dimer is eight as shown in Fig. 5.22.

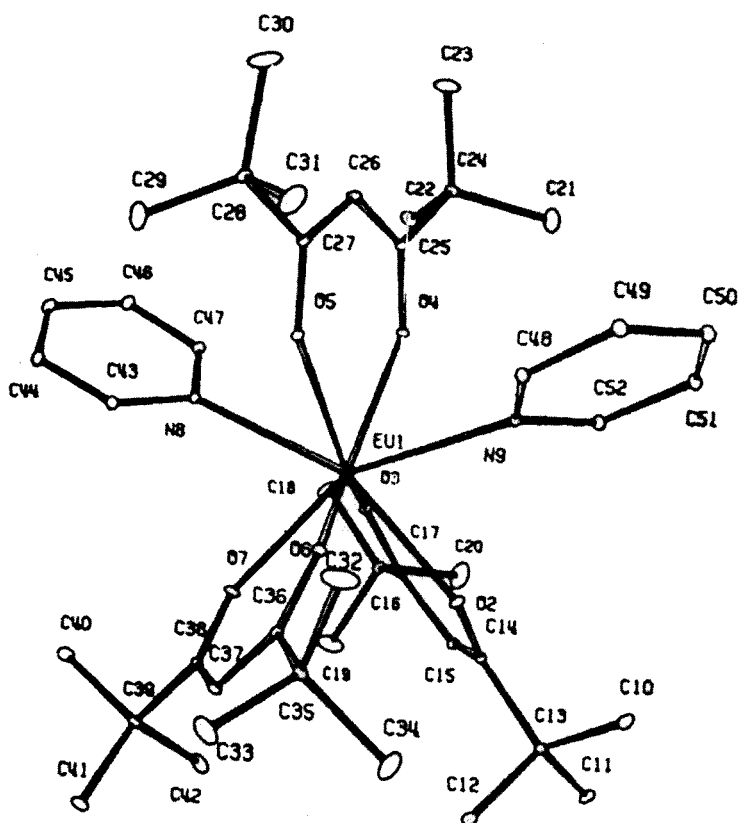


Fig. 5.20. The molecular structure of  $\text{Eu}(\text{DBM})_3(\text{py})_2$  (reprinted with permission from Cramer, R.E. and K. Seff, 1972, *Acta Crystallogr.* B28, 3281–3293).

The extensive hydrogen bonding of a three-dimensional nature stabilizes the structure. With ligands that closely resemble nicotinate but possessing different hydrogen bonding possibilities, the hydrogen bonding modes and packing can be altered. The crystal structures [96] of  $\{\text{Ho}(\text{C}_5\text{H}_4\text{NCO}_2\text{H})_3(\text{H}_2\text{O})_2(\text{NCS})_6\text{Cr} \cdot 2\text{H}_2\text{O}\}_\infty$  and  $\{\text{La}(\text{C}_5\text{H}_4\text{NCO}_2)_3(\text{H}_2\text{O})_2\}_\infty$  contain metal atoms chelated with nicotinic acid and isonicotinate ion, respectively. In both the compounds, adjacent metal ions are alternately bridged by four and two carboxylate groups. These compounds differ from the nicotinate complex in that they are polymeric in configuration. There are two coordinated water molecules with eight as the overall coordination number. The coordination polyhedra in all these cases is a distorted square antiprism.

The heavier rare earths form a second type of isonicotinate dihydrate structure typified by  $\{\text{Er}(\text{C}_5\text{H}_4\text{NCO}_2)_3(\text{H}_2\text{O})_2\}_\infty$  in which chains of erbium atoms are linked by pairs of bridging carboxylate groups. Eight-coordination is achieved at each metal atom by a chelating carboxylate and two water molecules [97].

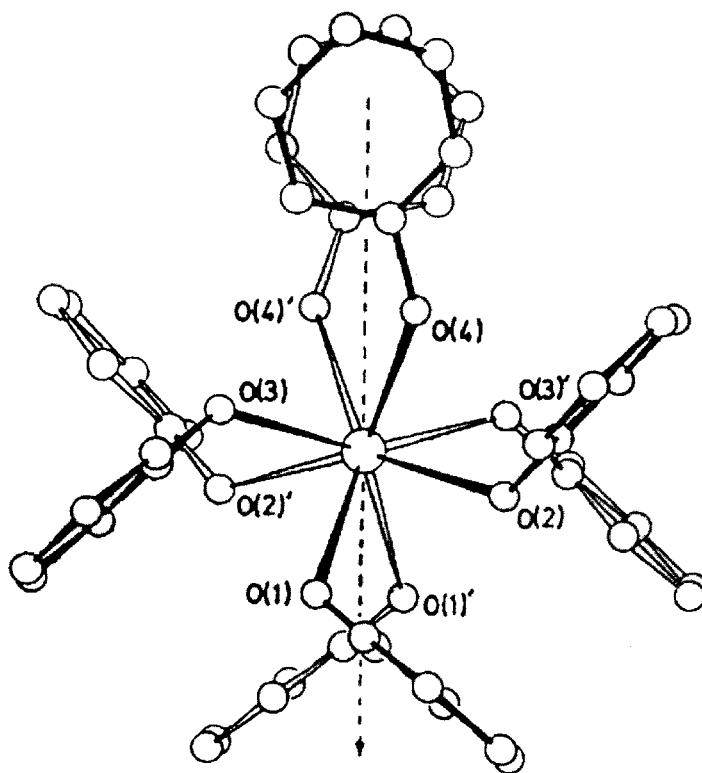


Fig. 5.21. The molecular structure of the octakis(pyridine-*N*-oxide) lanthanum(III) ion (reprinted with permission from A.R. Al-Karaghoulfi and J.S. Wood, 1972, *J. Chem. Soc., Chem. Comm.*, 516-517).

The crystal structure of  $\beta$ -Ce(acac)<sub>4</sub> has square antiprismatic geometry for the metal polyhedron [93] in the same isomeric form as in the case [129] of  $\alpha$ -Ce(acac)<sub>4</sub>. The mean Ce–O distance in the  $\beta$ -form is 2.32 Å which is shorter than 2.40 Å in the  $\alpha$ -form. The main difference between the two forms lies in molecular packing rather than stereoisomerism [130].

At times the distortion of the geometry of a complex can be an advantage. For example, the distortion of the coordination antiprism of the europium atoms in [Eu(acac)<sub>3</sub>phen] results in the reduction of the symmetry of the complex to such an extent that all the characteristic electronic transitions become allowed and the full multiplicities are seen in the emission spectrum of the complex [100].

### 8.3. Cubes

It has been suggested that cubic stereochemistry might be possible for discrete 8-coordinate complexes with monodentate ligands. As evidence for the stability, the cubic lanthanum coordination polyhedron in [La(C<sub>5</sub>H<sub>5</sub>NO)<sub>8</sub>](ClO<sub>4</sub>)<sub>3</sub> has been cited. This complex is in the form of a square antiprism distorted towards a cube rather than a dodecahedron [94].

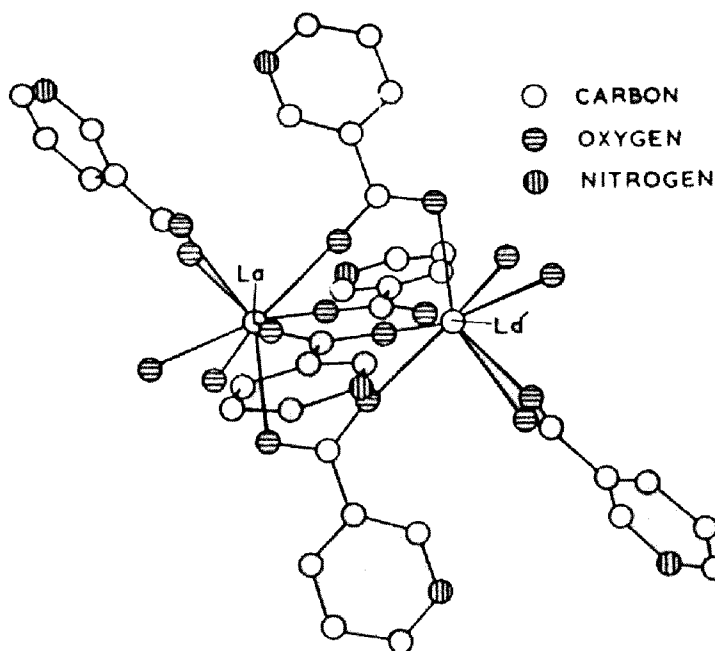


Fig. 5.22. Structure of the dimeric lanthanum nicotinate dihydrate (by courtesy of the American Chemical Society).

Certainly, more structural information on cubically coordinated metal complexes is needed to assess the role that intermolecular forces play in the determination of polyhedron geometry.

The electronic structure and chemical bonding in the 15-crown-5 complex of lanthanum trichloride having a coordination number of 8 has been studied. The molecular structure of  $\text{LaCl}_3(15\text{-crown-5})$  and the charge distribution of the complex, ligand and metal chloride are shown in Figs 5.23 and 5.24, respectively.

## 9. Coordination number 9

9-coordinate structures are common among complexes of larger lanthanides and some examples are given in Table 5.11. It can be expected from the calculated equal distance–equal charge repulsivities (EDEC) given in Table 5.12. The most common polyhedron for the complexes is the tricapped trigonal prism ( $D_{3h}$ ).

The hybridization of one s, three p and five d orbitals sustains the tricapped trigonal prismatic geometry. Less favorable capped square antiprismatic geometry is adopted by some lanthanide complexes. A variety of molecular structures are present in rare earth carboxylates with tricapped trigonal prismatic coordination. Trisdipicolinato [141,148–150] and trisdioxyacetato complexes are monomeric with ligands acting as tridentates. Trishydroxyacetato [131,143] and trisoxalato [139,158] complexes have polymeric structures with



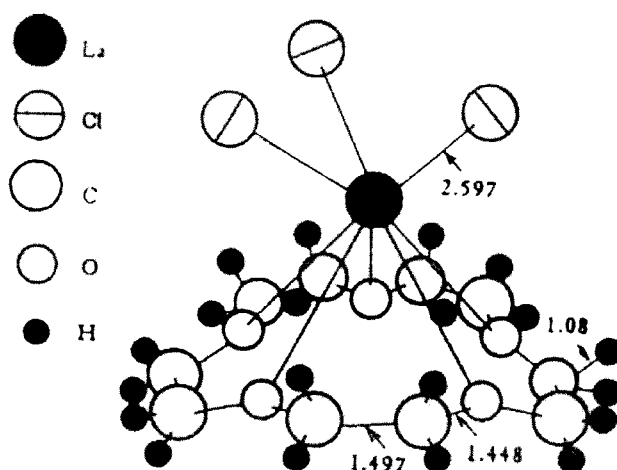


Fig. 5.23. Molecular structure of  $\text{LaCl}_3(15\text{-crown-}5)$  (numbers in the figure are bond lengths in Å). Ref.: Z. Li, J. Ni, G. Xu, J. Ren, Kexue Tongbao, 31, 956, 1986.

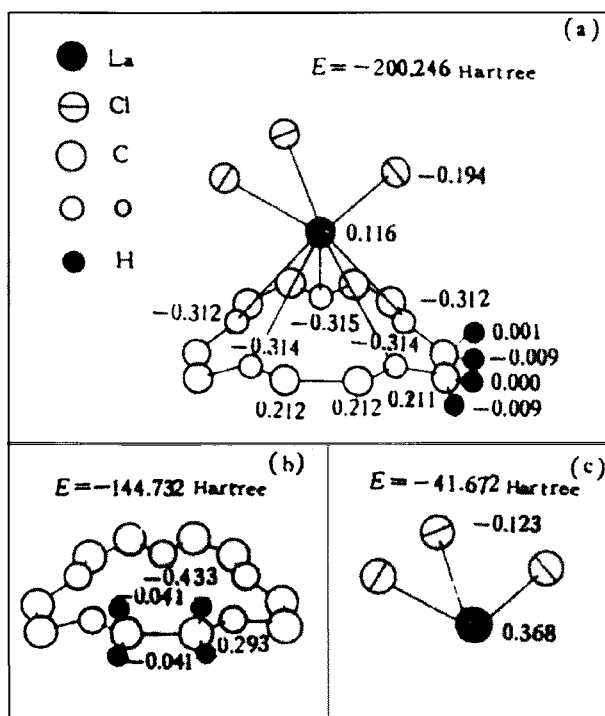


Fig. 5.24. Charge distribution of (a)  $\text{LaCl}_3(15\text{-crown-}5)$ , (b)  $15\text{-crown-}5$ , (c)  $\text{LaCl}_3$ . Ref.: Z. Li, J. Ni, G. Xu, J. Ren, Kexue Tongbao, 31, 956, 1986.

TABLE 5.11  
Structures incorporating nona-coordinate metal atoms.

Compound	Elements (M) for which structure is available	Reference
Tricapped trigonal prismatic		
M(HOCH <sub>2</sub> COO) <sub>3</sub> (orthorhombic)	La–Tb	[131]
M <sub>2</sub> (C <sub>2</sub> O <sub>4</sub> ) <sub>3</sub> · 10H <sub>2</sub> O	La, Ce, Pr, Nd	[132]
Na <sub>3</sub> [M(ODA) <sub>3</sub> ]2NaClO <sub>4</sub> · 6H <sub>2</sub> O	Ce–Lu	[133]
M <sub>2</sub> (SO <sub>4</sub> ) <sub>3</sub> · 9H <sub>2</sub> O	La–Ce	[134]
Ce <sub>2</sub> (SO <sub>4</sub> ) <sub>3</sub> · 4H <sub>2</sub> O		[135]
β-KCeF <sub>4</sub>		[136]
MCrSe <sub>3</sub>	La, Ce, Pr, Nd	[137]
MP <sub>3</sub> O <sub>9</sub> · 3H <sub>2</sub> O	La, Ce, Pr	[138]
Nd <sub>2</sub> (C <sub>2</sub> O <sub>4</sub> ) · 10.5H <sub>2</sub> O		[139]
Nd(IDA)Cl · 3H <sub>2</sub> O		[140]
Na <sub>3</sub> [M(PDC) <sub>3</sub> ] · 15H <sub>2</sub> O (triclinic)	Ce–Dy	[141]
Nd <sub>4</sub> W <sub>3</sub> O <sub>15</sub>		[142]
M(HOCH <sub>2</sub> COO) <sub>3</sub> (monoclinic)	Pr–Tb	[143]
[Eu(terpy) <sub>3</sub> ](ClO <sub>4</sub> ) <sub>3</sub>		[144]
Er(NO <sub>3</sub> ) <sub>3</sub> · 3DMSO		[145]
NH <sub>4</sub> M(C <sub>2</sub> O <sub>4</sub> ) <sub>2</sub> · H <sub>2</sub> O	Sm–Tm, Y	[146]
YFeCl <sub>2</sub> (OH) <sub>3</sub>		[147]
Na <sub>3</sub> [M(PDC) <sub>3</sub> ] · 14H <sub>2</sub> O (orthorhombic)	Dy–Lu	[148]
Na <sub>3</sub> [M(PDC) <sub>3</sub> ] · 13H <sub>2</sub> O (monoclinic)	Ho–Tm	[149]
Na <sub>3</sub> [M(PDC) <sub>3</sub> ]NaClO <sub>4</sub> · 10H <sub>2</sub> O (hexagonal)	Ho–Lu	[150]
Yb(NO <sub>3</sub> ) <sub>3</sub> · 3DMSO		[151]
Lu(NO <sub>3</sub> ) <sub>3</sub> · 3DMSO		[152]
Nd(NO <sub>3</sub> ) <sub>3</sub> · 3(antipyrene)		[153]
Nd(OCOCH <sub>2</sub> SCH <sub>2</sub> COO)Cl · 4H <sub>2</sub> O		[154]
Monocapped square antiprismatic		
M <sub>2</sub> O <sub>2</sub> Te	La–Dy	[155]
Pr(terpy)Cl <sub>3</sub> · (H <sub>2</sub> O) <sub>8</sub>		[156]
Cr(NCS) <sub>3</sub> · 7H <sub>2</sub> O		[157]
M(C <sub>2</sub> O <sub>4</sub> )(HC <sub>2</sub> O <sub>4</sub> ) · 3H <sub>2</sub> O	Dy, Er, Y, Yb	[158]
Nd <sub>2</sub> (malonato) <sub>3</sub> · 8H <sub>2</sub> O		
Intermediate and distorted polyhedra		
LaFeO <sub>3</sub>	Near regular shape(s)	[159]
LaF <sub>3</sub>		[160]
K <sub>2</sub> [Ce(CH <sub>3</sub> COO) <sub>5</sub> ] · H <sub>2</sub> O		[161]
Ce(CH <sub>3</sub> COO) <sub>3</sub> · 0.7H <sub>2</sub> O	CSA	[162]
NTAM(H <sub>2</sub> O) <sub>2</sub> · H <sub>2</sub> O (M = Pr–Tb)	TCTP–CSA	[163]
M <sub>2</sub> Si <sub>2</sub> O <sub>7</sub> (M = La–Sm)		[164]
7Gd <sub>2</sub> O <sub>3</sub> · 9SiO <sub>2</sub>		[65]

TCTP, symmetrically tricapped trigonal prism; CSA, monocapped square antiprism; IDA, iminodiacetato; ODA, oxydiacetato; T, tropolonato; NTA, nitrilotriacetato; PDC, pyridine-2,6-dicarboxylato(dipicolinato); Ox, 8-quinollinato; terpy, terpyridyl; DMSO, dimethylsulphoxide; DMF, *N,N*-dimethyl formamide.

TABLE 5.12  
Equal distance–equal charge repulsivities for 9 coordination (after King) [44].

Polyhedron		Repulsivity
Symmetrically tricapped trigonal prism	( $D_{3h}$ )	19.253
Capped square antiprism	( $C_{4v}$ )	19.780
Capped cube	( $C_{4v}$ )	21.181

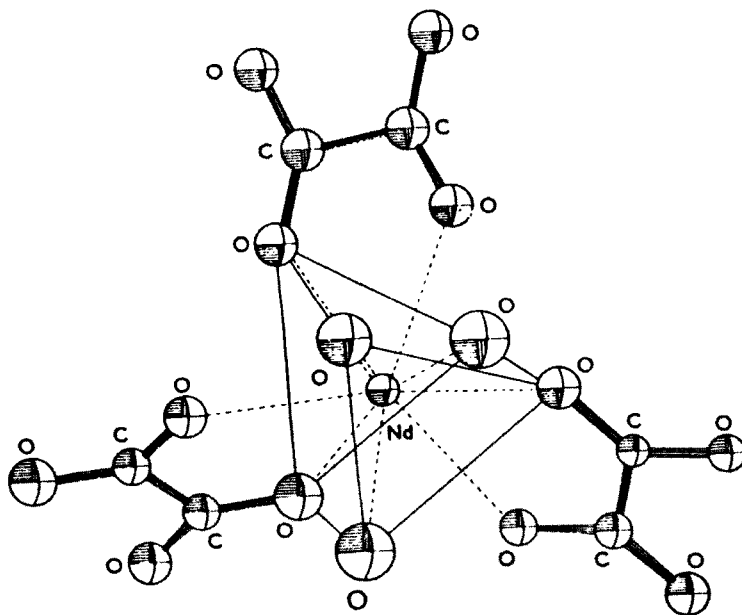


Fig. 5.25. Tricapped trigonal prismatic coordination in  $Nd_2(C_2O_4)_3 \cdot 10.5H_2O$ . From Hansson [139].

bridging ligands between metal ions. A characteristic feature of these complexes is polymorphism. For example, two forms of lanthanide trishydroxyacetate and three forms of lanthanide trispicolinate have been identified.

The basic polyhedron adopted by these structures is the tricapped trigonal prism ( $D_{3h}$ ). The coordination polyhedron of oxygen atoms around the neodymium atom in  $Nd(C_2O_4)_3 \cdot 10.5H_2O$  is shown in Fig. 5.25. The stability of the tricapped trigonal prism is confirmed by the large variety of ligand combinations around 9-coordinate metal ions (Table 5.9) which are best described by this polyhedron.

The tricapped trigonally prismatic coordination of europium in  $Eu(terpy)_3(ClO_4)_3$  is probably the first example of 9-coordination involving nitrogen donors [150]. Tricapped trigonal prismatic geometry is present in some simple hydrated compounds [165,166] such as  $Nd(H_2O)_9(BrO_3)_3$  and  $M(H_2O)_9(C_2H_5SO_4)_3$ , where  $M = Pr, Er, Ho, V$ . The structure of  $[Yb(DPC)_3]^{3-}$  is shown in Fig. 5.26.

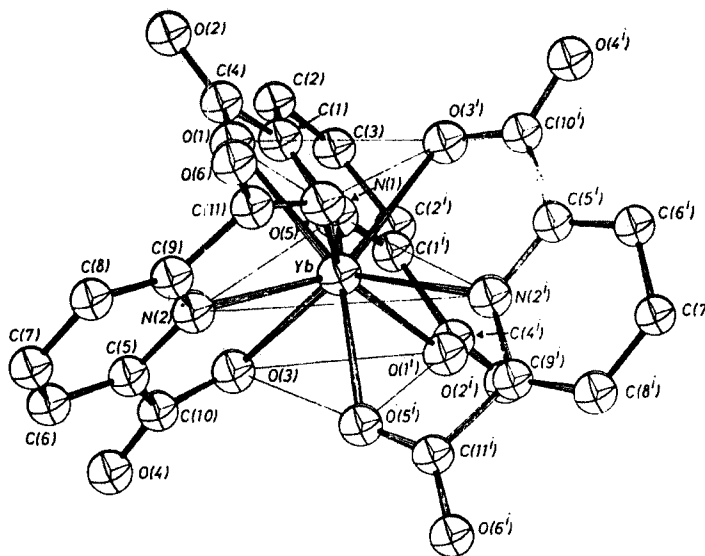


Fig. 5.26. The nine-coordinate structure of  $\text{Yb}(\text{DPC})_3^{3-}$  (reprinted with permission from Albertsson [148]).

The malonate complex of Eu(III),  $\text{Eu}_2(\text{malonate})_3 \cdot 8\text{H}_2\text{O}$  is interesting since there are two different coordination geometries, and only five of the water molecules are coordinated [167]. One of the Eu ions is eight-coordinate in the form of a distorted square antiprism and the other Eu ion is nine-coordinate, distorted tricapped trigonal prism. In the analogous neodymium complex, six water molecules are coordinated because of the difference in ionic radius. The neodymium complex is nine-coordinate with monocapped antiprismatic geometry [168].

A second form of  $\text{Nd}_2(\text{malonate})_3 \cdot 6\text{H}_2\text{O}$  complex has been reported [169]. In this complex neodymium is nine-coordinate surrounded by six carboxylate, and three water oxygen atoms and the geometry is intermediate between the distorted capped square antiprism and the distorted tricapped trigonal prism.

The structure of the dimethyl formamide adduct,  $(\text{facam})_3\text{Pr}(\text{DMF})_3\text{Pr}(\text{facam})_3$  contains three DMF molecules as bridging groups. The two praseodymium atoms are nine-coordinate with the oxygen atoms at the vertices of a distorted monocapped square antiprism [170]. The stability of this dimeric complex and its ability to accommodate three DMF ligands shows that factors such as nucleophilic strength of the substrate ligand, intermolecular packing mode, and hydrogen bonding are important in addition to intra molecular steric factors in determining the coordination number. The structure of the complex is important despite the previous notion that a coordination number greater than eight could not exist in these types of complexes [171].

The  $C_{4v}$  type stereoisomer exists for coordination polyhedra [158] of  $\text{M}(\text{C}_2\text{O}_4)(\text{HC}_2\text{O}_4) \cdot 3\text{H}_2\text{O}$ , where  $\text{M} = \text{Dy}, \text{Yb}, \text{Y}$  or  $\text{Er}$  and there seems to be no example of  $C_1$  stereoisomer of a capped square antiprism at present.

The polyhedron about praseodymium in  $\text{Pr}(\text{terpy})\text{Cl}_3 \cdot 8\text{H}_2\text{O}$  is a distorted capped square antiprism [156]. The middle nitrogen of terpyridine occupies the cap position. Two

nitrogens, one chlorine atom and one water oxygen atom occupy the square that is capped. The basal square is formed by four water oxygen atoms.

X-ray studies of  $\text{Ce}(\text{CH}_3\text{COO})_3 \cdot 0.7\text{H}_2\text{O}$  and  $\text{K}_2[\text{Ce}(\text{CH}_3\text{COO})_5]\text{H}_2\text{O}$  showed bridging acetate groups and the cerium atoms to be 9-coordinate with irregular coordination polyhedra [161,162].

Three crystallographically distinct groups of compounds of the general formula  $\text{LnNTA} \cdot n\text{H}_2\text{O}$  have been identified, when  $\text{Ln} = \text{La, Ce, } n = 5$ ;  $\text{Ln} = \text{Pr-Tb, } n = 3$ ;  $\text{Ln} = \text{Dy-Lu, } n = 4$ . The sudden change in thermodynamic properties of the compounds between the dysprosium group and the praseodymium group is reflected in the increase in the coordination number in the crystal [163]. Dysprosium in  $\text{DyNTA} \cdot 4\text{H}_2\text{O}$  is 8-coordinate and praseodymium in  $\text{PrNTA} \cdot 3\text{H}_2\text{O}$  is 9-coordinate. Praseodymium coordination can be described equally well as a distorted tricapped trigonal prism or as a distorted capped square antiprism. The removal of an atom at the cap of a distorted capped square antiprism results in a polyhedron resembling that of the dysprosium compound. The change in coordination at dysprosium may be explained by dependence on steric interaction between ligands within the coordination polyhedron.

In the orthorhombic perovskite-like compounds,  $\text{LaFeO}_3$ , the standard deviation of the average cation–oxygen bond distances has been used as a criterion for obtaining the coordination number [158]. For lanthanides Sm–Lu, there are eight oxygen atoms in the coordination sphere, and for lanthanum the coordination number is nine in the compound.

The neodymium complex of the formula,  $\text{Nd}(\text{NO}_3)_3(\text{Ph}_3\text{PO})_2(\text{C}_2\text{H}_5\text{OH})$  has been synthesized and the crystal structure shows it to be nine-coordinate [172].

## 10. Coordination number 10

The coordination polyhedra for ten-coordination is complex and has been discussed well [173]. The three polyhedra considered for this coordination are the bicapped square antiprism ( $D_{4d}$ ), the bicapped dodecahedron ( $D_2$ ) and a polyhedron of  $C_{2v}$  symmetry derived by sharing of a trans pair of the four equatorial B positions of a dodecahedron between two pairs of ligands as shown in Fig. 5.27.

When all the metal–ligand distances are the same, then the shape of the bicapped antiprism is defined by the angle of inclination,  $\theta$ , of the metal ligand bonds in the square antiprismatic set (positions A) to the four fold axis (the length ratio  $l/s$  should be defined). In the bicapped dodecahedron, the two trapezoidal planes BAAB are not constrained to be perpendicular as in the case of parent  $D_{2d}$  polyhedron, such that in addition to  $\theta_A$  and  $\theta_B$ , a third parameter  $\theta_C$  representing the relative orientation of the two planes must be defined. The third polyhedron ( $C_{2v}$ ) requires five angular parameters to define its shape if different angles are introduced for the non-equivalent planes BAAB and  $B'A'A'B'$ , where B is midpoint of edge C. The angular parameters are  $\theta_A, \theta_B, \theta'_A, \theta'_B$  and  $\theta_C$  which is the angular separation of the C position ligands.

The most favourable angular parameters for the polyhedra are:  $D_{4d}$ ,  $\theta = 64.8^\circ$ ;  $D_2$ ,  $\theta_A = 32.8^\circ$ ;  $\theta_B = 77^\circ$ ;  $\theta_C = 60^\circ$ ;  $C_{2v}$ ,  $\theta_A = 32.8^\circ$ ;  $\theta_B = 65.8^\circ$ ;  $\theta_{A'} = 34.9^\circ$ ;  $\theta_{B'} = 63.8^\circ$ ;  $\theta_C = 77.8^\circ$ .

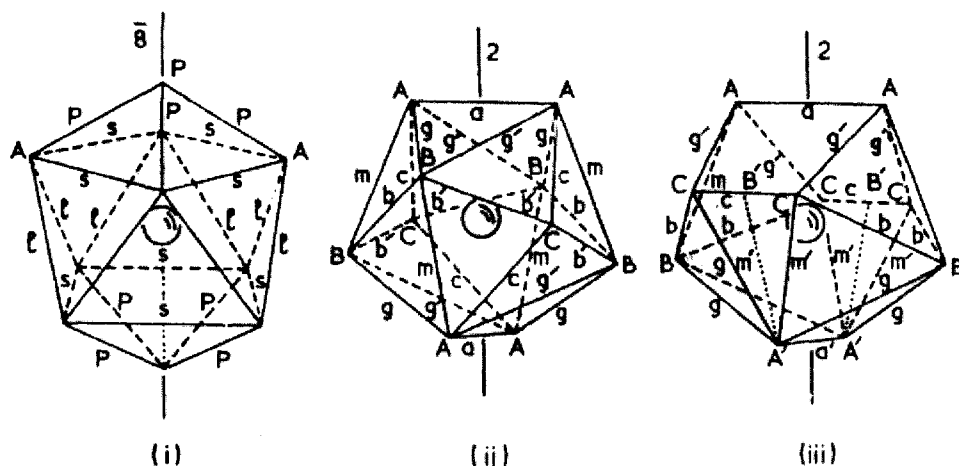


Fig. 5.27. Idealised 10-coordination polyhedra: (i) bicapped square antiprism ( $D_{4d}$ ); (ii) bicapped dodecahedron ( $D_2$ ); (iii)  $C_{2v}$  polyhedron based on a dodecahedron. The dotted lines  $A'B'$  in (iii) indicate the location of the original trapezoidal plane in the parent dodecahedron. (From Al-Karaghoulis and Wood, by courtesy of the American Chemical Society.)

The two different approaches to the calculation of repulsion energies [44,173] lead to the conclusion that the bicapped square antiprism is the most favourable geometry for ten coordination. There are complexes as examples of all the three types of polyhedra as shown in Table 5.13.

The complex  $H[La(EDTA)(H_2O)_4] \cdot 3H_2O$  involves severe restrictions placed on the polyhedron by the EDTA ligand, and overall the polyhedron may be considered to be approaching a bicapped square antiprism [174]. This is shown in Fig. 5.28. The coordination polyhedron in  $La(NO_3)_3 \cdot (bipy)_2$  has features belonging to all three geometries  $D_{4d}$ ,  $D_2$  and  $C_{2v}$ . Based on general shape criteria and adherence to various least squares best planes, the description would be in terms of  $D_2$  geometry [173].

A consideration of the complex  $Nd(NO_3)_3 \cdot 4DMSO$  shows that ten oxygen atoms are around the neodymium atom and the polyhedron is close to  $C_{2v}$  geometry [176]. The molecular structure and a simplified view of the  $C_{2v}$  coordination polyhedron is shown in Fig. 5.29. A similar geometry is adopted by  $La_2(CO_3)_3 \cdot 8H_2O$  compound and  $La(NO_3)_3 \cdot 4DMSO$  complex.

The importance of ionic radius is easily seen in that  $Yb(NO_3)_3 \cdot 3DMSO$  is a 9-coordinate tricapped trigonal prism [151].

The complexes  $[Ce(NO_3)_5]^{2-}$  and  $[Ho(NO_3)_3]^{2-}$  do not correspond to any idealized [190] polyhedra. The coordination polyhedron is nearly a pentagonal bipyramid if nitrate is unidentate. As ten coordinate complex,  $D_2$  bicapped dodecahedron is the best description as shown in Fig. 5.30.

The complex trinitrato-1,2-bis(pyridine-2-aldimino)ethane gadolinium(III) has the geometry approximating a pentagonal bipyramid if nitrate is unidentate with four of the five equatorial positions occupied by the nitrogen atoms of the tetradentate amine ligand and the remaining three positions by the three nitrate groups [191].

TABLE 5.13  
Coordination number 10.

Compound	Coordination polyhedron	Reference
HLa(EDTA) · 7H <sub>2</sub> O	Bicapped square antiprism	[174]
La(NO <sub>3</sub> ) <sub>3</sub> · 4DMSO	C <sub>2v</sub> based on dodecahedron	[175]
Nd(NO <sub>3</sub> ) <sub>3</sub> · 4DMSO	C <sub>2v</sub> based on dodecahedron	[176]
La(NO <sub>3</sub> ) <sub>3</sub> · (bipy) <sub>2</sub>	Bicapped dodecahedron	[177]
Tb(NO <sub>3</sub> ) <sub>3</sub> · (bipy) <sub>2</sub>	Bicapped dodecahedron	[178]
La <sub>2</sub> (CO <sub>3</sub> ) <sub>3</sub> · 8H <sub>2</sub> O	C <sub>2v</sub> based on dodecahedron	[179]
La <sub>3</sub> BO <sub>6</sub>		[180]
La <sub>4</sub> Re <sub>6</sub> O <sub>19</sub>	Tetracapped trigonal prism	[181,182]
La <sub>2</sub> Be <sub>2</sub> O <sub>5</sub>		[183]
[(C <sub>6</sub> H <sub>5</sub> ) <sub>3</sub> (C <sub>2</sub> H <sub>5</sub> )P] <sub>2</sub> [Ce(NO <sub>3</sub> ) <sub>5</sub> ]	Trigonal bipyramid*	[184]
Ce(NO <sub>3</sub> ) <sub>4</sub> (TPPO) <sub>2</sub>	Octahedral*	[185]
[GD][Ce(CH <sub>3</sub> COO) <sub>4</sub> ] · H <sub>2</sub> O	Octahedral*	[186]
Nd(BO <sub>2</sub> ) <sub>3</sub>		[187]
Gd(NO <sub>3</sub> ) <sub>3</sub> (DPAE)		[188]
DyBC		[189]

\*Polyhedra with chelate ligands considered to occupy a single coordination site.

DMSO, dimethyl sulphoxide; bipy, 2,2'-bipyridyl; TPPO, triphenyl phosphine oxide; GD, guanidinium; DPAE, 1,2-di(pyridine-2-aldimino)ethane; EPAE, ethylenediaminetetraacetate.

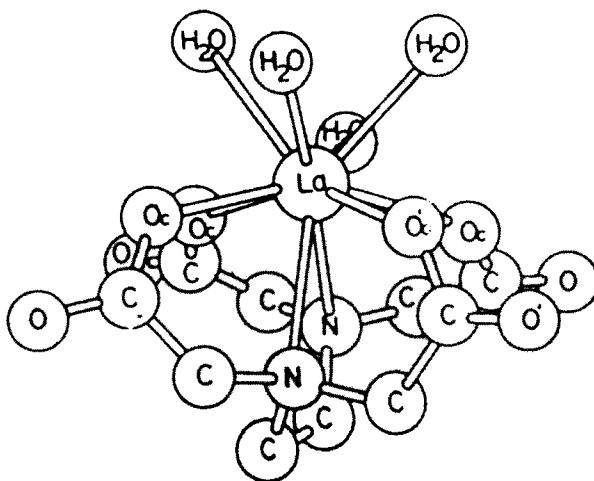


Fig. 5.28. The structure of the ten-coordinate cation in H[La(EDTA)(H<sub>2</sub>O)<sub>4</sub>] · 3H<sub>2</sub>O (reprinted with permission Lind, M.D., B. Lee and J.L. Hoard, 1965, J. Amer. Chem. Soc. 87, 1611–1612).

Many other ten-coordinate complexes cannot be described in terms of the three basic polyhedra. In some of these cases, appreciation of the molecular geometry is possible by considering groups which chelate with a small “bite” such as nitrate or acetate to be

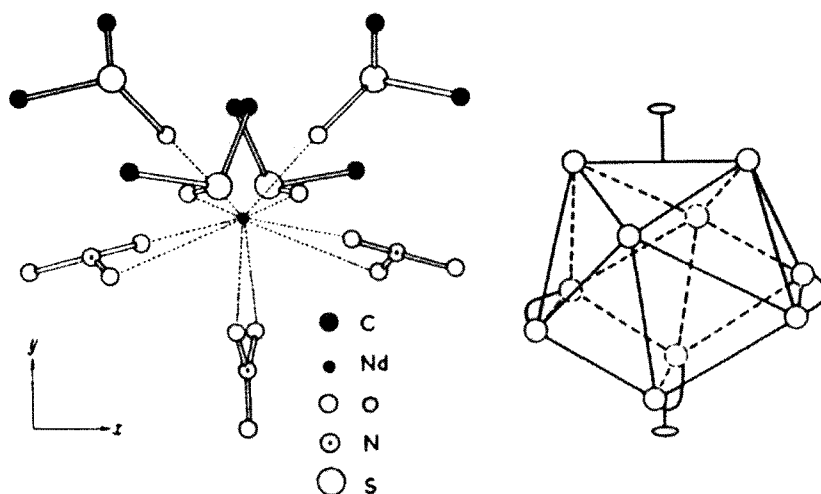


Fig. 5.29. Molecular structure of  $\text{Nd}(\text{NO}_3)_3(\text{DMSO})_4$  and (right) a simplified view of the  $C_{2v}$  coordination polyhedron (from Aslanov et al., by courtesy of the Soviet Academy of Sciences).

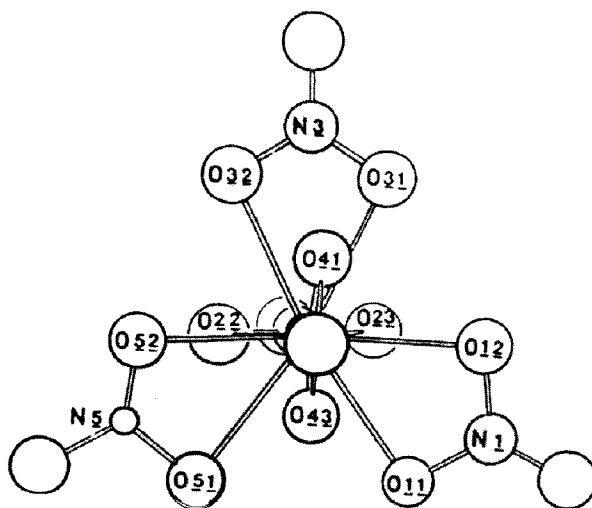


Fig. 5.30. The structure of the  $\text{Ho}(\text{NO}_3)_3^{2-}$  anion in  $(\text{NO})_2[\text{Ho}(\text{NO}_3)_5]$  (Toogood and Chieh, 1975) (reproduced by permission of the National Research Council of Canada, 1975, *Can. J. Chem.* 53, 831–835).

unidentate. By such considerations the following stereochemical assignments have been made.

$\text{Ce}(\text{NO}_3)_5^{3-}$	trigonal bipyramid
$\text{Ce}(\text{NO}_3)_4(\text{OPPh}_3)_2$	quasi-octahedral
$\text{Ce}_2(\text{H}_2\text{O})_2(\text{CH}_3\text{COO})_8$	quasi-octahedral



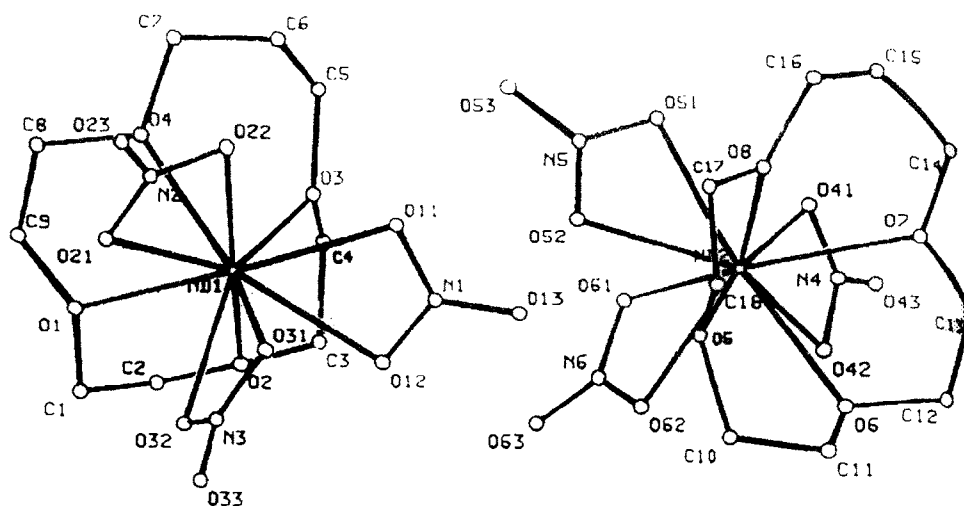


Fig. 5.31. The structure of  $\text{Nd(1)(NO}_3)_3 \cdot (13\text{-C-4})$  and  $\text{Nd(2)(NO}_3)_3 \cdot (13\text{-C-4})$ .

Lanthanide complexes of the formula  $\text{Ln(NO}_3)_3 \cdot (13\text{-C-4})$ , where  $\text{Ln} = \text{La to Lu}$  have been synthesized and the crystal structure of the Nd complex was determined [192]. The structure of the ten-coordinate complex is shown in Fig. 5.31.

## 11. Complexes of high coordination numbers

Lanthanide complexes formed with macrocyclic ligands in which the usual coordination number varies from 10 to 12 along with a few exceptions of coordination number 9, are given in Table 5.14. Some other lanthanide compounds are listed in Table 5.15.

Lanthanide complexes with macrocyclic ligands have metal:ligand ratios 4:3, 3:2, 2:1, 1:2, and 1:1. Some crystal structures of the complexes have been reported (Table 5.12). No definite analysis has been reported for complexes in which the lanthanide is coordinated with two or more macrocycles or one ligand is bonded to more than one lanthanide. The structures of 1:2 complexes, where  $\text{L} = 12\text{C4}$  or  $15\text{C5}$ , which are sandwich type have not been determined. In some complexes, no macrocycle is directly coordinated to the lanthanide. The coordination number is larger than 10 in macrocyclic complexes and even dodecacordinate complexes have been reported. The nondirectional bond between the lanthanide and the macrocyclic ligand and the relatively small space occupied by the coordinating atoms of the macrocycle lead to high coordination numbers. High coordination numbers are made possible when the small bidentate nitrate is the counter ion.

In the 1:1 complex of lanthanide nitrate with  $12\text{C4}$  or  $15\text{C5}$ , the polyether does not encapsulate the lanthanide ion in its cavity due to the small cavity size, but is coordinated as tetra- or pentadentate ligand on one side as shown in Fig. 5.32. The three nitrates are bonded on the other side of lanthanide as bidentate. Thus the lanthanide is 10- and 11-coordinate in  $12\text{C4}$  and  $15\text{C5}$  complexes, respectively. In the 1:2  $\text{Sm(ClO}_4)_3\text{-}15\text{C5}$

TABLE 5.14  
 Coordination number of rare earth elements in the complexes with macrocycles.

L	Ln	Anion	Ln:L	Species	CN <sup>a</sup>	Ref.
12C4	Y	NO <sub>3</sub> <sup>-</sup>	1:1	Y(NO <sub>3</sub> ) <sub>3</sub> L	10	[193]
	Eu	NO <sub>3</sub> <sup>-</sup>	1:1	Eu(NO <sub>3</sub> ) <sub>3</sub> L	10	[194]
MeOB15C5	Dy	NO <sub>3</sub> <sup>-</sup>	1:1	Dy(NO <sub>3</sub> )(H <sub>2</sub> O) <sub>3</sub>	9	[195]
15C5	Eu	NO <sub>3</sub> <sup>-</sup>	1:1	Eu(NO <sub>3</sub> ) <sub>3</sub> L	11	[196]
	Sm	ClO <sub>4</sub> <sup>-</sup>	1:2	[SmL(H <sub>2</sub> O) <sub>4</sub> ] <sup>3+</sup>	9	[197]
	Pr	TFA <sup>-</sup>	2:1	[Pr <sub>2</sub> (TFA) <sub>2</sub> (OH)L <sub>2</sub> ] <sup>2+</sup>	9	[198]
MeOB18C5	Sm	NO <sub>3</sub> <sup>-</sup>	1:1	Sm(NO <sub>3</sub> ) <sub>3</sub> L(H <sub>2</sub> O)	10	[199]
18C6	La	NO <sub>3</sub> <sup>-</sup>	1:1	La(NO <sub>3</sub> ) <sub>3</sub> L	12	[200]
	Nd	NO <sub>3</sub> <sup>-</sup>	1:1	Nd(NO <sub>3</sub> ) <sub>3</sub> L	12	[201,202]
	Gd	NO <sub>3</sub> <sup>-</sup>	1:1	Gd(NO <sub>3</sub> ) <sub>3</sub> (H <sub>2</sub> O) <sub>3</sub>	9	[200]
	Gd	Cl <sup>-</sup>	1:1	[GdCl <sub>2</sub> l(EtOH)] <sup>3+</sup>	9	[203]
	Nd	NO <sub>3</sub> <sup>-</sup>	4:3	[Nd(NO <sub>3</sub> ) <sub>2</sub> L] <sup>+</sup>	10	[204]
				1:1	[Nd(NO <sub>3</sub> ) <sub>6</sub> ] <sup>3-</sup>	12
DB18C6	Sm	ClO <sub>4</sub> <sup>-</sup>	1:1	Sm(ClO <sub>4</sub> ) <sub>3</sub> L	10	[205]
DC18C6	La	NO <sub>3</sub> <sup>-</sup>	1:1	La(NO <sub>3</sub> ) <sub>3</sub> L	12	[206]
	(2.2)	Eu	NO <sub>3</sub> <sup>-</sup>	1:1	[Eu(NO <sub>3</sub> ) <sub>3</sub> L] <sup>+</sup>	10
S <sub>2</sub> 18C6	La	ClO <sub>4</sub> <sup>-</sup>	1:1	(ClO <sub>4</sub> ) <sub>3</sub> L(H <sub>2</sub> O)	10	[208]
Py <sub>2</sub> Me <sub>2</sub> N <sub>3</sub> O <sub>3</sub> -18C6ene <sub>2</sub>	La	NO <sub>3</sub> <sup>-</sup>	1:1	La(NO <sub>3</sub> ) <sub>3</sub> L	12	[209]
Bicy(4.2B.2B)	La	Cl <sup>-</sup>	1:1	[LaCl(Cl,OH)L] <sub>2</sub> <sup>2+b</sup>	10	[210]
	(2.2.2)	Eu	ClO <sub>4</sub> <sup>-</sup>	1:1	[EuClO <sub>4</sub> ]L <sup>2+</sup>	10
	La	NO <sub>3</sub> <sup>-</sup>	4:3	[La(NO <sub>3</sub> ) <sub>2</sub> L] <sup>+</sup>	12	[212]
				[La(NO <sub>3</sub> ) <sub>6</sub> ] <sup>3-</sup>	12	
	Nd	NO <sub>3</sub> <sup>-</sup>	2:1	[Nd(NO <sub>3</sub> )L] <sup>2+</sup>	10	[213]
				[Nd(NO <sub>3</sub> ) <sub>5</sub> (H <sub>2</sub> O)] <sup>2-</sup>	11	
	Sm	NO <sub>3</sub> <sup>-</sup>	2:1	Sm(NO <sub>3</sub> )L <sup>2+</sup>	10	[214]
				[Sm(NO <sub>3</sub> ) <sub>5</sub> (H <sub>2</sub> O)] <sup>2-</sup>	11	
DOTA	Eu		1:1	[Eu(DOTA)(H <sub>2</sub> O)] <sup>-</sup>	9	[215]
Py <sub>2</sub> Me <sub>4</sub> N <sub>6</sub> -14C6ene <sub>4</sub>	Sm	NO <sub>3</sub> <sup>-</sup>	1:1	[Sm(NO <sub>3</sub> ) <sub>3</sub> (OH)L(H <sub>2</sub> O)] <sup>+</sup>	10	[216]
TETA	Tb		1:1	[Tb(TETA)] <sup>-</sup>	8	[217]
(aet) <sub>2</sub> N <sub>6</sub> 16C6c	La	TRIF	1:1	[La(TRIF) <sub>2</sub> L] <sup>+</sup>	10	[218]
	Yb	TRIF	1:1	[Yb(TRIF)L] <sup>2+</sup>	9	[218]
Py <sub>2</sub> Me <sub>4</sub> N <sub>6</sub> -18C6ene <sub>4</sub>	La	NO <sub>3</sub> <sup>-</sup>	1:1	La(NO <sub>3</sub> ) <sub>3</sub> L	12	[206]
	Ln	NO <sub>3</sub> <sup>-</sup>	1:1	Ln(NO <sub>3</sub> ) <sub>3</sub> L (Ln = La, Ce, Nd)	12	[219]

 TABLE 5.15  
 Lanthanide compounds with coordination numbers.

Compound	Coordination number	Polyhedron	Reference
(NH <sub>4</sub> ) <sub>2</sub> [Ce(NO <sub>3</sub> ) <sub>6</sub> ]	12	Icosahedron	[220]
(NH <sub>4</sub> ) <sub>2</sub> H <sub>6</sub> CeMo <sub>12</sub> O <sub>42</sub> · 12H <sub>2</sub> O	12	Icosahedron	[221]
[Nd(NO <sub>3</sub> ) <sub>3</sub> (18C6)]	12	Distorted icosahedron	[204]
[La(NO <sub>3</sub> ) <sub>3</sub> · (H <sub>2</sub> O)]	11	Pentacapped trigonal prism	[222]
[Eu(NO <sub>3</sub> ) <sub>3</sub> (15C5)]	11	Heptadecahedron	[196]
DyB <sub>2</sub> C	14		[189]
DyBC <sub>2</sub>	16		[189]

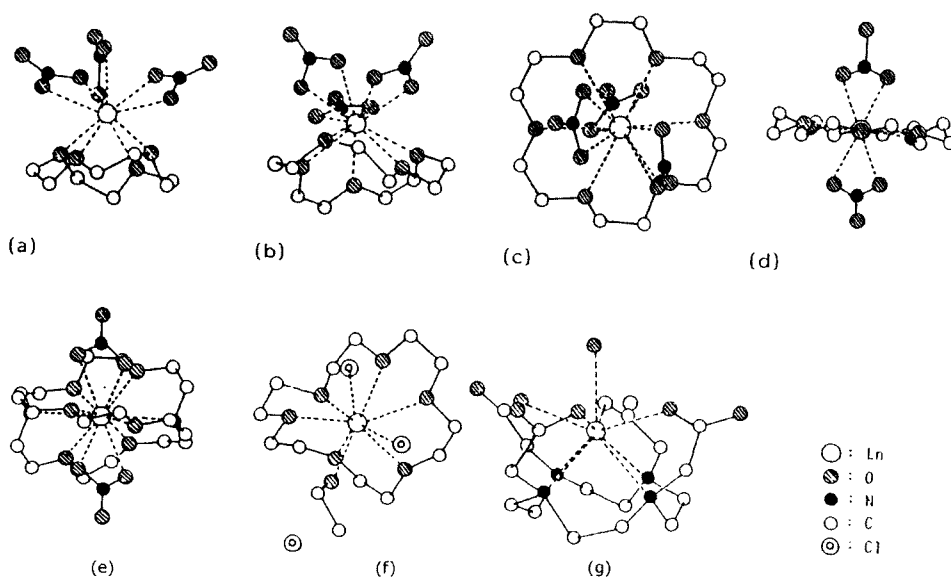


Fig. 5.32. Structures of some lanthanide complexes with macrocycles. Redrawn from (a) Bünzli et al. [196], (b) Bünzli et al. [194], (c) Backer-Dirks et al. [200], (d) Bünzli et al. [204], (e) Hart et al. [212], (f) Forsellini et al. [203], and (g) Spirlet et al. [217].

complex pentahydrate, Sm is coordinated to one 15C5 ligand and four water molecules and is thus 9-coordinate. The second 15C5 ligand is not bonded to Sm but bonded to the coordinated water molecules through hydrogen bonds. The perchlorate ion is not bonded to Sm [197]. The structures of  $[\text{LnX}_3(15\text{C}5)_2]$  were analyzed and speculated to be 1:2 sandwich complexes and the structure appeared to be highly distorted [223].

In the 1:1  $\text{La}(\text{NO}_3)_3$  or  $\text{Nd}(\text{NO}_3)_3$  complex with 18C6, the lanthanide is located near the center of the cavity of the polyether. One nitrate on one side of the polyether ring and two nitrates on the other side are coordinated to the lanthanide ion [200,204]. The lanthanide is 12-coordinate bonded to six oxygen atoms of the polyether and six oxygen atoms of the three nitrate ions. The ligand 18C6 is deformed so that metal–oxygen distances are suitable for coordination. One of the three nitrates is coordinated from the more crowded side resulting from the deformation to minimize the total steric repulsion. In the complex  $\text{Gd}(\text{NO}_3)_3 \cdot 18\text{C}6 \cdot 3\text{H}_2\text{O}$  the three nitrate groups and three water molecules provide nine oxygen bonding sites and the crown ether is held in lattice by hydrogen bonds between crown ether oxygen atoms and coordinated water. The structure of the Gd complex is not the same as those of La and Nd because of the steric hindrance originating from the smaller size of Gd. The hindrance is not due to the encapsulation of Gd by crown ether but due to the coordination of three nitrates together with the polyether. In fact, two nitrates besides 18C6 are coordinated to the lanthanide in the deca-coordinated cationic complex which is an ion of the components of the 4:3 complex. In another complex cation,  $[\text{GdCl}_2 \cdot 18\text{C}6 \cdot \text{EtOH}]^+$ , two chlorides and one ethanol molecule is coordinated to the metal [203]. The 1:1 complex cation  $[\text{Nd}(\text{NO}_3)_2 18\text{C}6]^+$  and the anion  $[\text{Nd}(\text{NO}_3)_6]^-$  without any polyether exist in the ratio of 3:1 in the crystal lattice of 4:3  $\text{Nd}(\text{NO}_3)_3 18\text{C}6$  complex [204]. In the

cation Nd is located near the center of the 18C6 cavity and bound to two nitrates with one above and the other below the polyether skeleton. Thus neodymium is bonded to six oxygen atoms of the ether and four oxygen of the two nitrate groups. The neodymium in the anion is 12-coordinate bonded to six bidentate nitrate groups but the placement of the nitrates appears to be hexacoordinated octahedral if each nitrate group is regarded as an atom.

The 1:1 complex of  $\text{Eu}(\text{ClO}_4)_3$  with cryptand (2.2.2) has six oxygen sites of the two nitrogen heteroatoms bonded to Eu in the cage and one bidentate perchlorate is bound between the oxyethylene chains [211]. The two perchlorate anions and the solvent,  $\text{CH}_3\text{CN}$  remain uncoordinated in the lattice. The structures of some 4:3 and 2:1 complexes of  $\text{Ln}(\text{NO}_3)_3$  with cryptand (2.2.2) have been determined. The composition of the 4:3  $\text{La}(\text{NO}_3)_3 \cdot (2.2.2)$  complex is  $[\text{La}(\text{NO}_3)_2 \cdot (2.2.2)]_3 [\text{La}(\text{NO}_3)_6]$ , which is similar to 4:3 18C6. Note that lanthanum is 10-coordinate in both the cationic and anionic units. In the 2:1 complexes of neodymium and samarium nitrates, the complex cation is  $[\text{Ln}(\text{NO}_3) \cdot (2.2.2)]^{2+}$ , similar to 1:1 complex, though the counter anion, nitrate, is not present as an uncoordinated species. The nitrates form an anionic part  $[\text{Ln}(\text{NO}_3)_5(\text{H}_2\text{O})]^{2-}$ , since a nitrate group is a better coordinating ligand than perchlorate.

The complex of other crown ethers and cryptands have structures similar to those 12C5, 15C5, or 18C6 crown ethers and the (2.2.2) cryptand. The structure analyses of hydrated crown ether complexes of heavier lanthanides reveal the presence of coordinated water molecules [224–229]. In some of these complexes, as many as eight water molecules are coordinated and neither the crown ether nor the counter anion is coordinated, but they are associated with the structure through hydrogen bonding with the coordinated water molecules. The studies on complexes of polyamino polyacetic acid macrocycles, DOTA and TETA containing no ether oxygen atom showed the interposing of lanthanides between two parallel tetragonals formed by the four nitrogen atoms of the 12- or 14-membered ring and by the four coordinating acetate oxygen atoms [217,230].

## References

- [1] D.H. Templeton, C.H. Dauben, *J. Am. Chem. Soc.* **76**, 5237, 1954.
- [2] W.H. Zacharisen, *Crystal chemistry of five f elements*, in: *The Actinide Elements*, ed. G.T. Seaborg, J.J. Katz, p 769, McGraw Hill Book Co., NY.
- [3] J.C.G. Banzli, D. Wessner, *Coord. Chem. Rev.* **60**, 191, 1984.
- [4] R.D. Shannon, *Acta Crystallogr.* **A32**, 751, 1976.
- [5] J.C.G. Banzli, in: *Rare Earths*, Dirigido por: Regino Sacre Puche Y Paul Caro, Madrid, 1998.
- [6] L. Helmholtz, *J. Am. Chem. Soc.* **61**, 1544, 1939.
- [7] T. Moeiler et al., *Chemical Reviews* **1**, 1965.
- [8] G. Anderegg, P. Nageli, F. Muller, G. Schwarzenbach, *Helv. Chim. Acta* **42**, 827, 1959.
- [9] G. Anderegg, *Helv. Chim. Acta* **43**, 825, 1960.
- [10] J.L. Hoard, B. Lee, M.D. Lind, *J. Am. Chem. Soc.* **87**, 1612, 1965.
- [11] P.T. Moseley, *Intl. Rev. Science, Inorg. Chem. Series 2*, Vol. 7, ed. K.W. Bagnak, Butterworths, London, 1975.
- [12] L.L. Martin, R.A. Jacobson, *Inorg. Chem.* **11**, 2785, 1972.
- [13] L.L. Martin, R.A. Jacobson, *Inorg. Chem.* **11**, 2789, 1972.
- [14] L.A. Aslanov, L.I. Soleva, M.A. Parikoshits, S.S. Goukhberg, *Zh. Strukt. Khim.* **13**, 655, 1972.
- [15] L.A. Aslanov, L.I. Soleva, M.A. Parikoshits, S.S. Goukhberg, *J. Struct. Chem. (USSR)* **14**, 998, 1973.
- [16] T. Meeller, *Int. Rev. Sci., Inorg. Chem. Ser. One*, Vol. 7, p. 275, Med. Tec. Publ. Co., 1972.

- [17] S.K. Ramalingam, S. Soundararajan, *J. Inorg. Nucl. Chem.* **29**, 1763, 1967.
- [18] K.J. Eisenstrant, R.E. Sievers, *J. Am. Chem. Soc.* **87**, 5254, 1965.
- [19] J. Selbin, N. Ahmad, N. Bhacca, *Inorg. Chem.* **10**, 1383, 1971.
- [20] L.R. Melby, N.J. Rose, E. Abramson, J.C. Caris, *J. Am. Chem. Soc.* **86**, 5117, 1964.
- [21] E. Hansson, On the Structure of Solid Rare Earth Exalates and Malonates, Thesis, Univer. of Lund, 1973.
- [22] D.C. Bradley, T.S. Ghotra, F.A. Hart, *J. Chem. Soc. Dalton Trans.* 1021, 1973.
- [23] J.S. Ghotra, M.B. Hursthouse, A.J. Welch, *J. Chem. Soc. Chem. Commun.* 669, 1973.
- [24] J. Ren, G. Xu, *Scientia Sinica, Series B* **30**, 337, 1987.
- [25] S.A. Cotton, F.A. Hart, M.B. Hursthouse, A.J. Welch, *J. Chem. Soc. Chem. Commun.* 1225, 1972.
- [26] J. Ren, G. Xu, *New Frontiers in Rare Earth Science and Applications*, ed. G. Xu, J. Xiao, pp. 273–277, Science Press, Beijing, China, 1985.
- [27] D.C. Bradley, J.S. Ghotra, F.A. Hart, M.B. Hursthouse, P.R. Raithby, *J. Chem. Soc. Chem. Commun.* 40–41, 1974.
- [28] J.L. Martin, L.C. Thompson, L.J. Radinovich, M.D. Glick, *J. Am. Chem. Soc.* **90**, 4493, 1968.
- [29] C.K. Jorgensen, B.R. Judd, *Mol. Phys.* **8**, 281, 1964.
- [30] J.P.R. de Villiers, J.C.A. Boyens, *Acta Crystallogr.* **B27**, 2335, 1971.
- [31] C.S. Erasmus, J.C.A. Boeyens, *Acta Crystallogr.* 1843, 1970.
- [32] V. Tazzoli, A. Della Giusta, M. Cola, A. Coda, B.C. Castellini, *Acta Crystallogr.* **28A**, 588, 1972.
- [33] R.W. Baker, J.W. Jeffrey, *Acta Crystallogr.* **25A**, 5161, 1971.
- [34] A. Stuhr, H. Jacobs, *Z. Naturforsch.* **26B**, 165, 1971.
- [35] C.D. Bradle, H. Steinfink, *Inorg. Chem.* **8**, 1320, 1969.
- [36] E.A. Kharakh, A.V. Chichagov, N.V. Belov, *Kristallografiya* **15**, 1064, 1970.
- [37] B.A. Maksimova, Yu.A. Kharitoner, V.V. Ilyukhin, N.V. Belov, *Dokl. Akad. Nauk SSSR* **183**, 1072, 1968.
- [38] N.G. Vatelietta, Yu.A.P. Yatenko, *Zh. Strukt. Khim.* **9**, 921, 1968.
- [39] H. Harris, H.L. Yakel, *Acta Crystallogr.* **22**, 354, 1967.
- [40] Yu.N. Smalin, Yu. Shepelev, *Izv. Akad. Nauk SSSR, Neorg. Mater.* **4**, 733, 1968.
- [41] H. Baernighausen, *Z. Anorg. Allg. Chem.* **374**, 201, 1970.
- [42] J.G. White, P.N. Yocom, S. Lierrier, *Inorg. Chem.* **6**, 1872, 1964.
- [43] J. Felsche, *Natur. Wissenschaften.* **57**, 669, 1970.
- [44] R.B. King, *J. Amer. Chem. Soc.* **92**, 6455, 1970.
- [45] R.J. Gillespie, *Can. J. Chem.* **38**, 818, 1960.
- [46] T.A. Claxton, G.C. Benson, *Can. J. Chem.* **44**, 157, 1966.
- [47] E.L. Mue Herties, C.M. Wright, *Quart. Rev. Chem. Soc.* **21**, 109, 1967.
- [48] C.S. Erasmus, J.C.A. Boeyens, *J. Cryst. Molec. Struct.* **1**, 83, 1971.
- [49] J.C.A. Boeyens, J.P.R. de Villiers, *Acta Crystallogr.* **28A**, 379, 1972.
- [50] J.C.A. Boeyens, J.P.R. de Villiers, *J. Cryst. Mol. Struct.* **1**, 297, 1971.
- [51] W.G. Mumme, A.D. Wadsley, *Acta Crystallogr.* **24B**, 1327, 1968.
- [52] C.T. Prewitt, A.W. Sleight, *Inorg. Chem.* **7**, 1090, 1968.
- [53] A.V. Chengor, N.V. Belov, V.S. Dkoralenko, V.I. Ponamarev, *Dokl. Akad. Nauk SSSR* **189**, 88, 1969.
- [54] A. Zalkin, D.H. Templeton, D.G. Karracker, *Inorg. Chem.* **8**, 2680, 1969.
- [55] M. Guillen, E.F. Bertant, *Bull. Soc. Fr. Ceram.* **72**, 57, 1966.
- [56] H. Beernighausen, N. Schultz, *Acta Crystallogr.* **25B**, 1104, 1969.
- [57] H.P. Beck, H. Beernighausen, *Z. Anorg. Allg. Chem.* **386**, 221, 1971.
- [58] Yu.I. Smelir, *Kristallografiya* **15**, 47, 1970.
- [59] J. Felsch, *Z. Kristallogr. Kristall geometric, Kristall Phys., Kristall Chem.* **133**, 364, 1971.
- [60] Yu.I. Smolin, Yu.I. Shepelov, *Khi. Vysokotemp. Mater., Tr. Vses. Sovesh., 2nd, Leningrad-90*, 1965; C.A. 69, 100636e.
- [61] W. Jeitschko, *Naturwissenschaften.* **57**, 544, 1970.
- [62] E.T. Keve, S.C. Abrahams, J.L. Bernstein, *J. Chem. Phys.* **54**, 3185, 1971.
- [63] A. Noerlund-Christensen, R.G. Hazell, *Acta Chem. Phys. Scand.* **26**, 1171, 1972.
- [64] D. Carre, P. Laruelle, P. Besancon, *Compt. Rend.* **270C**, 537, 1970.
- [65] Yu.I. Smolin, Yu.R. Shepelev, *Izv. Akad. Nauk SSSR, Neorg. Mater.* **5**, 1823, 1969.
- [66] F.A. Cotton, P. Legzdins, *Inorg. Chem.* **7**, 1777, 1968.

- [67] S.J.S. Wasson, D.E. Sands, R.F. Wagner, *Inorg. Chem.* **12**, 187, 1973.
- [68] J.A. Cunningham, D.E. Sands, W.F. Wagner, M.F. Richardson, *Inorg. Chem.* **8**, 22, 1969.
- [69] D.S. Dyer, J.A. Cunningham, J.J. Brooks, R.E. Sievers, R.E. Rondeau, Interactions of Nucleophiles with Lanthanide Shift Reagents, in: *Nuclear Magnetic Shift, Reagents*, ed. R.E. Sievers, pp. 21–51, Academic Press, New York, 1973.
- [70] D.L. Kepert, *J. Chem. Soc. Dalton Trans.* 617, 1974.
- [71] E. Bye, *Acta Chem. Scand.* **A28**, 731, 1974.
- [72] C. Huang, R. Xu, X. Xu, G. Xy, *J. Inorganic Chem. (China)* **1**, 103–112, 1985.
- [73] S.J. Lippard, *Prog. Inorg. Chem.* **8**, 109, 1967.
- [74] R.A. Penneman, R.R. Rayan, A. Rosenzweig, *Structure and Bonding* **13**, 1973.
- [75] J.L. Hoard, J.V. Silverton, *Inorg. Chem.* **2**, 235, 1963.
- [76] S.J. Lippard, B.J. Russ, *Inorg. Chem.* **7**, 1686, 1968.
- [77] D.G. Blight, D.Z. Kepert, *Inorg. Chem.* **11**, 1556, 1972.
- [78] D. Briown, D.G. Holah, C.E.E. Rickard, P.T. Moseley, *AERE Report*, R.6907, 1971.
- [79] J.H. Bwins, M.D. Danfor, *Inorg. Chem.* **8**, 1780, 1969.
- [80] F.H. Kruse, *J. Inorg. Nucl. Chem.* **33**, 1625, 1971.
- [81] D.P. Sinha, R. Prasad, *Indian J. Phys.* **45**, 435, 1971.
- [82] R.R. Ryan, R.A. Penneman, *Acta Crystallogr.* **27B**, 1939, 1971.
- [83] J.P.R. de Villiers, J.C.A. Boeyens, *Acta Crystallogr.* **27B**, 692, 1971.
- [84] J. Delannay, A. de Plognac, F. Fromage, J. Despujols, *Compt. Rend.* **273C**, 692, 1971.
- [85] J.V. Ugro, *Nucl. Sco. Abstr.* 30396, 1967.
- [86] V.W. Day, *Diss. Abstr.* **30B**, 4079, 1970.
- [87] L.A. Aslanov, E.F. Kerytni, M.A. Perai-Koshits, *Zh. Stukt. Khim.* **12**, 661, 1971.
- [88] I. Grenthe, *Acta Chem. Scand.* **25**, 3721, 1971.
- [89] I. Grenthe, *Acta Chem. Scand.* **23**, 1253, 1969.
- [90] P.B. Jamieson, S.C. Abrahams, J.L. Bernstein, *J. Chem. Phys.* **50**, 86, 1969.
- [91] E. Patscheke, H. Fuess, G. Will, *Chem. Phys. Lett.* **2**, 47, 1968.
- [92] A. Gieren, W. Hoppe, *Chem. Commun.* 413, 1971.
- [93] H. Titze, *Acta Chem. Scand.* **24**, 405, 1970.
- [94] A.R. Al-Kharaghoul, J.S. Wood, *Chem. Commun.* 516, 1972.
- [95] J.W. Moore, M.D. Glick, W.A. Baker, *J. Amer. Chem. Soc.* **94**, 1858, 1972.
- [96] J. Kay, J.W. Moore, M.D. Glick, *Inorg. Chem.* **11**, 2818, 1972.
- [97] L.A. Aslanov, I.K. Abdul-Minev, R.A. Cheupakhina, M.A. Porai-Koshits, *Zh. Strukt. Khim.* **12**, 936, 1971.
- [98] J. Albertsson, A. Okarsson, *Acta Chem. Scand.* **22**, 1700, 1968.
- [99] L.A. Aslanov, A.L. Ilinskii, P.I. Lazarev, M.A. Porai-Koshits, *Zh. Strukt. Khim.* **10**, 345, 1969.
- [100] W.H. Watson, R.J. Williams, N.R. Stemple, *J. Inorg. Nucl. Chem.* **34**, 501, 1972.
- [101] R.E. Cramer, K. Seff, *Acta Crystallogr.* **28B**, 3281, 1972.
- [102] A.L. Ilinskii, M.A. Porai-Koshits, L.A. Aslanov, P.I. Lazarev, *Zh. Strukt. Khim.* **13**, 277, 1972.
- [103] L.A. Butman, L.A. Aslanov, M.A. Porai-Koshits, *Zh. Strukt. Khim.* **11**, 46, 1970.
- [104] W. de Herrocks Jr., J.P. Sipe (III), J.P. Lubert, *J. Amer. Chem. Soc.* **93**, 5258, 1971.
- [105] L.P. Seoveva, S.V. Berisov, *Kristallografiya* **14**, 613, 1969.
- [106] S.C. Abrahams, J.L. Bernstein, *J. Chem. Phys.* **46**, 3776, 1967.
- [107] S.F. Bartram, *Act. Crystallogr.* **25**, 791, 1969.
- [108] L.A. Aslanov, M.A. Porai-Koshits, M.O. Dekaprilevich, *Zh. Strukt. Khim.* **12**, 470, 1971.
- [109] P.T. Lazarev, M.A. Porai-Koshits, L.A. Aslanov, V.S. Kuzin, *Zh. Strukt. Khim.* **12**, 1111, 1971.
- [110] L.A. Aslanov, V.B. Rybakov, V.M. Ionov, M.A. Porai-Koshits, V.I. Ivanov, *Dokl. Akad. Nauk SSSR* **204**, 1122, 1972.
- [111] I. Noerlund, C. Christenson, *Acta Chem. Scand.* **24**, 2440, 1970.
- [112] A.L. Ilinskii, L.A. Aslanov, V.I. Ivanov, A.D. Khalidov, C.M. Petrukhin, *Zh. Strukt. Khim.* **10**, 285, 1969.
- [113] O.E. Izotova, V.R. Aleksandrova, *Dokl. Akad. Nauk SSSR* **192**, 1037, 1970.
- [114] H. Brussett, F. Madaule-Aubry, R. Mahe, C. Boursier, *Compt. Rend.* **237**, 455, 1971.
- [115] J. Felsche, *Z. Kristallogr. Kristallgeometrie Kristall Phys. Kristall Chem.* **133**, 364, 1971.
- [116] K.K. Palkina, V.G. Kuznetsov, L.G. Muruga, *Zh. Strukt. Khim.* **13**, 341, 1972.
- [117] R.F. Klevtsova, V.A. Vinokurov, P.V. Klecstova, *Kristallografiya* **17**, 284, 1972.
- [118] K.A. Wilhelm, E. Lagerval, O. Muller, *Acta Chem. Scand.* **24**, 3406, 1970.
- [119] R.F. Klevtsova, S.V. Borisov, *Kristallografiya* **14**, 904, 1969.
- [120] J. Felsche, *Naturwissenschaften* **58**, 218, 1971.

- [121] T.N. Tarkhova, I.A. Grishin, N.N. Mironov, Zh. Neorg. Khim. **15**, 2584, 1970.
- [122] T.M. Ploanskaya, S.V. Berisov, N.V. Belov, Dokl. Akad. Nauk SSSR **193**, 83, 1970.
- [123] T.A. Kurova, V.B. Aleksandrov, Dokl. Akad. Nauk SSSR **201**, 1095, 1971.
- [124] J.G. Leipoldt, V.D.C. Bok, S.S. Basson, J.S. Van Vollenhoven, A.E. Laubscher, unpublished work, 1976.
- [125] V.W. Day, Diss. Abstr. Int. B **30**, 4079-4080, 1970.
- [126] A.J. McPhail, P.S.W. Tschang, J. Chem. Soc., Dalton Trans. 1165, 1974.
- [127] J.G. Leipoldt, L.D.C. Bok, A.E. Laubscher, S.S. Basson, J. Inorg. Nucl. Chem. **37**, 2477, 1975.
- [128] J.G. White, Inorg. Chim. Acta **16**, 159, 1976.
- [129] D. Grdenic, B. Matkovic, Acta Crystallogr. **12**, 817, 1969.
- [130] D. Grdenic, B. Matkovic, Acta Crystallogr. **16**, 456, 1973.
- [131] I. Grenthe, Acta Chem. Scand. **26**, 1479, 1972.
- [132] F.W. Ollendorf, F. Weigel, Inorg. Nucl. Chem. Litt. **5**, 263, 1969.
- [133] J. Albertsson, Acta Chem. Scand. **24**, 3527, 1970.
- [134] A. Dereigne, G. Pannetier, Bull. Soc. Chim. Fr. 174, 1968.
- [135] A. Dereigne, J.M. Manoli, G. Pannetier, P. Herpin, Bull. Soc. Fr. Mineral. Cristallogr. **95**, 269, 1972.
- [136] G.D. Brunton, Acta Crystallogr. **25**, 600, 1969.
- [137] N.Q. Duao, J. Etienne, P. Laruelle, Bull. Soc. Chim. Fr. 2433, 1971.
- [138] M. Bagieu-Beucher, I. Tordjman, A. Durif, Rev. Chim. Miner. **8**, 753, 1971.
- [139] E. Hansson, Acta Chem. Scand. **24**, 2969, 1970.
- [140] A. Oskarsson, Acta Chem. Scand. **25**, 1206, 1971.
- [141] J. Albertsson, Acta Chem. Scand. **26**, 1023, 1972.
- [142] T.M. Polyanskaya, S.V. Borisov, N.V. Belov, Kristallografiya **15**, 1135, 1970.
- [143] I. Grenthe, Acta Chem. Scand. **25**, 3347, 1971.
- [144] G.H. Frost, F.A. Hart, C. Heath, M.B. Hursthouse, Chem. Commun. 1421, 1969.
- [145] L.A. Aslanov, L.I. Soeva, S.S. Goukhberg, M.A. Porai-Koshits, Zh. Strukt. Khim. **12**, 1113, 1971.
- [146] T.R.R. McDonald, J.M. Spink, Acta Crystallogr. **23**, 944, 1967.
- [147] R.F. Klevtsova, P.V. Klevtsov, Zh. Strukt. Khim. **9**, 834, 1968.
- [148] J. Albertsson, Acta Chem. Scand. **24**, 1213, 1970.
- [149] J. Albertsson, Acta Chem. Scand. **26**, 985, 1972.
- [150] J. Albertsson, Acta Chem. Scand. **26**, 1005, 1972.
- [151] K.K. Bhandary, H. Manohar, K. Venkatesan, J. Chem. Soc., Dalton Trans. 288, 1975.
- [152] L.A. Aslanov, L.I. Soleva, M.A. Porai-Koshits, J. Struct. Chem. (USSR) **14**, 998, 1973.
- [153] K.K. Bhandary, H. Manohar, K. Venkatesan, Acta Crystallogr. **B32**, 861, 1976.
- [154] T. Malmberg, A. Oskarsson, Acta Chem. Scand. **27**, 2923, 1973.
- [155] P.M. Raccach, J.M. Longo, H.A. Eich, Inorg. Chem. **6**, 1471, 1967.
- [156] L.J. Radinovich, M.D. Glick, Inorg. Chem. **10**, 1463, 1972.
- [157] P.I. Lazarev, L.A. Aslanov, M.A. Porai-Koshits, V.I. Ivanov, Zh. Strukt. Khim. **13**, 543, 1972.
- [158] R.R. Ryan, R.A. Penneman, Inorg. Chem. **10**, 2637, 1971.
- [159] M. Marezio, P.D. Dernier, Mater. Res. Bull. **6**, 23, 1971.
- [160] A. Zalkin, D.H. Templeton, T.E. Hopkins, Inorg. Chem. **5**, 1466, 1966.
- [161] G.G. Sadikov, G.A. Kukina, M.A. Porai-Koshits, Zh. Strukt. Khim. **9**, 145, 1968.
- [162] G.G. Sadikov, G.A. Kukina, M.A. Porai-Koshits, Zh. Strukt. Khim. **8**, 551, 1967.
- [163] L.L. Martin, R.A. Jacobson, Inorg. Chem. **11**, 2785, 1972.
- [164] Yu.I. Smolin, Yu.F. Shepelev, I.K. Butikova, Kristallografiya **15**, 256, 1970.
- [165] L. Helmholz, J. Am. Chem. Soc. **61**, 1544, 1939.
- [166] D.R. Fitzwater, R.E. Rundle, Z. Krist. **112**, 362, 1959.
- [167] E. Hansson, Acta Chem. Scand. **27**, 2827, 1973.
- [168] E. Hansson, Acta Chem. Scand. **27**, 2441, 1973.
- [169] E. Hansson, Acta Chem. Scand. **27**, 2813, 1973.
- [170] J.A. Cunningham, R.E. Sievers, J. Amer. Chem. Soc. **97**, 1586, 1975.
- [171] W. de Herrocks Jr., NMR of Paramagnetic Molecules, p. 492, Academic Press, NY, 1973.
- [172] C. Huang, G. Li, Y. Zhou, T. Jin, G. Xu, Acta Sci. Univ. Peking **6**, 12, 1985.
- [173] A.R. Al-Kharaghoul, J.S. Wood, Inorg. Chem. **11**, 2293, 1972.
- [174] M.D. Lind, B. Lee, J.L. Hoard, J. Amer. Chem. Soc. **87**, 1611, 1965.
- [175] K.K. Bhandary, H. Manohar, Acta Cryst. **B29**, 1093, 1973.
- [176] L.A. Aslanov, L.I. Soleva, M.A. Porai-Koshits, S.S. Goukhberg, Zh. Strukt. Khim. **13**, 655, 1972.

- [177] V.B. Kravchenko, *Zh. Strukt. Khim.* **13**, 345, 1972.
- [178] D.S. Moss, S.P. Sinha, *Z. Phys. Chem. (Frankfurt Am Main)* **63**, 190, 1969.
- [179] D.B. Shim, H.A. Eick, *Inorg. Chem.* **7**, 1340, 1968.
- [180] J.S. Ysker, W. Hoffmann, *Naturwissenschaften* **57**, 129, 1970.
- [181] J.M. Longo, A.S. Sleight, *Inorg. Chem.* **7**, 108, 1968.
- [182] N.L. Morrow, L. Katz, *Acta Crystallogr.* **24B**, 1466, 1968.
- [183] L.A. Harris, H.L. Yakel, *Acta Crystallogr.* **24B**, 672, 1968.
- [184] A.R. Al-Karaghoul, J.S. Wood, *Chem. Commun.* 135, 1970.
- [185] G. Mazhar-ul-Haque, C.N. Caughlan, F.A. Hart, R. Van Nice, *Inorg. Chem.* **10**, 115, 1971.
- [186] G.G. Sadikov, G.A. Kukina, M.A. Porai-Koshits, *Zh. Strukt. Khim.* **12**, 859, 1971.
- [187] V.I. Pakhomov, G.I. Sil'nitskaya, A.V. Medvedev, B.F. Dzhurinskii, *Izv. Akad. Nauk SSSR, Neorg. Mater.* **8**, 1259, 1972.
- [188] Mazhar-ul-Haque, F.A. Hart, C.N. Caughlan, *Chem. Commun.* 1240, 1970.
- [189] J. Bauer, J. Debuigne, *Compt. Rend.* **274C**, 1271, 1972.
- [190] G.E. Toogood, C. Chieh, *Can. J. Chem.* **53**, 831, 1975.
- [191] G.D. Smith, C.N. Caughlan, Mazhar-ul-Haque, F.A. Hart, *Inorg. Chem.* **12**, 2654, 1973.
- [192] T. Lu, X. Wang, M. Tan, Y. Liu, Y. Inoue, T. Hakushi, *Helv. Chim. Acta* **76**, 241, 1993.
- [193] R.D. Rogers, L.K. Kurihara, *J. Inclusion Phenom.* **4**, 351, 1986.
- [194] J.-C.G. Bunzli, B. Klein, G. Dwessner, N.W. Alcock, *Inorg. Chim. Acta* **59**, 269, 1982.
- [195] G. Tomat, G. Valle, P. Di Bernardo, P.L. Zanorate, *Inorg. Chim. Acta* **110**, 113, 1985.
- [196] J.-C.G. Bunzli, B. Klein, G. Chapuis, K.J. Schenk, *Inorg. Chem.* **21**, 808, 1982.
- [197] T.T. Lee, H.R. Scheu, I.T. Chiu, C.T. Chang, *Acta Crystallogr. C* **39**, 1357, 1983.
- [198] D. Harrisson, A. Giorgetti, J.-C.G. Bunzli, *J. Chem. Soc., Dalton Trans.* 885, 1985.
- [199] G. Tomat, G. Valle, A. Cassoll, P. Di Bernardo, *Inorg. Chim. Acta.* **76**, L13, 1983.
- [200] J.D. Backer-Dirks, J.E. Cooke, A.M.R. Galas, J.S. Ghotra, C.J. Gray, F.A. Hart, M.B. Hursthouse, *J. Chem. Soc., Dalton Trans.* 2191, 1980.
- [201] J.-C.G. Bunzli, D. Wessner, *Inorg. Chim. Acta* **44**, L55, 1980.
- [202] G. Bombieri, G. De Pasli, F. Benetollo, A. Casol, *J. Inorg. Nucl. Chem.* **42**, 1417, 1980.
- [203] E. Forsellini, F. Benetollo, G. Bombieri, A. Casol, G. De Pasli, *Inorg. Chim. Acta* **109**, 167, 1985.
- [204] J.-C.G. Bunzli, B. Klein, D. Wessner, K.J. Schenk, G. Chapuis, G. Bombieri, G. DePasli, *Inorg. Chim. Acta* **54**, 143, 1981.
- [205] M. Ciampolini, N. Nardi, R. Chin, S. Mangani, P. Orisli, *J. Chem. Soc. Dalton Trans.* 1983, 1979.
- [206] *Cation Binding by Macrocycles*, eds Y. Inoue, G.W. Gokel, Marcel Dekker, Inc., NY.
- [207] J.-C.G. Bunzli, G.A. Leonard, D. Plancherel, G. Chapuis, *Helv. Chim. Acta* **69**, 288, 1986.
- [208] M. Ciampolini, P. Dapporto, N. Nardi, *J. Chem. Soc. Dalton Trans.* 1973, 1979.
- [209] A.M. Arif, C.J. Gray, F.A. Hart, M.B. Hursthouse, *Inorg. Chim. Acta* **109**, 179, 1985.
- [210] F. Benetollo, G. Bombieri, G. De Pasli, D.L. Hughes, D.G. Parsibsm, N.R. Truter, *J. Chem. Soc., Chem. Commun.* 425, 1984.
- [211] M. Ciampolini, P. Dapporto, N. Nardi, *J. Chem. Soc., Dalton Trans.* 974, 1979.
- [212] F.A. Hart, M.B. Hursthouse, K.M. Abdul Malik, S. Mourhouse, *J. Chem. Soc. Chem. Commun.* 549, 1978.
- [213] F. Benetollo, G. Bombieri, A. Cassol, G. De Pasli, J. Legendziewicz, *Inorg. Chim. Acta* **110**, 7, 1985.
- [214] J.H. Burns, *Inorg. Chem.* **18**, 3044, 1979.
- [215] M.R. Spirlet, J. Rebizant, J.F. Desreux, M.F. Loncin, *Inorg. Chem.* **23**, 359, 1984.
- [216] K.K. Abid, D.E. Fenton, U. Casellato, P.A. Vignato, R. Graziani, *J. Chem. Soc., Dalton Trans.* 351, 1984.
- [217] M.R. Spirlet, J. Rebizant, M.F. Loncin, J.F. Desreux, *Inorg. Chem.* **23**, 4278, 1984.
- [218] P.H. Smith, K.H. Raymond, *Inorg. Chem.* **24**, 3469, 1985.
- [219] A.M. Arif, J.D. Backer-Dirks, C.J. Gray, F.A. Hart, M.B. Hursthouse, *J. Chem. Soc., Dalton Trans.* 1665, 1987.
- [220] T.A. Beineke, J. Delgtaudio, *Inorg. Chem.* **7**, 715, 1968.
- [221] D.D. Dexter, J.V. Silverton, *J. Amer. Chem. Soc.* **90**, 3589, 1968.
- [222] B. Eriksson, L.O. Larsson, L. Niinisto, *J. Chem. Soc., Chem. Commun.* 616, 1978.
- [223] J.-C.G. Bunzli, W.D. Harrison, A. Giorgetti, G.O. Pradervand, N.W. Alcock, *Inorg. Chim. Acta* **109**, 59, 1985.
- [224] R.D. Rogers, *Inorg. Chim. Acta* **133**, 175, 1987.



- [225] R.D. Rogers, L.K. Kurihara, *Inorg. Chim. Acta* **116**, 171, 1986.
- [226] R.D. Rogers, L.K. Kurihara, *J. Inclusion Phenom.* **4**, 351, 1986.
- [227] R.D. Rogers, L.K. Kurihara, *J. Less Common Metals* **127**, 199, 1987.
- [228] R.D. Rogers, L.K. Kurihara, *Inorg. Chim.* **26**, 1498, 1987.
- [229] R.D. Rogers, E.J. Voss, *Inorg. Chem. Acta* **133**, 181, 1987.
- [230] M.R. Spirlet, J. Rebizant, M.F. Loncin, J.F. Desreux, *Inorg. Chem.* **23**, 4278, 1984.

chapter 6

---

## ORGANOMETALLIC COMPLEXES

---

---

# CONTENTS

---

1. Organometallic complexes of rare earths . . . . .	425
2. Tetrakis-cyclopentadienyl lanthanide ( $Cp_4Ln$ ) . . . . .	426
3. Triscyclopentadienyl lanthanides ( $LnCp_3$ ) and solvent coordinated complexes $LnCp_3S$ and $LnCp_32S$ . . . . .	426
4. Ten coordinate adducts, $LnCp_3 \cdot L$ . . . . .	429
5. Complexes with substituted cyclopentadienyls ( $Cp'_3Ln$ , $Cp'_3Ln \cdot L$ ) . . . . .	431
6. Complexes of the type $Cp_3MX$ . . . . .	433
7. Complexes of the type $Cp'_3MX$ ( $Cp' =$ substituted Cp) . . . . .	434
7.1. Complex types $Cp_2LnX$ , $Cp_2LnXY$ . . . . .	434
8. Compounds of the type $Cp_2Ln \cdot X$ ( $X = Ln-O, Ln-S, Ln-P$ ) . . . . .	436
9. Alkoxides, acetoxime and diketonate derivatives . . . . .	436
10. Compounds containing $Ln-N$ bonds in $Cp_2LnX$ . . . . .	437
11. Compounds $Cp_2LnX$ containing $Ln-P$ bond . . . . .	438
12. Compounds of the type $Cp'_2MX$ ( $Cp' =$ substituted Cp) . . . . .	439
13. Compounds of the type $Cp'_2LnX$ ( $Cp' =$ substituted Cp; $X =$ hydrocarbyl) . . . . .	439
14. Complexes of the type $Cp'_2LnX$ ( $X = O, S, Se, Te, N$ donor ligands) . . . . .	440
15. Cyclopentadienide complexes of lanthanides(II) . . . . .	441
16. Monocyclopentadienyl complexes . . . . .	442
17. Substituted monocyclopentadienyl complexes ( $Cp'LnX_2$ , $Cp'LnXY$ ) . . . . .	444
17.1. Low valent $LnCp_2^*$ complexes [ $Cp^* = C_5(CH_3)_5$ ] . . . . .	445
18. $Cp_2^*Ln$ halide complexes . . . . .	448
19. $Cp_2^*Ln$ hydrocarbyl complexes . . . . .	448
20. $Cp_2^*Ln$ complexes with O, S, Se, Te, N, As and Sb donors . . . . .	452
21. Complexes of the type $Cp^*LnX$ . . . . .	455
22. Ring bridged cyclopentadienyl lanthanide complexes . . . . .	458
23. Lanthanide indenyl complexes . . . . .	463
24. Lanthanide cyclooctatetraenyl complexes . . . . .	463
25. Lanthanide cyclopentadienyl hydride complexes . . . . .	468
26. Lanthanide-transition metal mixed organometallic complexes . . . . .	470
27. Lanthanide arene complexes . . . . .	470
28. Lanthanide complexes with other ligands . . . . .	473
References . . . . .	474

## 1. Organometallic complexes of rare earths

The first synthesis of tricyclopentadienyl complexes of rare earth metals was reported by Wilkinson and Birmingham [1]. Earlier attempts to prepare organo-lanthanide compounds, although unsuccessful, provided impetus for research activity in this fascinating subject. The availability of highly pure rare earth metals and the wide applications of this class of compounds has led to increased and intensive developments in organolanthanide chemistry during the past two decades. These developments have been well documented in the literature [2–16]. It is instructive to dwell a little on general aspects of lanthanides. The 4f orbitals in the lanthanides are well shielded and the metals do not experience as great an effective nuclear charge as the 5p, 6s or 5d orbitals. In spite of this, the 4f orbitals become more attractive with an increase in atomic number which results in a decrease in radius, also known as the “lanthanide contraction”.

By the loss of 4f electrons, La attains a stable electronic configuration giving rise to a trivalent oxidation state. Other oxidation states, such as two and four in some lanthanides, are possible when electronic configurations  $4f^0$ ,  $4f^7$  and  $4f^{14}$  are attained. The oxidation states and the oxidation–reduction potentials of some couples are given in Table 6.1. The lanthanides in 4+ oxidation state are strong oxidizing agents and an example is  $Ce^{4+}$ .

$Ln^{4+}$	Ce, Tb and Pr
$Ln^{3+}$	Common to lanthanides
$Ln^{2+}$	Eu, Sm, Yb, Lu

Oxidizing agents are in  $La^{4+}$ , and in 2+ oxidation state are strong reducing agents. In the lanthanides, the inner 4f orbitals are populated successively and these orbitals are

TABLE 6.1  
Redox potentials.

Couple	$E^0$ (V)
$Pr^{4+}/Pr^{3+}$	+3.2
$Ce^{4+}/Ce^{3+}$	+1.74
$Tb^{4+}/Tb^{3+}$	+3.10
$Eu^{3+}/Eu^{2+}$	–0.35
$Tm^{3+}/Tm^{2+}$	–2.10
$Yb^{3+}/Yb^{2+}$	–1.15
$Sm^{3+}/Sm^{2+}$	–1.55

well shielded by 5s and 5p orbitals and hence do not contribute significantly to bonding because of their limited radial extension. However, the f orbitals have some effect on the electronic properties of the metals. Lanthanides in oxidation state 3+ attain the noble gas configuration by the loss of 4f electrons. Sc and Y attain the configuration of Kr and Ar in 3+ oxidation state and hence behave like lanthanides.  $Y^{3+}$  and  $Sc^{3+}$  have similar chemistry as that of lanthanides. In general, lanthanides have strong affinity for oxygen as reflected by the high bond dissociation energies of LnO which range from 400 to 800 kJ/mol at 298 K.

In discussing lanthanide complexes, it is inevitable that a comparison to the actinide series shows that actinide complexes have more covalent bonding because 5f orbitals are not completely shielded by 6s and 6p electrons and thus have sufficient radial extension for some overlap with ligand orbitals. Some important features of organometallic compounds of lanthanides are: (a) organolanthanides are predominantly ionic due to the inability of f orbitals to overlap with ligand molecular orbitals, (b) because of the exceptional stability of the trivalent state of lanthanides, oxidative-addition reaction is not favoured, (c) the large radii of lanthanides require sterically demanding ligands to form discrete monomeric compounds, (d) due to the similarity in chemical behaviour with differences due to size differences, the lanthanide chemistry offers the possibility of using the same reaction conditions with different lanthanide metal ions, (e) because of the low covalent bonding contributions, the need for compatible orbital symmetries does not arise and this leads to the possibilities of new reactions, (f) lanthanides can have coordination numbers as high as 12, and give rise to coordinatively unsaturated species which can be used as catalysts. Most of the organometallic complexes of lanthanides contain one  $\pi$  donor/ $\pi$  acceptor type of ligand (cyclopentadienyl, cyclooctatetraenes) along with other ligands such as halides, hydrides, alkyls, etc. and the latter are the reactive centers of catalytic reactions.

The general major types of organometallic complexes of rare earths are listed in Table 6.2.

## 2. Tetrakis-cyclopentadienyl lanthanide ( $Cp_4Ln$ )

Tetrakis-cyclopentadienyl cerium ( $CeCp_4$ ) has been reported to be formed by the reaction of bis(pyridinium) hexachloroacetate with sodium cyclopentadienide [17]. Similarly indenyl and fluorenyl derivatives were prepared. Later work showed the same reactants in tetrahydrofuran to yield,  $Ce(Cp_3)$ , tricyclopentadienyl cerium complex instead of  $Ce(Cp_4)$  [18].

## 3. Tricyclopentadienyl lanthanides ( $LnCp_3$ ) and solvent coordinated complexes $LnCp_3S$ and $LnCp_32S$

$LnCp_3$  complexes, where Ln = Sc, Y, La, Ce, Pr, Nd, Sm, Gd, Dy, Er, and Yb have been synthesized by the reaction of anhydrous metal chloride with sodium cyclopentadienide in tetrahydrofuran at room temperature [1].

Another synthetic route involves ligand exchange between  $Sm(C_6F_5)_2$  with cyclopentadiene [19].  $LnCp_3$  (Ln = Er, Yb) has been synthesized by the reaction of  $LnCl_3$  with TICp in tetrahydrofuran or dimethoxy ethane [20].

TABLE 6.2  
General types of organometallic complexes of the rare earths\*.

Type	
Cyclopentadienyl compounds of the divalent rare earths	
$(C_5H_5)_2R$	(R = Eu, Yb)
$(C_5H_5)_2Sm \cdot OC_4H_8O$	
Cyclopentadienyl compounds of the trivalent rare earths	
Tricyclopentadienyl compounds	
$(C_5H_5)_3R$	(R = La–Lu, Y, Sc)
$(C_5H_5)_3R \cdot X$	(X = cyclo hexyliso-nitrile, THF, ammonia, triphenyl phosphine)
Dicyclopentadienyl compounds	
$(C_5H_5)_2RX$	(R = Sm–Lu)
$(CH_3C_5H_4)_2RX$	(R = Gd–Yb)
	(X = chloride, formate, acetate, benzoate, methoxy, phenoxy, iodide)
$(C_5H_5)_2RQ$	(Q = methyl, phenyl, phenylacetylde, allyl)
Indenyl compounds	
$(C_9H_7)_3R \cdot OC_4H_8O$	(R = La–Yb)
Cyclooctatetraenyl compounds	
$R(C_8H_8)$	(R = Eu, Yb)
$K[R(C_8H_8)_2]$	(R = La–Tb, Y)
$[R(C_8H_8)Cl \cdot 2C_4H_8O]_2$	(R = Ce–Sm)
$(C_5H_5)R(C_8H_8) \cdot THF$	(R = Nd, Sm, Ho, Er, Y)
$[Nd(C_8H_8)(OC_4H_8)][Nd(C_8H_8)_2]$	
Alkyl and aryl compounds	
$R(C_6H_5)_3$	(R = Sc, Y)
$[(CH_3)_3CCH_2]_3Sc \cdot 2THF$	
$[(CH_3)_3SiCH_2]_3Sc \cdot 2THF$	
$[o-CH_3OC_6H_4Si(CH_3)_2CH_2]_3SC$	
$\{[(CH_3)_3Si]_2CH\}_3Y$	
$\{[(CH_3)_3Si]_2CH\}_3R \cdot 2THF$	(R = Y, Sc)

\*L.C. Thompson, Handbook on the Physics and Chemistry of Rare Earths, eds K.A. Gschneidner, Jr., L. Eyring, Vol. 9, Chapter 25, North Holland, 1979.

The reaction of NaCp with  $(NH_4)_2[Ce(NO_3)_6]$  in a mole ratio 1:1 results in reduction of  $Ce^{4+}$  to  $Ce^{3+}$  while a molar ratio of 6:1 in tetrahydrofuran (THF) yields  $Cp_3Ce(THF)$  [21]. This may also be obtained by the reaction of  $LnCl_3$  (La = Ce, La, Nd) with four equivalents of NaCp [22]. NMR and IR data suggest the formulation  $[\eta^5(Cp)_3Ln(\mu-\eta^1-Cp)Na(THF)_n]$ .

In the  $Cp_3Ln$  complexes (i) increase in volatility and (ii) decrease in Ln–Cp bond energy with increasing atomic number have been observed. X-ray crystal structure determinations show monomeric structures in the case of Er, Tm and Yb complexes and polymeric structures in the case of La, Pr, Sm, Lu and Sc complexes. The two forms of  $Cp_3La$  with different crystal packing are shown in Fig. 6.1. One form has short La–C contacts between adjacent molecules in the form of  $\eta^5-(C_5H_5)_2La(\mu-\eta^5 : \eta^2-C_5H_5)$  units [23] and the other in the form of  $\eta^5-(C_5H_5)_2La(\mu-\eta^5 : \eta^1-C_5H_5)$  with one La–C short contact for the bridging  $C_5H_5$  to the adjacent molecule [24].

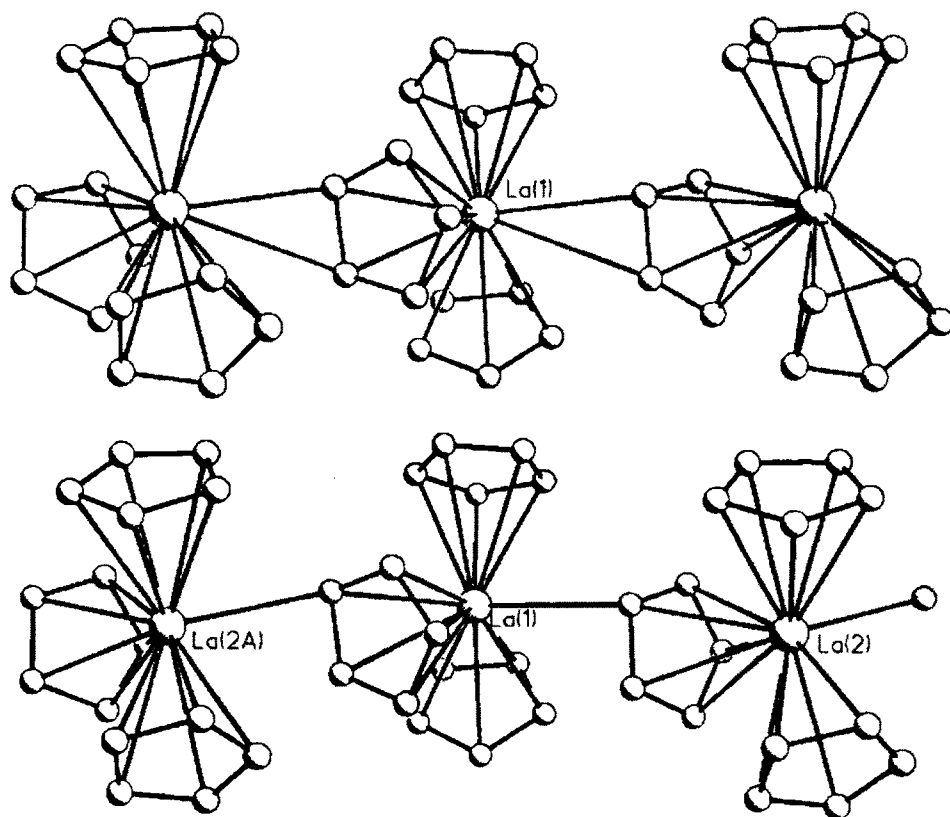


Fig. 6.1. Crystal structure of the two forms of [Cp<sub>3</sub>La] [26].

Sc and Lu derivatives are isomorphous and polymeric containing  $[\eta^5-(C_5H_5)_2Ln(\mu-\eta' : \eta'-C_5H_5)]_\infty$ . In the case of SmCp<sub>3</sub>, two crystallographically independent molecules bonded to each other by non-valence interactions has been observed [25].

The two forms of LaCp<sub>3</sub> are shown in Fig. 6.1. The structure of PrCp<sub>3</sub> consists of a singular polymeric chain in the solid state involving  $\eta^5$ -coordination of each Pr with three Cp ligands and  $\eta^x$  coordination ( $1 < x < 2$ ) with a fourth bridging Cp ligand [26]. This disposition is due to ionic interactions. The isostructural Y, Er, and Tm compounds are [27, 28] monomeric with closest Ln–C contacts, outside the three rings, greater than 3.14 Å. The Yb compound is monomeric but not isostructural with Tm and Lu compounds [29]. The contact distance of 4.139 Å between YbCp<sub>3</sub> units excludes the possibility of chemical interaction between the metal ion and carbon of closest YbCp<sub>3</sub> unit with the resulting nearly ideal D<sub>3h</sub> symmetry on the Yb ion.

The nature of bonding in LnCp<sub>3</sub> compounds is predominantly ionic as evidenced by (i) magnetic measurements, (ii) optical spectra, (iii) Raman spectra and (iv) NMR spectra. Magnetic susceptibilities of LnCp<sub>3</sub> compounds are nearly the same as those free lanthanide ions. UV-Vis spectra show sharp lines involving f–f electron transition with a nephelauxetic

effect smaller than transition elements but larger than lanthanide chlorides [30]. Raman spectra [31] show Cp ring vibrations involving  $\eta^5$  coordination and ionic interactions between metal and Cp rings. The unpaired f electrons give rise to paramagnetism and hence line broadening of NMR spectra. The isotropic shifts are composed of contact interactions of the unpaired f electron with the ligand and dipolar contributions or pseudo contact contributions and the latter contributions are important in  $\text{LnCp}_3$  compounds.

Some of the applications of  $\text{LnCp}_3$  compounds are (i) reduction of olefins by  $\text{LnCp}_3$  and NaH, (ii) reductive dehalogenation of aryl and vinyl halides with  $\text{LnCp}_3/\text{NaH}$ , (iii) reduction of  $\text{N}_2$  to  $\text{NH}_3$  with  $\text{LnCp}_3$  and sodium naphthalene in THF. When alkylhalides are used, alkylated derivatives were obtained which on hydrolysis gave alkyl cyclopentadienes involving an intermediate anion,  $[\text{Cp}_3\text{Ln}(\mu\text{-H})\text{LnCp}_3]$  [32].

#### 4. Ten coordinate adducts, $\text{LnCp}_3 \cdot \text{L}$

$\text{LnCp}_3$  compounds form adducts with Lewis bases, which are monomeric because the Lewis base prevents the formation of polymeric species by coordination to the metal and making the metal coordinatively saturated.  $\text{LnCp}_3 \cdot \text{THF}$  complexes, where Ln = Y, La, Pr, Nd, Gd and Lu are isostructural involving  $\eta^5$  coordination of Cp to the metal [33].  $\text{LnCp}_3 \cdot n\text{THF}$  where  $n = 2, 3$  are also known [34].  $\text{LnCp}_3 \cdot \text{L}$ , where L = THF or dimethoxyethane (DME), Ln = Ce, Nd, Sm, Gd, Er, were synthesized by the reaction of metal salt with thallos cyclopentadienides in THF or DME [35].  $\text{LnCp}_3 \cdot \text{THF}$  compounds containing La, Pr, Nd, Gd and Dy are isostructural and the molecule is coordinated to the metal such as Dy with Dy–O and Dy–C (Cp) bond distances of 2.522 Å and 2.649 to 2.816 Å, respectively [36].

With propionitrile as the base 1:1 and 1:2 adducts  $\text{Cp}_3\text{LnL}$ , where Ln = La, Pr, Yb, L =  $\text{CH}_3\text{CH}_2\text{CN}$  and  $n = 1, 2$  have been prepared. The Ln ion is  $\eta^5$  bonded to three Cp ligands and to a propionitrile nitrogen atom. The site symmetry around the lanthanide ion is nearly  $\text{C}_{3v}$ . This arrangement is typical of most  $\text{Cp}_3\text{LnX}$  compounds with ring centroid–metal–ring centroid angles,  $\text{C}_g\text{-M-C}_g$ , in the range of  $112^\circ\text{--}119^\circ$ . A significant feature observed in these complexes is the non-linearity of  $\text{Ln-N}\equiv\text{C-C}_2\text{H}_5$  with  $\text{Ln-N}\equiv\text{C}$  angles of  $168.3^\circ$  for La and  $171.0^\circ$  for Yb (Fig. 6.2). The pseudo-tetrahedral  $\text{Cp}_3\text{Ln-NCC}_2\text{H}_5$  system is able to add on an additional propionitrile to give 1:2 adducts, where the stereochemistry of Ln is trigonal bipyramidal with  $\text{D}_{3h}$  pseudo symmetry for Ln. The three Cp ligands are in the equatorial plane and the nitrile ligands in the trans-diaxial positions. A bending of about  $14^\circ$  is observed in the axial ligands probably due to steric reasons [37].

Transmetallation reactions of  $\text{TiCp}$  and  $\text{LnCl}_3$  in pyridine, acetonitrile and ether give rise to  $\text{Cp}_3\text{Ln} \cdot \text{L}$ , where Ln = Nd, Sm, Eu, Yb, L = pyridine; Ln = Nd, Sm, Yb; L = acetonitrile. Although the complexes  $\text{Cp}_3\text{Ln}(\text{Py})$  for Ln = Sm, Nd have the same composition, their crystal structures are different [38] with respect to pyridine coordination.

The adducts  $\text{Cp}_3\text{Ln} \cdot \text{L}$  have greater solubility in organic solvents than the parent  $\text{Cp}_3\text{Ln}$  base-free compounds.

$^{139}\text{La}$ -NMR studies on  $\text{Cp}_3\text{Ln} \cdot \text{L}$ , where L = DMSO, DMF,  $\text{OP}(\text{OMe})_3$  and  $\text{OCMe}_2$  have been reported [39]. Magnetic susceptibility data and EPR spectra of  $\text{Cp}_3\text{Yb} \cdot \text{L}$ , L =



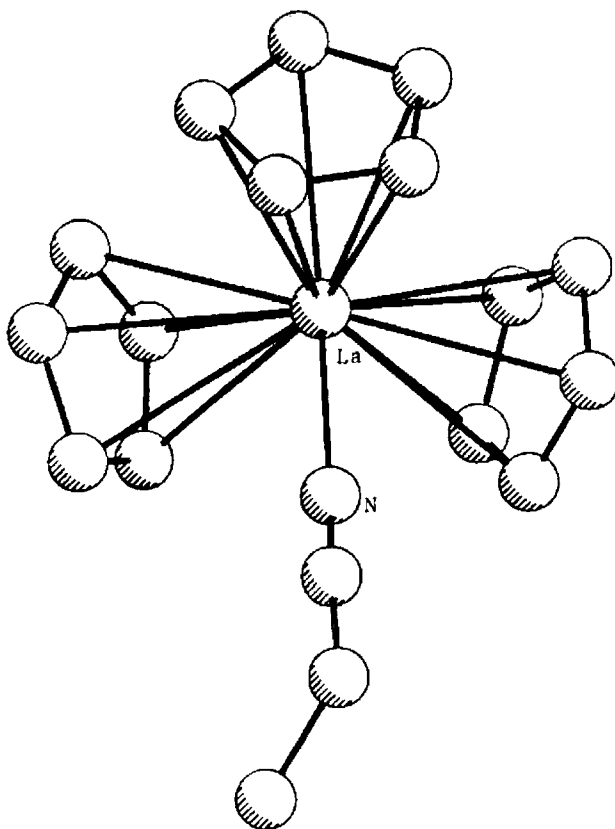
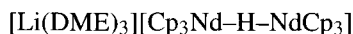
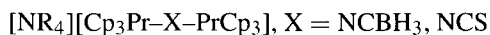
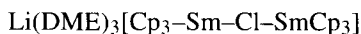
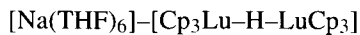


Fig. 6.2. Crystal structure of  $[\text{Cp}_3\text{LaNCCH}_2\text{CH}_3]$  [37].

THF,  $\gamma$ -picoline have been used to determine spin-orbit coupling constant and crystal field parameters [40].

The absorption spectrum of  $\text{Cp}_3\text{Nd}(\text{NCCH}_3)$  in a single crystal form at liquid nitrogen temperatures showed a truncated crystal field splitting pattern could be derived. The parameters of an empirical Hamiltonian were fitted [41] with the energies of 41 levels with a root mean square deviation of  $26\text{ cm}^{-1}$ .

Some complexes with bridging anions such as [41–45]



could be in the adducts class  $\text{Cp}_3\text{Ln} \cdot \text{L}$ . By reacting  $\text{Cp}_3\text{Sm} \cdot \text{THF}$  with lithium azide in dimethoxyethane (DME) the dimeric compound,  $[\text{Li}(\text{DME})_3][(\text{Cp}_3\text{Sm})_2(\mu-\text{N}_2)]$  with the

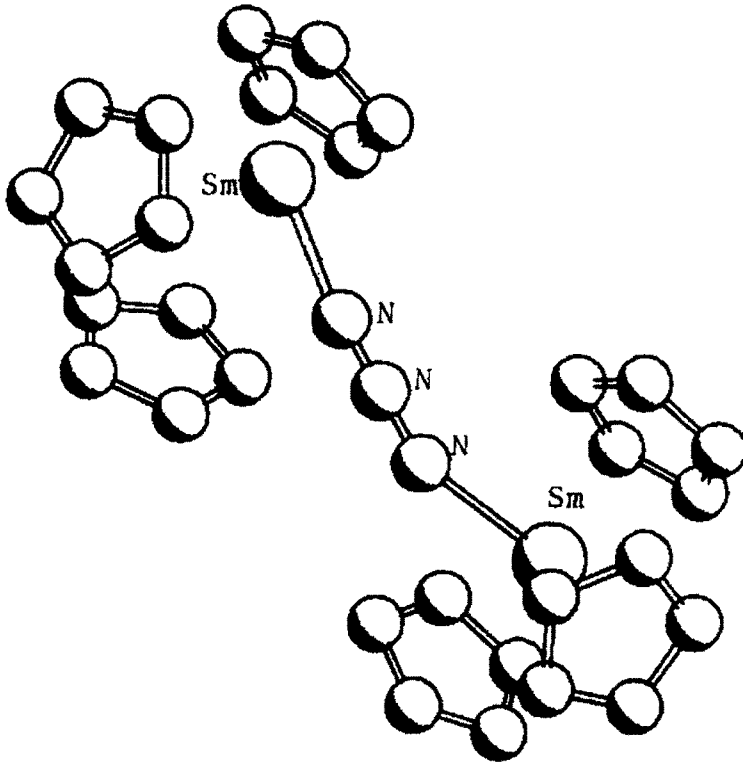
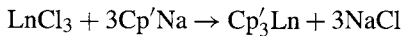


Fig. 6.3. Crystal structure of the anion  $\{[Cp_3Sm]_2(\mu-N_3)\}^-$  [42].

azido group bridging the two  $Cp_3Sm$  units can be obtained with the structure shown in Fig. 6.3.

### 5. Complexes with substituted cyclopentadienyls ( $Cp'_3Ln$ , $Cp'_3Ln \cdot L$ )

By introducing substituents into cyclopentadienyl ligands, steric hindrance takes place which might reduce the number of ligands bonded to the metal. The synthesis of  $Cp'_3Ln$  consists of the reaction



By reacting  $LaCl_3$  with excess  $Na(MeCp)$  in THF gives  $(MeCp)_3Ln$  which crystallizes as a tetramer. The structure differs from that of  $Cp_3Ln$ . The methyl substituent on the cyclopentadienyl ring forces the mode of coordination from an  $\eta^2 : \eta^5$  polymer for  $Cp_3Ln$  to a  $\eta^1 : \eta^5$  tetramer for  $(MeCp)_3Ln$ . The geometry of the tetrameric  $(MeCp)_3Ln$  is nearly identical with the compounds of Ce and Nd. The structure [46] of  $[(MeCp)_3Ce]_4$  is shown in Fig. 6.4.

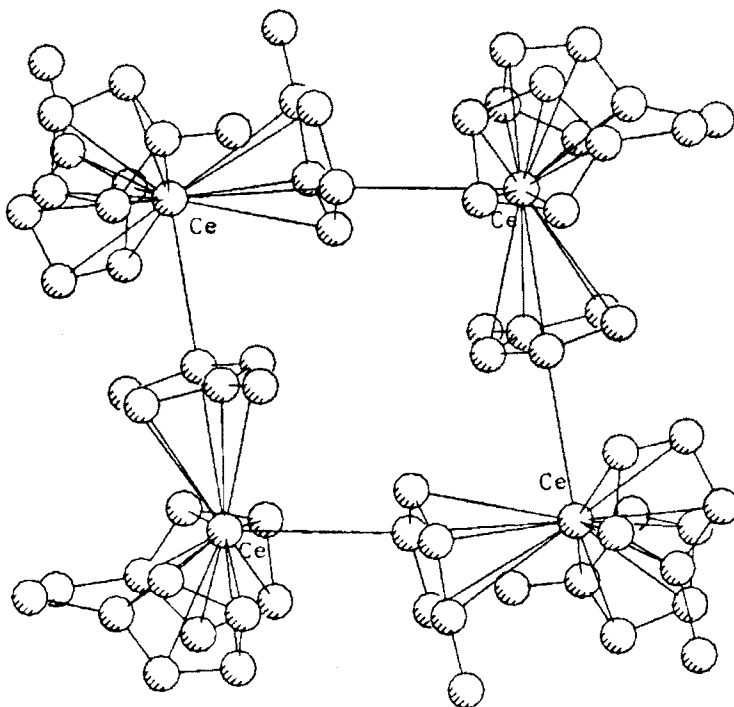


Fig. 6.4. Crystal structure of the tetramer  $[(\text{MeCp})_3\text{Ce}]_4$  [46].

The  $\eta^1\text{-C-Ln}$  distance is 3.018 Å for La, 3.03 Å for Ce and 2.984 Å for Nd. In contrast,  $(\text{MeCp})_3\text{Yb}$  is a monomer [47].

A mass spectral study of  $\text{Cp}'_3\text{Ln}$ , where  $\text{Cp}' = \text{MeC}_5\text{H}_4$ ,  $\text{Ln} = \text{La, Pr, Nd, Tm, Yb}$  shows the intramolecular migration of a methyl hydrogen atom to Ln or Ln-bonded  $\text{C}_5\text{H}_4$  resulting in possible ring enlargement [48] to  $\text{C}_6\text{H}_6$ .

All the substituted compounds  $(\text{RCp})_3\text{Ln}$  form adducts  $(\text{MeCp})_3\text{Ce}(\text{CNCMe}_3)$  and  $(\text{Me}_3\text{Si})_2\text{C}_5\text{H}_3]_3\text{Ce}(\text{CNCMe}_3)$  whose structures have been determined [46]. The trimethyl phosphine adduct,  $(\text{MeCp})_3\text{Ce} \cdot \text{PMe}_3$  has been obtained by the reaction of  $(\text{MeCp})_3\text{Ce} \cdot \text{THF}$  with  $\text{P}(\text{CH}_3)_3$  in ether [49]. The structure consists of Ce-centered mononuclear units in which the cerium atom is  $\eta^5$ -coordinated to three cyclopentadienyl rings and to the phosphorus of trimethyl phosphine. This compound is isomorphous with the U(III) analogue. The phosphite adduct shows nearly a tetrahedral geometry with three positions occupied by the ring centroids and the fourth position by the Lewis base.

Structural characterization of complexes of the type  $[(\text{Me}_3\text{Si})_2\text{C}_5\text{H}_3]_3\text{M}$  ( $\text{M} = \text{Sm, Ce, Th}$ ) shows that all the three complexes have a trigonal arrangement of the ligand centroids around the metal ion [50]. The Th and Sm complexes are isostructural. The Sm-C(Cp) distance varies from 2.698(5) to 2.807(5) Å with the longest distance involving a carbon atom between the two carbons containing the substituents,  $\text{Me}_3\text{Si}$ . Adducts are formed [46] with isocyanides giving rise to  $(\text{MeCp})_3\text{Ce}(\text{CNCMe}_3)$  and  $[(\text{Me}_3\text{Si})_2\text{C}_5\text{H}_3]_3\text{Ce}(\text{CNCMe}_3)$ .

The compound  $[(\text{Me}_3\text{C})_2\text{C}_5\text{H}_3]\text{Ce}$  has been obtained by the reaction of cerium triflate and  $[(\text{Me}_3\text{C})_2\text{C}_5\text{H}_3]_2$ . Lanthanum chloride reacts with  $\text{TiC}_5\text{H}_4\text{PPh}_2$  and  $\text{NaCp}$  to give  $\text{CpLa}(\text{C}_5\text{H}_4\text{PPh}_2)_2 \cdot \text{THF}$  and the structure of the compound indicates a distorted tetrahedral geometry around the La atom [51].

A more sterically hindered system is exemplified by the tris-pentamethyl-cyclopentadienyl samarium complex obtained in the reaction [52]



This complex is monomeric in the solid state.

Improved synthesis is achieved by the reaction [53]



and the resulting complex has trigonal planar symmetry around the Sm. Complexes of the type  $\text{LnCp}_3^0$  ( $\text{Cp}_3^0 = \text{H}_3\text{COCH}_2\text{CH}_2\text{C}_5\text{H}_4$ ), Ln = La, Pr, Nd, Sm, Gd have been synthesized. The La complex showed a trigonal bipyramidal geometry around La with formal coordination number of eleven [54,55].

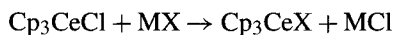
## 6. Complexes of the type $\text{Cp}_3\text{MX}$

The complex  $\text{Cp}_3\text{Ce}(\text{IV})\text{Cl}$  has been synthesized by reacting  $\text{NaCp}$  and bis(pyridinium) hexachlorocerate in THF. It may also be obtained [56] by the reaction of bis(pyridinium) hexachlorocerate and  $\text{Cp}_4\text{Ce}$ . These compounds,  $\text{Cp}_3\text{CeCl}$  may be used to prepare other compounds [57] like  $\text{Cp}_3\text{CeX}$ , where X = alkyl, aryl, pseudohalide, mercaptide, carboxylate.

The cerium compound  $\text{Cp}_3\text{Ce-R}$ , where R = hydrocarby group has been characterized after synthesis by the reaction [57] of  $\text{Cp}_3\text{CeCl}$  with  $\text{LiR}$  or Grignard reagent in THF.

The anionic complex  $[\text{Li}(\text{DME})_3]^+[\text{Cp}_3\text{Nd}(\text{C}_6\text{H}_5)]^-$  was prepared by reaction [58] of  $\text{NdCl}_3 \cdot 2\text{LiCl}$  with  $\text{NaCp}$  followed by treatment of the product  $\text{Cp}_2\text{NdCl} \cdot 2\text{LiCl}$  with  $\text{LiPh}$  at  $-78^\circ\text{C}$ . The structure consists of disconnected ion-pairs  $[\text{Li}(\text{DME})_3]^+$  and  $[\text{Cp}_3\text{Nd}(\text{C}_6\text{H}_5)]^-$ . The phenyl is  $\sigma$ -bonded to Nd and the arrangement on the whole is distorted tetrahedron [59] with  $\text{Nd-C}(\sigma)$  of 2.593 Å.

A number of compounds of the formula  $\text{Cp}_3\text{CeX}$ , where X = NCS, CN, NCO,  $\text{NO}_2$ ,  $\text{ONO}_2$ ,  $\text{SCH}_3$ ,  $\text{SC}_2\text{H}_5$ ,  $\text{SC}_3\text{H}_7$ ,  $\text{SCHMe}_2$ ,  $\text{Sn-}n\text{Bu}$ ,  $\text{Si-}i\text{Bu}$ ,  $\text{Si-}i\text{Pent}$ ,  $\text{O}_2\text{CH}$ ,  $\text{O}_2\text{CCH}_3$ ,  $\text{O}_2\text{CC}_2\text{H}_5$ ,  $\text{O}_2\text{CC}_3\text{H}_7$ ,  $\text{O}_2\text{CPh}$  have been prepared [57]



Electronic structure calculations at the non relativistic  $X\alpha$ -DVM level suggest non-negligible Ce-Cp for orbital covalency and give transition state ionization energies in good agreement with  $\text{He}^{\text{I}}/\text{He}^{\text{II}}$  photoelectron spectra.

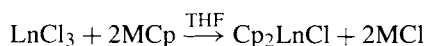
The reaction of  $\text{Ce}(\text{OCMe}_3)(\text{NO}_3)_3 \cdot \text{THF}$  with  $\text{NaCp}$  gives a mixture of  $\text{Cp}_2\text{Ce}(\text{OCMe}_3)_2$  and  $\text{Cp}_3\text{Ce}(\text{OCMe}_3)$ . The latter compound isolated by recrystallization from *n*-hexane has a distorted tetrahedral symmetry [60] around Ce(IV).

## 7. Complexes of the type $\text{Cp}'_3\text{MX}$ ( $\text{Cp}' = \text{substituted Cp}$ )

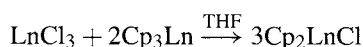
Lanthanide(IV) compounds with modified Cp are not known.

### 7.1. Complex types $\text{Cp}_2\text{LnX}$ , $\text{Cp}_2\text{LnXY}$

The reactions involved [57] in the preparation of  $\text{Cp}_2\text{LnCl}$  are

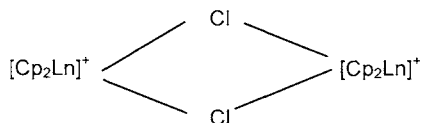


where Ln = Y, Sm, Gd, Tb, Dy, Ho, Er, Tm, Yb, Lu



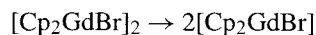
The compound  $\text{LnCp}_2\text{Cl}$  is dimeric in solid state, in solution, in gas phase and in non-coordinating solvents. In THF adducts of the type  $\text{Cp}_2\text{LnCl} \cdot \text{THF}$  are formed.

The structure of the dimer  $[\text{Cp}_2\text{Ln} \cdot \text{Cl}]_2$  consists of well-separated units connected by bridging chloride ions [61].



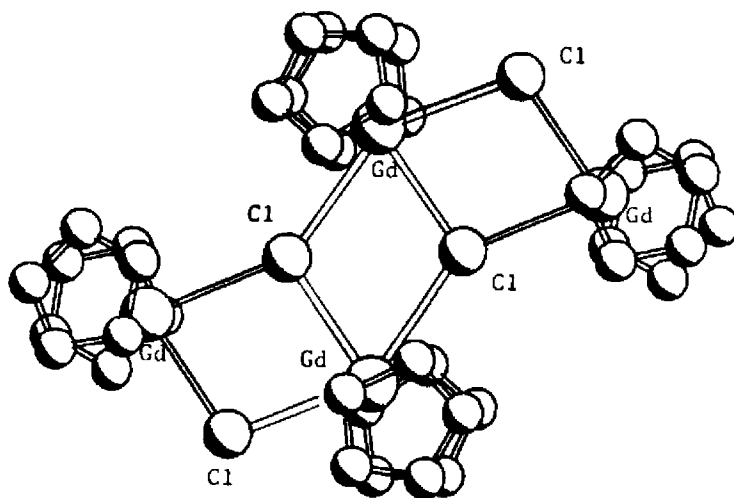
Similar dimeric structures are also encountered with bromides. In the case of Gd compound, tetramers have been reported containing two non-equivalent  $\text{Gd}^{3+}$  ions with formal coordination numbers of 8 and 9. These tetrameric units form the basic building blocks of compounds like  $[\text{Cp}_2\text{GdBr}]_\infty$  resulting in polymeric infinite double chains. The dysprosium compound  $[\text{Cp}_2\text{DyCl}]_\infty$  has also the polymeric structure. The structure [62] of tetrameric  $[\text{Cp}_2\text{GdCl}]_4$  is shown in Fig. 6.5.

A temperature dependent equilibrium between monomeric and dimeric bromo compounds has been confirmed by mass spectrometry



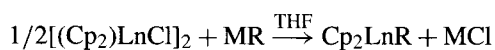
The dimeric  $[\text{Cp}_2\text{GdI}]_2$  compounds are poorly characterized [63] and the only fluoro compound [64] is the trimer  $[\text{Cp}_2\text{ScF}]_3$ .

The reaction of halide derivatives with Lewis bases causes cleavage of the dimer in some cases and in other cases the dimer forms an adduct with the Lewis base. The adduct  $\text{Cp}_2\text{LuCl}(\text{THF})$  as characterized by X-ray analysis shows a distorted tetrahedral disposition of the ligands around Lu, and conform to a 8-coordinate system. The isostructural dimer  $[\text{Cp}_2\text{Nd} \cdot \text{THF}]_2$  has asymmetrical chlorine bridges [65] in the solid state. Theoretical calculations involving the INDO method showed the compound  $\text{Cp}_2\text{NdCl}(\text{THF})$  to be covalent with a partial ionic character [66]. Also a cone angle model has been proposed for calculating the structural pattern of cyclopentadienyl compounds [67].

Fig. 6.5. Crystal structure of  $[\text{Cp}_2\text{GdCl}]_4$  [62].TABLE 6.3  
Compounds of the type  $\text{Cp}_2\text{Ln} \cdot \text{R}$ .

Compound		Reference
$\text{Cp}_2\text{Lu}(\text{CH}_2\text{SiMe}_3)\text{THF}$		[70]
$\text{Cp}_2\text{Lu}(\text{C}_6\text{H}_4\text{-4-Me})\text{THF}$		[70]
$\text{Cp}_2\text{Ln}(\text{p-tolyl})$	$\text{Ln} = \text{Gd, Yb, Er}$	[71]
$\text{Cp}_2\text{Ln}(\text{p-C}_6\text{H}_5\text{Cl})$	$\text{Ln} = \text{Gd, Yb, Er}$	[71]
$\text{Cp}_2\text{Yb} \cdot \text{R}$	$\text{R} = \text{C}_6\text{F}_5, \text{C}_6\text{Cl}_5, \text{C}\equiv\text{Cph}$	[72]
$\text{Cp}_2\text{SmCH}_2 \cdot \text{Ar}$	$\text{Ar} = \text{ph, O-}t\text{-BuC}_5\text{H}_4, 2,5\text{-Me}_2\text{C}_5\text{H}_3$	[73]
$\text{Cp}_2\text{Lu}(\text{CH}_2)_3\text{NMe}$	$\text{Lu-NMe}_2$ bond	[74]
$\text{Cp}_2\text{Er}(\mu\text{-CH}_3)_2\text{Li}(\text{tmed})$		[75]
$[\text{Cp}_2\text{ErC}\equiv\text{CCMe}_3]_2$		[76]
$\text{Cp}_2\text{LNC}\equiv\text{CPh}(\text{phen})$	$\text{Ln} = \text{La, Nd}$	[77]
$\text{Cp}_2\text{Ln}(t\text{-Bu})(\text{phen})$	$\text{Ln} = \text{La, Nd}$	[77]
$[\text{Cp}(\text{CH}_2)_3\text{Cp}]\text{NdC}\equiv\text{CPh}(\text{phen})$		[78]
$\text{Cp}_2\text{LuCH}_2\text{PMe}_2$		[78]
$\text{Cp}_2\text{LuR}'$	$\text{R}' = \text{methylene triorganophosphorane}$	[79]
$\text{Cp}_2\text{LuInd} \cdot \text{THF}$	$\text{Ln} = \text{Sm, Dy, Ho, Er, Yb}$	[80]
$\text{Na}(\text{diglyme})_2\text{Cp}_2\text{Lu}(\text{C}_{14}\text{H}_{10})$	$\text{C}_{14}\text{H}_{10} = \text{anthracene}$	[81]

Dicyclopentadienyl lanthanide alkyl and aryl complexes are prepared by the reaction [57]



where  $\text{M} = \text{Li}$  or  $\text{Na}$ ,  $\text{R} = \text{alkyl}$  or  $\text{aryl}$  group.

The compound  $\text{Cp}_2\text{YbMe}(\text{THF})$  may be used in the synthesis of complexes of the type  $[\text{Cp}_2\text{YbH}(\text{THF})]_2$  and  $[(\text{Cp}_2\text{YbMe})_3\text{H}(\text{THF})\text{Li}(\text{THF})]$  and  $\text{Yb}-\text{Me}$  distance is  $2.36(1) \text{ \AA}$ .

Compounds of the type  $\text{Cp}_2\text{LnR} \cdot \text{THF}$  have distorted tetrahedral geometry of the ligands around the metal. By coordination to a solvent molecule, the monomeric species is obtained. A heterometallic entity like aluminum alkyl or a bidentate ligand may stabilize the species. Stabilization may also occur through dimerization [69] as in  $[\text{Cp}_2\text{Y}(\mu\text{-Me})]_2$ . Other compounds that have been prepared and characterized are given in Table 6.3.

### 8. Compounds of the type $\text{Cp}_2\text{Ln} \cdot \text{X}$ ( $\text{X} = \text{Ln}-\text{O}, \text{Ln}-\text{S}, \text{Ln}-\text{P}$ )

Compounds of the type  $\text{Cp}_2\text{LnX}$  where X is an oxygen donor consist of: (i) carboxylic groups, (ii) alcohols, (iii) oximes, (iv) 1,3-diketones.

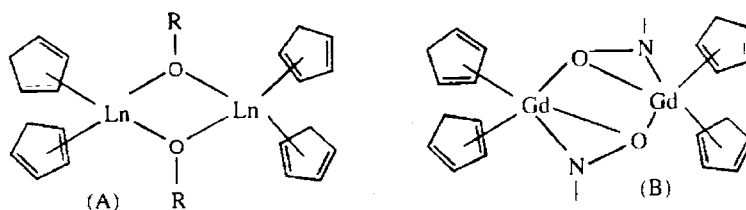
The reaction of  $\text{Cp}_2\text{LnCl}$  with sodium carboxylates yields the corresponding dicyclopentadienyl lanthanide carboxylates, which on the basis of molecular weight determinations are dimers with  $\mu$ -carboxylate bridges [57]. Some of the carboxylic acid complexes are summarized.

Compound		Reference
$\text{Cp}_2\text{Yb}(\text{O}_2\text{CR})$	$\text{R} = \text{Me}, \text{CF}_3, \text{Ph}, \text{C}_6\text{F}_5, \text{C}_6\text{Br}_5,$ $\text{MeO}_2\text{CC}_6\text{H}_4, \text{N}-\text{C}_5\text{H}_4$	[82]
$\text{CpYb}[\text{CO}(\text{O})\text{CH}=\text{CHC}(\text{O})\text{O}]$		[83]
$\text{Cp}_2\text{YbO}_2\text{CR}$	$\text{R} = \text{CMe}_3, \text{CCl}_3, \text{Et}, \text{CH}_2\text{Cl}$	[84]
$[\text{Cp}_2\text{YbO}_2\text{C}]_2\text{R}$	$\text{R} = \text{CH}_2, \text{CH}_2-\text{CH}_2, o\text{-C}_6\text{H}_4, p\text{-C}_6\text{H}_4$	[85]
$\text{Cp}_2\text{LnOAc}$	$\text{Ln} = \text{Sm}, \text{Gd}, \text{Tb}, \text{Dy}, \text{Ho}, \text{Tm}, \text{Lu}$	[86]
$\text{Cp}_2\text{LnOC}(\text{O})\text{CF}_3(\text{phen})_n$	$\text{Ln} = \text{Pr}, \text{Nd}, n = 1 \text{ or } 2$	[87]
	$\text{Ln} = \text{La}, \text{Ce}, n = 2$	
$[\text{Cp}_2\text{Ln}(\text{triflate})]_2$	$\text{Ln} = \text{Sc}, \text{Lu}$	[88]

The crystal structure [89] of  $[\text{Cp}_2\text{YbOSO}_2\text{CF}_3]_2$  is shown in Fig. 6.6.

### 9. Alkoxides, acetoxime and diketonate derivatives

The reaction of  $\text{Cp}_3\text{Ln}$  ( $\text{Ln} = \text{Dy}, \text{Yb}$ ) with alcohols,  $\text{ROH}$  in THF produces dimers  $[\text{Cp}_2\text{Ln}(\mu\text{-OR})]_2$  with symmetrical alkoxide bridges [90] (A) while with acetoxime dimeric complexes of the type  $[\text{Cp}_2\text{Ln}(\mu\text{-}\eta^2\text{-ONCMe})]_2$  ( $\text{Ln} = \text{Pr}, \text{Gd}, \text{Dy}, \text{Yb}$ ) are obtained. In the latter complex we have  $\text{Gd}-\text{O}-\text{N}-\text{Gd}$  (B) bonding (oximato bridge) [91].



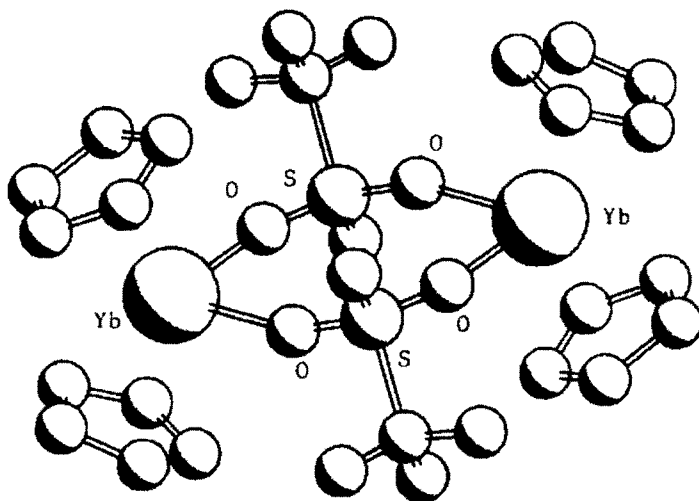


Fig. 6.6. Crystal structure of  $[\text{Cp}_2\text{YbOSO}_2\text{CF}_3]_2$  [89].

Monomeric complexes of the type  $\text{Cp}_2\text{Ln}(\text{THF})(\text{OR})(\text{F})$  are known [92] when  $\text{Ln} = \text{Nd}, \text{Sm}, \text{Yb}$ .

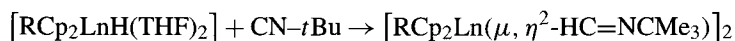
Complexes of the type  $\text{Cp}_2\text{Yb} \cdot \text{L}$  and  $\text{CpYb} \cdot \text{L}_2$ , where  $\text{L} = 1,3$ -diketone have been characterized and these complexes have chelated diketone [93].

Complexes of the type  $\text{Cp}_2\text{LuPPh}_2 \cdot \text{THF}$  on removal of THF give dimers of the type  $\{\text{Cp}_2\text{Lu}[\mu\text{-O}(\text{CH}_2)_4\text{PPh}_2]\}_2$ . The complex  $\text{Cp}_2\text{LuAsPh}_2(\text{THF})$  on hydrolysis yields an oxo-bridged dimer  $[\text{Cp}_2\text{Lu}(\text{THF})_2]_2(\mu\text{-O})$  with a linear  $\text{Lu-O-Lu}$  group [94].

Sulfur and selenium complexes are analogous to oxygen bearing complexes and the formula of  $\text{Cp}_2\text{Lu}(\mu\text{-SePh})_2\text{Li}(\text{THF})_2$ . This complex is obtained from  $\text{Cp}_2\text{Lu}(\mu\text{-Me})_2\text{Li}(\text{THF})_2$  and benzeneselenol [95]. The sulfur analogue of the same structure is obtained by using 2-methoxypropane-2-thiol in place of benzeneselenol. Dimeric thiolates  $[\text{Cp}_2\text{Yb}(\mu\text{-SR})_2]$ , where  $\text{R} = \text{propyl}, \text{butyl}$ ,  $\text{Ln} = \text{Dy}, \text{Yb}$  have been synthesized by reacting  $\text{Cp}_3\text{Ln}$  with  $\text{RSH}$  in THF. The X-ray structure of  $[\text{Cp}_2\text{Yb}(\mu\text{-S}(\text{butyl}))]$  shows the *n*-butyl group in anticonformation relative to the  $\text{Yb}_2\text{S}_2$  ring [96]. Monomeric  $\text{Cp}_2\text{Yb}(\text{THF})\text{SR}(\text{F})$  complex was prepared [92] by using a hindering thiolate anion  $[\text{R}(\text{F})\text{S}]^-$ , where  $\text{R}(\text{F}) = 2,4,6$ -tris(trifluoromethyl)phenyl group.

## 10. Compounds containing Ln-N bonds in $\text{Cp}_2\text{LnX}$

The first compound isolated in this class is  $\text{Cp}_2\text{ErNH}_2$  which has  $\text{Er-N}$  bond [97]. Tertiary butylisocyanide may be inserted into  $\text{RCp}_2\text{LnH}(\text{THF})_2$ , where  $\text{R} = \text{H}, \text{Me}$ .



$\text{Ln} = \text{Y}, \text{Er}$ . When  $\text{R} = \text{H}$  the structures of both  $\text{Er}$  and  $\text{Y}$  complexes are isostructural. The structure of the  $\text{Y}$  compound is shown in Fig. 6.7.



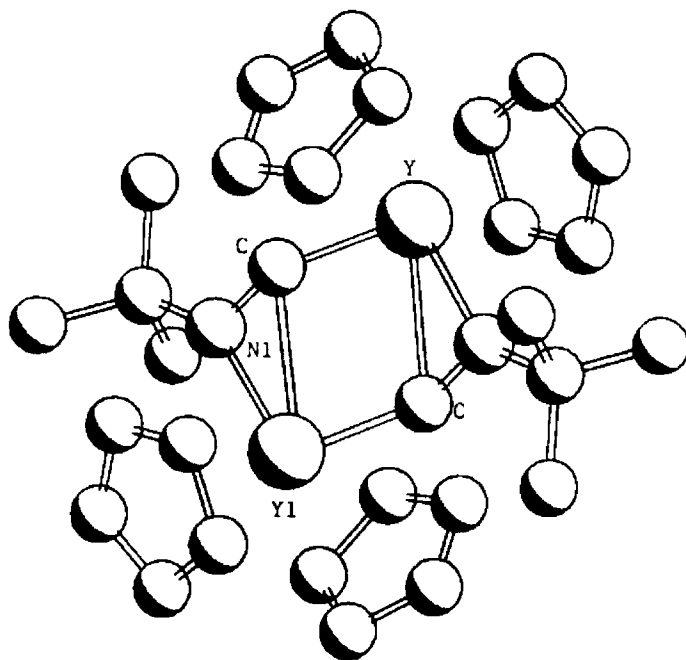


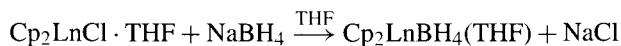
Fig. 6.7. Crystal structure of  $[\text{Cp}_2\text{Y}(\mu\text{-}\eta^2\text{-(HC=N'Bu)}_2)]_2$  [98].

Other derivatives containing the Ln–N bond are  $\text{Cp}_2\text{Y}(\mu\text{-N=CH-}t\text{Bu})_2$  containing two  $\text{Cp}_2\text{Y}$  units connected by two asymmetric Y–N bridges. Pyridine adducts  $\text{Cp}_2\text{Y} \cdot \text{Py}$  and  $\text{Cp}_2\text{Y}(\text{Py})_2$  have been characterized [99].

### 11. Compounds $\text{Cp}_2\text{LnX}$ containing Ln–P bond

Reaction of  $\text{Cp}_2\text{LnCl}$  with  $\text{LiPRR}'$  yielded [57]  $\text{Cp}_2\text{Ln} \cdot \text{PR}_3$ . When lithium cyclohexyl phosphide is used  $[\text{Cp}_2\text{YbPhC}_6\text{H}_{11}]$  is formed and  $[\text{Cp}_2\text{YbPPh}]$  is obtained with lithium phenylphosphide. These products are not stable in solution and decompose to yield polymeric compounds  $[\text{CpYbPC}_6\text{H}_{11}]_n$  and  $[\text{CpYbPPh}]_n$ . The compound  $[\text{Cp}_2\text{Lu}(\text{PPh})_2\text{Li}(\text{tmed}) \cdot 1/2\text{toluene}]$  has been characterized by X-ray analysis [100] with Lu–P distances of 2.782(1) Å and 2.813(2) Å. The arsenic compound analogous to the phosphorus compound has the same structure [101].

Borhydride complexes of lanthanides are prepared by the reaction



where Ln = Sm, Er, Yb, Lu. Evidence from IR spectra suggests the presence of tridentate borohydride bridges in the Sm complex and bidentate bridges in the smaller Er and Yb derivatives [70].

## 12. Compounds of the type $\text{Cp}'_2\text{MX}$ ( $\text{Cp}' = \text{substituted Cp}$ )

Use of the substituted cyclopentadienyl ligand can result in changes in structural, physical and chemical properties of the complexes. Substituted cyclopentadienyl ligand  $\text{Cp}' = \text{RC}_5\text{H}_4$ , where  $\text{R} = \text{Me}$ ,  $t\text{-Bu}$ ,  $\text{Me}_3\text{Si}$ ,  $\text{MeOCH}_2\text{CH}_2$ ,  $\text{Me}_2\text{PhSi}$  and  $\text{Cp}' = \text{R}_2\text{C}_2\text{H}_3$  ( $\text{R} = t\text{-Bu}$ ,  $\text{Me}_2\text{Si}$ ) has been used in the preparation of lanthanide complex. The resulting complexes have coordination geometry similar to those of unsubstituted parent cyclopentadienyl complexes.

Reaction of two equivalents of  $\text{Na}t\text{BuCp}$  with anhydrous  $\text{LnCl}_3$  yielded [102] dimeric  $[(t\text{BuCp})_2\text{LnCl}]_2$ , where  $\text{Ln} = \text{Sm}$ ,  $\text{Lu}$ . It is not possible to synthesize  $(t\text{BuCp})_3\text{Lu}$  but it is possible to obtain  $(t\text{BuCp})_3\text{LaTHF}$ ,  $(t\text{BuCp})_3\text{Sm}$  and  $[(t\text{BuCp})_2\text{SmCl}]_2$ .

Introduction of two  $t$ -butyl groups gives  $\text{Cp}' = 1,3\text{-}t\text{Bu}_2\text{C}_5\text{H}_3$  and with this ligand,  $[(\text{Cp}')_2\text{Nd}(\mu\text{-Cl})]_2$  dimer complex with  $\text{Nd-Cl}$  2.837 (1) and 2.841 (1) Å;  $\text{Nd-C}(\text{Cp}_{\text{av}})$  2.760(1) Å;  $\text{Nd-C}_g$  2.846 (1) Å ( $\text{C}_g = \text{C}_p$  ring centroid);  $\text{Nd-Cl-Nd}'$   $106^\circ(1)$  and  $\text{Cl-Nd-Cl}'$   $74.0(1)^\circ$  were obtained [103]. When the substituent in  $\text{Cp}$  is  $\text{Si-Me}_3$ , complexes of the type  $[\text{Cp}'_2\text{Ln}(\mu\text{-X})]_2$  and  $[\text{Cp}'_2\text{Ln}(\mu\text{-X})]_2\text{LiL}_2$ , where  $\text{Cp}' = \text{Me}_3\text{Si-C}_5\text{H}_4$ ;  $\text{Ln} = \text{Yb}$ ,  $\text{Yb}$ ,  $\text{Lu}$ ;  $\text{X} = \text{Cl}$ ,  $\text{I}$ ;  $\text{L} = \text{THF}$ ,  $\text{tmed}$ ,  $\text{Et}_2\text{O}$  have been obtained [57].

With disubstituted  $\text{Cp-R}_2$  ( $\text{R} = \text{Me}_3\text{Si}$ ) complexes of the type [104]  $[(\text{Me}_3\text{Si})_2\text{C}_5\text{H}_3]_2\text{-Ln}(\mu\text{-Cl})_2\text{Li}(\text{THF})_2$  have been obtained. X-ray crystal structures of  $[\text{Cp}''_2\text{Ln}(\mu\text{-Cl})]_2$ ,  $\text{Ln} = \text{Pr}$ ,  $\text{Yb}$  show distorted tetrahedral coordination around the metal ion. These complexes form adducts of the type  $[\text{Cp}''_2\text{LnCl}_2] \cdot \text{A}$ , where  $\text{A} = \text{N}(\text{PPh}_3)_2$ ,  $\text{PPh}_4$ ,  $\text{AsPh}_4$ ,  $\text{PPh}_3(\text{CH}_2\text{Ph})$ . With iodides,  $\text{Cp}'' = (\text{Me}_3\text{Si})_2$ , the complex  $[\text{K}(\text{THF})_x][\text{Cp}''_2\text{LnI}_2]$  is obtained which reacts with  $\text{CH}_3\text{CN}$  to yield  $\text{Cp}''_2\text{Ln}(\text{I})(\text{NCMe})_2$ , where  $\text{Ln} = \text{La}$ ,  $\text{Ce}$ .

When the substituent  $\text{R} = \text{MeOCH}_2\text{CH}_2$  the complex  $[(\text{MeOCH}_2\text{CH}_2\text{Cp})_2\text{Ln}(\mu\text{-Cl})]_2$  ( $\text{Ln} = \text{La}$ ,  $\text{Pr}$ ,  $\text{Nd}$ ) is obtained and the structure of the  $\text{La}$  complex is shown in Fig. 6.8.

The structure of the  $\text{La}$  complex showed [105] a chelating  $\text{MeOCH}_2\text{CH}_2\text{Cp}$  ligand  $\eta^5$  coordinated through the ring carbon atoms and forming an intramolecular Lewis acid-base adduct with the ether substituent and a pseudo octahedral coordination geometry. The monomeric complexes [106]  $(\text{MeO} \cdot \text{CH}_2 \cdot \text{CH}_2\text{Cp})_2\text{LnX}$  have pseudo trigonal bipyramidal geometry as revealed by X-ray studies. The formal coordination in these complexes is nine. The complex  $(\text{Me}_2\text{NCH}_2\text{CH}_2\text{Cp})_2\text{NdCl}$  is nine-coordinate with two  $\text{Nd-N}$  bonds.

## 13. Compounds of the type $\text{Cp}'_2\text{LnX}$ ( $\text{Cp}' = \text{substituted Cp}$ ; $\text{X} = \text{hydrocarbyl}$ )

Substituted cyclopentadienyl complexes have potential application in homogeneous ethylene polymerization. Some typical compounds which may be used are [108]  $\text{Cp}'_2\text{Ln}(\mu\text{-R})_2\text{AlR}_2$ ,  $\text{Cp}'_2\text{Ln}(\mu\text{-R})_2\text{LnCp}'_2$  ( $\text{R} = \text{CH}_3$ ,  $\text{C}_4\text{H}_9$ ,  $\text{C}_8\text{H}_{17}$ ,  $\text{C}_5\text{H}_3\text{CH}_3$ ;  $\text{Ln} = \text{Y}$ ,  $\text{Ho}$ ,  $\text{Er}$ ,  $\text{Yb}$ ;  $\text{Cp}' = \text{Cp} \cdot \text{CH}_3$ ,  $\text{Cp}(\text{CH}_3)_3\text{Si}$ ,  $\text{Cp}(\text{CH}_3)_4$ ).

Dimeric structures [109] with symmetric methyl bridges in  $[(\text{Me}_2\text{Cp})_2\text{YMe}]_2$  and asymmetrical methyl bridges in  $[(t\text{BuCp})_2\text{NdMe}]_2$  are found with  $\text{Y-C}(\sigma) = 2.161$  Å;  $\text{Nd-C}(\sigma) = 2.70(2)$ ,  $2.53(2)$  Å and  $\text{Nd-C}(\sigma)\text{-Nd}$  angles of  $94.7^\circ$  and  $87.3^\circ$ .

Complexes containing alkynyl bridges are known. Some examples are  $\text{Yb}$  and  $\text{Sm}$  in  $[(\text{MeCp})_2\text{Yb-C}\equiv\text{C-CMe}_3]_2$  and the  $\text{Sm}$  analogue. The structure of the  $\text{Sm}$  compound shows it to be centrosymmetric dimer with two  $(\text{MeCp})_2\text{Sm}$  units connected by

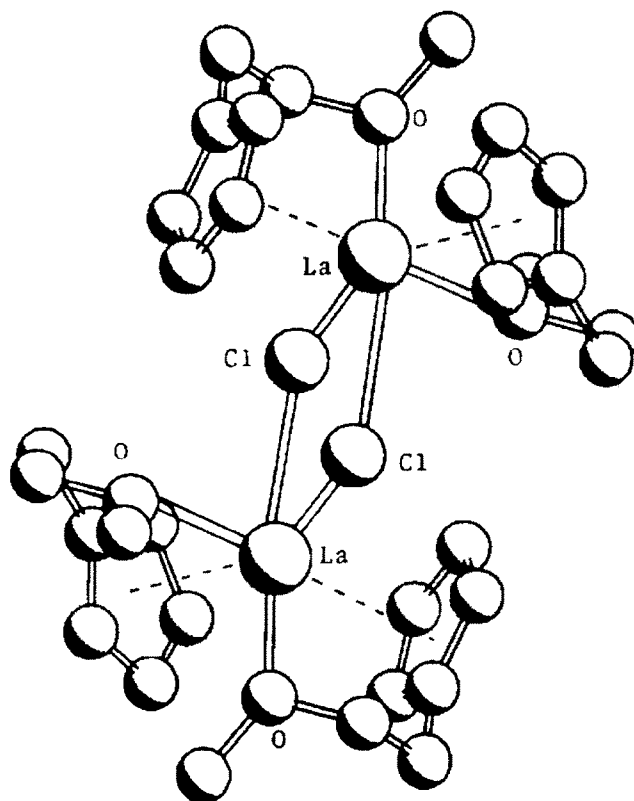


Fig. 6.8. Crystal structure of  $[(\text{MeOCH}_2\text{CH}_2\text{C}_5\text{H}_4)_2\text{LaCl}]_2$  [105].

alkynyl bridges. Monomeric compounds [72] of the type  $(\text{MeCp})_2\text{LnR}$ ,  $\text{Ln} = \text{Lu}$ ,  $\text{R} = \text{CH}_2\text{CHMeCH}_2\text{NMe}_2$ ,  $[\text{Li}(\text{THF})_4][(\text{C}_{14}\text{H}_{10})\text{CMe}_2\text{Cp}]_2\text{Nd}$  with the latter having pseudo tetrahedral coordination geometry [110] are well-characterized.

The complex containing 1,3-dithiane  $[(t\text{BuCp})_2\text{Ln}(\text{C}_4\text{H}_7\text{S}_2)]\text{LiCl} \cdot 2\text{THF}$ , where  $\text{Ln} = \text{Lu}$ , Y has been identified in which  $\sigma$  bonded and  $\eta^2$  coordinated 1,3-dithiane exists. The two structures are nearly the same type [111] with pseudotetrahedral coordination. An unusual 'pentagonal coordination ring' is observed between  $\text{Ln}$ -1,3-dithiane and a molecule of  $\text{LiCl}$ .

#### 14. Complexes of the type $\text{Cp}'_2\text{LnX}$ ( $\text{X} = \text{O}, \text{S}, \text{Se}, \text{Te}, \text{N}$ donor ligands)

Very few oxygen bonded complexes are known and the complexes are dimers [112] with the oxygen donor ligand forming the bridge. Complexes containing enolate bridges  $[(\text{MeCp})_2\text{Y}(\mu\text{-OCH}=\text{CH}_2)]_2$  and methoxide bridges,  $[(\text{Me}_3\text{SiCp})_2\text{Y}(\mu\text{-OMe})]_2$  are known. The structure of  $\{(\text{MeCp})_2\text{Yb}[(\mu\text{-O}(\text{C}_4\text{H}_7\text{O}))]\}_2$  is shown in Fig. 6.9. with two  $\text{Yb-O-Yb}$  bridges, which are bent.

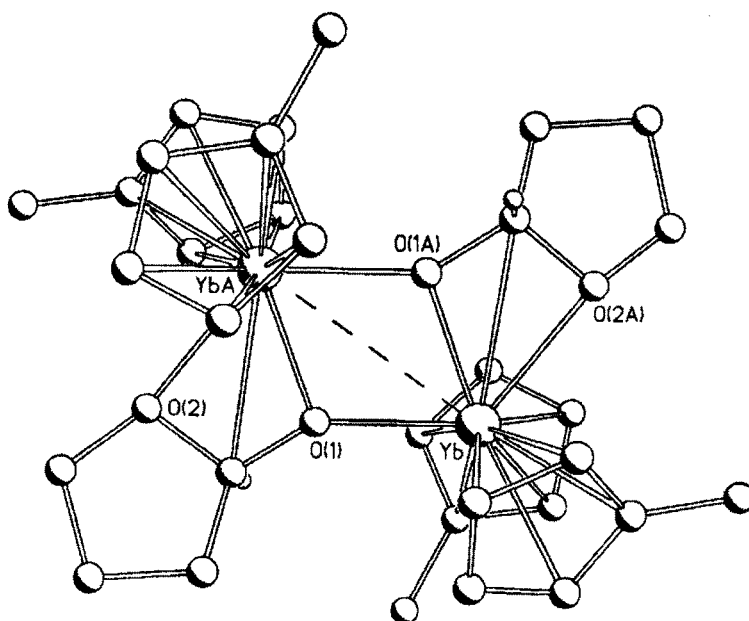


Fig. 6.9. Crystal structure of  $\{(\text{MeC}_5\text{H}_4)_2\text{Yb}[\mu\text{-O}(\text{C}_4\text{H}_7\text{O})]\}$  [113].

Other known oxygen, sulfur, selenium and tellurium derivatives are given below:

Alkoxide	$[(t\text{BuCp})_2\text{Ce}(\mu\text{-OR})_2]$	OR bridge	[114]
Hydroxide	$\{[(\text{Me}_3\text{Si})_2\text{Cp}]_2\text{Ln}(\mu\text{-OH})_2\}$	OH bridge	[115]
Sulfur	$[(\text{RCp})_2\text{Ce}(\mu\text{-SR}')_2]$	SR' bridge	[114]
Selenium	$[(t\text{BuCp})_2\text{Ln}(\mu\text{-SeR}')_2]$	SeR' bridge	[114]
Tellurium	$[(t\text{BuCp})_2\text{Y}(\mu\text{-TeMe})_2]$	TeMe bridge	[114]

Complexes containing nitrogen donor ligands such as  $[(\text{MeCp})_2\text{YbNH}_2]_2$  have been characterized and the complex is found to be a centro symmetric dimer in which the plane of  $\text{Yb}_2\text{N}_2$  part is nearly orthogonal to the plane of the two ring centroids and Yb atoms [116].

## 15. Cyclopentadienide complexes of lanthanides(II)

Complexes of the type  $\text{Cp}_2\text{Ln}$ ,  $\text{Ln} = \text{Yb}, \text{Eu}$  are obtained by dissolving the metal Yb or Eu in liquid ammonia in the presence of cyclopentadiene [117]. Another method consists of reduction of  $\text{Cp}_2\text{YbCl}$  with Na or Yb metal in THF. These compounds are air sensitive and ionic in character as evidenced by IR and Mössbauer spectral data [57].

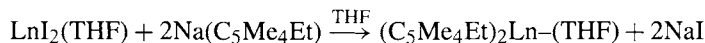
The equilibrium geometries of  $\text{Cp}_2\text{M}$  ( $\text{M} = \text{Yb}, \text{Eu}, \text{Sm}$ ) were studied by ab initio pseudopotential calculations at the Hartree–Fock (HF),  $\text{MP}_2$  and CSID levels. In the Hartree–Fock calculations [118] all the metallocenes favoured regular sandwich-type equilibrium structures with increasingly shallow potential energy surfaces for the bending motions along the series,  $\text{M} = \text{Ca}, \text{Yb}, \text{Sr}, \text{Eu}, \text{Sm}, \text{and Ba}$ .

Ab initio calculations on hypothetical organometallic cations  $\text{Cp}_2\text{Ln}^+$  ( $\text{Ln} = \text{Sc}, \text{La}$ ) show bent metallocene structures are favoured due to the covalent  $\sigma$  bonding contributions involving the totally symmetric metal  $d_\sigma$  orbitals which favor bent structures. Although the contribution of  $d_\sigma$  is lower than  $d_\pi$ , its involvement is sufficient to give bent structures [119].

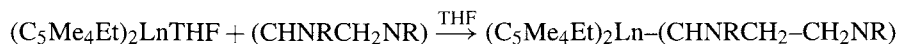
Phosphine oxide complex  $\text{Cp}_2\text{Yb}(\text{OPPh}_3)$  has been characterized [120] and the X-ray structure shows a pseudotetrahedral disposition of the Cp and  $\text{OPPh}_3$  ligands around  $\text{Yb}^{2+}$  ion with unusually short Yb–O distances at 2.30(2) and 2.33(2) Å. The complex  $(t\text{BuCp})_2\text{Yb}(\text{II})(\text{THF})_2$  has been prepared by reducing  $(t\text{BuCp})_2\text{YbCl}(\text{THF})$  with sodium and the complex has  $\text{C}_2$  symmetry with average bond distances Yb–C(Cp) 2.722(16); Yb–O 2.431(8) Å and angles  $\text{C}_g\text{–Yb–C}_g$  134°;  $\text{O}(1)\text{–Yb–O}(2)$  83.3°. The  $t\text{-BuCp}$  ligands are staggered [121]. Reaction of  $\text{SmI}_2$  with  $(t\text{-Bu}_2\text{Cp})\text{Na}$  in THF gives  $(t\text{Bu}_2\text{Cp})_2\text{Sm}(\text{THF})$  which is monomeric with pseudotrigonal coordination [122] and Sm–O distance of 2.57 Å and  $\text{C}_g\text{–Sm–C}_g$  angle of 132.5°.

Substituted cyclopentadienyl complex  $\text{Cp}''_2\text{SmTHF}$  ( $\text{Cp}'' = (\text{Me}_3\text{Si})_2\text{-1,3-C}_5\text{H}_3$ ) has been synthesized and is used as a catalyst in the polymerization of ethylene [50]. The polymeric lanthanocene(II) compounds are prepared by desolvation [123] of the monomeric diethyl ether adduct of Yb and THF adduct of Eu. The crystal structures of the complexes show a bent metallocene conformation with  $\text{C}_g\text{–Yb–C}_g$  angle of 138.0° and the distance between the metal center of one  $\text{Cp}''_2\text{Yb}$  unit and a methyl group of neighboring unit is Yb–C 3.091 Å. In the europium analogue Eu–C is 3.091 Å, Eu–H of 2.70 Å and  $\text{C}_g\text{–Eu–C}_g$  of 122°. In the Eu complex a conformation with a cyclopentadienyl ring bridging  $\eta^5 : \eta^3$  bridging two non equivalent Eu atoms is present.

The complexes  $(\text{C}_5\text{Me}_4\text{Et})_2\text{Ln}(\text{THF})$  are prepared by the reaction



where  $\text{Ln} = \text{Sm}, \text{Yb}$ . These complexes have trigonal structure with bent metallocene units. The carbene derivatives of  $\text{Ln} = \text{Sm}, \text{Yb}$  are obtained by the reaction [124]



where  $\text{R} = \text{Me}$  and  $\text{Ln} = \text{Sm}, \text{Yb}$ .

## 16. Monocyclopentadienyl complexes

In this class of complexes there is greater reactivity since the metal is coordinatively unsaturated. Thus substitution possibilities are numerous.

Lanthanides which are heavy form  $\text{Ln}(\text{Cp})\text{Cl}_2(\text{THF})_3$  complexes [57]. Other complexes of the type  $\text{CpLnCl}_2(\text{THF})_n$  of lighter lanthanides ( $\text{Ln} = \text{La}, \text{Tm}, n = 3$ ;  $\text{Ln} = \text{Eu}, n = 2$ ;  $\text{Ln} = \text{La}, \text{Sm}, \text{Eu}, \text{Tm}, \text{Yb}, n = 4$ ) have been synthesized and characterized [125].

The evidence for the monomeric nature of  $[\text{CpLnX}_2\text{S}_3]$  is obtained from the crystal structure [126,127] of isostructural complexes Er and Yb. The Yb complex has a distorted octahedral geometry of the type mer-trans (i.e.) trans chlorines and mer THF ligands. The

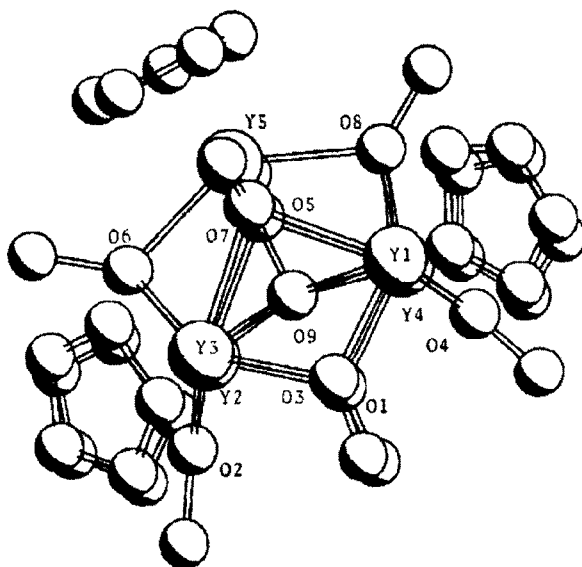


Fig. 6.10. Crystal structure of  $[(\text{CpY})_5(\mu\text{-OMe})_4(\mu^3\text{-OMe})_4(\mu^5\text{-O})]$  [130].

net result is major distortions in the form of bending of four equatorial ligands, two THF and two halides in the opposite direction to the bulk Cp ligand. This results in lengthening of the axial Ln–THF bond with respect to the equatorial Ln–THF bonds, associated with the steric effect of the Cp ligand trans to it.

The complexes  $[\text{Li}(\text{THF})_2]_2(\mu\text{-Cl})_4[\text{Cp} \cdot \text{Ln} \cdot \text{THF}]$ , where Ln = La, Nd have been characterized [128] and they are isomorphous. The Nd complex has a distorted octahedral geometry with Cp and THF occupying trans positions on one side and two bridging  $(\text{THF})_2\text{Li}(\mu\text{-Cl})_2$  on the other side.

The binuclear  $\text{CpSmCl}(\text{THF})_2(\mu\text{-Cl})_2\text{SmCl}_2(\text{THF})_3$  complex also has octahedral geometry [129] in which the CpSm unit is bonded through two chlorine atoms to the second Sm unit with pentagonal bipyramidal geometry.

The reaction of  $\text{Cp}_2\text{YCl}(\text{THF})$  with KOMe in THF yields both  $\text{Cp}_2\text{Y}(\text{OMe})$  and  $(\text{CpY})_5(\mu\text{-OMe})_4(\mu^3\text{-OMe})_4(\mu^5\text{-O})$  and the structure of the latter is shown in Fig. 6.10. The structure consists of a square pyramid of Y atoms each coordinated to one Cp ligand.

Each triangular face has a triply bridging methoxide ligand and a doubly bridging methoxide group is attached to each base. On the other hand, complexes of the type  $\text{Cp}_n\text{Ln}(\text{Sal})_{3-n}$  and  $\text{Cp}_n\text{Ln}(\text{fur})_{3-n}$ , where Ln = Nd, Yb,  $n = 1, 2$ ; Sal, salicyl aldehyde; fur = furfuryl alcohol have been synthesized and found to be susceptible to disproportionation [131].

Non-solvated complexes  $\text{CpLn}(\text{Cl})[\text{OCOC}_6\text{H}_4(\text{O-X})]$ , where Ln = Sm, Yb; X = H, F, Br, I,  $\text{OCH}_3$  have bridged dimeric structure as evidenced by IR, mass spectra and XPS data.

Since the triflate group can be replaced with ease, complexes containing triflate,  $\text{CpLu}(\text{OSO}_2\text{CF}_3)_2(\text{THF})_3$  and  $\text{Cp}_2\text{Lu}(\text{OSO}_2\text{CF}_3)\text{THF}$  are good starting materials for the synthesis of other complexes. The structure shows a pseudo octahedral disposition of the mer, trans type in the adduct with three THF molecules [88].

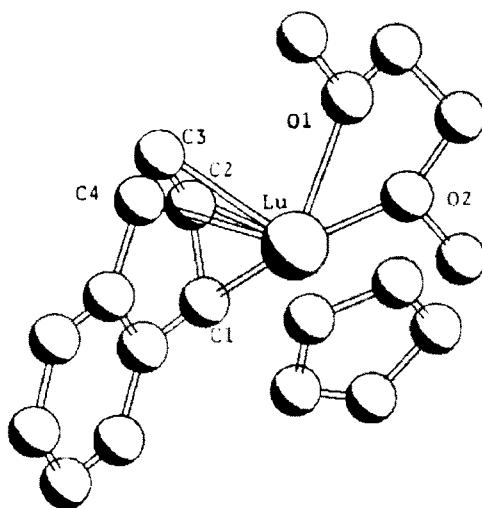


Fig. 6.11. Crystal structure of  $[\text{CpLu}(\eta^4\text{C}_{10}\text{H}_8)\text{-(MeO(CH}_2)_2\text{OMe)}]$  [132].

Treatment of  $\text{Cp}_2\text{Yb(THF)}$  with azobenzene in THF and toluene yields  $[\text{Cp(THF)Yb}]_2\text{-[N}_2\text{Ph}_2]_2$  which is a dimer with an overall geometry similar to  $[\text{Cp}^*(\text{THF)Sm}]_2\text{[N}_2\text{Ph}_2]_2$ .

Mixed complexes with cyclooctatetraenide (COT) and phenylacetylide in the case of heavier lanthanides,  $\text{CpLn(COT)(THF)}$ , Ln = heavy lanthanides and  $\text{CpHo (C}\equiv\text{CPh)}_2$  have been characterized [57].

Metathesis of  $\text{CpLuCl}_2(\text{THF})_3$  with  $\text{Li(CH}_3)_3\text{NMe}_2$  gives  $\text{CpLu}[(\text{CH}_2)_3\text{NMe}_2]\text{Cl(THF)}_2$  with a pseudo octahedral geometry and is an example of monomeric lanthanide complex with Lu-C  $\sigma$ -bond. Bulky naphthalide analogous to chelating effect stabilizes  $[\text{CpLu}(\eta^4(\text{C}_{10}\text{H}_8)\text{-MeO(CH}_2)_2\text{OMe})]$  whose structure is shown in Fig. 6.11.

The reaction of  $[\text{CpLu}(\text{C}_{10}\text{H}_8)(\text{DME})]$  with diphenyl acetylene yields a complex with C-C coupling and a dinuclear complex. The X-ray structure and diamagnetism of the compound suggest the presence of an dialkylidene bridge in the complex.

Other compounds of some interest are given below:

$[(\text{CpNd})_4(\mu^2\text{-Me})_2(\mu^4\text{-O})(\mu^2\text{-Cl})_6]$	stabilized by dioxygen anion	[133]
$\text{CpLu}[(\text{CH}_2)_3\text{AsR}_2]_2$	C-As chelate	[134]

## 17. Substituted monocyclopentadienyl complexes ( $\text{Cp/LnX}_2$ , $\text{Cp'/LnXY}$ )

Substitution of the cyclopentadiene ligand with bulky groups enables the facile synthesis of complexes of earlier members of the lanthanides. The general method of synthesis involves sodium salt of  $\text{RCp}$ , where R = Me, *t*Bu,  $\text{C}_5\text{H}_9$ ,  $\text{C}_3\text{H}_5$ ,  $\text{Me}_3\text{Si}$  or  $\text{MeOCH}_2\text{CH}_2$  with  $\text{LnCl}_3$ . The product of the reaction is  $\text{RCpLnCl}_2 \cdot \text{THF}$ . The reaction of  $\text{LnCl}_3 \cdot 2\text{LiCl}$  with  $\text{MeCpNa}$  in THF yields  $[(\text{THF})_2\text{Li}]_2(\mu\text{-Cl})_4 [(\text{MeCp})\text{Ln(THF)}]$ , where Ln = La, Nd. The crystal structure of the Nd complex [135] shows that the unit  $\text{Li}(\mu\text{-Cl})_2\text{Nd}(\mu\text{-Cl})_2\text{Li}$

is a stabilizing agent of the monocyclopentadienyl complex. The ligands around Nd are exhibiting a distorted octahedral arrangement with a coordination number of eight.

Transmetallation reactions have been used to obtain lanthanide complexes of the type  $[\text{Li}(\text{DME})_3][(\text{MeCp})\text{Ln}(\text{NPPH}_2)_3]$ , where  $\text{Ln} = \text{La, Pr, Nd}$  and were characterized by IR and NMR spectra. The crystal structure of the La complex shows distinct  $[(\text{MeCp})\text{Ln}(\text{NPPH}_2)_3]^-$  anions and  $[\text{Li}(\text{DME})_3]^+$  cations. Lanthanum has a distorted tetrahedral geometry. Steric effects of the MeCp ligand are reflected in the  $\text{C}_g\text{-Ln-N}$  angle range of  $106\text{--}121^\circ$ . The La-N distance (average value) is  $2.459 \text{ \AA}$ . This complex is the first example containing La-N  $\sigma$  bond.

The synthesis and X-ray crystal structure of  $(\text{Me}_3\text{SiCp})\text{Y}[(\mu\text{-OtBu})(\mu\text{-Me})\text{AlMe}_2]_2$  shows a heterometallic bridge stabilization and an unusual tetragonal pyramidal geometry for yttrium [135].

The reaction of  $\text{ErCl}_3$  with  $[\text{C}_5\text{H}_9\text{CpNa}]$  in THF gives the complex [136]  $[(\text{C}_5\text{H}_9\text{Cp})\text{Er}(\text{THF})_2(\mu^2\text{-Cl})_3(\mu^3\text{-Cl})_2[\text{Na}(\text{THF})_2]]$  which has a dimeric structure and Er--Er distance of  $3.876 \text{ \AA}$ . Each erbium atom is surrounded by one  $\text{C}_5\text{H}_9\text{Cp}$ , two  $\mu^3\text{-Cl}$ ,  $\mu^2\text{-Cl}$  and one THF molecule in a distorted octahedral arrangement. The average bond length of  $\text{Er}-\mu^3\text{-Cl}$ ,  $2.760 \text{ \AA}$  is longer than  $\text{Er}-\mu^2\text{-Cl}$ ,  $2.744 \text{ \AA}$ .

The complex  $(t\text{-BuCp})\text{SmI}_2 \cdot 3\text{THF}$  is a rare example of an iodide derivative and the Sm coordination polyhedron is a distorted octahedron [25]. The Sm-I bond distances are  $3.107(1)$  and  $3.186(2) \text{ \AA}$ . In the complex  $\text{Cp}^0\text{SmI}_2 \cdot 2\text{TfHf}$ , where  $\text{Cp}^0 = 2\text{-methoxyethyl cyclopentadienyl}$ , the  $\text{Cp}^0$  ligand forces the two iodine atoms into cis positions while the iodines are in the transpositions in the complex  $(t\text{-BuCp})\text{SmI}_2 \cdot 3\text{THF}$ .

The oxophilic character of lanthanide is evident from the characterization of the complex  $(\text{MeCp})_3\text{Yb}_4(\mu\text{-Cl})_6(\mu^3\text{-Cl})(\mu^4\text{-O})(\text{THF})_3$  by the reaction of  $\text{YbCl}_3$  and  $\text{YbOCl}$  with MeCp in THF. The crystal structure of the complex shows an oxygen-centred tetrahedral arrangement of Yb atoms with  $\mu\text{-Cl}$  bridging each edge and  $\mu^3\text{-Cl}$  over the triangular face formed by the  $(\text{MeCp})\text{Yb}$  units [137].  $\text{Yb-O}(\mu^4\text{-oxide})$  bond distance range is  $2.13(1)\text{--}2.29(1) \text{ \AA}$ .

Substituted cyclopentadienyl with the pentamethyl group results in: (i) increased covalent character of the metal-cyclopentadienyl bond, (ii) strong  $\pi$  donor and weak  $\pi$  acceptor properties, (iii) kinetic stabilization due to steric shielding of the metal ion, and (iv) increased thermal stability of the metal complexes, (v) decrease in tendency to form polymeric structures due to increase in intermolecular interactions, (vi) increased solubility in organic solvents, and (vii) increase in vapour pressure.

### 17.1. Low valent $\text{LnCp}_2^*$ complexes [ $\text{Cp}^* = \text{C}_5(\text{CH}_3)_5$ ]

The complex  $\text{SmCp}_2^*$  was synthesized by metal vapour reaction of samarium with  $\text{C}_5(\text{CH}_3)_5\text{H}$  as a green product or by desolvation of the red  $\text{SmCp}_2^* \cdot 2\text{THF}$  by sublimation. The crystal structure of the complex  $\text{SmCp}_2^*$  shows it to be decamethyl samarocene with bent metallocene disposition [138]. The  $\text{C}_g\text{-Sm-C}_g$  angle of  $140.1^\circ$  is greater than  $136.7$  in the desolvated analogue. The Sm-C bond distance is reduced,  $2.79(1) \text{ \AA}$  compared to  $2.86(3) \text{ \AA}$  and the structure of  $\text{SmCp}_2^*$  is shown in Fig. 6.12.

The analogous red  $\text{EuCp}_2^*$  has been prepared by the sublimation of the THF solvated complex. The Eu complex is isostructural with the Sn complex [139]. The bent structure



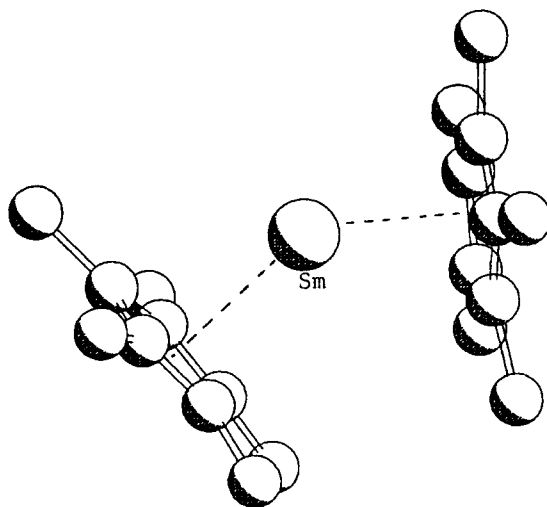


Fig. 6.12. Crystal structure of  $[\text{Cp}_2^*\text{Sm}]$  [138].

is supposed to optimize the polarization of the large cation by two anions which may give better total electrostatic bonding for the two rings. This explanation is not supported by electrostatic considerations or MO calculations or steric effects, and in fact favour two parallel  $\text{Cp}^*$  rings. A similar bent structure has been postulated for  $\text{YbCp}_2^*$  based on electron diffraction data [140].

The complex  $\text{SmCp}^*$  adds on  $\text{C}_5\text{H}_6$  forming a trivalent and mixed valent product  $\text{Cp}_2^*\text{SmCp}$ , and  $\text{Cp}_2^*\text{SmCpSmCp}_2^*$ , respectively. In the mixed valent product there is a deficiency of  $\text{C}_5\text{H}_6$ . In the complex  $\text{Cp}_2^*\text{Sm}^{\text{III}}(\mu\text{-Cp})\text{Sm}^{\text{II}}\text{Cp}_2^*$  the two valence states have been assigned on the basis of spectroscopy [141] which has been confirmed by X-ray analysis. The  $\text{Sm}(\text{III})$  coordination geometry is trigonal. The bridging Cp is symmetrically bound to  $\text{Sm}(\text{III})$  and two atoms are closer to  $\text{Sm}(\text{II})$  at distances of 2.986(8) and 3.180(9) Å, respectively.

The green complex  $\text{SmCp}_2^*$  DME has been synthesized from  $\text{SmCl}_2$  and  $\text{NaCp}^*$  in DME and characterized as monomeric with a pseudo tetrahedral ligand disposition [142].

The complex  $\text{Cp}_2^*\text{Sm}(\text{THF})_2$  may also be synthesized from  $\text{SmI}_2$  and  $\text{KCp}^*$  in the ratio of 1:2. When the ratio is 1:1,  $[\text{Cp}^*\text{Sm}(\mu\text{-I})(\text{THF})_2]_2$  is formed which can be used as starting material for the preparation of a series of alkyl complexes because of the ease of replacing iodide [143].

Substitution of THF in  $\text{Cp}_2^*\text{Sm}(\text{THF})_2$  yields  $\text{Cp}_2^*\text{SmL}_2$ , where  $\text{L}$  = dihydropyran or tetrahydropyran with  $\text{Sm}-\text{C}$  average distances of 2.842(4) Å and 2.816(3) Å in agreement with change in coordination number for Sm from 8 to 7.

In the case of ytterbium, the complexes  $\text{Cp}_2^*\text{Yb} \cdot \text{L}$  ( $\text{L} = \text{THF}, \text{Et}_2\text{O}$ ) have been characterized as monomeric [144] unlike the chain polymer structure of  $(\text{MeCp})_2\text{Yb} \cdot \text{THF}$  with bridging  $\text{MeCp}$  ligands. The pyridine complex  $\text{Cp}_2^*\text{Yb}(\text{Py})_2$  has approximate tetrahedral coordination geometry with predominantly  $\text{Yb}-\text{Cp}^*$  ionic bonding and  $\text{Cp}^*$  radius close to a value of 1.64(3) Å, for ionic bonding [145].

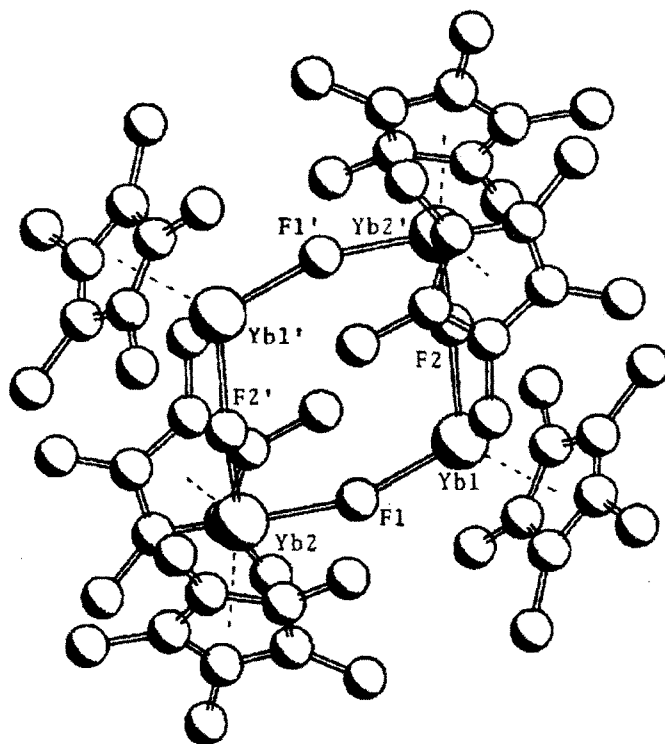


Fig. 6.13. Crystal structure of  $[\text{Cp}_6^*\text{Yb}_4\text{F}_4]$  [151].

Complexes of the type  $\text{Cp}_2^*\text{Ln}(\text{Me}_2\text{PCH}_2\text{CH}_2\text{PMe}_2)$ ,  $\text{Ln} = \text{Eu}, \text{Yb}$  are known to have a polymeric structure and are not soluble in organic hydrocarbon solvents. When the  $-\text{CH}_2-\text{CH}_2-$  bridge is replaced by  $-\text{CH}_2-$ , the complexes become soluble and possibly the  $\text{Cp}^*$  ligand reduces the tendency for polymerization [146]. The interactions between  $\text{Ln}$  and  $\text{Cp}^*$  in  $\text{Cp}_2^*\text{Ln}$  ( $\text{Ln} = \text{Sm}, \text{Eu}, \text{Yb}$ ) are ionic in nature as evidenced by XPS data and MO calculations [147].  $\text{Cp}_2^*\text{Sm}$  has been found to be a better reducing agent than  $\text{SmI}_2$ .

Adducts of  $\text{Cp}_2^*\text{Ln}$  ( $\text{Ln} = \text{Eu}, \text{Yb}$ ) with  $\text{NH}_3$  have been synthesized and crystallographically characterized [148].

Atom-abstractive addition of  $\text{Cp}_2^*\text{YbOEt}_2$  with alkyl and aryl halides give  $\text{Cp}_2^*\text{YbX}$  and  $\text{Cp}_2^*\text{YbX}_2$  where  $\text{X} = \text{halide}$  [149]. The side products of the reaction are  $\text{Cp}^*\text{H}$ ,  $\text{R}-\text{R}$ ,  $\text{RH}$ .

The mixed valence complex  $(\text{Cp}_2^*\text{Yb})_2(\mu-\text{F})$  in the solid state has a linear  $\text{Yb}^{\text{II}}-\text{F}-\text{Yb}^{\text{III}}$  asymmetric bridge with the different  $\text{Yb}-\text{F}$  distances  $\text{Yb}(1)-\text{F}$  2.317(2) and  $\text{Yb}(2)-\text{F}$  2.084(2) Å consistent with  $\text{Yb}^{\text{II}}$  and  $\text{Yb}^{\text{III}}$  formulation. This formulation is also supported by variable temperature data of magnetic susceptibility [150].

The tetramer  $\text{Cp}_6^*\text{Yb}_4(\mu-\text{F})_4$  consists of two  $\text{Cp}_2^*\text{Yb}(\mu-\text{F})\text{YbCp}_2^*$  units centrosymmetrically related and connected through fluoro bridges [151]. In the complex  $\text{Yb}^{\text{III}}$  is tetrahedral and  $\text{Yb}^{\text{II}}$  is trigonal as shown in Fig. 6.13.

The complex  $\text{Cp}_2^*\text{Yb}(\eta^2-\text{MeC}\equiv\text{CMe})$  has been characterized by spectroscopy and X-ray analysis and is the first example of  $\eta^2$ -acetylene complex of a lanthanide. The structure

has the acetylene plane, including Yb, about orthogonal ( $91.5^{\circ}$ ) to the centroids and Yb plane and a weak 2-butyne to  $\text{Cp}_2^*\text{Yb}$  interaction [151].  $[\text{K}(\text{THF})_n]_2[\text{Cp}_2^*\text{NdCl}_2]$ ,  $[\text{Cp}_2^*\text{NdCl}(\text{THF})]$  are some examples of Nd(II) complexes [152].

### 18. $\text{Cp}_2^*\text{Ln}$ halide complexes

As noted earlier, pentamethyl substitution in the cyclopentadienyl ligand confers some stability allowing ligand redistribution and the synthesis of chloride complexes of lanthanides. Stabilization also occurs by coordination with Lewis bases or alkali halides.

Solvent stabilized complexes  $\text{Cp}_2^*\text{Y}(\mu\text{-Cl})_2\text{Li}(\text{THF})_2$ , and  $\text{Cp}_2^*\text{YCl}(\mu\text{-Cl})\text{Li}(\text{THF})_3$  have been synthesized and the first complex has two bridging chlorine atoms and the second complex has one bridging chlorine and one terminal chlorine.

Complexes with other Lewis bases such as ether, acetone, pyridine, acetonitrile, are known. In the structure [146] of the complex  $\text{Cp}_2^*\text{Yb}(\text{Me}_2\text{PCH}_2\text{PMe}_2)$  the divalent Yb is oxidized by  $\text{YbCl}_3$  to the trivalent metallocene, Yb is coordinated to two  $\text{Cp}^*$  units, one chlorine and one phosphorus atom of dmpm ligand in a nearly tetrahedral manner with  $\text{Yb-Cl}$  2.532 Å and  $\text{Yb-P}$  2.941 Å. The complex  $[\text{Cp}_2^*\text{SmCl}]_3$  is trimeric and has three bridging chloride and forms a planar six-membered ring. The tetraglyme complex [153]  $\text{Cp}_{10}^*\text{Sm}_5\text{Cl}_5[\text{Me}(\text{OCH}_2\text{CH}_2)_4\text{OMe}]$  has four independent types of  $\text{Cp}_2^*\text{Sm}$  units. The structure of the cation  $\{\text{Cp}_2^*\text{ClSm}(\mu\text{-Cl})\text{SmCp}_2^*[\mu\text{-}\eta^4\text{Me}(\text{OCH}_2\text{CH}_2)_4\text{OMe}]\text{SmCp}_2^*\}$  is given in Fig. 6.14.

In the cation portion of the complex two Sm environments are nearly tetrahedral and the remaining  $\text{Cp}_2^*\text{Sm}$  unit is bound to three oxygen atoms of the tetraglyme molecule. The anion part is  $[\text{Cp}_2^*\text{ClSm}(\mu\text{-Cl})\text{SmClCp}_2^*]^-$ .

In the anionic portion of the complex, the  $\text{Cp}_2^*\text{Sm}$  units are twisted  $90^\circ$  with respect to each other. Other complexes synthesized and characterized are given below:

Complex		Reference
$[\text{Cp}_2^*\text{Sm}(\mu\text{-CN})(\text{CNC}_6\text{H}_{11})_3]$		
$\text{Li}[\text{Cp}^*\text{LnX}_3]$	$\text{Ln} = \text{Sm, Yb, X} = \text{Br}$	[57]
$\text{Li}[\text{Cp}_2^*\text{LnX}_2]$	$\text{Ln} = \text{Sm, Yb, X} = \text{I}$	[57]
$[\text{Cp}_2^*\text{LnX}]$		[57]
$\text{Cp}_2^*\text{YbF}(\text{OEt}_2)$	Tetrahedral $\text{Yb-F}$ 2.015 Å	[154]
$\text{Cp}_2^*\text{YbF}(\text{THF})$	Tetrahedral $\text{Yb-F}$ 2.026 Å	[154]

### 19. $\text{Cp}_2^*\text{Ln}$ hydrocarbyl complexes

The pentamethyl cyclopentadiene lanthanide complexes containing hydrocarbyl substituents have been studied extensively for their applications in homogeneous catalysis and C-H activation. The well-known catalyst of the Ziegler-Natta type  $\text{Cp}_2^*\text{LnMe}(\text{Et}_2\text{O})$  is typical of the large number of compounds [155] that have been studied. Solvent-free electrophilic alkyl derivatives serve as precursors of the majority of the compounds which have been studied.

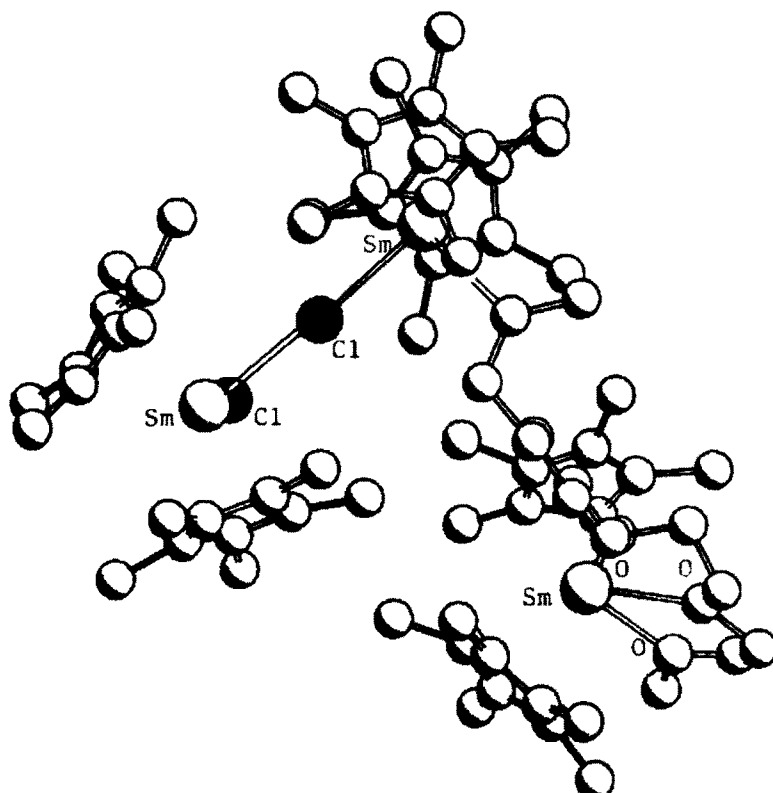
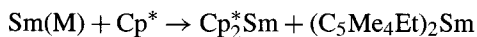
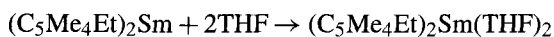
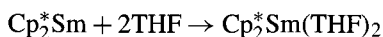


Fig. 6.14. Crystal structure of the cation  $[\text{Cp}_2^*\text{ClSm}(\mu\text{-Cl})\text{SmCp}_2^*(\mu\text{-}\eta^4\text{-Me}(\text{OCH}_2\text{CH}_2)_4\text{OMe})\text{SmCp}_2^*]$  [153].

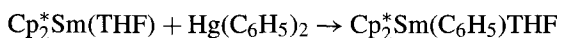
Synthesis of  $\text{Cp}_2^*\text{Sm}$  is achieved by reacting Sm metal vapour [143] with  $\text{Cp}^*$  at  $-110$ – $125^\circ\text{C}$ .



Further reaction with THF produces



Reaction with  $\text{Hg}(\text{C}_6\text{H}_5)_2$  gives [156]



The complex  $\text{Cp}_2^*\text{Sm}(\text{THF})_2$  reduces  $\text{Al}(\text{Me})_3$  in toluene giving rise to  $\text{AlMe}_4$  bridged complex  $\text{Cp}_2^*\text{Sm}[(\mu\text{-Me})\text{AlMe}_2(\mu\text{-Me})_2\text{SmCp}_2^*]$  which metallates C–H bonds of benzene, hexane and pyridine and catalyzes the polymerization of ethene. The structure of the complex shows [157] bent  $\text{Cp}_2^*\text{Sm}$  units, connected to two tetrahedral  $(\mu\text{-Me})_2\text{AlMe}_2$  units

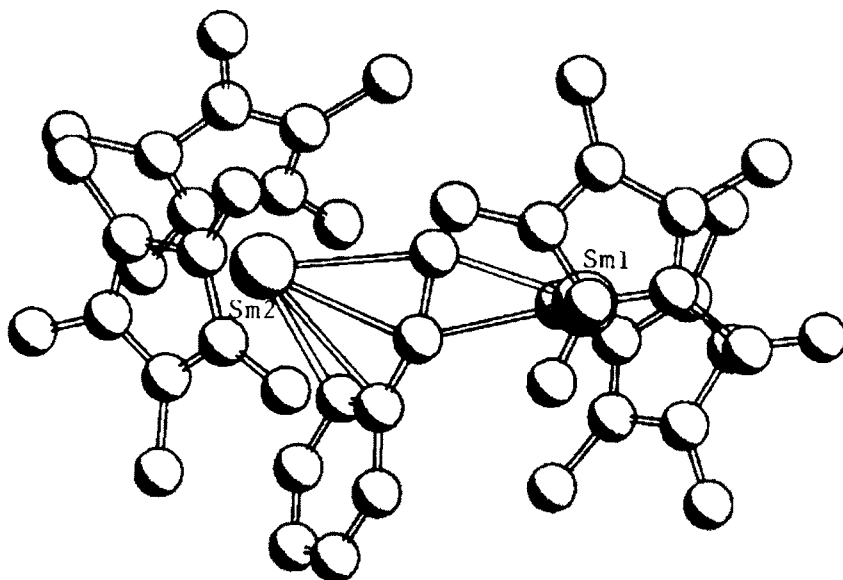


Fig. 6.15. Crystal structure of  $[(Cp_2^*Sm)_2(\mu-\eta^2:\eta^4-CH_2CHPh)]$  [158].

with nearly linear  $Sm(\mu-Me)Al$  bridges. The bridging methyl hydrogens are indicated to be equatorial with  $Sm-C$  (bridging methyl) distance of 2.75 Å.

Both unsaturated complexes  $Cp_2^*Sm$  and  $Cp_2^*Sm(THF)_2$  are extensively used in a variety of reactions and one example is the isomerization of *cis*-stilbene to *trans*-stilbene [158] with the production of  $[Cp_2^*Sm(\mu-\eta^2:\eta^4-PhCHCHPh)]$ .

The reaction of styrene with  $Cp_2^*Sm$  gives  $[Cp_2^*Sm]_2(CH_2CHPh)$  and the product's structure analyzed by X-ray method shows two  $Cp_2^*Sm$  units (Fig. 6.15) on the opposite sides of the alkene bond and the phenyl carbon atoms interacting with one of the Sm atoms. Sm(2) has a coordination number of ten due to the  $\eta^2$ -arene coordination, while Sm(1) has eight coordination resulting in lengthening in bond distances with respect to Sm(1) by about 0.07 Å for  $Sm-C_{ring}$ . This illustrates the bimetallic coordination of  $Cp_2^*Sm$  to stilbene, styrene and nitrogen.

The reactions of  $Cp_2^*Sm(THF)_2$  with a variety of alkenes in hexane or toluene solvent to produce allyl and alkene products have been studied. Binuclear Sm complexes have been synthesized [159] by the reaction of  $Cp_2^*Sm$  with pyrene, anthracene, 2,3-benzanthracene, 9-methylanthracene. The structure of the complex  $[(Cp_2^*Sm)_2(\mu-\eta^3:\eta^3-C_{10}H_{14})]$  is shown in Fig. 6.16.

The lanthanide complexes containing alkyne units,  $RC\equiv C$  have been well-characterized containing  $M-C$  bonds and this due to the strong  $\sigma$  bond and low steric congestion around the carbon donor atoms. Strong three centre  $M-C-M$  bridges are formed. Bimetallic bridges are also formed. The *t*-Bu-NC ligand can be inserted into bridging  $Ln-H$  bonds, where  $Ln = Er, Y$ , to give  $[Cp_2^*Ln(\mu, \eta^2-HC=NCtBu)(THF)]_2$ .

The complex  $[Cp_2^*LuMe]$  is an asymmetric dimer involving an agostic interaction between methyl (Me) and Lu compensating for the unsaturation of the complex [160].

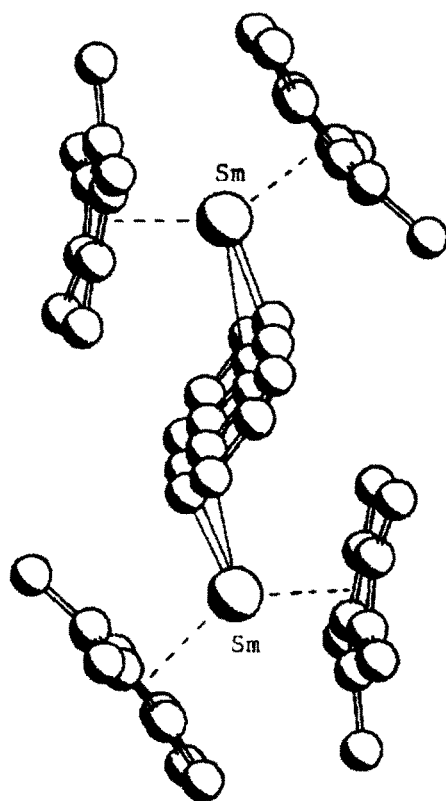


Fig. 6.16. Crystal structure of  $[(Cp^*_2Sm)(\mu-\eta^3:\eta^3-C_{10}H_{14})]$  [159].

Other complexes of the following type have been characterized.

Complex	Reference
$Cp^*_2LnCH(SiMe_3)_2$ , Ln = La, Nd, Sm, Lu	[160]
$(C_5Me_4Et)_2SmCH(SiMe_3)_2$	[161]
$\{Cp^*_3[C_5Me_3(CH_2CH_2)]Ce_2\}_2$	[162]
$Cp^*_2La(THF)(\mu-\eta', \eta^3-C_4H_6)LaCp^*_2$	[163]
$YbCp^*Sn(CH_2-tBu)_3(THF)_2$	[164]
$(Ph_3Sn_2)Yb(THF)_4$	[165]
$Ph_3SnYb(THF)_2(\mu-Ph)_3Yb(THF)_3$	[165]

In the Nd complex [160], the bent sandwich of  $Cp^*_2Nd$  is present, with a highly asymmetric  $CH(SiMe_3)_2$  fragment, and Nd–C  $\sigma$  bond distance of 2.517 Å and a secondary short contact Nd–C of 2.895 Å to a methyl carbon.

The structure of the cerium complex [162] consists of a centrosymmetric tetranuclear unit with a doubly metallated  $Cp^*$  group with  $\eta^5, \eta', \eta'$ ,  $C_5(CH_2)_2Me_3$  shared between three Ce atoms.

The Yb complex [165] has two Yb atoms with different coordination spheres [165]. One Yb is bonded to the  $\text{Ph}_3\text{Sn}$  unit with Yb–Sn bond length of 3.379 Å and two THF molecules. The second Yb atom has three THF molecules. The distorted octahedral coordination is present for both Yb atoms. The complex may be viewed as an association of two Yb units,  $\text{Ph}_3\text{SnYbPh}(\text{THF})_2$  and  $\text{Ph}_2\text{Yb}(\text{THF})_3$ . The Yb–C bridge is nearly symmetric with a distance range of 2.60 and 2.66 Å.

## 20. $\text{Cp}_2^*\text{Ln}$ complexes with O, S, Se, Te, N, As and Sb donors

The starting materials for the synthesis of the complexes are divalent species and alcoholysis of the alkyl or hydrides.

The oxygen bearing complex  $[\text{Cp}_2^*\text{Sm}]_2(\mu\text{-O})$  is synthesized by the reaction [166] of  $\text{Cp}_2^*\text{Sm}(\text{THF})$  with NO,  $\text{N}_2\text{O}$ ,  $\text{C}_4\text{H}_8\text{O}$  or  $\text{C}_5\text{H}_5\text{NO}$ . The product contains Sm–O–Sm linear bridges. The dimeric complex has  $S_4$  symmetry with the oxygen atoms lying at the centre of the rotation axis and the two bent metallocene units twisted  $90^\circ$  relative to each other. The  $\text{Cp}^*$  rings are in an eclipsed conformation on each samarium.

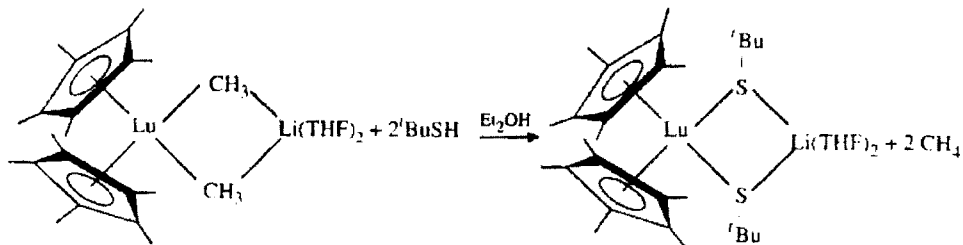
The reaction of  $\text{AgBPh}_4$  with  $\text{Cp}_2^*\text{Sm}(\text{THF})_2$  yields  $[\text{Cp}_2^*\text{Sm}(\text{THF})_2]^+[\text{BPh}_4]^-$  and the structure of the product by X-ray analysis showed eclipsed conformation of  $\text{Cp}^*$  rings while the  $\text{Cp}^*$  rings are staggered in the initial reactant complex [167].

That the complex  $\text{Cp}_2^*\text{Sm}(\text{THF})_2$  can activate CO and CH is demonstrated by the insertion of three CO molecules [168] to give  $[\text{Cp}_2^*\text{Sm}_2(\text{O}_2\text{CCO})(\text{THF})]_2$ . The complex  $[\text{Cp}_2^*\text{Sm}]_2\text{C}_2(\text{C}_6\text{H}_5)_2$  is formed by the reaction [169] of  $\text{Cp}_2^*\text{Sm}(\text{THF})_2$  with  $\text{C}_6\text{H}_5\text{C}\equiv\text{CC}_6\text{H}_5$ .

The reactivity of the samarium hydride complex is evidenced [170] by the formation of  $[\text{Cp}_2^*\text{Sm}(\text{THF})]_2[\mu\text{-}\eta^2\text{-(OSiMe}_2\text{OSiMe}_2\text{O)}]$  a bridged samarium siloxide, from  $[\text{Cp}_2^*\text{Sm}(\mu\text{-H})]_2$ . The samarium hydride complex is also used in the polymerization of methyl methacrylate [171].

The lanthanide carbyls  $\text{Cp}_2^*\text{LnCH}(\text{SiMe}_3)_2$ , where Ln = Ce, La react with acetone to give aldolates  $\text{Cp}_2^*\text{LnOCMe}_2\text{CH}_2\text{C}(=\text{O})\text{Me}$ . The structure of the cerium compound shows distinct differences in Ce–O distances, namely Ce–O of 2.182 Å of alkyl oxide and 2.506 Å to the carbonyl oxygen [172].

The complexes containing S, Se and Te donors are rare and this is easily understood because lanthanides are hard while S, Se, Te are soft. Zalkin [173] synthesized  $\text{Cp}_2^*\text{Yb}(\text{S}_2\text{NEt}_2)$  in which the Yb–S bond of 2.70 Å and S–Yb–S angle of  $67.1^\circ$  were noted. Another sulfur bearing complex has been synthesized by the scheme given below [174].



The product complex is a bridged dinuclear Lu–Li compound with a puckered LuS<sub>2</sub>Li unit and Lu–S distances of 2.709 and 2.723 Å. Complexes of the type Cp<sub>2</sub>\*Yb(ER)(L), where R = organic group, E = O, S, Se, Te, L = Lewis base have been characterized and the structure of the complex [Cp<sub>2</sub>\*Yb(SPh)(NH<sub>3</sub>)] shows the Yb atom is at the centre of a distorted tetrahedron, consisting of one sulfur, one nitrogen and the Cp\* ring centroids [175].

Other complexes containing S, Se, Te characterized are given below.

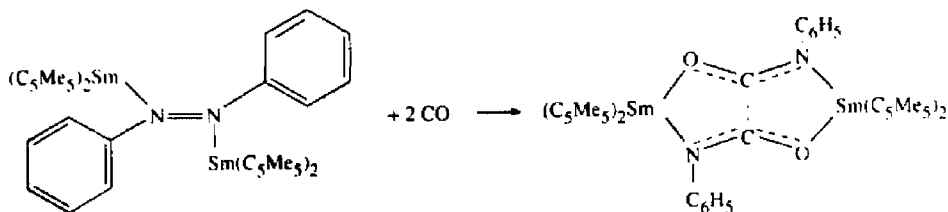
Complex	Reference
Cp <sub>2</sub> *Yb(TePh)(NH <sub>3</sub> )	[176]
(Cp <sub>2</sub> *Yb) <sub>2</sub> Te <sub>2</sub>	[177]
[Cp <sub>2</sub> *Yb] <sub>2</sub> (μ-L)	L = S, Se, Te [178]
Cp <sub>2</sub> *Sm(L)	L = S, Se, Te [179]
[Cp <sub>2</sub> *CeL <sub>2</sub> ]BPh <sub>4</sub>	L = THF, tetrahydrothiophene (THT) [180]

The ditelluride complex is a centrosymmetric dimer [177] and the Yb is tetrahedrally bonded to two Cp\* ligands and to the Te<sub>2</sub><sup>2-</sup> ion. The structure of Se complex [178] has a linear Se–Yb–Se bridge (170.1°) with two Cp<sub>2</sub>\*Yb units mutually staggered and the compound is seven coordinate. The structure of Ce complex [180] shows a rare example of Ce–S dative bond with Ce–S distances of 3.058 and 3.072 Å.

The amide complex of Cp<sub>2</sub>\*Ln such as Cp<sub>2</sub>\*LnN(SiMe<sub>3</sub>)<sub>2</sub>, where Ln = Nd, Yb has been characterized [181] and the Y complex was found to be roughly of trigonal planar geometry and coordinately unsaturated which favours the formation of weak Y–methyl contacts and a short Y–N distance due to the donation of lone-pair of electrons by nitrogen to yttrium.

Analogous derivatives of Y, Nd, Sm, Lu have been characterized [182] with modified C<sub>5</sub>Me<sub>4</sub>Et in place of Cp\* which is C<sub>5</sub>Me<sub>5</sub>.

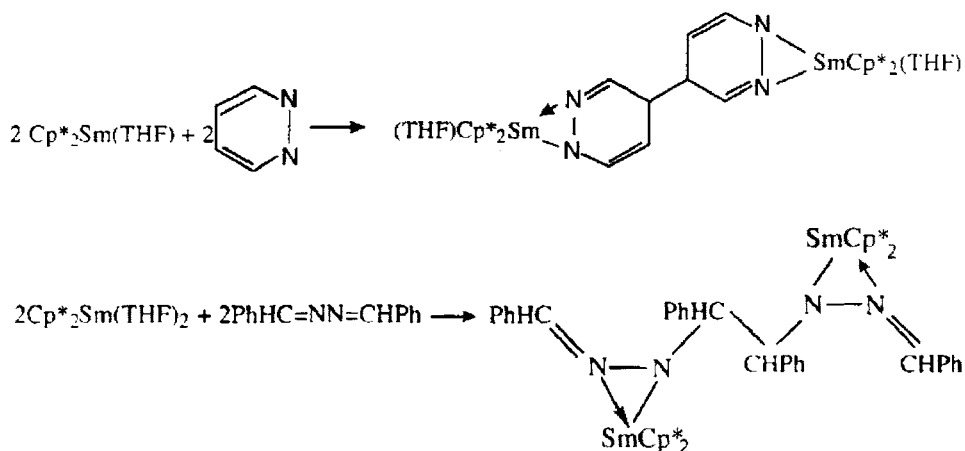
The complex Cp<sub>2</sub>\*Sm(THF)<sub>2</sub> reacts with azobenzene and the product adds on CO. The final product contains Sm bonded to one oxygen, one nitrogen as depicted below [183].



The complex Cp<sub>2</sub>\*Sm(THF)<sub>2</sub> causes multiple bond cleavage to produce multiple bonded species [182]. The complex reacts with CO, RC≡CR, RN=NR and R<sub>2</sub>C=CR<sub>2</sub> bearing compounds resulting in some useful transformations. The samarium complex Cp<sub>2</sub>\*Sm(THF)<sub>2</sub> reacts with azine containing C=N bond and reduces the azines by one electron per substrate. The reaction is illustrated below. With benzaldehydeazine the

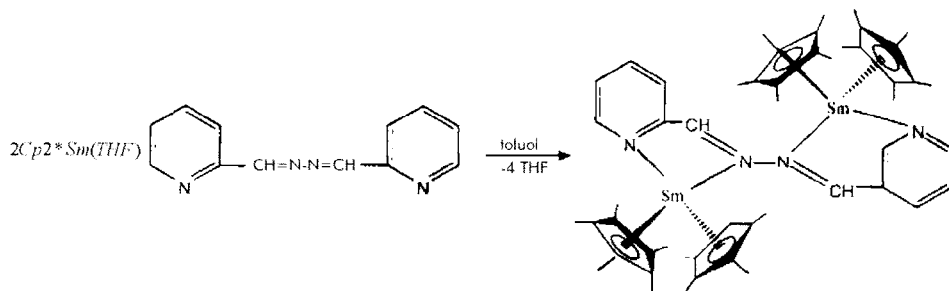


reductive coupling gives rise to an unsolvated dimeric complex as shown below [184].



The samarium is eight coordinate in these complexes. With bipyridine as a reactant the monometallic complex  $\text{Cp}^*_2\text{Sm}(\eta^2\text{N}_2\text{C}_{10}\text{H}_8)$  is obtained and the physicochemical evidence such as  $^{13}\text{C}$  NMR points to the presence of Sm(III) in the complexes.

The reaction scheme of  $\text{Cp}^*_2\text{Sm}(\text{THF})$  with pyridinealdazine is shown below.



The N heterocyclic dianions of quinoxaline and phenazine form bridged complexes and the structure [185] of the  $[\text{Cp}^*_2\text{La}]_2(\text{C}_{12}\text{H}_8\text{N}_2)$  is shown in Fig. 6.17.

Other complexes containing nitrogen, arsenic, antimony and bismuth are given below.

Complex	Reference
$\text{Cp}^*_2\text{LnR}$ Ln = La, Nd, Sm, Y, Lu; R = H, CH(TMS) <sub>2</sub> , N(TMS) <sub>2</sub>	[186]
$(\text{Cp}^*_2\text{Sm})_2(\mu\text{-}\eta^2 : \eta^2\text{-Bi}_2)$	[187]
$\text{Cp}^*_2\text{Sm}(\mu\text{-}\eta^2 : \eta^2 : \eta'\text{Sb}_3)(\text{THF})$	[188]
$\text{Cp}^*_2\text{YbMeBeCp}^*$	[151]
$\text{Cp}^*_2\text{Lu}(\mu\text{-AsPh}_2)_2\text{Li}(\text{tmed})$	[189]

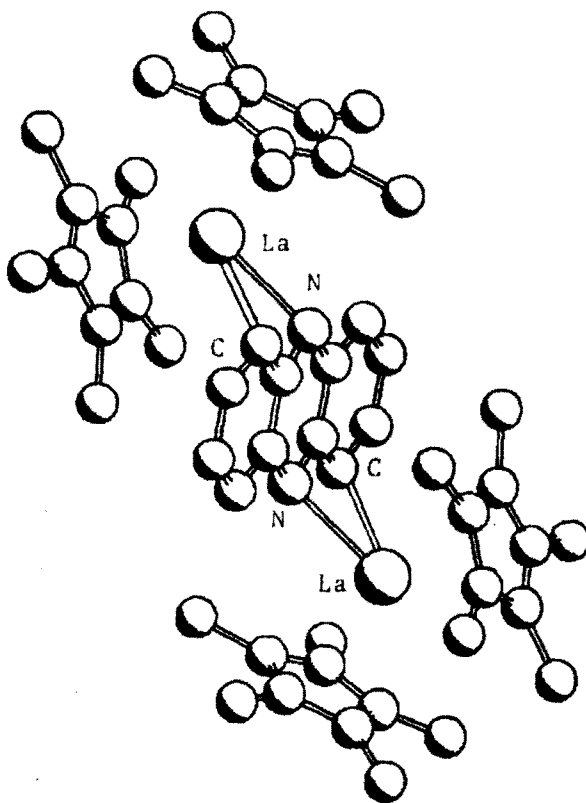


Fig. 6.17. Crystal structure of  $[\text{Cp}_2\text{La}]_2(\text{C}_{12}\text{H}_8\text{N}_2)$  [185].

The catalytic activity of the  $\text{Cp}_2^*\text{LnR}$  complexes in hydroamination/cyclization of aminoolefins has been documented in terms of lanthanide size and other factors [186].

The dibismuth complex happens to be the first example of an f element [187]. The bismuth unit,  $\text{Bi}_2$  is in planar coordination to two Sm atoms. The Bi–Bi distance is 2.851 Å with possible multiple bonding and the Bi–Sm distance of 3.29 Å.

In the antimony complex  $\text{Sb}_3^{3-}$  is bent [188] with an angle of 114.5° and an average Sb–Sb distance of 2.688 Å, further five of the Sm–Sb distances are in the range of 3.162–3.205 Å with the sixth one 3.686 Å. The Yb complex [151] shows a structure involving  $\text{MeBeCp}^*$  linearly bridged through the methyl group to the  $\text{Cp}_2^*\text{Yb}$  unit. The arsenic complex is the first of its kind [189] with Lu–As distances of 2.896 and 2.870 Å.

## 21. Complexes of the type $\text{Cp}^*\text{LnX}$

The first compound with one  $\text{Cp}^*$  ligand to be synthesized was the Yb complex. The complex  $\text{Cp}^*\text{Yb}(\mu^2\text{-I})_3\text{Li}(\text{Et}_2\text{O})_2$  was obtained by the reaction [190] of Yb metal with

Cp\*Li and LiI in ether. The corresponding chloro derivative was prepared by reacting YbCl<sub>3</sub> with Cp\*Li. This method has been used to prepare a series of chloro and iodo complexes of different lanthanides as ether solvates.

Some of the complexes characterized are as given below.

Complex	Reference
Cp*YbCl <sub>2</sub>	[191]
Cp*CeI <sub>2</sub> (THF) <sub>3</sub> Pseudotetrahedral, mer, trans geometry	[192]
Cp*Sm(μ-I)(THF) <sub>3</sub>	[193]
Cp*GdCl <sub>2</sub> (THF) <sub>3</sub>	[194]
{[Na(THF)[Cp*Gd(THF)] <sub>2</sub> Cl <sub>5</sub> ] · 6THF}	[194]
[K(DME) <sub>3</sub> ]{K[(Cp*Yb) <sub>3</sub> Cl <sub>8</sub> K(DME) <sub>2</sub> ] <sub>2</sub> }    Distorted octahedral geometry	[195]
[Yb <sub>5</sub> Cp* <sub>6</sub> (μ <sup>4</sup> -F)(μ <sup>3</sup> -F) <sub>2</sub> (μ <sup>2</sup> -F) <sub>6</sub> ]	[196]

The structure of the pentaytterbium cluster complex is shown in Fig. 6.18.

Complexes containing monopentamethyl cyclopentadiene as oxo, alkyl and aryloxides, β-diketones, hydrazine, dianionic carbollide derivatives have been characterized and are summarized below.

Complex	Reference
Cp* <sub>5</sub> Yb <sub>5</sub> O(C <sub>4</sub> H <sub>10</sub> O) <sub>2</sub> Cl <sub>8</sub> Cluster structure	[197]
Cp*Lu(CH <sub>2</sub> SiMe <sub>3</sub> )[CH(SiMe <sub>3</sub> ) <sub>2</sub> (THF)]	[198]
[Li(TMEDA)Cp*Lu[CH(SiMe <sub>3</sub> ) <sub>2</sub> (μ-Cl) <sub>2</sub> ]	[198]
Li(THF) <sub>3</sub> [Cp*Lu[(CH <sub>2</sub> SiMe <sub>3</sub> )(CH(SiMe <sub>3</sub> ) <sub>2</sub> Cl)]	[198]
Cp*La[(CH(SiMe <sub>3</sub> ) <sub>2</sub> ) <sub>2</sub> ]	[198]
[Li(tmed) <sub>2</sub> ][Cp*LuMe <sub>3</sub> ]	[79]
Cp*La[CH(SiMe <sub>3</sub> ) <sub>2</sub> ]BPh <sub>4</sub>	[200]
[Cp*Ce(μ-OCMe <sub>3</sub> ) <sub>2</sub> ] <sub>2</sub>	
Cp*Ce(OAr) <sub>2</sub> OAr = 2,6-di- <i>t</i> -butyl phenoxo	[135b]
Cp*Ce[CH(SiMe <sub>3</sub> ) <sub>2</sub> ] <sub>2</sub>	[201]
Cp*Ce[N(SiMe <sub>3</sub> ) <sub>2</sub> ] <sub>2</sub>	[201]
Cp*Y(acac) <sub>2</sub>	[202]
[(Cp*Sm) <sub>6</sub> Se <sub>11</sub> ]	[203]
[Cp*Sm <sub>4</sub> ] <sub>4</sub> (NHNH) <sub>2</sub> (NHNH) <sub>4</sub> (NH <sub>3</sub> ) <sub>2</sub>	[204]
{Cp*[(Me <sub>3</sub> Si) <sub>2</sub> CH]Sc(carbollide)} <sub>2</sub> Li(THF) <sub>3</sub>	[205]

The lutetium complexes containing alkyls are the first of its kind reported [198]. The structures of the precursor lutetium complexes [198] show them to be a three-legged stool coordination geometry. One of the complexes has a structure in which the lithium is bonded to lutetium through two bridging chlorides and through one chloride in the other complex. In the lanthanum complex [200], X-ray studies provide evidence for the presence of stabilization of unsaturated lanthanum through agostic Si–C bonds.

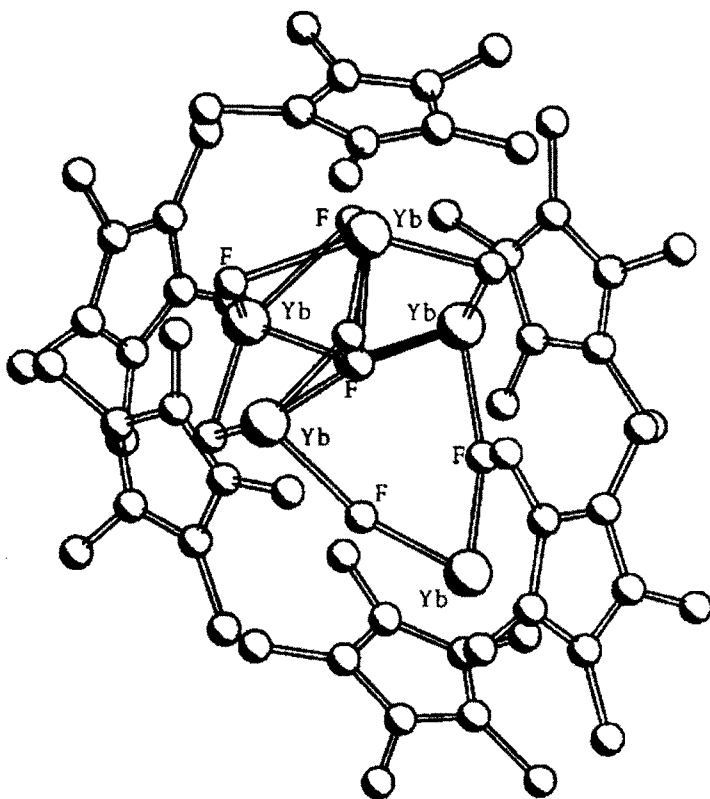
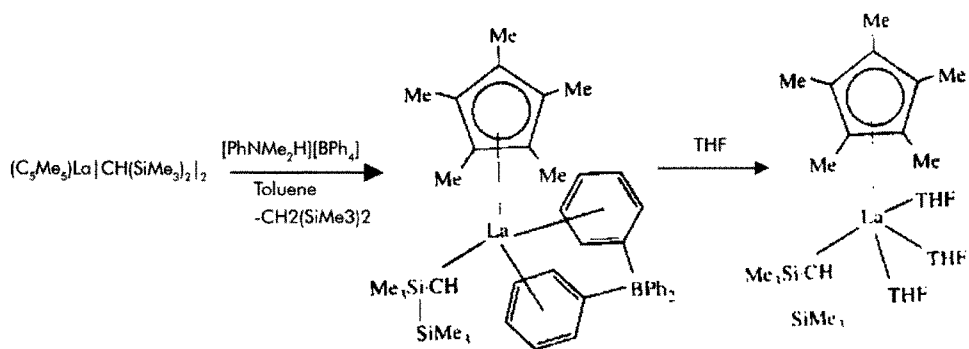


Fig. 6.18. Crystal structure of  $[\text{Cp}^*_2\text{Yb}_5(\mu^4\text{-F})(\mu^3\text{-F})_2(\mu^2\text{-F})_6]$  [196].

The coordination geometry of lutetium in the alkyl complex [79] is nearly tetrahedral with two long Lu–C bonds (2.575 Å) and one short Lu–C bond (2.39 Å).

The synthesis of the La complex containing  $\text{BPh}_4$  follows the scheme given below [200].



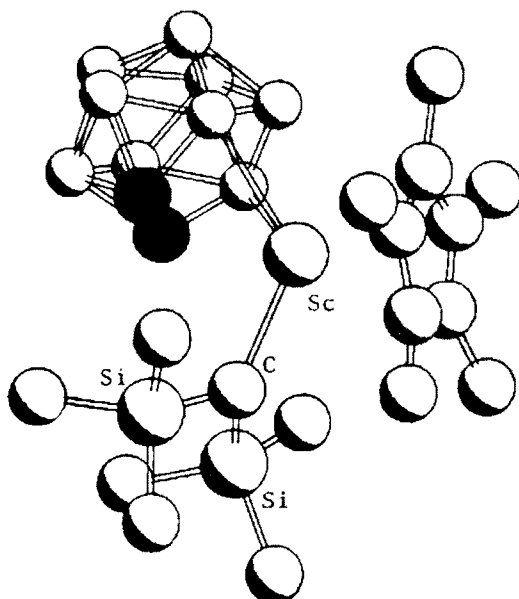


Fig. 6.19. Crystal of the fragment  $(\text{Cp}^*-(\text{MeSi})_2\text{CH})\text{Sc}(\text{carbollid})$  [205] (solid circles are the carbons of the carbollide ligand).

The cerium complexes given above [201] are monomeric, and Ce(III) is five-coordinated and the unsaturation of these complexes favours interactions with the available C–H and Si–C bonds.

The tetrameric samarium complex [204] has four Sm atoms in a tetrahedral disposition with bridging  $(\text{NHNH})^{2-}$  anions on each side of the tetrahedron with Sm–Sm distances of 3.563 and 3.552 Å. The two  $\text{NH}_3$  units are coordinated to two Sm centers at a distance of 2.664 Å.

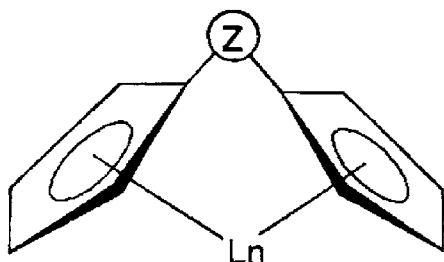
The crystal structure of Sc carbollide complex is shown in Fig. 6.19. In the complex, each Sc is  $\eta^5$  bonded to  $\text{Cp}^*$ ,  $\eta^5$  bonded to carbollide and to one- $\text{CH}(\text{SiMe}_3)_2$  group. The centers of the two  $\eta^5$  groups form an angle of  $137.8^\circ$  with Sc and two of such units share a Li atom to the B atoms of each carbollide resulting in a dimeric anion with  $\text{Li}(\text{THF})_3$  as the cation.

## 22. Ring bridged cyclopentadienyl lanthanide complexes

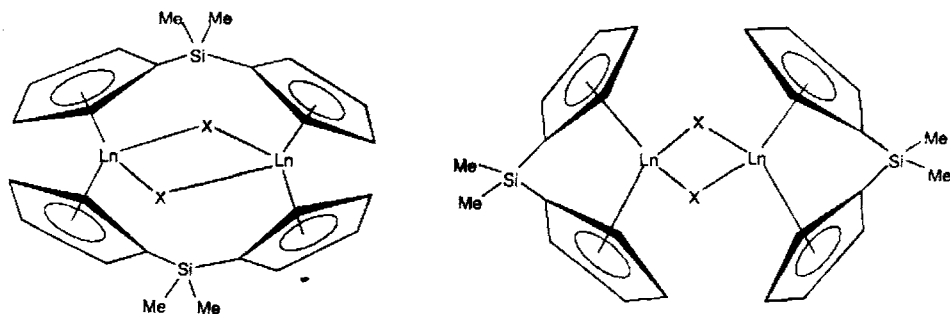
The difficulties in preparing dicyclopentadienyl lanthanide of lighter lanthanides, La, Ce, Pr and Nd are overcome by increasing the steric hindrance around Ln by using multisubstituted Cp ligand or by decreasing the mobility of the Cp ligand by catenation.

Bridged cyclopentadienyl ligands  $\text{RCp}_2$ , where  $\text{R} = \text{CH}_2$ ,  $\text{Me}_2\text{Si}$ ,  $\text{CH}_2\text{CH}_2\text{CH}_2$  have been used to confer stability with respect to redistribution of Cp ligands in the complexes.

Use of bridged Cp ligands in the complexes reduces the steric crowding around the Ln ion, a reduced  $C_g-Ln-C_g$  angle and an open opposite side of Ln for coordination for the facile approach of the incoming substrate as shown in the structure below.



In dimeric lanthanide complexes, substituted Cp ligands can act as either a bridge or as a chelate. The complexes  $Ln[1,3-(CH_2)_3(C_5H_4)_2]Cl$ , where  $Ln = La$  and  $Ce$ ,



and  $[Cp(CH_2)_3Cp]LnX(THF)$ , where  $Ln = Pr, Nd, Gd, Dy, Ho, Er, Lu$  and  $X = Cl$  have been characterized [206,207].

By the reaction  $YbCl_3$  with  $Na_2[Cp(SiMe_2)Cp]$  in THF gave rise [208] to a dimeric ligand bridged product  $[Yb(\mu-Cl)(\mu-Me_2SiCp_2)]_2$ . On the other hand, the reaction of NaH with  $[Yb(\mu-Cl)(\mu-Me_2SiCp_2)]_2$  yielded a monochloro monohydride complex  $\{[(\mu-Me_2SiCp_2)Yb(THF)]_2(\mu-H)(\mu-Cl)\}$  whose structure [209] is shown in Fig. 6.20. The corresponding Y complex has chelated dimeric structure consisting of hydride.

Complexes with other bridging ligands are codified below.

The Nd complexes [210,211] have a bridging mode as opposed to a chelating mode. The Yb complex [212] with tetramethylethylene bridge [212] has pseudotetrahedral geometry. The  $C_g-Yb-C_g$  angle is  $121^\circ$  and the  $Cl-Yb-Cl$  angle of  $97.1^\circ$  in the non-bridged complex. In the bridged complex, Cp rings are eclipsed and tetramethyl ethylene has a staggered conformation. Complexes with  $R_2Si$  bridges show a chemical behaviour different from normal bridged and chelated complexes which may be due to steric and electronic factors [213]. These complexes have poor catalytic activity.

Ligand	Lanthanide	Reference
$\text{Me}_2\text{Si}(\text{C}_5\text{H}_3\text{Bu})_2^-$	$\text{Nd}(\mu\text{-Cl})_2$	[210]
$\text{Me}_2\text{Si}(\text{C}_5\text{Me}_4)_2^{2-}$	$\text{Nd}(\mu\text{-Cl})_3$	[211]
$\text{Me}_2\text{Si}(\text{C}_5\text{Me}_4)_2$	$\text{Ln} = \text{Nd, Sm, Lu, } (\mu\text{-Cl})_2$	[212]
$\text{Me}_2\text{C}_2(\text{C}_5\text{H}_4)_2$	Yb	[212]
$[\text{R}_2\text{Si}(\text{C}_5\text{H}_4)\text{Me}_4\text{C}_5]$	Lu	[213]
$\text{R}_2\text{Si}$	$\text{Ln} = \text{Sc, Nd, Sm, Lu}$	[214]
$\text{Me}_2\text{Ge}(\text{C}_5\text{Me}_4)_2$	$\text{Ln} = \text{Nd, Ho}$	[215]
$\text{Me}_2\text{Si}(\text{C}_5\text{Me}_4)(\text{C}_5\text{H}_3\text{R}^*)$ $\text{R}^* = (-)\text{menthyl}$	$\text{Ln} = \text{Y, La, Nd, Sm, Lu}$	[186]
$[\text{O}(\text{CH}_2\text{CH}_2\text{C}_5\text{H}_4)_2]$	$\text{Ln} = \text{Nd, Gd, Ho, Er, Yb, Lu, Y}$	[216]
$\text{CH}_3\text{N}(\text{CH}_2\text{CH}_2\text{C}_5\text{H}_4)_2$	Ln	[217]
$(\text{C}_5\text{H}_4\text{CH}_2)_2\text{C}_5\text{H}_3\text{N}$	Ln	[218]
$(\text{C}_5\text{H}_4\text{SiMe}_2)_2\text{O}$	Ln	[219]

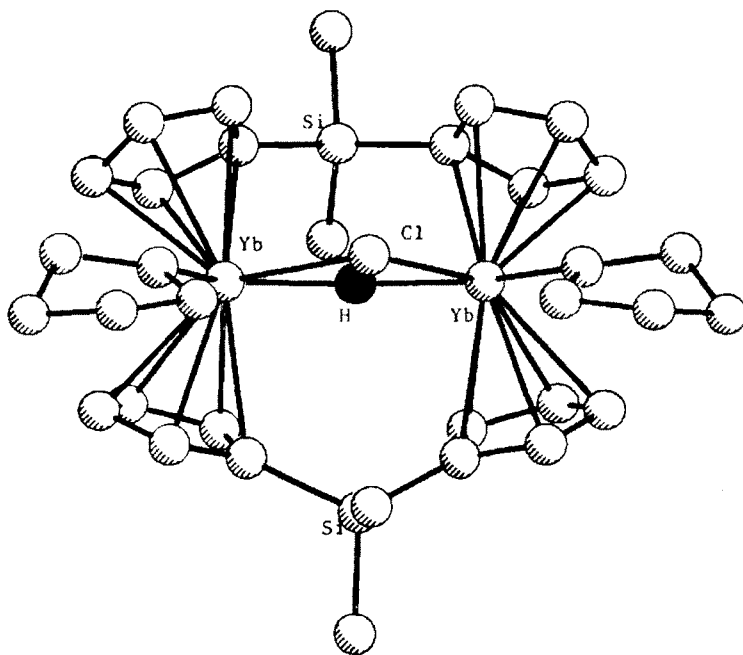


Fig. 6.20. Crystal structure of  $[(\text{Me}_2\text{SiCp}_2)\text{Yb}(\text{THF})_2](\mu\text{-H})(\mu\text{-Cl})$  [209].

The structure of the complex  $[\text{Et}_2\text{Si}(\text{C}_5\text{H}_4)(\text{Me}_4\text{C}_5)\text{Lu}]_2(\mu\text{-H})(\mu\text{-C}_2\text{H}_5)$  shown in Fig. 6.21 has an unusual coordination geometry of the  $\mu$ -ethyl ligand which bridges asymmetrically two Lu ions.

The complexes with chiral asymmetric ligands [186] are used for catalytic enantioselective olefin hydrogenation.

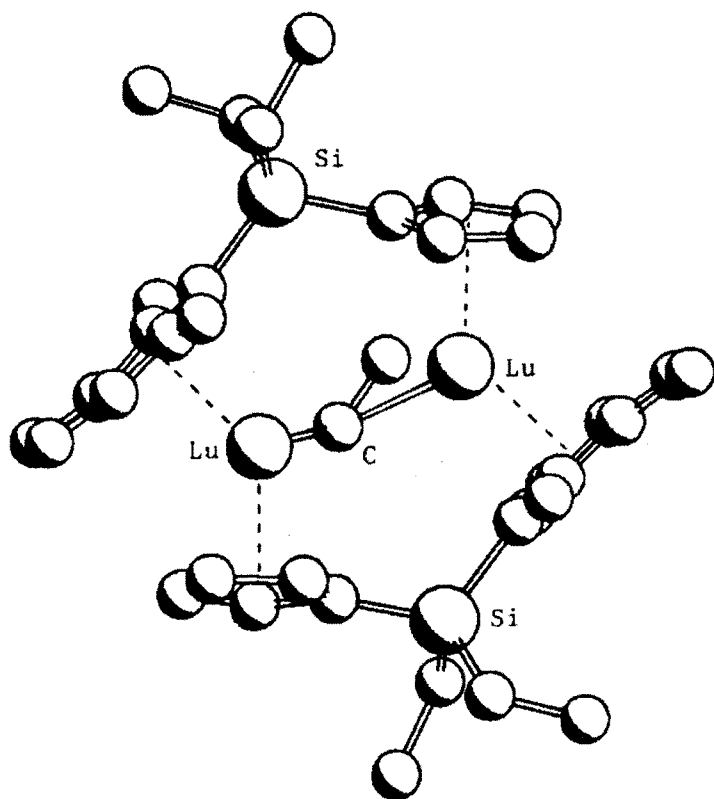
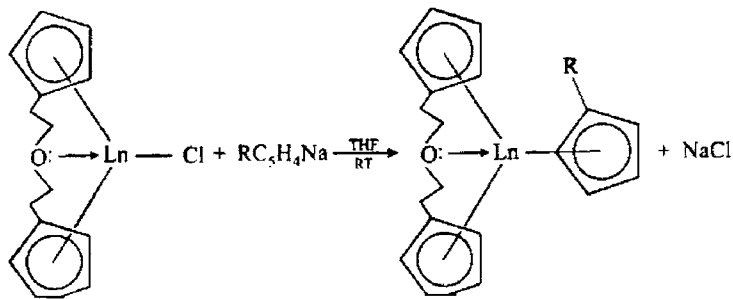


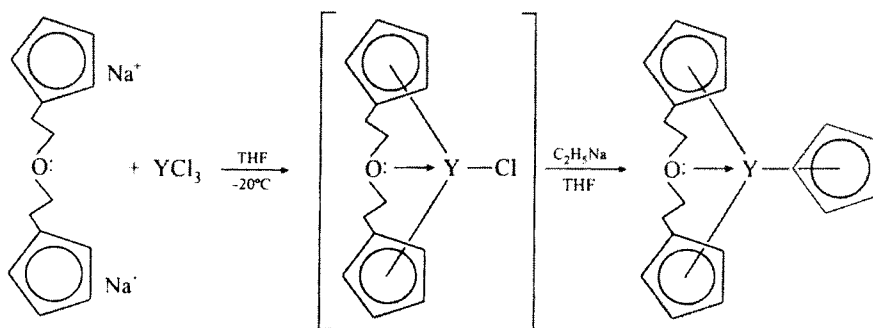
Fig. 6.21. Crystal structure of  $[\text{Et}_2\text{SiCp}^*\text{Lu}]_2(\mu\text{-H})(\mu\text{-Et})$  [213] ( $\mu\text{-H}$  is missing).

The complexes containing  $\text{O}(\text{CH}_2\text{CH}_2\text{C}_5\text{H}_4)_2$  are used to obtain other complexes by the reactions

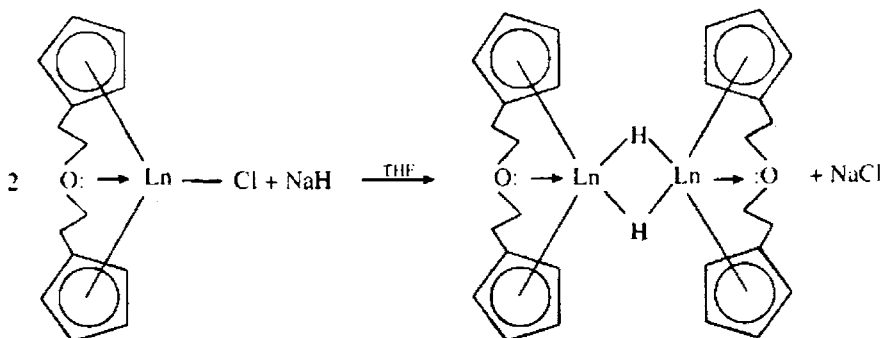




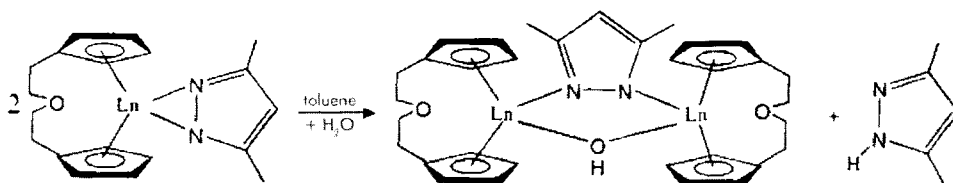
R = H, Ln = Nd, Gd, Er, Yb, Lu, Y; R = CH<sub>3</sub>, Ln = Yb, Y.



The dimeric complexes are obtained by the reaction [220]



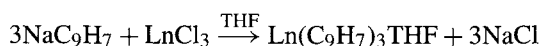
The monomeric complex  $\{[O(CH_2CH_2C_5H_4)_2]Ln(N_2C_5HMe_2)\}$  forms a dimer thus [215]



Sm(II), Y(II) have been stabilized in their complexes with the ligand  $O(CH_2CH_2C_5H_4)_2$  by THF solvation. The structure of Yb complex of  $O(CH_2CH_2C_5H_4)_2$  with DME is nearly trigonal pyramidal with an  $C_g-Yb-C_g$  angle of  $132.7^\circ$  as in the nonbridged complex thereby showing high conformational flexibility of the ligand.

### 23. Lanthanide indenyl complexes

Lanthanide indenyl complexes of Ln(III) are known. Ce(IV), Sm(II) also form indenyl complexes. Mixed cyclopentadienyl-indenyl complexes of lanthanides have been prepared by reacting CpLnCl with NaC<sub>9</sub>H<sub>7</sub>. Typical preparation involves the reaction [221]



where Ln = La, Sm, Gd, Tb, Dy, Yb.

The trisindenyl cerium pyridinate is an example of trihapto indenyl coordination [222]. A tetrahedral disposition of the ligands around Ce is formed by the centroids of the  $\pi$  bonded portion of the indenyl ligands and nitrogen of the pyridine. Trihapto indenyl coordination [223] is also seen in (IndGdCl<sub>2</sub> · 3THF) · THF and (Ind)<sub>3</sub>Ln(THF), where Ln = Nd, Gd, Er, with octahedral and tetrahedral arrangements, respectively. A linear chlorine bridge and pentahapto indenyl coordination [224] is noted in [Na(THF)<sub>6</sub>] [Nd(Ind)<sub>3</sub>( $\mu$ -Cl)Nd(Ind)<sub>3</sub>].

The NMR spectrum of the La complex is similar to ionic NaC<sub>9</sub>H<sub>7</sub> but the spectrum of the Sm complex showed a decrease in ionic character. The structure of Sm(Ind)<sub>3</sub> consists of symmetrical coordination by indenyl rings with an average Sm–C distance of 2.75 Å and the angle between Sm atoms and the normal to the planes of the indenyl rings is nearly 120°. There is no preference in bonding to the electron-rich C-1 position thus indicating the bonds to be primarily ionic in nature [225].

### 24. Lanthanide cyclooctatetraenyl complexes

Cyclooctatetraene, C<sub>8</sub>H<sub>8</sub><sup>2-</sup> (COT) forms a variety of complexes with lanthanides due to their large size and to the possible f orbital of suitable symmetry. The characterized complexes [226] are of sandwich-type or oligomeric with the COT units shared among like or different metals. Mixed complexes with Cp or similar ligands as well mono COT either with halides or neutral ligands or  $\sigma$ -bonded ligands such as alkyl, aryl, alkoxide, aryloxy and amide are known. Lanthanide complexes are more sensitive to oxygen and also undergo ligand exchange. The structure of mono COT complexes is usually monomeric and the number of ligands attached to the metal ion depends on steric factors and the ionic size of the metal ions.

Some typical complexes are noted in Table 6.3. COT ligands can in principle stabilize Ln(II), Ln(III) and Ln(IV) ions. The first complexes characterized were Ln(COT), where Ln = Eu(II), Yb(II) prepared by the reaction of metals with COT in liquid ammonia [227]. The complex (COT)Yb(Py)<sub>3</sub> · 0.5Py has a structure consisting of a three-legged stool for the coordinated ligands [228]. Other Ln(II) complexes are given below.

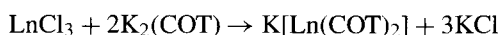
The anionic Yb(II) complexes [230,231] have planar parallel eclipsed COT rings, sandwiching a centrosymmetric Yb with Yb–C distance 2.74 Å. The potassium bound to DME is at the opposite side of each ring.

TABLE 6.4  
 Cyclooctatetraenyl complexes.

Compound	Colour	Magnetic moment (B.M.)
K[Y(C <sub>8</sub> H <sub>8</sub> ) <sub>2</sub> ]	Yellow	–
K[La(C <sub>8</sub> H <sub>8</sub> ) <sub>2</sub> ]	Green	–
K[Ce(C <sub>8</sub> H <sub>8</sub> ) <sub>2</sub> ]	Pale green	1.88
K[Pr(C <sub>8</sub> H <sub>8</sub> ) <sub>2</sub> ]	Yellow-gold	2.84
K[Nd(C <sub>8</sub> H <sub>8</sub> ) <sub>2</sub> ]	Pale green	2.98
K[Sm(C <sub>8</sub> H <sub>8</sub> ) <sub>2</sub> ]	Brown	1.48
K[Gd(C <sub>8</sub> H <sub>8</sub> ) <sub>2</sub> ]	Yellow	–
K[Tb(C <sub>8</sub> H <sub>8</sub> ) <sub>2</sub> ]	Yellow-brown	9.86
[Ce(C <sub>8</sub> H <sub>8</sub> )Cl · 2C <sub>4</sub> H <sub>8</sub> O] <sub>2</sub>	Yellow-green	1.79
[Pr(C <sub>8</sub> H <sub>8</sub> )Cl · 2C <sub>4</sub> H <sub>8</sub> O] <sub>2</sub>	Pale green	3.39
[Nd(C <sub>8</sub> H <sub>8</sub> )Cl · 2C <sub>4</sub> H <sub>8</sub> O] <sub>2</sub>	Bright green	3.37
[Sm(C <sub>8</sub> H <sub>8</sub> )Cl · 2C <sub>4</sub> H <sub>8</sub> O] <sub>2</sub>	Purple	1.36

Complex	Reference
[(Me <sub>3</sub> Si) <sub>3</sub> C <sub>8</sub> H <sub>5</sub> ]C <sub>8</sub> H <sub>5</sub> Sm(THF) <sub>3</sub>	[229]
[K(DME) <sub>2</sub> ] <sub>2</sub> Yb(COT) <sub>2</sub>	[230]
K <sub>2</sub> [Yb( <i>t</i> -BuCOT) <sub>2</sub> ]	[231]

The majority of complexes are Ln(III)–COT derivatives. A variety of complexes of the type Ln(COT)X, where X = halide, chalcogenide, pnictogenide, hydrocarbyl are known. Ionic complexes are obtained by the reaction



where Ln = Y, La, Ce, Pr, Nd, Sm, Gd, Tb.

A comparison of structural parameters of COT complexes shows the relevance of steric interactions, particularly with metals in higher oxidation states in determining metal–ligand distances giving evidence for possible covalent bonding in these complexes.

The structure of Yb(COT)<sub>2</sub><sup>–</sup> shows a shorter [232] metal–ring carbon distance to the uncapped COT(Yb–C 1.843 Å) than the capped Yb–C distance 1.902 Å. The structure [233] of Er–COT complex is shown in Fig. 6.22.

The complex has a tetralayer-sandwich structure with adjacent Er(III) and K(I) bridged by η<sup>8</sup>-cyclooctatetraenyl group. The Er–C bond lengths range is 2.569–2.660 Å and K–COT range is 3.024–3.284 Å. When the substituted COT ligand is used in the preparation of lanthanide complexes as is the case with [1,4-(Me<sub>3</sub>Si)<sub>2</sub>(C<sub>8</sub>H<sub>6</sub>)] bridging ligands are limited to halides (Cl) and solvents like THF (O-bridge).

In the case of iodide, monomeric COTLnI(THF)<sub>n</sub> complexes, where Ln = La, Ce, Pr; n = 3; Ln = Nd, n = 2; Ln = Sm, n = 1 have been characterized and the complex of Ce with a four-legged stool geometry [234]. Many complexes containing Cp and COT of lanthanides have been characterized and an approximately linear coordination (173°) of

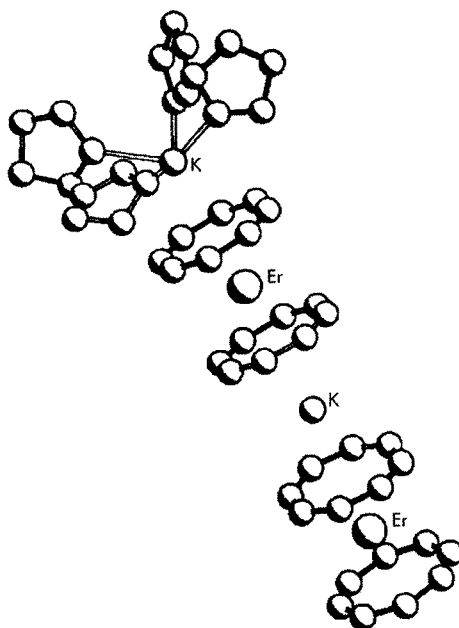


Fig. 6.22. Crystal structure of  $[(\text{COT})\text{-Er}(\mu\text{-COT})\text{K}(\mu\text{-COT})\text{Er}(\mu\text{-COT})\text{K}(\text{THF})_4]$  [233].

the ligand centroids around the metal is generally observed for non-solvated complexes as in the case of  $\text{Cp}^*\text{LuCOT}$  whose structure [235] is shown in Fig. 6.23.

Many substituted COT ligands have been used to characterize lanthanide complexes.

Complexing ligand	Lanthanides	Reference
$\text{C}_5\text{H}_9\text{Cp}$	$\text{Ln} = \text{Nd, Gd, 2THF}$ $\text{Ln} = \text{Gd; 1THF}$	[236] [236]
$\text{NaCp}$	$\text{Ln} = \text{Pr, Nd; 2THF}$ $\text{Ln} = \text{Gd; 1THF}$	[237] [237]
$\text{KC}_9\text{H}_7$	$\text{Ln} = \text{Pr, Nd, 2THF}$	[237]
Benzyl Cp	Gd	[238]
$\text{HC}_5\text{R}_4\text{PMe}_2$ ; R = H, Me	Sm	[239]
$(\text{CH}_2\text{SiMe}_3)$	$\text{Ln} = \text{Y, Sm, Lu}$	[240]
$[\text{N}(\text{SiMe}_3)_2]^-$	$\text{Ln} = \text{Y, Gd, Er, Lu}$	[241]
$[\text{Ph}_2\text{P}(\text{NSiMe}_3)_2]^-$		[242]
-OR	$\text{Ln} = \text{Y, Lu}$	[242]
Diaryl disulfide } Diaryl selenide }	$\text{Ln} = \text{Sm}$	[234]

The X-ray structure of the Nd complex [236] with COT and  $\text{C}_5\text{H}_9\text{Cp}$  shows distorted tetrahedral geometry while the Gd complex has triangular geometry when it has one THF molecule and tetrahedral geometry when there are 2 THF molecules in the complex.

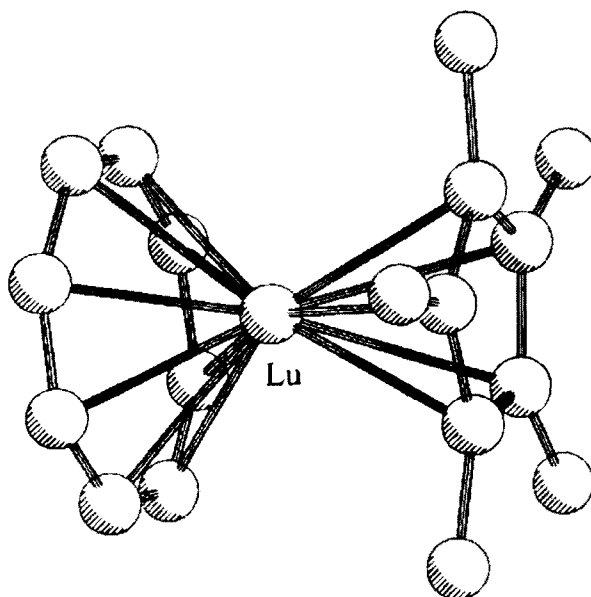


Fig. 6.23. Crystal structure of [(COT)-LuCp\*] [235].

The complexes CpPrCOT · 2THF and IndPrCOT · 2THF are characterized by non-parallel sandwich structures [237].

In the benzyl Cp complex of Gd, one benzyl Cp, one COT, and two DME oxygen atoms are coordinated making the formal coordination number ten [238]. The X-ray analysis [239] of COTSm(C<sub>5</sub>H<sub>4</sub>PPh<sub>2</sub>)(THF)<sub>2</sub> shows a pseudo-tetrahedral geometry around the metal ion.

The X-ray structure of {Sm[N(SiMe<sub>3</sub>)<sub>2</sub>]<sub>2</sub>} (μ-COT) has an unusual “inverse sandwich” structure [241], where the two Sm units are symmetrically bridged by the COT ligand, as shown in Fig. 6.24.

Lanthanum to nitrogen bonds are present in the mixed COT complexes [242]. Cerium(IV) forming stable complexes with COT, Ce(COT)<sub>2</sub> is characterized. Self-consistent field calculations showed [243] the ground state of cerocene to be almost entirely 4*f*' corresponding to the formula Ce<sup>3+</sup>(COT<sup>1.5</sup>)<sub>2</sub> rather than Ce<sup>4+</sup>(COT<sup>2</sup>)<sub>2</sub><sup>-</sup>. The methyl substituent in COT stabilizes the Ce(IV) complex which has a non-linear C<sub>g</sub>-Ce-C<sub>g</sub> angle of 176°. The two COT substituents are not staggered, and they are equidistant from cerium.

Substituted COT ligands have been used in the synthesis of cerocenes [246] starting from CeCl<sub>3</sub> and Ce(triflate)<sub>3</sub>. Cerocene reacts with Yb powder to give a complex [229] containing both Ce and Yb.

The molecular structure [245] of the contact ion pair [K(diglyme)][Ce(C<sub>8</sub>H<sub>8</sub>)<sub>2</sub>] is shown in Fig. 6.25. The significant feature is the symmetric coordination of the two C<sub>8</sub>H<sub>8</sub><sup>2-</sup> rings in a π fashion. The molecular symmetry is close to S<sub>8</sub>.

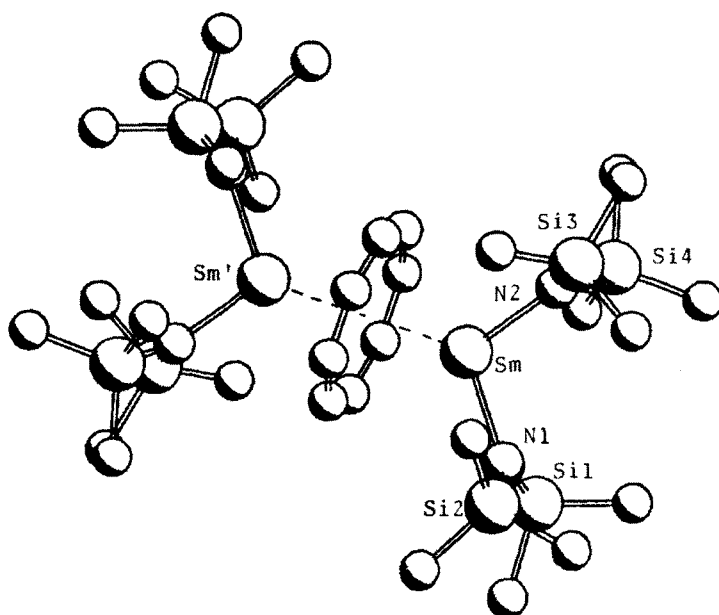


Fig. 6.24. Crystal structure of  $\{Sm[N(SiMe_3)_2]_2\}_2(\mu-COT)$  [241].

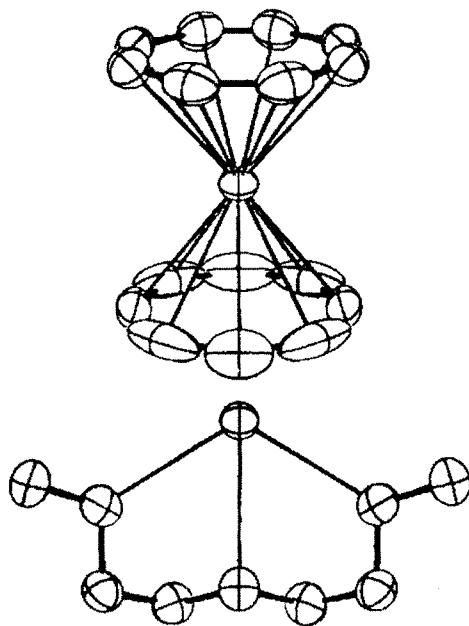
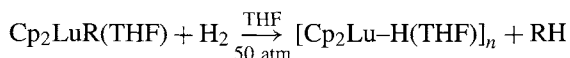


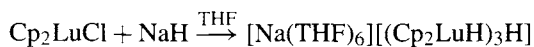
Fig. 6.25. The structure of the contact ion pair  $[K(diglyme)][Ce(C_8H_8)_2]$  (reprinted with permission from Hodgson, K.O. and K.N. Raymond, 1972, *Inorg. Chem.* 11, 3030–3035) [245].

## 25. Lanthanide cyclopentadienyl hydride complexes

The general method of synthesis of these complexes is hydrogenation of  $\text{Cp}_2\text{Y}$  or the corresponding alkyl derivatives



The products of hydrogenation are dimeric as evidenced by cryoscopic methods of determination of molecular weight and X-ray analysis [57]. Different hydrido complexes may be obtained by the reactions [246]



The structure of  $[\text{Na}(\text{THF})_6][(\text{Cp}_3\text{Lu})_2(\mu\text{-H})] \cdot 2\text{THF}$  shows a centrosymmetric dimeric anion with a single hydrogen bridge.

Other hydrido complexes that have been characterized are given below.

Complex		Reference
$[\text{Cp}_2^*\text{Sm}(\mu\text{-H})_2]$		[247]
$[\text{Cp}_2\text{ErH}]_3\text{Cl}[\text{Li}(\text{THF})_4]$		[248]
$[(\text{Me}_2\text{Cp})_2(\text{THF})\text{Y}(\mu\text{-H})_2]$		[248]
$[\text{Cp}_2\text{Y}(\mu\text{-OCH}_3)_3(\mu^3\text{-H})_2]$		[249]
$[(\text{Me}_3\text{Si})_2\text{C}_5\text{H}_3]_2\text{LnBH}_4(\text{THF})$	Ln = La, Pr, Nd, Sm	[250]
$[\text{Cp}_2\text{YCl}]_2[\text{AlH}_3\text{OEt}_2]$	Polymeric	[251]
$\text{Cp}_2\text{Y}(\mu\text{-Cl})_2\text{YCp}_2$	Y-H-Al bridge connected to $\text{AlH}_3 \cdot \text{OEt}_2$	[251]
$[\text{Cp}_2\text{Y}]_2\text{AlH}_4\text{Cl} \cdot \text{NEt}_3\text{C}_6\text{H}_6$		[252]
$[(t\text{Bu}_2\text{C}_5\text{H}_3)\text{LuH}]_4[\text{AlH}_4 \cdot \text{Et}_2\text{O}]_2[\text{AlH}_4]_2$		[253]
$[\text{Cp}_2\text{Sm}(\mu^3\text{-H})_2][(\mu^2\text{-H})_2\text{AlHNEt}_3]_2$		[254]
$\text{Cp}_2\text{LnRe}_2\text{H}_7(\text{PMe}_2\text{Ph})_4$	Ln = Y, Lu	[255]

The X-ray structure of the Sm complex [247] shows one of the  $\text{Cp}_2^*\text{Sm}$  units rotated with respect to the second one by  $87^\circ$  such that the molecule shows approximate  $S_4$  symmetry.

In the Er complex [248] there are cation-anion ion-pairs. In the anionic unit, three  $\text{Cp}_2\text{Er}$  units are connected by hydrogen and chlorine bridges in a triangular array with one  $\mu^3\text{-H}$  having  $\text{Er-H}_{\text{av}}$  2.18 Å, two ( $\mu^2\text{-H}$ ),  $\text{Er-H}_{\text{av}}$  of 2.34 Å.

The Y complex with ( $\mu\text{-H}$ ) is characterized by nearly square planar geometry for the four cyclopentadienyl centroids [248]. The structure of the methoxy complex of Y is a triangular arrangement of three  $\text{Cp}_2\text{Y}$  units bridged by methoxy groups [249].

In the case of Y, Yb and solvent free complex of Sc, the  $\text{BH}_4$  group behaves like a tridentate ligand.

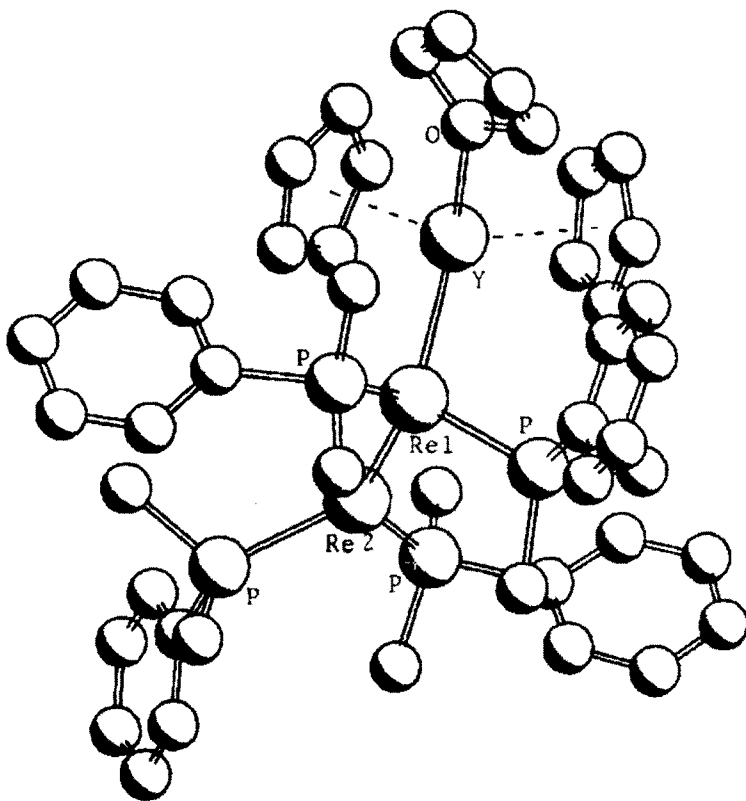


Fig. 6.26. Crystal structure of  $[\text{Cp}_2\text{Y}(\text{THF})\text{Re}_2\text{H}_7(\text{PMe}_2\text{Ph})_4]$  [255].

The potential use of non-solvated lanthanide cyclopentadienyl hydride complexes as catalysts in alkene C–H bond activation, hydrogenation of alkynes led to synthesis of aluminum hydride organo lanthanide complexes. Examples of such complexes with polymeric structure and chain structure have been characterized [251].

The X-ray analysis of the mixed Al and Y complex containing  $\text{NEt}_3$  group shows a trimetallic structure [252], in a triangular array in which the centre has a hydrogen  $\mu^3$ -bonded to the three metal ions and metal ions in turn are connected on the periphery by hydrogen and chlorine bridges.

The lutetium complex [253] has a structure characterized by a tetrahedral metal core of Lu atoms bound by bridging hydrogens, and tri- $\text{AlH}_4$  and tetradentate ( $\text{AlH}_4 \cdot \text{Et}_2\text{O}$ ) groups.

The Sm complex [254] is characterized by a formal twenty electron configuration. The Sm atom is coordinated by four hydrides. The heterometallic complex of Y and Re has an open triangular structure as shown in Fig. 6.26. The  $\text{Re}(2)\text{--Y}'$  distance is 4.186 Å and the other  $\text{Re}(1)\text{--Y}$  distance of 3.090 Å. This suggests the presence of a hydride bridge for  $\text{Re}(1)\text{--Y}$ . Short  $\text{Re}\text{--Re}$  distance of 2.576 is also accounted for by the earlier explanation. The bridging hydride structure is also supported by NMR data [255].



## 26. Lanthanide–transition metal mixed organometallic complexes

Organolanthanide complexes are coordinately unsaturated and as a result take part in forming mixed complexes with transition metal complexes containing nitrosyl or carbonyl groups. As a result, mixed complexes containing metal–metal bonds or lanthanide–isocarbonyl or isonitrosyl interactions have been characterized. Some typical complexes are given below.

Complex		Reference
$\text{Cp}_3\text{Ln}$ or $(\text{MeCp})_3\text{Ln}$	Ln = Sm, Gd, Dy, Ho, Er, Yb	[256]
+		
$\text{Co}_2(\text{CO})_8$ , $\text{MnCp}(\text{CO})_3$	M = Cr, Mo, W	[256]
$\text{CpM}(\text{CO})_2\text{NO}$		
$(\text{THF})\text{Cp}_2\text{Yb}(\mu\text{-OC})\text{Co}(\text{CO})_3$		[257]
$(\text{THF})\text{Cp}_2\text{Lu-Ru}(\text{CO})_2\text{Cp}$		[257]
$[\text{Cp}_2'\text{Ce}(\mu\text{-OC})\text{W}(\text{CO})\text{Cp}(\mu\text{-CO})_2]$		[258]
$\text{Cp}_2^*\text{Yb}(\mu\text{-OC})\text{Co}(\text{CO})_3\text{THF}$		[249]
Complexes with Ln-OC-M bridges		[259]
$[(\text{C}_5\text{H}_4\text{PPh}_2)_2\text{Yb}(\text{THF})_2\text{X}] \cdot n\text{PhMe}$	X = Ni(CO) <sub>2</sub> , Mo(CO) <sub>4</sub> , PtMe <sub>2</sub>	[260]
Mo–Sm, W–Sm		[261]

Isocarbonyl and isonitrosyl linkages to lanthanides are evident in the complexes noted above [256], confirmed by IR spectroscopy. In the Yb complex, an isocarbonyl bridge Yb–OC–Co has been confirmed while in the lutetium complex Lu–Ru metal–metal bond is present [257].

In the cerium complex an unusual 12-membered ring has been observed. The ring is formed by Ce–O=C–W units with the O–C–W angle nearly linear (178°) while the Ce–O–C angle is 154°. This structure has been found to be unstable [258].

X-ray analysis of the Yb complex [249] shows the two coordination tetrahedra around Yb and Ce are linked by a CO bridge. A large number of lanthanide complexes with Ln–OC–M bridges have been characterized [259]. Tetrathiometallate anions have been used for the synthesis of mixed metal [261], Mo–Sm, W–Sm complexes such as  $\{[\text{Cp}_2^*\text{Sm}]_2\text{Mo}(\mu\text{-S})_4\}\text{PPh}_4$ .

The structure of the mixed metal complex of Yb and Ni is shown in Fig. 6.27. In the complex Yb has a pseudotetrahedral geometry consisting of two THF molecules and Cp\* ring centroids of two  $\eta^5$ -diphenyl phosphino-cyclopentadienides which are also bonded through the phosphorus atom to Ni(CO)<sub>2</sub> units [260].

## 27. Lanthanide arene complexes

This is a relatively new area of lanthanide complexes. The first complex of this family  $\text{Sm}(\eta^6\text{-C}_6\text{Me}_6)(\text{AlCl}_4) \cdot 1.5\text{toluene}$  was synthesized from  $\text{SmCl}_3$ ,  $\text{AlCl}_3$  and hexamethyl

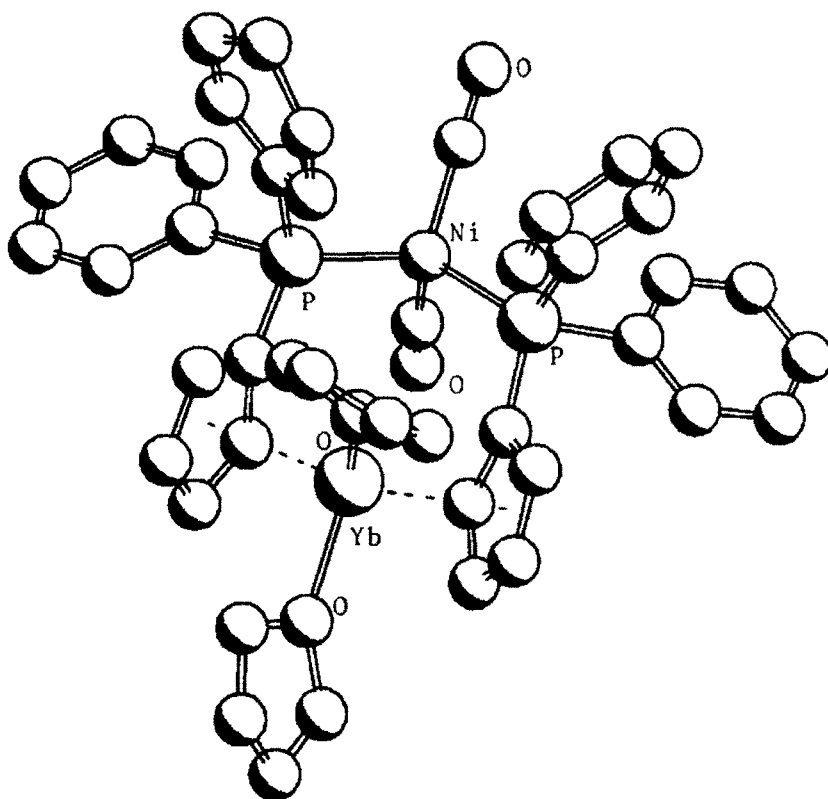


Fig. 6.27. Crystal structure of  $[\text{Yb}(\text{THF})_2(\text{C}_5\text{H}_4\text{PPh}_2)_2\text{Ni}(\text{CO})_2]$  [260].

benzene in toluene medium [262]. Some other complexes characterized are given below.

Complex		Reference
$[\text{Ln}^0(\eta^6\text{-}i\text{-Bu}_3\text{C}_6\text{H}_3)_2]$	$\text{Ln} = \text{Nd, Tb, Dy, Ho, Er, Lu}$	[263]
$\text{Ln}(\eta^6\text{-C}_6\text{H}_6)(\text{AlCl}_4)_3 \cdot \text{benzene}$	$\text{Ln} = \text{La, Nd, Sm}$	[264]
$\text{Yb}(\text{o-2,6-Ph}_2\text{C}_6\text{H}_3)_3$		[265]
$(\mu\text{-}\eta^4 : \eta^4\text{-C}_{10}\text{H}_8)[\text{LaI}_2(\text{THF})_3]_2$		[266]

The formation of  $\text{Ln}^0$  complexes is rationalized in terms of a bonding model [263] involving the promotion of energy from  $f^n s^2$  to  $f^{n-1} d^1 s^2$ . The structure of the Gd complex is shown in Fig. 6.28. The complex has a sandwich structure.

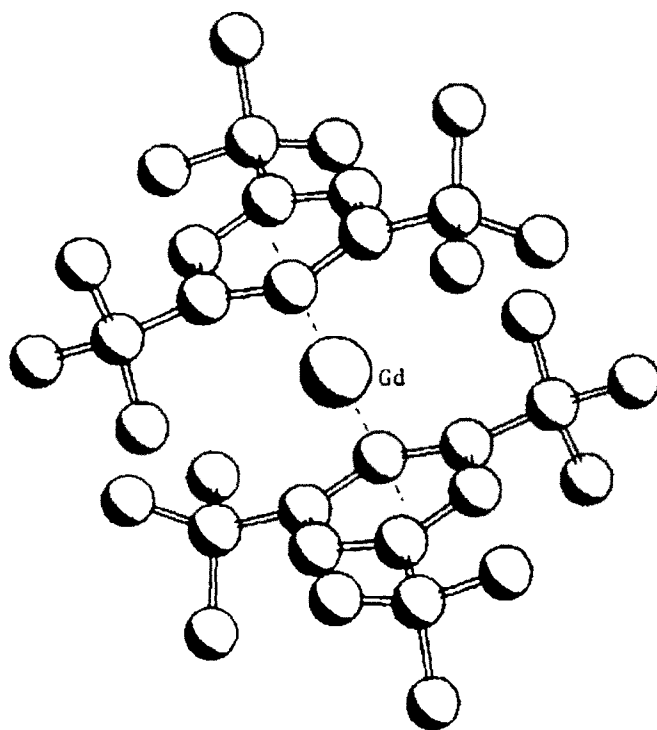
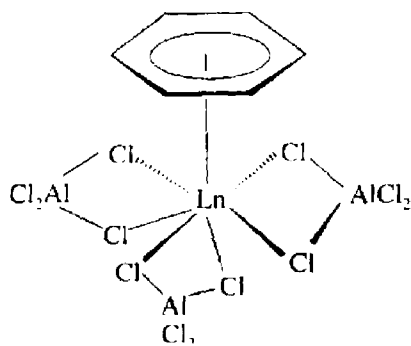


Fig. 6.28. Crystal structure of  $[(\eta^6\text{-C}_6\text{H}_3\text{Bu}_3)_2\text{Gd}]$  [263].

The lanthanide complexes containing benzene have a pentagonal bipyramidal geometry [264].



Intra molecular Yb- $\pi$  interaction [2.978(6) Å] from one of the phenyl substituents has been observed in the Yb complex [265]. A bridging naphthalene unit is present in the lanthanum complex connecting two  $\text{LaI}_2(\text{THF})_3$  units [266].

## 28. Lanthanide complexes with other ligands

Typical complexes of lanthanides with other ligands are noted below.

Complex		Reference
$(C_4Me_4X)_2Ln(THF)_2$	$Ln = Yb, Sm; X = P, As$	[267]
Complexes with carboranes	$Sm, Eu, Gd, Yb$	[268]
$[(Ph_3P)_2N][(\eta^5C_2B_9H_{11})_2Sm(THF)_2]$	$Sm$	[269]
Trinuclear carborane clusters	$Gd, Tb$	[268]

The similarity of carboranes to the cyclopentadienyl ligand gave impetus for the characterization of carborane complexes of lanthanides.  $Sm, Eu, Gd,$  and  $Yb$  complexes of both half-sandwich and sandwich structure have been characterized [268]. The structure of the complex  $[(\eta^5C_2B_9H_{11})_2Sm(THF)_2]$  is shown in Fig. 6.29.

With the ligand  $[C_2B_9H_{11}]^{2-}$  bivalent lanthanides form 1:1 half sandwich type complexes and trivalent lanthanides form bent sandwich complexes [269].

Trinuclear carborane clusters are formed [268,270] in the case of  $Gd$  and  $Tb$ .

The most important applications of organolanthanides are as Ziegler–Natta catalysts in polymerization of olefins and as reagents in stoichiometric organic synthesis. Organolanthanide compounds are also useful as volatile precursors for MOCVD applications in the

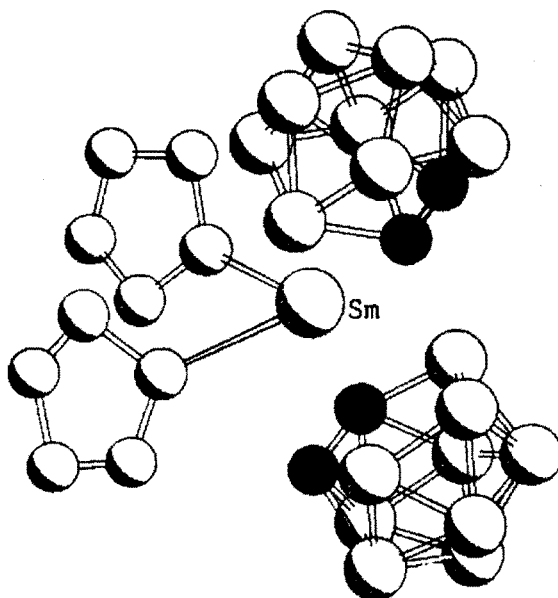


Fig. 6.29. Crystal structure of the anion of  $[(Ph_3P)_2N][(\eta^5C_2B_9H_{11})_2Sm(THF)_2]$  [269].

fabrication of semiconductors. Because of the interesting magnetic properties they are potentially useful for optoelectronic devices. The possible potential use of enantiomerically pure organolanthanide complexes in enantioselective catalytic hydrogenation, alkylation and hydroamination of prochiral unsaturated systems deserves attention.

At present, there is nearly a century of industrial applications and the future of this field is as promising as ever, both from the fundamental and applied points of view.

## References

- [1] G. Wilkinson, J.M. Birmingham, *J. Am. Chem. Soc.* **76**, 6210, 1954.
- [2] T.J. Marks, I.L. Fraglia, *Fundamental and Technological Aspects of Organo-f-element chemistry*, Reidel, Dordrecht, 1985.
- [3] M.N. Bochkarev, G.S. Kalina, L.N. Sacharov, S.Ya. Korshev, *Organic Compounds of the Rare Earths*, Nauka, Moscow, 1989.
- [4] T.J. Marks, R.D. Ernst, *Comprehensive Organometallic Chemistry*, Vol. 3, eds F.G.A. Stone, G. Wilkinson, E.W. Abel, Pergamon press, Oxford, 1982.
- [5] G.J. Palenik, *Systematics and the Properties of the Lanthanides*, ed. S.P. Sinha, Reidel, Dordrecht, 1983.
- [6] W.J. Evans, M.A. Hosborn, *J. Organomet. Chem.* **326**, 299, 1987.
- [7] T.J. Marks, M.R. Gangne, S.P. Nolan, L.E. Shock, A.M. Seyam, *D. Stern, Pure Appl. Chem.* **61**, 1665, 1989.
- [8] J.C. Green, *Struct. Bonding* **43**, 37, 1989.
- [9] C.J. Burns, B.E. Bursten, *Comments Inorg. Chem.* **9**, 61, 1989.
- [10] M. Ephriti Khine, *New J. Chem.* **16**, 451, 1992.
- [11] C.J. Schaverien, *Adv. Organomet. Chem.* **36**, 283, 1994.
- [12] F.T. Edelmann, *Angew. Chem.* **34**, 2466, 1995.
- [13] H. Schumann, J.A. Meese-Mercktscheffel, L. Esser, *Chem. Rev.* **95**, 865, 1995.
- [14] F.G.N. Clark, *Comprehensive Organometallic Chemistry II*, Vol. 4, eds E.W. Abel, F. Gordon, A. Stone, J. Wilkinson, Ch. 1, Pergamon Press, Oxford, 1995.
- [15] J. Richter, F. Edelmann, *Coord. Chem. Rev.* **147**, 373, 1996.
- [16] G.B. Deacon, Q. Shen, *J. Organomet. Chem.* **511**, 1-17, 1996.
- [17] B.L. Kalsotra, S.P. Anand, R.K. Multani, B.D. Jain, *J. Organomet. Chem.* **28**, 87, 1971.
- [18] D.B. Deacon, T.D. Tuong, D.G. Vince, *Polyhedron* **2**, 969, 1983.
- [19] Y. Zhongwen, M. Huaizhu, Y. Yonghfei, *J. Less Common Metals* **126**, 405, 1986.
- [20] G.B. Deacon, C.M. Forsyth, R.H. Newnham, T.D. Tuong, *Aust. J. Chem.* **40**, 895, 1987.
- [21] P.S. Gradeff, K. Yunlu, T.J. Deming, J.M. Olofson, J.W. Ziller, W.J. Evans, *Inorg. Chem.* **28**, 2600, 1989.
- [22] K. Jacob, J. Glanz, K. Tittes, K.H. Thiele, I. Parlik, A. Lycka, *Z. Anorg. Allg. Chem.* **577**, 145, 1989.
- [23] S.H. Eggers, J. Kopf, R.D. Fischer, *J. Organomet.* **5**, 383, 1986.
- [24] J. Rebizant, C. Apostolidis, M.R. Spirlet, B. Kanellakopulos, *Acta Crystallogr.* **C44**, 614, 1988.
- [25] V.K. Bel'skii, Yu.K. Gun'ko, G.D. Soloveichik, M.B. Bulychev, *Organomet. Chem. USSR* **4**, 281, 1991.
- [26] W. Hinrichs, D. Melzer, M. Rehwoldt, V. Jahn, R.D. Fischer, *J. Organomet. Chem.* **251**, 299, 1983.
- [27] M. Adam, G. Massarweh, R.D. Fischer, *J. Organomet. Chem.* **405**, C33, 1991.
- [28] S.H. Eggers, W. Hinrichs, J. Kopf, W. Jahn, R.D. Fischer, *J. Organomet. Chem.* **311**, 313, 1986.
- [29] S.H. Eggers, J. Kopf, R.D. Fischer, *Acta Crystallogr.* **C43**, 2288, 1987.
- [30] W.T. Carnall, in: *Organometallics of the f-Elements*, eds T.J. Marks, R.D. Fischer, Ch. 9, Reidel, Dordrecht, 1979.
- [31] V.T. Aleksanyam, G.K. Borisov, I.A. Garbuzova, G.G. Devyatykh, *J. Organomet. Chem.* **131**, 251, 1977.
- [32] C. Qian, D. Zhu, Y. Gu, *J. Organomet. Chem.* **398**, 251, 1991.
- [33] C. Ni, D. Deng, C. Qian, *Inorg. Chim. Acta* **110**, L7, 1985.
- [34] G.Z. Suleimanov, V.I. Bregadze, N.A. Koval'chuk, I.P. Baletskaya, *J. Organomet. Chem.* **235**, C17, 1982.
- [35] G.B. Deacon, A.J. Koplick, T.D. Tuong, *Aust. J. Chem.* **37**, 517, 1984.

- [36] Z. Ye, S. Wang, Y. Yu, L. Shi, *Inorg. Chim. Acta* **177**, 97, 1990.
- [37] M.R. Spirlet, J. Rebizant, C. Apostolodis, B. Kanellakopoulos, *Inorg. Chim. Acta* **139**, 211, 1987.
- [38] G.B. Deacon, B.M. Gatehouse, S.N. Platts, D.L. Wilkinson, *Aust. J. Chem.* **40**, 907, 1987.
- [39] M. Adam, E.T.K. Haupt, R.D. Fisher, *Bull. Mag. Reson.* **12**, 101, 1990.
- [40] H.D. Amberger, H. Schultze, H. Reddmann, G.V. Shalimoff, N.M. Edelstein, *J. Less Common Metals* **149**, 249, 1989.
- [41] H. Schulz, H. Reddmann, H.D. Amberger, *J. Organomet. Chem.* **440**, 317, 1992; **424**, 139, 1992.
- [42] H. Schumann, V. Genthe, E. Hahn, M.B. Hos-sain, D. Helm, *J. Organomet. Chem.* **299**, 67, 1986.
- [43] H. Schumann, S. Nickel, J. Loebel, J. Pickardt, *Organometallics* **7**, 2004, 1988.
- [44] W. Jahn, K. Yunlu, W. Oroschin, H.D. Am-berger, R.D. Fisher, *Inorg. Chim. Acta* **95**, 85, 1984.
- [45] Y. Sun, Q. Shen, S. Jin, Y. Lin, *Yingyong Huaxue* **8**, 23, 1991.
- [46] S.D. Stults, R.A. Andersen, A. Zalkin, *Organometallics* **9**, 115, 1990.
- [47] A. Hammel, W. Schwarz, J. Weidlein, *J. Organomet. Chem.* **363**, C29, 1989.
- [48] G. Paolucci, R.D. Fischer, H. Breitbach, B. Pelli, P. Traldi, *Organometallics* **7**, 1918, 1988.
- [49] S.D. Stults, A. Zalkin, *Acta Crystallogr.* **C43**, 430, 1987.
- [50] W.J. Evans, R.A. Keyer, J.W. Ziller, *J. Organomet. Chem.* **394**, 87, 1990.
- [51] H. Schumann, J.A. Meese-Marktscheffel, B. Gorella, F.H. Gorlitz, *J. Organomet. Chem.* **428**, C27, 1992.
- [52] W.J. Evans, S.L. Gonzales, J.W. Ziller, *J. Am. Chem. Soc.* **113**, 7243, 1991.
- [53] W.J. Evans, K.J. Forrestal, J. Leman, Y.W. Ziller, *Organometallics* **15**, 527, 1996.
- [54] C. Qian, B. Wang, D. Deng, G. Wa, P. Zheng, *J. Organomet. Chem.* **427**, C29, 1992.
- [55] D. Deng, C. Qian, F. Song, Z. Wang, G. Wu, P. Zheng, S. Jin, Y. Lin, *J. Organomet. Chem.* **458**, 83, 1993.
- [56] B.L. Kalsotra, S.P. Anand, R.K. Multani, B.D. Jain, *J. Organomet. Chem.* **28**, 87, 1971.
- [57] T.J. Marks, R.D. Ernst, in: *Comprehensive Organometallic Chemistry*, Vol. 3, eds F.G.A. Stone, G. Willinson, E.W. Abel, Ch. 21, p. 173, Pergamon Press, Oxford, 1982.
- [58] H. Gao, Q. Shen, J. Hu, S. Jin, Y. Lin, *Chinese Sci. Bull.* **34**, 614, 1989.
- [59] H. Gao, Q. Shen, J. Hu, S. Jin, Y. Lin, *J. Organomet. Chem.* **427**, 141, 1992.
- [60] W.J. Evans, T.J. Deming, J.W. Ziller, *Organometallics* **8**, 1581, 1989.
- [61] W. Lamberts, H. Lueken, B. Hessner, *Inorg. Chim. Acta* **134**, 155, 1987.
- [62] W. Lamberts, B. Hessner, H. Lueken, *Inorg. Chim. Acta* **139**, 215, 1987.
- [63] Z. Ye, H.M. & A. Y.J. Wu, *J. Less Common Met.* **126**, 405, 1986.
- [64] F. Bottomley, D.E. Paez, P.S. White, *J. Organomet. Chem.* **191**, 35, 1985.
- [65] Z. Jin, Y. Liu, W. Chen, *Sci. Sin. Ser. B* **30**, 1136, 1988.
- [66] Z. Li, W. Chen, G. Xu, J. Ren, W.H. Xue, **3**, 111, 1987.
- [67] X. Li, X. Feng, Y. Xu, H. Wang, P. Sun, J. Shi, *Kexue Tongbao* **32**, 1259, 1987.
- [68] W.J. Evans, R. Dominguez, T.P. Hanusa, *Organometallics* **5**, 236, 1986.
- [69] J. Holton, M.F. Lappert, D.G.H. Ballard, R. Pearce, J.L. Atwood, W.E. Hunter, *J. Chem. Soc., Dalton Trans.* **54**, 1979.
- [70] H. Schumann, W. Genthe, N. Bruncks, J. Pickardt, *Organometallics* **1**, 1194, 1982.
- [71] C. Qian, G. Ye, H. Lu, Y. Li, J. Zhou, Y. Ge, *J. Organomet. Chem.* **247**, 161, 1983.
- [72] G.B. Deacon, D.L. Wilkinson, *Inorg. Chim. Acta* **142**, 155, 1988.
- [73] J. Collin, J.L. Namy, C. Beid, H.B. Kagan, *Inorg. Chim.* **140**, 29, 1987.
- [74] H. Schumann, J.A. Meese-Marktscheffel, A. Dietrich, F.H. Gorlitz, *J. Organomet. Chem.* **430**, 299, 1992.
- [75] H. Schumann, H. Lauke, E. Hahn, M.J. Heeg, D. Vander Helm, *Organometallics* **4**, 321, 1985.
- [76] J.L. Atwood, W.E. Hunter, A.L. Wayda, W.J. Evans, *Inorg. Chem.* **20**, 4115, 1981.
- [77] C. Qian, Y. Ge, *J. Organomet. Chem.* **299**, 97, 1986.
- [78] H. Schumann, F.W. Reier, E. Palamidis, *J. Organomet. Chem.* **297**, C30, 1985.
- [79] H. Schumann, F.W. Reier, *Inorg. Chim. Acta* **95**, 43, 1984.
- [80] Z. Zhennan, W.Z. Zhik, D. Baohu, Y.Z. Wen, *Polyhedron* **8**, 17, 1989.
- [81] D.M. Roitershtein, L.F. Rybakova, E.S. Petrov, A.M. Ellern, M. Antipin, T. Struchov, *J. Organomet. Chem.* **460**, 39, 1993.
- [82] G.B. Deacon, D.L. Wilkinson, *Aust. J. Chem.* **42**, 845, 1989.

- [83] X. Wang, Z. Ye, *Youji Huaxue* 389, 1985.
- [84] Z. Ye, Z. Zhou, S. Yuan, Z. Luo, *Youji Huaxue* 119, 1984.
- [85] X. Wang, X. Zhou, J. Ren, J. Zhong, Y. Xia, R. Liu, S. Wang, *Huaxue Xuebo* 44, 1155, 1986.
- [86] Z. Ye, Z. Zhou, Z. Lou, X. Wang, F. Shen, *Huaxue Xuebo* 44, 707, 1986.
- [87] J. Zhou, Y. Ge, C. Qian, *Synth. React. Inorg. Met. Org. Chem.* 14, 651, 1984.
- [88] H. Schumann, J.A. Meese-Marktscheffel, A. Dietrich, *J. Organomet. Chem.* 377, C5, 1989.
- [89] J. Stehr, R.D. Fischer, *J. Organomet. Chem.* 430, C1, 1992.
- [90] Z. Wu, Z. Huang, R. Cai, Z. Xu, X. You, X. Huang, *Polyhedron* 15, 13, 1996.
- [91] Z. Wu, D. Pan, Z. Huang, R. Cai, *Polyhedron* 15, 127, 1996.
- [92] P. Poremba, M. Noltemeyer, H.G. Schmidt, F.T. Edelmann, *J. Organomet. Chem.* 501, 305, 1995.
- [93] L. Yang, L. Dai, H. Ma, Z. Ye, *Organometallics* 8, 1129, 1989.
- [94] H. Schumann, E. Palamidis, J. Loebel, *J. Organomet. Chem.* 384, C49, 1990.
- [95] H. Schumann, I. Albrecht, M. Gallagher, E. Hahn, C. Muchmore, J. Pickardt, *J. Organomet. Chem.* 349, 103, 1988.
- [96] Z. Wu, W. Ma, Z. Huang, R. Cai, *Polyhedron* 15, 3427, 1996.
- [97] R.E. Magin, S. Manastyrsky, M. Dubeck, *J. Am. Chem. Soc.* 85, 672, 1963.
- [98] W.J. Evans, J.H. Meadows, W.E. Hunter, J.L. Atwood, *Organometallics* 2, 1252, 1983.
- [99] W.J. Evans, J.H. Meadows, W.E. Hunter, J.L. Atwood, *J. Am. Chem. Soc.* 106, 1291, 1984.
- [100] H. Schumann, E. Palamidis, G. Schmid, R. Boese, *Angew. Chemie, Int. Engl. Edn.* 25, 718, 1986.
- [101] H. Schumann, E. Palamidis, J. Loebel, J. Pickardt, *Organometallics* 7, 1008, 1988.
- [102] A.L. Wayda, *J. Organomet. Chem.* 361, 73, 1989.
- [103] A. Recknagel, F. Knosel, H. Gornitzka, M. Noltemeyer, F.T. Edelmann, U. Behrens, *J. Organomet. Chem.* 417, 363, 1991.
- [104] M.F. Lappert, A. Singh, J.L. Atwood, W.E. Hunter, *J. Chem. Commun.* 1190, 1191, 1981; 69, 1983.
- [105] D. Deng, C. Qian, G. Wu, P. Zheng, *J. Chem. Soc. Chem. Commun.* 880, 1990.
- [106] D. Deng, B. Li, C. Qian, *Polyhedron* 9, 1453, 1990.
- [107] W.A. Herrmann, R. Anwander, P. Munk, W. Scherer, *Chem. Ber.* 126, 331, 1993.
- [108] D.G.H. Ballard, A. Courties, J. Holton, J. McMeeking, R. Pearce, *J. Chem. Soc. Chem. Commun.* 994, 1978.
- [109] Q. Shen, M. Qi, J. Guan, Y. Lin, *J. Organomet. Chem.* 406, 353, 1991.
- [110] Y. Chauvin, S. Heyworth, H. Olivier, F. Robert, J. Saussine, *J. Organomet. Chem.* 455, 89, 1993.
- [111] S.A. Vinogradov, A.E. Mistrukov, I.P. Beletskaya, *J. Chem. Soc., Dalton Trans.* 2679, 1995.
- [112] W.J. Evans, M.S. Sollberger, J.L. Shreeve, J.M. Olofson, J.H. Rein, W.J. Ziller, *Inorg. Chem.* 31, 2492, 1992.
- [113] G. Masserwech, R.D. Fischer, *J. Organomet. Chem.* 444, 67, 1993.
- [114] S.D. Stults, R.A. Andersen, A. Zalkin, *Organometallics* 9, 1623, 1990.
- [115] P.B. Hitchcock, M.F. Lappert, S. Prashar, *J. Organomet. Chem.* 413, 79, 1991.
- [116] A. Hammell, J. Weidlein, *J. Organomet. Chem.* 388, 75, 1990.
- [117] F.R. Calderazzo, R. Pappalardo, S. Losi, *J. Inorg. Nucl. Chem.* 28, 987, 1966.
- [118] M. Kaupp, P. Schleyer, M. Dolg, H. Stoll, *J. Am. Chem. Soc.* 114, 8202, 1992.
- [119] M. Kaupp, O.P. Charkin, P. Schleyer, *Organometallics* 11, 2765, 1992.
- [120] G.B. Deacon, B.M. Gatehouse, P.A. White, *Polyhedron* 8, 1983, 1989.
- [121] V.D. Makhav, Yu.B. Zvedov, N.G. Chernrukov, V.I. Berestenkov, *Vysokochist Veshchestva* 210, 1990.
- [122] V.K. Bel'skii, Yu.K. Gun'ko, B.M. Bulychev, A.I. Sizov, G.I. Soloveichik, *J. Organomet. Chem.* 437, 177, 1992.
- [123] P.B. Hitchcock, J.A.K. Howard, M.F. Lappert, S. Prashar, *J. Organomet. Chem.* 437, 177, 1992.
- [124] A. Schumann, M. Glanz, H. Hemiling, *New J. Chem.* 19, 491, 1995.
- [125] W. Chen, G. Yu, S. Xias, Y. Huang, X. Gao, *Kexue Tongbao* 28, 1043, 1983.
- [126] C.S. Day, V.W. Day, R.D. Ernst, S.H. Vollmer, *Organometallics* 1, 998, 1982.
- [127] D.B. Deacon, C.D. Fallon, D.L. Wilkinson, *J. Organomet. Chem.* 293, 45, 1985.
- [128] Z. Jin, N. Hu, Y. Yi, X. Xu, G. Liu, *Inorg. Chim. Acta* 142, 333, 1988.
- [129] G. Depaoli, P. Zanonato, G. Valle, *Inorg. Chim. Acta* 170, 109, 1990.
- [130] W.J. Evans, M.S. Sollberger, *J. Am. Chem. Soc.* 108, 6095, 1986.

- [131] Z. Wu, Z. Ye, Z. Zhou, *Polyhedron* **8**, 2109, 1989.
- [132] A.V. Protchenko, L.N. Zakharov, M.N. Bokharev, J.Y. Struchko, *J. Organomet. Chem.* **447**, 209, 1993.
- [133] Z. Jin, J. Guan, G. Wei, J. Hu, Q. Shen, *Jiegou Huaxue* **9**, 140, 1990.
- [134] H. Schumann, J.A. Meese-Markts Cheffel, A. Dietrich, J. Pickardt, *J. Organomet. Chem.* **433**, 241, 1992.
- [135] (a) J. Guan, S. Jin, Y. Lin, Q. Shen, *Organometallics* **11**, 2483, 1992; (b) W.J. Evans, T.J. Boyle, J.W. Ziller, *J. Organomet. Chem.* **462**, 141, 1993.
- [136] J. Jin, S. Jin, Z. Jin, W. Chen, *Polyhedron* **22**, 2873, 1992.
- [137] J. Zhou, H. Ma, Z. Wu, X. You, Z. Xu, X. Huang, *J. Organomet. Chem.* **503**, 11, 1995.
- [138] W.J. Evans, L.A. Hughes, T.P. Hanusa, *J. Am. Chem. Soc.* **106**, 4270, 1984.
- [139] W.J. Evans, L.A. Hughes, T.P. Hanusa, *J. Organometal.* **5**, 1285, 1986.
- [140] R.A. Andersen, J.M. Boncella, C.J. Burns, R. Blom, A. Haaland, H.V. Volden, *J. Organomet. Chem.* **312**, C49, 1986.
- [141] W.J. Evans, T.A. Ulibarri, H. Zhang, *J. Am. Chem. Soc.* **110**, 6877, 1988.
- [142] S.J. Swamy, J. Loebel, J. Pickardt, H. Schumann, *J. Organomet. Chem.* **353**, 27, 1988.
- [143] W.J. Evans, J.W. Grate, H.W. Choi, I. Bloom, W.E. Hunter, J.L. Atwood, *J. Am. Chem. Soc.* **107**, 941, 1985.
- [144] T.D. Tilley, R.A. Andersen, B. Spencer, A. Zalkin, *Inorg. Chem.* **21**, 2647, 1982.
- [145] K.H. Raymond, C.W. Eigenbrot, *Acc. Chem. Res.* **13**, 276, 1980.
- [146] T.D. Tilley, R.A. Andersen, A. Zalkin, *Inorg. Chem.* **22**, 856, 1983.
- [147] J.C. Green, D. Hohl, N. Roesch, *Organometallics* **6**, 712, 1987.
- [148] A.L. Wayda, J.L. Dye, R.D. Rogers, *Organometallics* **3**, 1605, 1984.
- [149] R.J. Finke, S.R. Keenan, P.L. Watson, *Organometallics* **8**, 263, 1989.
- [150] C.J. Burns, R.A. Andersen, *J. Chem. Soc., Chem. Commun.* 136, 1989.
- [151] C.J. Burns, R.A. Andersen, *J. Am. Chem. Soc.* **109**, 915, 941, 5853, 1987.
- [152] M. Wedler, A.K. Recknagel, P.T. Edelman, *J. Organomet. Chem.* **395**, C26, 1990.
- [153] W.J. Evans, D.K. Drummond, J.W. Grate, H. Zhang, J.L. Atwood, *J. Am. Chem. Soc.* **109**, 3928, 1987.
- [154] P.L. Watson, T.H. Tulip, I. Williams, *Organometallics* **9**, 1999, 1990.
- [155] P.L. Watson, D.C. Roe, *J. Am. Chem. Soc.* **104**, 6471, 1982.
- [156] W.J. Evans, I. Bloom, W.E. Hunter, J.L. Atwood, *Organometallics* **4**, 112, 1985.
- [157] W.J. Evans, L.R. Chamberlain, T.A. Ulibarri, J.W. Ziller, *J. Am. Chem. Soc.* **110**, 6423, 1988.
- [158] W.J. Evans, T.A. Ulibarri, J.W. Ziller, *J. Am. Chem. Soc.* **112**, 219, 1990.
- [159] W.J. Evans, S. L. Gonzales, J.W. Ziller, *J. Am. Chem. Soc.* **116**, 2600, 1994.
- [160] P.L. Watson, G.W. Parshall, *Acc. Chem. Res.* **18**, 51, 1985.
- [161] H. Schumann, E.C.E. Rosenthal, G. Kociok-Kohn, G.A. Molander, J. Winterfield, *J. Organomet. Chem.* **496**, 233, 1995.
- [162] M. Booi, A. Meetsma, J.H. Teuben, *Organometallics* **10**, 3246, 1991.
- [163] A. Scholz, A. Smola, J. Scholz, J. Loebe, H. Schumann, K.K. Thiele, *Angew. Chem.* **33**, 1171, 1991.
- [164] F.G.N. Cloke, I.C. Dalby, P.B. Hitchcock, H. Karamallakis, G.A. Lawless, *J. Chem. Soc. Chem. Comm.* 779, 1991.
- [165] M.N. Bochkarev, V.V. Khramenkov, Y.F. Rad'kov, L.N. Zakharov, Y.T. Struchkov, *J. Organomet. Chem.* **421**, 29, 1991.
- [166] W.J. Evans, J.W. Grate, I. Bloom, W.E. Hunter, J.L. Atwood, *J. Am. Chem. Soc.* **107**, 405, 1985.
- [167] W.J. Evans, T.A. Ulibarri, L.R. Chamberlain, J.W. Ziller, D. Alvarez, *Organometallics* **9**, 2124, 1990.
- [168] W.J. Evans, J.W. Grate, L.A. Hughes, H. Zhang, J.L. Atwood, *J. Am. Chem. Soc.* **107**, 3728, 1985.
- [169] W.J. Evans, D.K. Drummond, L.A. Hughes, H. Zhang, J.L. Atwood, *Polyhedron* **7**, 1693, 1988.
- [170] W.J. Evans, T.A. Ulibarri, J.W. Ziller, *Organometallics* **10**, 134, 1991.
- [171] H. Yasuda, H. Yamamoto, K. Yokota, S. Miyake, A. Nakamura, *J. Am. Chem. Soc.* **114**, 4908, 1992.
- [172] H.J. Heeras, M. Maters, J.H. Teuben, G. Helgeson, S. Jagner, *Organometallics* **11**, 350, 1992.
- [173] A. Zalkin, D.H. Templeton, W.D. Luke, A. Streitwieser, Jr., *Organometallics* **1**, 618, 1982.
- [174] H. Schumann, I. Albrecht, E. Hahn, *Angew. Chem.* **24**, 985, 1985.
- [175] A. Zalkin, T.J. Henly, R.A. Andersen, *Acta Crystallogr.* **C43**, 233, 1987.
- [176] D.J. Berg, R.A. Andersen, A. Zalkin, *Organometallics* **7**, 1858, 1988.



- [177] A. Zalkin, D.J. Berg, *Acta Crystallogr.* **C44**, 1488, 1988.
- [178] D.J. Berg, C.J. Burns, R.A. Andersen, A. Zalkin, *Organometallics* **8**, 1869, 1989.
- [179] A. Recknagel, A.M. Noltemeyer, D. Stalke, U. Pieper, H.G. Schmidt, F.T. Edelmann, J. *Organomet. Chem.* **411**, 347, 1991.
- [180] H.J. Heres, A. Meetsma, J.H. Teuben, J. *Organomet. Chem.* **414**, 351, 1991.
- [181] T.D. Tilley, R.A. Andersen, *Inorg. Chem.* **20**, 3267, 1981.
- [182] G. Bombieri, G. Paolucci, *Handbook on the Physics & Chemistry of Rare Earths*, Vol. 25, p. 342, 1998.
- [183] W.J. Evans, D.K. Drummond, L.R. Chamberlin, R.J. Doedens, S.G. Bott, H. Zhang, J.L. Atwood, *J. Am. Chem. Soc.* **110**, 4983, 1988.
- [184] A. Recknagel, M. Noltemeyer, F.T. Edelmann, *J. Organomet. Chem.* **410**, 53, 1991.
- [185] J. Scholz, A. Scholtz, R. Weimann, C. Janiak, H. Schumann, *J. Organomet. Chem.* **33**, 1171, 1994.
- [186] M.R. Gagne, C.L. Stern, T.J. Marks, *J. Am. Chem. Soc.* **114**, 275, 1992.
- [187] W.J. Evans, S.L. Gonzales, J.W. Ziller, *J. Am. Chem. Soc.* **113**, 9880, 1991.
- [188] W.J. Evans, S.L. Gonzales, J.W. Ziller, *J. Chem. Soc. Chem. Commun.* 1138, 1992.
- [189] H. Schumann, E. Palamidis, G. Schmid, R. Boese, *Angew. Chem.* **25**, 718, 1986.
- [190] P.L. Watson, J.F. Whitney, R.L. Harlow, *Inorg. Chem.* **20**, 3271, 1981.
- [191] R.G. Finke, S.R. Keenan, D.A. Schiraldi, P.L. Watson, *Organometallics* **5**, 598, 1986.
- [192] C.S. Day, V.W. Day, R.D. Ernst, S.H. Vollmer, *Organometallics* **1**, 998, 1982.
- [193] W.J. Evans, J.W. Grate, K.R. Levan, I. Bloom, T.T. Peterson, R.J. Doedens, H. Zhang, J.L. Atwood, *Inorg. Chem.* **25**, 3614, 1986.
- [194] Q. Shen, M. Qi, Y. Lin, *J. Organomet. Chem.* **399**, 247, 1990.
- [195] H. Schumann, I. Albrecht, M. Gallagher, E. Hahn, C. Janiak, C. Kolax, J. Loebel, S. Nickel, E. Palamidis, *Polyhedron* **7**, 2307, 1988.
- [196] P.L. Watson, T.H. Tulip, I. Williams, *Organometallics* **9**, 1999, 1990.
- [197] A. Zalkin, D.J. Berg, *Acta Crystallogr.* **C45**, 1630, 1989.
- [198] C.J. Schaverien, H. Heijden, A.G. Orpen, *Polyhedron* **8**, 1850, 1989.
- [199] N.J. Heres, J.H. Teuben, R.D. Rogers, *J. Organomet. Chem.* **364**, 87, 1989.
- [200] C.J. Schaverien, *Organometallics* **11**, 3476, 1992.
- [201] H.J. Heres, A. Meetsma, J.H. Teuben, R.D. Rogers, *Organometallics* **8**, 2637, 1989.
- [202] H. Schumann, J. Winterfeld, R.D. Kohn, L. Esser, J. Sun, A. Dietrich, *Chem. Ber.* **126**, 907, 1993.
- [203] W.J. Evens, G.W. Rabe, M.A. Ansari, J.W. Ziller, *Angew. Chem.* **106**, 2200, 1994.
- [204] K.G. Wang, E.D. Stevens, S.P. Nolan, *Organometallics* **11**, 1011, 1992.
- [205] G.C. Bazan, W.P. Schaefer, J.E. Bercaw, *Organometallics* **12**, 2126, 1993.
- [206] J. John, M. Tsutsui, *J. Coord. Chem.* **10**, 177, 1980.
- [207] C. Qian, C. Ye, H. Lu, Y. Li, Y. Huang, *J. Organomet. Chem.* **263**, 333, 1984.
- [208] N. Hock, W. Oroschin, G. Paolucci, R.D. Fischer, *Angew. Chem.* **25**, 738, 1986.
- [209] K. Qiao, R.D. Fisher, G. Paolucci, P. Traldi, E. Celon, *Organometallics* **9**, 1361, 1990.
- [210] L. Esser, *Doctoral Thesis (Tech. Univ., Berlin)*, 1991.
- [211] G. Jeske, L.E. Shock, P.N. Swepston, H. Schumann, T.J. Marks, *J. Am. Chem. Soc.* **107**, 8103, 1985.
- [212] P. Yan, N. Hu, Z. Jin, W. Chen, *J. Organomet. Chem.* **391**, 313, 1990.
- [213] D. Stern, M. Sabat, T.J. Marks, *J. Am. Chem. Soc.* **112**, 9558, 1990.
- [214] W.E. Piers, P.J. Shapiro, E.E. Bunel, J.E. Bercaw, *Synlett.* 74, 1990.
- [215] H. Schumann, L. Esser, J. Loebel, A. Dietrich, D. Helm, X. Ji, *Organometallics* **10**, 2585, 1991.
- [216] C. Qian, Y. Ge, D. Deng, Y. Gu, *Huaxue Xuebao* **45**, 210, 1987; *Acta Chim. Sin.* 431, 1989.
- [217] C. Qian, D. Zhu, *J. Organomet. Chem.* **445**, 79, 1993.
- [218] G. Paolucci, R. D'Ippolito, C. Ye, C. Qian, J. Graper, R.D. Fisher, *J. Organomet. Chem.* **471**, 87, 1994.
- [219] J. Grapper, R.D. Fischer, *J. Organomet. Chem.* **471**, 87, 1994.
- [220] Z. Xie, C. Qian, Y. Huang, *J. Organomet. Chem.* **412**, 61, 1991.
- [221] M. Tsutsui, H.J. Gysling, *J. Am. Chem. Soc.* **90**, 6880, 1969.
- [222] A. Zazetta, A. Greco, *Acta Crystallogr. B* **35**, 457, 1979.
- [223] G. Fuxing, W. Gecheng, J. Zhangsheng, C. Wenqi, *J. Organomet. Chem.* **438**, 289, 1992.
- [224] M. Chen, G. Wu, W. Wu, S. Zhaung, Z. Huang, *Organometallics* **7**, 802, 1988.
- [225] J.L. Atwood, J.H. Burns, P.G. Laubereau, *J. Am. Chem. Soc.* **95**, 1830, 1973.

- [226] A. Streitwieser, Jr., U. Muller-Westerheff, J. Am. Chem. Soc. **90**, 7364, 7368, 7528, 1968.
- [227] R.G. Hayes, J.L. Thomas, J. Am. Chem. Soc. **91**, 6876, 1969.
- [228] A.L. Wayda, I. Mukerji, J.L. Dye, R.D. Rogers, Organometallics **6**, 1328, 1987.
- [229] F.T. Edelman, New J. Chem. **19**, 535, 1995.
- [230] A.J. Kinsley, A. Streitwieser, Jr., A. Zalkin, Organometallics **4**, 52, 1985.
- [231] A.J. Kinsley, A. Streitwieser, Jr., A. Zalkin, Acta Crystallogr. **C42**, 1092, 1986.
- [232] T.R. Boussie, D.C. Eisenberg, J. Rigsbee, A. Streitwieser, A. Zalkin, Organometallics **10**, 1922, 1991.
- [233] J. Xia, Z. Jin, G. Lin, W. Chen, J. Organomet. Chem. **408**, 173, 1991.
- [234] K. Mashima, Y. Nakayama, A. Nakamura, N. Kaneshima, Y. Kai, H. Takaya, J. Organomet. Chem. **437**, 85, 1994.
- [235] H. Schumann, R.D. Koehn, F.W. Reier, A. Dietrich, J. Pickardt, Organometallics **8**, 1388, 1989.
- [236] J. Jin, X. Zhuang, Z. Jin, W. Chen, J. Organomet. Chem. **490**, C8, 1995.
- [237] K. Wen, Z. Yin, W. Chen, J. Chem. Soc., Chem. Commun. 680, 1991.
- [238] J. Xia, S. Yin, W. Chen, J. Chem. Soc., Chem. Commun. 680, 1991.
- [239] M. Visseaux, A. Dormond, M.M. Kubicki, C. Moise, D. Baudry, M. Ephrit Khine, J. Organomet. Chem. **433**, 95, 1992.
- [240] A.L. Wayda, R.D. Rogers, Organometallics **4**, 1440, 1985.
- [241] H. Schumann, J. Winterfield, L. Esser, G. Kociok-Kohn, Angew. Chem. **32**, 1208, 1993.
- [242] K. Kilimann, F.T. Edelmann, J. Organomet. Chem. **444**, C15, 1993; **496**, C5, 1995.
- [243] M. Dolg, P. Fulde, W. Kuchle, C.S. Neumann, H.J. Stoll, J. Chem. Phys. **94**, 3011, 1991.
- [244] K. Killimann, F.T. Edelmann, J. Organomet. Chem. **496**, C5, 1994.
- [245] H.O. Hodgson, K.N. Raymond, Inorg. Chem. **11**, 3030, 1972.
- [246] H. Schumann, U. Genthe, E. Hahn, M.B. Hos-sain, D. Helm, J. Organomet. Chem. **299**, 67, 1986.
- [247] W.J. Evans, I. Bloom, W.E. Hunter, J.L. At-wood, J. Am. Chem. Soc. **105**, 4101, 1983.
- [248] W.J. Evans, W.K. Drummond, T.P. Hanusa, R.J. Doedens, Organometallics **6**, 2279, 1987.
- [249] W.J. Evans, M.S. Sollberger, S.I. Khan, R. Bau, J. Am. Chem. Soc. **110**, 439, 1988.
- [250] E.B. Lobkoski, Yu.K. Gun'ko, B.M. Bulychev, G.L. Soloveichik, M.Y. Antipin, J. Organomet. Chem. **406**, 343, 1991.
- [251] E.B. Lobkoski, G.L. Soloveichik, A.B. Erofeev, B.M. Bulychev, V.K. Bel'skii, *ibid.* **235**, 151, 1982.
- [252] V.K. Bel'skii, A.B. Erifeev, B.M. Bulychev, G.L. Soloveichik, *ibid.* **365**, 123, 1984.
- [253] S.Ya. Knyazhanski, E.B. Lobkovski, B.M. Bulychev, V.K. Bel'skii, *ibid.* **419**, 311, 1991.
- [254] V.K. Bel'skii, Yu.K. Gun'ko, B.M. Bulychev, G.L. Soloveichik, *ibid.* **419**, 299, 1991.
- [255] D. Alvarez Jr., K.G. Caulton, W.J. Evans, J.W. Ziller, J. Am. Chem. Soc. **112**, 5674, 1990.
- [256] T.D. Tilley, R.A. Anderson, J. Am. Chem. Soc. **104**, 1772, 1982.
- [257] G.K. Magomedov, A.Z. Voskobolnikov, I.P. Beletskaya, Metal. Khim. **2**, 823, 1989; **3**, 706, 1990.
- [258] P.N. Hazin, J.C. Huffman, J.W. Bruno, J. Chem. Soc., Chem. Commun. 1473, 1988; Organomet. **9**, 416, 1990.
- [259] J.M. Boncella, R.A. Andersen, Inorg. Chem. **23**, 432, 1984; J. Chem. Soc., Chem. Comm. 809, 1984.
- [260] G.B. Deacon, A.J. Koplick, T.D. Tuong, Polyhedron **1**, 423, 1982.
- [261] W.J. Evans, M.A. Ansari, J.W. Ziller, S.I. Khan, Organometallics **14**, 3, 1995.
- [262] F.A. Cotton, W. Schwotzer, J. Am. Chem. Soc. **108**, 4657, 1986.
- [263] J.G. Brennen, F.G.N. Cloke, A.A. Sameh, A. Zalkin, J. Chem. Soc., Chem. Commun. 1668, 1987.
- [264] B. Fan, Q. Shen, Y. Lin, J. Organomet. Chem. **377**, 51, 1989.
- [265] G.B. Deacon, S. Nickel, P. Mackinnon, E.R.T. Tiekink, Aust. J. Chem. **43**, 1245, 1990.
- [266] L.I. Fedushkin, M.N. Bocharov, H. Schumann, L. Esser, G. Kociok-kohn, J. Organomet. Chem. **489**, 145, 1995.
- [267] F. Nief, F. Mathey, Synlett 745, 1991; Polyhe-dron **12**, 19, 1993.
- [268] H. Zhang, A.R. Oki, Y.A. Maguire, N.S. Hos-mane, Acta Crystallogr. **C51**, 635, 1995.
- [269] M.J. Manning, C.B. Knobler, M.F. Hawthorne, J. Am. Chem. Soc. **110**, 4458, 1988.
- [270] A.R. Oki, H. Zhang, N.S. Hosmane, Angew. Chem. **31**, 432, 1992.

chapter 7

---

**KINETICS AND MECHANISMS OF RARE  
EARTH COMPLEXATION**

---

---

# CONTENTS

---

1. Rate laws . . . . .	484
2. The tools of mechanistic analysis . . . . .	485
3. Rate laws . . . . .	485
4. Stereochemistry . . . . .	486
5. Variation of rate constant . . . . .	486
6. Encounters and outer-sphere complexation . . . . .	488
7. The study of reactions . . . . .	488
8. Fast reactions . . . . .	489
9. Flow methods . . . . .	490
10. Stopped-flow method . . . . .	492
11. Relaxation methods [9] . . . . .	493
12. Temperature-jump method . . . . .	494
13. Pressure-jump method . . . . .	494
14. Ultrasonics . . . . .	494
15. Magnetic resonance methods [10] . . . . .	496
16. Paramagnetic line broadening . . . . .	496
17. Kinetic expressions for chemical relaxation [13] . . . . .	498
18. Mechanisms of rare earth complex formation reactions . . . . .	514
19. Counterion coordination . . . . .	515
20. Solvent exchange in dimethyl formamide (DMF) . . . . .	517
21. Solvent exchange in water . . . . .	523
22. Complex formation in aqueous solutions . . . . .	526
23. Aminopoly carboxylate complexes . . . . .	527
24. Lanthanide–EDTA–5-sulphosalicylate mixed complexes . . . . .	532
25. Isotopic exchange reactions of LnEDTA complexes . . . . .	533
26. NMR studies of lanthanide macrocyclic complexes . . . . .	535
27. Dynamics of supramolecular complexes . . . . .	537
27.1. Tetraazaporphine complexes . . . . .	538
28. Isomerization reactions . . . . .	538
29. Interfacial catalysis of formation and dissociation of lanthanide complexes [83] . . . . .	539
30. Lanthanide catalysis in isomerization reactions [84] . . . . .	540
31. Electron transfer reactions [85] . . . . .	544
32. Inner-sphere redox reactions . . . . .	546
33. Thermal decomposition kinetics and mechanisms . . . . .	547

34. Photochemistry and photophysics of lanthanide complexes . . . . .	553
35. Photochemistry of lanthanides . . . . .	554
36. Photochemistry of Eu in aqueous solutions . . . . .	554
37. Photochemistry of cerium system . . . . .	555
38. Photosubstitution reactions . . . . .	557
39. Luminescence of lanthanide ions . . . . .	557
40. Determination of solvation state of lanthanides . . . . .	559
41. Ligand exchange rates . . . . .	561
42. Energy transfer from lanthanide ions . . . . .	563
References . . . . .	564

Reaction kinetics have been found useful in unraveling the mechanisms of reactions. There are two principal reasons for studying the rates of complexation reactions. The first is the practical importance of being able to predict how quickly a mixture of reactants reach an equilibrium state and the second reason for the study is how it can reveal the mechanism of the reaction. The mechanism of a reaction has two connotations. The first connotation may refer to a statement of all elementary steps in an overall reaction. The second meaning refers to individual steps themselves and their detailed nature.

### 1. Rate laws

It is not our purpose here to derive the rate laws. The integrated rate laws are summarized in Table 7.1. Most of the reactions can be broken down into a sequence of steps that involve either a unimolecular reaction or a bimolecular reaction. A reaction of a specified order can be accounted for in terms of a sequence of several unimolecular or bimolecular steps. Thus the order of a reaction is quite distinct from the molecularity of the individual steps. Order of a reaction is an empirical quantity obtained from the rate law while molecularity is characteristic of the underlying mechanism.

TABLE 7.1  
Integrated rate laws.

Order	Reaction	Rate law ( $x = [P]$ )	Integrated form	$t_{1/2}$
0	$A \rightarrow P$	$dx/dt = k_0$	$k_0 t = x$ for $x \leq [A]_0$	$[A]_0/2k_0$
1	$A \rightarrow P$	$dx/dt = k_1[A]$	$k_1 t = \ln \left\{ \frac{[A]_0}{[A]_0 - x} \right\}$	$(\ln 2)/k_1$
2	$A \rightarrow P$	$dx/dt = k_2[A]^2$	$k_2 t = \frac{x}{[A]_0([A]_0 - x)}$	$1/k_2[A]_0$
	$A + B \rightarrow P$	$dx/dt = k_2[A][B]$	$k_2 t = \left\{ \frac{1}{[B]_0 - [A]_0} \right\} \ln \left\{ \frac{[A]_0([B]_0 - x)}{([A]_0 - x)[B]_0} \right\}$	
	$A + 2B \rightarrow P$	$dx/dt = k_2[A][B]$	$k_2 t = \left\{ \frac{1}{[B]_0 - 2[A]_0} \right\} \ln \left\{ \frac{[A]_0([B]_0 - 2x)}{([A]_0 - x)[B]_0} \right\}$	
	$A \rightarrow P$ with autocatalysis	$dx/dt = k_2[A][P]$	$k_2 t = \left\{ \frac{1}{[A]_0 - x} \right\} \ln \left\{ \frac{[A]_0([P]_0 + x)}{([A]_0 - x)[P]_0} \right\}$	
3	$A + 2B \rightarrow P$	$dx/dt = k_3[A][B]^2$	$k_3 t = \frac{[A]_0 - [B]_0}{[A]_0[B]_0(2[A]_0 + [B]_0)} + \left\{ \frac{1}{2[A]_0 - [B]_0} \right\}^2 \ln \left\{ \frac{[A]_0([B]_0 - 2x)}{([A]_0 - x)[B]_0} \right\}$	
$n \geq 2$	$A \rightarrow P$	$dx/dt = k_n[A]^n$	$k_n t = \frac{1}{n-1} \left\{ \left( \frac{1}{[A]_0 - x} \right)^{n-1} - \left( \frac{1}{[A]_0} \right)^{n-1} \right\} \frac{2^{n-1} - 1}{(n-1)k_n[A]_0^{n-1}}$	

## 2. The tools of mechanistic analysis

The solution kinetics involves three fundamental types of experiment, namely: (i) rate law, (ii) stereochemistry and (iii) variation of rate constant with structure or environment. Each one permits the analysis of slightly different aspects of a reaction, and then develops a scheme of reaction classification which throws light on the behaviour of a reaction in each experimental situation. It is useful to briefly discuss the role of each of the three types of experimental investigation in the study of complex substitution reactions.

## 3. Rate laws

As a result of the 'solvent-cage' effect, any slow reaction occurring between two or more species in solution may be divided into two steps. The first step involves a diffusional encounter and the second step is a rearrangement of the encounter complex in the first step to yield a product [1,2]. If the overall rate is more than an order of magnitude slower than the diffusion-controlled limit, the first step may be treated as a pre-equilibrium process. The steps involved may be written as



where  $K_E$  is the encounter equilibrium constant,  $\text{MX} \cdot \text{Y}$  represents an encounter complex or an outer-sphere complex and  $k$  is the first-order rate constant for the slow-step of rearrangement of the encounter complex to give the product. Octahedral substitution pathways represented by scheme (7.1) are known as interchange pathways (I) [3]. It is clear that an understanding of outer-sphere complex formation (which is frequently ion-pairing) is important to interchange pathways.

Another pathway that is important in the discussions of octahedral substitution and distinct from interchange is considered below. In this pathway the encounter with the entering ligand does not precede but follows the slow step. The scheme of the pathway may be written as



The implication of an encounter following the slow step is that M is an intermediate of sufficiently long lifetime that competition between X and Y for a presence in the encounter complexes with M is possible. In octahedral complexes the intermediate M has a coordination number of five. The pathway (7.2) is called 'dissociative', D.

Both interchange (I) and dissociative (D) pathways represented by schemes (7.1), and (7.2) frequently lead to second-order rate expressions; first-order in complex and first-order in incoming or attacking ligand. In a dilute solution, the observed second-order rate constant for the interchange path (7.1) is

$$k_{\text{obs}} = K_E \cdot k$$

The observed rate constant may also be interpreted in terms of the [Y] dependence of the competition the  $k_{-1}$  and  $k_{-2}$  steps in pathway (7.2). Only when the rates have been analysed over a wide concentration range is it possible to distinguish between interchange (7.1) and dissociative (7.2) pathways. It is important to note that the encounter is perpetual when Y is the solvent and in such a case there may not be an operational distinction between interchange (7.1) and dissociative (7.2) pathways.

#### 4. Stereochemistry

The steric course of a reaction is also closely related to the type of encounter that occurs with the entering ligand. The steric course of an interchange is most likely determined by the encounter geometry, and may give very little information as to the nature of the transition-state geometry unless this can be explicitly related to the encounter geometry. Stereochemistry may be more informative when a dissociative (D) pathway is involved. An important point is that stereochemical rearrangements past the transition state may in certain instances identify an intermediate of the D-pathway type whose lifetime is too short to be detected by competition experiments involving X and Y.

#### 5. Variation of rate constant

Variation of the rate constant for substitution as a function of structure, environment, temperature or pressure gives, in the context of transition-state theory, information on the relationship between only two points on the reaction hypersurface. The two points on the hypersurface are ground state and transition state. The most important factor in the octahedral substitution process is the extent of specific bonding of the entering ligand in the transition state. When bonding to the entering group occurs, the energy of the transition state is lowered and the degree of lowering will vary as a function of choice of the entering ligand. The energy profiles of associative and dissociative types of reaction are shown in Figs 7.1 and 7.2, respectively.

If the entering ligand does not bond to the central metal atom in the transition state, there will be no decrease in activation energy due to the entering ligand. Under such circumstances, the activation energy is determined from the energetics of bond breaking. The activation energy must accumulate in the original metal complex by thermal fluctuation.

Classification of the ligand substitution mechanisms is given in Table 7.2a.

It is obvious that the dissociative (D) pathway implies no assistance from the entering ligand since the entering ligand is not a stoichiometric component of the transition state.



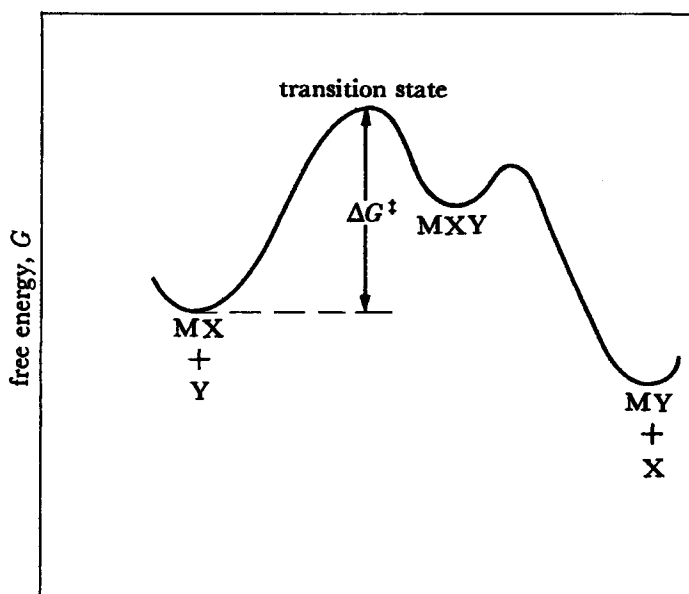


Fig. 7.1. Energy profile of an associative reaction.  $\Delta G^\ddagger$  is the free energy of activation.

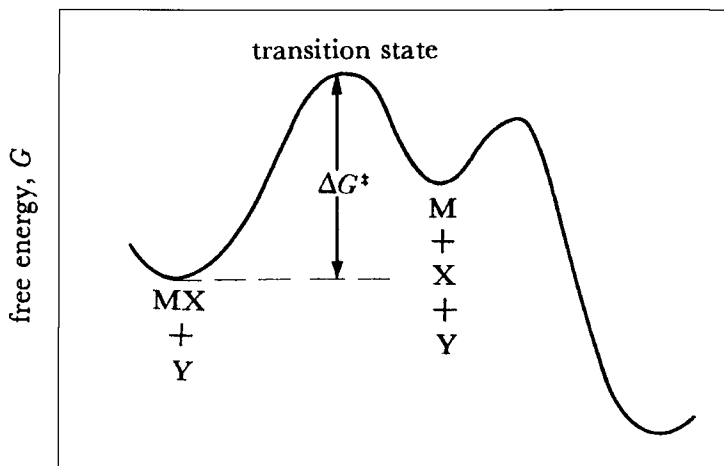


Fig. 7.2. Energy profile of a dissociative reaction.

TABLE 7.2a  
Classification of ligand substitution mechanisms.

Mode of activation	Intermediate of increased coordination number	One-step process	Intermediate of reduced coordination number
Associative	A	$I_a$	
Dissociative		$I_a$	D

Hence it is convenient to call this unassisted activation dissociative (referred as 'd'). The mode of approach to the transition state that is assisted by the entering ligand is known as associative ('a'). The true test that distinguishes between dissociative (d) and associative (a) modes of activation is the sensitivity of the rate constant to the nature of the entering ligand. Now it must be clear that an interchange (I) pathway may use either the a or d modes activation leading to  $I_a$  and  $I_d$  processes.  $I_d$  processes are those in which the "dissociated", transition state does not drop to an intermediate of reduced coordination number with lifetime longer than an average encounter complex. Similarly, the  $I_a$  process does not involve a transition state of a higher coordination number with a lifetime longer than an average encounter complex.

## 6. Encounters and outer-sphere complexation

The value of the equilibrium constant for an encounter is certainly of prime importance in the discussion of interchange pathways of complex formation. This was first suggested, in fact by Werner [4] as early as in 1912. Most of the work on ligand substitution in complexes is based on the assumption that encounter equilibria could be calculated from the ion-pairing equation of Fuoss [5] which was derived in turn from a consideration of diffusion-controlled reactions by Eigen [6]. At zero ionic strength, the encounter equilibrium constant,  $K_E$  is given as

$$K_E = \frac{4\pi a^3 N}{300} \exp\left\{\frac{-Z_1 Z_2 e^2}{\epsilon a k T}\right\} \quad (7.3)$$

where  $a$  is the distance of closet approach of two species,  $\epsilon$  the dielectric constant of the medium and the other symbols have the usual meaning [5]. Equation (7.3) can be corrected to finite ionic strength, by using Debye-Huckel equations. In practice 'a' is an adjustable parameter.

Whenever it is feasible, it is useful to study encounter equilibria experimentally, as in the case of Co(III) complexes in water and non-aqueous solvents [7]. There are some weaknesses in equation (7.3) as evidenced by: (i) the formation of anionic species by overcompensation of the original positive charge of the metal complex, (ii) lack of evidence of outer-sphere complexation in some cases like  $\text{Co}(\text{en})_3^{3+}$  with  $\text{Fe}(\text{CN})_6^{3-}$  and (iii) the fact that outer-sphere complexes are preferred over inner-sphere complexes in several systems.

It is to be noted that irrespective of the weaknesses of equation (7.3), it has been extensively used in kinetic studies, especially in kinetics of fast complex formation reactions. The above equation was tested for its applicability to outer-sphere association reactions by ultrasonic absorption methods [8].

## 7. The study of reactions

The basic data of chemical kinetics are the concentrations of reactants and products as a function of time. The method chosen for monitoring the concentrations depends on the nature of the species involved in the reaction, and on its rapidity.

Many reactions go to completion (i.e. attain thermodynamic equilibrium) over a period of minutes or hours, and may be monitored by classical techniques. One of the following methods is chosen.

- (a) Pressure changes: a reaction in the gas phase might result in a change of pressure, and hence its progress may be monitored by recording the pressure as a function of time.
- (b) Spectroscopy: a technique in which intensity of the absorption of visible light by the reactant or product may be monitored. This technique is particularly useful in the studies of transition metal complexes.
- (c) Polarimetry: when the optical activity of a mixture changes in the course of a reaction, it can be monitored by measuring the angle of optical rotation.
- (d) Electrochemical methods: when a reaction changes the number or nature of ions present in a solution, its course may be followed by monitoring conductivity of the solution. Another method involves the reactions occurring at electrodes.
- (e) Other methods: miscellaneous methods of determining composition include mass spectrometry and chromatography. In order to use these techniques, a small amount of reaction mixture is bled from the reacting system at a series of time intervals after the start of the reaction, and then analysed.

There are three main ways of applying these analytical techniques

- (i) Real time analysis: in this method the composition of the reaction system is analysed while the reaction is in progress.
- (ii) Quenching: in this method the reaction is frozen after a suitable interval of time, and then the composition is analysed by any suitable technique. Quenching can be normally done by a sudden lowering of temperature but this is applicable to slow enough reactions such that very little reaction occurs during the time it takes to cool the mixture.
- (iii) Flow method: in this method, solutions of the reagents are mixed as they flow together into a chamber as shown in Fig. 7.3. The reaction continues as the thoroughly mixed solutions flow through the outlet tube, and observations of the composition at different positions along the tube by spectroscopy is equivalent to observing the reaction mixture at different times after mixing. Reactions that are complete within a few milliseconds can be observed by this technique. But the main drawback of this technique is that large volumes of solution are necessary.

## 8. Fast reactions

All reactions are fast. At least, the individual steps of a reaction when molecules rearrange in a unimolecular step, or transfer atoms in a bimolecular encounter, occur on an atomic time scale and are complete in less than about  $10^{-9}$  s. The slowness of the net reaction is due to the slowness with which molecules get activated or come together. But even the net rate may become very fast when the activation energy can be provided very rapidly.

Recent developments in chemical kinetics have been in the study of rapid reactions. Chemical events with half-lives as short as  $10^{-7}$  seconds have been studied with reasonable accuracy. It is obvious that special methods must be used to study such labile reactions.

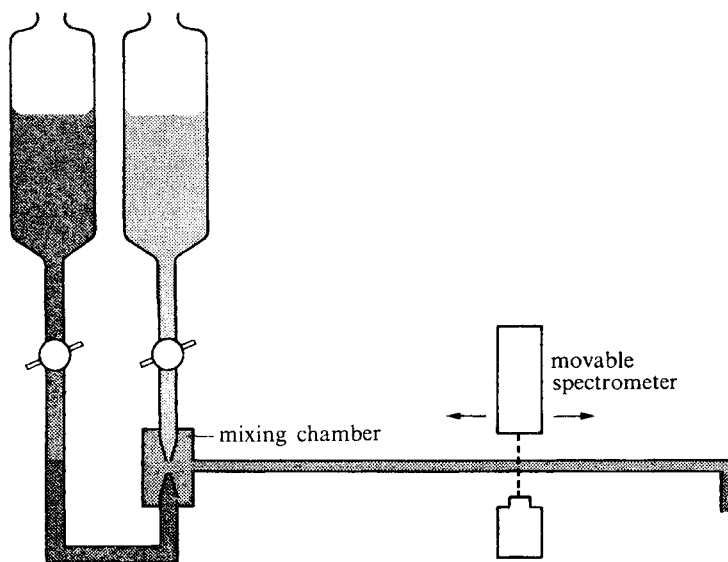


Fig. 7.3. Apparatus used in the flow technique.

A large part of the interest in rapid reactions results from the availability of electronic methods of measuring times in millisecond, microsecond and picosecond ranges.

Even though short times can be easily measured, there still lies the difficult problem of detecting a change in the system due to reaction in this time interval. Further, the problem of mixing together the reagents to initiate a reaction is a severe limitation in that a finite time of the order of milliseconds is required for homogeneous mixing. For shorter times, it is necessary to start with reactants already uniformly distributed and in a state of equilibrium. The equilibrium may be perturbed and subsequent events followed or alternatively the dynamic nature of a chemical equilibrium may be used. A simple and useful technique is to invoke some other time-dependent process or phenomenon, with a characteristic time of the same order as that of the half-life of the reaction. The interplay of these two times then produces observable results which depend on their relative values.

## 9. Flow methods

The flow method that has been briefly discussed sometimes offers special advantages in kinetic studies. The basic equations for flow systems with no mixing may be derived as follows: let us consider a tubular reactor space of constant cross-sectional area  $A$  as shown in Fig. 7.4 with a steady flow of ' $u$ ' of a reaction mixture expressed as volume per unit time. Now we will select a small cylindrical volume unit  $dV$  such that the concentration of component  $i$  entering the unit is  $C_i$  and the concentration leaving the unit is  $C_i + dC_i$ . Within the volume unit, the component is changing in concentration due to chemical reaction with a rate equal to  $r_i$ . This rate is of the form of the familiar chemical rate equation and is a function of the rate constants of all reactions involving the component  $i$

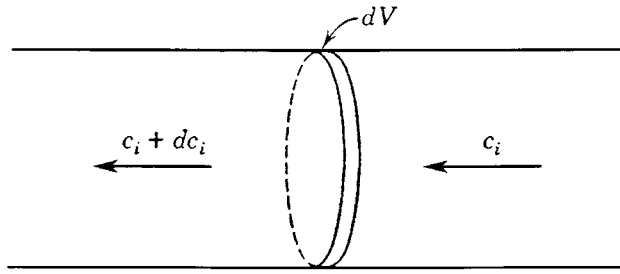


Fig. 7.4. Cylindrical volume element in a flow system.

and of the various concentrations in the volume unit. The change in the number of moles of the component  $i$  with time in the volume unit may be written as

$$\frac{dn_i}{dt} = r_i dV - u dC_i \quad (7.4)$$

After a certain time, the concentration will generally become constant for each component within the element. This means that a steady state is reached throughout the reactor volume such that the composition remains uniform with time at any point. However, the composition from point to point will be different. Under steady state conditions, we have

$$r_i dV = u dC_i \quad (7.5)$$

On integration of equation (7.5) we get

$$\frac{V}{u} = \int_{C_0}^C \frac{dC_i}{r_i} \quad (7.6)$$

where  $C_0$  is the concentration of the component entering the reaction space and  $V$  is the total volume of the reactor up to the point where the concentration is  $C$ . For a tubular reactor, volume is  $Al$ , where  $l$  is the distance from the entrance of the reactor to the point in question.

In order to use equation (7.6) we need a definite expression for rate  $r$  considering a first-order reaction



where the concentration of component A is equal to  $C$ .

$$r = \frac{dc}{dt} = -k_1 C \quad (7.8)$$

Using the value of  $R$  in equation (7.8) and substituting it in equation (7.6) followed by integration we get

$$k_1 = (u/V) \ln(C_0/C) \quad (7.9)$$

Thus equation (7.9) resembles the equation for a first-order reaction in a closed system

$$k_1 = (1/t) \ln(C_0/C) \quad (7.10)$$

Thus it can be generalized that the integrated equation for a reaction of any order in a flow system with no mixing is the same as for a closed system except for the time variable replaced by  $V/u$ .

In the case of a stirred flow reactor, the composition becomes uniform throughout the entire volume of the reactor as a result of stirring. The volume element  $dV$  may be replaced by  $V$ , the total volume in equation (7.4), and  $dC_i$  by  $(C - C_0)$ . Then dividing through by  $V$ , we get

$$\frac{dc}{dt} = r - (u/V)(C - C_0) \quad (7.11)$$

and this equation describes the approach to steady state. At steady state,  $dC/dt$  is zero and the composition becomes constant and stays like that independent of time. Then we may write

$$r = (u/V)(C - C_0) \quad (7.12)$$

A similar equation can be obtained for each component in the system by using a suitable expression for  $r$ . Analysis of  $C$  and  $C_0$ , where  $u$  and  $V$  are known gives the value of  $r$ , which is the rate. By changing the initial concentrations or the flow  $u$ , the rate can be found for other conditions. Considering a first-order reaction



in a stirred flow reactor, when B is initially not present, equation (7.12) becomes

$$k_1(a - x) = (u/V)x \quad (7.14)$$

Thus knowledge of  $a$  and  $x$  enables the evaluation of  $k_1$ .

Equation (7.12) can be extended to more complex rate equations. Some of the advantages of the stirred flow method are: (i) complicated rate expressions can be handled without integration, (ii) reaction can be carried out under constant conditions of solvent composition, ionic strength and transient intermediate can be built up in concentration, detected and measured.

## 10. Stopped-flow method

This method avoids the need for large volumes of solutions by focusing attention on the mixing chambers. The device is shown in Fig. 7.5. The two solutions are mixed very rapidly by injecting the material into a cavity. The cavity is fitted with a plunger that moves back

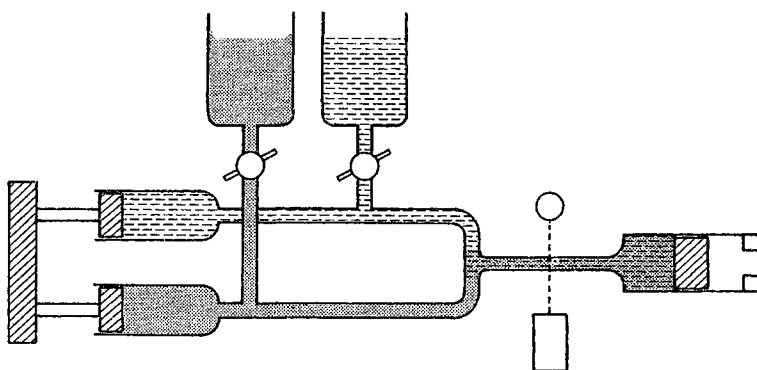


Fig. 7.5. Stopped-flow apparatus.

as the solutions flood in. The flow ceases when the plunger reaches a stop, and the reaction continues in the thoroughly mixed solutions. Observations, usually spectroscopic, are made on the mixed solution sample as a function of time. The important aspect of the apparatus is that it brings small amounts of reactants together in a thoroughly mixed form in a very short time, and then electronic techniques are used to resolve the time evolution of the reaction. This method is good for reactions with half-times of  $\sim 10$  ms.

Pulsed continuous flow is a method in which continuous flow is established for a short time. This method can reduce reagent consumption to  $\sim 5$  ml, and fast jet mixers have lowered the accessible reaction half-time to the  $10 \mu\text{s}$  range. Pulsed accelerated flow may be viewed as an adaptation of pulsed continuous flow in which the flow rate through the mixer and observation chamber is varied during the course of one kinetic run. This method can be used for reactions with half-times down to  $\sim 10 \mu\text{s}$ . This method is limited to first-order reaction conditions.

## 11. Relaxation methods [9]

Chemical relaxation techniques are the products of pioneering work of M. Eigen. In a relaxation measurement, it is necessary to perturb a system at equilibrium by a sudden change in a physical variable, such as temperature, pressure, or electric field strength. The experiment is carried out so that the time of the change to be applied is much shorter than that for the chemical reaction to shift to its new equilibrium state (i.e.) the alteration in the physical variable changes the equilibrium constant of the reaction. The concentrations then adjust to their values under the new conditions of temperature, pressure or electric field.

The kinetic data are obtained by monitoring over time a suitable property, such as absorbance or conductivity, that can be related to the incremental change in concentration. The experiment is designed so that the shift from one equilibrium position to another is not very large. The small size of the concentration adjustment requires sensitive detection, but results in considerable simplification in mathematics, in that the re-equilibration of a single-step reaction follows first-order kinetics.

The perturbation of the equilibrium normally is a change in temperature, pressure or concentration of one of the reagents and the methods are known as temperature jump, pressure jump and concentration jump, respectively. The advantage of these methods is that the perturbation, especially of temperature and pressure, can be applied very quickly and reactions with half-times in the microsecond range can be observed. The major limitation is that the equilibrium position of the reaction must involve significant concentrations of both reactants and products. Thus relaxation methods are not applicable to essentially irreversible reactions.

## 12. Temperature-jump method

The position of equilibrium should be properly poised such that the resulting signal change has a sufficient amplitude for detection. The magnitude of the perturbation must be large enough to produce a useful signal which depends on the sensitivity of detection of one component. Suppose the energy of the capacitor is discharged through the solution, suddenly raising its temperature by Joule heating. It is necessary that the solution and the capacitor's electrodes must be arranged to ensure the suddenness of this event. Temperature-jump apparatus is shown in Fig. 7.6 schematically.

The magnitude of the equilibrium displacement depends on  $\Delta T$  and  $\Delta H^\ddagger$  for the equilibrium. The sign of  $\Delta H^\ddagger$  determines the direction of the shift in accordance with the Van Hoff equation. A typical equipment might discharge 10–25 kV in 1 cm<sup>3</sup> of solution. Such a voltage discharge may produce about 45 J in 10<sup>-6</sup> s corresponding to  $4.5 \times 10^7$  W and temperature rise of 5–10°C.

The temperature change must occur much more rapidly than the chemical reactions can re-equilibrate. The timing of these events is illustrated in Fig. 7.7. There is generally more than one equilibrium that is perturbed to different extents by the temperature pulse. Sometimes the deliberate introduction of a second equilibrium can be advantageous. The second equilibrium may involve a pH indicator, which may have a higher equilibrium rate constant than the main reaction consuming acid or base. The change in the concentration of the indicator may be monitored colorimetrically, thus allowing the determination of very small changes in the reaction of interest.

## 13. Pressure-jump method

In this method the solution is pressurized to several thousand atmospheres. At a desired time a diaphragm is mechanically ruptured. The system then relaxes to the equilibrium position at atmospheric pressure. The magnitude of the concentration jump depends on the value of  $\Delta V^\ddagger$ . For an equilibrium reaction with  $\Delta V^\ddagger = 5 \text{ cm}^3 \text{ mol}^{-1}$ , the constant  $K$  will change by about 2 percent per 100 bars of pressure.

## 14. Ultrasonics

The absorption of ultrasonic waves has been used in the study of very rapid reactions such as intramolecular processes, interconversion of rotational isomers, formation and



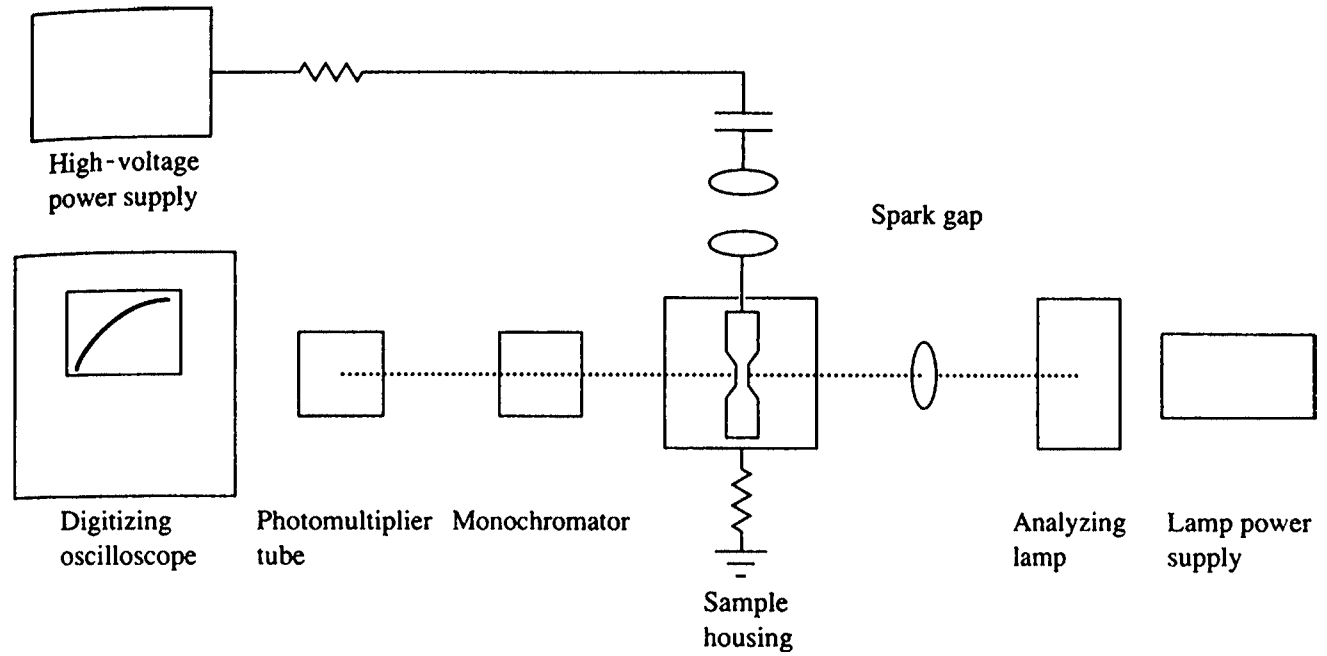


Fig. 7.6. Schematic drawing of a temperature apparatus. Shown are the analyzing lamp, observation cell, monochromator, photomultiplier, oscilloscope, spark gap, and high-voltage supply.

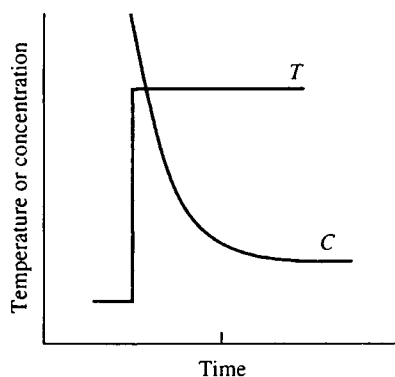


Fig. 7.7. A schematic representation of temperature and concentration profiles in a temperature-jump experiment. All scales are arbitrary, and the matter to be emphasized is that the temperature jump rapidly compared with the re-equilibrated reaction.

dissociation of hydrogen bonded species and outer-sphere ion association of transition metals and rare earth aquo ions.

### 15. Magnetic resonance methods [10]

Nuclear magnetic resonance (NMR) and electron paramagnetic resonance (EPR) are useful in studying very fast exchange reactions in an equilibrium system. It is necessary that at least two different environments be accessible to the magnetically active nucleus or electron. As a result of different environments, quite different spectra may be obtained for a system in each environment in the absence of exchange or slow exchange. Rapid exchange leads to an averaging of the spectra which is predicted by the solution of Bloch equations for magnetic resonance modified to include exchange phenomenon [11].

The effect of chemical exchange on NMR linewidth is shown in Fig. 7.8.

The spectrum is that of an equimolar mixture of hydrogen peroxide and water. Here  $\tau$  is the mean lifetime of a proton in each environment and  $\delta$  is the frequency difference in cycles per second between the two signals in the absence of exchange. In general, values of  $\tau$  of the order of  $1/\delta$  can be found. For  $\tau \gg 1/\delta$  two separate signals are observed and for  $\tau \ll 1/\delta$  one averaged signal is observed. Since  $\delta$  is generally of the order of 100 cycles per second,  $\tau$  is of the order of 0.01 seconds.

### 16. Paramagnetic line broadening

When one of the two environments for the nucleus gives a much broader line than the other, in the absence of exchange, then the important variables are the width of the broad line in cycles per second and  $\tau$  the exchange lifetime [12]. Such a broad line will result from a paramagnetic environment. A small amount of broad line environment will mix into a large amount of the narrow line environment to give an overall broadening. This line broadening

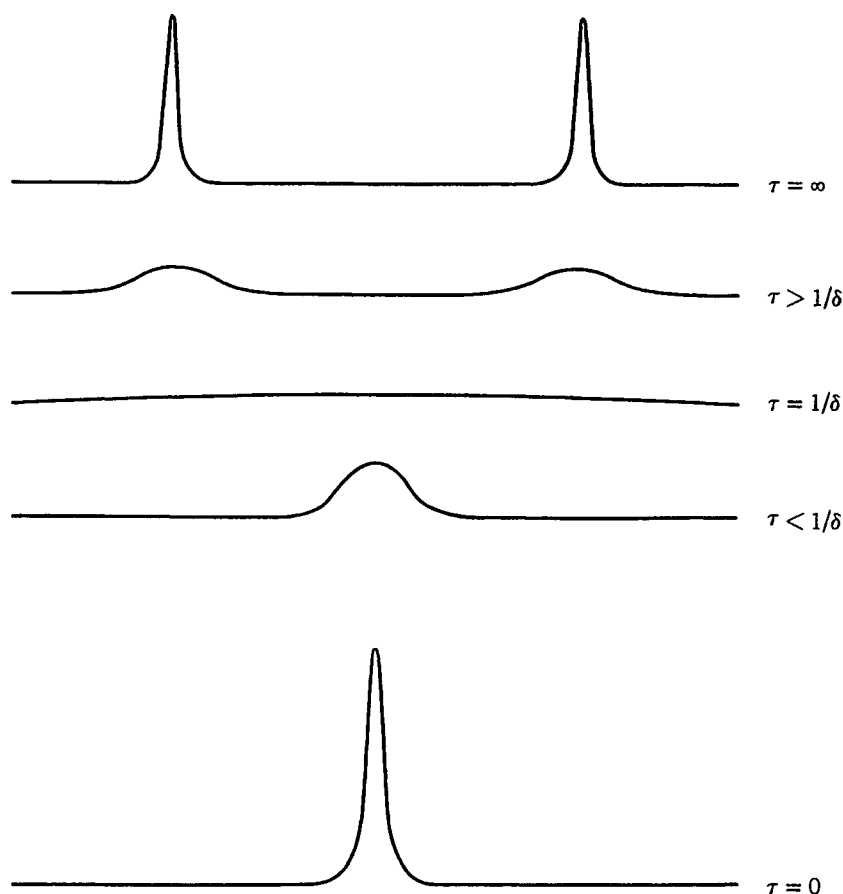


Fig. 7.8. The effect of chemical exchange on NMR line-width. Resonance frequency increasing from left to right.

has been used to determine mean lifetimes of ions and exchange times of a microsecond or less may also be determined.

The width of a resonance signal is related to the lifetime of a given magnetic state. The reciprocal of the half-width at half-height is the transverse relaxation time  $T_2$ . The line width is related to the exchange lifetime.

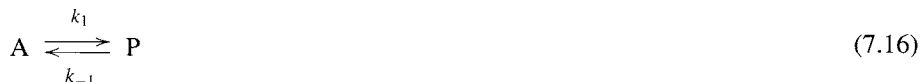
$$\frac{1}{T_2} = \frac{1}{T_2'} + \frac{1}{\tau} \quad (7.15)$$

In equation (7.15)  $T_2'$  is line width when there is no exchange taking place. It is to be recognized that line broadening is an example of Heisenberg's uncertainty principle.

A paramagnetic ion produces a very short relaxation time in nuclei closely associated with it. This results in a broad line. The overall effect depends both on the relaxation and on the rate of exchange. The slower rate process is the one that is measured.

### 17. Kinetic expressions for chemical relaxation [13]

Consider the reaction



Suppose the equilibrium is suddenly displaced. The re-equilibration follows first-order kinetics. Here  $\tau$  the relaxation time is defined as the reciprocal of the first-order rate constant for re-equilibration. Then we have

$$\tau^{-1} = k_e = k_1 + k_{-1} \quad (7.17)$$

Now consider the reaction



At the time of perturbation, the concentration of C or of any other component might be different from the equilibrium value. This difference does not matter because it is the displacement  $\delta$  from the equilibrium value that matters.

$$[C]_t = [C]_e - \delta \quad (7.19)$$

$$[A]_t = [A]_e + \delta \quad (7.20)$$

$$[B]_t = [B]_e + \delta \quad (7.21)$$

Then the rate equation is

$$\frac{-d\delta}{dt} = k_1([A]_e + \delta)([B]_e + \delta) - k_{-1}([C]_e - \delta) \quad (7.22)$$

Imposing the equilibrium condition

$$k_1[A]_e[B]_e = k_{-1}[C]_e \quad (7.23)$$

equation (7.22) becomes

$$\frac{-\delta}{dt} = k_1([A]_e + [B]_e)\delta + k_{-1}\delta + k_1\delta^2 \quad (7.24)$$

When the perturbation is small, the quadratic term is negligible and the reequilibration process is a first-order process. The relaxation time is

$$\tau^{-1} = k_e = k_{-1} + k_1([A]_e + [B]_e) \quad (7.25)$$

Let us consider a single-step relaxation represented by the scheme



whose rate is given by

$$-\frac{1}{a} \frac{d[A]}{dt} k_1 [A]^a [B]^b - k_{-1} [P]^p [Q]^q \quad (7.27)$$

If  $a\delta$  is the extent of perturbation in  $[A]$ , the concentrations are

$$[A]_t = [A]_e + a\delta = [A]_e (1 + a\delta[A]_e^{-1}) \quad (7.28)$$

$$[P]_t = [P]_e - p\delta = [P]_e (1 - p\delta[P]_e^{-1}) \quad (7.29)$$

After substitution of equations (7.28) and (7.29) into equation (7.27) and imposing the equilibrium condition

$$k_1 [A]_e^a [B]_e^b = k_{-1} [P]_e^p [Q]_e^q \quad (7.30)$$

we get for relaxation time

$$\tau^{-1} = k_e = k_1 [A]_e^a [B]_e^b \left\{ \frac{a^2}{[A]_e} + \frac{b^2}{[B]_e} \right\} k_{-1} [P]_e^p [Q]_e^q \left\{ \frac{p^2}{[P]_e} + \frac{q^2}{[Q]_e} \right\} \quad (7.31)$$

Expressions for the relaxation times of single-stage equilibria are given in Table 7.2b.

Systems showing more than two relaxation times means more than two steps are involved and these are complex systems. Consider the reaction



for which two relaxation times are expected. If  $\delta_1$ ,  $\delta_2$  and  $\delta_3$  are the perturbations

$$\delta_1 = [A]_t - [A]_e = [B]_t - [B]_e \quad (7.33)$$

$$\delta_2 = [I]_t - [I]_e \quad (7.34)$$

$$\delta_3 = [P]_t - [P]_e \quad (7.35)$$

Only two of the equations (7.33) to (7.35) are independent since

$$\delta_3 = -\delta_1 - \delta_2 \quad (7.36)$$

due to stoichiometry.

TABLE 7.2b  
Expressions for the relaxation times of certain reactions.

Reaction	Relaxation time
$A \xrightleftharpoons[k_{-1}]{k_1} P$	$\frac{1}{\tau} = k_1 + k_{-1}$
$A \xrightleftharpoons[k_{-1}]{k_1} P + Q$	$\frac{1}{\tau} = k_1 + k_{-1}([P]_e + [Q]_e)$
$2A \xrightleftharpoons[k_{-1}]{k_1} P$	$\frac{1}{\tau} = 4k_1[A]_e + k_{-1}$
$A + B \xrightleftharpoons[k_{-1}]{k_1} P + Q$	$\frac{1}{\tau} = k_1([A]_e + [B]_e) + k_{-1}([P]_e + [Q]_e)$
$A + B \xrightleftharpoons[k_{-1}]{k_1} P$	$\frac{1}{\tau} = k_1([A]_e + [B]_e) + k_{-1}$

The two independent rate equations are

$$-\frac{d\delta_1}{dt} = k_1([A]_e + \delta_1)([B]_e + \delta_1) - k_{-1}([I]_e + \delta_2) \quad (7.37)$$

$$\frac{d\delta_3}{dt} = k_2([I]_e + \delta_2) - k_{-2}([P]_e + \delta_3) \quad (7.38)$$

These two simultaneous equations are solved by finding the roots of the secular equation

$$\begin{pmatrix} a_{11} - \frac{1}{\tau} & a_{12} \\ a_{21} & a_{22} - \frac{1}{\tau} \end{pmatrix} = 0 \quad (7.39)$$

The  $a$ 's in equation (7.39) are coefficients of

$$\frac{-dC_i}{dt} = a_{11}\delta_1 + a_{12}\delta_3 \quad (7.40)$$

$$\frac{-d\delta_3}{dt} = a_{21}\delta_1 + a_{22}\delta_3 \quad (7.41)$$

The roots of equation (7.39) are the reciprocals of the relaxation times. The useful combinations are

$$\tau_I^{-1} \tau_{II}^{-1} = k_1([A]_e + [B]_e)(k_2 + k_{-2}) + k_{-1}k_{-2} \quad (7.42)$$

$$\tau_I^{-1} + \tau_{II}^{-1} = k_1([A]_e + [B]_e) + k_{-1} + k_2 + k_{-2} \quad (7.43)$$

Equations (7.42) and (7.43) give rate constants  $k_I$  and  $k_{II}$ .

In the event the first relaxation time is much smaller than the second, the first step is faster than the second and we have

$$\tau_I^{-1} \approx k_1([A]_e + [B]_e) + k_{-1} \quad (7.44)$$

$$\tau_{II}^{-1} \approx k_2 \left\{ \frac{k_1([A]_e + [B]_e)}{1 + k_1([A]_e + [B]_e)} \right\} + k_{-2} \quad (7.45)$$

Many other reaction schemes are also characterized by two relaxation times. Values of  $\tau$  can be obtained from the experiment. By changing concentrations, the  $\tau$  values change and thus facilitate the evaluation of the constituent rate constants.

Now we will illustrate the temperature-jump method with an example reaction such as complexation of lanthanides by anthranilic acid [15,16]. The conditions are: (i) the system is in equilibrium, (ii) the temperature perturbation applied to the system must be small so that the rate equations can be linearized, (i.e.)  $\Delta G/RT \ll 1$ . In such a case, we have

$$\frac{dC_i}{dt} = -(C_i - \bar{C}_i)/\tau \quad (7.46)$$

where  $C_i$  and  $\bar{C}_i$  are concentrations of  $i^{\text{th}}$  species in the perturbed and equilibrium state respectively and  $\tau$  is the relaxation time. By plotting the logarithm of a quantity related to  $C_i$  vs time,  $t$ ,  $\tau$  can be evaluated. The relaxation time is related to the rate constants and equilibrium concentrations of the species in the equilibrium state established after perturbation in a unique way depending on the mechanism. It is also necessary that  $\Delta H > 0$  for the reaction. In this system, the temperature change was  $5^\circ$  and the minimum observable relaxation time was about  $2 \mu\text{s}$ .

Lanthanum perchlorate, anthranilic acid and methyl red solutions of  $\mu = 0.2 \text{ M}$  are placed in the temperature jump cell and equilibrated. Since  $\Delta H$  is small, the indicator change of the system is also small. The wavelength region 470–525 nm was chosen for the temperature jump.

Typical kinetic data at  $20^\circ\text{C}$  and  $\mu = 0.2 \text{ M}$  are given in Table 7.3.

The data were found to be consistent with the mechanism



Since reactions of equations (7.47) and (7.49) are in rapid equilibrium in comparison to reaction of  $\text{Dy}^{3+}$  with anthranilate, the relaxation time,  $\tau$  is given by the equation

$$\frac{1}{\tau} = k_{23} \left\{ \frac{[\text{Dy}^{3+}]}{1 + a} + [\text{An}^-] \right\} + k_{32} \quad (7.50)$$

TABLE 7.3  
Typical kinetic data at 20°C and  $\mu = 0.2$  (NaClO<sub>4</sub>).

No.	10 <sup>4</sup> [Dy(III)] <sup>a</sup> (M)	10 <sup>4</sup> [HAn] <sup>a</sup> (M)	10 <sup>6</sup> [Hin] <sup>a</sup> (M)	pH	1/1000 $\tau$ (s <sup>-1</sup> )
1	0.0409	0.0203	4.38	5.57	13.2
2	26.7	0.860	8.77	6.08	46.3
3	16.0	0.860	8.77	5.84	36.0
4	10.7	0.860	8.77	6.03	33.0
5	5.33	0.860	8.77	5.82	28.3
6	2.67	0.430	4.38	5.75	28.5
7	21.3	0.860	8.77	5.88	42.0
8	0.0205	0.0041	4.38	6.03	19.9
9	0.0409	0.0081	8.77	6.90	20.4
10	0.0409	0.0215	4.30	4.62	14.8
11	0.0818	0.0215	4.30	5.58	17.5
12	1.07	0.0215	4.30	4.22	14.9
13	5.33	0.860	8.60	5.37	22.1
14	2.67	0.430	4.30	5.33	21.3
15	26.7	0.860	8.60	5.26	59.8
16	26.7	0.860	8.60	6.10	70.6
17	18.1	0.860	8.60	6.01	50.8
18	25.6	0.860	8.60	5.95	62.5

<sup>a</sup>Initial total concentrations.

$$a = \frac{[\text{H}^+]}{K_{\text{An}} + [\text{An}^-] \left\{ \frac{K_{\text{In}^+}[\text{H}^+]}{K_{\text{In}^+}[\text{H}^+] + [\text{In}^-]} \right\}} \quad (7.51)$$

$$K_{\text{In}} = \frac{[\text{H}^+][\text{In}^-]}{[\text{HIn}]} \quad (7.52)$$

A plot of  $1/\tau$  versus  $\{(\text{Dy}^{3+})/1 + a\} + [\text{An}^-]$  is shown in Fig. 7.9.

From Fig. 7.9 the slope obtained corresponds to the forward rate constant  $k_{23}$  and the intercept gives the reverse reaction rate constant,  $k_{32}$ .

Now the pressure-jump technique will be described with a system consisting of lanthanide oxalate complexes [17]. The technique used a sudden change in pressure to perturb the equilibrium and a conductivity bridge to detect and follow the changes in the system. The course of re-equilibration is recorded by the use of an oscilloscope and a camera.

A steel plunger was dropped which ruptured the phosphor bronze diaphragm to release the pressure. In addition to causing pressure release, the contact of the steel plunger with the diaphragm served to trigger a single sweep of the oscilloscope.

Using 0.1 M MgSO<sub>4</sub> solution which has a relaxation time less than 1  $\mu$ s. The time constant of the set-up was found to be  $60 \pm 6$   $\mu$ s. The relaxation times were measured over a range of concentrations of the reactants in order to determine the rate constants. The total ligand (oxalate) concentration was maintained at values which insured that only the first stage of complexation was important.



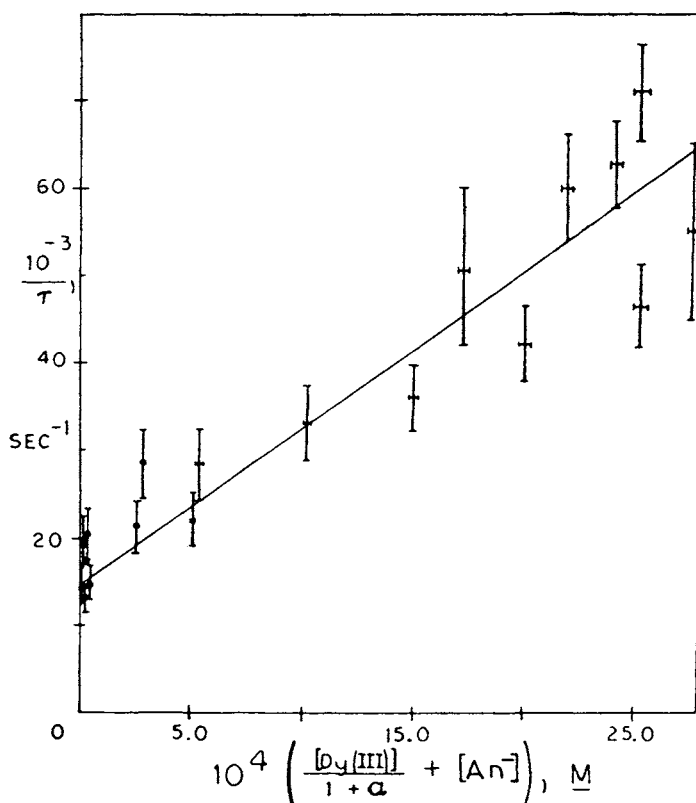


Fig. 7.9. Plot of  $1/\tau$  vs.  $\{[Dy(III)]/(1+\alpha) + [Au^-]\}$  at  $20^\circ C$  and  $\mu = 0.2$  ( $NaClO_4$ ).

The mechanism that is assumed for the formation of lanthanum oxalate complex is as follows [18]



The first step is the diffusion of the two aquo ions together. The second step is the partial loss of the solvent and the formation of an ion pair. The third step is the loss of water from

the inner hydration sphere of the metal ion and this step is much slower than the first two steps. The last step is the formation of the fully chelated complex. Assuming steady state for ML(aq) the rate equation is given by

$$\frac{d[\text{ML}(\text{aq})']}{dt} = \frac{K_1 K_2 k_{34} k_{45}}{k_{43} k_{45}} [\text{M}(\text{aq})][\text{L}(\text{aq})] - \frac{k_{43} k_{54}}{k_{43} + k_{45}} [\text{ML}(\text{aq})'] \quad (7.57)$$

where  $K_1$  and  $K_2$  are equilibrium constants for steps 1 and 2, respectively. Then we may write

$$k_f = \frac{K_1 K_2 k_{34} k_{45}}{k_{43} + k_{45}} \quad (7.58)$$

$$k_r = \frac{k_{43} k_{54}}{k_{43} k_{45}} \quad (7.59)$$

If  $k_{45} \gg k_{43}$  the measured forward and reverse rate constants may be written as

$$k_f = K_1 K_2 k_{34} \quad (7.60)$$

$$k_r = k_{43}/K_4 \quad (7.61)$$

Knowing  $K_1 K_2$  and  $K_4$  the forward and reverse rate constants can be obtained.  $K_1 K_2$  was obtained by the Bjerrum method [19] or the diffusion theory [20] of Eigen. The forward and reverse rate constants were determined using the relationship

$$\frac{1}{\tau} = k_f(C_M - C_L) + k_r \quad (7.62)$$

where  $\tau$  is the measured relaxation time and  $C_M$  and  $C_L$  are the overall metal and ligand concentrations, respectively. Since most of the ligand is complexed and  $C_M \gg C_L$  the equation takes the form

$$\frac{1}{\tau} = k_f(C_M - C_L) + k_r \quad (7.63)$$

The values of  $\tau$  are obtained experimentally at various concentrations and then  $1/\tau$  is plotted against the equilibrium concentrations of the reactants. The slope of the plot gives  $k_f$  and the intercept gives  $k_r$ . The kinetic data obtained are given in Table 7.4. A least square analysis of the data gave the values of  $k_f$  and  $k_r$  along with the stability constants (Table 7.5). Temperature dependence of the rate constants gave activation parameters (Table 7.6).

The rate constants for the reaction of murexide with lanthanides obtained by Geier [21] are of similar magnitude as those of oxalate complexes. The forward rate is insensitive to the nature of the entering ligand which provides support for the operation of the four-step mechanism proposed by Eigen [18]. The substitution reactions of lanthanides appear to be governed by the four-step mechanism. The rate determining step in this mechanism is the

TABLE 7.4  
Formation kinetics of some lanthanide oxalate complexes [22].

Metal ion	$C_M \times 10^5$ (M)	$C_L \times 10^5$ (M)	$\tau$ ( $\mu$ s)
La	7.3	2.2	240 $\pm$ 24
	9.1	2.3	178 $\pm$ 18
	12.0	2.1	126 $\pm$ 13
Nd	7.2	1.8	216 $\pm$ 22
	9.0	1.8	161 $\pm$ 16
	11.6	1.6	116 $\pm$ 12
Sm	6.0	1.0	230 $\pm$ 23
	9.9	1.2	140 $\pm$ 14
	12.3	1.3	103 $\pm$ 10
Eu	6.5	1.4	254 $\pm$ 25
	8.1	1.1	180 $\pm$ 18
	10.5	1.3	140 $\pm$ 14
Gd	6.6	1.2	402 $\pm$ 40
	8.3	1.3	309 $\pm$ 30
	14.5	1.5	167 $\pm$ 17
Tb	8.4	1.0	565 $\pm$ 56
	11.8	1.8	418 $\pm$ 42
	23.1	2.1	200 $\pm$ 20
Dy	11.0	1.4	800 $\pm$ 80
	16.5	1.5	515 $\pm$ 51
	22.1	2.1	383 $\pm$ 38
Ho	13.1	2.1	909 $\pm$ 91
	20.4	3.2	584 $\pm$ 58
	23.8	1.8	450 $\pm$ 45
Er	19.5	1.5	790 $\pm$ 79
	26.8	1.8	628 $\pm$ 62
	40.2	2.2	420 $\pm$ 42
Tm	17.6	1.6	990 $\pm$ 99
	21.8	1.8	790 $\pm$ 79
	27.3	2.3	635 $\pm$ 63

The temperature on each is 25°C.

TABLE 7.5  
Rate constants for lanthanides [22].

Ion	$k_f \times 10^{-7}$ ( $M^{-1} s^{-1}$ )		$k_r \times 10^{-6}$ ( $s^{-1} M^{-1}$ )	$k_f/k_r \times 10^{-6} M^{-1}$	Stability constant from literature
	Geier				
La	8.0	8.6	8.2	1.0	1.17
Nd	8.6	9.3	10.2	8.4	8.70
Sm	8.2	9.6	6.3	13.0	11.00
Eu	7.7	8.2	3.8	20.0	22.90
Gd	4.6	5.2	3.3	14.0	12.90
Tb	2.4	3.0	2.5	9.7	10.00
Dy	1.3	1.7	1.4	9.3	9.30
Ho	1.0	1.4	1.0	9.8	1.00
Er	0.63	1.0	6.3	1.0	
Tm	0.63	1.1	6.7	0.9	1.05

TABLE 7.6  
Temperature dependence of the rates [22].

Ion	$T$ ( $^{\circ}\text{C}$ )	$(C_M - C_L) \times 10^5$ (M)	$t$ ( $\mu\text{s}$ )	$k_f \times 10^{-7}$ ( $\text{M}^{-1} \text{s}^{-1}$ )	$E_a$ (kcal/mole)	$\Delta H^{\ddagger}$ (kcal/mole)	$\Delta S^{\ddagger}$ (e.u.)
La	15	5.1	$337 \pm 33$	5.72			
	25	5.1	$240 \pm 24$	8.03	6.1	5.5	-4-6
	35	5.1	$167 \pm 17$	10.15			
Nd	15	5.4	$301 \pm 30$	6.17			
	25	5.4	$215 \pm 21$	8.61	6.2	5.6	-4.4
	30	5.4	$158 \pm 16$	11.70			
Gd	15	7.0	$440 \pm 44$	3.26			
	25	7.0	$311 \pm 31$	4.61	6.5	6.0	-5.2
	35	7.0	$207 \pm 21$	6.92			
Tb	15	10.0	$611 \pm 61$	1.64			
	25	10.0	$415 \pm 41$	2.41	6.7	6.2	-4.9
	35	10.0	$280 \pm 28$	3.56			
Er	15	38.0	$636 \pm 64$	0.41			
	25	38.0	$420 \pm 42$	0.63	7.7	7.2	-4.2
	30	38.0	$332 \pm 33$	0.80			
Tm	15	25.0	$960 \pm 96$	0.42			
	25	25.0	$635 \pm 64$	0.63	7.5	7.0	-4.8
	35	25.0	$402 \pm 40$	1.00			

loss of a water molecule from the inner hydration sphere of the metal ion and therefore depends on the properties of the hydrated lanthanide ion.

The ultrasonic method involving pulse technique has been used in measuring the rates of complexation of lanthanides with sulphate [22]. Measurements of the absorption of ultrasonic energy were made at selected frequencies between 15 and 230 Mc/s using the pulse method [23]. The change in amplitude of a short pulsed sound wave is measured as the path length through the test solution is varied. The change in amplitude of such a pulse was compared with a pulse produced by a comparison oscillator, operating at the main transmitted frequency and passing through a standard attenuator system. Two units covering frequency ranges 15-75 and 70-230 Mc/s were used. This arrangement has the advantage of reducing the overall dimensions of the transducer-delay rod assembly at higher frequencies. The frequency overlap between the two units was a useful check on the consistency of measurement. The maximum path lengths were 2.5 and 1.00 cm for the low and high frequency ranges, respectively.

The relaxation spectra of lanthanide sulphate at 0.01 M are given in Fig. 7.10.

The excess sound absorption produced by the chemical reaction is denoted by  $Q\lambda$  and expressed by

$$Q\lambda = 2\alpha_{\text{chem}}\lambda/NC_i \quad (\text{cm}^3 \text{ molecule}) \quad (7.64)$$

where  $N$  is Avogadro's number,  $C_i$  the molar concentration of solute per ml. The attenuation of a plane progressive sound wave traversing a solution is given by

$$I = I_0 \exp(-2\alpha x) \quad (7.65)$$

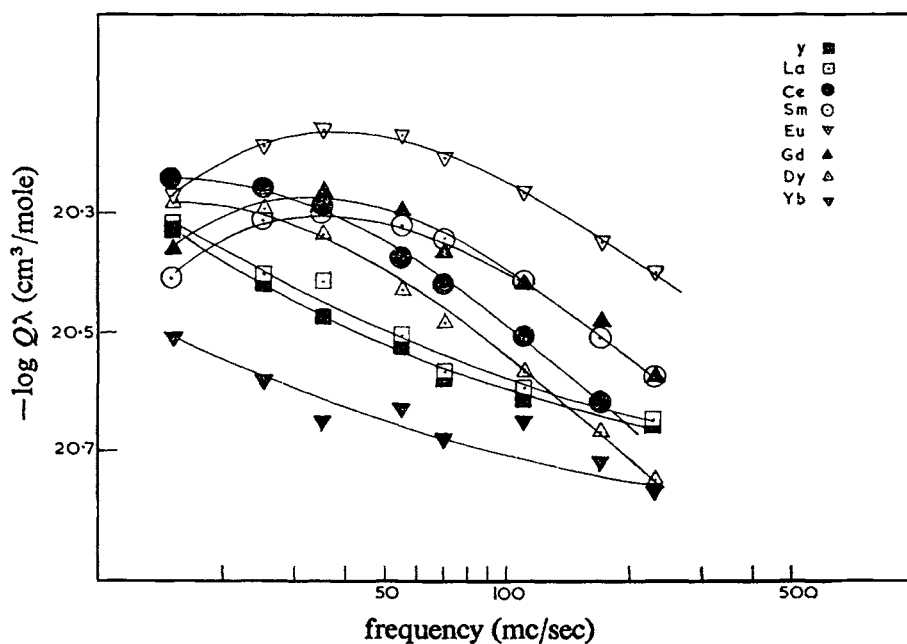


Fig. 7.10. Experimental log excess sound absorption against log frequency curves ( $\sim 0.01$  M solutions) [22].

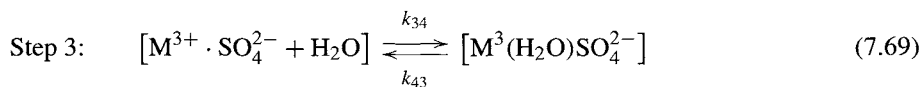
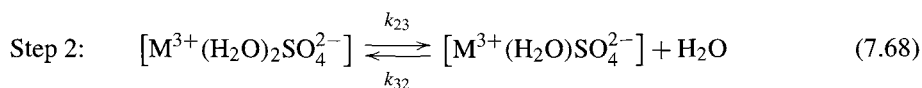
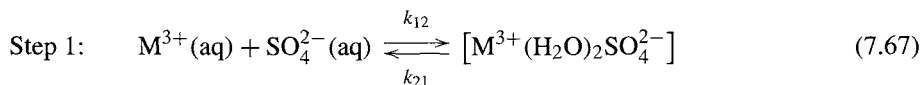
where  $I$  is sound intensity at a distance  $x$ ,  $I_0$  the sound intensity at zero distance, and  $\alpha$  is absorption coefficient for the solution. The experimentally measured absorption is  $\alpha$  and

$$\alpha_{\text{chem}} = \alpha_{\text{exp}} - \alpha_{\text{H}_2\text{O}} \quad (7.66)$$

where the units of  $\alpha_{\text{chem}}$  are nepiers/cm.

Concentration dependence of relaxations is shown in Fig. 7.11 for samarium sulphate.

The data were analysed in terms of a three-step complex formation mechanism of Eigen and Tamm [18]. The mechanism consists of successive removal of one water molecule from the solvation sheath of each ion in three reversible steps as the ions approach from infinite separation to ultimate contact.



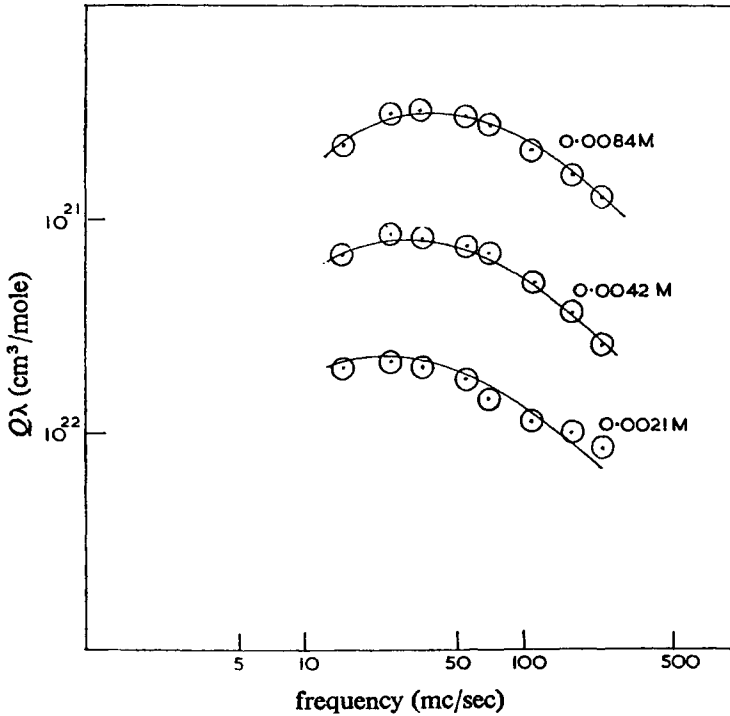


Fig. 7.11. Concentration dependence of characteristic frequency  $\nu_{m3}$  for samarium sulphate [22].

In order to find a solution to the problem, the relaxation spectra should consist of three distinct maxima with the corresponding relaxation times given by the equations:

$$\frac{1}{\tau_1} = 2\pi \nu_{m1} = k_{21} + k'_{12} \quad (7.70)$$

$$\frac{1}{\tau_2} = 2\pi \nu_{m2} = k_{32} + \left[ \frac{k'_{12}}{k'_{12} + k_{21}} \right] k_{23} = k_{32} + k'_{23} \quad (7.71)$$

$$\frac{1}{\tau_3} = 2\pi \nu_{m3} = k_{43} \left[ \frac{k'_{23}}{k'_{23} + k_{32}} \right] k_{34} = k_{43} + k'_{34} \quad (7.72)$$

where  $\tau_1$ ,  $\tau_2$ , and  $\tau_3$  are relaxation times for steps 1, 2 and 3, respectively,  $\nu_{m1}$ ,  $\nu_{m2}$  and  $\nu_{m3}$  are frequencies of maximum absorption for steps 1, 2 and 3, respectively. The value of  $k'_{12}$  is to be corrected for activities of ions. For small perturbations

$$k'_{12} = k_{12}^0 \pi_f \left\{ [M^{3+}] + [SO_4^{2-}] + [SO_4^{2-}] \left( \frac{\partial \ln \pi_f}{\partial \ln [M^{3+}]} \right) \right\} \quad (7.73)$$

where  $k_{12}^0$  is the rate constant at zero ionic strength,  $\pi_f$  is the activity quotient  $f_{3+}f_{2-}/f_{\ddagger}$  and  $[M^{3+}]$  and  $[SO_4^{2-}]$  are the equilibrium free ion concentrations.

If the solute concentration is  $C_i$  mole/l of  $M_2(SO_4)_3$ , the degree of association is  $\beta$  at equilibrium then the total concentration of associated species is  $2\beta C_i$  mole/l.

$$\text{Now } [M^{3+}] = 2(1 - \beta)C_i \quad \text{and} \quad [SO_4^{2-}] = (3 - 2\beta)C_i \quad (7.74)$$

We may then write

$$k'_{12} = k_{12}^0 \pi_f C_i \left\{ (5 - 4\beta) + \left[ (2\beta - 3) \frac{\partial \ln \pi_f}{\partial \ln \beta} \right]_{C_i} \right\} \quad (7.75)$$

The values of  $\beta$  for each  $C_i$  were obtained by iteration from the total thermodynamic equilibrium constants based on conductivity measurements. The activity coefficients  $f_{3+}$ ,  $f_{2-}$  and  $f_{\ddagger}$  were evaluated from the extended Debye-Hückel theory.

The rate expressions in terms of concentrations and equilibrium constants are

$$2\pi v_{m1} = k_{21} + k_{12}^0 [\theta(C)] \quad (7.76)$$

$$2\pi v_{m2} = k_{32} + \left[ \frac{\theta(C)}{K_{12} + \theta(C)} \right] k_{23} \quad (7.77)$$

$$2\pi v_{m3} = k_{43} + \left[ \frac{\theta(C)}{K_{12}K_{23} + (1 + K_{23})[\theta(C)]} \right] k_{34} \quad (7.78)$$

where  $K_{12}$ ,  $K_{23}$  and  $K_{34}$  are thermodynamic equilibrium constants for steps 1, 2, and 3, respectively, and defined as

$$K_{12} = k_{21}/k_{12}^0; \quad K_{23} = k_{32}/k_{23}; \quad K_{34} = k_{43}/k_{34} \quad (7.79)$$

and

$$\theta(C) = \pi_f C_i \left\{ (5 - 4\beta) + \left[ (2\beta - 3) \frac{\partial \ln \pi_f}{\partial \ln \beta} \right]_{C_i} \right\} \quad (7.80)$$

Experimentally the single relaxation observed was attributed to step 3 in the mechanism because: (a) theoretical calculation of  $k_{12}^0$  and  $k_{21}$  predicted an estimated relaxation frequency inaccessible to the equipment used and (b) step 2 is excluded since the rate of displacement of water from the primary hydration sphere of an anion is independent of the cation. The relaxation data were analyzed by the equation

$$\frac{\alpha}{v^2} = \frac{A}{1 + (v/v_m)} + B \quad (7.81)$$

The data follow a pattern illustrated in Fig. 7.12 for samarium sulphate. Fig. 7.12 is suggestive of the fact that the characteristic frequency approximates closely to that of the

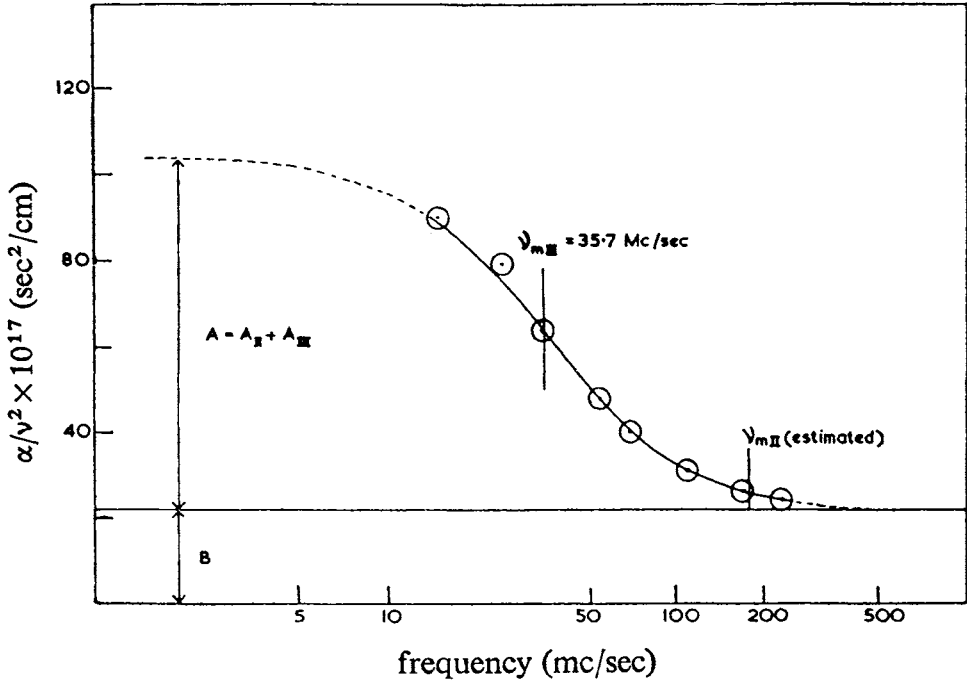


Fig. 7.12. Plot of  $\alpha/v^2$  against log frequency for samarium sulphate (0.0084 M) [22].

slowest relaxation  $\nu_{m3}$ . Analysis of the data in terms of two relaxations

$$\left(\frac{\alpha}{v^2}\right) = \frac{A_{II}}{1 + (\nu/\nu_{mII})} + \frac{A_{III}}{1 + (\nu/\nu_{mIII})} + B \quad (7.82)$$

$\nu_{mII}$  and  $\nu_{mIII}$  are two variables. Knowing  $\nu_{mIII}$  from the equation

$$2\mu_{\max III} = A_{III}\bar{C}\nu_{mIII} \quad (7.83)$$

when  $\nu = \nu_{mIII}$ ,  $\mu_{\max III} = Q\lambda_{III}$ ,  $\bar{C}$  is velocity of sound. The calculated  $A_{III}$  accounts for 95% of the change in  $\alpha/v^2$  with the estimated value of  $\nu_{mII} \sim 175$  Mc/s which indicates that step 2 is not responsible for intense absorption. Rearranging equation (7.82) gives

$$\left(\frac{\alpha}{v^2} - B\right) = \frac{(\alpha - Bv^2)}{v_{mIII}^2} + A \quad (7.84)$$

$(\alpha/v^2 - B)$  is plotted against  $(\alpha - Bv^2)$  as shown in Fig. 7.13. The slope  $= -1/v_{mIII}^2$  from which the characteristic frequency  $\nu_{\max III}$  is obtained. The  $\nu_{\max III}$  values are given in Table 7.7.

The kinetic parameters were derived from the relaxation data by making the following assumptions: (i) the equilibrium constant for step 1 is the same for all the lanthanides,



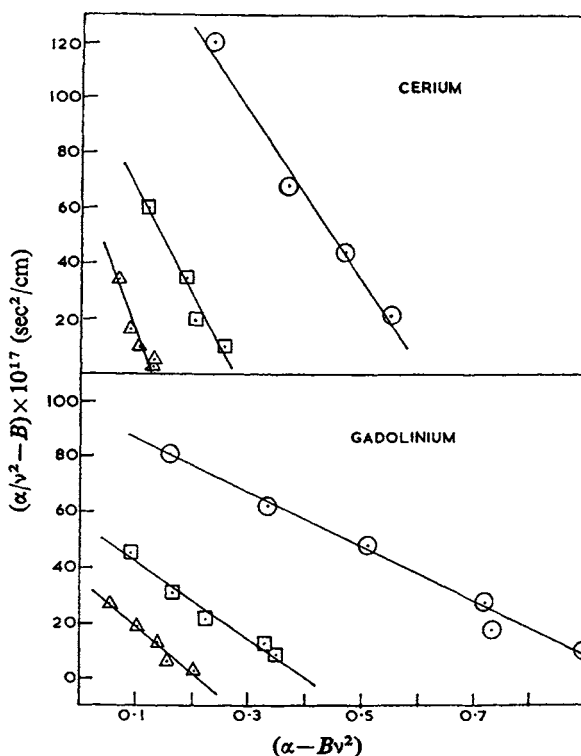


Fig. 7.13. Plot of  $(\alpha/v^2 - B)$  against  $(\alpha - Bv^2)$  for cerium(III) and gadolinium(III) sulphates. The slope is equal to  $-1/\nu_{\text{mIII}}$  [22].

$K_{12} = 0.0023 \text{ mole l}^{-1}$ , (ii) since it is impractical to analyse data for  $k_{23}$  and  $k_{32}$ , a value of  $K_{23} = 0.51$  for magnesium sulphate is used [24]. While it is unlikely that an increase in charge of the cation will have no effect on the equilibrium constant for step 2, the nature of the cation is of secondary importance in the elimination of water from the sulphate solvation sheath. Also the field of a magnesium ion is close to the field of a lanthanide ion, (iii) the term  $(\partial \ln \pi_f / \partial \ln \beta) C_i$  is evaluated according to the procedure in the literature [25]. The magnitude of this term is small, when the concentration is reduced, (iv) a plot of  $2\pi \nu_{\text{mIII}}$  against  $\{\theta_c / K_{12} K_{23} + (1 + K_{23})[\theta(c)]\}$  for various concentrations gives  $k_{43}$  as intercept and  $k_{34}$  as slope as shown in Fig. 7.14, (v) neither hydrolysis of lanthanide nor formation of higher sulphate complexes is important to interfere in the mechanism.

The resulting data for  $k_{34}$  and  $k_{43}$  are given in Table 7.8. It is to be noted that the values of  $k_{43}$  are not as reliable as those of  $k_{34}$  because of the long extrapolation involved. The thermodynamic association constant  $K_{\Sigma}$  is given by

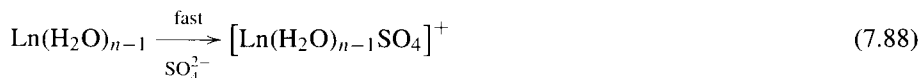
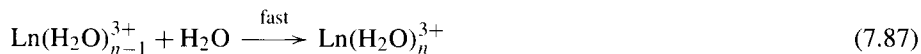
$$K_{\Sigma} = \frac{1 + K_{34} + K_{23}K_{34}}{K_{12}K_{23}K_{34}} \quad (7.85)$$

TABLE 7.7  
Relaxation frequency data.

Ion	Molar conc. $\times 10^2$	$2\pi \nu_{\text{vmlIII}}$ (Mc/s)
$\text{Y}^{3+}$	1.41	89
	0.71	73
	0.36	65
$\text{La}^{3+}$	0.88	99
	0.44	63
	0.22	52
$\text{Ce}^{3+}$	0.98	111
	0.49	89
	0.24	79
$\text{Sm}^{3+}$	0.84	225
	0.42	178
	0.21	148
$\text{Eu}^{3+}$	0.98	228
	0.49	185
	0.25	161
$\text{Gd}^{3+}$	0.95	207
	0.47	171
	0.24	143
$\text{Dy}^{3+}$	0.97	104
	0.65	93
	0.32	70
$\text{Yb}^{3+}$	3.57	48
	1.14	39
	0.94	41

The equilibrium constant values are in good agreement with the literature values with the exception of yttrium.

Similarity of  $k_{34}$  values for complexation between  $\text{Mg}^{2+}$  and  $\text{SO}_4^{2-}$ ,  $\text{CrO}_4^{2-}$  and  $\text{S}_2\text{O}_3^{2-}$  and solvent exchange rates of paramagnetic ions to the  $k_{34}$  values obtained by the present ultrasonic studies give evidence for a dissociative type of mechanism. The removal of a water molecule from the solvated lanthanide in step 3 is probably the rate-determining step. We may then write



Assuming lighter lanthanides have coordination number 8, the heavy lanthanides have a coordination number of 9 and the intermediate lanthanides with a coordination number

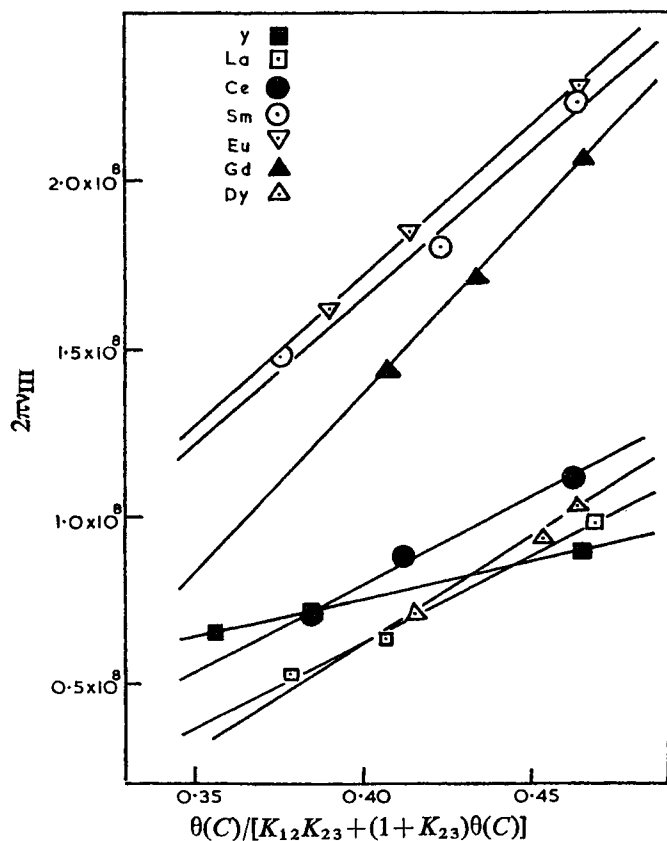

 Fig. 7.14. Plots of  $2\pi\nu_{III}$  against  $\theta(C)/[K_{12}K_{23} + (1 + K_{23})\theta(C)]$  [22].

 TABLE 7.8  
 Rate constants and equilibrium constants.

	$k_{34}$ ( $s^{-1}$ )	$k_{43}$ ( $s^{-1}$ )	$K$ ( $1 \text{ mole}^{-1}$ ) (kinetic)	$K$ ( $1 \text{ mole}^{-1}$ ) (conductimetric)
$Y^{3+}$	$\sim 2.6 \times 10^8$	$\sim 2 \times 10^8$	$12.4 \times 10^3$	$3.0 \times 10^3$
$La^{3+}$	$5.2 \times 10^8$	$1.4 \times 10^8$	$4.3 \times 10^3$	$4.2 \times 10^3$
$Ce^{3+}$	$5.5 \times 10^8$	$1.4 \times 10^8$	$4.6 \times 10^3$	$3.9 \times 10^3$
$Sm^{3+}$	$8.8 \times 10^8$	$1.9 \times 10^8$	$5.2 \times 10^3$	$4.6 \times 10^3$
$Eu^{3+}$	$9.2 \times 10^8$	$2.0 \times 10^8$	$(5.3 \times 10^3)$	$(3.6 \times 10^3)^{\#}$
$Gd^{3+}$	$10.5 \times 10^8$	$3.0 \times 10^8$	$4.3 \times 10^3$	$4.6 \times 10^3$
$Dy^{3+}$	$6.4 \times 10^8$	$1.9 \times 10^8$	$4.1 \times 10^3$	$(3.9 \times 10^3)^*$
$Yb^{3+}$	$\sim 10^8$			$3.9 \times 10^3$

$\#$ Obtained by distribution method.  $*$ Estimated.

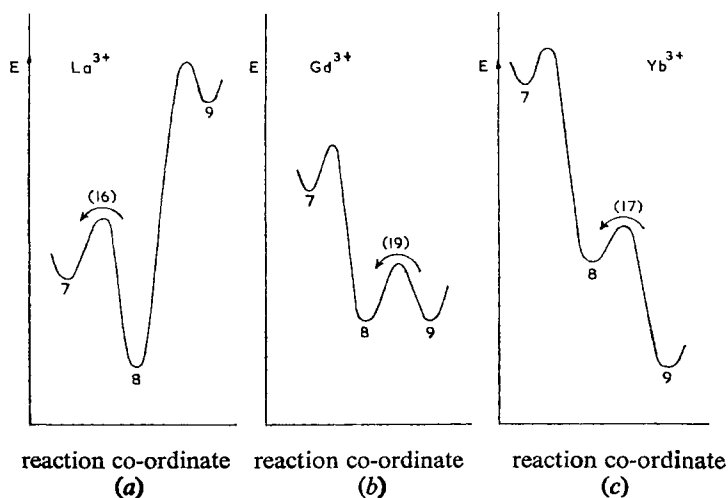


Fig. 7.15. Schematic representation of reaction showing proposed co-ordination number changes in the rate-determining steps for (a)  $\text{La}^{3+}$ ; (b)  $\text{Gd}^{3+}$ ; (c)  $\text{Yb}^{3+}$  [22].

between 8 and 9, the rate determining step for  $\text{La}^{3+}$  is



In the case of  $\text{Yb}^{3+}$



In the case of  $\text{Gd}^{3+}$ , the coordination number is between 8 and 9 with two possible rate-determining states assuming we have both  $\text{Gd}(\text{H}_2\text{O})_8^{3+}$  and  $\text{Gd}(\text{H}_2\text{O})_9^{3+}$



It is proposed that the reaction (7.92) will be faster than (7.91) and (7.89) and (7.90). The net result is that an enhanced rate of water elimination would be the consequence of two adjacent coordination numbers having similar energy levels. Energy profiles of  $\text{La}^{3+}$ ,  $\text{Gd}^{3+}$  and  $\text{Yb}^{3+}$  are shown in Fig. 7.15.

## 18. Mechanisms of rare earth complex formation reactions

In the case of transition metal complex formation reactions, model systems are established and the patterns of reactivity can be discussed in terms of model systems. For example, cobalt(III) and platinum(II) do serve as paradigm for octahedral and square planar

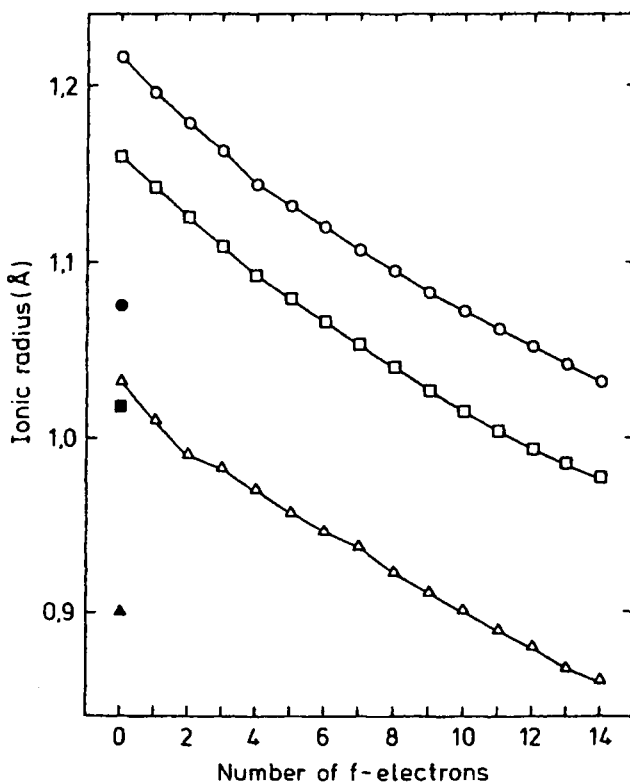


Fig. 7.16. Illustration of the lanthanide contraction for CN = 6 ( $\Delta$ ), 8 ( $\square$ ) and 9 ( $\circ$ ). Filled symbols are for  $Y^{3+}$  (ionic radii taken from diffraction data, as compiled by Shannon [2]).

complexes. Further, the substitution reaction rates of transition metal complexes of model systems are relatively slow and can be studied by conventional techniques like UV-Vis spectroscopy. In contrast to transition metals, lanthanides are characterized by progressive filling of 4f orbitals which are shielded by filled 5s and 5p orbitals, leading to very small crystal field splittings in the lanthanide complexes. The crystal field splittings in lanthanides is of the order of  $\sim 200\text{--}400\text{ cm}^{-1}$  and are small compared to  $\sim 10\,000\text{ cm}^{-1}$  in transition metals. Further, the coordination number (CN) also changes in the lanthanide series. The coordination properties of lanthanides mainly depend upon the steric nature of the ligands, as illustrated by the large variety of coordination numbers (primarily 6–12) observed in their complexes [26,27]. Another unique property is the lanthanide contraction. The ionic radii decrease in the series due to increase of nuclear electric field. This is true irrespective of the coordination numbers as shown in Fig. 7.16.

### 19. Counterion coordination

Anions which may be termed as 'innocent' from the point of coordination readily coordinate in organic solvents like methanol and acetonitrile [28–30]. Using  $^{139}\text{La}$  NMR,

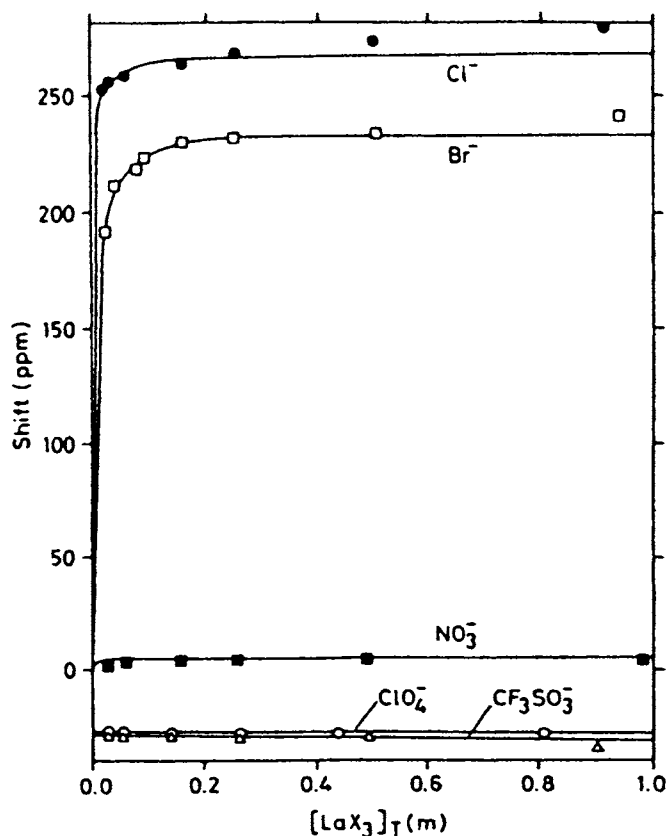


Fig. 7.17.  $^{139}\text{La}$  NMR chemical shifts as a function of  $\text{LaX}_3$  concentration in anhydrous methanol at  $23^\circ\text{C}$ . Solid lines are the results of fitting data.

counter ion coordination has been studied with  $\text{Cl}^-$ ,  $\text{Br}^-$ ,  $\text{NO}_3^-$ ,  $\text{ClO}_4^-$  and  $\text{CF}_3\text{SO}_3^-$  ions. The chemical shift  $\delta_{\text{obs}}$  measured in a solution of lanthanum compounds was very sensitive to the composition of the inner coordination sphere of La. The observed shifts of  $^{139}\text{La}$  are shown in Fig. 7.17 for various concentrations of lanthanum salts.

The stability constant  $K_X$  can be derived from equations (7.93) and (7.94)



$$\delta_{\text{obs}} = (1-x)\delta_{\text{La}^{3+}} + x\delta_{\text{LaX}^{2+}} \quad (7.94)$$

where  $x$  is the mole fraction of  $\text{LaX}^{2+}$ . The  $K_X$  values are given in Table 7.9. These values are in agreement with the values obtained from the reaction

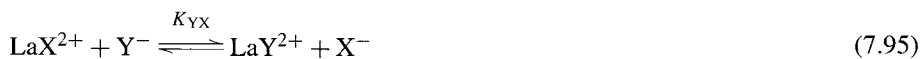


TABLE 7.9

Stability and relative stability constants for the equilibria  $\text{La}^{3+} + \text{X}^- = \text{LaX}^{2+}$  and  $\text{LaX}^{2+} + \text{Y}^- = \text{LaY}^{2+} + \text{X}^-$  in methanol at 23°C determined by  $^{139}\text{La}$ -NMR.

$\text{X}^-$	$K_X$	$\log K_X$	$\text{Y}^-$	$K_{YX}$	$\log K_{YX}$
$\text{ClO}_4^-$	$390 \pm 60$	$2.6 \pm 0.2$	$\text{Cl}^-$	3.82	0.58
$\text{CF}_3\text{SO}_3^-$	$450 \pm 60$	$2.7 \pm 0.1$	$\text{Br}^-$	1.06	0.02
$\text{Br}^-$	$460 \pm 70$	$2.7 \pm 0.2$	$\text{ClO}_4^-$	0.79	-0.10
$\text{Cl}^-$	$1500 \pm 200$	$3.2 \pm 0.1$	$\text{CF}_3\text{SO}_3^-$	0.31	-0.51

TABLE 7.10

Average number  $\bar{n}$  of associated perchlorate ions per  $\text{Ln}^{3+}$  and corresponding association constants in anhydrous acetonitrile measured by FT-IR. The solutions are 0.05 M in  $\text{Ln}(\text{ClO}_4)_3$ .

Ln	$\bar{n} (\pm 0.08)$	$\log K (\pm 0.3)$	Ln	$\bar{n} (\pm 0.08)$	$\log K (\pm 0.3)$
La	1.56	a	Tb	0.89	1.9
Pr	1.18	a	Dy	0.79	1.6
Nd	1.18	a	Er	0.93	2.1
Eu	0.87	1.8	Tm	0.87	1.8

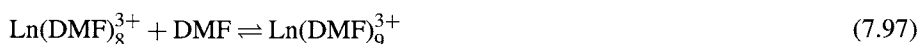
<sup>a</sup> $\log K$  for  $\text{Ln}(\text{ClO}_4)^{2+}$  is too large to be determined by this technique.

$$\delta_{\text{obs}} = x\delta_{\text{LaX}^{2+}} + (1-x)\delta_{\text{LaY}^{2+}} \quad (7.96)$$

It has been shown by FT-IR measurements that perchlorate which is normally thought to be 'innocent', forms inner-sphere complexes with lanthanides. Most of the bound perchlorate is a monodentate. In the case of  $\text{Eu}^{3+}$  and  $\text{Tb}^{3+}$  bidentate disposition of perchlorate was also observed. The value of association constants of perchlorate with lanthanides are given in Table 7.10.

## 20. Solvent exchange in dimethyl formamide (DMF)

The behaviour of lanthanum in dimethyl formamide (DMF) is quite different from that in methanol and acetonitrile. While perchlorate forms inner sphere complexes with lanthanides in acetonitrile [31], no such complexes are formed in DMF [32]. The coordination properties in DMF solutions were studied by NMR and UV-Vis spectroscopy techniques [33,34]. The rate of DMF exchange in the system ytterbium perchlorate–DMF– $\text{CD}_2\text{Cl}_2$  was slow enough that  $^1\text{H}$  NMR resonances permitted the determination of the mean coordination number to be  $7.8 \pm 0.2$ . Similar determination in the case of thulium(III) gave a mean coordination number of  $7.7 \pm 0.2$ . Thus it was concluded that the predominant species in heavy lanthanides is  $\text{Ln}(\text{DMF})_8^{3+}$  in DMF solutions. In the case of lighter lanthanides, the following equilibrium exists



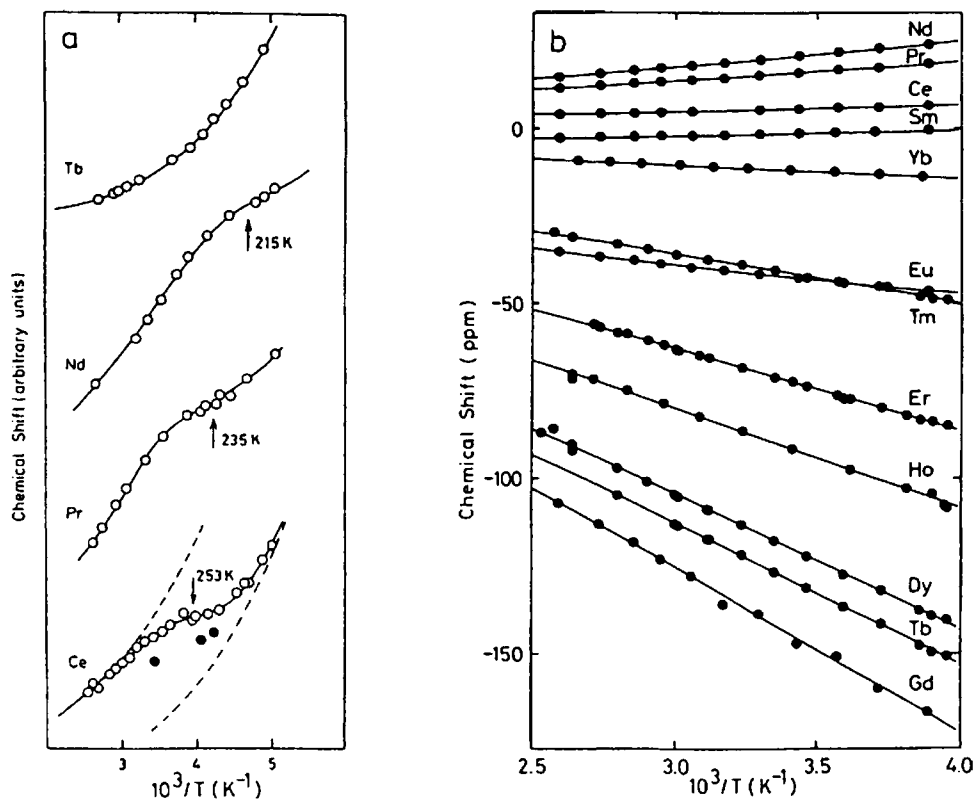


Fig. 7.18. Solvent NMR chemical shifts recorded in lanthanide perchlorate solutions. (a) DMF formyl  $^1\text{H}$  in pure DMF (open circles are for ambient pressure measurements; filled circles are for measurements done at 200 MPa). (b) Water  $^{17}\text{O}$  in 2.0 M  $\text{H}^+$  aqueous solutions [33].

The evidence for the increase in coordination number lies in  $^1\text{H}$  NMR formyl proton shifts for  $\text{Ce}^{3+}$ ,  $\text{Pr}^{3+}$  and  $\text{Nd}^{3+}$ . The proton shifts are seen in Fig. 7.18. The inflection observed in the case of  $\text{Ce}^{3+}$ ,  $\text{Pr}^{3+}$  and  $\text{Nd}^{3+}$  implies two different paramagnetic environments are responsible for contributing to the average  $^1\text{H}$  shift of the solvent in rapid exchange. The increase in coordination number is above 8 in the case of  $\text{Ce}^{3+}$ ,  $\text{Pr}^{3+}$  and  $\text{Nd}^{3+}$ . Since no inflection is observed in the  $\text{Tb}^{3+}$  to  $\text{Yb}^{3+}$  series, it is concluded that  $\text{Ln}(\text{DMF})_8^{3+}$  is the predominant species.

The visible absorption spectra of  $\text{Nd}(\text{ClO}_4)_3$  in DMF solutions were studied. In particular, the transition involved is  $^4\text{I}_{9/2} \rightarrow ^2\text{P}_{1/2}$ . This transition exhibits both temperature and pressure dependence. The visible spectra of  $\text{Nd}(\text{ClO}_4)_3$  solutions in DMF and in water are shown in Fig. 7.19.

The spectrum in DMF at 322 K approaches the spectrum of  $\text{Nd}(\text{DMF})_8(\text{ClO}_4)_3$  and the pressure and temperature dependence of the spectra coupled with  $^1\text{H}$  NMR shifts are indicative of the displacement of the equilibrium towards species of higher coordination



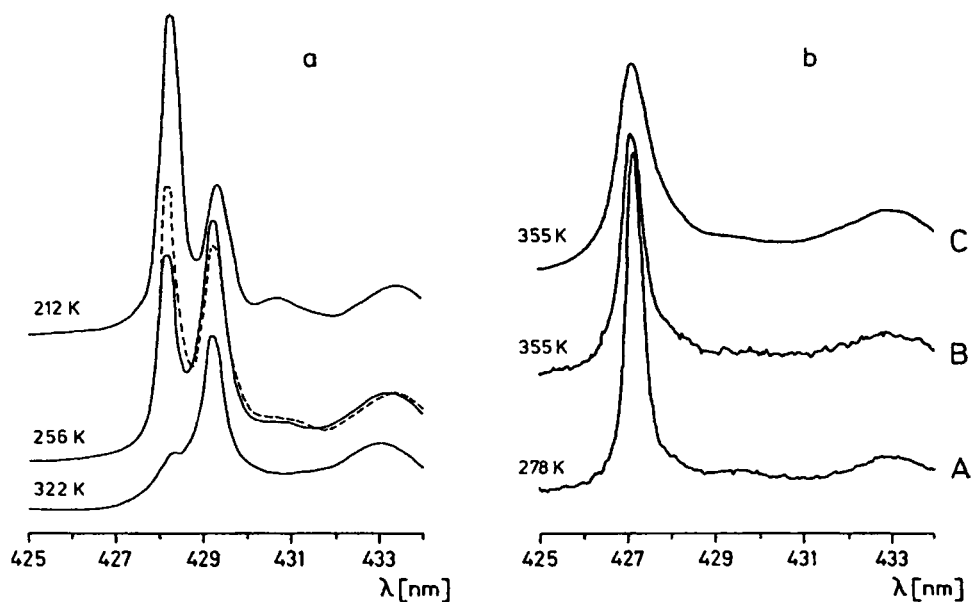


Fig. 7.19. Visible absorption spectra for  $\text{Nd}(\text{ClO}_4)_3$  solutions. (a) In DMF (dashed line at 120 MPa) and (b) in water (A, B:  $10^{-1}$  M  $\text{Nd}^{3+}$ ; C: 3 M  $\text{Nd}^{3+}$ ) [34].

number (i.e.) 9. The temperature and pressure dependencies of the spectra were analysed quantitatively leading to the following thermodynamic parameters for the reaction:



$\Delta H^\ddagger = -14.9 \pm 1.3$  kJ mol $^{-1}$ ,  $\Delta S^\ddagger = -69.1 \pm 4.2$  JK $^{-1}$  mol $^{-1}$ ,  $\Delta V^\ddagger = -9.8 \pm 1.1$  cm $^3$  mol $^{-1}$ . The activation volume of  $-9.8$  cm $^3$  mol $^{-1}$ , compared to molar volume of DMF of 72 cm $^3$  mol $^{-1}$  gives evidence for the formation of  $\text{Nd}(\text{DMF})_9^{3+}$  which is probably accompanied by lengthening of the eight Nd–DMF bonds.

The rate of solvent exchange of  $\text{Ln}(\text{DMF})_8^{3+}$  with DMF, where Ln = Tb, Dy, Ho, Er, Tm, and Yb was analysed [34,35] by using the relationships

$$\frac{1}{T_{2r}} = \frac{1}{P_m} \left( \frac{1}{T_2} - \frac{1}{T_{2A}^0} \right) = \frac{1}{\tau_m} \left[ \frac{T_{2m}^{-2} + (T_{2m}\tau_m)^{-1} + \Delta\omega_m^2}{(T_{2m}^{-1} + \tau_m^{-1})^2 + \Delta\omega_m^2} \right] + \frac{1}{T_{2os}} \quad (7.98)$$

$$\Delta\omega_r = \frac{\Delta\omega_B}{P_m} = \frac{\Delta\omega_m}{(\tau_m/T_{2m} + 1)^2 + \tau_m^2 \Delta\omega_m^2} + \Delta\omega_{os} \quad (7.99)$$

From equations (7.98) and (7.99), the kinetic parameters can be obtained using the observed NMR line-width and chemical shift of the free solvent signal. In equations (7.98) and (7.99),  $P_M$  is the mole fraction of the bound solvent,  $T_{2A}$ ,  $T_2$ ,  $T_{2m}$  and  $T_{os}$  are transverse relaxation times of pure, free, bound and outer sphere solvent,  $\Delta\omega_s$ ,  $\Delta\omega_m$  and  $\Delta\omega_{os}$  are chemical shifts relative to pure solvent of free, bound and outer sphere solvent,

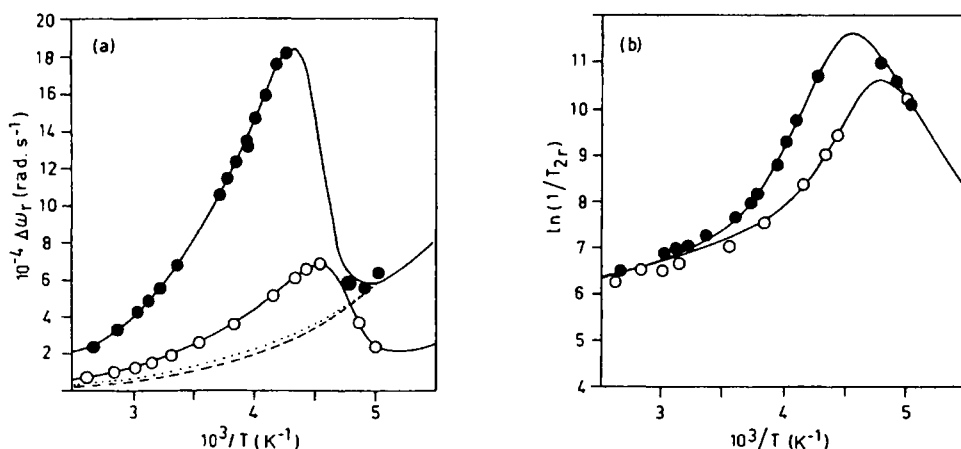


Fig. 7.20. Variable temperature  $^1\text{H}$  NMR data (formylic proton) for  $[\text{Tm}(\text{DMF})_8](\text{ClO}_4)_3$  in DMF: (a) reduced chemical shift, and (b) transverse relaxation rate. The measurements were performed at 60 MHz ( $\circ$ ) and 200 MHz ( $\bullet$ ) [35].

respectively, and  $\tau_m$  is the mean residence time of the coordinated solvent molecule, which is equal to the inverse of the exchange rate constant  $k$ . The pressure and temperature dependencies of  $k$  are given by

$$k = 1/\tau_m = k_B T/h \exp(\Delta S^\ddagger/R - \Delta H^\ddagger/RT) \quad (7.100)$$

$$\ln k = \ln k_0 - \Delta V_0^\ddagger P/RT + \Delta\beta^\ddagger P^2/2RT \quad (7.101)$$

where  $\Delta H^\ddagger$ ,  $\Delta S^\ddagger$ ,  $\Delta V^\ddagger$  and  $\Delta\beta^\ddagger$  are enthalpy, entropy, activation volume and compressibility coefficient, respectively.

A nonlinear multiparameter least squares fitting of experimental data obtained at various temperatures was done. An example for  $\text{Tm}^{3+}$  is given in Fig. 7.20. The exchange of  $\text{Tm}(\text{DMF})_8^{3+}$  with DMF as a function of time is given in Fig. 7.20. Note the change in chemical shift and transverse relaxation time as a function of temperature at three different frequencies.

The pressure dependence of the exchange of DMF with  $\text{Ln}(\text{DMF})_8^{3+}$  for Tb, Dy, Ho, Er, Tm, Yb, is shown in Fig. 7.21. The kinetic parameters are given in Table 7.11.

Reference to the data in Table 7.11 shows  $\Delta H^\ddagger$  progressively increases from Tb to Yb. On the other hand,  $\Delta S^\ddagger$  changes from negative to positive values. We have positive values of  $\Delta V^\ddagger$  indicating a dissociative mode of exchange [36]. Further increase in the values of  $\Delta V^\ddagger$  in going from Tb to Yb probably indicates a change in mechanism of the exchange reaction.

In order to explore the possible change in the mechanism, kinetics of DMF exchange were carried out in nitromethane as a diluent. The rate constants for the DMF exchange with  $\text{Ln}(\text{DMF})_8^{3+}$  in nitromethane are plotted as a function of  $[\text{DMF}]$  in the case of Tm,

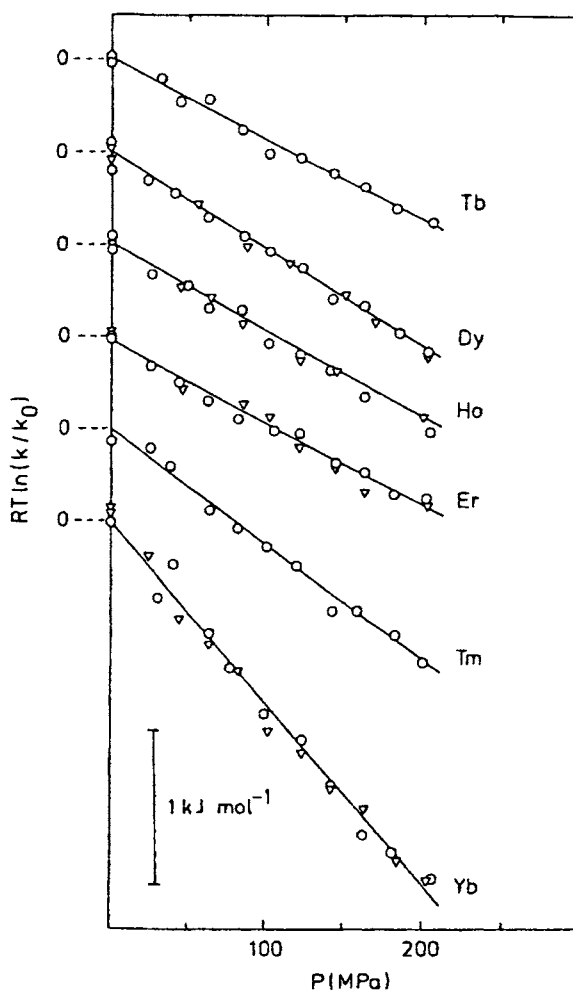


Fig. 7.21. Variable pressure data for DMF exchange on  $\text{Ln}(\text{DMF})_8^{3+}$  ions, in neat DMF [35].

TABLE 7.11  
Kinetic parameters for DMF exchange on  $\text{Ln}(\text{DMF})_8^{3+}$  [35].

$\text{Ln}^{3+}$	$K^{200} (10^{-5} \text{ s}^{-1})$	$K^{298} (10^{-5} \text{ s}^{-1})$	$\Delta H^\ddagger (\text{kJ mol}^{-1})$	$\Delta S^\ddagger (\text{JK}^{-1} \text{ mol}^{-1})$	$\Delta V^\ddagger (\text{cm}^3 \text{ mol}^{-1})$
Tb	$7.2 \pm 0.2$	$190 \pm 10$	$14.1 \pm 0.4$	$-58 \pm 2$	$+5.2 \pm 0.2$
Dy	$2.8 \pm 0.1$	$63 \pm 3$	$13.8 \pm 0.4$	$-69 \pm 2$	$+6.1 \pm 0.2$
Ho	$1.16 \pm 0.02$	$36 \pm 6$	$15.3 \pm 0.8$	$-68 \pm 4$	$+5.2 \pm 0.5$
Er	$0.80 \pm 0.03$	$130 \pm 40$	$23.6 \pm 1.8$	$-30 \pm 9$	$+5.4 \pm 0.3$
Tm	$0.29 \pm 0.01$	$310 \pm 30$	$33.2 \pm 0.5$	$+10 \pm 2$	$+7.4 \pm 0.3$
Yb	$0.28 \pm 0.01$	$990 \pm 90$	$39.3 \pm 0.6$	$+40 \pm 3$	$+11.8 \pm 0.4$

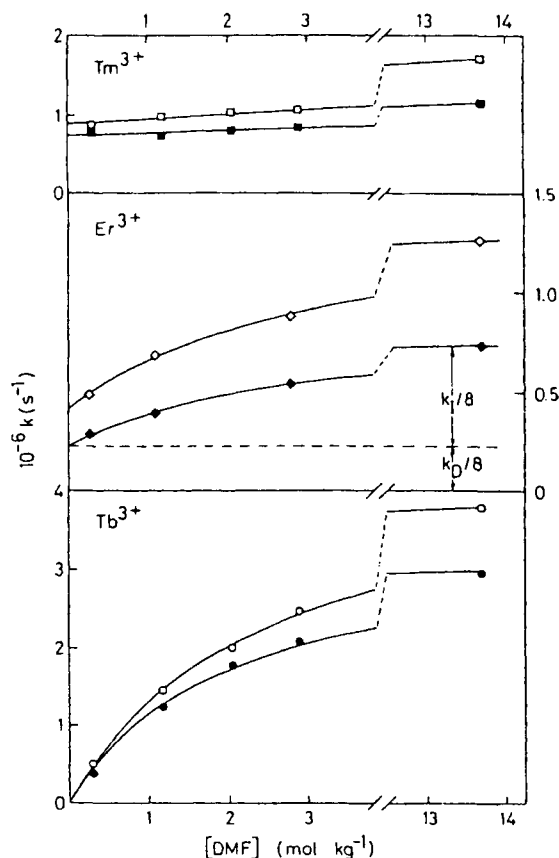
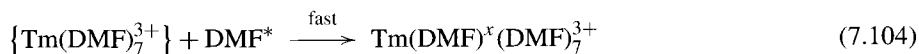


Fig. 7.22. Rate constant  $k$  for DMF exchange on  $\text{Ln}(\text{DMF})_8^{3+}$  in  $\text{CD}_3\text{NO}_2$  ( $\text{Ln} = \text{Tm}, \text{Er}$  and  $\text{Tb}$ ). (●) 231 K; (○) 239 K; (◆) 234 K; (◇) 244 K; (■) 248 K [35].

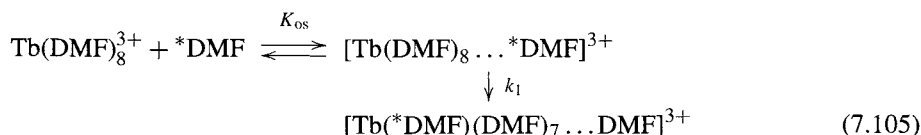
Er, and Tb in Fig. 7.22. It is obvious from this plot that the exchange rate constant for  $\text{Tm}(\text{DMF})_8^{3+}$  is independent of free DMF concentration. The observed first order rate law

$$-d[\text{Tm}(\text{DMF})_8^{3+}]/[\text{Tm}(\text{DMF})_8^{3+}]dt = 8k = k_D \quad (7.102)$$

can be explained by a dissociative mechanism involving an intermediate of a reduced coordination number. The positive values of  $\Delta S^\ddagger$  in the case of Tm and Yb and the similarity in  $\Delta V^\ddagger$  values to  $\text{Nd}^{3+}$  ( $+9.8 \text{ cm}^3 \text{ mol}^{-1}$ ) are indicative of the operation of a limiting dissociative D mechanism for DMF exchange in these ions.



Reference to Fig. 7.22 shows that the exchange rate constant increases in proportion to [DMF] for which the following scheme involving outer sphere association is proposed.



The rate law that is consistent with the mechanism is

$$-d[\text{Tb}(\text{DMF})_8^{3+}]/[\text{Tb}(\text{DMF})_8^{3+}]dt = 8k = k_1 K_{\text{os}}[\text{DMF}]/(1 + K_{\text{os}}[\text{DMF}]) \quad (7.106)$$

The  $K_{\text{os}}$  values obtained from equation (7.106) are:

La	$K_{\text{os}}$ (mol <sup>-1</sup> kg)	$T$ (K)
Er	0.37	234
	0.30	244
Tb	0.51	231
	0.42	239

and these values are in fair agreement with theoretically calculated values [37]. Reference to Table 7.11 shows the  $\Delta S^\ddagger$  and  $\Delta V^\ddagger$  values for  $\text{Tb}^{3+}$  to  $\text{Ho}^{3+}$  are anomalous. The negative  $\Delta S^\ddagger$  values are rationalized in terms of loss of degrees of freedom upon the formation of a nine-coordinate transition state. The positive  $\Delta V^\ddagger$  values are probably due to two effects: (i) increase in volume due to lengthening of the bond of the departing DMF molecule, (ii) decrease in volume due to entrance of the ninth DMF molecule. Thus  $\text{Tb}^{3+}$ ,  $\text{Dy}^{3+}$  and  $\text{Ho}^{3+}$  undergo DMF exchange by a dissociative interchange mechanism,  $I_d$ . The behaviour of  $\text{Er}^{3+}$  is totally different from other lanthanides. The net exchange rate constant is a composite of  $k_1$  and  $k_D$ . One of the rate constants  $k_D$  is independent of the DMF concentration and the other rate constant,  $k_1$  is dependent on free DMF concentration. Both dissociative and dissociative interchange mechanisms are operating in the case of  $\text{Er}^{3+}$ . In summary the mechanisms of DMF exchange are as follows:

Group 1: $\text{Tb}^{3+}$ , $\text{Dy}^{3+}$ , $\text{Ho}^{3+}$	Dissociative interchange, $I_d$
Group 2: $\text{Tm}^{3+}$ , $\text{Yb}^{3+}$	Dissociative, D
Group 3: $\text{Er}^{3+}$	Both dissociative, D and dissociative interchange, $I_d$

It is useful to note that in the lanthanides, more than one mechanism operates and hence it is difficult to find a paradigm based on which all the kinetic data can be systematized.

## 21. Solvent exchange in water

Solvent exchange rates in water are of crucial importance in understanding and interpreting kinetic data on complexation of lanthanides by other ligands. Before examining the solvent exchange data in water we digress to a discussion of coordination of lanthanides in

TABLE 7.12  
Metal-oxygen bond distances in solid lanthanide hydrates.

	$\delta(\text{Ln-O})$	Ref.		$\delta(\text{Ln-C})$	$\delta(\text{Ln-P})$	$\frac{\delta(\text{Ln-C})}{\delta(\text{Ln-P})}$	Ref.
$[\text{La}(\text{H}_2\text{O})_6](\text{ClO}_4)_3$	2.48	[39]	$[\text{La}(\text{H}_2\text{O})_9](\text{CF}_3\text{SO}_3)_3^f$	2.619	2.519	1.04	[45]
$[\text{Tb}(\text{H}_2\text{O})_6](\text{ClO}_4)_3$	2.35	[39]	$[\text{Pr}(\text{H}_2\text{O})_9](\text{BrO}_3)_3$	2.52	2.49	1.01	[46]
$[\text{Er}(\text{H}_2\text{O})_6](\text{ClO}_4)_3$	2.25	[39]	$[\text{Pr}(\text{H}_2\text{O})_9](\text{EtOSO}_3)_3$	2.592	2.470	1.05	[46]
			$[\text{Nd}(\text{H}_2\text{O})_9](\text{BrO}_3)_3$	2.51	2.47	1.02	[47]
			$[\text{Nd}(\text{H}_2\text{O})_9](\text{CF}_3\text{SO}_3)_3$	2.568	2.451	1.05	[48]
			$[\text{Sm}(\text{H}_2\text{O})_9](\text{BrO}_3)_3$	2.55	2.46	1.04	[49]
			$[\text{Gd}(\text{H}_2\text{O})_9](\text{CF}_3\text{SO}_3)_3$	2.546	2.402	1.06	[45]
			$[\text{Y}(\text{H}_2\text{O})_9](\text{EtOSO}_3)_3$	2.518	2.368	1.06	[50]
			$[\text{Y}(\text{H}_2\text{O})_9](\text{CF}_3\text{SO}_3)_3$	2.525	2.344	1.08	[45]
$[\text{Gd}(\text{H}_2\text{O})_8]\text{Cl}_3 \cdot (15-5)^a$	2.41 <sup>b</sup>	[40]	$[\text{Ho}(\text{H}_2\text{O})_9](\text{EtOSO}_3)_3$	2.474	2.373	1.04	[51]
$[\text{Dy}(\text{H}_2\text{O})_8]\text{Cl}_3 \cdot (18-6)$	2.38 <sup>c</sup>	[41]	$[\text{Ho}(\text{H}_2\text{O})_9](\text{CF}_3\text{SO}_3)_3$	2.526	2.367	1.07	[48]
$[\text{Y}(\text{H}_2\text{O})_8]\text{Cl}_3 \cdot (15-5)$	2.37 <sup>b</sup>	[42]	$[\text{Er}(\text{H}_2\text{O})_9](\text{EtOSO}_3)_3$	2.52	2.37	1.06	[52]
$[\text{Lu}(\text{H}_2\text{O})_8]\text{Cl}_3 \cdot (15-5)$	2.35 <sup>b</sup>	[40]	$[\text{Yb}(\text{H}_2\text{O})_9](\text{EtOSO}_3)_3$	2.518	2.321	1.08	[46]
$[\text{Lu}(\text{H}_2\text{O})_8][\text{Na}(12-4)_2]\text{Cl}_4$	2.34 <sup>d</sup>	[43]	$[\text{Yb}(\text{H}_2\text{O})_9](\text{BrO}_3)_3$	2.43	2.32	1.05	[46]
$[\text{Lu}(\text{H}_2\text{O})_8]\text{Cl}_3 \cdot 1.5(12-4)$	2.33 <sup>e</sup>	[44]	$[\text{Lu}(\text{H}_2\text{O})_9](\text{CF}_3\text{SO}_3)_3$	2.503	2.291	1.09	[45]

<sup>a</sup>(15-5), (18-6), (12-4) are crown ethers; <sup>b</sup>dodecahedron, <sup>c</sup>bicapped trigonal prism, <sup>d</sup>square antiprism, <sup>e</sup>bicapped trigonal prism, <sup>f</sup>nonhydrates are tricapped trigonal prisms; <sup>c</sup>capping and <sup>p</sup>prismatic oxygens.

aqueous solutions. It is still not certain that the coordination number changes or not in the lanthanide series, although many studies have been made [38]. The coordination number of lanthanides is fairly well established in solid state as evidenced in Table 7.12.

A coordination number of 9 with a tricapped trigonal prismatic geometry appears to be common as in  $[\text{Ln}(\text{H}_2\text{O})_9]\text{X}_3$ .

The question of coordination in aqueous solutions is not as clear as in solid state. Spedding's work [53] on the partial molar volumes of aquo ions of lanthanides and the irregular trends of these quantities in the lanthanides has been taken as evidence for change in coordination number in the lanthanide series [54]. The change in coordination from 9 to 8 in the lanthanide series has been confirmed by X-ray and neutron diffraction studies of  $\text{LnCl}_3$  solutions [55]. The coordination numbers of lanthanides determined in aqueous solutions by various techniques along with the coordination numbers obtained are given below:

Technique	$\text{Ln}^{3+}$	CN	Ref.
X-ray diffraction	La, Nd, Gd	8	[56]
X-ray diffraction	La, Sm, Tb, Er	8	[57]
Neutron scattering	Dy	8	[58]
	Yb	7.8	[58]
Fluorescence	Eu	9.6	[59]
	Tb	9.1	[59]
Fluorescence	Eu	9.0	[60]
	Tb	9.0	[60]
NMR	Tm, Yb	9.0	[58]
UV-Visible	Ce	8.9	[61]

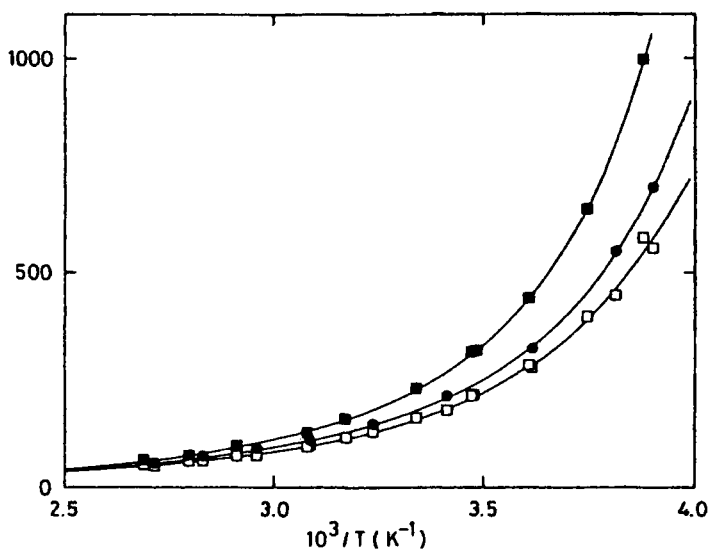


Fig. 7.23.  $^{17}\text{O}$  water relaxation data as a function of reciprocal temperature in a 0.3 M  $\text{Ho}(\text{ClO}_4)_3/1.9$  M  $\text{HClO}_4$  solution: ( $\square$ )  $1/T_1$  at 4.67 and 8.48 Tesla, ( $\bullet$ )  $1/T_2$  at 4.67 Tesla, ( $\blacksquare$ )  $1/T_2$  at 8.48 Tesla [62].

Early studies [62] on the solvent exchange rates of water with lanthanide aquo ions gave exchange rate limits between  $2.1 \times 10^7 \text{ s}^{-1}$  for  $\text{Tb}^{3+}$  to  $0.33 \times 10^7 \text{ s}^{-1}$  for  $\text{Tm}^{3+}$  determined by an analysis of lineshape of  $^{17}\text{O}$  NMR at 1.4 Tesla. Using high field NMR spectrometers (4.7 to 9.3 Tesla) the accessible time scale has been extended. By combining the measured  $^{17}\text{O}$  NMR chemical shifts,  $\Delta\omega_s$ , longitudinal and transverse relaxation rates  $1/T_1$  and  $1/T_2$ , respectively, water exchange kinetics of lanthanide aquo ions from  $\text{Tb}^{3+}$  to  $\text{Yb}^{3+}$  were studied [63]. The relevant equations are

$$(1/T_2 - 1/T_1)/P_m = (\Delta\omega_m)^2/k \quad (7.107)$$

$$\Delta\omega_s/P_m = \Delta\omega_m \quad (7.108)$$

The kinetic effect on  $(1/T_2 - 1/T_1)$  is proportional to  $(\Delta\omega_s)^2$  and also on the square of the magnetic field as shown in Fig. 7.23. From the temperature and pressure dependence, the kinetic parameters presented in Table 7.13 were obtained. The two activation parameters, namely the entropy and the volumes of activation, are negative and also are of the same magnitude for all the lanthanide ions. These activation parameters imply a common water exchange mechanism for all the lanthanides studied and possibly an associative activation path of exchange. The activation volume,  $\Delta V^\ddagger$  of  $-6.0 \text{ cm}^3 \text{ mol}^{-1}$  probably reflects the difference between a large negative contribution due to the transfer of a water molecule electrostricted in the second coordination sphere to the first coordination sphere and a positive contribution due to the difference in partial molar volumes of  $N + 1$  coordinated transition state and  $N$  coordinated aquo lanthanide ion. It should be noted that the latter difference (in partial molar volumes of  $\text{Ln}(\text{H}_2\text{O})_{N+1}$  and  $\text{Ln}(\text{H}_2\text{O})_N$  is due to the increase in Ln-O bond distance (Fig. 7.16).

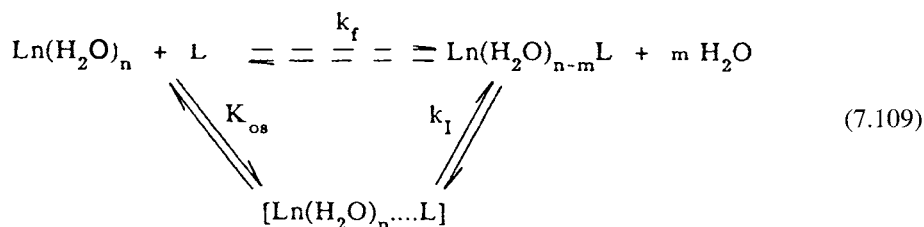
TABLE 7.13  
Kinetic parameters for water exchange on  $\text{Ln}(\text{H}_2\text{O})_8^{3+a}$  [63].

$\text{Ln}^{3+}$	$K^{298}$ ( $10^8 \text{ s}^{-1}$ )	$\Delta H^\ddagger$ ( $\text{kJ mol}^{-1}$ )	$\Delta S^\ddagger$ ( $\text{JK}^{-1} \text{ mol}^{-1}$ )	$\Delta V^\ddagger$ ( $\text{cm}^3 \text{ mol}^{-1}$ )
Gd	$11.9 \pm 1.0$	$12.0 \pm 1.4$	$-30.9 \pm 4.3$	
Tb	$5.58 \pm 0.13$	$12.1 \pm 0.5$	$-36.9 \pm 1.6$	$-5.7 \pm 0.5$
Dy	$4.34 \pm 0.10$	$16.6 \pm 0.5$	$-24.0 \pm 1.5$	$-6.0 \pm 0.4$
Ho	$2.14 \pm 0.04$	$16.4 \pm 0.4$	$-30.5 \pm 1.3$	$-6.6 \pm 0.4$
Er	$1.33 \pm 0.02$	$18.4 \pm 0.3$	$-27.8 \pm 1.1$	$-6.9 \pm 0.4$
Tm	$0.91 \pm 0.02$	$22.7 \pm 0.6$	$-16.4 \pm 1.9$	$-6.0 \pm 0.8$
Yb	$0.47 \pm 0.02$	$23.3 \pm 0.9$	$-21.0 \pm 3.3$	

<sup>a</sup>If a hydration number of nine is assumed:  $k$  is multiplied by a factor 8/9,  $\Delta S^\ddagger$  decreases by  $1.0 \text{ JK}^{-1} \text{ mol}^{-1}$ ,  $\Delta H^\ddagger$  and  $\Delta V^\ddagger$  do not change.

## 22. Complex formation in aqueous solutions

Now that we have data for water exchange rates, the complex formation reactions of lanthanides in aqueous media can be considered. Complex formation reactions of lanthanides usually involve initial formation of an outer-sphere complex followed by a loss of water molecule and the ligand taking the position of the leaving water molecule. The reaction scheme is as follows:



The overall rate constant  $k_f$  is measured by the relaxation methods. Assuming that the outer-sphere complex formation is faster than the water substitution by ligand L, the interchange rate constant  $k_1$  can be calculated using the equation

$$k_f = K_{os} k_1 \quad (7.110)$$

where  $K_{os}$  is obtained from Fuoss's relationship. The  $k_1$  values thus obtained when L = nitrate, sulphate and acetate by ultrasonic measurements are plotted against  $1/r_i$  of the lanthanide ion in Fig. 7.24. The  $k_1$  values for sulphate complexation are surprisingly similar to water exchange rate constants.

In the absence of data on water exchange rates for lighter lanthanides, it is difficult to say whether water exchange rates will be similar to sulphate complex formation rates for the lighter lanthanides.

The mechanism involving a fast outer-sphere complex formation step is not favoured by some schools of thought. If both the inner- and outer-sphere processes are of comparable



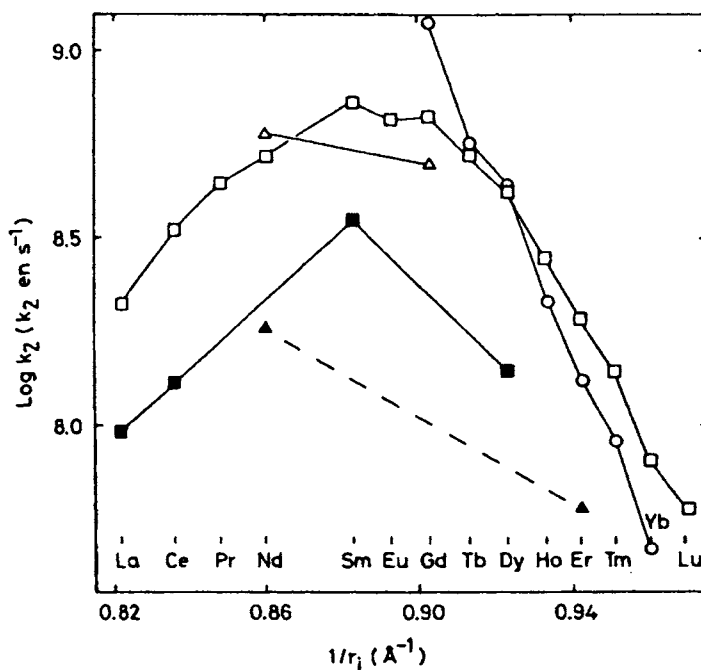


Fig. 7.24. Water exchange rate constant ( $\circ$ ), ref. [41] and interchange rate constants  $k_1$  from ultrasonic absorption results at 298 K for aqueous  $\text{Ln}^{3+}$  ions: ( $\square$ )  $\text{SO}_4^{2-}$  (ref. [69]); ( $\blacksquare$ ) acetate (ref. [70]); ( $\triangle$ ) nitrate (ref. [71]); ( $\blacktriangle$ ) nitrate (ref. [72]).

magnitude in lanthanide ions, then the evaluation of  $k_1$  values and their significance are questionable. This may be a possible reason for most of the researchers in reporting the overall complex formation rate constants,  $k_f$ . The overall complex formation rate constants,  $k_f$  for lanthanides with  $L =$  nitrate, murexide, anthranilate, xylenol orange, oxalate, methyl red and picolinate are plotted against  $1/r_i$  of lanthanide in Fig. 7.25. The interesting feature of the figure is there are three distinct groups. Group I consists of nitrate and picolinate with rate constants in the range  $7 \times 10^8$ – $9.1 \times 10^9 \text{ M}^{-1} \text{ s}^{-1}$ . Group II consists anthranilate, oxalate murexide and methyl red with rate constants similar in values for La to Tm for all the ligands with the exception anthranilate for Er, Yb, and Lu. There is only one member in group III namely xylenol orange with rate constants in the range  $7 \times 10^6$ – $1.0 \times 10^7 \text{ M}^{-1} \text{ s}^{-1}$ . At first sight it is tempting to state that there are three different mechanisms operating. It is reasonable to state that complex formation with group II ligands is probably occurring through dissociative substitution. Group II ligands are also bidentates and it is possible that ring closure is a crucial step.

### 23. Aminopoly carboxylate complexes

The dissociation kinetics of lanthanide–*N*-methylethylenediamine–*N,N',N''*-triacetate (MEDTA) in acetic acid–sodium acetate solutions using  $\text{Cu}^{2+}$  ion as a sequestering agent

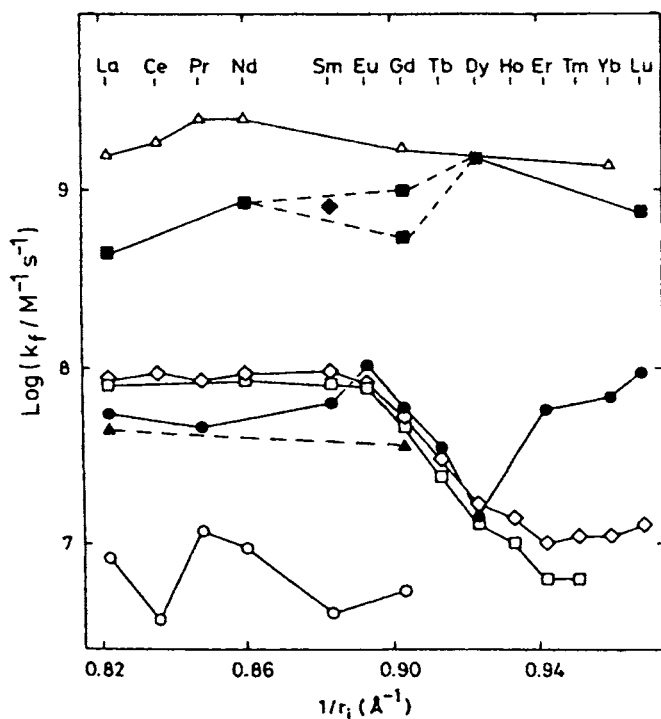


Fig. 7.25. Rate constants  $k_f$  for complex formation on  $\text{Ln}^{3+}$  in water. ( $\Delta$ ) Nitrate by ultrasonic absorption at 298 K (ref. [64]), ( $\diamond$ ) murexide by T-jump at 285 K (ref. [21]), ( $\blacklozenge$ ) murexide by E-jump at 298 K (ref. [65]), ( $\bullet$ ) anthranilate by T-jump at 285 K (ref. [16]), ( $\circ$ ) xylenol orange by T-jump at 298 K (ref. [66]), ( $\square$ ) oxalate by P-jump at 298 K (ref. [17]), ( $\blacktriangle$ ) methyl red by pH-jump at 293 K (ref. [67]), ( $\blacksquare$ ) picolinate by pH-jump at 293 K (ref. [68]).

have been studied [72]. The following reaction scheme has been postulated. The reverse reactions have been excluded because the exchange reaction goes to completion.

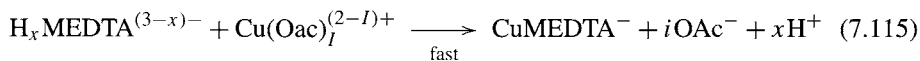
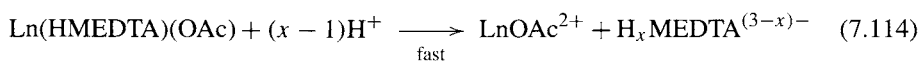


TABLE 7.14

Variation of the stability constant ( $K_M$ ) of the mixed LnMEDTA–acetate complexes, the dissociation rate constant ( $k_s K_M$ ) and the calculated formation rate constant for the lanthanides (except Pm) and yttrium at 0.5 M ionic strength,  $T = 25^\circ\text{C}$  [72].

Ln	$r$ (Å)	$K_M$ ( $\text{M}^{-1}$ )	$10^{-6} \times k_s K_H$ ( $\text{M}^{-1} \text{s}^{-1}$ )	$10^{-10} \times k_{\text{form}}$ ( $\text{M}^{-2} \text{s}^{-1}$ )
La	1.061	$10 \pm 1$	$7.9 \pm 1.4$	0.183
Ce	1.034	$7 \pm 1$	$7.0 \pm 1.0$	0.267
Pr	1.013	$10 \pm 1$	$4.8 \pm 0.7$	0.714
Nd	0.995	$9 \pm 2$	$3.2 \pm 0.7$	0.633
Sm	0.964	$42 \pm 8$	$0.82 \pm 0.19$	1.76
Eu	0.950	$36 \pm 2$	$0.86 \pm 0.38$	2.14
Gd	0.938	$29 \pm 3$	$1.02 \pm 0.14$	2.01
Tb	0.923	$33 \pm 4$	$0.69 \pm 0.11$	3.75
Dy	0.908	$38 \pm 4$	$0.50 \pm 0.06$	5.61
Ho	0.894	$58 \pm 10$	$0.252 \pm 0.050$	6.78
Er	0.881	$75 \pm 23$	$0.124 \pm 0.043$	7.15
Tm	0.869	$85 \pm 23$	$0.092 \pm 0.027$	11.3
Yb	0.858	$152 \pm 31$	$0.042 \pm 0.009$	11.9
Lu	0.848	$255 \pm 12$	$0.024 \pm 0.002$	14.3
Y	0.93	$37 \pm 6$	$0.7 \pm 0.2$	4.20

Assuming that  $K_m$  is large such that large amounts of mixed complex  $[\text{Ln}(\text{MEDTA})\text{-(OAc)}]^-$  exists in solution, the following rate expression is obtained

$$\text{Rate} = \frac{k_s K_M K_H [\text{H}^+][\text{OAc}^-] C_{\text{LnY}}}{1 + K_M [\text{OAc}^-]} \quad (7.116)$$

$$\frac{\text{Rate}}{C_{\text{LnY}}} = k_{\text{1 exp}} = \frac{k_s K_H K_M K_a [\text{H}^+][\text{Buffer}]}{K_a + K_M K_a [\text{Buffer}] + [\text{H}^+]} \quad (7.117)$$

Analysis of the experimental data by this scheme resulted in data given in Table 7.14.

The important difference between the dissociation mechanism of LnMEDTA complexes and the acid catalyzed dissociation of LnEDTA is the formation of mixed LnMEDTA–Ac<sup>−</sup> complex. The stability constants of such mixed complexes are small (1 to 10) and this may explain why such mixed complexes do not show up in the kinetics of dissociation or exchange of LnEDTA complexes. Further, in the present case  $[\text{LnMEDTA}]^0$  association with an acetate anion should be more favourable than  $[\text{LnEDTA}]^-$  with an acetate anion based on electrostatic theory. Reference to Table 7.14 shows that  $K_M$  values increase with increasing atomic number (decreasing radii) for heavy lanthanides but are independent for La–Nd series.

The values of  $k_s K_H$  decrease with increase in atomic number. The variation of  $k_s K_H$  for LnMEDTA with  $1/r$  and the rates of  $[\text{LnDCTA}]^-$  for acid dependent dissociation path show similarities as shown in Fig. 7.26.

The dissociation kinetics of lanthanide complexes with the macrocycle, 1,7-diaza-4,10,13-trioxacyclopentadecane-*N,N'*-diacetic acid (K21DA) were studied in acetic acid–acetate buffer with  $\text{Cu}^{2+}$  as the scavenger of the ligand [73]. The dissociation rates were

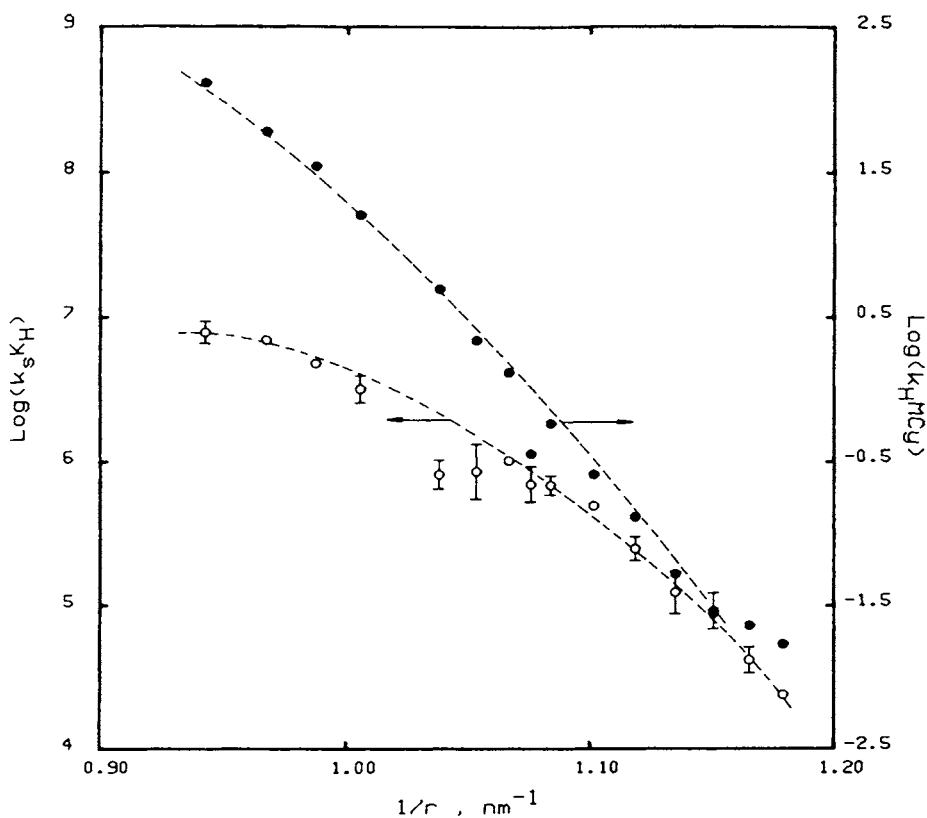


Fig. 7.26. Variation of the dissociation rate constant ( $k_s, K_H$ ) of the mixed complexes  $\text{Ln}(\text{MEDTA})(\text{OAc})^-$  and of  $\text{LnDCTA}^-$  ( $k_H^{\text{MCy}}$ ) versus the reciprocal ionic radii of the rare earth ions. (O)  $\text{Ln}(\text{MEDTA})(\text{OAc})^-$ , this work. (●)  $\text{LnDCTA}^-$  [72].

independent of  $[\text{Cu}^{2+}]$ . The decomposition kinetics involved two pathways namely acid-dependent and acid-independent pathways. The lighter lanthanides showed a first-order dependence on  $[\text{H}^+]$  and the heavier lanthanides yielded saturation curves with limiting rate constants at higher acid concentrations. The following mechanism has been proposed (Fig. 7.27).

The rate law obeyed by the lighter lanthanide may be written as

$$k_{\text{obs}} = k_d + k_H[\text{H}^+] + k_{\text{AC}}[\text{acetate}] \quad (7.118)$$

For the heavier lanthanides the rate law is of the form

$$k_{\text{obs}} = k_d + \frac{K'k_{\text{lim}}[\text{H}^+]}{1 + K'[\text{H}^+]} \quad (7.119)$$

The data on the rate constants are given in Table 7.15. Based on the experimental data on  $k_d$  and water exchange rate constant, it is surmised that self dissociation of the complex does

TABLE 7.15  
Resolved rate constants<sup>a</sup> for dissociation of Ln–K21DA complexes at 25°C [73].

Metal	$k'_d$ (s <sup>-1</sup> )	$k_H$ (M <sup>-1</sup> s <sup>-1</sup> )	$K'$ (M <sup>-1</sup> )	$k_{lim}$ (s <sup>-1</sup> )	$k_{AC}$ (M <sup>-1</sup> s <sup>-1</sup> )
La	$4.69 \times 10^{-2}$	$7.18 \times 10^2$			2.18
Pr	$4.14 \times 10^{-3}$	$8.19 \times 10$			
Eu	$1.76 \times 10^{-3}$	$3.11 \times 10$			$8.09 \times 10^{-2}$
Tb	$2.18 \times 10^{-3}$		$2.96 \times 10^3$	$1.46 \times 10^{-2}$	
Er	$3.32 \times 10^{-3}$		$6.64 \times 10^3$	$1.04 \times 10^{-2}$	
Yb	$8.76 \times 10^{-3}$		$9.39 \times 10^3$	$1.50 \times 10^{-2}$	
Lu	$1.08 \times 10^{-2}$		$1.22 \times 10^4$	$4.11 \times 10^{-2}$	

TABLE 7.16  
Activation parameters<sup>a</sup> for self-dissociation and acid-catalyzed of Ln–K21DA complexes [73].

Metal	$\Delta H_d^\ddagger$ (kcal/mol)	$\Delta S_d^\ddagger$ (cal/(deg mol))	$\Delta H_H^\ddagger$ (kcal/mol)	$\Delta S_H^\ddagger$ (cal/(deg mol))	$\Delta H_{lim}^\ddagger$ (kcal/mol)	$\Delta S_{lim}^\ddagger$ (cal/(deg mol))
La	4.7	-49.5	$6.5 \pm 0.3$	$-23.7 \pm 0.9$		
Eu	6.9	-48.6	$7.4 \pm 0.6$	$-26.9 \pm 2.1$		
Er	$-7.9 \pm 0.8$	$-43.4 \pm 2.6$			$-14.0 \pm 0.3$	$-20.8 \pm 1.1$
Lu	$-8.0 \pm 0.5$	$-40.5 \pm 1.8$			$-15.6 \pm 0.5$	$-12.6 \pm 1.5$

<sup>a</sup>Error limits correspond to standard deviations. The values of  $\Delta H_d^\ddagger$ , and  $\Delta S_d^\ddagger$ , listed for La and Eu complexes are crude, and hence no error limits are quoted. They have been calculated from  $k'_d$  values after subtracting the contribution from acetate catalysis. At 25°C the acetate catalysis (0.005 M acetate) corresponds to 23% of  $k'_d$  for both La and Eu complexes, and the same percent contribution was assumed at other temperatures (15, 35 and 45°C) as well.

not occur in one step. Instead it may involve a rate-determining distortion of the complex to give an intermediate that is rapidly scavenged by a hydrogen ion or cupric ion leading to products. The proposed reaction scheme may be written as



The activation parameters for both acid-dependent and acid-independent pathways are given in Table 7.16. The low enthalpy of activation and a large negative entropy of activation for the self-dissociation pathway may well be due to a rate-determining step of slow distortion of the complex to give an active intermediate. The  $\Delta H_H^\ddagger$  values for the acid-catalyzed pathway are much smaller than the values of lanthanide complexes with EDTA, CyDTA and MEDTA indicating lower thermodynamic stability of the K21DA complexes of lanthanides [73].

## 24. Lanthanide–EDTA–5-sulphosalicylate mixed complexes

Mixed complex formation kinetics between LnEDTA and L, where L stands for 5-sulphosalicylate [74], 8-hydroxy quinoline-5 sulfonate and picolinate [75] were studied and two pathways namely acid-dependent and acid-independent pathways have been identified. The overall reaction stoichiometry may be written as

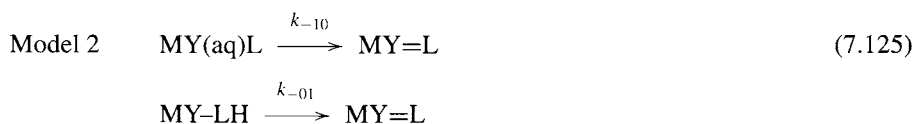
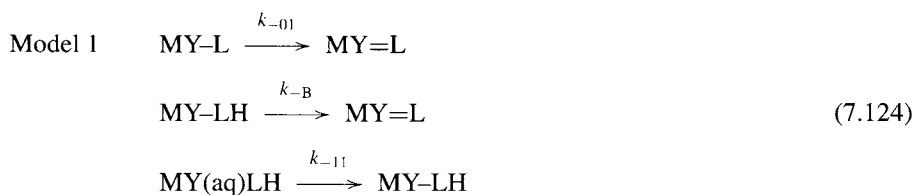


where L is ligand, BH/B is the buffer system with protonation constant  $\beta_B$ .

The observed rate constant,  $k_{\text{obs}}$  for the overall process is

$$k_{\text{obs}} = f_c f_k \quad (7.123)$$

where  $f_k$  is a function of rate constants, equilibrium constants and concentrations, while  $f_c$  depends on equilibrium concentrations and equilibrium constants.  $f_c$  is independent of the mechanism. The two mechanisms tested are: (i) two consecutive steps with parallel hydrogen ion dependent and hydrogen independent pathways. The two consecutive steps are ring closure/ring opening (I) and a unidentate association/dissociation step (II), (ii) the second mechanism [76] assumes that ring closure/ring opening step is much faster than other reactions, with an additional buffer catalyzed pathway. The values of association rate constants in both models 1 and 2 are given in Table 7.17. The various constants are associated with the following processes.



The values for the rate constant  $k_{-10}^*$  are nearly the same for the mixed complexes when L = picolinate, sulfosalicylate and 8-oxyquinoline-5-sulfonate indicating and hence it appears that they fit Model 1 (i.e.) Diebler–Eigen mechanism involving a dissociative pathway. This is true in the case of lighter lanthanides. In the case of heavier lanthanides,

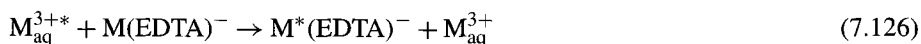
TABLE 7.17  
Values of association rate constants for the SULF systems [74].

Model 1	$\lg k_{-00}^* (s^{-1}M^{-1})$	$\lg k_{-B}^* (s^{-1}M^{-1})$	$\lg k_{-11}^* (s^{-1}M^{-1})$
Model 2	$\lg k_{-10}^* (s^{-1}M^{-1})$	$\lg k_{-B}^* (s^{-1}M^{-1})$	$\lg k_{-01}^* (s^{-1}M^{-3})$
La	7.5 ± 0.1		7.3 ± 0.1
Am		-2.7 ± 0.1	
Et		-2.9 ± 0.1	
Nd	7.1 ± 0.1		6.5 ± 0.1
Am		-2.8 ± 0.1	
Et		-3.1 ± 0.1	
Trim		-3.6 ± 0.1	
Gd	7.0 ± 0.1		6.2 ± 0.1
Am		-2.8 ± 0.1	
Et		-3.1 ± 0.1	
Trim		-3.7 ± 0.1	
Triet		-2.7 ± 0.1	
Er	6.3 ± 0.1		5.1 ± 0.1
Am		-3.6 ± 0.1	
Et		-3.8 ± 0.1	
Trim		-4.4 ± 0.1	
Lu	6.2 ± 0.1		4.3 ± 0.1
Am		-3.8 ± 0.1	
Et		-4.0 ± 0.1	

the mechanism is likely to change from dissociative to associative type [76]. The rate constants for ring opening/closure step for a given lanthanide are different for the quinoline and picolinate while for sulfosalicylate the values are close to those of picolinate. This is probably due to the similar geometry in sulfosalicylate and picolinate although they form 6 and 5 membered rings, respectively. On the other hand, quinolate is a bulkier ligand involving six membered rings and this may be the reason for the slower rates for the smallest lanthanides.

## 25. Isotopic exchange reactions of LnEDTA complexes

Isotopic exchange reactions of the type



do not involve any net chemical change in the system and can be expected to indicate the effect of 4f electron population or any possible change in coordination number on the exchange rate [77]. The exchange mechanism involves an acid dependent decomposition of the complex followed by a fast complexation reaction. The protonated complex undergoes auto-decomposition with and without the aid of the buffer anion. The buffer anion removes one water molecule from  $Ln(H_2O)_n^{3+}$  and promotes exchange of  $M_{aq}^{3+}$  in the  $[M_{aq}^{3+} - M(EDTA)^-]$  system. A plot of  $\log k$  (exchange),  $\log K$  vs atomic number is shown in

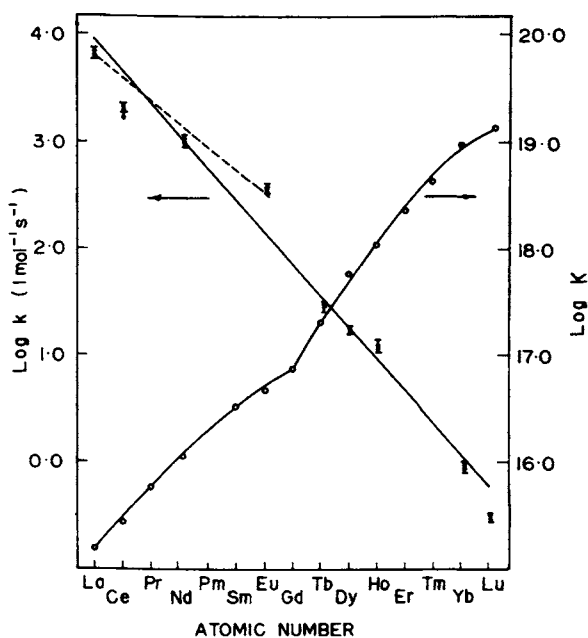


Fig. 7.27. Dependence of the isotopic exchange rate constants ( $k$ ) and the stability constants ( $K$ ) of the complexes R(EDTA) on the atomic number of the rare earths. The vertical bars shown in the figure represent the probable error in the  $k$  values. The dotted line describing the behavior of the elements lanthanum, neodymium and europium is from the comparison of exchange reactivity attempted by Fomin.

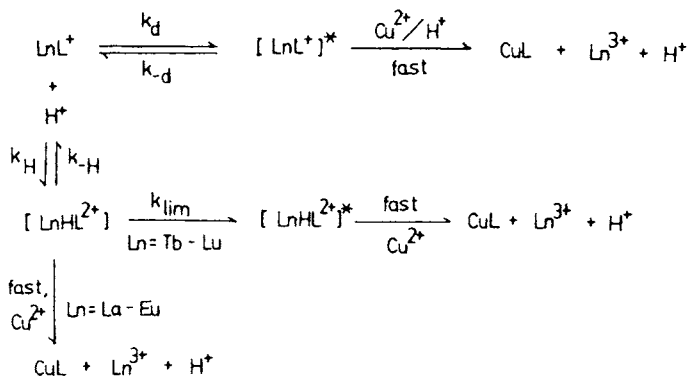


Fig. 7.27a. Proposed mechanisms for dissociation of Ln-K21DA complexes (coordinated water molecules omitted for clarity).

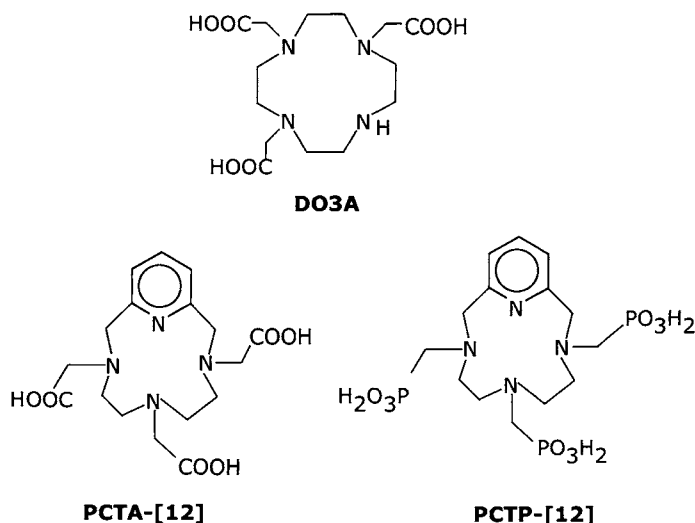
Fig. 7.27. It is seen from Fig. 7.27 that the rate constant for the exchange reaction  $[\text{Ce}_{\text{aq}}^{3+} - \text{Ce}(\text{EDTA})^-]$  is much lower than the expected value. It is to be noted that the crystal field stabilization energy including spin-orbit interaction reaches a maximum for cerium in the cerium sub group and the ligand field strength is in the order  $\text{H}_2\text{O} < \text{CH}_3\text{COO}^-$ . The



protonated  $M(\text{EDTA})^-$  complex, replacement of a water molecule in the complex by an acetate anion from the buffer may result in a crystal field stabilized complex leading to reduced value for the exchange rate constant in the case of cerium.

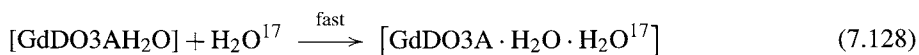
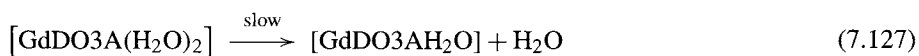
## 26. NMR studies of lanthanide macrocyclic complexes

NMR relaxometric studies of Gd(III) complexes with ligands DO3A, PCTA-[12] and PCTP-[12] whose structure are given below proved interesting [78].



The proton nuclear magnetic relaxation dispersion profiles as well as the  $^{17}\text{O}$  temperature dependency were analysed. Best-fit parameters are given in Tables 7.18 and 7.19.

All three complexes have a decreased lifetime of the coordinated water molecule as compared to octadentate ligands such as GdDOTA. In the case of GdDO3A and GdPCTA[12] complexes, coordinated water exchange is occurring by a dissociative mechanism

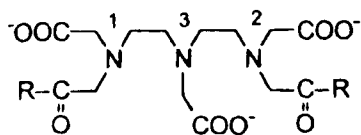


The exchange lifetime is short in GdPCTP, suggesting an associative mechanism of exchange of coordinated water

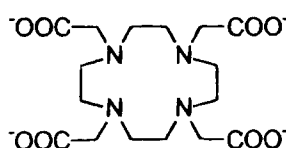


Associative mechanism of water exchange also occurs in the case of  $[\text{Gd}(\text{H}_2\text{O})_8]^{3+}$  and  $[\text{GdPD}(\text{H}_2\text{O})_2]^-$ . The practical significance of this fundamental work is that the  $\text{GdPCTP}[12]$  complex is a promising candidate as a contrasting agent in magnetic resonance imaging because of the high stability constant,  $K_f$ , and the fast water exchange rate.  $\text{Gd}(\text{III})$  complexes of the following ligands were studied by  $^{13}\text{C}$ ,  $^{17}\text{O}$  and  $^1\text{H}$  NMR [79].

### Structures of the Various Ligands Discussed

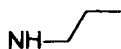


R = OH: **DTPA**

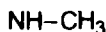


**DOTA**

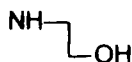
R:



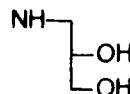
**BPA**



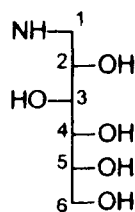
**BMA**



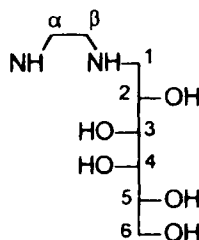
**BEA**



**BPDA**



**BGLUCA**



**BENGALAA**

The data on exchange rates and activation volume are given in Table 7.20.

Based on the kinetic parameters, a dissociative mechanism is proposed.



It is useful to note that the sugar moieties bound to the metal do not have influence on the relaxivities and hence on the water exchange rate constants.

TABLE 7.18  
 $^{17}\text{O}$  NMR best-fit parameters obtained from the analysis of the temperature dependence of  $R_{2p}^0$  for 50 mM aqueous solutions of the Gd(III) complexes [78].

Complex	$q$	$\Delta^2$ ( $\text{s}^{-2} \times 10^{19}$ )	$\tau_v$ (ps)	$\tau_m$ (ns)	$\Delta H_v$ ( $\text{kJ mol}^{-1}$ )	$\Delta H_M$ ( $\text{kJ mol}^{-1}$ )
Gd-DO3A	2	3.5	14	160	1.7	44
Gd-PCTA[12]	2	5.9	15	70	3.6	45
Gd-PCTP[12]	1	7.8	19	6.0	5.0	14

TABLE 7.19  
 [78].

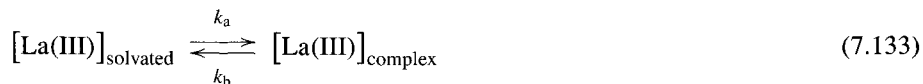
Complex	$q$	$\Delta^2$ ( $\text{s}^{-2} \times 10^{19}$ )	$\tau_v$ (ps)	$\tau_R$ (ns)	$r$ ( $\text{\AA}$ )
Gd-DO3A	2	4.6	14	66	3.15
Gd-PCTA[12]	2	2.8	28	70	3.10
Gd-PCTP[12]	1	7.8	19	106	3.06

TABLE 7.20  
 Exchange rates for water in Gd(III) complexes [79].

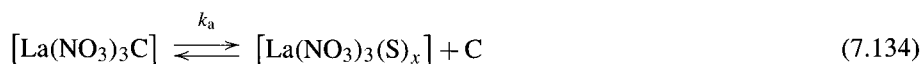
Complex	$k_{\text{ex}}$ ( $\text{s}^{-1}$ ) $\times 10^5$	$\Delta V^\ddagger$ ( $\text{cm}^3 \text{mol}^{-1}$ )
[Gd(DTPA-BPDA)(H <sub>2</sub> O)]	$3.6 \pm 0.3$	+6.7
[Gd(DTPA)-(BGLUCA)(H <sub>2</sub> O)]	$3.8 \pm 0.2$	+6.8
[Gd(DTPA-BENGALAA)(H <sub>2</sub> O)]	$2.2 \pm 0.1$	+5.6

## 27. Dynamics of supramolecular complexes

$^{139}\text{La}$ ,  $^1\text{H}$ ,  $^{13}\text{C}$  and  $^{17}\text{O}$  NMR studies [80] of lanthanum–crown ether complexes in acetonitrile showed the formation of 1:1 La(III)–18C6 complex. The stability constant  $\log K = 4.4$ . Similarly 1:1 complex was formed in the case B15C5. The coordination number in the complexes with B15C5, 15C5 and 18C6 in acetonitrile solution is 11 or 12. The exchange reaction studied is



NMR data show a dissociation/recombination mechanism in which the



exchange is due to a complete dissociation of the complex with the departure of the leaving ligand followed by recomplexation with another ligand. Using the relationship

$$k_a + k_b = k_{-1}(1 - \rho)^{-1} \quad (7.135)$$

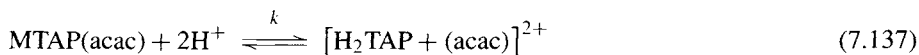
$k_{-1}$  value of  $2.4 \times 10^3 \text{ s}^{-1}$  was obtained.

The dissociation/recombination mechanism was further confirmed by studying the ligand facial exchange in  $[\text{La}(\text{III})(\text{NO}_3)_3 \cdot 18\text{C6}]$  with the value for  $k$  of  $35 \pm 5 \text{ s}^{-1}$  which is close to  $k_{-1}$  of  $50 \pm \text{s}^{-1}$ . The exchange equilibrium may be written as ligand facial exchange:



### 27.1. Tetraazaporphine complexes

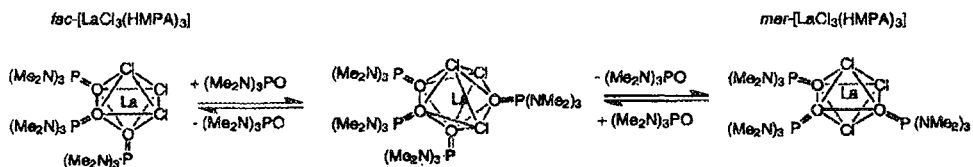
Kinetic studies [81] of tetraazaporphine acetylacetonate mixed complexes of Dy(III), Eu(III) and Nd(III) in aqueous and methanolic solutions show the stability to be in the order DyTAP(acac) > EuTAP(acac) > NdTAP(acac). These complexes undergo decomposition on protonation.



## 28. Isomerization reactions

Reversible fac–mer isomerization of the  $[\text{LaCl}_3(\text{HMPA})_3]$  complex studied by variable temperature  $^1\text{H}$  NMR spectroscopy gave evidence for an associative mechanism [82]. However it is not possible to distinguish between associative interchange mechanism and seven coordinate intermediate. An equilibrium mixture of  $[\text{LaCl}_3(\text{HMPA})_3]$  and  $[\text{LaCl}_3(\text{HMPA})_4]$  is also a possibility.

According to the proposed mechanism, both exchange of  $[\text{LaCl}_3(\text{HMPA})_3]$  with HMPA and fac–mer isomerization of  $[\text{LaCl}_3(\text{HMPA})_3]$  are second-order reactions and depend on the concentrations of the parent complex and free HMPA (hexamethyl phosphoramidate). The proposed mechanism may be represented as follows.

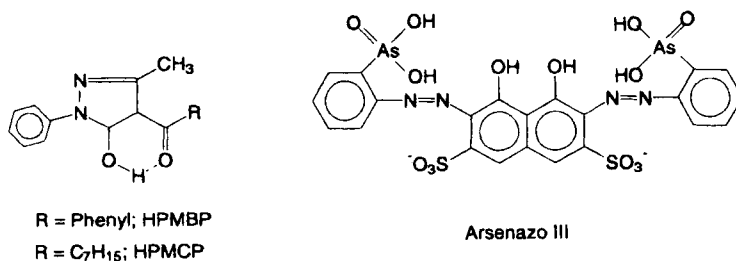


The proposed mechanism of *fac-mer* isomerization and HMPA exchange in  $[\text{LaCl}_3(\text{HMPA})_3]$ . The central seven-coordinate species is either an interchange transition state, an intermediate or a stable molecule.

The second order rate constant  $k_2$  (196 K) is  $1.0 \times 10^4 \text{ M}^{-1} \text{ s}^{-1}$  and  $\Delta G^\ddagger$  (196 K) is  $32 \pm 1 \text{ kJ mol}^{-1}$ .

## 29. Interfacial catalysis of formation and dissociation of lanthanide complexes [83]

Kinetics of formation and dissociation of lanthanide complexes [La(III) = Pr, Eu, Tb, Ho, and Yb] with 1-phenyl-3-methyl-4-benzoyl-5-pyrazolone (HPMBP) in toluene–water phase were studied by monitoring the fate of La<sup>3+</sup>–arsenazo III (AZ) complex (MAZ) in the aqueous phase with the hydrophilic separator. The structures of the ligands and AZ are given below:



The experimental data on the rate constants for formation of La(III)–HPMBP and La(III)–HPMCP are given in Table 7.21 and the reaction scheme is given below.



The dissociation of the complexes ML<sup>2+</sup> both uncatalyzed and catalyzed pathways may be written as



TABLE 7.21

Complexation rate constants for trivalent lanthanide–acylpyrazolone complexes in the toluene–water phase pair catalyzed by arsenazo III<sup>a</sup> [83].

Metal	HPMBP		HPMCP	
	log $k_1^i$	log $k_{\text{AZ}}^i$	log $k_1^i$	log $k_{\text{AZ}}^i$
Pr	4.15	3.79	5.77	4.03
Eu	4.70	3.67	6.07	4.49
Tb	4.80	3.47	6.13	4.52
Yb	5.05	2.84	6.35	3.89

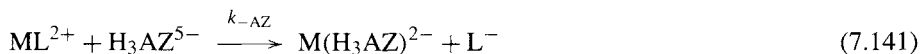
<sup>a</sup> $k_1^i$  and  $k_{\text{AZ}}^i$  in M<sup>-1</sup> s<sup>-1</sup>.

TABLE 7.22

Dissociation rate constants for lanthanide-acylpyrazolone complexes in the toluene-water phase pair and triton X-100 micelles<sup>a</sup> [83].

Metal	HPMBP			HPMCP						
	Toluene-water			Triton X-100		Toluene-water			Triton X-100	
	log $k_{-1}^i$	log $k_{-AZ}^i$	log $K_{-2}$	log $k_{-1}$	log $k_{-1}K_{-2}$	log $k_{-1}^i$	log $k_{-AZ}^i$	log $K_{-2}$	log $k_{-1}$	log $k_{-1}K_{-2}$
Pr	0.05	7.38	-4.51	2.91	-1.60	0.43	6.79	-5.34	3.41	-1.93
Eu	-0.03	7.34	-4.73	2.46	-2.27	0.33	7.15	-5.74	3.11	-2.63
Tb	-0.11	7.36	-4.91	2.49	-2.42	0.28	7.47	-5.85	2.62	-3.23
Ho					-2.71					-3.72
Yb	-0.21	6.88	-5.26	2.42	-2.84	0.15	6.99	-6.20	1.86	-4.34

<sup>a</sup> $k_{-1}^i$  and  $k_{-AZ}^i$  in  $M^{-1} s^{-1}$ ;  $K_{-2}$  in M.



The rate constants for dissociation of  $ML^{2+}$  complexes,  $k_{-1}$  and  $k_{-AZ}$  are given in Table 7.22.

The complex formation constants increase by a small amount in going from Pr to Yb. The opposite trend is observed for the dissociation rate constants. The rate constants for the formation  $M^{3+}$  HPMCP complexes are higher than the rate constants for  $M^{3+}$  HPMB complexes. The rate constants for dissociation of the complexes in micelles (Triton X-100) are three orders of magnitude larger than those at the toluene-water interface. This study is the first example where the complex formation and its dissociation reactions in a two-phase liquid system are catalyzed by a metallochromic indicator with the catalysis being predominantly an interfacial reaction. The complex formation and dissociation reactions show a high sensitivity to the structure of the ligand in the micellar pseudophase than in the two phase liquid-liquid system. The significance of these results lie in understanding the efficiencies of separations and improvement of such efficiencies toward complete resolutions of lanthanides using techniques such as centrifugal partition chromatography and micellar high-performance liquid chromatography. Log  $\beta_{LL}$  and log  $K$  of the complexes increase with increasing atomic number (Fig. 7.28).

### 30. Lanthanide catalysis in isomerization reactions [84]

Lanthanide(III) ions have been found to catalyze the geometric isomerization of *trans*-bis(oxalato)diaquochromate(III) and *trans*-bis(malonato)diaquochromate(III) to yield the corresponding *cis*-isomers. The proposed mechanism for the uncatalyzed and catalyzed pathway for the oxalato complex is shown in Fig. 7.29.

The catalytic rate constants and activation parameters are given in Table 7.23.

In Fig. 7.30 log  $k_{Ln}$  is plotted against log  $K_1$  for the *trans*-*cis* isomerization of the oxalato complex. Here  $k_{Ln}$  refers to catalytic rate constants and  $K_1$  is the complex formation constant for lanthanide propionate complexes. The linear free energy relationship holds

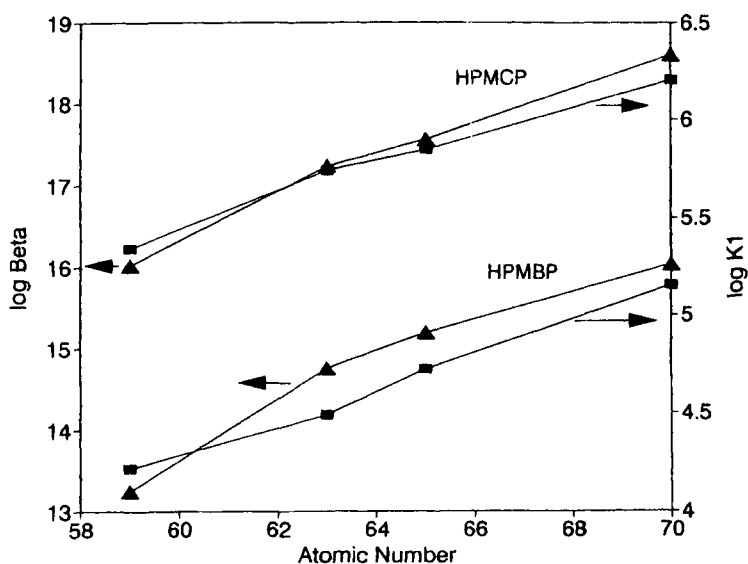


Fig. 7.28. Plot of  $\log \beta_{LL}$  and  $\log K_1^i$  vs atomic number of lanthanides for HPMBP and HPMCP [83].

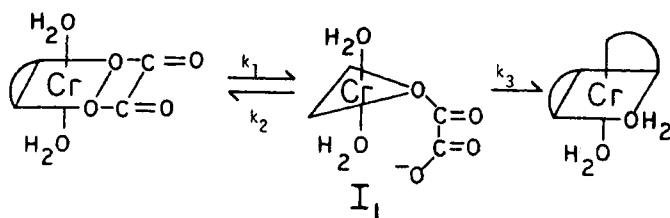
TABLE 7.23

Catalytic rate constants and activation parameters for the *trans-cis* isomerization of *trans*-bis(oxalato)diaquochromate(III) [84].

Lanthanide ion	$10^2 k_{Ln^{3+}} (M^{-1} s^{-1})$			$\Delta H^\ddagger$ (kcal/mol)	$\Delta S^\ddagger$ (cal/mol deg)
	15°C	25°C	30°C		
La <sup>3+</sup>	3.04	8.00	11.4	15.1	-13.0
Pr <sup>3+</sup>	4.56	9.75	16.0	13.7	-17.1
Nd <sup>3+</sup>	4.35	11.4	16.2	14.9	-12.8
Sm <sup>3+</sup>	4.44	11.4	16.2	14.7	-13.7
Eu <sup>3+</sup>	4.77	11.3	17.3	14.4	-14.6
Gd <sup>3+</sup>	4.12	9.94	14.8	14.3	-15.2
Tb <sup>3+</sup>	3.85	9.73	14.6	14.9	-13.1
Dy <sup>3+</sup>	2.79	9.27	14.3	18.6	-1.02
Ho <sup>3+</sup>	2.31	9.91	14.4	21.3	-7.87
Er <sup>3+</sup>	3.68	9.80	14.7	15.7	-10.6
Tm <sup>3+</sup>	3.08	9.64	15.0	17.9	-3.09
Yb <sup>3+</sup>	4.52	11.4	15.9	14.2	-15.2
Lu <sup>3+</sup>	3.24	10.8	16.4	18.5	-1.06
Y <sup>3+</sup>	2.11	7.78	12.2	20.1	3.54

good for lighter lanthanides La through Gd. For the lighter lanthanides, the predominant pathway is through  $I_3$  (Fig. 7.29). For the heavier lanthanides, the predominant pathway is probably through  $I_2$ . A plot of  $\log \Delta H^\ddagger$  against the ionic radii of the lanthanides shows a linear relationship for the lighter lanthanides and deviates from linearity in the case of

Uncatalyzed Pathway:



Catalyzed Pathway:

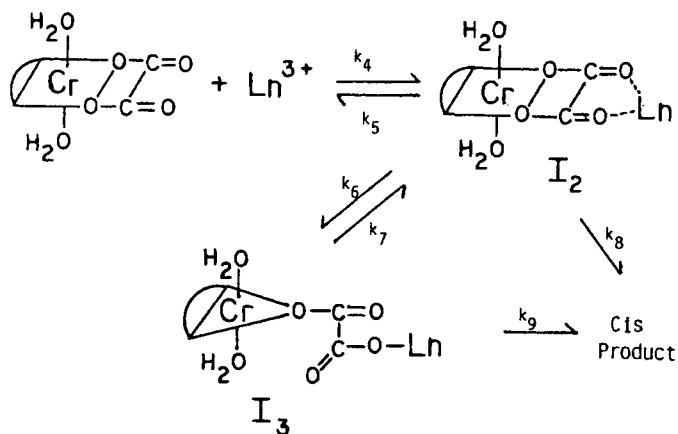


Fig. 7.29. Mechanism for the uncatalyzed and lanthanide ion catalyzed *trans-cis* isomerization of *trans*-bis(oxalato)-diaquochromate(III) [84].

heavier lanthanides. This observation also supports the notion that the lighter and heavier lanthanides catalyze the isomerization reaction pathways involving  $I_3$  and  $I_2$ , respectively. Yttrium is not a member of the lanthanide series. In spite of this, the chemistry of  $Y(III)$  is similar to that of  $La(III)$ . The catalytic rate constant with  $Y(III)$  is essentially the same as that with  $La(III)$  but smaller than  $Ho(III)$  by about 20%. This difference might indicate some participation of the f-orbitals in the intermediate complex.

The catalyzed isomerization of the malonate complex was found to proceed by a different mechanism from that of the oxalate complex. The rate constants and the activation parameters are given in Table 7.24. No linear free energy relationship was found to be valid in the malonate system.

A plot of  $\log k_{Ln}$  vs  $\log K_1$  for the malonate system is shown in Fig. 7.31. The catalyzed isomerization of the malonate complex proceeds by a different mechanism from that of the oxalato analogue because: (i) lack of linear free energy relationship between the catalytic rate constants and the complex formation constants, (ii) linear relationship between catalytic rate constants ( $\log k_{Ln}$ ) and formation constants of lanthanide malonate complexes ( $\log K_1$ ), (iii) catalytic rate constants for the malonate system are smaller than the corresponding rate constants for the oxalate system. The proposed mechanism for



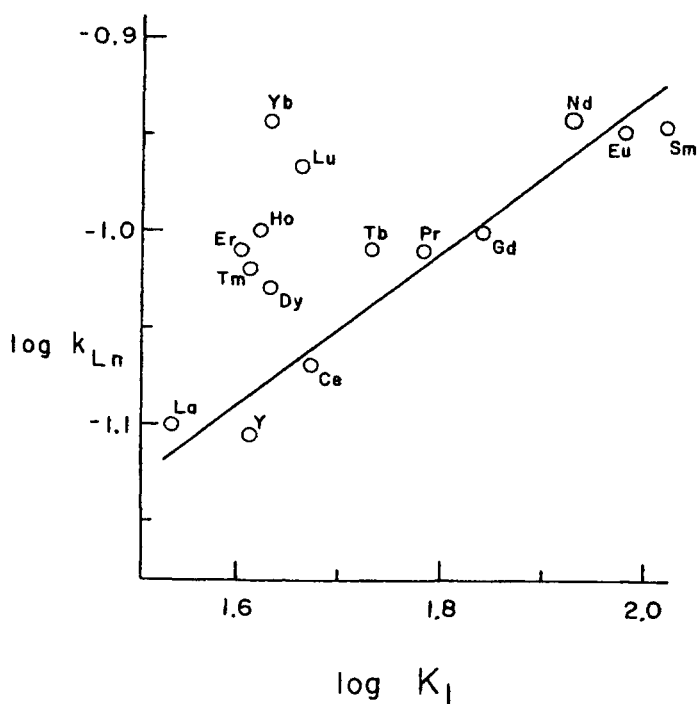


Fig. 7.30. log-log plot of the catalytic rate constants for the lanthanide ion catalyzed *trans-cis* isomerization of *trans*-bis(oxalato)diaquochromate(III) (25°C,  $I = 1.5$  M adjusted with  $\text{NaNO}_3$ ) vs. the formation constants for the lanthanide/propionate complexes (25°C,  $I = 2.0$  M) [84].

TABLE 7.24  
[84].

Lanthanide ion	$10^5 k_{Ln^{3+}} (\text{M}^{-1} \text{s}^{-1})$			$\Delta H^\ddagger$ (kcal/mol)	$\Delta S^\ddagger$ (cal/mol K)
	25°C	30°C	35°C		
$\text{La}^{3+}$	1.19	2.67	6.30	29.9	19.2
$\text{Pr}^{3+}$	1.36	2.77	4.52	21.2	-9.76
$\text{Nd}^{3+}$	1.64	3.10	4.96	19.7	-14.3
$\text{Sm}^{3+}$	1.57	2.53	3.82	15.7	-27.9
$\text{Eu}^{3+}$	1.61	2.78	5.29	21.0	-10.2
$\text{Gd}^{3+}$	1.87	2.74	4.12	13.7	-34.3
$\text{Tb}^{3+}$	1.44	2.29	3.18	13.9	-34.2
$\text{Dy}^{3+}$	2.00	2.52	2.84	5.84	-60.4
$\text{Ho}^{3+}$	1.57	2.16	3.94	16.2	-2.63
$\text{Er}^{3+}$	1.84	2.14	2.98	8.19	-52.8
$\text{Tm}^{3+}$	1.89	2.36	2.93	7.29	55.7
$\text{Yb}^{3+}$	2.26	2.62	3.27	6.20	-59.1
$\text{Lu}^{3+}$	1.63	2.27	3.29	12.2	-39.5
$\text{Y}^{3+}$	1.47	2.33	2.89	11.9	-40.8

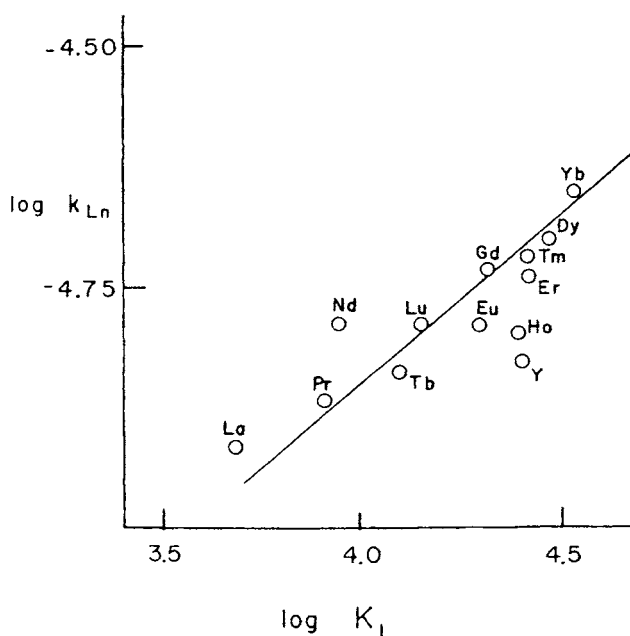


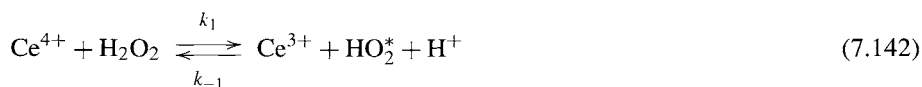
Fig. 7.31. log-log plot of the catalytic rate constants for the lanthanide ion catalyzed *trans-cis* isomerization of *trans*-bis(malonato)diaquochromate(III) (25°C,  $I = 1.5$  M adjusted with  $\text{NaNO}_3$ ) vs. the formation constants for the lanthanide/malonate complexes (25°C,  $I = 0.1$  M) [84].

the lanthanide ion catalyzed *trans-cis* isomerization of  $[\text{Cr}(\text{Mal})_2(\text{H}_2\text{O})_2]^-$  is shown in Fig. 7.32. The proposed mechanism is also supported by the observation the  $\log \Delta H^\ddagger$  vs  $1/r$  plot is linear.

As the ionic radii decrease, the acidity of the ion increases and hence the affinity for the malonate ligand. It is also to be noted that the catalytic rate constant increases with increasing acidity of the lanthanide ion, which is consistent with the proposed mechanism. If the metal ion acidity is a crucial factor in determining the reaction rate, Y(III) should give a rate similar to Ho(III) since both Y(III) and Ho(III) have nearly identical acidity properties. This is shown to be true by data in Figs 7.31 and 7.33.

### 31. Electron transfer reactions [85]

An extensively studied system is the kinetics of Ce(III)–Ce(IV) exchange reaction catalyzed by  $\text{H}_2\text{O}_2$ . In order to understand the mechanism of the exchange reaction it is necessary to have some idea of the catalyzed reaction. Kinetic study of Ce(IV) reaction with  $\text{H}_2\text{O}_2$  resulted in the postulation of the following mechanism for the reaction



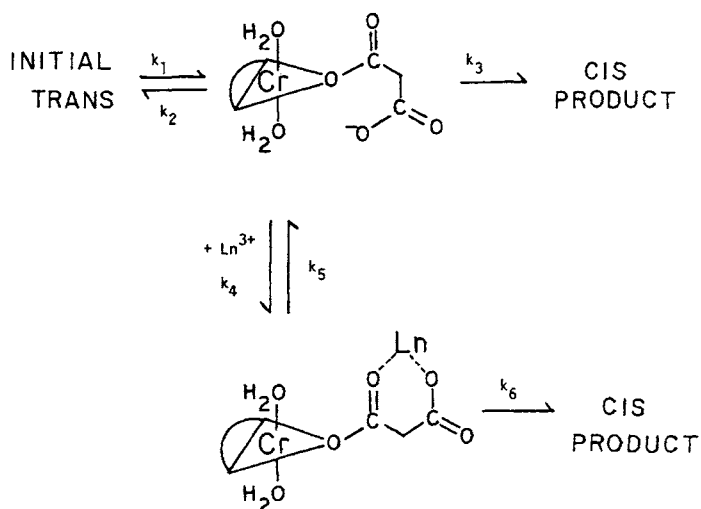


Fig. 7.32. Mechanism for the lanthanide ion catalyzed *trans-cis* isomerization of *trans*-bis(malonato)diaquochromate(III) [84].

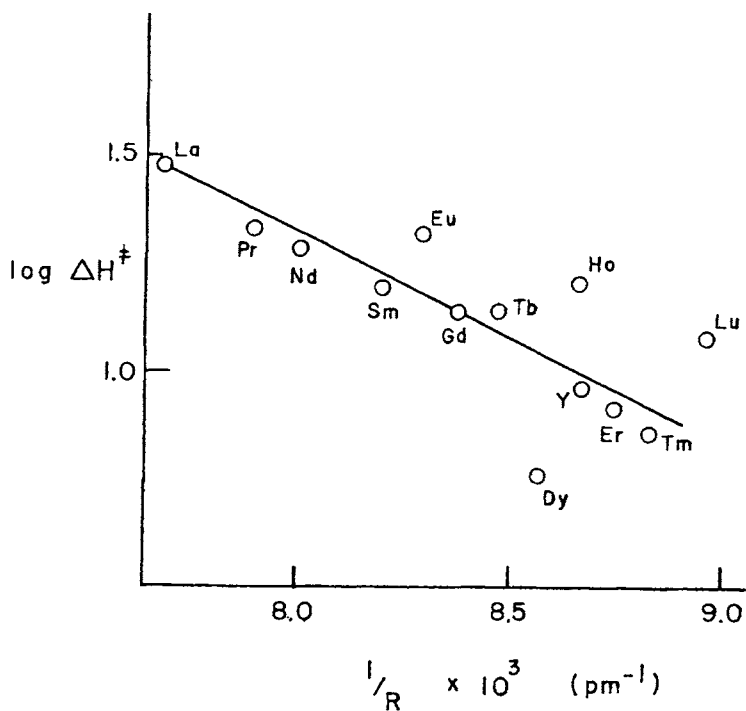


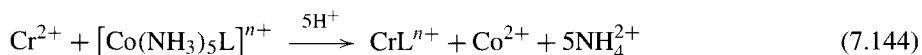
Fig. 7.33. Plot of  $\Delta H^\ddagger$  for each lanthanide ion catalyzed isomerization of *trans*-bis(malonato)diaquochromate(III) vs. the ionic radii of the corresponding lanthanide ions [84].



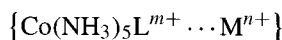
in which  $k_1 = 1.0 \times 10^6 \text{ M}^{-1} \text{ s}^{-1}$  and  $k_2/k_{-1} = 13$ . It is clear from these results that a considerable amount of  $\text{HO}_2^*$  is produced, at least for a short period, by mixing large amounts of  $\text{H}_2\text{O}_2$  ( $\sim 0.1 \text{ M}$ ) with a small amount of  $\text{Ce(IV)}$  ( $10^{-3} \text{ M}$ ), which is consumed in the first step (7.142) and thus cannot consume  $\text{HO}_2^*$  in step (7.143). By mixing the solutions efficiently and using electron spin resonance (ESR) within 10 ms of mixing the presence of an  $\text{HO}_2^*$  intermediate has been detected. This reaction illustrates the utility of direct detection and the study of intermediates which in turn helps confirm the rate law and a mechanism consistent with the rate law.

### 32. Inner-sphere redox reactions

The pioneering work of Taube and co-workers on the reduction of  $\text{Co(III)}$  complexes by  $\text{Cr(II)}$  led to many interesting aspects of developments in the elucidation of the bridging ligand and its role in inner-sphere electron transfer reactions. The most important aspect is to determine the nature of a good bridging group and its effect on the rate of the inner-sphere electron transfer reaction. Many bridging groups have been studied and rates of many orders of magnitude have been observed. Extensive data have been obtained on reactions of the type



In the place of  $\text{Cr}^{2+}$ , other reductants such as  $\text{V}^{2+}$ ,  $\text{Fe}^{2+}$  and  $\text{Eu}^{2+}$  have been used and the rates of the redox reactions determined. Designating the reductant as  $\text{M}^{n+}$ , the bridge that is formed during the course of the redox reaction may be represented as



Some data on the rate constants for the reduction of  $\text{Co(III)}$  complexes are given in Tables 7.25a and 7.25b. The rate constants vary depending upon the nature of the bridging ligand L. It is obvious that the better the bridge, the higher the rate constant for the redox reaction.

After the electron transfer,  $\text{Co}(\text{NH}_3)_5^{2+}$  decomposes rapidly into  $\text{Co}^{2+}$  and  $5\text{NH}_4^+$  in acid solutions. Precursor complex formation, intramolecular electron transfer or successor complex dissociation may be rate limiting. The reaction profiles for these alternatives are shown in Fig. 7.34. Many rate laws can arise from different rate-determining steps. A second-order rate law is common, but the second-order rate constant  $k_{\text{obs}}$  is probably composite. The situation in Fig. 7.34b is applicable in the case of  $\text{Cr}^{2+}$ ,  $\text{Eu}^{2+}$  and other ions (the redox rate constant is less than the substitution rate constant), and  $\Delta H_{\text{obs}}^\ddagger$  values are negative. The negative  $\Delta H_{\text{obs}}^\ddagger$  values are good evidence for the formation of precursor complexes.

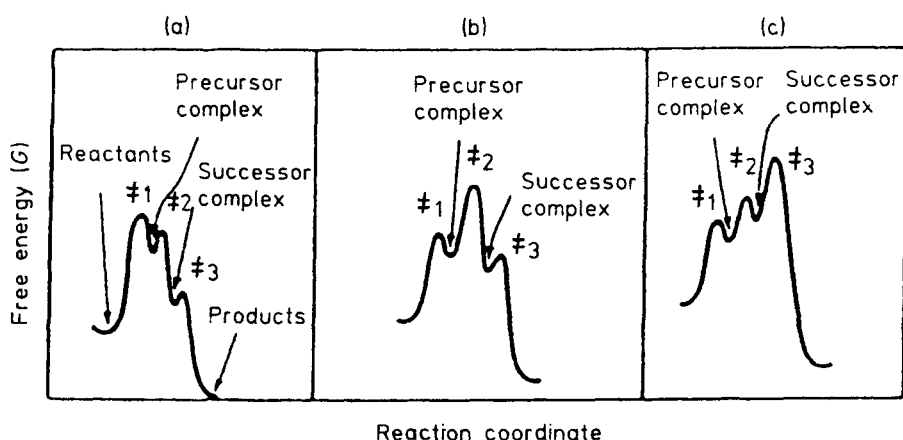


Fig. 7.34. Reaction profiles for inner-sphere redox reactions illustrating three types of behavior: (a) precursor complex formation is rate-limiting, (b) precursor-to-successor complex is rate-limiting and (c) breakdown of successor complex is rate-limiting. The situation (b) appears to be most commonly encountered [85].

TABLE 7.25a  
Rate constants ( $k$  ( $M^{-1} s^{-1}$ )) for the reduction of  $Co(NH_3)_5L^{n+}$  by a variety of reductants at  $25^\circ C$  [85].

L	$Cr^{2+}$	$V^{2+}$	$Fe^{2+}$	$Eu^{2+}$
$NH_3$	$8.0 \times 10^{-5}$	$3.7 \times 10^{-3}$		$2 \times 10^{-2}$
Py	$4.1 \times 10^{-3}$	0.24		
$H_2O$	$\leq 0.1$	0.53		0.15
$OCOCH_3$	0.35	1.2	$< 5 \times 10^{-5}$	0.18
$OCOCOOH$	$1.0 \times 10^2$	12.5	$3.8 \times 10^{-3}$	
$F^-$	$2.5 \times 10^5$	2.6	$6.6 \times 10^{-3}$	$2.6 \times 10^4$
$Cl^-$	$6 \times 10^5$	10	$1 \times 10^{-3}$	$3.9 \times 10^2$
$Br^-$	$1.4 \times 10^6$	25	$7.3 \times 10^{-4}$	$2.5 \times 10^2$
$I^-$	$3 \times 10^6$	$1.2 \times 10^2$		$1.2 \times 10^2$
$OH^-$	$1.5 \times 10^6$	$< 4$		$< 2 \times 10^3$
$N_3^-$	$\sim 3 \times 10^5$	13	$8.8 \times 10^{-3}$	$1.9 \times 10^2$
$NCS^-$	19 <sup>b</sup>	0.3	$< 3 \times 10^{-6}$	0.05
$SCN^-$	$1.9 \times 10^5$	30	0.12	$3.1 \times 10^3$
	$0.8 \times 10^5$			

The rate constants for the reduction of aquo cations by hydrated electrons and for the oxidation of aquo cations by hydroxyl radicals at  $25^\circ C$  are given in Tables 7.25b and 7.25c, respectively.

### 33. Thermal decomposition kinetics and mechanisms

Thermal decomposition kinetics of complexes have been studied by thermogravimetry and differential thermal analysis in order to understand the thermal stability and the mechanism

TABLE 7.25b

Second-order rate constants ( $10^{-8} k_2$  ( $\text{dm}^3 \text{mol}^{-1} \text{s}^{-1}$ )) for reduction of aquo cations by hydrated electrons at 25°C.

Na <sup>+</sup>	K <sup>+</sup>	Cs <sup>+</sup>	Ag <sup>+</sup>	Tl <sup>+</sup>					
0.0002	0.0003	0.0002	360	300					
Cr <sup>2+</sup>	Mn <sup>2+</sup>	Fe <sup>2+</sup>	Co <sup>3+</sup>	Ni <sup>2+</sup>	Cu <sup>2+</sup>	Zn <sup>2+</sup>			
420	0.8	3.5	120	220	300	15			
						Cd <sup>2+</sup>			
						520			
	Mg <sup>2+</sup>		Sn <sup>2+</sup>	Pb <sup>2+</sup>					
	<0.001		34 <sup>a</sup>	390					
Al <sup>3+</sup>	In <sup>3+</sup>	Cr <sup>3+</sup>							
20	560	600							
Y <sup>3+</sup>									
2									
La <sup>3+</sup>	Pr <sup>3+</sup>	Nd <sup>3+</sup>	Sm <sup>3+</sup>	Eu <sup>3+</sup>	Gd <sup>3+</sup>	Tb <sup>3+</sup>	Er <sup>3+</sup>	Tm <sup>3+</sup>	Yb <sup>3+</sup>
3.4	2.9	5.9	250	610	5.5	0.17	0.7	30	430
Am <sup>3+</sup>	Bk <sup>3+</sup>	Cf <sup>3+</sup>							
16	11	30							
Th <sup>4+</sup>									
190									

<sup>a</sup>At pH 11.

TABLE 7.25c

Second-order rate constants for oxidation of aquo cations by hydroxyl radicals in aqueous solution at 25°C<sup>a</sup>.

Reductant	$k_2$ ( $\text{dm}^3 \text{mol}^{-1} \text{s}^{-1}$ )	Reductant	$k_2$ ( $\text{dm}^3 \text{mol}^{-1} \text{s}^{-1}$ )	Reductant	$k_2$ ( $\text{dm}^3 \text{mol}^{-1} \text{s}^{-1}$ )
Ag <sup>+</sup> aq	$\geq 3 \times 10^9$				
Tl <sup>+</sup> aq	$7.6 \times 10^9$				
Zn <sup>2+</sup> aq	$< 5 \times 10^5$			VO <sup>2+</sup> aq	$5.0 \times 10^8$
Cd <sup>2+</sup> aq	$< 5 \times 10^5$				
Cr <sup>2+</sup> aq	$1.2 \times 10^{10}$				
Mn <sup>2+</sup> aq	$\geq 1.4 \times 10^7$	Pd <sup>2+</sup> aq	$5.1 \times 10^9$		
Fe <sup>2+</sup> aq	$4.4 \times 10^8$				
Co <sup>2+</sup> aq	$8 \times 10^5$	Ti <sup>3+</sup> aq	$3.0 \times 10^9$		
Ni <sup>2+</sup> aq	$< 5 \times 10^5$	Cr <sup>3+</sup> aq	$3.2 \times 10^8$		
Cu <sup>2+</sup> aq	$3.5 \times 10^{8b}$	Ce <sup>3+</sup> aq	$30/7.2 \times 10^7$	NpO <sub>2</sub> <sup>+</sup> aq	$4.5 \times 10^7$
Sm <sup>2+</sup> aq	$6.2 \times 10^9$	Pr <sup>3+</sup> aq	$4 \times 10^6$	PuO <sub>2</sub> <sup>+</sup> aq	$4 \times 10^{7d}$
PuO <sub>2</sub> <sup>+</sup> aq	$\sim 4 \times 10^{7d}$				
Eu <sup>2+</sup> aq	$1.3 \times 10^9$				
Tm <sup>2+</sup> aq	$7 \times 10^9$	U <sup>3+</sup> aq	$4.1 \times 10^8$	U <sup>4+</sup> aq	$8.6 \times 10^8$
Yb <sup>2+</sup> aq	$3.2 \times 10^9$	Pu <sup>3+</sup> aq	$1.8 \times 10^{9c}$	Pu <sup>4+</sup> aq	$\sim 1 \times 10^{8d}$

<sup>a</sup>Data for the actinides from C. Lierse, K.H. Schmidt, and J.C. Sullivan, *Radiochim. Acta*, 1988, 71.

<sup>b</sup>Or Ca  $10^{10}$  (P.V. Bernhardt, G.A. Lawrance, and D.F. Sangster, *Polyhedron*, 1991, 10, 1373).

<sup>c</sup>Predicted values for Np<sup>3+</sup>aq, Am<sup>3+</sup>aq, Bk<sup>3+</sup>aq and Cf<sup>3+</sup>aq are all about  $5 \times 10^8$ .

<sup>d</sup>Predicted values.

TABLE 7.26  
 Thermoanalytical data [86].

Temperature (°C)	% weight loss		Probable composition of the residues
	Found	Calculated	
Nd(phenobarbitone)Cl <sub>3</sub> · H <sub>2</sub> O			
100–120	3	3.2	Nd(phen)Cl <sub>3</sub>
600–700	63	66.0	Nd <sub>2</sub> O <sub>3</sub>
Nd(amylobarbitone)Cl <sub>3</sub> · H <sub>2</sub> O			
100–120	3	3.2	Nd(amylo)Cl <sub>3</sub>
600–700	65.5	66.0	Nd <sub>2</sub> O <sub>3</sub>
Nd(butabarbitone)Cl <sub>3</sub> · H <sub>2</sub> O			
100–120	3	3.7	Nd(buta)Cl <sub>3</sub>
600–700	63	65	Nd <sub>2</sub> O <sub>3</sub>
Nd(phen)(oxine) <sub>2</sub> Cl <sub>3</sub> · H <sub>2</sub> O			
100	2	2.5	Nd(phen)(oxine) <sub>2</sub> Cl
380	38	33	Nd(oxine) <sub>2</sub> Cl
500	52	52.4	Nd(oxine)Cl
900	77	76.6	Nd <sub>2</sub> O <sub>3</sub>
Nd(amylo)(oxine) <sub>2</sub> Cl <sub>2</sub> · H <sub>2</sub> O			
100	2	2.5	Nd(amylo)(oxine) <sub>2</sub> Cl
380	32	31.8	Nd(oxine) <sub>2</sub> Cl
500	51	52	Nd(oxine)Cl
900	73	76	Nd <sub>2</sub> O <sub>3</sub>
Nd(buta)(oxine) <sub>2</sub> Cl · H <sub>2</sub> O			
100	2	2.5	Nd(buta)(oxine) <sub>2</sub> Cl
400	31	30.4	Nd(oxine) <sub>2</sub> Cl
660	52	51	Nd(oxine)Cl
900	73	75.9	Nd <sub>2</sub> O <sub>3</sub>
Dy(DMG)Cl <sub>3</sub> · 4H <sub>2</sub> O			
160	14.0	15.1	Dy(DMG)Cl <sub>3</sub>
240	41.0	39.6	DyCl <sub>3</sub>
800	62.0	60.9	Dy <sub>2</sub> O <sub>3</sub>
Dy(DAMO)Cl <sub>3</sub> · 7H <sub>2</sub> O			
140	7.0	7.3	Dy(DAMO)Cl <sub>3</sub> · 5H <sub>2</sub> O
230	26.0	25.4	Dy(DAMO)Cl <sub>3</sub>
505	41.0	45.7	DyCl <sub>3</sub>
950	63.5	62.4	Dy <sub>2</sub> O <sub>3</sub>
Sm(phen) <sub>2</sub> Cl <sub>3</sub> · 2H <sub>2</sub> O			
100	2	2.75	Sm(Phen) <sub>2</sub> Cl <sub>3</sub> · H <sub>2</sub> O
170	4	5.51	Sm(Phen) <sub>2</sub> Cl <sub>3</sub>
520	33	33.08	Sm(Phen)Cl <sub>3</sub>
840	60	60.65	SmCl <sub>3</sub>
950	74	73.29	Sm <sub>2</sub> O <sub>3</sub>
Sm(NPU) <sub>3</sub> Cl <sub>3</sub> · 3H <sub>2</sub> O			
200	5.5	5.0	Sm(NPU) <sub>3</sub> Cl <sub>3</sub>
321	45.5	45.35	Sm(NPU)Cl <sub>3</sub>
450	61.5	64.26	SmCl <sub>3</sub>
822	76.0	75.74	Sm <sub>2</sub> O <sub>3</sub>
Sm(DPU) <sub>3</sub> Cl <sub>3</sub> · 2H <sub>2</sub> O			
135	2	1.94	Sm(DPU) <sub>3</sub> Cl <sub>3</sub> · H <sub>2</sub> O
150	4	3.87	Sm(DPU) <sub>3</sub> Cl <sub>3</sub>
260	27.5	26.69	Sm(DPU) <sub>2</sub> Cl <sub>3</sub>

TABLE 7.26  
(Continued.)

Temperature (°C)	% weight loss		Probable composition of the residues
	Found	Calculated	
315	50	49.52	Sm(DPU)Cl <sub>3</sub>
735	77.5	78.26	SmOCl
870	79	81.17	Sm <sub>2</sub> O <sub>3</sub>
Gd(DMG)(DPTU) <sub>3</sub> Cl <sub>3</sub> · 3H <sub>2</sub> O			
160	14	15.21	Gd(DPTU) <sub>3</sub> Cl <sub>3</sub>
180	23	25.40	Gd(DPTU) <sub>3-x</sub> Cl <sub>3</sub>
540	77	76.40	GdCl <sub>3</sub>
760	84	83.77	Gd <sub>2</sub> O <sub>3</sub>
Gd(TU) <sub>5</sub> (U) <sub>3</sub> Cl <sub>3</sub> · 3H <sub>2</sub> O			
80	2.05	2.5	Gd(TU) <sub>5</sub> (U) <sub>3</sub> Cl <sub>3</sub> · 2H <sub>2</sub> O
110	4.10	4.25	Gd(TU) <sub>5</sub> (U) <sub>3</sub> Cl <sub>3</sub> · H <sub>2</sub> O
160	6.15	5.60	Gd(TU) <sub>5</sub> (U) <sub>3</sub> Cl <sub>3</sub>
190–200	9.56	9.5	Gd(TU) <sub>5</sub> (U) <sub>3-n</sub> Cl <sub>3</sub>
260	37.14	37.0	Gd(TU) <sub>3</sub> (U)Cl <sub>3</sub>
440	65.6	65.0	Gd(TU) <sub>3-n</sub> Cl <sub>3</sub>
585	69.95	70.0	GdCl <sub>3</sub>
900	79.35	79.5	Gd <sub>2</sub> O <sub>3</sub>
Gd(DMG)(TU) <sub>3</sub> Cl <sub>3</sub> · 4H <sub>2</sub> O			
110	4	5.29	Gd(DMG)(TU)Cl <sub>3</sub> · 2H <sub>2</sub> O
130	9	10.59	Gd(DMG)(TU) <sub>3</sub> Cl <sub>3</sub>
170	18	19.2	Gd(DMG) <sub>1-n</sub> (TU) <sub>3</sub> Cl <sub>3</sub>
210	28	27.65	Gd(TU) <sub>3</sub> Cl <sub>3</sub>
310	51	50.01	Gd(Tu) <sub>2</sub> Cl <sub>3</sub>
510	60	61.19	GdCl <sub>3</sub>
990	72	73.33	Gd <sub>2</sub> O <sub>3</sub>

Note: pheno = phenobarbitone, buta = butabarbitalone, amylo = amylobarbitone, oxine = 8-hydroxyquinoline, DMG = dimethylglyoxime, DAMO = diacetylmonoxime, phen = 1,10-phenanthroline, NPU = N-phenylurea, DPU = diphenylurea, DPTU = diphenylthiourea, TU = thiourea, U = urea.

of decomposition. Some benefits of such studies are: (i) to distinguish between lattice water and coordinated water and (ii) to isolate some complexes which cannot be synthesized by conventional synthetic methods. Thermoanalytical data on some lanthanide complexes [86] are summarized in Table 7.26.

Reference to Table 7.26 shows the dysprosium diacetyl monoxime complex to have seven molecules of water. This complex loses two molecules of lattice water at 160°C. At 230°C, the remaining five coordinated water molecules are lost from the complex.

In the case of Gd–dimethylglyoxime thiourea complex, four molecules of lattice water are lost at 130°C followed by an endothermic peak at 170°C and a complete loss of dimethylglyoxime at 210°C. The residue was analyzed and found to be Gd(thiourea)<sub>3</sub>Cl<sub>3</sub>. Normally it is difficult to prepare the Gd thiourea complex by direct synthetic procedures. Thus this example shows that thermal decomposition kinetics is a suitable method for the synthesis of some complexes under favourable conditions. The thermal decomposition data on LnCr(tartrate)<sub>3</sub> · 2H<sub>2</sub>O, where Ln = La, Nd, Eu, Dy, and Er are given in Table 7.27. There are six to eight steps in the decomposition [87].



TABLE 7.27  
Thermal decomposition data on tartrate complexes [87].

Compound	Stage	$T_{\text{range}}^a$ (°C)	$T_{\text{max}}$ (°C)	Intermediate	Mass loss of %	
					Calcd.	Experim.
[LaCr(tartrate) <sub>3</sub> ] · 6H <sub>2</sub> O	I	59–128	78	LaCr(tartrate) <sub>3</sub> · 2H <sub>2</sub> O	13.97	13.82
	II	128–190	–	LaCr(tartrate) <sub>3</sub>	4.65	5.01
	III	190–293	263	LaCrOX <sub>3</sub>	22.51	23.14
	IV	283–322	299	LaCr(CO <sub>3</sub> ) <sub>5/2</sub> O <sub>1/2</sub>	13.71	13.33
	V	322–368	335	LaCr(CO <sub>3</sub> ) <sub>2</sub> O	2.84	3.01
	VI	368–434	–	LaCr(CO <sub>3</sub> ) <sub>3/2</sub> O <sub>3/2</sub>	2.84	3.14
	VII	434–547	482	LaCr(CO <sub>3</sub> ) <sub>1/2</sub> O <sub>5/2</sub>	5.69	5.01
	VIII	740–758	747	LaCrO <sub>3</sub>	2.84	2.77
Total loss				69.05	69.23	
[NdCr(tartrate) <sub>3</sub> ] · 8H <sub>2</sub> O	I	78–141	81	NdCr(tartrate) <sub>3</sub> · 2H <sub>2</sub> O	13.86	13.50
	II	141–199	–	[NdCr(tartrate) <sub>3</sub> ]	4.62	4.34
	III	199–295	268	NdCrOx <sub>3</sub>	22.35	22.07
	IV	295–330	301	NdCO <sub>3</sub> O <sub>2</sub>	22.10	22.63
	V	390–545	510	Nd(CO <sub>3</sub> ) <sub>1/3</sub> O <sub>8/3</sub>	3.76	4.00
	VI	688–720	719.5	NdCrO <sub>3</sub>	1.88	1.74
Total loss				68.57	68.37	
[EuCr(tartrate) <sub>3</sub> ] · 9H <sub>2</sub> O	I	81–143	83	EuCr(tartrate) <sub>3</sub> · 2H <sub>2</sub> O	15.67	15.40
	II	143–200	–	EuCr(tartrate) <sub>3</sub>	4.47	4.41
	III	200–263	–	EuCr(tartrate)(Ox) <sub>2</sub>	14.42	15.00
	IV	263–291	268	EuCr(CO <sub>3</sub> ) <sub>3</sub>	17.66	18.42
	V	360–440	400	EuCr(CO <sub>3</sub> ) <sub>2</sub> O	5.47	5.52
	VI	440–508	–	EuCr(CO <sub>3</sub> ) <sub>3/2</sub> O <sub>3/2</sub>	2.73	2.64
	VII	508–558	544	EuCr(CO <sub>3</sub> ) <sub>1/2</sub> O <sub>5/2</sub>	5.47	5.32
	VIII	726–751	747	EuCrO <sub>3</sub>	2.73	2.28
Total loss				68.62	69.63	
[DyCr(tartrate) <sub>3</sub> ] · 6H <sub>2</sub> O	I	85–153	108	DyCr(tartrate) <sub>3</sub> · 1H <sub>2</sub> O	11.83	12.05
	II	153–217	–	DyCr(tartrate) <sub>3</sub>	2.36	2.32
	III	217–300	269	DyCr(tartrate)(Ox) <sub>2</sub>	15.25	16.02
	IV	300–350	311	DyCr(CO <sub>3</sub> ) <sub>3</sub>	18.67	18.45
	V	490–605	–	DyCr(CO <sub>3</sub> ) <sub>1/2</sub> O <sub>5/2</sub>	14.46	13.90
	VI	682–755	739	DyCrO <sub>3</sub>	2.89	3.02
Total loss				65.46	65.76	
[ErCr(tartrate) <sub>3</sub> ]10H <sub>2</sub> O	I	88–160	130	ErCr(tartrate) <sub>3</sub> · 2H <sub>2</sub> O	17.19	16.32
	II	160–230	–	ErCr(tartrate) <sub>3</sub>	4.29	4.74
	III	230–308	268	ErCrOx <sub>3</sub>	20.78	19.95
	IV	308–359	318	ErCr(CO <sub>3</sub> ) <sub>1/2</sub> O <sub>5/2</sub>	23.17	23.60
	V	519–577	547	ErCr(CO <sub>3</sub> ) <sub>2/6</sub> O <sub>16/6</sub>	0.87	1.02
	VI	678–730	705	ErCrO <sub>3</sub>	1.75	1.68
Total loss				68.06	67.74	

<sup>a</sup> $T_1 - T_f^1$ .

TABLE 7.28

Phenomenological data for the thermal decomposition of lanthanide perchlorate complexes of AA [88].

Complexes	Stages of decomposition	TG plateau (°C)	DTG peak (°C)	% mass loss; found (calculated)
[La(AA) <sub>2</sub> (ClO <sub>4</sub> )](ClO <sub>4</sub> ) <sub>2</sub>	I	220–410	325	41.23 (41.00)
	II	410–560	505	8.75 (8.60)
	III	560–620	590	38.35(38.39)
[Pr(AA) <sub>2</sub> (ClO <sub>4</sub> )](ClO <sub>4</sub> ) <sub>2</sub>	I	220–420	320	41.40 (41.00)
	II	420–550	500	8.30 (8.56)
	III	550–650	610	38.50(38.20)
[Nd(AA) <sub>2</sub> (ClO <sub>4</sub> )](ClO <sub>4</sub> ) <sub>2</sub>	I	220–400	325	41.20 (41.00)
	II	400–560	510	8.40 (8.47)
	III	560–620	590	38.45(38.15)
[Sm(AA) <sub>2</sub> (ClO <sub>4</sub> )](ClO <sub>4</sub> ) <sub>2</sub>	I	220–400	320	41.50 (40.97)
	II	400–560	510	8.50 (8.40)
	III	560–630	600	38.50(38.15)
[Eu(AA) <sub>2</sub> (ClO <sub>4</sub> )](ClO <sub>4</sub> ) <sub>2</sub>	I	220–410	325	41.25 (40.90)
	II	410–560	500	8.55 (8.35)
	III	560–620	605	38.33 (38.05)
[Gd(AA) <sub>3</sub> ](ClO <sub>4</sub> ) <sub>3</sub>	I	180–252	210	8.60 (8.50)
	II	252–336	312	30.00 (30.50)
	III	336–690	508	48.00 (48.80)
[Dy(AA) <sub>3</sub> ](ClO <sub>4</sub> ) <sub>3</sub>	I	180–250	205	8.60 (8.50)
	II	250–340	320	30.00 (30.45)
	III	340–700	520	48.00 (48.20)
[Ho(AA) <sub>3</sub> ](ClO <sub>4</sub> ) <sub>3</sub>	I	180–260	200	8.60 (8.45)
	II	260–345	325	30.00 (30.40)
	III	345–690	525	48.00 (48.17)
[Er(AA) <sub>3</sub> ](ClO <sub>4</sub> ) <sub>3</sub>	I	180–255	205	8.70 (8.30)
	II	255–335	320	30.50 (30.35)
	III	335–700	520	48.50 (48.10)

The activation parameters such as activation energy and pre-exponential factor,  $A$  calculated by different methods show the decomposition rate is independent of the nature of the rare earth cation. The activation energies are in the range of 60–70 kJ mol<sup>-1</sup> with a reaction order in the range 1.4 to 1.6.

Thermal decomposition of lanthanide complexes of 4-*N*-(4'-antipyrylmethylidene)/amino antipyrine is found to occur in three stages [88] and the phenomenological data are given in Table 7.28. In the case of the lanthanum complex, the three stages of decomposition are as follows:

- Stage I: Loss of one ligand AA and conversion of non-coordinated perchlorate to chlorate.
- Stage II: Conversion of two chlorate groups to chloride.
- Stage III: Loss of second ligand AA and conversion of coordinated perchlorate to chloride. The behaviour of Pr, Nd, Sm and Eu complexes is similar to the La complex.

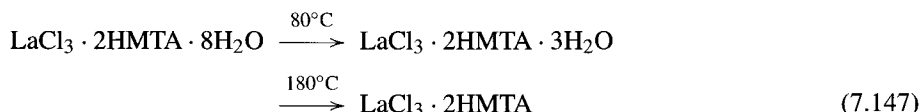
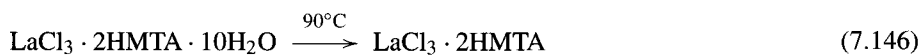
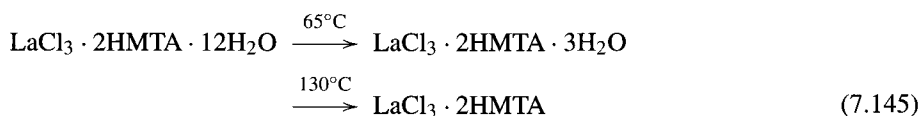
The three stages of decomposition of Gd, Dy, Ho and Er complexes are:

- Stage I: Conversion of perchlorate into chlorate.
- Stage II: Loss of one AA ligand and conversion of chlorate into chloride.
- Stage III: Loss of 2 AA ligands.

In general, lighter lanthanide complexes are thermally more stable than the heavy lanthanide complexes.

The activation energy for the various complexes is in the range of 32–237 kJ/mol. This low value probably indicates that the ligands are loosely bound to the metal ion. The negative values of  $\Delta S$  indicate more ordered structure in the activated complex than the reactants.

Thermal decomposition kinetics of  $\text{LnCl}_3 \cdot 2\text{HMTA} \cdot n\text{H}_2\text{O}$  complex, where  $\text{Ln} = \text{La}, \text{Pr}, \text{Nd}$ , HMTA = hexamethylenetetraamine and  $n = 8, 10, 12$  show essentially the two stages in which lattice and coordinated water molecules are removed from the complex in the temperature ranges 65–80° and 135–145°C, respectively. A typical reaction scheme may be written as follows [89].



Phenylacetic acid complexes of lanthanides of the formula  $\text{LnL}_3 \cdot n\text{H}_2\text{O}$ , where  $\text{Ln} = \text{Ce}, \text{Nd}, \text{Pr}, \text{Ho}, \text{Er}, \text{Yb}$  and  $\text{Y}$ ,  $n = 1-2$  have been studied. The complexes of Pr and Nd decompose in three stages:



The complexes of Ce, Y, Er, Ho, and Yb decompose in two steps.



### 34. Photochemistry and photophysics of lanthanide complexes

In the lanthanide series, we have 14 elements that result from the addition of electrons into the f orbitals. For the lanthanide series, the electron configurations are 4f (1–14). In the lanthanide series, the majority of the compounds are formed by trivalent  $\text{M}^{3+}$  ions. From a spectroscopic point of view, all the rare earth ions have a large spin-orbit coupling constants, resulting in electronic states being defined by the angular momentum

values  $J$ . The lanthanides form compounds that are primarily ionic in character, with coordination numbers of 8 or 9. Recently, complexes with coordination numbers of 11 and 12 have been synthesized. The compounds of lanthanides are substitution labile in aqueous solutions [91].

The influence of the ligand field on the electronic states of lanthanides is small and generally of the order of  $\sim 200 \text{ cm}^{-1}$ . Because the ligand field perturbation of  $J$  states are minimal, the  $f$ - $f$  electronic transitions are sharp. In addition to  $f$ - $f$  transitions, both  $4f \rightarrow 5d$  and charge transfer transitions are also observed in the spectra of lanthanides [92]. Lanthanide ions exhibit emission in the solid state, and in some cases in aqueous solutions. Energy transfer from the ligand or intermolecularly from an excited state can give rise to the emission from lanthanide ions.

The photochemistry of lanthanide ions is limited to photoredox reactions. Photo substitution has not been studied because of the lability of metal ions, and since ligand substitution reactions are rapid even under thermal conditions.

### 35. Photochemistry of lanthanides

Photoredox reactions are likely to take place when the metal complex has two oxidation states that are close in energy. In the majority of lanthanide elements the trivalent state is common and redox reactions are not as common as in the case of transition metal ions. The exceptions are  $\text{Ce}^{3+}/\text{Ce}^{4+}$  and  $\text{Eu}^{2+}/\text{Eu}^{3+}$  couples, wherein the stability of  $4f^7$  configuration or the xenon electronic configuration stabilizes the  $\text{Eu(III)}$  and  $\text{Ce(IV)}$ . In aqueous solutions  $\text{Ce(III)}$  and  $\text{Eu(III)}$  exist as aquo species of the type  $\text{Ce}(\text{H}_2\text{O})_n^{3+}$  and  $\text{Eu}(\text{H}_2\text{O})_n^{3+}$ , where  $n = 8$  or  $9$ . The nature of  $\text{Ce(IV)}$  in aqueous solutions is uncertain because it can undergo oligomerization [93].  $\text{Ce(IV)}$  ion is a strong one-electron oxidizing agent with a standard reduction potential  $E^0$  of  $1.7 \text{ V}$  [94]. The situation in the case of europium is different. The  $\text{Eu}^{2+}$  ion is a strong one-electron reducing agent with a standard reduction potential  $E^0$  of  $-1.99 \text{ V}$  [95].

### 36. Photochemistry of Eu in aqueous solutions

Acidified aqueous solutions of the  $\text{Eu}^{2+}$  ion on irradiation at  $366 \text{ nm}$  undergo photoreduction of hydrogen [96] to give molecular hydrogen with a quantum yield,  $\Phi$  of  $0.2$ . The reaction may be written as



The reverse reaction occurs upon photolysis at  $254 \text{ nm}$  [97].



The extinction coefficient of  $\text{Eu}^{2+}$  is much greater than  $\text{Eu}^{3+}$  and hence the reverse reaction becomes dominant as the  $\text{Eu}^{2+}$  concentration in solution increases.

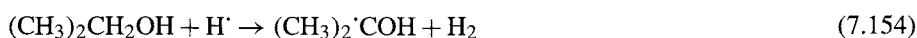
Aqueous solutions of  $\text{Eu}^{3+}$  on photolysis give rise to hydroxyl radicals thus



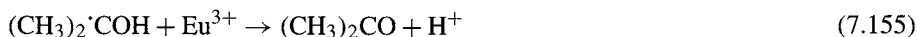
On addition of 2-propanol to the above system, hydrogen is evolved.



The hydrogen atoms abstract the methine hydrogen from 2-propanol to give hydrogen and 2-propanol radical



Finally the 2-propanol radical is oxidized to acetone by  $\text{Eu}^{3+}$  ion



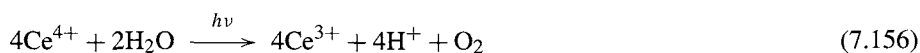
It is obvious that the whole process is catalytic in both  $\text{Eu}^{2+}$  and  $\text{H}^+$  ions and the net reaction is the photodecomposition of 2-propanol into acetone and hydrogen.

In the case of photolysis of acidic aqueous solutions of  $\text{Eu}^{2+}$  ion at 366 nm, the excited state results from  $4f \rightarrow 5d$  transitions localized on the metal centre. These excited states have also considerable MLCT character because of strong mixing of metal 5d orbitals with ligand orbitals. In the case of the reaction of  $\text{Eu}^{3+}$  with  $\text{H}_2$  which occurs on photolysis at 254 nm, the photo reaction is due to the formation of an LMCT excited state. This process has been successfully used in the photochemical separation of Eu from other members of the lanthanides because  $\text{Eu}^{2+}$  is the only member of the lanthanide series which is at suitably low energy that an LMCT state is accessible [98].  $\text{Yb}^{3+}$  and  $\text{Sm}^{3+}$  ions behave in a similar fashion to  $\text{Eu}^{3+}$  as far as their photochemical behaviour is concerned. Aqueous solutions of  $\text{Sm}^{3+}$  or  $\text{Yb}^{3+}$  containing 2-propanol on photolysis at 185 nm give hydrogen and acetone as products probably by a mechanism similar to  $\text{Eu}^{3+}$  ion.

### 37. Photochemistry of cerium system

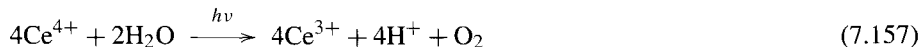
Aqueous solutions of  $\text{Ce}^{4+}$  ion are yellow in colour with a broad absorption band in the UV region extending into the visible region. This absorption band is due to an LMCT transition. Irradiation in this band region results in photo redox reactions between  $\text{Ce}^{4+}$ – $\text{Ce}^{3+}$  ions [99].

Photooxidation of solvent water occurs upon irradiation of aqueous solutions of  $\text{Ce}^{4+}$  yielding oxygen as a product [100].

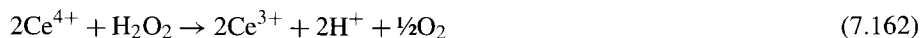


From the studies of measurement of quantum yields it is surmised that the photo active species in the above reaction involves  $\text{Ce}^{4+}$  dimers and the reduced  $\text{Ce}^{3+}$  ion

deactivates the reactive dimers. The dimers might act as two-electron acceptors. Further  $\text{Ce}^{3+}$  undergoes photoreaction in perchloric acid solutions to give hydrogen [101]. These two photo reactions lead to the possibility of photolytically splitting water into hydrogen and oxygen by a careful control of experimental conditions so that both the reactions involving  $\text{Ce}^{4+}$  and  $\text{Ce}^{3+}$  take place



An alternative explanation for the photooxidation of aqueous perchloric acid to give oxygen has been postulated [102]. This mechanism involves a photo reaction in which hydroxyl radicals are formed. The proposed reaction scheme is as follows:



Hydroxyl radicals have been detected in the photolysis of frozen solutions of  $\text{Ce}(\text{ClO}_4)_4$  in perchloric acid solutions [103].

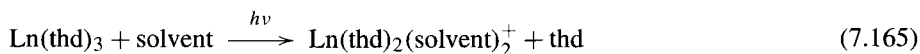
Photoreduction of  $\text{Ce}^{4+}$  to  $\text{Ce}^{3+}$  in aqueous sulphuric acid solutions is affected by the presence of other ions such as  $\text{Cl}^-$ ,  $\text{Br}^-$ ,  $\text{Tl}^+$  and compounds like formic acid [104]. Photoreduction quantum yields were higher in presence of  $\text{Cl}^-$ ,  $\text{Br}^-$ ,  $\text{Tl}^+$  and formic acid. It is surmised that the added ions trap the hydroxyl radical formed in the photoreduction of  $\text{Ce}^{4+}$  to  $\text{Ce}^{3+}$  and prevent the reverse reaction of  $\text{Ce}^{3+}$  with hydroxyl radical. If nitrate ion is initially present in the system, photolysis produces nitrate radicals [105]. The production of nitrate radicals may occur due to either the photolysis of  $\text{Ce}^{4+}$  [106] or due to the thermal oxidation of nitrate by hydroxyl radicals generated in the photolysis of  $\text{CeOH}^{3+}$  [107]. Photooxidation of organic compounds by  $\text{Ce}^{4+}$  ion is well established [108]. Photo oxidation of carboxylic acids by ceric ion at 254 nm or 350 nm gives rise to a cerous ion and carboxyl radical due to the oxidation of carboxylate ion. Acetic acid solutions of ceric ion on photolysis at 350 nm give rise to carbon dioxide and methane as major products along with higher homologues containing carbon-carbon bonds. This reaction follows the scheme given below:



The alkyl radicals combine with each other to give higher hydrocarbons. Evidence for the formation of alkyl radicals at 77 K by photolysis has been obtained although its formation from a free carboxyl radical has not been confirmed [109].

### 38. Photosubstitution reactions

Photo substitution reactions of Pr, Eu and Ho complexes with the ligand L = 2,2,6,6-tetramethyl-3,5-heptanedione (thd) of the formula  $\text{Ln}(\text{thd})_3$  have been studied by irradiation into the f-f bands [110]. The corresponding thermal reactions are slow. The ligand thd is replaced by solvent thus



The photo substitution pathway probably involves intramolecular energy transfer from an f-f excited state to an intraligand state leading to the dissociation of ligand thd from the complex. Excitation of ligand absorption bands of  $\text{Tb}(\text{thd})_3$  also leads to the same substitution reaction [111].

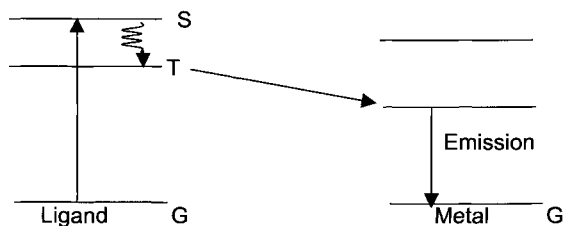
### 39. Luminescence of lanthanide ions

Among the lanthanides,  $\text{Sm}^{3+}$ ,  $\text{Eu}^{3+}$ ,  $\text{Gd}^{3+}$ ,  $\text{Tb}^{3+}$ , and  $\text{Dy}^{3+}$  ions exhibit luminescence in solutions because of favourable spectroscopic properties. In the case of these ions, the energy gap between the lowest level of emission and the highest energy ground state is considerably large such that emission occurs in preference to loss of energy by a nonradiative decay process. The emission levels of  $\text{Eu}^{3+}$  and  $\text{Tb}^{3+}$  are located at 580 and 488 nm respectively, above the ground state energy level as shown below:



The emission and corrected excited spectra for EDTA complexes of  $\text{Eu}^{3+}$  and  $\text{Tb}^{3+}$  complexes are shown in Fig. 7.35. Similar spectra are predicted for other  $\text{Eu}^{3+}$  and  $\text{Tb}^{3+}$  complexes because of very little change in f-orbital energy levels due to different ligands.

It has been shown in the case of  $\beta$ -diketonate complexes of lanthanides that the excited singlet state of the ligand goes to the ligand triplet by intersystem crossing and then energy is transferred from the ligand triplet to the metal ion manifold. Finally, the emission occurs from the excited state of the metal.



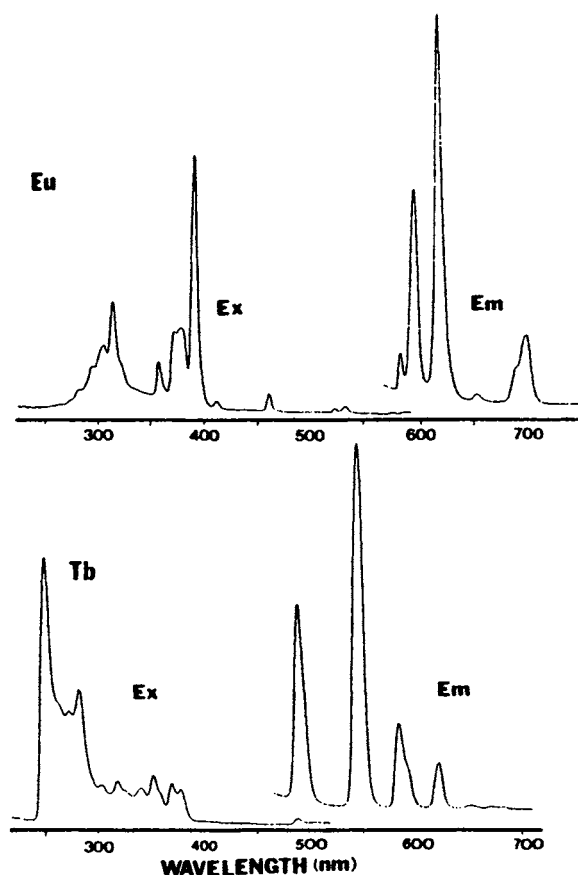


Fig. 7.35. Excitation and emission spectra of EDTA complexes of Eu(III) and Tb(III).

The luminescence yield increases with decreasing temperature and the rate of intramolecular transfer from the ligand triplet to the metal ion states is very fast. Quantum yields for emission increase with addition of neutral ligands and replacing hydrogen in the ligands by deuterium. An approximate energy level diagram for  $\text{Eu}^{3+}$  and  $\text{Tb}^{3+}$  is given in Fig. 7.36.

The photophysical properties of  $\text{EuL}_3$ , where  $\text{L} = 8\text{-hydroxyquinoline (8-hq)}$  and dibenzoylmethide [112] can be elucidated by reference to Fig. 7.36. In the case of  $\text{Eu(8-hq)}_3$  the ligand triplet state (C) lies below  ${}^5\text{D}_1$  state of  $\text{Eu(III)}$  and hence no emission from  ${}^5\text{D}_1$  state is observed. Emission from  ${}^5\text{D}_0$  state is observed. In the case of  $\text{Eu(dbm)}_3$  ligand triplet state (B) is above  ${}^5\text{D}_1$  and emission from both  ${}^5\text{D}_1$  and  ${}^5\text{D}_0$  states is observed. When the ligand is acetylacetonone (acac) we have  $\text{Eu(acac)}_3$  and the triplet level of the ligand is A. Transfer of energy from ligand triplet to the metal results in emission from both  ${}^5\text{D}_1$  and  ${}^5\text{D}_0$  states. Considering the complex  $\text{Tb(acac)}_3$  the triplet level (A) may undergo intersystem crossing to  ${}^5\text{D}_3$  although emission is observed from only  ${}^5\text{D}_4$  level. The quantum yields for emission in Eu complexes under ligand excitation is in the range 0.002–0.43 but higher (0.18–0.84) from a metal centred emissive level. On the other hand



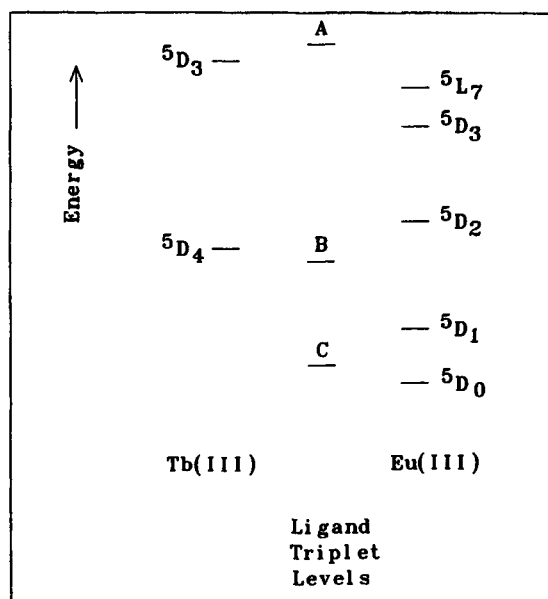


Fig. 7.36. Energy level diagram for Eu(III), Tb(III), and  $\beta$ -diketonate triplet levels.

the quantum yields for terbium complexes are low because of deexcitation of  $^5D_4$  level by coupling with closely spaced triplet level (B) of the ligand.

Luminescence has been observed from pyridine and bipyridine based complexes of Eu(III) and Tb(III). Lanthanide cryptate complexes have also been studied [113]. Eu(III) complexes having aminocarboxylate, substituted pyridines have been used as suitable labels in time-resolved luminescence-based bioaffinity analysis [114–116]. Chain nitrogen donor chelate complexes or macrocyclic ligands based on pyridine or bipyridine units have also been used in bioaffinity tests [117,118]. Chemiluminescence has been observed in Eu(III) complexes. Two such systems are (i) population of  $^5D_0$  state of  $[\text{Eu}(\text{dbm})_3(\text{pyridine})]$  complex<sup>119</sup> by energy transfer from electrogenerated singlet state exciplex benzophenone/tri-*p*-tolylamine<sup>++</sup>, (ii) thermal decomposition of trimethyl 1,2-dioxetane to a triplet state in the presence of  $\text{Eu}(\text{L})_3\text{Phen}$  complex [120].

#### 40. Determination of solvation state of lanthanides

A good understanding of the way or paths of deexcitation of lanthanide ion excited states in complexes with simple ligands like water can throw light on the coordination sphere of the lanthanide ion. Techniques based on this principle have been used in the determination of the number of water molecules coordinated to the lanthanide ion [121].

In the case of  $\text{Eu}^{3+}$  and  $\text{Tb}^{3+}$  aquo ions, the luminescence intensity in  $\text{D}_2\text{O}$  is higher than in  $\text{H}_2\text{O}$  solutions. The excited state lifetimes in  $\text{D}_2\text{O}$  are higher than  $\text{H}_2\text{O}$  [122]. Because of the smaller energy gap, the deuterium isotope effect is greater in  $\text{Eu}^{3+}$  than in  $\text{Tb}^{3+}$ . The energy gap refers to the separation of emission level and the highest  $J$

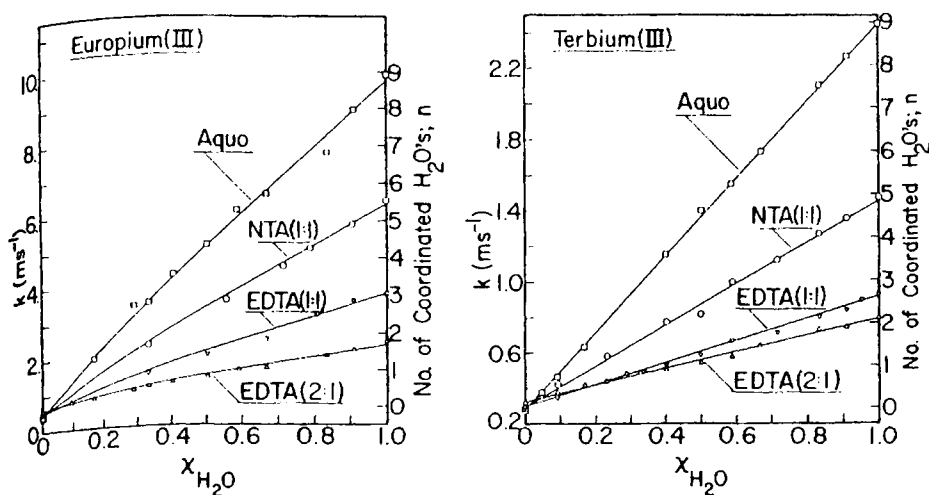


Fig. 7.37. Plots of lanthanide ion luminescence decay constants,  $k$  ( $\text{ms}^{-1}$ ), vs. mole fraction of  $\text{H}_2\text{O}$  ( $\chi_{\text{H}_2\text{O}}$ ) in  $\text{H}_2\text{O}$ – $\text{D}_2\text{O}$  mixtures for  $\text{Eu}(\text{III})$  and  $\text{Tb}(\text{III})$ . The number of coordinated  $\text{H}_2\text{O}$ 's,  $n$ , for the indicated complexes is given on the right-hand ordinates: aquo ions ( $\square$ ); NTA complexes (pH 6.0) ( $\circ$ ); EDTA (1:1) complexes (pH 6.0) ( $\nabla$ ); EDTA (2:1) complexes (pH 7.5) ( $\triangle$ ) [123].

level of ground state. The deexcitation of the excited state is due to vibronic coupling with high frequency ligand vibrations to enable crossing the energy gap. The reciprocals of lifetimes,  $\tau^{-1}$ , and intensities,  $I^{-1}$ , vary linearly with the mole fraction of water in mixtures of  $\text{H}_2\text{O}$  and  $\text{D}_2\text{O}$ . The enhancement of luminescence intensity decreases in the presence of complexing ligands. Nonaqueous solvents also decrease solvent isotope effect. The quenching of luminescence can be correlated with the number of OH oscillators.

From the lifetimes of the excited states of dilute solutions of  $\text{Eu}^{3+}$  and  $\text{Tb}^{3+}$  in  $\text{H}_2\text{O}$  and  $\text{D}_2\text{O}$  the number of coordinated water molecules can be obtained. A typical plot of the lanthanide ion luminescence decay constant against mole fraction of water in  $\text{H}_2\text{O}$ – $\text{D}_2\text{O}$  mixtures is shown in Fig. 7.37. The observed decay constant,  $k_{\text{obs}}$  is comprised of

$$k_{\text{obs}} = k_r + k_x + k_{\text{H}_2\text{O}}\chi_{\text{H}_2\text{O}} \quad (7.166)$$

where  $k_r$  is the inherent radiative decay constant,  $k_x$  is the decay constant for all nonradiative processes other than OH deexcitation and  $k_{\text{H}_2\text{O}}$  is the decay constant for deexcitation through water OH vibrations. The slopes in Fig. 7.37 are equal to  $k_{\text{H}_2\text{O}}$  which in turn is proportional to the number of water molecules,  $n$ , in the primary coordination sphere. The intercept,  $k_r + k_x$  is constant for the complexes under study and assuming  $n = 9$  for aquo ion, the approximate  $n$  values can be obtained from the intercept with the scale on the right-hand ordinates of the figure. This method has been extended to nitrilo trismethylene phosphonic acid (ntp), ethylenediamine tetrakis(methylene phosphonic acid) (edtp), hexamethylenediamine tetrakis(methylene phosphonic acid) (hntp), diethylenetriamine pentakis(methylene phosphonic acid) (dtp) complexes of  $\text{Eu}(\text{III})$  and the relevant data [123] are given in Table 7.29.

TABLE 7.29

Observed  ${}^7F_0 \rightarrow {}^5D_0$  excitation bands and excited-state lifetimes of the Eu(III) complexes of ntp, edtp, hdtp, and dtpp at pH values of 6.0 and 10.0 [123].

Complex (ratio)	$\lambda$ (nm)	$\tau_{H_2O}$ ( $\mu$ s)	$\tau_{D_2O}$ ( $\mu$ s)	$q^a$
pH 6.0				
ntp (1:1)	579.14	210	600	3.5
(1:2)	579.73	910	2400	0.7
edtp (2:1)	578.95	230	2480	4.1
(1:1)	579.35, 578.95	410	2480	2.1
hdtp (2:1)	578.52	370	2450	2.4
(1:1)	579.31, 578.52	530	2450	1.6
Dtpp (2:1)	579.17	370	2440	2.4
(1:1)	579.80, 579.17	940, 370	1320, 2400	0.3, 2.4
pH 10.0				
ntp (1:10)	579.15	200	600	3.5
edtp (1:1)	578.72, 579.49	420	2320	2.1
hdtp (1:1)	579.83, 579.26	300	2450	3.1
dtpp (1:1)	578.78, 579.21	280	2440	3.3

<sup>a</sup>The number of coordinated water molecules  $q = 1.05(\tau_{H_2O}^{-1} - \tau_{D_2O}^{-1}) \pm 0.5$ .

The association of  $Eu^{3+}$  and  $Tb^{3+}$  ions with micellar aggregates, vesicles and biopolymers has been studied using luminescence methods. Micelles consist of spherical aggregates formed by the association of hydrophobic fatty acid tail groups inside the sphere, with polar head groups on the surface which are surrounded by water molecules. Reversed micelles have head and tail groups in the opposite direction. In the spectroscopy of micelles, the medium helps to single out single excited state molecules and thus eliminates triplet-triplet annihilation [124–127]. The occluded triplet in the micelle can diffuse to the lanthanide ion before annihilation. Experiments with  $Tb^{3+}$  have shown that  $Tb^{3+}$  ion binds to the low affinity calcium binding sites on the outer surface of the inner membrane of rat liver mitochondrial membranes [128]. Energy transfer data have revealed the  $Tb^{3+}$  binding sites to be close to each other on a protein constituent of the membrane. This approach can be used in studying binding to ionophores, antibiotics, nucleotides, proteins and enzymes [129].

#### 41. Ligand exchange rates

The spectral-kinetic method has been proposed for studying ligand exchange rates [130]. Consider the case of Eu(III) and the spectroscopic excited state is  ${}^5D_0$  and this state is selectively excited by a pulsed dye laser. Let us consider the equilibrium



in which both the Eu complexes are in equilibrium and related by a ligand exchange reaction. The time dependence of the luminescence emission upon excitation depends on

the rate of chemical exchange, relative to the deexcitation rate. We have two scenarios. In the first case the exchange rate is slow in which case selective excitation of one complex is followed by a single-exponential decay of luminescence with the characteristic lifetime of this complex. If the exchange reaction is rapid, the luminescence also decays exponentially, but with a lifetime equal to the weighted average of the lifetimes of both the complexes. In these two cases, luminescence lifetime measurements do not give any information on the kinetics of ligand exchange reaction. If the ligand exchange occurs at a rate comparable to the deexcitation rate, the time dependence of the luminescence is more complicated and becomes a function of both the chemical interconversion rates and the lifetimes of the excited states [131].

Consider the ligand exchange reaction



In the above reactions  $\text{Eu}^*$  is the excited state of  $\text{Eu(III)-}^5\text{D}_0$ .

The rates may be expressed as

$$\frac{d[\text{Eu}^*\text{L}_a]}{dt} = k_b[\text{Eu}^*\text{L}_b] - (k_a + \tau_a^{-1})[\text{Eu}^*\text{L}_a] \quad (7.171)$$

$$\frac{d[\text{Eu}^*\text{L}_b]}{dt} = k_a[\text{Eu}^*\text{L}_a] - (k_b + \tau_b^{-1})[\text{Eu}^*\text{L}_b] \quad (7.172)$$

Now the solutions to the differential equations are

$$[\text{Eu}^*\text{L}_a] = ([\text{Eu}^*\text{L}_a]_0/2a)[(a+b-c)\exp(dt) + (a-b+c)\exp(et)] \quad (7.173)$$

$$[\text{Eu}^*\text{L}_b] = ([\text{Eu}^*\text{L}_a]_0/a)k_a[\exp(dt) - \exp(et)] \quad (7.174)$$

where

$$a = [(c-b)^2 + 4k_a k_b]^{1/2}; \quad b = k_b + \tau_b^{-1}; \quad c = k_a + \tau_a^{-1};$$

$$d = 1/2(a-b-c); \quad e = -1/2(a+b+c)$$

The luminescence intensity at a given wavelength  $I(\lambda)$  for the exchange reaction is composed of

$$I(\lambda) = Q_a(\lambda)[\text{Eu}^*\text{L}_a]/[\text{Eu}^*\text{L}_a]_0 + Q_b(\lambda)[\text{Eu}^*\text{L}_b]/[\text{Eu}^*\text{L}_b]_0 \quad (7.175)$$

where  $[\text{Eu}^*\text{L}_a]_0$  is the concentration of the excited complex at  $t = 0$  (initial).  $Q_a(\lambda)$  and  $Q_b(\lambda)$  are the fractional luminescence emissions of  $\text{Eu}^*\text{L}_a$  and  $\text{Eu}^*\text{L}_b$  complexes,

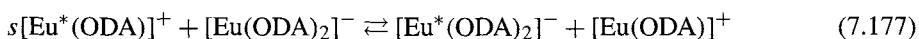
respectively. When the emission wavelengths do not overlap, selective monitoring of emission from  $\text{Eu}^*\text{L}_b$  results in the condition  $Q_a(\lambda) = 0$ ;  $Q_b(\lambda) = 1$ . The intensity of luminescence on selective excitation of  $\text{Eu}^*\text{L}_a$ , increases as  $\text{Eu}^*\text{L}_b$  is formed due to ligand exchange reaction, and then decays. If on the other hand  $Q_b(\lambda) = 0$ ,  $Q_a(\lambda) = 1$ , luminescence intensity will decrease rapidly initially due to the ligand exchange reaction followed by leveling off. When the emission wavelengths of  $\text{Eu}^*\text{L}_a$  and  $\text{Eu}^*\text{L}_b$  overlap, it is necessary to include  $Q_a(\lambda)$  and  $Q_b(\lambda)$  as parameters in the rate expressions.

Ligand exchange reactions of Ln complexes, where Ln = Eu, Sm, Tb and Dy have been studied by recording the luminescence [130,131]. In the case of Eu(III) and Tb(III) ligand exchange rates are on a time scale of NMR range. This method allows the study of faster exchange kinetics of Sm(III) and Dy(III) which have a shorter life time for the excited states. The complexes of Eu(III) with ligands like dipicolinate (DPA), oxidiacetate (ODA), iminodiacetate (IDA), and 1,2-diaminocyclohexane tetraacetate (DCTA) have been studied. The following reactions were investigated.



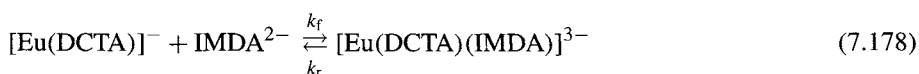
The exchange rate of DPA is slow with distinct  ${}^5\text{D}_0 \leftarrow {}^7\text{F}_0$  transitions and life times of  $[\text{Eu}(\text{DPA})]^+$  and  $[\text{Eu}(\text{DPA})_2]^-$  are 0.169 and 0.304 ms, respectively.

The rapid exchange of oxidiacetate between  $[\text{Eu}(\text{ODA})]^-$  and  $[\text{Eu}(\text{ODA})_2]^+$



also has two transitions  ${}^5\text{D}_0 \leftarrow {}^7\text{F}_0$  but with identical life times (0.248 ms). The lifetimes of  $[\text{Eu}(\text{ODA})]^+$  and  $[\text{Eu}(\text{ODA})_2]^-$  determined from a plot of  $\tau_F^{-1}$  vs intensity, I of  ${}^5\text{D}_0 \leftarrow {}^7\text{F}_0$  the excitation band are 7.20 and 2.83 ms, respectively.

The studies on the equilibrium by luminescence method



yielded lifetimes for  $[\text{Eu}(\text{DCTA})]^-$  and  $[\text{Eu}(\text{DCTA})(\text{IMDA})]^{3-}$  of 0.320 ms and 0.805 ms, respectively, with  $k_f = 1.6 \times 10^7 \text{ M}^{-1} \text{ s}^{-1}$  and  $k_r = 2.6 \times 10^3 \text{ s}^{-1}$ . Dissociation rate constants of some lanthanide complexes are given in Table 7.30.

## 42. Energy transfer from lanthanide ions

Chiral recognition techniques have been used in photoinduced electron transfer reactions and the differential formation of homochiral against heterochiral exciplexes. In the systems studied excited states of lanthanide complexes are quenched by transition metal complexes. The complexes with trigonal dihedral ( $\text{D}_3$ ) symmetry which can exist as enantiomers with either left handed ( $\wedge$ ) or right-handed ( $\Delta$ ) configurational chirality are chosen. The system consists of a mixture of racemic lanthanide complex and optically resolved

TABLE 7.30  
Dissociation rate constants of excited complexes of Ln(III) ions.

Ligand	Ln(III)	Solvent	$K_{\text{diss}}$ ( $\text{s}^{-1}$ )	Mechanism
1,10-phenanthroline	Eu	D <sub>2</sub> O	$2.7 \times 10^3$	Dissociative
2,2'-bipyridyl	Eu	D <sub>2</sub> O	$2.2 \times 10^4$	Dissociative
1-naphthoate	Eu	CD <sub>3</sub> OD-D <sub>2</sub> O (3:1)	$5.5 \times 10^5$	
	Sm	CD <sub>3</sub> OD-D <sub>2</sub> O (3:1)	$6.3 \times 10^5$	
	Sm	D <sub>2</sub> O	$4.4 \times 10^6$	Associative
Salicylate	Tb	D <sub>2</sub> O	$7.6 \times 10^9$ <sup>a</sup>	Acid catalysis
5-sulfosalicylate	Tb	D <sub>2</sub> O	$7.9 \times 10^9$ <sup>a</sup>	Acid catalysis
	Dy	D <sub>2</sub> O	$8.5 \times 10^9$ <sup>a</sup>	Acid catalysis

<sup>a</sup>Second-order rate constants in  $\text{s}^{-1} \text{M}^{-1}$ .

transition metal complex. On excitation of the lanthanide complex by unpolarized light, the lanthanide luminescence can be monitored for chiroptical activity as a function of time [132]. A typical system consists of  $[\text{Tb}(\text{dpa})_3]^{3-}$  and  $[\text{Ru}(\text{phen})_3]^{3+}$ . The rate constant for the differential excited state quenching reaction can be obtained from the differential emission of left and right circularly polarized light and the time dependence of the chiroptical luminescence. A series of pairs of complexes with different spectroscopic features have been studied, and variations in total achiral quenching rates and differential chiral discriminatory quenching rates have been observed. The structural and energetic factors have been found to play an important role.

## References

- [1] I. Amdur, G.G. Hammes, *Chemical Kinetics*, McGraw-Hill, New York, 1966.
- [2] C.H. Langford, *J. Chem. Educ.* **46**, 557, 1969.
- [3] C.H. Langford, H.B. Gray, *Ligand Substitution Processes*, W.A. Benjamin, New York, 1966.
- [4] A. Werner, *Ber.* **45**, 121, 1912.
- [5] R.M. Fuoss, *J. Am. Chem. Soc.* **80**, 5059, 1958.
- [6] M. Eigen, *J. Pure Appl. Chem.* **6**, 97, 1963.
- [7] C.H. Langford, W.R. Muir, *J. Am. Chem. Soc.* **89**, 3141, 1967.
- [8] A. Elder, S. Petrucci, *Inorg. Chem.* **9**, 19, 1970.
- [9] Investigation of Rates and Mechanisms of reactions, ed. C.F. Bernasconi, 4<sup>th</sup> edn., Vol. VI, Part II, *Techniques of Chemistry*, Wiley-Interscience, New York, 1986.
- [10] H.S. Gutowsky, D.W. McCall, C.P. Schlichter, *J. Chem. Phys.* **21**, 279, 1953.
- [11] H.M. McConnell, *J. Chem. Phys.* **28**, 430, 1958.
- [12] H.M. McConnell, S.B. Berger, *J. Chem. Phys.* **27**, 230, 1957.
- [13] C.F. Bernasconi, *Relaxation Kinetics*, Academic Press, New York, 1976.
- [14] E.L. King, *J. Chem. Edu.* **56**, 580, 1979.
- [15] H.B. Silber, J.H. Swinehart, *J. Phys. Chem.* **71**, 4344, 1967.
- [16] H.B. Silber, R.D. Farina, J.H. Swinehart, *Inorg. Chem.* **8**, 819, 1969.
- [17] A. Graffeo, J.L. Bear, *J. Inorg. Nucl. Chem.* **30**, 1577, 1968.
- [18] M. Eigen, K. Tamm, *Z. Electrochem.* **66**, 93, 107, 1962.
- [19] R. Fuoss, *J. Am. Chem. Soc.* **80**, 5059, 1958.
- [20] M. Eigen, *Z. Elektrochem.* **64**, 115, 1960.
- [21] G. Geier, *Ber. Bunsenges. Phys. Chem.* **69**, 617, 1965.
- [22] N. Purdie, C.A. Vincent, *Trans. Farad. Soc.* **63**, 2745, 1967.
- [23] M. Eigen, L. DeMaeyer, *Technique of Organic Chemistry*, Vol. VIII, Part 2, Chap. 18, Interscience, New York.
- [24] G. Atkinson, S.K. Kor, *J. Phys. Chem.* **69**, 128, 1965.
- [25] J. Steuhr, E. Yeager, *Physical Acoustics*, ed. Mason, Acad. Press, NY, 1965.

- [26] J.C.G. Bunzli, D. Wessner, *Coord. Chem. Rev.* **60**, 191, 1984.
- [27] R.D. Shannon, *Acta Cryst.* **A32**, 751, 1976.
- [28] J.C.G. Bunzli, C. Mabillard, *Inorg. Chem.* **25**, 2750, 1986.
- [29] E. Brucher, J. Glaser, I. Grenthe, I. Puigdomenech, *Inorg. Chim. Acta* **109**, 111, 1985.
- [30] J.C.G. Bunzli, A.E. Merbach, R.M. Nielson, *Inorg. Chim. Acta* **139**, 151, 1987.
- [31] D.L. Pisaniello, A.E. Merbach, *Helv. Chim. Acta* **65**, 573, 1982.
- [32] L.N. Lugina, N.K. Davidenko, L.N. Zabolina, K.B. Yatsimirskii, *Russ. J. Inorg. Chem.* **19**, 1456, 1974.
- [33] D.L. Pisaniello, P.J. Nichols, Y. Ducommun, A.E. Merbach, *Helv. Chim. Acta* **65**, 1025, 1982.
- [34] D.L. Pisaniello, L. Helm, P. Meier, A.E. Merbach, *J. Am. Chem. Soc.* **105**, 4528, 1983.
- [35] T.J. Swift, R.E. Connick, *J. Chem. Phys.* **37**, 307, 1962.
- [36] A.E. Merbach, *Pure Appl. Chem.* **54**, 1479, 1982; **59**, 167, 1987.
- [37] R.J. Fuoss, *J. Am. Chem. Soc.* **80**, 5059, 1958.
- [38] S.F. Lincoln, *Adv. Inorg. Bioinorg. Mechanisms* **4**, 217, 1986.
- [39] J. Glaser, G. Johansson, *Acta Chem. Scand.* **A35**, 639, 1981.
- [40] R.D. Rogers, L.K. Kurihara, *Inorg. Chim. Acta* **130**, 131, 1987.
- [41] R.D. Rogers, *Inorg. Chim. Acta* **133**, 347, 1987.
- [42] E.D. Rogers, L.K. Kurihara, *Inorg. Chim. Acta* **116**, 171, 1986.
- [43] R.D. Rogers, E.J. Voss, *Inorg. Chim. Acta* **133**, 181, 1987.
- [44] R.D. Rogers, *J. Coord. Chem.* **16**, 415, 1988.
- [45] J. Harrowfield, D.L. Kepert, J.M. Partick, A. White, *Aust. J. Chem.* **36**, 483, 1983.
- [46] J. Albertson, I. Elding, *Acta Cryst.* **B33**, 1460, 1977.
- [47] L. Helmholz, *J. Am. Chem. Soc.* **61**, 1544, 1939.
- [48] C.O. PaivaSantos, E.E. Castellano, L.C. Machado, G. Vincentini, *Inorg. Chim. Acta* **110**, 83, 1985.
- [49] S.K. Sikka, *Acta Cryst.* **A25**, 621, 1969.
- [50] R.W. Broach, J.M. Williams, G.P. Felcher, D.G. Hincks, *Acta Cryst.* **B 35**, 2317, 1979.
- [51] C.R. Hubbard, C.O. Quicksall, R.A. Jacobson, *Acta Cryst.* **B 30**, 2613, 1974.
- [52] D. Fitzwater, R.E. Rundle, *Z. Kristallogr.* **112**, 362, 1959.
- [53] F.H. Spedding, M.J. Pikal, B.O. Ayers, *J. Phys. Chem.* **70**, 2440, 1966.
- [54] T.W. Swaddle, *Adv. Inorg. Bioinorg. Mechanisms* **2**, 95, 1983.
- [55] A. Habenschuss, F.H. Spedding, *J. Chem. Phys.* **70**, 2797, 1979; **70**, 3758, 1979; **73**, 442, 1980.
- [56] L.S. Smith, D.L. Wertz, *J. Am. Chem. Soc.* **97**, 2365, 1975; **98**, 4424, 1976; *Inorg. Chem.* **16**, 1225, 1977.
- [57] G. Johansson, H. Wakita, *Inorg. Chem.* **24**, 3047, 1985.
- [58] C. Cossy, A.E. Merbach, *Pure Appl. Chem.* **60**, 1785, 1988.
- [59] W. Dew Horrocks, Jr., D.R. Sudnik, *J. Am. Chem. Soc.* **101**, 334, 1979.
- [60] S.P. Sinha, *NATO ASI Series*, **C109**, 451, 1970.
- [61] K. Miyakawa, Y. Kaizu, H. Kobayashi, *J. Chem. Soc. Farad. Trans* **184**, 1517, 1988.
- [62] J. Reuben, D. Fiat, *J. Chem. Phys.* **51**, 4918, 1969.
- [63] C. Cossy, L. Helm, A.E. Merbach, *Inorg. Chem.* **27**, 1973, 1988; *Inorg. Chim. Acta* **139**, 147, 1989.
- [64] G.S. Darbani, F. Fittipaldi, S. Petrucci, P. Hemmes, *Acustica* **25**, 125, 1971.
- [65] M.M. Farrow, N. Purdie, E.M. Eyring, *Inorg. Chem.* **13**, 2024, 1974.
- [66] K.B. Yatsimirskii, L.I. Budarin, *Coordination Chemistry*, Vol. 2, ed. A.E. Martell, ACS Monograph, 174, Chap. 1, pp. 1–194, 1978.
- [67] T.E. Eriksen, I. Grenthe, I. Puigdomenech, *Inorg. Chim. Acta* **121**, 63, 1986.
- [68] T.E. Eriksen, I. Grenthe, I. Puigdomenech, *Inorg. Chim. Acta* **126**, 131, 1987.
- [69] D. Fay, D. Litchinski, N. Purdie, *J. Phy. Chem.* **73**, 544, 1969.
- [70] V.L. Garza, N. Purdie, *J. Phys. Chem.* **74**, 275, 1970; R. Garnsey, D.W. Edbon, *J. Am. Chem. Soc.* **91**, 50, 1969.
- [71] H.B. Siiber, N. Scheinin, G. Atkinson, J.J. Gresek, *J. Chem. Soc. Farad. Trans. I* **68**, 1200, 1972.
- [72] M. De Jonghe, W. D'Olieslager, *Inorg. Chim. Acta* **109**, 7, 1984.
- [73] V. Chandrasekhar, C. Allan Chang, *Inorg. Chem.* **25**, 2061, 1986.
- [74] C.G. Ekstrom, L. Nilsson, I. Grenthe, *Inorg. Chim. Acta* **48**, 145, 1981.
- [75] C.G. Ekstrom, L. Nilsson, I.A. Duncan, I. Grenthe, *Inorg. Chim. Acta* **40**, 91, 1980.
- [76] M. Furrer, *Kinetik Von Schnellen Mischkomplexreaktionen der seltenen Erden Diss. Eidgenossischen Technischen Hochschule Zurich*, 1974.

- [77] K. Neelakantan, R.E. Jervis, *Inorg. Nucl. Chem. Letters* **7**, 131, 1971; *Can. J. Chem.* **52**, 1086, 1974.
- [78] S. Aime, M. Botto, S.G. Crich, G. Giovenzana, R. Pagliarin, M. Sisti, E. Terreno, *Magnetic Resonance in Chemistry* **36**, S200, 1998.
- [79] H. Lammers, F. Maton, D. Pubanz, M.W. Van Laren, H. Van Bekkum, A.E. Merbach, R.N. Muller, J.A. Peters, *Inorg. Chem.* **36**, 2527, 1997.
- [80] Z. Chen, L. Mercier, J.J. Tunney, C. Detel-lier, NATO ASI series, Series C, Mathematical and Physical Sciences, *Physical Supramolecular Chemistry*, eds L. Echevoyen, A.E. Kaifer, pp. 393–411, 1996.
- [81] O.G. Khelevina, A.A. Voinov, *Russ. J. General Chemistry* **70**, 778, 2000.
- [82] S. Petricek, A. Demsar, L. Golic, J. Kosmrlj, *Polyhedron* **19**, 199, 2000.
- [83] G. Ma, H. Freiser, S. Muralidharan, *Anal. Chem.* **69**, 2827, 1997.
- [84] D.H. Huchital, H.G. Brittain, L.K. Beutelman, X. Yang, *Inorg. Chim. Acta* **95**, 127, 1984.
- [85] R.G. Wilkins, *Kinetics and Mechanism of Reactions of Transition Metal Complexes*, VCH, Weinheim, 1991.
- [86] V. Ramachandra Rao, *ASTM Special Technical Publication*, 997, 1988.
- [87] V. Pocol, L. Patron, O. Carp, M. Brezeanu, E. Segal, N. Stanica, D. Crisan, *J. Thermal Analysis and Calorimetry* **55**, 143, 1999.
- [88] M. Nair, K. Muraleedharan, P.K. Radhakrishnan, *Thermochim. Acta* **292**, 115–122, 1997.
- [89] M. Zalewicz, *Thermochim. Acta* **149**, 133–140, 1989.
- [90] Z.L. Wang, C.J. Niu, Z.H. Liu, J.Z. Ni, *Thermochim. Acta* **282/283**, 353–358, 1996.
- [91] K. Kustin, J. Swinehart, *Prog. Inorg. Chem.* **13**, 107, 1970.
- [92] C.K. Jorgensen, J.S. Brinen, *Mol. Phys.* **6**, 629, 1963.
- [93] B.D. Blaustein, J.W. Gryder, *J. Am. Chem. Soc.* **79**, 540, 1957.
- [94] E. Wadsworth, F.R. Duke, C.A. Goetz, *Anal. Chem.* **29**, 1824, 1957.
- [95] F.A. Cotton, G. Wilkinson, *Advanced Inorg. Chemistry*, 5<sup>th</sup> edn, p. 956, Wiley, New York, 1988.
- [96] D.L. Douglas, D.M. Yost, *J. Chem. Phys.* **18**, 1687, 1950; D.D. David, K.L. Stevenson, G.K. King, *Inorg. Chem.* **74**, 2558, 1977.
- [97] Y. Haas, G. Stein, M. Tomkiewicz, *J. Phys. Chem.* **74**, 2558, 1970.
- [98] J. Donohue, *J. Chem. Phys.* **67**, 5402, 1977.
- [99] R.A. Sheldon, J.K. Kochi, *J. Am. Chem. Soc.* **90**, 6688, 1968.
- [100] L.J. Heidt, M.E. Smith, *J. Am. Chem. Soc.* **70**, 2746, 1948.
- [101] L.J. Heidt, A.F. McMillan, *J. Am. Chem. Soc.* **76**, 2135, 1954; *Science* **117**, 75, 1953.
- [102] M.G. Evans, N. Uri, *Nature* **166**, 602, 1950.
- [103] P.N. Moorthy, J.J. Weiss, *J. Chem. Phys.* **42**, 3127, 1965.
- [104] T.J. Sworski, *J. Am. Chem. Soc.* **77**, 3655, 1957.
- [105] T.W. Martin, R.E. Rummell, R.C. Cross, *J. Am. Chem. Soc.* **86**, 2595, 1964.
- [106] T.W. Martin, L.L. Swift, J.H. Venable, *J. Chem. Phys.* **52**, 2138, 1970.
- [107] L. Dogliotti, E. Hayon, *J. Phys. Chem.* **71**, 3802, 1967.
- [108] R.A. Sheldon, J.F. Kochi, *J. Am. Chem. Soc.* **90**, 6688, 1968; *ibid.* **88**, 1097, 1966.
- [109] D. Greatorex, T.J. Kemp, *Trans. Farad. Soc.* **67**, 1576, 1971; **68**, 121, 1972.
- [110] T. Donohue, *J. Am. Chem. Soc.* **100**, 7411, 1978.
- [111] H.G. Brittain, *J. Phys. Chem.* **84**, 840, 1980.
- [112] W.M. Watson, R.P. Zerger, J.T. Yardley, G.D. Stucky, *Inorg. Chem.* **14**, 2675, 1975.
- [113] N. Sabbatini, M. Guardigli, J.M. Lehn, *Coord. Chem. Rev.* **123**, 201, 1993.
- [114] H. Takalo, E. Hanniner, J. Kankare, *Helv. Chim. Acta* **76**, 877, 1993.
- [115] V.M. Mukkala, M. Kwiatkowski, J. Kankare, *Helv. Chim. Acta* **76**, 893, 1993.
- [116] V.M. Mukkala, M. Helenius, I. Hemmila, J. Kankare, H. Takalo, *Helv. Chim. Acta* **76**, 1361, 1993.
- [117] S. Wang, Q. Luo, Y. Zhan, Z. Heng, *Polyhedron* **12**, 1939, 1993.
- [118] N. Sabbatini, M. Guardigli, F. Bolletta, I. Manet, R. Ziessel, *New J. Chem.* **17**, 323, 1993.
- [119] R.E. Hemingway, S.M. Park, A.J. Bard, *J. Am. Chem. Soc.* **97**, 200, 1975.
- [120] E.H. White, P.D. Wildes, J. Wiecko, H. Doshan, C.C. Wei, *J. Am. Chem. Soc.* **95**, 7050, 1973.
- [121] W. Dew Horrocks, Jr., F. Schmidt, D.R. Sudnick, C. Kittrell, R.A. Bernheim, *J. Am. Chem. Soc.* **99**, 2378, 1977.
- [122] J.F. Kropp, M.W. Windor, *J. Chem. Phys.* **39**, 2769, 1963; **42**, 1599, 1965.
- [123] R.C. Holz, G.E. Meister, W. Dew Horrocks, Jr., *Inorg. Chem.* **29**, 5183, 1990.
- [124] J.R. Escabi-Perez, F. Nome, J.H. Fendler, *J. Am. Chem. Soc.* **99**, 7749, 1977.
- [125] F. Greiser, *J. Phys. Chem.* **85**, 928, 1981.
- [126] M. Alongren, F. Greiser, J.K. Thomas, *J. Am. Chem. Soc.* **101**, 2021, 1979.



- [127] G.D. Correll, R.N. Cheser, F. Nome, J.H. Fendler, *J. Am. Chem. Soc.* **100**, 1254, 1978.
- [128] R.B. Mickelsen, D.F.H. Wallach, *Biochim. Biophys. Acta* **433**, 674, 1976.
- [129] W. Dew Horrocks, Jr., M. Albin, *Prog. Inorg. Chem.* **31**, 1, 1983.
- [130] V.L. Eromolaev, V.P. Gruzdev, *Inorg. Chim. Acta* **95**, 179, 1984.
- [131] W. Dew Horrocks, Jr., V.K. Arkle, F.J. Liotta, D.R. Sudnick, *J. Am. Chem. Soc.* **105**, 3455, 1983.
- [132] D.H. Metcalf, S.W. Snyder, J.N. Demas, F.S. Richardson, *J. Am. Chem. Soc.* **112**, 5681, 1990.

chapter 8

---

SPECTROSCOPY OF LANTHANIDE  
COMPLEXES

---

---

# CONTENTS

---

1. Atomic theory . . . . .	572
2. Brief history of lanthanide crystal field theory . . . . .	575
2.1. Cubic point symmetry . . . . .	582
2.2. Hexagonal point symmetry . . . . .	583
3. Methods for determining crystal-field levels . . . . .	583
3.1. Miscellaneous methods . . . . .	589
4. Angular overlap model (AOM) . . . . .	589
5. Nephelauxetic effect . . . . .	593
6. Nephelauxetic series . . . . .	594
7. The intensities of intra 4f-4f transitions . . . . .	595
8. Judd-Ofelt theory . . . . .	596
9. Covalency model of hypersensitivity . . . . .	600
10. Role of symmetry . . . . .	604
11. Judd-Ofelt theory of hypersensitivity . . . . .	605
12. Dynamic coupling mechanism . . . . .	607
13. Absorption spectra of lanthanide ions . . . . .	610
14. Trivalent cerium . . . . .	613
15. Trivalent praseodymium . . . . .	614
16. Trivalent neodymium . . . . .	614
17. Trivalent promethium . . . . .	619
18. Trivalent samarium . . . . .	619
19. Trivalent europium . . . . .	619
20. Trivalent gadolinium . . . . .	624
21. Trivalent terbium . . . . .	624
22. Trivalent dysprosium . . . . .	625
23. Trivalent holmium . . . . .	627
24. Trivalent erbium . . . . .	627
25. Trivalent thulium . . . . .	632
26. Trivalent ytterbium . . . . .	632
27. Spectra of divalent lanthanides . . . . .	634
28. Some salient features of the absorption spectra of lanthanide complexes in solutions . . . . .	635
29. Determination of coordination number . . . . .	644
30. Study of chemical equilibria . . . . .	644
31. Structure of complexes . . . . .	645

32. Absorption spectra in aqueous media . . . . .	646
33. Absorption spectra in nonaqueous media . . . . .	647
34. Lanthanide complexes with carboxylic acids . . . . .	650
35. Oxydiacetate complexes . . . . .	651
36. Lanthanide alkoxides . . . . .	653
37. Lanthanide $\beta$ -diketonates . . . . .	653
38. Lanthanide complexes with nucleic acids . . . . .	656
39. Lanthanide complexes with nitrogen donor ligands . . . . .	659
40. Lanthanide amino acid complexes . . . . .	659
41. Lanthanide aminocarboxylate complexes . . . . .	660
42. Lanthanide diol complexes . . . . .	660
43. Miscellaneous complexes . . . . .	661
44. Energy levels of $f^2$ and $f^1$ configurations . . . . .	661
45. $f^2$ configuration . . . . .	662
45.1. Electron-repulsion perturbation . . . . .	662
45.2. Spin-orbit interaction perturbation . . . . .	668
45.3. The crystalline field perturbation . . . . .	676
45.4. Fitting of the crystalline field levels . . . . .	704
46. $f^1$ configuration . . . . .	706
46.1. Crystalline field of $D_{3h}$ symmetry . . . . .	707
46.2. Calculation of crystal field energies . . . . .	709
References . . . . .	710
Appendix . . . . .	717

The lanthanide series of elements differ from the transition metal series in that 4f shell inner electrons are shielded by the 5s<sup>2</sup>, 5p<sup>6</sup> closed shells. Consequently f shell electrons interact much less strongly with their environment than the d electrons in the transition series. The radial charge density for Pr<sup>3+</sup> is shown in Fig. 8.1. The electronic structure of the f<sup>n</sup> lanthanide ion is dominated by many different interactions than for more familiar d<sup>n</sup> transition metal ions.

### 1. Atomic theory

In the case of  $N$  electron atom with a nuclear charge  $Ze$ , where  $e$  is the charge on the electron,  $Z$  the atomic number, the non-relativistic Hamiltonian  $H$  may be written as

$$H = \sum_{i=1}^N \frac{p_i^2}{2m} - \sum_{i=1}^N \frac{Ze^2}{r_i} + \sum_{i<j}^N \frac{e^2}{r_{ij}} \quad (8.1)$$

with the assumption that the nuclear mass is infinite. The first term in equation (8.1) represents the kinetic energy of all the electrons, the second term the potential energy of all the electrons in the electric field of the nucleus, and the third term the repulsive coulomb potential between pairs of electrons. In order to solve equation (8.1) it is necessary to use central field approximation which assumes that: (i) each electron moves independently and (ii) each electron is moving in a spherically symmetric field or potential,  $-U(r_i)/e$ .

The central field Hamiltonian  $H_{CF}$  can be written as

$$H_{CF} = \sum_{i=1}^N \left[ \frac{p_i^2}{2m} + U(r_i) \right] \quad (8.2)$$

The central field Hamiltonian leads to the Schrödinger equation which can be solved in polar coordinates with wave functions having the form

$$\psi = r^{-1} R_{nl}(r) Y_{l_z}(\Theta, \phi) \quad (8.3)$$

The wave functions are products of radial function  $R_{nl}(r)$  and spherical harmonics  $Y_{l_z}(\Theta, \phi)$  and the energy levels are highly degenerate. The energy levels are labeled by the principal quantum number,  $n$  and the orbital quantum number  $l$ . This degeneracy is removed by perturbation effects. The properties of the electrons in an unfilled shell only are considered since electrons in filled subshells do not contribute to the electronic structure of the low-lying levels.

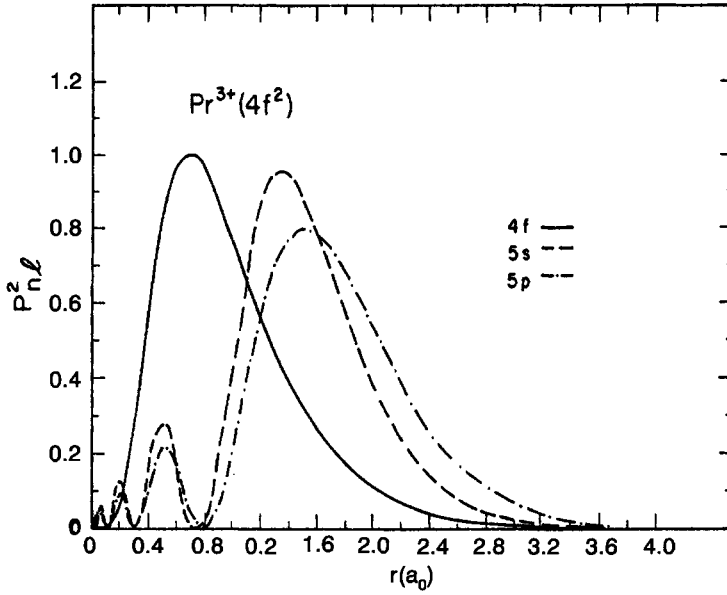


Fig. 8.1. Radial charge density for  $\text{Pr}^{3+}$ .

For f electrons, the significant perturbation is the resultant obtained by subtracting equation (8.2) from (8.1).

$$H - H_{\text{CF}} = \sum_{i=1}^N \left[ -\frac{Ze^2}{r_i} - U(r_i) \right] + \sum_{i<j}^N \frac{e^2}{r_{ij}} \quad (8.4)$$

The first summation term shifts all the levels in a given electron configuration equally and hence of no consequence. The second term

$$H_1 = \sum_{i<j}^N \left( \frac{e^2}{r_{ij}} \right) \quad (8.5)$$

represents the electrostatic coulomb repulsion between pairs of electrons.

Now we introduce the operators

$$L = \sum_i l_i \quad \text{and} \quad S = \sum_i s_i, \quad (8.6)$$

where  $l_i$  and  $s_i$  are orbital and spin angular momentum operators of the  $i^{\text{th}}$  electron.  $H_1$  is diagonal in  $L$  and  $S$  enabling the labeling of eigen states with eigen values  $L$  and  $S$  in the form  $2S+1L$  which is known as Russell-Saunders or  $L_i, S$  coupling. In order to allow for

relativistic corrections in the Hamiltonian, let us introduce  $H_2$ , the spin-orbit interaction

$$H_2 = \sum_i \xi(r_i) s_i l_i \quad \text{or} \quad H_2 = \zeta_{nl} S \cdot L \quad (8.7)$$

$$\text{where} \quad \xi(r) = \frac{\hbar^2}{2m^2 c^2 r} \frac{dU}{dr} \quad \text{and} \quad \zeta_{nl} = \int_0^\infty R_{nl}^2 \xi(r) dr$$

The spin-orbit interaction becomes more important as  $Z$  increases. The spin-orbit interaction is diagonal in  $J$ , where  $J = L + S$ . The  $^{2S+1}L$  multiplet is split into levels labeled by their  $J$  eigen values; for example

$$J = |L + S|, |L + S - 1|, \dots, |L - S|,$$

where each  $J$  level has a degeneracy of  $2J + 1$ . The interaction  $H_2$  will couple  $^{2S+1}L$  states whose values of  $S$  and  $L$  differ by not more than one.

If we consider a metal ion in a complex surrounded by ligands and assume that the ion is involved in purely electrostatic interactions with its surrounding ligands, we then have

$$H_3 = -e \sum_i Y(r_i, \Theta_i, \phi_i), \quad (8.8)$$

where the summation extends over all the electrons of the central metal ion and the term  $Y(r, \Theta, \phi)$  is the potential at the central ion from the surrounding ligands. On expansion of the potential in a series of spherical harmonies we have

$$H_3 = \sum_{i,k,q} D_k^q(r_i^k) Y_k^q(\Theta_i, \phi_i) \quad (8.9)$$

The number of terms that have to be considered in this series depends on the symmetry. The ligand field perturbation lifts the  $2J + 1$  degeneracy of a particular  $J$  level and the eigen values of the operator  $J_z$  are required to label the states.

The next perturbation to consider is the Zeeman operator

$$H_4 = \beta(L + 2S) \cdot H \quad (8.10)$$

The Zeeman operator (8.10) can be replaced by

$$H_4 = g_J \beta H \cdot J, \quad (8.11)$$

where  $g_J$  is the Landé  $g$  value which depends on  $L$ ,  $S$ , and  $J$ ,  $H$  is the external magnetic field and  $\beta$  is the Bohr magneton. This aspect is useful in understanding the results obtained by magnetic susceptibility and electron paramagnetic resonance.

The effects of the three perturbation Hamiltonians  $H_1$ ,  $H_2$  and  $H_3$  on the energy levels of a  $f^2$  electron configuration are shown in Fig. 8.2.

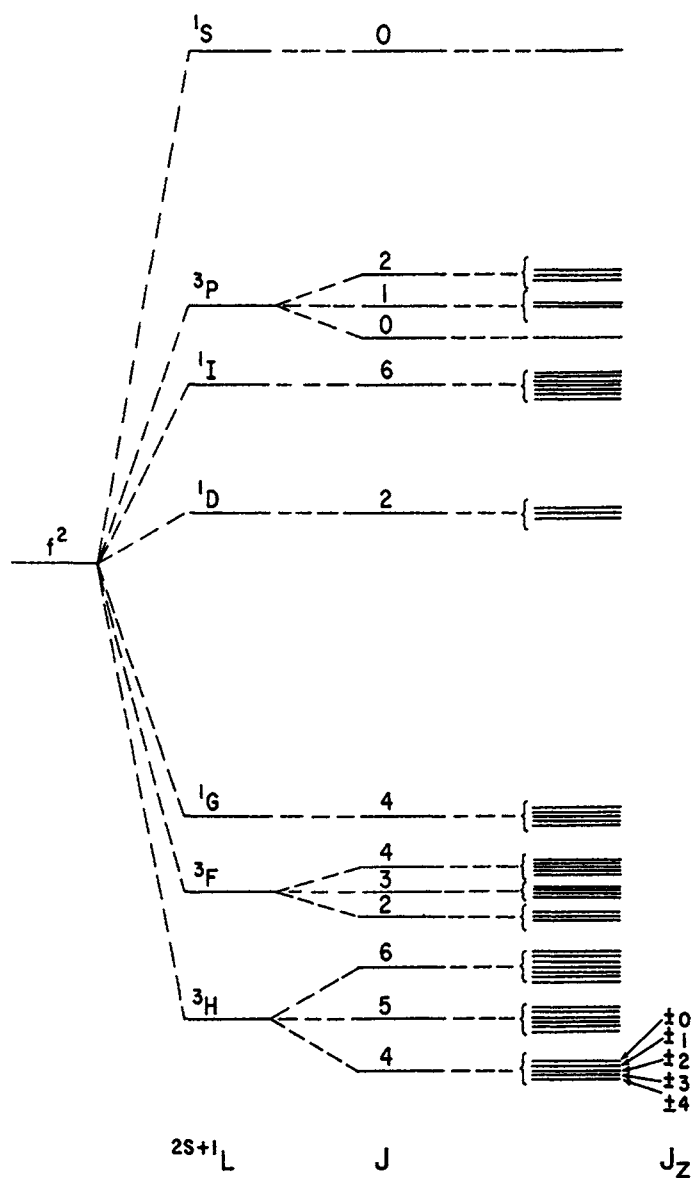


Fig. 8.2. Energy levels of the  $f^2$  configuration with the perturbation  $H_1$ ,  $H_2$ , and  $H_3$  applied successively.

## 2. Brief history of lanthanide crystal field theory

The birth of crystal field theory is due to Bethe who in 1929 showed that open-shell energy levels in a crystalline environment could be associated with the irreducible representation labels of the site point group. Little experimental work was done at that time because



obtaining pure rare earth salts and observing sharp spectra at low temperatures were difficult. However, the optical spectral transitions in trivalent lanthanides were identified as transitions within the 4f configuration by Freed in 1931. But the question remained as to why transitions should be observed between levels for which electric dipole transitions are forbidden. In fact Van Vleck referred to the lanthanide spectra as a 'puzzle' in 1937.

Lack of basic techniques for treatment of atomic spectra coupled with the fact that lanthanide crystal fields appear as small perturbations on the free ion levels hampered the developments of crystal field theory. Condon and Shortely provided the basic techniques for treating atomic spectra in 1935. These techniques were tedious for systems with more than two electrons. Then Racah came to the rescue in 1942 by developing techniques involving the use of non-symmetry continuous (Lie) groups to obtain a virtually complete classification of the states of  $f^n$  configurations. Racah's work has been significant in interpreting optical spectra of lanthanides as well as some consequences in nuclear theory and theory of elementary particles. Experimental work on obtaining good optical spectra of atoms with open shell ions in crystals by Hellwege in 1947 and Bleaney's contributions on lanthanides were the next significant advances. Using Wigner–Eckart theorem, Stevens simplified the problem of evaluating matrix elements of the crystal field potential in 1952. This was followed by first calculations of lanthanide crystal field parameters using electron spin resonance and magnetic susceptibility (Stevens, 1952–53). Later optical spectra were used to obtain crystal field parameters by Judd in 1955. The first intermediate coupling determination of crystal field parameters was done by Judd in 1957.

At about the same time, Dieke developed and published optical spectra of lanthanides in 1956. After 1960 the raw data were converted into crystal field parameters by the methods developed by Stevens, Elliot and Judd. This was followed by a large body of data on crystal field parameters derived from optical spectra of lanthanides from all parts of the world. The crystal field Hamiltonian as given in equation (8.9) for an f electron is

$$H_3 = \sum_{i,k,q} D_k^q(r_i^j) Y_k^q(\Theta, \phi) \quad (8.12)$$

The value of  $k$  is limited to  $k \leq 2l$ , where  $l$  is the orbital angular momentum of the electrons. For f electrons  $k \leq 6$ ;  $k$  must also be even based on parity of the matrix elements involved in the crystal field potential. Thus  $k = 2, 4$  or  $6$  for f electrons. Allowed values of  $q$  have to follow the rule  $|q| \leq k$ . Any further restrictions on  $q$  are dependent on the symmetry of the ligand field. When the highest symmetry axis on the quantization axis contains an  $n$ -fold rotation axis then  $|q| = \lambda n, \lambda, 0, 1, 2 \dots$ . When  $q$  is non-zero, then only  $J_z$  eigen states with eigen values that differ by  $\pm q$  can be mixed by the crystal field interaction. For a molecule with  $C_8$  axis only  $q = 0$  allowed. Then the non-zero crystal field parameters are  $D_2^0, D_4^0$  and  $D_6^0$ . Assuming that  $D_2^0 \gg D_4^0$  or  $D_6^0$ , the energy levels of the  $f^1$  system can be determined.

Stevens [4] developed an operator-equivalent method for evaluating crystal field matrix elements based on the Wigner–Eckart theorem. It was shown that within a particular  $J$  (or  $L$ ) manifold all operators of the same rank have matrix elements which are proportional to one another. The matrix elements of these operators along with proportionality constants for the ground terms of  $f^n$  ions have been tabulated [5].

TABLE 8.1

Matrix elements of the type  $\langle l, l_z | 0_k^0 | l, l_z \rangle$  for  $l = 3$  ( $l = 3$  for a single f electron) from Abragam and Bleaney. Each matrix element must be multiplied by  $(-2/45)A_2^0(r^2)$ .

$l_z$	0	$\pm 1$	$\pm 2$	$\pm 3$
0	-12	0	0	0
$\pm 1$	0	-9	0	0
$\pm 2$	0	0	0	0
$\pm 3$	0	0	0	15

The matrix element may be written as

$$\begin{aligned} \langle J, J_z | H_3 | J, J_z \rangle &= \sum_{k,q} D_k^q \langle r^k \rangle \langle J, J_z | y_k^q | J, J_z \rangle \\ &= \sum_{k,q} K_k A_k^q \langle r^k \rangle \langle J, J_z | 0_k^q | J, J_z \rangle, \end{aligned} \quad (8.13)$$

where  $0_k^q$  stands for the equivalent operators proportional to the spherical harmonic tensors of equation (8.12) with the proportionality constants  $K_k$  being  $\alpha$ ,  $\beta$  and  $\gamma$ , the second, fourth and sixth order operator equivalent factors. The  $A_k^q$  are treated as crystal field parameters.

The second order crystal field matrix elements for an  $f^1$  may now be evaluated. The equivalent operator is  $0_2^0 = 3J_z^2 - J^2$ . From the literature [5] we find  $J = 3$  or  $L = 3$  in this case and the  $L_z$  states are  $0, \pm 1, \pm 2, \pm 3$ . The matrix for this is shown in Table 8.1. From the literature [5] the second rank operator equivalent for an f electron is  $-2/45$ .

The energy levels are as follows:

$$\begin{aligned} E_{\pm 3} &= -\frac{2}{45} \times 15 \times A_2^0 \langle r^2 \rangle = -\frac{2}{3} A_2^0 \langle r^2 \rangle \\ E_{\pm 2} &= -\frac{2}{45} \times 0 \times A_2^0 \langle r^2 \rangle = 0 \\ E_{\pm 1} &= -\frac{2}{45} \times (-9) \times A_2^0 \langle r^2 \rangle = +\frac{2}{5} A_2^0 \langle r^2 \rangle \\ E_0 &= -\frac{2}{45} \times (-12) \times A_2^0 \langle r^2 \rangle = -\frac{8}{15} A_2^0 \langle r^2 \rangle \end{aligned} \quad (8.14)$$

The term  $\langle r^2 \rangle$  is the expectation value of the radial wavefunction. Since  $A_2^0$  and  $\langle r^2 \rangle$  are functions of radial wave functions, usually these parameters are empirically evaluated. The matrix elements and factors are dependent only on the angular parts of the wave functions and can be exactly evaluated.

The energy levels for  $l = 3$  with complete crystal field Hamiltonian given in equation (8.15) and literature data [5] with the notation  $A_k^0(r^k) = B_k^0$  come out to be (equa-

tion (8.16))

$$H_3 = \sum_{i,k=2,4,6} K_k A_k^0 \langle r^k \rangle_0^0(\Theta_i, \phi_i) \\ = \sum_i [\alpha A_2^0 \langle r^2 \rangle_0^0(\Theta_i, \phi_i) + \beta A_4^0 \langle r^4 \rangle_0^0(\Theta_i, \phi_i) + \gamma A_6^0 \langle r^6 \rangle_0^0(\Theta_i, \phi_i)] \quad (8.15)$$

$$E_{l_z=0} = -12\alpha B_2^0 + 360\beta B_4^0 - 3600\gamma B_6^0 \\ E_{l_z\pm 1} = -9\alpha B_2^0 + 60\beta B_4^0 - 2700\gamma B_6^0 \\ E_{l_z\pm 2} = 0\alpha B_2^0 + 420\beta B_4^0 - 1080\gamma B_6^0 \\ E_{l_z\pm 3} = 15\alpha B_2^0 + 180\beta B_4^0 - 180\gamma B_6^0 \quad (8.16)$$

From the literature [5] for  $l = 3$  we have

$$(3\|\alpha\|3) = \frac{-2}{45} \\ (3\|\beta\|3) = \frac{2}{11 \times 45} \\ (3\|\gamma\|3) = \frac{-4}{11 \times 13 \times 27} \quad (8.17)$$

Thus we have the expressions for the energy levels

$$E_{l_z=0} = +\frac{8}{15} A_2^0 \langle r^2 \rangle + \frac{16}{11} A_4^0 \langle r^4 \rangle + \frac{1600}{3 \times 11 \times 13} A_6^0 \langle r^6 \rangle \\ E_{l_z\pm 1} = +\frac{2}{5} A_2^0 \langle r^2 \rangle + \frac{8}{33} A_4^0 \langle r^4 \rangle + \frac{400}{11 \times 13} A_6^0 \langle r^6 \rangle \\ E_{l_z\pm 2} = 0 - \frac{56}{33} A_4^0 \langle r^4 \rangle + \frac{1600}{11 \times 13} A_6^0 \langle r^6 \rangle \\ E_{l_z\pm 3} = -\frac{2}{3} A_2^0 \langle r^2 \rangle + \frac{8}{11} A_4^0 \langle r^4 \rangle - \frac{80}{3 \times 11 \times 13} A_6^0 \langle r^6 \rangle \quad (8.18)$$

The list of Stevens factors  $\alpha_j$ ,  $\beta_j$  and  $\gamma_j$  and  $\langle r^l \rangle$  for the trivalent rare earth ions as codified by Elliot [6] and Freeman [7] are given in Tables 8.2 and 8.3, respectively.

We will digress here and examine spin-orbit interaction  $H_2$  which is important for  $f^1$  configuration. The basis set  $l, l_z$  can be used to evaluate exactly the angular part of this interaction. The  $J, J_z$  basis set that is diagonal in  $J$  may be used to calculate the energy of the states. It is then possible to draw a correlation diagram which starts from the limit of strong spin-orbit interaction to the limit of strong crystal-field interaction. Such a correlation is shown in Fig. 8.3. An estimated value of chi for the lanthanides is about 0.2 or 0.3. The higher the value of chi, the higher is the probability of covalent interaction.

TABLE 8.2  
List of Steven's factors  $\alpha_j$ ,  $\beta_j$ ,  $\gamma_j$ , for the trivalent RE-ions (from Elliot, 1972) [6].

Ions	$\alpha_j \times 10^2$	$\beta_j \times 10^4$	$\gamma_j \times 10^6$
Ce	-5.71	63.5	0
Pr	-2.10	-7.35	61.0
Nd	-0.643	-2.91	-38.0
Pm	0.771	4.08	60.8
Sm	4.13	25.0	0
Tb	-1.01	1.22	-1.12
Dy	-0.635	-0.592	1.03
Ho	-0.222	-0.333	-1.30
Er	0.254	0.444	2.07
Tm	1.01	1.63	-5.60
Yb	3.17	-17.3	148.0

TABLE 8.3  
 $\langle r^l \rangle$  for the different trivalent RE-ions (from Freeman, 1972) [7].

Ions	$\langle r^2 \rangle$	$\langle r^4 \rangle$	$\langle r^6 \rangle$
Ce	1.200	3.455	21.226
Pr	1.086	2.822	15.726
Nd	1.001	2.401	12.396
Sm	0.883	1.897	8.775
Eu	0.938	2.273	11.670
Gd	0.785	1.515	6.281
Dy	0.726	1.322	5.102
Er	0.666	1.126	3.978
Yb	0.613	0.960	3.104

We have so far considered the single f electron case. Now we turn to the case of the unfilled 4f shell. We have already shown that the electrostatic potential  $V(r)$  which a 4f electron experiences due to a charge distribution  $\rho(r)$  of its surrounding is of the form

$$V(r) = \sum_{l,m} \gamma_{lm} r^l Y_l^m(\theta, \phi) \quad (8.19)$$

provided there is no overlap between the charge distribution and the 4f electron and fulfills Laplace's equation  $\Delta V(r) = 0$ . Equation (8.19) is an expansion in terms of multipoles of 4f electron. It is also assumed that the spherical harmonics  $Y_l^m(\Theta, \phi)$  are normalized to  $\int d\cos\theta d\phi |Y_l^m(\Theta, \phi)|^2 = 1$ . It is to be noted that the summation of potential is restricted  $l \leq 6$  since  $l_{4f} = 3$  and  $2l_{4f} = 6$ .

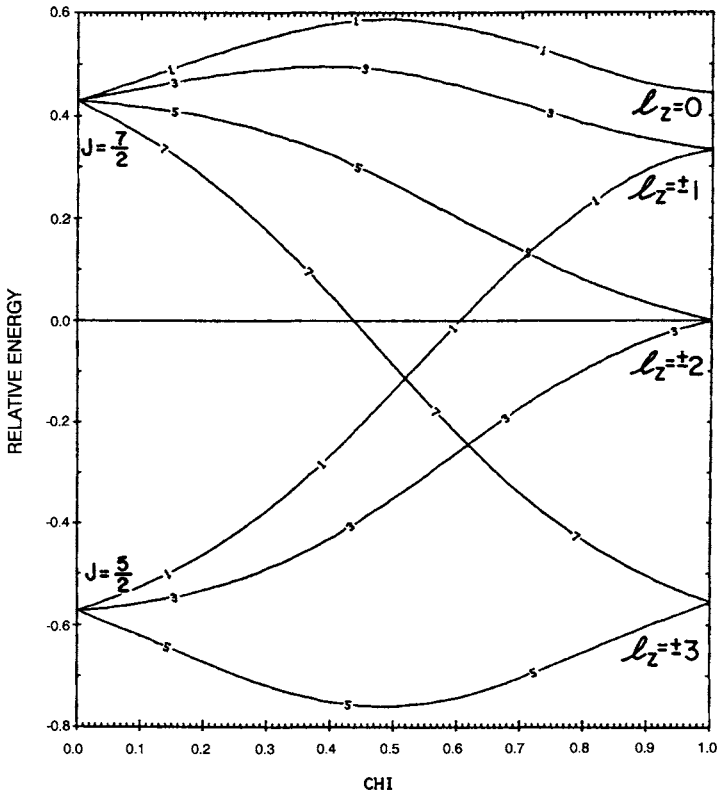


Fig. 8.3. Energy levels of the  $f^1$  configuration as a function of the relative strengths of the spin-orbit and crystal field interactions. For  $\chi = 0$ , only the spin-orbit interaction is considered; for  $\chi = 1$ , only the crystal field interaction is considered. The energy levels are numbered by  $2 \times J_z$ .

The potential  $V(r)$  may also be expanded in tesserial harmonics which has the advantage that the expansion is with respect to real functions. The expansion of  $V(r)$  in tesserial harmonics may be written as

$$V(r) = \sum_{l\alpha} \gamma_{l\alpha} r^l Z_{l\alpha}(\theta, \phi), \quad (8.20)$$

where the tesserial harmonics  $Z_{l\alpha}(\theta, \phi)$  are defined as

$$\begin{aligned} Z_{l0} &= Y_l^0, \\ Z_{lm}^c &= (2)^{-1/2} [Y_l^{-m} + (-1)^m Y_l^m] & Z_{lm}^s &= (2)^{-1/2} [Y_l^{-m} - (-1)^m Y_l^m] \end{aligned} \quad (8.21)$$

The subscript  $\alpha$  in equation (8.20) is such that for a given value of  $l$ ,  $Z_{l\alpha}$  spans over  $Z_{l0}$ ,  $Z_{lm}^c$ ,  $Z_{lm}^s$ . The  $Z_{l\alpha}$  and  $Y_l^m$  are tabulated in the literature [8]. The expansion coefficients  $Y_{l\alpha}$  are calculated from the charge distribution  $\rho(r)$

$$\gamma_{l\alpha} = \frac{4\pi}{2l+1} \int d^3r \frac{\rho(r)}{r^{l+1}} Z_{l\alpha}(\theta, \phi) \quad (8.22)$$

The point charge model is identified by assigning effective charges  $q_j$  to the neighboring sites of the lanthanide ion being considered. In such a case  $\rho(r)$  may be written as

$$\rho(r) = \sum_j q_j \delta(R_j - r), \quad (8.23)$$

where  $R_j$  values define the positions of the surrounding ions.

In the case of an unfilled 4f shell with more than one 4f electron, the potential energy of the ion in the crystal electric field may be written as

$$H_{\text{CEF}} = e \sum_i V(r_i), \quad (8.24)$$

where  $i$  spans over all 4f electrons. In the case of rare earth ions, the spin-orbit interaction energy is generally larger than the crystal field energy and hence it is necessary to restrict to the lowest  $J$  multiplet in calculating matrix elements of  $H_{\text{CEF}}$ . There are exceptions to this restriction which involve admixture of other  $J$  multiplets of importance [9,10]. Restricting to lowest  $J$  multiplet simplifies the calculations. It has been shown that the sum of polynomials  $X_i$ ,  $Y_i$ ,  $Z_i$  in equation (8.24) can be conveniently replaced by a sum of polynomials of  $J_x$ ,  $J_y$ ,  $J_z$  operators with the same transformation properties as the original expression. The advantage of the operators is that they act on the whole  $f^n$  configuration unlike the  $X_i$ ,  $Y_i$ ,  $Z_i$  polynomials which act on a single f electron. Rules for the transformation of  $\sum_i f(X_i, Y_i, Z_i)$  into operators are: (i) replace any product of  $x$ ,  $y$ ,  $z$  by product of  $J_x$ ,  $J_y$ ,  $J_z$  in a symmetrized form (i.e.) the sum of all different sequences of  $J_\mu$  as for example  $xy \rightarrow \frac{1}{2}(J_x J_y + J_y J_x)$ , (ii) the constants of proportionality depend on the degree of polynomial and on  $L$ ,  $S$  and  $J$ , (iii) the  $r_i^L$  operators are replaced by the averages  $\langle r^L \rangle$  over the 4f wavefunctions. Some examples are

$$\begin{aligned} \sum_i (x_i^2 - y_i^2) &\equiv \alpha_J \langle r^2 \rangle [J_x^2 - J_y^2] = \alpha_J \langle r^2 \rangle O_2^2 \\ \sum_i \frac{1}{2} \{ (x_i + iy_i)^4 + (x_i - iy_i)^4 \} &\equiv \beta_J \langle r^4 \rangle \frac{1}{2} [J_+^4 + J_-^4] = \beta_J \langle r^4 \rangle O_4^4 \\ \sum_i (x_i^6 - 15x_i^4 y_i^2 + 15x_i^2 y_i^4 - y_i^6) &\equiv \gamma_J \langle r^6 \rangle \frac{1}{2} [J_+^6 + J_-^6] = \gamma_J \langle r^6 \rangle O_6^6 \end{aligned} \quad (8.25)$$

The proportionality constants  $\alpha_j$ ,  $\beta_j$ , and  $\gamma_j$  are for polynomials of second, fourth and sixth degree [12] and  $O_n^m$  can be found in the literature [8]. The  $\alpha$ ,  $\beta$ ,  $\gamma$ , and  $\langle r^L \rangle$  are given

in Tables 8.2 and 8.3, respectively. Frequently the crystal field is described with respect to axes chosen such that  $\gamma_{l\alpha} = 0$  for  $\alpha$  corresponding to  $Z_{lm}^S$  (cf. equations (8.22), (8.21)) and in such a case we have

$$H_{\text{CEF}} = \sum_{l,m} A_l^m \langle r^l \rangle \theta_l O_l^m, \quad (8.26)$$

where  $\theta_l$  is equal to  $\alpha_l$ ,  $\beta_l$ ,  $\gamma_l$  for  $l = 2, 4, 6$ ,  $A_l^m$  numerical factors equal to  $Z_{lm}^C$  and the numerical factors are given in the literature [8].

The crystal field Hamiltonian is also written as

$$H_{\text{CEF}} = \sum_{l,m} B_l^m O_l^m \quad (8.27)$$

The crystal electric field Hamiltonian for some commonly encountered situations are as follows.

### 2.1. Cubic point symmetry

By choosing the four-fold axes in which the  $J$  operators are expressed in, we have

$$H_{\text{CEF}} = B_4^0 [O_4^0 + 5O_4^4] + B_6^0 [O_6^0 + 5O_6^4] \quad (8.28)$$

For a case of point charge model, expressions for  $B_4^0$  and  $B_6^0$  may be derived. Assuming the surrounding ions of charge  $q$  placed at a distance  $d$  from the rare earth ion we get

- eightfold coordination (cube)

$$B_4^0 = \frac{7}{18} \frac{|e|q}{d^5} \beta_J \langle r^4 \rangle \quad B_6^0 = \frac{1}{9} \frac{|e|q}{d^7} \gamma_J \langle r^6 \rangle$$

- sixfold coordination (octahedron)

$$B_4^0 = \frac{7}{16} \frac{|e|q}{d^5} \beta_J \langle r^4 \rangle \quad B_6^0 = -\frac{3}{64} \frac{|e|q}{d^7} \gamma_J \langle r^6 \rangle \quad (8.29)$$

The eigen values and eigen functions of the Hamiltonian in equation (8.28) have been tabulated for  $J = 5/2, 3, \dots, 8$  in the literature [13] by using the equation

$$H_{\text{CEF}} = W \left( \frac{x}{F(4)} (O_4^0 + 5O_4^4) + \frac{1 - |x|}{F(6)} (O_6^0 - 21O_6^4) \right), \quad (8.30)$$

where  $B_4^0 F(4) = Wx$  and  $B_6^0 F(6) = W(1 - |x|)$  with  $-1 < x < 1$ . The eigen values and eigen functions are given as a function of  $x$ . The factors  $F(4)$  and  $F(6)$  which depend on  $J$  are given. When the threefold axis  $Z$  is chosen as in the case of  $\text{Tb}^{3+}$  in  $\text{TbSb}$  we have

$$H_{\text{CEF}} = \bar{B}_4^0 [O_4^0 - 2^{1/2} 20 O_4^3] + \bar{B}_6^0 \left[ O_6^0 - \frac{35}{4} 2^{1/2} O_6^3 + \frac{77}{8} O_6^6 \right] \quad (8.31)$$

## 2.2. Hexagonal point symmetry

In this case the crystal field Hamiltonian is [8]

$$H_{\text{CEF}} = B_2^0 O_2^0 + B_4^0 O_4^0 + B_6^0 O_6^0 + B_6^0 O_6^0 \quad (8.32)$$

Since there are a large number of parameters there is a facile way to list the eigen values and eigen vectors.

The Hamiltonians for cubic, tetragonal and trigonal symmetry are given below:

$$\mathcal{H}_{\text{cubic}} = B_4(O_4^0 + 5O_4^4) + B_6(O_6^0 + 5O_6^4),$$

where  $B_4^4 = 5B_4^0$ ,  $B_6^4 = -21B_6^0$

$$\mathcal{H}_{\text{tetra}} = B_2^0 O_2^0 + B_4^0 O_4^0 + B_4^4 O_4^4 + B_6^0 O_6^0 + B_6^4 O_6^4 \quad (8.33)$$

$$\mathcal{H}_{\text{trig}} = B_2^0 O_2^0 + B_4^0 O_4^0 + B_4^3 O_4^3 + B_6^0 O_6^0 + B_6^3 O_6^3 + B_6^6 O_6^6$$

The calculation of crystal field parameters from  $B_l^m$  from a microscopic theory is very difficult and had limited success. For rare earth compounds a good deal of work and a semi-empirical understanding of the crystal field parameters have been achieved. Even here there are no successful ab initio calculations. It is surprising that the point charge model is valid in some rare earth compounds.

A basic assumption of crystal field theory is the vanishing overlap between the charges, which are responsible for the crystal field and 4f wave functions. Two observations that contradict this view are: (i) the measured  $B_l^m$  parameters divided by  $\langle r^l \rangle$  are not constant for a series of rare earth ions and (ii)  $B_6^m$  falls off less rapidly with increasing nuclear charge than expected from the corresponding variation of  $\langle r^6 \rangle$ . These two observations suggest that other electrons have an influence on the crystal field. The shielding effect of distorted filled s and d shells from the 4f electrons affect the electric field of the surrounding ligands. Thus a shielding factor is introduced [8]

$$A_l^m \langle r^l \rangle \text{ effective} = (1 - \sigma_l) A_l^m \langle r^l \rangle \text{ point charge} \quad (8.34)$$

Further overlap and covalency contributions need to be considered [7,14–16].

## 3. Methods for determining crystal-field levels

The most popular method for determining crystal-field levels of rare earth salts is spectroscopy [17,18]. The maximum number of energy levels (stark sublevels) generated in the various point groups are given in Table 8.4.

It is usually necessary to identify the electronic energy levels for free trivalent rare earth ions before analyzing the spectra of rare earths in crystals. Let us recall the equation for  $f^n$  configuration, the energy levels of the electrostatic interaction.

$$H_i = \frac{e^2}{r_{ij}} \quad (8.35)$$



TABLE 8.4  
Number of energy  $J$ -sublevels in a given point symmetry vs. the quantum number  $J$ .

Symmetry	$J$						
	0	1	2	3	4	5	6
Icosahedral	1	1	1	2	2	3	4
Cubic <sup>1</sup>	1	1	2	3	4	4	6
Hexagonal <sup>2</sup>	1	2	3	5	6	7	9
Pentagonal <sup>3</sup>	1	2	3	4	5	7	8
Tetragonal <sup>4</sup>	1	2	4	5	7	8	10
Low <sup>5</sup>	1	3	5	7	9	11	13

<sup>1</sup>O<sub>h</sub>, O, T<sub>d</sub>, T<sub>h</sub>, T.

<sup>2</sup>D<sub>6h</sub>, D<sub>6</sub>, C<sub>6v</sub>, C<sub>6h</sub>, C<sub>6</sub>, D<sub>3h</sub>, C<sub>3h</sub>, D<sub>3d</sub>, D<sub>3</sub>, C<sub>3v</sub>, S<sub>6</sub>, C<sub>3</sub>.

<sup>3</sup>D<sub>5h</sub>, C<sub>5h</sub>, C<sub>5v</sub>, C<sub>5</sub>, D<sub>5</sub>.

<sup>4</sup>D<sub>4h</sub>, D<sub>4</sub>, C<sub>4v</sub>, C<sub>4h</sub>, C<sub>4</sub>, D<sub>2d</sub>, S<sub>4</sub>.

<sup>5</sup>D<sub>2h</sub>, D<sub>2</sub>, C<sub>2v</sub>, C<sub>2h</sub>, C<sub>2</sub>, C<sub>s</sub>, S<sub>2</sub>, C<sub>1</sub>.

written in terms of the slater integrals

$$F^{(k)} = e^2 \int_0^\infty \int_0^\infty \frac{r_{<}^k}{r_{>}^{k+1}} [R_{nf}(r_i)R_{nt}(r_j)]^2 dr_i dr_j, \quad (8.36)$$

where  $r_{<}$  is the lesser and  $r_{>}$  is the greater of  $r_i$  and  $r_j$ . From Legendre polynomials' properties  $k$  must be even and  $k \leq 2l$  (i.e.)  $R = 0, 2, 4, 6$ . Related parameters which avoid the occurrence of fractional coefficients for  $F^{(k)}$  are

$$\begin{aligned} F_0 &= F^{(0)} \\ F_2 &= \frac{F^{(2)}}{225} \\ F_4 &= \frac{F^{(4)}}{1089} \\ F_6 &= \frac{25F^{(6)}}{184041} \end{aligned} \quad (8.37)$$

The parameters deduced from the crystal spectra of trivalent lanthanides are given in Table 8.5. The spin-orbit coupling parameter is seen to increase smoothly with atomic number while the  $F_k$  values increase erratically. This anomalous behavior is probably due to the use of hydrogenic approximation and ignoring of configuration interaction. By using the contribution of configuration interaction term  $\alpha L(L+1)$  to the energy matrices of Pr<sup>3+</sup> of  $f^2$  configuration the mean error decreased from 200 to 127 cm<sup>-1</sup>. The revised parameters for Pr<sup>3+</sup> are

$$\begin{aligned} F_2 &= 308.0, \quad F_4 = 50.92, \quad F_6 = 5.115, \\ Z &= 753.9, \quad \alpha = 14.77 \text{ cm}^{-1} \end{aligned}$$

TABLE 8.5  
Parameters deduced from the crystal spectra of the trivalent lanthanides.

Ion	$F_2$	$F_4$	$F_6$	$\zeta$	Reference*
Ce <sup>3+</sup>				644	[17]
Pr <sup>3+</sup>	305.4	51.88	5.321	729.5	
Nd <sup>3+</sup>	327.5	48.66	5.356	884.6	
Pm <sup>3+</sup>	346.2	47.68	5.232	1070	
Sm <sup>3+</sup>	370	51.08	5.591	1200	
Eu <sup>3+</sup>	401	55.36	6.059	1320	
Gd <sup>3+</sup>	406	56.05	6.135	1583	
Tb <sup>3+</sup>	434	59.91	6.558	1705	
Dy <sup>3+</sup>	420	57.98	6.346	1900	
Ho <sup>3+</sup>	414.6	68.80	7.272	2163	
Er <sup>3+</sup>	433.2	67.13	7.356	2393.3	
Tm <sup>3+</sup>	451.1	68.07	7.437	2656	
Yb <sup>3+</sup>				2882.7	

All values are in  $\text{cm}^{-1}$ .

TABLE 8.6  
Crystal field parameters for various lanthanide ions in  $\text{LaCl}_3$ .

Ion	$B_0^2$	$B_0^4$	$B_0^6$	$B_6^6$	Reference
Pr <sup>3+</sup>	95	-325	-634	427	[17]
Nd <sup>3+</sup>	195	-309	-710	466	
Sm <sup>3+</sup>	162	-182	-709	448	
Eu <sup>3+</sup>	178	-304	-816	521	
Tb <sup>3+</sup>	184	-320	-480	305	
Dy <sup>3+</sup>	182	-311	-371	271	
Er <sup>3+</sup>	188	-298	-424	279	

All values in  $\text{cm}^{-1}$ .

The crystal field parameters for various lanthanide ions in  $\text{LaCl}_3$  and lanthanide ethyl sulphates are given in Tables 8.6 and 8.7, respectively.

The crystal field parameters given in Tables 8.6 and 8.7 show an uneven variation with atomic number. The crystal field calculations are not of the same degree of reliability. In some cases, crystal field interactions between ion levels have been ignored. In other cases, the calculations included only levels derived from the ground multiplets while in some cases intermediate coupling effects have not been included. The validity of the data depends on whether all the available information has been used and the discrepancies are not due to incomplete treatment of the problem.

Crystal field levels in rare earth metals have been determined by measurements of properties such as: (i) specific heat, (ii) Van Vleck susceptibility, (iii) magnetization in high magnetic fields, (iv) paramagnetic resonance, (v) Mössbauer effect, (vi) inelastic neutron scattering and (vii) miscellaneous methods.

TABLE 8.7  
Crystal field parameters for various lanthanide ethylsulfates.

Ion	$B_0^2$	$B_0^4$	$B_0^6$	$B_6^6$	Reference
$\text{Pr}^{3+}$	31	-706	-778	578	[17]
$\text{Nd}^{3+}$	117	-568	-457	456	
$\text{Sm}^{3+}$	154	-385	-624	580	
$\text{Eu}^{3+}$	160	-505	-617	537	
$\text{Tb}^{3+}$	220	-598	-544	488	
$\text{Dy}^{3+}$	250	-208	-480	515	
$\text{Ho}^{3+}$	250	-630	-478	412	
$\text{Er}^{3+}$	252	-650	-496	407	
$\text{Tm}^{3+}$	195	-568	-457	456	

All values in  $\text{cm}^{-1}$ .

By measuring specific heat of a rare earth alloy, e.g.,  $\text{TmAl}_3$  along with the Schottky contributions, the different levels can be identified. The specific heat per mole of rare earth ions may be written as

$$C = R_0 Z^{-2} \left\{ Z \sum_i (\beta \delta_i)^2 \exp(-\beta \delta_i) - \left( \sum_i \beta \delta_i \exp(-\beta \delta_i) \right)^2 \right\}, \quad (8.38)$$

where  $i$  spans over all  $2J + 1$  crystal field states with energy  $\delta_i$ ;  $\beta = (k_B T)^{-1}$ ;  $k_B$ , Boltzman constant;  $T$ , temperature;  $Z$ , partition function  $= \sum_i \exp(-\beta \delta_i)$ ;  $R_0$ , gas constant.

Schottky anomaly is determined from the difference between an  $\text{RY}_n$  compound and  $\text{LaX}_n$  or  $\text{LuX}_n$  compound. Then the crystal field parameters are deduced from the Schottky anomaly data. The accuracy of the method is limited by spin-phonon interactions and exchange effects in rare earth ions which affect the Schottky effect. It is used to find crystal field parameters,  $W$ ,  $x$  which fit the specific heat data as shown in Fig. 8.4. The figure refers to a plot of  $C/R_0$  vs.  $T$  for  $\text{TmAl}_3$  [19].

Some information on crystal electric field levels can be obtained from the measurement of temperature-dependent Van Vleck susceptibility which can be described by the relationship

$$\chi(T) = N \mu_B^2 g^2 Z^{-1} \left\{ \sum_i \frac{|M_{ii}|^2}{T} \exp(-\beta \delta_i) + 2 \sum_{\delta_i \neq \delta_j} \frac{|M_{ij}|^2}{\delta_i - \delta_j} \exp(-\beta \delta_i) \right\} \quad (8.39)$$

In equation (8.39)  $g$  is Landé factor;  $\mu_B$ , Bohr magneton. The matrix elements  $M_{ij} = \langle i | J | j \rangle$ , where  $|n\rangle$  denote the different crystal field eigen states. The first term arising out of diagonal terms is the Curie term and the term arising out of off-diagonal contribution is the Van Vleck term. In the case of an impurity with a nonmagnetic ground state, there will be no Curie contribution at low temperature. For the case of silver with 0.5 atom percent

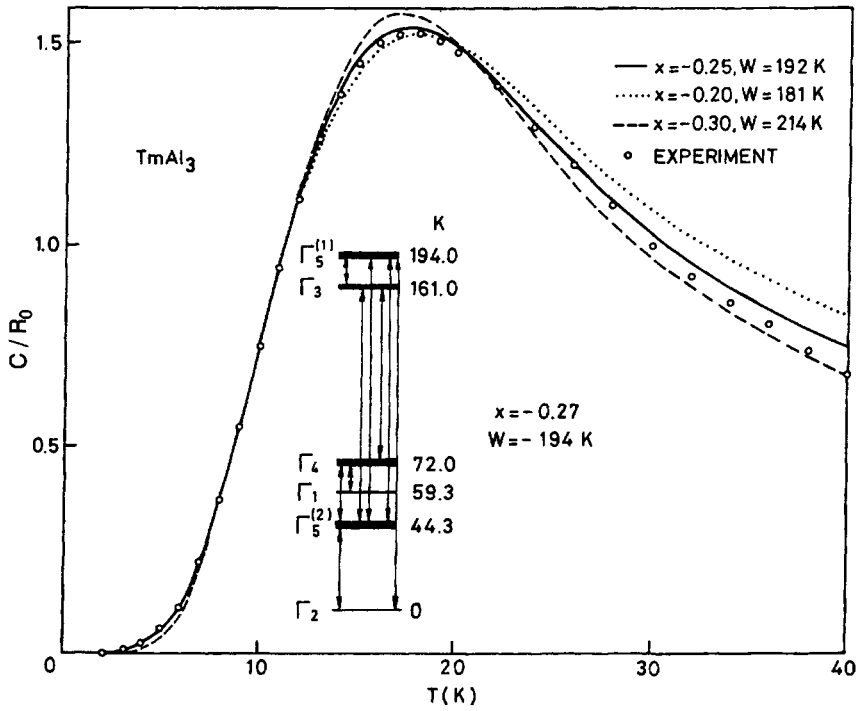


Fig. 8.4. Schottky anomaly and CEF-level sequence for  $\text{TmAl}_3$  [19].

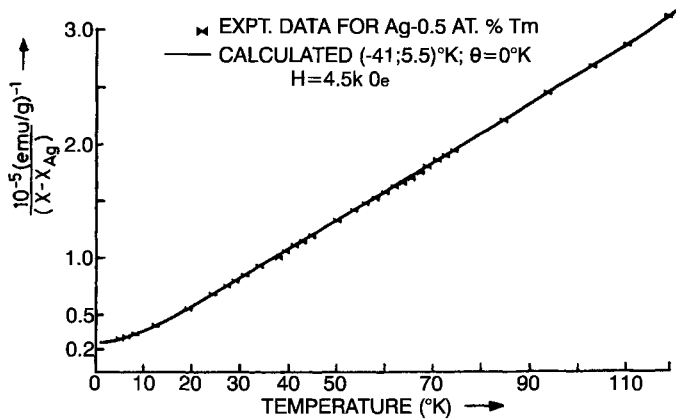


Fig. 8.5. Inverse susceptibility of Ag with 0.5 at% Tm [20].

$\text{Tm}$ , the variation of the susceptibility with temperature is shown in Fig. 8.5. Note the agreement between the calculated and measured susceptibility.

The inelastic neutron scattering method has been extensively used for studying crystal field effects in metals. The method involves scattering of monochromatic neutrons from

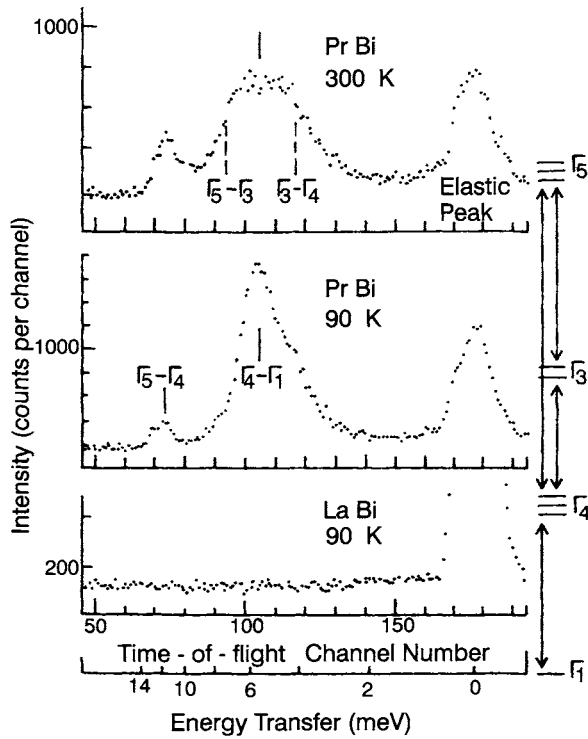


Fig. 8.6. Inelastic neutron scattering results on PrBi. The different inelastic peaks correspond to different transitions between the CEF-levels. For comparison LaBi does not show the inelastic scattering.

the sample which are then analyzed according to their energy and momentum. In such an experiment, the energy  $\omega$ , and momentum transfer  $|Q|$  are determined. The differential cross section for  $N$  non-interacting rare earth ions for a small momentum transfer is given by

$$\frac{d^2\sigma}{d\Omega d\omega} = N \left( \frac{1.91e^2g}{2mc^2} \right)^2 \frac{k_f}{k_i} f^2(Q) e^{-2w} \sum_{i,j} n_i |\langle j | J_{\perp} | i \rangle|^2 \delta_j - \delta_i - \omega \quad (8.40)$$

In equation (8.40)  $k_i$ ,  $k_f$  are moments of incident and outgoing neutrons,  $f(Q)$  the form factor of a single ion,  $e^{-2w}$  the Debye-Waller factor,  $n_i$  the occupational probability of the crystal electric field eigen state  $|i\rangle$ ,  $J_{\perp}$  perpendicular  $J$  component to the scattering vector  $Q$ . The crystal field transition is proportional to  $f^2(Q)e^{-2w}$  while the competing phonon scattering is proportional to  $Q^2e^{-2w}$ . The experimental data for PrBi and LaBi systems are shown in Fig. 8.6. The figure shows lack of interference of phonon effects on the scattering from the crystal electric field energy levels.

### 3.1. Miscellaneous methods

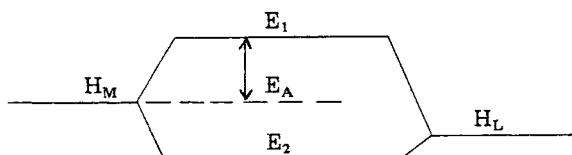
Some methods which have been used for the determination of crystal field parameters are given below:

- (a) magnetization in high magnetic fields [21],
- (b) Mössbauer effect studies [22],
- (c) electrical and thermal conductivity,
- (d) superconductivity.

Spectroscopic techniques of promise are super conducting tunneling spectroscopy and absorption of high-frequency phonons when the phonons are generated in super conduction tunneling junctions.

## 4. Angular overlap model (AOM)

In order to overcome the shortcomings of crystal field theory an alternate approach to the theory of bonding has been proposed by Jorgensen and coworkers known as the angular overlap model (AOM) [23–25]. The angular overlap model is one of the simplest yet fundamental approaches of the MO-LCAO (molecular orbital–linear combination of atomic orbitals) method. This model has been used to describe the lanthanide split levels in the presence of crystal fields. In this model, the magnitude of level splitting is measured by the antibonding energy,  $E_A$ , which is equal to the difference in the energies of the atomic,  $H_M$  and antibonding,  $E_1$  orbital with both the orbitals localized mainly on the metal ion.



According to the model, the antibonding energy of the  $nl$ -orbital of the metal in the complex is proportional to the square of its overlap integral with the ligand orbitals. The antibonding energy,  $E_A$  may be written as

$$E_A \cong \frac{H_L^2}{H_M - H_L} \cdot S^2, \quad (8.41)$$

where  $H_M$  and  $H_L$  are the coulomb integrals of the metal and ligand orbitals, respectively, and  $S$  is the overlap integral. The overlap integral  $S$  is assumed to be the product

$$S = \Xi S_R^*, \quad (8.42)$$

where  $\Xi$  and  $S_R^*$  are parameters which depend on the angular and radial parts of the interacting orbitals, respectively.

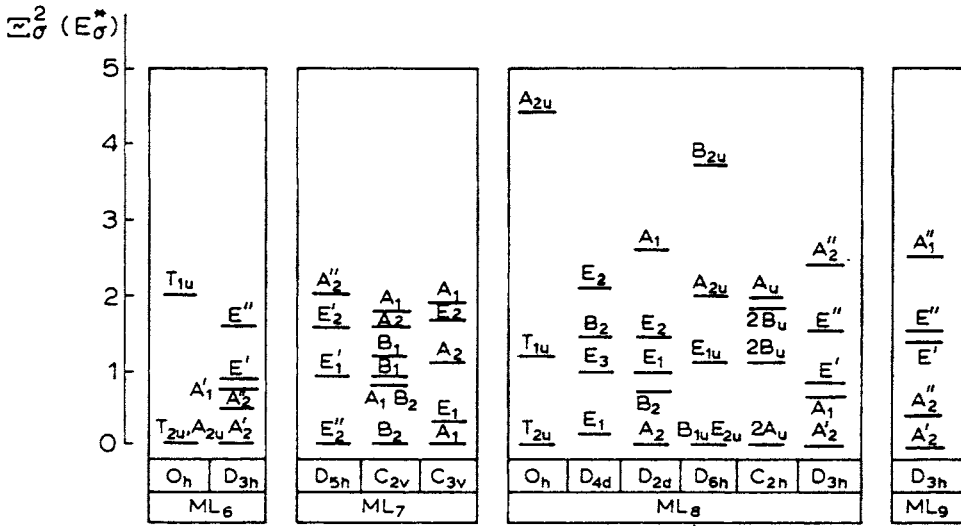


Fig. 8.7. Angular parameters,  $\Xi_{\sigma}^2$  of f-orbital overlap integrals in complexes of various composition and symmetry (in  $E_{\sigma}^* = 7I_{\sigma}^*$  units) [26].

Suppose that all the ligands in the complex are identical and are equidistant from the metal, then we have

$$E_A = e_{\lambda}^* \cdot \Xi_{\lambda}^2, \tag{8.43}$$

where

$$e_{\lambda}^* = \frac{H_L^2}{H_M - H_L} (S_R^*)^2 \tag{8.44}$$

In equation (8.44)  $\lambda$  denotes the type of overlap (i.e.)  $\sigma$  or  $\pi$ . The angular parameters  $\Xi_{\lambda}$  can be calculated accurately knowing the coordination number and symmetry of the complex.

The angular parameters of the overlap integrals of f-orbitals,  $\Xi_{\sigma}$  in the complexes of  $O_h$  and  $D_{3h}$  symmetry have been calculated by Jorgensen and coworkers [23]. The calculations have been extended to complexes of other point-group symmetries and the angular parameters for  $\pi$ -overlap integrals,  $\Xi_{\pi}$  have been estimated [26]. The results are depicted in Figs 8.7 and 8.8.

The coefficients,  $e_{\lambda}^*$  are assumed to be empirical parameters obtained from spectral data. On the basis of the model using only one empirical parameter  $e_{\lambda}^*$  (considering only  $\sigma$  overlap), the crystal fields have been successfully interpreted for lanthanide ions in ethylsulphates [23], for  $Er^{3+}$  in orthovanadate and orthophosphate and hydroxides.

Angular overlap treatment of  $\sigma$  and  $\pi$  bonding in f-orbital compounds has been done and results have been obtained for a number of geometries, especially those commonly

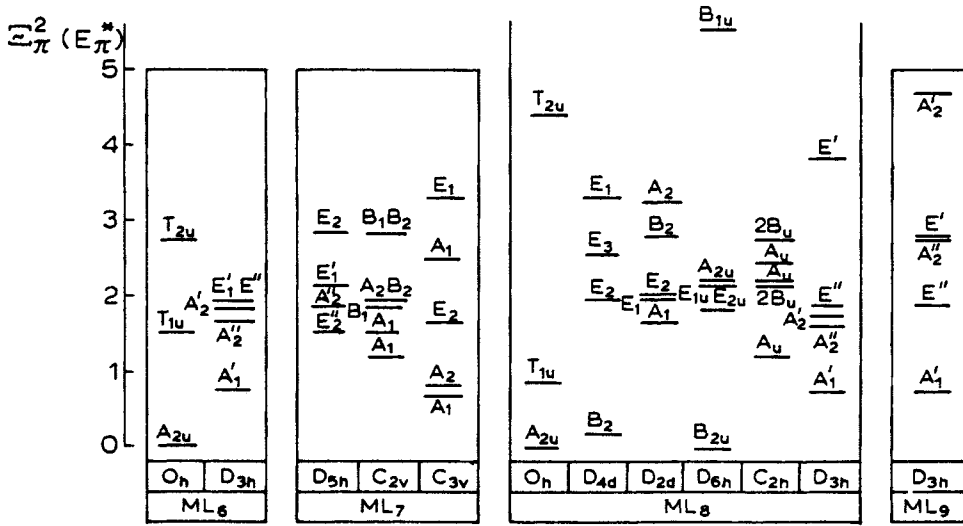


Fig. 8.8. Angular parameters,  $\Xi_{\pi}^2$  of f-orbital overlap integrals in complexes of various composition and symmetry (in  $E_{\pi}^* = 168e_{\pi}^*$  units) [26].

TABLE 8.8  
One-electron energies in  $\text{cm}^{-1}$  derived from experimental data.

	$\sigma(a_2'')$	$\pi(e')$	$\delta(e'')$	$\phi_1(a_2')$	$\phi_2(a_1')$
Ce(H <sub>2</sub> O) <sub>9</sub> (C <sub>2</sub> H <sub>5</sub> SO <sub>4</sub> ) <sub>3</sub>	-416	+250	-35	-425	+411
Pr(H <sub>2</sub> O) <sub>9</sub> (C <sub>2</sub> H <sub>5</sub> SO <sub>4</sub> ) <sub>3</sub>	-268	+113	+87	-323	+195
Pr(H <sub>2</sub> O) <sub>9</sub> (Gruber <sup>16</sup> )	-303	+122	+94	-268	+150
Pr <sup>III</sup> LaCl <sub>3</sub>	-164	+112	+39	-200	+64
Nd(H <sub>2</sub> O) <sub>9</sub> (C <sub>2</sub> H <sub>5</sub> SO <sub>4</sub> ) <sub>3</sub>	-255	+147	+61	-304	+144
Sm <sup>III</sup> LaCl <sub>3</sub>	-154	+149	-10	-220	+98
Tb(H <sub>2</sub> O) <sub>9</sub> (C <sub>2</sub> H <sub>5</sub> SO <sub>4</sub> ) <sub>3</sub>	-177	+121	+89	-294	+52
Dy(H <sub>2</sub> O) <sub>9</sub> (C <sub>2</sub> H <sub>5</sub> SO <sub>4</sub> ) <sub>3</sub>	-165	+118	+99	-317	+49
Dy <sup>III</sup> LaCl <sub>3</sub>	-96	+90	+42	-180	+12
Ho(H <sub>2</sub> O) <sub>9</sub> (C <sub>2</sub> H <sub>5</sub> SO <sub>4</sub> ) <sub>3</sub>	-160	+115	+100	-280	+12
Er(H <sub>2</sub> O) <sub>9</sub> (C <sub>2</sub> H <sub>5</sub> SO <sub>4</sub> ) <sub>3</sub>	-167	+119	+103	-277	+9
Tm(H <sub>2</sub> O) <sub>9</sub> (C <sub>2</sub> H <sub>5</sub> SO <sub>4</sub> ) <sub>3</sub>	-76	+115	+79	-294	+28

encountered in 4f and 5f metal complexes, in particular the relative contributions of  $\sigma$  and  $\pi$  interactions in octahedral hexahalo complexes [29].

The success of the AO model in explaining the spectral data of lanthanide compounds as aquo ions, aquo ethylsulphates and chlorides is illustrated by the data on one-electron energies derived from experimental results (Table 8.8) and the manner in which the one-electron energies vary with atomic number (Fig. 8.9).

Newman [31] proposed a model known as the 'superposition model' which simplified the calculations of different contributions to the crystal field parameters and facilitated their analysis. According to the superposition model, the crystal fields are built up from separate



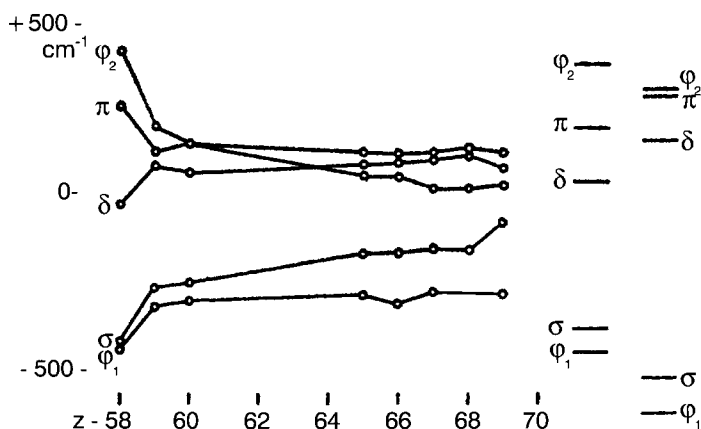


Fig. 8.9. One-electron energies (relative to the baricenter of the 4f shell) of lanthanide ennea-aqua ethylsulfates as function of the atomic number  $Z$ . At the right-hand side, the predicted results are indicated in terms of an arbitrary scaling factor [29].

contributions from each of the ions in the crystal. Each contribution may be represented as a cylindrically symmetric field described by three parameters  $\bar{A}_2\langle r^2 \rangle$ ,  $\bar{A}_4\langle r^4 \rangle$  and  $\bar{A}_6\langle r^6 \rangle$ . These parameters are distinguished from experimentally obtained parameters by denoting as  $\bar{A}_2(r)$ ,  $\bar{A}_4(r)$ , and  $\bar{A}_6(r)$  and usually referred to as 'intrinsic parameters'. The "intrinsic" and experimental parameters are related by the equation

$$A_n^m\langle r^n \rangle = \sum_i k_{nm}(i) \bar{A}_n(R_i), \quad (8.45)$$

where  $k_{nm}$  is a coordination factor which depends on the angular position of a single ion at a distance  $R_i$  from the central paramagnetic metal ion. In practice, it is assumed that only coordinated ions or ligands contribute significantly to the crystal field. If the ligands are equidistant we may write

$$A_n^m\langle r^n \rangle = k_{nm} \bar{A}_n(R_i) \quad (8.46)$$

The experimental data on crystal fields have been summarized [31] and shown that the overlap and covalency (charge transfer) contribute to a significant extent to the crystal field parameters when  $n = 4$  and 6. Analysis of the data on  $\text{PrCl}_3$  showed that the experimental parameters for  $A_6^0\langle r^6 \rangle$  and  $A_4^0\langle r^4 \rangle$  are in good agreement with the sum of the calculated electrostatic and covalent contributions. The values for  $A_2^0\langle r^2 \rangle$  showed poor agreement.

The semiempirical MO method has been used to calculate the ground level splitting of  $\text{Tm}^{2+}(\text{f}^{13})$  ion in the cubic field  $\text{CaF}_2$  taking into account  $\sigma$  and  $\pi$  interactions. The covalent contribution in the ground level splitting of the  $\text{Tm}^{2+}$  ion was found to be nearly 50 percent [32].

## 5. Nephelauxetic effect

The energy levels of lanthanide “free ions” in crystals and solutions determined from the absorption spectra differ somewhat from those of gaseous  $\text{Ln}^{3+}$  ions and depend on the environment [33–35]. In the presence of ligand fields, the whole  $4f^n$  structure appears to shorten as compared to gaseous ions. The mean  $J$  level in  $\text{Pr}^{3+}$  shifts by 5 percent [33] and by one percent in  $\text{Er}^{3+}$  [36]. The red shift observed in the absorption spectra of lanthanides has been termed as the nephelauxetic effect. The nephelauxetic effect has been discussed in detail [34].

The phenomenon of the nephelauxetic effect cannot be interpreted in the framework of an electrostatic model which considers exclusively first-order crystal field effects. The observed band shifts could be due to second-order crystal field effects. However, the theoretical values of the second-order crystal field effects are of the order of  $10 \text{ cm}^{-1}$  or so [40,41] and cannot account for the experimentally observed band shifts, which in some cases are as high as 100 to  $1000 \text{ cm}^{-1}$ .

At present there is consensus on the fact that the observed nephelauxetic effect in the spectra of lanthanide compounds is analogous to the phenomenon observed in the spectra of d-transition metal complexes. The nephelauxetic effect cannot be quantitatively interpreted by excluding the covalent interaction of lanthanide ions with surrounding ligands [34]. Jorgensen has proposed [38] two possible mechanisms of interaction for the observed nephelauxetic effect, namely: (i) direct participation of lanthanide  $4f$  orbitals in the formation of molecular orbitals also known as “symmetry restricted covalency”, (ii) transfer of some part of the ligand electron density to the unfilled  $6s$  and  $6p$  orbitals of the lanthanide also known as “central field covalency”.

The nephelauxetic effect is described quantitatively by parameter,  $\beta$ , which is equal to the ratio of the interelectron repulsion parameters (either Slater’s integrals,  $F_k$ , or Racah parameters,  $E^k$ ) in the complex and in the free ion. We may write

$$\beta = \frac{(F_k)_c}{(F_k)_f} \quad \text{or} \quad \beta = \frac{(E^k)_c}{(E^k)_f} \quad (8.47)$$

Since the nephelauxetic effect value  $(1 - \beta)$  is small in the lanthanide complexes, it can be defined to a first approximation as the ratio of wave number of  $f-f$  transitions in the complex and free ion

$$\beta \approx \frac{\nu_c}{\nu_f} \quad (8.48)$$

Since the energy levels of free lanthanide ions are not known, the relative nephelauxetic effect,  $\beta^1$  is usually determined from the experimental data using the spectra of the lanthanide aquo ions as reference or standards. In such a case

$$\beta' \approx \frac{\nu_e}{\nu_{\text{aq}}} \quad (8.49)$$

Jorgenson et al. [42] have proposed a relationship to define the nephelauxetic effect by taking into account ground state stabilization in the complex compared to the aquo ion. Accordingly we have

$$\sigma_c - \sigma_{aq} = d\sigma - (d\beta)\sigma_{aq}, \quad (8.50)$$

where  $\sigma_c$  and  $\sigma_{aq}$  represent spectral band baricentres of the complex and aquo ion, respectively,  $d\sigma$  is the ground state stabilization, and  $d\beta$  is the variation of the nephelauxetic parameter. The values of  $d\sigma$  and  $d\beta$  are usually obtained from a plot of  $\sigma_c - \sigma_{aq}$  against  $\sigma_{aq}$  for as large a number of levels as possible. It has been [43,44] shown that the experimentally obtained plots of  $\sigma_c - \sigma_{aq}$  vs.  $\sigma_{aq}$  can deviate from straight lines due to a relativistic nephelauxetic effect. The relativistic nephelauxetic effect is defined as the ratio of Landé parameters in the complex and free ion and equal to the spin-orbit coupling contribution to the energies of the ground and excited states.

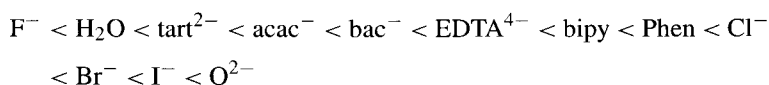
$$\beta_{rel} = \xi(4f_e)/\xi(4f)_f \quad (8.51)$$

Carnall proposed [45] using the energy levels of lanthanide ions in  $\text{LaF}_3$  as standards in defining  $\beta'$  and pointed out their advantages over the use of aquo ions

$$\beta' = \frac{\nu_e}{\nu_{\text{LaF}_3}} \quad (8.52)$$

## 6. Nephelauxetic series

The dependence of the nephelauxetic effect upon the nature of complexing ligands can be expressed as nephelauxetic series of ligands. For light lanthanides (Pr, Nd) the ligands can be arranged as follows according to the  $(1 - \beta')$  values:



The above series in general is similar to the ligand nephelauxetic series observed in the case of d-transition metals. The greatest nephelauxetic effect has been observed in sulphides [46], cyclopentadienides [47], and oxides [48] of lanthanides. However, attempts to formulate a common and general nephelauxetic series for the lanthanide series have been futile using aquo ions as reference standards. In the case of lanthanide complexes with the same ligand in aqueous solutions, the absorption band positions of light and heavy lanthanides shift in different directions. This unusual behavior of complexes may be due to the differences in structure of aquo ions and the complexes.

In efforts to explore the significance of the nephelauxetic effect, the possible relationship between the nephelauxetic absorption band shift and the structure of the complex has been investigated. The dependence of the nephelauxetic effect upon the coordination numbers in the complexes was recognized by Jorgensen and coworkers [49]. The nephelauxetic

effect has been attributed to a shortening of metal–ligand distance accompanied by a decrease in coordination number. This idea has been confirmed by the work of Laughlin and Conway [50] who studied the absorption spectra of  $\text{Pr}^{3+}$  in isostructural matrices:  $\text{CeCl}_3$ ,  $\text{NdCl}_3$ ,  $\text{SmCl}_3$ ,  $\text{GdCl}_3$ . The spectral data showed that with identical structure of the complexes (i.e.) coordination number of 9 and  $D_{3h}$  symmetry, a linear dependence of the wavenumbers of  ${}^3P_{0,1,2} \leftarrow {}^3H_4$  transition of  $\text{Pr}^{3+}$  on the praseodymium–ligand distance  $R$  has been observed.

An increase in  $R$  resulted in the band shift towards the short-wave region. Further, a linear correlation between the bond distance  $\bar{R}$  of Ln–O bond and the wave numbers of some f–f transitions in the absorption spectra of Pr(III) and Nd(III) complexes with different coordination numbers and symmetry was noted [51,52]. The complexes had oxygen donor ligands and  $\bar{R}$  (Ln–O) is the mean lanthanide–oxygen distance. This correlation has been examined in the light of the atomic overlap model.

An analyses based on the AO model examines the relationship between the nephelauxetic effect, and geometric and energy parameters. A parameter  $\eta$  proportional to nephelauxetic effect is defined as

$$\eta = (1 - \beta^{1/2})/\beta^{1/2} \quad (8.53)$$

The parameter  $\eta$  to a first approximation may written as

$$\eta \approx \frac{H_L^2}{(H_M - H_L)^2} (S_R^*)^2 N, \quad (8.54)$$

where  $N$  is the coordination number. For complexes with ligands containing identical donor atoms the equation may be written as

$$\eta \approx \text{constant} (S_R^*)^2 N, \quad (8.55)$$

where the constant is equal to

$$\frac{H_L^2}{(H_M - H_L)^2}$$

Equation (8.55) has two variables,  $S_R^*$  and  $N$  which vary with changes in the lanthanide–ligand distance in opposing directions. However, any variations in  $R$  have led to much more pronounced changes in  $(S_R^*)^2$  than in  $N$ . Thus the nephelauxetic effect increases when the coordination number decreases (i.e.) decrease in lanthanide–ligand distance in spite of the additive nature of  $\beta$  and decrease in the number of coordinated ligands.

## 7. The intensities of intra 4f–4f transitions

The first known work on the intensities of the intra 4f–4f transitions is that of Van Vleck [53]. This was followed by the work of Jurbner and coworkers [54,55]. In 1962 Judd [56] and Ofelt [57] independently proposed the theory of forced electric–dipole transition which enabled the compilation of oscillator strengths for lanthanide aquo ions.

### 8. Judd–Ofelt theory

The oscillator strength,  $P$ , of a spectral line for an electric dipole transition from the component  $|A\rangle$  of the ground state to the component  $|B\rangle$  of the excited state may be written as

$$P_{\text{ED}} = \chi \left\{ \frac{\left[ \frac{8\pi^2 mc\sigma}{h} \right]}{\langle A | D_q | B \rangle^2} \right\}, \quad (8.56)$$

where  $m$  is the mass of electron,  $c$  is the velocity of light,  $\chi$  is the Lorenz field correction for the refractive index, and  $D_q$  is the crystal field parameter connected with the electric dipole moment.

Mixing of configurations with opposite parity can occur if the contributions from  $V$  to the Hamiltonian contain terms with odd parity. The contribution from  $V$  arises due to the interaction of electrons of the ion with the crystal electric field which may be written as

$$V_{\text{CF}} = \sum_{tP} A_{tP} D_P^{(t)}, \quad (8.57)$$

where  $t$  is odd.

Considering the crystal electric field as a first-order perturbation, the mixing of states with higher energy and opposite parity,  $|nl\alpha''[S''L'']J''M''\rangle$  may be represented by  $|\psi''\rangle$  with  $|A\rangle$  and  $|B\rangle$  defined as

$$|A\rangle = |f^n \psi J M\rangle = \frac{\sum_k \psi | \langle f^n \psi J M | V_{\text{CF}} | \psi'' \rangle}{E(4f^n J) - E(\psi'')} \quad (8.58)$$

$$|B\rangle = |f^n \psi' J' M'\rangle = \frac{\sum_k \psi' | \langle f^n \psi' J' M' | V_{\text{CF}} | \psi'' \rangle}{E(4f^n J') - E(\psi'')} \quad (8.59)$$

The majority of the solution spectral studies have used the matrix elements given by Carnall [58,59] coupled with least squares analysis or statistical analysis [60–65]. The final expression is

$$P = \chi \left[ \frac{8\pi^2 mc}{3h} \right] \sigma \sum_{\lambda=2,4,6} T_\lambda [U^{(\lambda)}] (2J + 1) \quad (8.60)$$

In equation (8.60)  $T_\lambda$  represent phenomenological parameters which connect the ground state  $\langle f^n \psi J |$  and the final state  $\langle f^n \psi' J' |$  through the matrix of the square of the unit tensor operators  $U^{(\lambda)}$ . These quantities are sensitive to the accuracy of the oscillator strength and the nature of transitions used in their computation.

Lanthanides are class II metals [66] characterized by fast solvent exchange rates of aquo ion

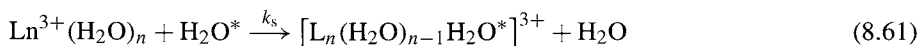


TABLE 8.9  
Hypersensitive transitions of lanthanides.

Ion (+3)	Transition	Energy (kK)	$E_{ff} \times (E_{ct})^{-3}$ ( $\times 10^4$ )	$E_{ff} \times (E_{fd})^{-3}$ ( $\times 10^4$ )
Pr	${}^3P_2 \leftarrow {}^3H_4$	22.5	2	4
	${}^1D_2 \leftarrow {}^3H_4$	17.0	1	3
Nd	$\left. \begin{matrix} {}^4G_{7/2} \\ {}^3K_{13/2} \end{matrix} \right\} \leftarrow {}^4I_{9/2}$	19.2	2	2
	$\left. \begin{matrix} {}^4G_{5/2} \\ {}^4G_{7/2} \end{matrix} \right\} \leftarrow {}^4I_{9/2}$	17.3	2	1
Sm	$\left. \begin{matrix} {}^6P_{7/2} \\ {}^4D_{1/2} \end{matrix} \right\} \leftarrow {}^6H_{5/2}$	26.6	6	2
	${}^4F_{9/2} \leftarrow {}^6H_{5/2}$	6.2	1	1/2
Eu	${}^5D_2 \leftarrow {}^7F_0$	21.5	15	1
Dy	${}^6F_{11/2} \leftarrow {}^6H_{15/2}$	7.7	1	1
	$\left. \begin{matrix} {}^4G_{11/2} \\ {}^4I_{15/2} \end{matrix} \right\} \leftarrow {}^6H_{15/2}$	23.4	4	1
Ho	${}^3H_6 \leftarrow {}^5I_8$	28.0	4	1
	${}^5G_6 \leftarrow {}^5I_8$	22.2	3	1
Er	${}^4G_{11/2} \leftarrow {}^4I_{15/2}$	26.5	3	1
	${}^2H_{11/2} \leftarrow {}^4I_{15/2}$	19.2	2	1
Tm	${}^3H_4 \leftarrow {}^3H_6$	12.6	2	1/2

Unlike the d transition metal ions, the crystal field stabilization energy for lanthanide ions is small, and the conversion of one geometry into another is very easy and common. Facile conversion of geometry in lanthanide ions affects the accuracy of the  $T_\lambda$  parameters as well as their interpretation. A decrease in the number of transitions is observed which have a large value for the  $T_\lambda$  matrix elements in the order  $T_2 > T_4 > T_6$ . Certain transitions with large values of  $T_2$  matrix elements are in general sensitive to the environment of the lanthanide ion. Such transitions are called hypersensitive transitions by Judd and Jorgensen [66]. Hypersensitive transitions are always associated with large values of the  $U^{(2)}$  matrix element. It is observed that  $T_2$  parameters vary widely for a great number of complexes with a distinctly different nature in both crystalline and solution media [67–72]. The hypersensitive transitions obey the selection rules and depend on  $U^{(2)}$ . Since these transitions involve dependence of intensities on the value of  $U^{(2)}$  matrix elements, they are known to be hypersensitive. Some hypersensitive transitions of lanthanides are given in Table 8.9.

- (i) When the lanthanide ion is at the centre of symmetry, the intensity of the hypersensitive transitions is zero.
- (ii) The intensities of hypersensitive transitions can be as large as 200 times the value of the aquo ions.
- (iii) The intensity seems to be in the order  $I^- \gg Br^- > Cl^- > H_2O > F^-$ .

- (iv) Hypersensitivity has been found to be proportional to the degree of involvement of 4f orbital in bonding indicated by a parameter  $b$

$$P \propto b; \quad b^{1/2} \left[ \frac{1 - \bar{\beta}}{2} \right]^{1/2} \quad (8.63)$$

$\bar{\beta}$  in equation (8.63) is defined as

$$\bar{\beta} = \left[ \frac{F_k^c}{F_k^f} \right] V \frac{\xi_{4fc}}{\xi_{4fi}} \quad (8.64)$$

In equation (8.64)  $F_k^f$  and  $F_k^c$  are interelectronic repulsion parameters of the free ion and the complex, respectively,  $k = 2, 4, 6$ ;  $\xi_{4fc}$  and  $\xi_{4fi}$  are spin-orbit interaction parameters for the complex and free ion, respectively [64].

- (v) The intensities of the hypersensitive transitions can be correlated with the  $pK_a$  of the ligands [74].
- (vi) In the presence of some ligands, the hypersensitivity can be found in some transitions which are not usually hypersensitive. For example,  ${}^3H_4 \rightarrow {}^3P_2$  and  ${}^3H_4 \rightarrow {}^1D_2$  in Pr(III);  ${}^4I_{9/2} \rightarrow {}^4G_{7/2}$ ,  ${}^4I_{9/2} \rightarrow {}^4F_{7/2}$ ;  ${}^4I_{9/2} \rightarrow {}^4F_{5/2}$ , and  ${}^4I_{9/2} \rightarrow {}^4F_{3/2}$ , in Nd(III). These transitions are known as ligand mediated pseudohypersensitive transitions.

Many attempts have been made to explain the origin and magnitude of hypersensitivity. The initial attempts focused on explanations based on crystal field theory. According to the crystal field theory model

$$T_\lambda \approx (r^{t+1})^2 R^{-2t-2} \quad (8.65)$$

when  $\lambda = 2, t = 1$  or  $3$ ;  $\lambda = 4, t = 3$  or  $5$ ;  $\lambda = 6, t = 5$  or  $7$ . Equation (8.65) suggests that  $T_\lambda$  parameters are sensitive to the immediate coordination environment with the order  $T_6 > T_4 > T_2$ . Unfortunately the observed order is the opposite of the predicted order. Thus crystal field theory cannot explain this anomaly as well as the hypersensitivity of octahedral lanthanide complexes.

According to Jorgensen and Judd, hypersensitivity may occur due to pseudoquadrupole transitions [66]. Consequently an ion embedded in an inhomogeneous dielectric would exhibit hypersensitive behavior. These normally weak electric quadrupole transitions are probably intensified and become hypersensitive transitions. Hypersensitivity can also occur in symmetries of spherical harmonics ( $Y_{mk}$ , with  $k = 1$ ) which form totally symmetrical representations. Thus this permits their inclusion in the crystal field potential.

Gruen [80] found that the vapor of  $NdI_3$  of  $D_{3h}$  symmetry with a spherical harmonic  $k = 1$  does not transform as a totally symmetric representation. This is a case that cannot be explained on the basis of symmetric representation of hypersensitivity. Since  $NdI_3$  vapor molecules are in a relatively homogeneous dielectric, the pseudoquadrupole mechanism is not operative. A vibronic mechanism including covalency has been advanced to explain the origin of hypersensitivity in lanthanide complexes.

Henrie et al. found a linear correlation between Judd–Ofelt parameters,  $T_\lambda$ , and the ligand basicity,  $pK_a$  [74]. The cyclopentadienide complexes show a high degree of hypersensitivity. The hypersensitivity increase when dibenzoylmethanide complexes of Eu(III) and Tm(III) formed adducts with Lewis bases. This is in accord with the fact that the base strength increases for both oxygen-containing bases and the nitrogen-containing adducts [90–93].

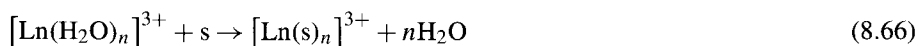
The  $T_2$  parameter has been related to hypersensitivity as well as to covalency. Studies of phosphate and germanate glasses have provided evidence for a static covalency mechanism consistent with the behaviors of  $T_2$  parameter [94]. But the results for Tm(III) and Er(III) seem to favor a vibronic mechanism. Comparison of the hypersensitivity behavior of Nd(III) doped in  $Y_2O_3$  and  $LaF_3$  crystals showed the hypersensitivity to be due to the change in symmetry [95]. Other points of interest are that non-hypersensitive transition intensities in the  $Y_2O_3$  lattice were twice as intense as those in  $LaF_3$  and the hypersensitive bands were seven times more intense in oxide than in  $LaF_3$ . The large difference in intensities is attributed to the greater basicity of the oxide lattice.

According to the nephelauxetic series, oxide ( $O^{2-}$ ) is the most basic and fluoride ( $F^-$ ) is the least basic [92]. Studies on Nd(III), Ho(III) and Er(III) anhydrous chlorides in solvents such as formamide showed evidence for the relationship between hypersensitivity and electron-donating ability of the solvent. The hexahalides of lanthanides give evidence for the role of symmetry and covalency in explaining the origin of hypersensitivity. The intensities of nonhypersensitive transitions of hexahalides are in the sequence  $LnCl_6^{3-} > LnBr_6^{3-} > LnI_6^{3-}$ .

In the case of Pr(III), the transition  $^3H_4 \rightarrow ^3F_2$  occurs at  $\sim 5200\text{ cm}^{-1}$  and shows hypersensitivity. The other two transitions  $^3H_4 \rightarrow ^3P_2$  and  $^3H_4 \rightarrow ^1D_2$  also show a marked sensitivity towards slight changes in the coordination environment of Pr(III) [73]. The latter two transitions in Pr(III) do not obey the selection rules and hence cannot be considered as hypersensitive transitions.

In the case of Nd(III) both  $^4I_{9/2} \rightarrow ^4G_{5/2}$ ,  $^4G_{7/2}$ , and  $^4K_{13/2}$  transitions [74] have been observed to be hypersensitive transitions although the later transitions have been questioned as to their hypersensitivity [73]. Another transition  $^4I_{9/2} \rightarrow ^4F_{5/2}$  of Nd(III) has been found to be hypersensitive, sometimes showing sensitivity higher than  $^4I_{9/2} \rightarrow ^4G_{5/2}$  and the reason for this anomaly is not clear. It is suggested that ligand mediated pseudohypersensitivity might explain the unusual hypersensitivity of the transition  $^4I_{9/2} \rightarrow ^4F_{5/2}$  [65].

One possible viewpoint is that the oscillator strength of the hypersensitive transitions might be affected by changes in the coordination sphere of the lanthanide ion. The aquo lanthanide ion on replacement of coordinated water by another solvent might affect the transition as in the case of substitution by a chromophore.



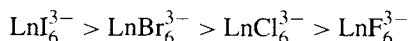
Thus solvent exchange might affect the oscillator strength of the transitions and in particular the hypersensitive transitions.



Some salient observations on hypersensitive transitions are as follows:

- (i) The intensity of hypersensitive transitions is zero when the lanthanide ion is at the center of symmetry [75,76]. Small deviations due to an inversion of the center of symmetry lead to an intensification of the hypersensitive transitions with little effect on other transitions [77–79].
- (ii) The intensities of the hypersensitive transitions can increase up to 200 times the intensity of the aquo ion and have been found to decrease in only these instances [77, 81,82].
- (iii) For a particular hypersensitive transition, the order of the ligands for a change in intensity is  $I^- \gg Br^- > Cl^- > H_2O > F^-$  [77,78,80,81]. Substitution of fluorine in  $\beta$ -diketonates results in considerable intensification of the hypersensitive band. Intensification of hypersensitive bands has also been observed in  $\beta$ -diketone [83], Schiff bases [84] and bipyridine–phenanthroline complexes [85,86].

It has been suggested [77] that this order shows that the iodide complexes are the least distorted from true octahedral symmetry. The hypersensitive transitions showed the sequence



which is exactly the opposite of the trend shown by non-hypersensitive transitions. The sequence shown for hypersensitive transitions parallels the behavior of  $LnX_6^{3-}$  in the vapor phase and also in keeping with the increasing electron-donating ability of the halide. It should be pointed out that this trend is opposite to the trend observed in distortion from  $O_h$  symmetry.

A linear correlation has been observed between the oscillator strengths of the hypersensitive transitions of Pr(III) and Nd(III) with the bonding parameter ‘b’ which represents the degree of mixing of the wave functions of metal and ligand. This observation implicates 4f metal orbitals in bonding. Correlation of oscillator strengths with the bonding parameter has been found to hold good for a number of complexes of Pr(III) and Nd(III) [87–89, 96–98]. It has also been observed that hypersensitivity in the form of intensification of bands is associated with a lowering in the coordination number of the lanthanide with an increased nephelauxetic effect resulting in shortening in metal–ligand distances. It is surmised that since the nephelauxetic effect causes intensification of the hypersensitive bands, the oscillator strengths of the hypersensitive bands may be sensitive to a lowering of the coordination number of the lanthanide ion [64].

## 9. Covalency model of hypersensitivity

The “covalent” model of hypersensitivity was developed by Choppin and coworkers [70,74] to explain (i) the observed order of sensitivity of the parameters to the environment is  $T_2 > T_4 > T_6 >$ , (ii) the general trend of the hypersensitive transition oscillator strength increases with estimated covalency, (iii) the observed hypersensitivity in octahedral complexes, (iv) the simultaneous occurrence of hypersensitivity and large splittings of

$J = 3/2$  levels, (v) the correlation between oscillator strength of hypersensitive transitions and ligand basicity.

Basically the procedure used by Choppin et al. [74] is analogous to that of Judd [56] and Ofelt [57] except to include charge transfer states in addition to  $f^{n-1}5d^1$  and  $f^{n-1}5g^1$  as the excited state to be mixed with  $f^n$ . The charge transfer states arise as one electron transfers from ligand orbitals to the f-orbitals on the metal. The problem reduces to describing the excited charge transfer states. If  $\phi$  represents the ligand wavefunction and  $m$  the number of ligand electrons, the  $f^n$  states are represented as

$$\sum_M a_M (\phi^m f^n \psi JM) \quad (8.67)$$

and the charge transfer states as

$$\sum_{M''} b_{M''} (\phi^{m-1} f^{n-1} \psi'' M'') \quad (8.68)$$

The perturbation is of the form

$$V = \sum_{t_p} [4\pi/(2t+1)]^{1/2} Y_{tp}(\phi_i \theta_i) F_{tp}(r_i) \quad (8.69)$$

will mix states of the  $f^n$  configuration with charge transfer states of differing parity. From the above the contribution of charge transfer states (equation (8.68)) to the electric dipole matrix element  $\langle B | D_q^{(1)} | B \rangle$  similar to the relationship obtained by Judd [56] has been derived. In an analogy to the results of Judd [56], the  $T_\lambda$ 's are proportional to  $\Delta E^{-2}$ , where  $\Delta E$  is the energy difference

$$\Delta E = E(\phi^{m-1} f^{n+1}) - E(\phi^m f^n) \quad (8.70)$$

$\Delta E$  is related to the optical electronegativity difference between the ligand and the metal

$$E = 30(\chi_M^{\text{opt}} - \chi_L^{\text{opt}}) + C^1(n)E^1 + C^3(n)E^3 + C^2(n)\xi_{nf}, \quad (8.71)$$

where  $\chi_M^{\text{opt}}$  and  $\chi_L^{\text{opt}}$  are the optical electronegativities of metal and ligand, respectively,  $E^1$  and  $E^3$  are Racah's interelectron repulsion parameters,  $\xi$  is the spin-orbit coupling constant, and  $C^1(n)$ ,  $C^2(n)$  and  $C^3(n)$  are coefficients. The ligand optical electronegativity is related quantitatively to the ligand  $pK_a$ . This leads to the correlation of oscillator strength,  $P$  with  $pK_a$ . Correlation of oscillator strength of hypersensitive transition in holmium complexes with  $pK_a$  of the ligand is shown in Fig. 8.10. The plot of optical electronegativity of ligand against oscillator strength of hypersensitive bands of Nd(III) and Ho(III) complexes is shown in Fig. 8.11. The correlation in Fig. 8.11 may be better if both parameters were determined from the same set of complexes.

By considering electron transfer states of the same parity as  $f^n$  (i.e.)  $f^{n+1}\phi^{m-1}$  (with  $\phi$  and  $f$  transforming as the same irreducible representations) mixed with  $f^n$  through

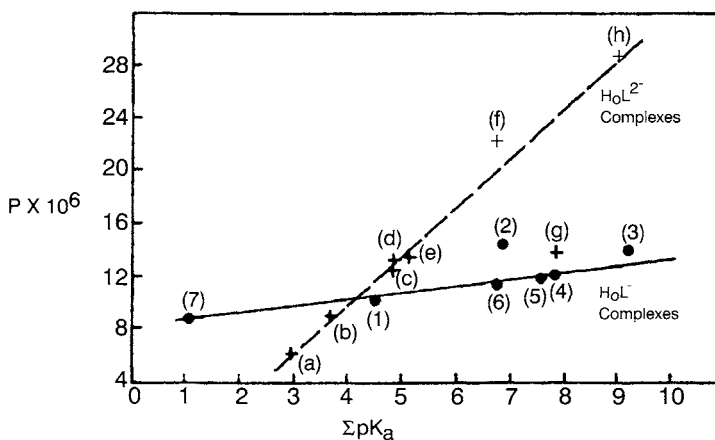


Fig. 8.10. Plot of oscillator strength  $P$  of the 1:1 complexes of  $Ho^{3+}$  with monobasic (+) and dibasic (●) ligands vs. the  $\Sigma pK_a$  of the ligand acid (from ref. [74]); (a) fluoride, (b) glycolate, (c) acetate, (d) propionate, (e)  $\alpha$ -picolinate, (f) tropolonate, (g) kojate, (h) acetylacetonate, (1) IMAD, (2) dipicolinate, (3) methyl succinate, (4) malonate, (5) maleate, (6) fumarate, (7) sulfate.

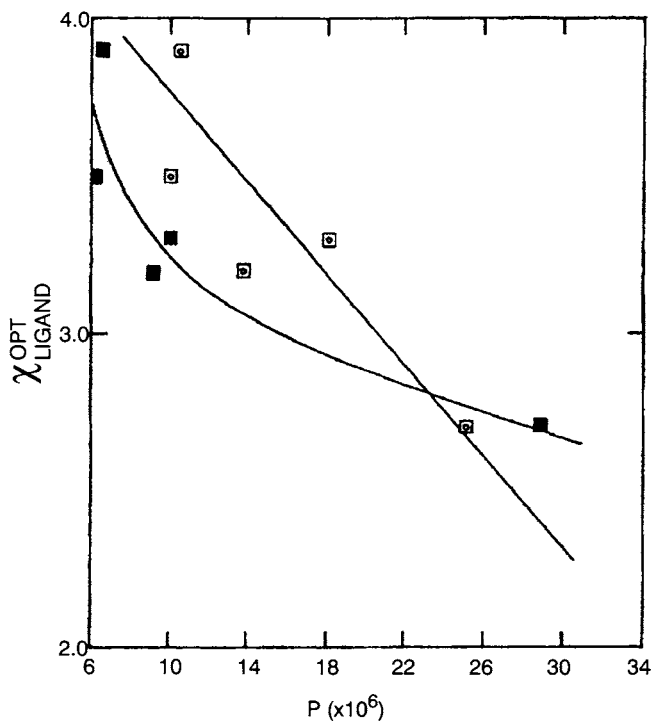


Fig. 8.11. Plot of optical electronegativities [74] ( $\chi_{ligand}^{opt}$ ) vs. hypersensitive band oscillator strengths for  $Nd^{3+}$  (□) and  $Ho^{3+}$  (■) complexes with various complexing ligands. The oscillator strengths are values for 1:1 complexes [74] while the ( $\chi_{ligand}^{opt}$ ) are for the varying degrees of ligand complexation.

configuration interaction, the correlation of the red shift of f-f transitions with increasing extent of covalency can be explained since the  $f^{n+1}\phi^{m-1}$  levels lie lower for more covalent ligands.

It is also known that the triplet levels in Pr(III) show a greater nephelauxetic effect than the singlet levels from compound to compound. This can be explained thus, the excited states arising from charge transfer from ligand to metal give rise to Pr(III) singlets with a baricentre higher than the triplets. Hence the triplet states arising from electron transfer shift the triplets of  $f^2$  to a greater extent than the singlets. The covalency model of Choppin can also explain the variations in the nephelauxetic effect as a function of  $Z$  for lanthanides.

In order to compare the  $T_\lambda$  parameters of Judd-Ofelt theory for different lanthanides, Carnell et al. [99] have removed the dependence of  $T_\lambda$  on the ground state multiplicity ( $2J + 1$ ) and defined a new set of parameters,  $T_\lambda$  given by

$$T_\lambda = T_\lambda(2J + 1)^C \quad (8.72)$$

The values of  $T_2$  have been calculated [100] using the oscillator strengths in the literature [101,102]. It is assumed that  $T_4$  and  $T_6$  are constant and equal to those of aquo ions.  $T_2$  values are correlated with  $pK_a$  values of the ligands for  $Nd^{3+}$  and  $Ho^{3+}$  showing that  $T_2$  is affected by the covalency of the M-L bond (Figs 8.12 and 8.13).

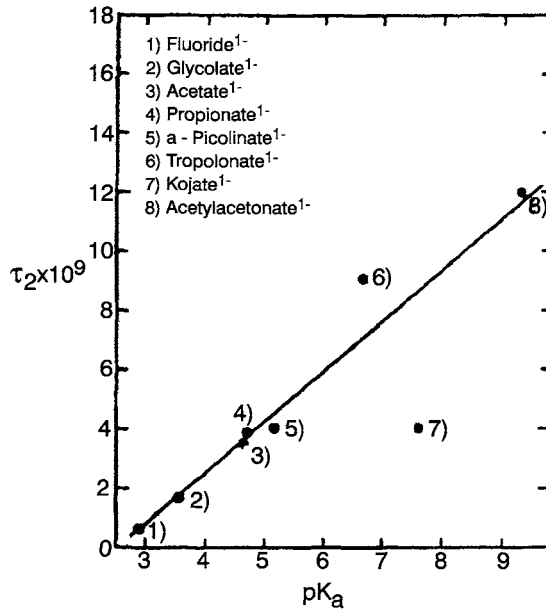


Fig. 8.12.  $T_2$  vs. ligand  $pK_a$  values for  $NdL^{2+}$  complexes.

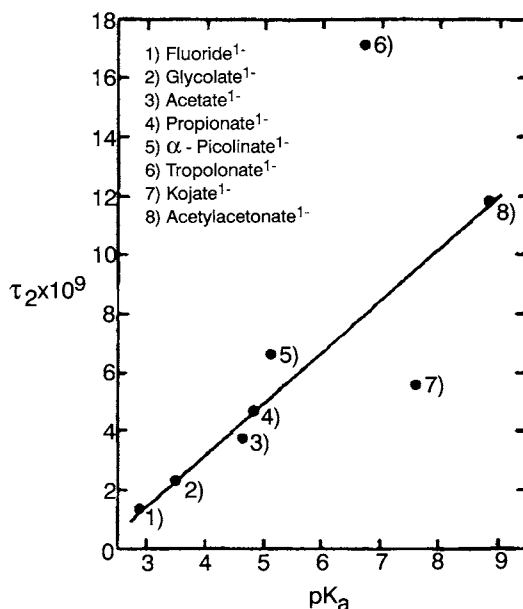


Fig. 8.13.  $T_2$  vs. ligand  $pK_a$  values for  $\text{HoL}^{2+}$  complexes.

## 10. Role of symmetry

The effect of symmetry on the spectral intensity is significant. All the observed  $f-f$  transitions have either  $U^{(4)}$  or  $U^{(6)}$  matrix elements and hence influenced by  $T_4$  and  $T_6$  parameters. Then the  $T_4$  and/or  $T_6$  parameters are expected to reflect the symmetry of the lanthanide environment. Nearly all the hypersensitive transitions also have  $U^{(4)}$  or  $U^{(6)}$  matrix elements which means that these transitions will be influenced the symmetry in the lanthanide complex. But hypersensitivity by itself cannot be due to a symmetry effect.

The hypersensitivity of the transitions given in Table 8.9 cannot be explained in the framework of the Judd–Ofelt theory since they have vanishing or very small  $U^{(2)}$  matrix elements. This is the case for the transitions  ${}^3P_2 \leftarrow {}^3H_4$  and  ${}^1D_2 \leftarrow {}^3H_4$  in  $\text{Pr}^{3+}$ . Similarly it has been noted that in a study of oscillator strengths and  $T_\lambda$  parameters of  $\text{Ln}(\text{NO}_3)_3$  salts, the normal transitions with vanishing  $U^{(2)}$  matrix elements showed variations in oscillator strengths similar to hypersensitive transitions. Such variations do not negate the Judd–Ofelt theory but indicate significant changes in symmetry around the lanthanide ion. A prime example of this phenomenon is the oscillator strength of  $\text{NdCl}_6^{3-}$  [103].

It is a usual practice to assume that the oscillator strengths of hypersensitive transitions are proportional to the  $T_2$  parameter. This assumption is reasonable for aqueous systems. In some hypersensitive transitions,  $U^{(4)}$  and  $U^{(6)}$  matrix elements are significant relative to the magnitude of  $U^{(2)}$ . Thus it is necessary to be careful when dealing with absolute values of oscillator strength alone, since symmetry may effect a significant contribution to the intensity of both hypersensitive and non-hypersensitive transitions. Caution should be

used when hypersensitive transitions for which  $U^{(2)}$  and either or both  $U^{(4)}$  and  $U^{(6)}$  are of comparable values.

It has been noted that the  ${}^7F_0 \leftarrow {}^5D_2$  hypersensitive transition in  $\text{Eu}^{3+}$  shows greater sensitivity to the environment than any other lanthanide ion. This phenomenon can be explained by possible mixing of the electron transfer character into the hypersensitive transition. The oscillator strength of an allowed electron transfer transition is given by

$$P_{\text{CT}} = RE_{\text{CT}} \langle \psi_0 | \nu | \psi_{\text{CT}} \rangle, \quad (8.73)$$

where  $P$  is the oscillator strength,  $k$  is a constant,  $E_{\text{CT}}$  is the energy of the charge transfer transition,  $\psi_0$  and  $\psi_{\text{CT}}$  are the ground and excited state wave functions, respectively. When an f-f transition "borrows" some intensity from the charge transfer transition, the contribution to the f-f oscillator may be written as

$$P_{\text{ff}} = a^2 E_{\text{ff}} (E_{\text{CT}})^{-3} P_{\text{CT}}, \quad (8.74)$$

where  $P_{\text{ff}}$  and  $P_{\text{CT}}$  are oscillator strengths of f-f and charge transfer transitions, respectively. 'a' represents matrix elements of asymmetrical vibrations or odd terms in the molecular field which mix the charge transfer level with the  $f^n$  level. Thus the oscillator strength should be sensitive to the charge transfer energy which in turn depends on the nature of the ligand in the lanthanide complex. The values of  $E_{\text{ff}} \times (E_{\text{CT}})^{-3}$  are given in Table 8.9 and obtained by calculation from  $\text{LnBr}_6^{3-}$  data [104,105]. It is seen from Table 8.9 that the value of  $E_{\text{ff}} \times (E_{\text{CT}})^{-3}$  is highest for Eu among the lanthanides exhibiting hypersensitive transitions. Thus a change in charge transfer energy should affect  $\text{Eu}^{3+}$  significantly. This is in agreement with the observation that  $\text{Eu}^{3+}$  is very sensitive to the environment. The greater sensitivity of  $\text{Ho}^{3+}$  and  $\text{Nd}^{3+}$  to the environment may also be explained by arguments similar to those advanced for  $\text{Eu}^{3+}$ .

In addition to mixing of charge transfer states with  $f^n$ , we also have f-d and f-g mixing, and an inverse third power dependence of the oscillator strength on the f-d or f-g transition energy. The lowest transition energies are observed for  $\text{Ce}^{3+}$ ,  $\text{Pr}^{3+}$  and  $\text{Tb}^{3+}$  and the f-d transitions have been observed for  $\text{LnBr}_6^{3-}$ , where Ln = Ce, Pr and Tb. The values of  $E_{\text{ff}} \times (E_{\text{fd}})^{-3}$  have been calculated and are given in Table 8.9. This value shows a smaller variation with atomic number than the corresponding parameter for charge transfer energies, and the maximum occurs in the case of  $\text{Pr}^{3+}$ . Some of the observations on the hypersensitivity of  $\text{Pr}^{3+}$  can be explained by invoking the variations in f-d energies. In general f-d energy varies much less than charge transfer energy with a change in ligand, and hence contribution to hypersensitivity is expected to be much less in most systems.

## 11. Judd-Ofelt theory of hypersensitivity

According to Judd and Ofelt, the hypersensitivity of a transition is due to the mixing of the excited states  $4f^{n-1} \rightarrow 5d^1$  and  $4f^{n-1} \rightarrow 5g^1$  with  $4f^n$  states. Henrie et al. added a partial charge transfer character to the above mixing of states in their covalency model in which

the electron is delocalized from the ligand orbital resulting in an intense hypersensitive band. The oscillator strength,  $P$  for an  $f$ - $f$  transition is given by [56,57]

$$P = \nu \sum_{\lambda=2,4,6} T_{\lambda} \langle f^n \psi J \| U^{(\lambda)} \| f^n \psi' J' \rangle \quad (8.75)$$

The above equation can be modified to give

$$\sum_m a_M (\phi^m f^n \psi J M) |, \quad (8.76)$$

where  $\phi$  is the ligand wave function and  $m$  the number of electrons in the ligand.

As shown before, the charge transfer can be represented as

$$\sum_{M''} b_M (\phi^{m-1} f^{n+1} \psi'' J'' M'') | \quad (8.77)$$

Then a perturbation of the form

$$V = \sum_{iP} \left[ \frac{4\pi}{(2t+1)} \right]^{1/2} Y_{iP}(\varphi_i \theta_i) F_{iP} / r_i \quad (8.78)$$

will result in mixing of  $f^n$  states with charge transfer states of different parity. Thus mixing of  $4f^n$  states with charge transfer states of the same parity,  $f^{n+1} \phi^{m-1}$  through coulombic and configuration interaction produces a red shift of the  $f$ - $f$  transition with increasing covalency since the  $f^{n+1} \phi^{m-1}$  levels are at lower energy for more covalent ligands.

The ligand wavefunction  $\phi$  can be the sum of renormalized radial functions multiplied by spherical harmonics, keeping the origin at the central metal ion and written as

$$\phi_{\text{ligands}} = \sum_K \alpha_K \sum_m Y_{Km}, \quad K = \text{odd} \quad (8.79)$$

The metal wave function,  $\phi$  is the sum of the original  $4f$  wave function and the ligand wavefunction weighted by a mixing coefficient  $b$  and may be written as

$$\phi_{\text{metal}} = (1-b)^{1/2} |4f\rangle - b^{1/2} |\phi_{\text{ligand}}\rangle \quad (8.80)$$

Using the matrix element  $\langle f \| C^{(f)} \| l \rangle$  we get

$$(1-b)^{1/2} \langle f \| C^{(t)} \| l \rangle - b^{1/2} \langle \phi_{\text{ligand}} \| C^{(t)} \| l \rangle \quad (8.81)$$

Hence the important term that affects  $T_{\lambda}$  is

$$-b^{1/2} \sum_k \alpha_k \langle Y_{km} \| C^{(t)} \| l \rangle$$

From this it is clear that when 4f–5d mixing occurs, then  $T_2$  will be affected,  $T_4$  affected to a lesser extent and  $T_6$  unaffected by the immediate coordination environment around the lanthanide ion. The  $4f^n \rightarrow 5d$  mixing may impart some sensitivity to  $T_6$  in some cases. Hypersensitivity involving  $T_4$  has not been identified in any transition.

## 12. Dynamic coupling mechanism

The original Judd–Ofelt theory is based on the idea that the ligands around the metal ion cause a perturbation which results in mixing of excited configuration with  $4f^n$  configuration. It is reasonable to envisage in this situation that the metal ion wavefunctions perturb the ligand wavefunctions and this idea has roots in Fajan's theory [106]. The dynamic coupling mechanism proposed by Mason [107] can be described thus. In a two-system model for lanthanide complexes, neglecting overlap, denoting the metal ground and excited state functions as  $|\text{Mo}\rangle$  and  $|\text{Ma}\rangle$ , respectively, and those of ligands as  $|\text{Lo}\rangle$  and  $|\text{La}\rangle$ , then the product function  $|\text{MoLo}\rangle$  represents the total system of lanthanide ion and ligand. The first-order perturbed ground state  $|\text{A}\rangle$  and excited state  $|\text{B}\rangle$  may be written as

$$|\text{A}\rangle = |\text{MoLo}\rangle - \sum_b (E_a + E_b)^{-1} \langle \text{MaLb} | V | \text{MoLo} \rangle |\text{MaLb}\rangle \quad (8.82)$$

$$|\text{B}\rangle = |\text{MaLo}\rangle + \sum_b (E_a - E_b)^{-1} \langle \text{MoLb} | V | \text{MaLo} \rangle |\text{MoLb}\rangle \quad (8.83)$$

where  $E_a$  refers to energy of  $|\text{Ma}\rangle \leftarrow |\text{Mo}\rangle$  and  $E_b$  that of  $|\text{Lb}\rangle \leftarrow |\text{Lo}\rangle$ . The f–f transition then can acquire a first-order electric dipole transition moment given by

$$e \langle \text{A} | Dq^{(1)} | \text{B} \rangle = e \sum_b 2E_b (E_b^2 - E_a^2)^{-1} \langle \text{MoMa} | V | \text{LoLb} \rangle \text{Lo} | Dq^{(1)} | \text{Lb} \rangle \quad (8.84)$$

Calculations of the crystal field and dynamic polarization contributions to the overall dipole strength of particular multiplet–multiplet  $|f^n J\rangle \rightarrow |f^n J^1\rangle$  transitions in the complexes  $[\text{Ln}(\text{H}_2\text{O})_9]^{3+}$  and  $[\text{Ln}(\text{oda})_3]^{3-}$  for  $\text{Ln} \equiv \text{Pr}, \text{Eu}, \text{Tb}$  and  $\text{Ho}$ , with a neglect of pseudo scalar cross [9] term of the anisotropic ligand polarizability contribution (equation (8.85)) show that the crystal field contribution is generally dominant, the dynamic polarization contribution being of comparable significance for the hypersensitive transitions [108]. Anisotropic ligand polarization contribution is given by the relation

$$\mu_{0m}^\gamma = - \sum_L \theta_{0m}^{\alpha\beta} G_{\alpha\beta\delta}^L \alpha_{\gamma\delta}^L(\nu_{0m}), \quad (8.85)$$

where  $\mu_{0m}^\gamma$  is the first-order electric dipole moment of the metal ion excitation  $\text{M}_0 \rightarrow \text{M}_m$ ,  $\Theta_{0m}^{\alpha\beta}$  the electric quadrupole moment,  $G_{\alpha\beta\delta}^L$  is geometric tensor representing the radial and angular terms governing the potential between the electric quadrupole moment centered on the metal ion and the induced dipole,  $\alpha_{\lambda\delta}^L(\nu_{0m})$  refers to the  $\gamma\delta$  component of the



polarizability tensor of the ligand L in the global coordinate framework of the complex at the transition frequency  $\nu_{0m}$ . The Greek subscripts and superscripts,  $\alpha, \beta, \gamma$ 's denote Cartesian components  $x, y, z$ , in the coordinate frame of the metal complex.

In the complexes  $[\text{Ln}(\text{H}_2\text{O})_9]^{3+}$ ,  $[\text{Ln}(\text{oda})_3]^{3-}$ , the dynamic polarization first-order electric dipole transition moment is minimized by negative interference due to the out-of-phase relation between the contributions of the  $[\text{ML}_3]$  and  $[\text{ML}_6]$  ligand sets [109,110]. For  $[\text{Ln}(\text{oda})_3]^{3-}$  and other  $D_3$  complexes, only the anisotropic polarizability contributions are non-zero for  $\Delta M_J = \pm 1$  transitions in the  $[\text{Eu}(\text{H}_2\text{O})_9]^{3+}$  and  $[\text{Eu}(\text{oda})_3]^{3-}$  complexes the contribution of the cross-term to the dipole strength of the  ${}^7F_0 \rightarrow {}^5D_2$  and  ${}^5D_0 \rightarrow {}^7F_2$  transitions has a magnitude comparable with that of the dominant crystal field or dynamic polarization contribution [111].

The eight-coordinate tetrakis(diethyldithiocarbamate) lanthanide complexes are isomorphous and the lanthanum complex has a quasi-tetrahedral configuration of the four  $\text{CS}_2$  chelate groups. The transition frequencies and dipole strengths of these complexes available over the accessible f-f manifold allowed the extraction of the Judd-Ofelt intensity parameters  $\Omega_\lambda$  for  $\lambda = 2, 4, 6$  by standard least squares methods [112,113]. The values of observed  $\Omega_\lambda$  and calculated  $\Omega_\lambda$  values are given in Table 8.10. The three components of  $\Omega_0$  are

$$\Omega_{\text{tot}} = \Omega(\text{CF}) + \Omega_\lambda(\text{LP}) + \Omega_\lambda(\text{CT}), \quad (8.86)$$

where  $\Omega(\text{CF})$  refers to the static crystal field,  $\Omega_\lambda(\text{LP})$  to the dynamic ligand polarization and  $\Omega_\lambda(\text{CT})$  to the pseudoscalar cross-term contributions to  $\Omega_\lambda(\text{TOT})$ . The dynamic polarization contributions recorded were calculated in the mean polarizability approximation, although the corresponding anisotropic ligand polarizability values do not differ significantly, as expected from the quasi-tetrahedral stereochemical disposition of the  $\text{CS}_2$  chelate groups [114].

The calculated intensity parameters show that the dynamic polarization mechanism is important mainly for the hypersensitive quadrupole f-f transitions as expected [115,116], due to the dependence of  $\Omega_\lambda(\text{LP})$  on  $R_L^{-2\lambda-4}$ . There are no major differences between the relative crystal field and ligand polarization contributions to  $\Omega_\lambda(\text{TOT})$  across the series of complexes from Pr(III) to Yb(III). In general, along the series the crystal field contribution to  $\Omega_\lambda(\text{TOT})$  increases from 5 to 57 to 98.5 percent for  $\lambda$  values of 2, 4 and 6, respectively, while the corresponding ligand polarization contribution decreases from 66 to 17 to 0.1 percent, respectively. The remaining cross-term component in equation (8.86) is significant for  $\lambda = 2$  and 4, contributing averages of 29 and 25 percent, respectively, over the series.

The dynamic coupling mechanism predicts that hypersensitivity should be observed when the point group of the lanthanide complex contains  $Y_{3m}$  spherical harmonics in the expansion of the point potential. The good agreement between the calculated and observed values for  $T_2$  or  $\Omega_2$  parameters shows that the dynamic coupling mechanism makes a significant contribution to the intensities of the quadrupole allowed f-electron transitions in lanthanide complexes. Qualitatively, the mechanism is allowed for all lanthanide group symmetries in which the electric quadrupole component  $\theta, \alpha, \beta$  and the electric dipole moment  $\mu, \alpha$  transform under a common representation.

TABLE 8.10  
The observed and calculated dipole strength parameters  $\Omega_\lambda$  of the f-f transitions in the series of Na[Ln((C<sub>2</sub>H<sub>5</sub>)<sub>2</sub>dtc.)<sub>4</sub>] complexes (IV) [112,113].

Ln <sup>3+</sup>	$\Omega_\lambda(\text{obs}) (\times 10^{-61} \text{ C}^2 \text{ m}^2)$			$\Omega_{\text{tot}}(\text{calc}) (\times 10^{-61} \text{ C}^2 \text{ m}^2)$						
	$\Omega_2$	$\Omega_4$	$\Omega_6$	$\Omega_2(\text{CF})$	$\Omega_2(\text{LP})$	$\Omega_2(\text{tot})$	$\Omega_4(\text{CF})$	$\Omega_4(\text{tot})$	$\Omega_6(\text{CF})$	$\Omega_6(\text{tot})$
Pr(f <sup>2</sup> )	7.19	3.83	2.56	1.31	18.72	27.83	2.04	4.13	2.92	2.98
Nd(f <sup>3</sup> )	10.73	2.87	2.77	1.35	16.83	25.60	1.25	3.06	1.80	1.84
Sm(f <sup>5</sup> )	4.71	3.71	1.27	0.82	13.89	19.94	1.11	2.23	1.37	1.40
Dy(f <sup>9</sup> )	9.50	1.22	1.17	0.87	10.32	15.74	1.17	1.89	1.40	1.41
Ho(f <sup>10</sup> )	9.75	2.85	1.16	0.74	9.73	14.60	0.96	1.60	1.12	1.13
Er(f <sup>11</sup> )	9.46	0.62	0.81	0.76	9.19	13.99	0.98	1.57	1.14	1.15
Tm(f <sup>12</sup> )	8.51	3.00	0.82	0.78	8.69	13.46	1.01	1.57	1.14	1.15
Yb(f <sup>13</sup> ) <sup>a</sup>				0.69	8.21	12.55	0.86	1.35	0.97	0.98

The observed  $\Omega_\lambda$  are minimized root mean square values based upon the spectroscopic data reported by Ciampolini et al. [66]. The individual crystal field contributions  $\Omega_\lambda(\text{CF})$  are listed for each calculated  $\Omega_\lambda$  together with the particular ligand polarization contribution  $\Omega_\lambda(\text{LP})$ . The calculated total  $\Omega_\lambda(\text{tot})$  sums the crystal field (CF) and ligand field (LF) contributions with the CF-LP cross-term.

<sup>a</sup>The observed and the calculated values of the total dipole strength of the  $^2\text{F}_{7/2} \rightarrow ^2\text{F}_{5/2}$  transition of the ytterbium(III) complex IV are  $3.67 \times 10^{-62} \text{ C}^2 \text{ m}^2$  and  $3.66 \times 10^{-62} \text{ C}^2 \text{ m}^2$ , respectively.

The lanthanide tribromides and triiodides in the vapor state have trigonal planar structures with  $D_{3h}$  symmetry. The triiodides have maximum oscillator strengths, and the dynamic coupling mechanism explains satisfactorily the observed oscillator strength of the hypersensitive transition and the associated  $T_2$  values [117]. Lanthanide triiodides have very high values of oscillator strength pertaining to the hypersensitive transition while lanthanide ions in a matrix of  $LaF_3$  have very low values of oscillator strength. The oscillator strengths of lanthanide  $\beta$ -diketonates for the hypersensitive transition lie between those of triiodides and lanthanides in  $LaF_3$  matrix. It is also surmised that the groups exocyclic to the chelate rings in complex contribute in different ways towards the observed oscillator strengths of the hypersensitive transitions.

Studies involving temperature dependence of the oscillator strengths of the hypersensitive transitions and circular dichroism (CD) and magnetic circular dichroism (MCD) of optically active complexes may give some useful information from which the relative contributions of static and dynamic coupling mechanisms to the observed oscillator strengths may be ascertained.

### 13. Absorption spectra of lanthanide ions

Having discussed the theoretical principles of crystal field theory, theories of intensity of the hypersensitive transitions, it is logical to examine the absorption spectral features of lanthanide ions in aqueous solutions. It is probably worthwhile looking into the historical development of the spectra of lanthanides. The most prominent era in the development is the 1930's. Prandtl and Scheiner [118] presented a complete collection of absorption spectra of trivalent lanthanides in solution. The covered region is 7000–2000 Å. An apparent symmetry in the region of absorption with band structure shifting toward the ultraviolet in approaching the centre of the series from both ends was observed.

Ce (colorless)  
Pr (yellow green)  
Nd (red violet)  
61 (unknown)  
Sm (yellow)  
Eu (essentially colorless)  
Gd (colorless)  
Tb (essentially colorless)  
Dy (light yellow green)  
Ho (brownish yellow)  
Er (pink)  
Tm (light green)  
Yb (colorless)

This apparent symmetry was also observed earlier by Main-Smith based on colour of the solutions alone [119]. Then followed the work of Van Vleck [53] which attributed the sharp absorption bands to transitions within the  $4f^n$  configuration. This interpretation was proposed by others as well [120–122].

Progress was made in the theoretical interpretation of the spectra of rare earth compounds and solutions in terms of energy level structure, in particular those of  $\text{Pr}^{3+}$  and  $\text{Tm}^{3+}$  with  $4f^2$  and  $4f^{12}$  configurations, respectively [123,124]. Differences in interpretation of the bands existed which were resolved in favour of f-f transitions [125]. Then the complex spectrum of  $\text{Nd}^{3+}(4f^3)$  was analyzed [126]. Jorgensen was one of the first to identify systematically the energy levels of lanthanide aquo ions [127].

The spectra of lanthanide ions are not as sensitive to the environment as the transition metal ions. The small changes in absorption spectra of  $\text{Eu}(\text{NO}_3)_3$  and  $\text{EuCl}_3$  were attributed to higher symmetry of the environment in the nitrate compound [128,129]. Later systematic investigations on the band intensities of the rare earth ions were made [130–135]. The procedure involving an intermediate coupling scheme was used in the calculation of energy levels [123,125].

Methods for obtaining high-purity rare earth salts combined with the availability of high resolution spectrophotometers led to comprehensive studies of the absorption spectra of lanthanides [136–141]. The experimental work on the spectra of single crystals of rare earth salts by Dieke was of immense value in the theoretical interpretation of the energy level structures of the lanthanide ions [142].

The Judd–Ofelt theory propounded in 1962 has been of immense value in the quantitative interpretation of the intensities of absorption spectral bands and continues to be the cornerstone of the field of absorption spectra of rare earth ions [56,57].

The absorption spectra of lanthanide ions with an unfilled  $4f$  level will now be examined. Some data on the terms of  $f^n$  configurations for trivalent lanthanide ions are given in Table 8.11. The configurations  $f^q$  and  $f^{14-q}$  are characterized by an identical set of terms. The number of terms becomes large as one goes from  $f^1$  ( $f^{13}$ ) to  $f^7$ . There is a systematic

TABLE 8.11  
Terms of  $f^q$  configuration of  $\text{Ln}^{3+}$  free ions.

Config.	$\text{Ln}^{3+}$	Terms	Number of terms	Number of levels with different $J$
$f^1, f^{13}$	$\text{Ce}^{3+}, \text{Yb}^{3+}$	$^2F$	1	2
$f^2, f^{12}$	$\text{Pr}^{3+}, \text{Tm}^{3+}$	$^1SDGI \quad ^3PFH$	7	13
$f^3, f^{11}$	$\text{Nd}^{3+}, \text{Er}^{3+}$	$^2PDFGHIKL \quad ^4SDFGI$ 2 2 2 2	17	41
$f^4, f^{10}$	$\text{Pm}^{3+}, \text{Ho}^{3+}$	$^1SDFGHI KLN \quad ^3PDFGHI KLM \quad ^5SDFGI$ 24 4 2 3 2      32 4 3 4 2 2	47	107
$f^5, f^9$	$\text{Sm}^{3+}, \text{Dy}^{3+}$	$^2PDFGHI KLMNO \quad ^4SPDFGHI KLM \quad ^6PFH$ 45 7 6 7 5 5 3 2      23 4 4 3 3 2 $^1SPDFGHI KLMNQ \quad ^3PDFGHI KLMNO$ 4 6 4 8 4 7 3 4 2 2      65 9 7 9 6 6 3 3	73	198
$f^6, f^8$	$\text{Eu}^{3+}, \text{Tb}^{3+}$	$^5SPDFGHIKL \quad ^7F$ 3 2 3 2 2	119	295
$f^7$	$\text{Gd}^{3+}$	$^2SPDF G HI KLMNOQ \quad ^4SPDFGHI KLMN$ 25 7 1 0 1 0 9 9 7 5 4 2      22 6 5 7 5 5 3 3 $^6PDFGHI \quad ^8S$	119	327

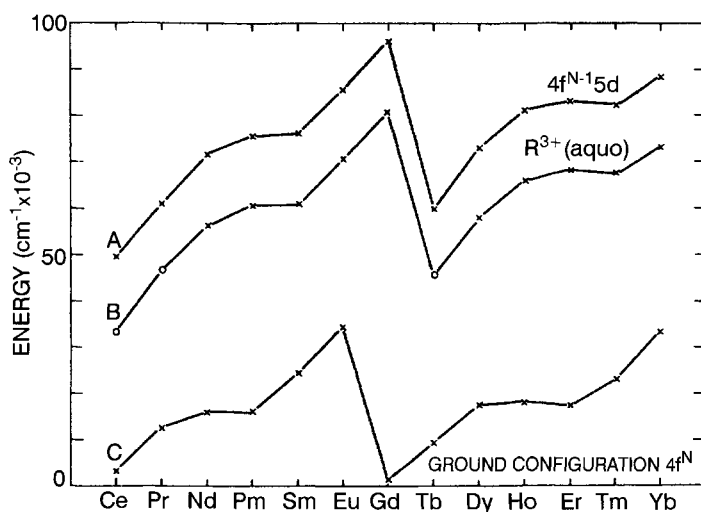


Fig. 8.14. Energy of the lowest level in the  $4f^{N-1}5d$  configuration relative to that of  $4f^N$  for the lanthanides. (A) Lanthanide 3+ gaseous ion spectra. (B) Data of (A) corrected to spectra observed in dilute acid solution. (C) Lanthanide 2+ gaseous ion spectra. For  $Gd^{2+}$ . The  $4f^7 5d$ -configuration lies lowest and  $4f^8$  is at  $1500\text{ cm}^{-1}$ .

variation in the energy differences between the lowest levels of the  $4f^n$  and higher-lying configurations in various ionized states of the lanthanides [143–145]. Emission spectroscopic data confirm  $4f^n$  as the ground state configuration of trivalent lanthanides. The lowest energy level corresponding to the next higher configuration ( $4f^{n-1}5d$ ) shows a trend depicted in Fig. 8.14.

In solutions, the energy of the  $4f \rightarrow 5d$  transitions is lowered by about  $15000\text{ cm}^{-1}$  as compared to gaseous ions and the corresponding parity allowed and relatively intense bands are observed in the ultraviolet region in  $Ce_{aq}^{3+}$ ,  $Pr_{aq}^{3+}$  and  $Tb_{aq}^{3+}$  ions. As shown in Fig. 8.14, the electronic absorption spectra of the majority of the trivalent lanthanides in the UV-vis spectral range involves only f–f transitions.

In several rare earth ions,  $Sc^{3+}$ ,  $Y^{3+}$ ,  $La^{3+}$ ,  $Ce^{4+}$  and  $Lu^{3+}$ , the core electronic structure has filled shells and as a result no absorption spectra at  $>200\text{ nm}$  is expected since high energies are required to promote an electron from filled shells. Broad absorption that increases exponentially in the UV region is observed in aquo ions of  $Eu^{3+}$ ,  $Yb^{3+}$  and  $Ce^{4+}$ . Intense bands are observed in complexes like  $CeCl_6^{2-}$  and  $CeBr_6^{2-}$  and these bands are thought to be due to electron transfer from the ligand molecular orbital to the central metal ion.

In the case of  $Sm^{2+}$  ( $4f^6$ ),  $Eu^{2+}$  ( $4f^7$ ) and  $Yb^{2+}$  ( $4f^{14}$ ) electronic absorption spectra have been observed because they have lower-lying  $4f^{n-1}5d$  configuration than the trivalent lanthanides with  $f^n$  configuration. In all the three cases, only f–d transitions are observed in solution. The weak f–f transitions of  $Sm^{2+}$  and  $Eu^{2+}$  are masked by the intense f–d bands.

In the absorption spectra of  $Ln^{3+}$  ions, the  $4f-4f$  transitions are located in the near infrared, visible and near ultraviolet regions. Only in the case of  $Eu^{3+}$  and  $Sm^{3+}$  is it possible to observe the transition from the first and second excited levels of the ground multiplet, having low energy values and populated at room temperature.

#### 14. Trivalent cerium

The  $\text{Ce}^{3+}$  ion with a single f electron can exist in two states differing in spin, namely,  $^2F_{5/2}$  (ground state) and  $^2F_{7/2}$ . The energy difference between the two states is  $2257 \text{ cm}^{-1}$  as obtained from the spectrum of gaseous  $\text{Ce}^{3+}$  ion [121]. The absorption bands are located in this region and hence make it difficult to observe the above transition in aqueous medium. The f–f transitions in the infrared region in  $\text{Ce}^{3+}$  containing crystals were studied. At room temperature, an unresolved band with a maximum at  $2200\text{--}2300 \text{ cm}^{-1}$  and a half-width of  $250\text{--}300 \text{ cm}^{-1}$  was observed. At low temperature, the band splits into some lines which are due to f–f transitions between sublevels of  $^2F$  term splittings in the crystal field and electron–vibronic transitions.

The  $\text{Ce}^{3+}$  ion has characteristic absorption in the near UV region due to 4f–5d transitions. In solution broad intense bands with half-width of  $1000\text{--}2000 \text{ cm}^{-1}$  and extinction coefficient of the order of  $10^2\text{--}10^3 \text{ l mol}^{-1} \text{ cm}^{-1}$  are observed due to 4f–5d transitions.

In the free  $\text{Ce}^{3+}$  ion, the energy of the two doublet terms corresponding to  $[\text{Xe}] 5d^1$  configuration equals  $49\,735 \text{ cm}^{-1}$  ( $^2D_{3/2}$ ) and  $52\,226 \text{ cm}^{-1}$  ( $^2D_{5/2}$ ). Because of the splitting of the D term the number and location of bands corresponding to f–d transitions depend strongly on the strength and symmetry of the ligand field surrounding the  $\text{Ce}^{3+}$  ion [151]. At low temperatures, the absorption bands have a fine structure in the form of narrow lines resembling the f–f transitions. The fine structure involving a series of narrow lines are mostly vibronic in origin [152].

The solution absorption spectrum of the  $\text{Ce}^{3+}$  aquo ion is shown in Fig. 8.15.

Trivalent cerium bands observed and their assignment is given below.

Observed $\text{Ce}^{3+}$ bands ( $\text{cm}^{-1}$ )	Assignment
33 800	
39 500	$^2D_{5/2}$
41 800	and
45 200	$^2D_{3/2}$
47 400	
49 800?	

Cerous magnesium nitrate exhibits strong anisotropy in the ground state g factors and the magnetic interaction between the magnetic moments of cerous ions in this crystal is small. Cerous magnesium nitrate has  $C_{3v}$  symmetry. The crystal field splittings in cerous magnesium nitrate suggest that the ionic model, which is normally considered to be suitable for the compound, is not sufficient to account for the observed data. The crystal field parameter values used are [153]:

$A_2^0(r^2)$	$-155 \pm 34$	$A_4^0(r^4)$	$5.8 \pm 7.7$
$A_6^0(r^6)$	$-43 \pm 9$	$A_4^3(r^4)$	$-1780 \pm 133$
$A_6^3(r^6)$	$4963 \pm 128$	$A_6^6(r^6)$	$2393 \pm 201$

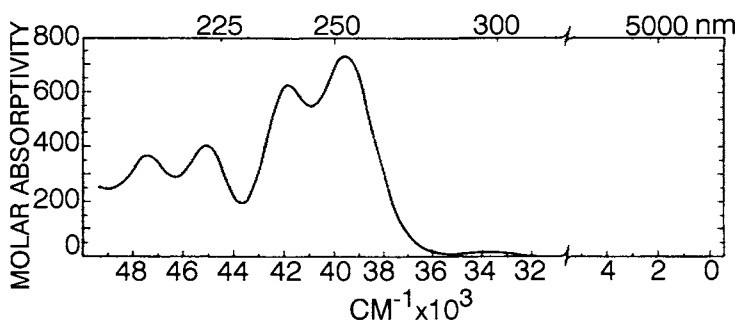


Fig. 8.15. Solution absorption spectrum of  $\text{Ce}^{3+}(\text{aq})$ . Jørgensen and Brinen (1963) report an additional band at 200 nm ( $50\,000\text{ cm}^{-1}$ ) not shown.

### 15. Trivalent praseodymium

The  $f^2$  configuration of the  $\text{Pr}^{3+}$  ion involves 13 energy levels. Their location is found experimentally by an analysis of the spectrum of gaseous  $\text{Pr}(\text{III})$  [154,155]. The ground term appears to be  $^3\text{H}_4$ . The energy level scheme for the free  $\text{Pr}^{3+}$  ion is given in Fig. 8.16. All the lines observed in the absorption spectra of  $\text{Pr}(\text{III})$  in solutions and crystals in the near infrared and visible regions are due to transitions from the ground state. The transition to the highest  $^1\text{S}_0$  level lying in the UV region cannot be observed since it is masked by the  $f-d$  transition [156].

The absorption spectra of  $\text{Pr}^{3+}$  in crystals have been studied [142]. At low temperatures, spectral bands show fine structure due to  $J$  level splitting in the crystal fields. For two pairs of levels  $^1\text{I}_6-^3\text{P}_1$  and  $^3\text{F}_4-^3\text{F}_3$  the split components may overlap. The absorption and fluorescence spectra of  $\text{Pr}^{3+}$  in  $\text{LaCl}_3$  and  $\text{LaBr}_3$  lattice provided accurate determination of the centers of gravity of  $\text{Pr}^{3+}$  energy levels. Experimental values [157,158] of the centers of gravity of  $\text{Pr}^{3+}$  in different environments are given in Table 8.12. The crystal field parameters used in these calculations are given in Table 8.13 along with the ethyl sulphate system [159].

The absorption spectra of  $\text{Pr}(\text{III})$  in solutions in the visible region have four bands due to the transitions from the ground state to  $^3\text{P}_2$ ,  $^3\text{P}_1$ ,  $^1\text{I}_6$ ,  $^3\text{P}_0$  and  $^1\text{D}_2$  levels. Relatively more complete spectra of  $\text{Pr}(\text{III})$  in dilute  $\text{DClO}_4$ , ethyl acetate and molten mixture of  $\text{LiNO}_3$  and  $\text{KNO}_3$  have been obtained [139]. So far, it has not been possible to resolve the crystal field components in the absorption spectra of  $\text{Pr}(\text{III})$  in solution. The aqueous absorption spectrum of  $\text{Pr}^{3+}$  ion is depicted in Fig. 8.17.

### 16. Trivalent neodymium

Trivalent neodymium has  $f^3$  configuration and has 41 energy levels. Because of the large number of levels, the absorption spectra of  $\text{Nd}(\text{III})$  in crystals and solutions contain many bands due to the transitions from ground state  $^4\text{I}_{9/2}$  to the excited levels [142]. The assignment of transitions of  $\text{Nd}^{3+}$  in the absorption spectrum of  $\text{Nd}_{\text{aq}}^{3+}$  ion is given in Fig. 8.18.

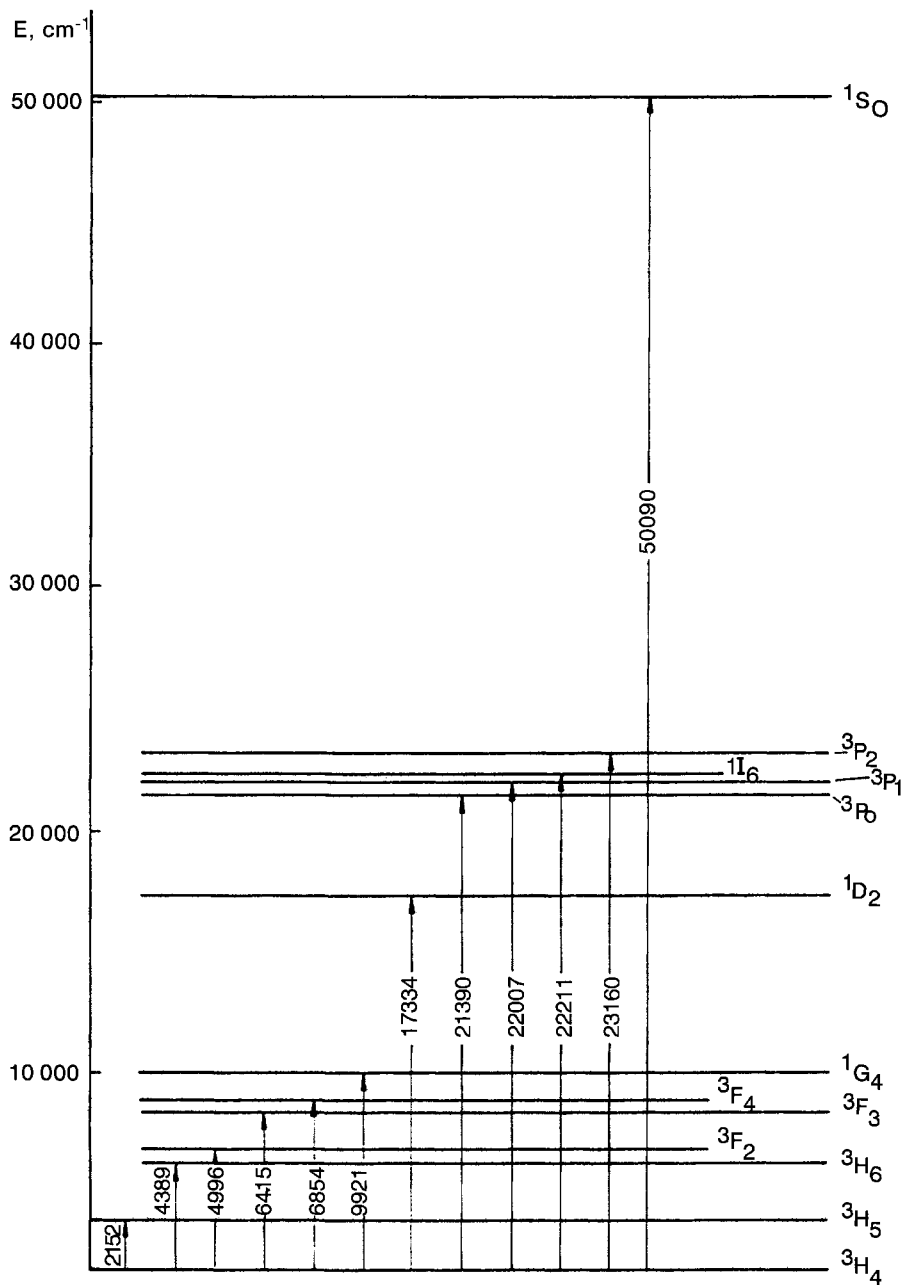


Fig. 8.16. Energy-level diagram for  $\text{Pr}^{3+}$  free ion [154].



TABLE 8.12

Experimental values of the centers of gravity of  $\text{Pr}^{3+}$  ion in different environment (wave numbers in  $\text{cm}^{-1}$ ) [157,158].

Free ion <sup>a</sup>	$\text{LaCl}_3$	$\text{LaBr}_3$	Ethyl sulfate	Assignment
23 160.9	22 141	22 045	22 304	$^3\text{P}_2$
22 211.6	21 310	21 269	21 401	$^1\text{I}_6$
22 007.6	20 986	20 889	21 148	$^3\text{P}_1$
21 390.1	20 385	20 287	10 551	$^3\text{P}_0$
17 334.5	16 641	16 579	16 731	$^1\text{D}_2$
9 921.4	9 700	9 669	9 684	$^1\text{G}_4$
6 854.9	6 670	6 659	6 702	$^3\text{F}_4$
6 415.4	6 234	6 202	6 216	$^3\text{F}_3$
4 996.7		4 848	4 816	$^3\text{F}_2$
4 389.1		4 166	4 174	$^3\text{H}_6$
2 151.2		2 117	2 086	$^3\text{H}_5$

TABLE 8.13  
Crystal field parameters [159].

	$\text{Pr}^{3+}$ in $\text{LaCl}_3$ ( $\text{cm}^{-1}$ )	$\text{Pr}^{3+}$ in $\text{LaBr}_3$ ( $\text{cm}^{-1}$ )		$\text{Pr}^{3+}$ in $\text{LaCl}_3$ ( $\text{cm}^{-1}$ )	$\text{Pr}^{3+}$ in $\text{LaBr}_3$ ( $\text{cm}^{-1}$ )
$A_2^0(r^2)$	47.26	54.18	$\zeta_{4f}$	729.5	715.2
$A_4^0(r^4)$	-40.58	-44.52	$F_2$	305.4	304.73
$A_6^0(r^6)$	-39.62	-35.43	$F_4$	51.88	51.57
$A_6^6(r^6)$	405.5	388.7	$F_6$	5.321	5.283
	$\text{Pr}^{3+}$ in ethyl sulfate ( $\text{cm}^{-1}$ )		$\text{Pr}^{3+}$ in ethyl sulfate ( $\text{cm}^{-1}$ )		
$A_2^0(r^2)$	15.31		$\zeta_{4f}$	727.9	
$A_4^0(r^4)$	-88.32		$F_2$	307.4	
$A_6^0(r^6)$	-48.76		$F_4$	49.44	
$A_6^6(r^6)$	548.48		$F_6$	5.138	

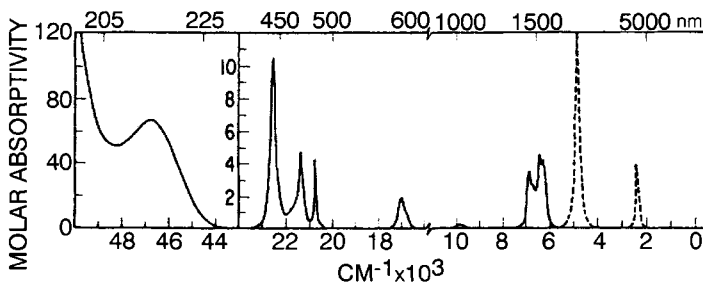


Fig. 8.17. Solution absorption spectrum of  $\text{Pr}^{3+}$  (aquo). Dashed lines indicate calculated curves.

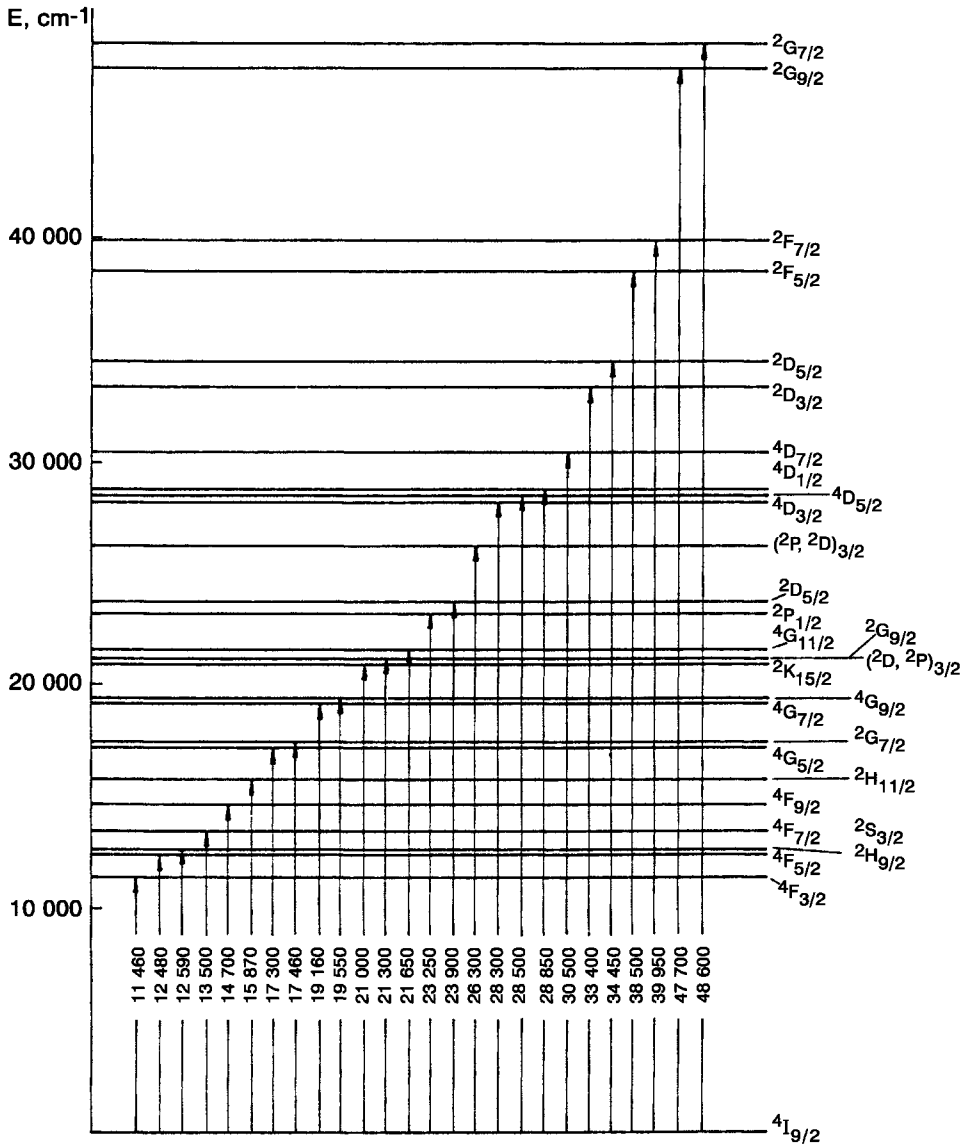


Fig. 8.18. Assignment of transition in near-IR, visible and near-UV regions of  $\text{Nd}^{3+}_{\text{aq}}$  absorption spectra [113].

The spectrum of  $\text{Nd}^{3+}$  in  $\text{LaCl}_3$  matrix [160], in double nitrates [161] such as  $\text{Nd}_2\text{Mg}_3(\text{NO}_3)_{12} \cdot 24\text{H}_2\text{O}$  and in ethyl sulphate [162] was analyzed leading to detailed interpretations. The energy levels of  $\text{Nd}^{3+}$  in  $\text{LaCl}_3$  and ethyl sulphate were calculated using the parameters given in Table 8.14.

The spectra of  $\text{Nd}(\text{III})$  in solutions reveal fine structure. But the splitting components belonging to different J-J transitions and the various complex species present in solution at

TABLE 8.14  
Parameters used to calculate energy levels of  $\text{Nd}^{3+}$  in  $\text{LaCl}_3$  [160,162].

	$\text{Nd}^{3+}$ in $\text{LaCl}_3$ ( $\text{cm}^{-1}$ )	Ethyl sulfate ( $\text{cm}^{-1}$ )
$A_2^0(r^2)$	97.59	58.4
$A_4^0(r^4)$	-38.67	-68.2
$A_6^0(r^6)$	-44.44	42.7
$A_8^0(r^8)$	443.0	595.0
$F_2$	327.49	331.33
$F_4$	48.665	47.956
$F_6$	5.356	5.3113
$\zeta_{4f}$	884.58	880.11

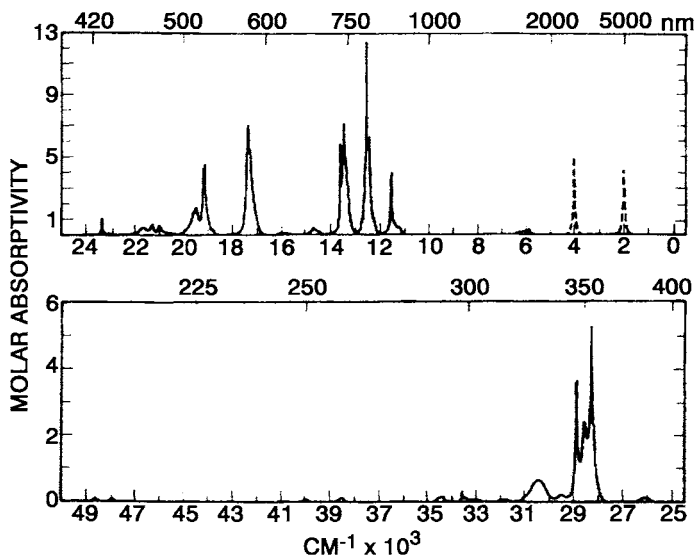


Fig. 8.19. Solution absorption spectrum of  $\text{Nd}^{3+}$  (aquo). Dashed lines indicate calculated curves.

equilibrium, generally overlap. The simple interpretation seems to be that the fine structure of the line corresponds to  ${}^2P_{1/2} \leftarrow {}^4I_{9/2}$  transition occurring at about  $\sim 23\,400\text{ cm}^{-1}$ . The upper level of this transition is not affected by the ligand field of any symmetry (Kramers doublet) and the observed splitting is that of the ground level. The maximum number ground level splittings for  $\text{Nd}(\text{III})$  is five. All the studies on the fine structure of bands of  $\text{Nd}(\text{III})$  involve this transition.

The intense band located at  $\sim 17\,500\text{ cm}^{-1}$  is due to the transition  ${}^4G_{5/2} \leftarrow {}^4I_{9/2}$  and this band is hypersensitive. This band overlaps with a less intense transition to  ${}^4G_{7/2}$  level occurring near  $\sim 17\,460\text{ cm}^{-1}$ . The band due to  ${}^4G_{5/2,7/2} \leftarrow {}^4I_{9/2}$  is generally used in solution chemistry for the determination of composition and stability of complexes. The

intensities of the hypersensitive bands can be explained by the Judd–Ofelt theory. Solution absorption spectrum of  $\text{Nd}^{3+}$  ion is given in Fig. 8.19.

### 17. Trivalent promethium

Promethium is a radioactive element which does not occur in nature. The isotope  $^{147}\text{Pm}$  with a half life of 2 years is used in the investigation of its chemical behavior. Some work on the measurement of absorption spectra is summarized in Table 8.14a.

The absorption spectrum of the aquo ion has been analyzed, the intensities of the bands can be explained by the Judd–Ofelt theory. The energy levels of  $\text{Pm}^{3+}$  ion are given in Table 8.15.

The solution absorption spectrum of  $\text{Pm}^{3+}$  aquo ion is depicted in Fig. 8.20.

### 18. Trivalent samarium

With  $f^5$  configuration, the number of multiplet terms of 73 and the number of J levels is 198 with the ground state  $^6\text{H}_{5/2}$ . The spectrum of  $\text{SmCl}_3$  in  $\text{LaCl}_3$  matrix has been analyzed and the energy levels have been calculated using the crystal field parameters [165]:

	( $\text{cm}^{-1}$ )		( $\text{cm}^{-1}$ )
$A_2^0\langle r^2 \rangle$	80.85	$A_6^0\langle r^6 \rangle$	-44.39
$A_4^0\langle r^4 \rangle$	-22.75	$A_6^0\langle r^6 \rangle$	425.7

Table 8.16 gives the observed and calculated energy levels of  $\text{Sm}^{3+}$  in  $\text{LaCl}_3$ .

In spite of a high number of levels, only a few characteristic transitions are necessary to identify  $\text{Sm}(\text{III})$  in solution. The visible region is devoid of transitions which are sensitive to the environment of  $\text{Sm}(\text{III})$ . Some transition to  $^6\text{F}$  multiplet are localized in the infrared region. The transition  $^6\text{F}_{1/2} \leftarrow ^6\text{H}_5$  is hypersensitive and occurs at  $6400 \text{ cm}^{-1}$ . The intensities of the bands have been analyzed [82,103].

The solution spectrum of  $\text{Sm}^{3+}$  aquo ion is given in Fig. 8.21.

### 19. Trivalent europium

Europium(III) with a configuration of  $f^6$  has ground state  $^7\text{F}_0$ . The splitting of  $^7\text{F}$  multiplets of  $\text{Eu}(\text{III})$  in ethyl sulphate has been analyzed by Judd [166] and good agreement between calculated and observed spectrum was obtained using the parameters:

	( $\text{cm}^{-1}$ )		( $\text{cm}^{-1}$ )
$A_2^0\langle r^2 \rangle$	80	$A_6^0\langle r^6 \rangle$	-38.6
$A_4^0\langle r^4 \rangle$	-63.1	$A_6^0\langle r^6 \rangle$	510

TABLE 8.14a

Medium	Range	Ref.
Pm(III) in aqueous solutions	300–1000 nm	[163]
2 transition to $^5G_2, ^5G_3$	$17\,700\text{ cm}^{-1}, 18\,260\text{ cm}^{-1}$	Hypersensitive
Pm(III) in DCl	Wide range	[164]
Pm(III) in $\text{DClO}_4$	Assigned bands up to $30\,000\text{ cm}^{-1}$	[141]
Molten $\text{LiNO}_3$	$^5I_8 \leftarrow ^5I_4, ^5I_7 \leftarrow ^5I_4$ observed	

TABLE 8.15  
Energy levels of  $\text{Pm}^{3+}$  ion (wavenumbers in  $\text{cm}^{-1}$ ) [163,164].

Observed	Calculated	Assignment	Observed	Calculated	Assignment
	0	$^5I_4$	24 910	24 849	$^3P_0$
	1586	$^5I_5$	25 840	25 373	$^1D_2$
	3305	$^5I_6$		26 439	$^3F_4$
	5101	$^5I_7$		26 736	$^3G_6$
	6934	$^5I_8$		27 120	$^3P_1$
12 146				27 514	$^3I_5$
12 412	12 288	$^5F_1$		27 838	$^3M_9$
12 484				28 094	$^3F_2$
12 781	12 731	$^5F_2$		28 429	$^3M_{10}$
13 611	13 650	$^5F_3$		28 654	$^3F_3$
13 982				28 719	$^3I_6$
14 247			29 070	29 128	$^3F_2$
14 327	14 369	$^5S_2$		29 221	$^3I_7$
14 624	14 602	$^5F_4$		29 319	$^1L_8$
	15 915	$^3K_6$	30 040	29 788	$^5D_0$
15 972	16 016	$^5F_5$	30 480	30 318	$^5D_1$
16 935	17 186	$^3K_7$	31 250	31 161	$^5D_2$
17 391	17 473	$^3H_4$	31 720		
17 609	17 719	$^5G_2$	31 990	31 989	$^5D_3$
18 262	18 095	$^5G_3$		32 290	$^1G_4$
18 355			32 530	32 552	$^3F_3$
	18 756	$^3K_8$		32 864	$^1D_2$
	19 881	$^3H_5$		32 930	$^3P_0$
20 272	20 274	$^5G_4$		33 019	$^5D_4$
	21 187	$^3G_3$		34 442	$^1I_6$
21 820	22 030	$^3D_2$		35 337	$^3H_4$
22 242	22 204	$^5G_5$		35 979	$^3F_4$
	22 208	$^3L_7$		35 983	$^3H_5$
	22 632	$^5G_6$		36 362	$^1H_5$
	23 154	$^3D_1$		36 962	$^1K_7$
236 663	23 353	$^3L_8$		38 013	$^3H_6$
	24 252	$^3G_4$	38 310	38 443	$^1D_2$
	24 253	$^3L_9$		39 684	$^3G_4$
	24 254	$^3M_8$		39 743	$^3G_3$
	24 369	$^3H_6$			
	24 765	$^3D_3$			

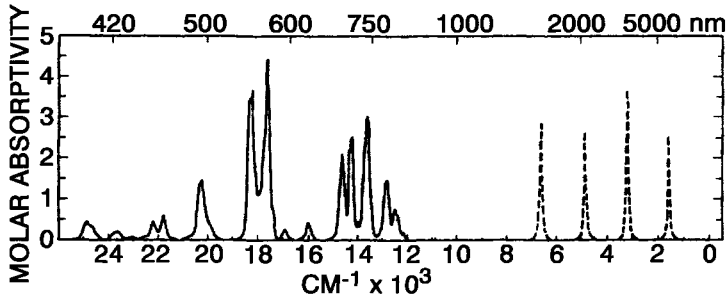


Fig. 8.20. Solution absorption spectrum of  $\text{Pm}^{3+}$  (aquo). Dashed lines indicate calculated curves.

TABLE 8.16

A comparison of the observed and calculated energy levels of  $\text{Sm}^{3+}$  ion in  $\text{LaCl}_3$  [165] (wavenumbers in  $\text{cm}^{-1}$ ) [165].

Levels	Observed	Calculated	Levels	Observed	Calculated	
${}^6\text{H}_{5/2}$	0.0	1.78	${}^6\text{H}_{15/2}$		6493.13	
	40.7	38.88			6494.56	
	66.1	66.13			6521.73	
${}^6\text{H}_{7/2}$	992.8	990.26			6524.52	
	1051.2	1050.67			6568.47	
	1104.7	1106.49			6586.29	
	1172.6	1173.89			6602.02	
					6616.38	
${}^6\text{H}_{9/2}$	2211.7	2213.83	${}^6\text{F}_{5/2}$		7049.33	
	2230.2	2228.96			7050.93	
	2308.0	2313.05			7050.34	
	2324.5	2324.00		7051.9	7050.34	
	2376.9	2371.46	${}^6\text{F}_{7/2}$		7873.77	
					7871.07	7873.77
					7900.94	7904.80
${}^6\text{H}_{11/2}$	3522.7	3517.43		7931.26	7928.32	
	3571.1	3571.05		7937.06	7933.41	
	3599.6	3597.89	${}^6\text{F}_{9/2}$		9049.63	
	3614.0	3616.83			9047.60	9049.63
	3646.0	3646.73			9052.76	9059.18
	3697.9	3701.40		9088.46	9088.46	
	${}^6\text{H}_{13/2}$	4957.38	4953.34		9114.20	9105.93
		4968.06	4968.87			9107.26
4988.0		4993.26	${}^6\text{F}_{11/2}$		10438.81	
4997.35		4997.49			10449.25	10452.56
5023.1		5021.10				10461.77
5034.0		5033.85			10468.15	10468.66
		5074.91			10478.83	10473.60
		5632.50		10480.17	10481.54	
${}^6\text{F}_{1/2}$		5404.84				
${}^6\text{F}_{3/2}$		5446.36				

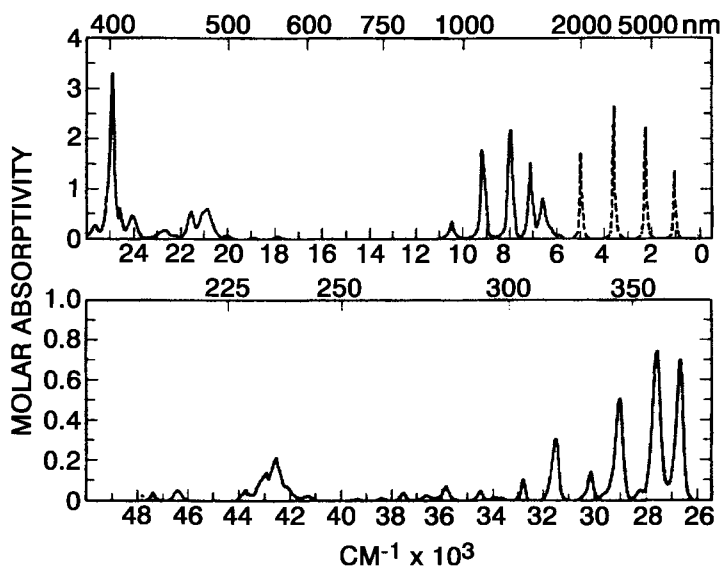


Fig. 8.21. Solution absorption spectrum of  $\text{Sm}^{3+}$  (aquo). Dashed lines indicate calculated curves.

Crystal field calculations for the absorption spectrum of  $\text{EuCl}_3$  in  $\text{LaCl}_3$  lattice [167] using the parameters

	( $\text{cm}^{-1}$ )		( $\text{cm}^{-1}$ )
$A_2^0(r^2)$	89	$A_6^0(r^6)$	-51
$A_4^0(r^4)$	-38	$A_6^6(r^6)$	495

gave good agreement for  ${}^7\text{F}$  multiplets. The assignment of bands in the absorption spectrum of  $\text{Eu}^{3+}$  aquo ion is given in Fig. 8.22. The ground state  ${}^7\text{F}$  does not overlap with the next multiplet  ${}^5\text{D}$ . The  ${}^5\text{D} \leftarrow {}^7\text{F}$  transition is located in the visible region. The excited levels of ground state  ${}^7\text{F}_1$  and  ${}^7\text{F}_2$  are located about  $360 \text{ cm}^{-1}$  and  $1000 \text{ cm}^{-1}$  above  ${}^7\text{F}_0$ . Hence these levels are populated at room temperature.

The solution absorption spectrum of  $\text{Eu}^{3+}$  aquo ion is given in Fig. 8.23. Although many transitions in the visible and UV region are possible, most of them are forbidden by selection rules based on  $\Delta J$ .

Since the ground state,  ${}^3\text{F}_0$  does not split in the presence of ligand fields, the transitions from it appear as narrow bands. Transitions from  ${}^7\text{F}_1$  and  ${}^7\text{F}_2$  appear as diffuse bands. In the aquo ion  ${}^3\text{H}_4 \leftarrow {}^7\text{F}_0$  transition at  $31250 \text{ cm}^{-1}$  is overlapped by  ${}^5\text{H}_5 \leftarrow {}^7\text{F}_1$  transition at  $31162 \text{ cm}^{-1}$ . Similarly  ${}^5\text{H}_2 \leftarrow {}^7\text{F}_0$  at  $33190 \text{ cm}^{-1}$  overlaps the  ${}^5\text{H}_4$  and  ${}^5\text{I}_4 \leftarrow {}^7\text{F}_1$ , located at  $33400 \text{ cm}^{-1}$ .

The  ${}^5\text{D}_0 \leftarrow {}^7\text{F}_0$  and  ${}^5\text{D}_1 \leftarrow {}^7\text{F}_0$  transitions are electric-dipole forbidden, [ $\Delta J(0 \leftrightarrow 0)$ ]. The transitions  ${}^5\text{D}_2 \leftarrow {}^7\text{F}_0$ ,  ${}^5\text{D}_0 \leftarrow {}^7\text{F}_0$ ,  ${}^5\text{D}_1 \leftarrow {}^7\text{F}_1$  and  ${}^5\text{D}_2 \leftarrow {}^7\text{F}_1$  are hypersensitive [168].

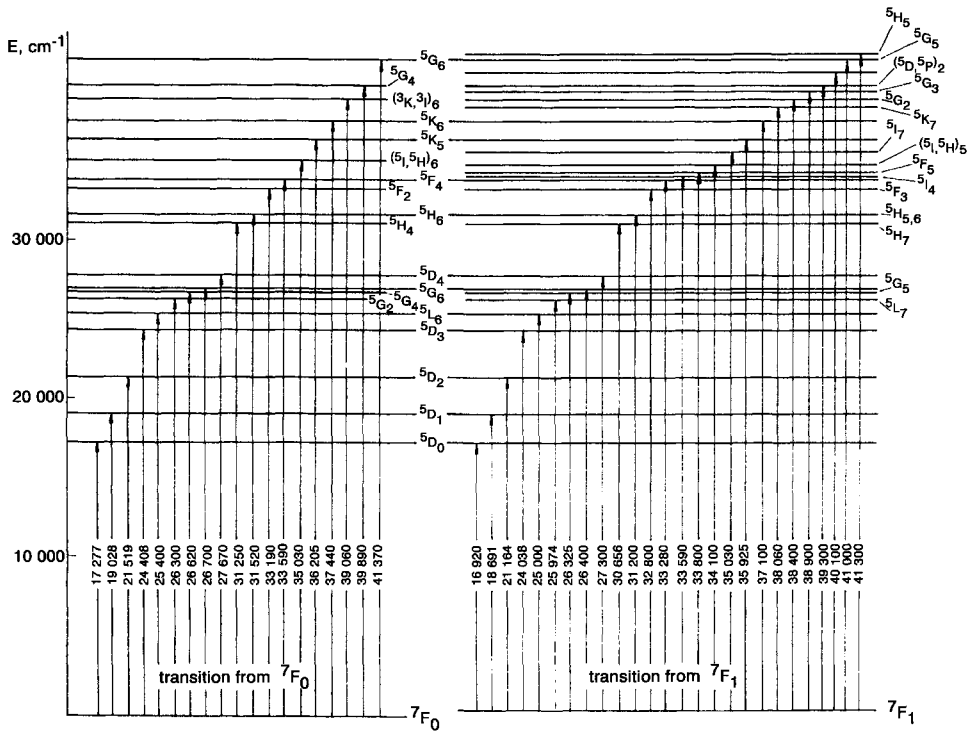


Fig. 8.22. Assignment of transitions in visible and near-UV regions of  $\text{Eu}^{3+}_{\text{aq}}$  absorption spectra [113].

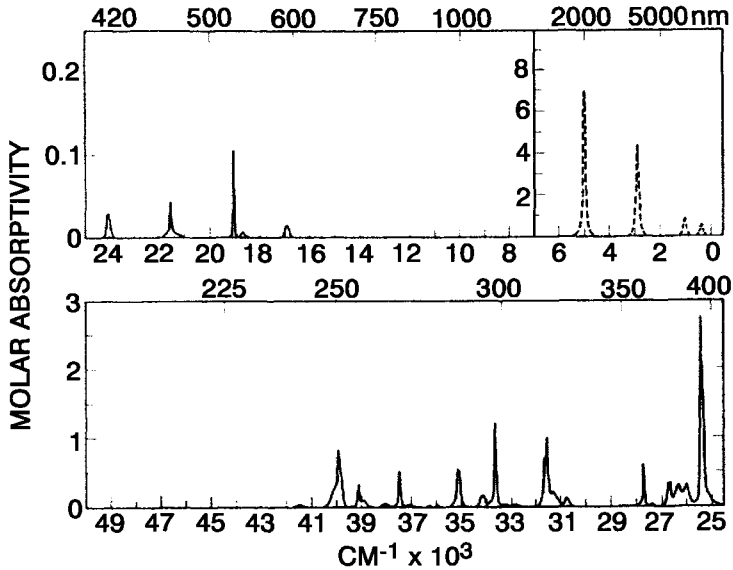


Fig. 8.23. Solution absorption spectrum of  $\text{Eu}^{3+}$  (aquo). Dashed lines indicate calculated curves.



TABLE 8.17  
The  ${}^6P$  multiplets in gadolinium salts (wavenumbers in  $\text{cm}^{-1}$ ) [113].

	$\text{GdCl}_3 \cdot 6\text{H}_2\text{O}$	$\text{Gd}(\text{Ac})_3 \cdot 4\text{H}_2\text{O}$	$\text{Gd}_2(\text{SO}_4)_3 \cdot 8\text{H}_2\text{O}$
${}^6P_{7/2}$	32 066.41	32 058.69	32 079.29
	32 091.44	32 069.69	32 107.91
	32 121.90	32 086.55	32 136.45
	32 145.29	32 098.75	32 162.97
${}^6P_{5/2}$	32 659.52	32 642.87	32 679.23
	32 699.10	32 671.77	32 717.49
	32 739.38	32 697.08	32 751.02
${}^6P_{3/2}$	Not observed	33 231.78	33 274.76
		33 251.41	33 307.53

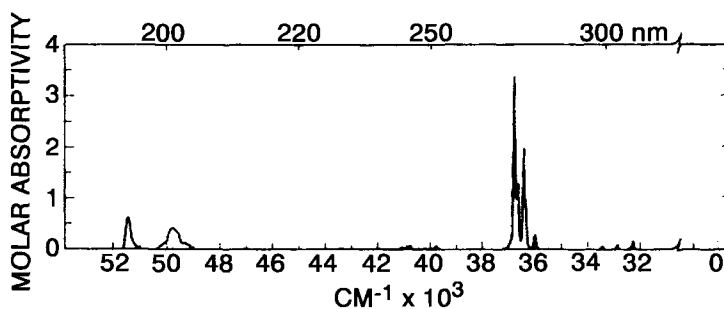


Fig. 8.24. Solution absorption spectrum of  $\text{Gd}^{3+}$  (aquo).

## 20. Trivalent gadolinium

Gd has  $f^7$  configuration with  ${}^8S_{7/2}$  as the ground state. From a study of crystal spectra  ${}^6P$  multiplets have been identified as shown in Table 8.17. The absorption spectrum lies in the UV region and the transitions correspond to components of  ${}^6P_{7/2}$  multiplets.

The intensities of the bands of the aquo ion have been analyzed [113] with the following identification and the solution spectrum is given in Fig. 8.24.

Most intense bands	${}^6I$ multiplet	$36\,000\text{--}37\,000\text{ cm}^{-1}$
Less intense bands	${}^6G$ multiplet	$50\,000\text{--}51\,000\text{ cm}^{-1}$
Less intense bands	${}^6D$ multiplets	$39\,000\text{--}40\,000\text{ cm}^{-1}$
Weak bands	${}^6P_{7/2}, {}^6P_{5/2}$	$32\,000\text{--}33\,000\text{ cm}^{-1}$

## 21. Trivalent terbium

Trivalent terbium with  $f^8$  configuration has energy levels similar to  $\text{Eu}^{3+}$  but in reverse order. The ground state is  ${}^7F_6$ . The highest level and the lowest excited level ( ${}^7F_5$ ) are separated from the ground state by  $16\,000\text{ cm}^{-1}$  and  $2080\text{ cm}^{-1}$ , respectively, and the

TABLE 8.18  
Energy levels of  $Tb^{3+}$  in  $LaCl_3$  [171].

Levels	Wavenumbers ( $cm^{-1}$ )	Levels	Wavenumbers ( $cm^{-1}$ )
${}^7F_6$	0.00	${}^7F_2$	4973.92
	56.83		5036.10
	90.56	${}^7F_1$	5037.55
	97.22		5440.14
	99.31		5487.78
	104.64	${}^7F_0$	5700.93
	112.80		${}^5D_4$
	117.99	20468.61	
2043.26	20472.29		
${}^7F_5$	2080.34		20490.21
	2096.76		20495.75
	2112.81		20496.06
	2151.53	${}^5D_3$	26267.30
	2167.79		26269.10
	2200.44		26270.33
${}^7F_4$	3266.42	${}^5L_{10}$	26280.51
	3354.21		26271.69
	3362.84		
	3373.27		
	3397.63		
	3437.69		
	4325.97		
${}^7F_3$	4346.65		
	4348.06		
	4363.97		
	4379.20		

excited levels of ground state are not populated at room temperature which is in contrast to  $Eu^{3+}$ . The following parameters gave the best agreement between calculated and observed energy levels of  $TbCl_3$  in  $LaCl_3$  matrix [171].  $A_2^0\langle r^2 \rangle$  92  $cm^{-1}$ ;  $A_4^0\langle r^4 \rangle$  - 40  $cm^{-1}$ ;  $A_6^0\langle r^6 \rangle$  - 30  $cm^{-1}$ ;  $A_6^6\langle r^6 \rangle$  290  $cm^{-1}$ .

The energy levels of  $Tb^{3+}$  are given in Table 8.18.

The solution absorption spectrum has been studied [113] up to 40 000  $cm^{-1}$  and is given in Fig. 8.25. The f-f transitions at 36 000  $cm^{-1}$  overlap with f-d bands at 38 000  $cm^{-1}$  and 46 000  $cm^{-1}$ .

## 22. Trivalent dysprosium

Dysprosium(III) with  $f^9$  has 73 multiplet terms with  ${}^6H_{15/2}$  as the ground state. Crystal spectrum of  $DyCl_3$  in  $LaCl_3$  matrix has been analyzed and the calculated and observed energy levels use the following parameters:  $A_2^0\langle r^2 \rangle$  91.30  $cm^{-1}$ ,  $A_4^0\langle r^4 \rangle$  - 38.97  $cm^{-1}$ ,  $A_6^0\langle r^6 \rangle$  - 23.17  $cm^{-1}$ ,  $A_6^6\langle r^6 \rangle$  257.8  $cm^{-1}$ . The energy levels of  $Dy^{3+}$  in  $LaCl_3$  are given

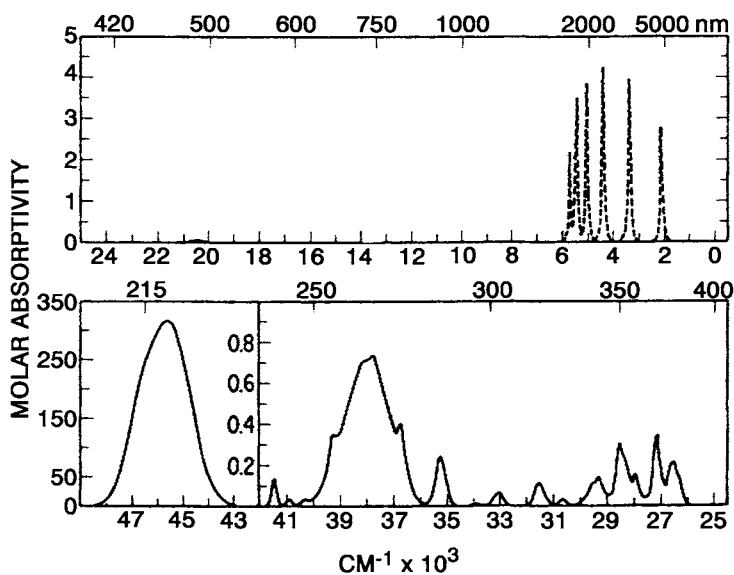


Fig. 8.25. Solution absorption spectrum of  $\text{Tb}^{3+}$  (aquo). Dashed lines indicate calculated curves.

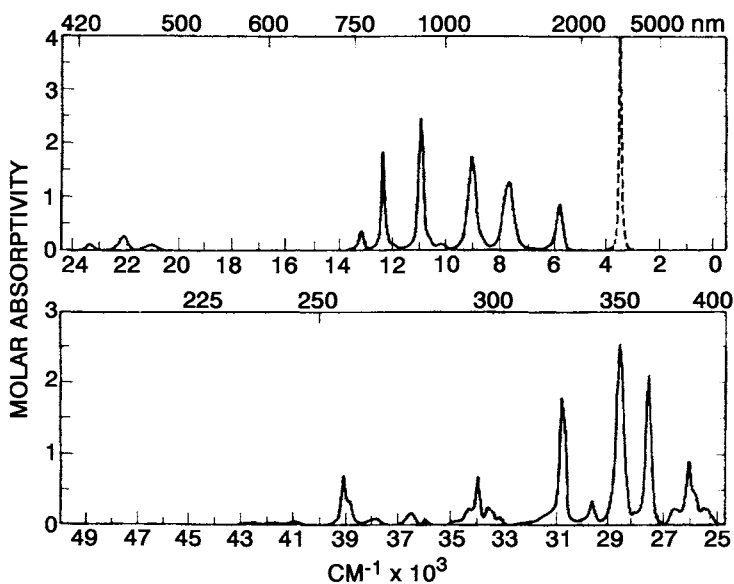


Fig. 8.26. Solution absorption spectrum of  $\text{Dy}^{3+}$  (aquo). Dashed lines indicate calculated curves.

in Table 8.19. Solution absorption spectrum [113] of  $\text{Dy}^{3+}$  aquo ion is given in Fig. 8.26. The f-f transitions located above  $36\,000\text{ cm}^{-1}$  are overlapped by more intense f-d bands. The only hypersensitive band [113] due to  ${}^6\text{F}_{11/2} \leftarrow {}^6\text{H}_{15/2}$  is located at  $7700\text{ cm}^{-1}$ .

TABLE 8.19

A comparison of the observed and calculated values of the levels of  $Dy^{3+}$  in  $LaCl_3$  (wavenumbers in  $cm^{-1}$ ) [172].

Levels	Observed	Calculated	Levels	Observed	Calculated
${}^6H_{15/2}$	0.0	0.99	${}^6F_{9/2}$	8952.14	8956.98
	9.82	8.29		8975.06	8980.41
	9.97	8.44		8981.14	8997.25
	15.65	14.29		8999.32	8998.52
	40.75	40.92		9011.78	9011.43
	80.48	82.81		9091.57	9086.85
	121.65	118.75			9107.48
140.51	146.30		9147.76		
${}^6H_{13/2}$	3457.03	3461.82		9175.24	
	3490.30	3489.54	${}^6H_{5/2}$	10 124.48	10 124.53
	3493.13	3494.63		10 151.57	10 151.54
	3522.31	3521.01		10 201.89	
	3546.62	3546.41	${}^6F_{7/2}$	10 913.36	10 913.10
	3551.93	3550.55		10 917.16	10 920.87
	3556.60	3553.97		10 922.23	10 920.88
${}^6H_{11/2}$	5793.28	5796.51		10 949.45	10 947.35
	5801.42	5800.84	${}^6F_{5/2}$	12 315.60	12 318.06
	5842.54	5840.54		12 317.87	12 320.46
	5850.29	5845.42		12 336.08	12 311.04
	5860.69	5859.15	${}^6F_{3/2}$	13 114.47	13 113.05
	5864.68	5870.47		13 116.84	13 118.25
${}^6H_{7/2}$	8937.14	8956.98			
	8944.40				
${}^6H_{9/2}$	7592.16		${}^6F_{11/2}$	7598.01	
	7593.59			7612.9	
				7660.33	
				7669.52	
				7675.08	
				7698.97	
				7746.5	

### 23. Trivalent holmium

Holmium(III) with  $f^{10}$  configuration has 47 multiplet terms and 107 levels of different J values due to spin-orbit coupling. The ground state is  ${}^5I_8$ . The energy levels of  $Ho^{3+}$  in  $LaCl_3$  matrix [173] are presented in Table 8.20.

The two hypersensitive bands at  $22\ 100\ cm^{-1}$  and  $27\ 700\ cm^{-1}$  are due to  ${}^5G_6 \leftarrow {}^5I_8$  and  ${}^3G_6 \leftarrow {}^3I_8$  transitions, respectively. The solution spectrum is shown in Fig. 8.27. Theoretical analysis of the spectrum has been made [113].

### 24. Trivalent erbium

Erbium(III) with  $f^{11}$  configuration has 17 multiplet terms with 41 levels due to spin-orbit coupling. The J energy levels are more separated than in  $Nd^{3+}$ . The energy level diagram

TABLE 8.20  
Energy levels of  $\text{Ho}^{3+}$  in  $\text{LaCl}_3$  [173].

Levels	Wave numbers ( $\text{cm}^{-1}$ )	Levels	Wave numbers ( $\text{cm}^{-1}$ )
$^5\text{I}_8$	0	$^5\text{G}'_2$	31 094
$^5\text{I}_7$	5087	$^3\text{M}_{10}$	33 296
$^5\text{I}_6$	8647	$^3\text{L}_8$	33 862
$^5\text{I}_5$	11 255	$^3\text{D}_3$	33 921
$^5\text{I}_4$	13 349	$^3\text{P}_1$	33 973
$^5\text{F}_5$	15 403	$^5\text{D}_4$	35 125
$^5\text{S}_2$	18 221	$^3\text{F}_3$	35 859
$^5\text{F}_4$	18 479	$^1\text{L}_8$	36 267
$^5\text{F}_3$	20 568	$^3\text{P}_0$	36 700
$^5\text{F}_2$	21 113	$^3\text{H}_4$	36 745
$^3\text{K}_8$	21 321	$^3\text{F}_2$	36 802
$^5\text{G}_6$	22 192	$^3\text{H}_5$	37 444
$^5\text{F}_1$	22 365	$^3\text{L}_7$	37 673
$^5\text{G}_5$	24 104	$^3\text{I}_7$	38 214
$^5\text{G}_4$	26 070	$^3\text{P}_2$	38 521
$^3\text{K}_7$	26 195	$^3\text{M}_9$	38 584
$^5\text{G}'_5$	28 040	$^3\text{I}_5$	39 215
$^3\text{H}_6$	28 391	$^3\text{F}_4$	39 226
$^3\text{L}_9$	28 421	$^3\text{I}_6$	39 654
$^5\text{G}_2$	28 620	$^5\text{D}_3$	40 255
$^5\text{G}_3$	28 953	$^5\text{D}_1$	40 424
$^3\text{K}_6$	30 261	$^3\text{F}_4$	41 858
$^3\text{F}_4$	30 721	$^5\text{D}_2$	42 051
			etc.

TABLE 8.20a

$\text{Er}^{3+}$ in	$\text{LaF}_3$ [174]	$\text{LaCl}_3$ [175]	$\text{Y}_2\text{O}_3$ [176]	Ethyl sulfate [177]
$\text{F}_2$	428.708	433.183	429.583	429.38
$\text{F}_4$	67.784	67.135	65.012	66.419
$\text{F}_6$	6.751	7.356	7.136	6.907
$\zeta_{4f}$	2389.60	2393.34	2383.17	2423.91

is given in Fig. 8.28. The transitions from the ground state,  $^4\text{I}_{15/2}$  to  $^2\text{H}_{11/2}$  at  $19\,200\text{ cm}^{-1}$  and to  $^4\text{G}_{11/2}$  at  $26\,500\text{ cm}^{-1}$  are hypersensitive [112]. The experimentally observed levels of  $\text{Er}^{3+}$  in  $\text{LaF}_3$ ,  $\text{LaCl}_3$ ,  $\text{Y}_2\text{O}_3$  and ethyl sulphate were fitted with the following best fit parameters ( $\text{cm}^{-1}$ ) (Table 8.20a).

The intensities of the absorption bands of coordination compounds have been studied [61,112,82,178]. A superposition model has been applied to the analysis of the spectrum of  $\text{Er}^{3+}$  in YGG and LuGG and the best-fit parameters obtained are given in Tables 8.21 and 8.22.

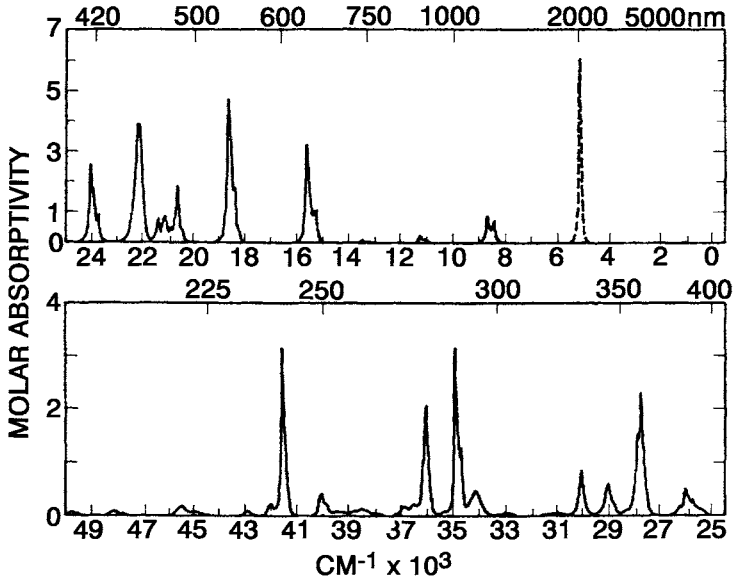


Fig. 8.27. Solution absorption spectrum of  $\text{Ho}^{3+}$  (aquo). Dashed lines indicate calculated curves.

TABLE 8.21  
Analysis of  $\text{Er}^{3+}$ : YGG parameters. ( $A_n^m(r^n)$  and  $\bar{A}_n$  are given in  $\text{cm}^{-1}$ ) [31].

	Experiment	No distortion	Angular distortion
$A_4^0(r^4)$	$-238 \pm 0.5$	-246	-238
$A_4^2(r^4)$	$255 \pm 2$	254	255
$A_4^0(R_1)$	$920 \pm 2$	860	916
$\bar{A}_4(R_1)$		96.6	95.6
$\bar{A}_4(R_2)$		58.9	55.4
$t_4$		13.2	14.5
$A_6^0(r^6)$	$33.0 \pm 0.1$	36	33
$A_6^2(r^6)$	$-58 \pm 2$	-24	-58
$A_6^4(r^6)$	$645 \pm 1$	636	642
$A_6^6(r^6)$	$-70 \pm 2$	-31	-70
$\bar{A}_6(R_1)$		22.8	23.1
$\bar{A}_6(R_2)$		22.3	18.1
$t_6$		0.5	6.6
$\Delta\theta_2$			$-0.2^\circ$
$\Delta\phi_2$			$9.1^\circ$

TABLE 8.22  
 Analysis of  $\text{Er}^{3+}$ : LuGG parameters ( $A_n^n(r^n)$  and  $\bar{A}_n$  are given in  $\text{cm}^{-1}$ ) [31].

	Experiment	No distortion	Angular distortion
$A_4^0(r^4)$	$-245 \pm 0.5$	-246	-238
$A_4^2(r^4)$	$175 \pm 2$	175	175
$A_4^4(r^4)$	$948 \pm 2$	864	946
$\bar{A}_4^0(R_1)$		93.2	90.7
$\bar{A}_4(R_2)$		65.9	63.1
$t_4$		9.0	9.5
$A_6^0(r^6)$	$33.8 \pm 0.1$	34.6	34.1
$A_6^2(r^6)$	$-83 \pm 2$	-54	-86
$A_6^4(r^6)$	$664 \pm 1$	663	662
$A_6^6(r^6)$	$-48 \pm 2$	-12	-52
$\bar{A}_6(R_1)$		24.9	25.8
$\bar{A}_6(R_2)$		21.9	16.9
$t_6$		3.4	11.1
$\Delta\theta_2$			$-0.0^\circ$
$\Delta\phi_2$			$7.9^\circ$

TABLE 8.23  
 Intrinsic parameters  $\bar{A}_4$ ;  $\bar{A}_6$  ( $\text{cm}^{-1}$ ) obtained using the superposition model for various systems. Values are given corresponding to the mean ligand distance in each host [31].

Ligand	$\text{F}^-$	$\text{F}^-$	$\text{Cl}^-$	$\text{O}^{2-}$	$\text{O}^{2-}$	$\text{S}^{2-}$
Host references	$\text{CaF}_2$	$\text{SrF}_2$	$\text{LaCl}_3$	Garnets	$\text{YVO}_4$ , $\text{YPO}_4$	Oxysulphides and sulphides
Ion						
$\text{Pr}^{3+}$			39; 16			
$\text{Nd}^{3+}$	129; 25	98; 31	38; 17			77; 21
$\text{Sm}^{3+}$			23; 17	89; 32		
$\text{Eu}^{3+}$			40; 20	60; 31	49; 27	47; 5
$\text{Gd}^{3+}$	87; 28	77; 23				
$\text{Dy}^{3+}$	78; 23		34; 10	91; 25		
$\text{Ho}^{3+}$			33; 11		41; 20	
$\text{Er}^{3+}$			37; 10	77; 21	57; 18	56; 11
$\text{Tm}^{3+}$				67; 17		
$\text{Yb}^{3+}$	60; 22			54; 30		
$\text{Dy}^{2+}$	76; 18	67; 16				
$\text{Ho}^{2+}$	83; 19	70; 16	34; 10			
$\text{Tm}^{2+}$	61; 16	53; 13				

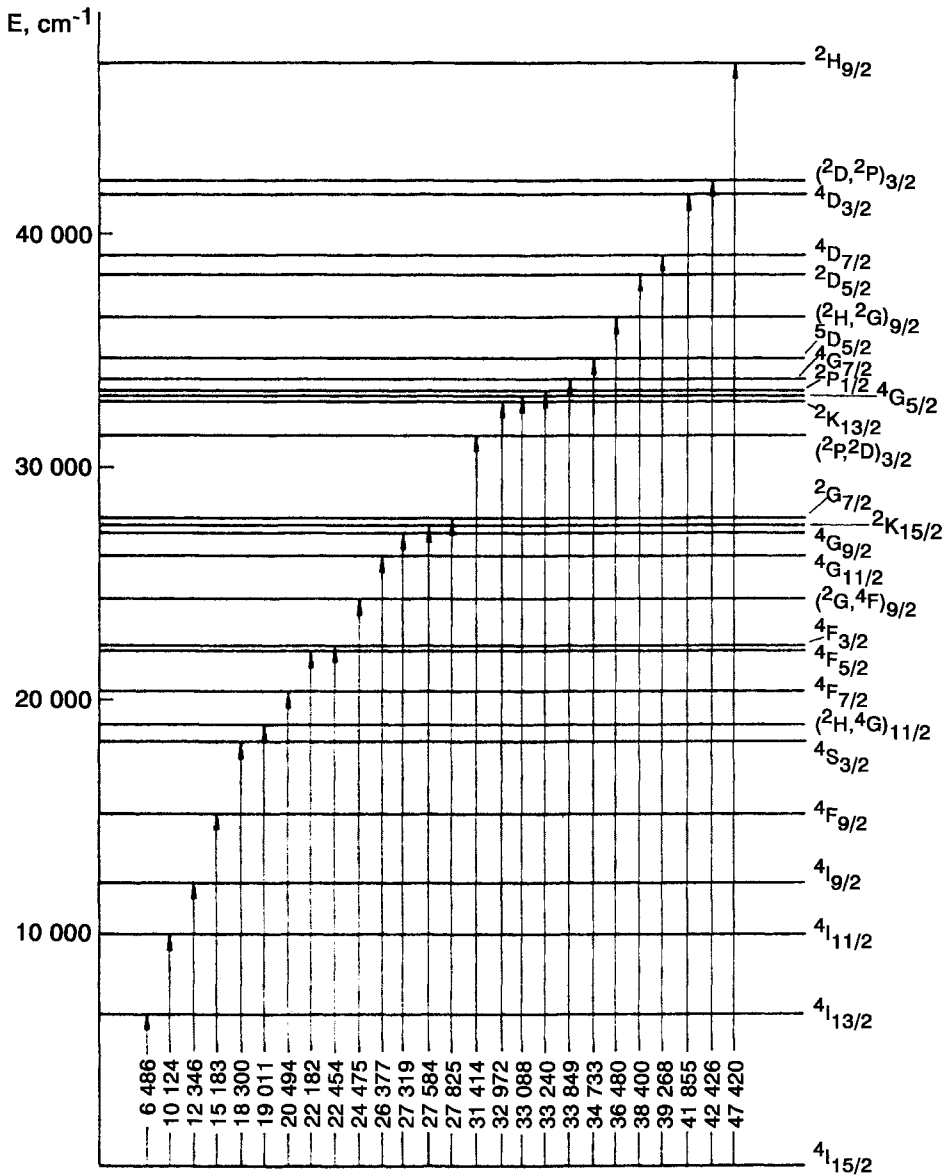


Fig. 8.28. Energy-level diagram for  $\text{Er}^{3+}$  free ion [112].

The superposition model has also been applied to experimental crystal field parameters obtained for lanthanides [31] substituted into host lattices of oxides, zircons, anhydrous trihalides, oxysulphides, alkaline earth fluorides and some other cubic crystals. The intrinsic parameters obtained from the analysis are given in Table 8.23. The solution spectrum of  $\text{Er}^{3+}$  aquo ion is given in Fig. 8.29.



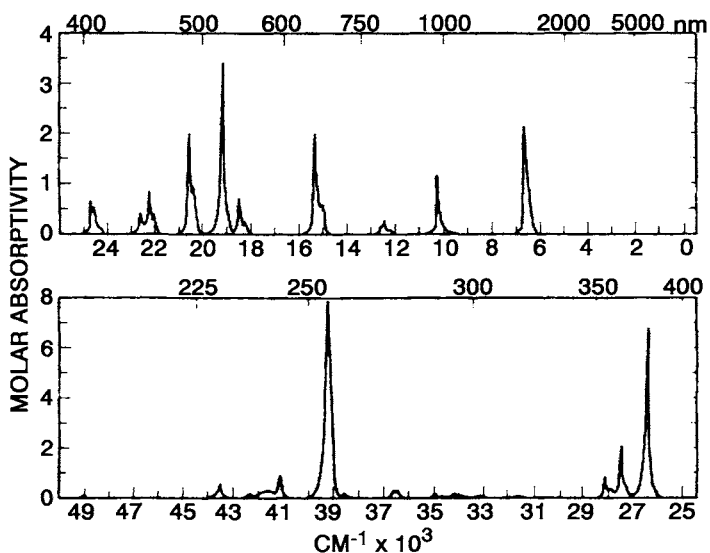


Fig. 8.29. Solution absorption spectrum of  $\text{Er}^{3+}$  (aquo).

## 25. Trivalent thulium

Thulium with  $f^{12}$  configuration has a ground state  $^3H_6$ . It resembles  $\text{Pr}^{3+}$  with  $f^2$  configuration except for the reversal of ground level multiplets. The energy levels of  $\text{Tm}^{3+}$  in lanthanum ethyl sulphate nonahydrate matrix have been calculated and observed using the best fit parameters [179]:  $A_2^0\langle r^2 \rangle$  129.8  $\text{cm}^{-1}$ ;  $A_4^0\langle r^4 \rangle$  - 71.0  $\text{cm}^{-1}$ ;  $A_6^0\langle r^6 \rangle$  - 28.6  $\text{cm}^{-1}$ ;  $A_6^6\langle r^6 \rangle$  432.8  $\text{cm}^{-1}$ .

Both the calculated and observed energy levels of Tm(III) in ethyl sulphate matrix are given in Table 8.24. Theoretical analysis of the spectrum of  $\text{Tm}^{3+}$  in  $\text{LaF}_3$  matrix has been done [180]. The absorption spectrum of the aquo ion has also been analyzed [113]. The  $^3H_4 \leftarrow ^3H_6$  transition is hypersensitive. The intensities of the bands have been well studied [61,112].

The solution absorption spectrum of  $\text{Tm}^{3+}$  aquo ion is given in Fig. 8.30.

## 26. Trivalent ytterbium

Ytterbium(III) has  $f^{13}$  configuration and resembles the  $\text{Ce}^{3+}$  ion. Ytterbium has a ground state of  $^2F_{7/2}$ . The separation of the two states  $^2F_{5/2} \leftarrow ^2F_{7/2}$  is approximately equal to  $7/2\zeta_{4f/2}$ , where  $\zeta$  is the spin-orbit coupling constant with a value of 2924  $\text{cm}^{-1}$ . The transition  $^2F_{7/2} \rightarrow ^2F_{5/2}$  occurs at 9700 Å. Theoretical analysis of the spectrum of Yb(III) in  $\text{LaF}_3$  matrix has been performed [180]. The solution spectrum of the aquo ion has also been analyzed [113]. The  $^3F_4 \leftarrow ^3F_6$  transition is hypersensitive. The observed absorption

TABLE 8.24  
 Calculated and observed energy levels of  $\text{Tm}^{3+}$  in ethyl sulfate host (wavenumbers in  $\text{cm}^{-1}$ ) [179].

Levels	Calculated	Observed <sup>a</sup>	
		W-R	G-C
$^3\text{H}_6$	0	0	
$^3\text{H}_4$	5634	5647	5900
$^3\text{H}_5$	8239	8061	8390
$^3\text{F}_4$	12587	12491	12673
$^3\text{F}_3$	14478	14313	14446
$^3\text{F}_2$	14982	14947	15092
$^1\text{G}_4$	21187	21109	21275
$^1\text{D}_2$	27778	27785	27926
$^1\text{I}_6$	32686	—	—
$^3\text{P}_0$	35262	35343	35074
$^3\text{P}_1$	36093	36329	36443
$^3\text{P}_2$	37955	38087	38100
$^1\text{S}_0$	—	—	—

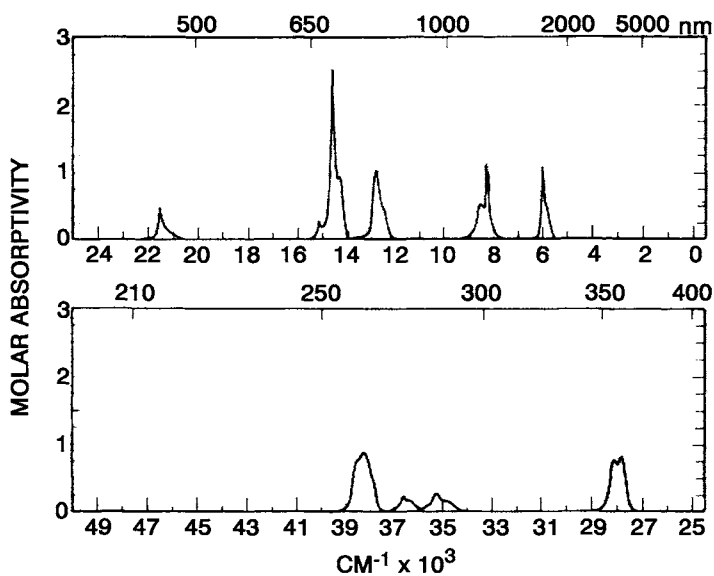


Fig. 8.30. Solution absorption spectrum of  $\text{Tm}^{3+}$  (aquo).

lines of  $\text{Yb}^{3+}$  in different site symmetry are given in Table 8.25. The solution absorption spectrum of aquo  $\text{Yb}^{3+}$  ion is given in Fig. 8.31.

The absorption bands of trivalent aquo rare earth ions with  $\epsilon > 0.2$  in the spectral range of 230–1700 nm are given in Table 8.26.

TABLE 8.25  
Observed absorption lines of  $\text{Yb}^{3+}$  ion in different site symmetry (wave numbers in  $\text{cm}^{-1}$ ) [181].

$\text{YbCl}_3 \cdot 6\text{H}_2\text{O}$		$\text{Yb}^{3+}$ in YGG	$\text{Yb}^{3+}$ in $\text{CaWO}_4$	$\text{Yb}(\text{C}_2\text{H}_5\text{SO}_4)_3 \cdot 9\text{H}_2\text{O}$
77 K	10 149	10 235	10 201	10 159
	10 163	10 320	10 240	10 199
	10 182	10 408	(10 264)	10 202
	10 193	10 443	10 278	10 218
		10 510	(10 352)	10 260
		10 562	10 370	
		10 604	(10 380)	
		10 632	10 405	
		10 703	(10 440)	
		10 753	(10 485)	
		10 778	(10 504)	
		10 811	(10 545)	
			10 595	
			(10 636)	
			10 652	
		(10 662)		
		(10 702)		
		10 716		
4 K	10 282	10 305		
	10 297	10 316		
	10 573	10 409		
	10 645	10 441		
	10 662	10 509		
		10 529		
		10 563		
		10 584		
		10 597		
		10 610		
		10 629		
		10 644		
		10 654		
		10 661		
		10 672		
		10 693		
		10 702		
		10 714		
	10 729			
	10 744			
	10 777			
	10 822			
	10 840			

## 27. Spectra of divalent lanthanides

The spectra of divalent rare earths Sm, Eu and Yb both in the solid state and solution have been reported. According to the nature of the ground state, the three types are (a) ions with  $f^n$  ground state, (b) ions with ground state from  $f^{n-1}d$  configuration, (c) ions in which

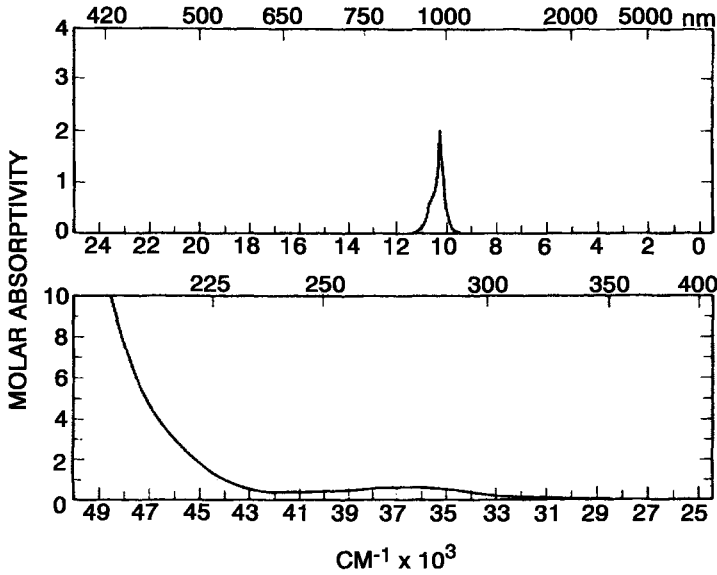


Fig. 8.31. Solution absorption spectrum of  $\text{Yb}^{3+}$  (aquo).

$f^{n-1}d$  and  $f^n$  states are close to each other. The spectra of divalent rare earths in  $\text{CaF}_2$  lattice are shown in Fig. 8.32. The energy levels of the three types of divalent rare earths differing in the ground state configurations are shown in Fig. 8.33. Note that this is only a rough energy level diagram and not drawn to scale.

Divalent  $\text{Sm}$  ( $4f^6$ ) is isoelectronic with  $\text{Eu}^{3+}$  and the spectra of these ions resemble each other very closely. Divalent europium ( $4f^7$ ) is colorless and all the absorption bands are located in the UV region like isoelectronic  $\text{Gd}^{3+}$  ion. Divalent thulium ( $4f^{13}$ ) has a strong absorption band in the visible region in  $\text{CaF}_2$  matrix due to  $4f-5d$  transition. The  $f-f$  transitions in  $\text{Tm}^{2+}$  are probably of magnetic dipole origin. No  $f-f$  transitions are possible in  $\text{Yb}^{2+}$  which has  $4f^{14}$  configuration. But  $4f-5d$  transitions are allowed and have been observed. The solution absorption spectra of  $\text{Sm}^{2+}$ ,  $\text{Eu}^{2+}$  and  $\text{Yb}^{2+}$  aquo ions are shown in Fig. 8.34.

The absorption spectra of  $\text{Tm}^{2+}$ ,  $\text{Gd}^{2+}$  and  $\text{Ho}^{2+}$  obtained by pulse radiolysis are shown in Fig. 8.35. This is the first spectroscopic evidence for  $\text{Gd}^{2+}$  and  $\text{Ho}^{2+}$ .

## 28. Some salient features of the absorption spectra of lanthanide complexes in solutions

Unlike in the solid state, solution chemistry is complicated by the existence of many complex species as a result of dissociation, solvolysis, polymerization, isomerization, etc. As a result, the central problem is to characterize the spectra of each individual species in solution.

TABLE 8.26  
Band register for R<sup>3+</sup> (aquo) ions in H<sub>2</sub>O-D<sub>2</sub>O with molar absorptivity ( $\epsilon$ ) > 0.2.

Band peak		Ion	$\epsilon$	Band peak		Ion	$\epsilon$
(cm <sup>-1</sup> )	(nm) <sup>a</sup>			(cm <sup>-1</sup> )	(nm) <sup>a</sup>		
5837	1713	Dy	0.84	15 608	641	Ho	3.19
5988	1670	Nd	0.25	16 000	625	Pm	0.44
6006	1665	Tm	1.04	16 920	591	Pm	0.26
6309	1585	Pr	4.18	16 980	589	Pr	1.88
6451	1550	Pr	4.51	17 373	576	Nd	7.20
6622	1510	Sm	0.79	17 605	568	Pm	4.43
6667	1500	Er	2.11	18 215	549	Er	0.21
6896	1450	Pr	3.60	18 235	548	Pm	3.68
7143	1400	Sm	1.54	18 315	546	Pm	3.45
7707	1297	Dy	1.22	18 399	544	Ho	1.81
8051	1242	Sm	2.02	18 477	541	Er	0.72
8278	1208	Tm	1.11	18 632	537	Ho	4.74
8417	1188	Ho	0.74	19 128	523	Er	3.40
8529	1172	Tm	0.50	19 198	521	Nd	4.33
8673	1153	Ho	0.87	19 522	512	Nd	1.76
9066	1103	Dy	1.72	20 242	494	Pm	1.47
9199	1087	Sm	1.77	20 375	491	Er	0.93
9876	1012	Pr	0.20	20 542	487	Er	2.02
10 262	974	Yb	2.03	20 614	485	Ho	1.84
10 262	974	Er	1.14	20 772	481	Pr	4.29
10 520	951	Sm	0.36	20 833	480	Ho	0.48
10 995	910	Dy	2.44	20 894	479	Sm	0.60
11 235	890	Ho	0.22	21 017	476	Nd	0.72
11 556	865	Nd	4.01	21 106	474	Ho	0.82
12 398	806	Dy	1.82	21 308	469	Nd	0.78
12 462	802	Er	0.27	21 349	468	Pr	4.59
12 472	802	Nd	6.42	21 377	468	Ho	0.82
12 484	801	Pm	0.74	21 533	464	Tm	0.48
12 586	794	Nd	12.5	21 580	463	Sm	0.54
12 804	781	Pm	1.46	21 668	462	Nd	0.52
12 820	780	Tm	1.02	21 786	459	Pm	0.63
13 210	757	Dy	0.35	22 056	453	Er	0.38
13 508	740	Nd	7.27	22 065	453	Dy	0.26
13 624	734	Pm	3.04	22 185	451	Ho	3.90
13 665	732	Nd	5.93	22 222	450	Pm	0.46
13 980	715	Pm	0.48	22 242	450	Er	0.88
14 239	702	Pm	2.54	22 522	444	Pr	10.4
14 347	697	Tm	0.92	22 624	442	Er	0.43
14 600	685	Nd	0.22	22 386	428	Nd	1.14
14 625	684	Pm	2.11	23 640	423	Pm	0.20
14 663	682	Tm	2.43	23 708	422	Ho	0.89
14 721	679	Nd	0.50	24 033	416	Ho	2.55
15 015	666	Er	0.54	24 096	415	Sm	0.47
15 179	659	Tm	0.27	24 570	407	Er	0.53
15 238	656	Ho	1.03	24 582	407	Sm	0.61
15 314	652	Ho	1.01	24 704	405	Er	0.67
15 328	652	Er	1.97	24 876	402	Pm	0.46
24 925	401	Sm	3.31	31 505	317	Eu	1.01

TABLE 8.26  
(Continued.)

Band peak				Band peak			
(cm <sup>-1</sup> )	(nm) <sup>a</sup>	Ion	$\epsilon$	(cm <sup>-1</sup> )	(nm) <sup>a</sup>	Ion	$\epsilon$
25 227	396	Dy	0.23	31 546	317	Sm	0.31
25 419	393	Eu	2.77	33 580	298	Dy	0.21
25 602	390	Sm	0.26	33 580	298	Nd	0.33
25 680	389	Ho	0.29	33 602	298	Eu	1.21
25 840	387	Dy	0.89	33 944	295	Dy	0.67
25 974	385	Ho	0.49	34 153	293	Ho	0.47
25 988	385	Eu	0.33	34 320	291	Dy	0.22
26 330	380	Eu	0.31	34 420	290	Nd	0.27
26 334	379	Dy	0.24	34 674	288	Ho	1.26
26 385	379	Er	6.68	34 891	287	Ho	3.16
26 510	377	Tb	0.21	35 100	285	Eu	0.57
26 624	376	Eu	0.36	35 211	284	Tm	0.27
26 702	374	Eu	0.36	35 223	284	Tb	0.25
26 752	374	Sm	0.70	35 920	278	Gd	0.29
27 137	368	Tb	0.34	35 997	278	Ho	2.07
27 427	365	Dy	2.11	36 258	276	Gd	0.92
27 457	364	Er	2.08	36 337	275	Gd	2.00
27 624	362	Sm	0.75	36 443	274	Er	0.31
27 678	361	Eu	0.64	36 536	274	Gd	1.38
27 716	361	Ho	2.27	36 550	274	Ho	0.20
27 809	360	Tm	0.80	36 576	273	Gd	1.22
27 932	358	Er	0.31	36 576	273	Tm	0.23
28 090	356	Tm	0.76	36 603	272	Er	0.30
28 120	356	Er	0.85	36 710	272	Gd	3.41
28 296	353	Nd	5.30	37 439	267	Eu	0.54
28 545	350	Tb	0.31	38 226	262	Tm	0.90
28 555	350	Nd	2.46	38 490	260	Nd	0.22
28 556	350	Dy	2.54	38 850	257	Dy	0.32
28 892	346	Nd	3.71	39 093	256	Dy	0.68
28 985	345	Ho	0.59	39 108	256	Eu	0.35
29 070	344	Sm	0.50	39 200	255	Er	7.89
29 410	340	Nd	0.21	39 872	251	Eu	0.80
29 595	338	Dy	0.34	40 064	250	Ho	0.39
30 039 <sup>b</sup>	333	Pm	4.73	41 152	243	Er	0.89
33 048	333	Ho	0.82	41 560	241	Ho	3.16
30 469	328	Nd	0.68	41 666	240	Er	0.31
30 478 <sup>b</sup>	328	Pm	4.96	42 016	238	Ho	0.21
30 798	325	Dy	1.78	42 553	235	Sm	0.22
31 250 <sup>b</sup>	320	Pm	2.53	43 525	230	Er	0.58
31 270	320	Eu	0.24				

<sup>a</sup>Measured center of observed band. The value in cm<sup>-1</sup> is the converted value [183].

Suppose we have  $n$  species in solution, with molar fractions  $\alpha_n$ ,  $\epsilon_n^{(\lambda)}$  as the unknown molar extinction coefficients, complexes of the type ML <sub>$n$</sub>  then the equation

$$\bar{\epsilon}^{(\lambda)} = \sum_n \alpha_n \epsilon_n^{(\lambda)}$$

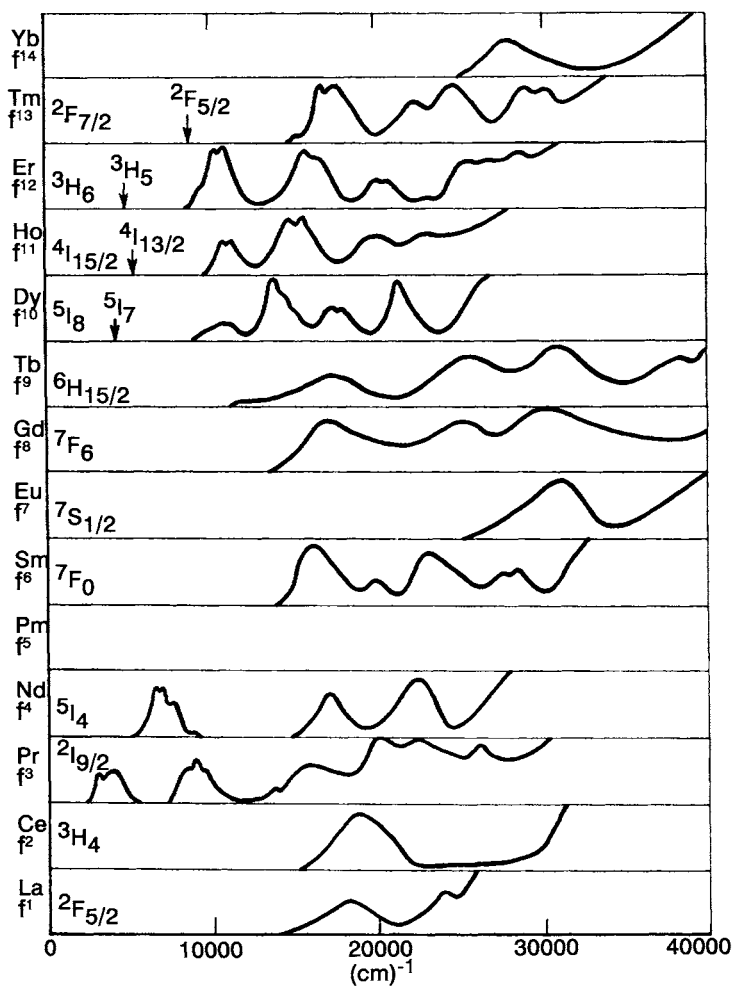


Fig. 8.32. Spectra of divalent rare-earth ions in  $\text{CaF}_2$  host crystal showing the  $f^n \rightarrow f^{n-1}d$  absorption bands. The arrows show the position of 4f internal transitions as found in the fluorescence measurements. (Reproduced from J. Chem. Phys. [182] with the kind permission of the American Institute of Physics.)

can be solved by measuring mean molar extinction coefficient  $\bar{\epsilon}(\lambda)$  at the wavelength  $\lambda$ . This is not so easy as in the cases of transition metal complexes because  $\epsilon_n$  values are low,  $\sim < 10 \text{ l mol}^{-1} \text{ cm}^{-1}$  and the  $\lambda$  wavelength shifts are low,  $< 10 \text{ cm}^{-1}$ .

In spite of the difficulties, some specific studies involving absorption spectra of complexes such as oxydiacetates of Pr(III), Nd(III), Eu(III) and Er(III), benzoylacetates of Eu(III) and monodiketonates of Eu(III) have been made with some success [184–186]. The experimental and calculated absorption spectra of oxydiacetate (ODA) complexes of Pr(III) are shown in Fig. 8.36.

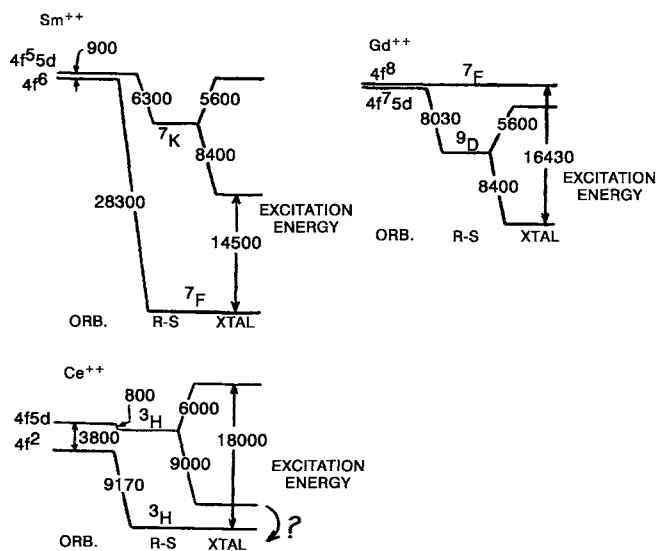


Fig. 8.33. The three typical cases of divalent rare-earth ions ground states. (i)  $\text{Sm}^{2+}$  ion representing the ions possessing  $f^n$  ground state, (ii)  $\text{Gd}^{2+}$  ion those of  $f^{n-1}d$  ground state and (iii)  $\text{Ce}^{2+}$  for the ions having  $f^{n-1}d$  state very close to  $f^n$  state. (Reproduced from J. Chem. Phys. with the kind permission of the American Institute of Physics.)

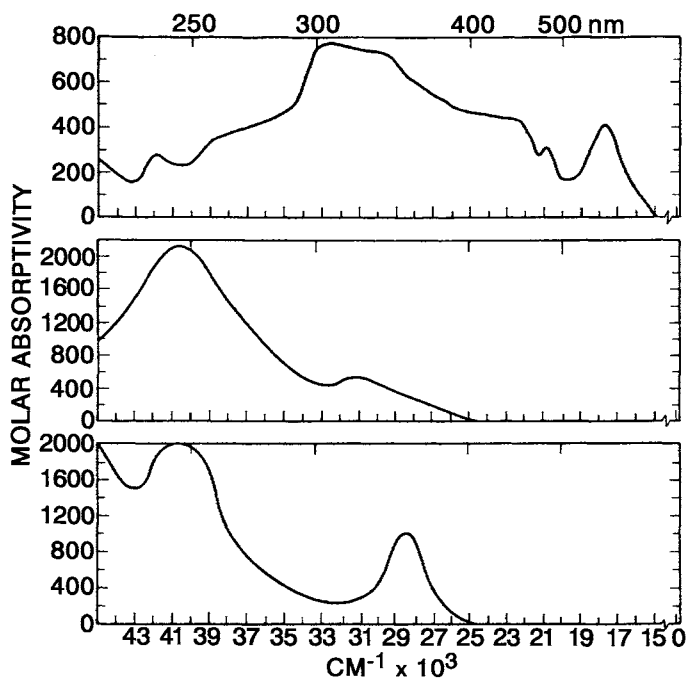


Fig. 8.34. Solution absorption spectra of  $\text{Sm}^{2+}$  (aquo),  $\text{Eu}^{2+}$  (aquo), and  $\text{Yb}^{2+}$  (aquo).



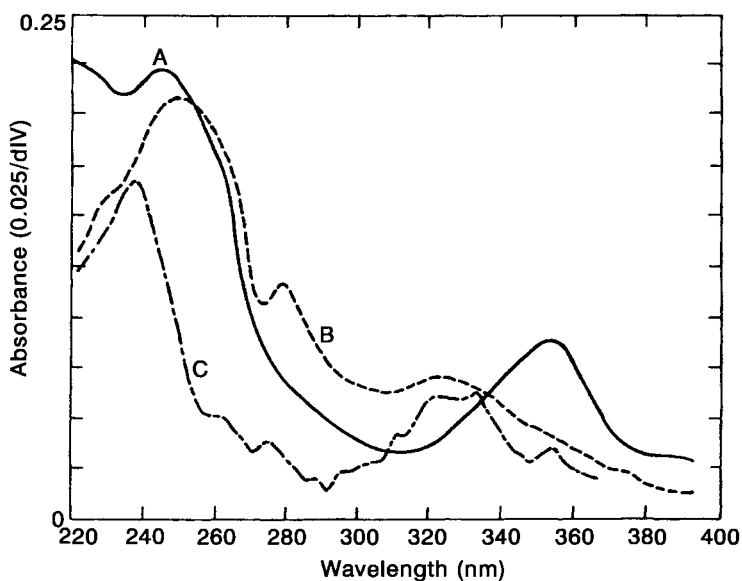


Fig. 8.35. Absorption spectra obtained by pulse radiolysis of lanthanide solutions. (A)  $\text{Tm}^{2+}$ , (B)  $\text{Gd}^{2+}$ , (C)  $\text{Ho}^{2+}$ .

Analysis of spectra is generally made to obtain (i) crystal field, ( $B_n^m$ ), (ii) nephelauxetic, ( $\beta$ ) and (iii) intensity parameters for a complex compound. These parameters are used in conjunction with relationships between spectroscopic, energy and geometry factors and deduce information on the structure of the complex.

Studies on solid complexes in single crystal form uses data on band splittings. As an example, we consider the spectra of centrosymmetric  $\text{Nd}^{3+}$ -hexakis-antipyrine triiodide single crystals. The calculated crystal field parameters are [187]:  $B_2^0 = 200 \text{ cm}^{-1}$ ;  $B_4^0 = -130 \text{ cm}^{-1}$ ;  $B_6^0 = 60 \text{ cm}^{-1}$ ;  $B_4^3 = 3250 \text{ cm}^{-1}$ ;  $B_6^3 = 1000 \text{ cm}^{-1}$ ;  $B_6^6 = 400 \text{ cm}^{-1}$ .

A comparison of the theoretical and experimental separations of  $\text{Nd}^{3+}$  is shown in Fig. 8.37.

Analysis of absorption spectra of complexes in solution is fraught with problems because splitting of the bands at room temperature is not high: (i) the ground state and excited ligand field sublevels of the ground J-levels can be populated according to the Boltzman distribution, (ii) only symmetry allowed transitions can be observed which can be obtained by group theory, (iii) lack of resolved bands in solution, (iv) broadening of bands due to electron-vibronic interaction with the solvent.

In principle, Gaussian analysis can resolve the bands with some assumptions about the shape, number and intensity of ligand-field bands. The analysis of the fine structure of the bands is limited (i.e.) bands which are split into the minimum number of ligand-field components. Such bands are listed in the literature [188].

The simplest system for the analysis of the fine structure of the absorption bands involves  $^5\text{D}_{0,1,2} \leftarrow ^7\text{F}_0$  transitions of  $\text{Eu}(\text{III})$ . The ground level is  $^7\text{F}_0$  and the transitions from the non-degenerate ground state appear as narrow bands in the spectra. Since the ground

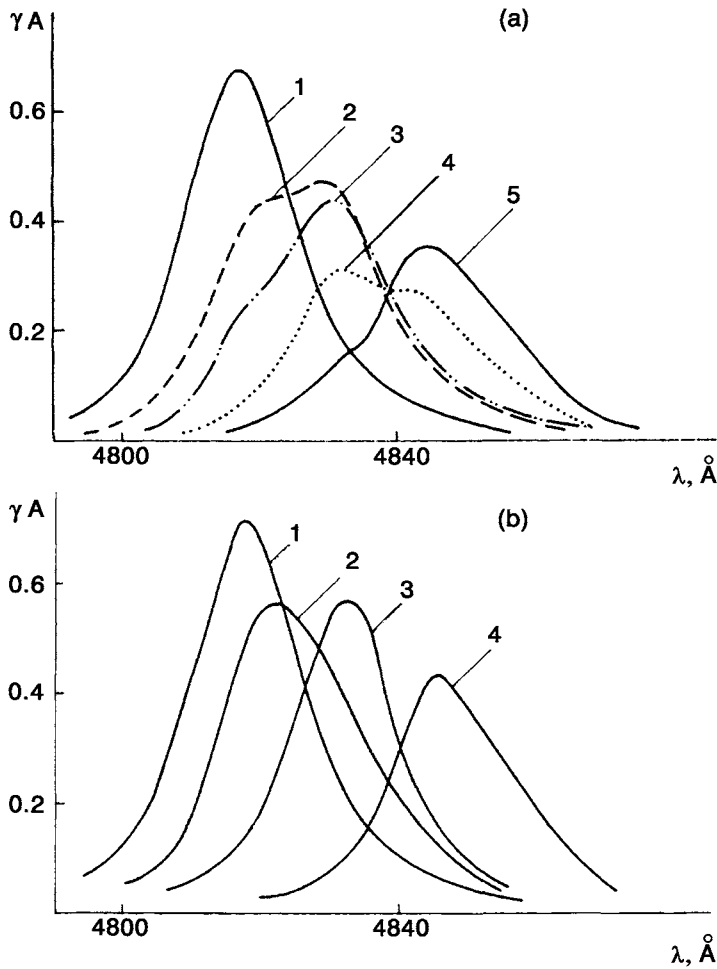


Fig. 8.36. (a) Absorption spectra of solutions involving  $\text{Pr}_{\text{aq}}^{3+}$ ,  $\text{Pr(OA)}_2^+$ ,  $\text{Pr(OA)}_3^{3-}$  and  $\text{Pr(OA)}_3^{3-}$  at ratios: (1) 1:100:0:0; (2) 5:61:34:0; (3) 1:34:61:4; (4) 0:2:54:44; (5) 0:0:11:89. (b) Absorption spectra of  $\text{Pr}_{\text{aq}}^{3+}$  (1) and calculated spectra of  $\text{Pr(OA)}_2^+$  (2),  $\text{Pr(OA)}_3^{3-}$  (3) and  $\text{Pr(OA)}_3^{3-}$  (4) [184].  ${}^3P_0 \leftarrow {}^3H_4$  transition;  $\gamma$  is the coefficient of contrast for the photographic plate [184–186].

state does not split in the ligand fields of any symmetry, the observed splitting must be due to excited states. In Table 8.28 the data on  ${}^5D_{0,1,2}$  level splitting and the activity of  ${}^5D_{0,1,2} \leftarrow {}^7F_0$  transitions in the spectra of Eu(III) in ligand fields of different systems are given. The splitting of these bands in the absorption spectra was used in the determination of the symmetry of the environment of Eu(III) in solutions of a variety of Eu(III) complexes [184,189,190]. In the case of Eu(III) only one band due to  ${}^5D_0 \leftarrow {}^7F_0$  transition is possible in this spectral region. When more than one band is observed in solution, it is possible to conclude that more than one species exists in solution. Such an observation has been made in solution for Eu(III) complexes with EDTA [191,192] and  $\beta$ -diketones [193].

TABLE 8.27  
Comparison of crystal field parameters of octahedral complexes.

Crystal	Ref.	Crystal-field parameters ( $\text{cm}^{-1}$ )	Comments
$\text{YCl}_3: \text{Er}^{3+}$	[19]	$B_4^0 = 175, B_6^0 = 0.4$	Approx. $O_h$ with $C_2$ distortion
$\text{Nd}_2\text{S}_3$	[15]	$B_4^0 = 274, B_6^0 = 85.5$	$O_h$ sym. assumed
$[(\text{C}_6\text{H}_5)_2\text{PH}]_3\text{NdCl}_6$	[16]	$B_4^0 = 282, B_6^0 = 74.7$	Approx. $O_h$ sym. predicted from observed spectra
$\text{Cs}_2\text{NaNdCl}_6$	[5]	$B_4^0 = 56.2, B_6^0 = 1.38$	$O_h$ symmetry
$\text{Pr}^{3+}\text{-HAPI}^a$	[11]	$B_4^0 = 295, (B_2^0 = 433)$	$D_{3d}$ symmetry
$\text{Nd}^{3+}\text{-HAPI}^a$	[9]	$B_2^0 = 200, B_4^0 = 195$ $B_6^0 = 16.8$	$D_{3d}$ symmetry

<sup>a</sup>The crystal-field parameters derived in this case have been converted in Steven's parameter scheme.

STATE	THEORETICAL SEPARATIONS ( $\text{cm}^{-1}$ )	EXPERIMENTALLY OBTAINED SEPARATIONS ( $\text{cm}^{-1}$ )
$4I_{9/2}$	$\text{————— } 421$ $\text{————— } 278$ $\text{————— } 218$  $\text{————— } 42$ $\text{————— } 0$	$\text{————— } 40$ $\text{————— } 0$
$2G_{7/2}$	$\text{————— } -67$ $\text{————— } -49$ $\text{————— } -17$ $\text{————— } 0$	$\text{————— } 201$ $\text{————— } 166$ $\text{————— } 138$ $\text{————— } 0(?)$
$4G_{5/2}$	$\text{————— } 272$ $\text{————— } 259$  $\text{————— } 0$	$\text{————— } 240$ $\text{————— } 199$  $\text{————— } 0$
$4F_{5/2}$	$\text{————— } 105$ $\text{————— } 93$ $\text{————— } 0$	$\text{————— } 117$ $\text{————— } 95$ $\text{————— } 0$
$4F_{3/2}$	$\text{————— } 63$ $\text{————— } 0$	$\text{————— } 94$ $\text{————— } 0$

Fig. 8.37. Comparison of theoretical and experimental separations of  $\text{Nd}^{3+}$  ion.

TABLE 8.28  
The splitting of  $^5D_0$ ,  $^5D_1$ , and  $^5D_2$  levels and the activity of  $^7F_0 \rightarrow ^5D_{0,1,2}$  transitions in the spectra of Eu(III)  
in ligand fields of different symmetry (according to the selection rules on symmetry only) [184,189,190].

Symmetry	$^5D_0$			$^5D_1$			$^5D_2$		
	Sublevel splitting	Active as <sup>a</sup>		Sublevel splitting	Active as <sup>a</sup>		Sublevel splitting	Active as <sup>a</sup>	
		ED	MD		ED	MD		Ed	MD
C <sub>s</sub>	A'	A'	A'	A' 2A''	A' 2A''	A' 2A''	3A' 2A''	3A' 2A''	3A' 2A''
C <sub>2</sub>	A	A	A	A' 2B	A 2B	A 2B	3A 2B	3A 2B	3A 2B
C <sub>2v</sub>	A <sub>1</sub>	A <sub>1</sub>	–	A <sub>2</sub> B <sub>1</sub> B <sub>2</sub>	B <sub>1</sub> B <sub>2</sub>	A <sub>2</sub> B <sub>1</sub> B <sub>2</sub>	2A <sub>1</sub> A <sub>2</sub> B <sub>1</sub> B <sub>2</sub>	2A <sub>1</sub> B <sub>1</sub> B <sub>2</sub>	A <sub>2</sub> B <sub>1</sub> B <sub>2</sub>
C <sub>2h</sub>	A <sub>g</sub>	–	A <sub>g</sub>	A <sub>g</sub> 2B <sub>g</sub>	–	A <sub>g</sub> 2B <sub>g</sub>	2A <sub>g</sub> A <sub>2</sub> 3B <sub>g</sub>	–	2A <sub>g</sub> 3B <sub>g</sub>
C <sub>3</sub>	A	A	–	A E	A E	A 2E	A 2E	A 2E	A 2E
C <sub>3v</sub>	A <sub>1</sub>	A <sub>1</sub>	–	A <sub>2</sub> E	E	A <sub>2</sub> E	A <sub>1</sub> 2E	A <sub>1</sub> 2E	2E
C <sub>3h</sub>	A'	–	A'	A' E''	–	A' E''	A' E' E''	E'	A' E''
C <sub>4</sub>	A	A	A	A E	A E	A E	A 2B E	A E	A E
C <sub>4v</sub>	A <sub>g</sub>	A <sub>1</sub>	–	A <sub>2</sub> E	E	A <sub>2</sub> E	A <sub>1</sub> B <sub>1</sub> B <sub>2</sub> E	A <sub>1</sub> E	E
C <sub>4h</sub>	A <sub>g</sub>	–	A <sub>g</sub>	A <sub>g</sub> E <sub>g</sub>	–	A <sub>g</sub> E <sub>g</sub>	A <sub>g</sub> 2B <sub>g</sub> E <sub>g</sub>	–	A <sub>g</sub> E <sub>g</sub>
D <sub>2</sub>	A	–	–	B <sub>1</sub> B <sub>2</sub> B <sub>3</sub>	B <sub>1</sub> B <sub>2</sub> B <sub>3</sub>	B <sub>1</sub> B <sub>2</sub> B <sub>3</sub>	2A B <sub>1</sub> B <sub>2</sub> B <sub>3</sub>	B <sub>1</sub> B <sub>2</sub> B <sub>3</sub>	B <sub>1</sub> B <sub>2</sub> B <sub>3</sub>
D <sub>2h</sub>	A <sub>g</sub>	–	–	B <sub>1g</sub> B <sub>2g</sub> B <sub>3g</sub>	–	B <sub>1g</sub> B <sub>2g</sub> B <sub>3g</sub>	2A <sub>g</sub> B <sub>1g</sub> B <sub>2g</sub> B <sub>3g</sub>	–	B <sub>1g</sub> B <sub>2g</sub> B <sub>3g</sub>
D <sub>2d</sub>	A <sub>1</sub>	–	–	A <sub>2</sub> E	E	A <sub>2</sub> E	A <sub>1</sub> B <sub>1</sub> B <sub>2</sub> E	B <sub>2</sub> E	E
D <sub>3</sub>	A <sub>1</sub>	–	–	A <sub>2</sub> E	A <sub>2</sub> E	A <sub>2</sub> E	A <sub>1</sub> 2E	2E	2E
D <sub>3h</sub>	A <sub>1</sub> '	–	–	A <sub>2</sub> ' E''	–	A <sub>2</sub> ' E''	A <sub>1</sub> ' E' E''	E'	E''
D <sub>3d</sub>	A <sub>1g</sub>	–	–	A <sub>2g</sub> E <sub>g</sub>	–	A <sub>2g</sub> E <sub>g</sub>	A <sub>1g</sub> 2E <sub>g</sub>	–	A <sub>1g</sub> E <sub>g</sub>
D <sub>4</sub>	A <sub>1</sub>	–	–	A <sub>2</sub> E	A <sub>2</sub> E	A <sub>2</sub> E	A <sub>1</sub> B <sub>1</sub> B <sub>2</sub> E	E	E
D <sub>4h</sub>	A <sub>1g</sub>	–	–	A <sub>2g</sub> E <sub>g</sub>	–	A <sub>2g</sub> E <sub>g</sub>	A <sub>1g</sub> B <sub>1g</sub> B <sub>2g</sub> E <sub>g</sub>	–	E <sub>g</sub>
D <sub>4d</sub>	A <sub>1</sub>	–	–	A <sub>2</sub> E <sub>3</sub>	–	A <sub>2</sub> E <sub>3</sub>	A <sub>1</sub> E <sub>1</sub> E <sub>2</sub>	E <sub>1</sub>	–
T <sub>d</sub>	A <sub>1</sub>	–	–	T <sub>1</sub>	–	T <sub>1</sub>	E T <sub>2</sub>	T <sub>2</sub>	–
O <sub>h</sub>	A <sub>1g</sub>	–	–	T <sub>1g</sub>	–	T <sub>1g</sub>	E <sub>g</sub> T <sub>2g</sub>	–	–

<sup>a</sup>ED = electric dipole; MD = magnetic dipole.

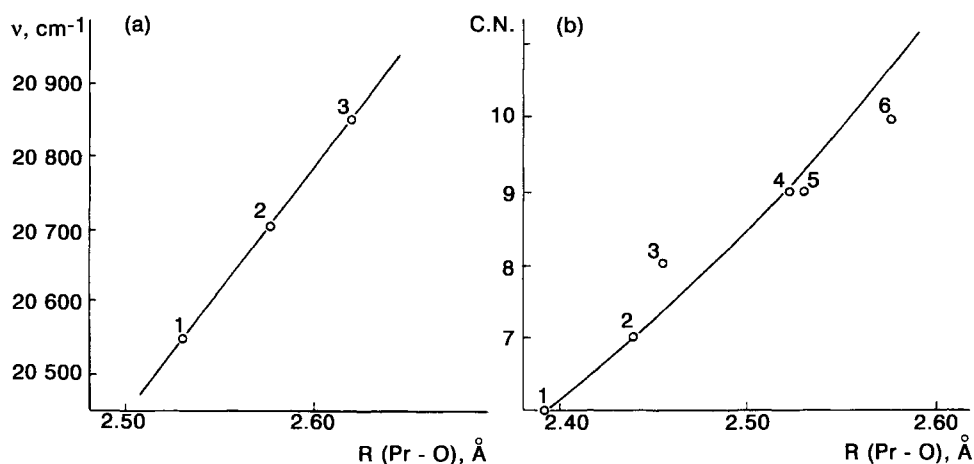


Fig. 8.38. (a) Dependence of  ${}^3P_0 \leftarrow {}^3H_4$  transition energy ( $\nu$ ) in the absorption spectra for Pr(III) complexes on mean Pr-O distances  $PrO_x$  chromophores: (1)  $Pr(C_2H_5SO_4)_3 \cdot 9H_2O$ ; (2)  $Pr(NO_3)_3 \cdot 6H_2O$ ; (3)  $Pr_2Mg_3(NO_3)_{12} \cdot 24H_2O$ ; ( $R_{Pr-O}$  is determined by extrapolation from  $Ce_2Mg_3(NO_3)_{12} \cdot 24H_2O$ ). (b) Interrelation between praseodymium coordination numbers (CN) and  $\bar{R}$  (Pr-O): (1) C- $Pr_2O_3$ ; (2)  $Pr_2(dpm)_6$ ; (3)  $NH_4Pr(tta)_4$ ; (4)  $Pr_2(C_2O_4)_3 \cdot 10H_2O$ ; (5)  $Pr-(C_2H_5SO_4)_3 \cdot 9H_2O$ ; (6)  $Pr(NO_3)_3 \cdot 6H_2O$  [196].

## 29. Determination of coordination number

It has been found that some of the J-J transitions in the absorption spectra bear a relationship with the metal-ligand distance in the rare earth metal ion complexes. This is particularly true in the case of Pr(III) and Nd(III) complexes. The correlation involves the energy of  ${}^3P_0 \leftarrow {}^3H_4$  transition of Pr(III) with the mean metal-ligand distance ( $R$ , Å) in a series of Pr(III) complexes. From such a correlation, the coordination number of Pr(III) in the complexes is estimated [194,195].

When the data on metal-ligand bond distances are available, it may be correlated with the energy of J-J transitions in the complexes. Such a correlation is depicted in Figs 8.38 and 8.39 for Pr(III) and Nd(III) complexes [196].

The relationships between  $\nu$  ( $cm^{-1}$ ) and  $R$  (M-O) and coordination number (CN) and  $R$  (M-O) are shown in Figs 8.38 and 8.39 for Pr(III) and Nd(III) complexes, respectively. The values of  $\nu$  are experimentally measured and the values of  $R$  (M-O) are taken from crystal structure data in the literature. Thus knowledge of  $\nu$  will give the value of  $R$  (M-O) from Figs 8.38a and 8.39a which in turn give values of coordination number (CN) by using the correlation in Figs 8.38b and 8.39b.

## 30. Study of chemical equilibria

Absorption spectra in the f-f region are in general not very sensitive to the ligand environment unlike the transition metal ions. In spite of this difficulty, the absorption spectroscopic method has been used in the determination of stability constants of Er(III) acetate [197] and Nd(III) glycolate complexes [198]. For complexes of low stability, a

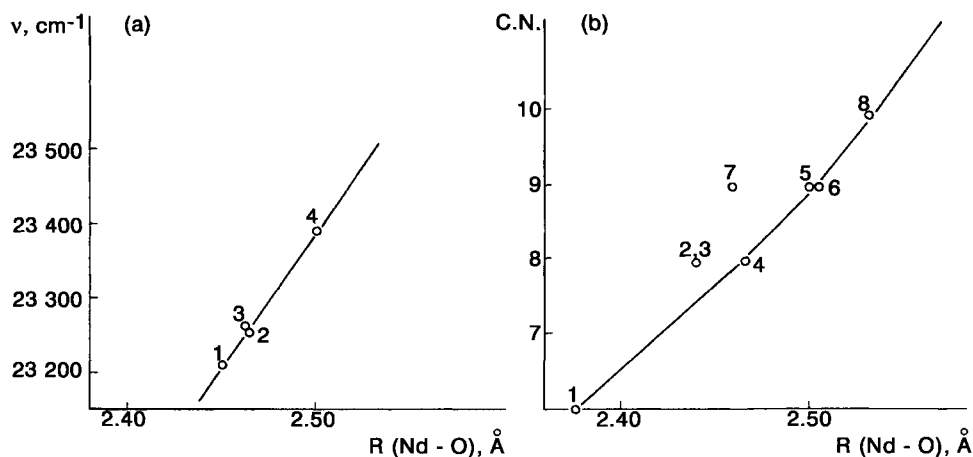


Fig. 8.39. (a) Dependence of  ${}^2P_{1/2} \leftarrow {}^4I_{9/2}$  transition energy in absorption spectra for Nd(III) complexes on mean Nd-O distances  $\text{NdO}_x$  chromophores: (1)  $\text{Nd}(\text{BrO}_3)_3 \cdot 9\text{H}_2\text{O}$  (2); (2)  $\text{Nd}(\text{aca})_3 \cdot 3\text{H}_2\text{O}$ ; (3)  $\text{K}_3\text{Nd}(\text{oda})_3 \cdot 2\text{NaClO}_4 \cdot 6\text{H}_2\text{O}$ ; (4)  $(\text{C}_5\text{H}_{11}\text{N})[\text{Nd}(\text{bac})_4]$ . (b) Interrelation between neodymium coordination numbers and  $\bar{R}(\text{Nd}-\text{O})$ : (1)  $\text{C}-\text{Nd}_2\text{O}_3$ ; (2)  $\text{Nd}(\text{tta})_3 \cdot 2\text{TPPO}$ ; (3)  $(\text{C}_5\text{H}_6\text{N})[\text{Nd}(\text{tta})_4]$ ; (4)  $\text{Nd}(\text{aca})_3 \cdot 3\text{H}_2\text{O}$ ; (5)  $\text{Nd}(\text{BrO}_3)_3 \cdot 9\text{H}_2\text{O}$ ; (6)  $\text{Nd}_2(\text{C}_2\text{O}_4)_3 \cdot 10\text{H}_2\text{O}$ ; (7)  $\text{Na}_3\text{Nd}(\text{oda})_3 \cdot 2\text{NaClO}_4 \cdot 6\text{H}_2\text{O}$ ; (8)  $\text{Nd}(\text{NO}_3)_3 \cdot 4\text{DMSO}$  [196].

differential approach involving the use of high concentrations of rare earth metal ions has been used [199]. Intensities of absorption band splitting components and their dependence on the ligand concentration have been used to determine the composition and stability of rare earth complexes [200]. Integrated band intensities have also been used in the determination of stability constants of some lanthanide complexes [201].

### 31. Structure of complexes

Empirical correlation of intensities of absorption bands with the structure of complexes in solutions have been made for lanthanide complexes. It has been recognized that forced electric-dipole transitions of low intensities, in some cases lower in intensity than those of magnetic-dipole transitions, may indicate that the ligand field has point group symmetry with a center of inversion. This criterion has been used in the determination of the ligand field by symmetry of  $\text{Eu}^{3+}$  aquo ion [202]. The absorption band intensity ratios have been used to show the octahedral structure [49] of lanthanide hexahalide complexes,  $\text{LnX}_6^{3-}$ .

Nd(III) hypersensitive transitions have been used to distinguish between inner and outer sphere complexes in solutions [203].

Coordination numbers of Nd(III), Ho(III) and Er(III) in  $\beta$ -diketone complexes in solutions were determined by a comparison of intensities of hypersensitive transitions with those of solid complexes of known structure [204].

Hypersensitive transition of Nd(III) and its intensity changes have been interpreted in the bonding of Nd(III) to protein either through carboxyl or the amino carboxyl group [205].

### 32. Absorption spectra in aqueous media

In aqueous solutions, lanthanide(III) ions are coordinated by water molecules. The hydration sphere of the lanthanide ions plays a vital role in the chemistry of the ion and also in several biochemical reactions involving isomorphous calcium(II) substitution reactions. The interpretation of the absorption spectra of lanthanide(III) ions in aqueous media is difficult because of the variability of the coordination number of the aquo ions along the lanthanide series. Kinetic and thermodynamic studies [206–210] on the lanthanide aquo systems led to the conclusion that the lighter lanthanides have a coordination number of 9, heavy lanthanides are octacoordinated and the middle members exist in an equilibrium mixture of octa and nonacoordinated aquo ions.

In chloride solutions, the variation of coordination number from 9 to 8 has been observed in aquo lanthanide ions [204]. This observation was negated by NMR studies. NMR studies show that La is nonacoordinated in chloride solutions while it is octacoordinated in  $\text{LaBr}_3$  solutions [211]. Thus the question of nonacoordination or octacoordination in La(III) still remains a puzzle and a plausible explanation is that an equilibrium mixture of both octa and nonacoordinated species is present in aqueous solutions with rapid interconversion of one into another. Both tricapped trigonal prismatic and dodecahedral structures may impart some stability to the two species with facile interconversion of one species into another. It will be useful to evaluate the energetics for the conversion of one structure into the other.

Complexation of Pr(III) by malic, tartaric and trioxylglutarate anions produced a systematic red shift of the band due to  $^3P_0 \leftarrow ^3H_4$  transition and the shift was additive. The additivity of the red shift suggests the individual contribution of each coordinate group. The individual contributions to the red shift were used in elucidating the structures and the coordination environment of Pr(III) ion.

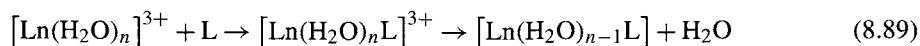
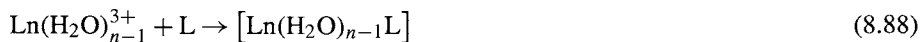
Studies on the acetate complexes of Nd(III) by Choppin et al. using the hypersensitive transition showed that the formation of the monoacetato complex did not alter the intensity of the band but produced a small red shift. Formation of the diacetato complex produced marked changes in intensity and red shift. These changes were interpreted as due to the penetration of the second acetate anion into the inner coordination sphere and causing a structural change [203]. These results may be interpreted as (i) initial addition of acetate forms an ion-pair complex, (ii) further addition of acetate results in entry of acetate into the inner coordination sphere of Nd(III) ion. Complex formation of Nd(III) with EDTA and NTA ligands was studied by the analysis of the bands due to  $^4G_{7/2} \leftarrow ^4I_{9/2}$  and  $^4G_{5/2} \leftarrow ^4I_{9/2}$  transitions as a function of ligand concentration and pH. Distinct changes in the shapes and intensities of the transitions were observed.  $T_2$  parameters changed significantly while  $T_4$  and  $T_6$  remained unaffected. The observed spectral changes and  $T_2$  parameters have been interpreted in terms of formation of Nd(III)–EDTA, Nd(III)–NTA complexes [214,215].

Absorption spectral analysis of 4f–4f bands in the adducts between lanthanide trifluoroacetates and 2-picoline *N*-oxide along with parametrization showed the existence of electrostatic interactions between lanthanides and ligand [216].

A comparison of the electric dipole transition intensity parameters for a series of complexes of  $\text{Nd}^{3+}$ ,  $\text{Ho}^{3+}$  and  $\text{Er}^{3+}$  with terdentate ligands having a common carboxyl group but differing in central donor and geometry of chelate ring has been

documented. Using the intensities of multiplet–multiplet transitions and Judd–Ofelt theory, the variations in  $\Omega_\lambda$  and  $T_\lambda$  parameters were interpreted to indicate small chemical and structural differences. Based on the changes in  $\Omega_\lambda$  parameters, terdentate coordination in the complexes has been proposed. The changes in intensity parameters showed that  $\Omega_2$  was affected by the differential ligand effect while  $\Omega_6$  was dependent on the nature of the lanthanide ion [217].

Complex formation of lanthanides is a rapid process. This is very obvious from the high rates for water exchange in lanthanide ions. Thus rapid motion of molecules of water in and around the lanthanide ion can be envisaged. Most of the time the relative positions with respect to one another and the cation are the same. The complexes have dynamic structures. Inner sphere complexation will certainly affect the water molecules in the outer spheres. Both dissociative and associative pathways of complex formation in aqueous media for lanthanides are possible.



The absolute partial molar volumes,  $V^0$  for  $[\text{Ln}(\text{H}_2\text{O})_n]^{3+}$  in  $\text{LnCl}_3$ , calculated value of  $V^0$  for 8 and 9 coordinate ions, rate constants for substitution by sulphate, water exchange, and activation volumes are shown for lanthanide series in Fig. 8.40. It is clear from the figure the nine coordination is valid from La to Nd, 8 coordination from Dy to Lu and intermediate between 8 and 9 for Pm to Tb. This type of change in coordination number causes further confusion in distinguishing inner sphere from outer sphere.

### 33. Absorption spectra in nonaqueous media

With the ionic mode of bonding in most of the complexes and the low values of ionic potential for lanthanides, very little direction is imparted to the lanthanide–ligand bond. The observed geometries and the primary coordination numbers of the lanthanide complexes are almost totally determined by the ligand characteristics such as conformational features, ligand donor–donor interaction, competition between ligand donor groups along with the number of solvent molecules available for coordination, chelating power of the ligand, the size of the chelate rings formed and the normalized bite of the ligand. The bond strength is less than in transition metal but greater than in alkali and alkaline earth metal compounds. The low polarizing ability of the  $\text{Ln}^{3+}$  ion together with the ionic interaction with the ligands induces slight changes in the electronic distribution in the metal–ligand binding site.

Literature covering the composition and structure of lanthanide complexes in nonaqueous media is not extensive [128,219]. Anhydrous  $\text{LnCl}_3$  in alcohol yielded crystalline tris-alcoholates. These compounds gave intense bands due to  ${}^3\text{H}_4 \leftarrow {}^3\text{P}_2$  transition in Pr(III) and  ${}^4\text{I}_{9/2} \leftarrow {}^4\text{G}_{5/2}$ ,  ${}^4\text{F}_{5/2}$  and  ${}^4\text{F}_{5/2}$  and  ${}^4\text{G}_{7/2}$  transitions in Nd(III) along with



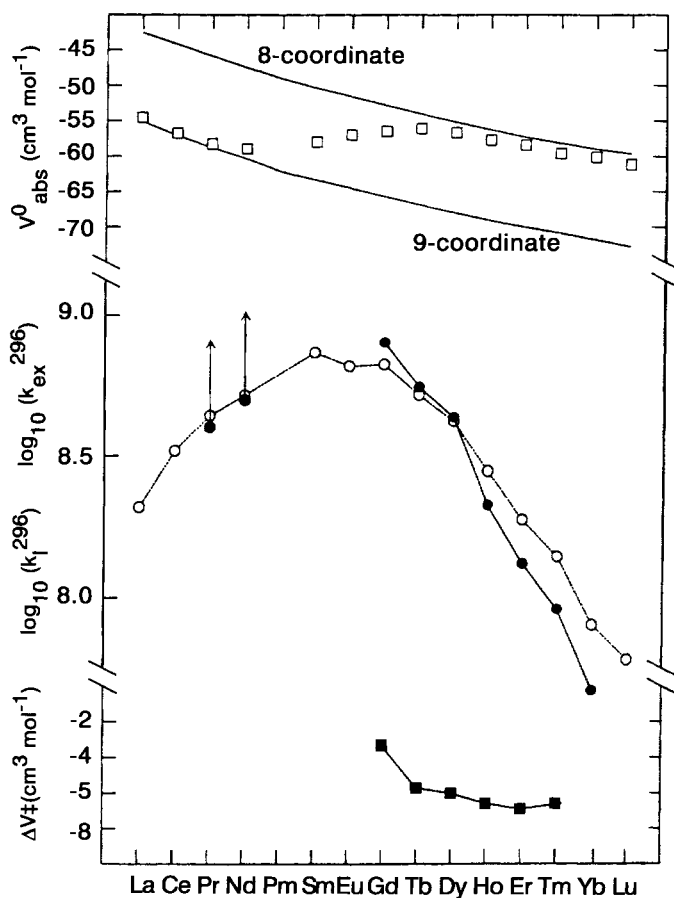


Fig. 8.40. Absolute partial molar volumes,  $V^0_{abs}$ , of  $[Ln(H_2O)_n]^{3+}$  in aqueous  $LnCl_3$  solutions ( $\square$ ), compared with the calculated values for  $[Ln(H_2O)_8]^{3+}$  and  $[Ln(H_2O)_9]^{3+}$  indicated by the upper and lower solid curves, respectively. Interchange rate constants,  $k_i$ , for the substitution of  $SO_4^{2-}$  on  $[Ln(H_2O)_n]^{3+}$  are shown as ( $\circ$ ), and water exchange rate constants (298 K) for  $[Ln(H_2O)_8]^{3+}$  are shown as ( $\bullet$ ). Activation volumes,  $\Delta V^\ddagger$ , are shown as ( $\blacksquare$ ) [218].

a red shift with respect to the band of aquo ion. Progressive small red shifts were observed in going from methanol to ethanol to isopropanol [220], along with considerable changes in intensity. The evidence obtained from IR and NMR showed the presence of alcohols in the coordination environment of Pr(III) and Nd(III). The marked red shift and significant increase in intensity in isopropanol is supported by conductivity data which showed poor ionization in isopropanol and high ionization in methanol.

The absorption spectra of  $LnCl_3$  in 4f–4f region in alcohol–water mixtures showed a red shift of the band with increase in the alcohol content. The coordination number in this media was thought to be six and this observation did not take into account the possibility of coordinated chloride [221,222]. The alcoholate adducts have been found to belong to the

$C_{2v}$  point group with a CN of 8 of lanthanide by an analysis of  ${}^5D_{0,1,2} \leftarrow {}^7F_0$  transition in Eu(III).

Many studies on the absorption spectra of lanthanides in alcoholic media have been made and the observations and anomalies have been explained in terms of entry of a chloride ion into the coordination sphere of the lanthanide ion. The composition and stability of halide complexes of lanthanides in alcohol and aqueous alcoholic solutions have been studied by spectral techniques. The halide ions have been found to cause marked changes in the spectra of lanthanides in alcoholic and aqueous media. The observed spectral changes may be attributed to changes in the immediate coordination environment of the lanthanide ion [223].

The shapes and intensities of spectral bands were used in complexation studies of lanthanide nitrates in organic solvents. The degree of complexation of nitrate was in the order water > methanol > acetonitrile. The tendency of the nitrate anion and the solvent molecules to compete for coordination followed the order DMF > TBP >  $NO_3^-$  >  $H_2O$  >  $C_2H_5OH$  > dioxane. The 4f–4f spectral band of  $Nd(ClO_4)_3$  in DMF, DMSO and DMSO– $H_2O$  mixtures split into two components whose relative intensities were attributed to different amounts of nona- and octacoordinated Nd(III) solvated ion. The major species are  $[Nd(DMF)_9]^{3+}/[Nd(DMSO)_9]^{3+}$  and the minor species are  $[Nd(DMF)_8]^{3+}/[Nd(DMSO)_8]^{3+}$ . Addition of water to the equilibrium mixture resulted in a shift of the equilibrium to predominantly nonacoordinated species due to substitution of DMF/DMSO by water along with a red shift of the spectral band [224,225].

Absorption spectral changes in the 4f–4f region of Pr(III) in 50/50 DMSO/ $H_2O$  mixtures led Borina [226] to conclude that  $[Pr(H_2O)_9]^{3+}$  is converted into  $[Pr(DMSO)_8]^{3+}$ . The observed red shift and intensification of the absorption band signified considerable covalent character in  $[Pr(DMSO)_8]^{3+}$  as compared to  $[Pr(DMSO)_9]^{3+}$ . The existence of  $[Ln(DMSO)_8]^{3+}$  and  $[Ln(DMF)_8]$  in DMSO and DMF, respectively, has been shown [227]. However, mixed solvato complexes of the type  $[Ln(solvent)_{8-n}]^{3+}$  have been identified in 50/50 mixtures DMF/ $H_2O$ , DMSO/ $H_2O$ , DMSO/ $H_2O$ ,  $CH_3CN/H_2O$  and dioxane/ $H_2O$ .

Absorption spectra of lanthanides in the 4f–4f region were used in the studies on complexation by haloacetates in DMF, DMSO, methanol and in mixtures of the solvents. Octacoordination in the solvents was inferred. The band intensities in pure solvents were higher than in solvent mixtures. Haloacetate appears to form an inner sphere complex in organic solvents and an outer sphere complex in aqueous media [227–231].

A spectroscopic procedure was used in the study of lanthanide complexes of dimethyl formamide and hexamethyl formamide in nitromethane [232]. The observed shifts in spectral bands along with IR data showed that the coordination number for Er(III) to be six and for Pr(III) and Nd(III) an equilibrium mixture of 8 and 9. The maximum number of hexamethyl phosphoramidate coordinated to Nd(III) is six with overall coordination number of 8.

The changes in the absorption spectrum due to the transition  ${}^2P_{1/2} \leftarrow {}^4I_{9/2}$  in water by the addition of DMSO to a solution of  $Nd(ClO_4)_3$  are shown in Fig. 8.41. For comparison purposes the spectrum of  $Nd(ClO_4)_3 \cdot 8DMSO$  is also shown. With progressive increase in DMSO in the solvent mixture  $H_2O$ –DMSO, the bands shift towards the spectrum of  $Nd(ClO_4)_3 \cdot 8DMSO$ . In mixed solvents two bands are seen which have been assigned to  $Nd(S)_9$  and  $Nd(S)_8$ .

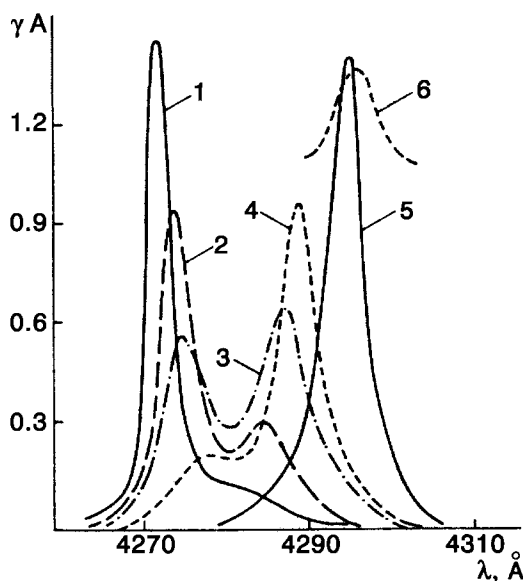


Fig. 8.41. Absorption spectra of 0.05 M  $\text{Nd}(\text{ClO}_4)_3$  in  $\text{H}_2\text{O}$  (1), DMSO (5) and in mixed  $\text{H}_2\text{O}$ -DMSO solvents at ratios (vol), 10:1 (2); 6:1 (3); 3.5:1 (4) and reflectance spectrum of  $\text{Nd}(\text{ClO}_4)_3 \cdot 8\text{DMSO}$  (6) [196], ( ${}^2\text{P}_{1/2} \leftarrow {}^4\text{I}_{9/2}$  transition).

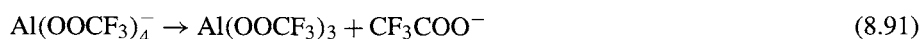
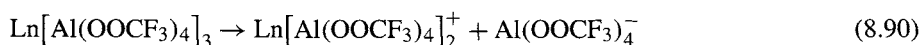
### 34. Lanthanide complexes with carboxylic acids

The detailed studies on the absorption spectral changes due to the formation of acetate complexes of Nd(III) showed that acetate addition in excess of M:L of 1:1 resulted in considerable changes in intensity of the hypersensitive transition  ${}^4\text{I}_{9/2} \leftarrow {}^4\text{G}_{5/2}$  along with a significant long wavelength shift [203]. This was interpreted as evidence for the second acetate group in the inner coordination sphere. The spectra of lanthanide haloacetates,  $\text{Ln}(\text{OOCR})_3$ , where  $\text{R} = \text{CH}_2\text{X}$ ,  $\text{CHX}_2$ ,  $\text{C}_3\text{X}$  and  $\text{X} = \text{F}$ ,  $\text{Cl}$ ,  $\text{Br}$  and  $\text{I}$  in both aqueous and nonaqueous media showed ionization in aqueous media to give  $\text{Ln}(\text{OOCR})_2^+$  and solvated product in nonaqueous media [233]. The spectra in aqueous media are similar to that of the aquo ion. But the intensities of the hypersensitive bands (Table 8.28a) were higher in haloacetate systems than in aquo ions. Further, the intensity of the bands is related to the  $\text{pK}_a$  values of the acid. In solution the haloacetates were monodentate although they can be bidentate in the solid state. The spectral characteristics together with the variations of parameters such as coulombic, spin-orbit, nephelauxetic, bonding, Judd-Ofelt intensity of the lanthanide halogenoacetate system in both solid state and solution showed the change of bidentate character in solid into monodentate in solution. The vacated position is occupied by solvent molecules. Such a conversion from bidentate into unidentate resulted in the intensification of bands. DMF caused greater intensification of the bands than DMSO. Solid complexes of the formula  $[\text{LnS}_8](\text{OOCR})_3$ , where  $\text{S} = \text{DMF}$ ,  $\text{DMSO}$ ,  $\text{CH}_3\text{OH}$ , were isolated and their spectra compared with solutions of lanthanide haloacetate in the appropriate solvent. The results showed the ionicity of the complexes with haloacetates in the outer sphere.

TABLE 8.28a

Pr(III)	$^3H_4 \rightarrow ^3P_2, ^1D_2$
Nd(III)	$^4I_{9/2} \rightarrow ^4G_{5/2}, ^4F_{5/2}$
Sm(III)	$^6H_{5/2} \rightarrow ^4F_{3/2}$
Eu(III)	$^4F_0 \rightarrow ^5D_2, ^3D_1, ^5D_0$
Ho(III)	$^5I_8 \rightarrow ^5G_6, ^3H_6$
Er(III)	$^5I_{15/2} \rightarrow ^4H_{11/2}, ^4G_{11/2}$

Bimetallic carboxylates of the formula,  $\text{Ln}[\text{Al}(\text{OOCR})_4]_3$  containing bidentate and bridging haloacetate groups have been shown to be ionized.



The absorption spectra of the bimetallic compounds showed intense 4f–4f bands along with a small nephelauxetic effect. The observed small nephelauxetic effect may be due to lowering of Slater–Condon ( $F_K$ ) and Racah ( $E^k$ ) interaction parameters which is in agreement with the ionic nature of the compounds in water and trifluoroacetic acid [234].

Lanthanides react with fatty acids such as lauric, palmitic and stearic acids to give compounds of the formula  $\text{Ln}(\text{COOR})_3$ . Lanthanide alkoxides react with fatty acids to yield mixed ligand soaps,  $[\text{Ln}(\text{OR})_n\text{A}_m]$ , where A is a fatty acid. Reaction of  $[\text{Ln}(\text{OR})_n\text{A}_m]$  with acetyl chloride or acetyl bromide yield lanthanide chloride- or bromide-mixed soaps. The spectral characteristics of the alkoxide-mixed soaps, chloride-mixed soaps, bromide-mixed soaps and quaternary-mixed soaps of Pr(III) and Nd(III) were studied and the spectral parameters were evaluated by regression analysis. The intensification of the bands and the nephelauxetic effect were in the order: quaternary soaps > alkoxide soaps > chloride-bromide-mixed soaps. The above order is in agreement with the calculated covalency due to the lowering of coulombic interaction parameters as well as the lower melting points of the mixed soaps.

More intense bands in the 4f–4f region were observed with lanthanide complexes of mandelic, salicylic, thiosalicylic, furoic, and thiophenic acids than the acetate and haloacetate analogues [235]. Both increase in intensity and nephelauxetic effect have been observed. It seems plausible that the aromatic groups in the hydroxy acids such as benzene, thiophene or furan contribute significantly to the intensity of the hypersensitive bands of the complexes. It appears that pH has an important role in determining the stoichiometry of the complex formed. Only ML species is formed up to pH 4 and both  $\text{ML}^{2+}$  and  $\text{ML}_2^+$  are formed at a pH of 6.0.

### 35. Oxydiacetate complexes

Absorption spectra of oxydiacetate complexes Ln(III), where Ln = Pr, Nd, Eu and Er were studied and some interesting results were obtained [184]. The band due to  $^5D_2 \leftarrow ^7F_0$  was well resolved in the case of Eu(III). Based on an analysis of the fine structure of the band

TABLE 8.29

Nephelauxetic effects ( $1 - \beta'$ ), mean lanthanide-ligand distances ( $\bar{R}$  (Ln-O)) and effective coordination numbers of lanthanides ( $CN_{\text{eff}}$ ) in Pr(III) and Nd(III) ODA complexes determined from baricentres ( $\sigma$ ) of spectral bands; ODA = oxydiacetate,  $^- \text{OOCCH}_2\text{OCH}_2\text{COO}^-$  [184].

Complex	Pr(III)				Nd(III)			
	$\sigma(^3\text{H}_4 \leftarrow ^3\text{P}_0)$ ( $\text{cm}^{-1}$ )	$(1 - \beta')$ $10^3$	$\bar{R}$ (Pr-O) ( $\text{\AA}$ )	$CN_{\text{eff}}$	$\sigma(^2\text{P}_{1/2} \leftarrow ^4\text{I}_{9/2})$ ( $\text{cm}^{-1}$ )	$(1 - \beta')$ $10^3$	$\bar{R}$ (Nd-O) ( $\text{\AA}$ )	$CN_{\text{eff}}$
$\text{Ln}^{3+}$ (aq)	20 750	—	2.590	11.2	23 393	—	2.500	9.0
$\text{Ln}(\text{ODA})^+$	20 719	1.5	1.584	11.0	23 348	1.9	2.486	8.6
$\text{Ln}(\text{ODA})_2^-$	20 689	3.1	2.572	10.5	23 313	3.4	2.476	8.3
$\text{Ln}(\text{ODA})_3^{3-}$	20 621	6.2	2.552	10.0	23 279	4.9	2.468	8.2
$\text{Na}_3\text{Ln}(\text{ODA})_3 \cdot 2\text{NaClO}_4 \cdot 6\text{H}_2\text{O}$	20 582	8.1	2.540	9.5	23 262	5.6	2.462	8.0

based on symmetry allowed selection rules, information on the ligand field symmetry in Eu(III) complexes was elicited. In the case of Pr(III), Nd(III) and Er(III) the fine structure was not resolved. Stepwise complexation of Pr(III) and Nd(III) resulted in progressive shift in long wavelength bands indicating a decrease in the mean Ln–O bond lengths due to substitution of water molecules in  $\text{Ln}(\text{H}_2\text{O})_n^{3+}$  oxydiacetate ligand. The data on  $\bar{R}$  (Ln–O), and effective coordination number  $\text{CN}_{\text{eff}}$  evaluated from the spectral information of Pr(III) and Nd(III) oxydiacetate complexes are given in Table 8.29. The coordination number of lanthanide dioxyacetate complexes is 9.

### 36. Lanthanide alkoxides

In this class of compounds the nature of the alkyl group appears to determine the polarizability of the alkoxy group. The volatility of the compounds depends on the alkyl group. Groups such as neopentyl, *t*-butyl and triphenyl carbinol cause covalency in the metal alkoxides and hence to their volatility.

Intense and broad absorption bands of Pr(III) and Nd(III) alkoxides in DMF show a red shift with respect to aquo ion. The intensity of the 4f–4f band and the magnitude of the nephelauxetic effect increased with increasing branching of the alkyl group. In addition to the usual intensification of the hypersensitive transitions  $^3\text{H}_4 \rightarrow ^3\text{P}_2$  in Pr(III) and  $^4\text{I}_{9/2} \rightarrow ^4\text{G}_{5/2}$  in Nd(III), additional bands due to  $^3\text{H}_4 \rightarrow ^3\text{P}_1$  and  $^3\text{H}_4 \rightarrow ^1\text{D}_2$  in Pr(III) and  $^4\text{I}_{9/2} \rightarrow ^4\text{G}_{7/2}$ ,  $^4\text{F}_{7/2}$ ,  $^4\text{F}_{5/2}$  and  $^4\text{F}_{3/2}$  in Nd(III) were sensitive to the nature of branching in the alkyl chain. This observation has been attributed to ‘pseudo-hypersensitive transitions’ and ‘ligand mediated pseudohypersensitivity’ [233].

### 37. Lanthanide $\beta$ -diketonates

This class of complexes has been studied extensively [236]. The spectroscopy of lanthanide  $\beta$ -diketonates was intensively studied during 1960’s and 1970’s because of their potential application in liquid lasers. Two species, viz., tetrakis  $\beta$ -diketonates  $[\text{Ln}(\text{diket})_4]^-$  and tris  $\beta$ -diketonates  $[\text{Ln}(\text{diket})_3]$ , have been characterized. The latter neutral complex accepts Lewis bases and forms compounds. The neutral  $[\text{Ln}(\text{diket})_3]$  complexes are both thermally and kinetically stable [237].

Comparative absorption spectrophotometry has been used in the studies of lanthanide  $\beta$ -diketonate complexes in solids as well as in solutions. The neutral hexacoordinated lanthanide tris diketonate on dissolution in a polar nonaqueous solvent, increased its coordination to eight by accepting two solvent molecules [204]. The addition of water or other oxygenated solvent to  $\text{Nd}(\text{diket})_3$  in solution resulted in significant changes in the shape and intensity of the band due to  $^4\text{I}_{9/2} \rightarrow ^4\text{G}_{15/2}$ , transition. These changes have been attributed to an increase in coordination number of Nd(III) from 6 to 8 by the coordination of two solvent molecules [238–241].

The absorption spectra of Pr(III) ( $^3\text{H}_4 \rightarrow ^3\text{P}_0$  transition), Nd(III) ( $^4\text{I}_{9/2} \rightarrow ^2\text{P}_{1/2}$  transition) and Eu(III) ( $^7\text{F}_0 \rightarrow ^5\text{D}_0$  transition) with several  $\beta$ -diketonates having alkyl and aryl radicals were studied [241]. The spectra of mono, bis, tris and tetrakis  $\beta$ -diketonates were analysed by comparative absorption spectrophotometry. In the stepwise complexation

with acetylacetonate of Pr(III) and Nd(III), the changes in the nephelauxetic effect, the mean Ln–O bond distance and the effective coordination number were obtained as shown in Table 8.30. The values of  $CN_{\text{eff}}$  for Nd(III) are in the acceptable range 8–9 while the values for Pr(III) are in the range of 10–11. The latter values are high and the discrepancy is yet to be explained.

Solution chemistry studies have shown [242] the pH dependence for the existence of  $\beta$ -diketonates as follows (Table 8.30a).

A linear correlation between the oscillator strength of the hypersensitive transition and molar refraction,  $P$  of the ligand in  $\beta$ -diketonate complexes has been established [243].

In the lanthanide- $\beta$  diketone system, when the stoichiometry of M:L is increased and at high levels of ligand, both hypersensitive transitions and non-hypersensitive transitions were intensified in Pr(III) and Nd(III) (Table 8.30b).

The possible explanation [233] for the environmental sensitivity of the transitions (nonhypersensitive) may be due to an increase in  $T_\lambda$  parameters which results in lowering of the excited states of the ions since the surrounding crystal field is influenced by the symmetric part of the crystal field. The observed changes in  $T_\lambda$  and the small nephelauxetic effect show that the nonsymmetric part of the crystal field affects  $T_\lambda$  values. The modifier ions distort the oxygen bonded to the lanthanide and thus lowers the site symmetry and increases the f–f transition probability.

Let us recall the relationship for  $T_\lambda$

$$T_\lambda = \chi \left[ \frac{8\pi^2 m}{3h} \right] (2\lambda + 1) \sum_{iip} A_{t,p} |2\Xi_2(t, \lambda),$$

where  $A_{t,p}$  ( $t$  odd) are parity terms in the crystal field expansion depending on site symmetry and  $\Xi(t, \lambda)$  contains the integral involving radial part of  $4f^n$  wave function. The energy difference between these two states is contained in the denominator of  $\Xi(t, \lambda)$  which also measures the symmetric part of the crystal field and changes with the type of chromophore but is unaffected by changes in the exocyclic part of the chromophore. The changes in this parameter are not significant when compared to the aquo lanthanide ion. The  $T_\lambda$  parameter is sensitive to the nature of the chromophore and to the nature of the group exocyclic to the chromophore skeleton. In the case of outersphere complexation in lanthanides  $T_\lambda$  varies significantly with negligible changes in coulombic, spin–orbit interaction and nephelauxetic effect. This then suggests that  $\Xi(t, \lambda)$  is not contributing significantly to  $T_\lambda$  and that the contribution of  $A_{t,p}$  ( $t$  odd) seems to dominate  $T_\lambda$  values. This term then contributes to the asymmetric terms in the crystal field expansion due to the distortion of the geometry around the lanthanide ion.

Absorption spectra of Pr(III) and Nd(III) complexes with alkyl, aryl, fluorine substituted  $\beta$ -diketonates and the associated hypersensitive transitions were studied in detail. Mono, bis, tris and tetrakis complexes in benzene, DMF, DMSO and ethanol were also studied. Spectra both in solids and solution permitted the interpretation of the state of  $\beta$ -diketonates based on the trends in the intensity and energy interaction parameters [238,244]. The various complexes were isolated and their IR,  $^1\text{H}$  NMR, stability constants were studied as well. Octacoordination in the tetrakis complex and tris complex associated with two solvent molecules was noted.

TABLE 8.30

Nephelauxetic effects ( $1 - \beta'$ ), mean lanthanide–ligand distances ( $\bar{R}$  (Ln–O)) and effective coordination numbers of lanthanides ( $CN_{\text{eff}}$ ) in Pr(III) and Nd(III) acac complexes determined from baricentres ( $\sigma$ ) of spectral bands; acac = acetylacetonate [241].

Complex	Pr(III)				Nd(III)			
	$\sigma(^3P_0 \rightarrow ^3H_4)$ ( $\text{cm}^{-1}$ )	$(1 - \beta')$ $10^3$	$\bar{R}$ (Ln–O) ( $\text{\AA}$ )	$CN_{\text{eff}}$	$\sigma(^2P_{1/2} \rightarrow ^4I_{9/2})$ ( $\text{cm}^{-1}$ )	$(1 - \beta')$ $10^3$	$\bar{R}$ (Nd–O) ( $\text{\AA}$ )	$CN_{\text{eff}}$
$\text{Ln}^{3+}$ (solv)	20 750	–	2.590	11.2	23 385	0.3	2.498	8.9
$\text{Ln}(\text{acac})^{2+}$	20 741	0.4	2.588	11.1	23 320	3.1	2.482	8.5
$\text{Ln}(\text{acac})_2^+$	20 681	3.3	2.570	10.5	23 298	4.1	2.473	8.3
$\text{Ln}(\text{acac})_3$	20 664	4.1	2.565	10.3	23 244	6.4	2.457	7.9
$\text{Ln}(\text{acac})_4^-$	20 596	7.4	2.542	9.8	23 217	7.6	2.450	7.7

<sup>a</sup>In mixed solvent with  $\text{H}_2\text{O}$ :  $\text{CH}_3\text{OH}$  ratio 1:4.



TABLE 8.30a

pH < 7.0	ML <sup>2+</sup> , ML <sub>2</sub> <sup>+</sup>
pH > 7.0	ML <sub>3</sub> <sup>0</sup> , ML <sub>4</sub> <sup>-</sup>

TABLE 8.30b

	Hypersensitive transition	Non-hypersensitive transition
Pr(III)	<sup>3</sup> H <sub>4</sub> → <sup>3</sup> P <sub>2</sub> ; <sup>4</sup> I <sub>9/2</sub> → <sup>4</sup> G <sub>5/2</sub>	<sup>3</sup> H <sub>4</sub> → <sup>3</sup> P <sub>1</sub> , <sup>3</sup> D
Nd(III)	<sup>4</sup> I <sub>9/2</sub> → <sup>4</sup> G <sub>5/2</sub>	<sup>4</sup> I <sub>9/2</sub> → <sup>4</sup> F <sub>7/2</sub> , <sup>4</sup> F <sub>5/2</sub> , <sup>4</sup> F <sub>3/2</sub>

Reaction of Pr(III), Nd(III) and Eu(III) with  $\beta$ -diketones in DMF, DMSO, EtOH and CH<sub>3</sub>CN favoured the formation of higher complexes. On the other hand, ML<sup>2+</sup> species is predominant in aqueous media irrespective of the ligand concentration. The band intensities and the nephelauxetic effect were significant in ML<sup>+</sup>, ML<sub>2</sub><sup>+</sup>, ML<sub>3</sub>, ML<sub>4</sub><sup>-</sup> complexes when the ligand L was a  $\beta$ -diketone with fluorine and aryl substituents [238,244].

The significant nephelauxetic effect in the spectra of Nd(III) hydroxyaquobisbenzoylacetonate was attributed to resonance in the  $\beta$ -diketone by Dutt [238], while the others interpreted this to the lower coordination number of six. Anhydrous lanthanide salts mixed with  $\beta$ -diketonates of the type (LnL<sup>I</sup>, L<sup>II</sup>, L<sup>III</sup>) show markedly greater nephelauxetic effect and intensity than the lanthanide tris  $\beta$ -diketonates in semiaqueous media which has been attributed to a lower coordination number in anhydrous  $\beta$ -diketonates [239,240].

The Eu(III) absorption band due to the transition <sup>7</sup>F<sub>0</sub> → <sup>5</sup>D<sub>0</sub> and the shifts in this band due to the nephelauxetic effect were studied for various  $\beta$ -diketones. A correlation between the energy of <sup>7</sup>F<sub>0</sub> → <sup>5</sup>D<sub>0</sub> transition and the sum of Taft's constants [186]  $\sigma_{RI}^* + \sigma_{RII}^*$  has been established as shown in Fig. 8.42.

Bimetallic fluoro  $\beta$ -diketonates of lanthanide and aluminum behave similarly to those of bimetallic alkoxides Ln[Al(OR)<sub>4</sub>]<sub>3</sub>. Both types of compounds show significant nephelauxetic effect and intense 4f–4f bands. The covalency parameters and nephelauxetic effect are higher in diketonates than in alkoxides. The high oscillator strengths of hypersensitive and pseudohypersensitive transitions of the fluoro  $\beta$ -diketonates are attributed to the chelating character of the ligands [244]. Plots of oscillator strengths of <sup>4</sup>I<sub>9/2</sub> → <sup>4</sup>G<sub>5/2</sub> and <sup>4</sup>I<sub>9/2</sub> → <sup>4</sup>F<sub>5/2</sub> versus bonding parameter b (or mixing coefficient) which describes the extent of mixing of 4f wave function with the ligand wave function showed a linear correlation with a positive slope. This correlation suggests the participation of 4f orbitals in bonding. The nephelauxetic effect results in shortening of the metal–ligand bond which will increase the probability of interaction between the metal and ligand orbitals. The nephelauxetic effect can also lower the coordination number.

### 38. Lanthanide complexes with nucleic acids

The lanthanides and divalent calcium are similar in size and have a tendency for high coordination numbers and these similarities make lanthanide ions as structural probes in biochemical reactions in place of calcium. Further, lanthanide ions can be used as markers

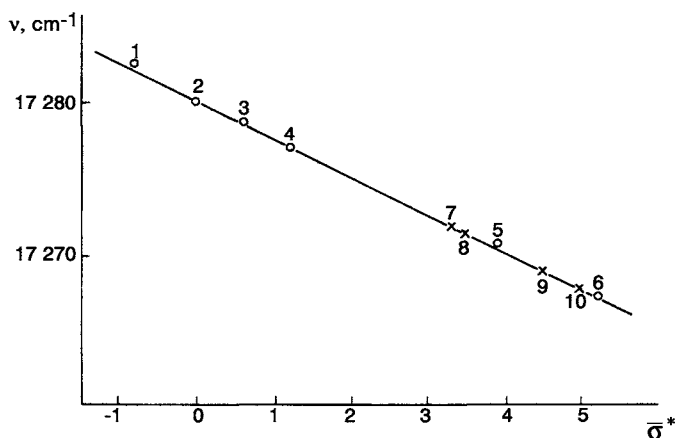


Fig. 8.42. Dependence of the  ${}^5D_0 \leftarrow {}^7F_0$  transition energy in the absorption spectra for Eu(III) mono- $\beta$ -diketonates on the sum of Taft's constants for RI and RII radicals in  $\beta$ -diketone: (1) Eu(dpm) $^{2+}$ ; (2) Eu(aca) $^{2+}$ ; (3) Eu(bac) $^{2+}$ ; (4) Eu(dbm) $^{2+}$ ; (5) Eu(tta) $^{2+}$ ; (6) Eu(hfa) $^{2+}$ ; (7) Eu(fod) $^{2+}$ ; (8) Eu(pdm) $^{2+}$ ; (9) Eu(tdpf) $^{2+}$ ; (10) Eu(tdm) $^{2+}$  [186].

because of  $4f^n$  configuration and the resulting paramagnetic properties. Natural biological molecules have centers of dissymmetry in molecular conformations and lanthanide complexes of these molecules behave as chiral lanthanide complexes [237].

The phosphate binds to Ln in a bidentate manner in nucleotide monophosphate. The terminal phosphate in adenosine diphosphate and triphosphate is involved in bonding to Ln [245]. The conformation of cytidine monophosphate and adenosine monophosphate in solution is similar. The spectral features of the interaction of nucleic bases (cytosine, guanine, uracil, substitute uracils, thiamide, adenine) and fluoronucleic bases (fluorouracil, fluorocytosine, fluorothymine, fluoroadenine) were studied in both aqueous media and in DMSO/DMF/dioxane–water mixtures. Outer sphere coordination was indicated in aqueous media by the weak  $4f-4f$  band intensities. In DMF/DMSO/dioxane–water mixture, higher intensities of the  $4f-4f$  bands along with red shifts were observed. Evidence through ultrasonic studies suggests that nucleic bases disrupt and weaken the structure of water which is reversed by the addition of the organic solvent. Nucleic bases attract water molecules and as a result interact weakly with aquo lanthanide ions. When an organic solvent is added, the interaction between nucleic bases and aquo lanthanide becomes stronger.

Fluorinated bases act as poor bases towards carbonyl oxygen and pyrimidine nitrogen in comparison to unsubstituted nucleic bases. If such is the case the intensities of the  $4f-4f$  bands of fluoronucleic base complexes of Ln have to be less than the intensities of the parent nucleic base complexes. This conclusion is not supported by experimental evidence. On the contrary, the intensity of  ${}^4I_{9/2} \rightarrow {}^4G_{5/2}$  and  ${}^4I_{9/2} \rightarrow {}^4F_{5/2}$  transition of Nd(III) and  ${}^3H_4 \rightarrow {}^3P_2$ ,  ${}^3P_1$  and  ${}^1D_2$  transition of Pr(III) complexes of fluoronucleic bases show increased intensity [233].

Nucleosides form stronger complexes with lanthanides than nucleic bases because of the presence of the ribose hydroxylic group. This is reflected in the intensity of the absorption bands. Cytidine, uridine and thymidine form stronger complexes than adenosine because

of the oxygen donor sites in uracil, thymine and cytosine. On the other hand, adenine has only a nitrogen donor. Ln–O is preferred to Ln–N. Fluorinated nucleoside produced more intense bands than nucleosides. Solid complexes of the type  $[\text{Ln}(\text{nucleic base})_4(\text{H}_2\text{O})_4]^{3+}$ ,  $[\text{Ln}(\text{nucleic base})_2(\text{H}_2\text{O})_3]^{3+}$  support the spectral studies that the nucleic base bonds through carbonyl oxygen. It is also shown that the two *cis*-hydroxyl groups of ribose sugar together with the carbonyl oxygen are involved in bonding as terdentate.

By examining space-fitting models it has been shown that several functional groups in adenosine and guanosine have many degrees of freedom. The base can rotate around the glycosidine bond without much difficulty. In the *syn*-conformation, the sugar oxygen and the base nitrogen approach closely to permit the formation of an inner sphere complex. In the *anti*-conformation the sugar oxygen and base nitrogen are far apart which does not allow bonding to the metal ion. Since the observed 4f–4f bands of the complexes are weak the metal is probably interacting with the *anti*-conformation of nucleoside. Further, the dimerization tendency of the *anti*-conformation nucleoside reduces the extent of complexation with lanthanide. Evidence obtained for stacking in nucleosides will further reduce the tendency for complex formation [233].

Fluorine substitution in nucleosides and nucleic bases resulted in stronger interaction between lanthanides and ligands as compared with unsubstituted nucleosides and nucleic bases. The analysis of the fine structure of the bands, based upon the selection rules for the symmetry allowed transitions enabled the understanding of ligand field symmetry in Pr(III) and Nd(III) complexes of fluorinated nucleosides and nucleic bases. The stepwise complexation of Pr(III) Nd(III) was studied by the red shift of the absorption band which indicated a decrease in Ln–O distance in the complex due to the substitution of water by the fluorinated nucleoside ligand.

Nucleotides bind to lanthanides more strongly than nucleosides. Conductivity data showed the nucleotide complexes behave like 1:1 electrolytes and to be more ionic in nature. Complexes of the type  $[\text{Ln}(\text{nucleic base})_2(\text{H}_2\text{O})_3]^-$  have been identified. The absorption spectra in aqueous solution do not change prominently; even the complex ionizes to form a 1:1 complex. In nonaqueous media, changes in spin–orbit parameters increase in oscillator strengths of 4f–4f transitions and increased intensity and progressive red shift of the bands occur. The analysis of the spectra of nucleotides AMP, GMP, CMP, IMP and UMP with Pr(III) and Nd(III) in 90/10 of DMSO/water solutions showed that nucleotides derived from bases having a carboxyl oxygen intensified the following transitions.

	Hypersensitive	Non-hypersensitive
Pr <sup>3+</sup>	$^3\text{H}_4 \rightarrow ^4\text{F}_4$	$^3\text{H}_4 \rightarrow ^3\text{P}_2, ^1\text{D}_2$
Nd <sup>3+</sup>	$^4\text{I}_{9/2} \rightarrow ^4\text{G}_{5/2}$	$^4\text{I}_{9/2} \rightarrow ^4\text{F}_{5/2}, ^4\text{G}_{7/2}, ^4\text{F}_{7/2}, ^4\text{F}_{3/2}$

The oscillator strength of  $^4\text{I}_{9/2} \rightarrow ^4\text{F}_{5/2}$  approached that of  $^4\text{I}_{9/2} \rightarrow ^4\text{G}_{5/2}$ . AMP containing nitrogen atom for coordinating gave the weakest 4f–4f bands. The intensification of the bands of Pr(III) and Nd(III) (both hypersensitive and non-hypersensitive bands) showed the trend AMP > ADT > ATP.

The above trend also reflects the increased ionic character. Greater ionization means a smaller red shift and weaker 4f–4f bands [233,246].

### 39. Lanthanide complexes with nitrogen donor ligands

Complexes of lanthanides with exclusively nitrogen donor ligands are not stable unlike oxygen donor ligands. Lanthanide complexes containing both oxygen and nitrogen donor ligands are known. When bipyridine or *o*-phenanthroline is present in the complex, the intensity of 4f–4f transitions in Ln(III), where Ln = Pr, Nd, Sm, Dy, Ho, Er increases considerably. Aqueous systems of Pr(III) or Nd(III) containing different amounts of bipyridine and *o*-phenanthroline do not show evidence of complexation and the 4f–4f bands remain unaffected. However, when the pH of the solution is increased to 5.0 the intensity of the 4f–4f bands increased significantly. The *o*-phenanthroline system showed greater hyperchromicity than the bipyridine system because of the additional phenyl group and associated  $\pi$  electrons. This suggests that the  $\pi$  electron density in *o*-phenanthroline is responsible for the observed hyperchromicity.

Trishaloacetates of lanthanides form 1:1 complexes with bipyridine and *o*-phenanthroline accompanied by marked changes in the energies and intensities of 4f–4f bands. Similarly 1:1 complexes of lanthanide tris  $\beta$ -diketonates with *o*-phenanthroline and bipyridine are known. The lanthanide is octacoordinated in these 1:1 complexes. Synthesis of mixed ligand complexes of lanthanides containing  $\beta$ -diketones and nitrogen bearing ligands and their spectral features to elucidate the nature of bonding in the complexes has received considerable attention [247–253]. Su et al. [254] interpreted the observed red shift for the spectral line  $^4I_{9/2}$  as due to the expansion of metal electronic cloud. It is suggested that a 4f orbital mixes with  $4f^{n-1}gd$  orbital of opposite parity and the resulting orbital takes part in bonding. The extent of red shift was in the order Nd–F < Nd–OH < Nd–OS( $\phi$ )<sub>2</sub> < Nd–O–P < Nd–OS(Me)<sub>2</sub> < Nd–O–Al. Further, the red shift in nonaqueous media was greater than in aqueous media.

The spectra of lanthanide mixed complexes of bipyridine/*o*-phenanthroline and carboxylate/ $\beta$ -diketone were studied both in solids and solution and were found to be octacoordinated. The shapes and intensities of the bands were nearly the same in solids and solution. The variation of  $T_{\lambda}$ , coulombic ( $F_k$ ,  $E^k$ ) and nephelauxetic ( $\beta$ ,  $\delta$ ,  $b$ ) parameters showed a similar trend. The complexes are ionized in dilute solutions ( $\sim 10^{-4}$  M) and unionized in 0.05–1.0 M solutions as revealed by an analysis of the spectral intensity [233,255].

Mixed ligand complexes of Pr(III) and Nd(III) with bipyridine/*o*-phenanthroline and diols (1,4-butane-, 1,4-butene-, 1,4-butyne-) in seminonaqueous media were studied with respect to  $^3H_4 \rightarrow ^3P_2$ ,  $^1D_2$  transitions in Pr(III) and  $^4I_{9/2} \rightarrow ^4F_{5/2}$ ,  $^4G_{7/2}$ ,  $^4F_{7/2}$ , and  $^4F_{3/2}$  transitions of Nd(III). The diols form seven membered rings along with two Ln–N bonds through bipyridine/*o*-phenanthroline. The intensity of the 4f–4f bands varied in the order butyne-1,4-diol > butene-1,4-diol > butane-1,4-diol.

These observations suggest an interaction between the  $\pi$  electron cloud located at second and third carbon atoms of the diols and the lanthanide metal orbitals. Similar behaviour was observed in the mixed complexes of lanthanide  $\beta$ -diketonates and the substituted diols [233].

### 40. Lanthanide amino acid complexes

The interactions between metals and amino acids/peptides/aminopolycarboxylates are of great interest in coordination chemistry [214,215]. These systems serve as model systems

in understanding the interactions involved in metal-protein chemistry. Coordination of amino acid to the metal has received some attention even in nonaqueous media [256–259].

Below pH, 5.0 the lanthanide amino acid interactions are weak as reflected in small changes in interelectronic repulsion and spin orbit interaction parameters and small nephelauxetic effect. Above pH 5.0, stronger complexes are formed as reflected by the changes in the spectral features. In anhydrous lanthanide complexes, amino acid is in inner sphere. Intense hypersensitive bands were observed in the complexes in solid state. IR spectra in the carboxylic and amino stretching frequency region indicated predominantly inner coordination through carboxyl oxygen and amino nitrogen. This is in keeping with the observed high oscillator strengths of the solid complexes. Upon dissolution in water, bidentate is converted into a unidentate.

The most important negative contributions to the enthalpies of chelation are due to the formation of Ln–N (amino) bonds. The enthalpies due to Ln–O (carboxyl) bonding are less favourable. Then chelate ring formation depends solely on the entropy increase due to the release of water molecules from aquo ion through the charge neutralization of metal and carboxyl group. Systematic analysis of the spectra of Pr(III) and Nd(III) in the visible and IR region showed that (i) up to pH 4.0 only  $ML^{2+}$  (L = amino acid) species is predominant, (ii) below pH 2.0 only carboxylate is bound to metal ion, (iii) below pH 2.0 the spectra resemble those of aquolanthanide, (iv) the presence of aromatic imidazole groups with secondary and tertiary nitrogen atoms in histidine and the sulfydryl group in cysteine intensify the 4f–4f bands considerably [256–259].

#### 41. Lanthanide aminocarboxylate complexes

Lanthanide–EDTA and lanthanide–NTA complexes, where Ln = Nd, Ho, Er at various Ln:L ratios in a broad pH range were studied by spectroscopy. Analysis of the data on oscillator strengths and  $T_{\lambda}$  parameters provided some clues on the nature of bonding in these complexes. Further  $T_2$  and  $T_6$  parameters showed a dependence on the ligand concentration. However, these studies could identify only one species  $[Nd(NTA)_2]^{3-}$  in solution [260].

#### 42. Lanthanide diol complexes

At pH 2.0 diols are not ionized and hence complexation occurs with neutral diol molecule. Above pH 2.0 diols are ionized and become bidentate complexing agent. The absorption spectra of lanthanide complexes with the following diols,

Ethane-1,2-	Butane-2,3-	Butene-1,4-	Pentane-1,5-
Propane-1,2-	Butane-1,3-	2-butyne-1,4-	Hexane-1,6-
Butane-1,2-	Butane-1,4-		

showed the complexes to be of varying stability. A correlation has been found between the stability constants of the complexes and the nephelauxetic effect as well as the oscillator

strengths of the 4f–4f transitions. The diols which formed either five or six membered rings with the lanthanide were the most stable and produced the greatest red shift and hence nephelauxetic effect. Among the diols studied butane 1,4-diol proved to be the least stable of the complexes as reflected by  $T_\lambda$ , oscillator strength,  $P$  and nephelauxetic parameter. As expected the spectral parameters showed complexes with five membered rings to be more stable than the six membered analogues.

2-butene and 2-butyne, 1,4-diols behaved in an unusual fashion. These diols formed strong complexes by way of seven-membered rings as reflected in intense bands, high nephelauxetic effect ( $1 - \beta$ ) and high mixing coefficient ( $b$ ). Probably  $\pi$  electron density of the double and triple bonds in butene and butyne, respectively, may be responsible for the observed effect. The 4f orbital may not be directly involved but a combination of 5d, 4f, and 6s orbitals might be interacting with the  $\pi$  electrons of the ligands. This observation is similar to the phenomenon observed in the mixed ligand complexes of  $\beta$ -diketones/phenanthroline of lanthanides with diols.

### 43. Miscellaneous complexes

Spectral data for miscellaneous complexes are available in the references cited in Table 8.31. The covalency parameters of some complexes are given in Table 8.50 (see Appendix).

### 44. Energy levels of $f^2$ and $f^1$ configurations

We will use  $f^2$  and  $f^1$  configurations to show the details in the theoretical calculation of energy levels and their fitting with the experimental data. The  $4f^2$  is the ground configuration of the ions  $\text{Pr}^{3+}$ ,  $\text{Ce}^{2+}$  and  $4f^1$  that of the  $\text{Ce}^{3+}$ . The theory is also applicable by hole formalism to the  $4f^{12}$  ( $\text{Tm}^{3+}$ ,  $\text{Er}^{2+}$ ) and  $4f^{13}$  ( $\text{Yb}^{3+}$ ,  $\text{Tm}^{2+}$ ) configurations. For the purpose of fitting the energy levels with the experimental data, we choose  $\text{Pr}^{3+}$  and  $\text{Ce}^{3+}$  ions both for free-ion levels and crystalline field levels. The crystalline field levels that we will use are for the host crystals  $\text{LaCl}_3$ . The spectrum of  $\text{Pr}^{3+}$  in  $\text{LaCl}_3$  is regarded as one of the best known of the rare earth spectra. We will be concerned with three major perturbations.

- (1)  $H^1$ , the Coulomb interaction between two electrons (also known as electrostatic or electron repulsion perturbation).
- (2)  $H^2$ , the spin–orbit interaction.
- (3)  $H^3$ , the crystalline field interaction.

There will be no electron repulsion perturbation in  $f^1$  configuration in which case we go directly to the  $H^2$  and  $H^3$  perturbations.

It is well-known that the electron repulsion perturbation gives rise to LS terms or multiplets (also known as Russell–Saunders terms) which in turn are split into LSJ spin–orbital levels by spin–orbit interaction. These spin–orbital levels are further split into what are known as Stark levels by the crystalline field. The energies of the terms, the spin–orbital levels and the crystalline field levels can be calculated by one of two methods, (1) the Slater determinantal method [310–313], (2) the Racah tensor operator method [314–316].

TABLE 8.31  
Lanthanide complexes with miscellaneous ligands.

Complexing ligand	Metal ( $M^{3+}$ )	Reference
Pyridine-2-aldehyde	Nd, Sm, Gd, Dy	[262]
Pyridine-2-aldehyde + oxime		
Primary ligand: oximes		
Secondary ligands: <i>o</i> -phenanthroline	La, Pr, Nd, Gd, Dy	[263]
Pyridine-2-aldoxime, oxime		
Pongamol ( $\beta$ -diketone)	Eu	[264]
	Sm, Dy, Yb	[265]
	Gd, Ho, Er	[274a]
Benzyl- $\alpha$ -monoxime	Sm, Eu, Dy	[266]
5-nitro-orotic acid	Nd	[267]
	La	[268]
	Pr, Sm	[269]
Benzoin- $\alpha$ -oxime	Pr, Nd, Sm	[270]
Dimethyl glyoxime	La, Pr, Nd, Sm, Dy	[271]
Curcumin	La, Pr, Nd, Sm	[272]
Anthranilic acid	Pr, Nd, Sm	[273]
3,4-dihydroxybenzaldehyde	Pr, Nd, Sm, Gd	[274b]
Hydroxy naphthoic acid	La, Ce, Pr, Nd, Sm	[275]
<i>o</i> -nitrobenzoic acid	Nd, Sm, Gd	[276]
Dihydroxy benzoic acid	La, Pr, Nd, Sm, Gd	[277]
Oximes	La, Ce, Pr, Nd, Sm, Gd	[278]
Dimethylglyoxime + bipyridine/anthranilic acid	Pr, Nd, Sm	[279]
Barbiturate	Pr, Nd, Sm	[280]
<i>o</i> -phenylenediamine	La, Pr, Nd, Gd	[281]
N-substituted anthranilic acid	La, Pr, Nd, Sm, Gd, Dy	[282]
Dimethylglyoxime + phenyl thiourea	La, Pr, Nd, Sm, Gd, Dy	[283]
Urea + <i>N</i> -phenyl thiourea	La, Pr, Nd, Sm, Gd, Dy	[284]
Oxime + thiourea	La, Pr, Nd, Sm, Gd, Dy	[285]
Urea/thiourea	La, Pr, Nd, Sm, Gd, Dy	[286,287]
Bipyridine + thiourea	La, Pr, Nd, Sm, Gd, Dy	[288]
$\beta$ -diketones	Lanthanides	[289]

Although in the case of  $f^2$ , either method can be applied with ease, the determinantal method becomes cumbersome for more than two-electrons and it is necessary to take recourse to the tensor operator method for  $f^N$ ,  $N > 2$ . We will show the derivation of energy levels by both methods in what follows:

## 45. $f^2$ configuration

### 45.1. Electron-repulsion perturbation

The  $f^2$  configuration gives rise to the terms  $^1I$ ,  $^3H$ ,  $^1G$ ,  $^3F$ ,  $^1D$ ,  $^3P$ , and  $^1S$ .

## 45.1.1. Calculation of electrostatic energies

45.1.1.1. Slater determinantal method Part of the microstate table for  $f^2$  is given in Table 8.32.

TABLE 8.32  
Partial microstate table for  $f^2$ .

$M_L$	$M_S$	
	+1	0
6		(3 <sup>+</sup> 3 <sup>-</sup> )
5	(3 <sup>+</sup> 2 <sup>+</sup> )	(3 <sup>+</sup> 2 <sup>-</sup> ) (3 <sup>-</sup> 2 <sup>+</sup> )
4	(3 <sup>+</sup> 1 <sup>+</sup> )	(3 <sup>+</sup> 1 <sup>-</sup> ) (3 <sup>-</sup> 1 <sup>+</sup> ) (2 <sup>+</sup> 2 <sup>-</sup> )
3	(3 <sup>+</sup> 0 <sup>+</sup> ) (2 <sup>+</sup> 1 <sup>+</sup> )	(3 <sup>+</sup> 0 <sup>-</sup> ) (3 <sup>-</sup> 0 <sup>+</sup> ) (2 <sup>+</sup> 1 <sup>-</sup> ) (2 <sup>-</sup> 1 <sup>+</sup> )
2	(3 <sup>+</sup> -1 <sup>+</sup> ) (2 <sup>+</sup> 0 <sup>+</sup> )	(3 <sup>+</sup> -1 <sup>-</sup> ) (3 <sup>-</sup> -1 <sup>+</sup> ) (2 <sup>+</sup> 0 <sup>-</sup> ) (2 <sup>-</sup> 0 <sup>+</sup> ) (1 <sup>+</sup> 1 <sup>-</sup> )
1	(3 <sup>+</sup> -2 <sup>+</sup> ) (2 <sup>+</sup> -1 <sup>+</sup> ) (1 <sup>+</sup> 0 <sup>+</sup> )	(3 <sup>+</sup> -2 <sup>-</sup> ) (3 <sup>-</sup> -2 <sup>+</sup> ) (2 <sup>+</sup> -1 <sup>-</sup> ) (2 <sup>-</sup> -1 <sup>+</sup> ) (1 <sup>+</sup> 0 <sup>-</sup> ) (1 <sup>-</sup> 0 <sup>+</sup> )
0	(3 <sup>+</sup> -3 <sup>+</sup> ) (2 <sup>+</sup> -2 <sup>+</sup> ) (1 <sup>+</sup> -1 <sup>+</sup> )	(3 <sup>+</sup> -3 <sup>-</sup> ) (3 <sup>-</sup> -3 <sup>+</sup> ) (2 <sup>+</sup> -2 <sup>-</sup> ) (2 <sup>-</sup> -2 <sup>+</sup> ) (1 <sup>+</sup> -1 <sup>-</sup> ) (1 <sup>-</sup> -1 <sup>+</sup> ) (0 <sup>+</sup> 0 <sup>-</sup> )

TABLE 8.33  
Coulomb and exchange integrals between  $f$  electrons expressed in Slater-Condor-Shortley parameters<sup>a</sup>.

$m_l$ values	$J$	$K$
±3	±3	$F_0 + 25F_2 + 9F_4 + F_6$
±3	∓3	$F_0 + 25F_2 + 9F_4 + F_6$
±3	±2	$F_0 - 21F_4 - 6F_6$
±3	∓2	$F_0 - 21F_4 - 6F_6$
±3	±1	$F_0 - 15F_2 + 3F_4 + 15F_6$
±3	∓1	$F_0 - 15F_2 + 3F_4 + 15F_6$
±3	0	$F_0 - 20F_2 + 18F_4 - 20F_6$
±2	±2	$F_0 + 49F_4 + 36F_6$
±2	∓2	$F_0 + 49F_4 + 36F_6$
±2	±1	$F_0 - 7F_4 - 90F_6$
±2	∓1	$F_0 - 7F_4 - 90F_6$
±2	0	$F_0 - 42F_4 + 120F_6$
±1	±1	$F_0 + 9F_2 + F_4 + 225F_6$
±1	∓1	$F_0 + 9F_2 + F_4 + 225F_6$
±1	0	$F_0 + 12F_2 + 6F_4 - 300F_6$
0	0	$F_0 + 16F_2 + 36F_4 + 400F_6$

<sup>a</sup>The  $F_K$  and the radial integrals  $F^K$  are related as follows:

$$F_0 = F^0$$

$$F_2 = F^2/225$$

$$F_4 = F^4/1089$$

$$F_6 = 25F^6/184041$$



Using the diagonal-sum rule (and the Coulomb and exchange integrals listed in Table 8.33)

$$\begin{aligned}
 E(^1I) &= J(33) = F_0 + 25F_2 + 9F_4 + F_6 \\
 E(^1I) + E(^3H) &= 2J(32) = 2F_0 - 42F_4 - 12F_6 \\
 E(^1I) + E(^3H) + E(^1G) &= 2J(31) + J(22) = 3F_0 - 30F_2 + 55F_4 + 66F_6 \\
 E(^1I) + E(^3H) + E(^1G) + E(^3F) &= 2J(30) + 2J(21) \\
 &= 4F_0 - 40F_2 + 22F_4 - 220F_6 \\
 E(^1I) + E(^3H) + E(^1G) + E(^3F) + E(^1D) &= 2J(3-1) + 2J(20) + J(11) \\
 &= 5F_0 - 21F_2 - 77F_4 + 495F_6 \\
 E(^1I) + E(^3H) + E(^1G) + E(^3F) + E(^1D) + E(^3P) \\
 &= 2J(3-2) + 2J(2-1) + 2J(10) = 6F_0 + 24F_2 - 44F_4 - 792F_6 \\
 E(^1I) + E(^3H) + E(^1G) + E(^3F) + E(^1D) + E(^3P) + E(^1S) \\
 &= 2J(3-3) + 2J(2-2) + 2J(1-1) + J(00) = 7F_0 + 84F_2 + 154F_4 + 924F_6
 \end{aligned}$$

From these equations we obtain the electrostatic energies for  $f^2$ :

$$\begin{aligned}
 E(^1S) &= F_0 + 60F_2 + 198F_4 + 1716F_6 \\
 E(^1D) &= F_0 + 19F_2 - 99F_4 + 715F_6 \\
 E(^1G) &= F_0 - 30F_2 + 97F_4 + 78F_6 \\
 E(^1I) &= F_0 + 25F_2 + 9F_4 + F_6 \tag{8.92} \\
 E(^3P) &= F_0 + 45F_2 + 33F_4 - 1287F_6 \\
 E(^3F) &= F_0 - 10F_2 - 33F_4 - 286F_6 \\
 E(^3H) &= F_0 - 25F_2 - 51F_4 - 13F_6
 \end{aligned}$$

Note that the energies of the triplet terms can be obtained independently using diagonal-sum rule with the microstates  $M_S = +1$

$$\begin{aligned}
 E(^3H) &= J(32) - K(32) = J(31) - K(31) = F_0 - 25F_2 - 51F_4 - 13F_6 \\
 E(^3H) + E(^3F) &= J(30) - K(30) + J(21) - K(21) \\
 &= J(3-1) - K(3-1) + J(20) - K(20) \\
 &= 2F_0 - 35F_2 - 84F_4 - 299F_6 \\
 E(^3H) + E(^3F) + E(^3P) &= J(3-2) - K(3-2) + J(2-1) - K(2-1) + J(10) - K(10) \\
 &= J(3-3) - K(3-3) + J(2-2) - K(2-2) + J(1-1) - K(1-1) \\
 &= 3F_0 + 10F_2 - 51F_4 - 1586F_6
 \end{aligned}$$

resulting in the energies:

$$E(^3F) = F_0 - 10F_2 - 33F_4 - 286F_6$$

$$E(^3P) = F_0 + 45F_2 + 33F_4 - 1287F_6$$

The energies of these terms can be expressed in terms of Racah parameters:  $E^0$ ,  $E^1$ ,  $E^2$ ,  $E^3$ , defined by the following relations:

$$\begin{aligned} E^0 &= F_0 - 10F_2 - 33F_4 - 286F_6 & F_0 &= 1/7(7E^0 + 9E^1) \\ E^1 &= 1/9(70F_2 + 231F_4 + 2002F_6) & F_2 &= 1/42(E^1 + 143E^2 + 11E^3) \\ E^2 &= 1/9(F_2 - 3F_4 + 7F_6) & F_4 &= 1/77(E^1 - 130E^2 + 4E^3) \\ E^3 &= 1/9(15F_2 + 18F_4 - 273F_6) & F_6 &= 1/462(E^1 + 35E^2 - 7E^3) \end{aligned}$$

giving

$$\begin{aligned} E(^1S) &= E^0 + 9E^1 \\ E(^1D) &= E^0 + 2E^1 + 286E^2 - 11E^3 \\ E(^1G) &= E^0 + 2E^1 + 260E^2 - 4E^3 \\ E(^1I) &= E^0 + 2E^1 + 70E^2 + 7E^3 & (8.93) \\ E(^3P) &= E^0 + 33E^3 \\ E(^3F) &= E^0 \\ E(^3H) &= E^0 - 9E^3 \end{aligned}$$

It is interesting to note that the triplet terms have only one parameter  $E^3$  other than the common additive constant  $E^0$ , similar to the d electron configurations where the terms of highest spin-multiplicity of a  $d^N$  configuration have only one parameter  $B$ .

Theoretical calculations employing 4f hydrogenic radial wavefunctions [315] give the ratios  $F_4/F_2 = 0.138$  and  $F_6/F_2 = 0.0151$ . However, it is possible to obtain  $F_4$ ,  $F_6$ , parameters along with  $F_2$  by fitting the experimental energy levels with the theoretical energy expressions.

*45.1.1.2. Energies of terms by tensor operators* The formulas for evaluating the electrostatic interaction matrix elements within a two electron configuration are given by

$$((nl)^2 SL | e^2/r_{12} | (nl)^2 SL) = \sum_K f_K(l, l) F^K(nl, nl) \quad (8.94a)$$

$$f_K(l, l) = (-1)^L (l \| C^{(K)} \| l)^2 \begin{Bmatrix} l & l & k \\ l & l & L \end{Bmatrix} \quad (8.94b)$$

$$(l \| C^K \| l') = (-1)^l [(2l+1)(2l'+1)]^{1/2} \begin{pmatrix} l & k & l' \\ 0 & 0 & 0 \end{pmatrix} \quad (8.94c)$$

where the  $\left\{ \begin{smallmatrix} l & l & k \\ l & l & l \end{smallmatrix} \right\}$  and  $\left( \begin{smallmatrix} l & k & l' \\ 0 & 0 & 0 \end{smallmatrix} \right)$  are the 6-j and 3-j symbols, respectively. The numerical values of the 3-j and 6-j symbols<sup>1</sup> have been tabulated by Rotenberg et al. [317].

$$(3\|C^k\|3) = -7 \begin{pmatrix} 3 & k & 3 \\ 0 & 0 & 0 \end{pmatrix}$$

$$(3\|C^k\|3)^2 = 49 \begin{pmatrix} 3 & k & 3 \\ 0 & 0 & 0 \end{pmatrix}^2$$

$$(3\|C^0\|3)^2 = 49 \begin{pmatrix} 3 & 0 & 3 \\ 0 & 0 & 0 \end{pmatrix}^2 = 49 \times 1/7 = 7$$

$$(3\|C^2\|3)^2 = 49 \begin{pmatrix} 3 & 2 & 3 \\ 0 & 0 & 0 \end{pmatrix}^2 = 49 \times 4/105 = 28/15$$

$$(3\|C^4\|3)^2 = 49 \begin{pmatrix} 3 & 4 & 3 \\ 0 & 0 & 0 \end{pmatrix}^2 = 49 \times 2/77 = 14/11$$

$$(3\|C^6\|3)^2 = 49 \begin{pmatrix} 3 & 6 & 3 \\ 0 & 0 & 0 \end{pmatrix}^2 = 49 \times \frac{100}{3003} = 700/429$$

$$\begin{aligned} E(^1S) &= (-1)^0 \left[ 7 \begin{Bmatrix} 3 & 3 & 0 \\ 3 & 3 & 0 \end{Bmatrix} F^0 + \frac{28}{15} \begin{Bmatrix} 3 & 3 & 2 \\ 3 & 3 & 0 \end{Bmatrix} F^2 \right. \\ &\quad \left. + \frac{14}{11} \begin{Bmatrix} 3 & 3 & 4 \\ 3 & 3 & 0 \end{Bmatrix} F^4 + \frac{700}{429} \begin{Bmatrix} 3 & 3 & 6 \\ 3 & 3 & 0 \end{Bmatrix} F^6 \right] \\ &= 7 \left( \frac{1}{7} \right) F^0 + \frac{28}{15} \left( \frac{1}{7} \right) F^2 + \frac{14}{11} \left( \frac{1}{7} \right) F^4 + \frac{700}{429} \left( \frac{1}{7} \right) F^6 \\ &= F^0 + \frac{4}{15} F^2 + \frac{2}{11} F^4 + \frac{100}{429} F^6 = F_0 + 60F_2 + 198F_4 + 1716F_6 \end{aligned}$$

$$\begin{aligned} E(^1D) &= (-1)^2 \left[ 7 \begin{Bmatrix} 3 & 3 & 0 \\ 3 & 3 & 2 \end{Bmatrix} F^0 + \frac{28}{15} \begin{Bmatrix} 3 & 3 & 2 \\ 3 & 3 & 2 \end{Bmatrix} F^2 \right. \\ &\quad \left. + \frac{14}{11} \begin{Bmatrix} 3 & 3 & 4 \\ 3 & 3 & 2 \end{Bmatrix} F^4 + \frac{700}{429} \begin{Bmatrix} 3 & 3 & 6 \\ 3 & 3 & 2 \end{Bmatrix} F^6 \right] \\ &= 7 \left( \frac{1}{7} \right) F^0 + \frac{28}{15} \left( \frac{19}{420} \right) F^2 + \frac{14}{11} \left( \frac{-1}{14} \right) F^4 + \frac{700}{429} \left( \frac{5}{84} \right) F^6 \\ &= F^0 + \frac{19}{225} F^2 - \frac{1}{11} F^4 + \frac{125}{1287} F^6 = F_0 + 19F_2 - 99F_4 + 715F_6 \end{aligned}$$

<sup>1</sup> The 3j and 6j symbols as well as the doubly reduced matrix elements needed in the calculation of crystalline field energies have been programmed for us by Gelio Alves and Chamindra Williams at Florida Atlantic University.

$$\begin{aligned}
 E(^1G) &= (-1)^4 \left[ 7 \begin{Bmatrix} 3 & 3 & 0 \\ 3 & 3 & 4 \end{Bmatrix} F^0 + \frac{28}{15} \begin{Bmatrix} 3 & 3 & 2 \\ 3 & 3 & 4 \end{Bmatrix} F^2 \right. \\
 &\quad \left. + \frac{14}{11} \begin{Bmatrix} 3 & 3 & 4 \\ 3 & 3 & 4 \end{Bmatrix} F^4 + \frac{700}{429} \begin{Bmatrix} 3 & 3 & 6 \\ 3 & 3 & 4 \end{Bmatrix} F^6 \right] \\
 &= 7 \left( \frac{1}{7} \right) F^0 + \frac{28}{15} \left( -\frac{1}{14} \right) F^2 + \frac{14}{11} \left( \frac{97}{1386} \right) F^4 + \frac{700}{429} \left( \frac{1}{154} \right) F^6 \\
 &= F^0 - \frac{2}{15} F^2 + \frac{97}{1089} F^4 + \frac{50}{4719} F^6 = F_0 - 30F_2 + 97F_4 + 78F_6
 \end{aligned}$$

$$\begin{aligned}
 E(^1I) &= (-1)^6 \left[ 7 \begin{Bmatrix} 3 & 3 & 0 \\ 3 & 3 & 6 \end{Bmatrix} F^0 + \frac{28}{15} \begin{Bmatrix} 3 & 3 & 2 \\ 3 & 3 & 6 \end{Bmatrix} F^2 \right. \\
 &\quad \left. + \frac{14}{11} \begin{Bmatrix} 3 & 3 & 4 \\ 3 & 3 & 6 \end{Bmatrix} F^4 + \frac{700}{429} \begin{Bmatrix} 3 & 3 & 6 \\ 3 & 3 & 6 \end{Bmatrix} F^6 \right] \\
 &= 7 \left( \frac{1}{7} \right) F^0 + \frac{28}{15} \left( \frac{5}{84} \right) F^2 + \frac{14}{11} \left( \frac{1}{154} \right) F^4 + \frac{700}{429} \left( \frac{1}{12012} \right) F^6 \\
 &= F^0 + \frac{1}{9} F^2 + \frac{1}{121} F^4 + \frac{25}{184041} F^6 = F_0 + 25F_2 + 9F_4 + F_6
 \end{aligned}$$

$$\begin{aligned}
 E(^3P) &= (-1)^1 \left[ 7 \begin{Bmatrix} 3 & 3 & 0 \\ 3 & 3 & 1 \end{Bmatrix} F^0 + \frac{28}{15} \begin{Bmatrix} 3 & 3 & 2 \\ 3 & 3 & 1 \end{Bmatrix} F^2 \right. \\
 &\quad \left. + \frac{14}{11} \begin{Bmatrix} 3 & 3 & 4 \\ 3 & 3 & 1 \end{Bmatrix} F^4 + \frac{700}{429} \begin{Bmatrix} 3 & 3 & 6 \\ 3 & 3 & 1 \end{Bmatrix} F^6 \right] \\
 &= - \left[ 7 \left( -\frac{1}{7} \right) F^0 + \frac{28}{15} \left( -\frac{3}{28} \right) F^2 + \frac{14}{11} \left( -\frac{1}{42} \right) F^4 + \frac{700}{429} \left( \frac{3}{28} \right) F^6 \right] \\
 &= F^0 + \frac{1}{5} F^2 + \frac{1}{33} F^4 - \frac{25}{143} F^6 = F_0 + 45F_2 + 33F_4 - 1287F_6
 \end{aligned}$$

$$\begin{aligned}
 E(^3F) &= (-1)^3 \left[ 7 \begin{Bmatrix} 3 & 3 & 0 \\ 3 & 3 & 3 \end{Bmatrix} F^0 + \frac{28}{15} \begin{Bmatrix} 3 & 3 & 2 \\ 3 & 3 & 3 \end{Bmatrix} F^2 \right. \\
 &\quad \left. + \frac{14}{11} \begin{Bmatrix} 3 & 3 & 4 \\ 3 & 3 & 3 \end{Bmatrix} F^4 + \frac{700}{429} \begin{Bmatrix} 3 & 3 & 6 \\ 3 & 3 & 3 \end{Bmatrix} F^6 \right] \\
 &= - \left[ 7 \left( -\frac{1}{7} \right) F^0 + \frac{28}{15} \left( \frac{1}{42} \right) F^2 + \frac{14}{11} \left( \frac{1}{42} \right) F^4 + \frac{700}{429} \left( \frac{1}{42} \right) F^6 \right] \\
 &= F^0 - \frac{2}{45} F^2 - \frac{1}{33} F^4 - \frac{50}{1287} F^6 = F_0 - 10F_2 - 33F_4 - 286F_6
 \end{aligned}$$

$$\begin{aligned}
 E(^3H) &= (-1)^5 \left[ 7 \begin{Bmatrix} 3 & 3 & 0 \\ 3 & 3 & 5 \end{Bmatrix} F^0 + \frac{28}{15} \begin{Bmatrix} 3 & 3 & 2 \\ 3 & 3 & 5 \end{Bmatrix} F^2 \right. \\
 &\quad \left. + \frac{14}{11} \begin{Bmatrix} 3 & 3 & 4 \\ 3 & 3 & 5 \end{Bmatrix} F^4 + \frac{700}{429} \begin{Bmatrix} 3 & 3 & 6 \\ 3 & 3 & 5 \end{Bmatrix} F^6 \right]
 \end{aligned}$$

$$\begin{aligned}
 &= -\left[7\left(-\frac{1}{7}\right)F^0 + \frac{28}{15}\left(\frac{5}{84}\right)F^2 + \frac{14}{11}\left(\frac{17}{462}\right)F^4 + \frac{700}{429}\left(\frac{1}{924}\right)F^6\right] \\
 &= F^0 - \frac{1}{9}F^2 - \frac{17}{363}F^4 - \frac{25}{14157}F^6 = F_0 - 25F_2 - 51F_4 - 13F_6
 \end{aligned}$$

Note:  $F_2 = F^2/225$ ,  $F_4 = F^4/1089$ ,  $F_6 = 25F^6/184041$ ,  $F_0 = F^0$ .

These energies are same as those derived by the Slater determinantal method.

#### 45.2. Spin-orbit interaction perturbation

Spin-orbit interaction splits the LS-terms into spin-orbital levels characterized by the total angular momentum  $J$ . The  $J$  values of a term are given by

$$J = (L + S), (L + S - 1), \dots, |L - S|$$

Each  $J$  level is  $(2J + 1)$  fold degenerate. This degeneracy is simply the total  $M_J$  values possible for a  $J$ .

Thus each of the three triplet terms  ${}^3H$ ,  ${}^3F$ , and  ${}^3P$  splits into three s-o levels whereas the singlet terms  ${}^1I$ ,  ${}^1G$ ,  ${}^1D$  and  ${}^1S$  do not split. The possible spin-orbital levels for  $f^2$  configuration are  ${}^3H_4$ ,  ${}^3H_5$ ,  ${}^3H_6$ ,  ${}^3F_2$ ,  ${}^3F_3$ ,  ${}^3F_4$ ,  ${}^3P_0$ ,  ${}^3P_1$ ,  ${}^3P_2$ ,  ${}^1I_6$ ,  ${}^1G_4$ ,  ${}^1D_2$  and  ${}^1S_0$ , a total of 13 levels.

##### 45.2.1. Calculation of spin-orbit energies

The diagonal elements can be calculated very simply either by the formula,

$$E(J) = \frac{\lambda}{2} [J(J + 1) - L(L + 1) - S(S + 1)] \quad (8.95)$$

or by making use of the Landé interval rule and the center of gravity principle. According to the Landé interval rule the energy difference between two adjacent levels  $J$  and  $(J - 1)$  of a term is given by  $J\lambda$ . The center of gravity implies  $\sum_J (2J + 1)E(J)$  of a term is zero.

The parameter  $\lambda$  here is a many-electron spin-orbit constant which is related to the one electron constant  $\zeta$  by  $N\lambda$ , where  $N$  is the number of f-electrons. For  $f^2$ ,  $\lambda$  is  $\zeta/2$ . As an example,  ${}^3H \Rightarrow L = 5, S = 1, J = 4, 5, 6$

$$E({}^3H_4) = -6\lambda = -3\zeta$$

$$E({}^3H_5) = -\lambda = -\zeta/2$$

$$E({}^3H_6) = 5\lambda = 5/2\zeta$$

Alternately, according to the Landé interval rule:  $E({}^3H_6) - E({}^3H_5) = 6\lambda$ ,  $E({}^3H_5) - E({}^3H_4) = 5\lambda$  and center of gravity means  $13E({}^3H_6) + 11E({}^3H_5) + 9E({}^3H_4) = 0$ . The solution of these three equations will give the same energies as above. Similarly,

$$E({}^3F_2) = -4\lambda = -2\zeta$$

$$E(^3F_3) = -\lambda = -\zeta/2$$

$$E(^3F_4) = 3\lambda = 3/2\zeta$$

$$E(^3P_0) = -2\lambda = -\zeta$$

$$E(^3P_1) = -\lambda = -\zeta/2$$

$$E(^3P_2) = \lambda = \zeta/2$$

$$E(^1I_6) = 0 = E(^1G_4) = E(^1D_2) = E(^1S_0).$$

Note that the above “energies” are actually the diagonal elements. In order to calculate the off-diagonals, it is necessary to take recourse to either the Slater determinantal method or the tensor operator method.

*45.2.1.1. Determinantal method* Derivation of  $|L, S, J, M\rangle$  (or simply  $|J, M\rangle$ ) functions as linear combinations of  $|L, S; M_L, M_S\rangle$  functions can be carried out either by using the tables of Wigner coefficients (the only table needed here is  $S = 1$ ) or by the use of the 3- $j$  symbols.

$$|j_1 j_2 j m\rangle = (-1)^{j_2-j_1-m} \sum_{m_1 m_2} (2j+1)^{1/2} \begin{pmatrix} j_1 & j_2 & j \\ m_1 & m_2 & -m \end{pmatrix} |j_1 j_2 m_1 m_2\rangle \quad (8.96)$$

Here the  $j_1, j_2$  that are coupled to give  $j$  are the  $L, S$  to give  $J$ . By either method the  $|JM\rangle$  functions that are needed at this point are  $M = J$ .

$$^3H_6: |5, 1; 6, 6\rangle = |5, 1; 5, 1\rangle$$

$$^3H_5: |5, 1; 5, 5\rangle = \sqrt{\frac{5}{6}}|5, 1; 5, 0\rangle - \sqrt{\frac{1}{6}}|5, 1; 4, 1\rangle$$

$$^3H_4: |5, 1; 4, 4\rangle = \sqrt{\frac{1}{55}}[3\sqrt{5}|5, 1; 5, -1\rangle - 3|5, 1; 4, 0\rangle + |5, 1; 3, 1\rangle]$$

$$^3F_4: |3, 1; 4, 4\rangle = |3, 1; 3, 1\rangle$$

$$^3F_3: |3, 1; 3, 3\rangle = \sqrt{\frac{3}{4}}|3, 1; 3, 0\rangle - \sqrt{\frac{1}{4}}|3, 1; 2, 1\rangle$$

$$^3F_2: |3, 1; 2, 2\rangle = \sqrt{\frac{1}{21}}[\sqrt{15}|3, 1; 3, -1\rangle - \sqrt{5}|3, 1; 2, 0\rangle + |3, 1; 1, 1\rangle]$$

$$^3P_2 = |1, 1; 2, 2\rangle = |1, 1; 1, 1\rangle$$

$$^3P_1 = |1, 1; 1, 1\rangle = \sqrt{\frac{1}{2}}|1, 1; 1, 0\rangle - \sqrt{\frac{1}{2}}|1, 1; 0, 1\rangle$$

$$^3P_0 = |1, 1; 0, 0\rangle = \sqrt{\frac{1}{3}}[|1, 1; 1, -1\rangle - |1, 1; 0, 0\rangle + |1, 1; -1, 1\rangle]$$

$${}^1I_6: |6, 0; 6, 6\rangle = |6, 0; 6, 0\rangle$$

$${}^1G_4: |4, 0; 4, 4\rangle = |4, 0; 4, 0\rangle$$

$${}^1D_2: |2, 0; 2, 2\rangle = |2, 0; 2, 0\rangle$$

$${}^1S_0: |0, 0; 0, 0\rangle = |0, 0; 0, 0\rangle$$

The above  $|J, M\rangle$  functions can also be obtained by the vector coupling method using ladder operator only. In this method we start with

$${}^3H_6: |5, 1; 6, 6\rangle = |5, 1; 5, 1\rangle$$

and obtain  $|5, 1; 6, 5\rangle$  and  $|5, 1; 6, 4\rangle$  by  $L_-$  operator. Then the  ${}^3H_5: |5, 1; 5, 5\rangle$  and  ${}^3H_4: |5, 1; 4, 4\rangle$  functions can be constructed by orthogonality. All the remaining functions of these levels follow by successive application of the lowering operator.

The  $|L, S; M_L, M_S\rangle$  wave functions in terms of microstates can be obtained either by 3-j symbols or ladder operators.

We will show the derivation of  ${}^3F: |3, 1; 3, 1\rangle$  by the 3-j method. In this method we will couple the two f-electrons ( $l_1 = 3, l_2 = 3$ ) to give  $|L, M\rangle$  function. The microstates that go into  ${}^3F |3, 1; 3, 1\rangle$  are (30) and (21). Using equation (8.96):

$$\begin{aligned} |3, 3; 3, 3\rangle &= (-1)^{3-3-3} \sqrt{7} \left[ \begin{pmatrix} 3 & 3 & 3 \\ 2 & 1 & -3 \end{pmatrix} (21) + \begin{pmatrix} 3 & 3 & 3 \\ 3 & 0 & -3 \end{pmatrix} (30) \right] \\ &= -\sqrt{7} \left[ \sqrt{\frac{1}{21}} (21) - \sqrt{\frac{1}{42}} (30) \right] = \sqrt{\frac{1}{6}} (30) - \sqrt{\frac{1}{3}} (21) \end{aligned}$$

Hence

$$|3, 1; 3, 1\rangle = \sqrt{\frac{1}{3}} (3^+0^+) - \sqrt{\frac{2}{3}} (2^+1^+)$$

As another example, consider  ${}^1G |4, 0; 4, 0\rangle$ . This function will have the microstates (31) and (22) (suppressing the spins), so that

$$\begin{aligned} |3, 3; 4, 4\rangle &= (-1)^{3-3-4} \sqrt{9} \left[ \begin{pmatrix} 3 & 3 & 4 \\ 3 & 1 & -4 \end{pmatrix} (31) + \begin{pmatrix} 3 & 3 & 4 \\ 2 & 2 & -4 \end{pmatrix} (22) \right] \\ &= \sqrt{9} \left[ \sqrt{\frac{1}{33}} (31) - \sqrt{\frac{5}{99}} (22) \right] = \sqrt{\frac{3}{11}} (31) - \sqrt{\frac{5}{11}} (22) \end{aligned}$$

Hence

$$|4, 0; 4, 0\rangle = \sqrt{\frac{3}{11}} \left[ \begin{pmatrix} + & - \\ 3 & 1 \end{pmatrix} - \begin{pmatrix} - & + \\ 3 & 1 \end{pmatrix} \right] - \sqrt{\frac{5}{11}} \begin{pmatrix} + & - \\ 2 & 2 \end{pmatrix}$$

In the vector coupling method, to derive  ${}^3F|3, 1; 3, 1\rangle$ , we start from  ${}^3H|5, 1; 5, 1\rangle = \begin{smallmatrix} + & + \\ 3 & 2 \end{smallmatrix}$  and obtain  $|5, 1; 4, 1\rangle$  and  $|5, 1; 3, 1\rangle$  by  $L_-$  operator. The  ${}^3F|3, 1; 3, 1\rangle$  function is constructed by orthogonality to  ${}^3H|5, 1; 3, 1\rangle$ . Similarly the  ${}^1G|4, 0; 4, 0\rangle$  is constructed by orthogonality to  ${}^1I|6, 0; 4, 0\rangle$  which is derived by lowering  ${}^1I|6, 0; 6, 0\rangle = \begin{smallmatrix} + & - \\ 3 & 3 \end{smallmatrix}$  twice.

The  $|L, S; M_L, M_S\rangle$  functions with  $M_L = L$  and  $M_S = S$  are listed below:

$${}^1I: |6, 0; 6, 0\rangle = \begin{smallmatrix} + & - \\ 3 & 3 \end{smallmatrix}$$

$${}^3H: |5, 1; 5, 1\rangle = \begin{smallmatrix} + & + \\ 3 & 2 \end{smallmatrix}$$

$${}^3F: |3, 1; 3, 1\rangle = \sqrt{\frac{1}{3}} \begin{smallmatrix} + & + \\ 3 & 0 \end{smallmatrix} - \sqrt{\frac{2}{3}} \begin{smallmatrix} + & + \\ 2 & 1 \end{smallmatrix}$$

$${}^3P: |1, 1; 1, 1\rangle = \sqrt{\frac{1}{14}} [\sqrt{3} \begin{smallmatrix} + & + \\ 3 & -2 \end{smallmatrix} - \sqrt{5} \begin{smallmatrix} + & + \\ 2 & -1 \end{smallmatrix} + \sqrt{6} \begin{smallmatrix} + & + \\ 1 & 0 \end{smallmatrix}]$$

$${}^1G: |4, 0; 4, 0\rangle = \sqrt{\frac{3}{11}} [\begin{smallmatrix} + & - \\ 3 & 1 \end{smallmatrix} - \begin{smallmatrix} - & + \\ 3 & 1 \end{smallmatrix}] - \sqrt{\frac{5}{11}} \begin{smallmatrix} + & - \\ 2 & 2 \end{smallmatrix}$$

$${}^1D: |2, 0; 2, 0\rangle = \sqrt{\frac{5}{42}} [\begin{smallmatrix} + & - \\ 3 & -1 \end{smallmatrix} - \begin{smallmatrix} - & + \\ 3 & -1 \end{smallmatrix}] - \sqrt{\frac{5}{21}} [\begin{smallmatrix} + & - \\ 2 & 0 \end{smallmatrix} - \begin{smallmatrix} - & + \\ 2 & 0 \end{smallmatrix}] + \sqrt{\frac{2}{7}} \begin{smallmatrix} + & - \\ 1 & 1 \end{smallmatrix}$$

$${}^1S: |0, 0; 0, 0\rangle = \sqrt{\frac{1}{7}} [\begin{smallmatrix} + & - \\ 3 & -3 \end{smallmatrix} - \begin{smallmatrix} - & + \\ 3 & -3 \end{smallmatrix} - \begin{smallmatrix} + & - \\ 2 & -2 \end{smallmatrix} + \begin{smallmatrix} - & + \\ 2 & -2 \end{smallmatrix} + \begin{smallmatrix} + & - \\ 1 & -1 \end{smallmatrix} \\ - \begin{smallmatrix} - & + \\ 1 & -1 \end{smallmatrix} - \begin{smallmatrix} + & - \\ 0 & 0 \end{smallmatrix}]$$

The other  $|L, S; M_L, M_S\rangle$  functions needed to calculate the spin-orbit energies are as follows:

$${}^3H: |5, 1; 5, 0\rangle = \sqrt{\frac{1}{2}} [\begin{smallmatrix} + & - \\ 3 & 2 \end{smallmatrix} + \begin{smallmatrix} - & + \\ 3 & 2 \end{smallmatrix}]$$

$$|5, 1; 5, -1\rangle = \begin{smallmatrix} - & - \\ 3 & 2 \end{smallmatrix}$$

$$|5, 1; 4, 1\rangle = \begin{smallmatrix} + & + \\ 3 & 1 \end{smallmatrix}$$

$$|5, 1; 4, 0\rangle = \sqrt{\frac{1}{2}} [\begin{smallmatrix} + & - \\ 3 & 1 \end{smallmatrix} + \begin{smallmatrix} - & + \\ 3 & 1 \end{smallmatrix}]$$

$$|5, 1; 3, 1\rangle = \sqrt{\frac{2}{3}} \begin{smallmatrix} + & + \\ 3 & 0 \end{smallmatrix} + \sqrt{\frac{1}{3}} \begin{smallmatrix} + & + \\ 2 & 1 \end{smallmatrix}$$

$${}^3F: |3, 1; 3, 0\rangle = \sqrt{\frac{1}{6}} [\begin{smallmatrix} + & - \\ 3 & 0 \end{smallmatrix} + \begin{smallmatrix} - & + \\ 3 & 0 \end{smallmatrix}] - \sqrt{\frac{1}{3}} [\begin{smallmatrix} + & - \\ 2 & 1 \end{smallmatrix} + \begin{smallmatrix} - & + \\ 2 & 1 \end{smallmatrix}]$$

$$|3, 1; 3, -1\rangle = \sqrt{\frac{1}{3}} \begin{smallmatrix} - & - \\ 3 & 0 \end{smallmatrix} - \sqrt{\frac{2}{3}} \begin{smallmatrix} - & - \\ 2 & 1 \end{smallmatrix}$$



$$\begin{aligned}
|3, 1; 2, 1\rangle &= \sqrt{\frac{2}{3}}(3^+ - 1) - \sqrt{\frac{1}{3}}(2^+ 0) \\
|3, 1; 2, 0\rangle &= \sqrt{\frac{1}{3}}[(3^+ - 1) + (\bar{3}^+ - 1)] - \sqrt{\frac{1}{6}}[(2^+ \bar{0}) + (\bar{2}^+ 0)] \\
|3, 1; 1, 1\rangle &= \sqrt{\frac{2}{3}}(3^+ - 2) - \sqrt{\frac{1}{3}}(1^+ 0) \\
{}^3P: |1, 1; 1, 0\rangle &= \sqrt{\frac{1}{28}}\{\sqrt{3}[(3^+ - 2) + (\bar{3}^+ - 2)] - \sqrt{5}[(2^+ - 1) + (\bar{2}^+ - 1)] \\
&\quad + \sqrt{6}[(1^+ \bar{0}) + (\bar{1}^+ 0)]\} \\
|1, 1; 1, -1\rangle &= \sqrt{\frac{1}{14}}[\sqrt{3}(\bar{3} - 2) - \sqrt{5}(\bar{2} - 1) + \sqrt{6}(\bar{1} \bar{0})] \\
|1, 1; 0, 1\rangle &= \sqrt{\frac{1}{14}}[3(3^+ - 3) - 2(2^+ - 2) + (1^+ - 1)] \\
|1, 1; 0, 0\rangle &= \sqrt{\frac{1}{28}}\{3[(3^+ - 3) + (\bar{3}^+ - 3)] - 2[(2^+ - 2) + (\bar{2}^+ - 2)] \\
&\quad + [(1^+ - 1) + (\bar{1}^+ - 1)]\} \\
|1, 1; -1, 1\rangle &= \sqrt{\frac{1}{14}}[\sqrt{3}(2^+ - 3) - \sqrt{5}(1^+ - 2) + \sqrt{6}(0^+ - 1)]
\end{aligned}$$

With these functions, it is a straightforward procedure to calculate the off-diagonal elements. Of course, the diagonal elements can also be calculated using these functions. As examples

$$\begin{aligned}
\langle {}^1I_6 | \sum_i l_i s_i | {}^1I_6 \rangle &= \langle 6, 0; 6, 6 | \sum_i l_i s_i | 6, 0; 6, 6 \rangle = \langle 6, 0; 6, 0 | \sum_i l_i s_i | 6, 0; 6, 0 \rangle \\
&= \langle (3^+ \bar{3}) | l_1 s_1 + l_2 s_2 | (3^+ \bar{3}) \rangle = \langle (3^+ \bar{3}) | l_1 s_1 | (3^+ \bar{3}) \rangle + \langle (3^+ \bar{3}) | l_2 s_2 | (3^+ \bar{3}) \rangle \\
&= \langle 3^+ | l_1 s_1 | 3^+ \rangle + \langle \bar{3} | l_2 s_2 | \bar{3} \rangle = \frac{3}{2} - \frac{3}{2} = 0 \\
\langle {}^1I_6 | \sum_i l_i s_i | {}^3H_6 \rangle &= \langle 6, 0; 6, 6 | \sum_i l_i s_i | 5, 1; 6, 6 \rangle = \langle 6, 0; 6, 0 | \sum_i l_i s_i | 5, 1; 5, 1 \rangle \\
&= \langle (3^+ \bar{3}) | l_1 s_1 + l_2 s_2 | (3^+ \bar{2}) \rangle = \langle (3^+ \bar{3}) | l_1 s_1 | (3^+ \bar{2}) \rangle + \langle (3^+ \bar{3}) | l_2 s_2 | (3^+ \bar{2}) \rangle \\
&= 0 + \langle \bar{3} | l_2 s_2 | \bar{2} \rangle = \frac{1}{2} \langle \bar{3} | l_{+s-} | \bar{2} \rangle = \frac{1}{2} \sqrt{6} \langle \bar{3} | \bar{3} \rangle = \frac{\sqrt{6}}{2} \zeta
\end{aligned}$$

We list below all the off-diagonal elements.

$$\langle {}^1\text{I}_6 | \vec{l} \cdot \vec{s} | {}^3\text{H}_6 \rangle = \frac{\sqrt{6}}{2} \zeta$$

$$\langle {}^3\text{H}_4 | \vec{l} \cdot \vec{s} | {}^3\text{F}_4 \rangle = 0$$

$$\langle {}^3\text{H}_4 | \vec{l} \cdot \vec{s} | {}^1\text{G}_4 \rangle = -\frac{\sqrt{30}}{3} \zeta$$

$$\langle {}^3\text{F}_4 | \vec{l} \cdot \vec{s} | {}^1\text{G}_4 \rangle = \frac{\sqrt{33}}{3} \zeta$$

$$\langle {}^3\text{F}_2 | \vec{l} \cdot \vec{s} | {}^3\text{P}_2 \rangle = 0$$

$$\langle {}^3\text{F}_2 | \vec{l} \cdot \vec{s} | {}^1\text{D}_2 \rangle = -\sqrt{6} \zeta$$

$$\langle {}^3\text{P}_2 | \vec{l} \cdot \vec{s} | {}^1\text{D}_2 \rangle = \frac{3\sqrt{2}}{2} \zeta$$

$$\langle {}^3\text{P}_0 | \vec{l} \cdot \vec{s} | {}^1\text{S}_0 \rangle = -2\sqrt{3} \zeta$$

A note on phases: it should be noted that the vector coupling method allows for an arbitrariness in the choice of phase for the wave functions. This choice of phase arises in the construction of functions by orthogonality. Here in the case of  $|J, M\rangle$  functions, the phase choice comes at

$${}^3\text{H}_5 : |5, 1; 5, 5\rangle, \quad {}^3\text{H}_4 : |5, 1; 4, 4\rangle$$

$${}^3\text{F}_3 : |3, 1; 3, 3\rangle, \quad {}^3\text{F}_2 : |3, 1; 2, 2\rangle$$

$${}^3\text{P}_1 : |1, 1; 1, 1\rangle, \quad {}^3\text{P}_0 : |1, 1; 0, 0\rangle$$

and in the case of  $|L, S; M_L, M_S\rangle$  functions the phase choice comes at  ${}^3\text{F}: |3, 1; 3, 1\rangle$ ,  ${}^3\text{P}: |1, 1; 1, 1\rangle$ ,  ${}^1\text{G}: |4, 0; 4, 0\rangle$ ,  ${}^1\text{D}: |2, 0; 2, 0\rangle$ , and  ${}^1\text{S}: |0, 0; 0, 0\rangle$ . Because of this phase choice, the off-diagonal matrix elements calculated by the determinantal method may not be identical to those obtained by the tensor operator method. Although the phases have no effect in the case of the free ion where we are concerned with only electrostatic and spin-orbit matrix elements, it is necessary to maintain the same phases, if these matrix elements are added on to a third perturbation, i.e., the crystalline field. In order to obtain identical results between the two methods, we have fixed the phases of the functions by the 3-j method to calculate the matrix elements in the determinantal method.

**45.2.1.2. Energies of spin-orbital levels by tensor operators** The matrix elements of spin-orbit interaction in an  $l^N$  configuration are shown to be

$$(l^N SLJM | \zeta \sum_i (s_i \cdot l_i) | l^N S' L' J M)$$

$$= \zeta(-1)^{J+L+S'} \left\{ \begin{matrix} LL'1 \\ S'SJ \end{matrix} \right\} \times (l^N SL | \sum (s_i \cdot l_i) | l^N S'L'), \quad (8.97a)$$

where

$$(l^N SL | \sum_i (s_i \cdot l_i) | l^N S'L') = [l(l+1)(2l+1)]^{1/2} (l^N SL \| V^{(11)} \| l^N S'L') \quad (8.97b)$$

The reduced matrix elements of  $V^{(11)}$  have been tabulated by Nielson and Koster [318].

$V^{(11)}$	${}^3\text{H}$	${}^3\text{F}$	${}^1\text{I}$	${}^1\text{G}$	${}^3\text{P}$	${}^1\text{D}$	${}^1\text{S}$
	$\frac{1}{2}\sqrt{\frac{165}{7}}$	0	$-\frac{1}{2}\sqrt{\frac{39}{14}}$	$\sqrt{\frac{15}{14}}$	0	0	0
		$\sqrt{\frac{3}{2}}$	0	$-\frac{1}{2}\sqrt{\frac{33}{7}}$	0	$\sqrt{\frac{15}{14}}$	0
			0	0	0	0	0
				0	0	0	0
					$\frac{1}{2}\sqrt{\frac{3}{7}}$	$-\frac{3}{2}\sqrt{\frac{5}{14}}$	$\sqrt{\frac{3}{7}}$
						0	0
							0

Using the reduced matrix elements, we obtain

$$(f^{2^3}\text{H} | \sum s_i l_i | f^{2^3}\text{H}) = \sqrt{84} \left( \frac{1}{2} \sqrt{\frac{165}{7}} \right) = 3\sqrt{55}$$

$$(f^{2^3}\text{H} | \sum s_i l_i | f^{2^1}\text{I}) = \sqrt{84} \left( -\frac{1}{2} \sqrt{\frac{39}{14}} \right) = -\frac{3}{2}\sqrt{26}$$

$$(f^{2^3}\text{H} | \sum s_i l_i | f^{2^1}\text{G}) = \sqrt{84} \left( \sqrt{\frac{15}{14}} \right) = 3\sqrt{10}$$

$$(f^{2^3}\text{F} | \sum s_i l_i | f^{2^3}\text{F}) = \sqrt{84} \left( \sqrt{\frac{3}{2}} \right) = 3\sqrt{14}$$

$$(f^{2^3}\text{F} | \sum s_i l_i | f^{2^1}\text{G}) = \sqrt{84} \left( -\frac{1}{2} \sqrt{\frac{33}{7}} \right) = -3\sqrt{11}$$

$$(f^{2^3}\text{F} | \sum s_i l_i | f^{2^1}\text{D}) = \sqrt{84} \left( \sqrt{\frac{15}{14}} \right) = 3\sqrt{10}$$

$$(f^{2^3}\text{P} | \sum s_i l_i | f^{2^3}\text{P}) = \sqrt{84} \left( \frac{1}{2} \sqrt{\frac{3}{7}} \right) = 3$$

$$(f^{2^3}\text{P} | \sum s_i l_i | f^{2^1}\text{D}) = \sqrt{84} \left( -\frac{3}{2} \sqrt{\frac{5}{14}} \right) = -\frac{3}{2}\sqrt{30}$$

$$\langle f^2 \ ^3P_1 | \sum s_i l_i | f^2 \ ^1S \rangle = \sqrt{84} \left( \sqrt{\frac{3}{7}} \right) = 6$$

Hence

$$E(^3H_4) = \zeta (-1)^{4+5+1} \left\{ \begin{matrix} 551 \\ 114 \end{matrix} \right\} 3\sqrt{55} = \zeta \left( -\sqrt{\frac{1}{55}} \right) 3\sqrt{55} = -3\zeta$$

$$E(^3H_5) = \zeta (-1)^{5+5+1} \left\{ \begin{matrix} 551 \\ 115 \end{matrix} \right\} 3\sqrt{55} = -\zeta \left( \sqrt{\frac{1}{1980}} \right) 3\sqrt{55} = -\frac{1}{2}\zeta$$

$$E(^3H_6) = \zeta (-1)^{6+5+1} \left\{ \begin{matrix} 551 \\ 116 \end{matrix} \right\} 3\sqrt{55} = \zeta \left( \sqrt{\frac{5}{396}} \right) 3\sqrt{55} = \frac{5}{2}\zeta$$

$$E(^3F_2) = \zeta (-1)^{2+3+1} \left\{ \begin{matrix} 331 \\ 112 \end{matrix} \right\} 3\sqrt{14} = \zeta \left( -\sqrt{\frac{2}{63}} \right) 3\sqrt{14} = -2\zeta$$

$$E(^3F_3) = \zeta (-1)^{3+3+1} \left\{ \begin{matrix} 331 \\ 113 \end{matrix} \right\} 3\sqrt{14} = -\zeta \left( \sqrt{\frac{1}{504}} \right) 3\sqrt{14} = -\frac{1}{2}\zeta$$

$$E(^3F_4) = \zeta (-1)^{4+3+1} \left\{ \begin{matrix} 331 \\ 114 \end{matrix} \right\} 3\sqrt{14} = \zeta \left( \sqrt{\frac{1}{56}} \right) 3\sqrt{14} = \frac{3}{2}\zeta$$

$$E(^3P_0) = \zeta (-1)^{0+1+1} \left\{ \begin{matrix} 111 \\ 110 \end{matrix} \right\} 3 = \zeta \left( -\frac{1}{3} \right) 3 = -\zeta$$

$$E(^3P_1) = \zeta (-1)^{1+1+1} \left\{ \begin{matrix} 111 \\ 111 \end{matrix} \right\} 3 = -\zeta \left( \frac{1}{6} \right) 3 = -\frac{1}{2}\zeta$$

$$E(^3P_2) = \zeta (-1)^{2+1+1} \left\{ \begin{matrix} 111 \\ 112 \end{matrix} \right\} 3 = \zeta \left( \frac{1}{6} \right) 3 = \frac{1}{2}\zeta$$

$$\langle ^3H_4 | l_i s_i | ^3F_4 \rangle = 0$$

$$\langle ^3H_4 | l_i s_i | ^1G_4 \rangle = \zeta (-1)^{4+5+0} \left\{ \begin{matrix} 541 \\ 014 \end{matrix} \right\} 3\sqrt{10} = -\zeta \left( \sqrt{\frac{1}{27}} \right) 3\sqrt{10} = -\sqrt{\frac{10}{3}}\zeta$$

$$\langle ^3H_6 | l_i s_i | ^1I_6 \rangle = \zeta (-1)^{6+5+0} \left\{ \begin{matrix} 561 \\ 016 \end{matrix} \right\} \left( -\frac{3}{2}\sqrt{26} \right) = -\zeta \left( \sqrt{\frac{1}{39}} \right) \left( \frac{-3\sqrt{26}}{2} \right) = -\sqrt{\frac{3}{2}}\zeta$$

$$\langle ^3F_2 | l_i s_i | ^3P_2 \rangle = 0$$

$$\langle ^3F_2 | l_i s_i | ^1D_2 \rangle = \zeta (-1)^{2+3+0} \left\{ \begin{matrix} 321 \\ 012 \end{matrix} \right\} 3\sqrt{10} = -\zeta \left( \sqrt{\frac{1}{15}} \right) 3\sqrt{10} = -\sqrt{6}\zeta$$

$$\langle ^3F_4 | l_i s_i | ^1G_4 \rangle = \zeta (-1)^{4+3+0} \left\{ \begin{matrix} 341 \\ 014 \end{matrix} \right\} (-3\sqrt{11}) = -\zeta \left( \sqrt{\frac{1}{27}} \right) (-3\sqrt{11}) = +\frac{\sqrt{33}}{3}\zeta$$

TABLE 8.34  
The electrostatic and spin-orbit energy matrices of  $f^2$ . [I, H, G, F, D, P, and S are the term energies, equation (8.92).]

$J = 5$	${}^3H_5 = H - \zeta/2$		
$J = 3$	${}^3F_3 = F - \zeta/2$		
$J = 1$	${}^3P_1 = P - \zeta/2$		
$J = 6$	${}^1I_6$	${}^3H_6$	
	${}^1I_6$	I	$\frac{\sqrt{6}}{2}\zeta$
	${}^3H_6$		$H + \frac{5}{2}\zeta$
$J = 4$	${}^3H_4$	${}^3F_4$	${}^1G_4$
	${}^3H_4$	$H - 3\zeta$	$\frac{-\sqrt{30}}{3}\zeta$
	${}^3F_4$		$F + \frac{3}{2}\zeta$
	${}^1G_4$		G
$J = 2$	${}^3F_2$	${}^3P_2$	${}^1D_2$
	${}^3F_2$	$F - 2\zeta$	$-\sqrt{6}\zeta$
	${}^3P_2$		$P + \frac{\zeta}{2}$
	${}^1D_2$		D
$J = 0$	${}^3P_0$	${}^1S_0$	
	${}^3P_0$	$P - \zeta$	$-2\sqrt{3}\zeta$
	${}^1S_0$	S	

$$\langle {}^3P_0 | l_i s_i | {}^1S_0 \rangle = \zeta (-1)^{0+1+0} \begin{Bmatrix} 101 \\ 010 \end{Bmatrix} 6 = -\zeta \left( \sqrt{\frac{1}{3}} \right) 6 = -2\sqrt{3}\zeta$$

$$\langle {}^3P_2 | l_i s_i | {}^1D_2 \rangle = \zeta (-1)^{2+1+0} \begin{Bmatrix} 121 \\ 012 \end{Bmatrix} \left( -\frac{3}{2}\sqrt{30} \right) = -\zeta \left( \sqrt{\frac{1}{15}} \right) \left( -\frac{3}{2}\sqrt{30} \right) = \frac{3\sqrt{2}}{2}\zeta$$

The electrostatic and spin-orbit energy matrices of  $f^2$  configuration applicable to a free-ion are given in Table 8.34.

### 45.3. The crystalline field perturbation

#### 45.3.1. Crystal field potential and crystal field parameters

Our aim is to derive theoretical crystalline field energy levels of  $f^2$  and fit the experimental levels of  $\text{PrCl}_3$ . According to the crystal structure proposed by Zachariasen [319], the nearest neighbors of the  $\text{Pr}^{3+}$  ion are nine  $\text{Cl}^-$  ions arranged in a tricapped trigonal

prismatic geometry resulting in  $D_{3h}$  symmetry<sup>2</sup>. Accordingly, we use  $D_{3h}$  symmetry for the crystal field potential,

$$H^3 = V_{D_{3h}}^{CF}$$

The nonvanishing terms in the crystal field potential in  $D_{3h}$  symmetry are

$$V_2^0, V_4^0, V_6^0, \text{ and } V_6^6$$

These can be expressed in terms of spherical harmonics:

$$V_{D_{3h}} = D_2^0 Y_2^0 + D_4^0 Y_4^0 + D_6^0 Y_6^0 + D_6^6 (Y_6^6 + Y_6^{-6}) \quad (8.98a)$$

or in terms of tensor operators:

$$V_{D_{3h}} = B_0^2 C_0^2 + B_0^4 C_0^4 + B_0^6 C_0^6 + B_6^6 (C_6^6 + C_{-6}^6) \quad (8.98b)$$

or in terms of Stevens' operator equivalents [320]:

$$\begin{aligned} V_{D_{3h}} = & A_2^0 (3z^2 - r^2) + A_4^0 (35z^4 - 30z^2 r^2 + 3r^4) \\ & + A_6^0 (231z^6 - 315z^4 r^2 + 105z^2 r^4 - 5r^6) \\ & + A_6^6 (x^6 - 15x^4 y^2 + 15x^2 y^4 - y^6) \end{aligned} \quad (8.98c)$$

The  $D$ ,  $B$ ,  $A$  are radial parameters.

Expression (8.98a) is also equivalent to

$$\begin{aligned} V_{D_{3h}} = & D_2^0 \cdot \frac{1}{4} \sqrt{\frac{5}{\pi}} (3z^2 - r^2) + D_4^0 \cdot \frac{3}{16} \sqrt{\frac{1}{\pi}} (35z^4 - 30z^2 r^2 + 3r^4) \\ & + D_6^0 \cdot \frac{1}{32} \sqrt{\frac{13}{\pi}} (231z^6 - 315z^4 r^2 + 105z^2 r^4 - 5r^6) \\ & + D_6^6 \cdot \frac{1}{32} \sqrt{\frac{3003}{\pi}} (x^6 - 15x^4 y^2 + 15x^2 y^4 - y^6) \end{aligned} \quad (8.98d)$$

Hence:

$$\begin{aligned} A_2^0 &= \frac{1}{4} \sqrt{\frac{5}{\pi}} D_2^0 \\ A_4^0 &= \frac{3}{16} \sqrt{\frac{1}{\pi}} D_4^0 \end{aligned}$$

<sup>2</sup> The actual site symmetry of the  $\text{Pr}^{3+}$  ion in the lattice is  $C_{3h}$ . However, the doubly degenerate levels of  $D_{3h}$  still retain their degeneracy in  $C_{3h}$  and the additional crystal-field parameter that arises in  $C_{3h}$  is not significant. The selection rules for electric dipole radiation in  $C_{3h}$  symmetry, however, are different.

$$\begin{aligned}
 A_6^0 &= \frac{1}{32} \sqrt{\frac{13}{\pi}} D_6^0 \\
 A_6^6 &= \frac{1}{32} \sqrt{\frac{3003}{\pi}} D_6^6
 \end{aligned}
 \tag{8.99}$$

Tensor operators and spherical harmonics are related by

$$C_M^L = \sqrt{\frac{4\pi}{2L+1}} Y_L^M \tag{8.100}$$

Hence:

$$\begin{aligned}
 D_2^0 &= B_0^2 \sqrt{\frac{4\pi}{5}} \\
 D_4^0 &= B_0^4 \sqrt{\frac{4\pi}{9}} \\
 D_6^0 &= B_0^6 \sqrt{\frac{4\pi}{13}} \\
 D_6^6 &= B_6^6 \sqrt{\frac{4\pi}{13}}
 \end{aligned}
 \tag{8.101}$$

so that the  $A$ 's and  $B$ 's are related by

$$\begin{aligned}
 A_2^0 &= \frac{1}{2} B_0^2 \\
 A_4^0 &= \frac{1}{8} B_0^4 \\
 A_6^0 &= \frac{1}{16} B_0^6 \\
 A_6^6 &= \frac{\sqrt{231}}{16} B_6^6
 \end{aligned}
 \tag{8.102}$$

#### 45.3.2. Crystal field splitting of spin-orbital levels

The character table for  $D_{3h}$  point group and the reduction to irreducible representations of  $D_{3h}$  of the  $(2J+1)$  states with a given  $J$  are presented in Tables 8.35 and 8.36. The  $|JM\rangle$  basis functions for six irreducible representations of  $D_{3h}$  are listed in Table 8.37.

Experimentalists use crystal quantum number,  $\mu$ , in place of the irreducible representation  $\Gamma_i$  to identify the experimental energy levels obtained by electric dipole polarization selection rules [322,323]. The correspondence between crystal quantum number  $\mu$  and the irreducible representations  $\Gamma_i$  of  $D_{3h}$  is given in Table 8.38 and the  $D_{3h}$  electric dipole selection rules in Table 8.39.

TABLE 8.35  
The character table for  $D_{3h}$  point group<sup>a,b</sup>

$D_{3h}$	E	$2C_3$	$3C'_2$	$\sigma_h$	$2S_3$	$3\sigma_v$		
$\Gamma_1$	1	1	1	1	1	1		$x^2 + y^2, z^2$
$\Gamma_2$	1	1	-1	1	1	-1	$R_z$	
$\Gamma_3$	2	-1	0	2	-1	0	$(x, y)$	$(x^2 - y^2, xy)$
$\Gamma_4$	1	1	1	-1	-1	-1		
$\Gamma_5$	1	1	-1	-1	-1	1	$z$	
$\Gamma_6$	2	-1	0	-2	1	0	$(R_x, R_y)$	$(zx, yz)$

<sup>a</sup>In Mulliken's notation  $\Gamma_1 = a'_1, \Gamma_2 = a'_2, \Gamma_3 = e', \Gamma_4 = a''_1, \Gamma_5 = a''_2, \Gamma_6 = e''$ .

<sup>b</sup>The  $\Gamma$  notation used by Margolis [321] is different from ours in that his  $\Gamma_3$  and  $\Gamma_5$  are our  $\Gamma_5$  and  $\Gamma_3$ , respectively.

TABLE 8.36  
The irreducible representations of  $D_{3h}$  spanned by the  $(2J + 1)$  states with a given  $J$  value.

$J$	$\Gamma_i$
0	$\Gamma_1$
1	$\Gamma_2 + \Gamma_6$
2	$\Gamma_1 + \Gamma_3 + \Gamma_6$
3	$\Gamma_2 + \Gamma_3 + \Gamma_4 + \Gamma_5 + \Gamma_6$
4	$\Gamma_1 + 2\Gamma_3 + \Gamma_4 + \Gamma_5 + \Gamma_6$
5	$\Gamma_2 + 2\Gamma_3 + \Gamma_4 + \Gamma_5 + 2\Gamma_6$
6	$2\Gamma_1 + \Gamma_2 + 2\Gamma_3 + \Gamma_4 + \Gamma_5 + 2\Gamma_6$

TABLE 8.37  
The  $|J, M\rangle$  basis functions for the irreducible representations of  $D_{3h}$  point group symmetry.

$\Gamma_1$ :	$ 0, 0\rangle;  2, 0\rangle;  4, 0\rangle; \frac{1}{2}[ 6, 6\rangle +  6, -6\rangle] + \sqrt{\frac{1}{2}} 6, 0\rangle; \frac{1}{2}[ 6, 6\rangle +  6, -6\rangle - \sqrt{\frac{1}{2}} 6, 0\rangle]$
$\Gamma_2$ :	$ 1, 0\rangle;  3, 0\rangle;  5, 0\rangle; \sqrt{\frac{1}{2}}[ 6, 6\rangle -  6, -6\rangle]$
$\Gamma_3$ :	$ 2, \pm 2\rangle;  3, \pm 2\rangle;  4, \pm 2\rangle;  4, \mp 4\rangle;  5, \pm 2\rangle;  5, \mp 4\rangle;  6, \pm 2\rangle;  6, \mp 4\rangle;$
$\Gamma_4$ :	$\sqrt{\frac{1}{2}}[ 3, 3\rangle +  3, -3\rangle]; \sqrt{\frac{1}{2}}[ 4, 3\rangle -  4, -3\rangle]; \sqrt{\frac{1}{2}}[ 5, 3\rangle +  5, -3\rangle]; \sqrt{\frac{1}{2}}[ 6, 3\rangle -  6, -3\rangle]$
$\Gamma_5$ :	$\sqrt{\frac{1}{2}}[ 3, 3\rangle -  3, -3\rangle]; \sqrt{\frac{1}{2}}[ 4, 3\rangle +  4, -3\rangle]; \sqrt{\frac{1}{2}}[ 5, 3\rangle -  5, -3\rangle]; \sqrt{\frac{1}{2}}[ 6, 3\rangle +  6, -3\rangle]$
$\Gamma_6$ :	$ 1, \pm 1\rangle;  2, \pm 1\rangle;  3, \pm 1\rangle;  4, \pm 1\rangle;  5, \pm 1\rangle;  5, \mp 5\rangle;  6, \pm 1\rangle;  6, \mp 5\rangle;$

TABLE 8.38  
Correspondence between crystal quantum number  $\mu$  and the irreducible representation  $\Gamma_i$  of  $D_{3h}$ .

$\mu$	$\Gamma_i$
0, 6, -6	$\Gamma_1, \Gamma_2$
$\pm 1$	$\Gamma_6$
$\pm 2$	$\Gamma_3$
3, -3	$\Gamma_4, \Gamma_5$



TABLE 8.39  
Electric dipole selection rules in  $D_{3h}$ .

	0		$\pm 2$	3		$\pm 1$
	$\Gamma_1$	$\Gamma_2$	$\Gamma_3$	$\Gamma_4$	$\Gamma_5$	$\Gamma_6$
0	{	$\Gamma_1$		$\sigma$		$\pi$
		$\Gamma_2$		$\sigma$	$\pi$	
$\pm 2$		$\Gamma_3$	$\sigma$	$\sigma$		$\pi$
3	{	$\Gamma_4$			$\pi$	$\sigma$
		$\Gamma_5$	$\pi$			$\sigma$
$\pm 1$		$\Gamma_6$		$\pi$	$\sigma$	$\sigma$

$\Gamma_1$ :	$12 \times 12$
$\Gamma_2$ :	$5 \times 5$
$\Gamma_3$ :	$16 \times 16$
$\Gamma_4$ :	$7 \times 7$
$\Gamma_5$ :	$7 \times 7$
$\Gamma_6$ :	$14 \times 14$

Thus the orders of secular determinants in  $D_{3h}$  for  $f^2$  configuration are: giving rise to a total of 61 Stark levels. Thirty of these ( $\Gamma_3$  and  $\Gamma_6$ ) are doubly degenerate which along with the other 31 nondegenerate levels will account for the total degeneracy of 91 for  $f^2$  given by the binomial coefficient  $\binom{14}{2}$ .

The complete crystal field energy matrices of  $f^2$  configuration in  $D_{3h}$  symmetry have been constructed by Margolis [321].

We will use the  $^3P$  multiplet to show the details in calculating the crystal field matrix elements.

### 45.3.3. Calculation of the crystal field energies

45.3.3.1. *Determinantal method* In this method it is necessary to calculate the one electron matrix elements of an  $f$  electron. These are, in terms of tensor operator parameters

$$\begin{aligned}
 (\pm 3|V|\pm 3) &= -\frac{1}{3}B_0^2 + \frac{1}{110}B_0^4 - \frac{5}{429}B_0^6 \\
 (\pm 2|V|\pm 2) &= -\frac{7}{33}B_0^4 + \frac{10}{143}B_0^6 \\
 (\pm 1|V|\pm 1) &= \frac{1}{5}B_0^2 + \frac{1}{33}B_0^4 - \frac{25}{143}B_0^6
 \end{aligned} \tag{8.103}$$

$$(0|V|0) = \frac{4}{15}B_0^2 + \frac{2}{11}B_0^4 + \frac{100}{429}B_0^6$$

$$(\pm 3|V|\mp 3) = -\frac{10}{13}\sqrt{\frac{7}{33}}B_0^6$$

The above expressions are obtained using the formula:

$$\begin{aligned} (l'm'|C_M^L|lm) \\ = (-1)^{-m'} [(2l'+1)(2l+1)]^{1/2} \begin{pmatrix} l' & L & l \\ -m' & M & m \end{pmatrix} \begin{pmatrix} l' & L & l \\ 0 & 0 & 0 \end{pmatrix} \end{aligned} \quad (8.104a)$$

which can be factored by the Wigner-Eckart theorem into two parts, one of which is independent of  $m'$ ,  $m$ , and  $M$  and is known as the reduced matrix element

$$(l'\|C^{(L)}\|l) = (-1)^{l'} [(2l'+1)(2l+1)]^{1/2} \begin{pmatrix} l' & L & l \\ 0 & 0 & 0 \end{pmatrix} \quad (8.104b)$$

so that

$$(l'm'|C_M^L|lm) = (-1)^{l'-m'} (l'\|C^L\|l) \begin{pmatrix} l' & L & l \\ -m'_l & M & m_l \end{pmatrix} \quad (8.104c)$$

from 3-j tables

$$(3\|C^2\|3) = (-1) \cdot 7 \begin{pmatrix} 3 & 2 & 3 \\ 0 & 0 & 0 \end{pmatrix} = -7 \left( \frac{2}{\sqrt{105}} \right) = -2\sqrt{\frac{7}{15}}$$

$$(3\|C^4\|3) = (-1) \cdot 7 \begin{pmatrix} 3 & 4 & 3 \\ 0 & 0 & 0 \end{pmatrix} = -7 \left( \frac{-2}{\sqrt{77}} \right) = \sqrt{\frac{14}{11}}$$

$$(3\|C^6\|3) = (-1) \cdot 7 \begin{pmatrix} 3 & 6 & 3 \\ 0 & 0 & 0 \end{pmatrix} = -7 \left( \frac{10}{\sqrt{3003}} \right) = \frac{-10\sqrt{7}}{\sqrt{429}}$$

$$(3, \pm 3|C_0^2|3, \pm 3) = (-1)^{3-3} (3\|C^2\|3) \begin{pmatrix} 3 & 2 & 3 \\ -3 & 0 & 3 \end{pmatrix}$$

$$= -2\sqrt{\frac{7}{15}} \left( \frac{1}{2}\sqrt{\frac{5}{21}} \right) = -\frac{1}{3}$$

$$(3, \pm 2|C_0^2|3, \pm 2) = (-1)^{3-2} (3\|C^2\|3) \begin{pmatrix} 3 & 2 & 3 \\ -2 & 0 & 2 \end{pmatrix} = -1 \left( -2\sqrt{\frac{7}{15}} \right) 0 = 0$$

$$(3, \pm 1|C_0^2|3, \pm 1) = (-1)^{3-1} (3\|C^2\|3) \begin{pmatrix} 3 & 2 & 3 \\ -1 & 0 & 1 \end{pmatrix} = -2\sqrt{\frac{7}{15}} \left( \frac{-1}{2}\sqrt{\frac{3}{35}} \right) = \frac{1}{5}$$

$$(3, 0|C_0^2|3, 0) = (-1)^{3-0}(3\|C^2\|3) \begin{pmatrix} 3 & 2 & 3 \\ 0 & 0 & 0 \end{pmatrix} = +2\sqrt{\frac{7}{15}} \left( \frac{2}{\sqrt{105}} \right) = \frac{4}{15}$$

$$(3, \pm 3|C_0^4|3, \pm 3) = (-1)^{3-3}(3\|C^4\|3) \begin{pmatrix} 3 & 4 & 3 \\ -3 & 0 & 3 \end{pmatrix} = +\sqrt{\frac{14}{11}} \left( \sqrt{\frac{1}{154}} \right) = \frac{1}{11}$$

$$(3, \pm 2|C_0^4|3, \pm 2) = (-1)^{3-2}(3\|C^4\|3) \begin{pmatrix} 3 & 4 & 3 \\ -2 & 0 & 2 \end{pmatrix} \\ = -\left( \sqrt{\frac{14}{11}} \right) \left( \frac{1}{3} \sqrt{\frac{7}{22}} \right) = -\frac{7}{33}$$

$$(3, \pm 1|C_0^4|3, \pm 1) = (-1)^{3-1}(3\|C^4\|3) \begin{pmatrix} 3 & 4 & 3 \\ -1 & 0 & 1 \end{pmatrix} = +\sqrt{\frac{14}{11}} \left( \frac{1}{3} \sqrt{\frac{1}{154}} \right) = \frac{1}{33}$$

$$(3, 0|C_0^4|3, 0) = (-1)^{3-0}(3\|C^4\|3) \begin{pmatrix} 3 & 4 & 3 \\ 0 & 0 & 0 \end{pmatrix} = -\left( \sqrt{\frac{14}{11}} \right) \left( -\sqrt{\frac{2}{77}} \right) = \frac{2}{11}$$

$$(3, \pm 3|C_0^6|3, \pm 3) = (-1)^{3-3}(3\|C^6\|3) \begin{pmatrix} 3 & 6 & 3 \\ -3 & 0 & 3 \end{pmatrix} \\ = \frac{-10\sqrt{7}}{\sqrt{429}} \left( \frac{1}{2\sqrt{3003}} \right) = -\frac{5}{429}$$

$$(3, \pm 2|C_0^6|3, \pm 2) = (-1)^{3-2}(3\|C^6\|3) \begin{pmatrix} 3 & 6 & 3 \\ -2 & 0 & 2 \end{pmatrix} \\ = -\left( \frac{-10\sqrt{7}}{\sqrt{429}} \right) \left( \sqrt{\frac{3}{1001}} \right) = \frac{10}{143}$$

$$(3, \pm 1|C_0^6|3, \pm 1) = (-1)^{3-1}(3\|C^6\|3) \begin{pmatrix} 3 & 6 & 3 \\ -1 & 0 & 1 \end{pmatrix} \\ = \frac{-10\sqrt{7}}{\sqrt{429}} \left( \frac{5}{2} \sqrt{\frac{3}{1001}} \right) = -\frac{25}{143}$$

$$(3, 0|C_0^6|3, 0) = (-1)^{3-0}(3\|C^6\|3) \begin{pmatrix} 3 & 6 & 3 \\ 0 & 0 & 0 \end{pmatrix} \\ = -\left( \frac{-10\sqrt{7}}{\sqrt{429}} \right) \left( \frac{10}{\sqrt{3003}} \right) = \frac{100}{429}$$

$$(3, +3|C_0^6|3, -3) = (-1)^{3-3}(3\|C^6\|3) \begin{pmatrix} 3 & 6 & 3 \\ -3 & 6 & -3 \end{pmatrix} \\ = \frac{-10\sqrt{7}}{\sqrt{429}} \left( \frac{1}{\sqrt{13}} \right) = -\frac{10}{13} \sqrt{\frac{7}{33}}$$

$$(3, -3|C_{-6}^6|3, 3) = -\frac{10}{13} \sqrt{\frac{7}{33}}$$

The above matrix elements can also be obtained by using the potential in spherical harmonics and the products of spherical harmonics given below [324].

$$\begin{aligned}
 Y_3^0 \cdot Y_3^0 &= \frac{1}{2\sqrt{\pi}} \left[ Y_0^0 + \frac{4}{3\sqrt{5}} Y_2^0 + \frac{6}{11} Y_4^0 + \frac{100}{33\sqrt{13}} Y_6^0 \right] \\
 Y_3^{\pm 1*} \cdot Y_3^{\pm 1} &= \frac{1}{2\sqrt{\pi}} \left[ Y_0^0 + \frac{1}{\sqrt{5}} Y_2^0 + \frac{1}{11} Y_4^0 - \frac{25}{11\sqrt{13}} Y_6^0 \right] \\
 Y_3^{\pm 2*} \cdot Y_3^{\pm 2} &= \frac{1}{2\sqrt{\pi}} \left[ Y_0^0 - \frac{7}{11} Y_4^0 + \frac{10}{11\sqrt{13}} Y_6^0 \right] \\
 Y_3^{\pm 3*} \cdot Y_3^{\pm 3} &= \frac{1}{2\sqrt{\pi}} \left[ Y_0^0 - \frac{\sqrt{5}}{3} Y_2^0 + \frac{3}{11} Y_4^0 - \frac{5}{33\sqrt{13}} Y_6^0 \right] \\
 Y_3^{\pm 3*} \cdot Y_3^{\mp 3} &= \frac{-1}{2\sqrt{\pi}} \frac{10\sqrt{7}}{\sqrt{429}} Y_6^{\mp 6}
 \end{aligned} \tag{8.105}$$

From the orthonormal properties of spherical harmonics, it follows immediately

$$\begin{aligned}
 (\pm 3|V|\pm 3) &= -\frac{1}{6}\sqrt{\frac{5}{\pi}} D_2^0 + \frac{3}{22\sqrt{\pi}} D_4^0 - \frac{5}{66\sqrt{13\pi}} D_6^0 \\
 (\pm 2|V|\pm 2) &= -\frac{7}{22\sqrt{\pi}} D_4^0 + \frac{5}{11\sqrt{13\pi}} D_6^0 \\
 (\pm 1|V|\pm 1) &= \frac{1}{2\sqrt{5\pi}} D_2^0 + \frac{1}{22\sqrt{\pi}} D_4^0 - \frac{25}{22\sqrt{13\pi}} D_6^0 \\
 (0|V|0) &= \frac{2}{3\sqrt{5\pi}} D_2^0 + \frac{3}{11\sqrt{\pi}} D_4^0 + \frac{50}{33\sqrt{13\pi}} D_6^0 \\
 (\pm 3|V|\mp 3) &= -5\sqrt{\frac{7}{429\pi}} D_6^0
 \end{aligned} \tag{8.106}$$

which will yield the same expressions (8.103) when  $D$ 's are substituted by  $B$ 's from (8.101).

The  $|JM\rangle$  functions of  $^3P$  levels and the  $|L, S; M_L, M_S\rangle$  functions of  $^3P$  term that are needed are listed below.

$$\begin{aligned}
 ^3P_2: |2, 2\rangle &= |1, 1; 1, 1\rangle \\
 |2, 1\rangle &= \sqrt{\frac{1}{2}} [|1, 1; 1, 0\rangle + |1, 1; 0, 1\rangle] \\
 |2, 0\rangle &= \sqrt{\frac{1}{6}} [|1, 1; 1, -1\rangle + |1, 1; -1, 1\rangle + 2|1, 1; 0, 0\rangle]
 \end{aligned}$$

$$\begin{aligned}
{}^3P_1: |1, 1\rangle &= \sqrt{\frac{1}{2}}[|1, 1; 1, 0\rangle - |1, 1; 0, 1\rangle] \\
|1, 0\rangle &= \sqrt{\frac{1}{2}}[|1, 1; 1, -1\rangle - |1, 1; -1, 1\rangle] \\
{}^3P_0: |0, 0\rangle &= \sqrt{\frac{1}{3}}[|1, 1; 1, -1\rangle + |1, 1; -1, 1\rangle - |1, 1; 0, 0\rangle] \\
{}^3P: |1, 1; 1, 1\rangle &= \sqrt{\frac{1}{14}}[\sqrt{3}(3^+ - 2^+) - \sqrt{5}(2^+ - 1^+) + \sqrt{6}(1^+ 0^+)] \\
|1, 1; 0, 1\rangle &= \sqrt{\frac{1}{14}}[3(3^+ - 3^+) - 2(2^+ - 2^+) + (1^+ - 1^+)] \\
|1, 1; -1, 1\rangle &= \sqrt{\frac{1}{14}}[\sqrt{3}(2^+ - 3^+) - \sqrt{5}(1^+ - 2^+) + \sqrt{6}(0^+ - 1^+)]
\end{aligned}$$

From the one-electron matrix elements of equation (8.103) and the fact that the crystal field potential is a one-electron operator, we can obtain

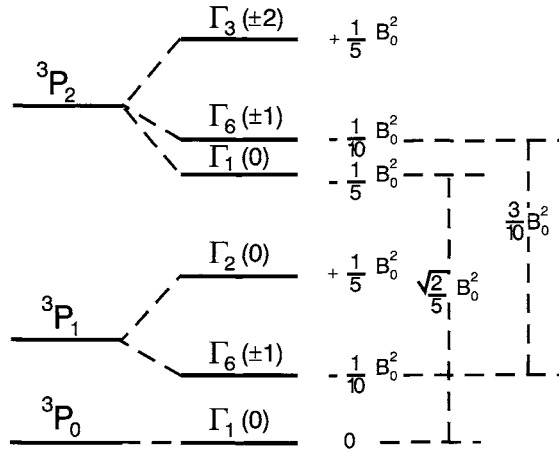
$$\langle(3-2)|V|(3-2)\rangle = \langle 3|V|3\rangle + \langle -2|V|-2\rangle = -\frac{1}{3}B_0^2 - \frac{4}{33}B_0^4 + \frac{25}{429}B_0^6$$

Similarly

$$\begin{aligned}
\langle(2-1)|V|(2-1)\rangle &= \frac{1}{5}B_0^2 - \frac{2}{11}B_0^4 - \frac{15}{143}B_0^6 \\
\langle(10)|V|(10)\rangle &= \frac{7}{15}B_0^2 + \frac{7}{33}B_0^4 + \frac{25}{429}B_0^6 \\
\langle(3-3)|V|(3-3)\rangle &= -\frac{2}{3}B_0^2 + \frac{2}{11}B_0^4 + \frac{10}{429}B_0^6 \\
\langle(2-2)|V|(2-2)\rangle &= -\frac{14}{33}B_0^4 + \frac{20}{143}B_0^6 \\
\langle(1-1)|V|(1-1)\rangle &= \frac{2}{5}B_0^2 + \frac{2}{33}B_0^4 - \frac{50}{143}B_0^6
\end{aligned} \tag{8.107}$$

Hence

$$\begin{aligned}
E|1, 1; 1, 1\rangle &= \frac{1}{14}[3\langle(3-2)|V|(3-2)\rangle + 5\langle(2-1)|V|(2-1)\rangle + 6\langle(10)|V|(10)\rangle] \\
&= \frac{1}{5}B_0^2 = E|1, 1; 1, 0\rangle = E|1, 1; 1, -1\rangle = E|1, 1; -1, 1\rangle \\
&= E|1, 1; -1, 0\rangle = E|1, 1; -1, -1\rangle \\
E|1, 1; 0, 1\rangle &= \frac{1}{14}[9\langle(3-3)|V|(3-3)\rangle + 4\langle(2-2)|V|(2-2)\rangle + \langle(1-1)|V|(1-1)\rangle] \\
&= \frac{-2}{5}B_0^2 = E|1, 1; 0, 0\rangle = E|1, 1; 0, -1\rangle
\end{aligned}$$

Fig. 8.43. Splittings of the  ${}^3P$  multiplet in  $D_{3h}$  crystalline field.

$${}^3P_2: \Gamma_1 = |2, 0\rangle E|2, 0\rangle$$

$$= \frac{1}{6}[E|1, 1; 1, -1\rangle + E|1, 1; -1, 1\rangle + 4E|1, 1; 0, 0\rangle] = -\frac{1}{5}B_0^2$$

$$\Gamma_6 = |2, \pm 1\rangle E|2, 1\rangle = \frac{1}{2}[E|1, 1; 1, 0\rangle + E|1, 1; 0, 1\rangle] = -\frac{1}{10}B_0^2$$

$$\Gamma_3 = |2, \pm 2\rangle E|2, 2\rangle = E|1, 1; 0, 1\rangle = \frac{1}{5}B_0^2$$

$${}^3P_1: \Gamma_2 = |1, 0\rangle E|1, 0\rangle = \frac{1}{2}[E|1, 1; 1, -1\rangle + E|1, 1; -1, 1\rangle] = \frac{1}{5}B_0^2$$

$$\Gamma_6 = |1, \pm 1\rangle E|1, 1\rangle = \frac{1}{2}[E|1, 1; 1, 0\rangle + |1, 1; 0, 1\rangle] = -\frac{1}{10}B_0^2$$

$${}^3P_0: \Gamma_1 = |0, 0\rangle E|0, 0\rangle = \frac{1}{3}[E|1, 1; 1, -1\rangle + E|1, 1; -1, 1\rangle + E|1, 1; 0, 0\rangle] = 0$$

The off-diagonals are:

$$\Gamma_6: \langle {}^3P_1 | {}^3P_2 \rangle = \frac{1}{2}[E|1, 1; 1, 0\rangle - E|1, 1; 0, 1\rangle] = \frac{3}{10}B_0^2$$

$$\Gamma_1: \langle {}^3P_0 | {}^3P_2 \rangle = \frac{1}{3\sqrt{2}}[E|1, 1; 1, -1\rangle + E|1, 1; -1, 1\rangle - 2|1, 1; 0, 0\rangle] = \frac{\sqrt{2}}{5}B_0^2$$

The splittings of the  ${}^3P$  multiplet by the crystal field is depicted in Fig. 8.43.

Note that the center of gravity of each of the spin-orbital levels is maintained, i.e.,  $E(\Gamma_1) + 2E(\Gamma_3) + 2E(\Gamma_6)$  of  ${}^3P_2 = 0$  just as the  $E(\Gamma_2) + 2E(\Gamma_6)$  of  ${}^3P_1 = 0$ .

Although the levels of the  ${}^3P$  term contain only the  $B_0^2$  parameter, both  $B_0^2$  and  $B_0^4$  are effective in splitting the levels of this multiplet because these levels and the levels of

the same representations of the other multiplets are connected by the off-diagonal matrix elements containing the  $B_0^4$  term.

45.3.3.2. *Crystal field energies by the tensor operator method* We may expand the potential in terms of the tensor operators  $C_q^{(K)}$  to give

$$V = \sum_{k,q,i} B_q^K (C_q^K)_i$$

where the summation involving  $i$  is over the two electrons.

For the  $f^2$  configuration the matrix elements of  $V$  are given by

$$\begin{aligned} & (f^2 SLJM | V | f^2 SL'J'M') \\ &= \sum_{k,q} B_q^K (f^2 SLJM | U_q^{(k)} | f^2 SL'J'M') (f \| C^{(K)} \| f) \end{aligned} \quad (8.108a)$$

The matrix elements of the tensor operator  $U_q^{(K)}$  which are diagonal in the spin  $S$  can be rewritten using the Wigner–Eckart theorem with the 3-j symbols and the reduced matrix elements

$$\begin{aligned} & (f^2 SLJM | U_q^{(K)} | f^2 SL'J'M') \\ &= (-1)^{(J-M)} \begin{pmatrix} J & K & J' \\ -M & q & M' \end{pmatrix} (f^2 SLJ \| U^{(K)} \| f^2 SL'J') \end{aligned} \quad (8.108b)$$

where the reduced matrix elements can be further expressed in terms of the doubly reduced matrix elements

$$\begin{aligned} & (f^2 SLJ | U^{(K)} | f^2 SL'J') \\ &= (-1)^{(S+L+J'+K)} [(2J+1)(2J'+1)]^{1/2} \begin{Bmatrix} J & J' & K \\ L' & L & S \end{Bmatrix} \\ & \times (f^2 SL \| U^{(K)} \| f^2 SL') \end{aligned} \quad (8.108c)$$

The doubly reduced matrix elements of  $U^{(K)}$  are tabulated by Nielson and Koster [318]. The necessary matrix elements needed here are given in Table 8.40.

${}^3P_0, {}^3P_1, {}^3P_2$  levels

Since the reduced matrix element  $(f^2 {}^3P \| U^K \| f^2 {}^3P) = 0$  for  $K = 4$  and  $6$ , the only term we need to evaluate is with  $K = 2$ .

Recall

$$(3 \| C^2 \| 3) = -2\sqrt{\frac{7}{15}}, \quad (3 \| C^4 \| 3) = \sqrt{\frac{14}{11}} \quad \text{and} \quad (3 \| C^6 \| 3) = -10\sqrt{\frac{7}{429}}$$

TABLE 8.40  
The doubly reduced matrix elements of  $U^{(K)}$  for  $f^2$ .

$U^2$	$^3P$	$^3F$	$^3H$	$^1S$	$^1D$	$^1G$	$^1I$
	$-\frac{3}{\sqrt{14}}$	$\sqrt{\frac{6}{7}}$	0	0	$\frac{2}{\sqrt{7}}$	0	0
		$-\frac{1}{3}$	$\frac{2}{3}\sqrt{\frac{11}{7}}$		$-\frac{11}{7\sqrt{6}}$	$\frac{2\sqrt{11}}{7}$	0
			$\frac{1}{3}\sqrt{\frac{143}{14}}$			$\frac{3}{7}\sqrt{\frac{3}{11}}$	$\sqrt{\frac{26}{77}}$
							$5\sqrt{\frac{13}{16}}$
$U^4$	$^3P$	$^3F$	$^3H$	$^1S$	$^1D$	$^1G$	$^1I$
	0	$-\sqrt{\frac{11}{21}}$	$\sqrt{\frac{10}{21}}$	0	0	$\sqrt{\frac{4}{7}}$	0
		$-\frac{1}{3}$	$\sqrt{\frac{65}{63}}$		$\frac{2\sqrt{55}}{21}$	$\frac{1}{7}\sqrt{\frac{15}{11}}$	$\frac{1}{3}\sqrt{\frac{130}{77}}$
			$-\sqrt{\frac{52}{63}}$			$-\frac{23\sqrt{13}}{77}$	$\frac{3}{11}\sqrt{\frac{195}{7}}$
							$2\sqrt{\frac{442}{33}}$
$U^6$	$^3P$	$^3F$	$^3H$	$^1S$	$^1D$	$^1G$	$^1I$
	0	0	$-\sqrt{\frac{3}{14}}$	0	0	0	$\frac{2}{\sqrt{7}}$
		$-\frac{1}{3}$	$-\frac{\sqrt{14}}{3}$		0	$\sqrt{\frac{10}{77}}$	$5\sqrt{\frac{5}{66}}$
			$-\frac{1}{3}\sqrt{\frac{85}{7}}$			$\frac{9}{11}\sqrt{\frac{15}{7}}$	$\frac{2\sqrt{34}}{11}$
							$\frac{1}{11}\sqrt{\frac{323}{21}}$

 $^3P_0$ 

$$\begin{aligned}
 \langle f^2\ ^3P_0\ 00 | V | f^2\ ^3P_0\ 00 \rangle &= (3 \| C^2 \| 3) \left[ (-1)^{0-0} \begin{pmatrix} 020 \\ 000 \end{pmatrix} \right] \\
 &\times \left[ (-1)^{1+1+0+2} \cdot 1 \cdot \begin{Bmatrix} 002 \\ 111 \end{Bmatrix} \right] \left( -\frac{3}{\sqrt{14}} \right) B_0^2 = 0
 \end{aligned}$$

 $^3P_1$ 

$$\begin{aligned}
 \langle f^2\ ^3P_1\ 10 | V | f^2\ ^3P_1\ 10 \rangle &= (3 \| C^2 \| 3) \left[ -\begin{pmatrix} 121 \\ 000 \end{pmatrix} \right] \left[ -3 \begin{Bmatrix} 112 \\ 111 \end{Bmatrix} \right] \left( -\frac{3}{\sqrt{14}} \right) B_0^2 \\
 &= -2\sqrt{\frac{7}{15}} \left( -\sqrt{\frac{2}{15}} \right) (-3) \left( \frac{1}{6} \right) \left( -\frac{3}{\sqrt{14}} \right) B_0^2 = \frac{1}{5} B_0^2 \\
 \langle f^2\ ^3P_1\ 11 | V | f^2\ ^3P_1\ 11 \rangle &= (3 \| C^2 \| 3) \left[ \begin{pmatrix} 121 \\ -101 \end{pmatrix} \right] \left[ -3 \begin{Bmatrix} 112 \\ 111 \end{Bmatrix} \right] \left( -\frac{3}{\sqrt{14}} \right) B_0^2 \\
 &= -2\sqrt{\frac{7}{15}} \left( \sqrt{\frac{1}{30}} \right) (-3) \left( \frac{1}{6} \right) \left( -\frac{3}{\sqrt{14}} \right) B_0^2 = -\frac{1}{10} B_0^2
 \end{aligned}$$



${}^3P_2$ 

$$\begin{aligned}
 (f^2 {}^3P_2 20|V|f^2 {}^3P_2 20) &= (3\|C^2\|3) \left[ \begin{pmatrix} 222 \\ 000 \end{pmatrix} \right] \left[ 5 \begin{Bmatrix} 222 \\ 111 \end{Bmatrix} \right] \left( -\frac{3}{\sqrt{14}} \right) B_0^2 \\
 &= -2\sqrt{\frac{7}{15}} \left( -\sqrt{\frac{2}{35}} \right) (5) \left( \frac{1}{10}\sqrt{\frac{7}{3}} \right) \left( -\frac{3}{\sqrt{14}} \right) B_0^2 = -\frac{1}{5} B_0^2 \\
 (f^2 {}^3P_2 21|V|f^2 {}^3P_2 21) &= (3\|C^2\|3) \left[ -\begin{pmatrix} 222 \\ -101 \end{pmatrix} \right] \left[ 5 \begin{Bmatrix} 222 \\ 111 \end{Bmatrix} \right] \left( -\frac{3}{\sqrt{14}} \right) B_0^2 \\
 &= -2\sqrt{\frac{7}{15}} \left( -\sqrt{\frac{1}{70}} \right) (5) \left( \frac{1}{10}\sqrt{\frac{7}{3}} \right) \left( -\frac{3}{\sqrt{14}} \right) B_0^2 = -\frac{1}{10} B_0^2 \\
 (f^2 {}^3P_2 22|V|f^2 {}^3P_2 22) &= (3\|C^2\|3) \left[ \begin{pmatrix} 222 \\ -202 \end{pmatrix} \right] \left[ 5 \begin{Bmatrix} 222 \\ 111 \end{Bmatrix} \right] \left( -\frac{3}{\sqrt{14}} \right) B_0^2 \\
 &= -2\sqrt{\frac{7}{15}} \left( \sqrt{\frac{2}{35}} \right) (5) \left( \frac{1}{10}\sqrt{\frac{7}{3}} \right) \left( -\frac{3}{\sqrt{14}} \right) B_0^2 = \frac{1}{5} B_0^2
 \end{aligned}$$

*Off-diagonals*

$$\begin{aligned}
 (f^2 {}^3P_2 20|V|f^2 {}^3P_0 00) &= (3\|C^2\|3) \left[ \begin{pmatrix} 220 \\ 000 \end{pmatrix} \right] \left[ \sqrt{5} \begin{Bmatrix} 202 \\ 111 \end{Bmatrix} \right] \left( -\frac{3}{\sqrt{14}} \right) B_0^2 \\
 &= -2\sqrt{\frac{7}{15}} \left( \sqrt{\frac{1}{5}} \right) (\sqrt{5}) \left( \sqrt{\frac{1}{15}} \right) \left( -\frac{3}{\sqrt{14}} \right) B_0^2 = \frac{\sqrt{2}}{5} B_0^2 \\
 (f^2 {}^3P_2 21|V|f^2 {}^3P_1 11) &= (3\|C^2\|3) \left[ -\begin{pmatrix} 221 \\ -101 \end{pmatrix} \right] \left[ -\sqrt{15} \begin{Bmatrix} 212 \\ 111 \end{Bmatrix} \right] \left( -\frac{3}{\sqrt{14}} \right) B_0^2 \\
 &= -2\sqrt{\frac{7}{15}} \left( \sqrt{\frac{1}{10}} \right) (-\sqrt{15}) \left( -\frac{1}{2\sqrt{5}} \right) \left( -\frac{3}{\sqrt{14}} \right) B_0^2 = \frac{3}{10} B_0^2
 \end{aligned}$$

These are identical to the matrix elements obtained by the determinantal method.

A note on simplification of calculating matrix elements in this method: equations (8.108a), (8.108b), and (8.108c) can be expressed as

$$\begin{aligned}
 (f^2 SLJM|V|f^2 SL'J'M') &= \sum_{k,q} (-1)^{(J-M)} \begin{pmatrix} J & K & J' \\ -M & q & M' \end{pmatrix} \\
 &\times (f\|C^{(K)}\|f) (-1)^{(S+L+J'+K)} [(2J+1)(2J'+1)]^{1/2} \begin{Bmatrix} J & J' & K \\ L' & L & S \end{Bmatrix} \\
 &\times (f^2 SL\|U^{(K)}\|f^2 SL') B_q^K
 \end{aligned} \tag{8.109}$$

The factor  $(-1)^{(J-M)} \begin{pmatrix} J & K & J' \\ -M & q & M' \end{pmatrix}$  gives the  $M$  dependence of the matrix element and the rest is the same for given  $J$  values of  $LSJ$ -levels. This latter part calculated separately can be called coefficients of the  $B^K$  parameters in the reduced matrix elements  $(J \| V \| J')$ . Once these are available, it is a very simple matter to obtain the  $M$  dependence of the matrix elements.

As an example

$$\begin{aligned} (f^2 {}^3P_2 2 | V | f^2 {}^3P_2 2) &= (f \| C^2 \| f) (-1)^{1+1+2+2} (5) \begin{Bmatrix} 222 \\ 111 \end{Bmatrix} \left( -\frac{3}{\sqrt{14}} B^2 \right) \\ &= -2 \sqrt{\frac{7}{15}} (5) \left( \frac{1}{10} \sqrt{\frac{7}{3}} \right) \left( -\frac{3}{\sqrt{14}} B^2 \right) = \frac{\sqrt{70}}{10} B^2 \end{aligned}$$

so that

$$(f^2 {}^3P_2 22 | V | f^2 {}^3P_2 22) = (-1)^{2-2} \begin{pmatrix} 222 \\ -202 \end{pmatrix} \left( \frac{\sqrt{70}}{10} B_0^2 \right) = \sqrt{\frac{2}{35}} \frac{\sqrt{70}}{10} B_0^2 = \frac{1}{5} B_0^2$$

$$\begin{aligned} (f^2 {}^3P_2 21 | V | f^2 {}^3P_2 21) &= (-1)^{2-1} \begin{pmatrix} 222 \\ -101 \end{pmatrix} \left( \frac{\sqrt{70}}{10} B_0^2 \right) \\ &= - \left( \sqrt{\frac{1}{70}} \right) \left( \frac{\sqrt{70}}{10} B_0^2 \right) = -\frac{1}{10} B_0^2 \end{aligned}$$

and

$$\begin{aligned} (f^2 {}^3P_2 20 | V | f^2 {}^3P_2 20) &= (-1)^{2-0} \begin{pmatrix} 222 \\ 000 \end{pmatrix} \left( \frac{\sqrt{70}}{10} B_0^2 \right) \\ &= \left( -\sqrt{\frac{2}{35}} \right) \left( \frac{\sqrt{70}}{10} B_0^2 \right) = -\frac{1}{5} B_0^2 \end{aligned}$$

We have tabulated these coefficients of  $B^K$  parameters in the reduced matrix elements  $(J \| V \| J')$  separately. They are given in Table 8.41. These tables will be useful in calculating the matrix elements of  $f^2$  configuration in any symmetry in which the crystal field potential has the terms containing the parameters  $B^2$ ,  $B^4$ , and  $B^6$ .

The complete crystal field energy matrices of  $f^2$  in  $D_{3h}$  are presented in Table 8.42.

#### 45.3.4. Checking the correctness of the crystal field matrix elements

Although we have insured the correctness of our crystal field matrix elements by calculating them by two different methods (determinantal and tensor operators), there are three interesting checks that one can make to insure that there are no errors in the calculated crystal field matrix elements<sup>3</sup>.

<sup>3</sup> The checks as well as the diagonalization of the matrices has been carried out by Chamindra Williams at Florida Atlantic University.

TABLE 8.41

Reduced crystal-field matrix elements for  $f^2$  configuration. (These matrices are not symmetric. The matrix elements satisfy the relation  $(J\|V\|J') = (-1)^{(J-J')}(J'\|V\|J)$ . Thus, these tables are to be read with the row label as  $J$  and the column label as  $J'$ .)

(a) Coefficients of $B^2$ in the reduced matrix elements ( $J\ V\ J'$ )									
	$^3P_0$	$^3P_1$	$^3P_2$	$^3F_2$	$^3F_3$	$^3F_4$	$^3H_4$	$^3H_5$	$^3H_6$
$^3P_0$	0	0	$\frac{1}{5}\sqrt{10}$	$-\frac{2}{15}\sqrt{30}$	0	0	0	0	0
$^3P_1$		$-\frac{1}{10}\sqrt{30}$	$-\frac{3}{10}\sqrt{10}$	$-\frac{2}{15}\sqrt{30}$	$-\frac{4}{15}\sqrt{15}$	0	0	0	0
$^3P_2$			$\frac{1}{10}\sqrt{70}$	$-\frac{2}{105}\sqrt{210}$	$-\frac{2}{15}\sqrt{30}$	$-\frac{6}{35}\sqrt{70}$	0	0	0
$^3F_2$				$\frac{4}{105}\sqrt{70}$	$-\frac{1}{15}\sqrt{10}$	$\frac{1}{315}\sqrt{210}$	$-\frac{4}{63}\sqrt{231}$	0	0
$^3F_3$					$\frac{1}{30}\sqrt{105}$	$-\frac{1}{18}\sqrt{15}$	$-\frac{2}{45}\sqrt{66}$	$-\frac{2}{15}\sqrt{66}$	0
$^3F_4$						$\frac{1}{42}\sqrt{385}$	$-\frac{2}{105}\sqrt{14}$	$-\frac{2}{45}\sqrt{66}$	$-\frac{4}{45}\sqrt{195}$
$^3H_4$							$-\frac{52}{825}\sqrt{385}$	$\frac{26}{225}\sqrt{15}$	$-\frac{1}{495}\sqrt{858}$
$^3H_5$								$-\frac{1}{50}\sqrt{4290}$	$\frac{1}{30}\sqrt{182}$
$^3H_6$									$-\frac{1}{66}\sqrt{10010}$
	$^1S_0$	$^1D_2$	$^1G_4$	$^1I_6$					
$^1S_0$	0	$-\frac{4}{15}\sqrt{15}$	0	0					
$^1D_2$		$\frac{11}{105}\sqrt{70}$	$-\frac{4}{105}\sqrt{1155}$	0					
$^1G_4$			$-\frac{6}{385}\sqrt{385}$	$-\frac{2}{165}\sqrt{4290}$					
$^1I_6$				$-\frac{1}{33}\sqrt{10010}$					

(b) Coefficients of $B^4$ in the reduced matrix elements ( $J\ V\ J'$ )									
	$^3P_0$	$^3P_1$	$^3P_2$	$^3F_2$	$^3F_3$	$^3F_4$	$^3H_4$	$^3H_5$	$^3H_6$
$^3P_0$	0	0	0	0	0	$-\frac{1}{3}\sqrt{2}$	$\frac{2}{33}\sqrt{55}$	0	0
$^3P_1$		0	0	0	$\frac{1}{2}$	$\frac{1}{6}\sqrt{15}$	$\frac{2}{33}\sqrt{66}$	$\frac{2}{11}\sqrt{11}$	0
$^3P_2$			0	$-\frac{1}{21}\sqrt{210}$	$-\frac{1}{6}\sqrt{15}$	$-\frac{1}{42}\sqrt{385}$	$\frac{2}{33}\sqrt{14}$	$\frac{2}{33}\sqrt{66}$	$\frac{2}{33}\sqrt{195}$
$^3F_2$				$-\frac{1}{63}\sqrt{70}$	$\frac{1}{9}\sqrt{5}$	$-\frac{1}{231}\sqrt{1155}$	$\frac{26}{231}\sqrt{42}$	$-\frac{13}{99}\sqrt{22}$	$\frac{2}{99}\sqrt{65}$
$^3F_3$					$-\frac{1}{198}\sqrt{154}$	$\frac{1}{66}\sqrt{330}$	$\frac{13}{33}\sqrt{3}$	$\frac{1}{18}\sqrt{143}$	$-\frac{35}{198}\sqrt{13}$
$^3F_4$						$-\frac{1}{54}\sqrt{2002}$	$\frac{1}{77}\sqrt{455}$	$\frac{1}{66}\sqrt{2145}$	$\frac{5}{66}\sqrt{195}$
$^3H_4$							$-\frac{2}{121}\sqrt{2002}$	$\frac{2}{33}\sqrt{78}$	$-\frac{2}{363}\sqrt{858}$
$^3H_5$								$-\frac{4}{99}\sqrt{286}$	$\frac{4}{99}\sqrt{182}$
$^3H_6$									$-\frac{8}{1089}\sqrt{17017}$
	$^1S_0$	$^1D_2$	$^1G_4$	$^1I_6$					
$^1S_0$	0	0	$\frac{2}{11}\sqrt{22}$	0					
$^1D_2$		$\frac{2}{21}\sqrt{70}$	$\frac{1}{77}\sqrt{210}$	$\frac{2}{33}\sqrt{65}$					
$^1G_4$			$-\frac{23}{847}\sqrt{2002}$	$\frac{3}{121}\sqrt{4290}$					
$^1I_6$				$\frac{4}{363}\sqrt{17017}$					

TABLE 8.41  
(Continued.)

(c) Coefficients of $B^6$ in the reduced matrix elements ( $J \  V \  J'$ )									
	$^3P_0$	$^3P_1$	$^3P_2$	$^3F_2$	$^3F_3$	$^3F_4$	$^3H_4$	$^3H_5$	$^3H_6$
$^3P_0$	0	0	0	0	0	0	0	0	$\frac{5}{429}\sqrt{858}$
$^3P_1$		0	0	0	0	0	0	$-\frac{5}{858}\sqrt{4290}$	$-\frac{5}{858}\sqrt{6006}$
$^3P_2$			0	0	0	0	$\frac{15}{143}\sqrt{26}$	$\frac{5}{858}\sqrt{6006}$	$\frac{5}{858}\sqrt{2730}$
$^3F_2$				0	0	$\frac{10}{1287}\sqrt{2145}$	$\frac{70}{1287}\sqrt{78}$	$-\frac{10}{429}\sqrt{2002}$	$\frac{10}{429}\sqrt{910}$
$^3F_3$					$-\frac{5}{858}\sqrt{3003}$	$-\frac{35}{2574}\sqrt{429}$	$\frac{70}{1287}\sqrt{390}$	0	$-\frac{140}{429}\sqrt{13}$
$^3F_4$						$\frac{5}{858}\sqrt{715}$	$\frac{70}{429}\sqrt{26}$	$\frac{20}{1287}\sqrt{6006}$	$\frac{20}{1287}\sqrt{4641}$
$^3H_4$							$\frac{136}{4719}\sqrt{715}$	$-\frac{34}{1287}\sqrt{1365}$	$\frac{10}{14157}\sqrt{510510}$
$^3H_5$								$\frac{1}{429}\sqrt{36465}$	$-\frac{5}{429}\sqrt{7735}$
$^3H_6$									$\frac{25}{4719}\sqrt{46189}$
	$^1S_0$	$^1D_2$	$^1G_4$	$^1I_6$					
$^1S_0$	0	0	0	$-\frac{20}{429}\sqrt{429}$					
$^1D_2$		0	$-\frac{10}{429}\sqrt{390}$	$-\frac{25}{429}\sqrt{910}$					
$^1G_4$			$-\frac{90}{1573}\sqrt{715}$	$-\frac{20}{4719}\sqrt{102102}$					
$^1I_6$				$-\frac{10}{4719}\sqrt{46189}$					

- (i) In the limit of zero spin-orbit interaction, i.e.,  $\zeta = 0$ ,  $f^2$  in  $D_{3h}$  symmetry gives rise to 33 Stark levels. Nineteen of these are the same levels from singlets. However, the 42 Stark levels of triplets become 14 if  $\zeta = 0$ . Thus, diagonalizing the matrices with a given set of  $F_K$  and  $B_q^K$  parameters and setting  $\zeta = 0$  should result in 33 eigenvalues. In addition, the 14 eigenvalues of the triplets can be independently checked by constructing the crystal field energy matrices of  $^3H$ ,  $^3F$ , and  $^3P$  terms in  $D_{3h}$  symmetry and diagonalizing them with the same set of parameters.
- (ii) In the limit of zero electron repulsions, i.e.,  $F_K = 0$ ,  $f^2$  in  $D_{3h}$  symmetry gives rise to 28 Stark levels which is the number obtained by assigning the two electrons of  $f^2$  to the seven Stark levels of  $f^1$  in  $D_{3h}$ . Thus, diagonalizing the matrices with a given set of  $\zeta$  and  $B_q^K$  parameters and setting the  $F_K = 0$  should result in 28 eigenvalues.
- (iii) Finally, in the limit of zero spin-orbit interaction and electron repulsions, i.e.,  $\zeta = 0$ ,  $F_K = 0$ ,  $f^2$  in  $D_{3h}$  gives rise to 15 Stark levels which is the number obtained by assigning the two electrons of  $f^2$  to the five Stark levels of  $f^1$  in  $D_{3h}$ . Thus diagonalizing the matrices with a given set of  $B_q^K$  parameters and setting  $\zeta = 0$ ,  $F_K = 0$  should result in 15 eigenvalues. In addition, these eigenvalues should agree with the values calculated directly for the 15 levels from the energy expressions.

TABLE 8.42

The energy matrices of  $f^2$  configuration in  $D_{3h}$  crystalline fields. (The capital letters, S, P, D, F, G, H, I stand for term energies.  $z = \zeta$ ,  $a = B_0^2$ ,  $b = B_0^4$ ,  $c = B_0^6$ ,  $d = B_6^6$ .)

(a) $\Gamma_1$ matrix				
	${}^3P_0$	${}^3P_2$	${}^3F_2$	${}^3F_4$
${}^3P_0$	$P - z$	$\frac{1}{5}\sqrt{2}a$	$-\frac{2}{15}\sqrt{6}a$	$-\frac{1}{9}\sqrt{2}b$
${}^3P_2$		$P + \frac{1}{2}z - \frac{1}{5}a$	$\frac{2}{21}\sqrt{3}(\frac{2}{5}a - b)$	$-\frac{12}{35}a + \frac{5}{63}b$
${}^3F_2$			$F - 2z - \frac{8}{105}a - \frac{2}{63}b$	$\frac{2}{7}\sqrt{3}(\frac{1}{45}a + \frac{5}{99}b + \frac{175}{1287}c)$
${}^3F_4$				$F + \frac{3}{2}z - \frac{5}{63}a - \frac{3}{77}b - \frac{25}{1287}c$
${}^3H_4$				
${}^3H_6^1$				
${}^3H_6^2$				
${}^1I_6^1$				
${}^1I_6^2$				
${}^1G_4$				
${}^1D_2$				
${}^1S_0$				

TABLE 8.42  
(Continued.)

	${}^3\text{H}_4$	${}^3\text{H}_6^1$	${}^3\text{H}_6^2$	${}^1\text{I}_6^1$
${}^3\text{P}_0$	$\frac{2}{99}\sqrt{55}b$	$\frac{5}{429}\sqrt{33}(c + \sqrt{2}d)$	$\frac{5}{429}\sqrt{33}(-c + \sqrt{2}d)$	0
${}^3\text{P}_2$	$\frac{1}{11}\sqrt{110}(-\frac{4}{99}b + \frac{15}{143}c)$	$\frac{5}{726}\sqrt{66}(2b - \frac{7}{13}c) + \frac{5}{429}\sqrt{33}d$	$-\frac{5}{726}\sqrt{66}(2b - \frac{7}{13}c) + \frac{5}{429}\sqrt{33}d$	0
${}^3\text{F}_2$	$\frac{1}{33}\sqrt{330}(-\frac{44}{105}a - \frac{52}{231}b + \frac{70}{429}c)$	$\frac{5}{121}\sqrt{22}(\frac{1}{9}b - \frac{14}{39}c) + \frac{20}{429}\sqrt{11}d$	$-\frac{5}{121}\sqrt{22}(\frac{1}{9}b - \frac{14}{39}c) + \frac{20}{429}\sqrt{11}d$	0
${}^3\text{F}_4$	$\frac{1}{11}\sqrt{110}(\frac{4}{315}a + \frac{3}{77}b - \frac{140}{1287}c)$	$-\frac{1}{198}\sqrt{66}(4a + \frac{25}{11}b - \frac{280}{143}c) + \frac{10}{429}\sqrt{33}d$	$\frac{1}{198}\sqrt{66}(4a + \frac{25}{11}b - \frac{280}{143}c) + \frac{10}{429}\sqrt{33}d$	0
${}^3\text{H}_4$	$H - 3z + \frac{104}{495}a - \frac{12}{121}b - \frac{1360}{14157}c$	$-\frac{1}{99}\sqrt{15}(\frac{1}{5}a - \frac{4}{11}b - \frac{140}{143}c) + \frac{5}{429}\sqrt{30}d$	$\frac{1}{99}\sqrt{15}(\frac{1}{5}a - \frac{4}{11}b - \frac{140}{143}c) + \frac{5}{429}\sqrt{30}d$	0
${}^3\text{H}_6^1$		$H + \frac{5}{2}z - \frac{2}{33}a - \frac{122}{1089}b - \frac{75}{3146}c + \frac{25}{429}\sqrt{2}d$	$-\frac{3}{11}a - \frac{10}{1089}b + \frac{775}{9438}c$	$\frac{1}{2}\sqrt{6}z$
${}^3\text{H}_6^2$			$H + \frac{5}{2}z - \frac{2}{33}a - \frac{122}{1089}b - \frac{75}{3146}c - \frac{25}{429}\sqrt{2}d$	0
${}^1\text{I}_6^1$				$I - \frac{4}{33}a + \frac{61}{363}b + \frac{15}{1573}c - \frac{10}{429}\sqrt{2}d$
${}^1\text{I}_6^2$				
${}^1\text{G}_4$				
${}^1\text{D}_2$				
${}^1\text{S}_0$				

TABLE 8.42  
(Continued.)

	${}^1I_6^2$	${}^1G_4$	${}^1D_2$	${}^1S_0$
${}^3P_0$	0	0	0	$-2\sqrt{3}z$
${}^3P_2$	0	0	$\frac{3}{2}\sqrt{2}z$	0
${}^3F_2$	0	0	$-\sqrt{6}z$	0
${}^3F_4$	0	$\frac{1}{3}\sqrt{33}z$	0	0
${}^3H_4$	0	$-\frac{1}{3}\sqrt{30}z$	0	0
${}^3H_6^1$	0	0	0	0
${}^3H_6^2$	$\frac{1}{2}\sqrt{6}z$	0	0	0
${}^1I_6^1$	$-\frac{6}{11}a + \frac{5}{363}b - \frac{155}{4719}c$	$-\frac{2}{11}\sqrt{3}(\frac{1}{3}a + \frac{5}{11}b + \frac{140}{429}c) - \frac{10}{143}\sqrt{6}d$	$\frac{5}{4719}\sqrt{2}\sqrt{11}(13b + 35c) - \frac{50}{429}\sqrt{11}d$	$-\frac{10}{429}\sqrt{66}c - \frac{20}{429}\sqrt{33}d$
${}^1I_6^2$	$I - \frac{4}{33}a + \frac{61}{363}b + \frac{15}{1573}c + \frac{10}{429}\sqrt{2}d$	$\frac{2}{11}\sqrt{3}(\frac{1}{3}a + \frac{5}{11}b + \frac{140}{429}c) - \frac{10}{143}\sqrt{6}d$	$-\frac{5}{4719}\sqrt{2}\sqrt{11}(13b + 35c) - \frac{50}{429}\sqrt{11}d$	$\frac{10}{429}\sqrt{66}c - \frac{20}{429}\sqrt{33}d$
${}^1G_4$		$G + \frac{4}{77}a - \frac{138}{847}b + \frac{300}{1573}c$	$-\frac{2}{33}\sqrt{66}(\frac{22}{35}a + \frac{5}{77}b + \frac{25}{143}c)$	$\frac{2}{33}\sqrt{22}b$
${}^1D_2$			$D - \frac{22}{105}a + \frac{4}{21}b$	$-\frac{4}{15}\sqrt{3}a$
${}^1S_0$				$S$

TABLE 8.42  
(Continued.)

(b) $\Gamma_2$ matrix					
	${}^3P_1$	${}^3F_3$	${}^3H_5$	${}^3H_6$	${}^1I_6$
${}^3P_1$	$P - \frac{1}{2}z + \frac{1}{5}a$	$-\frac{1}{7}\sqrt{7}\left(\frac{4}{5}a + \frac{1}{3}b\right)$	$\frac{1}{11}\sqrt{5}\left(\frac{2}{3}b + \frac{5}{13}c\right)$	$-\frac{5}{143}\sqrt{22}d$	0
${}^3F_3$		$F - \frac{1}{2}z - \frac{1}{15}a - \frac{1}{99}b + \frac{25}{429}c$	$-\frac{4}{105}\sqrt{35}a - \frac{1}{63}\sqrt{35}b$	$-\frac{10}{429}\sqrt{154}d$	0
${}^3H_5$			$H - \frac{1}{2}z + \frac{1}{3}a - \frac{8}{99}b - \frac{20}{429}c$	$-\frac{5}{429}\sqrt{110}d$	0
${}^3H_6$				$H + \frac{5}{2}z - \frac{1}{3}a - \frac{4}{33}b + \frac{25}{429}c$	$\frac{1}{2}\sqrt{6}z$
${}^1I_6$					$I - \frac{2}{3}a + \frac{2}{11}b - \frac{10}{429}c$
(c) $\Gamma_3$ matrix					
	${}^3P_2$	${}^3F_2$	${}^3F_3$	${}^3F_4^1$	
${}^3P_2$	$P + \frac{1}{2}z + \frac{1}{3}a$	$-\frac{1}{21}\sqrt{3}\left(\frac{4}{5}a + \frac{1}{3}b\right)$	$\frac{1}{21}\sqrt{105}\left(\frac{2}{5}a + \frac{1}{6}b\right)$	$-\frac{1}{14}\sqrt{15}\left(\frac{4}{5}a + \frac{1}{3}b\right)$	
${}^3F_2$		$F - 2z + \frac{8}{105}a - \frac{1}{189}b$	$\frac{1}{7}\sqrt{35}\left(\frac{1}{15}a - \frac{1}{27}b\right)$	$\frac{1}{14}\sqrt{5}\left(\frac{2}{45}a - \frac{2}{11}b + \frac{140}{1287}c\right)$	
${}^3F_3$			$F - \frac{1}{2}z + \frac{7}{594}b + \frac{5}{286}c$	$\frac{1}{14}\sqrt{7}\left(\frac{2}{9}a + \frac{5}{33}b - \frac{245}{1287}c\right)$	
${}^3F_4^1$				$F + \frac{3}{2}z - \frac{2}{63}a + \frac{1}{42}b + \frac{5}{234}c$	
${}^3F_4^2$					
${}^3H_4^1$					
${}^3H_4^2$					
${}^3H_5^1$					
${}^3H_5^2$					
${}^3H_6^1$					
${}^3H_6^2$					
${}^1I_6^1$					
${}^1I_6^2$					
${}^1G_4^1$					
${}^1G_4^2$					
${}^1D_2$					



TABLE 8.42  
(Continued.)

	${}^3F_4^2$	${}^3H_4^1$	${}^3H_4^2$	${}^3H_5^1$
${}^3P_2$	0	$\frac{1}{33}\sqrt{66}\left(\frac{2}{11}b + \frac{15}{143}c\right)$	$\frac{15}{143}\sqrt{2}d$	$-\frac{1}{33}\sqrt{21}\left(\frac{2}{3}b + \frac{5}{13}c\right)$
${}^3F_2$	$\frac{10}{1287}\sqrt{165}d$	$\frac{1}{11}\sqrt{22}\left(-\frac{22}{63}a + \frac{26}{77}b + \frac{70}{1287}c\right)$	$\frac{70}{1287}\sqrt{6}d$	$\frac{1}{33}\sqrt{7}\left(\frac{13}{9}b + \frac{20}{13}c\right)$
${}^3F_3$	$\frac{5}{1287}\sqrt{231}d$	$\frac{1}{11}\sqrt{770}\left(\frac{44}{1575}a + \frac{13}{462}b + \frac{70}{1287}c\right)$	$-\frac{20}{1287}\sqrt{210}d$	$\frac{1}{5}\sqrt{5}\left(-\frac{2}{5}a + \frac{5}{54}b\right)$
${}^3F_4^1$	$\frac{5}{1287}\sqrt{33}d$	$\frac{1}{11}\sqrt{110}\left(\frac{8}{1575}a - \frac{1}{42}b + \frac{14}{117}c\right)$	$\frac{28}{1287}\sqrt{30}d$	$\frac{1}{15}\sqrt{35}\left(\frac{2}{15}a + \frac{5}{22}b - \frac{40}{429}c\right)$
${}^3F_4^2$	$F + \frac{3}{2}z + \frac{1}{9}a - \frac{1}{33}b + \frac{5}{1287}c$	$\frac{28}{1287}\sqrt{30}d$	$\frac{1}{11}\sqrt{110}\left(-\frac{4}{225}a + \frac{1}{33}b + \frac{28}{1287}c\right)$	$\frac{4}{1287}\sqrt{1155}d$
${}^3H_4^1$		$H - 3z + \frac{208}{2475}a + \frac{2}{33}b + \frac{136}{1287}c$	$\frac{272}{14157}\sqrt{33}d$	$\frac{1}{33}\sqrt{154}\left(-\frac{13}{75}a + \frac{2}{11}b + \frac{34}{429}c\right)$
${}^3H_4^2$			$H - 3z - \frac{728}{2475}a - \frac{28}{363}b + \frac{272}{14157}c$	$-\frac{17}{1287}\sqrt{42}d$
${}^3H_5^1$				$H - \frac{1}{2}z + \frac{3}{25}a + \frac{4}{297}b + \frac{6}{143}c$
${}^3H_5^2$				
${}^3H_6^1$				
${}^3H_6^2$				
${}^1I_6^1$				
${}^1I_6^2$				
${}^1G_4^1$				
${}^1G_4^2$				
${}^1D_2$				

TABLE 8.42  
(Continued.)

	${}^3\text{H}_5^2$	${}^3\text{H}_6^1$	${}^3\text{H}_6^2$	${}^1\text{I}_6^1$
${}^3\text{P}_2$	$-\frac{5}{429}\sqrt{33}d$	$\frac{1}{363}\sqrt{2310}(\frac{2}{3}b + \frac{5}{13}c)$	$\frac{5}{429}\sqrt{3}d$	0
${}^3\text{F}_2$	$\frac{20}{429}\sqrt{11}d$	$\frac{2}{363}\sqrt{770}(\frac{1}{9}b + \frac{10}{13}c)$	$\frac{20}{429}d$	0
${}^3\text{F}_3$	0	$\frac{70}{363}\sqrt{22}(\frac{1}{9}b - \frac{1}{13}c)$	$\frac{10}{429}\sqrt{35}d$	0
${}^3\text{F}_4^1$	$-\frac{4}{143}\sqrt{55}d$	$-\frac{2}{33}\sqrt{154}(\frac{4}{15}a + \frac{5}{39}c)$	$\frac{10}{143}\sqrt{5}d$	0
${}^3\text{F}_4^2$	$-\frac{4}{225}\sqrt{3}\sqrt{5}a + \frac{1}{33}\sqrt{3}\sqrt{5}b + \frac{28}{1287}\sqrt{5}\sqrt{3}c$	$\frac{10}{1287}\sqrt{42}d$	$\frac{1}{33}\sqrt{165}(-\frac{4}{15}a + \frac{5}{11}b + \frac{140}{429}c)$	0
${}^3\text{H}_4^1$	$\frac{17}{143}\sqrt{2}d$	$-\frac{1}{33}\sqrt{35}(\frac{4}{75}a + \frac{10}{39}c)$	$\frac{25}{1573}\sqrt{22}d$	0
${}^3\text{H}_4^2$	$\frac{26}{2475}\sqrt{11}\sqrt{2}\sqrt{3}a + \frac{4}{363}\sqrt{11}\sqrt{2}\sqrt{3}b - \frac{119}{14157}\sqrt{11}\sqrt{2}\sqrt{3}c$	$\frac{10}{14157}\sqrt{1155}d$	$\frac{1}{33}\sqrt{6}(-\frac{1}{15}a - \frac{4}{11}b + \frac{350}{429}c)$	0
${}^3\text{H}_5^1$	$\frac{1}{143}\sqrt{77}d$	$\frac{1}{363}\sqrt{110}(-\frac{44}{25}a + \frac{20}{9}b + \frac{35}{13}c)$	$\frac{25}{429}\sqrt{7}d$	0
${}^3\text{H}_5^2$	$H - \frac{1}{2}z - \frac{3}{25}a + \frac{8}{99}b - \frac{8}{143}c$	$-\frac{5}{429}\sqrt{70}d$	$\frac{4}{165}\sqrt{11}a + \frac{4}{1089}\sqrt{11}b + \frac{175}{4719}\sqrt{11}c$	0
${}^3\text{H}_6^1$		$H + \frac{5}{2}z + \frac{5}{33}a - \frac{4}{297}b + \frac{25}{429}c$	$\frac{25}{4719}\sqrt{770}d$	$\frac{1}{2}\sqrt{6}z$
${}^3\text{H}_6^2$			$H + \frac{5}{2}z - \frac{1}{33}a + \frac{128}{1089}b + \frac{100}{4719}c$	0
${}^1\text{I}_6^1$				$I + \frac{10}{33}a + \frac{2}{99}b - \frac{10}{429}c$
${}^1\text{I}_6^2$				
${}^1\text{G}_4^1$				
${}^1\text{G}_4^2$				
${}^1\text{D}_2$				

TABLE 8.42  
(Continued.)

	${}^1I_6^2$	${}^1G_4^1$	${}^1G_4^2$	${}^1D_2$
${}^3P_2$	0	0	0	$\frac{3}{2}\sqrt{2}z$
${}^3F_2$	0	0	0	$-\sqrt{6}z$
${}^3F_3$	0	0	0	0
${}^3F_4^1$	0	$\frac{1}{3}\sqrt{33}z$	0	0
${}^3F_4^2$	0	0	$\frac{1}{3}\sqrt{33}z$	0
${}^3H_4^1$	0	$-\frac{1}{3}\sqrt{30}z$	0	0
${}^3H_4^2$	0	0	$-\frac{1}{3}\sqrt{30}z$	0
${}^3H_5^1$	0	0	0	0
${}^3H_5^2$	0	0	0	0
${}^3H_6^1$	0	0	0	0
${}^3H_6^2$	$\frac{1}{2}\sqrt{6}z$	0	0	0
${}^1I_6^1$	$-\frac{10}{4719}\sqrt{770}d$	$\frac{4}{33}\sqrt{7}\left(-\frac{2}{5}a + \frac{5}{13}c\right)$	$-\frac{20}{4719}\sqrt{231}d$	$\frac{2}{363}\sqrt{770}\left(\frac{1}{3}b - \frac{25}{13}c\right)$
${}^1I_6^2$	$I - \frac{2}{33}a - \frac{64}{363}b - \frac{40}{4719}c$	$-\frac{30}{1573}\sqrt{110}d$	$\frac{2}{11}\sqrt{30}\left(-\frac{1}{15}a + \frac{3}{11}b - \frac{70}{429}c\right)$	$-\frac{50}{429}d$
${}^1G_4^1$		$G + \frac{8}{385}a + \frac{23}{231}b - \frac{30}{143}c$	$-\frac{60}{1573}\sqrt{33}d$	$\frac{1}{11}\sqrt{110}\left(-\frac{22}{105}a + \frac{3}{77}b - \frac{10}{429}c\right)$
${}^1G_4^2$			$G - \frac{4}{55}a - \frac{46}{363}b - \frac{60}{1573}c$	$-\frac{10}{429}\sqrt{30}d$
${}^1D_2$				$D + \frac{22}{105}a + \frac{2}{63}b$

TABLE 8.42

(Continued.)

(d) $\Gamma_4$ matrix			
	${}^3F_3$	${}^3F_4$	${}^3H_4$
${}^3F_3$	$F - \frac{1}{2}z + \frac{1}{12}a - \frac{1}{198}b - \frac{5}{1716}c - \frac{5}{858}\sqrt{231}d$	$\frac{1}{4}\sqrt{3}\left(\frac{1}{9}a - \frac{10}{99}b + \frac{35}{1287}c\right) - \frac{5}{858}\sqrt{77}d$	$\frac{1}{33}\sqrt{330}\left(\frac{11}{75}a - \frac{13}{66}b - \frac{35}{429}c\right) + \frac{10}{429}\sqrt{70}d$
${}^3F_4$		$F + \frac{3}{2}z + \frac{1}{36}a + \frac{1}{22}b - \frac{85}{5148}c - \frac{5}{2574}\sqrt{231}d$	$-\frac{1}{11}\sqrt{110}\left(\frac{1}{225}a + \frac{1}{22}b + \frac{119}{1287}c\right) - \frac{14}{1287}\sqrt{210}d$
${}^3H_4$			$H - 3z - \frac{182}{2475}a + \frac{14}{121}b - \frac{1156}{14157}c - \frac{136}{14157}\sqrt{231}d$
${}^3H_5$			
${}^3H_6$			
${}^1I_6$			
${}^1G_4$			
	${}^3H_5$	${}^3H_6$	
${}^3F_3$	$\frac{1}{15}\sqrt{5}\left(-\frac{4}{5}a + \frac{5}{6}b\right)$	$\frac{35}{363}\sqrt{33}\left(\frac{1}{6}b + \frac{4}{13}c\right) - \frac{10}{429}\sqrt{7}d$	
${}^3F_4$	$\frac{1}{15}\sqrt{15}\left(\frac{4}{15}a + \frac{5}{66}b + \frac{280}{429}c\right) - \frac{4}{429}\sqrt{385}d$	$\frac{1}{33}\sqrt{11}\left(-\frac{8}{5}a + \frac{25}{22}b - \frac{140}{143}c\right) - \frac{10}{429}\sqrt{21}d$	
${}^3H_4$	$\frac{2}{99}\sqrt{66}\left(-\frac{13}{25}a + \frac{1}{11}b - \frac{119}{143}c\right) + \frac{17}{429}\sqrt{14}d$	$-\frac{2}{11}\sqrt{10}\left(\frac{1}{75}a + \frac{1}{33}b + \frac{35}{429}c\right) - \frac{5}{4719}\sqrt{2310}d$	
${}^3H_5$	$H - \frac{1}{2}z + \frac{1}{50}a + \frac{8}{99}b + \frac{29}{858}c + \frac{2}{429}\sqrt{231}d$	$\frac{1}{11}\sqrt{165}\left(-\frac{3}{50}a + \frac{4}{99}b - \frac{35}{858}c\right) - \frac{10}{429}\sqrt{35}d$	
${}^3H_6$		$H + \frac{5}{2}z + \frac{5}{66}a + \frac{8}{121}b + \frac{1075}{9438}c - \frac{50}{4719}\sqrt{231}d$	
${}^1I_6$			
${}^1G_4$			
	${}^1I_6$	${}^1G_4$	
${}^3F_3$	0	0	
${}^3F_4$	0	$\frac{1}{3}\sqrt{33}z$	
${}^3H_4$	0	$-\frac{1}{3}\sqrt{30}z$	
${}^3H_5$	0	0	
${}^3H_6$	$\frac{1}{2}\sqrt{6}z$	0	
${}^1I_6$	$I + \frac{5}{33}a - \frac{12}{121}b - \frac{215}{4719}c + \frac{20}{4719}\sqrt{231}d$	$\frac{1}{11}\sqrt{2}\left(-\frac{4}{5}a + \frac{15}{11}b + \frac{140}{143}c\right) + \frac{10}{1573}\sqrt{462}d$	
${}^1G_4$		$G - \frac{1}{55}a + \frac{23}{121}b + \frac{255}{1573}c + \frac{30}{1573}\sqrt{231}d$	

TABLE 8.42  
(Continued.)

(e) $\Gamma_5$ matrix			
	${}^3F_3$	${}^3F_4$	${}^3H_4$
${}^3F_3$	$F - \frac{1}{2}z + \frac{1}{12}a - \frac{1}{198}b - \frac{5}{1716}c + \frac{5}{858}\sqrt{231}d$	$\frac{1}{4}\sqrt{3}\left(\frac{1}{9}a - \frac{10}{99}b + \frac{35}{1287}c\right) + \frac{5}{858}\sqrt{77}d$	$\frac{1}{33}\sqrt{330}\left(\frac{11}{75}a - \frac{13}{66}b - \frac{35}{429}c\right) - \frac{10}{429}\sqrt{70}d$
${}^3F_4$		$F + \frac{3}{2}z + \frac{1}{36}a + \frac{1}{22}b - \frac{85}{5148}c + \frac{5}{2574}\sqrt{231}d$	$-\frac{1}{11}\sqrt{110}\left(\frac{1}{225}a + \frac{1}{22}b + \frac{119}{1287}c\right) + \frac{14}{1287}\sqrt{210}d$
${}^3H_4$			$H - 3z - \frac{182}{2475}a + \frac{14}{121}b - \frac{1156}{14157}c + \frac{136}{14157}\sqrt{231}d$
${}^3H_5$			
${}^3H_6$			
${}^1I_6$			
${}^1G_4$			
	${}^3H_5$	${}^3H_6$	
${}^3F_3$	$\frac{1}{15}\sqrt{5}\left(-\frac{4}{5}a + \frac{5}{6}b\right)$	$\frac{35}{363}\sqrt{33}\left(\frac{1}{6}b + \frac{4}{13}c\right) + \frac{10}{429}\sqrt{7}d$	
${}^3F_4$	$\frac{1}{15}\sqrt{15}\left(\frac{4}{15}a + \frac{5}{66}b + \frac{280}{429}c\right) + \frac{4}{429}\sqrt{385}d$	$\frac{1}{33}\sqrt{11}\left(-\frac{8}{5}a + \frac{25}{22}b - \frac{140}{143}c\right) + \frac{10}{429}\sqrt{21}d$	
${}^3H_4$	$\frac{2}{99}\sqrt{66}\left(-\frac{13}{25}a + \frac{1}{11}b - \frac{119}{143}c\right) - \frac{17}{429}\sqrt{14}d$	$-\frac{2}{11}\sqrt{10}\left(\frac{1}{75}a + \frac{1}{33}b + \frac{35}{429}c\right) + \frac{5}{4719}\sqrt{2310}d$	
${}^3H_5$	$H - \frac{1}{2}z + \frac{1}{50}a + \frac{8}{99}b + \frac{29}{858}c - \frac{2}{429}\sqrt{231}d$	$\frac{1}{11}\sqrt{165}\left(-\frac{3}{50}a + \frac{4}{99}b - \frac{35}{858}c\right) + \frac{10}{429}\sqrt{35}d$	
${}^3H_6$		$H + \frac{5}{2}z + \frac{5}{66}a + \frac{8}{121}b + \frac{1075}{9438}c + \frac{50}{4719}\sqrt{231}d$	
${}^1I_6$			
${}^1G_4$			
	${}^1I_6$	${}^1G_4$	
${}^3F_3$	0	0	
${}^3F_4$	0	$\frac{1}{3}\sqrt{33}z$	
${}^3H_4$	0	$-\frac{1}{3}\sqrt{30}z$	
${}^3H_5$	0	0	
${}^3H_6$	$\frac{1}{2}\sqrt{6}z$	0	
${}^1I_6$	$I + \frac{5}{33}a - \frac{12}{121}b - \frac{215}{4719}c - \frac{20}{4719}\sqrt{231}d$	$\frac{1}{11}\sqrt{2}\left(-\frac{4}{5}a + \frac{15}{11}b + \frac{140}{143}c\right) - \frac{10}{1573}\sqrt{462}d$	
${}^1G_4$		$G - \frac{1}{55}a + \frac{23}{121}b + \frac{255}{1573}c - \frac{30}{1573}\sqrt{231}d$	

TABLE 8.42  
(Continued.)

(f) $\Gamma_6$ matrix	${}^3P_1$	${}^3P_2$	${}^3F_2$	${}^3F_3$	${}^3F_4$
${}^3P_1$	$P - \frac{1}{2}z - \frac{1}{10}a$	$\frac{3}{10}a$	$\frac{2}{15}\sqrt{3}a$	$\frac{1}{42}\sqrt{42}(-\frac{8}{5}a + \frac{1}{2}b)$	$-\frac{1}{36}\sqrt{30}b$
${}^3P_2$		$P + \frac{1}{2}z - \frac{1}{10}a$	$\frac{1}{21}\sqrt{3}(\frac{2}{5}a + \frac{4}{3}b)$	$\frac{1}{42}\sqrt{42}(\frac{4}{5}a - \frac{5}{6}b)$	$\frac{1}{7}\sqrt{30}(-\frac{2}{5}a + \frac{1}{36}b)$
${}^3F_2$			$F - 2z - \frac{4}{105}a + \frac{4}{189}b$	$\frac{1}{14}\sqrt{14}(\frac{2}{15}a + \frac{5}{27}b)$	$\frac{1}{14}\sqrt{10}(\frac{2}{45}a + \frac{1}{33}b - \frac{280}{1287}c)$
${}^3F_3$				$F - \frac{1}{2}z - \frac{1}{20}a - \frac{1}{594}b - \frac{25}{572}c$	$\frac{1}{28}\sqrt{35}(\frac{1}{9}a + \frac{2}{11}b + \frac{245}{1287}c)$
${}^3F_4$					$F + \frac{3}{2}z - \frac{17}{252}a - \frac{3}{154}b + \frac{5}{5148}c$
${}^3H_4$					
${}^3H_5^1$					
${}^3H_5^2$					
${}^3H_6^1$					
${}^3H_6^2$					
${}^1I_6^1$					
${}^1I_6^2$					
${}^1G_4$					
${}^1D_2$					

TABLE 8.42  
(Continued.)

	${}^3\text{H}_4$	${}^3\text{H}_5^1$	${}^3\text{H}_5^2$	${}^3\text{H}_6^1$
${}^3\text{P}_1$	$-\frac{2}{99}\sqrt{33}b$	$\frac{1}{33}\sqrt{3}(2b - \frac{25}{26}c)$	$-\frac{5}{858}\sqrt{330}d$	$\frac{5}{858}\sqrt{231}c$
${}^3\text{P}_2$	$-\frac{2}{33}\sqrt{33}(\frac{1}{33}b + \frac{30}{143}c)$	$\frac{1}{33}\sqrt{3}(-\frac{4}{3}b + \frac{35}{26}c)$	$-\frac{5}{858}\sqrt{330}d$	$\frac{5}{1089}\sqrt{231}(2b - \frac{3}{26}c)$
${}^3\text{F}_2$	$-\frac{2}{33}\sqrt{11}(\frac{22}{21}a + \frac{13}{77}b + \frac{140}{429}c)$	$\frac{26}{297}b - \frac{70}{429}c$	$\frac{10}{429}\sqrt{110}d$	$\frac{10}{363}\sqrt{77}(\frac{1}{9}b - \frac{1}{13}c)$
${}^3\text{F}_3$	$\sqrt{154}(\frac{1}{315}a + \frac{13}{1694}b - \frac{175}{14157}c)$	$-\frac{1}{14}\sqrt{14}(\frac{4}{5}a + \frac{11}{54}b)$	0	$\frac{35}{363}\sqrt{22}(\frac{5}{36}b - \frac{4}{13}c)$
${}^3\text{F}_4$	$\frac{1}{11}\sqrt{110}(\frac{17}{1575}a + \frac{3}{154}b + \frac{7}{1287}c)$	$\frac{1}{10}\sqrt{10}(\frac{4}{45}a + \frac{5}{22}b - \frac{560}{1287}c)$	$-\frac{20}{429}\sqrt{11}d$	$\frac{1}{33}\sqrt{770}(-\frac{4}{15}a - \frac{5}{44}b + \frac{20}{429}c)$
${}^3\text{H}_4$	$H - 3z + \frac{442}{2475}a - \frac{6}{121}b + \frac{68}{14157}c$	$\frac{2}{11}\sqrt{11}(-\frac{13}{225}a + \frac{1}{11}b + \frac{238}{1287}c)$	$\frac{17}{429}\sqrt{10}d$	$\frac{2}{33}\sqrt{7}(-\frac{1}{15}a + \frac{1}{11}b + \frac{50}{429}c)$
${}^3\text{H}_5^1$		$H - \frac{1}{2}z + \frac{9}{50}a - \frac{16}{297}b - \frac{2}{143}c$	$\frac{1}{286}\sqrt{110}d$	$\frac{1}{363}\sqrt{77}(-\frac{11}{10}a + \frac{16}{9}b + \frac{50}{13}c)$
${}^3\text{H}_5^2$			$H - \frac{1}{2}z - \frac{3}{10}a - \frac{8}{99}b + \frac{5}{286}c$	$-\frac{5}{858}\sqrt{70}d$
${}^3\text{H}_6^1$				$H + \frac{5}{2}z + \frac{13}{66}a - \frac{256}{3267}b - \frac{250}{4719}c$
${}^3\text{H}_6^2$				
${}^1\text{I}_6^1$				
${}^1\text{I}_6^2$				
${}^1\text{G}_4$				
${}^1\text{D}_2$				

TABLE 8.42  
(Continued.)

	${}^3H_6^2$	${}^1I_6^1$	${}^1I_6^2$	${}^1G_4$	${}^1D_2$
${}^3P_1$	$\frac{5}{858}\sqrt{66}d$	0	0	0	0
${}^3P_2$	$\frac{5}{858}\sqrt{66}d$	0	0	0	$\frac{3}{2}\sqrt{2}z$
${}^3F_2$	$\frac{10}{429}\sqrt{22}d$	0	0	0	$-\sqrt{6}z$
${}^3F_3$	$\frac{10}{429}\sqrt{77}d$	0	0	0	0
${}^3F_4$	$\frac{10}{429}\sqrt{55}d$	0	0	$\frac{1}{3}\sqrt{33}z$	0
${}^3H_4$	$\frac{25}{429}\sqrt{2}d$	0	0	$-\frac{1}{3}\sqrt{30}z$	0
${}^3H_5^1$	$\frac{25}{858}\sqrt{22}d$	0	0	0	0
${}^3H_5^2$	$\frac{1}{11}\sqrt{5}\left(\frac{11}{30}a + \frac{4}{9}b - \frac{35}{78}c\right)$	0	0	0	0
${}^3H_6^1$	$\frac{25}{858}\sqrt{14}d$	$\frac{1}{2}\sqrt{6}z$	0	0	0
${}^3H_6^2$	$H + \frac{5}{2}z - \frac{1}{6}a + \frac{8}{99}b - \frac{125}{858}c$	0	$\frac{1}{2}\sqrt{6}z$	0	0
${}^1I_6^1$		$I + \frac{13}{33}a + \frac{128}{1089}b + \frac{100}{4719}c$	$-\frac{5}{429}\sqrt{14}d$	$-\frac{1}{11}\sqrt{35}\left(\frac{4}{15}a + \frac{3}{11}b + \frac{40}{429}c\right)$	$\frac{5}{363}\sqrt{77}\left(\frac{2}{3}b + \frac{5}{13}c\right)$
${}^1I_6^2$			$I - \frac{1}{3}a - \frac{4}{33}b + \frac{25}{429}c$	$-\frac{10}{143}\sqrt{10}d$	$-\frac{25}{429}\sqrt{22}d$
${}^1G_4$				$G + \frac{17}{385}a - \frac{69}{847}b - \frac{15}{1573}c$	$\frac{1}{11}\sqrt{55}\left(-\frac{44}{105}a - \frac{7}{11}b + \frac{40}{429}c\right)$
${}^1D_2$					$D - \frac{11}{105}a - \frac{8}{63}b$



TABLE 8.43  
Energy levels of  $\text{Pr}^{3+}$  ion.

Level	Experimental		Calculated		
	Free-ion	Centers of gravity of the LSJ levels in $\text{PrCl}_3$	$(\alpha = 0)^a$	$[\alpha L(L + 1)]^b$	$(\alpha \neq 0)^c$
${}^3\text{H}_4$	$0 \text{ cm}^{-1}$	$0 \text{ cm}^{-1}$	$0 \text{ cm}^{-1}$	$0 \text{ cm}^{-1}$	$0 \text{ cm}^{-1}$
${}^3\text{H}_5$	2152.09	2112	2026	2107	2112
${}^3\text{H}_6$	4389.09	4295	4167	4318	4320
${}^3\text{F}_2$	4996.61	4823	4735	4572	4591
${}^3\text{F}_3$	6415.24	6220	6088	5981	5997
${}^3\text{F}_4$	6854.75	6670	6774	6639	6639
${}^1\text{G}_4$	9921.24	9773	10002	9869	9828
${}^1\text{D}_2$	17334.39	16640	16973	16739	16701
${}^3\text{P}_0$	21389.81	20373	20406	20404	20356
${}^3\text{P}_1$	22007.46	20924	20983	21014	20975
${}^3\text{P}_2$	23160.61	22130	22210	22268	22233
${}^1\text{I}_6$	22211.54	21395	20896	21238	21299
${}^1\text{S}_0$			50680	49976	49484
$\sigma$			191	131	105

<sup>a</sup>Parameters:  $\zeta = 729.5$ ,  $F_2 = 305.4$ ,  $F_4 = 51.88$ ,  $F_6 = 5.321 \text{ cm}^{-1}$ .

<sup>b</sup>Parameters:  $\zeta = 753.9$ ,  $F_2 = 308.0$ ,  $F_4 = 50.92$ ,  $F_6 = 5.115$ ,  $\alpha = 14.77 \text{ cm}^{-1}$ .

<sup>c</sup>Parameters:  $\zeta = 755.1$ ,  $F_2 = 307.9$ ,  $F_4 = 50.23$ ,  $F_6 = 5.003$ ,  $\alpha = -0.6542 \text{ cm}^{-1}$ .

#### 45.4. Fitting of the crystalline field levels

Fitting of the crystalline field energy levels is carried out in two steps. The first step is to extract the Slater integrals  $F_K$  and the spin-orbit  $\zeta$  parameter by fitting the observed centers of gravity of the LSJ terms. These "free-ion" parameters are then used to obtain the crystal-field parameters  $B_q^K$  by fitting the observed energies of crystal-field levels. The reader is referred to the excellent paper by Margolis [321] for details of this procedure. The results of fitting the centers of gravity of the LSJ levels are presented in Table 8.43. The experimental centers of gravity of the LSJ levels in the Table 8.43 have been computed from the crystal-field levels identified [325,326] for  $\text{PrCl}_3$ . The three columns under calculated levels are as follows. The levels in the first column are calculated using  $\zeta$  and  $F_K$  parameters only. The second column of levels are obtained using an additional parameter  $\alpha$ , the so called Trees parameter, for orbit-orbit interaction which gives a correction term  $\alpha L(L + 1)$  to the electrostatic energies of the LS-terms. Finally, in order to improve the fitting of the free-ion terms, two other minor perturbations, spin-spin and mutual spin-orbit interactions, are added to the orbit-orbit interaction [321]. The energies in the third column are calculated with these minor perturbations. The standard deviations in these three levels of fitting are 191, 131, and 105, respectively. We have also included in this table the experimental free-ion levels of the  $\text{Pr}^{3+}$  ion [327–329] for a comparison.

TABLE 8.44

Experimental and calculated energy levels of  $\text{PrCl}_3$  (crystal-field parameters:  $B_0^2 = 94.52$ ,  $B_0^4 = -324.64$ ,  $B_0^6 = -633.92$ ,  $B_6^6 = 426.72 \text{ cm}^{-1}$ ).

Level	$\mu$	$\Gamma_i$	Exp.	Calc.
$^3\text{H}_4$	2	$\Gamma_3^1$	$0.0 \text{ cm}^{-1}$	$0.0 \text{ cm}^{-1}$
	3	$\Gamma_4$	33.1	28.2
	2'	$\Gamma_3^2$	96.4	99.3
	1	$\Gamma_6$	130.2	119.7
	3'	$\Gamma_5$	137.0	144.7
	0	$\Gamma_1$	—	199.6
$^3\text{H}_5$	3	$\Gamma_5$	2137.2	2132.9
	2	$\Gamma_3^1$	2169.8	2163.4
	1	$\Gamma_6^2$	2188.5	2192.5
	3'	$\Gamma_4$	2202.2	2197.6
	2'	$\Gamma_3^2$	2222.6	2224.2
	1'	$\Gamma_6^1$	—	2253.8
	0	$\Gamma_2$	—	2284.4
$^3\text{H}_6$	3	$\Gamma_4$	4230.4	4235.1
	2	$\Gamma_3^2$	4295.3	4293.6
	0	$\Gamma_1^2$	—	4349.5
	0'	$\Gamma_2$	—	4365.0
	3'	$\Gamma_5$	—	4378.8
	1	$\Gamma_6^2$	4423.1	4415.8
	2'	$\Gamma_3^1$	4431.0	4423.3
	1'	$\Gamma_6^1$	—	4505.1
	0''	$\Gamma_1^1$	—	4517.0
$^3\text{F}_2$	1	$\Gamma_6$	4922.6	4924.3
	0	$\Gamma_1$	—	4944.4
	2	$\Gamma_3$	4950.4	4948.9
$^3\text{F}_3$	0	$\Gamma_2$	6279	6283.9
	2	$\Gamma_3$	6303.5	6306.0
	3	$\Gamma_4$	6308.5	6306.2
	1	$\Gamma_6$	6352.1	6345.7
	3'	$\Gamma_5$	6367.2	6370.9
$^3\text{F}_4$	3	$\Gamma_5$	6700.6	6716.9
	3'	$\Gamma_4$	6751.5	6748.6
	2	$\Gamma_3^1$	6772.1	6764.3
	0	$\Gamma_1$	6782	6775.3
	1	$\Gamma_6$	6785.7	6778.6
	2'	$\Gamma_3^2$	6804.3	6803.1
$^1\text{G}_4$	3	$\Gamma_5$	—	9580.7
	0	$\Gamma_1$	9733.5	9745.4
	3'	$\Gamma_4$	9762.9	9757.5
	2	$\Gamma_3^2$	9772.2	9782.6
	1	$\Gamma_6$	9806.6	9817.1
	2'	$\Gamma_3^1$	9927	9921.5

TABLE 8.44  
(Continued.)

Level	$\mu$	$\Gamma_i$	Exp.	Calc.
$^1D_2$	0	$\Gamma_1$	16630.64	16649.6
	2	$\Gamma_3$	16730.9	16742.9
	1	$\Gamma_6$	16780.5	16759.8
$^3P_0$	0	$\Gamma_1$	20474.93	
$^3P_1$	1	$\Gamma_6$	21066.4	21066.6
	0	$\Gamma_2$	21096.16	21095.5
$^1I_6$	0	$\Gamma_2$	21298.96	21290.7
	0'	$\Gamma_1^1$	21301.02	21301.5
	1	$\Gamma_6^2$	—	21359.5
	0''	$\Gamma_1^2$	21395.6	21370.1
	1'	$\Gamma_6^1$	21411.35	21397.1
	2	$\Gamma_3^1$	—	21421.1
	3	$\Gamma_5$	—	21448.8
	2'	$\Gamma_3^2$	—	21474.6
	3'	$\Gamma_4$	—	21500.5
$^3P_2$	0	$\Gamma_1$	22207.0	22206.7
	1	$\Gamma_6$	22226.0	22227.3
	2	$\Gamma_3$	22246.7	22249.3
$^1S_0$	0	$\Gamma_1$	48800	

The results of the crystalline field calculations are given in Table 8.44. At the time Margolis did the fitting, 40 out of 61 Stark levels of  $\text{PrCl}_3$  were known. Since then, 6 more levels have been identified and a few of the previous levels have been slightly modified to within  $\pm 1 \text{ cm}^{-1}$ . We have listed these experimental values [322,330–332] along with our calculated values in this table. The crystal field parameters used were the same values derived by Margolis, i.e.,

$$B_0^2 = 94.52 \text{ cm}^{-1}, \quad B_0^4 = -324.64 \text{ cm}^{-1}, \quad B_0^6 = -633.92 \text{ cm}^{-1}$$

$$\text{and } B_6^6 = 426.72 \text{ cm}^{-1}$$

The free-ion parameters were

$$\zeta = 755.1 \text{ cm}^{-1}, \quad F_2 = 307.9 \text{ cm}^{-1}, \quad F_4 = 50.23 \text{ cm}^{-1} \quad \text{and} \quad F_6 = 5.003 \text{ cm}^{-1}$$

#### 46. $f^1$ configuration

There are no electron repulsions in  $f^1$  configuration. However, using term notation  $f^1$  can be considered as  $^2F$  which under spin-orbit interaction will split into a pair of levels  $^2F_{5/2}$

and  ${}^2F_{7/2}$  where  $5/2$  and  $7/2$  are the  $j$  values. The energies of these levels can be calculated by one of two ways. One is to use the formula

$$E_j = \frac{\zeta}{2} [j(j+1) - l(l+1) - s(s+1)]$$

which gives the values with  $l = 3$  and  $s = 1/2$

$$E_{5/2} = -2\zeta \quad \text{and} \quad E_{7/2} = \frac{3}{2}\zeta$$

Another is to use the Lande's interval rule

$$E_{j+1} - E_j = (j+1)\zeta$$

and the center of gravity of levels. Thus

$$E_{7/2} - E_{5/2} = \frac{7}{2}\zeta \quad \text{and} \quad 8E_{7/2} + 6E_{5/2} = 0,$$

where 8 and 6 are the degeneracies of  $7/2$  and  $5/2$  levels, respectively. These equations imply

$$E_{5/2} = -2\zeta \quad \text{and} \quad E_{7/2} = \frac{3}{2}\zeta$$

The experimental separation of the  ${}^2F$  pair of levels in  $\text{Ce}^{3+}$  has been found by Lang [333] to be  $2253 \text{ cm}^{-1}$  which gives a free-ion value for the spin-orbit constant parameter of  $644 \text{ cm}^{-1}$ .

#### 46.1. Crystalline field of $D_{3h}$ symmetry

The free-ion levels of an odd  $f^N$  configuration (which are half-integral  $J$ 's) in any noncubic symmetry are split by crystal field into levels that are doubly degenerate, the so-called Kramer's doublets. Thus each  $J$  level ( $j$  for one-electron) splits into  $(J + 1/2)$  Stark levels in  $D_{3h}$  symmetry.

We list in Table 8.45 the additional characters of the double group  $D_{3h}$  and in Table 8.46 the  $|J, M\rangle$  basis functions for the double group irreducible representations of  $D_{3h}$ .

TABLE 8.45  
Additional characters of double group  $D_{3h}$ .

$D'_{3h}$	$E$	$\bar{E}$	$2C_3$	$2\bar{C}_3$	$3C'_2, 3\bar{C}'_2$	$\sigma_h, \bar{\sigma}_h$	$2S_3$	$2\bar{S}_3$	$3\sigma_v, 3\bar{\sigma}_v$
$\Gamma_7$	2	-2	1	-1	0	0	$\sqrt{3}$	$-\sqrt{3}$	0
$\Gamma_8$	2	-2	1	-1	0	0	$-\sqrt{3}$	$\sqrt{3}$	0
$\Gamma_9$	2	-2	-2	2	0	0	0	0	0

TABLE 8.46  
The  $|J, M\rangle$  basis functions for the irreducible representations of  $D_{3h}$ .

Representation	$ J, M\rangle$ functions
$\Gamma_7$	$ 5/2, \pm 1/2\rangle,  7/2, \pm 1/2\rangle$
$\Gamma_8$	$ 5/2, \pm 5/2\rangle, \pm  7/2, \pm 5/2\rangle, \pm  7/2, \mp 7/2\rangle$
$\Gamma_9$	$ 5/2, \pm 3/2\rangle,  7/2, \pm 3/2\rangle$

TABLE 8.47  
The  $|J, M\rangle$  functions.

$ 7/2, 7/2\rangle = (3^+)$	
$ 7/2, 5/2\rangle = \sqrt{\frac{6}{7}}(2^+) + \sqrt{\frac{1}{7}}(3^-)$	$ 5/2, 5/2\rangle = -\sqrt{\frac{1}{7}}(2^+) + \sqrt{\frac{6}{7}}(3^-)$
$ 7/2, 3/2\rangle = \sqrt{\frac{5}{7}}(1^+) + \sqrt{\frac{2}{7}}(2^-)$	$ 5/2, 3/2\rangle = -\sqrt{\frac{2}{7}}(1^+) + \sqrt{\frac{5}{7}}(2^-)$
$ 7/2, 1/2\rangle = \sqrt{\frac{4}{7}}(0^+) + \sqrt{\frac{3}{7}}(1^-)$	$ 5/2, 1/2\rangle = -\sqrt{\frac{3}{7}}(0^+) + \sqrt{\frac{4}{7}}(1^-)$
$ 7/2, -1/2\rangle = \sqrt{\frac{3}{7}}(-1^+) + \sqrt{\frac{4}{7}}(0^-)$	$ 5/2, -1/2\rangle = -\sqrt{\frac{4}{7}}(-1^+) + \sqrt{\frac{3}{7}}(0^-)$
$ 7/2, -3/2\rangle = \sqrt{\frac{2}{7}}(-2^+) + \sqrt{\frac{5}{7}}(-1^-)$	$ 5/2, -3/2\rangle = -\sqrt{\frac{5}{7}}(-2^+) + \sqrt{\frac{2}{7}}(-1^-)$
$ 7/2, -5/2\rangle = \sqrt{\frac{1}{7}}(-3^+) + \sqrt{\frac{6}{7}}(-2^-)$	$ 5/2, -5/2\rangle = -\sqrt{\frac{6}{7}}(-3^+) + \sqrt{\frac{1}{7}}(-2^-)$
$ 7/2, -7/2\rangle = (-\bar{3})$	

TABLE 8.48  
Spin-orbit and crystal field energy matrices of  $f^1$  in  $D_{3h}$ .

$\Gamma_7$	$ 5/2, \pm 1/2\rangle$	$ 7/2, \pm 1/2\rangle$	
$ 5/2, \pm 1/2\rangle$	$-2\zeta + \frac{8}{35}B_0^2 + \frac{2}{21}B_0^4$	$-\frac{2\sqrt{3}}{7}(\frac{1}{15}B_0^2 + \frac{5}{33}B_0^4 + \frac{175}{429}B_0^6)$	
$ 7/2, \pm 1/2\rangle$		$\frac{3}{2}\zeta + \frac{5}{21}B_0^2 + \frac{9}{77}B_0^4 + \frac{25}{429}B_0^6$	
$\Gamma_8$	$ 5/2, \pm 5/2\rangle$	$\pm  7/2, \pm 5/2\rangle$	$\pm  7/2, \mp 7/2\rangle$
$ 5/2, \pm 5/2\rangle$	$-2\zeta - \frac{2}{7}B_0^2 + \frac{1}{21}B_0^4$	$\frac{\sqrt{6}}{7}(-\frac{1}{3}B_0^2 + \frac{10}{33}B_0^4 - \frac{35}{429}B_0^6)$	$-\frac{10}{13}\sqrt{\frac{2}{11}}B_0^6$
$ 7/2, \pm 5/2\rangle$		$\frac{3}{2}\zeta - \frac{1}{21}B_0^2 - \frac{13}{77}B_0^4 + \frac{25}{429}B_0^6$	$-\frac{10}{13}\sqrt{\frac{1}{33}}B_0^6$
$ 7/2, \mp 7/2\rangle$			$\frac{3}{2}\zeta - \frac{1}{3}B_0^2 + \frac{1}{11}B_0^4 - \frac{5}{429}B_0^6$
$\Gamma_9$	$ 5/2, \pm 3/2\rangle$	$ 7/2, \pm 3/2\rangle$	
$ 5/2, \pm 3/2\rangle$	$-2\zeta + \frac{2}{35}B_0^2 - \frac{1}{7}B_0^4$	$\frac{\sqrt{10}}{7}(-\frac{1}{5}B_0^2 - \frac{8}{33}B_0^4 + \frac{35}{143}B_0^6)$	
$ 7/2, \pm 3/2\rangle$		$\frac{3}{2}\zeta + \frac{1}{7}B_0^2 - \frac{3}{77}B_0^4 - \frac{15}{143}B_0^6$	

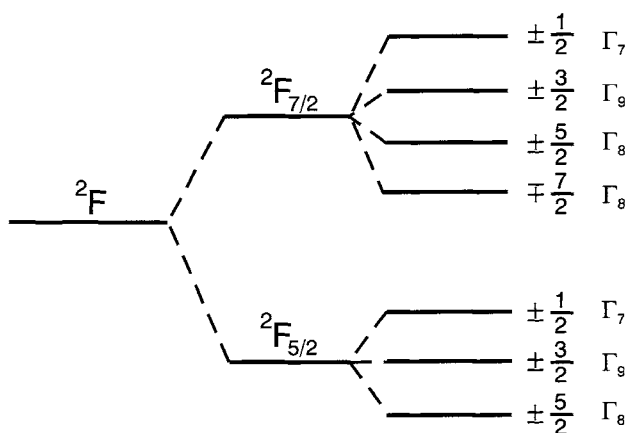


Fig. 8.44. Splittings of the  ${}^2F$  of  $f^1$  configuration under (a) spin-orbit interaction and (b) in  $D_{3h}$  crystalline field (schematic).

TABLE 8.49

Experimental and calculated energy levels of  $Ce^{3+}$  in  $LaCl_3$  (parameters:  $\zeta = 627$ ,  $B_0^2 = 129$ ,  $B_0^4 = -326$ ,  $B_0^6 = -997$ ,  $B_6^6 = 403 \text{ cm}^{-1}$ ).

Representation	Exp.	Calc.
$\Gamma_8  5/2, \pm 5/2\rangle$	$0 \text{ cm}^{-1}$	$0 \text{ cm}^{-1}$
$\Gamma_7  5/2, \pm 1/2\rangle$	37.5	36.1
$\Gamma_9  5/2, \pm 3/2\rangle$	110.0	111.1
$\Gamma_8  7/2, \mp 7/2\rangle$	2166.0	2166.8
$\Gamma_7  7/2, \pm 1/2\rangle$	2208.6	2212.2
$\Gamma_8  7/2, \pm 5/2\rangle$	2282.6	2280.7
$\Gamma_9  7/2, \pm 3/2\rangle$	2399.5	2393.9
$\sigma$		2.6

#### 46.2. Calculation of crystal field energies

The  $|J, M\rangle$  functions in terms of  $(l, m_l; s, m_s)$  functions can be obtained either by the lowering operator or by coupling coefficients tables. These are listed in Table 8.47.

With the basis functions of Table 8.46 and the one-electron matrix elements of equation (8.103), it is a simple matter to calculate the crystal field energies. We present in Table 8.48 the complete crystal-field and spin-orbit energy matrices of  $f^1$  in  $D_{3h}$ ; the splitting of the  ${}^2F$  of  $f^1$  configuration under spin-orbit interaction and further in  $D_{3h}$  crystalline field is shown in Fig. 8.44.

The experimental energy levels [334] of  $Ce^{3+}$  in  $LaCl_3$  have been fitted with these energy expressions and the fitting is given in Table 8.49.

## References

- [1] E.U. Condon, G.H. Shortley, *The Theory of Atomic Spectra*, Cambridge University Press, 1935.
- [2] B.R. Judd, *Operator Techniques in Atomic Spectroscopy*, McGraw-Hill, New York, 1963.
- [3] B.G. Wybourne, *Spectroscopic Properties of Rare Earths*, J. Wiley, New York, 1965.
- [4] K.W.H. Stevens, *Proc. Phys. Soc.* **A65**, 209, 1952.
- [5] A. Abragam, B. Bleaney, *Electron Paramagnetic Resonance of Transition Ions*, Clarendon Press, Oxford, 1970.
- [6] R.J. Elliot, R.T. Harley, W. Hayes, S.R.P. Smith, *Proc. Roy. Soc.* **A328**, 217, 1972.
- [7] A.J. Freeman, *Magnetic Properties of Rare Earth Metals*, ed. R.J. Elliot, Plenum Press, London and NY, 1972.
- [8] M.T. Hutchings, *Solid State Phys.* **16**, 227 (eds Seitz, Turnbull, Academic Press).
- [9] A. Furrer, *Proc. First Conf. On Crystal Elect. Fields Effects in Metals and Alloys*, ed. R. Devine, Univ. of Montreal, 1974.
- [10] H.W. De Wijn, A.M. Van Diepen, K.M.J. Buschow, *Proc. First Conf. On Crystal Elect. Fields Effects in Metals and Alloys*, ed. R. Devine, Universite de Montreal.
- [11] K.W.H. Stevens, *Rep. Prog. Phys.* **30**, 189, 1967.
- [12] R.J. Elliot, K.W.H. Stevens, *Proc. Roy. Soc.* **A215**, 437, 1953; **219**, 387, 1953.
- [13] K.R. Lea, M.G.M. Leask, W.P. Wolf, *J. Phys. Chem. Solids* **23**, 1381, 1962.
- [14] C.K. Jorgensen, R. Pappalardo, H.H. Schmidtke, *J. Chem. Phys.* **39**, 1422, 1963.
- [15] R.E. Watson, Freeman, *Phys. Rev.* **156**, 251, 1967.
- [16] M.M. Ellis, D.J.J. Newman, *J. Chem. Phys.* **47**, 1989, 1967.
- [17] B.G. Wybourne, *Spectroscopic Properties of Rare Earths*, Interscience, New York, 1965.
- [18] G.M. Dieke, *Spectra and Energy Levels of Rare Earth Ions in Crystals*, Interscience, New York, 1965.
- [19] E. Bucher, J.P. Maita, G.W. Hull, Jr., J. Sierro, C.W. Chu, B. Lüthi, *Proc. Int. Conf. On Cryst. Elect. Field Effects in Metals and Alloys*, ed. R.A.B. Devine, Montreal, 1974.
- [20] G. Williams, L.L. Hirst, *Phys. Rev.* **185**, 407, 1969.
- [21] L.W. Roeland, *Proc. Int. Conf. On Cryst. Elect. Fields in Metals and Alloys*, ed. R.A.B. Devine 1974, Montreal.
- [22] D.L. Ulrich, R.G. Barnes, *Phys. Rev.* **164**, 428, 1967.
- [23] C.K. Jorgensen, R. Pappalardo, H.H. Schmidtke, *J. Chem. Phys.* **39**, 1422, 1963.
- [24] C.K. Jorgensen, *J. Less Common Metals* **112**, 141, 1985.
- [25] C.K. Jorgensen, *Eur. J. Solid State Inorg. Chem.* **28**, 239, 1991.
- [26] K.B. Yatsimirskii, N.K. Davidenko, *Theor. Exper. Chem. (Russ.)* **5**, 10, 1969.
- [27] D. Kuse, C.K. Jorgensen, *Chem. Phys. Lett.* **1**, 344, 1967.
- [28] W. Urland, *Chem. Phys. Lett.* **50**, 445, 1977.
- [29] K.D. Warren, *Inorg. Chem.* **16**, 2008, 1977.
- [30] K.D. Warren, *Inorg. Chem.* **20**, 4223, 1981.
- [31] D.J. Newman, *Adv. Phys.* **20**, 197, 1971.
- [32] J.D. Axe, G. Burns, *Phys. Rev.* **152**, 341, 1966.
- [33] H.H. Crosswhite, G.H. Dieke, W.J. Carter, *J. Chem. Phys.* **43**, 2047, 1965.
- [34] C.K. Jorgensen, *Mat. Fys. Medd. Dan. Vid. Selsk. No. 22*, 30, 1956.
- [35] L.J. Katzin, M.L. Barnett, *J. Phys. Chem.* **68**, 3779, 1964.
- [36] W.J. Carter, *C.A.* **66**, 70635.
- [37] C.E. Schaffer, C.K. Jorgensen, *J. Inorg. Nucl. Chem.* **8**, 143, 1958.
- [38] C.K. Jorgensen, *Struct. Bonding* **1**, 3, 1966.
- [39] C.K. Jorgensen, *Oxidation Numbers and Oxidation States*, Springer-Verlag, Berlin, 1969.
- [40] D.A. Wensky, W.G. Moulton, *J. Chem. Phys.* **53**, 3957, 1970.
- [41] E.Y. Wong, I. Richman, *J. Chem. Phys.* **36**, 1889, 1962.
- [42] C.K. Jorgensen, R. Pappalardo, E. Rittershaus, *Z. Naturforsch. A* **19**, 424, 1964.
- [43] S.P. Sinha, H.H. Schmidtke, *Mol. Phys.* **38**, 2190, 1965.
- [44] S.P. Sinha, *Spectrochim. Acta* **22**, 57, 1966.
- [45] W.T. Cornall, *Proc. 14<sup>th</sup> ICCS, Toronto*, p. 367, 1972.
- [46] C.K. Jorgensen, R. Pappalardo, J. Flahaut, *J. Chim. Phys.* **444**, 1965.
- [47] R. Pappalardo, *Helv. Chim. Acta* **38**, 178, 1965.
- [48] C.K. Jorgensen, R. Pappalardo, E. Rittershaus, *Z. Naturforsch. A* **20**, 54, 1965.
- [49] J.L. Ryan, C.K. Jorgensen, *J. Phys. Chem.* **70**, 2845, 1966.
- [50] R.D. Laughlin, J.G. Conway, *J. Chem. Phys.* **38**, 1037, 1963.
- [51] K.B. Ytsimirskii, N.K. Davidenko, *Dokl. Akad. Nauk SSSR* **191**, 122, 1970.

- [52] N.K. Davidenko, K.B. Yatsimirskii, *Teor. Ex-  
perim. Chem. (Russ.)* **6**, 620, 1970.
- [53] J. Van Vleck, *J. Chem. Phys.* **11**, 67, 1937.
- [54] P. Franzen, J.P.M. Wondenberg, C.J. Jortner, *Physica* **10**, 693, 1943.
- [55] J. Hoogschagen, A.P. Snoek, C.J. Jortner, *Physica* **11**, 518, 1943.
- [56] B.R. Judd, *Phys. Rev.* **127**, 750, 1962.
- [57] G.S. Ofelt, *J. Chem. Phys.* **37**, 571, 1962.
- [58] W.T. Carnall, D.M. Gruen, R.L. McBeth, *J. Phys. Chem.* **66**, 2159, 1962.
- [59] W.T. Carnall, P.R. Fields, R. Sarup, *J. Chem. Phys.* **52**, 2587, 1969.
- [60] G.G. Gashurov, O.H. Sevens, *J. Chem. Phys.* **50**, 429, 1968.
- [61] K. Bukietynska, G.R. Choppin, *J. Chem. Phys.* **52**, 2875, 1970.
- [62] S.P. Tandon, P.C. Mehta, *J. Chem. Phys.* **52**, 4313, 1970; **53**, 414, 1971.
- [63] S.S.L. Surana, M. Singh, S.N. Misra, *J. Inorg. Nucl. Chem.* **42**, 61, 1980.
- [64] S.N. Misra, *J. Sci. & Ind. Res.* **44**, 366, 1985.
- [65] S.N. Misra, G.K. Joshi, *Indian J. Pure Appl. Phys.* **19**, 279, 1981; *J. Inorg. Nucl. Chem.* **43**, 205, 1981.
- [66] B.R. Judd, C.K. Jorgensen, *Mol. Phys.* **8**, 281, 1964.
- [67] S.N. Misra, G.G. Talela, N. Kiran, *Indian J. Chem.* **26A**, 309, 1987.
- [68] S.N. Misra, G. Joseph, K. Anjaiah, K. Venkata-  
subramanian, *ibid* **26A**, 919, 1987.
- [69] R.D. Peacock, *J. Chem. Soc. A* 2028, 1971.
- [70] D.E. Henrie, G.R. Choppin, *J. Chem. Phys.* **49**, 477, 1968.
- [71] K. Iftikar, M. Sayeed, N. Ahmed, *Inorg. Chem.* **21**, 80, 1982.
- [72] K. Bukietynska, A. Mondry, *Inorg. Chim. Acta* **110**, 1, 1985.
- [73] R.D. Peacock, *Struct. Bonding* **22**, 83, 1985.
- [74] D.E. Henrie, R.L. Fellows, G.R. Choppin, *Coord. Chem. Rev.* **18**, 199, 1976.
- [75] G. Blasse, A. Brit, W.C. Nienport, *J. Phys. Chem. Solid* **27**, 1587, 1966.
- [76] P. Kisleuk, W.F. Krupke, J.B. Gruber, *J. Chem. Phys.* **40**, 3606, 1964.
- [77] J.L. Ryan, C.K. Jorgensen, *J. Phys. Chem.* **70**, 2845, 1966.
- [78] J.L. Ryan, *Inorg. Chem.* **8**, 2053, 1969.
- [79] J.L. Martin, L. C. Thompson, L.J. Radvich, M.D. Glick, *J. Am. Chem. Soc.* **90**, 4494, 1960.
- [80] D.M. Gruen, C.W. Dekock, *J. Chem. Phys.* **45**, 455, 1965.
- [81] W.F. Krupke, *Phys. Rev.* **A145**, 325, 1966.
- [82] R.D. Peacock, *Mol. Phys.* **25**, 817, 1973.
- [83] S.N. Misra, G.K. Joshi, *J. Inorg. Nucl. Chem.* **43**, 205, 1981; *Indian J. Pure Appl. Phys.* **19**, 279, 1981.
- [84] S.N. Misra, G.K. Joshi, M.P. Bhutra, *J. Inorg. Nucl. Chem.* **43**, 525, 1981; *Indian J. Chem.* **23A**, 329, 1984.
- [85] N.G. Dzyubenko, L.I. Martynenko, *Zh. Neorg. Khim.* **31**, 1699, 1986.
- [86] V.S. Khomenko, M.O. Lozinskii, Y.A. Fil-  
alkov, L.I. Krasovskaya, T.A. Rasshinina, *Ko-  
ord. Khim.* **12**, 740, 1986.
- [87] G. Joseph, Ph.D. Thesis, Bhavnagar University, Bhavnagar, India, 1988.
- [88] K. Anjaiah, Ph.D. Thesis, Bhavnagar Univer-  
sity, Bhavnagar, India, 1989.
- [89] W.N. Cabaffin, Ph.D. Thesis, Bhavnagar Uni-  
versity, Bhavnagar, India, 1989.
- [90] R.G. Charles, R.C. Ohlman, *J. Inorg. Nucl. Chem.* **27**, 119, 1965.
- [91] N. Filipesine, N.N. McAvoy, *ibid.* **28**, 253, 1966.
- [92] S.P. Sinha, *ibid.* **28**, 189, 1966.
- [93] K. Iftikar, *Inorg. Chim. Acta.* **129**, 261, 1987.
- [94] R. Reisfield, Y. Eckstein, *Solid State Commun.* **13**, 265, 1973.
- [95] R. Reisfeld, *Struct. Bonding* **22**, 173, 1975.
- [96] S.N. Misra, A. Ahmed, A. Kothari, R.K. Jani, *J. Inorg. Nucl. Chem.* **43**, 2905, 1987.
- [97] S.N. Misra, A. Kothari, *Can. J. Chem.* **64**, 1975, 1983.
- [98] S.N. Misra, A. Kothari, *Indian J. Pure Appl. Phys.* **21**, 127, 1983.
- [99] W.T. Carnall, P.R. Fields, K. Rajnak, *J. Chem. Phys.* **49**, 4412, 1968.
- [100] D.M. Gruen, C.W. Dekock, R.L. McBeth, *Ad-  
van. Chem.* **71**, 102, 1967.
- [101] G.R. Choppin, R.L. Fellows, *J. Coord. Chem.* **3**, 209, 1973.
- [102] R.L. Fellows, G.R. Choppin, *J. Coord. Chem.* **4**, 79, 1974.
- [103] D.E. Henrie, B.K. Henrie, *J. Inorg. Nucl. Chem.* **36**, 2175, 1974.
- [104] L.J. Nugent, R.D. Baybarz, J.L. Burnett, J.L. Ryan, *J. Phys. Chem.* **77**, 1572, 1973.
- [105] L.J. Nugent, R.D. Baybarz, J.L. Burnett, J.L. Ryan, *J. Inorg. Nucl. Chem.* **33**, 2503, 1971.
- [106] K. Fajan, *Naturwissenschaften* **11**, 165, 1923; *Z. Elektrochem.* **34**, 502, 1928.
- [107] S.F. Mason, *J. Less Common Metals* **93**, 45, 1983.
- [108] F.S. Richardson, J.D. Saxe, S.A. Davis, T.R. Faulkner, *Mol. Phys.* **42**, 18, 1981.
- [109] R. Kuroda, S.F. Mason, C. Rosini, *Chem. Phys. Lett.* **11**, 11, 1980.



- [110] R. Kuroda, S.F. Mason, C. Rosini, *J. Chem. Soc., Farad. Trans., II* **77**, 1981.
- [111] S.F. Richardson, *Chem. Phys. Lett.* **86**, 47, 1982.
- [112] W.T. Carnall, P.R. Fields, B.G. Wynbourne, *J. Chem. Phys.* **42**, 3797, 1965.
- [113] W.T. Carnall, P.R. Fields, K. Rajnak, *J. Chem. Phys.* **49**, 4412, 4424, 4447, 4450, 1968.
- [114] S.F. Mason, G.E. Tranter, *Chem. Phys. Lett.* **94**, 29, 1983.
- [115] S.F. Mason, R.D. Peacock, B. Stewart, *Chem. Phys. Lett.* **29**, 149, 1974.
- [116] S.F. Mason, R.D. Peacock, B. Stewart, *Mol. Phys.* **30**, 1829, 1975.
- [117] M.J. Weber, T.E. Varitimos, B.H. Matsinger, *Phys. Rev.* **B8**, 47, 1973; *J. Appl. Phys.* **42**, 4996, 1971.
- [118] W. Prandtl, K. Scheiner, *Zeit. Anorg. Allgem. Chem.* **220**, 107, 1934.
- [119] J.D. Main-Smith, *Nature* **120**, 583, 1927.
- [120] S. Freed, *Phys. Rev.* **38**, 2122, 1931.
- [121] R.J. Lange, *Ann. D. Research* **14A**, 127, 1936.
- [122] P.C. Mukherji, *Indian J. Phys.* **10**, 319, 1936.
- [123] H.A. Bethe, F.H. Spedding, *Phys. Rev.* **52**, 454, 1937.
- [124] H. Lange, *Ann. D. Phys.* **31**, 609, 1938.
- [125] L.J.F. Broer, C.J. Gorter, *J. Hoogschagen, Physica* **11**, 231, 1945.
- [126] R.J. Satten, *J. Chem. Phys.* **21**, 637, 1953.
- [127] C.K. Jorgensen, *Dan. Mat. Phys. Medd.* **29**, No. 11, 1955.
- [128] S. Freed, S.I. Weissman, *J. Chem. Phys.* **6**, 297, 1938.
- [129] S. Freed, *Rev. Mod. Phys.* **14**, 105, 1942.
- [130] P. Franzen, J.P.M. Woudenberg, C.J. Gorter, *Physica* **10**, 365, 1943.
- [131] J. Hoogschagen, A.P. Snoek, C.J. Gorter, *Physica* **10**, 693, 1943.
- [132] J. Hoogschagen, *Physica* **11**, 513, 1946.
- [133] J. Hoogschagen, A.P. Snoek, C.J. Gorter, *Physica* **11**, 518, 1946.
- [134] J. Hoogschagen, Th.G. Scholte, S. Kruyer, *Physica* **11**, 504, 1946.
- [135] J. Hoogschagen, C.J. Gorter, *Physica* **14**, 197, 1948.
- [136] T. Moellor, J.C. Brantley, *Anal. Chem.* **22**, 433, 1950.
- [137] L. Holleck, C. Hartinger, *Angew. Chemie* **67**, 648, 1955.
- [138] C.V. Banks, D.W. Klingman, *Anal. Chim. Acta* **15**, 356, 1956.
- [139] W.T. Carnall, D.M. Gruen, R.L. McBeth, *J. Phys. Chem.* **66**, 2159, 1962.
- [140] W.T. Carnall, *J. Phys. Chem.* **67**, 1206, 1963.
- [141] W.T. Carnall, P.R. Fields, G.E. Toogood, *J. Phys. Chem.* **68**, 2351, 1964.
- [142] G.H. Dieke, *Spectra and Energy Levels of Rare Earth Ions in Crystals*, eds H.M. Crosswhite, H. Crosswhite, Wiley, New York, 1968.
- [143] L. Brewer, *J. Opt. Soc. Am.* **61**, 1101, 1666, 1971.
- [144] L.J. Nugent, K.L. Vandersluis, *J. Opt. Soc. Am.* **61**, 1112, 1971.
- [145] W.C. Martin, *J. Opt. Soc. Am.* **61**, 162, 1971.
- [146] P.P. Feofilov, *Opt. Spektrosk.* **6**, 234, 1959.
- [147] A.A. Kaplanskii, V.N. Mendvedev, P.P. Feofilov, *Opt. Spektrosk.* **14**, 664, 1963.
- [148] G. Mandel, R.P. Bauman, E. Banks, *J. Chem. Phys.* **44**, 4063, 1966.
- [149] Z.J. Kiss, *Phys. Rev.* **127**, 718, 1962.
- [150] R.A. Buchanan, H.E. Rast, H.H. Caspers, *J. Chem. Phys.* **44**, 4063, 1966.
- [151] C.K. Jorgensen, *Mat. Fys. Medd. Dan. Vid. Seisk. No.* **22**, 30, 1956.
- [152] W. Urland, *Chem. Phys. Lett.* **50**, 445, 1977.
- [153] Leask, Orbach, Powell, Wolf, *Proc. Roy. Soc. (London) A* **272**, 371, 1963.
- [154] H.H. Crosswhite, G.H. Dieke, W.J. Carter, *J. Chem. Phys.* **43**, 2047, 1965.
- [155] J. Sugar, *Phys. Rev. Lett.* **14**, 731, 1965.
- [156] C.K. Jorgensen, *Mol. Phys.* **5**, 271, 1962.
- [157] J. Margolis, *J. Chem. Phys.* **35**, 1367, 1961.
- [158] Wong, Richman, *J. Chem. Phys.* **36**, 1889, 1962.
- [159] Gruber, *J. Chem. Phys.* **38**, 946, 1963.
- [160] Eisenstein, *J. Chem. Phys.* **39**, 2134, 1963.
- [161] Tinsley, *J. Chem. Phys.* **39**, 3503, 1963.
- [162] Gruber, Satten, *J. Chem. Phys.* **39**, 1455, 1963.
- [163] G.W. Parker, P.M. Lantz, *J. Am. Chem. Soc.* **72**, 2834, 1950.
- [164] J.B. Gruber, J.G. Conway, *J. Inorg. Nucl. Chem.* **14**, 303, 1960.
- [165] Axe, Dieke, *J. Chem. Phys.* **37**, 2364, 1962.
- [166] Judd, *Mol. Phys.* **2**, 407, 1959.
- [167] Deshazer, Dieke, *J. Chem. Phys.* **38**, 2190, 1963.
- [168] N.A. Kazanskaya, *Opt. Spectrosk.* **29**, 1100, 1970.
- [169] Dieke, Leopold, *J. Opt. Soc. Amer.* **47**, 944, 1957.
- [170] Cook, Dieke, *J. Chem. Phys.* **27**, 1213, 1957.
- [171] Thomas, Singh, Dieke, *J. Chem. Phys.* **38**, 2180, 1965.
- [172] Crosswhite, Dieke, *J. Chem. Phys.* **35**, 1535, 1961.
- [173] Crozier, Runciman, *J. Chem. Phys.* **35**, 1392, 1961.
- [174] Krupke, Gruber, *J. Chem. Phys.* **39**, 1024, 1963; **41**, 1225, 1964.

- [175] Dieke, Singh, *J. Chem. Phys.* **35**, 555, 1961.
- [176] Kislink, Krupke, Gruber, *J. Chem. Phys.* **40**, 3606, 1964.
- [177] Rosenberger, *Z. Physik* **167**, 360, 1962.
- [178] S.P. Tandon, P.C. Mehta, *J. Chem. Phys.* **52**, 4313, 1970; **53**, 414, 1970.
- [179] Wong, Richman, *J. Chem. Phys.* **34**, 1182, 1961.
- [180] W.T. Carnall, P.R. Fields, J. Morrison, R. Sarup, *J. Chem. Phys.* **52**, 4054, 1970.
- [181] Dieke, Crosswhite, *J. Opt. Soc. Amer.* **46**, 885, 1956.
- [182] (a) McClure, Kiss, *J. Chem. Phys.* **39**, 3251, 1963;  
(b) Bubement, *Trans. Farad. Soc. (London)* **44**, 617, 1948;  
(c) S. Gordon, J.C. Sullivan, W.A. Mulac, D. Cohen, H. Schmidt, Pulse Radiolysis of Lanthanide and Actinide Elements, in: *Proc. 4<sup>th</sup> Symposium on Radiation Chemistry*, Kezthlley, Hungary, 1976.
- [183] J.B. Gruber, J.G. Conway, *J. Inorg. Nucl. Chem.* **14**, 303, 1960.
- [184] N.K. Davidenko, A.G. Goryushko, K.B. Yatsimirskii, *J. Inorg. Chem. (Russ.)* **18**, 1785, 1973.
- [185] A.G. Goryushko, N.K. Davidenko, *J. Inorg. Chem. (Russ.)* **19**, 1722, 1974.
- [186] A.G. Goryushko, N.K. Davidenko, *Theor. Experim. Chem. (Russ.)* **12**, 555, 1976.
- [187] A.K. Mukhopadhyay, M. Chowdhury, *Physical Rev., B* **16**, 3070, 1977.
- [188] K.B. Yatsimirskii, N.A. Kostromina, Z.A. Sheka, N.K. Davidenko, E.E. Kriss, V.I. Ermolenko, *Chemistry of Complex Compounds of Rare Earths (Russ.)*, Naukova Dumka, Kiev, 1966.
- [189] E.V. Sayre, D.S. Miller, S. Freed, *J. Chem. Phys.* **26**, 109, 1957.
- [190] K.B. Yatsimirskii, N.K. Davidenko, N. Kostromina, T.V. Ternovaya, *Theor. Experim. Chem. (Russ.)* **1**, 100, 1965.
- [191] N. Kostromina, N.N. Tananaeva, *J. Inorg. Chem. (Russ.)* **16**, 2356, 1971.
- [192] G. Geier, C.K. Jorgensen, *Chem. Phys. Lett.* **9**, 263, 1971.
- [193] A.G. Goryushko, N.K. Davidenko, *J. Inorg. Chem. (Russ.)* **19**, 1722, 1974.
- [194] K.B. Yatsimirskii, N.K. Davidenko, *Dokl. Akad. Nauk SSSR* **191**, 122, 1970.
- [195] N.K. Davidenko, K.B. Yatsimirskii, *Theor. Experim. Chem. (Russ.)* **6**, 620, 1970.
- [196] K.B. Yatsimirskii, N.K. Davidenko, *Coord. Chem. Rev.* **27**, 223, 1979.
- [197] A. Sonesson, *Acta Chem. Scand.* **12**, 1937, 1958.
- [198] A. Sonesson, *Acta Chem. Scand.* **13**, 998, 1959.
- [199] T.V. Maljkova, G.A. Shutova, K.B. Yatsimirskii, *J. Inorg. Chem. (Russ.)* **9**, 1833, 1964.
- [200] N.A. Kostromina, T.V. Ternovaya, K.B. Yatsimirskii, *Theor. Experim. Chem. (Russ.)* **2**, 673, 1966.
- [201] K. Bukietynska, A. Mondry, E. Osmeda, *J. Inorg. Nucl. Chem.* **39**, 483, 1977.
- [202] E.V. Sayre, D.S. Miller, S. Freed, *J. Chem. Phys.* **26**, 109, 1957.
- [203] G.R. Choppin, D.E. Henrie, K. Buijs, *Inorg. Chem.* **5**, 1743, 1966.
- [204] D.E. Karraker, *Inorg. Chem.* **6**, 1863, 1967.
- [205] E.R. Birnbaum, J.E. Gomez, D.W. Darnall, *J. Am. Chem. Soc.* **92**, 5287, 1970.
- [206] F.H. Spedding, M.J. Pikal, B.O. Ayers, *J. Phys. Chem.* **70**, 2430, 1966.
- [207] F.H. Spedding, D.A. Csejke, C.W. Dekock, *ibid.* **70**, 2423, 1966.
- [208] F.H. Spedding, L.E. Shier, J.A. Rard, *J. Chem. Eng. Data* **20**, 66, 1975.
- [209] W.M. Gildseth, A. Habenschuss, F.H. Spedding, *ibid.* **21**, 292, 1976.
- [210] F.H. Spedding, C.W. Dekock, G.W. Pepple, A. Habenschuss, *ibid.* **22**, 58, 1977.
- [211] J. Reuben, *J. Phys. Chem.* **71**, 2154, 1975.
- [212] N.K. Davidenko, K.B. Yatsimirskii, *J. Struct. Chem.* **7**, 700, 1968; *J. Inorg. Chem.* **13**, 138, 1968.
- [213] Y.A. Barbauland, N.K. Mikhaylova, *J. Inorg. Chem.* **18**, 699, 1973.
- [214] K. Bukietynska, A. Mondry, *Inorg. Chim. Acta* **110**, 1, 1985.
- [215] K. Bukietynska, A. Mondry, *Rare Earth Spectrosc., Proc. Int. Symp.*, 1984.
- [216] L. Zinner, H.F. Brito, *Inorg. Chim. Acta* **110**, 175, 1985.
- [217] M.T. Devlin, E.M. Stephene, F.S. Richardson, *Inorg. Chem.* **27**, 1517, 1988.
- [218] L.C. Smith, D.C. McCain, D.L. Wertz, *J. Am. Chem. Soc.* **98**, 5725, 1976.
- [219] N.L. Steele, D.L. Wertz, *Inorg. Chem.* **16**, 1225, 1977.
- [220] S.N. Misra, T.N. Misra, R.C. Mehrotra, *J. Inorg. Nucl. Chem.* **27**, 105, 1965; *J. Ind. Chem. Soc.* **42**, 351, 1965.
- [221] C.K. Jorgensen, N. Bjerrum, *Acta Chem. Scand.* **7**, 951, 1953.
- [222] P.K. Chernova, L.K. Sukhova, T.N. Yefinova, *Russ. J. Inorg. Chem.* **19**, 1249, 1974.
- [223] B. Jezowska, B. Trzebiatowska, B. Keller, *Bull. Acad. Pol. Sci.* **25**, 159, 1977; **24**, 763, 1976.

- [224] J. Abrahamner, Y. Marcus, *J. Inorg. Nucl. Chem.* **30**, 1563, 1968.
- [225] Y. Haas, G. Stein, *J. Phys. Chem.* **75**, 3668, 1971.
- [226] A.F. Borina, *Zh. Neorg. Khim.* **33**, 1969, 1988.
- [227] S.N. Misra, *J. Sci. Ind. Res.* **45**, 1986.
- [228] S.N. Misra, G. Joseph, K. Anjaiah, K. Venkata-subramanian, *Ind. J. Chem.* **28A**, 265, 1990.
- [229] B. Balar, Ph.D. Thesis, Bhavnagar University, Bhavnagar, India, 1989.
- [230] S.N. Misra, P.P. Vaishnav, M.P. Bhutra, M. Singh, *Bull. Chem. Soc., Japan* **51**, 389, 1978.
- [231] S.N. Misra, M. Singh, *Synth. React. Inorg. Org. Met. Chem.* **8**, 388, 1978; *J. Inorg. Nucl. Chem.* **40**, 1939, 1978.
- [232] L.N. Lugina, N.K. Davidenko, K.B. Yatsimirskii, *J. Inorg. Chem. (Russ.)* **19**, 2665, 1974.
- [233] S.N. Misra, S.O. Sommerer, *Appl. Spectr. Rev.* **26**, 151, 1991.
- [234] S.N. Misra, M. Singh, *Synth. React. Inorg. Org. Met. Chem.* **11**, 124, 1981.
- [235] S.S.L. Surana, M. Singh, S.N. Misra, *J. Inorg. Nucl. Chem.* **42**, 61, 1980.
- [236] R.C. Mehrotra, R. Bohra, D.P. Gaur, *Metal  $\beta$ -Diketonates*, Academic Press, 1982.
- [237] H.G. Brittain, *Coord. Chem. Rev.* **48**, 283, 1983.
- [238] N.K. Dutt, S. Rahut, *J. Inorg. Nucl. Chem.* **32**, 2905, 1970; **33**, 1715, 1971.
- [239] S.N. Misra, *Ind. J. Chem.* **19A**, 920, 1980.
- [240] S.N. Misra, G.K. Joshi, *J. Inorg. Nucl. Chem.* **42**, 205, 1981; *Indian J. Pure Appl. Phys.* **19**, 271, 1981.
- [241] A.G. Goryushko, N.K. Davidenko, *J. Appl. Spectrosc.* **8**, 74, 1968; **13**, 60, 1970.
- [242] I.M. Batiyev, G.M. Shilov, *Koord. Khim.* **9**, 64, 1983.
- [243] S.V. Belyukova, N.A. Nazenenko, T.B. Kravechenko, N.S. Polutkov, *Dokl. Akad. Nauk SSSR* **259**, 139, 1981.
- [244] S.N. Misra, W.N. Cabafin, *Chemica Scripta* **29**, 75, 1989.
- [245] R.J.P. Williams, *Structure and Bonding* **50**, 1, 1982.
- [246] S.N. Misra, P.P. Vaishnav, M.P. Bhutra, G.K. Joshi, *Indian J. Pure Appl. Phys.* **15**, 553, 1979.
- [247] K. Ifitkar, M. Sayeed, N. Ahmed, *Inorg. Chem.* **21**, 80, 1982.
- [248] S.V. Belyukova, N.A. Mazerenko, *Khim. Biol. Nauk* **5**, 40, 1980.
- [249] V.S. Khomenko, M.O. Lozinskii, Y.A. Fialko, L.I. Krasovskaya, T.A. Rasshimina, *Koord. Khim.* **12**, 740, 1986.
- [250] C. Gopinath, L. Ramamoorthy, S. Buddhudu, *Mater. Lett.* **4**, 279, 1986.
- [251] K. Ifitkar, *Inorg. Chim. Acta* **128**, 273.
- [252] R.C. Holz, L.C. Thompson, *Inorg. Chem.* **27**, 4640, 1988.
- [253] M.A. Tischenko, C.V. Melenleva, Z.A. Khafagi, M.P. Spirikhina, V.V. Tishenko, V.A. Shapkin, *Koord. Khim.* **14**, 763, 1988.
- [254] Q. Su, Y. Lu, *Huaxue Xueban* **43**, 697, 1984.
- [255] K. Bukietynska, P. Ngoethy, *Inorg. Chim. Acta* **132**, 21, 1987.
- [256] S. Misumi, T. Isobe, S. Kida, A. Inasmumi, *Bull. Chem. Soc. Japan* **41**, 25, 1968.
- [257] S.N. Misra, M.P. Bhutra, G.K. Joshi, *Indian J. Chem.* **21A**, 222, 1982.
- [258] A. Kothari, Ph.D. Thesis, Jodhpur University, Jodhpur, India, 1982.
- [259] B. Bhatia, M.P. Bhutra, S.P. Tandon, *Rev. Tec. Fac. Ing. Univ. Zulia* **11**, 69, 1988.
- [260] K. Bukietynska, A. Mondry, *Inorg. Chim. Acta* **130**, 145, 1987; **120**, 271, 1987.
- [261] W.N. Cabalfin, Ph.D. Thesis, Bhavnagar University, Bhavnagar, India, 1989.
- [262] S.D. Kulkarni, V. Ramachandra Rao, *Chemical Era* **XIV**, No. 9, 363, 1978.
- [263] S.P. Vasireddi, V. Ramachandra Rao, *J. Inorg. Nucl. Chem.* **39**, 311, 1977.
- [264] P. Radhakrishna Murty, V. Ramachandra Rao, *Ind. J. Chem.* **3**, 321, 1965.
- [265] P. Radhakrishna Murty, V. Ramachandra Rao, *Current Science* **35**, 12, 1966.
- [266] V. Ramachandra Rao, P. Radhakrishna Murty, *Current Science* **36**, 233, 1967.
- [267] S. Zakir Ali, V. Ramachandra Rao, *Marathwada University Journal* **7**, 11, 1965.
- [268] S. Zakir Ali, V. Ramachandra Rao, *Current Science* **37**, 254, 1968.
- [269] P. Radhakrishna Murty, S. Zakir Ali, V. Ramachandra Rao, *Marathwada University Journal* **VIII**, 1, 55, 1969.
- [270] V. Ramachandra Rao, P. Radhakrishnamurty, *Indian J. Chem.* **6**, 465, 1968.
- [271] V.H. Galgali, V. Ramachandra Rao, D.D. Khanol Kar, *Indian J. Chem.* **7**, 825, 1969.
- [272] P.V. Takalkar, V. Ramachandra Rao, *Indian J. Chem.* **7**, 943, 1969.
- [273] Y.H. Deshpande, V. Ramachandra Rao, *ibid.* **7**, 1051, 1969.
- [274] (a) D. Purushotham, V. Ramachandra Rao, *Curr. Sci.* **39**, 486, 1970;  
(b) S.F.M. Ali, M.P. Gawande, V. Ramachandra Rao, *Curr. Sci.* **42**, 817, 1973.
- [275] Y.H. Deshpande, V. Ramachandra Rao, *J. Inorg. Nucl. Chem.* **35**, 3626, 1973.

- [276] B.D. Sarje, B.K. Patil, V. Ramachandra Rao, *Science & Culture* **40**, 437, 1974.
- [277] S.F.M. Ali, V. Ramachandra Rao, *J. Inorg. Nucl. Chem.* **37**, 1041, 1975.
- [278] P.V. Takalkar, V. Ramachandra Rao, *J. Inorg. Nucl. Chem.* **37**, 2103, 1975.
- [279] J.N. Nandapurkar, V. Ramachandra Rao, *Curr. Sci.* **45**, 13, 483, 1976.
- [280] M.D. Pundlik, V. Ramachandra Rao, *Russ. J. Heterocyclic Chemistry* **6**, 837, 1976.
- [281] B.K. Patil, V. Ramachandra Rao, *Curr. Sci.* **45**, No. 19, 686, 1976.
- [282] B.K. Patil, V. Ramachandra Rao, *Indian Medical Gazette CXIII*, 375, 1979.
- [283] U.M. Meshram, V. Ramachandra Rao, *Chemical Era XVI*, 278, 1980.
- [284] P.V. Vaidya, V.D. Deshpande, V. Ramachandra Rao, *J. Indian Council of Chemists III*, 21, 1987.
- [285] U.M. Meshram, V. Ramachandra Rao, *Asian J. Chem.* **1**, 112, 1989.
- [286] C.V. Deshpande, V. Ramachandra Rao, *J. Indian Inst. Science* **69**, 329, 1989.
- [287] P.V. Vaidya, V.D. Deshpande, V. Ramachandra Rao, *Asian J. Chem.* **3**, 13, 1991.
- [288] Y. Subhedkar, V. Ramachandra Rao, *Asian J. Chem.* **6**, 277, 1994.
- [289] D. Purushothan, V. Ramachandra Rao, B.H.S.V. Raghava Rao, *Anal. Chim. Acta* **33**, 182, 1965.
- [290] S.P. Sinha, *Z. Anorg. Allg. Chem.* **434**, 277, 1977.
- [291] S.N. Misra, *Indian J. Chem.* **19A**, 1135, 1980.
- [292] M. Mohan, J.P. Tandon, N.S. Gupta, *Inorg. Chim. Acta* **111**, 187, 1986.
- [293] L.B. Zinner, G. Vicentini, *Am. Acad. Brasil Cienc.* **58**, 183, 1986.
- [294] D.L. Arora, K. Lal, S.P. Gupta, *J. Indian Chem. Soc.* **LXIII**, 836, 1986.
- [295] G. Singh, M.R. Srivastava, P.S.S.J. Sastry, T.R. Rao, *Proc. Ind. Acad. Sci.* **103**, 725, 1991.
- [296] R.K. Agarwal, A. Kumar, I. Chakraborti, *Oriental J. Chem.* **8**, 244, 1992.
- [297] J.L. Manzano, E. Rodriguez, M.A. Vincente, *Synth. React. Inorg. Met. Org. Chem.* **23**, 851, 1993.
- [298] R.K. Agarwal, R.K. Sarin, *Polish J. Chem.* **67**, 1925, 1993.
- [299] R.K. Agarwal, R.K. Sarin, *Polish J. Chem.* **67**, 1209, 1993.
- [300] R.K. Agarwal, R.K. Sarin, *Synth. React. Inorg. Met. Org. Chem.* **24**, 499, 1994.
- [301] T.R. Rao, P.A. Kumar, *ibid.* **24**, 239, 1994.
- [302] R.K. Agarwal, H. Agarwal, *ibid.* **25**, 715, 1995.
- [303] T.A. Khan, M.A. Khan, M.M. Haq, *ibid.* **26**, 1467, 1996.
- [304] G.F. Desa, B.D.B. Neto, R. Ferreira, *Inorg. Chim. Acta* **23**, 249, 1977.
- [305] B. Singh, P.K. Singh, V.P. Tiwari, *Proc. Indian Acad. Sci.* **103**, 701, 1991.
- [306] L.B. Zinner, C.A.A. ves de Corvalho, K. Zinner, *J. Alloys and Compounds* **180**, 343, 1992.
- [307] R.K. Agarwal, H. Agarwal, R. Prasad, *J. Indian Chem. Soc.* **73**, 605, 1996.
- [308] P.A. Kumar, *Synth. React. Inorg. Met. Org. Chem.* **27**, 577, 1997.
- [309] B. Singh, A.K. Srivastav, P.K. Singh, *Indian J. Chem.* **36A**, 72, 1997.
- [310] E.U. Condon, G.H. Shortley, *The Theory of Atomic Spectra*, Cambridge University Press, New York, 1957.
- [311] J.C. Slater, *Quantum Theory of Atomic Structure*, Vols I and II, McGraw Hill, New York, 1960.
- [312] C.J. Ballhausen, *Introduction to Ligand Field Theory*, McGraw Hill, New York, 1962.
- [313] J.S. Griffith, *The Theory of Transition-Metal Ions*, Cambridge University Press, New York, 1961.
- [314] B.G. Wybourne, *Spectroscopic Properties of the Rare Earths*, Interscience, New York, 1965.
- [315] B.R. Judd, *Operator Techniques in Atomic Spectroscopy*, McGraw-Hill, 1963.
- [316] (a) G. Racah, *Phys. Rev.* **62**, 438, 1942; (b) *ibid.* **63**, 367, 1943; (c) *ibid.* **76**, 1352, 1949; (d) U. Fano, G. Racah, *Irreducible Tensorial Sets*, Academic Press, New York, 1959.
- [317] M. Rotenberg, R. Bivins, N. Metropolis, J.K. Wooten, Jr., *The 3-j and 6-j Symbols*, M.I.T. Press, Cambridge, Mass, 1959.
- [318] C.W. Nielson, G.F. Koster, *Spectroscopic Coefficients for  $p^n$ ,  $d^n$  and  $f^n$  Configurations*, M.I.T. Press, Cambridge, Mass, 1964.
- [319] X. Zachariasen, *Acta Cryst.* **1**, 266, 1948.
- [320] K.W.H. Stevens, *Proc. Phys. Soc. (London)* **A65**, 209, 1952; R.J. Elliot, K.W.H. Stevens, *Proc. Phys. Soc. (London)* **A218**, 553, 1953.
- [321] (a) J.S. Margolis, *J. Chem Phys.* **35**, 1367, 1961; (b) J.S. Margolis, Ph.D. dissertation, University of California at Los Angeles, June 1960.
- [322] G.H. Dieke, *Spectra and Energy Levels of Rare Earth Ions in Crystals*, Interscience, New York, 1968.
- [323] K.H. Hellwege, *Ann. Physik* **6**, 4, 95, 1948.
- [324] J.R. Perumareddi, *Z. Naturforsch.* **36a**, 735, 1981.

- [325] E.V. Sayre, K.M. Sancier, S. Freed, *J. Chem. Phys.* **23**, 2060, 1955; **23**, 2066, 1955; **29**, 242, 1958.
- [326] G.H. Dieke, R. Sarup, *J. Chem. Phys.* **29**, 741, 1958.
- [327] NIST Atomic Spectra Database Data.
- [328] H.M. Crosswhite, G.H. Dieke, W.J. Carter, *J. Chem. Phys.* **43**, 2047, 1965.
- [329] J. Sugar, *J. Opt. Soc. Am.* **55**, 1058, 1965; **61**, 727, 1971.
- [330] J.W. Makovsky, W. Low, S. Yatsiv, *Phys. Letters* **2**, 186, 1962.
- [331] R. Sarup, H.M. Crozier, *J. Chem. Phys.* **42**, 371, 1965.
- [332] C. A. Morrison, R.P. Leavitt, in: *Handbook on the Physics and Chemistry of Rare Earths*, Vol. 5, eds K.A. Gschneider, Jr., L. Eyring, North-Holland, NY, 1982.
- [333] R.J. Lang, *Can J. Res.* **A13**, 1, 1935; **A14**, 127, 1936.
- [334] K.H. Hellwege, E. Orlich, G. Schaack, *Phys. Kondens. Materie* **4**, 196, 1965.

## Appendix

TABLE 8.50  
Spectral parameters of complexes.

Complexes	$\beta$	$\delta$	Complexes	$\beta$	$\delta$
Pr(HMPA) <sub>4</sub> (NO <sub>3</sub> ) <sub>3</sub>	0.994	0.603	Sm(TBP) <sub>2</sub> (Hsal) <sub>3</sub>	1.006	-0.59
Pr(HMPA) <sub>4</sub> (ClO <sub>4</sub> ) <sub>3</sub>	1.0908	-0.79	Dy(HMPA) <sub>4</sub> (NO <sub>3</sub> ) <sub>3</sub>	0.996	0.40
Pr(OMPA) <sub>3</sub> (ClO <sub>4</sub> ) <sub>3</sub> (OH <sub>2</sub> )	1.002	-0.2 <sup>a</sup>	Dy(HMPA) <sub>4</sub> (NO <sub>3</sub> ) <sub>3</sub>	1.009	-0.89
Pr(TBP) <sub>2</sub> (Hsal) <sub>3</sub>	1.004	-0.4	Ho(HMPA) <sub>4</sub> (NO <sub>3</sub> ) <sub>3</sub>	0.997	0.30
Nd(HMPA) <sub>4</sub> (NO <sub>3</sub> ) <sub>3</sub>	0.9919	0.816	Ho(HMPA) <sub>4</sub> (ClO <sub>4</sub> ) <sub>3</sub>	0.999	0.10
Nd(HMPA) <sub>4</sub> (ClO <sub>4</sub> ) <sub>3</sub>	0.991	0.908	Ho(OMPA) <sub>3</sub> (ClO <sub>4</sub> ) <sub>3</sub> (OH <sub>2</sub> ) <sub>4</sub>	1.001	-0.10 <sup>a</sup>
Nd(HMPA) <sub>6</sub> (ClO <sub>4</sub> ) <sub>3</sub>	0.992	0.806	Ho(OMPA) <sub>3</sub> (ClO <sub>4</sub> ) <sub>3</sub> (OH <sub>2</sub> ) <sub>4</sub>	1.005	-0.50 <sup>b</sup>
Nd(OMPA) <sub>3</sub> (ClO <sub>4</sub> ) <sub>3</sub> (OH <sub>2</sub> )	0.998	0.190 <sup>a</sup>	Er(HMPA) <sub>4</sub> (NO <sub>3</sub> ) <sub>3</sub>	0.994	0.60
Nd(OMPA) <sub>3</sub> (ClO <sub>4</sub> ) <sub>3</sub>	1.0012	-0.12 <sup>b</sup>	Er(HMPA) <sub>4</sub> (ClO <sub>4</sub> ) <sub>3</sub>	0.993	0.70
Nd(TBP) <sub>2</sub> (Hsal) <sub>3</sub>	0.9994	0.06	Er(OMPA) <sub>3</sub> (ClO <sub>4</sub> ) <sub>3</sub> (OH <sub>2</sub> ) <sub>2</sub>	1.005	-0.50 <sup>a</sup>
NdCl <sub>3</sub> in TBP	0.9959	0.41	Er(TBP) <sub>2</sub> (Hsal) <sub>3</sub>	1.006	-0.59
Sm(HMPA) <sub>4</sub> (NO <sub>3</sub> ) <sub>3</sub>	0.994	0.60	Yb(HMPA) <sub>4</sub> (NO <sub>3</sub> ) <sub>3</sub>	0.989	1.11 <sup>c</sup>
Sm(HMPA) <sub>6</sub> (ClO <sub>4</sub> ) <sub>3</sub>	0.995	0.50	Yb(HMPA) <sub>4</sub> (ClO <sub>4</sub> ) <sub>3</sub>	1.012	-1.20 <sup>c</sup>

<sup>a</sup>CH<sub>3</sub>OH solution, <sup>b</sup>Acetone solution. All others in CHCl<sub>3</sub> solution, <sup>c</sup>The calculated parameters are based on only one absorption band in the near infrared.

Nephelauxetic parameter ( $\beta$ ) and SINHA's covalency parameter of ( $\delta$ ) for the HMPA-complexes of the lanthanides, and a comparison with other complexes containing P → O donor ligands. TBP = tributylphosphate, OMPA = octamethylpyrophosphoramidate, HMPA = hexamethylpyrophosphoramidate. To emphasize the weak nephelauxetic effect produced by the P–O donor ligands, some of the  $\beta$  and  $\delta$  values are expressed with three or four places after the decimal without rounding off. Ref. [290].

Values of average nephelauxetic ratio ( $\bar{\beta}$ ), average covalency parameter ( $\bar{\delta}$ ) and average bonding parameter ( $\bar{b}^{1/2}$ ) of lanthanide 4-nicotinyltrifluoroacetates. Ref. [291].

Complex	$\bar{\beta}$	$\bar{\delta}$	$\bar{b}^{1/2}$
Pr(III)-4-NTFA*	0.9932	0.6846	0.0580
Nd(III)-4-NTFA	0.9946	0.6807	0.0367
Sm(III)-4-NTFA	0.9935	0.673	0.0556
Ho(III)-4-NTFA	0.9863	1.3894	0.0809
Er(III)-4-NTFA	0.9857	1.3586	0.0839

Ref. [292]		
[Pr(Hoaox) <sub>3</sub> (NO <sub>3</sub> ) <sub>2</sub> ](NO <sub>3</sub> ) $\beta = 0.9975$ $\delta = 0.2506$ $b^{1/2} = 0.02500$	[Dy(Hoaox) <sub>3</sub> (NO <sub>3</sub> ) <sub>2</sub> ](NO <sub>3</sub> ) <sub>2</sub> $\beta = 0.9925$ $\delta = 0.7498$ $b^{1/2} = 0.04330$	[Dy(Hoaox) <sub>3</sub> (Cl) <sub>2</sub> ](Cl) $\beta = 0.9923$ $\delta = 0.7734$ $b^{1/2} = 0.04387$
[Nd(Hoaox) <sub>3</sub> (NO <sub>3</sub> ) <sub>2</sub> ](NO <sub>3</sub> ) $\beta = 0.9932$ $\delta = 0.6753$ $b^{1/2} = 0.04123$	[Pr(Hoaox) <sub>3</sub> (Cl) <sub>2</sub> ](Cl) $\beta = 0.9975$ $\delta = 0.2506$ $b^{1/2} = 0.02500$	
[Sm(Hoaox) <sub>3</sub> (NO <sub>3</sub> ) <sub>2</sub> ](NO <sub>3</sub> ) $\beta = 0.9930$ $\delta = 0.7049$ $b^{1/2} = 0.04183$	[Nd(Hoaox) <sub>3</sub> (Cl) <sub>2</sub> ](Cl) $\beta = 0.9932$ $\delta = 0.6753$ $b^{1/2} = 0.04123$	[Sm(Hoaox) <sub>3</sub> (Cl) <sub>2</sub> ](Cl) $\beta = 0.9930$ $\delta = 0.7021$ $b^{1/2} = 0.04183$

Spectroscopic data (A) and oscillator strengths (B) for the neodymium complex. Ref. [293].

Transition	$\lambda$ (nm)	$\bar{\nu}$ (cm <sup>-1</sup> )	$\beta$	$\beta$	$b^{1/2}$	$\delta$
(A) $^4I_{9/2} \rightarrow ^2P_{1/2}$	429.5	23 282	0.992			
$I_{9/2} \rightarrow ^4G_{5/2}, ^2G_{5/2}$	582.85	17 157	0.990	0.991	0.063	0.81

Electronic spectral data (cm<sup>-1</sup>) of the complexes. Ref. [294].

Lanthanide ion	Level	Ln(NO <sub>3</sub> ) <sub>3</sub>	[LnLCl <sub>3</sub> (H <sub>3</sub> O) <sub>3</sub> ]Cl	$(1 - \beta) \times 10^3$	$\beta$	$\delta$	$b^1$	
Pr	$^3H_4 \rightarrow ^1D_2$	16 980	16 850		0.756	0.992	0.76	0.061
	$\rightarrow ^3P_0$	20 750	20 610					
	$\rightarrow ^3P_2$	22 470	22 280					
Nd	$^4I_{9/2} \rightarrow ^4F_{3/2}, ^3H_{9/2}$	12 470	12 300		0.757	0.992	0.76	0.061
	$\rightarrow ^4F_{9/2}$	14 640	14 520					
	$\rightarrow ^4G_{5/2}$	17 270	17 150					
	$\rightarrow ^4G_{9/2}$	19 460	19 300					
Sm	$^6H_{5/2} \rightarrow ^4I_{11/2}$	21 550	21 440		0.496	0.995	0.050	0.050
	$\rightarrow ^4P_{5/9}$	24 000	23 880					
	$\rightarrow ^4F_{9/2}$	24 870	24 750					

Nitrate in aqueous solution, complexes in DMF.  
L-adphH<sub>5</sub>.

Electronic spectral data\* and oscillator strengths of Ln(III) complexes of AINH. Ref. [295].

Complex	Band maxima (cm <sup>-1</sup> )		Assignments	Oscillator strength, $P \times 10^6$	Spectral parameters
	Nujol	DMSO			
[Pr(AINH) <sub>3</sub> Cl]Cl <sub>2</sub>	16 365–17 330	16 360–17 280	<sup>3</sup> H <sub>4</sub> → D <sub>2</sub>	8.36	$\bar{\beta} = 0.9661$
	20 200–20 445	20 190–20 750	→ <sup>3</sup> P <sub>0</sub>	6.89	$b^{1/2} = 0.1302$
	20 745–21 410	20 750–21 415	→ <sup>3</sup> P <sub>1</sub>	2.86	$\eta = 0.0174$
	21 415–22 725	21 420–22 690	→ <sup>3</sup> P <sub>2</sub>	3.45	$\delta\% = 3.5083$
[Nd(AINH) <sub>3</sub> Cl]Cl <sub>2</sub>	11 175–11 695	11 040–11 665	<sup>4</sup> I <sub>9/2</sub> → <sup>4</sup> F <sub>3/2</sub>	4.54	$\bar{\beta} = 0.9926$
	11 975–12 820	12 020–12 690	→ <sup>4</sup> F <sub>5/2</sub>	7.02	$b^{1/2} = 0.0615$
	12 935–13 795	13 020–13 660	→ <sup>4</sup> F <sub>7/2</sub> , <sup>4</sup> S <sub>3/2</sub>	6.46	$\eta = 0.0038$
	14 325–14 925	14 305–14 795	→ <sup>4</sup> F <sub>9/2</sub>	1.48	$\delta\% = 0.7463$
	16 395–17 480	16 475–17 535	→ <sup>4</sup> G <sub>5/2</sub> , <sup>2</sup> G <sub>7/2</sub>	29.26	
	18 520–19 610	18 585–19 800	→ <sup>4</sup> G <sub>7/2</sub> , <sup>4</sup> G <sub>9/2</sub>	5.46	
	20 704–21 850	–	→ <sup>2</sup> D <sub>3/2</sub>	–	
[Sm(AINH) <sub>3</sub> Cl]Cl <sub>2</sub>	20 410–21 365	–	<sup>6</sup> H <sub>5/2</sub> → <sup>4</sup> I <sub>9/2</sub>	–	$\bar{\beta} = 0.9973$
	21 365–21 980	21 365–21 970	→ <sup>4</sup> I <sub>11/2</sub>	–	$b^{1/2} = 0.0371$ $\eta = 0.0014$ $\delta\% = 0.2705$
[Eu(AINH) <sub>3</sub> Cl]Cl <sub>2</sub>	21 360–21 565	21 365–21 645	<sup>7</sup> F <sub>0</sub> → <sup>5</sup> D <sub>2</sub>	–	$\bar{\beta} = 0.9998$
	25 140–25 580	25 190–25 640	→ <sup>5</sup> L <sub>6</sub>	–	$b^{1/2} = 0.0105$ $\eta = 0.0001$ $\delta\% = 0.0201$

\*Spectral parameters calculated from nujol mull spectra.



Electronic spectral data ( $\text{cm}^{-1}$ ) and related bonding parameters of lanthanide(III) iodides complexes of MBAAP. Ref. [296].

Complex	$\text{LnI}_3$ electronic spectral bands	Complex electronic spectral bands	$J$ -level	$(1 - \beta)$	$b^{1/2}$	$\delta\%$	
$\text{PrI}_3 \cdot 3\text{MBAAP}$	22 470	22 290	$^4\text{H} \rightarrow ^3\text{P}_2$	0.0080	0.9919	0.0632	0.8065
	21 325	21 110	$\rightarrow ^3\text{P}_1$	0.0100	0.9899	0.0707	1.0102
	20 755	20 610	$\rightarrow ^3\text{P}_0$	0.0069	0.9930	0.0587	0.6948
	17 005	16 810	$\rightarrow ^1\text{D}_2$	0.0114	0.9885	0.0754	1.1532
$\text{NdI}_3 \cdot 3\text{MBAAP}$	19 555	19 475	$^3\text{H}_{9/2} \rightarrow ^3\text{G}_{9/2}$	0.0040	0.0059	0.0447	0.4016
	17 365	17 200	$\rightarrow ^4\text{G}_{5/2}$	0.0095	0.9904	0.0689	0.9592
			$\rightarrow ^3\text{G}_{7/2}$				
	13 665	13 350	$\rightarrow ^3\text{S}_{3/2}$	0.0230	0.9769	0.1072	2.3543
		$\rightarrow ^4\text{F}_{7/2}$					
	12 475	12 410	$\rightarrow ^4\text{F}_{5/2}$	0.0052	0.9947	0.0509	0.5227
			$\rightarrow ^4\text{H}_{9/2}$				
$\text{SmI}_3 \cdot 3\text{MBAAP}$	24 870	24 760	$^6\text{H}_{5/3} \rightarrow ^4\text{F}_{9/2}$	0.0044	0.9955	0.0469	0.4419
	24 000	23 710	$\rightarrow ^4\text{P}_{5/2}$	0.0120	0.9879	0.0774	1.2146
	21 555	21 505	$\rightarrow ^4\text{I}_{13/2}$	0.0023	0.9976	0.0339	0.2305
$\text{HoI}_3 \cdot 3\text{MBAAP}$	22 400	22 270	$^5\text{I}_3 \rightarrow ^5\text{G}_6, ^5\text{F}_1$	0.0058	0.9941	0.0538	0.5834
	19 300	19 000	$\rightarrow ^5\text{F}_4$	0.0155	0.9844	0.0880	1.5745
	15 750	15 610	$\rightarrow ^5\text{F}_4, ^5\text{S}_2$	0.0088	0.9911	0.0663	0.8879
	13 520	13 380	$\rightarrow ^5\text{I}_4$	0.0103	0.9896	0.0717	1.0408

Covalence parameters of the complexes. Ref. [297].

Complex	$\beta$	$\delta$	Assignments
Pr	1.0025	-0.25	$^3\text{H}_4 \rightarrow ^1\text{D}_2, ^3\text{P}_0, ^3\text{P}_1$ and $^3\text{P}_2$
Nd	1.0020	-0.20	$^4\text{I}_{9/2} \rightarrow ^4\text{F}_{5/2}, ^4\text{F}_{7/2}, ^4\text{F}_{9/2}, ^4\text{G}_{5/2} - ^2\text{G}_{7/2}$ and $^4\text{G}_{7/2}$
Sm	1.0094	-0.93	$^6\text{H}_{5/2} \rightarrow ^4\text{I}_{13/2}$
Dy	1.0024	-0.24	$^6\text{H}_{15/2} \rightarrow ^6\text{F}_{5/2}$
Ho	1.0005	-0.05	$^5\text{I}_8 \rightarrow ^5\text{F}_5, ^5\text{S}_2 - ^5\text{F}_4, ^5\text{F}_3$ and $^5\text{G}_6 - ^5\text{F}_1$

Calculated from the f-f diffuse reflectance spectra.

Electronic spectral data (cm<sup>-1</sup>) and related bonding parameters of the complexes. Ref. [298].

Ln <sup>3+</sup>	Complex electronic spectral bands		Energy levels	(1 - β)		β		b <sup>1/2</sup>		δ%		
	A	B		A	B	A	B	A	B	A	B	
Pr <sup>3+</sup>	22 320	22 380	<sup>3</sup> H <sub>4</sub> → <sup>3</sup> P <sub>2</sub>	0.00672	0.00400	0.99327	0.99599	0.04098	0.03162	0.67655	0.40161	
	21 200	21 250		→ <sup>3</sup> P <sub>1</sub>	0.00586	0.00351	0.99413	0.99648	0.03827	0.02962	0.58946	0.35223
	20 600	20 640		→ <sup>3</sup> P <sub>0</sub>	0.00722	0.00530	0.99277	0.99470	0.04248	0.03640	0.72725	0.53282
Nd <sup>3+</sup>	16 800	16 780	→ <sup>1</sup> D <sub>2</sub>	0.01176	0.01294	0.98823	0.98706	0.05422	0.05687	1.19000	1.31096	
	19 500	19 480	<sup>4</sup> I <sub>9/2</sub> → <sup>2</sup> G <sub>9/2</sub>	0.00510	0.00612	0.99489	0.99388	0.03570	0.03911	0.51261	0.61576	
	17 250	17 270		→ <sup>2</sup> G <sub>5/2</sub>	0.00747	0.00632	0.99252	0.99368	0.04321	0.03974	0.75262	0.63601
		13 610	13 630	→ <sup>2</sup> G <sub>7/2</sub>	0.00511	0.00365	0.99488	0.99635	0.03574	0.03020	0.51362	0.36633
				→ <sup>3</sup> S <sub>3/2</sub>								
				→ <sup>4</sup> F <sub>7/2</sub>								
12 400	12 420	→ <sup>4</sup> F <sub>5/2</sub>	0.00564	0.00400	0.99435	0.99600	0.03754	0.03162	0.5672	0.4016		
Sm <sup>3+</sup>	24 750	24 740	→ <sup>4</sup> H <sub>9/2</sub>	0.00482	0.00522	0.99517	0.99478	0.03471	0.03612	0.48433	0.52473	
			<sup>6</sup> H <sub>5/2</sub> → <sup>4</sup> F <sub>9/2</sub>									
			→ <sup>6</sup> P <sub>5/2</sub>									
			→ <sup>4</sup> I <sub>13/2</sub>									
23 700	23 710		0.01265	0.01208	0.98734	0.98792	0.05623	0.05495	1.28122	1.22277		
21 500	21 510		0.00232	0.00185	0.99767	0.99815	0.02408	0.02150	0.23254	0.18534		

A, Ln(ClO<sub>4</sub>)<sub>3</sub> · 4MBAAP.B, Ln(ClO<sub>4</sub>)<sub>3</sub> · 4HMBAAP.

Electronic spectral data ( $\text{cm}^{-1}$ ) and related bonding parameters of lanthanide nitrate complexes of MBAAP. Ref. [299].

Complex	$\text{Ln}(\text{NO}_3)_3$ electronic spectra bands	Complex electronic spectra bands	Energy levels	$(1 - \beta)$	$\beta$	$b^{1/2}$	$\delta\%$
$\text{Pr}(\text{NO}_3)_3 \cdot 2\text{MBAAP}$	22 470	22 300	$^3\text{H}_4 \rightarrow ^3\text{P}_2$	0.00756	0.99243	0.06148	0.76176
	21 280	21 100	$\rightarrow ^3\text{P}_1$	0.00845	0.99154	0.06500	0.85220
	20 830	20 680	$\rightarrow ^3\text{P}_0$	0.00720	0.99279	0.06000	0.72522
	16 950	16 800	$\rightarrow ^1\text{D}_2$	0.00884	0.99115	0.06648	0.89189
$\text{Nd}(\text{NO}_3)_3 \cdot 2\text{MBAAP}$	19 420	19 280	$^4\text{I}_{9/2} \rightarrow ^2\text{G}_{9/2}$	0.00720	0.99279	0.06000	0.72522
	17 390	17 200	$\rightarrow ^4\text{G}_{5/2}, ^2\text{G}_{7/2}$	0.01092	0.98907	0.07389	1.10406
	13 420	13 210	$\rightarrow ^2\text{S}_{3/2}, ^4\text{F}_{7/2}$	0.01564	0.98435	0.08843	1.5886
	12 500	12 340	$\rightarrow ^4\text{F}_{5/2}, ^4\text{H}_{9/2}$	0.01280	0.98720	0.08000	1.29659
$\text{Sm}(\text{NO}_3)_3 \cdot 2\text{MBAAP}$	24 850	24 730	$^6\text{H}_{5/2} \rightarrow ^4\text{F}_{9/2}$	0.00482	0.99517	0.04909	0.48433
	24 100	23 800	$\rightarrow ^6\text{P}_{5/2}$	0.01244	0.98755	0.07886	1.25968
	21 600	21 480	$\rightarrow ^4\text{I}_{13/2}$	0.00555	0.99444	0.05267	0.55810

Electronic spectral data ( $\text{cm}^{-1}$ ) and related bonding parameters of lanthanide(III) isothiocyanate complexes of MBAAP. Ref. [299].

Complex	Ln(NCS) <sub>3</sub> electronic spectra bands	Complex electronic spectra bands	Energy levels	(1 - $\beta$ )	$\beta$	$b^{1/2}$	$\delta\%$
Pr(NCS) <sub>3</sub> · 2MBAAP	22 400	22 240	<sup>3</sup> H <sub>4</sub> → <sup>3</sup> P <sub>2</sub>	0.00714	0.99285	0.05974	0.71914
			→ <sup>3</sup> P <sub>1</sub>	0.00894	0.99105	0.06685	0.90207
			→ <sup>3</sup> P <sub>0</sub>	0.00865	0.99134	0.06576	0.87255
			→ <sup>1</sup> D <sub>2</sub>	0.01006	0.98994	0.07092	1.01622
Nd(NCS) <sub>3</sub> · 3MBAAP	19 400 17 400 13 400 12 500	19 230 17 210 13 240 12 230	<sup>4</sup> I <sub>9/2</sub> → <sup>2</sup> G <sub>9/2</sub>	0.00876	0.99123	0.06618	0.88375
			→ <sup>4</sup> G <sub>5/2</sub> , <sup>2</sup> G <sub>7/2</sub>	0.01091	0.98908	0.07385	1.10304
			→ <sup>2</sup> S <sub>3/2</sub> , <sup>4</sup> F <sub>7/2</sub>	0.01194	0.98805	0.07726	1.20844
			→ <sup>4</sup> F <sub>5/2</sub> , <sup>4</sup> H <sub>9/2</sub>	0.02160	0.97840	0.10392	2.20768
Sm(NCS) <sub>3</sub> · 3MBAAP	24 900 24 000 21 600	24 730 23 810 21 470	<sup>6</sup> H <sub>5/2</sub> → <sup>4</sup> F <sub>9/2</sub>	0.00682	0.99317	0.05839	0.68669
			→ <sup>6</sup> P <sub>5/2</sub>	0.00791	0.99208	0.06288	0.79731
			→ <sup>4</sup> I <sub>13/2</sub>	0.00601	0.99398	0.05481	0.60463

Electronic spectral bands ( $\text{cm}^{-1}$ ) and related bonding parameters of lanthanide(III) nitrate complexes of HMBAAP. Ref. [300].

Complex	Complex electronic spectral bands	Energy levels	$(1 - \beta)$	$\beta$	$b^{1/2}$	$\delta\%$
Pr(NO <sub>3</sub> ) <sub>3</sub> · 2HMBAAP	22 300	<sup>3</sup> H <sub>4</sub> → <sup>3</sup> P <sub>2</sub>	0.00756	0.99243	0.04347	0.76176
	21 100	→ <sup>3</sup> P <sub>1</sub>	0.00845	0.99154	0.04596	0.85220
	20 680	→ <sup>3</sup> P <sub>0</sub>	0.00720	0.99279	0.04242	0.72522
	16 800	→ <sup>1</sup> D <sub>2</sub>	0.00884	0.99115	0.04701	0.89189
Nd(NO <sub>3</sub> ) <sub>3</sub> · 2HMBAAP	19 280	<sup>4</sup> I <sub>9/2</sub> → <sup>2</sup> G <sub>9/2</sub>	0.00720	0.99279	0.04242	0.72522
	17 200	→ <sup>4</sup> G <sub>5/2</sub> , <sup>2</sup> G <sub>7/2</sub>	0.01092	0.98907	0.05224	1.10406
	13 210	→ <sup>2</sup> S <sub>3/2</sub> , <sup>4</sup> F <sub>7/2</sub>	0.01564	0.98435	0.06252	1.58886
	12 340	→ <sup>4</sup> F <sub>5/2</sub> , <sup>4</sup> H <sub>9/2</sub>	0.01280	0.98720	0.05656	1.29659
Sm(NO <sub>3</sub> ) <sub>3</sub> · 2HMBAAP	24 730	<sup>4</sup> H <sub>5/2</sub> → <sup>4</sup> F <sub>9/2</sub>	0.00482	0.99517	0.03471	0.48433
	23 800	→ <sup>6</sup> P <sub>5/2</sub>	0.01244	0.98755	0.05576	1.25968
	21 480	→ <sup>4</sup> I <sub>13/2</sub>	0.00555	0.99444	0.03724	0.55810
Pr(NCS) <sub>3</sub> · 2HMBAAP	22 220	<sup>3</sup> H <sub>4</sub> → <sup>3</sup> P <sub>2</sub>	0.00803	0.99196	0.04480	0.80950
	21 030	→ <sup>3</sup> P <sub>1</sub>	0.00942	0.99057	0.04852	0.95096
	20 610	→ <sup>3</sup> P <sub>0</sub>	0.00913	0.99086	0.04777	0.92142
	16 720	→ <sup>1</sup> D <sub>2</sub>	0.01065	0.98934	0.05159	1.07647
Nd(NCS) <sub>3</sub> · 3HMBAAP	19 220	<sup>4</sup> I <sub>9/2</sub> → <sup>2</sup> G <sub>9/2</sub>	0.00927	0.99073	0.04814	0.93567
	17 200	→ <sup>4</sup> G <sub>5/2</sub> , <sup>2</sup> G <sub>7/2</sub>	0.01149	0.98851	0.05359	1.16235
	13 240	→ <sup>2</sup> S <sub>3/2</sub> , <sup>4</sup> F <sub>7/2</sub>	0.01194	0.98806	0.05463	1.20842
	12 230	→ <sup>4</sup> F <sub>5/2</sub> , <sup>4</sup> H <sub>9/2</sub>	0.02160	0.9784	0.07348	2.20768
Sm(NCS) <sub>3</sub> · 2HMBAAP	24 720	<sup>4</sup> H <sub>5/2</sub> → <sup>4</sup> F <sub>9/2</sub>	0.00722	0.99278	0.04248	0.72725
	23 800	→ <sup>6</sup> P <sub>5/2</sub>	0.00833	0.99167	0.04563	0.83999
	21 470	→ <sup>4</sup> I <sub>13/2</sub>	0.00601	0.99398	0.03878	0.60544

Electronic spectral data of Ln(III) complexes of Pyzh. Ref. [301].

Complexes	Band max. (cm <sup>-1</sup> )		S'L'J' <sup>†</sup>	Oscillator strength (P × 10 <sup>6</sup> )	Calculated parameters
	Nujol	MeOH			
[Pr(Pyzh) <sub>3</sub> Cl <sub>2</sub> ]Cl·EtOH	6329	—	<sup>3</sup> F <sub>3</sub>	—	$\bar{\beta} = 0.9947$
	6896	—	<sup>3</sup> F <sub>4</sub>	—	$b^{1/2} = 0.0513$
	9756	9569	<sup>1</sup> G <sub>4</sub>	3.86	$\% \delta = 0.5302$
	16 949*	16 949*	<sup>1</sup> D <sub>2</sub>	9.43	$\eta = 0.0026$
	20 833	20 964	<sup>3</sup> P <sub>0</sub>	3.67	
	21 212	—	<sup>3</sup> P <sub>1</sub> + <sup>1</sup> I <sub>6</sub>	2.11	
	22 366*	22 424*	<sup>3</sup> P <sub>2</sub>	4.15	
[Nd(Pyzh) <sub>3</sub> Cl <sub>2</sub> ]Cl·EtOH	12 375	12 578	<sup>4</sup> F <sub>5/2</sub> , <sup>2</sup> H <sub>9/2</sub>	16.16	$\bar{\beta} = 0.9990$
	13 496	13 477	<sup>4</sup> F <sub>7/2</sub> , <sup>2</sup> S <sub>3/2</sub>	14.59	$b^{1/2} = 0.0222$
	17 090*	17 294*	<sup>4</sup> G <sub>5/2</sub>	32.78	$\% \delta = 0.1001$
	18 823*	19 126*	<sup>4</sup> G <sub>7/2</sub>	0.86	$\eta = 0.0005$
	—	19 542	<sup>4</sup> G <sub>9/2</sub>	—	
	21 512	21 637	<sup>4</sup> G <sub>11/2</sub>	—	
	—	23 220	<sup>2</sup> P <sub>1/2</sub>	7.47	
[Sm(Pyzh) <sub>3</sub> Cl <sub>2</sub> ]Cl·EtOH	—	23 892	<sup>2</sup> D <sub>5/2</sub>	—	
	6289*	—	<sup>6</sup> F <sub>1/2</sub>	—	$\bar{\beta} = 0.9914$
	6389	—	<sup>6</sup> H <sub>15/2</sub>	—	$b^{1/2} = 0.0654$
	7142	—	<sup>6</sup> F <sub>5/2</sub>	—	$\% \delta = 0.8649$
	8000	—	<sup>6</sup> F <sub>7/2</sub>	—	$\eta = 0.0043$
	9174	9163	<sup>6</sup> F <sub>9/2</sub>	4.83	
	10 471	10 469	<sup>6</sup> F <sub>11/2</sub>	1.17	
[Eu(Pyzh) <sub>3</sub> Cl <sub>2</sub> ]Cl·EtOH	—	18 613	<sup>4</sup> F <sub>3/2</sub>	—	
	—	24 736	<sup>4</sup> F <sub>7/2</sub>	6.31	
	17 176	16 447	<sup>5</sup> D <sub>0</sub>	—	$\bar{\beta} = 0.9835$
	21 441*	21 412*	<sup>5</sup> D <sub>2</sub>	1.76	$b^{1/2} = 0.0908$
					$\% \delta = 1.6776$
[Dy(Pyzh) <sub>3</sub> Cl <sub>2</sub> ]Cl·EtOH					$\eta = 0.0083$
	9089	9091	<sup>6</sup> F <sub>9/2</sub>	2.41	$\bar{\beta} = 0.9976$
	10 873	10 967	<sup>6</sup> F <sub>7/2</sub>	2.86	$b^{1/2} = 0.0344$
	12 527	12 405	<sup>6</sup> F <sub>5/2</sub>	2.62	$\% \delta = 0.2385$
	13 072	13 182	<sup>6</sup> F <sub>3/2</sub>	0.87	$\eta = 0.0011$
	23 329	<sup>4</sup> G <sub>11/2</sub>	—		

<sup>†</sup>The ground state terms for the Pr(III), Nd(III), Sm(III), Eu(III) and Dy(III) complexes are, <sup>3</sup>H<sub>4</sub>, <sup>4</sup>I<sub>9/2</sub>, <sup>6</sup>H<sub>5/2</sub>, <sup>7</sup>F<sub>0</sub> and <sup>6</sup>H<sub>14/2</sub>, respectively.

\*Hypersensitive transition bands.

Electronic spectral data ( $\text{cm}^{-1}$ ) and related bonding parameters of lanthanide(III) nitrate complexes of CAAP. Ref. [302].

Complex	$\text{Ln}(\text{NO}_3)_3$ electronic spectra bands	Complex electronic spectra bands	Energy levels	$(1 - \beta)$	$\beta$	$b^{1/2}$	$\delta\%$	$\eta$
$\text{Pr}(\text{NO}_3)_3 \cdot 2\text{CAAP}$	22 470	22 320	$^3\text{H}_4 \rightarrow ^3\text{P}_2$	0.0066	0.9934	0.0408	0.6715	0.0033
	21 280	21 100	$\rightarrow ^3\text{P}_1$	0.0084	0.9916	0.0459	0.8613	0.0042
	20 830	20 650	$\rightarrow ^3\text{P}_0$	0.0086	0.9914	0.0464	0.8715	0.0043
	16 950	16 750	$\rightarrow ^1\text{D}_2$	0.0118	0.9882	0.0543	1.1930	0.0056
$\text{Nd}(\text{NO}_3)_3 \cdot 2\text{CAAP}$	19 420	19 250	$^4\text{I}_{9/2} \rightarrow ^2\text{G}_{9/2}$	0.0087	0.9913	0.0467	0.8827	0.0044
	17 390	17 200	$\rightarrow ^4\text{G}_{9/2}, ^2\text{G}_{7/2}$	0.0109	0.9891	0.0522	1.1040	0.0055
	13 420	13 200	$\rightarrow ^2\text{S}_{3/2}, ^4\text{F}_{7/2}$	0.0164	0.9836	0.0640	1.6663	0.0082
	12 500	12 350	$\rightarrow ^4\text{F}_{5/2}, ^4\text{H}_{9/2}$	0.0120	0.9880	0.0547	1.2145	0.0060
$\text{Sm}(\text{NO}_3)_3 \cdot 2\text{CAAP}$	24 850	24 720	$^4\text{H}_{5/2} \rightarrow ^4\text{F}_{9/2}$	0.0052	0.9948	0.0361	0.5257	0.0026
	24 100	23 820	$\rightarrow ^6\text{P}_{5/2}$	0.0116	0.9884	0.0538	1.1746	0.0058
	21 600	21 450	$\rightarrow ^4\text{I}_{13/2}$	0.0069	0.9931	0.0416	0.6988	0.0035

Electronic spectral data ( $\text{cm}^{-1}$ ) and related bonding parameters of lanthanide(III) perchlorate complexes of CAAP. Ref. [302].

Complex	$\text{Ln}(\text{ClO}_4)_3$ electronic spectra bands	Complex electronic spectra bands	Energy levels	$(1 - \beta)$	$\beta$	$b^{1/2}$	$\delta\%$	$\eta$
$\text{Pr}(\text{ClO}_4)_3 \cdot 4\text{CAAP}$	22 470	22 350	$^3\text{H}_4 \rightarrow ^3\text{P}_2$	0.0053	0.9947	0.0365	0.5368	0.0026
	21 325	21 200	$\rightarrow ^3\text{P}_1$	0.0058	0.9942	0.0382	0.5894	0.0029
	20 750	20 600	$\rightarrow ^3\text{P}_0$	0.0072	0.9928	0.0425	0.7272	0.0036
	17 000	16 860	$\rightarrow ^1\text{D}_2$	0.0082	0.9918	0.0453	0.8298	0.0041
$\text{Nd}(\text{ClO}_4)_3 \cdot 4\text{CAAP}$	19 460	19 650	$^4\text{I}_{9/2} \rightarrow ^2\text{G}_{9/2}$	0.0071	0.9929	0.0422	0.7191	0.0035
	17 380	17 260	$\rightarrow ^4\text{G}_{5/2}, ^2\text{G}_{7/2}$	0.0069	0.9931	0.0415	0.6948	0.0034
	13 680	13 600	$\rightarrow ^2\text{S}_{3/2}, ^4\text{F}_{7/2}$	0.0058	0.9942	0.0382	0.5874	0.0029
	12 470	12 400	$\rightarrow ^4\text{F}_{5/2}, ^4\text{H}_{9/2}$	0.0056	0.9944	0.0374	0.5641	0.0028
$\text{Sm}(\text{ClO}_4)_3 \cdot 4\text{CAAP}$	24 870	24 740	$^4\text{H}_{5/2} \rightarrow ^4\text{F}_{9/2}$	0.0052	0.9948	0.0361	0.5247	0.0026
	24 000	23 760	$\rightarrow ^6\text{P}_{5/2}$	0.0100	0.9900	0.0500	1.0101	0.0050
	21 550	21 450	$\rightarrow ^4\text{I}_{13/2}$	0.0046	0.9954	0.0340	0.4661	0.0023



Calculated spectral parameters. Ref. [303].

Complex	$\beta$	$b^{1/2}$	$\delta\%$	$\eta \times 10^{-3}$
[Pr(LH <sub>2</sub> ) <sub>2</sub> Cl · H <sub>2</sub> O]	0.9871	0.0803	1.3069	6.51
[Nd(LH <sub>2</sub> ) <sub>2</sub> Cl · H <sub>2</sub> O]	0.9880	0.0775	1.3069	6.05
[Sm(LH <sub>2</sub> ) <sub>2</sub> Cl · H <sub>2</sub> O]	0.9896	0.0721	1.0509	5.24
[Ho(LH <sub>2</sub> ) <sub>2</sub> Cl · H <sub>2</sub> O]	0.9913	0.0659	0.8776	4.37
[Er(LH <sub>2</sub> ) <sub>2</sub> Cl · H <sub>2</sub> O]	0.9926	0.0608	0.7455	3.72

Oscillator strengths for Nd(III) in aqueous solutions ( $P_{\text{exp}} \times 10^6$ ). Ref. [304].

Transition (assignment) <sup>a</sup>	Energy (cm <sup>-1</sup> )	[Nd(pya) <sub>3</sub> · 3H <sub>2</sub> O]				Aquo ion (25°C) <sup>b</sup>
		25.0 ± 0.5°C	50.0 ± 0.5°C	75.0 ± 0.5°C	9.0 ± 0.5°C	
<sup>4</sup> I <sub>9/2</sub> → <sup>4</sup> S <sub>3/2</sub> , <sup>4</sup> F <sub>7/2</sub>	13 000–14 100	11.4	11.1	10.8	10.6	8.78
<sup>4</sup> I <sub>9/2</sub> → <sup>4</sup> G <sub>5/2</sub> , <sup>2</sup> G <sub>7/2</sub>	16 600–18 200	18.2	18.0	17.9	17.6	9.34
<sup>4</sup> I <sub>9/2</sub> → <sup>2</sup> K <sub>13/2</sub> , <sup>4</sup> G <sub>7/2</sub> , <sup>4</sup> G <sub>9/2</sub>	18 600–20 200	9.8	9.6	9.5	9.3	6.82

Electronic spectral data for K [Nd(TCS)<sub>2</sub>]. Ref. [305].

Band max. (cm <sup>-1</sup> )	Assignment	Spectral parameters
11 425	<sup>4</sup> I <sub>9/2</sub> → <sup>4</sup> F <sub>3/2</sub>	$\bar{\beta} = 0.995$ $b^{1/2} = 0.050$ $\delta\% = 0.50$
12 420	→ <sup>4</sup> F <sub>5/2</sub>	
13 420	→ <sup>4</sup> F <sub>9/2</sub>	
17 095	→ <sup>4</sup> G <sub>5/2</sub> , <sup>2</sup> G <sub>7/2</sub>	
18 870		

Spectral parameters are calculated for hypersensitive transition <sup>4</sup>I<sub>9/2</sub> → <sup>4</sup>G<sub>5/2</sub>, <sup>2</sup>G<sub>7/2</sub>.Nd(III) trifluoroacetate complex of 3 picoline-*N*-oxide. Ref. [306].

$\beta = 0.989$	$b^{1/2} = 0.0735$	$\delta = 1.09$
-----------------	--------------------	-----------------

Electronic spectral data and related bonding parameters of lanthanide(III) chloride complexes of INH-BENZ. Ref. [307].

$\text{Ln}^{3+}$	$\text{LnCl}_3$ ( $\text{cm}^{-1}$ )	$\text{Ln}(\text{INH-BENZ})_2\text{Cl}_3$ ( $\text{cm}^{-1}$ )	J-level	$(1 - \beta)$	$\beta$	$b^{1/2}$	$\delta\%$	$\eta$	
Pr	22470	22350	$^3\text{H}_4 \rightarrow$	$^3\text{P}_2$	0.00534	0.99466	0.03655	0.53686	0.00268
	21325	21210		$^3\text{P}_1$	0.00539	0.99461	0.03670	0.54192	0.00270
	20750	20600		$^3\text{P}_0$	0.00722	0.99278	0.04248	0.72725	0.00363
	17000	16800		$^1\text{D}_2$	0.01176	0.98824	0.05422	1.18999	0.00593
Nd	19550	19450	$^4\text{I}_{9/2} \rightarrow$	$^2\text{G}_{9/2}$	0.00511	0.99409	0.03574	0.51362	0.00256
				$^4\text{G}_{5/2}$	0.00633	0.99367	0.03978	0.63703	0.00319
				$^2\text{G}_{7/2}$					
	13660	13620	$^2\text{S}_{3/2}$	0.00292	0.99708	0.02701	0.29285	0.00147	
	12470	12400	$^4\text{F}_{7/2}$						
			$^4\text{F}_{5/2}$		0.00561	0.99439	0.03744	0.56416	
Sm	24870	24800	$^6\text{H}_{5/2} \rightarrow$	$^4\text{F}_{9/2}$	0.00281	0.99719	0.02660	0.28179	0.00141
	24000	23800		$^6\text{P}_{5/2}$	0.00833	0.99167	0.04563	0.83999	0.00419
	21550	21500		$^4\text{I}_{13/2}$	0.00232	0.99768	0.02408	0.23253	0.00117

Electronic spectral data of Ln(III) complexes of dabbe. Ref. [308].

Complex	Band max (cm <sup>-1</sup> )		S'L/J'	P × 10 <sup>6</sup> Exptl. (calc.)	Bonding parameter
	Nujol	MeOH			
[Pr(dabbe) <sub>2</sub> Cl <sub>3</sub> ] · 4H <sub>2</sub> O	6323		<sup>3</sup> F <sub>3</sub>		β = 0.9924
	6875		<sup>3</sup> F <sub>4</sub>		b <sup>1/2</sup> = 0.0510
	9654	9563	<sup>1</sup> G <sub>4</sub>	3.81 (3.36)	%δ = 0.5322
	16955*	16794*	<sup>1</sup> D <sub>2</sub>	1.53 (1.58)	η = 0.0024
	20842	20661	<sup>3</sup> P <sub>0</sub>	2.50 (2.07)	
	22374*	22426	<sup>3</sup> P <sub>2</sub>	0.76 (1.34)	
[Nd(dabbe) <sub>2</sub> Cl <sub>3</sub> ] · 4H <sub>2</sub> O	11431	11427	<sup>4</sup> F <sub>3/2</sub>		β = 0.9946
	12474	12565	<sup>4</sup> F <sub>5/2</sub>	5.61 (5.74)	b <sup>1/2</sup> = 0.0322
	13284	13475	<sup>4</sup> F <sub>1/2</sub> , <sup>2</sup> S <sub>1/2</sub>	6.17 (16.34)	%δ = 0.5322
	17089*	17165*	<sup>4</sup> G <sub>5/2</sub> , <sup>2</sup> G <sub>1/2</sub>	31.54 (33.81)	η = 0.0031
	18889*	19095*	<sup>4</sup> G <sub>1/2</sub>	14.75 (14.31)	
		19568	<sup>4</sup> G <sub>9/2</sub>		
	21514	21668	<sup>4</sup> G <sub>11/2</sub>		
[Sm(dabbe) <sub>2</sub> Cl <sub>3</sub> ] · 4H <sub>2</sub> O	6254*		<sup>4</sup> F <sub>1/2</sub>		β = 0.9918
	6347		<sup>6</sup> H <sub>15/2</sub>		b <sup>1/2</sup> = 0.0656
	7166		<sup>4</sup> F <sub>5/2</sub>		%δ = 0.8456
	9174	9156	<sup>6</sup> F <sub>9/2</sub>	4.55 (4.83)	η = 0.0044
	10400	10444	<sup>4</sup> F <sub>11/2</sub>	1.57 (1.15)	
[Dy(dabbe) <sub>2</sub> Cl <sub>3</sub> ] · 4H <sub>2</sub> O	7655*		<sup>6</sup> H <sub>9/2</sub> , <sup>6</sup> F <sub>11/2</sub>		β = 0.9954
	9131	9089	<sup>6</sup> F <sub>9/2</sub>	2.23 (2.04)	b <sub>1/2</sub> = 0.0450
	10855	10961	<sup>4</sup> F <sub>7/2</sub>	3.26 (3.20)	%δ = 0.6713
	12448	12406	<sup>4</sup> F <sub>5/2</sub>	2.85 (2.77)	η = 0.0012
	13085	13156	<sup>6</sup> F <sub>5/2</sub>	0.73 (1.22)	
		32464	<sup>4</sup> G <sub>11/2</sub>		

\*Hypersensitive bands.

Electronic spectral data of heterobinuclear complexes. Ref. [309].

Complex	Band (cm <sup>-1</sup> )	Assignment	Bonding parameter
PrCl <sub>3</sub> Zn(aps) <sub>2</sub> (H <sub>2</sub> O) <sub>2</sub>	20 410	<sup>3</sup> H <sub>4</sub> → <sup>3</sup> P <sub>4</sub>	$\bar{\beta} = 0.997$ $b^{1/2} = 0.035$ $\delta\% = 0.251$ $\eta = 0.0015$
NdCl <sub>3</sub> Zn(aps) <sub>2</sub> (H <sub>2</sub> O) <sub>2</sub>	33 898	<sup>4</sup> I <sub>9/2</sub> → <sup>2</sup> D <sub>5/2</sub>	$\bar{\beta} = 0.993$
	27 778	→ <sup>2</sup> D <sub>3/2</sub>	$b^{1/2} = 0.059$
	17 241*	→ <sup>4</sup> G <sub>5/2</sub> , <sup>2</sup> G <sub>7/2</sub>	$\delta\% = 0.251$
	13 514	→ <sup>4</sup> S <sub>3/2</sub>	$\eta = 0.0035$
	12 500	→ <sup>2</sup> H <sub>9/2</sub>	
SmCl <sub>3</sub> Zn(aps) <sub>2</sub> (H <sub>2</sub> O) <sub>2</sub>	33 333	<sup>6</sup> H <sub>5/2</sub> → <sup>7</sup> F <sub>5/2</sub>	$\bar{\beta} = 0.991$
	28 169	→ <sup>4</sup> H <sub>7/2</sub>	$b^{1/2} = 0.066$
	26 667	→ <sup>4</sup> L <sub>17/2</sub>	$\delta\% = 0.888$
	22 727	→ <sup>4</sup> I <sub>15/2</sub>	$\eta = 0.0045$
EuCl <sub>3</sub> Zn(aps) <sub>2</sub> (H <sub>2</sub> O) <sub>2</sub>	27 778	<sup>7</sup> F <sub>1</sub> → <sup>5</sup> L <sub>9</sub>	$\bar{\beta} = 0.995$
	26 316	→ <sup>5</sup> G <sub>4</sub>	$b^{1/2} = 0.049$
	23 810	→ <sup>5</sup> D <sub>3</sub>	$\delta\% = 0.482$ $\eta = 0.0025$

chapter 9

---

PHOTOELECTRON SPECTROSCOPY OF RARE  
EARTHS

---

---

# CONTENTS

---

1. Basics . . . . .	735
2. Applications . . . . .	752
3. Oxidation . . . . .	762
4. Application in lanthanide complexes . . . . .	763
References . . . . .	776

## 1. Basics

The fundamental physical processes occurring in photoelectron spectroscopy are given in Table 9.1. The primary process is an ionization step induced by a photon. Photoionization produces an electron with discrete kinetic energy. The kinetic energy of the electron, KE is given by

$$E_{KE} = h\nu - E_b,$$

where  $h\nu$  is the energy of the incident photon and  $E_b$  is the binding energy of the electron. When X-ray sources such as Mg  $K_\alpha$  or Al  $K_\alpha$  are used, one has XPS or ESCA spectra which give low resolution of core levels. When ultraviolet sources such as He I and He II are used, one has PES or UPS spectra which gives high resolution of valence bands. Monochromatized synchrotron radiation bridges XPS and UPS and gives information on high resolution on many core levels.

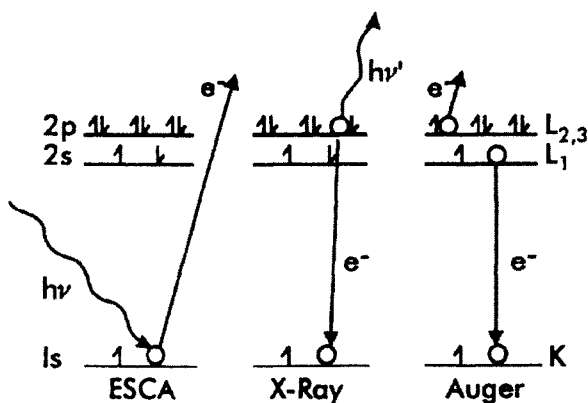
Electron ionization in an atom results in an excited ion and a second electron. Because of electron–electron repulsion interactions, electrons of discrete energies are not observed. In the secondary process the excited ion may give rise to photons which can lead to X-ray fluorescence. The excited ion may ionize further and emit an Auger electron of discrete energy. It is useful to note that photoionization may give rise to either an ESCA electron or an Auger electron. On the other hand, electron ionization can give rise to only Auger electrons. The kinetic energy of the Auger electrons is independent of photon energy while the kinetic energy of an ESCA electron depends on photon energy.

TABLE 9.1  
Fundamental physical processes in electron spectroscopy.

---

Primary processes
(A) Photoionization
$A + h\nu \rightarrow A^{+*} + e^-$ (discrete energy, ESCA)
$E(\text{kinetic}) = E(\text{photon}) - E(\text{binding})$
(B) Electron Ionization
$A + e_0^- \rightarrow A^{+*} + 2e^-$ (not discrete energy)
Secondary processes
(C) $A^{+*} \rightarrow A^+ + h\nu'$ (X-ray)
(D) $A^{+*} \rightarrow A^{++} + e^-$ (Discrete energy, Auger)
$E(\text{Auger})$ does not depend on photon energy
A = atom or molecule; $A^{+*}$ = excited ion

---



### ENERGETICS

$$\text{ESCA: } T_e = h\nu - E_B(1s)$$

$$\text{X-Ray: } h\nu = E_B(1s) - E_B(2p)$$

$$\text{Auger: } T_e = E_B(1s) - E_B(2s) - E_B'(2p)$$

Fig. 9.1.

The processes involved in ESCA, X-ray and Auger spectroscopy are illustrated in Fig. 9.1. The figure illustrates the photoionization of a 1s electron.

In ESCA the incident photon beam ejects a 1s electron from the atom. In the middle part of the figure, an electron from the 2p level, drops to the 1s level and emits photons in the process which can be  $K_{\alpha}$  X-rays. When a 2s electron drops to the 1s level with the simultaneous ejection of a 2p electron as shown on the right side of the figure, we have the KLL Auger process. It is useful to note that X-ray emission and the Auger process are competitive with each other and that the Auger process dominates at low energies (1000 eV) and X-ray emission is dominant at high energies (10 000 eV).

Fig. 9.2 is a block diagram of an ESCA photoelectron spectrometer.

The spectrometer consists of an X-ray source, a sample, an electron energy analyser, a detector, and a data display system. The electron energy analyser should have high resolution in order to obtain chemical information. It is necessary to have a vacuum of  $10^{-6}$  Torr or lower but  $10^{-10}$  Torr is preferable.

The analytical characteristics of ESCA are summarized in Table 9.2.

ESCA is capable of providing information on chemical bonding such as oxidation states of elements and structures of organic molecules. The technique can detect all elements except hydrogen and helium. In general there is very little overlap of spectral lines with some exceptions such as Pt 4f and Al 2p, Hg 4f and Si 2p.

Surface sensitivity is given by the intensity relationship

$$I = I_0(I - e^{-d/\lambda}),$$



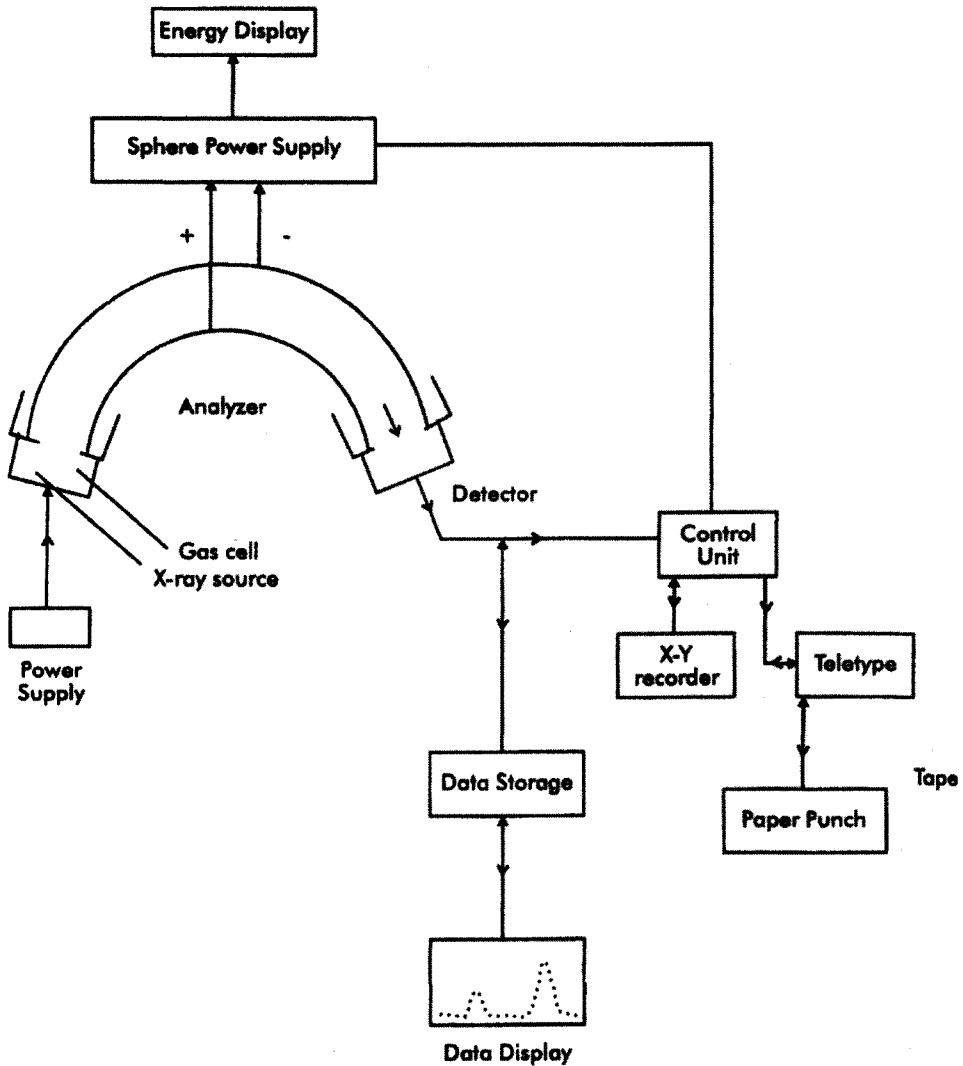


Fig. 9.2. Block diagram of McPherson ESCA photoelectron spectrometer.

where  $I$  is the intensity from an infinitely thick specimen ( $\sim 100 \text{ \AA}$ ),  $d$  is the thickness of analysed sample in  $\text{\AA}$ , and  $\lambda$  is the escape depth or mean free path of electrons in the sample. When  $d \approx 2\lambda$ , we have  $I \approx 80\% I_0$ . Thus in many cases monolayers and fractions of monolayers can be readily detected. ESCA is ideal for studying adsorption and other reactions on surfaces.

Core levels of all elements except hydrogen can be detected using an X-ray source. Valence bands can be obtained using a UV source. Core level binding energies are characteristic of the atom and the valence band spectrum of an adsorbed molecule is usually characteristic of the molecule. The spectra of adsorbed CO and C<sub>6</sub>H<sub>6</sub> resemble the gas

TABLE 9.2  
Analytical characteristics of ESCA.

---

Energy range
Kinetic energies: 100–1500 eV
Escape depth: 20 Å
Peak location: ±0.1 eV
Chemical information
Oxidation state
Organic structure
Bonding information
Elemental sensitivity
Elements $Z > 2$
Specificity: very good
Sensitivity variations: 50×
Quantitative analysis
Absolute ±30%
Relative ±5%
Detection limit: 0.1% monolayer
Matrix effects: some
Other aspects
Vacuum: $10^{-5}$ – $10^{-10}$ Torr
Depth profiling capability: yes, slow
$x$ - $y$ resolution: none
Speed: slow; typical run in 30 min
Sample destruction: none in 95% of the samples

---

phase spectra but are not identical. Core level binding energies for rare earths are given in Table 9.3.

The binding energies vary with the chemical environment, usually by about 10 eV for one element. The ESCA spectrum of trifluoroacetate shows the different peaks for  $\text{CH}_3$ ,  $\text{CH}_2$ , CO and  $\text{CF}_3$ . It is possible in the Is spectra to distinguish the peaks from oxygen in water and adsorbed molecular nitrogen from the adsorbed nitrogen atom.

It is possible to carry out semiquantitative or even quantitative analysis by ESCA using known or calculated cross-sections. The area of an ESCA peak is given by the relationship

$$A_x \propto n_x \sigma_x (\text{KE})_x^{1.7},$$

where  $n$  is the number of  $x$  atoms,  $\sigma$  is the probability of exciting a photoelectron (cross-section) and  $(\text{KE})_x^{1.7}$  reflects the sensitivity of the instrument.

The proportionality constant is not known but is a constant. We can then write

$$\frac{n_x}{n_y} = \frac{\sigma_y (\text{KE})_y^{1.7} A_x}{\sigma_x (\text{KE})_x^{1.7} A_y}.$$

The width and cross-sections of peaks vary greatly from one level to another. The cross-sections also vary with photon energy.

TABLE 9.3  
Binding energies (line positions for Al K<sub>α</sub> X-rays).

Atomic Number/Element	Photoelectron Lines																				
	3s	3p <sub>1/2</sub>	3p <sub>3/2</sub>	3d <sub>3/2</sub>	3d <sub>5/2</sub>	4s	4p <sub>1/2</sub>	4p <sub>3/2</sub>	4d <sub>3/2</sub>	4d <sub>5/2</sub>	4f <sub>5/2</sub>	4f <sub>7/2</sub>	5s	5p <sub>1/2</sub>	5p <sub>3/2</sub>	5d <sub>3/2</sub>	5d <sub>5/2</sub>	6s	6p <sub>1/2</sub>	6p <sub>3/2</sub>	
57 La	1208	1128	853	836	275	213	197	106		103			34								17
58 Ce	1272	1184	902	884	290	223	207		112	109			36								18
59 Pr	1339	1242	952	932	305	234	218			115 <sup>o</sup>			38								18
60 Nd		1301	1003	981	320	245	228			121			39								19
61 Pm			1060	1034	337	264	242			129			38								22
62 Sm			1108	1081	349	283	250			129			41								19
63 Eu			1155	1126	363	289	255			128			39								19
64 Gd			1218	1186	378	291	272			140			43								21
65 Tb			1276	1241	396	322	285			146		8	45								22
66 Dy			1333	1296	417	337	297			152		8	48								23
67 Ho			1393	1352	435	353	309			160		9	49	30							24
68 Er					451	368	321			167		9	52	31							24
69 Tm					470	384	333			175		8	53	32							25
70 Yb					482	389	341			182		3	51	30							24
71 Lu					509	413	360	206		196	9	7	57	34							27

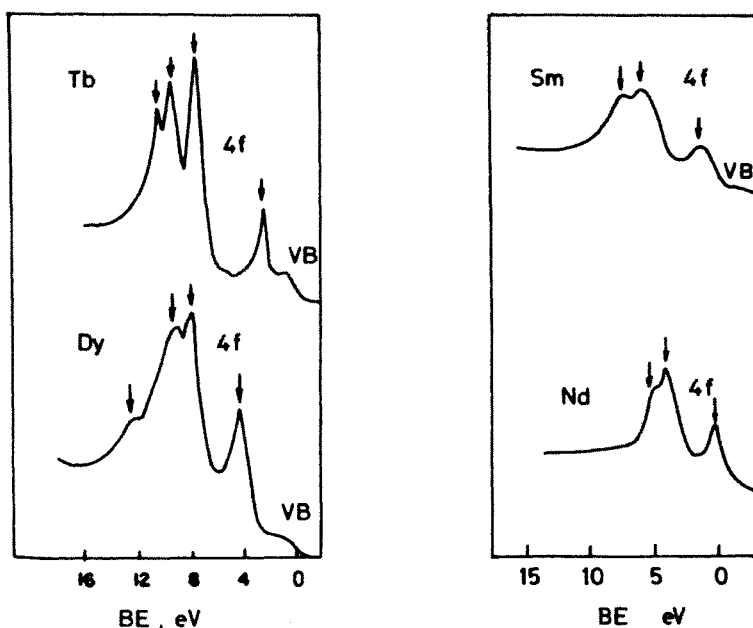


Fig. 9.3. Multiplet structure in 4f region of rare earth metals.

Photoelectron spectroscopy is useful for the study of solids and surfaces. In particular, X-ray and UV photoelectron spectroscopy has been used in studying rare earth systems. The important aspects such as valence band region and the core levels have been studied intensively in rare earth systems. The valence band region of rare earth metals and rare earth oxides have been studied well by photoelectron spectroscopy [1–8]. The final state multiplet structure of the 4f level has been studied both theoretically and experimentally [1–8]. The final 4f hole states of rare earth ions are given in Table 9.4. Typical multiplet structures are given in Fig. 9.3. The relative intensities of the multiplet peaks of the 4f level may be calculated by using the fractional parentage coefficients given by Cox [9].

The location of the 4f level in Ce has been found to be 1.9 eV below the Fermi edge from a study of the valence region of Ce and Cerium plus the oxygen system by ultraviolet photoelectron (UVPE) and X-ray photoelectron spectroscopy (XPES) [4,5]. This assignment finds confirmation by a study involving synchrotron radiation [6]. Steiner's studies of cerium alloys resulted in assigning a binding energy of 0.5 eV for the 4f level of  $\gamma$ -Ce. Such disparities can be attributed to the limitations of X-ray photoelectron spectroscopy (XPS) in the determination of ground state electronic properties.

The 4s and 5s core levels of rare-earth metals shown in Fig. 9.4 give a doublet structure instead of a single peak [10–13]. The doublet feature is due to the exchange interaction between the core-hole state of the s level and the localized unpaired 4f electrons. The splitting due to such exchange interaction is greater for 4s level than 5s level because the overlap of 4f orbital with 4s is greater than 4f orbital with 5s orbital. The splitting due to the exchange interaction is the same as the energy separation of the two peaks in the

TABLE 9.4  
States Arising in Ionization from  $f^n$  free-ion-configurations with first-order spin-orbit coupling [9].

Initial state		Final (LS) state and intensity		Multiplet components (J) and intensities	
$f^2$	$^3H_4$	$^2F$	2.000	5/2	1.714
				7/2	0.286
$f^3$	$^4I_{9/2}$	$^3H$	2.333	4	1.890
		$^3F$	0.667	5	0.424
$f^4$	$^5I_4$	$^4I$	2.545	2	0.563
				9/2	1.903
		$^4G$	0.955	11/2	0.599
				5/2	0.658
$^4F$	0.500	7/2	0.263		
		3/2	0.371		
$f^5$	$^6H_{5/2}$	$^5I$	2.758	5/2	0.114
				4	1.755
		$^5G$	1.266	5	0.919
				2	0.513
				3	0.575
				4	0.165
$^5F$	0.500	1	0.168		
		2	0.234		
$^5D$	0.476	0	0.149		
		1	0.224		
$f^6$	$^7F_0$	$^6H$	3.143	5/2	0.898
				7/2	2.245
		$^6F$	2.000	5/2	1.428
				7/2	0.571
$^6P$	0.857	5/2	0.816		
$f^7$	$^8S_{7/2}$	$^7F$	7.000	0	0.143
				1	0.429
				2	0.714
				3	1.000
				4	1.286
				5	1.571
$f^8$	$^7F_6$	$^8S$	1.143	6	1.857
				7/2	1.143
		$^6I$	1.857	15/2	0.303
				17/2	1.500
				11/2	0.101
				13/2	0.424
		$^6H$	1.571	15/2	1.030
				9/2	0.134
				11/2	0.434
				13/2	0.694
$^6G$	1.286	7/2	0.138		
		9/2	0.383		
		11/2	0.460		
$^6F$	1.000	9/2	0.383		
		11/2	0.460		

TABLE 9.4  
(Continued.)

Initial state		Final (L.S) state and intensity		Multiplet components (J) and intensities					
f <sup>9</sup>	<sup>6</sup> H <sub>15/2</sub>	<sup>6</sup> D	0.714	5/2	0.107				
				7/2	0.307				
				9/2	0.301				
		<sup>6</sup> P	0.429	5/2	0.230				
				7/2	0.199				
				7F	2.333	5	0.583		
		f <sup>10</sup>	<sup>5</sup> I <sub>8</sub>	<sup>5</sup> L	1.545	6	1.674		
						9	0.136		
						10	1.400		
						<sup>5</sup> K	1.364	8	0.211
								9	1.131
						<sup>5</sup> I	1.182	7	0.240
								8	0.913
						<sup>5</sup> H	1.000	6	0.233
7	0.739								
f <sup>11</sup>	<sup>5</sup> I <sub>8</sub>					<sup>5</sup> G	0.817	5	0.195
		6	0.605						
		<sup>5</sup> F	0.310	5	0.232				
				<sup>5</sup> D	0.454	4	0.454		
		f <sup>10</sup>	<sup>5</sup> I <sub>8</sub>	<sup>6</sup> H	2.800	11/2	0.138		
						13/2	0.646		
						15/2	2.004		
						<sup>6</sup> F	0.800	11/2	0.727
						<sup>4</sup> M	1.462	21/2	1.375
								<sup>4</sup> L	1.307
<sup>4</sup> K	1.189					19/2	1.167		
						15/2	0.161		
<sup>4</sup> I	1.000					17/2	1.018		
						13/2	0.154		
<sup>4</sup> H	0.379	15/2	0.837						
		13/2	0.318						
<sup>4</sup> G	0.692	11/2	0.611						
		<sup>4</sup> F	0.405	9/2	0.405				
f <sup>11</sup>	<sup>1</sup> I <sub>15/2</sub>	<sup>5</sup> I	3.182	6	0.169				
				7	0.736				
				8	2.263				
		<sup>5</sup> G	1.193	5	0.241				
				6	0.913				
		<sup>5</sup> F	0.625	5	0.550				
		<sup>3</sup> M	1.462	10	1.400				
				<sup>3</sup> L	1.307	9	1.206		
		<sup>3</sup> K	1.154	7	0.117				
				8	1.033				
<sup>3</sup> I	0.364	7	0.320						
<sup>3</sup> H	0.846	6	0.747						

TABLE 9.4  
(Continued.)

Initial state		Final (LS) state and intensity		Multiplet components (J) and intensities			
f <sup>12</sup>	<sup>3</sup> H <sub>6</sub>	<sup>3</sup> G	0.454	5	0.415		
		<sup>3</sup> F	0.382	4	0.382		
		<sup>4</sup> I	3.677	11/2	0.212		
				13/2	0.914		
				15/2	2.536		
		<sup>4</sup> G	1.688	7/2	0.106		
				9/2	0.419		
				11/2	1.157		
		<sup>4</sup> F	0.667	7/2	0.151		
				9/2	0.486		
				17/2	1.500		
		f <sup>13</sup>	<sup>2</sup> F <sub>7/2</sub>	<sup>2</sup> L	1.545	17/2	1.500
				<sup>2</sup> K	1.364	15/2	1.288
				<sup>2</sup> I	0.263	13/2	0.242
				<sup>2</sup> H	1.000	11/2	0.909
<sup>2</sup> G	0.396			9/2	0.359		
<sup>2</sup> F	0.470			7/2	0.436		
<sup>2</sup> D	0.296			5/2	0.296		
<sup>3</sup> H	4.714			4	0.321		
				5	1.375		
		6	3.018				
<sup>3</sup> F	3.000	2	0.357				
		3	0.875				
		4	1.768				
<sup>3</sup> P	1.286	0	0.107				
		1	0.375				
		2	0.804				
		<sup>1</sup> I	1.857				
		<sup>1</sup> G	1.286				
		<sup>1</sup> D	0.714				
		<sup>1</sup> S	0.143				

doublet band. The splitting or the energy separation of the two peaks is a function of the 4f<sup>n</sup> electron population (i.e.) increasing spin of the rare earth ion. The energy separation of the peaks reaches a maximum for f<sup>7</sup> configuration, followed by a decrease as we move along the series to f<sup>14</sup>. The energy separation of the two peaks ( $\Delta E$ ) as a function of f<sup>n</sup> is shown in Fig. 9.5.

Some metals like Eu and Yb show significant deviations from the smooth curve which are probably due to their divalent behaviour [12]. The splittings due to exchange interactions have been calculated [11] using Van Vleck's theorem [14]. The Slater integrals were evaluated by treating the 4f level as essentially core-like. Such calculations give good agreement for the 5s splittings but overestimate the 4s level splittings (Fig. 9.5). This disparity between calculated and observed splittings may be attributed to configuration interaction which becomes important in the case of 4s and 4f. Configuration interaction

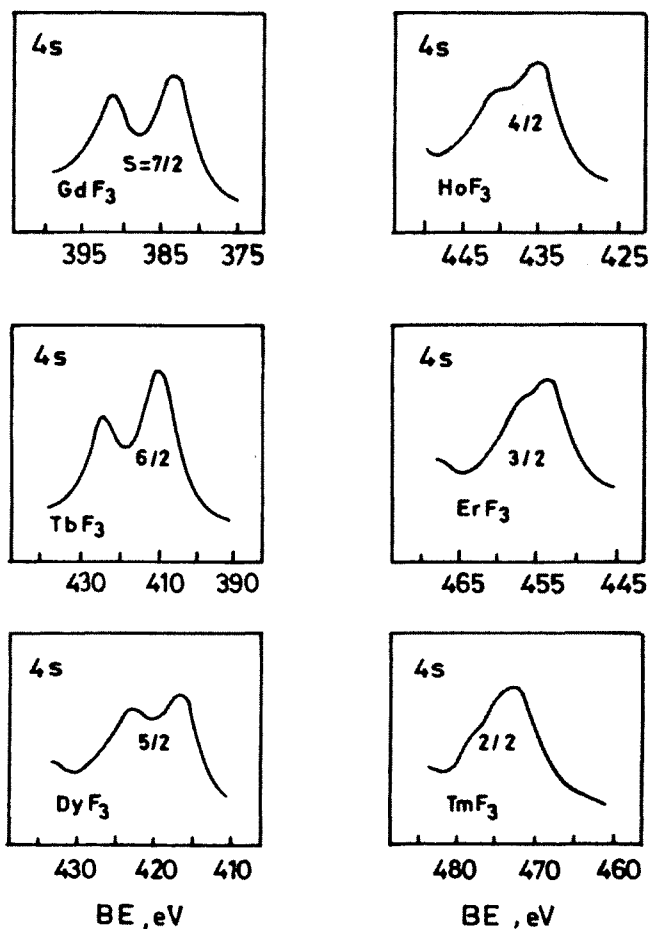


Fig. 9.4. XPS spectra of some rare earth trifluorides showing the doublet structure in the 4s region [50].

has been shown to play a dominant role in suppressing exchange interaction splittings in the case of first transition metal series [15].

In contrast to 4s and 5s levels, 4d levels of rare earth metals show [16–18] extended multiplet structures (Figs 9.6 and 9.7). La of  $4f^0$  and Lu of  $4f^{14}$  configurations give XPS spectra with a doublet structure due to spin–orbit interactions. This is the case in the metallic state as well as in their oxides. The doublet spectra of La 4d and Lu 4d are shown in Fig. 9.8.

Yb has a  $4f^{13}$  configuration and the metal gives a doublet structure due to spin–orbit interaction. On the other hand, oxidized Yb metal gives extended multiplet structure indicating the promotion of one of the f electrons to the valence shell. Fig. 9.9 shows the XPS spectrum of Yb metal, Yb metal with oxygen and  $Yb_2O_3$ . The multiple structure has been attributed to  $4f^n-4d^9$  interaction.



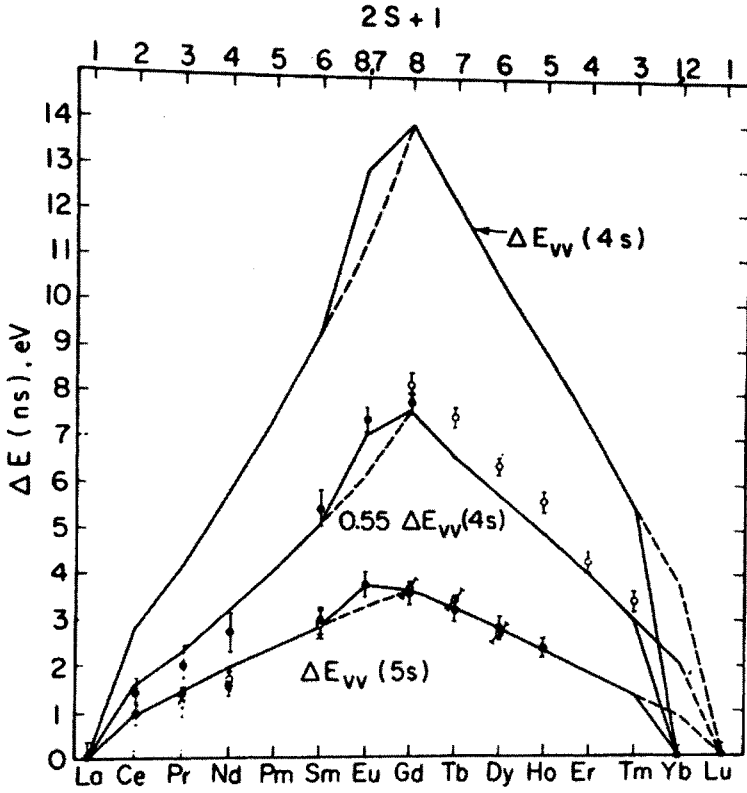


Fig. 9.5. The variation exchange splittings,  $\Delta E$ , in the 4s and 5s regions of rare earth metals and trifluorides through the lanthanide series. The lines drawn are the calculated exchange splittings, showing a good agreement with  $\Delta E_{5s}$  and a large overestimation for  $\Delta E_{4s}$ . Eu and Yb show deviations indicating their divalent nature [50].

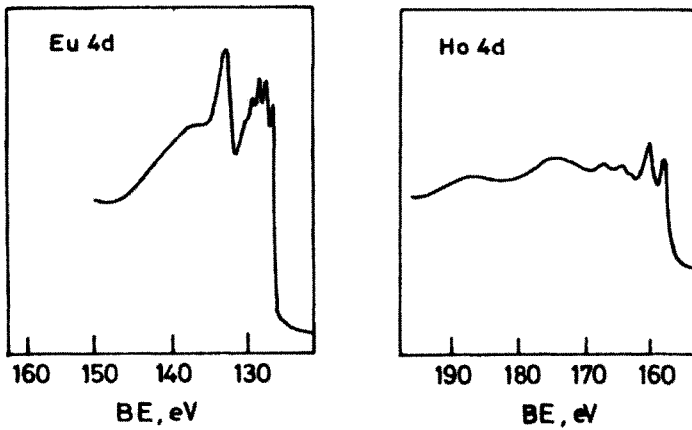


Fig. 9.6. Multiplet structure in XPE spectra of 4d region of rare earth metals [50].

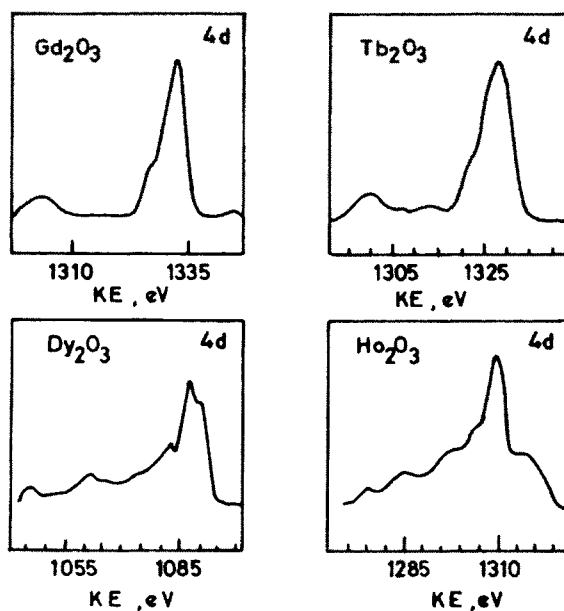


Fig. 9.7. Multiplet structure in the XPE spectra of 4d region of rare earth oxides.

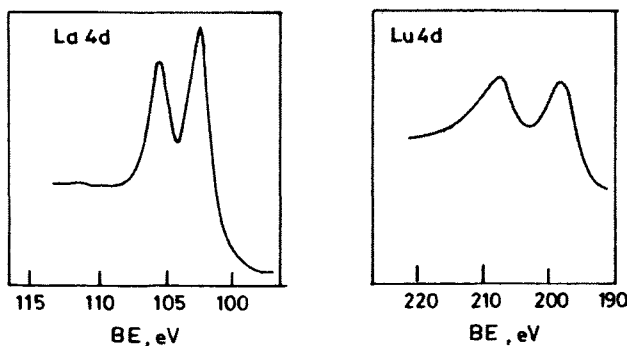


Fig. 9.8. XPE spectra of the 4d region of La and Lu showing the simple spin-orbit split doublet structure in  $4f^0$  and  $4f^{14}$  configurations, respectively [16,17].

Theoretical calculations on the rare earth oxide systems using an intermediate coupling scheme show good agreement with experimentally observed spectra [18,19].

The 3d levels in lanthanides are far removed from 4f levels and the overlap of these two levels if any is very small. As a result, multiplet structure in the 3d region is not expected. Although this is the case, XPS of some lanthanide compounds, particularly elements from lanthanum to neodymium, exhibit splitting in the bands apart from the doublet due to spin-orbit interaction. This type of structure is shown in Figs. 9.10, 9.11 and 9.12. These splittings are known as satellites and originate from multielectronic excitations. In general,

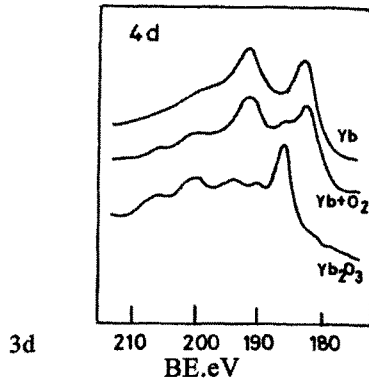


Fig. 9.9. XPE spectra of the region of Yb, Yb + O<sub>2</sub> and Yb<sub>2</sub>O<sub>3</sub>. Yb shows a simple spin-orbit doublet structure indicating a 4f<sup>14</sup> configuration, whereas Yb<sub>2</sub>O<sub>3</sub> shows an extended multiplet structure indicating the promotion of a 4f electron to the valence level [17].

it is common to have charge-transfer satellites. Compounds such as oxides and halides of elements from La to Nd give XPS peaks which are about 2–4 eV removed from the bands due to 3d level. The satellite peaks of lower intensity occur in other levels. The satellite peaks have been studied extensively [19–24] and appear to originate from the interatomic charge-transfer process. The 3d hole created by the ejected electron acts as an extra nuclear charge for the valence electrons resulting in the localization of electrons in the ligand nearer to the metal.

Assuming the 3d band signal to be due to 3d<sup>9</sup>4f<sup>*n*+1</sup>, X<sup>*m*</sup>, the charge transfer state may be written as 3d<sup>9</sup>, 4f<sup>*n*+1</sup>, X<sup>*m*-1</sup>, where *m* denotes the electrons on the ligand X. One of the two states is more stable and the satellite peak due to the charge transfer process can appear either on the lower energy side or higher energy side of the main peak. Usually the peaks due to charge transfer processes appear on the higher binding energy side of the main band and are known as shake-up satellites. When the charge transfer process results in bands located at the lower binding energy side of the main band, these bands are known as shake-down satellites. Shake-down satellites are illustrated in the case of praseodymium and neodymium oxides (Fig. 9.13).

In Fig. 9.12, more than one satellite is seen and these satellites are attributed to charge transfer from oxygen to higher empty levels 5d and 6p of the metal [19,23].

In the case of halides of La, Ce, Pr and Nd, the relative intensity of satellite peaks in comparison to the main peak was found to increase with an increase in the degree of covalent bonding [24]. In the case of lanthanum halides, the intensity of the satellite peaks varied in the order LaF<sub>3</sub> < LaCl<sub>3</sub> < LaBr<sub>3</sub>. On the other hand, the energy separation of the satellite peaks and the main peaks showed no particular trend indicative of the degree of covalency of the bond. In order to ascertain the charge transfer character of the satellite peaks, theoretical calculations involving MSX<sub>α</sub> approximation on clusters of La, Ce, Pr and Nd performed by Jorgenson showed that the Muffin-Tin approximated charge to be high around the metal site. The approximated charge near the metal site after the 3d hole is created, was higher than that before the photo release of the 3d electron. At the same time,

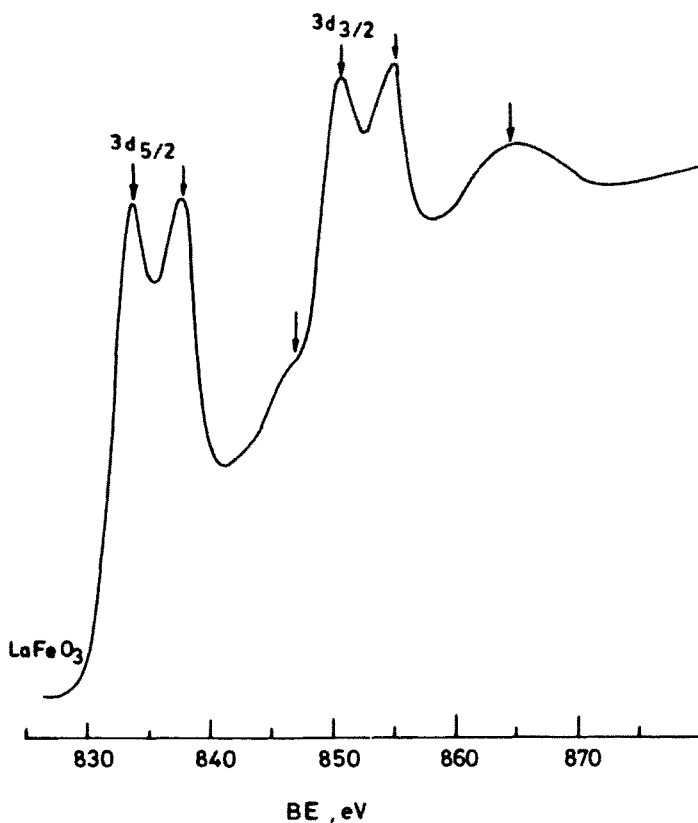


Fig. 9.10. XPE spectra of  $\text{LaFeO}_3$  in the  $\text{La}(3d)$  region showing the charge-transfer satellites at an energy separation of approximately 4 eV from  $3d_{5/2}$  and  $3d_{3/2}$  signals. The weaker satellites at an energy separation of 13–16 eV are attributed to energy loss processes [50].

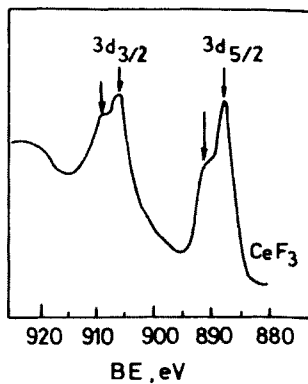


Fig. 9.11. XPE spectra of  $\text{CeF}_3$  in the  $\text{Ce}(3d)$  region showing the existence of charge transfer satellites along with the  $3d_{5/2}$  and  $3d_{3/2}$  signals [50].

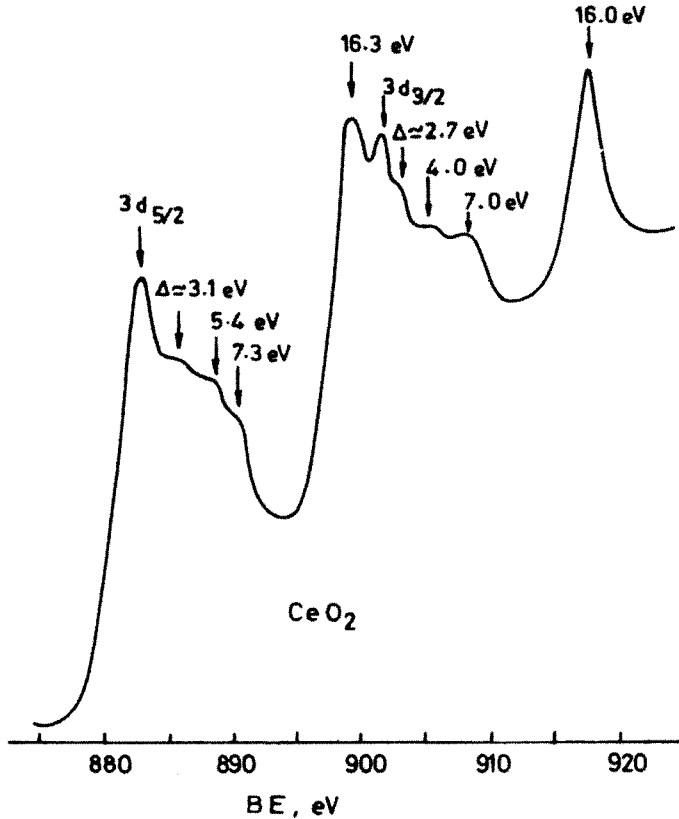


Fig. 9.12. XPE spectra of the 3d region of CeO<sub>2</sub> showing various satellite signals along with 3d<sub>5/2</sub> and 3d<sub>3/2</sub> peaks of Ce [50].

a decrease in charge on the ligand was also observed. Increased charge on the metal had a 4f character as evidenced by wave analysis. The theoretical calculations have been unable to predict the energy separation of the satellite peaks and the main peak accurately [25,26].

In the 3d region of lanthanum oxide (La<sub>2</sub>O<sub>3</sub>) a weak satellite structure removed from the main peak by 16 eV has been observed [27,28] (Fig. 9.10). This structure, having been observed in all other levels including O(1s), was attributed to energy loss. A similar but intense peak is seen in all levels of CeO<sub>2</sub> (Fig. 9.12) and this is also thought to be due to energy loss process. In the case of CeO<sub>2</sub>, the observed intense peak attributed to energy loss has been interpreted as the normal 3d signal (3d<sup>9</sup>4f<sup>0</sup>, X<sup>n</sup> state) with lower binding energy intense peak due to the shake-down charge transfer state with 3d<sup>9</sup>4f<sup>0</sup>, X<sup>n-1</sup>.

In the case of La, Ce, Pr and Nd, a weak band on the lower binding energy side of the 3d band has been observed. The XPS of Ba, La, Ce and Pr are shown in Fig. 9.14. The observed weak band has been attributed to charge transfer from the conduction band (6s, 5d) to the 4f level. In this case, the 3d hole is thought to stabilize the 4f level as compared to the conduction band (6s, 5d) thereby facilitating the intra-atomic charge transfer process.

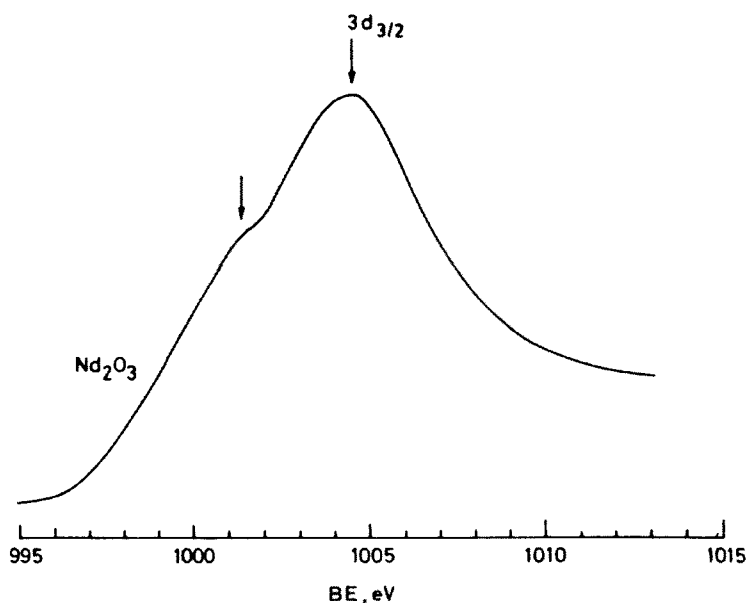


Fig. 9.13. XPE spectra of  $3d_{3/2}$  region of  $\text{Nd}_2\text{O}_3$  showing the existence of shake-down charge transfer satellite peak on the lower binding energy side of the main peak [50].

This interpretation is supported by an increase in energy separation of the satellite peak and main peak with increasing atomic number. It should also be noted that the energy separation of the 4f level and conduction band (6s, 5d) increases with increasing atomic number,  $Z$ .

The splitting of bands due to spin-orbit interactions of the 2p levels of first row transition metal oxides were found to vary linearly with atomic number  $Z$  contrary to the expected  $(Z-Z_0)^4$  dependence [30]. This disparity has been attributed to a drastic change in the screening constant,  $Z_0$ , with atomic number,  $Z$ . Similarly the band splittings due to spin-orbit interaction in rare earth oxides were fitted to the Dirac equation with a screened coulomb potential and a  $(Z-Z_0)^4$  in the non-relativistic limit, where a defect parameter accounts for the deviation from spherical potential [19]. It is to be noted that although spin-orbit splittings of the bands have  $(Z-Z_0)^4$  dependence, the non-spherical nature of the potential has significant effect on the splittings as shown in Fig. 9.15.

A possible relationship between binding energies and atomic number is revealed by plotting the logarithm of binding energies against the logarithm of atomic number ( $\ln E$  vs  $\ln Z$ ). Such a plot for rare earth oxides [19] and third row transition elements is shown in Fig. 9.16. A linear relationship is observed for rare earth oxides. However two distinct regions are seen when third row transition metal oxides are considered. This may be due to a profound change in the screening constant and the defect parameter as one sub shell is filled and electrons begin to occupy a new sub shell.

Some of the rare earths exhibit two different oxidation states in the same compound. A familiar example is  $\text{Tb}_4\text{O}_7$  which contains the +3 and +4 oxidation states. XPS bands due to trivalent and tetravalent oxidation states are seen in 4f, 4d and 5d bands [30]. The

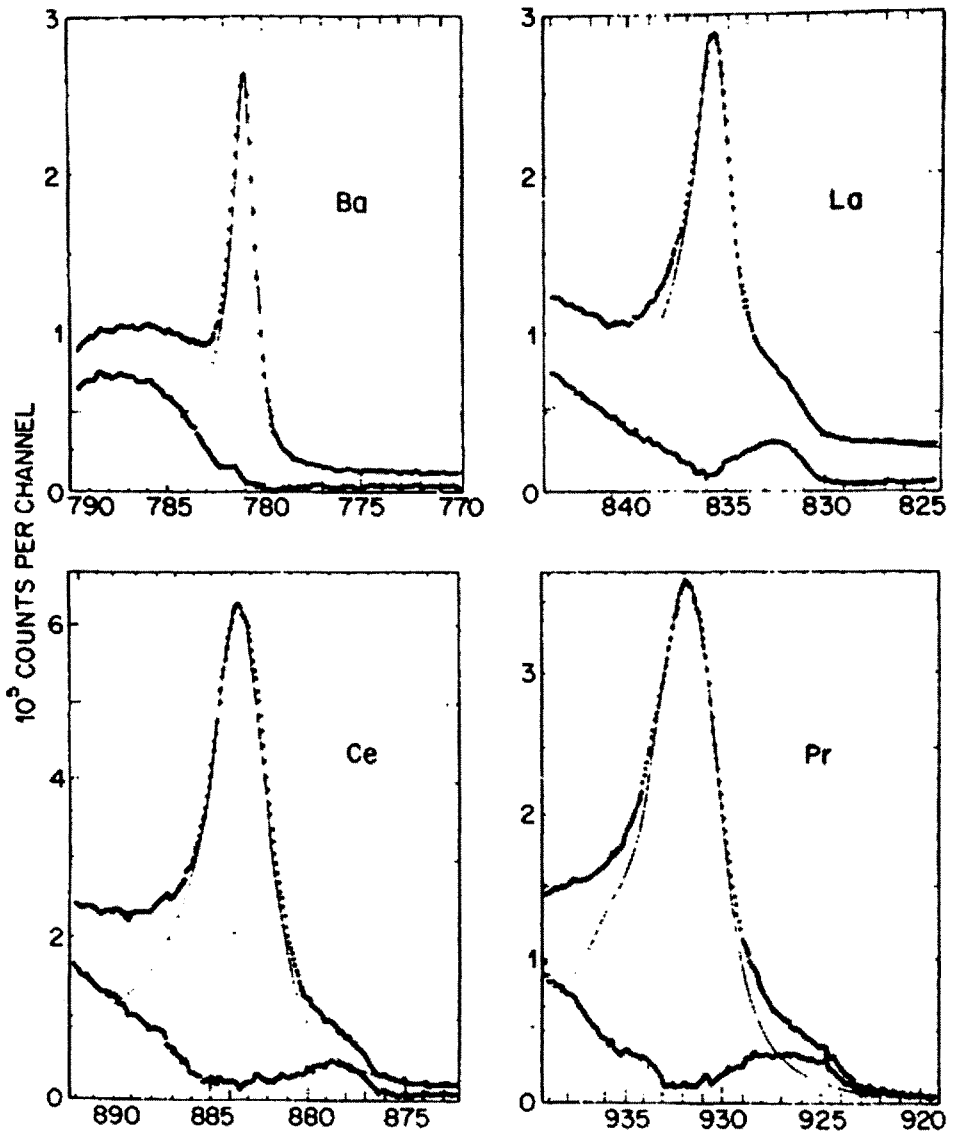


Fig. 9.14. XPE spectra of the 3d region of Ba and some rare earth metals showing the existence of the lower binding energy satellites due to electron transfer from conduction band to the core-hole stabilized 4f level. In the case of Ba, where no such satellite is seen, the empty 4f level lies above the Fermi edge and the 3d hole does not stabilize it below the Fermi level. The upper curves are the recorded spectra, the smooth lines are fits to the experimental data assuming single Doniach-Šunjić lines in Ba, La and Ce and multiplet-split lines in Pr. The lower solid curves are the difference spectra showing the existence of satellites [50].

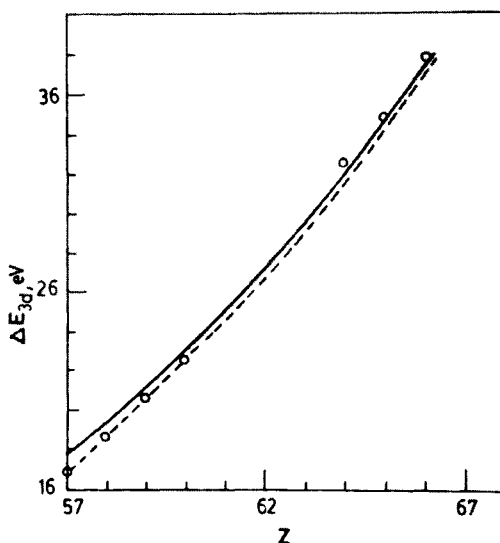


Fig. 9.15. Plot of the spin-orbit splittings,  $\Delta E_{3d}$ , in the case of rare earth sesquioxides against the atomic number,  $Z$ . The broken and full curves are according to a  $(Z - Z_0)^4$  and Dirac equation with screened Coulombic potential, respectively [50].

spectra of  $Tb_2O_3$ ,  $TbO_2$  and  $Tb_4O_7$  are given in Fig. 9.17. The 5p region in all the oxides shows a multiplet structure instead of a spin-orbit doublet and this is probably due to configuration interaction. In Fig. 9.17 the 5p region of the spectra of  $Tb_2O_3$ ,  $TbO_2$  and  $Tb_4O_7$  are shown. The 4d region of the spectra of the three oxides is shown in Fig. 9.18.

A comparison of XPS spectra of  $Tb_2O_7$  and  $TbO_2$  with those of  $Tb_4O_7$  in the 5p and 4d regions enables one to deduce the presence of both trivalent and tetravalent terbium in  $Tb_4O_7$ .

## 2. Applications\* [50]

Valence fluctuation, also known as inter configuration fluctuation, is exhibited by rare earth compounds and rare earth alloys. In valence fluctuation, an electron is promoted from the 4f level to the conduction band. Valence fluctuation occurs in less than  $10^{-11}$  s which is shorter than Mössbauer transitions but greater than XPS time scale (i.e.)  $10^{-16}$  s. Thus XPS is capable of detecting different valence states in compounds. On the other hand, other techniques having incompatible time scales give information on the time-averaged valence states. Theoretically, it is known that the 3d and 4d levels give rise to distinct peaks with a separation of about 7 eV in systems involving valence fluctuation. The energy differences between the XPS peaks of some rare earths exhibiting two different valencies in the 3d and 4d levels are given in Table 9.4.

Among the rare earth series, Ce, Sm, Eu, Tm, and Yb show valence fluctuation since they satisfy the condition

\* Major part of this topic is based on Ref. [50] for which the authors are grateful.



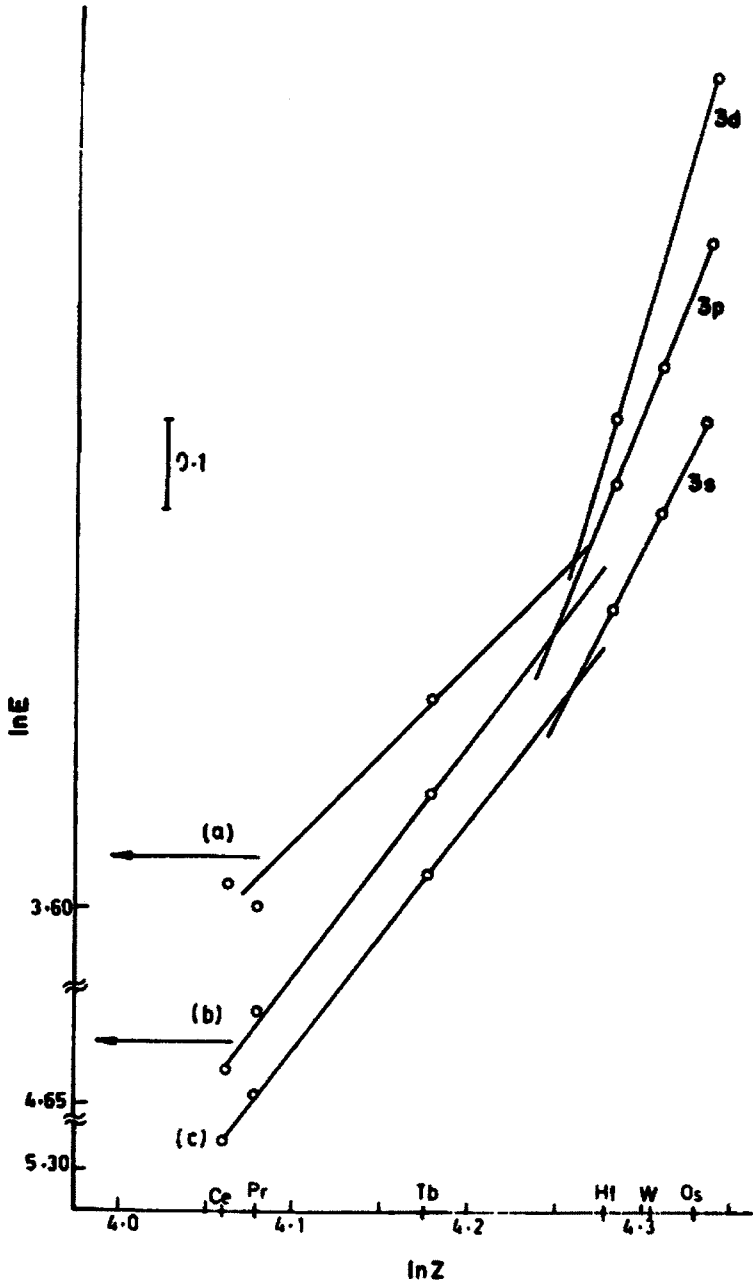


Fig. 9.16. Plot of  $\ln E$  against  $\ln Z$  for the dioxides of rare earth and third row transition metals showing two distinct linear regions [50].

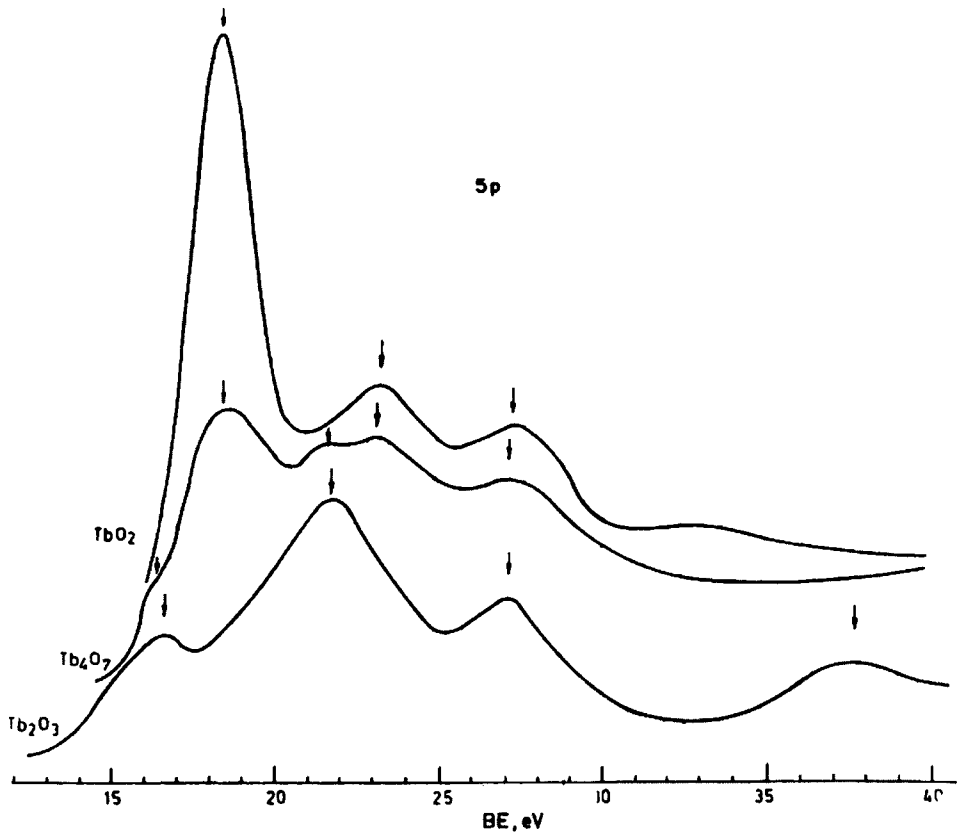


Fig. 9.17. The XPE spectra of  $Tb_2O_3$ ,  $TbO_2$  and  $Tb_4O_7$  in the 5p region showing the existence of mixed valency (3+ and 4+ states) of Tb in  $Tb_4O_7$ . The 5p region in all the oxides of Tb shows a multiplet structure, instead of a spin-orbit doublet, possibly due to configuration mixing [50].

TABLE 9.4a

Calculated energy difference between the XPE spectra of rare earth metals in two different valencies in the 3d and 4d regions.

	$m^*$	$\Delta E_{3d}$ (eV)	$\Delta E_{4d}$ (eV)
Ce	4	10.3	7.8
Sm	3	9.3	7.8
Eu	3	9.6	7.8
Tm	3	9.3	8.0
Yb	3	9.5	8.3

\*The higher of the two valencies of the metal.

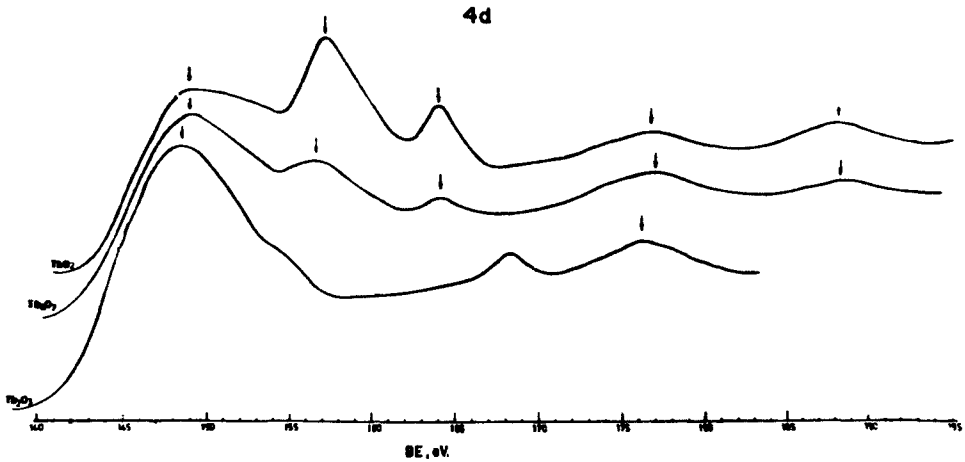


Fig. 9.18. The XPE spectra of  $Tb_2O_3$ ,  $TbO_2$  and  $Tb_4O_7$  in the 4d region showing the existence of mixed valency (3+ and 4+ states) in  $Tb_4O_7$ . In all these cases, 4d shows a multiplet structure [50].

$$E_{\text{EXC}} = E_n - (E_{n-1} + E_e) \approx 0,$$

where  $E_n - E_{n-1}$  is the energy difference between  $4f^n$  and  $4f^{n-1}$  levels and  $E_e$  is the energy of the promoted electron. XPS studies on  $SmB_6$  [31]  $SmS$  [32–34],  $EuCu_2Si_2$  [35, 36],  $EuRh_{2-x}Pt_x$  [37],  $YbAl_3$  [38] and thulium chalcogenide [38] have been done in detail. Other systems including  $CeN$  [39],  $CeAl_2$  and  $CePd_3$  [40] have been studied. The role of XPS studies in elucidating valence fluctuation has been reviewed [41].

By comparing the XP spectra of  $SmB_6$  [31] with the spectra of  $SmSb$  ( $Sm^{3+}$ ) and  $SmTe$  ( $Sm^{2+}$ ) in the 4d region, the peaks in  $SmB_6$  have been identified as due to  $Sm^{2+}$  and  $Sm^{3+}$ . The spectra of  $SmSb$ ,  $SmTe$  and  $SmB_6$  are given in Fig. 9.19. The 4f region of the spectrum of  $SmB_6$  shows agreement with the calculated multiplet structure for  $Sm^{2+}$  and  $Sm^{3+}$ . The observed and calculated spectra of  $SmB_6$  are shown in Fig. 9.20 [50].

In the case of  $CeN$ , the multiplet structure due to  $Ce^{3+}$  of  $4f^1$  configuration and spin-orbit doublet in the 4d region due to  $Ce^{4+}$  of  $4f^0$  configuration are seen in Fig. 9.21. Peaks distinctly different for +3 and +4 states of Ce are also seen in the 3d region (Fig. 9.22).

The X-ray photoelectron spectra of Ce,  $CeAl_2$ ,  $Ce_{0.8}Y_{0.2}Al_2$  and  $CePd_3$  in the 3d and 4d regions are shown in Figs. 9.23 and 9.24, respectively. Distinct signals for  $Ce^{3+}$  and  $Ce^{4+}$  in  $Ce_{0.8}Y_{0.2}Al_2$  are seen in the 3d and 4d regions. Only a trivalent cerium signal is present in  $CeAl_2$ . Valence fluctuation is seen in  $CePd_2$ .

In the case of thulium compounds  $TmSe$  and  $TmTe$  and  $YbAl_3$ , distinct multiplet structures due to divalent and trivalent thulium are seen in the 4f region [38]. The multiplet structure in  $TmTe$  is more distinct than in the case of  $TmSe$  in agreement with magnetic susceptibility data, (i.e.) magnetic moment of  $TmTe$  is smaller than that of  $TmSe$ .

X-ray photoelectron spectrum of  $EuCu_2Si_2$  along with the calculated spectrum for the compound are shown in Fig. 9.26. The spectrum clearly shows the presence of both divalent and trivalent europium in the alloy. The spectrum of  $YCu_2Si_2$  is also included in Fig. 9.26

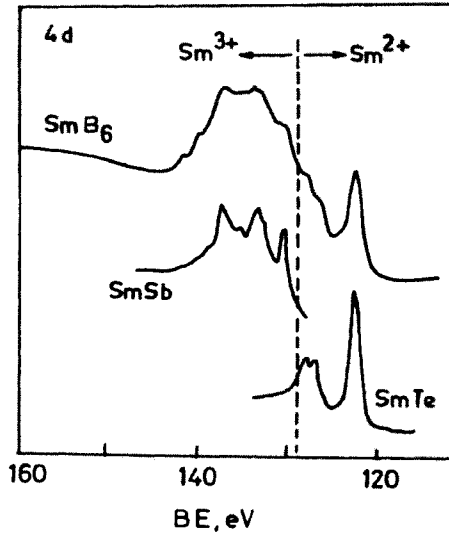


Fig. 9.19. XPE spectra of  $\text{SmSb}$  (Sm in  $3+$ ),  $\text{SmTe}$  (Sm in  $2+$ ) and  $\text{SmB}_6$  in the 4d region showing the signals due to the  $2+$  and  $3+$  states in valence fluctuating  $\text{SmB}_6$  [50].

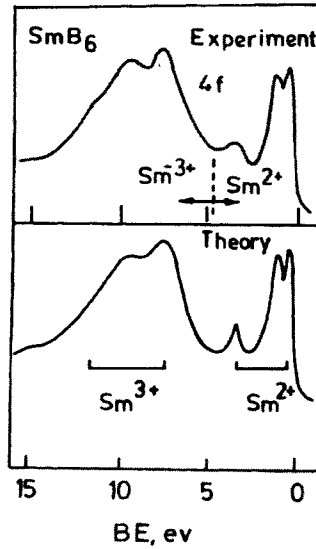


Fig. 9.20. XPE spectra of  $\text{SmB}_6$  in the 4f region compared with the combined multiplet structures calculated for  $\text{Sm}^{2+}$  and  $\text{Sm}^{3+}$  [50].

to show the contribution of Cu and Si in the valence region. In the case of  $\text{EuRh}_2$ , the 4d multiplet structure may be compared to the spectrum of  $\text{EuPt}_2$  where Eu is in divalent state and then conclude the presence of both divalent and trivalent states in  $\text{EuRh}_2$ . The spectrum

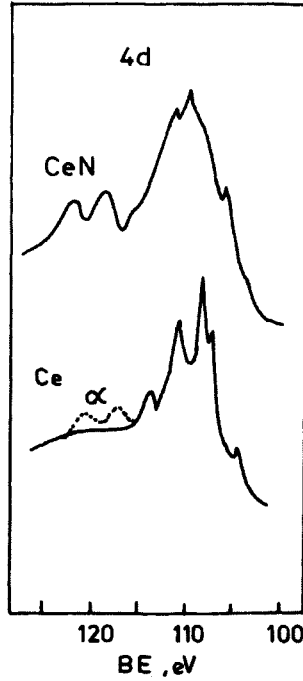


Fig. 9.21. XPE spectra of CeN in the 4d region compared with that of  $\gamma$ -Ce in  $4f^1$  configuration (full line) and that of the spin-orbit doublet structure of  $\alpha$ -Ce in  $4f^0$  configuration (broken line) [50].

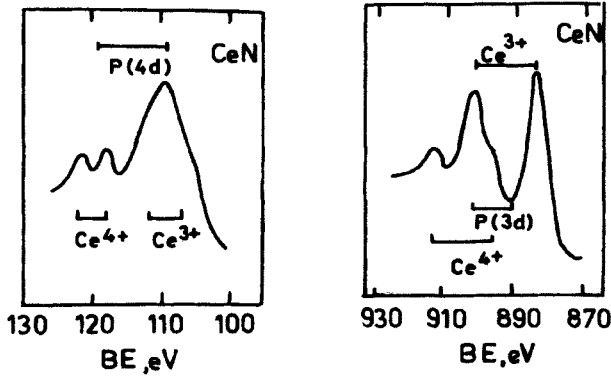


Fig. 9.22. XPE spectra of CeN in the 4d and 3d regions showing the existence of valence fluctuation in this compound.  $P(4d)$  and  $P(3d)$  are the calculated energy differences between the two valences,  $4f^0$  and  $4f^1$ , of Ce in XPE spectra of the corresponding levels [50].

of  $\text{EuRh}_{1.5}\text{Pt}_{0.5}$  showed a predominantly divalent europium component in agreement with Mössbauer findings.

It is useful to compare the results obtained by XPS studies with results obtained by other techniques. XPS is a highly surface-sensitive technique and a major portion of the intensity

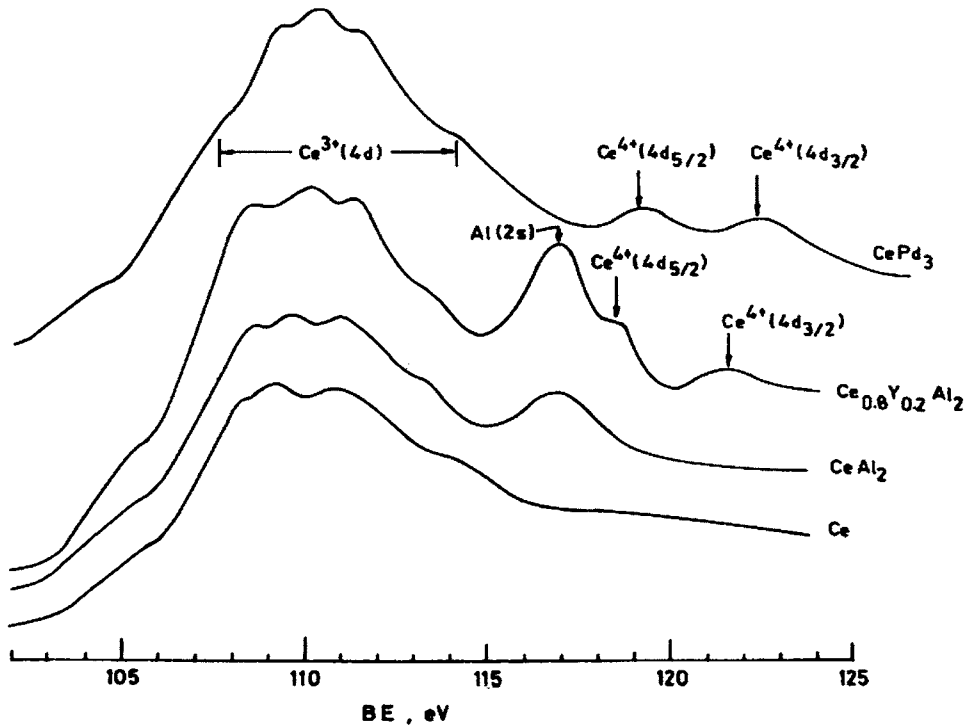


Fig. 9.23. XPE spectra of Ce, CeAl<sub>2</sub>, Ce<sub>0.8</sub>Y<sub>0.2</sub>Al<sub>2</sub> and CePd<sub>3</sub> in the 4d region indicating valence fluctuations in the cases of Ce<sub>0.8</sub>Y<sub>0.2</sub>Al<sub>2</sub> and CePd<sub>3</sub>, and the trivalent nature of CeAl<sub>2</sub> [50].

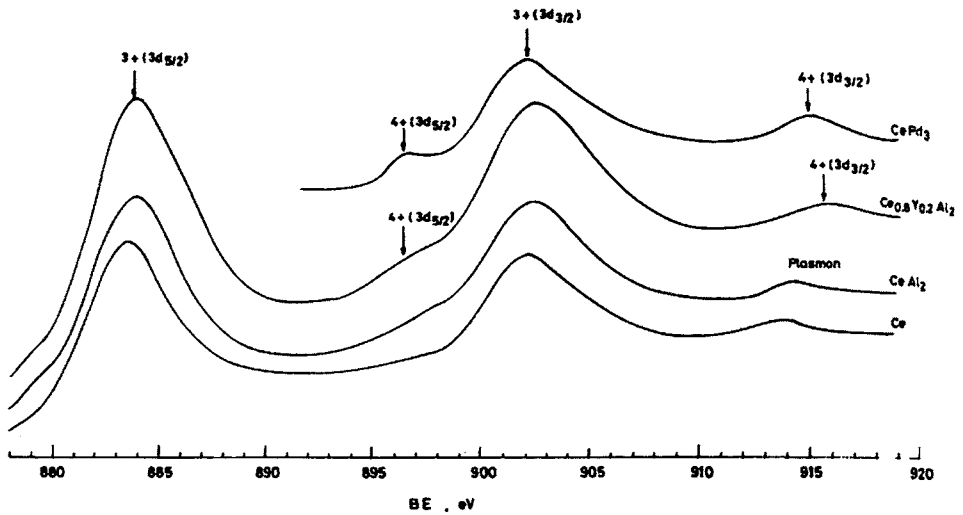


Fig. 9.24. XPE spectra of Ce, CeAl<sub>2</sub>, Ce<sub>0.8</sub>Y<sub>0.2</sub>Al<sub>2</sub> and CePd<sub>3</sub> in the 3d region indicating valency fluctuations in the cases of Ce<sub>0.8</sub>Y<sub>0.2</sub>Al<sub>2</sub> and CePd<sub>3</sub>, and the trivalent nature of CeAl<sub>2</sub> [50].

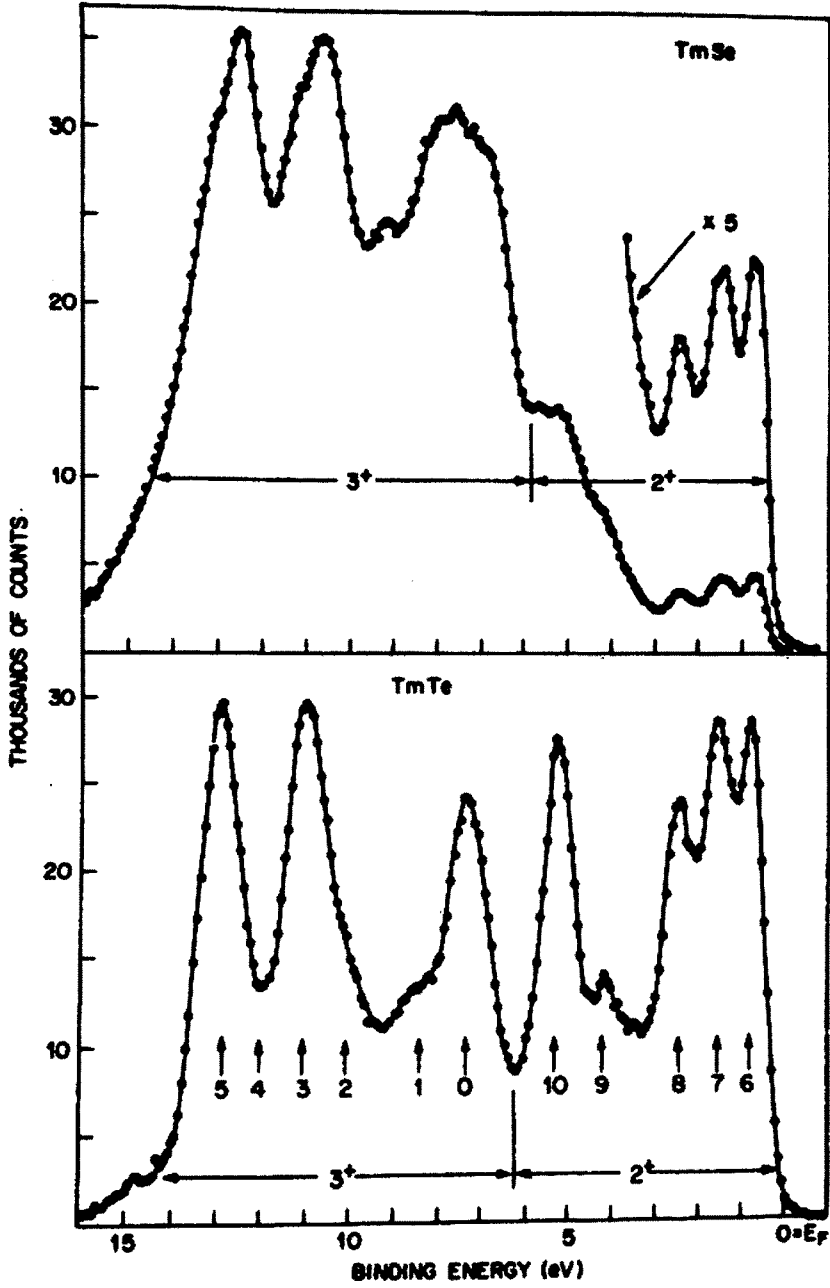


Fig. 9.25. The multiplet structure of the 4f region in the XPE spectra of TmSe and TmTe. Signals due to divalent as well as trivalent Tm can be seen clearly [38].

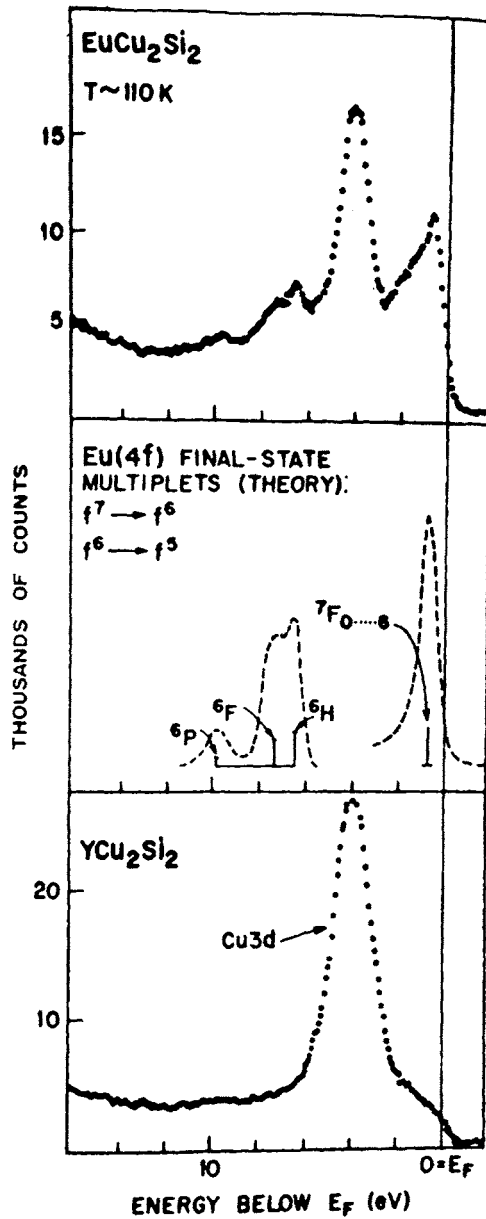


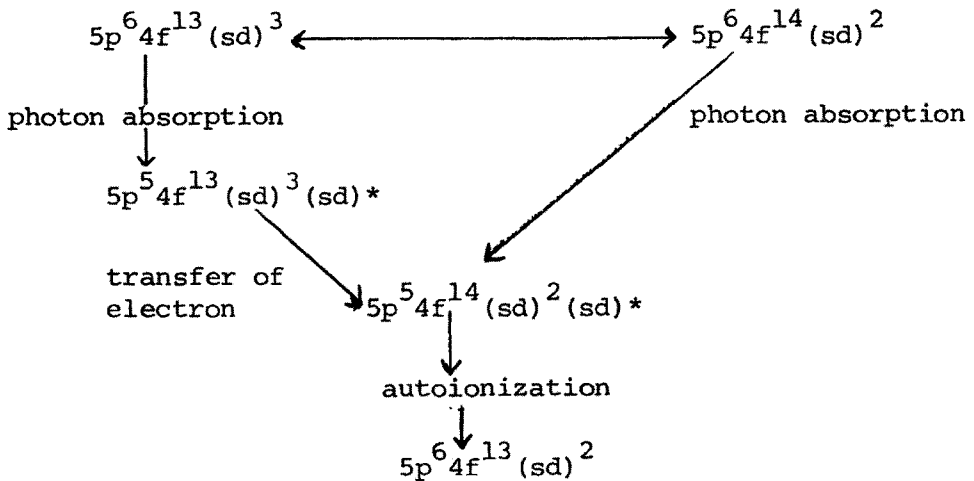
Fig. 9.26. XPE spectrum of 4f region of  $\text{EuCu}_2\text{Si}_2$  (upper curve) compared with the theoretical multiplet structure of divalent and trivalent Eu (middle curve), indicating the existence of valence fluctuation in this compound. The lower spectrum (for  $\text{YCu}_2\text{Si}_2$ ) shows the contribution of Cu and Si in the valence region.



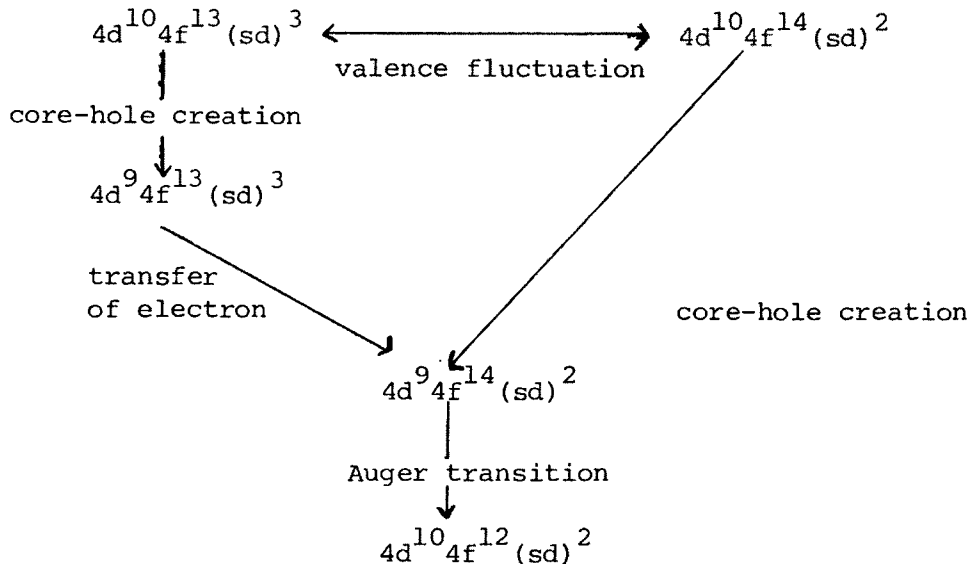
of peaks arises from the first few monolayers of the sample. On the other hand, Mössbauer spectroscopy, magnetic susceptibility and nuclear magnetic resonance (NMR) measure the bulk properties. Thus the results obtained by XPS may not always agree with the results obtained by other techniques which measure the bulk properties. Surfaces of alloys may be stabilized by one valency or other [35]. It should be borne in mind that some factors such as the absence of translational symmetry in a direction perpendicular to the surface and the surface strain may affect valence fluctuation. NMR studies [42] of  $Ce_{0.6}Cs_{0.4}Al_2$  show the presence of tetravalent cerium while XPS studies show the strong presence of trivalent cerium with a weak peak due to tetravalent cerium [43].

Surface stabilization of valency is also encountered in Sm. XPS of Sm in the 4f, 4d, and 3d regions show the presence of both divalent and trivalent metal [44,45]. The angular dependence of the relative intensities of the divalent and trivalent samarium peaks indicate the presence of divalent and trivalent samarium on the surface [45]. Another example of a surface stabilized system is ytterbium in  $YbAu_2$ . XPS of  $YbAu_2$  in 4f and 5p regions indicate surface-stabilized divalent Yb in total disagreement with the findings from the lattice volume of  $YbAu$  giving evidence for trivalent Yb [46]. Since XPS is a surface sensitive technique, it is needless to point out that surface cleanliness is of paramount importance and any minor surface impurity on the metal or alloy can give unexpected results.

The explanation that 4f level stabilization of rare earths by a core hole leads to some difficulties in the interpretation of XPS results in valence fluctuating systems [47]. In the case of  $YbAl_3$ , XPS data show clearly the presence of both divalent and trivalent states of Yb. On the other hand, ultraviolet photoelectron spectrum (UPS) showed the presence of only divalent Yb. The mechanism of ejection of the 4f electron in the low excitation energy range is one of autoionization of the 5p level. The 5p hole thus created stabilizes the  $4f^{13}$  so much that an electron is transferred fast enough from the valence level resulting in  $4f^{14}$  configuration. Following this, autoionization probably occurs giving rise to a peak corresponding to  $4f^{14}$  state. This process is schematically shown below [50].



The Auger spectrum of  $\text{YbAl}_3$  in the 4d–4f–4f region showed no significant difference from that of Yb metal with  $4f^{14}$  configuration. In this case the valence electron transfer is due to the 4d hole state and the processes involved in valence electron transfer are shown below.



The process of transfer of the valence electron to the 4f level suffers from some deficiencies. The 5p level being one of the outermost levels with binding energy  $\sim 25$  eV is unlikely to stabilize the 4f level to a significant extent. Further, the time scale involved in the electron transfer from valence level to 4f level is not compatible ( $< 10^{-16}$  s). Thus it is hard to explain the observed trivalent and tetravalent states in CeN. In the case of Ce, the 3d hole stabilizes the 4f level of Ce significantly below the Fermi edge. This leads to the notion that the electron transfer may not be as fast as  $< 10^{-16}$  s. If the electron transfer from valence band to the 4f level due to the core is fast, then it is difficult to explain the experimental observations on the XPS of 3d region of La, Ce and Pr (Fig. 9.14).

Another argument is based on mean free paths of electrons in Auger spectra of He II spectra [47]. In these spectra, the mean free path of electrons is about 3–4 Å, while in the case of 4f electrons released due to Mg  $K_{\alpha}$  radiations is about 17–18 Å. Thus the Auger technique senses the electrons in the outermost two monolayers while XPS is sensitive to about seven monolayers and in such a case, surface stabilization of the divalent state may very well be the case in accordance with the experimental findings [47].

### 3. Oxidation

There have been a few studies on the surface oxidation of cerium. Oxidation of cerium has been studied by UV photoelectron spectroscopy [48] and XPS [49]. From these studies, the formation of  $\text{Ce}_2\text{O}_3$  on the surface of the metal has been concluded along with evidence for

physisorbed oxygen. The earlier studies concluded that the cerium-oxygen system reached saturation very rapidly and longer exposure to oxygen had very little effect [49]. These studies were followed by a detailed examination of the cerium-oxygen system [50]. At low exposures of cerium to oxygen, immediate formation of  $\text{Ce}_2\text{O}_3$  takes place as evidenced by the spectrum in the 3d region shown in Fig. 9.27. No evidence of physisorbed oxygen on the metal was observed in the signal due to oxygen (1s) at low exposure as seen in Fig. 9.28. The XPS of the valence region also gives evidence for the formation of  $\text{Ce}_2\text{O}_3$ . Initial formation of  $\text{Ce}_2\text{O}_3$  is accompanied by physisorption of oxygen as evidenced by O(1s) signal showing a shoulder in the peak (Fig. 9.28). The formation of  $\text{Ce}_2\text{O}_3$  was nearly complete at about 30L of oxygen. The 3d peak of  $\text{Ce}_2\text{O}_3$  is seen to have a negative chemical shift with respect to the metal. The peak that was assigned to  $\text{Ce}_2\text{O}_3$  with a positive chemical shift [49] has been assigned later to charge transfer from O(1s) to Ce(4f) shake-up satellite. Above 30L of oxygen formation of  $\text{CeO}_2$  takes place as evidenced by the satellite in the 3d region at a binding energy of 317 eV (Fig. 9.27).

After the formation of  $\text{CeO}_2$ , the shoulder on O(1s) peak intensity decreased and the O(1s) peak shifted to a lower binding energy (Fig. 9.28) leading to the supposition that tetravalent cerium makes its appearance. It is surmised that adsorbed oxygen on  $\text{Ce}_2\text{O}_3$  provides sites for nucleation of tetravalent cerium. In order to ascertain the relative stabilities of  $\text{CeO}_2$  and  $\text{Ce}_2\text{O}_3$ , the cerium-oxygen system containing some tetravalent cerium was left for a certain period in the spectrometer and the spectrum was obtained. The resulting spectrum gave evidence for the conversion of  $\text{CeO}_2$  into  $\text{Ce}_2\text{O}_3$  by way of a decrease in intensity of the satellite at 917 eV as well as the reappearance of the O(1s) peak shoulder [50].

The surface oxidation of Ce was studied in the valence region by UV photoelectron spectroscopy [50] using He II radiation. Above 10L of oxygen, the bands in the 6s, 5d region disappeared, while the 4f band remained unaffected and O(2p) band intensity increased. These changes are seen in Fig. 9.29. The spectra in Fig. 9.29 show the formation of  $\text{Ce}_2\text{O}_3$  with  $\text{Ce}^{3+}(4f^1)$ . At an oxygen level of 3000L, the decrease in 4f band intensity indicates the presence of  $\text{Ce}^{4+}(4f^0)$ .

XPS and UV photoelectron studies [50] of the oxidation of La show the formation of  $\text{La}_2\text{O}_3$  as evidenced O(1s) peak and the charge transfer satellite in the 3d region. Also the 3d peaks of  $\text{La}_2\text{O}_3$  show negative chemical shift with respect to the metal. After  $\text{La}_2\text{O}_3$  is formed, the presence of adsorbed oxygen is seen as a shoulder on the O(1s) peak. On oxygen exposure, the valence bands nearly disappear both in XPS and UV photoelectron spectra. The system La-O<sub>2</sub> is illustrated in Fig. 9.30.

#### 4. Application in lanthanide complexes

X-ray photoelectron spectroscopy was used in the studies [51] of lanthanide complexation with macrocyclic ligand, 1,1-bis(quinoline-8-oxo)-3,6,9-trioxoundecane of the formula  $\text{La}(\text{NO}_3)_3 \cdot 2\text{C}_{26}\text{H}_{28}\text{N}_2\text{O}_5 \cdot 3\text{H}_2\text{O}$ . The macrocyclic ligand  $\text{C}_{26}\text{H}_{28}\text{N}_2\text{O}_5$  is abbreviated as CROD. XPS data for the complexes are given in Table 9.5. It is seen that oxygen bonded C 1s gives a signal of binding energy of 286.5 eV and O 1s peak of the ligand is located at 532.6 eV. The C 1s and O 1s bands in the ligand are shifted to lower energies when compared with C 1s: 286.4 eV and O 1s: 533.1 eV in benzo-15-crown-5 and dibenzo-18-crown-6 (C 1s: 286.6 eV, O 1s: 533.2 eV) providing evidence for greater electron density

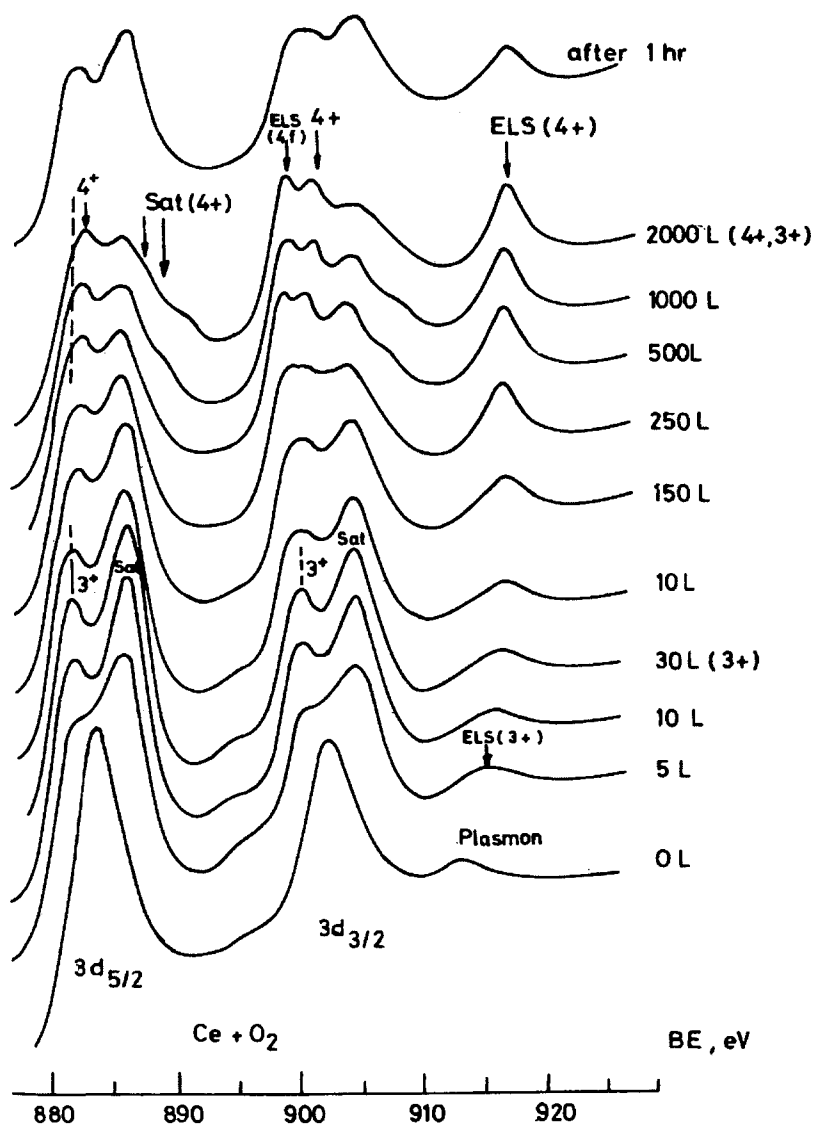


Fig. 9.27. XPE spectra of Ce + O<sub>2</sub> system in 3d region showing the formation of Ce<sub>2</sub>O<sub>3</sub> on the surface at low oxygen exposure. The completion of Ce<sub>2</sub>O<sub>3</sub> formation takes places at about 30L as indicated by the well defined satellite structure. Further oxygen exposure leads to the formation of CeO<sub>2</sub> as indicated by the growth of the energy loss (ELS) peak due to Ce<sup>4+</sup>. The uppermost plot indicates that CeO<sub>2</sub> reconverts into Ce<sub>2</sub>O<sub>3</sub> when left in vacuum as evidenced by changes in the satellite structure [50].

on carbon and oxygen in CROD. An overlap of signals for O 1s from nitrate, water and the ligand was observed. Oxygen bonded C 1s band shifts to higher binding energy in the complex than the free ligand. The shift is about 1.3 eV. A comparison of N 1s energies for

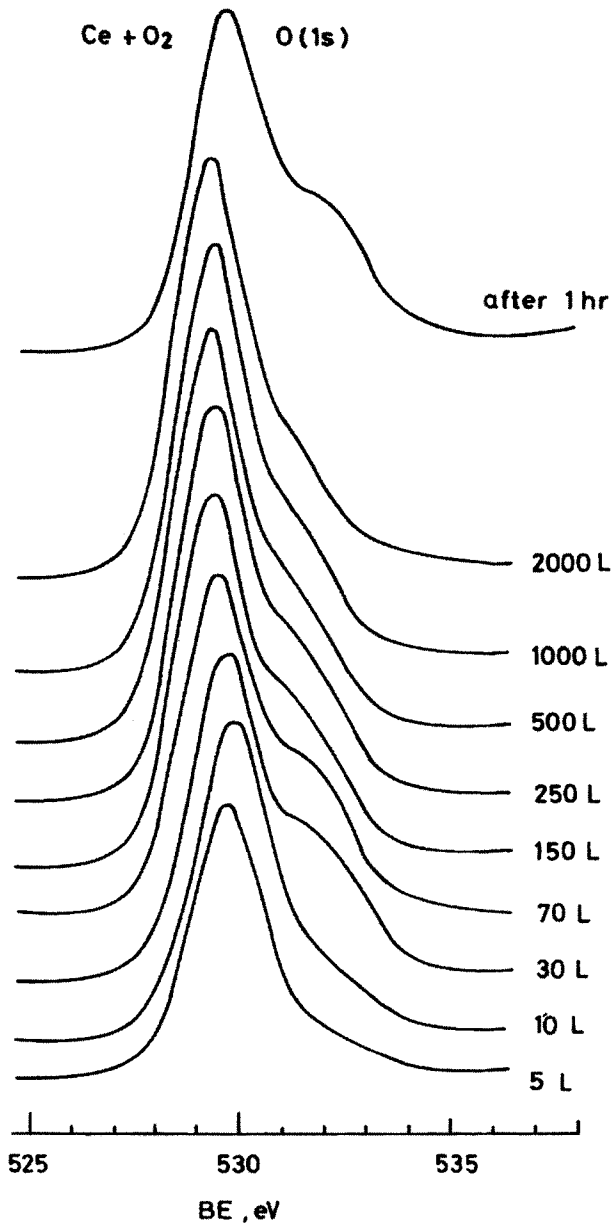


Fig. 9.28. XPE spectra of Ce + O<sub>2</sub> system in the O(1s) region at various exposures of oxygen. The uppermost curve shows the effect of leaving the Ce + O<sub>2</sub> system in vacuum after a large (2000L) oxygen exposure [50].

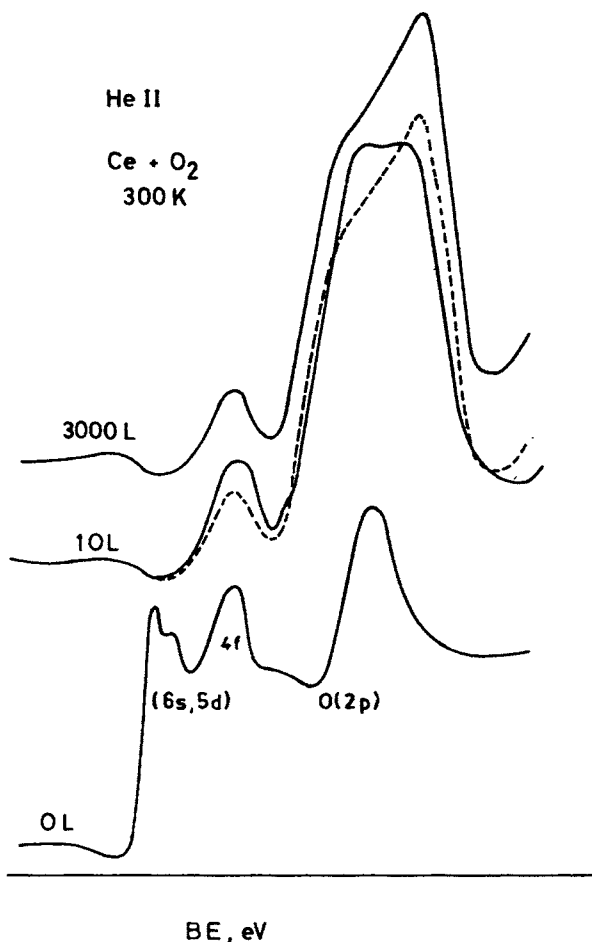


Fig. 9.29. UVPE spectra of Ce + O<sub>2</sub> system using He II radiation. The lowermost spectrum shows the sharp (6s, 5d) band as well as the 4f level of clean Ce metal with very small amount of oxygen on the surface. The middle curve shows the effect of small oxygen exposure (10L); the (6s, 5d) band disappears, whereas the 4f level remains unaffected and a clear O(2p) signal appears around 6–7 eV indicating the formation of Ce<sub>2</sub>O<sub>3</sub>. The upper curve shows the effect of a very large oxygen exposure (3000L); the 4f intensity decreases clearly as compared to the case of 10L oxygen exposure (as shown by the dotted line super-imposing the signal at 10L exposure) indicating the formation of CeO<sub>2</sub>. The O(2p) peak at 0L is due to adsorbed oxygen on a fresh metal surface [50].

nitrate shows the value was lower in the complex than in free nitrate. The spectra of O 1s peaks in the Pr complex and Pr(NO<sub>3</sub>)<sub>3</sub> are shown in Fig. 9.31.

O 1s peaks in CROD and the complex are located at 532.6 and 534 eV, respectively. O 1s peak in Pr(NO<sub>3</sub>)<sub>3</sub> shifts to lower binding energy upon complexation as shown in Fig. 9.31. These two observations show evidence for the formation of La–O (nitrate) bonding.

The binding energies of 3d<sub>5/2</sub> level are given in Table 9.5. Upon complexation, electron density of the valence levels of the lanthanide increases, and hence contributes to a decrease

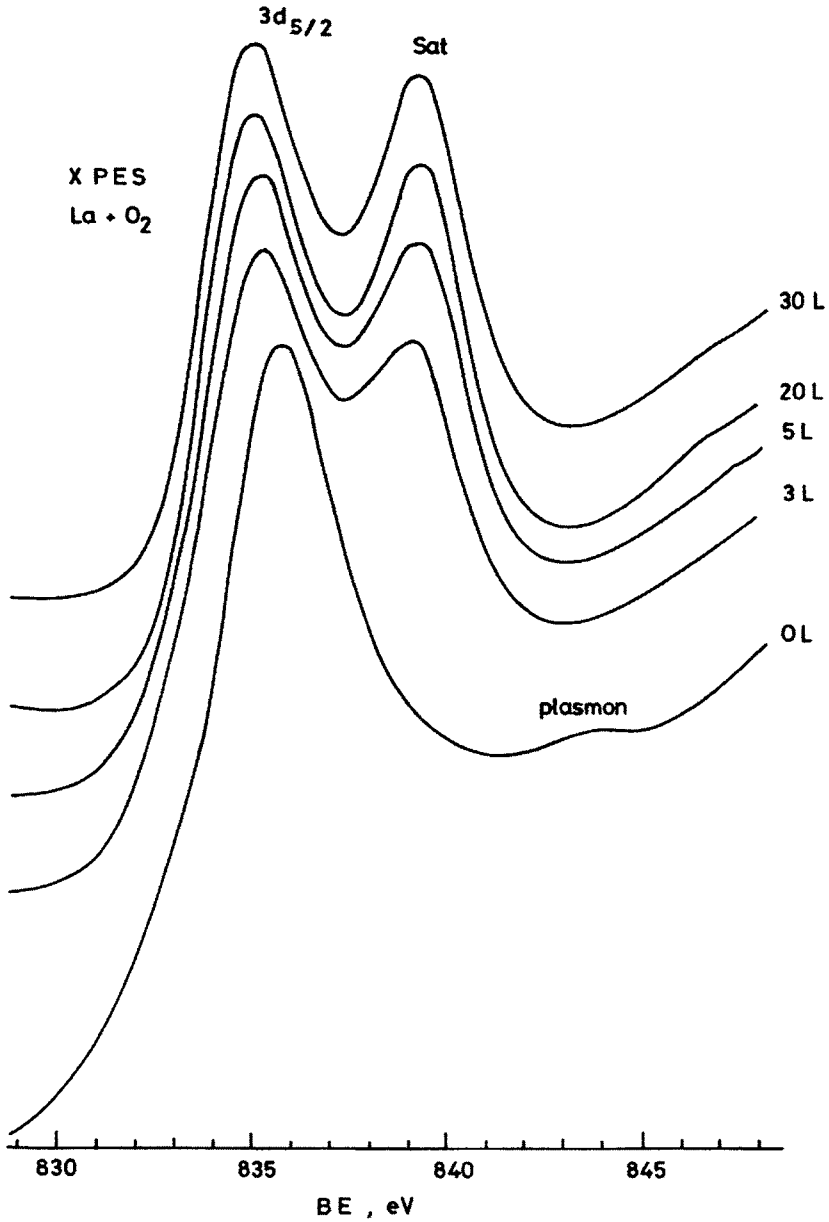


Fig. 9.30. XPS spectra of La + O<sub>2</sub> system in the 3d region at various oxygen exposures indicating the formation of La<sub>2</sub>O<sub>3</sub> at very low exposures [50].

TABLE 9.5  
XPS data for CROD and the complexes

Compound	Ln 3d <sub>5/2</sub> <sup>a</sup>	C 1s	O 1s	N 1s <sup>b</sup>
C <sub>26</sub> H <sub>28</sub> N <sub>2</sub> O <sub>5</sub>		285.0 285.6	532.6	339.2
3La(NO <sub>3</sub> ) <sub>3</sub> ·2C <sub>26</sub> H <sub>28</sub> N <sub>2</sub> O <sub>5</sub> ·3H <sub>2</sub> O	836.5 (837.5)	285.0 286.9		339.3 407.1 (408.1)
3Ce(NO <sub>3</sub> ) <sub>3</sub> ·2C <sub>26</sub> H <sub>28</sub> N <sub>2</sub> O <sub>5</sub> ·3H <sub>2</sub> O	883.3 (885.1)	285.0 286.9		339.2 406.7 (407.7)
3Pr(NO <sub>3</sub> ) <sub>3</sub> ·2C <sub>26</sub> H <sub>28</sub> N <sub>2</sub> O <sub>5</sub> ·3H <sub>2</sub> O	934.1 (935.2)	285.0 286.9		339.2 406.8 (407.8)
3Nd(NO <sub>3</sub> ) <sub>3</sub> ·2C <sub>26</sub> H <sub>28</sub> N <sub>2</sub> O <sub>5</sub> ·3H <sub>2</sub> O	984.9 (986.0)	285.0 285.8		339.3 407.1 (407.9)

<sup>a</sup>Values in parentheses are binding energies for Ln 3d<sub>5/2</sub> spectra of La(NO<sub>3</sub>)<sub>3</sub>·H<sub>2</sub>O, Ce(NO<sub>3</sub>)<sub>3</sub>·4H<sub>2</sub>O, Pr(NO<sub>3</sub>)<sub>3</sub>·3H<sub>2</sub>O and Nd(NO<sub>3</sub>)<sub>3</sub>·2H<sub>2</sub>O, respectively.

<sup>b</sup>Values in parentheses are binding energies for N 1s spectra of La(NO<sub>3</sub>)<sub>3</sub>·H<sub>2</sub>O, Ce(NO<sub>3</sub>)<sub>3</sub>·4H<sub>2</sub>O, Pr(NO<sub>3</sub>)<sub>3</sub>·3H<sub>2</sub>O and Nd(NO<sub>3</sub>)<sub>3</sub>·2H<sub>2</sub>O, respectively.

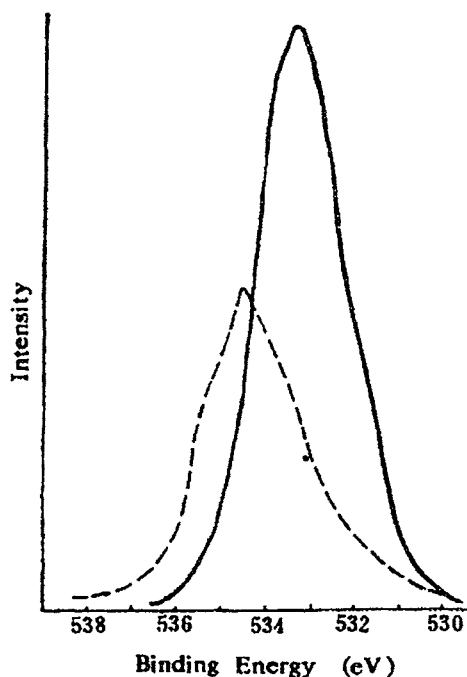


Fig. 9.31. O 1s XPS peaks. Solid line: 3Pr(NO<sub>3</sub>)<sub>3</sub>·2C<sub>26</sub>H<sub>28</sub>N<sub>2</sub>O<sub>5</sub>·3H<sub>2</sub>O; dotted line: Pr(NO<sub>3</sub>)<sub>3</sub>·3H<sub>2</sub>O.

in energy of the inner electron. Satellite peaks have also been observed on both sides of the Ln 3d<sub>5/2</sub> peak. The energies of satellite peak locations are given in Table 9.5a. The satellite peaks are attributed to O(2p) → Ln(4f) charge transfer process. It is also observed that the intensity of satellite peak decreases in going from La to Nd. The decrease in intensity of satellite peaks is due to progressive stabilization of 4f level below the O(2p) level. Further, the contraction of the 4f orbital along the lanthanide series, results in a lower overlap of



TABLE 9.5a

Ln 3d <sub>5/2</sub> (eV)	Satellite (eV)
La 836.5	839.4
Ce 883.3	886.1
Pr 934.1	930.3
Nd 984.9	981.8

4f and O(2p) orbitals of the ligand resulting in lower intensity of the satellite peaks in the lanthanide series. The intensity ratio of the satellite peak to main peak is given by

$$\frac{I_S}{I_0} = \frac{\langle \phi / \phi_{(i)}^* \rangle^2}{\langle \phi / \phi_{(i)} \rangle^2}$$

where  $\phi$  is the molecular orbital in the ground state and related to the shake-up or shake-down process,  $\phi_{(i)}$  and  $\phi_{(i)}^*$  are the occupied molecular orbital of core-ionized state and its antibonding counterpart, respectively. In the case of lanthanide complexes,  $\phi$  is mainly localized on the ligand and  $\phi^*$  the antibonding counterpart is essentially 4f orbital. After core-ionization, the occupied  $\phi_{(i)}$  orbital should gain 4f orbital character due to charge transfer from the ligand to the lanthanide 4f orbital. On the other hand, the antibonding orbital  $\phi_{(i)}^*$  in the core-ionized state should have ligand character.

MS X $_{\alpha}$  calculations on LaF<sub>3</sub> and CeF<sub>3</sub> show a large flow of electrons from the ligand to 4f shell upon core-ionization [52]. Thus, the intense satellite peaks of the La complex is probably due to the large overlap of  $\langle \phi / \phi_{(i)}^* \rangle$  and small overlap of  $\langle \phi / \phi_{(i)} \rangle$ . The consequence of this is that the metal–ligand bonding in the lanthanide complex has relatively large f-orbital covalency in its core-ionized state. As the 4f electron population increases, an electron influx into the vacant 4f orbital is interrupted leading to considerable diminution of mixing between the ligand and vacant 4f orbitals in  $\phi_{(i)}^*$  and  $\phi_{(i)}$  molecular orbitals of the core-ionized state and consequent smaller overlap  $\langle \phi / \phi_{(i)}^* \rangle$ . Hence the greater intensity of the satellite peak indicates stronger covalency of the complex.

The N 1s binding energy of the ligand CROD is due to the quinolyl nitrogen and does not undergo any shift upon complexation. Thus there is no bonding between lanthanide and nitrogen in the CROD ligand. In the complex 3Ln(NO<sub>3</sub>)<sub>3</sub>·2CROD·3H<sub>2</sub>O the nitrogen in nitrate and the nitrogen in the ligand CROD have two different environments and the N 1s spectra given in Fig. 9.32 show small differences. The peak at higher binding energy is due to nitrate nitrogen and the peak at lower binding energy is due to nitrogen in the ligand, CROD. The two peaks have area ratio of 9:4 corresponding to the nitrogens in the complex 3Ln(NO<sub>3</sub>)<sub>3</sub>·2C<sub>26</sub>H<sub>28</sub>N<sub>2</sub>O<sub>5</sub>·3H<sub>2</sub>O.

The binding energies of Ln 3d<sub>5/2</sub> peaks in various lanthanum compounds are given in Table 9.6. The first three sets of compounds refer to lanthanum nitrates and their complexes. In the next series, we have hydroxides, oxides and oxalate complexes. Plots of log(binding energy) vs atomic number in the La–Nd series are shown in Figs 9.33 and 9.34. Among related compounds, log(binding energy) appears to be a linear function of atomic number.

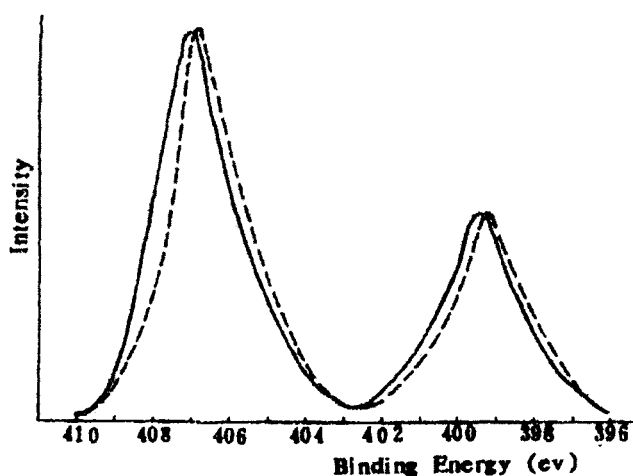


Fig. 9.32. N 1s XPS peaks. Solid line:  $3\text{Nd}(\text{NO}_3)_3 \cdot 2\text{C}_{26}\text{H}_{28}\text{N}_2\text{O}_5 \cdot 3\text{H}_2\text{O}$ ; dotted line:  $3\text{Pr}(\text{NO}_3)_3 \cdot 2\text{C}_{26}\text{H}_{28}\text{N}_2\text{O}_5 \cdot 3\text{H}_2\text{O}$ .

TABLE 9.6  
Data of Ln  $3d_{5/2}$  and  $\lg \text{BE}^a$ .

Compound	Ln $3d_{5/2}$ (eV)	$\lg \text{BE}$
$\text{La}(\text{NO}_3)_3 \cdot \text{H}_2\text{O}$	837.5	2.9230
$\text{Ce}(\text{NO}_3)_3 \cdot 4\text{H}_2\text{O}$	885.1	2.9470
$\text{Pr}(\text{NO}_3)_3 \cdot 3\text{H}_2\text{O}$	932.2	2.9709
$\text{Nd}(\text{NO}_3)_3 \cdot 2\text{H}_2\text{O}$	986.0	2.9939
$\text{La}(\text{NO}_3)_3 \cdot \text{C}_{14}\text{H}_{20}\text{O}_5$	835.9	2.9222
$\text{Ce}(\text{NO}_3)_3 \cdot \text{C}_{14}\text{H}_{20}\text{O}_5$	882.4	2.9457
$\text{Pr}(\text{NO}_3)_3 \cdot \text{C}_{14}\text{H}_{20}\text{O}_5$	933.5	2.9701
$\text{Nd}(\text{NO}_3)_3 \cdot \text{C}_{14}\text{H}_{20}\text{O}_5$	984.5	2.9932
$3\text{La}(\text{NO}_3)_3 \cdot 2\text{C}_{26}\text{H}_{28}\text{N}_2\text{O}_5 \cdot 3\text{H}_2\text{O}$	836.5	2.9225
$3\text{Ce}(\text{NO}_3)_3 \cdot 2\text{C}_{26}\text{H}_{28}\text{N}_2\text{O}_5 \cdot 3\text{H}_2\text{O}$	883.3	2.9461
$3\text{Pr}(\text{NO}_3)_3 \cdot 2\text{C}_{26}\text{H}_{28}\text{N}_2\text{O}_5 \cdot 3\text{H}_2\text{O}$	934.1	2.9704
$3\text{Nd}(\text{NO}_3)_3 \cdot 2\text{C}_{26}\text{H}_{28}\text{N}_2\text{O}_5 \cdot 3\text{H}_2\text{O}$	984.9	2.9934
$\text{La}(\text{OH})_3$	835.0	2.9217
$\text{Ce}(\text{OH})_3$	881.7	2.9453
$\text{Pr}(\text{OH})_3$	932.9	2.9698
$\text{Nd}(\text{OH})_3$	981.7	2.9920
$\text{La}_2\text{O}_3$	834.6	2.9215
$\text{Ce}_2\text{O}_3$	883.1	2.9460
$\text{Pr}_2\text{O}_3$	933.4	2.9701
$\text{Nd}_2\text{O}_3$	982.9	2.9925
$\text{La}_2(\text{C}_2\text{O}_4)_3$	837.0	2.9927
$\text{Ce}_2(\text{C}_2\text{O}_4)_3$	883.6	2.9463
$\text{Pr}_2(\text{C}_2\text{O}_4)_3$	935.6	2.9711
$\text{Nd}_2(\text{C}_2\text{O}_4)_3$	984.5	2.9932

<sup>a</sup>BE: binding energy.

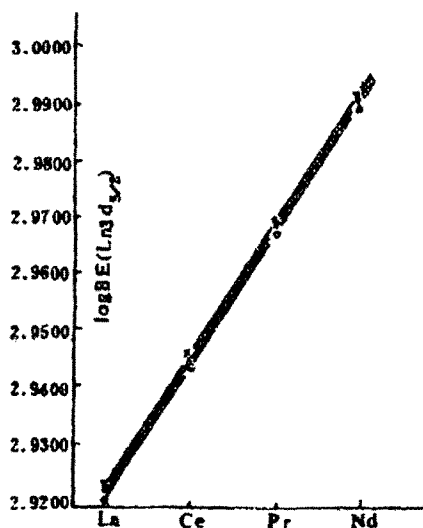


Fig. 9.33. Plot of log BE against atomic number. (●)  $\text{Ln}(\text{NO}_3)_2 \cdot n\text{H}_2\text{O}$ , (●)  $3\text{Ln}(\text{NO}_3)_3 \cdot 2\text{C}_{26}\text{H}_{28}\text{N}_2\text{O}_5 \cdot 3\text{H}_2\text{O}$ , (×)  $\text{Ln}(\text{NO}_3)_3 \cdot \text{C}_{14}\text{H}_{20}\text{O}_5$ .

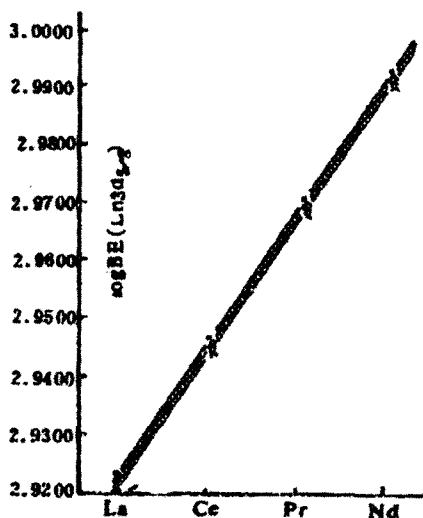


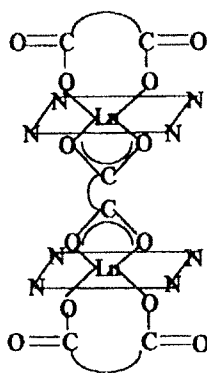
Fig. 9.34. Plot of log BE against atomic number. (●)  $\text{Ln}_2(\text{C}_2\text{O}_4)_3$ , (●)  $\text{Ln}_2\text{O}_3$ , (×)  $\text{Ln}(\text{OH})_3$ .

XPS data [53] on  $\text{Ln}_2(\text{phen})_4\text{L}_3$ , where L = D-camphoric acid, phen = 1,10-phenanthroline, Ln = La, Pr, Sm, Eu, Tb, and Ho are presented in Table 9.7. Because Pr, Sm, Eu, and Tb have variable oxidation states, there is overlap of XPS bands. The binding energies confirm the tetravalency of lanthanides in the complexes. The N 1s peak in the free ligand at 401.2 eV is shifted to 399.2 eV in the complexes. The O 1s peaks are asymmetric

TABLE 9.7  
XPS spectra data of the complexes and the ligands (BE, eV).

Compound	N 1s	C 1s (–COO <sup>–</sup> )	O 1s	Ln	Ac% <sup>a</sup> (Ln/C/N/O)
Phen·H <sub>2</sub> O	401.2				
Na <sub>2</sub> L		288.6	534.2		
La <sub>2</sub> (Phen) <sub>4</sub> L <sub>3</sub>	399.4	288.3,287.8	533.8br	3d <sub>5/2</sub> , 835.9	
Pr <sub>2</sub> (Phen) <sub>4</sub> L <sub>3</sub>	399.0	288.4,288.0	533.8br	933.5	2.0:78.5:8.1:12.1
Sm <sub>2</sub> (Phen) <sub>4</sub> L <sub>3</sub>	399.0	288.4,288.0	533.5br	1083.6	2.0:79.1:8.2:12.1
Eu <sub>2</sub> (Phen) <sub>4</sub> L <sub>3</sub>	399.1	288.2,287.8	533.6br	1137.0	2.0:79.3:8.4:12.0
Tb <sub>2</sub> (Phen) <sub>4</sub> L <sub>3</sub>	399.1	288.3,287.9	533.9br	4d <sub>3/2</sub> , 150.8	2.0:78.4:8.1:12.2
Ho <sub>2</sub> (Phen) <sub>4</sub> L <sub>3</sub>	399.2	288.3,287.9	534.0br	4d <sub>3/2</sub> , 162.4	2.0:78.7:8.1:12.1

<sup>a</sup>Atomic molar percent.



Scheme 9.1.

and deconvolution gives three components. The C 1s peak of carboxyl group gives two components with relative intensity of 2:1. The component with higher binding energy and greater is assigned to unidentate and the weaker component to a bidentate carboxyl. Based on IR spectra and magnetic moment, the following structure has been assigned to the complex (Scheme 9.1).

He(I) photoelectron spectra of lanthanum tris- $\beta$ -diketonate complexes have been studied and the spectra interpreted on the basis of quantum chemical calculations of ground and ionized states by  $X_{\alpha}$ -DV and ab initio methods [54]. The comparative analysis of the photoelectron spectra of Sc, and Lu tris-acetylacetonates showed that substitution of one oxygen atom by NH group shifts the two pairs of  $\pi$  and  $n$  orbitals to a different extent. The IE (ionization energy) values for  $\pi_3$  ( $e$ ) and  $\pi_3$  ( $a_1$ ) orbitals decreased by 0.8–1.0 eV. The  $n_-$  and  $n_+$  molecular orbital two pair bands showed a weak shift of 0.1 eV or less.

In  $D_3$ -symmetry all metal tris- $\beta$ -diketonates form the group orbitals

$$\pi_1, \pi_2, \pi_5: a_2 + e; a_1 + e$$

$$\pi_2, \pi_4: a_1 + e; n_-; a_2 + e$$

TABLE 9.8  
 IE values (eV) for metal tris- $\beta$ -diketonates of group III.

Compound	$\pi_3$		$n_-$		$n_4$			$\pi_{2+}$ others MO
	$a_2$	e	$a_2$	e	$a_1$	e		
M(acac) <sub>3</sub>								
M = Sc		8.31	8.9	9.25		10.11		11.45
	8.03	8.32	8.87	9.25	10.30		10.05	11.6
Y		8.18	8.9	9.07		9.97		11.6
	7.92	8.20*	8.88	9.14	10.26		9.94	11.6
Sm		8.0		9.0				11.5
Gd		8.1		9.0				
Tb, Dy		8.2		9.1			10.0	11.5
Ho		8.2	8.92	9.09	10.24		9.97	11.5
Er	8.02	8.20*	8.99	9.26	10.28		10.02	11.5
Yb	8.2			9.0	10.30		10.06	11.5
Lu	8.10	8.33*	8.89	9.22	10.30		10.01	11.5
M(dpm) <sub>3</sub>								
M = Sc	7.8	8.0	8.4	8.7	9.9		9.7	
Y	7.9	8.1	8.5	8.7	9.8		9.6	
Pr		7.7		8.5		9.3		
Nd	7.6	7.8		8.5	9.6		9.3	
Gd	7.6	7.8		8.5	9.7		9.4	
Tb	7.6	7.8	8.3	8.5	9.7		9.4	
Dy	7.9	8.1	8.4	8.6	9.8		9.5	
Ho	7.6	7.8	8.3	8.5	9.7		9.5	
Yb, Er	7.8	8.0		8.6	9.8		9.6	
Lu	7.8	8.0	8.5	8.7	9.8		9.6	
AlL <sub>3</sub>	7.6	7.8	8.3	8.5	9.7		9.4	
L = acacCl <sup>-</sup>		8.08		9.59		10.70		11.43-n <sub>Cl</sub>
AcacMe <sup>-</sup>		7.75		9.03		10.26		11.02
	7.76	7.84*	9.28	8.88		10.25		11.03
AcacSEt <sup>-</sup>		7.8		9.50		10.33		8.33-n <sub>p</sub> 11.02-n <sub>e</sub>
Eu(tfac) <sub>3</sub>	9.21	9.47*	9.91	10.18	11.2		11.5	
Eu(hfac) <sub>3</sub>		10.1		11.0		11.8		

Metal s, p and d atomic orbitals belong to  $a_1$ ,  $a_2 + e$ ,  $a_1 + e_t + e_e$ , respectively. The theoretical calculations by semi-empirical and  $X_\alpha$ -DV methods showed the following trends in  $ML_3$  complexes: (i) oxygen 2p-atomic orbital contribution to four high pairs of  $\pi$  and  $n$ -orbitals is 45–70%, (ii) a–e splitting values and signs for  $\pi_3$ -,  $n_-$ - and  $n_+$ -orbitals are determined by metal atomic orbital contribution, (iii)  $a_2(n_-)$ -e( $n_-$ ) splitting value and its sign serves as a criterion for M–L bond covalency.

The ionization energy values for rare earth complexes with acetylacetonate (acac) and  $M(dpm)_3$  are given in Table 9.8. Photoelectron spectra showed covalency of M–L bonds in the order  $ScL_3 > LuL_3 > YL_3$ . This order is based on the fact  $a_2(n_-)$ -e( $n_-$ ) splitting and ionization energies of  $n_-$  orbitals decreased in the same order.

Mixed complexes of lanthanides with substituted porphyrin and acetylacetonate ligands were characterized by UV-Vis, IR, NMR, XPS and conductivity [55]. XPS data are given

TABLE 9.9  
X-ray photoelectron spectroscopy data (eV).

Compound	N 1s <sup>1</sup>	N 1s <sup>2</sup>	N 1s <sup>3</sup>	Ln
H <sub>2</sub> TPP	398.00	400.06		
DyTPP(acac)	398.40			
H <sub>2</sub> NTPP	398.40	400.30	403.10	
NdNTPP(acac)	398.60	400.60	401.40	Nd 3d <sub>5/2</sub> 161.00
Eu NTTP(acac)	398.50	400.30	402.70	Eu 3d <sub>5/2</sub> 1135.30
Tm NTTP(acac)	398.70	400.30	401.20	Tm 4d 180.00
Lu NTTP(acac)	398.50	400.20	403.10	Lu 4d <sub>5/2</sub> 196.80

in Table 9.9. The binding energies of 398.4 and 400.3 eV are assigned to pyrrole nitrogen N–H and aza nitrogen. The N 1s at 403.10 is due to the nitro group. In DyTPD there is one N 1s band while in other lanthanide complexes there are two N 1s bands and this has been interpreted as four non-equivalent Ln–N bonds in LnNTPP(acac) and equivalent bonds Dy–N in DyTPP(acac).

The O 1s spectra of free ligand 5-fluorouracil-1-propionic acid and the corresponding rare earth complexes (RE = Y, La, Pr, Sm, Eu, Dy, Er) of the formula Re(FPA)<sub>3</sub>·*n*H<sub>2</sub>O are compared. The free ligand yielded a broad band which could be resolved into two bands due to carbonyl oxygen and carboxyl oxygen. Only one sharp O 1s peak was observed in the complex and this is attributed to bidentate bonding of COO<sup>−</sup> to lanthanide. In the 3d<sub>5/2</sub> band the weak satellite indicated very little participation of 4f orbital in the complex [56].

Ternary complexes of the type Ln(phen)L<sub>3</sub>, where L is 2-mercapto salicylic acid and Ln = La to Yb have been characterized [57] by XPS, IR, NMR, UV-Vis spectra and conductivity. The binding energies of N 1s, O 1s, S 2p, C 1s and Ln 3d states are summarized in Table 9.10.

The N 1s binding energies in the complexes are higher than the free ligand values showing reduced electron density on the metal bonded nitrogen. The O 1s spectra are asymmetric and on deconvolution gave two sets of four components with an intensity ratio of 1:1:2:2. The more intense set at 533.4 and 533 eV was assigned to carboxyl oxygen (C–O<sup>−</sup>) and the less intense set at 532.8 and 532.4 eV to carbonyl oxygen (C=O). This assignment is supported by C 1s and S 2p binding energies. C 1s spectrum is asymmetric and on deconvolution gives two components with an intensity ratio of 1:2. The asymmetric S 2p peak has two components with an intensity ratio of 1:2. The following structure for the complex has been suggested.

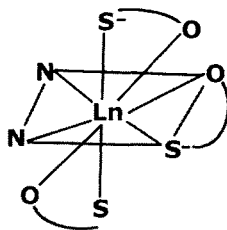


TABLE 9.10  
The binding energy of the N 1s, O 1s, S 2p, Ln, 3d, 4d electrons in Ln(phen)L<sub>3</sub> (eV).

Compound	N 1s	O 1s	S 2p	C 1s (-CO <sub>2</sub> <sup>-</sup> )	Ln
phen	401.2				
bipy	400.8				
L		533.6,533.2	162.9	288.6	
La(phen)L <sub>3</sub>	401.9	533.4,532.0	162.0	288.5	3d <sub>1/2</sub> 836.1
		532.9,532.6		288.3	
Nd(phen)L <sub>3</sub>	408.1	533.5,533.0	162.1	288.4	3d <sub>5/2</sub> 984.3
		532.8,533.0		288.0	
Eu(phen)L <sub>3</sub>	401.8	533.6,533.1	162.0	288.4	1136.0
		532.8,532.4		288.1	
Gd(phen)L <sub>3</sub>	401.8	533.4,533.0	162.1	288.3	1190.9
		532.8,532.4		288.0	
Tb(phen)L <sub>3</sub>	401.6	532.3,532.0	162.1	288.4	1245.6
		532.8,532.6		288.0	
Ho(phen)L <sub>3</sub>	401.8	533.4,533.0	162.0	288.2	4d 162.5
		532.8,532.4		288.1	
Yb(phen)L <sub>3</sub>	401.7	533.2,533.0	161.9	288.2	185.8
		532.7,532.4		287.9	
La(bipy)L <sub>3</sub>	401.0	533.4,533.0	162.1	288.5	3d <sub>1/2</sub> 836.2
		532.8,532.4		288.2	
Sm(bipy)L <sub>3</sub>	401.1	533.2,533.0	162.0	288.4	3d <sub>5/2</sub> 1084.1
		532.8,532.5		288.2	
Gd(bipy)L <sub>3</sub>	401.2	533.3,533.0	161.9	288.3	1191.4
		532.8,532.4		288.0	
Ho(bipy)L <sub>3</sub>	401.1	533.6,533.2	161.8	288.1	4d 162.3
		532.8,532.4		287.8	
Yb(bipy)L <sub>3</sub>	401.3	533.5,533.0	161.7	288.2	186.0
		536,532.3		279.8	

TABLE 9.11  
Ranges for the ligand-to-ligand Rydberg transitions of the Ln(fod)<sub>3</sub> in cm<sup>-1</sup>.

IP	3s	3p	3d
73 500	46 500–51 500	51 500–57 500	59 500–61 500
76 500	49 500–54 500	54 500–60 500	62 500–64 500
78 000	51 000–56 000	56 000–62 000	64 000–66 000
86 000	59 000–64 000	64 000–70 000	72 000–74 000
93 500	66 500–71 500	71 500–77 500	

The He I photoelectron and far UV absorption spectra of lanthanide heptafluoro dimethyl octanedione (fod) complexes exhibit bands only due to ligands. The bands due to ionization from the 4f orbitals of lanthanides were too weak to identify. The far UV spectra showed new bands in the region of 60 000–75 000 cm<sup>-1</sup> and these bands have been interpreted in terms of 5d ← 4f and higher charge transfer Rydberg transitions [58]. Ranges for the ligand–ligand Rydberg transitions of Ln(fod)<sub>3</sub> are given in Table 9.11.

## References

- [1] P.O. Heden, H. Lofgren, S.B.M. Hagsstrom, *Phys. Rev. Lett.* **26**, 432, 1971.
- [2] P.R. McFeely, S.P. Kowalezyk, L. Ley, D.A. Shirley, *Phys. Lett.* **45A**, 227, 1973.
- [3] Y. Baer, G. Busch, *J. Electron Spec. Rel. Phen.* **5**, 611, 1974.
- [4] Y. Baer, G. Busch, *Phys. Lett.* **31**, 25, 1973.
- [5] A. Platau, S.E. Karlsson, *Phys. Rev. B* **18**, 3820, 1978.
- [6] L.I. Johansson, J.W. Allen, T. Gustafsson, I. Lindau, S.B.M. Hagstrom, *Sol. St. Comm.* **28**, 53, 1978.
- [7] P. Steiner, H. Hochst, S. Hufner, *J. Phys.* **F7**, L145, 1977.
- [8] A.F. Orchard, G. Thornton, *J. Electron Spec. Rel. Phen.* **10**, 1, 1977.
- [9] P.A. Cox, *Structure and Bonding*, Vol. 24, p. 59, Springer-Verlag, 1975.
- [10] R.L. Cohen, G.K. Wertheim, A. Rosencwaig, H.J. Guggenheim, *Phys. Rev.* **B5**, 1037, 1972.
- [11] J.F. Herbst, D.N. Lowy, R.E. Watson, *Phys. Rev.* **B6**, 1913, 1972.
- [12] F.R. McFeely, S.P. Kowalezyk, L. Ley, D.A. Shirley, *Phys. Lett.* **A49**, 301, 1974.
- [13] J.F. Herbst, R.E. Watson, Y. Baer, *Phys. Rev.* **B16**, 2447, 1977.
- [14] J.H. Van Vleck, *Phys. Rev.* **45**, 405, 1934.
- [15] P.S. Bagus, A.J. Freeman, F. Sasaki, *Phys. Rev. Lett.* **30**, 850, 1973.
- [16] S.P. Kowalezyk, N. Edelstein, F.R. McFeely, L. Ley, D.A. Shirley, *Chem. Phys. Lett.* **29**, 491, 1974.
- [17] W.C. Lang, B.D. Padalia, L.M. Watson, D.J. Fabian, P.R. Norris, *Faraday Discussions, Chem. Soc.* **60**, 37, 1975; *Proc. Roy. Soc. London, Ser. A* **354**, 269, 1977.
- [18] A.F. Orchard, G. Thornton, *J. Electron Spec. Rel. Phen.* **13**, 27, 1978.
- [19] C.N.R. Rao, D.D. Sarma, *J. Electron Spec. Rel. Phen.* **13**, 1980.
- [20] C.K. Jorgenson, H. Berthou, *Chem. Phys. Lett.* **13**, 186, 1972.
- [21] A.J. Signorelli, R.G. Hayes, *Phys. Rev.* **B8**, 81, 1973.
- [22] S. Suzuki, T. Ishii, T. Sagawa, *J. Phys. Soc., Japan* **37**, 1334, 1974.
- [23] P. Burroughs, A. Hammett, A.F. Orchard, G. Thornton, *J. Chem. Soc. Dalton Trans.* **17**, 1686, 1976.
- [24] H. Berthou, C.K. Jorgenson, C. Bonnelle, *Chem. Phys. Lett.* **38**, 99, 1976.
- [25] J. Weber, H. Berthou, C.K. Jorgenson, *Chem. Phys. Lett.* **45**, 1, 1977.
- [26] J. Weber, H. Berthou, C.K. Jorgenson, *Chem. Phys.* **26**, 69, 1977.
- [27] W.Y. Houng, R.J. Thorn, *Chem. Phys. Lett.* **56**, 69, 1977.
- [28] W.H. Madhusudan, S. Kollali, P.R. Sarode, M.S. Hedge, P. Ganguly, C.N.R. Rao, *Pramana* **12**, 379, 1979.
- [29] G. Cretilius, G.K. Wertheim, D.N.E. Buchanan, *Phys. Rev.* **B18**, 6519, 1978.
- [30] C.N.R. Rao, D.D. Sarma, S. Vasudavan, M.S. Hedge, *Proc. Royal Soc. A* **367**, 239, 1979.
- [31] J.N. Chazalviel, M. Campagna, G.K. Wertheim, P.H. Schmidt, Y. Yafet, *Phys. Rev. Lett.* **37**, 919, 1976; *Sol. St. Comm.* **19**, 725, 1976; *Phys. Rev.* **B14**, 4586, 1976.
- [32] J.L. Freouf, D.E. Eastman, W.D. Gobman, F. Holtzberg, J.B. Torrance, *Phys. Rev. Lett.* **33**, 161, 1974.
- [33] M. Campagna, E. Bucher, G.K. Wertheim, L.D. Longinotti, *Phys. Rev. Lett.* **33**, 165, 1974.
- [34] R.A. Pollak, F. Holtzberg, J.L. Freeouf, D.E. Eastman, *Phys. Rev. Lett.* **33**, 820, 1975.
- [35] C.N.R. Rao, unpublished results.
- [36] K.H.J. Buschow, M. Campagna, G.K. Wertheim, *Sol. St. Comm.* **24**, 253, 1977.
- [37] I. Nowik, M. Campagna, G.K. Wertheim, *Phys. Rev. Lett.* **38**, 43, 1977.
- [38] M. Campagna, E. Bucher, G.K. Wertheim, D.N.E. Buchanan, L.D. Longinotti, *Phys. Rev. Lett.* **32**, 885, 1974.
- [39] Y. Baer, Ch. Zurcher, *Phys. Rev. Lett.* **39**, 956, 1977.
- [40] B.D. Padalia, W.C. Lang, P.R. Norris, L.N. Watson, D.J. Fabian, *Proc. Royal Soc. London, Ser. A* **354**, 269, 1977.
- [41] M. Campagna, G.K. Wertheim, E. Bucher, *Structure and Bonding*, Vol. 30, p. 99, Springer-Verlag, 1976.
- [42] L.C. Gupta, unpublished results.
- [43] K.H.J. Buschow, M. Campagna, G.K. Wertheim, *Solid St. Comm.* **24**, 253, 1977.
- [44] G.K. Wertheim, M. Campagna, *Chem. Phys. Lett.* **47**, 182, 1977.
- [45] G.K. Wertheim, G. Crecelius, *Phys. Rev. Lett.* **40**, 813, 1978.
- [46] G.K. Wertheim, J.H. Wernick, G. Crecelius, *Phys. Rev.* **B18**, 875, 1978.
- [47] W.F. Egelhoff, Jr., G.G. Tibbetts, *Phys. Rev. Lett.* **44**, 482, 1980.



- [48] C.R. Helms, W.E. Spicer, *Appl. Phys. Lett.* **21**, 237, 1972.
- [49] A. Platau, L.I. Johansson, A.L. Hagstrom, W.E. Karlsson, S.B.M. Hagstrom, *Surf. Sci.* **63**, 153, 1977.
- [50] C.N.R. Rao, D.D. Sarma, *Chemistry & Technology of Rare Earths*, Acad. Press, 1980.
- [51] J. Lippei, C. Botao, C. Daowen, W. Dianxan, Y. Xuezhong, *J. Mol. Sci.* **4**, 143, 1986.
- [52] J. Weber, *Chem. Phys. Lett.* **45**, 1, 1977.
- [53] S. Zhongxing, Y. Sheng, Z. Zhengzhi, D. Rewen, C. Hui, *Bull. Soc. Chim. Belg.* **106**, 261, 1997.
- [54] V.I. Vovna, I.B. Lvov, S.N. Slabzhenikov, A.Yu. Ustinov, *J. Electron Spec. and Related Phenom.* **88-91**, 109, 1998.
- [55] D.M. Li, Z. Jhao, H. Sun, G. Liu, T. Shi, X. Liu, S. Dong, *Synth. React. Inorg. Met.—Org. Chem.* **30**, 1899, 2000.
- [56] Y. Liu, J. Kang, Z. Wang, L. Wang, L. Gao, C. Xia, J. Cui, *J. Coord. Chem.* **52**, 1, 2000.
- [57] W. Bo, M. Hong Zhu, *Inorganic Communications* **3**, 243, 2000.
- [58] G. Richer, C. Sandorfy, *J. Molecular Structure (Theochem)* **167**, 413, 1988.

chapter 10

---

## LANTHANIDE NMR SHIFT REAGENTS

---

---

# CONTENTS

---

1. Introduction . . . . .	781
2. History of development of NMR shift reagents . . . . .	781
3. Chemical shifts in lanthanide complexes . . . . .	784
4. Contact shifts . . . . .	785
5. Temperature dependence . . . . .	789
6. Separation of contact and dipolar contributions . . . . .	790
7. Nuclear relaxation . . . . .	794
8. Kinetic factors . . . . .	796
9. Analysis of shift reagent equilibria . . . . .	796
10. Applications . . . . .	798
11. Conformational isomers . . . . .	805
12. Quantitative aspects . . . . .	805
13. Polymers . . . . .	806
14. Isotope effects . . . . .	806
15. Chiral shift reagents . . . . .	806
16. Applications to pharmaceuticals . . . . .	808
17. Application to coordination metal complexes . . . . .	810
18. Interaction at non-donor sites . . . . .	810
19. LSR interaction via donor atom . . . . .	810
20. Conformational studies . . . . .	812
21. Chiral studies . . . . .	813
22. Spin-lattice relaxation studies . . . . .	813
23. Kinetic studies . . . . .	817
24. Application of LIS to biological macromolecules . . . . .	818
25. Studies on $Mg^{2+}$ -ATP-dependent phosphoglycerate kinase . . . . .	821
26. $Ca^{2+}$ -binding protein, parvalbumin . . . . .	823
27. Studies on surfaces of proteins . . . . .	827
28. Applications to cells, tissues and organs . . . . .	828
29. Applications of lanthanides in biology . . . . .	832
30. New Ln(III) reagents . . . . .	834
31. Computer programs for simulation of induced shifts . . . . .	837
References . . . . .	840

## 1. Introduction

The effects of paramagnetism on nuclear magnetic resonances (NMR) of the ligand molecules have been studied from the early days of nuclear magnetic resonance spectroscopy [1]. This was followed by Hinckley's work on the use of lanthanide complexes to simplify unresolved proton resonances in low field NMR spectra [2]. The lanthanide induced shift (LIS) has been used in solving a variety of NMR problems. Some of the problems solved by this technique are: (i) qualitative spectral analysis and simplification, (ii) proving molecular stereochemistry, (iii) quantitative analysis of dynamic structures in solution, (iv) application to perfused tissues and organs, and (v) magnetic resonance imaging. All of these applications are based upon three fundamental properties of lanthanide ions, namely: (i) Lewis acid behaviour, (ii) presence of unpaired f electrons, and (iii) their ability to form complexes with coordination numbers in the range of 8 to 10. Consider the interaction of a Lewis base with a lanthanide cation. During such an interaction, NMR active nuclei in the Lewis base are affected by the unpaired electrons present in the f shell of the lanthanide cation, leading to paramagnetic relaxation or broadening of the resonance peak along with a shift of the NMR frequency in some cases. When the interaction between the cation and the Lewis base is electrostatic, the paramagnetic lanthanide ions with anisotropic distribution of f electrons give rise to lanthanide induced NMR pseudo contact shift. This type of LIS is useful in obtaining structural information.

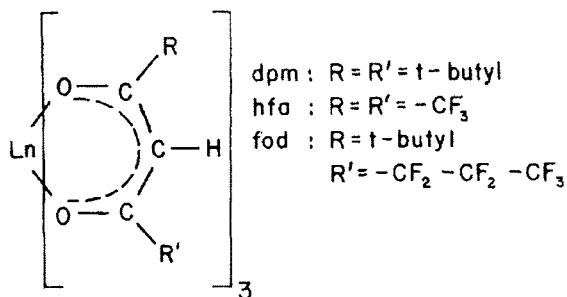
Trivalent gadolinium with  $f^7$  configuration has isotropic distribution of electrons and hence cannot produce pseudo contact shift. However, when the Lewis acid–base interaction is partly covalent, the unpaired electron spin density influences the molecular framework of the base and causes an LIS known as contact shift. Gd(III) is used to ascertain the contributions of contact shift to the measured LIS.

We will now proceed to a discussion of LIS methodologies, uses of lanthanides in complex NMR spectra, quantitative aspects of the LIS method such as testing and separation of shifts, use of pseudo contact shift in molecular structure, and use of aqueous cations and lanthanide complexes in biological systems.

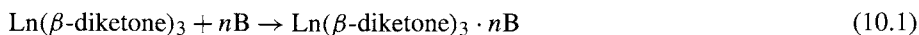
## 2. History of development of NMR shift reagents

Many lanthanide shift reagents are now available commercially which are soluble in common organic solvents. Most of the reagents are lanthanide complexes of  $\beta$ -diketones having the basic 2,4-pentanedione structure. Some common reagents are Pr(fod)<sub>3</sub>, Eu(tfa)<sub>3</sub>, Yb(hfa)<sub>3</sub> and also associated permutations. The shift reagents are tris- $\beta$ -diketonates of

lanthanides with a hexacoordinate structure and 3-fold symmetry axis. The metal ion in the  $\beta$ -diketonate complex

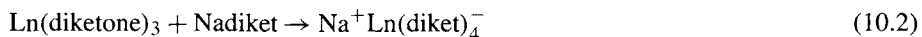


is coordinately unsaturated and hence forms an adduct with a base. The complex is soluble in dry 'inert' organic solvent.



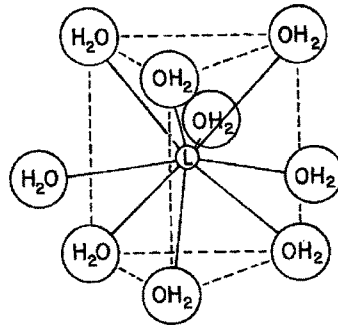
Upon dissolution in an organic solvent, the  $\beta$ -diketone complex forms an adduct with Lewis base B with weak interaction. The Lewis base molecule which is weakly bound enters into rapid exchange between the lanthanide site and bulk solution. Hence the observed LIS values in the NMR spectrum of Lewis base depend upon the equilibrium constants and the geometries of the acid-base complexes formed.

For the qualitative use of shift reagents to resolve overlapping resonance peaks, it is not necessary to titrate or analyze equilibrium constants. It is a normal practice to keep the shift reagent stored over a drying agent and add a few crystals to the sample whose NMR is being studied. In quantitative analysis, it is useful to know the purity of the reagent for it may be contaminated with excess ligand

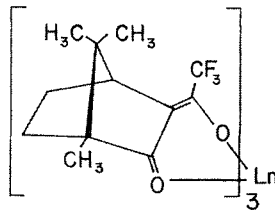


In such cases, the shift reagent must be purified such that it is pure tris  $\beta$ -diketonate of Ln. The purity of the shift reagent may be checked by <sup>1</sup>H NMR or mass spectrometry and purified by treating with CCl<sub>4</sub> and 0.1 M HCl.

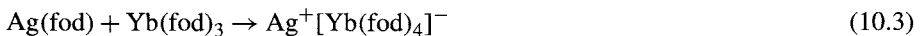
Other reagents that have been found useful in NMR spectroscopy are chiral shift reagents [4] and binuclear lanthanide-silver shift reagents [5]. Both these reagents are soluble in organic solvents. The chiral reagents are similar to  $\beta$ -diketonates except they also contain a bulky, rigid, asymmetric structure as part of the whole entity. The most common reagent is a derivative of D-camphor, such as 3-trifluoroacetyl-D-camphorato (facm). A typical shift reagent is the Eu<sup>3+</sup> bonded to three molecules of facm to give E(facm)<sub>3</sub> which binds to one substrate enantiomer with higher affinity than the other substrate enantiomer. Thus the normal chemical degeneracy of the enantiomeric mixture is removed leading to a method of determining enantiomeric purities. This method is

Fig. 10.1. Structure of  $\text{Nd}(\text{H}_2\text{O})_9^{3+}$ .

applicable only when the Lewis base site is near the asymmetric centre and the substrate should be a racemic mixture.



The binuclear lanthanide–silver reagent is formed by combining silver diketonate such as  $\text{Ag}(\text{fod})$  with a lanthanide tris diketonate like  $\text{Yb}(\text{fod})_3$  to give  $\text{Ag}^+[\text{Yb}(\text{fod})_3]^-$ .



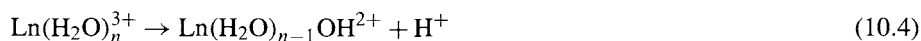
With this type of shift reagent, the silver ion binds to soft Lewis base donors, such as olefins, aromatics, phosphenes, and halogenated compounds. At the same time, silver remains as an ion pair with  $\text{Yb}(\text{fod})_4^-$  in a specific orientation such that a paramagnetic shift is induced in the resonances of NMR resonance peaks of cis and trans geometric isomer mixtures of long-chain alkenes and complex mixtures of aromatic molecules [5].

In 1971, the use of aqueous lanthanide cations as NMR shift reagents in biological systems was discovered by R.J.P. Williams and coworkers [6]. The principles of application of both lanthanide  $\beta$ -diketonates and lanthanide aquo cations are the same and the latter is somewhat complicated. The complex situation in the case of aquo lanthanide cations arises due to the dynamic equilibrium that exists in aqueous solutions of lanthanide ions. Considering aquo Nd(III) ion as an example, one finds that  $\text{Nd}(\text{H}_2\text{O})_9^{3+}$  exists as a tricapped trigonal prism structure in the solid state as shown in Fig. 10.1. The coordination number of aquo lanthanide ions for larger ions (La–Nd) is nine and eight for the smaller ions (Dy–Lu). For intermediate ions there exists a dynamic equilibrium [7] mixture of  $\text{Ln}(\text{H}_2\text{O})_8^{3+}$  and  $\text{Ln}(\text{H}_2\text{O})_9^{3+}$ . Because of the rapid water exchange equilibrium, the added ligand with active

NMR nuclei will enter into an exchange process in which the ligand will displace one or two molecules of water from an aquo lanthanide ion depending upon whether the ligand is a monodentate or bidentate. Thus a variety of mixed complexes are possible,  $\text{Ln}(\text{L})_n(\text{H}_2\text{O})_m$ . Hence NMR detects the averaged effects which varies from one lanthanide to another.

Unlike the lanthanide  $\beta$ -diketonates, aquo lanthanides can be obtained in high purity because of the commercially available rare earth oxides of high purity. Dissolution in HCl or  $\text{HNO}_3$  will give the lanthanide chloride or lanthanide nitrate solution and can be stored indefinitely because of their stability.

Because of the tendency of trivalent lanthanides to hydrolyse at pH 6–7



and eventual precipitation as hydroxide, it is combined with a chelating agent such as EDTA which prevents hydrolysis and yet provides coordination sites for ligands whose NMR spectral changes may be studied. An example of such an LIS complex is  $[\text{La}(\text{EDTA})(\text{H}_2\text{O})_3]^-$  whose structure is shown in Fig. 10.2.

Other ligands which are complexed with lanthanides and further used as LIS reagents are  $\text{DPA}^{2-}$ ,  $\text{NTA}^-$ ,  $\text{EDTA}^{4-}$ ,  $\text{NOTA}^{4-}$ , and  $\text{DOTA}^{4-}$  whose structure are shown in Fig. 10.3.

Shift reagent	Reference
$[\text{Ln}(\text{NTA})(\text{H}_2\text{O})_5]$	[8]
$[\text{Ln}(\text{EDTA})(\text{H}_2\text{O})_3]$	[9–13]
$[\text{Ln}(\text{NOTA})(\text{H}_2\text{O})_3]$	[13,14]
$[\text{Ln}(\text{DOTA})(\text{H}_2\text{O})]$	[13]

Aqua lanthanide water soluble shift reagents are soluble over a wide pH range but limit the number of additional ligands which can bind to the central lanthanide. Thus the number of possible exchanging structures being averaged in a LIS experiment is limited. Some possible applications of these reagents are given below.

Compound	Reference
Carboxylates	[13]
Amines	[13]
Alcohols	[13]
Amino acids	[12]
Mono-dinucleotides	[8,9,11]

### 3. Chemical shifts in lanthanide complexes

Nuclei of ligands in paramagnetic complexes are coupled to the electronic spin of the central ion by the electron-nuclear hyperfine interaction. As a result of this interaction,

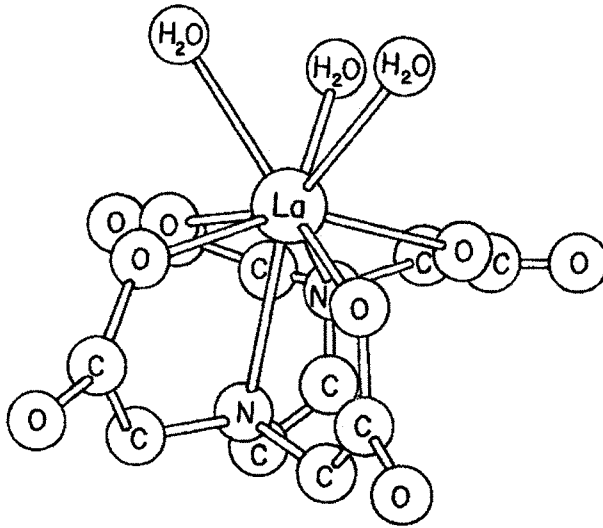


Fig. 10.2. Structure of  $\text{La}(\text{EDTA})(\text{H}_2\text{O})_3$ .

large chemical shifts (relative to the diamagnetic system) in the NMR spectra of the ligands are observed. There are two independent mechanisms of hyperfine interaction. (i) The contact interaction results from a finite probability of finding an unpaired electronic spin on an atomic  $s$  orbital, (ii) the dipolar interaction takes place via space and causes shifts only if the magnetic susceptibility of the central ion is anisotropic. Otherwise it is averaged out and no dipolar shifts are observed. This is the case with  $S$ -state ions such as  $\text{Gd}^{3+}$ . Hence the net shift,  $\Delta_b$  is a sum of two contributions, namely the contact shift,  $\Delta_c$  and the dipolar shift,  $\Delta_d$ .

$$\Delta_b = \Delta_c + \Delta_d \quad (10.6)$$

#### 4. Contact shifts

The first systematic study of chemical shifts in lanthanide complexes involved measurement and interpretation of oxygen-17 shifts of aquo complexes and the sign variation of the observed shifts in the series. The  $^{17}\text{O}$  shifts of  $\text{Dy}^{3+}$  and  $\text{Ho}^{3+}$  perchlorates conform to the Curie law of equation (10.8) and the corrections due to second order treatment for the ions are small [16].

Studies on proton shifts in aqueous solutions of lanthanide perchlorates showed irregular sign variation of the shifts in the series and quite different from  $^{17}\text{O}$  shifts. This observation led to the idea that proton shifts are predominantly due to dipolar contributions. Further the proton shifts departed from Curie's law significantly [17]. The relative dipolar shifts and their temperature dependence can be predicted by Bleaney's theory [18]. For now  $\text{Eu}^{3+}$  and  $\text{Sm}^{3+}$  are not considered.



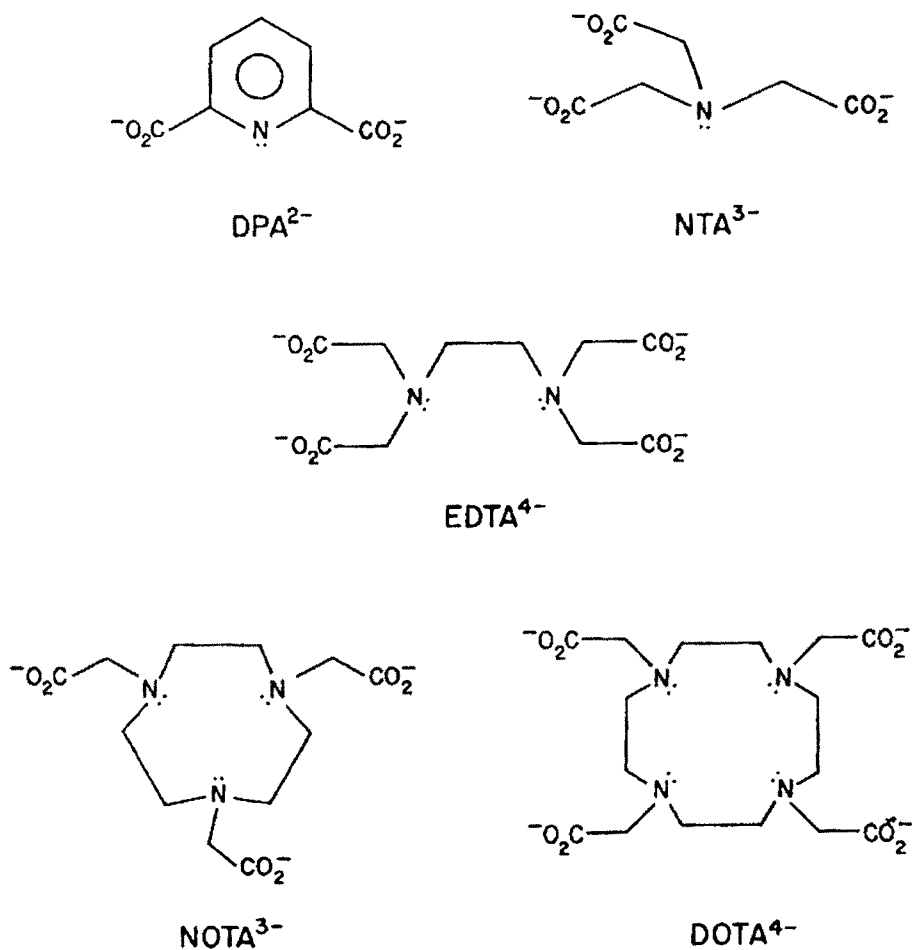


Fig. 10.3. Structure of some chelates used with lanthanide cations.

Bleaney's theory consists of two important points. (i) In a lanthanide complex the ground state of the ion has  $2J + 1$  levels split by the ligand field, which may be populated at room temperature. The magnetic properties of an isolated group of levels may be anisotropic. But the lifetime of the ion in any one of these levels is very short at room temperature. The estimated electron spin relaxation times from the nuclear relaxation measurements are of the order of  $10^{-13}$  s. Thus in an NMR experiment only the magnetic moment averaged over a time long compared with the electron relaxation time is to be considered since the reorientation time of the complex along the series suggested that there was no direct overlap between the 4f and the oxygen 2s wave function, but rather a promotion of a bonding electron into an empty antibonding orbital leaving a net spin at the oxygen nucleus. This

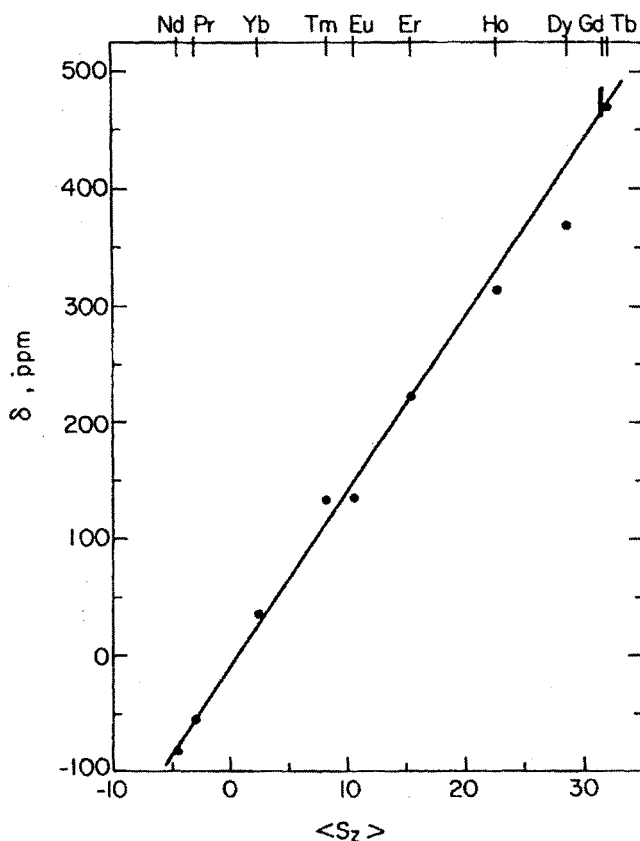


Fig. 10.4. The water oxygen-17 shift in 1 molal  $R(\text{ClO}_4)_3$  solutions plotted against  $\langle S_z \rangle$ .

mode of interaction is known as spin polarization in contrast to delocalization or direct overlap. The contact shift in frequency units may be written as

$$\Delta_c = A \langle S_z \rangle, \quad (10.7)$$

where  $A$  is the hyperfine coupling constant in frequency units and  $\langle S_z \rangle$  is the projection of the total electron spin magnetization of the lanthanide on the direction of the external magnetic field. To a first approximation we have

$$\langle S_z \rangle = g_L(g_L - 1)J(J + 1)(\beta H_0/3kT), \quad (10.8)$$

where  $g_L$  is the Lande'  $g$ -factor,  $J$  is the resultant electron spin angular momentum in  $\hbar$  units of ground level,  $\beta$  is the Bohr magneton, and  $H_0$  is the intensity of the external magnetic field. Equation (10.8) is applicable to all  $\text{Ln}^{3+}$  ions except  $\text{Eu}^{3+}$  and  $\text{Sm}^{3+}$  in which cases higher levels should be included. The  $\langle S_z \rangle$  values calculated using equation (10.8) are given in Table 10.1. A method involving a second order perturbation

TABLE 10.1  
 $\langle S_Z \rangle$  (in units of  $\beta H_0/3kT$ ) of trivalent lanthanide [15].

R <sup>3+</sup>	$\langle S_Z \rangle^a$	$\langle S_Z \rangle^b$
Pr	-3.200	-2.972
Nd	-4.909	-4.487
Eu	-	10.682
Gd	31.500	31.500
Tb	31.500	31.818
Dy	28.333	22.545
Ho	22.500	22.629
Er	15.300	15.374
Tm	8.167	8.208
Yb	2.571	2.587

<sup>a</sup>Calculated with equation (10.8).

<sup>b</sup>From [15].

treatment resulted in a correction of up to 10% in the  $\langle S_Z \rangle$  values with complex temperature dependence [15]. The latter values are also given in Table 10.1.

The O<sup>17</sup> shifts observed in 1 molal solutions of lanthanide perchlorates are plotted against  $\langle S_Z \rangle$  values given in Table 10.1. The resulting plot showed the correlation is reasonably good and it shows that the hyperfine coupling constant  $A$  for the oxygen in water of aquo complexes of lanthanides does not change significantly. The averaged magnetic moment is composed of the contributions of  $2J + 1$  levels of the ground  $J$  manifold, each weighted by the corresponding relative population. As an approximation, at the temperature of the NMR experiment  $kT \gg \Delta E_J$  where  $\Delta E_J$  is the energy span of the levels. Assuming equal distribution of population, equally-weighted average of the magnetic moments over the entire ground manifold of the lanthanide ion gives rise to isotropic magnetic susceptibility. Thus the dipolar shift in the first order disappears.

(ii) Higher order terms of the level populations consider deviations from equal population at a given temperature. This second order approximation gives a  $1/T$  dependent population distribution which serves as weighting factors in the calculation of the average magnetic moment. The average magnetic moment together with Curie's law gives an anisotropic,  $1/T^2$  dependent susceptibility. This in turn gives rise to dipolar NMR shifts in lanthanide complexes.

The dipolar shift for an axially symmetric complex may be written as

$$\Delta_d = \frac{\nu_0 \beta^2}{60kT^2} \cdot \frac{3 \cos^2 \theta - 1}{r^3} 2A_2^0(r^2) g_L^2 J(J+1)(2J-1)(2J+3) \langle J \parallel \alpha \parallel \rangle, \quad (10.9)$$

where  $\nu_0$  is the resonance frequency,  $T$  is the temperature,  $r$  is the distance between the central metal and ligand,  $\theta$  is the angle between the vector  $r$  and the principal axis of symmetry of the complex,  $A_2^0$  are ligand field coefficients which are constant for a given complex in the lanthanide series and the last term has been calculated by Bleaney. The relative dipolar shifts and their ratio to the contact shifts for lanthanide complexes at 300 K are given in Table 10.2. For isostructural complexes, these values give the relative shifts for the lanthanide series.

TABLE 10.2  
Relative dipolar shifts and their ratio to the contact shifts  
for lanthanide complexes (at 300 K).

R <sup>3+</sup>	<i>D</i> [18]	<i>D</i> / <i>S<sub>Z</sub></i> <sup>b</sup> [15]
Pr	-11.0	3.70
Nd	-4.2	0.94
Eu	4.0	0.37
Gd	0	0
Tb	-86	-2.70
Dy	-100	-3.50
Ho	-39	-1.72
Er	33	2.15
Tm	53	6.46
Yb	22	8.50

<sup>b</sup>*S<sub>Z</sub>* from Golding and Halton (1972).

For simplicity the dipolar shift may be written as

$$\Delta_d^i = DG_i, \quad (10.10)$$

where  $G_i = (3 \cos^2 \theta_i - 1)/r_i^3$  is the geometrical function for a ligand nucleus,  $i$ , and  $D$  is a temperature dependent factor characteristic of the lanthanide (Table 10.2). In Fig. 10.5 the observed shift,  $\Delta$  (ppm) is plotted against  $D$  values for pyridine, 2,6-dicarboxylates and its quinoline adducts. It is clear from the figure that the correlations are good.

Bleaney's treatment has been modified and a generalized treatment to include arbitrary ligand field components has been advanced [21]. The modified treatment gives results differing by 20% from Bleaney's results and the deviation from  $1/T_2$  dependence by 10%. Unfortunately, lack of available ligand field parameters for most of the systems presents difficulties in using the modified treatment.

## 5. Temperature dependence

The temperature dependence of contact and dipolar shifts can be written as

$$\Delta_b = A\langle S_Z \rangle' / T + D'G/T^2, \quad (10.11)$$

where  $\langle S_Z \rangle' \equiv T\langle S_Z \rangle$  and  $D' \equiv DT^2$ . The equation (10.11) shows that the temperature dependencies of the two contributions to NMR shift are different. The temperature dependence of the shifts can be analyzed by plotting  $\Delta_b T$  versus  $1/T$  and the intercept and slope of the resulting plot are the relative contact and dipolar contribution to the shift, respectively.

$$\Delta_b T = A\langle S_Z \rangle' + D'G/T \quad (10.12a)$$

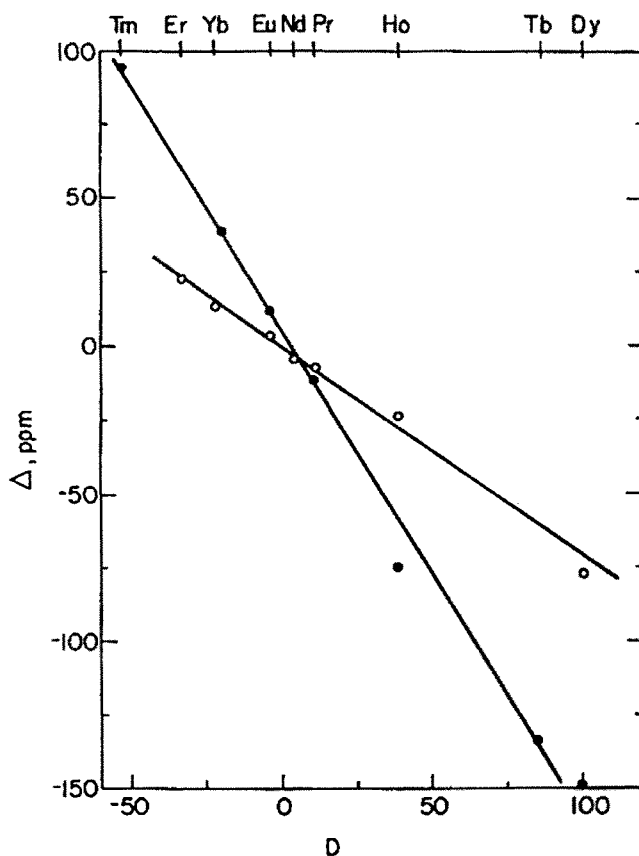


Fig. 10.5. The carbon-13 shift of  $C_{\alpha}$  in  $R(DPA)_3$  complexes (filled symbols) [19] and the proton shift of  $H_7$  in quinoline- $R(dpm)_3$  adducts (open symbols) [20] plotted against the corresponding  $D$  value.

A plot for the proton shift of acetone induced by  $Yb(fod)_3$  as a function of temperature is shown in Fig. 10.6.

The contact contribution to the shift induced by the ytterbium complex is minimal and a similar observation has been made for proton shifts in  $Tm(DPA)_3$  and  $Yb(DPA)_3$  complexes in aqueous solution [23].

## 6. Separation of contact and dipolar contributions

Substituting equations (10.7) and (10.10) into equation (10.6) the following general equation for the shifts in the lanthanide complexes may be written

$$\Delta_b^i = A_i \langle S_Z \rangle + DG_i, \quad (10.12b)$$

where  $i$  refers to the ligand nucleus. In the context when only the spin polarization mechanism is important,  $A_i$  will be a constant in the lanthanide series. When isostructural

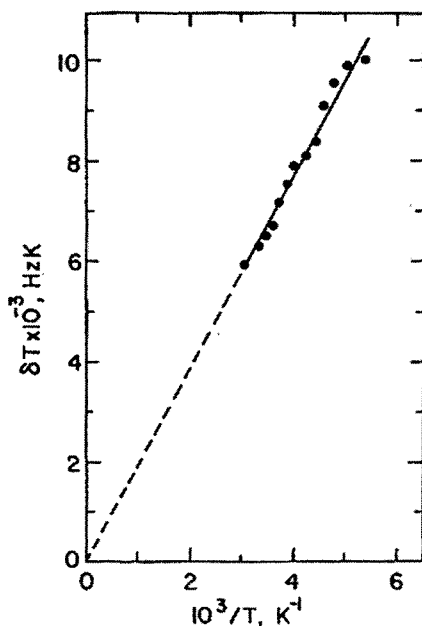


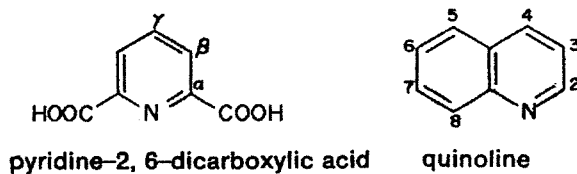
Fig. 10.6. The product of the temperature and the  $\text{Yb}(\text{fod})_3$  induced proton shift of acetone (in Hz at 90 MHz) plotted against the reciprocal temperature [22].

complexes are considered  $G_i$  will remain a constant. Now that  $A_i$  and  $G_i$  are constants we may write

$$\Delta_b^i / \langle S_Z \rangle = A_i + G_i (D / \langle S_Z \rangle) \quad (10.13)$$

The theoretical values of  $\langle S_Z \rangle$  and  $D / \langle S_Z \rangle$  are available as given in Tables 10.1 and 10.2. A plot of  $\Delta_b^i / \langle S_Z \rangle$  versus  $D / \langle S_Z \rangle$  for lanthanide–DPA complexes is shown in Fig. 10.7. It is clear from the figure that  $C_\gamma$  values are in keeping with the model. On the other hand the carboxyl carbon which is in  $\alpha$  position to the coordinating atoms does not conform to the model probably due to the operations of other shift mechanisms. Other nuclei in the ligand DPA conform to the model. It is useful to note that a maximum in structural imperfections in the lanthanide series will be shown by nuclei for which  $\theta = 45^\circ$  where the derivative of  $(3 \cos^2 \theta - 1)$  has a maximum. This may also contribute to the shifts of carboxyl carbon.

A plot of  $\Delta / \langle S_Z \rangle$  versus  $D / \langle S_Z \rangle$  for the  $\text{H}_2$  and  $\text{H}_3$  protons of quinoline adducts with  $\text{Ln}(\text{dpm})_3$  is shown in Fig. 10.8. The  $\text{H}_2$  proton that is in beta position shows some deviations from the model while the  $\text{H}_3$  and other nuclei conform to the model well.



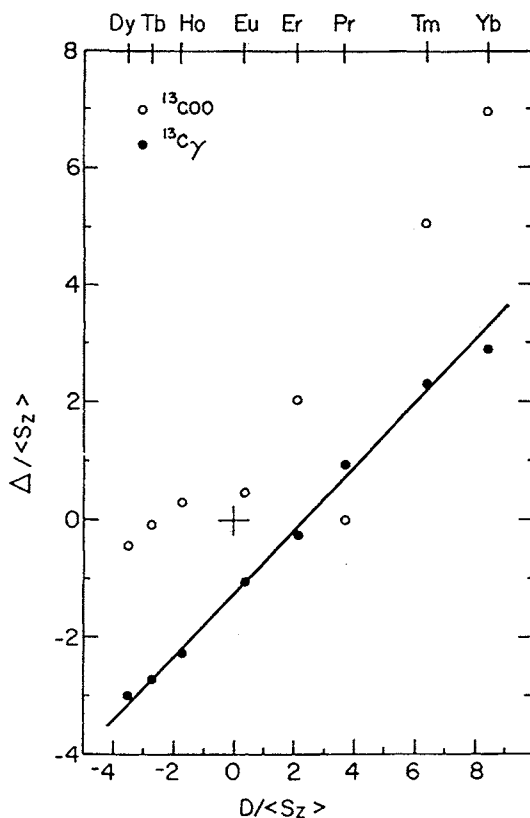


Fig. 10.7. The  $\langle S_Z \rangle$  normalised carbon-13 shifts of the carboxyl and  $\text{C}_{\gamma}$  in  $\text{R}(\text{dpm})_3$  complexes plotted against the corresponding  $D/\langle S_Z \rangle$  ratio [19].

Some salient points to note are: (i) the model is in accord with the experimental results, (ii) nuclei at  $\alpha$  and  $\beta$  positions to the coordinating atom show deviations from the model due to contributions of other shift mechanisms. Thus the best procedure for the elucidation of molecular structure by using lanthanide reagents consists of (i) to obtain the relative magnitude of geometrical function,  $G$  for different ligand nuclei from the slopes of  $\Delta_b^i T$  versus  $1/T$  plots, (ii) since temperature dependence of ytterbium complexes conforms to the model, use of ytterbium complexes is prudent, (iii) in cases where the temperature dependence is interfered with effects due to chemical equilibrium or exchange, data for a number of lanthanides at room temperature may be obtained and plots of equation

$$\Delta_b^i/\langle S_Z \rangle = A_i + G_i(D/\langle S_Z \rangle) \quad (10.14)$$

be made. The most suitable lanthanides for this purpose in order of  $D/\langle S_Z \rangle$  ratios are Yb, Tm, Pr, Dy, (iv) it is also necessary that the data be obtained for isostructural complexes, (v) the data for nuclei in  $\alpha$  and  $\beta$  positions of the coordinating atom are not considered relevant and hence can be ignored in the analysis.

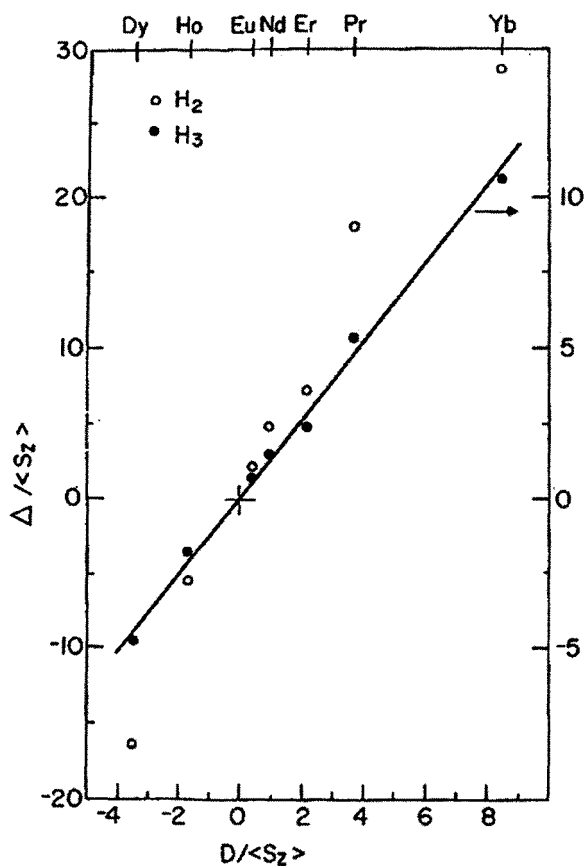


Fig. 10.8. The  $\langle S_z \rangle$  normalised proton shifts of  $H_2$  and  $H_3$  in quinoline- $R(dpm)_3$  adducts plotted against the corresponding  $D/\langle S_z \rangle$  ratio [20].

The discussion so far has centred on lanthanide complexes with axial symmetry. When lanthanide adducts are devoid of axial symmetry, the dipolar shift is given by the equation [18]

$$\Delta_d = r^{-3} [D_1 (3 \cos^2 \theta - 1) + D_2 \sin^2 \theta \cos \phi], \quad (10.15)$$

where  $D_1$  and  $D_2$  are temperature dependent constants for a particular lanthanide and  $\phi$  is the angle between the projection of the vector on the plane perpendicular to the magnetic axis of the complex and one of the axes on this plane. Non-axial symmetry is likely with non-chelating ligands like *N*-acetyl-L-3 nitrotyrosine ethyl ester and in such cases equation (10.15) is empirically fitted using the relative distances determined from relaxation measurements on the gadolinium complex [24]. Although the chelation is absent, effective axial symmetry is usually observed with shifts and this may be due to the averaging mechanisms. The ligand molecule rotates freely about an axis which passes



through the central ion of the complex. Such a motion will average out the second term [25] of equation (10.15). Another possible averaging mechanism is a situation when the lanthanide adduct in solution exists as an ensemble of many isomers rapidly undergoing interconversion [26]. This case is similar to ligand rotation.

## 7. Nuclear relaxation

Nuclear relaxation in paramagnetic complexes occurs due to the time dependent terms in the nuclear spin Hamiltonian. The amount of relaxation effect is dependent on the intensity of electron–nuclear interaction and the rate at which this interaction is interrupted. Thus the relaxation rates of ligand nuclei are determined by the two factors, namely, molecular structure and molecular dynamics in solution. Thus the relaxation rates of ligand nuclei shed light on molecular structure and dynamics in solution.

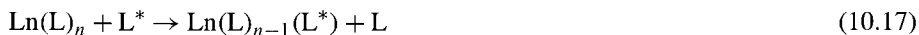
In the case of rapid reactions of lanthanide complexes if  $T_{1e}$  the electron spin relaxation time is short compared to the rotational reorientation time,  $\tau_r$ , the electron–nuclear dipolar interaction will give rise to nuclear relaxation rates given by [27]

$$\frac{1}{T_{1b}} = \frac{1}{T_{2b}} = \left(\frac{20}{15}\right) \gamma_N^2 g_N^2 \beta J(J+1) r^{-6} T_{1e}, \quad (10.16)$$

where  $T_{1b}$  and  $T_{2b}$  are longitudinal and transverse relaxation times, respectively, and  $\gamma_N$  is the nuclear magnetogyric ratio,  $r$  is the cation–nuclear distance which in some cases permits accurate determination of relative distances.

In the case of Gd(III) ion  $T_{1e}$  is large and is replaced by a function of the correlation time,  $\tau_c$  and the resonance frequency, where  $1/\tau_c = 1/T_{1e} + 1/\tau_r$ . Still the  $r^{-6}$  dependence holds good in the Gd<sup>3+</sup> complexes for the relative relaxation rates for different ligand nuclei.

In solutions, the exchange rates of bound and free ligand in the lanthanide complexes is so rapid on the NMR time scale that only the average signal is observed. The



relaxation rates are then weighted averages. But the transverse relaxation rate divided by  $\pi$  is equal to the line width at half-height which also contains an additional contribution arising from the uncertainty due to chemical shift difference,  $\Delta_b$ , between the bound state and free state of the ligand L. When a rapid exchange of ligand occurs, we have for relaxation rates

$$1/T_1 = P_f/T_{1f} + P_b/T_{1b} \quad (10.18)$$

$$1/T_2 = P_f/T_{2f} + P_b/T_{2b} + P_f^2 P_b^2 (\tau_f - \tau_b) (2\pi \Delta_b)^2 \quad (10.19)$$

where  $P_f$  and  $P_b$  are fractional populations in the magnetic environments of free and bound states, respectively, and  $\tau_f$  and  $\tau_b$  are mean residence times, respectively. If the ligand exchange is a first-order reaction,  $\tau_b$  as a constant,  $\tau_f$  will depend on concentration and may be written as [27]

$$\tau_f = \tau_b P_f/P_b \quad (10.20)$$

TABLE 10.3

Proton relaxation in aqueous solutions of lanthanides at  $21 \pm 1^\circ\text{C}$  and 22.1 MHz.

$\text{R}^{3+}$	$1/T_{1b}$ ( $\text{s}^{-1}$ )	$T_{1e}$ (ps)
Nd	116	0.096
Dy	3309	0.316
Ho	3255	0.313
Er	2467	0.291
Tm	2274	0.430
Yb	382	0.201

TABLE 10.4

Mean life-times and electron spin relaxation times of  $\text{R}(\text{fod})_3$ -pinacolone adducts obtained from line-broadening data at 90 MHz.

R	Temp. ( $^\circ\text{C}$ )	$\tau_b$ (ms)	$T_{1e}$ (ps)
Pr	0		0.12
Yb	0	0.22	0.34
Yb	27	0.11	0.22

Combining equations (10.19) and (10.20), letting  $P_f = 1 - P_b$ ,

$$1/T_2 = (1 - P_b)/T_{2f} + P_b/T_{2b} + P_b(1 - P_b)^2\tau_b(2\pi\Delta_b)^2 \quad (10.21)$$

Proton relaxation in aqueous lanthanide chloride solutions analyzed using equations (10.16) and (10.18) gave rise to results presented in Table 10.3. A coordination number of 9 and a proton-lanthanide distance of 3.1 Å were used in the calculation of  $1/T_{1b}$  and  $T_{1e}$ , respectively [28]. The electron relaxation times are  $\sim 10^{-13}$  s. For Gd(III)  $T_{1e} = 10^{-9} - 10^{-10}$  s and  $1/T_{1b}$  for aquo Gd(III) ion is  $9040 \text{ s}^{-1}$  and its relaxation effects are relatively strong [29].

It is not possible to relate lanthanide induced line broadenings to lanthanide-nuclear distances in a relatively simple way because of the contribution of the last term in equation (10.21). As a result of a detailed study of  $\text{Ln}(\text{fod})_3$  adducts with pinacolone, equation (10.21) is rearranged to give

$$(1/T_2 - 1/T_{2f})/P_b = \left( \frac{1}{T_{2b}} - \frac{1}{T_{2f}} \right) + 4\pi^2\Delta_b^2\tau_b(1 - P_b)^2 \quad (10.22)$$

and  $(1/T_2 - 1/T_{2f})P_b$  is plotted against  $(1 - P_b)^2$ . From the intercept and slope of the plot  $1/T_{2b}$  and  $\tau_b$  can be evaluated using the measured  $\Delta_b$  values. Typical results obtained by such a procedure are given in Table 10.4.

The significance and consequences of the term  $P_b(1 - P_b)^2\tau_b(2\pi\Delta_b)^2$  are: (i) larger line-broadenings at higher frequencies because of the frequency dependence of the shift, (ii) maximum broadening when  $P_b = 1/3$  because  $P_b(1 - P_b)^2$  is maximum, (iii) the ratio of lanthanide induced broadenings for different nuclei with the same ligand may depend on the lanthanide and its concentration [30].

TABLE 10.5  
Mean life-times of 1:2 R(fod)<sub>3</sub>-hexamethyl  
phosphoramidate adducts at 273.2 K.

R	$\tau_b$ (ms)
Pr	26.32
Eu	15.17
Tb	5.99
Ho	2.35
Er	1.42
Yb	0.39

## 8. Kinetic factors

Addition of a small amount of a paramagnetic lanthanide shift reagent to a solution of ligand results in chemical shift of the ligand NMR spectrum which is proportional to  $L_n/L$  ratio at low values. The condition of rapid chemical exchange must prevail when  $\tau_b$ , the mean lifetime of the complex is much shorter than  $1/\Delta_b$ . The condition is  $\tau_b \ll 1/2\pi \Delta_b$ .

But on the other hand when the exchange reaction is slow, two NMR signals, one unshifted due to a free ligand and one due to a metal–ligand bond are obtained. Conditions of slow exchange have been found in  $Ln(fod)_3$  with many ligands. The stoichiometry of the adducts has been obtained from the relative areas of the signals. An analysis of line shapes led to the evaluation of kinetics with chemical exchange being a first-order process.

The slow exchange may have some unforeseen effects on the temperature and frequency dependence of lanthanide induced shifts. Such effects must be borne in mind when deviations from expected behaviour are noted. When  $\tau_b \ll T_{2b}$  the induced shift  $\delta$  is given by

$$\delta = P_b \Delta_b / 1 + \omega_0^2 \Delta_b^2 \tau_b^2, \quad (10.23)$$

where  $\omega_0$  is the resonance frequency ( $s^{-1}$ ). When  $\omega_0^2 \Delta_b^2 \tau_b^2 = 1$ , the observed shift at lower frequency will be greater than at a higher frequency and temperature dependence of the observed shift will be different at the two frequencies. Thus when temperature dependence of chemical shifts in labile lanthanide complexes is being investigated, it is necessary to also study frequency dependence to unravel complications due to kinetic factors.

## 9. Analysis of shift reagent equilibria

The NMR spectra of most of the lanthanide shift reagents in solution involve rapid chemical exchange. In many situations one has 1:2 and 1:1 adducts and free ligand in solution. The observed lanthanide induced shift,  $\delta$  is the sum of two contributions

$$\delta = [LnL] \Delta_1 / L_t + 2[LnL_2] \Delta_2 / L_t, \quad (10.24)$$

where  $\Delta_1$  and  $\Delta_2$  are intrinsic shifts of  $\text{LnL}$  and  $\text{LnL}_2$ , respectively, subscript t is for total concentration and  $[\text{LnL}]$  and  $[\text{LnL}_2]$  are equilibrium concentrations. Rearranging equation (10.24) we get

$$\frac{[\text{LnL}]}{L_t \delta} = \frac{1}{\Delta_1} - \frac{2[\text{LnL}_2]}{L_t \delta} \cdot \frac{\Delta_2}{\Delta_1} \quad (10.25)$$

A plot of  $[\text{LnL}]/L_t \delta$  versus  $2[\text{LnL}_2]/L_t \delta$  should yield a straight line confined by the axes with intercepts of  $1/\Delta_1$  on the ordinate and  $1/\Delta_2$  on the abscissa. For a set of observed shifts and total concentrations, the values of dissociation constants  $K_1$  and  $K_2$  are chosen and the equilibrium



concentrations are calculated. The values that are obtained are used in equation (10.25) to obtain the values of  $\Delta_1$  and  $\Delta_2$  by a least-squares fit. Using the  $\Delta_1$  and  $\Delta_2$  values and equation (10.24), the  $\delta$  values are calculated and compared with the observed  $\delta$  values. The procedure is repeated by varying  $K_1$  and  $K_2$  values until minimum standard deviation is obtained. Two types of titration are done. In type I the ligand concentration  $L_t$  is kept constant with varying Ln and in type II, Ln concentration is kept constant while varying  $L_t$ . From computer simulations it has been shown that if  $4K_1 < K_2$ , type I titration will give accurate values of  $K_1$  and  $\Delta_1$ ; and type II titration will give accurate  $K_2$  but less accurate  $\Delta_2$  value. When  $4K_1 > K_2$  both types of titration give accurate value of  $K_2$  and  $\Delta_2$  and less reliable values of  $K_1$  and  $\Delta_1$ . Type I and II titrations are illustrated in Figs 10.9. and 10.10, respectively, for  $\text{Eu}(\text{fod})_3$ -DMSO system.

Equation (10.25) was used in the analysis of data and the resulting plot is shown in Fig. 10.11, assuming  $K_1 = 0.75$  mM,  $K_2 = 24.0$  mM. From the intercepts  $\Delta_1 = 447.0$  Hz and  $\Delta_2 = 275.4$  Hz values were obtained. The best-fit values obtained by the treatment are:  $K_1 = 0.75 \pm 0.06$  mM;  $K_2 = 24.0 \pm 1.7$  mM;  $\Delta_1 = 447 \pm 11$  MHz;  $\Delta_2 = 275 \pm 65$  MHz.

It follows from the above discussion that the systems of 1:2 stoichiometry are complex and that 1:1 systems are preferable for lanthanide induced shifts in the determination of structures of organic molecules. The 1:1 stoichiometry is encountered in the case of  $\text{Ln}(\text{dpm})_3$  in organic solvents [33],  $\text{Ln}(\text{fod})_3$  in  $\text{CHCl}_3$  [32],  $[\text{Ln}(\text{EDTA})]^-$  in aqueous solution [34].

An important method for measuring intrinsic shifts consists of measuring the shifts,  $\delta$ , relative to an internal standard like tetramethyl silane  $[\text{Si}(\text{CH}_3)_4]$  in organic solvents for two nuclei at two different lanthanide concentrations [35]. For two nuclei a and b we have

$$\delta^a = \delta_0^a + P_b \Delta_b^a \quad (10.28)$$

$$\delta^b = \delta_0^b + P_b \Delta_b^b \quad (10.29)$$

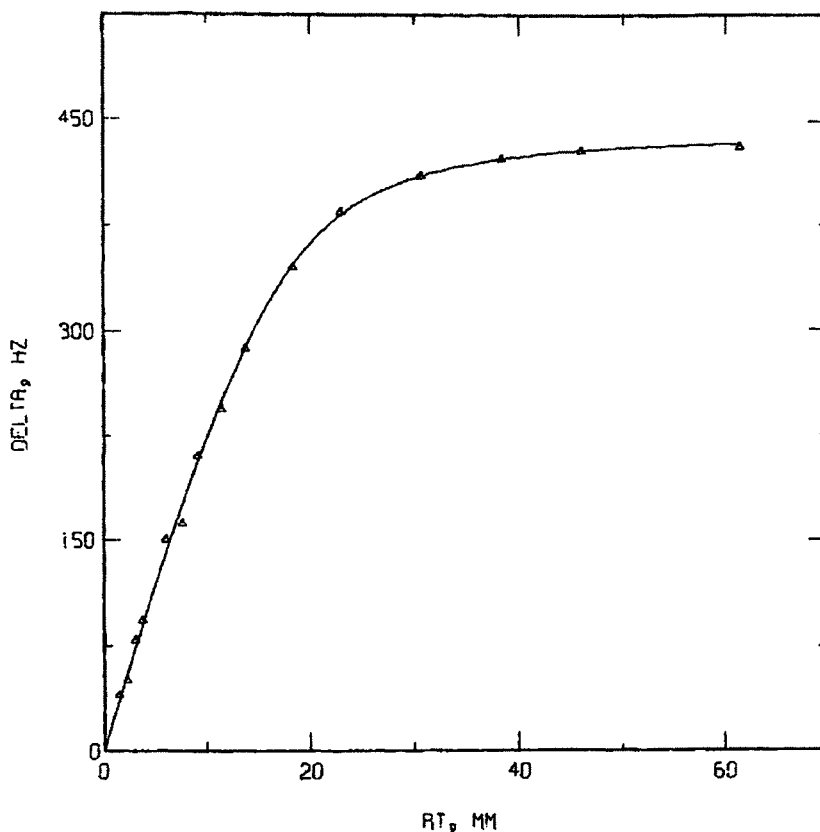


Fig. 10.9. Type I titration of the shift induced by  $\text{Eu}(\text{fod})_3$  ( $R_1$  in mM) in the proton resonance of DMSO (20 mM in  $\text{CCl}_4$ ). The curve is calculated with the parameters given in the text [28].

where  $\delta_0^a$  and  $\delta_0^b$  are shifts with respect to internal standard in the absence of lanthanide

$$\delta^a = \delta_0^a - (\delta_0^a + \delta_0^b) \frac{\Delta_b^a}{\Delta_b^a \Delta_b^b} + (\delta^a + \delta^b) \frac{\Delta_b^a}{\Delta_b^a + \Delta_b^b} \quad (10.30)$$

A plot of  $\delta^a$  versus  $(\delta^a + \delta^b)$  should give a straight line whose slope equals  $\Delta_b^a / \Delta_b^a + \Delta_b^b$ .

## 10. Applications

The most commonly used shift reagents are lanthanide  $\beta$ -diketonates. A large number of different combinations of  $\beta$ -diketonates and lanthanide metals can be used as shift reagents. The most commonly used metal chelates are those of  $\text{Eu}(\text{III})$  and  $\text{Yb}(\text{III})$  which usually induce downfield shifts, and  $\text{Pr}(\text{III})$ , which induces upfield shifts. The commonly used shift reagents are listed in Table 10.5a.

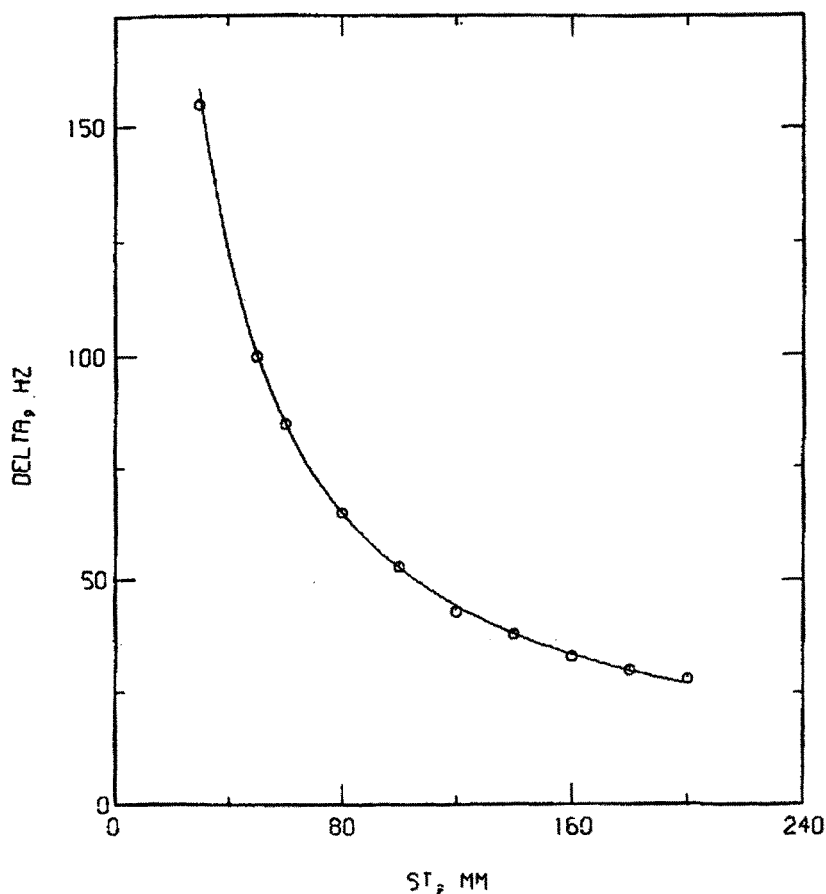


Fig. 10.10. Type II titration of the shift induced by 10 mM  $\text{Eu}(\text{fod})_3$  in the proton resonance of DMSO ( $\delta_1$  in mM). The curve is calculated with the parameters given in the text [28].

Initially non-fluorinated ligand like dipivaloyl methane (dpm) was used. Later on it was observed that fluorine substitution in the ligand resulted in greater resolution of the spectrum as in the case of di-*n*-butyl ether which is shown in Fig. 10.12.

Simplification and clarification of spectra often yield a good deal of information. An elegant example of the use of shift reagents is shown in Fig. 10.13. This figure shows the NMR spectrum of friedelan-3/ $\beta$ -ol with and without added shift reagent  $\text{Eu}(\text{thd})_3$ .

The spectrum of *cis*-4-*t*-butyl cyclohexanol in  $\text{CDCl}_3$  with the addition of increasing amounts of  $\text{Eu}(\text{thd})_3$  was studied, and the initial resonance positions of protons were determined by plotting the chemical shift versus moles of shift reagent added, and extrapolating the lines to zero concentration of the shift reagent (Fig. 10.14). This figure also illustrates the effect of concentration of shift reagent on the magnitude of the induced shifts.

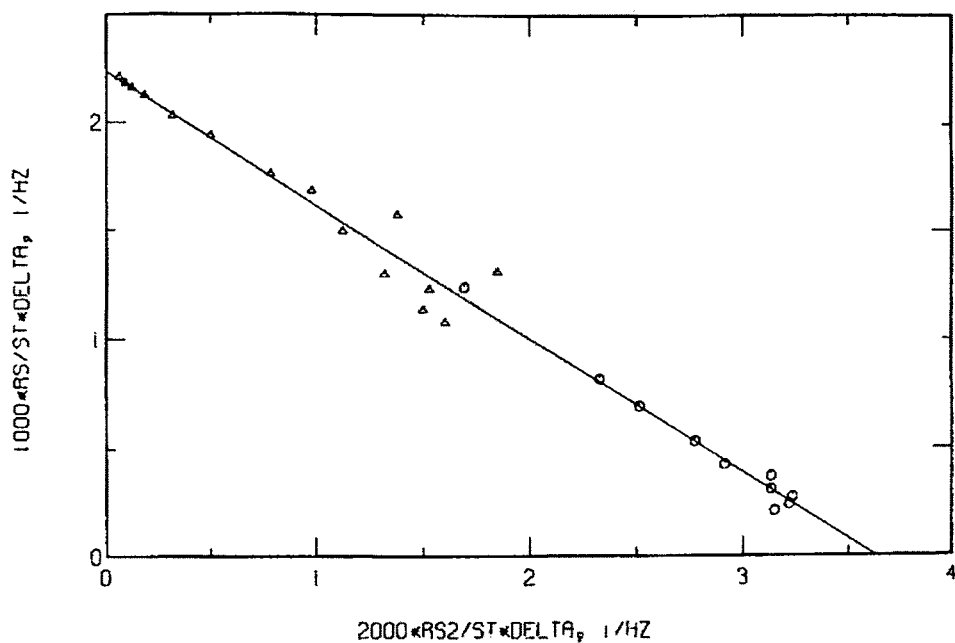


Fig. 10.11. A plot according to equation (38.21) of the data of Figs. 38.6 and 38.7 using values of  $[LnL_2]$  and  $[LnL_2]$  calculated with  $K_1 = 0.75$  mM and  $K_2 = 24.0$  mM [28].

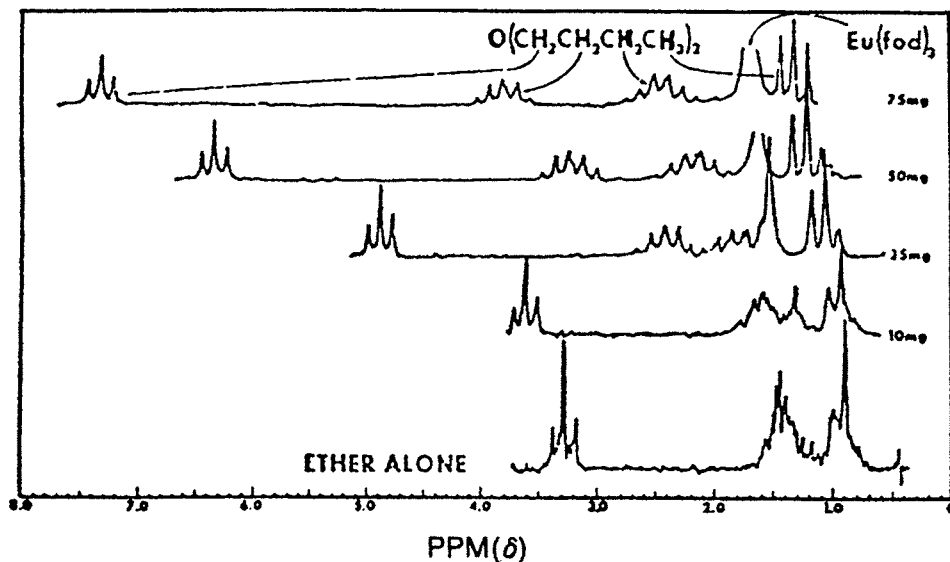


Fig. 10.12. Clarification of the spectrum of di-*n*-butyl ether by addition of  $Eu(fod)_3$  [36].

TABLE 10.5a  
 $\beta$ -Diketonates commonly employed as shift reagent ligands<sup>a</sup>.

Ligand	Abbreviation	Structure of anion
2,2,6,6-tetramethyl-3,5-heptanedione (dipivaloylmethane)	thd (tmhd) (dpm)	
6,6,7,7,8,8,8-heptafluoro-2,2-dimethyl-3,5-octanedione (1,1,1,2,2,3,3,3-heptafluoro-7,7-dimethyl-4,6-octanedione)	fod	
1,1,1,5,5,6,6,7,7,7-decafluoro-2,4-heptanedione (1,1,1,2,2,3,3,3,7,7,7-decafluoro-4,6-heptanedione)	dfhd	
3-trifluoroacetyl-D-camphor [3-(trifluoromethylhydroxymethylene)-D-camphor]	facam	
3-heptafluorobutyryl-D-camphor [3-(heptafluoropropylhydroxymethylene)-D-camphor]	hfbc	

<sup>a</sup>Less preferred names and abbreviations are given in parentheses.

Coupling constants which are usually difficult to measure because of peak overlap can be obtained by the addition of a shift reagent. It is necessary to keep in mind that the coupling constants obtained by addition of shift reagents are for complexed species and may not be the same for uncomplexed species. Decoupling or double irradiation experiments are feasible with addition of a shift reagent. An example where coupling constants and double irradiation were determined is the case of 7,8-*cis-endo*-diphenyl-2-oxabicyclo[4.2.0]octane. The spectrum on addition of Eu(fod)<sub>3</sub> is shown in Fig. 10.15.

Structural and stereo chemical information can be obtained by the application of the McConnell–Robertson equation [40]

$$\frac{\Delta\nu_i}{\nu_i} = \frac{K(3\cos^2\theta_i - 1)}{r_i^3} \quad (10.31)$$

which gives the relationship between the induced chemical shift of the  $i^{\text{th}}$  nucleus,  $\Delta\nu_i$  and the location of the nucleus. In equation (10.31)  $K$  is a constant,  $r_i$  is the distance between the  $i^{\text{th}}$  nucleus and Eu(III) ion, and  $\theta_i$  is the angle between the principal magnetic



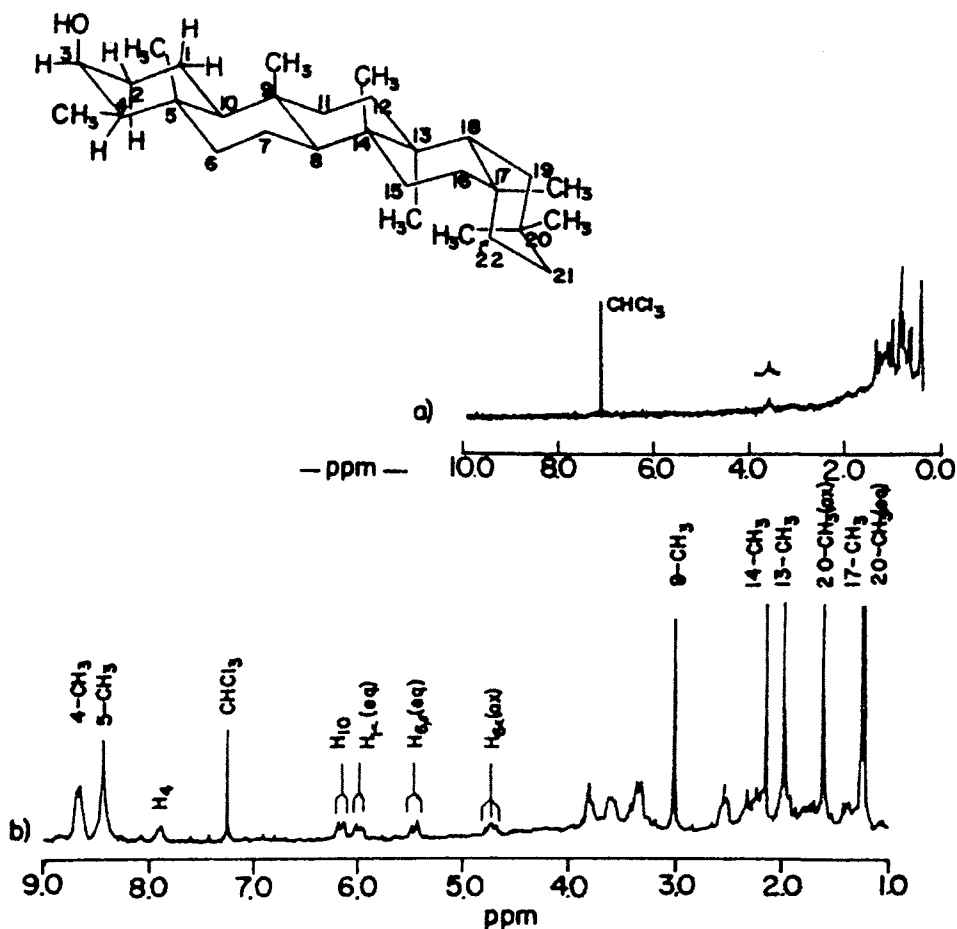


Fig. 10.13. NMR spectrum of friedelan-3 $\beta$ -ol (10 mg,  $0.24 \times 10^{-4}$  mol in 0.4 ml of  $\text{CDCl}_3$ ): (a) normal spectrum at 100 MHz, (b) partial 220-MHz spectrum of solution of friedelan-3 $\beta$ -ol containing one mol equivalent of  $\text{Eu}(\text{thd})_3$  (17 mg) [37].

axis of the complex and a line drawn from the nucleus of interest to the lanthanide ion. Some of the conditions under which equation (10.31) is applicable are: (i) the observed shifts are entirely of pseudo-contact in origin, (ii) only one stoichiometric species exists in equilibrium,  $(\text{LnL})$ , (iii) only one geometric isomer is present, (iv) the isomer is magnetically axially symmetric, so that the shifts are proportional to the geometric factor,  $K(3 \cos^2 \theta_i - 1)/r_i^3$ , (v) the principal magnetic axis has a known orientation with respect to the substrate ligand, (vi) the substrate ligand exists in a single conformation.

The angle term in equation (10.31) gives positive values, except when  $\theta > 55^\circ$  but  $\theta < 125^\circ$ . At these values of angle  $\theta$ , the induced shifts will be in the opposite direction of normal shifts, (i.e.) upfield for Eu and downfield for Pr. The reversal in the direction of the shifts is due to the term  $(3 \cos^2 \theta - 1)$  becoming negative for these angles.

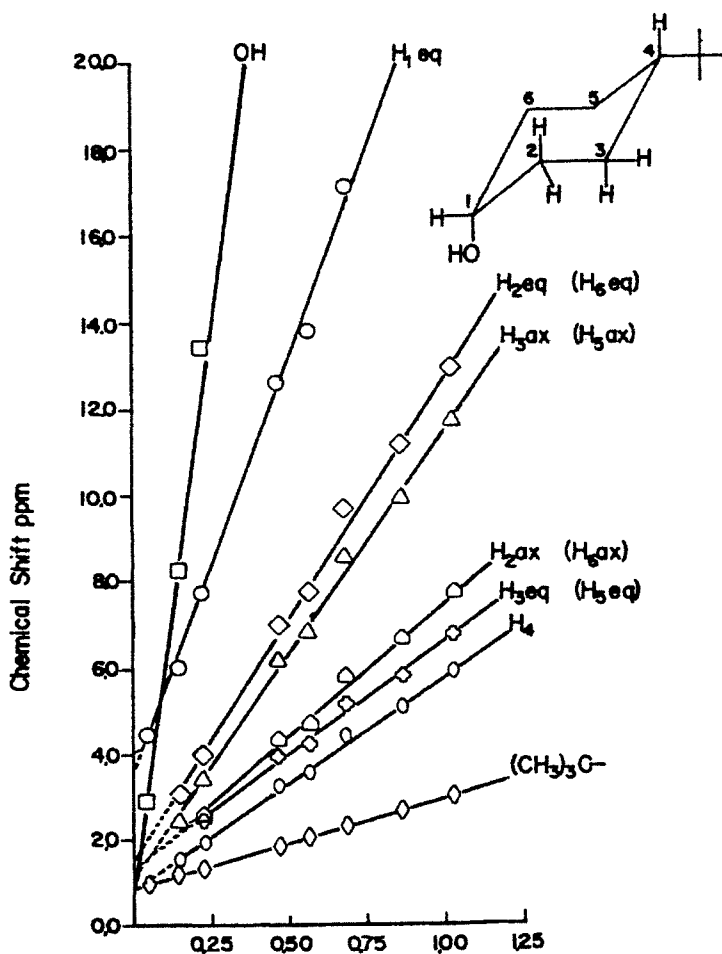


Fig. 10.14. Variations in the chemical shift for the different protons of *cis*-4-*t*-butylcyclohexanol with increasing concentration of Eu(thd) [38].

An example of angle dependence of shifts is illustrated by the isomeric mixture of *p,p'*-disubstituted azoxy benzenes to which Eu(fod)<sub>3</sub> is added. This is illustrated in Fig. 10.16. A scale model was used to estimate the H–Eu–O angle for the methoxy and methyl protons of one isomer as shown in Fig. 10.17.

Assuming Eu–O bond distance of 2 Å, the angle made with methoxy protons 84° and the angle with methyl protons is 40° for the isomer. Thus according to equation (10.31) the methyl peak is shifted downfield ( $\theta < 55^\circ$ ) and the methoxy peak is shifted upfield ( $\theta > 55^\circ$ ). Reference to the spectra of the isomers in Fig. 10.13 show degenerate peaks before Eu(fod)<sub>3</sub> was added. After addition of the shift reagent, the methyl peak of the least abundant isomer moves upfield and its methoxy peak moves downfield. The more abundant isomer shows the opposite behaviour.

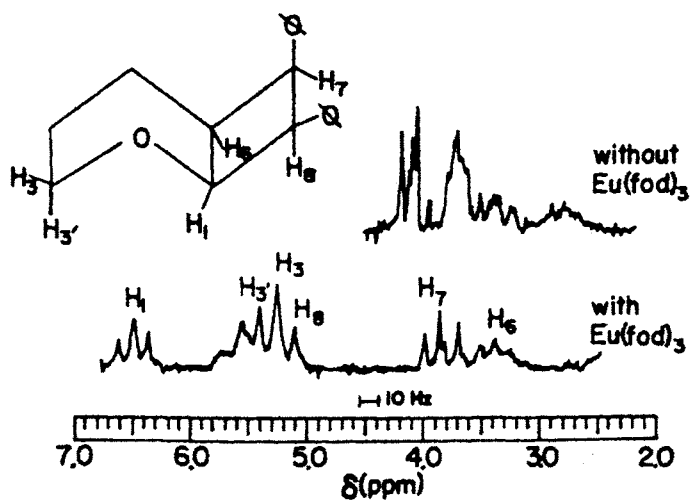


Fig. 10.15. Effect of  $\text{Eu}(\text{fod})_3$  on 7,8-*cis-endo*-diphenyl-2-oxabicyclo[4.2.0]octane [39].

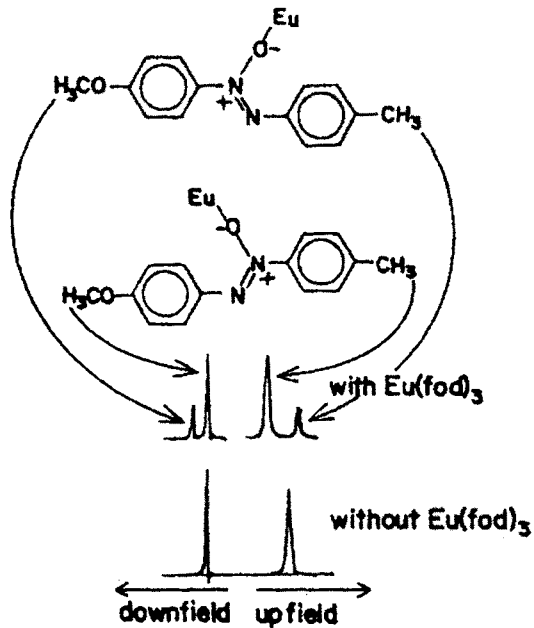


Fig. 10.16. Isomers of *p*-methoxy-*p'*-methylazoxybenzene and partial NMR spectra of the isomeric mixture showing upfield and downfield shifts induced by the addition of  $\text{Eu}(\text{fod})_3$ .

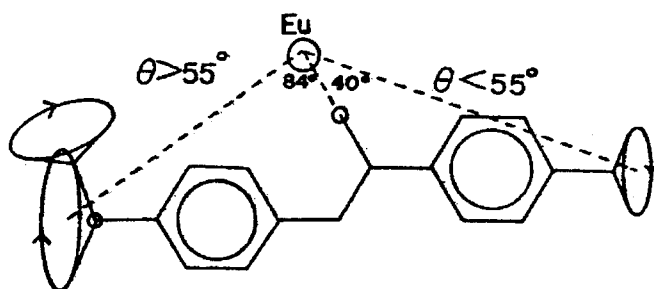


Fig. 10.17. Scale model of Eu-azoxybenzene adduct.

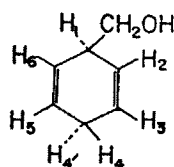


Fig. 10.18. 1,4-Dihydrobenzyl alcohol [41].

## 11. Conformational isomers

Both planar and boat conformations for 1,4-cyclohexadiene and its derivatives are possible. Addition of  $\text{Eu}(\text{fod})_3$  allowed the determination of the conformation of 1,4-dihydrobenzyl alcohol [41]. Addition of  $\text{Eu}(\text{fod})_3$  and double and triple irradiation experiments made the determination of coupling constants possible. The vicinal coupling constants  $J_{3,4}$  and  $J_{3,4'}$  were equal indicating planarity of the ring. Other coupling constants also indicated a planar conformation for the ring. Possible rapid boat-to-boat inversion was ruled out by measurement of coupling constants of 3-fluoro-1,4-dihydrobenzyl alcohol- $\text{d}_2$  from unaltered spectra and spectra obtained after addition of  $\text{Eu}(\text{fod})_3$ .

## 12. Quantitative aspects

Quantitative approaches for the analysis of lanthanide shifts by calculations have been made for some preferred conformations and compared with the experimentally observed shifts [42–44]. One of the approaches involves locating the molecule under study in a Cartesian coordinate system with the functional group at the origin. Then different positions of the lanthanide ion are examined by moving the ion over the surface of a sphere of radius  $d$ , the assumed Eu–heteroatom distance, through all angular values. At each lanthanide position, shifts for all protons are calculated using equation (10.31). (McConnell–Robertson). The calculated values are compared with the observed shifts and a best fit is determined. For oxygenated hydrocarbons, Ln–O distance was in the range of 2.5–3.5 Å which is close to 2.5 Å obtained for Eu–O by X-ray crystallography.

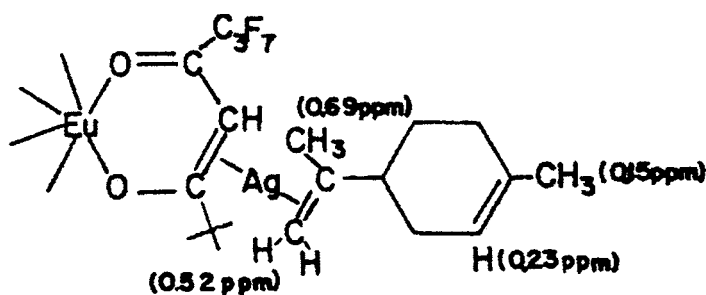


Fig. 10.19. Possible mode of interaction of lanthanide with alkene [0.1 M  $\text{Eu}(\text{fod-d}_9)_3$ , 0.1 M  $\text{C}_3\text{F}_7\text{CO}_2\text{Ag}$ , 0.2 M limonene in  $\text{CCl}_4$ ] [46].

Another method involves placing the structure of a molecule on a map of the dipolar field and reading predicted shifts which are scaled with the observed shifts. Some molecules studied by this method are pyridine, *cis*-4-*t*-butyl cyclohexanol, and 1-adamantanol [45].

Lanthanide shift reagents are hard Lewis acids and normally do not react with alkenes. But  $\text{Eu}(\text{fod})_3$  in combination with silver heptafluorobutyrate [46] alters the spectrum of alkenes by a type of interaction shown in Fig. 10.19.

### 13. Polymers

Shift reagents have been used in studies of polymers. For atactic poly(methyl methacrylate) addition of shift reagent resolved the three peaks of C-methyls in isotactic, heterotactic and syndiotactic triads [47]. The resolution of resonances of polypropylene oxide with  $\text{Eu}(\text{fod})_3$  is shown in Fig. 10.20. In the absence of a shift reagent, the triads of the methyl groups appear as three overlapping doublets. The figure shows how progressive addition of  $\text{Eu}(\text{fod})_3$  separated methyl as well as  $-\text{CH}=\text{}$  and  $-\text{CH}_2-$  resonances. The separation of these resonances was found useful in the molecular weight determination by end-group analysis [49].

### 14. Isotope effects

Deuterium isotope effect has been observed in alcohols upon addition of  $\text{Eu}(\text{fod})_3$ . Substitution of deuterium for hydrogen vicinal to the OH group resulted in increased shifts for other protons in the substituted alcohol. This effect may be due to: (i) deuterium involved in greater hydrogen bonding with the oxygen of  $\text{Eu}(\text{fod})_3$  than hydrogen and thus increasing complex stability, (ii) deuterium might also increase the basicity of the oxygen in the alcohol [50].

### 15. Chiral shift reagents

Chiral shift reagents are used for the determination of enantiomeric purity by NMR. Resonances of enantiomers give rise to different chemical shifts in the chiral environment,

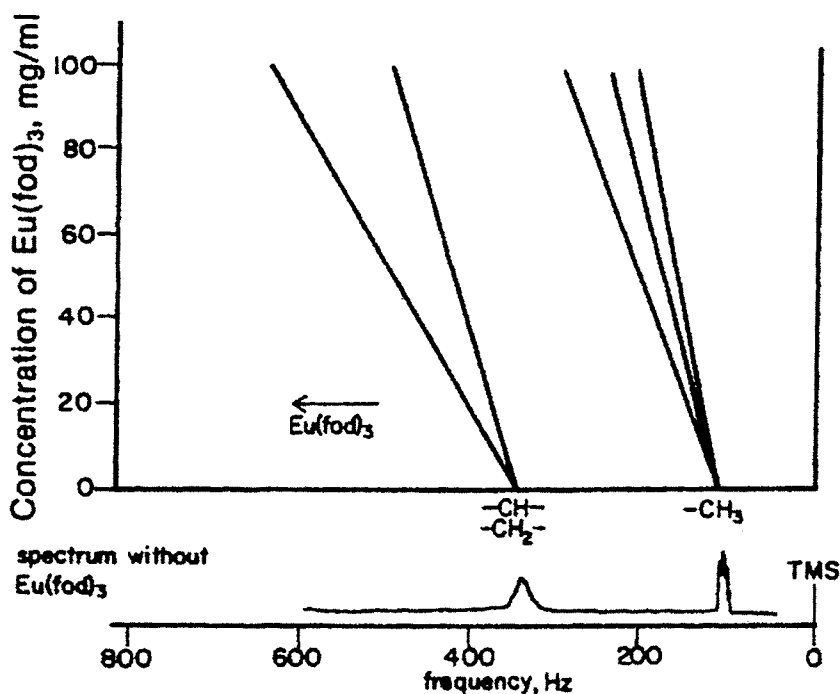


Fig. 10.20. Effect of progressive addition of  $\text{Eu}(\text{fod})_3$  on the spectrum of polypropylene oxide [47].

leading to the determination of enantiomeric relative abundances [51]. Thus chiral shift reagents can be used to determine whether reactions have occurred with retention of configuration, inversion or racemization or a combination. Protons and groups which are enantiotropic by internal comparison also show separation of resonances in the presence of a chiral shift reagent, and this effect can be used to distinguish meso from D,L-diastereomers [52].

The reagent tris[3-*t*-butylhydroxymethylene]-D-camphorato]Eu(III) was used initially to separate the resonances of R and S enantiomeric amines [53]. The fluorinated reagent tris[3-trifluoroacetyl-D-camphorato]Eu(III),  $\text{Eu}(\text{facam})_3$  was used in the separation of resonances of enantiomers of 2-phenyl-2-butanol. The spectra of 2-phenyl-2-butanol on addition of  $\text{Eu}(\text{thd})_3$  and  $\text{Eu}(\text{facam})_3$  are shown in Fig. 10.21. As seen in the figure,  $\text{Eu}(\text{thd})_3$  did not cause changes in the resonances while  $\text{Eu}(\text{facam})_3$  caused separation of  $\alpha$ -methyl resonances into two peaks, and resolved the  $\beta$ -methyl triplets into a quintuplet and thus distinguishing the two isomers [54].

The shift reagent  $\text{Eu}(\text{facam})_3$  has also been successfully used to determine the enantiomeric composition of a sample of D,L-3-methyl-3-phenyl-2-pentanone. The chiral shift reagent caused separation of some of the peaks arising from the two enantiomers. The spectrum of D,L-3-methyl-3-phenyl-2-pentanone in the presence of added  $\text{Eu}(\text{facam})_3$  is shown in Fig. 10.22. The acyl methyl protons are well resolved as seen on the left side of the figure and their relative areas may be integrated. The optical purity of this sample

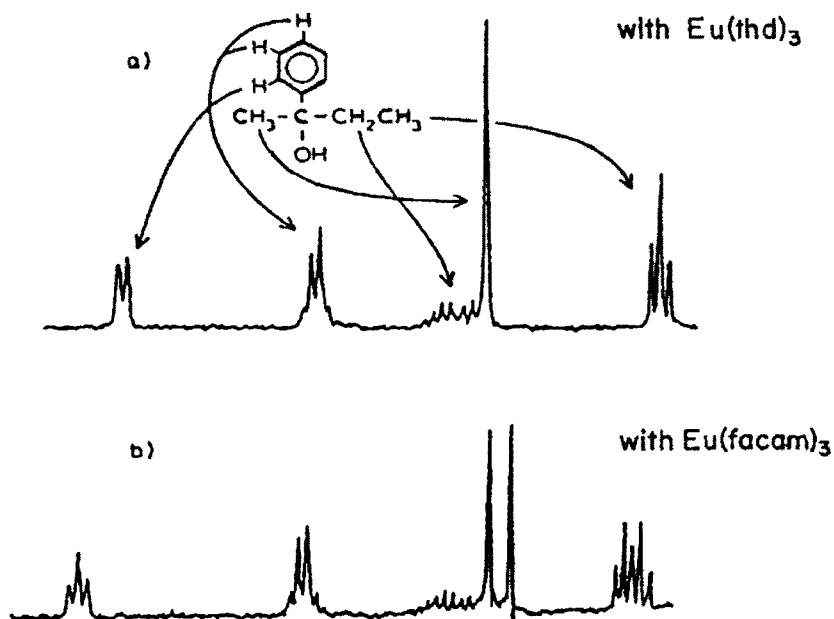


Fig. 10.21. Differences in shifts of enantiomers induced by adding a chiral shift reagent. Spectra of 0.54 M 2-phenyl-2-butanol in  $\text{CCl}_4$  in the presence of (a) 0.13 M  $\text{Eu}(\text{thd})_3$ , and (b) 0.42 M  $\text{Eu}(\text{facam})_3$  [54].

determined by NMR is 27.3% which is comparable to 25.4% determined by polarimetry [54].

For closely related compounds, absolute configuration has been determined from NMR spectra in the presence of chiral shift reagents [55]. For compounds with greater structural differences there are many difficulties and uncertainties to overcome before concrete results can be obtained. One of the problems is the manner of variation of induced differential shift,  $\Delta\Delta\delta$  of resonances of protons as a function of reagent-substrate molar ratio as shown for 2-phenyl-2-butanol in Fig. 10.23. It is clear from the figure that  $\Delta\Delta\delta$  for  $\alpha$ -methyl resonances increase steadily, while for  $\beta$ -methyl protons reaches a maximum, then declines and reaches plateau. For the ortho protons, a reversal in the sense of non-equivalence occurs at a molar ratio of approximately unity. Some of the implications of such a behaviour are both theoretical and practical. If the complex formation constants for enantiomers are different, then the sense of non-equivalence should be the same for all the proton resonances, and  $\Delta\Delta\delta$  should increase to a maximum and level off. Since this is not the case, different magnetic environments or stoichiometries of shift reagent-substrate adducts may be the factors for the observed anomalous variation of  $\Delta\Delta\delta$ .

The most common chiral lanthanide shift reagents are given in Table 10.6.

## 16. Applications to pharmaceuticals [58]

Chiral lanthanide shift reagents represent the most important NMR method for optical purity determination. The potential importance of configuration for chiral drugs has

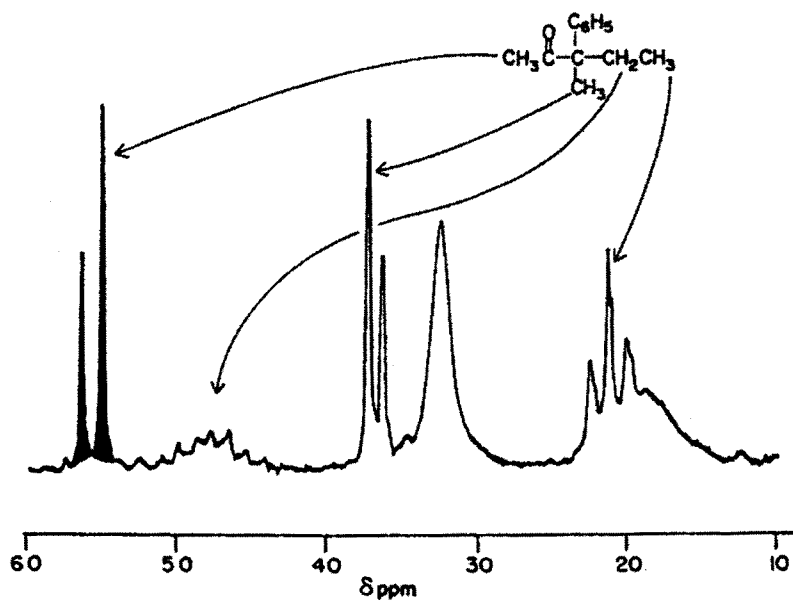


Fig. 10.22. Spectrum of a  $\text{CCl}_4$  solution of D,L-3-methyl-3-phenyl-2-pentanone in 0.5 M  $\text{Eu}(\text{facam})_3$  [54].

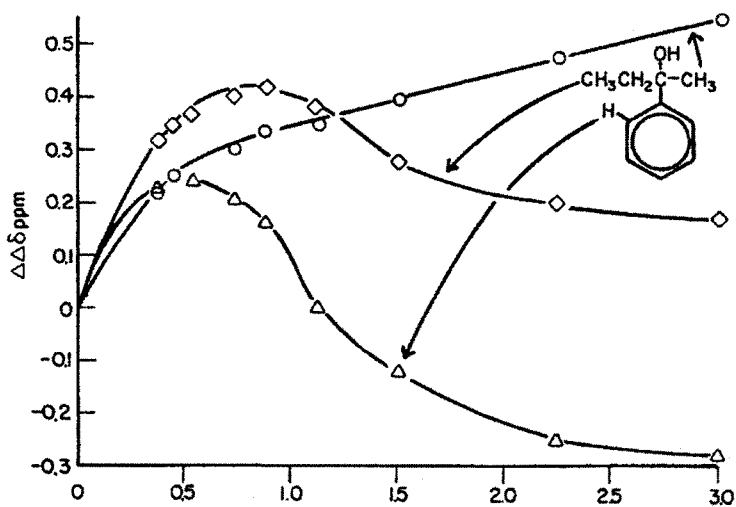
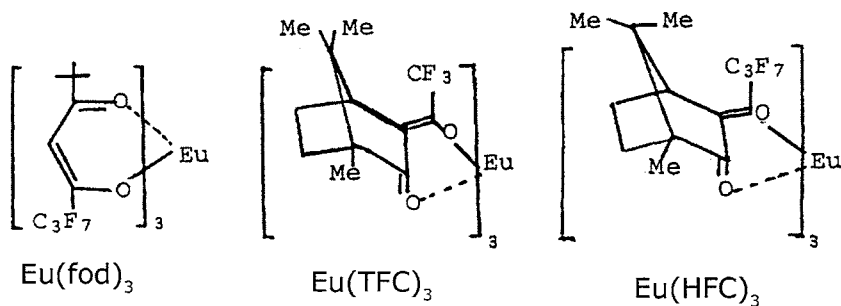


Fig. 10.23. Plots of  $\Delta\Delta\delta$  vs. reagent-substrate molar ratio for three sets of protons of 2-phenyl-2-butanol; in 0.3 M  $\text{Eu}(\text{hfbc})_3$  [56].

resulted in increased interest in both enantioselective synthesis and in methods for the determination of enantiomeric excess. The reagents of interest are given below.





The list of drugs analyzed for optical purity by  $^1\text{H}$  NMR spectroscopy with lanthanide shift reagents is given in Table 10.7.

### 17. Application to coordination metal complexes [89]

The application of lanthanide induced shift reagents to studies involving organic compounds is extensive. A similar approach to the NMR studies involving classical coordination complexes is less common. Lanthanide shift reagents (LSR) have been used to: (i) detect the bonding mode through LSR interaction at non-donor sites, (ii) LSR interaction via donor atom bridge formation, (iii) conformational studies using LSR, (iv) chiral studies, (v) spin-lattice relaxation studies, (vi) non-dilute fast exchange kinetics, (vii) slow exchange kinetics, (viii) thermodynamics of slow exchange reactions.

### 18. Interaction at non-donor sites

$\text{Eu}(\text{fod})_3$  has been used to distinguish between N-bonded and S-bonded thiocyanate ligands. The LSR binds to uncoordinated nitrogen when the thiocyanate is S-bonded to the metal ion and shifts in proton resonances of suitable attached organic ligands are observed. When the thiocyanate is N-bonded, no significant interaction occurs. This procedure is useful for deciding the bonding mode of thiocyanato complexes and hence also for distinguishing the linkage isomers in complexes [90].

Addition of  $\text{Eu}(\text{III})$  perchlorate to the disulphide complex of  $\text{Co}(\text{III})$  resolves [91] the NMR signals of the methyl group because  $\text{Eu}(\text{III})$  binds to the pendant acetate group as shown in Fig. 10.24.

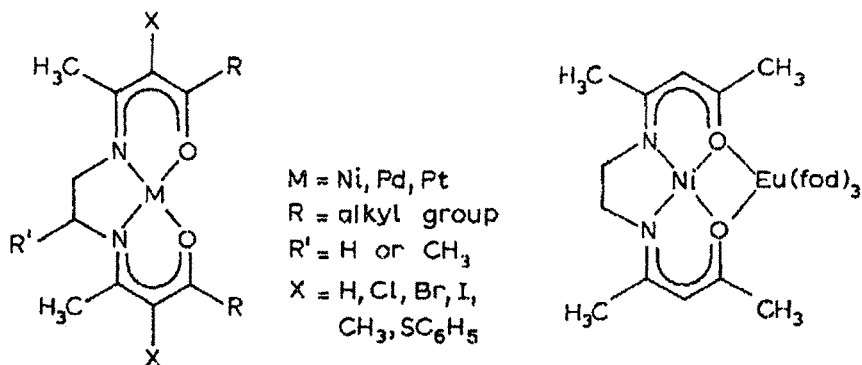
### 19. LSR interaction via donor atom

Studies on the interaction of  $\text{Ln}(\text{fod})_3$  where  $\text{Ln} = \text{Eu}, \text{Pr}$  with diamagnetic metal complexes of the type shown below yielded 1:1 adducts through bonding of  $\text{Ln}(\text{fod})_3$  with *cis* oxygen donors [92]. However the  $\text{Eu}(\text{III})$  ion may be out of plane in the adduct [93].

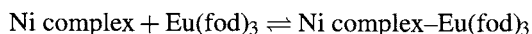
TABLE 10.6  
 Common chiral lanthanide shift reagents.

Structure of L in LnL <sub>3</sub>	Lanthanon	Abbreviation <sup>a</sup>	Ref.	
	Eu	Eu[pvc] <sub>3</sub>	[57]	
	R = CF <sub>3</sub>	Eu	Eu[tfc] <sub>3</sub>	[57]
	R = CF <sub>3</sub>	Pr	Pr[tfc] <sub>3</sub>	[57]
	R = CF <sub>3</sub>	Yb	Yb[tfc] <sub>3</sub>	[57]
	R = C <sub>3</sub> F <sub>7</sub>	Eu	Eu[hfc] <sub>3</sub>	[57]
	R = C <sub>3</sub> F <sub>7</sub>	Pr	Pr[hfc] <sub>3</sub>	[57]
	R = C <sub>3</sub> F <sub>7</sub>	Yb	Yb[hfc] <sub>3</sub>	[57]
	Eu	Eu[dcm] <sub>3</sub>	[57]	

<sup>a</sup>pvc = pivaloyl-D-camphorato; tfc = trifluorohydroxymethylene-D-camphorato; hfc = heptafluorohydroxymethylene-D-camphorato; dcm = dicamphoyl-D-methanato.



Progressive addition of Eu(fod)<sub>3</sub> to the nickel complex in CDCl<sub>3</sub> showed shifts depicted in Fig. 10.25. It is clear that 1:1 adduct is formed with an adduct formation constant of  $K \sim 10^3 \text{ M}^{-1}$  as estimated from the equilibrium



The observed shifts did not obey the McConnell–Robertson equation. It has been found from <sup>13</sup>C NMR that a contact (through-bond) mechanism was found to be significant in

TABLE 10.7

List of drugs analyzed for optical purity by  $^1\text{H-NMR}$  spectroscopy with lanthanide shift reagents.

Drugs	Reference
Hexobarbital	[59]
Cocaine	[60]
Substituted amphetamines	[61]
Dextro & levomethorphan	[62]
Thiohexital	[63]
Methamphetamine	[64]
Amphetamine	[65,66]
Glutethimide	[67]
Mephentyoin	[68]
Methohexital	[69]
Mephobarbital	[70]
Ethotoin	[71]
Thiamylal	[72]
3,4-Methylenedioxyamphetamine	[73]
Vinclozolin	[74,75]
Tranylcypromine	[76]
Indacrinone precursor	[77]
Ethosuximide and other analogs, e.g. phensuximide, methsuximide and paramethadione	[78]
Thiopental, and other barbiturates, e.g. secobarbital, talbutal, butabarbital and pentobarbital	[79]
2,5-Dimethoxy-4-ethyl amphetamine	[80]
Ketazolam	[81]
Aminoglutethimide	[82]
Meparfynol	[83]
Metapramine	[84]
Levamisole and dexamisole	[85]
Penicillamine	[86]
Benoxaprofen	[87]
Ephedrine	[88]
Propranolol	[88]
Various non-steroidal antiinflammatory agents, e.g. ibuprofen, naproxen and analogs	[88]

this system. The presence of a contact term implies some covalency in Eu–O bond. When R in the complex is bulky *t*-butyl group adduct formation was inhibited because of steric hindrance to the approach of Eu(fod)<sub>3</sub> towards the complex. When R = CF<sub>3</sub>, an electron-withdrawing group, Lewis basicity of oxygen donor atoms is reduced and no adduct is formed. When the complex has sulfur atoms in place of oxygen atoms, no adduct forms due to the lower affinity of ‘soft’ sulphur atoms for Eu(III) [94].

## 20. Conformational studies

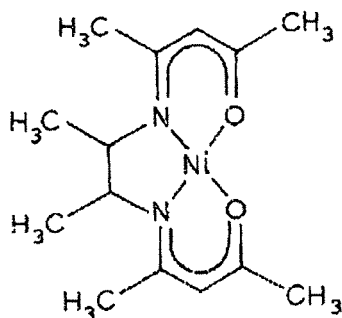
The diamagnetic Ni complex cited earlier with a backbone derived from propylenediamine was studied by the addition of Eu(fod)<sub>3</sub>. On addition of LSR, the resonances shifted and when LSR:complex ratio of 0.3 was reached, a first-order pattern consisting of a five peak multiplet, a four peak multiplet and a doublet were observed.

This pattern corresponds to the first-order coupling scheme shown in Fig 10.26. In this scheme, the coupling constants between  $H_f$  and  $H_d$  was assumed to be zero as predicted by the Karplus relationship since the dihedral angle between these protons is  $90^\circ$ . From the LSR spectrum, the different coupling constants were measured. The chemical shifts were extrapolated to zero concentration of  $\text{Eu}(\text{fod})_3$ . Using these chemical shifts and the coupling constants from the shifted spectra, the original overlapping spectrum was simulated by a computer. The agreement obtained between the experimental and simulated spectra confirms the validity of the first-order coupling scheme and the  $-\text{CH}_3$  group of propylene-diamine occupies an axial position.

## 21. Chiral studies

Addition of chiral LSR such as (+)tris[3-heptafluoropropyl hydroxymethylene]-D-[camphorato]Eu(III),  $\text{Eu}[(+)\text{fpc}]_3$  to a racemic mixture of diamagnetic Ni complex with propylenediamine backbone results in a composite of two overlapping spectra [92]. The changes in the methyl doublet are shown in Fig. 10.27. Combined with spectral integration, this technique may be used for the analysis of mixtures of optically active complexes.

Another example studied is the isomers of the complex derived from racemic and meso forms of 2,3-diaminobutane. The complex is depicted below. With the racemic addition of  $\text{Eu}[(+)\text{fpc}]_3$  gives the two sets of resonances due to *R,R*- and *S,S*-diastereomers. With meso form, a doubling of each spectral peak was observed. The doubling is due to the presence of a meso plane in the molecule which makes each half of the molecule enantiotropic.



Addition of  $\text{Eu}[(+)\text{fpc}]_3$  to  $\beta\text{-[Ru}_2\{\text{S}_2\text{CN}(\text{CH}_3)_2\}_5\text{]BF}_4$  resulted in distinguishing  $\Delta\Delta$  and  $\lambda\lambda$  stereoisomers in  $\text{CDCl}_3$  solution [95].

## 22. Spin-lattice relaxation studies [93]

The  $^1\text{H}$  and  $^{13}\text{C}$  NMR spin-lattice relaxation rates in the nickel complex cited earlier in LSR interaction via donor atom were reduced when  $\text{Gd}(\text{fod})_3$  was added.  $\text{Gd}(\text{III})$  was found to bind to the two oxygen atoms of the metal complex with  $\text{Gd}(\text{III})$  ion located

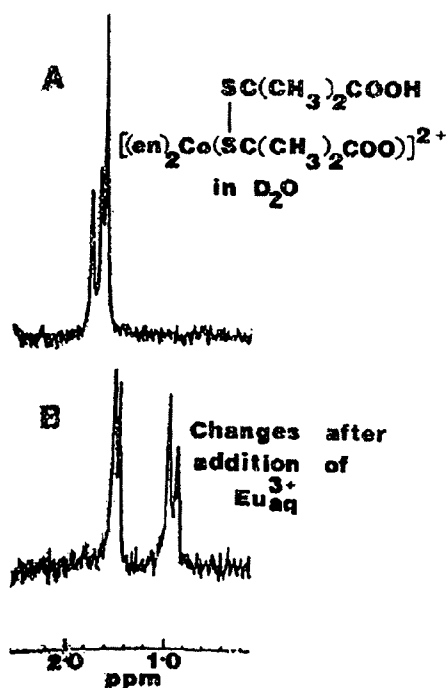


Fig. 10.24. The methyl multiplet in the NMR spectrum of the cobalt complex. (B) The separation of the methyl signals after addition of excess europium perchlorate.

about 1.8 Å out of the plane of the complex.  $\text{Gd}(\text{NO}_3)_3$  was used in place of  $\text{Gd}(\text{fod})_3$  and the complex gave the same results (i.e.) confirming the out-of-plane bonding by the Gd(III) ion. Steric interactions between the methyl groups of the complex and the fod ligands of Gd(III) were thought to be responsible for the out-of-plane binding to Gd(III) in which the  $\text{Eu}(\text{fod})_3$  is bonded through two cis oxygen atoms and terminal nitrogen of the azido group fits the experimental data. Lifetimes of the order of  $10^{-3}$  to  $10^{-4}$  s were estimated which are by far smaller than  $10^5$  s observed for the nickel complexes.

The variation of line-widths of the methyl resonances as a function of  $\text{Eu}(\text{fod})_3$  concentrations is shown in Fig. 10.28. It is clear that the maximum line-width occurs when  $\text{Eu}(\text{fod})_3$ :complex ratio of 1:3. This is in agreement with the predicted value for  $\text{Eu}(\text{fod})_3$ :complex ratio of 0.33 by differentiating equation (10.32).

On the other hand the interaction of  $\text{Eu}(\text{fod})_3$  with  $M(\beta\text{-diketonate})_3$  complexes of the type showed the reaction to be slow with respect to NMR time scale [98]. As  $\text{Eu}(\text{fod})_3$  is added, the intensity of original signals decrease while new signals appear. When the ratio of complex: $\text{Eu}(\text{fod})_3$  is 1:1 further changes in the spectrum do not occur.

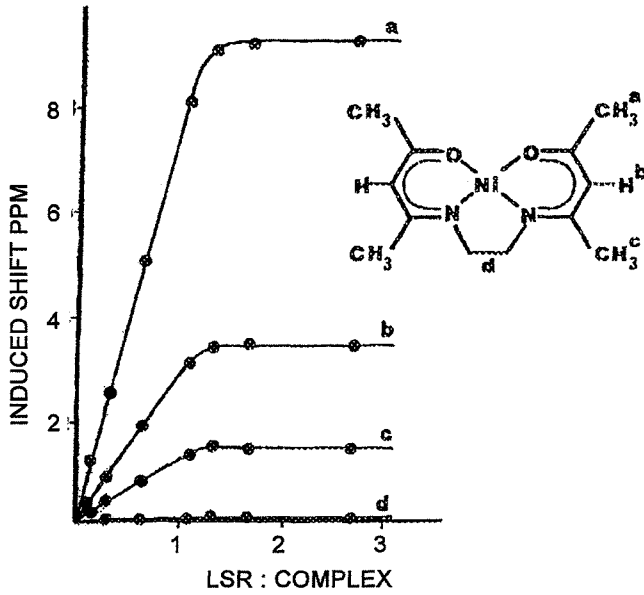


Fig. 10.25. The lanthanide-induced shifts induced by  $\text{Eu}(\text{fod})_3$  in the  $^1\text{H}$  NMR spectrum of 4 ( $M = \text{Ni}$ ,  $R = \text{CH}_3$ ,  $R' = \text{H}$ ,  $X = \text{H}$ ).

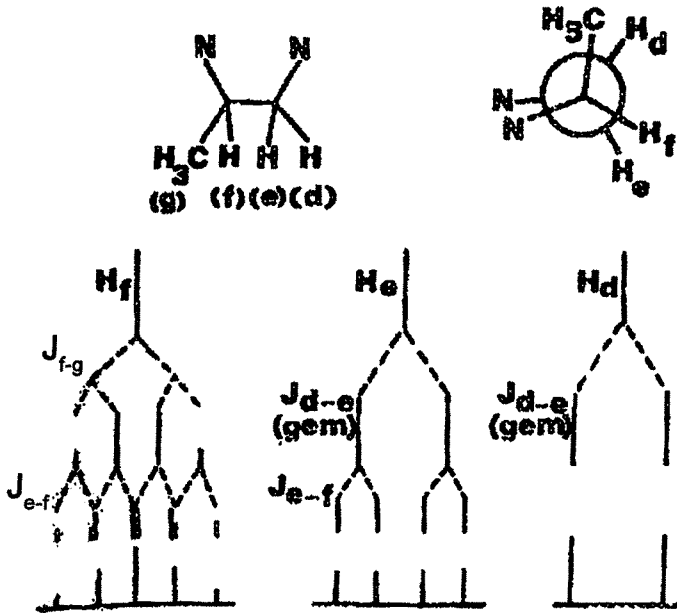


Fig. 10.26. First-order NMR coupling scheme for the propylenediamine backbone of 4 ( $M = \text{Ni}$ ,  $R = \text{CH}_3$ ,  $R' = \text{CH}_3$ ,  $X = \text{H}$ ).



Fig. 10.27. Changes in the propylenediamine methyl resonance of a racemic mixture of 4 ( $M = \text{Ni}$ ,  $R = \text{CH}_3$ ,  $R' = \text{CH}_3$ ,  $X = \text{H}$ ) on addition of  $\text{Eu}(++)\text{fpc}_3$ : (a) original methyl doublet; (b-f) changes on addition of LSR.

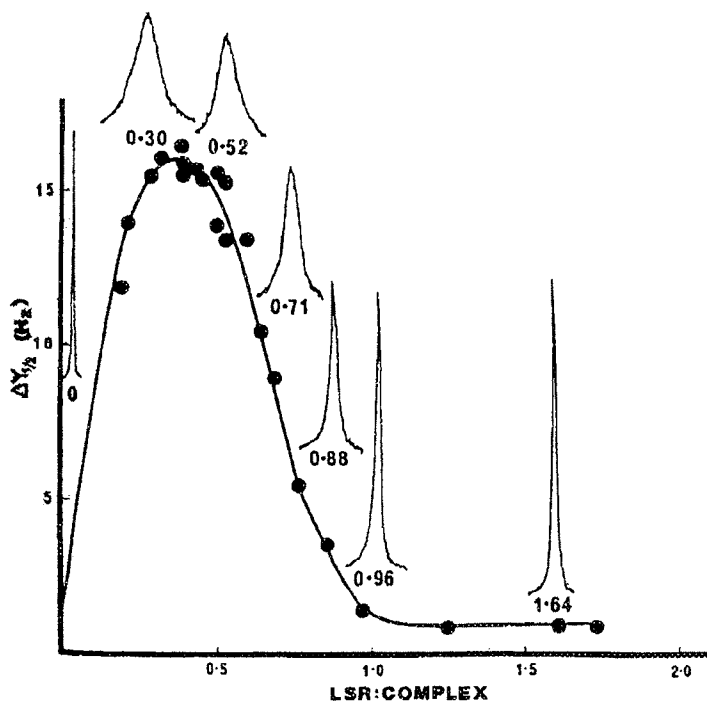
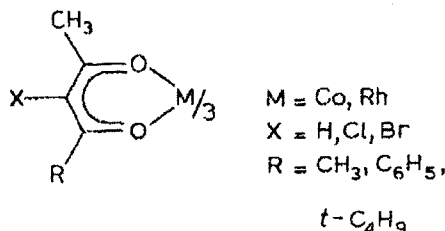


Fig. 10.28. Changes in the linewidth of the resonance corresponding to the methyl groups adjacent to the imine functions of 4 ( $M = \text{Ni}$ ,  $R = \text{CH}_3$ ,  $R' = \text{H}$ ,  $X = \text{H}$ ) on addition of  $\text{Eu}(\text{fod})_3$ ,  $\Delta\nu_{1/2}$  = half width of resonance at half height.



### 23. Kinetic studies [96]

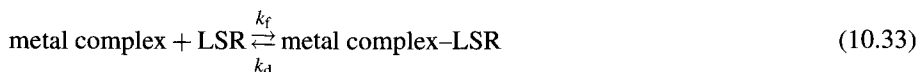
Kinetics of adduct formation between Ni complexes of the type referred to under interactions via donor atom and  $\text{Eu}(\text{fod})_3$  were studied which showed changes in line-widths of the proton resonances in addition to induced chemical shifts. From the concentration dependence of the chemical shifts and line-width, the lifetime of the adduct and  $k_f$  (formation rate constant),  $k_r$  (reverse rate constant) can be determined using the relationship

$$\Delta\nu_{1/2} = f_A \Delta\nu_A + f_B \Delta\nu_B + f_A^2 f_B^2 \tau_B^2 \pi \delta^2, \quad (10.32)$$

where  $\Delta\nu_{1/2}$  is the half-width of the observed resonance at half height,  $\Delta\nu_A$  is half-width of the metal complex in the absence of LSR,  $\Delta\nu_B$  is half-width of the adduct,  $f_A$  is mole fraction of metal complex,  $f_B$  is the mole fraction of the metal complex as the LSR adduct,  $\tau_B$  is the lifetime of the adduct and  $\delta$  is the difference in Hz between the original chemical shift and the limiting chemical shift on complete adduct formation.

From experimental data  $\tau_B$  of  $2.3 \times 10^{-5}$  s for Ni complex– $\text{Eu}(\text{fod})_3$  and  $2.2 \times 10^{-5}$  s for Pt complex– $\text{Eu}(\text{fod})_3$  were obtained. It is useful to note that the last term in the equation (10.32) has a significant effect on the line-broadening.

The equilibrium may be written as

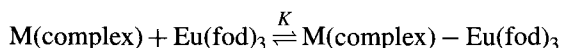


and we have  $k_d = \tau_B^{-1}$ ,  $K = k_f/k_d$ . The second-order rate constant  $k_f$  of  $10^7 \text{ M}^{-1} \text{ s}^{-1}$  was obtained for the Ni and Pt complexes with  $\text{Eu}(\text{fod})_3$ .

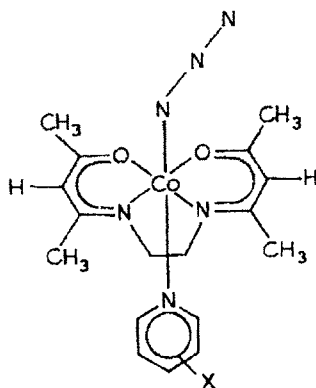
Interaction of deuterated  $\text{Eu}(\text{fod})_3$  with cobalt (III) complexes of the type [97] showed the formation of 1:1 adduct and IR data showed that  $\text{Eu}(\text{fod})_3$  is bonded through the azido group. Both NMR and IR data gave evidence for 1:1 adduct formation (Scheme 10.1).

A model with X-ray diffraction studies of the solid 1:1 adduct show a structure in which the octahedron of oxygen atoms of cobalt share a face with a tricapped trigonal prismatic arrangement of oxygens around the  $\text{Eu}(\text{III})$  ion. The adduct has  $\text{C}_3$  symmetry.

In the case of slow exchange reactions, NMR data can be used to calculate the equilibrium constants for the adduct formation







Scheme 10.1.

TABLE 10.8

Thermodynamic data for the interaction of  $\text{Eu}(\text{fod})_3$  with the cobalt(III) complexes of  $\beta$ -diketones [99].

Adduct system	Calorimetry <sup>a</sup>		<sup>1</sup> H NMR <sup>b</sup>
	$-\Delta H^0$ (kJ M <sup>-1</sup> )	$K$ (M <sup>-1</sup> )	$K$ (M <sup>-1</sup> )
[Co(acac) <sub>3</sub> ] + [Eu(fod) <sub>3</sub> ]	30.5 ± 1.2	10 <sup>4</sup>	≥ 10 <sup>4</sup>
[Co(bzac) <sub>3</sub> ] + [Eu(fod) <sub>3</sub> ]	1 ± 1		≥ 10 <sup>3</sup>
[Co(dbm) <sub>3</sub> ] + [Eu(fod) <sub>3</sub> ]	— <sup>c</sup>		~ 0

<sup>a</sup>In C<sub>6</sub>H<sub>6</sub> at 30 °C.<sup>b</sup>In C<sub>6</sub>D<sub>6</sub> at 33 °C.<sup>c</sup>No heat change detected.

Calorimetric studies in which the complex is titrated with  $\text{Eu}(\text{fod})_3$  have been done and the data on  $K$  and  $\Delta H$ , enthalpy were obtained [99]. Some data thus obtained are given in Table 10.8. Electron-withdrawing groups in the ligand of the complexes resulted in lower binding constants. Further substitution of Rh in place of cobalt resulted in lower  $K$  values. For the Rhodium complexes, X-ray structural data [100] indicate the donor oxygen atoms will be slightly more separated than in the cobalt complexes and this may be a factor for the observed weaker binding of the Rh(III) complexes to  $\text{Eu}(\text{fod})_3$ .

## 24. Application of LIS to biological macromolecules

Application of the LIS method to study the structure of biologically important macromolecules is fraught with some difficulties which are not usually encountered for small molecules. Poor spectral resolution, lack of resonance assignments and the availability of multiple lanthanide binding sites are some of the difficulties in probing the structures of macromolecules. Some LIS studies [101] have been reported for *t*-RNA. But most of the studies involve low molecular weight proteins which contain one or more lanthanide binding sites. Lanthanide ions bind in normal Ca(II) sites on proteins, such as amylases, ther-

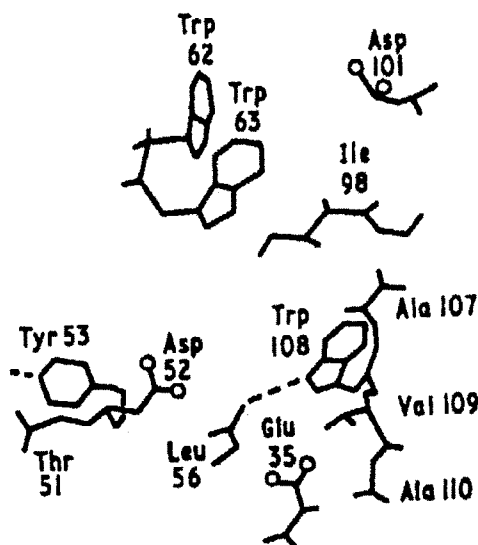


Fig. 10.29. Schematic illustration of the active site region of lysozyme as determined by X-ray crystallography (reprinted with permission from Ref. [106]).

molysin, calmodulin, or parvalbumin or may be conveniently located near two carboxyl groups such as in concanavalin A or lysozyme. The  $\text{Ln}^{3+}$ -ATP complexes have been used as a substitute for  $\text{Mg}^{2+}$ -ATP in the kinases [104]. It is useful if the substitution of  $\text{Ln}^{3+}$  for  $\text{Ca}^{2+}$  or  $\text{Mg}^{2+}$  is isomorphous so that the system retains its normal activity and the results may have relevance to biological structure or function. Unfortunately this is not the case. It has been suggested that if  $\text{Ln}^{3+}$  substituted protein is active,  $\text{Ca}^{2+}$  or  $\text{Mg}^{2+}$  has a structural role and if the  $\text{Ln}^{3+}$  containing protein is inactive, the ion plays a catalytic role [105].

Hen egg lysozyme is a small enzyme, having a single polypeptide chain of 129 aminoacid residues and a molecular mass of approximately 14 400 Da, that catalyzes the hydrolysis of glycosidic linkages in bacterial cell walls. The schematic illustration of the active sites of lysozyme is shown in Fig. 10.29.

Lysozyme binds with lanthanide ions in a weak manner ( $K_{\text{assoc.}} \approx 10^3 \text{ M}^{-1}$  at the carboxyl groups of Glu-35 and Asp-52. Other weak binding sites ( $K_{\text{assoc.}} \leq 10 \text{ M}^{-1}$ ) are also available. Conformational perturbations resulting from binding are small. Overlap of shifted and unshifted resonances was a major problem. Addition of incremental amounts of  $\text{Gd}^{3+}$  and generating NMR difference spectrum after each addition circumvented the problem of overlap of resonances [107]. Since  $\text{Gd}^{3+}$  induces line-broadening of resonances nearest the binding site, the resonances that appear in each new difference spectrum reflect nuclei further removed from the  $\text{Gd}^{3+}$  binding site. Ions which produce paramagnetic shift are then added along with  $\text{Gd}^{3+}$  to obtain LIS values for the previous assigned resonances near the lanthanide binding region which could not be resolved earlier. The difference spectra of the methyl region of lysozyme are shown in Fig. 10.30.

Some of the observed LIS values and relaxation rate enhancements of CH resonances of hen egg white lysozyme with various lanthanides [108] are given in Table 10.9.

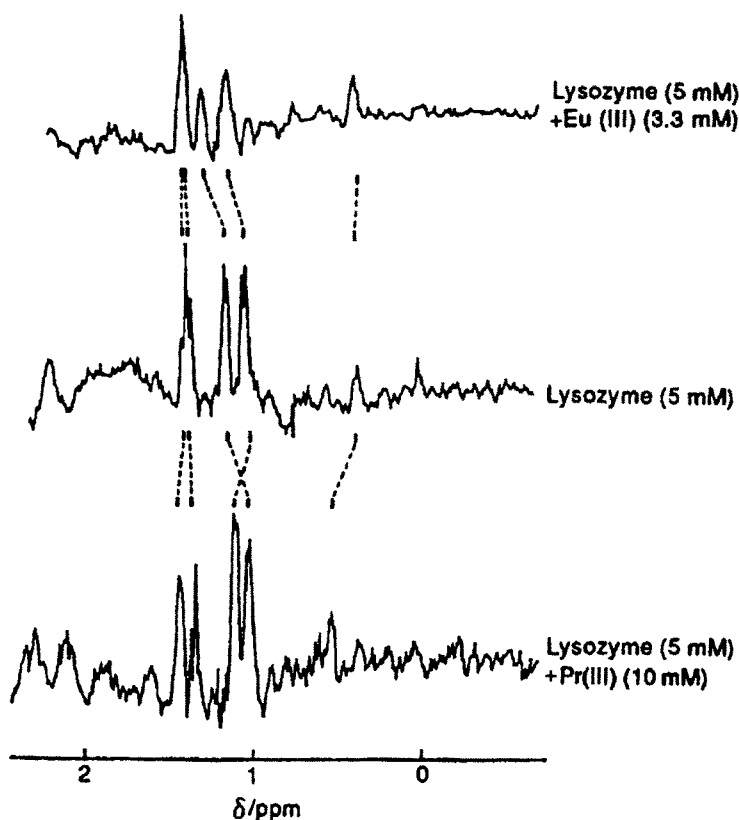


Fig. 10.30.  $\text{Gd}^{3+}$  difference spectra of the methyl region of lysozyme in the absence and presence of shift probes [107].

A semiquantitative correlation of the structure of the protein in solution with the crystal was attempted. Since the relative relaxation of resonances induced by  $\text{Gd}^{3+}$  is proportional to the relative values of  $1/r^6$  for the different nuclei, where  $r$  is the distance between the lanthanide and the nucleus of interest, a plot of the calculated distances and experimental values from the X-ray structure was made [108]. Allowance has been made for the rotation of methyl groups and for flipping of tyrosine residues. The correlation of NMR data with X-ray crystal structure data shown in Fig. 10.31, is reasonably good, with the exception of resonances for val-109 and others at longer distances ( $r \geq 14 \text{ \AA}$ ).

The observed LIS data (Table 10.9) (i.e.) LIS ratios are independent of the nature of the lanthanide with the exception of  $\text{Tm}^{3+}$ . The ratios  $(3 \cos^2 \theta - 1)/r^3$  for each nucleus were calculated and found to agree reasonably with the observed ratios. There is a general agreement between the crystal structure and the solution structure as determined by the LIS method. The agreement between the calculated ratios of  $(3 \cos^2 \theta - 1)/r^3$  for each nucleus and the observed ratios confirms the general agreement between the crystal structure of lysozyme and the solution structure determined by the LIS method. This suggests that the conformation of the enzyme near the metal binding site is unique and well defined.

TABLE 10.9  
Proton shift and relaxation data for lanthanide(III) ions in hen egg white lysozyme<sup>a</sup> [109].

Resonance	Gd <sup>3+</sup>		Shift ratios		Calculated
	Observed	<i>r</i> <sup>h</sup> (Å)	Observed		
	broadening ratio		Pr <sup>3+</sup>	Nd <sup>3+</sup>	
Val-109 C <sup>γ</sup> 1H <sub>3</sub>	2300	8.81	73	-110	65
Val-109 C <sup>γ</sup> 2H <sub>3</sub>	2300	6.02	-109	-380	175
Ala-110 CH <sub>3</sub>	1750	6.26	59	64	-80
Trp-108 C <sup>γ</sup> H	1200	6.87	-117	-55	-137
Trp-108 N H	-	-	-45	-	-21
Ala-31 CH <sub>3</sub>	163	10.44	-	-69	-
Thr-51 CH <sub>3</sub>	140	9.61	151	100	111
<i>o</i> -Tyr-53	100	10.90	100	100	100
<i>m</i> -Tyr-53	100	9.87	160	-	144
Leu-56 C <sup>γ</sup> 1H <sub>3</sub>	95	11.85	0	12	-1
Leu-56 C <sup>γ</sup> 2H <sub>3</sub>	95	9.60	-9	-	-19
Ile-98 C <sup>γ</sup> 2H <sub>3</sub>	75	13.3	-32	-11	-23
Met-105 CH <sub>3</sub>	35	12.6	-14	5	-25
Met-12 CH <sub>3</sub>	25	14.7	-2	7	-6
Leu-17 C <sup>γ</sup> 1H <sub>3</sub>	25	17.2	-	12	-
Leu-17 C <sup>γ</sup> 2H <sub>3</sub>	25	15.8	-	-	-
<i>o</i> -Tyr-20	-	-	0	-	-3
<i>o</i> -Tyr-23	-	-	-14	-	-10
Trp-63 C <sup>γ</sup> H	-	-	53	-	42
Ala-107	-	-	-68	-	-49

A solution structure map of the region surrounding the lanthanide binding site as generated from the experimental studies [107] is depicted in Fig. 10.32.

## 25. Studies on Mg<sup>2+</sup>-ATP-dependent phosphoglycerate kinase

Yeast 3-phosphoglycerate kinase (PGK), a glycolytic enzyme which catalyzes the reversible phosphorylation of 3-phosphoglycerate (PGA) by ATP, is a monomer with a molecular weight of about 45 kDa. The crystal structure of PGK shows that the polypeptide chain has two structurally independent domains that are joined by a short helical hinge consisting of two chains [109,110]. More than fifty percent of the residues are in the form of two large  $\beta$  sheets and there are 14 strands and 13  $\alpha$  helices between the sheets. The catalytic mode of Mg<sup>2+</sup>-ATP/Mg<sup>2+</sup>-ADP binding to PGK is to the C-terminal domain, where a hydrophobic depression binds the adenine group. The phosphate chain of the cofactor points towards the N-terminal domain but away from the C-terminal domain. It is probable that C-domain carries the cofactor and the N-domain the PGA substrate and a catalyst.

Paramagnetic difference spectroscopic technique was used [111,112] in determining the perturbations of the enzyme resonances in line-broadening inhibitor Gd<sup>3+</sup>-ATP and the substrate Mn<sup>2+</sup>-ATP. Identical perturbations were induced. The difference spectra of the PGK are given in Fig. 10.33. The perturbations are specific in nature corresponding to

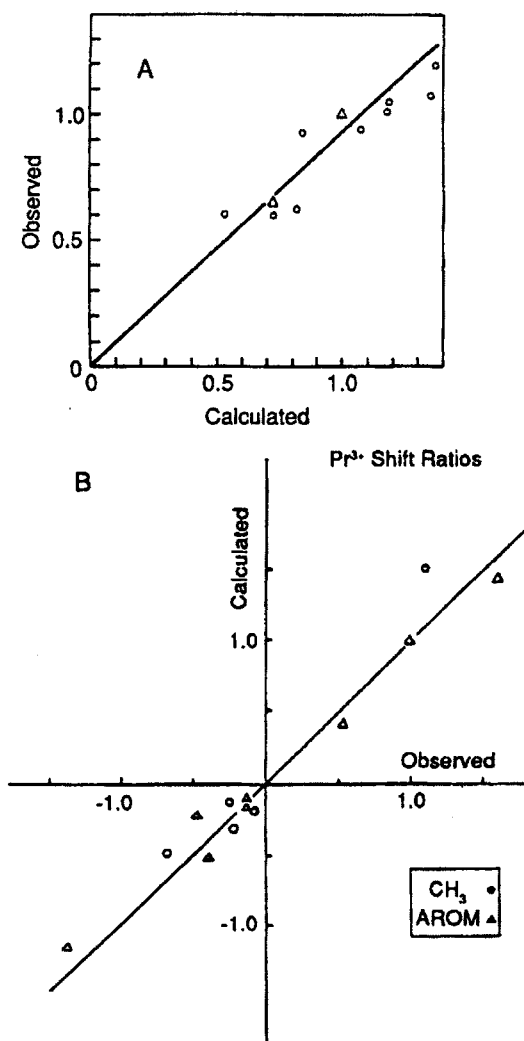


Fig. 10.31. Correlation of calculated and observed (A) relative distances from the  $\text{Gd}^{3+}$  ion in lysozyme and (B) relative shifts induced by the  $\text{Pr}^{3+}$  ion in lysozyme (reprinted with permission from Ref. [107]).

the basic patch of N-domain, His-62 (peak 3 in Fig. 10.30a), His-167-peaks 4.15; His-170-peak 5; C-domain, Tyr-193-peak 14 and phe-342-peak 12. The effects of shift probes  $\text{Ln}^{3+}\text{-ATP}$ , where  $\text{Ln}^{3+} = \text{Pr}^{3+}, \text{Eu}^{3+}$  were found to agree with line-broadening data. Largest LIS values were observed for His-167, His-62 and His-170. The broadening probe  $\text{Gd}^{3+}\text{-P}_2$  ( $\text{P}_2 = \text{pyrophosphate}$ ) and the shift probe  $\text{Eu}^{3+}\text{-P}_2$  produced similar effects as those of  $\text{Ln}^{3+}\text{-ATP}$ .

The broadening and shift data obtained from  $\text{Ln}^{3+}\text{-ATP}$  probe were used to map [111] geometrically the active site of the enzyme, including the conformation of ATP,

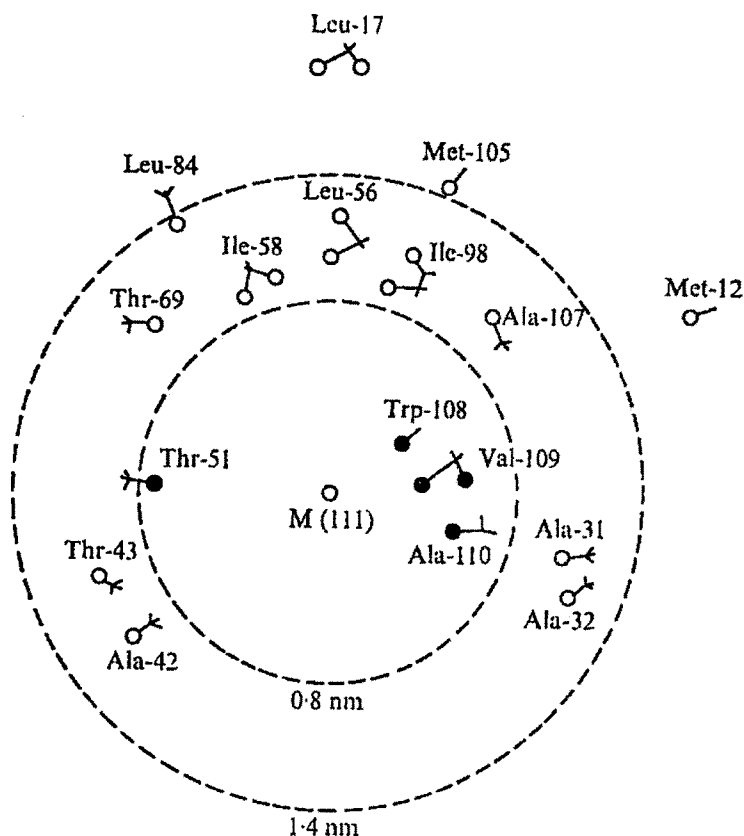


Fig. 10.32. Two-dimensional representation of the amino acid residues around the active site of lysozyme (from Ref. [107]).

the positions of various enzyme side-chain residues and an approximate position for the substrate PGA. The resulting map is shown in Fig. 10.34. There are differences between crystal structure and the structure in solution obtained by NMR. In solid form the basic histidine patch is separated by at least 12 Å from the ATP binding site. The observed proximity of the two binding sites in the two domains is supported by a hinge-bending movement hypothesis postulated to explain the catalytic mechanism of this enzyme [109].

## 26. $\text{Ca}^{2+}$ -binding protein, parvalbumin

This protein has been studied in detail by the LIS method [113,114]. The protein binds two equivalents of  $\text{Ca}^{2+}$  in two distinct binding domains known as "CD and EF hands." Each of the domains consists of a short  $\alpha$ -helical structure, a loop around the  $\text{Ca}^{2+}$  site which contains regularly spaced carboxyl, carbonyl, and hydroxyl side-chain ligands for the metal ion, followed by a second  $\alpha$ -helical region. The binding domains have a very high affinity

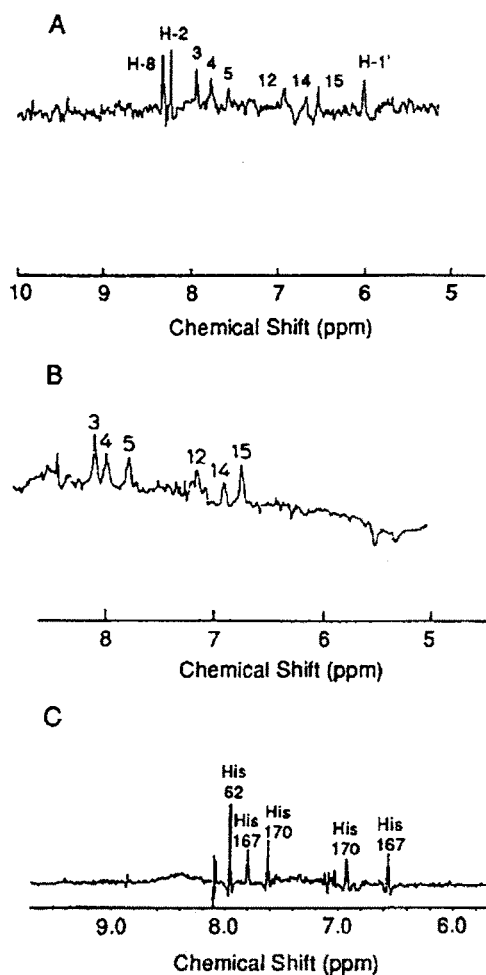


Fig. 10.33. Paramagnetic difference spectra of the PGK aromatic proton region in the presence of (A) 20  $\mu\text{M}$   $\text{Gd}^{3+}$ -ATP; (B) 40  $\mu\text{M}$   $\text{Gd}^{3+}$ - $\text{P}_2$ ; (C) 2  $\mu\text{M}$   $[\text{Cr}(\text{CN})_6]^{3-}$  [111,112].

for  $\text{Ca}^{2+}$  and even higher affinity for  $\text{Ln}^{3+}$  ions. Studies have shown the CD domain to have higher affinity for  $\text{Ln}^{3+}$  ions than the EF domain [113]. This situation permits preferential loading of the EF site by the smaller paramagnetic  $\text{Yb}^{3+}$  or diamagnetic  $\text{Lu}^{3+}$  ions at low  $\text{Ln}^{3+}$ /protein ratios.

The complex NMR spectrum of calcium saturated carp parvalbumin and parvalbumin with 0.8 eq. of  $\text{Yb}^{3+}$  is shown in Fig. 10.35. The spectrum is more complex than lysozyme. When  $\text{Yb}^{3+}$  is added progressively to the protein, several of the proton resonances disappear from the original positions and several new resonances appear both upfield and downfield from the original diamagnetic positions.

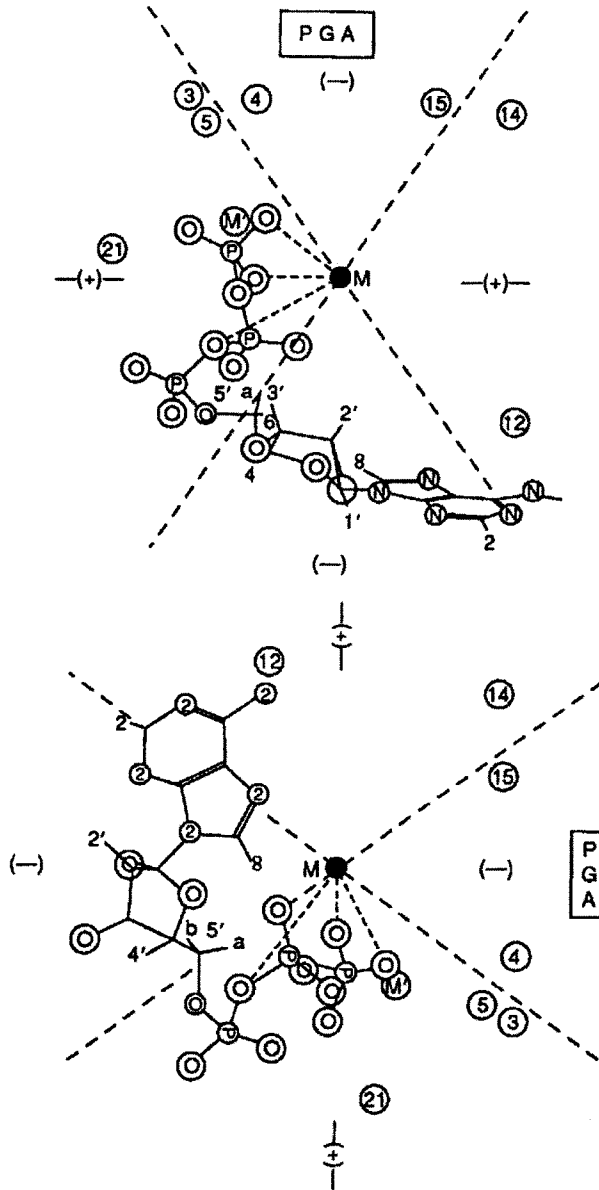


Fig. 10.34. Schematic of the active site of PGK showing the relative coordination of the enzyme and ATP protons to the lanthanide (designated M). The protons are located spatially on the basis of the NMR data. The dashed lines represent the dipolar cone of the LIS, and the plus signs (+) define the symmetry axis (PGA, 3-phosphoglycerate: 3, His-62; 4, 15, His-167; 5, His-170; 12, Phe-342; 14, Tyr-193). (Adapted with permission from Ref. [111]).



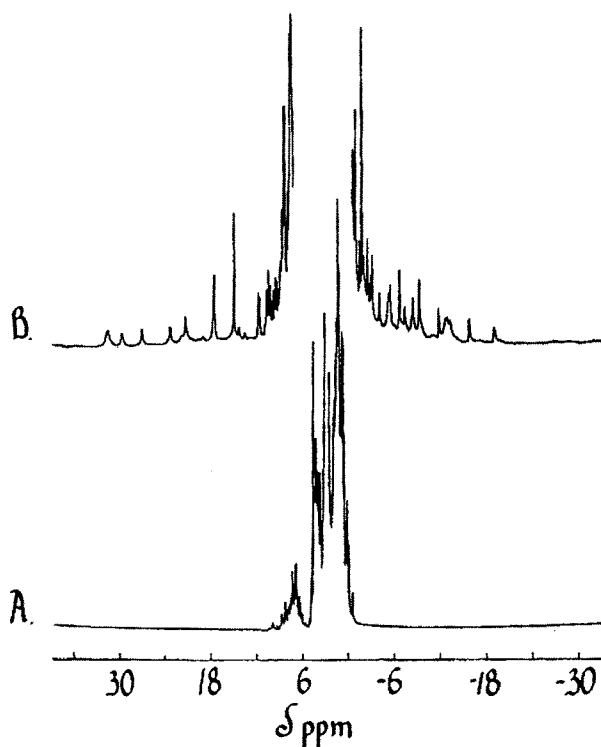


Fig. 10.35. 270 MHz  $^1\text{H}$  spectrum of (A) calcium saturated carp parvalbumin and (B) parvalbumin with 0.8 equivalents of  $\text{Yb}^{3+}$  (from Ref. [113]).

Some of the resonances are due to  $\text{Yb}^{3+}$  binding in the EF site and others due to the binding in the CD site as shown in Fig. 10.36. This behaviour is characteristic of a slow exchange reaction and is difficult to interpret since the correspondence between the diamagnetic and paramagnetic resonances is not known. Proper assignments may be estimated from the temperature dependence of the shifted resonances, extrapolated to high temperatures. The second problem is to determine the direction and magnitude of magnetic susceptibility tensors which define the values of  $D'$  and  $D'_2$  in the equation

$$\text{LIS} = D'(3 \cos^2 \theta - 1)/r^3 + D''(\sin^2 \theta \cos 2\phi)/r^3 \quad (10.34)$$

Axial symmetry cannot be assumed as in the case of lysozyme, since data are available only for one lanthanide ion. Data with other lanthanide ions were not obtained because selectivity of the EF site over the CD site varies with increase in cation size and hence it is not possible to test for axial symmetry.

Only five of the resonances listed in Table 10.10 could be assigned with certainty and these were to locate the direction and magnitude of the  $\text{Yb}^{3+}$  magnetic susceptibility tensors using coordinates for the five nuclei from the X-ray structural data. Using the values in Table 10.10, LIS values for other nuclei could be predicted and other resonances

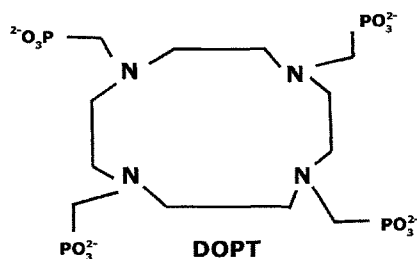
TABLE 10.10  
Comparison of calculated vs. observed LIS's in parvalbumin (from [114]).

Nucleus	LIS <sub>obs</sub> (ppm)	LIS <sub>calc</sub> (ppm)
<sup>1</sup> H His-26 C2H	0.485	0.475
<sup>1</sup> H His-26 C4H	0.343	0.332
<sup>1</sup> H N-acetyl CH <sub>3</sub>	0.033	0.082
<sup>113</sup> Cd CD metal site	-0.270	-0.286
<sup>13</sup> C Arg-75 ξ-carbon	0.318	0.351

assigned. The calculated LIS values for protons close to the EF site were generally larger than the observed shifts indicating less compact structure in solution in the EF region than in solid state.

## 27. Studies on surfaces of proteins [115]

The resonances of <sup>13</sup>C introduced in the fd gene 5 DNA protein by reductive methylation without disrupting its ability to bind single-stranded DNA were studied by NMR [115]. Three of the modified lysine resonances out of a total six lysyl residues containing <sup>13</sup>C enriched methyl groups were affected by the binding of oligo nucleotides. For the purpose of assigning resonances, the protein was titrated with the chelate Tb(DOTP)<sup>5-</sup>, to act as an extrinsic LIS probe [117]. The structure of DOTP is shown below.



The spectrum of <sup>13</sup>C enriched protein before and after addition of DOTP is shown in Fig. 10.37. It is seen that resonances 1, 2 and 5 shifted to higher frequency while resonances 3 and 4 shifted to lower frequency, throughout the titration until one equivalent of chelate per protein dimer had been added.

Further additions of Tb(DOTP)<sup>5-</sup> did not affect the spectrum. Competition experiments between Tb(DOTP)<sup>5-</sup> and an oligonucleotide showed their binding to be mutually exclusive, suggesting that the binding site for phosphonate chelate overlaps the DNA binding sites. This system has a single, specific lanthanide complex binding site which may be saturated at concentrations used in NMR experiment with prevailing rapid chemical exchange conditions. This allows the direct determination of stoichiometry along with the evaluation of the diamagnetic chemical shift of each of the resonances. Further, Tb(DOTP)<sup>5-</sup> structure is axially symmetric [118] and the LIS data fit the axial symmetry

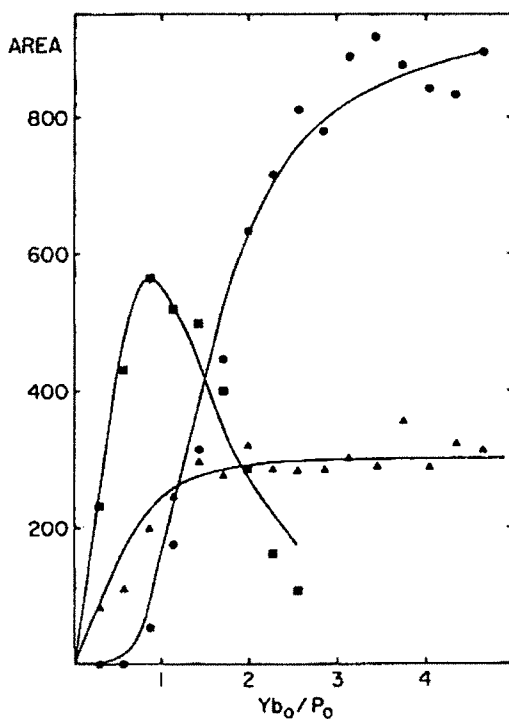


Fig. 10.36. Areas of three different resonances in parvalbumin as a function of total added  $\text{Yb}^{3+}$  (from Ref. [113]).

TABLE 10.11  
Some proteins studied by Ln(III) reagents

Protein	Study
Lysozyme	Ln(III) probes established structure in solutions
Neurotoxins	Uncovering of hydrophobic surface
Protease inhibitors	Assignment of resonances
Cytochrome-c	Assignment of resonances
Transferrin [55]	Ln(III) probes established the Fe(III) binding sites
Calmodulins	Uncovering of Ca(II) binding sites

model. This is an example of a chelate that is useful in monitoring protein structures in solution by NMR. Some proteins studied by Ln(III) reagents are given in Table 10.11.

## 28. Applications to cells, tissues and organs

The application of LIS reagents to studies of cells, tissues or organs involves lifting the normal degeneracy of NMR signals of molecules or ions in different compartments. This may be accomplished by a paramagnetic shift reagent which while remaining extracellular,

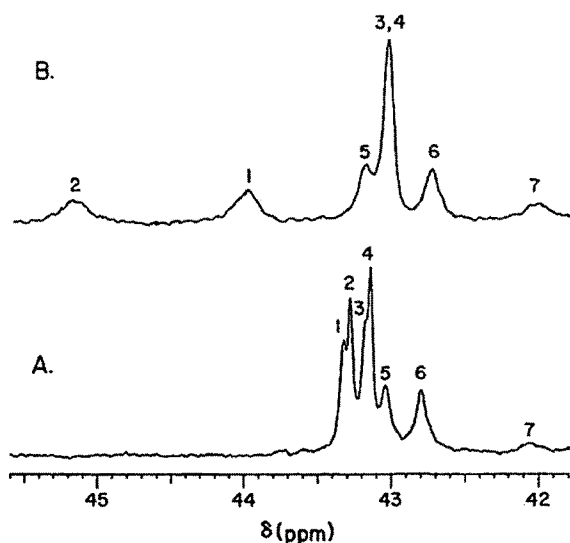


Fig. 10.37. 50.1 MHz  $^{13}\text{C}$  NMR spectrum of [ $^{13}\text{C}$ -methyl] gene 5 protein (A) before and (B) after the addition of  $\text{Tb}(\text{DOTP})^{5-}$  (from Ref. [115]). Resonances 1–6 correspond to the six dimethyllysyl residues while resonance 7 is the partially modified N-terminal dimethylmethionyl residue [115].

binds to the molecules or ion of interest and induces LIS (pseudo contact or contact) in those nuclei. Nuclei in other compartments would remain unaffected unless there is a rapid exchange of molecules or ions between the two compartments.

Most of the LIS studies of this type involve  $^{23}\text{Na}$  and or  $^{39}\text{K}$  measurements. These ions are present in large concentrations in biological systems and their NMR sensitivities are favourable and they play an important role in maintaining transmembrane electrical potentials. Transmembrane transport [119] and compartmentalization [120] have been discussed. The topic of interest here is the chemistry and development of lanthanide shift reagents for biological studies which are important because of their potential applications in magnetic resonance imaging and magnetic resonance spectroscopy of humans.

Studies on the use of anionic complexes of lanthanides,  $[\text{LnX}]^{n-}$  which induce significant shifts in  $^{23}\text{Na}$  resonances through the formation of ion-pair complexes of the type  $\text{Na}^+[\text{LnX}]^{n-}$  have been made [13,121,122]. The sodium ion forms ion-pairs with the complexing or pendant charged groups in the chelate and produces  $^{23}\text{Na}$  LIS shift. The most effective agent in inducing LIS per unit concentration [123] is dysprosium bis(tripolyphosphate),  $\text{Dy}(\text{PPP})_2^{7-}$ . The structure of this complex in solution is obtained from  $^{17}\text{O}$ ,  $^{31}\text{P}$ ,  $^{23}\text{Na}$  LIS and relaxation data [124] and is shown in Fig. 10.38.

The corrected pseudo contact shift values fit the axial symmetry model with the principal symmetry axis bisecting the two coordinated tripolyphosphate groups. The  $\text{Na}^+$  ions are to a large extent associated with the two terminal charged oxygen atoms on each phosphate group at an average distance of 5.8 Å from the  $\text{Ln}^{3+}$  ion. The spectrum of  $^{23}\text{Na}$  resonances of human erythrocytes with  $\text{Dy}(\text{PPP})_2^{7-}$  as a shift reagent is shown in Fig. 10.39. The intra- and extracellular resonances of  $^{23}\text{Na}$  are well resolved with 2 mM  $\text{Dy}(\text{PPP})_2^{7-}$ . There are

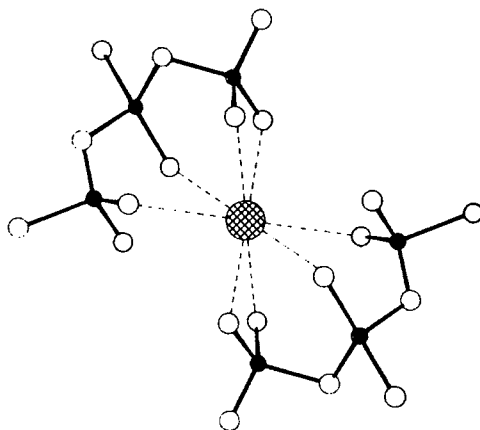


Fig. 10.38. The structure of  $\text{Dy}(\text{PPP})_2^{7-}$  (from Ref. [124]). The cross-hatched circle represents  $\text{Dy}^{3+}$ , the dark circles phosphorous, and open circles oxygen.

two drawbacks in the use of  $\text{Dy}(\text{PPP})_2^{7-}$  as a shift reagent for  $^{23}\text{Na}$ . The first drawback is that  $\text{Ca}^{2+}$  ions compete with  $\text{Na}^+$  ions to form the ion-pair complex and thus reduce the LIS to zero. It has been reported that it is difficult to maintain [125] viable perfused heart preparations in the presence of  $\text{Dy}(\text{PPP})_2^{7-}$ . The second problem is that the thermodynamic stability of the complex is too low for it to remain stable in most tissues. The complex was shown to dissociate into  $\text{Dy}^{3+}$  and phosphate after exposure to rat abdominal muscle for 5 hours.

Another reagent  $\text{Dy}(\text{TTHA})^{3-}$  was suggested by Springer et al. [122,123,125] which has: (i) high stability constant, (ii) is less sensitive to divalent ions, and (iii)  $^{23}\text{Na}$  shifts are independent of pH in the range of 5.5–12.0. One of the drawbacks of this reagent is that it requires five times the concentration (10 mM) to induce shifts in  $^{23}\text{Na}$  resonances in different cellular compartments [126,127].

The schematic structure of  $\text{Dy}(\text{TTHA})^{3-}$  is shown in Fig. 10.40. A concentration of 10 mM of  $\text{Dy}(\text{TTHA})^{3-}$  is required to produce a shift of  $^{23}\text{Na}$  of the same magnitude as that of 2 mM of  $\text{Dy}(\text{PPP})_2^{7-}$ . The two complexes  $\text{Dy}(\text{PPP})_2^{7-}$  and  $\text{Dy}(\text{TTHA})^{3-}$  induce  $^{23}\text{Na}$  shifts in opposite directions. Thus  $\text{Na}^+$  ions must associate in different spatial regions of the ligands with respect to the principal axis of symmetry in the two complexes. We have noted that  $\text{Dy}(\text{PPP})_2^{7-}$  “effective” axial symmetry but  $\text{Dy}(\text{TTHA})^{3-}$  probably has a non-axial component which might render it an ineffective shift reagent.  $\text{Dy}(\text{TTHA})^{3-}$  probably has two unbound carboxyl groups available for ion-pair formation with  $\text{Na}^+$  ions but the carboxyl groups may be farther than bound phosphates in  $\text{Dy}(\text{PPP})_2^{7-}$  from the lanthanides. The negative charge in  $\text{Dy}(\text{TTHA})^{3-}$  is lesser than in  $\text{Dy}(\text{PPP})_2^{7-}$  which will affect both the amount and affinity of contact ion pairs. The value of LIS depends upon the ligand field term  $D'$ , the angle  $\theta$  and  $r$ , the distance in axial symmetry in equation (10.34). Thus it is possible to maximize the  $^{23}\text{Na}$  LIS by selecting a lanthanide chelate which permits positioning  $\text{Na}^+$  binding sites precisely along the perpendicular direction to the highest-fold symmetry in a compact structure and also maximize  $D'$ .

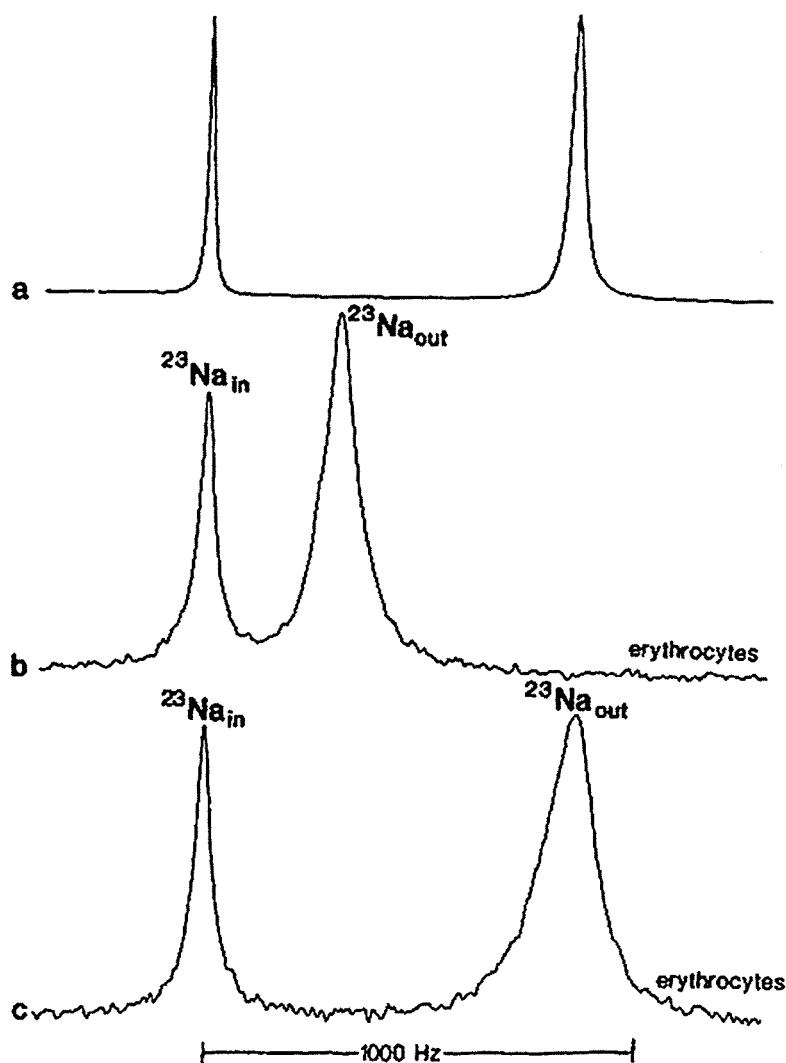


Fig. 10.39.  $^{23}\text{Na}$  NMR spectra of gently packed human erythrocytes in a medium containing 140 mM  $\text{Na}^+$ , 10 mM  $\text{K}^+$ , and 2 mM (spectrum b) or 5 mM (spectrum c)  $\text{Dy}(\text{PPP})_2^{7-}$ . Spectrum a was obtained on a 140 mM  $\text{Na}^+$  solution in a concentric tube with the outer compartment containing 5 mM  $\text{Dy}(\text{PPP})_2^{7-}$  (from Ref. [121]).

Sherry et al. [129] developed and studied a new reagent,  $\text{Tm}(\text{DOTP})^{5-}$ . The structure of the ligand is shown in Fig. 10.41. The  $\text{Dy}(\text{DOTP})^{5-}$  is comparable to  $\text{Dy}(\text{PPP})_2^{7-}$  in inducing  $^{23}\text{Na}$  shifts but the shifts are reversed [129] by  $\text{Ca}^{2+}$ . On the other hand the reversal of shifts with  $\text{Tm}(\text{DOTP})^{5-}$  are less than in the case of  $\text{Dy}(\text{DOTP})^{5-}$ .  $\text{Tm}(\text{DOTP})^{5-}$  is thermodynamically stable and not hydrolysed by phosphates or acids.

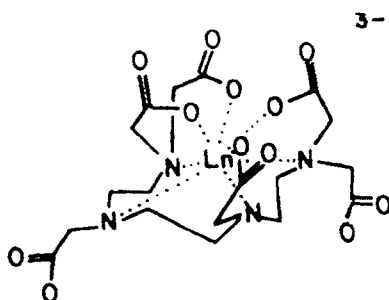


Fig. 10.40. Proposed structure of  $\text{Dy}(\text{TTHA})^{3-}$  (from Ref. [123]).

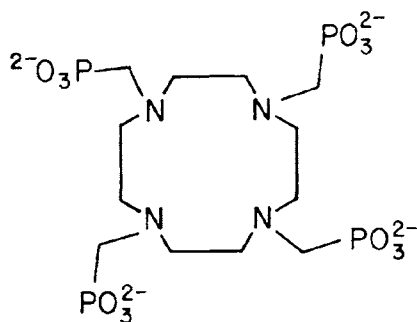


Fig. 10.41. Structure of the macrocyclic chelating agent,  $\text{DOTP}^{8-}$ .

The DOTP complexes are axially symmetrical and the values and direction of  $^{23}\text{Na}$  LIS for the various lanthanides indicate that  $\text{Na}^+$  binding region is near the 4-fold axis of symmetry in the complex. The NMR spectra of  $^{23}\text{Na}$  in perfused rat heart are shown in Fig. 10.42. The large extracellular  $\text{Na}^+$  resonances shifted upon the progressive addition on  $\text{Tm}(\text{DOTP})^{5-}$  and the heart rate was normal. After the addition of 3.75 mM of  $\text{Tm}(\text{DOTP})^{5-}$ , a small  $\text{Na}^+$  resonance appeared near the diamagnetic chemical shift position of  $\text{Na}^+$ . This resonance increased in intensity in response to the interval as shown in Fig. 10.43 and was assigned to intracellular  $\text{Na}^+$ .  $\text{Tm}(\text{DOTP})^{5-}$  has been found very useful in monitoring  $\text{Na}^+$  levels on normal and damaged heart tissue.

## 29. Applications of lanthanides in biology

Lanthanide ions can be used to study the potential properties of the A-sub group ions such as  $\text{Na}^+$ ,  $\text{K}^+$ , and  $\text{Ca}^{2+}$ . Some of the uses are: (i) heavy atom “stains” in electron microscopy or X-ray diffraction, (ii) lanthanide ions as competing ions for  $\text{Ca}^{2+}$  sites, (iii) kinetic properties-fluxional properties, (iv) structural features.  $\text{Ln}(\text{III})$  can be used as a scattering element replacement for  $\text{Ca}(\text{II})$  or  $\text{Mg}(\text{II})$ . Some examples are the structures of concanavalin A and *t*-RNA. The replacement is not always isomorphous and the data should be interpreted with care. Some proteins bind  $\text{Ln}(\text{III})$  although they function without

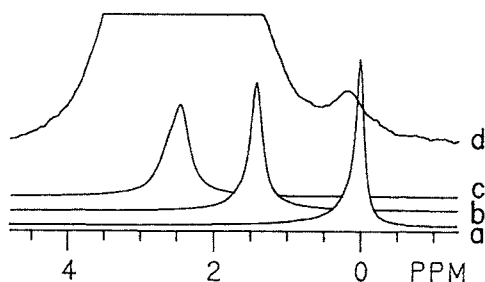


Fig. 10.42.  $^{23}\text{Na}$  NMR spectra at 11.75 Tesla of a Langedorff perfused rat heart with (a) no shift reagent, (b) 2.5 mM  $\text{Tm}(\text{DOTP})^{5-}$ , or (c) 3.75 mM  $\text{Tm}(\text{DOTP})^{5-}$ . Spectrum (d) is a  $10\times$  expansion of (c) showing the small intracellular  $\text{Na}^+$  resonance [129].

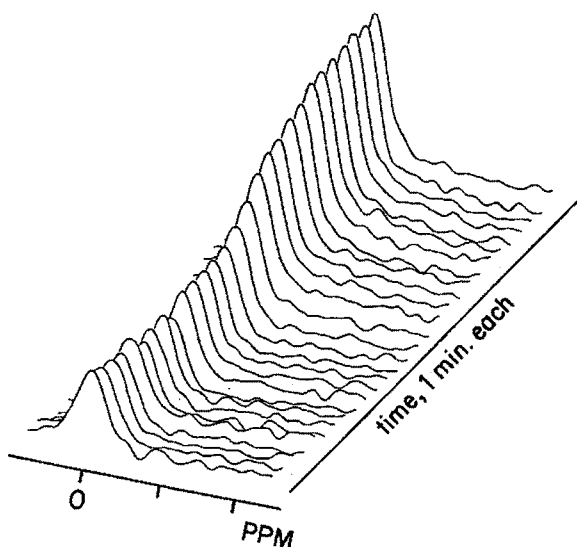


Fig. 10.43. Changes in the intracellular  $^{23}\text{Na}^+$  resonance in a rat heart during global ischemia. Each spectrum represents a one minute interval (the large extracellular resonance has been omitted for clarity) [129].

metal ions. Cations have been used in the X-ray studies of lysozyme as discussed earlier.  $\text{Gd}(\text{III})$  has been used as a probe in the NMR studies of the enzyme.

Lanthanide ions stain anionic surfaces as, for example, in membranes and this property has been used in electron microscope studies. NMR studies have shown that the membranes are perturbed slightly but not significantly at the electron microscopic level. It is possible to use  $\text{Ln}(\text{fod})_3$  as a staining agent which stains the membrane internally since it is hydrophobic. An example of the use of the  $\text{Gd}(\text{FOD})_3$  in staining vesicles is shown in Fig. 10.44. NMR studies have shown that the staining reagent does not perturb the membrane grossly [116].



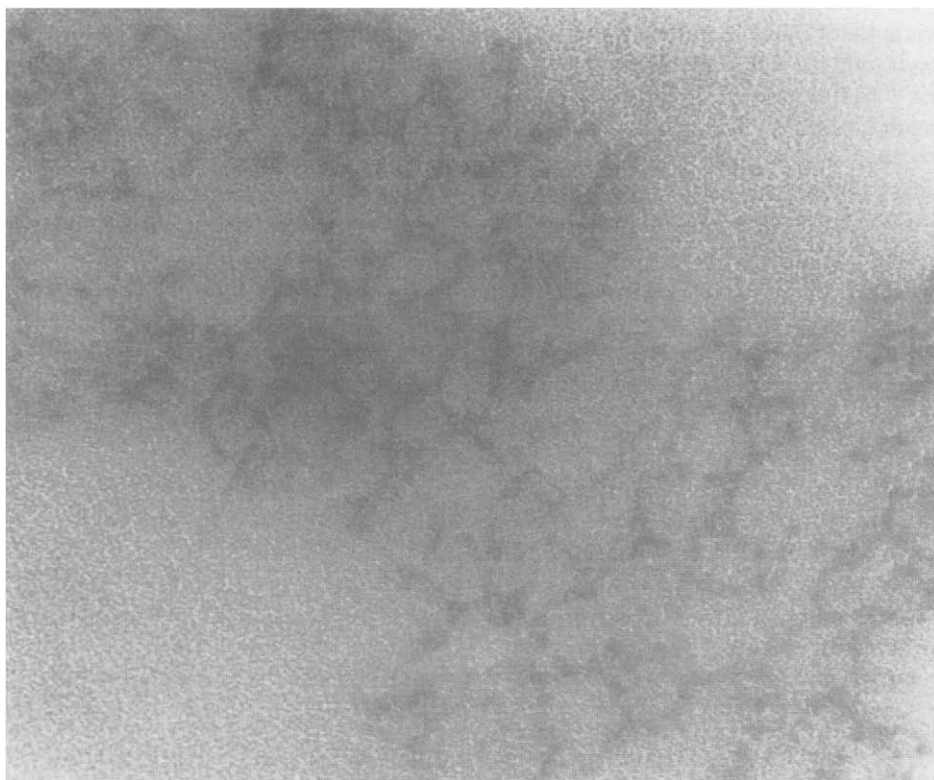
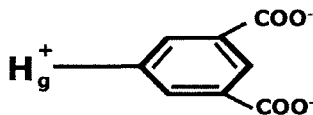


Fig. 10.44. Electron microscope picture of vesicles (500 Å radius) stained with  $Gd(fod)_3$ ; magnification  $5 \times 10^5$ .

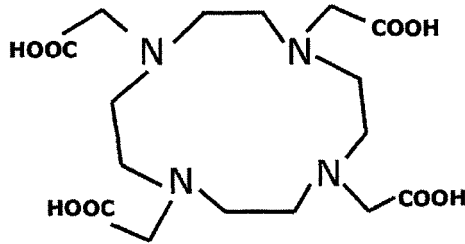
### 30. New Ln(III) reagents

Thus far Ln(III) aquo cations or  $Ln(fod)_3$  complexes have been used in the studies of both small and large molecules [116].  $Ln(EDTA)$  complexes have been found to be useful for anionic centers and  $Ln(dipicolinate)_3^{3-}$  for cationic centers. A reagent of promise is given below. This reagent binds to the sulphhydryl (Scheme 10.2) groups and so locating the dicarboxylate Ln(III) binding group. As an alternate, one can use the reagent (Scheme 10.3).

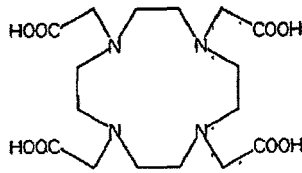
Some promising reagents for the development of Ln(III) probes as specific reagents are given in Fig. 10.45. It is possible to add functional groups so that they can be linked to specific substrates. Thus the reagents will probe specific sites instead of general hydrophobic regions.



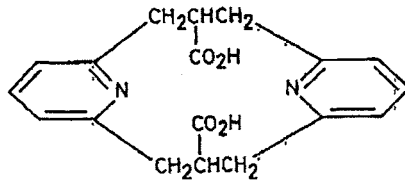
Scheme 10.2.



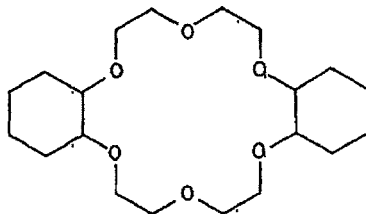
Scheme 10.3.



(I)



(II)



(III)

Fig. 10.45. The formulae of possible chelating agents for the development of Ln(III) probes as specific reagents.

Lipid bilayers have been studied in vesicles of about 500 Å diameter. The bilayers can be made of many lipids. The most common lipid is lecithin, phosphatidyl choline (PC). Packing the lipids in the vesicle results in two-thirds of the lipid head groups on the external face about one-third on the internal face. The head group of the lipid PC is phosphocholine  $-O-PO_2^- -O-CH_2-CH_2-N^+(CH_3)_3$  and the head group is studied by P, H, D or C NMR and the long fatty chains by C, H, or D NMR. Conformational studies of the molecules by conventional de-coupling, nuclear Overhauser effects and by Ln(III) probes

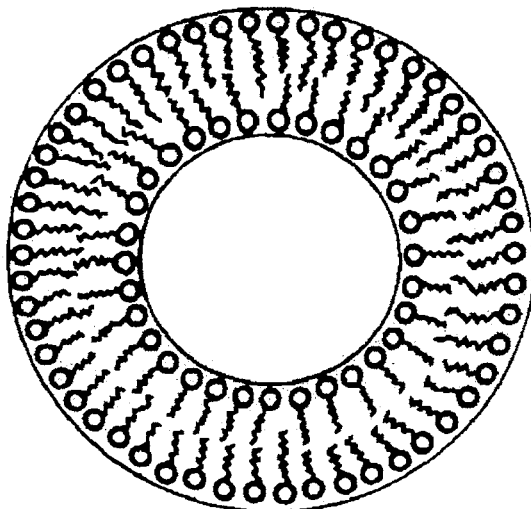
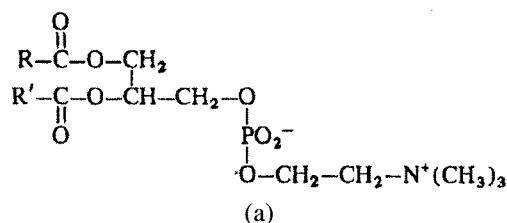


Fig. 10.46. Phosphatidyl choline vesicles. (a) The formula of the lipid, where R and R' are long chain alkyl groups, and (b) the structure of the vesicle.

show close agreement between solution and X-ray structure was found only in the absence of Ln(III) since Ln(III) cations altered the conformation of the head group. The metal ions bind to the  $-\text{PO}_2^-$  groups and repel the  $-\text{N}^+(\text{CH}_3)_3$  groups away from the lipids [130,131]. Phosphatidyl choline Vesicles, both formula and structure are shown in Fig. 10.46.

The paramagnetic shifts and relaxation changes induced by Ln(III) on the resonances can be used to obtain binding constants. The binding of a cation to a bilayer surface is not the same as the binding to a monomer head group in solution since the bilayer carries a charge. The charge on the bilayer changes with Ln(III) binding and the binding is then anti-cooperative. Thus the initial binding constant  $K$  of Ln(III) is larger than to glycerol-phospho-choline, an isolated head group. The binding constants fall with occupancy as the charge builds up

$$K_x = K \cdot e^{-xc},$$

where  $x$  is fractional occupancy and  $c$  is a constant. This type of binding is probably important in biology [132-134].

The shift ratios are constant (i.e.) independent of Ln(III) ions for the head groups of the bilayer but vary significantly for glycerol-phospho-choline in the second half of the lanthanide series as opposed to the first half of the series. This probably reflects the differences in hydration of cations in the head groups and at the membrane surface.

The biological significance of the work is the effect of calcium ions on the membrane structure. We note that about  $< 10^{-7}$  M of  $\text{Ca}^{2+}$  ions inside the cell and about  $> 10^{-3}$  M outside the cells are present. Thus the binding is more likely to the outside of the bilayer which in turn stabilizes the lipids on the outside and also affects the geometry of the lipid on two sides of the membrane leading to differences in binding of other reagents and even curvature of the bilayer. Ln(III) cations can be placed either inside or outside the bilayer since they cannot cross the membrane [135]. Using Pr(III), the inside and outside signals were followed differentially on changing the bathing solution which permitted studies of transport across the lipid bilayer.

Studies of the properties of the lipid layer were made by incorporating the shift reagent,  $\text{Ln}(\text{fod})_3$  in the membrane. This enabled the study of partitioning of molecules into the bilayer as for example chloroform, or the binding of protein to the bilayer surface. This approach might lead to finding the special parts of proteins which bind to membranes [116]. The structure of the lipid in the vesicle as obtained from Ln(III) shift and relaxation data is shown in Fig. 10.47.

### 31. Computer programs for simulation of induced shifts

Since the advent of NMR-LSR studies, many computer programs have been written for the simulation of induced shifts. Most of the programs are no-name programs and are not easily available. Some of the programs and their uses are listed below.

CHMSHIFT	Finds the optimum geometry of the complex. The direction of the magnetic axis need not be collinear to the Ln-L bond [136,137]
PDIGM	Finds the optimum geometry of the complex [138]
OPLIS	Finds the optimum geometry of the complex [139]
MAXI	Finds the optimum geometry of the complex, by modifying the conformation during computation to obtain a better fit [140]
LANTHAMATIC	Finds the optimum geometry of the complex [141]
(APSIMON)	Newton's method is used for searching for the optimum lanthanide position [142]
Other no-name (generic)	Search for optimum lanthanide position [143]

Three programs have been written [143] and they are: (i) SIMULATION, (ii) PGM 1, and (iii) PGM 2.

The program SIMULATION involves the simplest use of the subroutines. It takes as input the molecular geometry of the lanthanide-substrate complex and gives a relative induced shift for each of the protons. The program PGM 1 takes as input two possible geometries for the lanthanide complex and gives relative weighted induced shifts for different weightings.

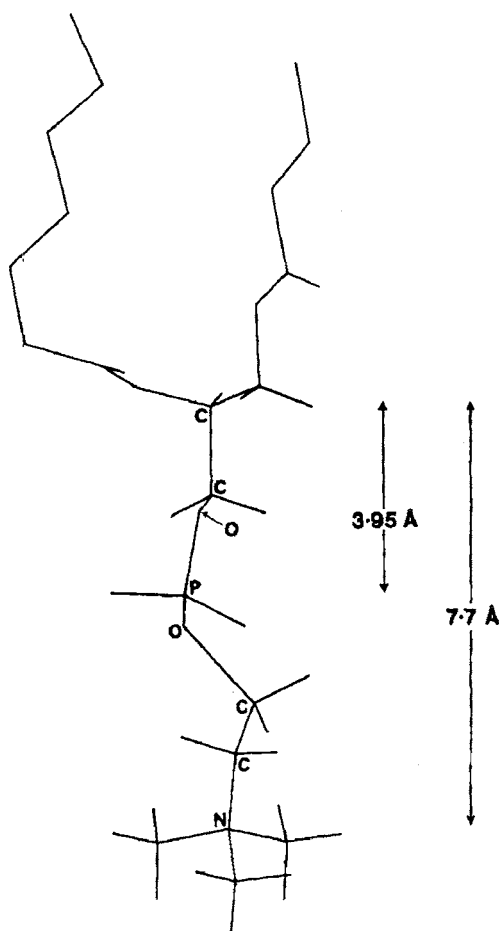


Fig. 10.47. The structure of the lipid in the vesicle as derived from Ln(III) shift and relaxation data.

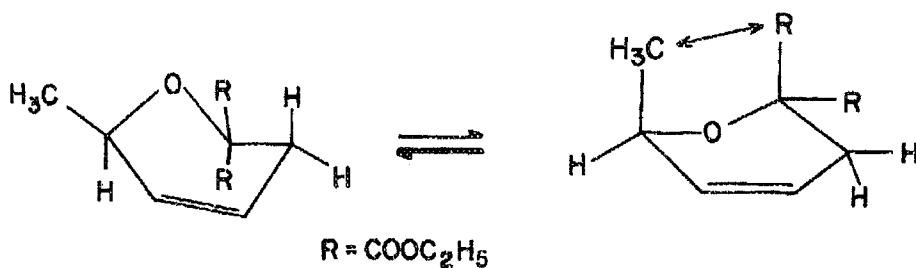
The program PGM 2, finds the ranges for the induced shifts if the lanthanide is allowed to move in a cube centred on a given position.

To illustrate the practical use of the three programs [143], a dihydropyran derivative, ethyl-2-methyl-5,6-dihydro- $\alpha$ -pyran-6,6-dicarboxylate has been chosen as an example. This unsaturated, sugar-related compound in solution exists in an equilibrium of two conformations.

The equilibrium is shown in Fig. 10.48.

SIMULATION program for induced shifts for DIAX (1 – HC) was used. Methyl group protons are represented by six rotamer positions, 6, 7, 8, 9, 10 and 11 (Scheme 10.4).

The induced shifts of six protons 1 to 6 as a result of calculation by the program are as follows.



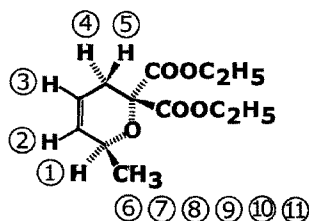
HC - I

I - HC

DIEQ

DIAX

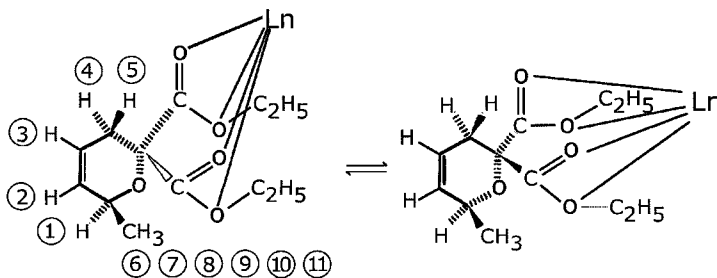
Fig. 10.48. Conformations of ethyl 2-methyl-5,6-dihydro- $\alpha$ -pyran-6,6-dicarboxylate.



Scheme 10.4.

Proton	Induced shift
1	4.15360
2	3.43982
3	4.02928
4	7.63056
5	10.00000
6	5.53857

Simulation of induced shifts for different equilibria between DIEQ (HC - I) and DIAX (I - HC) by PGM 1 was done considering the equilibrium



The data on relative induced shifts using PGM1 program are as follows.

Molar fraction (first form)	Relative induced shifts					
	1	2	3	4	5	ME
0.00	10.00	8.28	9.70	18.37	24.08	13.33
0.10	10.00	7.81	9.16	17.91	22.23	11.99
0.20	10.00	7.38	8.67	17.49	20.58	10.78
0.30	10.00	6.99	8.24	17.12	19.08	9.69
0.40	10.00	6.65	7.84	16.78	17.73	8.70
0.50	10.00	6.33	7.48	16.47	16.50	7.81
0.60	10.00	6.04	7.15	16.19	15.38	6.99
0.70	10.00	5.77	6.85	15.93	14.34	6.23
0.80	10.00	5.53	6.57	15.69	13.39	5.54
0.90	10.00	5.30	6.31	15.47	12.51	4.90
1.00	10.00	5.09	6.07	15.27	11.70	4.30

Ranges for the induced shifts when the lanthanide moves in a cube as calculated by program PGM 2 are as follows.

Proton	Minimum	Induced shift	Maximum
1	6.4027	6.5498	6.6719
2	3.2805	3.3342	3.3806
3	3.9343	3.9763	4.0167
4	10.0000	10.0000	10.0000
5	7.6125	7.6627	7.7243
6	2.7412	2.8169	2.8842

## References

- [1] N. Bloembergen, E.M. Purcell, R.V. Pound, *Phys. Revs.* **73**, 679, 1948.
- [2] C.C. Hinckley, *J. Am. Chem. Soc.* **91**, 5160, 1969.
- [3] J.A. Peters, A.P.G. Kieboom, *Recl. Trav. Chim. Pays-Bas* **102**, 381, 1983.
- [4] G.R. Sullivan, in: *Topics in Stereochemistry*, eds E.I. Eliel, N.L. Allinger, J. Wiley, Vol. 10, pp. 287–329, NY, 1978.
- [5] T.J. Wenzel, in: *Lanthanide Shift Reagents in Stereochemical Analysis*, eds T.C. Morrill, Vol. 5, pp. 151–173, V.C.H. Publishers, Inc., New York, 1986.
- [6] C.D. Barry, J.A. Glasel, A.C.T. North, R.J.P. Williams, A.V. Xavier, *Nature* **232**, 236, 1971.
- [7] A. Habenschuss, F.H. Spedding, *J. Chem. Phys.* **44**, 73, 1980.
- [8] R.E. London, A.D. Sherry, *Biochemistry* **17**, 3662, 1978.
- [9] C.M. Dobson, R.J.P. Williams, A.V. Xavier, *J. Chem. Soc., Dalton* 2662, 1972.
- [10] G.A. Elgavish, J. Reuben, *J. Am. Chem. Soc.* **98**, 4755, 1976.
- [11] C.F.G.C. Geraldes, R.J.P. Williams, *Eur. J. Biochem.* **97**, 93, 1979.
- [12] A.D. Sherry, C.A. Stark, J.R. Ascenso, C.F.G.C. Geraldes, *J. Chem. Soc., Dalton* 2078, 1981.
- [13] C.C. Bryden, C.N. Reilley, J.F. Desreux, *Anal. Chem.* **53**, 1418, 1981.

- [14] C.F.G.C. Gerald, M. Singh, A.D. Sherry, *J. Less Common Metals* **112**, 255, 1985.
- [15] R.M. Golding, M.P. Halton, *Aust. J. Chem.* **25**, 2577, 1972.
- [16] J. Reuben, D. Fiat, *J. Chem. Phys.* **51**, 4909, 1969.
- [17] J. Reuben, D. Fiat, *J. Chem. Phys.* **47**, 5440, 1967.
- [18] B. Bleaney, *J. Mag. Res.* **8**, 91, 1972.
- [19] C.N. Reilley, B.W. Good, J. Desreux, *Anal. Chem.* **47**, 2110, 1975.
- [20] A.A. Chalmers, K.G.R. Pachler, *J.C.S. Perkins II*, 748, 1974.
- [21] R.M. Golding, P. Pykko, *Mol. Phys.* **26**, 1389, 1973.
- [22] G.A. Elgavish, J. Reuben, *J. Mag. Res.* **16**, 360, 1974.
- [23] J.F. Desreux, C.N. Reilley, *J. Am. Chem. Soc.* **98**, 2105, 1976.
- [24] T.D. Marinetti, G.H. Snyder, B.D. Sykes, *J. Am. Chem. Soc.* **97**, 6562, 1975.
- [25] J.M. Briggs, G.P. Moss, E.W. Randall, K.D. Sales, *J.C.S. Chem. Comm.* 1180, 1972.
- [26] W. Dew Horrocks, Jr., *J. Am. Chem. Soc.* **96**, 3022, 1974.
- [27] J. Reuben, J. Fiat, *J. Chem. Phys.* **51**, 4918, 1969.
- [28] J. Reuben, G.A. Elgavish, in: *Handbook on physics and chemistry of Rare Earths*, eds K.A. Gscheidner, L. Eyring, North-Holland Publishing Co., 1979.
- [29] J. Reuben, *J. Chem. Phys.* **63**, 5063, 1975.
- [30] J. Reuben, *J. Am. Chem. Soc.* **98**, 3726, 1976.
- [31] R.E. Lenkinski, J. Reuben, *J. Mag. Res.* **21**, 47, 1976.
- [32] D.F. Evans, M. Wyatt, *J.C.S. Dalton* 765, 1974.
- [33] G.A. Cattin, F.A. Hart, G.P. Moss, *J.C.S. Dalton* 208, 1976.
- [34] G.A. Elgavish, J. Reuben, *J. Am. Chem. Soc.* **98**, 4755, 1976.
- [35] K.L. Servis, J. Bowler, *J. Am. Chem. Soc.* **95**, 3392, 1973.
- [36] R.E. Rondeau, R.E. Sievers, *J. Am. Chem. Soc.* **93**, 1522, 1971.
- [37] P.V. Demarco, T.K. Elzey, R.B. Lewis, E. Wenkert, *J. Am. Chem. Soc.* **92**, 5737, 1970.
- [38] P.V. Demarco, T.K. Elzey, R.B. Lewis, E. Wenkert, *J. Am. Chem. Soc.* **92**, 5734, 1970.
- [39] P. Serve, R.E. Rondeau, H.M. Rosenberg, *J. Heterocycl. Chem.* **9**, 721, 1972.
- [40] H.M. McConnell, R.E. Robertson, *J. Chem. Phys.* **29**, 1361, 1958.
- [41] J.W. Paschal, P.W. Rabideau, *J. Am. Chem. Soc.* **96**, 272, 1974.
- [42] M.R. Willcott, R.E. Lenkinski, R.E. Davis, *J. Am. Chem. Soc.* **94**, 1742, 1972.
- [43] R.E. Davis, M.R. Willcott, *ibid.* **94**, 1744, 1972.
- [44] M.R. Willcott, R.E. Davis, R.W. Holder, *J. Org. Chem.* **40**, 1952, 1975.
- [45] R.M. Wing, T.A. Early, J.J. Uebel, *Tetrahedron Lett.* 4153, 1972.
- [46] D.F. Evans, J.N. Tucker, G.C. Devillard, *Chem. Comm.* 205, 1975.
- [47] A.R. Katritzky, A. Smith, *Tetrahedron Lett.* 1765, 1971.
- [48] A.R. Katritzky, A. Smith, *Rubber J.* **154**, 30, 1972.
- [49] F.F.L. Ho, *J. Polym. Sci., Part B* **9**, 491, 1971.
- [50] K.A. Kime, R.E. Sievers, *Aldrichimica Acta* **10**, 55, 1977.
- [51] W.H. Pirkle, S.D. Beare, *J. Am. Chem. Soc.* **91**, 5150, 1969.
- [52] K. Mislou, M. Raban, *Top. Stereochem.* **1**, 7, 1967.
- [53] G.M. Whitesides, D.W. Lewis, *J. Am. Chem. Soc.* **92**, 6979, 1970.
- [54] H.L. Goering, J.N. Eikenberry, G.S. Koerner, *J. Am. Chem. Soc.* **93**, 5313, 1971.
- [55] K. Ajisaka, M. Kamisaku, M. Kainosho, *Chem. Lett.* 857, 1972.
- [56] H.L. Goering, J.N. Eikenberry, G.S. Koerner, C.J. Lattimer, *J. Am. Chem. Soc.* **96**, 1493, 1974.
- [57] D. Parker, *Chem. Rev.* **91**, 1441, 1991.
- [58] H.Y. Aboul-Enein, *Analytical Letters* **21**, 2155, 1988.
- [59] J. Knabe, V. Gradmann, *Arch. Pharmacol.* **310**, 468, 1977.
- [60] J.A. Kroll, *J. Forensic Sci.* **24**, 303, 1979.
- [61] R.V. Smith, P.W. Erhardt, D.B. Rusterholz, C.F. Barfknecht, *J. Pharm. Sci.* **65**, 412, 1976.
- [62] I.W. Wainer, M.A. Tischler, E.B. Shencin, *J. Pharm. Sci.* **69**, 459, 1980.
- [63] F.I. Carroll, A. Philip, D.M. Naylor, H.D. Christensen, W.C. Goad, *J. Med. Chem.* **24**, 1241, 1981.
- [64] J.H. Liu, S. Ramesh, J.T. Tsay, W.W. Ku, M.P. Fitzgerald, S.A. Angelos, C.L.K. Lins, *J. Forensic Sci.* **26**, 656, 1981.
- [65] J.H. Liu, J.T. Tsay, *Analyst* **107**, 544, 1982.
- [66] I.W. Wainer, L.C. Schneider, J.D. Weber, *J. Assoc. Off. Anal. Chem.* **64**, 848, 1981.
- [67] S. Eberhart, R. Rothchild, *Appl. Spectroscopy* **37**, 292, 1983.
- [68] J. Avolio, R. Rothchild, *J. Pharm. Biomed. Anal.* **2**, 403, 1984.
- [69] R. Rothchild, P. Sinons, *Spectrochimica Acta* **40A**, 881, 1984.



- [70] J. Avolio, R. Rothchild, *J. Mag. Reson.* **58**, 328, 1984.
- [71] J. Avolio, R. Rothchild, *Appl. Spectrosc.* **38**, 734, 1984.
- [72] S. Eberhart, R. Rothchild, *Appl. Spectrosc.* **38**, 74, 1984.
- [73] J. Avolio, R. Rothchild, *Appl. Spectrosc.* **39**, 604, 1985.
- [74] A. Hatzis, R. Rothchild, *Spectroscopy Letters* **19**, 617, 1986.
- [75] A. Hatzis, R. Rothchild, *Appl. Spectrosc.* **40**, 743, 1986.
- [76] A. Hatzis, R. Rothchild, *J. Pharm. Biomed. Anal.* **4**, 451, 1986.
- [77] A. Hatzis, R. Rothchild, *J. Pharm. Biomed. Anal.* **4**, 443, 1986.
- [78] J. Avolio, S.T. Eberhart, R. Rothchild, P. Simons, *Appl. Spectrosc.* **40**, 531, 1986.
- [79] S.T. Eberhart, A. Hatzis, J. Jimenez, R. Rothchild, P. Simons, *J. Pharm. Biomed. Anal.* **5**, 233, 1987.
- [80] A. Hatzis, R. Rothchild, *J. Pharm. Biomed. Anal.* **5**, 119, 1987.
- [81] R. Martin, C. Myers, R. Rothchild, *Spectroscopy Letters* **20**, 645, 1987.
- [82] A. Hatzis, R. Rothchild, P. Simons, *Anal. Chim. Acta* **194**, 211, 1987.
- [83] W.C. Myers, R. Rothchild, *Spectroscopy Letters*, in press.
- [84] C. Myers, R. Rothchild, *Spectroscopy Letters* **20**, 945, 1987.
- [85] N. Buyuktimkin, W. Schunack, *Arch. Pharm. (Weinheim, Ger.)* **316**, 1042, 1983.
- [86] A.F. Cockerill, G.L.O. Davies, R.G. Harrison, D.M. Rackham, *Org. Magn. Reson.* **6**, 669, 1974.
- [87] S.M. Browner, A.F. Cockerill, R.J. Maidment, D.M. Rackham, G.F. Snook, *J. Pharm. Sci.* **65**, 1305, 1976.
- [88] G.H. Dewar, J.K. Kwakye, R.T. Parfitt, R. Sibson, *J. Pharm. Sci.* **71**, 802, 1982.
- [89] L.F. Lindoy, *Coord. Chem. Rev.* **48**, 83, 1983.
- [90] S.J. Anderson, A.H. Newbury, *J. Chem. Soc. Chem. Commun.* **48**, 1975.
- [91] J.D. Lydon, R.C. Elder, E. Deutsch, *Inorg. Chem.* **21**, 3186, 1982.
- [92] L.F. Lindoy, W.E. Moody, *J. Am. Chem. Soc.* **99**, 5863, 1977.
- [93] T.Y. Lee, D.A. Hanna, G.W. Everett, *Inorg. Chem.* **20**, 2004, 1981.
- [94] T.C. Morrill, R.A. Clark, D. Bilobran, D.S. Young, *Tetrahedron Lett.* **397**, 1975.
- [95] A.R. Hendrickson, J.M. Hope, R.L. Martin, *J. Chem. Soc., Dalton Trans.* **2032**, 1976.
- [96] J.K. Beattie, L.F. Lindoy, W.E. Moody, *Inorg. Chem.* **15**, 3170, 1976.
- [97] L.F. Lindoy, H.W. Louie, *Inorg. Chem.* **20**, 4186, 1981.
- [98] L.F. Lindoy, H.W. Louie, *J. Am. Chem. Soc.* **101**, 841, 1979.
- [99] D.P. Graddon, L. Muir, L.F. Lindoy, H.W. Louie, *J. Chem. Soc., Dalton Trans.* **2596**, 1981.
- [100] J.C. Morrow, E.B. Parker, *Acta Crystallogr. Sect. B* **29**, 1145, 1973.
- [101] C.R. Jones, D.R. Kearns, *Proc. Natl. Acad. Sci. USA* **71**, 4237, 1974.
- [102] C.F.G.C. Geraldès, *Methods in Enzymology*, Vol. 227, p. 43, Academic Press, NY, 1993.
- [103] D. Sherry, C.F.G.C. Geraldès, in: *Lanthanide Probes in Life, Chemical and Earth Sciences*, eds J.C.G. Bunzli, G.R. Choppin, p. 93, Elsevier, 1989.
- [104] P. Tanswell, E.W. Westhead, R.J.P. Williams, *FEBS Letters* **48**, 61, 1974.
- [105] R.B. Martin, F.S. Richardson, *Q. Revs. Biophys.* **12**, 181, 1979.
- [106] K.G. Morallee, E. Niebor, F.J.C. Rossotti, R.J.P. Williams, A.V. Xavier, *Chem. Commun.* **1132**, 1970.
- [107] I.D. Campbell, C.M. Dobson, R.J.P. Williams, A.V. Xavier, *Ann. NY Acad. Sci.* **222**, 163, 1973.
- [108] I.D. Campbell, C.M. Dobson, R.J.P. Williams, *Proc. Roy. Soc. London A* **345**, 41, 1975.
- [109] R.D. Banks, C.C.F. Blake, P.R. Evans, R. Haser, D.W. Rice, G.W. Handy, M. Merrett, A.W. Philips, *Nature* **279**, 773, 1979.
- [110] H.C. Watson, N.P.C. Walter, *EMBO J.* **1**, 1635, 1982.
- [111] P. Tanswell, E.W. Westhead, R.J.P. Williams, *Eur. J. Biochem.* **63**, 249, 1976.
- [112] H.R. Wilson, R.J.P. Williams, J.A. Littlechild, H.C. Watson, *Eur. J. Biochem.* **170**, 529, 1988.
- [113] L. Lee, D.D. Sykes, *Biochemistry* **20**, 1156, 1981.
- [114] L. Lee, D.D. Sykes, *Biochemistry* **22**, 4366, 1983.
- [115] D.M. Gray, A.D. Sherry, J. Teherani, J.W. Kansy, *J. Biomol. Struct. Dynam.* **2**, 77, 1984.
- [116] R.J.P. Williams, *Structure and Bonding* **50**, 81, 1982.
- [117] L.R. Dick, C.F.G.C. Geraldès, A.D. Sherry, C.M. Gray, D.M. Gray, *Biochemistry* **28**, 7896, 1989.
- [118] A.D. Sherry, C.F.G.C. Geraldès, W.P. Cacheris, *Inorg. Chim. Acta* **139**, 137, 1987.
- [119] C.S. Springer, *Ann. NY Acad. Sci.* **508**, 130, 1987.

- [120] P.S. Belton, R.G. Ratcliff, *Prog. Nucl. Magn. Reson. Spectrosc.* **17**, 241, 1985.
- [121] R.K. Gupta, P. Gupta, *J. Magn. Reson.* **47**, 344, 1982.
- [122] M.M. Pike, C.S. Springer, *J. Magn. Reson.* **46**, 348, 1981.
- [123] S.C. Chu, M.M. Pike, E.T. Fossel, T.W. Smith, J.A. Balschi, C.S. Springer, *J. Magn. Reson.* **56**, 33, 1983.
- [124] M.S. Nieu Wenhuizen, J.A. Peters, A.P.G. Kieboom, H. Van Bekkam, *J. Am. Chem. Soc.* **107**, 12, 1985.
- [125] C.S. Springer, *Ann. Rev. Biophys. Chem.* **16**, 375, 1987.
- [126] N.A. Matwiyoff, C. Gasprovic, R. Wenk, J.D. Wicks, A. Rath, *Magn. Reson. Med.* **3**, 164, 1986.
- [127] M.M. Pike, J.C. Frazer, D.F. Dedrick, J.S. Ingwall, P.D. Allen, C.S. Springer, T.W. Smith, *Biophys. J.* **48**, 159, 1985.
- [128] C.S. Springer, in: *NMR Techniques in the Study of Cardiovascular Structure and Function*, eds M. Osbakken, J. Haselgrove, p. 289, Futura Publ. co., Mount Kisco, NY, 1989.
- [129] A.D. Sherry, C.R. Malloy, F.M.H. Jeffray, W. Cacheris, C.F.G.C. Geraldès, *J. Magn. Reson.* **76**, 528, 1988.
- [130] H. Hauser, M.C. Phillips, B.A. Levine, R.J.P. Williams, *Nature* **261**, 390, 1976.
- [131] M.F. Brown, J. Seelig, *Nature* **269**, 721, 1977.
- [132] G. Buidt, J. Seelig, *Nature* **271**, 182, 1978.
- [133] H. Hauser, B.A. Levine, R.J.P. Williams, *Biochim. Biophys. Acta* **508**, 450, 1978.
- [134] J. Westman, L.E.G. Eriksson, *Biochim. Biophys. Acta* **557**, 62, 1979.
- [135] V.F. Bystrov, N.I. Dubrovina, L.T. Bavsukov, L.D. Bergelson, *Chem. Phys. Lipids* **6**, 343, 1971.
- [136] G.E. Hawkes, D. Leibfritz, D.W. Roberts, J.D. Roberts, *J. Am. Chem. Soc.* **95**, 1659, 1973.
- [137] J.D. Roberts, G.E. Hawkes, J. Husar, A.W. Robert, D.W. Roberts, *Tetrahedron* **30**, 1833, 1974.
- [138] M.R. Willcott III, R.E. Lenkinski, R.E. Davis, *J. Am. Chem. Soc.* **94**, 1742, 1972.
- [139] I. Kordova, A.F. Fomichev, V.P. Zvolinski, *Zh. Struct. Khim.* **22**, 27, 1971.
- [140] G.R. Sullivan, *J. Am. Chem. Soc.* **98**, 7162, 1976.
- [141] A.J. Rafaiski, J. Barciszewski, M. Karonski, *J. Mol. Struct.* **19**, 223, 1973.
- [142] J.W. Apsimon, H. Beierbeck, *Tetrahedron Lett.* 581, 1973.
- [143] J.B. Chiasson, K. Jankowski, in: *Lanthanide Shift Reagents in Stereochemical Analysis*, ed. Morrill, VCH Publishers, 1986.
- [144] V. Schurig, *Kontakte (Darmstadt)* **2**, 22, 1985.
- [145] J. Passivirta, in: *Lanthanide Shift Reagents in Stereochemical Analysis*, ed. Morrill, p. 107, VCH Publishers, 1986.
- [146] D.J. Raber, in: *Lanthanide Shift Reagents in Stereochemical Analysis*, ed. Morrill, pp. 55-105, VCH Publishers, 1986.
- [147] F. Inagaki, T. Miyazawa, *Progress in NMR Spectroscopy* **14**, 67-111, 1981.

## chapter 11

---

# ENVIRONMENTAL, ECOLOGICAL, BIOLOGICAL ASPECTS

---

---

# CONTENTS

---

1. Introduction . . . . .	847
2. Techniques used in probing biochemical reactions . . . . .	850
3. Absorption spectra . . . . .	850
4. Fluorescence . . . . .	852
5. Circularly polarized luminescence (CPL) . . . . .	854
6. Nuclear relaxation methods . . . . .	855
7. Nuclear magnetic resonance (NMR) . . . . .	856
8. Gd(III) EPR as a probe . . . . .	857
9. Mössbauer spectroscopy . . . . .	857
10. X-ray diffraction . . . . .	858
11. Lanthanide interactions with proteins . . . . .	858
12. Nucleotides . . . . .	862
13. Nucleic acids . . . . .	864
14. Carbohydrates . . . . .	865
15. Other molecules . . . . .	866
16. Phospholipids and membranes . . . . .	866
17. Environmental behavior of lanthanides . . . . .	867
17.1. Weathering . . . . .	870
18. Rare earth distribution in soils . . . . .	872
19. Speciation of rare earth elements . . . . .	873
20. $E_h$ -pH diagrams . . . . .	878
21. Predominance diagrams . . . . .	879
22. Migration of lanthanides in environment . . . . .	883
23. Metabolism and toxicity of lanthanides . . . . .	883
23.1. Metabolism . . . . .	883
23.2. Toxicity . . . . .	884
23.3. Medical uses . . . . .	885
24. Ecological aspects . . . . .	886
24.1. Sedimentation and erosion . . . . .	887
24.2. Ant behaviour . . . . .	887
24.3. Sorption by aquatic insects . . . . .	887
24.4. Root sorption . . . . .	888
References . . . . .	888

## 1. Introduction

Intensive research into the studies of biochemical aspects of lanthanides began when it was recognized that due to the similarities in the ionic radii of  $\text{Ca}^{2+}$  and  $\text{La}^{3+}$ , lanthanum can be used in place of  $\text{Ca}^{2+}$  in some biological reactions. Some pertinent chemical properties of lanthanides, calcium and yttrium are noted in Table 11.1. Based on this similarity, sound theoretical principles of these aspects have been developed [3]. Lanthanides and calcium ions are similar in ionic radii as well as in their coordination behaviour and the mode of bonding. The properties of biochemical relevance are given in Table 11.2.

The similarities cited permit  $\text{Ln}^{3+}$  ions to take the place of  $\text{Ca}^{2+}$  ions in biological reactions. Many  $\text{Ca}^{2+}$  binding sites exclude competing  $\text{Mg}^{2+}$  although the former might be present at lower concentrations. This selectivity is due to the small ionic radius (0.72 Å) and coordination number of 6 (inflexible coordination geometry) and affinity for N atoms of  $\text{Mg}^{2+}$ . It has also been observed that  $\text{Ln}^{3+}$  ions can occupy  $\text{Mg}^{2+}$  sites in t-RNA and some  $\text{Mg}^{2+}$  requiring enzymes.  $\text{Ln}^{3+}$  ions can also substitute for  $\text{Fe}^{3+}$ ,  $\text{Fe}^{2+}$  and  $\text{Mn}^{2+}$  in some cases.

It is generally assumed that  $\text{Ca}^{2+}$  sites cannot be designed to exclude  $\text{Ln}^{3+}$  ions. There are a number of exceptions to this generality. Some examples are:  $\text{Ln}^{3+}$  ions cannot replace  $\text{Ca}^{2+}$  in scallop myosin [4], concanavalin A [5];  $\text{Ca}^{2+}$  ions cannot displace  $\text{Gd}^{3+}$  from  $\text{I}_g\text{G}$  [6]. Sometimes the reduced oxidation state of the Ln ion is useful. An example of this is the binding of  $\text{Eu}^{2+}$  to concanavalin A and restore biological activity to the apoprotein [7].

Steric factors and hydrophobicity are thought [8] to play a role in the substitution of  $\text{Ca}^{2+}$  ion by  $\text{Ln}^{3+}$  ions. The flexibilities of intracellular  $\text{Ca}^{2+}$  binding proteins are different from the rigid extra-cellular  $\text{Ca}^{2+}$  dependent enzymes in the sense that the  $\text{Ca}^{2+}$  ion sits in the rigid hole in the latter [9].

The effect of change in ionic radius in going from  $\text{La}^{3+}$  to  $\text{Lu}^{3+}$  showed in some cases no systematic trend. While in other cases two types of trend have been observed: (i) systematic increase from  $\text{La}^{3+}$  to  $\text{Lu}^{3+}$  for the activation of  $\alpha$ -amylase [10], (ii) decrease in effect from  $\text{La}^{3+}$  to  $\text{Lu}^{3+}$  in the case of inhibition of  $\text{Ca}^{2+}/\text{Mg}^{2+}$ -ATPase of skeletal muscle sarcoplasmic reticulum [11].

The above observations have been rationalized based on the decrease in free energy upon binding interaction. The three forms of energy involved are: (i) hydration energy, (ii) free energy of interaction between the  $\text{Ln}^{3+}$  ion and the negative site and (iii) the energy involved in possible deformations of the binding site necessary to achieve binding. Ignoring the last energy factor, binding sites with very low field strengths cannot overcome the hydration energy. Hence larger and more weakly hydrated  $\text{Ln}^{3+}$  will bind easily. With strong field site, small, strongly hydrated  $\text{Ln}^{3+}$  ions will bind easily. Consideration of the geometry of the binding site shows that under spatial restrictions, large ions

TABLE 11.1  
Some pertinent chemical properties of the lanthanides, calcium, and yttrium<sup>a</sup>.

Element	Symbol	Atomic number	Atomic weight	Outer electronic configuration													Ionic radius (Å)				$\sum I^a$ (eV)
				Atomic (Ln <sup>0</sup> )								Ionic (Ln <sup>3+</sup> )					CN6	CN7	CN8	CN9	
				4s	4p	4d	4f	5s	5p	5d	6s	4f	5s	5p							
Calcium	Ca	20	40	c													1.00	1.06	1.12	1.18	–
Lanthanum	La	57	139	2	6	10		2	6	1	2		2	6	1.03	1.10	1.16	1.22	36.2		
Cerium	Ce	58	140	2	6	10	2	2	6		2	1	2	6	1.01	1.07	1.14	1.20	36.4		
Praseodymium	Pr	59	141	2	6	10	3	2	6		2	2	2	6	0.99	–	1.13	1.18	37.55		
Neodymium	Nd	60	144	2	6	10	4	2	6		2	3	2	6	0.98	–	1.11	1.16	38.4		
Promethium	Pm	61	147	2	6	10	5	2	6		2	4	2	6	–	–	–	–	–		
Samarium	Sm	62	150	2	6	10	6	2	6		2	5	2	6	0.96	1.02	1.08	1.13	40.4		
Europium	Eu	63	152	2	6	10	7	2	6		2	6	2	6	0.95	1.01	1.07	1.12	41.8		
Gadolinium	Gd	64	157	2	6	10	7	2	6	1	2	7	2	6	0.94	1.00	1.05	1.11	38.8		
Terbium	Tb	65	159	2	6	10	9	2	6		2	8	2	6	0.92	0.98	1.04	1.10	39.3		
Dysprosium	Dy	66	162.5	2	6	10	10	2	6		2	9	2	6	0.91	0.97	1.03	1.08	40.4		
Holmium	Ho	67	165	2	6	10	11	2	6		2	10	2	6	0.90	–	1.02	1.07	40.8		
Erbium	Er	68	167	2	6	10	12	2	6		2	11	2	6	0.89	0.95	1.00	1.06	40.5		
Thulium	Tm	69	169	2	6	10	13	2	6		2	12	2	6	0.88	–	0.99	1.05	41.85		
Ytterbium	Yb	70	173	2	6	10	14	2	6		2	13	2	6	0.87	0.93	0.99	1.04	43.5		
Lutetium	Lu	71	175	2	6	10	14	2	6	1	2	14	2	6	0.86	–	0.98	1.03	40.4		
Yttrium	Y	39	89	2	6	1		2							0.90	0.96	1.02	1.08	–		

<sup>a</sup>From Faktor and Hanks [1]; ionic radii from Shannon [2].

<sup>b</sup> $\sum I$  = sum of the first three ionization potentials.

<sup>c</sup>Outer electronic configuration:  $3s^2 3p^6 3d^0 4s^2$ .

<sup>d</sup>Outer electronic configuration:  $4s^2 4p^6$ .

TABLE 11.2  
Salient properties of  $\text{Ca}^{2+}$  and  $\text{Ln}^{3+}$ .

Property	$\text{Ca}^{2+}$	$\text{Ln}^{3+}$
Coordination number	6–12 reported 6 or 7 favored	6–12 reported 8 or 9 favored
Coordination geometry	Highly flexible	Highly flexible
Donor atom preference	$0 \gg N \gg S$	$0 \gg N \gg S$
Ionic radius (Å)	1.00–1.18 (CN 6–9)	0.86–1.22 (CN 6–9), depending on species
Type of bonding	Ionic	Ionic
Hydration number	6	8 or 9
Water exchange rate constant ( $\text{s}^{-1}$ )	$\sim 5 \times 10^8$	$\sim 5 \times 10^7$
Diffusion coefficient ( $\text{cm}^2/\text{s} \times 10^5$ )	1.34	$\text{La}^{3+}$ , 1.30
Crystal-field stabilization	None	Negligible

TABLE 11.3

The lanthanides whose ionic radii equal or are closest to that of calcium at different coordination numbers<sup>a</sup>.

Coordination number of calcium	Coordination number of lanthanide			
	6	7	8	9
6	Ce–Pr	Sm–Eu	Er	<Lu <sup>b</sup>
7	>La <sup>c</sup>	Ce–Pr	Eu–Gd	Er
8	>La	>La	Pr–Nd	Eu
9	>La	>La	>La	Pr

<sup>a</sup>Based upon the ionic radii of Shannon (1976).

<sup>b</sup>>Lu:  $\text{Ca}^{2+}$  smaller than all  $\text{Ln}^{3+}$  at these coordination numbers.

<sup>c</sup>>La:  $\text{Ca}^{2+}$  bigger than all  $\text{Ln}^{3+}$  at these coordination numbers.

would be sterically hindered and small ions cannot coordinate to all ligands in the binding site. Thus maximum binding can occur with the  $\text{Ln}^{3+}$  ion of optimum ionic radius. The data on lanthanides with optimum ionic radius to that of  $\text{Ca}^{2+}$  are given in Table 11.3.

The interpretation based on the ionic radii of the ions must be done taking into account the limitations such as the radii given are crystal radii which differ from those of solvated ions in solutions. The variation of flexible coordination geometries of the ions results in adjustment of the radii according to the binding site. By increasing the coordination number, the smaller lanthanide ions expand their radii and approach the value of  $\text{Ca}^{2+}$  ion. As the CN increases from 6 to 9, the lanthanide ion whose radius is close to that of  $\text{Ca}^{2+}$  ion changes. Under conditions designated as >La, the  $\text{Ca}^{2+}$  ion is bigger than all the  $\text{Ln}^{3+}$  ions (i.e.) six coordinate  $\text{Ca}^{2+}$  ions are smaller than nine coordinated  $\text{Ln}^{3+}$  ions. In general, the  $\text{Ca}^{2+}$  has a CN of 6 or 7 while  $\text{Ln}^{3+}$  ions have a CN of 8 or 9. Thus the ionic radii of  $\text{Ln}^{3+}$  ions span a range which includes  $\text{Ca}^{2+}$  ions.

Some differences between  $\text{Ca}^{2+}$  ions and  $\text{Ln}^{3+}$  are noted below.

	$\text{Ca}^{2+}$ ions	$\text{Ln}^{3+}$ ions
1	No absorption spectra	Absorption spectra
2	No colour	Coloured ions
3	Diamagnetic	Paramagnetic
4	Non-luminescent	Luminescent
5	Stable complexes	Complexes more stable than those of $\text{Ca}^{2+}$
6	Small charge/size ratio	High charge/size ratio
7	CN = 6	CN = 8, 9, >9

The differences cited above between  $\text{Ca}^{2+}$  and  $\text{Ln}^{3+}$  does not preclude the substitution of the  $\text{Ca}^{2+}$  ion by  $\text{Ln}^{3+}$  in biologically important molecules. The greater stability of  $\text{Ln}^{3+}$  complexes is illustrated [13] by Fig. 11.1.

It is obvious from the figure that lanthanide complexes in general are more stable than the corresponding calcium complexes which is in keeping with the higher ionic potential of lanthanides, and greater coordination numbers. In the range of concentration of 1 mM to 1 nM there is a linear correlation, with the  $\text{Ln}^{3+}$  binding is greater by a factor of  $10^4$  to  $10^5$ . For denticities greater than 6, the  $\text{Ln}^{3+}$  complexes are more stable than  $\text{Ca}^{2+}$  with an opposite trend,  $\text{Ca}^{2+} > \text{Ln}^{3+}$  for weak complexes. Another difference between  $\text{Ln}^{3+}$  and  $\text{Ca}^{2+}$  ions is that the ligand exchange rate (for or water) of  $\text{Ca}^{2+}$  ions is higher than  $\text{Ln}^{3+}$  ions.

It is useful to note that lanthanides act as catalysts in some biochemical reactions like (i) depolymerization of RNA [14], (ii) cleavage of yeast tRNA [15], (iii) cleavage of phosphate group [14] from ATP in presence of  $\text{Ce}^{3+}$ , (iv) increase in amide proton exchange in aspartyl-phenylalanine [16].

## 2. Techniques used in probing biochemical reactions

It is useful to recognize that only trace amounts of lanthanides are present in living organisms. Lanthanides do not partake in any metabolic process. The interest in lanthanides in probing biochemical reactions arises because they can be used as probes to unravel the interactions between  $\text{Ca}^{2+}$  and biologically important molecules. As pointed out earlier the absorption spectra, paramagnetism and luminescence of lanthanides can be profitably used in probing the interactions of  $\text{Ca}^{2+}$  with biological molecules.

## 3. Absorption spectra

As noted in Chapter 8 the absorption spectra of lanthanides are characterized by sharp but complicated absorption spectra of low intensity. It is also to be noted that the spectral features are generally not sensitive to the surrounding environment, at least not as much as the transition metals. That is, the f orbitals are well shielded from the environment.

However, the hypersensitive transitions of some lanthanides may be used with some success in probing the metal-biological molecules' interactions as pointed out in Chapter 8.  $\text{Nd}^{3+}$  is particularly suited for such studies with spectral lines in the region 500–600 nm



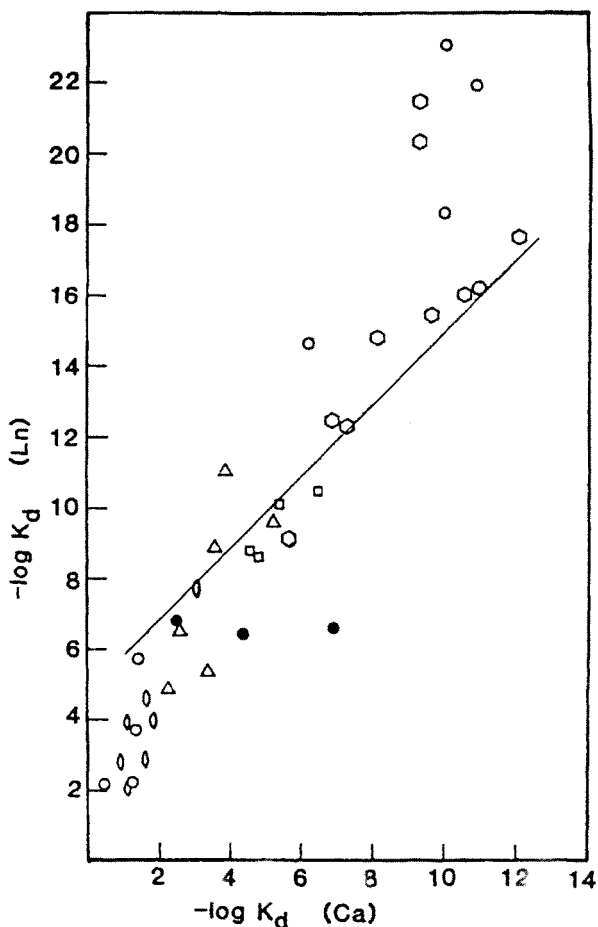


Fig. 11.1. Comparison of the affinities of lanthanide ions for a variety of ligands. Ligand densities: (O) 1; (◊) 2; (Δ) 3; (◻) 4; (○) 6; (●) cryptate ligands [13].

associated with the  $^4I_{9/2} \rightarrow ^4G_{5/2}, ^2G_{7/2}$  transitions. These transitions are sensitive to formation of complexes. There are many studies involving lanthanides and molecules of biological significance [17–19]. Typical difference spectra with EDTA and trypsin as ligands are given in Fig. 11.2.

Although the spectra are alike, the spectral intensity depends upon pH indicating the extent of the bound  $Nd^{3+}$  ion, and this may be useful in the determination of  $pK$ 's of the protein ligands at the binding site [18].

The lanthanides modify the UV absorption spectra of proteins when aromatic chromophores are present at the binding site. Sharp maxima at 245 and 295 nm in the difference spectrum of transferrin saturated with  $Tb^{3+}$  ion as opposed to that of metal free protein were observed [20]. The shape of the spectrum is suggestive of lanthanide induced

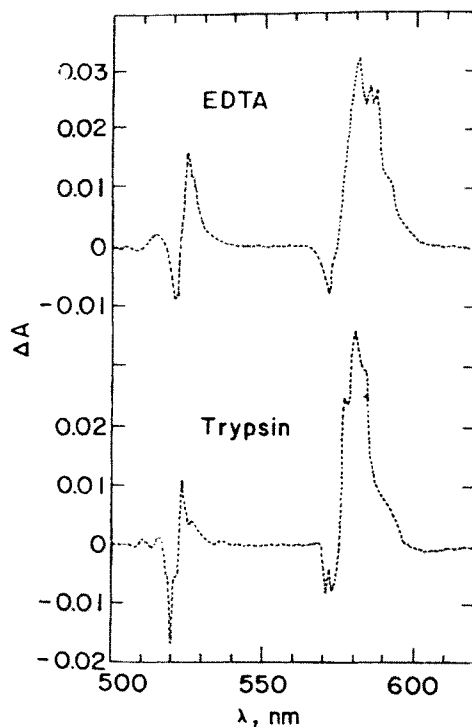


Fig. 11.2. Neodymium(III) difference absorption spectra with EDTA and with trypsin at pH 5.6. Reconstructed from Darnall et al. (1971). Concentrations:  $\text{Nd}^{3+}$  3.74 mM, EDTA 87.5 mM;  $\text{Nd}^{3+}$  26 mM, trypsin 0.37 mM.

modification of the local environment of tyrosine residues. Some other similar studies have been done on lacto-ferrin [21].

#### 4. Fluorescence

Many lanthanides in the form of complexes emit fluorescence when excited with light absorbed by ligands. Lanthanide ions in crystals or in solution also exhibit fluorescence. The fluorescence observed due to energy transfer from the triplet state of the ligand to excited state of  $\text{Ln}^{3+}$  is known as enhanced fluorescence. The fluorescence emission spectra of  $\text{Tb}^{3+}$  aquo ion in the absence and presence of porcine trypsin at pH 6.3 is shown in Fig. 11.3.

The considerable enhancement in fluorescence emission is evident. The transition involved is  $^5\text{D}_4 \rightarrow ^7\text{F}_5$  transition. The enhancement of fluorescence also depends on the excitation wavelength. From the value of the excitation wavelength,  $\lambda_{\text{exc}}$  giving rise to the maximum emission enhancement, the residue involved in the energy transfer can be usually identified.

The fluorescence enhancement can be profitably used in quantifying of  $\text{Tb}^{3+}$  ion bound to macromolecules. The displacement of bound  $\text{Tb}^{3+}$  by other cations for the same site

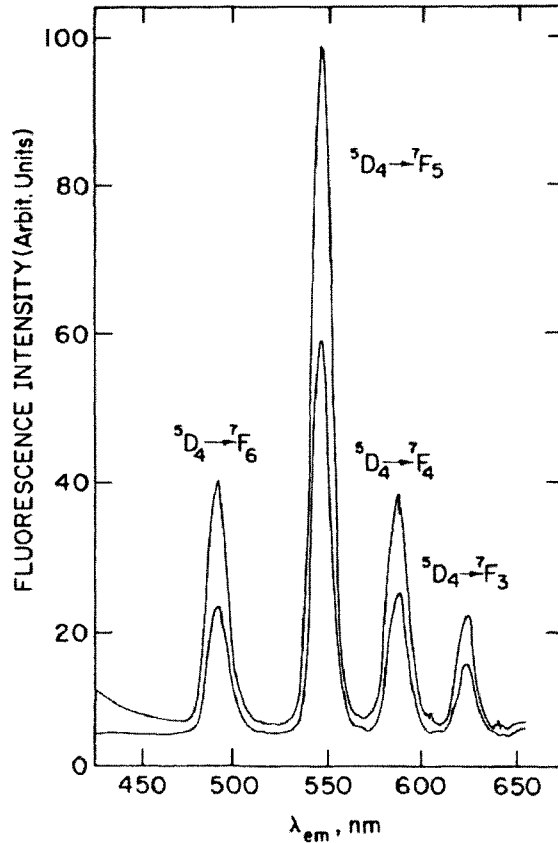


Fig. 11.3. Fluorescence emission spectra with  $\lambda_{ex} = 265$  nm of 0.1 M  $TbCl_3$  in the presence (upper curve) and the absence (lower curve) of  $1.25 \times 10^{-5}$  M porcine trypsin at pH 6.3 [22].

results in quenching of the fluorescence, and the amount of quenching can be used to monitor the binding of the competing cations



The biological macromolecule has inherent fluorescence which is quenched upon binding to the  $Ln^{3+}$  ion. For example the fluorescence of porcine trypsin is quenched by 21% upon binding to  $Tb^{3+}$  ion, while  $Ca^{2+}$  does not give rise to quenching. The extent of quenching of the fluorescence of the macromolecule can be useful in identifying the residues involved in energy transfer from high lying triplet of the residue to low-lying  $Ln^{3+}$  excited state. The fluorescence spectral data for macromolecular complexes [30] of  $Tb^{3+}$  ion are given in Table 11.4.

TABLE 11.4  
Abilities of various proteins to enhance the luminescence of  $Tb^{3+}$  a,b.

Protein	Equiv. of $Tb^{3+}$	Excitation	TE <sup>c,d</sup>	CPE <sup>d,e</sup>
Parvalbumin, carp	1	Phe	s	m
Troponin C, rabbit skeletal	1	Tyr	s	m
Troponin C, bovine cardiac	1	Tyr	s	m
Trypsinogen	1	Trp	m	n
Trypsin	1	Trp	m	n
Chymotrypsinogen	1	Trp	m	n
$\alpha$ -chymotrypsin	1	Trp	m	n
$\delta$ -chymotrypsin		Trp	m	n
Subtilisin Carlsberg	1	Tyr	m	n
Subtilisin BPN	2	Tyr	m	n
Pronase		Trp	s	w
Elastase, porcine	1	Trp	vs	s
Collagenase, bacterial	~20	Tyr + Trp	s	s
Prothrombin, bovine	11	Trp + Tyr	s	n
Prothrombin, fragment I	7	Trp	m	n
S-100, calf brain	2	Trp	w	n
Phospholipase A, porcine	1	Tyr	m	n
Phospholipase A, porcine and equine	1	Tyr	m	n
Phospholipase A rattlesbake	1	Tyr	m	n
Phospholipase A, honeybee	1	Trp	m	n
Vitamin D Ca-binding protein, porcine	1	Tyr	m	n
$\alpha$ -amylase, bacterial	2	Trp	s	m
$\alpha$ -amylase, porcine	2	Trp	s	w
Lysozyme, hen egg	1	Trp	w	n
Lactalbumin, bovine	1	Trp	w	n
Deoxyribonuclease, bovine	2	Trp + Tyr	s	n
Pyruvate kinase, rabbit	4	Trp	w	n
Creatine phosphokinase, rabbit		Trp	w	n
Pyrophosphatase, yeast	2	Trp	w	n
$Ca^{2+}$ -ATPase, rabbit	2	Trp	m	n
Thermolysin	1	Trp	s	w
Concanavalin A		Trp	m	n

<sup>a</sup>From Brittain et al. (1976), with permission.

<sup>b</sup> $\beta$ -amylase phosphitin, thrombin, rabbit myosin light chains, soybean trypsin inhibitor, and chicken ovomucoid trypsin inhibitor were inactive.

<sup>c</sup>TE: terbium emission.

<sup>d</sup>vs, very strong; s, strong; m, medium; w, weak; n, none.

<sup>e</sup>CPE: circularly polarized emission.

## 5. Circularly polarized luminescence (CPL)

The J sublevels of rare earths are split by ligand fields of low symmetry. These splittings may be observed in circularly polarized luminescence (CPL) but not in the fluorescence spectrum. Hence CPL spectra provide information on the rare earth ion and thus throw light on the binding site. The emission and CPL spectra of  $Tb^{3+}$  bound to transferrin and cobalbumin were found to be similar leading to the conclusion that the structure and

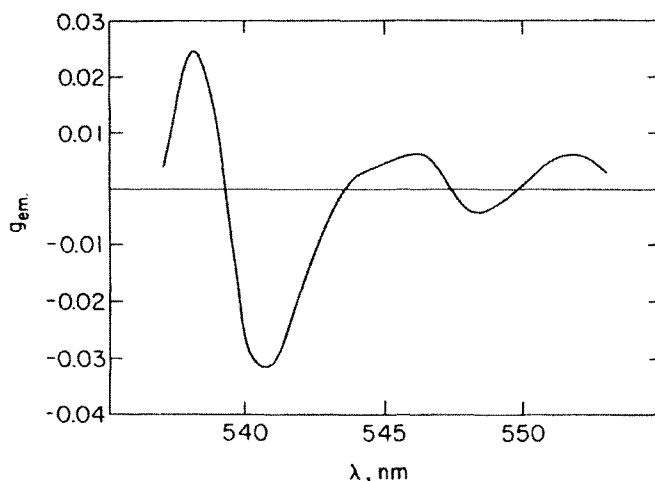
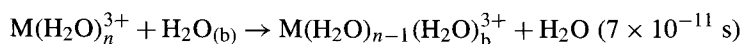


Fig. 11.4. Part of the circularly polarized luminescence spectrum of the  $\text{Tb}^{3+}$ -porcine trypsin complex showing the  $^5\text{D}_4 \rightarrow ^7\text{F}_5$  transition [22].

conformation of the metal ion binding site of the two proteins must be similar [23]. The detailed studies on the CPL spectra of  $\text{Eu}^{3+}$  and  $\text{Tb}^{3+}$  in carboxylic acid and amino acid complexes led to some interesting results [24]. The CPL was expressed in terms of an anisotropy factor,  $g_{\text{em}}$  which is defined as twice the ratio between the intensity of circularly polarized component of the luminescence and the total luminescence at the same wavelength. The CPL spectrum of  $\text{Tb}^{3+}$  ion bound to porcine trypsin shown in Fig. 11.4. clearly indicates splitting into three components of the transition  $^5\text{D}_4 \rightarrow ^7\text{F}_5$ . This method is the most sensitive in probing the interaction of  $\text{Ln}^{3+}$  with weak ligands [25,26].

## 6. Nuclear relaxation methods

Unpaired electrons in nuclei lead to paramagnetism and the large magnetic moments due to spin enhance the relaxation rates of nuclei in their vicinity through electron-nuclear hyperfine interaction. In this respect, ions with S states are particularly effective, because of long electron relaxation time. Among the rare earths, the prominent member is the  $\text{Gd}^{3+}$  ion which is involved in electron-dipolar interaction. The longitudinal relaxation rate of a nucleus due to electron-dipolar interaction,  $1/T_{1M}$  shows a  $1/r^6$  dependency, where  $r$  is the distance. Because of the  $1/r^6$  dependence, it is natural that nuclei in close proximity are affected to a high extent. In aqueous solution, free water molecules exchange with coordinated water of the metal ion, and one observes an average effect in the form of an increase in relaxation rate,



The increase in relaxation rate is given by

$$1/T_p = P_M/T_M$$

TABLE 11.5  
Water proton relaxation rate enhancement at 24.3 MHz for  $Gd^{3+}$ -protein complexes.

Ligand	$\epsilon_b$	Temp. ( $^{\circ}C$ )	Reference
Alk. phosphatase	5.9	25	[31]
$\alpha$ -amylase	3.4	25	[32]
Bovine serum albumin	5.9	35.7	[29]
Concanavalin A	7.1 <sup>a</sup>	24	[33]
Ig G (strong sites)	9.5 <sup>b</sup>	19	[34]
Inorg. pyrophosphatase	9.3	25	[35]
Lysozyme	11.0 <sup>c</sup>	24	[36]
Phospholipase A <sub>2</sub>	16.4	22	[37]
Prophospholipase A <sub>2</sub>	5.8	22	[37]
Pyruvate kinase	12.0	28	[38]
Pyruvate kinase-ATP	9.5	28	[38]
Trypsin	1.4	25	[39]

<sup>a</sup>At 35 MHz.

<sup>b</sup>At 20 MHz.

<sup>c</sup>At 48 MHz.

where  $P_M$  is the fractional population of the given nuclei in the vicinity of the ion. For water proton relaxation rates (PRR)

$$P_M = n[M]/55.5$$

where  $[M]$  is the molar concentration of metal ion of hydration number  $n$  and 55.5 is the molarity of water.

In the case of  $Gd^{3+}$ , there is a rapid water exchange with respect to the relaxation  $T_{1M}$  [28]. For water exchange reaction of  $Gd^{3+}$  aquo ion the water tumbling time is  $\sim 7 \times 10^{-11}$  s. When  $Gd^{3+}$  is bound to a macromolecule, part of the hydration sphere is substituted by a protein molecule, the effective correlation changes (i.e.) effectively it becomes the electron relaxation time [29] which is about  $10^{-9}$  s. By virtue of binding to a macromolecule, a net enhancement in proton relaxation rate,  $E_0$  is observed which is characteristic of the  $Gd^{3+}$  complex and depends on the resonance frequency and temperature. Some data on the enhancements obtained for  $Gd^{3+}$  protein complexes are given in Table 11.5.

The water PRR enhancement can be used to obtain the number of water molecules attached to the Gd-macromolecular complex which in turn gives information on the sites bound to the macromolecule.

## 7. Nuclear magnetic resonance (NMR)

Paramagnetic lanthanides induce chemical shifts in the NMR spectrum of the ligands in their vicinity. The origin of the shift is the dipolar interaction of the nuclear magnetic

moment and the anisotropic magnetic moment of the unpaired 4f electrons. The shift for complexes of axial symmetry is given by

$$\Delta_M = D(3 \cos^2 \theta - 1)/r^3$$

where  $D$  is a constant and depends on temperature characteristic of the lanthanide and complex,  $r$  is the distance between the nucleus and ion, and  $\theta$  is the angle between the vector  $r$  and the principal axis of symmetry. The induced shift is sensitive to molecular geometry. Lanthanides have been used as shift reagents in: (i) the determination of mononucleotide conformation in solution [40], (ii) studies of phospholipid bilayer vesicles [41], (iii) studies on t-RNA [42].

The  $^{139}\text{La}$  NMR has been used for obtaining relaxation rates at different frequencies and hence correlation times which have been applied to  $\text{La}^{3+}$ -bovine serum albumin [43].

## 8. Gd(III) EPR as a probe

The EPR linewidths of Gd(III) complexed with cacodylate buffer and bovine albumin serum have been obtained which were consistent with the action of Gd(III) as a paramagnetic relaxation probe with the same protein [44]. A host of inorganic and organic ligands including amino acids and nucleotides complexed with Gd(III) were studied and two types of peaks were observed (i.e.) narrow symmetric peaks and broad asymmetric peaks [45].

EPR provides a sensitive test for Gd(III)-biological buffer interactions [46]. The EPR spectral studies have proved to be useful in biological systems where Gd(III) substitutes for Ca(II) sites. Gd(III) EPR spectra of Gd(III) phospholipase A<sub>2</sub> complex were compared with those of aquo Gd(III) and Gd(III) bound to zymogen or pro-phospholipase A<sub>2</sub> [47]. The two metal protein complexes differ by a heptapeptide fragment. The line narrowing and its relative effect in the two complexes appears to be a reflection of the change in symmetry of the metal-binding site caused by the removal of a heptapeptide fragment.

Other studies using Gd(III) EPR probe involve Ca(II)AT Pase [48] and to characterize, Ca(II) binding site on  $\alpha$ -lactalbumin [49]. Gd(III) EPR probe has also been used as a probe for Fe(III) sites in human serum transferrin [50,51]. The data on Gd(III)-transferrin indicate a highly anisotropic site for Gd(III) in the complex, a conclusion reached by both the groups [50,51].

## 9. Mössbauer spectroscopy

Lanthanides have isotopes which may be used in this technique. The principle consists of measuring resonant  $\gamma$ -ray absorption as a function of relative velocity between the source and the sample. The spectral line shifts and splittings give information on the chemical nature and symmetry of the site of ion.  $\text{Eu}^{3+}$ -transferrin [53] and tumor metabolism studies [54] with  $^{153}\text{Sm}$  have not proved to be particularly informative.

TABLE 11.6  
Biological macromolecules studied by  
X-ray method using lanthanides.

Macromolecules	Reference
Thermolysin	[54,55]
Lysozyme	[56]
Concanavalin A	[57]
Ferredoxin	[58]
Flavodoxin	[59]
tRNA	[60,61]

## 10. X-ray diffraction

Lanthanides have been used in X-ray crystallography because they give rise to anomalous scattering components of X-radiation in the determination of structures of macromolecules. In particular  $\text{Sm}^{3+}$ ,  $\text{Nd}^{3+}$  and  $\text{Eu}^{3+}$  give large scattering. In thermolysin,  $\text{Ln}^{3+}$  ions occupy  $\text{Ca}^{2+}$  binding sites. The enzyme lysozyme is devoid of  $\text{Ca}^{2+}$  and the function and nature of the site is not known.  $\text{Mg}^{2+}$  ions in tRNA are replaced by  $\text{Ln}^{3+}$  ions. The studies in general show that  $\text{Ca}^{2+}$  ions are substituted by  $\text{Ln}^{3+}$  ions in macromolecules without marked disruption. Some data on macromolecules are given in Table 11.6. Neutron diffraction studies of macromolecules appear to be promising.

Luminescence immuno assays have been discussed in detail in Chapter 12. Some other techniques are listed below with pertinent references:

- cytochemical detection techniques [62,63],
- electron microscopy [64,65],
- extraction and precipitation [66,67],
- lanthanide enhanced affinity chromatography [68],
- magnetic techniques [69].

## 11. Lanthanide interactions with proteins

Amino acids are the building blocks of proteins. In aqueous solutions of pH range 3–8, amino acids are present in the zwitter ionic form  $^+\text{NH}_3\text{CH}(\text{X})\text{COOH}$ , where X is the amino acid side chain. The bonding is primarily through the carboxyl group. The possible participation of amino nitrogen in coordinating to the metal although controversial, it is possible, in view of the synthesis of many macrocyclic complexes with some containing nitrogen donor atoms. The data on dissociation constants of some amino acid complexes are given in Table 11.7.

Higher complexes of stoichiometries 1:2 and 1:3 have also been reported. It has been suggested that at pH values above 7 amino acid:  $\text{Ln}^{3+}$  stoichiometry might change from 1:1 to 1:2. It has also been suggested that paramagnetic lanthanides could be used in sequencing peptides from their C-termini [78].

Small peptides containing amino acids found at the  $\text{Ca}^{2+}$  binding sites of proteins have been synthesized and studied. *N*-acetyl-asp formed 1:1 complexes with  $\text{Ln}^{3+}$  ( $\text{Ln} =$



TABLE 11.7  
Dissociation constants of 1:1 lanthanide–amino acid complexes.

R <sup>3+</sup>	Amino acid	K <sub>D</sub> (M)	pH	Temp. (°C)	Method	Ref.
La	Sarcosine	0.25	3–8	25	NMR	[70]
Nd	Alanine	0.23	–	22	Potent.	[71]
Nd	Alanine	0.15	4.0	22	NMR	[71]
Nd	Histidine	0.50	4.0	22	NMR	[71]
Nd	Serine	0.10	–	22	Potent.	[71]
Nd	Serine	0.08	4.0	22	NMR	[71]
Nd	Threonine	0.13	4.0	22	NMR	[71]
Pr	Alanine	0.30	4.6–5.0	39	NMR	[72]
Pr	Ampicillin	6.13	4.0–4.6	25	NMR	[73]
Eu	Glycine	0.20	3.6	25	Partition	[74]
Eu	Glycine	0.08	3.8	–	NMR	[75]
Eu	Alanine	0.18	3.6–4.5	25	Partition	[76]
Eu	Azetidine-2-carboxylate	0.28	4.6–5.0	37	NMR	[77]
Lu	Sarcosine	0.13	3–8	25	NMR	[70]

Yb, Tm, Er, Ho, Dy) with  $K_d$  values in the range 0.15–0.3 mM. The *N*-acetyl-asp and *N*-acetyl-Asp-Gly-aspartylamide are associated with the EF Ca<sup>2+</sup> binding site of parvalbumin [79].

Thermolysin is a zinc metallo enzyme which binds Ca<sup>2+</sup> ions. It consists of a single polypeptide chain of M.W. 34 600 containing 316 amino acid residues. Four Ca<sup>2+</sup> ions per molecule give thermal stability to the enzyme. The crystal structure of both Ln<sup>3+</sup> substituted and unsubstituted enzyme has been determined [54].

Ca <sup>2+</sup> (S1)	} Bound to carboxyl groups Glu-177, Asp-185, Glu-180
Ca <sup>2+</sup> (S2)	
Ca <sup>2+</sup> (S3)	Singly bound Asp-57, Asp-59, C=O of Glu-61 + 3 water molecules
Ca <sup>2+</sup> (S4)	Singly bound-C=O of Tyr-193, Thr-194, Ile-197; OH of Thr-194; COO <sup>-</sup> of Asp-200; 2 water molecules.

Affinity of Eu<sup>3+</sup> for sites S1 and S2 is greater than Ca<sup>2+</sup> and for sites S3 and S4 Ca<sup>2+</sup> binds more strongly than Eu<sup>3+</sup>. Ligand distances are given in Table 11.8.

An independent study [81] consisted of inserting Tb<sup>3+</sup> probe in site(1) and an acceptor Ln<sup>3+</sup> ion (Ln = Pr, Nd, Ho or Er) into sites S(3) and S(4). Energy transfer occurred between S(1) and S(4). Lifetimes of emission from Tb<sup>3+</sup> and Eu<sup>3+</sup> in H<sub>2</sub>O and D<sub>2</sub>O led to one water molecule at site(1). Similarly 3.1 and 4 water molecules at sites S(3) and S(4) were obtained. These data are consistent with X-ray crystallographic data. A distance of 10.9–11.8 Å between S(1) and S(4) was calculated and is close to 10.9 Å obtained from crystallography.

The “E–F hand” proteins parvalbumin, troponin C, calmodulin, calbindin and oncomodulin have been studied with respect to lanthanide interactions. The crystal structure of parvalbumin [82] consists of six  $\alpha$ -helical regions labeled as A–F. One Ca<sup>2+</sup> ion is bound in the loop joining C and D helices and the second ion in the loop of E–F. Calcium ion is bound to six protein ligands in the CD site. Ca<sup>2+</sup> in the EF site is bound to seven protein ligands and a water molecule.

TABLE 11.8  
Calcium and europium distances in thermolysin<sup>a</sup>.

Ligand	Distance (Å)		
	Ca 1	Eu 1	Ca 2
Sites S(1) and S(2)			
Asp 185	3.6	3.3	
	2.7	2.4	2.4
Glu 177	2.1	2.1	
	2.6	2.4	2.1
Glu 190	1.9	2.1	
	2.6	2.6	2.1
Glu 187	2.0	2.1	
Asn 183			2.1
Asp 138	3.0	3.3	
H <sub>2</sub> O 1	2.9	2.7	
H <sub>2</sub> O 2			2.9
H <sub>2</sub> O 3			2.6
	Ca 3	Eu 3	
Site S(3)			
Asp 57	3.5	3.6	
	2.6	3.0	
Asp 59	2.0	2.4	
	3.4	3.3	
Glu 61	2.6	3.2	
H <sub>2</sub> O	12.3	2.0	
H <sub>2</sub> O	2.1	1.8	
H <sub>2</sub> O	2.1	1.7	
	Ca 4	Eu 4	
Site S(4)			
Tyr 193	2.5	2.4	
Thr 194	1.8	1.9	
	2.2	2.7	
Ile 197	3.0	2.9	
Asp 200	2.5	2.8	
H <sub>2</sub> O	2.5	2.2	
H <sub>2</sub> O	2.2	1.8	
H <sub>2</sub> O		2.8	

The dissociation constants of lanthanides in parvalbumin are noted in Table 11.9.

The data show that lanthanides bind to parvalbumin more strongly than calcium ions.

X-ray crystallographic studies show that lanthanides can replace Ca<sup>2+</sup> in these proteins isomorphously. The match may not be perfect but the perturbations are small. In general lanthanides bind to the proteins more strongly than Ca<sup>2+</sup> because of the higher ionic potential of the lanthanides. It is interesting to note that some enzymes also associate with lanthanides although the enzymes do not require Ca<sup>2+</sup> for their enzymatic activity. In this regard, lanthanide substitution gives structural information and also inhibits the activity. Some data for lysozyme and trypsin are given in Tables 11.10 and 11.11, respectively.

TABLE 11.9  
Dissociation constants of various lanthanides for the two  
Ca<sup>2+</sup>-binding sites of parvalbumin.

Ln <sup>3+</sup>	K <sub>d</sub> (M × 10 <sup>-11</sup> )		Reference
	CD site	EF site	
La <sup>3+</sup>	2.0	4.8	[83]
Ce <sup>3+</sup>	3.2	4.8	[83]
Gd <sup>3+</sup>	5.0	5.0	[83]
	0.5	0.5	[84]
Tb <sup>3+</sup>	600	2.0	[85]
Yb <sup>3+</sup>	52	4.0	[83]
Lu <sup>3+</sup>	36	4.8	[83]

TABLE 11.10  
Calculated association constants for Ln<sup>3+</sup> and lysozyme [86].

Ln <sup>3+</sup>	K <sub>a</sub> (M <sup>-1</sup> × 10 <sup>3</sup> )
La <sup>3+</sup>	5.0 ± 1.4
Pr <sup>3+</sup>	7.5 ± 3.7
Nd <sup>3+</sup>	3.7 ± 2.1
Gd <sup>3+</sup>	7.0 ± 2.6
Tb <sup>3+</sup>	4.0 ± 1.7
Dy <sup>3+</sup>	8.7 ± 4.0
Er <sup>3+</sup>	6.6 ± 1.5
Tm <sup>3+</sup>	4.1 ± 1.9

In some proteins like concanavalin A Ln<sup>3+</sup> ions do not bind to the Ca<sup>2+</sup> site. In some cases metal ions such as Mg<sup>2+</sup>, Mn<sup>2+</sup> and Fe<sup>3+</sup> may be displaced by lanthanides. Certain proteins like lysozyme and concanavalin A have unique binding sites which may be occupied by lanthanides. The association or binding constants of lanthanides with different protein span a wide range. The affinities of lanthanides for proteins increase in general with increase in charge at the binding site and decrease in hydration. The smaller Ln<sup>3+</sup> ions close to Ca<sup>2+</sup> ion size are good candidates for binding proteins.

Lanthanides substitution in proteins also provide structural and functional aspects of proteins. The techniques which provide such useful information are NMR and luminescence techniques. NMR helps assignment of peaks and also provides conformational analysis (i.e.) in identification of acid residues in the vicinity of the binding site. A useful situation arises when the lanthanum binding site is in proximity to the active site. Luminescence spectroscopy gives the number of water molecules bound and also the interionic distance in cases where two binding sites are present.

Lanthanides are better cofactors than Ca<sup>2+</sup> for the activation of trypsinogen by trypsin. Proteins like calmodulin retain their biochemical activity even after substitution by a lanthanide. This is due to the same degree of conformational changes produced by Ca<sup>2+</sup> and Ln<sup>3+</sup> ions. But most Ca<sup>2+</sup> requiring proteins function less effectively on substitution

TABLE 11.11  
Association constants of lanthanide–trypsin complexes<sup>a</sup> [87].

$\text{Ln}^{3+}$	$K_a (\text{M}^{-1})$
$\text{La}^{3+}$	180
$\text{Pr}^{3+}$	372
$\text{Nd}^{3+}$	540
$\text{Sm}^{3+}$	668
$\text{Gd}^{3+}$	360
$\text{Tb}^{3+}$	900
$\text{Ho}^{3+}$	750
$\text{Er}^{3+}$	962
$\text{Tm}^{3+}$	1630
$\text{Yb}^{3+}$	1860
$\text{Lu}^{3+}$	2110
$\text{Y}^{3+}$	823

by  $\text{Ln}^{3+}$  ions. The role of  $\text{Ca}^{2+}$  in the proteins can be elucidated by lanthanide substitution, and an example of this is the case of staphylococcal nuclease.

## 12. Nucleotides

Nucleotides in the form of metal ion complexes are involved in a variety of enzymatic reactions either as substrates or as cofactors. These may also be viewed as monomers of DNA and RNA. Lanthanide complexes of nucleotides have been extensively studied because (i) the conformation of nucleotides in solution can be elucidated from lanthanide induced NMR chemical shifts and line-broadenings [40] and (ii) lanthanide nucleotide complexes may act as competitive inhibitors in enzymatic reactions [88] and hence can be used as paramagnetic probes in the mapping of their binding site on the enzyme [89].

Complex formation constants for lanthanide nucleotide complexes are given in Table 11.12.

It has been shown that phosphate in nucleotide monophosphates acts as a bidentate ligand. The disposition of  $\text{Ln}^{3+}-\text{PO}_4^{3-}$  is shown in Fig. 11.5.

In the ATP complexes, the lanthanide ion interacts with the terminal  $\beta$  and  $\gamma$  phosphates which act probably as tetradentate ligand.

At pH values above 7.0 the nucleotides are fully ionized and complex formation with lanthanides is more favourable. At pH 5.6 a dissociation constant of the order of 1 mM is estimated for  $\text{Tb}^{3+}$  complexes of nucleotide monophosphates from fluorescence measurements [93]. At pH 7.0  $\text{Eu}^{3+}$ –ADP complex gave a value  $10^{-7}$  M for  $K_D$  [96]. The dissociation constants of Ln–ATP complexes obtained by Morrison and Cleland [97] are given in Table 11.13.

The effect of increased pH is obvious from the data on the dissociation constants for Ln–ATP complexes.

Lanthanides have been used to afford spectral resolution in NMR studies of cyclic nucleotides. The magnitudes of lanthanide induced chemical shifts and line-broadenings

TABLE 11.12  
Association constants for lanthanide complexes of mono- and dinucleotides.

Nucleotide	pH	Ln <sup>3+</sup>	$K_a$ ( $M^{-1}$ )	Ref.
5' AMP	2	Ho	$6 \pm 2$	[40]
5' AMP	2	Eu	$10 \pm 2$	[40]
5' AMP	1.5-1.8	Eu	10	[90]
5' A.G.CMP	2	Eu, Pr	$15 \pm 5$	[91]
5' AMP	6.7	Eu	$4.2 \times 10^5$	[92]
5' A.G.C.UMP	5.6	Tb	$\sim 10^3$	[93]
5' GMP	1.5-1.8	Eu	14	[90]
5' TMP	1.5-1.8	Eu	17	[90]
5' TMP	2	Eu	$17 \pm 3$	[40]
3',5'-cAMP	4.9	Ho	$13 \pm 1.7$	[94]
2',3'-cAMP	2.3	Eu	$7.9 \pm 1.2$	[95]
2',3'-cCMP	2.3	Eu	$8.6 \pm 1.01$	[95]
5'-ADP	7	Eu	$(58 \pm 3) \times 10^4$	[96]
5'-ADP	8	Eu	$(7.7 \pm 0.3) \times 10^4$	[96]
5'-ADP	6.7	Eu	$7.1 \times 10^6$	[92]

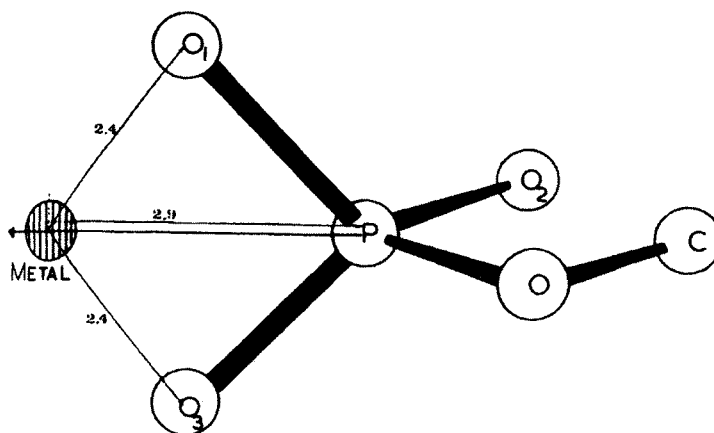


Fig. 11.5. Diagram showing the Ln<sup>3+</sup>-binding position with respect to the phosphate group of AMP and TMP. Interatomic distances are shown in Å.

have been analyzed in terms of molecular structure of mononucleotides [40,90], cyclic nucleotides [94], dinucleotide phosphates [90] and ATP [89]. The conformation of AMP in dimethyl sulphoxide was found to be different from that in water [40].

Polynucleotides bind lanthanides more strongly than mononucleotides and tRNA providing stronger ligands than DNA. This difference is reflected in the data on  $K_a$  values for Tb<sup>3+</sup> complexes given in Table 11.14.

TABLE 11.13  
Dissociation constants of Ln-ATP complexes at pH 8 [97].

Ln of Ln-ATP complex	Dissociation constant ( $\mu\text{M}$ )
La	$0.33 \pm 0.06$
Ce	$0.35 \pm 0.06$
Pr	$0.31 \pm 0.07$
Nd	$0.29 \pm 0.05$
Sm	$0.22 \pm 0.01$
Eu	$0.16 \pm 0.04$
Gd	$0.087 \pm 0.005$
Tb	$0.094 \pm 0.024$
Dy	$0.049 \pm 0.009$
Ho	$0.099 \pm 0.010$
Er	$0.086 \pm 0.019$
Tm	$0.038 \pm 0.010$
Yb	$0.024 \pm 0.006$
Lu	$0.044 \pm 0.011$

TABLE 11.14  
Binding parameters for  $\text{Tb}^{3+}$  complexes of DNA and polynucleotides.

Polynucleotide or DNA	$K_a$ ( $M^{-1}$ )	$n$ (residues/ $\text{Tb}^{3+}$ )	Ref.
Poly(c)	$8.2 \times 10^5$	3.7	[98]
Poly(c)	$8.2 \times 10^5$	3.7	[99]
Oligo(dG) <sub>6</sub>	$2.8 \times 10^4$	1.3	[100]
Oligo(dG) <sub>8</sub>	$2.9 \times 10^4$	1.5	[100]
Poly(dG) <sup>a</sup>	$3.0 \times 10^4$	3.3	[100]
Poly(dA-dT)	$7.0 \times 10^4$	5.0	[98]
Poly(A,G)	$5.0 \times 10^6$	2.6	[98]
E. coli DNA	$4.1 \times 10^4$	3.7	[100]
Plasmid, supercoiled DNA	$1.2 \times 10^5$	5.5	[100]
Calf thymus DNA <sup>a</sup>	NA <sup>b</sup>	3	[101]
Calf thymus DNA (27 mM NaCl)	$10^7$	NA	[102]
Calf thymus DNA (133 mM NaCl)	$1.6 \times 10^5$	NA	[102]
Calf thymus DNA (200 mM NaCl)	$1.2 \times 10^4$	NA	[102]
Calf thymus DNA (400 mM NaCl)	$3.5 \times 10^3$	NA	[102]

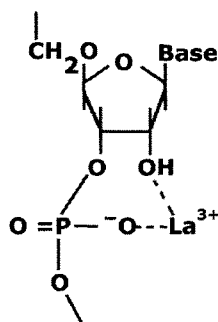
<sup>a</sup>Determined with  $^{160}\text{Tb}^{3+}$ . All others determined by  $\text{Tb}^{3+}$  luminescence enhancement.

<sup>b</sup>Not available.

### 13. Nucleic acids

Nucleic acids are known to be responsible for the storage and transcription of genetic information in living cells and are involved in protein synthesis. Nucleic acids are polymers of nucleoside phosphates and hence negatively charged in neutral solutions. Nucleic acids interact strongly with metal ions. Such an interaction with metal ions helps to maintain the conformational stability of nucleic acids and their function. The formation of a complex

between  $\text{La}^{2+}$  and ribonucleic acids is probably occurring by chelate formation between phosphate and 2-hydroxyl group [103].



The interaction between DNA and  $\text{Tb}^{3+}$  in the solid state studied by fluorescence showed that one cation was present for each phosphate group [104]. Later it was shown that DNA precipitates after  $\text{Ln}^{3+}$ :DNA ratio reaches 1:3. Lanthanides also induce conformational changes in DNA including the adaptation of Z configuration.

Both fluorescence and NMR techniques have been used in studies involving lanthanide–RNA interactions. Fluorescence enhancement of several hundred fold was observed on interaction of  $\text{Tb}^{3+}$  and  $\text{Eu}^{3+}$  with tRNA from *E. coli*. Enhancement was not observed in the case tRNA from yeast. From the fluorescence measurements the conclusion [105] that there are four tight equivalent sites for  $\text{Eu}^{3+}$  per tRNA molecule containing approximately 80 nucleotides with  $K_D$  of  $6 \times 10^{-6}$  M. X-ray studies [61] also indicate four lanthanide binding sites on tRNA.

Protein biosynthesis occurs on ribosomes which are small organelles composed of proteins and ribosomal RNA (tRNA). Fluorescence and dialysis techniques have been used to study the interaction of  $\text{Tb}^{3+}$  with tRNA. The relative fluorescence was found to be proportional to the amount of bound  $\text{Tb}^{3+}$  ion. Intact ribosomes produced similar effects on those of tRNA indicating the primary sphere for lanthanide binding is that of ribosomes.

#### 14. Carbohydrates

Lanthanides have been used as NMR shift reagents for carbohydrates in solution [106]. Carbohydrates and polyols can bind metal ions provided they have three *cis* hydroxyl groups with axial–equatorial–axial arrangement. A typical binding is illustrated below.

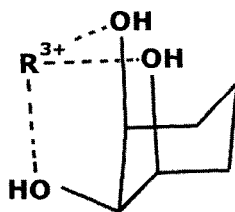


TABLE 11.15  
Dissociation constants (at 52°C) of  $\text{Ca}^{2+}$  and  $\text{La}^{3+}$  complexes with sugars

Sugar	$K_D^{\text{Ca}}$ (M)	$K_D^{\text{La}}$ (M)
$\beta$ -D-lyxopyranose	$1.25 \pm 0.15$	$1.0 \pm 0.1$
$\alpha$ -D-ribofuranose	$0.45 \pm 0.05$	$0.18 \pm 0.01$
$\alpha$ -D-ribofuranose	$0.71 \pm 0.05$	$0.28 \pm 0.01$
$\beta$ -D-ribofuranose	$1.45 \pm 0.2$	$1.1 \pm 0.1$

The complex formation [107] with D-allose is in the order  $\text{Na}^+ < \text{Y}^{3+} < \text{Ca}^{2+} < \text{La}^{3+}$ . NMR studies on metal ions – sugar complexation where the sugars involved are D-lyxose and D-ribose gave rise to data given in Table 11.15.

NMR has been used in studies of chelation by the anions of D-galacturonic acid and its derivatives. The data showed the formation of 3:1 complexes [109]. Proton relaxation studies using  $\text{Gd}^{3+}$  on mono- and disaccharides, and effect of  $\text{Gd}^{3+}$  on  $^1\text{H}$  and  $^{13}\text{C}$  spectra of uronic acids showed the method to be useful for distinguishing between anomeric forms [110,111].

## 15. Other molecules

Lanthanides also interact with porphyrins, [112] Vitamin  $B_{12}$  [113], the  $\text{Ca}^{2+}$  ionophores A 22 187 and X537A [114,115], bilirubin [116], high-density lipoproteins [117], melanin [118], and amphetamines [119] which are of interest to biochemists.

## 16. Phospholipids and membranes

Membranes are much more organized in the molecular sense among biological systems than their constituents, proteins and phospholipids. The physiological and pharmacological action of lanthanides probably involves interaction of lanthanides with membranes. Initial pioneering work of Mines [120] in this regard should be noted. Subsequently it was noted that  $\text{La}^{3+}$  should bind strongly at  $\text{Ca}^{2+}$  binding sites and serve the purpose of a nerve blocking agent [121]. Since biological membranes are complex, artificial membranes have been used to study the interactions of lanthanides and phospholipids. The major phospholipid in biological membranes is phosphatidylcholine (lecithin) and hence this is chosen as the model system. Phosphate groups in these systems are the binding sites for  $\text{La}^{3+}$  ions. The formation constants of lanthanide–phosphatidylcholine complexes are given in Table 11.16.

The estimates of the binding constants show a large variation. The large variations may be attributed to the experimental difficulties involved in the determination. Binding of lanthanides is independent of pH in the range 3–7 but increases in the presence of anions in the order  $\text{Cl}^- < \text{Br}^- < \text{NO}_3^- < \text{SCN}^- < \text{I}^- < \text{ClO}_4^-$ .

Lanthanide ions also affect the conformation of the artificial membranes as reflected in the increase in width [128] of the bilayer by 6 Å and the polar head groups are oriented



TABLE 11.16  
Affinities of lanthanide ions for phosphatidylcholine bilayer membranes.

Lanthanide ion	Approximate $K_a$ ( $M^{-1}$ )	Comment	Reference
La	120	Values obtained by different methods	[122]
Tb	565		[123]
Various	715	Calculated range, given different theoretical concentration of binding sites	[124]
	30		
Nd	120–1000		[125]
Eu	284–9400		[126]
Pr	2	Low-affinity, T-site	[127]
	3000	High-affinity, R-site	

perpendicular to the surface [125]. The inner and outer polar head groups in bilayer vesicles can be distinguished by paramagnetic lanthanides in conjunction with NMR [41].

In general the physiological responses of cells, tissues and organs to lanthanides are due to the interactions between  $Ln^{3+}$  and the outer surface of their plasmalemmae. Lanthanides interact with cellular membranes strongly with association constants in the  $\mu M$  range [129]. Lanthanides can bind to membrane proteins, membrane glycoproteins and to the phospholipid bilayer but the question which of these function as lanthanum receptors on intact cells remains unresolved. Physiological studies suggest that the outer surfaces of  $Ca^{2+}$  channels are likely binding sites for lanthanide ions [130]. Lanthanides do not penetrate artificial phospholipid bilayers and probably cannot enter healthy cells. There is some possibility that lanthanides enter some specific types of cells under some conditions [131]. Lanthanides present in aggregates are internalized through phagocytosis [132]. Lanthanides stabilize phospholipid membranes (i) by increasing rigidity, (ii) making the surface charge more positive and (iii) and promoting aggregation and membrane fusion at high concentrations. In the case of biological membranes, additional effects such as increase in membrane potential, membrane resistance and changes in transmembrane  $Ca^{2+}$  fluxes are observed. It has been observed that high concentrations of lanthanides can effectively inhibit all the exchange of  $Ca^{2+}$  between many types of cells and their external media.

Since lanthanides usually block cellular uptake of  $Ca^{2+}$ , they also naturally inhibit physiological processes that depend on  $Ca^{2+}$  influx. Some of the inhibited functions are nerve impulses, contraction of muscles, and hormonal responses.

Mitochondrial membranes have high affinity for lanthanides [133], and contain two binding sites. Lanthanides inhibit the uptake of  $Ca^{2+}$  by mitochondria, and hence prevent the associated physiological responses.

## 17. Environmental behavior of lanthanides

The earth's crust is made up of minerals and a few of these occur in sufficient abundance and constitute rocks. The three types of rocks are: (i) igneous, (ii) metamorphic rocks (95% of earth's crust), (iii) sedimentary rocks (5% of earth's crust).

Igneous rocks: (i) originate from silica melt 'magma', (ii) major elements (>1%); minor elements (0.01–1%); trace elements (<0.01%).

Igneous rocks can be: (i) ultra basic rock, (ii) basic rock, (iii) intermediate rock, (v) acid rock.

Metamorphic rock is the product of solid state process such as crystallization due to heat and pressure. The rock is generally left unchanged chemically. Sedimentary rocks are formed from pre-existing rocks by a number of processes known as denudation. Denudation consists of weathering, transportation and erosion.

Sedimentary rocks: (i) argillaceous rocks, 77% (shale); (ii) arenaceous rocks, 13% (limestone/dolomite).

Minerals may be defined as units of definite chemical composition formed by natural processes.

Rock-forming minerals				
Feldspars (58%)	Ferro- magnesian (16%)	Micas (3%)	Quartz (13%)	Limestone, dolomite
Alkaline earth/ alkaline silicates (K,Na)AlSi <sub>3</sub> O <sub>8</sub> (Ca,Ba)Al <sub>2</sub> Si <sub>2</sub> O <sub>8</sub>	Silicates of Fe/Mg (Mg,Fe,Mn,Ca)SiO <sub>4</sub> (Mg,Fe)SiO <sub>3</sub> (Ca,Mg,Fe,Al) <sub>2</sub> (Al,Si) <sub>2</sub> O <sub>6</sub>	KAl <sub>2</sub> (Si,Al) <sub>4</sub> O <sub>10</sub> (OH) <sub>2</sub>	SiO <sub>2</sub>	CaCO <sub>3</sub> (Ca,Mg)(CO <sub>3</sub> ) <sub>2</sub>

In addition to the rock-forming minerals which form more than 95% of the earth's crust, many accessory minerals are known which have different geochemical origin and are widely distributed.

Rare earths with the exception of promethium are widely distributed in nature and are highly disseminated in crustal formations. The rare earth contents in the earth's crust and in the major types of rocks are given in Table 11.17. The total lanthanide content in different types of rocks is given by the sum of  $\sum$  La–Lu, Y which varies from a value of 100 mg kg<sup>-1</sup> in basic rocks to three times the value in acid rocks. The global abundances in the earth's crust are also given in the table and these values are calculated [134] as the weighted averages of the rock composition, namely, 45% granite, 35% granodionite, 5% diorite and 15% basalts.

Many minerals containing rare earths are known [135] and since lanthanides have similar properties, then each mineral that contains one lanthanide also contains other lanthanides. Table 11.17 shows the rare earth elements to have undergone differentiation during geochemical processes although they have similar chemical behaviour.

The lanthanide contraction is probably the reason why the natural processes lead to fractionation and give rise to cerium group elements containing mainly the larger rare earth elements of lower atomic numbers, and to yttrium earth minerals containing mainly smaller rare earth elements with higher atomic numbers. Yttrium, although not a rare earth element, its atomic number 39 is low and its radius is similar to that of Ho. Thus yttrium appears with heavy rare earth elements.

The distinction between the two groups, lighter and heavier lanthanides is a consequence of magmatic differentiation and due to the small differences in ionic sizes. The ratio of light rare earth to heavy rare earths,  $\sum$  La–Eu/ $\sum$  Gd–Lu, Y is different and depends on the type

TABLE 11.17

Global abundances and average concentrations of rare earth elements in different rocks in  $\text{mg kg}^{-1}$ .

Element	Atomic number	Earth crust	Basic rock (Ba salts)	Intermediate rock	Acid rock (granites)
La	57	42	6.1	31	55
Ce	58	81	16	60	104
Pr	59	10	2.7	7.4	12
Nd	60	40	14	31	47
Sm	62	7.6	4.3	6.2	8
Eu	63	1.5	1.5	1.3	1.1
Gd	64	7.2	6.2	6.8	7.4
Tb	65	1.1	1.1	1.1	1.1
Dy	66	5.8	5.9	6.1	6.2
Ho	67	1.4	1.4	1.5	1.5
Er	68	3.9	3.6	3.9	4.2
Tm	69	0.62	0.60	0.65	0.69
Yb	70	3.7	3.2	3.8	4.3
Lu	71	0.61	0.55	0.62	0.68
Y	39	35	32	35	38
$\sum$ La–Lu, Y		241	100	196	290
$\sum$ La–Eu		182	45	137	226
$\sum$ Gd–Lu, Y		59	55	59	64
$\sum$ La–Eu		3.1	0.8	2.3	3.5
$\sum$ Gd–Lu, Y					

of rock. The ratio  $\sum \text{La–Eu} / \sum \text{Gd–Lu, Y}$  has a value of 0.8 ( $\sim 1.0$ ) in basic rock and 3.5 in acid rock.

It is also seen from Table 11.17 the crustal content of even-numbered elements is consistently higher than for odd-numbered elements. This observation is consistently higher than for the Oddo–Harkins rule according to which nuclei with equal numbers of protons and neutrons are inherently more stable than those which have an unpaired proton or neutron.

Geochemically, lanthanides are lithophilic with the tendency to form silicates [136]. The chemical bond is of the ionic type. Lanthanide minerals can be divided into three distinct groups. The first group consists of minerals containing major quantities of rare earth elements. These are formed by crystallization from magmatic mother liquors and are located mainly in pegmatites. The process of differential crystallization in the case of one type of mineral favoured the smaller RE(III) ions and gave rise to cerium earth minerals such as bastnaesite ( $\text{CeFCO}_3$ ), monazite ( $\text{CePO}_4$ ) and cerite [ $\text{Ce}_3(\text{Ca,Fe})\text{H}_3\text{Si}_3\text{O}_{13}$ ] while in other types, larger RE(III) ions were favoured giving rise to yttrium earth minerals such as euxenite [ $\text{RE}(\text{Nb,Ta})\text{TiO}_6 \cdot n\text{H}_2\text{O}$ ], xenotime ( $\text{REPO}_4$ ) and gadolinite [ $\text{RE}_2(\text{Fe,Be})\text{Si}_2\text{O}_{10}$ ].

The second group includes minerals in which lanthanides are in trivalent state but form a minor constituent. Such minerals arise through the partial substitution of RE(III) ions for large divalent ions like Ca(II), Sr(II) and Pb(II). This substitution is known as diadochy and depends on three factors, namely ionic size, valence and the type of bonding. The ionic sizes must not differ by more than 15% from each other. RE ions (0.85 Å–1.14 Å),  $\text{Ca}^{2+}$

(0.99 Å),  $\text{Sr}^{2+}$  (1.13 Å) and  $\text{Pb}^{2+}$  (1.19 Å) are well within the range of each other. The minerals calcite, fluorite and apatite belong to this group.

The third group consists of minerals in which RE ions are divalent,  $\text{Eu}^{2+}$  (1.25 Å) and  $\text{Sm}^{2+}$  (1.27 Å). These ions by diadochy replace large ions like  $\text{K}^+$  (1.33 Å),  $\text{Sr}^{2+}$  (1.13 Å) and  $\text{Pb}^{2+}$  (1.19 Å). Some typical minerals are strontianite, fluorite and potassium feldspars.

### 17.1. Weathering

Rocks and minerals breakdown due to physical, biological and chemical weathering and only a few minerals remain chemically unchanged.

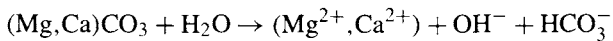
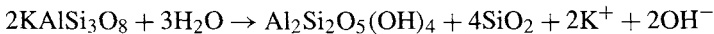
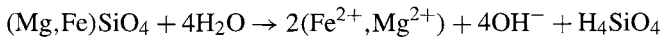
Weathering:

- Physical weathering: rocks are fragmented; little or no chemical changes; plays a role in rugged topography and special climates.
- Biological weathering: due to living organic species; least conspicuous form of weathering.
- Chemical weathering: dominant form; breakdown of rocks and minerals at moderate pressures and temperatures due to combined action of water, carbon dioxide and oxygen.

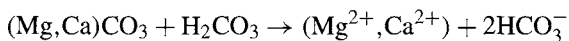
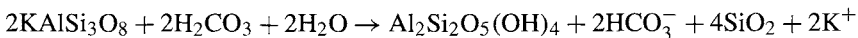
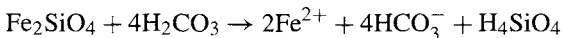
The four basic processes involved in chemical weathering are: (i) formation of carbonic acid from water and carbon dioxide, (ii) ionization, (iii) hydrolysis and (iv) oxidation.

The various rocks and associated minerals show different degrees of resistance to chemical weathering and the order of resistance is: carbonates, sulphides < silicates < oxides.

The chemical weathering of silicates and carbonates occurs through hydrolysis

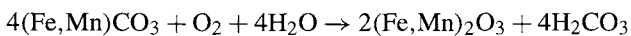
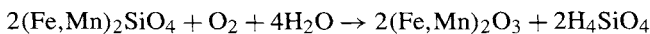


Atmospheric carbon dioxide in rain water produces carbonic acid of pH ~5.7 and attacks the minerals

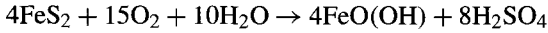


The above reaction scheme shows the  $\text{K}^+$ ,  $\text{Fe}^{2+}$ ,  $\text{Mg}^{2+}$ ,  $\text{Ca}^{2+}$  are set free along with the trace elements associated with them bound due to diadochy. In all the above reactions the pH increases towards alkalinity and to a maximum of 9.0.

Oxidation reaction in chemical weathering is important in the case of iron and manganese bearing minerals.



In the process of degradation, trace elements are set free. There are no sulphide minerals of concern in rare earths. In spite of this, the oxidation of sulphide minerals is shown below



The product acid aids in further attack of the mineral, releasing all the trace metals in the mineral.

The initial products of chemical weathering are: (i) simple soluble constituents with further dependence on the species and the existing physico-chemical conditions, (ii) insoluble minerals such as clay minerals, iron-and manganese oxides and precipitates of ionically dissolved elements and (iii) highly resistant residual minerals.

The rare earth elements in the parent rocks associated with minerals are fairly resistant to weathering. But to the extent the weathering of rare earth minerals occurs, rare earths are released as  $\text{M}^{3+}$  ions. In the case of minerals containing  $\text{Sm}^{2+}$  and  $\text{Eu}^{2+}$  the ions are easily oxidized to trivalent state and their further speciation depends on the following secondary reactions. In principle meteoric water is capable of setting free rare earth ions or as a soluble  $\text{M}^{3+}$  complex.

The concentration levels of lanthanides [137] in fresh/ground water is less than  $2 \mu\text{g l}^{-1}$  and in sea water  $0.02 \mu\text{g l}^{-1}$ . The lanthanides in sea water are to a degree associated with suspended particles and the concentration of free  $\text{M}^{3+}$  ions is below the solubility products of insoluble hydroxides and carbonates [138]. However, soluble  $\text{M}^{3+}$  complexes may be present [133].

The residence time for lanthanides in sea water varies from 200 years for the lighter lanthanides and 50 years for the heavier lanthanides. The difference in residence times among the lanthanides may be due to higher stability and hence higher mobility of the heavier lanthanides [133].

The mobility of rare earth elements on weathering is very restricted and they remain in place by the formation of insoluble hydroxides or carbonates. They may also be associated with clay minerals or iron and manganese oxide which are formed during the weathering process [139,140]. The entire group of insoluble minerals formed due to weathering are collectively known as soils and sediments. These consist mostly of argillaceous materials like shales and clays, with minor amounts of iron and manganese oxides, hydroxides, carbonates and phosphates of ionic nature. Average rare earth contents of products formed due to weathering are given in Table 11.18. A comparison of the data in Tables 11.17 and 11.18 shows that the values of the total lanthanides,  $\sum \text{La-Lu, Y}$  and the ratios of lighter lanthanides to heavier lanthanides,  $\sum \text{La-Eu}/\sum \text{Gd-Lu, Y}$  have similar values in the earth's crust, shales, sandstones, clays and sediments demonstrating that lanthanide fractionation in natural matter, is unchanged by weathering. However there are some variations which depend upon the physico-chemical conditions of the weathering environment. The presence of water and pH are the important conditions.

In arid climates, neither leaching nor fractionation of the lanthanides from weathering occurs. Under humid conditions, there are indications of leaching of heavier lanthanides in particular probably due to the higher stability of complexes of heavier lanthanides. Cerium is an exception to the general lanthanide behaviour probably because in geochemical conditions it is in the tetravalent state.

TABLE 11.18  
Average contents of rare earth elements in materials formed after weathering given in  $\text{mg kg}^{-1}$ .

	Sediment	Shales	Sandstone	Limestone	Clays	Manganese nodules
La	41	40	42	10	31	160
Ce	83	79	78	20	56	720
Pr	9.7	10	11	2.5	9.6	50
Nd	32	36	38	9	35	190
Sm	6.4	7.1	8.4	2.1	6.2	90
Eu	1.2	1.4	2	0.4	1.8	14
Gd	5.6	6.1	7.1	2.7	7.4	6.4
Tb	1	0.87	2	0.44	1.1	10
Dy	5.4	5.2	6.9	2.1	6	42
Ho	1.6	1	2	0.28	1.2	8
Er	3.8	3	4.9	1.7	3	19
Tm	0.6	0.5	1	0.16	0.56	2.4
Yb	3.6	3	4.4	1.6	2.9	6.4
Lu	0.7	0.5	0.8	0.16	0.8	
Y	40	41	54	23	32	310
$\sum$ La-Lu, Y	236	228	263	53	195	1628
$\sum$ La-Eu	173	173	179	44	140	1224
$\sum$ Gd-Lu, Y	62	54	83	9	45	404
$\sum$ La-Eu	2.8	3.2	2.2	4.9	3.1	3.0
$\sum$ Gd-Lu, Y						

The environmental pH also plays a role. The lanthanides are immobilized by precipitation at  $\text{pH} > 7$ , but they are more soluble at lower pH, and can be easily removed.

Weathering of limestone produces a lanthanide depleted product and the heavier lanthanides are leached to higher degree than the lighter lanthanides. This is probably due to the formation of soluble carbonato complexes. The lanthanides are highly concentrated in manganese nodules consisting of manganese oxides. The manganiferrous nodules are located in deep ocean floors which also contain other metals. Manganese nodules should be considered and treated as mineral deposits.

## 18. Rare earth distribution in soils

Soils are heterogeneous both in the physical and chemical sense. Soils can be classified into four groups [137]: (i) the soil-fraction constitutes 5–90% soil dry matter and contains inorganic matter with particle size  $> 200$  nm. It contains resistant minerals and is chemically inert because of few functional groups. Sieving gives gravel, sand and silt. The second soil fraction consists of inorganic colloidal particles with particle diameters of  $< 200$  nm. They constitute 10–80% of soil dry matter, and are chemically active. This fraction contains clay minerals and hydrous oxides of Fe, Al, Mn.

Clay minerals are aluminosilicates with layer structures. The basic constituent elements Si and Al are substituted by other elements by diadochy. Clay minerals swell in water and

act as cation exchangers since they carry a negative charge in the range  $4 < \text{pH} < 10$ .

		Cation exchange capacity (meq/100 g)
Kaolinite	$\text{Al}_4\text{Si}_4\text{O}_{10}(\text{OH})_8$	3–15
Mica, illite	$(\text{Na}, \text{Ca}, \text{Mg}, \text{Fe}^{2+}, \text{Fe}^{3+})_{1-1.5}\text{Al}_4(\text{Si}_{7-6.5})\text{O}_{20}(\text{OH})_4$	10–40
Montmorillonite	$(\text{Na}, \text{Ca})_{0.33}(\text{Al}, \text{Mg})_2\text{Si}_4\text{O}_{10}(\text{OH})_2 \cdot n\text{H}_2\text{O}$	80–15

Clay minerals being negatively charged act as cation exchangers. Kaolinite is common in temperate climates with frequent rainfall, while illite and montmorillonite are present in arid climates.

The hydrous oxides of Fe, Al, and Mn have ion exchange properties. At low pH hydrous oxides act as anion exchangers and at  $\text{pH} \geq 7$  they act as cation exchangers [141]. The oxides generally form a thin coating on clay particles. The third soil fraction known as humus, consists of organic matter, and is the result of bio-activity. Organic matter is composed of soluble low-molecular weight, polyfunctional organic acids of short residence time in soils, fulvic acids and insoluble humic acids. Fulvic and humic acids are weather resistant organic polymers with carboxyl hydroxyl and phenolic functional groups. Fulvic and humic acids form complexes with metal ions and also have ion exchange property [142]. Although variable, soil organic matter is about 1–3% of soil dry matter.

The fourth soil fraction is known as the soil solution, which consists of moisture held by capillary action in the soil particles. The soil solution may be separated by centrifugation. The soil solution contains the ions, which are mobile in soils and is thought to be the main nutrient medium for sustaining plant roots and micro-organisms. The soil is in dynamic equilibrium with the soil solution and the exchange time is of the order of seconds. The movement of the soil solution through the soil after rainfall is responsible for the layered structure of soils.

Soil also contains living matter, which is mostly unicellular and takes part in controlling pH and redox potential of the soil.

The number of determinations on the distribution of rare earths in soils are limited. A set of representative data [139,140] are given in Table 11.19.

Reference to Tables 11.19 and 11.17 shows that the total lanthanide content ( $\sum \text{La-Lu}$ , Y) and the ratio of lighter rare earths to heavier rare earth's ( $\sum \text{La-Eu} / \sum \text{Gd-Lu}$ , Y) have similar values both in the earth's crust and soils. The values obtained for soils of different origin do not differ significantly [133,140] and are always similar to the values of parent materials [143].

It appears unlikely, that lanthanides are mobile. They appear to remain 'in situ' as insoluble precipitates or bound to insoluble materials formed during weathering, as for example, clay minerals [139], iron, manganese oxide minerals [133] and possible soil organic materials.

The speciation of lanthanides and the various concentrations of the species in soils are not available in the literature [140].

## 19. Speciation of rare earth elements

The speciation of rare earth elements and the interest in the topic arose due to the need for such information in the case of actinides. Both sets are f elements and the need

TABLE 11.19  
Mean content and average range of rare earth elements in soils of variable origin in  $\text{mg kg}^{-1}$ .

Element	Mean	Range
La	37	2.1–183
Ce	84	9.8–300
Pr	6.5	3.4–2
Nd	44	4.1–300
Sm	6.0	0.6–23
Eu	1.3	0.1–2.6
Gd	3.5	1.7–6.2
Tb	0.85	0.11–1.7
Dy	5.7	2.2–12
Ho	0.80	0.39–1.8
Er	3.0	1.4–6.2
Tm	0.62	0.34–1.2
Yb	3.9	0.04–50
Lu	0.46	0.1–0.95
Y	28	5–200
$\sum$ La–Lu, Y	226	
$\sum$ La–Eu	179	
$\sum$ Gd–Lu, Y	47	
$\sum$ La–Eu	3.8	
$\sum$ Gd–Lu, Y		

for speciation of actinides and its disposal in the form of radioactive waste resulted in some activity in this regard. Since most of the actinides are artificial, it is difficult to study their environmental behaviour. The need for such information led to the activity in environmental behaviour of naturally occurring lanthanides which are f elements. It is thought that knowledge on speciation of lanthanides might prove useful in the case of actinides.

Rare earth elements are capable of forming various species on exposure to varied and complex environmental conditions. Studies of physicochemical behaviour of rare earth elements under various environmental conditions require a knowledge of the formation and behaviour of various lanthanide species as a function of pH, redox conditions, nature and concentration of ligands present and the solubilities of the lanthanide complexes formed.

Trivalent oxidation state is a common oxidation state of lanthanides in solution. Tetravalent Ce and divalent Eu and Sm are also known to exist in solution. The standard electrode potentials [144] for some lanthanide couples are given in Table 11.20.

The standard electrode potentials for all the rare earths have similar values and are comparable with the redox potentials of alkaline earth metals [144]. Thus the lanthanides are strong reducing agents, and form trivalent ions easily. Both europium and samarium can exist in both trivalent and divalent states and the divalent states are not stable in aqueous solutions. Cerium can exist in both tetravalent and trivalent states in solution but Ce(III) is the most stable.

Trivalent lanthanides are favoured under normal environmental conditions and many lanthanide(III) compounds are known. Many of the compounds are soluble but the hydroxide, carbonates, fluorides and phosphates are insoluble. Solubility products of some



TABLE 11.20  
Standard electrode potentials for lanthanide couples given in volts.

Reaction	Volts
$\text{La}^{3+} + 3\text{e}^- + \text{La}^0$	-2.37
$\text{Ce}^{3+} + 3\text{e}^- + \text{Ce}^0$	-2.34
$\text{Nd}^{3+} + 3\text{e}^- + \text{Nd}^0$	-2.25
$\text{Sm}^{3+} + \text{e}^- + \text{Sm}^{2+}$	-1.55
$\text{Eu}^{3+} + \text{e}^- + \text{Eu}^{2+}$	-0.43
$\text{Ce}^{4+} + \text{e}^- + \text{Ce}^{3+}$	+1.44
$\text{La}(\text{OH})_3 + 3\text{e}^- + \text{La}^0 + 3\text{OH}^-$	-2.76
$\text{Ce}(\text{OH})^{3+} + \text{H}^+ + \text{e}^- + \text{Ce}^{3+} + 3\text{OH}^-$	+1.71

Temperature 250°C.

All substances are at unit activity.

TABLE 11.21  
Solubility products of insoluble simple lanthanide compounds.

Chemical reactions	Temp.	Solubility product
$\text{La}(\text{OH})_3 + \text{La}^{3+} + 3\text{OH}^-$	25°C	$2.0 \times 10^{-21}$
$\text{Eu}(\text{OH})_3 + \text{Eu}^{3+} + 3\text{OH}^-$	25°C	$2.5 \times 10^{-26}$
$\text{La}_2(\text{CO}_3)_3 + 2\text{La}^{3+} + 3\text{CO}_3^{2-}$	25°C	$4.7 \times 10^{-34}$
$\text{Sm}_2(\text{CO}_3)_3 + 2\text{Sm}^{3+} + 3\text{CO}_3^{2-}$	25°C	$3.2 \times 10^{-33}$
$\text{LaPO}_4 + \text{La}^{3+} + \text{PO}_4^{3-}$	25°C	$3.7 \times 10^{-23}$

compounds are given in Table 11.21. The naturally-occurring hydroxyl and carbonate ions combine with lanthanide ions to form corresponding lanthanide hydroxides and carbonates, which precipitate as soon as the solubility product is exceeded.

Rare earths form mostly ionic types of complexes with inorganic ligands. The formation constants of some inorganic complexes of europium and lanthanum are given in Table 11.22. In general the formation constants of rare earth elements are similar such that the missing values can be obtained through interpolation from known values. But there are minor differences with the heavier lanthanides tending to form complexes of higher stability.

The lanthanides show ability to form complexes with hydroxide and carbonate ions. Although the lanthanide hydroxides and carbonates are very insoluble, some soluble complexes like  $\text{Eu}(\text{OH})_4^-$  and  $\text{Eu}(\text{CO}_3)_2^-$  may be formed. Although  $\text{HCO}_3^-$  is the predominant species in the pH range studied, bicarbonate complexes are not formed [147, 148].

The thermodynamic stability of lanthanide complexes with inorganic ligands  $\text{OH}^-$  and  $\text{F}^-$  increases slightly with increase in atomic number. The formation constants for  $\text{MOH}^{2+}$  and  $\text{MF}^{2+}$  formation

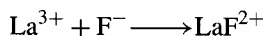
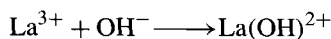


TABLE 11.22  
Stability constants of lanthanides with simple inorganic ligands at 298 K.

Chemical reactions	Ionic strength	log <i>K</i>
$\text{Eu}^{3+} + \text{OH}^- + \text{Eu}(\text{OH})^{2+}$	0	6.2
$\text{Eu}^{3+} + 2\text{OH}^- + \text{Eu}(\text{OH})_2^+$	0	11.4
$\text{Eu}^{3+} + 3\text{OH}^- + \text{Eu}(\text{OH})_3$	0	16.4
$\text{Eu}^{3+} + 4\text{OH}^- + \text{Eu}(\text{OH})_4^-$	0	20.7
$\text{Eu}^{3+} + \text{CO}_3^{2-} + \text{Eu}(\text{CO}_3)^+$	1	5.9
$\text{Eu}^{3+} + 2\text{CO}_3^{2-} + \text{Eu}(\text{CO}_3)_2^-$	1	10.7
$\text{Eu}^{3+} + \text{Cl}^- + \text{EuCl}^{2+}$	1	-0.1
$\text{Eu}^{3+} + 2\text{Cl}^- + \text{EuCl}_2^+$	1	-0.7
$\text{Eu}^{3+} + \text{NO}_3^- + \text{Eu}(\text{NO}_3)^{2+}$	0	0.2
$\text{Eu}^{3+} + 2\text{NO}_3^- + \text{Eu}(\text{NO}_3)_2^+$	0	-0.6
$\text{La}^{3+} + \text{H}_2\text{PO}_4^- + \text{La}(\text{H}_2\text{PO}_4)^{2+}$	0.5	1.61
$\text{Eu}^{3+} + \text{F}^- + \text{EuF}^{2+}$	1	3.19
$\text{Eu}^{3+} + \text{SO}_4^{2-} + \text{Eu}(\text{SO}_4)^+$	0.1	1.87
$\text{Eu}^{3+} + 2\text{SO}_4^{2-} + \text{Eu}(\text{SO}_4)_2^-$	0.1	2.73

TABLE 11.23  
Formation constants of the  $\text{M}(\text{OH})^{2+}$  and the  $\text{MF}^{2+}$  species of the lanthanides.

Element	$\text{M}^{3+} + \text{OH}^- = \text{M}(\text{OH})^{2+}$	$\text{M}^{3+} + \text{F}^- = \text{MF}^{2+}$
La	5.5	2.67
Ce	5.7	2.81
Pr	5.9	3.01
Nd	6.0	3.09
Sm	6.1	3.12
Eu	6.2	3.19
Gd	6.0	3.31
Tb	6.1	3.42
Dy	6.0	3.46
Ho	6.0	3.52
Er	6.1	3.54
Tm	6.3	3.56
Yb	6.3	3.58
Lu	6.4	3.61

for all the lanthanides are given in Table 11.23. As one progresses in the series, the formation constants increase from 5.5 to 6.4 in the case of the  $\text{LaOH}^{2+}$  complex and 2.67 to 3.61 in the case of the  $\text{LaF}^{2+}$  complex [145].

Lanthanides in oxidation state (III) form complexes with organic ligands with oxygen donor groups and some data for Eu(III) complexes are given in Table 11.24.

At  $\text{pH} > 3$ , Eu(III) forms 1:1 complexes with fulvic and humic acids [142] with  $\log \beta$  values greater than 6.

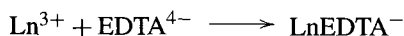
In the treatment of nuclear waste for disposal, the practice has been to scavenge the radioactive nuclides by using multidentate complexing agents such as ethylenediaminete-

TABLE 11.24

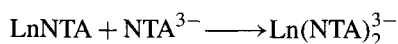
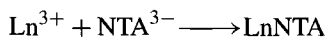
Stability constants of mononuclear of Eu(III)-complexes with selected organic ligands at 295 K and at the indicated ionic strengths.

Formula	Name	Species	log <i>K</i> <i>I</i> variable	log $\beta$ <i>I</i> = 0.5
CH <sub>3</sub> COOH	(acetic acid)	ML <sup>2+</sup>	1.90–1.94–2.13	
		ML <sub>2</sub> <sup>+</sup>	3.19–3.46	
HOOC–COOH	(oxalic acid)	ML <sub>3</sub>	3.75–4.24	
		ML <sup>+</sup>	5.04–5.36	
		ML <sub>2</sub> <sup>–</sup>	8.70–9.04	
		ML <sub>3</sub> <sup>3–</sup>	11.45	
		ML <sub>3</sub> <sup>5–</sup>	13.09	
HOOC–CH <sub>2</sub> –COOH	(malonic acid)	ML <sub>4</sub> <sup>+</sup>	3.72–4.30	
		ML <sub>2</sub> <sup>–</sup>	6.24	
HOOC–CH <sub>2</sub> OH	(glycolic acid)	ML <sup>2+</sup>	2.52–2.57–2.93	
		ML <sub>2</sub> <sup>+</sup>	4.56–4.61–5.07	
		ML <sub>3</sub>	5.91–6.52	
HOOC–CH <sub>2</sub> –CHOH–COOH	(malic acid)	ML <sub>4</sub> <sup>–</sup>	6.4	
		ML <sub>4</sub> <sup>+</sup>	4.85	
HOOC–CHOH–CHOH–COOH	(tartaric acid)	ML <sub>2</sub> <sup>+</sup>	4.33	2.76
HOOC–CH <sub>2</sub> –C(OH)(COOH)–CH <sub>2</sub> COOH	(citric acid)	ML	7.91	6.70
		ML <sub>2</sub> <sup>3–</sup>		10.95
CH <sub>2</sub> NH <sub>2</sub> COOH	(glycine)	ML <sup>2+</sup>	0.70	
HOOC–CH <sub>2</sub> –CH(NH <sub>2</sub> )–COOH	(aspartic acid)	ML <sup>+</sup>	5.62	5.09
HS–CH <sub>2</sub> –CHNH <sub>2</sub> COOH	(cysteine)	ML <sub>2</sub> <sup>–</sup>	9.80	5.13

traacetic acid (EDTA) belonging to the groups of polyaminocarboxylic acids. The lanthanides form EDTA complexes with high stability constants



and these complexes are introduced into the environment in waste disposal areas. These complexes represent radioactive mobile species and the formation constants of these complexes are given in Table 11.25. Nitrilotriacetic acid (NTA) is also used for scavenging purposes and the data for such a complex



are given. The complexing agent NTA appears to be more favorable than EDTA because it is easily biodegradable [149].

TABLE 11.25  
Stability constants of europium(III)-complexes with EDTA and NTA.

Chemical reaction	Ionic strength	Temp.	log <i>K</i>
$\text{Eu}^{3+} + \text{EDTA}^{4-} + \text{Eu}(\text{EDTA})^{-}$	0.1	20–25°C	17.35
$\text{Eu}^{3+} + \text{NTA}^{3-} + \text{Eu}(\text{NTA})^{-}$	0.1	20–25°C	11.33
$\text{Eu}^{3+} + 2\text{NTA}^{3-} + \text{Eu}(\text{NTA})_2^{3-}$	0.1	20–25°C	20.69

## 20. $E_h$ -pH diagrams

The predominant valence state of lanthanides is Ln(III). Europium, however, can be present as Eu(II) and Eu(III). Cerium in the state Ce(IV) is not lanthanide-like.

The migration of lanthanides in natural environments is thought to simulate Am(III). The ligands of interest in this regard are  $\text{OH}^-$ ,  $\text{SO}_4^{2-}$ ,  $\text{Cl}^-$ ,  $\text{F}^-$ ,  $\text{HCO}_3^-$  and  $\text{CO}_3^{2-}$  which are invariably present in fresh water, sea water and ground water. Low-molecular weight organic acids of soil organic matter and added complexing agents such as EDTA are also present.

A knowledge of the chemical behaviour coupled with physico-chemical data can be useful in predicting chemical species of a metal ion that is likely to be present in a given environment. The stability of the various chemical species in aqueous medium can be represented in the form of a stability diagram. Such diagrams are constructed by plotting  $E_h$  versus pH. These diagrams show the equilibrium presence of various species as regions relative to pH and  $E_h$  or  $pE$  related to  $E_h$  by the equation

$$pE = [nF/2.303RT]E_h.$$

The behaviour of europium which can exist as Eu(II) or Eu(III) in nature determined by pH,  $E_h$ , temperature, pressure, ionic strength and the anions present is considered. Using the formation constants, europium speciation is shown in Fig. 11.6 when the anion is hydroxide ion. The diagram is calculated according to the procedure given in the literature. Europium(III) forms hydroxide species in a stepwise manner and the formation constants given in Table 11.22 have been used. The values for the formation constant of  $\text{Eu}(\text{OH})^+$  are not available. An estimated value was obtained from the corresponding alkaline earth species taking into account the close similarities of the chemistry of Eu(II) and Ca(II). It is assumed that the formation constants of  $\text{Eu}(\text{OH})^+$  and  $\text{Ca}(\text{OH})^+$  are of the same magnitude [145].

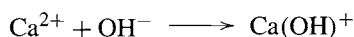


Fig. 11.6 shows the regions in which the indicated species are present to an extent of 50% or more of the total species under the given conditions. Eu(III) is the main species over a pH range of acidic-neutral. Above pH 7, between pH 8 and 9  $\text{Eu}(\text{OH})^{2+}$  is predominant. Above

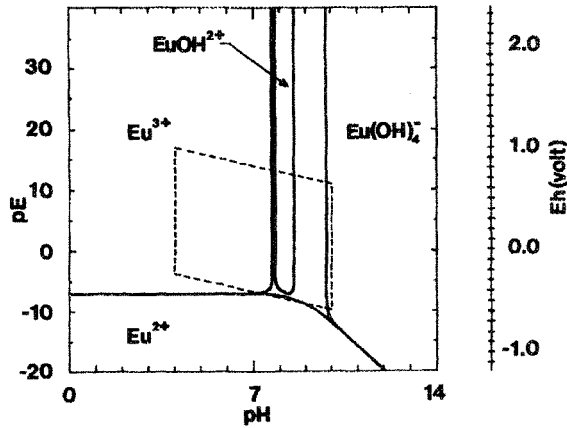


Fig. 11.6. Europium speciation in the presence of hydroxide ions.

pH 10 we have  $\text{Eu(OH)}_4^-$  as the dominant species. Eu(II) is predominant under strongly reducing conditions with no sign of  $\text{Eu(OH)}^+$  in the figure. Within the parallelogram representing geochemical conditions existing in the real world, only Eu(III) is of interest. We have

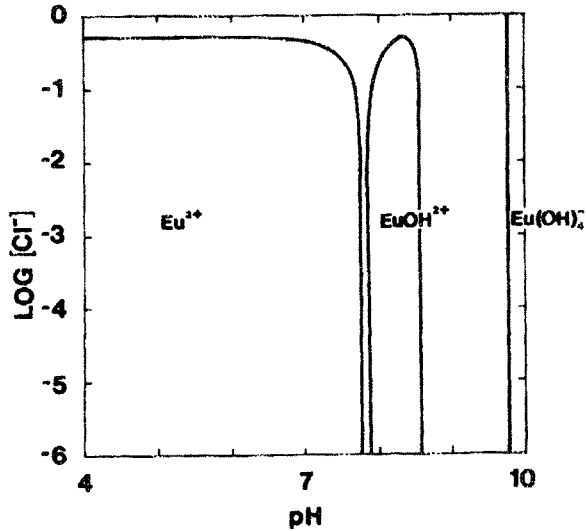
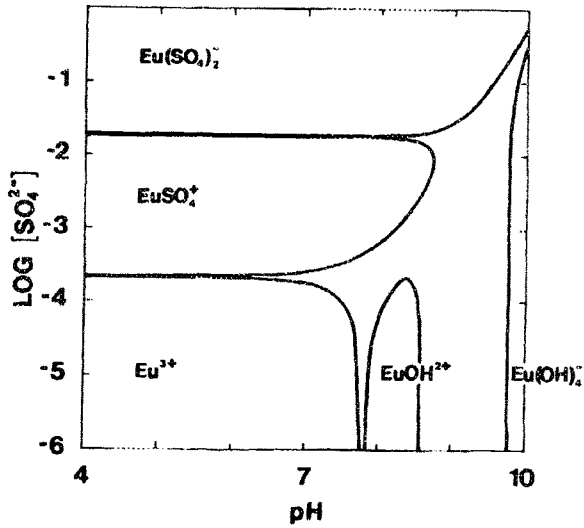
- pH 0–7,  $\text{Eu}^{3+}$
- pH 8–9,  $\text{Eu(OH)}^{2+}$
- pH 10,  $\text{Eu(OH)}_4^-$

## 21. Predominance diagrams

A more simple approach in speciation is to construct a predominance diagram in which the logarithm of anion concentration is plotted against pH. The data on complex formation constants, hydrolytic reactions are taken into account in constructing predominance diagrams. These diagrams represent a laboratory solution. These diagrams clearly indicate the various species likely to exist under conditions and in turn determine the migration behaviour of the element of interest. The predominance diagram consists of a plot of  $\log[C_A]$  vs the logarithm of anion concentration as the ordinate and pH as the abscissa. These diagrams show domains where different species dominate. The domains are defined as areas where the species are more than 50% of the total concentration of the metal ion. It is easy to read the diagrams and identify the dominating species under given conditions. The concentration of the rare earth ion is about  $\sim 10^{-6}$  M and the formation of polynuclear complexes is considered to be negligible.

The ligands of interest are those present in ground water, namely,  $\text{HCO}_3^-$ ,  $\text{CO}_3^{2-}$ ,  $\text{SO}_4^{2-}$ ,  $\text{Cl}^-$ ,  $\text{F}^-$ ,  $\text{OH}^-$  and low-molecular weight organic acids. Environmental concentrations of these ions [150] and the procedure for constructing a predominance diagram are given in the literature [151].

The predominance diagram given in Fig. 11.7 shows that in the chloride concentration range  $10^{-6}$  M to 1.0 M, no chloro complexes are formed. But in strong saline ground

Fig. 11.7. Predominance diagram for the Eu(III)/Cl<sup>-</sup> system.Fig. 11.8. Predominance diagram for the Eu(III)/SO<sub>4</sub><sup>2-</sup> system.

waters (i.e.)  $[\text{Cl}^-] > 1.8 \text{ M}$   $\text{EuCl}_2^+$  is formed [142]. We notice above pH 7,  $\text{EuOH}^{2+}$  ion is formed followed by  $\text{Eu(OH)}_4^-$  at pH  $\sim 10$ . Below pH 7  $\text{Eu}^{3+}$  is the predominant species.

Predominance diagram for Eu(III)-SO<sub>4</sub><sup>2-</sup> system is given in Fig. 11.8. At low sulphate concentrations ( $\sim 10^{-4} \text{ M}$ ) and pH range 4 to 7.5,  $\text{Eu}^{3+}$  is the dominant species. Above  $10^{-4} \text{ M}$  and below  $10^{-2} \text{ M}$  sulphate concentration and pH range of 4–8,  $\text{EuSO}_4^+$  is the

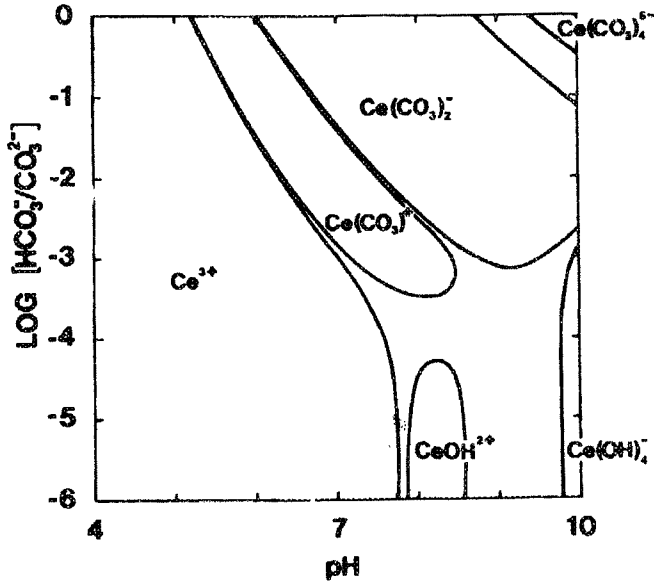


Fig. 11.9. Predominance diagram for the Ce(III)/CO<sub>3</sub><sup>2-</sup> system.

dominant species. Above  $10^{-2}$  M of sulphate, we have  $\text{Eu}(\text{SO}_4)_2^-$ . Above pH 7.5 and at comparable  $\text{OH}^-$  and  $\text{SO}_4^{2-}$  concentrations,  $\text{EuOH}^{2+}$  and  $\text{Eu}(\text{OH})_4^-$  are formed.

Cerium(III) is considered to be a representative element for trivalent lanthanides and carbonate ions. Lanthanide carbonates are insoluble and the experimental data for the formation constants of the various carbonato species are available for Ce(III)-CO<sub>3</sub><sup>2-</sup> system [148].

The predominance diagram for Ce(III) and the carbonate system has been given in Fig. 11.9. It is obvious from the diagram that ionic  $\text{Ce}^{3+}$  is the dominant species in acidic pH (<5.0) in the entire carbonate concentration range of  $10^{-6}$ - $10^0$  M. As the pH approaches 7 and carbonate concentration range of  $5 \times 10^{-3}$  and 1.0 M, carbonate complexes of the type  $\text{Ce}(\text{CO}_3)^+$ ,  $\text{Ce}(\text{CO}_3)_2^-$  and  $\text{Ce}(\text{CO}_3)_3^-$  are formed. Above pH 7 and below  $10^{-4}$  M carbonate,  $\text{Ce}(\text{OH})^{2+}$  and  $\text{Ce}(\text{OH})_4^-$  are formed.

Soil organic matter contains chelating agents such as  $\alpha$ -hydroxy acids. Typical acids are tartaric and citric acids. The predominance diagram for Eu(III)-tartaric acid is shown in Fig. 11.10. Ionic europium is present below pH 7, and ligand concentration of  $<10^{-3}$  M. At ligand concentrations greater than  $10^{-3}$  M,  $\text{Eu}(\text{tartrate})^+$  is formed. At pH >6.0 and  $[\text{L}] = 10^{-5}$ - $10^0$  M,  $[\text{Eu}(\text{tartrate})(\text{OH})]$  and  $[\text{Eu}(\text{tartrate})(\text{OH})_2]^-$  complexes are formed [151].

The predominance diagram for Eu(III)-citric acid system is shown in Fig. 11.11.

- pH < 5, L =  $10^{-5}$ - $10^{-6}$  M,  $\text{Eu}^{3+}$  species
- pH 4-10, L =  $10^{-6}$  M,  $\text{Eu}(\text{citrate})$
- pH 4-10, L =  $10^{-4}$ - $10^{-2}$  M,  $\text{Eu}(\text{citrate})_2^{3-}$
- pH ~10, L =  $10^{-6}$  M,  $\text{Eu}(\text{OH})^{2+}$

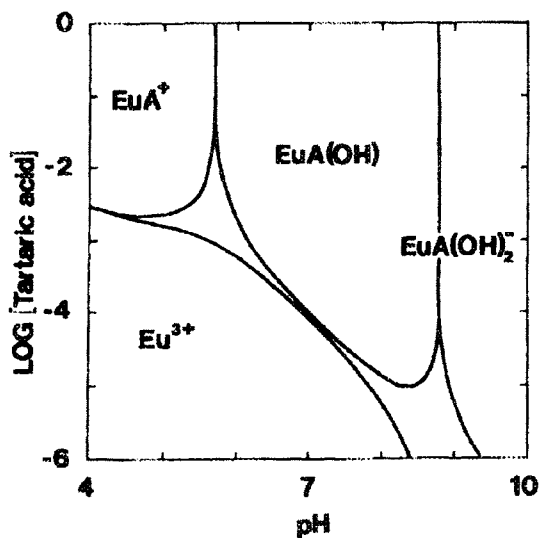


Fig. 11.10. Predominance diagram for the Eu(III)/tartaric acid system.

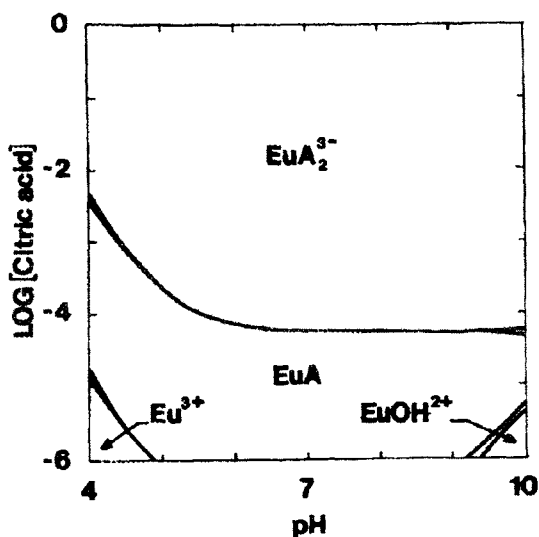


Fig. 11.11. Predominance diagram for the Eu(III)/citric acid system.

Citric acid is a very good ligand and  $\text{Eu}(\text{citrate})$ ,  $\text{Eu}(\text{citrate})_2^{3-}$  species dominate over the pH range 4–10 and  $L = 10^{-6}$  to  $10^{-2}$  M.

Lanthanide speciation can be summarized as follows, considering the behaviour of Eu(III) and Ce(III) as representative of lanthanides. Eu(III) is present as ionic species in the acidic pH range excepting when citric acid is present in the system in which case Eu–citrate



complexes are formed. Eu forms  $\text{Eu}(\text{OH})^{2+}$  and  $\text{Eu}(\text{OH})_4^-$  at high pH when citric acid is absent. Trivalent lanthanides form  $\text{Ln}(\text{OH})^{2+}$ ,  $\text{Ln}(\text{OH})_4^-$ ,  $\text{LnCO}_3^+$ ,  $\text{Ln}(\text{CO}_3)_3^{3-}$  complexes with  $\text{OH}^-$  and  $\text{CO}_3^{2-}$  and organic complexes in the concentration range present under natural conditions. Lanthanides form strong 1:1 complexes with humic and fulvic acids at pH values greater than 3.0. Lanthanides are present as complexes when chelating agents like EDTA occur in solution.

## 22. Migration of lanthanides in environment

Considering the pH range 4–10 as the geochemical range, the redox potential due to the breakdown of water due to redox processes, the rare earths are predominantly present as Ln(III). Since the anions  $\text{OH}^-$  and  $\text{CO}_3^{2-}$  are present in natural environments, rare earths combine with these anions to form insoluble hydroxides and carbonates and hence immobilized. At lower pH, rare earth ions are adsorbed on clays, which are natural ion exchangers. The interactions of rare earth ions with humic and fulvic acids in soils, and Fe/Mn oxides are so strong, that they become immobile.

But as noted, earlier rare earths form soluble hydroxide and carbonate like  $\text{Ln}(\text{OH})^{2+}$ ,  $\text{Ln}(\text{OH})_4^-$ ,  $\text{LnCO}_3^+$ ,  $\text{Ln}(\text{CO}_3)_3^{3-}$  with  $\text{OH}^-$  and  $\text{CO}_3^{2-}$ . These complexes are formed above pH 8. Some complexes are anionic and these complexes can migrate. The few anomalies noted in the natural distribution of rare earths may be due to the possible removal as soluble hydroxy or carbonate complexes. Lanthanides form complexes with organic acids. Organic acids are present in soils and there is no information readily available on the existence of the migration of rare earth organic complexes. The geochemical findings and the experimental data are consistent with each other. It is reasonable to conclude that trivalent rare earths are immobile in geochemical environments, but there is the possibility of mobility when rare earths are present as hydroxide, or carbonate or organic complexes, due the presence of organic acids in soil organic matter.

## 23. Metabolism and toxicity of lanthanides

### 23.1. Metabolism

As noted earlier the abundance of rare earths in the earth's crust is over 100 ppm. It was also noted that the migration potential of rare earths in natural environmental conditions is not high because of the formation of insoluble hydroxides and carbonates. The migration potential depends upon the concentrations of  $\text{LnOH}^{2+}$ ,  $\text{Ln}(\text{OH})_4^-$ ,  $\text{LnCO}_3^+$  and  $\text{Ln}(\text{CO}_3)_3^{3-}$ . In areas rich in lanthanide ores, the soils may contain as much as 1 mg per gram of dry soil. Lanthanides probably find their way to the formation of atmospheric dusts. Industrial exposure results in inhalation of atmospheric dusts. Industrial exposure results in inhalation of fumes and external contamination of existing wounds. Lanthanides have a limited ability to traverse through the food chain. Even though some soils may contain high levels of lanthanides [152], the concentration in the ground waters is very low. Some plants absorb relatively large amounts while others do not [153]. Very poor

absorption by vertebrates limits the assimilation of lanthanides from food and this is seen from the low concentrations detected in mammalian organs [154].

The surface binding of trivalent lanthanides to microorganisms is strong [155]. Lanthanides are probably not transported into bacteria, algae or yeast. Poor intestinal absorption may be due to: (i) insoluble nature of salts, (ii) binding to digesta and (iii) inability of lanthanides to make use of  $\text{Ca}^{2+}$  transporting mechanism. The efficiency of absorption varies from 1% to 100% when administered orally or intravenously. Most of the distribution is in the liver and skeleton. Lanthanide sequestering may also occur in the spleen, lung and endocrine glands [156].

Excretion from the liver occurs fecally. Excretion of lanthanide complexes occurs through urine.

The lighter lanthanides preferentially accumulate in the liver while heavier lanthanides prefer bone [157]. This trend is particularly evident when lanthanide citrate complexes are administered. When lanthanides are introduced as chelate complexes, the absorption by the body is complete and the excretion rates also increase [158]. The excretion depends upon the stability of the chelate complex. If there is no exchange with the physiological ligands the excretion is rapid and complete.

### 23.2. Toxicity

The toxic and pharmacological aspects of lanthanides have been reviewed [159–161]. Many studies have been made on the effect of lanthanides on microorganisms. Lanthanides inhibit the growth of bacteria, fungi and yeast. Concentrations of  $\text{Ln}^{3+}$  as low as  $10^{-4}$  to  $10^{-5}$  M are required for inhibition. Concentrations of  $\text{Ln}^{3+}$  as low as  $10^{-5}$  M were found to stimulate bacterial growth [162]. The mode of inhibition appears to be suppression of bacterial respiration. Toxicity of lanthanides depends upon the chemical form and mode of administration. Oral administration is not effective because of poor absorption from the gastrointestinal tract (G.I.) [163]. The  $\text{LD}_{50}$  values were in the range of several grams per kilogram of body weight in the case of oral administration. At high doses, growth of rats was suppressed. Gastric hemorrhage and slight structural changes in the hepatocytes have been observed. Subcutaneous injection gave minimum lethal doses [159,164] in the range of 100–1000 mg/kg. Contact of abraded skin with lanthanides produces ulcers. Intradermally injected lanthanides produce granulomas and calcification. Lanthanides cause ocular irritation, conjunctivitis and sometimes ulceration.

Intraperitoneally injected lanthanides are more toxic [160] with  $\text{LD}_{50}$  values in the range of 50–500 mg/kg. Guinea pigs are more sensitive than rats and mice [165]. Weak complexing agents like citrate increase lethality by making lanthanide available. Strong complexing agents like EDTA facilitate excretion and reduce lethality. Lanthanides cause internally peritonitis, adhesions and ascites. Chronic exposure to lanthanide fumes result in emphysema, pneumonitis, bronchitis and pulmonary fibrosis. It is also reported that pulmonary reticulosarcoma might occur. Rare earth pneumoconiosis has been detected on humans exposed to rare earth oxide fumes [166]. Lanthanides showed embryotoxicity. Calcification and sterility result on intratesticular injection of lanthanides.

Intravenously injected lanthanides are most toxic [160] with  $\text{LD}_{50}$  values in the range of 10–100 mg/kg. Death occurs due to cardiovascular collapse and respiratory failure [167]. Pharmacological response into intravenously (I.V.) injected lanthanides are

TABLE 11.26  
Effects of Pr NAA and Sm NAA on the testis and epididymis of rats.

Parameter	Control (3)	Pr NAA (3)	Sm NAA (3)
Average testis length (cm)	19 ± 0.07	1.4 ± 0.18 <sup>a</sup>	1.7 ± 0.28 <sup>a</sup>
Average testis width (cm)	1.4 ± 0.12	1.3 ± 0.24 <sup>b</sup>	1.2 ± 0.14 <sup>b</sup>
Average testis weight (g)	19 ± 0.23	0.9 ± 0.06 <sup>a</sup>	1.2 ± 0.05 <sup>b</sup>
Relative germinal cell number	6–8	4–6	3–5
Relative interstitial cell number (low power field)	30–40	20–30	20–30
Number of seminiferous tubule cut ends	++++	+++	+++
Number of spermatozoa in epididymal tubules	++++	+	+

<sup>a</sup>  $P > 0.1$  or  $P < 0.1$ ;

<sup>b</sup>  $P > 0.01$  or  $P < 0.01$ .

++++ = numerous, +++ = fairly good, + = poor.

Numbers in parentheses indicate number of animals used.

TABLE 11.27  
Effects of Pr NAA and Sm NAA on the weight and secretory activity of rat accessory.

	Parameter	Control (3)	Pr NAA (3)	Sm NAA (3)
Average weight (g)	Epididymis	0.513	0.439	0.427
	Seminal vesicles	0.921	0.843	0.735
	Prostate glands	0.310	0.290	0.250
	Cowpers glands	0.030	0.020	0.030
Relative amount of secretion	Epididymis	++++	+++	++
	Seminal vesicles	++++	++	++
	Prostate glands	++++	++	++
	Cowpers glands	+++	+	+

++++ = numerous, +++ = fairly good, ++ = moderate, + = poor.

Numbers in parentheses indicate the number of animals used.

calcification [168], hypotension, hypoglycemia and increased clotting times. Another response is rare earth fatty liver produced by the lighter lanthanides resulting in massive hepatic accumulation of triglycerides [169]. Lanthanides have anticoagulant properties by virtue of interference in clotting reactions which require  $\text{Ca}^{2+}$  ions [170]. Rao et al. [171] studied the effect of intravenously administering Pr and Sm nicotines into rats and the resulting data are given in Tables 11.26 and 11.27. These findings are significant from the point of view of extending to clinical trials for treating prostate problems.

### 23.3. Medical uses

An excellent review on this aspect appeared in the literature [172]. Cerium salts have proved to be a useful antiseptic for external application to wounds [162]. Treatment of burns was achieved by using a mixture of cerium nitrate and silver sulfadiazine [173].

Lanthanide salts are known for anticoagulant properties [170]. Some undesirable side effects have also been observed when lanthanide salts are used [174]. Complexes of

rare earths with 3-sulfoisonicotinic acid [175] and  $\beta$ -acetyl propionic acid and nicotinic acid [171] do not appear to have side effects [176] and clinical use of these compounds seems promising.

Surgical implantation of  $^{90}\text{Y}$  has been used in almost all radio therapeutic treatment of human tumors. The method has been successfully used in the treatment of Nelson's syndrome [177], Cushing's syndrome [178] and breast cancer [179].

There are many reports in the literature about the affinity of lanthanides for tumors in vivo. Among the lanthanides Tm shows the greatest specificity. But  $^{167}\text{Tm}$  can be obtained with the aid of a cyclotron.  $^{169}\text{Yb}$  is readily available and has been successfully used in place of Tm [180]. Studies on humans with  $^{169}\text{Yb}^{3+}$ -citrate confirmed good imaging of lung cancers, primary and secondary brain tumors and bone metastases of various origins [181].

For purposes of cisternography, lanthanide complex of diethylene-triaminepentaacetic acid (DTPA) which is highly stable ( $K \approx 10^{22}$ ) is used. This complex  $^{169}\text{Yb}$ -DTPA has been used in the measurement of spinal fluid kinetics [182], as markers of the efficiency of urinary excretion [183], digesta markers and scintigraphic detection of synovial cysts [185]. Magnetic resonance imaging has been discussed at length elsewhere (Chapter 12).  $\text{Gd}^{3+}$  complexes are best suited for this technique,  $\text{Gd}$ -DTPA complex gives good images of tumors especially cerebral tumors, hepatic tumors, and transition cell carcinoma of the bladder [186]. Good imaging has also been obtained for imaging meningiomas [187], intracranial tumors [188] and mammary tumors [189]. MRI has now become the most important diagnostic technique in the field of medicine all over the world [190].

Computed tomography (CT) has been found useful in detecting tumors when lanthanide oxides were injected [191]. Cranial tumors have also been studied using  $\text{Gd}$ -DTPA by this technique [188].

Synovium is a tissue which lines all diarthrodial joints and this tissue under arthritic conditions becomes inflamed and causes pain, swelling and loss of motion. Medical destruction using radioisotopes is known as radiosynvectomy.  $^{90}\text{Y}$ ,  $^{169}\text{Er}$ ,  $^{165}\text{Dy}$  and  $^{177}\text{Lu}$  have been used in radiosynvectomy [192–195].

Plaques are formed on the internal surfaces of arteries during the development of atherosclerosis. The plaques consist of collagen, elastin, cholesterol, and calcium.  $\text{LaCl}_3$  was tested at 20–40 mg/kg of body weight in animals and was found to be effective in reducing coronary atherosclerosis [196,197].

Anti-inflammatory properties of lanthanides have been recognized for the past forty years, although the mechanism is not clearly known [198]. It was also predicted that lanthanides and their complexes might be eventually used in the treatment of arthritis [199].

## 24. Ecological aspects

Ecological studies involving rare earth elements although not as extensive as biochemical studies, shows some promise in studies involving: (i) sedimentation and erosion, (ii) ant behaviour, (iii) sorption by aquatic insects and (iv) root sorption.

### 24.1. Sedimentation and erosion

Short term (0.5 to 3 y) accretion rates have been estimated by extrapolation from sedimentation taking place over 25 y periods or longer [200]. Dy and Sm radioisotopes have been used for direct measurements over short accretion periods without interfering with natural wetland biological and physical processes. This application in wetland sedimentary studies estimates yearly changes and obviates problems of wetland deposition estimates which occurred many decades ago [201].

### 24.2. Ant behaviour

Fire ants are a major pest in sugarcane fields in the southern United States. There exists a controversy over the positive or negative role, that fire ants play in agroecosystems. Radiotracer studies of early times [202] although economical to carry out, cannot be used in croplands because of possible radioactive contamination of food. Studies involving Sm-labeled fire ants prevented food contamination problems and resulted in information on ant behaviour that was previously not available [203].

### 24.3. Sorption by aquatic insects

As spawning salmonid fishes die in headwaters of streams, the resulting decay products released into the water, became useful nutrients to ecosystems. Dy and Sm were perfused into the tissues of 4–5 kg salmon *gairdnerii* and these served as analogues of nutrients. These were then released into a stream with fish decay products over several months. The

TABLE 11.28  
Yield increment range of crops by RE application.

Crop	Average range (%)
Apple	10–15
Rice	5–10
Grape	8–12
Corn	6–11
Cotton	7–10
Banana	8–15
Soya bean	5–10
Tomato	10–15
Cucumber	8–15
Orange	5–10
Sugar cane	10–15
Rubber tree	8–14
Chinese cabbage	10–20
Wheat	6–12
Flue cured tobacco	8–10
Tea	8–12
Sugar beet	6–10
Water melon	8–10
Peanut	8–12
Green pepper	8–15

importance of fish decay products was inferred from the rate of capture and the extent of retention of the stable tracers associated with the decay products by the aquatic insects collected at various distances below the release site.

#### 24.4. Root sorption

Biological indicator species such as fresh water sponges, clams, mussels, insect larvae that sorb water-borne pollutants are difficult to assess over time periods of years. The lanthanides may be used as indicator species utilizing the adventitious roots of stream-side trees [204–206]. The ability of tree roots to sorb both chelated and non-chelated lanthanides from water indicate that aquatic roots accumulate, concentrate and retain lanthanides to such an extent that the roots can be used as indicators of aquatic pollution, and that lanthanides can be studied as analogues of toxic elements and compounds.

Rare earth elements such as La and Ce stimulate crop rooting, germinating and increase crop chlorophyll content [207]. Chinese scientists have pioneered in this field [208] and use a product known as CHANGLE which contains La and Ce nitrates. Yield increase range for various crops is shown in Table 11.28.

#### References

- [1] M.M. Faktor, R. Hanks, J. Inorg. Nucl. Chem. **31**, 1649, 1969.
- [2] R.D. Shannon, Acta Crystallogr., Sec. A **32**, 751, 1976.
- [3] R.J.P. Williams, Biochem. Soc. Trans. **7**, 481, 1970.
- [4] P.D. Chantler, J. Biol. Chem. **258**, 4702, 1983.
- [5] C.E. Richardson, W.D. Behnke, Biochim. Biophys. Acta **534**, 267, 1978.
- [6] S.K. Dower, R.A. Dwek, A.C. McLaughlin, L.E. Mole, E.M. Press, C.A. Sunderland, Biochem. J. **149**, 73, 1975.
- [7] R.B. Homer, B.D. Mortimer, FEBS Lett. **87**, 69, 1978.
- [8] H.B. Silber, FEBS Lett. **41**, 303, 1974.
- [9] B.A. Levine, R.J.P. Williams, in: The Role of Calcium in Biological Systems, eds. L.J. Anghileri, A.M. Tuffett-Anghileri, Vol. 1, pp. 3–26, CRC Press, Boca Raton, FL.
- [10] G.E. Smolka, E.R. Birnbaum, D.W. Darnall, Biochemistry **10**, 4556, 1971.
- [11] G.G. Dos Remedios, Nature **270**, 750, 1977.
- [12] W.P. Tew, Biochem. Biophys. Res. Commun. **78**, 624, 1977.
- [13] W. Dew Horrocks, in: Advances in Inorganic Biochemistry, eds. G.L. Eichorn, L.G. Marzilli, Vol. 4, p. 201, Elsevier, NY.
- [14] G.L. Eichorn, J.J. Butzow, Biopolymers **3**, 79, 1965.
- [15] B.F. Rordorf, D.R. Kearns, Biopolymers **15**, 1491, 1976.
- [16] H.E. Bleich, J.A. Glasel, J. Am. Chem. Soc. **97**, 6585, 1975.
- [17] E.R. Birnbaum, J.E. Gomez, D.W. Darnall, J. Am. Chem. Soc. **92**, 5287, 1970.
- [18] E.R. Birnbaum, D.W. Darnall, Bioinorg. Chem. **3**, 15, 1973.
- [19] D.W. Darnall, E.R. Birnbaum, J.E. Gomez, G.E. Smolka, Proc. 9th Rare Earth Res. Conf., Blacksberg, VA, ed. P.E. Field, Vol. 1, pp. 278–291.
- [20] C.K. Luk, Biochemistry **10**, 2838, 1971.
- [21] B. Teuwissen, P.L. Mason, P. Osinski, J.F. Heremans, Eur. J. Biochem. **31**, 239, 1972.
- [22] M.A. Epstein, A. Levitzki, J. Rueben, Biochemistry **13**, 1777, 1974.
- [23] A. Gafni, I.G. Steinberg, Biochemistry **13**, 800, 1974.
- [24] C.K. Luk, F.S. Richardson, J. Am. Chem. Soc. **97**, 6666, 1975.
- [25] S.A. Davis, F.S. Richardson, J. Inorg. Nucl. Chem. **42**, 1973, 1980.
- [26] F.S. Richardson, Chem. Rev. **82**, 541, 1982.
- [27] M. Epstein, J. Rueben, A. Levitzki, Biochemistry **16**, 2449, 1977.
- [28] J. Reuben, J. Chem. Phys. **63**, 5063, 1975.
- [29] J. Reuben, Biochemistry **10**, 2834, 1971; J. Phys. Chem. **75**, 3164, 1971.

- [30] H.G. Brittain, F.S. Richardson, *Bioinorg. Chem.* **7**, 233, 1977.
- [31] G.L. Cottam, A.D. Sherry, K.M. Valentine, in: *Proc. 11th Rare Earth Conf. Traverse City, Michigan*, eds J.M. Hascke, H.A. Eick, Vol. 1. p. 204, 1974.
- [32] A. Levitzki, J. Reuben, *Biochemistry* **12**, 41, 1973.
- [33] B.H. Barber, B. Fuhr, J.P. Carver, *Biochemistry* **14**, 4075, 1975.
- [34] S.K. Dower, R.A. Dwek, A.C. McLaughlin, L.E. Mole, E.M. Press, C.A. Sunderland, *Biochem. J.* **149**, 73, 1975.
- [35] B.S. Cooperman, N.Y. Chin, *Biochemistry* **12**, 670, 1973.
- [36] R. Jones, R.A. Dwek, S. Forsen, *Eur. J. Biochemistry* **47**, 271, 1974.
- [37] R.D. Hershberg, G.H. Reed, A.J. Slotboom, G.H. Dettaas, *Biochemistry* **15**, 2268, 1976.
- [38] K.M. Valentine, G.L. Cottam, *Arch. Biochem. Biophys.* **158**, 346, 1973.
- [39] M. Epstein, A. Levitzki, J. Reuben, *Biochemistry* **13**, 1777, 1974.
- [40] C.D. Barry, A.C.T. North, J.A. Glasel, R.J.P. Williams, *Nature* **232**, 236, 1971.
- [41] V.F. Bystrov, N.I. Dubrovina, L.I. Barsukov, L.D. Bergelson, *Chem. Phys. Lipids* **6**, 343, 1971.
- [42] C.R. Jones, D.R. Kearns, *J. Am. Chem. Soc.* **96**, 3651, 1974.
- [43] J. Reuben, Z. Luz, *J. Phys. Chem.* **80**, 1357, 1974.
- [44] J. Reuben, *J. Phys. Chem.* **75**, 3164, 1971.
- [45] E.C.N.F. Gerald, R.J.P. Williams, *J. Chem. Soc. Dalton* **18**, 1721, 1971.
- [46] E.M. Stephens, C.M. Grisham, *Biochemistry* **18**, 4678.
- [47] G.H. Reed, R.D. Hershberg, G.H. Dettaas, in: *NMR in Biochemistry*, eds S. Opella, P. Lu, Marcel Dekker, NY, 1979.
- [48] E.M. Stephens, Ph.D. Thesis, University of Virginia, 1980.
- [49] G. Musici, G.H. Reed, L.J. Berliner, *J. Inorg. Biochem.* **26**, 229, 1986.
- [50] P.B. O'Hara, S.H. Koenig, *Biochemistry* **25**, 1445, 1986.
- [51] O. Zak, P. Aisen, *Biochemistry* **27**, 1075, 1988.
- [52] K. Spartalian, W.T. Oosterhuis, *J. Chem. Phys.* **59**, 617, 1973.
- [53] A.M. Friedman, J.C. Sullivan, S.L. Ruby, A. Lindenbaum, J.J. Russell, B.S. Zabransky, G.V.S. Rayudu, *J. Nucl. Med. Biol.* **3**, 37, 1976.
- [54] P. Coleman, L.H. Weaver, B.W. Mathews, *Biochem. Biophys. Res. Commun.* **46**, 1999, 1972.
- [55] B.W. Mathews, L.H. Weaver, *Biochemistry* **13**, 1719, 1974.
- [56] K. Kurachi, L.C. Sicker, L.H. Jensen, *J. Biol. Chem.* **250**, 7663, 1975.
- [57] J.W. Becker, G.N. Reeke, Jr., J.L. Wang, B.A. Cunningham, G.M. Edelman, *J. Biol. Chem.* **250**, 1513, 1975.
- [58] L.C. Sicker, E. Adman, L.H. Jensen, *Nature* **235**, 40, 1972.
- [59] K.D. Watenpugh, L.C. Sicker, L.H. Jensen, J. Legall, M. Dubourdiou, *Proc. Nat. Acad. Sci. USA* **69**, 3915, 1972.
- [60] S.H. Kim, G.J. Quigley, F.L. Suddath, A. McPherson, D. Sneden, J.J. Kim, J. Weinzierl, P. Blattmann, A. Rich, *Proc. Nat. Acad. Sci. USA* **69**, 3746, 1972.
- [61] J.D. Robertus, J.E. Ladner, J.T. Finch, D. Rhodes, R.S. Brown, B.F.C. Clark, A. Klug, *Nature* **250**, 546, 1974.
- [62] R.T. Briggs, D.B. Drath, M.L. Karnovsky, M.J. Karnovsky, *J. Cell Biol.* **67**, 566, 1975.
- [63] T. Fujimoto, K. Inomato, K. Ogawa, *Histochem. J.* **14**, 87, 1982.
- [64] F. Calvet, B.M. Siegel, K.G. Stern, *Nature* **162**, 305, 1948.
- [65] M. Shaklai, M. Tavassoli, *J. Histochem. Cytochem.* **30**, 1325, 1982.
- [66] R.M. Mason, R.W. Mayes, *Biochem. J.* **131**, 535, 1973.
- [67] P.J. Roughley, M. Hatt, R.M. Mason, *Biochem. Biophys. Acta* **539**, 445, 1978.
- [68] B.C. Furie, B. Furie, *J. Biol. Chem.* **250**, 601, 1975, *ibid.* **248**, 5821, 1973.
- [69] C.H. Evans, W.P. Tew, *Science* **213**, 653, 1981.
- [70] N.A. Kostromina, *Zhur. Neorg. Khim.* **16**, 2966, 1971.
- [71] A.D. Sherry, G.L. Cottam, *Arch. Biochim. Biophys.* **156**, 665, 1973.
- [72] G.A. Elagavish, J. Reuben, 1978.
- [73] C.M. Dobson, G.R. Moore, R.J.P. Williams, *FEBS Lett.* **51**, 60, 1975.
- [74] S.P. Tanner, G.R. Choppin, *Inorg. Chem.* **7**, 2046, 1968.
- [75] E. Nieboer, W.P. Flora, M. Podolski, H. Falter, *Proc. 10th Rare Earth Conf.*, eds C.J. Kevane, T. Moeller, Vol. 1, Arizona, 1973.
- [76] A. Aziz, S.J. Lyle, J.E. Newbery, *J. Inorg. Nucl. Chem.* **33**, 1757, 1971.
- [77] F.S. Inagaki, M. Takahashi, M. Tasumi, T. Miyazawa, *Bull. Chim. Soc. Japan* **48**, 853, 1975.

- [78] J.H. Bradbury, L.R. Porown, M.W. Crompton, B. Warren, *Anal. Biochem.* **62**, 30, 1974.
- [79] J.G. Shelling, M.E. Bjornson, R.S. Hodges, A.K. Taneja, B.D. Sykes, *J. Magn., Reson.* **57**, 99, 1984.
- [80] B.W. Mathews, L.H. Weaver, W.R. Kester, *J. Biol. Chem.* **249**, 8030, 1974.
- [81] A.P. Snyder, D.R. Sudnick, V.K. Arkle, W. Dew Horrocks, *Biochemistry* **20**, 3334, 1981.
- [82] P.C. Moews, R.H. Kretsinger, *J. Mol. Biol.* **91**, 229, 1975.
- [83] T.C. Williams, D.C. Corson, B.D. Sykes, *J. Am. Chem. Soc.* **106**, 5698, 1984.
- [84] A. Cave, M.F. Dares, J. Parello, A. Saint-Yves, R. Sempere, *Biochimie* **61**, 755, 1979.
- [85] L. Lee, B.D. Sykes, *Biochemistry* **20**, 1156, 1981.
- [86] F. Ostroy, R.A. Gams, J.D. Glickson, R.E. Lenkinski, *Biochim. Biophys. Acta* **527**, 56, 1978.
- [87] M. Epstein, A. Levitzki, J. Reuben, *Proc. 10th Rare Earth Conf.*, Vol. 1, p. 124, Plenum, NY, 1973.
- [88] P. Tanswell, E.W. Westhead, R.J.P. Williams, *FEBS Lett.* **48**, 60, 1974.
- [89] P. Tanswell, E.W. Westhead, R.J.P. Williams, *Eur. J. Biochem.* **63**, 249, 1976.
- [90] C.D. Barry, J.A. Giasel, A.C.T. North, R.J.P. Williams, A.V. Xavier, *Biochim. Biophys. Acta* **262**, 101, 1972.
- [91] C.M. Dobson, C.F.G.C. Geraldles, G. Ratcliffe, R.J.P. Williams, *Eur. J. Biochem.* **88**, 259, 1978.
- [92] J. Galea, R. Beccaria, G. Ferroni, J.P. Belaich, *Electrochim. Acta* **23**, 647, 1978.
- [93] C. Formoso, *Biochem. Biophys. Res. Commun.* **53**, 1084, 1973.
- [94] D.K. Lavalley, A.H. Zeltman, *J. Am. Chem. Soc.* **96**, 5552, 1974.
- [95] C.F.G.C. Geraldles, R.J.P. Williams, *Eur. J. Biochem.* **85**, 1978.
- [96] K.J. Ellis, J.F. Morrison, *Biochim. Biophys. Acta* **362**, 201, 1974.
- [97] J.F. Morrison, W.W. Cleland, *Biochemistry* **22**, 5507, 1983.
- [98] T. Haertle, J. Augustyniak, W. Gusehlbauer, *Nucleic Acids Res.* **9**, 61, 91, 1981.
- [99] M.D. Topal, J.R. Fresco, *Biochemistry* **19**, 5531, 1980.
- [100] D.S. Gross, H. Simpkins, *J. Biol. Chem.* **256**, 9593, 1981.
- [101] G. Yonuschot, G. Robey, G.W. Mushrush, D. Helman, G. Van de Woude *Bioinorg. Chem.* **8**, 397, 1978.
- [102] D.E. Draper, *Biophys. Chem.* **21**, 91, 1985.
- [103] E. Bamann, H. Trapmann, F. Fischler, *Biochem. Z.* **328**, 89, 1954.
- [104] G. Yonuschot, G.W. Mushrush, *Biochemistry* **14**, 1677, 1975.
- [105] M.S. Kayne, M. Cohn, *Biochemistry* **13**, 4159, 1974.
- [106] S.J. Angyal, *Carbohydr. Res.* **26**, 271, 1973; *Tetrahedron* **30**, 1695, 1974.
- [107] S.J. Angyal, *Aust. J. Chem.* **25**, 1957, 1972.
- [108] R.E. Lenkinski, J. Reuben, *J. Am. Chem. Soc.* **98**, 3089, 1976.
- [109] T. Anthonsen, B. Larsen, O. Smidsrod, *Acta Chem. Scand.* **26**, 2988, 1972; **27**, 2671, 1973.
- [110] B. Casu, G. Gatti, N. Cyr, A.S. Perlin, *Carbohydrate Res.* **41**, C6, 1975.
- [111] L.D. Hall, C.M. Preston, *Carbohydrate Res.* **41**, 53, 1975.
- [112] W. Dew Horrocks, C.P. Wong, *J. Am. Chem. Soc.* **98**, 7157, 1976.
- [113] G.T. Bratt, H.P. Hogen Kamp, *Arch. Biochem. Biophys.* **218**, 225, 1982.
- [114] B.P. Shastri, M.B. Shankaran, K.R. Easwaran, *Biochem.* **26**, 4925, 1987.
- [115] F.S. Richardson, A.D. Gupta, *J. Am. Chem. Soc.* **103**, 5716, 1981.
- [116] R.A. Velapoldi, O. Menis, *Clin. Chem.* **17**, 1165, 1971.
- [117] G. Assmann, E.A. Sokoloski, H.B. Brewer, *Proc. Natl. Acad. Sci. USA* **71**, 549, 1974.
- [118] T. Sarna, J.S. Hyde, H.M. Swartz, *Science* **192**, 1132, 1976.
- [119] R.V. Smith, P.W. Erhardt, D.B. Rusterholz, C.F. Barfknecht, *J. Pharm. Sci.* **65**, 412, 1976.
- [120] G.R. Mines, *J. Physiol. (London)* **40**, 327, 1910; **42**, 309, 1911.
- [121] J.Y. Lettvin, W.F. Pickard, W.S. McCulloch, W. Pitts, *Nature* **202**, 1338, 1964.
- [122] H. Akutsu, J. Seelig, *Biochemistry* **10**, 7366, 1981.
- [123] H. Grasdalen, L.E.G. Eriksson, J. Westman, A. Ehrenberg, *Biochim. Biophys. Acta* **469**, 151, 1977.
- [124] H. Hauser, M.C. Phillips, B.A. Levine, R.J.P. Williams, *Eur. J. Biochem.* **58**, 133, 1975.
- [125] H. Hauser, M.C. Phillips, B.A. Levine, R.J.P. Williams, *Nature* **261**, 390, 1976.
- [126] Y.K. Levine, A.G. Lee, N.J.M. Birdsall, J.C. Metcalfe, J.D. Robinson, *Biochim. Biophys. Acta* **291**, 592, 1973.
- [127] A. Chrzyszczek, A. Wishnia, C.S. Springer, *Biochim. Biophys. Acta* **648**, 28, 1981.
- [128] T.J. McIntosh, *Biophys. J.* **29**, 237, 1980.
- [129] R.G. Canada, *Biochem. Biophysics. Res. Commun.* **111**, 135, 1983.



- [130] E. El-Fakahny, J.R. Lopez, E. Richelson, J. Neurochem. **40**, 1687, 1983.
- [131] S.J. Dunbar, Comp. Biochem. Physic. **72A**, 199, 1982.
- [132] R.T. Briggs, D.B. Drath, M.L. Karnovsky, M.J. Karnovsky, J. Cell. Biol. **67**, 566, 1975.
- [133] M. Crompton, I. Heid, C. Baschera, E. Carafoli, FEBS Lett. **104**, 352, 1979.
- [134] K.H. Wedepohl, Handbook of Geochemistry, II-2/57-71, Springer Verlag, Berlin.
- [135] P. Pascal, Nouveau Traite de Chimie Minerale, Tome VII, Masson et Cie, Paris, 1959.
- [136] H.J. Rosler, H. Large, Geochemical Tables, Elsevier, 1972.
- [137] H.J.M. Bowen, Environmental Chemistry of Elements, Academic Press, 1979.
- [138] J.D. Burton, Radioactive Nuclides in the Marine Environment, in: Chemical Oceanography, eds J.P. Riley, G. Skirrow, Vol. 3, pp. 91-191, Academic Press, 1975.
- [139] A.M. Ure, M.L. Berrow, Environmental Chemistry **II**, 114-118, 1982.
- [140] P.J. Coughtrey, M.C. Thorne, Radionuclide Distribution and Transport, in: Terrestrial and Aquatic Ecosystems, Vol. 2, p. 455, Balkema, Rotterdam, 1983.
- [141] R.E. Meyer, D.A. Palmer, W.D. Arnold, F.I. Case, in: Geochemical Behaviour of Disposed Radioactive Waste, eds G. Scott Barney, J.D. Naurtil, W.W. Schulz, ACS Ser. **246**, pp. 76-94, 1984.
- [142] L. Carlsen, Radionuclide-Soil Organic Matter Interactions, CEC, 1984.
- [143] J.R. Bacon, A.M. Ure, Anal. Chim. Acta **105**, 163, 1979.
- [144] Handbook of Physics and Chemistry, The Chemical Rubber Co., USA.
- [145] R.M. Smith, A.E. Martell, Critical Stability Constants, Vol. 4, Inorg. Complexes, 1976.
- [146] C.F. Baes Jr., R.E. Mesmer, The Hydrolysis of Cations, J. Wiley & Sons, NY, 1976.
- [147] L. Ciavatta, D. Ferri, I. Grenthe, F. Salvatore, K. Spahio, Acta Chem. Scand. A **35**, 403, 1981.
- [148] D. Ferri, I. Grenthe, S. Hietanen, F. Salvatore, Acta Chem. Scand. A **37**, 359, 1983.
- [149] J.L. Means, T. Kucak, D.A. Crerar, Env. Pollution, Ser. B. **45**, 1980.
- [150] B.S. Jensen, Migration Phenomena of Radionuclides into the Geosphere, Harwood Acad. Publ., 1982.
- [151] B.S. Jensen, Complex Formation of Selected Radionuclides with Ligands Commonly Found in Groundwater: Low Molecular Organic Acid., CEC.
- [152] W.O. Robinson, H. Bastron, K.J. Murata, Geochim. Cosmochim. Acta **14**, 55, 1958.
- [153] C. Milton, K.J. Murata, M.K. Knechtel, Am. Mineral. **29**, 92, 1944.
- [154] E.S. Gladney, Anal. Chim. Acta. **118**, 385, 1980.
- [155] J.M. Sobek, D.E. Talburt, J. Bacteriol. **95**, 47, 1968.
- [156] K. Takada, Health Phys. **35**, 537, 1978.
- [157] P.W. Durbin, M.H. Williams, M. Gee, R. Newman, J.G. Hamilton, Proc. Soc. Exp. Biol. Med. **91**, 78, 1956.
- [158] H. Hart, in: Rare Earths in Biochemical and Medical Research, eds G.C. Kyker, E.D. Anderson, pp. 118-135, US Atomic Energy Commission Report ORINS-12, 1956.
- [159] T.J. Haley, J. Pharm. Sci. **54**, 663, 1965: Handbook of Physics and Chemistry of Rare Earths, eds K.A. Gscheidner, L.R. Eyring, Vol. 4, North-Holland, Amsterdam.
- [160] B. Venugopal, T.D. Luckey, Metal Toxicity in Mammals, Vol. 2, Chemical Toxicity of Metals and Metalloids, Chapter 3, pp. 101-173, Plenum Press, NY.
- [161] P. Arvela, Prog. Pharmacol. **2**, 71-114, 1979.
- [162] A. Muroma, Am. Med. Exp. Biol. Fenn. **36** (Suppl. 6), 1-54, 1958.
- [163] D.W. Bruce, B.E. Heitbrink, K.P. DuBois, Toxicol. Appl. Pharmacol. **5**, 750, 1963.
- [164] D. Lazlo, D.M. Ekstein, R. Lewin, K.G. Stern, J. Natl. Cancer Inst. **13**, 559, 1952.
- [165] J.G. Graca, E.L. Garst, W.E. Lowry, A.M.A. Arch. Ind. Health **15**, 9, 1957.
- [166] M.H. Husain, J.A. Dick, Y.S. Kaplan, J. Soc. Occup. Med. **30**, 15, 1980.
- [167] T.J. Haley, K. Raymond, N. Komesu, H.C. Upham, Br. J. Pharmacol. **17**, 526, 1961.
- [168] T.J. Haley, H.C. Upham, Nature **200**, 271, 1963.
- [169] B. von Lehmann, E. Oberdisse, O. Grajewski, H.R. Arntz, Arch. Toxicol. **34**, 89, 1975.
- [170] R.B. Hunter, W. Walker, Nature **178**, 47, 1956.
- [171] V. Ramachandra Rao, K.V.B. Rao, R. Nagabhusanam, An Indo-United States symposium on 'Bioactive Compounds from Marine Organisms' with emphasis on Indian Ocean, ed. M.F. Thompson, Oxford & IBH Publishing Co., New Delhi, 1991.
- [172] K.J. Ellis, Inorg. Perspect. Biol. Med. **1**, 101-135, 1977.
- [173] L. Manafo, Panminerva Med. **25**, 151, 1983.
- [174] S.B. Beaser, A. Segel, L. Vandam, J. Clin. Inves. **21**, 447, 1942.
- [175] E. Vineke, E. Sucker, Arch. Exp. Pathol. **187**, 594, 1950.

- [176] S. Divald, M.M. Joulie, in: *Medicinal Chemistry*, ed. Burger, 3<sup>rd</sup> edn, Part II, pp. 1092–1122, Wiley Inter Science, New York, 1970.
- [177] J. Cassar, F.H. Doyle, P.D. Lewis, K. Mashiter, S. van Noorden, G.F. Joplin, *Br. Med. J.* **2**, 269, 1976.
- [178] C.W. Burke, F.H. Doyle, G.F. Joplin, R.N. Arndt, D.P. Macerlean, T.R. Fraser, *Quart. J. Med.* **42**, 693, 1973.
- [179] W. Fasching, G. Wense, A. Zangl, *Bull. Soc. Int. Chir.* **2**, 81, 1974.
- [180] K. Hisada, N. Tomami, T. Hiraki, A. Ando, *J. Nucl. Med.* **15**, 210, 1974.
- [181] J.E. Chatal, B.P. LeMevel, R. Guihard, E. Guihard, C. Moigneteau, *J. Radiol. Electrol.* **56**, 401, 1975.
- [182] F.H. Deland, A.E. James, H.N. Wagner, F. Hosain, *J. Nucl. Med.* **12**, 683, 1971.
- [183] C.D. Russell, P.G. Bischoff, F.N. Katzen, K.L. Rowell, M.U. Yester, L.K. Lloyd, W.N. Tauxe, E.V. Dubovsky, *J. Nucl. Med.* **26**, 1243, 1985.
- [184] D.P. Hutcheson, B. Venugopal, D.H. Gray, T. Luckey, *J. Nutr.* **109**, 702, 1979.
- [185] N. Adiseshan, F.L. Johnson, I.H. Butfield, *Aust. NZ J. Med.* **5**, 256, 1975.
- [186] D.H. Carr, J. Brown, G.M. Bydder, R.E. Steiner, H.J. Weinmann, U. Speck, A.S. Hall, I.R. Young, *Am. J. Radiol.* **143**, 215, 1984.
- [187] G.M. Bydder, D.P. Kingsley, J. Brown, H.P. Niendorf, I.R. Young, *J. Comput. Assist. Tomogr.* **9**, 690, 1985.
- [188] C. Clausen, M. Laniado, E. Kazner, W. Schorner, R. Felix, *Neuro Radiology* **27**, 164, 1985.
- [189] S.H. Heywang, D. Hahn, H. Schmidt, I. Krischke, W. Eiermann, R. Bassermann, J. Lissner, *J. Comput. Assist. Tomogr.* **10**, 199, 1986.
- [190] C.S. Springer, W.D. Rooney, *Proc. Int. Soc. Magn. Reson. Med.* **9**, 2241, 2001.
- [191] A. Havron, M.A. Davis, S.E. Selter, A.J. Paskins-Hurlburt, S.J. Hessel, *J. Comput., Assist. Tomogr.* **4**, 642, 1980.
- [192] P.F. Spooen, J.J. Rasker, R.P. Arens, *Eur. J. Nucl. Med.* **10**, 441, 1985.
- [193] C.J. Menkes, A. LeGo, P. Verrier, M. Aignan, F. Delbarre, *Am. Rheum. Dis.* **36**, 254, 1977.
- [194] C.B. Sledge, J.D. Zuckerman, M.R. Zalutsky, R.W. Atcher, S. Shortkroff, D.R. Lionberger, H.A. Rose, B.J. Hurson, P.A. Lankener, R.J. Anderson, W.A. Bloomer, *Arthritis Rheum.* **29**, 153, 1986.
- [195] D.R. Bard, C.G. Knight, T.D.P. Page, *Clin. Exp. Rheumatol.* **3**, 237, 1985.
- [196] D. Kramsh, A.J. Aspan, C.S. Apstein, *J. Clin. Invest.* **65**, 967, 1980.
- [197] R. Ginsberg, K. Davis, M.R. Bristow, K. Mckennet, S.R. Kodsi, M.E. Billingham, J.S. Schroeder, *Lab. Invest.* **49**, 154, 1983.
- [198] H. Jancso, *J. Pharmacol.* **13**, 577, 1962.
- [199] C.H. Evans, *Orthop. Surv.* **3**, 63, 1979; *Eur. J. Biochem.* **151**, 29, 1985.
- [200] R.D. Deloune, J.S. Whitcomb, W.H. Patrick, J.H. Pardue, R.S. Pezeshki, *Estuaries* **12**, 247, 1989.
- [201] R.M. Knaus, D.L. Van Gent, *Estuaries* **12**, 269, 1989.
- [202] A.T. Showler, R.M. Knaus, T.E. Reagan, *Agri. Ecosystems Environ.* **30**, 97, 1990.
- [203] A.T. Showler, R.M. Knaus, T.E. Reagan, *Insectes Sociaux* **36**, 235, 1989.
- [204] R.M. Knaus, L.R. Curry, *Bull. Environ. Contam. Toxicol.* **21**, 388, 1979.
- [205] R.M. Knaus, *Environ. Sci. Technol.* **15**, 809, 1981.
- [206] R.M. Knaus, A.H. El-Fawari, *Environ. Exptl. Bot.* **21**, 217, 1981.
- [207] B. Guo, X. Tang, Q. Zhou, *Eur. J. Solid State Inorg. Chem.* **28**, 393, 1991.
- [208] H.L. Zheng, Z.Q. Zhao, C.G. Zhang, J.Z. Feng, Z.L. Ke, M.J. Su, *Biomaterials* **13**, 157–163, 2000.

chapter 12

---

APPLICATIONS

---

---

# CONTENTS

---

1. Role of rare earths in steels . . . . .	896
2. Cathodic inhibition by rare earth metal compounds . . . . .	898
2.1. Electrochemical studies . . . . .	898
2.2. Film characteristics . . . . .	900
2.3. Mechanism of inhibition . . . . .	900
3. Rare earths as catalysts . . . . .	902
3.1. Function of lanthanides . . . . .	902
3.2. Fluid catalytic cracking (FCC) . . . . .	905
3.3. Automotive pollution control . . . . .	905
3.4. Polymerization catalysts . . . . .	906
3.5. Other applications . . . . .	906
3.6. Further applications . . . . .	906
3.7. Pollution control . . . . .	906
3.8. Catalytic (flameless) combustion . . . . .	906
3.9. Polymer production . . . . .	907
3.10. Alternative fuels technology and chemicals manufacture . . . . .	907
4. Use of rare earths in paints and pigments . . . . .	907
5. Use of rare earths in cinema arc carbons . . . . .	908
6. Rare earths in alloys . . . . .	909
6.1. Misch metal . . . . .	909
6.2. Titanium alloys . . . . .	909
6.3. Nickel–iron–cobalt-base superalloys . . . . .	910
6.4. Chromium-base alloys . . . . .	911
6.5. Rapidly solidified alloys . . . . .	913
7. Rare earth magnets . . . . .	916
7.1. Applications [42] . . . . .	917
7.2. DC motors . . . . .	918
7.3. AC motors . . . . .	919
7.4. Other miscellaneous applications . . . . .	920
7.5. Dental applications . . . . .	920
8. Nd–Fe–B powders for bonded magnets . . . . .	920
9. Rare earths in lasers . . . . .	921
9.1. Rare earth ions . . . . .	921
9.2. Lasers . . . . .	922

10. Hi-tech applications [45] . . . . .	924
10.1. Hydrogen fuel storage for automobiles . . . . .	924
10.2. Chemical heat pump . . . . .	924
10.3. Metal hydride battery . . . . .	925
10.4. Perpendicular magneto-optical disk as high density storage media . . . . .	925
10.5. Magnetic refrigeration in cryogenics . . . . .	926
10.6. Magneto-strictive alloys . . . . .	926
10.7. Outlook for rare earth based metal hydrides and NiMH rechargeable batteries . . . . .	927
11. Photonics, electronics and related applications [48] . . . . .	928
11.1. Photonics . . . . .	929
11.2. Electronics . . . . .	930
12. Applications in ceramics . . . . .	931
12.1. Stabilized zirconia . . . . .	933
12.2. Oxygen sensors . . . . .	933
13. Applications in fiber optics, luminescent solar concentrators . . . . .	936
13.1. Fiber optics . . . . .	936
13.2. Crystal lasers . . . . .	938
13.3. Single-mode fibre lasers [115] . . . . .	939
13.4. Luminescent solar concentrators (LSC) . . . . .	939
14. Rare earth substituted garnet films for magnetic bubble memory applications . . . . .	940
15. Rare earth phosphors [130] . . . . .	941
15.1. Emission of rare earth ions . . . . .	941
15.2. Phosphors for fluorescent lamps . . . . .	941
15.3. Phosphors for CRTs . . . . .	943
15.4. Phosphors for vacuum UV excitation . . . . .	943
15.5. Rare earth phosphors in semiconducting light emitting diodes . . . . .	944
16. Rare earths in superconductors . . . . .	948
17. Rare earth complexes in organic synthesis . . . . .	952
17.1. Reactions involving the carbon-carbon bond formation . . . . .	952
17.2. Carbon-oxygen bond formation . . . . .	958
17.3. Carbon-nitrogen bond formation . . . . .	958
17.4. Lanthanide based organometallic compounds . . . . .	960
18. Rare earths in radionuclide therapy . . . . .	961
19. Applications of luminescent lanthanide complexes . . . . .	962
19.1. Emission properties of lanthanide chelates . . . . .	964
19.2. The dissociative enhancement principle . . . . .	966
19.3. Future prospects . . . . .	969
20. Rare earth compounds in imaging applications . . . . .	970
20.1. Magnetic resonance imaging . . . . .	970
20.2. Application . . . . .	973
20.3. Progress in contrast reagents . . . . .	974
References . . . . .	977

The current and potential uses or applications of rare earth elements are given in Table 12.1. Ref. [1].

### 1. Role of rare earths in steels

Rare earths have been used in steels as deoxidizers and desulphurizers since the 1920s. Addition of rare earths to steels improves physical, mechanical and chemical properties of steels. Some examples are cleanliness, toughness, grain refinement, directionality of mechanical properties, weldability, hydrogen damage, aqueous corrosion and high temperature corrosion of steels. In physical properties such as melting points and vapor pressures, rare earths differ from iron to such an extent that problems of dissolution or vaporization during addition to molten steel are not likely to occur. The lower vapor pressures of rare earths at steel-making temperatures is a major advantage over alternative elements like calcium and magnesium. Rare earth metals are very reactive and readily combine with oxygen, sulphur and nitrogen to form oxides, sulphides and nitrides, respectively. Rare earths do not readily form carbides in iron and steels. Thus rare earths are useful in ferrous process metallurgy for deoxidation and desulphurization of steels and cast iron.

Free energies of formation of rare earth compounds are in the order: oxides > oxysulphides > sulphides > nitrides > carbides. Thermodynamically, the addition of rare earths in steel-making should favour deoxidation and desulphurization.

In other words, the deoxidation and desulphurization are complex processes which depend upon the corresponding 'solubility products' when rare earths are added to steels.

- (i) Rare earths can reduce oxygen levels in steel to values obtained with other deoxidizers such as carbon. Refractories used in steel-making or melting that are compatible with rare earths as deoxidizers are compounds such as magnesia. Desulphurization of steels is effective with rare earths at low oxygen contents. Addition of rare earths to steel eliminates the deleterious effects of impurities like lead, tin, and arsenic which concentrate at the grain boundary and thereby decrease the hot workability of steels.
- (ii) Non-metallic inclusions in steels act as nucleating sites for void formation in the ductile fracture of steels and consequent deleterious effect on ductility and toughness of steels. The volume fraction of inclusions is related to the ductility of steels. Directionality of mechanical properties such as toughness and formability of hot-rolled steels are affected by the presence of elongated MnS inclusions which are oriented parallel to the plane of fracture in the transverse specimens. Directionality can be reduced by shape control of inclusions such as globular MnS inclusions instead of elongated inclusions. Shape control of inclusions has been achieved by adding rare earth elements such as cerium with a Ce/S ratio greater than 4.

TABLE 12.1  
The rare earth elements—current and potential uses.

Element	Atomic number	Chemical symbol	Uses
Yttrium	39	Y	High-temperature alloys, metallurgy, red phosphor, optical glasses, ceramics, catalysts, lasers, microwave devices
Lanthanum	57	La	Misch metal*, high-refraction low-dispersion glasses, arc light carbons, petroleum cracking catalysts
Cerium	58	Ce	Polishing powders, opacifier for porcelain coatings, glass decolouriser and melting accelerator, photographic materials, textiles, arc lamps, ferrous and non-ferrous alloys including high-temperature Mg alloys, automotive catalytic converters, misch metal*
Praseodymium	59	Pr	Alloys, didymium glass (for protective goggles), yellow ceramic pigments, cryogenic refrigerant, misch metal*
Neodymium	60	Nd	Electronics, steel manufacture, glazes and coloured glass (including didymium glass), lasers, magnets, petroleum cracking catalysts, misch metal*
Promethium	61	Pm	(All isotopes are radioactive and synthetically prepared.) Miniature batteries for harsh environments
Samarium	62	Sm	Reactor control and neutron shielding, magnets, luminescent and infra-red absorbing glasses, catalysts, ceramics, electronic devices, magnetostrictive alloys, misch metal*
Europium	63	Eu	Phosphor activator, electronic materials, neutron absorber
Gadolinium	64	Gd	Electronic materials, high-temperature refractories, alloys, cryogenic refrigerant, thermal neutron absorber, superconductor, magnetic materials, bubble memory substrates
Terbium	65	Tb	Lasers, electronic materials, erasable optical memory substrate, magnetostrictive alloys
Dysprosium	66	Dy	Catalysts, electronic materials, phosphor activators, magnetic refrigeration, magnetostrictive alloys
Holmium	67	Ho	Electronic devices, catalysts, refractories, magnetic materials, magnetostrictive alloys
Erbium	68	Er	Infrared-absorbing glasses, phosphor activator
Thulium	69	Tm	Portable X-ray units
Ytterbium	70	Yb	Research applications
Lutetium	71	Lu	Research applications

\*Misch metal is an alloy of about 50% cerium, 25% lanthanum, 15% neodymium and 10% other rare earth metals. Uses include manufacture of a pyrophoric alloy with iron and deoxidizer in metallurgical applications, getter for removal of oxygen from vacuum tubes, high strength magnesium alloys.

- (iii) Addition of rare earths results in grain refinement of steels through the formation of rare earth compounds facilitating heterogeneous nucleation during solidification.
- (iv) Addition of rare earths to cast iron modify the microstructure and improve ductility and toughness of samples. As a result of rare earths addition to the product, cast irons of high wear resistance, high strength, reduced brittleness, increased bending strength, and impact strength, improved machinability, improved corrosion resistance and damping capacity and a product devoid of pinholes and microporosity can be obtained.

Steels and steel structures in service can fail by many modes. One major mode of failure is hydrogen embrittlement cracking. High strength steels are particularly sensitive to hydrogen embrittlement. Additions of Ce or La to high strength steels improve their resistance to hydrogen embrittlement mode of failure through a microstructure consisting of continuous grain boundary inclusions which trap the hydrogen and inhibit its transport to the crack tip. Cerium in steels reduces the permeability of hydrogen through high strength steels and consequently reduce the flow of hydrogen from bulk metal to the crack tip.

Rare earth elements such as La on addition to ferritic stainless steels show improved creep strength over steels devoid of lanthanum. High strength steels are extensively used in the aerospace industry. Welding is an important step in the fabrication of steel structures. Welding can result in some problems such as (a) burning and tearing in the heat affected zone, (b) hydrogen-induced heat affected zone cracking, (c) heat affected zone cracking during heat treatment, (d) brittle fracture, (e) knife line attack. Rare earth additions to steels are generally found to suppress the problems encountered in the welding process used in the fabrication of steel structures.

## 2. Cathodic inhibition by rare earth metal compounds

The mitigation of corrosion can be achieved economically by the use of corrosion inhibitors. Chromate has been extensively used in an aqueous environment for the protection of aluminium, zinc and steel. Although chromates are cheap and effective, they are not acceptable because of their toxicity. Alternate inhibitors such as molybdates, organic inhibitors such as phosphonates, mixtures of phosphates, borates and silicates and surfactants like sulfonates have been used in place of chromates. Chromates are anodic inhibitors and help to form passive oxide on the metal surface.

In recent years, the use of rare earth metal salts as inhibitors has been gaining attention. Rare earth metal salts have been found to be effective inhibitors for the protection of aluminium alloys, mild steel and zinc.

### 2.1. Electrochemical studies

Potentiodynamic polarization studies [4] on aluminum alloy AA 7075 in air saturated 0.1 M NaCl solution with and without the addition of 1000 ppm each of  $\text{CeCl}_3$ ,  $\text{PrCl}_3$  and  $\text{YCl}_3$ , yielded the polarization curves shown in Fig. 12.1.

It is seen from the figure that in a 0.1 M NaCl solution, the corrosion potential,  $E_{\text{corr}}$  and pitting potential,  $E_{\text{pit}}$ , are identical with a value of  $-0.72$  V (vs SCE). The cathodic branch of the curve shows the current density to be independent of potential. This shows oxygen reduction to be the main cathodic reaction. When the inhibitor is added, the cathodic branch of the curve shifts to more negative potentials and lower current densities indicating a reduction in the rate of oxygen reaction.  $E_{\text{corr}}$  is shifted away from  $E_{\text{pit}}$  and into the cathodic region. The potential shifts are about 160 mV in the case of  $\text{CeCl}_3$  and  $\text{PrCl}_3$  and 50 mV in the case of  $\text{YCl}_3$ . The widening of the gap between  $E_{\text{corr}}$  and  $E_{\text{pit}}$  is attributed to increased resistance to pitting. The suppression of the cathodic reaction is due to the formation of a rare earth metal oxide film during polarization at cathodic potentials. Similar observations [5] have been made in the inhibition of Al-Zn-Mg alloy in NaCl solutions when the alloy



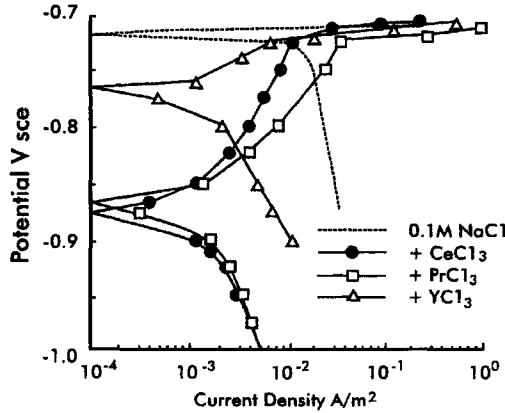


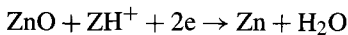
Fig. 12.1. Polarization curves for 7075 Al in 0.1 M NaCl and in 0.1 M NaCl with 1000 ppm of various REM chlorides (from R.B.W. Hinton in: Corrosion Inhibitor Science and Technology (1993), edited by A. Raman and P. Labine, I-11-1. © Copyright by NACE International. All rights reserved by NACE; reprinted with permission).

tested had 0.2% cerium. In this case, cerium oxide may be present in the aluminium oxide or may be initially dissolved and later precipitated on the surface of the alloy.

Polarization curves obtained [6] for 7075 aluminium in 0.1 M NaCl alone and with the addition of different amounts of  $\text{CeCl}_3$  showed that  $E_{\text{corr}}$  shifts away from  $E_{\text{pit}}$  in a gradual manner as a function of  $\text{CeCl}_3$  concentration. At 0–10 ppm of  $\text{CeCl}_3$ , the coverage of the metal surface with cerium oxide increases, along with reduction in current density. At 10–1000 ppm of  $\text{CeCl}_3$ , the alloy is completely covered with cerium oxide along with inhibition of oxygen reduction reaction. There is no significant effect above 1000 ppm  $\text{CeCl}_3$ .

Cathodic polarization curves for mild steel exposed to air-saturated tap water and tap water containing 200 ppm of  $\text{CeCl}_3$  [7] showed that oxygen reduction is the primary cathodic reaction in aerated solutions devoid of  $\text{CeCl}_3$  and the current density is considerably reduced by the addition of  $\text{CeCl}_3$ . A pale yellow film was also observed on the sample.

Cathodic polarization characteristics of zinc in 0.1 M NaCl with and without  $\text{CeCl}_3$  addition showed that reduction of oxygen is the primary cathodic reaction. Addition of  $\text{CeCl}_3$  reduces the rate of cathodic reaction. The observed peak in 0.1 M NaCl at  $-1300$  mV has been attributed to the reduction of ZnO film



The reaction is pH dependent and is described by the equation

$$E = E^0 - 0.059\text{pH}$$

The calculated pH of the sample at  $-1300$  mV is 10.5 which is higher than the value of 8.3 obtained in  $\text{CeCl}_3$  solution at a peak value of  $-1170$  mV. The lower pH in  $\text{CeCl}_3$  solution is evidence of inhibition of the cathodic reaction by  $\text{CeCl}_3$ . The polarization curve obtained after 64 h shows a further reduction in current density, which suggests the presence of surface film responsible for inhibition of the cathodic reaction.

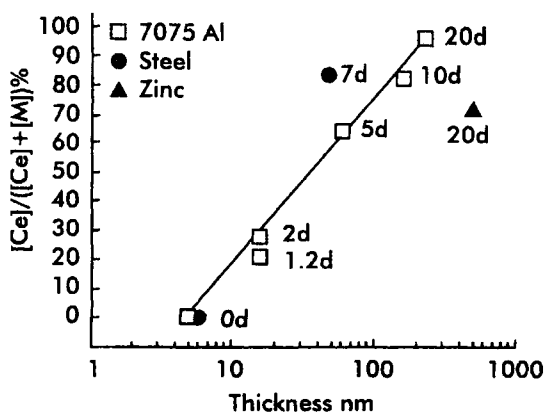


Fig. 12.2. The surface atom concentration ratio [Ce] to ([Ce] + [M]), in which M is either Al, Zn, or Fe, as a function of thickness of cerium oxide film, both determined by AES profiling, for alloys immersed in solution for the number of days indicated (from R.B.W. Hinton in: Reviews on Corrosion Inhibitor Science and Technology (1993), edited by A. Raman and P. Labine, I-10-1. © Copyright by NACE International. All rights reserved by NACE; reprinted with permission).

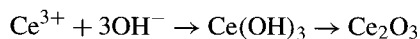
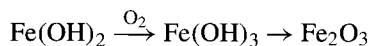
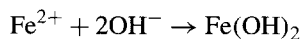
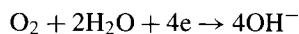
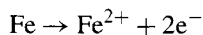
## 2.2. Film characteristics

The formation of a rare earth metal oxide on the metal surface, impedes the cathodic reduction of oxygen and thus cathodic inhibition is achieved by the addition of a rare earth metal salt to a system. The surface atom concentration ratio,  $[Ce/Ce + M]$ , where M is Fe, Al or Zn, is a function of cerium oxide film thickness determined by AES depth profiles as shown in Fig. 12.2.

The metal surface is covered with cerium oxide and the thickness of the film increases with time of immersion of the sample in the  $CeCl_3$  solution. Deposition and growth of islands of rare earth oxide have been observed. The islands may be associated with anodic and cathodic sites located in the microstructure of the metal.

## 2.3. Mechanism of inhibition

Based on the electrochemical polarization and surface analytical data available, it is possible to surmise the following mechanism for inhibition by rare earth metal salts:



### 2.3.1. Corrosion inhibition by rare earth metal salts

Studies on the corrosion inhibition of aluminium alloys, mild steel and zinc by rare earth metal salts are summarized in Table 12.1a.

Rare earth metal salts have been found to be effective inhibitors for various forms of corrosion as illustrated in Table 12.1b.

TABLE 12.1a

Metal	Conditions	Reference
Al AA7075 (Al-Zn-Mg-Cu)	0.1 M NaCl; CeCl <sub>3</sub> , LaCl <sub>3</sub> , YCl <sub>3</sub> inhibitors (0–10 000 ppm)	[6]
AA2024 (Al-Cu-Mg)	0.1 M NaCl; CeCl <sub>3</sub> , LaCl <sub>3</sub> , YCl <sub>3</sub> inhibitors (0–10 000 ppm)	[8]
Al alloy	0.6 M NaCl; 500 ppm CeCl <sub>3</sub>	[9]
AA 2014	Aerated 3.5% NaCl; 1375 ppm Y(NO <sub>3</sub> ) <sub>3</sub>	[10]
Al	CeCl <sub>3</sub> · 7H <sub>2</sub> O	[8]
AA7075	0.1 M NaCl; 1000 ppm	[8]
AA7075	0.1 M NaCl; CeCl <sub>3</sub> , LaCl <sub>3</sub> , YCl <sub>3</sub>	[10]
Mild steel	3.5% NaCl solution; 1 mM of cerium or lanthanum nitrate	[10]
Mild steel	Quiescent soft tap water; CeCl <sub>3</sub> · 7H <sub>2</sub> O inhibitor	[8]
Mild steel	Hard water containing high chloride concentration; CeCl <sub>3</sub> · 7H <sub>2</sub> O inhibitor	[8]
Zinc	0.1 M NaCl; CeCl <sub>3</sub> inhibitor in 0–10 000 ppm	[8]
Galvanized steel	Range	
Zinc, electroplated	Soft tap water	[8]
Zinc washers	CeCl <sub>3</sub> inhibitor	

TABLE 12.1b

Type of corrosion	Conditions	Reference
Galvanic corrosion	Cu-steel	[8]
	Cu-Al in 0.1 M NaCl; 1000 ppm CeCl <sub>3</sub> La, Nd, Pr chlorides	
	Cu-mild steel in tap water, 200 ppm CeCl <sub>3</sub>	[7]
	Cu-mild steel, Cu/Al, 7075/D6 AC 7075/CF, Al/CF in 0.1 M NaCl, 1000 ppm CeCl <sub>3</sub>	
Crevice corrosion	A7075 with rubber O ring in OAM NaCl CeCl <sub>3</sub> inhibitor	[6]
Differential aeration corrosion	Mild steel; CeCl <sub>3</sub> inhibitor 0–200 ppm in tap water	[7]
Stress corrosion cracking	AA7075 in 0.1 M NaCl; 1000 ppm of CeCl <sub>3</sub> , LaCl <sub>3</sub> , YCl <sub>3</sub> at stress levels 250 MPa and 338 MPa 7075 alloy in 0.1 M NaCl; 1000 ppm CeCl <sub>3</sub>	[6]
	Al-Zn-Mg alloy in NaCl solutions cerium/yttrium salts 0.4 to 0.2 wt percent	[11]
	SAE 4340 steel in dry air, moist air and 100% RH; NO <sub>3</sub> /borate La(NO <sub>3</sub> ) <sub>3</sub> , cerium ammonium nitrate	[12]
Corrosion fatigue	A 7075 alloy in air, OAN NaCl and OAM NaCl + 1000 ppm CeCl <sub>3</sub>	[6]

TABLE 12.1c

Inhibitor	Application	Reference
Rare earth metal salts	Aircraft industry. Effective for pitting corrosion, stress corrosion cracking, corrosion fatigue, galvanic corrosion and crevice corrosion by using rare earth metal salts in waters for washing aircraft. Disposal of the waters is environmentally safe	[4,6]
Rare earth metal salts	Recirculating water systems	
Cerium oxide	Conversion coatings, cerium oxide coatings on aluminium alloys and aluminium/silicon carbide metal matrix composites	[13,14]
Rare earth metal oxide coating	Coating on aluminium alloys	[14]
Rare earth metal compounds	Inhibiting pigments in paints. Silica, alumina, iron oxide or tin oxide with adsorbed rare earth metal cation in alkyd resin-based paints	[15]

Some of the possible practical applications of rare earth metals in corrosion inhibition in industrial situations are summarized in Table 12.1c.

### 3. Rare earths as catalysts

During the period 1960–1980, the petroleum and chemical industries have been one of the largest consumers of rare earth compounds. This trend began with the development of zeolite catalysts for petroleum refining in the mid 1960s. Since then the demand for rare earth catalysts has increased steadily. By 1980 catalytic applications amounted to about 41% of rare earths used in U.S.A. (as percentage of total rare earth oxide market share). This figure rose to 55% by 1983. About 90% of rare earth compounds used as catalysts are consumed in the production of cracking catalysts for petroleum refining. The remaining 10% are shared between a variety of catalyst systems used in (i) automotive emission control, (ii) manufacture of polymers and (iii) production of specialty chemicals.

The patenting activity in the field of rare earth catalysts during 1970 and 1985 is illustrated in Fig. 12.3a. The vertical scale is arbitrary and is based on a total of 580 publications in 1985. As compared to 1970, the total published papers increased by four times and the patents by three times. Further, the patent activity showed a shift in emphasis from petroleum refining to pollution control activity. Other commercial catalyst systems are ammoxidation and dehydrogenation in which rare earths play a crucial role.

In Tables 12.2 to 12.5 the lanthanide component used as the catalyst and the corresponding purpose are given.

#### 3.1. Function of lanthanides

- (i) Redox behaviour of cerium consists of facile interconversion of Ce(III) and Ce(IV) states. This is further supported by the high oxidizing power of Ce(IV). In addition to this the redox behaviour of praseodymium has been profitably used.

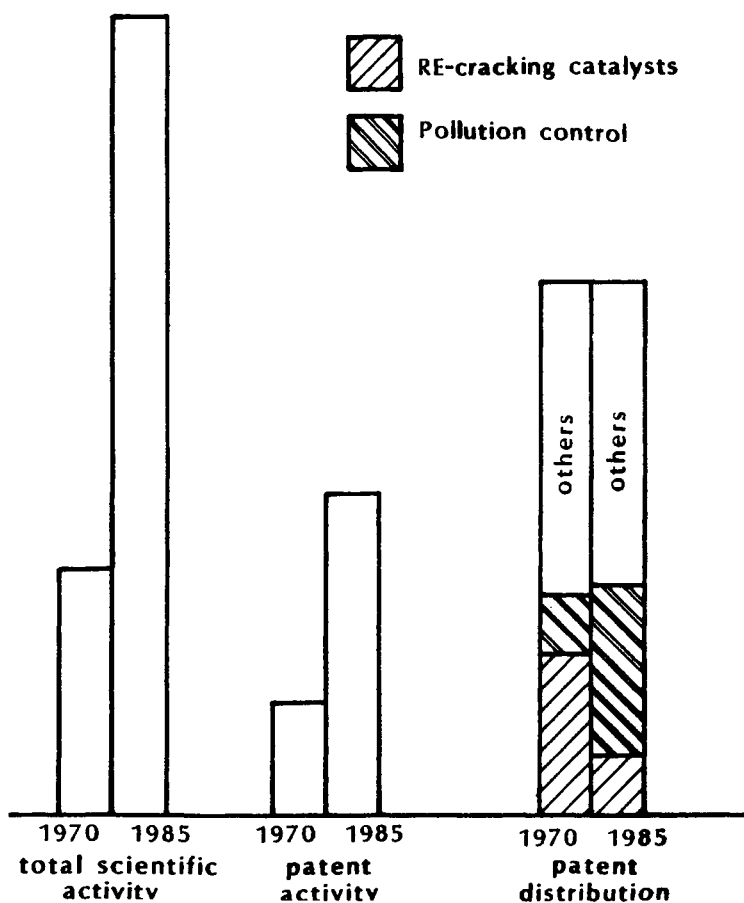


Fig. 12.3a.

TABLE 12.2  
Catalyst systems containing lanthanides; lanthanide oxides as the majority component.

Form	Purpose
Lanthanides alone	For oxidation/combustion For double bond isomerization For dehydration/dehydrogenation For synthesis gas (CO-H <sub>2</sub> ) reactions For sulfur oxides (SO <sub>x</sub> ) control
Lanthanide oxides as the bulk phase supporting dispersed metals	For synthesis gas (CO-H <sub>2</sub> ) reactions For carbon oxide methanation
Supporting other oxides, supporting cluster molecules	For carbon oxide methanation

TABLE 12.3  
Catalytic systems containing lanthanides; lanthanide as the minority component in simple oxides.

Form	Purpose
Lanthanides as modifiers to other oxides in aluminas	To maintain surface area To increase oxidation rates To increase methanation rates
In zirconias	For conduction in electrocatalysis
In iron oxide	For ammonia synthesis promotion
Lanthanide oxides in mixed oxides	
With aluminas	To provide sulfur oxides (SO <sub>x</sub> ) control
With iron oxides	For dehydrogenation in carbon monoxide reactions
With other transition metal oxides	For oxidation

TABLE 12.4  
Catalytic systems containing lanthanides; lanthanides in complex oxide and oxy-anion system.

Form	Purpose
Lanthanides as components in complex oxide systems	
In perovskites	For conduction in electrocatalysis For oxidizing properties For hydrogenation properties For synthetic gas (CO-H <sub>2</sub> ) reactions To provide sulfur oxides (SO <sub>x</sub> ) control
In oxysulphides	
In other systems	
Lanthanides in oxy-anion systems	
In aluminosilicates	For cracking reactions
In molybdates	For ammoxidation reactions
In phosphates	For hydrolysis of chlorinated aromatics
In other systems	

TABLE 12.5  
Catalytic systems containing lanthanides; lanthanides in non-oxide and homogeneous systems.

Form	Purpose
Lanthanides as components in non-oxide systems	
As halides	With co-catalysts for olefin polymerization in mixed halides for oxychlorination as supports
Lanthanides in homogeneous systems	
As organometallics	For olefin polymerization For olefin hydrogenation
As cerium(IV) salts	For free radical polymerization
As coordination complexes	For Diels-Alder reactions For olefin polymerization
As nitrates, chlorides, alkoxides etc.	In organic synthesis

- (ii) The large size together with high charge of lanthanides leads to novel stable crystal structures such as perovskites. Lanthanides also provide resistance to crystal structure degradation at high temperatures of species such as zeolites and alumina.
- (iii) Lanthanide–carbon bonds can initiate polymerization of active olefins and the success of the process depends upon the relative stability of propagating steps to terminating steps. In this function the lanthanides resemble the early transition metals.
- (iv) The large size of lanthanides together with high coordination numbers leads to non-directional metal–ligand bonds. No specific geometry is imposed on the lanthanide coordination complex. Therefore a transition between different coordination environments does not involve difficulty and hence the lanthanide complexes can function as templates for catalyzed reactions.
- (v) The oxidative ability of cerium(IV) is used commercially. The required Ce(IV) is often formed indirectly. For example a cerium derivative is converted in situ to cerium oxide which is the probable active species.
- (vi) The reaction of carbonaceous materials with oxygen or air is catalyzed by metal oxides. Cerium additives are used in the combustion of fuel oils or in diesel operations. For example cerium carboxylates reduce particulate emission (act as smog suppressant) and enhance the performance of particulate traps in diesel fuel engines.
- (vii) Lanthanide oxides when added to support active metals tend to modify the course of reactions such as oxygenation. The dissociation of CO is assisted by transient bonding between carbonyl oxygen and lanthanide ion. This factor may be important in complex catalysts in which lanthanides act as modifiers.

### 3.2. Fluid catalytic cracking (FCC)

This is by far the most important process utilizing rare earth catalysts. Petroleum refineries all over the world are trying to maximize yields of gasoline and middle distillates. The predominant technique of refining to achieve maximum yields is fluid catalytic cracking which converts high-boiling point fractions such as vacuum oils and residues into lower-boiling point products like gasoline and diesel oil. The addition of zeolites–crystalline aluminosilicates with a defined pore structure of molecular dimensions, 0.4 to 1.0 nm containing rare earths to the conventional amorphous silica alumina catalysts used in catalytic cracking, results in higher yields and longer lifetime. The total rare earth content varies between 1 and 7 wt percent. Initially rare earth chloride solutions consisting of natural distribution were used as FCC catalysts, but currently cerium-depleted solutions are preferred since cerium-free catalysts exhibit improved thermal stability.

### 3.3. Automotive pollution control

Cerium is an important component of the three-way catalyst (TWC) technology used to control atmospheric pollution from internal combustion engines. Addition of ceria helps (i) to stabilize the alumina washcoat which supports the catalytically active phases of platinum and rhodium and thus minimize the thermal degradation of the catalyst layer, (ii) to provide for oxidation of hydrocarbons and carbon monoxide during the fuel rich/low air cycle. Without this capacity for oxygen storage, three-way catalysts would be confined to a narrower operating window requiring more precise and expensive control devices.

Lanthana is supposed to be superior to ceria as a washcoat stabilizer, but for oxygen storage, ceria is most effective. The market for auto exhaust catalysts is extensive with over several million units being produced each year in the world, but the rare earth content is only of the order of several grams.

### 3.4. *Polymerization catalysts*

Rare earth halide (in particular  $\text{NdCl}_3$ )-based compounds are very active catalysts for polymerization of dienes. The products are polymers with improved elastic and thermoplastic properties caused by high stereo regularity. The polymerization process is highly efficient (i.e.) 60 000 moles of butadiene are polymerized by one atom of rare earth. Hence the demand for rare earth compounds as polymerization catalysts is low.

### 3.5. *Other applications*

Rare earths are used as catalysts and catalyst promoters in a variety of processes such as oxidation, synthesis of alcohol, dehydration and production of specialty chemicals. Complex oxides containing rare earths are also used as electrode materials in electrochemical systems.

### 3.6. *Further applications*

The potential of rare earth compounds as catalytically active phases and promoters in pollution control, catalytic combustion, polymer production and in the fuel and chemical manufacture and thermal stabilizers for catalyst supports (alumina, silica–alumina, titania) need to be mentioned. Application of rare earths in alternate fuels technology (Fischer–Tropsch Processes, natural gas to transport fuel pathways) is also promising.

### 3.7. *Pollution control*

Complex oxides of the perovskite structure containing rare earths like lanthanum have proved effective for oxidation of CO and hydrocarbons and for the decomposition of nitrogen oxides. These catalysts are cheaper alternatives than noble metals like platinum and rhodium which are used in automotive catalytic converters. The most effective catalysts are systems of the type  $\text{La}_{1-x}\text{Sr}_x\text{MO}_3$ , where M = cobalt, manganese, iron, chromium, copper. Further, perovskites used as active phases in catalytic converters have to be stabilized on the rare earth containing washcoat layers. This then leads to an increase in rare earth content of a catalytic converter unit by factors up to ten compared to the three way catalyst.

Rare earth containing catalysts are useful in stationary pollution control devices as for example lanthanum titanate catalysis in the reduction of sulphur dioxide with carbon monoxide to yield carbon dioxide and elemental sulphur. The disposal of elemental sulphur is far less hazardous than that of effluent from an  $\text{SO}_2$  scrubber.

### 3.8. *Catalytic (flameless) combustion*

This process is attractive for many applications. Heat can be directly produced on the walls of heat exchangers and  $\text{NO}_x$  pollution is significantly reduced. Perovskites of the type effective in pollution control are good combustion catalysts.



### 3.9. Polymer production

New and more effective polymerization catalysts such as the lutetium complex  $(C_5H_5)_2LuCH_3$  is the fastest soluble ethylene polymerization catalyst for producing high density polyethylene.

### 3.10. Alternative fuels technology and chemicals manufacture

Rare earth oxides are useful for partial oxidation of natural gas to ethane and ethylene. Samarium oxide doped with alkali metal halides is the most effective catalyst for producing predominantly ethylene. In syngas chemistry, addition of rare earths has proven to be useful to catalyst activity and selectivity. Formerly thorium oxide was used in the Fisher–Tropsch process. Recently ruthenium supported on rare earth oxides was found selective for lower olefin production. Also praseodymium–iron/alumina catalysts produce hydrocarbons in the middle distillate range. Further unusual catalytic properties have been found for lanthanide intermetallics like  $CeCo_2$ ,  $CeNi_2$ ,  $ThNi_5$ . Rare earth compounds (Ce, La) are effective promoters in alcohol synthesis, steam reforming of hydrocarbons, alcohol carbonylation and selective oxidation of olefins.

## 4. Use of rare earths in paints and pigments

Rare earths are used in the paints and pigments industry (i) as coating materials for pigments to enhance their durability and performance characteristics, (ii) in the manufacture of ceramic pigments and (iii) in the manufacture of driers for organic coatings.

Some of the important inorganic pigments such as lead chromes and titanium dioxide, are subjected to surface treatment to enhance their pigmentary properties, particularly light fastness, weathering fastness, heat resistance and chemical resistance. Many organic and inorganic compounds are used in the surface treatment of pigments. Compounds of cerium both with or without hydrous oxides of aluminum or silicon are widely used to coat lead chrome paints so that the light fastness and other properties are improved substantially. In an analogous manner titanium dioxide pigment is treated with cerous acetate to improve resistance to sunlight and outdoor durability, in particular for the pigments used in synthetic fibres, molding composition of high polymers, paints, powder coatings, and wire coatings.

In solid solutions, rare earths impart colour to the solutions due to their electronic configurations. This property has been profitably used in the manufacture of ceramic pigments which are extensively used in colouring of wall and floor tiles, table-ware and sanitary-ware. Cerium and praseodymium are extensively used in ceramics pigments. The shades that result due to the use of cerium and praseodymium are yellow, orange and green.

Metallic soaps are prepared by reacting an inorganic metal salt with an organic acid such as naphthenic acid and these are then used as paint driers to induce or accelerate the setting and solidification of a varnish or paint film. There are two types of paint driers, namely (i) active or surface driers and (ii) auxiliary or through driers. Some examples of active driers are cobalt and manganese bearing driers which are in wide use. Some commonly used through driers contain lead and zinc. Cerium naphthenate may also be used as an auxiliary or through drier. Cerium naphthenate is more active than lead as an auxiliary drier. It has been noted that cerium naphthenate imparts a yellow colour to the film in addition

to exhibiting an increase in skinning tendency. A rare earth naphthenate consisting of 50% cerium with the remaining consisting of lanthanum, praseodymium and neodymium has been evaluated for its performance and was found to give better toughness and hardness to the film along with improved colour retention and water and soap resistance.

Another noteworthy development is an inorganic fluorescent pigment consisting of manganese activated yttrium oxide for artificial teeth. On exposure to UV light, natural teeth exhibit yellowish white fluorescence. Artificial teeth with comparable optical behaviour in the UV-Vis region can be produced by using an inorganic fluorescent pigment containing yttrium or gadolinium or lanthanum besides cerium and terbium.

### **5. Use of rare earths in cinema arc carbons**

Cinema arc carbons or electrodes are used in projecting motion pictures on a screen. The necessary radiation is produced through an electric arc struck between two carbon rods. The two carbon rods are connected to a current source and are separated by a small gap known as an arc gap. At the point of separation, a very high concentration of energy initiates volatilization of carbon and thus provides the ionized vapour needed for continuous electrical conductance. Continuous flow of current through the vapour produces ions in excited states which emit energy of discrete wavelengths. Thus the radiating arc forms the light source for motion picture projection.

For the production of white light, a temperature of  $>1500^{\circ}\text{C}$  is required. The incandescent carbon volatilizes above  $3600^{\circ}\text{C}$  and hence reasonable brightness can be obtained from the arc produced from carbon electrodes.

The arc light source produced from pure carbon electrodes is of low intensity and cannot be used for the projection of technicoloured films on a wide screen. Thus there is need for the development of a much brighter source of light with a specified spectral quality. Then cored carbon electrodes were developed. The new carbon electrodes consist of two parts namely the shell and core, each of which has its distinct function. The shell forms the outer wall and is made of various forms of carbon. The core contains the flame material (carbon powder). Further, metal salts are also added to the core material to improve the brightness of the arc. The metal salts provide a steady flow of ions to ensure steady flow of electric current. The flame material produces volatile atoms in the arc stream which due to deexcitation produces radiation of different wavelengths. Thus the brightness of arc light from the cored carbon electrode is the result of radiating energy of carbon and the characteristic emission from the flame material added to the core.

Rare earth compounds mostly of the cerium group have been used in the core in order to obtain high emission of spectral energy. It is a common practice to use a combination of cerium, lanthanum and neodymium compounds. The carbon electrodes used for the production of high brightness light have generally large cores rich in rare earth compounds. High intensity light is due to high current density and efficient conversion of electrical energy into radiant energy with proper spectral distribution. When an arc is formed by striking high intensity cored carbon electrodes, a very bright crater results at the tip of the positive carbon electrode and a tail flame appears. The crater of the high intensity arc is the source of the radiant energy.

When a stable arc is formed due to the flow of high currents, the rare earth compounds vaporize from the cup shaped positive crater. During this process, the rare earth atoms absorb energy and get excited. The electrons of rare earths in excited high energy states revert to lower energy ground states by emitting radiant energy, with characteristic wavelengths. The emission of radiant energy by the rare earth ions adds to the brightness of the crater region.

The path of least resistance for the electric current is from negative carbon to the positive core. Hence most of the electrons forming the high current density in the arc stream travel from the positive core. At this point the energy is high such that the core vaporizes faster than the shell, thus forming a cup on the face of the positive carbon, which is the main source of light.

Rare earth compounds in the form of oxides and fluorides are mixed with carbon powder and introduced into the core of the positive arc carbon electrode. The amounts of rare earth compounds used and the size of the core are dependent on the operational requirements.

The demand for a brighter light source with a specific spectral range has been on the increase due to a continuing need for the projection of colour movies on wide screens. Rare earth compounds have thus become essential in the cinema industry.

## 6. Rare earths in alloys

### 6.1. *Misch metal*

This is an alloy of about 50% cerium, 25% lanthanum, 15% neodymium and 10% other rare earth metals.

Some of the uses are: (i) manufacture of pyrophoric alloy with iron, (ii) deoxidizer in metallurgical applications, (iii) as a getter for the removal of oxygen from vacuum tubes, (iv) manufacture of high strength magnesium alloys, (v) the thermal stability and creep strength are some of the most important requirements in the automotive industry. A new heat resistant magnesium alloy containing aluminum, zinc, calcium and rare earths (Misch Metal) has been developed. This alloy shows good cast properties and corrosion resistance, (vi) manufacture of lighter-flints, (vii) steel manufacture, (viii) manufacture of nodular cast iron, (ix) manufacture of aluminum wire with improved elongation for overhead wiring.

### 6.2. *Titanium alloys*

Addition of rare earths to Ti-base alloys results in a profound effect on recrystallized grain size and other microstructural features as shown in Table 12.6.

Some of the benefits of the addition of rare earths to titanium alloys are: (i) effect on recrystallized grain size, (ii) refinement in the alpha colony size caused by yttrium results in increased strength and percentage elongation, (iii) improved stress rupture life due to dispersion strengthening of  $CeO_2$ , stabilization of dislocation substructure and purification of grain boundaries. Oxidation resistance of Ti alloys can be improved by the addition of rare earths as shown in Fig. 12.3b. Among the rare earths, gadolinium is the most effective in improving oxidation resistance. The decreased oxidation rate in the presence of rare earths is ascribed to improved adhesion of oxide scale to the substrate. Addition of Tb to VT-5L alloy increases its tensile strength at 500°C by about 60 percent. Hot workability can be improved by the addition of rare earth metals. Addition of 25 ppm of Y to the

TABLE 12.6  
Effects of RE additions on the microstructure and mechanical properties of Ti alloys.

Alloy	RE addition (wt%)	Recrystallized grain size ( $\mu\text{m}$ )	Room temperature		Stress rupture life (h) ( $500^\circ\text{C}/55 \text{ kg}/\text{mm}^2$ )	Remarks
			Y.S. (MPa)	% elongation		
Ti	—	200	—	—	—	1
Ti	1.0 Er	10	—	—	—	
Ti-6Al-4V (as-cast)	—	—	738	7	—	RE addition resulted in refinement of $\alpha$ -colony size, while prior beta grain size remained unchanged
Ti-6Al-4V (as-cast)	0.03 Y	—	769	14	—	2
ZT3 (Ti-5Al-5Mo-2Sn-0.25Si)	—	—	—	—	140	ZT3 Chinese origin high temperature Ti-base alloy
ZT3	0.025 La	—	—	—	500	3

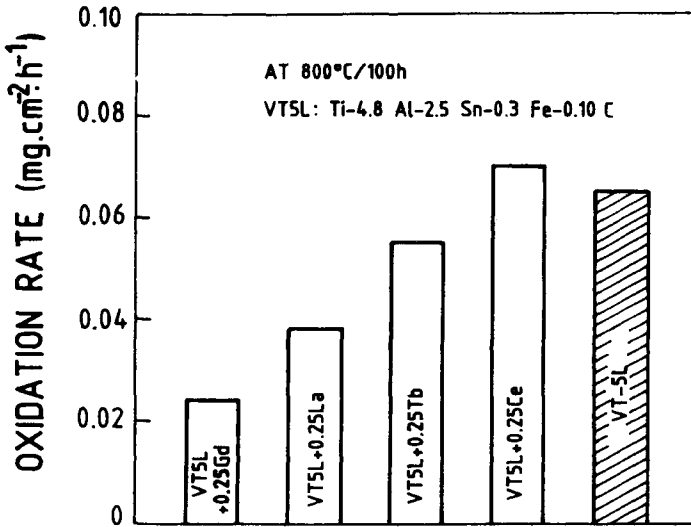


Fig. 12.3b. Effect of RE additions on oxidation rate of VT5L alloy [28].

Ti-5Al alloy plates reduces rolling edge cracks significantly. Addition of  $\text{Y}_2\text{O}_3$  results in affecting grain refinement and thus improved superplastic formability.

### 6.3. Nickel-iron-cobalt-base superalloys

Addition of rare earths improves the high temperature oxidation resistance of heat-resistant alloys. The improved resistance is observed in terms of reduction in weight gain and

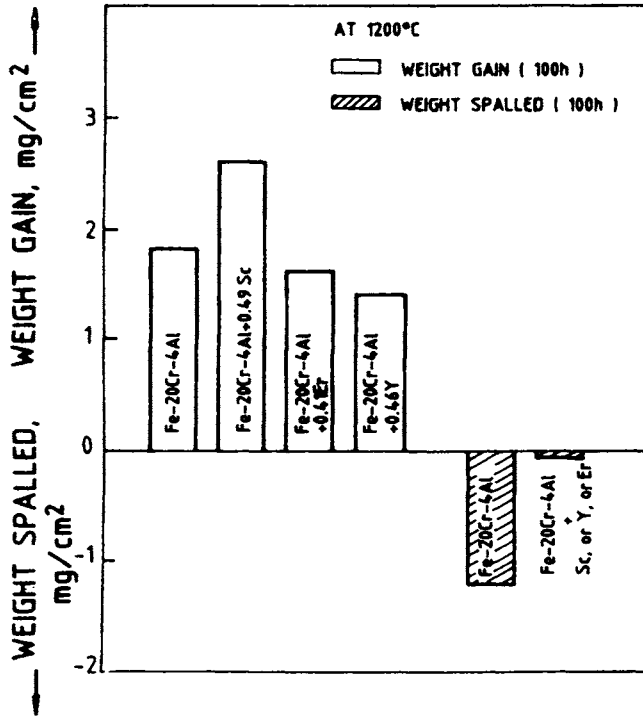


Fig. 12.4. Effect of RE additions on isothermal oxidation and spalling behaviour [29].

improved adherence of the surface oxide. The effect of Sc, Y and Er on the isothermal oxidation and spalling behaviour of Fe-20Cr-4Al alloys is shown in Fig. 12.4. Addition of rare earths has a dramatic effect on the spalling behaviour. The effect of addition of Y on the isothermal and cyclic oxidation behaviour of Co-10Cr-11Al alloy is shown in Fig. 12.5. It is clear that there is 2-fold improvement in oxidation resistance under isothermal conditions and a 13-fold improvement under cyclic conditions. Many explanations have been proposed to explain the improvement in oxide adhesion and these are summarized in Table 12.7.

The presence of Y in the coatings improves the oxidation resistance of  $\text{Al}_2\text{O}_3$  scale. Thus, MCrAlY coatings outperform diffusion aluminides significantly in oxidation tasks as shown in Table 12.8.

Microalloying of Ni-base alloys with rare earths improves ductility, stress rupture life and creep resistance as shown in Table 12.9. The improved properties are due to desulphurisation caused by rare earths. Addition of cerium to Inconel 600 and Hastalloy improves their hot workability.

#### 6.4. Chromium-base alloys

These are potentially useful high-temperature materials. Chromium is moderately resistant to oxidation but absorbs nitrogen from air and loses structural stability. Addition of

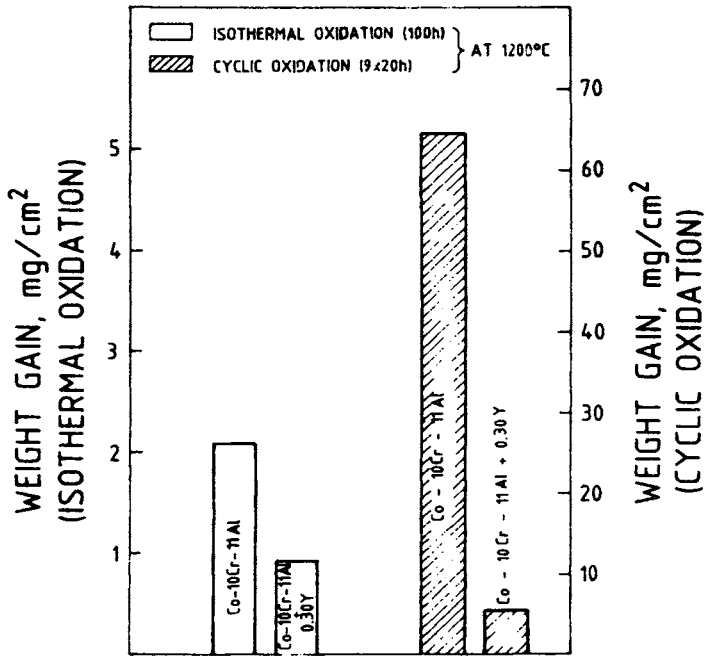


Fig. 12.5. Isothermal and cyclic oxidation behaviour of Co-10Cr-11Al alloy containing 0.30 wt% Y [30].

TABLE 12.7  
Models of Al<sub>2</sub>O<sub>3</sub> scale adherence in superalloys [31,32].

Nomenclature	Effect of RE
Pegging	Peg is produced by the selective oxidation of the RE at the scale alloy interface causing mechanical keying of scale
Vacancy sink	Provides sites for vacancy condensation by the internal oxide particles of REs and thus eliminates interfacial porosity
Scale plasticity	Modification of the oxide scale plasticity due to finer Al <sub>2</sub> O <sub>3</sub> grains, thus allowing accommodation of the thermally induced stresses
Graded seal	Formation of a compound oxide layer between scale and substrate which has graded thermal expansion coefficient
Chemical bond	Sulfur "bond poison" is gettered by RE elements
Growth stress	Al <sup>3+</sup> counter diffusion and growth within existing oxide is prevented and thus suppresses the tendency to develop convoluted morphology

TABLE 12.8  
Oxidation resistance of coating on Ni-base superalloy.

Coating	Coating life at 1190°C (h)
Aluminide	100
Pt-aluminide	250
NiCoCrAlY	> 1000

TABLE 12.9  
Effects of Re additions on the mechanical properties of Ni-base superalloys.

Alloy	Re addition	Elongation ( $\Delta L/L_6$ at 750°C)	Stress rupture life, h 650°C/ 620 MPa	% creep strain in 100 h (650°C/ 586 MPa)	Suggested mechanism	Reference
Ni-20Cr	0	0.35	–	–	RE addition results in reduction in free S & O content, increase in interfacial energy and grain boundary mobility,	[33]
Ni-20Cr	60 ppm Ce	0.90	–	–	low cavitation rate, transition from brittle intergranular to ductile transgranular fracture mode	
Unitemp 901 (Ni-Fe-Cr- Mo-Ti)	0	–	87	0.15		[34]
Unitemp 901	30 ppm La	–	115.5	0.055	Decrease in free S content of alloy; S-induced embrittlement tendency is suppressed	[34]

yttrium or other rare earths increases the oxidation resistance of Cr base alloys at 1260°C significantly, and the amount of nitrogen absorbed is considerably decreased as shown in Fig. 12.6. The positive effect of La on heat resistance of Cr is due to the formation of a barrier oxide film comprised of Cr<sub>2</sub>O<sub>3</sub> and LaCrO<sub>3</sub>. In addition, LaCrO<sub>3</sub> distributed along the grain boundaries forms diffusion barriers and changes the oxidation law from parabolic to logarithmic law.

Chromium shows no ductility at room temperature and hence it is difficult to obtain desirable shapes with useful properties. But microalloying of Cr with Y, La, or other light rare earths results in improved yield strength and ductility. On the other hand addition of heavy rare earths such as Er, Dy, and Lu makes Cr more brittle.

Addition of rare earths to Cr results in (i) improved stress rupture life, (ii) improved hot plasticity and (iii) decrease in ductile–brittle transition temperature.

## 6.5. Rapidly solidified alloys

### 6.5.1. Al-base alloys

The typical features of the phase diagram of Al–rare earth alloys are high liquid solubility, low solid solubility of rare earths and relatively low liquidus temperatures. The low diffusivity of rare earths in these alloys is an attractive feature from the point of view of the thermal stability of the dispersoids.

Addition of Ce to rapidly solidified alloys of Al–Fe produces a product suitable for use at high temperatures. The heat treatable ingot metallurgical products are used up to 175°C.

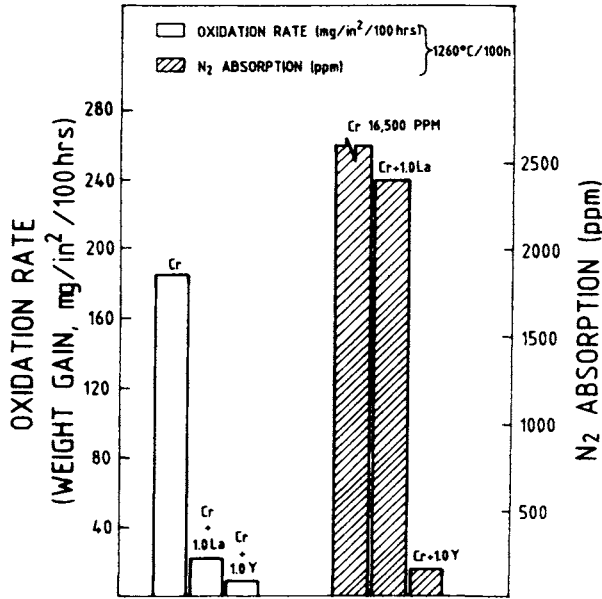


Fig. 12.6. Effects of RE additions on oxidation and nitrogen absorption of Cr [35].

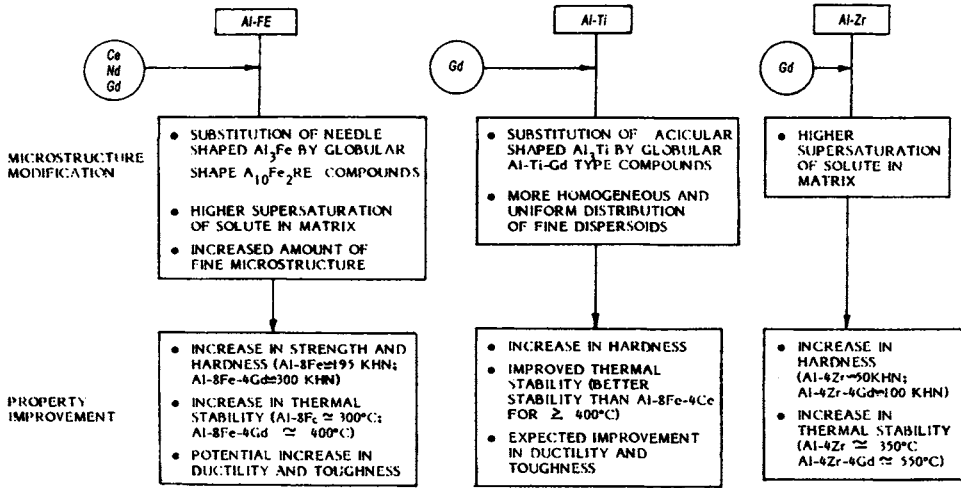


Fig. 12.7. Effect of RE addition on the microstructure and mechanical properties of Al-transition metal alloys [35-37].

On the other hand, rapidly solidified Al-Fe-Ce alloy retains its high strength up to 340°C. Addition of rare earths to Al-transition metal alloys shows a notable modification of micro structure resulting in improved strength and thermal stability as shown in Fig. 12.7.



TABLE 12.10

Effects of RE additions on the microstructure and mechanical properties of rapidly solidified Ti alloys.

Alloy	RE addition (wt%)	0.2% Y.S. (MPa) RT	0.2% Y.S. (MPa) 55°C	Stress rupture life (h) (600°C/19 MPa)	% creep strain (538°C/210 MPa)	Nature of dispersoids	Reference
Ti	—	250	75	—	—	—	[39]
Ti	1.8% Y	250	175	—	—	Y <sub>2</sub> O <sub>3</sub>	
Ti	—	—	—	12.5	—	—	
Ti	1.5% Nd	—	—	68	—	50–150 nm Nd <sub>2</sub> O <sub>3</sub>	[40]
Ti	1.0% Er	—	—	288	—	50–150 nm Er <sub>2</sub> O <sub>3</sub>	
Ti–6Al–2Sn– 4Zr–2Mo	—	—	—	—	0.421	—	[41]
Ti–6Al–2Sn– 4Zr–2Mo	1.7% Ce– 0.5% S	—	—	—	0.167	CeS, Ce <sub>2</sub> S <sub>3</sub>	

TABLE 12.11

Effect of rare earths in long range ordered alloys [27].

Alloy	Formula	Steady state creep rate (h <sup>-1</sup> )	Rupture [time (h)]	Creep rupture ductility (%)
551 MPa, 650°C				
LRO-20	(Fe <sub>50</sub> Ni <sub>50</sub> ) <sub>3</sub> V	$1.3 \times 10^{-2}$	0.9	4.8
LRO-42	(Fe <sub>50</sub> Ni <sub>50</sub> ) <sub>3</sub> (V <sub>98</sub> Ti <sub>2</sub> ) + 0.1 wt% Ce	$6.2 \times 10^{-5}$	451	8.0
413 MPa, 760°C				
LRO-1	(Fe <sub>22</sub> Co <sub>78</sub> ) <sub>3</sub> V	$2.9 \times 10^{-3}$	2.3	4.0
LRO-61	(Fe <sub>22</sub> Co <sub>78</sub> ) <sub>3</sub> V V <sub>93</sub> Ti <sub>4</sub> Nb <sub>3</sub> + 0.04 wt% Ce	$7.5 \times 10^{-4}$	90	13

### 6.5.2. Ti-base alloys

Rare earths have low solubilities in  $\alpha$ -Ti and hence can function as dispersion-strengthening agents. Rapid solidification and deformation processing of Ti-base alloy containing rare earths was used to obtain a fine dispersoid of rare earth oxides, sulphides and oxysulphides. The data on improved strength, stress rupture life and creep resistance of Ti-base alloys with added rare earths are given in Table 12.10.

### 6.5.3. Intermetallics

Titanium aluminides are ordered intermetallics and hence have lower diffusivity and high elastic modulus. These compounds are stronger than the conventional titanium alloys and are suitable for high temperature applications. But these compounds have low ductility due to the planarity of slip in these compounds.

Rare earth addition and rapid solidification processing might result in (i) grain refinement and (ii) development of fine incoherent dispersoids leading to dispersed slip. Addition of dispersoids such as Er<sub>2</sub>O<sub>3</sub> and Ce<sub>2</sub>S<sub>3</sub> to Ti<sub>3</sub>Al(Nb) alloys produces refinement

of grain size. The grain size refinement reduces cracking in indenter ductility tests without improving fracture toughness.

Long-range ordered alloys like  $(\text{Fe},\text{Co})_3\text{V}$ ,  $(\text{Fe},\text{Ni})_3\text{V}$  and  $(\text{Fe},\text{Co},\text{Ni})_3\text{V}$  are suitable alloys for high temperature applications. Addition of as little as  $<0.1\%$  Ce along with Ti to these alloys increases rupture ductility by two fold, lowers the creep rate and increases the rupture life of the  $(\text{Fe},\text{Ni})_3\text{V}$  alloy. The creep resistance of long range ordered alloys is increased by the addition of Nb and Ti/Ce.

## 7. Rare earth magnets

Permanent magnets in the form of Alnico were introduced in the 1940's and soon Alnico replaced electromagnets and the uses of permanent magnets extended to motors, generators and loudspeakers. Discovery of ferrite magnets has led to use of permanent magnets in every day life. In 1970 samarium-cobalt family of hard magnetic materials with high magnetic energy densities were introduced. This revolution accelerated with the discovery of a new generation of rare earth magnets based on neodymium, iron and boron with higher magnetic energy densities than the samarium-cobalt system. Because of the high energy densities, both Sm-Co and Nd-Fe-B based magnets can replace electromagnets and are also likely to be used in tiny stepper motors in wristwatches, and the sound transducers in Walkman type headsets. The magnetic energy densities of magnetic materials are depicted in Fig. 12.8. It is clear from the figure that rare earth based magnets have the highest values for maximum energy product  $BH_{\text{max}}$ .

The Nd-Fe-B magnets are based on the intermetallic compound of the formula  $\text{Nd}_2\text{Fe}_{14}\text{B}$ . The interest in these magnets is due to the fact they are stronger than other materials and of low cost. The magnetic energies and costs of the most common magnetic materials as of 1986 are presented in Table 12.12.

Analogous to the Sm-Co magnet, the price of Nd-Fe-B is expected to decrease and may fall below \$100/kg. The cost per joule is the important factor and with the cost of \$100/kg of Nd-Fe-B it will be cheaper than Sm-Co and Alnico and competitive with ferrites.

The world market in 1986 for permanent magnets was about \$2 billion with a growth rate of about 10% per annum. By the end of 2000, the world market for permanent magnets was probably about \$5 billion. As the market matures, NdFeB magnets will have a market of about \$2.5 billion or so available to it.

Fabrication of Nd-Fe-B magnets is done by two methods. One of the methods involves powder metallurgy. An ingot of the alloy is ground to a particle size of 3–5  $\mu\text{m}$ , aligned and pressed in a magnetic field and sintered at about 1200°C. All these operations are conducted in an inert atmosphere. The second method involves hot pressing. The molten alloy is ejected in a stream onto the rim of a rotating copper wheel (i.e. melt spinning) where it freezes into a fine-grained friable ribbon. The ribbon is coarsely ground and hot pressed at 700°C to produce an isotropic magnet. Plastic deformation at 700°C produces alignment of the magnetic axis normal to the direction of flow and the resulting magnet has similar properties as those of sintered magnets.

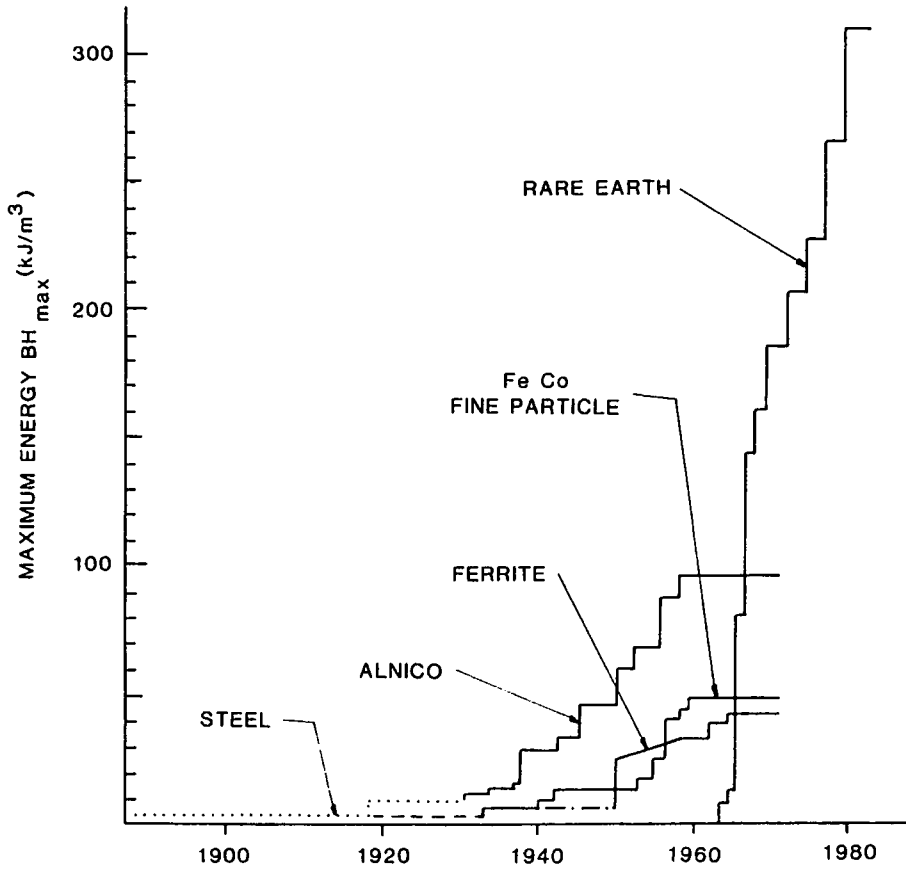


Fig. 12.8. [42].

TABLE 12.12  
Comparison of magnets [42].

Magnet type	Magnetic energy $BH_{max}$ (kJ/m <sup>3</sup> )	1986 (\$/kg)	Density (kg/m <sup>3</sup> )	Cost/joule (\$/J)
Hard ferrite	29	12	4400	1.8
Alnico	45	30	7200	4.9
SmCo	220	335	8200	12.5
NdFeB	290	335	7400	8.5

7.1. Applications [42]

One of the largest applications of permanent magnets is in electric motors and generators. In electrical machines permanent magnets provide a steady magnetic flux in a region occupied by moving conductors. The magnetic properties of the major types of permanent

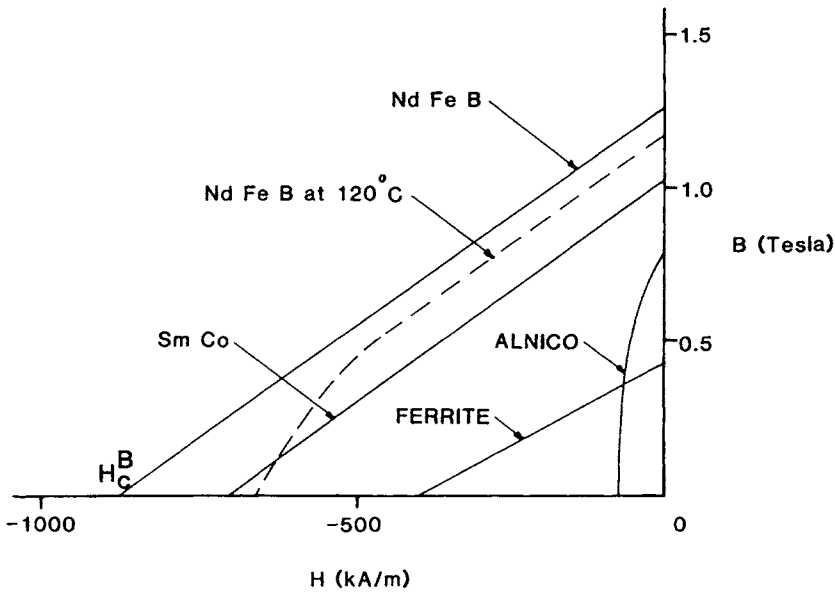


Fig. 12.9. Flux density ( $B$ ) versus magnetizing field ( $H$ ) for the important classes of permanent magnets [43].

magnets at room temperature are compared in Fig. 12.9, where flux density  $B$  (Tesla) is plotted against demagnetizing field  $H$  (kA/m). The two important technical parameters are coercivity ( $H_C^B$ ) and remanence ( $B_R$ ). It is clear that NdFeB is superior to all other products. The elevated temperature behaviour of NdFeB is shown by a dashed line. The maximum magnetic energy product ( $BH_{\max}$ ) occurs at the point on each line where the product of  $B$  and  $H$  is a maximum and determines the maximum magnetic energy available in the external field. A magnetic circuit consists of permanent magnet, iron and an air gap and the working point on the  $B$  vs  $H$  curve is determined by the relative dimensions of the components. As a rule of thumb, as the air gap increases, the working point of the magnet moves from  $B_R$  towards  $H_C^B$ . In general from the economic point of view, the working point should be close to  $BH_{\max}$ .

## 7.2. DC motors

The two types are (i) brushed and (ii) brushless. The major features of brushed DC motors are shown in Fig. 12.10. The coils are wound on a slotted iron rotor with mechanical commutation. In Fig. 12.10a ferrite is used and in Fig. 12.10b a NdFeB magnet is used. The size and weight is reduced in the latter scheme. By using permanent magnets, the iron rotor, which is a source of eddy-current and hysteresis losses, is totally eliminated in disk geometry as shown in Fig. 12.10c. In the second type, brushless motors, the rotor position is detected by Hall or optoelectronic sensors and the current is commuted electronically. The brushless DC motors consisting of multipole design and low-inertia disk geometry are shown in Fig. 12.11. In Fig. 12.11a the “inside-out” geometry permits mounting the permanent magnets on the rotor surface allowing the heat-generating coils on the outside to be

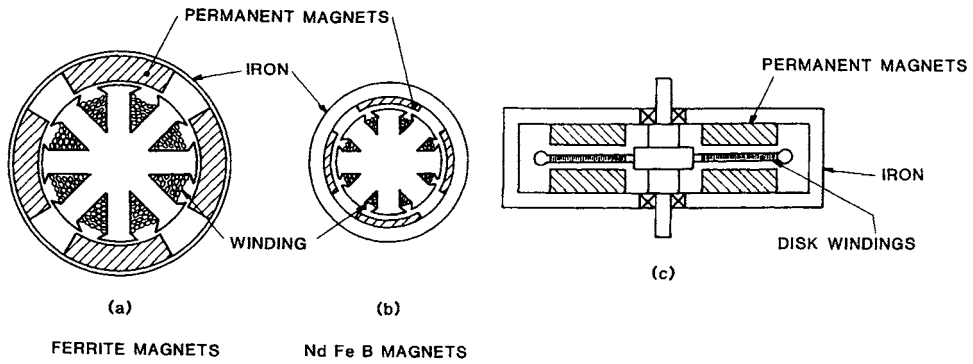


Fig. 12.10. Brushed DC motors of similar ratings using ferrite (a) or NdFeB (b) permanent magnets are compared. The disk geometry is illustrated in (c) [43].

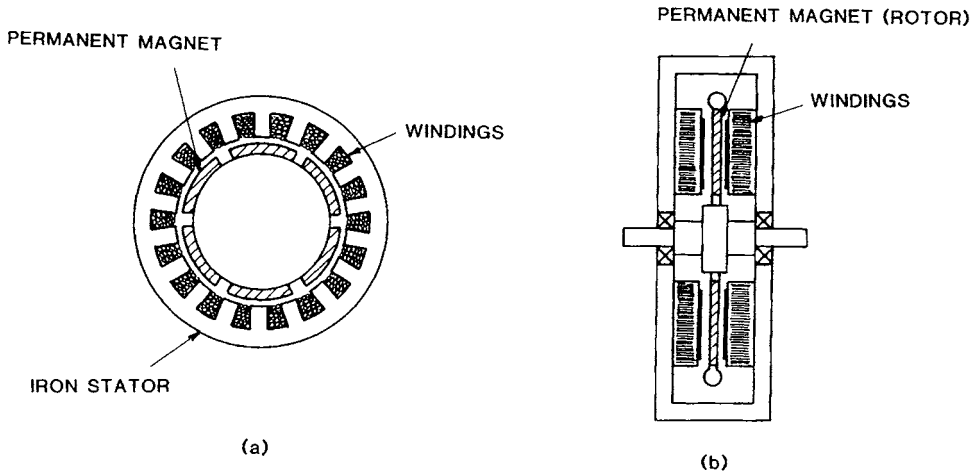


Fig. 12.11. Brushless DC motors. (a) 6-pole, 3-phase, 18-slot design. (b) Low-inertia disk geometry [43].

effectively cooled. The low-inertia disk geometry in Fig. 12.11b is favored for servomotors in robots.

The specific power of rare earth permanent magnet motors can exceed 1 kW/kg. The combination of reliable, low-cost, solid-state controllers and brushless permanent magnet motors will find applications in (i) computer accessories like disk drives, printers, x-y plotters, (ii) consumer goods like hand tools, fans, and air-conditioners, (iii) robotics, traction motors, steel mills, lift motors, and (iv) aerospace flight control actuators.

### 7.3. AC motors

Three-phase induction motors operating at a fixed speed are used industrially. By using permanent magnets in the induction motors, it is possible to attain reduction in size and weight and improved efficiency.

The major limitations for extensive use of NdFeB alloys in motors are (i) cost and (ii) restricted operating temperature range. Improved alloys with linear  $B$  vs  $H$  behaviour up to 150°C would satisfy the requirements.

#### 7.4. Other miscellaneous applications

- Loudspeakers. The conventional design of a fixed magnet and moving coil can be inverted.
- Magnetic resonance imaging. For flux densities of up to 0.3 Tesla permanent magnets are superior to superconducting magnets in terms of operating costs and negligible stray fields.
- Magnetic bearings. The force between two magnetic components increases as the square of the flux density. Magnetic bearings are subject to large demagnetizing fields and require high-coercivity magnets.
- Mineral separators. Permanent magnets can replace electromagnets resulting in reduced operating costs and size and improved efficiency.
- Sonar transducers and laser mounts. Alloys of Tb, Dy, and Fe exhibit magnetostrictive properties (i.e.) change shape under applied magnetic field. These alloys are used in sonar transducers and laser mounts.

#### 7.5. Dental applications

Initially during the 1950s Alnico magnets were used for enhancing retention of dentures. These products were large and the repelling forces were mechanically and physiologically unfavorable and were superseded by Sm/Co magnets. Sm-Co magnets are small and fitted into root-canal treated (root filled) tooth roots, and opposite polarity magnets in dentures, to hold dentures against the roots by magnetic attraction with forces of around 150 grams.

Australian manufacturer Innovadent produces Nd-Fe-B alloy magnets of two sizes namely "mini" magnet (case size of  $3 \times 3 \times 4 \text{ mm}^3$ ) providing 500 grams of retention and "Maxi" magnet (case size  $4 \times 4.5 \times 6.5 \text{ mm}^3$ ) with about 1000 grams of retention.

Other applications in dentistry are: (i) magnetic retention of vital teeth, (ii) magnetically-retained removable bridges, (iii) for use in artificial tooth implants which are fitted with magnetisable caps, (iv) applications in orthodontics.

### 8. Nd-Fe-B powders for bonded magnets

The rapidly solidified Nd-Fe-B powders are the basis of bonded magnets. Rapid solidification is exclusively done by melt spinning. The product consists of flakes with highly stable and magnetically hard microstructure. The flake-like particles are comminuted into powder and later processed into bonded magnets. The powders are magnetically isotropic with coercivities in the range of 4 to 16 Oe; anisotropic powder made by hydrogen decomposition desorption process has also been used in bonded magnets. Some applications of bonded Nd magnets are given in Table 12.12a.

TABLE 12.12a  
Bonded neodymium applications.

Mature	Growth	Developing
Camera shutter	Spindle motor Hard disk drive CD Rom CD player	Automotive
Electric view finder	Pick up motor CD Rom	Major appliance
Clock/watch	Pager	Magnetic roller bar
Stepper motor	Stepper motor	Factory automation
VCR	Laser printer	
Fax machine		
Dot matrix printer		
Camcorder		
Actuator	Mini disk	Speaker
Floppy disk driver		Telephone/cellular Consumer electric Head phone Spindle motor Floppy disk drive Optical disk drive Small appliance "High Tech" kitchen appliance Cordless power tool

## 9. Rare earths in lasers

Lasers based on electronic transitions in rare earth ions have extensive applications in technology. It is believed that the solution to the energy crisis may well be controlled thermonuclear fusion in which neodymium lasers might play a vital role. The world's most powerful laser, NOVA, located in Livermore, California is a neodymium-in-glass laser used in fusion research. NOVA can deliver more than 100 kJ of energy in a three nanosecond pulse of focused infra-red light. Other areas of application of neodymium lasers are for cutting, welding, heat treatment of materials, fabrication of microelectronic circuits in semiconductor industry, medical applications, such as ophthalmic and surgical fields, military applications of range finding and target designating, active surveillance and communications, and in air-borne laser bathymeter for speedy data gathering to map depths of coastal waters.

The neodymium laser is popular because it is a solid state laser. Trivalent neodymium ions are incorporated in a host crystal or glass, at about one atomic percent doping. In the solid state, high concentrations of ions are available as opposed to the gaseous state. Further the host crystal provides mechanical strength and chemical inertness.

### 9.1. Rare earth ions

The rare elements are suited for incorporation into crystals or glasses as active lasers due to their electronic configuration. The outer most electrons of the rare earths form a complete

TABLE 12.13  
Electronic configuration of some rare earth ions.

Trivalent ion	Outer electronic structure			
Cerium, Ce <sup>3+</sup>	4d <sup>10</sup>	4f <sup>1</sup>	5s <sup>2</sup>	5p <sup>6</sup>
Praseodymium, Pr <sup>3+</sup>	4d <sup>10</sup>	4f <sup>2</sup>	5s <sup>2</sup>	5p <sup>6</sup>
Neodymium, Nd <sup>3+</sup>	4d <sup>10</sup>	4f <sup>3</sup>	5s <sup>2</sup>	5p <sup>6</sup>
Ytterbium, Yb <sup>3+</sup>	4d <sup>10</sup>	4f <sup>13</sup>	5s <sup>2</sup>	5p <sup>6</sup>
Xenon, Xe	4d <sup>10</sup>	–	5s <sup>2</sup>	5p <sup>6</sup>

noble gas shell, namely a xenon shell which is optically inactive. Inside the xenon shell, the 4f orbitals are successively filled with electrons from cerium to ytterbium. Rare earths are incorporated into the hosts as trivalent compounds. The electron configuration of some rare earth ions is given in Table 12.13.

## 9.2. Lasers

The first requirement is that a number of active rare earth ions be excited such that the 4f electrons remain in higher energy states. When the number of rare earth ions in the higher energy excited states are greater than the number in ground or normal state, population inversion is achieved. Population inversion can be achieved by optical pumping in which the atoms in the ground state are excited to higher states by absorption of pump light. The electrons in the excited levels decay by non-radiative transitions to a metastable level which is the upper laser level. The pump light source may be a flash lamp emitting a broad band of visible radiation.

The second requirement of laser activity is known as stimulated emission in which a photon of electromagnetic radiation interacts with an excited ion resulting in an electronic transition and emission of another photon exactly similar to the original photon in frequency, polarization, phase and direction. Thus an assembly of photons can be amplified by passage through an excited medium. The electronic transition is then from metastable upper laser level to the lower laser level. The lower laser level can be either the ground state or a level above the ground state which is usually unpopulated and decays quickly to the ground state. The first type of laser system involving pump, upper and ground level is known as a three-level laser system. The second type involving pump, upper, lower and ground levels is known as a four-level laser system. In the three-level system, population inversion condition can be achieved by exciting more than half of the ions whereas any degree of excitation achieves population inversion in the four-level laser system. The lasing threshold can be reached with much less pump energy in a four-level system as compared to a three-level system.

The trivalent neodymium ion is a good example of a four-level laser system. The trivalent Nd<sup>3+</sup> system is illustrated in Fig. 12.12 in a schematic fashion.

Trivalent neodymium absorbs strongly in broad bands in the green, red and near infra-red with reasonable coincidence in the output of a xenon flash lamp. Nearly all the electrons excited into the pump bands revert to the metastable upper level <sup>4</sup>F<sub>3/2</sub> through non-radiative decay which has a lifetime of 230 μs. Radiative transition then occurs to a set of lower energy levels <sup>4</sup>I<sub>15/2</sub>, <sup>4</sup>I<sub>13/2</sub>, <sup>4</sup>I<sub>11/2</sub>, <sup>4</sup>I<sub>9/2</sub>. All these levels are multiplets and the lowest of <sup>4</sup>I<sub>9/2</sub> is



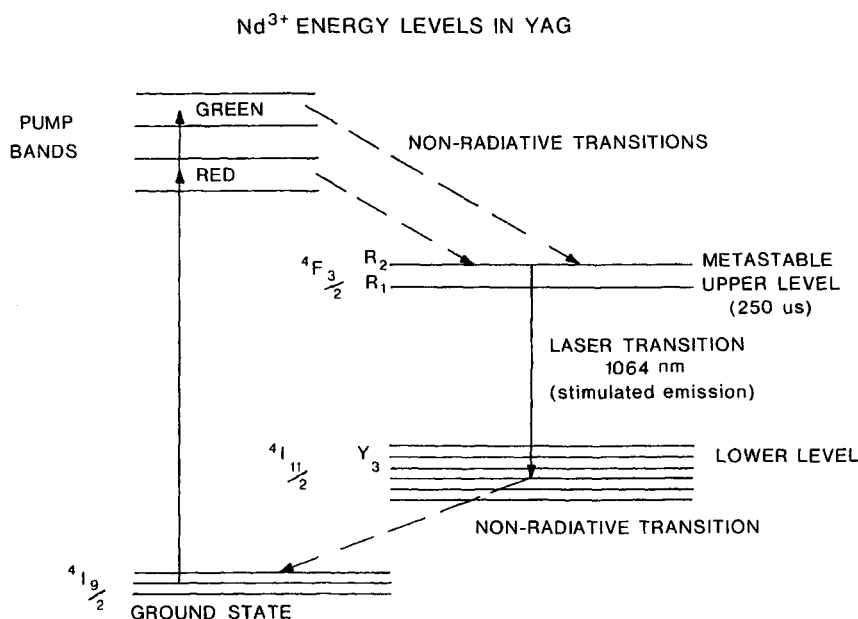


Fig. 12.12.

the ground state. The transition with the largest stimulation emission cross-section is from the upper  $4F_{3/2}$  level at  $11\,502\text{ cm}^{-1}$  in Nd-doped yttrium–aluminium garnet, Nd:YAG, to  $4I_{11/2}$ , level at  $2111\text{ cm}^{-1}$  with a wavelength of 1064 nm. This is the normal lasing transition in Nd:YAG although lasing on many other transitions can be produced by deliberately introducing losses for the 1064 nm transition in the optical resonator. The lower laser level is sufficiently higher in energy than the ground state, so that it is not populated at room temperature ensuring a true four-level scheme of lasing in the  $\text{Nd}^{3+}$  system.

The laser scheme is modified when neodymium is placed in other host environments in that the electronic levels have slightly different energies with different stimulated emission cross sections which may vary with the polarization of the stimulating radiation. As an example, Nd in lanthanum beryllate host (Nd:BeL), the major laser transition is at 1079 nm and 1070 nm for two different polarizations. YAG is the most common and versatile host for neodymium but glass has advantages for high energy applications such as fusion research. Other crystal hosts such as YAP, YLF and BeL have some unique features.

A third and important requirement for lasing action is to have sufficient optical gain irrespective of the active medium. The optical gain is achieved by multiple passes of the photons through the population-inverted medium. Multiple passes of photons is achieved by placing the active medium in an optical resonator. The optical resonator consists of two or more mirrors. A typical optical arrangement for a laser system is shown in Fig. 12.13.

Lasing action has been observed with other rare earths. The lower laser level in holmium is close to the ground state and can operate as a four level laser at liquid nitrogen temperatures. Erbium is similar to holmium. With other rare earths, alternate wavelengths can be obtained. Both Ho and Er operate in a region greater than  $1.5\ \mu\text{m}$ . Erbium can also

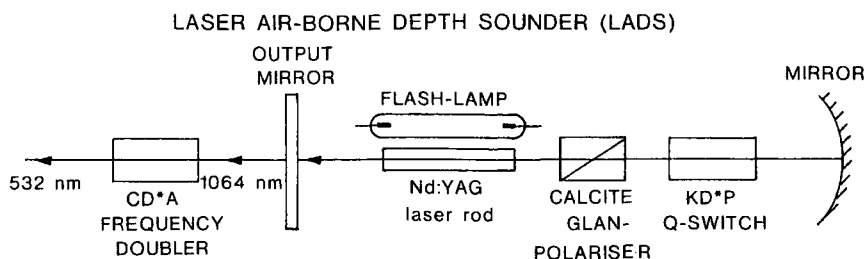


Fig. 12.13. Typical optical arrangement for a laser air-borne depth sounder (LADS).

operate at  $2.94 \mu\text{m}$  which can be absorbed by human tissue (in surgical operations) and efficiently transmitted by optical fibres.

## 10. Hi-tech applications [45]

The four major areas of applications of rare-earths in the high-tech field are (i) metal-hydride systems for energy storage, (ii) perpendicular magneto-optical disks for high density storage, (iii) magnetic refrigerators for cryogenic applications, (iv) magnetostrictive alloys for transducers for conversion of magnetic energy into mechanical energy.

Kawasaki Heavy Industry made one of the largest hydrogen storage vessels using metal hydrides and some of the activity in metal hydride systems in Japan is detailed in Table 12.14 as an example. The vessel has a capacity of  $175 \text{ Nm}^3$  corresponding to 25 high pressure hydrogen cylinders (150 atm). The lanthanum rich misch metal–nickel–aluminium alloy is used. This alloy can absorb and discharge hydrogen at a lower pressure and temperature than other conventional alloy systems. The vessel carries 1000 kg of the alloy and operates at 7 atm storage pressure (at  $30^\circ\text{C}$ ). The weight of the vessel is about 70% of the weight of a high pressure vessel of the same capacity and occupies only about 1/7ths of the volume of the latter. In one cycle of operation of absorption–desorption, hydrogen purity is upgraded from 99.99% to 99.99999%.

### 10.1. Hydrogen fuel storage for automobiles

Industrial research is focused on the development of the hydrogen fuelled engine as a substitute for the gasoline engine for automobiles. The hydride of La–MM–Ni–Al alloy has been studied for fuel storage. This alloy hydride was found to take up to  $80 \text{ Nm}^3$  of hydrogen. This system has been successfully tested on a Toyota Wagon ( $2000 \text{ cm}^3$ , 4 cylinders) by driving a distance of 200 km at a speed of 100 km/h.

### 10.2. Chemical heat pump

The reaction between hydrogen and a rare earth alloy generates heat, and hydrogen desorption occurs with absorption of heat. On this basis, an air-conditioning system has been developed. A chemical heat pump has been developed by Nihon Steel using 800 kg of MM–Ni–Ca–Al alloy with a capacity of 150 000 kcal/h. This was used as an air conditioner for a room. Such a device has been installed in a house containing a spa which is operated

TABLE 12.14  
Metal hydride systems in Japan.

Field	Companies, Institute	Work capacity	Operation	Alloys
H <sub>2</sub> fuel storage for automobile	GIRI Kawasaki	H <sub>2</sub> storage cap. 84 Nm <sup>3</sup>	1985	La-MMNiAl 480 kg
H <sub>2</sub> storage	Kawasaki	H <sub>2</sub> storage cap. 175 Nm <sup>3</sup>	1984	La-MMNiAl 1000 kg
	Kogakuin Univ. Japan	H <sub>2</sub> storage cap. 220 Nm <sup>3</sup>	1984	MMNiFe LaMMNiAl 1200 kg
Chemical heat pump	Chemi Eng. Kubota	3000 kcal/h	1983	LaNi 45 kg
	Toyobo			
	Sekisui	1400 kcal/h	1983	LaNi 90 kg
	Nihon Jyuka	1500 kcal/h	1983	MMNiAl 38 kg
	Kogakuin Univ			
	Nihon steel	150 000 kcal/h	1984	MMNiAlCa 800 kg
	Chiyoda Eng	300 000 kcal/h	1986	MMNiAlCa 3500 kg
	Nihon steel			
	Sekisui Chuo.	66 400 kcal/h	1986	MMNiAlFe
	Denki Japan			LaNiAl
	Chemi Eng.			2600 kg

MM, misch-metal.

with the input energy of the spa hot water for cooling in summer and warming in winter at total of 18 rooms occupied by 52 persons. The largest chemical heat pump facility with a capacity of 300 000 kcal/h using 3500 kg of MM-Ni-Ca-Al alloy was developed in Japan in 1986. Many more developments have followed.

### 10.3. Metal hydride battery

A metal hydride battery similar to the nickel-cadmium battery has been developed by Sharp corporation. The battery is shaped in the form of a button of 20 mm diameter and can give 1.2 V. The anode in the battery is made of La-Ni-Sn alloy hydride, and the cathode is nickel oxide. Potassium hydroxide solution in polyamide-resin is the electrolyte. The battery exhibits high energy density (i.e.) 1.5 to 2.0 times that of the Ni-Cd battery, good cycling life and superior low temperature behaviours.

### 10.4. Perpendicular magneto-optical disk as high density storage media

The reproduction of musical notes or sounds by the new digital recorders known as CD's is not sufficient to discern the notes clearly. In the digital process, the heights of sound peaks and valleys are measured and converted into binary (zero and ones) numbers of bits which in turn are reconverted into waves, and the waves into sound by the audio system.

In a similar way, the video disk reconverts the signal produced by the Kerr effect on a thin film of an amorphous substance such as Tb-Fe sputtered on a substrate disk made of plastic or glass. The Tb-Fe film functions like a perpendicular magneto-optical memory

system and provides the most suitable high density storage medium. In this system, the perpendicular magneto-optical recording can be erased, followed by recording and presenting the video picture like any other video tape recorder. The perpendicular magneto-optical disk has a large storage capacity 100 times conventional video disks such as CED, VHD, MCA, Laser disk, Video disk. Some of the promising materials for the amorphous film are Tb–Fe, Tb–Co, Dy–Fe, Gd–Fe and Gd–Co.

The perpendicular magneto-optical disks have gained importance in the world and continue to enjoy a good market.

### *10.5. Magnetic refrigeration in cryogenics*

Magnetic refrigeration has received considerable attention because it offers higher efficiency and reliability than the conventional helium gas refrigerator. Superfluid helium in the temperature region near 2 K is a very effective coolant for superconducting devices including superconducting coils. A rotating type of refrigerator with gadolinium sulphate as the working substance was developed and with this device, a minimum temperature of 2.10 K and a useful cooling power of  $<0.1$  W at 2.16 K were obtained. A new rotating magnetic refrigerator using super fluid helium based on the principle of the Carnot cycle was developed. Sinusoidal magnetization and demagnetization of the working substance is accomplished by rotating a superconducting coil in the persistent current mode. This prototype refrigerator uses Gd-Ga-garnet (GGG) as the working substance. Also heat switches which utilize heat transfer modes of helium and free of moving parts are used. A minimum temperature of 1.90 K and useful cooling power of 1.5 W at 2.10 K were obtained by this procedure [46].

Scientists at Ames laboratory have developed magnetic refrigeration as an alternative to traditional cooling systems which emit gases that contribute to global warming. The new refrigerator uses a special wheel made of gadolinium which heats up when exposed to a magnetic field, then cools when the field is removed. The only energy is the electrical energy for the motors to spin the wheel and drive the water pumps. Magnetic refrigeration could power air conditioners, freezers and other systems. Astronautics corporation of America, Madison, Wisconsin is actively involved in commercialization ventures.

### *10.6. Magneto-strictive alloys*

Rare earth metals such as Tb, Sm, and Dy when alloyed with Fe exhibit properties of giant magneto-striction. The  $\text{Tb}_{0.3}\text{Dy}_{0.7}\text{Fe}_{1.9}$  Laves phase alloy exhibits outstanding magneto-strictive properties and is receiving a great deal of attention as a transducer material for the conversion of magnetic energy into mechanical energy. The characteristics of a typical magnetostrictive alloy, and its potential applications are detailed below.

- Magnetomechanical strain 1800  $\mu\text{m}$ .
- Forces equivalent to 500–700 MPa.
- High frequency mechanical response.

- Controllable sound velocity.
- Larger relative permeability change in response to applied mechanical stress.

Potential applications:

- Valve control.
- Active antivibration.
- Impact printers.
- Clamping action.
- Micro-pump.
- High mechanical impedance drivers, etc.

Potential applications of active magnetic refrigeration.

1. Liquefaction of gases	
Hydrogen slush	15 K
Hydrogen	20 K
Natural gas (methane)	109 K
Propane	231 K
Ammonia	240 K
Butane	273 K
2. Sub-room temperature refrigeration	
Supermarket chillers (refrigeration & frozen foods)	
Food processing plants	
Frozen vegetables, fruits, meat, dairy products	265 K
Refrigeration	275 K
Chemicals (Cl <sub>2</sub> , NH <sub>3</sub> , ethylene, polyethylene)	170–250 K
Air conditioning/heat pumps	
Large scale systems (buildings)	288–300 K
Motor vehicles	288–300 K
Homes	288–300 K
3. Industrial low-level heat (heat pumps)	
Sugar refining, liquor distilling	300–470 K
4. Agriculture	
Grain drying	295–315 K
5. Waste separation and treatment	
Chemical	70–370 K
Nuclear	250–370 K
Agriculture (hog lots, etc.)	70–295 K

### 10.7. Outlook for rare earth based metal hydrides and NiMH rechargeable batteries

The rare earth based metal hydrides AB<sub>5</sub> have proven to be best suited for use in the negative electrode in NiMH batteries. The market demand for the nickel–metal hydride battery is high because of the rapid demand for portable electronics goods such as video cameras, shavers, power tools, cellular phones, lap-top computers which use high performance batteries.

The world's rechargeable battery market is shown below. The projected growth rate of NiMH from 1994 to 2000 is shown below.

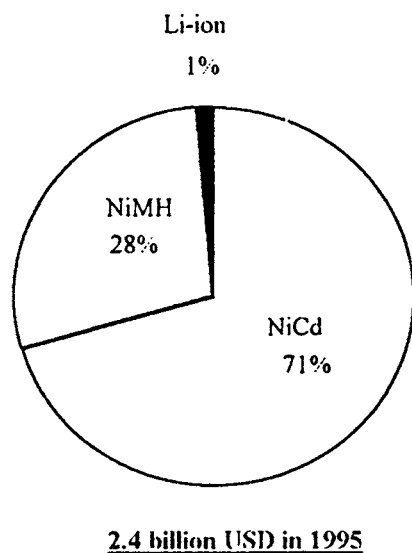


Fig. 12.14. World rechargeable battery market.

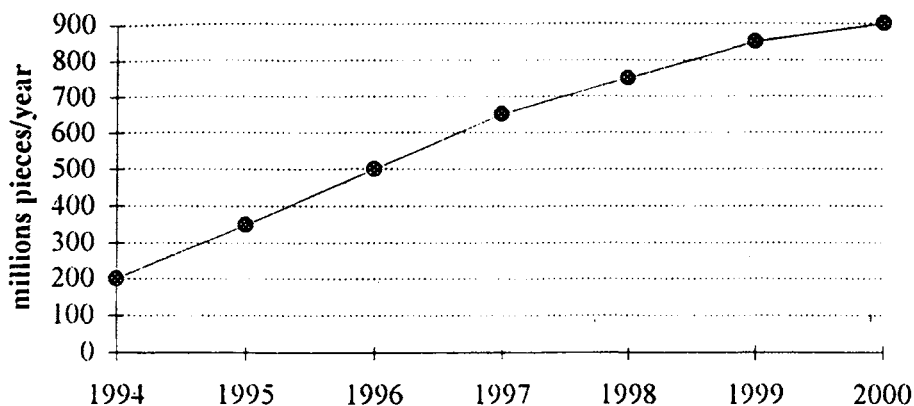


Fig. 12.15. NiMH battery production forecast.

## 11. Photonics, electronics and related applications [48]

A sensor is a device that detects and quantifies some property by providing an external signal such as electrical, in response to that property. As an example the yttria-stabilized zirconia (YSZ) sensors give a voltage output that depends on the partial pressure of oxygen in the exhaust gas of an automobile. A sensor responds to some form of energy and may be thought of as a transducer converting one form of energy into another. In a sense, although extreme, devices that modify energy may be considered as transducers. Neodymium-colored filter glass falls into this category.

In specifying a 'sensor/transducer', it is necessary to identify the input and output energy. As for example,

	Input	Output
YSZ sensors	Chemical	Electrical
CRT phosphors	Electrical	Radiation
Optical filter	Radiation	Radiation

Sometimes the transducers utilize an auxiliary source of energy as in some electrical device with electrical energy as input and output forms, but the output signal is determined by an auxiliary form such as thermal or radiation energy. The transducers need to be specified by input, output and auxiliary forms and in such a case, they are known as self-modulating transducers. When no auxiliary form of energy is involved one has self-regulating transducers.

### 11.1. Photonics

The technology involving light and other forms of radiant energy with a fundamental unit, the photon, is known as photonics. Transducers which have visible light as output are widely used. Examples are phosphors, which emit light. Uses of lanthanides in luminescence transducers are listed in Table 12.15. The list includes CRT Phosphors and fluorescent lamps.

Some phosphors are self-generating and others are stimuable phosphors involving modulating transducers to delay the output. Some examples of lanthanides in luminescence transducers are listed in Table 12.16.

The dose to which personnel is exposed can be read off the film badge by using thermoluminescence. The thulium-doped calcium sulphate phosphor can measure low doses precisely. The X-ray image in photo stimuable luminescence (PSL) can be processed digitally by stimulating the exposed phosphor with a light source different from the actual exposure. The PSL intensity has a linear response with respect to X-ray energy.

#### 11.1.1. Radiation transducers

Because of the novel spectral behaviour, there are numerous applications of lanthanides involving conversion or modification of the input energy in the visible and near-visible region. Some examples of this process are neodymium ion lasers in yttrium aluminum garnets (YAG) or gadolinium scandium gallium garnet (GSSG). Further samarium-doped filter glass can absorb unnecessary UV and IR radiation and strengthen the Nd pumping bands.

Transparency to the incident radiation is a trait of a transducer. Yttrium oxide, doped with lanthanum oxide is transparent to IR radiation. Blocking of undesired UV radiation is achieved by cerium doped glasses. Some examples of modulating transducers are given in Table 12.17.

Devices based on lanthanum lead zirconate titanate (PLZT) using polarized light can be switched from transparent to opaque in microseconds. Welding goggles and aircraft windows offer protection from sudden flashes of intense light.

TABLE 12.15  
Lanthanides in luminescence transducers (visible radiation).

Input energy	Material	Application	Reference
Gamma, neutron	Ce-doped glass	Particle detection	[50]
X-ray	Tb; Gd <sub>2</sub> O <sub>2</sub> S, etc.	Screen phosphors	[51]
UV	Several	Fluorescent lamps	[52]
IR	Yb, Er; LnF <sub>3</sub>	Laser monitoring	[53]
Electron	Eu; Y <sub>2</sub> O <sub>2</sub> S, etc.	CRT-TV red, etc.	[54]
Electrical	Ce, Sm, Tb; etc.	Flat-panel displays	[55]
Mechanical	Eu salts		[56]

TABLE 12.16  
Lanthanides in luminescence (visible radiation).

Input energy	Auxiliary	Material	Application	Reference
Gamma, etc.	Thermal	Tm, Dy; CaSO <sub>4</sub>	Dosimetry	[57]
Visible	Thermal	Eu, Etc.	Temperature measurement	[58]
X-ray	Visible	Eu, BaFCl	Computer X-ray	[59]

TABLE 12.17  
Lanthanides in radiation uses transducers.

Input/output	Auxiliary	Material	Application	Reference
Visible	Electrical	PLZT	Displays, protections	[60]
Infra-red	Magnetic	Ce, Tb, glass	Faraday rotators	[61]
Visible	Magnetic	Ln, GIG	Displays, printers	[62]
Micro, radio	Magnetic	YIG/GIG	Communications	[63]

A different type of protection is provided by cerium or terbium containing fluorophosphate glasses used in laser-based fusion research. The lasers need to be protected from back reflected light and it is done using the Faraday effect. A glass with a high loading of ions and which has magnetic moments provides the necessary Faraday rotation in an applied magnetic field. The Faraday effect can be used for sensing the magnetic field using a long suitably-doped fiber for detecting the rotation of the polarized light.

Modulated transducers are used in optical information processing. Faster, and smarter devices are required to control displays, printers and communication equipment. Thin garnet films, with individual pixels, that can be addressed independently and be switched from transparent to opaque can be used in this technology. Light switching arrays (LISA) are composed of bismuth substituted gadolinium iron garnets (GIG).

### 11.2. Electronics

The field of transducer matrices for electrical properties covers many devices containing lanthanides. For example, capacitors are miniaturized and new dielectric compositions



TABLE 12.18  
Lanthanides in magnetic devices as transducers.

Magneto-technology	Notation	Material	Application	Reference
Optic	(radiation, magnetic)	Gd/Tb/Fe	Data recording	[64]
Optic	(magnetic, magnetic)	Ln/GGG	Bubble memory	[65]
Strictive	(magnetic, mechanical)	Terfenol	Sonar	[66]
Caloric	(magnetic, thermal)	Gd alloys	Refrigeration	[67]

are used to meet performance requirements. A desirable property is that the value of capacitance be independent of temperature. The negative-positive-zero (NPO) material is based on neodymium/barium titanate system. Some lanthanide oxides are also incorporated into the dielectric compositions for improved performance. The multilayer ceramic capacitors consume large amounts of lanthanide oxides.

Magnetic properties are important in the function of electronic devices. An example is the use of yttrium iron garnet (YIG) in microwave devices. On applying an external magnetic field to a YIG disk, the input, say energy of one particular frequency selectively passes to the output. Thin films based of YIG within which magnetic waves can pass have proven to be useful. The use of lanthanides in magnetic devices as transducers is listed in Table 12.18.

The non-volatile bubble memories used for data storage are based on the principle of formation of magnetic domains in thin films grown on a gadolinium gallium garnet crystal substrate. Molecular engineering creates the precise film compositions for optimum performance.

A technique has been developed for data storage based on the magnetic behaviour of thin magnetizable Ln-alloy films. The fact that gadolinium has a curie point at room temperature and can be driven above this point by local heating is used.

Magnetic energy can be converted into mechanical energy by magnetostrictive alloys of which Terfenol Tb/Dy/Fe is a good example. This material is mainly in sonar transducers which have a sound-power output that is 25 times greater than ceramic transducers. Magnetostrictive alloys may be useful in vibrational control in the case of 'soft' structures that are rigid, as for example, in positioning of tools.

Since the input and output can be interchanged in a symmetrical three dimensional transducer, this interchange principle can be effectively used in magnetic refrigeration. The operating temperature range determines the working material and the Gd Metal is most suitable for ambient conditions.

## 12. Applications in ceramics

Traditionally ceramics are solid inorganic substances obtained by employing high temperatures of naturally derived substances like clay. Because of the similarities in materials and production processes, the field of glasses is also included in ceramics. Thus ceramics include both crystalline inorganics and amorphous substances [68].

TABLE 12.19

Yellow stain based on Pr oxide (%)		Orange stain based on Y oxide (%)		Light purple pigment based on Nd oxide (%)	
ZrO <sub>2</sub>	60	ZrO <sub>2</sub>	96	ZrO <sub>2</sub>	60
SiO <sub>2</sub>	30	NH <sub>4</sub> VO <sub>3</sub>	3	SiO <sub>2</sub>	1
NaF	3	Y <sub>2</sub> O <sub>3</sub>	1	NaF	6
NaCl	4			Nd <sub>2</sub> O <sub>3</sub>	33
Pr <sub>6</sub> O <sub>11</sub>	3				

TABLE 12.20  
World market for ceramic tiles, 1982 [68].

Consumption (10 <sup>6</sup> m <sup>2</sup> )		Consumption per capita (m <sup>2</sup> )	
Europe	450	Italy	3.0
South America	200	Brazil	1.0
Asia-Africa	130	Japan	0.5
North America	60	United States	0.2

An advanced ceramic is characterized by (i) synthesis of materials of defined composition, (ii) manufacture under controlled conditions of pressure and temperature, and (iii) those that provide some special functions.

High technology ceramics can be used in (i) components in automobile engines, (ii) electronic devices, and as (iii) bio-compatible parts.

In traditional areas such as ceramic tiles, praseodymium oxide in a zirconium silicate matrix is used as a yellow stain. Cerium oxide is used as an opacifier or to give esthetic effects in the glaze. Other pigment colours, such as orange with yttrium oxide and light purple with neodymium oxide can be prepared. The compositions of these pigments are given in Table 12.19.

Very highly pure cerium oxide is also used in serigraphy (i.e.) silk screen printing. The product is mixed in the printing oil and then applied through a silk screen. Although the data are not current, the world market for ceramic tiles, as of 1982 is given in Table 12.20. The projected figure for 2000 is 1.2 billion m<sup>2</sup>.

The various materials used, along with the lanthanide additive and the applications, are given in the form of tables based on the properties such as mechanical, chemical, electrical and magnetic, emission of radiation and interaction with electromagnetic radiation. The applications based on the mechanical and nuclear properties are given in Table 12.21.

Ceramic components such as turbine blades, piston caps, turbocharger rotors and valves for heat engines are important. The ceramics that are useful for this application are silicon nitride (Si<sub>3</sub>N<sub>4</sub>), zirconia (ZrO<sub>2</sub>), silicon carbide (SiC) and SiAlON ("sialons"). Yttrium or lanthanide oxide is added as an additive to produce the desired properties. The yttrium or lanthanide additives act as sintering aids and produce different effects such as (i) a second phase Y<sub>2</sub>Si<sub>3</sub>O<sub>3</sub>N<sub>4</sub> which is crystalline and resists crack growth, (ii) production of crystalline yttrium aluminum garnet which has high strength and oxidation resistance, (iii) stabilization of cubic ZrO<sub>2</sub>.

TABLE 12.21  
Mechanical and nuclear properties.

Application	Material	Additive	Reference
High-temperature strength (structural parts, cutting tool tips, wear resistance)	Si <sub>3</sub> N <sub>4</sub>	Y <sub>2</sub> O <sub>3</sub> , Ln <sub>2</sub> O <sub>3</sub>	[70,71]
	SiAlON	Y <sub>2</sub> O <sub>3</sub> , Ln <sub>2</sub> O <sub>3</sub>	[72]
	ZrO <sub>2</sub>	Y <sub>2</sub> O <sub>3</sub> , Ln <sub>2</sub> O <sub>3</sub>	[73]
	AlN	Y <sub>2</sub> O <sub>3</sub> , Ln <sub>2</sub> O <sub>3</sub>	[86]
High-temperature strength superrefractories	CeS		[87]
	Y <sub>2</sub> O <sub>3</sub>		[88]
Dispersion strengthener for metals	Ni	Y <sub>2</sub> O <sub>3</sub>	[74]
	Al	CeO <sub>3</sub>	[89]
	Ti	Er <sub>2</sub> O <sub>3</sub> , Nd <sub>2</sub> O <sub>3</sub>	[75]
Polishing powder for silicate glass	CeO <sub>2</sub>		[90]
Neutron absorber for reactor control	EuB <sub>6</sub>		[91]
	Gd <sub>2</sub> O <sub>3</sub>		[92]

### 12.1. Stabilized zirconia

By the addition of 11%, Y<sub>2</sub>O<sub>3</sub> fully stabilized zirconia is obtained. The resulting system is cubic. With lower amounts of Y<sub>2</sub>O<sub>3</sub>, one obtains partially stabilized zirconia (PSZ). Use of Y<sub>2</sub>O<sub>3</sub> in zirconia results in production of (i) synthetic gems (15 wt% Y<sub>2</sub>O<sub>3</sub> in ZrO<sub>2</sub>), (ii) engineering ceramics (5–6 wt% of Y<sub>2</sub>O<sub>3</sub> in ZrO<sub>2</sub>) which are used in the production of knives, scissors, etc., (iii) PSZ can be used in a cylinder liner or for protection of piston heads in automobiles.

### 12.2. Oxygen sensors

PSZ containing 9 wt% Y<sub>2</sub>O<sub>3</sub> is used in the sensor. The sensor is used to control automotive engine exhaust gas to reduce emission of CO, nitrogen oxides and hydrocarbons. At high temperatures, the ceramic becomes conductive to oxygen and generates a potential difference used to optimize air/fuel ratio. This helps the three-stage catalyst system to operate at maximum efficiency. Exhaust gas emission and the voltage signal are shown in Fig. 12.17.

The applications based on chemical properties are given in Table 12.22.

There is an obvious overlap among various applications categories. An example of the overlap is alumina which is both a structural refractory ceramic as well as a catalyst support. The additives modify the interconversion of various Al<sub>2</sub>O<sub>3</sub> phases and the high surface area of  $\gamma$ -Al<sub>2</sub>O<sub>3</sub> is maintained by the added 3 wt% ceria or lanthana. Additives like yttria stabilize zirconia with respect to inertness and mechanical stability. Addition of yttrium or lanthanide to Fe–Cr–Al alloys reduces the spallation of oxide film.

The applications based on electrical and magnetic properties are given in Table 12.23.

The vast growth in electronic equipment owes to capacitors which are essential in almost all the devices. Barium titanate forms the heart of the capacitors. The perovskite structure contains a small ion of high charge at the centre of an MO<sub>6</sub> octahedron. The high polarizability is the basis of a high dielectric constant in the capacitor. The addition of Nd to the mixed titanate gives a stable capacitance over a wide temperature range.

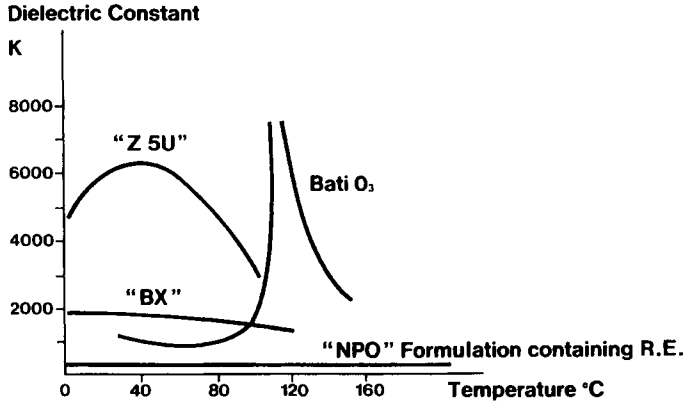


Fig. 12.16. Dielectric constant evolution of several MLC.

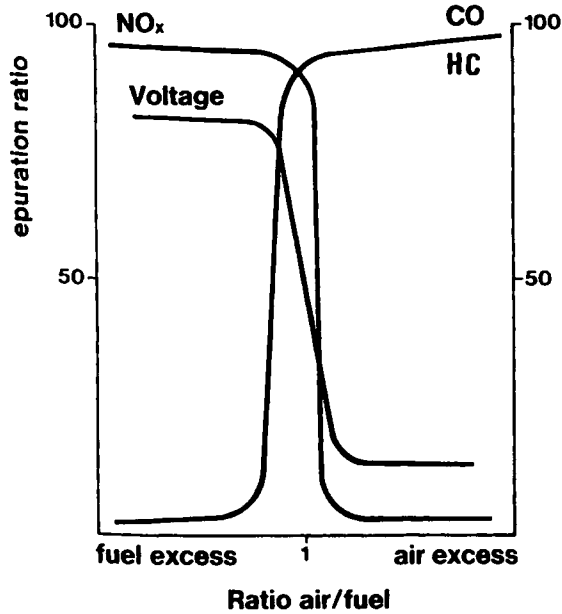


Fig. 12.17. Exhaust gas emission.

Another interesting system is Pb/La/Zr/Ti/O with about 10 at% La. By a sintering process, a transparent ceramic is obtained. By applying voltage across such a ceramic, the plane of polarization is altered within microseconds. This feature is used in information display systems.

Dielectric constant evolution of multilayer capacitors (MLC) is shown in Fig. 12.16.

It is clear that in the case of barium titanate, the dielectric constant is not steady in the temperature range (−55 to +125°C). Addition of neodymium carbonate in a “NPO”

TABLE 12.22  
Chemical properties.

Application	Material	Additive	Reference
Decolorizing	Glass	Ce	[92]
Catalyst support	Al <sub>2</sub> O <sub>3</sub>	Ln <sub>2</sub> O <sub>3</sub>	[76,77]
Oxidation catalyst	CeO <sub>2</sub>		[84]
Cracking catalyst	Zeolites	Ln(3+)	[85]
Protective coatings	Fe-Cr-Al	Y etc.	[79]
	ZrO <sub>2</sub>	Y <sub>2</sub> O <sub>3</sub> , Ln <sub>2</sub> O <sub>3</sub>	[78]
Sensors	ZrO <sub>2</sub>	Y <sub>2</sub> O <sub>3</sub>	[96]
	LnO <sub>2</sub> , LnF <sub>3</sub>		[97,98]

TABLE 12.23  
Electrical and magnetic properties.

Application	Material	Additive	Reference
Ionic conductivity	ZrO <sub>2</sub>	Y <sub>2</sub> O <sub>3</sub>	[96]
	CeO <sub>2</sub>	Pr, Gd	[97]
Electronic conductivity	LaCrO <sub>3</sub>		[99]
	LaMnO <sub>3</sub>		[99]
Resistors	LnB <sub>6</sub>		[100]
Electron emission	LaB <sub>6</sub>		[101]
Dielectric capacitors	Nd/Ba/Ti/O	Ln	[80]
	Pb/La/Zr/Ti/O		[102]
Thermistors	BaTiO <sub>3</sub>	La, Y	[103]
Varistors	ZnO <sub>2</sub>	Pr <sub>6</sub> O <sub>11</sub>	[104]
Electro-optic	Pb/La/Zr/Ti/O		[81]
Information storage	Gd <sub>3</sub> Ga <sub>5</sub> O <sub>12</sub>	Ln	[105]

formulation stabilizes the system with a deviation of less than  $30 \times 10^{-6}/^{\circ}\text{C}$  over the temperature range. The capacitor life is also increased by 400–500 times by the addition of lanthanum in the ceramic body.

Small amounts of Y or La are used to dope BaTiO<sub>3</sub> which is the main component of all PTCs (positive temperature coefficient). Demand for PTC thermistors is high. Yttrium iron garnets are used in soft ferrites at very high frequencies (microwave region) for radar equipment.

Applications based on emission of electromagnetic radiation are given in Table 12.24.

The lasing action of Nd<sup>3+</sup> ion in YAG or glass is well known and Sm is used in glass surrounding lasing rods to absorb unwanted UV light.

The red television phosphor is based on europium. This phosphor is also used in trichromatic fluorescent lamps where a blend of red, blue and green phosphors gives white light.

The applications due to interaction with electromagnetic radiation are listed in Table 12.25.

TABLE 12.24  
Emission of electromagnetic radiation.

Application	Material	Additive	Reference
Lasers	YAG, glass	Nd, Sm	[82]
	Glass	Er, Ho	[106]
Phosphors, CRT	Y <sub>2</sub> O <sub>2</sub> S	Eu	[107]
	Various	Ce, Tb, Eu	[107]
Phosphors, X-ray	LaOBr	Tb, Tm	[108]
	Gd <sub>2</sub> O <sub>2</sub> S		
Phosphors, lamp	SCAP	Eu	[83]
	Y <sub>2</sub> O <sub>3</sub>	Eu	[83]
	Various	Ce/Tb	[83]
Pigments	ZrSiO <sub>4</sub>	Pr	[109]

TABLE 12.25  
Interaction with electromagnetic radiation.

Application	Material	Additive	Reference
Lens glass	La/Zr/B/O		[110]
IR transparency	CaLa <sub>2</sub> S <sub>4</sub>		[111]
	Y <sub>2</sub> O <sub>3</sub> /La <sub>2</sub> O <sub>3</sub>		[112]
Radiation control	Glass	Ce	[113]
UV absorption	Pigments, etc.	Ce	[84]
Antireflection	Pr <sub>6</sub> O <sub>11</sub>	Ln	[114]
Microwave	Y <sub>3</sub> Fe <sub>5</sub> O <sub>12</sub>	Ln	[85]

Lanthanum has been used extensively in camera lenses to give high refractive indices with low dispersion. Cerium oxide absorbs UV light strongly and hence prevents degradation of pigments.

Yttrium iron garnet (YIG) is used in devices that process microwaves. Growing YIG and LnIG films on perfect crystals obtained from gadolinium gallium garnet (GGG) is involved in ceramics which have technological applications.

### 13. Applications in fiber optics, luminescent solar concentrators

#### 13.1. Fiber optics

The development of fiber optics together with semiconductor lasers and rare earth lasers is useful in simple broadband communications over varied distances, in computers, switching systems, aircraft and space craft [115]. There has been an increase in the types of fiber wave guides based on fluoride glasses. Glasses doped with rare earth ions show emission in the range of maximum transparency of the fibers. Glasses doped with rare earth ions with the desired emission are drawn into fibers which are part of long fibers made of undoped glass. The intrinsic lasers form part of integrated fiber optics.

The laser action of a glass or crystal depends on the laser peak cross-section and the threshold power for lasing. The peak cross-section  $\sigma$  is given by [116]

$$\sigma = \frac{\lambda^4 A}{8\pi C n^2 \Delta\lambda},$$

where  $\lambda$  is the emission wavelength,  $\Delta\lambda$  is full width at half height of emission band,  $n$  the refractive index,  $A$  is the radiative transfer probability in  $s^{-1}$ . The threshold power,  $P_{thr}$  ( $W/cm^2$ ) for transverse pumping is given by

$$P_{thr} = \frac{hc(L_0 + L_{res}) \times 10^{-7}}{2\lambda_p l F \sigma \alpha_p},$$

where  $L_{res}$  is the resonant power loss due to self-absorption at the laser wavelength and is given by

$$L_{res} = 2l\sigma N\beta_Y/Z,$$

where  $N$  is the number of lasing ions,  $\beta_Y$  is Boltzmann factor for the terminal laser level,  $Z$  is partition function and  $l$  the length of the laser. In the case of Nd(III) the terminal level  $^4I_{11/2}$  for the 1060 nm luminescence is positioned at  $\approx 2000\text{ cm}^{-1}$ , then  $\Delta E/kT = 10$  at room temperature, and the Boltzmann factor is  $4.5 \times 10^{-5}$ . For 1 cm long minilaser at representative values of  $N$  and  $\sigma$ :  $L_{res} = 0.2\text{--}0.1\%$ ;  $L_0$  is the nonresonant loss which is mainly due to the absorption of the medium and loss at mirrors and is taken to be  $0\text{--}1.5\%$ ;  $\lambda_p$ , the pumping wavelength, for Nd(III) it is at 806 nm of LED having 25 nm bandwidth;  $\tau_f$ , the lifetime of lasing level;  $F$ , the Boltzmann population function of the lasing level which in cases of glasses have an inhomogeneous broadening and is taken as 1;  $\alpha_p$ , the absorption coefficient of the pumped level and equal to optical density/thickness.

Rare earth doped lasers of Nd(III), and Ho(III), and Er(III) are available and in use [117]. The threshold powers have been calculated for these ions in various glasses and are as follows.

Nd (mol%)	Transition	$P_{thr}$ ( $W/cm^2$ )
0.5–2.0	$^4F_{3/2}\text{--}^4I_{11/2,13/2}$	11–450
Ho 0.125–2.0	$^5I_7\text{--}^5I_8$	24.2–5815
	$^5I_6\text{--}^5I_8$	
	$^5I_7\text{--}^5I_8$	
Er 0.125–2.66	$^4I_{11/2}\text{--}^4I_{15/2}$	4.9–2118
	$^4I_{11/2}\text{--}^4I_{13/2}$	

The threshold powers can be lowered by transferring energy from other ions. The effect of added ions on threshold power is obvious from the data given below.

	$\lambda$ ( $\mu\text{m}$ )	$P_{\text{thr}}$ ( $\text{W}/\text{cm}^2$ )
Er [+Yb (5 mol%)]	2.80	0.35–0.55
Er [+Yb (5 mol%)]	0.98	13.80–15.40
Ho [+Er (5 mol%)]	2.00	10.00
Ho [+Yb (5 mol%)]	1.20	13.30
Ho [+Yb (5 mol%)]	2.90	0.86

### 13.2. Crystal lasers

Energy transfer in crystal lasers allows lasing at room temperature.

#### 13.2.1. Holmium

Codoping dielectric crystals by Er(III), Tm(III) and Yb(III) allows Ho(III) lasing [118]. Lasing at 2.12  $\mu\text{m}$  of  $(\text{Y}_{0.89}\text{Tm}_{0.1}\text{Ho}_{0.01})(\text{Al}_{0.99}\text{Cr}_{0.01})$  codoped by Tm(III) and Cr(III) [119] Ho(III) lasing at 2.086  $\mu\text{m}$  in Cr,Tm,Ho:YAlSc garnet and Cr,Tm,Ho:YSc Ga garnet [120].

Effective energy pumping is supplied by Cr(III) as shown in Fig. 12.18.

Fluoride hosts have been preferred over oxide hosts for Ho(III) since the lifetime of  $^5\text{I}_7$  in  $\text{YLiF}_4$  is 12 ms [121,122].

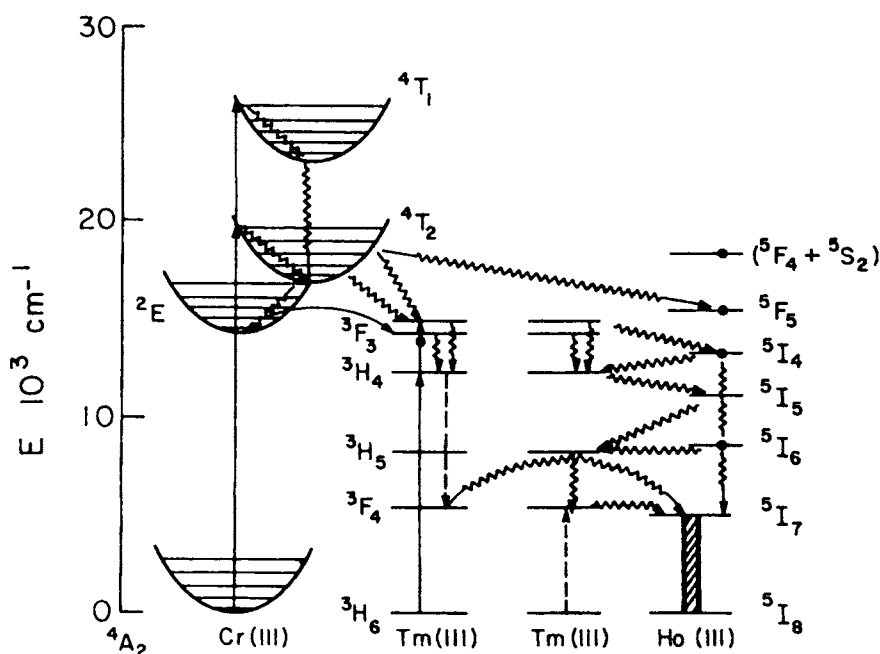


Fig. 12.18. A scheme of triple energy transfer  $\text{Cr(III)} \rightarrow \text{Tm(III)} \rightarrow \text{Ho(III)}$ .



### 13.2.2. Erbium

Er(III) in  $\text{YLiF}_4$  is a room temperature solid state laser lasing at  $1.73 \mu\text{m}$ .

Er(III) in  $\text{YAlO}_3$  at  $1.7 \mu\text{m}$  due to  ${}^4\text{S}_{3/2} \rightarrow {}^4\text{I}_{9/2}$ .

Er(III) in garnets at  $2.80 \mu\text{m}$  due to  ${}^4\text{I}_{9/2} \rightarrow {}^4\text{I}_{13/2}$ .

### 13.2.3. Thulium

A tunable Q switched thulium-doped single mode silica fiber laser has been described [123].

### 13.3. Single-mode fibre lasers [115]

Preparation of fluoride active fibres doped with rare earths has been achieved. Active fibres based on silica are known. Single-mode fibre lasers can operate at low threshold and high gain and continuous operation. When silicate fiber was doped with Nd(III), a lasing threshold of 100 mW was achieved. A gain of 17 dB in a short length of Nd(III) doped fibre has been observed indicating the way to high gain optical fiber amplifiers.

Q switching of the fibre lasers by lasers using an acousto-optic modulator/rotating chopper results in peak powers of several watts in pulses in the range of 50 ns to  $1 \mu\text{s}$ .

Transmission loss is probably the most important single performance parameter of optical fibres and hence it remains as an active area of research and development. Activity on low-loss fibres has focused on mid-IR-fibres. Fibres based on fluoride glasses can transmit light 10–100 times more efficiently than silicate glasses. Zirconium fluoride optical glass is being used which transmits light up to  $5\text{--}7 \mu\text{m}$  with very little loss of transmission. Losses lower than 1 dB/km at  $2.55$  or  $2.6 \mu\text{m}$  have been achieved. An application of this is in repeaterless transoceanic cable systems. Other applications are sensing, spectroscopy, power-delivery for medicine and industrial processing.

### 13.4. Luminescent solar concentrators (LSC)

The principle of operation of the luminescent solar operator involves the absorption of solar radiation in a collector containing fluorescent species whose emission bands do not overlap with the absorption bands. The fluorescence emission is trapped by total internal reflection and concentrated at the edges of the thin plate acting as a collector [124]. Some of the advantages of LSCs over conventional solar collectors are (i) collection of both direct and diffuse light, (ii) effective heat dissipation on non-utilized energy by the large area of the collector plate in contact with air allowing essentially 'cold-light' to reach the photovoltaic cells, (iii) it is not necessary to track the sun, (iv) the luminescent species is so chosen to allow matching of the concentrated light to the maximum sensitivity of the photovoltaic cell [124,125].

The performance of LSCs which absorb light in a large area plate, and convert it into luminescence and further concentration at the edges of the plate has been well described.

The optical efficiency of an LSC is given by

$$\eta_{\text{opt}} = \eta_{\text{tr}}\eta_{\text{abs}}\eta_{\text{fl}}\eta_{\text{st}}\eta_{\text{par}},$$

where:  $\eta_{\text{tr}}$  = efficiency of trapped fluorescence due to internal reflections;  $\eta_{\text{abs}}$  = efficiency of the absorbed light;  $\eta_{\text{fl}}$  = fluorescence efficiency;  $\eta_{\text{st}}$  = stokes efficiency;  $\eta_{\text{par}}$  = efficiency including parasitic losses.

The choice of a material for LSC depends obviously on the optical efficiency which in the case of rare earth ions may be obtained from the calculated absorption and fluorescence efficiency. An efficiency of 12% for Nd doped tellurite glass has been observed [126].

The intrinsic absorption of rare earth ions is low because the electronic transitions involved are parity forbidden. Thus alternate ways [127] of increasing the efficiency of an LSC doped by inorganic ions by non-radiative and radiative trapping of strong luminescence by organic dyes incorporated in a thin polymer or glass films covering the plates was studied. This technique helped to attain 40% efficiency in the case of a Nd doped plate covered by an organic dye [128]. The mechanism is that the dye absorbs the solar light efficiently and then fluoresces which is trapped by the glass. The high concentration of emitting photons amplifies the absorption of Nd(III) which then gives intense luminescence.

#### 14. Rare earth substituted garnet films for magnetic bubble memory applications

Rare earth substituted thin iron garnet films are of considerable technical importance as basic materials for magnetic bubble memory devices. Iron garnet films required for use in the devices are grown as thin films on non-magnetic substances like  $Gd_3Ga_5O_{12}$ ,  $Sm_3Ga_5O_{12}$  using liquid phase epitaxy technique. In order for a film to support magnetic bubbles (cylindrical domains) and be useful in the devices, it must possess uniaxial anisotropy perpendicular to the plane of the film. Further, the saturation magnetic moment of the material must be small when the materials are grown as thin films on non magnetic single crystal substrate. It is also necessary that the mismatch between lattice parameters of the film and the substrate should be small. In order to achieve the above conditions, rare earths such as Sm, Eu, Lu, Gd, Yb are substituted in the prototype yttrium iron garnet (YIG) compositions.

LPE technique has been used in the growth of films. Thin films of the composition  $Y_{3-x}Sm_xFe_{3.8}Ga_{1.0}O_{12}$  ( $x = 0.4, 0.46$ ),  $Y_{3-x}Eu_xFe_{4.0}Ga_{1.0}O_{12}$  ( $x = 0.2-1.2$ ) and  $(Y, Eu, Yb)_3(FeAl)_5O_{12}$  were grown. The suitability of these films with respect to resonance, relaxation properties and anisotropy has been studied.

Bubble memories may be viewed as solid state integrated analogs of rotating electro-mechanical memories such as disks, drums and tape recorders. In both rotating and integrated versions, information is stored in the form of magnetized regions. In the integrated version (bubble memory) the magnetic regions are cylindrical domains (bubbles) stabilized in a thin layer of a magnetic material whose magnetisation is opposite to that of surrounding area. The presence and absence of the magnetic regions at specific locations correspond respectively to binary digits 1 and 0 stored at these locations. These bits are made accessible by moving the domains within the solid layer to an access device, as opposed to physically moving the storage medium as in the case of a disk or tape.

Memory systems based on magnetic bubble technology have many significant applications for commercial and military systems. In commercial applications, bubble memories are used as micro peripherals. As far as military applications are concerned, bubble memory systems offer (i) a high quality and (ii) high reliability as compared to other available storage media. Further advantages for bubble memory systems are compact size, fast random access, physical ruggedness and inherent nonvolatility. The present estimated market is in the billions of dollars.

## 15. Rare earth phosphors [130]

Phosphors are mostly solid inorganic materials consisting of a host lattice doped with impurities. The absorption of energy occurs through either the host lattice or the impurities and the emission invariably originates from the impurities.

### 15.1. Emission of rare earth ions

Emission of rare earth ions is due to the optical transition involving f levels ( $\text{Tb}^{3+} 4f^8$ ;  $\text{Gd}^{3+} 4f^7$ ;  $\text{Eu}^{3+} 4f^7$ ). The f electrons are well shielded from the chemical environment and f–f emission spectra consist of sharp lines. These optical transitions are generally slow within a time scale of microseconds to milliseconds because the f–f transitions are partially forbidden along with spin forbiddenness of many transitions.

Sometimes broad emission bands are observed as in the case of  $\text{Eu}^{2+}$  and  $\text{Ce}^{3+}$ . In these cases the emission is due to 5d–4f transitions. The d–f emission spectra are broad because of the (i) participation of the d electrons, (ii) d–f transitions are allowed and have a time scale of microseconds. Typical f–f and d–f emission spectra are shown in Figs 12.19 and 12.20, respectively.

Many transition metal ions are known as luminescent centers as for example  $\text{Mn}^{2+}$  in  $\text{Zn}_2\text{SiO}_4:\text{Mn}$  with a broad emission band due to the electronic transition  ${}^4\text{T}_1(t_{2g}^4 e_g^1) \rightarrow {}^6\text{A}_1(t_{2g}^3 e_g^2)$ . The emitted light is green. On the other hand, the emission band of  $\text{Mn}^{4+}$  in  $\text{Mg}_4\text{GeO}_{5.5}\text{F}:\text{Mn}$  is narrow with some vibronic interaction structure. The emission in this compound is due to a spin flip transition in  $t_{2g}^3$  without any change in chemical bonding.

Emission from  $\text{CaWO}_4$  gives broad bands and the transition involved is a charge transfer transition. In this case, there is a strong variation in chemical bonding.

The unique properties of rare earth ions are (i) the spectral positions of the emission lines are independent of the host lattice, (ii) some of the ions,  $\text{Tb}^{3+}$ ,  $\text{Eu}^{3+}$  emit at spectral positions, enabling high lumen efficacies along with a very good quality of white light.

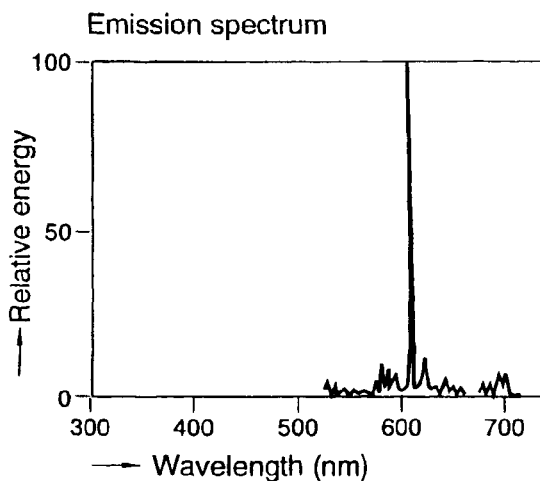
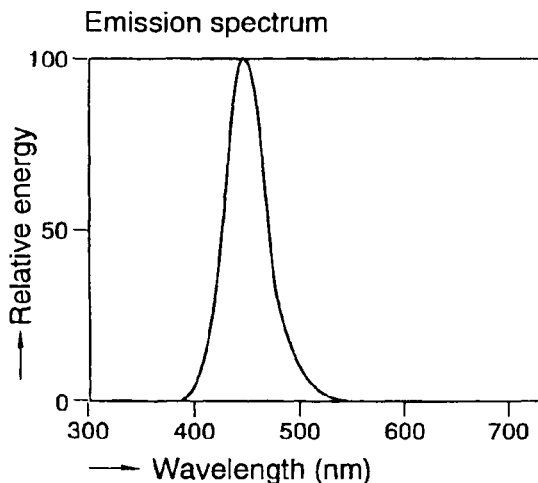
### 15.2. Phosphors for fluorescent lamps

The characteristics of fluorescent lamps for general illumination must be efficiency of generating of white light and the ability to reproduce all colours in a natural way along with the colour temperature of the generated light. These factors are determined by the phosphors used. The colour temperature equals the temperature of the black body radiator whose emission spectrum has the same colour coordinates. The colour rendering index (CRI) is determined by comparison of the emission spectrum of the lamp with that of a black body radiator having the same colour temperature. By definition, the CRI of a black body radiator and an incandescent lamp is 100.

Some time ago  $\text{Ca}_5(\text{PO}_4)_3(\text{F},\text{Cl}):(\text{Sb}, \text{Mn})$  (halophosphate CHP) was used in fluorescent lamps. Lamps based on CHP have moderate energy efficiency (75 lm/W) and CRI of 50–60.

Rare earth phosphors based lamps have efficiency of 100 lm/W and CRI of >80.

$\text{BaMgAl}_{10}\text{O}_{17}$  doped with  $\text{Eu}^{2+}$  (BAM) is used as blue emitting phosphor in fluorescent lamps. Photons are absorbed by  $\text{Eu}^{2+}$  ions and causes 4f–5d transition. Emission from  $\text{Eu}^{2+}$  occurs.

Fig. 12.19. Emission spectrum of  $\text{Y}_2\text{O}_3:\text{Eu}$ .Fig. 12.20. Emission spectrum of  $\text{BaMgAl}_{10}\text{O}_{17}:\text{Eu}$ .

Red emission in lamps is due to  $\text{Y}_2\text{O}_3:\text{Eu}$ . Excitation involves charge transfer transition from  $\text{O}^{2-}$  ions to  $\text{Eu}^{3+}$  and then emission occurs due to f-f transitions in  $\text{Eu}^{3+}$  ions.

An example of green emitting phosphor is  $(\text{Ce},\text{Tb})\text{MgAl}_{11}\text{O}_{19}$  in which  $\text{Ce}^{3+}$  ions absorb the light and then energy transfer to  $\text{Tb}^{3+}$  occurs. This is shown in the emission spectrum of  $(\text{Ce},\text{Tb})\text{MgAl}_{11}\text{O}_{19}$  in Fig. 12.21. Note the emission from  $\text{Tb}^{3+}$  along with some UV emission from  $\text{Ce}^{3+}$ . Another phosphor involving energy transfer from  $\text{Ce}^{3+}$  to  $\text{Tb}^{3+}$  via  $\text{Gd}^{3+}$  is  $(\text{Ce},\text{Gd},\text{Tb})\text{MgB}_5\text{O}_{10}$ .

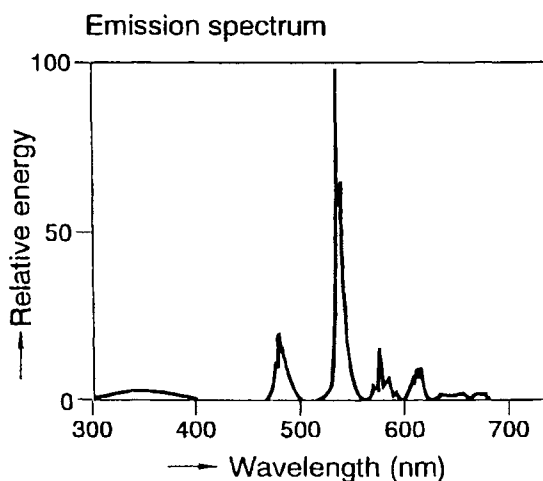


Fig. 12.21. Emission spectrum of  $(\text{Ce,Tb})\text{MgAl}_{11}\text{O}_{19}$ .

### 15.3. Phosphors for CRTs

The only rare earth phosphor used is red emitting  $\text{Y}_2\text{O}_2\text{S}:\text{Eu}$ . The line emission of the  $\text{Eu}^{3+}$  ions contributes to the high luminous efficiency of the phosphor in spite of its low energy efficiency. It is necessary to have line emitting phosphors in the red region in view of the rapid decrease in eye sensitivity for light of wavelength greater than 600 nm. In CRTs used in projection television,  $\text{Y}_2\text{O}_3:\text{Eu}$  is applied as red emitting phosphor because of its better saturation behaviour than  $\text{Y}_2\text{O}_2\text{S}:\text{Eu}$ . The green phosphor  $\text{Y}_2\text{SiO}_5:\text{Tb}$  is used.  $\text{ZnS}:\text{Ag}$  is used for the blue region.

### 15.4. Phosphors for vacuum UV excitation

The performance of many phosphors under VUV excitation is known. For display applications, blue emitting barium magnesium aluminates doped with  $\text{Eu}^{2+}$  show good performance, although some degradation occurs during the operation of the device. The degradation results in a colour point shift of the plasma display panels. Although the reasons for the degradation are not yet clear, coatings on  $\text{BaMgAl}_{10}\text{O}_{17}:\text{Eu}$  have proven to be promising [131].

The green primary for plasma display panels is based on  $\text{Mn}^{2+}$ . There are disadvantages to this system. For lamps,  $\text{Tb}^{3+}$  emission is preferred in view of the requirement of high colour quality.

Red light is obtained by either  $\text{Y}_2\text{O}_3:\text{Eu}$  or  $(\text{Y,Gd})\text{BO}_3:\text{Eu}$ , the VUV absorption of  $\text{Y}_2\text{O}_3:\text{Eu}$  is weaker than that of  $(\text{Y,Gd})\text{BO}_3:\text{Eu}$  but the emission spectrum of  $\text{Y}_2\text{O}_3:\text{Eu}$  better matches the EBU requirements for display applications. The emission spectrum of  $\text{Y}_2\text{O}_3:\text{Eu}$  has a maximum at 611 nm while that of the borate system is at 595 nm. This illustrates the point that although the emission spectrum of  $\text{Eu}^{3+}$  is due to optical f-f transitions, the detailed shape of the emission spectrum depends on the crystal host. Emission in  $\text{Y}_2\text{O}_3:\text{Eu}$  at 611 nm is due to an electric dipole transition while in the case of

the borate system at 595 nm the emission is due to magnetic dipole transition. The electric dipole transitions in the borate system are symmetry forbidden and the emission in this system is rather slow (3 ms) which is a disadvantage when applied in displays.

### 15.5. Rare earth phosphors in semiconducting light emitting diodes

The popularity of the blue light emitting diode (LED) based on GaN is well known. There are two ways of generating white light. The blue, green and red diodes can be combined to generate white light. Cluster lamps consisting of blue, green and red LEDs are already available. A single LED can be obtained by combining a blue LED with green, yellow and/or red emitting phosphor materials which absorb and convert part of the blue incident light. Some recent development work on combining a blue LED emitting at 470 nm and a broad band phosphor which can be excited at 470 nm with emission at 555 nm shows the feasibility of creating white light composed of blue, and yellow–green emissions. An example of such a system uses  $(Y_{1-x}Gd_x)_3(Al_{1-y}Ga_y)_5O_{12}:Ce^{3+}$  (YAG:Ce) as a broad band phosphor. The variation of  $x$  and  $y$  causes YAG:Ce emission shift between 510 and 570 nm which allows adjustment of white colour temperatures from 8000 to 3000 K. The CRI reaches 85 and the luminous efficiency is 5 lm/W. This system has been chosen for commercialization in Japan. The emission spectrum of a white LED consisting of a blue LED and yellow emitting YAG:Ce is given in Fig. 12.22.

The major drawback of the system YAG:Ce is the decrease in overall efficiency upon lowering the colour temperature.

Some of the conditions to be satisfied by phosphor material are (i) the phosphor should absorb at the emission wavelength of the diode, (ii) the quantum yield should be high and (iii) the full width at half maximum of the emission band should be small to achieve high luminous output. Some of the promising phosphor systems containing  $Eu^{3+}$  and  $Tb^{3+}$

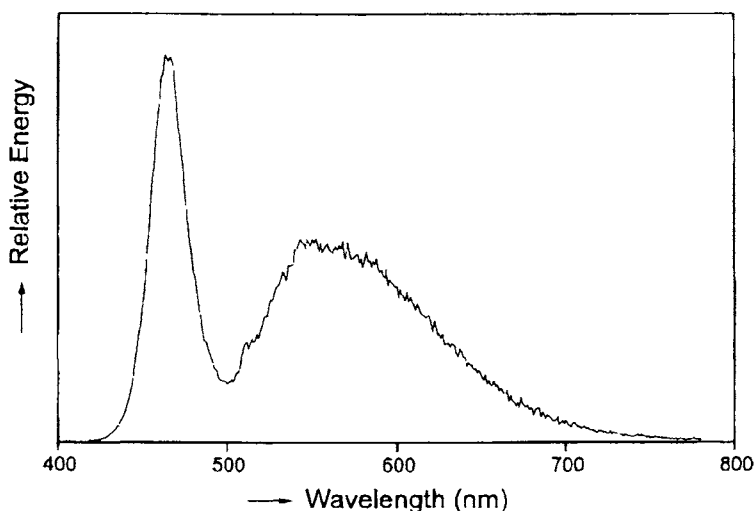


Fig. 12.22. Emission spectrum of a white LED consisting of a blue LED and yellow emitting YAG:Ce.

are  $\text{Y}_2\text{O}_3:\text{Eu}^{3+}$ ,  $\text{Y}(\text{V,P,B})\text{O}_4:\text{Eu}^{3+}$ ,  $(\text{Ce,Tb,Gd})\text{MgB}_5\text{O}_{10}$  (CBT),  $\text{Eu}^{3+}$ ,  $\text{Tb}^{3+}$  complexes with ligands like acetylacetone and phenanthroline [132]. Some systems in which emission occurs with quantum efficiencies of the order of 140–200% are  $\text{Pr}^{3+}$  in  $\text{YF}_3$  or  $\text{SrAl}_{12}\text{O}_{19}$  and  $\text{Eu}^{3+}$  in  $\text{LiGdF}_4:\text{Eu}$ . These systems need to be explored further for applications in LEDs or phosphors showing high quantum efficiency [133].

The role of rare earths in electroluminescent and field emission display phosphors has been of much interest and activity [134]. Flat panel displays unite all non-cathode ray tube (CRT) direct view displays.

Flat panel displays:

- Liquid crystal displays, 90% of the market, not suitable for military applications, medical instruments, vehicles and dusty environments.
- Emissive displays.
  - Electro luminescent (EL).
    - \* AC driven thin films EL (AC-TFEL).
    - \* AC driven powder EL (AC-PEL), application in lighting.
    - \* Original EL.
  - Field emission (FED).
  - Plasma (PD).

The structure of an AC-TEFL device is shown in Fig. 12.23. AC-TFEL devices:

- Hybrid multicolor structure based, two substrates, too expensive.
- Color by white structure, use of white phosphor, lack of efficient phosphor.
- Use of three phosphors, disadvantage—too many processing steps.

The present approach to multicolored EL devices is color by white based on stacked  $\text{ZnS}:\text{Mn}/\text{SrS}:\text{Ce}$  phosphors, which is due to the improvements [135] in the development of  $\text{SrS}:\text{Ce}$ .

Some data on composition, luminance, efficiency of rare earth AC TFEL phosphors are given in Table 12.26.

Although development work has focused on phosphors containing various rare earth ions, the stacked  $\text{SrS}:\text{Ce}/\text{ZnS}:\text{Mn}$  ‘white’ phosphor is by far the most suitable EL phosphor for a ‘color by white’ fullcolor approach and the emission spectrum covers the whole visible region (Fig. 12.24).

The cross sectional view of field emission display is shown in Fig. 12.25.

The composition, color and efficiency of some selected FED phosphors are given in Table 12.27.

Field emission is still a flat panel technology in its infancy. The technology is beset with many unsolved problems. Development of phosphors for FED has been slow. Some of the problem areas are (i) how different the surface may be as compared to the bulk, (ii) degree of conductivity of the phosphor, (iii) optimum particle size, (iv) comparative performance of thin films and powders and the reasons for the weak performance of the thin films.

#### 15.5.1. Rare earth phosphors used in medical radiography

The following are the needs for more efficient X-ray intensifying screens:

- (a) Reduce patient exposure to damaging X-rays.

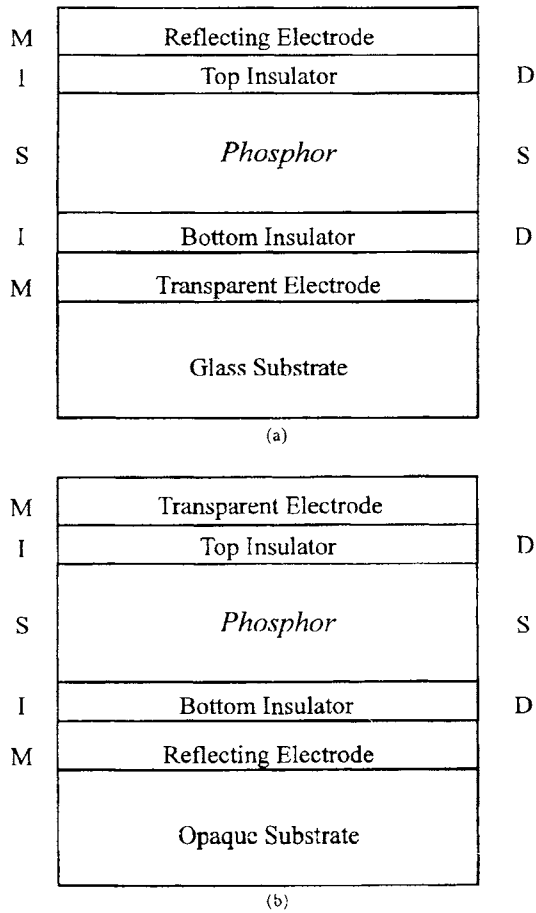


Fig. 12.23. Cross-sectional view of (a) normal and (b) inverted AC-TFEL device structure.

TABLE 12.26

Composition, color, luminance, efficiency and color coordinates of rare earth ACTFEL phosphors [136,137].

Composition	Color	Luminance $L_{40}$ at 60 Hz ( $\text{cd m}^{-2}$ )	Efficiency ( $\text{lm W}^{-1}$ )	CIE coordinates	
				$x$	$y$
CaS:Eu	Red	12	0.05	0.68	0.31
CaS <sub>0.5</sub> Se <sub>0.5</sub> :Eu	Red	25	0.25	0.66	0.33
ZnS:Sm,Cl	Red	12	0.08	0.64	0.35
ZnS:TbOF	Green	100	1.3	0.30	0.60
ZnS:Tb	Green	70	0.6	0.30	0.60
CaS:Ce,Cl	Green	10	0.10	0.27	0.53
SrS:Ce	Blue-green	100	0.80	0.30	0.50
SrS:Ce/filter	Blue	10	0.10	0.13	0.18
ZnS:Tm	Blue	0.2	< 0.01	0.15	0.15
CaGa <sub>2</sub> S <sub>4</sub> :Ce	Blue	10	0.04	0.15	0.19



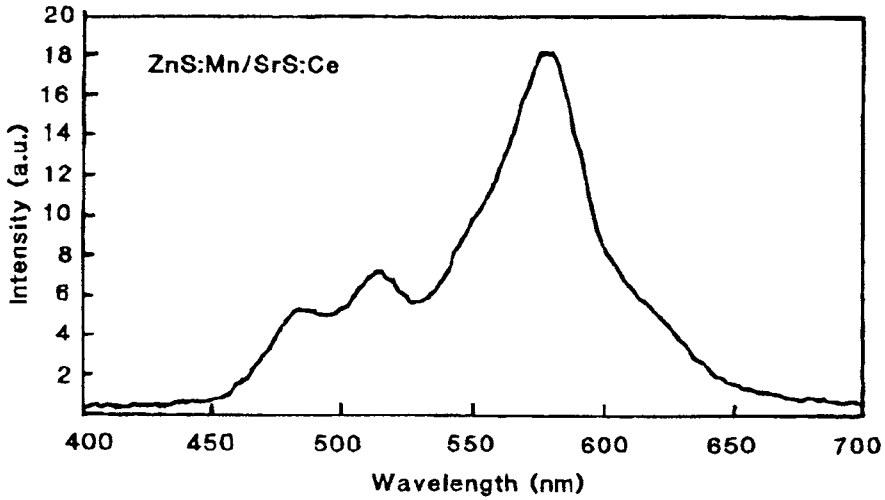


Fig. 12.24. EL emission spectrum of a SrS:Ce/ZnS:Mn device.

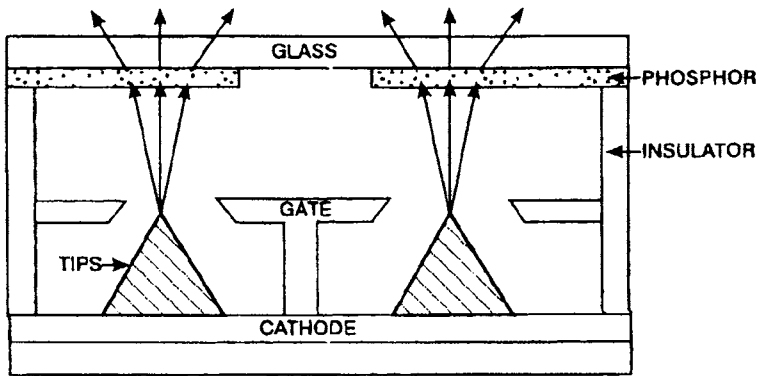


Fig. 12.25. Cross-sectional view of a field emission display.

- (b) Reduce motion unsharpness by shorter exposure times.
- (c) Reduce focal spot size by using lower powered X-ray generators.
- (d) Use of slower, finer grain film for higher contrast and less cross over unsharpness.
- (e) Reduce quantum noise by higher X-ray absorption.
- (f) Improve image quality by using thinner screens and smaller particle sized phosphors.

The phosphors which are efficient under X-ray excitation and have been studied are  $\text{La}_2\text{O}_2\text{S:Tb}$ ,  $\text{Gd}_2\text{O}_2\text{S:Tb}$ ,  $\text{BaFCl:Eu}$ ,  $\text{LaOBr:Tb}$ ,  $\text{LaOBr:Tm}$ . The final image quality depends on (i) X-ray absorption, (ii) phosphor absolute density, (iii) particle size, (iv) conversion efficiency and (v) emission characteristics. The studies showed that rare earth phosphors are useful in intensifying X-ray screens because of (i) their higher absolute densities, (ii) higher conversion efficiencies and (iii) higher X-ray absorptions.

TABLE 12.27  
Composition, color and efficiency at low-voltage operation of selected FED phosphors [134].

Composition	Color	Efficiency (lm W <sup>-1</sup> )
500 V [130]		
ZnO:Zn	Green	10.7
Gd <sub>2</sub> O <sub>2</sub> S:Tb	Green	7.9
Y <sub>3</sub> Al <sub>5</sub> O <sub>12</sub> :Tb	Green	2.0
Y <sub>2</sub> O <sub>2</sub> S:Eu	Red	3.5
Y <sub>2</sub> O <sub>3</sub> :Eu	Red	2.2
YVO <sub>4</sub> :Eu	Red	0.4
300 V, 131 μA		
CaS:Ce	Green	3.10
SrGa <sub>2</sub> S <sub>4</sub> :Eu	Green	3.00
La <sub>2</sub> O <sub>2</sub> S:Tb	Green	5.20
Gd <sub>2</sub> O <sub>2</sub> S:Tb	Green	3.52
Y <sub>2</sub> O <sub>2</sub> S:Eu	Red	2.20
Y <sub>2</sub> O <sub>3</sub> :Eu	Red	1.57
Y <sub>2</sub> SiO <sub>5</sub> :Ce	Blue	0.25
Y <sub>2</sub> SiO <sub>5</sub> :Tb	Green	1.05
LaOBr:Tb	Green	1.95
LaOCl:Tb	Green	0.36
LaOBr:Tb	Blue	0.54
LaOBr:Tm	Blue	0.17

## 16. Rare earths in superconductors

Research activity in the field of superconductivity has been extensive and continues to be of interest globally. As a result of the discovery of the property of superconductivity, mercury was observed to conduct an electrical current without resistance. This observed state of zero resistance and perfect diamagnetism and the nature of magnetic flux penetration into superconducting materials have continued to draw the attention of materials scientists and solid state scientists.

In spite of the high scientific activity during 1960s and 1970s, the actual engineering applications of superconducting materials were confined to some specific fields like magnets for particle accelerators, fusion energy research activity, and nuclear magnetic resonance imaging technology. One of the important reasons is that superconductors are far too expensive in spite of the advances made over several decades of intensive research. The most important parameter, the critical temperature,  $T_c$  below which superconductivity occurs, never reached beyond 20 K or so, making it necessary for the use of liquid helium as a refrigerant.

Later on, the scenario changed, the important "liquid nitrogen barrier" was broken, and the superconducting technology began to rely on liquid nitrogen as a refrigerant. The material consists of mixed metal oxide of the general formula R-M-Cu-O, where R stands for a rare earth metal atom and M is calcium or strontium or barium. The first compound [139] is La<sub>2</sub>BaCuO<sub>4</sub> with superconductivity at 40 K. This was followed by the discovery

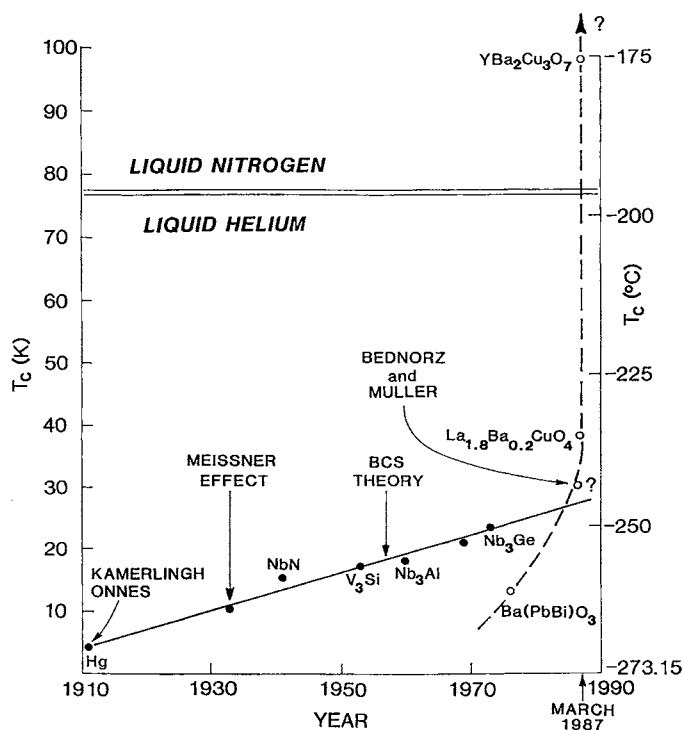


Fig. 12.26. A plot of the maximum superconducting critical temperature with time showing, in addition, the important discoveries of the Meissner effect, the microscopic Bardeen, Cooper and Schrieffer (BCS) theory and the temperature barrier, set by the boiling point of liquid nitrogen. (Reproduced by courtesy of Dr. J.M. Bell, C.S.I.R.O., Division of Applied Physics.)

[140] of  $\text{YBa}_2\text{Cu}_3\text{O}_7$  with superconductivity at 90 K. The first compound has a structure as that of  $\text{K}_2\text{NiF}_4$ .

The compounds of the type  $\text{YBa}_2\text{Cu}_3\text{O}_7$  are broadly known as a family of 1,2,3-compounds. These are compounds consisting of multiple phases. It is also disturbing to note that the precise composition and constitution of these compounds and their role in exhibiting the properties are not completely clear. It also appears that the properties of the compound are independent of the rare earth present in the compound. Superconductivity has been observed at relatively high temperature in the case of all the rare earths in 1,2,3-compounds. One of the stringent requirements is that the starting materials from which the 1,2,3-compounds are synthesized have to be pure.

A plot of  $T_c$  with time is shown in Fig. 12.26 to illustrate the developments.

Superconductivity in the multiphase quaternary borocarbide system Y-Ni-B-C has been recently reported [141,142]. Earlier work on valence fluctuations in ternary borides  $\text{RENi}_4\text{B}$  were studied and in the case of  $\text{YNi}_4\text{B}$ , a weak but reproducible signal of superconductivity at  $T_c$  of 12 K was observed. This is the first report or discovery of a ternary superconducting phase of the elements Y, Ni and B with a high  $T_c$  value (Fig. 12.27).

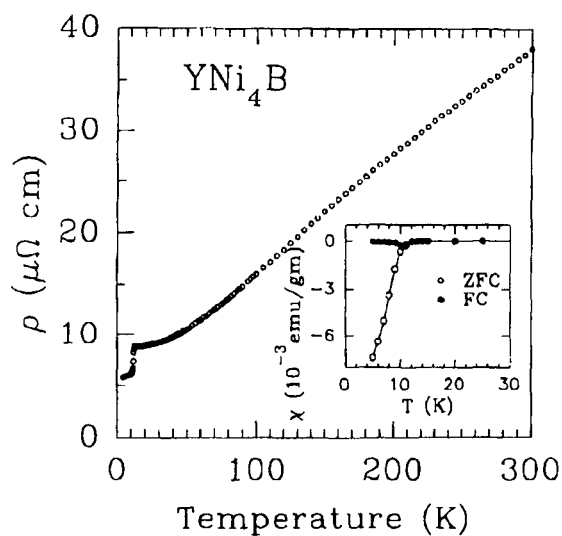


Fig. 12.27. Superconductivity at  $\sim 12$  K in samples of nominal composition  $\text{YNi}_4\text{B}$ . There is a sharp drop in resistivity and the material exhibits diamagnetism (inset) [141].

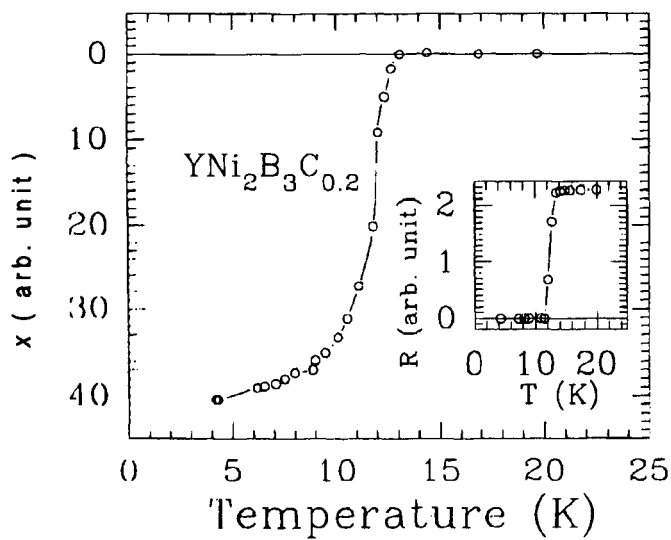


Fig. 12.28. Superconductivity in  $\text{YNi}_2\text{B}_3\text{C}_x$ . The diamagnetic response and the drop in resistivity (inset) start at  $T \sim 13$  K [142].

These initial observations of superconductivity in  $\text{YNi}_4\text{B}$  led to the synthesis of borocarbides of the formula  $\text{YNi}_x\text{B}_y\text{C}_z$  with varying values of  $x$ ,  $y$ ,  $z$ . This led to the discovery [142] of super conductivity in  $\text{YNi}_2\text{B}_3\text{C}_{0.2}$  (Fig. 12.28).

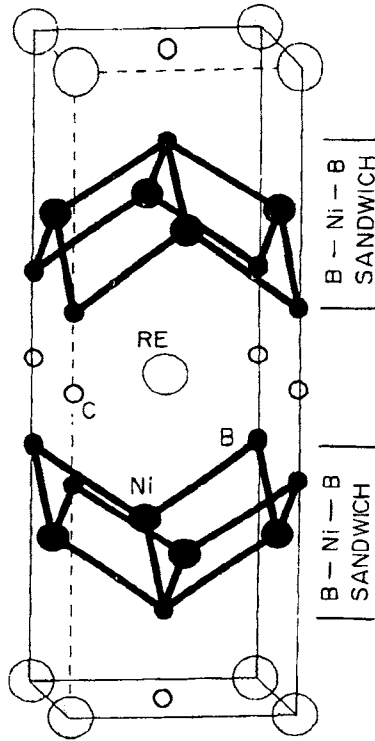


Fig. 12.29. Unit cell of the structure of  $\text{RENi}_2\text{B}_2\text{C}$  [142].

Other quaternary borocarbides studied are  $\text{Y-Pd-B-C}$  with  $T_c \approx 22$  K, 10 K,  $\text{YNi}_2\text{B}_2\text{C}$  with  $T_c \approx 23$  K and  $\text{Y-Ni-B-C}$  with  $T_c \approx 24$  K.

The unit cell structure of  $\text{RENi}_2\text{B}_2\text{C}$  (where  $\text{RE} = \text{Lu, Ho, Er, Tm}$ ) as determined by Cava et al. is shown in Fig. 12.29. The structure is essentially a stack of  $\text{RE-C}$  sheets and  $\text{Ni}_2\text{B}_2$  ( $\text{B-Ni-B}$  sandwiches) layers arranged in alternating sequence along the  $c$ -axis. The short  $\text{B-C}$  bonds provide contact between  $\text{RE-C}$  planes and  $\text{Ni}_2\text{B}_2$  layers and also provide a conducting path along the  $c$ -axis.

Quaternary borocarbides,  $\text{RENi}_2\text{B}_2\text{C}$  have rather high  $T_c$  and  $T_N$  values as is evident from the data given in Table 12.28.

The interesting feature is that the series of borocarbides represent all combinations of  $T_c$  and  $T_N$  and that both superconductivity and magnetism coexist at the highest ever reported temperature. This class of compounds led to further detailed studies to understand the interplay of superconductivity and magnetism, in addition to identifying new superconducting materials.

Much science still needs to be done, such as the current carrying capacity or the critical current density of the materials. Critical current density is an extrinsic property of superconducting materials which strongly depends upon microstructure and hence on the way materials are prepared. Such studies impact on the technology because of the need to produce a sample of suitable form on which the critical current density can be measured. There

TABLE 12.28

Superconducting ( $T_c$ ) and anti-ferromagnetic transition  $T_N$  temperatures in superconducting quaternary Ni-containing borocarbides.

RENi <sub>2</sub> B <sub>2</sub> C	$T_c$ (K)	$T_N$ (K)	Remarks
DyNi <sub>2</sub> B <sub>2</sub> C	6 [145–148]	11 [144,145]	$T_c < T_N$
HoNi <sub>2</sub> B <sub>2</sub> C	8 [143]	8.5 [144]	$T_c \approx T_N$
ErNi <sub>2</sub> B <sub>2</sub> C	11 [143]	6.5 [144]	$T_c > T_N$
TmNi <sub>2</sub> B <sub>2</sub> C	10.6 [143]	1.5 [149–152]	$T_c > T_N$
YbNi <sub>2</sub> B <sub>2</sub> C	< 2 [148]	< 2 [148]	

has been a widespread interest in the measured critical current densities of some materials. Some of the values are too low for them to be of use for conductors of high-field magnet applications, but improvements are possible with better control over microstructure. In some applications, achieving high critical current densities may not be necessary.

Technology as we have witnessed over the years has been outpacing any other development. Some of the developments in technology such as co-extrusion in copper, sintered material objects of required shapes, use of thin-film techniques to produce a tape for electrical connections and the fabrication of tapes and wires of superconductor Nb<sub>3</sub>Sn lend hope for future technological developments in superconducting rare earth materials such as borocarbides and YBa<sub>2</sub>Cu<sub>3</sub>O<sub>7</sub>.

## 17. Rare earth complexes in organic synthesis

Metal mediated reactions play an important role in organic chemistry. It has recently been found that rare earth trifluoromethane sulfonate complexes may be substituted for conventional Lewis acids in a variety of organic reactions.

Lanthanide(III) trifluoromethane sulfonates in the hydrated form can be prepared by reacting the rare earth oxide with triflic acid in aqueous solution. The product is hydrated salt which is heated under vacuum to produce an anhydrous rare earth trifluoromethane sulfonate. The anhydrous salts are used in organic reactions. Some of the advantages of using rare earth triflates over conventional Lewis acids are (i) they act as catalysts rather than stoichiometric reagents, (ii) they are effective catalysts in aqueous solutions and (iii) they can be easily recovered without any loss of catalytic activity for subsequent use.

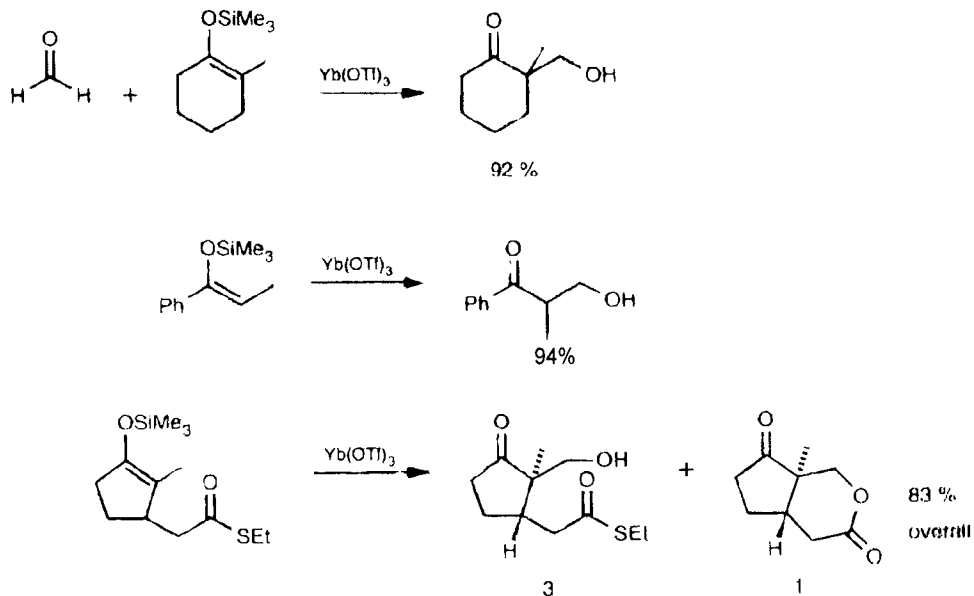
The rare earth triflates are used in three types of organic reactions, namely (i) carbon–carbon bond formation, (ii) carbon–oxygen bond formation and (iii) carbon–nitrogen bond formation.

### 17.1. Reactions involving the carbon–carbon bond formation

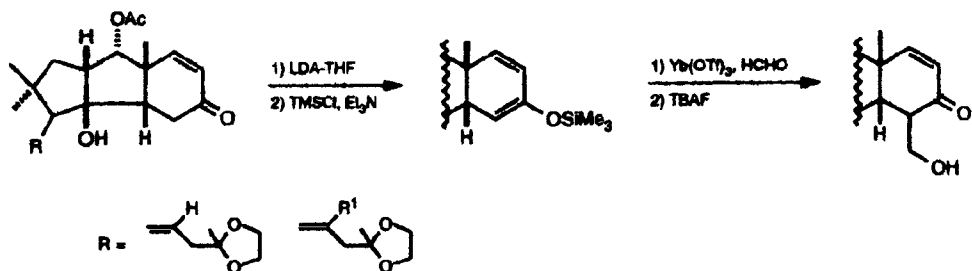
#### 17.1.1. Aldol condensation

Silyl enol ether of 2-methyl cyclohexanone reacts readily in the presence of ytterbium triflate to form 2-hydroxymethyl-2-methyl cyclohexanone [153,154]. Yields ranged from

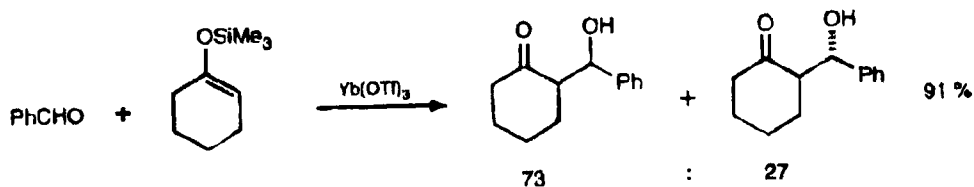
77 to 94% with various silyl enol ethers and the reactions were conducted in 1:1 THF–water mixture with Yb triflate as catalyst.



Total synthesis of A-seco taxane was accomplished using aldol condensation route using Yb triflate as the catalyst [155].

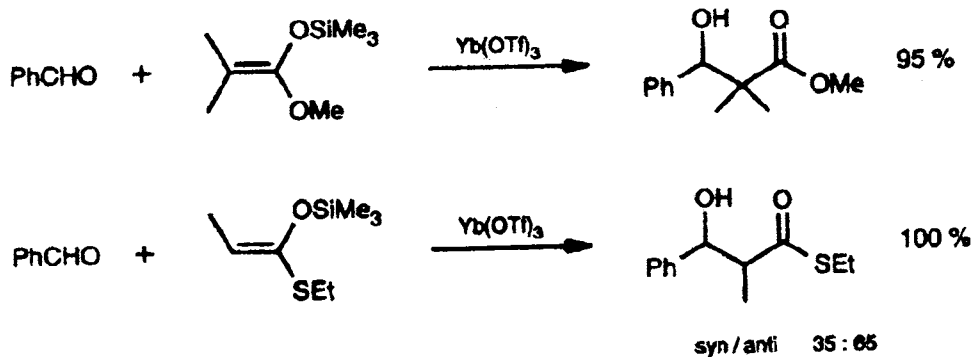


Reaction of 1-trimethyl siloxy cyclohexene with benzaldehyde gave high yield when Ln(OTf)<sub>3</sub>, where Ln = Yb, Lu or Gd were used as catalysts with modest diastereoselectivities averaging 75% syn and 25% anti forms.



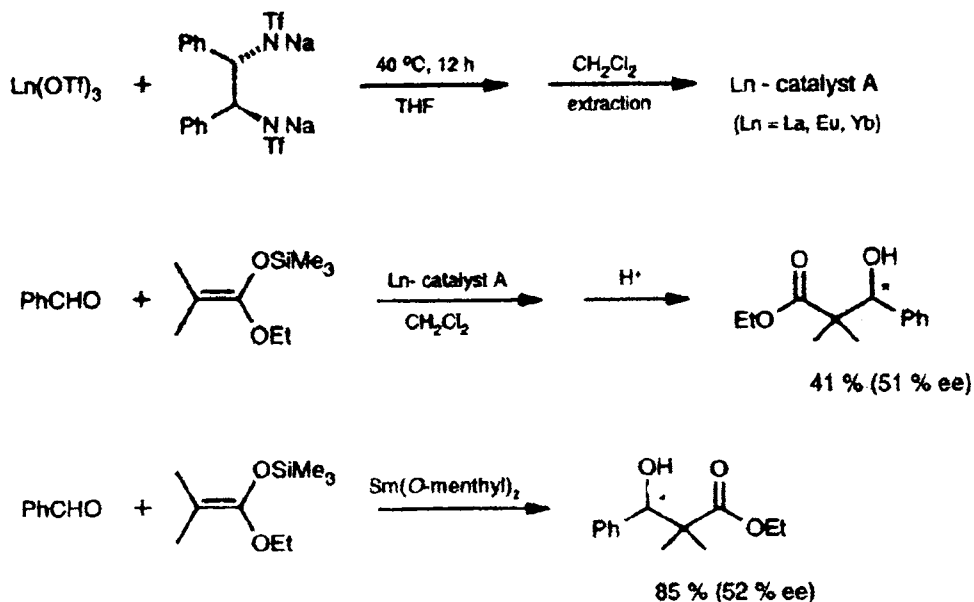
Salicylaldehydes and 2-pyridine carboxaldehyde which cannot be normally used with Lewis acids because of their coordination to metal may be used as substrates with Lu triflate as a catalyst [156].

Another interesting aspect is that Ln triflates can be used both in aqueous and nonaqueous media as shown below [157].



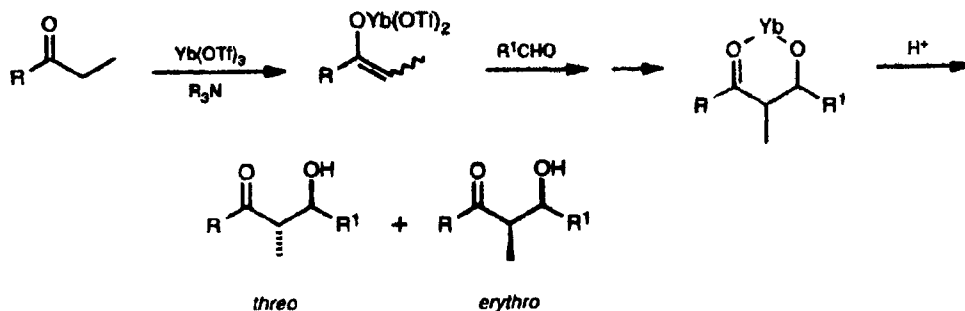
Some chiral Lewis acids for use in enantioselective reactions have been prepared. Reaction of Ln triflates with deprotonated form of (1*S*,2*S*)-1,2-diphenylethylenediamine in THF yields the chiral catalyst [158].

Reaction of (*E*)-silyl ketene acetals with benzaldehyde involves using Yb triflate as catalyst and the reaction scheme is shown below [159].



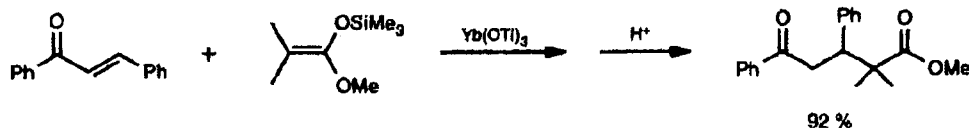
Cross-aldol reactions between ketones and aldehydes use Yb triflate as a stoichiometric reagent [160]. The reaction sequence is shown below.





### 17.1.2. Michael reaction

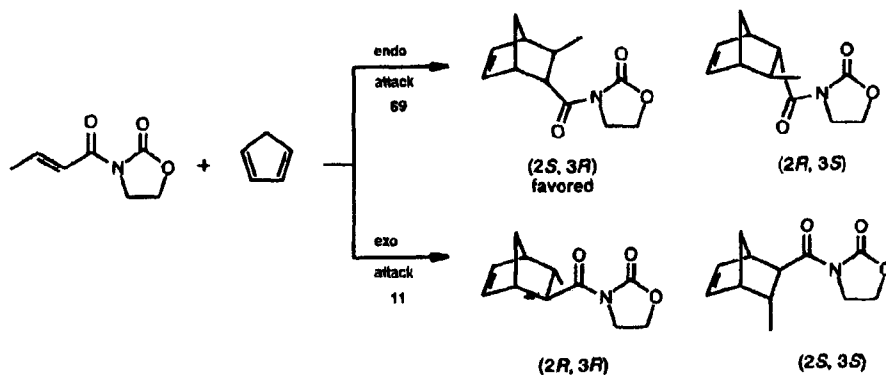
The conjugate addition of silyl enolates to  $\alpha, \beta$ -unsaturated ketones to yield 1,5-dicarbonyl compounds uses Yb triflate as a catalyst [161].



### 17.1.3. Diels–Alder reaction

Lewis acid catalysts are used in these reactions to improve regioselectivity and endo addition. Rare earth triflates are used in this type of reaction. Typical data are given in Table 12.29 detailing the percent yield and endo and exo yields [161].

A chiral Diels–Alder catalyst has been prepared from Yb or Sc triflate, (*R*)-(+)-binaphthol with a tertiary amine (trimethyl piperidine) catalyzing the reaction of crotonoyl-1,3-oxazolidin-2-one with cyclopentadiene as shown below [162,163].



The structure of the catalyst as determined by  $^{13}\text{C}$  NMR involves the bonding of binaphthol to the metal through oxygen atoms along with two hydrogen bonds to the nitrogen of the trimethyl piperidine as shown below [164].

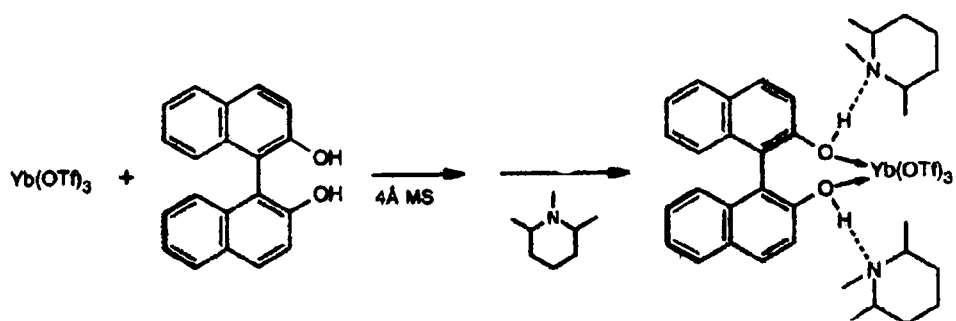
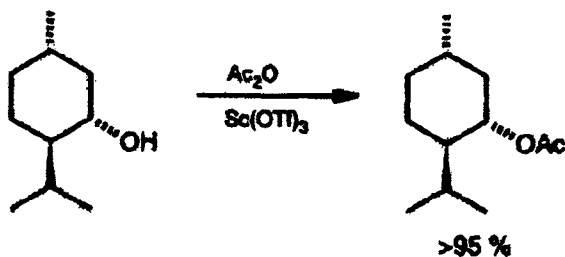
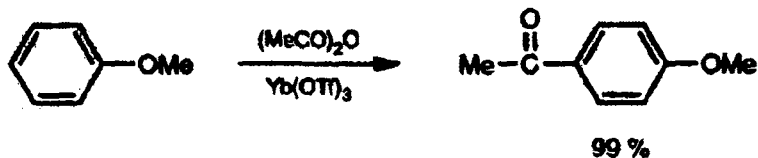


TABLE 12.29  
Rare earth triflates used as catalysis in Diels–Alder reactions [161].

				Yield	endo	exo	$\frac{\text{M}(\text{OTf})_3}{\text{M}}$
	+			76 %	7	93	Yb
	+			86 %	90	10	Yb
	+			93 %, 89 %	100	0	Yb, Sc
	+			91 %			Sc
	+			95 %	87	13	Sc
	+			83 %	> 95	< 5	Sc

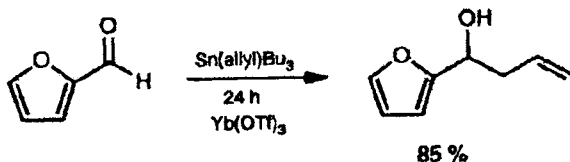
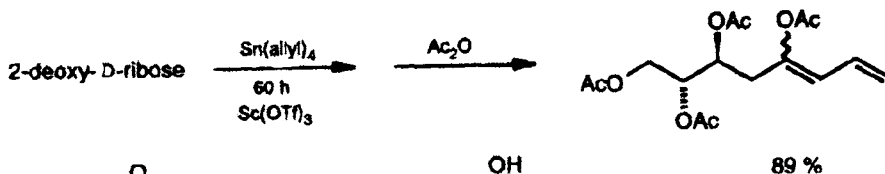
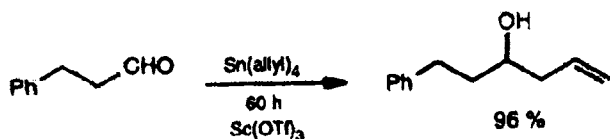
## 17.1.4. Acylation

In place of  $\text{AlCl}_3$ , Yb triflate in nitromethane promotes the acylation of anisole, thioanisole and *N,N*-dimethylaniline to the corresponding acetophenones as shown below [165].



## 17.1.5. Allylation

Lewis acids are required in stoichiometric amounts in allylation of aldehydes. On the other hand Sc and Yb triflates catalyze allylation of aldehydes as shown below [166].



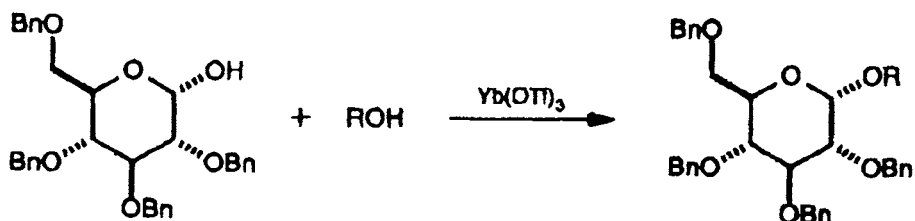
## 17.1.6. Pinacol coupling reactions [167]

$\text{Sm(OTf)}_3$  reduced with ethylmagnesium bromide at  $-78^\circ\text{C}$  promotes the reductive homocoupling of aldehydes and ketones to give pinacols.

## 17.2. Carbon–oxygen bond formation

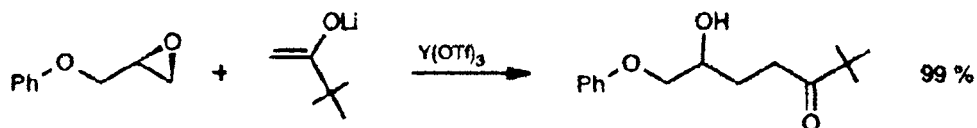
### 17.2.1. Glycosylation [168]

A mixture of  $\text{Yb}(\text{OTf})_3$  and methoxyacetic acid is used as a catalyst for the reaction of 1-hydroxy sugar with alcohols to form glycosides. The glycosylation in general is stereoselective.



### 17.2.2. Ring opening [169]

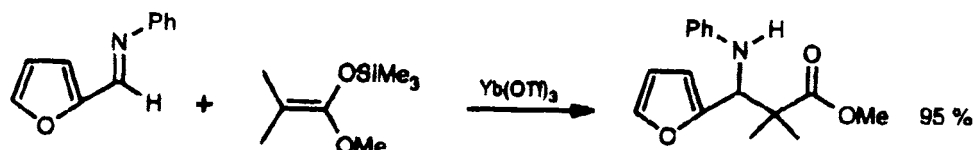
Yttrium triflate catalyzes the reaction of lithium enolates with epoxides to form  $\gamma$ -hydroxy ketones.



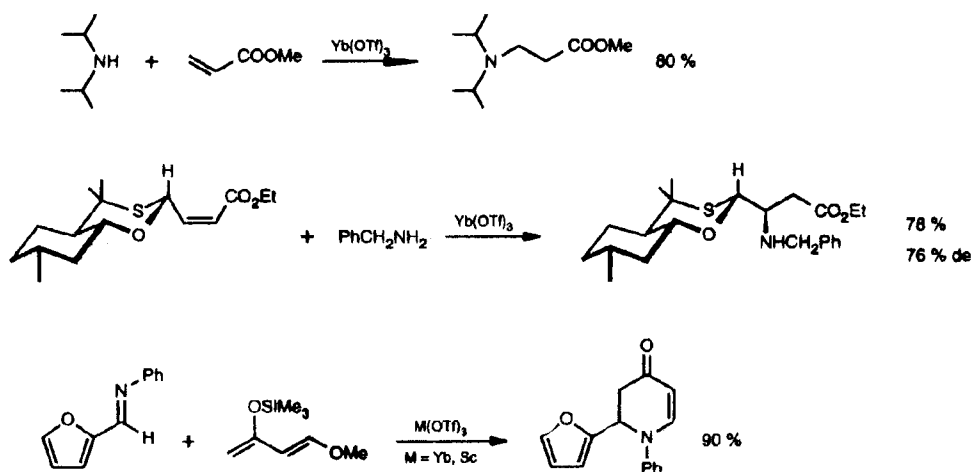
## 17.3. Carbon–nitrogen bond formation

### 17.3.1. Enolates and esters [170]

Preparation of  $\beta$ -amino ketones and  $\beta$ -amino esters which lead to  $\beta$ -lactam compounds involves the reaction of imines with enolates catalyzed by  $\text{Ln}(\text{OTf})_3$ , where  $\text{Ln} = \text{Y}, \text{Yb}, \text{Sc}$ .

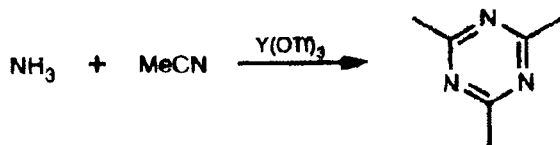


Other reactions catalyzed by  $\text{Yb}(\text{OTf})_3$  involving C–N bond formation are shown below [171].



### 17.3.2. Nitriles [172,173]

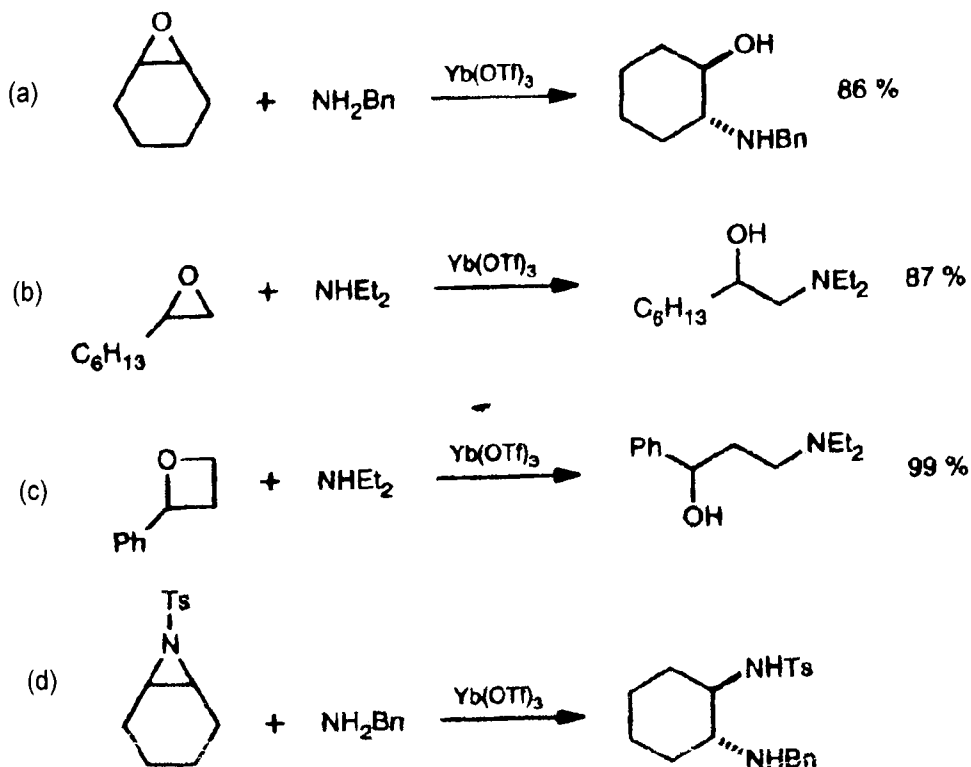
Monoamines, primary diamines and secondary amines react with nitriles to give amidines, cyclic amidines and pyrimidines, respectively, in the presence of  $\text{Yb}(\text{OTf})_3$  as a catalyst. Reaction of ammonia with acetonitrile is shown below.



### 17.3.3. Ring opening reactions [174–176]

- Cyclohexene oxide reacts with benzylamine in presence of  $\text{Yb}(\text{OTf})_3$  to give  $\beta$ -amino alcohols.
- Aminolysis of 1,2-epoxides to give  $\beta$ -amino alcohols in presence of  $\text{Yb}(\text{OTf})_3$ .
- Aminolysis of oxetanes to give  $\gamma$ -amino alcohols is catalyzed by  $\text{Ln}(\text{OTf})_3$ , where  $\text{Ln} = \text{Yb, Nd, Gd}$ .
- Aziridines react with amines in presence of  $\text{Yb}(\text{OTf})_3$  to give 1,2-diamines.

All the above four types of reactions are illustrated below.



#### 17.4. Lanthanide based organometallic compounds

Some of the applications of the organometallic compounds of lanthanides are as catalysts for (i) stereo specific polymerization of diolefins and in particular to obtain high yields of 1,4-*cis*-polybutadiene and 1,4-*cis*-polyisoprene and copolymer of the two monomers. The order of effectiveness of the rare earths as catalysts is  $\text{Nd} > \text{Ce}$ ,  $\text{Pr} < \text{Sm}$ ,  $\text{Eu}$ . The nature of halogen of the Lewis acid affecting the catalytic activity is in the order  $\text{Br} > \text{Cl} > \text{I} > \text{F}$ . Detailed work on the activity of cerium octanoate- $\text{AlR}_3$ -halide showed stereo specificity with cerium as the primary regulator. Cerium is thought to form  $\pi$ -allyl or  $\pi$ -crotyl complexes with butadiene.

Lithium lanthanum  $\pi$ -allyl complexes,  $\text{LiLn}(\text{All})_4$  dioxane, where  $\text{Ln} = \text{Ce}$ ,  $\text{Nd}$ ,  $\text{Sm}$ ,  $\text{Gd}$ ,  $\text{Dy}$  have been synthesized and used as catalysts in the polymerization of butadiene. The data show the predominance of 1,4-*trans* product. The catalytic activity of the lanthanides was nearly the same as evidenced by the percent yield in the range 78–90.

On the other hand using  $\text{LiLn}(\text{Allyl})_4$  dioxane in combination with Lewis acids like  $\text{AlBr}_3$  or base like TMEDA or THF, where  $\text{Ln} = \text{Ce}$ ,  $\text{Nd}$ ,  $\text{Sm}$ ,  $\text{Gd}$  gives yields in the range of 70–94 percent. When a Lewis base is involved, the vinyl content of the product is about 80 percent.

Organometallic compounds like  $\text{Ce}(\text{COT})_2$ ,  $\text{Ce}_2(\text{COT})_3$  have been used in polymerization of ethylene. Dimerization of propylene is catalyzed by a mixture of rare earth acetyl

TABLE 12.30  
Antiknock properties of lanthanides derivatives.

Additive	(g/gal)	(mmols of metal/gal)	Octane number (res. met.)
Pr(THD) <sub>3</sub>	0.447	0.65	102.0
Nd(THD) <sub>3</sub>	0.451	0.65	102.0
Yb(THD) <sub>3</sub>	0.470	0.65	102.3
Ce(THD) <sub>3</sub>	0.568	0.65	103.7
Pb(C <sub>2</sub> H <sub>5</sub> ) <sub>4</sub>	–	0.65	101.6
Isooctane	–	–	100.0

THD: 2,2,6,6-tetramethyl-3,5-heptanedione.

acetates and aluminum alkyl halides. Some rare earth heptanedione complexes show antiknock properties as shown in Table 12.30.

### 18. Rare earths in radionuclide therapy

The developments in radionuclide therapy with radio labeled antibodies and bone-seeking radiopharmaceuticals have been extensive. This necessitates more accuracy in radiation absorbed dose estimates. Many radionuclides attached to various targeting agents have been studied. Some rare earth radionuclides used in internal emitter therapy are listed below.

Radionuclide	Half life	$E_{\beta}$ max (MeV)	$E_{\gamma}$ (MeV)
<sup>153</sup> Sm	1.9 d	0.81	0.103 (29%)
<sup>177</sup> Lu	6.8 d	0.50	0.21 (6%)
<sup>166</sup> Ho	26.8 h	1.84	0.081 (6.2%)
<sup>153</sup> Sm EDTMP	1.9 d	0.81	0.103 (29%)
<sup>166</sup> Ho DOTMP	26.8 h	1.84	0.081 (6.2%)
<sup>177</sup> Lu DOTA·Tyr	6.8 d	0.50	0.21 (6%)

In general, radiation absorbed dose estimates are required in deciding if the patient should undergo therapy and also the levels of activity to be administered. There already exists the limits on dose estimates for diagnostic studies with radionuclides. Accurate dose estimates in patients are relevant in establishing dose–response relationships for toxicity and efficacy of radioimmunotherapy.

The relationship that is used in the estimation of organ doses is [178]

$$D_{t \leftarrow s}[\text{rad}] = S_{t \leftarrow s} \left[ \frac{\text{rad}}{\mu\text{Ci-h}} \right] \tilde{A}_s[\mu\text{Ci-h}], \quad (12.1)$$

where  $S_{t \leftarrow s}$  is a rectangular matrix giving the dose to a target organ  $t$  per unit time activity in a source organ  $S$ . There are two parts in the equation. The first part  $S$  refers to geometric

factors. The second part  $\tilde{A}_s$ , the cumulated activity, refers to the area under the curve obtained on plotting  $A_s$  versus time. It is to be noted that  $D$  and  $\tilde{A}_s$  are column vectors and the various elements of the vectors refer to the source and target organs for any specific radio nuclide. If  $A_0$  is the injected activity, and using this in division, one obtains  $\tau$ , the residence time and the dose per unit injected activity is  $S \cdot \tau$ . Thus estimated doses are given in terms  $S \cdot \tau$ .

If the elements of  $S$  matrix represent other geometric positions, then  $\tilde{A}$  vector will represent integrated activities in the organ.

Thus the calculation by equation (12.1) gives the mean dose to the target organ. The left hand side of equation (12.1) amounts to the ratio of total energy absorbed divided by the mass of the target. In addition to this dose–volume histograms may be used for internal beta emitters in both normal organs and tumors.

Radionuclide therapy involved the use of

- 1940's  $\text{Na}_3^{32}\text{PO}_4$
- 1985  $^{89}\text{SrCl}_2$
- 1990's  $^{153}\text{SmEDTMP}$  and  $^{186}\text{ReHEDP}$

These are involved in therapy for palliation of bony metastases which are found in breast and prostate cancer.

Radiation synovectomy involves therapy of rheumatic synovitis in knees inflicted with rheumatoid arthritis. Treatment involves the use of Dy-165 FMHA (270 mCi) or Ho-166 FMHA (10 mCi).

The treatment is also applicable to the shoulder and ankle.

## 19. Applications of luminescent lanthanide complexes

Immunological assays are classified according to several criteria. When the assay involves a separation step, the assay is heterogeneous and when no separation step is involved, the assay is supposed to be homogeneous [180]. Both types of assays are compared in Table 12.31. Up to now, heterogeneous assays have been used more because of high sensitivity, obtained through the physical separation of the fraction carrying the labeled immunoreagent from other interfering biological species in the sample. Schematic illustration of heterogeneous immunoassays is given in Fig. 12.30. The assay system consists of a liquid phase containing the antigen to be analyzed and a solid phase.

TABLE 12.31  
Comparison between homogeneous and heterogeneous assays [180].

Homogeneous assays	Heterogeneous assays
Simple performance	More complicated performance
Easy automatization	Difficult mechanization
Limited sensitivity	High sensitivity
Limited dynamic range	Wide dynamic range
Limited menu (small antigens)	General applicability
Background interferences	Reduced interferences



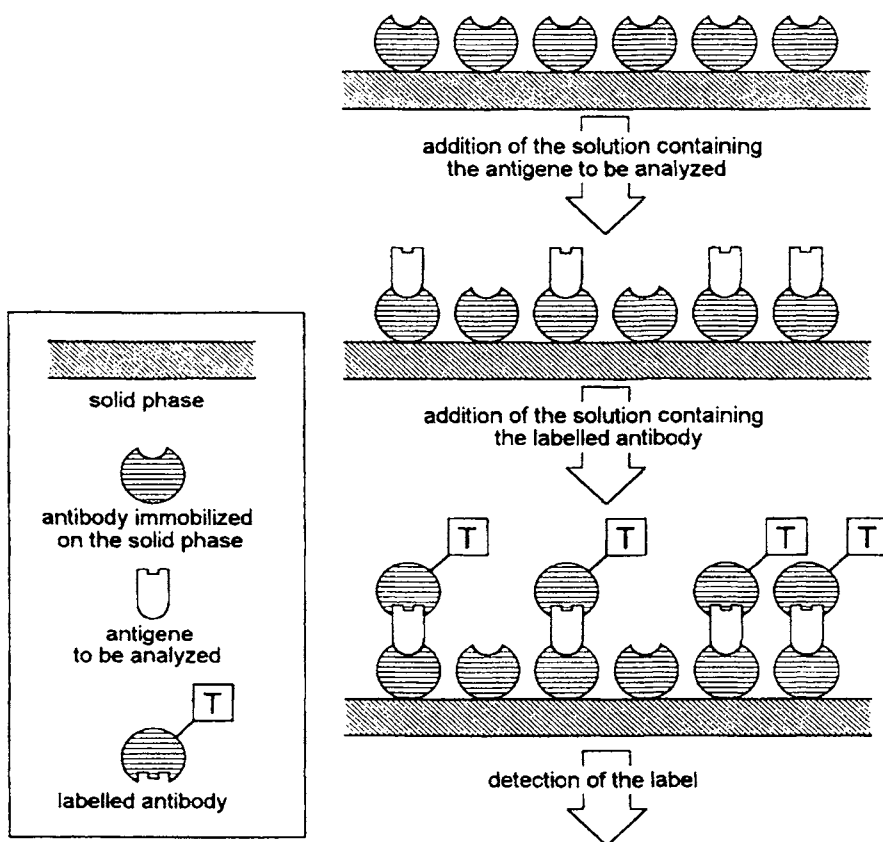


Fig. 12.30. Heterogeneous immunoassays [180].

A specific antibody immobilized on the solid phase binds the antigen; this is then washed to remove other biological species present in the sample, which can interfere in the form of background in the detection step. A solution of a labeled antibody specific for the antigen is added to mark the antigen. Thus the antigen is captured between the antibody immobilized on the solid phase and the labeled antibody.

The field of immunoassays is large in terms of variety of compounds to be analyzed and the concentrations involved such as millimoles to subpicomoles. One of the optimum requirements is high sensitivity. Immunoassays involving labeling with radio isotopes have been popular in clinical analyses [181]. Some of the advantages and disadvantages of radioimmunoassays are listed in Table 12.32.

The number of disadvantages outweigh the advantages of radioimmunoassays and this leads to development of non-radioisotopic immunoassay methods. Many substances can be firmly attached to the antibody without changes in binding properties towards the antigen. This principle has been used in some methods to be competitive with radioisotopic methods. In order for alternate methods to function as alternatives to radioisotopic

TABLE 12.32  
Advantages and disadvantages of radioimmunoassays.

Advantages	Disadvantages
High sensitivity: low and stable background	Short lifetime of radioisotopes
Robust detection: not sensitive to background interferences and to environmental factors	Radiation hazard: handling, legal, purchase and waste problems
Small size of radioisotopes: minimal effect on immunoreaction	Expensive production
Radiation counting well established	Negative public attitude

methods, it is necessary that they detect the labeled immuno reagent at a level of  $10^{-15}$ – $10^{-18}$  moles.

There are two alternative methods based on (i) enzymatic labels and (ii) luminogenic labels. The sensitivity and the principles on which these methods are based have been outlined below.

Alternative tracers:

- Enzymatic [182]. Based on high turn-over of enzyme-catalyzed reaction. Detection signal depends on (i) incubation time, (ii) temperature, (iii) other physical and chemical conditions during substrate incubation. Disadvantages are (i) interferences from endogenous enzymes or inhibitors, (ii) steric repulsions due to the enzyme in the coupling of antibody to antigen.
- Luminogenic. These are known as fluoroimmuno assays (FIAs) [183,184]. Some features are (i) labeling is inexpensive and not dangerous, (ii) luminescence detection is simple and rapid. Three types of labels are (i) photo-luminescent species, (ii) bioluminescent species, (iii) chemiluminescent species.

Photoluminescent labels are of interest because they involve rare earth complexes, in particular complexes of  $\text{Eu}^{3+}$ ,  $\text{Sm}^{3+}$ ,  $\text{Tb}^{3+}$  and  $\text{Dy}^{3+}$ . Of course there are disadvantages in this method when compared to the radioisotope method. Some disadvantages are (i) decreased sensitivity due to light scattering and (ii) short life times of fluorescent species (i.e.) of the order of nanoseconds. Major improvement has been accomplished through time-resolved measurements. The use of labels with long-lived luminescent states helps to minimize the interference due to background fluorescence. In particular  $\text{Eu}^{3+}$  and  $\text{Tb}^{3+}$  complexes are best suited for time resolved FIAs because (i) their luminescence states are long-lived (lifetimes of the order of milliseconds) and (ii) their line-like emission bands are positioned in the visible region so that the emission can be easily discerned from the broad background fluorescence bands in the UV region.

### 19.1. Emission properties of lanthanide chelates

Some lanthanide ions when complexed with UV-absorbing ligands, can efficiently accept energy from the excited state of the ligand and produce highly enhanced emission characteristics of the metal ion. Rare earth complexes have some advantages over organic fluorescent probes such as fluorescein, rhodamines, umbelliferones such as

- (i) The energy transfer from the ligand to lanthanide occurs with high efficiency.

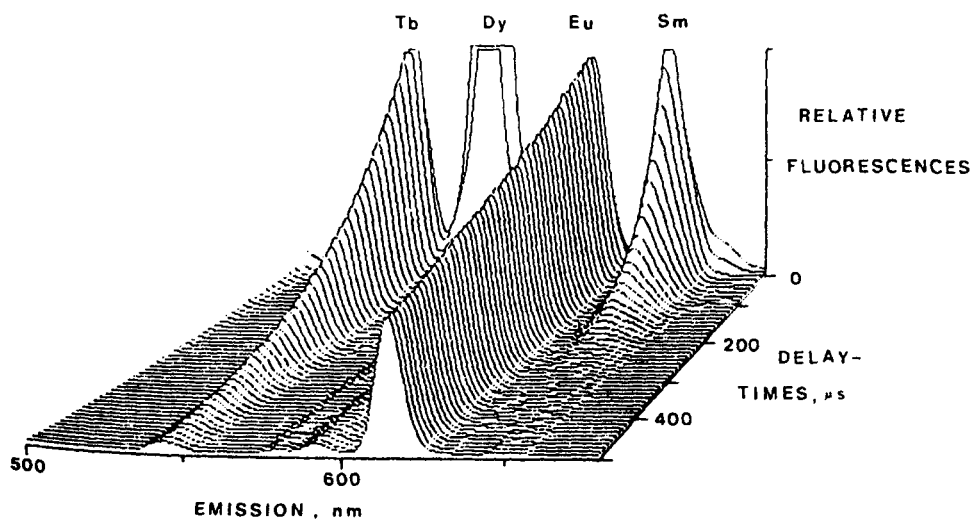


Fig. 12.31. The emission-decay profiles of  $Tb^{3+}$ ,  $Dy^{3+}$ ,  $Eu^{3+}$  and  $Sm^{3+}$  chelated with pivaloyltrifluoroacetone [181].

- (ii) The absorption and emission bands are line-like and well separated ( $\sim 250$  nm).
- (iii) The narrow emission band can be collected by narrow bandwidth filters; effective and easy filtering helps to distinguish the emission from the background and also from the emission of other lanthanides used as labels in double- or multiple label assays.
- (iv) Long lifetimes of excited states helps to separate the lanthanide emission from biological and instrumental interferences.

The emission-decay profiles of  $Tb^{3+}$ ,  $Dy^{3+}$ ,  $Eu^{3+}$  and  $Sm^{3+}$  complexes of pivaloyl trifluoroacetone are shown in Fig. 12.31. A sketch of time resolved fluorometry of  $Eu^{3+}$  with spectral filters and temporal resolution (time windows) is shown in Fig. 12.32.

#### 19.1.1. Chelate labelling

The applications of lanthanides in the biomedical field are due to the studies on chelate complexes which can simultaneously complex the lanthanide ion and also form a bond with the bioanalytical reagent such as an antibody. The labeled reagent must form a highly stable chelate and must also be biocompatible for it to be used in bioassays. Further labeling of antibodies with lanthanide ions must not affect other biological properties such as affinity, specificity and solubility or other properties such as binding non-specifically to other reagents or test tube surfaces. Some of the requirements are high hydrophilicity, suitable net charge, thermodynamic and kinetic stability, and applicability of the coupling reaction with the target. The most suitable complexing reagents that satiate the requirements for antibody labeling are polyaminopolycarboxylates, activated with a suitable reactive amino group. The chelating moiety has to be thermodynamically stable to enable its storage as a stock solution for up to years. Because of its kinetic stability, it can withstand the influence of a high excess of ions and other competing complexing agents present in biological samples. Each biological application has its own stability requirement. Considerable stability of

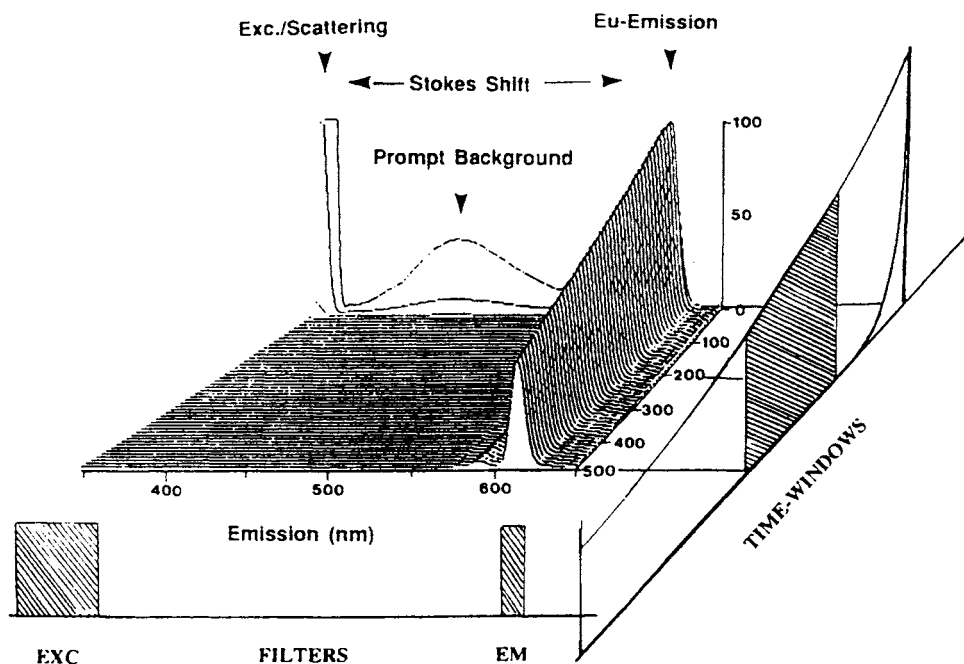


Fig. 12.32. Time-resolved fluorometry of  $\text{Eu}^{3+}$  with combination of spectral (filters) and temporal (time windows) resolution [181].

the labeling chelate is required in vitro immunoassays and even greater stability for DNA hybridization cellular assays in in vivo applications such as radioimmunotherapy or imaging requiring extreme chelate stability to avoid side toxic effects or concentrations of label ions in liver. The chelates used in labeling are given in Fig. 12.33.

The coupling of the stable chelate to the biological moiety should be a mild, facile, efficient and reproducible reaction. In antibodies, the free amino groups of lysins are reactive and their modification has no ill effects on the affinity and specificity. Isothiocyanato groups can be used for modification purposes without affecting the high affinity, solubility and specificity of the most tested monoclonal antibodies.

### 19.2. The dissociative enhancement principle

The chelates of lanthanides are suitable for use in FIAs. These assays fall into three groups depending upon the way lanthanide chelates are used: (i) assays relying on a separate fluorescence enhancement step, (ii) assays using stabilization techniques and (iii) assays using in situ fluorescent stable chelates. Among these, the fluorescence enhancement assays, lanthanide chelate based fluoroimmunoassays are practical. There are two ways by which the fluorescence enhancement may be achieved, namely (i) by forming mixed ligand chelate, (ii) completely dissociating labeled chelate before forming a fluorescent chelate. An acidic solution is used to dissociate the labeled chelate into ions followed by the addition of an enhancement solution containing a luminogenic ligand. Commercially

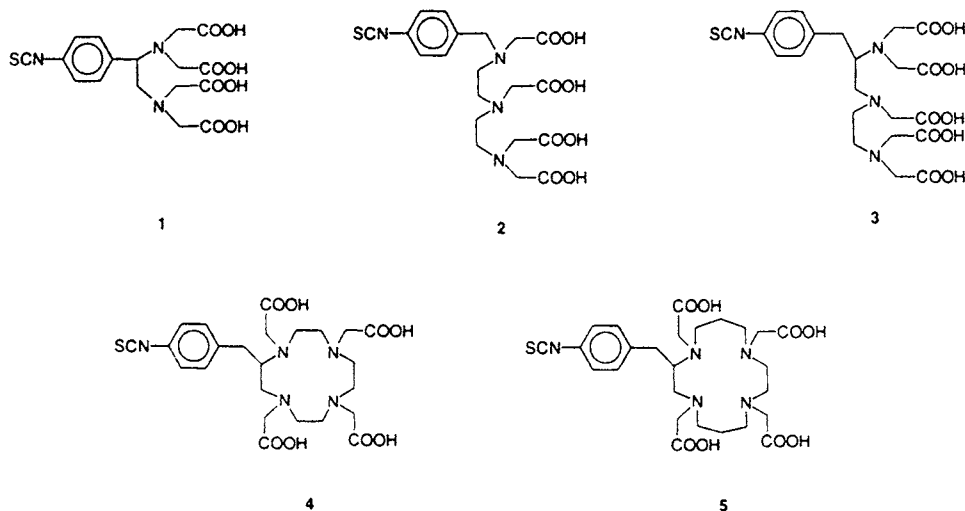


Fig. 12.33. Bifunctional chelating agents used in lanthanide labelling: isothiocyanatophenyl derivatives of EDTA (1), DTTA (2), DTPA (3), TETA (4) and DPTA (5).

this technique is known as DELFIA (dissociation-enhanced lanthanide fluoro immuno-assay). The fluorescence enhancement solution performs (i) ion dissociation at low pH of 3.2, simultaneously entrapping the formed  $\beta$ -diketone-TOPO chelates into a micellar phase preventing possible back reaction in equilibrium, (ii) formation of a new chelate complex with added luminogenic ligands ( $\beta$ -diketones and TOPO) and additives (synergistic ligands, detergents and  $Y^{3+}$  chelates) as well as luminescence optimization and stabilization.

One of the main advantages of DELFIA is that the method can be used with any chelate optimized for the particular labeling. In acidic conditions, luminescence is not interfered with because of the inability of complexing agents to complex lanthanides. The added luminogenic ligands must be optimized according to the energy levels of the lanthanide used. By appropriate choice of the ligand, dual-triple- and quadruple-label applications are possible with the simultaneous use of up to four different lanthanides as labels [185,186].

The excited triplet level of the ligand in the enhancement system must lie above the emissive level of the lanthanide ion for efficient transfer of energy. The emission levels of  $Eu^{3+}$  (613 nm) and  $Sm^{3+}$  (643 nm) are at lower energy than  $Tb^{3+}$  (545 nm) and  $Dy^{3+}$  (573 nm) and hence it is difficult to have one optimum universal ligand for energy transfer in the case of all four lanthanides. Emission levels of lanthanides along with the triplet levels of aliphatic and aromatic  $\beta$ -diketones are shown in Fig. 12.34.

A great number of enhancement solution constituents have been studied [185–188] including fluorinated aliphatic, and aromatic  $\beta$ -diketones and dipicolinic acid derivatives. Fluorination of  $\beta$ -diketone helps chelate formation at the low pH used for ion dissociation.

The emission of luminescent chelates can be increased by having a large excess of structurally identical non-emissive chelates. An example of non-emissive chelates are those of  $Gd^{3+}$ ,  $Y^{3+}$ . For example, the luminescence of  $Eu^{3+}$ - $\beta$ -diketone can be increased by 1000-fold by the addition of  $Gd^{3+}$  chelates.



TABLE 12.33

Decay-times and detection limits of some lanthanides measured with time-resolved fluorometry using different types of enhancement solution.

Lanthanide		Normal $\beta$ -NTA	Enhancement system and ligands		
			PTA	CO-flour PTA + Y	Sequential $\beta$ -NTA + TMP-DPA
Decay ( $\mu$ s)	Eu <sup>3+</sup>	730	900	948	730
	Sm <sup>3+</sup>	50	40	48	50
	Tb <sup>3+</sup>	-	100	239	1154
	Dy <sup>3+</sup>	-	<1	11	16
Detection limit (pM)	Eu <sup>3+</sup>	0.05	0.4	0.02	0.05
	Sm <sup>3+</sup>	3.5	20	4.0	3.5
	Tb <sup>3+</sup>	-	3.0	0.3	0.4
	Dy <sup>3+</sup>	-	1000	20	20

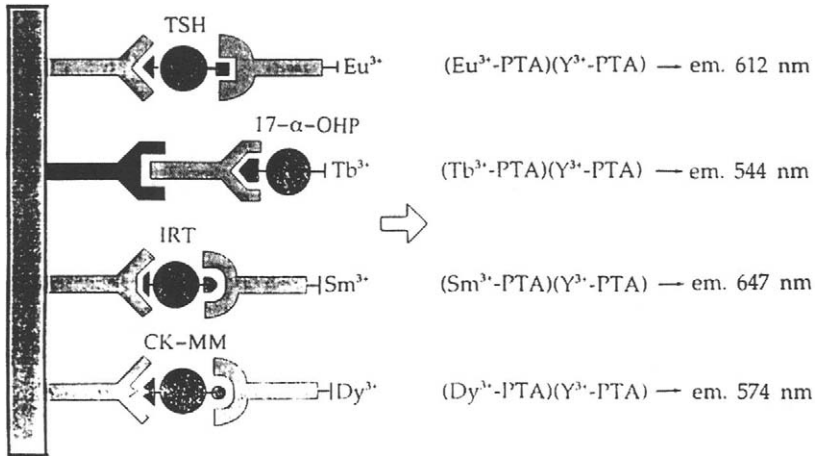


Fig. 12.35. Quadruple-label immunoassays of four analytes (thyroid stimulating hormone, 17 $\alpha$ -hydroxyprogesterone, immunoreactive trypsin and creatine kinase) in a single assay cuvette with four different lanthanide labels [190].

are DNA hybridization assays involving lanthanide-labelled DNA probes as in detection of gene mutation after PCR amplification. DELFIA finds applications not only in immunology and molecular biology but also in cellular immunology, receptor-binding assays and enzymatic assays.

19.3. Future prospects

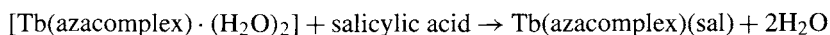
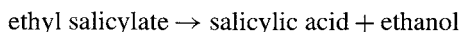
Intensive research in various groups is in progress in developing (i) luminogenic ligand-labelled secondary reagents, (ii) precipitating luminogenic chelate-based substrates for in-situ assays, (iii) lanthanide-doped phosphors. All these have some drawbacks.

The ideal situation is when the complex should have (i) high emission intensity, (ii) high hydrophilicity, (iii) small size and (iv) high stability. Although many research investigations are focused on the development of new luminescent chelates the two types of complexes that satisfy the requirements are based on cryptates [193,194] and polyamino carboxylates [195], and the energy absorbing and mediating groups are pyridine derivatives.

The development of new technologies depends upon the development of new lanthanide chelates like  $\text{Eu}^{3+}$ -cryptate and energy transfer to allophycocyanin [196]. Another technology of interest is the coupling of immunological recognition reaction, specific label technology and a fibre optics sensor. Development of a single microscopic multiparametric technology [197] for all possible analytes related to a certain disease, multiparametric micro imaging system and similar systems depends on the time-resolved fluorimetry of lanthanide complexes.

### 19.3.1. Salicylic acid recognition

Terbium(III) complexes of tetraazacyclodecane containing two labile water molecules bound to the lanthanide ion gives rise to larger increase in luminescence when the lanthanide chelates to salicylate ion. The mechanism is as follows:



The emission from the terbium aza-sal complex occurs well after the fluorescence from the surrounding biological proteins (Chem. Commun. 2134, 2002).

## 20. Rare earth compounds in imaging applications

Imaging techniques are in common use in diagnostic medicine. Spatially resolved images of the human body provide useful information. In diagnostic imaging procedures some chemical substances are used known as contrast reagents, the fate or behaviour of which on introduction into the body cavities gives useful information in the form of images. This in turn gives information on normal and diseased tissues. For example, the rate of excretion of a contrast agent into urine may provide useful information on the kidneys (Table 12.33a).

### 20.1. Magnetic resonance imaging

Modern magnetic resonance imaging (MRI) techniques use contrast reagents (CR) to enhance images and pharmacokinetic information is obtained by monitoring an image's temporal response to contrast reagent injection. In most cases, the signal from the contrast reagent is detected directly but the case of magnetic resonance imaging is somewhat different. In MRI, the images are constructed from the nuclear magnetic resonance signal arising from the proton magnetic moments of hydrogen atoms in water molecule (i.e.)  $^1\text{H}_2\text{O}$ , which forms the main constituent of most tissues. The natural variation of the proton density (i.e.) the amount of water per volume in tissues is not sufficient for high contrast. It is not



TABLE 12.33a  
Imaging techniques

Nuclear imaging [198]	X-ray imaging [199,200]	Nuclear magnetic resonance [200,201]
Use of radioactive substance	Use of X-rays	Use of radiofrequencies
Gamma ray detection	Counter detector	Nuclear magnetic resonance spectrum is analyzed by a computer and give digital images
Detection $10^{-6}$ – $10^{-9}$ M	Digitized images of tissues. Tissue absorption gives background.	Final output: 3-dimensional images
Monitoring in-vivo biochemical reactions	Contrast agent has to be of heavy elements, (e.g.) $\text{BaSO}_4$ and also insoluble $\text{Lu}^{3+}$ , $\text{Yb}^{3+}$ complexes of DTPA have been used. Tolerance of La compounds is not favourable. In dual energy subtraction radiography, lanthanide complexes may be used.	Contrast agents used are gadolinium complexes $\text{Gd}(\text{DTPA})$ , $\text{Gd}(\text{DOTA})$ , $\text{Gd}(\text{BOPTA})$ , $\text{Gd}(\text{HP-DO3A})$ ; $\text{Gd}(\text{III})$ complexes are well tolerated and excreted well from the body.
Lanthanides used as radio-pharmaceuticals in nuclear imaging of tumors, kidneys.	Desirable properties of contrast agent: X-ray absorption, biological safety and in intravenous agents—high water solubility and low viscosity and osmolality.	Dosage given is of the order of millimoles.

advisable to practically alter this quantity significantly by external intervention. Thus, an MRI pulse sequence is used such that the proton density does not limit the strength of the  $^1\text{H}_2\text{O}$  signal. By the use of a paramagnetic contrast reagent, the magnetism of its unpaired electrons affects the  $^1\text{H}_2\text{O}$  signal and the contrast reagent is detected indirectly through its ability to influence the strength of the signal. The mechanism of this effect is shown in Fig. 12.36. The figure shows the equilibrium interchange of a water molecule bound to the paramagnetic Gd ion in the common contrast reagent  $\text{Gd}(\text{DTPA})^{2-}$  with free water molecule in bulk water [204]. DTPA stands for diethylene triamine pentaacetate. This contrast reagent is also known as Magnevist. The seven unpaired electrons of  $\text{Gd}(\text{III})$  through its magnetism affect the proton signal of the bound water molecule of the contrast reagent.

After perturbation by a resonant radio frequency pulse, the tissue  $^1\text{H}_2\text{O}$  signal relaxes or returns to equilibrium. The paramagnetism of the  $\text{Gd}(\text{III})$  ion catalyzes the relaxation of the tissue  $^1\text{H}_2\text{O}$  signal. The equilibration of the component of the  $^1\text{H}_2\text{O}$  vector along the direction of the instrument's magnetic field is known as longitudinal relaxation and is identified by the longitudinal relaxation time,  $T_1$ . The value of  $T_1$  is decreased by the contrast reagent and with the suitable  $T_1$  weighted pulse sequence, the  $^1\text{H}_2\text{O}$  signal detected increases. Thus, tissue regions containing the injected contrast reagent appear brighter in the post contrast reagent image.

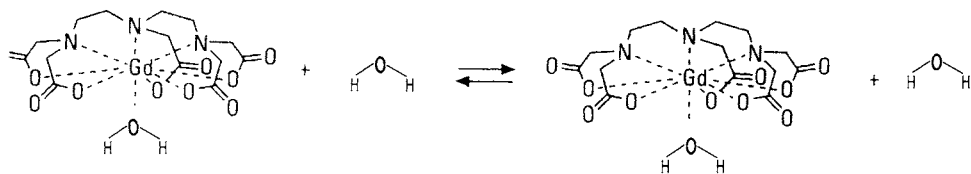


Fig. 12.36.

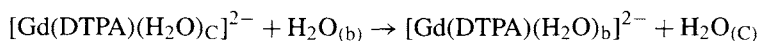
TABLE 12.34  
Clinically relevant gadolinium(III) chelates [204].

Chemical name	Generic name	Brand name	Company	Classification
$[\text{Gd}(\text{DTPA})(\text{H}_2\text{O})]^{2-}$	Gadopentetate dimeglumine	Magnevist <sup>a</sup>	Schering (Germany)	Extracellular
$[\text{Gd}(\text{DOTAX} \text{H}_2\text{O})]^{1-}$	Gadoterate meglumine	Dotarem <sup>a</sup>	Guerbet (France)	Extracellular
$[\text{Gd}(\text{DTPA-BMA})(\text{H}_2\text{O})]$	Gadodiamide	Omniscan <sup>a</sup>	Nycomed-Amersham (U.K.)	Extracellular
$[\text{Gd}(\text{HP-DO3A})(\text{H}_2\text{O})]$	Gadoteridol	ProHance <sup>a</sup>	Bracco (Italy)	Extracellular
$[\text{Gd}(\text{DO3A-butrol})(\text{H}_2\text{O})]$	Gadobutrol	Gadovist <sup>a</sup>	Schering (Germany)	Extracellular
$[\text{Gd}(\text{DTPA-BMEA})(\text{H}_2\text{O})]$	Gadoversetamide	OptiMARK <sup>b</sup>	Mallinckrodt (U.S.)	Extracellular
$[\text{Gd}(\text{BOPTA})(\text{H}_2\text{O})]^{2-}$	Gadobenate dimeglumine	MultiHance <sup>a</sup>	Bracco (Italy)	Hepatobiliary/extracellular
$[\text{Gd}(\text{EOB-DTPA})(\text{H}_2\text{O})]^{2-}$	Gadoxetic acid disodium	Eovist <sup>b</sup>	Schering (Germany)	Hepatobiliary
MS-325	Gadophostriamine trisodium	AngioMARK <sup>b</sup>	EPDC/Mallinckrodt (U.S.)	Llood pool

<sup>a</sup> Approved.

<sup>b</sup> In clinical trials.

### The water exchange reaction



is very rapid and the average lifetime of a water molecule bound to  $\text{Gd}(\text{DTPA})^{2-}$  is 130 ns at 37°C. The rapid exchange rate helps all water molecules that can chemically access the Gd complex to be influenced by the paramagnetism of the Gd complex (CR) during a short time. This is significant since it facilitates the detection of the contrast reagent where the ratio of contrast reagent to water molecules is  $2:10^6$ .

Clinically relevant Gd(III) chelates are given in Table 12.34.

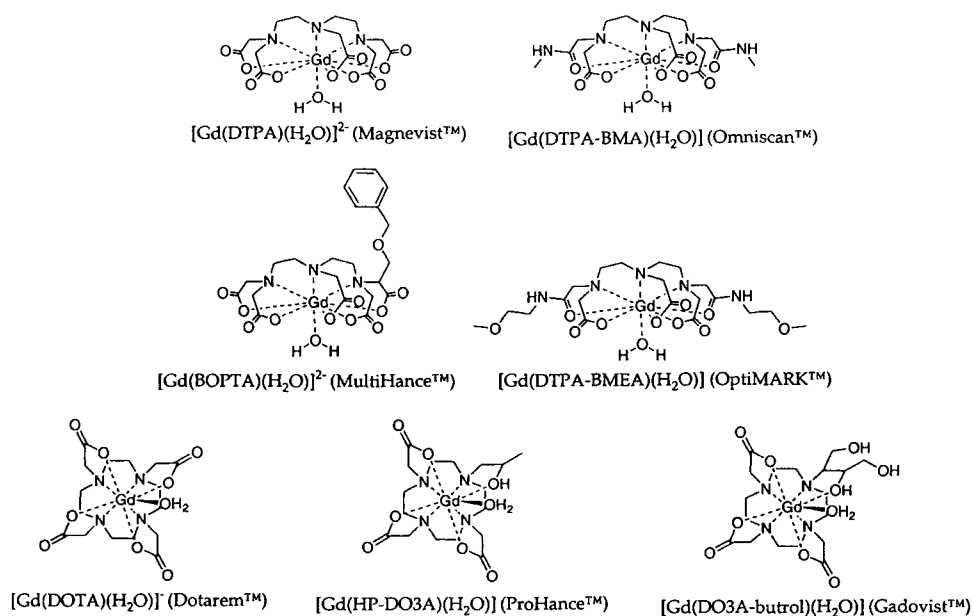


Fig. 12.37.

The structures of some gadolinium chelates used as contrast reagents are shown in Fig. 12.37.

## 20.2. Application

The contrast reagent is generally injected intravenously and then arrives at the region of interest dissolved in the blood plasma. Thus the enhancement rate is used to measure perfusion, which is defined as  $CR_p$ . It is generally accepted that  $Gd(DTPA)^{2-}$  type contrast reagents (CR) do not cross cell membranes including those of blood cells. When CRs leave a blood vessel, they are thought to leave through the junctions between endothelial cells lining the vessel wall, which are nearly totally closed in most regions of the healthy brain, otherwise known as the blood-brain barrier. Thus CRs serve as excellent tracers of even a slightly compromised blood-brain barrier, such as the one found in multiple sclerosis lesions and in some tumors as a result of angiogenesis.

When CRs are in extra vascular volume, they occupy extra cellular space, and are designated as  $CR_0$  (outside) where they directly bind with extra cellular water.  $^1H_2O_0$ . Since the transverse relaxation time,  $T_1$  is an intensive property of  $^1H_2O$ , its CR induced change depends directly on the molar ratio of  $CR_0$  to  $H_2O_0$ . Thus measurement of  $T_1$  allows the direct determination of the concentration of CR (i.e.)  $[CR]_0$  in the space in which CR is distributed. Further, because most of the water is intracellular ( $^1H_2O_i$ ), the change in the tissue  $^1H_2O$   $T_1$  from the entire voxel by CR allows the determination of the kinetics of water movement across the cell membrane. The kinetics is characterized by the average lifetime of a water molecule inside a cell,  $\tau_1$ , and is inversely proportional

to the cytolemmal water permeability, which is affected by aquaporin regulation. These parameters together permit measurement of intra- and extra cellular volume fractions which are intravoxel quantities. Thus the determination of voxel quantities in each pixel in the field of view leads to intra- and extra cellular volume maps as well as a cytolemmal water permeability map.

### 20.3. Progress in contrast reagents

The CR  $\text{Gd}(\text{DTPA})^{2-}$  is modified by attaching diphenyl cyclohexyl-phosphodiester residue, and its structure is shown in Fig. 12.38. The attached diester residue is a ligand for serum albumin binding sites [204].

This modified CR is targeted for blood. This modified CR designated as MS-325 exploits the relaxivity,  $r_1$ , the coefficient which relates the  $^1\text{H}_2\text{O}$   $T_1$  to the concentration of CR in vitro. The  $r_1$  of free MS-325 is  $6.6 \text{ (mM)}^{-1} \text{ S}^{-1}$  but the value increases to  $30\text{--}50 \text{ (mM)}^{-1} \text{ S}^{-1}$  when the CR is bound to albumin. This means that the CR is reversibly activated on binding to human serum albumin and is very much more effective in reducing  $^1\text{H}_2\text{O}$   $T_1$  value. Hence the detection is made easy at much lower levels. This effect, known as proton relaxation enhancement (or the receptor-induced magnetization enhancement), is due to the reduced rate of rotation of CR molecule bound to a macromolecule, and in this case, the rotation rate may be reduced by two orders of magnitude.

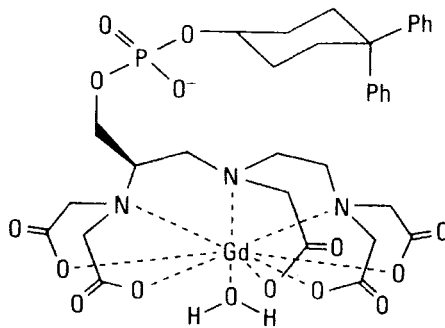


Fig. 12.38.

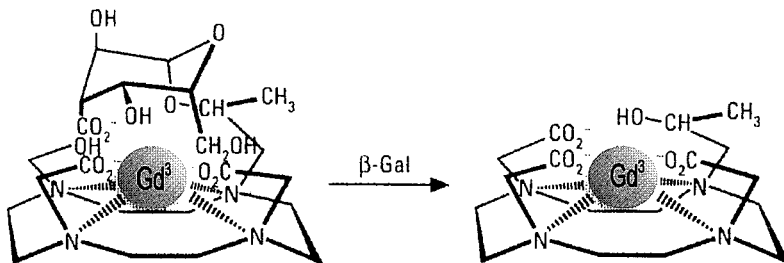
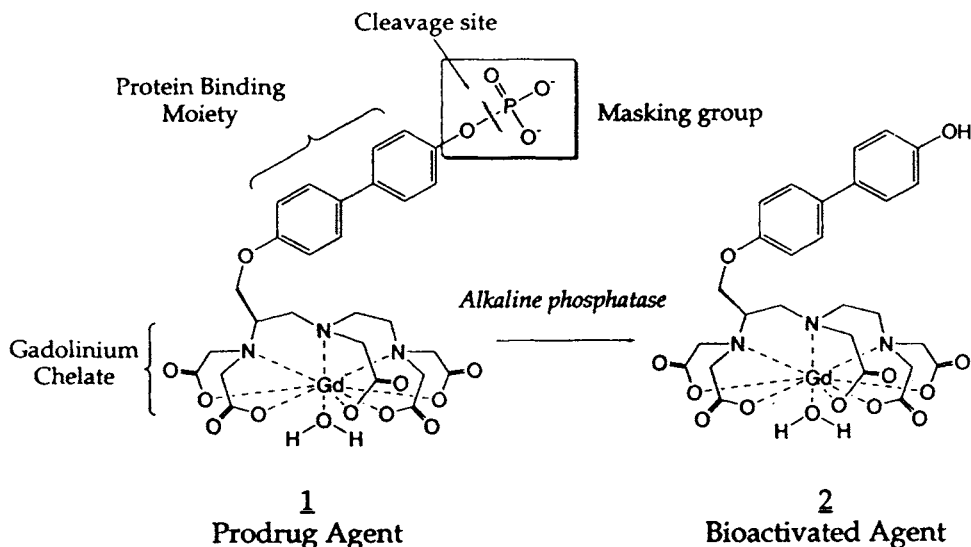


Fig. 12.39.

The chelate  $\text{Gd}(\text{DOTA})^-$  is modified by attaching a galactopyranose ring and as a result, the water binding site is blocked. Hence it is a poor CR since the water exchange reaction is inhibited. But the adduct undergoes cleavage when used for the common marker enzyme  $\beta$ -galactosidase ( $\beta$ -gal). The resulting product exposes the Gd site to water [205]. This method of producing improved CR is very promising since it shows 20% increase in relaxivity. The sequence is shown in Fig. 12.39.

Relaxivity increase has been achieved by using protein binding changes and the scheme is shown below.



A substrate for alkaline phosphatase, prodrug agent 1 was selected for its low binding affinity for HSA. Reaction of prodrug 1 with enzyme gave 70% increase in  $1/T_1$  in 4.5% HSA. Hydrolysis of phosphate moiety increased the hydrophobicity of the aryl group resulting in greater HSA binding affinity. Higher binding of bioactivated agent 2 showed increased relaxivity [204].

The calcium-responsive agent,  $\text{Gd}(\text{DOPTA})$  based on calcium-chelating EGTA fluorophores has been synthesized. When low concentrations of calcium are present, the aromatic iminoacetate groups may coordinate to  $\text{Gd}(\text{III})$  ion in some way, giving low relaxivity. As the calcium concentration increased to micro molar levels, the EGTA group binds to calcium, possibly releasing the  $\text{Gd}(\text{III})$  coordinated iminoacetates, with attendant increase in relaxivity from  $3.26$  to  $5.76 \text{ mM}^{-1} \text{ S}^{-1}$ . The mechanism of increase in relaxivity in the system is not definitive.

The chemical factors which contribute to the stability of contrast reagents are (i) multidentate ligands, (ii) high thermodynamic stability, (iii) kinetic inertness in some cases. In future, efforts need to be directed towards the search and synthesis of new CRs with balanced higher relaxivity and acceptable stability.

Applications of blocking principle based contrast reagents are many and wide-ranging. The application in gene expression and as a method of study of embryonic development will be briefly described. The contrast reagent, 1,4,7,10-tetraazacyclododecane-

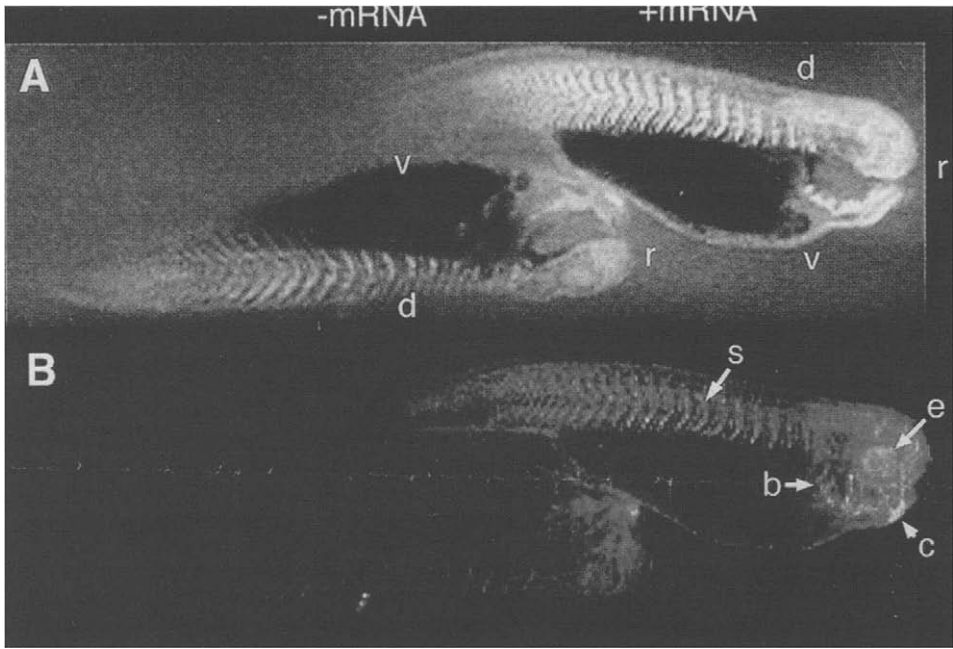


Fig. 12.40.

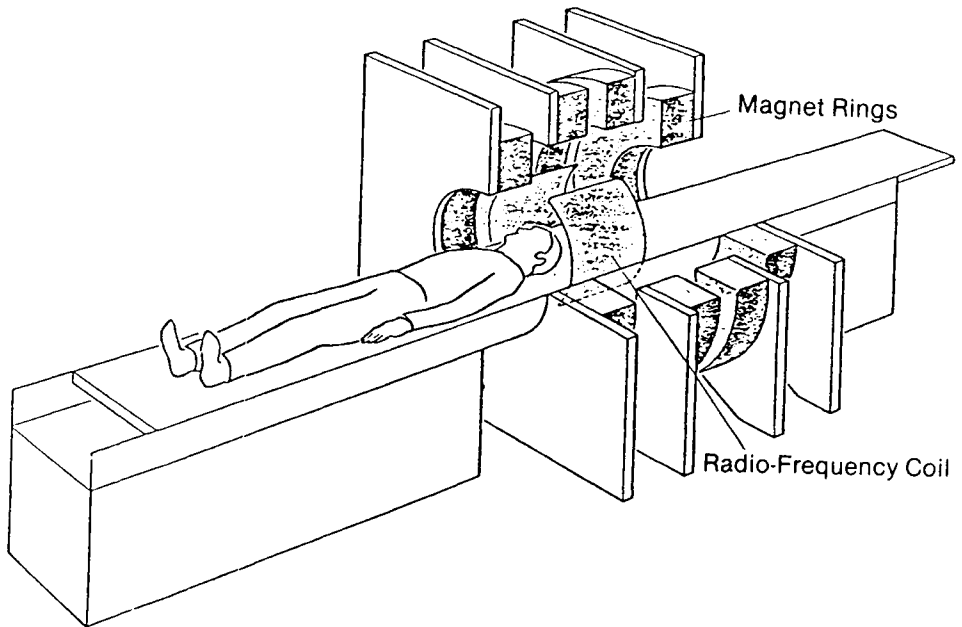


Fig. 12.41. Schematic of an NMR imager showing the approximate size and relative position of the patient, magnet, and radiofrequency coils in one of several arrangements possible.

$N,N',N'',N'''$ -tetraacetate complex of Gd(III), Gd(DOTA)<sup>-</sup> is attached to a galactopyranose ring and is termed as Egad Me. This modified contrast reagent as noted earlier blocks the water exchange reaction but on reaction with enzyme  $\beta$ -galactoside, the cleavage of the galactopyranose ring occurs resulting in a CR with improved properties.

The CR, Egad Me solution was injected into each cell of the embryo at the two-cell stage in tadpoles. But for one embryo, one cell was injected with  $\beta$ -gal mRNA. As this organism develops, half the cells should be expressing  $\beta$ -gal while the other half should not. The differences in MRI images are clearly seen in Fig. 12.40 [205].

A schematic of an NMR imaging set up is shown in Fig. 12.41.

## References

- [1] A. McCulloch, *Materials Australasia*, p. 5–7, May 1987.
- [2] V.S. Arunachalam, S. Ramachandran, *Rare earths in steel technology*, in: *Science and Technology of Rare Earth Materials*, eds E.C. Subba Rao, W.E. Wallace, Academic Press, New York, 1980.
- [3] H. Nagai, *Rare earths in steels*, in: *Handbook of the Physics and Chemistry of Rare Earths*, Vol. 25, eds K.A. Gscheidner, Jr., L. Eyring, Elsevier, Amsterdam, 1998.
- [4] D.R. Arnott, B.R.W. Hinton, N.E. Ryan, *Materials Performance* **26**, no. 8, 42, 1987.
- [5] E. Lichtenberger-Bajza, I. Boczor, *Mitteilung des Planungs und Forschungsinstitutes der Aluminiumindustrie*, Budapest, 119/137, 1977.
- [6] B.R.W. Hinton, N.E. Ryan, D.R. Arnott, P.N. Trathen, L. Wilson, B.E. Wilson, *Corrosion Australasia* **10**, no. 3, 12, 1985.
- [7] B.R.W. Hinton, P.N. Trathen, L. Wilson, N.E. Ryan, *Proc. 28th Australasian Corrosion Association Conference*, Perth, Australia, Nov. 1988.
- [8] B.R.W. Hinton, N.E. Ryan, P.R. Trathen, unpublished results.
- [9] P.L. Lane, *Royal Aircraft Establishment Technical Report*, 87046, Aug. 1987.
- [10] B.P.F. Goldie, J.J. McCarroll, *Australian patent*, AU-32947184, 1984.
- [11] E. Lichtenberger-Bajza, I. Boczor, *Aluminium* **56**, no. 10, 653, 1980.
- [12] V.S. Agarwala, *Proc. Int. Conf. on Corrosion Inhibition*, Preprint Vol. 1, Dallas, TX, May 1983.
- [13] B.R.W. Hinton, D.R. Arnott, N.E. Ryan, *Materials Forum* **9**, no. 3, 162, 1986.
- [14] F. Mansfeld, S. Liu, K. Kim, H. Shih, *Corrosion Science* **27**, no. 9, 997, 1987.
- [15] B.P. Goldie, J.J. McCarroll, *Australian Patent*, AU-A-12527/83, 1983.
- [16] B.T. Kilbourn, *Proc. 17<sup>th</sup> Rare Earth Research Conference*, McMaster University, Hamilton, Ontario, Canada, June 9–12, 1986.
- [17] K. Foger, *Materials Australasia*, p. 24, May 1987.
- [18] G.N. Sauvion, P. Ducros, *J. of Less Common Metals* **111**, 23–35, 1985.
- [19] G.C. Desai, *Materials Science Forum*, Vol. 30, p. 259, 1988.
- [20] K. Franz, W. Jager, *U.S. Patent* 4,167,417, Reuder-de-Haen AG, Germany.
- [21] H. Parker, *Principles of Surface Coating Technology*.
- [22] Payne, *Organic Coating Technology*.
- [23] *Inorganic Pigments-Manufacturing Process-Chemical Technology*, Review No. 166, ed. M.H. Gutcho, Noyes Data Corporation, U.S.A.
- [24] D.C. Bagchi, *Materials Science Forum*, Vol. 30, p. 265, 1988.
- [25] B.B. Rath, B.A. MacDonald, S.M.L. Sastry, R.J. Lederich, J.E. O'Neal, C.R. Whitsett, in: *Titanium 80-Science and Technology*, Proc. 4th International Conf. on Ti, Kyoto, Japan, May 19–22, 1980, p. 1185, eds H. Kimura, O. Izumi, Vol. II, TMS of AIME, Warrendale, 1980.
- [26] S.R. Seagle, G.S. Hall, H.B. Bomberger, *ibid.*, 2169.
- [27] Y. Li, S. Zhang, C. Li, T. Zhang, *Acta Met. Sinica* **20**, A131, 1984.
- [28] V.A. Kaschuk, M.B. Svetlov, in: *Titanium and Titanium Alloys—Scientific and Technological Aspects*, Proc. 3rd Int. Conf. on Ti, Moscow, May 18–21, 1976, p. 2201, eds J.C. Williams, A.F. Below, Vol. III, Plenum Press, New York, 1982.
- [29] T. Amano, Z. Yajima, Y. Saito, *Proc. JIMIS-3 (1983)*, High Temperature Corrosion, Trans. Japan Inst. of Metals, Supplement, 247, 1983.

- [30] I.M. Allam, D.P. Whittle, J. Stringer, J. Oxidation of Metals **12** (1), 35, 1978.
- [31] A.M. Huntz, *Mat. Sci. & Eng.* **87**, 251, 1987.
- [32] J.G. Smeggil, *Mat. Sci. & Eng.* **87**, 261, 1987. Superalloys II, eds C.T. Sims, N.S. Stoloff, W.C. Hagel, p. 371, John Wiley & Sons, New York, 1987.
- [33] F. Cosandey, J. Kandra, *Met. Trans. A* **18A**, 1239, 1987.
- [34] R. Bailey, R.R. Shiring, R.-U. Anderson, in: Superalloys Metallurgy and Manufacture, Proc. 3rd Int. Symp., Sept. 12–15, 1976, eds B.H. Kear, et al., p. 109, Claitors Publishing Division, Baton Rouge, 1976.
- [35] J.W. Semmel, Jr., in: Refractory Metals and Alloys, Proc. of Met. Soc. of AIME Conf. Vol. II, eds M. Semchyshe, J.J. Harwood, p. 119, Interscience Publishers, New York, 1961.
- [36] Y.R. Mahajan, Y.W. Kim, F.H. Froes, *J. Mat. Sci.* **22**, 202, 1987.
- [37] Y.R. Mahajan, S.D. Kirchoff, F.H. Froes, *Scripta Met.* **20** (5), 643, 1986.
- [38] Y.R. Mahajan, S.D. Kirchoff, *Scripta Met.* **21** (8), 1125, 1987.
- [39] S. Naka, M. Marty, H. Octor, *J. Mat. Sci.* **22**, 887, 1987.
- [40] S.M.L. Sastry, P.J. Meschter, J.E. O'Neal, *Met. Trans. A* **15A**, 1451, 1984.
- [41] M.B. Vordahl, U.S. Patent No. 3,179,522, Apr. 23, 1968.
- [42] J.S. Cook, R.K. Day, J.B. Dunlop, *Materials Australasia*, p. 20, May 1987.
- [43] B.R.D. Gillings, *Materials Australasia*, p. 22, May 1987.
- [44] V. Panchanathan, *Rare Earths, Science, Technology and Applications*, p. 137, The Minerals, Metals & Materials Society, 1997.
- [45] R. Omachi, *Materials Sciences Forum*, Vol. 30, p. 147, 1988.
- [46] K.A. Gschneidner, Jr., V.K. Pecharsky, *Rare Earths, Sciences, Technology and Applications*, Vol. III, eds R.G. Bautista, C.O. Bounds, T.W. Ellis, B.T. Kilbourne, 1997.
- [47] L.Y. Zhang, *ibid.*, p. 235, 1997.
- [48] B.T. Kilbourn, *Inorg. Chim. Acta* **140**, 335, 1987.
- [49] S. Middlehock, D.J.W. Noorlag, *Sensors Actuators* **2**, 29, 1981–82.
- [50] R. Ruchti et al., *IEEE Trans. Nucl. Sci.* **NS-33** (1), 151, 1986.
- [51] J.G. Rabatin, in: *Industrial Applications of Rare Earth Elements*, ed. K.A. Gschneidner, A.C.S. Symposium Series, Vol. 164, p. 203, 1981.
- [52] J.M.P.J. Versteegen, D. Radielovic, L.E. Vrenken, *J. Illum. Eng. Soc.* **4**, 90, 1975.
- [53] J.L. Sommerdijk, A. Brill, *Philips Tech. Rev.* **34** (1), 24, 1974.
- [54] J.R. McColl, F.C. Palilla, in: *Industrial Applications of Rare Earth Elements*, ed. K.A. Gschneidner, A.C.S. Symposium Series, Vol. 164, p. 177, 1981.
- [55] M. Yokoyama, *Thin Film A.C. Electroluminescence for Automobile Instruments*, SAE Tech. Paper 850144, Soc. Autom. Eng., Warrendale, PA, 1985.
- [56] C.R. Hurt, N. McAvoy, S. Bjorklund, N. Filipescu, *Nature (London)* **212**, 179, 1966.
- [57] A.S. Pradhan, *Radiat. Protection Dosim.* **1** (3), 153, 1981.
- [58] M.R. Cates et al., *Proc. Med. Biol., Opt. Tech. Meas. Control, Spectrosc., Photochem. Sci. Meas. Symp. ICALEO 185*, p. 142, 1986.
- [59] K. Takahashi, J. Miyahara, Y. Shibahara, *J. Electrochem. Soc.* **132** (6), 1492, 1985.
- [60] G.H. Haertling, in: *Ceramic Materials for Electronics*, Vol. 3, ed. R.C. Buchanan, *Am. Ceram. Soc.*, p. 139, 1986.
- [61] Y. Asahara, T. Izumitani, *Proc. Tech. Program Electro-opt. laser 78 Conf Expo.*, p. 16, 1978.
- [62] P. Paroii, *Thin Solid Films* **114**, 187, 1984.
- [63] G. Schiefer, *Philips Tech. Rev.* **36** (9), 255, 1976.
- [64] M. Hartmann, B.A. Jacobs, J.J.M. Braat, *Philips Tech. Rev.* **42** (2), 37, 1985.
- [65] D.J. Breed, F.H. de Leeuw, W.T. Stacy, A.B. Voermans, *Philips Tech. Rep.* **38** (7/8), 211, 1978/79.
- [66] A.E. Clark, in: *Handbook on the Physics and Chemistry of Rare Earths*, ed. K.A. Gschneidner, Chap. 15, p. 231, North-Holland, Amsterdam, 1979.
- [67] W.E. Keller, *Magnetic Refrigeration: The Basis for a New Refrigeration Technology*, LALP-82-34, Los Alamos National Laboratory Report, 1982.
- [68] B.T. Kilbourn, *J. Less Common Metals* **111**, 1–8, 1985.
- [69] G. Yoldjian, *J. Less Common Metals* **111**, 17–22, 1985.
- [70] F.F. Lange, *Ceram. Bull.* **62**, 1369, 1983.
- [71] W.A. Sanders, D.M. Mieskowski, *Ceram. Bull.* **64**, 304, 1985, *Tech. Note, Lanthology 520*, available from Molycorp.
- [72] K.H. Jack, *Met. Technol. (NY)* **9**, 297, 1982.
- [73] F.F. Lange, *J. Mater. Sci.* **17**, 240, 1982.
- [74] G.A.J. Hack, *Powder Metall.* **27**, 73, 1984.



- [75] S.M.L. Sastry, P.J. Meschter, J.E. O'Neal, *Metall. Trans. A* **15**, 1451, 1984.
- [76] G. Kim, *Ind. Eng. Chem. Prod. Res. Dev.* **21**, 267, 1982.
- [77] H. Schaper, E.B.M. Doesburg, L.L. van Reijnen, *Appl. Catal.* **7**, 211, 1983.
- [78] C.H. Liebert, R.A. Miller, *Ind. Eng. Chem. Prod. Res. Dev.* **23**, 344, 1984.
- [79] R.B. Herchenroeder, G.Y. Lai, K.V. Rao, *J. Met.* **35**, 16, 1983; H. Nagai, M. Okabayashi, *Trans. Jpn. Inst. Met.* **23**, 334, 1982.
- [80] D. Kolar, Z. Stadler, S. Gaberscek, D. Suvorov, *Ber. Dtsch. Keram. Ges.* **55**, 346, 1978; K. Wakino, K. Minai, H. Tamura, *J. Am. Ceram. Soc.* **67**, 278, 1984.
- [81] G.H. Haertling, *Ferroelectrics* **50**, 389, 1983; *Am. Chem. Soc. Symp. Ser.* **164**, 265, 1981.
- [82] R.J. Pressley, *Opt. Ind. Syst. Purch. Dir. B538*, 1980; *Tech. Literature KSF filter Material*, Kigre Inc., Toledo, OH.
- [83] W.A. Thornton, *Am. Chem. Soc. Symp. Ser.* **164**, 195, 1981.
- [84] B. Barnard, U.K. Pat. 2,042,573, 1980; H.W. Jacobson, U.S. Pat. 4,461,810, 1984; *Tech. Note, Lanthology 515*, available from Molycorp.
- [85] J.-P. Castera, *J. Appl. Phys.* **55**, 2506, 1984; R.C. Booth, E.A.D. White, *J. Phys. D* **17**, 579, 1984.
- [86] K. Anzai, N. Iwase, Y. Sugiura, *Toshiba Rev.* **39**, 500, 1984.
- [87] E.D. Eastman, L. Brewer, L.A. Bromley, P.W. Gilles, N.L. Lofgren, *J. Am. Chem. Soc.* **72**, 2248, 1950; *J. Am. Ceram. Soc.* **34**, 128, 1951.
- [88] Y. Tsukuda, *J. Can. Ceram. Soc.* **52**, 14, 1983.
- [89] Alcoa Data sheet: Alloy CU78; P.P. Millan, Jr., *J. Met.* **35**, 76, 1983; U.S. Pat. 4,379,719, 1983.
- [90] R.V. Horrigan, *Am. Chem. Soc. Symp. Ser.* **164**, 95, 1981; *Tech. Note, Lanthology, 527*, available from Molycorp.
- [91] K. Schwetz, A. Lipp, *ATW, Atomwirtsch., Atomtech.* **15**, 531, 1973.
- [92] H. Assmann, W. Doerr, M. Peehs, *J. Am. Ceram. Soc.* **67**, 631, 1984.
- [93] T.C. Schutt, G.A. Barlow, *Ceram. Bull.* **51**, 155, 1972.
- [94] Application Reps. 7101b and 7907, available from Molycorp.
- [95] D.N. Wallace, *Am. Chem. Soc. Symp. Ser.* **164**, 101, 1981.
- [96] F.L. Kennard, III, *Am. Chem. Soc. Symp. Ser.* **164**, 251, 1981.
- [97] C.M. Mari, *Solid State Ionics* **12**, 419, 1984.
- [98] S. Kuwata, N. Miura, N. Yamazoe, T. Seiyama, *Chem. Lett.* **981**, 1295, 1984.
- [99] S.F. Palguev, V.I. Zemtov, V.K. Gilderman, A.D. Neujmin, *Solid State Ionics* **13**, 65, 1984.
- [100] P.C. Donohue, *Eur. Pat.* 0,008,437, 1980.
- [101] E.K. Storms, *J. Appl. Phys.* **54**, 1076, 1983.
- [102] G. Maher, *Proc. Electron. Compon. Conf.* **33**, 173, 1983.
- [103] B.M. Kulwicki, *Am. Ceram. Soc. Adv. Ceram.* **1**, 138, 1981.
- [104] K. Mukae, I. Nagasawa, *Am. Ceram. Soc. Adv. Ceram.* **1**, 331, 1981.
- [105] R. Blunt, *Chem. Br.* **19**, 740, 1983.
- [106] V.P. Gapontsev, S.M. Matitsin, A.A. Isineev, V.B. Kravchenko, *Proc. Int. Conf Lasers 1135*, 1982.
- [107] J.R. McColl, F.C. Palilla, *Am. Chem. Soc. Symp. Ser.* **164**, 177, 1981.
- [108] J.G. Rabatin, *Am. Chem. Soc. Symp. Ser.* **164**, 203, 1981.
- [109] R.A. Eppler, *Ceram. Bull.* **56**, 213, 1977; *Tech. Note, Lanthology 525*, available from Molycorp.
- [110] W.H. Price, *Sci. Am.* **72**, 1976.
- [111] W.B. White, D. Chess, C.A. Chess, J.V. Biggers, *Trans. SPIE* **297**, 38, 1981.
- [112] W.H. Rhodes, *J. Am. Ceram. Soc.* **64**, 13, 1981.
- [113] H.-G. Byhan, *Silikattechnik* **33**, 359, 1982.
- [114] Ricoh Co. Ltd., *Jpn. Pat.* 57,112,701, 1982.
- [115] R. Reisfeld, *Inorganica Chimica Acta* **140**, 345, 1987.
- [116] R. Reisfeld, C.K. Jorgensen, *Lasers and Excited States of Rare Earths*, Springer-Verlag, Berlin/N.Y., 1977.
- [117] E.P. Chicklis, *Proc. Conf. On Lasers and Electrooptics*, San Francisco, June 1986.
- [118] A.A. Kaminskii, A.G. Petrosyan, V.A. Federov, S.E. Sarkisov, *Sov. Phys. Dokl.* **26**, 846, 1981.
- [119] B.M. Antipenko, *Sov. Tech. Phys. Lett.* **11**, 284, 1985.
- [120] E.W. Duczynskie, *Appl. Phys. Lett.* **48**, 1562, 1986.
- [121] T.M. Pollak, W.F. Wing, R.G. Grasso, E.P. Chicklis, H.P. Jentsen, *IEEE, J. Quant. Electron.* **QE-18**, 159, 1982.
- [122] B. Dischler, W. Wettling, *J. Phys. D* **17**, 1115, 1984.
- [123] P. Myslinski et al., *Optical Engineering* **32**, 2025, 1993.
- [124] R. Reisfeld, C.K. Jorgensen, *Struct. Bonding* **49**, 1, 1982.
- [125] R. Reisfeld, *Inorg. Chim. Acta* **95**, 69, 1984.
- [126] R. Reisfeld, *J. Less Common Metals* **93**, 243, 1983; *ibid.* **112**, 9, 1985.
- [127] R. Reisfeld, *Chem. Phys. Lett.* **95**, 95, 1983; *ibid.* **114**, 306, 1985.

- [128] R. Reisfeld, Ann. Rep. to Israel Ministry of Energy and Belfer Foundation 1983, 1984, 1986 (available from Israel Ministry of Energy), Hybrid Luminescent Solar Concentrators.
- [129] C.M. Srivastava, B. Uma Maheswar Rao, Materials Science Forum **30**, 227, 1988.
- [130] C.R. Ronda, T. Justel, H. Nikol, J. Alloys and Compounds **275–277**, 669–676, 1998.
- [131] H. Beehtel, W. Czarnojan, W. Mayr, T. Justel, H. Nikol, C. Ronda, German Patent 19727607.5, 1997.
- [132] V. Balzani, F. Scandola, Supramolecular Chemistry, Ellis Howood, New York, 1991.
- [133] A.M. Srinivastava, W.W. Beers, J. Lumin. **71**, 285, 1997.
- [134] M. Leskela, J. Alloys and Compounds **275–277**, 702–708, 1998.
- [135] R. Tomqvist, SID 97, Digest **28**, 855, 1997.
- [136] C.N. King, J. SID **4**, 153, 1996.
- [137] M. Godlewski, M. Leskela, Crit. Rev. Solid State Mater. Sci. **19**, 199, 1994.
- [138] J. Rabatin, 12<sup>th</sup> Rare Earth Conference, July 1976, Vail, Colorado, p. 819.
- [139] J.G. Bednorz, K.A. Muller, Z. Phys. B **64**, 18, 1986.
- [140] M.K. Wu, J.R. Ashburn, C.J. Torng, P.H. Hor, R.L. Meng, L. Gao, Z.J. Huang, Y.Q. Wang, C.W. Chu, Phys. Rev. Lett. **58**, 908, 1987.
- [141] C. Mazumdar, R. Nagarajan, C. Godart, L.C. Gupta, M. Latroche, S.K. Dhar, C. Levy-Clement, B.D. Padalia, R. Vijayaraghavan, Solid State Commun. **87**, 413, 1993.
- [142] R. Nagarajan, C. Mazumdar, Z. Hossain, S.K. Dhar, K.V. Gopalakrishnan, L.C. Gupta, C. Godart, B.D. Padalia, R. Vijayaraghavan, Phys. Rev. Lett. **72**, 274, 1994.
- [143] R.J. Cava, H. Takagi, H.W. Zandbetgen, J.J. Krajewski, W.F. Peck, T. Siegrist, B. Batlogg, R.B. Van Dover, R.J. Felder, K. Mizuhashi, J.O. Lee, I.I. Eisaki, S. Uchida, Nature **367**, 252, 1994.
- [144] H. Eisaki, H. Takagi, R.J. Cava, K. Mizuhashi, J.O. Lee, B. Batlogg, J.J. Krajewski, W.F. Peck, Jr., S. Uchida, Phys. Rev. B **50**, 647, 1994.
- [145] Z. Hossain, S.K. Dhar, R. Nagarajan, L.C. Gupta, C. Godart, R. Vijayaraghavan, IEEE Trans. Magn. **31**, 4133, 1995.
- [146] C.V. Tomy, M.R. Lees, L. Afalfiz, G. Balakrishnan, D. McK Paul, Phys. Rev. B **52**, 9186, 1995.
- [147] B.K. Cho, P.C. Canfield, D.C. Johnston, Phys. Rev. B **52**, R3844, 1995.
- [148] Z. Hossain, L.C. Gupta, R. Nagarajan, S.K. Dhar, C. Godart, R. Vijayaraghavan, Physica B **194/196**, 1975, 1996.
- [149] J.W. Lynn, S.K. Sinha, Z. Hossain, L.C. Gupta, R. Nagarajan, C. Godart, Physics B **224**, 66, 1996.
- [150] J.W. Lynn, S. Skan Thakumar, Q. Huang, S.K. Sinha, Z. Hossain, L.C. Gupta, R. Nagarajan, C. Godart, Phys. Rev. B **55**, 6584, 1997.
- [151] B.K. Cho, Xu. Ming, P.C. Canfield, L.L. Miller, D.C. Johnston, Phys. Rev. B **52**, 3676, 1995.
- [152] D.W. Cooke, J.L. Smith, S.I. Blundell, K.H. Chow, P.A. Pattenden, F.L. Pratt, S.F.J. Cox, S.R. Brown, A. Morrobel Sosa, R.L. Lichti, L.C. Gupta, R. Nagarajan, Z. Hossain, C. Mazumdar, C. Godart, Phys. Rev. B **52**, R3864, 1995.
- [153] S. Kobayashi, Chem. Lett. 2087, 1991.
- [154] S. Kobayashi, I. Hachiya, J. Org. Chem. **59**, 3590, 1994.
- [155] S. Arseniyadis, Q. Wang, D.V. Yashunsky, T. Kaoudi, R. Brondi Alves, R. Potier, Tetrahedron Lett. **36**, 1633, 1995.
- [156] S. Kobayashi, I. Hachiya, Tetrahedron Lett. **33**, 1625, 1992.
- [157] S. Kobayashi, I. Hachiya, T. Takahori, Synthesis **371**, 1993.
- [158] S. Kobayashi, I. Hachiya, H. Ishitani, M. Araki, Synlett **472**, 1993.
- [159] K. Uotsu, H. Sasai, M. Shibasaki, Tetrahedron: Asymmetry **6**, 71, 1995.
- [160] T.K. Hollis, B. Bosnich, J. Am. Chem. Soc. **5**, 117, 4570, 1995.
- [161] S. Kobayashi, I. Hachiya, T. Takahori, M. Araki, H. Ishitani, Tetrahedron Lett. **33**, 6815, 1992.
- [162] S. Kobayashi, H. Ishitani, I. Hachiya, M. Araki, Tetrahedron **50**, 11623, 1994.
- [163] S. Kobayashi, I. Hachiya, H. Ishitani, M. Araki, Tetrahedron Lett. **34**, 4535, 1993.
- [164] S. Kobayashi, H. Ishitani, M. Araki, I. Hachiya, Tetrahedron Lett. **35**, 6325, 1994.
- [165] A. Kawada, S. Mitamura, S. Kobayashi, J. Chem. Soc. Chem. Commun. 1157, 1993.
- [166] I. Hachiya, S. Kobayashi, J. Org. Chem. **58**, 6958, 1993.
- [167] S. Fukuzawa, T. Tsuchimoto, T. Kanai, Kodorui **24**, 206, 1994; Chem. Lett. 1981, 1994.
- [168] J. Inanaga, Y. Yokoyarna, T. Hanamoto, J. Chem. Soc. Chem. Commun. 1090, 1993.
- [169] P. Crotti, V. Di Bussolo, L. Favero, F. Macchia, M. Pineschi, Tetrahedron Lett. **35**, 6537, 1994.
- [170] S. Kobayashi, M. Araki, H. Ishitani, S. Nagayama, I. Hachiya, Synlett **233**, 1995.
- [171] S. Matsubara, M. Yoshioka, K. Utimoto, Chem. Lett. 827, 1994.

- [172] J.H. Forsberg, V.T. Spaziano, T.M. Balasubramanian, G.K. Liu, S.A. Kinsley, C.A. Duckworth, J.J. Poteruca, P.S. Brown, J.L. Miller, *J. Org. Chem.* **52**, 1017, 1987.
- [173] J.H. Forsberg, V.T. Spaziano, S.P. Klump, K.M. Sanders, *J. Heterocycl. Chem.* **25**, 767, 1988.
- [174] M. Meguro, N. Asao, Y. Yamamoto, *J. Chem. Soc. Perkin Trans.* 2597, 1994.
- [175] M. Chini, P. Crotti, L. Favero, F. Macchia, M. Pineschi, *Tetrahedron Lett.* **35**, 433, 1994.
- [176] P. Crotti, L. Favero, F. Macchia, M. Pineschi, *ibid.* **35**, 7089, 1994.
- [177] A. Mazzei, in: *Organo-metallics of 'f' Elements*, eds T.J. Marks, R.D. Fisher, D. Reidel Publishing Co., Dordrecht, Holland, 1979.
- [178] AAPM Report No. 71, April 2001.
- [179] G.V.S. Rayudu et al., *Application of lanthanides in tumor interactions*, *J. Nucl. Med.* **15**, 526, 1974; *J. Nucl. Med.* **16**, 528, 1975; *Int. J. Nucl. Med. and Biol.* **2**, 44, 1975; *Eu. J. Nucl. Med.* **9**, 1982; *J. Label. Comp. Radiopharm.* **21**, 1039, 1984.
- [180] L. Stryer, *Biochemistry*, Freeman, New York, 1988.
- [181] L.E.M. Miles, C.N. Hales, *Nature* **219**, 186, 1968.
- [182] K.E. Rubenstein, R.S. Scheider, E.F. Ullman, *Biochem. Biophys. Res. Commun.* **47**, 846, 1972.
- [183] H.R. Schroeder, P.O. Vogelhut, R.J. Carrico, R.C. Bogulaski, R.T. Buckler, *Anal. Chem.* **48**, 1933, 1976.
- [184] I.A. Hemmila, *Chemical Analysis*, eds J.D. Winefordner, I.M. Kolthoff, Vol. 117, Wiley, New York, 1991.
- [185] I. Hemmila, *Scand. J. Clin. Lab. Invest.* **48**, 388, 1988.
- [186] I. Hemmila, R. Harju, in: *Bioanalytical Applications of Labelling Technologies*, eds I. Hemmila, T. Stahlberg, P. Mottram, pp. 83, 195, 263, *Wallas, Turku*, 1994.
- [187] I. Hemmila, *Anal. Chem.* **57**, 1676, 1985.
- [188] I. Hemmila, V.M. Mikkala, M. Latva, P. Kilholma, *J. Biochem. Biophys. Meth.* **26**, 283, 1993.
- [189] I. Hemmila, *J. Alloys and Compounds* **225**, 480, 1995.
- [190] Y.Y. Xu, K. Pettersson, K. Blomberg, I. Hemmila, H. Mikola, T. Lovgren, *Clin. Chem.* **38**, 2038, 1992.
- [191] P. Hurskainen, P. Dahlen, J. Ylikoski, M. Kuratowski, H. Siitari, T. Lovgren, *Nucleic Acids Res.* **19**, 1057, 1991.
- [192] K. Blomberg, *J. Immunol. Meth.* **168**, 267, 1993.
- [193] N. Sabbatini, M. Guardigli, J.M. Lehn, G. Mathis, *J. Alloys & Compounds* **180**, 363, 1992.
- [194] O. Prat, E. Lopez, G. Mathis, *Anal. Biochem.* **195**, 283, 1991.
- [195] V.M. Mikkala, C. Sund, M. Kuratowski, P. Pasenen, M. Hogberg, J. Kankare, H. Takalo, *Helv. Chem. Acta.* **75**, 1621, 1992; **76**, 1361, 1993.
- [196] G. Mathis, *Clin. Chem.* **391**, 1953, 1993.
- [197] R.P. Ekins, F. Chu, E. Biggart, *Ann. Biol. Clin. (Paris)* **48**, 655, 1990.
- [198] *Radiopharmaceuticals: Progress and Clinical Perspectives*, 2 volumes, ed. A.R. Fritzberg, CRC Press, Boca Raton, FL, 1986.
- [199] P.K. Knoefel, *Radiopaque Diagnostic Agents*, Charles C. Thomas Publ., Springfield, IL, 1961.
- [200] J.E. Potchen, P.R. Kochler, D.O. Davis, *Principles of Diagnostic Radiology*, McGraw-Hill, NY, 1971.
- [201] C.L. Partain, A.E. James, F.D. Rollo, P.R. Price, *Nuclear Magnetic Resonance Imaging*, W.B. Saunders, Philadelphia, PA, 1983.
- [202] P. Mansfield, P.G. Morris, *NMR Imaging in Biomedicine, Supplement 2, Advances in Magnetic Resonance*, ed. J.S. Waugh, Academic Press, NY, 1982.
- [203] J.C. Sullivan, A.M. Friedman, G.V.S. Rayudu, E.W. Fordham, P.C. Ramachandran, *Int. J. Nucl. Med. Biol.* **2**, 44, 1975.
- [204] P. Caravan et al., *Chem. Rev.* **99**, 2293, 1999.
- [205] A.Y. Louie et al., *Nat. Biotechnol.* **18**, 321, 2000.
- [206] C.S. Springer, *Physicochemical Principles influencing magneto pharmaceuticals*, in: *NMR in Physiology and Bio Physics*, ed. R.J. Gillies, Academic Press, San Diego, 1994.
- [207] C.S. Springer, W.D. Rooney, *Proc. Int. Soc. Magn. Reson. Med.* **9**, 2241, 2001.

---

## Subject Index

---

- $E_h$ -pH diagrams, 878  
 $\beta$ -diketonates, 801  
 $\beta$ -diketonates ligands, 293  
 $\beta$ -diketones, 781  
*t*-butyl groups, 293  
1,3-diketones, 436  
1,3-diketones as oxygen donors, 292  
18C6 complexes, 169  
4*f* orbitals, 111  
4*f* valence electrons, 262  
4*p* orbitals, 111  
4*s* orbitals, 111
- A-sub group ions, 832  
absolute hardness, 117  
absorption spectra, 610  
absorption spectra in aqueous media, 646  
absorption spectra in nonaqueous media, 647  
absorption spectra of lanthanide complexes in solutions, 635  
absorption spectra of lanthanides, 850  
AC motors, 919  
acetate complexes, 646  
acetonitrile, 264, 298, 310, 318  
acetonitrile solution, 283  
acetoxime, 436  
actinide complexes, 426  
actinide series, 97  
actinides, 873, 874  
actinium, 92, 96  
actuators, 338  
acylation, 957  
Adachi, Gin-Ya, 327  
adduct compounds, 294  
agostic Si-C bonds, 456  
Ahrland, 114  
air-conditioning system, 924  
Al-transition metal alloys, 914  
Al-base alloys, 913  
alcoholates, 293  
alcohols, 436  
alcohols as oxygen donors, 293  
aldehydes, 957  
aldol condensation, 952  
aldolates, 452  
Alizarin Red S, 139  
alkali metal ions, 327  
alkaline earths, 92  
alkoxides, 293, 436  
alkoxy group, 653  
alkyl chain structure, 165  
alkyl group, 653  
alkynide units, 450  
allophycocyanin, 329  
allosteric effect, 336  
allylation, 957  
Alnico, 916  
Alnico magnets, 920  
alternative fuels technology, 907  
aluminum hydride organo lanthanide complexes, 469  
ambidentate ligand, 282  
amine groups, 169  
amino acid complexes, 659, 858  
amino acids, 265  
aminocarboxylate complexes, 167, 660  
aminocarboxylic acids, 20  
aminoolefins, 455  
aminopolycarboxylate complexes, 166, 527  
aminopolycarboxylic acids, 299  
analogous selenocyanate complexes, 298  
analysis of lanthanide shifts, 805  
analytical chemistry of rare earths, 47  
analytical sensors, 338  
angular overlap model (AOM), 589  
anhydrous diketonate complexes, 267  
anhydrous lanthanide complexes, 660  
anhydrous salts, 263  
anion exchangers, 26  
ant behaviour, 886, 887  
anti-inflammatory properties, 886  
antiknock properties, 961  
antimony complex, 455  
aquated ion, 277  
aquatic pollution, 888  
aqueous aliquots, 269

- aquo cations, 547  
aquo complexes, 785  
aquo ions, 524  
ARS, 140, 143  
arsenic complex, 455  
arthritis, 886  
association constants of rare earth cations, 20  
associative reaction, 487  
atomic absorption, 66  
atomic theory, 572  
Auger technique, 762  
auto exhaust catalysts, 906  
automotive pollution control, 905  
axial ligands, 429  
axial symmetry, 793
- Baekeland, Leo Henrik, 308  
Bakelite, 308  
Bardeen, Cooper and Schrieffer (BCS) theory, 949  
baricentre energies, 122  
baricentre polynomial model, 125  
barium, 121  
barium magnesium aluminates, 943  
barium titanate, 933  
bastnasite, 11, 12, 32, 46  
benzoates, 167  
bibracchial lariat ethers, 341, 342  
bicapped square antiprism, 411  
bidentate bridges, 438  
bidentate configuration, 282  
bidentate donor ligands, 297  
bidentate nitrates, 283, 291  
bidentate phenanthroline, 298  
bimolecular reaction, 484  
binuclear lanthanide-silver shift reagents, 782  
bioanalytical applications, 329  
biochemical aspects of lanthanides, 847  
biological macromolecules, 818  
biological membranes, 866  
biology, 334  
biomedical analysis, 329  
bipyridine based complexes, 559  
bispicolinato complexes, 155  
Bjerrum method, 136  
Bleaney's theory, 785, 786  
Bloch equations, 496  
blood-brain barrier, 973  
Böhmer, Volker, 360  
bonded magnets, 920  
bonded neodymium applications, 921  
bony metastases, 962  
borhydride complexes, 438  
borocarbides, 951  
bridged cyclopentadienyl ligands, 458  
bridging ligand, 546  
bromo complexes, 282  
butadiene, 960  
butylbenzo substitutes, 168
- calcium reduction, 46  
calix-crowns, 361  
calix-cryptands, 361  
calixarenes, 307, 311, 312, 316, 350–352, 356, 357, 359, 360, 368  
camera lenses, 936  
capacitors, 933  
carbohydrates, 865  
carbon-carbon bond formation, 952  
carbon-nitrogen bond formation, 958  
carbon-oxygen bond formation, 958  
carbonates, 263  
carbonyl groups, 292  
carbonyl ligands, 294  
carbonyl oxygen donors, 291  
carborane complexes, 302, 473  
carboxyl groups, 166  
carboxylate groups, 166, 290  
carboxylates, 167  
carboxylic acid complexes, 436  
carboxylic acids, 265, 289, 650  
carboxylic groups, 436  
Cartesian coordinate system, 805  
catalysis, 334  
catalyst systems, 903  
catalytic (flameless) combustion, 906  
catalytic enantioselective olefin hydrogenation, 460  
catalytic systems, 904  
cathodic inhibition, 898  
cation exchangers, 26  
cells, 828  
central field approximation, 572  
central field covalency, 593  
ceramics, 931  
cerium, 38, 121, 122, 871  
cerium carboxylates, 905  
cerium complexes, 334, 451, 458, 470  
cerium group, 156, 158–160  
cerium salts, 885  
cerium subgroup, 154, 155  
cerium-oxygen system, 763  
cerocene, 466  
chalcophilic, 113  
chalcophilic elements, 112  
charge-transfer satellites, 747  
chelate complexes, 160  
chelate labelling, 965  
chelate rings, 164, 165

- chelating agents, 315  
chelation, 160, 277  
chemical equilibria, 644  
chemical heat pump, 924  
chemical polarizability, 112  
chemical shifts, 518, 784  
chemicals manufacture, 907  
chemiluminescence, 559  
chiral asymmetric ligands, 460  
chiral dicarboxylic acids, 335  
chiral drugs, 808  
chiral lanthanide complexes, 657  
chiral lanthanide shift reagents, 811  
chiral recognition techniques, 563  
chiral shift reagents, 782, 806–808  
chiral studies, 813  
chiroptical luminescence, 564  
chloro complexes, 280, 282  
chromate, 898  
chromium-base alloys, 911  
chromophores, 130  
chronopotentiometric method, 150  
chronopotentiometry, 149  
cinema arc carbons, 908  
circularly polarized luminescence, 854  
classification of rare earths, 3  
cobalt complexes, 818  
colligative properties, 132  
commercial ion exchangers, 19  
common earths, 3  
comparison of magnets, 917  
competitive reaction technique, 130  
complex formation, 377  
complex formation in aqueous solutions, 526  
complex formation reactions, 526  
complex forming agents, 176  
complex oxides, 906  
complex substitution reactions, 485  
complexation reactions, 277, 484  
complexes in non-aqueous solutions, 278  
complexes of the type  $Cp_2^{\prime}LnX$ , 434  
complexes of the type  $Cp_3LnX$ , 433  
complexometric titration, 263  
complexometric titration methods, 39  
computer programs, 837  
Condon–Shortley theory, 171  
conductimetry, 277  
configuration interaction, 743  
conformational isomers, 805  
conformational studies, 812  
consumption of rare earths, 9  
contact shifts, 781, 785  
continuous variations method, 140  
contrast reagents, 970, 973, 974  
coordination metal complexes, 810  
coordination number 4, 382  
coordination number 5, 383  
coordination number 6, 383  
coordination number 7, 387  
coordination number 8, 394  
coordination number 9, 405  
coordination number 10, 410  
coordination number,  $N$ , 110, 111  
coordination numbers, 153, 277, 378, 781  
coordination polyhedra, 378  
core levels, 740  
coronands, 316, 322, 329, 332, 341, 346, 360, 368  
coronary atherosclerosis, 886  
coronates, 318–320, 325–327, 368  
corrosion inhibition, 901  
corrosion inhibitors, 898  
counterion coordination, 515  
coupling, 573  
covalency model of hypersensitivity, 600  
 $Cp_2^{\prime}LnX$ , 439, 440  
 $Cp_2^{\prime}MX$ , 439  
 $Cp^{\ast}LnX$ , 455  
 $Cp_2^{\ast}Ln$  complexes, 452  
 $Cp_2^{\ast}Ln$  halide complexes, 448  
 $Cp_2^{\ast}Ln$  hydrocarbyl complexes, 448  
 $Cp_2LnX$ , 436  
 $Cp_2LnX$  containing Ln–P bond, 438  
crown ether complexes, 306, 307  
crown ethers, 169, 177, 305, 310, 311, 316–318, 329  
cryptands, 169, 306, 310–312, 315, 322, 329, 332  
cryptate complexes, 559  
cryptates, 322, 324–327, 342, 368, 970  
crystal field effects, 153  
crystal field energies, 680, 686, 709  
crystal field parameters, 576, 585, 589, 616, 642  
crystal field splitting, 678  
crystal field stabilization, 153  
crystal field theory, 158, 583  
crystal lasers, 938  
crystal radii, 152  
crystal structures, 110  
crystal–field interaction, 578  
crystalline complex, 266  
crystalline field levels, 583, 704  
crystalline field of  $D_{3h}$  symmetry, 707  
crystalline field perturbation, 676  
cubes, 404  
cubic point symmetry, 582  
cyclen, 311  
cyclen derivatives, 312, 343, 344  
cyclohexanediamine tetraacetate, 155  
cyclooctatetraene, 463

- cyclooctatetraenyl complexes, 464  
cyclopentadiene ligand, 444  
cyclopentadienide complexes, 441, 599  
cyclopentadienyl centroids, 468  
cyclopentadienyl complexes, 439  
cyclopentadienyl compounds, 434  
cyclopentadienyl derivatives, 325  
cyclopentadienyl ligands, 431, 439, 448, 473
- d-transition metal complexes, 593  
DACDA, 170  
DAPDA, 170  
data storage, 931  
DC motors, 918  
Debye–Hückel equations, 488  
Debye–Hückel theory, 509  
density functional theory, 117  
dental applications, 920  
denticity, 313  
deprotonation, 118, 267  
Desreux, Jean François, 344  
determinantal method, 669, 680  
determination of coordination number, 644  
deuterium isotope effect, 806  
diacetato complex, 646  
diadochy, 869  
dialkylidene bridge, 444  
diazacrown ethers, 169  
dibenzo-18-crown-6 ether, 305  
dibenzoylmethanide complexes, 599  
dibismuth complex, 455  
dicyclopentadienyl lanthanide alkyl complexes, 435  
dicyclopentadienyl lanthanide carboxylates, 436  
Diebler–Eigen mechanism, 532  
Diels–Alder reactions, 955, 956  
dienes, 906  
diethylenetriamine pentaacetate, 155  
diketonate derivatives, 436  
diketones, 266  
dimeric anion, 400  
dimetallic gadolinium complex, 313  
dimethyl formamide (DMF), 517  
dimethyl formamide adduct, 409  
diol complexes, 660  
dioxyacetate complexes, 653  
diphosphazane dioxide complexes, 301  
dipivoyl methane complexes, 380  
discovery of rare earths, 3  
displacement chromatography, 22  
dissociation kinetics, 529  
dissociative enhancement principle, 966  
dissociative pathways, 486  
dissociative reaction, 487  
distribution constants, 143  
ditelluride complex, 453  
divalent rare earths, 634  
DMF exchange, 521  
DMSO, 169  
dodecacordinate complexes, 414  
dodecahedron, 397  
DOTA, 311  
DOTA complexes, 170  
Dotarem, 345, 346  
DOTP complexes, 832  
double symmetry, 172  
double–double effect, 170, 172–175  
drugs analyzed for optical purity, 812  
dynamic coupling mechanism, 607  
dynamic ion-exchange chromatography, 68, 69  
dynamic structures in solution, 781  
dysprosium, 153  
dysprosium diacetyl monoxime complex, 550  
dysprosium group, 410
- ecological aspects, 886  
EDPDA, 166, 167  
EDTA, 134, 160, 167, 176, 266  
EDTA complexes, 159, 557, 558  
Eigen, M., 493  
Eigen–Tamm mechanism, 315  
electrical resistivity, 107  
electrochemical studies, 898  
electrochromic materials, 334  
electrolysis, 46  
electromagnetic radiation, 935  
electron configurations, 84–86, 91, 96  
electron ionization, 735  
electron repulsions, 87, 90  
electron spectroscopy, 735  
electron transfer reactions, 544  
electron-repulsion perturbation, 662  
electronegativity, 113  
electronic chemical potential, 117  
electronic configurations, 90, 92–95, 97, 119, 922  
electronic devices, 931  
electronics, 930  
electrophilic alkyl derivatives, 448  
electrostatic bonds, 262  
electrostatic energies, 663  
electrostatic model, 314  
electrostatic theory, 152  
electrothermal atomization, 66  
eluting agents, 26  
elution chromatography, 23  
emission of rare earth ions, 941  
emission properties of lanthanide chelates, 964  
emission spectroscopic methods of analysis, 45

- emission spectroscopy, 63, 64  
emissive displays, 945  
enantiomeric excess, 809  
enantiomeric relative abundances, 807  
enantiomers, 808  
enantioselective catalytic hydrogenation, alkylation,  
  hydroamination of prochiral unsaturated systems, 474  
enantioselective synthesis, 809  
encounter complex, 485  
encounter equilibria, 488  
encounters, 488  
energies of spin-orbital levels, 673  
energy levels of  $f^2$  and  $f^1$  configurations, 661  
energy transfer from lanthanide ions, 563  
enolate bridges, 440  
enolates, 958  
enthalpy, 161  
entropy, 165  
entropy factor, 277  
environmental behavior of lanthanides, 867  
enzymatic labels, 964  
equilibrium constant, 488  
erbium, 939  
erbium complex, 384  
erosion, 886, 887  
erythrocytes, 831  
ESCA, 738  
ESCA photoelectron spectrometer, 737  
esters, 958  
ethanol, 282  
ether solvates, 456  
ethylene, 960  
ethylenediamine complexes, 297  
ethylenediamine tetraacetic acid, 155  
europium, 878  
europium complexes, 152, 291, 353  
europium(III)-complexes, 878  
exchange reactions, 496  
extended networks, 361  
extraction and separation processes, 327, 360  
extrastabilization energy, 153, 156, 158  
  
 $f^1$  configuration, 706  
 $f^2$  configuration, 662  
Fajan's theory, 607  
fast reactions, 489  
ferrous process metallurgy, 896  
fiber optics, 936  
field emission, 945  
Fisher, Emil, 309  
flame emission, 66  
flow methods, 490  
fluid catalytic cracking (FCC), 905  
fluorescence, 852  
fluoro complexes, 286  
formation, 488  
formation constants, 150, 153  
four-level laser system, 922  
fractional crystallization, 19, 176  
fractional precipitation, 20  
fractionation separation, 176  
Fronaeas, 148  
frontier orbitals, 115, 116  
  
gadolinium, 152–154, 160  
gadolinium chelates, 973  
gadolinium complex, 339  
gadolinium cryptate, 332  
gadolinium gallium garnet, 936  
gadolinium(III) chelates, 972  
Gd(III) EPR as a probe, 857  
geological environments, 7  
Gibbs energy, 314  
Gibbs free energy, 326  
glycolate ligands, 400  
glycolic acid complexes, 290  
glycosylation, 958  
graphite-furnace atomic-absorption spectrometry, 56  
gravimetric determination of rare earth elements, 36  
Gutmann's donor number, 326  
Gutsche, C.D., 308  
  
H-bonds, 313  
halide complexes, 280, 649  
halide derivatives, 434  
halides, 113, 163, 285  
Hall effect, 107  
haloacetate complexes, 163  
hard and soft acid base principle, 113  
hard-hard interaction, 116  
Hartree-Fock, 441  
Hartree-Fock calculations, 119  
heart tissue, 832  
heat-resistant alloys, 910  
heavy earths, 3  
heavy metal recycling, 311  
heavy rare earths, 136  
HEDTA, 167  
Heisenberg's uncertainty principle, 497  
hematoporphyrin derivatives, 338  
heme complexes, 307  
heptanedione complexes, 961  
heteroatoms, 364  
hexagonal point symmetry, 583  
hexahalide complexes, 645  
hexahalides, 599



- hexathiocyanato complexes, 384  
hi-tech applications, 924  
high coordination numbers, 414  
high density storage media, 925  
high pressure liquid chromatography, 68, 69  
Hirst's model, 105  
hole formalism, 91  
holmium, 152, 153, 938  
holmium complexes, 601  
HOMO, 115  
homogeneous ethylene polymerization, 439  
homogeneous fluoroimmunoassays, 330  
homogeneous precipitation, 20  
host-guest interaction, 309  
HSAB principle, 119  
human serum transferrin, 857  
Hund's rules, 86, 90  
hydrated lanthanide salts, 263  
hydration sphere, 160, 277  
hydrocarbyl substituents, 448  
hydrochloric acid digestion, 16  
hydrogen embrittlement cracking, 898  
hydrogen fuel storage for automobiles, 924  
hydrogen storage vessels, 924  
hydroxy lanthanide ions, 268  
hydroxy lanthanides, 262  
hydroxycarboxylic acids, 290  
hypersensitive transitions, 597, 599, 604, 850
- igneous rocks, 868  
imaging applications, 970  
imaging techniques, 971  
imines, 267  
iminocryptand, 332  
iminodiacetic acid complex, 299  
induced fit, 312  
induced fit principle, 311, 312, 315, 341  
inductively coupled mass spectrometry, 66  
inductively coupled plasma mass spectrometry, 68  
inelastic neutron scattering, 588  
inner orbitals, 262  
inner sphere, 163, 279  
inner-sphere complexes, 488  
inner-sphere electron transfer reactions, 546  
inner-sphere redox reactions, 546  
inorganic ligands, 276  
integrated rate laws, 484  
integration constant, 131  
interaction at non-donor sites, 810  
interchange pathways, 485, 488  
interconfigurational fluctuations, 104–107  
interelectronic repulsion, 172  
interelectronic repulsion parameter, 122, 125  
interfacial catalysis, 539
- intermediate elements, 112  
intermetallic compounds, 104, 105  
intermetallics, 915  
intra 4f–4f transitions, 595  
intraligand charge polarization, 167  
intramolecular repulsions, 169  
inverse sandwich, 466  
iodo complexes, 282  
ion exchange chromatography, 22  
ion exchange method, 148, 149, 151  
ion exchange retention, 143  
ion-dipole bonds, 309  
ion-exchange media, 26  
ionic complexes, 152  
ionic radii, 110  
ionophores, 304  
Irving, H.M.N.H., 137  
isomerization reactions, 538, 540  
isostructural complexes, 788, 791  
isothermal oxidation, 911  
isotope effects, 806  
isotopic exchange reactions, 533
- J–J transitions, 644  
Jorgensen, C.K., 124  
Judd–Ofelt theory, 596, 604, 611  
Judd–Ofelt theory of hypersensitivity, 605
- K21DA complexes, 531  
Kimball's concept, 111  
kinetic approach, 129  
kinetic expressions for chemical relaxation, 498  
kinetic factors, 796  
kinetics, 314  
kinetics of adduct formation, 817  
kinetics of formation, 354  
Kirin, I.S., 307  
Klopman, G., 115  
Knight shifts, 109  
Kramer's doublets, 707
- L quantum number, 170  
La(III)–ARS system, 139  
La/ARS, 140  
labile reactions, 489  
labile systems, 130  
Landé parameter, 120  
Langmuir–Blodgett film technology, 338  
lanthanide  $\beta$ -diketonates, 653, 798  
lanthanide alcoholates, 265  
lanthanide alkoxides, 653  
lanthanide arene complexes, 470  
lanthanide catalysis, 540

- lanthanide chlorides, 429  
lanthanide complexation with macrocyclic ligand, 763  
lanthanide complexes in solutions, 275  
lanthanide contraction, 103, 104, 425  
lanthanide crystal field theory, 575  
lanthanide cyclooctatetraenyl complexes, 463  
lanthanide cyclopentadienyl hydride complexes, 468  
lanthanide fractionation, 871  
lanthanide halides, 264  
lanthanide indenyl complexes, 463  
lanthanide induced shift, 781  
lanthanide interactions with proteins, 858  
lanthanide nitrates, 264  
lanthanide NMR shift reagents, 779  
lanthanide nucleotide complexes, 862  
lanthanide ores, 8  
lanthanide oxalate complexes, 502  
lanthanide oxides, 903, 905  
lanthanide perchlorates, 264  
lanthanide processes, 100  
lanthanide propionate complexes, 540  
lanthanide salts, 885  
lanthanide series, 97  
lanthanide speciation, 882  
lanthanide supramolecular complexes, 270  
lanthanide triflates, 264  
lanthanide trifluoromethane sulfonates, 264  
lanthanide-acylpyrazolone complexes, 539, 540  
lanthanide-amino acid complexes, 859  
lanthanide-carbon bonds, 905  
lanthanide-EDTA-5-sulphosalicylate mixed complexes, 532  
lanthanide-organic ligand interaction, 161  
lanthanide-transition metal mixed organometallic complexes, 470  
lanthanide-doped phosphors, 969  
lanthanides in biology, 832  
lanthanides in magnetic devices, 931  
lanthanum, 19, 92, 95, 96  
lanthanum complex, 384  
lanthanum nitrate, 307  
lanthanum reduction, 46  
ariat crown ethers, 341, 342  
Larmor precision frequency, 108  
lasers, 921, 922  
lattice constant, 107  
lawrencium, 92, 96  
Lehn, Jean-Marie, 306  
Lewis acid behaviour, 781  
Lewis acid catalysts, 955  
Lewis acids, 309  
Lewis bases, 267, 429, 434, 448  
ligand exchange rates, 561  
ligand titration curve, 136  
ligand-ligand repulsion energies, 395  
light earths, 3  
limestone, 872  
lipophilicity, 351  
lipid solubility, 304  
lipophilicity, 360  
liquid crystal displays, 945  
liquid-liquid ion-exchange chromatography, 26  
lithophilic, 113  
lithophilic elements, 112  
Ln HMPA complexes, 294  
Ln(III) probes, 835  
Ln(III) reagents, 834  
Ln-EDTA system, 166  
Ln-H<sub>2</sub>O bond, 161  
Ln-K21DA complexes, 531, 534  
Ln-N bonds, 167  
Ln-N bonds in Cp<sub>2</sub>LnX, 437  
Ln-O bonds, 161, 166, 167  
LnCp<sub>3</sub> compounds, 429  
LnEDTA, 167  
LnEDTA complexes, 533  
LnMEDTA complexes, 529  
location of the major rare earth deposits, 6  
lock-and-key principle, 309, 310, 312, 315, 318  
long-range ordered alloys, 916  
low coordination number, 380  
low oxidation states, 325  
LSR interaction via donor atom, 810  
luminescence, 358, 970  
luminescence decay constants, 560  
luminescence of lanthanide ions, 557  
luminescence spectroscopy, 283  
luminescence transducers, 929  
luminescent chelates, 970  
luminescent complexes, 316  
luminescent lanthanide complexes, 962  
luminescent polymers, 327  
luminescent probes, 357  
luminescent rare earth compounds, 295  
luminescent solar concentrators, 939  
luminogenic labels, 964  
luminogenic ligand-labelled secondary reagents, 969  
LUMO, 115  
lutetium, 92, 95, 96, 119, 154  
lutetium complexes, 315, 456, 469, 470, 907  
lysozyme, 819-823, 826  
Mössbauer spectroscopy, 107, 857  
macrobicyclic effect, 169  
macrocycles, 168, 169, 303, 311, 312  
macrocyclic complexes, 168, 268, 303, 308, 535  
macrocyclic compounds, 177, 327

- macrocyclic effect, 319  
macrocyclic ligands, 168, 309, 351  
macrocyclic polyethers, 268  
macromolecules, 269  
macrotricyclic ligands, 329  
Madelung potential, 111  
magnetic bubble memory devices, 940  
magnetic refrigeration, 926, 927  
magnetic refrigerators, 924  
magnetic resonance images, 345  
magnetic resonance imaging, 311, 316, 330, 360, 781, 829, 970  
magnetic resonance methods, 496  
magnetic resonance spectroscopy, 829  
magnetic susceptibility measurements, 107  
magneto-optical disks, 924, 925  
magneto-strictive alloys, 924, 926, 931  
Magnevist, 971  
malignant tumours, 338  
malonate complex, 409, 542  
malonate groups, 290  
manufacturers, 15  
materials science, 334  
mechanism of inhibition, 900  
mechanisms of rare earth complex formation reactions, 514  
mechanistic analysis, 485  
medical imaging, 345  
medical radiography, 945  
medical uses, 885  
medicine, 334  
MEDTA, 167  
Meissner effect, 949  
membranes, 866  
memory systems, 940  
metabolism, 883  
metal chelates, 798  
metal fullerene complexes, 302  
metal hydride battery, 925  
metal hydride systems, 924, 925  
metal hydrides, 927  
metal ions, 364  
metal mediated reactions, 952  
metal separation, 327  
metal-cyclopentadienyl bond, 445  
metal-ligand bonding, 172  
metal-ligand titration curve, 136  
metal-oxygen bond distances, 524  
metal-hydride systems, 924  
metal-ion coordination chemistry, 303  
metal-template synthesis, 268  
metallacalixarenes, 366  
metallacrowns, 364, 366, 368  
metallacyclic complexes, 366  
metallocene structures, 442  
metallurgical applications of rare earths, 9  
metamorphic rock, 868  
methanol, 168, 281, 282  
methoxide bridges, 440  
micelles, 561  
Michael reaction, 955  
microorganisms, 884  
microstate table, 663  
microstates, 86, 89  
microwave digestion, 52, 53  
middle earths, 3  
migration of lanthanides, 883  
Mikulin-Sergievskii-Dannus model, 30  
miscellaneous complexes, 661  
misch metal, 897, 909  
mitochondrial membranes, 867  
mixer-settlers, 28  
modulating transducers, 929  
molar absorptivity of rare-earth ions, 41  
mole ratio method, 139, 140  
molecular orbital-linear combination, 589  
molecular stereochemistry, 781  
monazite, 8, 11, 12, 16, 32, 33, 46  
monoacetato complex, 646  
monobromo complexes, 282  
monocyclopentadienyl complexes, 442, 444, 445  
monodentate configuration, 282  
monodentate ligand, 352  
monomeric complexes, 437  
mononuclear complexes, 129-131  
monopentamethyl cyclopentadiene, 456  
motors and generators, 917  
Mulliken bond order, 382  
multidentate complexing agents, 876  
multidentate ligands, 156, 298, 314, 315  
multilayer capacitors, 934  
multiphase quaternary borocarbide system, 949  
multiplet structures, 119, 745, 752, 740  
  
natural abundance of rare earth elements, 4  
Nd complexes, 459  
neodymium, 394  
neodymium complexes, 338, 409, 410, 718  
neodymium lasers, 921  
nephelauxetic action, 174  
nephelauxetic effect, 172, 428, 593  
nephelauxetic series, 594  
Nernst-Peter equation, 326  
nerve blocking agent, 866  
neutral bidentate complexes, 395  
neutron activation analysis, 63  
nickel, 111

- nickel–iron–cobalt-base superalloys, 910
- nicotinate complex, 403
- NiMH rechargeable batteries, 927
- nitrate, 283
- nitrate complexes, 288, 289
- nitrile ligands, 429
- nitriles, 959
- nitrioloacetate complexes, 161
- nitrioloacetic acid, 379
- nitrilotriacetic acid complexes, 379
- nitrogen donor ligands, 441, 659
- nitrogen donors, 295
- nitrogen–oxygen donors, 299
- NMR imager, 976
- NMR shift reagents, 781
- non-ionizable ligands, 267
- non-solvated lanthanide cyclopentadienyl hydride complexes, 469
- nona-coordinate metal atoms, 407
- nonactin, 303, 304
- nonactin potassium complex, 304
- noncyclic ligands, 168
- NTA, 176, 266
- nuclear imaging, 971
- nuclear magnetic resonance, 971
- nuclear relaxation, 794
- nuclear relaxation methods, 855
- nuclear waste management, 311, 327
- nucleic acids, 656, 864
- nucleoside phosphates, 864
- nucleotides, 862
  
- octa-coordinate metal atoms, 398
- octahedral complexes, 156, 642
- octahedral lanthanide complexes, 598
- octahedral substitution, 485
- octakis lanthanum(III) ion, 404
- octakis perchlorate, 402
- olive oil aroma, 338
- optical isomers, 262
- optical purity, 810
- optical purity determination, 808
- optical spectral transitions, 576
- optoelectronic devices, 474
- orbital energy, 90
- orbitals, 78, 79, 81–83, 85, 92
- organic acids, 883
- organic synthesis, 952
- organolanthanide chemistry, 425
- organolanthanide complexes, 470, 474
- organolanthanides, 473
- organometallic complexes, 423, 425
- organometallic compounds, 960
- organs, 828
  
- outer sphere, 163
- outer-sphere complexation, 284, 488
- outer-sphere complexes, 279, 488
- oxalate complexes, 290, 504, 505, 542
- oxalato complex, 540
- oxidation of cerium, 762
- oxidation states, 96
- oxide adhesion, 911
- oximate bridge, 436
- oximes, 436
- oxyanions, 288
- oxydiacetate (ODA) complexes, 638
- oxydiacetate complexes, 651
- oxygen bearing complexes, 437
- oxygen bonded complexes, 440
- oxygen donor ligands, 276
- oxygen donors, 289, 294
- oxygen sensors, 933
- oxygen-17 shifts, 785
- oxynitrates, 264
  
- paints and pigments, 907
- para-sulfonated-calixarenes, 362
- paramagnetic complexes, 784, 794
- paramagnetic lanthanides, 856, 867
- paramagnetic line broadening, 496
- paramagnetic relaxation probe, 857
- paramagnetic species, 345
- paramagnetism, 781
- parvalbumin, 823, 824, 827, 828
- Pauli's exclusion principle, 84, 123
- Pauli's hole-equivalence, 123
- Pedersen, Charles J., 305
- pegmatites, 9, 869
- pentahapto indenyl coordination, 463
- pentamethyl cyclopentadiene lanthanide complexes, 448
- pentaytterbium cluster complex, 456
- perchlorate, 289
- perchlorate complexes, 278, 280
- perchlorate complexes of AA, 552
- perchlorate vibrations, 279
- perfused heart preparations, 830
- perfused tissues and organs, 781
- permanent magnets, 916, 917
- perovskites, 110, 906
- perturbation energy, 115
- petroleum refining, 902
- phagocytosis, 867
- pharmaceuticals, 808
- phenyl ring, 169
- phenylacetic acid complexes, 553
- phosphatidylcholine, 866

- phosphatidylcholine bilayer membranes, 867  
 phosphinamides, 295  
 phosphine oxide complex, 442  
 phosphoglycerate kinase, 821  
 phospholipid membranes, 867  
 phospholipids, 866  
 phosphor systems, 944  
 phosphors, 929, 941, 946  
 phosphors for CRTs, 943  
 phosphors for fluorescent lamps, 941  
 phosphors for vacuum UV excitation, 943  
 phosphorus acids, 265  
 photo stimulable luminescence, 929  
 photochemistry of cerium system, 555  
 photochemistry of Eu, 554  
 photochemistry of lanthanide complexes, 553  
 photochemistry of lanthanides, 554  
 photodynamic treatment, 340  
 photoelectron spectroscopy, 733, 735, 740  
 photoionization, 735  
 photoluminescent labels, 964  
 photonics, 929  
 photonics, electronics, 928  
 photophysics of lanthanide complexes, 553  
 photoredox reactions, 554  
 photosubstitution reactions, 557  
 phthalocyanine complexes  $\text{LnPc}_2$ , 307  
 phthalocyanine triple decker complexes, 337  
 phthalocyanines, 307, 316, 334, 338, 368  
 pinacol coupling reactions, 957  
 podands, 312, 315  
 podates, 319, 320  
 point charge model, 583  
 polarographic methods, 40, 150  
 polarography, 130, 135, 136, 149  
 pollution control, 906  
 polyamino carboxylates, 970  
 polyamino polyacetic acids, 266  
 polyaminocarboxylic acids, 877  
 polyaminopolycarboxylates, 965  
 polycyclic ethers as oxygen donors, 294  
 polydentate inorganic anions, 262  
 polydentate ligands, 314  
 polyether ring, 169  
 polymer production, 907  
 polymerization catalysts, 906  
 polymers, 806  
 polymetallic assemblies, 368  
 polynuclear complexes, 130, 137  
 polynuclear macrocyclic complexes, 268  
 polyols, 865  
 population inversion, 922  
 porphyrins, 269, 307, 316, 334, 368  
 potassium complex, 304  
 potentiometric method, 148, 149  
 potentiometric technique, 136  
 potentiometric titration, 151  
 potentiometry, 130, 133, 277  
 praseodymium, 122  
 praseodymium complex, 301, 379  
 praseodymium group, 410  
 precipitating luminogenic chelate-based substrates, 969  
 precipitation, 19, 176  
 precipitation reactions, 40  
 precursor complexes, 546  
 predisposed ligands, 311  
 predominance diagrams, 879  
 preparation of rare earth metals, 46  
 pressure-jump method, 494  
 pressure-jump technique, 502  
 pricing pattern, 15  
 principle of hole formalism, 90  
 probing biochemical reactions, 850  
 production, 14  
 production of rare earth metals, 33  
 production of rare earths chloride from bastnasite, 17  
 propylene carbonate, 168  
 protein biosynthesis, 865  
 proteins, 828  
 proton relaxation, 795  
 proton resonances, 781  
 proton shifts, 785  
 protonation constant, 265  
 pseudohalides, 285, 287  
 pseudohypersensitive transitions, 598  
 pseudohypersensitivity, 599  
 pseudoquadrupole transitions, 598  
 PTC thermistors, 935  
 pulsed continuous flow, 493  
 pyridine based complexes, 559  
 pyridine derivatives, 970  
 pyridine groups, 335  
 pyridine-*N*-oxide complexes, 295  
 quadrupole transitions, 598  
 qualitative analytical reagents, 49  
 qualitative reagents for rare earth elements, 35  
 qualitative spectral analysis, 781  
 quantum mechanical perturbation method, 115  
 quantum mechanics, 75  
 quantum numbers, 78, 79, 84  
 quaternary borocarbides, 951  
 quinuclidine complex, 390  
 R(EDTA), 534  
 R-G bonds, 309

- Racah parameters, 90, 99, 100, 123, 172  
Racah's theory, 123  
radar equipment, 935  
Radecka-Paryzek, Wanda, 332  
radial function, 77  
radial wave functions, 78  
radiation synovectomy, 962  
radiation transducers, 929  
radioimmunoassays, 964  
radioimmunotherapy, 966  
radionuclide therapy, 961  
radiosynovectomy, 886  
rapid reactions, 490  
rapidly solidified alloys, 913  
rare earth catalysts, 902  
rare earth deposits in India, 7  
rare earth distribution in soils, 872  
rare earth elements, 897  
rare earth extraction, 27  
rare earth magnets, 916  
rare earth markets, 5  
rare earth metal salts, 898, 900, 901  
rare earth naphthenate, 908  
rare earth oxide systems, 746  
rare earth phosphors, 945  
rare earth reserves, 5  
rare earth sources, 10  
rare earth substituted garnet films, 940  
rare earth triflates, 952, 956  
rare earth trifluorides, 744  
rare earth/cerium oxide, 28  
rare earths, 14  
rare earths as catalysts, 902  
rare earths consumption, 10  
rare earths in alloys, 909  
rare earths in steels, 896  
rate constant, 485, 486, 488  
rate laws, 484, 485  
reaction classification, 485  
reagents for rare earths elements, 34  
rechargeable battery market, 928  
recovery of rare earths from monazite, 33  
recovery of rare earths from ores, 16  
recovery of rare earths from xenotime, 18  
recycling, 327  
redox potentials, 425  
redox reactions, 547  
refined spin-pairing energy theory, 124  
relaxation methods, 493  
reserves of rare earths, 5  
rhodium complexes, 818  
ribosomes, 865  
ring bridged cyclopentadienyl lanthanide complexes, 458  
ring opening, 958  
ring opening reactions, 959  
ring size, 165  
rock-forming minerals, 868  
root sorption, 886, 888  
Rossotti, 137  
Russell-Saunders, 573  
Russell-Saunders coupling, 120  
Rydberg, J., 119, 121  
  
salicylic acid recognition, 970  
samarium complexes, 152, 453  
samarium hydride complex, 452  
sandwich complexes, 318  
sandwich compounds, 334  
satellite peaks, 747, 768  
Sato, Nariaki, 357  
Sc carbollide complex, 458  
scandium, 92, 93  
scandium group, 92  
Schiff base derivatives, 307  
Schiff base macrocyclic ligands, 311  
Schiff bases, 266, 267  
Schrödinger equation, 75, 77–79, 119  
sedimentary rocks, 868  
sedimentation, 886, 887  
selenocyanate complexes, 288  
self-assembly processes, 312  
semiconducting light emitting diodes, 944  
semiconductors, 474  
sensors, 928  
separation factors, 26, 30, 33  
separation of contact and dipolar contributions, 790  
separation of rare earths, 19  
separation of rare earths by ion exchange, 22  
sepulchrand, 315  
serigraphy, 932  
Sessler, John, 339  
shake-down satellites, 747  
shake-up satellites, 747, 763  
shift reagent equilibria, 796  
shift reagent ligands, 801  
shift reagents, 781, 782, 798, 799, 810, 812  
Shinkai, Seiji, 335, 357  
silicates, 869  
simulation of induced shifts, 837  
single-mode fibre lasers, 939  
Slater's rules, 104  
Slater-Condon-Shortley parameters, 123  
soft character, 112  
soft-soft interaction, 117  
soils, 872  
solid rare earth complexes, 285

- solvation state, 559  
solvent exchange, 517  
solvent exchange in water, 523  
solvent extraction, 28, 31, 176, 177  
solvent extraction reagents, 26  
solvent separated complexes, 163  
solvent-cage effect, 485  
some physical properties of rare earth metals, 4  
sorption by aquatic insects, 886, 887  
spalling behaviour, 911  
speciation of rare earth elements, 873  
specific guests, 270  
spectra of divalent lanthanides, 634  
spectral parameters of complexes, 717  
spectral-kinetic method, 561  
spectrophotometric analysis of rare earths with organic reagents, 43  
spectrophotometric method of analysis, 61  
spectrophotometric methods, 176  
spectrophotometric methods for the rare earth elements, 42  
spectrophotometric studies, 272  
spectrophotometry, 277  
spin density oscillations, 104  
spin multiplicity, 86  
spin polarization, 787  
spin-lattice relaxation studies, 813  
spin-orbit energies, 668  
spin-orbit interaction, 578  
spin-orbit interaction perturbation, 668  
spin-orbit splittings, 752  
spin-orbital levels, 678  
spin-orbit coupling, 91  
spin-orbit levels, 88  
spin-pairing energies, 122, 170, 173  
square antiprismatic geometry, 401  
stability constants, 129, 130, 134, 136, 140, 151, 158, 168, 173, 265  
stability of complexes, 127  
stability of rare earth complexes in solution, 150  
stabilized zirconia, 933  
staphylococcal nuclease, 862  
steels, 896  
stereochemistry, 485, 486  
steric effects, 160, 277  
steric factors, 153  
steric hindrance, 152  
Stetter, H., 343  
Steven's factors, 579  
stoichiometry, 262  
stopped-flow apparatus, 493  
stopped-flow method, 492  
structure of complexes, 645  
substituted cyclopentadienyls, 431, 445  
sugars, 866  
sulfoxide group, 295  
sulfuric acid digestion, 16  
sulphide minerals, 871  
sulphuric acid process, 16  
superalloys, 912  
superconducting devices, 926  
superconductors, 948  
supramolecular complexes, 537  
surface oxidation, 762  
symmetry, 604  
synthesis of lanthanide complexes, 265  
tartrate complexes, 551  
temperature apparatus, 495  
temperature dependence of contact and dipolar shifts, 789  
temperature-jump experiment, 496  
temperature-jump method, 494, 501  
template effect, 332  
ten coordinate adducts, 429  
tensor operator method, 686  
tensor operators, 673  
terbium complexes, 559  
ternary complexes, 774  
terpyridyl, 298  
tetraazaporphine complexes, 538  
tetraglyme complex, 448  
tetrakis acetylacetonate complex, 395  
tetrakis complexes, 267, 395, 654  
tetrakis lutetium complex, 382  
tetrakis yttrate ion, 401  
tetrakis-cyclopentadienyl lanthanide, 426  
tetrakis-dibenzoyl methane complexes, 380  
tetrakis-hexafluoro acetylacetonates, 400  
tetrameric samarium complex, 458  
tetrameric units, 434  
tetramethylethylene bridge, 459  
tetrapyrrole derivatives, 334  
tetrapyrrole-based ligands, 335  
texaphyrins, 339  
thallous cyclopentadienides, 429  
thermal decomposition kinetics, 547, 550  
thermal reactions, 19  
thermodynamic considerations, 160, 314  
thermodynamic equilibrium, 489  
thermoluminescence, 929  
thiocyanate, 282  
thiocyanate complexes, 287, 288  
thiocyanato complexes, 282, 283  
thorium, 94  
three-level laser system, 922  
three-way catalysts, 905

- thulium, 152, 939  
Ti-base alloys, 915  
tissues, 828  
titanium alloys, 909  
titanium aluminides, 915  
TMDTA, 167  
TMEDTA, 167  
toxicity, 884  
transducers, 928, 929, 931  
transmetallation reactions, 445  
tribracchial lariat ethers, 341  
tricapped trigonal prism, 405  
tricapped trigonal prismatic coordination, 408  
tricyclopentadienyl complexes, 425  
tridentate borohydride bridges, 438  
trifluoromethane sulfonate, 279, 280  
trifluoromethane sulfonate complexes, 952  
trihapto indenyl coordination, 463  
triisopropoxides, 293  
trinuclear carborane clusters, 473  
triphenyl arsine oxide complexes, 295  
tris complex, 654  
tris-chelates, 380  
tris-dipivaloylmethane complexes, 384  
triscyclopentadienyl lanthanides, 426  
trisdioxyacetato complexes, 405  
trisdipicolinato, 405  
trisdipivoyl methane complexes, 380  
trishaloacetates, 659  
trishydroxyacetato complexes, 405  
trisindenyl cerium pyridinate, 463  
trisoxalato complexes, 405  
trivalent cerium, 613  
trivalent dysprosium, 625  
trivalent erbium, 627  
trivalent europium, 619  
trivalent gadolinium, 345, 624  
trivalent holmium, 627  
trivalent lanthanides, 111, 576, 784  
trivalent neodymium, 614, 922  
trivalent praseodymium, 614  
trivalent promethium, 619  
trivalent rare earth ions, 377  
trivalent rare earths, 883  
trivalent samarium, 619  
trivalent terbium, 624  
trivalent thulium, 632  
trivalent ytterbium, 632  
tumor therapy, 329  
tumors, 886  
ultrasonics, 494  
unidentate ammonia, 296  
unimolecular reaction, 484  
unpaired f electrons, 781  
UV-vis spectroscopy, 130  
valence band region, 740  
valence fluctuation, 752  
valence shell electron-pair repulsion, 111  
van der Waals interactions, 309  
variation exchange splittings, 745  
variation of rate constant, 486  
vibrational spectroscopy, 283  
volumetric methods of analysis of rare earth elements, 38  
von Baeyer, Adolf, 307  
water exchange rates, 526  
water proton relaxation rates, 856  
wave functions, 75, 77, 103  
weathering, 870  
Werner, Alfred, 303  
Wigner-Eckart theorem, 576  
Wimpenny, Richard, 366  
X-ray absorption edge studies, 109  
X-ray absorption spectroscopy, 107  
X-ray crystallography, 271  
X-ray diffraction, 858  
X-ray fluorescence analysis, 65  
X-ray imaging, 971  
X-ray photoelectron emission spectroscopy, 107  
X-ray photoelectron spectroscopy, 740, 763  
X-ray spectroscopy, 65  
xenotime, 11, 12, 16  
ytterbium, 92, 338  
ytterbium complexes, 792  
yttria-stabilized zirconia, 928  
yttrium, 13, 15, 20, 49, 50, 57, 69, 92, 93, 152  
yttrium complex, 400  
yttrium earths, 19  
yttrium group, 156, 158–160  
yttrium iron garnet, 931, 936, 940  
yttrium subgroup, 154, 155  
yttrium triflate, 958  
Zeeman operator, 574  
Ziegler, Erich, 308  
Ziegler-Natta catalysts, 473  
Ziegler-Natta type, 448  
Zinke, Alois, 308  
zirconium fluoride optical glass, 939